PIERS 2014 Guangzhou

Progress In Electromagnetics Research Symposium

Abstracts

August 25–28, 2014
Guangzhou, CHINA

www.emacademy.org
www.piers.org

PIERS 2014 Guangzhou Abstracts

Published by

The Electromagnetics Academy
777 Concord Avenue, Suite 207
Cambridge, MA 02138

www.emacademy.org
www.piers.org

ISSN: 1559-9450
ISBN: 978-1-934142-27-1

Welcome to PIERS 2014 Guangzhou,

where microwave and lightwave communities meet

It is our great pleasure to invite you to participate in Progress in Electromagnetics Research Symposium (PIERS) 2014 and share the latest findings in the electromagnetic wave spectrum (including microwave and lightwave, and beyond).

This year is a special year because it marks the 150 years of Maxwell's Equations. James Clerk Maxwell presented his important finding to the British Royal Society in 1864. Both microwave and lightwave are governed by the same Maxwell's equations. However, many people in microwave rarely read papers in optics journals and "reinvented the wheel" from time to time, while many other people in optics rarely read papers in microwave journals and keep "reinventing the wheel". It is therefore very worthwhile to encourage the microwave community and the lightwave community to meet and talk (or listen) to each other in a conference. PIERS 2014 is a great event as a Family Reunion of Electromagnetic Waves, where microwave and lightwave communities meet.

PIERS 2013 Stockholm was a great success with 1,650 paper submissions and 1,135 registered/paid participants from 67 countries and many top-notch keynote/invited speakers of the areas. PIERS 2014 Guangzhou is setting a new record with over 2,000 paper submissions.

Like PIERS 2013 Stockholm, this year's conference will feature the following five tracks:

SC 1. Computational Electromagnetics, Electromagnetic Compatibility, Scattering and Electromagnetic Theory;

SC 2. Metamaterials, Plasmonics and Complex Media;

SC 3. Optics and Photonics;

SC 4. Antennas and Microwave Technologies;

SC 5. Remote Sensing, Inverse Problems, Imaging, Radar and Sensing.

PIERS 2014 Guangzhou features a full suite of plenary, keynote, invited, and contributed talks given by international academic and industrial researchers who are leaders in their respective fields.

The plenary Session is scheduled on the morning of Monday, August 24, with five outstanding speakers. Prof. Sir John Pendry (Imperial College London, UK) will give a plenary talk on metamaterials. Prof. David Miller of Stanford University will discuss low-energy integrated photonics for information processing. Prof. Akira Ishimaru (University of Washington, Seattle, USA) will talk about "Statistical Electromagnetic Theories Applied to Imaging in Geophysical and Biological Random Media". Prof. Federico Capasso of Harvard University will give a plenary talk "Flat Optics Based on Metasurfaces: Molding Wavefronts and Surface Waves". Prof. Lihong Wang (Washington University in St. Louis, USA) will give a presentation entitled "Photoacoustic Tomography: Ultrasonically Beating Optical Diffusion and Diffraction".

A sesquicentennial anniversary session to commemorate 150 years of Maxwell's equations is organized at PIERS 2014, with the following nine distinguished senior speakers of the electromagnetics community: Jean-Charles Bolomey, Federico Capasso, Weng Cho Chew, Raymond W. Chiao, Giorgio Franceschetti, Prabhakar H. Pathak, John B. Pendry, Donald R. Wilton, and Arthur D. Yaghjian.

Two mini-symposia have been organized in PIERS 2014, with many excellent keynote/invited speakers. One is on "Photovoltaics, LEDs and Other Optoelectronics in Energy" organized by Wallace C. H. Choy and Mario Dagenais. It consists of 6 sessions with different organizers. The other mini-symposium is on "Microwave Photonics" (organized by Christina Lim and Chao Wang) with 3 sessions on various related topics.

The feature of Focus sessions introduced in PIERS 2013 Stockholm continues this year. PIERS 2014 has about 20 focus sessions on various hot topics, such as Casimir Effect and Heat Transfer, Photoacoustic Tomography and Sensing, Disordered Photonics, Tunable and Reconfigurable Metamaterials and Plasmonics, etc..

In addition to the regular technical sessions, several pre-conference short courses have been planned for PIERS 2014.

Best Student Paper Awards will be given to students who are first authors and presenters of excellent contributed talks. Awards will be presented during the Banquet on August 27.

To encourage participants to meet with the authors and discuss technical issues in-depth, free beer will be provided at the poster session area around the coffee break time of the first three days.

A Welcome Reception will be held in the evening of August 24 on the 3rd floor of the conference hotel (the Langham Place Guangzhou).

If you want to visit any local Guangzhou institutions, organizations and companies, you may contact our local organizer, South China Normal University. They will be glad to assist you for any request you may have.

It is an enormous task to organize this big conference and it is impossible to succeed without the dedicated efforts of many supporters and volunteers. We are indebted to the entire Technical Program Committee, particularly, the Technical Program Committee Chairs, the Subcommittee Chairs, and the Session organizers who have worked persistently throughout the year to invite speakers and organize the technical sessions which results in the present excellent technical program.

We thank all the contributors and authors for making PIERS 2014 a truly unique, outstanding global event.

Sincerely,

Prof. Sailing He,

The Royal Inst. of Technology, Sweden
and JORCEP (Sino-Swedish Joint Research Center of Photonics), China, Lead General Co-chair

Prof. Kazuya Kobayashi

Chuo University, Japan, General Co-chair

Prof. Raj Mittra

Pennsylvania State University, USA, General Co-chair

Prof. Ke Wu

Ecole Polytechnique, University of Montreal, Canada, General Co-chair

THE ELECTROMAGNETICS ACADEMY

The Progress in Electromagnetics Research Symposium (PIERS) is sponsored by The Electromagnetics Academy.

The Electromagnetics Academy is devoted to academic excellence and the advancement of research and relevant applications of the electromagnetic theory and to promoting educational objectives of the electromagnetics profession. PIERS provides an international forum for reporting progress and advances in the modern development of electromagnetic theory and its new and exciting applications.

Founded by the late Professor Jin Au Kong (1942–2008) of MIT in 1989, The Electromagnetics Academy is a non-profit organization registered in USA.

JOURNAL:
PROGRESS IN ELECTROMAGNETICS RESEARCH

Progress In Electromagnetics Research (PIER) publishes peer-reviewed original and comprehensive articles on all aspects of electromagnetic theory and applications. This is an open access, on-line journal PIER (E-ISSN 1559-8985). It has been first published as a monograph series on Electromagnetic Waves (ISSN 1070-4698) in 1989. It is freely available to all readers via the Internet.

PIER is a non-profit organization.

WWW.JPIER.ORG

Contact Email: work@jpier.org

Progress In Electromagnetics Research Symposium
August 25–28, 2014
Guangzhou, CHINA

PIERS 2014 GUANGZHOU ORGANIZATION

PIERS 2014 Guangzhou General Co-chairs

Sailing He, Royal Institute of Technology, SWEDEN; JORCEP, CHINA

Kazuya Kobayashi, Chuo University, JAPAN

Raj Mittra, Pennsylvania State University, USA

Ke Wu, University of Montreal, CANADA

PIERS Chair

Leung Tsang, University of Washington, USA

PIERS 2014 Guangzhou Technical Program Committee Co-chairs

Yang Hao, University of London, UK

Iam-Choon Khoo, Pennsylvania State University, USA

Joshua Li, University of Electronic Science and Technology, CHINA

Ari Sihvola, Aalto University, FINLAND

Sune Svanberg, Lund University, SWEDEN

PIERS 2014 Guangzhou Subcommittee 1
(CEM, EMC, Scattering and Electromagnetic Theory)

Weng Cho Chew, University of Illinois, USA, Lead Co-Chair
Qiang Chen, Tohoku University, Japan, Co-Chair
Jin-Fa Lee, Ohio State University, USA, Co-Chair
Qing Huo Liu, Duke University, USA, Co-Chair
Yoichi Okuno, Kumamoto University, Japan, Co-Chair

Mauro Antezza	Lei Bi	Yangjian Cai	Georgi Nikolov Georgiev
Eva Gescheidtova	Brahim Guizal	Satoru Kurokawa	Shinichiro Ohnuki
Rafal Przesmycki	Yury V. Shestopalov	Mei Song Tong	Jan Vrba
Zheng Wang	Ying Wu		

PIERS 2014 Guangzhou Subcommittee 2
(Metamaterials, Plasmonics and Complex Media)

Che Ting Chan, Hong Kong University of Science and Technology, China, Co-Chair
Tie Jun Cui, Southeast University, China, Co-Chair
Yongmin Liu, Northeastern University, USA, Co-Chair
Din Ping Tsai, Taiwan University, Taiwan, Co-Chair
N. Asger Mortensen, Technical University of Denmark, Denmark, Co-Chair

Hongsheng Chen	Nicholas X. Fang	Zheyu Fang	Lei Gao
Aaron Ho-Pui Ho	Zubin Jacob	Krzysztof Kempa	Yuri Kivshar
Geoffroy Lerosey	Jensen Li	Xiaofeng Li	Zhi-Yuan Li
Cun-Zheng Ning	Willie J. Padilla	Ilya V. Shadrivov	Ranjan Singh
Shumin Xiao	Baile Zhang	Han Zhang	Lei Zhou

PIERS 2014 Guangzhou Subcommittee 3
(Optics and Photonics)

El-Hang Lee, Fellow of Korean Academy of Science and Technology, South Korea, Lead Co-Chair
Katarina Svanberg, Lund University, Sweden, Co-Chair
Benjamin Eggleton, University of Sydney, Australia, Co-Chair
Mario Dagenais, University of Maryland, USA, Co-Chair

Alexander Argyros	Gilberto Brambilla	Giulio Cerullo	Jiajia Chen
Ray Chen	Xuewen Chen	Hyuck Choo	Wallace C. H. Choy
Xin Da	Vladimir Falko	Zuyuan He	Kazuo Hotate
Darren Hudson	Peter Uhd Jepson	Wei Jin	Mikhail Lapine
Kwang-Sup Lee	Jianfeng Li	Christina Lim	Liu Liu
David Marpaung	Oliver Muecke	Dragomir Neshev	Andrew Poon
Cees Ronda	Ali Serpenguzel	Zhimin Shi	Xuewen Shu
Fabien Sorin	Nelson Tansu	Chao Wang	Yiping Wang
Lech Wosinski	Siyuan Yu		

PIERS 2014 Guangzhou Subcommittee 4
(Antennas and Microwave Technologies)

Kamal Samanta, Milmega/Teseq, UK, Co-Chair
Maurizio Bozzi, University of Pavia, Italy, Co-Chair
Xun Gong, University of Central Florida, USA, Co-Chair
Xiaodong Chen, Queen Mary College, University of London, UK, Co-Chair
Zhongxiang Shen, Nanyang Technological University, Singapore, Co-Chair

Elisenda Bou Balust	Dau-Chyrh Chang	Albert Chin	Masahiro Horibe
Wenxing Li	Yungui Ma	Chong Kim Ong	Oscar Quevedo-Teruel
Nian-Xiang Sun	Tsuyoshi Uchiyama	John Y. C. Vardaxoglou	Yuan Yao
Qiaowei Yuan	Lei Zhu		

PIERS 2014 Guangzhou Subcommittee 5
(Remote Sensing, Inverse Problems, Imaging, Radar and Sensing)

Leung Tsang, University of Washington, USA, Lead Co-Chair
Kun-Shan Chen, Institute of Remote Sensing and Digital Earth, CAS, China, Co-Chair
Mats Gustafsson, Lund University, Sweden, Co-Chair
Matti Lassas, University of Helsinki, Finland, Co-Chair
Jianchen Shi, University of California, Santa Barbara, USA, Co-Chair

Xudong Chen	Shuanggen Jin	Lai Bun Lok	Sven Nordebo
Rocco Pierri	Raffaele Solimene	Xiaobing Wang	

PIERS 2014 Guangzhou Local Organizing Committee

Sailing He (Co-chair)	Jun Li (Co-chair)

Xianyu Ao	Kun Cai	Erik Forsberg	Changjian Guo
Xuezhi Hong	Wen Huang	Jin Liu	Liu Liu
Ziqian Luo	Li Peng	Chunlin Tan	Qiuqiang Zhan
Yuan Zhang	Bin Zhou	Huilin Zhu	Wanlin Zhu

PIERS 2014 GUANGZHOU SESSION ORGANIZERS

M. Antezza
E. B. Balust
M. Bozzi
P. K. L. Chan
K.-S. Chen
S.-Y. Chen
Z. Chen
W.-Y. Choi
T. J. Cui
R. E. De Araujo
Z. Fang
L. Gao
M. N. Georgieva-Grosse
B. Guizal
B. S. Ham
A. H.-P. Ho
D. D. Hudson
S. Jin
H.-L. Kao
S. Kurokawa
D. Lei
W. Li
A. Liang
Q. H. Liu
T. C. Lu
R. Mittra
D. N. Neshev
S. Ohnuki
W. J. Padilla
S. Popov
O. Quevedo-Teruel
L. Sakhnini
L. Shao
Z. Shi
R. Singh
Y. Su
S. Svanberg
D. P. Tsai
J. Vrba
L. H. V. Wang
Z. Wang
L. Wosinski
Y. Wu
D. Xing
T. Yamasaki
R. Yang
J. Yu
Q. Yuan
X. Zhang
H. Zhu

A. Argyros
N. Behdad
G. Brambilla
D.-C. Chang
N. Chen
X. D. Chen
Q. Cheng
H. Choo
M. M. Da Silva
S. Du
S.-P. Feng
S. Gao
E. Gescheidtova
L. J. Guo
J. Hao
M. Horibe
Z. Jacob
W. Jin
I.-C. Khoo
Y. Lai
G. Lerosey
X. Li
D. Liang
Y. Liu
Y. Ma
N. A. Mortensen
C.-Z. Ning
Y. Okuno
D. Payne
R. Przesmycki
C. C. Renaud
K. K. Samanta
Z. Shen
J. Shibayama
R. Solimene
N.-X. Sun
N. Tansu
T. Uchiyama
C. Wang
W. Wang
P. R. Watekar
B. Wu
F. Xia
C. Xu
L. Yan
T.-J. Yang
S. Yu
H. Zeng
G. Zhou
L. Zhu

M. H. Asghari
L. Bi
Y. Cai
H. Chen
Q. Chen
X. D. Chen
W. C. Chew
W. C. H. Choy
M. Dagenais
H. Duan
M. Fleischer
P. D. Garcia
N. C. Giebink
Y. J. Guo
Y. Hao
K. Hotate
B. Jalali
B. L. G. Jonsson
Y. S. Kivshar
Y.-C. Lan
J. Li
Z. Li
H. Liu
Y. M. Liu
D. Marpaung
O. D. Mücke
S. Nordebo
C. K. Ong
R. Pierri
J. Qian
H. Rogier
A. Serpenguzel
Y. V. Shestopalov
X. Shu
F. Sorin
S. Sun
M. S. Tong
J. Y. C. Vardaxoglou
C. W. Wang
Y. C. Wang
Z. Wei
C.-J. Wu
S. Xiao
K. Xu
J. K. W. Yang
Y. Yao
W. Yu
B. Zhang
J. Zhou
T. Zhu

S. Ates
G. G. E. Bjork
D. Cao
J. Chen
K.-P. Chen
X. W. Chen
A. Chin
Q.-X. Chu
D. Dai
N. X. Fang
J. Gao
G. N. Georgiev
A. A. Glazunov
M. Gustafsson
Z. He
Y.-Z. Huang
L. J. Jiang
J.-H. Jou
K. Kobayashi
J.-H. Lee
J. F. Li
Z.-Y. Li
L. Liu
Z. Liu
A. E. Miroshnichenko
H. Murata
L. Nowosielski
H. Ou
A. W. O. Poon
Q. Quan
C. Ronda
I. V. Shadrivov
J.-C. Shi
A. Sihvola
E. Sousa
K. Svanberg
M. R. Tripathy
F. Vollmer
F. Wang
Y. P. Wang
L. Wosinska
W. Wu
D. Xie
X. Xu
L. Yang
H.-L. Yip
L. X. Yuan
H. Zhang
Z. Zhou

PIERS 2014 GUANGZHOU ORGANIZERS AND SPONSORS

- ☐ South China Normal University
- ☐ JORCEP (Sino-Swedish Joint Research Center of Photonics), China
- ☐ Centre for Opt. & Electromagn. Res., South China Academy of Advanced Optoelectronics, South China Normal University
- ☐ ZJU Institute for Opto-electronic Technology Commercialization (IOTEC)
- ☐ Development & Research Academy for Global Optical Neo-technology (DRAGON)
- ☐ Shanghai Key Laboratory of Electromagnetic Environmental Effects for Aerospace Vehicle, China
- ☐ Asian Office of Aerospace Research and Development (AOARD)
- ☐ Office of Naval Research Global
- ☐ Bureau of Science and Information Technology of Guangzhou Municipal Government
- ☐ Shanghai Ideaoptics Instrument Co., Ltd., China
- ☐ The Electromagnetics Academy at Zhejiang University, China
- ☐ The Electromagnetics Academy

PIERS 2014 GUANGZHOU EXHIBITORS

- ☐ Simpleware Ltd., UK
- ☐ Altair Engineering Software (Shanghai), China
- ☐ Biaoqi Electronics/Ocean Optics, China
- ☐ Luster LightTech, China
- ☐ Shanghai Ideaoptics Instrument Co., Ltd., China
- ☐ Jiangsu DragonNova Optoelectronics Technologies Ltd., China

simpleware converting 3D images into models

FEKO Comprehensive Electromagnetic Solutions

DRAGON

复享 光谱改变生活

标旗 BIAOQI Ocean 海洋 Optics 光学

凌云光子 LUSTER

E³LAB 上海市航空航天器电磁环境效应重点实验室 Shanghai Key Laboratory of Electromagnetic Environmental Effects for Aerospace Vehicle

DRAGON: DRAGON/IOTEC can help you commercialize your ideas in China or help your existing company establish itself on the Chinese market. Visit our booth in the exhibit area for a discussion on how we can help you realize your ambitions in China.

PIERS 2014 SESSIONS

Session 1A1
Plenary Session

Flat Optics Based on Metasurfaces: Molding Wavefronts and Surface Waves

Federico Capasso
School of Engineering and Applied Sciences, Harvard University, USA

Abstract— Metasurfaces based on sub-wavelength patterning have major potential for realizing arbitrary control of the wavefront of the diffracted light by achieving local control of the phase amplitude and polarization [1]. We discuss novel devices based on this technique; a salient feature is the ability to create often with a single digital mask an arbitrary analog phase profile. A variety of flat optical components, including lenses, polarizers, vortex plates, coatings, holograms and couplers with polarization invariant coupling efficiency will be presented.

REFERENCES

1. Yu, N. and F. Capasso, *Nature Materials*, Vol. 13, 139, 2014.

Low-energy Integrated Photonics for Information Processing

David A. B. Miller
Stanford University, USA

Abstract— Optical interconnects are likely to be essential for future high-performance information processing and switching machines because of the need to reduce energy consumption and increase bandwidth density [1, 2]. Though the increasing use of optics may be the only viable physical approach to achieving both of these goals, the necessary optoelectronic devices and associated integration technology are nonetheless very challenging. Very low operating energies are required in the optoelectronic devices, into the 10's of femtojoules and ideally even below such levels; such energies strain the abilities of standard approaches to many optoelectronic devices, such as lasers and modulators. Integration with the electronics is essential if overall capacitances (and hence operating energies) are to be minimized, again posing many device technology challenges.

In optoelectronic devices, operating energies in the scale of $\sim 10\,\mathrm{fJ}$ have been demonstrated (see, e.g., [3] and references therein), and the first sub-fJ devices are emerging [3–5], some [3, 4] with serious prospects of integration in silicon integrated circuit processes. There are arguably many opportunities for optoelectronic devices with even lower energies. We can exploit nanoresonators, such as photonic crystal structures, to reduce volumes to allow very low threshold lasers [6] or very low energy modulators [5]. The quantum-confined Stark effect [7] is so strong that it can demonstrate sub-fJ modulator operation [3, 4] without even using any resonators. Nanometallic structures can concentrate and manipulate light at wavelength and subwavelength scales [8–10], allowing detectors with very low capacitance, for example; such low-capacitances can allow the elimination of receiver circuits and their power dissipation [11].

This talk will discuss some of these approaches and the prospects for future optoelectronic devices that could allow the continued scaling to higher capacities in handling information.

REFERENCES

1. Miller, D. A. B., "Device requirements for optical interconnects to silicon chips," *Proc. IEEE*, Vol. 97, 1166–1185, 2009.
2. Keckler, S. W., W. J. Dally, B. Khailany, M. Garland, and D. Glasco, "GPUs and the future of parallel computing," *IEEE Micro*, Vol. 31, No. 5, 7–17, Sep.–Oct. 2011.
3. Miller, D. A. B., "Energy consumption in optical modulators for interconnects," *Opt. Express*, Vol. 20, A293–A308, 2012.
4. Ren, S., Y. Rong, S. A. Claussen, R. K. Schaevitz, T. I. Kamins, J. S. Harris, and D. A. B. Miller, "Ge/SiGe quantum well waveguide modulator monolithically integrated with SOI waveguides," *IEEE Photonics Technol. Lett.*, Vol. 24, 461–463, 2012.
5. Shambat, G., B. Ellis, M. A. Mayer, A. Majumdar, E. E. Haller, and J. Vuckovic, "Ultra low power fiber coupled gallium arsenide photonic crystal cavity electro optic modulator," *Optics Express*, Vol. 19, 7530–7536, 2011.
6. Ellis, B., M. A. Mayer, G. Shambat, T. Sarmiento, J. Harris, E. E. Haller, and J. Vuckovic, "Ultralow-threshold electrically pumped quantum-dot photonic-crystal nanocavity laser," *Nature Photonics*, Vol. 5, 297–300, 2011.
7. Kuo, Y.-H., Y.-K. Lee, Y. Ge, S. Ren, J. E. Roth, T. I. Kamins, D. A. B. Miller, and J. S. Harris, "Strong quantum-confined stark effect in germanium quantum-well structures on silicon," *Nature*, Vol. 437, 1334–1336, 2005.
8. Tang, L., S. E. Kocabas, S. Latif, A. K. Okyay, D.-S. Ly-Gagnon, K. C. Saraswat, and D. A. B. Miller, "Nanometre-scale germanium photodetector enhanced by a near-infrared dipole antenna," *Nature Photonics*, Vol. 2, 226–229, 2008.
9. Ly-Gagnon, D.-S., K. C. Balram, J. S. White, P. Wahl, M. L. Brongersma, and D. A. B. Miller, "Routing and photodetection in subwavelength plasmonic slot waveguides," *Nanophotonics*, Vol. 1, 9–16, 2012.
10. Balram, K. C., R. M. Audet, and D. A. B. Miller, "Nanoscale resonant-cavity-enhanced germanium photodetectors with lithographically defined spectral response for improved performance at telecommunications wavelengths," *Opt. Express*, Vol. 21, 10228–10233, 2013.

11. Debaes, C., A. Bhatnagar, D. Agarwal, R. Chen, G. A. Keeler, N. C. Helman, H. Thienpont, and D. A. B. Miller, "Receiver-less optical clock injection for clock distribution networks," *IEEE J. Sel. Top. Quantum Electron.*, Vol. 9, 400–409, 2003.

Statistical Electromagnetic Theories Applied to Imaging in Geophysical and Biological Random Media

Akira Ishimaru, Ce Zhang, and Yasuo Kuga
Department of Electrical Engineering, University of Washington, USA

Abstract— Maxwell's Equations are the cornerstone of our profession. One of the important areas of the work of our profession is the statistical electromagnetic theories, which have a wide range of practical applications such as microwave remote sensing of the earth, object detection in clutter, medical optics and ultrasound imaging, characterization of metamaterials and composite materials, and wireless communications through clutter environments.

There have been great progress made in understanding statistical multiple scattering theories in random media and rough surfaces, which have been benefitted greatly from many studies made in quantum electrodynamics and astrophysics such as Feynman Diagrams, Wigner Distributions, Anderson Localizations and Dyson and Bethe-Salpeter equations. Tatarskii, Kong, Tsang and others made important contributions to the development of the statistical Electromagnetic theories.

This paper gives a review of statistical wave theories applied to problems of imaging in geophysical and biological random media including turbulence, particulate matter,and rough surfaces, and remote sensing. Important applications of the statistical EM are the remote sensing and imaging of objects in random media. There may be several recent developments which are important to advance the imaging technologies in clutter. They include the development of the coherence in multiple scattering. It may be normally expected that multiple scattering tends to decrease coherence and the waves become incoherent. However recent work revealed that the coherence can be maintained even under multiple scattering. Examples are the enhanced coherent backscattering, the memory effects and super resolution. These theories are applied to imaging in random media.

This paper discusses these effects to be used for imaging of objects including the time reversal in random media. It has been observed that the wave scattered by an object in random medium can trace and back propagate along the same path and form an image. It is also noted that multiple scattering can produce an equivalent larger input aperture to produce super resolution. Another interesting phenomenon is that even under multiple scattering the direction of the incident wave is remembered and strong correlation can be observed under certain conditions. This is called the "Memory Effects".

This paper discusses recent studies of the applications of these phenomena in imaging of objects in clutter environments, including integrations of signal processing and scattering for imaging, wireless channel capacity in random media, random media effects on OCT, seismic coda, photon density waves, porosity, Stokes vector emissivity and ocean wind direction,rough surface flattening transformation, and optical and ultrasound biological imaging.

Metamaterials

J. B. Pendry
Imperial College London, UK

Abstract— The recent advances in the field of metamaterials show the rich variety of effects that can be brought into play by micro-structuring a medium. Although studies of the effect of internal structure on material properties goes back at least to Maxwell, the potential for introducing truly radical properties is a recent development. I shall review some of the advances made in the field which include the expansion of the concept into acoustics, and finally make some speculations about what we might see in the future.

Photoacoustic Tomography: Ultrasonically Beating Optical Diffusion and Diffraction

Lihong V. Wang
Optical Imaging Lab, Department of Biomedical Engineering
Washington University, St. Louis, USA

Abstract— Photoacoustic tomography has been developed for *in vivo* functional, metabolic, molecular, and histologic imaging by physically combining non-ionizing electromagnetic and ultrasonic waves. Broad applications include early-cancer detection and brain imaging. Unlike ionizing x-ray radiation, non-ionizing electromagnetic waves — such as optical and micro-/radio waves — pose no health hazard andreveal new contrast mechanisms. Unfortunately, electromagnetic waves in the non-ionizing spectral region do not penetrate biological tissue in straight paths as x-rays do. Consequently, high-resolution tomography based on optical waves alone — such as confocal microscopy, two-photon microscopy, and optical coherence tomography — is limited to superficial imaging within approximately one optical transport mean free path (~ 1 mm in the skin)of the surface of scattering tissue. Ultrasonic imaging, on the contrary, provides good image resolution but suffers strong speckle artifacts as well as poor contrast in early-stage tumors. Ultrasound-mediated imaging modalities that combine electromagnetic and ultrasonic waves can synergistically overcome the above limitations. The hybrid modalities provide relatively deep penetration at high ultrasonic resolution and yield speckle-free images with high electromagnetic contrast.

In photoacoustic computed tomography, a pulsed broad laser beam illuminates the biological tissue to generate a small but rapid temperature rise, which leads to emission of ultrasonic waves due to the rmoelastic expansion. The short-wavelength pulsed ultrasonic waves are then detected by unfocused ultrasonic transducers. High-resolution tomographic images of optical contrast are then formed through image reconstruction. Endogenous optical contrast can be used to quantify the concentration of total hemoglobin, the oxygen saturation of hemoglobin, and the concentration of melanin. Melanoma and other tumors have been imaged *in vivo*. Exogenous optical contrast can be used to provide molecular imaging and reporter gene imaging.

In photoacoustic microscopy, a pulsed laser beam is focused into the biological tissue to generate ultrasonic waves, which are then detected with a focused ultrasonic transducer to forma depth resolved 1D image. Raster scanning yields 3D high-resolution tomographic images.Super-depths beyond the optical diffusion limit have been reached with high spatial resolution.Super-resolution beyond the optical diffraction limit has also been achieved recently. The following skin image was acquired in vivo in a mouse using optical-resolution photoacoustic microscopy.

The annual conference on this topic has been doubling in size approximately every three years since 2003 and has become the largest in SPIE's Photonics West as of 2010.

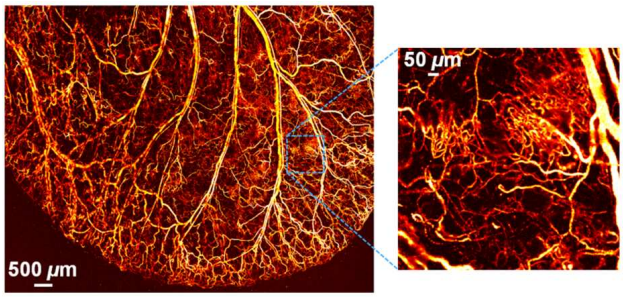

REFERENCES

1. *Nature Biotechnology*, Vol. 21, 803, 2003.
2. *PRL*, Vol. 92, 033902, 2004.
3. *PRL*, Vol. 96, 163902, 2006.
4. *Nature Biotechnology*, Vol. 24, 848, 2006.
5. *Nature Protocols*, Vol. 2, 797, 2007.

6. *PRL*, Vol. 99, 184501, 2007.
7. *Nature Photonics*, Vol. 3, 503, 2009.
8. *Nature Materials*, Vol. 8, 935, 2009.
9. *Nature Photonics*, Vol. 5, 154, 2011.
10. *Nature Materials*, Vol. 10, 324, 2011.
11. *Nature Photonics*, Vol. 5, 154, 2011.
12. *Science*, Vol. 335, 1458, 2012.
13. *Nature Medicine*, Vol. 18, 1297, 2012.
14. *PNAS*, Vol. 110, 5759, 2013.
15. *PRL*, Vol. 111, 204301, 2013.
16. *PNAS*, Vol. 111, 21, 2014.
17. *PRL*, Vol. 112, 014302, 2014.

Session 1P1
FocusSession.SC1: Casimir Effect and Heat Transfer

Casimir Forces between Monolithic Silicon Structures with Nonconventional Shapes

H. B. Chan[1], **J. Zou**[1, 2], **Z. Marcet**[1, 2], **A. W. Rodriguez**[3, 4], **M. T. H. Reid**[5], **A. P. McCauley**[6], **I. I. Kravchenko**[7], **T. Lu**[1], **Y. Bao**[2], **and S. G. Johnson**[4]

[1]Department of Physics, The Hong Kong University of Science and Technology
Clear Water Bay, Kowloon, Hong Kong, China
[2]Department of Physics, University of Florida, Gainesville, Florida 32611, USA
[3]School of Engineering and Applied Sciences, Harvard University, Cambridge, Massachusetts 02138, USA
[4]Department of Mathematics, Massachusetts Institute of Technology
Cambridge, Massachusetts 02139, USA
[5]Research Laboratory of Electronics, Massachusetts Institute of Technology
Cambridge, Massachusetts 02139, USA
[6]Department of Physics, Massachusetts Institute of Technology, Cambridge, Massachusetts 02139, USA
[7]Center for Nanophase Materials Sciences, Oak Ridge National Laboratory
Oak Ridge, Tennessee 37830, USA

Abstract— The Casimir force refers to the interaction between electrically neutral bodies that originates from the quantum fluctuations of the electromagnetic field. For two flat metallic plates separated by a vacuum gap, the Casimir force is attractive and the magnitude increases rapidly with decreasing separation. With the continual trend of miniaturization, such quantum electrodynamical effects could play an important role in future nanomechanical devices. Nevertheless, utilization of the Casimir force on the chip level remains a challenge because all experimental observations of the Casimir force so far require an external object to be manually positioned close to the mechanical element. To avoid difficulties in alignment at small separations, one of the interacting surfaces is commonly chosen to be spherical.

We present measurement of the Casimir force between single-crystalline silicon components on a semiconductor chip, in the absence of external objects. The structure consists of two microfabricated beams with near-square cross sections fabricated on a silicon-on-insulator wafer. One of the beams acts as the forcesensing element. The force gradient exerted on this beam is measured using magnetomotive transduction. The distance between the two beams can be decreased from 1.8 μm to $\sim$ 260 nm using a comb actuator integrated on the same substrate, where electrostatic forces push the second beam towards the force-sensing beam. Since both the shape and the separation of the interacting bodies are defined in a single lithographic step, no external alignment is required. Furthermore, this scheme allows us to measure the force between surfaces with complex shapes. Calculations indicate that the Casimir force on such structures display nonconventional distance dependence.

Electromagnetic Diffraction from Nanostractured Objects: Numerical Challenges

B. Guizal, A. Noto, R. Messina, and M. Antezza
Laboratoire Charles Coulomb, UMR 5221 du CNRS, University Montpellier 2, France

Abstract— Very recently, the electromagnetic scattering problem from nanostructured objects, and in particular gratings, become one of the central issues for the Casimir force and the heat transfer community; both on theory and experimental sides [1–5]. The scattering problem presents several non trivial numerical issues, especially for metallic materials. If not correctly handled numerical results can lead to artifactual phenomena. I will present the state of the art on such a problem and propose a strategy towards safe and rigorous computations.

REFERENCES

1. Chan, H. B., et al., *Phys. Rev. Lett.*, Vol. 101, 030401, 2008.
2. Bao, Y., et al., *Phys. Rev. Lett.*, Vol. 105, 250402, 2010.
3. Intravaia, F., et al., *Nature Communication*, 2013, DOI: 10.1038/ncomms3515.
4. Lambrecht. A., et al., *Phys. Rev. Lett.*, Vol. 101, 160403, 2008.
5. Guerout, R., et al., *Phys. Rev. B*, Vol. 85, 180301, 2012.

Three-body Radiative Heat Transfer and Casimir-Lifshitz Force Out of Thermal Equilibrium for Arbitrary Bodies

R. Messina and M. Antezza
Laboratoire Charles Coulomb, UMR 5221 du CNRS, University Montpellier 2, France

Abstract— We study the Casimir-Lifshitz force and the radiative heat transfer in a system consisting of three bodies held at three independent temperatures and immersed in a thermal environment, the whole system being in a stationary configuration out of thermal equilibrium. The theory we develop is valid for arbitrary bodies, i.e., for any set of temperatures, dielectric and geometrical properties, and describes each body by means of its scattering operators. For the three-body system we provide a closed-form unified expression of the radiative heat transfer and of the Casimir-Lifshitz force (both in and out of thermal equilibrium), generalizing our previous theory for two arbitrary bodies [1, 2]. This expression is thus first applied to the case of three planar parallel slabs. In this context, we discuss the apmplification of heat transfer on one of the external slabs due to the presence of the intermediate one and without any additional energy source [3]. Finally, we consider the force acting on an atom inside a planar cavity. We show that, differently from the equilibrium configuration, the absence of thermal equilibrium admits one or more positions of minima for the atomic potential. While the corresponding atomic potential depths are very small for typical ground state atoms, they may become particularly relevant for Rydberg atoms, becoming a promising tool to produce an atomic trap [4].

REFERENCES

1. Messina, R. and M. Antezza, *Europhys. Lett.*, Vol. 95, 61002, 2011.
2. Messina, R. and M. Antezza, *Phys. Rev. A*, Vol. 84, 042102, 2011.
3. Messina, R., M. Antezza, and P. Ben-Abdallah, *Phys. Rev. Lett.*, Vol. 109, 244302, 2012.
4. Messina, R. and M. Antezza, Preprint, 2014, arXiv:1402.2506.

On the Quantitative Measurement of Heat Transfer at Nanoscale by Means of the Near Field Scanning Thermal Microscope

A. Kittel, **D. Hellmann**, **K. Kloppstech**, **N. Könne**, **and L. Worbes**
University of Oldenburg, Germany

Abstract— Experimental investigations of the near field transfer down to sub-nanometer distances make an important contribution to the understanding of the involved mechanisms. A Near Field Scanning Thermal Microscope (NSThM) is able to image the heat transfer mediated by evanescent modes with a lateral resolution of a few nanometer. A precise calibration is essential in order to compare the measurements not only in a qualitative but also in a quantitative way with predictions of theory. An in situ calibration procedure is presented which gives reliable numbers of the heat transfer for each individual sensor used in the experiments under identical conditions. The influence of ultrathin films of NaCL deposited on a substrate of Au(111) on the heat transfer will be presented under variation of the film thickness ranging from a single layer to a few atomic layers. Already the single layer has a pronounced increase of the heat transfer and, therefore, on the coupling of two nanoscale objects.

Near-field Thermal Radiation Transistor Based on Phase Change Materials

Svend-Age Biehs[1] and Philippe Ben-Abdallah[2]

[1]Institut für Physik, Carl von Ossietzky Universität, Oldenburg D-26111, Germany
[2]Laboratoire Charles Fabry, UMR 8501, Institut d'Optique, CNRS
Université Paris-Sud 11, 2, Avenue Augustin Fresnel, Palaiseau Cedex 91127, France

Abstract— We introduce the analog of a field-effect transistor which is able to control the flow of heat exchanged in near-field by thermal photons between two bodies. This device is composed by a block of three separated solid elements, a thermal source, a drain and an intermediate layer made of a phase-change material which plays the role of the gate. The source and the drain are assumed to be made of silica. We show that by changing the temperature around its critical value of the gate while keeping the temperatures of the source and the drain fixed the radiative heat flux exchanged between the thermal source (hot body) and the thermal drain (cold body) can be reversibly switched, modulated and even amplified by a tiny action on the gate. Hence, this device has the same functionality as a usual field-effect transistor. Such a near-field thermal transistor could find important applications in the domain of nanoscale thermal management.

Effective Thermal Conductivity of Metal/Organic Semiconductor Nanocomposites

Xinyu Wang and Paddy K. L. Chan
Department of Mechanical Engineering, The University of Hong Kong, Hong Kong, China

Abstract— Due to the outstanding electrical and thermal properties, nanocomposites have been used in electronic devices and thermoelectric materials widely. By controlling the structure of nanocomposites, we can modulate the electrical-performance and thermoelectric figure of merit of the organic semiconductors. Organic thin film transistors (OTFTs) have attracted more attention because of the high compatibility with large-area fabrication techniques and low fabrication cost. Sumei Wang et al. found that the memory window of pentacene OTFT-based organic memory device could be improved significantly by embedding silver nanoparticles into pentacene thin films. Xiaochen Ren et al. demonstrated that an organic temperature sensor based on organic thermistor and OTFT showed a high thermal resolution by adding silver nanoparticles. However, thermal property of metal/organic semiconductor nanocomposites also plays a remarkable role in the device performance but have not been investigated in detailed. Effective medium approximation (EMA) is an approach to predict the effective thermal conductivity of nanocomposites. J. Ordonez-Miranda et al. introduced a modified EMA model to calculate the effective thermal conductivity by involving thermal boundary resistance (TBR) and electron-phonon coupling. Here we apply effective medium approximation to predict the effective thermal conductivity of metal/organic semiconductor nanocomposites.

In the calculations, we consider the effects of nanoparticle diameter, thermal boundary resistance, and electron-phonon coupling on the effective thermal conductivity of nanocomposites. We find that for fixed electron-phonon coupling, if we consider the thermal boundary resistance between Ag nanoparticle and pentacene, the thermal conductivity will decrease firstly and then increase with the increasing nanoparticle diameter. The larger thermal boundary resistance, the more obvious is the decreasing trend. If thermal boundary resistance is equal to zero, the effective thermal conductivity will show a continuous increasing trend. The explanation for this case is as follows. When thermal boundary resistance is considered, the phonon scattering between the organic material and metal nanoparticles will be strengthened when the nanoparticle diameter becomes larger, and it will reduces the effective thermal conductivity. When the nanoparticle diameter is very large, high Ag thermal conductivity's contribution will exceed the effect of phonon scattering, and the effective thermal conductivity will increase. In addition, for the fixed thermal boundary resistance, $R_{int} = 2 \times 10^{-8}\mathrm{m}^2\cdot\mathrm{K/W}$, higher electron-phonon coupling will give a higher effective thermal conductivity, which is due to the fact that higher electron-phonon coupling means fast energy transport between electron and phonon of Ag. And results in this condition shows that electron-phonon coupling only plays a role when the nanoparticle diameter is larger than 20 nm. These findings suggest the thermal boundary resistance and nanoparticle diameter of the metal/organic nanocomposites should be carefully controlled to achieve the desired thermal conductivity. This work provides important information to thermal management and fabrication of nanocomposites in the organic electronic devices.

A Tutorial on Casimir Interactions between Nanostructured Materials

Diego A. R. Dalvit
Theoretical Division, MS B213, Los Alamos National Laboratory, Los Alamos, NM 87545, USA

Abstract— I will discuss the influence of systematic patch effects in Casimir force measurements. I will first review the the state-of-the-art theoretical approaches to model electrostatic patch effects in metallic Casimir samples, describe the results of a recent experimental effort to measure potential distributions using Kelvin probe force microscopy, and finally describe their implications in the theory-experiment comparison in Casimir physics.

QED Effects Involving Non-reciprocal Media

J. Klatt and S. Y. Buhmann
University of Freiburg, Germany

Abstract— Non-reciprocal media violate time-reversal invariance, be it through the influence of an applied magnetic field, internal magnetisation, bulk motion or some other mechanism. This is manifest in the electromagnetic response via anisotropic, asymmetric permittivity, permeability or conductivity tensors or, for an isotropic medium, via non-chiral cross-polaris abilities. As a consequence, Onsager's theorem which states that optical paths can be reversed, is not valid in these media. This can have surprising consequences.

We have recently formulated macroscopic quantum electrodynamics as a theory to study quantum effects in such media. Possible examples include the following: (i) Casimir force: It is well know that while the Casimir force between two perfectly conducting plates is attractive, that between a perfectly conducting and an infinitely permeable plate is repulsive and somewhat weaker. The model of a perfect electromagnetic conductor allows to continuously switch between these two extremes and understand the transition between attractive and repulsive regimes. (ii) Casimir-Polder force: Dispersion interactions with non-reciprocal media can be sensitive to the time-reversal invariant properties of atoms and molecules. The most prominent of these is CP violation. (iii) Quantum friction: An example where motion breaks the time-reversal symmetry is the quantum friction force between an atom and a flat surface. We explore new regimes of the phenomenon by considering parallel and normal motion at retarded and non-retarded distances.

REFERENCES

1. Scheel, S. and S. Y. Buhmann, "Casimir-Polder forces on moving atoms," *Phys. Rev. A*, Vol. 80, No. 4, 042902, 2009.
2. Buhmann, S. Y., D. T. Butcher, and S. Scheel, "Macroscopic quantum electrodynamics in nonlocal and nonreciprocal media," *New J. Phys.*, Vol. 14, 083034, 2012.
3. Buhmann, S. Y., *Dispersion Forces II — Many-body Effects, Excited Atoms, Finite Temperature and Quantum Friction*, Springer, Heidelberg, 2012.

Transformation Optics Makes van der Waals Force Calculation Easier

Rongkuo Zhao
The Blackett Laboratory, Department of Physics, Imperial College London, London SW7 2AZ, UK

Abstract— Electromagnetic waves in one coordinate system can be exactly described in a different one, based on the fact that Maxwell's equations are form-invariant under coordinate transformations (with the permittivity and permeability tensors properly modified) [1]. This technique is called transformation optics. It offers us a strategy to start from a 'mother' system that is easy to solve, and then transform to a desired 'daughter' one that is difficult to handle. Through mapping nearly touching geometries into desired ones [2], powerful analytical formulae have been developed to calculate the spectra of singular and nearly singular two-dimensional metallic structures. By extending the two-dimensional transformation optics framework to the three-dimensional one and mapping two separated spheres into an annulus (see Fig. 1), we have recently developed accurate and extremely efficient approaches for calculating the absorption and scattering spectra, field enhancement performance, modal frequencies and spatial distribution for nanospherical dimers [3]. Using this technique, we have not only achieved fast convergence of exact van der Waals forces between spherical nanoparticles made of realistic metals at arbitrary separation but also obtained very accurate universal analytical expressions [4]. These analytical results enable us to shed physical insight into the sophisticated behavior of van der Waals forces in extremely small gaps.

If the extremely small gap goes to a sub nanometre scale, the classical electrodynamics picture which describes the dielectric response in terms of local parameters fails to predict the optical properties of metallic surfaces due to the inherent quantum nature of electrons [5]. The surface electrons induced by an applied electric field are not located precisely on the surface but are smeared across the boundary in a layer whose thickness is about 0.1 nm in a typical metal. This is the so-called nonlocal effect. It will alter the van der Waals forces in the small gap limit. Our new technique of the three-dimensional inversion transformation optics paves a way for exact analysis of the nonlocal effect on the van der Waals forces between three-dimensional nanostructures. We have used this technique to study the van der Waals force between two metallic spheres, with considering the nonlocal effect.

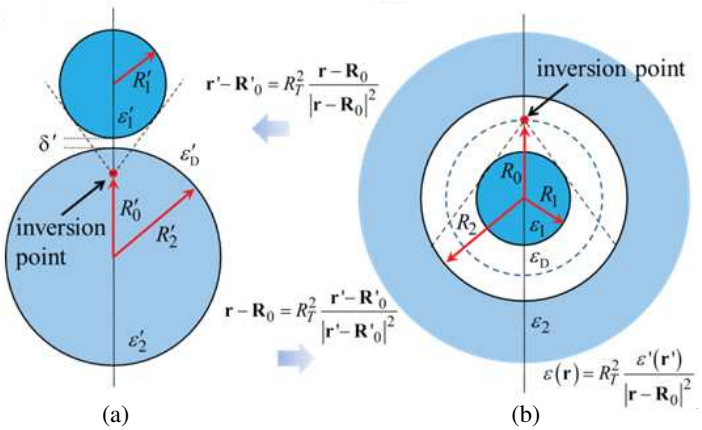

Figure 1: Applying an inversion transformation $\mathbf{r} - \mathbf{R}_0 = R_T^2(\mathbf{r}' - \mathbf{R}'_0)/|\mathbf{r}' - \mathbf{R}'_0|^2$ about the point R'_0, (a) two separated spheres are mapped into (b) an annulus, and vice versa. The annulus geometry comprises an inner solid sphere and an outer hollow one. The geometric inversion is accompanied by a transformation of the permittivities given by $\varepsilon(\mathbf{r}) = R_T^2|\mathbf{r} - \mathbf{R}_0|^{-2}\varepsilon'(\mathbf{r}')$. The small gap inside the cone indicated by the two dashed lines in (a) is enlarged in the annulus and is located further from the inversion point in (b). The opening angle of the cone in (a) is unchanged under the conformal transformation.

ACKNOWLEDGMENT

RZ thanks the support from Royal Commission for the Exhibition of 1851.

REFERENCES

1. Ward, A. J. and J. B. Pendry, *Journal of Modern Optics*, Vol. 43, 773, 1996.
2. Pendry, J. B., et al., *Science*, Vol. 337, 549, 2012.
3. Pendry, J. B., A. I. Fernández-Domínguez, Y. Luo, and R. Zhao, *Nat. Phys.*, Vol. 9, 518, 2013.
4. Zhao, R., Y. Luo, A. I. Fernández-Domínguez, and J. B. Pendry, *Phys. Rev. Lett.*, Vol. 111, 033602, 2013.
5. Fernández-Domínguez, A. I., et al., *Phys. Rev. Lett.*, Vol. 108, 106802, 2012.

Dispersion Interaction of Highly Excited Systems

Stefan Scheel
Institut of Physics, University of Rostock, Universitätsplatz 3, D-18055 Rostock, Germany

Abstract— Dispersion forces such as Casimir and Casimir-Polder forces arise due to fluctuations of the quantized electromagnetic field. In thermal equilibrium, these forces can be computed by envoking the linear fluctuation-dissipation theorem which leads to the well-known Lifshitz formalism. If, however, an atom is prepared in some energy eigenstate, this constitutes an out-of-equilibrium nonstationary state. In most experimental realizations involving cold atoms and room temperature surfaces, this is typically the case. This requires a dynamical theory of dispersion interactions which we have developed recently.

In this talk I will focus on a few examples of Casimir-Polder and van der Waals interactions of highly excited systems. For atoms in Rydberg states, the Casimir-Polder forces scales quartically in the principal quantum number, thereby making this interaction dominant even at moderate distances [1]. This effect can be used to construct hybrid quantum systems that combine cold atoms with graphene membranes. I will show that it is possible, by driving an atom cyclically through a Rydberg state, to create a backaction force on a graphene sheet that is strong enough to excite ripples [2]. At such large interaction strengths, the perturbative approach to calculating dispersion interactions is no longer valid, and one has to resort to exact Fano-type digitalization methods [3].

The van der Waals interaction between Rydberg atoms leads to the well-known effect of Rydberg blockade which prohibits the Rydberg excitation of an atom in the vicinity of an already excited atom. We have recently found experimental evidence of Rydberg blockade between excitons in the semiconductor cuprous oxide [4] which opens up novel opportunities to study Rydberg physics in semiconductor systems.

REFERENCES

1. Crosse, J. A., S. A. Ellingsen, K. Clements, S. Y. Buhmann, and S. Scheel, *Phys. Rev. A*, Vol. 82, 010901(R), 2010.
2. Ribeiro, S. and S. Scheel, *Phys. Rev. A*, Vol. 88, 052521, 2013.
3. Ribeiro, S. and S. Scheel, in preparation.
4. Kazimirczuk, T., D. Fröhlich, S. Scheel, H. Stolz, and M. Bayer, 2014, submitted for publication.

How Does Casimir Energy Fall?

K. A. Milton[1], **K. V. Shajesh**[2], **S. A. Fulling**[3], **and Prachi Parashar**[1]

[1]University of Oklahoma, USA
[2]Southern Illinois University, USA
[3]Texas A&M University, USA

Abstract— Several years ago we demonstrated that the Casimir energy for perfectly reflecting and imperfectly reflecting parallel plates gravitated normally, that is, obeyed the equivalence principle. At that time the divergences in the theory were treated only formally, without proper regularization, and the coupling to gravity was limited to the canonical energy-momentum-stress tensor. Here we strengthen the result by removing both of those limitations. We consider, as a toy model, massless scalar fields interacting with semitransparent (δ-function) potentials defining parallel plates, which become Dirichlet plates for strong coupling. We insert space and time point-split regulation parameters, and obtain well-defined contributions to the self-energy of each plate, and the interaction energy between the plates. (This self-energy does not vanish even in the conformally-coupled, strong-coupled limit.) We also compute the local energy density, which requires regularization near the plates. In general, the energy density includes a surface energy that resides precisely on the boundaries. This energy is also regulated. The gravitational interaction of this well-defined system is then investigated, and it is verified that the equivalence principle is satisfied.

Resonant Interaction Energy between Two Identical Atoms in a Photonic Crystal

T. Fukuta[1], **R. Incardone**[2], **V. Notararigo**[2], **R. Passante**[2], **T. Petrosky**[3], **L. Rizzuto**[2], **and S. Tanaka**[1]

[1]Department of Physical Science, Osaka Prefecture University
Gakuen-cho 1-1, Sakai 599-8531, Japan
[2]Dipartimento di Fisica e Chimica, Università degli Studi di Palermo and CNISM
Via Archirafi 36, Palermo I-90123, Italy
[3]Center for Complex Quantum Systems, The University of Texas at Austin
Austin, Texas 78712, USA

Abstract— We consider the resonant interaction energy between two identical atoms, one in an excited state and the other in the ground state, placed inside a photonic crystal. We consider two different models of a photonic crystal: a one-dimensional crystal and an isotropic three-dimensional crystal. The two atoms, having the same orientation of their transition dipole moment, are supposed prepared in their entangled symmetrical state and interacting with the quantum electromagnetic field in the multipolar coupling scheme. We consider both the case of an atomic transition frequency outside the photonic band gap and the case of a transition frequency inside the gap. When the transition frequency is outside the photonic band gap and close to its edge, so that the effective mass approximation can be used, we show that the resonant interatomic energy and force can be strongly enhanced by the presence of the photonic crystal, in both cases of 1D crystal and isotropic 3D crystal, as a consequence of the modified dispersion relation and density of states. The distance dependence of the force is however the same as for atoms in the vacuum space. Differences among the two models considered of photonic crystal are discussed in detail, as well as comparison with the analogous system of two impurity atoms in a quantum semiconductor wire. A numerical estimate of the effect in a realistic situation is also discussed. When the atomic transition frequency is inside the band gap, we find that strength of the resonant interaction force is reduced and that it decreases more rapidly with the distance compared to the case of atoms in the vacuum space. However, in this case, the spontaneous decay of the atoms is strongly inhibited, so that the state considered has a much longer lifetime. This could make easier the experimental measurement of the interatomic resonant force, which requires maintaining for a sufficiently long time the coherence of the correlated state of the two atoms.

A Varicap Based Microwave Parametric Amplifier for the Study of the Dynamical Casimir Effect

C. Braggio[1, 2], G. Carugno[2], F. Della Valle[3], G. Galeazzi[4], A. Lombardi[4], G. Ruoso[4], D. Zanello[5], and V. V. Dodonov[6]

[1]Dip. di Fisica e Astronomia, Via F. Marzolo 8, Padova I-35131, Italy
[2]INFN, Sez. di Padova, Via F. Marzolo 8, Padova I-35131, Italy
[3]Dip. di Fisica and INFN, Sez. di Trieste, Via A. Valerio 2, Trieste I-34127, Italy
[4]INFN, Laboratori Nazionali di Legnaro, Viale dell'Università 2, Legnaro I-35020, Italy
[5]INFN, Sez. di Roma, Piazzale A. Moro 1, Roma I-00185, Italy
[6]Instituto de Física, Universidade de Brasília, CP 04455, Brasília, Distrito Federal 70910-900, Brazil

Abstract— We are developing an apparatus to observe the so called dynamical Casimir effect [1, 2] in microwave cavities with time-dependent properties of boundaries. We expect to detect microwave quanta generated due to the parametric amplification of the initial thermal (in perspective — vacuum) fluctuations in the fundamental field mode [3]. Therefore a novel type of parametric amplifier has been used to study the single mode thermal field inside a resonator [4]. This amplifier is based on a microwave resonant cavity whose proper frequency can be modulated by means of a variable capacitance diode (varicap). By proper tuning of the varicap, a parametric amplification process can be initialized and will lead to different results depending on the amount of power used to drive the varicap.

Thanks to the presence of secondary resonances in the pumping system, our parametric amplifier can be used both in the degenerate and non-degenerate modes. Moreover, by using the system in a pulse mode, it is possible to study the time evolution of the energy present in the fundamental mode of the resonator. It is of particular interest to study this behavior for a cavity loaded with thermal photons, i.e., for the thermal radiation kept at some temperature Θ.

In the pulse mode the amplification is kept only for a finite amount of time t_F, that can be chosen at will. By performing repeated measurements it is possible to make an histogram of the measured energy values $E^i(t_F)$ reached inside the cavity at the time t_F: these values are each time different since the input power has the thermal Planck (Bose-Einstein) distribution with the average energy $k_B\Theta$ (which is much bigger than the energy of microwave quanta $\hbar\omega$ for the temperatures higher than 1 K). In this way we are able to study the "coarse-grained" energy distribution in the amplified cavity mode (since we cannot resolve discrete energy levels) [5].

The aim of this presentation is to show our recent experimental results and their theoretical explanation.

REFERENCES

1. Dodonov, V. V., *Phys. Scripta*, Vol. 82, 038105, 2010.
2. Wilson, C. M., G. Johansson, A. Pourkabirian, M. Simoen, J. R. Johansson, T. Duty, F. Nori, and P. Delsing, *Nature*, Vol. 479, 376, 2011.
3. Braggio, C., G. Bressi, G. Carugno, C. D. Noce, G. Galeazzi, A. Lombardi, A. Palmieri, G. Ruoso, and D. Zanello, *Europhys. Lett.*, Vol. 70, 754, 2005.
4. Braggio, C., G. Carugno, F. Della Valle, G. Galeazzi, A. Lombardi, G. Ruoso, and D. Zanello, *New J. Phys.*, Vol. 15, 013044, 2013.
5. Galeazzi, G., A. Lombardi, G. Ruoso, C. Braggio, G. Carugno, F. Della Valle, D. Zanello, V. V. Dodonov, *Phys. Rev. A*, Vol. 88, 53806, 2013.

Session 1P2a
MS-2.3: Focus Session on Integrated Microwave Photonics

THz Bandwidth RF-photonic 2D/3D Integrated Circuits for Optical Arbitrary Waveform Generation and Measurements

S. J. Ben Yoo
Department of Electrical and Computer Engineering, University of California, Davis, USA

Abstract— We will discuss 2D and 3D photonic integrated systems designed for coherent synthesis, processing, and detection of optical waves in time, space, and frequency domains. The talk will be in three parts addressing applications in future communication, computing, and imaging systems including chip-scale LIDAR, satellite communication, and data systems. The 3D photonic integrated circuit (PIC) platform exploits direct inscribing of arbitrarily shaped waveguides using femtosecond lasers. In one example, such a 3D PIC allows arbitrary beam forming for spatial division multiplexing using orbital angular momentum states. We will further discuss 2D integrated photonic technologies based on InP, silicon, and silica material platforms. Examples at UC Davis include > THz coherent optical transmitters and receivers on a monolithically integrated InP platform, silicon photonic RF-photonic lattice filters, and orbital-angular-momentum (OAM) MUX/DEMUXes. Dynamic optical arbitrary waveform generation and measurement (OAWG and OAWM) technologies enable > THz scale coherent optical transmission systems with arbitrary modulation formats and bandwidth. Integrated 3D OAM devices can realize arbitrary spatial beam forming. Finally, we will address future prospects of the new 2D/3D RF-photonic integration circuits towards realizing future communication, computing, and imaging systems.

Recent Progress in Silicon Nitride Waveguide-based Integrated Microwave Photonics

Leimeng Zhuang[1,2], **Caterina Taddei**[1,4], **Marcel Hoekman**[3], **Ruud M. Oldenbeuving**[5], **Klaus-J. Boller**[4], **and Chris G. H. Roeloffzen**[1,5]

[1]Telecommunication Engineering Group
University of Twente, P. O. Box 217, Enschede, AE 7500, The Netherlands
[2]Monash Electro-Photonics Laboratory
Monash University, Clayton, VIC 3168, Australia
[3]LioniX BV, P. O. Box 456, Enschede, AL 7500, The Netherlands
[4]Laser Physics and Nonlinear Optics Group, P. O. Box 217, Enschede, AL 7500, The Netherlands
[5]SATRAX BV, P. O. Box 456, Enschede, AL 7500, The Netherlands

Abstract— In the past decade, silicon nitride waveguide circuits attracted a significant amount of attention for their applications in the field of integrated microwave photonics. An obvious reason for this is the capability of silicon nitride waveguides to realize devices featuring simultaneously low loss, compactness, and low cost possibility for high-volume production. This is regarded as the essential need for the proliferation of integrated microwave photonics in the future RF/microwave engineering. Silicon nitride waveguide-based devices using TriPleX^{TM} technology [1] demonstrated a systematic propagation loss of 0.1 dB/cm and a bend radius of 70 μm. The devices were fabricated using CMOS-based deposition and etching equipment. Based on this technology, a wide variety of on-chip functionalities have been demonstrated in the context of microwave photonics in the recent years [2], including tunable delay line, true-time-delay-based beamforming network, spectral filter, separate carrier-phase tuning, frequency discriminator, pulse shaper, differentiator, fractional Hilbert transformer, hybrid coupler, and modulation transformer. All of them are achieved by combining basic build blocks such as directional couplers, Mach-Zehnder interferometers, and ring resonators. In the RF/microwave regime, those functionalities require the circuits to have delay lines of ns or higher, which translate to path lengths in the order of tens of cm. This makes us believe that TriPleX^{TM} can serve as an enabling technology for the realization of on-chip, low-loss, complex microwave photonic signal processors. In line with this goal, efforts are currently being made to address two challenges in the development of the technology. One challenge is to achieve the so-called programmable microwave photonic signal processors, which are supposed to be composed of a number of generic processing units and are able to be reconfigured into arbitrary circuit architectures according to the functionality requirement. The other is to realize fully integrated microwave photonic systems, where a critical step is the chip-level integration of the processers in TriPleX^{TM} technology with active on-chip functionalities such as lasers, modulators and/or photodiodes. This photonic hybrid integration is aimed to establish a promising photonic subsystem platform, which will enable the creation of a new category of microwave photonic functionalities and their applications. A picture of an integrated photonic beamformer developed for a K_u-band phased array receive antenna is shown in Fig. 1(a). In this platform, a hybrid integration of an edge-coupled optical beamforming network chip in TriPleX^{TM} technology and a chip containing an array of

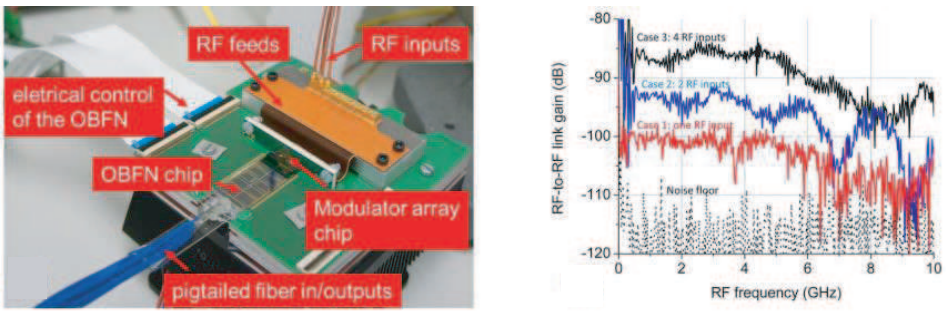

(a) (b)

Figure 1: (a) A photo of an integrated photonic beamformer developed for a K_u-phased array receive antenna; (b) measurements on beamforming effects of up to 4 simultaneous RF inputs applied to the modulators.

surface-coupled electoabsorption modulators based on InGaAs/InAlAs quantum wells is successfully achieved. For the system functionality verification, a number of RF S_{21} measurements were performed using a probe signal sweeping up to 10 GHz. The probe signal was split equally to drive 4 modulators, which emulates 4 RF inputs to the beamformer. In the beamformer, the RF signals from different inputs were synchronized and constructively combined. To demonstrate the beamforming effect, the measured beamformer outputs for different number of simultaneous RF inputs are shown in Fig. 1(b), where an output gain of 6 dB by doubling the number of inputs is measured in agreement with the theory.

REFERENCES

1. Zhuang, L., D. A. I. Marpaung, M. Burla, W. P. Beeker, A. Leinse, and C. G. H. Roeloffzen, "Low-loss, high-index-contrast Si_3N_4/SiO_2 optical waveguides for optical delay lines in microwave photonics signal processing," *Opt. Express*, Vol. 19, No. 23, 23162–23170, 2011.
2. Roeloffzen, C. G. H., L. Zhuang, C. Taddei, A. Leinse, R. G. Heideman, P. W. L. van Dijk, R. M. Oldenbeuving, D. A. I. Marpaung, M. Burla, and K.-J. Boller, "Silicon nitride microwave photonic circuits," *Opt. Express*, Vol. 21, No. 19, 22937–22961, 2013.

Ultrafast Photonic Differentiator and Integrator Employing Integrated Silicon Microring or MZI

Jianji Dong, Shasha Liao, Aoling Zheng, and Ting Yang
Wuhan National Laboratory for Optoelectronics, School of Optical and Electronic Information
Huazhong University of Science and Technology, Wuhan 430074, China

Abstract— Integrated microwave photonics is becoming one of the most promising topics due to the compact size, light weight, and low power consumption. In this paper, we will demonstrate several schemes of ultrafast photonic differentiator and integrator employing integrated silicon microring resonators. By tuning the carrier density (thus refractive index) of mirroring resonators with electrodes, fractional photonic differentiation is implemented at the through port due to the variable phase hop. On the other hand, the drop port of microring resonator shows an integrator feature with internal losses, corresponding to differential equation solver. Both first order and second order linear ordinary differential equation solvers are demonstrated using two cascaded microring resonators. This finding may motivate the development of integrated optical signal processors and further extend optical computing technologies.

Photonic Crystal Structures for Integrated Coherent FIR Microwave Filter

Jérôme Bourderionnet[1], **S. Combrié**[1], **Z. Han**[2], **X. Chécoury**[2], **and A. De Rossi**[1]

[1]Thales Research & Technology, 1 Avenue Augustin Fresnel, Palaiseau, France
[2]Institut d'Électronique Fondamentale (UMR CNRS 8622), Université Paris-Sud 11, Orsay, France

Abstract— Photonics is now part of the heart of modern radar systems, with already hundreds of optical links implemented in latest generation of radars. Beside signal transportation, a decisive objective for radar and communication systems is to exploit photonics properties to perform more complex signal processing functions [1].

Photonics has proved for years its remarkable potential for manipulations of optically carried microwave signals, such as delaying, weighting, routing or sampling,which are enabling building blocks for signal processing implementations such as finite impulse response (FIR) filters. A classical multi-tap FIR filter implementation requires to weight time-delayed replicas of an incident signal by both positive and negative weighting coefficients [2]. The incoherent addition of the replicas reconstructs the impulse response of the filter [3, 4]. Negative weighting coefficients are however extremely difficult to obtain in an integrated platform and usually requires single-sideband format and optical carrier phase tuning [5]. When the whole system is integrated on a single device, the tap-to-tap optical phase distribution within the chip can be easily stabilized. It is then possible to add the signal replicas coherently in the optical domain and to use the optical phase distribution to program the filter weighting coefficients. These coefficients result from phase interference products and can be arbitrarily positive or negative. We currently implement this concept on a Silicon On Insulator platform, using a photonic crystal directional coupler network to generate the multiple taps. Each tap then includes a fixed delay section (spiral waveguide) and a tunable delay section (photonic crystal thermally tunable waveguide). In this structure, the tunable delay line is used for the dual purpose of delaying the optically carried RF modulation envelope (the RF signal), and to adjust the carrier optical phase.

REFERENCES

1. Capmany, J. and D. Novak, *Nature Photonics*, Vol. 1, 319–330, 2007.
2. Candy, J. V., *Signal Processing, the Modern Approach,* McGraw-Hill, 1988.
3. Huang, T. X. H., X. Yi, and R. A. Minasian, *Optics Express*, Vol. 19, 6231–6242, 2011.
4. Sancho, J., J. Bourderionnet, J. Lloret, S. Combrié, I. Gasulla, S. Xavier, S. Sales, P. Colman, G. Lehoucq, D. Dolfi, J. Capmany, and A. De Rossi, *Nature Communications*, Vol. 3, 1075, 2012.
5. Pu, M., L. Liu, W. Xue, Y. Ding, H. Ou, K. Yvind, and J. M. Hvam, *Optics Express*, Vol. 18, 6172–6182, 2010.

Waveguide Bragg Gratings for Integrated Microwave Photonics Signal Processing

Maurizio Burla and José Azaña
Institut National de la Recherche Scientifique — Énergie, Matériaux et Télécommunications (INRS-EMT)
1650 boulevard Lionel-Boulet, Varennes, QC, J3X 1S2, Canada

Abstract— Recently, integrated microwave photonics (IMWP) signal processing using photonic integrated circuits (PICs) has attracted a great deal of attention as an enabling technology for a number of functionalities not attainable by purely microwave solutions. In this context, integrated waveguide Bragg grating (WBG) devices constitute a particularly attractive approach, thanks to their high compactness and exibility in producing arbitrarily defined amplitude and phase responses, by directly acting on perturbations of the grating profile. In this talk, I will first give a brief overview of recent advances in the field of integrated WBGs applied to microwave photonics (MWP). The current MWP activities at INRS-EMT will then be described. A number of recent demonstrations by our group of the use of WBGs for MWP and ultrafast optical signal processing will be provided, for applications such as reconfigurable filters for RF signals, broadband delay lines and phase shifters, pulse shapers and analog optical links. Finally, a perspective on the exciting possibilities offered by the silicon photonics platform in the field of MWP will be given, potentially enabling integration of highly-complex active and passive functionalities with high yield on a single chip, with a particular focus on the use of WBGs as basic building blocks.

Wireless Millimeter-wave to Lightwave Signal Converters Using Simple Planar Antennas on $LiNbO_3$ Optical Crystal

Y. N. Wijayanto[1], **A. Kanno**[1], **T. Kawanishi**[1], **H. Murata**[2], **and Y. Okamura**[2]

[1]National Institute of Information and Communication Technology, Japan
[2]Graduate School of Engineering Science, Osaka University, Japan

Abstract— The wireless communication has attracted much interest in past decade, owing to its high mobility. Since mobile devices are developed rapidly and high quality data are required, the wireless communication should be developed furthermore to obtain high capacity data communication. In order to enhance the capacity, the operational frequency of the microwave can be increased to millimeter-wave bands. By increasing the operational frequency, the bandwidth becomes large. Now, 60 GHz millimeter-wave band is one candidate for future wireless communication for providing high capacity. However, the millimeter-wave bands have large transmission loss in the air and millimeter-wave metal cables.

The large transmission loss in metal cable can be solved using optical fiber, where lightwave is used for carrying the millimeter-wave signal. Many short coveraged wireless links with pico/femto cell are required for solving large propagation loss of the millimeterwave signal in the air. Therefore, optical fiber links are promising to contribute in the high capacity wireless communication with millimeter-wave signals. The important device in the systems is a converter from wireless millimeter-wave to lihtwave signals.

We have studied and developed wireless microwave/millimeter-wave to lightwave signal converters using patch antennas embedded with narrow gaps. The antennas were fabricated on an electro-optic crystal such as $LiTaO_3$ or $LiNbO_3$. The prototype devices were successfully fabricated on a $LiTaO_3$ optical crystal for microwave and millimeter-wave bands. The $LiTaO_3$ optical crystal has relatively high dielectric constant of about 42. Conversion efficiency of the devices is obtainable using larger antenna size for increasing antenna gain and microwave/millimeter-wave interaction length. The larger antenna size can be achieved by using an electro-optic crystal with low dielectric constant such as a $LiNbO_3$ optical crystal with relatively dielectric constant about 30.

In this paper, we propose a wireless millimeter-wave to lightwave signal converters using simple planar antennas fabricated on a $LiNbO_3$ optical crystal. The proposed device is composed of a straight optical waveguide and patch antennas embedded with a narrow gap. Large antenna size and long millimeter-wave interaction length can be obtained. As a result, the conversion efficiency from wireless millimeter-wave to lightwave signals becomes larger. The proposed device has a simple planar structure. It can be also operated with no external power supply.

Generation of 90-GHz Millimeter Wave Using Quantum Dot Two-mode Laser

Kouichi Akahane, Naokatsu Yamamoto, Atsushi Kanno, Keizo Inagaki, Toshimasa Umezawa, and Tetsuya Kawanishi
National Institute of Information and Communications Technology
4-2-1, Nukui-Kitamachi, Koganei, Tokyo 184-8795, Japan

Abstract— Millimeter and terahertz waves can be generated by irradiating high-speed photodiodes or photoconductive materials with a two-wavelength emission laser. Electromagnetic waves at such frequencies have recently become important for high-speed wireless communication and accurate sensing. We have developed a quantum dot (QD)-based wavelength-tunable two-wavelength emission laser (two-mode laser) with a narrow linewidth and stable emission wavelength. In this study, we investigate the generation of 90-GHz millimeter waves (MMWs) by using the QD two-mode laser and high-speed uni-traveling carrier photodiode (UTC-PD). The laser structure with highly stacked InAs QDs was grown on InP(311)B substrates through solid-source molecular beam epitaxy. The ridge waveguide was fabricated subsequent to the growth of the QD laser wafer. An external cavity laser system was constructed using the QD gain chip, an optical band-pass filter, and an etalon filter. We observed two-mode lasing with a frequency separation of 90 GHz, which is in good agreement with the free spectral range of the etalon filter. Because a clear beat signal was observed in the interference measurements, laser emission can be considered to have occurred simultaneously at the two wavelengths. Mode hopping and competition were largely suppressed by using QDs as the gain medium because the QDs have a delta-function-like density of states; thus, the QDs individually contributed to the laser emission, stabilizing the laser-emission wavelength. Such two-mode lasing was introduced in the UTC-PD, and its output was evaluated by using a spectrum analyzer. This evaluation revealed a generation of MMWs at 89.2715 GHz with a full width at half maximum of 10 MHz.

Applications of FWM in Millimeter-wave Signal Generation — Integration Perspectives

Borja Vidal
Nanophotonics Technology Center, Universitat Politècnica de València
Camino de Vera, sn, Valencia 46022, Spain

Abstract— The growing demand for additional wireless broadband spectrum to accommodate bandwidth-hungry services has led to the unleashing of underused spectral bands and the exploration of higher frequency regions both for wireless access and backhaul. Spectral bands over 60 GHz offer plenty of bandwidth for communications. However, this region has remained basically unused because of the complexity and cost of electronic components. Photonic signal generation can be used jointly with electronics to develop high bit rate wireless transmission in the sub-THz band [1].

Practical exploitation of the millimeter-wave region requires further developments to simplify the system and achieve competitive cost targets with market potential. Photonic integration is a key element to address these issues, not only for digital transmission but also for microwave photonics applications [2]. Nonlinear optics also offers different approaches to simplify microwave and THz signal generation. Four-Wave Mixing is a versatile phenomenon that can be exploited to generate millimeter-wave signals from low microwave oscillators with good rejection of undesired harmonics [3].

In this work, the use of Four-Wave Mixing for the generation of millimeter-waves is analyzed and the potential for developing integrated photonic millimeter-wave signal generation systems based on parametric processes is discussed.

ACKNOWLEDGMENT

This work was partially supported by the Spanish Ministerio de Economia y Competitividad under project TEC2012-35797.

REFERENCES

1. Koenig, S., et al., *Nature Photonics*, Vol. 7, 977–988, Dec. 2013.
2. Marpaung, D., et al., *Lasers & Photonics Review*, Vol. 7, No. 4, 506–538, Jul. 2013.
3. Vidal, B., *Opt. Lett.*, Vol. 37, No. 24, 5055–5057, Dec. 2013.

Nonlinear Integrated Microwave Photonics

David Marpaung
CUDOS, School of Physics, University of Sydney, NSW 2006, Australia

Abstract— Harnessing nonlinear optical effects in a photonic chip scale has been proven useful for a number of key applications in optical communications. Microwave photonics (MWP) can also benefit from the adoption of such a technology, creating a new concept of nonlinear integrated microwave photonics. Here, we look at the potential of using nonlinear optical effects in a chip scale to enable RF signal processing with enhanced performance. We review a number of recent results in this field, with particular focus on the creation of frequency agile and high suppression microwave bandstop filters using on-chip stimulated Brillouin scattering (SBS). We also discuss the future prospect of nonlinear integrated MWP to enable a general purpose, programmable analog signal processor, as well as compact, high performance active microwave filters with enhanced energy efficiency.

Session 1P2b
SC3: Solid-state Quantum Photonics

The Photonic Nanowire: An Emerging Platform for a Highly Efficient Quantum Light Source

N. Gregersen[1], **J. Claudon**[2], **M. Munsch**[2], **J. Bleuse**[2], **A. Delga**[2], **J. Mørk**[1], **and J. M. Gérard**[2]

[1]DTU Fotonik, Department of Photonics Engineering, Technical University of Denmark, Denmark
[2]CEA-CNRS-UJF Joint Group 'Nanophysique et Semiconducteurs', CEA, INAC, SP2M, France

Abstract— The single-photon source capable of emitting single indistinguishable photons on demand represents a key component in quantum information applications. The photonic nanowire represents an attractive platform to construct a source with near-unity efficiency.

Introduction: An optically or electrically triggered quantum light emitter, e.g., a semiconductor quantum dot (QD), embedded in a solid-state semiconductor host material appears as an attractive platform for deterministic generation of single photons. However, for a QD in bulk material, the large index contrast at the semiconductor-air interface leads to a collection efficiency of only 1–2%, and efficient light extraction thus poses a major challenge in single-photon source engineering [1].

The photonic nanowire is a vertical GaAs cylinder with an embedded InAs QD placed on a substrate with an emission wavelength of $\approx 950\,\text{nm}$. By choosing a proper nanowire radius, the spontaneous emission into radiation modes can be strongly suppressed, and the probability for an on-axis QD of emitting photons into the fundamental HE_{11} mode can be close to unity. The design features no cavity and does not rely on resonant cQED effects, meaning that efficient coupling from the QD to the guided mode is obtained over a broad spectral range. No spectral alignment between the emitter line and a narrow cavity line is required, which represents a huge practical advantage in the fabrication.

To control the light emission and ensure a high collection efficiency, two additional elements must be included. While photons are efficiently funneled into the nanowire fundamental mode, half of the light will propagate towards the substrate due to the nanowire mirror symmetry. It is thus necessary to implement a bottom metal mirror to reflect this light back towards the top. Furthermore, the optimum nanowire diameter is only $\approx \lambda/4$ leading to a narrow mode waist and a highly divergent far field emission pattern of the truncated nanowire. A conical tapering strategy is thus required allowing for an adiabatic expansion of the fundamental mode and narrow output beam waist.

The original optically pumped photonic nanowire design implements regular conical taper, and its first experimental demonstration featured an efficiency of 0.72. However, for applications, electrical contacting is desired, and a novel photonic trumpet design based on an inverted conical tapering compatible with the implementation of a top metal contact has recently been proposed. The trumpet features a strongly Gaussian far-field emission, and a first implementation of this strategy [2, 3] has very recently lead to an ultra-bright single-photon source with a first-lens external efficiency of 0.75 and a predicted coupling to a Gaussian beam of 0.61.

ACKNOWLEDGMENT

This work was funded by project SIQUTE (contract EXL02) [4] of the European Metrology Research Programme (EMRP). The EMRP is jointly funded by the EMRP participating countries within EURAMET and the European Union.

REFERENCES

1. Gregersen, N., P. Kaer, and J. Mørk, "Modeling and design of high-efficiency single-photon sources," *IEEE J. Sel. Top. Quantum Electron.*, Vol. 19, 9000516, 2013.
2. Munsch, M., N. S. Malik, J. Bleuse, E. Dupuy, A. Delga, J. M. Gérard, J. Claudon, N. Gregersen, and J. Mørk, "Dielectric GaAs antenna ensuring an efficient broadband coupling between an InAs quantum dot and a Gaussian optical beam," *Phys. Rev. Lett.*, Vol. 110, 177402, 2013.
3. Munsch, M., N. S. Malik, J. Bleuse, E. Dupuy, A. Delga, J. M. Gérard, J. Claudon, N. Gregersen, and J. Mørk, "Erratum," *Phys. Rev. Lett.*, Vol. 111, 239902, 2013.
4. http://www.ptb.de/emrp/siqute-home.html.

Controlling On-chip Microwave Photons for Quantum Information Processing

Haohua Wang
Zhejiang University, China

Abstract— The superconducting microwave resonator is an important device for quantum information processing. However, it is experimentally challenging to generate pure photon state in the resonator with a well-defined excitation number n, also known as a Fock state. By interposing a highly non-linear superconducting phase qubit between a resonator and a classical signal, we have successfully demonstrated the generation of the Fock states and the arbitrary states in the resonator. Furthermore, we demonstrate a circuitry architecture involving a frequency-tunable resonator coupled to a phase qubit. By frequency-tuning the microwave photons stored in the resonator, we can coherently shuffle energy quanta between the qubit and a microscopic two-level defect. We also discuss our recent demonstration of a quantum error detection protocol, which improves the on-chip storage time of a quantum state, in a circuit consisting of three phase qubits coupled to a common resonator.

Towards Deterministic Generation of Bright Stream of Single Photons

Xuewen Chen
School of Physics, Huazhong Unviersity of Science and Technology, Wuhan, China

Abstract— Single-photon sources based on single emitters have been discussed for applications in cryptography, quantum computation, quantum networking, spectroscopy, and metrology. The success of all these proposals will crucially rely on the efficient generation of photons into well-defined modes. To achieve this, researchers have recently considered various photonic structures. However, despite of impressive progress, the existing realizations fall short of achieving near-unity efficiency in generating single photons. In this talk, I will present our theoretical proposals and experimental verifications of optical antenna structures to achieve beyond 99% efficiency in collecting emissions from a single solid-state quantum emitter. Our work paves the way towards deterministic generation of bright stream of single photons.

Towards Quantum Computing and Quantum Networking with Solid-state Single Spins and Single Photons

Chao-Yang Lu
University of Science and Technology of China, China

Abstract— Single-photon sources based on semiconductor quantum dots offer distinct advantages for quantum information, including a scalable solid-state platform, ultrabrightness and interconnectivity with matter qubits. A key prerequisite for their use in optical quantum computing and solid-state quantum networks is a high level of efficiency, tunability, indistinguishability, and robustness. In this talk, I will our recent experiments on generating deterministic, highly indistinguishable, robust and tunable single photons from a single quantum dot. The methods used include pulsed resonance fluorescence, adiabatic rapid passage, and spin-flip Raman scattering. Two-photon interference was observed from the same dot with an indistinguishablity up to 99.5% and remotes dots up to 87%. I will discuss our more recent results of generating Greenberger-Horne-Zeilinger-type spin-photon entanglement and quantum state transfer between single photons and single spins.

REFERENCES

1. Pan, et al., *Rev. Mod. Phys.*, Vol. 84, 777, 2012.
2. Cai, et al., *Phys. Rev. Lett.*, Vol. 110, 230501, 2013.
3. He, et al., *Nature Nanotechnology*, Vol. 8, 213, 2013.
4. He, et al., *Phys. Rev. Lett.*, Vol. 111, 237403, 2013.

Self-assembled Low Density Quantum Dot and Quantum Dot-in-nanowire Structures for Quantum Photonics

Guo-Wei Zha[1, 2], **Zhi-Chuan Niu**[1, 2], **Ying Yu**[1, 2], **Xiang-Jun Shang**[1, 2], **Jian-Xing Xu**[1, 2], **Si-Hang Wei**[1, 2], **Li-Juan Wang**[1, 2], **and Hai-Qiao Ni**[1, 2]

[1]State Key Laboratory of Superlattices and Microstructures
Institute of Semiconductors, Chinese Academy of Sciences, Beijing 100083, China
[2]Synergetic Innovation Center of Quantum Information and Quantum Physics
University of Science and Technology of China, Hefei, Anhui 230026, China

Abstract— Self-assembled III-V quantum dots (QDs) are of particular attractive as solid quantum light emitters owing to their stability, narrow spectral linewidth, and short radiative lifetime. Semiconductor nanowires (NWs) have appeared as promising building blocks for future nanoscale electronic and photonic devices owing to their high crystalline quality and integration possibilities.

Our recent works on the epitaxial growth and characteristics of self assembled QDs and QDs-in-NWs structures are reported. Firstly, we have successfully fabricated single InAs QD decorating at the corner of gold-free branched GaAs/AlGaAs grown on silicon substrate [1]. The photolumine scence intensity is ~ 20 times stronger than that on the facets of the straight NW. Sharp excitonic emission is observed at 4.2 K with a linewidth of 101 μeV and a vanishing two-photon emission probability of $g^2(0) = 0.031(2)$ [2]. Secondly, two types of quantum nanostructures based on self-assembled GaAs quantum dot embedded into GaAs/AlGaAs hexagonal nanowire systems are also presented, one is sandwiched in two $Al_{0.7}Ga_{0.3}As$ barrier shells and the other is in the center of $Al_{0.58}Ga_{0.42}As$ quantum ring and covered by $Al_{0.7}Ga_{0.3}As$ barrier shell. Sharp and enhanced excitonic emission is observed at liquid nitrogen temperature (77 K) with a emission rate of 8 MHz and a two-photon emission probability of $g^2(0) = 0.15(2)$ [3]. Thirdly, we have reported on the fabrication of single quantum rings (QR) on the sidewall of bottom-up GaAs nanowires for the first time [4]. These new nanostructures may open a new avenue to the fabrication of highly efficient single-photon sources, novel quantum optics experiments, as well as designing robust quantum optoelectronic devices operating at higher temperature required for practical applications.

Bright Single-photon Emission by Solid-state Sources in Engineered Nanophotonic Devices

L. Sapienza[1, 2], **M. Davanço**[1], **S. Ates**[1, 2], **K. C. Balram**[1, 2], **A. Badolato**[3], **and K. Srinivasan**[1]

[1]Center for Nanoscale Science and Technology, NIST, Gaithersburg, MD 20899, USA
[2]Maryland NanoCenter, University of Maryland, College Park, MD 20742, USA
[3]Department of Physics and Astronomy, University of Rochester, Rochester, NY 14627, USA

Abstract— Solid-state quantum emitters are promising light sources for quantum information protocols relying on the storage, manipulation, and transmission of the information encoded in single photons through optical cavities and waveguides. Epitaxially grown, self-assembled InAs/GaAs quantum dots have proven to be a particularly promising system, and a lot of effort has been devoted to the efficient extraction of the emitted single photons by fabricating engineered nanophotonic structures. Among those, we have developed circular dielectric Bragg grating cavities, planar structures that provide directional vertical emission with a near-Gaussian far-field pattern, along with moderate (few nm) bandwidth and Purcell enhancement (< 10) of the radiative rate of the embedded single quantum dots [1, 2]. Furthermore, in order to boost the collection efficiency of single emitters in nanofabricated photonic structures and control the light-matter interaction, we have developed an all-optical positioning technique that allows achieving deterministic light-matter coupling on a chip, an essential requirement for the implementation of quantum information protocols in devices.

REFERENCES

1. Davanço, M., M. T. Rakher, D. Schuh, A. Badolato, and K. Srinivasan, *Appl. Phys. Lett.*, Vol. 99, 041102, 2011.
2. Ates, S., L. Sapienza, M. Davanço, A. Badolato, and K. Srinivasan, *IEEE Journal of Selected Topics in Quantum Electronics*, Vol. 18, 1711, 2012.

Quantum Dot Cavity Quantum Electrodynamics Using a Photonic Crystal Nanocavity with High Q and Small V

Yasutomo Ota[1], **Satoshi Iwamoto**[2], **and Yasuhiko Arakawa**[2]

[1]NanoQuine, University of Tokyo, Japan
[2]NanoQuine, IIS, University of Tokyo, Japan

Abstract— Photonic cavities containing semiconductor quantum dots provide an attractive testbedfor studying cavity quantum electrodynamics (cavity QED) in the solid state. Such studies are expected to play an important role for understanding the physics in semiconductor nanolasers — an ultimate form of semiconductor lasers that could be useful for realizing on-chip classical data communication with low energy consumption, as well as for developing future optical quantum information devices. So far, various types of resonators have been used for fabricating quantum dot cavity QED systems, including micropillars, microdisks and point defect photonic crystal nanocavities. However, almost all these resonators have failed in simultaneously realizing high quality factors (Qs) and small cavity mode volumes (Vs), in experiments for quantum dot cavity QED, and have provided limited ranges of key parameters that govern the physics: emitter-cavity coupling strength g, cavity decay rate κ, emitter decay rate γ. This limitation posed on the obtainable system parameters has restricted the range of the cavity QED studies from weak coupling ($g < \kappa + \gamma$) only up to shallow strong coupling regime ($g \sim \kappa + \gamma$).

In this presentation, we will report quantum dot cavity QED systems using a novel photonic crystal nanocavity that experimentally supports a high Q factor and small V at the same time. Using this cavity, we achieved the highest g/κ value ever reported for quantum dot based systems. This novel system will allow ones to quest into deeper strong coupling regimes of quantum dot cavity QED ($g \gg \kappa + \gamma$) and opens the possibility to realizing various nanophotonic devices including single photon switches and transistors, single photon generators based on photon blockade, as well as N-photon bundle generators.

Numerical Study on Single Crystalline Diamond Waveguide-based Single Photon Emitter

Yunxiao Li, Yanfeng Zhang, Yujie Chen, Hui Chen, Siyuan Yu, and Zelin Ma
State Key Laboratory of Optoelectronic Materials and Technologies
School of Physics and Engineering, Sun Yat-sen University, Guangzhou 510275, China

Abstract— A color center in a diamond can be used as a single solid-state qubit which can be probed by optical means. As a qubit, a color center in a single crystalline diamond has better performance than one in a nano-crystalline diamond. However, the poor photon collection efficiency limits its application. To improve the photon collection efficiency, several approaches have been proposed. For example, fabricating solid immersion lens or nanowires with color center embedded at the interface or collecting photons from the edge of a diamond chip via total internal reflection have been demonstrated to be able to greatly improve the photon collection efficiency.

In this work, we have designed a structure based on a single crystalline diamond waveguide in order to improve the photon collection efficiency. We design a 10-μm long rectangular diamond waveguide on a silica substrate (the upper cladding is air), putting a dipole source at the center of the designed waveguide to represent the color center and collecting photons at both ends of the designed waveguide. In the case that the dipole is oriented parallel to the waveguide longitudinal axis, only few photons can be collected (about 1%), hence we only consider the situation that the dipole is oriented in the transverse plane. Using finite-difference time-domain (FDTD) method for simulation, we have done extensive research to study the optimum aspect ratio of the waveguide and find that the optimum cross-section of the waveguide is about $0.2\,\mu m \times 0.2\,\mu m$. In the best case scenario, the photon collection efficiency can exceed 60% in theory. We then put a grating at one end of the waveguide to further increase the photon collection efficiency by collecting photons from another end.

This method have the benefit of higher single photon collection efficiency while keeping the integrated quantum photonics concept, so that a number of single photon sources integrated on one chip.

Session 1P3a
MS-1.1&MS-1.8: Inorganic & Semiconductor Photovoltaics

III-V Compound Semiconductor Quantum Dot and Nanowire Solar Cells

C. Jagadish
Department of Electronic Materials Engineering, Research School of Physics and Engineering
The Australian National University, Canberra, ACT 0200, Australia

Abstract— Photovoltaics (PVs) is no doubt one of the leading technologies under enormous growth in recent years to address the growing issues of global warming, climate change and energy shortage. Along with the ongoing research activities and industry developments to reduce the cost of conventional PV devices such as Si-based solar cells, a lot of research efforts have now been focused on exploring new concepts and approaches for high efficiency solar cells. The fast emerging nanotechnology has opened up great opportunities to produce solar cells with lower cost and/or improved performance by employing the unique properties of nanostructures, such as self-assembled quantum dots (QDs) and nanowires (NWs). By incorporating multiple layers of self-assembled QDs into the intrinsic region of a standard p-i-n solar cell structure during the epitaxial growth, the low energy photons (lower than the energy gap of the host material) in the solar spectrum can be absorbed by the QD layers, leading to an extended photoresponse to longer wavelengths and thus larger photocurrent. Different QD structures based on GaAs p-i-n structures have been investigated [1, 2] with the demonstration of improved short circuit current (I_{sc}) (compared with the GaAs reference cell). Quantum dot solar cells (QDSCs) have also shown promise in further improving the performance of the most efficient multi-junction solar cell devices due to the flexibility in bandgap engineering which provides better current-matching and hence the increased output current of the entire device, leading to efficiencies $> 40\%$ under solar concentration [3]. On the other hand, nanowire research is also a new and emerging field growing at a fast pace [4]. The excitement in this field is due to the unique electronic and optical properties of the one-dimensional nanowire structures. By incorporating the superior photovoltaic properties of III-V semiconductors into nanowire structures, it is expected that further enhancement in the solar cell efficiency can be achieved with significant cost reduction due to much less material usage in nanowires.

In this talk, nanostructure solar cells based on III-V compound semiconductor quantum dots (InGaAs/GaAs) and nanowires (GaAs) are demonstrated. Experimental results based on material and device studies will be presented and discussed in terms of basic concepts, current limitations and future prospects for high efficiency photovoltaic applications.

REFERENCES

1. Guimard, D., R. Morihara, D. Bordel, K. Tanabe, Y. Wakayama, M. Nishioka, and Y. Arakawa, "Fabrication of InAs/GaAs quantum dot solar cells with enhanced photocurrent and without degradation of open circuit voltage," *Applied Physics Letters*, Vol. 96, 203507-3, 2010.
2. Jolley, G., H. F. Lu, L. Fu, H. H. Tan, and C. Jagadish, "Electron-hole recombination properties of $In_{0.5}Ga_{0.5}As$/GaAs quantum dot solar cells and the influence on the open circuit voltage," *Applied Physics Letters*, Vol. 97, 123505-3, 2010.
3. Valdivia, C. E., S. Chow, S. Fafard, et al., "Measurement of high efficiency $1\,cm^2$ AlGaInP/InGaAs/Ge solar cells with embedded InAs quantum dots at up to 1000 suns continuous concentration," *35th IEEE Photovoltaic Specialists Conference (PVSC)*, 001253–001258, Hawaii, 2010.
4. Li, Y., F. Qian, J. Xiang, and C. M. Lieber, "Nanowire electronic and optoelectronic devices," *Materials Today*, Vol. 9, 18–27, 2006.

Challenges to the Realization of Intermediate Band Solar Cells Using InAs/GaAs Quantum Dots

Tian Li and Mario Dagenais
Department of Electrical and Computer Engineering, University of Maryland, College Park, USA

Abstract— Quantum dot (QD) solar cells are "third generation" photovoltaic (PV) devices Quantization effects in QD devices potentially can lead to higher conversion efficiencies than what has been predicted by the Shockley-Queisser detailed balance analysis. Interest in III-V quantum dots (QDs) has been raised following the recent proposal for the introduction of an intermediate band solar cell (IBSC) by Marti and Luque which promises conversion efficiency as high as 63.2% under concentration. Our work focuses on experimental and theoretical studies aimed at establishing a basic understanding of the principal electrical and optical processes governing the operation of quantum dot solar cell to determine its feasibility for the realization of IBSC.

Uniform performance QD solar cells with high conversion efficiency have been fabricated using carefully calibrated processes. Before coating with Si_3N_4, the QD sample has a current density of 24.8 mA/cm^2, compared with 23.2 mA/cm^2 for the reference structure. Clearly, we generate a higher short circuit current in our quantum dot devices as compared to the bulk solar cell. After depositing an AR coating, we measured a short circuit current of 29.9 mA/cm^2 (record) for the quantum dot sample with an open circuit voltage of 0.77 V, lower than that of the reference GaAs sample which had an open circuit voltage of 0.92 V. This value is also similar to the highest short circuit current that has been generated in bulk GaAs. The overall efficiency for our quantum dot solar cell is 17.8% (near record for a QD solar cell device), even though the Voc has been reduced by about 157 mV as compared to our bulk sample.

In our work, we found that the incorporation of self-assembled QDs interrupts the lattice periodicity and introduces a greatly broadened tailing density of states extending from the bandedge towards mid-gap. Through careful investigation of the origin of the enhancement of the short circuit current density (Jsc), a below-bandgap density of states (DOS) model with an extended Urbach tail has been developed. The extended Urbach tail was found to contribute to as much as 45% of the total 5.5% Jsc enhancement in our QD device compared with its reference bulk device. Meanwhile, the existence of this extended tail also explains the observed Voc degradation in a QD device due to a lower chemical potential separation between electrons and holes.

The key to a successful IBSC prototype requires the optimization of a sequential two-step photon absorption via the intermediate states. However, a broadened background tailing density of states can function as an efficient carrier relaxation and collection pathway, competing with the process for the second photon absorption. Based on our two-photon measurements, we conclude that it is not likely that a true two photon photogenerated current can lead to appreciable photocurrent increase at room temperature, even under sun concentration. Our results demonstrate that the enhancement of Jsc comes mostly from a single photon process. No evidence for intermediate-band contributions is detected in our measurements.

Prospects and Requirements for 30% Efficient Thin-film on Silicon Tandem Cells

Thomas P. White, **Niraj N. Lal**, **and Kylie R. Catchpole**
Centre for Sustainable Energy Systems, Research School of Engineering
The Australian National University, Canberra 0200, Australia

Abstract— With the rapid rise of new thin film PV materials such as perovskites [1] in recent years, there is growing interest in combining low-cost thin film solar cells with crystalline silicon technology to create high efficiency silicon based tandem cells. This approach has the potential to achieve efficiencies well above the existing single junction c-Si record of 25%, while benefitting directly from the global investment in silicon cell manufacturing. It would also provide a pathway for new PV materials to enter the market without competing directly against silicon.

This presentation will review our recent work to identify the requirements for a thin film top cell to be used in tandem with silicon, and to establish material and cell performance targets for reaching efficiencies of 30%. These targets provide clear guidelines for the selection of suitable top cell materials and technologies, and directions for future material and cell research.

In the first instance, an estimate of the required top cell efficiency can be made by considering the performance of a high efficiency c-Si bottom cell under the reduced solar spectrum transmitted through a top cell with band gap E_g (see Fig. 1(a)). The inset in Fig. 1(b) shows the predicted output power from a 25% efficient c-Si PERL cell on the bottom of a two-cell stack, as a function of the top cell band gap. Here we assume that all photons with energy $h\nu > E_g$ are absorbed in the top cell, and all photons with energy $h\nu < E_g$ are transmitted to the Si cell. The main axis in Fig. 1(b) shows the top cell efficiency required to recover the 25% efficiency of the bottom cell (blue curve), and to reach 27.5% (green) and 30% (red) tandem cell efficiencies. It is clear that relatively efficient top cells are essential to make this approach worthwhile: assuming no optical losses, a 1.5 eV band gap top cell must be ∼17% efficient to break even (recover the 25% efficiency of the bottom cell), or 22% to reach a tandem efficiency of 30%. These requirements drop to ∼9% and 14% respectively for a top cell bandgap of 2 eV.

To further investigate these requirements, we apply a simple model for a four-terminal tandem cell based on material characteristics of the top cell, including band gap, absorption coefficient, carrier diffusion length and luminescence efficiency [2]. In particular, we evaluate top cells with strong absorption and poor electronic quality; typical characteristics of low-cost earth-abundant semiconductors. Our results show that with careful light management, efficiencies of 30% are achievable using thin film absorbers in the top cell with carrier diffusion lengths on the order of 100nm and luminescence efficiencies of 10^{-5}.

This analysis establishes clear research targets for high-bandgap semiconductor materials and novel thin film solar cell concepts that can be combined with existing c-Si technology. Such

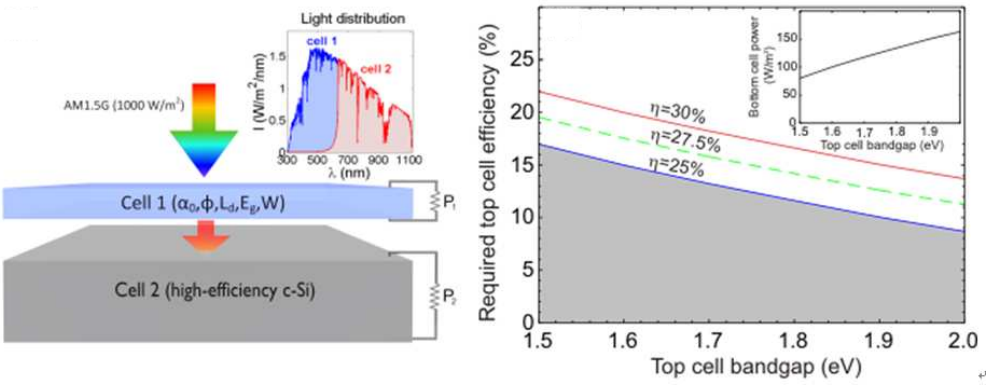

Figure 1: (a) Schematic of the tandem configuration. Cell 1 is a thin film cell (absorber thickness W) with bandgap E_g. Cell 2 is a 25% c-Si cell. Inset in (a): absorption in an idealized tandem. (b) Top cell efficiency required to reach a tandem efficiency of $\eta = 25\%$, 27.5% and 30%. Shaded area shows $\eta < 25\%$. Inset in (b): bottom cell output power when the top cell absorbs all photons with energy $h\nu > E_g$.

tandem approaches could enable the rapid development of a new generation of low cost, high efficiency cells.

REFERENCES

1. Snaith, H. J., *J. Phys. Chem. Lett.*, Vol. 4, 3623–3630, 2013.
2. White, T. P., N. N. Lal, and K. R. Catchpole, *IEEE J. Photovolt.*, Vol. 4, 208–214, 2014.

Fully Automated Development Process for High Efficiency CIGS Solar Cells

Sven Lindstrom
Midsummer AB, Elektronikhöjden 6, Järfälla SE-175 43, Sweden

Abstract— The investment cost for production of thin film solar cells must be lowered to spread the technology and gain the benefits of scale of operation. The step from laboratory to mass production must also be addressed as only two companies in the world has achieved GW scale of thin film solar cell production. Midsummer has developed an "OpenSource" development platform for CIGS solar cell R&D. With this low cost platform, any university, institute or company will gain access to a world-class CIGS process and equipment. The platform will enable results to be shared and improved between different research groups. The platform already has a proven, fully developed solution for mass production of thin film solar cells.

The production solution for CIGS solar cells developed by Midsummer is an all-sputtering process for Cd-free solar cells on stainless steel substrates measuring $156 \times 156\,\mathrm{mm}$. The aperture area efficiency achieved on a whole cell ($225\,\mathrm{cm}^2$) is $> 16\%$ without anti-reflective coating. All the materials in the cell are sputtered, including the buffer layer. The stainless steel substrate used allows rapid heating and cooling as well as deposition at high temperatures. Unlike roll-to-roll solutions, Midsummer choose a process that produces individual cells on $156 \times 156\,\mathrm{mm}$ stainless steel substrates, this allows for making flexible modules while keeping cell uniformity and performance at an optimum to reduce manufacturing and development costs.

Thanks to an automated development tool in an all-vacuum process, most of the development work is done in a stable environment without operator interference. This way, also small deviations in sample performance can be detected. This is especially important when most of the large efficiency improvements ($> 0.5\%$) has been made. With a fast and automated development process, large amounts of cells can be produced at low cost and with statistical analytical tools, continuous improvements can be made without having the cost and scale of mass production.

Surface Morphology-dependent Photoelectrochemical Responses of Silicon Nanowire Arrays Prepared by Chemical Etching

Shaolong Wu[1], **Xiaofeng Li**[1], **Yaohui Zhan**[1], **Rui-Ting Zheng**[2], **and Guo-An Cheng**[2]

[1]Institute of Modern Optical Technologies
& Collaborative Innovation Center of Suzhou Nano Science and Technology
Key Lab of Advanced Optical Manufacturing Technologies of Jiangsu Province
& Key Lab of Modern Optical Technologies of Education Ministry of China
Soochow University, Suzhou 215006, China
[2]Key Laboratory of Beam Technology and Material Modification of Ministry of Education
College of Nuclear Science and Technology, Beijing Normal University, Beijing 100875, China

Abstract— Maximizing the optical absorption of one dimensional semiconductor nanostructure arrays (1DSNSAs) is desirable for high performance of 1DSNSA-based optoelectronic devices. However, a quite large surface-to-volume ratio and enhanced surface roughness are usually introduced by tailoring the morphology of the 1DSNSAs prepared in a top-down method to improve the optical absorption. Surface recombination is mainly determined by the surface characteristics and significantly affects the photogenerated carrier collection. Herein, we systematically investigated the photoelectrochemical (PEC) characteristics of silicon nanowire arrays (SiNWAs) with various morphologies prepared by the metal-assisted chemical etching of Si wafers. First, PEC responses of two kinds of SiNWAs with either smooth or rough surfaces were performed under the irradiation of white light (wavelength range of 420–760 nm). Although the average optical absorption properties of the two samples within 420–760 nm wavelengths were comparable and much better than the planar silicon, the saturation photocurrent density of the rough-surface (smooth-surface) SiNWAs was obviously smaller (larger) than that of the planar Si. Second, we intensively studied the PEC behaviors of the SiNWs prepared by different etching time under the irradiation of quasi-monochromatic ($\sim$ 590 nm) light for clearing up the reasons for the above disparities. Experimental results show that the saturation photocurrent density and photoresponsivity of the SiNWAs first increased and then gradually decreased with an increasing etching time, while the reflection spectrum was gradually suppressed to the measurable minimum. Finally, we demonstrated the PEC stability and photoresponsivity of SiNWAs can be effectively enhanced through coating carbon film shell. We proposed that the directions for the design of nanostructure-based optoelectronic devices should include not only strong optical absorption but also low surface/bulk carrier recombination. High-sensitivity optoelectronic devices could be obtained only by balancing the requirements for light absorption and photogenerated carrier collection.

Solution-processed Silver Mesh as Transparent Conductive Electrode for Application in Solar Cell

Yuanlin Huang[1], **Han Bing**[1], **Krzysztof Kempa**[2], **and Jinwei Gao**[1]

[1]Institute for Advanced Materials (IAM), Academy of Advanced Optoelectronics
South China Normal University, Guangzhou 510006, China
[2]Department of Physics, Boston College, Chestnut Hill, Massachusetts 02467, USA

Abstract— A solution-processed and inexpensive method for silver micro-size mesh as transparent conductive electrode is experimentally demonstrated, which based on simple photolithography, selective silver particle deposition, and sintering method. This micro-size mesh electrodes show good opto-electrical properties with the sheet resistances as low as $2.1\,\Omega$/sq and the low optical reflectance of $\sim 10\%$, which is comparable to commercial screen-printed conductive bar, but with a lower fabrication cost, can be potentially used in crystalline silicon solar cell.

Development of Quantum Wire Intermediate Band Solar Cells

V. Kunets[1], **C. Furrow**[1], **M. Ware**[1], **Y. Hirono**[1], **M. Benamara**[1], **V. Dorogan**[1], **Y. Mazur**[1], **M. Mortazavi**[1], **N. Al Saqri**[2], **D. Jameel**[2], **D. Taylor**[2], **M. Henini**[2], **and G. Salamo**[1]

[1]Institute for Nanoscience and Engineering, University of Arkansas, Fayetteville, Arkansas, USA
[2]School of Physics and Astronomy, University of Nottingham, Nottingham, UK

Abstract— We present a study on intermediate band (IB) solar cells using one-dimensional InGaAs coupled quantum wires (QWRs) grown on the GaAs (311). A plane by molecular beam epitaxy as the IB structure. Using this structure, we have demonstrated a $\sim$ 12% enhancement in solar energy conversion efficiency as compared to a reference pin GaAs solar cell device. This enhancement results from an increase in short circuit current I_{sc}, and an only insignificant degradation of the open circuit voltage, V_{oc}, of 20 mV as shown in Fig. 1. This is in contrast to many other previously designed quantum dot IB solar cells in which the gain in I_{sc} is offset by the comparatively large decrease in V_{oc}. This discrepancy between nanostructure based IB solar cells will be discussed. These solar cell devices were probed by structural, optical and electrical measurement techniques. Detailed structural studies by AFM (Fig. 2(a)) and TEM demonstrate high quality growth. Low temperature photoluminescence (PL) shown in Fig. 2(b), resulting

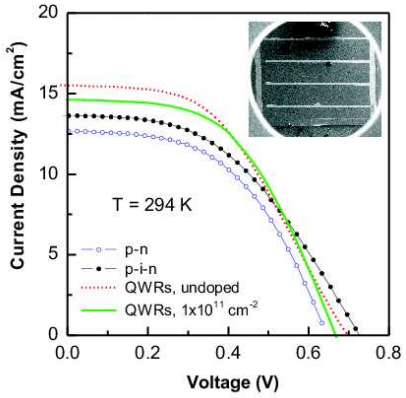

Figure 1: Room temperature efficiency measurements for four different solar cells. SEM image of the device is shown in inset.

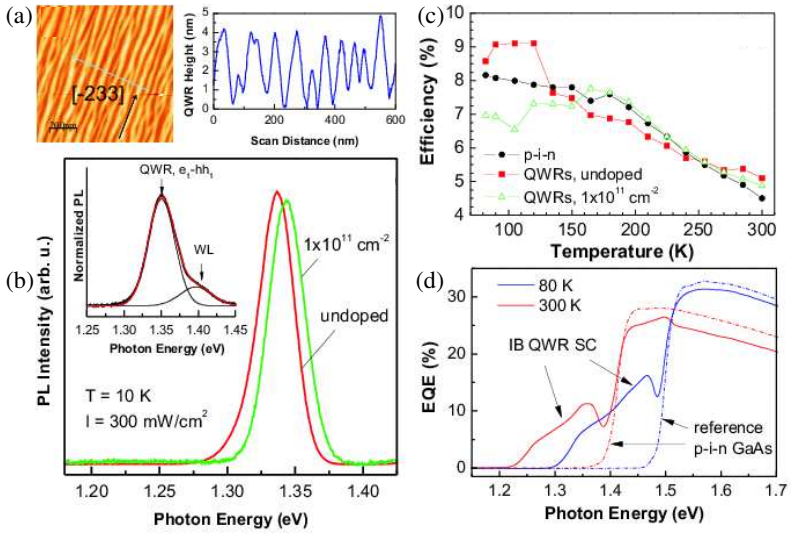

Figure 2: (a) AFM image and QWR height profile taken across [−110]. (b) PL measurements at 10 K. Inset represents PL at high excitation intensity (3000 W/cm^2). (c) Total efficiency vs. temperature. (d) EQE spectra for QWR and reference solar cells at 80 K and 300 K.

from optical transitions between ground states of the QWRs, reveals the electronic structure of the IB which correlates with the enhanced optical absorption due to the IB at room temperature. The effects of doping on this IB structure were studied in detail through external quantum efficiency (EQE) (Fig. 2(d)), direct photocurrent measurements with multiband excitation, and temperature dependence of the total conversion efficiency (Fig. 2(c)). In addition, deep states affecting solar cell performance, mainly caused by strained layer epitaxy were probed by deep level transient spectroscopy (DLTS). These demonstrated reasonable correlation with EQE of the solar cells at different temperatures.

Session 1P3b
MS-1.9: Light Management for Photovoltaics

Solar Rectifying Antennas: A New Distinct Paradigm for Power Conversion

Jeffrey Gordon
Department of Solar Energy & Environmental Physics, Blaustein Institutes for Desert Research
Ben-Gurion University of the Negev, Sede Boqer Campus, 84990, Israel

Abstract— We explore the tantalizing prospect of using rectifying antennas for *solar* power conversion. This approach is fundamentally distinct from photovoltaic or solar thermal power converters principally because antennas harvest only *coherent* radiation. We evaluate the fundamental limits for this novel solar power conversion strategy from basic principles of optics and thermodynamics.

Rectifying antennas constitute an established, high-efficiency power conversion technology for radio-frequency, microwave and, most recently, terahertz frequencies. Although sunlight is commonly viewed as incoherent — therefore ostensibly not suitable for antenna collection — all radiation exhibits spatial coherence on a sufficiently small scale.

The latest advances in thetheory and experimental confirmation of basic performance bounds for aperture antenna harvesting, based on the partial coherence of broadband solar radiation, will be reviewed. This includes the first-ever direct measurement of the spatial coherence of sunlight. The ramifications for using optical concentrators that can effectively replace orders of magnitude of antenna and rectifier elements will be discussed.

Even if the antenna harvesting of unpolarized, wide-spectrum solar radiation can be tackled, the question remains whether an incoherent, continuous, broadband signal can be rectified at reasonable efficiencies. Accordingly, we derive a basic upper bound on the ability to rectify any continuous broadband spectrum — including blackbody (most notably solar) radiation and white noise — and thereby confirm the promising potential for high-efficiency solar rectification.

Finally, a fundamental thermodynamic limit for *coherence-limited* solar converters at arbitrary optical concentration is derived — a generalization of the eponymous Landsberg limit for solar power conversion. In the process, the device dimensions and potential efficiency for high-performance solar rectifying antennas are established.

Record Efficient Upconverter Solar Cell Devices

Jan Christoph Goldschmidt[1], **Stefan Fischer**[1], **Barbara Herter**[1], **Benjamin Fröhlich**[1], **Karl W. Krämer**[2], **Bryce S. Richards**[3], **Aruna Ivaturi**[3], **Sean K. W. MacDougall**[3], **Jose Marques Hueso**[3], **Elena Favilla**[4], **and Mauro Tonelli**[4]

[1]Fraunhofer Institute for Solar Energy Systems, Heidenhof Str. 2, Freiburg 79110, Germany
[2]Department of Chemistry and Biochemistry, University of Bern, Freiestrasse 3, Bern 3012, Switzerland
[3]School of Engineering and Physical Sciences, Heriot-Watt University, Edinburgh EH14 4AS, Scotland
[4]NEST, Dipartimento di Fisica, Universitá di Pisa, Largo B. Pontecorvo, 3, Pisa I-56127, Italy

Abstract—

Introduction: For silicon solar cells, the 20% of the energy incident from the sun carried by sub-band-gap photons are lost. Upconversion — the generation of one high energy photon out of at least two lower energy photons — can reduce these losses. Despite theoretical limits close to 40% for ideal silicon solar cells with attached upconverters [1, 2] real devices stayed far below those limits [3–6]. While especially the early works performed experiments with monochromatic excitation, upconversion has been increasingly investigated under broad spectrum illumination to determine its potential for solar energy harvesting and efficiencies have increased considerably [7–10].

In this paper, we present measurements of upconverter solar cell devices (UCPVDs) showing world-record values for the relative increase in short-circuit current density due to upconversion, and first time ever outdoor characterization of UCPVDs. To further increase upconversion performance, we apply photonic structures that combine local irradiance enhancement and resonant emission amplification.

Approach: The microcrystalline upconverter materials β-$NaYF_4$:25% Er^{3+} and Gd_2O_2S:10% Er^{3+} embedded in perfluoro-cyclobutyl (PFCB), and mono-crystalline samples of BaY_2F_8:30% Er^{3+} were attached to planar silicon solar cells that featured broad-band anti-reflection coatings by an index matching liquid (IML). The created UCPVDs were characterized using concentrated light of a solar simulator and outdoors under direct sun illumination. A spectral mismatch correction [9] was applied to the results of the solar simulator measurements. Multilayer photonic structures were realized via plasma enhanced chemical vapor deposition (PECVD) of amorphous silicon carbides with two different refractive indices, and nanoparticles of β-$NaYF_4$:25% Er^{3+} embedded into polymethylmethacrylate (PMMA) were integrated into the photonic structures. Upconversion luminescence of these systems was measured using an integrating sphere setup under 1523 nm laser excitation.

Results and Conclusions: In measurements with a solar simulator, we determined a maximum additional short-circuit current density due to upconversion $\Delta j_{SC,UC}$ of 17 mA/cm^2 at illumination with 94 suns for an UCPVD with an mono-crystalline BaY_2F_8:30% Er^{3+} upconverter. This translates into a record relative enhancement of 0.5%, considering the 33.4 mA/cm^2 short-circuit current density of the used silicon solar cell with 17.6% efficiency. A $\Delta j_{SC,UC}$ of 8 mA/cm^2 at 70 suns and 5 mA/cm^2 at 67 suns were achieved with the micro-crystalline upconverter materials β-$NaYF_4$:25% Er^{3+} and Gd_2O_2S:10%Er^{3+}, respectively. Both samples, featured 84.9 w/w% concentration of the upconverter material in the PFCB. In outdoor measurements, a $\Delta j_{SC,UC}$ of 3.7 mA/cm^2 suns and 3.1 mA/cm^2 both at 55 suns were achieved using again β-$NaYF_4$:25% Er^{3+} and Gd_2O_2S:10%Er^{3+}. The solar simulator measurements agree well with these first of its kind outdoor measurements, especially considering that the β-$NaYF_4$:25% Er^{3+} sample used in the outdoor measurements featured only 75.7 w/w% concentration and therefore suffered from slightly reduced absorption. These values demonstrate the huge progress that has been made in the last years and constitute a nearly 40 fold increase compared to the only 3 year old best values [7]. Continued progress along this path makes significant efficiency enhancements due to upconversion to appear in reach.

The incorporation of upconverter material into multi-layer photonic structures increased upconversion luminescence by about a factor of 2. The presence of a back-reflector that increases the local irradiance has a stronger positive impact than the presence of a cavity around the upconverter that is designed to increase emission of upconversion luminescence. These findings are in agreement with theoretical studies that will be presented in detail alongside a more detail experimental investigation at the conference.

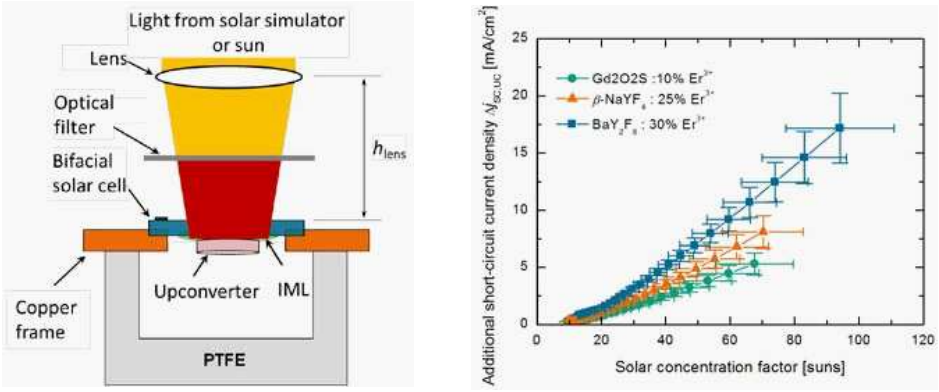

(a) (b)

Figure 1: (a) The $\Delta j_{SC,UC}$ was measured for UCPVD both with a solar simulator and outdoors. The incident light was concentrated with a Fresnel lens and the concentration level adjusted by the height of the lens above the UCPVD. Photons with energies above the band-gap were blocked from reaching the solar cell to facilitate the detection of $\Delta j_{SC,UC}$. (b) In the solar simulator measurements mono-crystalline BaY_2F_8:30% Er^{3+} showed the highest $\Delta j_{SC,UC}$ and record values of 17 mA/cm^2 at 94 suns.

REFERENCES

1. Johnson, C. M. and G. J. Conibeer, "Limiting efficiency of generalized realistic c-Si solar cells coupled to ideal up-converters," *Journal of Applied Physics*, Vol. 112, No. 10, 2012.
2. Trupke, T., et al., "Efficiency enhancement of solar cells by luminescent up-conversion of sunlight," *Solar Energy Materials & Solar Cells*, Vol. 90, No. 18–19, 3327–3238, 2006.
3. Shalav, A., et al., "Application of $NaYF_4$:Er^{3+} up-converting phosphors for enhanced near-infrared silicon solar cell response," *Applied Physics Letters*, Vol. 86, No. 1, 13505, 2005.
4. Richards, B. S. and A. Shalav, "Enhancing the near-infrared spectral response of silicon optoelectronic devices via up-conversion," *IEEE Transactions on Electron Devices*, Vol. 54, No. 10, 2679–2684, 2007.
5. Fischer, S., et al., "Enhancement of silicon solar cell efficiency by upconversion: Optical and electrical characterization," *Journal of Applied Physics*, Vol. 108, No. 4, 044912, 2010.
6. Ivaturi, A., et al., "Optimizing infrared to near infrared upconversion quantum yield of beta-$NaYF_4$:Er^{3+} in fluoropolymer matrix for photovoltaic devices," *Journal of Applied Physics*, Vol. 114, No. 1, 013505, 2013.
7. Goldschmidt, J. C., et al., "Experimental analysis of upconversion with both coherent monochromatic irradiation and broad spectrum illumination," *Solar Energy Materials and Solar Cells*, Vol. 95, No. 7, 1960–1963, 2011.
8. MacDougall, S. K. W., et al., "Ultra-high photoluminescent quantum yield of b-$NaYF_4$:10% Er^{3+} via broadband excitation of upconversion for photovoltaic devices," *Opt. Express*, Vol. 20, No. S6, A879–A887, 2012.
9. Fischer, S., et al., "Absolute upconversion quantum yield of β-$NaYF_4$ doped with Er^{3+} and external quantum efficiency of upconverter solar cell devices under broad-band excitation considering spectral mismatch corrections," *Solar Energy Materials and Solar Cells*, Vol. 122, 197–207, 2014.
10. Fischer, S., et al., "Upconverter silicon solar cell devices for efficient utilization of sub-band-gap photons under concentrated solar radiation," *IEEE Journal of Photovoltaics*, Vol. 4, No. 1, 183–189, 2014.

Photonic Architectures for Beating Light Trapping and Efficiency Limits in Solar Cells

Jeremy N. Munday
University of Maryland, USA

Abstract— Based on thermodynamic arguments, limitations can be placed on both the amount of light a semiconducting slab can absorb and the maximum solar energy conversion efficiency such a device can attain. However, by careful photonic design these limits can be circumvented. In this talk, I will present classes of photonic structures for photovoltaics that have the potential to surpass these limits. The first class is designed to improve the cell's current based on anti-reflection coatings, scattering, and light trapping. The second class is designed to improve the voltage characteristics of the device through either optical concentration or an effective modification of the semiconductor bandgap.

To improve the current, three processes that need to be considered. First, high-quality antireflection coatings are necessary to ensure that the incident solar flux enters the cell. We have recently developed a simple, scalable, and inexpensive paper-based coating that can reduce reflections at all angles of illumination, which leads to an efficiency improvement of 24% for a GaAs solar cell. Second, light that enters the device must be efficiently scattered to increase the optical path for thin, weakly absorbing devices. Rather than using textured surfaces, we recently explored the use of quantum dots, which are able to absorb incident photons and efficiently re-emit them into waveguide modes of the solar cell. Such a scheme has been shown to increase the efficiency of a polymer solar cell by 28%. Third, the overall structure should be designed in such a way that the average local density of optical states (LDOS) within the absorber is higher than it would be for a bulk material. When this condition is met, the thin film absorption limit can be significantly increased.

To improve the voltage characteristics, two approaches are taken. First, we consider optical concentration in nanophotonic structures, such as nanowires. The increased optical concentration leads to increased carrier concentration, and hence higher cell voltages. As a second approach, we use photonic crystals to modify the absorption and emission properties of solar cells. Using the principle of detailed balance, we show that the semiconductor bandgap can be effectively modified, allowing us to improve the cell's open circuit voltage.

By combining these strategies, we will layout a pathway to achieving ultra-high efficiency solar cells based purely of photonic design considerations.

Light Management and Optical Requirements for Thin-film on Silicon Tandem Cells

Thomas P. White, **Niraj N. Lal**, **and Kylie R. Catchpole**
Centre for Sustainable Energy Systems, Research School of Engineering
The Australian National University, Canberra 0200, Australia

Abstract— Tandem solar cells that combine novel thin-film photovoltaic materials with high efficiency crystalline silicon technology have the potential to reach efficiencies above 30% [1]. Perovskite solar cells are emerging as the leading thin-film contender for such tandem devices, with reported efficiencies above 16%, and open circuit voltages $> 1\,\mathrm{V}$ in stand-along cells [2]. However, integrating these two cell technologies without reducing the performance of either cell will be a significant challenge.

There are two essential requirements for a top cell in a tandem: first, the cell must absorb the short wavelength part of the solar spectrum and produce current at a higher voltage than the bottom cell; second, the cell must transmit the long wavelength part of the spectrum to the cell below (Fig. 1(a)). These requirements place strict conditions on the optical properties of the top cell both in terms of short wavelength absorption, and long-wavelength transmission.

In this work, we analyse the optical requirements for thin-film on silicon tandems. In particular we quantify the effects of parasitic optical loss in transparent electrode layers and sub-bandgap absorption in the top cell, and identify the critical importance of long wavelength transparency in the top cell (Fig. 1(a)). We also investigate the requirements and opportunities for light trapping in the top cell (Figs. 1(b), (c)) and use a combined optical and electrical tandem cell model to show that any scheme to increase short wavelength absorption in the top cell must have excellent wavelength selectivity. Furthermore, planar selective intermediate reflectors such as Bragg stacks are found to be detrimental to the tandem cell performance in most situations [3].

Through this analysis, we show that the very high quantum efficiency and optimized performance of existing silicon technology places very strict optical performance requirements on thin-film top cells. Achieving tandem cell efficiencies approaching 30% will require improved transparent electrodes, reduced sub-bandgap absorption in active layers, and novel wavelength-selective light trapping schemes.

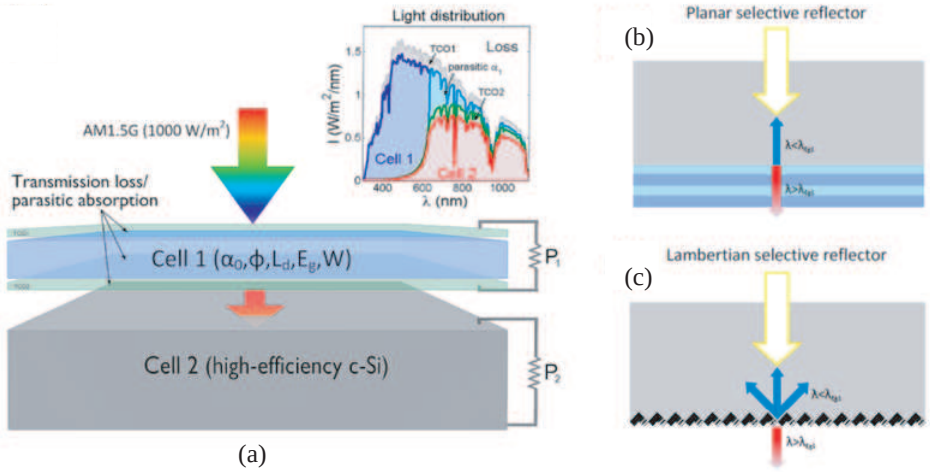

Figure 1: (a) Schematic of a four-terminal tandem cell consisting of a thin-film cell on top of a silicon cell. Inset: distribution of the absorbed solar spectrum in each part of the cell. (b), (c) Schematics of two intermediate light trapping schemes considered in this work: (a) planar selective reflector, and (b) a Lambertian selective reflector.

REFERENCES

1. White, T. P., N. N. Lal, and K. R. Catchpole, *IEEE J. Photovolt.*, Vol. 4, 208–214, 2014.
2. Snaith, H. J., *J. Phys. Chem. Lett.*, Vol. 4, 3623–3630, 2013.
3. Lal, N. N., T. P. White, and K. R. Catchpole, in preparation.

Ultrathin Metal-semiconductor Nanocomposites as Resource Efficient Light Absorbers for Photovoltaics

Carl Hägglund
Ångström Solar Center/Division of Solid State Electronics
Department of Engineering Sciences, Uppsala University, Sweden

Abstract— The light absorbing semiconductor layers of solar cells are traditionally made to absorb nearly all photons with energies exceeding the bandgap, more or less through choice of thickness according to the inverse of the absorption coefficient. A drastically different approach is to design a nanocomposite material with effective optical constants such that they approach the ideal conditions for light absorption for a given, very small thickness. By combining semiconducting layers suitable for solar energy conversion with noble metal nanoparticles supporting localized surface plasmon resonances in the visible to near infrared range, it has been theoretically and experimentally demonstrated that such conditions can readily be accomplished with mass equivalent thicknesses on the nanoscale. Effective absorption coefficients exceeding $1\,\mathrm{nm}^{-1}$, or an order of magnitude higher than for bulk metals, were observed [1]. In order to exploit the light absorption in such nanocomposites for efficient solar energy conversion, several important challenges must be successfully addressed. Firstly, the absorption must cover a broad spectral range, typically between 2 and 3 eV in width depending on bandgap. Further, losses in the form of Joule heating of the metal component must be minimized. Finally, efficient charge carrier separation must be accomplished. One approach that may prove useful in these regards is to exploit plasmon near-field induced absorption in a strongly coupled, highly damped semiconductor material [2]. A high damping of the plasmon resonance both broadens the absorption peak and causes a high fraction of the absorption to take place in the semiconductor layer, thus avoiding Joule heating and producing more long lived electron hole pairs that can feasibly be separated with higher yield. Recent experimental results in this area, based on ultrathin semiconductor layers grown on metal nanoparticle arrays by atomic layer deposition, will be presented.

REFERENCES

1. Hägglund, C., G. Zeltzer, R. Ruiz, I. Thomann, H.-B.-R. Lee, M. L. Brongersma, and S. F. Bent, "Self-assembly based plasmonic arrays tuned by atomic layer deposition for extreme visible light absorption," *Nano Lett.*, Vol. 13, 3352–3357, 2013, DOI: 10.1021/nl401641v.
2. Hägglund, C. and S. P. Apell, "Plasmonic near-field absorbers for ultrathin solar cells," *The Journal of Physical Chemistry Letters*, Vol. 3, 1275–1285, 2012, DOI: 10.1021/jz300290d.

Photon Management with Lanthanides: Up and Down

A. Meijerink and R. Martin Rodriguez
CMI, Debye Institute, P. O. Box 80 000, TA Utrecht 3508, The Netherlands

Abstract— Spectral conversion using up- and downconversion have received increasing attention in the past 20 years. Triggered by the development of mercury free fluorescent tubes, the invention of downconversion has now spread to other applications, including solar cells. State-of-the-art commercial crystalline Si (c-Si) solar cells dominate the market and have energy efficiencies around 15%. The main energy losses (over 70%) are related to the spectral mismatch [1]. IR photons with energies lower than the bandgap are not absorbed while for photons with energies exceeding the bandgap, the excess energy is lost as heat during the fast thermalization. Two methods are capable of reducing spectral mismatch losses: upconversion (UC) and downconversion (DC) [2, 3]. In case of UC, two infrared photons are 'added up' to give one higher energy photon that can be absorbed. The opposite process, downconversion, involves 'cutting' of one high energy photon into two lower energy photons. This process can reduce energy losses related to thermalization.

In this presentation, we will discuss recent progress for both UC and DC. For DC both resonant two-step energy transfer and cooperative energy transfer can be used to split one high energy photon into two lower energy photons [4]. It is not always trivial to distinguish between the two processes and approaches to identify the DC mechanism will be discussed. In the field of upconversion, Er^{3+} has been the ion of choice due to the equally spaced energy levels in the IR spectral region, allowing efficient IR to NIR UC or, in combination with Yb^{3+}, NIR to visible UC. Here a new strategies for IR to NIR UC will be discussed based on alternative lanthanide ions (including Ho^{3+} and Tm^{3+}). Also, Gd_2O_2S:Er^{3+} will be shown to be an attractive host for efficient upconversion, with UC quantum yield above 10% at moderate excitation powers ($700\,W/m^2$). Finally, challenges in the field of UC and DC materials will be addressed like concentration quenching and sensitization.

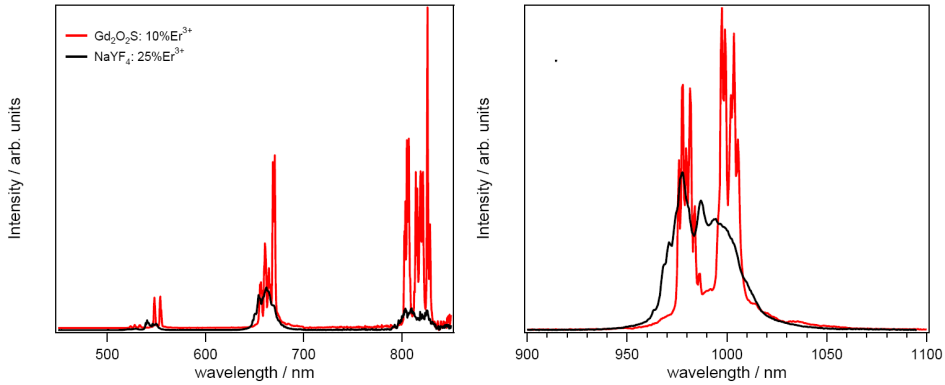

Figure 1: Upconversion spectra of Gd_2O_2S: 10%Er^{3+} and $NaYF_4$:25%Er^{3+} after $^4I_{13/2}$ excitation at 1510 and 1523 nm, demonstrating the higher efficiency of Gd_2O_2S:Er under monochromatic IR.

REFERENCES

1. Richards, B. S., *Sol. En. Mat. Sol. Cells*, Vol. 90, 2329–2337, 2006.
2. Trupke, T., M. A. Green, and P. Würfel, *J. Appl. Phys.*, Vol. 92, 1668, 2002.
3. Trupke, T., M. A. Green, and P. Würfel, *J. Appl. Phys.*, Vol. 92, 4117, 2002.
4. Van der Ende, B., L. Aarts, and A. Meijerink, *Advanced Mater.*, Vol. 21, 3073–3077, 2009.

The Up-conversion Process in Quantum Cutting Phosphors: Ce^{3+}-Yb^{3+} Co-doped YAG

Huiqi Ye[1, 2], **Liang Tang**[1, 2], **and Dong Xiao**[1, 2]

[1]National Astronomical Observatories/Nanjing Institute of Astronomical Optics & Technology
Chinese Academy of Sciences, Nanjing, Jiangsu 210042, China
[2]Key Laboratory of Astronomical Optics & Technology
Nanjing Institute of Astronomical Optics & Technology, Chinese Academy of Sciences
Nanjing, Jiangsu 210042, China

Abstract— The up-conversion process, converting two NIR photons into one visible photon, is found in the Ce^{3+}-Yb^{3+} co-doped YAG phosphors, which are a kind of NIR quantum cutting materials with promising application in improving silicon solar cell efficiency by converting one visible photon into two NIR photons. Under 457 nm excitation of 5d level of Ce^{3+}, the NIR emissions ($\sim$ 1030 nm) due to Yb^{3+}: $^2F_{5/2}$-$^2F_{7/2}$ are obtained in addition to the visible emissions ($\sim$ 540 nm) of Ce^{3+}; while under 915 nm excitation of Yb^{3+}, the visible emissions ($\sim$ 540 nm) of Ce^{3+} are also observed. The results show that the energy could be transferred between Ce^{3+} and Yb^{3+} in both direction as a result of quantum cutting and up-conversion. The intensities of luminescence are dependent on the excitation power and follow a power law ($I \sim P^n$). The n is about 1 for Ce^{3+} emissions, however between 1 and 1/2 for Yb^{3+} emissions under excitation of Ce^{3+}; and between 1 and 2 for Ce^{3+} emissions under excitation of Yb^{3+}. The existence of up-conversion process in the quantum cutting materials would seriously affect NIR emission efficiency because of the possible energy drawback. It should be one reason for low quantum yields of these materials in the experiment although the theoretical prediction. In the view of improving solar cell efficiency, the up-conversion process not only affects the quantum cutting efficiency but also adds extra absorption in the NIR range, where the silicon solar cell is at its most efficiency. So it is very important to study the process carefully and find a solution.

Luminescent Manipulation of Sunlight for Photovoltaics and Biofuels

Chris Giebink
Department of Electrical Engineering, The Pennsylvania State University, USA

Abstract— Optical concentration is a powerful and near-term strategy to lower the cost of electricity produced from established solar cell technologies because it reduces the cell area needed to generate a given amount of power. Whereas passive geometric optical concentrators are invariably bound by the sine limit, luminescent solar concentrators (LSCs) can in principle achieve high concentration ratio ($> 100x$) without tracking the Sun. These devices traditionally consist of a luminescent slab that absorbs sunlight and emits it into modes confined by total internal reflection, where it is subsequently absorbed by photovoltaic cells attached to the edges. Despite their promise, however, practical LSCs have so far failed to achieve useful concentration for photovoltaics due to limited solar spectrum absorption and optical losses within the slab.

We are exploring opportunities to improve LSC performance and diversify their application by photonically controlling the luminescent etendúe. Leveraging highly directional luminescence together with a generalized nonimaging optical framework, we demonstrate routes to both increase concentration ratio for photovoltaics and alternatively to optimize the distribution of light within closed photobioreactors for enhanced algal biofuel productivity. Our approach, which is based on the use of macroscopic freeform waveguides, leads to the formation of optical pseudo-potentials that act like in-plane graded index variations, channeling the flow of light and localizing it at particular points to dramatically boost concentration ratio.

Enhancing the Efficiency of Photovoltaics via Thin Photonics

Rajesh Menon
Department of Electrical and Computer Engineering
University of Utah, Salt Lake City, Utah 84112, USA

Abstract— The relatively high cost of solar energy is the primary factor limiting its widespread adoption. This cost can be decreased substantially with a concomitant increase in system efficiency as it affects not just the device costs but all other balance-of-systems costs as well. The efficiency of a photovoltaic device is fundamentally limited by the inability of a single bandgap absorber to convert the broad solar spectrum into electric power. In this presentation, I will describe an approach that utilizes broadband diffractive optics to spectrally separate sunlight and concentrate these spectral bands onto appropriate single-bandgap photovoltaic devices in order to substantially increase the overall device efficiency [1]. We applied nonlinear optimization to design these optics [2], grayscale lithography to fabricate them and combined them with a variety of solar cells to demonstrate significant increases in overall efficiency. Compared to multijunction cells, the single-junction devices as well as the planar micro-optics can be manufactured at low cost.

We have also applied nonlinear optimization techniques for light-management in thin-film photovoltaic devices [3, 4]. Specifically, we designed nanophotonic structures in ultra-thin organic absorbers sandwiched between high-index cladding layers (GaP or ITO) [5]. Using the multiple coupled resonances enabled via subwavelength structures, we can enhance light absorption beyond the conventional ergodic limit [6]. Recently, we also applied our design methodology to account for the motion of the sun, thereby allowing for high system efficiencies under non-tracking conditions [5, 7].

In this presentation, I will describe both areas of research, and **emphasize the rich opportunity for innovation at the intersection of numerical electromagnetics, nanophotonics, nanofabrication and photovoltaics.**

REFERENCES

1. Kim, G., J.-A. Dominguez-Caballero, H. Lee, D. Friedman and R. Menon, "Increased photovoltaic power output via diffractive spectrum separation," *Phys. Rev. Lett.*, Vol. 110, 123901, 2013.
2. Kim, G., J.-A. Dominguez-Caballero, and R. Menon, "Design and analysis of multi-wavelength diffractive optics," *Opt. Exp.*, Vol. 20, No. 2, 2814–2823, 2012.
3. Wang, P. and R. Menon, "Simulation and optimization of 1-D periodic dielectric nanostructures for light-trapping," *Opt. Exp.*, Vol. 20, No. 2, 1849–1855, 2012.
4. Wang, P. and R. Menon, "Optimization of periodic nanostructures for enhanced light-trapping in ultra-thin photovoltaics," *Opt. Exp.*, Vol. 21, No. 5, 6274–6285, 2013.
5. Shen, B., P. Wang, and R. Menon, "Optimization and analysis of 3D nanostructures for power-density enhancement in ultra-thin photovoltaics under oblique illumination," *Opt. Exp.*, Vol. 22, No. 52, A311–A319, 2014.
6. Yu, Z., A. Raman, and S. Fan, "Fundamental limit of nanophotonic light trapping in solar cells," *Proc. Natl. Acad. Sci.*, Vol. 107, No. 41, 17491–17496, USA, 2010.
7. Wang, P. and R. Menon, "Simulation and analysis of the angular response of 1D dielectric nanophotonic light-trapping structures in thin-film photovoltaics," *Opt. Exp.*, Vol. 20, No. S4, A545–A553, 2012.

Session 1P4a
SC2: Plasmonic Nanophotonics 1 — Experiment, Measurement and Fabrication

THz Sensor Based on the Principle of Plasmon-induced Radiation Force

Kosei Ueno, **Hiroko Itoh**, **Wakako Nakano**, **Sho Nozawa**, **and Hiroaki Misawa**
Research Institute for Electronics Science, Hokkaido University
N21, W-10, Kita-ku, Sapporo, Hokkaido 001-0021, Japan

Abstract— Terahertz waves (THz) have received considerable attention for use in many applications such as transmission imaging and fingerprint spectra with an important contribution in the bioengineering and security field. Here, we have successfully demonstrated volume phase transition of polyacrylamide gel using plasmon-induced radiation force that is working on the nanometer-sized gap region of a plasmonic optical antenna based on the localization of THz wave on it. Finally, a primitive camera sensing for the THz wave has been successfully proposed using a conventional CCD camera and the plasmon-induced radiation force.

Closely-spaced gold nanochain structures whose plasmon resonant wavelength is far-infrared region were fabricated by electron beam lithography and lift-off techniques on non-doped silicon substrate. To induce volume phase transition of polymer gel owing to radiation force working on nanogap, polyacrylamide gel was deposited on the closely-spaced gold nanostructures and subsequently continuous wave (CW) laser beam 10.6 μm (28.3 THz) was irradiated on the gold nanostructured substrate.

Scanning electron microscope (SEM) image of gold nanochain structure and its extinction spectrum are shown in Figs. 1(a) and 1(b). Plasmon resonance band peaking at 10.6 μm is clearly observed. When the polyacrylamide gel was placed on closely-spaced gold nanoparticles and subsequently laser beam was irradiated on them, the volume phase transition of polyacrylamide gel was clearly observed even with an irradiation power of 10 kW/cm^2 under the incident polarization parallel to the nanochain structure as shown in Fig. 1(c). On the other hand, we have confirmed that the volume phase transition of polyacrylamide gel was not observed under the incident polarization perpendicular to the nanochain structure as shown also in Fig. 1(c). Here, we discuss about the mechanism that the volume phase transition of polyacrylamide gel was induced since the balance of the osmotic pressure in polyacrylamide gel collapsed due to intense plasmoninduced radiation force at nanogap. In this system, especially, there was a possibility that the volume phase transition was induced by the rise in heat on gold nanostructures based on the plasmon excitation. However, we confirmed that the volume phase transition of polyacrylamide gel was not induced by temperature up to 95°C as a separate experiment. On the

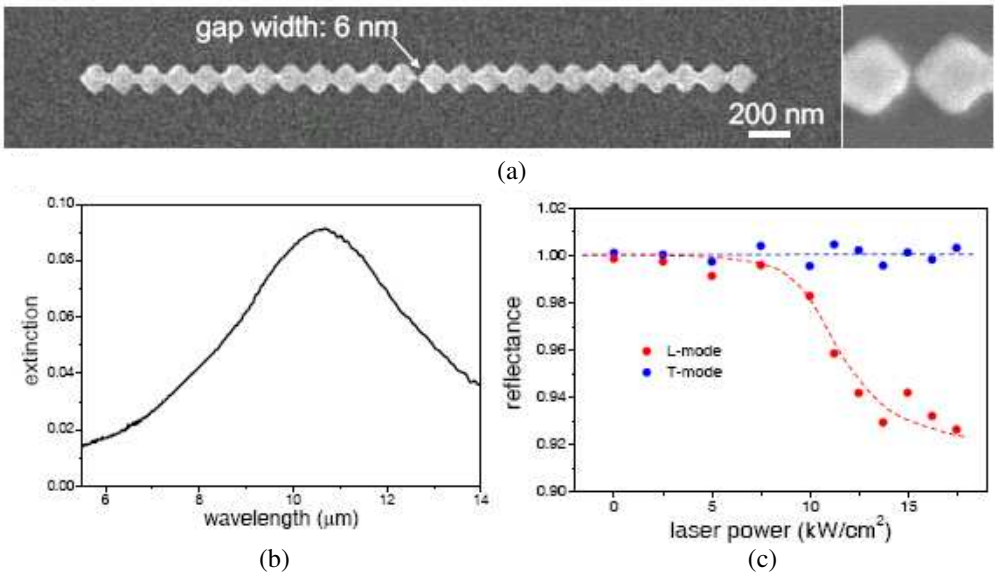

Figure 1: (a) SEM image of gold nanochain structure. (b) Extinction spectrum of gold nanochain structure. (c) Laser power dependence of reflectance of the probe beam (550 nm) to pursue the volume phase transition of polyacrylamide gel utilizing refractive index change based on the phase transition.

basis of the principle, the phenomenon was applied to THz imaging camera using a conventional visible wavelength CCD camera. The detailed principle of the sensor will be exhibited in this presentation.

Optical Trapping with Plasmonic Nano-islands

Zhiwen Kang, Jiajie Chen, Shu-Yuen Wu, and Ho-Pui Ho
Department of Electronic Engineering, The Chinese University of Hong Kong
Shatin, N.T., Hong Kong SAR, China

Abstract— Plasmonic tweezers are devices that harness the enhanced optical gradient force exerted on targets (micro- and nano-objects) using tightly localized near-field of surface plasmons. Typically, these devices require high-precision fabrication techniques such as electron-beam lithography, focused-ion beam milling, or colloidal lithography to generate the desired surface patterns. This renders the fabrication process time-consuming, expensive and low yield, which drastically diminish the prospect of using plasmonic tweezers for large-scale applications. We demonstrate herein that speckle optical tweezers that utilize random interference light field may be a possible choice. Inspired by this concept, we show that the use of plasmonic random/disordered systems can generate speckles in the near-field, thus readily leading toplasmonic tweezers with ease. Such random structures are easily obtained via metal deposition (thermal evaporation or sputtering) followed by thermal annealing. Typically a sample may take the form of gold nanoisland substrate (AuNIS). Our experiments have revealed that two-dimensional trapping, manipulation, and three-dimensional stacking of polystyrene spheres (nm to μm in size) are achievable with very low power densities (several $\mu W/\mu m^2$). The collective near-field from the localized surface plasmons of the nano-islands has enhanced the trapping force considerably. Moreover, plasmonic heating also results in convective flow near the illuminated spot, and it plays a positive role by bringing far-field targets into the hot zone. The net force is towards the surface, thus making the trap stable. Trapping of *Escherichia coli* has also been demonstrated. Our results show that the plasmonicnano-islands system provides highly practical substrate for optical tweezers. Users can simply focus a laser beam at the AuNIS surface to activate the trap. This is a major step forward since until now all plasmonic tweezers are based on well-defined metallic structures. We also see that the AuNIS reported here may find application as advanced optical manipulation devices for biochemistry, biophysics, biomedicines, and on-chip target delivery in microfluidic systems.

Light Propagation in High Aspect Metal Structures Prepared Using Ordered Anodic Porous Alumina

Hideki Masuda and Toshiaki Kondo
Department of Applied Chemistry, Tokyo Metropolitan University
1-1 Minamiosawa, Hachioji, Tokyo 192-0397, Japan

Abstract— For the preparation of the functional optical devices based on surface plasmon resonance (SPR), the use of the self-ordered structures is a promising process because of capability of formation of highly controlled metal structures [1]. The anodic porous alumina, which is formed by anodization of Al in acidic electrolyte, is a typical self-ordered hole array material [2]. This material has highly ordered hole array structures composed of a close-packed array of cylindrical cells with a straight hole. We have been studying the application of the ordered high aspect structure of anodic porous alumina as a starting structure for the fabrication of various types functional optical devices based on the SPR [3, 4]. The two or three dimensional ordered metal structures prepared using highly ordered anodic porous alumina show unique optical properties originating from the SPR, which was strongly dependent on the sizes and shapes of the obtained metal structures. In the present report, the fabrication of new types of functional optical devices based on SPR and their light propagation properties are described. Ordered hole array structures could be used for the fabrication of metal waveguide and coaxial cables array structures with high aspect ratios. The metal coaxial cable arrays showed unique light propagation properties beyond the restriction of the transmission wavelength due to their geometrical structures. In addition to this, ordered hole array structures of anodic porous alumina could be also applied to the fabrication of the metamaterials composed of ordered metal fine structures. The metal wire or dot array structures with high aspect ratios showed negative refractive indexes for incident light. The light propagation properties in the samples were analyzed by the calculations using FDTD (Finite-Difference Time-Domain) and RCWA (Rigorous Coupled Wave Analysis) methods. The fabrication processes described in the present report make it possible to prepare an ordered array of geometrically controlled nanostructures of metals, which allow the effective light propagation in the high aspect features.

REFERENCES

1. Kondo, T., K. Nishio, and H. Masuda, *Appl. Phys. Express*, Vol. 2, 032001, 2009.
2. Masuda, H. and K. Fukuda, *Science*, Vol. 268, 1466, 1995.
3. Kondo, T., F. Matsumoto, K. Nishio, and H. Masuda, *Chem. Lett.*, Vol. 37, 466, 2008.
4. Kondo, T., H. Masuda, and K. Nishio, *J. Phys. Chem. C*, Vol. 117, 2531, 2013.

Improving Light Emission by Plasmonic Lattice Coupled to Waveguide

Yuntian Chen[1] **and A. F. Koenderink**[2]

[1]School of Optical and Electronic Information
Huazhong University of Science and Technology, Wuhan, China
[2]Center for Nanophotonics, FOM Institute AMOLF
Science Park 104, Amsterdam 1098 XG, The Netherlands

Abstract— Mankind has long pursued the realization of bright and efficient sources of light, on basis of thermal and incandescent light sources, gas phase fluorescence, and most recently on basis of solid state lighting by light emitting diodes (LED). In LEDs based on III-V and III-nitride semiconductors the key problem is that the large refractive index contrast between air and the semiconductor limits light out-coupling. A large number of surface patterning techniques have been proposed to improve overall light extraction [1, 2], external and internal quantum efficiency, as well as directivity. The surface structures include random and periodic surface texturing [3], metallic thin films with and without air holes, and periodic metallic spheres/cylinders [1, 2]. Among those techniques, a particularly interesting scheme involves coupling the emission to waveguide modes, and then scattering the waveguide mode into freely propagating photons using periodic structures [4]. Here we set up a simple yet rigorous model that allows to assess the performance of this generic idea in two distinct scenarios. The first is extraction of light from GaN light emitting diodes, the second is conversion of blue light into white light through a phosphor conversion layer put directly on an LED, as sketched in Figs. 1(a), (b), respectively.

Under the approximation that the dipole response of, and coupling between, the particles dominates, we model the plasmonic lattice using a rigorous electrodynamic point dipole model that contains all retarded multiple scattering interactions between plasmon antennas self consistently, accounting analytically for the slab waveguide. The purpose of introducing a coupled waveguide-lattice system is to channel the emission from the active layer to the waveguide mode, and subsequently to 'redirect' bounded light to freely propagating photons.

As an example, we calculate the angle-dependent emission rate enhancement for GaN LED and phosphor based LED, shown in Figs. 1(c), (d). As can be seen, the waveguide modes are folded into the radiation cone by the plasmonic lattice. With lattice constant of 0.75λ (λ vacuum wavelength), we estimate that the radiated power from a dipole source embedded in the active layer, into the upper half space is enhanced by a factor of 8 for GaN based LEDs. As the lattice constant increases, the higher diffraction order of the folded guided mode falls into the radiation cone. However, the overall scattering efficiency from the plasmonic lattice is decreased, due to the lower particle density for larger lattice constant. Hence, it is necessary to optimize the coupled waveguide-lattice structure to extract light as much as possible. Compared with numerical methods, i.e., FDTD or FEM, our point dipole model is efficient to find the optimal waveguide lattice structure in such a large parameter space, which is of relevance for LEDs.

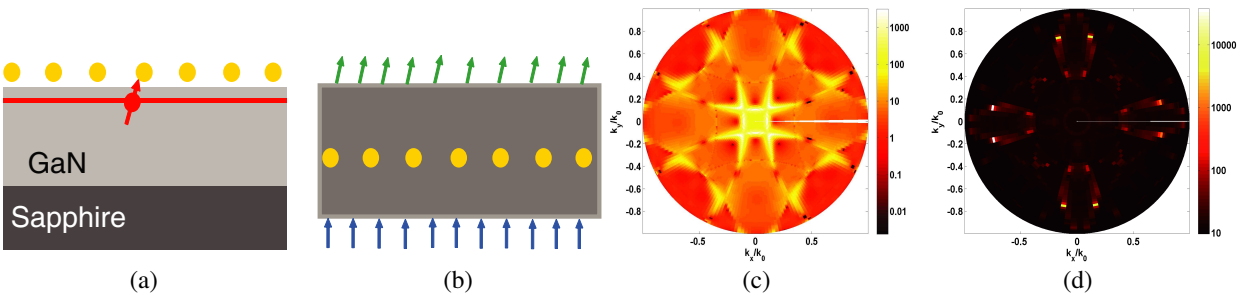

Figure 1: Nanophotonic structures patterned on (a) GaN material based LED system, and (e) Phosphor based LED system (Ceirum YAG). Angle-dependent emission rate enhancement for (c) GaN based LED, and for (d) Phosphor based LEDs.

REFERENCES

1. Yeh, D. M., C. F. Huang, C. Y. Chen, Y. C. Lu, and C. C. Yang, *Nanotechnology*, Vol. 19, 345201, 2008.
2. Henson, J., J. DiMaria, E. Dimakis, T. D. Moustakas, and R. Paiella, *Opt. Lett.*, Vol. 37, 79, 2012.
3. Schnitzer, I., E. Yablonovitch, C. Caneau, T. Gmitter, and A. Scherer, *Appl. Phys. Lett.*, Vol. 63, 2174, 1993.
4. Rigneault, H., F. Lemarchand, A. Sentenac, and H. Giovanini, *Opt. Lett.*, Vol. 24, 148, 1999.

Ultracompact On-chip Long-wave Photodetector Based on Hybrid Plasmonic Waveguides

Hao Wu, **Xiaowei Guan**, **and Daoxin Dai**
State Key Laboratory for Modern Optical Instrumentation
Centre for Optical and Electromagnetic Research
Zhejiang Provincial Key Laboratory for Sensing Technologies
Zhejiang University, Zijingang Campus, Hangzhou 310058, China

Abstract— Photo-detection plays an important role for many applications, like optical interconnects, optical sensing, etc.. Photodiode is very popular for high-speed photo-detection. However, the operation wavelength range of a photodiode is limited by the bandgap of the semiconductor. In recent years, silicon photonics for long-wave (like mid-infrared) is attracting lots of attention, particularly for optical sensing. However, the long-wave photo-detection on silicon is still a challenge. In this paper, we propose an ultrasmall on-chip long-wave photodetector by utilizing the thermal resistance effect of the metal strip on a hybrid plasmonic waveguide structure, which consists of a metal strip, a silicon core and a sandwiched nano low-index layer. When light propagates along a hybrid plasmonic waveguide, the metal strip is heated due to the light absorption. In this case, there is a temperature increase which depends on the power of the incident light. Accordingly, the resistance of the metal strip increases due to the thermal-resistance effect of metal. Here a Wheatstone bridge is applied to measure the resistance change accurately so that the photodetector is with very high sensitivity. Owing to the nano-scale confinement of light in a hybrid plasmonic waveguide, the temperature increase of metal due to the metal absorption is enhanced in comparison with the conventional long-range plasmonic waveguide. For example, the theoretical responsivity is as high as 60 mV/mW (at a bias voltage of 1 V) when the metal strip is with the dimension of 500 nm × 10 nm × 10 μm. Here the thickness of the low-index (SiO_2) layer and the high-index (Si) layer are 50 nm and 340 nm, respectively. The corresponding sensitivity is ∼ 5 nW. This hybrid-plasmonic-waveguide photodetector also enables a fast response because of very short thermal conduction path. More importantly the present on-chip photodetector is available for an ultra-braod wavelength range, which makes it useful for optical sensing system in different wavelength band.

Near-field Confinement in 3D SRR Metamolecules for Optical Refractive Index Sensor

Pin Chieh Wu[1], **Hsiang Lin Huang**[2], **Wei Ting Chen**[1], **Kuang-Yu Yang**[3], **Ta-Jen Yen**[4], **Din Ping Tsai**[1, 3], **and Hai Pang Chiang**[2, 3, 5]

[1]Graduate Institute of Applied Physics, Taiwan University, Taipei 10617, Taiwan
[2]Institute of Optoelectronic Sciences, Taiwan Ocean University, Keelung 20224, Taiwan
[3]Research Center for Applied Sciences, Academia Sinica, Taipei 11529, Taiwan
[4]Department of Materials Science and Engineering, Tsing Hua University, Hsinchu 30013, Taiwan
[5]Institute of Physics, Academia Sinica, Taipei 11529, Taiwan

Abstract— The localized surface plasmon resonance (LSPR) has found a lot of applications in detecting environmental materials and local refractive index changes. For sensor application, the sensitivity, defined as the ratio between resonance wavelength change and refractive index change ($\Delta\lambda/\Delta n$, where n is the refractive index of surrounding material) is an important factor to examine the sensor performance. To increase the sensitivity of a plasmonic sensor, one can do is the increase of the plasmon-enhanced fields or the effective area between enhanced fields and surrounding materials. In recent years, the use of SPR nanostructures as biochips is very popular, and sensitivity as high as 10^{-8} RIU can be obtained by changing the laser wavelength or structure. However, the general planar metamaterials including split-ring resonator (SRR) structures always have a large connection between induced fields and substrate which resulting in fraction of enhanced field embedded into substrate. As a result, the effective surface for sensing is dramatically decreased for planar metamaterials. One can do is to lift the metamaterials above substrates with dielectric material that is able to increase the spatial region with enhanced fields into environment. In this work, we experimentally and numerically study the refractive index sensing characteristics of plasmonic arrays composed of three-dimensional (3D) split ring resonators (SRRs) at optical region. Due to the strong near-field enhancement in free space, it is demonstrated that the sensitivity of 3D SRR structures (with 60 nm prong length) is at a high value as 796.9 nm and 603.3 nm per refractive index unit in simulation and experiment, respectively. In addition, the sensitivity can be further actively controlled by the feature prong length of 3D SRRs. An ultrahigh sensitivity about 1500 can be numerically approached while 3D SRR with 140 nm prong length. In addition, not only the sensitivity but also the FOM value is increased even though the metallic Joule loss is increased with increased prong length. These results pave a promising candidate for label-free sensor chips with ultrahigh sensitivity and biophotonics.

REFERENCES

1. Wu, P. C., et al., *Nanophotonics*, Vol. 1, 131–138, 2012.
2. Luk'yanchuk, B., et al., *Nat. Mater.*, Vol. 9, 707–715, 2010.
3. Chen, W. T., et al., *Optics Express*, Vol. 19, 12837–12842, 2011.
4. Linden, S., et al., *Science*, Vol. 306, 1351–1353, 2004.
5. Chiang, H. P., et al., *Appl. Phys. Lett.*, Vol. 88, 141105, 2006.
6. Peng, T. C., et al., *Plasmonics*, Vol. 6, 29, 2011.

UV and Visible Plasmonics of Topological Insulator

Jun-Yu Ou[1], **Jin-Kyu So**[1], **Zilong Wang**[2], **Jun Yin**[1], **Giorgio Adamo**[2], **Azat Sulaev**[3], **Cesare Soci**[2], **Lan Wang**[3], **and Nikolay I. Zheludev**[1, 2]

[1]Optoelectronics Research Centre & Centre for Photonic Metamaterials
University of Southampton, SO17 1BJ, UK
[2]Centre for Disruptive Photonic Technologies, Nanyanag Technological University, Singapore
[3]School of Physical and Mathematical Sciences, Nanyang Technological University, 637371, Singapore

Abstract— Plasmonic resonances in absorption spectra and cathode-luminescence are observed in metamaterials made of a topological insulator, $Bi_{1.5}Sb_{0.5}Te_{1.8}Se_{1.2}$, at the UV and visible frequencies due to the material's interband transition and nontrivial surface conducting state. We also report on infrared nonlinear properties of this material as a prospective platform for switchable broadband plasmonic devices.

Session 1P4b
SC2&3: Nano-focusing and Applications

Optical Manipulation with Nanostructured Plasmonic Fields

Keiji Sasaki
Research Institute for Electronic Science, Hokkaido University, Sapporo 001-0020, Japan

Abstract— Plasmonic trapping has attracted significant attention because of its applicability to nanoparticle manipulations such as single-molecule trapping and quantum-dot sorting. In this presentation, we report super-resolution trapping where nanoparticles are optically manipulated in nanoscale space smaller than the diffraction limit [1]. We performed two-dimensional mapping of optical trapping potentials experienced by a 100-nm dielectric particle above a plasmon resonant gold nanoblock pair with a gap of several nanometers. The experimental results demonstrated that the potentials have nanometer-sized spatial structures that reflect the near-field landscape of the nanoblock pair. When an incident polarization parallel to the pair axis is rotated by 90°, a single potential well turns into multiple potential wells separated by a distance of approximately 230 nm ($< \lambda/2$). We show that the trap stiffness can be enhanced by approximately 3 orders of magnitude compared to that with conventional far-field trapping. In addition, we propose new concept for controlling spatial profiles of gap-mode localized plasmonic fields toward the flexible nanomanipulation. We theoretically and experimentally show that the field distributions within hot spots are formed by constructive and destructive interferences of dipolar, quadrupolar, and higher-order multipolar plasmonic modes, which can be drastically altered by adjusting parameters of the excitation optical system [2, 3]. Optical switching of hot spots separated by an 80-nm distance is also demonstrated using a double-nanogap plasmonic structure.

REFERENCES

1. Tanaka, Y., S. Kaneda, and K. Sasaki, "Nanostructured potential of optical trapping using a plasmonic nanoblock pair," *Nano Lett.*, Vol. 13, 2146, 2013.
2. Tanaka, Y., A. Sanada, and K. Sasaki, "Nanoscale interference patterns of gap-mode multipolar plasmonic fields," *Sci. Rep.*, Vol. 2, 764, 2012.
3. Tanaka, Y., K. Sasaki, et al., "Direct imaging of nanogap-mode plasmon-resonant fields," *Opt. Express*, Vol. 19, 7726, 2011.

Reproducible Ultrahigh SERS Enhancement in Gold Nanoparticle-plane Junctions under Radially Polarized Excitation

Tian Yang, Jing Long, Hui Yi, and Hongquan Li
The University of Michigan, Shanghai Jiao Tong University Joint Institute
800 Dongchuan Rd, Shanghai 200240, China

Abstract— Detection of Raman scattering from single molecules requires ultrahigh electromagnetic SERS enhancement, which can be achieved by broadband intense focusing of photons in the nanometer sized hot spots of localized surface plasmon resonance (LSPR) structures. Suffering from the lack of efficient top-down fabrication techniques at sub-nanometer scale, ultrahigh SERS enhancement factors have been typically achieved by using metallic nanoparticle colloids in which the hot spots are randomly located with an uncontrolled distribution of intensities, resonance wavelengths and polarizations. To address this problem, we have demonstrated vertical optical antennas that are efficiently excited by focusing a radially polarized (RP) laser beam, and have achieved electromagnetic SERS enhancement factor of almost 10^{10} in a well-controlled and well-reproduced scheme.

Each vertical optical antenna is consisted of a 60 nm diameter gold nanosphere on top of an atomically flat gold surface [1]. A monolayer of malachite green isothiocyanate (MGITC) molecules is adsorbed onto the nanosphere. By focusing an RP laser beam at 633 nm onto the nanosphere at normal incidence, the vertically polarized LSPR mode is efficiently excited so that an intense hot spot in the sub-nanometer nanosphere-plane junction gap is formed and the Raman scattering of the MGITC molecules in the gap is significantly enhanced. Fig. 1(a) is a schematic illustration of the vertical optical antenna and focusing the RP laser beam. A full vectorial profile of the focal spot of the laser beam has been obtained and confirmed to have a strong vertically polarized component by raster scanning a 100 nm diameter gold nanosphere on an aerogel substrate [2]. Raman scattering is collected by the same objective. Collection of Raman scattering is further assisted by etching rings into the gold surface around the nanosphere so as to scatter surface plasmon polaritons at the Stokes frequencies. Fig. 1(b) is an SEM micrograph of the device. Fig. 1(c) shows the collected Raman scattering spectrum from this device. Comparison with the Raman spectra from a monolayer of MGITC molecules on an atomically flat gold surface indicates an electromagnetic SERS enhancement factor of around 0.7×10^{10} which has been reproducibly observed for different nanospheres with a variation as small as ±15% (for the small amount of experiments that we have conducted to date). Under a weak laser power of 300 nW, no degradation of the Raman signals has been observed for over five minutes.

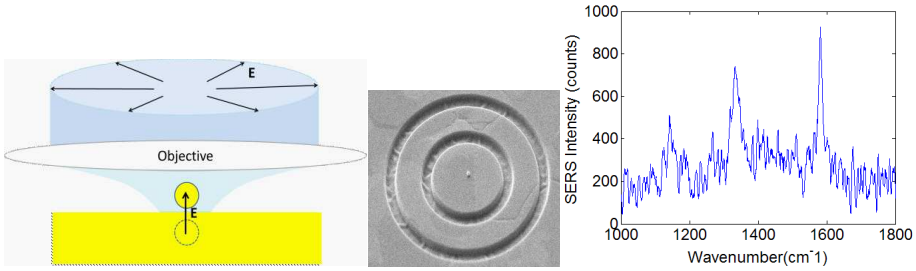

(a) (b) (c)

Figure 1: (a) A schematic of the SERS experiment. (b) An SEM micrograph of a SERS device. (c) The Raman spectrum from a monolayer of MGITC molecules in the gold nanoparticle-plane junction gap, under an RP laser power of 300 nW at 633 nm and an integration time of 2 s.

REFERENCES

1. Liu, B., D. Wang, C. Shi, K. B. Crozier, and T. Yang, "Vertical optical antennas integrated with spiral ring gratings for large local electric field enhancement and directional radiation," *Optics Express*, Vol. 19, 10049–10056, 2011.
2. Yi, H., J. Long, H. Li, X. He, and T. Yang, "Sub-wavelength full-vectorial profiling of optical focus," *Frontiers in Optics*, FW4F.3, Orlando, Florida, USA, 2013.

Recent Progresses on Silicon Hybrid Nanoplasmonics for Ultra-dense Photonic Integration

Daoxin Dai
Centre for Optical and Electromagnetic Research
State Key Laboratory for Modern Optical Instrumentation
Zhejiang Provincial Key Laboratory for Sensing Technologies
Zhejiang University, Zijingang Campus, Hangzhou 310058, China

Abstract— Hybrid plasmonic waveguides, which consist of a high-index region, a metal region and a low-index nano-slot between them, have been paid intensive attention in the past years. Since the hybrid plasmonic waveguide has the potential to achieve a nano-scale light confinement as well as relatively long propagation distance simultaneously, it becoming very attractive as a promising candidate to realize next-generation ultra-dense photonic integrated circuits. The hybrid plasmonic waveguides also offer a platform to merge photonics and electronics so that one can realize ultra-small optoelectronic integrated circuits (OEICs) for high-speed signal generation, processing as well as detection. In this paper, we give a review for the recent progresses on silicon hybrid nanoplasmonic waveguides as well as ultrasmall functionality devices, including sub-μm^2 power splitters/couplers, micro-resonators, as well as polarization handling devices.

Microfiber Bragg Grating Sensors

Bai-Ou Guan, Yang Ran, Jie Li, and Long Jin
Institute of Photonics Technology, Jinan University, Guangzhou 510632, China

Abstract— Microfibers are optical fibers with micron-scale diameters, which guide light based on the total internal reflection effect at the silica-air interface. In recent years microfibers have attracted a great attention because of its superiority in providing high fraction of evanescent fields, manageable large waveguide dispersion, high nonlinearity, compact and flexible structure [1]. Fiber gratings are one of the most importance photonic devices in fiber optic communication and sensing, which are formed by introducing a periodic refractive-index modulation along an optical fiber. The presence of microfibers not only provide a new platform for developing fiber grating based devices, but also enrich the concept of fiber gratings.

In this paper, we briefly review our most recent works on fiber Bragg gratings in optical microfibers and their applications as sensors [2–7]. High effective inscription of Bragg gratings in microfibers with 193 nm excimer laser is demonstrated. Temperature and refractive-index response of microfiber Bragg gratings are characterized. Temperature-independent refractive-index sensing is realized by using a single Bragg grating in microfiber. Surface-functionalized microfiber Bragg grating based biosensor for specific DNA detection is also demonstrated.

ACKNOWLEDGMENT

This work is supported by the National Science Fund for Distinguished Young Scholars of China (61225023), the Research Fund for the Doctoral Program of Higher Education (20114401110006), the Planned Science and Technology Project of Guangzhou (2012J5100028), the Project of Science and Technology New Star of Zhujiang in Guangzhou city (2012J2200062), and the Guangdong Natural Science Foundation (S2013030013302).

REFERENCES

1. Tong, L. M., F. Zia, X. Guo, and J. Y. Lou, "Optical microfibers and nanofibers: A tutorial," *Opt. Commun.*, Vol. 285, No. 23, 4641–4647, 2012.
2. Guan, B.-O., J. Li, L. Jin, and Y. Ran, "Fiber Bragg gratings in optical microfibers," *Opt. Fiber Technol.*, Vol. 19, No. 6B, 793–801, 2013.
3. Ran, Y., L. Jin, Y.-N. Tan, L.-P. Sun, J. Li, and B.-O. Guan, "High-efficiency ultraviolet-inscription of Bragg gratings in microfibers," *IEEE Photon. J.*, Vol. 4, No. 1, 181–186, 2012.
4. Ran, Y., L. Jin, L.-P. Sun, J. Li, and B.-O. Guan, "Bragg gratings in rectangular microfiber for temperature independent refractive index sensing," *Opt. Lett.*, Vol. 37, No. 13, 2649–2651, 2012.
5. Gao, S., L. Jin, Y. Ran, L. P. Sun, J. Li, and B.-O. Guan, "Temperature compensated microfiber Bragg gratings," *Opt. Express*, Vol. 20, No. 16, 18281–18286, 2012.
6. Ran, Y., L. Jin, L.-P. Sun, J. Li, and B.-O. Guan, "Bragg gratings in rectangular microfiber for temperature independent refractive index sensing," *Opt. Lett.*, Vol. 37, No. 13, 2649–2651, 2012.
7. Ran, Y., L. Jin, L.-P. Sun, J. Li, and B.-O. Guan, "Temperature-compensated refractive index sensing using a single Bragg grating in an abrupt fiber taper," *IEEE Photon. J.*, Vol. 5, No. 2, 7100208, 2013.

High Efficiency Compact SiN Focusing Grating Coupler with a Metal Reflector for Visible Light

Yaoran Sun, **Yuguang Zhang**, **Pengxin Chen**, **Yaocheng Shi**, **and Daoxin Dai**
Centre for Optical and Electromagnetic Research
State Key Laboratory for Modern Optical Instrumentation
Zhejiang University, East Building No. 5, Zijingang Campus, Hangzhou 310058, China

Abstract— Grating couplers (GCs) are widely used in integrated optical devices as a building block to couple light from fibers to optical waveguides, or vice versa. The design and fabrication of compact GCs working for infrared and near infrared light have been systematically investigated on silicon-on-insulator (SOI) platforms. However, on one hand, for visible light, not much work on high efficiency compact GC has been reported; on the other hand, integrated optical devices for visible light are prominent for molecule sensing and biophotonic imaging. In this paper, a compact TE-polarization SiN focusing grating coupler (GC) whose working wavelength is around 635nm is proposed and demonstrated to achieve high coupling efficiency between a standard single mode fiber (SMF) and the chip. The GC coupling efficiency is comprehensively analyzed with a three-dimensional finite-difference time-domain (3D-FDTD) method, and an optimized design strategy is also given. High coupling efficiency is achieved by properly choosing the thickness of the buried oxide (BOX) layer, the incident angle, and the grating pitch. By introducing a metal (e.g., Al) reflector beneath the silicon oxide layer, the coupling efficiency is as high as 60% theoretically. The SiN GCs are fabricated with an E-Beam lithography process and an ICP etching process. The measured results agree well with the calculated ones.

Exploiting Plasmonic Confinement for High-resolution Structural Colors and Sub-wavelength Nanolithography

L. Jay Guo
Department of Electrical Engineering and Computer Science
The University of Michigan, Ann Arbor, MI 48109, USA

Abstract— Light interacting with metallic nanostructures can produce various interesting effects. Such properties can be exploited for making structural colors [1] — artificial structures that can produce colors without using colorant pigments; which may find potential applications in future display and e-book devices that offers more energy saving. It can also be exploited for nanolithography applications. In this context, surface plasmon-based nanostructures are attractive due to their small dimensions and the ability of efficient light confinement and manipulation. Here we show that, by selective conversion between the free-space waves and spatially confined modes in plasmonic nano-resonators formed by the periodic subwavelength metal-insulator-metal (MIM) structures, the transmission [2] or reflection [3] spectra from such arrays can be well controlled by using simple design rules. High efficiency color filters based on these plasmonic resonators are capable of transmitting arbitrary colors with transmission greater than 80%, or reflecting colors with high contrast. By combining MIM nanostructures with different dimensions, arbitrary nano-micrometer-scale colorful patterns can be obtained. At present, this lateral dimension is 1–2 orders of magnitude smaller than the best high-definition color filters currently available. Furthermore, these plasmonic devices have longitudinal thickness 1∼2 orders of magnitude thinner than the colorant pigment, which is very attractive to the design of ultrathin panel display devices.

Stacking an array of MIM structures could form hyperbolic metamaterials capable of supporting high-k photonic modes. This property can be exploited for lithographic patterning based on the interference of such high-k modes. We present the analyses of propagation of surface plasmon wave due to the MIM waveguide coupling, and techniques to improve the performance of subwavelength nanolithography [4]. The new understandings provide useful guidelines and design criteria for plasmonic lithography. In practice much of the fabricated metal/dielectric multilayer stack structures cannot be approximated by effective media [5], due to the relatively thick layers used in deposition. Especially it is very difficult to obtain thin and smooth Ag film on dielectrics. We describe a new approach of introducing small amount of dopant atoms to make ultra-thin and smooth Ag films. Multilayer stack structure was fabricated to show the effective medium behavior.

REFERENCES

1. Xu, T., H.-F. Shi, Y.-K. Wu, A. F. Kaplan, J. G. Ok, and L. J. Guo, "Structural colors: From plasmonic to carbon nanostructures," *Small*, Vol. 7, 3128, 2011.
2. Xu, T., Y.-K. Wu, and X.-G. Luo, and L. J. Guo, "Plasmonic nano-resonators for color filtering and spectral imaging," *Nat. Comm.*, Vol. 1, 59, 2010.
3. Wu, Y.-K., A. E. Hollowell, C. Zhang, and L. J. Guo, "Angle-insensitive structural colours based on metallic nanocavities and coloured pixels beyond the diffraction limit," *Scientific Reports*, Vol. 3, 1194, 2013.
4. Zhu, P., H. Shi, and L. J. Guo, "SPPs coupling induced interference in metal/dielectric multilayer waveguides and its application for plasmonic lithography," *Opt. Exp.*, Vol. 22, 12521–12529, 2012.
5. Zhu, P., P. Jin, and L. J. Guo, "Insight of limitations of effective media theory for metal-dielectric multilayer metamaterials," *Opt. Comm.*, Vol. 305, 8–12, 2013.

Aperture-independent Nano Focusing of Light by Surface and Bulky Plasmonic Structures

Changtao Wang, **Xiangang Luo**, **Jiayu He**, **Na Yao**, **and Zeyu Zhao**
State Key Lab of Optical Technologies on Nano-Fabrication and Micro-Engineering
Institute of Optics and Electronics, Chinese Academy of Sciences, P. O. Box 350, Chengdu 610209, China

Abstract— Benefiting from the localized surface plasmon resonance (LSPR) effect, a number of novel nano-aperture structures, including fiber aperture, bow-tie and bull eyes etc., are proposed and demonstrated for nano focusing of light. One common feature of these methods is the strong dependence of focus width on the apertures' geometrical size, like the gap size of bowtie and diameter of bull eye's central transparent hole. This delivers great challenges for fabrication and practical application.

In our investigation, surface plasmon in propagation manner instead of localized surface plasmon is employed to design plasmonic structures for aperture-independent nano focusing of light. For instance, multiple concentric transparent rings illuminated by circular polarization light help to excite surface plasmons inside a metal-insulator-metal cavity structure, which could be superimposed constructively and focused to about 50 nm FWHM size with 365 nm light wavelength in vacuum. This idea could be extended to the case of bulky plasmonic structures composed by alternatively stacked metal-dielectric films. Surface plasmons between adjacent metal films could be coupled one by one and form a bulk plasmonic field. In our design and numerical simulations, it is demonstrated that appropriate one dimensional and two dimensional apertures, such as slits or circular apertures, help to excite bulky surface plasmon which could focus at specific distance inside the multiple films. By adding a photoresist layer to the focusing region, a resist line of about 60 nm width is observed in the lithography experiment, which is believed to be exposed by the focused light line of a 100 nm wide slit aperture above the 6 layers of Ag/SiC and each layer is 15 nm. On the other hand, we found that metal-insulator-metal structure could help to manipulate and localize the focus of surface plasmon with enhanced intensity, reduced focus size and elongated focus depth inside the insulator region. The method of aperture-independent nano focusing of light by surface and bulky plasmonic structures is believed to find potential applications like nano lithography, high density optical storage and nanoscope etc..

Engineered Highly Efficient Nanofocusing Plasmonic Waveguides

Hyuck Choo
Department of Electrical Engineering, Division of Engineering and Applied Science
California Institute of Technology, USA

Abstract— Scientific and commercial applications of optical nanofcousing devices have attracted a lot of research efforts in recent years. Sub-diffraction-limited microscopy, nano-photolithography, tipbased nanofabrication, and heat-assisted magnetic recording (HAMR) for achieving data density beyond 1 Tbits/in^2 are a few examples. To realize these applications, nanofocusing devices must be able to confine light into sub-50-nm space (sub-20 nm for HAMR applications) at high efficiency. Previously, researchers have achieved nanofocusing using scanning-tunnelingmicroscope (STM) tips, tapered plasmonic pins, enhanced transmission apertures, and tapered fiber probes [1–4].

As a potential solution, we have explored a highly efficient nanofocusing device [5]. The fabricated device is a nanoplasmonic waveguide composed of Au/SiO_2/Au layers and is fabricated using electron-beam induced deposition, focused ion-beam milling, and e-beam metal evaporation [6]. The waveguide dimensions linearly taper in 3D to form an efficient focusing tip. The thickness of the SiO_2 layer decreases from 200 nm in the body down to 14 nm in the tip.

We optimized the design of the device by running a series of FEM and FDTD simulations. To fabricate the device, we first deposit a 50-nm-thick gold layer. The dielectric material, which is SiO_2, is deposited using electron-beam induced deposition. The tapering geometry is achieved by controlling the scan (deposition) area and the dose of the electron beam and by performing multilayer depositions. The process has enabled us to obtain tapering angles between 5–45 degrees and deposit layers as thin as 5 nm. Following the SiO_2 deposition, another 50-nm-thick gold layer is deposited. The final shape of the transformer is defined by performing focused ionbeam milling.

To measure its nanofocusing efficiency, we used 120-fs Ti-sapphire-laser pulses at 830 nm (focused down to a diffraction limited spot, FWHM $\sim$ 500 nm) and excited at the base of the transformer. Then we collected the two-photon emission only from the tapered tip. From our optical measurements, we have experimentally estimated that the structure focuses light within the 80-by-14-nm area in the tip and enhances the electric field by a factor 400. The transmission efficiency was over 70%.

REFERENCES

1. Novotny, L., et al., "Theory of nanometric optical tweezers," *Physical Review Letters*, Vol. 79, 645–648, 1997.
2. Ruppin, R., "Effect of non-locality on nanofocusing of surface plasmon field intensity in a conical tip," *Physics Letters A*, Vol. 340, 299–302, 2005.
3. Barnes, W. L., et al., "Surface plasmon subwavelength optics," *Nature,* Vol. 424, 824–830, 2003.
4. Yatsui, T., et al., "Increasing throughput of a near-field optical fiber probe over 1000 times by the use of a tripletapered structure," *APL*, Vol. 73, 2090–2092, 1998.
5. Choo, H., et al, "Nanofocusing in a metal-insulator-metal gap-plasmon waveguide with a 3D dimensional linear taper," *Nature Photonics*, Vol. 6, 838–844, December 1, 2012.
6. Utke, I., et al., "Gas-assisted focused electron beam and ion beam processing and fabrication," *JVST B*, Vol. 26, 1197–1276, 2008.

Dynamic Plasmonic Trapping and Manipulation of Metallic Particles for SERS Application

Changjun Min[1], **Yuquan Zhang**[1], **Junfeng Shen**[1], **Wei Shi**[1], **and X.-C. Yuan**[2]

[1]Key Laboratory of Optical Information Science & Technology, Institute of Modern Optics
Ministry of Education of China, Nankai University, Tianjin 300071, China
[2]Institute of Micro & Nano Optics, College of Optoelectronic Engineering
Shenzhen University, Shenzhen 518060, China

Abstract— We propose a novel dynamic plasmonic tweezers for trapping and manipulating metallic particles and demonstrate its application on Surface-enhanced Raman scattering (SERS). In the first part, we discuss the interaction mechanism between metallic particles and the sharp peak of surface plasmons (SPs) in the plasmonic tweezers excited by a highly focused radially polarized beam. We show that metallic particles of nanometer to micrometer sizes can be attracted and trapped in such plasmonic tweezers instead of being repulsed by a conventional optical tweezers due to high scattering force. Through numerical analysis, we find that the resultant total force in the plasmonic tweezers is the result not of a stronger gradient force dominating an opposing scattering force, but instead of a dominant gradient force assisted by a weak scattering force acting in the same direction. Next we consider manipulating the metallic particles by modifying the properties of incident beam in the plasmonic tweezers. The optical vortices (OV) are chosen to excite the plasmonic vortices and rotate particles in the plasmonic tweezers. We show that metallic particles in plasmonic vortices can be trapped and rotated in a certain radius depending on the OV's topological charge, due to the optical force provided by the orbital angular momentum (OAM) of OV. Finally, we introduce the application of the plasmonic tweezers in SERS. By trapping and dragging a single gold nanoparticle with the plamonic tweezers, we demonstrated a dynamic single-particle-film SERS system, which produces a high SERS enhancement factor of $\sim 10^9$, and therefore provides a promising approach to controllable SERS detection and imaging.

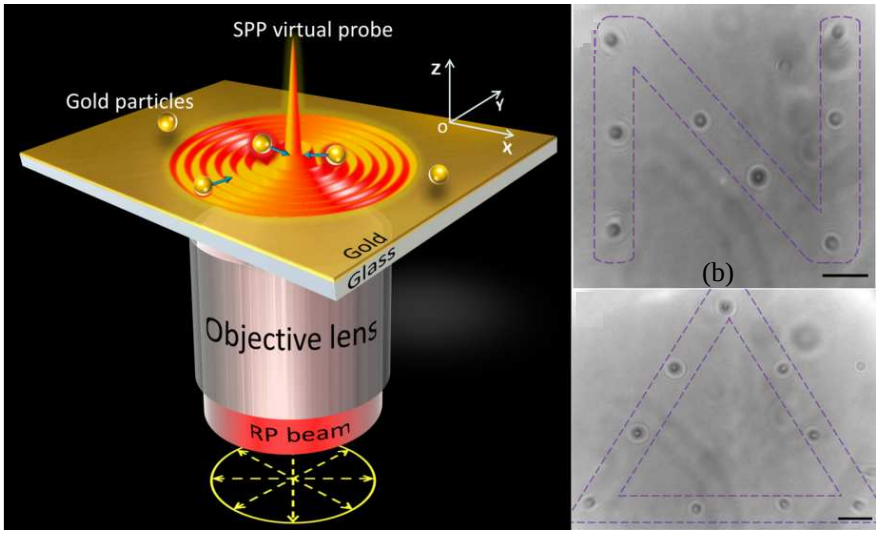

Figure 1: (a) Schematic of trapping metallic particles by the plasmonic tweezers. (b), (c) Patterns of the letter 'N' and triangle 'Δ' constructed by 1 μm gold particles through the plasmonic tweezers.

Plasmon Coupling in Gold Nanostructures

Huanjun Chen[1, 2, 3, 4], **Lei Shao**[4], **and Jianfang Wang**[4]

[1]State Key Laboratory of Optoelectronic Materials and Technologies
Sun Yat-sen University, Guangzhou 510275, China
[2]Guangdong Province Key Laboratory of Display Material and Technology
Sun Yat-sen University, Guangzhou 510275, China
[3]School of Physics and Engineering, Sun Yat-sen University, Guangzhou 510275, China
[4]Department of Physics, The Chinese University of Hong Kong, Shatin, Hong Kong SAR, China

Abstract— Gold nanocrystals, well known for their extraordinary localized surface plasmon resonances associated with the collective free electron oscillations, have attracted more and more interests in recent years. While an individual gold nanocrystal's plasmonic properties are strongly dependent on its size, shape, and surrounding environment, assembly of gold nanocrystals into nanostructures will give rise to distinct plasmonic properties that are different from those of the isolated ones. The field enhancement in the gaps among different gold nanocrystals will function as 'hot spot' for surface enhanced spectroscopies. The ordered assemblies would also give rise to collective plasmonic behaviors and form the building blocks for metamaterials. Moreover, clusters composed of ordered gold nanocrystals provide a platform for studying the transition from the localized plasmon resonance associated with isolated nanocrystals to the propagating one associated with metal/dielectric interfaces. In this report we would like to introduce some of our recent studies in the plasmon coupling in gold nanostructures.

The plasmon resonances in gold nanocube clusters are strongly dependent on both the number of nanocubes in the clusters and their orderings. Generally, as a cluster became larger and more asymmetric, it exhibited additional scattering peaks towards longer wavelengths while maintained a nearly fixed resonance at c.a. 550 nm. Finite difference time domain (FDTD) calculations revealed that the nearly fixed plasmon resonance was originated from the vertical coupling of nanocube clusters with the substrate, while the horizontal coupling among different nanocubes produced those multiple scattering peaks at longer wavelengths.

Gold nanorods exhibit both the transverse and longitudinal plasmon modes due to their anisotropy nature The plasmon coupling between two nanorods is therefore strongly dependent on their orientations. We have studied the coupling in nanorod dimers of different nanorod angles. Both the antibonding and bonding modes have been observed in the scattering spectra of the dimers and their intensity ratio decreases exponentially as the nanorod angle increases. These observations are consistent with the FDTD calculations and have been understood using a quasi-static dipolar coupling model.

Plasmon coupling in heterodimers composed of two closely adjacent nanocrystals differing in size or shape will be so different from that of homodimers due to the symmetry breaking. We have studied the plasmon coupling in nanorod-nanorod heterodimers composed of two nanorods of the same widths while different lengths. The dimers are arranged into linear fashion and anticrossing behavior is observed in the coupling energy diagram. This behavior is further confirmed by the FDTD calculations. Moreover, systematic calculations have indicated that the anticrossing behavior is strongly dependent on the interparticle distance and head shape of the nanocrystals. In addition, the numerical results also reveal Fano resonances between two nanorods of different longitudinal plasmon energies, which is originated from the coupling between the dipole and quadrupole resonances in each nanorod. We have also studied the plasmon coupling in heterodimers composed of nanorod and nanosphere. It is found that the coupling can induce a Fano like resonance, which is strongly dependent on the relative position of the nanorod and nanosphere. We believe that these results will further our understanding on the plasmon coupling of metal nanostructures as well as pave the way for the development of complex plasmon-based photonic devices and ultrasensitive plasmonic sensors.

On the other hand, nowadays state-of-the-art plasmonic devices require fabricating different metal nanostructures onto various substrates. Incorporation of substrates can bring in inhomogeneous electromagnetic environment surrounding the metal nanostructures, which can strongly modify the plasmonic properties from their free-space counterparts. We also cultivate the effects of various substrates, including the metals, semiconductors, and insulators, on the plasmonic properties of the gold nanorods. Our results indicate that the presence of the substrates will strongly modify

the far-field scattering patterns as well as scattering spectra of the supported nanorods. Specifically, Fano type resonance can be observed for large nanorods supported on substrate with high dielectric constant.

Session 1P5
FocusSession.SC2: Tunable and Reconfigurable Metamaterials and Plasmonics 1

Optical Properties on Demand: Reconfigurable and Coherently Controlled Metadevices

Nikolay I. Zheludev[1, 2]

[1]Centre for Photonic Metamaterials and Optoelectronics Research Centre
University of Southampton, UK
[3]Centre for Disruptive Photonic Technologies, NTU, Singapore

Abstract— Metamaterials, artificial electromagnetic media achieved by structuring on the subwavelength scale, were initially suggested as negative index material for the "superlens" and for transforming electromagnetic space to control propagation of waves. The research agenda is now shifting to achieving tunable, switchable, nonlinear, gain and sensing functionalities using metamaterials. We show how engaging the changing balance of forces, structural transformation, light confinement and coherent optical effects at the nanoscale brings about the emerging field of metadevices that we define as devices with unique and useful on-demand functionalities achieved by structuring of functional matter on the subwavelength scale.

Reconfigurable Plasmonic and Metamaterial Devices Using Liquid Metals

Jinqi Wang, Shuchang Liu, and Ajay Nahata
Department of Electrical and Computer Engineering, University of Utah, Salt Lake, UT, USA

Abstract— The field of plasmonics has developed rapidly over the last decade, in large part, because surface plasmon-polaritons (SPPs) offer unique capabilities for controlling and manipulating the propagation properties of electromagnetic radiation. While much of the work in this area has focused on passive device implementations, there is great need for the development of active devices. In recent years, there have been a number of studies describing active control of the propagation properties of SPPs using a variety of different techniques. These approaches have employed optically active materials, transient optical nonlinearities, and application of an external magnetic field. In each of these cases, a basic tuning capability in either the transmission amplitude or resonance frequency was demonstrated. However, the fractional change in each of these cases was relatively small. In this submission, we demonstrate that liquid metals are an attractive material system for plasmonic applications at terahertz (THz) frequencies.

To illustrate this, we show several different examples associated with enhanced transmission through subwavelength apertures using eutectic gallium indium (EGaIn) as the liquid metal. In each case, we started by fabricating an elastomeric polydimethylsiloxane (PDMS) mold with the appropriate microchannel geometry using standard soft lithography. The liquid metal could then be injected into or withdrawn from individual microchannnels. In the latter case, this could be done without leaving any metal residue. THz time-domain spectroscopy (THz TDS) was used to measure the optical transmission properties of each device. In addition to characterizing the device properties, we also characterized the complex dielectric properties of EGaIn through measurement of reflected THz spectra from both an EGaIn film and a Au film, where Au was used as the reference. The dielectric constant of EGaIn, ε, was found to be $\sim -300 + 25i$ in the spectral range of 0.1–0.5 THz, demonstrating that the EGaIn behaved as a metal in this spectral range. We also measured the refractive index of PDMS and found that it had a value of $\sim 1.57 + 0.04i$ over the same spectral range. Using the dielectric properties of both materials, we were able to account for all of the resonances in the transmission spectra.

In general, plasmonic devices, such as the ones described here, could be fabricated on the same substrate, allowing for reconfigurability using appropriate electrical signals to drive micro-pumps that can inject or withdraw the liquid metal. Thus, this approach offers significant promise for developing active devices. Finally, we note that that this general idea may be extended to develop active device that can operate in other regions of the electromagnetic spectrum.

Liquid Crystal Controlled and Tunable Metamaterials

A. E. Miroshnichenko, M. Decker, I. Staude, A. Minovich, D. Neshev, and Y. S. Kivshar
Nonlinear Physics Centre, The Australian National University, Australia

Abstract— Many important applications of photonic structures require the ability to change their properties all-optically through a nonlinear change of their optical response. However, in materials occurring in nature, a sizable optical nonlinearity requires the use of ultra-high light intensities and powers, hindering the practical use of optical nonlinearities. One of the important and practically achievable approaches is to engineer metamaterial response by infiltrating them with with liquid crystals to achieve tunable linear or strongly nonlinear response of their transmission. As the phase transition of liquid crystals can affect the refractive index over the whole optical wavelength spectrum and even into the microwave range, it is therefore possible to tune the magnetic response of metamaterials through the whole optical range.

We fabricated fishnet and coupled split-ring resonantor structures using gold and MgF2 as metal and dielectric layers deposited on a glass substrate. For nanostructuring of the metal-dielectric layers, they use focused ion beam milling, fabricating a typical fishnet structure as shown in the scanning electron microscope. This sample is then infiltrated with E7 nematic LC (from Merck) making sure that the LC completely fills the holes of the fishnet. The presence of the LC inside the structure is verified by transmission measurements where the shift of the hole mode manifesting the infiltration is observed. Furthermore, bias electric field can be applied between the top ITO electrode and the gold film for electrical control of the LC molecular alignment. This interplay between the optical and the bias electric field induced liquid crystal reorientation demonstrates an important mechanism of electrically controlled optical non-linearity in metamaterials.

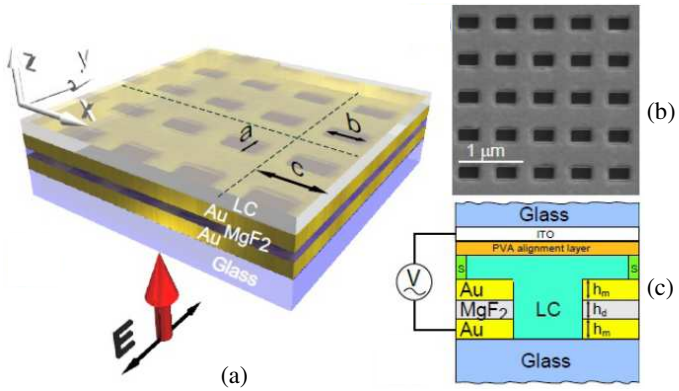

Figure 1: (a) Schematic of the fishnet metamaterial structure infiltrated with nematic liquid crystal. (b) Scanning electron microscope image (top view) of the fabricated fishnet metamaterials. (c) Side view of the liquid-crystal cell.

ACKNOWLEDGMENT

This work is supported by ARC Future Fellowships and Super Science projects.

Spontaneous Chiral Symmetry Breaking in Magneto-elastic Metamaterials

Mingkai Liu[1], **David. A. Powell**[1], **Ilya. V. Shadrivov**[1], **Mikhail Lapine**[2], **and Yuri. S. Kivshar**[1]

[1]Nonlinear Physics Centre, Research School of Physics and Engineering
Australian National University, ACT 0200, Australia
[2]CUDOS @ Sydney, School of Physics, University of Sydney, NSW 2006, Australia

Abstract— Spontaneous chiral symmetry breaking is a prominent effect closely related to the fundamental phenomena in a wide range of areas. Here we show theoretically and experimentally that this effect can also be available in magneto-elastic metamaterial systems, in which enantiomeric nonlinear meta-molecules with opposite handedness are electromagnetically coupled. Our study provides a new possibility for creating and designing artificial phase-transition effects in metamaterials.

Introduction: Spontaneous symmetry breaking is an underlying mechanism of many fundamental phenomena in nature, such as spontaneous magnetization [1], the homo-chirality of biomolecules [2, 3], the bulk of mass of nucleons [4], and the recently discovered Higgs bosons [5], etc.. We show that this effect can be found in magneto-elastic metamaterials [6].

Results: We explored the nonlinear effect of a system where enantiomeric chiral meta-molecules are electromagnetically coupled [Fig. 1(a)]. Each meta-molecule consists of a pair of twisted split-ring resonators (SRRs), connected with an elastic wire. The mutual twist angles θ of meta-molecules can be changed due to electromagnetic (EM) torque. Intuitively, the chiral symmetry of the system should be preserved if all the meta-molecules are excited evenly, and the net chirality of the system should be zero. However, due to the inter-molecular interaction, the system stability changes and as such the symmetry can be broken spontaneously ($\theta_1 + \theta_2 \neq 0$) when the pump power surpasses a certain threshold [Fig. 1(b)]. This results in the sudden occurrence of energy localization and giant polarization rotation [Fig. 1(c)]. Our theoretical prediction was also confirmed with experiment.

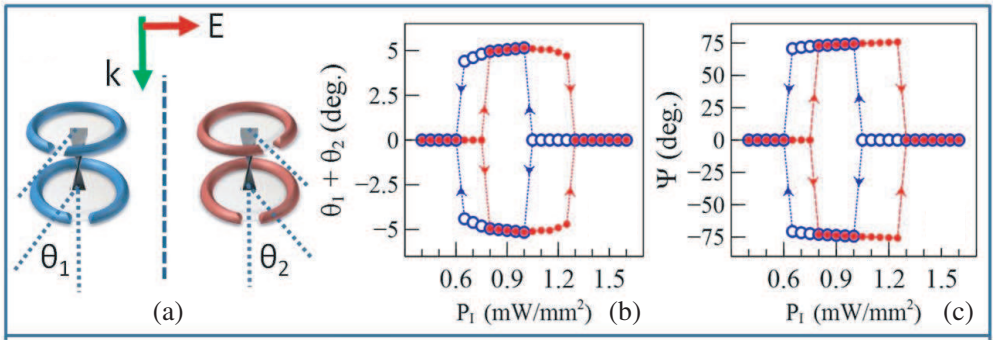

Figure 1: Schematic of a pair of enantiomeric torsional meta-molecules. (b) The asymmetry of twist angles, defined by $\theta_1 + \theta_2$, and the corresponding (c) polarization rotation Ψ of forward scattered waves, as functions of incident power density P_I.

REFERENCES

1. Yang, C. N., *Phys. Rev.*, Vol. 85, 808, 1952.
2. Avetisov, V. and V. Goldanskii, *PNAS*, Vol. 93, 11435–11442, 1996.
3. Nambu, Y. and G. Jona-Lasinio, *Phys. Rev.*, Vol. 122, 345–358, 1961.
4. Nambu, Y. and G. Jona-Lasinio, *Phys. Rev.*, Vol. 124, 246–254, 1961.
5. Higgs, P., *Phys. Rev. Lett.*, Vol. 13, 508, 1964.
6. Lapine, M., I. V. Shadrivov, D. A. Powell, and Y. S. Kivshar, *Nat. Mater.*, Vol. 11, 30–33, 2012.

Near-dispersionless, Broadband Transmission Enhancement in Plasmonic Quasicrystals

Venu Gopal Achanta, V. J. Yallapragada, Sachin Kasture, and P. R. Ajith
DCMP & MS, Tata Institute of Fundamental Research, Mumbai, India

Abstract— Near dispersionless plasmonic modes and related transmission enhancement would be useful in light harvesting applications and material characterization studies especially if one could achieve broadband response. Both the Kretschmann and grating geometries, in general, have incident angle dependence based on energy and momentum conservation [1]. We showed that in 2-d grating patterns, one could achieve near-dispersionless plasmon modes [2]. That is, a particular plasmon resonance is launch angle independent and thus can be excited by light incident at any angle. However, these near-dispersionless modes are narrow and thus have limited applications. It would be advantageous if one could get broadband and designable spectral response that is near-dispersionless. Especially, if one could get transmission enhancement over broad band then it would be useful in light harvesting applications. In addition, the plasmon mediated field localization at the metal-dielectric interface would be useful in nonlinear optical studies among others.

We demonstrate 2-dimensional patterned gold films in which the spectral response can be designed to achieve broadband, near-dispersionless transmission enhancement [3]. With plasmonic structures conforming to quasicrystal air hole patterns in gold film, we achieved an order of magnitude transmission enhancement over 500–750 nm wavelength range. This is extended in bigrating structures to a wavelength range of 500–1200 nm. In addition to broadband and designable, near dispersionless transmission enhancement, these structures show polarization independence. The local field enhancement leads to broadband second harmonic generation (SHG) though the metal surface nonlinearity is weak. We estimate the second order nonlinear susceptibility of gold over broad wavelength region from the SHG [4].

To summarize we demonstrate plasmonic quasicrystals in which broadband transmission enhancement that is launch angle and launch polarization independent. We demonstrate designable spectral response for the dispersionless transmission enhancement due to the dense k-space of the plasmonic quasicrystal. The plasmon mediated local field enhancement over broadband wavelength range is used to generate SHG and estimate the second order susceptibility of gold surface nonlinearity.

REFERENCES

1. Raether, *Surface Plasmons on Smooth and Rough Surfaces and on Gratings*, Springer, New York, 1986.
2. Kasture, S., P. Mandal, A. Singh, A. Ramsay, A. S. Vengurlekar, S. Dutta Gupta, V. I. Beletelov, and A. V. Gopal, "Near dispersion-less surface plasmon polariton resonances at a metal-dielectric interface with patterned dielectric on top," *Appl. Phys. Lett.*, Vol. 101, 091602, 2012.
3. Kasture, S., P. R. Ajith, V. J. Yallapragada, R. Patil, V. V. Nikesh, G. Mulay, and A. V. Gopal, "Plasmonic quasicrystals for designable ultrabroadband transmission enhancement and second harmonic generation," 2013, arXiv:1309.3286.
4. Dick, B., A. Gierulski, and G. Marowsky, "Determination of the nonlinear optical susceptibility $\chi^{(2)}$ of surface layers by sum and difference frequency generation in reflection and transmission," *Appl. Phys. B*, Vol. 38, 107–116, 1985.

Making Structured Metals Transparent for White Light by Surface Plasmons

Ru-Wen Peng, Ren-Hao Fan, Xiang Xiong, and Mu Wang
National Laboratory of Solid State Microstructures, Department of Physics
Nanjing University, Nanjing 210093, China

Abstract— In this talk, we present our recent work on making structured metals transparent for broadband electromagnetic waves by surface plasmons (SPs) or spoof surface plasmons (SSPs). First, we demonstrate that the interference between localized and propagating SPs plays the important role on the optical transmission through subwavelength-hole arrays. The observed phenomena belong to plasmonic Fano effects. Second, we show that the transmission enhancement originates not only from the coupling between the incident light and the excited SPs, but also from the coupling among those SPs in multiple nanoaperture stacks. Third, we demonstrate that the metallic plates with narrow slit arrays can become transparent within extremely broad spectral bandwidths, and high transmission efficiency is insensitive to the thickness of metal. This phenomenon explicitly shows the conversion between light and SPs. The investigations provide a guideline to develop many novel materials and devices, such as transparent conducting panels, antireflective solar cells, and other broadband metamaterials.

REFERENCES

1. Fan, R. H., J. Li, R. W. Peng, X. R. Huang, D. X. Qi, D. H. Xu, X. P. Ren, and M. Wang, "Oblique metal gratings transparent for broadband terahertz waves," *Appl. Phys. Lett.*, Vol. 102, 171904, 2013.
2. Fan, R. H., L. H. Zhu, R. W. Peng, X. R. Huang, D. X. Qi, X. P. Ren, Q. Hu, and M. Wang, "Broadband antireflection and light-trapping enhancement of plasmonic solar cells," *Phys. Rev. B*, Vol. 87, 195444, 2013.
3. Qi, D.-X., R.-H. Fan, R.-W. Peng, X.-R. Huang, M.-H. Lu, X. Ni, Q. Hu, and M. Wang, "Multiple-band transmission of acoustic wave through metallic gratings," *Appl. Phys. Lett.*, Vol. 101, 061912, 2012.
4. Huang, X.-R., R.-W. Peng, and R.-H. Fan, "Making metals transparent for white light by spoof surface plasmons," *Phys. Rev. Lett.*, Vol. 105, 243901, 2010.
5. Fan, R. H., R.-W. Peng, X.-R. Huang, J. Li, Y. Liu, Q. Hu, M. Wang, and X. Zhang, "Transparent metals for ultrabroadband electromagnetic waves," *Advanced Materials*, Vol. 24, 1980, 2012.
6. Bao, Y. J., R. W. Peng, D. J. Shu, M. Wang, X. Lu, J. Shao, W. Lu, and N. B. Ming, "Role of Interference between Localized and propagating surfacewaves on the extraordinary optical transmission through a subwavelength-aperture array," *Phys. Rev. Lett.*, Vol. 101, 087401, 2008.
7. Tang, Z. H., R. W. Peng, Z. Wang, X. Wu, Y. J. Bao, Q. J. Wang, Z. J. Zhang, W. H. Sun, and M. Wang, "Coupling of surface plasmons in nanostructured metal/dielectric multilayers with subwavelength hole arrays," *Phys. Rev. B*, Vol. 76, 195405, 2007.

3D Gyroid Networks Inspired by Butterfly Wings

Min Gu
Centre for Micro-Photonics and CUDOS, Faculty of Science, Engineering and Technology
Swinburne University of Technology, Hawthorn, Victoria 3122, Australia

Abstract— Three-dimensional chiral (3D) photonic crystals and meta-materials have recently received much attention because they provide a platform to manipulate optical circular dichroism. Here we demonstrate a novel class of 3D gyroid microstructures inspired by a recent finding in butterfly wing-scales and show that these 3D gyroid structures nano-engineered by direct laser writing have the ability to redirect circularly polarized light as a chiral beamsplitter. If these nano-structures are coated with metals, they become 3D chiral meta-materials.

Design and Implementation of Synthetic Multi-spectral Materials

David R. S. Cumming, Iain J. H. McCrindle, James Grant, and Timothy D. Drysdale
School of Engineering, University of Glasgow, Glasgow, G12 8LT, UK

Abstract— Structured optical materials, usually consisting of subwavelength structures etched into metal films, have been shown to be good alternatives to typical optical components, due to the capability to engineer their optical characteristics over a large wavelength range. At visible and NIR wavelengths, subwavelength hole arrays etched into a metal film have been shown to filter incident light and enhance transmission due to surface plasmon (SP) at the metal-dielectric interface [1]. At THz frequencies, where the metal does not support SPs, and can be considered to be a perfect electric conductor, subwavelength features can still lead to engineered optical properties through the creation of a metamaterial (MM) [2]. In our work we have hybridised optical plasmonic filters and MMs to create multi-spectral materials that combine the visible and NIR characteristics of plasmonic filters with THz MMs.

We have etched a MM filter and 16 optical plasmonic filters into an aluminium film [3]. The resultant multi-spectral filter can filter 15 optical and 1 NIR wavelength over different regions of the film surface, whilst simultaneously filtering a single THz frequency. The MM filter component consists of a complementary electric ring resonator (cERR) with an engineered effective plasma frequency corresponding to the THz peak.

We have also integrated plasmonic filters with a THz MM absorber [4]. The multi-spectral absorber-filter consists of 16 plasmonic filters etched into the ground plane of a MM absorber, which is designed to absorb a single THz frequency. Multi-spectral materials could lead to the creation of coaxial multi-spectral imaging systems.

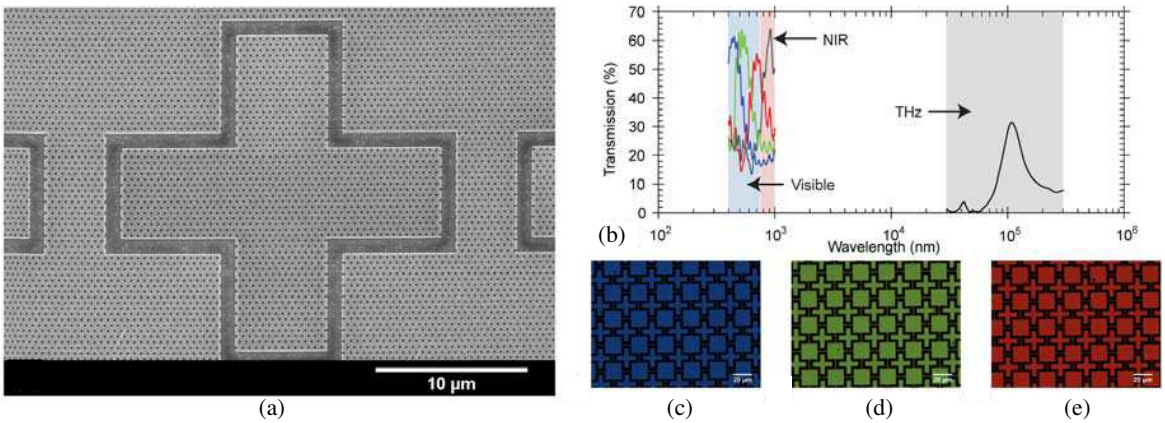

Figure 1: (a) Scanning electron micrograph of the multi-spectral filter, showing the cERR unit cell with a nanohole array. (b) Transmission spectra of the multi-spectral filter, showing RGB and NIR plasmonic filters, and the THz MM component. (c)–(e) Transmission microscope images of the multi-spectral filter-absorber, showing different plasmonic filter regions with ERRs.

REFERENCES

1. Ebbesen, T. W., H. J. Lezec, H. F. Ghaemi, T. Thio, and P. A. Wolff, *Nature*, Vol. 391, 667, 1998.
2. Padilla, W. J., M. T. Aronsson, C. Highstrete, M. Lee, A. J. Taylor, and R. D. Averitt, *Phys. Rev. B*, Vol. 75, 041102, 2007.
3. McCrindle, I. J. H., J. Grant, T. D. Drysdale, and D. R. S. Cumming, *Opt. Express*, Vol. 21, 19142, 2013.
4. McCrindle, I. J. H., J. Grant, T. D. Drysdale, and D. R. S. Cumming, *Adv. Optical Mater.*, Vol. 2, 149–153, 2014.

Controlling Surface Plasmon Polaritons Using Magneto-optical Cavities

D. A. Bykov[1, 2] **and L. L. Doskolovich**[1, 2]

[1]Image Processing Systems Institute of the Russian Academy of Sciences, Samara 443001, Russia
[2]Samara State Aerospace University, Samara 443001, Russia

Abstract— In recent years, considerable attention has been given to the investigation of nanoscale structures for the excitation and manipulation of surface plasmon polaritons (SPP). In a number of papers, a variety of geometries for the SPP excitation and steering were proposed [1]. Of great interest is the use of magneto-optical (MO) materials for magnetic-field-tunable excitation and manipulation of the SPP. Usually the variation of the optical properties due to external magnetic field is relatively small. However, it was recently shown that the use of resonant structures allows one to significantly enhance the MO effects observed [2]. This effect can be explained in terms of structure eigenmodes excitation [2].

In this work we look into the possibility of controlling the SPP's intensity by means of resonant magneto-optical cavities located on metal interface. Two closely related problems are investigated: the magneto-optically-controlled excitation of the SPP by a plane wave [3] and magneto-optically-controlled transmission of the SPP through the cavity. Both problems are solved by designing optimal geometry of the cavity, taking eigenmodes symmetry and polarization properties into account. We used the temporal coupled-mode theory and the scattering matrix formalism to present simple theoretical model that describes resonant effects in considered structures. The presented theoretical predictions are in good agreement with the rigorous computations based on the generalized Lorentz reciprocity theorem and aperiodic Fourier modal method. The magnetization-induced relative SPP intensity variation demonstrated in numerical computations varies from a few percent to 100%. The large value of intensity variation opens new possibilities for ultrafast SPP modulation.

ACKNOWLEDGMENT

The work was financially supported by Russian Science Foundation (RSF) grant 14-19-00796, Russian Foundation for Basic Research (RFBR) grants 12-07-00495, 13-07-00464, by the ministry of education and science of the Russian Federation (RF), and by RF Presidential scholarship SP-1665.2012.5.

REFERENCES

1. Liu, H., P. Lalanne, X. Yang, and J.-P. Hugonin, "Surface plasmon generation by subwavelength isolated objects," *J. Sel. Top. Quant. Electr.*, Vol. 14, No. 6, 1522–1529, 2008.
2. Belotelov, V. I., L. Kreilkamp, I. A. Akimov, A. N. Kalish, D. A. Bykov, et al., "Plasmon-mediated magneto-optical transparency," *Nature Commun.*, Vol. 4, 2128, 2013.
3. Bykov, D. A. and L. L. Doskolovich, "Magneto-optically-controlled surface plasmon excitation," arXiv:1310.4738, 2013.

Reconfigurable THz Chiral Metamaterials and Tunable Hyperbolic Metamaterial Cavities

Junsuk Rho[1, 2, 3, 4] **and Xiang Zhang**[3, 4]

[1]Department of Mechanical Engineering
Pohang University of Science and Technology (POSTECH), Pohang, Korea
[2]Department of Chemical Engineering
Pohang University of Science and Technology (POSTECH), Pohang, Korea
[3]NSF-Nanoscale Science and Engineering Center, University of California
Berkeley, CA 94720, USA
[4]Materials Sciences Division, Lawrence Berkeley National Laboratory
Berkeley, CA 94720, USA

Abstract— Metamaterials, artificially structured nanomaterials, have enabled unprecedented phenomena such as negative refraction. Especially, hyperbolic metamaterials also known as indefinite metamaterials have unique dispersion relation where the principal components of its permittivity tensors are not all with the same signs and magnitudes. Such extraordinary dispersion relation results in hyperbolic dispersion relations which lead to a number of interesting phenomena, such as super-resolution effect which transfers evanescent waves to propagating waves at its interface with normal materials and, the propagation of electromagnetic waves with very large wavevectors comparing they are evanescent waves and thus decay quickly in natural materials. In this abstract, I will show a unique application of metamaterials for miniaturizing optical cavity, a key component to make lasers, into the nanoscale for the first time. Figure 1 shows the cavity array which not only successfully captured light in 20 nm dimension and show very high figure of merit experimentally, but also tune the refractive index based on the size of the cavities and the number of multilayer at optical frequencies. We achieved it goes up to 45 theoretically and 17.4 experimentally [1]. Second, I will show the recent achievements of terahertz photo-induced switching of reconfigurable negative index metamaterial device and large scale negative index metasurface with anomalous spinhall effect shown in Figure 2 [2, 3]. Finally, I will discuss recent development of scalable fabrication techniques for metamaterial and plasmonic structures. I believe our efforts in sub-wavelength metamaterials having such extraordinary optical properties will lead to further advanced nanophotonics research.

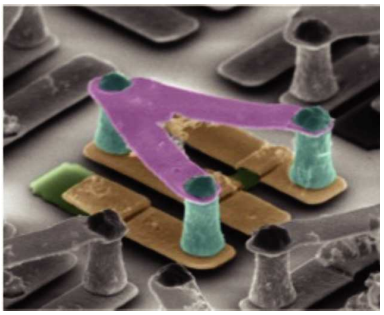

Figure 1: Switchable chiral metamaterial.

Figure 2: Tunable refractive index cavities.

ACKNOWLEDGMENT

This work has been supported by the U. S. Department of Energy, Office of Basic Energy Sciences under contract No. DE-AC02-05CH11231 at the University of California Berkeley and Lawrence Berkeley National Laboratory. J. Rho acknowledges fellowships from the U. S. Department of Energy and the Samsung Scholarship Foundation, Republic of Korea.

REFERENCES

1. Rho, J., et al., "Experimental realization of three-dimensional indefinite cavities at the nanoscale with anomalous scaling laws," *Nature Photonics*, Vol. 6, 450–454, 2012.

2. Zhang, S., J. Rho, et al., "Photoinduced handedness switching in terahertz metamolecules," *Nature Communications*, Vol. 3, 946, 2012.
3. Yin, X., J. Rho, et al., "Photonics spin hall effect at metasurfaces," *Science*, Vol. 339, 1405–1407, 2013.

Tailoring Artificial Plasmonic Nanostructures to Visible-near IR Regime: Towards Versatile and Ultrasensitive Plasmonic Biosensors

Qihua Xiong[1, 2]

[1]School of Physical and Mathematical Sciences, Nanyang Technological University, Singapore
[2]School of Electrical and Electronic Engineering, Nanyang Technological University, Singapore

Abstract— In this talk, I will present our recent effort of pushing artificial plasmonic nanostructures to visible-near infrared regime by nanofabrication. By intelligent design and tuning of the fundamental unit (bow-tie antenna, split-ring resonator or nanorod arrays) and arrangement, such, we were able to push the Ag- or Au-based "metamaterials" to resonant at visible-near infrared frequency regime, on either opaque and rigid substrates like silicon or glass or transparent plastic substrates. We will also show that such photonic devices provide unconventional advantages in ultrasensitive detection of chemical and biological species, based upon both the frequency shift of the resonance due to local effective refractive index change and the surface enhanced Raman spectroscopy signal, which carries the molecular fingerprint information. A wide range of analytes can be detected, such as DNA molecules, cancer markers, food and drink contaminants (plasticizers and melamines), and heavy metal ions. Our works suggest the extremely bright future of top-down metamaterials towards plasmonic sensing platform that implement the conventional colloidal particle approaches.

REFERENCES

1. Zhang, J., et al., "Tailoring alphabetical metamaterials in optical frequency: Plasmonic coupling, dispersion, and sensing," *ACS Nano*, DOI: 10.1021/nn500527f, 2014.
2. Wen, X. L., et al., "Near-infrared active metamaterials and their applications in tunable surface-enhanced Raman scattering," *Opt. Express*, Vol. 22, 2989–2995, 2014.
3. Wen, X. L., et al., "Transparent free-standing metamaterials and their applications in surface-enhanced Raman scattering," *Nanoscale*, Vol. 6, 132–139, 2014.
4. Zhang, Q., et al., "Multiple magnetic mode-based Fano resonance in split-ring resonator/disk nanocavities," *ACS Nano*, Vol. 7, 11071–11078, 2013.
5. Cao, C., et al., "Metamaterials-based label-free nanosensor for conformation and affinity biosensing," *ACS Nano*, Vol. 7, 7583–7591, 2013.
6. Dodson, S., et al., "Optimizing electromagnetic hotspots in plasmonic bowtie nanoantennae," *J. Phys. Chem. Lett.*, Vol. 4, 496–501, 2013.
7. Peng, B., et al., "Vertically aligned gold nanorod monolayer on arbitrary substrates: Self-assembly and femtomolar detection of food contaminants," *ACS Nano*, Vol. 7, 5993–9000, 2013.
8. Peng, B., et al., "Fluorophore-doped core-multishell spherical plasmonic nanocavities: Resonant energy transfer toward a loss compensation," *ACS Nano*, Vol. 6, 6250–6259, 2012.
9. Xu, X. L., et al., "Flexible visible-infrared metamaterials and their applications in highly sensitive chemical and biological sensing," *Nano Lett.*, Vol. 11, 3232–3238, 2011, highlighted by Nature Asia Materials and Nanowerk.com.

Surface Wave on Graphene by a Moving Charged Particle

Xihang Shi[1] **and Baile Zhang**[1, 2]

[1]Division of Physics and Applied Physics, School of Physical and Mathematical Sciences
Nanyang Technological University, Singapore
[2]Centre for Disruptive Photonic Technologies, Nanyang Technological University, Singapore

Abstract— The near field of a moving charged particle can be coupled into surface waves on graphene, which is well known as surface plasmon polaritons. It has been verified that the water waves excited by a moving boat can have strong shock waves at the edge and weak plane waveswith fronts moving parallel to the motion of the boat. We show in this paper that similar surface waves on graphene can be excited by a moving charged particle.

Introduction: Phenomenon in electromagnetic waves can find their analogs in classical mechanical waves, e.g., the Cherenkov radiation is analogous to the shock wave excited by a supersonic plane, transition radiation to the water wave by dropping a stone in the lake, electromagnetic surface wave to seismic surface wave. When a boat moves in the water, it leaves behind a complicated field pattern; at the outside, it is a shock wave with wave propagating forward but skew to the boat's motion direction, inside, a weak plane waves with fronts moving parallel to the motion of the boat is also generated. In this paper, we show that similar results can be excited by a charged particle moving parallel to the graphene. The result is not only interesting, but most importantly, deepening our understating of SPPs. The paper contains the numerical result and asymptotic analytical solution to each part of the waves.

Active THz Phase Modulators Based on Graphene Metamaterials

Ziqi Miao, **Qiong Wu**, **Xin Li**, **Qiong He**,
Zhenghua An, **Yuanbo Zhang**, **and Lei Zhou**
State Key Laboratory of Surface Physics and Physics Department
Fudan University, Shanghai 200433, China

Abstract— According to Fermat-Huygens principle, the phase distribution of electromagnetic (EM) wave on a certain plane essentially determines the wave-front of EM wave radiated from that plane to the far field. Therefore, controlling the local phase of EM wave freely can help create any far-field wave-front as desired, which is the key aim for many photonic researchers. By using ultra-thin metamaterials (meta-surfaces) to manipulate the local phases of reflected/refracted waves, many amazing wave-manipulation effects have been realized, such as polarization control [1], light bending/reflection satisfying a generalized Snell's law [2], holographic imaging [3], light harvesting and focusing [4, 5], and even propagating-wave to surface wave conversion [6]. In all these systems, the most important element is the local phase modulator, either transmittive or reflective, that can modulate the phase of transmitted/reflected wave in a pre-designed manner.

However, so far the realized/adopted phase modulators are all *passive* elements, which means that they cannot be actively tuned by external means once fabricated. Here, we demonstrate that an actively tunable THz phase modulator can be realized by combining graphene with a particular metamaterial structure. By tuning the carrier densities of the graphene via external gating, we experimentally demonstrate that a maximum phase change of 180 degrees can be achieved at certain frequencies, whereas in previously realized THz modulators such phase-change is limited to 65 degrees [7]. Our experimental results are in good agreement with full wave simulations and a simple coupled-mode theory is adopted to explain the intrinsic physics of such a dramatic effect. Our discovery paves the road for many applications in THz domain where active wave-manipulation devices are generally lacking, some of which will be discussed in more details during the conference.

REFERENCES

1. Hao, J. M., et al., *Phys. Rev. Lett.*, Vol. 99, 063908, 2007.
2. Yu, N. F., et al., *Science*, Vol. 334, 333, 2011.
3. Larouche, S., et al., *Nature Materials*, Vol. 11, 450, 2012.
4. Xiao, S. Y., et al., *Phys. Rev. B*, Vol. 85, 085125, 2012.
5. Li, X., et al., *Opt. Lett.*, Vol. 37, 4940, 2012.
6. Sun, S. L., et al., *Nature Materials*, Vol. 11, 426, 2012.
7. Lee, S. H., et al., *Nature Materials*, Vol. 11, 936, 2012.

Optically Controlled Active Terahertz Meta-surfaces

Abul K. Azad, **Dibakar Roy Chowdhury**, **Hou-Tong Chen**, **and Antoinette J. Taylor**
Center for Integrated Nanotechnologies, Material Physics Application Division
Los Alamos National Laboratory, New Mexico, NM-87545, USA

Abstract— Metamaterials have enabled many unprecedented electromagnetic phenomena including negative refraction, invisible cloaking, super lensing, and magnetism at optical frequencies, which are not accessible with naturally occurring materials [1]. The fundamental building blocks of metamaterials are typically composed of sub-wavelength metallic resonators periodically patterned on dielectric substrates and these composites exhibit electromagnetic properties that are fundamentally different than those of the composing materials. The bulk properties of metamaterials are mostly determined by resonant interactions of these mesoscopic elements with the incident electromagnetic waves. A single layer planar metamaterial, called meta-surface, is often employed to yield specific electromagnetic properties using a co-designed, bottom-up approach. The field of metamaterial may greatly improve the terahertz (THz) technology, which is still suffering from severe lack of compact and efficient devices.

Metamaterials have enabled many unprecedented electromagnetic phenomena including negative refraction, invisible cloaking, super lensing, and magnetism at optical frequencies, which are not accessible with naturally occurring materials [1]. The fundamental building blocks of metamaterials are typically composed of sub-wavelength metallic resonators periodically patterned on dielectric substrates and these composites exhibit electromagnetic properties that are fundamentally different than those of the composing materials. The bulk properties of metamaterials are mostly determined by resonant interactions of these mesoscopic elements with the incident electromagnetic waves. A single layer planar metamaterial, called meta-surface, is often employed to yield specific electromagnetic properties using a co-designed, bottom-up approach. The field of metamaterial may greatly improve the terahertz (THz) technology, which is still suffering from severe lack of compact and efficient devices.

REFERENCES

1. Chen, H.-T., et al., *Laser & Photonic Reviews*, Vol. 5, No. 4, 513, 2011.
2. Chowdhury, D. R., et al., *Applied Physics Letters*, Vol. 99, 231101, 2011.
3. Chowdhury, D. R., et al., *Applied Physics Letters*, Vol. 102, 011122, 2013.
4. Gu, J., R. Singh, et al., *Optical Materials Express*, Vol. 2, 1617, 2012.

Optical Control of Plasmonic Structures and Metasurfaces at THz Frequencies

G. Georgiou[1], **A. Bhattacharya**[1], **M. C. Schaafsma**[1], **T. Steinbusch**[1], **H. K. Tyagi**[1], **and J. Gómez-Rivas**[1, 2]

[1]Center for Nanophotonics, FOM Institute AMOLF, Amsterdam, The Netherlands
[2]COBRA Research Institute, Eindhoven University of Technology, The Netherlands

Abstract— Resonant plasmonic structures and metasurfaces hold a great promise as the building blocks for future optical devices. In this contribution we investigate the photo-excitation of such structures on semiconductor surfaces using a patterned optical illumination. Using this approach we are able to actively tune localized surface plasmon resonances (LSPRs) both spatially and temporally. Furthermore, the concept of beam-steering for THz waves using photo-generated carriers in semiconductors is explored both theoretically and experimentally.

Introduction: Semiconductors are promising materials for THz opto-electronics. Their versatile nature, with a permittivity that can be controlled by the free carrier density, makes them excellent candidates for active plasmonics, metamaterials and metasurfaces. Structures made out of these materials can give rise to LSPRs at THz frequencies. The precise response of these structures depends on their geometry and permittivity; parameters that we can actively tune in our experiments.

Results: In this work we explore the photo-generation of resonant plasmonic structures at THz frequencies. An optical pump beam in a conventional time-resolved THz time domain spectrometer (TRTS) is spatially patterned using a spatial light modulator (SLM) to contain several plasmonic structures. Consequently, these structures are projected on to the surface of a 1 µm thick GaAs. Using a band-to-band excitation, we photo-generate free carriers and therefore change the permittivity of GaAs from an insulating to a metallic state only at selected areas of illumination defined by the SLM. After the excitation a single cycle THz pulse drives the free electrons into a coherent oscillation giving rise to LSPRs. To verify this we have performed far-field extinction measurements on THz plasmonic antennas of varying length, demonstrating the excitation of the fundamental resonant mode $\lambda/2$ [1].

Moreover, this work is extended towards the photo-generation of THz circuit elements such as capacitors and inductors. By optically exciting loaded dimer antenna structures, we are able to drive LC circuit resonances at THz frequencies using surface plasmon polaritons. Furthermore, the idea of metasurfaces for active beam steering is investigated experimentally using optically excited blazed gratings. Our measurements show beam steering of THz waves in the range of $\pm 30°$.

Conclusion In conclusion we have demonstrated the photo-excitation of resonant plasmonic structures at THz frequencies using a SLM. This method suggests that a single semiconductor surface can be used to define patterns and resonant structures that could be useful for THz sensing, opto-electronic circuits, as well as for active beam-steering in imaging systems.

ACKNOWLEDGMENT

This work has been supported by the ERC through Grant No. 259727 THZ-PLASMON, by the Netherlands Foundation for Fundamental Research on Matter (FOM) and the Netherlands Organisation for Scientific Research (NWO).

REFERENCES

1. Georgiou, G., H. K. Tyagi, P. Mulder, G. J. Bauhuis, J. J. Schermer, and J. Gómez-Rivas, "Photo-generated THz antennas," *Sci. Rep.*, Vol. 4, No. 3854, 2014.

Session 1P6
FocusSession.SC3: Photoacoustic Tomography and Sensing

Mid-infrared Trace Gas Detection in Exhaled Breath for Disease Diagnostics and Monitoring

Frank K. Tittel, **Wei Ren**, **Wenzhe Jiang**, **Yingchun Cao**, **and Dongfang Jiang**
Department of Electrical and Computer Engineering, Rice University, Houston, TX 77005, USA

Abstract— This talk will focus on recent advances in the development of trace gas sensor technologies, based on infrared semiconductor lasers for the ultra-sensitive detection, quantification and monitoring of trace gas species and their application in medical diagnostics, life sciences, public health and atmospheric chemistry [1–3]. Identification and quantification of potential disease biomarkers for asthma, renal failures, diabetes and caner has been the driving force for the development of analytical instruments based on laser spectroscopy. For example, breath gas analysis is a method for obtaining non-invasive accurate, and rapid information on the clinical state of an individual by monitoring volatile organic compounds present in exhaled breath instead of performing blood tests The development of novel compact trace gas sensors based on interband cascade and quantum cascade lasers permits the targeting of strong fundamental rotational-vibrational transitions in the mid-infrared, which are one to two orders of magnitude more intense than overtone transitions in the near-infrared spectral region. Specifically, the spectroscopic detection and monitoring of six molecular gas species of interest in medical diagnostics, such as ammonia (NH_3), nitric oxide (NO), carbon monoxide (CO), sulfur dioxide (SO_2), methane (CH_4), nitrous oxide (N_2O) and hydrogen peroxide (H_2O_2) will be described [1–4]. These molecules were detected using conventional photoacoustic spectroscopy (PAS), quartz-enhanced photoacoustic spectroscopy (QEPAS) and laser absorption spectroscopy with a novel, compact multipass absorption cell [1]. PAS and QEPAS can achieve minimum detectable absorption coefficient in the range from 10^{-8} to $10^{-11}\,\mathrm{cm}^{-1}/\sqrt{\ }\mathrm{Hz}$.

REFERENCES

1. Lewicki, R., et al., *Current Status of Mid-infrared Semiconductor Laser-based Sensor Technologies for Trace-gas Sensing Applications,* Chapter 23, 597–632, SPIE Press, 2013.
2. Tittel, F. K., et al., *Tunable Mid-infrared Laser Absorption Spectroscopy,* Chapter 15, 579–629, Woodhead Publishing Limited, 2013.
3. Tittel, F. K., et al., *Emerging Infrared Laser Absorption Spectroscopic Techniques for Gas Analysis,* Chapter 4, 71–109, John Wiley and Sons, 2013.
4. Ren, W., et al., "Hydrogen peroxide detection with quartz-enhanced photoacoustic spectroscopy using a distributed-feedback quantum cascade laser," *Appl. Phys. Lett.*, Vol. 104, 041117, 2014.

Coregistered Functional-anatomical Mapping of Live Tissue with Laser Optoacoustic Ultrasonic Imaging System (LOUIS)

Alexander Oraevsky
TomoWave Laboratories, Inc. and University of Houston, Texas, USA

Abstract—

Introduction: We review 2D and 3D tomography systems combining advantages of laser optoacoustics and ultrasound as a dual-modality. The optoacoustic sub-system can provide anatomical images based on combined distribution of the major molecular chromophores in the body absorbing near-infrared light, functional images of the total hemoglobin [Hb] and blood oxygen saturation [SO_2] as well as molecular images of targeted contrast agents [1]. The laser ultrasound sub-system can provide images of the speed of sound (SoS), ultrasonic attenuation (UA) and ultrasonic reflection (UR), which have morphological significance and provide means for iterative reconstruction of more accurate optoacoustic images. The system was first tested and optimized using tissue mimicking phantoms. Then *in vivo* images of nude mice were obtained to demonstrate the system capabilities in a number of preclinical research applications. Finally, we adopted the preclinical system for the clinical utility in diagnostic imaging of breast cancer.

Methods: LOUIS-3D uses ns laser pulses from a Ti:Sapphire laser tunable in the near-infrared spectral range and operating at 10 Hz to illuminate a mouse placed on computer controlled rotational stage and generate optoacoustic images of the optical absorption (OA) coefficient through the entire body and head of a nude mouse using an arc shaped ultrasonic array of 96 1×1 mm transducers. Slightly modified system design with rotating imaging module with two orthogonally placed linear probes each having 48 ultrawide-band ultrasonic transducers was used in clinical breast imaging. The system also uses ns pulses from a Nd:YAG laser operating at 1064 nm to illuminate a strongly absorbing polymer layer that emits wide-band ultrasound pulses used to generate laser ultrasonic images. The two types of images are coregistered in space. This permitted inclusion of SoS and UA images into our algorithm of optoacoustic image reconstruction to improve contrast and resolution of volumetric OA images. As a preliminary step in clinical evaluation, 2D optoacoustic and ultrasonic images were acquired through a hand-held linear probe that allowed automatic coregistration (in space and time) of morphological images based on ultrasound and functional images based on optoacoustics.

Preclinical Results: 3D OA images of soft tissues were produced through the whole body and brain of a nude mouse with resolution of ~ 0.28 mm. We demonstrated that through proper signal filtering and image processing either larger anatomy (organs or major veins and arteries) or the smaller structures (kidney medullas, ovarian arteries) and even microvasculature can be visualized. This system was also employed to generate functional images of hemoglobin and oxyhemoglobin in the organs and vasculature. Injection of optoacoustic contrast agents based on strongly absorbing nanoparticles allowed to improve image contrast and study biodistribution of gold and carbon nanoparticles in the mouse organs.

Clinical Results: Co-registered optoacoustic and ultrasound imaging was tested as a method of enhancement of diagnostic specificity for breast cancer at the level of detection sensitivity of 98%. The total hemoglobin and its level of oxygen saturation was initially estimated with physiologically relevant accuracy in computer models and in tissue mimicking gel phantoms. After the system was validated and calibrated in phantoms, a pilot clinical study was performed on patients with breast masses having ambiguous classification based on x-ray mammography followed by conventional ultrasound. We will present examples of clinical images depicting coregistered functional anatomical maps of breast cancer and benign mass. One can appreciate increased concentration of the total hemoglobin associated with higher density of the tumor microvasculature and decreased level of blood oxygen saturation in a cancerous lesion compared with a benign mass. Noninvasive diagnosis from the co-registered OA/US images was compared with the gold standard of core biopsy. Based on the preliminary data of the initial 100 patients, the co-registration of optoacoustic functional and ultrasound morphological images provides $> 15\%$ greater specificity of noninvasive diagnosis of breast masses relative to specificity of the diagnostic ultrasound alone. With $\sim 1,500,000$ negative biopsies performed in the USA annually, this means 225,000 less of unnecessary biopsies at $3,000 each.

Conclusions: Coregistered volumetric images of the optical absorption coefficient and the speed of sound allow reconstruction of accurate anatomical and functional images in small laboratory

animals such as mice. Each type of images, laser optoacoustic and laser ultrasonic, has its own merit in preclinical research, while each of the two images helps to improve quantitative accuracy of the other image. Initial clinical studies using 2D laser optoacoustic ultrasonic imaging system validated its clinical utility as a more accurate modality for noninvasive diagnosis. Based on preliminary clinical data we believe that translation of the developed 3D system to the clinical application as a 2-in-1 screening and diagnostic imaging modality for breast cancer care has significant potential.

Real-time Interleaved Ultrasound and Photoacoustic Imaging System

Matthew O'Donnell[1], **Chen-Wei Wei**[1], **Thu-Mai Nguyen**[1], **Bastien Arnal**[1], **and Ivan Pelivanov**[1, 2]

[1]Department of Bioengineering, University of Washington
3720 15th AVE NE, Seattle, WA 98195, USA
[2]International Laser Center, Moscow State University
Leninskie Gory, 1, bld. 2, Moscow 119991, Russian Federation

Abstract— Clinical ultrasound (US) provides excellent image quality with multi-centimeter penetration depths, sub-millimeter spatial resolution, good cost effectiveness, and high flexibility. It suffers, however, from poor contrast resolution. Photoacoustic (PA) imaging combines optical absorption contrast with US resolution, and typically delivers penetration up to a few centimeters. It complements US imaging by providing molecular information using the same transducers and imaging electronics. US-guided PA imaging could have a number of clinical applications related to imaging the microvasculature (exploiting hemoglobin contrast), detecting molecularly-targeted, nanoscale contrast agents, and guiding interventional procedures. An integrated scan format in which US and PA image frames are interleaved at traditional real-time frame rates is needed to optimally translate this technology to the clinic.

Integrated US/PA systems have been developed as a research tool. However, for clinical applications, these systems are not practical due to the high-cost, large size, and low repetition-rate laser source. High pulse energy Q-switched lasers produce high signal-to-noise ratio (SNR) PA signals induced by nanosecond pulses. However, they are generally bulky, expensive, and hard to operate and maintain. In addition, their low pulse repetition rate can severely limit image frame rates for real-time operation. To facilitate clinical translation of interleaved US/PA imaging, we propose to use a low-cost, portable, and flexible laser source that should be applicable to a number of applications.

In this paper, an integrated US/PA imaging system is presented, with image frame rates > 30 Hz. By employing a portable, low-cost, low pulse-energy (1 mJ/pulse), high repetition rate (1 kHz), 1064-nm laser, and a rotating galvo-mirror system enabling rapid laser beam scanning over the imaging area, integrated US/PA imaging is demonstrated for potential applications requiring a few centimeters of penetration. We acquired integrated PA (by combining multiple single-shot sub-images covering the scan region) and US images of a 2-mm-diameter cylindrical absorber (absorption coefficient $5\,\mathrm{cm}^{-1}$) embedded in a tissue-mimicking gelatin phantom at 8-mm depth. The imaging area is 2 cm $\times$ 1 cm (depth $\times$ lateral). An SNR of 16 dB for the absorber was obtained, comparable to conventional PA methods using high energy, low repetition rate lasers. The frame rate of the current system produces an integrated US/PA frame at 32 Hz, and 100 Hz operation is envisioned with an upgraded US imaging system. Examples of potential clinical application using this system will be presented.

Recent Advancements in Photoacoustic Tomography Image Reconstruction

Mark A. Anastasio
Department of Biomedical Engineering, Washington University in St. Louis, USA

Abstract— Photoacoustic computed tomography (PACT) is an emerging soft-tissue imaging modality that has great potential for a wide range of preclinical and clinical imaging applications. It can be viewed as a hybrid imaging modality in the sense that it utilizes an optical contrast mechanism combined with ultrasonic detection principles, thereby combining the advantages of optical and ultrasonic imaging while circumventing their primary limitations. In this talk, we review our recent advancements in practical image reconstruction approaches for PACT. Such advancements include physics-based models of the measurement process and associated inversion methods for reconstructing images from limited data sets in acoustically heterogeneous media. Applications of PACT to transcranial brain imaging and breast cancer detection will be presented.

Photoacoustic Image Features of Breast Carcinoma with Conventional Imaging and Pathological Validation

Michelle Heijblom[1], **Daniele Piras**[1], **Johan van Hespen**[1], **Ton van Leeuwen**[1], **Wiendelt Steenbergen**[1], **Srirang Manohar**[1], **Frank van den Engh**[2, 3], **Margreet van der Schaaf**[2, 3], **Joost Klaase**[2, 3], **and Mariël Brinkhuis**[4]

[1]Biomedical Photonic Imaging Group, Faculty of Science and Technology
MIRA, Institute for Biomedical Technology and Technical Medicine
University of Twente, Enschede, The Netherlands
[2]Department of Radiology, Medisch Spectrum Twente, Enschede, The Netherlands
[3]Department of Surgery, Medisch Spectrum Twente, Enschede, The Netherlands
[4]Laboratory for Pathology East Netherlands, P. O. Box 377, AJ, Enschede 7500, The Netherlands

Abstract— Photoacoustic imaging brings together advantages of optical imaging and ultrasound imaging. The technique measures ultrasound excited by pulsed light illumination of optically absorbing structures in tissue. This allows the development of images of pathologies such as cancer that are endowed with higher absorption due to enhanced vascularization. We will look at selected latest results obtained using the improved Twente Photoacoustic Mammoscope (PAM 1) in imaging symptomatic and suspect breasts.

Methods: PAM 1 uses a parallel plate geometry with mild compression of the breast when the subject is in prone position. Pulsed laser excitation uses 1064 nm with a beam size of approximately 65 mm and a radiant exposure of 10 mJ cm^{-2}. Forward-mode detection is performed using a 2D ultrasound detector array acoustically coupled to the caudal side of the breast using gel. The detector array has 572 PVDF elements with a central frequency at 1 MHz and covers roughly 80×80 mm.

IN the period from April 2012 to date technically acceptable measurements on highly suspect and suspect breasts of 39 patients were made. PA images are compared with imaging results from x-ray mammography, ultrasound imaging and in a sub-set of patients with Magnetic Resonance Imaging (MRI). In a sample set of patients, post-surgical tumor specimens were subjected to an extended histopathology protocol where whole-mount coupes were stained for endothelial cells.

Results and Conclusions: In 31 of the 32 cases of malignancy we could visualize high-contrast regions at the expected lesion depths and positions. In the subset of patients where pre-operative MRI and extended histopathology have been applied, we find good correspondence with spatial features of photoacoustic images. This suggests that the high photoacoustic contrast at 1064 nm is indeed largely the consequence of tumor vascularization. Further, the PA contrast is higher than observed on x-ray mammography and appears independent of breast density. The results provide strong evidence for the potential that photoacoustic mammography has for clinical translation.

ACKNOWLEDGMENT

The research was financially supported by the Agentschap NL Innovation-Oriented Research Programmes Photonic Devices under the HYMPACT Project (IPD083374).

Full Aberration Correction towards High-resolution Deep Clinical Multimodal Optoacoustic and Ultrasound Imaging

Michael Jaeger, Hidayet Günhan Akarçay, Michael Grünig, Gerrit Held, Sara Peeters, Tigran Petrosyan, Stefan Preisser, and Martin Frenz
Institute of Applied Physics, University of Bern, Switzerland

Abstract— Optoacoustic (OA) imaging will experience broadest clinical application if implemented in epi-style with the irradiation optics and the acoustic probe integrated in a single probe, for flexible imaging of the human body in combination with echo ultrasound (US). In such a multimodal combination, OA imaging is promising to improve diagnostic accuracy via the display of small blood vessels and local blood oxygenation within the anatomical context shown on US. To be clinically most successful, the OA modality should in addition provide an adequate imaging depth of several centimetres, where it could help diagnose and monitor breast cancer, cardiovascular disease, or vascular recovery after severe trauma or burns. Clutter signals, that emerge at the site of tissue irradiation close to the acoustic probe, are a significant obstacle to deep imaging when using an epi-style setup; however, the development of clutter reduction techniques has brought us close to the theoretical limit given by transducer noise and optical penetration depth.

At the stage of getting close to a clinically suitable imaging depth of several centimetres, a further important obstacle to deep imaging are acoustic aberrations. The unknown wavefront distortions of OA transients, when propagating from deep tissue structures through tissue with an unknown distribution of speed of sound, degrade the spatial resolution of these structures if not compensated for during image reconstruction. Acoustic aberrations are even more limiting to OA imaging than to conventional pulse-echo US: OA image contrast mostly relays on the display of sparsely distributed blood vessels, rather than spatially distributed diffuse signals. Loss of spatial resolution therefore comes with simultaneously reduced signal intensity from such sparse sources, potentially leading to their invisibility. Full contrast and imaging depth of epi-OA imaging will therefore only be achieved when, in addition to clutter reduction, the true distribution of speed of sound is taken into account for image reconstruction. To be clinically relevant for implementation in a freehand combined OA and US system, such an attempt should be real-time, and it should not make use of any a priori knowledge.

In this paper we present a novel technique, in which imaging of the spatial distribution of speed of sound is possible with high spatial resolution based on pulse-echo US: Computed ultrasound tomography in echo mode (CUTE). The measurement of speed of sound relies on the changing phase of reconstructed pulse-echoes when changing the steering angle of the echo generating pulse. In any point of the image, the echo phase as a function of transmit steering angle directly measures the effect of acoustic aberration along different propagation directions towards that point. A real-time capable Fourier domain algorithm then allows the reconstruction of the 2D sound speed distribution from the 2D map of local echo phase shifts measured in 2D US images obtained with a linear probe. In a combined epi-OA and US system, knowledge of the speed of sound allows in a subsequent step for full aberration correction of both the US and the OA image. Phantom results demonstrate that this technique allows spatially invariant diffraction-limited resolution in presence of a strong aberrator, with consequently improved contrast.

Enhanced Plasmonic Photothermal Therapy by Combining Targeted Delivery of Gold Nanoparticles with Sonoporation

Yu-Hsin Wang, **Si-Ping Chen**, **and Pai-Chi Li**
Department of Electrical Engineering, Institute of Biomedical Electronics and Bioinformatics
Taiwan University, Taiwan

Abstract— Plasmonic photothermal therapy (PPTT) using gold nanoparticles (AuNPs) as efficient photoabsorbing agents has been proposed. One critical step in PPTT is to effectively deliver AuNPs into the cells. In this study, we demonstrate that the AuNP delivery can be greatly enhanced by combining the following mechanisms: AuNPs encapsulation with microbubbles (AuMBs), molecular targeting and sonoporation employing acoustic cavitation of microbubbles (MBs). Both in *vitro* and *in vivo* tests are performed. For molecular targeting, these AuMBs are modified with anti-VEGFR2 and their angiogenesis targeting capabilities are confirmed by ultrasound imaging. Once bound to the angiogenesis markers, the MBs are destructed by ultrasound to release the AuNPs. The ultrasound-assisted release is also confirmed by photoacoustic measurements. In addition, acoustic cavitation is induced during MB destruction for increased transient cellular permeability (also known as sonoporation). Inertial cavitation dose is measured and found positively correlated with the temperature rise at the tumor site. The concentration of AuNPs delivered into the cells is also measured based on optical absorbance. The AuNPs delivered into the cells are observed using third harmonic generation microscopy and two photon fluorescence microscopy. A temperature elevation of 20°C is achieved *in vitro*. PPTT results *in vivo* also show sufficient temperature increase (> 45°C) for hyperthermia. Therefore, it is confirmed that efficacy of PPTT can be enhanced by combing targeted delivery of AuNPs with sonoporation.

Photoacoustic and Ultrasound Dual-modality Imaging for Inflammatory Arthritis

Xueding Wang[1], **Guan Xu**[1], **David Chamberland**[2], **and Gandikota Girish**[1]

[1]Department of Radiology, University of Michigan School of Medicine, Ann Arbor, MI, USA
[2]Division of Rheumatology, Department of Internal Medicine
University of Michigan School of Medicine, Ann Arbor, MI, USA

Abstract— Arthritis is a leading cause of disability, affecting 46 million of the population in the U.S. Although arthritis is serious, potentially crippling, and commonly disabling, comprehensive diagnosis and optimized therapies of these disorders are hindered drastically by lack of cost efficient and powerful joint imaging technologies. Development and application of new imaging technologies for the discovery of biomarkers of arthritic disease onset, progression, and response to therapy are of broad interest and are common goals of physicians and medical researchers. Rendering new optical contrast in articular tissues at high spatial and temporal resolution, emerging photoacoustic imaging (PAI) combined with more established ultrasound (US) technologies provides unique opportunities for diagnosis and treatment monitoring of arthritis. In addition to capturing peripheral bone and soft tissue images, PAI has the capability to quantify hemodynamic properties including regional blood oxygenation and blood volume, both abnormal in synovial tissues affected by arthritis. Therefore, PAI, together with US, should be of considerable help for further understanding the pathophysiology of arthritis as well as assisting in therapeutic decisions, including assessing the efficacy of new pharmacological therapies. We will review our work on the development of photoacoustic arthritic imaging technology during the last six years at the University of Michigan School of Medicine. We will present the first imaging findings on animal models of arthritis, including both chronic and acute inflammation models. Validation of its performance in monitoring and objective evaluation of pharmacological therapy on animal model of arthritis will also be presented. Moreover, our resent work on PAI and US real-time imaging of human peripheral joints realized with a commercial US platform will also be presented.

The Application of Nonlinear Photoacoustic Cavitation

Xinmai Yang
Bioengineering Research Center and Department of Mechanical Engineering
The University of Kansas, Lawrence, KS 66045, USA

Abstract— Photoacoustic (PA) effect describes a phenomenon where the acoustic signal is generated by the absorbed optical energy. When the locally absorbed optical energy is low, the acoustic signal can be generated through a linear thermal expansion process. When the optical energy absorbed by a target is high, photoacoustic effect may transit from linear to nonlinear regime, and acoustic cavitation can be induced. The induction of acoustic cavitation has a lot of applications in both diagnosis and therapy. Especially, when a PA system is combined with high intensity focused ultrasound (HIFU) system, significantly improved therapeutic effect can be expected.

This presentation will review our recent work on the combination of nonlinear photoacoustics and HIFU for therapeutic purpose. The combination of nonlinear photoacoustics and HIFU can significantly enhance cavitation activities, especially activities related to inertial cavitation. The enhanced cavitation activities have a number of potential clinical applications. One potential application is to enhance HIFU heating. During HIFU thermal therapy, in addition to monitoring the outcome of thermal therapy, a PA system can significantly improve the induced tissue temperature by a process called cavitation-enhanced heating. Our in vivo results shows that the heating enhancement is maximized in the middle range HIFU pressures, while heating enhancement is relatively low when the HIFU pressure is high. The other potential application is to enhance ultrasound-aided thrombolysis process. The combination of photoacoustics and HIFU can provide well defined and controlled cavitation region. When a blood clot is targeted, the induced cavitation can quickly dissolve the clot, while the damage to the surrounding region can be minimized. Our ex vivo results demonstrates that when a PA system and HIFU are combined, significantly better treatment outcome is achieved than using ultrasound technique alone.

Dual-modal Whole Eye Photoacoustic Imaging

Ning Wu, Qiushi Ren, and Changhui Li
Department of Biomedical Engineering, Peking University, Beijing, China

Abstract— We developed a prototype dual-modal ocular imaging system integrating photoacoustic and ultrasound imaging modalities. This system successfully imaged the murine eyes in vivo, including iris, retina, retinal pigment epithelium, and choroid. Our results demonstrated that this system has a great potential in the diagnosis of human's various ocular diseases.

Introduction: Ophthalmic disease has been one of the major causes which threaten our daily life, which can be divided into anterior and posterior ophthalmic diseases. All of these diseases are associated with structural and functional changes. Therefore, high resolution ocular imaging modality that can provide accurately co-registered structural and functional imaging is highly desired.

In ophthalmology, various methods are widely used to acquire both anatomical and functional images. Besides these clinically used optical methods, several ocular imaging methods based on the emerging photoacoustic tomography (PAT) have gained increasing interest in recent years [1, 2], and demonstrated great potential for clinical applications. However, previous high resolution ocular imaging systems based on photoacoustic imaging can only image part of the ocular tissue. Here, we presented a novel system which can be used to image from iris to fundus with the high-resolution capability.

Methods: The schematic diagram of our ocular imaging system is shown in Fig. 1. It employs a reflection mode configuration, where the light source and the ultrasonic detection are set in the same side of the sample. The irradiation laser pulses generated by a pulsed laser system was coupled into a single-mode fiber, and then focused by two objective lenses. A glass slide which permits the light transmission but reflects ultrasound was obliquely placed in a water cube at 45 degrees. Thus the light and ultrasound waves can share the same route within the eye. A focused transducer was used to detect PA signal. The ultrasonic signal was amplified by two amplifiers, and then recorded by an acquisition card.

Results: Both anterior and fundus of the murine eye have been successfully imaged by this system, as seen in Fig. 2. Since blood vessels generate high signal in PAT, vessels in iris and

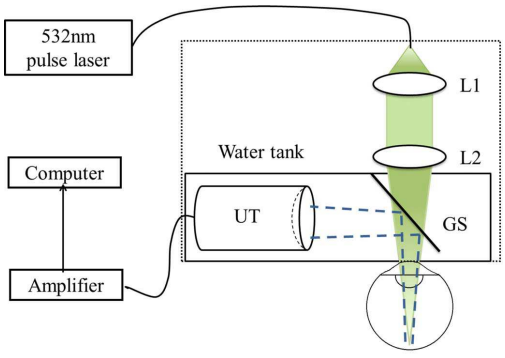

Figure 1: System setup.

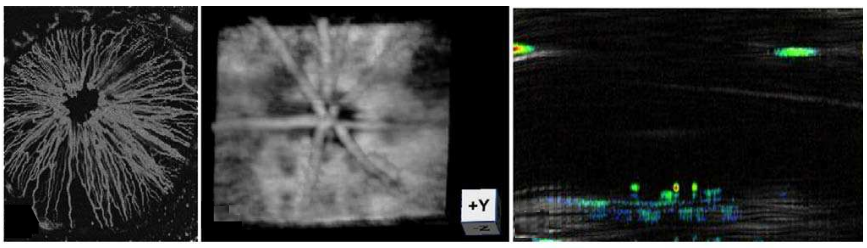

(a) (b) (c)

Figure 2: Imaging results. (a) and (b) are the photoacoustic imaging of iris and fundus, respectively, (c) photoacoustic and ultrasound imaging coregistration.

fundus have been clearly imaged in Figs. 2(a) and 2(b). Besides the photoacoustic imaging, ultrasound imaging provide structural information. Finally, these two imaging results can be fused with high spatial accuracy, as seen in Fig. 2(c).

Besides animal study, this system has a great potential to investigate pathological mechanism of many ocular diseases, such as glaucoma, DR, and AMD.

ACKNOWLEDGMENT

Research supported by National Science Foundation of China (61078073).

REFERENCES

1. Jiao, S., et al., "Photoacoustic ophthalmoscopy for in vivo retinal imaging," *Optics Express*, Vol. 18, No. 4, 3967, 2010.
2. Hu, S., et al., "Label-free photoacoustic ophthalmic angiography," *Optics Letters*, 1–3, 2010.

In Vivo Photoacoustic Tomography: Systems and Contrast Agents

Chulhong Kim
Creative IT Engineering, Pohang University of Science and Technology (POSTECH), Republic of Korea

Abstract— High-resolution volumetric optical imaging modalities, such as confocal microscopy, two-photon microscopy, and optical coherence tomography, have become increasing important in biomedical imaging fields. However, due to strong light scattering, the penetration depths of these imaging modalities are limited to the optical transport mean free path ($\sim 1\,\mathrm{mm}$) in biological tissues. Photoacoustic imaging, an emerging hybrid modality that can provide strong endogenous and exogenous optical absorption contrasts with high ultrasonic spatial resolution, has overcome the fundamental depth limitation while keeping the spatial resolution. The image resolution, as well as the maximum imaging depth, is scalable with ultrasonic frequency within the reach of diffuse photons. In biological tissues the imaging depth can be up to a few centimeters deep.

In this presentation, the following topics of photoacoustic imaging will be discussed; (1) multiscale multiview whole body spectroscopic photoacoustic imaging, (2) virtual intraoperative surgical photoacoustic mircoscopy, (3) multimodal photoacoustic tomography, and (4) contrast agents for photoacoustic imaging.

Multi-scale Biomedical Imaging with Acoustic- and Optical-resolution Photoacoustic Tomography

Liang Song
Research Laboratory for Biomedical Optics and Molecular Imaging
Institute of Biomedical and Health Engineering
Shenzhen Institutes of Advanced Technology, Chinese Academy of Sciences
1068 Xueyuan Boulevard, Nanshan, Shenzhen 518055, China

Abstract— While super-resolution imaging has broken through the optical diffraction limit to enable our visualization of the sub-cellular world in live cells, photoacoustic tomography (PAT) has broken through the optical diffusion limit to allow us seeing intact biological tissue *in vivo* at an unprecedented depth (up to several cm) with rich optical contrasts. As a result, PAT can provide anatomic, functional, and molecular information on biological tissue at multiple scales from organelles to organs. In this talk, we will present our development of multi-scale photoacoustic tomography technologies in both the microscopy and endoscopy forms. While acoustic-resolution photoacoustic microscopy and endoscopy can penetrate deep to provide a macroscopic view on disease status, their optical-resolution counter-parts can offer optical-diffraction limited spatial resolution to visualize microscopic changes locally. Example applications of the developed technologies in molecular and functional imaging of cancer and intravascular imaging of atherosclerosis will be discussed.

Multiscale Photoacoustic Microscopy for Brain Imaging

Bowen Jiang[1, 2], **Xiaoquan Yang**[1, 2], **Hui Gong**[1, 2], **and Qingming Luo**[1, 2]

[1]Britton Chance Center for Biomedical Photonics, Wuhan National Laboratory for Optoelectronics
Huazhong University of Science and Technology, 1037 Luoyu Road, Wuhan 430074, China
[2]Key Laboratory of Biomedical Photonics of Ministry of Education
Huazhong University of Science and Technology, 1037 Luoyu Road, Wuhan 430074, China

Abstract— Photoacoustic microscopy is capable of multiscale imaging in biological tissues from organelles to organs. We developed an acoustic-resolution photoacoustic microscope (OR-PAM) for cortex imaging in rats. The results suggested the OR-PAM could be used to monitor the hemodynamic changes of cortex in physiological and pathological status. An optical-resolution photoacoustic microscope (OR-PAM) is also developed. It was used in the assessing the effect of drug on single cerebral microvessels. The results demonstrated that the OR-PAM revealed not only the hemodynamic changes of the vessels but also the changes of the morphology of the vessels. To fully explore the potential of multiscale capability of PAM, a new method was used to integrate the OR-PAM and AR-PAM in one system. The lateral resolution of the system can be continuously tuned from diffraction limited size of optics to the limited resolution of acoustic to fulfill different requirements of the system. The system can be used in the multiscale imaging with arbitrary resolution from OR to AR as the user's wish.

Light Focusing and Imaging through Turbid Media Using the Photo-acoustic Transmission-matrix

Thomas Chaigne[1,2], **Jérôme Gâteau**[1,2], **Ori Katz**[1,2], **Emmanuel Bossy**[1], **and Sylvain Gigan**[1,2]

[1]Institut Langevin, ESPCI ParisTech, CNRS UMR 7587, INSERM ERL U979
1 rue Jussieu, Paris 75005, France
[2]Laboratoire Kastler Brossel, Université Pierre et Marie Curie, Ecole Normale Supérieure
CNRS, 4 Place Jussieu, 75252 Paris Cedex 05, France

Abstract— We report the implementation of the photo-acoustic transmission-matrix (PATM) method with a linear ultrasound array. The PATM allows optimizing light delivery to specified regions of the image and revealing features otherwise hidden.

Focusing light to the micron scale is the enabling element in many important biomedical and industrial applications such as optical microscopy and laser nano-surgery. However, the inherent inhomogeneity of biological tissues results in light scattering, which limits effective focusing to shallow depths of a few hundred microns [1]. As a result, optical microscopy, perhaps the most important tool in biological discovery and medical investigation, is currently restricted to superficial investigation. In 2007, a seminal work by Vellekoop et al. [2] demonstrated that it is possible to focus light through highly scattering, nearly opaque samples by shaping the incident wavefront using Spatial Light Modulators (SLM) and iterative optimization of a feedback signal. Following the demonstration by Vellekoop et al., wavefront-shaping has been exploited in numerous works to achieve various sought-after goals, from surpassing the diffraction limit in scattering media to improving imaging [3]. In most of these works the feedback signal was obtained from a camera placed *behind* the scattering medium, thus limiting the applicability of this technique to scenarios where one has access to both input/output sides of the scattering medium. However, a highly desired goal is to focus light inside a heterogenous, scattering sample, such as biological tissue. Utilizing a photoacoustic signal as the feedback signal can overcome these limitations, enabling controlled focusing at an arbitrary variable position *inside* a scattering medium [4]. Here we study experimentally the potential of photoacoustic-guided wavefront shaping for controlled focusing inside scattering biological media. We extend previous recently published 1-D images obtained with a single element transducer [5] to 2-D images obtained with a commercial linear ultrasound array.

The photoacoustic transmission-matrix method previously is demonstrated with 2D photoacoustic images. On the one hand, this approach provides a powerful way to focus light through scattering media. On the other hand, photoacoustic imaging can benefit from the optimization of light delivery to increase signals, and features otherwise invisible with conventional reconstruction approach may be retrieved [6] from the information contained in the PATM.

REFERENCES

1. Ntziachristos, V., "Going deeper than microscopy: The optical imaging frontier in biology," *Nat. Meth.*, Vol. 7, 603–614, 2010.
2. Vellekoop, I. M. and A. P. Mosk, "Focusing coherent light through opaque strongly scattering media," *Opt. Lett.*, Vol. 32, 2309–2311, 2007.
3. Mosk, A. P., A. Lagendijk, G. Lerosey, and M. Fink, "Controlling waves in space and time for imaging and focusing in complex media," *Nat. Photon.*, Vol. 6, 283–292, 2012.
4. Kong, F., et al., "Photoacoustic-guided convergence of light through optically diffusive media," *Opt. Lett.*, Vol. 36, 2053–2055, 2011.
5. Chaigne, T., O. Katz, A. C. Boccara, M. Fink, E. Bossy, and S. Gigan, "Controlling light in scattering media noninvasively using the photo-acoustic transmission-matrix," *Nat. Photon.*, Vol. 8, 58–64, 2014.
6. Gâteau, J., T. Chaigne, O. Katz, S. Gigan, and E. Bossy, "Improving visibility in photoacoustic imaging using dynamic speckle illumination," *Opt. Lett.*, Vol. 38, No. 23, 5188–5191, 2013.

Co-registered Photoacoustic and Ultrasound on Humans with a Range of High Frequency Probes

Martin J. Leahy, **Haroon Zafar**, **Sean O'Gorman**,
Aedán Breathnach, **and Hrebesh M. Subhash**
Tissue Optics & Microcirculation Imaging Group, School of Physics
National University of Ireland, Galway, Ireland

Abstract— Co-registered photoacoustic and ultrasound imaging (PAI) using multi-element linear transducer array, combined with multichannel collecting system was used for in vivo volumetric imaging of the structure and blood microcirculation within human tissue. 3D photoacoustic and high frequency ultrasound volumetric scans, measured 10 mm (length) × 14.1 mm (width) × 30.5 mm (depth) were acquired from the forearm skin using 15, 21 and 40 MHz frequency transducers at 860 nm and 1060 nm wavelength. 3D co-registered structural and functional (microcirculation) maps of the forearm skin were obtained from normal subjects. Some preliminary clinical data will also be presented. The linear array based PAT with co-registered high frequency ultrasound has been found promising in terms of resolution, imaging depth and imaging speed for in vivo microcirculation imaging within human skin. However, significant challenges remain, particularly with the penetration depth.

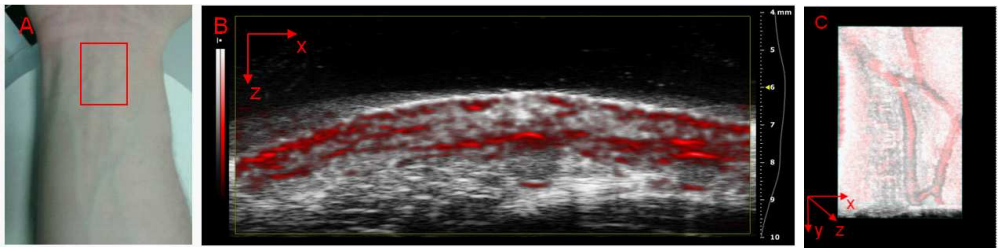

Figure 1: 3D photoacoustic and ultrasound imaging of the volar aspect of human wrist.

Conclusion: Co-registered photoacoustic and ultrasound imaging with a linear array-based probe provides a convenient means of imaging the microcirculation within its native structural context and adds functional information. The depth and resolution are dependent on the frequency such that the best resolution is worse than 200 times smaller than imaging depth.

ACKNOWLEDGMENT

This study was supported by Science Foundation Ireland and NBIP Ireland funded under the Higher Education Authority PRTLI Cycle 4, co-funded by the Irish Government and the EU - Investing in your future and IRCSET, the Science Foundation Ireland (SFI). Haroon Zafar is supported by a Hardiman Fellowship from NUI Galway.

Session 1P7
FocusSession.SC3: Nonlinear Optics: Structured Materials, Functional Devices and Applications 1

Towards Metamaterials with Efficient Second-order Nonlinear Optical Response

R. Czaplicki[1], **H. Husu**[1, 2], **J. Mäkitalo**[1], **R. Siikanen**[1], **J. Lehtolahti**[3], **J. Laukkanen**[3], **M. Kuittinen**[3], **and M. Kauranen**[1]

[1]Department of Physics, Tampere University of Technology, P. O. Box 692, Tampere FI-33101, Finland
[2]Centre for Metrology and Accreditation (MIKES), P. O. Box 9, Espoo FI-02151, Finland
[3]Institute of Photonics, University of Eastern Finland, Joensuu FI-80101, Finland

Abstract— We investigate arrays of gold nanoparticles with different shapes by second-harmonic generation. Efficient second-order nonlinear optical response can be obtained through various mechanisms related to plasmon resonances. In addition to resonances, the geometry of the particles plays significant role, leading to unexpected results.

Introduction: The optical properties of metal nanostructures depend strongly on plasmonic resonances, which are sensitive to geometrical parameters of the nanoparticles (NPs) and the surrounding environment. The geometry is particularly important for second-order nonlinear effects, which require symmetry breaking. The metallic NPs give rise to strong local fields through plasmons leading to enhanced nonlinear optical interactions. We show that in contrast to recent interpretations [1], second-harmonic generation (SHG) from metal nanostructures cannot be explained solely by the plasmonic resonance enhancement. Instead, the character of plasmon oscillations supported by the geometry plays a crucial role.

Experiment and Results: Arrays of **L** and **T**-shaped gold NPs were fabricated by electron-beam litography and lift-off techniques. In the fabrication process, a 0.5 mm fused silica substrate was covered by 3 nm Cr adhesion layer on top of which 20 nm thick gold nanoparticles were deposited. The final 20 nm thick glass layer was added on top to protect the particles.

The extinction spectra revealed strong dichroism with pronounced plasmonic resonances at different wavelengths for the light polarized along (y) and orthogonal (x) to symmetry axes.

The nonlinear optical properties were determined by detecting SHG from the samples irradiated by the beam from an Nd:glass laser (200 fs, 1060 nm, 80 MHz). The input and SHG polarizations were controlled by high-quality polarizers and a half-wave plate. The SHG response obeys the symmetry rules in the case of all samples and the resonance conditions are obeyed for the case of **L** NPs [2]. They are compromised, however, in the case of **T** NPs. When the incident field is x-polarized, the SHG signal is weak. This is due to the specific geometry of the **T** NPs, which makes coupling to the allowed y-polarized SHG difficult. In order to overcome this difficulty, polarization containing x- and y-polarized incident field can be used. As a result, the allowed x-polarized component of SHG is very strong, even if only one input polarization component is resonant.

Conclusion: We have shown that the nonlinear optical responses from metal NPs of diverse geometries don't necessarily follow the plasmonic resonance conditions. Instead, the geometry of the NPs plays an important role in the enhancement of the optical nonlinearity. Such results suggest that the nanostructures are not optimized yet. In the new designs of efficient nonlinear optical metamaterials, the geometry should support both plasmon resonances and local fields.

REFERENCES

1. Niesler, F. B. P., N. Feth, S. Linden, and M. Wegener, "Second-harmonic optical spectroscopy on split-ring resonator arrays," *Opt. Lett.*, Vol. 36, 1533–1535, 2011.
2. Czaplicki, R., M. Zdanowicz, K. Koskinen, J. Laukkanen, M. Kuittinen, and M. Kauranen, "Dipole limit in second-harmonic generation from arrays of gold nanoparticles," *Opt. Express*, Vol. 19, 26866–26871, 2011.

Low-threshold Optical Bistabilities in Ultra-thin Plasmonic Films

Shiwei Tang[1], **Baocheng Zhu**[1], **Shiyi Xiao**[1], **Jung-Tsung Shen**[2], **and Lei Zhou**[1]

[1]State Key Laboratory of Surface Physics
Key Laboratory of Micro and Nano Photonic Structures (Ministry of Education)
Fudan University, Shanghai 200433, China
[2]Department of Electrical and Systems Engineering, Washington University in St. Louis, USA

Abstract— Optical bistability (OB) is a nonlinear optical phenomenon that can provide the necessary light control in many optoelectronic applications. However, the optical thicknesses of these devices must be comparable to wavelength in order to sustain a Fabry-Perot (FP) mode or the power of incident light is extremely high to obtain OB [1]. For practical applications, it is highly desired to find a mechanism to achieve the OB at a low input power using a device with a miniaturized size.

Here we describe an approach to achieve this goal. We employed finite-difference-time-domain (FDTD) simulations to study the optical transmission behaviors of metallic plates with array of subwavelength fractal apertures filled with nonlinearly active materials. We found that OB can occur at a low input power even when the film thickness and linear refraction index are very small, and the OB threshold is nearly independent no the film thickness, which quite is different from an FP slab. We can further reduce the threshold by narrowing the aperture line width. A simple model is established to reproduce all salient features of FDTD simulations, showing the crucial role of lateral resonance in understanding these anomalous effects [2].

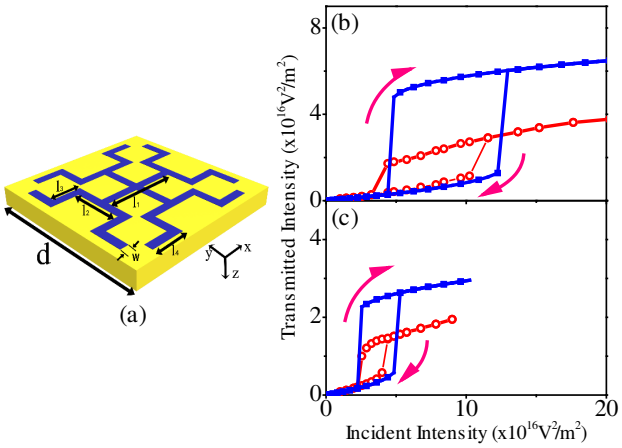

Figure 1: (a) Unit cell structure of fractal-like holey metallic plate; Bistability loops in the fractal-like HMP with $\lambda = 1.55\,\mu$m obtained by both FDTD calculations (circle lines) and theoretical calculation (solid line): (b) $w = 20\,$nm, $h = 60\,$nm (c) $w = 15\,$nm, $h = 60\,$nm.

REFERENCES

1. Chen, W. and D. L. Mills, *Phys. Rev. B*, Vol. 35, 524, 1987.
2. Tang, S. W., J. T. Shen, S. Y. Xiao, and L. Zhou, unpublished.

Sub-wavelength Linear and Nonlinear Localized Discrete Modes in Arrays of Coupled Metallic Nanowires

Fangwei Ye[1], **Boris Malomed**[2], **Dumitru Mihalache**[3], **Nicolae Panoiu**[4], **and Xianfeng Chen**[1]

[1]Department of Physics and Astronomy, Shanghai Jiao Tong University, Shanghai 200240, China
[2]Department of Physical Electronics, School of Electrical Engineering, Faculty of Engineering
Tel Aviv University, Tel Aviv 69978, Israel
[3]Department of Theoretical Physics
"Horia Hulubei" National Institute for Physics and Nuclear Engineering
407 Atomistilor, Magurele-Bucharest 077125, Romania
[4]Department of Electronic and Electrical Engineering, University College London
Torrington Place, London WC1E7JE, UK

Abstract— In this presentation, we will report our two very recent works on arrays of coupled metallic nanowires.

In the first work, we study the effect of structural disorder on the spatial distribution of the plasmonic field and its dynamics upon propagation in a system consisting of one- and two-dimensional (1D and 2D) arrays of optically coupled metallic nanowires. In its regular form, the plasmonic system is composed of identical, periodically distributed metallic nanowires, which form 1D or 2D plasmonic crystals. We find that a random distribution of radii of the nanowires leads to transverse spatial localization of surface-plasmon-polaritonic collective excitations (i.e., plasmonic supermodes of the array). Depending on parameters, the characteristic spatial confinement of the plasmonic field can be significantly smaller than the optical wavelength, which demonstrates that the plasmonic nanostructures can be effectively employed to explore a new physical regime of the subwavelength Anderson's localization of the electromagnetic field. To facilitate a possible experimental observation of such extreme localization of light, we have studied their possible excitations in the realistic (lossy) metallic arrays.

In the second work, and connected to the previous topic, we show that a periodic metallic nanowires embedded into a dielectric medium with the Kerr nonlinearity supports subwavelength plasmonic lattice solitons (PLS). The properties and existences of PLS are studied in detail. Our analysis shows that the transition from a weak to strong optical coupling between plasmonic nanowires results in the formation of PLS with markedly different characteristics of their optical power and field distributions. According to this, we are able to identify three qualitatively different regions for PLS formations.

In both works, the properties of the localized modes (the Anderson modes and PLS) are studied in detail by solving the full set of the vectorial Maxwells equations. Thus we present the first demonstration of both the Andersons localization of light and the discrete solitons beyond the conventional coupled-mode-theory (CMT) and paraxial approximations. In both works, the full solutions are compared with predictions of the CMT. Compensation of metal losses by a background optical gain is analyzed too, revealing that the gain coefficient required to balance the losses is much smaller than the loss parameter of the metallic components of the plasmonic array.

Iridium(III) Complexes as Nonlinear Absorbing Materials

Wenfang Sun, **Yuhao Li**, **Rui Liu**, **Zhongjing Li**, **Naveen Dandu**, **and Svetlana Kilina**
Department of Chemistry and Biochemistry
North Dakota State University, Fargo, ND 58108-6050, USA

Abstract— Organic materials with broadband nonlinear absorption in the visible to the near-IR region are desired for a variety of photonic device applications. Due to the broadband excited-state absorption in the visible to the near-IR region in many of the Ir(III) complexes, and the heavy metal induced intersystem crossing (which induces very weak transitions from the ground state to the triplet excited state in the visible to the NIR region), Ir(III) complexes are promising candidates as broadband nonlinear absorbing materials. In addition, the octahedral geometry of the Ir(III) complexes can prevent intermolecular interactions, which reduces the quenching of the excited state. Moreover, the ease of structural modifications makes them the ideal candidates for structure-property correlation study.Although many Ir(III) complexes have been widely studied for OLED application, exploration of Ir(III) complexes as nonlinear optical materials has been scarce. Therefore, we have designed and synthesized several series of heteroleptic cationic Ir(III) complexes with different diimine ligands, and different degrees of π-conjugation on the diimine ligand and/or cyclometalating ligands. The UV-vis absorption, emission, and transient absorption of the complexes were systematically investigated. Reverse saturable absorption of the complexes was demonstrated at 532 nm using ns laser pulses. It was revealed that the different diimine ligands influence the triplet excited-state lifetime significantly. Extending the π-conjugation on the diimine ligand via attaching the benzothiazolylfluorenyl component on the diimine ligand can prolong the triplet excited-state lifetime and broaden the triplet excited-state absorption band dramatically; while introducing the same component on the cyclometalating C^N ligands decreases the triplet excited-state lifetime and reduce the triplet excited-state absorption significantly.

Widely Wavelength Tunable Femtosecond Laser Resources Based on Nonlinear Optical Processes

Ming-Lie Hu
Ultrafast Laser Laboratory, College of Precision Instruments and Opto-electronics Engineering
Key Laboratory of Opto-electronic Information Science and Technology of Ministry of Education
Tianjin University, Tianjin 300072, China

Abstract— It has been shown by intensive research activities in the laser and photonics fields that many novel properties unimaginable with conventional optical fibers can result from the photonic crystal fibers (PCFs). Recently, based on some of these properties, photonic crystal fiber has been successfully applied in femtosecond laser technology and greatly improve the performance of femtosecond laser. A brief review of recent work on high power femtosecond laser based on PCF is demonstrated. Furthermore, garmonic generation and optical parametric process based on the high power femtosecond fiber laser can generate new wavelengths of femtosecond pulses from the ultraviolet to mid-infrared. And the wavelength tunable femtosecond laser have a tremendous impact on physics in subwavelength structure, Chemics and Bioglogy.

New Frontiers in Chip-based Nonlinear Optics

Benjamin J. Eggleton
ARC Centre of Excellence, School of Physics, University of Sydney, Australia

Abstract— My talk reviews our recent progress in developing revolutionary photonic circuits that exploit nanophotonics and optical nonlinearity to generate and manipulated photons at the single photon level. I will review our recent progress in developing silicon and chalcogenide based dispersion engineered photonic crystal circuits that offer exquisite control of light with a particular emphasis on slow-light enhancements. Highlights of this work include the first demonstration of optical solitons in silicon, integrate spatial multiplexing of heralded photons and ultra-compact optical switches.

REFERENCES

1. Blanco-Redondo, A., et al., "Observation of soliton compression in silicon photonic crystals," *Nature Communications*, Vol. 5, 3160, 2014, doi:10.1038/ncomms4160.
2. Collins, M. J., et al., "Integrated spatial multiplexing of heralded single-photon sources," *Nature Communications*, Vol. 4, 2582, 2013, doi:10.1038/ncomms3582.
3. Eggleton, B. J., B. Luther-Davies, and K. Richardson, "Chalcogenide photonics," *Nature Photonics*, Vol. 5, 141–148, 2011, doi:10.1038/nphoton.2011.309.
4. Corcoran, B., et al., "Green light emission in silicon through slow-light enhanced third-harmonic generation in photonic-crystal waveguides," *Nature Photonics*, 2009, doi:10.1038/nphoton.2009.28.

Silicon-on-insulator Optical Circuits with High Q, Small Mode Volume Photonic Crystal Slot Microcavities: Nonlinear Response and Optical Trapping of Nanoparticles in Various Solvent Environments

Jeff F. Young and S. Hamed Mirsadeghi
Advanced Materials and Process Engineering Laboratory, Department of Physics and Astronomy
University of British Columbia, Vancouver, BC V6T1Z1, Canada

Abstract— A silicon-on-insulator (SOI) based planar photonic circuit is described that comprises a set of input/output grating couplers connected via channel and photonic crystal 1D waveguides to a 3D microcavity formed in a photonic crystal-clad slot waveguide. The circuits are designed to offer high quality factor (Q), small mode volume (V) resonances with the corresponding cavity mode antinodes localized primarily in the background solvent environment in which the circuits are immersed. These circuits, which do not require undercutting of the buried oxide layer in the SOI structure, exhibit Q factors over 7500, and can be used to detect refractive index unit (RUI) changes of $\sim 2 \times 10^{-5}$ RIU[1]. They can be cleaned and reused many times.

Here we will present the nonlinear transmission properties of these cavities in isopropyl alcohol (IPA) and methanol, using CW excitation near 1600 nm. We also report the behaviour of these circuits when immersed in IPA solutions containing ~ 30 nm diameter Au nanoparticles. These small nanoparticles strongly perturb the cavity resonance (backaction) when in proximity to the antinodes, so particle motion in the cavities gets imprinted on the transmission time series data. Using less than 1 mW of waveguide-coupled CW power, we observe a rich array of optical trapping dynamics of these nanoparticles, which can be quantitatively explained using a self-consistent model for the trapping forces and backaction effects on the cavity resonance. For a fixed optical power, the time series data can clearly distinguish trapping dynamics associated with particles differing in diameter by a single nanometre.

REFERENCES

1. Hamed Mirsadeghi, S., E. Schelew, and J. F. Young, *App. Phys. Lett.*, Vol. 102, 131115, 2013, doi: 10.1063/1.4799963.

Graphene, Topological Insulator and Other 2-dimensional Layered Materials for Microwave and Terahertz Photonics Applications

Shuangchun Wen
Hunan University, Changsha, China

Abstract— The emergence of graphene and graphene-like two-dimensional layered materials provides plenty of chances to the exploration of new microwave/terahertz materials and devices. We experimentally found that beyond graphene, other two-dimensional layered materials such as topological insulators, MoS_2 etc. also possess wideband nonlinear optics response ranging from the visible, mid-infrared to the terahertz and microwave. Particularly, we experimentally demonstrated for the first time that graphene and topological insulators may be novel microwave- and terahertz-absorbing materials, suggesting their potential applications in electromagnetic interference shielding, cloaking, stealth coating in military jets, and so on. In this presentation, we will review some research advances in microwave and terahertz properties of two-dimensional layered materials, and outlook their applications in, especially, microwave and terahertz photonics.

Coherent Anti-Stokes Raman Holography

Zhiwen Liu[1], **Kebin Shi**[2], **Perry S. Edwards**[1], **Nikhil Mehta**[1], **Alexander S. Cocking**[1], **and Demetri Psaltis**[3]

[1]Department of Electrical Engineering, The Pennsylvania State University
University Park, PA 16802, USA
[2]Institute of Modern Optics, Peking University, Beijing, China
[3]School of Engineering, Ecole Polytechnique Fédérale de Lausanne, Lausanne, Switzerland

Abstract— Coherent anti-Stokes Raman holography merges the unique chemical selective capability of coherent anti-Stokes Raman scattering spectroscopy (CARS) with the amplitude and phase detection capability of holography, to result in a label-free three-dimensional (3D) imaging modality. In CARS holographic imaging, a sample is excited by a pump/probe beam and a Stokes beam to produce an anti-Stokes wide field image signal, where the frequency difference between the pump and the Stokes beams matches the molecular vibrational frequency of the sample. The coherent anti-Stokes signal is then holographically recorded by interfering with a frequency-matched reference beam on a charge coupled device camera. The resulted digital CARS hologram captures both the amplitude and the phase of the complex anti-Stokes image field, from which 3D label-free imaging can be realized. In this presentation, we review both the off-axis and the inline digital CARS holography, as well as the application to imaging biological cells. Digital processing approaches including both digital diffractive propagation and compressive sensing based methods are also discussed.

Domain Engineered Lithium Niobate, a Versatile Platform for Multifunctional Photonic Devices

Yan-Qing Lu
National Laboratory of Solid State Microstructures
College of Engineering and Applied Sciences, Nanjing University, Nanjing 21093, China

Abstract— Periodically poled lithium niobate (PPLN) is a highly efficient material for nonlinear frequency conversion including second harmonic generation, difference frequency generation, sum frequency generation, optical parametric oscillation, and other nonlinear processes. Due to the opposite signs of nonlinear optical coefficients in different ferroelectric domains, a nonlinear grating is written in a PPLN, and then the quasi-phase-matching (QPM) could be realized at room temperature over the crystal's whole transparent range. In addition to nonlinear optical coefficients, other third-rank tensors such as the piezoelectric and electro-optic coefficients are also modulated along with the periodic domains, results in some interesting properties. Some coupling effects with two or more processes involved are also founded.

In this talk, I will revisit the history of PPLN, especially the key research activities in the past two decades in our group from materials fabrication, domain characterization, physical properties to related applications. We will see how the coupling effects in PPLN induce polariton excitation with an observable negative dielectric constant. The concepts of "domain engineering" and "function integration" are thus discussed based on PPLN photonic chips, where the electro-optically and acousto-optically controlled nonlinear processes could be realized. Applications of tunable optical diode, low-voltage modulator and polarization insensitive frequency convertor are discussed. Some recent progresses in our group are also introduced, for example, the new patterned poling techniques and frequency conversion of optical vortices. We believe the domain engineered Lithium Niobate should be a versatile platform for various multifunctional photonic devices from solid state lasers to photonic integrated circuits in both the classic and quantum optic worlds.

REFERENCES

1. Ming, Y., et al., "Tailoring entanglement through domain engineering in a Lithium Niobate waveguide," *Scientific Reports*, to be published, DOI: 10.1038/srep04812.
2. Shao, G. H., et al., "Nonlinear frequency conversion of fields with orbital angular momentum," *Phys. Rev. A*, Vol. 88, 063827, 2013.
3. Hu, X. K., et al., "Mimicing surface phonon polaritons in microwave band based on ionic-type phononic crystal," *Appl. Phys. Lett.*, Vol. 101, 151109, 2012.
4. Wu, Z. J., et al., "Optical frequency comb generation through quasi-phase matched quadratic frequency conversion in a micro-ring resonator," *Opt. Express*, Vol. 20, 17192–17200, 2012.
5. Shao, G. H., et al., "Optical parametric amplification of arbitrarily polarized light in periodically poled $LiNbO_3$," *Opt. Express*, Vol. 20, 19343–19348, 2012.

Four-wave Mixing Response of a Graphene Layer Covered on a Tapered Fiber

Jiamei Lu, Qiang Jin, Xibin Li, Qiang Yan, Qianyu Gao, and Shiming Gao
Centre for Optical and Electromagnetic Research
State Key Laboratory of Modern Optical Instrumentation
Zhejiang University, Hangzhou 310058, China

Abstract— Nonlinear optical materials are always expected to be of smaller-size and higher nonlinear coefficient. Graphene, which is of a single atomic layer thickness and whose nonlinear coefficient is five orders higher than silicon [1], has the potential to be an ideal ultra-compact nonlinear material. When a graphene layer overlaps a tapered fiber, the evanescent field ensures the sufficient interaction between graphene and light filed. As a result, such a scheme is expected to extend the interaction distance and enhance the nonlinear effect. On the other hand, graphene also introduces a heavy absorption loss through linear loss [2], two-photon absorption and free-carrier absorption. By considering these effects, four-wave mixing (FWM) is numerically investigated in a tapered fiber covered by a monolayer graphene in telecommunication band. The numerical model is established and the conversion efficiency for a particular graphene length and incident pump power is calculated. By varying the pump power and length of this structure, the optimum length and pump power are obtained. The dispersion of the structure is relatively large, which will lead to a large phase mismatch. However, the structure length is only around 50 μm, much shorter than the conventional nonlinear media such as silicon nanowire. Therefore, the conversion bandwidth is still kept on a wide level. By comparing the graphene composite structure with that without graphene, one can find that the graphene composite structure has much higher nonlinear Kerr coefficient than the pure tapered fiber, and high conversion efficiency can be achieved through much shorter interaction length.

REFERENCES

1. Hendry, E., P. J. Hale, J. Moger, et al., "Coherent nonlinear optical response of graphene," *Phys. Rev. Lett.*, Vol. 105, No. 9, 097401, 2010.
2. Yang, H., X. Feng, Q. Wang, et al., "Giant two-photon absorption in bilayer graphene," *Nano Letters*, Vol. 11, No. 7, 2622–2627, 2011.

Reconfigurable All-optical Logic Operation Based on Semiconductor Optical Amplifiers

Xinliang Zhang
Wuhan National Laboratory for Optoelectronics, School of Optical and Electronic Information
Huazhong University of Science and Technology, Wuhan 430074, China

Abstract— All-optical logic operation can be used for functions in optical network such as header recognition, coding and decoding, etc. and in optical computing such as solving differential equations and some complex operation functions. Comparing with electronic based technology, all-optical counterparts can avoid the optical/electrical/optical conversion process and decrease the power consumption greatly.

There are many different nonlinear effects in semiconductor optical amplifiers, such as cross-gain modulation, cross-phase modulation, four-wave mixing, transient cross-phase modulation effect and so on. We can easily realize different logic operations with different nonlinearities. For example, we can get AND gate based on four-wave mixing effect, and we can get different logic operation with different filter detuning based on transient cross-phase modulation effect. Based on one semiconductor optical amplifier, we have demonstrated five different logic operation functions at 40 Gb/s.

With the help of pre-coding process based on demodulation process of DPSK signal, logic minterms and maxterms can be easily realized based on cross-gain modulation effect in semiconductor optical amplifiers. All-optical minterms and maxterms generation for two input signals, three input signals and four input signals at 40 Gb/s have been demonstrated. Based on these minterms or maxterms, arbitrary logic functions could be constructed. Basic idea for the scheme is illustrated and experimental results for some combinational logic functions are introduced in this talk.

We also presented a novel approach to design a programmable logic array (PLA) exploiting minterms and maxterms. Based on minterms and maxterms, both sum-of-products (SOP) and product-of-sums (POS) typed PLAs are exhibited through six important logic functions.

Session 1P8a
FocusSession.SC2&3: Plasmonic, Metallic, or Dielectric Nanolasers

Integration of InP Nanowire Lasers on (001) Silicon Substrate by Selective Epitaxial Growth

Zhechao Wang[1], **Clement Merckling**[2], **Bin Tian**[1], **Weiming Guo**[2], **Marianna Pantouvaki**[2], **Joris Van Campenhout**[2], **Dries Van Thourhout**[1], **and Philippe Absil**[2]

[1]INTEC-Department, Ghent University-IMEC, Sint-Pietersnieuwstraat 41, Ghent 9000, Belgium
[2]IMEC, Kapeldreef 75, Heverlee 3001, Belgium

Abstract— The co-integration of nanolasers with silicon photonic circuit could potentially solve the most challenging obstacle of silicon photonics, i.e., a lack of light sources due to the indirect bandgap of the silicon material. Although a wide range of IIIV-on-Si nanolasers demonstrations could be found in literature, in most of the cases, nanolasers are first processed on III-V substrates, and then removed to be placed on a silicon substrate. This complex and low-yield integration strategy makes these nanolasers practically infeasible. Selective epitaxial growth could be the optimal approach, which provides precise position control and very high yield.

To implement such epitaxial integration method, a fundamental scientific problem has to be solved, that is the huge lattice constant mismatch between IIIVs and silicon (8.1% for InP on silicon) and also the polarity difference at the interface. Previously we reported a polytypic InP nano-cavity laser which is epitaxially grown on (001) Silicon by using step-surface-germanium seed layer [1]. However, the yield is lower than expected, mainly due to the incomplete annihilation of anti-phase-boundaries (APBs). In this work, we present the further improved of yielding and material quality by using 'V-groove' templates, in which APBs can only form at the trench corners which will be blocked by burring the corner before heteroepitaxy. Sub-pJ lasing threshold at room temperature has been achieved.

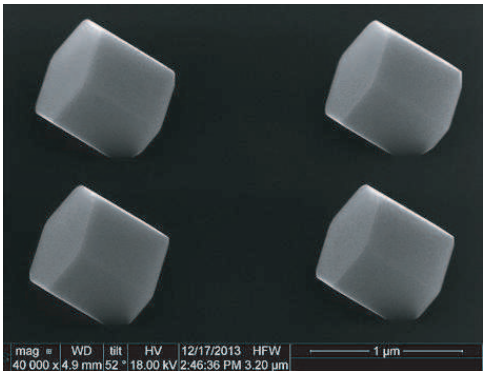

Figure 1: A tilted SEM picture of an array of InP nanowires selectively grown on silicon. Good uniformity in terms of wire diameter and length could be easily identified.

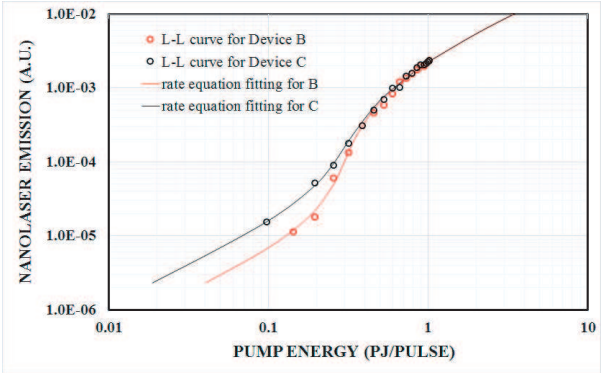

Figure 2: The light in-light out curve of two InP/Si nanolasers measured at room temperature. The circles are measured points and the solid curves are the rate equation fittings, from which the threshold are derived as 0.26 pJ and 0.19 pJ, respectively.

REFERENCES

1. Wang, Z., B. Tian, M. Paladugu, M. Pantouvaki, N. Le Thomas, C. Merckling, W. Guo, J. Dekoster, J. Van Campenhout, P. Absil, and D. Van Thourhout, "Polytypic InP nano-laser monolithically integrated on (001) silicon," *Nano Letters*, Vol. 13, 5063–5069, 2013.

Semiconductor Plasmonic Nano-cavity Laser on Silicon: Simulation, Design and Fabrication

Qian Wang, Chee Wei Lee, and Kim Peng Lim
Agency for Science, Technology and Research, Data Storage Institute
5 Engineering Drive 1, 117608, Singapore

Abstract— Semiconductor plasmonic nano-cavity lasers on silicon including nano-disk, nano-ring and coaxial laser are studied. A self-consistent 2.5 dimensional finite difference time domain (FDTD) incorporating the Drude-Lorentz model for the metal and multilevel and multi-electron semiconductor gain media model is developed to give a spatial and temporal electromagnetic simulation of the nanolaser. The three types of nano-cavity laser are designed and compared numerically regarding the modal volume and threshold material gain. The outputs of the in-plane nano-disk and nano-ring are designed for integration with other devices on chip. Fabrication of the designed nano-cavity lasers on silicon is also presented and discussed.

Mode and Polarization Control in Gallium Nitride Nanowire Lasers

George T. Wang[1], **Jeremy B. Wright**[1, 2], **Huiwen Xu**[2], **Antonio Hurtado**[3], **Changyi Li**[2], **Steven R. J. Brueck**[2], **Qiming Li**[1], **Ting-Shan Luk**[1], **Jeffery J. Figiel**[1], **and Igal Brener**[1]

[1]Sandia National Laboratories, Albuquerque, NM 87185, USA
[2]Center for High Technology Materials, University of New Mexico, Albuquerque, NM 87106, USA
[3]University of Essex, Wivenhoe Park, Colchester, CO4 3SQ, UK

Abstract— III-nitride nanowires are gaining interest as potential ultracompact and low-power nanoscale lasers in the UV-visible wavelengths [1]. While GaN nanowire lasers typically operate in a combined multi-longitudinal and multi-transverse mode state, single-mode lasing is desired for applications needing high beam quality and spectral purity. Here we introduce multiple schemes for controlling the optical mode and the polarization of GaN nanowires lasing under optical pumping. GaN nanowires were synthesized by a two-step "dry plus wet" top-down technique to create nanowires with precisely controlled geometries. The length and the diameter of the nanowires could be controlled by the thickness of the GaN epilayer and the wet etch time, respectively. As the dimensions were reduced to a critical value, the nanowire lasing behavior transitions from multiple- to single-mode [2]. For nanowires with larger dimensions, we demonstrate three alternative methods to realize single mode lasers. The first method involves placing two nanowires side-by-side in contact using a nanoprobe. The resulting coupled cavity generates a Vernier effect, which dramatically increases the free spectral range between adjacent resonant modes, giving rise to the single-mode operation [3]. For the second method, single-mode lasing is achieved by placing GaN nanowires onto gold substrates. The nanowire-gold contact generates a mode-dependent loss, which can strongly attenuate higher modes and ensure single-mode operation [4]. Additionally, the coupling of the GaN nanowires to an underlying gold substrate allows for lasing polarization control. The substrate breaks the symmetry of the nanowire geometry and generates an inherent polarization-sensitive loss. Finally, in a third method, we demonstrate distributed feedback mode selection in a single gallium nitride nanowire by coupling the nanowire to an external dielectric grating [5]. Single-mode nanowire lasing was achieved when the nanowire was oriented to align the spectral location of the stop-band to the optical gain bandwidth of GaN. Sandia National Laboratories is a multi-program laboratory managed and operated by Sandia Corporation, a wholly owned subsidiary of Lockheed Martin Corporation, for the U.S. Department of Energy's National Nuclear Security Administration under contract DE-AC04-94AL85000.

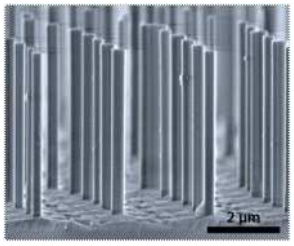

Figure 1: Top-down fabricated *c*-axis GaN nanowires.

REFERENCES

1. Arafin, S., X. Liu, and Z. Mi, "Review of recent progress of III-nitride nanowire lasers," *Journal of Nanophotonics*, Vol. 7, doi:10.1117/1.jnp.7.074599, 2013.
2. Li, Q., et al., "Single-mode GaN nanowire lasers," *Optics Express*, Vol. 20, 17873–17879, 2012.
3. Xu, H. W., et al., "Single-mode lasing of GaN nanowire-pairs," *Appl. Phys. Lett.*, Vol. 101, doi:10.1063/1.4751862, 2012.
4. Xu, H. W., et al., "Gold substrate-induced single-mode lasing of GaN nanowires," *Appl. Phys. Lett.*, Vol. 101, 221114, doi:10.1063/1.4768300, 2012.
5. Wright, J. B., et al., "Distributed feedback gallium nitride nanowire lasers," *Appl. Phys. Lett.*, Vol. 104, doi:10.1063/1.4862193, 2014.

Metal-clad Nanolasers for Dense Chip-scale Integration

Qing Gu and Yeshaiahu Fainman
Department of Electrical and Computer Engineering
University of California at San Diego, La Jolla, CA 92093, USA

Abstract— This paper presents recent progress in metal-clad nanolasers, in particular, the metallo-dielectric and coaxial designs for applications in dense chip-scale integration. By understanding the interplay of various temperature-dependent parameters, we study their effects on nanolaser performance and perform cavity designs by jointly considering optical, electrical, thermal, and temperature dependent material properties.

III-V Semiconductor Nanowire Lasers

C. Jagadish
Department of Electronic Materials Engineering, Research School of Physics and Engineering
The Australian National University, Canberra, A.C.T. 0200, Australia

Sizes Controllable Periodical Nanoslits Array for Surface Enhanced Raman Scattering (SERS)

Yunfei Zhu, Guofu Zhou, and Mingliang Jin
Electronic Paper Display Institute, South China Academy of Advanced Optoelectronics
South China Normal University, China

Abstract— The first observation of SERS was reported when the high quality Raman spectra of monolayer pyridine was obtained. The signal enhancement was related to the electrochemically roughed Ag electrode surface [1]. According to the SERS mechanism, the localized surface Plasmon resonance (LSPR) makes the major contribution to the electromagnetic field enhancement on the metal nano-roughed surface which domain the contribution to SERSthe LSPR strength can be influenced by the morphology of the substrate, like the gap between the nano-objects [2, 3]. The dimension of the gap is an important factor to tune the LSPR [4]. However, the particle-based substrates are lack of the controlling of the gap distance and orientation. As the explosive development of nanotechnology, more and more researches were focused to improve the controllability of making nanogaps. Nanofabrication techniques like electron beam lithography currently provide the good resolution to fabricate highly ordered arrays [5]. The only limitation is the small working area, which is at micron scale, of e-beam lithography. In this paper, we present a new nanogaps surfaces fabricated by laser interference lithography (LIL), which is a "top down" fabrication strategy, to realize the large area metal nanoslits (NS). The edge to edge distance of the nanoslits can be controlled by the thickness of the deposited gold layer. The periodicity of the nanoslits can be tuned by LIL. The LSPR wavelength on this nanoslits surface can be precisely tuned to match the excitation source and providing optimal local electromagnetic field enhancement. Au nanoslits arrays are presented with high-density $\sim 10^4$ NSs cm^{-1}, slits distance down to ~ 10 nm. A SERS analytical enhancement factor of $1.4 * 10^7$ is obtained using 632.8 nm laser as a light source from a benzenethiol monolayer chemisorbed on the Au nanoslits substrate with 10 nm gap and 500 nm periodicity.

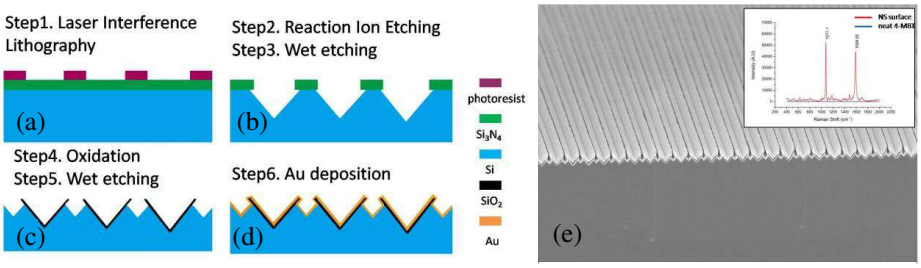

Figure 1: Schematic of the nanoslits fabrication process. (a) Patterned mask fabricate with Laser Interference Lithography. (b) Photoresist and SiN removed with Reaction Ion Etching, triangular undercut profile formed after the anisotropic wet etching process. (c) Si oxidation and a second etching process after the mask removed. (d) Au deposition process. (e) SEM figure of the nanoslits. Scale bar is 100 nm.

REFERENCES

1. Fleischmann, M., P. J. Hendr, and A. J. McQuillan, "Raman spectra of pyridine adsorbed at a silver electrode," *Chemical Physics Letters*, 163–166, 1974.
2. Jain, P. K., X. Huang, I. H. El-Sayed, and M. A. El-Sayed, "Review of some interesting surface plasmon resonance-enhanced properties of noble metal nanoparticles and their applications to biosystems," *Plasmonics*, 2007.
3. Kubo, W. and S. Fujikawa, "Au double nanopillars with nanogap for plasmonic sensor," *Nano Lett.*, Vol. 11, 8–15, 2011.
4. Wu, H.-Y., C. J. Choi, and B. T. Cunningham, "Plasmonic nanogap-enhanced raman scattering using a resonant nanodome array," *Small*, 2012.
5. Le, T. N. L., M. Jin, J. Wiedemair, A. van den Berg, and E. T. Carlen, "Large area metal nanowire arrays with tunable sub-20 nm nanogaps," *ACS Nano*, Vol. 7, 2013.

Single-mode Single-nanowire FP Laser

Xiaowei Liu, Jiabei Li, Zongyin Yang, and Qing Yang
State Key Laboratory of Modern Optical Instrumentation, Department of Optical Engineering
Zhejiang University, Hangzhou 310027, China

Abstract— Semiconductor nanowires have been widely studied as nanoscale lasers due to their attractive properties, such as serving as high gain media and resonance cavity themselves [1]. However, in most endface-reflecting single-nanowire cases, we can only obtain multimode output for the small FSR (free spectral range) whereas large width of the spontaneous emission [2]. The FSR can be expanded when decreasing the nanowire length but leading higher threshold so that lasing could be impossible before pump power burned the nanowire. From now on, single-mode emission can be achieved only if the vernier effect has been introduced, which means two or more cavities being coupled together [3, 4]. In 2011, Xiao, et al. fold a single nanowire to form two loop mirrors such that four cavities have been coupled [3]. In 2013, Gao, et al. cut a single nanowire in order to get two nanowires being placed head to head, so two cavities have been coupled [4]. However, in the former case, the loop's diameter and shape can affect the lasing mode heavily and in the latter, the distance between the two nanowires are determining. What's more, folding nanowire to the precise shape is too challenging to be repeatable, and cutting the nanowire using FIB (focused ion beam milling) is very expensive and may destroy the crystal structure and optical quality of the nanowire. Consequently, highly stable, easily fabricated, low threshold, and low cost single-mode output nanowire lasers have been a huge challenge as well as an attracting task. Recently, we have successfully realized a single-mode single-nanowire FP laser on the basis of fabricating a kind of Zinc doped CdS nanowire with excellent photoluminescence property. By cutting the nanowire with appropriate diameter about 300 nm down to 5.95 μm, the marked interference figure has been watched and 10 dB side-mode suppression ratio has been obtained. The single mode lasing arises from proper reflectivity on the end face and the outstanding gain property of the nanowire. This simple method to achieve monochromatic nanoscale laser with high repeatability will show perspective in laser-based remote sensing, optical data storage, and long-distance optical communication.

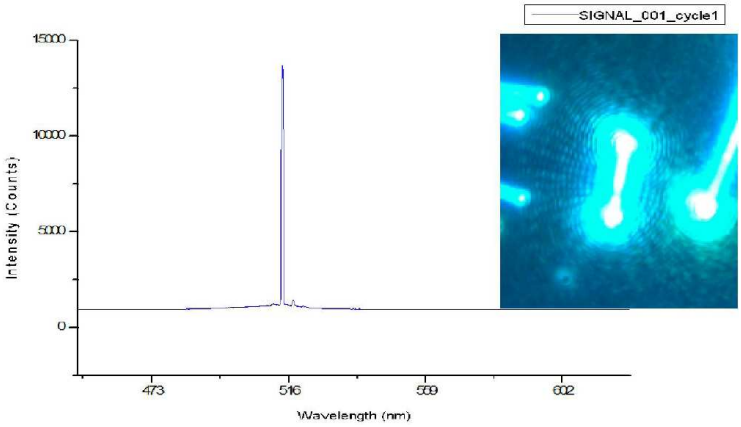

REFERENCES

1. Duan, X., Y. Huang, R. Agarwal, and C. M. Lieber, "Single-nanowire electrically driven lasers," *Nature*, Vol. 421, 241–245, 2003.
2. Johnson, J. C., H.-J. Choi, et al., "Single gallium nitride nanowire lasers," *Nat. Mater.*, Vol. 1, 106–110, 2002.
3. Xiao, Y., C. Meng, P. Wang, et al., "Single-nanowire single-mode laser," *Nano. Lett.*, Vol. 11, No. 3, 1122–1126, 2011.
4. Gao, H., A. Fu, S. C. Andrews, and P. Yang, "Cleaved-coupled nanowire lasers," *PNAS*, Vol. 110, 865–869, 2013.

Strong Light-matter Coupling in ZnO Based Microcavities

Yu-Hsun Chou, **Ying-Yu Lai**, **Shing-Chung Wang**, **and Tien-Chang Lu**
Department of Photonics, Chiao Tung University, Hsinchu, Taiwan

Abstract— In this letter, we systematic analysis the room-temperature strong-coupling effects of ZnO microcavity from relaxation to polariton lasing. Semiconductor microcavities (MCs), which offer good optical confinement with a small mode volume for the photonics portion and an excitonic layer for the matter portion of the strong coupling, are regarded as promising candidates for demonstrating and manipulating strong light-matter coupling in solid-state systems [1]. Because the semiconductor MCs undergo a strong coupling regime, the coupling rate between the bared exciton modes and the confined photon modes is faster than their dissipation rates. Compared with weakly coupled MCs, the rapid exchange rate in strongly coupled MCs renders the energy transfer between the excitons and photons reversible and reduces the possibility of energy dissipation through non-radiative channels, which results in a higher internal quantum efficiency. The new eigenstates generated from the strong exciton-photon coupling are called exciton-polaritons. Exciton-polaritons are quasi-particles, which behave as composite bosons with very light effective mass and controllable dispersions. Due to the bosonic properties, the polaritons tend to condense at ground state through several relaxation processes. Recently, the strong light-matter interaction in ZnO-embedded microcavities has received great attention, due to its ability to generate the robust bosonic quasiparticles, exciton-polaritons, at or above room temperature [2]. Given the aforementioned properties, many phenomena have been extensively studied in polariton systems, including ultra-low threshold polariton lasing [3], polariton parametric oscillation [4] and polaritonic circuits [5]. The matter characteristic of the polaritons allows them to scatter with electrons, phonons and polaritons, then to condense in the coherent ground state. The stable room temperature operation of polaritonic effects in a ZnO microcavity promises a wide range of practical applications in the future, such as ultra-low power consumption coherent light emitters in the ultraviolet region, polaritonic transport, and other fundamental of quantum optics in solid-state systems.

REFERENCES

1. Vahala, K. J., "Optical microcavities," *Nature*, Vol. 424, 839–846, 2003.
2. Chen, J.-R., et al., *Appl. Phys. Lett.*, Vol. 94, 061103, 2009.
3. Huang, R., Y. Yamamoto, R. André, J. Bleuse, M. Muller, et al., *Phys. Rev. B*, Vol. 65, 165314, 2002.
4. Baumberg, J. J., P. G. Savvidis, R. M. Stevenson, A. I. Tartakovskii, M. S. Skolnick, et al., *Phys. Rev. B*, Vol. 62, 16247–16250, 2000.
5. Liew, T. C. H., A. V. Kavokin, and I. A. Shelykh, "Optical circuits based on polariton neurons in semiconductor microcavities," *Phys. Rev. Lett.*, Vol. 101, 016402, 2008.

Session 1P8b
SC3: Semiconductor Lasers

Epitaxially Re-grown Photonic Crystal Surface Emitting Lasers

R. A. Hogg

Department of Electronic and Electrical Engineering, Centre for Nano-science and Technology
University of Sheffield, Sheffield, S3 7HQ, UK

Abstract— Photonic crystal surface emitting lasers (PCSELs) [1] offer the ultimate in control in semiconductor lasers. The photonic crystal causes light waves propagating in various 2D directions to be coupled with one another and a 2D standing wave (cavity mode) is constructed over a broad area. PCSELs have been shown to have high power scaling with area, high single-mode powers [2], large scale coherent emission, control of the beam shape and polarization with design of the photonic crystal geometry [3, 4], as well as beam steering [5]. Williams et al., demonstrated GaAs all semiconductor PCSELs based on epitaxial regrowth [6], as shown schematically in Fig. 1. These all semiconductor PCSELs have been shown to give high coupling values similar to their void containing counterparts [6, 7] due to a strong mode overlap of the photonic crystal with the in-plane guided mode. In this presentation I shall review the development of epitaxially regrown PCSEL's, describing results from latest devices which demonstrate broad area coherent emission.

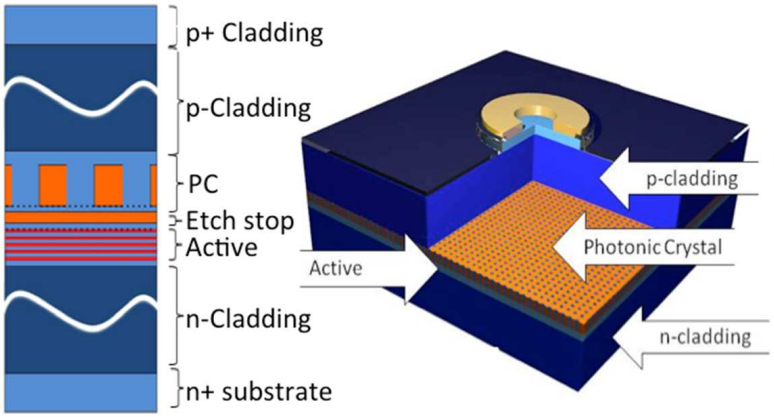

Figure 1: Schematic of the epitaxial layer structure and cut-away of the final device.

REFERENCES

1. Imada, M., et al., *Appl. Phys. Lett.*, Vol. 75, 316, 1999.
2. Hirose, K., et al., *Nature Photonics*, Vol. 8, 406, 2014.
3. Miyai, E., et al., *Nature*, Vol. 441, 946, 2006.
4. Kurosaka, Y., et al., *Optics Express*, Vol. 16, No. 22, 18485, 2008.
5. Kurosaka, Y., et al., *Nature Photonics*, Vol. 4, 447, 2010.
6. Williams, D. M., et al., *IEEE PTL*, Vol. 24, 11, 2012.
7. Taylor, R. J. E., et al., *IEEE JSTQE*, Vol. 19, 4900407, 2013.

Semiconductor Nanostructure-based Photonic Devices for Ultrafast, Power-efficient Systems

Osamu Wada[1, 2]

[1]JSPS Beijing Office, Beijing, China
[2]Kobe University, Japan

Abstract— In order to support the ever increasing bandwidth demand in communication networks and signal processing systems, ultrafast, high-performance photonic devices are prerequisite. On the other hand, power consumption of signal switching/routing systems is considered to become a serious bottleneck in scaling up the bandwidth. The development of high-performance, power-efficient photonic devices are therefore crucial in tackling this problem. This talk first reviews the present status and issues of photonic systems and devices and then discusses recent technical developments of photonic devices based on semiconductor nanostructures, with a particular focus on ultrafast signal processing devices based on quantum dot (QD) materials which include QD-based semiconductor optical amplifiers (SOAs) and QD-based vertical cavity all-optical switches.

Photonic Temporal Integrator Based on Semicondcuctor Lasers Under Lasing Condition

Ming Li[1,*], **Ningbo Huang**[1], **Reza Ashrafi**[2], **Xin Wang**[1], **Wei Li**[1], **Lixian Wang**[1], **José Azaña**[2], **and Ninghua Zhu**[1]

[1]Institute of Semiconductors, Chinese Academy of Sciences
No. 35, Tsinghua East Road, Beijing 100083, China
[2]Institut National de la Recherche Scientifique-Énergie
Matériaux et Télécommunications (INRS-EMT)
1650 Boulevard Lionel-Boulet, Varennes, QC J3X 1S2, Canada

Abstract— In the past tens of years, information technology has witnessed a tremendous progress in optical communication systems, which are superior to electronic systems in many applications [1]. As a result of their severe speed limitation, traditional electronic systems cannot afford a high signal processing speed, and thus they are limited to offer a broad operation bandwidth. Fortunately, all-optical signal processing techniques could be used to overcome these limitations compared to their electronic counterparts. An all-optical processor inherently has the outstanding features of high signal processing speed, low power consumption and broad operation bandwidth.

A photonic temporal integrator is a basic building block to create more complex signal-processing and computing optical platforms. Such a device performs the temporal integral of an arbitrary input optical signal, which has many important applications such as optical dark soliton detection [2], pulse-shaping [3], optical memory [4] and photonic analog-to-digital conversion [5]. Several kinds of photonic temporal integrators have been proposed and experimentally demonstrated based on different optical components and systems, including fiber Bragg grating (FBG), ring resonator and a time-spectrum convolution system. N. Q. Ngo reported a photonic integrator based on a phase-shifted FBG working in transmission [6]. Y. Park et al. used a uniform FBG working in reflection to implement a photonic integrator which could integrate an optical pulse with a time width down to a few picoseconds ($\sim$ 6 ps) [3]. M. Ferrera et al. reported a photonic integrator using a microring resonator compatible with CMOS technology and experimentally proved that the temporal integration window could reach as long as 800 ps with an operation bandwidth of 200 GHz [7]. In addition, a real-time and single-shot ultra-fast photonic time-intensity integrator for arbitrary temporal waveforms has been proposed and demonstrated based on a time-spectrum convolution system [8]. These reported photonic temporal integrators are implemented based on passive components, which necessarily translates into a limited and fixed integration time window. However, for an ideal integrator, the integration time windows should be infinite. This feature is crucial for many practical applications, particularly to create all-optical memory units with sufficiently long hold/storage times. Since a limited temporal integration window of a passive photonic integrator is mainly caused by the loss of the cavity, a loss-compensation mechanism should be introduced. As a strong demand for a large temporal integration time, an optical filter with gain medium (i.e., an active resonator) is required. Experimental realization has been demonstrated by using an all-fiber active filter based on superimposed fiber Bragg gratings [9].

In this paper, a photonic temporal integrator based on an integrated *active Fabry-Perot* (FP) cavity is proposed and theoretically investigated. The gain medium in the FP cavity is a semiconductor optical amplifier (SOA) with high gain coefficient. A key feature of the proposed photonic integrator is that the length of its integration time window can be widely tunable and could be ideally extended to be infinitely long by simply changing the injection current. In addition, SOAs can be easily integrated with other semiconductor devices, such as laser, modulator and photodetector in photonic integrated circuits, which is another critical feature for achieving integrated all-optical signal processing circuits with complicated functionality. Based on the use of an FP cavity with practically feasible parameters, a photonic temporal integrator with an integration time window of 160 ns and an operation bandwidth of 180 GHz is successfully demonstrated through numerical simulations. The time-bandwidth product of the simulated photonic temporal integrator is 28,800, which is about two-orders of magnitude higher than any previously reported results.

*Corresponding author: Ming Li (ml@semi.ac.cn).

REFERENCES

1. Azaña, J., "Ultrafast analog all-optical signal processors based on fiber-grating devices," *IEEE Photon. J.*, Vol. 2, No. 3, 359–386, 2010.
2. Ngo, N. Q., "Optical integrator for optical dark-soliton detection and pulse shaping," *Appl. Opt.*, Vol. 45, No. 26, 6785–6791, 2006.
3. Park, Y., T. J. Ahn, Y. Dai, J. Yao, and J. Azaña, "All-optical temporal integration of ultrafast pulse waveforms," *Opt. Express*, Vol. 16, No. 22, 17817–17825, 2008.
4. Asghari, M. H. and J. Azaña, "Photonic integrator-based optical memory unit," *IEEE Photon. Technol. Lett.*, Vol. 23, No. 4, 209–211, 2011.
5. Jin, Y., P. Costanzo-Caso, S. Granieri, and A. Siahmakoun, "Photonic integrator for A/D conversion," *Proc. SPIE*, Vol. 7797, 1–8, 2010.
6. Ngo, N. Q., "Design of an optical temporal integrator based on a phase-shifted fiber Bragg grating in transmission," *Opt. Lett.*, Vol. 32, No. 20, 3020–3022, 2007.
7. Ferrera, M., Y. Park, L. Razzari, B. E. Little, S. T. Chu, R. Morandotti, D. J. Moss, and J. Azaña, "On-chip CMOS-compatible all-optical integrator," *Nat. Commun.*, Vol. 1, 1–5, 2010.
8. Malacarne, A., R. Ashrafi, M. Li, S. LaRochelle, J. P. Yao, and J. Azaña, "Single-shot photonic time-intensity integration based on a time-spectrum convolution system," *Opt. Lett.*, Vol. 37, No. 8, 1355–1357, 2012.
9. Slavik, R., Y. Park, N. Ayotte, S. Doucet, T. J. Ahn, S. Larochelle, and J. Azaña, "Photonic temporal integrator for all-optical computing," *Opt. Express*, Vol. 16, No. 22, 18202–18214, 2008.

Plasmon Lasers: Development, Features and Applications

Renmin Ma
School of Physics, Peking University, Beijing 100871, China

Abstract— Plasmon lasers are a new class of coherent optical frequency electromagnetic wave amplifiers that deliver intense and coherent surface plasmons well below the diffraction barrier. In this talk, I will review our recent works on the development, features and applications of plasmon lasers.

Tunable V-cavity Semiconductor Laser and Modules

Jian-Jun He[1], **Xiaohai Xiong**[1], **Jianjun Meng**[1], **Sen Zhang**[1], **Xiaolu Liao**[1], **Hongli Zhu**[1], **Lin Wu**[1], **Li Zou**[2], **Lei Wang**[2], **and Guoping Li**[2]

[1]State Key Laboratory of Modern Optical Instrumentation
Centre for Integrated Optoelectronics, Department of Optical Engineering
Zhejiang University, Hangzhou 310027, China
[2]Lightip Technologies (Hangzhou) Co. Ltd.
11 Xiyuan Eighth Road, Suite D-502, Hangzhou 310030, China

Abstract— We present the principle, design, packaging and measurement results of widely tunable V-cavity lasers. By using a novel half-wave coupler, single-mode lasing with high side-mode-suppression-ratio is achieved. Single-electrode controlled wide-band wavelength tuning with Vernier effect is realized. The full-band tuning of 50 channels with 100 GHz spacing is demonstrated by further employing temperature induced gain spectrum shift. The laser is packaged into a small-form-factor 9-pin TOSA, and the electronic driver has been developed for the wavelength tuning and direct modulation. The advantages of compactness, fabrication simplicity, and easy wavelength control offer great potential for the tunable laser to be used in low-cost access and data center networks.

The Proposal of Pulse Synchronous Laser Signal Source Based on Coupled-microdisk Photonic Molecules

Bo-Wen Liu, Yue-De Yang, Xiu-Wen Ma, and Yong-Zhen Huang
State Key Laboratory on Integrated Optoelectronics
Institute of Semiconductors, Chinese Academy of Sciences, Beijing 100083, China

Abstract— During the past twenty years, photonics molecules (PMs) which consist of clusters of electromagnetically coupled optical microcavities have been drawing a great attention for their distinctive optical properties. Photonic molecules with different configurations or patterns are applied to realize variety kinds of photoelectronic devices, such as microlasers, tunable filters and switches, compact photo information processing, and sensors, et al.. On the other hand, in the radar system, transmitter utilize pulse synchronous signals to control different amplifier chains and trigger modulation switches of different amplifier chains at different triggering time. These pulse synchronous signals must keep a strict sequential relationship to make sure the transmitters operate properly. In addition, the synchronization between transmitter and indicator depends on pulse synchronous signals. With the determination range, especially the speed determination, is continuously expanded, pulse synchronous signals with higher pulse repetition frequency (PRF) are needed. Here we propose a model to generate pulse synchronous laser signals based on two waveguide coupled microdisk photonic molecules. Through the beating between symmetric mode and antisymmetric mode in the microdisk photonic molecules, two pulse synchronous laser signals are coupled out by two waveguides. We simulate the light field of the structure via Finite Difference Time Domain (FDTD) method and compute the frequency differences between the symmetric mode and antisymmetric mode of different TM modes. The frequency differences, which represent the PRF of pulse synchronous laser signals, can reach from dozens of GHz to about 1 THz in theory. Meanwhile, we calculate the Q factors of different modes with different symmetry. The numerical results show that the proposed model can generate two pulse synchronous laser signals with fixed pulse widths and complementary phase which can act as a pulse synchronous laser signal source.

Simulation of Thermal Tuning in V-coupled Cavity Laser with an On-chip Thin-film Heater

Haoyu Deng, **Jianjun Meng**, **and Jian-Jun He**
State Key Laboratory of Modern Optical Instrumentation, Center for Integrated Optoelectronics
Department of Optical Engineering, Zhejiang University, China

Abstract— V-coupled cavity laser (VCCL) is a compact, reliable and gratingless widely-tunable semiconductor laser that is highly promising for reconfigurable optical communication network as well for laser sensing. Thermal tuning accomplished by an on-chip thin-film strip resistor acting as a heater is a simple way of achieving wide wavelength-tuning without complicated fabrication process. This paper introduces a thermal model based on finite-element method (FEM) of VCCL with an on-chip heater to calculate the transient and steady-state temperature distribution in the laser and its tuning behavior.

We simulated the heat transfer in the cross-section perpendicular to the waveguide of the laser with top-heating structure, fabricated on a 5 quantum-well (QW) wafer. The result indicates that the active region in the heated waveguide obtains a temperature increase of 15 K when 100 mW heating source power is provided on the heater. Through transient calculation, the time duration to reach a thermal balance is around 2 ms, which gives sufficiently high tuning speed for many applications.

Thermal crosstalk between the two V-shaped coupled waveguides is also evaluated, which reaches as high as 26.9% when heated by the heater on the waveguide top. That means, when the power in the heater is set to 100 mW, the temperature will rise by an average of 4 K in the waveguide that is not directly heated. Considering the 0.1 nm/K temperature induced wavelength tuning, the 11 K temperature difference will cause 1.1 nm difference between the resonant wavelength peak of the two cavities and 22 nm wavelength shift of the output laser in consequence due to the Vernier effect of the VCCL with 5% difference in cavity lengths. This theoretical tuning rate of 0.22 nm/mW is much more power-efficient than tuning by thermal-electric cooler (TEC).

Thermal insulating groove to suppress the thermal crosstalk mentioned above is designed and analyzed. It is found that the crosstalk cannot be reduced to below 20% unless the groove is deeper than 37 μm. With the etching depth of the groove increased to 50 μm, the crosstalk decreases to 17%, and the tuning rate increases to 0.28 nm/mW.

Dynamical Characteristics for Semiconductor Microdisk Laser Subject to Optical Injection

Ling-Xiu Zou, Yong-Zhen Huang, Bo-Wen Liu, Xiao-Meng Lv, Yue-De Yang, Jin-Long Xiao, and Yun Du
State Key Laboratory on Integrated Optoelectronics
Institute of Semiconductors, Chinese Academy of Sciences, Beijing 100083, China

Abstract— In this paper, the dynamic characteristics of four-wave mixing, period-one and period-two oscillations, and optical injection locking state are demonstrated for a 8-μm-radius directional-emission microdisk laser subject to optical injection. For the microdisk laser biased at 7 mA, the 3 dB bandwidth of the small signal modulation response is increased from 3.4 to 13.7 GHz due to the optical injection locking with an injected optical power of 0.5 mW.

Session 1P9a
SC3: Functional Optical Fiber Devices

Regeneration and Fibre Gratings: Towards the Penultimate High Temperature Sensor

J. Canning
Interdisciplinary Photonics Laboratories, School of Chemistry
The University of Sydney, 222 Madsen Building F09, Sydney 2006, Australia

Abstract— Regeneration [1–9] is a process that transforms glass structure and stabilizes such transformation on a local scale introduced by a seed structure. That change is aided by localized differences in internal strain within the glass network,introduced by a combination of a seed-patterned change and a gas such as active hydrogen or traditionally inert helium. Regeneration can be assisted by chemically enhanced strain such as OH formation with hydrogen which raises the internal pressure in a glass. Typically this process is carried out at high temperature and, with additional annealing, leads to ultra-high temperature performance of glass components. In germanosilicate glass, temperature performances in excess of 1200°C have been reported [2]. Both fibre Bragg gratings and long period gratings have been demonstrated. Even femtosecond laser written gratings and draw tower gratings have been regenerated to boost their performance [8, 9]. At such high temperatures, viscoelastic tuning allows novel control of the process to generate arrays from a single phase mask [10] and chirped regenerated gratings [11]. Viscoelastic stretching of glass at high temperatures requires special packaging to avoid drift of the grating response over time [12, 13].

Despite some curious observations since the mid-1990s onwards from various groups that may be related but were entirely misunderstood, their fundamental process was only recognised in 2008 [1, 13] and optimization quickly followed [2–9]. Today, regeneration is being studied by groups worldwide in significant numbers and has been applied extensively to a range of applications spanning pressure sensors [14], high temperature fibre lasers [15], the study of the MCVD process [16], diesel train engine monitoring [17], plant monitoring [18], aerospace applications [19] and industrial electroplating [20].

REFERENCES

1. Bandyopadhyay, S., J. Canning, M. Stevenson, and K. Cook, "Ultra-high temperature regenerated gratings in boron codoped germanosilicate optical fibre using 193 nm," *Opt. Lett.*, Vol. 33, No. 16, 1917–1919, 2008.
2. Canning, J., M. Stevenson, S. Bandyopadhyay, and K. Cook, "Extreme silica optical fibre gratings," *Sensors*, Vol. 8, 6448, 2008.
3. Laffont, G., R. Cotillard, and P. Ferdinand, "9000 hours-long high temperature annealing of regenerated fiber Bragg gratings," *Fifth European Workshop on Optical Fibre Sensors, SPIE*, 87941X, 2013.
4. Canning, J., S. Bandyopadhyay, M. Stevenson, P. Biswas, J. Fenton, and M. Aslund, "Regenerated gratings," *J. Eur. Opt. Soc.*, Vol. 4, 09052, 2009.
5. Wang, T., L.-Y. Shao, J. Canning, and K. Cook, "Regeneration of fiber Bragg gratings under strain," *Appl. Optics*, Vol. 52, 2080–2085, 2013.
6. Shao, L. Y., J. Canning, T. Wang, K. Cook, and H. Y. Tam, "Viscosity of silica optical fibres characterized using regenerated gratings," *Acta Materialia*, Vol. 61, 6071–6081, 2013.
7. Gao, S., J. Canning, and K. Cook, "Ultra-high temperature chirped fiber Bragg gratings produced by gradient stretching of viscoelastic silica," *Opt. Lett.*, Vol. 38, No. 24, 5397–5400, 2013.
8. Cook, K., C. Smelser, J. Canning, G. Garff, M. Lancry, and S. Mihailov, "Regenerated femtosecond fibre gratings," *Proceedings of SPIE*, Vol. 8351, 835111, 2012.
9. Lindner, E., J. Canning, C. Chojetzki, S. Brückner, M. Becker, M. Rothhardt, and H. Bartelt, "Post-hydrogen-loaded draw tower fiber Bragg gratings and their thermal regeneration," *Appl. Optics*, Vol. 50, No. 17, 2519–2522, 2011.
10. Wang, T., L.-Y. Shao, J. Canning, and K. Cook, "Regeneration of fiber Bragg gratings under strain," *Appl. Optics*, Vol. 52, 2080–2085, 2013.
11. Gao, S., J. Canning, and K. Cook, "Ultra-high temperature chirped fiber Bragg gratings produced by gradient stretching of viscoelastic silica," *Opt. Lett.*, Vol. 38, No. 24, 5397–5400, 2013.

12. Barrera, D., V. Finazzi, J. Villatoro, S. Sales, and V. Pruneri, "Packaged optical sensors based on regenerated fiber Bragg gratings for high temperature applications," *IEEE Sensors J.*, Vol. 12, No. 1, 107–112, 2012.
13. Shao, L.-Y., J. Canning, T. Wao, K. Cook, and H.-Y. Tam, "The viscosity of silica optical fibers characterized using regenerated gratings," *Acta Materiala*, Vol. 61, 6071–6081, 2013.
14. Chen, T., R. Chen, C. Jewart, B. Zhang, K. Cook, J. Canning, and K. P. Chen, "Regenerated gratings in air-hole microstructured fibers for high-temperature pressure sensing," *Opt. Lett.*, Vol. 36, 3542–3544, 2011.
15. Chen, R., A. Yan, M. Li, T. Chen, Q. Wang, J. Canning, K. Cook, and K. P. Chen, "Regenerated distributed Bragg reflector fiber lasers for high-temperature operation," *Opt. Lett.*, Vol. 38, No. 14, 2490–2492, 2013.
16. Åslund, M. L., J. Canning, A. Canagasabey, R. A. de Oliveira, Y. Liu, K. Cook, and G.-D. Peng, "Mapping the thermal distribution within a silica preform tube using regenerated fibre Bragg gratings," *Int. J. of Heat and Mass Transfer*, Vol. 55, Nos. 11–12, 3288–3294, 2012.
17. Mezzadri, F., F. C. Janzen, C. Martelli, J. Canning, and K. Cook, "Monitoramento de temperaturaemturbina de motor diesel de locomotiva com sensor a fibra óptica," *MOMAG 2012 — 15th Brazilian Symposium for Microwaves and Optoelectronics (SBMO) and the 10th Brazilian Congress for Electromagnetics (CBMag)*, Brazil, 2012.
18. Willsch, R., W. Ecke, M. W. Rothhardt, and H. Bartelt, "Advanced optical FBG sensor systems and examples of their application in energy facility monitoring," *OSA Advanced Photonics Congress, (Optical Society of America)*, paper BTu4E.1, 2012.
19. Adamovsky, G., D. Varga, and B. Floyd, "Development and performance evaluation of optical sensors for high temperature engine applications" *AII Meeting*, Atlanta, USA, 2010.
20. Tu, Y. and S.-T. Tu, "Fabrication and characterization of a metal-packaged regenerated fiber Bragg grating strain sensor for structural integrity monitoring of high-temperature components," *Smart Mater. Struct.*, Vol. 23, 035001, 2014.

Optically Controllable Fiber Device

Vincent K. S. Hsiao
Department of Applied Materials and Optoelectronic Engineering
Chi Nan University, Nantou 54561, Taiwan

Abstract— We demonstrate an optically controllable fiber device by using organic (liquid crystal, LC) and inorganic (chalcogenide, ChG) photo-active materials. The fiber designs are the photonic crystal fiber (PCF) and side-polished fiber (SFP). The demonstrated photo-active LC-SPF can achieve fiber attenuator, polarizer, sensor and switch. The photo-active LC-PCF can achieve fast fiber polarization switch which has response time of less than 100 ms. The ChG-SPF fiber polarizer has insertion loss of less than 0.2 dB that the 70 degree phase modulation can be achieved.

ACKNOWLEDGMENT

This work is supported by the National Science Council, Taiwan, under project No. 100-2628-E260-003-MY3.

Plasma-modified Optical Fiber Bio-sensors

Mateusz Smietana[1], **Marcin Koba**[2], **and Wojtek J. Bock**[2]

[1]Institute of Microelectronics and Optoelectronics
Warsaw University of Technology, Koszykowa 75, Warsaw 00-662, Poland
[2]Centre de Recherche en Photonique, Université du Québec en Outaouais
101 rue Saint-Jean-Bosco, Gatineau J8X 3X7, QC, Canada

Abstract— Plasma is a fundamental state of matter containing positive and negative particles, i.e., ions and electrons. The ionization process responsible for existence of plasma is typically induced by strong electromagnetic field. Plasma is widely applied for deposition, etching or surface functionalization of a number of materials. It is difficult to imagine fabrication of novel microelectronic and optoelectronic devices without using plasma-based deposition of thin films, their selective etching or functionaliation of their surfaces for subsequent selective binding of chemical or biological molecules. Depending on plasma process parameters, i.e., generator frequency and power, composition of gases, pressure, temperature and applied substrates, different effects of the process can be obtained. Fabrication of materials with different structure (from amorphous to crystalline, porous, multilayers), optical properties (absorption, refractive index) and surface activity, as well as their processing is discussed. The paper focuses on application of the plasma methods for enhancing sensing properties of long-period gratings (LPGs). The LPG is a periodic modulation of refractive index within the fiber resulting in coupling of core and cladding modes. Thanks to coupling of the cladding modes, the LPGs are sensitive to variation of external refractive index and modification of the fiber surface. That is why the gratings can be applied for label-free bio-sensing, where receptor bio-molecules are attached to sensor's surface. The LPG can detect variation of bio-film density and thickness. Using plasma methods, namely Radio Frequency Plasma Enhanced Chemical Vapor Deposition (RF PECVD) and Reactive Ion Etching (RIE), it is possible to maximize sensitivity of the LPG by deposition of a thin high-refractive-index overlay or reduction of the fiber diameter. Both the processes are highly controllable and repeatable. Proper selection of the process parameters allows for tuning uniformity of the reactions around the fiber and their effectiveness.

Special Functions of Modified Optical Microfiber

Xueliang Zhang, **Yang Yu**, **Zhangqi Song**, **Yuzhong Chen**, **and Zhou Meng**
College of Optoelectronic Science and Engineering
National University of Defense Technology, Changsha 410073, China

Abstract— A common optical microfiber has usually been required to have very low loss so as to satisfy the research of optical microfiber based components. On the contrary, optical microfibers with special characteristics and a little higher loss are experimentally studied in this paper, just by modifying some of the parameters related to the optical microfiber fabrication system. Some optical microfibers have high backscattering characteristic, some have a little higher absorption loss. We have fabricated a kind of OM with high backscattering and no more than 5 mm waist region length, which can be evaluated as a reflector with low reflectance. The reflection function has been demonstrated by using the OM reflector as one of the two reflectors in a Fabry-Perot interferometer. We have also controlled the size and loss of OM to enhance its optical induced thermal effect. The OM is injected with intensity-modulated 980 nm light with average light power of about several milliwatts, the optical phase in the OM at 1550 nm wavelength is measured to be modulated while the OM is inserted into a Michelson interferometer. The result show that the OM acts as a kind of optical modulating material based on the optical induced thermal effect. In conclusion, OMs have been studied to evaluate reflection function and thermal modulation function, OM will become a kind of functional fiber and have potential value on research of new OM components.

Polarisation Dynamics in Carbon Nanotube Mode Locked Ultrafast Fibre Lasers

Chengbo Mou[1], **Sergey Sergeyev**[1], **Raz Arif**[1], **Aleksey Rozhin**[1], **Tatiana Habruseva**[1], **Veronika Tsatourian**[1, 2, 3], **and Sergei Turitsyn**[1]

[1]Aston Institute of Photonic Technology (AIPT), Aston University, Birmingham, B4 7ET, UK
[2]National Physical Laboratory, Hampton Road, Teddington, Middlesex, TW11 0LW, UK
[3]School of Engineering and Physical Sciences, Heriot-Watt University, Edinburgh, EH14 4 AS, UK

Abstract— Ultrafast fibre lasers are regarded as the next generation light sources. They have wide applications in the fields of optical communication, metrology, sensing, imaging etc.. Intensive studies have been done on the generation of short pulses (i.e., sub 100 fs, few cycle), high power, high energy and different wavelength window. While, polarisation, as an important property of light pulses, has rarely been exploited. This is due to the polarisation dependency of the approaches that used to achieve ultrashort pulses such as nonlinear polarisation rotation, and nonlinear interferometry. Recently, the development of carbon nanotube (CNT) and graphene as low cost, compact, and polarisation independent saturable absorber has offered us a more convenient approach to achieve ultrafast fibre lasers. Using the CNT mode locked fibre laser, by properly adjusting the intracavity polarisation controller, we have observed various polarisation patterns in the format of Poincare sphere under a number of mode locking regimes such as soliton, soliton molecues, stretch pulse and harmonic mode locking. A unique spiral attractor have been observed for the first time. Using a home developed fast polarimeter, we have also resolved the pulse to pulse polarisation dynamics which highlighted by a triangular or linear pattern.

Fabrication and Applications of D-shaped Fiber Based Graphene Saturable Absorber and Polarizer

Lilin Yi[1], **Ran Zheng**[1], **Weixiong Li**[1], **Haiyan Nan**[2], **Zhenghua Ni**[2], **and Weisheng Hu**[1]

[1]The State Key Lab of Advanced Optical Communication Systems and Networks
Shanghai Jiao Tong University, Shanghai 200240, China
[2]Department of Physics, Southeast University, Nanjing, China

Abstract— Graphene has shown its outstanding optical characteristics in many applications such as saturable absorber [1] and polarizer [2] attributed to wavelength independent, easy combination with fiber and low-cost fabrication. For both applications, graphene covered on D-shape is preferred for longer light-graphene interaction length [3, 4] to achieve higher modulation depth and optical-coupling respectively. In this paper, we present the fabrication and applications of graphene saturable absorber (GSA) and graphene polarizer on D-shape fiber.

Two kind of D-shape fiber (DF) fabrication method shown in Fig. 1, the single-mode fibre (SMF) was fixed on (Fig. 1(a), Type I) or bent and embedded into (Fig. 1(b), Type II) a glass substrate and then polished by machine. Spin-coated polymethyl methacrylate (PMMA) layer (Type I) or deposited 100-nm thick gold film (Type II) [5] on the high-quality CVD graphene were transferred on the DF. For Type II, we kept the gold cover to enhance the light-graphene interaction as shown in Figs. 1(c) and (d) to improve the nonlinear effects, meanwhile simplify the process.

After the DF based GSAs were made, we characterized them with IL, polarization dependent loss (PDL), and modulation depth (ΔR). And then we inserted the GSAs into mode-locked fiber laser as graphene mode-lockers (GML), different types of ultra-short pulse were achieved as shown in Table 1. For the gold coated graphene, the PDL is much higher. And it is a result of rough manual measurement and the real value must be higher, therefore it serves as both polarizer and saturable absorber for better mode-locking performances.

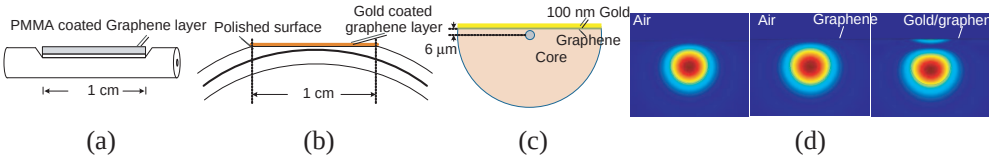

Figure 1: Two types of D-shape fiber based GSA. (a) PMMA coated graphene covered; (b), (c) gold coated graphene covered; (d) optical-field simulation with COMSOL.

Table 1: GSAs characteristics and mode-locking results.

GSA	Description	DF without graphene		DF with graphene layer			Mode-locking results		
		IL (dB)	PDL (dB)	IL (dB)	PDL (dB)	ΔR	τ_{pulse}	E_{pulse}	P_{peak}
Type I	PMMA-coated	8	1.2	13	3	3%	303 fs (DM)	12 nJ	40 kW
Type II	Gold-coated	7	1.24	8	> 12	14%	263 fs (soliton)	13.65 nJ	51 kW

REFERENCES

1. Bao, Q., et al., "Atomic-layer graphene as a saturable absorber for ultrafast pulsed lasers," *Adv. Funct. Mater.*, Vol. 19, 3077, 2009.
2. Bao, Q., et al., "Broadband graphene polarizer," *Nature Photonics*, Vol. 5, No. 7, 411, 2011.
3. Song, Y., et al., "Graphene mode-lockers for fiber lasers functioned with evanescent field interaction," *Appl. Phys. Lett.*, Vol. 96, 51122, 2010.
4. Yi, L., et al., "High-peak-power femtosecond pulse generation using graphene as saturated absorber and dispersion compensator," *Proc. ECOC*, We.2.A.2, London, 2013.
5. Song, L., et al., "Transfer printing of graphene using gold film," *ACS Nano*, Vol. 3, 1353, 2009.

Nonlinear Effect in Carbon-nanotube-coated Optical Fiber Grating

Li-Yang Shao
Center for Information Photonics & Communications
School of Information Science & Technology
Southwest Jiaotong University, Chengdu, Sichuan 610031, China

Abstract— Four-wave mixing (FWM) in single-walled carbon nanotubes (SWCNTs) deposited on the cladding of a tilted fiber Bragg grating (TFBG) is demonstrated. A thin SWCNT film floating on the surface of pure water is wrapped on the cladding of the fiber manually. FWM is generated between a probe and a pump by TFBG-induced interaction of the core mode with the SWCNT deposited on the outer cladding.

Miniaturized Fiber Interferometers and Their Applications as Fiber Sensors

Bo Dong, **Banghong Zhang**, **Junhong Ng**, **and Yixin Wang**
Institute for Infocomm Research (I2R), Singapore 138632, Singapore

Abstract— Recently, much attention has been focused on the miniaturized fiber interferometers devices due to their advantages of compact structure, small size and low cost. In this paper, we introduce two types of miniaturized fiber Mach-Zehnder interferometer (FMZI) and fiber Fabry-Perot interferometer (FFPI) and their applications as fiber sensors. An in line miniaturized FMZI could be fabricated by discharge or a point hydrogen flame. Here, we demonstrate its application as a fiber temperature sensor. A miniaturized FFPI can be fabricated by discharge when a single mode fiber is connected to a hollow core photonic crystal fiber. Here, we demonstrate its application as a liquid refractive index sensor.

Session 1P9b
SC3-workshop: Integrated Nanophotonics for Optical Interconnects in Data Centers

Integrated Nanophotonic Devices for Optical Interconnections

Yidong Huang, Xue Feng, Dengke Zhang, Hai Yan, Xiangdong Li, and Kaiyu Cui
Department of Electronic Engineering, National Lab. for Information Science and Technology
Tsinghua University, Beijing 100084, China

Abstract— Nanostructure is an effective solution for realizing optoelectronic devices with compact size and high performances simultaneously. This paper reports our research progress on integrated nanophotonic devices for optical interconnections.

To improve the integration density and promote the data rate of on-chip optical interconnections, wavelength division multiplexing (WDM) is a natural solution. One of the key components in a WDM transmission link is optical add-drop multiplexer (OADM), which allows flexible addition and extraction of WDM signals. We proposed and demonstrated a parent-sub microring structure for OADM with compact footprint, large free spectral range, and uniform channel spacing simultaneously. The thermal tuning efficiency is as high as 0.27 nm/mW. For dropping state, all four channels can be de-multiplexed to the drop ports with 2 dB drop loss, 18 dB through port extinction, and less than −20 dB channel crosstalk [1, 2].

On the other hand,the optical orbital angular momentum (OAM), as a new degree of light, can carry an infinite amount of data and increase the transmission data rate dramatically. Here we proposed an optical OAM coding and decoding method.According to this idea, we designed a OAM coder/decoder and partly demonstrated with experiments [3]. Furthermore, we proposed a simple on-chip integrated structure to generate OAM beams, where only silicon waveguides and couplers are involved, and OAM with charge numbers of 1 or −1 can be selectively generated with mode purity large than 90%. The proposed device is very compact with footprint of less than 120 µm × 50 µm and can be easily fabricated with CMOS technology [4].

As the development of the silicon light source, the transmission waveguide becomes a main challenge since the output of silicon emitter would be highly absorbed by silicon-wire waveguide, which is now widely adopted in photonic integrated circuits. One of the solutions is adopting silicon slot waveguide. In this paper, the transmission loss of silicon slot waveguide is investigated by the finite element method, and a solution to optimize the structure of slot waveguide is proposed. Within the wavelength range of 800–1100 nm, the minimum transmission loss of optimized slot waveguide can be as low as 0.05–6.5 dB/mm. Typically, the value is about 3–4 dB/mm at wavelength of 900 nm [5].

REFERENCES

1. Yan, H., et al., "Integrated optical add-drop multiplexer based on a compact parent-sub microring-resonator structure," *Optics Communications*, Vol. 289, 53, 2013.
2. Yan, H., et al., "Compact optical add-drop multiplexers with parent-sub ring resonators on SOI substrates," *IEEE Photo. Tech. Lett.*, Vol. 25, No. 15, 1462, 2013.
3. Zhang, D., et al., "Ecoding and decoding of orbital angularmomentum for wireless optical interconnects onchip," *Optics Express*, Vol. 20, 26986, 2012.
4. Zhang, D., et al., "Generating in-plane optical orbital angularmomentum beams with silicon waveguides," *IEEE Photo. J.*, Vol. 5, No. 2, 2201206, 2013.
5. Li, X., et al., "Designing low transmission loss silicon slot waveguide at wavelength band of high material absorption," *Optics Communications*, Vol. 306, 131, 2013.

Silicon and Hybrid Silicon Photonics for Optical Interconnects in Datacenters

Andrew W. Poon, Yu Zhang, Yu Li, and Lei Zhang
Photonic Device Laboratory, Department of Electronic and Computer Engineering
The Hong Kong University of Science and Technology, Clear Water Bay, Hong Kong SAR, China

Abstract— In this talk we will briefly review three of our latest experimental works in silicon and hybrid silicon photonics and their potential applications for optical interconnects in 1550 nm in data centers, including (i) hybrid silicon unidirectional-emission microspiral disk lasers with direct modulation, (ii) silicon sub-band gap linear-absorption-based adaptively tuned microring-based switch arrays, and (iii) hybrid silicon wavelength-division-multiplexed (WDM) photo detector arrays.

For hybrid silicon unidirectional-emission microspiral disk lasers, we employ the conventional die-to-die polymer-based bonding technique to bond an InAlGaAs/InP multiple-quantum-well (MQW) gain medium shaped into a microdisk onto a patterned silicon-on-insulator (SOI) wafer. The laser cavity in the shape of a microspiral disk is patterned on the SOI wafer, which is evanescently coupled to the gain medium bonded on top. The silicon microdisk is directly butt-coupled to a silicon waveguide for unidirectional laser output-coupling to a single waveguide port. We employ spatially selective injection into the MQW gain medium by using a ring-shaped p-contact on top of the III-V microdisk rim region in order to selectively inject current to the whispering-gallery-like modes of the microspiral cavity, and thus help enhance the laser performance. Our on-going experimental works suggest that such a hybrid silicon microdisk laser structure should enable an on-chip integration of an array of unidirectional-emission lasers with direct modulation at a high data rate.

In the front of on-chip optical routers, we propose and demonstrate the use of silicon microring resonators with an integrated silicon sub-band gap linear-absorption-based p-i-n photodiode detector for monitoring the microring internal power, and thus monitoring the spectral alignment between the optical carrier and the microring resonance, as an adaptively tuned switching element. We consider this as a paradigm shift in making silicon microring resonators a potentially practical device in the presence of dynamic fluctuations of the on-chip conditions. We enhance the sub-band gap linear responsivity by introducing defect states using an after-process implantation and annealing Our on-going experiments reveal that a sub-band gap linear responsivity of $\sim 10\,\mathrm{mA/W}$ at $-1\,\mathrm{V}$ can be attained in a small-size silicon microring. Our experiments also demonstrate adaptive tuning of the microring resonance wavelength using the photocurrent as a feedback signal to an off-chip microprocessor to tune either an electro optical or thermo-optical tuner integrated along the microring.

Furthermore, we propose to integrate on-chip a hybrid silicon WDM photo detector array using the same die-to-die bonding as the hybrid silicon microdisk lasers. Together with the hybrid silicon microdisk lasers and the adaptively tuned silicon microring switch arrays, we envision a holistic view of hybrid silicon and silicon photonic integrated circuits that will find immediate applications for data centers and beyond.

Optical Interconnects for Datacenter Networks: Progress and Challenges

Xuezhi Hong[1], **Matteo Fiorani**[2], **and Jiajia Chen**[2]

[1]ZJU-SCNU Joint Research Center of Photonics
South China Normal University (SCNU), Guangzhou 510006, China
[2]School of Information and Communication Technology
KTH Royal Institute of Technology, Kista 16443, Sweden

Abstract— In the "information age" a substantial amount of data are stored, processed, computed, transmitted and instantly made available upon request. Users of these data range from large organizations (e.g., big enterprises, government, universities, etc.) to individual customers, who are increasingly relying on the "cloud" services. This has led to a significant growth of global datacenter traffic (including within data center, data center-to-data center and data center-to-user). According to Cisco[1], the amount of such traffic was already 2.6 zettabytes[2] per year in 2012 and will triple to reach 7.7 zettabytes per year in 2017, which represents a 25% compound annual growth rate. On the other hand, due to thermal dissipation constraints the power consumption that can be afforded by the network equipment is only allowed to increase at a much lower rate (e.g., 2 times every 4 years, 1 MW in 2016 and 2 MW in 2020 accepted for the network equipment within a datacenter [1]). Current data center networks, which are based on electronic switching, are not able to scale to future traffic requirements in a sustainable manner.

high capacity for telecommunication networks [2]. It has been also widely considered as a promising transmission technology for future datacenter solutions [3]. In this paper, an overview is provided for the recent progress on optical interconnects for datacenter networks, based on which we would also identify the challenges posed by extremely dynamic traffic within a datacenter. The major focus will be on mapping these challenges to the requirements of physical layer in order to provide some guidelines for component design. For instance, in high-capacity optical interconnect applications, spatial multiplexing with duplicated hardware is often considered as an effective way to meet the large bandwidth requirement. However, such a solution enlarges the footprint of the system and might not be a power-efficient way especially when a huge number of channels are required. Spectral multiplexing, where advanced modulation formats with multiple bits per symbol can be employed, could be a good solution to reduce the number of spatial channels while keeping the total number of channels in the same level. On the other hand, digital signal processing (DSP) technology is needed in the system with advanced modulation formats, which may reduce the effective computation power at the servers dedicated to the carried applications (e.g., cloud computing). Therefore, a trade-off needs to be carefully investigated to verify whether there are gains or losses to use very advanced modulation formats in data center networks, i.e., the benefits of the improved spectral utilization for communications are able to compensate the computation power sacrificed by DSP or not.

REFERENCES

1. Kachris, C., et al., "Optical interconnection networks in data centers: Recent trends and future challenges," *IEEE Communications Magazine*, Vol. 14, 39–45, Sep. 2013.
2. Kilper, D. C., et al., "Power trends in communication networks," *IEEE Journal of Selected Topics in Quantum Electronics*, Vol. 17, 275–284, Mar.–Apr. 2011.
3. Kachris, C., et al., "A survey on optical interconnects for data centers," *IEEE Communications Surveys & Tutorials*, Vol. 14, 1021–1036, Fourth Quarter, 2012.

[1]Cisco Global Cloud Index: Forecast and methodology, 2012–2017, Cisco White Paper, 2013.
[2]1 zettabytes = 10^{21} bytes.

Hybrid AlGaInAs/InP on Silicon Lasers for Optical Interconnects

Yue-De Yang, **Shao-Shuai Sui**, **Ming-Ying Tang**, **Jin-Long Xiao**, **and Yong-Zhen Huang**
State Key Laboratory on Integrated Optoelectronics
Institute of Semiconductors, Chinese Academy of Sciences, China

Abstract— Silicon based photonic links have been proposed to replace electrical links for the optical interconnects. The CMOS compatible silicon photonic links have the advantage of low power consumption and high bandwidth density, but the indirect-band-gap material silicon are usually not suitable for realizing low-power-consumption light sources due to the ultralow light-emission efficiency. Hybrid integration of III-V material with direct band gap on silicon is attracting great attention for realizing high efficiency on-chip light source. We propose and demonstrate metal confined hybrid AlGaInAs/InP whispering gallery microcavity and Fabry-Pérot (FP) lasers on a silicon-on-insulator (SOI) wafer with bisbenzocyclobutene (DVS-BCB) assisted bonding and standard planar fabrication technology. The p-electrode metals covered on the laser resonators lasers are used for enhancing the mirror reflectivity, while the laser emission is evanescently coupled to a silicon waveguide. Such hybrid silicon lasers have a large optical confinement factor in the active layer, yet still realize laser output from the silicon waveguide. Room temperature electrical injection lasing is realized for the hybrid microdisk lasers with radii from 7 μm to 20 μm and microring lasers with outer radius of 20 μm and inner radii from 10 to 15 μm. Multiple wavelength microdisk laser arrays with radii around 12 μm are demonstrated with threshold current densities about 4 kA/cm^2. For a hybrid silicon laser with the Fabry-Pérot (FP) resonator length of 415 μm and width of 6 μm, the continuous-wave and pulsed threshold current densities are 2.0 and 1.4 kA/cm^2, respectively. The lasing spectra show oscillations of the envelope of the longitudinal modes due to the encasing of the metallic layer. We also measure the near- and far-field patterns, which are consistent with the lasing spectra upon multiple transverse modes.

Group-IV Light Emitting Materials and Devices for Optical Interconnect

Buwen Cheng, Zhi Liu, Chao He, Dongliang Zhang, Xu Zhang, Wenqi Huang, Chunlai Xue, Chuanbo Li, and Qiming Wang
State Key Laboratory on Integrated Optoelectronics
Institute of Semiconductors, Chinese Academy of Sciences, Beijing 100083, China

Abstract— To meet the requirements of high performance and low cost of the optical interconnect, a lot of efforts have been made on Si-based photonics in the last decade. Although most Si-based optical devices have been demonstrated, the light emitter is still an open question due to the inherent performance limitations of silicon. Supplying light from external sources or bonding III-V emitters onto silicon is a good choice for the near term. But, for the future application, group-IV laser on silicon compatible with CMOS technology is necessary and crucial.

Germanium has unique light emitting property due to the small separation of 0.14 eV between the absolute minimum ofthe conduction band at the L-point of the Brillouin zone and the Γ-point local minimum. Tensile strain can further decrease the separation, hence enhance the luminescence of the direct band-gap transition. N-type doping can also improve the luminescence of Ge by increasing the electron occupying probability at Γ valley. If we alloy Sn into Ge to form GeSn alloy, the band structure will be tuned. When the composition of Sn is higher than about 8%, the energy band will transform from indirect to direct band gap. It means that GeSn is promising for group-IV laser on Si. Pb has the similar effect to Sn when alloyed into Ge. The predicated transitional concentration from indirect to direct band-gap of GePb is much lower than that of GeSn alloys.ThisresultindicatesthatGePballoycouldbea significant alternative for group-IV light emitting material with high efficiency. In this paper, we will introduce our study on light emitting materials and devices on Si substrate. Ge, GeSn and GePb will be involved.

Silicon Multimode Photonic Integrated Devices for On-chip Optical Interconnects

Daoxin Dai
Centre for Optical and Electromagnetic Research
State Key Laboratory for Modern Optical Instrumentation
Zhejiang Provincial Key Laboratory for Sensing Technologies, Zhejiang University
Zijingang Campus, Hangzhou 310058, China

Abstract— Multimode spatial-division multiplexing (SDM) technology has attracted much attention for its potential to enhance the capacity of an optical-interconnect link with a single wavelength carrier, which is promising for low-cost on-chip optical interconnects (photonic network-on-chip). For a mode-multiplexed optical-interconnect link, the functional elements are quite different from the conventional ones as multiple modes are involved. The higher-order mode handling has to be very meticulous to avoid any undesired mode coupling/conversion so that the channel crosstalk can be low. In this paper we give a review and discussion on multimode photonic integrated devices for mode-multiplexed optical-interconnects. First the analysis and discussion on light propagation and mode conversion in tapered waveguides as well as bent waveguides is given. Recent progress on mode converter/(de)multiplexers in our group is then reviewed, including the mode evolution in adiabatic tapered structures and the mode-selection in asymmetrical directional couplers. Finally the demands of some functional devices used for mode-multiplexed optical-interconnects is discussed.

Optical Routers for Photonic Networks-on-chip

Lin Yang, Fanfan Zhang, Qiaoshan Chen, Jianfeng Ding, Ruiqiang Ji, and Rui Min
State Key Laboratory on Integrated Optoelectronics
Institute of Semiconductors, Chinese Academy of Sciences, Beijing 100083, China

Abstract— The performance of chip multiprocessor (CMP) is determined not only by the number of the processor cores integrated on a die, but also by how efficiently they collaborate with each other. With CMP continuously requiring more communication bandwidths, metallic-based electrical NoC gradually becomes the bottleneck for improving the performance of CMP due to its high power consumption, limited bandwidth and long latency. Photonic NoC is considered as a potential solution to overcome the limitations of its electrical counterpart. Optical router is a key device in photonic NoC, which is responsible for routing data from one optical link to another optical link.

In this paper, we will review the status of the optical routers for photonic networks-on-chip and introduce our efforts on this topic. Firstly, we will introduce several demonstrated optical routers based on microring or Mach-Zehnder optical switches. Then, we will introduce a universal method for constructing an N-port non-blocking optical router for photonic NoC. The optical router constructed by this method has minimum optical switches, in which the number of the optical switches is reduced about 50% compared to the reported optical routers based on microring optical switches and about 30% compared to the reported optical routers based on Mach-Zehnder optical switches, and therefore is more compact in footprint and more power-efficient. Finally, we will introduce the fabricated 4-port optical router constructed by this method.

REFERENCES

1. Ji, R. Q., L. Yang, et al., "Five-port optical router for photonic networks-on-chip," *Optics Express*, Vol. 19, No. 21, 20258–20268, 2011.
2. Ji, R. Q., L. Yang, et al., "Microring-resonator-based four-port optical router for photonic networks-on-chip," *Optics Express*, Vol. 19, No. 20, 18945–18955, 2011.
3. Ji, R. Q., J. Xu, and L. Yang, "Five-port optical router based on microring switches for photonic networks-on-chip," *IEEE Photonics Technology Letters*, Vol. 25, No. 5, 492–495, 2013.
4. Min, R., R. Q. Ji, Q. S. Chen, et al., "A universal method for constructing N-port nonblocking optical router for photonic networks-on-chip," *Journal of Lightwave Technology*, Vol. 30, No. 23, 3736–3741, 2012.

A Universal Method for Constructing *N*-port Non-blocking Optical Router Based on 2 × 2 Optical Switch

Qiaoshan Chen, Fanfan Zhang, Ruiqiang Ji, Lei Zhang, and Lin Yang
State Key Laboratory on Integrated Optoelectronics
Institute of Semiconductors, Chinese Academy of Sciences, China

Abstract— With CMP continuously requiring more communication bandwidth, metallic-based electrical network-on-chip (NoC) gradually becomes the bottleneck for improving the performance of CMP due to its high power consumption, limited bandwidth and long latency. Photonic NoC is considered as a potential solution to overcome the limitations of its electrical counterpart. Many topologies for photonic NoCs have been widely studied, such as Mesh, Torus, Crossbar, Fat-Tree and Clos. The optical router is located at each node of photonic NoC and connects the local processing core with other processing cores.Several nonblocking optical routers have been proposed or even demonstrated, which are not scalable. High-radix non-blocking optical routers have potential applications in the future on-chip optical interconnects,

In this paper, we propose a universal method for constructing N-port non-blocking optical router for photonic networks-on-chip, in which all MR optical switches or M-Z optical switches behave as 2 × 2 optical switch. The optical router constructed by this method has the lowest power consumption and requires the least theoretical optical switches, in which the number of the optical switches is reduced about 50% compared to the reported optical routers based on MR optical switches and more than 30% compared to the reported optical routers based on M-Z optical switches, and therefore is more compact in footprint. We also present a strict mathematical proof of the non-blocking routing of the proposed N-port optical router and the insertion loss and power consumption comparisons of the proposed optical routers with the reported optical routers. Based on the comparisons, we can conclude that fully adopting 2 × 2 optical switches in the optical router can reduce its average power consumption and footprint without sacrificing its insertion loss.

Energy-efficient and Fast Thermal-response in Silicon Hybrid Nanoplasmonic Waveguides

Xiaowei Guan, Hao Wu, and Daoxin Dai
State Key Laboratory for Modern Optical Instrumentation
Centre for Optical and Electromagnetic Research
Zhejiang Provincial Key Laboratory for Sensing Technologies
Zijingang Campus, Zhejiang University, Hangzhou 310058, China

Abstract— Silicon hybrid nanoplasmonic waveguides, which consist of a high-index region (silicon), a metal region and a low-index nano-slot between them, enable a nano-scale light confinement as well as long propagation distance simultaneously. For silicon hybrid nanoplasmonic waveguides, the metal strip can play a role of electrical heater as well as nanoplasmonic waveguide. In this paper, the thermal response of silicon hybrid nanoplasmonic waveguides is investigated for the first time, including the response time and the energy efficiency. When using a silicon hybrid nanoplasmonic waveguide, the heating volume is extremely small because of the nano-scale cross section of the waveguide, which enables low power-consuming operation, as shown by the numerical simulation. Furthermore, since the low-index nano-slot of a silicon hybrid nanoplasmonic waveguide has a thickness in the nano-scale ($10 \sim 100\,\text{nm}$), the thermal conduction becomes very fast. Our numerical simulation also shows that the thickness of the buried-oxide (BOX) layer of the silicon-on-insulator (SOI) structure influences the thermal performance. The response time decreases exponentially as the BOX thickness decreases. One should note that the BOX thickness for a regular SOI nanowire should be thick enough ($2 \sim 3\,\mu\text{m}$) to avoiding the substrate. Fortunately, it is allowed to choose a thin BOX (e.g., $1\,\mu\text{m}$) for silicon hybrid nanoplasmonic waveguide. On basis of the numerical analysis, we obtain a 100 nm-wide optimal silicon hybrid nanoplasmonic waveguide with a $1\,\mu\text{m}$-thick BOX and the propagation loss is about $0.09\,\text{dB}/\mu\text{m}$. The theoretical response time is sub- ($\sim 500\,\text{ns}$) for a temperature increase of 100°C in the silicon core when the heating power is only 0.61 mW. It can be seen that a silicon hybrid nanoplasmonic waveguide is very promising for thermal nanophotonic integrated devices.

Novel Hybrid Plasmonic Devices on Silicon Platform

Lech Wosinski[1, 2], **Fei Lou**[1, 2], **and Lars Thylen**[1, 2]

[1]School of Information and Communication Technology
KTH Royal institute of Technology, Kista 16440, Sweden
[2]JORCEP (Joint Research Center of Photonics of the Royal Institute of Technology, Sweden and Zhejiang University), Zhejiang University, Hangzhou 310058, China

Abstract— Existing electrical interconnects in data centers, mainly between cabinets and at larger distances are being replaced by optical active cables giving much lower power dissipation (no ohmic losses), incomparably higher bandwidth, especially when using wavelength division multiplexing (WDM) of optical signals, as well as much higher speed of data transmission. The trend of replacing electrical connections by optical ones is evolving towards smaller distances including intra-cabinet (board to board connections), which is presently proposed using different technological solutions and in the near future will be realized for inter- and intra-chip communication, where ultra-small feature size of the optical components and very high level of integration are demanded.

Silicon nanophotonics has been identified as technology of choice for these applications as the photonic components can be, in principle, CMOS compatible and fabricated together with processor structures in microelectronic fabs as an integrated solution. Although it appeared to be not so straight-forward as one estimated in the beginning, many examples to solve compatibility problems have been presented. Nevertheless the limitation of classical optics, the diffraction limit of light, does not allow to make the feature size of Si nanophotonic components comparable to electronic ones. The minimal modal field of light in a silicon waveguide is about half of the light wavelength in the material, which means about 220 nm for $\lambda = 1550$ nm. For downscaling of photonic components, different solutions based on surface plasmon waveguiding along metal-dielectric interfaces have been proposed, that allows for deep sub-wavelength confinement, but at the expense of tremendous propagation losses.

Hybrid plasmonic waveguides are a novel type of plasmonic structures, where a hybrid mode can be propagated partially as photonic one in low refractive index dielectric and partially as plasmonic mode at the metal boundary. This results in a trade-off, which can be optimized differently for different applications, but in most cased allowing for relatively low losses and subwavelength confinement simultaneously.

In this paper we present a number of different solutions, both simulated and fabricated and evaluated for hybrid plasmonic components for future interconnects applications.

ACKNOWLEDGMENT

This work was supported by "the Swedish Research Council (VR) through its Linnæus Center of Excellence ADOPT", as well as project VR-621-2010-4379.

Session 1P10a
SC3: Advances in Optical Networking: Parts 1

Photonic Networks in Big Data Era

Ken-ichi Kitayama
Osaka University, Suita, Osaka 565-0871, Japan

Abstract— A vision of photonic network in 2020 is presented, which envisages "smart photonic cloud" in the Big Data era. The smart photonic cloud is referred to as an atmosphere which serves as a universal infrastructure, providing with connectivities to machine-to-machine communications such as networked high-performance computing and intra- and inter data center networks. To cope with strong demands for network virtualization without any physical and logical constraint, its photonic layer 2 virtualization will becomes feasible, which differentiates from the conventional one in terms of the number of slices and the dynamic range of the bandwidth of each slice. For the starter, the guiding principle and the objectives of the vision will be addressed. Next, three "Ss" key enabling technologies, including smart photonic networking, synthetic transport platform, and scale-free photonics will be presented. A key building block to the above three enabling technologies is the photonic network processor, which can synthesize desired functions of the switch node and the transmission link. The photonic network processor leverages on a recent progress of digital signal processing for coherent optical transmission systems an optical interconnect based upon silicon photonics, and it allows software-defining its functions.

Multi-domain Software Defined Optical Networks for Data Center Migration

Jie Zhang and Yongli Zhao
State Key Lab of Information Photonics and Optical Communications
Beijing University of Posts and Telecommunications, China

Abstract— Cloud infrastructure, generally consisting of geographically distributed large-scale data centers interconnected over WDM based optical networks, has become the key enabler and one of the most significant components for the Future Internet. The increasing cloud centered services requires the orchestrated provisioning of network resources with a consideration of bandwidth-on-demand allocation. Nevertheless, the present optical networks are statically configured and can only provide lightpaths with rigid bandwidths. The emergence of Software defined optical networks separates the control plane and turn it into a centralized and flexible solution. It enables data center operators to control and program network functions such as bandwidth provisioning with QoS guarantees. A practical problem should be discussed under the centralized control of software defined optical networks, that a vendor or a network operator may be unwilling to share its own topology information due to some policies or security reasons. Furthermore, a large-scale network operator may divide its network into several domains to limit the computing and management complexity. These result in the absence of a control entity knowing the global network topology. However, multi-domain softerware defined optical network frameworks merely aggregate information from each controller to form a global topology, without considering the multi-controller collaboration between controllers under information isolation.

Transformable Optical Circuit and Packet Switching for Data Center Network

Weisheng Hu and Weiqiang Sun
State Key Laboratory of Advanced Optical Communication Systems and Network
Department of Electronic Engineering, Shanghai Jiao Tong University, Shanghai, China

Abstract— Data center is considered as the "brain of the Internet" which provides accessible information for a variety of end users and devices connecting to the Internet at any time and place. Until now, the data centers consume much electrical power, which brings worry to the society, and peoples generally prefer to relocate the larger data centers in cooler place in the world as an alternatively good choice. It is well-accepted that the architecture of data center network is the key factor to decide the electrical power consumption lever and so attracts a lot of attention from both academia and industrial societies.

In today's electrically-switched data center network, researchers typically puts several tens of servers in one rack with an aggregated TOR (Top of Rack) switch in each, and connects the TOR switches with core switches. For a larger data center with rapidly growing traffic volume and increasing number of TORs, the scalability to support high bisection bandwidth is important and challenging, since the overall server utilization may suffer if insufficient bandwidth occurs. Researchers have been exploring different kinds of data center network topologies to provide high bisection bandwidth by using commodity Ethernet switches-examples include Fat trees, DCell, and BCube.

On the other hand, more recently, researchers have proposed to use optical circuit switches (OCS) to deliver reconfigurable bandwidth throughout the data center network, which is expected to reduce some of the expense and power consumption. Fortunately, the characteristics of many data center workloads suggest that many data center applications may not need full bisection bandwidth at the packet granularity, and show evidence of ON-OFF traffic behavior with most of their traffic going to a few other ToRs with paired connections of a subset of the paths. Therefore, the optical components and systems, such as Micro-electro-mechanical System (MEMS) matrix, Wavelength Selective Switch (WSS), Arrayed Waveguide Grating Router (AWGR) as typical examples, are proposed to be used in the data center network to reduce the complexity and power consumption overall together with the electrically-switched network in parallel.

In this paper, we will discuss several optical switching patterns which are potentially used in data center network, and, in particularly, we will report a transformable optical circuit and packet switching (TOCAPS) scheme for data center network. Much detail will be presented in the conference.

ACKNOWLEDGMENT

This work is supported by the 863 Program, the university research fund for the doctoral program of priority development areas (20110073130006), the NSFC (61221001), and 973 program of China (2010CB328204/5).

Optical Networks for Energy-efficient Data Centers

Lena Wosinska
KTH Royal Institute of Technology, Sweden

Abstract—

Survivable Techniques for Flex-grid Elastic Optical Networks

Gangxiang Shen
Soochow University, China

Abstract— Flex-grid elastic optical networks receive much research interest due to its better spectrum efficiency and more flexibility in bandwidth allocation for lightpaths compared to the traditional fixed-grid based Wavelength Division Multiplexing (WDM) networks. There has existed much research effort on spectrum assignment and resource optimization for the elastic optical network in the literature. However, it is just beginning to consider the survivability issue for the elastic optical network. Survivability is of paramount importance to the elastic optical network, especially in which each fiber carries even higher bandwidth than the traditional WDM networks when its spectrum efficiency is improved. In this paper, we will consider various network protection techniques, including ring cover, p-Cycles, span restoration (SR), 1+1 path protection, and shared backup path protection (SBPP). We will present the corresponding integer linear programing (ILP) models for each of the protection techniques, in which two unique constraints of the elastic optical network, i.e., spectrum continuity and contiguity, are incorporated. We will also compare these protection techniques from the perspectives of restoration speed, operational simplicity, and spare capacity efficiency. In addition, considering the importance of spectrum conversion for enhancing the spectrum utilization of the elastic optical network, we evaluate how different spectrum conversion capabilities show their impacts on the survivable elastic optical network design.

Software Defined Networking (SDN) Enabled Optical as a Service (OaaS) with Dynamic Network Provisioning

Yongli Zhao and Jie Zhang
State Key Laboratory of Information Photonics and Optical Communications
Beijing University of Posts and Telecommunications, Beijing 100876, China

Abstract— Optical network has been deployed widely as one of the most important physical infrastructure because of the advantages of high capacity, long transmission distance, and low energy consumption. Then how to exploit the potentiality of optical networks gets more and more attention, especially in the current data center networks. Optical as a service (OaaS) is proposed and designed to provide the optical network resources directly for the data centers with considering both data center resources and network resources, which can be implemented with software defined networking (SDN). Under SDN enabled OaaS architecture, a new concept of network provisioning is proposed different from legacy connection (lightpath) provisioning, because the client's requests may include not only one end-to-end connection, but also several end-to-end connections, even a network with edge application resources.

Virtualization technology is a key issue for the network provisioning in data center networks. A virtualization control architecture is designed in SDN enabled OaaS to efficiently complete the network provisioning, and different resource mapping algorithms considering survivability is proposed and simulated in this architecture. As a generalized optimization strategy in SDN enabled OaaS, the cross stratum optimization (CSO) strategy is involved considering both data center resource and network resource. Finally, SDN enabled OaaS testbed implemented with Open Day Light will be described with some experimental results.

Software-defined Elastic Optical Networking in Temporal, Spectral and Spatial Domains

S. J. Ben Yoo
Department of Electrical and Computer Engineering, University of California, Davis, USA

Abstract— We discuss elastic optical networking (EON) in temporal, spectral, and spatial domains, and a new control and management framework in future software-defined-networking (SDN). In EON, flexible amounts of spectral bandwidth may be allocated to each data channel without requiring adherence to a fixed wavelength grid. Such an approach is well-suited for supporting a wide range of dynamic traffic demands in a bandwidth-efficient manner. Adding a new dimension in space division multiplexing (SDM) with elasticity using orbital angular momentum (OAM) together with dynamic optical waveform generation and measurement (OAWG and OAWM), will enable 3D EON in the temporal, frequency and space domain by dividing the spectrum on each spatial state (OAM state) into slices and dynamically processing information at lower rates compatible with CMOS electronics. We leverage these technologies together with 2D and 3D photonic integrated circuits to demonstrate, for the first time, an elastic optical networking in temporal, spectral, and spatial domains. A new 3D EON-SDN testbed has been setup at UC Davis to investigate and test (1) optical transmission systems based on integrated OAM technology, (2) approaches for statically and dynamically allocating network and spatial/spectral resources to meet user demands in a cost-effective and spectrally-efficient manner, (3) traffic grooming and defragmentation techniques for improving the utilization of spatial and spectral resources in EONs, (4) a new supervisory channel signaling method to make possible optical performance monitoring necessary for cross-layer QoS-aware and impairment-responsive networking, and (5) a network control and management system that will enable the dynamic provisioning of routes and spectral resources for EONs. We will discuss the newly developed concepts and technologies towards realizing spectrally-efficient, QoS-aware, adaptive, and resilient 3D EON-SDN.

Session 1P10b
SC3: Onchip Multiplexing Technologies and Devices for Optical Interconnects

Si-photonic Based Optical OFDM Demultiplexer for Tb/s Transmission Links

L. Zimmermann[1], **A. Rahim**[2], **S. Schwarz**[3], **J. Bruns**[4], **K. Voigt**[4], **G. Winzer**[1], **C. G. Schäffer**[3], **and K. Petermann**[4]

[1]IHP, Im Technologiepark 25, 15236 Frankfurt (Oder), Germany
[2]Université Laval, Centre d'optique, Photonique et Laser, Québec, G1V 0A6, Canada
[3]Helmut-Schmidt-Universität, Institut für Hochfrequenztechnik
Holstenhofweg 85, 22043 Hamburg, Germany
[4]TU-Berlin, Institut für Hochfrequenz-und Halbleiter-Systemtechnologien
Einsteinufer 25, 10587 Berlin, Germany

Abstract— Optical orthogonal frequency-division multiplexing (OFDM) format employs multiple orthogonal sub-carriers and has attracted great attention over the last few years mainly due to its high spectral efficiency and large tolerance to optical fiber impairments. This makes the optical OFDM approach an excellent candidate for data rates up to Tb/s. However, it has been recognized that the realized OFDM systems are limited by the speed of the electrical components and their power consumption. Therefore, it would be very convenient to process the OFDM signal purely in the optical domain. Regarding this requirement we focus here on an optical device for demultiplexing of OFDM signals. The device should provide serial-to-parallel conversion as well as discrete Fourier transform (DFT). On the transmitter side we would have to implement the inverse functionalities

We use the Si-Photonics platform for the realization of an 8 channel optical OFDM demultiplexer. The device is realized by using 180° (2-port MMIs) and 90° (4-port MMIs) optical hybrids (offering accurate phase relations, low imbalance and large fabrication tolerances), plus delay lines and phase shifters. We started from 4 µm silicon-on-insulator (SOI) technology for first devices and afterwards migrated to SOI nanotechnology. The change from 4 µm to nanotechnology can be considered as an evolution towards considerably more compact devices (factor of reduction in size ~ 60) and scalable architectures due to the high material index contrast. Realized MMI couplers in both technologies show comparable performances. The waveguide loss in SOI nanotechnology is slightly higher compared to 4 µm SOI technology ($\sim$ 0.8 dB/cm instead of 0.1 dB/cm) but tolerable due to the use of significantly shorter waveguides. In case of nanotechnology we use grating couplers for fiber chip coupling. We could demonstrate coupling losses of 1.5 dB/coupler by use of enhanced gratings. The electrical control of the optical OFDM demultiplexer in Si nanotechnology requires a factor of ten less power compared to the 4 µm platform.

The fabrication of the Si-based OFDM demultiplexer was done in a SiGe:CBiCMOS pilot line at IHP which is one of the leading manufacturers of high-performance BiCMOS. Beside the compatibility and manufacturability of Si based PLCs, the use of BiCMOS tool set offers potential for further opto-electronic integration which is an important requirement for future realizations of high-speed photonic applications. By means of OFDM this could be, for instance, opto-electric signal conversion by photo detectors and further electrical signal processing. The measured responses for each channel of the fabricated OFDM demultiplexers in 4 µm SOI technology and SOI nanotechnology indicate good agreement with the ideal transmission responses. The crosstalk is better than 16 dB and 22 dB, respectively. An emulation test shows that the measured filter responsesare able to demultiplex all 8 separately QPSK modulated sub-carriers. The Q-value for QPSK demodulation in 4 µm SOI technology (37.5 GBaud) has an average of 12.7 dB. The Q-value in Si nanotechnology has a minimum Q-value 14.5 dB (13.5 GBaud).

III-V Quantum-dot Lasers Monolithically Grown on Si Substrates for Silicon Photonics

Siming Chen and Huiyun Liu
Department of Electronic and Electrical Engineering, University College London, London WC1E 7JE, UK

Abstract— The merger of photonics and electronics into a dual-function platform, the optoelectronic integrated circuit (OEIC) fabricated with existing Si infrastructure can overcome interconnection issue for Si chips while pushing forward the silicon microelectronics beyond the classical complementary metal-oxide-semiconductor (CMOS) era. Although great efforts have been devoted for Si-based light generation and modulation technologies in the last 30 years, monolithic growth of electrically pumped laser on Si remains a 'holy grail' for Si photonics. Due to the nature of indirect bandgap of group IV materials, only optically pumped lasers have been demonstrated for the devices using Si and Ge as optical gain materials. Monolithic integration of semiconductor III-V compound lasers on Si platform has long attracted a great deal of attention with the ultimate goal — high-speed and low-powerconsumption optoelectronic circuits — to achieve for Si photonics. III-V quantum dots (QDs) — semiconductor nanosized crystals — are one of the most promising candidates for producing such devices with the advantages of lower threshold current density and less sensitivity to defects over conventional semiconductor quantum-well devices. Here, we report the development of Si-based 1300-nm InAs/GaAs QD laser diodes monolithically grown on Si, Ge, and Ge/Si substrates for silicon photonics. A very low RT pulsed Jth of 63.4 A/cm^2, a cw RT Jth of 163 A/cm^2, RT output power of $\sim$ 93 mW, and lasing up to 84°C have been demonstrated III-V quantum-dot laser grown on silicon substrates, as shown in Figure 1 [1–3]. This study could ultimately form the basis for the monolithic integration of 1300-nm InAs/GaAs QD lasers on Si platform to realize the long-dreamed of III-V/Si optoelectronic integrated circuit.

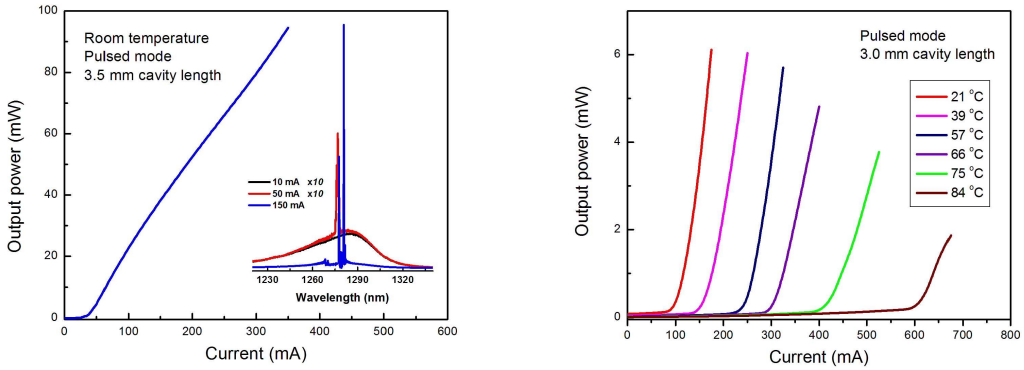

Figure 1: (a) Light output power versus current for 5-layer InAs/GaAs QD laser diodes grown on a Si substrate. The inset shows the emission spectra of InAs/GaAs quantum dot laser for different drive currents below and above threshold. (b) Light output against current for Si-based InAs/GaAs QD laser diode at various substrate temperatures.

REFERENCES

1. Lee, A., Q. Jiang, M. Tang, Y. Zhang, A. J. Seeds, and H. Liu, *IEEE J. Sel. Topic Quantum Electron.*, Vol. 19, 1901107, 2013.
2. Lee, A., Q. Jiang, M. Tang, A. Seeds, and H. Liu, *Optics Express*, Vol. 20, 22181–22187, 2012.
3. Liu, H., T. Wang, Q. Jiang, R. Hogg, F. Tutu, F. Pozzi, and A. Seeds, *Nature Photonics*, Vol. 5, 416, 2011.
4. Wang, T., H. Liu, A. Lee, F. Pozzi, and A. Seeds, *Optics Express*, Vol. 19, 11381, 2011.
5. Tang, M., S. Chen, J. Wu, Q. Jiang, V. G. Dorogan, M. Benamara, Y. I. Mazur, G. J. Salamo, A. Seeds, and H. Liu, *Optics Express*, Vol. 22, 11528, 2014.

Recent Progress in On-chip Multiplexing/Demultiplexing Silicon Photonic Devices and Technologies

Jian Wang
Wuhan National Laboratory for Optoelectronics, School of Optical and Electronic Information
Huazhong University of Science and Technology, Wuhan, Hubei 430074, China

Abstract— In this paper, we review our recent works in on-chip multiplexing/demultiplexing silicon photonic devices and technologies. On-chip demultiplexing of polarization and wavelength multiplexed OFDM/OQAM 64/128-QAM signals using silicon 2D grating coupler and microring resonators and on-chip two/three mode (de)multiplexing of OFDM 64/128/256-QAM signals using tapered silicon asymmetrical directional couplers are demonstrated in the experiments.

Reconfigurable Two-mode Mux/Demux Device for Optical Interconnects

Hau Ping Chan and Wai Ying Chan
Department of Electronic Engineering, City University of Hong Kong
23 Tat Chi Avenue, Hong Kong, China

Abstract— Optical interconnects is a promising solution to relief the pressing demands on the data-link bandwidth requirement between system-to-system, board-to-board and even chip-to-chip. Multiplexing, along with a modulation technique, has been employed to further expand the capacity of optical link. Wavelength division multiplexing, space division multiplexing are some of the possible approaches. Recently, the mode division multiplexing technique has attracted attention as an alternative for expanding transmission capacity. This technique uses modes in multimode fiber or waveguide to carry sets of modulated signals. Therefore, the capacity of this technique becomes multiples of that in a single-mode waveguide. Mode multiplexer/demultiplexer (mux/demux) is the key device for handling such mode multiplexing and demultiplexing processes. In this talk, we will review our recently proposed two-mode mode mux/demux device that can multiplex and demultiplex signals carried by the fundamental and the first-order modes in a waveguide. The device is implemented in planar lightwave circuit platform, and is originally designed for long haul optical communication systems. However, we find our design has no fundamental limits to its application to optical interconnects for expanding link capacity. The device is based on an interleaver structure which consists of an unbalanced Mach-Zehnder interferometer cascaded with a two-mode interferometer. One advantage of our design is that the device has reciprocal characteristic between its input and output ports, thus adds flexibility in different applications. In addition, the device can also be operated as a reconfigurable mux/demux routing device by adding a suitable electrode. We have demonstrated its functionality by realizing the device in polymer platform. The two routes carried by the fundamental mode and the first-order mode of the device can be dynamically swapped through the thermo-optic effect of the polymer. Moreover, our design can be applied to other materials platforms. The device is easy to implement and should have potential applications in optical interconnects.

Low-crosstalk 8-channel Silicon Mode Demultiplexer with Grating Polarizers

Jian Wang, **Pengxin Chen**, **Sitao Chen**, **Yaocheng Shi**, **and Daoxin Dai**
State Key Laboratory for Modern Optical Instrumentation
Centre for Optical and Electromagnetic Research
Zhejiang Provincial Key Laboratory for Sensing Technologies
Zhejiang University, Zijingang Campus, Hangzhou

Abstract— An 8-channel silicon hybrid demultiplexer is proposed and demonstrated with significantly reduced crosstalk by introducing TE-type and TM-type grating polarizers. This 8-channel hybrid multiplexer enables polarization and mode-division multiplexing simultaneously by combining a polarization beam splitter (PBS) and six cascaded asymmetrical directional couplers so that one can (de)multiplex eight channels for the fundamental TE/TM mode (i.e., TE_0, and TM_0) and six higher order modes (i.e., the TE_1, TE_2, TE_3, TM_1, TM_2, and TM_3 modes). In this paper, we give a comprehensive analysis for the crosstalk of our previous 8-channel silicon mode demultiplexer with a three-dimensional finite-difference time-domain (3D-FDTD) method, and it is shown that the polarization crosstalk for some mode-channels is the dominant source for the mode-channel crosstalk. Fortunately the polarization crosstalk can be reduced greatly with polarization selective devices including PBSs or polarizers as proposed in this paper. As an example, TE-type and TM-type shallowly-etched grating polarizers are introduced at the output ends, which also serve as fiber-chip couplers simultaneously. The designed TE and TM-type polarizers have a period of 0.63 μm and 1.0 μm, respectively, with a 0.5 duty cycle and 70 nm etched depth. In order to characterize the mode demultiplexer, a photonic integrated circuit including a mode multiplexer, 100 μm-long multimode waveguide, and a mode demultiplexer are fabricated on the silicon-on-insulator platform with a standard fabrication process. The experimental results show that the polarization crosstalk of the fabricated 8-channel mode multiplexer is reduced greatly and the crosstalk for all the eight channels are about ~ -20 dB with a $\sim$80 nm wavelength bandwidth.

Higher-order Ring Resonators and Delayed Interferometers Based on 300-mm SOI Technology for WDM Applications

Seok-Hwan Jeong, Yu Tanaka, and Ken Morito
Photonics Electronics Technology Research Association (PETRA)
AIST West-7SCR, 16-1 Onogawa, Tsukuba, Ibaraki 305-8569, Japan

Abstract— Recently, total bandwidth per central processing unit in high-performance servers reaches to a few Tbit/s, which requires advanced optical interconnect technologies based on Si photonics that would be able to surpass the limits of transmission bandwidth and power consumption by electric wirings. Wavelength division multiplexing (WDM) would be one of promising technologies to enhance the aggregate bandwidth and to reduce the assembly cost for connecting to optical fibers. WDM optical interconnect normally requires Si-nanowire optical multiplexers/demultiplexers, from the viewpoint of monolithic integration with compact and energy-efficient Si-nanowire optical modulators and photo-detectors. In almost cases, WDM devices work with the help of the lightwave interference based on the splitting and remixing at multiple optical paths. Thus, their operational performances strongly depend on the controllability of the relative phase relation between all of the optical paths. The phase controllability is mainly determined by the sidewall roughness of Sinanowire waveguides. 300-mm silicon-on-insulator (SOI) wafer-scale ArF-immersion lithography technologies could be attractive for markedly reducing the phase errors in Si-nanowire waveguides. In this talk, we will introduce highperformance Si-nanowire waveguide based WDM devices such as higher-order microring resonators and multi-stage delayed interferometer demultiplexers fabricated by phase controllable and highly productive 300-mm SOI wafer-scale ArF-immersion CMOS process. For the two kinds of WDM devices, we will theoretically analyze and experimentally demonstrate low insertion loss, spectral flatness and low crosstalk properties, together with high manufacturing tolerances. High-performance WDM devices having much complicated configurations could be realized by using these high-precision fabrication technologies with finer phase controllability.

Photonic Crystal Cavities for Optical Interconnects

Liam O'Faolain
School of Physics and Astronomy, University of St Andrews
Scottish Universities Physics Alliance (SUPA), North Haugh, St Andrews, KY16 8QP, UK

Abstract— Photonic Crystal (PhC) resonators are the ultimate means of confining light in space and time (i.e., they give the highest Q to mode volume ratio). Such high spatial confinement enables devices with footprints of less than $100\,\mu m^2$ and mode areas of approximately $1\,\mu m^2$, translating into optical modulators with some of the lowest capacitances reported [1]. High Q-factors enhance the light matter interaction and allow modulation with high extinction ratios to be achieved. They also require low driving voltages and provide new routes to silicon photo-detection [2]. Furthermore, the high optical finesse of PhC resonators provides very large free spectral range maximizing the channels available for Wavelength Division Multiplexing. This makes PhC cavities extremely attractive for the realization of the high integration density, highly scalable and low power consumption optical links required to provide high bandwidth interconnects for the next generation of computers. However, in order to maximize compatibility with electronics a number of key issues must be addressed.

It is well known that extremely precise fabrication processes are required for the realization of high performance PhCs. Not only must the etched sidewalls be vertical and smooth (similar to Photonic Wire based devices), positioning accuracies at the nanometre level are also required. To date, this combination has prevented the realization of high Q-factor devices using Deep Ultraviolet Lithography, a key prerequisite for the mass manufacture of silicon based optical devices [3]. In this work, we use a recently developed PhC resonator design that shows increased tolerance to fabrication imperfections and improved compatibility with DUV patterning to realize the highest silicon-based optical Q-factor yet realized using optical lithography.

Additionally, date most work in silicon photonics is based on the silicon on insulator platform, which provides a low material losses and high refractive index contrasts However SOI limits the integration of electronic and photonics components, as the thick lower cladding required for optical isolation from the substrate compromises transistor performance. Deposit silicon provides a range of options in this regard [4], I will present our recent work on photonic crystals in this system.

REFERENCES

1. Debnath, K., L. O'Faolain, F. Y. Gardes, A. G. Steffan, G. T. Reed, and T. F. Krauss, *Optics Express*, Vol. 20, 27420–27428, 2012.
2. Debnath, K., F. Y. Gardes, A. P. Knights, G. T. Reed, T. F. Krauss, and L. O'Faolain, *Applied Physics Letters*, Vol. 102, 171106, 2013.
3. Bogaerts, W., R. Baets, P. Dumon, V. Wiaux, S. Beckx, D. Taillaert, B. Luyssaert, J. Van Campenhout, P. Bienstman, and D. Van Thourhout, *Journal of Lightwave Technology*, Vol. 23, 401, 2005.
4. Biberman, A., K. Preston, G. Hendry, N. Sherwood-Droz, J. Chan, J. S. Levy, M. Lipson, and K. Bergman, "Photonic network-on-chip architectures using multilayer deposited silicon materials for high-performance chip multiprocessors," *Journal of Emerging Technology in Computing Systems*, Vol. 7, 7:1–7:25, 2011.

Silicon Reflective-type Arrayed-waveguide Grating (De)multiplexers with Micro Reflectors

Sitao Chen and Daoxin Dai
Centre for Optical and Electromagnetic Research
State Key Laboratory for Modern Optical Instrumentation
East Building No. 5, Zijingang Campus, Zhejiang University, Hangzhou 310058, China

Abstract— An arrayed waveguide grating (AWG) (de)multiplexer is one of the key components in wavelength-division-multiplexed (WDM) optical communication networks. Particularly, for on-chip optical interconnect systems, compactness is undoubtedly the desire for the elements so that large-scale photonic integration can be realized. For AWG (de)multiplexers, various material platforms have been developed, including silica-on-silicon, III-V platform, silicon-on-insulator (SOI), etc.. Among them, SOI nanowires have been attractive in the past years to make ultra-small photonic integrated devices by utilizing the ultra-high index-contrast. The AWG size can be reduced again by half at least without sacrificing the fabrication complexity when employing the reflective-type layout. In this paper, we design and demonstrate ultra-compact SOI-nanowire AWG (de)multiplexers by introducing micro-reflectors at the end of each arrayed waveguide. Here two types of micro-reflectors are considered. One is Bragg-grating reflectors and the other is loop-mirrors. The Bragg-grating reflector with an ultrasmall footprint enables high efficiency for TE polarization, which is very useful for the case when only TE polarization is involved. The reflectivity of a Bragg-grating reflector is around 90% over 300 nm wavelength band. However a Bragg-grating reflector does not work well for TM polarization. Alternatively, a loop-mirror is a potential candidate for TM polarization as well as TE polarization. In this paper, the loop-mirror is designed with a Y-branch and a micro-bend, which enable a reflectivity of 90% over a 150 nm wavelength band. These two types of micro-reflectors have been realized for the reflective AWG (de)multiplexers. Our demonstrated ultrasmall reflective-type AWGs have 8 channels and the channel-spacing is 400 GHz.

Session 1P11
SC4: Recent Progress on Magnetic and Multiferroic Materials

Tunable Bandpass Filters with Magnetodielectric and Multiferroic Materials

Guo-Min Yang[1] and Nian-Xiang Sun[2]

[1]Key Laboratory of Information Science of Electromagnetic Waves
Department of Communication Science and Engineering
Fudan University, Shanghai 200433, China
[2]Department of Electrical and Computer Engineering
Northeastern University, Boston, MA 02115, USA

Abstract— With the continuous growth of wireless communication technologies, design and manufacturing of low cost and tunable microwave components are among most critical issues in communication systems. As one of the basic components in the RF front-end, the need for compact and low insertion loss tunable bandpass filters (BPF) has been continuously growing in modern communication systems and radar systems. Basically, there are four major technologies for achieving tunability in bandpass filters, including electronically tunable bandpass filters, magnetically tunable bandpass filters, mechanically tunable bandpass filters, and dual H- and E-field tunable bandpass filters.

In this work, new designs of electronically tunable bandpass filters with magnetodielectric materials are investigated. A new self-biased ferrite film of NiCo-ferrite is investigated and adopted for the Ferrite/Dielectric/Ferrite (F/D/F) sandwich structures, which is successfully applied in the miniaturized and tunable bandpass filter designs. Novel bandpass filter designs with F/D/F sandwich structure with one layer to five layers are compared and a maximum frequency shift of 240 MHz with respect to the unperturbed condition has been achieved [1].

A magnetically tunable bandpass filter (BPF) with a yttrium iron garnet (YIG) film deposited on the gadolinium gallium garnet (GGG) substrate have been designed, fabricated, and characterized. Single-crystal YIG films at their ferromagnetic resonance are adopted as the resonator, which is coupled to a T-shaped microstrip coupling structure to form a bandpass filter design. The operating frequency of the BPF can be tuned via a bias magnetic field, and a large tunability of the operation frequency of 190–840 MHz with relatively small bias fields of 50–250 Oe, together with a low insertion loss of 2 dB. This is equivalent to 12%–54% of the central frequency of the bandpass filter [2]. A clear E-field induced operation frequency shift of 200 MHz, or $\sim 10\%$ was demonstrated on the multiferroics based bandpass filter having a YIG/PZN-PT heterostructure [3]. These demonstrated new magnetodielectric and multiferroic tunable bandpass filters with dual H- and/or E-field tunability are very compact and energy efficient, which could have many applications in RF front and other microwave circuits.

ACKNOWLEDGMENT

This work is sponsored by NFSC under Grant 61201063, DPHE of China under Grant 20120071120020.

REFERENCES

1. Yang, G. M., O. Obi, G. Y. Wen, and N. Sun, "Design of tunable bandpass filters with ferrite sandwich materials by using a piezoelectric transducer," *IEEE Trans. Magn.*, Vol. 47, No. 10, 3732–3735, Oct. 2011.
2. Yang, G. M., J. Wu, J. Lou, M. Liu, and N. X. Sun, "Low loss magnetically tunable bandpass filters with YIG films," *IEEE Trans. Magn.*, Vol. 49, No. 9, 5063–5068, Sep. 2013.
3. Yang, G. M., J. Lou, J. Wu, G. Y. Wen, Y. Q. Jin, and N. Sun, "Dual H- and E-field tunable multiferroic bandpass filters with yttrium iron garnet film," *The IEEE Microwave Theory & Techniques Society International Microwave Symposium 2011*, Baltimore, MD, USA, Jun. 5–10, 2011.

Magnetoelectric and Magnetic Thin Film Microwave/RF Components

X. Yang[1], **Y. E. Wang**[1], **and N. Sun**[2]

[1]University of California, Los Angeles, Los Angeles, CA 90095, USA
[2]Northeastern University, Boston, MA 02115, USA

Abstract— Multiferroic composite materials consisting both magnetic and ferroelectric phase are of great interests, as its magnetoelectric (ME) coupling property may lead to novel RF devices. Compared to conventional tunable microwave magnetic devices that are tuned by magnetic field, these dual H- and E-field tunable microwave multiferroic devices are much more energy efficient, compact, and light-weight.

To reduce the device's profile factor and the tuning power expense, a voltage tunable phase shifter without external magnetic biases is demonstrated. The phase shifter consists of an yttrium iron garnet (YIG)/lead magnesium niobate-lead titanate (PMN-PT) magnetoelectric (ME) heterostructure. To maximize the mechanical deformation being transferred from the piezoelectric phase to the magnetic phase, a stacked double layer PMN-PT transducer operating in bending mode is proposed. Accordingly, the devices show great improvement on the phase shift output by over 20% compared to the output from a single layer PMN-PT transducer. A maximum of 120 degree is obtained under an electric field of 11 kV/cm.

Integration of magnetic metals and oxides into RFIC show great potential in modern microwave circuits. We present the simulation of a three port Y-junction circulator with bandpass behavior using high quality sputtered YIG thin film. The total thickness of the devices is less than 10 microns and the area is less than 2.5 mm square. HFSS simulations show the insertion loss (S_{21}) is 2.3 dB with a high Q-factor of 130, and the off-band rejection are all below 20 dB. In addition, the isolation (S_{12}) at resonant frequency is 25 dB. The operating central frequency can be tuned by varying the external magnetic bias which is perpendicular to the device surface.

Magnetic Field Tuned Semiconducting Properties in Ferromagnetic/Semiconducting Composites

Junyi Zhai, Mingzeng Peng, Ming Song, and Liu Yudong
Beijing Institute of Nanoenergy and Nanosystems, Chinese Academy of Sciences, China

Abstract— With the requirements of minimization of volume and multifunctional of devices, materials with magnetic, optical, electric and mechanical properties and/or coupling between two or more of these properties will useful in designation of state of the art devices. However, only a few single phase materials have these multifunctional properties in nature. An alternative method is to fabricate multilayer composites, by using the strain transition between each layer to realize the properties coupling between each layer. This method made big progress in magnetoelectric cooping in ferroelectric/ferromagnetic composites. Recently, more and more studies showed that the semiconductor properties can be tuned by applied force or strain in piezoelectric semiconductors. Here, we fabricated magnetostrictive/semiconductor composites. By using the strain transition between magnetostrictive materials and piezoelectric semiconductors, the composites will have magnetic, semiconductor properties, magnetic and mechanical tuned semiconductor properties, includes but not limited in investigations of I-V properties in schottky diode and optical properties in p-n junction changed by applied force and magnetic field. These works will help understand multi-field coupling in new composites and design of new multifunctional devices.

Self-assembly and Field-directed Assembly of Ferrite-ferroelectric Core-shell Nanocomposites: Studies on Magneto-electric Interactions

G. Sreenivasulu[1], **Ferman Chavez**[2], **and G. Srinivasan**[1]

[1]Physics Department, Oakland University, Rochester, Michigan 48309, USA
[2]Chemistry Department, Oakland University, Rochester, Michigan 48309, USA

Abstract— Multiferroic composites with ferroelectric and ferromagnetic phases have attracted considerable attention in recent years for studies on the nature of mechanical strain mediated magneto-electric (ME) interactions. Core-shell particulate and fibers are of particular interest since one expects strong ME coupling due to large surface-to-volume ratio. Here we discuss self-assembly and magnetic field directed assembly of core-shell ferrite-ferroelectric nanoparticles and coaxial nano-wires and evidence for strong ME interactions.

For self-assembly of core-shell nanoparticles, nickel ferrite (NFO) (10–100 nm) and barium titanate (BTO) (50–100 nm) particles were coated with complementary coupling groups and allowed to assemble with the aid of a catalyst. In one strategy we attached carboxylate groups bearing an alkyne functionality to BTO and alkyl azide groups to NFO nanoparticles. Using the "click" reaction, the two groups were linked together (Fig. 1). Magneto-electric characterization of these composites by magnetic field induced polarization and magneto-dielectric effect indicate strong ME coupling [1].

We synthesized ferrite-ferroelectric core-shell nano-fibers by electrospinning and allowed them to assemble in a magnetic and/or electric field. Systems studied include nickel ferrite and BTO or PZT. Fibers with 1–2 micron in diameter and 0.2–0.4 micron ferrite of ferroelectric core with lengths ranging from 10–100 micron were prepared. Electron microscopy studies show the anticipated core-shell structure for the nanowires (Fig. 2). The fibers were assembled into rings, parallel wires and mats in a static magnetic field gradient and ac or dc electric fields. The effects of the field strength and frequency on the structure of the resulting assembly were investigated. Studies over 16–42 GHz show evidence for strong ME coupling in the composites [2].

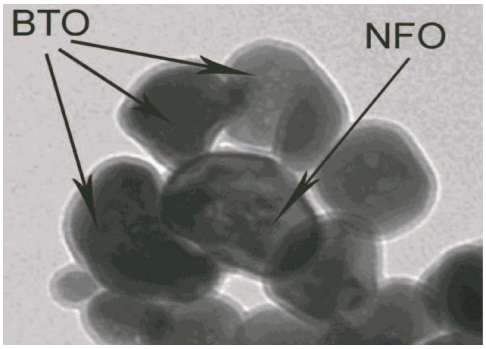

Figure 1: TEM micrograph showing chemically self-assembled nanoparticles of nickel ferrite (NFO) core-barium titanate shell [1].

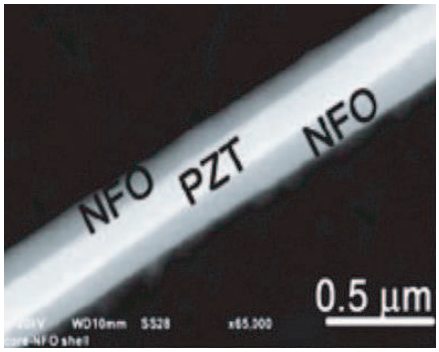

Figure 2: SEM image showing a PZT core-NFO shell coaxial nanowire [2].

REFERENCES

1. Sreenivasulu, G., M. Popov, F. A. Chavez, et al., *Appl. Phys. Lett.*, Vol. 104, 052901, 2014.
2. Popov, M., G. Sreenivasulu, R. Zhang, et al., Vol. 104, 052910, 2014.

Multiferroics and Magnetoelectric Coupling Effects in Metal-organic Frameworks

Y. Sun, **Y. Tian**, **J.-Z. Cong**, **S.-P. Shen**, **Y.-S. Chai**, **and L.-Q. Yan**
Beijing National Laboratory for Condensed Matter Physics
Institute of Physics, Chinese Academy of Sciences, Beijing 100190, China

Abstract— Multiferroics and magnetoelectric (ME) effects have attracted considerable interest in recent years. While most work are currently focusing on inorganic oxides, organic materials could open up new routes to multiferroics and ME effects. The hybrid metal-organic frameworks (MOFs) that combine magnetism of metal ions with hydrogen-bond ferroelectricity represent a new type of multiferroic materials. Since 2009, there have been several reports on the multiferroic behaviors in MOFs [1, 2]. However, the cross coupling between magnetic and electric orders (the ME effects) has been rarely observed in MOFs.

In this talk, we report on both the direct and converse ME effects in a series of multiferroic MOFs with a perovskite-like structure. Single-crystal samples of MOFs were prepared by solvothermal condition method. These MOF samples show a magnetic ordering at 5–20 K [3], depending on the magnetic ions (Cu^{2+}, Mn^{2+}, or Fe^{2+}). Meanwhile, they also exhibit a ferroelectric/antiferroelectric transition between 165–260 K due to the ordering of hydrogen bonds. We find strong evidences for the ME effects in these MOFs. In the Mn-based MOF, the high-temperature ferroelectric state can be modified by applying a high magnetic field. Such a ME coupling in the paramagnetic state is probably related to the magnetoelastic effect that modifies the hydrogen bonding and the local magnetic interaction [4]. In the Fe-based MOF, the low-temperature magnetic state can be controlled by applying a moderate electric field of a few kV/cm. This converse ME effect is likely related to electric field modification of hydrogen-bond orientation [5]. Our study suggests that the perovskite MOFs are promising organic multiferroic materials with strong ME effects.

REFERENCES

1. Jain, P., et al., *J. Am. Chem. Soc.*, Vol. 131, 13625, 2009.
2. Xu, G. C., et al., *J. Am. Chem. Soc.*, Vol. 133, 14948, 2011.
3. Tian, Y., et al., *Phys. Rev. Lett.*, Vol. 112, 017202, 2014.
4. Wang, W., et al., *Sci. Rep.*, Vol. 3, 2024, 2013.
5. Tian, Y., et al., *Phys. Status Solidi RRL*, Vol. 8, 91, 2014.

Composition-graded Magnetic Thin Films with Tunable Microwave Performance Controlled by Electrical Field

Nguyen N. Phuoc[1] and C. K. Ong[2]

[1]Temasek Laboratories, National University of Singapore
5A Engineering Drive 2, Singapore 117411, Singapore
[2]Center for Superconducting and Magnetic Materials, Department of Physics
National University of Singapore, 2 Science Drive 3, Singapore 117542, Singapore

Abstract— Soft magnetic thin films used for high-frequency applications have recently received much attention as they offer a much better microwave performance compared to the bulk counterparts. For the applications operating at high frequency in GHz range, a magnetic thin film needs to have a high in-plane magnetic anisotropy as well as high saturation magnetization. Recently, composition-graded magnetic thin films have been found to possess attractive advantages for microwave applications such as high resonance frequency and good thermal stability [1–3]. We also found that such composition-graded magnetic thin films have a peculiar behavior of the magnetic anisotropy increased with temperature, which may be useful for other applications [2, 3]. In this work, we will investigate multiferroic heterostructures based on piezoelectric crystal (such as PMN-PT or PZN-PT) and composition-graded magnetic thin films (such as FeCoTa, FeCoHf or FeCoZr). We found that the resonance frequency can be tuned by the applied electric field from 7 GHz up to 9 GHz through the change of the magneto-elastic anisotropy. The experimental results will be discussed in conjunction with the theoretical analysis with a model put forward. Our results also suggest a novel way to enhance the microwave performance of magnetic thin films through an electric field treatment.

REFERENCES

1. Li, S., Z. Huang, J-G. Duh, and M. Yamaguchi, *Appl. Phys. Lett.*, Vol. 92, 092501, 2008.
2. Phuoc, N. N. and C. K. Ong, *Adv. Mater.*, Vol. 25, 980, 2013.
3. Phuoc, N. N. and C. K. Ong, *Appl. Phys. Lett.*, Vol. 102, 212406, 2013.

Thin Film Magnetoelectric Composites as Biomagnetic Sensors

Andre Piorra, Christine Kirchhof, Erdem Yarar, Volker Röbisch, Dirk Meyners, and Eckhard Quandt
Inorganic Functional Materials, Institute for Materials Science
Faculty of Engineering, University of Kiel, Kaiserstr. 2, Kiel 24143, Germany

Abstract— Composites constisting of piezoelectric and magnetostrictive constituents exhibit magnetoelectric coefficients that are larger than that of natural magnetoelectrics by several orders of magnitude. These composites have high potential for applications as extremely sensitive ac magnetic field sensors. Special features of these magnetic field sensors are their passive nature, their good limit of detection beyond $\mathrm{pT/Hz^{1/2}}$, and their large dynamic range with linear response.

The thin film magnetoelectric 2-2 composites of this work consist of AlN or different ferroelectrics as the piezoelectric component and different magnetostrictive layers, either amorphous FeCoSiB single or multilayer films. These thin film composites show an extremely high magnetoelectric coefficient of up to 20 kV/cmOe at mechanical resonance in vacuum [1]. However, almost all magnetoelectric composites require the presence of an external d.c. magnetic bias field, which limits their use as compact, highly sensitive magnetic-field sensors. An induced exchange bias using multilayers with the sequence $\mathrm{Ta/Cu/Mn_{70}Ir_{30}/FeCoSiB}$ overcomes this limitation and provides maximum magnetoelectric effect size at zero magnetic bias field [2].

In this presentation different magnetoelectric thin film composites will be discussed in view of the used piezoelectric material, of the employed different electrode concepts [3] and of the used magnetostrictive component in view of their use as very sensitive magnetic field sensors for biomagnetic applications.

ACKNOWLEDGMENT

Funding via the DFG Collaborative Research Center SFB 855 is gratefully acknowledged.

REFERENCES

1. Kirchhof, C., M. Krantz, J. Teliban, R. Jahns, S. Marauska, B. Wagner, R. Knöchel, M. Gerken, D. Meyners, and E. Quandt, "Giant magnetoelectric effect in vacuum," *Appl. Phys. Lett.*, Vol. 102, 232905, 2013.
2. Lage, E., C. Kirchhof, V. Hrkac, L. Kienle, R. Jahns, R. Knöchel, E. Quandt, and D. Meyners, "Exchange biasing of magnetoelectric composites," *Nature Materials*, Vol. 11, No. 6, 523–529, 2012.
3. Piorra, A., R. Jahns, I. Teliban, J. L. Gugat, M. Gerken, R. Knöchel, and E. Quandt, "Magnetoelectric thin film composites with interdigital electrodes," *Appl. Phys. Lett.*, Vol. 103, 032902, 2013.

Strain-mediated Control of Magnetic Properties in Flexible Multilayered MagnetostrictiveFeGa Films

Qingfeng Zhan, Guohong Dai, Xiaoshan Zhang, Yiwei Liu, Zhenghu Zuo, Xing Rong, and Run-Wei Li
Key Laboratory of Magnetic Materials and Devices
Ningbo Institute of Material Technology and Engineering
Chinese Academy of Sciences, Ningbo 315201, China

Abstract— Flexible magnetic devices, i.e., magnetic devices fabricated on flexible substrates, are very attractive in applications such as detection of magnetic field in an arbitrary surface, non-contact actuators, and microwave devices, due to their stretchable, biocompatible, lightweight, portable, and low cost properties. Flexible magnetic films are essential for the realization of various functionalities of flexible magnetic devices. On various flexible substrates, including polyethylene terephthalate (PET), polydimethylsiloxane (PDMS), and Polyvinylidene difluoride (PVDF), we have fabricated flexible magnetic films, exchange biased heterostructures, spin-valve multilayers, and composite multiferroics based on magnetostrictive $Fe_{81}Ga_{19}$ alloys. The magnetic anisotropy in FeGa films can be enhanced by deposited on a flexible bowed-substrates, which leads to a high ferromagnetic resonance frequency. On the other hand, the metallic and photoresist buffer layers could effectively smoothen the rough surface of flexible substrates and reduce the stress-induced magnetic anisotropy and the coercive field. Mechanical strains produced by bending of the films can effectively modulate the magnetic properties of flexible magnetic films and exchange-biased heterostructures. The spin-valve multilayers grown flexible substrates by using FeGa as the magnetic layers exhibit a significant stress dependence of giant magnetoresistant. For FeGa films and spin-valve structures grown on flexible ferroelectric polymers of PVDF, the strains caused by the piezoelectric effect under an electric field or the anisotropic thermal expansion of PVDF at various temperatures give rise to a modulation of their magnetic behaviors, which can be understood based on a modified Stoner-Wohlfarth model calculation.

Magnetization Dynamics of Ni-Fe Elliptical Dot Arrays Measured by the FMR Measurement with a CPW

Yasushi Endo and Masahiro Yamaguchi
Department of Electrical Engineering, Graduate School of Engineering
Tohoku University, 6-6-05 Aoba, Aramaki, Aoba-ku, Sendai 980-8579, Japan

Abstract— The magnetization dynamics of nanomagnets have attracted much attention for the spintronics devices such as magnetic random access memories (MRAMs), magnetic logic devices and so on. The dynamics significantly depends on the damping constant α, which determines the strength of damping torque in nanomagnets. α can be obtained from various ferromagnetic resonance (FMR) measurement techniques such as microwave cavities and coplanar waveguides (CPWs). FMR measurements with CPW have the following advantages: (1) The samples are excited over a very wide range of radio frequencies upon the changing external magnetic field intensity. (2) The highly sensitive measurements allow samples to be downsized to the micron scale. Herein, to clarify the dynamics of nanomagnets in detail, we employed the FMR measurement with CPW to evaluate α in 50-nm-thick Ni-Fe elliptical dot arrays. Effective in-plane anisotropy field increases markedly with decreasing the dot size, which may be attributed to the enhancement of the magnetostatic energy. Effective saturation magnetization decreases slightly as the dot size is decreased. The reason for this is that the demagnetization field coefficient changes with the decreases of the dot size. In addition, α increases monotonically from 0.01 to 0.02 with decreasing the dot size at the external magnetic field of 500 Oe applying in the longitudinal axial direction of the dots. Their values are higher than that of the Ni-Fe film ($\alpha = 0.009$). This may be caused by inhomogeneity of demagnetization field distribution near dot edges. These results suggest that the extrinsic damping significantly influences on the dynamics of nanomagnets. These results also demonstrate that the FMR measurement with the CPW can evaluate the dynamics of nanomagnets in detail.

Multifunctional Materials for Electronics and Photonics

Federico Rosei
UNESCO Chair, Centre for Energy, Materials and Telecommunications, INRS
1650 Boul. Lionel Boulet, Varennes, QC J3X 1S2, Canada

Abstract— The bottom–up approach is considered a potential alternative for low cost manufacturing of nanostructured materials [1]. It is based on the concept of self-assembly of nanostructures on a substrate, and is emerging as an alternative paradigm for traditional top down fabrication used in the semiconductor industry. We demonstrate various strategies to control nanostructure assembly (both organic and inorganic) at the nanoscale. Depending on the specific material system under investigation, we developed various approaches, which include, in particular: (i) control of size and luminescence properties of semiconductor nanostructures, synthesized by reactive laser ablation [2]; (ii) we developed new experimental tools and comparison with simulations are presented to gain atomic scale insight into the surface processes that govern nucleation, growth and assembly [3–7]; (iii) we devised new strategies for synthesizing multifunctional materials for electronics and photovoltaics [8–18].

REFERENCES

1. Rosei, F., *J. Phys. Cond. Matt.*, Vol. 16, S1373, 2004.
2. Riabinina, D., et al., *Phys. Rev. B*, Vol. 74, 075334, 2006.
3. Dunn, K., et al., *Phys. Rev. B*, Vol. 80, 035330, 2009.
4. Ratto,F., et al., *Small*, Vol. 2, 401, 2006.
5. Ratto, F., et al., *Phys. Rev. Lett.*, Vol. 96, 096193, 2006.
6. Ratto, F., et al., *Nanotechnology*, Vol. 19, 265703, 2008.
7. Ratto, F., et al., *Surf. Sci.*, Vol. 602, 249, 2008.
8. Ratto, F. and F. Rosei, *Mater. Sci. Eng. R*, Vol. 70, 243, 2010.
9. Moutanabbir, O., et al., *Phys. Rev. B*, Vol. 85, 201416, 2012.
10. Yan, C., et al., *Adv. Mater.*, Vol. 22, 1741, 2010.
11. Yan, C., et al., *J. Am. Chem. Soc.*, Vol. 132, 8868, 2010.
12. Nechache, R., et al., *Adv. Mater.*, Vol. 23, 1724, 2011.
13. Nechache, R., et al., *Appl. Phys. Lett.*, Vol. 98, 202902, 2011.
14. Aïssa, B., et al., *Appl. Phys. Lett.*, Vol. 99, 183505, 2011.
15. Chen, G., et al., *Chem. Comm.*, Vol. 47, 6308, 2011.
16. Chen, G., et al., *Chem. Comm.*, Vol. 48, 8009, 2012.
17. Dembele, T., et al., *J. PowerSources*, Vol. 233, 93, 2013.
18. Li, S., et al., *Chem. Comm.*, Vol. 49, 5856, 2013.

Enhanced Sensitivity in Magnetoelectric Laminate Sensors Based on Magnetoelectric Nonlinearity

Jie Jiao, **Yuting Liu**, **Jiashuai Ma**, **Xiangyong Zhao**, **and Haosu Luo**
Key Laboratory of Inorganic Functional Material and Device
Shanghai Institute of Ceramics, Chinese Academy of Sciences, Shanghai 201800, China

Abstract— In this work, the models of responsivity and noise in magnetoelectric (ME) laminate sensors based on ME nonlinearity were established. Metglas/PMNT multi-push-pull mode ME laminate with high performances and charge pre-amplifier with super low intrinsic noise were designed and fabricated. The nonlinear and linear properties in ME composites under DC bias magneitc field were investigated via a frequency conversion technique. It was found that the major noise near the carrier frequency is caused by the driven magnetic field source, and both linear ME coefficient and noise floor near carrier frequency (bandwidth of noise measurement was 10 Hz) was dependent on DC bias magneitc field while the nonlinear ME coefficient was independent. In the end, an enhanced magnetic field sensitivity of 20 pT at 1 Hz and 200 pt at 10 MHz were obtained by optimizing the operating parameters like modulation amplitude, modulation frequency and DC bias magneitc field.

Magnetoelasticity and Electrical Performances of Laminated ME Materials Used for Magnetic Anomaly Sensors

Haosu Luo, **Jie Jiao**, **Yuting Liu**, **Jiashuai Ma**, **and Xiangyong Zhao**
Key Laboratory of Inorganic Functional Material and Device
Shanghai Institute of Ceramics, Chinese Academy of Sciences, Shanghai 201800, China

Abstract— In this work, the properties of magnetoelectric (ME) responsivity and intrinsic electric noise in laminated ME composite were studied. The established models of detectivity and detectivity figure of merits (FOMs) of magnetoelectric composite as the sensing material of the magnetic anomaly sensor were used to direct the design and fabrication of L-T mode and multi-push-pull mode ME composite based on Metglas alloy and relaxor ferroelectric single crystals. A charge amplifier with super low intrinsic noise was fabricated to measure the output properties of ME composites precisely. The measured detectivity of magnetic anomaly sensors were in accordance with the theoretical predictions. The noise equivalent magnetic induction of sensor has been achieved as $5\,\mathrm{pT/Hz^{1/2}}$@1 Hz, $1\,\mathrm{pT/Hz^{1/2}}$@10 Hz, $0.1\,\mathrm{pT/Hz^{1/2}}$@1 kHz and $10\,\mathrm{fT/Hz^{1/2}}$@EMR.

Low Loss Magnetodielectric Composites for RF and Microwave Applications

Hong Wang
Electronic Materials Research Laboratory, Key Laboratory of Ministry of Education
Xi'an Jiaotong University, Xi'an 710049, China

Abstract— Advances in composites have led to a variety of new materials with strong potential applications to electronics. Low loss magnetodielectric composites with high permittivity and permeability will benefit the miniaturization and multifunction for microwave and RF electronic devices. In this work, the ceramic based low loss magnetodielectric oxide composites were successfully developed by hybrid process technology and solid solution process technology with the aim of integrating the dielectric properties and magnetic properties. The hybrid processing technology exhibits the advantage of lowered sintering temperatures for the oxide composites while maintaining good microstructure and high performance. The pure single phase electromagnetic oxide ceramics have been obtained by suitable solid solution composition design and process. With introducing elastomer as matrix, flexible low loss magnetodielectric ceramic-polymer composites were prepared and studied. To understand the function inheriting in the composites, the useful measures to tailor the properties of the multifunctional composites were proposed and discussed.

Multiferroic Co_2Z Hexaferrite-$BaTiO_3$ Particulate Composites for Microwave Absorption Applications

Xian Wang, Qifan Li, Yan Nie, Zekun Feng, and Rongzhou Gong
School of Optical and Electronic Information
Huazhong University of Science and Technology, Wuhan 430074, China

Abstract— Microwave absorber has been attracting a great amount of research interest due to its extensive application. According to the fundamental principles of microwave absorption, multiferroic materials, with a combination of ferroelectricity and ferromagnetism, provides great opportunities for realizing good impedance matching and high attention ability so as to achieve good absorption performances. In this work, multiferroic $(Ba_{0.52}Sr_{0.48})_3Co_2Fe_{24}O_{41}(Co_2Z)/BaTiO_3$ particulate composites were prepared by the procedures as follows: the magnetic and ferroelectric phases were mixed with mass ratios of $Co_2Z/BaTiO_3$ = 100/0 (labeled as S0), 90/10 (S1), 80/20 (S2), 70/30 (S3), and 60/40 (S4); sintered at 1000°C for 4h; and then milled into micron size of particles. Successively, their structure, magnetic and microwave absorption properties within 2–18 GHz were investigated, respectively. The X-ray diffraction patterns reveal the coexistence of pure ferroelectric and magnetic phases in the composites. The SEM morphologies show that the uniform distribution and well combination of the two phases are conducive to the interaction between them. The saturation magnetization proportionally decreases while the coercivity increases with increasing $BaTiO_3$ content. It is founded that the ferroelectric phase presents a strong tunability of permeability and permittivity with frequency, which can be attributed to the simultaneous effects of electrical polarization and magnetization, and even magnetoelectric coupling in the composites. Compared with single phase of Co_2Z ferrite, the multiferroic composites exhibit enhanced microwave absorbing properties in a wide frequency range due to the improved magnetic and dielectric properties. Furthermore, the optimal working frequency can be manipulated by modifying mass ratio of the two phases. The present work leads us to suggest that multiferroic composites have great potential to be used as microwave absorbers.

REFERENCES

1. Zhang, H. F., S. W. Derek, and H. L. W. Chan, *J. Appl. Phys.*, Vol. 104, 104109-1–6, 2008.
2. Mandal, A. and C. K. Das, *J. Appl. Polym. Sci.*, 39926-1–9, 2014.
3. Li, B. W., Y. Shen, Z. X. Yue, and C. W. Nan, *Appl. Phys. Lett.*, Vol. 89, 132504-1–3, 2006.

Session 1P12a
SC4: Si-based Microwave Devices and ICs

Widely Tunable Inductors Utilizing Transmission-line with Variable Distributed Load Capacitor for Millimeter-wave Applications

Yixiao Wang, **Xiucheng Hao**, **Le Ye**, **and Huailin Liao**
Institute of Microelectronics, Peking University, Beijing 100871, China

Abstract— This paper proposes a widely tunable inductor realized by transmission lines (T-Line) for applications under 60 GHz. The proposed inductor is conceptually realized by T-Line and a variable distributed capacitor, which is added into the conventional equivalent RLGC model of the T-Line. However, in practical design, it would be impossible to add real distributed load capacitor to T-Line segments of unity length. Therefore, we make an approximation by limiting the segment length of the T-Line and dividing the T-Line into N parts, which makes each segment is far smaller than the wavelength. Apparently, while N is set larger tending to infinite, the approximation comes much nearer to the real situation. What's more, the simulation results show the inductance approximation is quite match while $N \geqslant 4$. As a result, the inductor consists of several short T-Line segments ($N = 4$) and shunt variable distributed load capacitors. With the changeable load capacitors, the equivalent inductance of whole T-Line could be tuned. For conceptual demonstration, a prototype T-Line-C VCO is implemented to compare with the conventional LC VCO formed by fixed inductors. For the same $\pm 50\%$ capacitance variation rate, the conventional LC VCO with fixed inductors only achieves 11.6% frequency tuning range from 60.5 GHz to 67.6 GHz; In contrast, the demonstrated VCO based on the proposed tunable T-Line inductors achieves a 23.7% frequency tuning range from 50.7 GHz to 65.44 GHz, which could cover worldwide 60 GHz bands. Meanwhile, the simulated output power is about -5 dBm to -20 dBm, which is sufficient for on-chip applications. The proposed T-Line based inductor is appropriate for 60 GHz applications. It gives us a potential to achieve large frequency tuning range for MMW modules, such as VCO, LNA, PA, which utilize T-Lines as the passive network.

Investigation of a Miniature and High Gain On-chip V Band Microstrip Antenna

Li-Yan Xie[1], **Jia-Qi Liu**[1, 2, 3], **Yu-Bo Wang**[1], **Chenghsin Chuang**[4], **Albert Chin**[4], **Joshua Le-Wei Li**[1, 2, 3], **and Kai Kang**[1]

[1]Institute of Electromagnetics and School of Electronic Engineering
University of Electronic Science and Technology of China, Chengdu, China
[2]Advanced Engineering Platform and School of Electronic Engineering
Monash University, Selangor, Malaysia
[3]Advanced Engineering Platform and School of Electronic Engineering
Monash University, Victoria, Australia
[4]Department of Electronic Engineering, Chiao Tung University, Hsinchu, Taiwan

Abstract— Recently, the research on high performance and compact volume in V band with 40 to 75 GHz devices has been increasing widespread, which brings great chance to reduce the size of complementary metal oxide semiconductor (CMOS) circuit for the less work in the impedance match with antenna. However, high dielectric constant and low-resistivity in Si material and thin substrate make it difficult to design and fabricate a high performance on-chip antenna in standard CMOS technology. Different kinds of methods have been approached to solve the problem. Some researchers [1] tried to solve the problem by adopting a silicon lens at the backside of the chip but what changed the standard CMOS technology and cost a lot. Others improved the antenna performance by doing the research of antenna radiation mechanism. And different structures of antenna such as dipole [2], inverted F [3], yagi [4] and slot [5] has been designed to fit with the circuits. Unfortunately, the radiation efficiency and gain in on-chip antenna still can't achieve a high level. Nowadays, the microstrip antenna with a ground plane on metal layer 1 shielding the wave from penetrating into the low-resistivity Si substrate what can give a new approach to improve the performance in on-chip antenna. Considering the great occupation of the patch and thin substrate which is only about one-five-hundredth of a wavelength (around 10 μm), the investigation of patch radiation mechanism has to be done to obtain a miniature and high gain on-chip V band microstrip antenna.

The main parameters in the investigation are the patch length, the spacing between the patch and the edge, and the thickness from the patch to the ground plane. Other parameters such as the arguments of the feed-line are predetermined by demanded 50 Ω output impedance matching of the circuit and the chosen technology. This structure was simulated with the finite element method software HFSS from Ansoft Corporation.

In this paper, a smaller occupation and higher gain on-chip antenna is designed and fabricated by making detail analysis on the parameters of the structure. The finally designed patch with 0.87 mm × 1.22 mm occupies half of the area of the same patch antenna through traditional design method. The peak gain of the designed antenna is −2.87 dBi and the efficiency of the designed on-chip antenna is 11.6% in simulation results from HFSS software.

REFERENCES

1. Babakhani, A., X. Guan, A. Komijani, A. Natarajan, and A. Hajimiri, "A 77-GHz phased-array transceiver with on-chip antennas in silicon: Receiver and antennas," *IEEE Journal of Solid-State Circuits*, Vol. 41, No. 12, 2795–2806, 2006.
2. Shamim, A., L. Roy, N. Fong, and N. G. Tarr, "24 GHz on-chip antennas and balun on bulk Si for air transmission," *IEEE Transactions on Antennas and Propagation*, Vol. 56, No. 2, 303–311, 2008.
3. Zhang, Y. P., M. Sun, and L. H. Guo, "On-chip antennas for 60-GHz radios in silicon technology," *IEEE Transactions on Electron Devices*, Vol. 52, No. 7, 1664–1668, 2005.
4. Chuang, H.-R., L.-K. Yeh, P.-C. Kuo, K.-H. Tsai, and H.-L. Yue, "A 60-GHz millimeter-wave CMOS integrated on-chip antenna and bandpass filter," *IEEE Transactions on Electron Devices*, Vol. 58, No. 7, 1837–1845, 2011.
5. Pan, S. and F. Capolino, "Design of a CMOS on-chip slot antenna with extremely flat cavity at 140 GHz," *IEEE Antennas and Wireless Propagation Letters*, Vol. 10, 827–830, 2011.

An Ultra-wideband and Low Phase Noise LC-VCO Using NMOS Varactor with MOM Digital Capacitor Switching Arrays

Mohammed Aqeeli, Zhirun Hu, Xianjun Huang, Abdullah Alburaikan, and Cahyo Muvianto
School of Electrical and Electronic Engineering
The University of Manchester, Manchester M13 9PL, UK

Abstract— An ultra-wideband, low phase-noise, low power and fully integrated CMOS VCO was realised in 130-nm CMOS technology, in order to fulfil the increasing requirements of Worldwide Interoperability for Microwave Access (WiMAX) technology and the recent exponential demand for higher capacity, more channels and greater distance wireless local area networks (WLANs) currently dominating the industrial world. This work presents a novel design at a 5.74 GHz centre frequency, with high-performance varactors composed of a body-grounded NMOS tuneable varactor based on accumulation mode and digital tuneable capacitors. These were designed using the series circuits of adequate metal-oxide-metal (MOM) capacitors, thereby taking advantage of their high quality factor, high capacitance density, low parasitic capacitance, narrow spacing and thinner dielectric layers and a novel switching device known as a MOM digital capacitor switching array (MOMDCSA). In addition, a self-biasing current source was implemented to avoid major obstacles, resulting in higher power supply sensitivity, higher up-conversion of flicker noise, due to higher harmonic distortion, and high power consumption. This structure produces a higher quality factor and lower phase noise in comparison to metal-oxide-semiconductor (MOS) varactors, and it also solves high phase noise variations, due to a wider tuning range, and minimises the sensitivity of the VCO effect of noise by optimising the gain. Therefore, the proposed VCO has an output frequency which varies linearly with control voltage through approximately fixed phase noise values for every bandwidth frequency. The high performance VCO specifications include a (3.56–6.98) GHz frequency range, which is approximately 59%. The measured phase noise of -131.7 dBc/Hz at 1 MHz offset from the centre frequency, figure of merit (FOM) of -202.38 dBc/Hz and total power consumption of the VCO core is 2.35 mW from 3.3 V supply voltage. The output peak-to-peak voltages of the VCO is 2.8 V with excellent spurious harmonics at < -32 dBm. For CMOS, there were no published VCO designs featuring this topology before prior to this work. As proof of the concept, the performance of the novel VCO was compared to other state-of-the-art designs in 0.09 µm, 0.13 µm, 0.18 µm and 0.25 µm CMOS technologies, the results showing clearly that the novel VCO is the best in terms of phase-noise, power dissipation, ultra bandwidth and FOM, not only for fabricated work but also with simulated designs as well.

Dual-band Bandpass Filter Based on GaN MMIC

Zhi Xia Du[1], **Xiu Yin Zhang**[1], **and Hsuan-Ling Kao**[2]

[1]School of Electronic and Information Engineering, South China University of Technology
Guangzhou 510640, China
[2]Department of Electronic Engineering, Chang Gung University, Taoyuan, Taiwan

Abstract— Dual-band bandpass filter using stub-loaded resonators based on GaN MMIC (Monolithic Microwave Integrated Circuit) is presented in this paper. The proposed circuit consists of two symmetric stub-loaded resonators, which are folded and coupled to each other. Every stub-loaded resonator is composed of a conventional microstrip half-wavelength resonator and an open stub. In order to reduce the mutual coupling between the two open stubs at the high frequencies, the open stubs are arranged at outside of the open loop while are still located at the midpoint of the main microstrip line. The ports are directly tapped at the resonators. According to the even- and odd-mode analysis, the second passband can be controlled by the stubs while the first passband is fixed. Therefore, the dual passbands can be tuned individually. Furthermore, open stubs are added to the 50-ohm feed lines, which are used to not only improve the selectivity of the filter, but also to couple with the resonators that can improve the performance of the filter. Benefitting from the integrated circuit technology, the design occupies a small size.

For demonstration, a dual-band bandpass filter based on MMIC is designed and the simulated result shows good performance. The center frequencies of the passbands are located at 40 and 60 GHz, with 3dB bandwidth of 15% (37 to 43 GHz) and 13.3% (56 to 64 GHz). The insertion losses are 3.3 and 3.8 dB at the lower and upper passbands and the return losses within the two passbands are better than 17 dB. Three transmission zeros are generated, resulting in high selectivity.

The Experimental Study of THz Power Detector Design in 0.18 μm CMOS Technology

Chih-Wei Lai[1], **Wei-Cheng Chen**[1], **Tzu-Chao Yan**[1], **Chun-Hsing Li**[1], **Ming-Ching Kuo**[2], **and Chien-Nan Kuo**[1]

[1]Chiao-Tung University, Hsinchu 300, Taiwan
[2]The Information and Communications Research Laboratories (ICL)
Industrial Technology Research Institute (ITRI), Hsinchu 310, Taiwan

Abstract— In this abstract, the experimental study of four THz power detector test-keys in 0.18 μm CMOS technology will be presented.

The implement methods of THz power detector in CMOS technology include quasi-static self-mixing, diode-connected NMOS, and Schottky diode. Due to the circuit model limitation, the silicon-verification of THz CMOS power detector is an essential step in circuit design flow.

In this study, two different bias conditions are designed at the output node of both common-gate and common-source topologies. The first condition is feeding a fixed dc bias value via 100 kohm resistor, and the second condition is without dc bias at output node. The differential-input type power detector is used to suppress fundamental signal and reject common-mode noise. For measurement consideration, the on-chip patch antenna is used to receive input power from signal source and generate differential signal for each power detector cell.

From the measurement results, the responsivity of common-gate with dc bias, common-gate without dc bias, common-source with dc bias, and common-source without dc bias are 23.2 kV/W, 10.5 kV/W, 435 kV/W and 19 kV/W at 332 GHz. The measured noise equivalent power of common-gate with dc bias, common-gate without dc bias, common-source with dc bias, and common-source without dc bias are 24.2 nW/$\sqrt{\text{Hz}}$, 0.952 nW/$\sqrt{\text{Hz}}$, 514 pW/$\sqrt{\text{Hz}}$ and 526 pW/$\sqrt{\text{Hz}}$ at 332 GHz.

In brief, four power detector test-keys are realized in 0.18 μm CMOS technology and measured at 332 GHz. The ratio of responsivity between common-source and common-gate is about 18, and the responsivity could be improved 22 times by feeding dc bias at the output node. Based on the experiment result and comparison, the suggested topology for THz image application is common-source with dc bias.

Study of Response of PIN Diode to Electromagnetic Pulse

Yong Li[1], **Haiyan Xie**[1], **Chun Xuan**[1], **Hongfu Xia**[1], **and Jian-Guo Wang**[1, 2]

[1]Northwest Institute of Nuclear Technology, Xi'an 710024, China
[2]School of Electronic and Information Engineering, Xi'an Jiaotong University, Xi'an 710049, China

Abstract— Response of PIN diode is numerically simulated by a self-developed 2D semiconductor device simulation GSRES to study the response behavior of PIN diode limiter under electromagnetic pulse (EMP). Current overshoot phenomena of PIN diode during the rise time of EMP, which is validated to be due to the capacitive performance of PIN diode under high frequency, are analyzed. Shorter rise time of EMP causes higher current peak value. Overshoot current is affected by the impurity doping concentration of PIN diode. Higher doping concentration of impurity in the P layer and N layer causes higher peak of current and sooner attenuation of overshoot current. Doping concentration of the I layer affects the overshoot current too, but not as salient as concentration of the P and N layers. These results can be used in radiation hardening for PIN diode limiter.

Amplifier Design Using 0.18 µm CMOS Technology

Yuan Chun Li[1] and Hsuan-Ling Kao[2]

[1]Department of Electronic Engineering, City University of Hong Kong, Hong Kong, China
[2]Department of Electronic Engineering, Chang Gung University, Tao-Yuan, Taiwan

Abstract— This paper presents a radio frequency amplifier using 0.18 µm CMOS technology. It is designed for global positioning system. In order to obtain high gain, the proposed amplifier is composed of three stages. The first two stages are signal end. They use cascade structure which means common gate-common source structure. The final stage uses active balun, which transforms signal from single end to differential signal. The supply voltage is 3.3 V. The simulation is carried out in ADS software. And the layout is finished in Cadence software. The proposed three stage amplifier is tapped out and measured. The area of the die including DC and RF pads is $1.5 \times 1.1\,\mathrm{mm}^2$. The measurement is performed on probe. The working frequency is from 3.6 GHz to 5.1 GHz. In this frequency range, the gain of small signal is 20 dB and the gain flatness is smaller than 1 dB. S_{11} is smaller than −15 dB. The measured saturation output power is −12 dBm at −20 dBm input power. The power consumption is 10 mW. Because the output signal is differential signal, the amplitude and phase difference are also tested. The amplitude difference between the two ports is smaller than −0.3 dB and the phase difference is 180°. The unbalance of phase difference is smaller than 3°. The comparison between simulation and measurement is carried out. The good agreement confirms the validity of the proposed method. With these good measured results, the proposed amplifier can be utilized as a radio frequency buffer amplifier in the receiver of the global positioning system.

Session 1P12b
Specialty Optical Fibers: Design, Applications, Devices, and Process

THz False-color Imaging with Flexible Tube-lattice Fiber Probe

Wenliang Lu[1, 2], **Shuqin Lou**[1], **Xin Wang**[1], **and Alexander Argyros**[2]

[1]School of Electronic and Information Engineering, Beijing Jiaotong University, Beijing 100044, China
[2]Institute of Photonic and Optical Science (IPOS), School of Physics
The University of Sydney, NSW 2006, Australia

Abstract— A flexible tube-lattice fiber is introduced into a THz-TDS system to implement a THz false-color imaging system. The fiber, which has three low-loss transmission windows in the frequency range of 0.1–1 THz, can lead THz radiation out of the system and lead back to the detector. It can be used as a probe to break the spatial limit of the THz-TDS system and widen the range of applications. A cuvette filled with two different kinds of white powder was used as a sample in the experiment. One end of the fiber was fixed and the other end near the sample was scanned by a 2D translation stage across the sample. THz radiation from the fiber passes through the sample and is reflected by a mirror at the back of the cuvette. The reflected THz radiation contains the sample's THz spectral information. Thus, the entire sample can be investigated by scanning the fiber. Three-primary colors (red, green and blue) are defined by spectral intensities of the fiber transmission windows. A 13×16 pixels false-color image was generated with the mix of values of the primary colors. In the false-color image, the two kinds of powder, the cuvette and the background present different colors and saturation which indicate different materials and the concentration, respectively. The resolution was also investigated by scanning slits in a metal sheet. The resolution of the imaging system is approximately 1 mm.

Simulation of Temperature Profile of Soot Preform during Sintering Process

Ramesh Behera and Sham Nagarkar
Sterlite Technologies Ltd, Aurangabad, India

Abstract— Sintering process in optical fiber manufacturing technology densifies the soot preform to glass preform which is used for drawing optical fiber. The analysis of temperature profile of the soot preform during sintering has been studied using Computational Fluid Dynamics (CFD) simulation tool. The temperature profile inside the soot preform is discussed by changing the preform diameter during sintering process.

Introduction: Sintering is an important process to convert soot preform to glass preform by densification phenomena. The quality of densification depends on the temperature profile of the preform which is controlled by furnace temperature and gas flow rate.

The article presents a Computational Fluid Dynamics (CFD) calculation to find out the temperature of soot preform during sintering process. In this study, the temperature inside the soot preform has been discussed with varying the preform diameter following to a validation study.

Theoretical Calculation: ANSYS FLUENT [1] software is used to solve the governing equations, which is a finite volume method (FVM) based CFD code. As part of the CFD calculation, a 3D engineering drawing of the sintering apparatus is prepared, a good quality mesh is generated in the 3D drawing and the governing equations of mass conservation, Naiver-Stokes, turbulence and species transport, energy conservation and radiation are solved.

Results: The validation study was carried out inside the sintering apparatus in stand by condition (i.e., in absence of soot preform) before discussing the soot temperature profile calculated using CFD. The simulation result depicts that the temperate is maximum in furnace region as compared to other part of the apparatus (Figure 1(a)). The simulated temperature profile matches with the experiments (Figure 1(b)).

The temperature profile is calculated using CFD of soot preforms with two different diameters. The diameter of the second soot preform is 4 times larger than the first soot preform. Temperatures are calculated using the conduction, convection and radiation phenomena in between the furnace muffle tube and soot preform & the conduction inside the soot preform respectively. The densification and gas diffusion inside the soot was not considered. It has been reported that the heat transfer through conduction inside the soot is faster than the gas diffusion [2].

Simulation results suggest that the temperature drop in between the furnace muffle tube and soot surface is negligible in both sizes of soot preforms (Figure 2). However, the temperature drop inside second preform (Figure 2(b)) is 3 times more than the first preform (Figure 2(a)) which should be considered in the process design.

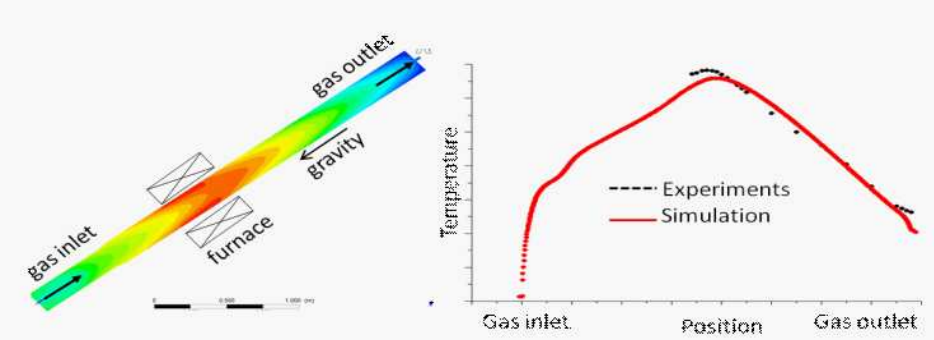

(a) (b)

Figure 1: (a) Temperature field inside the sintering apparatus in standby condition and (b) temperature comparison plot.

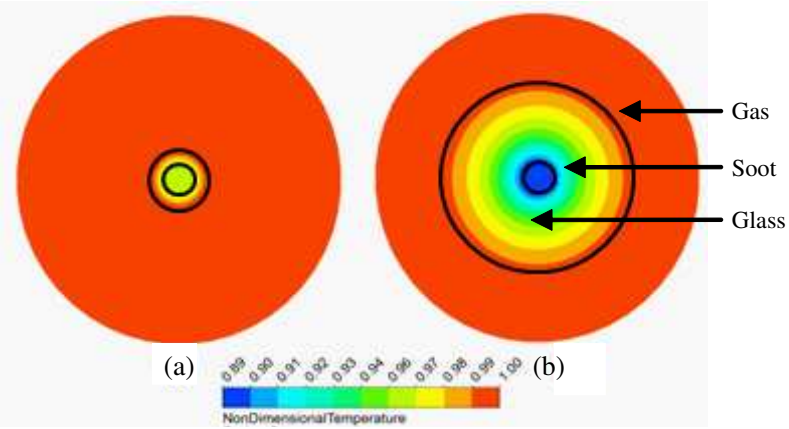

Figure 2: Temperature field in a cross section positioned at center of furnace in sintering apparatus: (a) first preform and (b) second preform.

REFERENCES

1. FLUENT v13.0, *Theory Guide and Users Manual*, ANSYS Inc..
2. Doorwar, S., S. Chakraborty, and S. Neogi, "A multiscale model for quantifying helium diffusion in porous unsintered glass," *The Canadian Journal of Chemical Engineering*, Vol. 88, April 2010.

Yield Improvement of Optical Fiber Manufacturing through Redesign of ACVD Burner

Ramesh Behera and Datta Pasare
Sterlite Technologies Ltd., Aurangabad, India

Abstract— A burner design has been proposed to improve the manufacturing yield of optical fiber. The burner is an important device to fabricate the silica soot preforms in ACVD process of manufacturing optical fiber. The glass formation in the tip of fumes tube of burner is a common problem which leads to block the fumes tube exit and scrap soot preform. The burner has been redesigned using Computational Fluid Dynamics (CFD) simulation tool to understand the interaction of silica precursor, hydrogen and oxygen gas flow paths and to avoid the glass formation. Using the redesigned burner, the scrap of soot preform due to glass formation has been lowered.

Introduction: The ACVD is a well known technology for manufacturing glass performs used for drawing optical fibers. A burner is an important device in ACVD manufacturing process and it is used for formation of silica particles from combustion of hydrogen and oxygen and silica precursors. Silica particles hence produced are deposited on a bait/glass rod in the form of soot preform. There are many defects such as glass formation in burner tip, wart on soot preform and bad interface on soot prefrom in the ACVD process which leads to scrap soot preform. The overall manufacturing cost of optical fiber increases if the soot performs is scrapped. It has been a challenging task to decrease the optical fiber manufacturing cost due to current competitive market. To understand and remove the defects, engineers explore to use of smart engineering tools which is a cost effective solution. The Computational Fluid Dynamics (CFD) simulation tool has been used to understand the one defect, known as glass formation in the tip of burner.

The article presents a CFD calculation of interaction of gas flow paths of silica precursor, hydrogen and oxygen in the generic and redesigned burners. In this study, the gas velocities resulted from CFD calculation have been discussed and experimented to access the improvement.

Theoretical Calculation: ANSYS FLUENT [1] software is used to solve the governing equations, which is a finite volume method (FVM) based CFD code. As part of the CFD calculation, a 3D engineering drawing of the burner was prepared, a good quality mesh is generated in the 3D drawing and the governing equations of mass conservation, Naiver-Stokes, turbulence and species transport are solved.

Results: The velocity vectors are shown in Figure 1 for both burners as part of CFD results. Figures 1(a) and 1(b) represent for generic and redesigned burners respectively. The axis shown in Figure 1 represents for fumes tube of burners. The pitch circle diameters of redesigned burner

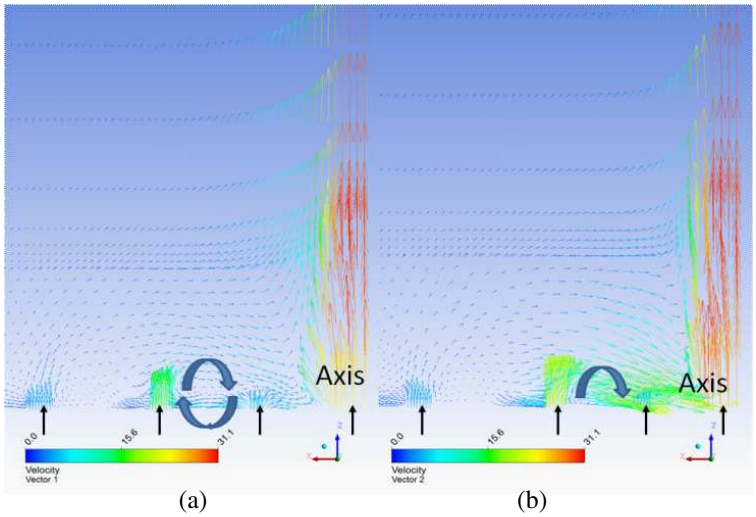

(a) (b)

Figure 1: Non-dimensional velocity vectors: (a) "generic" burner, (b) redesigned burner.

are decreased by 4 units as compared to the generic burner keeping all other inputs constant. The gas injection locations are marked in arrow.

The velocity field causes for glass formation in tip of fumes tube in the generic burner due to less gas flow between first and second injections and a recirculation zone between second and third injections (Figure 1(a)). Whereas the velocity field generated in the redesigned burner does not allow for glass formation as the gas flows are directed towards the first and second injections from the second and third injections respectively (Figure 1(b)).

REFERENCES

1. FLUENT v14.0, *Theory Guide and Users Manual*, ANSYS Inc..

Core Profile Based Dispersion Optimization in Trench Assisted Bend-insensitive Optical Fibers

Pramod R. Watekar, Archi Bhattacharya, and Nagaraju Bezawada
Sterlite Technologies Ltd., Aurangabad 431016, India

Abstract— We present a new design method to optimize the performance of bend insensitive optical fibers based on core profile optimization. The experimental results will also be discussed.

Introduction: With the increasing deployment of FTTx applications all over the world, bend insensitive optical fibers are gaining commercial and scientific attention. This has resulted in commercial availability of a range of bend insensitive optical fibers (G.657A1, A2, B2, B3) [1]. However, realization of ultra low bending loss fibers for home deployment has posed many challenges; one of them is the dispersion failure. It is well known that the decrease in the macro-bending loss causes the cable cutoff wavelength and the dispersion at 1550 nm to increase beyond the recommendations suggested by ITU-T for G.657 category (especially B3) fibers. Thus, the tradeoff between high bend insensitivity and the limited dispersion at 1550 nm has to be understood and addressed to obtain optimized parameters. In the current communication, we present a design methodology based on the core profile optimization. We justify our method by presenting experimental results.

Discussion: The trench assisted profile under consideration is shown in Fig. 1. Firstly, we select trench dimensions and its position to get minimum macro-bending loss, which may affect the dispersion properties, still it is not disturbed. Secondly, the shape of the core profile is changed and optical parameters are calculated. Finally, the optimum alpha profile is chosen so that all required optical parameters are obtained.

We choose a typical profile with core relative index difference of 0.412%, trench relative index difference of −0.484% and where the core is of 8.4 µm diameter (d), trench is separated by $0.72d$ distance from the core edge and the trench width is $0.6d$. As shown in Fig. 2, the dispersion is over 18 ps/km·nm for the non-optimized profile of the core and reduces further with change in the value of alpha. However, this also increases the bending loss and hence, alpha has to be chosen optimally.

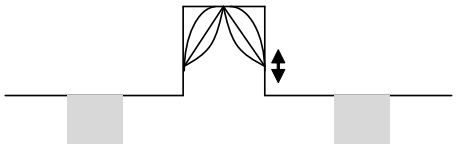

Figure 1: Trench assisted bend insensitive fiber at different alpha values.

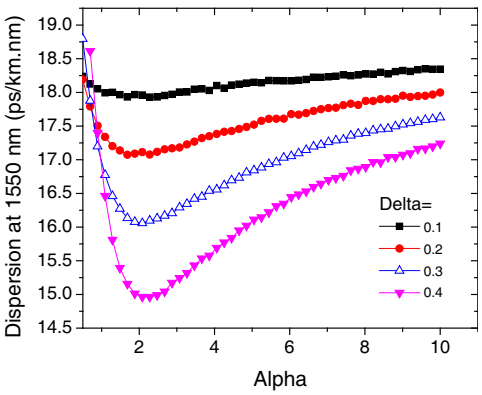

Figure 2: Effects of alpha on the dispersion at 1550 nm.

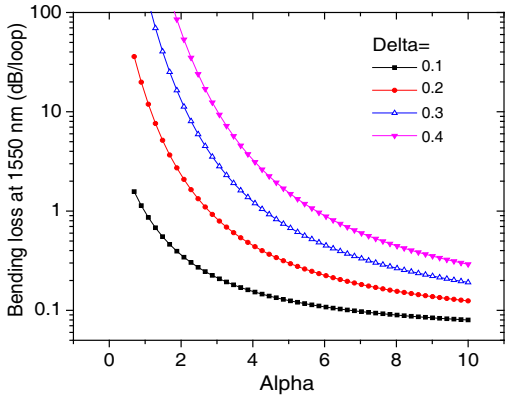

Figure 3: Effects of alpha on the bending loss at 5 mm radius.

REFERENCES

1. www.sterlitetechnologies.com.

Experimental Investigation of Modal Noise in Ultra Bend-insensitive Fibers

Nagaraju Bezawada, Manoj Gupta, and Pramod R. Watekar
Center of Excellence, Sterlite Technologies Limited, Aurangabad, India

Abstract— We experimentally investigate the modal noise characteristics of short length ultra bend-insensitive optical fibers with different splice conditions using broadband source/OSA technique.

Introduction: As the fiber penetrates indoor for FTTH, it needs to have very high bend resistance [1]. Harsh conditions like sharp turns, staples, and reduced storage space are very common in indoor applications. As the macro-bend loss of conventional matched clad fibers cannot be reduced beyond certain extent without disturbing mode field diameter (MFD) and dispersion, a trench in cladding design has been proposed. Fibers with trench in cladding design can achieve ultra low bend losses without compromising on MFD and dispersion. However, these fibers typically have higher cutoff wavelengths than matched clad fibers due to more confinement of optical power. Also, the existence of trench in these fibers results in the existence of higher order mode beyond cutoff wavelength. The existence of this higher order mode can cause modal noise and needs to be investigated in short length bend insensitive fibers.

In this paper, we present measurement results of modal noise in a 2 m length ultra bend-insensitive fiber with different splice conditions.

Experimental Setup: Our measurement method is based on wideband light source/OSA technique and monitors transmitted optical power through the short length fiber under test as a function of wavelength. A schematic of the apparatus used for this test is shown in Fig. 1.

Results and Discussion: The fiber sample used for measuring multipath interference (MPI) is a G.657 B3 category fiber with a macrobend loss of 0.07 dB/turn at a bend radius of 5 mm and cable cutoff wavelength of 1240 nm.

MPI of the sample is measured at both 1260 and 1310 nm by inserting the sample and switching on the polarization scrambler. OSA was set into MAX and MIN hold mode and Max and Min power was measured for 15 minutes. This time was sufficient for the scrambler to explore all the polarization states on Poincare sphere. Fig. 2 shows measured Max and Min power curves at 1310 nm for an insertion loss of 1.49 dB. MPI is calculated using this Max and Min data using the formula given in [2]. MPI dependence on insertion loss (due to offset splices) is shown in Fig. 3. Measured MPI values as a function of insertion loss are plotted at both 1260 nm and 1310 nm.

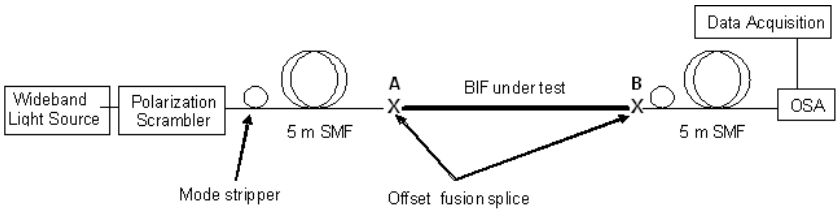

Figure 1: Experimental setup.

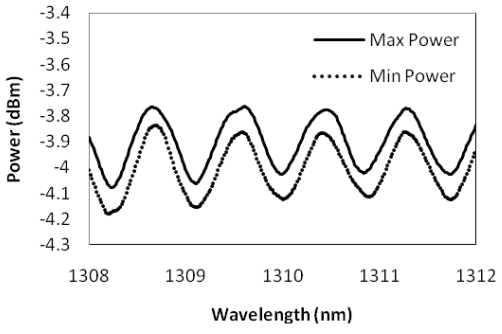

Figure 2: Measured Max and Min power curves at 1310 nm for an insertion loss of 1.49 dB.

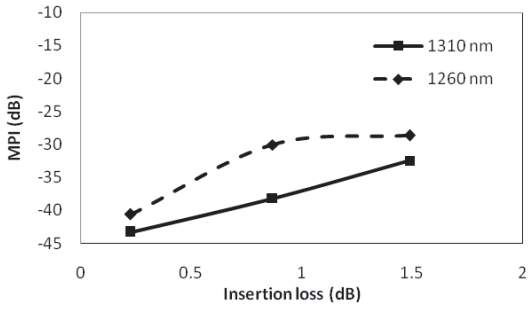

Figure 3: Dependence of MPI on insertion loss at 1260 nm and 1310 nm.

REFERENCES

1. Himeno, K., et al., "Low-bending-loss single-mode fibers for fiber-to-the-home," *J. Lightwave Technol.*, Vol. 23, 3494–3499, 2005.
2. Ramachandran, S., et al., "Measurement of multipath interference in the coherent crosstalk regime," *Photon. Technol. Lett.*, Vol. 15, 1171–1173, 2003.

Measurement of Nonlinear Coefficient of Ultra Bend-insensitive Optical Fiber

Manoj Gupta, **Nagaraju Bezawada**, **and Pramod R. Watekar**
Center of Excellence, Sterlite Technologies Limited, Aurangabad, India

Abstract— We present measurement of nonlinear coefficient of bend insensitive fibers at 1550 nm by direct continuous wave method. Measured nonlinear coefficient for G.657A2 fiber is 1.25 $(\text{W-km})^{-1}$.

Introduction: Nowadays, the whole world is witnessing the fast and rapid optical communication because of dense wavelength division multiplexing (DWDM) networks. These networks carry high power densities and the rapid increase in the power put into an optical fiber gives rise to such phenomena as nonlinear optical effects. Nonlinear optical interaction will become prominent when optical power density is high and interaction takes place for longer distance. The intensity dependent refractive index (n_2) leads to variety of nonlinearity effects such as self-phase modulation (SPM), cross-phase modulation (XPM) and four wave mixing (FWM) in the optical fibers and is thus a critical parameter for long haul networks. Typically, G.652 D fibers are used in long haul networks. However, G.657 A fibers, which are designed for access networks,are expected to see applications outside access network in future. This is due to their improved microbending performance and compatibility with G.652 D. So, it is important to understand nonlinear characteristics of these fibers.There are various approaches proposed in the literature to measure the nonlinear coefficient [1, 2]. However, we have used cw-SPM method.

In this paper, we present nonlinear coefficient measurement for Sterlite's Bowlite G.657 A2 optical fiber.

Result and Discussion: Two continuous signals centered at 1550.06 nm and 1550.23 nm were launched having power of 10 dBm each. The launch polarization of signals was adjusted using polarization controllers. These two signals are combined using a 50 : 50 splitter. The combined signal is amplified using a high power EDFA and launched into the fiber under test. A band pass filter (BW: 3.2 nm) is used to filter the noise. Output power spectrum was recorded by using optical spectrum analyzer (OSA). Resolution bandwidth of OSA was 0.02 nm. The recorded spectra at different launch powers are shown in Figure 1. An attenuator of 20 dB loss was inserted before OSA for controlling power going to OSA input port. Figure 2 shows the variation of nonlinear phase shift with input launch power. Nonlinear coefficient is measured using methodology given in [2].

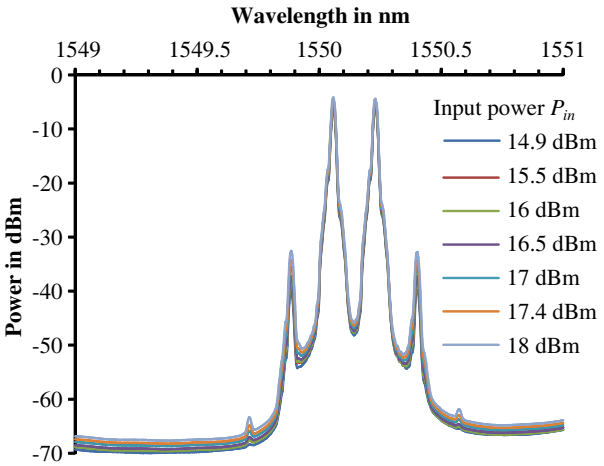

Figure 1: Output power spectrum at different input lauching power level into fiber sample of bend insensitive fiber G.657 A2.

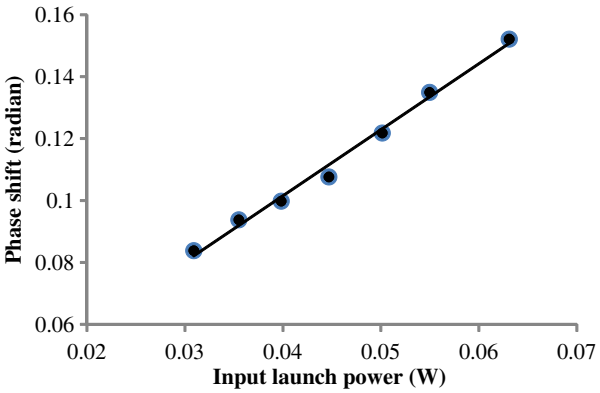

Figure 2: Phase shift variation due to changing the launching power for G.657 A2.

REFERENCES

1. Boskovic, A., S. V. Chernikov, and J. R. Taylor, "Direct continuous-wave measurement of $n2$ in various type of telecommunication fiber at 1.55 mm," *Optics Letters*, Vol. 21, No. 24, 1996.
2. Namihira, Y., et al., "A comparison of six techniques for nonlinear coefficient measurements of various single mode optical fibers," *NIST*, 1–5, 2002.

Surface Plasmon Resonance of Tapered Au Nano-particles Cladding-doped Optical Fiber

Seongmin Ju, **Seongmook Jeong**, **Youngwoong Kim**, **Sang-Hyun Lee**, **and Won-Taek Han**
School of Information and Communications/Department of Physics and Photon Science
Gwangju Institute of Science and Technology, 123 Cheomdan-gwagiro, Buk-Gu
Gwangju 500-712, South Korea

Abstract— To improve the SPR sensitivity of the Au nano-particles cladding-doped optical fiber, effect of taper-waist diameter with tapered angle on the SPR sensitivity was investigated. As the diameter of the tapered optical fiber decreased from 125 μm to 70 μm, the SPR sensitivity increased from 407 nm/RIU to 800 nm/RIU.

Fiber optics surface plasmon resonance (SPR) sensor based on tapered optical fiber using novel metals such as Cu, Ag, and Au as a sensitive layer has drawn much attention due to its sensing capability for various sensor applications [1]. The taper-waist diameter is an adjustment parameter for sensor sensitivity because tapering makes the evanescent fields spread out into cladding and reach the external environment. Also, it is possible to make the angle of incidence light more close to the critical angle of the sensing region and thus penetration of the evanescent wave inside the sensing region increase [1, 2].

In this paper, to improve the SPR sensitivity of the Au nano-particles cladding-doped optical fiber, effect of taper-waist diameter with tapered angle on the SPR sensitivity was investigated. A part of the optical fiber was stripped off and then tapered into smaller diameter fibers of 100 μm, 80 μm, and 70 μm with uniform sensing region of 20 mm as well as down/up tapering lengths of 5 mm each with the fiber length of 20 cm by the graphite heating system (Vytran, GPX series) [1]. To examine a refractive index sensing property of the tapered Au nano-particles cladding-doped optical fiber, SPR spectrum was measured by putting small drops of the refractive index matching oil with various refractive indices ($n = 1.418$–1.448). The SPR absorbance was measured by the optical spectrum analyzer with the white light source as an input broadband light. The SPR was found to occur at a particular wavelength around 400 nm for the corresponding refractive index, increased with the increase of the index. The position and the width of the SPR peak were slightly red-shifted and increased with the increase of the refractive index, respectively. The measured SPR sensitivities (wavelength/RIU) of the tapered Au nano-particles cladding-doped optical fiber was estimated to be 460 nm/RIU, 556 nm/RIU, and 800 nm/RIU with tapered diameter of 100 μm, 80 μm, and 70 μm, respectively as shown in Fig. 1. For a comparison, the measured SPR sensitivity of the Au nano-particles cladding-doped optical fiber without tapering was estimated to be 407 nm/RIU. As the diameter of the tapered optical fiber decreased from 125 μm to 70 μm, the SPR sensitivity increased from 407 nm/RIU to 800 nm/RIU because the coupling between the evanescent wave and the surface plasmon wave became much stronger by increasing the penetration depth (angle of the ray) and the number of reflections of incident rays per unit length of the fiber in the sensing region.

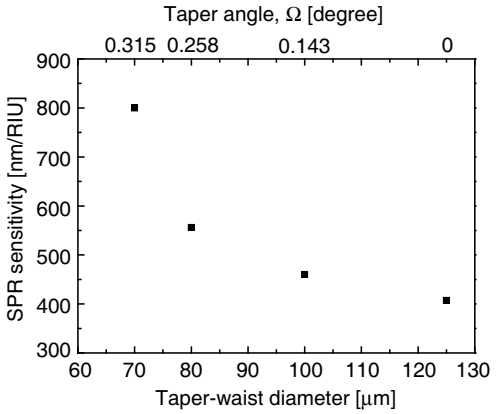

Figure 1: Variation of the SPR sensitivity with different taper-waist diameters of 70 μm, 80 μm, 100 μm, and 125 μm as well as uniform length of the waist taper region of 20 mm and down/up tapering regions of 5 mm each.

ACKNOWLEDGMENT

This work was partially supported by the New Growth Engine Industry Project of the Ministry of Trade, Industry and Energy, Basic Science Research Program through the National Research Foundation of Korea (NRF) funded by the Ministry of Education (No. 2013R1A1A2063250), the Korea government (MSIP) (No. 2011-0031840), the Brain Korea-21 Plus Information Technology Project through a grant provided by the Gwangju Institute of Science and Technology, South Korea.

REFERENCES

1. Ju, S., S. Jeong, Y. Kim, P. Jeon, M.-S. Park, H. Jeong, S. Boo, J.-H. Jang, and W.-T. Han, "Experimental demonstration of surface plasmon resonance enhancement of the tapered optical fiber coated with Au/Ti thin film," *Journal of Non-Crystalline Solids*, Vol. 383, 146–152, 2014.
2. Villatoro, J., D. Monzón-Hernández, and E. Mejía, "Fabrication and modeling of uniform-waist single-mode tapered optical fiber sensors," *Applied Optics*, Vol. 42, 2278–2283, 2003.

Gamma-ray Irradiation Effect on Non-resonant Third-order Optical Nonlinearity of Germano-silicate Glass Optical Fiber

Youngwoong Kim[1], **Seongmin Ju**[1], **Seongmook Jeong**[1], **Jong-Yeol Kim**[2], **Nam-Ho Lee**[2], **Hyun-Kyu Jung**[2], **and Won-Taek Han**[1]

[1]Department of Physics and Photon Science, School of Information and Communications
Gwangju Institute of Science and Technology, 123 Cheomdan-gwagiro
Buk-Gu, Gwangju, Republic of Korea
[2]Nuclear Convergence Technology Development Department
Korea Atomic Energy Research Institute, 989-111 Daedeok-daero
Yuseong-gu, Daejeon, Republic of Korea

Abstract— A number of studies have been conducted to examine the effects of radiation exposure on optical properties of various glass optical fibers to evaluate their feasibility for photonic devices in radiation-harsh environments. The radiation-induced changes in optical properties of silica-based glass optical fiber such as absorption (or attenuation), optical refractive index, and luminescence are mainly explained by varied structures of the radiation-induced defects in the glass network. It was also been found that the gamma-ray irradiation affected nonlinear optical phenomenon of some bulk glasses or optical fibers due to the formation of radiation-induced defects [1]. However, to the best our knowledge, there has been no experimental measurement for the non-resonant optical nonlinearity of gamma-ray irradiated optical fiber. In this paper, the effect of gamma-ray irradiation on the non-resonant third optical nonlinearity of the germano-silicate single mode optical fiber (Corning® SMF-28e+) was investigated.

The optical fiber was irradiated by gamma-ray from a Co^{60} radiation source (MSD Nordion, pencil type/C-188 sealed). The irradiation was carried out at different dose rates (10.3 Gy/min, 20.4 Gy/min, and 41.4 Gy/min) for 60 minutes to investigate dose dependence of the optical nonlinearity. The non-resonant third optical nonlinearity of the optical fiber was measured by the continuous wave self-phase modulation (cw-SPM) method. To determine the non-resonant optical nonlinear refractive index, n_2, the nonlinear phase shift, φ_{SPM}, was measured experimentally. The φ_{SPM} increased linearly with the input signal power and the n_2 of the optical fiber was estimated to be $2.31\times10^{-20}\,\mathrm{m^2/W}$, $2.43\times10^{-20}\,\mathrm{m^2/W}$, $2.48\times10^{-20}\,\mathrm{m^2/W}$, and $2.54\times10^{-20}\,\mathrm{m^2/W}$ for the gamma-ray dose of 0 Gy (no γ-ray irradiated), 617 Gy, 1,222 Gy, and 2,468 Gy, respectively, as shown in Fig. 1. The n_2 of the optical fiber increased with the gamma-ray irradiation dose, but the rate of increase became decreased with increasing the dose. This is because the saturation of formation of the radiation-induced defects was reaching at higher gamma-ray dose. The radiation-induced defects in the optical fiber such as Ge/Si-related non-bridging oxygen hole centers (NBOHCs) may contribute the $\chi^{(3)}$ hyper-polarizabilities which are responsible for the non-resonant optical nonlinearity [2], thus the increase in the n_2 of the optical fiber was thought to be closely related to the formation of the radiation-induced defect centers.

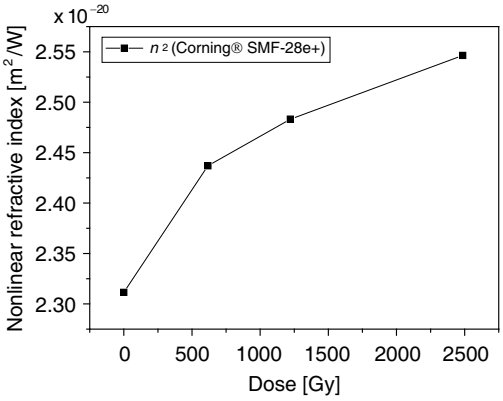

Figure 1: Variation of the nonlinear refractive index, n_2, of the optical fiber with respect to gamma-ray dose.

ACKNOWLEDGMENT

This work was partially supported by the New Growth Engine Industry Project of the Ministry of Trade, Industry and Energy, Basic Science Research Program through the National Research Foundation of Korea (NRF) funded by the Ministry of Education (No. 2013R1A1A2063250), the Korea government (MSIP) (No. 2011-0031840), the Brain Korea-21 Plus Information Technology Project through a grant provided by the Gwangju Institute of Science and Technology, South Korea.

REFERENCES

1. Isbi, Y., S. Sternklar, E. Granot, and L. Boehm, "Enhanced $\chi^{(3)}$ in γ-ray irradiated bulk glass," *Optics Communications*, Vol. 194, 213–216, 2001.
2. Ju, S., P. R. Watekar, S. Jeong, Y. Kim, and W.-T. Han, "Effect of Zn addition on non-resonant third-order optical nonlinearity of the Cu-doped germano-silicate optical glass fiber," *Journal of Nanoscience and Nanotechnology*, Vol. 12, 629–634, 2012.

Bending Effect on Optical Emission Properties of Yb/Al Doped Optical Fiber with Depressed Cladding Structure

Seongmook Jeong[1], **Seongmin Ju**[1], **Youngwoong Kim**[1], **Yune Hyoun Kim**[2], **Swook Hann**[2], **and Won-Taek Han**[1]

[1]Department of Physics and Photon Science, School of Information and Communications
Gwangju Institute of Science and Technology
123 Cheomdan-gwagiro, Buk-Gu, Gwangju 500-712, South Korea
[2]Laser-IT Research Center, Korea Photonics Technology Institute
9 Cheomdan venture-ro, Buk-Gu, Gwangju 500-779, South Korea

Abstract— Large core optical fiber and double-cladding fiber are used to apply for high power fiber laser due to their compensating limited lasing efficiency and low launching efficiency of pump power. However, the large core optical fiber has high bending loss and therefore it's difficult to make compact size fiber laser system [1]. Bending loss of optical fiber can be reduced by addition of depressed cladding structure around the fiber core due to reduction of effective refractive index of cladding under bending condition [2].

In this paper, an Yb/Al doped optical fiber with depressed cladding structure was fabricated by using modified chemical vapor deposition (MCVD) and drawing process. During the drawing process, the fiber was coated with the lower refractive index polymer (UVF PC-375 AP) for double-cladding effect with protection of the fiber. Core and cladding diameter of the fabricated fiber were 29.7 µm and 633.3 µm, respectively and the optical attenuation measured by cut-back method was estimated to be 1,250 dB/m at 975 nm. To evaluate emission properties of the fiber (length = 1 meter) under bending condition from 100 mm to 10 mm in diameter, the 975 nm laser diode (COSET, CM0001C) was used for pumping and launched into the fiber. In case of launching the laser onto the core and the depressed cladding layer, the intensity of the emission band appearing from 1,000 nm to 1,100 nm did not change much with the bendings, because almost pumping power went through the fiber core due to effect of depressed cladding structure. However, in the case of launching onto the depressed cladding layer and low-index polymer coating, the emission intensity at 1,060 nm increased with the decrease of bending diameter until 50 mm and then decreased. With the fabricated Yb/Al doped optical fiber with depressed cladding structure, the optimum bending diameter for a laser application was found to be 50 mm.

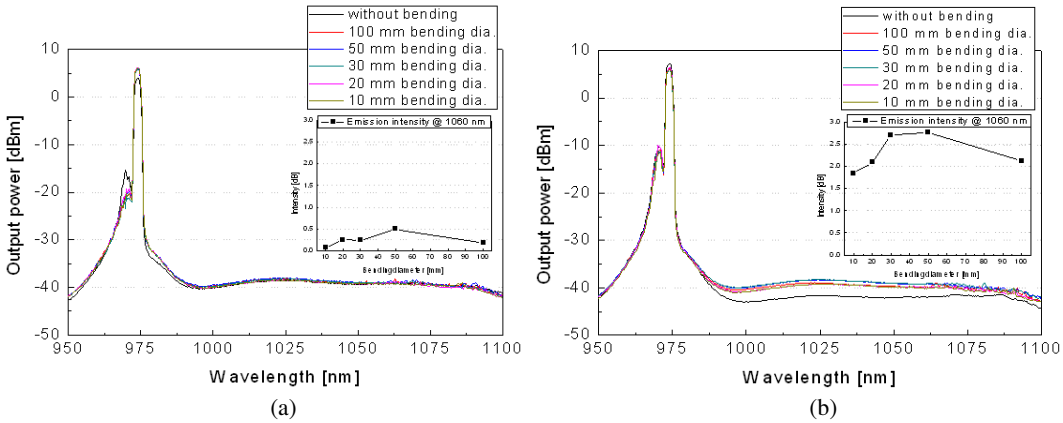

Figure 1: Emission spectra with and without bending of the fiber upon pumping with the 975 nm laser diode, (a) launching onto the core and depressed cladding layer, (b) launching onto the depressed cladding layer and the low-index polymer coating. The insets are the output powers at 1060 nm with bending diameters.

ACKNOWLEDGMENT

This work was partially supported by the New Growth Engine Industry Project of the Ministry of Trade, Industry and Energy, Basic Science Research Program through the National Research

Foundation of Korea (NRF) funded by the Ministry of Education (No. 2013R1A1A2063250), the Korea government (MSIP) (No. 2011-0031840), the Brain Korea-21 Plus Information Technology Project through a grant provided by the Gwangju Institute of Science and Technology, South Korea.

REFERENCES

1. Lin, Z., G. Ren, S. Zheng, W. Jian, J. Zheng, and S. Jian, "Analysis and characterization of Er–Yb codoped depressed inner cladding fiber," *Applied Optics*, Vol. 52, 5856–5861, 2013.
2. Watekar, P. R., S. Ju, and W.-T. Han, "Design and development of a trenched optical fiber with ultra-low bending loss," *Optics Express*, Vol. 17, 10350–10363, 2009.

Session 1P13a
FocusSession.SC4: Optimal Antennas

Bandwidth Limitations and Trade-off Relations for Wide- and Multi-band Array Antennas over a Ground Plane

B. L. G. Jonsson
School of Electrical Engineering, KTH Royal Institute of Technology, Stockholm, Sweden

Abstract— There has been a recent drive to find fundamental limitations of bandwidth performance. Such results include Rozanovs (2000) bandwidth performance of absorbers, and Gustafssons (2007) limitation for single port antennas, similar bounds on transmission coefficients through a frequency selective screen and high-impedance surfaces are also known. In the present work we show a related bound for array antennas over a ground plane. We illustrate how this bound can be formulated as an array figure of merit, weighting impedance bandwidth, return loss, scan range and material and size information against each other.

The derivation of the array figure of merit is based on Bode-Fano theory for a scattering passive object, and is related to the Rozanov bound of absorbers. This result is essentially a sum-rule result that only requires that the element is a scattering passive, time-invariant and linear. The bound is derived for linearly polarized arrays over an infinite planar ground-plane.

The array figure of merit can both be used to evaluate existing antennas, and we illustrate the performance for some recent arrays. It can also be used as a prediction tool and hence as an a-priori assessment of impedance bandwidth limitations for a given antenna element. The array figure of merit contains return-loss, impedance bandwidth, scan range, and element specific information. We show how to use the array figure of merit to investigate trade-off between, e.g., return-loss and bandwidth or bandwidth versus thickness. Several cases are illustrated.

Different approaches to bandwidth measurement for wide-band array antennas are also discussed. We note that the array figure of merit easily extend to multi-band antennas.

Low-cost Solutions for Optimal Antenna Design

Amalendu Patnaik
Department of Electronics and Communication Engineering
Indian Institute of Technology Roorkee, Roorkee 247667, India

Abstract— Design of optimal antennas has been gaining much attention because of the number of unconventional demands by the wireless communication engineers. The usual process of the antenna design starts with a rough model in a simulator, where the dimensions are chosen using the available closed-form formulas. The performance of the initial designed antenna is observed and if it is not meeting the requirement of the user, then the antenna engineer has to play with all the design parameters until getting the desired response. This change of parameters, while simulating an antenna structure, is performed basically in a hit-and-trial way. As there are number of parameters involved in this process, so it makes the antenna design process a cumbersome one.

Looking the entire process from a mathematical point of view, observing the response for a specific model of an antenna is nothing but correlating a set of response parameters with a set of design parameters or in other words is a function mapping problem. Similarly, changing each parameter of the antenna in a hit-and-trial manner, until getting the desired response, is a kind of solving an optimization problem. In the present work, we have proposed to solve these two problems using soft-computing based approaches. A trained neural network (NN) is used to solve the function mapping problem, whereas, particle swarm optimization (PSO) technique is used to solve the optimization problem. The job of the NN is to correlate the design parameters of the antenna like with its response parameters, such as, resonant frequency, input impedance etc. A feed-forward NN trained in the back-propagation mode is used for this purpose. The job of the PSO is to systematize the hit-and-trial way of changing the antenna design parameters in order to reach the user defined goal. Although any other soft-computing based optimizer can be used for solving the task in hand, the reason of using PSO is: it is simple to apply, easy to code and is a high performance evolutionary computational technique. The performance of these soft-computing tools has already been verified in many microwave engineering applications.

Many typical antenna design problems are solved using the developed methodology, such as design of custom-made fractal antennas, stacked patch antennas and frequency selective surfaces. The performance of the designed structures is cross verified with the experimental results. Although at the developer level the process is very much time consuming, but at the user level the response of the developed methodology is very fast.

Determining Physical Bounds for Antennas above Ground Planes

Doruk Tayli and Mats Gustafsson
Department of Electrical and Information Technology, Lund University, Lund, Sweden

Abstract— Mobile phone antenna design poses a big challenge for antenna engineers. This is a result of integrating new communication standards and capabilities into a single terminal. The antenna performance is limited when the terminal is restricted to have smaller physical size.

To convert the antenna design procedure from an intuition based one to a scientific approach; the antenna engineer should know the quantitative value of the potential of the structure that they are working with. The main parameter of importance for small antenna design is the Q-factor and radiation efficiency. The antenna Q-factor is inversely proportional to the bandwidth and determines its bandwidth potential. The Q-factor has been rigorously investigated in [1–5].

Here we extend the results in [6] to find the physical bounds for antennas above ground planes using convex optimization. With the formulations in [7, 8] and the results from [5] the stored energies are written as quadratic forms. These are further expanded using basis functions, similar to the method of moments MoM. The resulting quadratic form can be written as a convex optimization problem for the ratio between gain and the Q-factor.

The physical bounds for different antennas above a ground plane are investigated. FEKO [9] simulation results show that the different antennas conform to the physical bounds. The results verify that convex optimization is an effective tool for computing the limits for the Q-factor.

REFERENCES

1. Wheeler, H. A., "Fundamental limitations of small antennas," *Proc. IRE*, Vol. 35, No. 12, 1479–1484, 1947.
2. Chu, L. J., "Physical limitations of omni-directional antennas," *J. Appl. Phys.*, Vol. 19, 1163–1175, 1948.
3. Volakis, J., C. C. Chen, and K. Fujimoto, *Small Antennas: Miniaturization Techniques & Applications*, McGraw-Hill, New York, 2010.
4. Gustafsson, M., C. Sohl, and G. Kristensson, "Physical limitations on antennas of arbitrary shape," *Proc. R. Soc. A*, Vol. 463, 2589–2607, 2007.
5. Gustafsson, M. and S. Nordebo, "Optimal antenna currents for Q, superdirectivity, and radiation patterns using convex optimization," *IEEE Trans. Antennas Propagat.*, Vol. 61, No. 3, 1109–1118, 2013.
6. Gustafsson, M., "Efficiency and Q for small antennas using Pareto optimality," *2013 IEEE International Symposium on Antennas and Propagation*, 2013.
7. Gustafsson, M. and B. L. G. Jonsson, "Stored electromagnetic energy and antenna Q," *Tech. Rep. LUTEDX/(TEAT-7222)/1-25/(2012)*, Lund University, 2012.
8. Vandenbosch, G. A. E., "Reactive energies, impedance, and Q factor of radiating structures," *IEEE Trans. Antennas Propagat.*, Vol. 58, No. 4, 1112–1127, 2010.
9. FEKO, "EM simulation software," https://www.feko.info/.

Further Research on the Stored Energies and Radiation Q

Geyi Wen
Research Center of Applied Electromagnetics
Nanjing University of Information Science and Technology, Nanjing, China

Abstract— This paper discusses the methods for evaluating the stored electromagnetic energies and the radiation Q for an arbitrary lossless antenna. It has been demonstrated that the most general expressions for the stored electric energy $\tilde{W}_e$ and magnetic energy $\tilde{W}_m$ around a radiator characterized by source distributions $\mathbf{J}$, ρ in a region V are given by

$$\begin{aligned}
\tilde{W}_e &= \frac{\eta v}{16\pi}\iint_v\iint_v \bar{\rho}(\mathbf{r})\rho(\mathbf{r}')\frac{\cos kR}{R}dV(\mathbf{r})dV(\mathbf{r}') \\
&\quad+\frac{\omega\eta}{32\pi}\iint_v\iint_v \left[\bar{\rho}(\mathbf{r})\rho(\mathbf{r}')-\frac{1}{v^2}\bar{\mathbf{J}}(\mathbf{r})\cdot\mathbf{J}(\mathbf{r}')\right]\sin kR dV(\mathbf{r})dV(\mathbf{r}') \\
&\quad-\frac{\omega\eta v}{16\pi}\iint_v\iint_v \mathrm{Im}\left[\bar{\rho}(\mathbf{r})\frac{\partial\rho(\mathbf{r}')}{\partial\omega}\right]\frac{\sin kR}{R}dV(\mathbf{r})dV(\mathbf{r}') \\
&\quad+\frac{\omega\eta v}{16\pi}\iint_v\iint_v \frac{1}{v^2}\mathrm{Im}\left[\bar{\mathbf{J}}(\mathbf{r})\cdot\frac{\partial\mathbf{J}(\mathbf{r}')}{\partial\omega}\right]\frac{\sin kR}{R}dV(\mathbf{r})dV(\mathbf{r}'). \\
\tilde{W}_m &= \frac{\eta v}{16\pi}\iint_v\iint_v \frac{1}{v^2}\bar{\mathbf{J}}(\mathbf{r})\cdot\mathbf{J}(\mathbf{r}')\frac{\cos kR}{R}dV(\mathbf{r})dV(\mathbf{r}') \\
&\quad+\frac{\omega\eta}{32\pi}\iint_v\iint_v \left[\bar{\rho}(\mathbf{r})\rho(\mathbf{r}')-\frac{1}{v^2}\bar{\mathbf{J}}(\mathbf{r})\cdot\mathbf{J}(\mathbf{r}')\right]\sin kR dV(\mathbf{r})dV(\mathbf{r}') \\
&\quad-\frac{\omega\eta v}{16\pi}\iint_v\iint_v \mathrm{Im}\left[\bar{\rho}(\mathbf{r})\frac{\partial\rho(\mathbf{r}')}{\partial\omega}\right]\frac{\sin kR}{R}dV(\mathbf{r})dV(\mathbf{r}') \\
&\quad+\frac{\omega\eta v}{16\pi}\iint_v\iint_v \frac{1}{v^2}\mathrm{Im}\left[\bar{\mathbf{J}}(\mathbf{r})\cdot\frac{\partial\mathbf{J}(\mathbf{r}')}{\partial\omega}\right]\frac{\sin kR}{R}dV(\mathbf{r})dV(\mathbf{r}').
\end{aligned}$$

These new expressions contain frequency derivative terms for the source distributions, and have been compared with previous theories and are validated by numerical examples. The minimization of radiation Q is also investigated. There exists an optimal current distribution that minimizes the radiation Q for specified antenna geometry. The optimized Q and the optimal current distribution may be determined by solving a generalized eigenvalue equation obtained from the Rayleigh quotient for the radiation Q.

Computational Challenges in Convex Optimization for Antenna Analysis

Sven Nordebo[1] and Mats Gustafsson[2]

[1]Department Physics and Electrical Engineering
Linnæus University, Växjö 351 95, Sweden
[2]Department Electrical and Information Technology
Lund University, Box 118, Lund SE-221 00, Sweden

Abstract— Current optimization provides performance bounds and suggestions for the distribution of optimal currents on antennas [1, 2]. Many current optimization problems can be solved efficiently by formulating them as convex optimization problems [3]. The formulations as convex optimization problems are also advantageous as they are easily generalized to specific antenna problems by inclusion of additional convex constraints.

In this presentation, we present an algorithm based on relaxation for the maximization of the gain Q-factor quotient. The algorithm is efficient for large problems as the relaxed problem is solved by inversion of a linear system. We present a derivation of the algorithm and several numerical examples.

REFERENCES

1. Gustafsson, M. and S. Nordebo, "Optimal antenna currents for Q, superdirectivity, and radiation patterns using convex optimization," *IEEE Transactions on Antennas and Propagation*, Vol. 61, No. 3, 1109–1118, 2013.
2. Cismasu, M. and M. Gustafsson, "Antenna bandwidth optimization with single frequency simulation," *IEEE Transactions on Antennas and Propagation*, Vol. 62, No. 3, 1304–1311, 2014.
3. Boyd, S. and L. Vandenberghe, *Convex Optimization*, Cambridge University Press, 2004.

Antenna Lenses from Transformation Optics

R. C. Mitchell-Thomas[1] and O. Quevedo-Teruel[2]

[1]Department of Physics and Astronomy
University of Exeter, EX4 4QL, England, UK
[2]School of Electrical Engineering
KTH Royal Institute of Technology, Stockholm SE-10044, Sweden

Abstract— Transformation optics is a novel method that creates a mathematical link between material properties and a set of coordinate systems [1, 2]. Using this technique, it is possible to calculate the material properties that need to be implemented so that commonly used electromagnetic devices, such as lenses, can have their physical shape changed whilst retaining their functionality. However, the exact analytical route to calculating these properties requires anisotropic media that have complex structure and severely limit the bandwidth due to the resonant materials used to create them [3]. A route to overcome this problem was proposed, and utilises a quasi-conformal transformation [4]. This involves an approximation which defines purely isotropic devices. Provided that each individual discrete cell is not severely stretched in one dimension, or is heavily twisted, the accuracy of this method is high.

Quasi-conformal transformations have previously been employed to re-design standard lenses to that they are either planar or conformal to given surfaces [5]. This presentation will explore the possibility to create bespoke lenses for common antenna feed types, such as a microstrip patch, to create highly directive beams. This differs from the previous work as it does not rely on an existing lens, but will simply redirect the radiated wave fronts using a graded index lens. During the presentation, a number of examples will be shown, and numerical simulations will be used to evaluate the performance.

ACKNOWLEDGMENT

This work was funded by the Engineering and Physical Sciences Research Council (EPSRC), UK under a Programme Grant (EP/I034548/1) "The Quest for Ultimate Electromagnetics using Spatial Transformations (QUEST)".

REFERENCES

1. Pendry, J. B., D. Schurig, and D. R. Smith, "Controlling electromagnetic fields," *Science*, Vol. 312, 1780, 2006.
2. Leonhardt, U., "Optical conformal mapping," *Science*, Vol. 312, 1777, 2006.
3. Schurig, D., J. J. Mock, B. J. Justice, S. A. Cummer, J. B. Pendry, A. F. Starr, and D. R. Smith, "Metamaterial electromagnetic cloak at microwave frequencies," *Science*, Vol. 314, 977, 2006.
4. Li, J. and J. B. Pendry, "Hiding under the carpet: A new stratergy for cloaking," *Physical Review Letters*, Vol. 101, 203901, 2008.
5. Quevedo-Teruel, O., W. Tang, R. C. Mitchell-Thomas, A. Dyke, H. Dyke, L. Zhang, S. Haq, and Y. Hao, "Transformation optics for antennas: Why limit the bandwidth with metamaterials?," *Scientific Reports*, Vol. 3, 1903, 2013.

Quality Factor for Antennas: A Tutorial

Arthur D. Yaghjian
Electromagnetics Research Consultant, 115 Wright Road, Concord, MA 01742, USA

Abstract— After a review of the theory of antenna bandwidth and quality factor (Q), the lower-bound formulas for the Q of electrically small antennas in an arbitrarily shaped volume are derived for combined electric and magnetic dipole moments excited by both electric and magnetic surface currents as well as by electric surface currents alone. With either excitation, separate formulas are found for the dipole antennas containing only lossless (or "nondispersive-conductivity") material and "highly dispersive lossy" material. The formulas involve the quasi-static electric and magnetic polarizabilities of the associated perfectly conducting volume of the antenna, the ratio of the powers radiated by the electric and magnetic dipoles, and the efficiency of the antenna. The talk introduces a universally valid formula for antenna impedance bandwidth, then discusses the associated formula for the Q of antennas with lossless or nondispersive-conductivity material, and finally generalized this formula to antennas with highly dispersive lossy material. This general formula for Q is made possible by the development of a surprisingly simple formula for energy density in material that can be highly dispersive and lossy. Comparisons of energy density obtained with the simple formula are made with previously postulated possibilities for energy density in highly dispersive lossy material. With the help of the general formula for Q, the lower bounds on Q are found for linear, single-port, passive antennas tuned to an isolated resonance or antiresonance with a series capacitor or inductor. Examples of antennas are given that approach the derived Q lower bounds.

An Overview of Current Optimization and Physical Bounds on Antennas

Mats Gustafsson
Department of Electrical and Information Technology
Lund University, Box 118, Lund SE-221 00, Sweden

Abstract— Optimization is used in antenna technology to improve and construct new designs [7]. Global optimization based on random search algorithms, such as genetic algorithms [6] and particle swarm dominate the field of antenna design due to the non-linearity and non-convexity of most antenna problems. Optimization of the current density is fundamentally different and many antenna problems are convex in the current density [3, 5]. The formulations as convex optimization problems are very powerful as there are many efficient algorithms and dual problems can be used for error estimates [1]. For antennas, we can formulate many optimization problems relevant for antenna problems by combining the stored energy, radiated power, near-and far fields, and induced currents [4, 5].

Current optimization provides physical bounds on antenna performance and examples of optimal current distributions. The physical bounds are useful because they provide a bound on the performance solely based on the shape and size of the design volume. The concept of physical bounds for electrically small antennas was first introduced more than half a century ago by Chu and Wheeler [2, 8]. In this presentation, an overview of current optimization for small antennas is presented.

REFERENCES

1. Boyd, S. P. and L. Vandenberghe, *Convex Optimization,* Cambridge University Press, 2004.
2. Chu, L. J., "Physical limitations of omni-directional antennas," *J. Appl. Phys.*, Vol. 19, 1163–1175, 1948.
3. Cismasu, M. and M. Gustafsson, "Antenna bandwidth optimization with single frequency simulation," *IEEE Trans. Antennas Propagat.*, Vol. 62, No. 3, 1304–1311, 2014.
4. Gustafsson, M., M. Cismasu, and B. L. G. Jonsson, "Physical bounds and optimal currents on antennas," *IEEE Trans. Antennas Propagat.*, Vol. 60, No. 6, 2672–2681, 2012.
5. Gustafsson, M. and S. Nordebo, "Optimal antenna currents for Q, superdirectivity, and radiation patterns using convex optimization," *IEEE Trans. Antennas Propagat.*, Vol. 61, No. 3, 1109–1118, 2013.
6. Haupt, R. L. and D. H. Werner, *Genetic Algorithms in Electromagnetics,* Wiley-IEEE Press, 2007.
7. Rahmat-Samii, Y. and E. Michielssen, "Electromagnetic optimization by genetic algorithms," *Wiley Series in Microwave and Optical Engineering*, John Wiley & Sons, 1999.
8. Wheeler, H. A., "Fundamental limitations of small antennas," *Proc. IRE*, Vol. 35, No. 12, 1479–1484, 1947.

Session 1P13b
SC4: THz Antennas and Systems

A Simple Experimental Method to Analyze the Properties of Terahertz-wave Propagation in Complex Atmosphere

X. Q. Lin[1, 2], P. Mei[2], X. F. Yang[1], J. W. Yu[2], Y. Jiang[2], and Y. Fan[2]

[1]State Key Laboratory of Complex Electromagnetic Environment Effects on Electronic and Information System, Luoyang Electronic Equipment Center of China, Luoyang 471003, China
[2]EHF Key Laboratory of Science, School of Engineering
University of Electronic Science and Technology of China, Chengdu 611731, China

Abstract— Terahertz-wave has received considerable attention in both scientific and engineering communities for its higher communication speed, better imaging resolution and less harm medical care. More recently, satisfactory achievements are obtained in designing terahertz source and detector equipments. But the advancement of researches on terahertz-wave propagation properties is still poor. The main analysis method is given by ITU-R [1] which is only suitable for idea atmospheric as only the oxygen, nitrogen and water vapor are considerable. For real complex atmosphere, experimental method is preferred. However, the presented experimental systems are extremely complicated and expensive [2, 3]. They are difficult to be copied by common fabricated technology.

In this paper, a much simple experimental method is proposed to analyze the terahertz-wave propagation properties. The schematic diagram and process of parameter retrieval are shown in Figs. 1(a) and (b), respectively. Two terahertz-wave transmission paths are presented in one vacuum chamber but with different lengths. Two switches are required to selected different transmission paths in a short time by which the measurement errors such as assembling error and instrumental error can be ignored. Different complex atmosphere can be injected into the vacuum chamber and its equivalent electromagnetic parameters such as relative permittivity and permeability can be retrieved. Then the detailed propagation properties can be further calculated. The above method is certificated in full-wave simulation and the error is less than 3% when isotropic material is used to simulate the atmosphere.

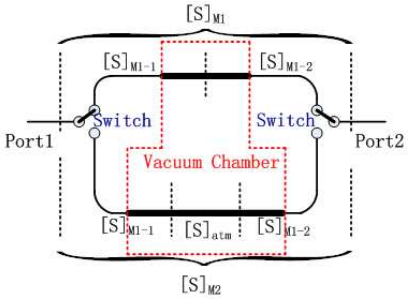

(a)

Retrieval Process:
Step 1: Inject the atmosphere;
Step 2: Measure the $[S]_{M1}$;
Step 3: Calculate the $[S]_{M1-1}$ and $[S]_{M1-1}$;
Step 4: Measure the $[S]_{M2}$;
Step 5: Calculate the $[S]_{atm}$;
Step 6: Retrieve the equivalent medium parameters;
Step 7: Calculate the propagation properties.

(b)

Figure 1: The schematic diagram and process of parameter retrieval. (a) Schematic diagram. (b) Retrieval Process.

REFERENCES

1. International Telecommunications Union, Radiocommunications Bureau, "Attenuation by atmo-spheric gases," *Recommendation ITU-R*, 676-9, February 2012.
2. Meshkov, A. I. and C. D. L. Frank, "Laboratory measurements of dry air atmospheric absorption with a millimeter wave cavity ringdown spectrometer," *Journal of Quantitative Spectroscopy and Radiative Transfer*, Vol. 108, No. 2, 256–276, 2007.
3. Yang, Y., M. Mandehgar, and D. Grischkowsky, "Determination of the water vapor continuum absorption by THz-TDS and molecular response theory," *Optics Express*, Vol. 22, No. 3, 4388–4403, 2014.

A General and Effective Clutter Filtering Strategy for Quiet Zone Evaluation in Tri-reflector Compact Range

Jingjuan Wang[1], **Cheng Yang**[1], **Yuan Yao**[1], **Xiaoming Liu**[1], **Junsheng Yu**[1], **and Xiaodong Chen**[2]

[1]School of Electronic Engineering
Beijing University of Posts and Telecommunications, Beijing, China
[2]School of Electronic Engineering and Computer Science
Queen Mary University of London, London, UK

Abstract— Nowadays, millimeter and sub-millimeter wave technique is broadly applied in fields such as remote sensing, radio astronomy. In order to verify the performance of millimeter and sub-millimeter system, accurate measurement should be performed. Compact antenna test range (CATR) is a promising method for electrically large antenna measurement due to that it can generate a pseudo-plane wave region, which is often referred to as quite zone.

The performance of CATR mainly depends on the amplitude and phase ripple in the quiet zone. Various sources may affect the performance of the quiet zone, including environment clutter, especially in millimeter and sub-millimeter band. Method of moment is widely used to reduce clutter noise because of its simple principle. However, in the case of CATR, this method has to simulate all the processes like wave packet generation, diffraction, absorption which cause complexity and large calculating quantity. Besides, all the properties have to be simulated all over again for each new project. The aim of this paper is to provide a brief and general method to deduce quiet zone clutter noise of a CATR, using the theory of digital signal processing.

A clutter filtering strategy is presented to enhance the performance of the quiet zone of a tri-reflector compact antenna test range. The method is based on the band limitation properties of the scattered fields to filter the noise in quiet zone. Priori information on the source, such as its size, geometry, and position are required in this approach. By exploiting a simple low-pass filter, this filtering strategy can partially filter out the environmental clutter. Numerical results will be presented in the full-length paper. A flowchart is shown below:

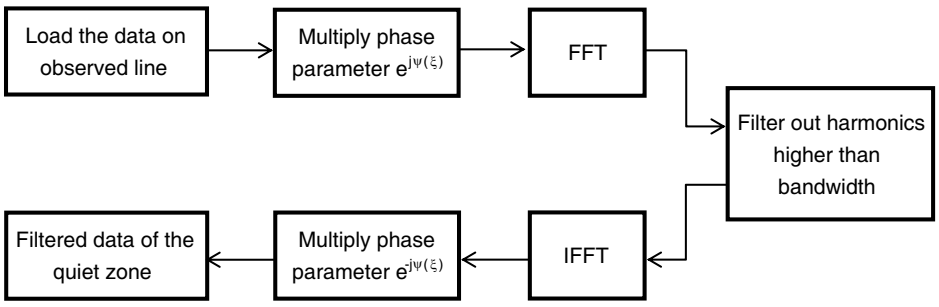

Figure 1: Flowchart of filtering algorithm in case of CATR.

Implementation of Three-dimensional Diffractive Gaussian Beam Analysis Method

Fangyuan Cheng[1], **Zejian Lu**[1], **Xiaoming Liu**[1], **Hai Wang**[1], **Junsheng Yu**[1], **and Xiaodong Chen**[2]

[1]School of Electronic Engineering, Beijing University of Posts and Telecommunications
279 Box, 10 Xi Tu Cheng Road, Haidian District, Beijing 100876, China
[2]School of Electronic Engineering and Computer Science, Queen Mary University of London
Mile End Road, London El 4NS, UK

Abstract— This paper reports a 3-dimensional Diffractive Gaussian Beam Analysis (DGBA) method for the analysis of electrically large reflector antennas. Many numerical calculation methods can be employed to predict the diffracted fields of reflector antennas such as Physical Optics (PO) and Geometrical Optics (GO). Unfortunately,GO does not account for the effects of boundary diffraction, which is however, very important in some antenna systems. PO is an accurate and modular method for analyzing reflector antennas, but it is expensive in terms of computation time and storage for electrically large system. In this connection, a faster method, namely diffracted Gaussian beam analysis, combines the numerical efficiency of GO in terms of beam-modes analogous to rays in GO, and the rigor of PO, has been developed. Nevertheless, the current 2-Dimensional DGBA requires the incident wave and reflector to be symmetrical about a certain plane, such that the optical centers of the feed and all of the reflectors must lie on the same plane. To overcome this limitation, this paper introduces the approach of full plane expansion, where the field over the whole input plane is decomposed to a series of GBs. This method can be applied to stereoscopic system in some practical applications. An preliminary analysis have been conducted for the reflected field and the diffracted filed, as shown in Fig. 1. The future work will focus on the integration of the reflection and diffraction to a complete method.

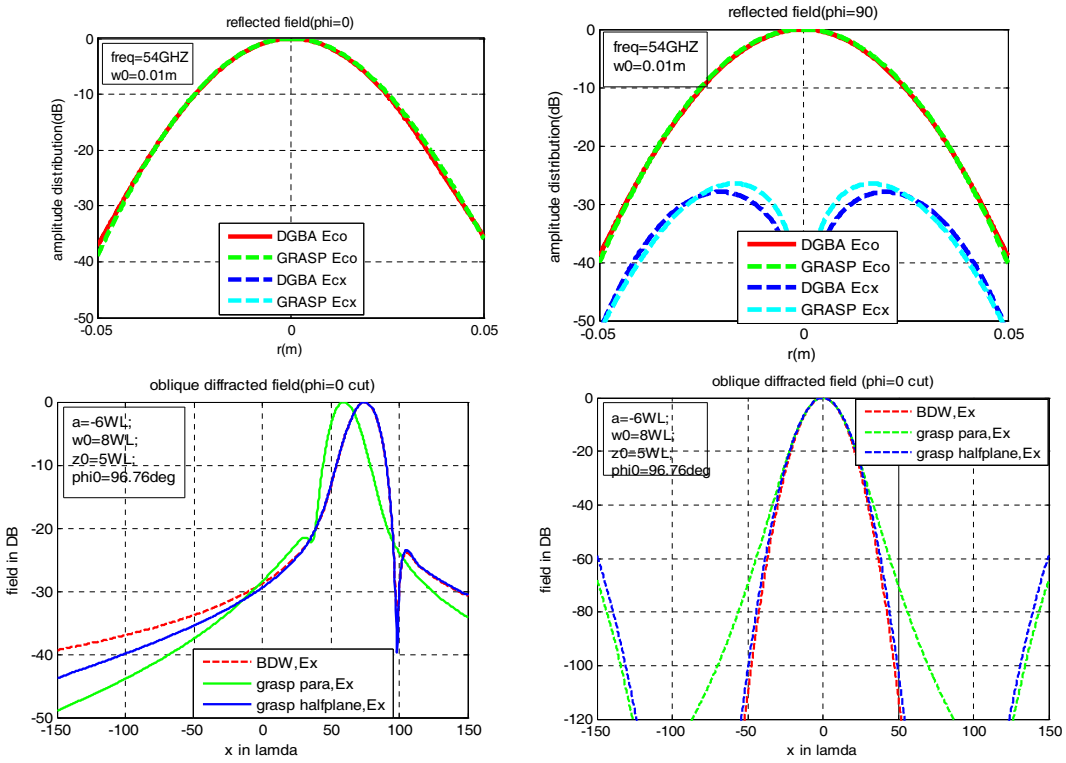

Figure 1: The reflected field and the diffracted filed.

A Fast Gaussian Beam Tracing Method for Quasi-optical System Analysis Based on Gabor Frame Expansion

Hai Wang[1], **Zejian Lu**[1], **Fangyuan Cheng**[1], **Junsheng Yu**[1], **Xiaodong Chen**[2], **Xiaoming Liu**[1], **and Yuan Yao**[1]

[1]School of Electronic Engineering
Beijing University of Posts and Telecommunications, Beijing 100876, China
[2]School of Electronic Engineering and Computer Science
Queen Marry University of London, E1 4NS, UK

Abstract— Quasi-optical system has been the topic of research in the past decades. With the increase of frequency, Gaussian beam analysis method becomes more accurate and practical, and takes advantage of analytical simplicity with respect to Physical Optics (PO) or Geometrical Optics (GO) especially calculating unsymmetrical and large electrically reflector antenna. The conventional modeling approaches in multi-reflector quasi-optical system analysis are constituted by two aspects: expansion techniques and tracking techniques. Gaussian Beam (GB) is traced into a reflector where reflection or diffraction occur and emergent beam fields can be obtained via superimposing all GBs. However, beams of radiation in quasi-optical are effectively confined near optical axis, which can be considered as focused pure GB. Based on this conclusion, a fast quasi-optical analysis method is proposed on the assumption that the diffraction on the reflector edge is rare thus can be neglected if the reflector size is four times larger than the beam width for incident GBs. In this method, the field pattern of feed is expanded into sets of sub-GBs using Gabor frame expansion method, and near area of specular reflection point is approximated as parabolic model to solve out reflection wave parameters according to the incident wave and mirror parameters. A multi-reflector quasi-optical system can be performed by introducing the astigmatic GB, which well represents characterization of electromagnetic propagation and makes a very quick evaluation of the system performance. Feed pattern have been successfully expanded into sub-GBs and recovered signal after propagation distance 0.5 m as showed in Figure [1] and some numerical simulation result of reflection an astigmatic GB on a curved surface is provided from Figure [2]. Numerical and experimental comparison reveal a good trade-off between the accuracy and the computational effort.

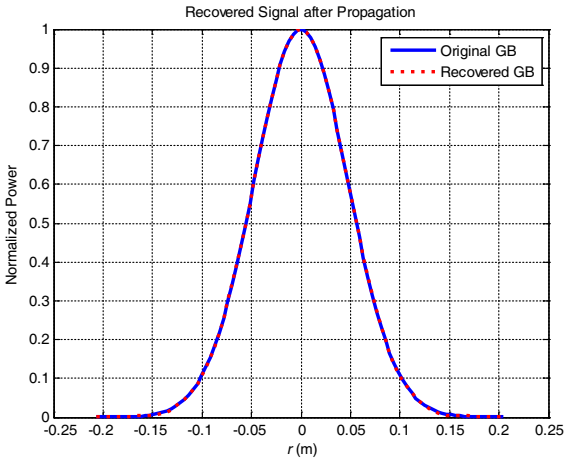

Figure 1: Far field pattern of feed (solid line) and is expanded into sets of sub-GBs using Gabor frame expansion method and its recovered field pattern (dotted line) after propagation distance 0.5 m.

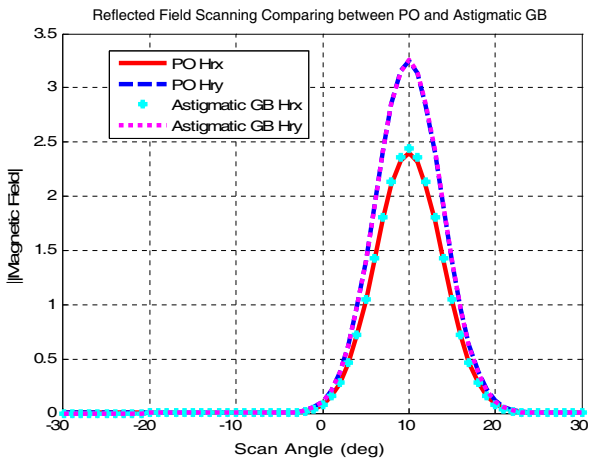

Figure 2: A single astigmatic GB oblique incidence on the reflector, reflected field scanning comparing between PO and astigmatic GB.

Evaluation of the Fast Scanning THz-TDS Unit Using Voice Coil Motor

Yuma Nanba, Yasumasa Matsuoka, Kenji Sakai, Toshihiko Kiwa, and Keiji Tsukada
Graduate School of Natural Science and Technology, Okayama University
3-1-1 Tsushima-naka, Kita-ku, Okayama-Shi, Okayama Prefecture 700-8530, Japan

Abstract— In recent years, terahertz (THz) technology has been advanced rapidly by the development of technology such as laser and semiconductor technology. The terahertz wave which has the characteristics of light and radio wave is expected to apply to quality inspection of chemical and non-destructive testingdetection of illegal drugs and explosives at the airport. Among various types of THz technology, THz time-domain spectroscopy (THz-TDS) is one of the promised tools for materials research by analyzing the amplitude and phase, since a lot of information of inter-molecules are existed in the THz regions. The optical sampling methods are generally used to detect the time-domain waveforms of THz waves and thus mechanically-driven time-delays are required for measurement. Thus it generally takes about 5 min. for measure a single THz waveform.

In this work, a voice coil driven time-delay derived from Kyowa Fine Tech Co. Ltd., Japan was applied for fast scanning. The reflection mirror and the core of the voice coil were simultaneously vibrated in counter derations, therefore, the vibration were not transferred to the optical setups. As the result, a single waveform can be obtained in approximately 250 ms by vibrating the voice coil at 2 Hz. We can simultaneously display the THz wave on an oscilloscope by acquiring waveform quickly and the frequency spectrum of the THz wave by using the FFT conversion function. In addition, the signal-to-noise ratio can be increased by integrating THz waveform.

Here, the signal-to-noise ratio as a function of measurement time was evaluated.

Session 1P14a
SC5: Inverse Problems: Theories, Computations, and Applications

Simultaneous Reconstruction of the PEC and Dielectric Scatterers Via Inverse Scattering Method

Xiuzhu Ye
Beihang University, Beijing 100191, China

Abstract— The methods for reconstructing perfect electric conductor (PEC) or dielectric scatterers individually, have already been well studied in the inverse society. However, the problem of reconstructing the two kinds of scatterers together is not often addressed in the literature. The difficulty comes mainly from the modelling method. Due to different boundary conditions, the PEC is commonly modeled by the surface based pixel while the dielectric is usually modeled by the volume based pixel, which poses difficulty in modeling them together. Another difficulty comes from lack of physical parameter that can represent the two kinds of scatterers simultaneously. One existing method is to approximate the PEC into highly lossy scatterer. Thus the PEC and dielectric are both represented by the permittivity. However, this method cannot distinguish the PEC and lossy scatterer due to the approximation taken.

In this paper, the dielectric scatterer and PEC are both modeled by T-matrix, which serves as the physical parameter representing both dielectric and PEC. The T-matrix is derived directly from the boundary condition. The two kinds of scatterers are successfully modeled by the volume based pixel, and the classification criterion is derived from the asymptotic series of the T-matrix. The subspace based optimization method (SOM) is applied to realize the iterative process.

Examples are given to prove the reconstruction ability of the proposed method. Apart from the synthetic data, the algorithm is also tested by the experimental data from Fresnel Institut. The numerical results show that the T-matrix method is able to simultaneously reconstruct the dielectric and PEC scatterers. Besides, the proposed method is also able to differentiate the highly lossy dielectric scatterer from the PEC scatterer.

Subspace-based Optimization for Inverse Scattering Problems at Oblique Incidence

Qingyang Meng, **Dexin Ye**, **Qinyi Lv**, **and Lixin Ran**
Laboratory of Applied Research on Electromagnetics (ARE)
Zhejiang University, Hangzhou 310027, China

Abstract— Inverse scattering problems, i.e., reconstructing the permittivities of scatterers by utilizing the information of scattering data, has found its wide applications in many areas, such as biomedical imaging, non-destructive testing and remote sensing. The subspace-based optimization method (SOM) has been found an effective method for solving inverse scattering problems which is fast convergent and robust against noise. In this paper, we investigate the subspace-based optimization method applied on inverse scattering problems at oblique incidence. Compared with general 2-D problems, electric vectors in oblique incident occasion have more components and complicated coupling between different components. Furthermore, it is hard to measure all electric vector components in experiments. To overcome such difficulties, we modify the SOM and reconstruct the permittivities of scatterers with only axial electric component. By choosing the number of singular values that is used to span signal space carefully, our method shows to be effective in large range of angles.

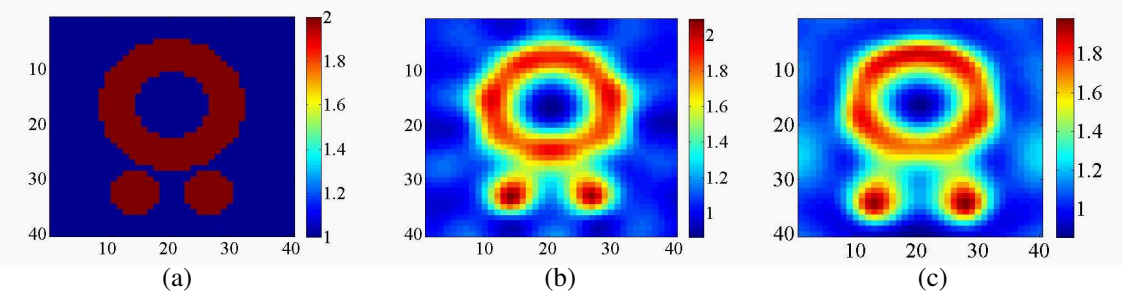

Figure 1: The numerical simulation results, (a) original profile, (b) reconstructed profile with oblique angle 20 degrees and SNR 20 dB, (c) reconstructed profile with oblique angle 40 degrees and SNR 20 dB.

Doppler Radar Sensor Based Small- and Large-scale Motion Imaging

Qinyi Lv[1], **Dexin Ye**[1], **Qingyang Meng**[1], **Shan Qiao**[2], **and Lixin Ran**[1]

[1]Laboratory of Applied Research on Electromagnetics (ARE)
Zhejiang University, Hangzhou 310027, China
[2]Zhejiang University City College, Hangzhou 310015, China

Abstract— Doppler radar sensor has widely used in non-contact movement monitoring. Previously, small-scale physiological signals such as human respiration and heartbeat rates are the primary interest of study. In this paper, we propose a comprehensive approach that can be used to improve the demodulation linearity of microwave Doppler radar sensors, such that detailed time-domain motion information ranging from micro- to large-scales can be accurately reconstructed. Experiments show that based on digital-IF receiver architecture, dynamic DC offset tracking, and the extended differentiate and cross-multiply (DACM) arctangent algorithm, the displacement and velocity of both micrometer-scale cardiac motion and meter-scale human walking can be accurately recovered. Our work confirms that substantial time-domain motion information is carried by the signals backscattered from moving objects. Retrieval of such information using Doppler radar sensor can be potentially used in a wide range of healthcare and biomedical applications, such as motion pattern recognition and bio-signal measurements.

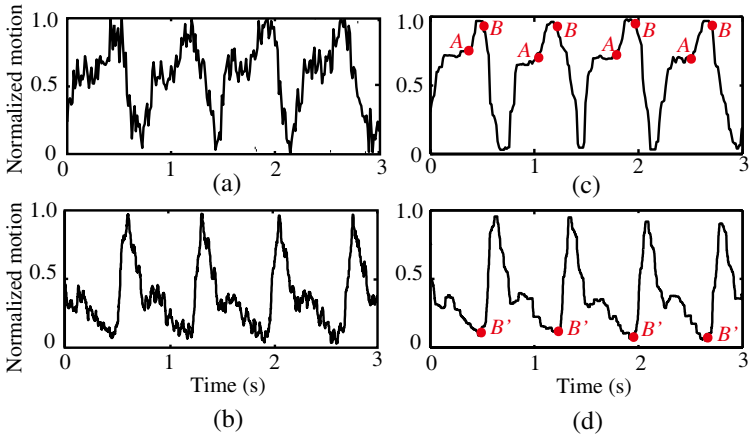

Figure 1: The experimental results when the subject held the breath: (a) time domain cardiac motion reconstructed by the extended DACM algorithm, (b) artery pressure captured by the contact sensor, (c) median filtering result of the time domain cardiac motion, and (d) median filtering result of the artery pressure, all of which comply with the descriptions in the popular medical textbook.

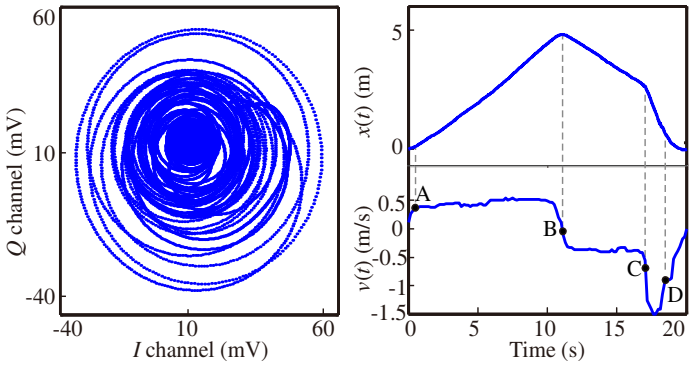

Figure 2: The experimental results of 5-meter human walking. The subject jumped in his return trip at around 18 seconds. The recovered displacement and velocity clearly demonstrates this jump with velocity change from $-0.4\,\mathrm{m/s}$ to $-1.5\,\mathrm{m/s}$.

Imaging Dielectric Objects by Limited Diversity of Scattering Data

C. X. Yang, R. P. Chen, Y. J. Zhang, C. N. Xu, S. C. Yan, and M. S. Tong
Department of Electronic Science and Technology, Tongji University
4800 Cao'an Road, Shanghai 201804, China

Abstract— Solving inverse scattering problems is challenging because the involved governing equations are nonlinear and the solutions are inherently nonunique. This is particularly true when measuring conditions are unfavorable and diverse scattering data are not available. Usually, the inverse problems are solved by linearizing governing equations and gradually minimizing the mismatch between calculated data and measured data in an iterative scheme. In the integral equation approach (IEA) for reconstructing dielectric objects, there are forward scattering integral equation (FSIE) and inverse scattering integral equation (ISIE) and we need to alternatively solve them in the context of distorted Born iterative method (DBIM) or its variations. The solution of permittivity from the ISIE can reveal the profile of unknown object in the imaging domain.

The ISIE is insolvable by direct inversion because the matrix equation is inherently ill-posed and the diversity of measured data with noise contamination is usually limited. One has to transform the inversion of measured data into an optimization problem and the best solution is chosen by minimizing a cost functional. The optimization problem can be solved by different approaches and we apply the DBIM-like Gauss-Newton minimization approach (GNMA) in this work since it can be conveniently incorporated with the multiplicative regularization method (MRM) and line search method (LSM) to enhance the inversion quality. The MRM was proposed for gradient-type algorithms and was used for the inversion by the finite difference time domain (FDTD) approach, but we use it for the IEA in this work. The MRM can adaptively vary the regularization parameter as the iteration proceeds so it is unnecessary to perform a large number of numerical experiments for choosing the regularization parameter. We also incorporate the LSM which can optimize the search of step size in each iteration and accelerate the convergence of inversion process. The use of MRM and LSM is essential when we consider the reconstruction with a poor measurement condition which may be encountered in many applications. A numerical example for reconstructing a two-dimensional (2D) dielectric object with a limited view is presented to illustrate the approach.

Time Reversal Imaging Using Minimum Norm Iterative Type Partial Noise Subspace Method

Qiang Gao, **Wei Gao**, **Xiao-Hua Wang**, **and Bing-Zhong Wang**
School of Physical Electronics, University of Electronic Science and Technology of China
No. 4, Section 2, North Jianshe Road, Chengdu 610054, China

Abstract— Orthogonality between the signal subspace and noise subspace is the foundation of the time reversal operator (TRO) based imaging techniques. The TRO-based methods have better performance than the traditional time reversal wave back propagation method, which benefits from the spatial and temporal focusing properties of the time reversal waves. The decomposition of time reversal operator (DORT) method and time reversal multiple signal classification (TR-MUSIC) method are the well-known two types of TRO-based imaging algorithm widely used in optics and electromagnetics. DORT and TR-MUSIC methods employ signal and noise subspaces, respectively. DORT method is more stable than TR-MUSIC method in the noise cases, while the TR-MUSIC has higher resolution than DORT method. TR-MUSIC method costs more computing resources than DORT method because the vector numbers of noise subspace is greater than that of the signal subspace in most cases. And in noise case, the eigenvalues of the eigenvalue decomposition of the multi-static response (MSR) matrix are hard to distinguish the zero and non-zeros, then the undesirable error is inevitable in the division of the signal subspace and noise subspace. To overcome this flaw, a signal subspace based entropy minimization method is developed, the method eliminates the estimation of a cutoff in signal versus noise subspaces.

In the direction-of-arrival (DOA) estimation, the well-known MUSIC method used the whole noise subspace, while the minimum norm method used one vector to reduce the computing resource. In the original minimum norm method, a polynomial with special properties is constructed by the eigenvectors of the covariance matrix, the zeros of the polynomial give estimations of the angle of arrival. In addition, a required minimum norm function is calculated by the special power basis instead of eigenvector basis, this method provides a substantial saving compared with the computing resources of eigenvalue decomposition based minimum norm algorithm when the number of multiple sources is much lower than that of the array sensors. And the case also is a huge challenge to the MUSIC method. By analyzing the mean square error of MUSIC method and minimum norm method, the results show that the relative performance of MUSIC method and the minimum norm method depends on the ratio of their parameter sensitivities.

In this paper, a minimum norm iterative type partial noise subspace imaging method is proposed to estimate the locations of targets in free space. Compared with the TR-MUSIC method of using all noise subspace vectors, the imaging precision of the minimum norm method has declined in a certain degree. To solve this problem, an iterative process is introduced. Thus, the proposed method avoids the difficulty of distinguishing the signal subspace with noise subspace while providing stable imaging of the targets. In multiple scattering case, the singular value decomposition of the MSR matrix is employed to generate the signal subspace vectors (signal vectors) and noise subspace vectors (noise vectors). Actually, the tow subspaces need not to be divided. Finally, similar to the minimum norm type method, the single noise vector in noise-well case and the partial noise subspace (bottom noise vectors) in high-level noise case are used to compute the imaging pseudo-spectrum, respectively. Numerical simulation results show the proposed method provides stable imaging and reduces the computing resources than the TR-MUSIC method, whilemaking up the shortfall of the minimum norm method and possessing similar imaging precision as well as the TR-MUSIC method. The iterative partial noise subspace method can replace the TR-MUSIC method in many cases without any loss. It is a good method for fast detection and imaging of targets.

Contrast Source Inversion Method Using the Wavelet Basis

Oguz Semerci[1], **Maokun Li**[1], **and Aria Abubakar**[2]

[1]Schlumberger-Doll Research, Cambridge, MA, USA
[2]Schlumberger, Houston, TX, USA

Abstract— Wavelet transform has been applied to electromagnetic modeling and inversion due to the multiscale nature of wavelet basis. It decomposes an image into a coarse representation plus a sequence of refinements, where wavelets at different levels represent details of the image at different scales. In this work, we present a contrast source inversion (CSI) algorithm which employs truncated wavelet representations of the inversion domain. Specifically, we represent both the unknown contrast sources and the contrast function in the wavelet domain, and we control the resolution of reconstruction by constraining the number of levels in the wavelet representation. Therefore, our method can be considered as a multi-scale approach.

In order to reduce the number of wavelet coefficients for these unknowns, we apply a progressive multi-scale truncation scheme based on the reconstructed contrast function. First, we solve the inverse problem using only the low-scale wavelet representations. This step provides a smooth, nevertheless stable, reconstruction of the contrast sources and the contrast distribution. In the second step, we first determine the locations of significant higher scale wavelet representations from the wavelet representation at a lower level using a nonlinear transform. The nonlinear transform we developed for this purpose utilizes the scale-location relationships between levels. Then, we solve another inverse problem using this extended set of wavelet coefficients.

The aim of employing a truncation scheme is to eliminate the redundancy in the full wavelet representation as well as improving the efficiency of the CSI algorithm especially for the case where the number of measurement data points is significantly less than the number of unknowns in the spatial domain contrast sources and contrast distribution. Secondly, our approach automatically correlates the locations of the wavelet coefficients that represent the real and the imaginary parts of the contrast function, which in turn improves the accuracy of the inversion.

We tested the wavelet-domain CSI method using both synthetic and experimental data. The numerical experiments show that the wavelet-domain CSI method can reconstruct better images compared to conventional CSI method when the number of measurement data points is smaller than the number of unknowns in the contrast function. In conclusion, our method increases the robustness of the CSI algorithm for noisy or limited data, and decreases the computation time as well as the memory usage.

Non-contact Thermoacoustic Imaging

Xiong Wang[1], **Yexian Qin**[2], **Tao Qin**[1], **Huan Meng**[1], **Russell S. Witte**[2], **and Hao Xin**[1]

[1]Department of Electrical and Computer Engineering, University of Arizona, Tucson AZ 85721, USA
[2]Department of Medical Imaging, University of Arizona, Tucson, AZ 85724, USA

Abstract— Microwave-induced thermoacoustic imaging (TAI) has been actively researched in the past decade [1–4] and shown to be a promising non-ionizing technology for various applications, such as breast cancer imaging, brain imaging, foreign body detection, renal calculi detection and prostate cancer imaging, to name but a few. TAI develops an image indicative of the internal features of a dielectrically lossy sample by exploiting emanated acoustic waves from absorbed pulsed microwave energy in the sample due to the thermoacoustic effect [5]. As a hybrid modality, TAI integrates several attractive merits, including large contrast, high spatial resolution and low cost of implementation.

In conventional TAI modalities, some acoustic coupling medium (usually oil [1, 3, 4] or water [2]) is required to couple the generated acoustic waves from sample to receiving acoustic transducers. However, this contacting modality limits some potential applications of TAI, in which a physical contact with the sample or patient is undesired or impractical. For example, brain surgery, retinal screening, burn diagnosis, living small animal imaging and explosive detection. Therefore, developing non-contact TAI technique, which obviates the use of coupling medium and detects the needed thermoacoustic signals through air, is certainly beneficial to applying TAI to these new areas. In addition, non-contact TAI is also favorable to breast cancer screening, adding one more advantage to its translation to the clinic.

Non-contact modality of photoacoustic imaging (PAI) [6–8], which is similar to TAI but uses optical excitations, has been demonstrated by several groups. It employs a vibrometer to remotely acquire the photoacoustic signals, namely displacements at the surface of the sample induced by the mechanical vibrations associated with the acoustic waves launched inside the sample. Similar to acoustic pressures measured in conventional TAI or PAI, the obtained displacements also contain useful information for reconstructing images of the sample. Accordingly, non-contact TAI can be established by direct analogy with non-contact PAI. Compared to non-contact PAI, non-contact TAI lends itself to deeper penetration into the sample and is more suitable to some applications.

In this work, non-contact TAI is proposed and some facets of it are introduced in details. One of the most important features affecting the performance of non-contact TAI is the magnitude of the displacements. Numerical models specifically for non-contact TAI are built to simulate time-domain acoustic wave propagation and displacement generation subject to the input microwave signal. An experimental system is also explored based on different vibrometer technologies. Preliminary results indicate that simulated displacements are in good agreement with those measured in experiments. Proof-of-concept demonstration of non-contact TAI is achieved.

REFERENCES

1. Wang, L. V., X. Zhao, H. Sun, and G. Ku, "Microwave-induced acoustic imaging of biological tissues," *Rev. Sci. Instrum.*, Vol. 70, No. 9, 3744–3748, September 1999.
2. Kruger, R. A., K. D. Miller, H. E. Reynolds, W. L. Kiser, D. R. Reinecke, and G. A. Kruger, "Breast cancer in vivo: Contrast enhancement with thermo-acoustic CT at 434 MHz — Feasibility study," *Radiology*, Vol. 216, No. 1, 279–283, July 2000.
3. Nie, L., D. Xing, D. Yang, L. Zeng, and Q. Zhou, "Detection of foreign body using fast thermoacoustic tomography with a multielement linear transducer array," *Appl. Phys. Lett.*, Vol. 90, 174109, 2007.
4. Wang, X., D. R. Bauer, R. Witte, and H. Xin, "Microwave-induced thermoacoustic imaging model for potential breast cancer detection," *IEEE Trans. Biomed. Eng.*, Vol. 59, No. 10, 2782–2791, Oct. 2012.
5. Bell, A. G., "Production of sound by radiant energy," *J. Franklin Inst.*, Vol. 111, 401–426, 1881.
6. Carp, S. A., A. Guerra, III, S. Q. Duque, Jr., and V. Venugopalan, "Optoacoustic imaging using interferometric measurement of surface displacement," *Appl. Phys. Lett.*, Vol. 85, No. 23, 5772–5774, Dec. 2004.

7. Rousseau, G., B. Gauthier, A. Blouin, and J. Monchalin, "Non-contact biomedical photoacoustic and ultrasound imaging," *J. Biomed. Opt.*, Vol. 17, No. 6, 061217-1–061217-7, June 2012.
8. Berer, T., A. Hochreiner, S. Zamiri, and P. Burgholzer, "Remote photoacoustic imaging on solid material using a two-wave mixing interferometer," *Opt. Lett.*, Vol. 35, No. 24, 4151–4153, Dec. 2010.

A Microwave Radiation Interferometry Method Based on Adaptive Super-sparse Sampling

Suhua Chen, **Lu Zhu**, **and Yuanyuan Liu**
School of Information Engineering, East China Jiaotong University, Nanchang 330013, China

Abstract— The Interferometry Synthetic Aperture Imaging Radiometers (SAIRs) is to sample visibility function based on the Nyquist theory of space interferometry measurement, which do not need the mechanical scanning and can directly image. Due to the complex structure of the imaging system and low imaging resolution, the SAIRs practical application is limited seriously. According to the characteristic of the image is sparse or can be sparse representation in transform domain, the Compressed Sensing (CS) can project the high-dimensional signal to low-dimensional space, so the quantity of the projection measurement data is far less than that by the Nyquist sampling method. Also the microwave radiation interferometry conducted in the frequency domain, which has the characteristics of low frequency information less and high frequency information richer, and the distribution of them is centralized; at the same time, the microwave radiation image itself have the specialty of the gradient sparsity and the local smoothness, it can be sparse representation in differential domain. On the basis of the priori information about the observation and the sparse domain, we establish the incoherent optimization model between the observation matrix and the sparse matrix according to the principle of the two matrixes satisfying the irrelevant in the CS. Using the incoherent optimization model, we can adaptively obtain the spatial measurement with different probability, to realize super sparse interferometry. The adaptive super-sparse sampling method can overcome the disadvantage of equal probability of the Fourier random sampling methods. In order to reconstruct the microwave radiation image, we establish the imaging model based on total variation regularization constraint, and use the alternating iterative algorithm to realize the reconstruction. The simulation and experiment results show that it is fast to reconstruct microwave radiation image with the adaptive super-sparse sampling method, and it can greatly improve the quality of the microwave radiation image in the case of the same sampling rate.

Reconstructing 2D Perfectly Electric Conductors

Xudong Chen[1] and Xiuzhu Ye[2]

[1]Department of Electrical and Computer Engineering, National University of Singapore, 117576, Singapore
[2]Electromagnetic Lab., Beihang University (BUAA), Beijing 100191 China

Abstract— In this paper, we reconstruct the locations, contours and the exact number of perfectly electric conductors (PEC) objects by utilizing the information of scattering data. Two-dimensional (2D) setup is considered. The reconstruction of PEC has found wide applications, such as biomedical imaging, remote sensing, and non-destructive testing.

In this inverse scattering problem, no *a priori* information, such as the number of the objects and their approximate locations or centers, is needed. In addition, PEC scatters can be of both closed-contour and line-shape. There are mainly three challenges in this problem. The first is common to both PEC and dielectric scatterer inverse scattering, that is, ill-posedness and nonlinearity. The second and the third ones are unique to PEC inverse scattering problem. The second deals with the parameterization of PEC scatterers, whereas the third one deals with constructing the objective function. For the parameterization, it is difficult to represent PEC scatterers, which can be of both closed-contour and line-shape, without *a priori* information on the number of the scatterers and their approximate locations. For the construction of the objective function, it is much more difficult in PEC case than in dielectric case. In dielectric case, both scatterers and background can be represented by permittivity, and subsequently, the Lippmann-Schwinger equation can be applied to the whole domain of interest. In comparison, in PEC case, the electric-field-integral-equation (EFIE) is only applicable to the boundary of PEC scatterer that is however unknown in inverse problem.

We start from the transverse magnetic (TM) case. To tackle the difficulty in parameterization, we propose that the background medium, together with scatterers of arbitrary number and arbitrary shapes, is effectively expressed as line-segments that take binary values, with zero being background and one being PEC boundary. In building up the objective function, we use the fact that the electric field is zero at the boundary of PEC and at the same time the induced current is zero at the background medium. Once the objective function is built up, we apply existing optimization methods to minimize it. Here we adopt the continuous-type subspace-based optimization method (SOM).

Next we consider the reconstruction of perfectly electric conductor (PEC) scatterers with transverse electric (TE) wave illumination. Compared with the transverse magnetic (TM) counterpart, the TE case is not only mathematically more complex, but also numerically more demanding in the sense that the triangular basis is used to represent induced electric current due to the fact the current follow is a vector instead of a scalar. Moreover, although the longitudinal magnetic field is usually used in the wave equation in the TE forward scattering problem, we adopt the transverse electric field in the wave equation in the inverse problem for the reason that the boundary condition at the PEC surface can be easily added to the objective function.

Multi-input Localized Electrical Property Retrieval — Theories and Numerical Examples

Shao Ying Huang
Singapore University of Technology and Design, Singapore

Abstract—

Introduction: Knowledge of the spatial distribution of electrical properties, namely dielectric constant (ε_r) and conductivity (σ) is valuable for *in vivo* specific absorption rate (SAR) mapping in high-field magnetic resonance imaging (MRI) and to various diagnostic and therapeutic technologies. The retrievals of electrical properties (EP's) of human tissues based on B_1^+- or B_1^--maps from a MRI scanner have become an interesting research topic. EP's are retrieved by solving Maxwell's equations directly, e.g., the method named electric properties tomography (EPT) [1] and Localized Electrical Property Retrieval (LEPR) [2]; or by solving a linear system formed based on Maxwell's equations, e.g., local Maxwell tomography (LMT) [3]; or by numerical approaches using volume integral equation (VIE) or finite element method (FEM) [4]. On top of the aforementioned analytic and numerical approaches, iterations are used for the optimization of the retrievals [5, 6]. Among these methods, some approaches such as EPT need absolute phase of B_1^+ and it works based on the assumption that $\varphi^+/2 = \varphi^-/2$ at 3 T or below. There are other methods such as LMT that have no phase assumption. In our work, we propose a new method to retrieve the electrical properties of tissues when the half phase assumption holds. It works with multiple input B_1 maps. It is termed Multi-input Localized Electrical Property Retrieval (MLEPR). For this method, no integration is needed. Furthermore, only B_1^+-maps are needed in the calculation, meaning it does not require the z-component of the magnetic field, which is similar to EPT or LEPR. In this abstract, the theory of MLEPR is presented in detail. For MLEPR, LEPR, and EPT that work for 3 T or below, under the tested simulation data where ground-truth is known, the ε_r-map using MLEPR shows very high accuracy, which out-performs the other two methods.

$$\nabla \times \vec{H}(\vec{r}) = i\omega\varepsilon_c \vec{E}(\vec{r}) \tag{1}$$

$$-\nabla^2 \vec{B}(\vec{r}) = \left(\frac{\nabla\varepsilon_c}{\varepsilon_c}\right) \times \left(\nabla \times \vec{B}(\vec{r})\right) + \omega^2\varepsilon_c\mu\vec{B}(\vec{r}) \tag{2}$$

$$-\nabla^2 B_x(\vec{r}) = \left(\frac{\partial B_y}{\partial x} - \frac{\partial B_x}{\partial y}\right)\frac{\partial\varepsilon_c/\partial y}{\varepsilon_c} + \left(\frac{\partial B_z}{\partial x} - \frac{\partial B_x}{\partial z}\right)\frac{\partial\varepsilon_c/\partial z}{\varepsilon_c} + \omega^2\varepsilon_c\mu B_x(\vec{r}) \tag{3}$$

$$-\nabla^2 B_y(\vec{r}) = \left(\frac{\partial B_z}{\partial y} - \frac{\partial B_y}{\partial z}\right)\frac{\partial\varepsilon_c/\partial z}{\varepsilon_c} - \left(\frac{\partial B_y}{\partial x} - \frac{\partial B_x}{\partial y}\right)\frac{\partial\varepsilon_c/\partial x}{\varepsilon_c} + \omega^2\varepsilon_c\mu B_y(\vec{r}) \tag{4}$$

$$-\nabla^2 B_z(\vec{r}) = -\left(\frac{\partial B_z}{\partial x} - \frac{\partial B_x}{\partial z}\right)\frac{\partial\varepsilon_c/\partial x}{\varepsilon_c} - \left(\frac{\partial B_z}{\partial y} - \frac{\partial B_y}{\partial z}\right)\frac{\partial\varepsilon_c/\partial y}{\varepsilon_c} + \omega^2\varepsilon_c\mu B_z(\vec{r}) \tag{5}$$

$$\begin{aligned}-\nabla^2(B_x + B_y + B_z) &= \frac{\partial\varepsilon_c/\partial y}{\varepsilon_c}\left(\frac{\partial B_y}{\partial x} - \frac{\partial B_x}{\partial y} - \frac{\partial B_z}{\partial y} + \frac{\partial B_y}{\partial z}\right)\\ &+\frac{\partial\varepsilon_c/\partial z}{\varepsilon_c}\left(\frac{\partial B_z}{\partial x} - \frac{\partial B_x}{\partial z} + \frac{\partial B_z}{\partial y} - \frac{\partial B_y}{\partial z}\right) + \frac{\partial\varepsilon_c/\partial x}{\varepsilon_c}\left(-\frac{\partial B_y}{\partial x} + \frac{\partial B_x}{\partial y} - \frac{\partial B_z}{\partial x} + \frac{\partial B_x}{\partial z}\right)\\ &+\omega^2\varepsilon_c\mu(B_x + B_y) + \omega^2\varepsilon_c\mu B_z\end{aligned} \tag{6}$$

$$\begin{aligned}&\left(\frac{\partial B_y}{\partial x} - \frac{\partial B_x}{\partial y} + \frac{\partial B_y}{\partial z}\right)\frac{\partial\varepsilon_c/\partial y}{\varepsilon_c} + \left(-\frac{\partial B_x}{\partial z} - \frac{\partial B_y}{\partial z}\right)\frac{\partial\varepsilon_c/\partial z}{\varepsilon_c} + \left(-\frac{\partial B_y}{\partial x} + \frac{\partial B_x}{\partial y} + \frac{\partial B_x}{\partial z}\right)\frac{\partial\varepsilon_c/\partial x}{\varepsilon_c}\\ &+\left[-\frac{\partial B_z}{\partial y}\frac{\partial\varepsilon_c/\partial y}{\varepsilon_c} + \left(\frac{\partial B_z}{\partial x} + \frac{\partial B_z}{\partial y}\right)\frac{\partial\varepsilon_c/\partial z}{\varepsilon_c} - \frac{\partial B_z}{\partial x}\frac{\partial\varepsilon_c/\partial x}{\varepsilon_c} + \nabla^2 B_z(\vec{r}) + \omega^2\varepsilon_c\mu B_z\right]\\ &(B_x + B_y)\omega^2\varepsilon_c\mu = -\nabla^2(B_x + B_y)\end{aligned} \tag{7}$$

$$\text{NRMSE} = \frac{100 \times \|M_{\text{Retrieved}} - M_{\text{True}}\|_2}{\|M_{\text{True}}\|_2} \tag{8}$$

Methods: Time convention of $e^{i\omega t}$ is used. When $\mu\nabla\times$ both sides of Ampere's law in (1) and substitute in both Ampere's law and Faraday's law, with the identity $\nabla\times\nabla\times\vec{H} = \nabla(\nabla\cdot\vec{H}) - \nabla^2\vec{H}$,

we have Equation (2) where $\varepsilon_c = \varepsilon_r - i\sigma/\omega$. The x-, y-, and z-components of (2) are expressed in (3), (4), and (5), respectively. Eqs. (3)–(5) are summed and expressed in (6). Eq. (6) can be rearranged in (7) in a way that the known quantity is on the right hand side and the unknown with known coefficients are on the left hand side. The highlighted parts in (7) are unknowns. There are five unknowns in (7) thus five independent B_1^+-maps are needed to form a $Ax = b$ system to solve the unknowns where A has a size of 5×5. The 5th unknown, $\omega^2\mu\varepsilon_c$ gives information on ε_r and σ. The method is validated in a 3-compartment numerical spherical phantom (Figs. 1 and 2) comprising cerebrospinal fluid (CSF), white matter (WM), and grey matter (GM). SEMCAD based on FDTD is used for full-wave simulations. B_1^+-maps are calculated for the phantom at 128 MHz ($B_0 = 3$ T). The ε_r and σ of the tissues at 128 MHz are tabulated in Table 1 [7]. The background is air. The excitation sources are planes waves in five different directions ($\hat{k}_i$ in Fig. 1). The half phase assumption is held. ε_r- and σ-maps are obtained using different methods and compared.

Results: Figures 3(a)–(d) show the true ε_r- and σ-maps, and the retrieved ones using MLEPR, LEPR, and EPT, respectively. The signal to noise ratio (SNR) of the B_1^+-maps is 100. The 1st and 2nd rows show the ε_r- and σ-maps, respectively. The third order Savitsky-Golay (SG) smoothing filter with a window size of 7 in three directions around each voxel and median filtering were applied. The normalized root-mean-square errors (NRMSEs) for the points within the sphere (radius = 95 mm) are calculated using (8). NRMSEs arise from both tissue boundaries effects and the accuracy of the retrieval in the homogeneous area.

Table 1: Electrical properties.

Tissue	ε_r,	σ (S/m)
CSF	84.0	2.1
WM	52.5	0.3
GM	73.5	0.6

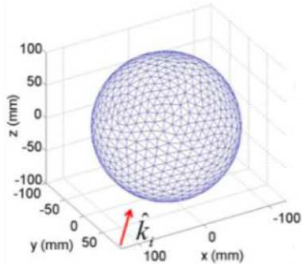

Figure 1: The spherical phantom.

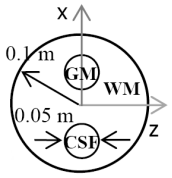

Figure 2: The spherical phantom with compartments.

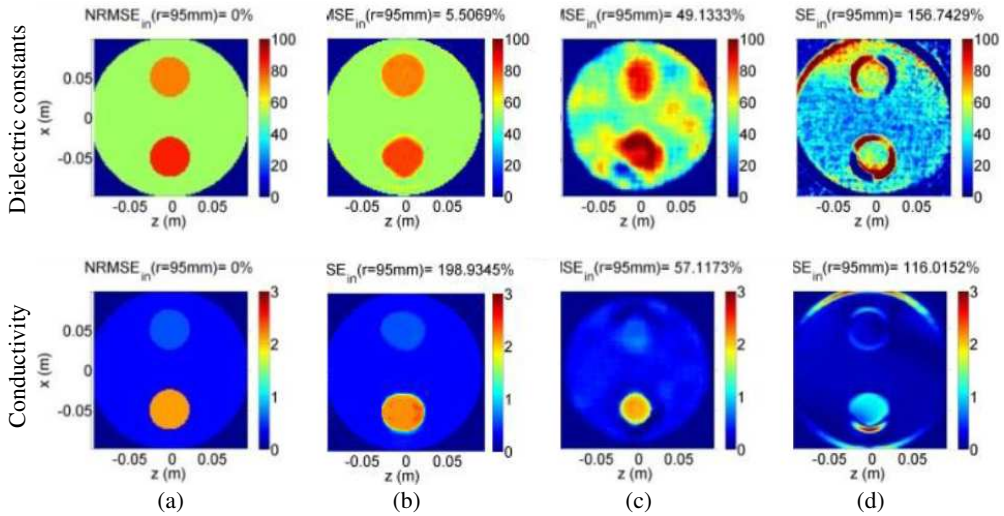

Figure 3: True maps and the retrieved electrical property maps on $y = 0$ xz-planes. (a) True maps. (b) MLEPR (the proposed). (c) LEPR. (d) EPT [1].

Discussion and Conclusion: As shown in Fig. 3, with SNR = 100, the proposed method shows an NRMSE of 5.5% for ε_r which is much lower than either the previously proposed LEPR (49.1%) or EPT (156.7%). The same smoothing filter is used. This indicates the accuracy of the retrievals and the smaller area of inaccuracy at the tissue boundaries using MLEPR. It also implies the smaller sensitivity of MLEPR to noise. The retrieved conductivity is reasonably accurate. The proposed Multi-input Localized Electrical Property Retrieval provides an alternative to retrieve electrical properties of tissues, especially dielectric constants, using multiple B_1^+-maps. Five independent maps are needed for the algorithm. It shows high retrieval accuracy (especially for ε_r) which implies reduced inaccurate area near the tissue boundaries with B1 maps of the same resolution, subject to SNR constraints. It will serve as a good base for further optimizations such as those taking iterative approaches.

REFERENCES

1. Katscher, U., et al., *IEEE Trans. Med. Imaging*, Vol. 28, 1365, 2009.
2. Huang, S. Y., et al., *ISMRM*, 4177, 2013.
3. Sodickson, D. K., et al., *ISMRM*, 387, 2012.
4. Chew, W. C., *Waves and Fields in Inhomogeneous Media*, IEEE Press, 1995.
5. Lee, J., et al., *ISMRM*, 4183, 2013.
6. Balidemaj, E., et al., *ISMRM*, 4185, 2013.
7. http://niremf.ifac.cnr.it/tissprop.

Fast Forward and Inverse Solution Methods for Magnetodielectric Materials

Qing Huo Liu, **Wenji Zhang**, **Zhiru Yu**, **Yunyun Hu**, **Yuan Fang**, **and Jianyang Zhou**
Department of Electrical and Computer Engineering
Duke University, Durham, North Carolina 27708, USA

Abstract— Magnetodielectric materials are those having both permittivity and permeability values different from those in the vacuum. They have many emerging applications, but their forward and inverse scattering problems are challenging to solve with the integral equation formulism because of the complexity. In this work, the forward problem via the coupled volume integral equations is solved by the stabilized bi-conjugate gradient FFT (BCGS-FFT) method for magnetodielectric objects. The traditional discretization using the cell-center method is first investigated. We found that the accuracy of this method is good for low contrast objects, but it deteriorates as the object size and contrast become larger. Here we use the volumetric roof-top functions as both basis and testing functions for the electric and magnetic flux densities (D, B). However, we found that a new set of basis functions must be utilized for the electric and magnetic vector potentials (F, A). Unlike the conventional weak form BCGS-FFT methods for pure dielectric objects, this BCGS-FFT method needs to use the second order curl conforming basis functions for these vector potentials to make the solver efficient and accurate. Once the forward problem is efficiently solved, the inverse scattering problem of inhomogeneous magnetodielectric materials will be investigated by using the Born iterative method, distorted Born iterative method, and variational Born iterative method. Applications in microwave frequency and other frequency bands will be presented.

Session 1P14b
SC5: Microwave Imaging: Detection, Localization and Profiling

Introduction to the Researches on Radar Conducted in MIRSL/CAS

Yunhua Zhang, **Xiaojin Shi**, **Xiang Gu**, **Wenshuai Zhai**,
Xueyan Kang, **Yuan Deng**, **Dong Li**, **Xiao Dong**, **Jiefang Yang**,
Qilun Yang, **Qingshan Yang**, **Yueying Tang**, **Xiangkun Zhang**, **and Jingshan Jiang**
The Key Laboratory of Microwave Remote Sensing, Center for Space Science and Applied Research
Chinese Academy of Sciences, No. 1 Nanertiao, Zhongguancun, Haidian, Beijing 100190, China

Abstract— In this paper, we give an introduction to some of the research activities on radar for both the hardware and signal processing algorithms conducted in recent years in the key lab of microwave remote sensing (MIRSL), Chinese Academy of Sciences (CAS). The works focus on the following aspects: (1) wide band and interferometric radar systems; (2) radar signals and processing; (3) polarimetric radar remote sensing; (4) radar image registration; (5) super resolution algorithms; (6) ground moving target indication/imaging; (7) compressive sensing in radars.

In aspect (1), we have developed Ku-band and Ka-band radar systems/subsystems with bandwidth up to 4 GHz, ground based and airborne experiments were carried out with these systems; in aspect (2), we designed high-performance chaotic radar signal, stepped-frequency chirp signal (SFCS), and stepped-frequency noise signal (SFNS), as well as high efficiency processing algorithms were developed; in aspect (3), we put our efforts on extending the Huynen dichotomy to the Huynen canonical dichotomy and further to the generalized Huynen dichotomy based on the wave dichotomy and N-target invariance, which can be applied to the scattering scenarios of irregularity and non-symmetry for unsupervised terrain classification; in aspect (4), we developed fast registration algorithm for InSAR image pair through solving an optimization problem, as well as an accurate algorithm based on weak affine transformation; in aspect (5), we mainly focus on MUSIC, ESPRIT, and Super-SVA super-resolution algorithms; in aspect (6), we developed computer simulation system for GMTI based on array radar, we also developed algorithms for ground moving target imaging based on Keystone and other transforms; in aspect (7), we developed the 2D-double CS (chirp scaling and compressive sensing) algorithm for SAR imaging, as well as the Maximum a Posteriori Estimation (MAPE) algorithm based on multiplicative speckle model for SAR imaging of complex scenarios, we also developed compressive sensing based pulse compression algorithms for SFCS and SFNS.

Both simulation and experiment results are presented to show the works.

Nanoscale Imaging of a Transmission Mode Scanning Microwave Microscope Investigated by a 3D Finite-element Method

Abiola O. Oladipo[1, 2], **Andrea Lucibello**[3], **Manuel Kasper**[4], **Spyros Lavdas**[2], **Giovanni M. Sardi**[3], **Emanuela Proietti**[3], **Ferry Kienberger**[5], **Romolo Marcelli**[3], **and Nicolae C. Panoiu**[2]

[1]Bio-Nano Consulting, 338 Euston Road, London NW1 3BT, UK
[2]Department of Electronic and Electrical Engineering, University College London Torrington Place, London WC1E 7JE, UK
[3]Institute of Microelectronics and Microsystems, National Research Council via del Fosso del Cavaliere, 100, 00133 Rome, Italy
[4]Johannes Kepler University Linz, Gruberstrasse 40, 4020 Linz, Austria
[5]Agilent Technologies Austria GmbH, Gruberstrasse 40, 4020 Linz, Austria

Abstract— Imaging at the nanoscale have proved to be a major driving force for recent advancements in many fields of science and technology, which include biology, medicine, material science and electronics. As a result of the ever increasing amounts, complexity and diversity of nano-samples that require imaging and characterization, the need to develop fast, accurate and versatile broadband microscopy techniques has become more pressing than ever before. Scanning microwave microscopy (SMM) uniquely combines the speed, versatility and accuracy of the well-established vector network analyser with the high sensitivity of the atomic force microscopy technique.

In this study, we developed an analytical model to calculate and relate the total impedance of the transmission mode scanning microwave microscope (Tx-SMM) to the S-matrix scattering parameters and investigated the sensitivity of the system. Also we performed 3D advanced finite-element analysis of the electromagnetic interactions between the probes and the sample in the Tx-SMM. We compared our analytical and computational results and studied the influence of variations in the conductivity of the bulk silicon substrate on the system characteristics. Moreover, we investigated the effect of variations of the permittivity of both the sub-surface constituents and the covering material of the sample on the scattering parameters. Our numerical simulations results showed that the Tx-SMM leads to larger sensitivity (from twofold to as much as 5× increase) as compared to the system sensitivity in the re ection mode operation. In particular, our analysis revealed that the sensitivity of the phase of the S_{21} parameter was 3× larger than that of its magnitude. Our findings underline the increased sensitivity of the Tx-SMM system against small variations in the sample parameters, which has important experimental implications by shedding a new light on the overall performance of the Tx-SMM system.

Comparison of the Time-reversal MUSIC and BP Algorithms in Multi-target Detection

Bing Li and Bin-Jie Hu
School of Electronic and Information Engineering
South China University of Technology, Guangzhou 510641, China

Abstract— Multi-target detection based on the time-reversal imaging with multiple signal classification (TR-MUSIC) and back-projection (BP) algorithms is presented in this paper. In the TR-MUSIC, firstly, the backscatter of a signal transmitted into a scattering environment is recorded. Secondly, the time reversal operator is obtained with the use of transfer matrix, and the eigenvalues and eigenvectors of the time reversal operator are calculated. Finally, the targets can be located through back-propagation of the eigenvectors of time reversal operator. In the BP, the imaging region is divided into grids and each grid represents a pixel. The electric field of each pixel is able to be obtained by recorded electromagnetic wave propagation time from the transmitters to each pixel in imaging region and from each pixel in imaging region to receivers. At last, the targets can be located by calculating the sum of amplitudes of electric field of each pixel in imaging area. The imaging methodology and basic theory of TR-MUSIC and BP algorithms are outlined. In order to illustrate the performance of these two algorithms in detail, numerical simulations for three ideal point-like targets are conducted and analyzed. Here, we consider two versions of the simulation: targets detection with enough detection elements which provide enough echo signals or not, and for each version, compare two approaches: TR-MUSIC and BP algorithms. Results show that the targets can be located accurately by using TR-MUSIC algorithm in both versions and BP algorithm with enough detection elements, while there are some ghost pixels by using BP algorithm under the condition of few detection elements. Thus, the TR-MUSIC approach has a better performance than BP approach.

Development of Magnetic Phase Mapping for Analyzing the Internal Structure of the Spot Welding

Song Nannan, Keisyu Shiga, Yuya Tsukamoto, Kenji Sakai, Toshihiko Kiwa, Weiying Cheng, and Keiji Tsukada
Graduate School of Natural Science and Technology, Okayama University, Japan

Abstract— Resistance spot welding technologies are widely used in industry. A highly reliable monitoring method is needed to effectively weld and create a robust structure. In the previous study, we have developed an ECT (Eddy Current Test) method for spot weld evaluation. In this method, the generated nugget could be evaluated using the magnetic field intensity detected by the detection coil, and it was able to evaluate the nugget size of spot welding. However, the influence of lift-off caused by the depression on the surface of the spot weld is not negligible. Therefore, in order to reduce the influence of lift-off, the spot welded structure was evaluated not only by the magnetic field intensity, but also by the phase of magnetic field with multiple frequencies. The samples were measured at 20-points of 1 mm intervals in the center line of spot weld. Both magnetic field intensity and phase were measured by changing frequency and the obtained data was shown as two dimensional mapping. This mapping indicates the depth information of welding because the penetrated depth of magnetic field depends on the frequency. When the lift-off was increased, the mapping of magnetic field intensity was significantly decreased, and the change of the magnetic field intensity was not detected. Meanwhile, the magnetic field phase does not affected by the change of lift-off and the obtained mapping was correlated with the nugget shape. This result suggests that the nugget of spot welding can be evaluated by the magnetic field phase when the lift-off increased. Thus, the influence of depression on the surface of the spot weld can be eliminated and the evaluation method using magnetic phase mapping is suitable for spot welding monitoring.

Session 1P15a
Oral Presentations for Best Student Paper Awards — SC4: Antennas and Microwave Technologies

A Novel Parallel Double Helix Loop Resonator for Magnetic Coupled Resonance Wireless Power Transfer

Cheng Yang and Koichi Tsunekawa
Department of Computer Science Engineering
Chubu University, Kasugai-shi, Aich, Japan

Abstract— Magnetic coupled resonance wireless power transfer (WPT) technology is expected to the next generation wireless power charging system, because of its advantage of mid-range power transfer distance and high efficiency. There are two most important performances of this technology always be focus on which are: long power transfer distance and high power transfer efficiency. To achieve this, it is necessary to improve the resonator quality factor and the coupling efficiency. The quality factor is proportional to the resonance frequency and self-inductance of the resonator and inversely proportional to the resonator resistance. Therefore, it is necessary to reduce the resistance in order to improve the resonator quality factor.

A traditional structure helix loop resonator is widely used for magnetic resonance WPT system as shown in Fig. 1(a). In this paper a novel parallel double helix loop resonator is proposed which could reduce the resistance without sacrifice resonator self-inductance as shown in Fig. 1(b). The loop is made by copper wire with 0.55 [mm] diameter. The experimentally demonstrates that the resistance loss of parallel double helix loop resonator is smaller than the traditional structure helix loop resonator about 48%. On the other hand, the maximum power transfer efficiencies at critical coupling point of parallel double helix loop and traditional type helix loop are 87% and

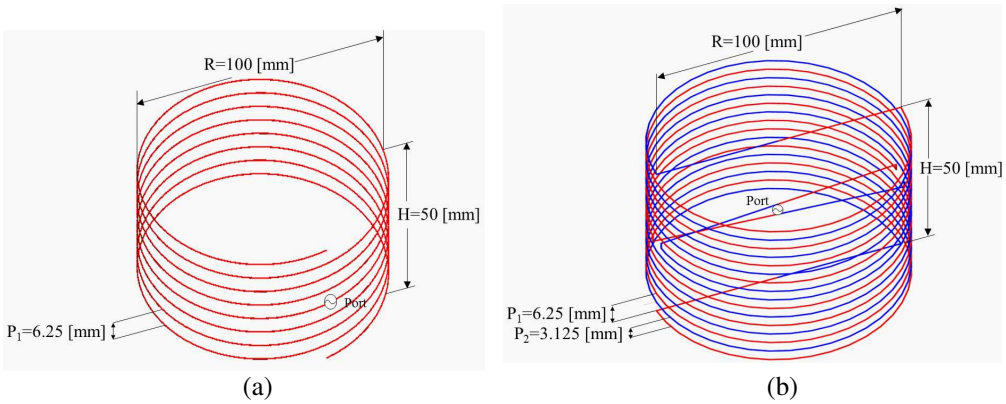

Figure 1: Resonator configuration. (a) Traditional structure helix loop resonator. (b) Parallel double helix loop resonator.

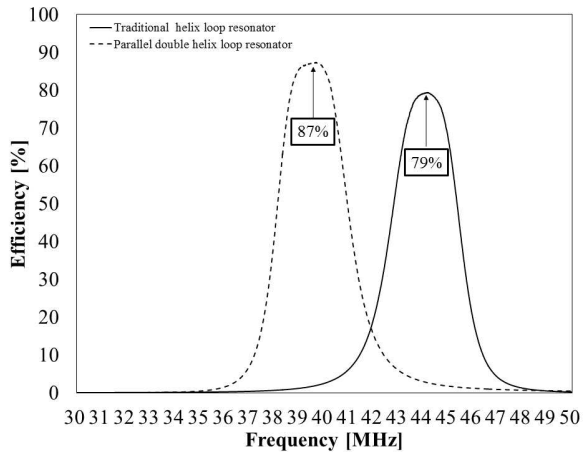

Figure 2: The wireless power transfer efficiency experiment result comparison of traditional helix loop resonator and parallel double helix loop resonator at critical coupling point.

79% with 50 Ohms port impedance as shown in Fig. 2. Then the power transfer characteristic as a function of distance is investigated, and we found out that the coupling efficiency between two parallel double helix loop resonators is also improved. At last, for extend the power transfer distance, a pair of matching loops are used to match the transmitting and receiving resonator to the optimal port impedance at varying power transfer distance and the measurement result shows that the power transfer efficiency of traditional type helix loop resonator could only achieve to 34% but the parallel helix loop resonator could achieve to 57% at the transfer distance of 20 [cm].

Parabolic Strip Telescope

V. Kosejk, G. Chadzitaskos, and J. Červený
Department of Physics, Faculty of Nuclear Sciences and Physical Engineering
Czech Technical University, Břehová 7, Prague CZ-115 19, Czech Republic

Abstract— This contribution is focused on the development of special astronomical telescope, and particularly on processing of images produced by it. We propose a special kind of astronomical telescopes that use parabolic strip instead of the classical parabolic mirrors as a primary mirror. Structurally, it is a flexible strip of reflective material which is curved into parabola along one axis. Scanned image of a point on the sky appears in the focus as a line, which is an integral of the reflected intensity of the observed point. For a perfect reconstruction of image the telescope has to rotate around the optical axis in 180 degrees. During rotation series of images is made. Then the reconstruction algorithms are used in order to present the final image of the subject.

For the computer reconstruction of images we use 3 different types of algorithms. The basic algorithm is the filtered back projection; it is based on Radon transformation. This algorithm is also used in image reconstruction of computer tomography. Another developed procedure is the multiplication algorithm. Third reconstruction algorithm is based on a census of individual projections.

Each reconstruction algorithms can be used for different requirements. Summation algorithm is suitable for fast image reconstruction. However the main disadvantage of this algorithm is relatively strong noise. Multiplication algorithm uses mutual multiplication of individual projections (sub-images). The reconstruction process achieves very good results. Rear-projection filtered multicast algorithm is similar but it includes filtering of each projection in the frequency spectrum. The Rampl filters have been used for filtration.

When comparing the rotational and Newtonian telescope, the main advantage of the rotating telescope is simple design, thus simple to produce high-resolution with the same objective area. Disadvantage in relation to other is a need of one more rotational moving and subsequent image reconstruction. With a sufficiently large telescope would be theoretically possible a direct observation of exoplanets of a size comparable to Jupiter.

Frequency Tunable Antenna with Zeroth Order Resonator for UHF Near-field RFID Systems

Xiao-Dong Wei, Hong-Lin Zhang, and Bin-Jie Hu
School of Electronic and Information Engineering
South China University of Technology, Guangzhou, China

Abstract— Recently ultra-high frequency (UHF) near-field radio frequency identification-(RFID) technology has gained much attention due to its excellent performance in item-level RFID applications, such as drugs, bottles of water, clothes, and retail goods. In UHF RFID systems, the reader emits signals through reader antennas. The performance of the reader antenna affects the reading distance and reading rate. The key point in UHF near-field RFID reader antenna design is to generate strong and uniform magnetic field in an adequate interrogation zone. In this letter, we present a frequency tunable antenna with epsilon negative (ENG) zeroth order resonator (ZOR) for ultra-high frequency (UHF) near-field radio frequency identification (RFID) systems. The ENG ZOR unit cell is composed of a toroidal inductor, a metal pin, a variable capacitor and an additional ground plane. The additional ground plane is connected to ground plane of the antenna through the variable capacitor. The additional ground and the variable capacitor affect the shunt right-handed capacitance of the ENG unit cell. By changing the capacitance of the variable capacitor, the resonant frequency of the antenna can be swept from 834 MHz to 1046 MHz. A comparative study with other UHF near-field RFID reader antennas shows that the left-handed loop achieves stronger near H-field with good impedance matching. The measured maximum reading distance is 85 mm at 30 dBm input power. And the minimum input power for successful detecting of detect the near-field tag with lower than -12 dBm, which is much lower than the conventional UHF near-field RFID reader antennas. The measurement results agree well with the simulated ones. The proposed antenna is suitable for UHF near-field RFID systems.

Electrical Lumped Model for Implemented RF-MEMS Capacitive Switch on Semi-suspended Coplanar-waveguide

Amin Khalili Moghaddam, Joon Huang Chuah, and Harikrishnan A/L Ramiah
Department of Electrical Engineering, University of Malaya, Kuala Lumpur 50603, Malaysia

Abstract— A novel electrical lumped model for an RF MEMS capacitive switch which is implemented on a semi-suspended coplanar-waveguide is proposed and studied. The quality factor is mathematically studied taking the effects of air-gaps and substrate resistance into consideration. Results indicate that increasing the equivalent resistance of transmitting line and the switch, series resistance, in down-state has negative effect and can considerably decrease the quality factor. Increasing the capacitance of the switch also has a negative effect on the quality factor. Increasing the substrate resistance improves the quality factor. Lower capacitance can allow the switch to operate with a wider bandwidth of high quality factors and larger capacitance can make the bandwidth narrower.

Edge Effects in a Strongly Coupled Dipole Element Array in Triangular Lattice

C. I. Kolitsidas and B. L. G. Jonsson
Electromagnetic Engineering, School of Electrical Engineering
KTH Royal Institute of Technology, Sweden

Abstract— Wideband antenna arrays for wireless communications is a topic that has always attracted a lot of interest. Future wireless base stations are envisioned to support all commercially available bands. Furthermore, it is expected to offer advanced coverage characteristics, like dedicated user beams. It is the path towards implementing a multi-user multiple input multiple output (MU-MIMO) system for commercial applications. This generates the need for a wideband and wide-scan antenna array suitable for base station applications.

Over the last decade, a new class of antenna array systems has been developed that is able to utilize strong inter-element coupling. It was shown that these elements are able to provide wideband $(5:1)$ performance while keeping a relatively low profile ($d \approx \lambda_{highfreq}/2.5 - \lambda_{highfreq}/3$, d is the distance from the ground plane to the radiating structure). Thus it is an attractive approach with the possibility for communication applications. In the case of base station application a mid-sized array is in need in order to keep a low profile. An important factor that appears during the finite array design procedure is the performance variance of the elements with respect to their position in the array. These variances are mainly caused by the "edge effects" in the finite array. Thus it is expected that the outer elements in the finite array will have degraded performance when compared with the central array elements. Another important factor that impacts the scanning performance of the array is the array lattice selection. It known that arrays in triangular lattices have better scanning performance.

In this study the focus is on the impact of edge effects in the triangular lattice of a strongly coupled antenna array. Our analysis is based the finite $\times$ infinite approach for both E- and H-plane with multiple rows taken into account in order to capture the effects on the different edges that appear in triangular grids.

The Multiple Periodic Structure Antenna Design

Z. L. Ma, L. J. Jiang, S. Gupta, and W. E. I. Sha
Department of Electrical and Electronic Engineering, The University of Hong Kong, Hong Kong, China

Abstract— Periodic structures have been playing a significant role in modern physics and engineering. In past decades, they were widely applied in both optics and microwave areas, such as Bragg grating, leaky-wave antennas, filters and so on. However, most studies on periodic structures were focused on the single periodicity that single unit cell periodically repeats along the structure. In the meantime, metamaterials with its fundamental right/left-handed characteristics have attracted attentions in recent years. Different from conventional materials, the metamaterial is normally a dispersive material whose refractive index is frequency dependent.

In this talk, a more general concept of the multiple periodic (MP) structure is proposed. In this structure, the periodically loaded element is replaced by a supercell which is formed by cascading several different unit cells. The dispersion relations of one dimensional MP structures are analyzed from both layered media and lumped circuits aspects. Regarding each aspect, both non-dispersive (conventional) and dispersive (composite right/left-handed (CRLH)) materials are discussed. It is found that with the increase of the periodicity, multiple stopbands appear. While for the effective dispersion relation of the supercell, the space harmonic modes' separation distance is reduced. It leads to simultaneously dualistic (right- and left-handed) radiation performance and multibeam property. And more abundant radiation modes are excited at relatively lower frequencies comparing with conventional periodic structures. Besides, a general dispersion relation formula and a general Bragg condition for MP structures are derived. The dispersion relation is simply described by the former, and the latter helps to indicate the stopbands' locations and engineer the dispersion relation consequently. Applications of MP structures to phase reversal (PR) antennas are also presented. They experimentally verifies both transmission and radiation characteristics of the proposed MP structures. In each analysis, single (SP), double (DP) and triple periodic (TP) structures are presented and compared. Due to the multi-beam property, MP PR antennas can realize the transmission to multiple separated targets.

A Dual-band Circularly Polarized Antenna with Novel Feeding Method for BDS, GPS and GLONASS Application

J. Zhang, X. Q. Lin, L. Y. Nie, F. Cheng, Z. Y. Kang, Y. Jiang, and J. W. Yu
EHF Key Lab of Fundamental Science, School of Electronic Engineering
University of Electronic Science and Technology of China, Chengdu 611731, China

Abstract— Dual-band or tri-band circularly polarized antennas has been widely used in a compatible navigation systems. It has been reported that a multiband antenna can be realized by patches stacked [1] and cutting slots on the patch will achieve circularly polarization under the condition of single feed [2]. Based on this idea, we design a dual-band circularly polarized antenna. One of the bands operates at the BDS B3 (1268.52 ± 10 MHz). The other band concludes the GPS L1 (1575.42 ± 10 MHz) and GLONASS L1 (1602 ± 8 MHz). The antenna structure is shown in Fig. 1(a). By changing the length and width of four slots on each patch, its circular polarization performance and working bandwidth can be adjusted. The thickness of upper substrate is appropriately increased to improve the high frequency bandwidth. The multistacked patches fed through two coaxial probes which provide two different input signal. In this paper, we improve the method of the probe feed on the lower patch. The probe do not connect the lower patch but solder to a small disc on the upper patch. The radius of the disc and the gap width has small impact on the input impedance of two frequency band. By adjusting these parameters, we will obtain better impedance matching performance. The simulated S-parameter of the proposed antenna is shown in Fig. 2(b).

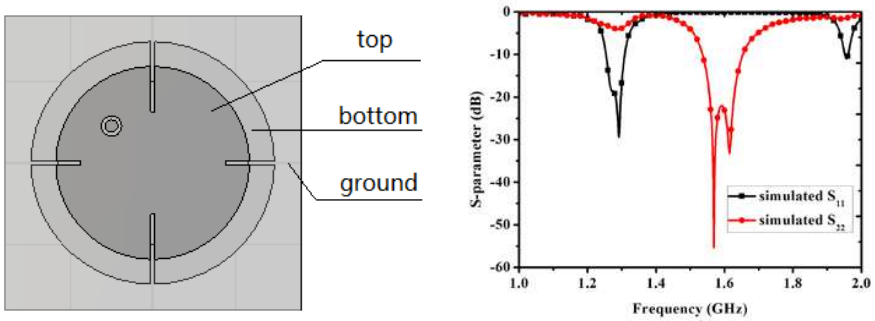

(a) (b)

Figure 1: The top view of proposed antenna and S-parameter simulation result. (a) Antenna structure of top view. (b) Simulated S-parameter of proposed antenna: $S_{11} < -10$ dB frequency band is 1.254–1.308 GHz, $S_{22} < -10$ dB frequency band is 1.536–1.653 GHz.

REFERENCES

1. Falade, O. P., "Single feed stacked patch circular polarized antenna for triple band GPS recievers," *IEEE Transaction on Antennas and Propagation*, Vol. 60, No. 10, 4479–4484, 2012.
2. Agarwal, K., "RIS-based compact circularly polarized microstrip antennas," *IEEE Transaction on Antennas and Propagation*, Vol. 61, No. 2, 547–554, 2013.

Broadband Circularly Polarized Loop Antenna Based on High-pass and Low-pass Filters for Handheld RFID Reader Applications

Bo Xu, **Qi Liu**, **and Yusha Liu**
Centre for Optical and Electromagnetic Research
Zhejiang University, China

Abstract— Recent researches on portable circular polarized Radio Frequency Identification (RFID) reader have 3 dB axial-ration (AR) bandwidth below 80 MHz. In order to cover all the Ultra-High Frequency (UHF) RFID bands including U.S. (902 MHz–928 MHz), Japan (952 MHz–955 MHz), Europe (866 MHz–869 MHz) and P. R. China (840.5 MHz–844.5 MHz and 920.5 MHz–924.5 MHz) simultaneously, this paper present a novel broadband handheld circular polarized RFID reader antenna. The proposed antenna consists of a square-loop radiating element with 2 feed ports and a broadband feeding network in the same plane, measuring 95 mm × 95 mm × 1.6 mm. The feeding network, which achieves broadband AR bandwidth, is composed of a wilkinson power divider, a high-pass filter and a low-pass filter. The feed port of the power divider is connected to a 50 Ω SMA port. The two output ports of the wilkinson power divider are connected to the high-pass filter and the low-pass filter respectively. The T-topology is chosen for the high-pass network and the pi-topology is chosen for the low-pass network using discrete chip capacitors and inductors. By selecting suitable capacitors and inductors and adjusting the resonant frequency of two networks to 910 MHz, the simulated phase difference between the two networks is $90^\circ \pm 2^\circ$ from 645 MHz to 977 MHz, which connect to radiating element leading to a broadband right-hand circular polarization in z direction and left-hand circular polarization in $-z$ direction. The simulated broad impedance bandwidth ($S_{11} < -10$ dB) is from 801 MHz to 1232 MHz. The simulated 3 dB axial-ratio bandwidth of the proposed antenna is from 800 MHz to 960 MHz. The estimated gain in the maximum radiation direction is about 3 dBic. The measured result will be reported in the full-length paper.

Session 1P15b
Oral Presentations for Best Student Paper Awards — SC1: CEM, EMC, Scattering & EM Theory

Electromagnetic Heat-induced of Nanowire in Liquid: Computation of the Bubble Shape

A. Chaari, T. Grosges, L. Giraud-Moreau, and D. Barchiesi
Project Group for Automatic Mesh Generation and Advanced Methods
Gamma3 Project (UTT-INRIA), University of Technology of Troyes, France

Abstract— The study of the cross sections of diffraction and absorption by particles has shown the ability to produce complex electromagnetic field patterns at short distance. These physical effects have open the experimental and theoretical way of designing efficient systems in various new applications (sensors, imaging and burning biomedicine applications, data storage ...) [1–3]. In this contribution, we develop a method to study the bubble forming around nanowire in a liquid from the computation of a coupled electromagnetic-thermal process.

To detect the presence of nanowire in a liquid, an indirect method consists in detecting the bubble produced by photo-thermal process around the nanowire. Under an intense laser illumination, the electromagnetic energy absorbed by the nanowire acts like a thermal source in the liquid and induces a local increase of the temperature around the nanowire. When the temperature elevation overpass the vaporization threshold of the liquid, a bubble is forming. To solve the coupled photo-thermal equations, the computational domain is represented by a mesh. The adaptation of the mesh is required, even with analytical models, to reach convergence, with confidence and to control the accuracy of the computation of the field [4, 5].

Here, the numerical solution of the absorption of light by a nanowire is computed by a Finite Element Method. The intensity of the electric field E, the derived heat source Q and the temperature T are computed at each spatial node of the computational domain. The spatial node coordinates, where the computation is achieved, are selected through an optimized adaptive remeshing process. This remeshing is governed by a mesh element size map ensuring the conformity with the underlying geometry domain as well as the accuracy of the physical solution of interest. This size map results from an a posteriori estimation of the interpolation error on the physical field of interest (H, E, Q and T). Therefore, the problem is reduced to a characterization of meshes on which the interpolation error is limited by a threshold [6]. The influence of the laser source and the geometrical parameters (wavelength, size and shape of the nanowire) related to the size and shape of the bubble are analyzed. We show that the aspect ratio and the volume of the bubble can be expressed as function of the aspect ratio and the volume of the nanowire. By solving the inverse problem two functions are obtained enabling to find the size and shape of the nanowire from the size and shape of bubble.

REFERENCES

1. Barchiesi, D., D. Macías, L. Belmar-Letellier, D. van Labeke, M. Lamy de la Chapelle, T. Toury, E. Kremer, L. Moreau, and T. Grosges, "Plasmonics: Influence of the intermediate (or stick) layer on the efficiency of sensors," *Appl. Phys. B — Lasers Opt.*, Vol. 93, No. 1, 177–181, 2008.
2. Grosges, T., D. Barchiesi, T. Toury, and G. Gréhan, "Design of nanostructures for imaging and biomedical applications by plasmonic optimization," *Opt. Lett.*, Vol. 33, No. 23, 2812–2814, 2008.
3. Grosges, T., S. Petit, D. Barchiesi, and S. Hudlet, "Numerical modeling of the subwavelength phase-change recording using an apertureless scanning near-field optical microscope," *Opt. Express*, Vol. 12, No. 24, 5987–5995, 2004.
4. Barchiesi, D., T. Grosges, E. Kremer, and M. Lamy de la Chapelle, "Electromagnetic heat-induced in meso-structures: Computation of temperature in metallic dimers," *PIERS Online*, Vol. 7, No. 5, 406–410, 2011.
5. Grosges, T., H. Borouchaki, and D. Barchiesi, "New adaptive mesh development for accurate near-field enhancement computation," *J. Microscopy*, Vol. 229, No. 2, 293–301, 2008.
6. Grosges, T., H. Borouchaki, and D. Barchiesi, "Improved scheme for accurate computation of high electric near-field gradients," *Opt. Express*, Vol. 15, No. 3, 1307–1321, 2007.

Computation of the Field Enhancement by Small Facet Angles of Metallic Nanoparticles: Adaptive Remeshing for Finite Element Method

F. Mezghani, D. Barchiesi, A. Cherouat, T. Grosges, and H. Borouchaki
Project Group for Automatic Mesh Generation and Advanced Methods
Gamma3 Project (UTT-INRIA), University of Technology of Troyes, France

Abstract— The synthesis of metal nanoparticles with well-defined size and shape distributions has reached a high level of control [1–3]. Under illumination, these particles are useful for biology and nanotechnology applications such as cancer therapy, drug delivery, fluorescence or spectroscopy enhancement. For all these applications, the design of nanoparticles benefits of accurate electromagnetic calculations involving their actual shape [4–6]. In some experimental cases, the shape of gold nanoparticles exhibits facets that are related to their mode of elaboration [1–3]. We propose a finite element approach to evaluate accurately the field enhancement near facets with small angles. An adaptive remeshing or refinement method is necessary to have a high accuracy while ensuring the convergence of calculation with limited IT resources (RAM and CPU time). An adaptive refinement method uses the h-adaptation and a physics a posteriori error estimator based on the L2 norm (residual method) [7]. The proposed method differs from the classical refinement techniques. It is based on the unit remeshing (h-adaptation) and a geometry a posteriori error estimator with the interpolation method of physical field of interest [5]. The strategy of this method is to remesh the structure on the basis of the map of the physical and geometrical size that will ensure compliance with the initial geometry and the accuracy of the physical solution [4–6]. A loop of calculation was established with a stopping criteria providing an accuracy rate of the solution and the convergence. The 3D calculations of the intensity of the electric field near a polyhedron are shown in Fig. 1. After four remeshing the field enhancement near the small change of angles between two facets of polyhedron appears in the results of computation. The induced field enhancement cannot be neglected as it reaches 12% for angle of tilt between the two facets of 5°. The classical refinement techniques are not able to reveal this change.

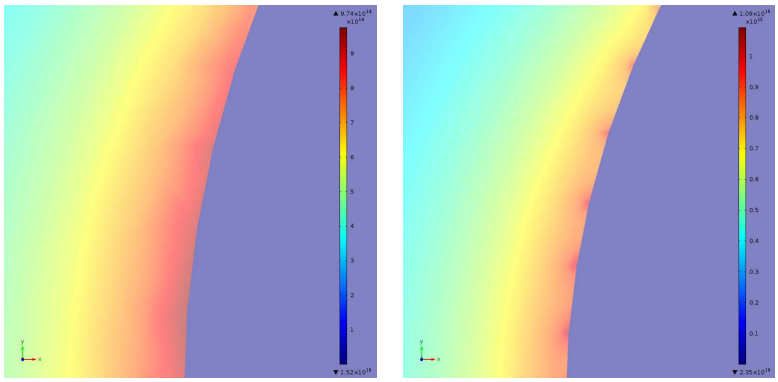

(a) (b)

Figure 1: Cut plane of the 3D intensity of the total electric field around the faceted particle. (a) First mesh (on geometry). (b) Fourth iteration of remeshing.

REFERENCES

1. Hu, M., J. Chen, Z.-Y. Li, L. Au, G. V. Hartland, X. Li, M. Marquez, and Y. Xia, "Gold nanostructures: Engineering their plasmonic properties for biomedical applications," *Chem. Soc. Rev.*, Vol. 35, 1084–1094, 2006.
2. Liu, B., J. Xie, J. Y. Lee, Y. P Ting, and J. P. Chen, "Optimization of high-yield biological synthesis of single-crystalline gold nanoplates," *J. Phys. Chem. B*, Vol. 109, 15256–15263, 2005.
3. Daniel, M.-C. and D. Astruc, "Gold nanoparticles: Assembly, supramolecular chemistry, quantum-size-related properties, and applications toward biology, catalysis, and nanotechnology," *Chem. Rev.*, Vol. 104, 293–346, 2004.

4. Grosges, T., H. Borouchaki, and D. Barchiesi, "Improved scheme for accurate computation of high electric near-field gradients," *Opt. Express*, Vol. 15, No. 3, 1307–1321, 2007.
5. Borouchaki, H., T. Grosges, and D. Barchiesi, "Improved 3D adaptive remeshing scheme applied in high electromagnetic field gradient computation," *Finite Elements in Analysis and Design*, Vol. 46, 84–95, 2010.
6. Grosges, T., H. Borouchaki, and D. Barchiesi, "New adaptive mesh development for accurate near-field enhancement computation," Vol. 229, No. 2, 1365–2818, 2008.
7. Verfürth, R., *A Review of a Posteriori Error Estimation and Adaptive Mesh-Refinement Techniques*, Teubner Verlag and J. Wiley, Stuttgart, 1996.

A Unified Field Analysis Method for IR/MMW Beam Splitter

Yi Tian[1, 2, 3], **Hui Yan**[1, 3], **Xin Wang**[1, 3], **Li Zhang**[2], **and Zhuo Li**[1, 3]

[1]School of Opto-Electronics, Beijing Institute of Technology, Beijing 100081, China
[2]Shanghai Institute of Electro-Mechanical Engineering, Shanghai 201109, China
[3]Beijing Key Lab for Precision Optoelectronic Measurement Instrument and Technology
Beijing 100081, China

Abstract— Infrared (IR)/millimeter wave (MMW) beam splitter is a key component of dual-mode compound guidance system. The beam splitter is tilted by 45° along the main axis and it transmits MMW signals and reflects IR signals at the same time. The insertion of a beam splitter in the dual-mode compound guidance system will affect the uniformity of the MMW field. Simultaneously, the insertion also affects the IR imaging quality. Moreover, the detecting and tracking precision will be limited by the distortion of the filed received by MMW and IR sensors. Therefore, it is necessary to build a theoretical model to analyze the MMW and IR field distribution. Generally, the calculation of electrical field in a MMW sensor aperture is a near field diffraction problem. However the calculation of optical field focused on an IR field plane array through an IR lens is a far field diffraction problem. Nevertheless, both IR and MMW are electromagnetic wave, and they can be described by Maxwell-Equations. So the MMW near field and IR far field problem can be solved by a unified method derived from integral formulation of Maxwell-Equations. Thus, aperture field integration method (AFIM) is proposed and utilized to efficiently compute the field distributions of IR/MMW beam splitter including the MMW near field distribution and IR far field distribution. In order to validate the AFIM, a single dielectric layer beam splitter is proposed. It is analyzed by AFIM and multilevel fast multi-pole method (MLFMM). Compared to MLFMM, the memory requirement and CPU time consumption are reduced drastically from 4.6 GB and 2141 seconds to 1.2 MB and 58 seconds, respectively. In order to meet the far field condition a scale factor is proposed to transform the focal plane into a far field plane, when the IR far field in a focal plane is computed. The IR far field calculation accuracy is better than 97% compared to the analytical solutions. The simulation results show that the AFIM as a unified method can be applied to both beam splitters' MMW near field and IR far field engineering estimation.

Conductor Modeling Based on Volume Integral Equations

J. Zhang and M. S. Tong
Department of Electronic Science and Technology
Tongji University, Shanghai, China

Abstract— Accurate solution of electromagnetic (EM) problems with lossy conductors requires to consider the finite conductivity of the conductors. The loss of the conductors may not be ignored when the frequency is low or the conductivity is small since the skin depth is large. In the integral equation approach for solving the problem, one usually uses surface integral equation (SIE) approach with an approximate surface impedance when the skin depth is small. For large skin depth caused by low frequency or small conductivity, one treats the conductors as dielectric-like objects and uses a two-region scheme to formulate the SIEs. The SIEs are solved by the method of moments (MoM) with the Rao-Wilton-Glisson (RWG) basis function. However, the solutions may not be valid for a wide range of frequency and conductivity because the integral kernels include those parameters and the conditioning of SIEs is susceptible to the frequency.

In this work, we also treat the conductors as dielectric-like objects but use volume integral equations (VIEs) to formulate the problem. The VIEs are the second-kind of integral equation, so they are well-conditioned in general. Also, the VIEs only have one unknown function (electric current density) for dielectric (nonmagnetic) objects while two unknown functions appear in the SIEs. To solve the VIEs, we do not use the traditional MoM with the Schaubert-Wilton-Glisson (SWG) basis function but propose a point-matching scheme which does not use any basis and testing functions and allows a geometric discretization of nonconforming meshes, resulting in much convenience in implementation. Moreover, the scheme can choose current densities as unknowns so that the integral kernels are free of material parameters and the solutions can endure a wide change of frequency and conductivity. The scheme requires an accurate evaluation of hypersingular integrals resulting from the double gradient operation in the dyadic Green's function but we have developed a robust technique to handle them. We present a numerical example for EM scattering by a conductive sphere to illustrate the approach and good results can be observed.

Session 1P15c
Oral Presentations for Best Student Paper Awards — SC5: Remote Sensing, Inverse Problems, Imaging, Radar and Sensing

Localisation of Motionless Persons in 3D Space by UWB Radar

P. Kazimir[1], **D. Kocur**[1], **J. Fortes**[1], **and R. Zetik**[2]

[1]Technical University of Kosice, Park Komenskeho 13, Kosice 04210, Slovakia
[2]Ilmenau University of Technology, Ehrenbergstrasse 29, Ilmenau 98693, Germany

Abstract— In the last decade, several ultra wideband (UWB) radars assigned for the support of the emergency event solving have been developed. Usually, they provide short-range through wall localisation of human beings in 2-dimensional space (2D). However, according to security experts, person positioning not only in 2D but also in 3D is needful. Following this demand, we have focused on motionless human being localisation problem in 3D.

In this paper, a new method of static person localisation in 3D by UWB radar will be introduced. This approach is based on the application of multistatic UWB radar using one transmitting and four receiving antennas. The novel localisation method is based on the approximation of 3D localisation problem by the solution of two 2D localisation tasks. Here, the localisation of motionless human beings is based on the detection of the slow motion (frequency band: 0.2–0.5 Hz) of his or her thorax caused by breathing. Then, for the static person localisation in 2D, a signal processing procedure including signal processing phases such as background subtraction (exponential averaging method), power spectrum estimation (method of the periodogram), estimation of the total energy of signal in the frequency band 0.2–0.5 Hz corresponding to human beings breathing (integration method), target detection (CFAR detector application), time-of arrival estimation and target localisation (trilateration method based on direct computation method) is applied.

A proper lay-out of the radar antenna system will be introduced for the considered UWB radar, too. The proposed antenna system of the radar consists of one transmitting and four receiving antennas located in the same plane. The receiving antennas are located in the vertex of the square, whereas the transmitting antenna is put in the intersection of the diagonals of the same square. The localisation of the target in 2D by using the outlined radar antenna array provides the estimate of the target coordinates in the x-y and y-z planes. Then, by the proper combinations of these coordinates, the estimate of the target coordinates in 3D will be obtained.

The performance properties of the outlined concept of 3D localisation system have been evaluated by the experiments intent on indoor line-of-sight localisation of a person and on through-the wall localisation, too. The obtained preliminary experimental results are illustrated in Fig. 1. The comparison of the true target positions (represented by a human torso) and estimated target positions (represented by the red cross) show that the novel method introduced in this paper is capable to provide good estimate of the static person position in 3D.

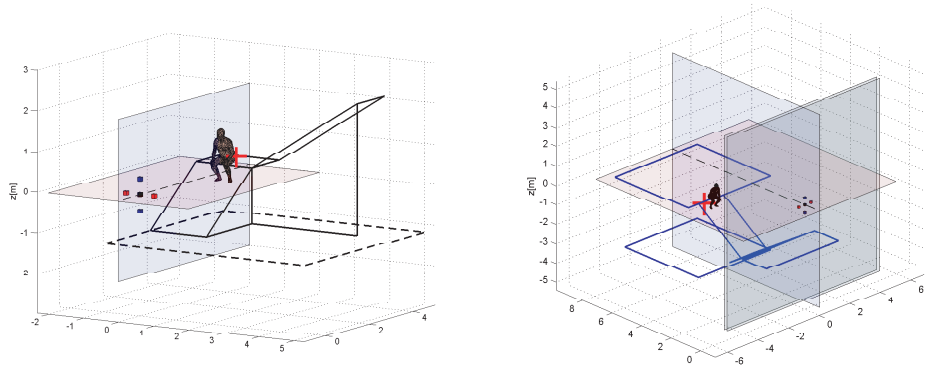

(a) (b)

Figure 1: Experimental results: (a) indoor line-of-sight localisation, (b) through-the wall localisation.

Research of Composite Electromagnetic Scattering from Targets and Rough Surface Basing on the Efficient Numerical Algorithm

Yu Liang[1], **Li-Xin Guo**[2], **Xiang-Hua Zeng**[1], **and Zhen-Sen Wu**[2]

[1]College of Physics Science and Technology, Yangzhou University, Yangzhou, Jiangsu, China
[2]School of Physics and Optoelectronic Engineering, Xidian University, Xi'an, Shaanxi, China

Abstract— Some studies of composite electromagnetic scattering from targets and rough surface are implemented by using the Propagation-Inside-Layer-Expansion (PILE) combined with the Forward-Backward Method (FBM) hybrid scheme. Multiply target and rough surface cases are considered, that is, not only the single buried target is referred to, but also the targets both above and below the rough surface are aimed at, and different spectral (Gaussian, exponential, and PM spectrum) types of rough surface are included. The composite scattering integral equations are bulit. The formation mechanisms of the EPILE+FBM scheme including the self- and multal coupling inductions between targets and rough surface are analyzed. The accuracy and efficiency of the hybrid algorithm are verified. The applications of this scheme for the specific type of targets are carried out. The scattering results under different parameters, such as different roughness, different moisture, different temperature, different target size and height, etc., are investigated, the important scattering phenomena and characteristics are discussed and corresponding conclusions are obtained. The presented hybrid scheme will make sense to the domains of electromagnetics, remote sensing, radar surveillance, target recognition, optics, material science, etc..

ACKNOWLEDGMENT

This work was supported by the National Natural Science Foundation of China (Grant No. 11347182), by the University Science Research Project of Jiangsu Province (Grant No. 13KJB140020), by the National Natural Science Foundation for Distinguished Young Scholars of China (Grant No. 61225002) and by the Science Foundation of Yangzhou University (Grant No. 2012CXJ009). The authors would like to thank the reviewers for their helpful and constructive suggestions.

REFERENCES

1. Tsang, L. and J. A. Kong, *Scattering of Electromagnetic Waves — Numerical Simulations*, 114–176, Wiley, New York, 2000.
2. Jandhyala, V., E. Michielssen, S. Balasubramaniam, and W. C. Chew, "A combined steepest descent-fast multipole algorithm for the fast analysis of three-dimensional scattering by rough surfaces," *IEEE Trans. on Geosci. Remote Sens.*, Vol. 36, No. 3, 738–748, May 1998.
3. Liang, Y., L. X. Guo, and Z. S. Wu, "The fast EPILE combined with FBM for electromagnetic scattering from dielectric targets above and below the dielectric rough surface," *IEEE Trans. on Geosci. Remote Sens.*, Vol. 49, No. 10, 3892–3905, 2011.
4. Liang, Y., L. X. Guo, and Z. S. Wu, "The EPILE combined with the generalized-FBM for analyzing the scattering from targets above and on a rough surface," *IEEE Antennas Wireless Propag. Lett.*, Vol. 9, 809–813, 2010.

FPGA-based Real-time Generator of Combination Chaotic Frequency-modulated Signal for Noise Radar

Qilun Yang[1,2], **Yunhua Zhang**[2], **and Bingjie Li**[1,2]

[1]University of Chinese Academy of Sciences, Beijing 100049, China
[2]The Key Laboratory of Microwave Remote Sensing, Chinese Academy of Sciences, Beijing 100190, China

Abstract— Noise radars acquire the ECCM capability and the LPD/LPI characteristics by transmitting random waveforms. This paper proposes a scheme for generating the combination chaotic frequency-modulated (CCFM) signal for noise radar in real-time based on FPGA. The exploited CCFM signal can overcome the effect of limited quantization length destroying the chaotic property of chaotic signal, so it can get lower sidelobe of auto-correlation.

The FPGA-based real-time generator can generate the CCFM signal by embedding the Bernoulli map into the Logistic map, i.e., the Logistic map is used to produce the parameters needed for the Bernoulli map, and the resulted Bernoulli sequences under different parameters are combined to obtain the combination map. The combination map is then used to modulate the signal frequency to finally obtain the CCFM signal. Fig. 1 shows the software structure which is realized by FPGA.

Figure 2 shows the hardware structure. The analog to digital converter (ADC) gives FPGA the initial value of the chaotic map, and then the FPGA generates the inphase and quadrature (I/Q) components of the CCFM. After that, the digital I/Q signals are sent to digital to analog converter (DAC) followed by a low-pass filter (LPF) to get the analog I/Q signals, which are input of the quadrature modulator to obtain the intermediate frequency signal. The experiment demonstrates that the real-time generated CCFM signal has good random characteristic and low PSLR of auto-correlation.

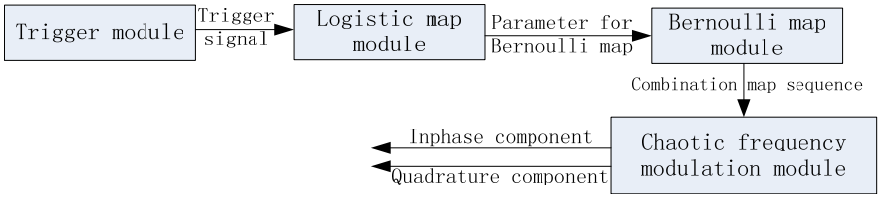

Figure 1: The software structure of the FPGA-based real-time generator of CCFM signal.

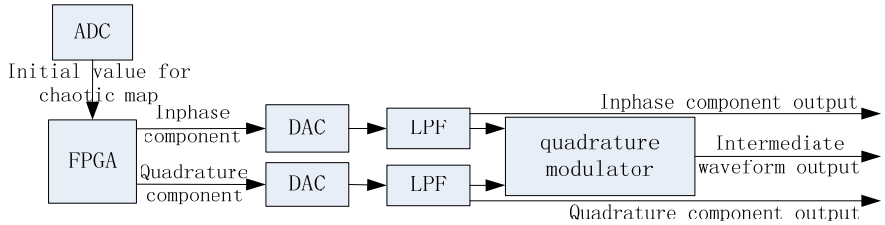

Figure 2: The hardware structure of the FPGA-based real-time generator of CCFM signal.

Uncertainty Estimation in Vector Wind Retrievals from Satellite-based Polarimetric Microwave Radiometer Measurements

Xiaolin Tong[1, 2, 3], **Zhenzhan Wang**[2], **and Qingxia Li**[3]

[1]School of Physics and Electronics, Henan University, Kaifeng 475001, China
[2]Key Laboratory of Microwave Remote Sensing
National Space Science Center/Center for Space Science and Applied Research
Chinese Academy of Sciences, Beijing 100190, China
[3]Department of Electronics and Information Engineering
Huazhong University of Science and Technology, Wuhan 430074, China

Abstract— The main characteristic of wind vector is circularity in any reference direction, which creates problems when analyzing the data statistically. Due to this periodicity, standard statistical techniques cannot be used to analyze circular data. For example, (1) in the regions including upwind/downwind ambiguity, the STD obtained from the linear statistics approach is about 60–80°. However, we couldn't deduce that it is upwind/downwind ambiguity from the STD. (2) The Cramer-Rao bound (CRB) has been widely used as sensitivity estimation. The precondition of the CRB approach is the possibility distribution is normal one. Since the model of wind direction reveres is non-linear, the angel distribution is not normal. A problem appeared for wind-vector sensitivity estimation. The STD obtained from closest solution is lower than the sensitivity obtained from CRB. In this paper, we introduce the directional statistics approach for evaluating the uncertainty. The circular STD is always between zero and one inclusive, making it very different from its linear analog, which can have any positive value. It is indicative of the spread in a data set. If all samples point into the same direction, the circular STD will be small. If the samples are spread out evenly, the circular STD will be close to one. Importantly, however, a circular variance of 1 does not imply a uniform distribution around the circle. If all samples either point towards 0° or 180°, the circular variance is 1, yet the data is not distributed uniformly around the circle. The sensitivity is reassessed based on the directional statistics approach, and compared with CRB. The sensitivities of CRB are high where the derivatives of the brightness temperatures changing rapidly. The incorrect results come from the effect of nonlinearity. When the directional statistics approach is used, the peak disappeared where the derivatives of the brightness temperatures changing rapidly. In addition, the directional statistics approach can be used to estimate the characterization of uncertaintys in wind vector retrievals from Scatterometry.

Session 1P0
Poster Session 1

Backward Angular Distribution of Air Lasing Induced by Femtosecond Laser Filamentation

T. Zeng[1], **J. Y. Zhao**[1], **W. W. Liu**[1], **and S. L. Chin**[2]

[1]Key Laboratory of Optical Information Science and Technology, Ministry of Education
Institute of Modern Optics, Nankai University, Tianjin 300071, China
[2]Centre d'optique, Photonique et Laser (COPL), Département de physique, de genie physique et d'optique,
Université Laval, Québec, QC, G1V 0A6, Canada

Abstract— Angular distribution of the back scattered nitrogen fluorescence induced by femtosecond laser filamentation in air has been studied. The experimental results demonstrate that the fluorescence intensity forms multiple rings and is amplified in the backward direction through amplified spontaneous emission (ASE). More important, ASE signal features angular dependent gain coefficient. The results are valuable for optimization of the remote-sensing setup by filamentation in air.

A Novel Knowledge-aided Approach for Training Data Selection

Su-Dan Han, Chong-Yi Fan, Xiao-Tao Huang, and Zhi-Min Zhou
School of Electronic Science and Engineering, National University of Defense Technology, China

Abstract— Space-time adaptive processing (STAP) is an important technique for suppressing strong clutter in airborne radar systems. Traditional STAP employs training data near the range under test to estimate interference covariance matrix and generate the optimal weight vector under the assumption that they are independent and identically distributed with the tested data. However, realistic clutter environments usually appear heterogeneous and non-stationary thereby violating the assumption, leading to covariance estimation errors, adaptive weight vector mismatch and consequently, degradation in STAP performance. Clutter heterogeneity generally consists of clutter power differences, target-like signals, clutter discretes and spectral dissimilarities. One useful approach to mitigate the effect of clutter heterogeneity is screening the training data before covariance estimation. Lots of screening metrics have been proposed, and among these, using a prior knowledge is regarded as one of the most promising ways.

In this paper, a novel knowledge-aided screening metrics is proposed and its performance in heterogeneous environment is analyzed. We choose the distance between covariance matrix of training data and tested data as screening metrics to measure the statistical similarity. Euclidean distance, Riemannian distance and distance between the covariance matrix of whitened training data and identity matrix is taken into consideration. Prior knowledge of radar system parameters and platform movement parameters are used to construct the covariance matrix of tested data using clutter model, and prior knowledge of white noise spectral density is employed to generate a positive-definite covariance matrix of training data which is necessary in calculating the distance. Compared with the approach exploiting the sample covariance matrix as the estimation of the covariance matrix of tested data, our knowledge-aided approach can achieve a much better performance in training data selection and consequently, a improvement in detection performance.

Novel Design and Implementation of Ultra-wideband Pulse Generator Based on Avalanche Transistor

Y. Guo and G. Zhu
School of Electronic Science and Engineering
National University of Defense Technology, Changsha, China

Abstract— Based on the avalanche multiplication effect of the avalanche transistor, a novel ultra-wideband (UWB) pulse generator has been designed. The UWB pulse technologies are described, and then different approaches for UWB pulse are analyzed and compared. The considered pulse generation technologies are based on logic gates, Step-Recovery Diodes (SRD), and avalanche transistors. The basis of the proposed generator is a logic component to generate the trigger pulse, an avalanche transistor to generate the high avalanche pulse, and an unique pulse-shaping circuit composed of the SRD and Schottky diode, which is used to reduce the pulse width and maintain the pulse amplitude high. Every component in the UWB pulse generator should be picked, and the radio-frequency (RF) characteristics of the circuit must be considered. Finallythe UWB pulse generator generates periodic negative pulse, whose pulse full width is 410 ps, pulse amplitude is −3.1 V, and pulse ringing level is −29.5 dB in the simulation mode. Then the circuit is fabricated on an FR-4 glass epoxy substrate, and a kind of UWB pulse with pulse duration of 416 ps, pulse amplitude of 3.0 V and ringing level of −12.6 dB is achieved. The measured result agrees with the simulation, and it shows that the design is reasonable. Besides, the measured result is analyzed and the expectation is presented. With the features such as simple structure, stable performance and low cost, the proposed design is ideal for the UWB wireless communication system.

An Efficient Algorithm for the Calculation of Quantum Radar Cross Section of Flat Objects

Yun Lin, Liangshuai Guo, and Kun Cai
Science and Technology on Electromagnetic Scattering Laboratory, China

Abstract— The quantum information technology has experienced significant progress in the past decade. The developments in the related fields such as quantum computation and quantum communication provide the theoretical and practical bases for the realizing of the quantum radar, although there is still a long way to go for an operational quantum radar system [1–3]. The quantum radar has been proposed as a candidate for the next generation detection method [4], since the quantum radar system has some potential advantages over the classical radar system based on some preliminary studies. For example, the quantum radar is able to recognize the intercept-resend jamming by utilizing the entangled photon pairs [5]. There are many research topics related to quantum radar such as the characteristics of signal channel in a quantum radar system, the physical design and realization of a quantum radar system, the signal processing technology in a quantum radar system, and the estimation of the quantum radar cross section. Among all these topics, the quantum radar cross section has little dependence on the physical realization of the system. Furthermore, the study of the quantum radar cross section can provide useful information for the design of the quantum radar system. The quantum radar cross section should be investigated in advance.

The quantum radar cross section is a measurement of the visibility of targets with the illumination of the quantized electromagnetic wave (photon). The definition of the quantum radar cross section is similar as the classical radar cross section [6]. The quantum radar cross section can be calculated with the help of photon wave function. Following the definition of the quantum radar cross section expressed in [6], we present an efficient algorithm for calculating the quantum radar cross section utilizing the analytical photon wave function. The proposed algorithm is much more efficient than the one mentioned in [6]. The algorithm is able to simulate arbitrary flat structures. We calculate the quantum radar cross section of flat rectangular and elliptical plates. The simulated results have good agreement with reference results, and with much less computational costs. The algorithm is extended to deal with homogeneous dielectric object with the cooperation of the reflection coefficients. The proposed algorithm shows the potential to simulate the quantum radar cross section of a much more complex system.

REFERENCES

1. Lanzagorta, M. and Q. Radar, *Synthesis Lectures on Quantum Computing,* Morgan & Claypool Publishers Series, 2012.
2. Tan, H. and Z. Dai, "Key technology research in the quantum radar," *Journal of Huazhong Normal University*, Vol. 46, No. 3, 2012.
3. Lin, P., Z. Yu, and C. Li, "Review and forecast of quantum radar," *2013 Asia-Pacific Conference on Synthetic Aperture Radar (APSAR)*, 2013.
4. Allen, E. H. and M. Karageorgis, "Radar systems and methods using entangled quantum particles," US Patent 7375802, 2008.
5. Malik, M., O. S. Magana-Loaiza, and R. W. Boyd, "Quantum-secured imaging," *Physics Letters*, Vol. 101, 241103, 2012.
6. Lanzagorta, M., "Quantum radar cross sections," *Proceedings of the Quantum Optics Conference, SPIE Photonics Europe*, 2010.

A Real Time 3D Multi Target Data Fusion for Multistatic Radar Network Tracking

El-Sayed Abdoul Moaty El-Badawy, Tarek Reda Abd-ElShahid, and Alaa El-Din Sayed Hafez
Faculty of Engineering, Alexandria University, Egypt

Abstract— The paper is devoted to propose a data fusion algorithms into multistatic radar network to improve its tracking capability. The proposed data fusion algorithm is based on using common measurement architecture gives state estimates with relatively low and medium uncertainty followed by cumulative measurement fusion (CMF) or cumulative state vector fusion (CSVF) algorithm which is very simple, easy to implement and can be used in real time. Extended Kalman Filter (EKF) is used as a non-linear tracking and predictor algorithm. The system is simulated using Matlab program to compare the performance of the estimation routines of both fusion algorithms and the targets scenario is simulated using Monte Carlo simulation. Simulation results have shown that these cumulative fusion algorithms improve the multistatic radar network tracking capability and produce a significant reduction in the root sum square error (RSSE), absolute error, and root sum square variance (RSSV) than achieved from monostatic radar.

In a multistatic-multi-target environment, where each radar processes its own observations and sends the resulting tracks to a data fusion center, the first step is to determine whether or not two or more tracks, coming from different radar systems with different accuracies, represent the same target (track-to-track association). The next step is to combine the radar tracks when it is determined that they indeed represent the same target (track fusion). Both problems arise when several radars carry out surveillance over a common volume (overlapping sensor coverage). A survey of the current research in this area has been presented in [1–8]. Furthermore, the goal of data fusion is to operate on a combination of radar sensor measurements, features, track states, and object type and identification likelihoods to produce a single integrated air picture of the air space to a high degree of accuracy. Technologies that enable this synergistic fusion and interpretation of data at several levels from disparate, distributed radars and other sensors should enhance system acquisition, tracking and discrimination of threat objects in a cluttered environment and provide enhanced battle space awareness. There are two approaches for fusion of multiple radar data: measurement fusion and state vector fusion. In the first approach, the radar measurements are combined and an optimal estimate of the target state vector is obtained. State vector fusion is preferable for implementation in a variety of practical systems. In this approach, each radar employs an estimator to extract a target track state vector and its associated covariance matrix from its respective sensor measurement, that are then transmitted over a data link to a fusion center. At the fusion center, track-to-track correlation and state vector fusion are performed to obtain a composite target state vector [9].

The proposed method uses current radars data for track-to-track association using cumulative measurement fusion, and cumulative state vector fusion in order to produce an accurate target estimation and prediction with the multistatic radar network. Results based on Monte Carlo simulations are presented. The proposed method is able to perform track correlation and fusion with low root sum square error (RSSE), absolute error, and root sum square variance (RSSV) than achieved from monostatic radar. The remainder of this paper is organized as follows. Section 2 describes the target tracking algorithms and the extended Kalman filter. Section 3 presents a brief overview of data association and fusion methods in the tracking systems. In Sections 4 present the proposed comulative track-to-track association and track fusion. Simulation results and discussion are presented in Section 5. Finally, Section 6 concludes the paper.

A New FPGA Prototype for Synchro to Digital Converter Using CORDIC Algorithm

Mohamed Rizk, Ahmed Hossin, and Alaa El-Din Sayed Hafez
Faculty of Engineering, Alexandria University, Alexandria, Egypt

Abstract— This paper introduce a new approach to FPGA implementation of synchro to digital converter using Co-ordinate Rotation Digital Computer CORDIC algorithm. This algorithm was the best replacement of analog conversion system by the high resolution digital. CORDIC algorithm used for the fast calculation of elementary functions like multiplication, division, trigonometric functions. The approach is based on receiving the synchro signals S1, S2, and S3 from the synchro motor, and converts them to two perpendicular signals sin signal and cosine signal using solid state Scott-t transformer. Then the a CORDIC circuit receive this signals after converting them to digital and produce the azimuth angle in digital format. This prototype of hardware implementation of CORDIC algorithm used Spartan-III series FPGA, with constraint to area efficiency and throughput architecture. The prototype results show that the conversion time is less than 1 µs which is suitable for real time applications in radar and missile control applications.

Introduction: CORDIC is the abbreviation of Co-ordinate Rotation Digital Computer. The first description for iterative approach of this algorithm is firstly provided by Jack E. Volder in 1959 [1]. CORDIC algorithm provides an efficient way of rotating the vectors in a plane by simple shift add operation to estimate the basic elementary functions like trigonometric operations, multiplication, division and some other operations like logarithmic functions, square roots and exponential functions. Most of the applications either in wireless communication or in digital signal processing are based on microprocessors which make use of a single instruction and a bunch of addressing modes for their working. As these processors are costs efficient and offer extreme flexibility but yet are not suited for some of these applications. During the last 50 years the CORDIC algorithm has emerged in a wide variety of applications. The CORDIC algorithm has received increased attention after a unified approach is proposed for its implementation [2].

The CORDIC arithmetic processor chip is designed and implemented to perform various functions possible in rotation and vectoring mode of circular, linear, and hyperbolic coordinate systems [3]. Since then, CORDIC technique has been used in many applications [4], such as single chip CORDIC processor for DSP applications [5, 6]. Recently several researches applied CORDIC algorithm in radar pulse compression, rotary encoders, and waveform generation [7–12]. This paper implement CORDIC S/D converter to convert synchro signals into high resolution digital azimuth angle. This achieves a high precision S/D conversion with low propagation delay compared with that implemented using microcontroller or analog processing.

Improved Design of Ku Band High Power Rectangular Waveguide Directional Coupler

Chao Wang, **Gaofeng Guo**, **and En Li**
University of Electronic Science and Technology of China, Chengdu, China

Abstract— This paper demonstrates an effective designing method of the high power rectangular waveguide directional coupler. The coupler designed using this method has wide band, high directivity, flat coupling, low voltage standing ratio and manufacturing accuracy. According to the required technology parameter, and the engineering design method based on the modified Bethe aperture coupling theory, the relevant parameters of equally spaced waveguide directional coupler are preliminarily designed. On the basis of this, using simulation software HFSS to do the simulation and optimization of the space between three outside coupling holes of the head end and the tail end, the performance of isolation is improved. A directional coupler at Ku waveband is designed in this paper, the error between the simulation value of coupling and the required value −10 dB is less than 0.6 dB, and after optimization, the isolation is less than −47 dB in the whole operating frequency band.

Magnetic Field Controlled Diffraction Grating

Guojing Huang, Henghe Jiang, Bin Zhou, and Zhuo Chen
Centre for Optical and Electromagnetic Research, South China Academy of Advanced Optoelectronics
South China Normal University, Guangzhou 510631, China

Abstract— A novel magnetically tunable diffraction grating based on photoresist solidified magnetic nanoparticles is proposed and demonstrated experimentally. We mixed the ferro fluid and the photoresist at room temperature on a silica wafer and then the mixture was heated at 90°C for solidification and formed a thin film. The refraction index and the absorption coefficient of the film are sensitive to surrounding magnetic field. The diffraction grating was fabricated by etching the magnetic film periodically. The grating's period we made was 10 μm, and the grooves and the convex groove were both 5 μm respectively. We demonstrated the magnetically tenability of this grating by measuring the changing of the diffraction angle of the high order diffraction light. Here we applied a He-Ne laser as the light source. The diffracted light was received far away from the grating (several meters) and to enhance the sensitivity as a small change of the diffraction angel would lead to a detectable movement of the laser spot. This approach is a good candidate for the following applications: magnetic sensors, magnetic controlled optical switches, modulator and so on. This is a new method to fabricate the magnetically tunable diffraction grating. Compared with some other present diffraction grating, the proposed magnetically tunable diffraction grating is with a more simple configuration and is easier to be produced. The period of this magnetically diffraction grating can be tuned to adapt to the different application needs by the external magnetic field strength. All of these are in favor of its practical applications.

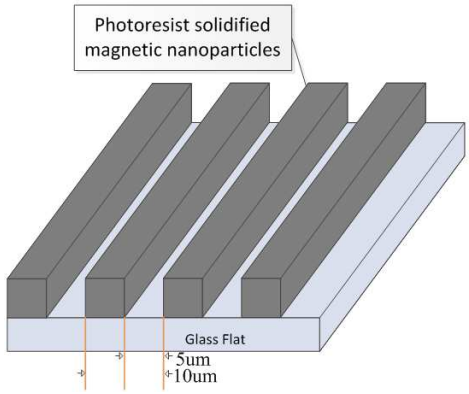

Figure 1: Structure of the magnetic controlled diffraction grating.

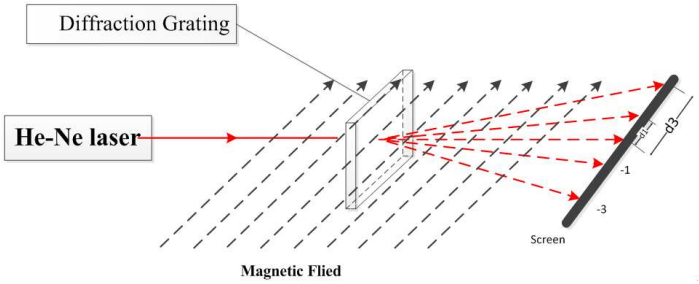

Figure 2: Schematic diagram of the experimental system.

Analysis of Immunity by RF Wireless Communication Signals

Hongsik Keum[1], **Jungyu Yang**[2], **and Heung-Gyoon Ryu**[3]

[1]EletroMagneticwave Technology Institute, RAPA, South Korea
[2]Department of Radio Environment Safety, Radio Research Agency, South Korea
[3]Department of Electronic Engineering, Chungbuk National University, South Korea

Abstract— Despite of widespread use of new digital wireless communications,the radiated immunity test based on IEC 61000-4-3 only has been performed with using AM signal. In this study, we have analyzed the radiated immunity test method that is going on recent standardization activity to investigate close proximity fields from RF wireless communications and have investigated the impact of digitally modulated signals. The results show that the devices were influenced much more by digital modulation signal than by AM or PM signal. Also it shows that we need to investigate the depth research on radiated immunity testing for the environment of modern communication technology.

Resonant Properties of HE_{111} Mode of a Complicated Microwave Cavity for a New Type of Rubidium Clock

Xiao Xiao Li, **Shang Lin Hou**, **Yanjun Liu**, **and Jing Li Lei**
School of Science, Lanzhou University of Technology, Gansu, China

Abstract— The microwave cavity is one of the most important microwave components in the rubidium clock, which directly has an impact on the properties of atom frequency standard. Placing a glass bubble filled with rubidium gas in the microwave cavity, microwave radiation field provided by microwave cavity can interact with rubidium gas inside the glass bubble and make rubidium atomic level transition occur. To miniaturize the cavity, materials are often filled in the microwave cavity. Glass bubble can be seen as a type of media filled inside the cavity. Sometimes, other materials are often used to further miniaturize the cavity. For some applications, it is desirable that microwave radiation field changes with the energy of rubidium gas at a certain frequency such as 6.835 GHz. Generally, the resonant frequency is related to material property and rubidium gas parameters. Therefore they are extremely critical for rubidium frequency standard design because of the effect of material property and rubidium gas parameters on resonant frequency.

In this paper, resonant properties of HE_{111} mode of a complicated microwave cavity with ceramic material, used in rubidium clock, are studied by mode matching method. The microwave cavity works at a certain frequency such as 6.835 GHz by accommodating a glass bubble containing rubidium vapour. To make electromagnetism focus on the centre of the cavity for energy exchange and further miniaturize the cavity to a large extent, a ceramic dielectric ring is installed in the inner layer of the glass bubble. In order to study main factors influencing resonant characteristics, resonant frequencies of HE_{111} mode are calculated through eigen equation and compared with simulated results. The results show that theoretical computations are in good agreement with finite element simulations. In addition, the effects of loaded dielectric and rubidium vapour on resonant frequency are also analyzed. This work is of great significance for the miniaturizing of the cavity and theory perfection in atomic clock.

Dielectric Properties of Rice Husk/Carbon Nanotubes Composites in Ku-band

Y. S. Lee[1], **F. Malek**[2], **E. M. Cheng**[3], **Wei-Wen Liu**[4], **F. H. Wee**[1], **M. N. Iqbal**[1], **L. Zahid**[1], **M. S. Mezan**[2], **F. S. Abdullah**[2], **and M. Othman**[2]

[1]School of Computer and Communication Engineering, Universiti Malaysia Perlis (UniMAP)
Pauh Putra Campus, Arau, Perlis 02600, Malaysia
[2]School of Electrical Systems Engineering, Universiti Malaysia Perlis (UniMAP)
Pauh Putra Campus, Arau, Perlis 02600, Malaysia
[3]School of Mechatronic Engineering, Universiti Malaysia Perlis (UniMAP)
Pauh Putra Campus, Arau, Perlis 02600, Malaysia
[4]Institute of Nano Electronic Engineering (INEE), Universiti Malaysia Perlis (UniMAP)
Kangar, Perlis 01000, Malaysia

Abstract— This paper presents the dielectric properties of rice husk and carbon nanotubes (RHCNTs) composites materials. The RHCNTs composites materials prepared with various weight ratios of rice husk with CNTs 0%–10% length, width, and thickness of each RHCNTs composite sample are 15.799 mm, 7.899 mm, and 5 mm was fabricated. First, the rice husk and CNTs were mix with polyester resin and methyl ethyl ketone peroxide (MEKP) harden agent. Then, stir the mixture for 1 hour. The RHCNTs mixtures were stir for 1 hour shown in Figure 1(a). After the composition, the RHCNTs composite were filled into waveguide sample holder to fabricate the rectangular shape sample for WR-62 waveguide. The RHCNTs samples were fabricated by using WR-62 sample holder mould shown in Figure 1(b). The RHCNTs samples were prepared in rectangular shapes, which fit into WR-62 waveguide sample holders. Before conduct to the measurement, calibration technique TRL (through-reflect-line) of waveguide flanges must be applied before conduct the measurement. The calibration technique is to minimize the residual errors of the measurements. The rectangular waveguide technique was used to measure the Dielectric properties of the RHCNTs composites materials. The Dielectric properties were measured using rectangular waveguide transmission line technique. A pair of coaxial cable was connected to Agilent E8362B performance network analyzer and the two waveguide adaptors were connected with coaxial cables. The sample holder was place between the two waveguide adaptors. The conversion of s-parameters to complex dielectric parameter is computed by using 85071E Agilent technology software which using a transmission line technique consists of a network analyzer to perform the conversion to Dielectric properties, ε_r. The 85071E software is originally developed by NRW to calculate the permittivity from transmission and reflection coefficient. The Dielectric properties are represented in terms of both the real and imaginary parts of permittivity in Ku-band frequency. The conductivity of RHCNTs shows increasing when the ratio of CNTs mixture increases. The materials, their dielectrics properties measurement result over 12.4–18 GHz frequency range are discussed.

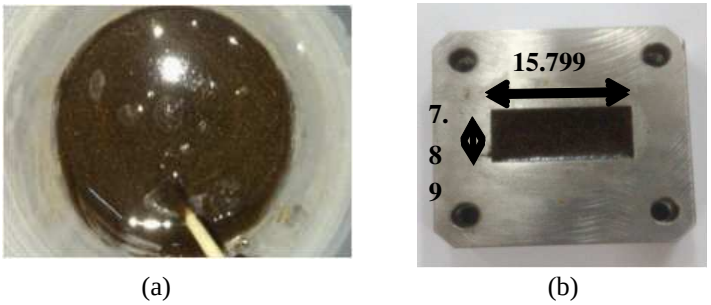

Figure 1: (a) RHCNTs after stir with polyester and MEKP. (b) Ku-Band sample holder fit with RHCNTs sample.

Contribution of Evanescent Waves to Vortex Vector Field with Inhomogeneous Polarization in Near Field

Yin-Long Feng[1] **and Rui-Pin Chen**[1, 2]

[1]School of Sciences, Zhejiang A & F University, Lin'an, Zhejiang 311300, China
[2]Department of Physics, Zhejiang Sci-Tech University, Hangzhou 310018, China

Abstract— We study the evanescent wave of a vortex vector optical field with inhomogeneous states of polarization in the cross section of the field. The TE and TM terms of the evanescent wave and the propagating wave of a cylindrical vortex vector optical field with inhomogeneous states of polarization in the cross section of the field are derived by the vector angular spectrum method. The vector structure of the evanescent wave and propagating wave components of the cylindrical vector field is demonstrated. The ratio of the evanescent wave and the propagating wave of a cylindrical vector optical field with different states of polarization with different vortex charges n and polarization charges m as a function of propagation distance in near field is described. Comparison between the contribution of TE and TM terms of both the propagating and the evanescent waves of the cylindrical vortex vector field in free space is demonstrated. The intensity (squared modulus) distributions of the TE and TM terms of the propagating and evanescent waves are described to compare the contributions of the propagating and the evanescent waves associated with the cylindrical vector field with inhomogeneous states of polarization in the cross section of the field. These results, therefore, provide useful information on how to spatially manipulate the evanescent waves of a vortex vector cylindrical optical field in near field by choosing appropriate vortex charges n and states of polarization in the cross-section of the field.

VEMC Computing System for Electromagnetic Compatibility of Integrated Circuits

Boyuan Zhu[1], **Hengxu Li**[1], **Junwei Lu**[1], **Haiyan Sun**[2], **Ling Sun**[2], **and Lingling Yang**[2]

[1]School of Engineering, Griffith University, Brisbane, Australia
[2]College of Electrical Engineering, Nantong University, Nantong, China

Abstract— This paper introduces a newly developed virtual electromagnetic compatibility (VEMC) computing system and related techniques for electromagnetic compatibility (EMC) computer modelling, simulation and optimisation in integrated circuit (IC). The system is a high performance computation and collaborative visualisation platform which provides researchers and engineers with an integrated and flexible computation environment in modeling, simulation and optimisation of IC EMC issues. It meets various computation needs and increases machine usage and computation efficiency of computation resources. A case study presents computational models of interested issues in IC-level EMC modelled, simulated and optimised by the developed system.

Introduction: In modern IC-level EMC, computational electromagnetic (CEM) modelling and visualization techniques become most significant considerations. They are now an integral part of design in engineering practice and implemented to solve real life EMC problems which is proved extremely important for this high EMC risks industry. Traditional "build then test" procedure for EMC was proved time consumed and very expensive in terms of cost. CEM modelling and visualization allows designer to investigate, monitor and modify the interested area of the design at an early stage, which makes it play an important role in scientific research and industry applications of IC.

Visualization and high performance computation are closely related that utilizes visualization techniques to deal with the complicated dynamic electromagnetic problems [1]. Due to the variety and complexity of different IC EMC problems, it always requires engineers from different disciplines work collaboratively to analyse and optimize the solution together. Using interactive and collaborative visualization techniques provide an alternative solution to achieve best performance and efficiency of teamwork. However, current CEM products and systems are still dominated by single user oriented designs. The VEMC computing system is a high performance distributed and parallel computation and visualization system designed for requirements of high-load EMC modelling, simulation and optimisation tasks. The overall structure is shown in Figure 1. It integrates a full electromagnetic modelling and simulation environment with various pre-defined model libraries and templates. The system uses cloud computing concept to offer users a remote working environment on the modelling and simulation. The cost of entire system is well controlled comparing to professional supercomputing cluster structure.

Comparing to traditional procedure of IC design, modern design requires more collaborative work when considering IC-level EMC. In Figure 2, it demonstrates EMC computer modelling

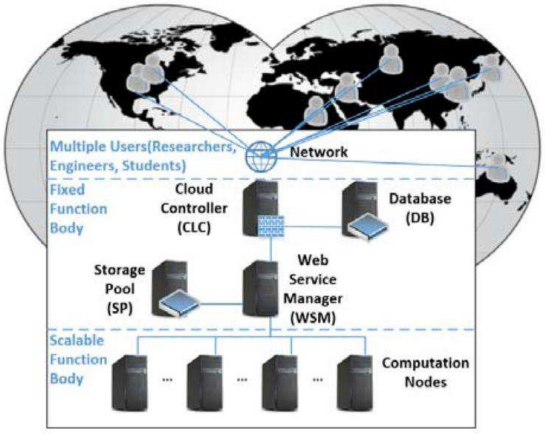

Figure 1: VEMC computing system structure.

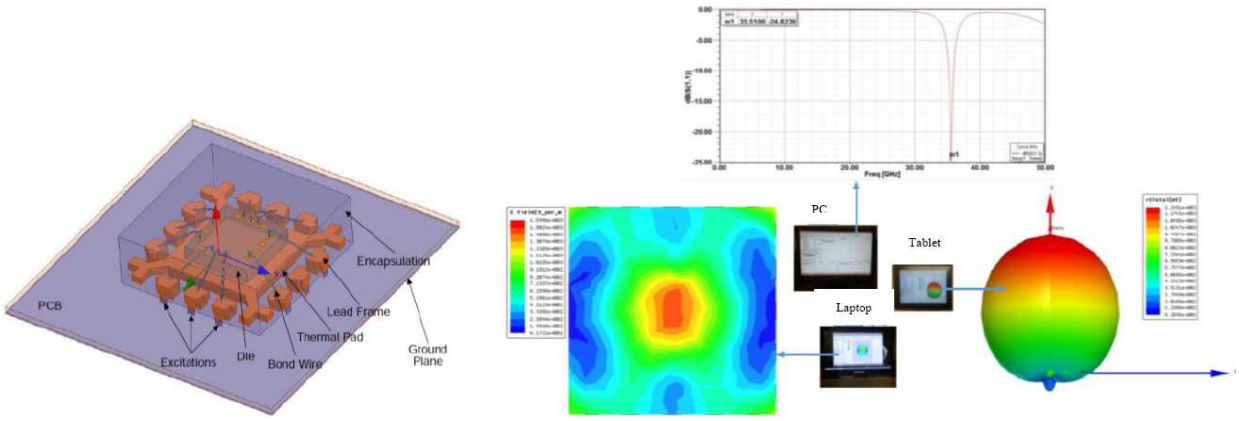

Figure 2: EMC computer modelling and simulation of a MMIC.

and simulation of a monolithic microwave integrated circuit (MMIC) and how three users work on the same project and look at different results from different terminals simultaneously via VEMC system. Some parallel optimisation work is also done which can not be shown due to the limitation of length. Details will be provided in the full paper. To conclude, this makes VEMC computing system necessary by using its CEM modelling and collaborative visualisation technology in modern IC-level EMC.

REFERENCES

1. Lu, J., "High performance computation and interactive visualization of electromagnetics for engineering eductaion programs," *IEEE Transactions on Magnetics*, Vol. 48, No. 2, 299–302, Feb. 2012.

Wide-angle Polarization-independent Planar Magnetic Metamaterials Based on Dielectric Resonators

Jiafu Wang[1], **Shaobo Qu**[1, 2], **Zhuo Xu**[2], **Hua Ma**[1], **Hongliang Du**[1], **Jun Wang**[1], **and Hongya Chen**[1]

[1]College of Science, Air Force Engineering University, Xi'an, Shaanxi 710051, China
[2]Electronic Materials Research Laboratory, Key Laboratory of the Ministry of Education Xi'an Jiaotong University, Xi'an, Shaanxi 710049, China

Abstract— Based on dielectric resonators, the theory, design and implementation of planar magnetic metamaterials made of dielectric blocks were investigated. By etching simple metallic patterns on surface of the dielectric blocks, field distributions of the desired resonance modes can be enhanced while those of the undesired suppressed. In this way, the resonance frequency of the desired mode can be tuned down to lower frequency range. A wide-angle polarization-independent planar magnetic metamaterial based on short cylindrical dielectric resonators was proposed and analyzed. Due to its polarization-independence, wide incident angle, the magnetic metamaterial is ready to be used in various microwave components, such as antenna radomes, microwave filters and frequency selective surfaces.

High-efficiency Anomalous Reflection Characteristics of an Ultra-thin Gradient Meta-surface Based on SRRs

Hong Ya Chen, Jia Fu Wang, Hua Ma, Shao Bo Qu,
Jie Qiu Zhang, Yong Feng Li, Ming Bao Yan, and Yong Qiang Pang
College of Science, Air Force Engineering University, Xi'an, Shaanxi 710051, China

Abstract— Metasurfaces are the planar version of metamaterials that are engineered to control and tailor EM waves in unconventional ways. An alternative approach is to use gradient meta-surfaces (GMs). By designing the phase gradients delicately on GMs, additional wave vectors are pre-defined to redirect the reflected and refracted waves to desired directions. Hence, GMs can realize both negative refraction (a typical effect realized by metamaterials) and negative reflection. This leads to the finding of the Generalized Snell's Law. Although the unique properties of GMs are so attractive, the realization of GMs is not easy. Equal amplitudes and strict gradient phase changes of scattered waves must be satisfied simultaneously to get a high-efficiency GM. To achieve this, the unit cell of GM must be designed so delicately that a minor variation may lead to drastic reduction of the efficiency. Nevertheless, it is comparatively easier to design a reflective GM since equal amplitudes can be realized by a backing metallic sheet. The design of reflective GMs is reduced to the design of phase gradients.

In this paper, we focus our research on the manipulation of EM wave reflection using reflective GMs under normal incidence. The theory and design method are briefly described and then one GM sample is presented. Both simulation and experiment results demonstrate that a carefully designed gradient meta-surface based on the square ring resonators (SRRs) supports high-efficiency anomalous reflections at the designed frequency, which agree quite well with theoretical predictions. For the ease of manipulating the reflected waves at will through the phase gradient, such GMs are very attractive for application in high directivity antennas, RCS reduction, flat focusing, etc..

Microwave Plasma Reactor Based on Microwave Oven

R. Pongsopon, **T. Chim-Oye**, **and M. Fuangfoong**
Department of Physics, Faculty of Science and Technology
Thammasat University, Rangsit Center, Pathum Thani 12120, Thailand

Abstract— In this paper, a simple compact size microwave plasma reactor (MPR) based on 2.45 GHz 700 W home used microwave oven has been design and constructed for use in laboratory. Main design criteria were low cost and available of parts and components in home country, in order to make it easy to use, to repair, to move and no leak of microwave radiation. This system consists of reactor vessel, mini air pump and solution container with heater. The reactor vessel is made from 800 ml Pyrex beaker with two pipes mounted on the aluminum cover plate of vessel for injection and exhaust gas. The quarter wavelength electrode unit consisting of five tungsten rods is placed on a circular aluminum plate with diameter $\lambda/2$ for used to generating plasma. Currently the microwave plasma reactor built is being used to be microwave plasma chemical vapor deposition system (MPCVD). However, such a system can easily be adapted to serve as surface cleaner of substrate.

An Experimental Investigation of the Concentration of KCl in Liquid Electrode of Atmospheric Pressure DBD

F. Manu[1], **C. Tawee**[1], **F. Pollawat**[2], **and F. Wasana**[3]

[1]Department of Physics, Faculty of Science and Technology
Thammasat University, Rangsit Center, Thailand
[2]Sirinthorn International Institute of Technology
Thammasat University, Rangsit Center, Thailand
[3]Faculty of Science and Technology
Thammasat University, Rangsit Center, Thailand

Abstract— In this paper, the high voltage power supply for dielectric barrier discharge (DBD) have been design and constructed by using a function generator, power amplifier and twin car's ignition coil. Three different types of electrode configurations namely, cylindrical-cylindrical, cylindrical-plate and parallel-parallel were used in the experiment. The air discharge gap between the dielectric layers was fixed at 3 mm. The main objective of this study is to study the effect of the concentration of potassium chloride (KCl) in liquid electrode of the DBD at atmospheric pressure on the uniform discharge and number of electrode on the discharge voltage. Finally, we investigate the usage of DBD system with cylindrical-cylindrical electrode for waste water treatment.

Study on Permittivity and Optimal Design of Metamaterial

Zihao Fu[1], **Yanfang Li**[2], **and Guizhen Lu**[1]

[1]Information School, Communication University of China, Beijing, China
[2]Materials and Machinery School, Jiangxi Science & Technology Normal University, Nanchang, China

Abstract— Artificial electromagnetic materials in the recent years develop rapidly, both in the military aspects about stealth technology and in daily life to absorb harmful electromagnetic waves in nature. As the environmental impact of electromagnetic radiation become terrible. The importance of artificial electromagnetic materials becomes more prominent. Artificial electromagnetic materials have great potential in the antenna and microwave devices and other research fields, because Metamaterials can be produced by the restructure of traditional materials in nature. We use new technology to prepare artificial electromagnetic materials. Therefore, for the study of Metamaterials has become very urgent. This paper analyses the characteristics of the Metamaterials. By the homogenization method we can effectively deal with the periodic structure situation, therefore, faced a similar problems, we can generally use the method of homogenization to solve. Firstly, considering the scope of its application, a frequency selective surface structure was verified. For the homogenization method, scattering parameters results were obtained to compare with the original structure. Target structure uses S-parameter inversion to obtain equivalent electromagnetic parameters. The paper analyses the absorbing properties of the structure, it also pays attention to the energy dissipation. On this basis, using the honeycomb structure instead of the original structure, better absorbing effect can be obtained. As is known, honeycomb structure not only has absorbing effect but also with good mechanical properties. The absorbing materials can effectively absorb the incident electromagnetic wave and make it decay. Cause electromagnetic loss so that electromagnetic energy is converted into thermal energy or other energy forms. Finally, this paper proposes a kind of absorbing structure with better performance.

Independently Tunable Multichannel Terahertz Filtering in a Defect Resonator Embedded with Graphene Sheets

Fenghua Shi and Yihang Chen
Laboratory of Quantum Information Technology
School of Physics and Telecommunication Engineering
South China Normal University, Guangzhou 510006, China

Abstract— Novel terahertz filters with independently tunable transmission channels are constructed by embedding voltage-gated graphene sheets into a defect resonator of a one-dimensional photonic crystal. The frequency of each high-transmission defect mode can be separately tuned by changing the electrode voltage of the corresponding graphene sheet. We show that the influence of graphene sheets on defect modes depend on the positions where the graphene sheets are embedded. We also find that the graphene sheet can hardly influence the defect mode when it is inserted at the antinode of the standing-wave-like electric field corresponding to the defect mode. Based on these properties, two- and three-channel independently tunable filters are designed. Our proposed structures provide an efficient way to manipulate the terahertz waves.

Concentration Measurements of Atmospheric CH_4, N_2O and H_2O Vapor Using a Quantum Cascade Laser-based QEPAS Sensor

Hongming Yi[1, 2], **Olivier Laurent**[3], **Weidong Chen**[1], **Michel Ramonet**[3], **Rabih Maamary**[1], **Eric Fertein**[1], **and Xiaoming Gao**[2]

[1]Laboratoire de Physicochimie de l'Atmosphère, Université du Littoral Côte d'Opale, Dunkerque, France
[2]Laboratory of Atmospheric Physico-Chemistry, Anhui Institute of Optics and Fine Mechanics, China
[3]Laboratoire des Sciences du Climat et de l'Environnement, 91191 Gif sur Yvette, China

Abstract— In the present work, a sensor based on quartz-enhanced photoacoustic absorption spectroscopy (QEPAS) incorporating a mid-IR external cavity quantum cascade lasers (EC-QCL) operating around 8 µm was developed for simultaneously monitoring atmospheric CH_4, N_2O and water vapor H_2O. Under optimal condition, minimum detection limits of 50 ppb for CH_4, 30 ppb for N_2O, and 500 ppm for H_2O, were achieved (with lock-in time constant of 1 s and a laser power of ~ 50 mW). The achieved measurement precisions (peak-peak value) were 100 ppb for CH_4 and 30 ppb for N_2O, respectively, with the help of real-time Kalman filtering.

Due to the photoacoustic (PA) relaxation effect [1–3], water vapor present in the atmosphere provide a positive effect by speeding-up the relaxation rate to increase PA signal of CH_4. This is a very important specific issue in PA-based sensor for system calibration and stability. In the present work, the impact of present atmospheric water vapor on CH_4 and N_2O measurements has been investigated, for the first time in the mid-IR.

Recent researches [4] show that N_2O emission currently is the single most important ozone-depleting emission and is expected to remain the largest throughout the 21st century. This further emphasizes the importance of long-term measurements of N_2O. The developed QEPAS sensor fulfills this need and it is well adapted for simultaneous monitoring of CH_4 and N_2O emission from various sources.

Experimental detail and preliminary results will be presented. The problems encountered by the QEPAS technique applied for trace gas monitoring and the further improvements will be discussed.

ACKNOWLEDGMENT

The financial supports from the IRENI program and the CaPPA project (under contract ANR-10-LABX-005) are acknowledged.

REFERENCES

1. Schilt, S., J.-P. Besson, and L. Thévenaz, *Appl. Phys. B*, Vol. 82, 319–329, 2006.
2. Barreiro, N., A. Peuriot, G. Santiago, and V. Slezak, *Appl. Phys. B*, Vol. 108, 369–375, 2012.
3. Yi, H., W. Chen, A. Vicet, et al., *Appl. Phys. B*, 2013, DOI: 10.1007/s00340-013-5713-x.
4. Ravishankara, A. R., J. S. Daniet, R. W. Portmann, *Science*, Vol. 326, 123–125, 2009.

Nitrous Acid Detection with Quartz-enhanced Photoacoustic Spectroscopy Using an External Cavity Quantum Cascade Laser

Hongming Yi[1, 2], **Rabih Maamary**[1], **Xiaoming Gao**[2], **Markus W. Sigrist**[3], **and Weidong Chen**[1]

[1]Laboratoire de Physicochimie de l'Atmosphère, Université du Littoral Côte d'Opale, Dunkerque, France
[2]Laboratory of Atmospheric Physico-Chemistry
Anhui Institute of Optics and Fine Mechanics, Hefei, China
[3]Laser Spectroscopy and Sensing Laboratory, Institute of Quantum Electronics, ETH Zurich, Switzerland

Abstract— It is well known that nitrous acid (HONO) acts as an important source of hydroxyl free radical (OH). However, despite its importance and several decades of research, the sources and sinks of HONO as well as their formation mechanism in the atmosphere are still not completely defined and understood. Field observations show that modeled HONO concentrations are often significantly below observed values, suggesting a large missing source of HONO [1–3]. This is due to the difficulty in measuring this highly reactive short-lived species. Assessment of HONO concentration is very challenging, because the reactivity and solubility of HONO combined with its fast photolysis process makes it subject to sampling-induced artifacts and losses, which requires: (1) ultrahigh sensitivity and measurement precision (typical HONO concentration varies from 30 pptv to several ppbv in the early morning), (2) fast time response and high spatial resolution (its atmospheric lifetime is a few minutes), (3) residence time as short as possible to minimize the losses due to its reaction with other species and/or wall surfaces within the sampling system and hence to ensure higher measurement accuracy. A number of analytical techniques have been developed for HONO monitoring in the atmosphere. They can be classified into two categories: 1) analysis of HONO in the aqueous phase after chemical conversion by wet chemical methods or 2) analysis of HONO in the gas phase using spectroscopic techniques. However, each of these techniques suffers from various limitations in terms of detection limit, sampling approach, and potential interference effects.

In the present work, we report our first attempt to realize high sensitivity and high selectivity detection of gaseous HONO with ultrashort residence time using modern quartz-enhanced photoacoustic spectroscopy (QEPAS). A spectrophone involving off-beam coupled QEPAS [4] excited with an external cavity quantum cascade lasers (EC-QCL) was developed which allowed us to probe the strong absorption lines in the ν_3 H-O-N bending mode of the trans-HONO near 1255 cm^{-1}. With the photodetector-free QEPAS sensing platform we monitored HONO within a very small gas-sample volume (of few mm^3) with high sensitivity. This permits a significant reduction of air sampling residence time. The developed QEPAS sensor was evaluated using HONO concentrations varying from 70 ppmv down to 1 ppmv. As no standard gas reference is commercially available, the QEPAS sensor calibration was performed by means of lab-generated HONO samples calibrated by direct absorption spectroscopy using the spectral data reported in Ref. [5]. The absorption line located at 1254.85 cm^{-1} with a line intensity of $\sim 10^{-20}$ $cm^{-1}/(molecule \cdot cm^{-2})$ was used for interference-free HONO detection. A minimum detection limit (MDL) of 100 ppbv HONO was achieved at 70 mbar using a laser output power of 50 mW and a lock-in time constant of 1 s. The corresponding power normalized MDL is 5 ppbW.

A further improvement in photoacoustic detection sensitivity could be realized by using higher exciting optical power at ∼W level [6] in combination with intracavity enhanced QEPAS [7], which could allow detection of HONO at the ∼pptv level. This work demonstrates the potential of using QEPAS for the detection of highly reactive HONO species in ambient air, which enables an improved insight into atmospheric chemical processes related to HONO.

REFERENCES

1. Stemmler, K., M. Ammann, C. Donders, J. Kleffmann, and C. George, "Photosensitized reduction of nitrogen dioxide on humic acid as source of nitrous acid," *Nature*, Vol. 440, 195–198, 2006.
2. Zhou, X., N. Zhang, M. TerAvest, D. Tang, J. Hou, S. Bertman, M. Alaghmand, P. B. Shepson, M. A. Carroll, S. Griffith, S. Dusanter, and P. S. Stevens, "Nitric acid photolysis on forest canopy surface as a source for tropospheric nitrous acid," *Nature Geosci.*, Vol. 4, 440–443, 2011.

3. Su, H., Y. Cheng, R. Oswald, T. Behrendt, I. Trebs, F. X. Meixner, M. O. Andreae, P. Cheng, Y. Zhang, and U. Pöschl, "Soil nitrite as a source of atmospheric HONO and OH radicals," *Science*, Vol. 333, 1616–1618, 2011.
4. Yi, H., K. Liu, W. Chen, T. Tan, L. Wang, and X. Gao, "Application of a broadband blue laser diode to trace NO_2 detection using off-beam quartz-enhanced photoacoustic spectroscopy," *Opt. Lett.*, Vol. 36, 481–483, 2011.
5. Becker, K. H., J. Kleffmann, R. Kurtenbach, and P. Wiesen, "Line strength measurements of trans-HONO near $1255\,cm^{-1}$ by tunable diode laser spectrometry," *Geophys. Res. Lett.*, Vol. 22, 2485–2488, 1995.
6. Ma, Y., R. Lewicki, M. Razeghi, and F. K. Tittel, "QEPAS based ppb-level detection of CO and N_2O using a high power CW DFB-QCL," *Opt. Express*, Vol. 21, 1008–1019, 2013.
7. Borri, S., P. Patimisco, I. Galli, D. Mazzotti, G. Giusfredi, G. Scamarcio, P. de Natale, and V. Spagnolo, "Intracavity quartz-enhanced photoacoustic sensor," *Appl. Phys. Lett.*, Vol. 104, 091114, 2014.

A Side Information Free PTS-PAPR Reduction in Coherent Optical OFDM Systems Using Superimposed Training

Changjian Guo, **Haipeng Liu**, **and Han Zhang**
South China Normal University, Guangzhou 510006, China

Abstract— In this paper, we report a side information free partial transmit sequence (PTS) technique to reduce the peak-to-average power ratio (PAPR) for coherent optical OFDM systems. The key idea is that the side information of PTS is considered as a part of channel frequency response. Based on superimposed training (ST) channel estimation, where the training sequence is arithmetically added onto the information symbols in frequency domain, the combined channel response with the phase factors of PTS can be estimated within each interleaved PTS sub-block. Therefore, the proposed scheme does not need to reserve bits for submitting side information, resulting in an increase in the data rate. Furthermore, to enhance the performance of bit error rate (BER), a side information recovery is performed across the interleaved PTS sub-blocks at receiver to enable an improvement on the combined estimation over the whole sub-blocks. Simulation results demonstrate the advantages of the proposed method over the conventional superimposed training coherent optical OFDM systems.

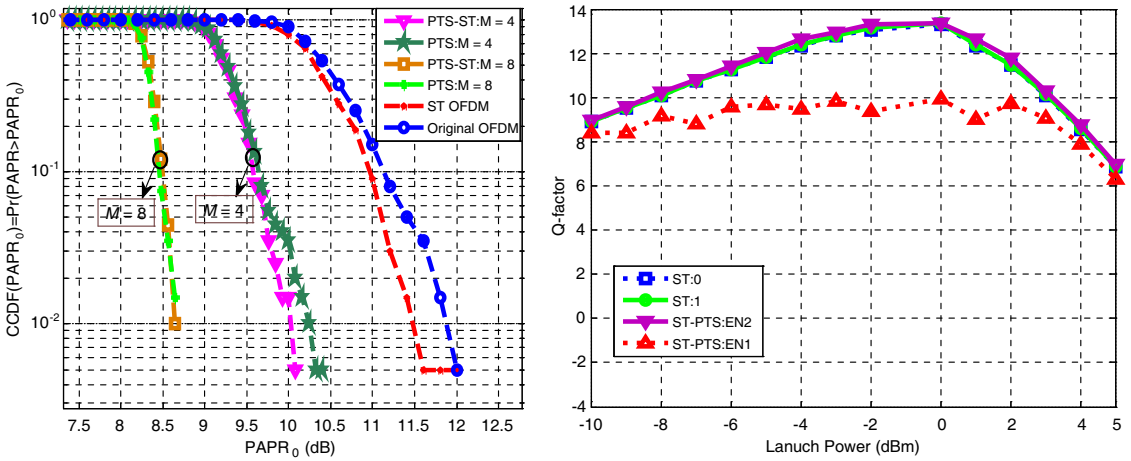

Figure 1: (a) The PAPR performance of the ST-PTS scheme; (b) the Q-factor as a function of the launched optical power for ST and ST-PTS based CO-OFDM systems after 2000 km of standard single mode fiber transmission.

Photoelectrochemical Solar Cells Based on Micro/Nano-structured Silicon

Kangkang Dang, Wenbin Huang, Yali Xue, Xuyue Wang, Yang Yang, and Xianyu Ao
Centre for Optical and Electromagnetic Research
South China Normal University, Guangzhou 510006, China

Abstract— Micro/nanostructures on siliconsuch as wires, cones, and holes, have attracted broad interests for prospective applications in solar energy harvesting due their good anti-reflection and light-trapping properties. On the other hand, some new device concepts were developed, such as radial pn-junctions. However, the increased surface area arising from the micro/nanostructures can also increase photocarrier recombination. Actually there is some controversy in the literature over whether such texture can really enhance the conversion efficiency of solar cells.

Herein we will present photovoltaic properties of three kinds of black silicon in photoelectrochemical cells, to assess the influence of increased light absorption and increased surface area on conversion efficiency, relative to the behavior of a planar silicon wafer. The three kinds of black silicon were all prepared by wet chemical etching, namely, nanowire structure [1] and nanoporous structure [2] by metal-assisted electroless etching, and macroporous structure [3] by electrochemical etching. Among them, the macroporous silicon has the smallest surface area.

REFERENCES

1. Peng, K. Q., X. Wang, X. L. Wu, and S. T. Lee, "Platinum nanoparticle decorated silicon nanowires for efficient solar energy conversion," *Nano Letters*, Vol. 9, 3704, 2009.
2. Oh, J., H.-C. Yuan, and H. M. Branz, "An 18.2%-efficient black-silicon solar cell achieved through control of carrier recombination in nanostructures," *Nature Nanotechnology*, Vol. 7, 743, 2012.
3. Ao, X., X. Tong, D. S. Kim, L. Zhang, M. Knez, F. Mueller, S. He, and V. Schmidt, "Black silicon with controllable macropore array for enhanced photoelectrochemical performance," *Applied Physics Letters*, Vol. 101, 111901, 2012.

Dual-polarized FSS with Wide Frequency Tunability and Simple Bias Network

Hang Zhou[1], **Xinhua Wang**[1], **Shaobo Qu**[1], **Lin Zheng**[1], **Hangying Yuan**[1], **Mingbao Yan**[1], **Yongfeng Li**[1], **Jiafu Wang**[1], **Hua Ma**[1], **and Zhuo Xu**[2]

[1]College of Science, Air Force Engineering University, Xi'an 710051, China
[2]Electronic Materials Research Laboratory, Key Laboratory of the Ministry of Education
Xi'an Jiaotong University, Xi'an 710049, China

Abstract— In this paper, a dual-polarized frequency selective surface (FSS) with wide frequency tunability and simple bias network is presented. The FSS is composed of two-layered metallic structures. The top layer is etched with Jerusalem crosses and metallic grids. Varactor diodes are positioned between the grids and the Jerusalem crosses. The bottom layer is etched with crossed metallic lines. The two-layered structures are connected to each other with an array of plated vias. Based on this configuration, a DC path is created for biasing the varactors with the grids and crossed metallic lines. The FSS exhibits dual polarized performances using such a simple bias network. Numerical results obtained by full wave simulation method show that by altering the capacitance of the varactors from 0.2 to 1.0 pF, wide frequency tunability from 6.85 GHz to 3.7 GHz can be achieved. Design procedure and results of the FSS are presented and discussed.

ACKNOWLEDGMENT

This work was supported Project supported by the National Natural Science Foundation of China (Grant Nos. 61302023, 11274389, 11204378).

Study and Design of the Novel Shunt Liner Active Power Filter for a Superconducting Magnet Power Supply

Jinglin Wu and Xiaoning Liu
University of Science and Technology of China, Hefei, Anhui, China

Abstract— The superconducting outsert of the 40 T hybrid-magnet in High Magnetic Field Laboratory (HFML) of Chinese Academy of Sciences (CAS) requires a highly stabilized low-voltage high-current power supply. One of the design is a switching power supply with active DC power filter. As the current flowing through a Shunt Active Power Filter (SAPF) is only the ripple current, the power loss caused by the filter can be very low, so SAPF is more and more applied in high-current devices. Usually, a shunt PWM converter can be used to generate current which is equal but oppositely phased to the ripple current. However, EMI noises caused by PWM have great influence on the circuit and the speed of response is limited by the switching frequency. Meanwhile, the load voltage variation makes it very difficult to design parameters of the filter. In this paper, a novel shunt liner active power filter (SLAPF) is designed to overcome the disadvantages of existing dc active filter schemes. Structurally, SLAPF can be divided into two components, one is the current compensator, and the other is the auxiliary power supply. The current compensator is composed of a power supply with fixed output voltage and two parallel branches, each of which consists an adjusting transistor. The auxiliary power supply is used to ensure the voltage across the adjusting transistors keep in a proper range, so the transistors can always operate in the saturation region. Based on the on-resistance variability of adjusting transistors, just as the series linear regulator, the output current of the current compensator can accurately track the oppositely phased out ripple current of main circuit, which leads to a good filter effect. In the paper, the detail structure and working principle of SLAPF are presented at first, then the design flow is described, which includes the control method of the current compensator, the analysis of topology chosen for auxiliary power supply. At last, the experimental results show that the filtering effect of SLAPF is good enough to make the power supply meet the technical requirements.

Design of Ku-band Dielectric Resonator Filter for Satellite Applications

Seyi Stephen Olokede, Nor Muzlifah Mahyuddin, Majid Rafiee, and Enoch Adama Jiya
School of Electrical & Electronic Engineering
Universiti Sains Malaysia, Nibong Tebal, Penang 14300, Malaysia

Abstract— Advances in technologies and continued growth of wireless devices has continue to challenge the community to design and produce new alternative but smaller and more multifunctional filters that are suitable and relevant to the current technology. It is evident that the traditional filter such as waveguide filter is no longer significant, efficient, nor adequate for today's technology that demands small, compact, easy integration and cheap solution to almost every electronic device. Although, alternative filter solution employing microstrip technology where such filter design consist of only a few rows of parallel-coupled transmission lines has been ground breaking and remarkable. However, such filter becomes unrealizable as the frequency of the filter increases. The gap between the two neighbouring microstrip lines becomes narrower resulting to a very tight coupling. The strait spacing between the rows of parallel-coupled transmission lines complicates the fabrication process of the filter as the printing machine only supports etch limitation up to a minimum trace and gap of about 0.3 mm.

To overcome this serious challenge therefore, it is contingent to investigate the possibility of an alternative novel-fed dielectric resonator filter for Ku-band applications. Dielectric resonators (DRs) offer more flexibility in filter design. The proposed design is such that three identical cylindrical DRs are excited by four microstrip lines of certain dimensions. The dimensions that are multiples of quarter wavelengths of the centre frequency of which the filter operates are calculated to coincide with maximum radiation of the transmission lines based on the standing wave ratio formation of the voltage allocation on shorted microstrip transmission line. Besides, these stubs and the DRs were configured in such a way that the DRs were positioned in a manner that their various resonances overlap constructively. In effect, wideband impedance bandwidth was achieved. Instead of the conventional direct side proximity-coupled microstrip feed line common among series feed array, the proposed utilizes the same principle, but rather with broken or piecewise segmented transmission stubs such that each stub is of a dimension of a multiple of quarter wavelength. The widths are determined by their characteristic impedance equivalency. Not only was the transmission line broken into stubs, the stubs were also offset from each other by the diameter of the cylindrical DRs.

By this arrangement, it is therefore evident that each DR is placed in between two transmission lines, and as such, the first DR coupled electromagnetic energy from the input port to the next transmission stub, and so on until the output port. Essentially, the proposed feed will mitigate the effect of unnecessary reflection, and thus deliver a better match, good reflection coefficient, improved bandwidth and performance as it is expected that a good impedance match will naturally improve the filter efficiency. In effect, the proposed will efficiently coupled the signal energy from one microstrip to the other while providing a good performance and low insertion loss.

The proposed design is modeled using finite integration technique (FIT) full-wave CST commercial solver, and the resulting design is fabricated on the Duroid RO4003C microwave laminate board of permittivity of 3.38, with a substrate thickness of 0.813 mm, $\tan(\delta)$ of 0.0027, and a metal thickness of 0.035 mm. Subsequently, the fabricated design is measured, and the measure and simulated results is plotted to determine the degree of agreement. Preliminary work shows a good filter response with acceptable insertion loss within the Ku-band of applications.

Deriving the Geometry of Frequency Selective Surfaces (FSS) and Metamaterials (MTM) Elements from Transmission Lines by Using Surrogate Meta-modeling Techniques

Fabrizia Ghezzo, **Loris Serafino**, **Chunlin Ji**, **Xigeng Miao**, **and Ruopeng Liu**
Kuang-Chi Institute of Advanced Technology
Gaoxin Zhong 1st Road, High-Tech Industrial Park, Shenzhen 518057, China

Abstract— Since the 1970s there has been an extensive effort to generalize transmission line (TL) networks for modeling and predicting the electromagnetic response of frequency selective surfaces (FSS) and recently also for metamaterials (MTM). However, given the complexity of the physical phenomena involved which influence the electromagnetic response of these periodic unit cells, in almost all the cases the equivalence of the TL-model with a specific FSS or MTM element can be found only for simple geometries.

Currently, most of the unit cell elements studied in the literature, both in the case of FSS and MTM are generally derived by using an intuitive way to predict their electromagnetic response. The procedure often consists in designing a structure by changing some of the geometrical features of elements already studied in the literature. By doing so a new element is found and a series of simulations must be carried out to characterize its behavior at varying frequency. This process is generally time consuming and computationally very expensive.

Even though the application of TL represents a potential powerful tool for the design of FSS and MTM with complex shape, it can be said that it is quite difficult to find the correspondence between TL circuit and the element geometry especially in the cases of oblique incidence, different polarization angles and multilayer configurations.

In this work we propose a method based on the Kriging surrogate modeling technique for the generation of a multi response model which determines the correspondence between the resistance, capacitance, inductance, and admittance (RCLG) of a generalized transmission line and the dimensions of the geometrical features of a specific frequency selective surface (FSS) or metamaterial structure (MTM) — expressed in parametric form — operating in predefined frequency ranges. Specifically, in this study we consider the model for the application in the microwave frequency range.

The method presented in this work is meant to overcome the difficulties connected to the equivalence between TL models and the geometry of the FSS or MTM element. To demonstrate the potentiality of the newly developed methodology, an example of design of a metamaterial structure in the case of perpendicular incidence and single layer configuration will be analyzed and the preliminary results obtained will be discussed. The method can be further generalized for the design and the optimization of periodic sub-wavelength structures in the general case of arbitrary incidence and polarization angles as well as for multilayer material systems.

Analysis and Design of Ku Band Coaxial-waveguide Transition

Chao Wang[1], **Gaofeng Guo**[1], **Junhu Wang**[2], **and En Li**[1]

[1]University of Electronic Science and Technology of China, Chengdu 611731, China
[2]Aerospace Research Institute of Materials and Processing Technology, Beijing 100076, China

Abstract— Coaxial-waveguide transition plays an important role in microwave system. Based on the influence of waveguide ladder exerted on transmission performance of electromagnetic wave in guided wave system, this paper demonstrates the situations of this structure applied in Ku band coaxial-waveguide converter designation. The reflected wave and insertion loss have been reduced by using a multi-steps structure with the coaxial probe excitation. The effectiveness of impedance matching is well-improved, and the transmission performance of coaxial-waveguide converter is highly-advanced. Simulation results proved the effectiveness of waveguide ladder in designing coaxial-waveguide converters. The VSWR of coaxial-waveguide transition designed in this paper is less than 1.04 in the 12.4–18 GHz octave bandwidth, and the high modulus produced is very small.

A Novel Monopulse Microstrip Antenna Array with Compound Feed Network

Feng-Wei Yao, Xiao-Qing Tian, Li-Li Zhu, Yuan-Bo Shang, and Xing-Zuo Dai
Shanghai Key Laboratory of Electromagnetic Environment Effects for Aerospace Vehicle
Shanghai 200438, China

Abstract— For most monopulse microstrip antenna array, a radiator array is divided to four sub-arrays, every sub-array has his own feed network in E-plane and H-plane. Every line array is fed at the center side, therefore the E-plane feed network is placed between adjacent two patches of two sub-arrays, this small distance may bring the significant near coupling between feed lines and sub-arrays, which will deteriorate the side lobe and lower the efficient of antenna.

In this paper, a novel feed network design is presented, with which every microstrip line array of monopulse antenna can be fed at the edge side with the middle of the row shorted. At the same time, the sub-arrays in E-plane are fed with 180 degree phase difference to suppress the higher order modes. Furthermore in order to decrease the substrate loss especially in high frequency, a waveguide one-plane feed network and a waveguide comparator are used, which is connected with every line array by SMA-waveguide connector. This proposed feed network can solve the problem of near coupling, higher order modes and minish substrate loss. By using this compound feed network, a X-band monopulse antenna array is fabricated and tested, -20 dB side-lobe level for the sun pattern and 35 dB null depth for difference pattern have achieved in experiment, which is most similar with simulated in software.

Development of Narrowband Filter Based on S-shaped Resonators for Terahertz Frequency Range

E. A. Sedykh, **A. V. Vedeneev**, **and M. K. Khodzitsky**
ITMO University, Saint Petersburg, Russia

Abstract— Structure constituted of stacked layers of single side paired S-shaped resonators for terahertz frequency range (0.1–2 THz) is studied. Transmission spectra of that structure indicate that it can be used as a stopband filter for THz frequency range.

Introduction: Devices based on metamaterials are now of great interest for THz biomedicine, spectroscopy and tomography applications. Present work focuses on S-shaped single side paired resonators because they can be used to implement filters, superlenses, negative index materials in terahertz frequency range [1]. Similar structure (2D array of aforementioned resonators) has been theoretically and experimentally studied in GHz frequency range [2]. In the present work narrowband filter based on stacked 2D arrays of single side paired S-shaped resonators (Fig. 1) is studied for terahertz frequency range.

Results and Conclusion: The structure under study has been analytically described using equivalent circuit model to obtain formulae for its effective permittivity and permeability dispersion characteristics [3]. Transmission spectra of the structure were numerically simulated using CST Microwave studio time domain solver for different combinations of structure dimensions for tangential (H-vector is perpendicular to the substrate plane) direction of excitation wave propagation. The results obtained by CST MW simulation and by analytical model show good agreement. Following the simulation the considered structure was fabricated on sitall (glass-ceramic) substrates coated with copper using laser engraving technique. Transmission spectra obtained for the sample were experimentally studied using terahertz time-domain spectroscopy. These spectra feature resonant transmission peaks associated with LC and plasmon resonances which shift to lower frequencies with an increase of resonator dimensions.

Transmission spectra of the considered structure indicate that such structures can be used as both narrowband stopband filter and negative index media in different regions of terahertz frequency band.

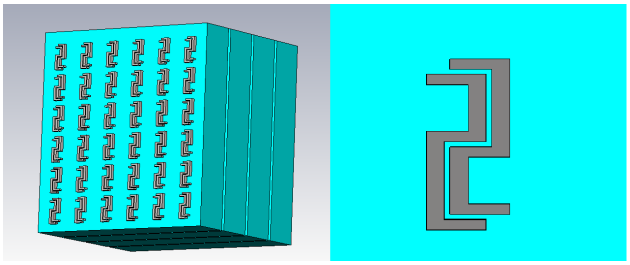

Figure 1: Structure under study (a) consists of four sitall/metasurface layers, (b) with metasurface being a 2D array of single side paired S-shaped resonators.

ACKNOWLEDGMENT

This work was financially supported by Government of Russian Federation, Grant 074-U01.

REFERENCES

1. Chen, H., L. Ran, and J. Huangfu, "Left-handed materials composed of only S-shaped resonators," *Phys. Rev. E*, Vol. 70, 057605, 2004.
2. Wang, D., L. Ran, and H. Chen, "Experimental validation of negative refraction of metamaterial composed of single side paired S-ring resonators," *Appl. Phys. Lett.*, Vol. 90, 254103, 2007.
3. Chen, H., L. Ran, and J. Huangfu, "Equivalent circuit model for left-handed metamaterials," *J. of Appl. Phys.*, Vol. 100, 024915, 2006.

IME-HF Instrument on Board TARANIS Satellite Dedicated to the Measurement of the EM Thunderstorm Lightning and TLEs Signatures

J. L. Rauch[1], **O. Santolik**[2], **I. Kolmasova**[2], **A. Millet**[1], **M. Chabassiere**[1], **R. Lan**[2], **and L. Uhlír**[2]

[1]LPC2E, 3A av. de la Recherche Scientifique, 45071 Orléans Cedex 2, France
[2]Institute of Atmospheric Physics AS CR, Prague, Czech Republic

Abstract— The observations of red sprites, blue jets, elves, sprite halos, gigantic jets, etc., named Transient Luminous Events (TLEs) and the observations of Terrestrial Gamma ray Flashes (TGFs) have pointed out the existence of impulsive transfers of energy between the Earth atmosphere and the space environment. Possible electromagnetic signatures of electron acceleration processes have been investigated. Many authors have shown that relativistic runaway electron beams driven by intense lightning-generated Quasi-Electrostatic (QE) fields may undergo intense interactions with the background magnetospheric plasma, leading to rapid nonlinear growth of Langmuir waves. Intense radio emissions in the range of several MHz up to tens of MHZ are predicted to be produced by runaway electrons or by a simultaneous effect of runaway breakdown and extensive atmospheric showers. Plasma physics offer other interactions and so other potential signatures like the production of lower hybrid waves. TIPPs (Trans Ionospheric Pulse Pairs) have been frequently observed by the FORTE satellite.

TARANIS is a satellite of the french space agency (CNES) dedicated to study the thunderstorm lightings and TLEs to have a comprehensive understanding of the energy transfer between atmosphere-ionosphere and magnetosphere region. TARANIS scientific payload consists in a complex package of instruments, in particular the (Instrument de Mesure Electrique Haute Frequence) IME-HF experiment proposed to measure the wave electric field in the frequency range from 100 kHz up to 35 MHZ. The aim of IME-HF experiment is to characterize the properties of lightnings and TLEs signatures. The experiment is composed of electric sensors and on board analyzer. Several kinds of signals can be recorded as waveform and filters bank. In this presentation, we propose to described the capability of the IME-HF experiment and the strategy of measurement and how TARANIS payload is integrated taken as a whole.

Design of Signal Source without External Reference for Fiber Optical Comb System

Changqi Yang
School of Science, Xi'an Shiyou University, Xi'an 710065, China

Abstract— Femtosecond frequency comb is a great invention in the field of metrology at the end of the last century. It can simply and effectively synchronize the phases for optical signals of different wavelengths or RF signals. Erbium doped fiber optical comb has many advantages. The National Time Service Center of Chinese Academy of Sciences has launched a project on the new type erbium-doped fiber femtosecond optical comb research. This paper introduces the signal source which is designed for this project. DDS chip AD9854 is used as the signal source. The signal source output has a wideband from 1–80 MHz. Test result for the signal source is discussed.

RF Shielded Hat for Protecting Cameraman from EMF Exposure

N. Hisham[1], **H. A. Rahim**[1], **F. Malek**[2], **M. Jusoh**[1],
F. A. A. Fuad[1], **F. S. Abdullah**[2], **and M. S. Mezan**[2]

[1]Embedded, Networks and Advanced Computing Research Cluster (ENAC)
School of Computer and Communication Engineering, Universiti Malaysia Perlis, Perlis, Malaysia
[2]School of Electrical System Engineering, Universiti Malaysia Perlis, Perlis, Malaysia

Abstract— This paper presents a new layer of absorber for RF Shielded Hat. The objective of this studied is to create and develop a new layer of absorber for RF Shielded Hat made from Microwave Absorbing Sheet that can protect the cameraman from electromagnetic field (EMF). The Microwave Absorbing Sheet is used because of super light weight, good microwave shielding, high absorption and no problem for skin contact. Three different types of protective hat are chosen: back of the hat with no protection to allow adjustment of size, rear hat that covers the neck and hat that covers head and thyroid region. All hats are sewn with microwave absorber sheet. The investigation was aimed to study whether the types of hat worn reduce the electromagnetic exposure to human head. The measurement campaign was carried out in the anechoic chamber to completely absorb reflections of either sound or electromagnetic waves. The wireless video camera operated in frequency of 2.45 GHz. The position of the wireless video camera was fixed on the right of the cameraman shoulder where this position is much closer to our heads. The experiment was investigated in two different situations, while being exposed in the sham condition and also 2.45 GHz signal. Both of the measurement will be undertaken during the pre, during and after the experiments. The results showed that the measured sham condition during the pre, during and after the experiments recorded similar readings.

Reflection Loss Performance and Performance Assessment of Pyramidal Microwave Absorber Using Agriculture Waste

M. S. Mezan[1], **M. F. A. Malek**[2], **M. S. Jusoh**[1], **F. S. Abdullah**[2], **and N. A. M. Affendi**[2]

[1]School of Business Innovation and Technopreneurship, Universiti Malaysia Perlis
Jalan Kangar-Alor Setar, Kangar, Perlis 01000, Malaysia
[2]School of Electrical System Engineering, Universiti Malaysia Perlis
Pauh Putra Campus, Arau, Perlis 02600, Malaysia

Abstract— Agricultural product is one of the major revenue incomes for Malaysia. The large scale production of agricultural product lead to a new by product which is known as agricultural waste. The estimate annual production of agricultural waste and residues for Malaysia is 42 million tonnes. Oil palm waste and rice production waste are among the highest production of agriculture waste. Agricultural wastes materials can be applied for many applications as for this research, four types of materials has been used; rice husks, banana leaves, sugarcane bagasse and mixture of rice husks and rubber tire dusts. This research highlighted microwave absorber application as the output using proposed agricultural wastes. Microwave absorber is the most important element in anechoic chamber to deny signals reflection. Each different waste will be fabricated as the main materials for each microwave absorber. Compared with commercial product, the product developed in this research used almost 100% natural resources rather than chemicals. The proposed shape for the microwave absorbers is square base pyramidal shape absorber. The measurement technique will involve two factors which are the microwave absorber electromagnetic properties and free space measurement to measure the reflectivity performances. For differentiation, each fabricated material will go through reflection loss performance to measure the absorption performance. Its performance is analyzed in term of reflection loss performance using the free space measurement technique. To answer the measurement goodness in this research, Rasch measurement model is applied. To indicate the goodness of RCS measurement technique, Rasch measurement model may determine the three major criteria for evaluating good measurement which are validity, reliability and significance.

Grounding Microstrip Lines with Via Holes and General Reformulation of the Iterative Method F.W.C.I.P.

Sameh Toumi, Fethi Mejri, and Taoufik Aguili
Syscom Laboratory, Engineers' National School of Tunis, Tunisia

Abstract— Grounding microstrip circuits with via holes are an established technology and modelling isolated via holes with analytical model is well known. However, the availability of electromagnetic field solvers provides an opportunity to model via holes and the metalization surrounding them in a more realistic fashion.

The via hole ground has many applications in the synthesis of microstrip microwave circuits. Indeed, it can be used for the realization of stub, the parallel insertion of lumped element and the photonic gap structures. . ..

The high cost of technology and time implemented for the realization of a function of analog electronics make impossible the traditional approach to test several models for testing arrive at the necessary improvements. The designer of microwave circuit must have a simulation tool to predict the performance of a component or a circuit operating in different conditions.

In our work we used the iterative method FWCIP (Wave Concept Iterative Process), this method is based on the concept of wave using a fast Fourier transform which is developed for the study of planar circuits of arbitrary geometry.

Many studies have been done with the iterative method FWCIP for the study of planar structures homogeneous, single or multilayer and arbitrary or complex shape. But in this case, the sample studied is complicated because the guide presented is crossed by a current wire which means the modal base will be modified from the standard case. That's why several efforts should be made about this subject, for this reason we introduce our research that requires an implementation of a new iterative method equation modeling a planar structure integrating a via hole.

In this paper we propose a model of an electromagnetic planar structure consists of a microstrip connected to the ground through a via-hole placed on the upper side of a dielectric substrate. Electromagnetic modeling of the new problem is to calculate all of the fields present in the structure and write the new formulation of the iterative process that expresses the relationship between the incident and reflected waves. The results provided by this reformulated method are in good agreement with the data determined by the software HFSS approach (Electromagnetic Field Simulation Software).

An Effective Optimization of Reliability of Co-phase Power Supply Device

H. Xu, S.-F. Xie, and W.-L. Zhao
School of Electrical Engineering, Southwest Jiaotong University
Chengdu, Sichuan 610031, China

Abstract— In this paper, the structure and principle of a kind of co-phase power supply system is proposed. The co-phase power supply devices based on two-level quadruple modular topology structure and three-level duplicate topology structure are studied and the former one is chosen as a computational example. According to the analysis of high power electronic elements in power system, a k/n(G) reliability model of the co-phase power supply device, based on two-level quadruple modular topology structure, is established. Then, the reliability of the co-phase power supply device is calculated. With the failure rate and Mean Time To Failures (MTTF) presented, the reliability of the co-phase power supply device is quantificationally evaluated. In order to promote the reliability of the device, two optimized schemes, which include increasing internal components of converter cells and increasing the standby branches of the device, are presented. Compared with the original scheme, the optimized schemes show the promotion of the reliability. Finally, to demonstrate, the computational method is adopted. The results agree well with the proposed schemes.

Tunable Single Bandpass Filter Based on Fluid-filled PCFs

Shengnan Wu and Chengliang Wang
Centre for Optical and Electromagnetic Research
State Key Laboratory of Modern Optical Instrumentation, Zhejiang University, Hangzhou 310058, China

Abstract— Lots of tunable all-fiber filters with various properties have been explored. A spot of scheme have been proposed such as optical bragg fiber grating, all-fiber Fabry-Perot interferometers and so on. However, fiber bragg grating is sensitive to external perturbations including strain and bend. Recently, photonic crystal fiber (PCF) has been used in filters as well. Due to their multi bandpass properties and poor tunable ability, most of the filters are not practical

In this paper, we proposed a tunable single band pass filter with large tunable scales of bandwidth and center wavelength. The filter consists of two cascaded PCFs with high thermo-optic fluid filling in the air rods. By changing the refractive index of the fluid as well as adjusting the fill-rate of cladding, the PCF can realize only one band gap at certain wavelength of interest. The temperatures of the two PCFs were tuned by accurate temperature controller, respectively. Due to the refractive index variation of the fluid, the transmission spectra of the PCFs will red or blue shift. As a result, the overlap part of the spectra can be tuned by simply setting the PCF at different temperatures. Numerical simulation was carried out by using the BandSolve module of Rsoft. The refractive index and the thermo-optic coefficient of the fluid were 1.58, -4.79×10^{-4}°C, respectively. By tuning a total temperature range of $0 \sim 100$°C, the center wavelength can shift more than 100 nm and the bandwidth can be tuned more than 200 nm. Moreover, this kind of all fiber structure is robust and insensitive to strain and bending, which renders it as an ideal tunable single band pass filter in optical communication and sensing systems.

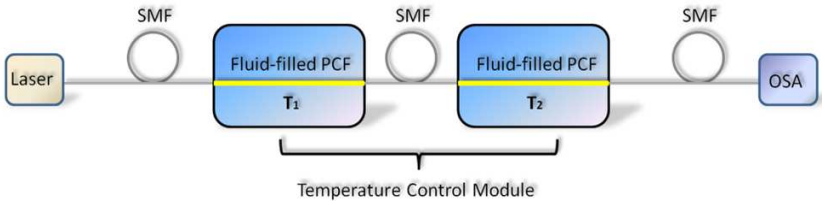

Figure 1: Experimental set up.

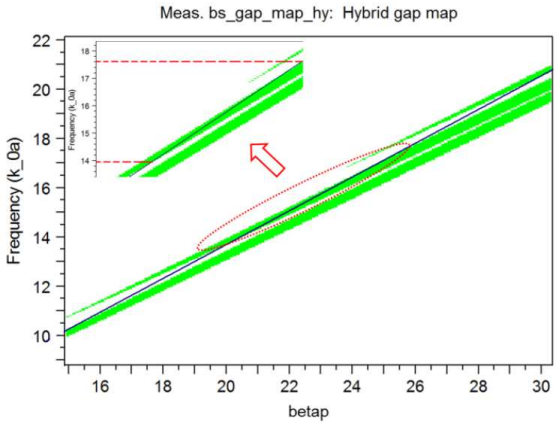

Figure 2: Calculated bandgap maps (The fill-rate is 0.7 and the refractive index of the filling fluid and the fused silica are 1.58, 1.4607, respectively). betap is the product of propagation constant and the lattice constant a ($a = 4.0\,\mu$m). Frequency is the product of vacuum wave number and lattice constant a. The black line is the so called air-line whose value of X-axis is the product of value of Y-axis and the refractive index of core. It was shown that there is a bandgap ($1.435\,\mu\text{m} \sim 1.804\,\mu$m) between $1.214\,\mu$m and $2.452\,\mu$m.

Beam Forming Antenna for WLAN

Ho-Jun Lee[1], **Min-Ki Woo**[2], **Nae-In Lee**[2], **and Gene Yoo**[2]

[1]Convergence Communication Components Research Center
Korea Electronics Technology Institute, Republic of Korea
[2]Innonet Co., Ltd., Republic of Korea

Abstract— This paper present analysis, design, and simulation of dual feed dual polarization microstrip patch antenna for WLAN applications. The proposed antenna configuration is shown in Figure 1. Antennas in this paper are simulated by using the Ansoft simulation software high-frequency structure simulator (HFSS). A prototype of this antenna was fabricated on FR4 substrate with thickness $h = 1$ mm and dielectric constant $\varepsilon_r = 4.4$. The dimensions of the fabricated antenna, which is etched on $100 \times 260 \times 5$ mm substrate. The measurements of electrical characteristics such as radiation patterns, VSWR, and return loss of the implemented antenna were conducted in an anechoic chamber equipped with a HP 8510C network analyzer and far field measurement system. The measured gain of the antenna is from 11.98 to 12.49 dBi. Figure 2 shows a photograph of the fabricated antenna. We manufactured the antenna based on the results of optimized simulation results and measured characteristics of the suggested antenna in the anechoic chamber. Details of the proposed antenna designs are described, and typical experimental results are presented and discussed.

Table 1: Antenna electrical specification.

Frequency Range		2400 ~ 2500 MHz
Polarization		± 45°
Band Width		100 MHz
Array		1*4 Array
Gain		≤ 6 dBi
Beam width	Horizontal	≥ Nominal 60°
	Vertical	≥ Nominal 50°
F-B ratio		≥ 10 dB
VSWR		≤ 1 : 2.0
Impedance		50 Ω
Maximum input power		≤ 10 W

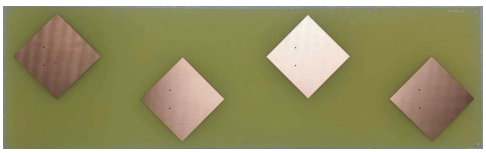

Figure 1: Proposed antenna.

Figure 2: Photograph of the fabricated antenna.

REFERENCES

1. Stutzman, W. L. and G. A. Thiele, *Antenna Theory and Design*, 2nd Edition, Hohn Wiley & Sons, New York, 1998.
2. Balanis, C. A., *Antenna Theory Analysis and Design*, 2nd Edition, Wiley & Sons, 1997.

Wireless Power Transfer and NFC System Using Loop Antenna

Ho-Jun Lee[1] and Sek-Byoung Chae[2]

[1]Convergence Communication Components Research Center
Korea Electronics Technology Institute, Republic of Korea
[2]Cenotech Co., Ltd., Republic of Korea

Abstract— In this paper, we proposed a new design method to design a wireless power transfer and NFC (Near-field Communications) system using loop antenna for mobile handsets. The proposed antenna configuration is shown in Figure 1. Figure 2 shows a measured photograph of the fabricated antenna. The measurements of electrical characteristics such as thickness, reading range and coil impedance of the implemented antenna were conducted with RFID smart reader and network analyser. The measured total thickness of the antenna is 187 mm, coil impedance is 0.5 Ω, and reading range more than 10 cm. This antenna have a dimension of $48 \times 55\,\text{mm}^2$. We manufactured the antenna based on the results of optimized wireless power transfer and NFC systems characteristics of the suggested antenna. Details of the proposed antenna designs are described, and typical experimental results are presented and discussed.

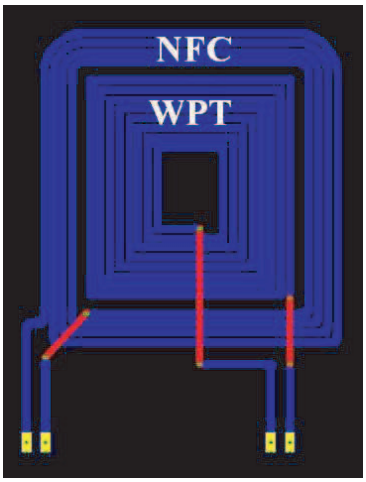

Figure 1: Proposed antenna.

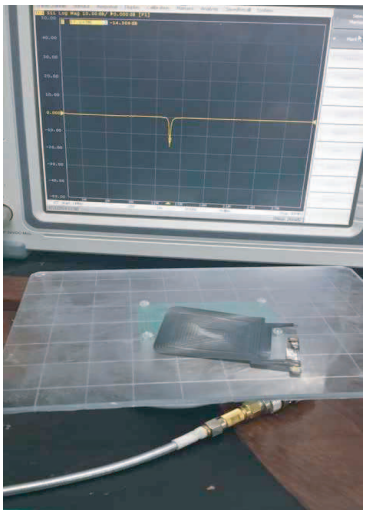

Figure 2: Photograph of the fabricated antenna measure.

REFERENCES

1. Lee, J. and S. Nam, "Fundamental aspects of near-field coupling small antennas for wireless power transfer," *IEEE Trans. Antennas Propag.*, Vol. 58, No. 11, 3442–3449, Nov. 2010.

Criss-Cross Metamaterial Based Radiating Structures for C-band Applications

Kirti Inamdar[1], **Y. P. Kosta**[2], **and S. Patnaik**[3]

[1]ECED, SVNIT, Surat, Gujarat, India
[2]MEFGI, Rajkot, Gujarat, India
[3]St. Xavier's Institute of Engineering, Mumbai, India

Abstract— In this paper, we present the design of a metamaterial based microstrip patch antenna, optimized for bandwidth and multiple frequency operations. A Criss-Cross structure has been proposed, this shape has been inspired from the famous Jerusalem Cross. The theory and design formulas to calculate various parameters of the proposed antenna have been presented. Design starts with the analysis of the proposed unit cell structure, and validating the response using software — HFSS Version 13, for obtaining negative response of ε and μ-metamaterial. The software analysis of the proposed unit cell structure has been validated experimentally thus giving negative response of ε and μ. Following this, a metamaterial-based-microstrip-patch-antenna is designed. A detailed comparative study is conducted exploring the response of the designed patch made of metamaterial and that of the conventional patch. Finally, antenna parameters such as gain, bandwidth, radiation pattern and multiple frequency responses are investigated and optimised for the same and presented in table and response-graphs. It is also observed that the physical dimension of the metamaterial based patch antenna is smaller compared to its conventional counterpart operating at the same fundamental frequency. The challenging part was to develop metamaterial based on some signature structures and techniques that would offer advantage in terms of bandwidth and multiple frequency operation, which is demonstrated in this paper. The unique shape proposed in this paper gives improvement in bandwidth without reducing the gain of the antenna. The C-band of the frequency spectrum has been chosen for all the above mentioned exercise as it is the most popular band for commercial, satellite and radar applications. The proposed metamaterial based antenna can be utilized for higher gain and bandwidth requirements in any of these applications.

Microstrip Patch Antenna Design with Criss-Cross Metamaterial Based Radome Cover

Kirti Inamdar[1], **Y. P. Kosta**[2], **and S. Patnaik**[3]

[1]ECED, SVNIT, Surat, Gujarat, India
[2]MEFGI, Rajkot, Gujarat, India
[3]St. Xavier's Institute of Engineering, Mumbai, India

Abstract— A high gain microstrip patch antenna with a metamaterial cover over it has been proposed in this paper. A new design namely Criss-Cross metamaterial is being used here. The Criss-Cross unit cell comprises of a cross printed on one face of dielectric substrate and the same cross rotated by 45° is being printed on the other face of the same substrate. The DNG behavior, i.e., both ε and μ are simultaneously negative for this metamaterial is obtained at 6 GHz; the patch also operates on the same frequency. The radome cover is constructed by stacking three layers made up of a 3×3 Criss-Cross metamaterial array. A 3×3 array of Criss-Cross metamaterial unit cell is printed on FR4 substrate. This arrangement of radome cover increases the gain of a simple patch antenna up to 7.8 dB. The radome cover over the antenna is used to protect the structure from environmental hazards. However due to use of conventional dielectric materials as radome, the performance of the antenna degrades. When a metamaterial in printed on such dielectric material, its properties and behavior changes. This leads to improvement of performance of patch antenna along with its physical protection. The directivity of the proposed patch antenna also improves due to the lens behavior of the radome cover over the patch. A conventional radome cover will scatter the EM radiations emitted by the patch antenna. But the metamaterial cover acts as a lens which focuses the EM radiations. This action is once again due to the unusual properties of the metamaterials.

A Multi-channel Digital Temperature Acquisition System Based on SOPC

W. He, Q.-Y. Feng, and D.-H. Jia
School of Information Science and Technology
Southwest Jiaotong University, Chengdu, Sichuan 610031, China

Abstract— In this paper, a multi-channel digital temperature acquisition system is proposed. Based on System on a Programmable Chip (SOPC) and 1-wire bus technologies, the temperature acquisition node is designed. The data acquired is transferred to the host computer through RS232 serial interface. The software on the computer analyzes and processes the received data to achieve the real-time monitoring and display of the temperature through the User Interface (UI). Programmable resolution 1-wire digital thermometer DS18B20 is adopted in this design. The acquisition node is configured by NIOS soft core CPU using Verilog HDL and C language, meanwhile, the UI on the PC is designed in Visual Basic language. The temperature sensor has an operating temperature range of $-55°$C to $125°$C. The resolution of the acquisition is $0.0625°$C and the display resolution is $0.01°$C. All simulations in the design are done in Quartus and Modelsim tools. Finally, the operation of the temperature acquisition system is validated on an Altera Cyclone II series FPGA chip. The measure results are displayed on both the local LCD module of the acquisition node and the UI of the host computer. The system can also give out alarm signals when the temperature acquired exceeds the threshold set through software. Due to the use of SOPC technology, the system is of high integration, high design flexibility, small volume and low power consumption. The system can be widely used in areas such as intelligent greenhouses, temperature monitoring systems inside storehouses, equipment, or machinery, and process control systems.

A High Precision and Externally Synchronous CMOS Relaxation Oscillator

Y.-Y. Deng, Q.-Y. Feng, and D.-H. Jia
School of Information Science and Technology
Southwest Jiaotong University, Chengdu, Sichuan 610031, China

Abstract— A high precision and externally synchronous relaxation oscillator with simple structure is proposed in this paper. The oscillator consists of the current circuits, a capacitor, two comparators, a RS flip-flop and other components. In the current circuits, positive and negative temperature coefficient current are obtained. With the current temperature compensation, a low temperature current is used to charge and discharge the capacity. By optimizing the delay of the comparators the oscillator has a good ability of control linearity In this method a high precision oscillator is obtained. Based on 0.5 µm OKI technology library, HSPICE and Cadence software is used to circuit simulation the simulation results show that the oscillator has stable output frequency and wide range of external synchronization. Under the environment of typical applications in the chip system the frequency of the oscillation is 500.1 kHz, With the power supply temperature changing from −40°C to 125°C, the frequency migration ranges from −0.3% to +1.3%.

A Novel Algorithm of Landmine Detection

Xin-Yun Wang, **Qian Song**, **Han-Hua Zhang**, **and Zhi-Min Zhou**
College of Electronic Science and Engineering
National University of Defense Technology, Changsha, Hunan 410073, China,

Abstract— In complex environments, detection of weak body-of-revolution (BOR) targets, such as landmines, is a difficult task, primarily due to the weak presence of targets. A novel algorithm which exploits aspectual invariance and local contrast to discriminate landmines from other man-made targets and natural clutter in SAR image is proposed in this paper. Aspectual invariance is the most significant and the most robust characteristic of BOR targets such as landmines, which can be used to detect landmines. Firstly, azimuth scattering entropy (ASE), which measures the characteristic of aspectual invariance, is extracted as a detection feature. The detection threshold is then acquired from the histogram of the ASE image with auto-adaptation method. The ultimate detection result is obtained by fusing results from aspectual invariance detection and Constant False Alarm Rate (CFAR) detection of the full aperture image.

The algorithm proposed in this paper concerns with the use of priori information of the to-be-detected targets. Compared with traditional methods, which are mainly based on the Automatic Target Detection/Recognition (ATD/R) scheme proposed by the Lincoln Laboratory of MIT, our algorithm makes detection more specific. The proposed algorithm can effectively eliminate the clutter which cannot be eliminated in the full aperture image, which increases the accuracy of the extraction of Region of Interest (ROI). In that case, the amount of calculation of the later discrimination stage will significantly be reduced. So although the extra aspectual invariance detection and fusion operation increase the amount of calculation, the whole ATD/R runtime won't add up. This paper takes the background of detecting metal anti-tank mines with Airship Mounted Ultra-wide Band SAR (AMUSAR). The results of experimental data demonstrate the effectiveness and practicability of the proposed algorithm.

TDLAS Based Early-stage Forest Fire Detection System

Jiawei Zhang[1], **Mingbao Li**[2], **Wei Li**[3], **and Hongli Zhang**[1]

[1]College of Mechanical and Electrical Engineering, Northeast Forestry University, China
[2]College of Civil Engineering, Northeast Forestry University, China
[3]Traffic College, Northeast Forestry University, China

Abstract— The commonly used forest fire detection method is insufficient to detect the early-stage forest fire. To cover this disadvantage, this paper tried a new method of detecting early-stage forest fire by using TDLAS (Tunable Diode Laser Absorption Spectroscopy) technique. By virtue of high sensitivity and rapid response, TDLAS can be used to detect trace characteristic gas CO from the early-stage forest fire. A new system was constructed consisting of light source and driver unit, optical path unit and detection and receiving unit. Based on the LabVIEW platform, a reliable and intelligent CO detection system with well favorable man-computer interface was developed. To determine the performance of light source, tuning characteristic of tunable diode laser on temperature and current was debugged. From the test results of second-harmonic spectrum for different CO concentrations the analysis, it was shown that there is a good linearity between CO concentration and spectrum intensity and the system had a good accuracy. The detection system was calibrated at normal temperature and pressure and modified considering the effect of temperature and pressure. It can be concluded that it is feasible to detect early-stage forest fire by measuring CO concentration and it helps to highly improve the performance of the forest fire detection system.

N(h)-profiles of the Ionosphere and Values of the Total Electron Content

O. Maltseva[1], **G. Zhbankov**[1], **and G. Ma**[2]

[1]Institute for Physics Southern Federal University, Stachki, 194, Rostov-on-Don 90, 344090, Russia
[2]National Astronomical Observatories, Chinese Academy of Sciences
20 A Datun Road, Chaoyang District, Beijing 100012, China

Abstract— Values of the total electron content TEC are defined by distribution of electron density in the ionosphere, i.e., by its N(h)-profile, and thus carry the information about this profile. It is important for testing of model TEC values and other applications. In the report of authors presented on XXXI URSIGASS2014 [1], it is shown that if to divide the N(h)-profile into three parts (bottom side, topside and plasmaspheric ones) then it is possible to coordinate completely the model N(h)-profile and the experimental value TEC(obs). In the report [1], the bottom side part of a profile was fixed by means of the experimental critical frequency foF2, the topside part was fixed with engaging of plasma frequencies fne(sat) of two satellites, a plasmaspheric part by introduction of coefficient K(PL), modifying this part of a profile up to the full coincidence between TEC(obs) and the model TEC. On an example of the South East Asia area and conditions of the high solar activity, it is shown that values of K(PL), the closest to 1, correspond to TEC of a grid-based method (GBM). In the present paper, similar research is fulfilled according to data of 2006. Features of this case are the low solar activity, presence of the data only of one satellite CHAMP, absence of the foF2 data. For determination of foF2 for four stations (Nanning, Guangzhou, Xiamen, Fuzhou), the experimental values of TEC for these stations and the experimental values of a median of the equivalent slab thickness of an ionosphere for the Guangzhou station and 2004 were used. As the model, IRI-Plas was used, allowing us to define the N(h)-profile including the plasmaspheric part and corresponding to the experimental value TEC(obs). As the experimental values of TEC(obs), IGS and GBM values were used. In both cases, the profiles transiting through fne (sat) of one satellite are very close each other and have the more essentially underestimated density of electrons in the topside ionosphere than the profiles transiting only through foF2. The main distinction belongs to the plasmaspheric part. Coefficients K(PL) are much higher than in case of the high solar activity. This can be result of a greater influence of measurement errors of TEC. The answer to a question that else is at the reason of distinctions (underestimated Ne or overestimated TEC) can be obtained comparing with independent measurements of density in the topside and plasmaspheric parts. Examples of redistribution of ionization between these parts both in quiet, and in disturbed conditions are given.

Forced Solitary Wave in Water Wave Basin under the Earth's Gravity Field

Shigehisa Nakamura
Kyoto University, Japan

Abstract— Monitoring of solitary wave on water surface is introduced. For this purpose, a water basin for a hydraulic modeling is used. Under a given boundary condition of a hydraulic model, a sinusoidal wave is propagates to pass a slit to diffract just like a case of Fresnel diffraction of optical ray. A specific linkage of boundary conditions, bathymetry, and a generated sinusoidal wave with a specific period is found for producing a solitary water wave in the basin. Some experiments are helpful for basic understanding of a process of solitary wave formation at a generated sinusoidal wave. Then, the author tends to consider whether this solitary wave might suggest that the strange peak observed during the monitoring tsunami waves accompanied by the 2011 earthquake in the northwest Pacific.

Parameterized Dynamic Range Reduction for UWB SAR Image

Chao Li and Yue-Li Li
College of Electronic Science and Engineering
National University of Defense Technology, Changsha, China

Abstract— The visualization of ultra wide bandwidth synthetic aperture radar (UWB SAR) data involves the mapping from high dynamic range amplitude values to gray values which have a lower dynamic rang. While UWB SAR image often display in gay scale and usually are coded in 8 bit, it's necessary to propose a useful method of dynamic range compression.

In this letter, first of all we examine the characteristic statistic between UWB SAR image and ordinary SAR image. We can know the log-normal distributing is more suitable for UWB SAR image. Secondly, for rapidly obtaining the image suitable for human observation, a new method of visualization for single look complex SAR image is proposed. The proposed method is a parameterized method based on the characteristic statistic of the UWB SAR data. In this method we got a global function which is used to map the amplitude values to [0, 1]. The result is then linearly mapped to gray levels, i.e., to 8 bit values. So, how to select the transformation functions will be discussed further. Lastly, we compare the visualization results between ones based on the proposed method and ones obtained by the traditional sorting based algorithm. We could know that the proposed method need low computational cost.

After these discussion, we could conclusion that the new adaptive method for dynamic range compression is more suitable for the characteristic statistic of UWB SAR image. It's parameterized and cost low computation. Visibility of details, especially strong reflectors, is improved in the displayed result. We believe it will make more contribution to the visualization of UWB SAR image.

The Mikaelian's Magnetic Lens for Static Magnetic Field Enhancement

Fei Sun[1, 2] **and Sailing He**[1, 2]

[1]Centre for Optical and Electromagnetic Research
Zhejiang Provincial Key Laboratory for Sensing Technologies, JORCEP
East Building #5, Zijingang Campus, Zhejiang University, Hangzhou 310058, China
[2]Department of Electromagnetic Engineering, School of Electrical Engineering
Royal Institute of Technology (KTH), Stockholm S-100 44, Sweden

Abstract— Traditional lenses for static magnetic field concentration are often closed structures and the enhanced DC magnetic fields are inside these structures. The static magnetic flux diverges very quickly in the free space outside these closed lenses. In this paper, we extend the Mikaelian's lens which has been widely used for focusing the light wave to design a non-closed DC magnetic lens which can concentrate the DC magnetic field and give a good DC magnetic field enhancement in free space regions even after a certain distance from the back surface of the lens. This magnetic ML will have many potential applications in magnetic sensors, wireless energy transmission and drug delivery by magnetic particles.

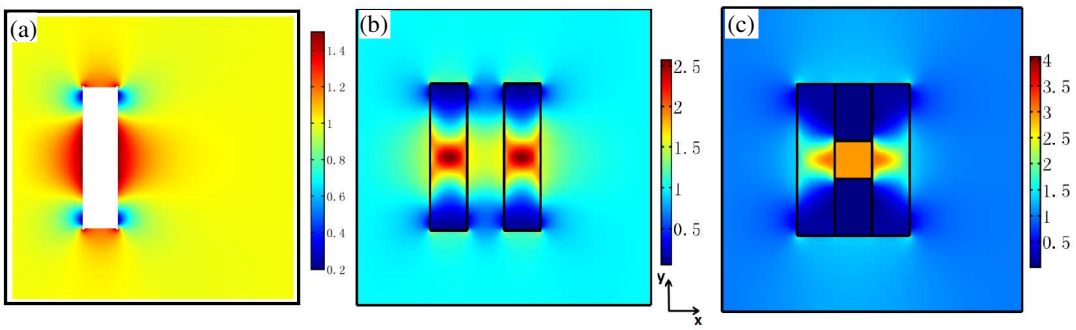

Figure 1: 2D FEM simulation results: the amplitude of total static magnetic field distribution when a uniform background DC magnetic field with amplitude 1 T is normally imposed onto the lens from $-x$ to $+x$ direction. (a) The white rectangular region is the magnetic ML. The parameters of the magnetic ML are $H = 0.4\,\mathrm{m}$, $d = 1\,\mathrm{cm}$, $\mu_c = 10$ and $g = 30\mathrm{m}^{-1}$. (b) The structure is two identical magnetic MLs with the same parameters of the one in (a) separated by 10 cm. In this case the DC magnetic field enhancement on the center axis 5 cm after the back surface of the first lens is about 1.54 (one single lens can only achieve a 1.25 time field enhancement in (a)). (c) The structure is composed of two diamagnetic materials with height 15 cm in y direction, width 10 cm in x direction and permeability $\mu = 0.01$ placed between two identical MLs used in (b). In the middle of our two identical MLs, we get a nearly uniform 2.83 time of magnetic field enhancement in a 10 cm plus 10 cm rectangle air region.

Skin Color Measurements: Usefulness of the Metric Hue Angle of Uniform Color Spaces for Dermatological Treatment

Makio Akimoto[1], **Yurika Koshiishi**[1], **Hikari Ikeda**[1], **Kazuhisa Maeda**[1], **and Mieko Hata**[2]

[1]Tokyo University of Technology, 1404-1, Katakura, Hachioji, Tokyo 192-0982, Japan
[2]Takano Medical Clinic, 6-4-23, Aoto, Katsushika-ku, Tokyo 125-0062, Japan

Abstract—

Background/Aims: Skin color is predominantly determined by pigments such as hemoglobin, melanin, carotene and bilirubin. Those skin color determing components can be altered significantly by UV light and several substances. The quantification of experimentally induced color changes is widely used method in dermatology and cosmetics since the color response can be used as an indicator of skin properties, drug properties and skin protection properties. Conventionally, Munsell color system and CIE color space have been used in the evaluation of skin color. However, these methods may not correspond to the subjective feeling has been pointed out. Therefore, the present study, we examined the usefulness of hue angle was calculated from the uniform color space. Metric hue angle is expected to correspond well to the appearance of skin color than the chromaticity coordinates or tristimulus values. The focus areas of this work are as follows: a) examined the differences in the various color spaces using a standard skin color samples, and b) measuring the skin color such as cheeks and forehead of subjects by using a commercially available instruments.

Methods: Colorimeter and digital camera were used in this study. A Minolta Chromameter CR-200 was used to take skin color measurements in CIE XYZ tristimulus values with 2° standerd observer. The illuminant was set to the CIE standard C and D_{65} to simulate skin color in a day light condition. Measuring geometry was diffuse illumination/0° viewing specular component excluded. The measured area is 8 mm in diameter. In vitro color parameters were taken with instrument standerdized skin color charts in order to evaluate accuracy and skin color range. Healthy male and fimail volunteers aged 10–50 years were included in the study. The skin colors collected from different positions on face and diffirent continents. Written informed consent was obtained from each volunteer and the protocol was approved. Skin color recorded value was the mean of three consecutive measurements. Color was expressed using $L^*a^*b^*$ and $L^*u^*v^*$ 1976 CIE systems.

Results: Two uniform colour spaces CIELAB and CIELUV were simultaneously adopted by CIE to approximate human vision. CIELAB and LUV are an opponent colour systems. It correlates with a fact that somewhere between the optical nerve and the brain retinal colour stimuli are translated into distinctions between light and dark, red and green, and blue and yellow. The color gamut and distribution of each subjects are plotted on a^*-b^*, u^*-v^* and L^*-metric hue angle planes. An imaging system based on digital camera which has been developed as a colorimeter and applied to measure colors in terms of tristimulus values within an image. In comparison with colorimeter, the digital camera system is an non contact instrument which is not only able to convey the whole design via accurate images but also measures texture surface.

Conclusion: Measured CIE-$L^*a^*b^*$, CIE-$L^*u^*v^*$ and metric hue angle parameters enable the unique identification of every color that may be visually distinguished and their use is proposed for the unambiguous communication of skin color information for clinical or scientific purposes. Hue angle were found to correspond well to the appearance of skin color. However, the subjects are too few to make a general conclusion, and the authors would like to add additional observers in the not-too distant future.

New Method for Automated Disk Diffusion Test

Pavel Krepelka[1], **Robert Kadlec**[3], **Karel Bartusek**[2], **and Martin Jakubec**[3]

[1]Department of Theoretical and Experimental Electrical Engineering
Faculty of Electrical Engineering and Communication
Brno University of Technology, Technicka 12, Brno 616 00, Czech Republic
[2]Institute of Scientific Instruments of the ASCR v.v.i.
Kralovopolska, 147, Brno 612 00, Czech Republic
[3]Vyzkumny Ustav Mlekarensky s.r.o, Ke Dvoru 12a, Prague 160 00, Czech Republic

Abstract— Microbial resistence to antibiotics is a very important parameter in the selection of a proper therapy and in the control of resistence spreading. One of the most used methods for measuring microbial susceptibility is the disk diffusion test. The test is based on diffusion of concentrated antibiotics from paper disk into agar. Concentration of antibiotics in the agar is dependent on distance from the center of the disc. Near antibiotic disc is concentration much higher due difficult permeation of antibiotics in agar. The diffused antibiotics then inhibit growth of sensitive strains. The zones are usually measured manually or by electronic calipers. Several aproaches for automatic inhibition zone detection have been introduced in recent years. Nevertheless, most of the algorithms are based on a similar radial profile analysis. We have designed a novel image-processing algorithm for measuring the size of inhibition zones of antibiotics based on an analysis of corrected image and rated this image with multicriterial algorithms (based on an observation of the radius profile). The algorithm was tested on 100 clinical isolates, resulting in calculation accuracy of 89% (ratio of success computed radii). If we include alternative radii (to be selected manually), the precision of the calculation rises to 98% (tolerance deviations between manual and automatic measurements were 2 mm). The achieved accuracy was independent of the culture medium (e.g., Muller-Hinton, blood agar, chocolate agar). The main advantage of the algorithm is the invariantness to the tested bacterial strain and culture medium. The new algorithm offers an alternative way to determine inhibition zones and evaluate antimicrobial susceptibility.

The Study of the Growth of Tissue Cultures under a Layer of Nanotextiles

M. Pokludova and P. Křepelka
Department of Theoretical and Experimental Electrical Engineering
Brno University of Technology, Technická 3082/12, Brno 612 00, Czech Republic

Abstract— Nowadays nanotextiles are very popular due to their unique properties (antibacterial, very light weight, thin, solid, high porosity, transparency, good mechanical properties, etc.). These characteristics bring new possibilities of classification in the various fields of human activity. For example, the filtration of air and water through the nanofiber membranes whose structure is similar to the construction of tissue that supports the growth of cells in their natural environment. Carbon nanofibers have their application in treating the effects of myocardial infarction. Nanotextiles consist of nanofibers with a diameter in the range from 50 to 500 nm. Production of such a fabric is much more complex than classical woven fabric. This material is not possible hold by any device. Production is carried out using the electrospinning. The nanotextile produced spinning method was used on the samples of spruce embryos and concluded (with samples) in the plastic Petri's dishes. Spruces embryos were selected for their rapid growth, their biggest increase is till the fifteenth day then they are growth-stabilized. The aim of this paper is to determine the influence of the nanotextiles to the tissue cultures and whether the embryos will be able to growth under this structure. The samples were periodically removed from the magnetic field and moved in an isolated box throughout the outdoor environment into the room with NMR tomograph for obtaining the images of individual tissue cultures. After fifteen days the last measurement was carried out and the results of all measurements were evaluated using the programs Marevisi and Matlab. Observed parameters of individual samples were processed into graphs.

Plasmonic Focusing of Metallic Probe Patterned with Periodic Structure

Qinbai Qian, Fuchun Xi, Peng Gou, Jie Xu, and Zhenghua An
State Key Laboratory of Surface Physics, Key Laboratory of Micro and Nano Photonic Structures (Ministry of Education), Department of Physics, Fudan University, Shanghai 200433, China

Abstract— A tip with the ability of high efficient near-field enhancement plays a significant role insurface analysis technologies such as near-field scanning microscopy and tip-enhanced Raman spectroscopy. Generally, for aperatureless or scattering type SNOMs equipped with no-patterned metallic probes, one high power laser is required to excite longitudinal local field enhancement. However, the necessity of using intense lasers brings limitations to real applications and is also likely to damage the samples. Here we propose a new design of probe patterned with periodic structure, which causes the surface plasmons induced by incident light to focus at the tip markedly, and then a highly enhanced field is generated. It is therefore possible to relieve high power requirement and even reach pure passive mode for some applications such as near-field infrared emission spectroscopy.

In this work, we simulate a metallic scattering probe (cone angle of 90°) with periodic and concentric wedged rings (Figs. 1(a), (b)). When the linearly polarized incident light beam reaches the metal surface, one two-way propagating surface plasmons would be excited. The upward ones finally focus at the tip [1], leading to high electromagnetic field density of states around the needlepoint. Simulation results show that spectral line of E-field intensity at the tip apex have seveal peaks whose resonant frequencies exhibit strong dependence on wedge period (Fig. 1(c)) but little dependence (Fig. 1(d)) on shape of wedged rings, suggesting propagating plasmons dominate in the field enhancement. We discuss the field enhancement performance for various cone angles of ideal PEC and real lossy metal tips.

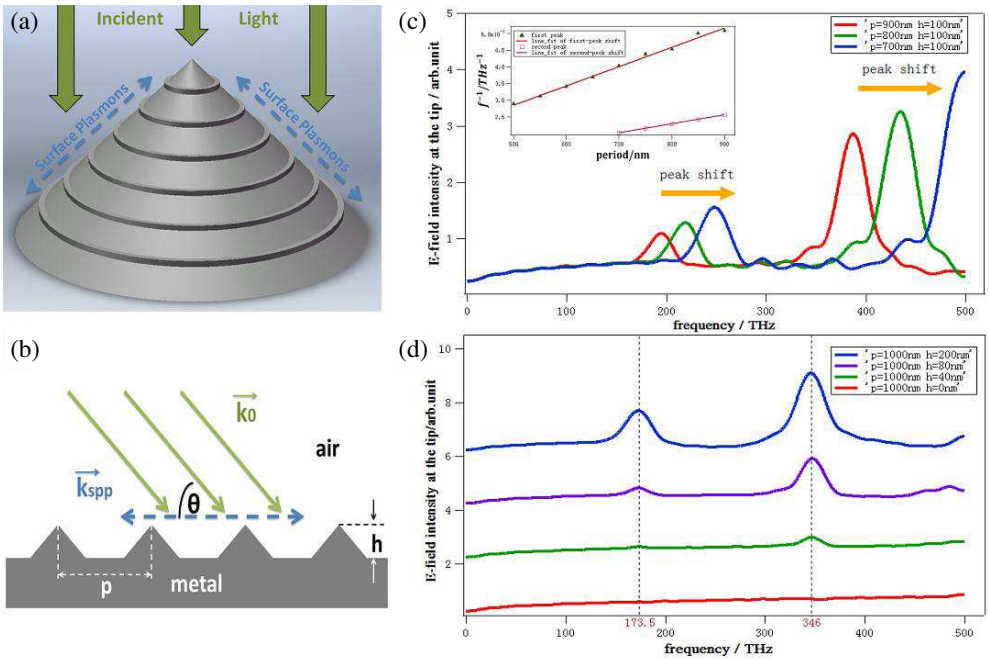

Figure 1: (a) Sketch of metallic probepatterned with periodic structure, the cone angle is set to 90°. (b) View of cross section along the slope. (c) Spectral line of E-field intensity at the tip apex when keeping the wedge height of 'h' as 100 nm and changing 'p' from 700 nm to 900 nm. The insert picture shows the reciprocals of these peaks' corresponding frequencies are linearly related to the wedge period. (d) Spectral line of E-field intensity at the tip apex when keeping 'p' as 1000 nm and changing 'h' from 0 nm to 200 nm.

REFERENCES

1. Lindquist, N. C., P. Nagpal, A. Lesuffleur, D. J. Norris, and S. H. Oh, *Nano Lett.*, Vol. 10, 1369-73, 2010.

Characterization of Ultrashort Pulse Laser by Using $KNbO_3$ Nanoneedles Based Frequency-resolved Optical Gating (FROG)

Jiaxin Yu and Fuhong Cai
Centre for Optical and Electromagnetic Research
Zhejiang Provincial Key Laboratory for Sensing Technologies
JORCEP [Joint Research Center of Photonics of the Royal Institute of Technology, Lund University and Zhejiang University], Zhejiang University, Zijingang Campus, Hangzhou 310058, China

Abstract— Frequency-Resolved Optical Gating (FROG) is nowadays one of the most powerful techniques in ultrashort pulse characterization. An autocorrelation-type measurement can be used for FROG as long as the autocorrelator signal beam is spectrally resolved. The frequency-resolved intensity autocorrelation of a FROG trace can provide adequate frequency and time information to reconstruct the original pulse. In a SHG based FROG system, it is common to use a piece of bulk crystal as nonlinear medium. An angle dithering apparatus for the crystal have to be involved in order to satisfy the phase matching conditions under different excitation wavelengths, thus it is always space consuming and complicated to modulate. In this paper, we demonstrate a approach of SHG-FROG measurement using potassium niobate ($KNbO_3$) nanoneedle clusters, instead of bulk crystal, as nonlinear medium. The $KNbO_3$ nanoneedles have been reported as a kind of excellent nonlinear nano-material. Using the $KNbO_3$ nanoneedles clusters, we obtained a comparable measurement of the pulse time/frequency-dependent intensity. Our approach is implemented on a conventional SHG-FROG system by replacing the bulk crystal with nanoneedle clusters at focus. This replacement is promising in several aspects: First, due to the nanometer scale, the phase matching constraints can be automatically satisfied even over a wide band of wavelength, and the angle dithering can be eliminated, which will largely reduce the system volume. Meanwhile, a lower complexity of phase matching modulation makes the FROG system more accessible for common users. Therefore, our $KNbO_3$ nanoneedles based SHG-FROG approach significantly enhances choices for existent pulse characterization systems.

FDTD-based CAD Simulator for Coaxial Applicator — Biomedical Application

C. W. Lee[1], **K. Y. You**[1], **and C. Y. Lee**[2]

[1]Department Communication Engineering, Faculty of Electrical Engineering
Universiti Teknologi Malaysia, Skudai 81310, Malaysia
[2]Faculty of Bioscience and Medical Engineering
Universiti Teknologi Malaysia (UTM), Johor 81310, Malaysia

Abstract— This paper presents development of FDTD-based CAD simulator using MATLAB graphic user interface feature for solving the coaxial slot radiator problem. The capability of the CAD is to visualize the 2D and 3D electromagnetic field and bio-heat distribution. The CAD is competitive with commercial simulator in term of learning curve and simplicity in the program algorithm. In this paper, the creation steps of the CAD are described in detail. In addition, the comparison result between the CAD and commercial simulator are intensively discussed and analyzed. Some of the limitations of this CAD are also presented.

To Elaborate the Low Observable Characteristic of Stealth Aircrafts

Faran Awais Butt[1], **Ijaz Haider Naqvi**[2], **and Ali Imran Najam**[3]

[1]School of Engineering, University of Management and Technology (UMT), Lahore, Pakistan
[2]Syed Babar Ali School of Science and Engineering (SSE)
LUMS, Sector U, D.H.A., Lahore Cantt, Pakistan
[3]National Electronics Complex (NECOP Design Centre), Islamabad, Pakistan

Abstract— The stealth aircrafts diffract and scatter very low power electromagnetic radiations owing to its special geometry and highly absorbent material. However, if the electromagnetic wave is incident at certain angles, significant scattering can be expected at certain angles. Hence, stealth aircrafts though low observable cannot be called as invisible because if the aircraft is energized at proper angle of incidence, significant scattering can be observed in a range of aspect angles.

The measure of an ability to scatter the incident wave depends upon a factor known as radar cross section which is the ratio of scattered electric field to the incident electric field. It is the minimum radar cross section property of the stealthy machine that makes it look like invisible to the radar. The radar cross section is dependent upon many factors like shape, orientation, material of the stealth aircraft which is related to the electromagnetic features of the stealth material like its thickness, permittivity, permeability and type of polarization. All the properties that somehow influence the radar cross section although can reduce the cross section to a great level but by no means can make the machine 'invisible'. More over the vulnerabilities of stealth aircrafts can be exploited as well.

Stealth aircraft is designed to diffract the incident coming wave into specific directions so if there is a properly placed receiver on the other side of the aircraft it can receive enough scattering to detect the target threat. The paper shows that stealth target can be exploited as although less intense, it always scatter electromagnetic waves in some directions. Hence, a multi-static radar approach can be suitable under such conditions instead of traditional monostatic radar.

Sidelobe Blanking in Phased Array Radar System for Countering Radar Jamming

Faran Awais Butt and Madiha Jalil
School of Engineering, University of Management and Technology (UMT), Lahore, Pakistan

Abstract— Electronic warfare systems deploying effective Electronic counter measures are a big threat to the modern radar systems. Noise jamming and deception jamming are the two main types of electronic countermeasure techniques used by the modern air craft's. Jammers mostly target the radar from the side lobes of the radar's receiving antenna.

Side lobe blanking systems can be very effective against the jamming ECM systems. Radars use a highly directive antenna which can come under influence of the target threat's ECM system. In side lobe blanking system an omni directional antenna is set up near the main radar antenna. The purpose of this antenna is to alert the system about the presence of jamming. In presence of jamming, the omni directional antenna which has higher gain then the radar antenna's side lobes, detects more powerful radar return then the main lobe of the antenna, this would indicate the presence of the jamming. This jamming can be effective if the jamming signal has the same polarization which the radar's receiver is expecting. The jamming signal can lose its effectiveness if it does not have the same polarization as the expected radar's return.

In phased array radar, there are group of antennas in which the signals supplied to each antenna element is varied in such a pattern that the radiation pattern of the radar is re enforced in a particular direction. Recently phased array radars have gained some serious attention owing to their effectiveness in detection. The proposed suggestion is to make dynamic phased array radar with side lobe blanking system. Frequency hopping accompanying with the cross polarized antennas in each respective array can be very effective against all type of jammers especially against the side lobe jammers.

Shielding and Mutual Coupling Effect of Ground Penetrating Radar Antenna

M. N. A. Karim[1, 2], **M. F. A. Malek**[2], **M. F. Jamlos**[2], **F. S. Abdullah**[2], **H. A. Halim**[2], **and H. Nornikman**[3]

[1]School of Computer and Communications Engineering, Universiti Malaysia Perlis
Main Campus UniMAP, Pauh Putra, Arau 02600, Malaysia
[2]School of Electrical System Engineering, Universiti Malaysia Perlis
Main Campus UniMAP, Pauh Putra, Arau, Perlis 02600, Malaysia
[3]Department of Telecommunication Engineering
Faculty of Electronic and Computer Engineering, Universiti Teknikal Malaysia, Melaka, Malaysia

Abstract— This paper discusses the shielding and mutual coupling effect of ground penetrating radar (GPR) antenna for buried object detection. In this study, bi-static radar system is considered. The antenna used in this system is designed at wide operational frequency, 0.5 GHz to 3.0 GHz. To observe the shielding effect and mutual coupling between antennas, two antennas with the same operating frequency are placedin an individual shielded box. The study is accomplished using Computer Simulation Technology (CST) software. The antenna is designed using substrate Taconic TLY-5 with dielectric constant of 2.2 andthicknessof 1.57 mm. The study and discussion includes the simulated results of radiation pattern, current distribution and reflection coefficient.

Introduction: Ground penetrating radar (GPR) is one of the non-destructive detection methods that have been tremendously exploredmainly in the area of research and development. One of

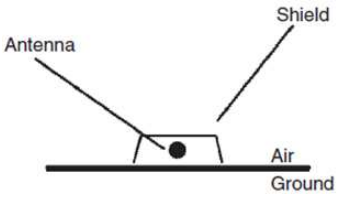

Figure 1: A shielded ground penetrating radar (GPR) antenna.

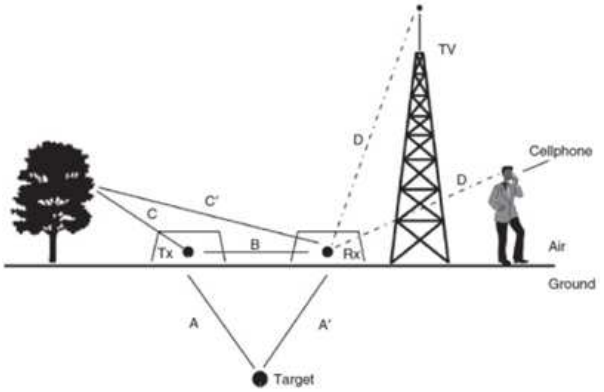

Figure 2: A ground penetrating radar (GPR) system emits and detects radio wave signals. There are many possible signals and paths and the objective to maximize the target response and minimize others.

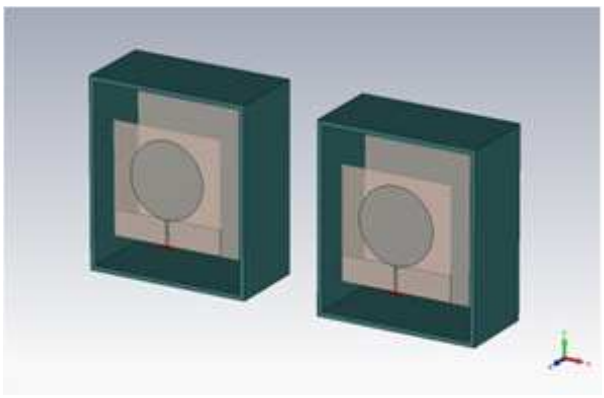

Figure 3: CST layout of shielded GPR antenna.

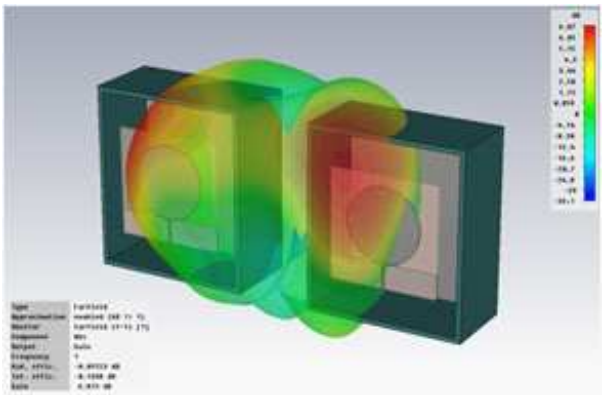

Figure 4: Coupling effect of the shielded antenna.

the important parts in the GPR system is the antenna itself. In a bi-static radar system, two antennas with the same specificationsare used fortransmitting and receiving the signal. When the transmitter sends the radio wave signal into the ground, the receiver will capture the reflected signal from the ground. Generally, the antenna performance usually affected by mutual coupling and signal from other sources. As a result, the position or the distances between two antennas need to be considered. Fig. 1 shows the proposed GPR antenna. The antenna is shielded to minimize the coupling effect between antennas and isolate the antenna fromundesired signals in the air.

As shown in Fig. 2, the signal is travelling from a transmitter to a receiver along a number of paths. The purpose of shielding is to selectively enhance some signals and supress others. This study leads to the objectives of:

a. Maximize the energy on the path AA' to and from subsurface target (i.e., focus on direct signal downward)
b. Minimize the direct transmitter to receiver energy on path B
c. Minimize the energy that escape into the air as on path CC'
d. Minimize external EM noise as indicated by signal D

Detection of Low-level Electromagnetic Signal of Partial Discharge by Means of Disturbed Acquisition Discrimination

P. Drexler[1], **M. Cap**[1], **P. Fiala**[1], **M. Steinbauer**[1], **M. Kaska**[2], **and L. Kocis**[3]

[1]Brno University of Technology, Czech Republic
[2]TES, Trebic, Czech Republic
[3]EGU HV Laboratory, Praha, Czech Republic

Abstract— The proposed article will present a new approach to detection of very weak electromagnetic signal, which is generated by partial discharge (PD). This approach is a part of radio frequency method, known as ultra-high frequency (UHF) method. The UHF method is utilized for detection, activity quantization and localization of PD in high-voltage power transformers. The UHF method is the most advancing method for this type of transformer diagnostic. The state of the art in instrument technology allows real-time acquisition and processing of pulsed broad band signals together with 3D localization of PD occurrence. The UHF method is based on measurements of electromagnetic waves in UHF spectrum produced by PD. Typical spectrum of the PD UHF signal ranges from hundreds of MHz to units of GHz. The UHF signal is detected by sensing heads that enter the transformer through its casing. Sensing heads, which were developed at Brno University of Technology (BUT), contains antennas and a set of high-frequency components, which adapt the signals from the antennas. The signals from the sensing heads are processed by a digitizer and real-time evaluated by a custom-made software developed at BUT also. The measurement of PD activity has been made on eight power transformers in the Dukovany nuclear power plant in the Czech Republic. The initial experimental measurement, which was under full working arrangements, has been accompanied by some issues. The recorded signals contained strong interference. It has been estimated that the source of the interference is probably situated in the high voltage bushings, which feed the transformer from a turbo-generator. The interfering signal in form of electromagnetic waves has propagated through the air vicinity and it has coupled to the sensing heads. It has been found that the proper shielding is a crucial factor, while the PD signal level is far below the level of the interference. An improved shielding has been developed and it has significantly reduced the level of interference. However, the signal level of expected PD activity was still below the level of the interference. Therefore, a new method for weak PD signal detection has been proposed, developed and verified. The method is based on the discrimination of signal acquisitions, which are disturbed by the interference, while the acquisitions of the desired weak signal are passing to further processing. The method was verified within an experiment, when very short electrical pulses were injected in the transformer vessel by antenna. The pulses closely simulated the spectral composition, time characteristic and the magnitude of real weak PD. The weak pulse signals were successfully detected in the presence of high level interference.

The detailed principle of the method will be described in the paper and the report on the results of the experimental measurement will be given also.

Dynamics of Radiative Heat Exchange between Parallel Plates of Silicon Carbide: The Role of Near Field

S. A. Dyakov[1], **J. Dai**[1], **M. Yan**[1], **and M. Qiu**[1, 2]

[1]Department of Materials and Nano Physics, School of Information and Communication Technology
Royal Institute of Technology, Electrum 229, Kista 16440, Sweden
[2]State Key Laboratory of Modern Optical Instrumentation
Department of Optical Engineering, Zhejiang University, Hangzhou 310027, China

Abstract— In this work we consider the dynamics of radiative heat exchange between parallel plates of silicon carbide. When the distance between the objects is much smaller than the thermal de Broglie wavelength, the heat transfer intensity can be sufficiently enhanced. The enhancement of the radiative heat transfer intensity in the near field is due to the coupling of evanescent photons which correspond to the surface states such as plasmon-polaritons and phonon-polaritons. In this case, thermal radiation between two bodies exceeds that between two blackbodies in the far field by orders of magnitude.

We determined the characters of time evolutions of temperatures of plates, namely, time which it takes for plates to reach thermal equilibrium, τ, and temperature of plates in thermal equilibrium, T_{eq}. Parameters τ strongly depends on the distance between plates, d, and their thicknesses, h. We have shown that for d and h, varying from 1 nm to 1 mm, the which it takes for plates to reach thermal equilibrium changes from 10^{-8} to 10^{2} sec. The dependence of τ and T_{eq} from the distance between plates is shown in Fig. 1 for $h = 100$ nm.

When the separation distance between plates, is small (near field regime), the parameter τ is proportional to proportional to thickness of plates and square of the distance between plates. In this case the temperature of the sink reaches the temperature of the heat source. When the separation distance is large (far field regime), τ does not depend on the distance between plates and the equilibrium temperature of the sink is less than the temperature of the source.

The method of simulation of time evolutions can be applied to more complicated planar structures other than the described system of two SiC plates. We believe that the results of this work can be useful for design of more complex systems where the heating time is important such as an absorber and emitter in solar thermophotovoltaic devices.

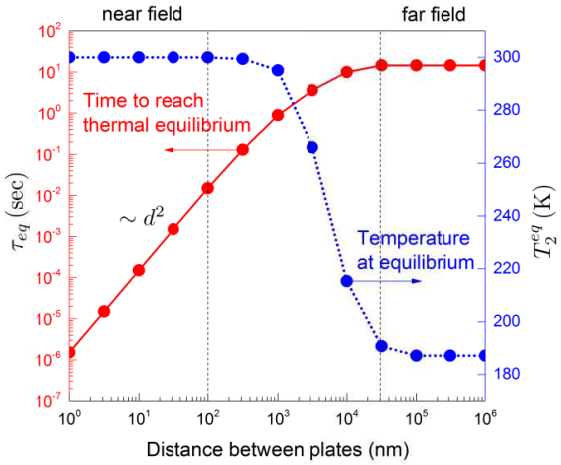

Figure 1: Time which it take for cold plate to reach thermal equilibrium, and temperature of cold plate at thermal equilibrium as a function of the distance between plates.

A Novel Design of Ku Band Coaxial-waveguide Directional Coupler Used for the Measurement of the Short-circuited Line Method

Qijia Liu, Chao Wang, Binjie Tao, and En Li
University of Electronic Science and Technology of China, Chengdu, China

Abstract— An effective method was proposed to design a high power coaxial-waveguide directional coupler applied to the short-circuited line method. In this paper, the coupler designed using the proposing method has wide band, high directivityflat coupling coefficient, lower SWR, and low requirement for machining accuracy. According to the required technology parameter, preliminary designed the aperture waveguide directional coupler and the adapter. In order to achieve the more excellent indices, we simulate and optimize the distance between the two hole and the two ends hole size of the coupler, the step size of the adapter. The VSWR of coaxial-waveguide transition designed in this paper is less than 1.06 in the 12.4–18 GHz octave bandwidth, and the high modulus produced is very small. Therefore, coaxial-waveguide directional coupler of the directivity and the coupling coefficient are improved.

Frequency-tunable Circular Polarization Beam Splitter Using a Graphene-dielectric Sub-wavelength Film

Tuo Chen[1, 2] **and Sailing He**[1, 3]

[1]State Key Laboratory of Modern Optical Instrumentations
Centre for Optical and Electromagnetic Research, JORCEP
Zhejiang University, Hangzhou 310058, China
[2]Department of Physics, Zhejiang University, Hangzhou 310058, China
[3]Department of Electromagnetic Engineering, School of Electrical Engineering
Royal Institute of Technology, S-100 44 Stockholm, Sweden

Abstract— Manipulating the circular polarization of light is of great importance in chemistry and biology, as chiral molecules exhibit different physiological properties when exposed to different circularly polarized waves. Here we suggest a graphene/dielectric-stacked structure, which has both the properties of a epsilon-near-zero material and the high Hall conductivity of graphene. The proposed sub-wavelength structure demonstrates efficient manipulation of circular polarization properties of light. In a quite broad frequency range and at a large oblique incidence angle, the present magnetically active structure is transparent for one circularly polarized wave, and opaque for another. Such an effect can be further tuned by changing the magnitude of the applied magnetic field and chemical potential of graphene.

Nanoscale Plasmonic Switch at Far Infrared Frequencies Using Graphene

Jieer Lao[1], **Jin Tao**[2, 3], **Qi Jie Wang**[2, 3], **and Xu Guang Huang**[1]

[1]Laboratory of Photonic Information Technology
South China Normal University, Guangzhou 510006, China
[2]OPTIMUS & NOVITAS, School of Electrical and Electronic Engineering
Nanyang Technological University, 50 Nanyang Avenue, Singapore 639798, Singapore
[3]CDPT, Centre for Disruptive Photonic Technology, School of Physical and Mathematical Sciences
Nanyang Technological University, Singapore 637371, China

Abstract— The electro-optical switches using graphene have been the subject of much interest both theoretically and experimentally in the recent years [1, 2]. However, most of them are based on electro-absorption, which is relied on the modulation of the interband or intraband transition of graphene. Less work has been done in the electro-refraction with different Fermi level, which can also be employed in the modulation mechanism.

In this paper, we report a different modulation principle and method, the gate-voltage-controlled mode-guiding switching/mode-cutoff mechanism, to achieve the modulation function [3]. The proposed structure of the graphene 2D waveguide at far infrared frequencies is designed. The complex surface conductivity is estimated within the random-phase approximation in Ref. [4]. By altering the voltages applied to the graphene to form different Fermi level pattern, in the on state, the SPP waves will be confined within the core region due to higher effective index of the core than the surrounding cladding layers. In the off state, by decreasing the Fermi level in the cladding, the vast majority of energy will diffuse to the cladding, only small fraction of energy remains in the core. The finite-difference time-domain (FDTD) method is used to evaluate the optical performance. Up to 21.5 dB/μm modulation depths and more than 20 THz bandwidth can be achieved. 3-dB modulation depth can be satisfied as short as 139.8 nm. This plasmonic graphene-based switch can be used to promote the performance of current modulators in the integrated optical field, providing another method for interconnect in ultrahighly integrated photonic circuits.

REFERENCES

1. Lu, Z. L. and W. S. Zhao, *J. Opt. Soc. Am. B*, Vol. 29, 1490–1496, 2012.
2. Gosciniak, J. and D. T. H. Tan, *Nanotechnology*, Vol. 24, 185202, 2013.
3. Lao, J., J. Tao, Q. J. Wang, and X. G. Huang, *Laser & Photon. Rev.*, 2014, doi:10.1002/lpor.201300199.
4. Falkovsky, L. A. and S. S. Pershoguba, *Phys. Rev. B*, Vol. 76, 153410, 2007.

Digital Multi-channel High Resolution Phase Locked Loop under Influence of Potential System Uncertainties

Mohamed Rizk, Shawky Shaaban, Usama Aboul-Nadar, and Alaa El-Din Sayed Hafez
Alexandria University, Alexandria, Egypt

Abstract— This paper is devoted to present a multi-channel, high resolution, fast lock phase locked loop (PLL) for surveillance radar applications under influence of system noise. Phase detector based PLLs are simple to design, suffer no systematic phase error, and can run at the highest speed. Reducing loop gain can proportionally improve jitter performance, but also reduces locking time and pull-in range. The system is studied under influence of system noise in the range from 5 to 30 dB to reflect the reliability of the system under these conditions. The results perform a comparison of noise power, VCO control input, Lock time, ISE and ITSE Performance indices for three selective channels among 38 channels operated in the desired frequency range. The results show superiority of the system in difficult operating conditions.

Introduction: Phase-locked loops (PLLs) are used in surveillance radar wave formers to implement a radar waveform synthesis. The major concerns in the design of PLLs are noise or jitter performance and the lock time. G. David [1], describe two simply implemented frequency detectors which, when added to the traditional phase detector, can improve acquisition even for very small loop bandwidths and large initial frequency offsets. Kurt M. Ware, et al. [2] presents a numerical system simulation program that explores the time-domain behavior of an idealized model based on the phase-locked loop design. Faster lock is attained while maintaining the PLL's gain/phase margin characteristics by B. David et al. [3]. Kent Kundert [4], presents a methodology for predicting the jitter performance of a PLL using simulation. Several researches introduce an improvement for the jitter and frequency lock time [5–11] but not consider multi-channel, high resolution PLLs Digital phase-locked loop (DPLL) design one of most active research topics in complex digital communication systems. It replaces traditional PLL designs, a charge-pump and voltage controlled oscillator (VCO) [12]. A new method for tracking narrowband signals acquired via compressive sensing is designed in Ref. [13]. This paper presents a multi-channel, high resolution PLL for surveillance radar systems based on developing the charge pump by a digital adaptive gain processor to achieve fast lock times while improving jitter performance in lock. Section 2 provides a theoretical analysis of the frequency synthesis and the phase locked loop. Section 3 briefly describes the proposed PLL architecture. Section 4 discusses the results and a summary is in Section 5.

Localization in One-dimensional Structures with Power-law Correlated Heterogeneity

Sepideh. S. Zakeri[1], **Stefano Lepri**[2, 3], **and Diederik S. Wiersma**[1, 3, 4]

[1]European Laboratory for Non-linear Spectroscopy (LENS)
Universita di Firenze, Sesto Fiorentino (FI) 50019, Italy
[2]Consiglio Nazionale delle Ricerche, Istituto dei Sistemi Complessi
via Madonna del Piano 10, Sesto Fiorentino I-50019, Italy
[3]Istituto Nazionale di Fisica Nucleare, Sezione di Firenze
via G. Sansone 1, Sesto Fiorentino I-50019, Italy
[4]Dipartimento di Fisica e Astronomia, Universita di Firenze, Sesto Fiorentino (FI) 50019, Italy

Abstract— For many years, multiple scattering of light in heterogeneous structures has been basis of numerous applied and fundamental researches. One of the recent studies reports on observation of Lévy flights [1, 2] for photons passing through some engineered materials with controlled heterogeneity named Lévy glasses [3, 4]. Spatial distribution of heterogeneity in these structures follows α-stable Lévy distributions ($0 < \alpha < 2$) which are characterized by power-law tails and diverging moments. Using these α-stable distributions provides a more general framework to model photon transport processes where anomalous laws like super diffusion can arise. Unlike diffusive samples, in a Lévy glass, there is a non-vanishing probability for light at an arbitrary depth inside the medium to be coupled to its surrounding environment [5]. This property can result in complex interference effects for light scattered by these structures.

In this work, we aim to numerically study effect of large-scale heterogeneities on localization in one dimensional Lévy structures. Using transfer matrix technique, we numerically solve discrete wave equation for one-dimensional lattices with Lévy-spaced defects. We then calculate Lyapunov exponents as inverse of the localization length.We statistically study frequency dependence of Lyapunov exponent versus different parameters of the system such as degree of heterogeneity (α), disorder strength, number of defects, etc.. Thus far, we have focused on one dimensional structures but our model can be further expanded to 2D.

In addition, we also study how energy and moments of a wavepacket spreading through Lévy structures with different degree of heterogeneity (α) varies in time. Tail behavior of the asymptotic energy profile is also investigated.

REFERENCES

1. Mandelbrot, B. B., *The Fractal Geometry of Nature*, W. H. Freeman, San Francisco, California, 1982.
2. Shlesinger, M., G. M. Zaslavsky, and J. Klafter, *Nature*, Vol. 363, 31, 1993.
3. Barthelemy, P., J. Bertolotti, and D. S. Wiersma, *Nature*, Vol. 453, 495, 2008.
4. Bertolotti, J., K. Vynck, L. Pattelli, P. Barthelemy, S. Lepri, and D. S. Wiersma, *Advanced Functional Materials*, Vol. 20, 965, 2010.
5. Burresi, M., V. Radhalakshmi, R. Savo, J. Bertolotti, K. Vynck, and D. S. Wiersma, *Phys. Rev. Lett.*, Vol. 108, 110604, 2012.

TM Wave Mode Analysis of Circular Dielectric Resonator with Anisotropic Permittivity

Hepi Ludiyati[1, 2], **Andriyan Bayu Suksmono**[1], **and Achmad Munir**[1]

[1]Radio Telecommunication and Microwave Laboratory
School of Electrical Engineering and Informatics, Institut Teknologi Bandung, Indonesia
[2]Department of Electrical, Politeknik Negeri Bandung, Indonesia

Abstract— This paper presents the theoretical analysis of transverse magnetic (TM) wave mode for circular dielectric resonator with anisotropic permittivity. The analysis which is emphasized on its resonant frequency is required to investigate specific properties of resonator in TM wave mode which are useful for microwave application. By introducing the anisotropic permittivity, the resonator is expected to have the property with unique characteristic compared to the conventional one. To determine the resonant frequency of resonator for TM wave mode, Maxwell's equations with proper boundary condition are applied for circular waveguide that encapsulates an anisotropic circular dielectric resonator. The anisotropic permittivity is established by assuming the different values of relative permittivity in each axis of cylindrical coordinate, i.e., ε_ρ, ε_ϕ and ε_z. The analysis result shows that the circular dielectric resonator with anisotropic permittivity in z axis, i.e., propagation direction, has significantly changed the resonant frequencies of TM wave mode which can be applicable for resonance mode selection.

Adaptive Optimal Polarization Detection of Target in Clutter Background Based on Generalized Rayleigh Quotient

S. Lei[1], **Z. Zhao**[1], **Z. Nie**[1], **and Q. H. Liu**[2]

[1]School of Electronic Engineering, University of Electronic Science and Technology of China, China
[2]Department of Electrical and Computer Engineering, Duke University, USA

Abstract— Detection of a target in clutter background is a challenging problem for target detection system when the target and the clutter are closely spaced in angle and Doppler domains. Polarization information has been widely used to improve the detection performance. It has been demonstrated that polarization information is as important as amplitude, phase and frequency. Especially, when the polarization states of transceiver match target scattering characteristics well and mismatch clutter scattering characteristics, detection performance would be substantially improved. In this paper, the optimal polarized waveform is designed to match target scattering characteristics and therefore to improve detection target in clutter background.

Most current methods on polarization targets detection assume the target echoes to be ascertained in signal model during the detection period. But in practice, the target echo may obey a kind of distribution and the distribution relates with the polarizations. Aiming to study a more realistic problem, an adaptive generalized likelihood ratio (AGLR) polarization detector is proposed. Different to existing methods, the detector assumes the target echo to be a non-zero mean Gaussian distribution with respect to the polarization states of transceiver. The prominent advantage of the proposed detector is that it can adaptively adjust the polarization states of transceiver according to the variation of the polarization properties of target and clutter to maximize signal to clutter and noise ratio (SCNR).

The problem of maximizing the SCNR is converted to a problem of maximizing a generalized Rayleigh quotient (GRQ). By solving the GRQ problem, the AGLR detector always optimally selects the polarization state that can maximize the SCNR. The performance of the AGLR detector is numerically validated through some numerical experiments. Compared with two conventional GLR detectors, the AGLR detector achieves a 3 dB to 10 dB improvement.

Scattering of a Partially Coherent Pulse on a Deterministic Sphere with Semisoft Boundaries

Haixia Wang, **Chaoliang Ding**, **and Liuzhan Pan**
Department of Physics, Luoyang Normal University, Luoyang 471022, China

Abstract— In recent years the statistical properties of the light generated by scattering have been studied extensively due to their considerable interest in medical diagnostics and imaging, remote sensing of the atmosphere and ocean, and so on. However, in most cases, the treatment of scattering of the field was confined to the case that the incident field is statistically stationary. Using the model of partially coherent pulses proposed by Friberg et al., we investigate the scattering of a partially coherent plane-wave pulse on deterministic sphere with semisoft boundaries. The analytical expressions for the intensity profile and the degree of temporal coherence of the scattered field are derived. The effect of summation index M and effective radius σ on the intensity profile and the degree of temporal coherence of the scattered field is emphasized.

Calculation of Shielding Effectiveness of an Apertured Rectangular Cavity Against Planar Electromagnetic Pulses

Xiaoning Shi, Chongqing Jiao, and Shuai Niu
State Key Laboratory of Alternate Electrical Power System with Renewable Energy Sources
North China Electric Power University, Beijing 102206, China

Abstract— Based on the equivalent circuit method and the Fourier transform technique, an approximate analytical model for calculating the shielding effectiveness of an apertured rectangular cavity against planar electromagnetic pulse is presented. The validity of the theoretical model is verified by the comparison with the full-wave electromagnetic simulation software CST. The effects of the aperture's shape and size, and pulse width on the pulse shielding effectiveness are analyzed.

Parametric Inversion of 2-D Dielectric Rough Surface Based on SVM

Qiyuan Zou, Qinghe Zhang, and Fei Xu
School of Science, Three Gorges University, Yichang, Hubei 443002, China

Abstract— Inverse scattering is one of the most challenging problems in electromagnetic field due to its nonlinear and probabilistic characteristics which belong to the question instinctively. However, it is still gaining a considerable amount of attention in theory circle and engineering circle because of its numerous applications in seismology, target identification, ground-penetrating radar, geophysical sensing and so on. Present paper mainly focuses on support vector machine (SVM) optimization approach to estimate the parameters of random dielectric rough surface with microwave remote sensing data. Several observation points are setted above the random rough surface to acquire the scattering signal, while numerical solutions based on method of moment (MoM) are used to compute scattering field at the observation points. In MoM, the rough interface of finite size is modeled in the simulation and a taped incident field is used to avoid surface edge scattering effects. With the help of support vector regression (SVR), it is able for us to transform the original problem into a problem of regression estimation,scattering data acquired above serves as training sample. After that, by training the support vector machines, then we establish the inverse scattering model to reconstruct the geometries (root-mean-square height δ and relevant length ℓ) of the rough surface. By comparing the numerical results from training sample and testing sample, it shows the validity and veracity of SVM approach. We also care about the error analysis and investigate the relative importance and sensitivity of various physical parameters of the random rough surface as well as the incident field to the final result.

Electormagnetic Field-focusing EBG Lens

G. A. Balykov[1], **V. A. Kaloshin**[2], **A. N. Semenov**[1], **and A. P. Smirnov**[1]

[1]Lomonosov Moscow State University, Moscow, Russia
[2]Kotelnikov Institute of Radio Engineering and Electronics, Moscow, Russia

Abstract— The electromagnetic field focusing capabilities of non-continuous periodic Mikaelian lens is considered. Theoretical continuous Mikaelian lens has the electromagnetic field focusing properties and concentrates incident wave field in one point on the border. Also this lens has sophisticated structure and cannot be implemented using current technologies. The alternative way to implement similar structure is by using periodic layers of constant permittivity which are separated by the periodic layers of air. The idea is to replace continuous lens with the another one, which structure could be easily implemented in practice. Continuous lens has permittivity reducing from 2.56 on the axis of symmetry to 1.0 at the borders. The new lens is a periodic structure, that does not have the same redundancy of permittivity as the continuous one. Such lens has layers containing both the non-conductor and the air, and the ratio of thickness of air to thickness of material increases in the direction from axis of symmetry towards the borders. Thickness ratio of air to thickness of material in each layer is calculated according to the permittivity in the continuous lens on the same distance from the axis of symmetry. Material and air create necessary permittivity in total. It is shown, that the ratio of wavelength to the one period length should be higher than specific value. FDTD method is used for the numerical simulation. The thickness of one layer expressed in the number of grid points is important numerical parameter. When this number is too small, structure of lens close to the axis of symmetry cannot be resolved, and this leads to loss of focusing capabilities. To avoid this, the number of grid points per layer should be at least equal to 10, but the higher this number is the better result would be achieved. The problem with increasing the number is that grid size should also be increased, and the amount of needed memory will also significantly rise. Number of computational experiments is performed and electromagnetic-field focusing capability of layered lens is obtained.

Performance Analysis of Parallel FDTD Algorithm on IBM BlueGene Supercomputer Series

A. P. Smirnov[1], **A. N. Semenov**[1], **and A. V. Pozdneev**[2]

[1]Lomonosov Moscow State University, Moscow, Russia
[2]IBM East Europe/Asia Ltd., Moscow, Russia

Abstract— The advances in high performance computing nowadays have increased the need of the computational resources to solve the large-scale problems. The large-scale electromagnetic and optical problems with the size of the order of 400 wavelengths in every dimension for a problem with arbitrary complex geometry structure can be solved. One of the most widespread numerical methods for Maxwell equations solving is Finite Difference Time Domain (FDTD) method. FDTD is based upon Yee lattice and Maxwell equations in integral form and differentional relations from which finite difference approximation is obtained. In this paper, IBM BlueGene/P and BlueGene/Q performance is compared to calculate the large electromagnetic problem using parallel Finite Difference Time Domain method. Introduced early EMWSolver3D was implemented on Lomonosov Moscow State University IBM BlueGene/P supercomputer. Using 1D data decomposition for the highly elongated spatial domains together with the asynchronous transfer operations between nodes of supercomputer it is allows to solve problems up to 10^{10} computational cells on more than a thousand nodes. Parallel implementation of FDTD algorithm based on hybrid MPI/OpenMP approach is used in this paper. The scalability of the algorithm on both BlueGene/P and BlueGene/Q systems that runs in different parallel modes is considered. Parallel processing performance comparison of both systems shows that the IBM BlueGene/Q supercomputer gives near linear speedup and the great efficiency on FDTD algorithm.

Analytical Formulation for Electromagnetic Leakage from an Apertured Rectangular Cavity

Y. Y. Li and C. Q. Jiao
State Key Laboratory of Alternate Electrical Power System with Renewable Energy Sources
North China Electric Power University, Beijing 102206, China

Abstract— With the rapid development of electronic technologies and the wide applications of wireless communication technologies, electromagnetic environment becomes more and more subtle and complex. So, various protection measures to prevent electromagnetic interference from both conducting and field coupling mechanisms have been studied and developed. An analytical formulation has been developed for the electromagnetic leakage from an apertured rectangular cavity excited internally by an electric dipole. The formulation consists of three parts: the interior problem of determining the field distribution within a closed cavity with the eigen-mode expansion method; the problem of characterizing the leakage mechanism of aperture by using the Bethe's small hole coupling theory; the exterior problem of determining the transmission field by using antenna theory. Theoretical values of shielding effectiveness are in good agreement with full-wave simulations. Analytic approaches, disregarding limited scope of application, are still of realistic interest in both science and engineering aspects due to clear physical meaning, high computation efficiency and easy to be programmed. In this paper, an analytic formulation is implemented to investigate the electromagnetic leakage from an aperture rectangular cavity. The formulation is based on the Bethe's small aperture coupling theory, which uses equivalent electric and magnetic dipoles to describe the relationship between the internal field of a closed cavity excited by an internal source and the leakage field from apertures. This Bethe's theory had been employed by some authors in earlier papers, and it is shown that the approach can work very well provided that the size of aperture is much smaller than one wavelength.

Transient Electromagnetic Topology Method for Complex Wiring Consisting of Random and Nonuniform Transmission Lines

Haiyan Xie[1], **Yong Li**[1], **Hongfu Xia**[1], **Chun Xuan**[1], **and Jianguo Wang**[2]

[1]Northwest Institute of Nuclear Technology, P. O. Box 69-12, Xi'an, Shaanxi 710024, China
[2]Northwest Institute of Nuclear Technology, P. O. Box 69-1, Xi'an, Shaanxi 710024, China

Abstract— The transient electromagnetic topology (TEMT) method is improved to include random and nonuniform transmission lines first and then is applied for the analysis of a car with complex wiring inside, which is composed by two random and a nonuniform transmission lines, under an electromagnetic pulse (EMP). In the TEMT method, the SPICE model for the nonuniform transmission line is composed by cascading the SPICE models for the segments of uniform lines, which compose the nonuniform transmission line. For the random transmission line, the average parameters are computed first and then the SPICE model is developed as the usual transmission line. For the car with complex wiring inside, a three dimensional finite-difference time-domain method is applied to compute the electromagnetic fields at the average positions of the transmission lines. For the nonuniform transmission line, an interpolation is needed to get the exact excitation fields. Then based on the excitation fields and the line parameters, the SPICE models for the two random and one nonuniform transmission lines are developed. At last, a SPICE software is employed to obtain the induced voltage generated by the EMP on the devices within the car. The study on the car with complex wiring show that the improved TEMT method can deal well with the nonuniform and random transmission lines and the induced voltages of the devices generated by the EMP can be up to 100 V, which may cause upsets or damages to the devices.

A Low Power PLL Synthesizer for ICD System

Jin-Sup Kim and Se-Hwan Choi
Convergence Communication Components Research Center
Korea Electronics Technology Institute, Korea

Abstract— Medical devices for monitoring the patient's medical status have been continuously evolved from the body-attached wearable form to the implant form. Such medical implant devices include cardiac pacemakers, insulin dispensers, neuro-stimulators, and bladder controllers. Implantable cardiac defibrillator (ICD) system is one of the most important implant devices. In this paper, a low power PLL synthesizer for ICD system is proposed and implemented using 0.18 μm CMOS technology. The architecture of the proposed one is shown in Figure 1. Conventional PLL synthesizer requires a level converter because of the signal swing difference between current mode logic (CML) and CMOS logic. The level converters are typically very high current demanding circuits. In this work, we design and fabricate the PLL synthesizer with fully digital prescaler for low current consumption except voltage control oscillator. Also, the prescaler uses the latch with clocked inverter which is basic block of D flip-flop. The clocked inverter is used to reduce the delay time in the latch and retain the stable set-up time. The phase noise is −87.5 dBc/Hz at 10 kHz offset frequency. The frequency tuning range is from 382 to 433 MHz. The supply voltage is 1.8-V.

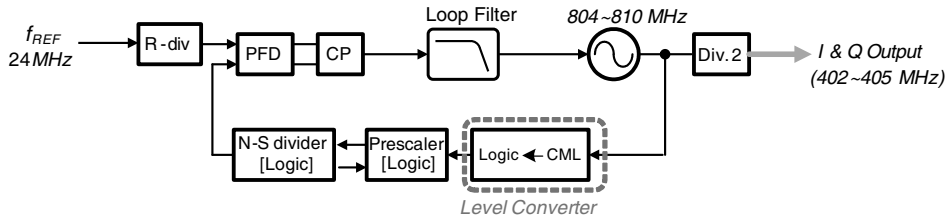

Figure 1: Block diagram of the proposed PLL synthesizer.

Influence of the Socket on Chip-level ESD Testing

Yu Xiao[1], **Jiancheng Li**[2], **Jianfei Wu**[2], **Yunzhi Kang**[3], **and Jianwei Su**[1]

[1]P. O. Box 9010, Xiangtan University, Xiangtan, Hunan 411105, China
[2]National University of Defense Technology, Changsha, Hunan 410073, China
[3]Freescale Semiconductor Inc., TEDA, TianJin 300457, China

Abstract— This paper introduces a method of IC-level Electrostatic Discharge (ESD) testing and discusses the influence of the socket on Chip-Level ESD testing. During the powered ESD (PESD) testing, welding the chip to the PCB is a necessary process which can be a repetitive process and time consuming. In order to solve this problem, a ball grid array (BGA) test socket is used during the test. The socket is built from copper-clad pogo pin and is pinned in an 8×8 mm array with 121 pins on a 0.65-mm pitch. As the test results suggest, there is little difference between testing with the socket and without. So in this study we take such factors into account as the pan angle range between ESD gun and PCB, the ESD gun, etc.. It is found in this study that the difference value (D-value) percentage between socketed ESD testing and non-socketed ESD testing is within 6.4%, the D-value percentage that the pan angle range of the ESD gun produces is within 5.8%, and the D-value percentage that the ESD GUN produces is within 5.8%. Based on these findings, it is concluded that work efficiency can be greatly improved by using the socket in PESD testing.

Solitary Wave Induced in a Sinusoidal Water Surface Wave Field of Hydrodynamics

Shigehisa Nakamura
Kyoto University, Japan

Abstract— Monitoring for nonlinear processes of water surface waves is introduced in brief. It was found a kind of nonlinear water surface waves which had a single crest wave with an infinitely long wave in a water tank. This wave was named as solitary wave on water surface in an experiment first. Then, a solitary wave had been led in a mathematical formulation. Another nonlinear wave known as a cnoidal wave was found in a form of cn function mathematically. An extensive experiment in an water tank has led to see a process in which an input function of linear sinusoidal wave induced a nonlinear wave quite similar to the solitary wave.

The Casimir Force and Heat Conduction Viewed as Exclusion of Natural Spatial Energy and Lateral EM Coupling between the Walls of a Waveguide

Michael J. Underhill
Underhill Research Ltd., Lingfield, UK

Abstract— The proposal here is that the Casimir attractive force and the heat conduction between two closely spaced plane surfaces are related processes each with more than one sub-process component. One main process is 'Electromagnetic (EM) coupling' [1–9]. The second main process is the exclusion of 'natural spatial energy' between the surfaces. Both contribute to the Casimir attractive force and to heat conduction but vary differently with distance and temperature.

EM coupling is an essential concept for the Physical EM Model proposed as the basis for an Electromagnetic Theory of Everything (EMToE) [1, 8, 9]. 'Natural spatial energy' is taken to have two components both with a white noise (flat) spectrum. One is thermal noise kT the other is the noise fluctuations of what can be called Zero-Point-Energy (ZPE) which is assumed to have a white noise spectrum, but to be independent of temperature. (Here the ZPE process is preferred rather than the 'virtual photon' quantum process as the explanation for the Casimir force. A previous paper showed that photons in free-space at room temperature are unstable below about 300 THz or one micron wavelength [10]). The stability frequency decreases as the square root of absolute temperature ($\sqrt{T}$) down to an expected ZPE fluctuation limit that remains to be established, arguably by measurements of the two Casimir effects.

A Transverse Electric (TE) wave can travel between two uniformly spaced finite parallel plane conducting plates in any direction in the plane. If energy is supplied uniformly into the gap h between the two planes from all directions energy is stored between the planes in the form of standing wave modes. A TE waveguide has a lower cut-off frequency $f_c = c/2h$ where $c = 3 \times 10^8$ m/s is the free-space wave velocity. Any noise or fluctuation energy below this frequency is therefore excluded from exerting an outward pressure between the plates. There is thus a nett attractive force between the plates. The excluded energy per unit area is proportional to the distance h and inversely proportional to the TE waveguide cut-off frequency. Thus we can predict a $1/h^2$ law for the Casimir force.

The 'natural spatial energy' available for exclusion is assumed to be a combination of heat energy and 'Zero-Point-Energy' ZPE. Heat energy (radiance) in space has a flat 'white noise' spectrum of spectral density kT watts/Hz/m^{-2} (where k is Boltzmann's constant). ZPE white noise is assumed to have a constant spectral envelope that is independent of temperature.

An initial assumption is that EM coupling impedance is the primary cause of excess heat conduction over radiant energy coupling. EM coupling is inversely proportional to the distance h and inversely to the square root of frequency, but with a lower cut-off frequency at which the coupling becomes constant and does not increase any more with decreasing distance. This can be shown to imply a $1/h$ distance law down to a saturation distance at which the heat conductance becomes the same as if the plates were touching.

REFERENCES

1. Underhill, M. J., "A Physical model of electro-magnetism for a theory of everything," *PIERS Online*, Vol. 7, No. 2, 196–200, 2011; *PIERS Proceedings*, 1665–1669, Marrakesh, Morocco, March 20–23, 2011.
2. Underhill, M. J., "Maxwell's transfer functions," *PIERS Proceedings*, 1766–1770, Kuala Lumpur, Malaysia, March 27–30, 2012.
3. Underhill, M. J., "A local ether lens path integral model of electromagnetic wave reception by wires," *PIERS Proceedings*, 1005–1008, Moscow, Russia, August 19–23, 2012.
4. Underhill, M. J., "Novel analytic EM modelling of antennas and fields," *PIERS Proceedings*, 1771–1775, Kuala Lumpur, Malaysia, March 27–30, 2012
5. Underhill, M. J., "Antenna pattern formation in the near field local ether," *PIERS Proceedings*, 1009–1012, Moscow, Russia, August 19–23, 2012.

6. Underhill, M. J., "Wideband small loop-monopole HF transmitting antenna with implications for Maxwell's equations and the Chu criterion," *PIERS Proceedings*, 764–768, Taipei, March 25–28, 2013.
7. Underhill, M. J., "Coupled electromagnetic wave propagation in space and around surfaces and interfaces," *PIERS Proceedings*, 394–398, Stockholm, Sweden, August 12–15, 2013.
8. Underhill, M. J., "Electromagnetic structures and inertias of particles including the higgs boson," *PIERS Proceedings*, 401–405, Taipei, March 25–28, 2013.
9. Underhill, M. J., "The stability of EM particles and predicted mass ratios," *PIERS Proceedings*, 399–404, Stockholm, Sweden, August 12–15, 2013.
10. Underhill, M. J., "The phase noise spectrum and structure of photons?" *Proc. 16th EFTF*, 1–8, Noordwijk, Netherlands, April 13–16, 2010.

Induced Polarization Method 3D Forward Modeling in Time Domain by Using Laplace Transformation

Wei Deng[1], **Hideki Mizunaga**[1], **and Jingsong Shen**[2]

[1]Department of Earth Resources Engineering, Faculty of Engineering
Kyushu University, Fukuoka 819-0395, Japan
[2]College of Geophysics and Information Engineering
China University of Petroleum (Beijing), Beijing 102200, China

Abstract— The induced polarization (IP) responses of a three-dimensional (3D) body in the earth can be calculated using finite difference method (FDM). But it is difficult to get apparent resistivity of different time in time domain. So firstly a numerical scheme in Laplace domain applying the algorithm of the singularity removal of LOWRY al. (1989) has been developed for the dipole-dipole modeling in a half space. In the program, large sparse matrix is saved and solved using Incomplete Cholesky Conjugate Gradient method (ICCG). The computer program can be used more flexible electrode configuration and the higher accuracy can be achieved in numerical than the conventional computer program based on the direct finite difference method (FDM). Secondly Gaver-Stehfest method is developed to do inverse Laplace transformation to obtain apparent resistivity in time domain. Gaver-Stehfest method is one of the best numerical inversion of Laplace transforms. In this paper, Cole-Cole model is used to simulate the rock electrical properties. The numerical solution using this method in a simple homogeneous medium is given to compare with analytic solution. It proves this program is effective and accurate. Numerical results for some examples are shown the IP responses which is influenced by parameters including chargeability, time constant and frequency dependency based on Cole-Cole model.

The Beam-wave Interaction for Different Modes in Three-gap Coupled Cavity Output Circuit

Jian Cui[1], **Jirun Luo**[2], **Wenkai Liu**[1], **Haiyan Sun**[1], **Zhi Liu**[1], **and Ming Huang**[1]

[1]North China University of Technology, Beijing 100144, China
[2]Institute of Electronics, Chinese Academy of Sciences, Beijing 100190, China

Abstract— Extended-interaction klystron (EIK) is invented to achieve a large power, wide frequency bandwidth and high gain in the millimeter/sub-millimeter wave length range. There is a great difference of the electric field intensity on the gap for different modes in a multi-gap coupled cavity chain. The mechanism of the beam-wave synchronization and coupling of these modes is the key technology for the investigation of modes stablity and modes overlaping.

The analytical expressions of the conversion efficiencies for the electron beam in a multi-gap coupled cavity chain are derived based on kinematics theory. Through calculating the conversion efficiencies of the electron beam for modes 2π, π and $\pi/2$, the mechanism of the beam-wave synchronization and coupling in the three-gap coupled cavity are discussed. The analytic result of 2π mode shows that the high efficiency region appears on the right of the bisector and the maximum efficiency $\eta = 80\%$ is obtained upon the transit angle of the first drift tube $\theta_{12} = 1.26\pi$ and the second drift tube $\theta_{23} = 0.66\pi$. Compared with 2π mode, there are four high efficiency regions with different distribution for π mode. When the efficiency η is over 80%, the corresponding parameter θ_{23} is too small to realize in structure. Therefore, it is practical to choose $\theta_{12} = 0.42\pi$ and $\theta_{23} = 1.32\pi$ in the upper left region with maximum efficiency $\eta = 78.48\%$. Considering the beam-wave interaction on two gaps for $\pi/2$ mode, it can be regarded as a special π mode of double-gap cavity with a longer drift distance. The maximum efficiency is less than that of 2π mode and π mode. In this case, the maximum efficiency η is only 60% with a fixed value of $\theta_{12} + \theta_{23} = 1.47\pi$.

The results show that the maximum efficiency depends on the optimal combination of the lengths of the first tube and second drift tube respectively, which have a great difference for modes 2π, π and $\pi/2$. However, under the same total modulation coefficient, there is no significant difference in the maximum conversion efficiency of these modes.

Efficient Electromagnetic Scattering Simulation Approach of the Rotating Moving Complex Targets

Guoqing Zhu[1], **Chunzhu Dong**[1, 2], **Kainan Qi**[1], **Jing Huang**[1], **and Hongcheng Yin**[1, 2]

[1]Science and Technology on Electromagnetic Scattering Laboratory, Beijing 100854, China
[2]Information Engineering School, Communication University of China, Beijing 100024, China

Abstract— The detection and recognition of moving target is focused by lots of research scholars greatly. However, the algorithms for detection and recognition have to be Testing and verification by a great deal of radar echo data. Efficient electromagnetic scattering simulation becomes an effective and economic method for achieving it. The design of appropriate moving target electromagnetic scattering simulation for computer-generated bots poses serious challenges as they have to satisfy stringent requirements that include computation and execution efficiency. This paper discusses a novel efficient high-frequency electromagnetic scattering simulation approach of the rotating moving complex targets. Based on the wide-adopted high-frequency asymptotic methods, such as Physical Optics (PO), Equivalent Edge Currents (EEC) and Shooting Bouncing Ray (SBR), a novel efficient approach is proposed by employing the adaptable NVIDIA OPTIX ray-tracing engine to solve scattering problems of rotating moving complex targets. High accuracy and efficiency of the hidden-surface-removal (HSR) in PO/EEC and the ray-tracing in SBR are realized at the same time with the state-of-art GPU computation technology. The precise scattering modulation effects of rotating moving target are therefore achieved. Experiments show the effectiveness of the approach.

The Research of Methods Based on Traveling Wave Suppression

Yongfeng Wang[1, 2], **Xiaonan Zhang**[2], **and Kainan Qi**[1, 2]

[1]College of Information Engineering, Communication University of China, China
[2]Science and Technology on Electromagnetic Scattering Laboratory, Beijing 100854, China

Abstract— The theory of traveling-wave scattering and two kinds of methods for restraining the traveling-wave scattering are represented in the paper. The traveling-wave scattering could be declined by shaping and radar absorbing material (RAM). The experimental results prove that inhibition effect of traveling-wave scattering using the above methods is prominent.

A traveling-wave current comes into being, when a long, thin body is illuminated by grazing incident electromagnetic wave. The flowing traveling-wave current is reflected when it encounters the end of the truncation, and the traveling-wave scattering contributes a lot to the radar cross section (RCS) of the target. The traveling-wave scattering can be researched by making use of the existing concepts of antenna theory.

In this paper, a sample of traveling-wave broad was manufactured. Firstly, we restrained the traveling-wave scattering by shaping. The end edge of traveling-wave broad was transformed into saw-tooth or circular arc shape, and measured results proved the shaping method could reduce the RCS of the traveling-wave broad by 10 dB at X-band. Moreover, we restrained the traveling-wave scattering by coating radar absorbing material on the surface of the broad. And the measured results showed that the method of radar absorbing material could reduce the RCS of the traveling-wave broad by more than 10 dB at X-band.

Fan-shaped Patch Element Wideband Terahertz Metamaterial Perfect Absorber

Xiaodong Hao and Weiping Qin
School of Electronic Science and Engineering
Nanjing University of Posts and Telecommunications, Nanjing 210003, China

Abstract— The wide-band absorbance of the absorber made from the well-known metallic dipole patch has been realized by modifying geometrical shape of conventional rectangular bars in single periodic cell. The increase of relative bandwidth of this new absorptive structure with fan-shaped patch can reach and exceed 100% with respect to the centre frequency comparing with conventional dipole patch geometry. The new structure of absorber exciting a new broadband resonant modes results in the bandwidth expanding. The work presented here provides an efficient method to decrease the number of elements and layers of multi-layer metamaterial absorber compared to conventional element structures used previously.

A Novel Tunable Dual-band Microwave Metamaterial Absorber Based on Split Ring Resonant

Jialin Yuan[1], **Shaobin Liu**[1], **Borui Bian**[1], **Xiangkun Kong**[1, 2], **Haifeng Zhang**[1], **Ben Ma**[1], **Zhiwen Mao**[1], **and Beiyin Wang**[1]

[1]Key Laboratory of Radar Imaging and Microwave Photonics
Ministry of Education, College of Electronic and Information Engineering
Nanjing University of Aeronautics and Astronautics, Nanjing 210016, China
[2]Jiangsu Key Laboratory of Meteorological Observation and Information Processing
Nanjing University of Information Science and Technology, Nanjing 210044, China

Abstract— we present the design simulation fabrication and measurement of a tunable metamaterial at microwave frequencies by embedding varactor diodes as an active elements inside metamaterial units. we use a pair of feed lines to control the reverse bias voltage on the diode. The proposed absorber can perform absorption peaks at two resonant frequencies. The lower resonant frequency can be tuned in a wide range by tuning the value of the diodes while the higher resonant frequency keeps unchangeable. In addition, the absorber with the thickness of $\lambda/74$ at the lowest fundamental resonant frequency is ultra-thin. We also find the absorber is insensitive to the polarization of incident waves under both TE and TM polarizations.

A Broadband Terahertz Metamaterial Absorber Based on Square Ring Resonators

Guo-Dong Wang, **Jun-Feng Chen**, **Xi-Wei Hu**, **and Ming-Hai Liu**
State Key Laboratory of Advanced Electromagnetic Engineering and Technology
School of Electrical and Electronic Engineering
Huazhong University of Science and Technology, Wuhan 430074, China

Abstract— A simple design of broadband metamaterial absorber (MA) is numerically investigated at terahertz frequencies in this paper. The unit cell of this absorber consists of two square rings with different geometric dimensions, a dielectric substrate and continuous metal film. A wide frequency band ranging from 2.95 THz to 3.71 THz with absorption rate of over 90% is obtained. Distributions of surface current density on the front and back metallic layers are illustrated. The loss contributions of metallic structures and dielectric substrate are also discussed. Finally, the multi-reflection interference theory is introduced to interpretate the absorption mechanism. The calculated absorption rates coincide well with the simulated results at wide angles of incidence for both transverse electric (TE) and transverse magnetic (TM) waves. The proposed absorber is an ideal candidate as absorbing elements in many applications, such as thermal detectors, terahertz imaging, and stealth technology.

Plasmonic Butterfly-shaped Photocoupling in Charge Sensitive Infrared Phototransistors

Jie Xu, Qinbai Qian, Peng Gou, Le Yang, and Zhenghua An
State Key Laboratory of Surface Physics, Key Laboratory of Micro and Nano Photonic Structures (Ministry of Education), Department of Physics, Fudan University, Shanghai 200433, China

Abstract— Semiconductor has provided mankind a revolutionary microelectronic technology which enters our modern daily life, essentially due to the extraordinary electronic tunablity by biasing or gating [1]. Under photo-excitation, photo-carriers in semiconductors can be efficiently generated, manipulated and collected, which leads to a successful optoelectronic industry, particularly in visible light range. Coming into longer infrared or terahertz wavelength ranges, however, the photocoupling and its combination with pixel-scale electronic biasing becomes nontrivial. The independent design for photocoupling efficiency and electronic biasing becomes correlated and challenging particularly when (sub)wavelength-sized scale is needed [2]. Here we propose a metallic butterfly grating (BSG) which allows efficient photo-coupling and simultaneous gating in subwavelength-scale, and demonstrate its application to a highly sensitive infrared detector called charge sensitive infrared phototransistor (CSIP) [3]. The BSG arrays deposited on top of the photo-active area of CSIPs (wavelength of 14 μm) to induces strong electric fields at the QW located at 100 nm below the crystal surface, while the central strip can be biased to isolate photo-generated holes, thereby realizing $a > 3$ orders longer lifetime and boosting the infrared photo-responsivity to be much higher than conventional infrared detectors. The resonance is different between the incidence radiation of electric field polarization Ex and Ey, which gives a moderate polarization selectivity.

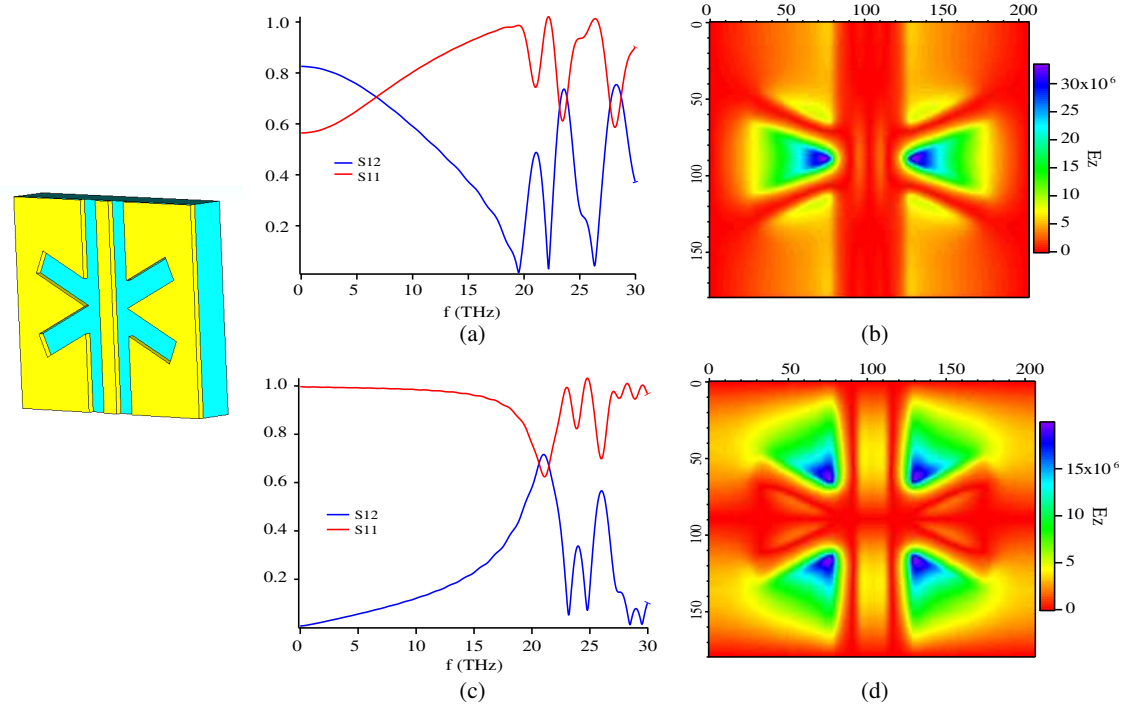

Figure 1: The electric field distribution of direction Z of different polarition by using the FDTD simulation.

REFERENCES

1. Ebbesen, T. W., H. J. Lezec, H. F. Ghaemi, T. Thio, and P. A. Wolff, "Extraordinary optical transmission through sub-wavelength hole arrays," *Nature*, Vol. 391, 667–669, 1998.
2. Schuller, J. A., E. S. Barnard, W. Cai, Y. C. Jun, J. S. White, and M. L. Brongersma, "Plasmonics for extreme light concentration and manipulation," *Nat. Mater.*, Vol. 9, 193–204, 2010.
3. An, Z., J.-C. Chen, T. Ueda, and S. Komiyama, *Applied Physics Letters*, Vol. 86, 172106, 2005.

Plasmonic Antenna Enhanced Spin Rectification

Peng Gou, Fuchun Xi, Jie Xu, Qinbai Qian, Ziyi Zhao, and Zhenghua An
State Key Laboratory of Surface Physics, Key Laboratory of Micro and Nano Photonic Structures (Ministry of Education), Department of Physics, Fudan University, Shanghai 200433, China

Abstract— Spin rectification is an important electric detection tool of spin dynamics, which is one of the significant effects in the system of ferromagnetic thin film. The DC voltage generated by the spin rectification is proportional to the product of microwave electric and magnetic field components. It has potential applications in microwave detector, nondestructive detection, dielectric measurement and so on. However, the signal of the spin rectification is too small for broad applications. So we introduce the plasmonic antenna [1] which can not only enhance the electric field but also the magnetic field to the spintronic devices, that we achieve a high signal amplification.

Here we design a novel Plasmonic Antenna (PA) [2], which could be considered as two back-to-back Split Ring resonators (Figure 1(a)). This PA is like the LC circuit and has its intrinsic resonant frequency which is determined by its dimension. At the resonant frequency, the PA can largely enhance both the electric and magnetic components of electromagnetic wave in its near-field region (Figure 1(b)). This character satisfies the need of spin rectification, and of course, the PA could be designed to match many different demands, which is one of its advantages.

First, we use the FDTD method to simulate the performance of the antenna (Figure 1(b)), we can get a high enhancement of the electric field and the magnetic field, lead to a three orders of magnitude amplification of the spin rectification photovoltage. Then in the experiment, the PA is used to harvest microwave energy to assist the spin rectification to generate an enhanced DC voltage, and the enhancement could reach two orders more (Figure 1(c)). At last, we also find that the photovoltage signal will decrease sharply while the thickness of PET increase.

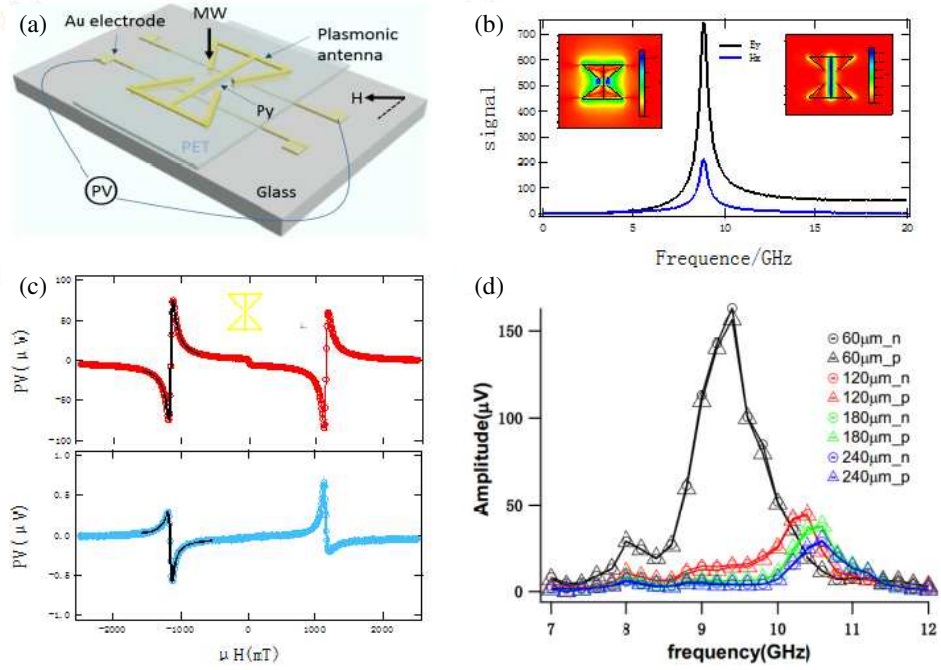

Figure 1: (a) Experimental setup in which the top is antenna and the spintronic layer (Py and Au electrode) is separated by PET spacer. Glass is used as the substrate for whole device. (b) The enhancement of electric and magnetic field in our antenna simulated by FDTD method. (c) The measurement of the microwave photovoltage in experiment, and the red one is measured using an antenna, and the blue one is without antenna. The enhancement could reach two orders. (d) The photovoltage dependence on the thickness of PET spacer.

REFERENCES

1. Grosjean, T., M. Mivelle, F. I. Baida, et al., "Diabolo nanoantenna for enhancing and confining the magnetic optical field," *Nano Letters*, Vol. 11, No. 3, 1009–1013, 2011.
2. Xi, F., L. Zhang, J. Xu, et al., "Electromagnetic field enhancement and its application in spin rectification," *Applied Physics Express*, Vol. 6, No. 10, 103002, 2013.

Session 2A1
Focus Session: Education for Electromagnetics

When 'Light' Dawns upon Them: Mapping the Conceptual Understanding of Electromagnetism Students

S. Y. Buhmann
University of Freiburg, Germany

Abstract— Electromagnetism teaching has recently been facing external and internal challenges: Externally, the place of electromagnetism within the physics core curriculum worldwide faces competition from subjects such as nano-electronics, photonics and computer science. Internally, electromagnetism suffers from its students' perception as difficult and unexciting, creating a need to incorporate topical issues to raise interest and motivation. This leads to the question: What is really essential within the electromagnetism curriculum?

To answer this question, the reported study focusses on the student's conceptual understanding of the core concept of electromagnetism teaching, 'light'. Its relevance has recently been stressed by the United Nation's announcement of an International Year of Light in 2015. First-year MSc and BSc students at Imperial College London have been asked to draw a concept map of 'light'. Such a concept map, as introduced by Novak, is a hierarchical arrangement of physics concepts which linked by labelled lines. The maps have been analysed with respect to their structure, morphology and content and have been compared with an expert concept map as prepared by the instructors of the Year 2 Electromagnetism course at Imperial College. The maps reveal that students at the beginning of their university education have remarkably homogeneous concepts of 'light' which include wave–particle duality as well as common optical phenomena and which are firmly rooted in experiments and normal-life experience. MSc students have a much more abstract concept of 'light', in line with Nespor's chain of mobilisations model for physics learning. In addition, their understanding is more individual, relating to both their learning history and specialisation. This begs the question: Do different physicists really see the same thing when they 'see light'?

REFERENCES

1. Novak, J. D. and B. D. Gowin, *Learning How to Learn*, Cambridge University Press, Cambridge, 1984.
2. Nespor, J., *Knowledge in Motion: Space, Time and Curriculum in Undergraduate Physics and Management*, Routledge Falmer, London, 1994.

Electromagnetic Education: Is There a Magic Bullet to Fix the Crisis?

Raj Mittra
EMC Lab, The Pennsylvania State University, 319 EE East, University Park, PA 16802, USA

Abstract— It is no secret that EM education is facing a crisis of sorts, at least in the *developed* countries. Unfortunately, while there is a lot of talk, and a plethora of ideas for solving the problem, there does not appear to be a magic bullet to 'fix' the crisis.

In this presentation, we will propose two possible approaches to addressing the problems we face in recruiting undergraduates, and in training graduate students at the Ph.D. level. Not unexpectedly, the two recipes we propose are very different from each other, because they are separately tailored for undergraduate and graduate students, respectively. Though they are not magic bullets by any stretch of our imagination, they are nonetheless time-tested ideas that are worth our consideration, as we grasp for ways to mitigate the EM education problem at hand.

We will begin the presentation by describing a program, which has been in existence at the Penn State University for quite some time now, and which is geared toward attracting undergraduate students in science and engineering to "space science" and related fields. The program works with a selected group of undergraduate students and gives them an opportunity to have a hands-on experience in designing 'real' rockets that are launched in space with the help of NASA, which partially sponsors the project at Penn State, as well as at other institutions.

The second strategy, which deals with the issue of training graduate-level students, is more conceptual in nature, and is in contrast to the hands-on experience type of program described above, for the undergraduate students. It teaches the graduate students how to handle the information they gather from the existing literature by examining the material critically, rather than simply accepting this information on blind faith, as they often have a tendency to do, especially when dealing with emerging fields. It also teaches the graduate students how to connect the material which they have learned in their classes to practical real-world problems, of the type they would be expected to tackle when they enter the job market following their graduation.

Flux-cutting and Electromotive Force: How to Motivate Students into Electrodynamics

A. Sihvola
Department of Radio Science and Engineering
Aalto University School of Electrical Engineering, Espoo, Finland

Abstract— Efforts in teaching electromagnetics culminate often in attempts to cover Maxwell equations. A challenging task indeed, it requires several stages of focus on varying aspects and character of electric and magnetic fields. The divergence laws (electric and magnetic), Coulomb/Gauss relations, which talk about static field effects of sources and the flow of fluxes, can be visualized with some success on blackboard or computer screen with lines, arrows, and colors, although vector fields (especially in three dimensions) do not easily transform into flat images. However, trying to transmit the meaning of the dynamic equations (generalized Ampre's law and the Faraday law) require a considerably larger amount of efforts. In this presentation, I try to discuss ways of classroom behavior which I personally feel most efficient and rewarding from the viewpoint of an electromagnetics teacher. Some of the methods that I use have also been described in my earlier articles [1].

REFERENCES

1. Sihvola, A., J. Leppävirta, and H. Kettunen, "Signs, curls, and time variations: Learning to appreciate Farady's law," *Advanced Electromagnetics*, Vol. 1, No. 1, 1–5, 2012.

Alignment of Student Activities, through Exercises, Quizzes, Demonstrations, and Lectures, Applied to Electromagnetic Teaching

B. L. G. Jonsson
KTH Royal Institute of Technology, Stockholm, Sweden

Abstract— My teaching in electromagnetic theory consists of several different parts, aiming in the direction of the constructive alignment (Biggs 2007). The course goals are described as specific active verbs (required at KTH). The underlying assumption in my course design is that the students own work is the basis for his/her learning. Thus my designing of lectures, homework, quizzes and mid-term exams are aiming to direct the students own activities to be in course alignment, while focusing them to the key areas. I will illustrate my interpretation of course alignment by two examples, lectures with quizzes and with the homework/class-room demonstration exam chain.

The classes in electromagnetic theory, begins with 2×45 minute lectures on electromagnetic theory, each such a lecture is interrupted by 2–4 class-room Mazur (1996) inspired quizzes. These quizzes are directly focused on what was just taught in the class, and often requires the student to apply, test, or use the recently demonstrated theory or demonstrated experiment. These quizzes are rather informal. A quiz is stated as a short question, with a (3–4) multiple choice answers. The students are requested to select an answer, through a quick show of hands. This is followed by a subsequent student-to-student discussion for a few additional minutes, ended with a new show of hands. Often but not always it converges to the right answer. An important feedback loop for me is that I circulate among the students to engage in a short discussion with probing questions and encouragements during the work with the quiz. These few-to-one students to teacher interaction often indicate weak and strong points of the students initial understanding of the theory. The quiz ends with a demonstration of a method to arrive to the correct answer.

The above quizzes as a teaching element were introduce in the response of that a high level attention of the students are typically limited to 10–15 minutes (Bligh 1972). What was also clear from the study was that a high level attention can return if the students are engaged in another activity. This other activity tested here is the student-to-student discussion and problem solving during the quizzes. The quizzes are aligned with the course, by focusing on applying the just illustrated electromagnetic ideas and theories.

The homework, demonstrations and exam-chain of alignment begins with using old exams as training material. Apart from the above described lectures, we have class-room demonstrations on problem solving. The problems are both introductory problems, and exam-level questions. The demonstrations apply and exemplify the methods used to solve electromagnetic problems. They illustrate only a few of the recommended tasks per class. There is a large amount of old-exam questions available to the students. They are used as homework problems and training material along the course, and in particular for the two mid-term exams. These 2 h class-room exams on problem solving can yield a small bonus for the student towards the final exam. However they are mainly used to provide feedback both to the lecturer and to the student on the student knowledge and problem solving ability at the present stage of the course.

The electric engineering students taking the course are, at the end of the course, requested to provide feedback. This feedback shows that the quizzes and the experimental demonstrations are the most appreciated activities during the course. For me as a lecturer, the quizzes and mid-term exams provide a direct feedback of their present level knowledge, which enables me to make adjustment during the subsequent teaching in response to the observed level of understanding. This may include additional information focusing on a problem area and when it is required we insert additional classes focused on the students own problem-solving often through a small group student-to-student discussion, with a teacher circulating between several such small groups, to help along the discussion.

One of the key important parts in a successful teaching of electromagnetic theory is that the prerequisite mathematics is well integrated. To further this observation we have across courses discussion between mathematic and electromagnetic lecturers about mutual requirements and observed results of the present knowledge. In preparation for autumn 2014 and an updated electromagnetic course, such mutual exchange between vector algebra and electromagnetic has been emphasized, and we look forward to evaluating the result.

Electrical Engineering Education Systems in Finnish and Chinese Universities

Jiaran Qi
Department of Microwave Engineering
Harbin Institute of Technology, Harbin 150080, China

Abstract— In this presentation, the electrical engineering education systems at the university level in Finland and China are introduced and compared according to the author's personal education experiences in these two countries. The focus of this presentation will cover curriculum design for undergraduate students, eligibility examination (trail lectures to a group of experienced educators as the audience) for new lecturers, lecturer evaluation system, and most importantly, the response and the suggested modifications to the current education systems from undergraduate students. In addition, I will share with the audience several simple yet effective in-class demonstrative experiments/tools, which have been applied in fundamental electromagnetic education for undergraduate students.

Using Popular Science Summaries to Improve Writing Skills in Master Theses

Daniel Sjöberg
Electrical and Information Technology, Lund University, Box 118, Lund 221 00, Sweden

Abstract— The Swedish Higher Education Authority has recently launched a quality assurance system which focusses on the learning outcomes of the educational programmes. In particular, the final theses of the students have been given significant attention, leading to an increased interest in the thesis writing process, and the development of writing skills in general.

In Sweden, it is common that the students, in addition to the technical presentation of the thesis, write a popular summary. Often, this summary is written as the last part of the thesis project. In this presentation, I discuss how this kind of popular summary can be used as a means to develop the students' skills in written communication, by introducing it as an early component in the thesis instead of as the final part.

In a reasonably sized department, many students can be expected to do their master theses projects at more or less the same time. Indeed, the current Swedish trend is to aim for a limited number of presentation dates at faculty level, which makes it possible to synchronize several master the- sis students with respect to a written assignment like a popular summary of each thesis project, and use peer review techniques to let the students improve each others written works. The peer review has the additional benefit of demonstrating to the students the importance of analyzing the target group of the text.

Practices and Explorations on Introducing New Scientific Research Achievements into Electromagnetics Teaching for Undergraduates

Jing Liu, **Jun Zhang**, **and Hanwu Yang**
College of Optoelectronic Science and Engineering
National University of Defense Technology, Changsha 410073, China

Abstract— In accordance with the "Outline of China's National Plan for Medium and Long-term Education Reform and Development (2010–2020)", the raising of education quality is appointed at the heart of task for the present Chinese higher education reform and development. Furthermore, the fostering of young talents or professionals shall command a central position in college work, and no effect shall be spared to produce high-caliber professionals and top-notch innovators with steadfast faith, more integrity, rich knowledge, and superb abilities. Consequently, course teaching, as the most important activity in university, has become the top concerned and hot discussed subject. Actually, since from the beginning of the 20th century, many educational experts and scholars has suggested to introduce the latest scientific research achievement into undergraduate teaching, and then putted it into practice. This paper analyses and sums up these practices coming from some famous Chinese universities, and integrates with our own in the National University of Defense and Technology, during the past nearly 10 years. Based on these, several good ideas and reliable approaches are discussed and concluded, which we think are useful to effectively improve student's research ability and creative thinking in the courses such as electromagnetic, electromagnetic field and wave, and electrodynamics for undergraduates. At last, some special impediments and outstanding problems are addressed with the expectation to have a deeper discussion with international colleagues.

Study of Fraunhofer Diffraction Pattern Using Frequency Image Processing

Jimy Alexander Cortés and Jairo Alberto Mendoza Vargas
Universidad Tecnológica de Pereira, Colombia

Abstract— Any type of energy that travels in a waveform is capable of bending around obstacles, but this is more evident when the obstacle is comparable in size to the energy's wavelength. Light, as a wave, is diffracted and its analysis is a hot topic in engineering due to its applications in scientific instrumentation and the foundation of quantum theory and its particle wavelength properties. This paper introduces an alternative classroom way to present the link between far-field diffraction of an incident plane wave, called Fraunhofer diffraction and the Fourier Transform using image processing techniques in the laboratory and classroom to undergraduate physics and engineering students using Freemat, a free clone of the highly popular scientific numerical analysis software, Matlab. We propose experiments for a single slit and a circular aperture (Airy Disk) which are analyzed using a digital photographic camera as the instrument and three different wavelength (650 nm red, 532 nm green and 405 nm violet) low cost, low power (5 mW) laser pointers as light samples. These experiments offer an alternative laboratory and classroom implementation which allows evaluation of Fraunhofer diffraction with a relative error of less than 3% compared to the ideal two dimensional Fast Fourier Transform and present a cross-relation between two apparently separate topics for physics and engineering students. Even though this kind of didactic strategies are applicable for all countries for teaching Fraunhofer Diffraction, they are more suitable for third world countries where complex and expensive laboratory setups cannot be afforded.

Session 2A2
MS-2.2: Focus Session on Radio-over-Fiber Systems

High-speed Photo-detectors for Millimeter-wave RoF Applications

Toshimasa Umezawa, Atsushi Kanno, and Tetsuya Kawanishi
National Institute of Information and Communications Technology, Koganei, Tokyo 184-8795, Japan

Abstract— A radio-over-fiber-based distributed cell system, which consists of 90-GHz radar cell sites connected to a base station through an optical fiber network, is an attractive candidate for creating a real-time foreign object debris imaging system for railways and airport runways [1]. The 90-GHz band is suitable and can be extended to detect small signals at a high spatial resolution because it has low atmospheric attenuation. A high-speed photodetector with a high sensitivity, a high conversion gain, and a high signal-to-noise ratio (SNR) in the millimeter-wave region is a key device in allimaging systems. In this report, we present the basic properties of a PIN photodiode with respect to the photocurrent linearity, and a high-conversion-gain, high-SNR photoreceiverin the 30–45-GHz range that can becombined with an RF doubler or tripler.

High-linearity PIN photodiodes were designed with an extremely low carrier concentration in the intrinsic depletion layer. The photodiodes, which have a surface-illuminated PIN structure based on an InGaAs absorption layer, were fabricated using a standard semiconductor process that included a mesa dry etching process. The maximum 3-dB cutoff frequency ($f_{3\,\mathrm{dB}}$) of 60 GHz was determined for a small photodetective area of 10 µm in diameter. Because of the largerinternal electric field with a low carrier concentration in the depletion layer, highlinearity in the photocurrent and RF power can be achieved in an optical input power range from −20 dBm to +17 dBm. Introducing passive components such as inductors between the 50-Ω load and the photodiodes as a frequency compensation technique [2], we measured an RF gain of several dB in the millimeter-wave region (30–40 GHz). This result is in good agreement with the simulated RF gain. Moreover, this technique can be applied when developing millimeter-wave, high-SNR photoreceivers integrated with low-noise RF amplifiers of 24 dB in the 24–34-GHz range. A high conversion gain of 1000 V/W and single side band phase noise of −103 dBc/Hz can be achieved in the 30–33-GHz range (Fig. 1). Also, ahigh sensitive photodetector having avalanche multiplication effect have been developed by using InAs quantum dot absorption layer. The avalanche multiplication factor of 12 could be achieved (Fig. 2).

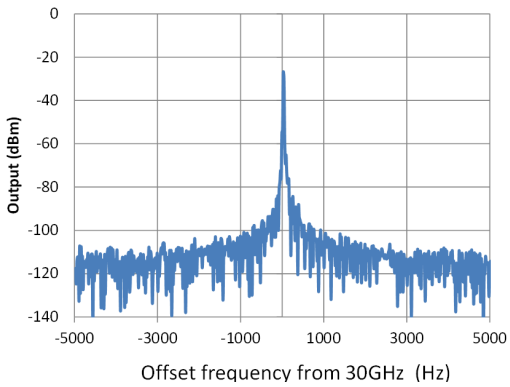

Figure 1: Measured SSB phase noise spectrum.

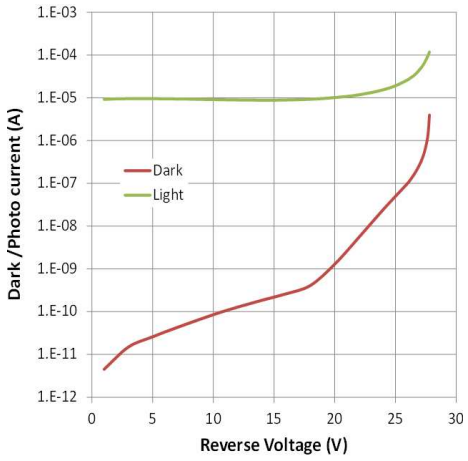

Figure 2: Multiplied photocurrent and dark current.

REFERENCES

1. Kohmura, A., S. Futatsumori, N. Yonemoto, and K. Okada, "Optical fiber connected millimeter-wave radar for FOD detection on runway," *Proceedings of the 10th European Radar Conference*, 41–44, 2013.
2. Umezawa, T., A. Kanno, and T. Kawanish, "Development of photodiodes for millimeter-wave small signal detection," *AP-RACS Tech. Dig.*, 2013.
3. Umezawa, T., K. Akahane, A. Kanno, and T. Kawanishi, "Investigation of 1.5 µm wavelength InAs quantum dots absorption layer for high speed photodetector," *Applied Physics Express*, Vol. 7, 032201, 2014.

The Convergence of Wireless and Radio-over-Fiber Systems

Wai Pang Ng
Northumbria University, UK

Abstract— The talk will focus on how convergence of mobile wireless systems and optical fiber communications can support the growth of the mobile wireless technology. The talk will include recent advances in the field of fiber-wireless convergence such as cloud radio-over-fiber (RoF) and point-to-point RoF system architectures.

The need for more bandwidth is driving the growth of femtocells within the mobile networks, in 4G and possibly in 5G networks. Optical fiber technology (radio-over-fiber) can provide a reliable and high speed channel between the macrocells and femtocells. Therefore the convergence of mobile wireless and optical fibre will be essential to accommodate the growth of bandwidth requirements, thus enabling a high speed channel at the access network.

In-home Fiber Wireless Networks Incorporating Optical Microwave Beam Steering: System Architecture and Integrated Device

Z. Cao, **A. M. J. Koonen**, **Y. Jiao**, **Q. Wang**, **H. P. A. van den Boom**, **and E. Tangdiongga**
COBRA Research Institute, Eindhoven University of Technology, The Netherlands

Abstract— The current explosion of communication traffic volume is driven by an insatiable appetite for high speed internet connectivity and video-based content delivery to wireless and mobile terminal users, especially for in-home scenarios. A lot of research has been carried out to exploit wireless capacity. In the spatial domain, spatial multiplexing, spatial isolation (pico/femto-cells), and spatial filtering (beam-steering) attract lots of attention due to their abilities to boost capacity immensely. Spatial isolation requires many wireless access points and its successful deployment depends on building structures. These features limit its applications. Unlike spatial multiplexing which requires complicated digital signal processing, beam-steering (BS) directs signals to the desired user with minimum interference. Phased array antennas (PAAs) are widely considered as the best candidate for microwave beam-steering due to their fast steering and compactness [1]. The operational bandwidth of a conventional PAA is limited. Specifically, a severe limitation is often caused by the use of phase shifters to scan the beam, which results in beam deformations ("squint") in the measured antenna pattern. The use of true time delay (TTD) technology potentially eliminates such bandwidth restriction, as it provides a theoretically frequency-independent time delay on each channel of the array [2]. Standard TTD technology typically consists of digitally-switched transmission line sections wherein weight, loss and cost increase rapidly with increased operational frequency and/or phase tuning resolution. These issues can be avoided by adopting optical TTD microwave beam steering (OTTD-MBS). However, most OTTD-MBS schemes are investigated mainly for radars rather than wireless broadband data communications. No experimental results reveal the system performance for the latter applications. Recently, we have proposed and investigated radio-over-fiber systems incorporating optical true-time-delay microwave beam steering [3, 4]. However, the employed optical tunable delay lines (OTDLs) based on bulk-optics components limit their further applications [3, 4]. Obviously an integrated solution is the key to future successfull implementation. To pave the way for its final applications, a compact and fabrication-tolerant OTDL based on a silicon-on-insulator (SOI) generic platform is proposed and characterized. Such OTDL is based on a re-circulating symmetric arrayed waveguide grating loop (AWG-loop) and is passively controlled by tuning the wavelength of the input optical signal. In this talk, we will review our current research on both advanced system architecture for in-home fiber wireless networks with optical microwave beam steering and the novel realization of integrated optical tunable delay lines.

REFERENCES

1. Mailloux, R., *Phased Arrya Antenna Handbook*, Artech House, 2005.
2. Vidal, B., et al., *IEEE Microw. Wireless Compon. Lett.*, Vol. 13, 238–240, 2003.
3. Cao, Z., et al., *Photon. Technol. Lett.*, Vol. 25, 1932–1935, 2013.
4. Cao, Z., et al., *ECOC2013*, Tu.1.F.2, 2013.

High Capacity Radio over Fiber System at the 75–110 GHz Band

Lei Deng[1, 2], **Songnian Fu**[1, 2], **Ming Tang**[1, 2], **Deming Liu**[1, 2], **and Ping Shum**[3]

[1]National Eng. Laboratory for Next Generation Internet Access System, Wuhan 430074, China
[2]School of Optical and Electronic Information
Huazhong University of Science and Technology, Wuhan 430074, China
[3]School of Electrical and Electronic Engineering
Nanyang Technological University, Singapore 637553, Singapore

Abstract— Recently, W-band (75–110 GHz) signal over fiber technique has attracted more and more attention due to its larger available transmission, and wider wireless coverage. In this paper, we focus on realizing high capacity radio over fiber system at the W-band by using photonic heterodyne up-conversion technique. In our experiment, a net bit rate of 42.13 Gb/s 16QAM-OFDM signal at 86 GHz RF carrier frequency is transmitted over fiber and wireless hybrid channel by using optical I/Q modulator, optical comb generator, and optical heterodyne beating based W-band signal generator. Results show that the system performance is significantly deteriorated by the beating noise, and the channel nonlinearity. To address these issues, efficient phase noise compensation algorithm and improve channel estimation algorithm are proposed and designed to successfully transmit the 42.13 Gbit/s 16QAM-OFDM signals at 86 GHz over 0.6 m air distance. Moreover, to resolve the high system requirement about linear amplifier and modulator due to the high PARP of OFDM signal, and to avoid the deterioration influence of the laser phase noise, a nonlinearity and phase noise tolerant OFDM W-band signal over fiber system based on optical phase modulation has been proposed. In this way, constant envelope OFDM W-band wireless signal with 0 dB PAPR is obtained to suppress the nonlinear impairments. In addition, the phase noises of the beating lasers appear as additive terms to the desired signal, and could be easily filtered out without complex phase noise estimation and compensation algorithms. In our experiment, 8 Gb/s 16QAM -OFDM signal is successfully transmitted over 2.3 m air distance and 22.8 km single mode fiber. The proposed systems have potential application in future fiber-wireless system which can obtain high speed, high bandwidth and large transmission distance.

Wireless Backhaul Challenge: Optical-wireless Network Integration as a Solution

Thas Ampalavanapillai Nirmalathas, Chathurika Ranaweera, Yizhuo Yang, Elaine Wong, and Christina Lim
Department of Electrical and Electronic Engineering, Melbourne School of Engineering
The University of Melbourne, Parkville VIC 3010, Australia

Abstract— As the demand for mobile data explodes, the mobile networks need to build capacity and coverage to cope with this. Small cells are considered as a key part of the network operator strategy to build capacity. Small cells are faced with a backhaul challenge in providing high capacity communication network to deal with the projected traffic growth. In this paper, we will examine the optical-wireless network integration as an effective solution to this challenge and will consider a range of issues in relation to such converged optical-wireless network architecture. Optical networks combined with special techniques for trasnporting radio-frequency signals can address the capacity requirements of future wireless networks while offering cost-effectiveness and improved energy efficiency. This paper will also highlight the latest research into energy efficiency of optical transport of wireless signals and optimisation of fiber-fed wireless network deployment including physical as well as protocol layer integration issues.

All-optical Frequency Conversion Techniques for Radio-over-fiber Applications

Jong-In Song
School of Information and Communications, GIST
261 Cheomdan-gwagiro, Buk-gu, Gwangju 500-712, Korea

Abstract— Radio-over-fiber (RoF) technology is attractive for future wireless access network to support increasing demands for broadband wireless services including high-speed wireless local area networks, telemedicine, and digital multimedia broadcasting since it can transmit broadband wireless signals having high radio-frequency (RF) carrier frequencies over an optical fiber having ultra-low loss and ultra-wide bandwidth characteristics.

The RoF system utilizes microwave photonics technology that has advantages including ultra-low loss, ultra-wide bandwidth, and compatibility with other optical networks. All-optical frequency up-conversion technique, which generates an optical radio frequency (RF) signal by mixing an optical intermediate frequency (IF) signal with an optical local oscillator (LO) signal, is one of the key technologies for RoF systems. All-optical frequency up-conversion techniques offer large bandwidth and compatibility with wavelength division multiplexing (WDM) technique, which is suitable for broadband wireless systems with high carrier frequencies.

In this paper, various frequency conversion techniques including electrical, photonic, and all-optical frequency conversion schemes are compared with an emphasis on all-optical frequency conversion schemes utilizing the nonlinearities including cross gain modulation (XGM), cross phase modulation (XPM), four wave mixing (FWM), cross polarization modulation (XPolM), coherent population oscillation (CPO) effects in a semiconductor optical amplifiers (SOA), semiconductor optical amplifier Mach-Zehnder interferometer (SOA-MZI), and nonlinear SOA. All-optical frequency conversion schemes for generation of optical single sideband signals for transmission over a single mode fiber (SMF) in order to overcome power fading problem associated with the fiber chromatic dispersion will also be addressed.

Multi-dimensional Digital Predistortion for Multi-band Radio-over-fiber Systems

Jianqiang Li, **Hao Chen**, **Yinqing Pei**, **Chunjing Yin**, **and Kun Xu**
State Key Laboratory of Information Photonics and Optical Communications
Beijing University of Posts and Telecommunications, Beijing, China

Abstract— The global mobile data traffic is undergoing explosive growth. However, the average revenue per user (ARPU) for mobile operators is not growing at the same rate, since the traditional radio access network (RAN) architecture suffers from severe problems in service quality, power consumption, and cost efficiency. Therefore, an evolved network concept C-RAN has been envisioned by China Mobile and well recognized by the wireless communications community. As for the network architecture, the C-RAN concept replies on distributed antenna systems (DAS) where the traditional base transceiver station (BTS) processing functions are centralized in a central unit (CU) and thereby the remote antenna units (RAUs) are much simplified. The so-called fronthaul connections between CU and RAUs are commonly enabled by optical fiber links to meet the requirements in bandwidth, distance and delay. Radio-over-fiber (ROF) links can serve as a promising option to make fronthaul connections between CU and RAUs.

It has been realized that the legacy and emerging wireless communication standards will coexist for a long time to support diverse user terminals and demands. At the same time, different standards are working at different discrete allocated frequency bands. Therefore, most of the major mobile operators worldwide are facing a multi-band multi-standard environment in practical RAN deployment. In this respect, the C-RAN framework suggests a unified network solution for smooth evolution and good compatibility, which prevents deploying multiple wireless communication systems over separate network infrastructures. Under the framework of C-RAN, it is necessary to investigate multi-band multi-standard ROF systems for future RAN.

However, ROF systems suffer from the inherent nonlinearities from either directly-modulated lasers or external optical modulators. Unlike single-band ROF systems, the modulation nonlinearities in multi-band ROF systems can result in both in-band and cross-band nonlinear distortions, which ultimately limit the link performance and radio-frequency (RF) power transmitting efficiency. In order to address this issue, we have recently developed and experimentally investigated a series of multi-dimensional digital predistortion (DPD) techniques based different models for linearizing multi-band RoF systems. This talk will specify these techniques, review the recent experimental results, discuss practical implementation issues, and raise several open questions.

Fiber-wireless System Techniques for Next-Gen Multi-Gb/s Wireless Applications

Anthony Ng'oma[1], **Hejie Yang**[1], **and Po-Tsung (Boris) Shih**[2]

[1]Science and Technology Division, Corning Incorporated, Corning, NY 14831, USA
[2]Corning Taiwan Research Center, Hsinchu, Taiwan

Abstract— Wireless data continues to grow exponentially — driven by the high proliferation of smart mobile devices and the popularity of video-centric mobile applications. Because of limitations in the capabilities and performance of current wireless communication systems the gap between demand and supply of wireless bandwidth is widening. The industry is working on multiple technologies to meet the growing demand for wireless bandwidth — including 4G Cellular, Next-Gen Wi-Fi, and mm-wave-based systems, including 60 GHz.

Since fundamentally, wireless communication uses a shared medium, future high data rate wireless systems will rely on a few fundamental techniques to achieve the needed growth in wireless data capacity. These include the use of small wireless cells, increased spectral efficiency through more complex modulation formats (including MIMO), and the use of mm-wave frequencies, which offer large amounts of unused spectrum.

The aforementioned techniques come with their own technical challenges. For instance, the utilization of large numbers of smaller cells requires extensive backhaul infrastructure networks, which increases both deployment and operation costs, in addition to more complex system management.

Fiber-based infrastructure solutions can help alleviate many of the technical and deployment challenges faced by current and future wireless systems. To begin with, fiber offers enormously large bandwidth, which could be exploited to significantly increase the performance of wireless systems or to simplify their deployment and management complexity. The large fiber bandwidth can be used to integrate distribution systems for both analog and digital signals. Furthermore, analog Radio-over-Fiber transmission can be utilized as a powerful protocol-agnostic platform for distributing cost-effectively signals of multiple wireless standards.

This paper investigates a wide-range of technical challenges and proposes solutions for RoF-based distribution systems capable of supporting advanced wireless technologies including MIMO and mm-waves. We experimentally demonstrate the efficacy of simple and practical RoF system techniques and methods for realizing ultra high-capacity systems supporting > 70 Gb/s wireless data transmission.

Photonic-assisted Ultrafast THz Wireless Access

Xianbin Yu[1], **Ying Chen**[1, 2], **Michael Galili**[1], **Toshio Morioka**[1], **Peter Uhd Jepsen**[1], **and Leif K. Oxenløwe**[1]

[1]DTU Fotonik, Department of Photonics Engineering
Technical University of Denmark, Kgs. Lyngby DK-2800, Denmark
[2]Department of Information Science & Electronic Engineering
Zhejiang University, Hangzhou, China.

Abstract— THz technology has been considered feasible for ultrafast wireless data communication, to meet the increasing demand on next-generation fast wireless access, e.g., huge data file transferring and fast mobile data stream access. This talk reviews recent progress in high-speed THz wireless communications enabled by photonics technologies, as well as the needed technical breakthroughs for achieving ultrafast data rates beyond 100 Gbit/s.

Session 2A3
MS-1.5: Organic and Hybrid Solar Cells 1

Organic and Hybrid-perovskite Photovoltaic Cells with High Performance

Yang Yang[1, 2]

[1]Department of Materials Science and Engineering, University of California
Los Angeles, California 90095, USA
[2]California NanoSystems Institute, University of California
Los Angeles, California 90095, USA

Abstract— Solution-processed organic solar cells and organic-inorganic hybrid solar cells are among the most promising photovoltaic technologies for ultimatelow-costmanufacture. In this presentation, I will briefly report our recent works: small molecule, polymer and perovskite photovoltaics.

(1) Small molecule OPV. Small molecule organic semiconductors have attracted increasing interest due to the advantages of its well-defined structures, facile synthesis and purification, and generally high charge carrier mobility. In the first part of my presentation, I will report high performance single junction and double junction OPV device based on DOR3T-BDTT. Using the solution spin-coating fabrication process, the certified power conversion efficiency (PCE) of 8.02% from single junction device was obtained. A homo-tandem solar cell was constructed with a novel solution processed interlayer (or tunnel junction), demonstrating an unprecedented PCE of 10.1%.

(2) The second part of my presentation is on polymer solar cell. Recently, we demonstrate two families of NIR conjugated polymers (Eg $\sim$ 1.4 eV) specifically suitable for tandem structure. One is based on alternating benzodithiophene/diketopyrrolopyrrole units and the other is based on alternating dithienopyran/diflourobenzothiadiazole units. In the single-layer devices, power conversion efficiencies (PCE) of 7 $\sim$ 8% were achieved. When the polymers were applied to tandem solar cells, we demonstrated PCE of 10.6% (under the AM 1.5G solar condition). Furthermore, the tandem devices show excellent stability due both to the intrinsic stability of the polymer and the advanced device structure.

(3) The third part of my presentation is on the organic-inorganic hybrid perovskite based solar cells, particularly $CH_3NH_3PbX_3$ (X = Cl, Br, I). We demonstrate a novel low temperature vapor assisted solution process to fabricate organic-inorganic hybrid perovskite films (e.g., $CH_3NH_3PbX_3$, X = Cl, Br, I) and the corresponding photovoltaic devices. The perovskite films derived from this approach exhibit superior film quality, with full surface coverage, uniform grain structure with grain size up to micron scale, and a complete precursor transformation. Facilitated by the excellent film quality, the $CH_3NH_3PbI_3$ materials enable a PCE over 12% in a planar architecture. We have further improved device engineering, and our latest perovksite solar cell has reached the best efficiencies in the range of 15–19%[1]. We believe by further research in film formation, better device architecture, and interface engineering will lead to continuous improvement of perovskite solar cells.

[1]Un-certified results.

Light Harvesting and Charge Separation with Semiconductor Quantum Dots

Andrey L. Rogach
Department of Physics and Materials Science & Centre for Functional Photonics
City University of Hong Kong, Tat Chee Avenue, Kowloon, Hong Kong S.A.R., China

Abstract— Semiconductor nanocrystal quantum dots of different sizes, shapes and compositions can nowadays be synthesized in large quantities by inexpensive and versatile solution based approaches. They are attractive as building blocks of different functional nanostructures. We provide an overview of semiconductor nanocrystals of different sizes and shapes synthesized in our labs and demonstrate several approaches for nanocrystal's assembly. Advanced optical spectroscopy provides important insights into fundamental photophysical properties of semiconductor quantum dots. Different application aspects of functional structures based on semiconductor nanocrystals related to the light harvesting, energy transfer and charge separation are discussed.

Dynamic Donor: Acceptor and Electrode Interfaces in Organic Bulk-heterojunction and Perovskite Solar Cells under Device-operating Condition

Bin Hu[1, 2]

[1]Huazhong University of Science and Technology, Wuhan 430074, China
[2]University of Tennessee, Knoxville, TN 37996, USA

Abstract— Organic bulk-heterojunction and perovskite solar cells have shown surprisingly high photovoltaic actions with the efficiencies reaching 15% from simple device designs. These quick advancements bring a fundamental demand to the field: revealing deeper internal photovoltaic processes at dynamic donor : acceptor (D : A) and electrode interfaces under-device-operating condition. At this moment, the deeper internal photovoltaic processes at the dynamic D : A and electrode interfaces still remain largely un-revealed, forming a great challenge to further advance the field of organic solar cells. To respond to this great challenge, we have investigated the dynamic D : A and *electrode interfaces* under device-operating condition by using our previously defined unique experimental methods: magnetic field effects of photocurrent and photoinduced capacitance. Our fundamental studies have focused on two timely-important issues: (i) *controlling the electron-hole binding energies at D : A interface through polarization and energy parameters and* (ii) *enhancing the charge collection at electrode interface through dielectric effects* in both bulk-heterojunction and perovskite solar cells. This presentation will discuss the critical understanding and effective knowledge base on controlling the useful and non-useful photovoltaic processes at both D : A and electrode interfaces towards further photovoltaic advancements in bulk-heterojunction and perovskite solar cells.

Film Morphology Control for High Efficiency Perovskite Solar Cells

Liyuan Han, Xudong Yang, Chuanjiang Qin, Yongzhen Wu, and Jian Liu
Photovoltaic Materials Unit, National Institute for Materials Science
Sengen 1-2-1, Tsukuba 305-0047, Japan

Abstract— Organo lead trihalide perovskites ($CH_3NH_3PbX_3$, X = I, Br or Cl) as light absorption materials have attracted great attention recently in photovoltaic research. By virtue of their high absorptivity and long carrier diffusion length, the power conversion efficiency (PCE) was rapidly increased from 3.8% to above 15% within the short five years. In this presentation, I will report some our latest researches in this field.

Firstly, uniform, highly crystalline perovskite film is important for sequential deposition processed perovskite solar cells. We develop a new method to enable an efficient deposition of perovskite film with enhanced conversion rate and surface morphology. By this approach, the energy conversion efficiency of mesoporous-free perovskite solar cells was twice as high as that of using traditional method.

Secondly, the hole-blocking layer is required to prevent holes formed in the perovskie or HTL layer from reaching the FTO electrode, which would otherwise short-circuit the cell. Optimization of the blocking layer is a key factor for improving the device performance of perovskite solar cells. We systematically examined the different blocking layer fabricated by three different methods. The surface morphology and film resistance shows that atomic layer deposition (ALD) based TiO_2 compact layer contains much lower density of nano-scaled pinholes with respect to spin-coating and spray pyrolysis ones. The ALD-TiO_2 layer acts as an efficient hole-blocking layer in perovskite solar cells, which offers a large shunt resistance and enables a high power conversion efficiency of 12.56%.

REFERENCES

1. Park, N., *J. Phys. Chem. Lett.*, Vol. 4, 2423–2429, 2013.
2. Kojima, A., K. Teshima, Y. Shirai, and T. Miyasaka, *J. Am. Chem. Soc.*, Vol. 131, 6050–6051, 2009.
3. Lee, M. M., J. Teuscher, T. Miyasaka, T. N. Murakami, and H. J. Snaith, *Science*, Vol. 338, 643–647, 2012.

Nickel Oxide Electrode Interlayer in $CH_3NH_3PbI_3$ Perovskite/PCBM Planar-heterojunction Hybrid Solar Cells

Jun-Yuan Jeng, Kuo-Cheng Chen, Tsung-Yu Chiang, Tzung-Fang Guo, and Peter Chen
Department of Photonics, Advanced Optoelectronic Technology Center
Research Center for Energy Technology and Strategy, Cheng Kung University
No. 1, Ta-Hsueh Rd., Tainan 701, Taiwan

Abstract— The work successfully presented the application of nickel oxide as the p-contact to fabricate the decent perovskite-based photovoltaics [1, 2] The p-contact nickel oxide exhibits several optical, electrical, and chemical advantages being the potential electrode-interlayer. A respectful solar to electrical PCE of 7.8% with a $V_{OC} = 0.92\,\mathrm{V}$, a $J_{SC} = 12.43\,\mathrm{mA/cm^2}$, and a FF = 0.68 has been achieved with the device configuration of the glass/ITO/NiO_x/$CH_3NH_3PbI_3$ perovskite/PCBM/BCP/Al structure under standard 1 sun AM 1.5G simulated solar irradiation, as shown in Fig. 1 [1]. In addition, the device composed of the mesoscopic nanocrystalline NiO/peroskite/PCBM configuration exhibits a $V_{OC} = 1.04\,\mathrm{V}$, a $J_{SC} = 13.24\,\mathrm{mA/cm^2}$, and a FF = 0.69, corresponding to a higher magnitude of PCE to 9.51% [2]. To the best of our knowledge, this is the highest magnitude of PCE for perovskite-based solar cells applying p-contact metal oxide electrode interlayer. NiO electrode interlayer is a p-type semiconductor of high work function of 5.4 eV, which is close to the valence band edge level of $CH_3NH_3PbI_3$ perovskite (5.4 eV). The alignment of energy level minimizes the interfacial energy losses for the hole transfer and optimizes the photovoltage output of device. Additionally, the higher magnitude of J_{SC} and PCE also results from the better surface coverage (93%) of $CH_3NH_3PbI_3$ perovskite film on the glass/ITO/NiO_x substrate. The efficient hole transfer at perovskite/NiO heterojunction was verified by photo-induced absorption spectroscopy, showing a broad spectral feature above 800 nm, the long-lived charge-separation state of NiO^+/P^- [2]. The success of this new style device configuration of p-type metal oxide material has the advantages of providing robust perovskite-based thin film solar cells in future. Our findings reveal the design principle for enhancing the photovoltaic performance of $CH_3NH_3PbI_3$ perovskite/PCBM hybrid PHJ [3, 4] solar cells through the judicious selection of the metal oxide electrode interlayer.

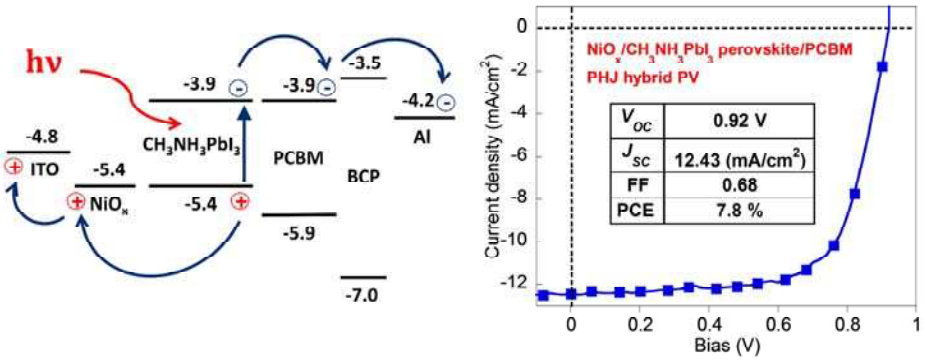

Figure 1: The energy diagram and J-V curves of $CH_3NH_3PbI_3$ perovskite-based solar cell applying inorganic p-type nickel oxide (NiO_x) as the electrode interlayer.

REFERENCES

1. Jeng, J.-Y., K.-C. Chen, T.-Y. Chiang, P.-Y. Lin, T.-D. Tsai, Y.-C. Chang, T.-F. Guo, and P. Chen, "Nickel oxide electrode interlayer in $CH_3NH_3PbI_3$ perovskite/PCBM planar-heterojunction hybrid solar cells," *Adv. Mater.*, 2014, in press.
2. Wang, K.-C., J.-Y. Jeng, P.-S. Shen, Y.-C. Chang, E. W.-G. Diau, C.-H. Tsai, T. Y. Chao, H.-C. Hsu, P.-Y. Lin, P. Chen, T.-F. Guo, and T.-C. Wen, "p-type mesoscopic nickel oxide/organometallic perovskite heterojunction solar sells," 2014, under the review.
3. Jeng, J.-Y., Y.-F. Chiang, M.-H. Lee, S.-R. Peng, T.-F. Guo, P. Chen, and T.-C. Wen, "$CH_3NH_3PbI_3$ perovskite/fullerene planar-heterojunction hybrid solar cells," *Adv. Mater.*, Vol. 25, 3727, 2013.

4. Chiang, Y.-F., J.-Y. Jeng, M.-H. Lee, S.-R. Peng, P. Chen, T.-F. Guo, T.-C. Wen, Y.-J. Hsu, and C.-M. Hsu, "High voltage and efficient bilayer heterojunction solar cells based on organic-inorganic hybrid perovskite absorber with low-cost flexible substrate," *Phys. Chem. Chem. Phys.*, Vol. 16, 6033, 2014.

Organic and Hybrid Photovoltaics Based on Conjugated Polymers and Organo-lead Halides

Chih-Ping Chen
Department of Materials Engineering, Ming Chi University of Technology
84 Gunjuan Road, Taishan, New Taipei City 243, Taiwan

Abstract— We will report the indacenodithiophene (**IDT**) based alternating conjugated polymers and the organo-lead halides as the donor materials for organic photovoltaic (OPV) application, repectively. We investigate the molecular structures, device architectures, morphological, and performance of OPV based on these blended films. The constructed OPV devices exhibit power conversion efficiency over 7% under AM 1.5G simulated solar light (100 mW cm^{-2}) and are highly durable under accelerated condition.

ACKNOWLEDGMENT

We thank the National Science Council (NSC101-2113-M-131-001-MY2) of Taiwan for financial support.

REFERENCES

1. Chen, C.-P., Y.-C. Chen, and C.-Y. Yu, *Polym. Chem.*, Vol. 4, 1161, 2013.
2. Chen, C.-P. and H. L. Hsu, *Macromol. Rapid Commun.*, Vol. 34, 1623, 2013.
3. Chen, C.-P., Y.-D. Chen, and S.-C. Chuang, *Adv. Mater.*, Vol. 23, 3859, 2011.
4. Chen, C.-P., Y.-W. Lin, J.-C. Horng, and S.-C. Chuang, *Adv. Energy Mater.*, Vol. 1, 776, 2011.

P-type Solar Cells Based on Organometal Halide Perovskites Sensitized Mesoporous NiO Photocathodes

Xianwei Zeng and Wei Chen

Michael Grätzel Centre for Mesoscopic Solar Cells, Wuhan National Laboratory for Optoelectronics
College of Optoelectronic Science and Engineering, Huazhong University of Science and Technology
Wuhan 430074, China

Abstract— To significantly improve the performance of p-type half cells is prerequisite for the realization of highly efficient pn tandem cells in the future. Since the seminal work of Miyasaka et al. in 2009, organometal halide perovskites have attracted great attention as a new class of light absorbers due to their high molar extinction coefficient and specific ambipolar charge transfer property. Herein, for the first time we report highly efficient p-type solar cells based on organometal halide perovskites ($CH_3NH_3PbBr_3$, $CH_3NH_3PbI_3$ and $CH_3NH_3PbI_2Cl$) sensitized mesoporous NiO photocathodes, which are deposited on top of a about 50 nm thick NiO compact layer. It is particularly necessary to point out that the compact NiO blocking layer deposited by spray pyrolysis holds the key on the "p-type" current flow in the perovskites sensitized NiO solar cells. Among those three different sensitizers, $CH_3NH_3PbI_2Cl$ sensitized device shows remarkably higher efficiency than the other two sensitizers, which is mainly due to its higher hole injection efficiency at the perovskite/NiO interface and the higher hole collection efficiency through the mesoporous NiO network. Time-resolved photoluminescence spectroscopy and transient photocurrent/photovoltage decaymeasurements have been carried out to characterize the kinetics of the related interfacial processes. A close to 100% internal photon to current conversion efficiency has been approved in $CH_3NH_3PbI_2Cl$ sensitized NiO solar cell, despite the light harvesting loss caused by glass substrate and NiO film. Additionally, the compatibility with the iodine based electrolyte of these perovskites sensitized p-type solar cells makes them very promising to combine with efficient n-type dye-sensitized solar cells, to construct efficient pn tandem cells.

High-performance Planar Heterojunction Perovskite Solar Cells: Preserving Long Charge Carrier Diffusion Lengths and Interfacial Engineering

Yizheng Jin[1] and Baoquan Sun[2]

[1]State Key Laboratory of Silicon Materials, Department of Materials Science and Engineering
Zhejiang University, Hangzhou 310027, China
[2]Jiangsu Key Laboratory for Carbon-based Functional Materials & Devices
Institute of Functional Nano & Soft Materials (FUNSOM), Soochow University
199 Ren'ai Road, Suzhou 215123, China

Abstract— Methylammonium lead halide perovskites are promising absorbers for solution-processed thin film photovoltaics owning to the unique combination of good optical absorption characteristics and long charge carrier diffusion lengths. Here we show that the charge carrier diffusion lengths of two classes of perovskites, $CH_3NH_3PbI_{3-x}Cl_x$ and $CH_3NH_3PbI_3$, are both highly sensitive to film processing conditions and optimal processing procedures are critical to preserving the long carrier diffusion lengths of the perovskite films. This understanding, together with the improved cathode interface by integrating ZnO nanocrystal electron-transporting interlayers, lead to the successful fabrication of highly efficient, stable and reproducible planar heterojunction $CH_3NH_3PbI_{3-x}Cl_x$ solar cells with a remarkably high fill factor of 0.80 and impressive power-conversion efficiencies (PCEs) up to 15.9%. A 1-square-centimeter device yielding a PCE of 12.3% has been realized, demonstrating that this simple planar structure is promising for large-area devices.

Interface Engineering and Morphology Control for High Performance Perovskite/Fullerene Planar Heterojunction Solar Cells

Hin-Lap Yip, Qifan Xue, Chen Sun, Zhicheng Hu, Fei Huang, and Yong Cao
State Key Laboratory of Luminescent Materials and Device
South China University of Technology, Guangzhou, China

Abstract— Solar cells based on organometal trihalide perovskites (e.g., $CH_3NH_3PbI_3$) as light absorbers are emerging as a low-cost and high performance photovoltaic technology that may fulfil the requirements for large-scale deployment of solar energy. Over the past few years, significant progress was made in pervoskite solar cells with power conversion efficiencies (PCE) shot up from 3% to 18%. Recent studies revealed that organometal trihalide pervoskites exhibit several desired properties for photovoltaic applications including facile tunable bandgaps, high absorption coefficient, long carrier-diffusion lengths, high ambipolar mobilities and low exciton binding energy, making them a very appealing class of material for new generation photovoltaic technology.

In this talk we will present two strategies to improve the performance of perovskite/fullerene planar heterojunction solar cells. First, the growth kinetic of the perovskite films was tuned by introducing chemically-tailored processing additives. Depending on the choice of the additives, the crystallinity and coverage of the perovskite films can either be enhanced or suppressed and we found that the solar cell performance was strongly depending on the morphology of the perovskite films. Second, novel interfacial materials were introduced to improve the contact between the fullerene electron transport layer and the metal cathode interface, resulted in Ohmic contact with reduced interfacial resistance and a significant improvement on the fill factor. Combining these two strategies high performance perovskite solar cells with over 15% PCE were achieved.

Room-temperature Near-infrared/Wide-band Pervoskite Whispering-gallery Planar Nanolasers

Qing Zhang[1], **Son Tung Ha**[1], **Xinfeng Liu**[1, 2], **Tze Chien Sum**[1, 2, 3], **and Qihua Xiong**[1, 3, 4]

[1]Division of Physics and Applied Physics, School of Physical and Mathematical Sciences
Nanyang Technological University, Singapore 637371, Singapore
[2]Energy Research Institute @ NTU (ERI@N)
Nanyang Technological University, 50 Nanyang Drive, Singapore 637553, Singapore
[3]Singapore-Berkeley Research Initiative for Sustainable Energy, 1 Create Way, Singapore 138602, Singapore
[4]NOVITAS, Nanoelectronics Centre of Excellence, School of Electrical and Electronic Engineering
Nanyang Technological University, Singapore 639798, Singapore

Abstract— Near-infrared (NIR) solid-state micro/nanolasers are important building blocks for true integration of optoelectronic circuitry. Although significant progress has been made in III-V nanowire lasers with achieving NIR lasing at the room-temperature, challenges remain including low quantum efficiencies and high Auger losses. Importantly, the obstacles towards integrating 1-D nanowires on the planar ubiquitous Si platform need to be effectively tackled. Here we demonstrate a new family of planar room-temperature NIR nanolasers based on organic-inorganic perovskite $CH_3NH_3PbI_2X$ (X = I, Br, Cl) nanoplatelets. Well-defined polygonal crystalline perovskite nanoplatelets are grown on mica substrates by chemical vapour methods, which naturally forms high-Q whispering-gallery-mode cavity. Their large exciton binding energies, long diffusion lengths and naturally formed high-quality planar whispering-gallery mode cavities ensure adequate gain and efficient optical feedback for low-threshold optically pumped in-plane lasing. Further, we synthesize pervoskite nanoplateletes with varied bandgap from ultra-violet to near-infrared and demonstrate wide-band tunable lasing based on the structures. We show that these remarkable wavelength tunable whispering-gallery nanolasers can be easily integrated onto conductive platforms (Si, Au and indium tin oxide, etc.). Our findings open up a new class of wavelength tunable planar nanomaterials potentially suitable for on-chip integration.

Two-dimensional Conjugated Benzo[1,2-b:4,5-b′]dithiophene-based Photovoltaic Polymers

Jianhui Hou
State Key Laboratory of Polymer Physics and Chemistry
Beijing National Laboratory for Molecular Sciences
Institute of Chemistry, Chinese Academy of Sciences, Beijing 100190, China

Abstract— Polymer solar cell (PSC) has attracted much attention due to its potential application in production of large area, light weight and flexible panels. In order to improve power conversion efficiency (PCE) of PSC, more and more new materials were designed and synthesized and their properties, like molecular energy levels and band gaps, can be tuned effectively. In these new materials, benzo[1,2-b:4,5-b′]dithiophene (BDT) based conjugated polymers exhibited very promising photovoltaic properties.

In our recent works, photovoltaic properties of BDT-based conjugated polymers were tuned through molecular structure design. Functional groups or conjugated components with strong electron-withdrawing effect were introduced into the BDT-based polymers, and HOMO level of the BDT-based polymers can be lowered effectively without sacrificing absorption area and hole mobility. Therefore, higher open circuit voltage (Voc), good short circuit voltage (Jsc) and fill factor (FF) were recorded, and hence $\sim$ 9% PCE can be realized. Moreover, we used varied types of conjugated side groups to modulate the molecular energy levels of the BDT-based polymers. For example, *para*-alkylphenyl, meta-alkoxy-phenyl, fluorine-substituted thiophene groups were used to construct the two-dimensional conjugated structures. The results show that the fluorinations on the donor and the acceptor moieties in these polymers has little influence on their optical absorption properties but exhibit synergistic effect on lowering their HOMO and LUMO levels. The Voc of the PSC based on the trifluorinated polymer is 0.22 V higher than the PSC based on the non-fluorinated analog polymer. Accordingly, the PSC based on PBT-3F showed an enhanced PCE of 8.6%.

In this presentation, the synthesis process and photovoltaic properties of these newly designed BDT-based materials will be introduced in detail.

Session 2A4
SC2: Plasmonic Nanophotonics 2 — Design, Modeling and Simulation

Effective Model for Plasmonic Coupling

Meng Qiu, Bin Xi, Shiyi Xiao, Hao Xu, and Lei Zhou
State Key Laboratory of Surface Physics
Key Laboratory of Micro and Nano Photonic Structures
Fudan University, Shanghai, China

Abstract— Plasmonic couplings between nanoparticles generate fascinating physical phenomena, which can be utilized to realize certain applications [1, 2]. However, theoretical understandings on such problems are relatively behind experimental developments. Most theoretical efforts are based full wave simulations, which are not only computational complicated but also physically less transparent [3]. A complete effective model accounting for both electric and magnetic dipole terms in plasmonic nanoparticles, derived from a rigorous ground, is highly desired and is the key motivation of present work [4].

Based on the generalized tight-binding method for dispersive photonic media [5] and a multiple-expansion technique, we derived an analytical model for plasmonic coupling coefficient $t_{1,2}$ between two NPs, which includes all interacting terms between electric and magnetic dipoles of the NPs,

$$t_{1,2} = t_{pp} + t_{pp}^{rad} + t_{pm} + t_{mm} \tag{1}$$

where

$$t_{pp} = (f_0/8\pi\varepsilon_0\langle\Phi|\Phi\rangle)\cdot\left[\vec{p}_1^{\,*}\cdot\vec{p}_2 - 3(\vec{p}_1^{\,*}\cdot\hat{d})(\vec{p}_2\cdot\hat{d})\right]/d^3 \tag{2}$$

and

$$t_{mm} = (f_0\mu_0/8\pi\langle\Phi|\Phi\rangle)\cdot\left[\vec{m}_1^{\,*}\cdot\vec{m}_2 - 3(\vec{m}_1^{\,*}\cdot\hat{d})(\vec{m}_2\cdot\hat{d})\right]/d^3 \tag{3}$$

are the standard dipolar interactions between electric and magnetic dipoles in different NPs.

$$t_{pp}^{rad} = -(f_0/16\pi\varepsilon_0\langle\Phi|\Phi\rangle)\cdot(kd)^2\cdot\left[\vec{p}_1^{\,*}\cdot\vec{p}_2 + (\vec{p}_1^{\,*}\cdot\hat{d})(\vec{p}_2\cdot\hat{d})\right]/d^3 \tag{4}$$

is the electric dipolar interaction contributed from radiation effect.

$$t_{pm} = i(f_0/8\pi\varepsilon_0 c\langle\Phi|\Phi\rangle)\cdot(kd)\cdot\vec{p}_1^{\,*}\cdot(\vec{m}_2\times\hat{d})/d^3 \tag{5}$$

describes the interaction between electric and magnetic dipoles [4].

We performed extensive full-wave simulations on particular plasmonic coupled systems to verify the effective model presented in Eq. (1)–(5). Computations show that our effective model can well describe the plasmonic coupling behaviors in general cases. In particular, when the NP is large enough so that a quasi-static approximation is no longer valid, one has to take the radiation correction term t_{pp}^{rad} into account (see Figs. 1(e), (f)) to reasonably describe the plasmonic coupling behaviors, and the EM cross-interaction term t_{pm} is crucial to explain an intriguing mode-sequence reversal effect discovered in a particular coupled NP systems (see Fig. 1(k)). In addition, we found that the coupling strength between certain plasmonic nanoparticles can be tuned through varying the orientations of NPs, leading to interesting phenomena such as ultra-slow-wave plasmon propagation.

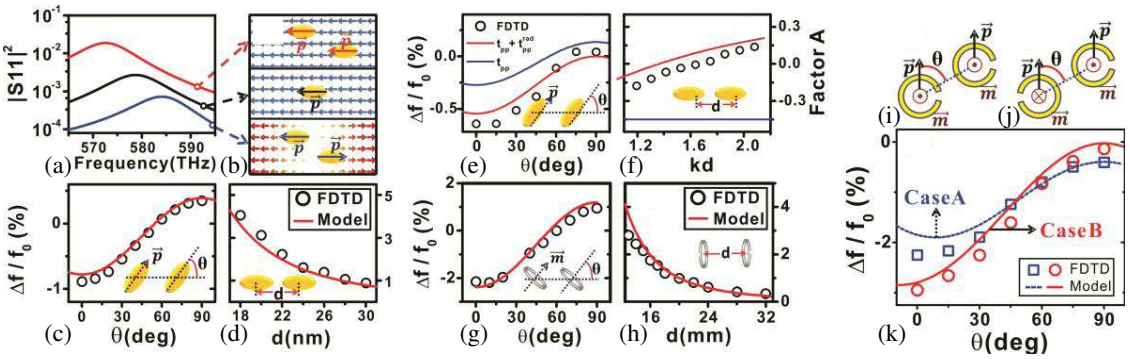

Figure 1: (a), (b) The simulation method to measure the "Dark mode", and (c), (d) the compare between the FDTD simulation result and our model in frequency splitting when the nanoparticles are small nano-ellipsoid, (e), (f) large nano-ellipsoid, (g), (h) BC-SRR and (i), (k) split ring.

REFERENCES

1. Rycenga, M., C. M. Cobley, J. Zeng, W. Li, C. H. Moran, Q. Zhang, D. Qin, and Y. Xia, *Chemical Reviews*, Vol. 111, 3669, 2011.
2. Halas, N. J., S. Lal, W. S. Chang, S. Link, and P. Nordlander, *Chemical Reviews*, Vol. 111, 3913, 2011.
3. Zuloaga, J., E. Prodan, and P. Nordlander, *Nano Letter*, Vol. 9, 887, 2009.
4. Xi, B., M. Qiu, S. Xiao, H. Xu, and L. Zhou, *Physical Review B*, 2014, in press.
5. Xi, B., H. Xu, S. Xiao, and L. Zhou, *Physical Review B*, Vol. 83, 165115, 2011.

Plasmonic Nanoantennas as Coherent Perfect Absorbers on SOI Waveguides for Modulators and All-optical Switches

Roman Bruck and Otto L. Muskens
Physics and Astronomy, Faculty of Physical Sciences and Engineering
University of Southampton, Southampton SO17 1BJ, UK

Abstract— Absorption in integrated optics is generally seen as a parasitic effect, which needs to be minimized. However, the control of absorption is also an opportunity to actively influence the propagation of light in waveguides. An example of this is critical coupling, where light can be coupled with 100% efficiency from a waveguide into a ring resonator by matching losses.

Related to the phenomenon of critical coupling, coherent perfect absorption (CPA) was recently predicted and demonstrated [1, 2]. In the context of integrated waveguides, CPA can be achieved by loading waveguides with absorbers of sub-wavelength dimensions in the propagation direction [3]. We investigate arrays of plasmonic nanoantennas on top of silicon on insulator (SOI) waveguides as CPA structures. In a scenario (see Fig. 1(a)), where two counterpropagating waves of same wavelength and amplitude form up a standing wave in the waveguide with spatially constant nodes of minimum and maximum average energy density, the absorbance strongly depends on the position of the antennas relative to the nodes of the standing wave.

We propose to integrate the CPA structure in the middle of an evanescent X-coupler, as depicted in the inset in Fig. 1(b). Two counterpropagating waves inserted into the X-coupler will form a standing wave in the middle section of both waveguides, where 50% of each individual wave is transferred to the adjacent waveguide. The characteristics of gold nanoantenna array-loaded X-couplers made from SOI waveguides were investigated by means of 3D finite-difference time-domain simulations.

In the on-state (antennas in **minimum** nodes of standing wave), the losses of the X-coupler with CPA absorbers are only 1.1%. In the off-state (antennas in **maximum** nodes of standing wave) transmission is smaller than 0.3% (see Fig. 1(b)), resulting in an extinction ration of better than 25 dB ($\lambda = 1.55\,\mu$m, TE).

The proposed modulator and all-optical switch can find applications in telecommunication applications, in coherent networks as well as in sensing or in increasing nonlinear effects. The large absorption means that light can be efficiently removed from the optical circuit. The calculated absorbers have a length of only 740 nm and show a flat and broadband spectral characteristic throughout telecommunication bands.

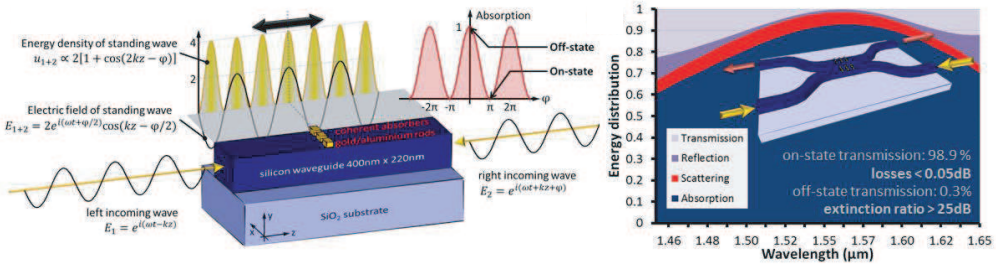

(a) (b)

Figure 1: Concept of coherence perfect absorption by plasmonic nanoantennas on top of silicon waveguides. Depending on the position of the antennas relative to the nodes of a standing wave in the waveguide, composed by two counterpropagating waves, absorption can be suppressed or maximized. (b) Off-state (minimum transmission) spectra of CPA structures on each waveguide of an evanescent X-coupler. The insets show the simulated structures.

REFERENCES

1. Chong, Y. D., L. Ge, H. Cao, and A. D. Stone, "Coherent perfect absorbers: Time-reversed lasers," *Phys. Rev. Letters*, Vol. 105, 053901, 2010.
2. Wan, W., Y. Chong, L. Ge, H. Noh, A. D. Stone, and H. Cao, "Time-reversed lasing and interferometric control of absorption," *Science*, Vol. 331, 889, 2011.

3. Bruck, R. and O. L. Muskens, "Plasmonic nanoantennas as integrated coherent perfect absorbers on SOI waveguides for modulators and all-optical switches," *Opt. Exp.*, Vol. 21, 27662–27671, 2013.

Perfect Optical Imaging in the Quasi-static Regime

David J. Bergman
Tel Aviv University, Israel

Abstract— A new approach is applied to the discussion of perfect imaging in the quasi-static regime. This is based upon the quasi-static eigenstates of Maxwell's equations. Exact results for the local electric potential are obtained for an ε_2, ε_1, ε_2 three parallel slabs micro-structure, which is relevant for the perfect imaging phenomenon. Among the surprising results is that, in the limit where $\varepsilon_1/\varepsilon_2 = -1$ and ε_1, ε_2 are both real, the electric field always diverges in some parts of the system. Moreover, the dissipation rate sometimes also diverges. The strongest focusing of a point charge object is achieved not at the geometric optics focus, but at a point on the ε_1, ε_2 planar interface that is furthest from the object point. An extension of these results to the non-quasi-static regime will also be described.

Second-order Surface Plasmon Enhanced Photoresponse in Ge Photodetectors with Bull's Eye Antennas

F.-F. Ren[1, 2], **H. Lu**[2], **H. H. Tan**[1], **and C. Jagadish**[1]

[1]Department of Electronic Materials Engineering, Research School of Physics and Engineering
The Australian National University, Canberra, ACT 0200, Australia
[2]School of Electronic Science and Engineering, Nanjing University, Nanjing 210093, China

Abstract— Bull's eye antennas have demonstrated the ability to enhance the absorption of nanometer-scale photodetectors by converting input light into the fundamental Bloch surface plasmons (SPs) and inducing extremely strong optical intensity inside an ultra-small region. So far, few reports focus on the plasmonic antennas which support higher order modes, mainly due to their weak near-field intensity and confinement. However, higher orders have the unique advantage of being able to be excited with a much longer grating period, since they have a larger wave vector and thus the effective wavelength of SPs is smaller than the grating period. Here, we conduct a comprehensive study of the second-order Bloch SP mode in a nanometer-scale Ge metal-semiconductor-metal photodetector with a basic or split bull's eye antenna. Particular emphasis is given to the geometrical optimization to understand how such plasmonic antennas enhance and focus the transmitted light, which is essential for energy buildup in an ultra-small absorbing area. It was found that the variation of geometrical parameters or periodicity in the breaking of bull's eye structure will lead to different changes in the extraordinary optical transmission spectra as compared to the fundamental modes, including the spectral position and transmissivity. The collective response features of higher-order modes and the effect of light trapping/absorption have also been analyzed by comparing them to the fundamental modes or other geometrical designs. Finally, we observed the area-normalized responsivity can be enhanced up to 3.8 times at 2 V bias for a 780 nm light at normal incidence with a grating period of 1500 nm due to the contribution of second-order SP mode. It suggests an easier fabrication for sub-wavelength applications where optically denser materials are required.

New Optical Properties of Nanoapertures and Their Applications

Vasily Klimov
Lebedev Physical Institute, Russian Academy of Sciences, Russia

Abstract— Many interesting properties of nanoholes and nanoapertures in metal filmshave been already discovered (see e.g., [1–3]). However this geometry is very rich and one can expect a lot of new interesting effects there. In my talk, I will discuss several new optical effect related with nanoapertures in metal film.

I will start with discussion of new mechanisms of extraordinary transmission provided by an optical Tamm state which is formed between metal film and planar metamaterials (see Fig. 1(a)).

We have shown that total transmission due to optical Tamm states can be as large as 800% and even more. I also will discuss nonreciprocal and nonlinear properties of light in presence of nanoapertures.

Then I will discuss molecule fluorescence near nanoapertures. Here I will present new analytical and numerical results, whichallow to understand clearly this complicated phenomenon.

In final part of my talk I will discuss how optical fields near nanoaperture can be used for control of atom dynamics (atom nano-optics).

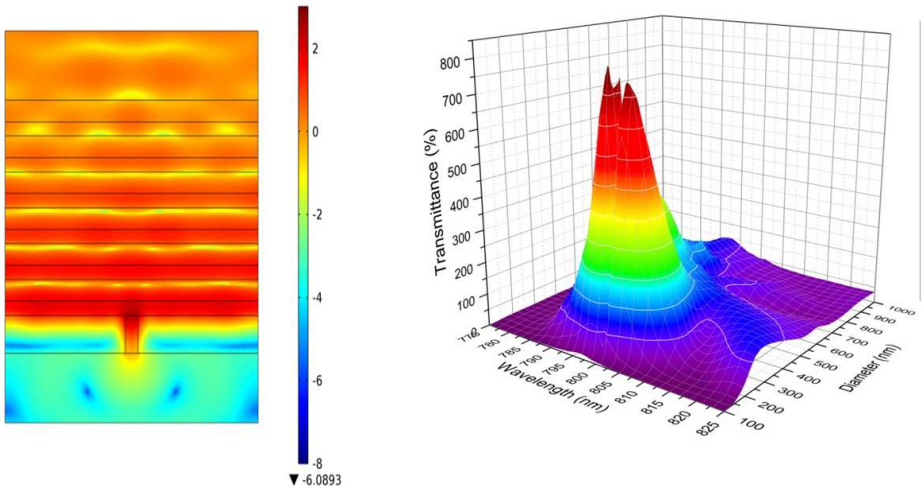

Figure 1: (a) Field distribution in transversal cross-section; (b) Transmission through nanoholes array as a function of wavelength and aperture diameter.

ACKNOWLEDGMENT

I would like to thank the Russian Foundation for Basic Research (grant No. 14-02-00290), the Presidium of the Russian Academy of Sciences, the Russian Quantum Center and the Skolkovo foundation for financial support of this work.

REFERENCES

1. Bethe, H. A., "Theory of diffraction by small holes," *Phys. Rev.*, Vol. 66, 163, 1944.
2. Ebbesen, T. W., H. J. Lezec, H. F. Ghaemi, T. Thio, and P. A. Wolff, "Extraordinary optical transmission through sub-wavelength hole arrays," *Nature*, Vol. 391, 667, 1998.
3. Cakmakyapan, S., A. E. Serebryannikov, H. Caglayan, and E. Ozbay, "One-way transmission through the subwavelength slit in nonsymmetric metallic gratings," *Opt. Lett.*, Vol. 35, 2597, 2010.

Magnetic Toroidal Moment in Coupled Plasmonic Nanodisks and Their Properties

Qiang Zhang, **Sheng Lei Wang**, **Fei Fei Qin**, **and Jun Jun Xiao**
College of Electronic and Information Engineering, Shenzhen Graduate School
Harbin Institute of Technology, Shenzhen, Guangdong 518055, China

Abstract— In addition to many intriguing properties reported so far, metamaterial is a good platform to study special physical phenomenon that is usually difficult to be observed in atomic and condensed matter system. Toroidal dipole moment is such an example. Strongly coupled plasmonic nanodisks have been found to support both magnetic multipoles and magnetic toroidal moment that can be excited easily. We systematically study the magnetic-resonance-associated optical characteristics based on such metamaterials and explored their robustness to geometry perturbation. We also examine the optomechanical effects with respect to the toroidal moment. It is shown that the magnetic toroidal mode is distinct to magnetic multipole modes in various aspects.

Plasmonics: Evolution from Sensors to Nanowire Waveguides for Interconnect Applications

Lech Wosinski[1, 2], **Fei Lou**[1, 2], **and Lars Thylen**[1, 2]

[1]School of Information and Communication Technology
KTH Royal Institute of Technology, Kista 16440, Sweden
[2]JORCEP (Joint Research Center of Photonics of the Royal Institute of Technology (Sweden) and Zhejiang University), Zhejiang University, Hangzhou 310058, China

Abstract— Optical properties of metals and plasmonic phenomena have been known and exploited for decades, but main applications have been concentrated to sensing using refractive index changes based on surface plasmon resonances (SPRs), local field enhancement in different surface-enhanced Raman spectroscopy (SERS) methods including tip-enhanced Raman spectroscopy (TERS), and other sensing principles. Possibility to apply plasmonics for guiding of light has been discussed since mid-eighties [1], but only recently its advantages have been seriously considered.

Silicon photonics has been chosen as technology of choice for integration with electronic circuits due to sub-micron feature size and compatibility to microelectronic fabrication on common Si platform, allowing for high accuracy, high yield and possibility for mass production. With continuous down-scaling and performance increasing of integrated circuits, nanophotonic interconnects have been proposed for inter- and intra-chip communication, as traditional metal-based interconnects are no longer sufficient with limited bandwidth, delay, power dissipation and cross-talk. Nanophotonic components based on silicon, although much smaller than traditional integrated photonic structures have their limitations as well, mainly due to the diffraction limit of light which does not allow to decrease a light modal field below $\lambda/2n$ (half of the light wavelength in the material). This means that with a Si nanowire waveguide cross section of the order of $200 \times 500\,\mathrm{nm}$ silicon-based devices are still an order of magnitude larger than their electronic counterparts.

Here plasmonics comes with an alternative solution to pure photonic waveguiding, allowing for sub-wavelength light confinement. A large variety of different plasmonic structures for waveguiding have been explored. When single metal-dielectric interfaces, so-called long-range plasmon waveguides do not fulfil the sub-wavelength guiding conditions, different metal-insulator-metal structures can confine the modal field to the insulator area allowing for deep sub-wavelength confinement if insulator is enough thin. Strip-line, slot-line [2] and v-grove [3] structures have been examined by different authors, as well as more sophisticated multi-layered systems [4] and quantum dot arrays [5]. Although there are many structures and plasmonic components based on these solutions, all of them are suffering huge losses due to the proximity of metal surfaces.

Recently a new type of plasmonic waveguide structure has been proposed [6–8] and experimentally confirmed [9, 10], which can solve this problem, allowing for quite free adjustment of trade-off between the modal confinement (below the diffraction limit of light) and propagation length. In the so-called hybrid plasmonic waveguide light is confined in a low refractive index material in between metal layer on the one side and high refractive index material (ex. silicon) on the other side.

In this paper, we present principles of plasmonic and hybrid plasmonic waveguiding as well as a number of fabricated and evaluated hybrid plasmonic components for future interconnect applications.

ACKNOWLEDGMENT

This work was supported by "The Swedish Research Council (VR) through its Linnæus Center of Excellence ADOPT", as well as project VR-621-2010-4379.

REFERENCES

1. Stegeman, G. I., J. J. Burke, and D. G. Hall, *Opt. Lett.*, Vol. 8, 383, 1983.
2. Liu, L., Z. Han, and S. He, *Opt. Express*, Vol. 13, 6645, 2005.
3. Bozhevolnyi, S., et al., *Nature*, Vol. 440, 508, 2006.
4. Yan, M., L. Thylén, and M. Qiu, *Opt. Express*, Vol. 19, 3818, 2011.

5. Holmström, P., L. Thylen, and A. Bratkovsky, *Appl. Phys. Lett.*, Vol. 97, 073110, 2010.
6. Alam, M. Z., J. Meier, J. S. Aitchison, and M. Mojahedi, *CLEO/QELS*, Paper ID: JThD112, 2007.
7. Oulton, R. F., V. J. Sorger, D. A. Genov, D. F. P. Pile, and X. Zhang, *Nat. Photonics*, Vol. 2, 496, 2008.
8. Dai, D. and S. He, *Opt. Express*, Vol. 17, No. 19, 16646, 2009.
9. Wu, M., Z. Han, and V. Van, *Opt. Express*, Vol. 18, 11728, 2010.
10. Wang, Z., D. Dai, Y. Shi, G. Somesfalean, P. Holmstrom, L. Thylen, S. He, and L. Wosinski, *Technical Digest of OFC/NFOEC*, Paper JThA017, 2011.

Universal Eigenvalue Analysis for 2D Periodic Plasmonic Nanostructures

Wei E. I. Sha[1], **Hui Wang**[2], **Wallace C. H. Choy**[1], **and Weng Cho Chew**[3]

[1]Department of Electrical and Electronic Engineering
The University of Hong Kong, Pokfulam Road, Hong Kong, China
[2]The Key Laboratory of Intelligent Computing and Signal Processing
Anhui University, Ministry of Education, Hefei, China
[3]Department of Electrical and Computer Engineering
University of Illinois, Urbana-Champaign, Illinois, USA

Abstract— We developed a universal eigenvalue analysis for 2D arbitrary nanostructures comprising dispersive and lossy materials. The complex Bloch band structures (BS) of plasmonic crystals and gratings are rigorously calculated by the finite-difference discretization of wave equation. Given a frequency of interest, the eigenvalue algorithm solves one Bloch wavenumber as the eigenvalue via fixing another. (1) For plasmonic crystals, the influence of ohmic (metallic) loss on the complex BS and eigenmodes is investigated. Regarding a TE polarization with H_z field, the ohmic loss strongly affects the BS and eigenmodes at plasmonic resonance frequencies. Both the fast oscillation of dispersion curve and strong field confinement of eigenmodes are damped due to the high ohmic loss. Regarding a TM polarization with E_z field, the introduction of ohmic loss twists the vertical dispersion curve at the bandgap and breaks the symmetry of eigenmodes. Regarding both polarizations, the high ohmic loss lowers the quality factor of eigenmodes. (2) For plasmonic gratings, the abnormally large group velocity is observed at a plasmonic band edge with a large attenuation constant. Interestingly, we found the abnormal group velocity is caused by the leaky (radiation) loss, not by metallic absorption (ohmic) loss. The periodically modulated surface of the grating significantly modifies the original BS of the semi-infinite dielectric-metal structure and induces the extraordinarily large group velocity, which is different from the near-zero group velocity at photonic band edge. The work is fundamentally important to the design of plasmonic nanostructures.

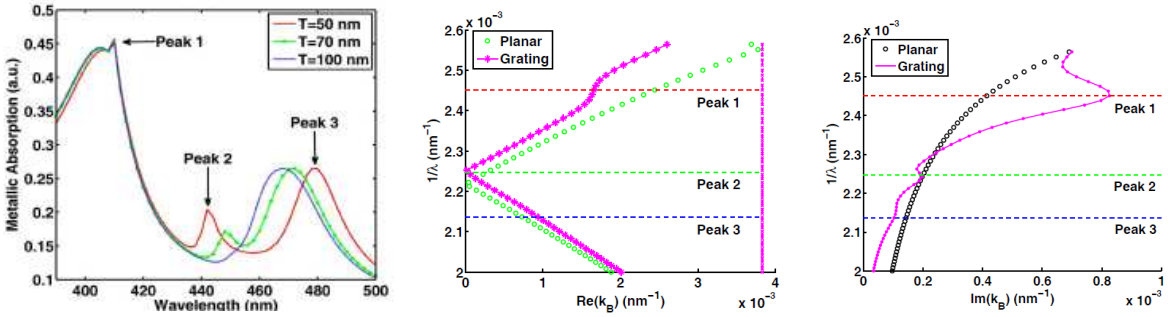

(a) (b) (c)

Figure 1: The plasmonic band gap (PBG) and plasmonic band edge (PBE) effects. (a) The absorbance as a function of grating thickness T. Peak 1 and 3 relate to PBEs. Peak 2 relates to PBG. (b), (c) Plasmonic BS of the grating. The anomalous group velocity is found at a PBE (peak 1 in (b)) with a large attenuation (peak 1 in (c)). The original BS of planar air-metal structure is strongly perturbed.

Near-field Surface Plasmon Effects on Au-double-slit Diffraction for Polychromatic Light

Pin Han
Graduate Institute of Precision Engineering, Chung Hsing University
250 Kuo Kuang Road, Taichung 402, Taiwan

Abstract— The surface plasmon effects on near-field diffraction for polychromatic light are studied. An Au-double-slit is used as the model and Fresnel integral is employed to perform the theoretic analysis. The results are illustrated with numerical examples and they show that, compared with the normal double-slit, the plasmon effect changes the spectral shift from redshift to blueshift and also enhances the intensity peak.

A Lagrange RLC Circuit Model for Split-ring Resonators

Hsun-Chi Chan and Guang-Yu Guo
Department of Physics, Taiwan University
No. 1, Sec. 4, Roosevelt Road, Taipei 10617, Taiwan

Abstract— Metamaterials are the artificially fabricated materials with unusual optical properties. In particular, left-handed metamaterials that have simultaneously negative electric permittivity ε and magnetic permeability μ have many exotic properties such as negative index of refraction [1]. Above all, metallic wires [2] and split-ring resonators (SRRs) [3] are two key structures to achieve negative ε and μ respectively. Together with these two structures, the first negative-index metamaterials (NIMs) were experimentally verified in the microwave region [4]. Different designs were proposed such that the working bands are pushed toward the visible region [5]. Liu et al. in 2010 proposed a Lagrange model for stereo-metamaterials (metamaterials that have same constituent units but with different orientation) to investigate its chiral optical properties [6]. Aside from usual numerical simulation methods such as finite-difference time-domain method (FDTD) and finite element method (FEM), the Lagrange model provides us a deeper insight into the mechanism of a metamaterial system. Inspired by this work [6], here we introduce a Lagrange model for a single SRR interacting with an incident electromagnetic (EM) wave. First, we consider single SRR as an RLC circuit. In an SRR, the metal ring and the slit correspond to an inductor (L) and a capacitor (C), respectively. Depending on the orientation and polarization of the incident EM wave, we also take the electric and/or magnetic dipole interaction into account, which is the origin of the presence of the effective ε and μ. Then we take the oscillating charge Q and induced current $\dot{Q}$ as two independent generalized coordinates. By substituting the Lagrangian into the Euler-Lagrange equation and solving the equation of motion, we obtain the frequency-dependent Q and hence the effective ε and μ. Most significantly, we find that the forms of ε and μ are just the Lorentzian line shapes as described in the literatures [3, 7]. Finally, we use our model to fit two well-know examples, the fishnet structure [8] and single SRR [9]. The benchmark numerical results agree well with our model. This method can also be used to investigate other more complicated systems.

REFERENCES

1. Veselago, V. G., "The electrodynamics of substances with simultaneously negative values of ε and μ," *Soviet Physics Uspekhi*, Vol. 10, 509, 1968.
2. Pendry, J. B., A. J. Holden, W. J. Stewart, and I. Youngs, "Extremely low frequency plasmons in metallic mesostructures," *Physical Review Letters*, Vol. 76, 4773, 1996.
3. Pendry, J. B., A. J. Holden, D. J. Robbins, and W. J. Stewart, "Magnetism from conductors and enhanced nonlinear phenomena," *IEEE Transactions on Microwave Theory and Techniques*, Vol. 47, 2075, 1999.
4. Shelby, R. A., D. R. Smith, and S. Schultz, "Experimental verification of a negative index of refraction," *Science*, Vol. 292, 77, 2001.
5. Soukoulis, C. M., S. Linden, and M. Wegener, "Negative refractive index at optical wavelengths," *Science*, Vol. 315, 47, 2007.
6. Liu, H., J. X. Cao, S. N. Zhu, N. Liu, R. Ameling, and H. Giessen, "Lagrange model for the chiral optical properties of stereometamaterials," *Physical Review B*, Vol. 81, 241403, 2010.
7. Smith, D. R., W. J. Padilla, D. C. Vier, S. C. Nemat-Nasser, and S. Schultz, "Composite medium with simultaneously negative permeability and permittivity," *Physical Review Letters*, Vol. 84, 4184, 2000.
8. Zhang, S., W. Fan, K. J. Malloy, S. R. Brueck, N. C. Panoiu, and R. M. Osgood, "Near-infrared double negative metamaterials," *Opt. Express*, Vol. 13, 4922, 2005.
9. Linden, S., C. Enkrich, M. Wegener, J. Zhou, T. Koschny, and C. M. Soukoulis, "Magnetic response of metamaterials at 100 Terahertz," *Science*, Vol. 306, 1351, 2004.

Optical Multiple Bistability in Metal-insulator-metal Plasmonic Waveguides Side-coupled with Twin Resonators

Ruei-Cheng Shiu[1], **Guang-Yu Guo**[1], **and Yung-Chiang Lan**[2]

[1]Department of Physics, Taiwan University
No. 1, Sec. 4, Roosevelt Road, Taipei 10617, Taiwan
[2]Department of Photonics, Cheng Kung University
No. 1 University Road, Tainan 701, Taiwan

Abstract— Nonlinear and switchable metamaterials, two kinds of the emergent materials of great interest [1], have widely been applied in nano-devices such as optical switches, rewritable memories, and logic operators. Metal-insulator-metal (MIM) plasmonic waveguides are a fundamental structure for surface plasmon polariton propagation, and provide low-loss propagation in a wide range of frequency. Therefore, several investigations based on MIM plasmonic waveguides to realize bistable effect in switchable systems with a nonlinear optical material have been reported recently [1–4]. In this paper, we build up a structure composed of a MIM plasmonic waveguide and two racetracks filled with optical Kerr nonlinear material to realize the multi-bistable effect. Such property may have valuable applications in multi-switches, optical logic operations.

We consider two racetrack resonators side-coupled to a silver MIM plasmonic waveguide as shown as Fig. 1. The resonators are filled with a Kerr nonlinear material, whose relative permittivity ($?_d$) depends on the local intensity of electric field $|E|^2$: $?_d = ?_0 + \chi^{(3)}|E|^2$, where $?_0$ and $\chi^{(3)}$ are linear relative permittivity and third-order nonlinear susceptibility. In our simulations, the Drude model with the plasma frequency (ω_p) and electron collision frequency ($?_d$) set to 1.255×10^{16} and 0.68×10^{14}, is used to describe the dielectric response of Ag, i.e., the relative permittivity of Ag is given by $?_{ag}(\omega) = 1 - \omega p^2/(\omega^2 - 2i\omega?_d)$. A TM-polarized plane wave (input-signal), of which the magnetic field is perpendicular to the x-y plane, is incident onto the waveguide from one end (Fig. 1), and the wavelength is 1540 nm.

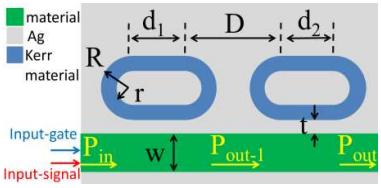

Figure 1: Illustration of our proposed plasmonic waveguide.

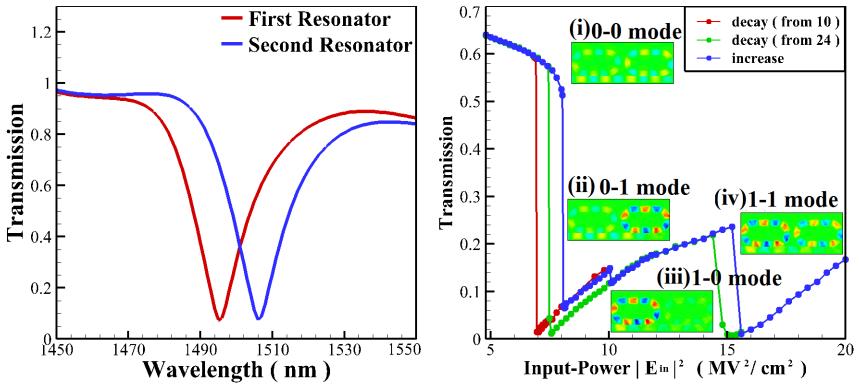

Figure 2: (a) Transmission spectra of the first (red line) and second (blue line) racetrack resonators. (b) Transmission efficiency as a function of the power of input. The blue (green and red) line and points indicate that the power of input-signal increases from 0 (decreases from 24 MV^2/cm^2 and decreases from 10 MV^2/cm^2). (i), (ii), (iii), and (iv) are the contours of $|H_z|^2$ as $|E_{in}|^2$ = 7.8, 8.6, 12, and 16.4 MV^2/cm^2 on the blue line, respectively.

First of all, we find that the eigen-wavelength of the first and second resonators are 1506 nm and 1495 nm respectively, as shown in Fig. 2(a). In addition, such structure has a strong resonance, $Q_1 = Q_2 = 72$, in the nonlinear resonators at the signal wavelength, which can enhance the nonlinear Kerr effect. As a result, we choose 1540 nm as the signal wavelength. Based on our FDTD simulations, the multi-bistable effect is presented in Fig. 2(b), and the blue (green and red) line and points indicate that the power of the input-signal increases from 0 (decreases from $24\,\mathrm{MV}^2/\mathrm{cm}^2$ and decreases from $10\,\mathrm{MV}^2/\mathrm{cm}^2$). In Fig. 2(b), (i), (ii), (iii), and (iv) are the contours of $|H_z|^2$ normalized by the input power when the signal power increases to 7.8, 8.6, 12, and $16.4\,\mathrm{MV}^2/\mathrm{cm}^2$, respectively.

In this study, we have investigated the optical multi-bistable effect in two racetracks filled with an optical Kerr material on one side of a MIM plasmonic waveguides by two-dimensional FDTD simulations. Because of its multi-bistable effect, such system may find technological applications in multi-switches, optical logic operations, or even optical devices.

REFERENCES

1. Zheludev, N. I., *Science*, Vol. 328, 582–583, 2010.
2. Wang, X., H. Jiang, J. Chen, P. Wang, Y. Lu, and H. Ming, *Opt. Express*, Vol. 19, 19415–19421, 2011.
3. Shen, Y. and G. P. Wang, *Opt. Express*, Vol. 16, 8421–8426, 2008.
4. Lin, X. S., J. H. Yan, Y. B. Zheng, L. J. Wu, and S. Lan, *Opt. Express*, Vol. 19, 9594–9599, 2011.

Session 2A5
FocusSession.SC2: Transfromation Optics 1

Broadband Collection and Concentration of Light: A Transformation Optics Approach

Yu Luo and J. B. Pendry
The Blackett Laboratory, Department of Physics
Imperial College London, London SW7 2AZ, UK

Abstract— The ability of harvesting light and efficiently concentrating its energy into a nanoscale active center is highly desired for many applications, such as fluorescence, Raman scattering, single-molecule detection, and nonlinear effect. Surface plasmons have made these applications possible through a strong interaction between the incident light and free electrons in the metal. Critical to these goals is an ability to fully characterize and model the plasmonic properties of metallic nanostructures. In this contribution, a systematic strategy is proposed, based on transformation optics, to investigate a broad variety of plasmonic nanostructures. We exploit the fact that a finite nanoparticle with sharp geometrical features (such as edges or corners) can behave like an infinite plasmonic system and can exhibit a continuous light absorption property over a broadband spectrum [1]. Comprehensive discussions are provided on how the effects of nonlocality [2] and edge rounding [3] affect the local field enhancement as well as the energy and bandwidth of each plasmonic resonance. Generalization of this method to three-dimensional situations will also be discussed [4]. The largely analytic approach gives physical insights into the processes involved and suggests the way forward to study a wide variety of plasmonic nanostructures.

REFERENCES

1. Luo, Y., R. Zhao, A. I. Fernandez-Dominguez, S. A. Maier, and J. B. Pendry, *Sci. China Inf. Sci.*, Vol. 56, 120401, 2013.
2. Luo, Y., A. I. Fernandez-Dominguez, A. Wiener, S. A. Maier, and J. B. Pendry, *Phys. Rev. Lett.*, Vol. 111, 093901, 2013.
3. Luo, Y., D. Y. Lei, S. A. Maier, and J. B. Pendry, *Phys. Rev. Lett.*, Vol. 108, 023901, 2012.
4. Pendry, J. B., A. I. Fernandez-Dominguez, Y. Luo, and R. Zhao, *Nature Physics*, Vol. 9, 518, 2013.

Unusual Geometrical Optics and Geodesic Lenses

A. J. Danner[1], **A. Akbarzadeh**[1], **H. L. Dao**[1], **and T. Tyc**[2]

[1]Department of Electrical and Computer Engineering
National University of Singapore, 117583, Singapore
[2]Faculty of Science and Faculty of Informatics, Masaryk University
Kotlářská 2, Brno 61137, Czech Republic

Abstract— Geometrical optics is highly useful for many tasks in optics, and when used for ray tracing purposes it allows visualization of the flow of energy through media. In certain circumstances, however, even if all of the normal conditions under which geometrical optics is assumed to be accurate are met, there are situations in which geometrical optics can spectacularly fail. For example, in anisotropic lenses with graded permittivity, and under conditions where spatial changes in permittivity are significantly larger than the wavelength (when geometrical optics would normally be expected to be accurate for ray tracing), there exist certain circumstances where results from ray optics cannot be trusted. Additional constraints on the use of geometrical optics are thus necessary when applied to anisotropic media. There are also situations in absolute optical instruments where rays can traverse regions of complex refractive index but still form geodesics, as well as situations where surface maps of geodesic lenses yield can only exist if they have complex (not real) coordinate axes.

Manipulating Electromagnetic Energy Flux via Transformation Devices and Metasurfaces

Bo Hou
School of Physical Science and Technology, Soochow University
1 Shizi Street, Suzhou 215006, China

Abstract— Transformation optics (TO) is a brand new methodology of controlling electromagnetic energy flux and can realize many exotic electromagnetic phenomena, e.g., cloaking, with metamaterials implementation. However, the fancy TO devices suffer from single working frequency or narrow bandwidth limitation and bulky volume disadvantage, which seriously constrain the relevant practical applications. On the other hand, the metallic structure with periodical subwavelength slits has exhibited multiple frequencies of extraordinary optical transmission (EOT), a consequence of Fabry-Perot (FP) resonance inside the slits. Furthermore, newly proposed flat optics materials, which are termed metasurfaces, enable the optical design within deeply subwavelength thickness scale and are receiving intense attentions. In this talk, I will review our recent work at microwave frequencies on manipulating electromagnetic energy flux by employing the EOT structures and the metasurfaces. They include (1) a type of TO devices with multiple frequencies of zero scattering cross-sections induced by FP resonance; (2) the unidirectional propagation of energy flux in metasurface-loaded waveguides; (3) the ultra-broadband coherent perfect absorption of ultrathin conductive films. Our work will be beneficial to mitigate the limitation and the disadvantage of the TO-based energy flux controlling devices.

Metamaterial Stacked Transformation Optics Lens for Subwavelength Imaging

Lian Shen and Hongsheng Chen
The Electromagnetics Academy at Zhejiang University
Zhejiang University, Hangzhou 310027, China

Abstract— Transformation optics lens has been designed, realized and characterized. The lens, which was composed of ultrathin sheet metamaterials, has the ability to achieve subwavelength imaging in the far field in real time. The sheet metamaterials involves extreme value which can be achieved by metallic rod array at its plasma frequency. Analysis was illustrated that integrating ultrathin sheet metamaterials into macroscopic metamaterials not only preserve optical properties of sheet metamaterials but also show good flexibility. The transformation optics lens can be bent, stretched, and twisted without breaking its optical properties. Such fabrication approach constitutes a further important step towards real world applications of subwavelength imaging.

Artificial Riemann Sheets: When the Two Science Work Meet

Lin Xu and Huanyang Chen
School of Physical Science and Technology, Soochow University, Suzhou, Jiangsu 215006, China

Abstract— Here we put the two original approaches of transformation optics [2, 3] into a more general concept — transformation optics with artificial Riemann sheets, where several new kinds of cloaks can be designed.

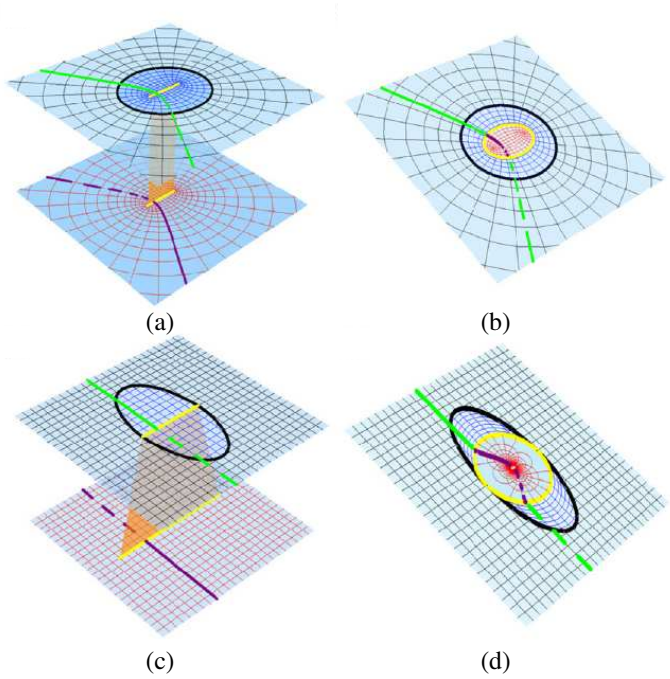

Figure 1: Two mappings with artificial Riemann sheets in virtual space. Panels (a) and (b) are virtual space and physical space through the mapping on an elliptical coordinate system. Panels (c) and (d) are virtual space and physical space through the mapping on a Cartesian coordinate system.

REFERENCES

1. Xu, L. and H. Chen, "Transformation optics with artificial Riemann sheets," *New J. Phys.*, Vol. 15, 113013, 2013.
2. Leonhardt, *Science*, Vol. 312, 1777–80, 2006.
3. Pendry, et al., *Science*, Vol. 312, 1780–2, 2006.

Controlling Transformation Optics through Enhanced Photon Thermal Effect

H. Liu
National Laboratory of Solid State Microstructures & Department of Physics
Nanjing University, Nanjing 210093, China

Abstract— In this work, a method is reported to control transformation optical effects by light through an enhanced photon thermal effect. A central potential transformation optical waveguide is fabricated to mimicking gravitational field. The strong laser is focused on the waveguide and the curvature of the effective space around the center is reduced due to photon thermal effect. We experimentally demonstrated that the deflection angle of gravitational lensing effect is dynamically controlled through this process. And the calculated result based on the theory of general relativity and full wave simulation fit our experiment results well. The combination transformation optics and the nonlinear medium offers a new degree to control the interaction between light and matter.

Phase Preservation in Transformation Optics. II

Baile Zhang[1] and Yuan Luo[2]

[1]School of Physical and Mathematical Sciences, Nanyang Technological University, Singapore
[2]Center for Optoelectronic Medicine, Taiwan University, Taiwan

Abstract— This is a following up talk after the one of "Phase preservation in transformation optics" we presented in PIERS 2013 in Stockholm. We thus entitle it as "Phase preservation in transformation optics. II."

The outstanding wave manipulation capability of transformation optics comes from its unique property in recovering both ray trajectory and optical path length. In PIERS Stockholm we demon- strated the unique phase preservation in transformation optics by using a very simple macroscopic transformation-optics device that achieves one-directional compression and can virtually lift an optical image by a macroscopic distance.

Here we go one step further to demonstrate phase-preserved macroscopic invisibility cloaking in an almost three dimensional (3D) space for visible light. This almost 3D cloak can have 3D invisibility performance within a limited field of view, and the wide angle (e.g., very large field of view) invisibility performance is achieved in multiple 2D planes intersecting in the 3D space. The phase preservation is verified with incoherent white-light interferometry without ambiguity and phase unwrapping.

The cloak is designed with a simplified 3D model. A perfect 3D model requires magnetism that is difficult for visible light. Therefore we give up the full 3D invisibility performance but preserve its performance in a limited field of view and multiple 2D planes. We then emphasize the fundamental role of phase preservation in 3D invisibility cloaking and experimentally verify it. The interference measurement is done with various oblique incidence from different angles. We consider this work as a solid demonstration that phase preserved transformation-optics invisibility cloaking is possible in 3D.

Electromagnetic Invisibility Cloaks Based on Inverse Design Methodology

Su Xu[1], **Qinghui Yan**[1], **Xiangxiang Cheng**[1], **Yuyu Jiang**[1], **Baile Zhang**[2], **and Hongsheng Chen**[1]

[1]The Electromagnetics Academy at Zhejiang University, Zhejiang University, Hangzhou 310027, China
[2]Division of Physics and Applied Physics, School of Physical and Mathematical Sciences
Nanyang Technological University, Singapore 637371, Singapore

Abstract— Inverse-design invisibility cloaks, inspired from the thoughts of forward-design cloaking techniques, have experience a period of remarkably fast development in the past few years. Here we report an inverse design method of invisibility cloaks based on the Mie scattering theory. The anisotropic profile of cloaking layers is optimized to minimize the total scattering cross section of the cloak-core system by adopting the genetic algorithm. As examples, an invisible dipole antenna is demonstrated experimentally and an omnidirectional spherical invisibility cloak design is proposed.

Electromagnetic Wavefront Control Using Subwavelength Dielectric Particles

Zongqi Xiao[1], **Qian Zhao**[1], **Fuli Zhang**[2], **Junming Ma**[1], **Ming Qiao**[1], **Yonggang Meng**[1], **Chuwen Lan**[3], **Bo Li**[3], **and Ji Zhou**[3]

[1]State Key Laboratory of Tribology, Department of Mechanical Engineering
Tsinghua University, Beijing 100084, China
[2]Key Laboratory of Space Applied Physics and Chemistry
Ministry of Education and Department of Applied Physics
School of Science, Northwestern Polytechnical University, Xi'an 710072, China
[3]State Key Laboratory of New Ceramics and Fine Processing
School of Materials Science and Engineering, Tsinghua University, Beijing 100084, China

Abstract— Subwavelength dielectric medium based on Mie resonance theory can be equivalent to an electric dipole or magnetic dipole, making it possible to control electromagnetic (EM) wave phase drastically. Differing from the metal-structured medium, any EM waves emitted from a zero-index medium keep the same constant phase inside the medium, which results in a uniform wavefront outside the medium. In this paper, we achieved the isotropic zero-permeability. The interaction between dielectric particles and the EM wave as well as the strong directional scattering are visually observed using the field distribution measurement. Through the mechanism above, an isotropic almost zero-index subwavelength medium based on Mie-magnetic-resonance dielectric medium sample is designed and constructed. The phase modulation of the cylindrical wave inside and outside the medium are theoretically and experimentally studied. Using the active control of temperature, the operating frequency range of zero-index effect is effectively tuned. This subwavelength particle modulates EM wave with the wavelength longer than 10 times of its own size, which provides an effective approach to the miniaturization, integration and high frequency of the device, and also contributes more to the intellectualization of EM device.

Control of Microwaves Using Metamaterials and Metasurfaces

Tie Jun Cui
State Key Laboratory of Millimeter Waves, Southeast University, Nanjing 210096, China

Abstract— In this talk, I will present the control of microwaves using metamaterials and metasurfaces towards the goal of real applications or potential applications in the near future. The presentation will be focused on gradient refractive index (GRIN) metamaterials, anisotropic zero-index (AZI) metamaterials, spoof surface plasmon (SP) metasurfaces, and holographic metasurfaces.

In GRIN metamaterials, the three-dimensional (3D) ground-plane invisibility cloak and 3D flattened Luneburg lens based on the transformation optics (TO), 3D GRIN flat lenses based on geometrical optics (GO), and 2D and 3D GRIN cylindrical lenses for super-resolution imaging based on TO are firstly introduced. Then I will present some new results on 3D anisotropic GRIN metamaterials to control differently-polarized waves independently and to realize multiple microwave functionalities using a single lens.

I propose and experimentally demonstrate two types of AZI metamaterials in the Cartesian and cylindrical coordinates, respectively. The spatial Cartesian AZI metamaterials (such as z component of permittivity or permeability tensor equals zero) are shown to generate perfectly plane waves in the z direction, resulting in high-directivity antennas. On the contrary, the radially AZI metamaterials (radial component of permittivity or permeability tensor in the cylindrical coordinate equals zero) will always produce omnidirectional radiations with high-efficiency spatial power combination regardless the numbers and positions of sources. When the Cartesian AZI metamaterials are placed inside waveguide, I show perfect bending, total transmission, and super reflection phenomena of microwaves.

Finally I present two kinds of metasurfaces to control microwaves: SP metasurfaces to manipulate spoof SP waves and holographic metasurfaces to manipulate spatial waves. For the SP metasurfaces, I propose a bi-functional Luneburg-fisheye lens and TO-based flattened Luneburg metasurface lens. For the holographic metasurfaces, I report some extreme controls of radiation patterns and scattered fields. I will also present complicated controls of both SP waves and spatial waves using combined metasurfaces.

Session 2A6
FocusSession.SC3&2: Disordered Photonics

Imaging through Scattering Media

J. Bertolotti[1], **E. G. van Putten**[2, 3], **C. Blum**[4], **A. Lagendijk**[2], **W. L. Vos**[2], **and A. P. Mosk**[2]

[1]Department of Physics & Astronomy, Electromagnetic & Acoustics Materials Group
University of Exeter, Exeter, Devon EX4 4QL, England
[2]Complex Photonic Systems (COPS), MESA+ Institute for Nanotechnology
University of Twente, P. O. Box 217, Enschede 7500 AE, The Netherlands
[3]Philips Research Laboratories, Eindhoven 5656 AE, The Netherlands
[4]Nanobiophysics (NBP), MESA+ Institute for Nanotechnology
University of Twente, P. O. Box 217, Enschede 7500 AE, The Netherlands

Abstract— Non-invasive imaging requires the ability to form sharp pictures even when an opaque material act as a screen between the object and the detector. Light scattering scrambles the spatial information of the object, thereby blurring the picture and making imaging impossible. The typical distance that light can traverse in a turbid medium before its direction is scrambled varies from tens of meters in fog, to a fraction of a millimeters in skin, to microns in paint. Gated imaging methods such as optical coherence tomography can separate the small amount of ballistic light that did not change direction from the scattered background, and diffuse tomography methods offer high-depth imaging at low resolution even if no ballistic light is present at all. It has been theoretically suggested that a complete knowledge of the scattering screen will allow one to image objects hidden behind it, and major steps in this direction were achieved using ultrasound and electromagnetic waves in both the microwave and in the optical regime. Yet to obtain the required knowledge of the scattering screen, it is necessary to access its back, thus severely limiting the usefulness of these approach.

We have recently demonstrated a reference-free imaging method that can obtain an image of a fluorescent object behind a thin layer that scatters all incident light. The incident laser light is scrambled by a diffuser which transmits negligible ballistic light. The speckles that hit the object excite fluorescence, that appear as a diffused blob on the front side of the diffuser. However the optical memory effect allows deterministic scanning of this overlap when the scattering layer has a physical thickness that is small compared to the distance to the object. By varying the incident angle, an angle-dependent intensity is measured from which the autocorrelation of the object can be extracted. Subsequently the shape of the object can be retrieved from the autocorrelation. We demonstrated imaging through a thin, strongly scattering screen based on fluorescence contrast.

Guiding a Non-classical State of Light Propagating through a Multiply Scattering Medium

Hugo Defienne[1, 2], **Marco Barbieri**[3], **Benoit Chalopin**[4], **Beatrice Chatel**[4], **Ian Walmsley**[3], **Brian Smith**[3], **and Sylvain Gigan**[1, 2]

[1]Institut Langevin, ESPCI ParisTech, CNRS UMR 7587, INSERM ERL U979
1 rue Jussieu, Paris 75005, France
[2]Laboratoire Kastler Brossel, Université Pierre et Marie Curie, Ecole Normale Supérieure
CNRS, 4 Place Jussieu, Paris Cedex 05 75252, France
[3]Clarendon Laboratory, University of Oxford, Parks Road, Oxford, OX1 3PU, United Kingdom
[4]Laboratoire de Collisions, Agrégats, Réactivité (CNRS UMR 5589), IRSAMC
Université Paul Sabatier, Toulouse 31062, France

Abstract— We investigate the possibility to use wavefront shaping techniques in order to generate and control non-classical states of light propagating through a multiply scattering medium. We experimentally show efficient guiding of a single-photon into a single-mode fiber placed at arbitrary positions after propagation in the medium, and demonstrate generation of an entangled state by focusing the single photons into two fibers simultaneously.

Quantum random walks offer an interesting playground for applications ranging from quantum simulation to computing. Complex media are a promising platform, since they naturally provide coherent coupling between a huge number of modes [1]. However, losses and scattering severely reduce their efficiency and such a system is generally considered unpractical for quantum applications. Recently, wavefront shaping techniques have been proposed to control the light propagating through a complex media [2]. Working with a linear non-absorptive medium, we can learn the scattering matrix of the medium and use it to control the output field [3]. This method permits for instance to focus classical light in one or more output modes using a spatial light modulator.

In our experiment [5], we generate a single-photon state of light using an heralding process based on a spontaneous parametric down conversion pair-generation setup. The scattering matrix is measured using a bright classical light in the same mode as the heralded single-photon, which means the medium is characterized for this specific optical mode [3].

First, we show that we can use the scattering matrix to strongly enhance the probability to detect a single photon in one specific output mode of our system, namely a single mode fiber. Moreover, the knowledge of the scattering matrix allows us to focus light in two different fibers with a well-controlled relative phase. By this mean, we generate the one-photon entangled state $|0\rangle_A|1\rangle_B + e^{i\phi}|1\rangle_A|0\rangle_B$ with a complete control of the position of the output modes A and B and of the phase ϕ. We characterize the purity of the entangled state generated by observing single-photon interferences on a beam splitter and by measuring the concurrence.

This experiment shows that the wavefront shaping methods in complex media can be applied to non-classical light and can be used to generate an arbitrary one-photon entangled state, with potential applications in quantum information.

REFERENCES

1. Peeters, W. H., J. J. D. Moerman, and M. P. van Exter, *Physical Review Letters*, Vol. 104.17, 173601, 2010.
2. Mosk, A. P., et al., *Nature Photonics*, Vol. 6.5, 283–292, 2012.
3. Popoff, S. M., et al., *Physical Review Letters*, Vol. 104.10, 100601, 2010.
4. Huisman, T. J., et al., arXiv preprint, arXiv:1210.8388, 2012.
5. Defienne, et al., arXiv:1401.3239 [quant-ph].

Making Materials to Engineer Generation and Transport of Light

Ceferino López Fernandez
Instituto de Ciencia de Materiales de Madrid (CSIC), Spain

Abstract— Light generation and light transport can be strongly affected by the detailed structure of the media where they take place. Materials Science has developed many tools to tweak light-matter interaction most of which can be labelled as *assembly* and *templating*. These involve allowing or inducing small particles to arrange themselves into photonic structures and infiltrating materials into the structures thus formed. When identical or similar spheres are involved photonic crystals and photonic glasses can be obtained and most often the techniques used are colloidal. Other techniques dispensing with the liquid are being explored. The mechanical properties [1] of these packings are dependent on their water content and largely determined by the surface hydrophobicity [2]. Templating often involves the synthesis of host materials in the pores of preassembled structures or around the particles before assembling. The former has proven useful for building lasers both Bloch mode-based and random as well as for tuning the transport. Non-spherical particles are less prone to control but still offer great possibilities [3]. The use of FRET coupling between dyes [4] can expand their potential as laser sources and their tunability can then be achieved by their chemical balance or tuning through their photonic environment [5].

REFERENCES

1. Gallego-Gómez, F., V. Morales-Flórez, Á. Blanco, N. de la Rosa-Fox, and C. López, "Water-dependent micromechanical and rheological properties of silica colloidal crystals studied by nanoindentation," *Nano Lett.*, Vol. 12, 4920-4, 2012.
2. Blanco, A., F. Gallego-Gómez, and C. López, "Nanoscale morphology of water in Silica colloidal crystals," *J. Phys. Chem. Lett.*, Vol. 4, 1136–1142, 2013.
3. Leonetti, M., C. Conti, and C. Lopez, "Non-locality and collective emission in disordered lasing resonators," *Light Sci. Appl.*, Vol. 2, e88, 2013.
4. Ibisate, M., J. F. Galisteo-López, V. Esteso, and C. López, "FRET-mediated amplified spontaneous emission in DNA-CTMA complexes," *Adv. Opt. Mater.*, Vol. 1, 651–656, 2013.
5. Galisteo-Lopez, J. F., M. Ibisate, and C. Lopez, "FRET-tuned resonant random lasing," *J. Mater. Chem. C*, 2014, in Press.

Subradiant Out-of-plane Scattering in Strongly Confined 2D Disordered Modes

Filippo Pratesi[1], **Kevin Vynck**[3], **Matteo Burresi**[1,2], **and Diederik S. Wiersma**[1,2]

[1]European Laboratory for Non-linear Spectroscopy (LENS), University of Florence
Via N. Carrara 1, Sesto Fiorentino, Firenze 50019, Italy
[2]Istituto Nazionale di Ottica (CNR-INO), Largo Fermi 6, Firenze 50125, Italy
[3]Laboratoire Photonique, Numerique et Nanosciences (LP2N), Institut d'Optique d'Aquitaine
CNRS-IOGS-University Bordeaux, UMR 5298, Talence 33400, France

Abstract— The study of wave propagation in disordered systems is tackled in various areas of science, e.g., from classical to quantum waves, from biology to solid state physics. In recent years, a rising interest is aimed toward the presence of different structural correlations and how these affect the propagation of waves. For example, in short-range correlated systems the opening of band-gaps was theoretically predicted [1], as well as the formation of localized states at the band edge of disordered photonic crystals [2].

In this work, we show that in correlated-disordered quasi-2D systems short-range order not only modifies the inplane multiple scattering, inducing a strong localization of light [3], but also dominates the out-of-plane coupling mechanism (Figures 1(a), (b) inset). As the volume of these localized modes reduces, the vertical loss concurrently decreases, leading to the counterintuitive effect of having a better 'cavity mode' in a smaller volume (Figure 1(c)). We show that this effect is induced by the coherent scattering involving nearest-neighbor scattering elements which inhibits the out-of-plane coupling.

To study this effect we calculated the lifetime associated with a random and correlated patterns of holes in a thin slab, using the 3D Finite-Difference Time-Domain (FDTD) method and a fitting procedure after spectral filtering. The thickness of the film was $t = 0.1\,\mu\text{m}$, radius $r = 0.23 * d_{av}$ with $d_{av} = 0.46\,\mu\text{m}$ average distance between holes, and dielectric constant $\varepsilon = 12$. However, while for the random system (not shown) the lifetime is directly proportional to the transport mean free path [3], this is not true when short-range correlations are present (Figure 1(a)). In particular a decrease of the lifetime would be expected, due to the increase of the in-plane scattering strength and the modulation of the density of photonic states (DOS) around the frequency $0.073t/\lambda$ (Figure 1(a) inset), numerically calculated for the analogous 2D system in the effective medium approximation [4]. The number of resonances above the light line was also obtained from this calculation (Figure (b)) and its comparison with the average lifetime shows

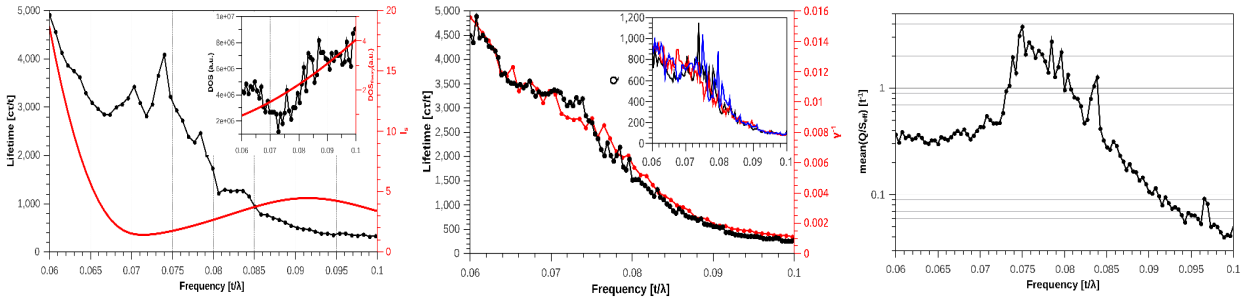

(a) (b) (c)

Figure 1: (a) Lifetime as a function of adimensional frequency of the correlated-disordered system calculated with 3D FDTD (black). Transport mean free path (red) calculated with the semi analytical approach developed in [3] for the purely 2D system. ((a) inset) Numerical (2D FDTD) and semi-analytical density of states for 2D system with effective refractive index in order to take into account the finite thickness of the slab and the presence of the holes (Maxwell-Garnett mixing rule). (b) Lifetime averaged over six disorder realizations (black) for the correlated disordered system (3D FDTD) and inverse number of resonances above the light line (2D FDTD) (red) [4]. ((b) inset) Quality factor of three disorder realizations. (c) Average quality factor of the localized modes divided by their effective spatial extention calculated from the Inverse Participation Ratio.

how out-of-plane losses of the 3D system can be predicted from the correlated disordered 2D system and how these are closely related to disorder in plane. The out-of-plane losses, T_{out}, for one and two holes in a slab was also calculated with 3D FDTD and showed how these are different in the two cases, having a minima at $0.073t/\lambda$ when the two holes are detached by d_{av}. This suggest that a coherent scattering mechanism is acting between neighbouring holes to reduce the out-of-plane losses.

REFERENCES

1. Liew, S. F., et al., *Phys. Rev. A*, Vol. 84, 063818, 2011.
2. Huisman, S. R., et al., *Phys. Rev. B*, Vol. 86, 155154, 2012.
3. Conley, G. M., et al., *Phys. Rev. Lett.*, 2014, accepted for publication.
4. Vynck, K., et al., *Nature Materials*, Vol. 11, 1017–1022, 2012.

Anderson Localization of Electromagnetic Waves in Randomly-stratified Metamaterials

Kihong Kim
Department of Energy Systems Research, Ajou University, Suwon, Korea

Abstract— We study the propagation and Anderson localization of electromagnetic waves in a randomly-stratified metamaterial slab, where both the dielectric permittivity ϵ and the magnetic permeability μ depend on one spatial coordinate z in a random manner. We assume a δ-function-correlated Gaussian randomness and consider three cases. In the first case, the randomness of ϵ and that of μ are uncorrelated. In the second case, both ϵ and μ are random, but the impedance $Z(=\sqrt{\mu/\epsilon})$ is uniform, while the refractive index $n(=\sqrt{\epsilon\mu})$ is random. In the third case, n is uniform, while Z is random. Using the invariant imbedding theory of wave propagation generalized to random media, we calculate the transmittance and the localization length of s and p waves incident obliquely on the slab, as a function of the incident angle θ and the strength of randomness in a numerically exact manner. When ϵ and μ are independently random, we find a generalized version of the Brewster anomaly phenomenon, where the localization length takes an extremely large value at a certain finite incident angle. In the second case where Z is uniform and n is random, the waves incident perpendicularly on the slab are delocalized, as expected in impedance-matched cases. Obliquely incident waves, however, are found to be localized. As the incident angle increases from zero, the inverse localization length increases from zero monotonically to some finite value at $\theta = 90°$. We find an intriguing behavior that for a fixed incident angle, the localization length depends nonmonotonically on the strength of disorder. In the third case where n is uniform and Z is random, the waves are localized at all incident angles smaller than 90°. The inverse localization length decreases monotonically as θ increases from zero to 90°. The dependence on the disorder parameter is monotonic in this case.

Random Distributed Feedback Fiber Laser Employing Erbium-doped Fibers

Lulu Wang and Xinyong Dong
Institute of Optoelectronic Technology, China Jiliang University, Hangzhou 310018, China

Abstract— An erbium-doped fiber (EDF) based random laser is demonstrated for the first time with a half-opened cavity structure formed by using a fiber Bragg grating (FBG) reflector and a long-distance (5–30 km) single-mode fiber (SMF). Under the pump of a 1480-nm laser diode, typical random laser radiation grounded on the random distributed feedback of backward Rayleigh scattering of the long-distance SMF is achieved with an obvious threshold behavior as a function of pump power. Thanks to the half-opened cavity design and the efficient gain from the pumped EDF, the measured threshold power, 10 mW, is about two orders lower in magnitude than that of previously reported conventional random fiber lasers amplified through distributed Raman effects. Dual-wavelength random lasing operation is also achieved by using two FBGs with different reflection wavelengths as reflector.

The Role of Disorder in Plasmonic Hole Arrays

Ajay Nahata[1] and Z. Valy Vardeny[2]

[1]Department of Electrical and Computer Engineering, University of Utah, Salt Lake City UT, USA
[2]Department of Physics and Astronomy, University of Utah, Salt Lake City UT, USA

Abstract— The physics of periodic systems is of fundamental importance and results in a variety of phenomena governing wave transport and interference. However, deviations from periodicity may result in higher complexity and give rise to surprising effects. One such deviation is realized in the class of structures referred to as photonic quasicrystals (QC), where the building blocks are arranged using well-designed patterns, but lack translation symmetry. Nevertheless, these structures, which lie between periodic and disordered or random structures, still show sharp diffraction patterns that attest to the existence of wave-interference resulting from long-range order [1]. We studied the properties of surface plasmon polaritons (SPP) on metallic foils using terahertz (THz) transmission measurements through a variety of two-dimensional (2D) QC hole arrays that include: Penrose structure [2], dodecagonal QC, deterministic 2D Fibonacci and Prouhet-Thue-Morse structures [3], as well as QC approximates and fractals [4]. We describe the obtained enhanced transmission resonances (and Fano-type anti-resonances) as due to SPP interference on the surfaces of the underlying geometry which contains discrete Fourier components, or reciprocal vectors in **k**-space, that govern the structure factor [1]. Comparison of the transmission resonances strength of the plasmonic QC with that in periodic hole arrays is used to investigate the *correlation length* of SPP in the QC structures [3].

REFERENCES

1. Vardeny, Z. V., A. Nahata, and A. Agrawal, "Optics of photonics quasicrystals," *Nature Photonics*, Vol. 7, 177, 2013.
2. Matsui, T., A. Agrawal, A. Nahata, and Z. V. Vardeny, "Transmission resonances through quasicrystal arrays of subwavelength apertures," *Nature*, Vol. 446, 517, 2007.
3. Nguyen, T. D., A. Nahata, and Z. V. Vardeny, "Measurement of surface plasmon correlation length differences using Fibonacci deterministic hole arrays," *Opt. Express*, Vol. 20, 15222, 2012.
4. Agrawal, A., T. Matsui, Z. V. Vardeny, and A. Nahata, "THz spectroscopy of plasmonic fractals," *Phys. Rev. Lett.*, Vol. 102, 113901, 2009.

Optical Materials by Design for Enhancing Light Harvesting in Dye Solar Cells

G. Lozano, C. Lopez-Lopez, F. E. Galvez, S. Colodrero, A. Jiménez, M. E. Calvo, H. Míguez
Institute of Materials Science of Seville, Spanish National Research Council, Seville, Spain

Abstract— In order to enhance light harvesting efficiency (the useful fraction of the incident light absorbed) in dye solar cells, different light-trapping mechanisms based on nanostructures compatible with the electrochemical device have been investigated. Due to the complexity involved in preparing and describing theoretically such nanostructured materials, most of the time, the analysis of the actual solutions employed is based on practical issues, rather on theoretical modelling. In this talk we will review different approaches to the optical design of dye solar cells to maximize light absorption. They comprise from methods based on photonic crystals or periodic surface patterns to those based on the inclusion of diffuse scattering particles randomly arranged in different configurations. Our work provides a theoretical framework in which the response of solar cells containing optical materials by design can be rationalized. The effect of these designs on the photovoltaic performance will be discussed, as well as the interplay with the semitransparency of the device, of interest for building-integrated photovoltaic devices.

REFERENCES

1. Gálvez, F. E., P. R. Barnes, J. Halme, and H. Míguez, "Dye sensitized solar cells as optically random photovoltaic media," *Energy & Environ. Sci.*, Vol. 7, 689, 2014.
2. Gálvez, F. E., E. Kemppainen, H. Míguez, and J. Halme, "Effect of diffuse light scattering designs on the efficiency of dye solar cells: An integral optical and electrical description," *J. Phys. Chem.*, Vol. 116, 11426, 2012.
3. Colodrero, S., A. Forneli, C. López-López, L. Pellejà, H. Míguez, and E. Palomares, "Efficient transparent thin dye solar cells based on highly porous 1D photonic crystals," *Adv. Funct. Mater.*, Vol. 22, 1303, 2012.
4. Colonna, D., S. Colodrero, H. Lindström, A. Di Carlo, and H. Míguez, "Introducing structural colour in DSCs by using photonic crystals: Interplay between conversion efficiency and optical properties," *Energy & Environ. Sci.*, Vol. 5, 8238, 2012.
5. López-López, C., S. Colodrero, S. R. Raga, H. Lindström, F. Fabregat-Santiago, J. Bisquert, and H. Miguez, "Enhanced diffusion through porous nanoparticle optical multilayers," *J. Mater. Chem.*, Vol. 22, 1751, 2012.
6. Lozano, G., S. Colodrero, O. Caulier, M. E. Calvo, and H. Míguez, "Theoretical analysis of the performance of one-dimensional photonic crystal-based dye-sensitized solar cells," *J. Phys. Chem. C*, Vol. 114, 3681, 2010.

Anderson Localization in Low-dimensional Structures to Enhance Light-matter Interaction

P. Lodahl and P. D. García
Quantum Photonics Group, Niels Bohr Institute, University of Copenhagen
Blegdamsvej 17, Copenhagen DK-2100, Denmark

Abstract— Introducing disorder in low-dimensional structures like photonic crystal waveguides (Figure 1(a)) or photonic crystals (Figure 1(b)) leads to Anderson localization of light (see insets). Light in these structures is efficiently trapped by random multiple scattering from the lattice imperfections. These disorder-indiuced optical modes are promising for cavity-quantum electrodynamics (QED) experiments where the radiative emission rate of single quantum emitters can be controlled when tuned through resonance with one of these random cavities, both in photonic crystal waveguides [1] and photonic crystals [2]. In addition, by using quantum dots as internal light sources reveals new physiscs in the form of *nonuniversal* intensity correlations between the different scattered paths within the structure. These novel correlations imprint the local QED properties deep inside the complex structure onto the far-field intensity pattern [2].

Finally, embedding quantum wells in a disordered photonic crystal waveguide allows the observation of random nanolasing where the cavity feedback is provided by the intrinsic disorder, which enables highly efficient, stable, and broadband tunable lasers with very small mode volumes [3].

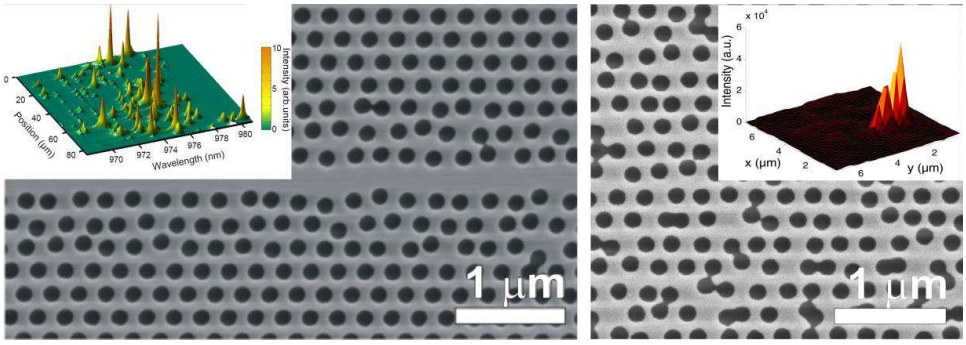

(a) (b)

Figure 1: (a) Scanning electron micrograph of a photonic crystal waveguide (top view) where the holes are deliberately displaced with respect to the ideal position. Inset: Spectral signature of Anderson localization of light in a disordered photonic crystal waveguide. The sharp optical resonances appear randomly distributed along the waveguide at frequencies in the slow-light regime of the waveguide. (b) Scanning electron micrograph of a photonic crystal with disorder in the holes position. Inset: quantum dot photoluminescence spectra collected while scanning the samples for a wavelength, $\lambda = (903 \pm 1)\,\mathrm{nm}$. The bright peaks are signatures of Anderson-localized modes.

REFERENCES

1. Sapienza, L., H. Thyrrestrup, S. Stobbe, P. D. Garcia, S. Smolka, and P. Lodahl, "Cavity quantum electrodynamics with Anderson-localized modes," *Science*, Vol. 327, 1352, 2010.
2. García, P. D., S. Stobbe, I. Soellner, and P. Lodahl, "Nonuniversal intensity correlations in two-dimensional Anderson-localizing random medium," *Physical Review Letters*, Vol. 109, 253902, 2012.
3. Liu, J., P. D. Garcia, S. Ek, N. Gregersen, T. Suhr, M. Schubert, J. Mørk, S. Stobbe, and P. Lodahl, "An Anderson-localized random nanolaser," to appear in *Nature Nanotechnology*, 2014.

Light Propagation in 3D Deterministic Aperiodic Tilings

Georg von Freymann[1, 2] **and Michael Renner**[2]

[1]Department of Physics and Research Center OPTIMAS
University of Kaiserslautern, Kaiserslautern 67663, Germany
[2]The Fraunhofer Institute for Physical Measurement Techniques, Germany

Abstract— Deterministic aperiodic structures provide the possibility to study light propagation in specific potential landscapes whose Fourier components are determined by the underlying aperiodic sequence. In accordance with Lebesgues spectral theorem the Fibonacci, Thue-Morse and Rudin-Shapiro sequences are examples of the three basic spectral measures, namely pure-point, singularly-continuous and absolutely-continuous, respectively. The Rudin-Shapiro sequence is closely related to uncorrelated disorder as it was designed to have a white noise power spectrum [1].

For the structure design we follow a common scheme to obtain so-called cubic tilings which are derived from a simple cubic crystal [2]. In these tilings the distances between lattice planes along the Cartesian axes take one of two different values. Which value the distance takes is determined by one of the above mentioned binary sequences. When choosing the Fibonacci sequence and a ratio of the two distances equal to the golden mean one ends up with a cubic Fibonacci tiling which is classified as a quasicrystal.

The tilings are fabricated by writing rods along the Cartesian axes using direct laser writing (DLW) in a negative-tone resist. Fabricating such complex structures with reasonable size requires galvanometric scanners to reduce the writing time. Furthermore, one has to employ an index-matched resist to avoid writing depth dependent aberrations.

We fabricate sets of samples of increasing generation number (up to the 10th Fibonacci generation along each axis) to study the scaling of the optical properties with system size (total transmission, mode pattern distributions). By measuring the effective width of a light beam traversing structures of different heights we deduce sub-diffusive behavior for all sequences in the near-infrared spectral range. For Rudin-Shapiro, the lateral mode profile shows an exponential decay indicating the existence of laterally localized states [3].

REFERENCES

1. Baake, M. and U. Grimm, "Surprises in aperiodic diffraction," *J. Phys. Conf. Ser.*, Vol. 226, 012023, 2010.
2. Lifshitz, R., "The square Fibonacci tiling," *J. Alloys Compd.*, Vol. 342, 186–190, 2002.
3. Renner, M. and G. von Freymann, "Transverse mode localization in three-dimensional deterministic aperiodic structures," *Adv. Opt. Mater.*, Vol. 2, 226–230, 2014.

Transmission Matrix Approach to Spatio-temporal Focusing of Light through Complex Media

Daria Andreoli[1, 2], **Giorgio Volpe**[1, 2], **Ori Katz**[1, 2], **Sébastien Popoff**[1, 2], **Samuel Gresillon**[1], **and Sylvain Gigan**[1, 2]

[1]Institut Langevin, ESPCI ParisTech, CNRS UMR 7587
INSERM ERL U979, 1 rue Jussieu, Paris 75005, France
[2]Laboratoire Kastler Brossel, Université Pierre et Marie Curie
Ecole Normale Supérieure, CNRS, 4 Place Jussieu, 75252 Paris Cedex 05, France

Abstract— Correcting for the spatial and temporal distortions of light induced by a strongly scattering medium is the focus of many applied topics in physics and biology. Recently, several techniques achieved this goal by relying on phase-conjugation or optimization methods. Here, we describe the possibility of deterministically focusing an ultrashort pulse in space and time on multiple points at the far side of a scattering medium. This can be made possible by the measurement of the multispectral transmission matrix of the medium, controlling only the spatial degrees of freedom of the incident light.

Focusing light in space and time through complex media is paramount in many applied topics in biology, imaging and nanomanipulation. However, light is strongly scattered when propagating through inhomogeneous media, thus preventing the achievement of this goal. Recently, active wavefront shaping techniques have emerged as a powerful way to control light propagation through complex media by relying on the use of spatial light modulators (SLM). The first approaches used phase-conjugation or optimization methods to either spatially focus light and/or to correct for the temporal distortion of an ultrashort pulse after propagating through the scattering medium. An alternative solution to the problem is a matricial approach, where the transmission matrix of the medium is measured. While optimization or phase-conjugation techniques have been shown to allow some degree of temporal control, the matrix approach has been monochromatic so far. Here, we propose to measure and use the transmission matrix to not only focus in space and in time through a complex medium, but to generate an arbitrary spatiotemporal distribution. In essence, we operate a femtosecond laser in CW mode around 800 nm, and measure the monochromatic transmission matrices at several wavelengths that composes the spectrum of the pulse. Once this 3D spatio-spectral matrix is known, we show that it is possible to use only spatial degrees of control on a SLM to deterministically control the pulse propagation through the medium and to focus in space and time at its far side. This approach opens up opportunities to have a full deterministic control of a nano-object through a complex medium.

Random Laser with Er/Yb-codoped Fiber Grating

Lulu Wang and Xinyong Dong
Institute of Optoelectronic Technology, China Jiliang University, Hangzhou 310018, China

Abstract— A random fiber laser is demonstrated based on a 25-mm-long multi-phase shifted fiber Bragg grating, which was fabricated in a highly Er/Yb-codoped fiber with the beam-scanning method. By inserting twenty phase errors with random amplitudes between 0 and 2π along the grating and end-pumping the Er/Yb co-doped fiber with a 980-nm laser diode, we achieved low threshold (38 mW) either single or dual-wavelength random lasing operations of changeable wavelengths depending on the power of pump laser.

Session 2A7
SC3: Optical Resonances and Microresonators

Influence of External Optical Injection on Small-signal Modulation Response for AlGaInAs/InP Microring Lasers

Yong-Zhen Huang, Xiao-Meng Lv, Ling-Xiu Zou, Bo-Wen Liu, Yue-De Yang, Heng Long, Jin-Long Xiao, and Yun Du
State Key Laboratory on Integrated Optoelectronics
Institute of Semiconductors, Chinese Academy of Sciences, Beijing 100083, China

Abstract— Direct modulated microlasers have the merits of small footprints and low power consumption compared with the light source integrated with an external optical modulator. However, the direct modulated speeds are usually limited by the relaxation oscillation frequency for semiconductor lasers. To further improve the modulation speed, optical injection locking was investigated for semiconductor distributed feedback lasers, vertical-cavity surface-emitting lasers and photonic crystal lasers. In this paper, we investigate the steady and dynamic characteristics for a microring laser subject to external optical injection. Microring lasers can have lower threshold current and better high speed modulation characteristics than the microdisk lasers, due to the smaller cavity volume and less effect of carrier spatial hole burning and diffusion. The dynamic characteristics are investigated for a microring laser with a radius of 12 μm and a ring width of 7 μm connected with a 2-μm-wide output waveguide subject to external optical injection. Single mode operation is realized with a side mode suppression ratio of 33.4 dB at a biasing current of 25 mA and a temperature of 290 K, and the corresponding 3 dB bandwidth of the small signal modulation response is 12.4 GHz. Under the optical injection from a tunable laser, the improvements of the small signal modulation response curves are observed for the microring laser with an additional resonance peak around the frequency of the beat frequency between the lasing mode and the injecting light. Furthermore, the optical generation of microwave signal by light beating between the lasing mode and the injecting light is demonstrated using a high-speed photodetector and a spectrum analyzer. The microring lasers are suitable to be a part of photonic integrated circuits fabricated by planar technology processes, which makes it available to realize enhanced high-speed modulation as well as the optical generation of microwave signal based on the optical injection operation in the photonic integrated circuit with a small footprint.

The Application of Optical Resonators in Biosensing

Qimin Quan
Rowland Institute at Harvard University, Cambridge, MA 02142, USA

Abstract— I will present two platforms for label-free biosensing, towards the goal of single cell analysis and single protein detection, both based on optical resonators. I will focus on how the sensitivity, multiplexability and *in situ* detection can benefit from nano- and micro-resonators.

The first platform is a surface plasmon resonance bioprobe. The bioprobe comprises of a tapered optical fiber with 50 nm tip size. A single gold nanorod is attached to the end of the tip, surface of which is functionalized with antibodies specific to the target analyte. The collective oscillation of the conductive electrons at the surface of the gold nanorod couples strongly to the polarized light in the visible wavelength range, generating a localized surface plasmon resonance (LSPR) signal, and is sensitive to small perturbations to its optical mode near its surface. I will demonstrate that this bioprobe can be inserted into a living single cell and detect intracellular proteins without affecting the cell viability.

The second platform is an on-chip SOI micro-cavity sensor. Light is strongly confined due to the constructive interference by the optimally designed photonic crystal. The high-Q factor generates a sharp resonance feature, whose shift indicates the binding of proteins on the cavity surface. I will discuss the prospect for detecting single proteins with these sensors.

High-performance Microcavity Optical Sensor Connected with a Waveguide

Shuai Liu[1], **Zhiyuan Gu**[1], **Nan Zhang**[1], **Shumin Xiao**[2], **and Qinghai Song**[1, 3]

[1]Department of Electrical and Information Engineering, Shenzhen Graduate School
Harbin Institute of Technology, Shenzhen 518055, China
[2]Department of Material Science and Engineering, Shenzhen Graduate School
Harbin Institute of Technology, Shenzhen 518055, China
[3]State Key Laboratory on Tunable Laser Technology, Institute of Opto-Electronics
Harbin Institute of Technology, Harbin 158015, China

Abstract— The traditional microcavity sensors suffer from the precise control of the gap between microcavity and tapered fiber. Here we demonstrate new sensing mechanism with waveguide connecting with the microcavity directly which can solve this problem. By inputting light through the waveguide, the high-Q whipering-gallery modes are excited. From the reflection spectrum of the waveguide, more than 10^5 modes are received and 10^{-5} refractive index change can be detected. In addition, a 20 nm-radius nano particle is detected from the corresponding change of reflection spectrum.

Compact Multi-channel Cascaded-ring Optical Sensor with High Sensitivity

Mao Mao, Sitao Chen, and Daoxin Dai
Centre for Optical and Electromagnetic Research
State Key Laboratory for Modern Optical Instrumentation
East Building No. 5, Zijingang Campus, Zhejiang University, Hangzhou 310058, China

Abstract— We propose and demonstrate a novel digital optical sensor which consists of a ring-based $1 \times N$ wavelength-selective power splitter and N cascaded microring-resonators. These cascaded microring-resonators are used as the transducer elements for N channels. And the $1 \times N$ wavelength-selective power splitter, which serves as a $1 \times N$ power splitter and N wavelength-selective optical filters, is realized by a single microring resonator with $N+1$ directional couplers. One of these $N+1$ directional couplers is used to couple the light from the input waveguide to the microring-resonator while the other N directional couplers are couple light from the microring-resonator to the N output waveguides individually. These $N+1$ directional couplers are designed optimally to achieve a high extinction ratio by choosing the gap width appropriately so that the N output waveguides will have uniform outputs. Such a microring-based $1 \times N$ wavelength-selective power splitter is much more compact than a conventional way of using a $1 \times N$ power splitter and N micro-rings. For the transducer elements, the N cascaded microring-resonators are with identical designs and their FSR are slightly different from that of the wavelength-selective power splitter. When the ambient refractive index changes the resonance peak of the transducer ring shifts slightly, which introduces a significant wavelength shift for the major peak of the cascaded-ring system due to a Vernier effect. In this way, this helps to achieve an ultra-high sensitivity (at the order of 10^5 nm/RIU). In this paper, we present this novel design and the experimental results for our compact multi-channel optical sensor with high sensitivity.

Coherent Phase Control in Microresonators and Its Application in Optical Signal Processing

Linjie Zhou, Liangjun Lu, Jingya Xie, and Jianping Chen
State Key Laboratory of Advanced Optical Communication Systems and Networks
Department of Electronic Engineering, Shanghai Jiao Tong University, Shanghai 200240, China

Abstract— Microresonators are basic building blocks for a variety of optical signal processing functions. The frequency and time domain responses need to be carefully designed to satisfy specific application requirements. Coherent phase control in resonators is an effective way to tailor the resonance transmission spectrum. Here we present our recent work of using coherent phase control in two devices for optical switching and pulse reshaping.

The first device is a double-ring assisted Mach-Zehnder interferometer (DR-MZI). The DR-MZI combines the merits of resonance enhancement in microring resonators (MRRs) and the coherent interference in MZIs. The microrings are over-coupled to MZI arms with a π phase shift across the resonance wavelength. When the two microrings resonate at the same wavelength, the device transmission is at the cross state. When one microring experiences a slight refractive index change, the phase difference of the two MZI arms equals to π in between the resonance wavelengths, switching the transmission to the bar state. As a result of the coherent interference between the two resonance arms of MZI, the switching is more power efficient than individual MZIs and MRRs. In our design, p-i-n diodes and resistive microheaters are both integrated into the MRRs for electrical tuning and phase error correction, respectively. Experimental results show that the insertion loss of our device is within -3.4 dB and the crosstalk is better than -20 dB. Upon phase error correction with thermal power consumption of 2.31 mW, the switching power consumption is only 0.69 mW. High-throughput data transmission up to 25 Gbps has also been demonstrated at both bar and cross states with no observable deterioration on eye-diagrams. Based on the DR-MZI, more complex 4×4 and 16×16 switching fabrics can be constructed with compact size and superior performance.

The second device is a self-coupled optical waveguide (SCOW). The SCOW resonator differs from a single microring resonator in terms of resonance modes and transmission spectrum. Because of the coherent interference between the CW and CCW modes in the resonator, the output transmission spectrum exhibits double-notch resonances. The notch separation and the central transparency peak can be freely set by tuning the two coupling coefficients. This particular feature can be utilized to transform the input pulse to various forms. Our study shows that a Gaussian input pulse can be reshaped into a flat-top square-like pulse or two consecutive pulses in phase. A square pulses can also be converted to a Gaussian-like pulse upon truncating the spectral sidelobes. Around the transmission notch, the SCOW resonator can work as a first- or second-order temporal differentiator, which is particularly useful for optical computing. An odd-symmetry Hermite-Gaussian (OS-HG) waveform can be derived from the original Gaussian pulse.

Silicon Based Optical Matrix Processor for Parallel Computing

Lin Yang, Jianfeng Ding, Lei Zhang, and Ruiqiang Ji
State Key Laboratory on Integrated Optoelectronics
Institute of Semiconductors, Chinese Academy of Sciences, Beijing 100083, China

Abstract— Matrix-vector multiplication is a fundamental operation in modern digital signal processing fields. Inspired by the intrinsic spatial parallelism of optics, much effort has been made to develop optical apparatuses that can perform such a parallelizable operation. The Stanford multiplier [1] is one of the most notable demonstrations, which is composed of light source array, optical lens, spatial light modulator (SLM) matrix and photodetector array. Almost all implementations are large in volume and high in power consumption. Moreover, many removable elements adopted make them extremely sensitive to the environmental vibration. To overcome these limitations, we propose an on-chip optical matrix-vector multiplier (MVM) [2, 3], which is composed of laser-modulator array, multiplexer, splitter, microring modulator matrix and photodetector array. The fan-out and fan-in with optical lenses in the traditional optical MVMs are replaced by the power splitting and wavelength multiplexing with waveguide devices in the proposed optical MVM, which greatly reduces the complexity and size of the system. The discrete components in the traditional optical MVMs are replaced by the integrated ones in the proposed optical MVM, which improves the stability and power efficiency of the system. 8×10^8 multiplications and accumulations per second is implemented by a demo system with a 4×4 microring modulator matrix [2, 3].

REFERENCES

1. Goodman, J. W., A. R. Dias, and L. M. Woody, "Fully parallel, high-speed incoherent optical method for performing discrete Fourier transforms," *Optics Letters*, Vol. 2, 1–3, 1978.
2. Yang, L., R. Q. Ji, L. Zhang, J. F. Ding, and Q. F. Xu, "On-chip CMOS-compatible optical signal processor," *Optics Express*, Vol. 20, 13560–13565, 2012.
3. Yang, L., L. Zhang, and R. Q. Ji, "On-chip optical matrix-vector multiplier," *Proceedings of SPIE*, Vol. 8855, 88550F-1, 2013.

Random Lasing by Chosen Resonances in Disordered Microcavities

Ceferino López Fernandez
Instituto de Ciencia de Materiales de Madrid (CSIC), Spain

Abstract— Optical resonances are most often identified with localized excitations in highly isolated microcavities. When identical resonators are coupled and their resonances interact they can lead to bands like electrons in solids (photonic bonds in photonic crystals) if ordered or to random resonances (photonic glasses) otherwise. Additionally if the resonators are all different only in very special circumstances (highly coupled) individual resonances survive to be identified. Disorder is typically lossy in this respect and only by providing gain to the system can one profit from disorder and resonance at the same time like in random lasers. We present results where resonances facilitate lasing in disordered systems with one [1] or two dyes [2] and show how these resonances can be made to interact to reveal both individual [3] and collective behaviours [4].

REFERENCES

1. Gottardo, S., et al., "Resonance-driven random lasing," *Nat. Photonics*, Vol. 2, 429–432, 2008.
2. Galisteo-Lopez, J. F., M. Ibisate, and C. Lopez, "FRET-tuned resonant random lasing," *J. Mater. Chem. C*, in press, 2014.
3. Leonetti, M., C. Conti, and C. López, "Switching and amplification in disordered lasing resonators," *Nat. Commun.*, Vol. 4, 1740, 2013.
4. Leonetti, M., C. Conti, and C. Lopez, "Non-locality and collective emission in disordered lasing resonators," *Light: Sci. Appl.*, Vol. 2, e88, 2013.

Making Microwave Radiation Visible: Phase-matching in Non-linear Crystalline Whispering Gallery Mode Resonators

Harald G. L. Schwefel[1, 2]

[1]Max Planck Institute for the Science of Light, Erlangen 91058, Germany
[2]Institute for Optics, Information and Photonics
University of Erlangen-Nuremberg, Erlangen 91058, Germany

Abstract— Efficient coherent conversion of microwave or THz radiation into the visible or near infrared is a challenging but worthwhile endeavor. With coherent detection, large detector arrays are possible to detect for example weak variations in the cosmological background radiation. Furthermore, where the microwave photon is fragile due to its low photon energy to environmental noise, the optical photon is more resistive and can be transported through long distances. Still in the microwave domain integrated microwave circuits are the most likely route towards the quantum computer. In order to communicate with such a quantum computer and distribute the results these states need to be converted coherently into optical photons that are more resilient and can live at room temperature. Nonlinear parametric sum-frequency generation is a process that conserves both the phase and amplitude of the initial state and is thus ideal for such an attempt. Phase-matching in second order non-linear interactions is critical for efficient conversion. In crystalline whispering gallery mode (WGM) resonators, where the light is confined by total internal reflection along the equator of a convex dielectric this requirement can be achieved by considering the angular momentum of the interacting modes.

Here we report on a room-temperature converter of near THz radiation based on a crystalline lithium niobate WGM resonator. Its high nonlinear $\chi^{(2)}$ coefficient together with its high optical quality factors ($Q > 10^8$) allows one to overcome the usually low efficiencies of such nonlinear processes. Geometric phase-matching and novel coupling techniques for the microwave radiation into the WGM resonator will be discussed and a first outlook for the ultimate experiment given.

Demonstration of a 3-bit Digital-to-analog Convertor Based on Silicon Microring Resonators

Jianfeng Ding, Fanfan Zhang, Qiaoshan Chen, and Lin Yang
State Key Laboratory on Integrated Optoelectronics
Institute of Semiconductors, Chinese Academy of Sciences, Beijing 100083, China

Abstract— Because of the advantage of large-capacity transmission and high-speed processing for digital signals over analog signals, the analog-to-digital convertor (ADC) and digital-to-analog convertor (DAC) have been widely used in many applications. The ADC converts the analog signal from the sensors into the digital signals. Then the digital signals are disposed by the computers or digital signal processors. The feedback signal is generated and converted into the analog signal by a DAC. As the electrical circuits become faster and faster, the bottleneck of sampling accuracy and aperture jitter will be more and more serious. Optical structures for ADC and DAC are considered as a potential solution to this problem. Silicon photonics has the advantage of integrating optical devices and electrical circuits in the same platform and is considered as a candidate to solve the problems of the future ADC/DAC.

We propose an N-bit optical DAC based on silicon microring resonators. A multiple-wavelength lightwave is coupled into the waveguide. The lightwaves with different wavelengths have different optical powers. The lightwave with the wavelength of λ_i has an optical power of $P/2^i$, where P is a constant optical power. The optical powers of the lightwave with different wavelengths are set as the reference weight for different digital bits, which is similar with that in the electrical DAC. There are N silicon microring resonators sharing the same bus waveguide, whose resonance wavelengths are corresponding to the input wavelengths. a_i is the electrical signal applied to the microring resonator. So the final output power is $\sum_{i=0}^{n} a_i \frac{P}{2^i}$ which is the digital-to-analog converting result of a digital sequence. As a proof of concept, a 3-bit DAC is fabricated and works well at a sampling speed of 500 Msample/s.

Laser from Localized Modes on a Conical Surface

Xing Lin, Yuan Niu, Yingxin Xu, and Wei Fang
State Key Laboratory of Modern Optical Instrumentation
Department of Optical Engineering, Zhejiang University, Hangzhou 310027, China

Abstract— In classical ray optics model, light propagating along the surface of a cone is bounded on narrower side and unbounded on the wider side, indicating that no stable orbit exists. However, when wave nature is taking into consideration, it has been shown that there exist localized whispering-gallery modes along conical surface when the cone angle is small. In this work we demonstrate, for the first time, lasing behavior from a silica conical surface whose surface was coated with colloidal semiconductor nanocrystals (NCs) as gain media.

The sample was prepared by melting the tip of a tapered fiber. A microsphere was formed on the tip, and the transition section between microsphere and the attached stem fiber naturally forms a conical surface. The microsphere sample was immersed into CdSe/CdS core/shell NC solution for several seconds, and dried in air to form a NC film on it. The sample was then pumped by a 532 nm nanosecond pulse laser operating at a repetition rate of 10 kHz. The emission from the sample was collected by an objective lens, and the image of the sample was projected on the entrance slit of a spectrometer equipped with a 2-dimentional CCD detect, so that spatial resolved spectrum could be measured.

Though microsphere has extremely high-Q whispering-gallery modes on the equator, to our amazement, we found that the majority samples first lased at the conical region rather than equator region, which were confirmed both from photoluminescence images of the sample and spatial resolved spectrum. We attributed this abnormal behavior to higher optical gain and localization of optical modes on a conical surface, after inspecting the NC film thickness and conducting numerical simulations.

Thermally-tuned Silicon Double Ring Resonator for External Cavity Tunable Laser

Lei Ding, Xianxin Jiang, Chang Yang, and Jian-Jun He
State Key Laboratory of Modern Optical Instrumentation
Centre for Integrated Optoelectronics, Department of Optical Engineering
Zhejiang University, Hangzhou 310027, China

Abstract— Silicon photonics has been considered a promising technology for large-scale and low-cost integration of photonic devices. To date, many optical devices have been demonstrated on silicon-on-insulator (SOI) platform, which are compatible with CMOS technology. For a compact and low power consumption tunable filter, silicon waveguide based ring resonator is attractive, owing to strong optical confinement and efficient thermal-optical effect of silicon. This paper presents a thermally-tuned silicon double ring resonator (DRR), using SOI with a 250 nm silicon top layer and a 2 μm buried oxide (BOX) layer. We used two racetrack ring resonators of slightly different optical path lengths to realize a wide tuning range based on Vernier effect. Numerical simulations based on the heat-transport equation are performed to show the temperature distribution in the tuning resonator and the performance of micro-heaters is optimized based on material thermal properties. The variation of effective refractive index of about 0.015 is achieved when the temperature changes by 80 K, corresponding to a wavelength shift in the order of 10 nm, which can be amplified by an order of magnitude using the Vernier effect. The resonator structure with micro-heaters is fabricated and the wavelength tuning is experimentally demonstrated. The DRR footprint is $\sim$ 700 μm × 400 μm. The free spectral ranges (FSRs) of the two racetrack ring resonators are 400 GHz and 500 GHz, respectively. The electrical properties of heaters and thermo-optical properties of the DRR are investigated. Using this DRR as a wavelength-tunable filter, a III-V/SOI external cavity tunable laser with narrow emission linewidth is designed and fabricated. The laser consists of an InP based gain section, the DRR and a free-space transmission section. The latter uses graded-index lenses to couple the gain chip with the DRR, constructing a long external cavity. Preliminary experimental results of the laser will be presented.

Session 2A8
SC2&1: Effective Medium Theories and Homogenization

From Acoustic Metamaterials to Functional Metasurfaces

Nicholas X. Fang
Department of Mechanical Engineering, Massachusetts Institute of Technology
77 Massachusetts Ave, Cambridge MA, USA

Abstract— By guiding and controlling the wave path through a deformed space, metamaterial devices that display distinctive response to light, acoustic waves and heat waves have opened up a new field of considerable interest. However, current challenge issues such as high loss and complex geometries are hampering the development of metamaterial technology. Is it possible to tailor the field information contained by a complex volumetric object with a thin metamaterial structure, so the observer from afar would not tell the difference?

In this invited talk, we will present our research progress toward tailoring the edge rays and creeping rays with acoustic metasurfaces. The tailored metasurface could lead to two pronounced effects: redirecting the reflected rays by spatial impedance gradient and reducing the strength of the edge rays. In fact our recent study suggest such illusional effects by embedding wedges in a transformed acoustic medium, and we will present theoretical analysis and experimental study of such engineered components with acoustic metasurface. The potential application of such novel device concept in underwater communication and medical ultrasound will be also discussed.

Generalized Effective Medium Theory for Metamaterials Beyond the Long-wavelength Limit

Baocheng Zhu, Shiwei Tang, Shiyi Xiao, and Lei Zhou
State Key Laboratory of Surface Physics
Key Laboratory of Micro and Nano Photonic Structures (Ministry of Education)
Physics Department, Fudan University, Shanghai 200433, China

Abstract— Metamaterials (MTMs) are man-made electromagnetic (EM) materials composed by subwavelength microstructures with tailored properties so that the whole system can be viewed as a homogeneous medium with effective properties dictated by the local structures. Many fascinating wave-manipulation effects were proposed based on MTMs, some of which were subsequently realized experimentally. Typically, those predictions were first obtained based on hypothetical systems with some effective ε and μ distributions, and MTMs were then designed and fabricated according to the assumed effective-medium properties. Therefore, effective medium theory (EMT) plays a crucial role in the MTM development, since a good EMT can better guide people to design appropriate MTMs to realize the predicted phenomena. In the past years, many versions of EMTs were successfully developed, but many of them suffer different limitations in different aspects [1].

Here, we proposed an alternative version of EMT, which is particular suitable for determining the effective parameters of a periodic structure involving *dispersive* metallic structures. Our EMT can be viewed as a generalization of a previously developed homogenization scheme first proposed in [2] derived based on the mode-expansion method, which can only be applicable to systems involving perfect electric conductors (PEC). We applied the newly developed EMT to study the effective-medium properties of a composite material with periodic array of metallic cylinders possessing arbitrary cross sections. The obtained results show that our generalized EMT is valid in the entire parameter region inside which the permittivity ε_M of the metallic object takes value, supported by excellent agreements achieved by comparing with full-wave numerical simulations. In particular, our theory recovers the standard volume-average results when ε_M is very small (real long-wavelength limit), and recovers the previous homogenization results (valid for PEC systems) when ε_M is infinitely negative. Moreover, our theory can yield accurate results when ε_M takes arbitrary values where the previous theories cannot work. We will introduce in the conference more details of our theoretical establishment and some applications of our newly developed EMT.

REFERENCES

1. Choy, T. C., *Effective Medium Theory: Principles and Applications*, Clarendon Press, Oxford, 1999.
2. Garcia-Vidal, F. J., L. Martín-Moreno, and J. B. Pendry, *J. Opt. A: Pure Appl. Opt.*, Vol. 7, S97, 2005.
3. Zhu, B. C., S. Tang, S. Xiao, and L. Zhou, Unpublished.

Angle Dependent Effective Medium Theory for 2D Photonic Crystals

Meng Xiao, Xueqin Huang, Anan Fang, and C. T. Chan
Department of Physics, Institute for Advanced Study
The Hong Kong University of Science and Technology
Clear Water Bay, Kowloon, Hong Kong, China

Abstract— We build an effective medium theory for a two dimensional (2D) photonic crystal comprising a square lattice of dielectric cylinders with the incident electric field polarized along the axis of the cylinders. In particular, we discuss the feasibility of constructing an effective medium theory for the case where effective wave vector is far away from the center of Brillouin Zone. When the k-vector is far away from the Brillouin Zone, the optical response of system is necessarily anisotropic, implying that effective medium description becomes inevitability angle dependent. The effective medium parameters have to depend on the direction of incident light. We employ scattering theory and treat the two-dimensional system as a large stack of one-dimensional (1D) arrays. While traditional effective medium theory is good for small wave vectors, we can extend to a much larger region of k-space if we consider only the zero-order inter-layer diffraction and all the higher order diffraction terms of inter-layer scattering involving evanescent modes can be ignored. Scattering theory enables the calculation of transmission and reflection coefficients of a finite sized slab, and we can extract effective parameters such as the effective impedance (Z_{eff}) and effective refractive index (n_{eff}) using a parameter retrieval method. We note that effective refractive index is uniquely defined only in a very limited region of k-space ($n_{eff}k_0a \ll 1$, where k_0 is the wave vector in side vacuum and a is the lattice constant), but Z_{eff} is uniquely defined and has a well-defined meaning inside a much larger domain in k-space. The effective impedance Z_{eff} is purely real for the pass band and purely imaginary in band gaps. Using the sign of imaginary part of Z_{eff}, we can classify the band gaps into two groups and this classification explains why there is usually no surface state on the boundary of typical fully gapped photonic crystals comprising of a lattice of dielectric cylinders. This effective medium approach also allow us to predict the dispersion of surface states of photonic crystals for surface wave vectors that are well beyond the zone center.

Nonlocal Effective Medium Model for Periodic Layered Metamaterials

Ruey-Lin Chern
Institute of Applied Mechanics, Taiwan University, Taipei 106, Taiwan

Abstract— In this study, the author proposes a nonlocal effective medium model for periodic layered metamaterials. The effective permittivity tensor of the layered structure is extracted by Taylor's expansion on the dispersion relation up to fourth order in the long wavelengths. The effective permittivity exhibits drastic variations in the wave vector domain, showing a typical feature of nonlocal resonance. In particular, strong spatial dispersion is found in the frequency range where surface plasmon polaritons are excited. Due to the nonlocal effect, additional waves appear in the medium and are identified as the bonding or antibonding modes with symmetric or antisymmetric surface charge alignments. The additional wave can be a forward wave with negative refraction or a backward wave with ordinary refraction, but with a very different feature from that in a local anisotropic medium with opposite signs of the permittivity components. Due to the nonlocal effect, negative refraction and backward wave occur even when the effective permittivity components are all positive. From the viewpoint of the effective medium, the periodic layered metamaterials are considered a special type of medium with the elliptic-like, hyperbolic-like, parabolic-like, or mixed type of dispersion, depending on the frequency range. These characters come in part from the anisotropy and in part from the nonlocal nature of the layered structure, and are in correspondence with the variety of the effective permittivity components. Basic attributes of the effective permittivity tensor are categorized into four frequency ranges for the in-plane components and two ranges for the out-of-plane component, which are closely related to the dispersion characteristics of the layered structure for TM and TE polarizations, respectively. These attributes are analyzed in each frequency range to give a perspective on the spatial dispersion or nonlocal effect in the layered metamaterials.

ACKNOWLEDGMENT

This work was supported in part by National Science Council of the Republic of China under Contract No. NSC 102-2221-E-002-202-MY3.

A Homogenization Scheme for Acoustic Metamaterial

Min Yang[1], **Guancong Ma**[1], **Ying Wu**[2], **Zhiyu Yang**[1], **and Ping Sheng**[1]

[1]Department of Physics, Hong Kong University of Science and Technology
Clear Water Bay, Kowloon, Hong Kong, China
[2]Division of Mathematical and Computer Science and Engineering
King Abdullah University of Science and Technology (KAUST)
Thuwal 23955-6900, Saudi Arabia

Abstract— The metamaterials have made possible a broad horizon for wave manipulations beyond natural materials. The exotic effective material parameters of metamaterials are based on the collective behaviors of the locally resonant micro-heterogeneities. The presence of resonant scatterings represents a challenge to the classical homogenization theory, such as the coherent potential approximation, which is based on the philosophy of adjusting the effective parameter values so as to minimize scattering at the long wavelength limit. While such a philosophy is intrinsically consistent with Rayleigh scatterings, with the scattering cross section vanishing at the long wavelength limit, here the presence of resonant scatterings no longer guarantees weak scattering in the long wavelength limit.

Here, we present a homogenization scheme for acoustic metamaterials that is based on reproducing the lowest orders of scattering amplitudes from a finite volume of the metamaterials. With the aid of metamaterials' eigenstates, the effective parameters such as mass density and elastic modulus can be obtained by matching the surface responses of a metamaterial's structural unit cell with a piece of homogenized material. From the Green theorem applied to the exterior domain problem, matching the surface responses is noted to be the same as reproducing the scattering amplitudes. We verify our scheme by applying it to three different wave-types: elastic shear waves, acoustic pressure waves, and decorated-membrane system who is the coupling of the former two. It is shown that the predicted characteristics and wave fields agree almost exactly with numerical simulations and experiments, and the scheme's validity is constrained by the number of dominant surface multi-poles instead of the usual long wavelength assumption. In particular, the validity extends to the full band in one dimension and to regimes near the boundaries of the Brillouin zone in two dimensions.

1D Photonic Crystals as Nonlocal Photonic Media

Zhong Qi Yao, Jie Luo, and Yun Lai
School of Physical Science and Technology, Soochow University, Suzhou, China

Abstract— Photonic crystals and metamaterials have shown us the ability to control electromagnetic waves in an almost arbitrary manner, leading to unprecendented applications. Metamaterials, with the size of unit structure usually much smaller than the working wavelength, can often be regarded as an homogeneous effective media with unusual parameters, such as the double negative media in negative refraction and the anisotropic media in invisibility cloaks. On the other hand, photonic crystals, with the size of unit structure comparable to the working wavelength, usually do not work as effective media, but as band-gap materials.

In this work, we propose a new theory the obtain the effective parameters of 1D photonic crystals when the wave vector is far away from the Brillouine Zone center, even to the Brillouine Zone edge. We find that in this case certain photonic crystals can still be regarded as good effective media, but become nonlocal, i.e., the parameters of the effective medium being not only dependent on the frequency but also on the wave vector. Such a class of nonlocal photonic media opens up many new possibilities. Our work reveals new physics in a mesoscopic scale between photonic crystals as band gap materials and metamaterials as local effective media.

REFERENCES

1. Yao, Z. Q., J. Luo, and Y. Lai, to be submitted.

Topological Photonic Band Engineering of Zero-refractive-index Materials

Z. H. Hang, Y. T. Yang, and S. S. Wang
School of Physical Science and Technology, Soochow University
1, Shizi Street, Suzhou 215006, China

Abstract— Using two-dimensional photonic crystals, we successfully constructed a zero-index material, with both permittivity and permeability equal to zero [1]. By carefully tuning the properties of photonic crystal cylinders, a triply-degenerate state at the Brillion zone center can be formed and with the help of effective medium theory, the effective parameter of this photonic crystal can be described.

Though our major previous works concentrated on the interesting wave propagation properties inside this homogeneous zero-refractive-index photonic crystal, the accidental degeneracy induced triply-degenerate states have very fruitful physics to be discussed. We will show, by breaking the rotational symmetry of the zero-index photonic crystal, we can engineer the photonic band diagram and configure the electromagnetic wave propagation properties. The equi-frequency contours can be of various shapes and thus various topologies. The peculiar equi-frequency contours can be understood with the help of the boundary effect medium theory developed. Our theoretical analysis is further verified by our microwave experiments and a new type of beam steering devices is designed. As no extra degeneracy is introduced to the band diagram, our beam steering devices has a wide configurability and is thus easy to be fabricated. We will also show some optical device designs based on this new type of anisotropic photonic crystal.

REFERENCES

1. Huang, X., Y. Lai, Z. H. Hang, H. Zheng, and C. T. Chan, "Dirac cones induced by accidental degeneracy in photonic crystals and zero-refractive-index materials," *Nature Materials*, Vol. 10, 582, 2011.

Retrieving Effective Constitutive Parameters for Bulk Magnetic Metamaterials and Surface Charged Dielectric Nanoparticles

Shiyang Liu[1], **Neng Wang**[2, 3], **Zhifang Lin**[4], **and S. T. Chui**[5]

[1]Institute of Information Optics, Zhejiang Normal University, Jinhua, Zhejiang 321004, China
[2]State Key Laboratory of Surface Physics (SKLSP), Fudan University, Shanghai 200433, China
[3]Department of Physics, Fudan University, Shanghai 200433, China
[4]Key Laboratory of Micro and Nano Photonic Structures (Ministry of Education)
Fudan University, Shanghai 200433, China
[5]Bartol Research Institute, University of Delaware, Newark, DE 19716, USA

Abstract— Metamaterials are structured materials made of delicately designed subwavelength resonant building blocks, which can be considered to homogeneous materials with the effective permittivity ε_{eff} and the effective magnetic permeability μ_{eff}. Metamaterials exhibit a lot of exotic EM properties and give rise to many unprecedented phenomena and potential applications. To gain insight into all these results and characterize metamaterials, we need to develop effective-medium theory (EMT) to retrieve the effective constitutive parameters ε_{eff} and μ_{eff}. There are also works on the design of composite scattering particles, some of which can also be regarded as an equal-size homogeneous scattering particle. Retrieving the corresponding effective parameters is of also great importance for the understanding of the EM properties and the optimization of the design. As a consequence, an appropriate effective-medium theory is required.

In this presentation, we present an EMT based on the coherent-potential approximation, which is developed particularly for the retrieval of the effective constitutive parameters of metamaterials composed of an array of periodically arranged ferrite rods. Combined with extended Mie theory, we can obtain the anisotropic effective parameters. With this EMT, we can also obtain the effective parameters for the surface charged dielectric nanoparticles (CDNPs) in the long wavelength limit when a homogenous CDNP is treated as an equivalent conventional absorbing neutral particle of the same size. It is demonstrated that while the surface charge induces negligible change of magnetic permeability in particle, it gives rise to a significant change of electric permittivity. The change in permittivity depends on the charge, the particle size, and the working frequency but is independent of the constituent material. Therefore, based on EMT we can tailor the optical properties of CDNPs by optimizing their parameters, allowing for many exotic phenomena, such as vanishing scattering efficiency, great enhancement of light absorption e?ciency, and surface charge induced surface plasmon resonance.

Double Dirac Cones in Phononic Crystals and Zero Refractive Index Material

Jun Mei and Yan Li
Department of Physics, South China University of Technology, China

Abstract— In a two dimensional phononic crystal (PC) composed of a periodic array of rubber coated steel cylinders placed in water host, double Dirac cones can be obtained at the Brillouin zone center by utilizing the accidental degeneracy, where the geometrical parameters of each cylinder are deliberately adjusted so that a doubly-degenerate dipolar mode and a doubly-degenerate quadrupolar mode meet at exactly the same frequency. In such a situation, two identical pairs of isotropic linear cones are formed around the Brillouin zone center, which is shown to be an inevitable result of the spatial symmetry of the involved eigen modes. The linear behavior and even the slopes of the bands can be predicted by a perturbation theory similar to k.p method in quantum mechanics. With the help of the retrieval method, it is found that at the very vicinity of the cones' vertex, the PC can be described with an effective medium with zero refractive index. By tailoring the surface impedance of the PC, nearly total transmission of incident wave can be achieved with zero phase change inside the PC. As a further demonstration, such a zero index material can be also used to squeeze and tunnel the wave energy through a narrow waveguide channel.

Homogenizations of Micropolar Elastic Metamaterial Using Field Averaging

C. N. Weng and T. Chen
Department of Civil Engineering, Cheng Kung University, Tainan, Taiwan

Abstract— Micropolar elasticity, also called Cosserat elasticity, is a generalized continuum theory which is extensively used to describe the mechanical behavior of materials with intrinsic microstructure effects. Recently, inspired by electromagnetic metamaterials, the research of elastic metamaterials have attracted considerable interest, and micropolar theory is appropriate to analyze the metamaterial model than traditional continuum theory due to the complex local resonant effect within the microstructures. In this paper, we introduce an approximation in homogenization of heterogeneous elastic metamaterials by a homogeneous equivalent micropolar media whose effective parameters are determined by average theory. Explicit formulations of averaged physical fields over the representative volume element (RVE) are presented in the text. It is mentioned that the average strain is an asymmetric tensor while the average curvature tensor can be symmetric or not which depends on the geometric size of unit cell. The average stress is basically identical to that in classical elasticity whereas the average couple stress appears the contributions from the couple stresses together with stresses of each local point. We illustrate a simple model with cubic periodically arranged structures to demonstrate the calculation processes and the dispersion relation of plane wave propagation. The presented methodology can be applied to homogenize any periodic structure with unit cells having arbitrary chiral inclusions.

Homogenization Model of Aligned Spheres in a Host Sphere

F. Mangini[1], **F. Frezza**[1], **and A. Sihvola**[2]

[1]Department of Information Engineering, Electronics and Telecommunications
"La Sapienza" University of Rome, Via Eudossiana 18, Rome 00184, Italy
[2]Department of Radio Science and Engineering, Aalto University, Otakaari 5A, Espoo 00076, Finland

Abstract— In the present paper, we propose a homogenization model of a series of aligned spheres embedded in a host dielectric sphere, i.e., we present a static analysis of a series of aligned inclusions inside a dielectric sphere in order to deduce the properties of the electrical external field as for a homogenized sphere, afterwards the study is extended to the quasi-static case, providing the quasi-static rule for this particular case. Moreover we use the quasi-static approach in order to calculate the scattered field, the polarizability and the effective permittivity of this spherical system. The effective-medium analysis of a composite sphere has been previously attempted in [1]. We consider a similar situation, but our purpose is to extend the model to N spheres and to understand the role of the geometrical behavior of the inclusions on the effective-medium parameters, i.e., we want to understand how the number, the position and the dimensions of the spherical inclusion affect the scattered field. Moreover, we are interested in the determination of the plasmon resonances when the sphere has a plasmonic behavior. The plasmon resonances of a plasmonic sphere with one eccentric inclusion have been studied in the literature and play an important role in the metamaterial design [2, 3]. We present the plasmon behavior in our case of complex system. For the validation and to obtain the results we excite the model with a uniform electric field along the direction of the aligned spheres in order to obtain an axial symmetric problem. Before proceeding to the validation of the model, we discuss the convergence of the series to obtain a rule for our particular case and we show the dependence of the truncation criterion on the number, radii and dimension of the spheres. For the validation, each obtained result is compared with the simulations implemented on a commercial software based on the Finite Element Method, the validation is effectuated in the cases of two and four spherical inclusions. From the studies we can affirm that the polarizability of the system is affected mostly by the radius of the internal sphere and weakly by the internal spheres' position and number.

REFERENCES

1. Chýlek, P. and G. Videen, "Scattering by a composite sphere and effective medium approximations," *Opt. Commun.*, Vol. 146, No. 1–6, 15–20, 1998.
2. Yun, B., Z. Wang, G. Hu, and Y. Cui, "Theoretical studies on the near field properties of non-concentric coreshell nanoparticle dimers," *Opt. Commun.*, Vol. 283, No. 14, 2947–2952, 2010.
3. Pea-Rodrguez, O. and U. Pal, "Enhanced plasmonic behavior of bimetallic (Ag-Au) multilayered spheres," *Nanoscale Res. Lett.*, Vol. 6, 279–283, 2011.

Dynamic Effective Medium Theory for Anisotropic Photonic Crystals

Xiujuan Zhang and Ying Wu
Division of computer, Electrical and Mathematical Science and Engineering
King Abdullah University of Science and Technology, Saudi Arabia

Abstract— We propose an effective medium theory (EMT) from coherent potential approximation for two dimensional anisotropic photonic crystals composed of a rectangular array of elliptical cylinders embedded in air. The theory can give the isotropic effective permittivity and anisotropic effective permeability beyond the long wavelength limit. To verify the theory, we performed the band structure simulations for several kinds of anisotropic photonic crystals. The presented theory can reproduce the band structure very well not only at long wave-length limit, but also towards the high frequency regime with wavelength in background medium comparable or even smaller than the smallest spacing between scatterers. The theory predicts the existence of a semi-Dirac point in a particular photonic crystal, which is again verified by the band structure simulations. At the semi-Dirac point, both the effective permittivity and one component of the effective permeability vanish, while the other component of the effective permeability is non-zero. This combination well explains the topological transition in the iso-frequency surface from a closed ellipse to an open hyperbola and indicates the photonic crystal is zero-refractive-index material along one direction and epsilon-near-zero material along the perpendicular direction.

Session 2A9
SC3: Optical Fiber Sensing Devices

Micro/Nano Fiber-based Photonic Devices and Sensors

Wei Jin, **Wa Jin**, **Chao Wang**, **and Hoi Lut Ho**
Department of Electrical Engineering
The Hong Kong Polytechnic University, Hong Kong, China

Abstract— Novel in-line photonic microcells based on encapsulated micro/nano optical fibers are reported. The photonic microcells are made by post-processing conventional single mode optical fibers or photonic crystal fibers, which overcome the fragility and contamination problems associated with bare micro/nano optical fibers. The applications of these microcells for in-fiber wavelength and polarization filters, amplifying and absorption cells, high sensitivity refractive index sensors and accelerometers are demonstrated.

Polarimetric Heterodyning Fiber Grating Laser Magnetic Field Sensors

Bai-Ou Guan, Linghao Cheng, and Long Jin
Institute of Photonics Technology, Jinan University, Guangzhou 510632, China

Abstract— Polarimetric heterodyning fiber grating laser sensor translates the measurands into a change in the intra-cavity birefringence of fiber grating laser [1]. The detection of external perturbations is realized by monitoring the laser polarization-mode beat frequency in the radio-frequency domain, usually in the range from several hundreds of MHz to several GHz. Compared to the wavelength-coded fiber grating laser sensor which converts measurrands into a shift in the lasing wavelength, the polarimetric heterodyning sensor has distinctive advantages of ease of interrogation and avoidance of expensive wavelength measurement. We have previously demonstrated that polarimetric heterodyning sensor can measure a variety of parameters including strain, hydrostatic pressure, acoustic wave, electric current, displacement, and acceleration, etc..

In this paper, we present a brief review of our most recent works on polarimetric heterodyning fiber grating laser magnetic field sensors. Two types of polarimetric heterodyning magnetic field sensor are demonstrated: one is based on Ampere force [2], the other is based on Faraday effect [3, 4]. The Ampere-force-based sensor shows an inherent immunity to environment disturbances. An approach for enhancing the response sensitivity of Faraday-effect-based sensor is also demonstrated.

ACKNOWLEDGMENT

This work is supported by the National Natural Science Foundation of China (61235005, 61177074), the Planned Science and Technology Project of Guangzhou (2012J5100028), the Project of Science and Technology New Star of Zhujiang in Guangzhou city (2012J2200043), and the Guangdong Natural Science Foundation (S2013030013302).

REFERENCES

1. Guan, B. O., L. Jin, Y. Zhang, and H. Y. Tam, "Polarimetric heterodyning fiber grating laser sensors," *J. Lightwave Technol.*, Vol. 30, No. 8, 1097–1112, 2012.
2. Cheng, L. H., Z. Z. Guo, J. L. Han, L. Jin, and B. O. Guan, "Ampere force based magnetic field sensor using dual-polarization fiber laser," *Opt. Express*, Vol. 21, No. 11, 13419–13424, 2013.
3. Cheng, L. H., J. L. Han, Z. Z. Guo, L. Jin, and B. O. Guan, "Faraday-rotation-based miniature magnetic field sensor using polarimetric heterodyning fiber grating laser," *Opt. Lett.*, Vol. 38, No. 5, 688–690, 2013.
4. Cheng, L. H., J. L. Han, L. Jin, Z. Z. Guo, and B. O. Guan, "Sensitivity enhancement of Faraday effect based heterodyning fiber laser magnetic field sensor by lowering linear birefringence," *Opt. Express*, Vol. 21, No. 25, 30156–30162, 2013.

Femtosecond-laser-micromachined Optical Fiber In-line Interferometers

Changrui Liao[1], **Lei Xu**[2], **Yiping Wang**[1], **D. N. Wang**[3], **Shen Liu**[1], **Zhengyong Li**[1], **Xiaoyong Zhong**[1], **Jiangtao Zhou**[1], **Qiao Wang**[1], **and Kaiming Yang**[1]

[1]Key Laboratory of Optoelectronic Devices and Systems of Ministry of Education and Guangdong Province College of Optoelectronic Engineering, Shenzhen University, Shenzhen 518060, China
[2]Department of Computing, The Hong Kong Polytechnic University, Hong Kong, China
[3]Department of Electrical Engineering, The Hong Kong Polytechnic University, Hong Kong, China

Abstract— Optical fiber is typically made of silica glass and functions as a waveguide, which is small in dimension, only slightly larger than that of human hair. Thus, it is difficult to process optical fibers by using conventional manufacturing techniques. Femtosecond lasers exhibit excellent capability in performing three-dimensional material processing in micron scale and even in sub-micron scale for some special materials, which makes it a powerful tool for micromachining optical fibers. Recently, femtosecond laser micromachining techniques have been used in a broad range of optical fiber sensors. In this talk, we summarize the fiber in-line interferometers those are fabricated by femtosecond laser micromachining in our past works.

ACKNOWLEDGMENT

This work was supported by the National Science Foundation of China (Nos. 11174064, 61308027, 61377090), National Science Foundation of SZU (No. 00036401), Science & Technology Innovation Commission of Shenzhen (Nos. KQCX20120815161444632 and JCYJ20130329140017262), Distinguished Professors Funding from Shenzhen University and Guangdong Province Pearl River Scholars.

REFERENCES

1. Ma, J., W. Jin, H. L. Ho, and J. Y. Dai, "High-sensitivity fiber-tip pressure sensor with graphene diaphragm," *Opt. Lett.*, Vol. 37, 2493–2495, 2012.
2. Wang, Y., D. N. Wang, C. Wang, and T. Y. Hu, "Compressible fiber optic micro-Fabry-Perot cavity with ultra-high pressure sensitivity," *Opt. Express*, Vol. 21, 14084–14089, 2013.
3. Ma, J., J. Ju, L. Jin, and W. Jin, "A compact fiber-tip micro-cavity sensor for high-pressure measurement," *IEEE Photon. Technol. Lett.*, Vol. 23, 1561–1563, 2011.
4. Liao, C., T. Y. Hu, and D. N. Wang, "Optical fiber Fabry-Perot interferometer cavity fabricated by femtosecond laser micromachining and fusion splicing for refractive index sensing," *Opt. Express*, Vol. 20, 22813–22818, 2012.
5. Liao, C., L. Xu, C. Wang, D. N. Wang, Y. Wang, Q. Wang, K. Yang, Z. Li, X. Zhong, J. Zhou, and Y. Liu, "Tunable phase-shifted fiber Bragg grating based on femtosecond laser fabricated in-grating bubble," *Opt. Lett.*, Vol. 38, 4473–4476, 2013.

Highly Hygroscopic Polymer Microcavity Fiber Fizeau Interferometer for Humidity Sensing

Yan-Wun You, Jia-Heng Dai, and Cheng-Ling Lee
Department of Electro-Optical Engineering, United University, Miaoli 360, Taiwan

Abstract— This work demonstrates a highly hygroscopic polymer microcavity fiber Fizeau interferometer (PMFFI) that uses a single-mode fiber (SMF) tip with very little polymer attached. The polymers with specific porous structures have good hygroscopicity which is very useful for the humidity sensing application. The structures of the fabricated PMFFIs and reflection spectra are shown in Fig. 1. In the inset of Fig. 1, L is microcavity of the polymer. The arc shape of the fabricated polymer surface is created because the cohesion force of monomer liquid material. Adhesive force between the SMF and the polymer would be very well if it was fully cured and well aged.

In the measurement, to reduce cost of the system for the sensor, we just utilized a general laser diode (LD) that replaced the broadband light source, BLS. The LD with the optical power of about 0.58 mW and central wavelength of 1531.5 nm inputs the fiber sensor. It can be predicted that a very cheap photodetector (PD) can be used to measure the optical power of the LD. The sensitivity with 0.192 dBm/%RH of the LD peak power responses to the RH has been achieved, as plotted in Fig. 2. Inset shows the reflection spectra of the proposed PMFFI with increase of humidity measured by the LD light source. Experimental results show that a good linear response of sensitivity and the rise of peak power with increase of the humidity have been performed. Additionally, the ease of fabrication and lack of fiber alignment for the all-fiber devices are distinctive in the humidity sensing technology.

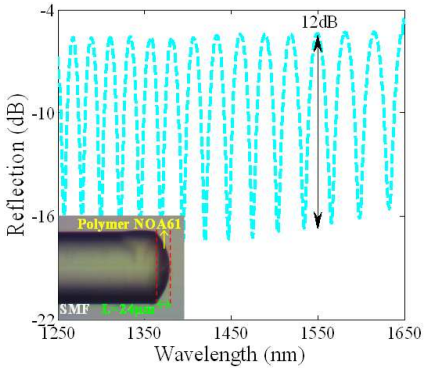

Figure 1: Interference spectra of the fabricated PMFFI measured by broadband light source. Inset presents the sensor head with microcavity of $L = 24\,\mu$m.

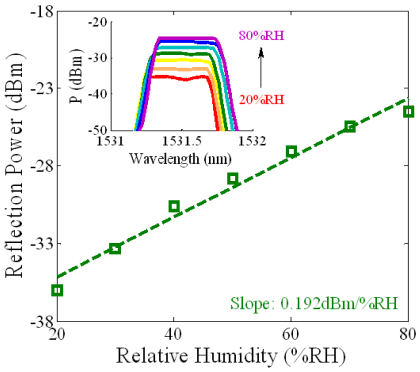

Figure 2: Humidity sensitivities of the LD peak power to the increase of humidity. Inset shows the spectral variations of the LD peak power.

Side-polished Fiber Sensing for Determination of Nematic Liquid Crystal Orientation

Yuqi Han[1], **Zhe Chen**[1, 2], **Jianhui Yu**[1, 2], **Haozhi Li**[1], **Xiaoli He**[1], **Jun Zhang**[1, 2], **Yunhan Luo**[1, 2], **Huihui Lu**[1, 2], **and Jieyuan Tang**[1, 2]

[1]Department of Optoelectronic Engineering, Jinan University, Guangzhou 510632, China
[2]Key Laboratory of Optoelectronic Information and Sensing Technologies
Guangdong Higher Education Institutes, Jinan University, Guangzhou 510632, China

Abstract— The orientation change of nematic liquid crystal (NLC) can be used in biosensor. The sensing characteristics of side-polished fiber (SPF) for determination of NLC orientation have been investigated. The relationship between the theoretical formula of liquid crystal refractive index and the optical transmission power in SPF was derived by empirical approach. The mechanical rotating method is designed to change the orientation of NLC on the polished surface. Experimental results show that the orientation transition of liquid crystal can indeed be sensed by monitoring the output optical power transmitted through the SPF. With mechanical rotation, when the rotation angle increased from 0° to 90°, the output optical power increased by 28.10 dB. Within the angle range from 0° to 30°, the response is almost linear. The average response slope is about 0.359 dB/°, which indicates relatively high sensitivity. Experiments indicate that SPF can be used in determination of the orientation transition of NLC. It would be used for a new fiber optical biosensor based on the SPF and NLC.

Magnetic Field Sensing with Up-taper Fiber-optic Structure

Shengli Pu and Shaohua Dong
College of Science, University of Shanghai for Science and Technology, Shanghai 200093, China

Abstract— Optical fiber sensors have attracted a great deal of attention over the past decades due to their particular characteristics, such as anti-interference, compactness, and high sensitivity. On the other hand, magnetic fluid (MF) is an attractive material that possesses versatile magneto-optic properties, such as tunable refractive index [1, 2], magneto-volume variation [3] and so on. Due to the fluidity of MFs, they are easy to be integrated with fibers. Therefore, fiber-optic magnetic field sensors based on magneticfluid have attracted increasing research interests. The most popular schemes include infiltrating the MFs into the air holes of the photonic crystal fiber (PCF), and using MFs as the claddings of the special fiber or fiber structures. Their fundamental principles are based on adjusting fiber mode field with magnetic field.

In this work, a novel and low costsensing structure was fabricated by fusion splicing of a segment of single mode fiber (SMF) with a commercial electric-arc fusion splicer (AV4671). Schematic diagram of the proposed sensing structure is shown in Fig. 1. After applying arc discharge, the fiber diameter is gradually enlarged due to the large overlap and push force. Two up-taper joints will be produced. Between the joints, the section of SMF_2 acts as the sensing arm (see Fig. 1). MF is used as the sensing material, which surrounds SMF_2. High-order cladding modes are excited within the cladding of SMF_2 through the up-taper joint, which are sensitive to the external environmental disturbance. The interference between the core and cladding modes and transmission loss of the sensing structure are sensitive to the external magnetic field, which is utilized for magnetic field sensing. The sensitivities can be up to 32.53 pm/Oe and -0.01964 dB/Oe, respectively.

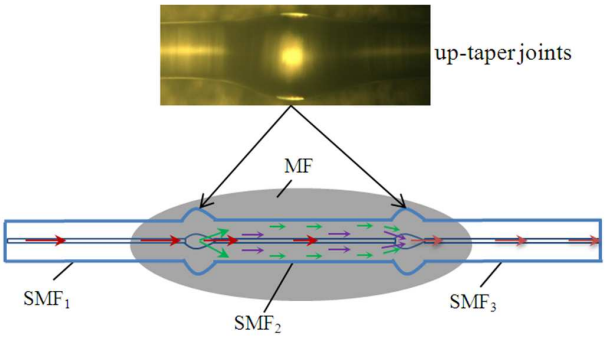

Figure 1: Schematic diagram of the proposed sensing structure. The insets show the microscopic images of the up-taper splicing joint.

REFERENCES

1. Wang, H., S. Pu, N. Wang, S. Dong, and J. Huang, "Magnetic field sensing based on singlemode-multimode-singlemode fiber structures using magnetic fluids as cladding," *Opt. Lett.*, Vol. 38, 3765–3768, 2013.
2. Lin, W., Y. Miao, H. Zhang, B. Liu, Y. Liu, and B. Song, "Fiber-optic in-line magnetic field sensor based on the magnetic fluid and multimode interference effects," *Appl. Phys. Lett.*, Vol. 103, 151101, 2013.
3. Dong, S., S. Pu, and J. Huang, "Magnetic field sensing based on magneto-volume variation of magnetic fluids investigated by air-gap Fabry-Pérot fiber interferometers," *Appl. Phys. Lett.*, Vol. 103, 111907, 2013.

High Sensitivity Micro Fabry-Perot Interferometer with Encapsulated Optical Liquid

Yu-Cheng Li[1], **Tsai-Chia Lung**[2], **and Nan-Kuang Chen**[3]

[1]Department of Electro-Optical Engineering
United University, Miaoli 360, Taiwan
[2]Optoelectronics Research Center, United University, Miaoli 360, Taiwan
[3]Department of Electronic Engineering
Taiwan University of Science and Technology, Taipei 106, Taiwan

Abstract— Fabry-Perot interferometers (FPI) have been widely used in precision optical sensing application such as temperature, index, and strain due to its high Q cavity [1]. Usually, the FPI can be made using Bragg grating or two parallel mirrors [2]. In this work, we propose a new structure based on a hollow core fiber (HCF) with encapsulated optical liquid [3]. The HCF is spliced between two singlemode fibers and tiny optical liquid is well confined in the middle of HCF, shown in Fig. 1. The length of the HCF is about 0.4 cm whereas the length of optical liquid is about 350 μm. The air core diameter of HCF is 20.5 μm. In measurement, the broadband light source over 1250–1650 nm form super luminescent diodes (SLD) is launched into the singlemode fiber. The index of liquid is 1.46 and the liquid forms a high efficient reflection interface for guiding lights. The transmission spectra for the device when the length of liquid is 4 mm and 5 mm are shown in Fig. 2 and Fig. 3, respectively. The HCF is further heated by a TE cooler to significantly change the output interference spectral patterns. This device is simple and Impact on the temperature.

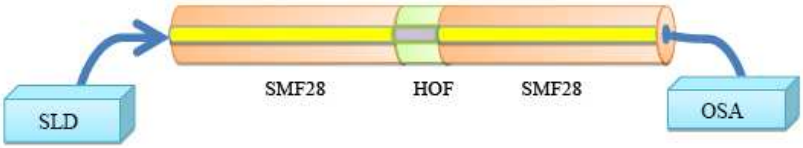

Figure 1.

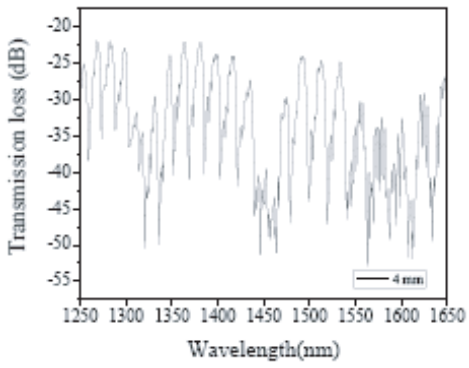

Figure 2.

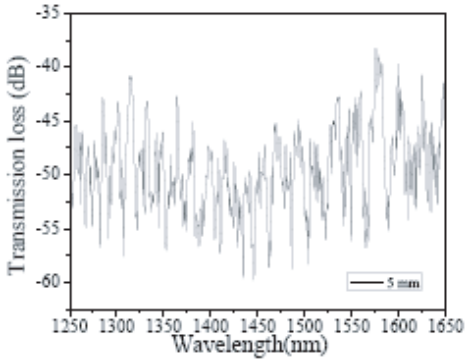

Figure 3.

REFERENCES

1. Rao, Y. J., "Recent progress in fiber-optic extrinsic Fabry-Perot interferometric sensors," *Opt. Fiber Technol.*, Vol. 12, 227–237, 2006.
2. Bhatia, V., K. A. Murphy, R. O. Claus, M. E. Jones, J. L. Grace, T. A. Tran, and J. A. Greene, "Optical fiber based absolute extrinsic Fabry-Perot interferometric sensing system," *Meas. Sci. Technol.*, Vol. 7, 58–61, 1996.
3. Zhang, Y., X. Chen, Y. Wang, K. L. Cooper, and A. Wang, "Microgap multicavity Fabry-Pérot biosensor," *J. Lightwave Technol.*, Vol. 25, 1797–1804, 2007.

Optical Fiber Flowmeter Using Silver-coated FBG Cascaded by Waist-enlarged Bitaper

Xinhuai Wang, Xinyong Dong, and Yan Zhou
Institute of Optoelectronic Technology, China Jiliang University, Hangzhou 310018, China

Abstract— A novel hot-wire flowmeter based on a silver-coated optical fiber Bragg grating (FBG) cascaded by waist-enlarged bitaper is proposed and experimentally demonstrated. The silver coating deposited on the surface of the FBG absorbs light of a pump laser, which is coupled into the fiber cladding by the specially-fabricated fiber waist-enlarged bitaper, to generate heat. Thus, the temperature of the FBG increases to a certain level, while air flow cools down the FBG by taking heat away. Bragg wavelength of the FBG changes with velocity of air flow according to a certain relationship. Experimental results show that a large measurement range up to 13.7 m/s is realized.

Compact Tunable Multibandpass Filters Based on Liquid-filled Photonic Crystal Fibers

Yingjie Liu, **Yiping Wang**, **Bing Sun**, **and Changrui Liao**
Key Laboratory of Optoelectronic Devices and Systems of Ministry of Education and Guangdong Province
Shenzhen University, Shenzhen 518060, China

Abstract— We demonstrated a compact tunable multi-bandpass filters based on liquid-filled photonic crystal fibers with a short size of about 9 mm and a high wavelength-tuning sensitivity of up to $-2.194\,\mathrm{nm}/^{\circ}\mathrm{C}$ by means of filling a liquid with a high refractive index of 1.7000 into air holes of a photonic crystal fiber (PCF). Such a PCF-based filter remains an almost constant bandwidths and a large extinction ratio of more than 40 dB within the whole wavelength-tuning range. Moreover, we investigate the response of the PCF based filter to strain, and bend, the transmission spectrum of the PCF-based filter is insensitive to the stretch force and the curvature of the fiber. Thus, our proposed filter could find wide application in all-fiber optical communication systems.

ACKNOWLEDGMENT

This work was supported by National Natural Science Foundation of China (grants No. 11174064, 61308027, and 61377090), Science & Technology Innovation Commission of Shenzhen (grants No. KQCX20120815161444632, and JCYJ20130329140017262), and Distinguished Professors Funding from Shenzhen University and Guangdong Province Pearl River Scholars.

Reflective Optical Fiber Refractometer Based on Fiber Bragg Grating in Thin-core Fiber

Yebin Zhang[1], **Chenliang Wang**[1], **Bin Zhou**[2], **and Sailing He**[1]

[1]State Key Laboratory of Modern Optical Instrumentation
Centre for Optical and Electromagnetic Research
Zhejiang University, Hangzhou 310058, China
[2]South China Academy of Advanced Optoelectronic
Centre for Optical and Electromagnetic Research
South China Normal University, Guangzhou 510631, China

Abstract— A compact reflective refractometer based on a fiber Bragg grating (FBG) inscribed in a short section of thin-core fiber (TCF) is proposed and experimentally demonstrated. As shown in Fig. 1(a), a short section of TCF was fusion spliced to the single-mode fiber (SMF). The core of the TCF is $\sim 3\,\mu$m. Then an FBG was inscribed in the TCF using the phase-mask method. The length of the FBG is ~ 8 mm. When the incident light reaches the hetero-core interface between the SMF and TCF, part of the core mode is coupled to the cladding modes. All these cladding modes and core mode in the TCF are reflected back when they reach the FBG. Different modes are reflected at different wavelengths, which are determined by the specific effective refractive index of these modes and the pitch of FBG. When the reflected light reaches the hetero-core interface again, these cladding modes are partly coupled into the core of the SMF. The reflected spectrum of the proposed refractometer is shown in Fig. 1(b).

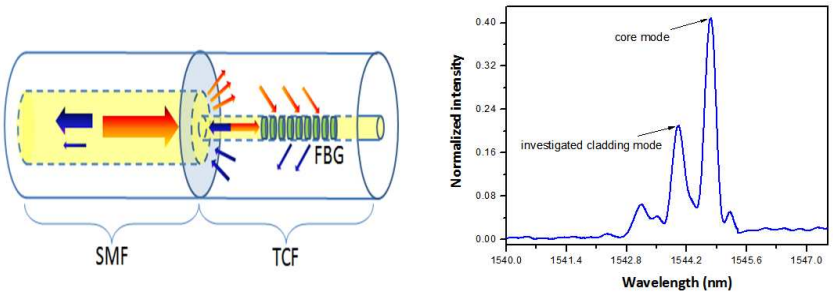

(a) (b)

Figure 1: (a) Schematic configuration of the reflective refratometer and (b) its reflected spectrum.

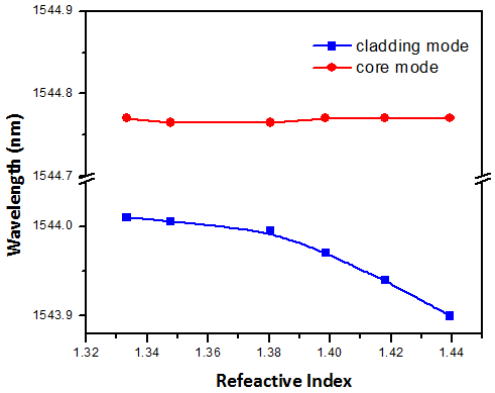

Figure 2: Measured wavelength responses of the core mode and cladding mode.

As the effective refractive index of the cladding mode depends on the refractive index of the surrounding medium, the refractive index of the surrounding medium can be deduced by the wavelength of the cladding mode reflection. In order to investigate the refractive index sensing capability, the proposed sensor is immersed into a series of glucose solutions with different

mass concentrations corresponding to different refractive index values. The wavelength shifts of the core mode and the cladding mode labeled in the Fig. 1(b) are investigated. The measured wavelength shifts versus the refractive index are shown in Fig. 2. As the refractive index of the surrounding solution increases from 1.3333 to 1.4394, the wavelength of cladding mode reflection experiences 110 pm blue shift, while the wavelength of the core mode reflection remains nearly unchanged. That means the wavelength of the core mode reflection can be used as the reference to achieve the temperature-insensitive refractive index sensing. Experimental results show this compact refractometer can provide wavelength-referenced reflective refractive index measurement, making it a good candidate for sensing in biological and chemical application.

Micro-tapered Fiber Mach-Zehnder Interferometers for Picoliter Index Sensing

Shu-Wei Chuang[1], **Jian-Wei Zheng**[1], **Wen-Chuan Lin**[1], **and Nan-Kuang Chen**[1, 2]

[1]Department of Electro-Optical Engineering, United University, Miaoli 360, Taiwan
[2]Optoelectronics Research Center, United University, Miaoli 360, Taiwan

Abstract— We demonstrate all-fiber micro-abrupt-tapered fiber Mach-Zehnder interferometers (MMZI) with a device length of 600 µm using two micro-abrupt-tapers in a cladding-reduced highly germanium doped single-mode fiber (Ge-doped SMF). This method is simple and low cost.

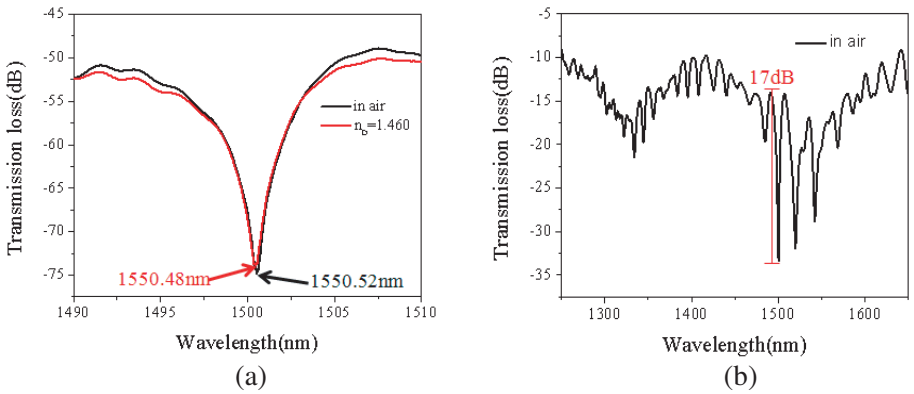

Figure 1: (a) Spectral responses of MMZI with different refractive indices. (b) Spectral responses of MMZI with uniform tapered length and taper waist of 370 µm and 30.19/30.54 µm, respectively.

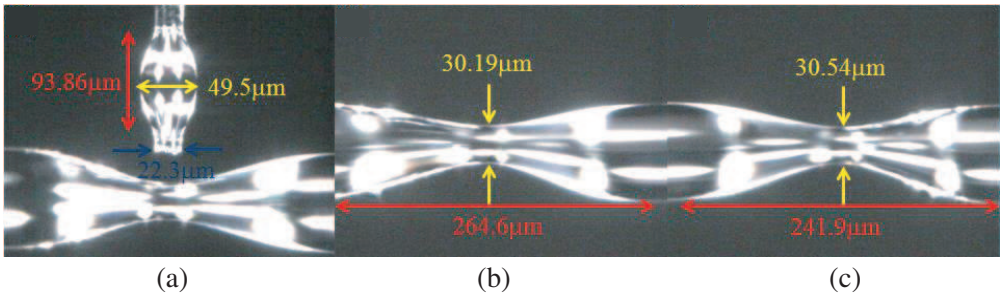

Figure 2: (a)–(c) Each part of the parameters shown above.

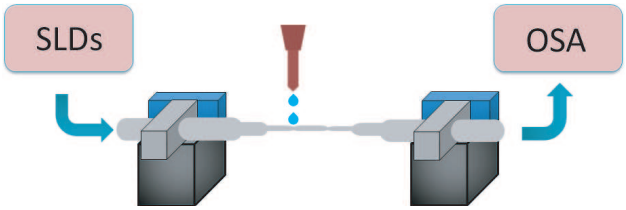

Figure 3: The configuration of the experimental setup for the SLD, superluminescent diodes. OSA, optical spectral analysis.

REFERENCES

1. Li, Y. and L. Tong, "Mach-Zehnder interferometers assembled with optical microfibers or nanofibers," *Opt. Lett.*, Vol. 33, 303–305, 2008.
2. Chen, N. K. and Z. Z. Feng, "Effect of gain-dependent phase shift for tunable abrupt-tapered Mach-Zehnder interferometers," *Opt. Lett.*, Vol. 35, 2109–2111, 2010.
3. Wang, X., Y. Li, and X. Bao, "C- and L-band tunable fiber ring laser using a two-taper Mach-Zehnder interferometer filter," *Opt. Lett.*, Vol. 35, 3354–3356, 2010.
4. He, M., J. S. Kuo, and D. T. Chiu, "Electro-generation of single femtoliter- and picoliter-volume aqueous droplets in microfluidic systems," *Appl. Phys. Lett.*, Vol. 87, 031916, 2005.

Temperature-insensitive Refractive Index Sensor Based on In-fiber Michelson Interferometer

Zhengyong Li, **Yiping Wang**, **and Changrui Liao**
Key Laboratory of Optoelectronic Devices and Systems of Ministry of Education and Guangdong Province
Shenzhen University, Shenzhen 518060, China

Abstract— A novel intensity-modulated refractive index sensor based on an in-fiber Michelson interferometer is experimentally demonstrated by splicing a section of thin core fiber between two standard single mode fibers with a commercial fusion splicer. We investigate the response to refractive index and temperature after the interferometer principle of the new structure being derived and analyzed. The analysis results show that the interferometer sensor could be considered as the superposition of Michelson interferometer. The experimental results indicate that such a refractive index sensor exhibits an ultrahigh sensitivity of −208.24 and 125.44 dB/RIU at the refractive index of 1.440 and 1.500, respectively. The refractive index sensor is insensitive to temperature and thus solves the cross-sensitivity problem between temperature and surrounding refractive index. Moreover, the promising RI sensor has the advantages of short size (less than 2 mm) and easy fabrication which can find potential applications in the fields of chemical and biomedical sensing, and environmental monitoring.

ACKNOWLEDGMENT

This work was supported by National Natural Science Foundation of China (grants Nos. 11174064, 61308027, and 61377090), Science & Technology Innovation Commission of Shenzhen (grants Nos. KQCX20120815161444632, and JCYJ20130329140017262), and Distinguished Professors Funding from Shenzhen University and Guangdong Province Pearl River Scholars.

Session 2A10
SC3: Advances in Optical Networking: Parts 2

Optical Performance Monitoring for Flexible Optical Networks

Calvin C. K. Chan
Department of Information Engineering
The Chinese University of Hong Kong, Shatin, N.T., Hong Kong, China

Abstract— In future optical networks, high bandwidth flexibility and high spectral efficiency are the most desirable capabilities to cope with the heterogeneous nature of the traffic demand. The networks have to be equipped with flexible transceivers and bandwidth flexible optical cross-connects to provision the heterogeneous traffic on flexible grid. To date, optical orthogonal frequency division multiplexing (OFDM) format is one of the feasible and promising signal formats to support such flexible optical networks. It has shown superior tolerance to transmission impairments as well as its signal bandwidth can be adjusted by accommodating different number of optical subcarriers to cope with different traffic needs. To assure the quality of the service provisioning, optical performance monitoring (OPM) is an indispensable element in network management. The signal quality and the working status of various network elements can be continuously monitored so as to facilitate the network control. The monitoring information can also be used to enable optimal compensation of various optical impairments, thus assures good signal quality in data delivery. OPM includes monitoring of various common system parameters of the transmission system, including optical signal-to-noise ratio (OSNR), accumulated chromatic dispersion (CD), polarization mode dispersion (PMD), etc. In this talk, the various OPM requirements and techniques for different key aspects of network and signal monitoring in future flexible optical network will be discussed.

An Efficient Regenerator and Wavelength Assignment Approach for $1+1:1$ and $1:1:1$ Protected Lightpath Services

Gangxiang Shen[1], **Chuanjun Wu**[2], **and Jixiong Dong**[2]

[1]School of Electronic and Information Engineering, Soochow University, Suzhou 215006, China
[2]Huawei Technologies, Shenzhen 518129, China

Abstract— Signal regeneration is expensive because it requires a pair of transponders. Thus, minimizing signal regeneration is an important topic in the design of optical transport networks. A comprehensive survey on signal regeneration planning has been performed in [1], in which most of the studies are found to focus on planning for unprotected lightpaths. Few are dedicated to the protected services such as $1+1$ or $1:1$ services, not mentioning the services ensured with dual-failure recovery [2] such as $1+1:1$ and $1:1:1$ ones.

Network connections ensured with dual-failure recovery are important for many users that need connections to support mission-critical services such as financial and military applications. $1+1:1$ and $1:1:1$ protection types provide sufficient survivability for services through establishing three lightpaths between each pair of source and destination nodes. For the $1+1:1$ service, in addition to $1+1$ protection which provides a pair of "working" and "first protection lightpaths," one more protection path (called "the second protection lightpath") is also reserved in case that both the first two paths fail simultaneously. Here colon ":" means that the protection resources on the second protection path can be shared. $1:1:1$ protection is similar to $1+1:1$ protection. The only difference is that the protection resources of the first protection lightpath of a $1:1:1$ service is also allowed to be shared (note that protection resources can only be shared in the same categories; the protection resources of a first protection lightpath and a second protection lightpath cannot be shared).

For the first time, we jointly consider the lightpath routing, wavelength assignment, and regenerator placement (RWA-RP) problem for the $1+1:1$ and $1:1:1$ services. We develop an efficient waveplane-based approach that integrates the steps of lightpath routing, wavelength assignment, and regenerator placement to optimize the total numbers of required regenerators and used wavelengths.

REFERENCES

1. Azodolmolky, S., et al., "A survey on physical layer impairments aware routing and wavelength assignment algorithms in optical networks," *Computer Communications*, Vol. 53, No. 7, 926–944, May 2009.
2. Clouqueur, M. and W. D. Grover, "Availability analysis of span-restorable mesh networks," *IEEE Journal on Selected Areas in Communications*, Vol. 20, 810–821, May 2002.

Dark Fiber Monitoring System for Ring-and-Spur Long-Reach Passive Optical Networks

Min Cen[1], **Jiajia Chen**[2], **Patrice Mégret**[1], **Véronique Moeyaert**[1], **and Marc Wuilpart**[1]

[1]Université de Mons, Service d'Electromagnétisme et de Télécommunications
Boulevard Dolez 31, 7000 Mons, Belgium
[2]School of ICT, KTH Royal Institute of Technology, Isafjordsgatan 22, 16440 Kista, Sweden

Abstract— Long-Reach Passive Optical Networks (LR-PONs) allows for extending the distance between the central office (CO) and end users from a few kilometers to several tens of kilometers and beyond, which offers high capacity and large coverage. It in turn enables node consolidation driven by the operators recently, reducing a large amount of COs and hence potentially achieving a significant operational cost save. Among different topologies proposed for LR-PONs, "ring and spur", where a ring is employed for feeder section followed by several sub-trees for distribution segments, is currently receiving an extensive investigation due to low infrastructure cost and high reliability. However, most of the existing PON monitoring systems are for purely tree-based topology and cannot be directly applied for ring-based networks. Therefore, an adequate supervision system is highly required in order to detect and localize faults occurring in the ring-and-spur LR-PONs. In this paper, we propose a monitoring system using "dark fiber" and multi-wavelength bi-directional Transmission Reflection Analysis (TRA) system, which measures the transmitted and backscattered powers with multiple wavelengths in both clockwise and counter-clockwise directions of the feeder ring in LR-PON.

In LR-PONs, optical amplifiers, e.g., erbium doped fiber amplifiers (EDFA), may need to be installed in the feeder ring to compensate optical power loss caused by the long distance fiber. These devices typically work for a specific spectrum (e.g., C-band only), which may block the monitoring signals in different band (e.g., U-band). Therefore, many existing monitoring solutions are not capable of fault supervision in the ring system. In order to address this issue, in our proposed system, a "dark fiber" (i.e., a fiber that has been deployed in the same cable as the working fibers but does not carry any data signals) is utilized for monitoring purpose. Moreover, this novel idea makes the TRA based monitoring system more precise and flexible since one can choose any set of monitoring wavelengths for supervision without affecting data signals as well as increasing the measuring accuracy.

Moreover, another challenge for LR-PON monitoring is long measuring time. Many existing monitoring schemes based on reflectometry techniques, e.g., Optical Time Domain Reflectometry (OTDR), have a quite long averaging process of the reflected signals, which could spend time in the magnitude of several minutes per line (e.g., $2 \sim 3$ minutes for the OTDR). Our proposed TRA technique only requires the measurement of power variations and consequently could significantly reduce the measurement time to $2 \sim 3$ seconds per line. Besides, the TRA technique uses an un-modulated light source that could makes the overall monitoring system simple and low cost.

Capacity Constraints for Phase Noise Influenced Coherent Optical DnPSK Systems

Gunnar Jacobsen[2], **Sergei Popov**[1], **Tianhua Xu**[1, 2], **and Sergey Sergeyev**[3]

[1]Royal Institute of Technology, Stockholm, SE-16440, Sweden
[2]Acreo Swedish ICT AB, Electrum 236, Kista, SE-16440, Sweden
[3]Aston University, Birmingham, B4 7ET, UK

Abstract— We present a comparative study of the influence of dispersion induced phase noise for n-level PSK systems. From the analysis, we conclude that the phase noise influence for classical homodyne/heterodyne PSK systems is entirely determined by the modulation complexity (expressed in terms of constellation diagram) and the analogue demodulation format. On the other hand, the use of digital signal processing (DSP) in homodyne/intradyne systems renders a fiber length dependence originating from the generation of equalization enhanced phase noise. For future high capacity systems, high constellations must be used in order to lower the symbol rate to practically manageable speeds, and this fact puts severe requirements to the signal and local oscillator (LO) linewidths. Our results for the bit-error-rate (BER) floor caused by the phase noise influence in the case of QPSK, 16PSK and 64PSK systems outline tolerance limitations for the LO performance: 5 MHz linewidth (at 3-dB level) for 100 Gb/s QPSK; 1 MHz for 400 Gb/s QPSK; 0.1 MHz for 400 Gb/s 16PSK and 1 Tb/s 64PSK systems.

Using our analysis, we also consider some design constrains for the phase noise impact in distributed-feed-back (DFB) or distributed-Bragg-reflector (DBR) semiconductor lasers, that would allow moving the system capacity from 100 Gb/s system capacity to 400 Gb/s in 3 years (1 Tb/s in 5 years).

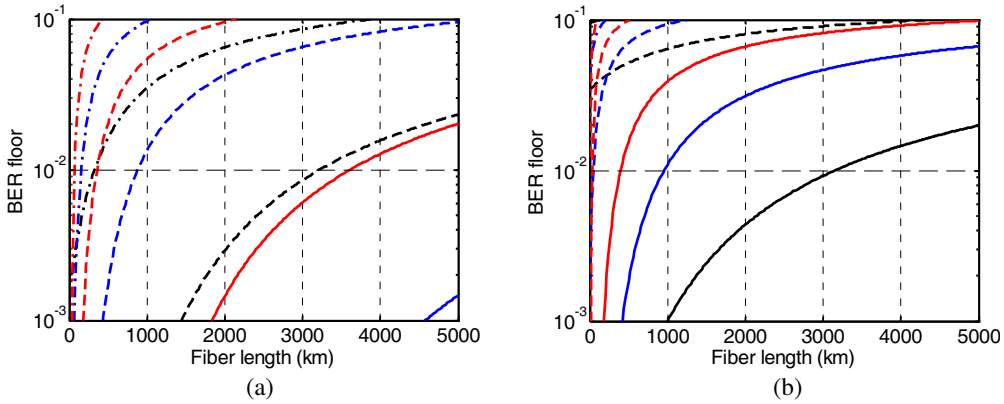

Figure 1: BER_{floor} as a function of transmission distance (fiber length L, km) for dual polarization (a) D16PSK, and (b) D64PSK systems. Total systems capacities are indicated by colors: 100 Gb/s (black), 400 Gb/s (blue) and 1 Tb/s (red). Linewidths of transmitter (Tx) and local oscillator lasers are equal and shown by line styles: 5 MHz (dash-dotted), 1 MHz (dashed) and 0.1 MHz (solid).

ACKNOWLEDGMENT

Work supported by FP7-PEOPLE-2012-IAPP GRIFFON project (No. 324391).

Secure Optical Communication System with Orthogonal CSK/DPSK Modulation Scheme

Bo Dai[1], **Zhensen Gao**[2], **Naoya Wada**[3], **and Xu Wang**[1]

[1]Institute of Photonics and Quantum Sciences, School of Engineering and Physical Sciences
Heriot-Watt University, Edinburgh EH14 4AS, UK
[2]Bell Laboratories, Alcatel-Lucent Shanghai Bell, Shanghai 201206, China
[3]Photonic Network Research Institute
National Institute of Information and Communications Technology (NICT), Tokyo 184-0015, Japan

Abstract— Secure optical communication has attracted great research interests to meet the military or commercial demands of high-speed secure transmission. Many advanced modulation schemes have been proposed to enhance the security of the communication system. In this paper, we will review secure communication systems using a variety of security enhancement techniques, including code-hopping technique, steganography and symbol overlapping technique.

A recently proposed secure communication system, which is based on the advanced orthogonal differential phase-shift keying (DPSK) and code-shift keying (CSK) modulation and public-key cryptography scheme, is also introduced. The security performance of the system is investigated by using two different eavesdropping methods: one-bit delay interference detection and differential detection. The results show that the security vulnerability exists only in the CSK channel while the DPSK channel can thwart these attacks. Therefore, public-key cryptography can be introduced into the system to efficiently use these two orthogonal channels for both public key distribution and encrypted data transmission. The privacy of the transmitted data can be double guaranteed by public-key cryptography scheme logically and optical code-processing techniques physically.

New Development in Critical Components for 40 Gbit/s Long-reach Passive Optical Networks

Xin Yin[1], **Xingzhi Qiu**[1], **Guy Torfs**[1], **Romain Brenot**[2], **Fabrice Blache**[2]
Mohand Achouche[2], **and Johan Bauwelinck**[1]

[1]IMEC/INTEC, Ghent University, Sint Pietersnieuwstr 41, Ghent 9000, Belgium
[2]III-V Lab, Route de Nozay, Marcoussis 91460, France

Abstract— The presentation shows the recent progress of the development of 40 Gbit/s downstream components in European Framework 7 Integrated Project "DISCUS". The DISCUS project aims to analyse, design, and demonstrate a complete end-to-end architecture and technologies for an economically viable, energy efficient and environmentally sustainable future-proof optical network. The access network proposed in DISCUS reference architecture is a long-reach passive optical network (LR-PON), which maximises infrastructure sharing, thus massively reducing cost and power consumption per customer. In order to support increasing capacity in the downstream direction, a 40 Gbit/s downstream upgrade from a 10 Gbit/s LR-PON is being investigated which will enable downstream data-rate switching between the two rates via wavelength selection.

Speed upgrade from 10 Gbit/s towards 40 Gbit/s is challenging and poses a few substantive technical issues: firstly, the distortions which are induced by chromatic dispersion grow with the square of the bit rate (i.e., 16× with 4× rate increasing). Secondly, while APDs have been used extensively in 10 Gbit/s PON downstream to improve the receiver sensitivity, no high-speed APD devices are commercially available for 40 Gbit/s NRZ operation. Finally, ONU electronics operating at 40 Gb/s line rate leads to significant increase in power consumption.

The development of new components and technologies is required in order to be able to support such evolution. A single carrier 40 Gbit/s downstream scheme in C-band is proposed based on a 3-level electrical duobinary modulation of a high-power, external cavity laser, monolithically integrated with an electro-absorption modulator and booster semiconductor optical amplifier. The novel solution relaxes the downstream channel bandwidth requirement and improves the chromatic dispersion tolerance. It also enables using a 25-Gbit/s back-side illuminated APD compatible with low-cost assembly in ONUs, thus reducing the cost and power consumption. In order to overcome the problem of high power consumption, we will use a new bit-interleaving multiplexing PON concept, capable of reducing the power consumption of downstream protocol processing ONU electronics by almost an order of magnitude.

Towards a Framework for Small-cell Network Planning

Elaine Wong, **I. Akhtar**, **S. Abeywickrama**, **C. Ranaweera**, **C. Lim**, **and A. Nirmalathas**
Department of Electrical and Electronic Engineering, The University of Melbourne, Australia

Abstract— The recent surge in smartphone and mobile tablet use has placed a tremendous strain on mobile bandwidth. To address this exponential growth, heterogeneous networks have been proposed whereby numerous small-radius microcells commonly referred to as "small cells" are placed alongside traditional macrocells [1]. A small cell Base Station (BS) has much smaller coverage radius range than that of a traditional macrocell, typically at 50 m–300 m. It is designed to achieve a small footprint with features such as low-cost and low power, and is to be deployed in a plug-and-play fashion that requires minimal regular maintenance.

However, the practical rollout of small cells is not without its challenges. For example, the effects of land terrain and urban geography on cellular mobile RF signal propagations significantly influence transmission quality and coverage. Varying geographical terrain posing obstructions for direct line-of-sight signal path between the transmitting BS and receiving mobile station, initiates significant signal loss and causes Non line-of-sight propagation. Further, street orientation and building blocks especially in urban areas, cause signal reflections which in turn, lead to significantly weakened signal reception for cell areas with smaller radius. The BS antenna height also influences cell positioning by affecting coverage. Thereby, appropriate cell location planning for placing small cell sites with optimal antenna height especially in urban areas, is essential. Meanwhile, recent studies have shown that BSs contribute to nearly 60% of the total energy consumption in cellular networks [2]. Hence, considering the potentially high BS density in small-cell networks, it is imperative that rigorous studies be undertaken on energy efficient power control mechanisms which account for the radiating power and required capacity enhancements that SCs can offer.

In this paper, we describe a small cell planning framework that exploits the effects of land terrain variation and urban geography. For illustration purposes, we choose a part of the Melbourne Central Business District (CBD) urban area for cell planning [3]. In our proposed framework, the relatively higher geographic elevations are first selected as potential locations for a small cell deployment. A common radius for all cell sites is then chosen within the typical urban area small cell radius range. For the selected cell radius, the signal strength and coverage ability for each cell site is then tested taking into account an antenna height of just below average building height. Finally, redundant cell locations are discarded from the initial planning to satisfy the maximum limit of cell sites per km^2 urban area. Our framework is shown to utilize fewer cells than the maximum limit of 30 cell sites/km^2 in urban area for LTE 1800 MHz network [4]. Further, we formulate a Linear Program (LP) to obtain the optimal operating power of SCs whilst constrained by the power and capacity requirements and subjected to daily capacity demand variations [5]. Even though some related studies in this area have studied energy efficiency of small-cell networks via several network models, to the best of our knowledge, a deduction to LP for the problem at hand is performed for the first time by our team. The formulation of the LP and the datasets and model parameters used in our evaluations will be presented. Our results show that our proposed traffic dependent transmit power regulation, an average power savings of 14.6% can be achieved throughout the day, as compared to using fully powered SCs.

REFERENCES

1. Hoydis, J., et al., *IEEE Veh. Technology Magazine*, Vol. 6, No. 1, 37–43, Mar. 2011.
2. Hasan, Z., et al., *IEEE Communications Surveys Tutorials*, Vol. 13, No. 4, 524–540, 2011.
3. Akhtar, I., et al., "Small-cell network site planning: A framework based on terrain effects and urban geography characteristics," submitted to *OECC/ACOFT*, 2014.
4. Holma, H. and A. Toskala, *WCDMA for UMTS: HSPA Evolution and LTE*, LibreDigital, 2010.
5. Abeywickrama, S. and E. Wong, "Estimation of transmit power for small cell networks, framework based on terrain effects and urban geography characteristics," submitted to *OECC/ACOFT*, 2014.

Availability Analysis for Elastic Optical Networks with Multi-path Virtual Concatenation Technique

Xiaoling Wang[1], **Limei Peng**[2], **and Gangxiang Shen**[1]

[1]School of Electronic and Information Engineering, Soochow University, China
[2]Department of Industrial Engineering, Ajou University, Suwon, South Korea

Abstract— Due to high spectrum efficiency and flexibility in bandwidth allocation, elastic optical networks receive an increasing research interest in recent years. Availability is one of important Service Level Agreement (SLA) metrics in telecommunication networks. Virtual Concatenation (VCAT) technique that can integrate the sub-bandwidths on multiple different paths to make up an end-to-end lightpath service can be applied to enhance the availability of the elastic optical network, because the distribution of sub-bandwidths on multiple different paths enables partial bandwidth to survive when a network incurs a failure.

This paper evaluates the benefit of applying the VCAT technique in enhancing the availability of elastic optical networks. We study three cases: the first one considers a single node pair, between which multiple parallel links connect, the second one also considers a single node pair, between which multiple disjoint end-to-end paths are employed for provisioning VCAT sub-bandwidths, and the last one considers a general mesh network, in which the second case is applied for any node pair and a network-wide average service availability is calculated. Based on the assumption that all the remaining capacity can be considered as available when one (or multiple) paths of a multi-path VCAT service is affected, we develop availability evaluation formulae for the aforementioned three study cases. Our study indicates that the VCAT technique can greatly enhance the availability of elastic optical networks, and different distributions of sub-bandwidths (i.e., numbers of frequency slots (FSs)) on multiple paths of a VCAT service can greatly impact the network availability. For the first case, under the assumption that the lengths of all links are same, an even distribution of FSs on different links is expected to achieve the highest availability. For the rest two cases, the distribution of FSs that can achieve highest availability depends on the structure of the network. In addition, a higher availability can be expected for a smaller VCAT sub-bandwidth granularity.

Optimal Time-dependent Spectrum Sharing between Neighboring Channels in Elastic Optical Networks

Xiaowei Zhao[1], **Gangxiang Shen**[1], **and Sanjay K. Bose**[2]

[1]School of Electronic and Information Engineering, Soochow University, Suzhou, Jiangsu, China
[2]Department of EEE, Indian Institute of Technology, Guwahati, India

Abstract— In recent years, the rapid growth of high-bit-rate applications such as cloud computing and multimedia video services has led to a tremendous increase in the volume of Internet traffic. It has therefore become important to design very efficient and flexible networks which will perform better than the traditional ITU-T [1] based Wavelength Division Multiplexing (WDM) optical networks. A typical WDM optical network used for optical communications is inflexible and inefficient because of its fixed grid and coarse granularity. Elastic optical networks based on the Orthogonal Frequency Division Multiplexing (OFDM) technology can solve most of these problems and are considered promising for next-generation optical networking. The elastic optical transmission technique allows flexible bandwidth and spectrum allocation [2] along with efficient spectrum utilization. This adapts well to real networks where the traffic demand changes dynamically in different time periods. In [3], the authors proposed the concept of time-dependent optical spectrum sharing which adapts elastic optical channels to carry time-dependent traffic demands. In [4], we had applied this concept to a single fiber link and our simulation studies showed that elastic optical channels can successfully handle the time-dependent uncertainty of traffic demand on each optical channel while still achieving high spectrum efficiency.

This paper extends the concept of time-dependent optical spectrum sharing to a general mesh-network. We present two different ILP optimization models from different perspectives for efficiently assigning spectra for lightpaths in a general mesh-network so as to achieve high spectrum efficiency in supporting time-dependent traffic demands. When assigning spectra for lightpaths, one model considers a fixed center frequency of each lightpath between SD pairs in all the time slots, while the other does not consider such a constraint. The tradeoff between them is that the model with a fixed center frequency can make the reconfiguration of lightpaths simpler as we do not need to change the channel center frequency from time slots to time slots, while it may suffer from poorer spectrum utilization compared to the case without such a constraint. Both optimizations have the same objective to minimize the maximal index of the used frequency slots (FSs) on the fiber links in the entire network where we assume that the time-dependent traffic demand of each lightpath between SD pairs is given in advance.

REFERENCES

1. ITU-T Recommendation G694.1, "Spectral grids for WDM applications: DWDM frequency grid," v2.0, 2012.
2. Zhang, G., et al., "A survey on OFDM-based elastic core optical networking," *IEEE Commun. Surv. Tut.*, Vol. 15, No. 1, 65–87, 2013.
3. Shen, G., et al., "Maximizing time-dependent spectrum sharing between neighbouring channels in CO-OFDM optical networks," *Proc. ICTON*, 2011.
4. Zhao, X., et al., "Optimal time-dependent spectrum sharing between neighboring elastic optical channels over a single link," *Proc. ACP*, 2013.

Session 2A11a
SC4: Recent Advances in Magneto-impedance Sensors

Development of Low Noise MI Sensor and Its Applications

N. Hamada, A. Shimode, C. M. Cai, and M. Yamamoto
Aichi Steel Corporation, 1 Wano-Wari Arao-machi, Tokai 476-8666, Japan

Abstract—

Introduction: The demand for magnetic sensor increases for tinier magnetic field detection. Low noise MI sensor with 20 pT/Hz$^{0.5}$ at 10 Hz has been commercialized in 2006, and was reported in 2008 [1]. In 2010, this sensor was improved to noise of 10 pT/Hz$^{0.5}$ at 10 Hz, and was reported [2]. Furthermore, this sensor was improved, and the development of lower noise sensor than current sensor was succeeded. Here we present this sensor of 3 pT/Hz$^{0.5}$ at 10 Hz and its applications.

Development of Low Noise MI Sensor: Low noise MI sensor was test-produced. There are 3 technical points. First point is that amorphous wire (UNITIKA) is treated to reduce the noise. Second point is wire length of amorphous wire from 6 mm to 10 mm due to decrease the demagnetizing field. Third point is number of wire from 1 to 4 due to increase the sensitivity. This sensor noise spectrum is measured by FFT as shown in Fig. 1, compared with current low noise sensor. This sensor shows 3 pT/Hz$^{0.5}$ at 10 Hz and has the 1/3 lower than current sensor reported in 2010 and 1/20 lower than FG sensor.

As applications, PP noise is one of practical property, and shown in Fig. 2. This sensor shows PP noise of less than 0.3 nT in applied frequency field.

The Applications: By this development, the expansion of the foreign body detection, the entry into the security gate for MRI and detecting the vehicle at parking lot are expected. In addition, the biomagnetic measurement is expected due to the detection of sub-nano-tesler level.

In the presentation, we will introduce the example of these applications.

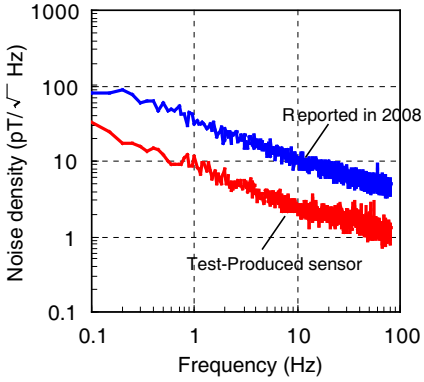

Figure 1: Noise spectrum.

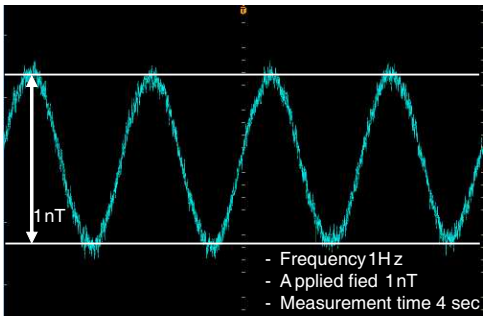

Figure 2: Noise level.

REFERENCES

1. Hamada, N., et al., "Abstract of the 32th meeting of the magnetic society of Japan," 2008.
2. Hamada, N., et al., "Abstract of international workshop on magnetic wires," *IWMW2010*, 2010.

Test-production of High Sensitivity Multi-core MI Element and Its Characteristics

N. Hamada, A. Shimode, S. Tatematsu, and M. Yamamoto
Aichi Steel Corporation, 1 Wano-Wari Arao-machi, Tokai 476-8666, Japan

Abstract— A small and highly sensitive magnetic sensor (AMI 306) based on the MI (Magneto Impedance) effect and used as an electromagnetic compass mainly in mobile phones, smart phones and tablets etc. has been developed and commercialized by Aichi Steel Corporation. Although it shows magnetic resolution in the micro Tesla order, higher performance in sensitivity and noise level is required. On the other hand, a specialized high sensitivity analog output magnetic sensor (nT sensor) with wound coil which shows magnetic resolution of under 1 nano Tesla, has also been commercialized for use in detecting AC magnetic fields. Recently, in this nT sensor, it has been reported the sensitivity is improved by adopting a multi core type sensor head with two or more magneto-sensitive amorphous wires (hereafter called wire) [1, 2]. In this paper, we present the development of an MI element showing high sensitivity and low noise by adopting the above mentioned multi structure and its characteristics

The effect of the magnetic properties (especially anisotropy feild) of wire, the length of the wire and multi type MI element for MI properties were investigated and the newly designed MI element was developed. The developed multi structure MI element, which is produced with photolithography and plating processes, is shown in Fig. 1. Its size is $1.9 \times 1.3 \times 0.5$ mm, and the pickup coil, which transforms the magnetic spin change of the wire surface corresponding to external magnetic field into voltage, is wound around a wire. In addition, the wires and pickup coils of each MI element in the multi MI element are connected in series.

The MI sensor is composed of an MI element combined with an electric circuit which excites a wire and an electric circuit which processes signals from a pickup coil. The noise density of the MI sensor is measured by FFT analyzer at zero magnetic fields with magnetic shielding. As shown in Fig. 2, the noise level of the developed MI sensor shows 0.1 nT at 10 Hz with magnetic shielding, 1/100 of the current MI element (AMI 306) noise level.

This developed MI sensor is expected to be used not only as an electromagnetic compass which require increasingly higher levels of performance, but also in automobile or industrial markets.

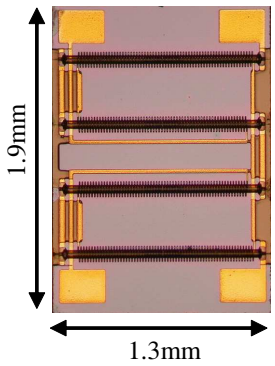

Figure 1: Developed multi MI element.

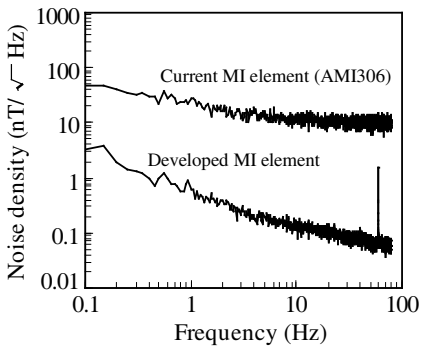

Figure 2: Noise density of developed MI element.

REFERENCES

1. Hamada, N., et al., *Intermag 2011*, FF-08, Taipei, 2011.
2. Uchiyama, T., et al., *Intermag 2013*, DG-05, Chicago, 2013.

Arousal Effect of ELF Magnetic Stimulus on Car Driver's Spine Evaluated with Occipital Electro-encephalogram and Back Magneto-cardiogram

Yoshiyuki Mohri[1], **Muneo Yamada**[1], **Wataru Kato**[1], **Tsuyoshi Uchiyama**[2], **and Kaneo Mohri**[3]

[1]Faculty of Science and Technology, Meijo University, Nagoya 468-8502, Japan
[2]Graduate School of Engineering, Nagoya University, Nagoya 464-8603, Japan
[3]Nagoya Industrial Science Research Institute, Nagoya 464-0819, Japan

Abstract— We have developed an effective and safe method for the arousal of car drivers with application of an extremely low frequency (ELF) magnetic field stimulation on their spine position without so-called "rebound phenomena of the re-drowsiness" in other methods [1, 2]. We have evaluated the arousal level for around 50 subjects with the electro-encephalogram (EEG) using a defined arousal index of $(\alpha + \beta)/(\theta + \delta)$ (α: 8–14 Hz, β: 14–40 Hz, θ: 4–8 Hz, and δ: 0.2–4 Hz) measured and FFT analyzed in the driving simulation system.

We newly investigated a physiological mechanism of the arousal with the ELF magnetic field stimulation using the magneto-cardiogram (MCG) measurements at the left shoulder blade bottom of the subject with the pico-Tesla resolution magneto-impedance sensor [3] in addition to the EEG measurements. The results suggest a strong relation between the brainstem with the arousal center and the heart-aorta system via the vagus nerve connecting the brainstem and the aorta corpuscula. The ELF magnetic stimulation on the spine simultaneously activates both the arousal center and the heart-aorta system with the blood flow promotion.

REFERENCES

1. Mohri, K., T. Uchiyama, M. Yamada, T. Watanabe, Y. Inden, T. Kato, and S. Iwata, "Arousal effect of physiological magnetic stimulation on elder person's spine for prevention of drowsiness during car driving," *IEEE Trans. Magn.*, Vol. 47, No. 10, 3066–3069, Oct. 2011.
2. Mohri, K., T. Uchiyama, M. Yamada, Y. Mohri, and W. Kato, "Physiological magnetic stimulation for arousal of elderly car drivers evaluated with electro-encephalogram and spine magnetic field," *IEEE Trans. Magn.*, Vol. 48, No. 11, 3505–3508, Nov. 2012.
3. Uchiyama, T., K. Mohri, Y. Honkura, and L. V. Panina, "Recent advances of Pico-Tesla resolution magneto-impedance sensor based on amorphous wire and CMOS IC MI sensor," *IEEE Trans. Magn.*, Vol. 48, No. 11, 3833–3839, 2012.

Detection of Back Magneto-cardiogram for Heart Disease Using Pico-Tesla Resolution Amorphous Wire Magneto-Impedance Sensor

Yoshiyuki Mohri[1], **Tsuyoshi Uchiyama**[2], **Muneo Yamada**[1], **and Kaneo Mohri**[3]

[1]Faculty of Science and Technology, Meijo-University, Nagoya 468-8502, Japan
[2]Graduate School of Engineering, Nagoya University, Nagoya 464-8603, Japan
[3]Nagoya Industrial Science Research Institute, Nagoya 464-0819, Japan

Abstract— New diagnosis methods for heart diseases having a higher disease sensitivity than the Electrocardiography (ECG) with similar usability have been required on the World Health Statistics 2012 by the WHO predicting the maximum number of the human death on 2030.

We newly found an intrinsic waveform of the healthy human bio signal showing the double peak pulses (DP) in the magneto-cardiogram (MCG) at the left shoulder blade bottom (LSBB) detected with the pico-Tesla Magneto-Impedance sensor [1, 2]. The DP signal is commonly observed in the LSBB-MCG of four healthy subjects disappeared for two subjects with the angina pectoris.

The DP signal partially recovered in the LSBB-MCG of the two angina pectoris subjects after stimulation with an ELF magnetic field which is applied with stroking by the subject a magnetized crashed stone crammed pipe on the body surface in 30 min. The FFT frequency spectrum of the LSBB-MCG for all subjects changed their distribution pattern to more lumped pattern gathering the blood flow system energy to the basic heart beat frequency band after the ELF magnetic stimulation which may improve the hypertension [3]. The DP signal may reflect the activity of the aorta located behind the heart.

REFERENCES

1. Uchiyama, T., K. Mohri, Y. Honkura, and L. V. Panina, "Recent advances of Pico-Tesla resolution magneto-impedance sensor based on amorphous wire and CMOS IC MI sensor," *IEEE Trans. Magn.,* Vol. 48, No. 11, 3833–3839, 2012.
2. Uchiyama, T., K. Mohri, and S. Nakayama, "Human bio-magnetic field measurement using Pico-Tesla sensitive amorphous wire magneto-impedance sensor," *Sensor Letters*, Vol. 11, No. 1, 191–194, 2013.
3. Nishimura, T., H. Tada, X. Guo, K. Mohri, and M. Fukushima, "A 1 μT extremely low frequency electromagnetic fields vs. sham control for mild-to-moderate hypertension: A double blind randomized study," *Hypertension Research*, Vol. 34, No. 3, 372–377, 2011.

Biomagnetic Field Detection of Cellular Organizations Using Improved Gradio-type MI Magneto Sensor

Shinsuke Nakayama[1], **Satoshi Atsuta**[2], **and Tsuyoshi Uchiyama**[3]

[1]Graduate School of Medicine, Nagoya University, Japan
[2]Fujidenolo Corporation, Japan
[3]Graduate School of Engineering, Nagoya University, Japan

Abstract— Electric current propagates in numerous biological tissues and organs to achieve their functions. A magnetic sensor applicable to measure corresponding magnetic fields will be a convenient tool in biological research and medical examinations.

In this presentation, we show quasi-real-time measurements of biomagnetic fields using an improved gradio-type magneto-impedance (MI) sensor. This magnetic sensor device was made of a magnetic amorphous wire and a pair of fine detector coils mounted in both ends of the wire. One end (MI1) was used to measure biomagnetic fields, while the other (MI2) was used to cancel environmental noise. For quasi-real-time measurements of biomagnetic fields, excitation pulses were repeated at $\sim$2 µs. The peak amplitudes of induction potentials in paired coils were measured by a pair of sample-hold-circuits, and subtracted. This gradio-type magneto sensor system provided the sensitivity of $\sim$25 µV/nT and firmly detected changes in magnetic fields of subnano-Tesla.

Spontaneously oscillating magnetic fields were recorded in several smooth muscle musculature preparations isolated from guinea-pigs. Especially, in gut musculatures which is known to generate propagating electric activity in the muscle layer, we examined the effect of changing the rotation of magneto-sensor and muscle layer on recorded direction of magnetic activity. The measurements indicated that the spontaneous magnetic waves reflected propagating electric currents in gut musculatures. Also, we coincidently measured magnetic waves corresponding to premature ventricular magnetic waves in a healthy subject (Uchiyama and Nakayama, 2013). All animal experiments were carried out in accordance with the Animal Experimental Guides of Nagoya University Graduate School of Medicine. Also, all procedures of human magnetic field measurements were approved by an institutional committee in Nagoya University.

Promotion Rate Index in ELF Magneto-protonics

Kaneo Mohri[1,3], **Masanori Fukushima**[2], **Yuko Mohri**[1,4], **and Yoshiyuki Mohri**[1]

[1]MI Institute, Nagoya 468-0028, Japan
[2]Foundation for Biomedical Research and Innovation, TRI-Kobe, Kobe 650-0047, Japan
[3]Nagoya Industrial Science Research Institute, Nagoya 464-0819, Japan
[4]Faculty of Science and Technology, Meijo University, Nagoya 468-8502, Japan

Abstract— We have proposed a principle named Magneto-Protonics [1, 2] in which free protons generated in the water with application of an extremely low frequency (ELF) magnetic field activate the organisms with promotion of the adenosine-tri-phosphate (ATP) generation at the mitochondria [3]. We have also developed a method for creation of the high strength concrete using magnetized coarse aggregate based on the Magneto-Protonics [4] in which the density and strength of the periodical alternative pulse distributed magnetic field for the bio activation are reinforced with the concrete hardening. The pulse train magnetic field is measured with the magneto-impedance sensor.

We newly found a common index for the evaluation of the bio-growth rate and the concrete hardening rate in an ELF magnetic field as "1 $\sim$ 2% per week," on the basis of an overall analysis of some experimental results of a goldfish culture experiment through three years, two cultivation experiments for the strawberry through two years and the komatsuna vegetable, and also three concrete kneading tests with magnetized coarse aggregate using the olivine stone and the oxidized slag stone.

REFERENCES

1. Mohri, K. and M. Fukushima, "Gradual decreasing characteristics and temperature stability of electric resistivity in water triggered with milligauss AC field," *IEEE Trans. Magn.*, Vol. 38, No. 5, 3353–3355, 2002.
2. Mohri, K. and M. Fukushima, "Milligauss magnetic field triggering reliable self organization of water with long range ordered proton transport through cyclotron resonance," *IEEE Trans. Magn.*, Vol. 39, No. 5, 3328–3330, 2003.
3. Fukushima, M., T. Kataoka, N. Sugiyama, and K. Mohri, "Milligauss magnetic field applied water exert and induce firefly luciferine-luciferase luminescence and induce intracellular calcium elevation of CHO cells without ATP," *IEEE Trans. Magn.*, Vol. 41, No. 10, 4188–4190, 2005.
4. Mohri, K., M. Sasaki, T. Uemura, Y. Mohri, M. Yamada, and T. Kato, "Pulse train distributed magnetic field generated from high strength concrete using magnetized olivine stone aggregate," *PIERS Proceedings*, 1057–1060, Taipei, March 25–28, 2013.

Session 2A11b
SC4: Advanced Magnetic Materials for Microwave Applications

Rotatable Anisotropy in Magnetic Thin Films

Guozhi Chai[1], **Nguyen N. Phuoc**[2], **and C. K. Ong**[3]

[1]Key Laboratory for Magnetism and Magnetic Materials of the Ministry of Education
Lanzhou University, Lanzhou 730000, China
[2]Temasek Laboratories, National University of Singapore, 117411, Singapore
[3]Center for Superconducting and Magnetic Materials, Department of Physics
National University of Singapore, 117542, Singapore

Abstract— Rotatable anisotropy in magnetic thin films is a special type of anisotropy that can only be detected by high frequency measurement other than the traditional VSM B∼H loops measurement. Up to now, it can be found in three types of magnetic thin films: (1) thin film with rotatable stripe domain structure, (2) antiferromagnetic/ferromagnetic multilayers, (3) thin film with strong exchange coupling interactions. The following types of magnetic thin films with rotatable anisotropy have been studied. In ferrite doped CoFe thin films, the resonance frequency with 4.5 GHz can be achieved in any direction of the film plane. The high resonance frequency is driven by the rotatable magnetic anisotropy propagated from the exchange coupling between rotatable ferrimagnetic spins and the ferromagnetic grains[4]. Combine with the rotatable stripe domain structure, the resonance frequency of the film possess zero-field ferromagnetic resonance frequency above 5 GHz after increasing the thickness of thin film larger than 180 nm. By using the Ta buffer layer, the in plane high frequency permeability can further be optimized to 22 and the resonance frequency will reach 6.4 GHz for films with the optimization parameters. As the direction in rotatable anisotropy are angular tunable, we combine the rotatable anisotropy and uniaxial anisotropy (arising from the oblique deposition) in the CoFeBSm thin film. The direction of easy axis can be rotated and the value of resonance frequency can been tuned from 3.8 GHz to 6.4 GHz and by applying a saturated magnetic field in film plane. These results may have a great implication for the tunable microwave magnetic devices.

ACKNOWLEDGMENT

Dr. Chai thanks the financial support from National Natural Science Foundation of China (NSFC) (No. 51107055).

Double Resonance Peaks of FeCo Thin Films with NiFe Underlayer

Xiaoxi Zhong[1], **Wee Tee Soh**[1], **Nguyen N. Phuoc**[2], **and C. K. Ong**[1]

[1]Center for Superconducting and Magnetic Materials, Department of Physics
National University of Singapore, 2 Science Drive 3, 117542, Singapore
[2]Temasek Laboratories, National University of Singapore, 5A Engineering Drive 2, 117411, Singapore

Abstract— Double resonance peaks were observed in the dynamic permeability spectra of the sputtering growth FeCo thin films with NiFe underlayer in which the thickness is varied up to 20 nm. A comprehensive investigation of the source of each resonance peak along with the field-dependent dynamic magnetization of the films was conducted. It was found that both of dynamic magnetic anisotropy and saturation magnetization of the two resonance peaks were different and the values of them were close to those of NiFe and FeCo, respectively. Moreover, triple resonance peaks were observed when the thickness of NiFe reached 50 nm, and the exchange coupling theory was applied to explain the additional peak. In addition, the behaviors of dynamic magnetic anisotropy and rotatable magnetic anisotropy as a function of external in-plane magnetic field at various angles were presented and discussed in details.

Application of Electromagnetic Waves in Softmaterials

Shengyong Xu
Department of Electronics, Peking University, China

Abstract— We will discuss latest experimental results on detection of both structural and electromagnetic properties of softmaterials (e.g., a fluidic channel) under a cover of dielectric layer (up to nearly two hundred micron thick), i.e., getting the information of subsurface, with a near-field microwave scanning microscope. This offers a unique approach for *in-situ* and non-invasive detection of conducting patterns and ionic fluids in a sealed system.

We will also discuss a novel theory on softmaterial electromagnetic waveguide, which can be constructed with a dielectric material merged in liquids. We have recognized several kinds of natural softmaterial electromagnetic waveguide structure in biosystems, which may play critical roles in transmission of bio-electric signals. We have confirmed by experiments that softmaterial waveguides at large scales work well for transmission of electromagnetic waves.

Tunable In-plane Uniaxial Magnetic Anisotropy of Nanocrystalline Fe-N Thin Films for High Frequency Application

Xiaoyu Li, **Jianbo Wang**, **and Qingfang Liu**
Key Lab for Magnetism and Magnetic Materials of Ministry of Education
Lanzhou University, Lanzhou 730000, China

Abstract— Nanocrystalline Fe-based thin films have been widely studied for high frequency application because of good soft magnetic properties [1, 2]. In this work, the high-frequency magnetic permeability spectra of as-sputtered Fe-N films with various N_2 flow ratio (N_2/N_2+Ar) were investigated. Meanwhile, oblique sputtering was used to adjust the in-plane uniaxial magnetic anisotropy (IPUMA) of Fe-N thin films.

Good soft magnetic properties with well-fined IPUMA can be obtained with the nitrogen gas flow ratio in the range from 3% to 5% because of the formation of amorphous and nanocrystalline iron nitride. The permeability spectra measured were well fitted based on the phenomenological Landau-Lifshitz-Gilbert equation. With the increase of N_2 flow ratio, the saturation magnetization $4\pi M_s$, the IPUMA field H_k, resonance frequency f_r continuously decrease, while the damping factor α and resonant frequency linewidth Δf_r increase. The increase of damping factor α can be ascribed to the increase of interatomic spacing and imperfection with increasing nitrogen content as a function of the increasing of N_2 flow ratio.

When the nitrogen gas flow ratio is fixed at 5%, the TEM results indicate the irregular randomly oriented fcc FeN0.056 fine particles uniformly disperse in the amorphous iron nitride matrix, so the samples show the typical nanocrystalline structure. The IPUMA field H_k of the Fe-N nanocrystalline thin films can be adjusted by changing the oblique angle θ and the deposition time t. H_k increases with increasing θ for the same deposition time t, and H_k increases with increasing t for the same oblique angle θ. For the typical samples with $t = 30$ min, H_k can be tuned increasing from 156 to 360 Oe, hence, the resonance frequencies increase from 2.87 to 6.05 GHz, which implies that the films have potential applications in high frequency field.

ACKNOWLEDGMENT

The authors thank for the support from National Basic Research Program of China (2012CB933101) and National Science Fund of China (51171075, 51371092).

REFERENCES

1. Hayakawa, Y., A. Makino, H. Fujimori, and A. Inoue, *J. Appl. Phys.*, Vol. 81, 3747, 1997.
2. Seemann, K., H. Leiste, and C. Ziebert, *J. Magn. Magn. Mater.*, Vol. 316, e879, 2007.

Microwave Tunable Ferromagnetic Microwires-filled Polymer under External Stimuli

F. X. Qin[1, 2], **J. Tang**[1], **H. X. Peng**[2], **and C. Brosseau**[3]

[1]1D Nanomaterials Group, National Institute for Materials Science
1-2-1 Sengen, Tsukuba, Ibaraki 305-0047, Japan
[2]Advanced Composite Centre for Innovation and Science, Department of Aerospace Engineering
University of Bristol, University Walk, Bristol, BS8 1TR, UK
[3]Université Européenne de Bretagne, Université de Brest, Lab-STICC
CS 93837, 6 Avenue Le Gorgeu, 29238 Brest Cedex 3, France

Abstract— In the present talk, we have troughed through the most recent advances on the microwave tunable composites in our group, i.e., the composites with electromagnetic behaviours sensitively modulated by the external stimuli [1]. We will present the effect of magnetic field, tensile stress and dc current on the electromagnetic properties of several sets of composites with varying wires, matrices and mesostructure, such as continuous-wire against short-cut wire, periodical against random. Two types of wires have been used as fillers, namely, glass-coated microwires prepared by Taylor-wire technique and the melt-extraction microwires prepared by the melt-extraction method. These composites were characterized by a modified frequency-domain microwave spectroscopy which is capable of measuring precisely the permittivity and permeability under external stimuli, i.e., in-situ microwave characterization. The focus is placed upon the presentation and analyses of the roles of dc magnetic field [2–4], tensile stress (strain) [5, 6], dc current [7] on the formulation of the electromagnetic spectra via delineating the relations between microstructure/mesostructure-macroscopic properties. We have shown here some unique dielectric behaviour such as cross-over phenomenon conditioned by specific geometry or microstructure and wide range of magnetic field, which are underpinned by the coupling between magnetostatics and electrodynamics of microwire(s). On the same footing, the mechanism accounting for the complex stress dependence of permittivity and unusual current effect are discussed. The particular role of polymer matrix and interface is also elucidated to explain some unexpected characteristics in the electromagnetic spectra. In addition to these foundational insights, the practical significance in the domains of e.g., microwave devices and high-performance sensing are concluded in the end corresponding to the discussed functionalities. Overall, this talk is expected to provide some general principles in designing, fabricating and characterizing such type of filled polymer by elongated magnetic fillers and inspire the development of next-generation multifunctional microwave devices.

REFERENCES

1. Qin, F. X. and H. X. Peng, *Prog. Mater. Sci.*, Vol. 58, 183, 2013.
2. Qin, F. X., et al., *Appl. Phys. Lett.*, Vol. 100, 192903, 2012.
3. Qin, F. X., et al., *Appl. Phys. Lett.*, Vol. 101, 152905, 2012.
4. Qin, F. X., et al., *Appl. Phys. Lett.*, Vol. 102, 122903, 2013.
5. Qin, F. X., et al., *Appl. Phys. Lett.*, Vol. 97, 153502, 2010.
6. Qin, F. X., et al., *Appl. Phys. Lett.*, Vol. 99, 252902, 2011.
7. Qin, F. X., et al., *Appl. Phys. Lett.*, Vol. 104, 012901, 2014.

Monte-Carlo Simulation of Magnetic Domain Structures in Nanomagnets

Xingsen Gao[1], **Jipei Chen**[1], **Guo Tian**, **Xiao Song**, **and Junming Liu**[2]

[1]Institute for Advanced Materials and Laboratory of Quantum Engineering and Quantum Materials
South China Normal University, Guangzhou 510006, China
[2]Laboratory of Solid State Microstructures, Nanjing University, Nanjing 210093, China

Abstract— Nanomagnets have attracted intensive interests due to their rich domain structures as well as a wide range of application potentials in ultrahigh-density magnetic recording, sensors, and microwave source or resonator devices. In this work, the domain states in nanomagnets were tailored by various parameters such as geometry, temperature, external field, and magnetic anisotropy, as simulated by Monte-Carlo method.

The magnetic domain states in ultrathin nanostructures was simulated based on a Heisenberg model involving the short-range exchange coupling, long-range dipole-dipole interaction, and perpendicular anisotropy. An intriguing thermally driven magnetic structural transition from perpendicular stripe domain to flux closure (planar vortex) state, accompanied by an apparent thermal hysteresis effect and typical characteristics of the first-order phase transition, is revealed. More interesting, it is found that the domain state evolution can be remarkably modulated by perpendicular anisotropy, which not only alters the vortex-striped transition behaviors, but also leads to various intriguing domain patterns such as bubble, skymion-like, and window-like domains in a controllable manna. Besides that, we also simulated the magnetic domains in nanodisck and nanoring structures with further including of Dzyalosinskii-Moriya interaction. By proper adjusting the geometric and anisotropy parameters, the nanoring can exhibit either vortex or skyminon lattice ring domain structure. A domain state phase diagram based on anisotropy and magnetic field was also derived, which may offer a guideline for further designing of domain states for certain applications.

Finally, we will also demonstrate an experimental example on how to develop ordered spinel ferrites nanodot arrays by using porous anodized alumina (AAO) template assist pulsed laser deposition process. The as deposited nanodots can exhibit various nanodomains, in association with geometric confinement.

ACKNOWLEDGMENT

The authors like to acknowledge the NSFC (Grant Nos. 51031004, 51272078, 51332007), NSFC-Guangdong (S2011040003205), and PCSIRT (Grant No. IRT1243) for financial supports.

Session 2A12
SC4: Array Antenna for Wireless Communication

Dual-band A-sandwich Radome Design for Airborne Applications

Licheng Zhou, Yongmao Pei, and Daining Fang
State Key Lab for Turbulence and Complex Systems, College of Engineering
Peking University, Beijing 100871, China

Abstract— A dual-band radome with A-sandwich structure is proposed for airborne applications. The radome is designed in a tangent ogive configuration with the wall structure of A-sandwich structure, aiming at excellent aerodynamic performance and a better strength-to-weight ratio. The skin layer of the A-sandwich wall structure is made of glass composite with relative permittivity of 4.0 and loss tangent of 0.015, while the core layer is a foam core with relative permittivity of 1.1 and loss tangent of 0.003. The thickness of each layer of the wall structure is dimensioned in 1/12 of the wavelength within each layer corresponding to a design frequency. The flat wall structure is demonstrated by the transfer matrix method that it exhibits dual-band performance with two pass-bands of 0–1.55 and 4.46–7.57 times of the design frequency. The geometry of the antenna-radome system is of typical dimensions for airborne applications, with the height of the radome to be 1.0 meter and the base diameter to be 0.5 meter. As for the EM performance of the antenna-radome system, the 3D ray-tracing method is applied to the analysis. Numerical results indicate that the tangent ogive radome with a design frequency of 5.5 GHz for the wall structure presents dual pass-bands of 8.4–8.8 GHz and 35.7–37.1 GHz, while one with a design frequency of 6.0 GHz presents dual pass-bands of 9.2–9.7 GHz and 39.0–40.0 GHz. Results show that the nose-cone radome exhibits dual-bands over 1.53–1.60 and 4.49–6.75 times of the design frequency for the wall structure. The dual-band A-sandwich radome proposed is demonstrated to be feasible for X-band and Ka-band applications.

Nonuniform Phase Reversal Antennas with Double-side near Field Focusing Beams

Z. L. Ma, L. J. Jiang, and S. Gupta
Department of Electrical and Electronic Engineering
The University of Hong Kong, Hong Kong, China

Abstract— Recently, the demand for near-field focusing antennas is continuously increasing in fields of radio frequency identification (RFID) systems, microwave inspection, sensing systems and so on. Some applications require the antenna has capability of concentrating radiated electromagnetic waves at a small spot. To achieve this goal, a large number of studies have been conducted. Various methods such as tapered microstrip antennas, patch array antennas and slot array waveguides were presented. However, the existing methods still have disadvantages of complicated antenna structures and feeding networks for array elements. At the same time, a phase reversal antenna is reported recently. This antenna is a periodic structure antenna. In each unit cell, a transmission part (guiding waves) and a crossover section (radiating waves) are included. It has very simple structure and simple radiation mechanism. However, currently presented phase reversal antennas are all arranged in uniform manner.

In this presentation, a novel nonuniform phase reversal antenna is proposed to realize the near field focusing. The crossover sections are arranged to obtain focusing beams by adjusting the electric lengths of transmission parts between each two adjacent crossovers. Detailed design method and mathematic calculations are presented. Due to the property of axially symmetric radiation of phase reversal antenna, the proposed antenna has two focusing beams in front and back sides, respectively. To achieve more sharp focusing performance and enhance the field strength at the focusing spot, a four-branch linearly polarized array is presented and examined. In summary, comparing with existing counterparts, the proposed antenna features simple structure, easy fabrication, low cost, no complicated feeding network and negligible cross-polarization.

A Dual Band Center-fed Sleeve Dipole Array for IEEE 802.11a/b Application

Dau-Chyrh Chang[1], **Yi-Ci Su**[1], **Chih-Hung Lee**[2], **and Chang-Hsuan Kao**[1]

[1]Oriental Institute of Technology, CRC, Taiwan
[2]Electronics Testing Center, Yuan Ze University, Taiwan

Abstract— For the IEEE 802.11 a/b application, a three by one dual bands printed sleeve dipole antenna array with center-fed as shown in Figure 1 has been investigated. The current distribution should be considered by the symmetry and asymmetry of the excitation mode in center-fed transmission line as shown in Figure 2. The optimized center-fed structure on the FR4 substrate can provide the high efficiency, high gain and ommi-directional antenna pattern. The simulation results by using GEMS are shown in Figure 3. The size of sleeve dipole antenna array is 220 mm by 8 mm by 0.4 mm. The efficiency, directivity, and gain are 84.24%, 5.69 dBi and 4.94 dBi at 2.45 GHz respectively. And the efficiency, directivity, and gain are 70.55%, 8.36 dBi, and 6.84 dBi at 5.8 GHz.

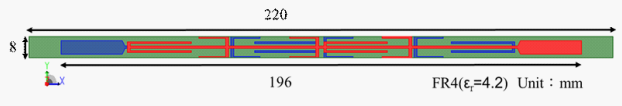

Figure 1: Dual bands sleeve dipole antenna array.

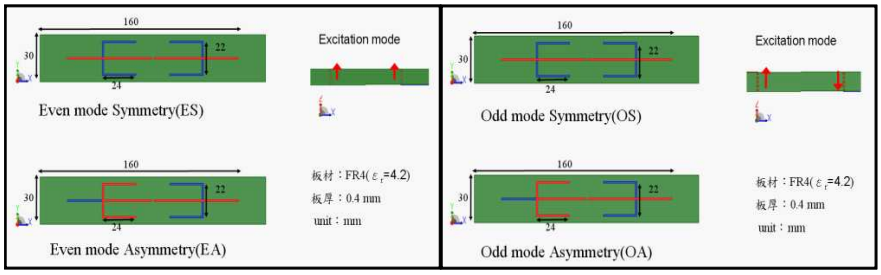

(a) (b)

Figure 2: Excitation mode of the transmission line. (a) Even mode. (b) Odd mode.

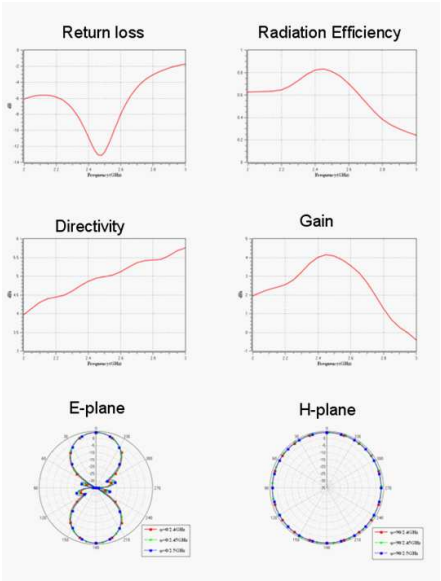

Figure 3: Simulation results.

Patch Antenna Array for IEEE 802.11a/n MIMO Application

Dau-Chyrh Chang[1], **Ming-Ching Yen**[1], **Chih-Hung Lee**[2,3], **and Yau-Jyun Tsai**[1]

[1]Oriental Institute of Technology, Taiwan
[2]Yuan Ze University, Taiwan
[3]Electronics Testing Center, Taiwan

Abstract— A dual polarization of patch antenna array for IEEE 802.11 a/n MIMO applications are proposed and experimentally studied in this paper. The four by one patch antenna array (200 mm by 70.5 mm by 0.4 mm) combine a wide band power divider with a reflector (210 mm by 75 mm by 0.4 mm) is show as in Figure 1. Due to the existence of the two resonators extended from the patch structure of the micro-strip feed line, good impedance matching across a very wide operating bandwidth can be achieved (5.18 GHz∼5.81 GHz). Figure 2 shows the equivalent circuit matching by ADS software. The results of simulation are shown in Figures 3 to 5. The efficiency and gain of the horizontal polarization are 70% and 14 dBi. The efficiency and gain of the vertical polarization are 65% and 12 dBi.

To design high gain and high directivity patch antenna array, the effectives of mutual coupling, throughput and Envelope Correlation Coefficient (ECC) of MIMO will be descriptions in the full paper.

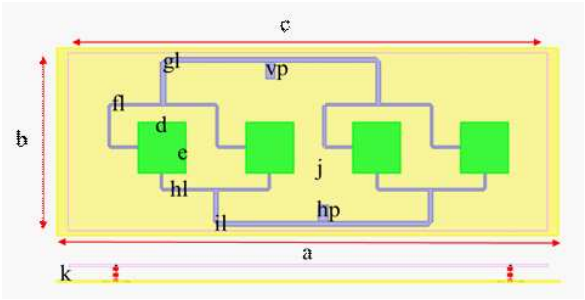

a	210	hl	48.5
b	71	il	58
c	200	j	21
d	20	k	2.5
e	20	vp	4 x 6
fl	27	hp	4 x 6
gl	42	Unit: mm	

Figure 1: Dual polarization of patch antenna array.

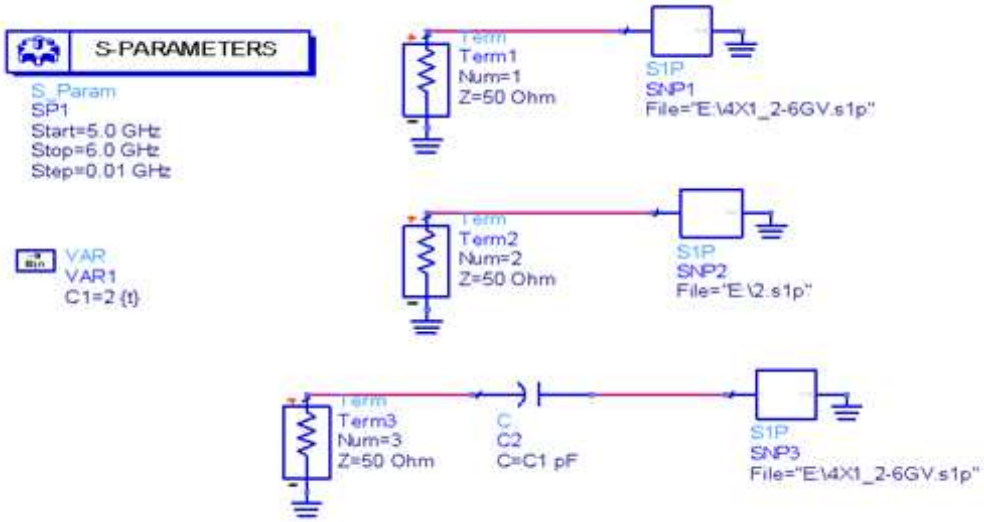

Figure 2: Equivalent circuit matching by ADS.

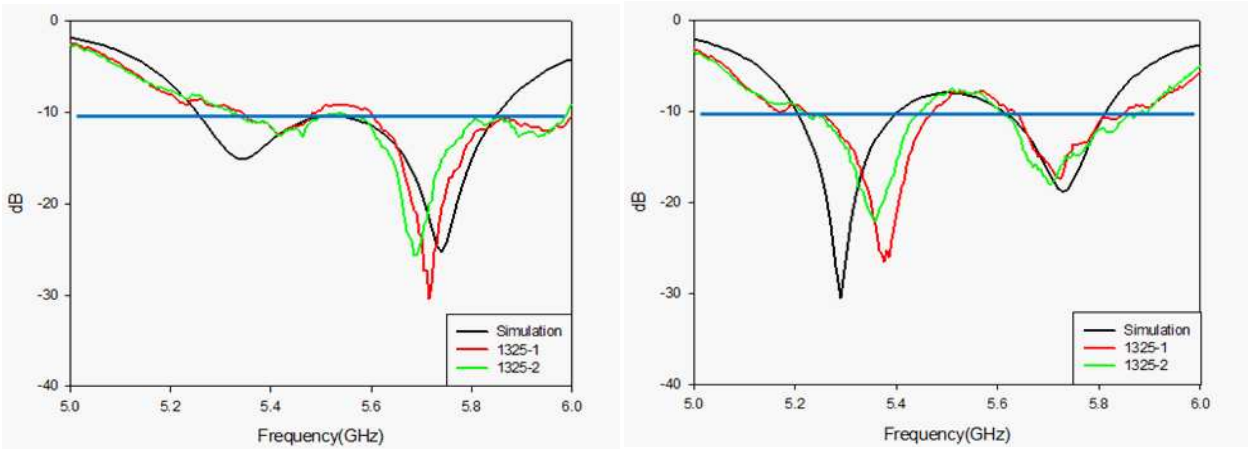

Figure 3: Return loss by simulation. (a) Horizontal, (b) vertical.

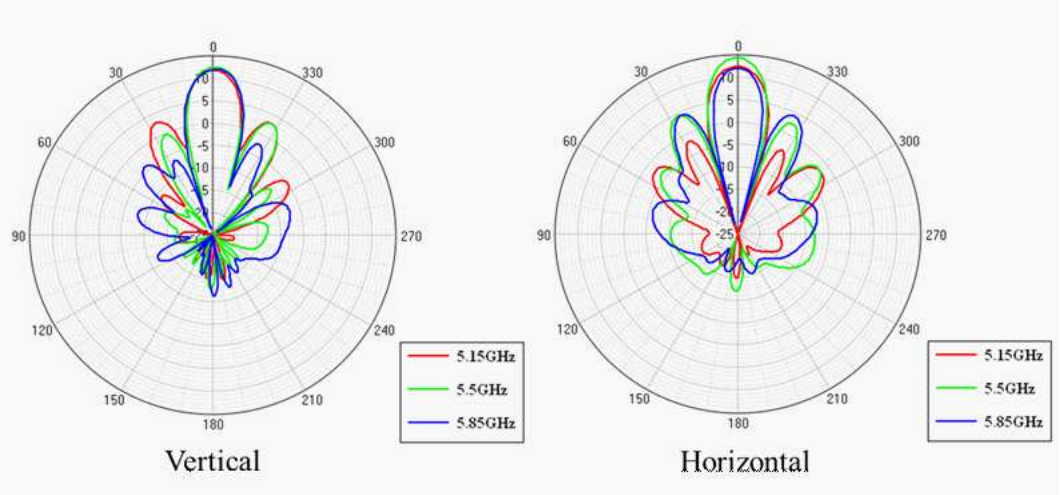

Figure 4: E-plane pattern by simulation.

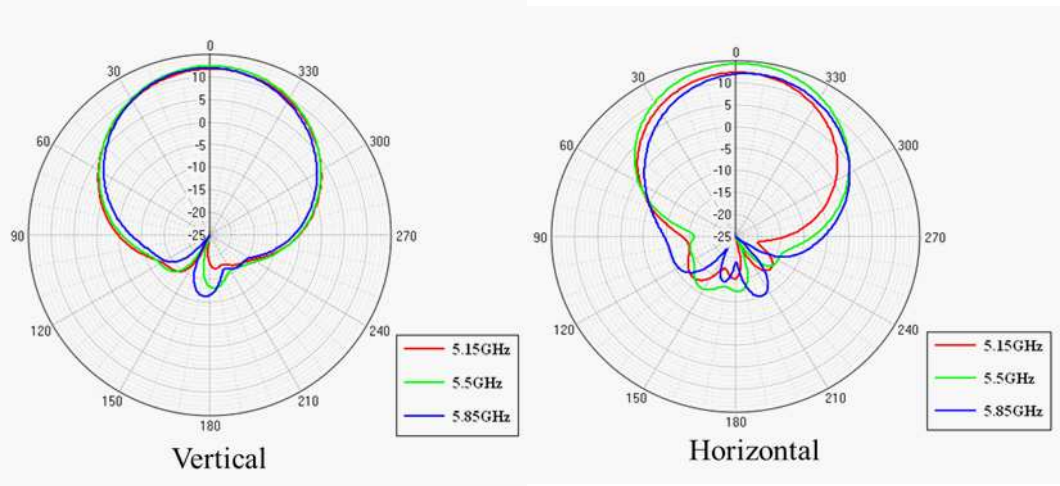

Figure 5: H-plane pattern by simulation.

Rectangular DRA Reflectarray with an Inclined Top-loading Micostrip Patch

Eng-Hock Lim, Hong Yik Wong, and Fook Loong Lo
Department of Electrical and Electronic Engineering
Universiti Tunku Abdul Rahman, Kuala Lumpur, Malaysia

Abstract— In this paper, the feasibility of using a rectangular dielectric resonator antenna (DRA) as the reflectarray unit element is explored. It has been shown that a loading rectangular strip stuck on top of a rectangular DRA can function as a phase shifter when it is inclined with a certain angle. The loss of the DRA reflectarray is usually lower than that for the microstrip patch because of the absence of conductive loss, especially in the millimeter-wave ranges. To demonstrate, a C-band rectangular waveguide (5.85 GHz–8.20 GHz) is used in the model. The unit element here is a DRA ($\varepsilon_r = 7$, $\tan\delta = 0.01$, $L_d = 14$ mm and $H_d = 6$ mm) with a top-loading metallic strip. The DRA is placed at the center of the ground plane. In this case, no substrate is used and the DRA is directly placed on a ground plane. It is found that inclining the strip angle (θ) can cause the incident wave to scatter with different phases; therefore, it is used as the phase shifter for the reflectarray. Commercial software CST Microwave Studio is used to simulate the model. The loss peaks at -0.4 dB at the inclined angle of $\theta = 25°$. The total phase shift introducible by the strip rotation is measured to be 162.29°.

Decoupled Hepta-band MIMO Antenna with a Neutralization Line for Smartphone Applications

Zhong-Xiang Chen and Yong-Ling Ban
Institute of Electromagnetics, University of Electronic Science and Technology of China
2006 Xi-Yuan Avenue, Western High-Tech District, Chengdu, Sichuan 611731, China

Abstract— A Hepta-band MIMO antenna incorporating a neutralization line (NL) for port decoupling for smartphone applications is proposed. The U-shape NL is applied to reduce the mutual coupling for the lower-band, which is lower than −10 dB for 824–960 MHz. In addition, the addition of the NL has no adverse effects on the bandwidth, and an LC matching circuit as well as on-ground slits are employed to cover the Hepta-band operation. A prototype is fabricated and tested, with S parameters, radiation efficiencies, envelope correlation coefficient (ECC) and mean effective gain (MEG) presented.

Transmission Line Type Circularly Polarized Series Patch Array for UHF RFID Applications

M. Chen[1], **L. Jiang**[1], **J. Xi**[2], **and Terry Ye**[2]

[1]The University of Hong Kong, Hong Kong, China
[2]Hong Kong LSCM, Hong Kong, China

Abstract— Two novel transmission line type series patch arrays are proposed for UHF RFID applications, especially, smart shelves. The proposed patch arrays are of low profile, low cost, and suitable for book shelves. A traditional series patch array is considered as a periodic structure with the periodicity of one guided wavelength. It scans through the broadside if the generally known stopband is closed. It can be shown that for the traditional series patch array, the stopband can be closed when a Q-balanced condition is achieved. Under this circumstance, the shunt and series Q factors are identical. One drawback for such patch array when applied to the RFID system is that its cross polarization is very low. As a result, a linearly polarized tag cannot be properly read when it is placed along the transversal direction. In fact, a circularly polarization is preferred for RFID systems since a blind zone could be minimized to accomodate different tag directions.

In this talk, two novel series patch arrays with the circular polarization will be demonstrated. One is to trim one corner of a typical rectangular patch and the other one is to introduce a slot in a square patch. Both of these approaches will perturb the current distribution and a desired polarization can be achieved by adjusting the amount of perturbation. Furthermore, in accordance with the Q-balanced method, the final resonance that is along two perpendicular directions also helps to balance the structure. Both of the novel arrays are simulated in a full-wave simulator. It has been shown that the proposed structures can be more easily balanced with the circular polarization. S parameters are measured by VNA. The reading ability is tested by using the UHF RFID reader. Success reading time can be estimated in this system by injecting power to the proposed reader antenna. Tags placed along various directions can be tested to verify the reliability of the proposed antenna.

A Compact Triple-band MIMO Antenna for Wimax/WLAN Application

Huifen Huang, Yuanhua Hu, and Wei Zhao
School of Electronic and Information Engineering
South China University of Technology, Guangzhou, China

Abstract— A compact printed triple-band inverted-F antenna suitable for WLAN and WiMAX multiple-input-multiple-output (MIMO) system is proposed in the paper.

The presented antenna consists of a folded-strip radiator and a parasitic radiation element. The main radiation element is evolved from simple inverted-F antenna, works at 2.4 GHz, 3.5 GHz, What differ from the traditional inverted-F antenna is the inversion of the position between the feeding point and the short-circuit point, and with the consideration of compact dimension, the short-circuit strip curves the Z-shaped structure, the open stub curves the L-shaped structure. Which can excite the mode of 2.4 GHz and high-order mode, but it still can't cover the Wimax frequency. So a L-shaped open stub is introduced in the Z-shaped short-circuit strip. Through the adjustment and deformation of the sequence of the structure, it can be observed that the main radiator actually is a inverted-F antenna with two open stub. In order to further cover the higher-frequency WLAN frequency. In the left of the main radiator, a L-shaped parasitic stub is added. As we know that inverted-F antenna is dependent of the length of the ground plane strongly, to reduce the whole size, a slit which can lengthen the current path then to improve the impedence match is added. The whole antenna only occupies $30 \times 25\,\mathrm{mm}^2$, suitable to be MIMO antenna. In order to reduce coupling among antenna elements, every element should be placed in a orthogonal way, simultaneously every corner should be truncated into cicular and a slit is added. The four-element MIMO antenna occupies $60 \times 60\,\mathrm{mm}^2$, operating at the following frequency bands: 2.36–2.56, 3.45–3.74, 4.95–6.33 GHz.

Session 2A13
SC4: Wireless Power Transfer

Power Transfer k-Q Product Explored for a Variety of Two-port LCR Circuit Topologies

Naoki Sakai and Takashi Ohira
Toyohashi University of Technology, Japan

Abstract— Power transfer efficiency is an important objective in designing wireless power transfer (WPT) systems. To improve power transfer efficiency, WPT engineers have to reduce both reflection loss and internal loss. While the reflection loss can be mitigated by employing appropriate matching circuits after source and before load, the internal loss of the system can never be recouped by tuning any external passive circuit. Therefore, it has the first priority for WPT engineers to develop the internal structure having minimum power loss. In designing the internal structure, they use maximum power transfer efficiency ($\eta_{\max}$). This is the power transfer efficiency when maximized by perfect impedance matching for the source and load simultaneously. It is commonly known that $\eta_{\max}$ depends uniquely on k-Q product [1, 2]. Coupling coefficient k and resonant Q factor could be easily derived in magnetic coupling WPT systems composed of simple two coils. However, in WPT systems of complicated topologies, k and Q become rather ambiguous. To solve this problem, a rigorous formula on k-Q product of two-port systems in an arbitrary topology was presented [3] in terms of immittance matrix parameters.

This paper applies the formula to various topologies consisting of lumped-constant resistors, inductors, and capacitors. We particularly explore those of all the combinations of one, two, and three passive elements. Derived formulas are systematically tabulated for engineers to get a lucid vista onto k-Q product at a glance. The resultant look-up table will work as a powerful handbook to find a brilliant way for high-$\eta_{\max}$ WPT system developments.

REFERENCES

1. Kurs, A., A. Karalis, R. Moffatt, J. D. Joannopoulos, P. Fisher, and M. Soljacic, "Wireless power transfer via strongly coupled magnetic resonators," *Science*, Vol. 317, 83–86, July 2007.
2. Awai, I., "Basic characteristics of magnetic resonance wireless power transfer system excited by a zero ohm power source," *IEICE Electronics Express*, Vol. 10, No. 21, Nov. 2013.
3. Ohira, T., "Angular expression of maximum power transfer efficiency in reciprocal two-port systems," *IEEE Wireless Power Transfer Confarence 2014*, Jeju, May 2014.

Three-phase Symmetrical Inductive Coupled Structure for Wireless EV Charging System

Jia-You Lee[1], **Hung-Yu Shen**[1], **and Shan-Jen Chao**[2]

[1]Department of Electrical Engineering, Cheng Kung University, Tainan, Taiwan
[2]Department of Power SBG, Lite-On Technology Corporation, New Taipei, Taiwan

Abstract— In this paper, a three-phase symmetrical inductive coupled structure is proposed for wireless electric vehicle charging system. This proposed inductive coupled structure is three-phase symmetric and consists of two identical windings, which separate on the primary and secondary sides with a certain air gap. Comparing to traditional power transmission technique, higher convenience and higher reliability are able to achieve when the wireless power transfer technique is applied in electric vehicles charging. Two possible methods for EV wireless charging could be to use plug-in paddle or stationary pad. The stationary pad seems to be a suitable solution for charging EV more freely than plug-in paddle. However, the charging pads both on the primary and secondary sides have to be aligned exactly. The objective of this research is to investigate the wireless power transfer technique for charging EV with high efficiency and high convenience.

Therefore, the three-phase symmetrical inductive coupled structure is proposed in this research to obtain a uniform distribution of flux over the charging area and to address the issue of alignment between the primary and secondary windings. Two shapes of coil, round and hexagon, are discussed in this paper to clarify the distribution of their magnetic field. Moreover, the strip core with low reluctance is applied to secondary winding for guiding more flux to go through. FEA software, Maxwell, is adopted to analyze the flux distribution of the proposed three-phase symmetrical inductive coupled structure and to design the arrangement of each coil unit and strip core. Fig. 1(a) shows the flux distribution of one hexagonal coil unit with strip core.

A 900 W laboratory scale prototype with three-phase symmetrical inductive coupled structure for EV wireless charging is implemented and tested to validate the feasibility of proposed system. Experimental results demonstrate that the measured transfer efficiency is 87.3% for an air gap of 2 cm between the two three-phase symmetrical windings when an 8.4 Ah lithium iron phosphate battery is charged. Fig. 1(b) represents the photo of the proposed wireless EV charging system with three-phase symmetrical inductive coupled structure. It includes three-phase full-bridge inverter, three-phase symmetrical inductive coupled structure, secondary charging circuit, and LiFePO4 battery module.

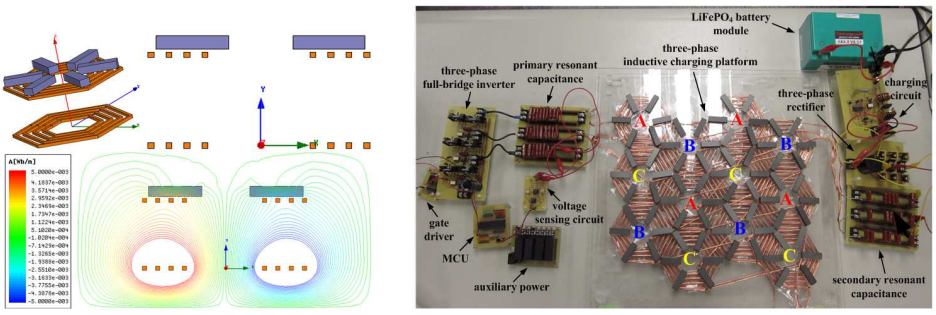

(a) (b)

Figure 1: (a) The flux distribution of one hexagonal coil unit with strip core and (b) the photo of the proposed wireless EV charging system with three-phase symmetrical inductive coupled structure.

On Frequency Optimization of Assymetric Resonant Inductive Coupling Wireless Power Transfer Links

Nuria Egidos[1], **Elisenda Bou**[1], **Raymond Sedwick**[2], **and Eduard Alarcon**[1]

[1]UPC BarcelonaTech, Barcelona, Spain
[2]University of Maryland, College Park, MD, USA

Abstract— Resonant Inductive Coupling Wireless Power Transfer (RIC-WPT) is a leading field of research due to the growing number of applications that can benefit from this technology: from biomedical implants to consumer electronics, fractionated spacecraft and electric vehicles amongst others. However, current applications are limited to symetric point-to-point-links. New challenges and applications of RIC-WPT emphasize the necessity to explore, predict and optimize the behavior of these links for different configurations: multi-point RIC-WPT networks and assymetrical systems. In this work a design methodology oriented towards the optimization of assymetric RIC-WPT links is presented, resulting in a closed analytical formulation of the optimal frequency at which an assymetrical RIC-WPT link should operate. Finally, the resulting efficiency-optimized link si explored and compared to previous results obtained in RIC-WPT symetric configurations [1, 2].

REFERENCES

1. Sedwick, R., "Long range inductive power transfer with superconducting oscillators," *Annals of Physics*, 2010.
2. Sedwick, R., "A fully analytic treatment of resonant inductive coupling in the far field," *Annals of Physics*, 2012.
3. Bou, E., E. Alarcon, and R. Sedwick, "Maximizing efficiency through impedance matching from a circuit-centric model of non-radiative resonant wireless power transfer," *Proceedings of 2013 IEEE International Symposium on Circuits and Systems*, June 2013.
4. Balanis, C. A., *Antenna Theory Analysis and Design*, Wiley, 2005.
5. Kiani, M. and M. Ghovanloo, "The circuit theory behind coupled-mode magnetic resonance-based wireless power transmission," *IEEE Transactions on Circuits and Systems I: Regular Papers*, Vol. PP, No. 99, 1, 2012.
6. Bou Balust, E., E. Alarcon, and J. Gutierrez, "A comparison of analytical models for resonant inductive coupling wireless power transfer," *PIERS Proceedings*, 689–693, August 19–23, Moscow, Russia, 2012.

Input and Output Impedance Matching Conditions and Maximum RF-to-DC Rectification Efficiency in Wireless Power Transfer System

Qiaowei Yuan[1], **Shinji Abe**[1], **Satoshi Suzuki**[1], **and Takashi Ohira**[2]

[1]Sendai National College of Technology, Japan
[2]Toyohashi University of Technology, Japan

Abstract— Power transfer and rectification efficiency are the first priority issues in developing WPT systems. Linear part of the system was elegantly formulated in terms of efficiency angle tangent [1], and considered from the aspect of coupled dipole antenna elements [2]. We still need more theoretical work for nonlinear part, e.g., RF inverters and rectifiers to achieve ultimate system performance [3]. This paper presents input and output impedance matching conditions and maximum RF-to-DC rectification efficiency in wireless power transfer systems. We assume an RF source having a finite available power and arbitrary output impedance, and a DC load with arbitrary resistance. We also involve intrinsic power loss due to diode's nonlinear parasitic resistance and capacitance. For such internal power loss factors given, we seek the optimum set of RF output impedance and DC load resistance simultaneously to maximize the overall power transfer efficiency which is the ratio of P_2 to P_1 as defined in Fig. 1. We consequently give a numerical example of the absolute maximum efficiency for a simple topology of diode rectifier.

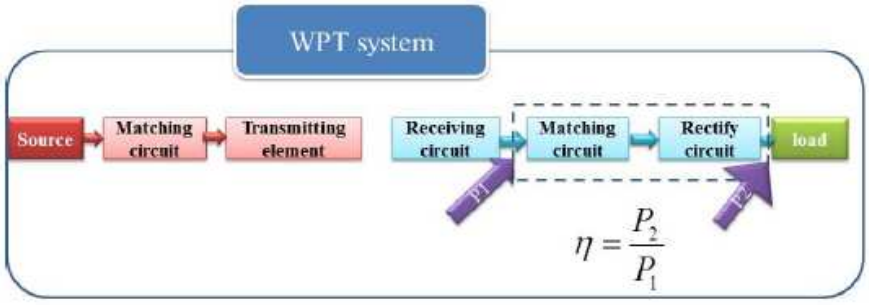

REFERENCES

1. Sakai, N., et al., "Power transfer k-Q product explored for a variety of two-port LCR circuit topologies," *Progress In Electromagnetics Research Symposium*, Guangzhou, China, August 25–28, 2014.
2. Chen, Q., K. Ozawa, Q. W. Yuan, and K. Sawaya, "Antenna characterization for wireless power-transmission system using near-field coupling," *IEEE Antennas and Propagation Magazine*, Vol. 54, No. 4, 108, 2012.
3. Ohira, T., "Power efficiency and optimum load formulas on RF rectifiers featuring flow-angle equations," *IEICE Electronics Express, ELEX*, Vol. 10, No. 11, 1–9, June 2013.

Development of Gallium Nitride Schottky Barrier Diode for Microwave Rectification

Jin-Ping Ao
Institute of Technology and Science, The University of Tokushima
2-1 Minami-Josanjima, Tokushima 770-8506, Japan

Abstract— The technology of wireless power transmission using microwave has been attracting much attention owing to the increasing demands for the various wireless technologies, such as electric vehicle power charging, energy harvesting, ubiquitous power source, and wireless power distribution within a building. In a microwave power transmission system, it normally consists of a DC/RF conversion, a microwave transmission path and a RF/DC conversion. In the receiving terminal, a so-called rectenna circuit is adopted to complete the RF to DC conversion [1]. The conversion efficiency strongly depends on the performance of the Schottky barrier diode (SBD) used in the rectenna circuit, such as on-resistance, off-capacitance and turn-on voltage. Silicon- and gallium arsenide-based SBD had already commercialized for application in this area. However, the breakdown voltage or the operation frequency is still limited due to the limitation of the material properties. As a wide bandgap semiconductor, gallium nitride (GaN) is regarded as a promising semiconductor material to realize high-voltage, high-speed, and low-resistance devices. In this presentation, the development of GaN SBDs will be reported to achieve low resistance, low capacitance with certain breakdown voltage for the application in microwave power transmission system.

The GaN SBDs are designed and fabricated for microwave power rectification with specialized device structure and fabrication process [2, 3]. The active layers include a drift layer and an access layer which are deposited on a sapphire substrate. The thickness and doping concentration of the drift layer are designed to get trade-off between the on-resistance and the breakdown voltage [4]. The access layer with a sheet resistance of about 25 Ω/square is designed to reduce the series resistance. Finger- and dot-type device were adopted to reduce the capacitance from the drift layer. The number of the finger and dot can be adjusted to fit the requirements of the operation frequency and the handling power. To reduce the capacitance from the anode pad, a trench isolation structure was developed by etching the active layer to the sapphire substrate. Furthermore, in order to reduce the turn-on voltage, TiN Schottky electrode with lower work function was synthesized by reactive sputtering of Ti pure metal in a mixture gas ambient of Ar and N_2 [5, 6]. The TiN SBDs showed comparable reverse leakage current and breakdown voltage but much lower turn-on voltage as the normally-used Ni electrode [7]. GaN SBDs can be expected to improve the RF/DC conversion efficiency of a rectenna circuit for microwave power transmission system.

REFERENCES

1. Shinohara, N., *IEEE Microwave Magazine*, Vol. 12, 64, 2011.
2. Fukui, K., et al., *IMWS-IWPT*, Kyoto, Japan, May 2012.
3. Takahashi, K., et al., *Jpn. J. Appl. Phys.*, Vol. 48, 04C095, 2009.
4. Ao, J.-P., et al., *CSICS 2010*, Monterey, USA, Oct. 2010.
5. Ao, J.-P., et al., *Vacuum*, Vol. 84, 1439, 2010.
6. Li, L. A., et al., *J. Vac. Sci. Technol. A*, Vol. 32, 02B116, 2014.
7. Kishi, A., et al., *SSDM 2013*, Fukuoka, Japan, Sep. 2013.

Design and Implementation of Wireless RF Power Transfer Circuit for Implantable Neurostimulator

Jia-You Lee[1], **Hung-Yu Shen**[1], **and Che-Li Lin**[2]

[1]Department of Electrical Engineering, Cheng Kung University, Tainan, Taiwan
[2]Department of N20 Process Integration, TSMC Ltd., Tainan, Taiwan

Abstract— In this paper, a wireless RF power transfer circuit is proposed for supplying energy to the implantable neurostimulator. For the implantable medical electronic devices, the main problem is that how to deliver enough power for this device. Embedding a disposable battery into the implantable device is the most common way. However, it still possesses some potential risk, i.e., leakage of battery electrolyte and replacement of battery. The purpose of this paper is to investigate the wireless RF power transfer technique to overcome the drawbacks of supplying power to implantable neurostimulator.

FEA software, Maxwell, is adopted in this paper to analyze and to design the appropriate coil for the proposed wireless RF power transfer system. The delayed pseudomonophasic pulse (DPS), as the electrical stimulation waveform of the proposed neurostimulator, is generated by the constant current circuit to prevent the tissue from self-heating. Besides, the phase locked loop (PLL) circuit and voltage sensor are applied to the proposed wireless RF power transmitter to realize the resonant frequency tracking control.

A small-size prototype with the proposed wireless RF power transfer circuit for functional neurostimulator is implemented. The fundamental experiments are carried out to verify the feasibility of proposed prototype, including the horizontal displacement test, perpendicular displacement test, and measurement of power transfer efficiency. A maximum efficiency of 55.6% can be obtained at an air gap of 20 mm between the transmitter and receiver. Although the air gap is enlarged to 35 mm, the receiving coil can still induce enough power for operating the implantable neurostimulator normally. Fig. 1 displays the photo of the proposed wireless RF power transfer circuit for implantable functional neurostimulator. Fig. 1(a) shows the wireless RF power transmitter, including class E RF exciting source, gate driver, RF oscillator, PLL circuit, and transmitting coil. Fig. 1(b) represents the implantable neurostimulator with area of $32 \times 30\,\mathrm{mm}^2$, including receiving coil, bridge rectifier, voltage regulator, DAC, microcontroller, and constant current circuit.

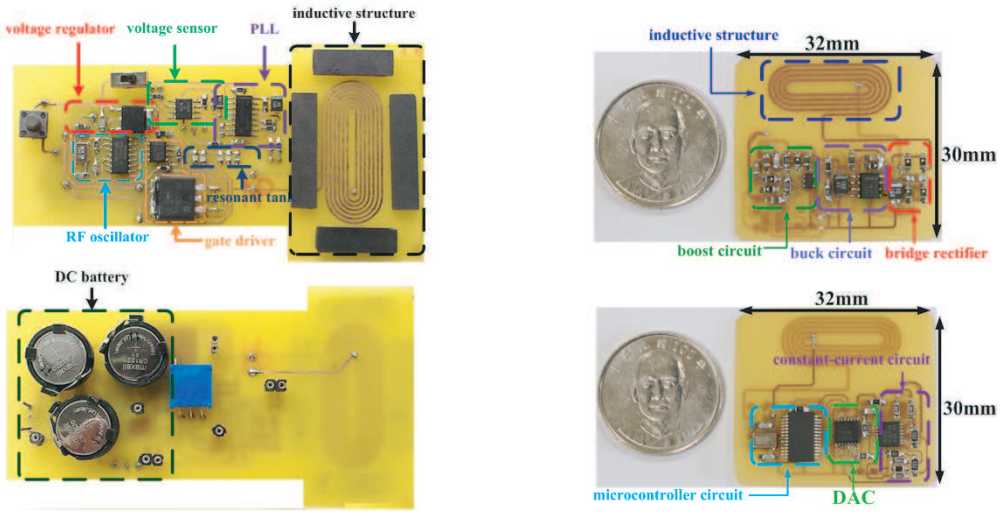

(a) (b)

Figure 1: The photo of the proposed (a) wireless RF power transmitter and (b) implantable neurostimulator.

Wireless Power Supply for ICP Devices with Hybrid Supercapacitor and Battery Storage

Aiguo Patrick Hu, **Fu-yu Beverly Chen**, **Yee Wen You**, **Daniel McCormick**, **and David Budgett**
The University of Auckland, New Zealand

Abstract— Hydrocephalus patients need Intracranial Pressure (ICP) devices to be implanted in brains to monitor the internal fluid pressure levels. ICP devices powered by non-rechargeable batteries would need to be replaced through surgery once they are fully discharged. A solution to frequent surgery is to use a rechargeable battery and replenish it wirelessly using inductive power transfer technology. However, a rechargeable battery requires long charging time and has limited charging cycles. A new energy storage element, supercapacitor, has been introduced which offers a high power density and longer lifespan, but has low energy density. Therefore, a hybrid energy storage system that combines the advantageous features of both rechargeable battery and supercapacitor would be ideal to power the ICP device. In this research we have proposed and developed a charging circuitry for the hybrid system based on inductive power transfer. An energy management scheme has also been developed to drive the device automatically using the two energy storage elements to meet both short and long term operation requirements. The operation modes are determined based on the duration that the primary coil is coupled to secondary implants. The proposed hybrid wireless power supply and storage system is practically implemented and tested, and the voltage levels of the supercapacitor and rechargeable battery are continuously monitored to evaluate the charging and system discharging characteristics. It has demonstrated that it takes only about 3 seconds to charge up the supercapacitor for 1 minute operation of ICP (with about 32 mW of power consumption), and 45 min to charge up the battery for 75 min operation.

On-chip CMOS RF Energy Harvesting System Using Parasitic Capacitance Compensation Technique

Junsik Park[1], **Jaeyeon Kim**[1], **Namsik Ryu**[2], **Sutae Kim**[3], **and Yongchae Jeong**[1]

[1]Chonbuk National University, Republic of Korea
[2]Electronics and Telecommunications Research Institute (ETRI), Republic of Korea
[3]Samsung Electronics, Republic of Korea

Abstract— Recently, RF energy harvesting technology has become an important research issue for one of the eco-friendly energy reusing technologies. If RF energy harvesting system using CMOS process technology is applied into power transmission terminal and wireless communication, it will be great help to overcome the problem of battery efficiency. Since the RF energy floating in the air is the power of −30 dBm or less, generally it is not sufficient power to operate rectifier circuit in the RF energy harvesting system. Therefore, generally the rectifier circuit uses a Schottky diode having a low threshold voltage to minimize the loss of voltage and efficiency. However, the implementation of RF energy harvesting system using the Schottky diodes in CMOS process is difficult due to manufacturing cost and process technology. Therefore, the different design and research direction is necessary. Figs. 1 and 2 show the schematic and layout of the proposed high efficiency on-chip RF harvesting system using a 0.13 µm CMOS process, respectively. Since return loss (S_{11}) is better than −15 dB in overall operating bandwidth as shown in Fig. 3 due to the matching network, the input signal can enter into the rectifier smoothly. In this work, the rectifier circuit is a Villard Voltage doubler structure using a MOSFET diode connection. The PMOS has a floating body structure in order to reduce body effect losses. Since the parasitic capacitance of MOSFET can cause the degradation in conversion efficiency, it is necessary to compensate these parasitic components. For this purpose, the inductor was used which can provide a form of virtual series resonant circuit with parasitic capacitance of both transistors. Furthermore, it is possible to increase the conversion efficiency by suppressing the harmonic components generated by the MOSFET and flattening DC signal using a off-chip low pass filter. The load resistor value was optimized for maximum conversion efficiency. Fig. 4 shows simulation results of conversion efficiency and output DC voltage. From the simulation, the efficiency of 25% or more is obtained for an input power of 10 ∼ 20 dBm which can significantly affect in battery efficiency enhancement of near field communication systems.

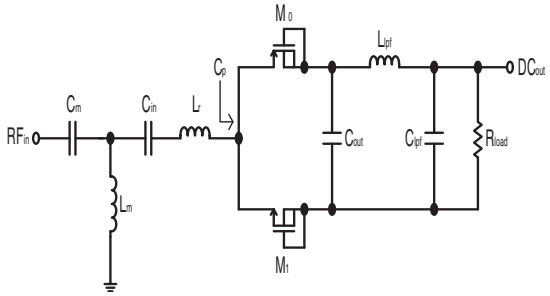

Figure 1.

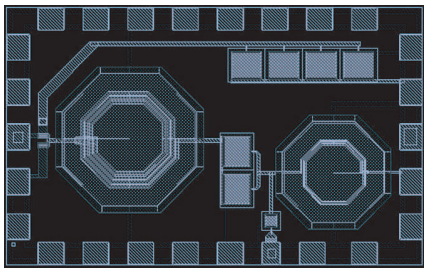

Figure 2.

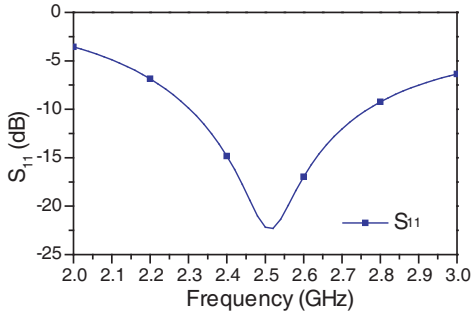

Figure 3.

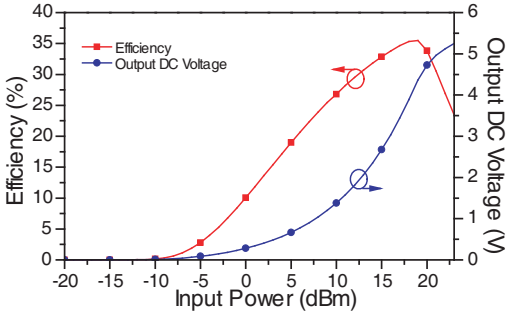

Figure 4.

Graphical Interactivity in Power Device and Circuit *S*-parameter Measurement Exploiting Möbius Transformation

K. Yamada, S. Sakihara, and T. Ohira
Toyohashi University of Technology, Japan

Abstract— Power transmission employing RF waves or what is called WPT (Wireless Power Transfer) is one of the most attractive research topics recently. A WPT system mostly involves inverter and rectifier modules, which work at a frequency ranging from hundreds of kilohertz to tens of megahertz for applications treating power levels from watts to megawatts. Inverters or rectifiers contain nonlinear elements such as FETs or diodes, therefore nonlinear measurements are necessary to design high-power, high-efficiency inverter/rectifier modules. There are some ways to model nonlinear behavior of an element. One choice is to make its equivalent circuit from small signal *S*-parameters measured at every bias point. In this case, however, it is time-consuming, as well as we cannot know the real behavior stimulated by large signals. On the other hand, load- and source-pull methods can observe the real behavior as it is working in the circuits. But it also needs a long time to find the matching point by a tuner. Nonlinear vector network analyzers are also available to get elements' real behavior. However, these methods cannot deal with sufficient power such as hundreds of watts or more. Above of all, the equipment is expensive and delicate.

To realize speedy, high-power, and low-cost measurement, we propose a novel *S*-parameter measurement method by using an oscilloscope. Because our method can use high-impedance port of oscilloscope, it can suit high-power. And it is much less expensive than existing *S*-parameter measurement systems. *S*-parameter is mathematically calculated from the measured waveforms via discrete Fourier transform and Möbius transformation. Additionally, time-domain measurement facilitates harmonics observation. We fabricated a one-port demonstrational system and developed its graphical user interface to enhance its utility. The demonstrated system can measure the reflection coefficient of the device under test excited with a very high power signal, and has as high operability as usual vector network analyzers.

Session 2A14
SC5: Remote Sensing

Removal of Synthetic Aperture Effect in Stepped Frequency Radar

Yake Li and Siu O'Young
Memorial University of Newfoundland, Canada

Abstract— Recent years have seen great advancement in radar theory and technology. With the development of solid state devices, low profile, low weight, low cost and high resolution radar has been made possible by employing continuous wave (CW) technique. Stepped frequency (SF) radar is one of the high resolution CW radars that have very simple structure. A stepped frequency radar is simply composed of a voltage controlled oscillator (VCO) which generates frequency modulated continuous wave (FMCW) according to a linearly varied control voltage; a mixer that mixes the received signal with the transmitted signal to obtain the intermediate frequency (IF) signal; and an antenna which transmits and receives the radar signal. Therefore, it is very suitable to be used on small unmanned aerial vehicles (UAVs) which performs short range surveillance and observation. However, the simple way realizing high range resolution of SF radar causes synthetic aperture effect (SAE) in the return echo, which lowers the range resolution and weakens the target detection ability. A method to remove the SAE is proposed here and the effect of the algorithm is verified by simulation.

Refinement of the X and Ku Band Dual-polarization Scatterometer Snow Water Equivalent Retrieval Algorithm

Jiancheng Shi and Chuan Xiong
Institute of Remote Sensing and Digital Earth, Chinese Academy of Sciences, Beijing, China

Abstract— Snow water equivalent is an important parameter for natural science studies, such as hydrology, climatology and water cycle studies. Active microwave remote sensing is the most promising tool for large scale snow water equivalent monitoring. However, according to the past studies, the sensitivity of radar measurements to dry snow water equivalence is in general relatively weak at C-band. X-band radars such as Cosmo-Skymed and TerraSAR-X have been shown to have stronger sensitivity compared to C-band sensors. However, even higher-frequency radar needs to be added to provide reliable measurements for quantitative retrieval of snow water equivalence; one proposed configuration for this purpose was CoreH2O. We proposed a preliminary algorithm for snow water equivalent retrieval using X and Ku band dual-polarization radar in a previous paper. In the meantime, in the past years there has been progress in both ground experiment techniques and electromagnetic scattering modeling of snow cover. This enables us to make a further refinement and improvement of the retrieval algorithm based on the new experimental data and newly developed electromagnetic scattering models in this study.

In this paper, we use both electromagnetic modeling and ground radar measurement data to further improve the snow water equivalent inversion algorithm using X and Ku band radar. The electromagnetic model for terrestrial snow microwave scattering is a hybrid discrete dipole approximation/radiative transfer model with bicontinuous medium, in which the complex microstructure, near field scattering and multiple scattering of snow are considered. The polarization and frequency characteristics of snow scattering at X and Ku band is intensively investigated to support the dual-frequency dual-polarization radar SWE inversion algorithm development. The data from experimental campaign NoSREx (Nordic Snow Radar Experiment) is used for forward model validation and inversion algorithm validation. Finally we demonstrate the detail and validation of the inversion algorithm.

A Soil Moisture Downscaling Algorithm for the SMAP Mission

Jiancheng Shi, **Peng Guo**, **Tianjie Zhao**, **and Jinyang Du**
State Key Laboratory of Remote Sensing Science
Jointly Sponsored by Institute of Remote Sensing and Digital Earth, Chinese Academy of Sciences, and Beijing Normal University, China

Abstract— Global measurements of the soil moisture are very important to understanding the components and interactions between the global water, energy, and carbon cycles. Satellite-based microwave remote sensing is one of the most promising techniques to monitor global near surface soil moisture, with frequent revisit and independence on the effects of clouds and solar illumination. Soil moisture retrieval using active and passive microwave remote sensing has been explored for several decades. The passive radiometric remote sensing is very sensitivity to soil moisture, even under vegetated conditions while the spatial resolution is typically low (tens kilometer). The active radar is capable of high spatial resolution but highly influenced by surface roughness, vegetation canopy structure. To combine the individual advantages of the passive and active approaches, the SMAP (Soil Moisture Active and Passive) was selected for development by NASA. The mission is targeted for launch in 2014. One of the main scientific objectives of SMAP is to enhance the spatial resolution and accuracy of soil moisture products through the combining use of radiometer and radar observations.

In this study, a downscaling algorithm to disaggregate the radiometer brightness temperature using the radar backscatter observations for SMAP mission was developed. The algorithm is based on the spectral downscaling which combines both phase and amplitude information in Fourier domain. Using the information from radar measurements at finer resolution, a new way to estimate the Fourier phase was proposed. The algorithm has been successfully applied to the PALS datasets from SMEX02. It is producing better results than radiometer-only inversions. The RMSE (Root Mean Square Error) of the downscaling brightness temperature are 3.26 K and 6.12 K for the Vertical and Horizontal polarization, respectively. Medium resolution soil moisture was retrieved from disaggregated/downscaled brightness temperature. The accuracy of the downscaling soil moisture retrievals is $0.0459\,m^3/m^3$, which is very close to SMAP science requirement of $0.04\,m^3/m^3$. The results indicate that the downscaling algorithm presented in this study is a promising approach to achieve finer resolution and more accurate soil moisture retrievals for the upcoming SMAP mission.

Application of Backscattering Models in Active-passive Microwave Remote Sensing of Ocean Salinity

J. Zhu[1, 2], **X. K. Zhang**[2], **H. Liu**[2], **and Y. J. Cai**[1, 2]

[1]Center for Space Science and Applied Research
University of Chinese Academy of Science, CAS, China
[2]The CAS Key Laboratory of Microwave Remote Sensing
Center for Space Science and Applied Research, CAS, Beijing, China

Abstract— In the combined active-passive microwave remote sensing of ocean salinity, the radiometer is used to measure the brightness temperature of the ocean surface and the scatterometer is used to measure the backscattering coefficient. The sea surface brightness temperature is a function of SSS (Sea Surface Salinity), SST (Sea Surface Temperature) and SSR (Sea Surface Roughness). So we can inverse the salinity through brightness temperature; however, the brightness temperature is influenced by various error sources at the same time, the leading part of which is sea surface roughness. Therefore, a crucial step of the inversion of SSS by brightness temperature is to eliminate the excess brightness temperature engendered by sea surface roughness. The elimination can be implemented by the sea surface backscattering coefficient, which is directly influenced by roughness. Thus the relevant backscattering models of empirical or analytical types corresponding to roughness can be a good choice to associate the excess brightness temperature with backscattering coefficient. The purpose of this paper is to assess the performance of empirical, semi-analytical and analytical models in roughness correction of surface brightness temperature. In the assessment, we show how to choose different models in various conditions and how a model can build a relationship between excess brightness temperature and backscattering coefficient through roughness. The relationship is considered as a model function to obtain pairs of the two parameters. Through this model function, the backscattering coefficient measurements can be used to correct the brightness temperature data obtained by radiometer and then the inversion of SSS will be more accurate and precise.

REFERENCES

1. Liu, H., X. K. Zhang, et al., "A combined L-band synthetic aperture radiometer and fan-beam scatterometer for soil moisture and ocean salinity measurement," *Geoscience and Remote Sensing Symposium (IGARSS)*, 4644–4647, 2012.
2. Le Vine, D. M., G. S. E. Lagerloef, F. R. Colomb, et al., "Aquarius: An instrument to monitor sea surface salinity from space," *IEEE Transactions on Geoscience and Remote Sensing*, Vol. 45, No. 7, 2040–2050, 2007.
3. Lagerloef, G., F. R. Colomb, et al., "The aquarius/SAC-D mission," *Oceanography*, Vol. 21, No. 1, 68–81, 2008.
4. Hwang, P. A., D. M. Burrage, et al., "An advanced roughness spectrum for computing microwave L-band emissivity in sea surface salinity retrieval," *IEEE Geoscience and Remote Sensing Letters*, Vol. 8, No. 3, 547–551, 2011.

Coherent and Multiple Scattering in Radar Scattering of Vegetated Surfaces at L band for SMAP Applications

Huangting Huang[1], **Shurun Tan**[1], **Leung Tsang**[1],
Xiaolan Xu[2], **Seung-Bum Kim**[2], **and Simon Yueh**[2]

[1]Department of Electrical Engineering, University of Washington, Seattle, WA 98195, USA
[2]Jet Propulsion Laboratory, California Institute of Technology, Pasadena, CA 91109, USA

Abstract— NASA's Soil Moisture Active Passive (SMAP) mission [1], will deploy an L-band space borne radar to provide global soil moisture observations at 3-km resolution. One of the active algorithms is the data cube approach with pre-computed results of backscattering as a function of rms heights, VWC and soil moisture. Vegetation canopies are divided into classes, such as corn, soya bean, wheat etc. Time series retrieval algorithm using data cubes have been applied and were demonstrated to be successful for field campaigns such as SMAPVEX 12 [2]. The current data cubes were based on the distorted Born approximation [3]. In the distorted Born approximation, the backscattering enhancement is accounted for in the double bounce term.

In this distorted Born approximation approach, each cylinder and disk is assumed to scatter with a scattering amplitude and the absolute value squared of the scattering amplitudes are added. This is labeled as incoherent addition of scattering amplitudes. The first order incoherent addition of scattering amplitudes was initially applied to each of the vegetation class. However, it was found that for the soybean field, where the overall VWC is generally small, the incoherent models do not account for the magnitudes of backscattering nor the polarization ratios [4]. Meanwhile, for the full grown corn field, where the overall VWC is quite large, the optical thickness becomes appreciable. The first order distorted Born approximation becomes inappropriate and the multiple scattering effects should be included. In this paper we address these two problems by (1) applying coherent addition model of scattering amplitudes for soya bean field and (2) applying vector radiative multiple scattering effects with cyclical corrections for corn field.

We use the coherent model for L band radar remote sensing of soya bean fields. Analytic methods and Monte Carlo simulations are used. The novel feature of the analytic model consists of introducing mutual exclusion functions to eliminate the overlap effects of branches in the former branching model [5]. To validate the new results, Monte Caro simulations are also used by generating samples of soya bean fields and calculating the scattered field for each sample. The Monte Carlo simulations are in good agreement with proposed analytic model. Backscattering coefficients are illustrated for a variety of scenarios with varying VWC and soil moisture conditions. The results show that HH are significantly different based on the coherent model versus that of the distorted Born approximation or first order radiative transfer model. The results of the analytic model are compared with experimental data measured at SMAPVEX 12 field campaign in both the absolute values of backscattering versus time series as well as the polarization ratio between VV and HH.

For crops such as corn, the VWC increases during a season, so that the optical thickness increases and multiple scattering effects should be considered. In the forward scattering model validation with L-band SMAP backscattering data [4], both the optical thickness and the scattering albedo of full-grown corn field are found to be high for v-pol. In this paper, we study the multiple scattering effects in radar backscattering from a corn vegetation layer overlying soil surface at L band. The multiple scattering effects are accounted for by solving the radiative transfer equation using an iterative approach. The inclusion of the cyclical terms [6, 7] is done for each iteration. The approach is carried out iteratively up to the fourth order. The physical model results including multiple scattering effects are validated against the SMAPVEX12corn backscattering data. In many cases the contribution from second order scattering and third order scattering are important for v-pol. The important scattering mechanisms in the second order and third order scattering are also identified for scattering from typical corn structures in L band. The relative contribution from multiple scattering depends both on the optical thickness and scattering albedo. In L band, the corn leaves mainly impose an attenuation effects to the larger cylindrical stalk structure scattering. The multiple scattering results are compared to the SMAP L-band corn scattering data for each field. The scatter plot of physical model versus measurements reveals a stronger correlation and a smaller root mean square error (RMSE) when multiple scattering effects are included.

REFERENCES

1. Entekhabi, D., E. G. Njoku, P. E. O'Neill, K. H. Kellogg, W. T. Crow, W. N. Edelstein, J. K. Entin, S. D. Goodman, T. J. Jackson, J. Johnson, J. Kimball, J. R. Piepmeier, R. D. Koster, N. Martin, K. C. McDonald, M. Moghaddam, S. Moran, R. Reichle, J. C. Shi, M. W. Spencer, S. W. Thurman, L. Tsang, and J. V. Zyl, "The soil moisture active passive (SMAP) mission," *Proceedings of the IEEE*, Vol. 98., No. 5, 704–716, May, 2010.
2. Kim, S. B., M. Moghaddam, L. Tsang, M. Burgin, X. Xu, and E. G. Njoku, "Models of L-band radar backscattering coefficients over the global terrain for soil moisture retrieval," *IEEE Trans. Geosci. Remote. Sens.*, Vol. 52, No. 2, 1381–1396, Feb. 2013.
3. Lang, R. H. and J. S. Sidhu, "Electromagnetic backscattering from a layer of vegetation: A discrete approach," *IEEE Trans. Geosci. Remote. Sens.*, Vol. 21, No. 1, 62–71, Jan. 1983.
4. Liao, T.-H., X. Xu, L. Tsang, H. Huang, S.-B. Kim, and E. G. Njoku, "Validation of physical models for active remote sensing at L-band from vegetated surfaces for SMAP mission," *IEEE International Geoscience & Remote Sensing Symposium*, Melbourne, Australia, July 21–26, 2013.
5. Yueh, S. H., J. A. Kong, J. K. Jao, R. T. Shin, and T. L. Toan, "Branching model for vegetation," *IEEE Trans. Geosci. Remote. Sens.*, Vol. 30, No. 2, 390–402, Mar. 1992.
6. Tsang, L. and A. Ishimaru, "Theory of backscattering enhancement of random discrete isotropic scatterers based on the summation of all ladder and cyclical terms," *J. Opt. Soc. Am. A*, Vol. 2, No. 8, 1331–1338, Aug. 1985.
7. Tsang, L. and A. Ishimaru, "Backscattering enhancement of random discrete scatterers," *J. Opt. Soc. Am. A*, Vol. 1, No. 8, 836–1338, Aug. 1984.

Development of a Radiative Transfer Model for the Soil Media with Including Vertical Profile Effects and Its Application in AMSR2

Hui Lu[1, 2], **Toshio Koike**[3], **and Ziwei Xu**[4]

[1]Ministry of Education Key Laboratory for Earth System Modeling, Center for Earth System Science
Institute for Global Change Studies, Tsinghua University, Beijing 100084, China
[2]Joint Center for Global Change Studies, Beijing, 100875, China
[3]The Department of Civil Engineering, The University of Tokyo, Tokyo 113-8658, Japan
[4]State Key Laboratory of Remote Sensing Science, School of Geography
Beijing Normal University, Beijing 100875, China

Abstract— Soil moisture is an important status variable that controls the interactions between land surface and atmosphere. Reliable estimation of soil moisture, especially in regional and global scale, is essential for climatic, meteorological and hydrological researches. This study presents the development of a microwave radiative transfer model (RTM) inside soil media with including the soil profile effects. In situ observations of soil moisture and temperature profile, measured during HIWater Experiment IOP, were used to formulate profile functions. The RTM is used in the AMSR2 soil moisture retrieval algorithm to improve soil moisture estimate in dry regions. By comparing the results of new algorithm against ground observations, the feasibility and capability of the revised algorithm were verified. The application of this algorithm in wide regions also demonstrated that our method could alleviate the overestimation-in-desert problem of original JAXA AMSR2 soil moisture products.

Active and Passive Remote Sensing of Bare Soil from L-band to Ku-band Using NMM3D

T. H. Liao[1], **L. Tsang**[1], **S. Tanelli**[2], **N. Niamsuwan**[2], **and S. Jaruwatanadilok**[2]

[1]Department of Electrical Engineering, University of Washington, Seattle, USA
[2]Jet Propulsion Laboratory, California Institute of Technology, Pasadena, USA

Abstract— The Global Precipitation Measurement (GPM) mission and Soil Moisture Active Passive (SMAP) mission include goals to understand the water cycle system in nature which involve land, atmosphere, and ocean. Both missions include active and passive sensors. The SMAP operates at L-band. For GPM, in addition to the passive microwave sensors of the usual AMSR frequencies, there are Ku-band and Ka-band radar. Two dimensional scattering problem of rough soil surface has been studied from L-band to Ka-band [1]. However for real life applications, numerical simulations need to be conducted for 3D problems. In this paper, we study 3D electromagnetic models of rough soil surface scattering and emission from L-band to Ku-band using three dimensional Numerical Methods of Maxwell's equations (NMM3D) for both active and passive remote sensing. In developing the models, we use the same physical parameter of rms heights and correlation lengths for all active and passive frequencies. Exponential correlation functions are used throughout as it has been established that the soil surface have exponential correlation functions. Gaussian correlation functions are too smooth to be of practical use for soil surfaces.

This presents a significant challenge because a physical rms height is much smaller than a wavelength at L-band and become comparable to wavelength at Ku-band. In previous works we illustrate numerical results of NMM3D results forms height up to 3.47 cm at L-band of 1.26 GHz which is 0.146λ [2]. However 0.146λ is only 0.32 cm at Ku-band of 13.6 GHz which is too small for rough soil surface at Ku band. In this paper, we extend the simulations for rms height up to 0.45λ which is 1 cm at Ku-band of 13.6 GHz. rms height of 1 cm is sufficiently large for soil surface including grassland and crop land as found in various field campaigns such as SGP99, SMEX02, and SMAPVEX12. Previously NMM3D was accelerated by hybrid UV/PBTG/SMCG method [2]. Here we also apply near field precondition to accelerate the convergence for iterative solver done by GMRES. We perform precondition in terms of block matrix along the diagonal of impedance matrix of MoM based NMM3D. By computing precondition matrix, the number of iterations is reduced. Since we perform Monte-Carlo simulation for preconditioned NMM3D, many realizations are required. A case with 32-by-32 square wavelengths for moderate heights takes less than 20 iterations for achieving precision of 0.01 in GMRES for each polarization in each realization. Various cases come of soil moisture, incident angle, frequency, rms height, and correlation lengths are illustrated. For numerical results, the dependence of backscattering coefficients and emissivities with same physical parameters of rms heights, correlation lengths and soil moistures are studied for the frequency range from L-band to Ku-band. We also compare results with the measurements data from field campaign such as POLARSCAT (LCX) and ***SEAC*^{4}*RS*** (Ku) for co-polarized backscattering coefficients. Also, energy conservation and reciprocity checks are applied to ensure the reliability.

REFERENCES

1. Xu, P., K. Chen, and L. Tsang, "Analysis of micriwave emission of exponentially correlated rough soil surfaces from 1.4 GHz to 36.5 GHz," *Progress In Electromagnetic Research*, Vol. 108, 205–219, 2010.
2. Huang, S. and L. Tsang, "Electromagnetic scattering of randomly rough soil surfaces based on numerical solutions of Maxwell equations in three-dimensional simulations using a hybrid UV/PBTG/SMCG method," *IEEE Transactions on Geoscience and Remote Sensing*, Vol. 50, No. 10, 4025–4035, 2012.

Polarimetric Properties of Randomly Rough Surfaces at L-band Using Numerical 3D Solutions of Maxwell Equations

Kuan-Liang Chen[1], **Kun-Shan Chen**[1], **Leung Tsang**[2], **and Tien Hao Liao**[2]

[1]Institute of Space Sciences, Central University, Jhongli, Taiwan
[2]Department of Electrical Engineering, University of Washington, Seattle, WA 98195, USA

Abstract— It is well known that fully polarimetric statistics can be derived from the modified Mueller matrix in which the elements of the matrix are related to the scattering matrix elements for co-polarization and cross-polarization in terms of linear polarizations. In numerical simulation of rough surface scattering, this requires a very accurate estimation of the complex scattering amplitudes, and poses challenges for accurate computation of cross-polarized returns. In this paper, we use NMM3D to perform simulations of polarimetric rough surface scattering at L band to calculate the scattering matrix for each realization. The NMM3D numerical scheme adopted in this paper has proven to be a very effective and yet efficient method to tackle the high-accuracy demanding in simulation of polarimetric statistics. Simulations of random rough surface scattering has been performed using surface size up to 32 wavelengths by 32 wavelengths. The rough surfaces are characterized by exponential correlation functions that are mostly better to characterize the bare surface. Because in numerical solutions of Maxwell equations, the electric fields of the scattered wave are calculated for each realization, thus scattering matrices can be simulated by NMM3D and such simulations are performed in this paper. For a given *rms* height, correlation length, soil permittivity and incident angle, we calculated the radar scattering matrix up to 958 independent realizations. For each realization, the components of scattering matrix, S_{HH}, S_{VV}, S_{HV} and S_{VH} are calculated. The computed scattering matrix over many realizations are then used to calculate the speckle statistics and the coherency matrix and for studying polarimetric SAR. The *rms* heights are from 0.5 cm to 6 cm. Also for selected cases, we have calculated results up to 1000 realizations and surface area of 32 by 32 square wavelengths. Results were computed incidence angles 20 degrees, 30 degrees, 40 degrees, and 50 degrees.

Using the simulated scattering matrices, we calculate the polarimetric speckle statistics (amplitude and phase difference), followed by a comparison with theoretical distributions. For fully developed speckle from the homogeneous rough surface, the results are examined and validated to ensure the simulated data quality as far as polarimetric properties is concerned. The simulations results of co-polarization and cross polarization backscattering coefficients were in good agreement with experimental measurements of bare soils at L band. It is also confirmed that the simulated data is fully agreed with theoretical Wishart distributions for homogeneous rough surface. By taking ensemble averages of combinations of scattering matrix elements, the coherency matrix are calculated. In characterization of three polarimetric descriptors, the entropy increases as roughness increases meaning more depolarization occurs, while the anisotropy displays a nonlinear effect versus *ks* — it increases for small values of *ks*, and turns to decrease when *ks* further increases, implying that the relationship between anisotropy and *surface rougnes* is not linear. We also observe that the alpha angle is not so sensitive to *ks*, as expected. It would be highly suggestive that by saying surface smooth or rough, special attention must be paid. From our simulation study, it is found even for a small set of *kl* and *ks*, significant depolarization due to multiple scattering may be occurred in exponentially correlated surface. Scattering symmetry, including reflection, rotation, and azimuthal symmetries, is also investigated. For exponentially correlated surface, even for small roughness scale, conditions of reflection symmetry generally are not met. We also describe the NMM3D methods of SAR simulations, noting that the cross polarization were in good agreement with experimental data. Accuracy of cross polarization is an important criterion for polarimetric SAR simulator. In the simulations in this paper, each realization of random rough surface is independent of the other. In the future we can generate a large random rough surface and perform rough surface scattering on adjacent samples to examine cases of correlated samples. With the advent of numerical solutions of Maxwell equations, we will continue to improve the computational efficiency, accuracy as well as going to higher frequencies such as C band and X band polarimetric SAR. We are also applying NMM3D simulations to calculate the scattering matrices of random discrete scatterers and volume-surface scattering interactions. Finally, it would be both theoretically and practically interesting to study the effect of the dielectric properties (or soil moisture content). Investigating the assumptions made in well-known parameter inversion algorithms from POLSAR data should also be explored.

ACKNOWLEDGMENT

The research in this paper were partially supported by the following: AFOSR, Asian Office of Aerospace Research & Development, grant FA2386-13-1-4017, National Science Council of Taiwan for Leung Tsang's sabbatical appointment and NASA SMAP project.

Session 2A15a
Oral Presentations for Best Student Paper Awards — SC3: Optics and Photonics

Guided-mode Resonance Enhanced Near-infrared-to-visible Upconversion Fluorescence in a Resonant Waveguide Grating

Hao Yu Liou[1], **Jian Hung Lin**[1], **Zhen-Dao Wang**[2], **Chun-Yen Tseng**[3], **Ching-Ting Lee**[3], **Chu-Chi Ting**[2], **Hung-Chih Kan**[1], **and Chia Chen Hsu**[1, 2]

[1]Department of Physics, Chung Cheng University
Ming Hsiung, Chia Yi 621, Taiwan
[2]Graduate Institute of Opto-Mechatronics, Chung Cheng University
Ming Hsiung, Chia Yi 621, Taiwan
[3]Institute of Microelectronics, Department of Electrical Engineering
Cheng Kung University, Tainan 701, Taiwan

Abstract— Guided mode resonance (GMR) enhanced near-infrared (near-IR)-to-visible upconversion fluorescence (UCF) from a rare-earth doped polymer resonant waveguide grating (RWG), comprised of a $NaYF_4$:Yb/Tm nanocrystals doped poly-methyl-methacrylate ($NaYF_4$:Yb/Tm-PMMA) thin layer on top of a textured SU8 substrate with a thin intervening layer of TiO_2. Strong UCF is observed by matching either incoming near-IR excitation or out-going UCF extraction to the GMR wavelengths of the rare-earth doped polymer RWG. The intensity of the UCF can be enhanced up to 10^4 times in visible range and 10^3 times in near-IR range compared with that from a flat area. According to the rigorous coupled-wave analysis calculations, high enhancement of UCF is attributed to the strong local field generated at the TiO_2 waveguide layer due to the resonance between the near-IR excitation light and the GMR. The extraction of the UPF is further promoted when the wavelengths of the UPF resonate with the GMRs.

Novel Tunable Multi-passband Microwave Photonic Filters Based on Fiber Mach-Zehnder Interferometer and Fiber Delay Lines

Hao Chen, Zuowei Xu, Hongyan Fu*, and Dan Zhang
Department of Electronic Engineering
School of Information Science and Engineering, Xiamen University, Xiamen 361005, China

Abstract— Microwave photonic filters (MPFs) have been under constant research in the last two decades. Compared with the traditional electronic filters, MPFs enjoy the advantages of broad bandwidth, low loss, good tunability, and the immunity to the electromagnetic interference, etc. Many techniques have been reported to realize functional MPFs, among which MPFs based on continuous sampling of a broadband optical source and dispersive medium have drawn much attention, since its free spectrum range is infinite in the theory, and thus resulting in a single passband frequency response, as well as its good tunability. Although the single-passband MPF has shown good application potential, in many practical applications, multi-passband MPFs with freely tunable central frequencies are more desirable. Most techniques in literature to realize MPFs are not applicable for this kind of multi-passband MPFs, since most of them have periodic frequency responses and their passbands move simultaneously when tuning the MPFs, while their free spectrum ranges keep the same. In this article, we report the demonstration of two new approaches to implement MPFs with multi passbands based on the sliced broadband optical source (BOS) with fiber Mach-Zehnder interferometer (FMZI) and fiber delay lines. The proposed MPFs are simple in construction, easy to implement, and show good tunibility and reconfigurability, which is very desirable in practical applications.

The first approach is to utilize an FMZI as a slicing filter and a multi-path fiber delay line to implement the multi-passband MPF. In our experiment, dual-passband has been demonstrated by using the dual-path fiber delay line. The light from a BOS is transmitted through the FMZI to obtain the continuous optical samples, and then the light is modulated by the electro-optic modulator (EOM) by microwave signals to be processed, and launched into the dual-path fiber delay line which is composed of two 3 dB optical couplers and has different lengths of fiber in two paths. After that, the light is recombined and detected by the photodiode (PD), and measured by the vector network analyzer (VNA). In our experiment, the frequency response with dual passbands has been achieved and by adjusting the length of the tunable optical delay line (TODL) in one arm of the FMZI, the central frequencies of both passbands can be tuned. By adding the paths of the optical delay line, multi-passband MPF can be realized with this method.

In the other method, paralleled FMZIs and a dispersive medium have been employed to realize the multi-passband MPF. In the experiment demonstration, two paralleled MZIs are used as the slicing filter to obtain the optical samples, after which the light is modulated by microwave signals to be processed through an EOM. Then, the modulated light is launched into a dispersive medium which in our experiment is coil of single mode fiber, and recovered by the high speed PD. Frequency response with dual passbands has been measured by the VNA, and the central frequencies of the passbands can be tuned freewill by adjusting the optical path difference of each FMZI. Multi-passband MPF with desirable number of passbands can be realized by introducing more FMZIs in this technique.

In conclusion, our proposed approaches to realize multi-passband MPFs are easy to implement, exhibit good tunability, flexibility, and show good application potential in the wireless communication and measurement systems.

*Corresponding author: Hongyan Fu (fuhongyan@xmu.edu.cn).

Sub-5 nm Lanthanide Doped ZrO_2 Upconversion Nanoparticle for Protein Targeted Biomaging

Jing Liu and Qiuqiang Zhan*
Centre for Optical and Electromagnetic Research, South China Normal University
Guangzhou 510006, China

Abstract— Lanthanide-doped upconversion nanoparticles (UCNPs) area promising new generation of imaging agents for bioimaging due to no auto-fluorescence, large penetration depth and non-blinking [1–3]. But it is a challenge to synthesize both ultra small and brilliant luminescence UCNPs because of the high nonradiative transition in the small size. In this paper an efficient ultra small core-shell UCNP was synthesized using a hydrothermal method and a thermal decomposition procedure. A new inorganic host — ZrO_2 was used for its low phonon energy ($470\,cm^{-1}$) and high absorption coefficient [4]. The core was synthesized through a hydrothermal method and the shell ($NaYF_4$:2%Yb^{3+}) was synthesized by a thermal decomposition procedure. The as-synthesized core-shell nanoparticles has a diameter smaller than 5 nm. By transferring the nanoparticles from hydrophobic to hydrophilic, a ligand free method [5] was used and then the nanoparticles was capped with water soluble polymers by a layer-by-layer method. UCNPs were characterized by transmission electron microscope (TEM) X-ray diffraction (XRD) analysis, and Fourier transform infrared (FTIR) spectroscopy. And also the relatively high quantum yield proves the remarkable luminescence efficiency. Because of the small size and high efficiency, the nanoparticle can be targeted to the membrane proteins of interest, such as nucleolin or prion protein (PrPC) [6]. An aptamer was employed as a recognizer for protein recognition. Firstly, the streptavidin (SA) was cultivated to the surface of UCNPs (SA-UCNPs) and the aptamer was integrated with SA-UCNPs via the interaction between biotin and streptavidin. The aptamer has specific recognition tothe protein of interest and thus can implement the single protein imaging. We also use the efficient water soluble poly(ethylene glycol) (PEG)-coated UCNPs to subcutaneous injection into a nude mouse to perform *invivo* imaging [7]. Therefore, the small and efficient core-shell nanoparticles was fabricated to achieve the single protein targeted imaging as well as the *in vivo* bioimaging.

*Corresponding author: Qiuqiang Zhan (qiuqiang.zhan@coer-scnu.org).

New Scaling of Electron Thermionic Emission from Single-layer Graphene

Shi-Jun Liang[1], **L. K. Ang**[1] **and Gang Chen**[2]

[1]Engineering Product Development, Singapore University of Technology and Design, Singapore
[2]Department of Mechanical Engineering, Massachusetts Institute of Technology
Cambridge, MA 02139, USA

Abstract— In this work, a simple model is developed to explore the electron thermionic emission from a single-layer graphene. This study is based on our prior efforts in showing that electron emission mechanisms from single-layer graphene is quite different from the traditional models, such as graphene field emission, and graphene laser-induced over-barrier emission, etc.. Now, we establish a new scaling for thermionic emission from graphene, quite different from the conventional Richardson's law responsible for bulk materials. Our analytical formula obtained in this work is demonstrated to agree well with numerical results. In addition, we estimate the contribution from tunneling effect, and found that it can be neglected, compared with the thermionic emission. The established scaling may be useful to interpreting some recent experimental results about vertical transport through atomic graphene devices and to developing a new generation of graphene-based thermionic energy converter.

ACKNOWLEDGMENT

This work was supported by SUTD (SRG EPD 2011014) and SUTD-MIT IDC grant (IDG21200106 and IDD21200103). L. K. Ang would like to acknowledge the support of a USA AFOSR AOSRD grant (11-4069).

1 Gbps Directed Optical Decoder Based on Two Cascaded Microring Resonators

Qiaoshan Chen, **Fanfan Zhang**, **Lei Zhang**, **Yonghui Tian**,
Ping Zhou, **Jianfeng Ding**, **and Lin Yang**
State Key Laboratory on Integrated Optoelectronics
Institute of Semiconductors, Chinese Academy of Sciences, China

Abstract— Directed logic is a paradigm which employs the optical switch network to perform the logical operation. Silicon microring switch is an attractive structure owing to its outstanding performances, such as compact size, ultra-low power consumption and CMOS-compatible fabrication process. Therefore, the directed logic based on silicon microring switches is easy to realize large-scale integration and low-cost manufacture in a high-volume CMOS-photonics foundry. A series of optical directed logic circuits have been proposed and even demonstrated.

We have demonstrated a directed optical decoder, whose speed is 10 kbps due to the thermo-optic modulation scheme. In this paper, we report the implementation of the decoder operations using an electro-optic circuit, which is fabricated by CMOS-compatible process in the silicon-on-insulator (SOI) platform. The circuit consisting of two cascaded microring switches, which are both modulated through the carrier-injection modulation in forward biased PN junctions embedded in the ring waveguides. The inherent resonance wavelength mismatch between two microring switches caused by fabrication errors is compensated by the microheaters fabricated on the top of the microring switches. Two non-return-to-zero electrical signals with a period of 8 bits generated by two pulse pattern generators are used to modulate the PN diodes embedded in the device. The results are presented by optical signals detected at four output ports of the device. The working wavelength and driving voltages of two MRRs are measured and analyzed by the static response spectra of the device. Dynamic experimental results show that the device can implement the decoding function from a 2-bit electrical signal to a 4-bit optical signal correctly. Bitwise operations at 1 Gbps are demonstrated successfully.

All-optical Wavelength Conversion Using Optical Injection Induced Wavelength Switching in V-cavity Laser

Yingchen Wu, Xiaohai Xiong, Yu Zhu, Jianjun Meng, and Jian-Jun He
State Key Laboratory of Modern Optical Instrumentation, Centre for Integrated Optoelectronics
Department of Optical Engineering, Zhejiang University, Hangzhou 310027, China

Abstract— All optical wavelength converters are key functional elements for large scalable wavelength routers. They usually employ power-hungry semiconductor optical amplifiers (SOAs) and tunable lasers involving complex structures such as non-uniform gratings and multiple epitaxial regrowth. In this paper, we present a simple, efficient, and cost-effective all-optical wavelength converter using injection-induced wavelength switching in widely tunable V-cavity laser. The widely-tunable V-cavity laser, which consists of two Fabry-Perot cavities coupled through a half-wave coupler, operates in single longitudinal mode with a high side-mode suppression ratio (SMSR) over 35 dB and offers simple and efficient wavelength switching with 100 GHz ITU channel spacing. When an external signal beam is injected at a wavelength corresponding to one of the sidemodes, the lasing wavelength is switched from the original main mode to the side mode. By filtering out the main mode of the V-cavity laser, a data-inverted wavelength conversion is achieved. The power of the injected signal beam is about −4 dBm. A small wavelength detuning of about 0.1 nm from the side mode is found to produce more stable converted signal. Using the chirp management method (CMM), a lager extinction ratio can be achieved. A 2.5 Gb/s non-return-to-zero (NRZ) conversion is experimentally demonstrated with an extinction ratio over 4 dB and SMSR of 36 dB. This wavelength converter can offer a channel-to-channel conversion, with converted signal approximately at a multiple of 100 GHz away from the input signal. Due to its device simplicity and power efficiency, it has great potential for applications in all-optical wavelength routing systems.

Ultracompact Adiabatic Tapered Coupler for the Si/III-V Heterogeneous Integration

Qiangsheng Huang[1], **Jianxin Cheng**[2], **Liu Liu**[2], **Yongbo Tang**[4], **and Sailing He**[1, 2, 3]

[1]Centre for Optical and Electromagnetic Research
JORCEP [Sino-Sweden Joint Research Center of Photonics]
Zhejiang Provincial Key Laboratory for Sensing Technologies, Zhejiang University, Zijingang Campus
East Building No. 5, Hangzhou 310058, China
[2]ZJU-SCNU Joint Research Center of Photonics
Centre for Optical and Electromagnetic Research, South China Academy of Advanced Optoelectronics
South China Normal University, Guangzhou 510006, China
[3]Department of Electromagnetic Engineering, Royal Institute of Technology, Stockholm 100 44, Sweden
[4]ArtIC Photonics Inc., Ottawa K2M 2C7, Canada

Abstract— Photonics based on Si/III-V heterogeneous integration through the DVS-BCB adhesive wafer bonding method or molecular direct wafer bonding method [1, 2] have been extensively investigated for many applications, due to its feasibility in combining active and passive photonic submodules onto one silicon substrate. Adiabatic taper has been considered to be a promising structure for this purpose due to its low insertion loss, low reflection, and good fabrication tolerance. However, in order to guarantee an adiabatic behavior, the proposed tapered structure was sufficiently long.

Here, we propose an ultracompact bi-sectional adiabatic tapered coupler, which is suitable for an adiabatic mode transformation between a common single mode SOI strip waveguide and a Si/III-V hybrid waveguide. Since the bi-sectional tapered coupler mimics a semi-3D taper and avoids exciting unwanted high-order modes in the thick p-InP cladding layer (which is removed in the first tapered section), the length of the adiabatic mode coupler can be dramatically shortened. Taking into account the mask design and reduce the complexity of the taper, we also design the tapered structure only in the III/V structure, while keeping the SOI wire waveguide straight. This makes it more flexible in the post III-V fabrication process without considering the alignment of the tapered structure in the light propagation direction. In order to design this bi-sectional adiabatic tapered structure, we use three-dimensional finite-difference time-domain method to analyze the performance of the first and second taper coupler, respectively, with different taper length and bonding layer thickness. In the proposed structure, the length of the bi-sectional tapered coupler can be as short as 9.5 μm with a large fundamental mode-coupling ratio (over 95%) in a bandwidth of $\sim$ 100 nm, and provides $\pm$100 nm tolerance to misalignment, even when the bonding layer is as thick as 50 nm.

REFERENCES

1. Roelkens, G., L. Liu, D. Liang, R. Jones, A. Fang, B. Koch, and J. Bowers, "III-V/silicon photonics for on-chip and inter-chip optical interconnects," *Laser Photon. Rev.*, Vol. 4, No. 6, 751–779, 2010.
2. Liu, L., G. Roelkens, J. Van Campenhout, J. Brouckaert, D. Van Thourhout, and R. Baets, "III-V/silicon-on-insulator nanophotonic cavities for optical network-on-chip," *Journal of Nanoscience and Nanotechnolog*, Vol. 10, 1461–1472, 2010.

Session 2A15b
Oral Presentations for Best Student Paper Awards — SC2: Metamaterials, Plasmonics and Complex Media

Tunable Rejections of Metamaterial Filter Based on Spoof Surface Plasmon Polaritons

Bai Cao Pan and Tie Jun Cui
State Key Laboratory of Millimetre Waves, School of Information Science and Engineering
Southeast University, Nanjing 210096, China

Abstract— According to the dispersion property, spoof surface plasmon polaritons (SPPs) can be supported within a low-pass propagating band. When the operating frequency rises to approach the asymptotic limit, which is also known as the surface plasma frequency, the spoof SPP modes vanish and the propagation cuts off. In this paper, we propose a method to achieve tunable rejections of spoof SPPs by producing independent absorptions. A spoof SPP waveguide consisting of corrugated microstrip line and matching convertors is introduced and electrically resonant metamaterials, the electric-field-coupled-LCs (ELCs), are employed and arranged along both sides of the waveguide. Since the electric field around the SPP waveguide excites strong and tight coupling to ELCs at resonant frequencies and their relative impedance keeps matching within a broadband, the propagating SPP modes are absorbed by such metamaterial particles and SPP filters with broad propagating band and significant rejection are achieved. Furthermore, the transmissions of the SPP filter with a series of ELCs scaled by different factors are investigated to clarify that the resonant frequency is directly controlled by the dimension of the metamaterial particles and that the coupling effect between different ELCs are weak enough to be ignored. As a result, it is convenient to control the absorptions by simply modulating the scaling factors of ELCs to construct a multiple rejection filter. Simulation results prove that the filter exhibits several significant rejections of -15 dB within a broad high-efficient propagating band. The proposed highly-efficient ultrathin planar filter is able to play an important role of filtering SPP waves in plasmonic circuits and systems.

A Planar Broadband Metamaterial Absorber with the Polarization Insensitive and Omnidirectional Absorption in the Min-infrared Regime

Nan Zhang, Linbo Zhang, Guorui Zhang, Peiheng Zhou, Xiaolong Weng, Jianliang Xie, and Longjiang Deng
National Engineering Research Center of Electromagnetic Radiation Control Materials
State Key Laboratory of Electronic Thin Film and Integrated Devices
University of Electronic Science and Technology of China, China

Abstract— Metamaterial perfect absorbers (MPAs) have recently gained considerable attention due to their potential applications in research of microbolometers, sensitive sensors, solar cells, and thermal emitters. MPAs are artificially constructed "atoms" that composed of sandwiched multilayers, where the top layer is the metallic patterns separated from the bottom metallic film by a dielectric interlayer. The great absorption works relying on the coupling between metallic components of the sandwiched structure at the resonant frequency. The tunable and controllable effects of MPAs afford them incomparable advantages to the naturally existing materials. However, MPAs also suffer from many disadvantages such as narrow operating waveband, sensitive to the polarization state and incident angle.

In this paper, we present the design, fabrication and characterization of a polarization insensitive and omnidirectional broadband planar metamaterial perfect absorber in the min-infrared regime. Multi-sized resonant patterns are employed to excite the broadband absorption, and the absorption bandwidth is efficiently broadened compared with the single-sized absorber. Geometric effects on the resonance wavelengths and the absorption spectra are studied in detail by using the equivalent circuit model. Experiment result shows that greater than 70% absorption is obtained within a waveband of 0.8 μm, which is in reasonable agreement with the simulation. The electromagnetic response of the MPA is theoretically investigated to reveal the intrinsic absorption mechanism. The broadband planar MPA is polarization insensitive and the absorption retains quite high even at large incident angles. The proposed structure holds promise for many applications, such as sensitive detecting, energy harvesting, and thermal modulating.

Efficient Generation of Second Harmonic from a Kind of Nonlinear Magnetic Metamaterial Composite

Shang Sun[1] and Shumin Xiao[2]

[1]Key Lab of Micro-Optics and Photonic Technology of Heilongjiang Province
Department of Physics, Harbin Institute of Technology, Harbin 158001, China
[2]Department of Material Science and Engineering, Shenzhen Graduate School
Harbin Institute of Technology, Shenzhen 518055, China

Abstract— We present a numerical investigation of efficient generation of second harmonic from a kind of nonlinear magnetic metamaterial composite. The analysis is focused on a structure consisting of periodic arrays of paired thin silver strips with second-order nonlinear material filled in the gap. The sandwich shaped periodic structure exhibits remarkable advantage in the generation of second harmonic signal. We, first, make an introduction to this sandwich structure, summarize the linear resonant properties and then investigate the wavelength dependence of the field enhancement in the gap. Next, we analyze about second-harmonic generation (SHG) from composite structure doping with isotropic nonlinear material by comparing with that from single layer nonlinear material and several other conditions. The results figure out that the magnetic resonance property of this nonlinear metamaterial composite makes a great contribution to the energy localization and gives rise to strong inhomogeneous field inside the gap. As a result, the strength of SHG is almost two orders larger than that of a pure nonlinear layer with comparable dimensions. Finally, we change the material property from isotropic to anisotropic, and investigate the impact combining with field enhancement, field profiles and linear and nonlinear polarization considerations, showing that most of the fundamental-harmonic electric field in the gap polarize along y direction, which is the power giving rise to the second-harmonic generation of the composite. This work leads to deeper understanding of singular nonlinear response in metamaterials.

Design and Fabrication of Acoustic Rotator Based on Extremely-anisotropic Metamaterials

Xue Jiang, **Bin Liang**, **and Jian-Chun Cheng**
Key Laboratory of Modern Acoustics, MOE, Department of Physics
Institute of Acoustics, Nanjing University, Nanjing 210093, China

Abstract— The field rotator is a fascinating device which can be regarded as a special kind of acoustic illusion, with the capability of making the object covered by it appears like a rotated one. By exploiting acoustic metamaterials with extremely anisotropic parameters, we have theoretically designed and experimentally realized anacoustic field rotator that can rotate the acoustic wavefront by a certain angle. For airborne sound,the designed field rotator simply consists of an array of identical plates made of acrylonitrile but adiene styrene plastic (ABS). Both the numerical and experimental demonstrations of the rotation effect illustrate that the resulting device has a broadband functionality. A nearly perfect agreement is observed between the numerical simulation and experimental results. The influence of the structural parameters on its performance has also been investigated. Moreover, we inspect the frequency dependence of rotation effect and it shows that the designed device can work effectively within a broad band, as long as the effective medium approximation is valid. In addition, it turns out that by elongating each plate the increase of anisotropy of metamaterial can be conveniently attained, which contributes to enhance the rotation effect. With the known relationship between the rotated angle and the structural parameters, the rotation angle can be manipulated conveniently. The application of the proposed device for non-plane wave has also been discussed and the possibility of extending the proposed scheme to three-dimensional cases has been considered. With the capability of rotating acoustic wavefront in a controlled manner, the realization of acoustic field rotator has open up a new avenue for the versatile manipulations on the acoustic waves and may have potential application in various situations that require special acoustic controls.

Session 2A0
Poster Session 2

Multi-band Microwave Metamaterial Perfect Absorber Based on Mie Resonance Theory

Jun-Feng Chen[1], **Guo-Dong Wang**[1], **Zhao-Quan Chen**[2, 3], **Ming-Hai Liu**[1], **and Xi-Wei Hu**[1]

[1]State Key Laboratory of Advanced Electromagnetic Engineering and Technology
School of Electrical and Electronic Engineering
Huazhong University of Science and Technology
Wuhan 430074, China
[2]University ITMO, Kronverkskiy pr. 49, St. Petersburg 197101, Russia
[3]College of Electrical and Information Engineering
Anhui University of Science and Technology
Huainan 232001, China

Abstract— A multi-band metamaterial absorber (MA) with near-unity absorption based on Mie resonance theory is proposed in the microwave region. It is composed of an array of dielectric cubes with different geometric parameters and a metallic ground plane. The simulated results show that four absorption peaks at 7.31 GHz, 7.58 GHz, 7.90 GHz and 8.19 GHz with the corresponding absorption rates of 99.05%, 99.37%, 99.65% and 99.16%, respectively. In addition, the composite MA is polarization-insensitive at the normal incidence and maintains high absorption rates at wide angles of incidence for both TE and TM wave. The influences of the permittivity and the side length of the dielectric cubes on its absorption characteristics are also investigated. This MA would be a promising candidate as absorbing elements in scientific and technical applications, such as cloaks, perfect lens and filters.

A Compact Plasmonic 4-way Wavelength Splitter for Planar Circuits

Yong Jin Zhou[1, 2] **and Bao Jia Yang**[1]

[1]Key Laboratory of Specialty Fiber Optics and Optical Access Networks
School of Communication and Information Engineering, Shanghai University, Shanghai 200072, China
[2]State Key Laboratory of Millimeter Waves, Southeast University, Nanjing 210096, China

Abstract— The structural metallic surface provides an effective method to guide and manipulate electromagnetic (EM) surface waves, which are called plasmonic metamaterials [1]. Domino plasmons for subwavelength terahertz circuitry have been proposed, where the waveguiding elements are based on plasmonic metamaterials and consist of an easy-to-manufacture periodic chain of metallic box-shaped elements protruding out of a metallic surface [2]. The dispersion relation of the corresponding EM modes is rather insensitive to the waveguide width, preserving tight confinement and reasonable absorption loss even when the waveguide transverse dimensions are well in the subwavelength regime. We have proposed a multidirectional frequency splitter with band-stop plasmonic filters based on similar waveguiding elements. However, such waveguiding elements have some defects for integrated planar circuits since the grating slot depths are tens of micrometers at THz frequencies. In this paper, we propose a compact plasmonic 4-way wavelength splitter at microwave and terahertz (THz) frequencies based on specially designed plasmonic structures which behave like metal-insulator-metal (MIM) plasmonic waveguide at optical frequencies. The specially designed structures placed on the dielectric substrate consist of two metal gratings with corrugated grooves in the inner surface, which are called spoof MIM plasmonic structures and are suitable for planar circuits since the whole structures can be easily manufactured by existing printed circuits board (PCB) technologies. A double-period spoof MIM structure is adopted to produce band-stop filtering features, which can improve the isolations between different branches at low frequencies. The splitter is investigated numerically based on the CST microwave studio (CST). The simulation results have been given at microwave and THz frequencies to verify such 4-way wavelength splitter. Electromagnetic waves at the designed frequencies are confined and guided along different branches with good isolations. Physical experiments will be done later.

REFERENCES

1. Cakamakyapan, S., H. Caglayan, A. E. Serebryannikov, and E. Ozbay, *Appl. Phys. Lett.*, Vol. 98, 051103, 2011.
2. Martin-Cano, D., M. L. Nesterov, A. I. Fernandez-Dominguez, F. J. Garcia-Vidal, L. Martin-Moreno, and E. Moreno, "Domino plasmons for subwavelength terahertz circuitry," *Optics Express*, Vol. 18, 754, 2010.

All-optical Diode Based on a Nonsymmetrical Coupled System of Microcavity Mode and Tamm States

Jian-Xia Hu and Yun-Tuan Fang
School of Computer Science and Telecommunication Engineering
Jiangsu University, Zhenjiang 212013, China

Abstract— We design a one-dimensional photonic crystal with a nonlinear microcavity and two metal films coated at its two sides. We study the transmission properties of the struture through the nonlinear transfer matrix method. Due to the coupling of two nonsymmetric optical Tamm states and nonlinear microcavity, the structure shows one-way transmission feature and an all-optical diode action occurs with the designed structure. We use two characteristic parameters to describe the performance of diode. The performance of diode is dependent on the thickness of nonlinear microcavity as well as the thickness of the metal. The results help us to optimize the design of all-optical diode.

The Influence of Air-hole Filling Fraction of Photonics Crystal Fibers on Stimulated Brillouin Scattering Slow Light

Shanglin Hou, Ji Sun, Weiqing Ge, Yanjun Liu, Jingli Lei, and Xiaoxiao Li
School of Science, Lanzhou University of Technology, Lanzhou, Gansu 730050, China

Abstract— The Stimulated Brillouin Scattering (SBS) is a kind of nonlinear optical phenomena. In this process, an acoustic wave which has a high-frequency is generated in the material via the electrostriction for the density of material increases under the high light power. The slow light technology based on SBS has some advantages in comparison with other slow light technologies, such as electromagnetic induction transparent (EIT), coherent population oscillation (CPO). It has great potential applications in fiber delay line, optical buffer and fiber optical sensor.

Photonic crystal fiber (PCF) is a new type of optical fiber with periodic arrangement of air hole in cladding. Its characteristics can be changed flexibly due to the periodic cladding structures. The cladding-core reflective index difference of PCF is much larger than traditional doped fiber and the effective model field area of PCF can be designed smaller. Both of them can improve the nonlinear properties of PCF then enhance the SBS effect.

In this letter, we numerically simulated the Stimulated Brillouin Scattering (SBS) slow light under the different structural parameters of the photonic crystal fiber (PCF) through the finite difference time domain method. SBS slow light is studied in time delay and broadening factor of the pulse for different air-hole filling fractions. The results indicated that time delay increases and broadening factor decreases with the increase of the air-hole filling fractions. The air-hole filling fraction has less effect on time delay and broadening factor under the same core diameter of the PCF.

Investigation on Slow Light of Nonuniform Photonic Crystal Fiber Bragg Gratings

Shanglin Hou, Weiqing Ge, Yanjun Liu, Daobin Wang, Jingli Lei, and Xiaoxiao Li
School of Science, Lanzhou University of Technology, Lanzhou, Gansu 730050, China

Abstract— The ability to slow down and delay optical pulses is an intriguing phenomenon with significant applications in telecommunications. Slow light has been observed in a wide variety of physical systems, varying from metal vapors with and without electromagnetically induced transparency, rare-earth-doped materials, Raman and Brillouin fibers, photonic crystal waveguides, and fiber Bragg gratings (FBGs). Compared with others, an FBG offers a much simpler and more practical alternative because it relies on a passive resonant effect and thus does not need low temperature and an optical pump. In many of these pioneering FBG slow light results, apodization plays an important role. So it's meaningful to investigate the influence of apodization and chirp on FBG slow light. Compared to traditional FBG, photonic crystal fiber grating (PCFG) has many advantages, such as easier tailoring design, endless single-mode transmission and adjustable dispersion characteristics, which has wider potential application in optical fiber communication, optical fiber sensing and optical information processing.

In this letter, we investigate the influences of Gaussian apodization on slow light in PCFGs by improved full vector effective index method (IEIM) and transmission matrix method. The results indicate that when 'dc' index change is large enough, the minimum value of group velocity first decreases and then increases as the apodization coefficient increases, which means that there is an optimum apodization coefficient that minimizes the group velocity; but when the 'dc' index change is small, the minimum value of group velocity increases as the apodization coefficient increases.

Research on the Controllable Frequency Octupling Technology for Generating Optical Millimeter-wave by External Modulator

Jianming Shang, Yanjun Liu, Daobin Wang, Weiqing Ge, Jingli Lei, Xiaoxiao Li, and Shanglin Hou

School of Science, Lanzhou University of Technology, Lanzhou, Gansu 730050, China

Abstract— With rapid development in information construction all over the world, mm-wave radio-over-fiber (ROF) has been the general trend in the development of wireless communication, owing to its portability, wireless, datamation and broadband. The key technology about optical mm-wave generation is to simplify the base station and reduce system cost. It is mm-wave communication that is also one of the academic focuses, which has important application in the future communication, military and other fields. Schemes for generating millimetre-wave, based on the nonlinear of Mach-Zehnder modulator (MZM), have a very wide range of applications and have been extensively studied. Due to this, several mm-wave solutions have been put forward.

Schemes mainly can be divided into two types according to whether using optical or electrical filter, while these without filter will become the dominant. However, the filter is necessary to remove the undesired sidebands which are not well suppressed. Therefore, the high quality generation of mm-wave signal without filter is of great interest for the frequency octupling scheme. Recently, it still has the problem of low redundant sideband suppression efficiency, complex system, high cost and so on.

In this letter, a novel scheme is proposed for frequency octupling mm-wave generation based on an integrated triple-parallel MZM without filter. Two kinds of redundant sidebands are well eliminated by adopting 90 degrees of the electric phase-difference about two sub Mach-Zehnder modulators (sub-MZMs), driven by radio frequency (RF) signal. Moreover, bias of the third sub-MZM is tailored to get best signal. The results indicate that the radio frequency spurious suppression ratio (RFSSR) is as high as 38.887 dB under the condition of conventional extinction ratio (30 dB). Furthermore, optical sideband suppression ratio (OSSR) can reach as high as 61.22878 dB at ideal extinction ratio (100 dB). Compared with previous schemes, it not only optimizes the method but get high RFSSR in the conventional condition.

Temperature Dependence of Liquid Filled Photonic Crystal Fibers

Jingli Lei, Shanglin Hou, Yanjun Liu, and Xiaoxiao Li
School of Science, Lanzhou University of Technology, Lanzhou, Gansu 730050, China

Abstract— Photonic crystal fiber (PCF), also called microstructrued fiber (MF), or holey fiber (HF), has air holes arranging according to a certain rule in the cross section, and constant along the length of the fiber. Compared with the conventional fiber, photonic crystal fiber structure has many unique characteristics due to flexible design, for example, endless single mode transmission, dispersion tailoring, high nonlinearity etc..

Dispersion is one of the key factors affecting the performance of optical fiber transmission and transmission distance, near zero dispersion fiber and broadband ultra flattened dispersion characteristic have potential applications. Along with solving the loss problem, the dispersion becomes important limiting factors in large capacity optical fiber communication system. Because PCF can be flexibly designed, the dispersion tailoring is much easier than conventional optical fiber. The structural parameters and optimization of optical fiber are tailored to achieve nearly zero ultra flattened dispersion, in addition, liquid such as water, ethanol, polymer etc is filled in the air holes to tailor its characteristics.

In this letter, the effects of temperature on dispersion, effective area and nonlinearity of an index-guiding hexagon photonic crystal fiber filled by ethanol are described by using the vectorial beam propagation method, and a nearly zero ultra flattened dispersion fiber is optimized design, the dispersion coefficients ranges from $0 \pm 0.5\,\mathrm{ps/(nm \cdot km)}$ at the wavelength of $1.46\,\mu\mathrm{m}$ to $1.65\,\mu\mathrm{m}$. The results indicate that increasing temperature could leads to increase dispersion and nonlinearity, but decrease the dispersion slope so as to flatten the dispersion. The result provides theoretical base for designing continuously tailoring dispersion optical communication components or optical sensing devices.

Dependence of Grating Length of Fiber Gragg Gratings on Slow Light

Chunlian Hu[1], **Yanjun Liu**[2], **Jingli Lei**[2], **and Shanglin Hou**[2]

[1]Alloy Powder Co., Ltd, Lanzhou University of Science & Technology, Lanzhou 730050, China
[2]School of Science, Lanzhou University of Technology, Lanzhou 730050, China

Abstract— Fiber Bragg grating has developed dramatically and performed an important role in fiber communications and optical fiber sensing in recent 30 years. Recently, the introduction of slow light with a wide range of novel properties results in unique spectral characteristics of fiber Bragg gratings, especially slow light delay of fiber Bragg grating is studied emphatically. K. B. Rochford and S. D. Dyer reported reconstruction of minimum-phase group delay from fiber Bragg grating transmittance or reflectance measurements. The results indicate that phase reconstruction is compared to exact solutions using the reflectance from a uniform grating. An intermediate windowing process improves the recovery accuracy. J. T. Mok, etc. observed 0.68 ns pulses delayed by 4.7 pulse widths in a 30 cm silica FBG without pulse broadening. Improved slow-light delay performance of a broadband SBS system using fiber Bragg grating was reported. Tunable delay slow-light in an active fiber Bragg grating was also studied. These studies provide a very simple approach to control the light group delay. However, this approach requires very high power signal, which limits its practical implications.

The influence of grating length of uniform fiber Bragg grating on delay is discussed by using numerical simulation method based on the coupled mode theory and slow light delay characteristics is studied by parameters optimization. The calculated result shows that grating length has a remarkable impact on the delay, when $L < 42.5008$ cm, the delay $_{\max}$ increases with L increasing, when L tends to 42.5008 cm have a maximum delay $_{\max}$, the value increased to 3.797 ps, but when $L > 42.5008$ cm, delay $_{\max}$ decreases with L increasing. This provides basis references for designing slow light components based on fiber Bragg gratings.

Integrated Optical Chemical Sensor Based on an SOI Ring Resonator Using Phase-interrogation

Xi Zhou[1], **Zhi Qiao**[1], **Chenzhao Zhang**[1], **Jianhao Zhang**[1, 2], **Tuowen Xiang**[1], **Yaocheng Shi**[2], **and Liu Liu**[1]

[1]South China Academy of Advanced Optoelectronics
South China Normal University, Guangzhou 510006, China
[2]Centre for Optical and Electromagnetic Research
JORCEP [Sino-Sweden Joint Research Center of Photonics]
Zhejiang Provincial Key Laboratory for Sensing Technologies
East Building No. 5, Zijingang Campus, Zhejiang University, Hangzhou 310058, China

Abstract— An integrated optical chemical sensor based on a silicon-on-insulator micro ring resonator is proposed and demonstrated. A novel phase interrogation approach is used to determine the resonance shift of the ring resonator with respect to the refractive index change of the cladding layer. A detection limit of 2.5×10^{-6} RIU is measured.

Optical refractive index sensors employing optical resonators and cavities have gain increasing research interests [1]. Recently, planar structures based on CMOS technologies and silicon photonic has shown their advantages of compact size, low cost, multi-functional integration. The basic idea of such refractive index sensor is that the effective index of the waveguide guided mode follows the change of the cladding material due to the evanescent field that leaks into the cladding. In a resonator or cavity structure, this will result in a shift of the resonant wavelength. With a ring resonator built by silicon-on-insulator nanowire waveguide, a sensitivity of 70 nm/RIU has been demonstrated initially [2], and this figure was improved to 2169 nm/RIU by using a cascaded-ring configuration [3]. In the above demonstrations, wavelength or power interrogation method is used to determine this wavelength shift, which is vulnerable to noises, such as, alignment stability, wavelength scanning accuracy and repeatability. This limits the smallest detectable refractive index change (defined as detection limit) that can be achieved.

In this paper, we proposed and demonstrate a phase interrogation approach to determine the wavelength shift of a SOI ring resonator. Figure 1(a) shows a sketch of the experimental setup, which is basically a 40 GHz single-side-band signal generation and detection scheme [4]. The rapid phase change around the resonance waveguide of an 40-μm-diameter over-coupled ring resonator impose a large phase difference [cf. Figs. 1(b) & 1(c)] to the two wavelength peaks of the single-side-band signal, which is then detected by a network analyzer. Fig. 1(d) shows the measured phase with different refractive indices of the cladding by using aqua-NaCl solution of different concentrations. A theoretical fit to the data give a peak sensitivity of $3.47 \times 10^{5°}$/RIU. The system stability for the phase measurement is 0.86° (3σ). This gives a detection limit of 2.5×10^{-6} RIU.

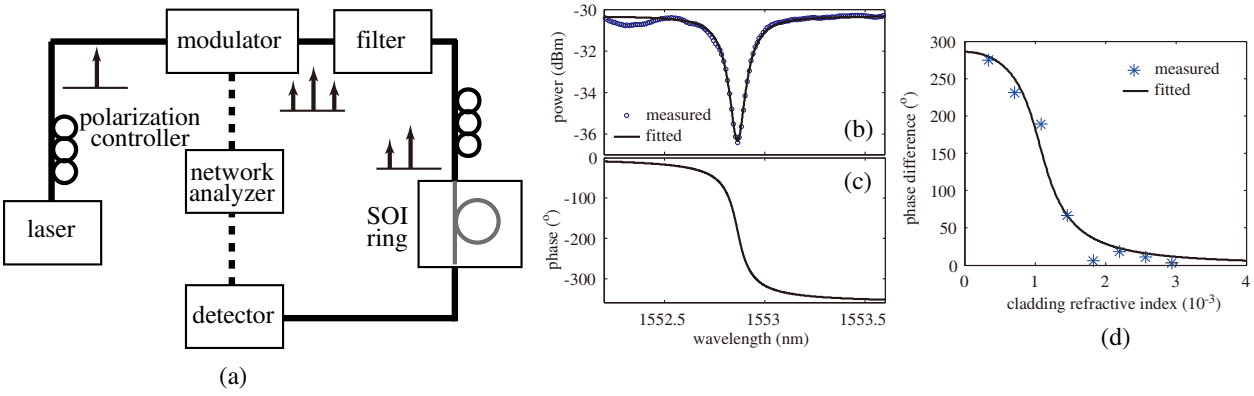

Figure 1: (a) Sketch of the experimental setup; (b) Power and (c) phase response of the measured SOI ring resonator; (d) Measured and fitted phase difference of the single-side-band signal.

REFERENCES

1. Fan, X., I. M. White, S. I. Shopova, H. Zhu, J. D. Suter, and Y. Sun, "Sensitive optical biosensors for unlabeled targets: A review," *Anal. Chim. Acta*, Vol. 620, 8–26, 2008.
2. Claes, T., J. G. Molera, K. De Vos, E. Schacht, R. Baets, and P. Bienstman, "Label-free biosensing with a slot-waveguide-based ring resonator in silicon on insulator," *IEEE Photon. J.*, Vol. 1, 197–204, 2009.
3. Claes, T., W. Bogaerts, and P. Bienstman, "Experimental characterization of a silicon photonic biosensor consisting of two cascaded ring resonators based on the Vernier-effect and introduction of a curve fitting method for an improved detection limit," *Opt. Express*, Vol. 18, 22747–22761, 2010.
4. Pu, M., L. Liu, W. Xue, Y. Ding, L. H. Frandsen, H. Ou, K. Yvind, and J. M. Hvam, "Tunable microwave phase shifter based on silicon-on-insulator microring resonator," *IEEE Photon. Technol. Lett.*, Vol. 22, 869–871, 2010.

Neural Correlates of Feigned Memory Impairment with Different Motivations: A Functional Near-infrared Spectroscopy (FNIRS) Study

Fang Li[1, 2], **Qianqian Gao**[1, 2], **Huilin Zhu**[1, 2], **Guixiong Xu**[1], **Xinge Li**[2], **Ziqiang Hu**[1, 2], **and Sailing He**[1]

[1]Centre for Optical and Electromagnetic Research, ZJU-SCNU Joint Research Center of Photonics South China Normal University (SCNU), Guangzhou 510006, China
[2]School of Psychology, South China Normal University (SCNU), Guangzhou 510631, China

Abstract— Feigned memory impairment is a common deceptive behavior in everyday life and forensic evaluation. However, few researches have examined the neural correlates of feigned memory impairment with different motivations: obtaining more reward or avoiding punishment. Functional near-infrared spectroscopy (FNIRS) has proved to be a cost-effective brain-imaging technique which can examine hemodynamic activities of cortical regions, and could have a great potential to probe the neural process of deception in the future.

In this study, 42 channels of FNIRS were adopted to investigate neural activities in the prefrontal cortex under three conditions: feigning memory impairment to obtain more reward, feigning memory impairment to avoid punishment and telling truth as the control condition. 12 healthy adults were recruited to perform a facial recognition task. When they performed the tasks in the two feigned memory impairment conditions, they were instructed to deceive the computer by telling lies and truths in order to improve the credibility that they really had memory defect. Moreover, they were told that in the condition of obtaining more reward, if they could convince the computer that their memory were impaired, they would get more money. In contrast, in the condition of avoiding punishment, if they could not convince the computer, they would lose some money. When they performed the tasks in the control condition, they were instructed to tell the truth all the time without any reward or punishment.

Results indicated that the condition of feigning memory impairment to avoid punishment would cause a significant increase in HbO or a significant decrease in Hb than the control condition in bilateral inferior prefrontal cortex, and the condition of feigning memory impairment to obtain more reward showed a significant increase in HbO or a significant decrease in Hb than the control condition in left middle prefrontal cortex and bilateral inferior prefrontal cortex. In addition, lying trials in the condition of feigning memory impairment to avoid punishment led to a significant increase in HbO or a significant decrease in Hb than telling-truth trials in the control condition in bilateral inferior prefrontal cortex, and lying trials in the condition of feigning memory impairment to obtain more reward showed a significant increase in HbO or a significant decrease in Hb than telling-truth trails in the control condition in left middle prefrontal cortex and bilateral inferior prefrontal cortex. These results demonstrate that feigned memory impairment with two different motivations can cause some different patterns of neural activities in the prefrontal cortex and FNIRS could be a useful technique for the detection of deception.

A Low-cost CCD-based Imager for Mapping Venous Oxygenation

Jun Li and Xiao Zhang
Centre for Optical and Electromagnetic Research
South China Normal University, Guangzhou 510006, China

Abstract— A low-cost imaging system is developed for mapping skin venous oxygen saturation. The system consists of a black-and-white CCD camera and cheap LED light sources working at 660 nm and 800 nm wavelength. To obtain venous oxygen saturation, a low cuff pressure is applied to alter the venous blood volume. With the two wavelength light sources alternately illuminating the skin, the CCD camera collects images carrying signals of diffuse reflectance before and after the occlusion. Using the Monte Carlo method, the relationship between the saturation value and the diffuse reflectance is determined. Therefore images captured can be converted into the venous saturation map. Experiments on human arms show that the measured data is in line with previous published data, demonstrating the effectiveness of the system on monitoring blood oxygenation in local tissues.

A Novel Compact Tri-band Bandpass Filter with Good Selectivity

D.-H. Jia, Q.-Y. Feng, X.-G. Huang, and Q.-Y. Xiang
School of Information Science and Technology
Southwest Jiaotong University, Chengdu, Sichuan 610031, China

Abstract— A novel tri-band bandpass filter (BPF) based on multi-mode resonators is presented. The resonant modes of the resonators can be analyzed by the even- and odd-mode analysis method. The bandwidths of first and second passbands can be independently controlled. Furthermore, five transmission zeros (TZ) are introduced at the adjacent of the passbands in a narrow frequency range to improve the selectivity, resulting sharp skirts. The design procedure is also given. Due to the small multi-mode resonator and tight coupling structure, the overall size of the proposed filter is really compact ($0.19\lambda_0 \times 0.18\lambda_0$). λ_0 is the wavelength of the center frequency of first passband in the substrate. Finally, a prototype to demonstrate the performance of the filter is designed and fabricated. The measured 3-dB fractional bandwidths for the three passbands (2.22, 2.98 and 3.5 GHz) are found to be 8.4%, 2.7% and 6.1%, respectively. The measurement shows good agreement with the simulation.

Dual-band Antenna Using Composite Right/Left-handed Transmission Lines for MICS and ISM Application

Yemin Hein and Sehwan Choi
Korea Electronics Technology Institute, Republic of Korea

Abstract— Metamaterials are artificial structures that can be designed to exhibit specific electromagnetic properties not commonly found in nature. Metamaterials having negative permittivity and permeability, are more commonly referred as left-handed materials (LHMs). The LHMs are considered as the general model of composite right/left hand (CRLH) structures. Recently, a small-size dual band implantable antenna for continuous glucose-monitoring applications was proposed. The design of dual-band components using composite Right/Left-handed transmission lines CRLH TLs with $\lambda/4$ short/open-circuit stub was studied. Beside a four-unit-cell flexible antenna in the coplanar waveguide line configuration was designed. Although previously studied antenna's structures can generate dual band function, their overall dimensions are too large to be applied in commercial products.

The proposed antenna is a miniaturized dual-band antenna using Right/Left-Handed transmission lines. The antenna size is 45% smaller in foot print area comparing the existing dual antenna because its wavelength is reduced by zero-order resonator. The operating frequencies of this antenna are 394–404 MHz for medical implant communication service (MICS) and 2.4–2.48 GHz for industrial, scientific, and medical (ISM) band.

Dual-band Bandpass Filter with Good Selectivity and Stopband Rejection

Daotong Li[1], **Yonghong Zhang**[1], **Kaida Xu**[1], **Kaijun Song**[1], **and Le-Wei Li**[2]

[1]EHF Key Lab of Science, University of Electronic Science and Technology of China, Chengdu, China
[2]Institute of Electromagnetics, University of Electronic Science and Technology of China, Chengdu, China

Abstract— As one of the essential microwave components, dual-band bandpass filters with good performance are highly desired in modern dual-band wireless communication systems. Microstrip ring resonators have been used to design various microwave circuits such as filters and mixers, due to the characteristics of compact size, high-Q factors, and sharp rejection skirt [1]. By using the coexisting of the two degenerate orthogonal modes, a dual-band passband filter can be achieved.

Although two transmission poles are generated in each passband and two transmission zeros are placed between the two passband by using rectangular ring resonator in [1], the out-of-band rejection and the selectivity are not good enough. The dual-band passband filter with good performance by utilizing the circular ring resonator is presented in Fig. 1(a). A good agreement is achieved between simulated and measured results (See Fig. 1(b)). The measured minimum insertion loss achieves 1.0 dB in the first passband and 1.6 dB in the second passband. Five transmission zeros are observed at 1.01, 4.62, 4.85, 9.85 and 10.32 GHz, respectively. A 20 dB rejection in the frequency range of 6.78 to 12.25 GHz is obtained. The dual operating frequencies can be adjusted by forming a non-uniform ring resonator with periodically-loaded stubs or stepped impedance configuration.

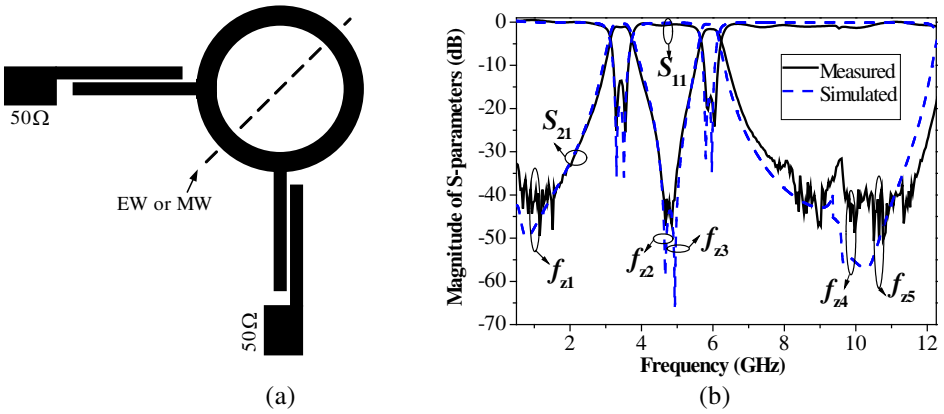

Figure 1: (a) The layout of the proposed dual-band bandpass filter. (b) Measured and simulated results.

ACKNOWLEDGMENT

This work was supported by the National Key Scientific Instrument and Equipment Development Projects (Grant No. 2013YQ200503).

REFERENCES

1. Sun, S., "A dual-band bandpass filter using a single dual-mode ring resonator," *IEEE Microwave and Wireless Components Letters*, Vol. 21, No. 6, 298300, 2011.

A Multi-layer Inductive Frequency Selective Surface for Use in the Ka and Ku Frequency Bands

Jonathan M. Rigelsford and Andrea Vallecchi
Department of Electronic & Electrical Engineering, The University of Sheffield
Mappin Street, Sheffield S1 3JD, United Kingdom

Abstract— This paper presents an interleaved multi-layer inductive frequency selective surface (FSS). The inductive dichroic surface presented is suitable for use as a sub-reflector in a tri-band satellite communications antenna system. The proposed design is capable of reflecting the frequency range 10.7–12.75 GHz, situated in the Ku band, while being transmissive at the two Ka sub-bands 17.3–20.2 GHz and 28.295–30 GHz and provides improved operational performance when compared to previously published designs [1].

The large bandwidths of operation in the transmission bands and the requirement of fast roll-off characteristics constitute the challenging aspects of the design of this type of FSS. A single element unit cell, which only has one transmittance band, does not provide enough degree of freedom to tailor the response of the FSS to be reflective in the Ku sub-band and transmissive in two Ka sub-bands. Multi-resonant unit cells with multiple perforations of variable shape have been therefore developed for the inductive FSS.

An image of prototype Ku/Ka frequency selective surface obtained using a digital microscope, is shown in Fig. 1. The designed unit cell incorporates a small Jerusalem-cross shaped perforation interleaved with larger interwoven Brigid's cross slots [2]. Interweaving the arms of the Brigid's cross slots leads not only to broadening the array operational bandwidth at the lower Ka sub-band but also to reducing the unit cell size. The resulting densely packed arrangement of the Jerusalem cross slots contributes in turn to achieving sufficiently large bandwidth also at the transmission frequencies of the higher Ka sub-band. Due to the symmetry of the unit cell, the FSS response is identical at both TE and TM polarized incident waves. All analysis of the proposed design has been carried out using the frequency domain solver available in CST Microwave Studio [3].

The FSS development process will be reported in detail in the full paper, followed by the presentation of simulated and measured results of the final design, fulfilling reflectivity and transmissivity specifications in the different frequency bands. In the full paper it will be also demonstrated how the performance of the FSS can be improved by using multiple layers.

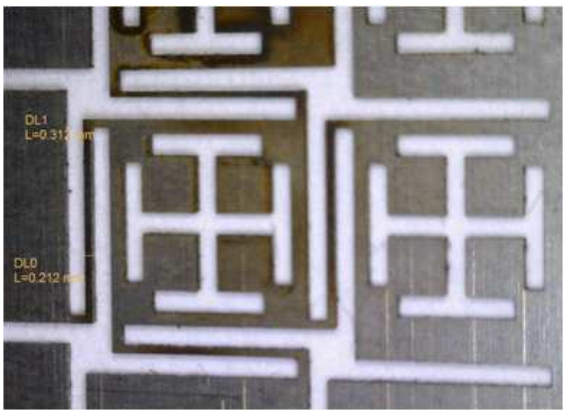

Figure 1: Microscope image of prototype Ku/Ka frequency selective surface.

REFERENCES

1. Rigelsford, J. M., S. Martin Benito, and A. Vallecchi, "A tri-band inductive frequency selective surface sub-reflector for satellite communications systems," *Proc. EuCAP 2014*, The Hague, The Netherlands, Apr. 6–11, 2014.
2. Vallecchi, A. and A. G. Schuchinsky, "Metasurfaces with intertwined conductor patterns," *Proc. Metamaterials' 2011*, Barcelona, Spain, Oct. 10–15, 2011.
3. CST Microwave Studio, http://www.cst.com.

New Design of Low Cost and Easy Tuning Compact GPS Microstrip Antenna

Chanjuan Li, Shiqiang Fu, Te Shao, and Hongmei Liu
School of Information Science and Technology, Dalian Maritime University, Dalian, Liaoning 116026, China

Abstract— A new low cost and easy tuning compact GPS microstrip antenna structure has been proposed. RHCP (right-hand circular polarized) radiation is realized with corner truncated on a square patch as the radiating element. The size of the antenna is reduced by cutting the central slot and marginal slits, which force the current to follow extra paths. Coaxial single-probe center feed loaded with microstrip stub is used to achieve impedance matching. The best operating frequency tuning can be achieved by varying the marginal slits. The design and tuning method is given. The final optimized antenna dimension has been obtained after a large of electromagnetic simulations. The simulated results show that the antenna has a good matching and CP radiation performance.

In this paper, a new single probe feed CP microstrip antenna with low-cost FR4 as substrate for GPS applications has been designed. Variations in FR4 electrical permittivity can shift the operating frequency. So one microstrip stub is used to achieve impedance matching and two marginal slits are introduced for the best operating frequency tuning. The purpose is to get the

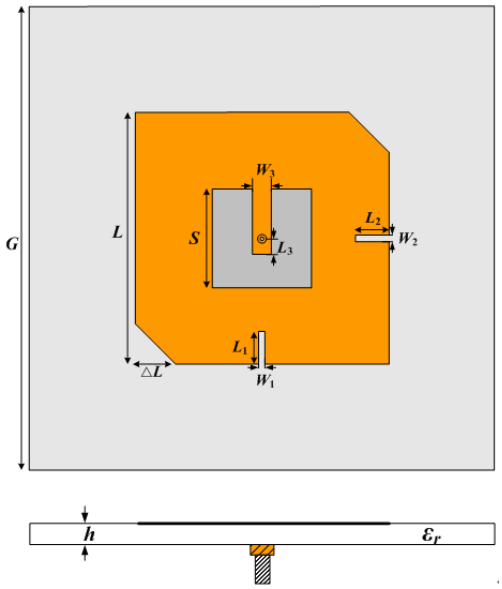

Figure 1: Configuration of the proposed antenna.

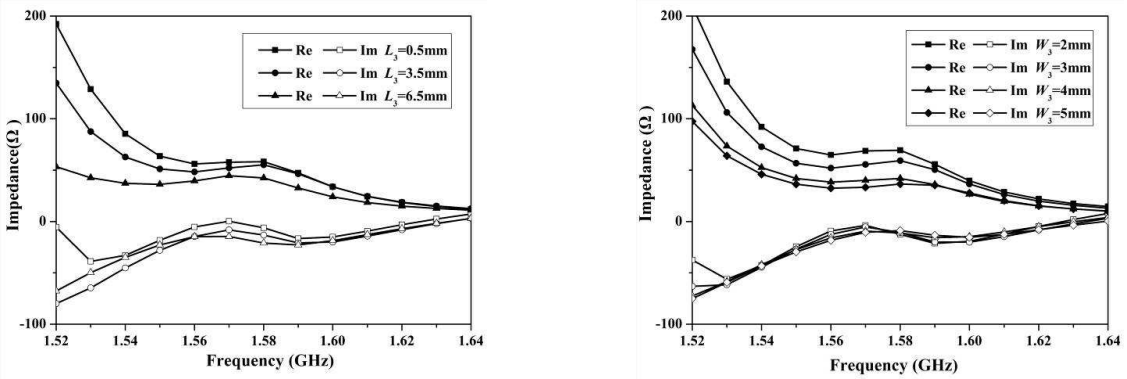

Figure 2: Input impedance as a function of matching stub length and width. (a) Impedance curve as a function of L_3. (b) Impedance curve as a function of W_3.

best axial-ratio and the return loss at the fixed frequency. Design concepts and procedures are introduced, followed by simulations and discussions.

The configuration of the proposed antenna element is shown in Fig. 1.

Throughout the studies, it is found that the real part of the antenna input impedance can be controlled by changing W_3 and L_3, while the imaginary part of the antenna input impedance can be adjusted mainly by changing L_3, which can be seen in Fig. 2. So we can first change L_3 to get a real input impedance (zero imaginary part), and then change W_3 to get the input resistance that we need. The impedance matching can be achieved without major modification of the radiator and the CP characteristic is also not so sensitive to the changing of the matching stub.

As mentioned before, the use of low-cost FR4 as substrate causes the frequency deviations due

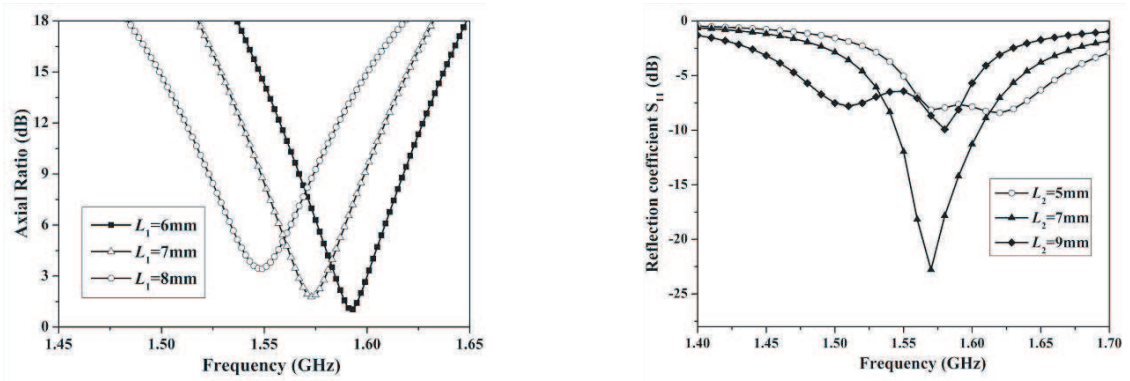

(a) (b)

Figure 3: The operating frequency deviations by varying the slit length. (a) Axial ratio curve as a function of L_1. (b) Reflection coefficient curve as a function of L_2.

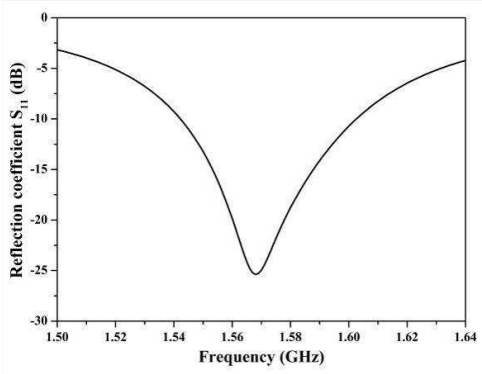

Figure 4: Simulated reflection characteristics versus frequency.

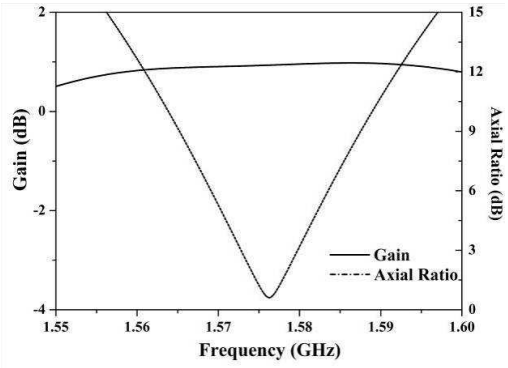

Figure 5: Gain and axial ratio characteristics of the antenna.

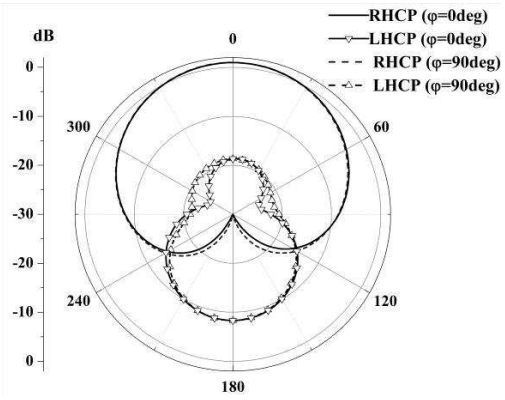

Figure 6: Simulated radiation pattern of antenna in two orthogonal planes at the center frequency.

to the inaccuracy of its relative permittivity. The proposed antenna configuration to compensate this effect has two narrow slits, as shown in Fig. 1. Cutting properly the slits length, frequency deviations can be compensated. It is shown in Fig. 3 that by adjusting the inserted slit length L_1 (the slit width fixed to be $W_1 = 1\,\text{mm}$), the CP axial ratio can be tuned. Meanwhile, the input reflection coefficient can be tuned by adjusting the inserted slit length L_2 (the slit width fixed to be $W_2 = 1\,\text{mm}$). It gives a convenient tuning option for the best operating frequency by varying the slit length.

The proposed antenna has been optimized for operation in the L_1 band with the centre frequency of 1575.42 MHz. The commercial simulation tool HFSS has been used in this study. After extensive simulations, the following values are selected: $L = 37\,\text{mm}$, $\Delta L = 4.4\,\text{mm}$, $S = 15\,\text{mm}$, $L_1 = 7\,\text{mm}$, $W_1 = 1\,\text{mm}$, $L_2 = 7\,\text{mm}$, $W_2 = 1\,\text{mm}$, $L_3 = 2.5\,\text{mm}$, $W_3 = 3\,\text{mm}$, $h = 2\,\text{mm}$, $\varepsilon_r = 4.4$, $G = 70\,\text{mm}$. The simulation results show that the final antenna displays good input impedance matching and excellent circular polarization radiation pattern, as can be seen from Fig. 4–Fig. 6.

Solitary Wave Induced in a Water Surface Wave Field

Shigehisa Nakamura
Kyoto University, Japan

Abstract— A problem on solitary wave induced in a water surface wave field is introduced for obtaining an analytical solution in a manner of mathematical science. By this time, it was recorded offshore at the case of the tsunamis generated by the earthquake in March 11, 2011 in the northwest Pacific. Adding to the above, a hydraulic experiment had been confirmed a couple of solitary waves induced in a field of water surface wave field artificially generated in a basin. Then, a problem is raised to solve in a manner of analytical mathematics for the solitary wave in a water surface wave field under some specific conditions.

Chaotic FM Signals for Circular SAR Imaging

Lingjuan Yu[1], **Xiaochun Xie**[2], **and Lingling Xiao**[1]

[1]Jiangxi University of Science and Technology, Ganzhou 341000, China
[2]Gannan Normal University, Ganzhou 341000, China

Abstract— Noise radar has low probability of intercept and high resistance to electronic countermeasures, which improves the ability of radar to survive in a complex environment. The ambiguity function of ideal noise signal has an approximate thumbtack shape, which makes noise radar with the ability of non-ambiguous measurement of range and velocity. Because of these excellent features, noise radar has broad application prospects in the military and civilian areas. On the other hand, circular SAR (CSAR) has high two-dimensional ground range resolution and a certain three-dimensional imaging capability. The combination between noise radar and CSAR can achieve the complementary strengths, which has significance for target detection and high resolution imaging.

In this paper, Ulam map chaotic FM signal is used as the transmitted signals for two-dimensional and three-dimensional CSAR imaging. All these imaging results are compared with other imaging results when the transmitted signals are chirp and Ulam map chaotic AM signals respectively. Simulation results of point-target show that when the transmitted signal is Ulam map chaotic FM signal, two-dimensional and three-dimensional resolution is higher and side-lodes except integral sidelobe ratio are lower than results of other two kinds of transmitted signals, because the effective bandwidth of Ulam map chaotic FM signal is wider than chirp and Ulam map chaotic AM signals. In addition, Ulam map chaotic AM and FM signals for CSAR imaging have stronger anti-interference ability.

Improve Compressive Sensing Radar Imaging Performance by Optimizing Measurement Matrix

Xiao-Chun Xie[1] and Ling-Juan Yu[2]

[1]School of Physics and Electronics Information, Gannan Normal University, Ganzhou 341000, China
[2]Faculty of Information Engineering, Jiangxi University of Science and Technology, Ganzhou 341000, China

Abstract— High-resolution radar images requires large signal bandwidth and needs high-speed data acquisition, storing, and transmission devices, which brings about big challenge for imaging radar development. Compressive sensing technique allows recovering an unknown sparse signal with overwhelming probability from very limited samples. Because the scattering field of the target is usually composed of only a limited number of strong scattering centers, representing strong spatial sparsity in high resolution radar application, there has been increased concern over compressive sensing in radar imaging.

The samples used in compressive sensing correspond to linear projections obtained by a sensing projection matrix. It has been shown that a random sampling matrix satisfies the fundamental theoretical requirements of compressive sensing. On the other hand, by increasing the amount of information of observational data, a projection sensing matrix that is optimally designed for a certain class of signals can further improve the reconstruction accuracy or further reduce the necessary number of samples.

In this paper, a framework is introduced for the design and optimization of the echo dictionary and the sensing projection matrix of compressive sensing high-resolution imaging radar. In this framework, a tight frame is constructed by shifting sequences of radar range echo to represent radar raw data sparsely. Then, a sensing projection matrix is optimized by constrain the mutual coherence between the sparsity tight frame and the sensing projection matrix minimum. Simulation results show that this optimization outperforms the use of random sensing matrices and the propose framework can demonstrates better performance than conventional compressive sensing radar imaging methods.

Compact Microstrip Diplexer for 4G Wireless Communication

Fangqi Yang[1], **Xuehui Guan**[1], **Lei Zhu**[2], **and Haiwen Liu**[1]

[1]School of Information Engineering, East China Jiaotong University, Nanchang 330013, China
[2]Faculty of Science and Technology, University of Macau, Macau SAR, China

Abstract— A novel compact microstrip diplexer for 4G wireless communication is proposed in this paper. The diplexer is composed of two stub-loaded dual-mode resonators (SLDMRs). As a few attractive advantages, this constructed SLDMR can be easily used to achieve a narrow passband, to have a compact size, and to self-contain a transmission zero that is very useful in enhancement of the isolation between two channels. Meanwhile, an additional coupling between the source and load is introduced by extending the feed lines, thereby further increasing the isolation of our concern. Two transmission zeroes are produced in each single passband by adjusting the length of the feed-lines. Two SLDMRs are then connected to a common port by the feed lines with two long fingers. This kind of diplexers are suitable for the system have two closely passbands. The diplexer is in final designed at 2.35 and 2.59 GHz for 4G wireless communication. Coupling scheme of the diplexer is obtained for analysis and design. Experimental results verify the proposed design approach and the predicted frequency response.

A High Gain Slot Antenna Based on Surface Plasmon Polaritons

Hongjuan Han, **Huiping Guo**, **Xueguan Liu**, **and Ying Wang**
School of Electronic Information Engineering, Soochow University, Suzhou, China

Abstract— Surface Plasmon Polaritons (SPPs) are charge density waves that propagate along the surface of a conductor and have the property of near-field enhancement. In the past a period of time, most studies of SPPs focus on the visible and infrared frequency ranges. The principles and novel effects of SPPs have been attracting the interest of researchers. Nowadays, there has been increasing interest in the studies of SPPs in the microwave regime. Control and manipulate electromagnetic wave using SPPs in the microwave regime exhibit significant advantages in directional antenna. It not only can improve the gain of the antenna, but also can adjust the direction of electromagnetic radiation. In this paper, firstly, we discuss the existence of SPPs in the surface of metal in microwave regime. We also analysis the motivation of SPPs. Secondly, we introduce a high gain slot antenna with single-layer director briefly. Thirdly, a four-layered slot antenna with compact size and high gain is proposed. This antenna is based on the previous antenna. The different between them is that a dielectric grid structure is added to last one. The dielectric grid structure make the incident electromagnetic wave scattered, which make the wave vector of the incident electromagnetic matched with the Surface Plasmon Polaritons in horizontal direction, so that the incident electromagnetic wave can couple with SPPs. The simulated gain of the previous antenna is 12.0 dBi at 5.6 GHz and measured gain is 10.5 dBi at 5.57 GHz. The simulated gain of the last antenna is 13.5 dBi at 5.6 GHz and measured gain is 11.4 dBi at 5.57 GHz. The 2 dBi dropped for the measured and simulated gain can be caused by the loss of dielectric. By motivating SPPs, the simulated and measured gain of the antenna enhances nearly 1.5 dBi and 0.9 dBi separately. The overall size of both the antenna is $100 \times 100 \times 19\,\mathrm{mm}^3$.

A Compact Circular Polarized Tag Antenna in UHF Band for Metallic Object Application

Yusha Liu, **Qi Liu**, **Bo Xu**, **and Jun Hu**
Centre for Opt. & EM Research, Zhejiang Provincial Key Lab for Sensing Technologies
Zhejiang University, Hangzhou, China

Abstract— In recent years, applications for radio frequency identification (RFID) systems in the ultra-high frequency (UHF) band has been receiving much interest in several service industries, purchasing, distribution logistics, and animal tracking applications. For a commercial RFID system, it usually consists of a reader and many tags. The reader antenna generally has a circular polarization radiation pattern to increase the orientation diversity, however, most of RFID tags are linear polarization (LP) in the UHF frequency band. In this paper, a tag antenna with excellent circular polarization is presented. The tag antenna is designed in UHF band. The radiating patch is loaded with four slits to achieve a circular polarization radiation. In order to reduce the size of the antenna, other slits are added to lengthen the resonant length. Then the antenna with four cross-shaped slits will present a better circular polarization radiation. A quarter-wave microstrip line connected to a tag chip is used to feed the radiating patch. The input impedance of the proposed antenna is matched to the tag chip at approximately the center frequency 915 MHz. The circular polarization radiation is obvious in z direction. Thus, the 10-dB impedance bandwidth and the 3-dB circular polarization bandwidth of the tag antenna are expected to be wider. Considering the Friis transmission equation, the reading range for the proposed antenna is calculated to verify that the antenna is indeed circularly polarized. Further experiment will demonstrate that the proposed tag antenna can provide better performance when mounted on a metallic surface as compared with the free space condition.

A Miniaturized Unidirectional Moxon Antenna for UHF RFID Tags

Q. Liu, S. Zhang, and B. Xu
Center for Optical and Electromagnetic Research, Zhejiang University, Hangzhou 310027, China

Abstract— In this letter, a miniaturized unidirectional moxon antenna for UHF RFID tags is proposed. The moxon antenna is a parasitic dual-element array with the ends of each element folded back towards each other for additional coupling. The ends are separated to create a gap, which is mostly responsible for the unidirectional pattern. Meander lines and an inductively coupled feeding loop are applied in this structure for the size reduction and the impedance match between the antenna and the chip, respectively. Our proposed antenna has an overall size of 80 mm × 60 mm, the maximum gain is 4.48 dB and the front-to-back ratio is 17.7 dB at 915 MHz. The measured maximum reading range is 18.5 m with a total transmitted power of 4.0 W EIRP at 915 MHz. In addition, the front-to-back ratios are all above 15 dB in FCC band. With a simulated gain of 4.48 dB in the front direction and −15.6 dB in the back direction, the simulated front-to-back ratio is 20 dB at 915 MHz. The measured front-to-back ratio is 17.7 dB, and the measured reading range is 18.5 m in the front direction and 2.4 m in the back direction at 915 MHz. The measured half power beamwidth is 70° in the x-y plane and 150° in the y-z plane while the half power beamwidth of the dipole antenna is about 70° in usage plane. The proposed antenna can be applied in some specific situations such as manual searching and RFID location, as it gives a much longer reading range in the required direction than in other directions.

Optimization of Machine Learning Parameters for Spectrum Survey Analysis

R. Urban and M. Steinbauer
Department of Theoretical and Experimental Electrical Engineering
Brno University of Technology, Technicka 12, Brno 612 00, Czech Republic

Abstract— In the modern wireless communication there is nearly no idle frequency spectrum capacity. The most suitable frequency bands are already allocated or sold out. The newly incoming wireless system has to be moved to higher frequency bands or to share spectrum with existing system. Nowadays two main approaches of spectrums sharing [1, 2] are discussed. The first one is called the underlay spectrum sharing which is using limited radiation power to minimize interference with existing systems like UWB technology. The second one is called overlay spectrum which is sharing technique using utilization of the unused spectrum parts of the particular frequency band. All of these techniques are applied in cognitive radio system for spectrum allocation [2]. In this paper we are focusing mainly on the frequency spectrum data evaluation based on the real measurement [3], which is used predominantly for overlay spectrum sharing. Firstly, the occupied parts of the frequency spectrum need to be detected and the threshold level needs to be set up. Afterwards, the measured frequency points are mapped into the channels of the particular examined service. This paper targets the reinforcement algorithms for channel assignment in cognitive radio. Reinforcement learning [4] is a technique using agent to learn from direct interaction with the environment maximizing its reward and perform specific action. Generally, agent has no additional information and his purpose is to discover which action yield to highest reward. This paper is comparing different parameters of the weight functions of the algorithm. Reward and punishment is optimized in order to get the most reliable results for the shortest time (learning time). These obtained data are subsequently compared with simplified reinforcement learning algorithm — in the moment when the energy levels get over the threshold level the interference are counted for the particular channel. Only the linear reward/punishment is used. The learning starts with randomly selected part of the measured data. Over the learning time, the channel table is updated by particular score either as a reward or as a punishment computed for that time. Finally, after the learning time, the verification channel table is built from all measured data and compared with obtained results.

ACKNOWLEDGMENT

This work was supported by the project CZ.1.07/2.3.00/30.0005 of Brno University of Technology.

REFERENCES

1. Yan, Z., "Dynamic spectrum access in cognitive radio wireless networks," *IEEE International Conference on Communications (ICC'08)*, 4927–4932, 2008.
2. Berlemann, L. and S. Mangold, *Cognitive Radio and Dynamic Spectrum Access*, John Wiley & Sons, 2009.
3. Urban, R., T. Korinek, and P. Pechac, "Broadband spectrum survey measurements for cognitive radio applications," *Radioengineering*, Vol. 21, 2012.
4. Sutton, R. S. and A. G. Barto, *Reinforcement Learning: An Introduction*, The MIT Press, 1998.

Novel Miniaturized Satellite Navigation Antennas Based on Substrate Integrated Waveguide

Shunyu Fang, Tailei Wang, and Shouzheng Zhu
Department of Communications Engineering, East China Normal University, Shanghai, China

Abstract— In this paper, two novel miniaturized satellite navigation antennas based on substrate integrated waveguide are proposed in this paper. A single-layer SIW annular slot antenna is studied and designed at first. Then through overlay a patch on top layer, a multi-layer SIW antenna is designed. Two antennas use broadband 3-branch coupler to realize 3 dB power split and phase quadrature. The first antenna covers the BDS B1I band with circular polarization and the second one covers the BDS B1I band and BDS B2I band with dual circular polarization. Performance has been proved to be better than microstrip antenna in gain and Front-Back Ratio. Both simulation and test results are given respectively with performance analysis.

Figure 1 shows the configuration of the first antenna, the single-layer SIW annular slot antenna.

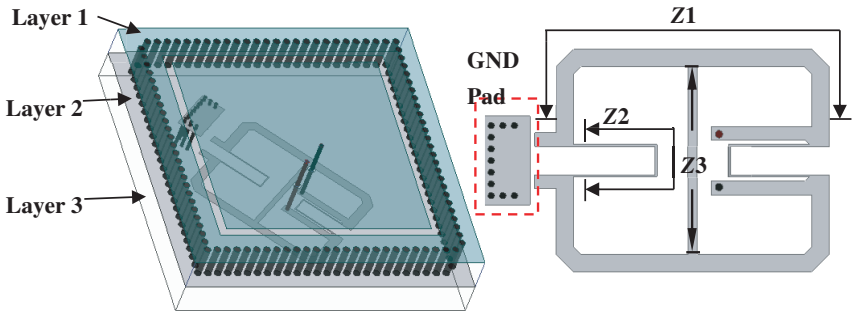

Figure 1: Configuration of the first antenna and the coupler and their geometrical parameters.

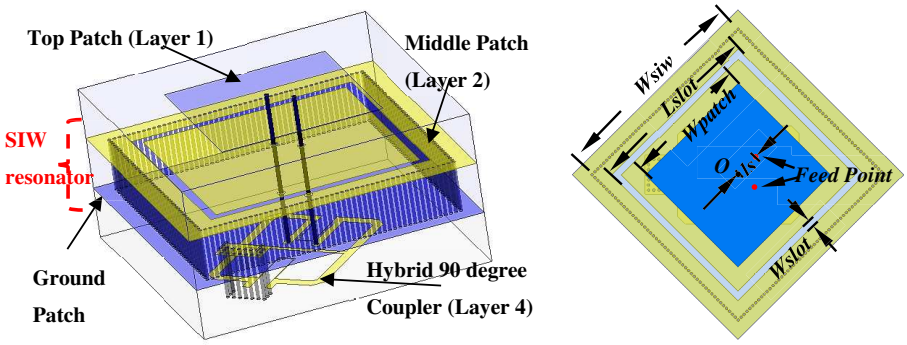

Figure 2: Configuration of the second antennas. (a) 3-D view. (b) Top view.

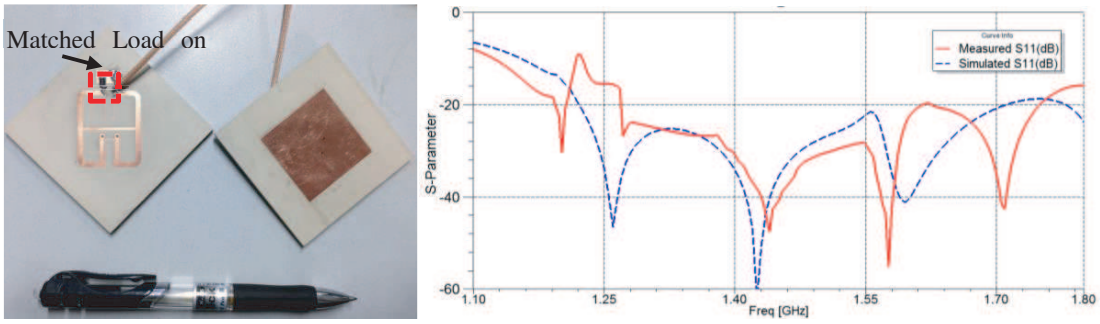

Figure 3: Photograph of fabricated antenna and its measured and simulated S-parameter .

In this antenna, an annular slot is etched on the SIW cavity. Radiation can realize through the slot.

Figure 2 shows the configuration of the second antenna. Through overlay a patch on top layer, the second antenna realizes dual band operation.

Figure 3 gives the Photograph of fabricated antenna (the second one).

A Novel Phase Measurement System Based on Six Port Reflectometer and LabVIEW

Tyler Wang, Jiajun Bian, and Shouzheng Zhu
School of Information Science and Technology, East China Normal University, 200241, China

Abstract— In this paper, a novel six port reflectometer (SPR) measurement system based on LabVIEW and a simple calibration method used to reducing the drastic complication of the calibration algorithms is proposed. This novel measurement system improves the efficiency of manual device measuring and handles easily. Experimental results are provided to demonstrate the performance of the developed SPR.

Six port technology was first used to microwave and millimeter wave measurement and network analyzer. During the 1970s, Engen and Hoer began to investigate the six-port technique as the heart of a simpler and less expensive network analyzer. Since then, there has been considerable work in the analysis, design, and testing of six-port systems.

Six port measurement system's calibration was the core of six port technology. Among the calibration methods proposed, the Engen's six port to four-port reduction is the most popular. However, the iterations required by the W-plane calibration algorithm tend to be lengthy and may fail because of drastic complication of the calibration algorithms. So we put forward a simple calibration method.

With the development of computer communication and measurement and control technology, LabVIEW has been turned into main tool in automatic measurement development system.

We build a novel measurement system based on LabVIEW, it improves the efficiency of manual device measuring and handles easily. The Section 1 is introduction and in Section 2, we first highlight the SPR working theory, then we present our novel calibration method and device model based on LabVIEW. In Section 3, experimental results are provided to demonstrate the performance of the developed SPR.

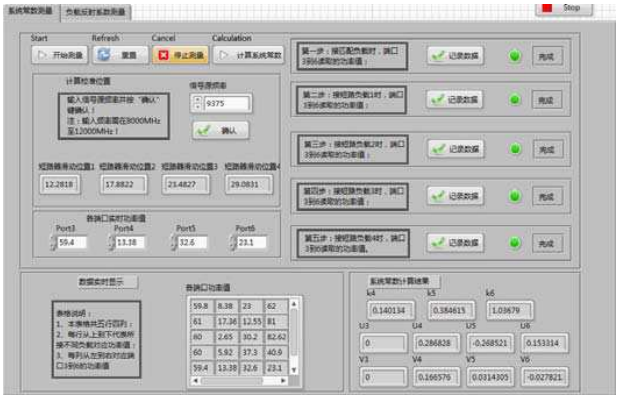

TD-LTE Antenna Array Smart Cover Study

Feng Gao[1], **Runhong Shan**[2], **Wentao Zhu**[1], **Kai He**[1], **and Zhiyuan Song**[1]

[1]China Mobile Group Design Institute, Beijing 100080, China
[2]Copyright Protection Center of China, China

Abstract— This paper integrated the antenna array analysis with differential evolution algorithm to optimize weights of antenna ports efficiently based on the customers' expected pattern, which could form the special broadcast beam to cover weak coverage cell. The broadcast beams were optimized by this method coincide with expected pattern through antenna anechoic chamber test. The LTE network experiment shows that the RSRP (Reference Signal Receiving Power) of communication network are improved 5% averagely after optimized by this method.

Investigation on Electromagnetic Scattering form Dielectric Soil Rough Surface with a PEC Object Embedded in It

Hongmei Miao[1] and Pengju Yang[2]

[1]College of Physics and Electronic Information, Yanan University, Yan'an 71600, China
[2]School of Physics and Optoelectronic Engineering, Xidian University, Xi'an 710071, China

Abstract— In this paper, electromagnetic (EM) scattering from one-dimensional dielectric soil rough surface with a perfect electric conductor (PEC) embedded in it is investigated by method of moments (MoM) for HH polarization. The soil rough surfaces are modeled as realizations of a Gaussian random process with the exponential spectrum, while the tapered incident wave is chosen to reduce the truncation error. Several numerical results are presented to investigate the impact of rough surface parameters of rms height and correlation length on the bistatic scattering coefficient (BSC), while the influence of the size and position of the object on the BSC is discussed.

Design and Development of a One Layer Planar Slot Antenna for Secondary Surveillance Radar

Maziar Hedayati, **Gholamreza Askari**, **Parisa Moslemi**, **and Hamid Mirmohammad Sadeghi**
Information and communication technology institute (ICTI)
Isfahan University of Technology (IUT), Isfahan 84156, Iran

Abstract— Secondary surveillance radar (SSR) is a system that installed on the top of the radar to be used in the air traffic control. It can detect the objects like an aircraft, in the air and represent the needed information such as the aircraft position and its identity. The SSR mechanism is based on sending a pair of signals at the frequency of 1030 MHz for interrogation and receiving a pair of signals as an answer at 1090 GHz [1]. SSR radars are built in the form of planar or cylindrical array antenna [2]. Reflector and multi layer antennas are the most common SSR antennas in the literatures that have some disadvantages like complexity and being bulky [3, 4] One layer microstrip array antennas which is proposed in this work, are the useful antennas in mass production because of their many advantages like easily printed, light weight and low cost which makes they suitable for radar applications. However they have some disadvantages like narrow bandwidth and high side lob level which is solved in this paper. To enhance the bandwidth, many attempts have been done in microstrip field. One method of increasing the bandwidth for the microstrip antennas is using stacked elements [5]. [6] proposed an stacked patch array of 1×8 elements with 14 dBi gain and the SLL of -14 dB, which is not enough low to provide the Side Lobe Suppression (SLS) for the SSR [1]. In addition using stacked element increase the complexity of the system. In this paper A useful, low cost, low complexity, and one layer microstrip slot L band antenna for secondary surveillance Radar (SSR) application is presented. The feed network of antenna is a rat-race divider to create sum and difference ports and sixteen unequaled power dividers to satisfy the Chebyshev distribution with -30 dB SLL. The feed network has an special structure that create constant group delay in all output ports and wide frequency bandwidth. The antenna gain for the sum pattern is 18.5 dB and 19 dB at 1030 MHz and 1090 MHz, respectively (Fig. 1) with a 3 dB beam width of 52° in elevation and 9.5° in azimuth. The difference has a -19 dB null at the peak of the sum pattern and an acceptable pattern against the sum pattern for SSR applications. Furthermore, the antenna has no need of the back fill antenna to eliminate the back lobe, which is critical for SSR applications. The total characteristics of the proposed antenna are shown in Table 1. A $2:1$ VSWR bandwidth of 9.4% is achieved with the presented geometry in simulation to cover the 1030 ± 10 MHz transmit and the 1090 ± 10 MHz receive frequency band (Fig. 2). Its low complexity structure makes it appropriate for many radar applications.

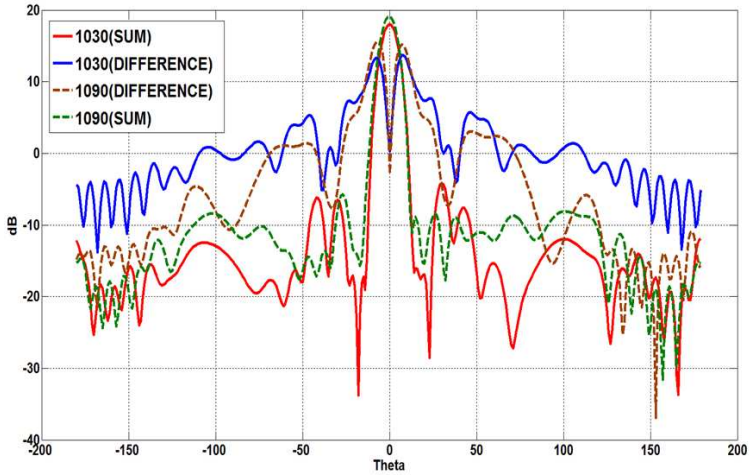

Figure 1: The radiation pattern of the array antenna with the center frequency of 1030, 1090 MHz.

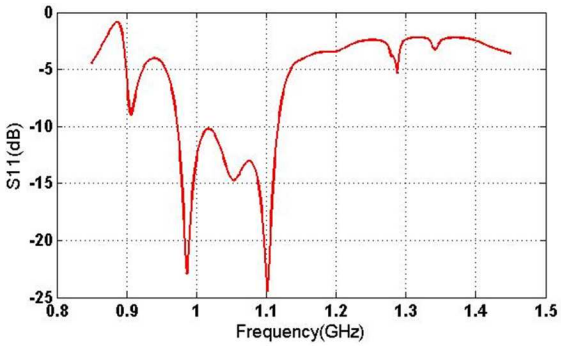

Figure 2: Simulated S11 of the 2×8 SSR antenna.

Table 1: Total characteristics of the proposed antenna.

Features	Unit	Value
#Channels	-	2 (Sum/Difference)
Frequency Range	MHz	1030±5, 1090±5
Polarization	-	Vertical
Sum Gain	dB	18.5
Sum Azimuth SLL	dB	−23
Sum Azimuth BLL	dB	−28
Difference Null	dB	19
Difference Coverage	dB	> 4
Sum Azimuth B.W	Degree	9.5
Sum Elevation B.W	Degree	52
Size	cm^3	$200 \times 10 \times 60$
Gain at Elevation Angle $(-20°, -40°) + 5\,dB >$ maximum Gain		
Gain at Elevation Angle$(\pm 60) + 12\,dB <$ maximum Gain		
Gain at Elevation Angle$(\pm 90) + 18\,dB <$ maximum Gain		
Gain at Elevation Angle$(\pm 145) + 28\,dB <$ maximum Gain		
Back lobe $+ 30\,dB <$ maximum Gain		

REFERENCES

1. Schejbal, V., et al., "Secondary surveillance radar antenna antenna designer's notebook," *Antennas and Propagation Magazine*, IEEE 55.2, 2013.
2. Stevens, M. C., *Secondary Survillance Radar*, Artech House, 1936.
3. Silver, A., *Microwave Antenna Theory and Design*, Sec. 5.7, Mcgraw-Hill, New York, 1949.
4. Stutzman, W. L. and W. A. Davis, *Antenna Theory*, John Wiley & Sons, Inc., 1998.
5. Lee, R. Q., K. F. Lee, and J. Bobinjak, "Characteristic of a two layer electromagnetically coupled rectangular patch antenna," *Electron. Lett.*, Vol. 23, No. 20, 1070–1072, Sept. 1987.
6. Kumar, S. A., C. K. Kumar, and A. Mittal, "EM coupled L-band antenna array for secondary surveillance radar," *European Microwave Conference 2009, EuMC 2009*, 1465, 1467, Sept. 29 2009–Oct. 1, 2009.

Study on the Characteristics of Long-wave Radiation over China Area

Y. T. Ma[1, 2], **L. S. Sun**[1], **and H. Ding**[1]

[1]School of Civil Engineering, Shenyang Jianzhu University, Shenyang, China
[2]School of Resource & Civil Engineering, Northeastern University, Shenyang, China

Abstract— The main kind of outgoing radiation on the surface of the Earth is the long-wave radiation outwards, which owns regional and seasonal characteristics. There are some serious natural disasters which can cause changes of the long-wave radiation. As a result, to forecast and alert disasters, it is essential to establish the OLR (Outgoing Long-wave Radiation) regional and seasonal background fields and monitor the radiation changes. Based on the OLR data which was provided by the satellite of NOAA, the regional and seasonal background fields in Chinese mainland and its surrounding areas were established. The data adopted is monthly average data (400 points per month), the investigation area covers between $17.5^\circ \sim 55^\circ$N north geographic latitude and $71.25^\circ \sim 133.75^\circ$E east geographic longitude, The time range is from 1991 to 2010, the spatial resolution is $2.5^\circ \times 2.5^\circ$. The variation characteristics of OLR which are influenced by latitude and longitude, time and region respectively were analyzed.

The research results showed that: the value of OLR changed obviously with the variation of latitude which also owned seasonality. There was a characteristic location at 35°N in which a point of inflexion on the OLR trend curve emerged; The value of OLR varied slightly with the change of longitude; The regionality characteristics were manifested as the low value of OLR in area of Qinghai-Tibet Plateau and northeast at all seasons, the relatively high value of OLR in Taiwan, Hainan, southern Yunnan and north Xinjiang in spring and winter, and the relatively high value of OLR in eastern Xinjiang and western part of Inner Mongolia in summer and autumn; the time characteristics showed that in most parts of Chinese region the value of OLR advanced while in other regions, the value of OLR unchanged.

The Study of the Generalized Stereopair Matching Method

L. S. Sun[1], **Y. T. Ma**[1,*], **and H. Wang**[2]

[1]School of Civil Engineering, Shenyang Jianzhu University, China
[2]School of Resource & Civil Engineering, Northeastern University, China

Abstract— The data of traditional images matching are remote sensing images obtained from the same sensor in different times. If the region can't be covered by the field view of one satellite sensor, stereo pair can't be acquired. It is necessary to match images from different satellites for getting the same overlap region. This method is called the generalized matching stereo pair. More images may be selected by the generalized stereo pair matching. The generalized stereo pair matching technical process has been studied in this article. The process is divided into five steps. First step is the selection of images with overlap regions; second step is the standardization processing of images for that images were consistent in resolution and color; third step is the image pyramid creation by Haar wavelet transform with matlab program; fourth step is the matching of correlation coefficient which is calculated by the value of pixels between target area and search area; fifth step is the least squares matching for acquiring the geometric parameters which can be used to compensate the geometric differences between two windows and the radiation transformation parameter which is used to compensate the radiation differences in pixels of two window. Two images were selected for verifying the generalized stereo pair matching. One was QuickBird image, the other was Spot image. Twenty six control points with same places in two images were selected for verifying the experimental results. The rate of success matching points was 88.5%. The experiment result showed the technical process of the generalized stereo matching in this article was feasible and reliable.

*Corresponding author: Yuntao Ma (mayuntao7@163.com).

Study on Surface Albedo of Different Land Cover Types in Liaoning Province

J. L. Wang[1], **Y. T. Ma**[1, 2, *], **and L. S. Sun**[1]

[1]School of Civil Engineering, Shenyang Jianzhu University, Shenyang, China
[2]School of Resource & Civil Engineering, Northeastern University, Shenyang, China

Abstract— On behalf of the reflectivity of the solar radiation on the earth's surface, Surface albedo is one of the key factors to influence the Earth's climate system. Therefore, the accurate surface albedo parameters and its relative factors are important parts of researching the regional climate change. Surface albedo is mainly affected by the solar elevation angle, the underlying surface conditions, soil moisturemeteorological conditions, etc.. The underlying surface conditions include land cover types, the proportion of surface features, water content and so on. Different land cover types which make up the Earth's surface have a great impact on surface albedo. In order to study the albedo characteristics of different land cover types, NDVI was introduced as a factor affecting surface albedo. This paper analyzed the relationship between surface albedo and NDVI from the different land cover types and the relationship between surface albedo and NDVI from the same land cover types in Liaoning Province adopting MOD43B3, MOD13A2, MOD12Q1 from MODIS data on August 12, 2012. The results showed that the sequence of features based on their values of NDVI was the following: woodland > cropland > grassland > urban area > wetlands > water, the sequence of features based on their values of surface albedo was the following: urban area > grassland > cropland > woodland > wetlands > water. NDVI and surface albedo of the different land cover types (except wetlands and water bodies) showed a significant negative correlation. In the same land cover types, NDVI and surface albedo of water, wetlands, urban and cropland were a positive linear correlation, NDVI and surface albedo of grassland and woodland were a negative linear correlation. This study provided a reference for feature extraction and regional climate change monitoring in Liaoning Province.

*Corresponding author: Yuntao Ma (mayuntao7@163.com).

Study on the Variation of Vegetation in Shenyang City Based on MODIS Data

Y. T. Ma[1,2], **J. L. Wang**[1,*], **and L. S. Sun**[1]

[1]School of Civil Engineering, Shenyang Jianzhu University, Shenyang, China
[2]School of Resource & Civil Engineering, Northeastern University, Shenyang, China

Abstract— Urban vegetation is an important composition factor of urban ecosystem and plays a key role on the protection of urban ecological environment, such as relieving urban heat island effect, purifying air and improving regional climate. So it's significant to carry out the study of urban vegetation.

The distribution characteristics and interannual variation of vegetation in Shenyang city from 2001 to 2011 were analyzed according to vegetation index products MOD13A3 from MODIS provided by NASA Earth Observing System (EOS). The following was the processing method: Normalized Difference Vegetation Index (NDVI) was taken as the indicator of vegetation growth, vegetation index in 2001 was as benchmark, the differences were calculated by subtracting vegetation index in other years with the benchmark and were graded according to NDVI classification standards, and then the analysis was performed.

The results showed that the vegetation density increased gradually from the city center to the periphery, the overall trend of vegetation variation in whole city was degraded from 2001 to 2011, the vegetation around the outskirt of town were slightly degraded and other parts of the vegetation showed moderate and slight improvement from 2002 to 2004, then since 2005, the vegetation degradation around the outskirt of town had been serious, the vegetation in the town and in the periphery areas of Shenyang such as southeast Dongling district, southeast Sujiatun district, southwest Shenbei new district and southeast Yuhong district were ameliorated more or less.

This paper also analyzed the influence factors of vegetation variation in Shenyang including natural factors and artificial factors. The natural factors had certain influence on vegetation variation, but the main effect was still the influence of artificial factors including urban expansion and urban greening. Urban expansion reduced the vegetation around the outskirt of town and urban greening increased the vegetation in the city center.

*Corresponding author: Jingli Wang (13898803180@163.com).

Oil Spill Detection Based on Characteristic Parameters and HAC

Honglei Zheng, Yanmin Zhang, and Yunhua Wang
College of Information Science and Engineering, Ocean University of China, Qingdao, China

Abstract— Segmentation of polarimetric Synthetic Aperture Radar (SAR) images is a crucial stage in the oil spill detection on the sea. The common image segmentation algorithms can hardly achieve satisfactory results. Conventionally, Hierarchical Agglomerative Clustering (HAC) theorem was applied to intensity of SAR images. In this paper, an oil spill detection method combining characteristic parameters and HAC is presented. A set of characteristic parameters depicting the physical features of ocean surface are evaluated based on a full polarimetric SAR image. And then, we apply the HAC theorem to the characteristic parameters rather than intensity images to classify the polarimetric SAR image into different types of regions. HAC takes advantages of multi-resolution segmentation to maintain effectively the shape properties of oil spill paths. After the segmentation, we extract the feature information of the oil spill regions and compared the feature information with those of the surrounding sea. Segmentation experiments of SAR images which include potential oil spill regions have been conducted with Radarsat-2 full polarimetric SAR images. In order to validate the applicability of this presented algorithm, we compared our results with other approaches, such as OTSU (method of maximum classes square error), K-means clustering etc.. The comparisons demonstrate that the segmentation method based on characteristic parameters has a better performance in recognizing the oil spill regions. Moreover, this method can effectively reduce the influences of small paths and it is helpful to improve the accuracy of oil spill detection in SAR imagery.

The Damping Model for Sea Waves Covered by Oil Films of Finite Thickness

Yunhua Wang[1] Yanmin Zhang[2], and Honglei Zheng[2]

[1]Ocean Remote Sensing Institute
Ocean University of China, Qingdao 266100, China
[2]College of Information Science & Engineering
Ocean University of China, Qingdao 266100, China

Abstract— The oil film of finite thickness viscous dampening model in combination with the action balance equation of sea surface wave spectrum is given in present work. The effects induced by physical parameters of oil film such as kinematic viscosity, film thickness, etc., and by environment parameters such as wind speed, wind direction, factional filling factor, etc., are all taken into account. From the results, it is found that we can see that the damping ratios are insensitive to the oil density, surface/interfacial tension and surface/interfacial viscosity for the waves whose wave numbers are smaller than 300 rad/m. However, the damping ratios would be obviously affected by the kinematic viscosity, surface/interfacial elasticity and thickness of oil film. Meanwhile, the simulated results also show that the damping ratio is also closely related to wind speed, the wind direction, and the fractional filling factor. And we find the damping ratio decreases with increasing wind speed, and increases with the wave spread azimuth angle. One reason for this phenomenon is that the higher the wind speed, the higher the wind input energy, hence, the weaker the Marangoni damping effect. The other reason is that the wave interaction becomes stronger when wave spread azimuth angle is small. Furthermore, fifteen ENVISAT ASAR Wide Swatch Mode images which were acquired in Gulf of Mexico during the 2010 BP oil spill accident are used to confirm the validity of the damping ratio evaluated by our approach. And the comparison shows that our theoretical damping ratios can agree with the measured data well, when we choose suitable fractional filling factor for different wind speeds. Conclusions obtained in this work would be meaningful for oil spill remote sensing.

Optimization of Pickup Coil in Compact Magnetometer with DC/AC Unit Employing High-T_c SQUID

Yuichi Ishihara, **Mohd Mawardi Saari**, **Toki Kusaka**, **Yuya Tsukamoto**, **Kenji Sakai**, **Toshihiko Kiwa**, **and Keiji Tsukada**
Graduate School of Natural Science and Technology, Okayama University
3-1-1 Tsushimanaka, Kitaku, Okayama, Okayama Prefucture 700-8530, Japan

Abstract— Magnetic susceptibility is a specific characteristic of substances and can be used to identify and analyze the amount of materials. Although a magnetometer is used to measure magnetic susceptibility, high sensitivity is required to evaluate various samples, such as paramagnetic and diamagnetic materials. In this study, we report a compact and highly sensitive magnetometer with a DC/AC unit using HTS-SQUID. This system can measure two characteristics: M-H characteristic by applying a DC magnetic field, and AC magnetic susceptibility by applying an AC magnetic field. In the measurement, a sample is placed in a magnetic field generated from an electromagnet. A secondary magnetic field from the sample is detected by the first order differential pickup coil located under the sample. For DC measurement, a pickup coil of which the sensitive axis is parallel to the DC magnetic field was used. Then, the sample is vibrated above the pickup coil and the detected secondary magnetic field is converted into an AC signal. Meanwhile for AC measurement, the pickup coil of which the sensitive axis is perpendicular to the AC magnetic field was used. The detected AC signal is transferred to the HTS-SQUID by a superconducting input coil that is connected in series to the pickup coil. Although the developed system could measure the M-H characteristic using the DC measurement unit, the measurement of AC magnetic susceptibility was difficult because the signal to noise (S/N) ratio is low when using the AC measurement unit. Therefore, optimization of the pickup coil for the AC measurement unit was investigated in this study. When the baseline of the pickup coil for AC measurement changed, the output signal intensity increased. However, the effect of the applied AC magnetic field could not be eliminated. Thus, a compensation coil was added to the pickup coil of which the sensitive axis is parallel to the applied magnetic field. As a result, the effect of the applied AC magnetic field could be reduced significantly and the S/N ratio increased. Therefore, using this developed system, both the M-H characteristic and AC magnetic susceptibility can be measured for various samples.

ACKNOWLEDGMENT

This work is supported by the "Strategic Promotion of Innovative R&D" of the Japan Science and Technology Agency (JST).

Microwave Radiation Image Reconstruction Method Based on Adaptive Multi-structural Dictionary Learning

Lu Zhu, **Jiangfeng Liu**, **Yuanyuan Liu**, **and Suhua Chen**
School of Information Engineering
East China Jiaotong University, Nanchang 330013, China

Abstract— Due to the complicated structure of microwave radiometric imaging system and the massive amount of data collection in one snapshot, it is difficult to achieve the high spatial resolution image by conventional microwave radiation imaging method based on the Nyquist sampling. In this paper, according to the priori information of the compressible multi-structural information of microwave radiation image, we adopt the Fourier random observation matrix to sparsely project the microwave radiation image, reducing the amount of data collection, and lowering the complexity of the system. Considering the multi-structural information of microwave radiation image, such as multi-sparsity in different domains, piecewise smoothness, etc., it is difficult to sparsely represent microwave radiation image in complex scene by the traditional orthogonal basis, but the piecewise smoothness ingredients of microwave radiation image meet the constraint condition of total variation, and the mixed orthogonal basis can sparsely represent the sparsity information of microwave radiation image. We make use of the sparse representation of the mixed orthogonal basis and the constraint condition of total variation regularization to construct the reconstruction model of microwave radiation image based on adaptive multi-structural sparsifying dictionary learning. We integrate dictionary learning technique to adaptively learn the multi-structural sparsifying dictionary, and the sparsifying dictionary is adapted to sparsely represent the microwave radiation image, and solve the convex programming problem of microwave radiation image reconstruction, and design the reconstruction method. The simulation results show that reconstructing microwave radiation image by the proposed algorithm achieves better reconstruction performance than that by the DLMRI algorithm.

The EMC Impact due Household Appliances in Smart Grid Networks

Stefania Sousa[1], **C. E. Capovilla**[2], **and H. X. Araujo**[1]

[1]Universidade Federal de São João Del Rei — UFSJ, Brazil
[2]Universidade Federal do ABC — UFABC, Campus Alto Paraopeba
Rodovia MG 443, Km 7, Ouro Branco/MG, Brazil

Abstract— The Smart Grid technology has become a reality day by day due its clean proposal which can provide, for example, the link between wind and solar power with electric cars. However, the "smart" factor of the technology is obtained through electronic components, which are in general, the major responsible of unintentional emissions and coupling. Therefore, in this work, the EMC — Electromagnetic Compatibility of household appliances is deal with the use of a conducted emission technique. The obtained results are compared to the existing standards.

Having as main goal improve the grid reliability, power quality and energy efficiency, the Smart Grid technology has become a subject of study nowadays [1]. However, the smartness of the grids is provided by electronics, which are in general the major responsible of unintentional emissions.

Due to the increase of the microelectronic and embedded electronic systems, every electronic device must be submitted to stricter EMC measurement, and their entries in the market are directly related to it responses on these test. However, only in the late 70s that the problems related to EMC — Electromagnetic Compatibility became of public knowledge, in general, due to the problems presented by TVs, communication devices, audio and video displays, among many other applications [2].

Basically, as far as the smart grid control is developed with microelectronic components, the conducted emission levels from the household appliance should be carefully observed, in order to guarantee the correct operation of the network. Moreover, the grid behavior must also be certified in order to ensure the correct operation of the devices connected to it in terms of electromagnetic compatibility. In this work, only the household devices will be investigated. This is extremely important because with no disturbances the voltage quality is perfect, otherwise not.

In order to analyze the conduct emission phenomena in some household appliance that are normally connected to the residential grid, the EMC Pre-Compliance Board — EPCB built in [3], and a LISN — Line Impedance Stabilization Network were employed.

The test setup, was performed in accordance to CISPR and FCC — Federal Communications Commission, agency in charge of standardization of radio communications and cable in the U.S.. The preliminary results were compared to CISPR 14-1 [4] and CISPR 22 [5], depending on the class of the household appliance DUT.

In this work, the conducted emission levels from the household appliance are observed in order to ensure the correct operation of the devices connected to grid in terms of EMC. The preliminary obtained results were compared to the regulatory standard and it can be observed that most of the devices are out of it, thus compromising the performance of the grid as a whole.

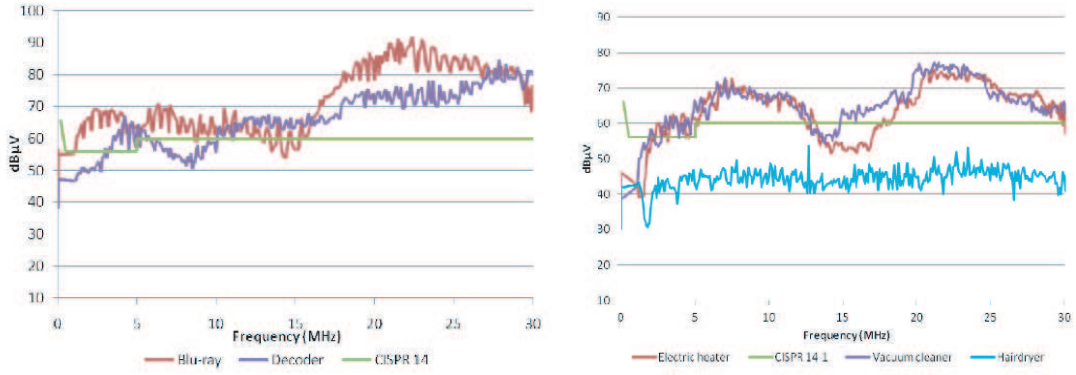

Figure 1: Measurement results of some household appliance: Preliminary results.

REFERENCES

1. Gunnar, A., K. Dursun, B. G. Hauge, and B. Bremdal, "Establishing sustainable and reliable Smart Grids," *2013 IEEE International Workshop on Applied Measurements for Power Systems (AMPS)*, 138–143, Aachen, Germany, 2013.
2. Montrose, M. I. and E. M. Nakauchi, *Testing for EMC Compliance*, New York, 2004.
3. Silva, F. R. L., L. R. Ribeiro, L. P. Dias, W. J. Santos, C. E. Capovilla, and H. X. Ee Araujo, "The design and implementation of an EMC pre-compliance board," *PIERS Proceedings*, 1267–1270, Stockholm, August 12–15, 2013.
4. CISPR 14-1 Ed 5.1, *Electromagnetic Compatibility — Requirements for Household Appliances, Electric Tools and Similar Apparatus — Part 1: Emission*, International Electrotechnical Commission, 2009.
5. CISPR 22 Ed 6.0, *Information Technology Equipment — Radio Disturbance Characteristics — Limits and Methods of Measurement,* International Electrotechnical Commission, 2008.

Determination of Microwave Conductivity of Electrolyte Solutions from Debye-Drude Model

Shuo Li, **Sucheng Li**, **Shahzad Anwar**, **Fa Tian**, **Weixin Lu**, **and Bo Hou**
School of Physical Science and Technology, Soochow University
1 Shizi Street, Suzhou 215006, China

Abstract— The solvation of ions in aqueous media is a fundamental process in biology and chemistry, and the characterization of dielectric constant of aqueous electrolyte solutions at microwave frequencies composes a powerful way to understand the dynamical process in aqueous media. In this work, we have combined the classical Debye and Drude models to determine the microwave conductivity of the salt (NaCl) solution by measuring its dielectric constant.

First, we assume that the permittivity of the electrolyte solution has a compound dielectric constant model which is the sum of the Debye model explained as the water background and the Drude model accounting for the conductive ions in the solution. Next, we use an Agilent network analyzer to measure the complex permittivity of the pure water and the NaCl solution at the microwave frequencies, 0.1–20 GHz. The Drude model's contribution from the conductive ions is calculated to be the difference value between the permittivity of the electrolyte and the permittivity of the pure water. Finally, the microwave conductivity is obtained from the Drude model $\varepsilon \approx i\sigma/\omega$. By employing this approach, we determine the microwave conductivity spectrum, which at lower frequencies maintains a constant, matching the direct current (DC) value acquired by a conductivity meter at the considerately low concentration case. In particular, we notice there is the slight difference between the microwave and DC conductivities as increasing the salt concentration.

As a justification of the Drude model, the damping coefficient, γ, for the conductive ions need be far greater than the angular frequency ω. From the DC conductivity, we derive the damping coefficient of the conductive ions and prove the applicability of the Drude model in our experimental microwave regime.

Numerical Simulations of a Complete GTEM Chamber

H. X. Araujo[1], **C. E. Capovilla**[2], **and L. C. Kretly**[3]

[1]Universidade Federal de São João Del Rei — UFSJ, Brazil
[2]Universidade Federal do ABC — UFABC, Brazil
[3]Universidade Estadual de Campinas — UNICAMP, Brazil

Abstract— With the advance of the digital and integrated technology and the use of electronic devices in several systems, the occurrence of interferences at the same environment becomes increasingly. Therefore, the use of techniques and specific tools to analyze the behavior of a certain device in an electromagnetic environment becomes indispensable. Among the methodologies found in the literature, the GTEM cell shows a higher frequency range, and the capability to realize both EMI — Electromagnetic Interference and EMS — Electromagnetic Susceptibility test.

The use of GTEM cells for EMI verification test is normally applied to identify the power magnitude that propagates on the TEM mode from the DUT. As the analysis is qualitative, the verification is done from the signal levels along the frequency range. On the other hand, the EMS tests are performed to identify the immunity of the DUT concerning interference provided by other devices.

Thus, a "lab-made" GTEM chamber was designed and implemented to perform EMC/EMI/EMS test. In this work, it will be shown some strategies to simulate the chamber. It is also shown the basic concepts to design this versatile chamber, employed in pre-compliance tests and Electromagnetic Compatibility for automotive, electronic boards and integrated circuits. Experimental results are compared to the simulated ones.

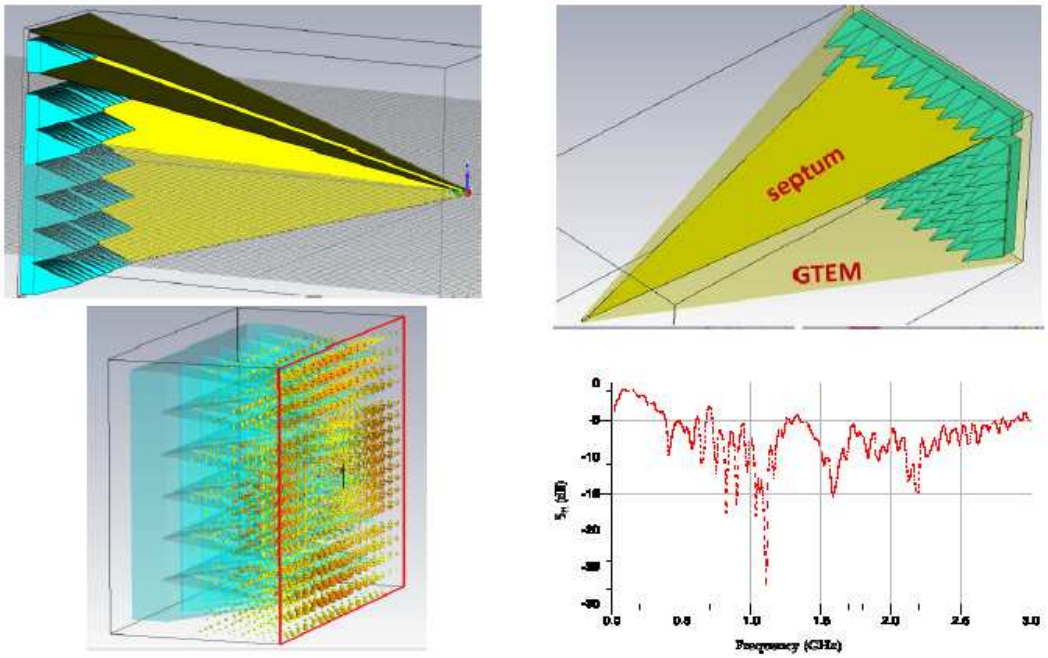

Figure 1: GTEM chamber on the simulator and return loss result.

Stacked Metamaterials Enables Ultranarrow and Directional Thermal Emission

Yongkang Gong, Kang Li, Jungang Huang, J. J. Martinez, and Nigel Copner
Faculty of Computing, Engineering and Science, University of South Wales, CF37 1DL, UK

Abstract— A thermal radiation source, such as a blackbody or an incandescent light bulb, is usually omnidirectional and broadband in nature, in marked contrast to a laser which is both temporally and spatially coherent. The desire to convert thermal emission from broadband to narrowband has long been a research topic of interest for scientists in the last decades, such as using luminescent bands of rare earth oxides, and tailoring photon density of states of photonic crystals. It has been recently noted that plasmonic nanophotonics offer exceptional opportunities to tailor absorption of a target material so as to modify its thermal emission spectrum on the basis of Kirchhoff's law. We proposed a novel metamaterials based on stacked gratings (SGs) which allows for thermal emission with ultranarrow spectrum and antenna-like spatial directivity. The SGs are composed of a metallic grating (MG) followed by a Bragg grating (BG). We observe that both the MG and the BG are highly reflective to the light but when they are combined together, interestingly, zero reflection occurs at the wavelengths located in the BG bandgap and gives rise to thermal emission in anomalous and intriguing ways. Numerical and analytical results demonstrate that the SGs are able to radiate light within narrow angular lobe as an antenna and its operating wavelength can be effectively tuned by varying BG bandgap position. More interestingly, the full width at half maximum of the SG's emission spectrum is tunable and can be significantly narrowed by narrowing the BG bandgap. We also demonstrate that multi-wavelength emission with near-unity peak and ultranarrow bandwidth can be achieved. These are the key results which open immense possibilities for novel infrared source, pertinent to applications such as thermal analysis, imaging, security, biosensing and medical diagnoses.

Microwave Coherent Perfect Absorption Based on Ultrathin Conductive Films

S. C. Li[1], **J. Luo**[1], **S. Anwar**[1], **S. Li**[1], **W. X. Lu**[1], **Z. H. Hang**[1], **Y. Lai**[1], **B. Hou**[1], **M. R. Shen**[1], **and C. H. Wang**[2]

[1]School of Physical Science and Technology, Soochow University
1 Shizi Street, Suzhou 215006, China
[2]Institute of Modern Optical Technologies
& Collaborative Innovation Center of Suzhou Nano Science and Technology
Jiangsu Key Lab of Advanced Optical Manufacturing Technologies
Soochow University, 1 Shizi Street, Suzhou 215006, China

Abstract— The absorption of microwave by metallic conductors is almost exclusively inefficient due to the huge impedance mismatch between metal and free space. The ultrathin conductive film may improve the absorbing efficiency up to the maximal 50% limit. In our previous work [1], we show ~ 5 nm thick Au film can achieve the 50% limit absorption. In addition, a methodology based on metallic mesh structure is proposed to design a kind of frequency-independent ultrathin absorbers. We perform a design of such absorbers with 50% absorption, which is verified by numerical simulations.

Recently, a new concept called coherent perfect absorption (CPA) which can accomplish 100% perfect absorption has attracted a lot of research interest [2–4]. Being regarded as the time-reversal process of laser generation, CPA takes place when a Fabry-Perot (FP) dielectric cavity is illuminated by two counter-propagating light beams satisfying coherence conditions, and all input EM energy is trapped and dissipated inside the cavity, resulting in 100% absorption. In this work, we show CPA can be realized on a single layer of ultrathin conductive film illuminated coherently by two microwave beams. Not involving resonance effects, the 100% absorption exhibits the frequency-independent characteristic and peculiarly occurs on an extremely subwavelength scale, $\sim \lambda/10000$, the film thickness. Distinctive from the conventional ways of engineering absorber's structure and/or substrate, the microwave coherent perfect absorption breaks the 50% limit with super structural simplicity and high performance.

Furthermore, we numerically and experimentally demonstrate that CPA can take place under single beam illumination as well. In fact, a perfect magnetic conductor (PMC) boundary, which behaves as a mirror boundary, can replace the second illuminated microwave beam. In real case, high impedance surfaces employing mushroom structure can realize this kind of PMC boundary at one or more specific working frequencies, which gives rise to the CPA phenomenon under single beam illumination.

REFERENCES

1. Li, S. C., et al., *AIP Advances*, Vol. 4, 017130, 2014.
2. Chong, Y. D., L. Ge, H. Cao, and A. D. Stone, *Phys. Rev. Lett.*, Vol. 105, 053901, 2010.
3. Wan, W. J., et al., *Science*, Vol. 331, 889–892, 2011.
4. Pu, M. B., et al., *Opt. Express*, Vol. 20, 2246–2254, 2012.

A Metamaterial-based Probe for EMC Measurements

M. F. P. Tartaglia[1], **A. V. Cardoso**[1], **C. E. Capovilla**[2], **and H. X. Araujo**[1]

[1]Universidade Federal de São João Del Rei — UFSJ, Brazil
[2]Universidade Federal do ABC — UFABC, Brazil

Abstract— In this work, planar probes for EMC — Electromagnetic Compatibility measurements are designed with metamaterials structures in order to improve its gain, bandwidth and resonance. Basically, three topologies are used (Jerusalem cross pair, fractal array and CSRR — complementary split ring resonator), in two different topologies: circular and square models. Experimental results are compared to the simulated ones.

The electrical circuit of any electronic device produces some kind of noise, which can reach levels of power that interfere in undesired ways on the operation of the equipment around and the environment as a whole. Each device generates a characteristic noise, due to its electrical circuit [1]. Depending on the electromagnetic emission of these noises, other electronic devices can then receive the interference by a path of radiation or, much less frequently a direct electrical connection.

The necessity to control the electromagnetic emissions and interference between circuits and electronic devices becomes a crucial point to assure its correct operation inside an electromagnetic environment. Some approaches were designed to support the pre-compliance tests (EMC/EMI/EMS) setups. In this work, is shown the design of low cost planar probes with metamaterial patterns for EMC measurements.

Actually, metamaterial is a macroscopic composite of periodic or non-periodic structure, whose function is due to both the cellular architecture and the chemical composition [2]. Therefore, the behavior of a material, in the presence of an electric field, is determined by the macroscopic parameters, permittivity ε and permeability μ. Several metamaterial structures have been investigated along the last years. In particular, ones those are capable to provide artificial magnetic responses and electric walls. The artificial magnetic conductors can be obtained when a plane wave focus on the capacitive gap, while the artificial electric conductor is obtained through the opposite way.

In fact, the metamaterial pattern is applied to physical devices aiming to obtain specific responses. In [3] a CSRR structure is employed to a UWB antenna in order to provide a rejection characteristic in a desired frequency. On the other hand, in [4] metamaterial structures are applied to an UHF antenna and a better gain is obtained, while in [5] the periodic is structures are applied to the septum of a GTEM — Gigahertz Transverse Electromagnetic chamber, expecting a shift on the resonance frequencies.

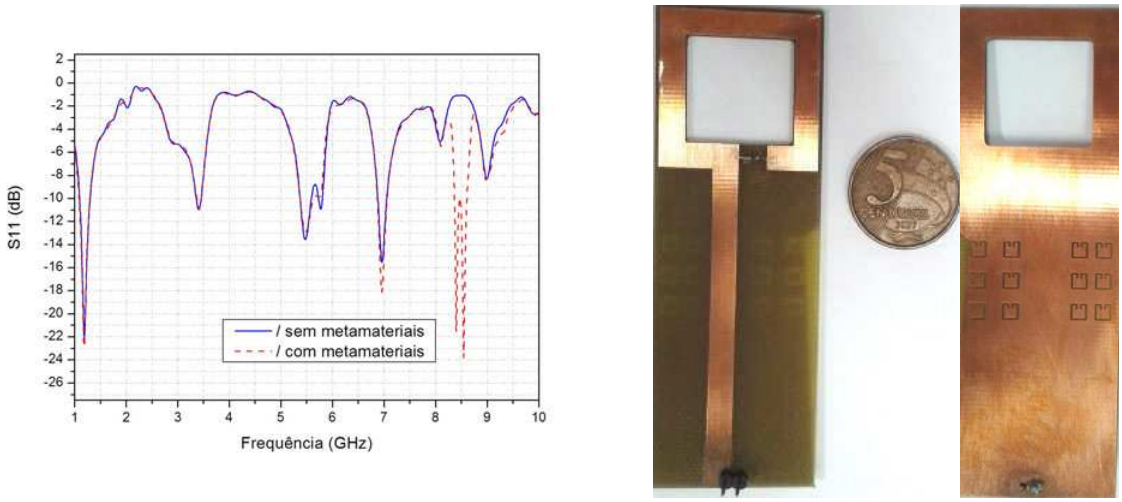

Figure 1: (a) Simulated result of one planar probe: Preliminary results, (b) built prototype.

In this context, to improve the performance in terms of gain, bandwidth, resonance, and provide a rejected band, three different topologies are employed in planar probes.

REFERENCES

1. Montrose, M. I. and E. M. Nakauchi, *Testing for EMC Compliance*, New York, 2004.
2. Cui, T. J., "Electromagnetic metamaterials: Recent advances on the theory, experiments, and applications," *IEEE Antennas Propag. Mag.*, 2008.
3. Jo, N.-I, D.-O. Kim, and C.-Y. Kim, "A compact band notched UWB antenna for mobile applications," *PIERS Online*, Vol. 6, No. 2, 177–180, 2010.
4. Araujo, H. X., S. E. Barbin, and L. C. Kretly, "Metamaterial cell patterns applied to quasi-Yagi antenna for RFID applications," *Radio and Wireless Symposium — RWS*, Santa Clara, USA, 2012.
5. De Araujo, H. X. and L. C. Kretly, "The effect of metamaterial patterning to improve the septum GTEM chamber performance," *PIERS Proceedings*, 1224–1228, Marrakesh, Morocco, March 20–23, 2011.

Design of Base Station Antenna for RF Energy Harvesting

Jung-Ick Moon, In-Kui Cho, Seong-Min Kim, Jae-Hun Yun, and Woo-Jin Byun
Radio Technology Research Department
Electronics and Telecommunications Research Institute (ETRI), Korea

Abstract— Generally the base stations or repeaters are transmitted with very high power. However, some of the transmitted power is radiated backward and dissipated [1]. In this paper, a base station antenna changing the backward radiation energy into the renewable RF energy is proposed. As shown in Figure 1, this antenna is composed of the array radiator and RF harvesters using slots on the ground plane. The main radiator having a dipole type covers LTE-band in Korea and several RF harvesters on the ground plane are used to renew the RF energy from the main radiators. Because the surface current on the ground plane flows into the RF harvesting port in the slot, the main radiator's electrical performance is not at all disturbed.

Moreover, the ground plane has a rectangular structure with vertical metallic walls in order to improve the gain and harvest the non-critical radiation of the antenna. The several harvesting ports are connected with the RF combiner by coaxial cables and the harvested energy is changed into the DC voltage through the rectifier circuit.

As a result, the amount of the harvested energy from this base station antenna is approximately 0.2% of the originally radiated power. The simulated radiation performances of the proposed antenna are shown in Figure and are almost same with that of the antenna without the harvester.

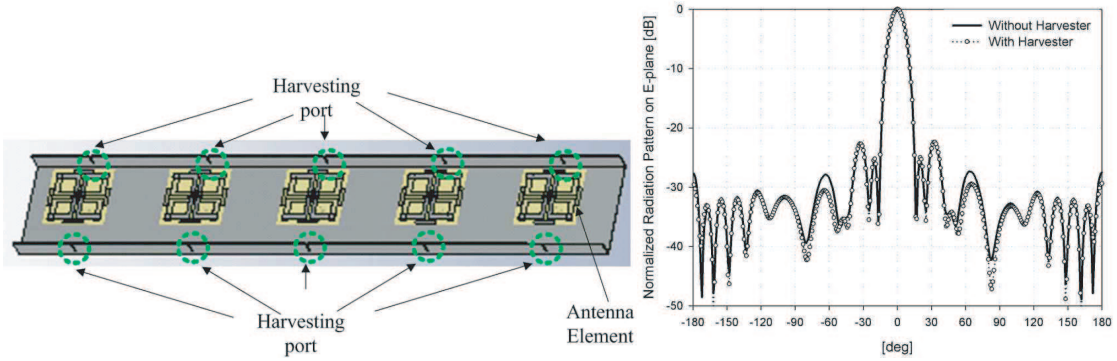

Figure 1: The proposed array antenna structure and its radiation patterns on E plane.

ACKNOWLEDGMENT

This research was funded by the MSIP (Ministry of Science, ICT & Future Planning), Korea in the ICT R&D Program 2013.

REFERENCES

1. Siu, L. and K.-M. Luk, "Unidirectional antenna with loaded dielectric substrate," *IEEE Antenna and Wireless Propagation Letters*, Vol. 7, 2008.

Design of Compact Passive Tag Antenna for Practical RFID Applications

Zihan Chen[1], **Sailing He**[1, 2], **Dongdi Zhu**[3], **and Chengcheng Du**[3]

[1]Department of Optical Engineering, Zhejiang University, Hangzhou 310027, China
[2]Department of Electromagnetic Engineering
School of Electrical Engineering, S-100 44 Stockholm, Sweden
[3]Department of Information Science & Electronic Engineering
Zhejiang University, Hangzhou 310027, China

Abstract— The communication quality between an RFID tag and a reader in a RFID network, especially the parameters of the passive tag antenna such as reading range, directivity and return loss, is affected by several factors from the environment. For practical RFID application, since the environment is complex and volatile, these factors include metallic surface of products, absorptions and impacts from neighbor tag antennas like scattering and mutual coupling. In this paper, it consists of the analysis of impacts caused by these factors and the design of passive tag antennas with resonant frequency 915 MHz able to be used in practical RFID applications against those impacts. Comparing with former ones, the proposed antenna reduces the size of the tag antenna to approximately commercial standard ($18\,\text{mm} \times 48\,\text{mm} \times 3\,\text{mm}$) by using certain structures applied in the unit cell of metamaterial or HIS, while the properties including directivity, return loss and input impedance are still appropriate for RFID applications. Simulation results from HFSS indicates that at 915 MHz, the return loss can be about -21 dB, as most of the power can be radiated into the space towards the receiver. Meanwhile, the input impedance $Z_0 = 9.4738 + j143.9189\,\Omega$, perfectly matching the impedance of the RFID chip placed on the top surface of the antenna. The above improved parameters play an important role in prolonging the reading range.

Statistical Characterization of Multiple Antennas Dynamic Body-to-body Radio Propagation Channel

H. A. Rahim[1], **F. Malek**[1], **V. Ganesan**[1], **K. K, Goh**[1], **F. A. A. Fuad**[1], **N. A. A. Talib**[2], **and F. S. Abdullah**[2]

[1]Embedded, Network and Advanced Computing Research Cluster (ENAC)
School of Computer and Communication Engineering, Universiti Malaysia Perlis
P. O. Box 77, d/a Pejabat Pos Besar, Kangar, Perlis 01000, Malaysia
[2]School of Electrical System Engineering, Universiti Malaysia Perlis
P. O. Box 77, d/a Pejabat Pos Besar, Kangar, Perlis 01000, Malaysia

Abstract— This paper presents the dynamic body-to-body diversity channel modeling of radio propagation channel in an indoor environment by utilizing quarter-wave planar textile monopole (TM) antennas at 2.45 GHz. The transmitting antenna is mounted on left chest of first human body. Two receiving antennas are placed in different locations; right chest and left upper arm (RC-LUA), left chest and left back (LC-LB) and right chest and right ankle (RC-RA). The diversity measurement systems use a Rohde & Schwarz signal generator (model SMBV100A) and an Agilent Network Analyzer (model PNA E8362B) to generate (transmit) continuous wave and measure (receive) the S_{21} parameters. During each measurement, two users are positioned at a 1 m distance where several body movements are performed, such as walking, running, bending and rotation of arms. For each location and measurement performed in the study, the S_{21} parameters are captured and statistically analyzed. Three combining techniques, maximal ratio combining (MRC), selection combining (SC) and equal gain combining (EGC) are applied. A statistical characterization of dynamic body-to-body diversity channels is derived. The results showed that log-normal distribution fits very well to the measured combined signal envelopes.

A Novel Idea of Evaluating Non-ionizing 2.45 GHz Wireless Body Area Network (WBAN) RF Radiation on Human Cognitive Performance Using Wearable Textile Monopole Antennas

H. A. Rahim[1], **F. Malek**[1], **P. J. Soh**[1], **F. A. A. Fuad**[1], **N. Hisham**[1], **N. A. A. Talib**[2], **and F. S. Abdullah**[2]

[1]Embedded, Network and Advanced Computing Research Cluster (ENAC)
School of Computer and Communication Engineering, Universiti Malaysia Perlis
P. O. Box 77, d/a Pejabat Pos Besar, Kangar, Perlis 01000, Malaysia
[2]School of Electrical System Engineering, Universiti Malaysia Perlis
P. O. Box 77, d/a Pejabat Pos Besar, Kangar, Perlis 01000, Malaysia

Abstract— This paper presents a very novel idea of evaluating the non-ionizing 2.45 GHz WBAN radio frequency electromagnetic fields exposure effect on human cognitive performance. The study aims at determining whether exposure of non-ionizing 2.45 GHz WBAN radio electromagnetic fields (EMF) may affect the cognitive performance of human being. Twenty healthy and right-handed volunteers (10 males and 10 females) are involved in the test and exposed to 2.45 GHz WBAN, emitted by a pair of planar textile monopole antennas in 1-hr per-session, with two separate sessions; EMF exposure and sham exposure (no exposure). Paired Associates Learning (PAL) task using CANTAB eclipse v4.0 cognitive software, is performed by each subject to assess the visual memory during the exposure of on-body textile monopole (TM) antennas positioned on right-upper-arm-to-left-chest link. The subjects are required to memorize specific patterns locations assigned by the task that are randomly placed in the allocated boxes, starting from 1 pattern to 8 patterns. Three trials are allowable if error is made. A total of two outcome measures are selected in measuring PAL which are PAL Total errors (adjusted), measuring the total number of errors across all assessed problem and all stages, with an adjustment for each stage not attempted due to previous failure) and PAL Mean errors to adjusted, measuring mean number of errors made before the stage is successfully completed. The result showed that both PAL outcome measures give no significant difference between exposure sessions (EMF and sham exposures), p's > 0.05. Thus, PAL performance (cognitive) is not affected by non-ionizing 2.45 GHz WBAN EMF exposure.

Fractal Etched Bow-tie Antenna Loading Zero-index Metamaterials

Kai Ma, Hui Feng Ma, Qiang Cheng, and Tie Jun Cui
State Key Laboratory of Millimeter Waves, Southeast University, Nanjing 210096, China

Abstract— Characterized by its wide impedance bandwidth and relatively stable radiation pattern, the bow-tie antenna has been widely utilized in the microwave as a suitable radiator. However, the comparatively limited radiation gain will constrain this type of antenna from more extensive applications when requiring high gain performance. In this paper, a bow-tie antenna etched with different types of fractal patterns is proposed, which can enlarge the current path for radiation thus minimize the overall dimensions of the radiator to further increase its impedance bandwidth. Moreover, for the sake of gain-enhancement, an artificial structure consisting of inhomogeneous and anisotropic zero-index metamaterials (ZIM) unit is carefully designed and adopted in the fractal pattern etched antenna. The ZIM structure processes a unique property that only one component of its permittivity or permeability tensor approaches to zero. This kind of metamaterials device featured by its zero-index is capable of transforming the conical or spherical wave front into near plane-wave front. Taking this advantage, we load the ZIM structure in the design of bow-tie antenna, which enhances the radiation gain. Each type of fractal pattern etched antenna loaded with ZIM is simulated using the commercial electromagnetic simulation software, CST Microwave Studio, and the simulated results are in good agreement to the analysis.

Validating Generalized Nonlocal Optics by First Principles Calculations

Pu Zhang, Martijn Wubs, and N. Asger Mortensen
DTU Fotonik, Department of Photonic Engineering, Technical University of Denmark, Denmark

Abstract— Recently hydrodynamic model of nonlocal optics has been generalized to include both convection and diffusion of electrons, allowing for complex parameter β. The comparatively simple model competes with much more sophisticated quantum models by predicting frequency shifts and spectrum broadening in transition from bonding dipolar to charge transfer modes. We validate the generalized nonlocal optics (GNO) by comparing with first principles calculations. With the nanoparticles of a dimer approximated by jellium model, a series of spectra of the dimer is calculated by time-dependent density functional theory (TDDFT), which serves as one of the most sophisticated theories innanoplasmonics. Since tunneling effect is not considered in GNO, to provide a fair comparison we also simulate the dimer with infinite barrier model (IBM) within TDDFT framework. Electrons spill-out and tunneling are thus completely suppressed by the infinitely high barrier outside jellium boundary. Electron density decays to zero at jellium boundary from inside, which is similar to the hard boundary of GNO. For both IBM and GNO, tunneling effect is excluded, and the spectra are greatly blue shifted. GNO turns out to predict qualitatively correct spectra when comparing with TDDFT, and agrees even better with TDDFT-IBM.

Inefficient tunneling effect in sub-nanometer gap between nanoparticles is an important assumption of GNO. In addition to spectrum, electron tunneling is also evaluated in TDDFT calculations. According to the spectrum, tunneling is clearly observable at 1 angstrom gap. The efficiency of tunneling is quantified by the number of electrons transferred in the plasmonic resonance. With jellium model charge transfer is found not dominating and justifies the assumption of GNO.

An Ultra-dense Optical Comb Based DWDM-OFDM-PON System

R. Lin[1], **M. Tang**[1], **R. Wang**[1], **Z. Feng**[1],
S. Fu[1], **D. Liu**[1], **J. Chen**[2], **and P. Shum**[3]

[1]Next Generation Internet Access National Engineering Lab (NGIA)
School of Optical and Electronic Information
Huazhong University of Science and Technology, Wuhan, China
[2]School of ICT, The Royal Institute of Technology (KTH), Kista, Sweden
[3]School of EEE, Nanyang Technological University, Singapore

Abstract— The bandwidth demand for end-to-end connectivity of broadband access services is expected to grow tremendous in the coming decades. To meet this requirement, dense wavelength multiplexing-passive optical network (DWDM-PON) has been widely investigated for high data rate services. On the other hand, due to its contribution in high spectrum efficiency, orthogonal frequency-division multiplexing (OFDM) is considered as a strong candidate for future access network. Although the spectrum efficiency would be enhanced dramatically, accounting of system cost and complexity, coherent OFDM (CO-OFDM) will be limited its application in long-haul communication but not the last kilometer access network. We proposed a DWDM-OFDM-PON scheme based on multi-wavelength COMB generation and experimentally demonstrated the feasibility of the downstream transmission. At the optical line terminal (OLT), an optical frequency comb generator (OFCG) is employed as the multi-wavelength optical source. 10 channels with 25 GHz spacing is provided at the transmitter, 2.5 GB/s DSB OFDM signal is uploaded into arbitrary waveform generator (AWG), and a Mach-Zehnder modulator is employed to convert the OFDM signal to DSB optical signal. The optical distribution network is emulated with 25.7 km single mode fiber (SMF) and a variable optical attenuator. At the receiver side, direct detection OFDM (DD-OFDM) scheme is utilized. The target channel is filtered by a tunable optical filter (TOF) and the OFDM signal is detected by a photo-diode before sampled by a real-time digital storage oscilloscope. The sampled OFDM signal is decoded and processed offline. In the wired link, error free OOK transmission has been realized. And power penalty is less than 0.5 dB for 2.5-GB/s OFDM-quadrature phase shift keying (QPSK) downlink. The proposed scheme can be applied to provide multiple independent services for the next generation optical access network.

Enhancing Plasmonic Photocatalytic Activity Using Silver Nanobeads

Jia Shiuan Wu, Wayne Yang, and Yuan-Fong Chau
Department of Electronic Engineering, Chien Hsin University of Science and Technology
No. 229, Jianxing Rd., Zhongli City, Taoyuan County 32097, Taiwan

Abstract— A novel plasmonic photocatalytic reactor which composed of silver nanobeads photodeposited onto a Titanium dioxide (TiO_2) thin film in a multilayer rotating-disk system has been numerically investigated using three-dimensional finite element method. Results show that the proposed structure can confine the field in a volume well below the diffraction limit and exhibit much higher photocalytic activity in a wide range of incident angle of light and broaden wavelength ranging in near-UV, visible and near-infrared that are not observed for the same case without the silver nanobeads on TiO_2 surface. The enhanced electric field region, intensity and peak wavelength resonance could be expanded as the inner permittivity filled inside the silver nanobeads and incident angle of light increased in the range of 30°.

ACKNOWLEDGMENT

This work was supported by Ministry of Science and Technology of the Republic of China (Taiwan) under Grant No. NSC 102-2112-M-231-001-.

Giant Enhancement of Nonreciprocity Using Hybrid Plasmonic-photonic Crystals

Kexin Liu[1], **Wei Jiang**[1], **and Sailing He**[1, 2]

[1]Centre for Optical and Electromagnetic Research
State Key Laboratory of Modern Optical Instrumentation, Zhejiang University, Hangzhou, China
[2]Division of Electromagnetic Theory, School of Electrical Engineering
Royal Institute of Technology, Stockholm S-100 44, Sweden

Abstract— Nonreciprocal propagation of light has been widely applied in many photonic systems such as isolators in optical fiber communication system. These nonreciprocal devices are indispensable for preventing unwanted reverse propagation of optical signals, but they are typically bulky due to the weak nonreciprocal effect of available magneto-optical materials. The growing research endeavor in integrated optics demands giant nonreciprocity.

Recently, the extensive research in plasmonics takes advantage of the coupling of light to charges like electrons in metals to enhance light-matter interaction by nanostructures that could localize light and alter the field distribution at sub-wavelength scale. In this work, we theoretically demonstrate a giant enhancement of the Kerr rotation in hybrid plasmonic-photonic crystals. The hybrid structure consists of plasmonic nanowire arrays on a magneto-optical thin film magnetized perpendicular to its plane and a one-dimensional photonic crystal as a substrate. We utilize three resonance mechanisms to enhance the magneto-optical effect in this structure. Firstly, the magneto-optical thin film produces TM-TE mode conversion and it enables the TE-mode waveguide resonance. Secondly, the plasmonic nanowire arrays enable the plasmon resonance for TM-polarized incident light, which hybridizes with the waveguide resonance. Thirdly, the one-dimensional photonic crystal plays as a total reflector in its band gap and makes the light bounce back and forth inside the film like a Fabry-Pérot resonator. Calculations, based on a rigorous coupled-wave analysis and a finite difference time domain method, demonstrate that in such structures above 10-time enhancement of the Kerr rotation could be achieved by making those resonances match with each other.

Magnetic Tuning Ferrite-dielectric Left-handed Material

Bai Du, **Jun Wang**, **Zhuo Xu**, **Song Xia**
Electronic Materials Research Laboratory, Key Laboratory of the Ministry of Education
International Center for Dielectric Research, Xi'an Jiaotong University, Xi'an 710049, China

Abstract— We chose ferrite and a special ceramic material to design an ferrite-dielectric LHM that could be tuned by magnetic bias. Lamellar ferrite and dielectric rods were used in the structure. In the X-band, the dielectric rods could provide a wide negative permittivity band and the dielectric produced negative effective permeability. The negative effective permeability frequency range could be tuned from 8.4 GHz to 11 GHz when the magnetic bias changed. The S parameters and the retrieved effective electromagnetic parameters showed a wide frequency tuning range of this ferrite-dielectric LHM.

Two Dimensional Polarization Independent All-dielectric Left-handed Metamaterial in Free Space

Jun Wang[1], **Shaobo Qu**[1], **Mingde Feng**[1], **Bai Du**[2], **and Zhuo Xu**[2]

[1]College of Science, Air Force Engineering University, Xi'an, Shaanxi 710051, China
[2]Electronic Materials Research Laboratory, Key Laboratory of the Ministry of Education
International Center for Dielectric Research, Xi'an Jiaotong University
Xi'an, Shaanxi 710049, China

Abstract— In this paper, we proposed a type of all-dielectric metamaterial (ADM) with quasi-continuous structure, which can inspire quasi-continuous electric and magnetic responses to acquire left-handed properties in free space. The proposed model utilizing dielectric rods and cubes as sub-wavelength inclusions. A two dimensional polarization independent left-handedness can be achieved with the frequencies at C band. The rods resonant under characteristic modes can generate negative permittivity and permeability, whereas the cubes are used in the non-resonant modes to assure the continuity of the displacement currents in dielectric inclusions. The simultaneously double negative properties can be interpreted by electric and magnetic fields distributions of the dielectric inclusions near 7.6 GHz under normal incidence with polarization angle 45°. The further study on transmission spectra and effective refractive indexes of the model with different polarization angles shows that the left-handed property is insensitive to different polarization angles due to the $\pi/2$ rotation symmetry of the ADM. The proposed ADM can be easily realized at infrared and optical frequencies with dielectric inclusions.

Compact SU8-silica Hybrid Thermo-optic Switch with Low Power Consumption

Wei Peng, **Pengxin Chen**, **and Yaocheng Shi**
Centre for Optical and Electromagnetic Research
State Key Laboratory of Modern Optical Instrumentation
Zhejiang University, Zijingang Campus, East Building No. 5, Hangzhou 310058, China

Abstract— We propose a novel MachCZehnder interferometer (MZI) type thermo-optic switch based on SU8-silica hybrid waveguide structures. The switch consists of a 1×2 power splitter, two transmission arms and a 2×1 power combiner. The input/output waveguides and the power splitter/combiner are realized by the conventional silica waveguides, while the two arms for the MZI consist of SU8 strip waveguides. Such hybrid SU8-Silica waveguide strucutures combines the advantages of the low propagation loss of the silica waveguides and the large thermo-optic coefficient of SU8. Due to the high thermo-optic coefficient of SU8, the length of the transmission arm can be dramatically reduced.

Controlled Growth of ZnO Nanorods via Coprecipitation Method with Application to Dye-sensitized Solar Cells

Ru Chen[1, 2], **Lei Miao**[1], **Haoliang Cheng**[1], **Chengyan Liu**[1], **and Hui Gu**[3]

[1]Key Laboratory of Renewable Energy
Guangzhou Institute of Energy Conversion, Chinese Academy of Sciences, Guangzhou 510640, China
[2]University of Chinese Academy of Sciences, Beijing 100049, China
[3]State Key Laboratory of High Performance Ceramics and Superfine Microstructure
Shanghai Institute of Ceramics, Chinese Academy of Sciences, Shanghai 200050, China

Abstract— As a new generation of solar cells, dye-sensitized solar cells (DSCs) have caused widespread concern in the scientific community. Photo-anode materials are decisive on the power conversion efficiency. As the best alternative photo-anode material of TiO_2, ZnO has a similar band gap with TiO_2, but smaller dielectric constant and faster electron mobility. In this paper, hexagonal prism-like ZnO nanorods were successfully prepared through coprecipitation method (followed by annealing). The effects of Al doping and annealing atmosphere on microstructure and optical properties of ZnO nanorods were systematically studied. X-ray diffraction results showed that the synthetic nanorods have a pure hexagonal wurtzite structure and good crystallinity. Field emission scanning electron microscope and transmission electron microscope experiments confirmed the rod morphology (hundreds of nanometers in diameter and several micrometers in length), single crystal and c-axis preference growth of ZnO nanomaterial. Energy Dispersive X-Ray Spectroscopy, Raman and UV-VIS-NIR spectra analysis indicated the successful substitutional doping of Al in the ZnO lattice. Diffuse reflectance at near-ultraviolet and visible wavelengths analysis indicated the suppression of the optical absorption for Al-doped ZnO compared to pristine ZnO, which may be related to the resistance to color center formation. The optimal optical properties Al-doped ZnO nanorods (high near-infrared absorption and no formation of the yellow coloration) are reached by combining H_2 atmosphere annealing with Al doping. Finally, the ITO glass coated with suspension of ZnO nanorods was used as photo-anodes for evaluating the DSCs performance. Compared with pure ZnO nanorods, Al-doped ZnO nanorods calcined with H2 atmosphere show higher dye adsorption ratio and conversion efficiency.

Optical Transmission through Ultrathin Metal Films with Sub-wavelength Hole Arrays: Experiments and Simulations

Shanshan Wu[1], **Jinfeng Zhu**[1], **Jiaye Li**[1], **Yanqiang Bai**[1], **and Qinghuo Liu**[2]

[1]Institute of Electromagnetics and Acoustics, Xiamen University, Xiamen, China
[2]Department of Electrical and Computer Engineering, Duke University, Durham, NC 27708, USA

Abstract— Metallic films are intensively studied as an alternative to indium tin oxide (ITO) used in optoelectronic devices and organic solar cells, in view of the limited reserves of indium and brittleness of ITO. Since the extraordinary optical transmission through sub-wavelength hole arrays was proposed, the research work has been focused on relatively thick metallic films, while ultrathin films are neglected. In this paper, the optical transmission through hexagonal arrays of sub-wavelength holes in ultrathin gold films is studied experimentally and theoretically. In experiments, the nanostructured gold films are fabricated using nanosphere lithography, reactive ion etching and electron beam evaporation technique. We prepare five kinds of gold ultrathin films with various sub-wavelength hole diameters, a constant periodicity of 530 nm and the same film thickness of 20 nm. Both optical transmission and reflection are measured using a UV-visible-NIR spectrometer (300 nm–2000 nm). Scanning electronic microscopy is used to characterize the surface morphology of the films and the size distribution of the hole arrays. The exact thickness of the gold film is measured using an atomic force microscope. To estimate the transmission efficiency of the optical absorber, we perform numerical computations using a finite different time-domain method and a spectral element method. The results from both measurement and simulation demonstrated significant coherency, which proved the rationalization of the design. One can observe that the resonant absorption wavelength can be altered over a broad spectral range by changing the diameter of the hole. As etching time increases, the holes'diameter deceases, and the transmission valleys induced by surface plasmon resonance are red shifted. The nanostructured ultrathin films can be designed to demonstrate novel photoelectric properties and promise many potential applications.

Study of an Agar Medium Using Terahertz Chemical Microscope

Akihiro Nakamura, Hiroyuki Nino, Kenji Sakai, Toshihiko Kiwa, and Keiji Tsukada
Graduate School of Natural Science and Technology, Okayama University
3-1-1 Tsushima-naka, Kita-ku, Okayama-Shi, Okayama Prefecture 700-8530, Japan

Abstract— Study of living cells is one of the key targets to understanding disease, and diverse types of methods has been proposed and developed.

On the other hand, Terahertz (THz) wave has been attracted by a lot of researchers since THz waves has a plenty of information on the bio-related materials such as inter-molecules reactions. However, there is strong water absorption in the THz region, so that few researches success in measuring living cells.

In our group, a THz chemical microscope (TCM) has been proposed and developed in order detect the bio-related materials in the water solutions using THz technology. The TCM generally detects the electric and/or chemical potential distributions on the sensing plate. Here, the prototype TCM is introduced in detail and the detection of the agar media, which is generally used for the cell cultivation, is demonstrated.

Metallohalide Perovskite-polymer Composite Film for Hybrid Planar Heterojunction Solar Cells

Hin-Lap Yip
South China University of Technology, Guangzhou, China

Abstract— Polymer with tailored chemical functionality was introduced as a processing additive to control the film formation kinetic of $CH_3NH_3PbI_3$ perovskite structure, leading to enhanced photovoltaic performance in a PEDOT : PSS/perovskite/PCBM-based planar heterojunction solar cell. By adjusting the polymer doping content, the grain size, film coverage and also the bandgap of the perovskite films can be effectively tuned. At optimized conditions, the planar heterojunction solar cell composed of a thin layer of perovskite film (∼50 nm) exhibits a PCE 6.35% with a V_{oc} of 1.07 V, a J_{sc} of 8.95 mA/cm^2 and a FF of 0.66, which are much higher than those of the control device with pristine perovskite film (PCE = 2.47%). The higher performance was attributed to the improved coverage of the perovskite film, which reduced the undesired contact between PEDOT : PSS and PCBM and minimized the shunting paths in the device. In addition, since the fabrication process for the perovskite solar cells can be proceeded at low temperature, flexible cells built on plastic substrate can therefore be realized with a PCE of 4.35%.

Typical Activation but Atypical Connectivity in Prefrontal Cortex of Children with Autism Spectrum Disorder under Rehabilitation during Joint Attention: A fNIRS Study

Jun Li[1], **Huilin Zhu**[1, 2], **Huan Guo**[2], **Heyon Shen**[2], **Lan Gao**[2], **Ziqiang Hu**[1, 2], **Qianqian Gao**[1, 2], **and Sailing He**[1]

[1]Centre for Optical and Electromagnetic Research
ZJU-SCNU Joint Research Center of Photonics
South China Normal University (SCNU), Guangzhou 510006, China
[2]School of Psychology, South China Normal University (SCNU), Guangzhou 510631, China

Abstract— Autism spectrum disorder (ASD) is a neuro-developmental disorder, characterized by delays or abnormal functioning of brain. Joint attention occurs when individual shares his/her attention with others by the means of language, gestures, or eye sights, which includes both initiating behavior and responding to the third. Typical developing (TD) infants develop the ability of joint attention at the stage of 8–15 months, and the establishment of joint attention will play an important role as the foundation for the babies' later language acquisition, mother-infant relationship and social skills. Joint attention is proved to be one of the main defects of infant or children with ASD, and thus joint attention skills are usually the compulsory training in the invention and rehabilitation of ASD children. In this study, functional near infrared spectroscopy (fNIRS) was used to study the pattern of activation and connectivity of brain during joint attention, with ASD children under rehabilitation and TD children. A joint/non-joint attention paradigm was adopted to detect the effect of the social information (gaze) on the executive functional area (including the superior frontal gyrus and the middle frontal gyrus) of the brain. Results showed that children with ASD who was enrolled in the rehabilitation since 3–6 years old could show the same pattern and strength of activation in the left middle frontal gyrus as TD children when performing some joint attention task, which indicated that the brain of those children with ASD actually could response to social information (gaze). However, children with ASD showed reduced connectivity between the left middle frontal gyrus and other brain regions in executive function area. This study supported the feasibility of using the fNIRS to assess atypical development of brain of ASD and its potential application to evaluate the effect of rehabilitation on the brain of patients with ASD.

Highly Integrated Microfluidic Chip for Immunoassays Based on Phase-sensitive Surface Plasmon Resonance Biosensing

Li Jiang, Gaoao Ye, and Sailing He
Centre for Optical and Electromagnetic Research
Zhejiang Provincial Key Laboratory for Sensing Technologies
JORCEP, Zhejiang University, Zijingang Campus, Hangzhou 310058, China

Abstract— We have designed and fabricated a novel highly integrated microfluidic chip for the phase-sensitive surface plasmon resonance biosensor which can be used to detect antibody-antigen recognition and binding events with high sensitivity. Our microfluidic chip in an area of $25.4 \times 25.4\,\mathrm{mm}^2$ contains three layers, including the gold sensing layer, the PDMS flow layer and the PDMS control layer. The bottom layer is the gold sensing layer integrated with 240 gold spots which can be functionalized with biomolecules for various immunoassays based on surface plasmon resonance sensing. Each gold spot is the sensing area where the incident light can couple with the surface plasmon wave, which contributes to changing the phase of the reflected light. The middle layer is the PDMS flow layer containing one inlet flow channel, one outlet flow channel, 10 main flow channels and 60 minor flow channels, which can deliver biological reagent to the gold spot. The upper layer is the PDMS control layer composed of 5 main microvalves and 8 minor microvalves, which are used to open or close the flow channels beneath. One channel can be individually selected to work while other channels are closed when applying pressure to 2 main microvalves and 4 minor microvalves. Sixty different samples can be detected simultaneously on the microfluidic chip. This microfluidic chip offers three main advantages: (1) 240 gold spots are highly integrated and 60 different samples can be detect simultaneously; (2) reaction time and sample consumption can be drastically reduced because of low volume; and (3) utilize the logic gate to control only one channel opening at a time.

Tungsten Selective Emitter Based on Core-shell Nanospheres

Lei Mo[1, 2], **Liu Yang**[1], **and Sailing He**[1]

[1]Centre for Optical and Electromagnetic Research, Zhejiang University, Hangzhou 301158, China
[2]Department of Physics, Zhejiang University, Hangzhou 301158, China

Abstract— For a typical photovoltaic (PV) solar cell, the power conversion efficiency is limited by the Shockley-Queisser (SQ) limit. Solar photons with their energies below the bandgap of the semiconductor cannot be absorbed or be converted into electricity either; while solar photons with their energies above the bandgap will likely lose their energies through thermalization due to the fast relaxation process. To overcome the SQ limit, solar thermo-photovoltaics (STPVs) were proposed, where, a selective absorber and selective emitter pair is inserted in front of a photovoltaic (PV) cell, serving the purpose of absorbing the broad solar radiation and generating heat (selective absorber) and thermally emitting the bandgap photons via conducted heat (selective emitter). Selective emitter plays an important role in narrowing the radiation spectrum so as for the narrow-band radiation to be fully absorbed and efficiently converted by the back PV cell. Therefore, it is vital to have a sharp emittance drop at the cut-off wavelength (corresponding to the semiconductor bandgap), below which very high emittance must be maintained.

In this presentation, we demonstrate a novel 3-dimensional tungsten selective emitter based on a core-shell nano-sphere structure. A new spectral efficiency is defined to effectively evaluate our selective emitters, considering both the emission suppression of the sub-bandgap photons and the emission enhancement of the above-bandgap photons. Based on this parameter, we achieved an optimized broadband selective emitter with a high spectral efficiency, whose emittance is high covering the wavelength range shorter than cut-off wavelength and owning sharp cut-off property around cut-off wavelength. It is very promising to be used in a high-efficiency planar STPV system.

Solution-grown Organic Single-crystalline p-n Junctions with Ambipolar Transport

Congcheng Fan, Hongzheng Chen, and Hanying Li
State Key Laboratory of Silicon Materials
MOE Key Laboratory of Macromolecular Synthesis and Functionalization
Department of Polymer Science and Engineering, Zhejiang University, Hangzhou, Zhejiang 310027, China

Abstract— Single crystals of organic semiconductors have the highest degree of order and purity, exhibiting superior electronic performance such as high charge carrier mobility among organic semiconductors. Typically, high-performance single-crystal electronic devices consist of one type of crystal, favoring either hole or electron transport. Devices composed of both hole and electron transporting single-crystals, such as single-crystalline p-n junctions, are expected to show ambipolar charge transport that is desirable for complementary circuits, organic light emitting diodes, and organic solar cells. However, it is challenging to prepare organic single-crystalline p-n junctions on which there are only a few reports. Here we demonstrate the growth of single-crystalline p-n junctions in a single step from a mixed solution of 2,7-dioctyl[1]benzothieno[3,2-b][1]benzothiophene (C8-BTBT) (p-type) and C_{60} (n-type), using the droplet-pinned crystallization (DPC) method previously reported. The single crystallinity of the p-n junction was confirmed by selected area electron diffraction with a single set of spot patterns for both components of the junction respectively. Field-effect transistors based on the junctions showed ambipolar charge transport characteristics, with the most balanced performance of $0.16\,cm^2V^{-1}s^{-1}$ for hole mobility and $0.17\,cm^2V^{-1}s^{-1}$ for electron mobility that are among the highest reported mobility of single-crystal-based ambipolar organic transistors. This work provides a new platform to study organic single-crystalline p-n junctions.

Study on Accuracy and Efficiency of the Numerical Algorithm for Electromagnetic Scattering from Targets and Rough Surface

Yu Liang[1], **Li-Xin Guo**[2], **Xiang-Hua Zeng**[1], **Jing-Guo Hu**[1], **and Zhen-Sen Wu**[2]

[1]College of Physics Science and Technology, Yangzhou University, Yangzhou, Jiangsu, China
[2]School of Physics and Optoelectronic Engineering, Xidian University, Xi'an, Shaanxi, China

Abstract— Some studies about the accuracy and efficiency of the Propagation-Inside-Layer-Expansion (PILE) combined with the (Generalized) Forward-Backward Method ((G) FBM) hybrid scheme for electromagnetic scattering from targets and rough surface are carried out. Many types of rough surface and targets are aimed at, such as, the Gaussian, exponential, and PM spectrum rough surface, and the simple cylinder-like, the complex missile-like targets, etc.. Many of rough surface and target parameters, for examples, the correlation length, the RMS height, the permittivity, the rough surface/target size, etc., are involved. The Relative Residual Error (RRE), that is set as the important evaluation criterion of algorithm accuracy is evaluated. The computational complexity and CPU time, which have been seemed as two key criterions for evaluation of algorithm efficiency are investigated. The numerical results demonstrate that, for different rough surface and multiply targets with multi-parameters cases, only needing a few iteration orders, the aformentioned Propagation-Inside-Layer-Expansion (PILE) combined with the (Generalized) Forward-Backward Method ((G) FBM) hybrid algorithm can reach enough accuracy, meanwhile, it can also improve the computational efficiency, compared with some classical numerical methods.

ACKNOWLEDGMENT

This work was supported by the National Natural Science Foundation of China (Grant No. 1134718 2), by the University Science Research Project of Jiangsu Province (Grant No. 13KJB140020), by the National Natural Science Foundation for Distinguished Young Scholars of China (Grant No. 61225002) and by the Science Foundation of Yangzhou University (Grant No. 2012CXJ009). The authors would like to thank the reviewers for their helpful and constructive suggestions.

REFERENCES

1. Tsang, L. and J. A. Kong, *Scattering of Electromagnetic Waves-numerical Simulations*, 114–176, Wiley, New York, 2000.
2. Liu, Q. H., L. Jiang, and W. C. Chew, "Large-scale electromagnetic computation for modeling and applications," *Proc. IEEE*, Vol. 101, No. 2, 223–226, 2013.
3. Jandhyala, V., E. Michielssen, S. Balasubramaniam, and W. C. Chew, "A combined steepest descent-fast multipole algorithm for the fast analysis of three-dimensional scattering by rough surfaces," *IEEE Trans. Geosci. Remote Sens.*, Vol. 36, No. 3, 738–748, 1998.
4. Liang, Y., L. X. Guo, and Z. S. Wu, "The fast EPILE combined with FBM for electromagnetic scattering from dielectric targets above and below the dielectric rough surface," *IEEE Trans. on Geosci. Remote Sens.*, Vol. 49, No. 10, 3892–3905, 2011.
5. Liang, Y., L. X. Guo, and Z. S. Wu, "The EPILE combined with the generalized-FBM for analyzing the scattering from targets above and on a rough surface," *IEEE Antennas Wireless Propag. Lett.*, Vol. 9, 809–813, 2010.

Application of S-UTD-CH Model into Multiple Diffraction Scenarios at 900 MHz

Mehmet Baris Tabakcioglu[1] and Doruk Ayberkin[2]

[1]Electrical and Electronics Engineering Department, Engineering Faculty
Bayburt University, Bayburt 69000, Turkey
[2]Computer Programming Department, Bayburt Vocational School
Bayburt University, Bayburt 69000, Turkey

Abstract— In this study, propagation prediction models based on ray tracing in coverage estimation for broadcasting systems are compared with respect to computation time and accuracy. Uniform Theory of Diffraction (UTD), Slope Diffraction (S-UTD) and Slope UTD with Convex Hull (S-UTD-CH) models are compared for computation time and propagation path loss. Moreover in this study, effects of transmitter height to relative path loss at the receiver are analyzed. S-UTD-CH model is optimum model with respect to computation time and relative path loss.

Analysis of Changing of Building Parameters via S-UTD-CH Model in Multiple Diffractions

Mehmet Baris Tabakcioglu[1] and Doruk Ayberkin[2]

[1]Electrical and Electronics Engineering Department
Engineering Faculty, Bayburt University, Turkey
[2]Computer Programming Department
Bayburt Vocational School, Bayburt University, Turkey

Abstract— To make more efficient and more reliable digital terrestrial broadcasting system a lot of electromagnetic wave propagation model has been introduced. Some of these models are numerical and so computation complexity and computation time is large. In addition to this accuracy of predicted electric field strength is high. The other introduced models are ray tracing based models and computation time, complexity and accuracy of predicted field is less than numerical ones. There is a trade-off between accuracy and computation time. S-UTD-CH model, ray tracing based, is optimal with respect to computation time and accuracy of predicted field [1–5]. Relative permittivity constant of obstacles affects the relative path loss at the receiver [6, 7]. Thanks to UHF, buildings and hills can be modeled as knife edge and wedge, respectively [8]. Types of structure of obstacles and inner angle of wedge affect the relative path loss, too. Moreover polarization types (vertical or horizontal) affects path loss. In this study, how inner angle, structure type and relative permittivity constant of obstacle and polarization type of electromagnetic wave change the relative path loss at the receiver is discussed.

ACKNOWLEDGMENT

This work partially supported by Bayburt University Scientific Research Support Unit under grant 2013-1/14.

REFERENCES

1. Tabakcioglu, M. B. and A. Kara, "Comparison of improved slope UTD method with UTD based methods and physical optic solution for multiple building diffractions," *Electromagnetics*, Vol. 29, No. 4, 303–320, 2009.
2. Tabakcioglu, M. B. and A. Kara, "Improvements on slope diffraction for multiple wedges," *Electromagnetics*, Vol. 30, No. 3, 285–296, 2010.
3. Tabakcioglu, M. B. and A. Cansiz, "Application of S-UTD-CH model into multiple diffraction scenarios," *International Journal of Antennas and Propagation*, Paper ID:285304, 2013.
4. Tabakcioglu, M. B. and A. Kara, "On the improvements in the multiple edge transition zone diffraction," *EuCAP'2007*, 2007.
5. Tabakcioglu, M. B., D. Ayberkin, and A. Cansiz, "Comparison and analyzing propagation models," *Asia-Pasific Conference on Antennas and Propagation*, Singapore, 2012.
6. Luebbers, R. J., "A general, uniform double wedge diffraction coefficient," *IEEE Trans. Antenna Propagation*, Vol. 39, No. 1, 8–14, 1991.
7. Tajvidy, A. and A. Ghorbani, "A new uniform theory-of-diffraction-based model for the multiple building diffraction of spherical waves in microcell environments," *Electromagnetics*, Vol. 28, No. 5, 375–387, 2007.
8. Andersen, J. B., "UTD multiple-edge transition zone diffraction," *IEEE Trans. Antennas and Prop.*, Vol. 45, 1093–1097, 1997.

Broadband Analysis and Characterization of Noise for In-door Power-line Communication Channels

M. Mosalaosi and Thomas J. O. Afullo
Department of Electrical, Electronic and Computer Engineering
University of KwaZulu-Natal, Private Bag X54001, Durban 4001, South Africa

Abstract— Powerline communication (PLC) has emerged as an alternative solution for connectivity at home and offices in recent times [1]. Its development for multimedia broadband applications thus requires an extensive knowledge of the major peculiarities which influences communication over this channel. PLC channels are susceptible to noise inherent in power networks, leading to performance degradation. In this work, we have set-up a measurement system designed to capture the noise both in frequency and time domain for real power networks. The main observable components of the indoor PLC noise are: background noise, impulsive noise, and narrowband interferences. The impulsive components of PLC noise are observed to be time variant, random in nature, have high power spectral density (PSD) and lasts for very small time durations. A greater portion of the impulsive noise has cyclostationary behaviour, though with different amplitudes and widths. The repetition rates of these impulses are synchronous with the mains harmonics of 50 Hz and 100 Hz, the supply frequency in Africa. Others have irregular occurrences and much higher repetition rates; hence they are unpredictable in nature. This noise is referred to as asynchronous impulsive noise [2].

These noise terms are key design parameters for modulation schemes in broadband PLC, popularly orthogonal frequency division multiplexing (OFDM), with its conventional receivers assuming additive white Gaussian noise (AWGN) [3]. The time variability of PLC noise is presented alongside its statistical analysis based on a series of measurements performed on numerous power-line scenarios. The relevance of this time variance is evaluated in actual channels. The significant difference in amplitudes of the impulsive noise is taken into account by modelling its statistical variation. The PSD for both the background and impulsive noise is presented. Finally, we present the results of the noise PSD captured with a parametric model and compare our results with findings from other parts of the world.

REFERENCES

1. Al Mawali, K. S., "Techniques for broadband power line communications: Impulse noise mitigation and adaptive modulation," Doctoral Thesis, RMIT University, Jul. 2011.
2. Cortes, J. A., L. Diez, F. J. Canete, and J. J. Sanchez-Matinez, "Analysis of the indoor broadband power-line noise scenario," *IEEE Transections on Electromagnetic Compatibility*, Vol. 52, No. 4, Nov. 2010.
3. Lin, J. and B. L. Evans, "Cyclostationary noise mitigation in narrowband powerline communications," *Proc. APSIPA Annual Summit and Conference*, Dec. 2012.

Design of All-fiber Coupled Electro-optic Sensors for High Power Microwave

Lili Song, Juntao He, Junpu Ling, Tao Jiang, and Danni Zhu
College of Optoelectronic Science and Engineering
National University of Defense Technology, Changsha, Hunan 410073, China

Abstract— A novel design of all-fiber coupled Electro-Optic (EO) sensors is introduced. Special fiber apparatus is used instead of free-space-coupling using bulk optics such as conventional lenses.

Due to different configurations and species of crystals, EO sensors often work as amplitude modulators, phase modulators or polarization state modulators. It's apparent that the design and optimization of EO sensors are crucial to achieving high-quality microwave sensing. Fabry-Perot (F-P) cavity is efficient to improve the sensitivity, fortunately, without reduction of the spatial resolution as the volume of the crystal does not increase. This paper displays detailed analysis and design progress of an F-P cavity based EO sensor with the application of $LiTaO_3$ crystal.

The reflectance dependence on some parameters of the sensor is analyzed, such as the incident angle, the thickness of the crystal, the space between collimator and crystal, the under tested E-field, etc.. According to the analysis, the exact thickness of $LiTaO_3$ crystal is calculated when attached to the collimator, which can make the reflectance and sensitivity to maximum. Based on the analysis using $LiTaO_3$ as the EO crystal, total reflectance appears when the incident angle is close to $43.34°$. Reflectance can get the maximum value when $h = 365.8076k_1$, $k_1 = 1, 2, 3 \ldots$ when the crystal is attached to the collimator. The sensitivity can be maximal when $h = 0.1227 + 0.3658k_2$ (μm), $k_2 = 1, 2, 3 \ldots$ in the same structure.

Investigation of Novel Waveguide Phase Shifters for High Power Applications

Yiming Yang, **Chengwei Yuan**, **Qiang Zhang**, **Danni Zhu**, **Shengren Peng**, **and Longzhou Yu**
College of Optoelectronic Science and Engineering
National University of Defense Technology, Changsha 410073, China

Abstract— High-power phase shifter that can on-line adjust the transmit phase of high-power microwave (HPM) is of great interest. It has an extensive application in mode converter, high power array antenna and other fields. However, the traditional phase shifters can not satisfy the power capacity requirement. There is a pressing need to come up with new alternative phase shifters. In this paper, three kinds of waveguide phase shifters are investigated. To increase the power capacity, no dielectric is introduced, and they are all mechanical phase shifters. The first one named waveguide-inserting-fin phase shifter. The inserting-fin changes the transmission constant of the microwave. 360 degree phase shift can be obtained by adjusting the length of the inserting metal fin. The advantage of this phase shifter is that the microwave propagation keeps on the same direction but with longer longitudinal length. The second one named narrow side slot-waveguide phase shifter. It is designed based on 3 dB power divider of waveguide Slot Bridge. The difference is using adjustable metal choke piston at the terminal position of the power divider. Then, it can realize 360 degree phase shift by adjusting the choke piston position. The last one named folded rectangular waveguide phase shifter. It includes E-bend phase shifter and H-bend phase shifter. The output phase is changed by adjusting the position of the bend waveguide. The advantage of this phase shifter is that it can achieve 360 phase degree with smaller size. All the phase shifters are with high transmission efficiency over 99% and high power capacity over 300 MW in the vacuum.

Compact Microstrip Patch Antenna with Parasitic Loading for X & Ku Band Applications

Mohit Barthwal[1], **Sohaib Abbas Zaidi**[1], **M. R. Tripathy**[1], **and S. S. Pattnaik**[2]

[1]Department of ECE, Amity University, Noida, India
[2]ETV Department, National Institute of Technical Teachers Training and Research, Chandigarh, India

Abstract— Microstrip patch antennas are becoming popular day by day because of the various advantage offered by them such as low cost, less weight, low profile and ease of fabrication [1]. Popularity of patch antenna can be known from the fact that they found their application in various fields like aircraft, space technology [2, 3], mobile communication, biomedical, broadcasting etc.. However narrow bandwidth of patch antenna is one of the major limitation, that researcher around the world have been trying to overcome. Many techniques have been suggested in the past in order to overcome this problem [4]. One such technique is employed in this paper in which parasitic elements are used along with driven patch excited with the help of coax feed for X & Ku band. An equivalent circuit of the proposed antenna is also developed and analyzed. The antenna is designed on FR4 substrate with permittivity 4.4 and having dimension of ground plane $17 \times 19\,\text{mm}^2$. The patch has a dimension of $6 \times 6\,\text{mm}^2$ which is loaded with parasitic elements. The proposed antenna is able to achieve impedance bandwidth of 1.8 GHz from 10.8 GHz to 12.6 GHz thus, covering Ku band as well and has a maximum gain of 3.9 dBi. Comparison between simulated and fabricated results would be presented. The return loss, electric field distribution, radiation pattern of the proposed antenna is presented in this paper. All simulations are done by using HFSS software.

REFERENCES

1. Garg, R., P. Bhartia, I. Bahl, and A. Ittipiboon, *Microstrip Antenna Design Handbook*, Artech House Inc., 2001.
2. Bugaj, M., R. Przesmycki, L. Nowosielski, and K. Piwowarczyk, "Active microstrip antennas operating in X band," *PIERS Online*, Vol. 7, No. 3, 221–225, 2011.
3. Motin, M. A., et al., "Design and simulation of a low cost three band microstrip patch antenna for the X-band, Ku-band and K-band applications," *7th International Conference on Electrical and Computer Engineering*, 397–400, Dec. 20–22, 2012.
4. Fernández González, J. M., P. Padilla, G. Expósito-Domínguez, and M. Sierra-Castañer, "Lightweight portable planar slot array antenna for satellite communications in X-band," *IEEE Antennas and Wireless Propagation Letters*, Vol. 10, 1409–1412, 2011.
5. Joshi, J. G., S. S. Pattnaik, and S. Devi, "Geo-textile based metamaterial loaded wearable microstrip patch antenna," *International Journal of Microwave and Optical Technology*, Vol. 8, No. 1, Jan. 2013.

Accurate Numerical Solutions for Electromagnetic Scattering by Strongly Anisotropic Structures

G. Z. Yin, Y. Q. Zhang, Z. G. Zhou, J. X. Hong, and M. S. Tong
Department of Electronic Science and Technology, Tongji University, Shanghai, China

Abstract— Electromagnetic (EM) analysis for anisotropic structures relies on the accurate solution of volume integral equations (VIEs) in the integral equation approach. Traditionally, the VIEs are solved by the method of moments (MoM) with the divergence-conforming Schaubert-Wilton-Glisson (SWG) basis function or curl-conforming edge basis function. These basis functions are defined over a pair of tetrahedral elements with a common face or common edge and require conforming meshes in geometric discretization, resulting in a higher preprocessing cost. Also, the basis functions have to assume a homogeneous material in each tetrahedron and disregard the possible directional difference of material, so they may not be suitable for highly anisotropic materials. In this work, we present a point-matching method which may be more appropriate to solve such problems because of its different features. The method uses a collocation procedure to transform integral equations into matrix equations and possesses several merits, i.e., the simple mechanism of implementation, use of nonconforming meshes, and removal of basis and testing functions. The method represents unknown functions at discrete points with directional components and usually includes more degrees of freedoms than the MoM. Furthermore, the method allows the use of JM-formulation which does not explicitly include material property in the integral kernels in the VIEs. These characteristics indicate that it is very suitable for solving anisotropic problems and also very friendly to the incorporation of fast algorithms like multilevel fast multipole algorithm (MLFMA). Although the method has to handle the hypersingular kernels resulting from the dyadic Green's function, the robust treatment techniques developed in recent years make it become a good alternative to the MoM, especially for highly anisotropic problems. A typical numerical example is presented to demonstrate the method and good performance can be observed.

Aharonov-Bohm Effect, Poincaré Lemma and Gauge Invariance

Peter A. Meleshenko[1, 2], **Hang T. T. Nguyen**[3], **Mikhail E. Semenov**[1, 2, 4], **and Alexander F. Klinskikh**[2]

[1]Zhukovsky-Gagarin Air Force Academy, Russia
[2]Voronezh State University, Russia
[3]Institute of Technology, Vietnam National University — Ho Chi Minh City, Vietnam
[4]Voronezh State University of Architecture and Civil Engineering, Russia

Abstract— The Aharonov-Bohm (AB) effect [1] is of more than fifty years history and remains relevant even in the present days (see, e.g., [2–5] and related references). Main object in the AB effect is an infinitely thin solenoid with the finite magnetic flux (AB flux). While the force field is absent the vector potential of the magnetic field confined in the solenoid is non-zero and can produce observable effects because the relative phase of the electron wave function depends on the AB flux. In other words, the AB flux affects the quantum state of an electron. Such an affection leads eventually to the observable effects.

As is known, there is a close "relationship" between the AB effect and the topology of the two-dimensional space (see, e.g., [6]). One of the most important result in this field is the Poincaré lemma which claims that on a contractible manifold, all closed forms are exact. We show by straightforward calculations (these calculations are based on the theory of generalized functions [7]) that in the presence of the AB effect the Poincaré lemma violates (more general, the Poincaré lemma can not be applied to the AB problem due to the fact that the space is not simply-connected). The obtained results allow us to "reformulate" the definition of the gauge invariance, namely:

$$\mathbf{A} \to \mathbf{A} + \nabla f, \quad \varphi \to \varphi - \frac{\partial f}{\partial t},$$

where f is an arbitrary ***single-valued*** function of the spatial coordinates and time.

Our consideration is based on a simple example. Let us consider the vector potential of the uniform magnetic field $\mathbf{A}_H$ and AB vector potential $\mathbf{A}_{AB}$:

$$\mathbf{A}_H = \frac{Hr}{2}\mathbf{e}_\theta = \frac{\Phi_H}{2\pi r}\mathbf{e}_\theta, \quad \mathbf{A}_{AB} = \frac{\Phi_{AB}}{2\pi r}\mathbf{e}_\theta,$$

where $\Phi_H = \pi r^2 H$ is the magnetic flux through the area of a ring with radius r, and Φ_{AB} is the AB flux. Formally, $\mathbf{A}_H$ and $\mathbf{A}_{AB}$ look similar. So, we can pose the following question: Does the gauge transformation (non-singular) which connects $\mathbf{A}_{AB}$ and $\mathbf{A}_H$ exist? The answer is: no, it does not. In our calculations we use the following expression for the derivative of the homogeneous functions with the homogeneity parameter $\lambda = -n+1 = -1$ (here $n = 2$ is a space dimension of the AB system) [7]:

$$\frac{\partial f}{\partial x_i} = \left(\frac{\partial f}{\partial x_i}\right)\Big|_G + (-1)^{i-1}\delta\left(x_1, x_2, \ldots, x_n\right) \times \int_\Gamma f\, dx_1 dx_2 \ldots dx_{i-1} dx_{i+1} \ldots dx_n.$$

REFERENCES

1. Aharonov, Y. and D. Bohm, "Significance of electromagnetic potentials in the quantum theory," *Phys. Rev.*, Vol. 115, 485–491, 1959.
2. Berry, M. V., "Asymptotics of the many-whirls representation for Aharonov-Bohm scattering," *J. Phys. A: Math. Theor.*, Vol. 43, 354002, 2010.
3. Kaufherr, T. and Y. Aharonov, "Nonlocal quantum dynamics of the Aharonov-Bohm effect," *J. Phys. A: Math. Theor.*, Vol. 43, 354012, 2010.
4. Klinskikh, A. F., P. A. Meleshenko, et al., "Radiative attenuation of the electron in the Aharonov-Bohm effect," *Nuovo Ciment. B*, Vol. 125, 1161–1171, 2010.
5. Meleshenko, P. A., H. T. T. Nguyen, and A. F. Klinskikh, "Spectroscopic peculiarities in a 2D Coulomb potential under Aharonov-Bohm effect," *Eur. Phys. J. D*, Vol. 67, 209, 2013.
6. Evans, M. W., "Physical optics, the sagnac effect, and the Aharonov-Bohm effect in the evans unified field theory," *Found. Phys. Lett.*, Vol. 17, 301–322, 2004.
7. Gel'fand, I. M. and G. E. Shilov, *Generalized Functions: Properties and Operations*, Academic Press, New York, 1964.

Analysis of Arrangement Structure for Metal Fiber in Blended Electromagnetic Shielding Fabric

Zhe Liu, **Xing Rong**, **Qianxue Zheng**, **Ruili Sun**, **Yuna Chen**, **and Xiuchen Wang**
Zhongyuan University of Technology, China

Abstract— In order to study shielding characteristics of electromagnetic shielding fabric, a method based on computer image analysis is proposed to build an arrangement model of metal fiber. At firstly, some important parameters about shielding effect are summarized, and then a new algorithm based on threshold segmentation for fabric texture extracting is putted forward. By ascertaining an optimization threshold, the fabric image is divided and a feature cluster gray image is established. Furthermore, the feature matrix of metal fiber comprising only two gray values which are threshold value and feature value is founded by using normalized method. At last, calculation formulas about metal fiber content per unit area and equivalent thickness are established and the arrangement model of metal fiber is built. Experiments and analysis show that the method given in this paper is able to describe accurately the arrangement of metal fiber in fabric and it will provide a reference for studying properties of electromagnetic shielding fabric.

Shielding Effectiveness Fitting of Local Electromagnetic Shielding Clothing Based on Human Figure

Xiuchen Wang, Xing Rong, Qianxue Zheng, Ruili Sun, Yuna Chen, and Zhe Liu
Zhongyuan University of Technology, China

Abstract— This study proposes a new method of shielding effectiveness (SE) based on NURBS curve, which aims to address current non- effective method to describe the SE distribution of electromagnetic shielding (EMS) clothing. Moreover, the SE of local clothing can be fitted with the curve to observe the distribution. A testing method of key points is introduced to test the SE of the local clothing. Some concrete functions and program steps of curve fitting are listed. And then a distribution image of the SE on arm position is drawn. Results show that the proposed algorithm can accurately draw a 3D image of the SE of the local clothing and can reveal the distribution of electromagnetic wave on the local human body.

On the Treatment of Hypersingularity for Solving Volume Integral Equations

P. C. Wang, Z. G. Zhou, J. H. Zhou, X. F. Yin, and M. S. Tong
Department of Electronic Science and Technology, Tongji University
4800 Cao'an Road, Shanghai 201804, China

Abstract— Volume integral equations are indispensable for solving electromagnetic (EM) problems with inhomogeneous or anisotropic media by an integral equation approach. The VIEs are usually solved by the method of moments with the divergence-conforming Schaubert-Wilton-Glisson (SWG) basis function or curl-conforming edge basis function. These basis functions require conforming meshes for geometrical discretization, resulting in a high cost for preprocessing. Aiming to reduce the cost of meshing or remeshing geometries, point-matching methods like Nyström method and meshless methods were proposed and have been widely used in practice. In these methods, we need to accurately evaluate singular volume integrals involving derivatives of the Green's function. Although many techniques have been developed for evaluating weakly and strongly singular integrals, the techniques for evaluating hypersingular integrals which come from the double gradient of the dyadic Green's function are very limited. Previously, we developed a treatment technique which uses a numerical integration for line integrals based on the analytical formulas of surface integrals. The treatment is valid but it may not be convenient in implementation. In this work, we present new formulas for evaluating the hypersingular volume integrals over a cylindrical domain so that the implementation can be greatly simplified. We demonstrate the new formulas by solving an EM scattering problem and good results have been observed.

Simulation for Flat-plate Bounded Wave EMP Simulator with Distributed Terminator and Plane Source

Xiangqin Zhu[1], **Jianguo Wang**[1, 2], **Guowei Zhang**[1], **and Weiqing Chen**[1]

[1]State Key Laboratory of Intense Pulsed Radiation Simulation and Effect (Northwest Institute of Nuclear Technology), Xi'an, Shaan'xi 710049, China
[2]School of Electronic and Information Engineering
Xi'an Jiaotong University, Xi'an, Shaan'xi 710049, China

Abstract— Lots of bounded wave electromagnetic pulse (EMP) simulator, which can produce transverse electromagnetic (TEM) waves, have been widely applied to effect experiments of electromagnetic compatibility, interference and damage of complicated electronic systems. Flat-plate bounded wave EMP simulator with distributed terminator has been widely adopted because it can afford EMP with fast rise-time. On the other hand, the size of simulators become bigger and bigger in order to satisfy the needs of general systematic experiments. So it's necessary to simulate the medium-sized or large flat-plate bounded wave EMP simulator with distributed terminator in time-domain. Parallelized finite-difference time-domain (FDTD) method for simulating the near-fields of flat-plate bounded wave EMP simulator (whose height is 22 m) with distributed terminator and plane source is presented in this paper. The effects of some simulator's model-parameters to the vertical electric fields of the testing points at the half-height in the simulator are simulated and analyzed. The results show that (1) if the ratio of the transitional line's maximum width to the maximum height (that is the simulator's ratio of width to height) is 2, the smallest rise-times of E_z at testing points can be got; (2) The bigger the simulator's ratio of width to height, the bigger the peak-value of E_z at the same testing-point; (3) If the simulator's ratio of width to height is 2 and the width of below PEC plate is equal to the transitional line's maximum width, the biggest FWHM of E_z at testing points can be gained;. (4) As the projection length of transitional line along x-axis increases, the peak-values of E_z at the points with the same distance from the source along x-axis increase while the rise-times of E_z decrease, but the decrease of rise-time tends stable.

H-polarized Plane Wave Diffraction by an Acute-angled Dielectric Wedge: A Time Domain Solution

M. Frongillo[1], **G. Gennarelli**[2], **and G. Riccio**[1]

[1]D.I.E.M. — University of Salerno, Via Giovanni Paolo II 132, Fisciano, SA 84084, Italy
[2]Institute for Electromagnetic Sensing of the Environment
National Research Council, Via Diocleziano 328, Naples 80124, Italy

Abstract— Time domain (TD) diffraction problems are currently receiving great attention from both the research community and industry because of the widespread use of ultra wide band (UWB) communication and radar systems. It is commonly accepted that, due to the large bandwidth of the UWB signals, the analysis of the wave propagation mechanisms in the TD framework is preferable to the frequency domain (FD) data processing. Furthermore, the analysis of transient scattering phenomena is also of importance for predicting the effects of electromagnetic pulses (EMPs) on civil and military structures.

Diffraction by penetrable wedges in the TD framework is a challenging problem from the analytical point of view, and numerical discretization techniques represent useful tools to support the research activity. Unfortunately, these methods become rapidly intractable when considering excitation pulses with high frequency content. Analytical TD solutions are not available in literature for penetrable wedges apart from those reported in [1, 2], where the TD counterparts of the frequency domain Uniform Asymptotic Physical Optics (FD-UAPO) solutions for the diffraction coefficients related to right- and obtuse-angled dielectric wedges were obtained by the authors. FD-UAPO solutions for evaluating the diffracted field in the dielectric region and the surrounding free-space were recently derived in the case of an acute-angled lossless wedge illuminated by H-polarized plane waves at normal incidence [3]. They were expressed in closed form and given in terms of the Geometrical Optics (GO) response of the structure and the UTD transition function [4].

This work deals with the TD diffraction by an acute-angled dielectric wedge when illuminated by a plane wave at normal incidence. In particular, the H-polarization case is here considered. The TD-UAPO diffraction coefficients are first determined in closed form via an inverse Laplace transform of the corresponding FD-UAPO ones by taking advantage of their UTD-like formulation. Then the transient diffracted field originated by an arbitrary function plane wave can be evaluated via a convolution integral.

REFERENCES

1. Gennarelli, G. and G. Riccio, "Time domain diffraction by a right-angled penetrable wedge," *IEEE Trans. Antennas Propag.*, Vol. 60, 2829–2833, 2012.
2. Gennarelli, G. and G. Riccio, "Obtuse-angled penetrable wedges: A time domain solution for the diffraction coefficients," *Journal of Electromagnetic Waves and Applications*, Vol. 27, No. 16, 2020–2028, 2013.
3. Frongillo, M., G. Gennarelli, and G. Riccio, "Diffraction by an acute-angled dielectric wedge: The H-polarization case," *PIERS Proceedings*, 846–849, Stockholm, Aug. 12–15, 2013.
4. Kouyoumjian, R. G. and P. H. Pathak, "A uniform geometrical theory of diffraction for an edge in a perfectly conducting surface," *Proc. of IEEE*, Vol. 62, 1448–1461, 1974.

Calculation of the Reflection and Transmission of Finite Sized Beams through Layered Uniaxial Anisotropic Media Accelerated by Plane Wave Spectrum Algorithm

Shihao Ji, **Ming Bai**, **Zhao Liu**, **Yao Ma**, **and Xiuzhu Ye**
Electromagnetics Laboratory, Beihang University, Beijing 100191, China

Abstract— Calculation of electromagnetic waves through layered anisotropic media has been a problem encountered in many cases, such as radome design, optical design and ferromagnetic materials. Existing research have discussed infinite plane waves through layered anisotropic media. However, in case of finite sized beam or different orientation structured beam through layered anisotropic media, such as laser beam or antenna radiation limited in size, there is a greater need to calculate refracted and reflected fields of arbitrary oriented finite beams. In this case, a calculation method is required, especially during design beam radiation. There are solution for such task, usually performed by numerical ways, such as the Finite-Difference Time-Domain (FDTD) method and the method of moment (MoM), which can be time and memory consuming.

This paper presents a method for calculating arbitrary oriented finite beams through layered anisotropic media. The method combines general transmitting matrix (GTM) method and optical fast-Fourier-transform based angular spectrum (FFT-AS) method. It can calculate full vectorial fields of electromagnetic beam refracted and reflected by the multilayer can within several seconds. In the calculation, the FFT-AS Method is first used to calculate the propagation between initial plane and temporary plane parallel to the surface plane. The angular spectrum method also converts arbitrary oriented finite beams into superposition of plane waves with different directions. Thus the general transmitting matrix method can be used to calculate the result of every single plane wave through layered anisotropic media. Each plane wave is decomposed to the parallel and perpendicular components, the refracted plane wave and the reflected plane wave can be calculated separately. Finally the refracted plane waves and the reflected plane waves can be combined at target plane. With this method, the result of arbitrary oriented finite beams through layered anisotropic media can be obtained accurately within seconds.

This method implemented and well verified a technique which can be used in the design process of the multilayer with big amount of parameter adjustment such as radome design and optical design.

Impact on the Performance of Compact Antenna Test Range due to Surface Deviation of the Reflector

Zhao Liu, Ming Bai, Shihao Ji, Xiao Fang, and Xiuzhu Ye
Electromagnetics Laboratory, Beihang University, Beihang 100191, China

Abstract— Compact antenna test range (CATR) technology is key measurement technology of antenna pattern test and target RCS test, which is such a system that converts the spherical wave generated from the feed into quasi plane wave. The output quasi plane wave is named "quiet zone", which could be seen as ideal plane wave. With the development of microwave technology, the microwave frequency band we use ranges to millimeter wave or even sub-millimeter wave, which makes high precision CATR technology becomes cumulatively important in basic microwave scientific research.

For high performance millimeter wave antenna test and large size object RCS test, CATR is necessary for it can economize test field compared to outdoor test. It can also save much more time than near field scanning test. Usually, the performance of quiet zone is judged by several technical indicators as the follows: the ripple and taper of amplitude, the ripple of phase, and the cross polarization. So the property of quiet zone is key specification of CATR. When design CATR, we expect the ripple of amplitude and phase to be as low as possible. During the assembly and debugging of millimeter wave CATR, these factors have unwanted influence on quiet zone, such as accuracy of machining, deformation of the reflector, and so on.

However, research had been conducted about the effect generated during manufacture is only on account of pattern of parabolic dish antenna, which causes limited influence. In this paper, we study effects of these factors and shows considerable guidance for further microwave technique development in the future, which is crucially significant for millimeter wave CATR construction.

Electromagnetic Waves Described with the Complex Quaternion

Zi-Hua Weng
School of Physics and Mechanical & Electrical Engineering, Xiamen University, Xiamen 361005, China

Abstract— J. C. Maxwell represented the physical feature of electromagnetic field with the quaternion analysis and the vector terminology. In 1843 W. R. Hamilton invented the quaternion. And J. T. Graves and A. Cayley invented the octonion independently. Later the scientists and engineers separated the quaternion into the scalar part and vector part. Maxwell mingled naturally the quaternion and vector to describe the electromagnetic feature in his works. Recently some scholars begin to study the physics feature of gravitational field with the quaternion.

The ordered couple of quaternions compose the octonion. On the contrary, the octonion is able to be separated into two parts, the quaternion and the S-quaternion (short for the second quaternion), while their coordinates are able to be complex numbers. The quaternion space is suitable to depict the gravitational features, and the S-quaternion space is proper to describe the electromagnetic features. Further it can directly deduce the wave equations in the electromagnetic and gravitational fields described with the complex octonion.

In the quaternion space, it is able to infer the field strength and field source etc in the gravitational field, and deduce the gravitational field equations and wave equation etc.. The Newton's law of universal gravitation in the classical gravitational theory can be reduced from one of gravitational field equations described with the quaternion. And the gravitational waves are transverse waves in a vacuum. In the S-quaternion space, it is able to deduce the field strength and field source etc in the electromagnetic field. Further the Maxwell's equations and electromagnetic wave equation etc can be inferred directly. The wave equation is identical with that in the classical electromagnetic theory with the vector terminology.

ACKNOWLEDGMENT

The authors are grateful for the financial support from the National Natural Science Foundation of China under grant number 60677039.

Methods for the Sensing and Evaluation of Ionosphere Changes and Their Impact on the Human Organism

M. Hanzelka[1], **J. Dan**[2], **P. Fiala**[1], **M. Friedl**[1], **and Vladan Holcner**[3]

[1]Department of Theoretical and Experimental Electrical Engineering
Brno University of Technology, Technická 3082/12, Brno 616 00, Czech Republic
[2]Rector's Office, Personnel Management Office, Masaryk University
Žerotínovonám, 9, Brno 601 77, Czech Republic
[3]Faculty of Economics and Management, University of Defence
Kounicova 65, Brno 662 10, Czech Republic

Abstract— The impact of the environment upon living organisms constitutes a crucial problem examined by today's science. In this context, research institutes worldwide have analyzed diverse positive and negative factors affecting the biological system of the human body. One such factor consists in the influence of the surrounding electromagnetic field. This paper presents the results of an investigation focused on ionosphere parameter changes and their impact on the basic function of the nervous system. It is a well-known fact that the frequency of the alpha waves of brain activity [1] ranges within 6–8 Hz. Changes in the electromagnetic and chemical structure of the Earth's surface may cause variation of signals in the above-defined frequency region of 6–8 Hz. Detailed examination of the overall impact of environmental factors upon the human organism is performed within a large number of medical disciplines. The research presented in this paper is concentrated on the sensing and detection of changes in the region of very low frequencies of the electromagnetic field; the authors use both theoretical and experimental procedures to define the effects that influence brain activity.

ACKNOWLEDGMENT

The research described in the paper was financially supported with a grant of the Czech Science Foundation (GACR 13-09086S), a project of the BUT science fund, No. FEKT-S-11-5/1012, and projects from the Education for Competitiveness Operative Programme (Nos. CZ.1.07.2.3.00.20.0175 and CZ.1.07/2.3.00/30.0005).

REFERENCES

1. Ferris, J., "The brain generates an electric field that influences its own activity," *Scientific American Mind*, Vol. 21, 10, October 28, 2010, published online: doi:10.1038/scientificamericanmind1110-10a.
2. Scorretti, R., N. Burais, L. Nicolas, and A. Nicolas, "Modeling of induced current into the human body by low-frequency magnetic field," *IEEE Transactions on Magnetics*, Vol. 41, No. 5, May 2005, doi: 10.1109/TMAG.2005.846276.
3. Carrubba, S. and A. A. Marino, "The effects of low-frequency environmental-strength electromagnetic fields on brain electrical activity: A critical review of the literature," *Electromagnetic Biology and Medical*, Vol. 27, No. 2, 83–101, Department of Orthopaedic Surgery, LSU Health Sciences Center, P. O. Box 33932, Shreveport, LA 71130-3932, United States, 2008.
4. Hashish, A. H., M. A. El-Missiry, H. I. Abdelkader, and R. H. Abou-Saleh, "Assessment of biological changes of continuous whole body exposure to static magnetic field and extremely low frequency electromagnetic fields in mice," Department of Physics, Faculty of Science, University of Mansoura, Mansoura 35516, Egypt, available online, February 21, 2008, doi:10.1016/j.ecoenv.2007.10.002.

Applications of Noise Spectroscopy in the Analysis of Periodic Material Structures

Z. Szabo, **P. Drexler**, **J. Seginak**, **D. Nešpor**,
M. Friedl, **P. Marcoň**, **and P. Fiala**
Department of Theoretical and Experimental Electrical Engineering
Brno University of Technology, Technická 12, Brno 616 00, Czech Republic

Abstract— The authors discuss the application of broadband noise signal in the research of periodic structures and present the basic testing related to the described problem. The aim is to find a metrological method utilizable for the investigation of metamaterials in the frequency range between 100 MHz and 10 GHz; this paper therefore characterizes the design of a suitable measuring technique based on noise spectroscopy and introduces the first tests conducted on a periodic structure (metamaterial). In this context, the applied equipment is also shown to complement the underlying analysis.

ACKNOWLEDGMENT

The research described in the paper was financially supported with a grant of the Czech Science Foundation (GACR 13-09086S), a project of the BUT science fund, No. FEKT-S-11-5/1012, and projects from the Education for Competitiveness Operative Programme (Nos. CZ.1.07.2.3.00.20.0175 and CZ.1.07/2.3.00/30.0005).

REFERENCES

1. Maslovski, S., S. Tretyakov, and P. Alitalo, "Near-field enhancement and imaging in double planar polariton-resonant structures," *J. Appl. Phys.*, Vol. 96, 1293, 2004.
2. Freire, M. and R. Marques, "Near-field imaging in the megahertz range by strongly coupled magnetoinductive surfaces: Experiment and ab initio analysis," *J. Appl. Phys.*, Vol. 100, 063105, 2006.
3. Machac, J., P. Protiva, and J. Zehentner, "Isotropic epsilon-negative particles," *2007 IEEE MTT-S Int. Microwave Symp. Dig.*, Honolulu, USA, TH4D-03, June 2007.
4. Protiva, P., J. Mrkvica, and J. Macháč, "Universal generator of ultra-wideband pulses," *Radio Engineering*, Vol. 17, No. 4, 74–79, 2008.
5. Oppenheim, A. V., R. W. Schafer, and J. R. Buck, *Discrete-time Signal Processing*, Prentice Hall, Upper Saddle River, N.J., ISBN 0-13-754920-2, 1999.
6. Brigham, E. O., *The Fast Fourier Transform*, Prentice-Hall, New York, 2002.
7. Addisson, P. S., *The Illustrated Wavelet Transform Handbook*, Institute of Physics Publishing, 400 pages, Bristol, 2002.
8. Bell, B. M. and D. B. Percival, "A two step Burg algorithm," *IEEE Transactions on Signal Processing*, Vol. 39, No. 1, 1991.

A Interdigital Slot-loaded Directional Coupler Design Based on Substrate Integrated Waveguide

Jie Cao, Lu Fu, and Shou-Zheng Zhu
School of Information, East China Normal University, Shanghai 200241, China

Abstract— A novel design method of low profile directional coupler based on substrate integrated waveguide (SIW) is presented in this paper. The directional coupler is designed based on a composite right/left-handed structure, which is realized by etching interdigital capacitor slots on the SIW directional coupler surface. The conventional directional coupler based on SIW has no slots, the metal surface and the ground are connected by metal via-walls, and the shunt inductance of equivalent circuit is generated by via-walls. In this design, the interdigital capacitor has been introduced into the model as a series capacitance, which is a multifinger periodic structure, an interdigital capacitor is made of some gaps, which are essentially very long and folded to use a small amount of area, and the gap meanders back and forth in a rectangular area forming two sets of fingers that are interdigital. And the detailed configuration of the proposed CRLH SIW directional coupler is shown in Fig. 1.

This design method has been validated by simulation results. Compared with those of a conventional SIW directional coupler, solution frequency has been reduced from 10.35 GHz to 6.8 GHz by introducing interdigital capacitor slots. Thus, directional coupler miniaturization is achieved. Meanwhile, the directional coupler has a stabilized value of S_{21} as well as S_{31} in a further wider frequency bandwidth (6.9 GHz–7.3 GHz), which all approaches to −4 dB, it could be applied to the equivalence of power between the output and coupled ports of directional coupler in the mentioned bandwidth. And the simulated S-parameters of the CRLH SIW directional coupler are shown in Fig. 2.

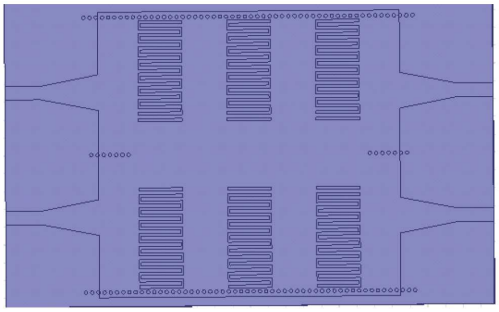

Figure 1: The detailed configuration of the proposed CRLH SIW directional coupler.

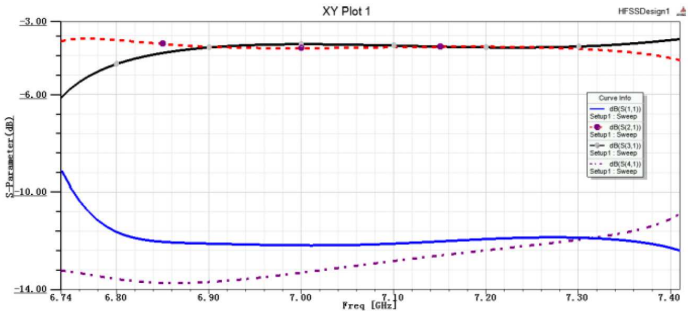

Figure 2: The simulated S-parameters of the CRLH SIW directional coupler.

A Tunable Microwave Absorber Based on Active Frequency Selective Surface

Kainan Qi[1, 2], **Xiaofeng Yuan**[1, 2], **and Yongfeng Wang**[1, 2]

[1]College of Information Engineering
Communication University of China, Beijing 100854, China
[2]Science and Technology on Electromagnetic Scattering Laboratory, Beijing 100854, China

Abstract— A novel microwave absorber is presented in this paper. The absorber is a single layer structure based on the topology of a Salisbury screen, but in which the conventional resistive layer is replaced by an active frequency selective surface (AFSS) controlled by PIN diodes. The reflectivity response of the tunable microwave absorber can be controlling by adjusting the current in PIN diodes. Experimental results are presented and prove the working mechanism of the new absorber, which show that the reflectivity response can be modulated over the frequency band from 10 GHz to 12 GHz.

Nonreciprocal Perfect Absorber Consisting of Nonlinear Plasma and Matching Metamaterials

Xiang-Kun Kong[1, 2], **Shao-Bin Liu**[1], **Hai-Feng Zhang**[1, 3], **Bo-Rui Bian**[1], **and Jia-Lin Yuan**[1]

[1]Key Laboratory of Radar Imaging and Microwave Photonics, Ministry of Education
Nanjing University of Aeronautics and Astronautics, Nanjing 210016, China
[2]Jiangsu Key Laboratory of Meteorological Observation and Information Processing
Nanjing University of Information Science and Technology, Nanjing 210044, China
[3]Nanjing Branch, Artillery Academy of the PLA, Nanjing 211132, China

Abstract— A novel, compact and multichannel nonreciprocal absorber through a wave tunneling mechanism in epsilon-negative and matching metamaterials is theoretically proposed. Nonreciprocal absorption properties are acquired via the coupling together of evanescent and propagation waves in an asymmetric configuration, constituted of nonlinear plasma alternated with matching metamaterial. The absorption channel number can be adjusted by changing the periodic number. Due to the positive feedback between nonlinear permittivity of plasma and the inner electric field, bistable absorption and reflection are achieved. Moreover, compared with some designs proposed before, our design is more compact and independent of incident angle or polarization. This kind of multilayer structure offers additional opportunities to design novel ormidirectional EM wave absorbers.

Minimum Variance Variable Constrain DOA Algorithm

Ahmed Khairy Aboul-Seoud, Ahmed Khairy Mahmoud, Alaa Hafez, and Ali Gaballa
Faculty of Engineering, Alexandria University, Alexandria, Egypt

Abstract— This work proposes a new direction-of-arrival (DOA) estimation algorithm for Smart antenna. The proposed algorithm is based on MVDR algorithm through the introduction of a new optimization problem, which aims to maintain the array gain in the 'look direction', so that the DOA can be estimated correctly using Smart antenna array. To verify the performance of the proposed algorithm, computer simulations are performed and then the results obtained are compared with the MVDR algorithm. The results show that the proposed algorithm outperforms the MVDR algorithm.

The use of electrostatic MEMS switches is attractive because of its advantages, such as very low power consumption and high isolation. However, MEMS switches have their share of problems, such as, high driving voltage, relatively low speed and low power handling. Many previous researches focus on RF MEMS switch, which presents a good performance at microwave frequency. This result an increasing use of RF MEMS switches for telecommunication purpose in the last ten years. This paper purposes is to use RF MEMS series switch for Switched beam array creates a group of overlapping beams that together result in 0° to 180° coverage. The beam pattern is generated using combines of MEMS phase shifters that feed networks into a highly integrated multifunctional chip, which can then be connected to the antenna array and T/R modules, Adaptive arrays allow the antenna to steer the beam to any direction of interest while simultaneously nulling interfering signals. Beamdirection can be estimated using direction-of-arrival (DOA) estimation methods.

Session 2P1
FocusSession.SC1: Advances in Multiscale, Multiphysics Computation

Some Recent Progress on the Discontinuous Galerkin Time Domain Method for Multiscale Electormagnetics

Qing Huo Liu, **Qiang Ren**, **Qingtao Sun**, **and Luis Tobon**
Department of Electrical and Computer Engineering
Duke University, Durham, North Carolina 27708, USA

Abstract— Multiscale electromagnetic problems are becoming commonplace in engineering applications. In this talk, we discuss some recent progress on the discontinuous Galerkin time domain (DGTD) method in computational electromagnetics. In the past few years, both discontinuous Galerkin finite element time domain (DG-FETD) and discontinuous Galerkin spectral element time domain (DG-SETD) methods have received considerable attention. Moreover, they have been combined together to improve their capabilities to simulate large scale and multiscale electromagnetic problems [1]. These methods usually use both the electric (E) and magnetic (H) field intensity vectors as the unknown field variables in the discontinuous Galerkin scheme to make use of the flux conditions at the interface between subdomains. However, unfortunately, it has been discovered that E and H must have different orders of basis functions to avoid spurious modes. This makes the number of degrees of freedom significantly larger than the traditional FETD method in a single domain. This problem is recently resolved by a new discontinuous Galerkin time domain method based on the E field and B (magnetic flux density) field having the same order of basis functions [2]. This method can significantly reduce the number of unknowns and computation load. Here we will discuss some recent progress in this new DGTD method for multiscale electromagnetics problems.

REFERENCES

1. Chen, J. and Q. H. Liu, "Discontinuous Galerkin time-domain methods for multiscale electromagnetic simulations: A review," *Proc. IEEE*, Vol. 101, No. 2, 242–254, 2013.
2. Ren, Q., L. Tobon, and Q. H. Liu, "A new 2D non-spurious discontinuous Galerkin finite element time domain (DG-FETD) method for Maxwell's equations," *Progress In Electromagnetics Research*, Vol. 143, 385–404, 2013.

Efficient Wide-band Analysis of GPR Antenna Around a Platform Using the Best Uniform Rational Approximation Technique

Ji Ma, **Guangyou Fang**, **and Yicai Ji**
Key Laboratory of Electromagnetic Radiation and Sensing Technology
Chinese Academy of Sciences, Beijing 100190, China

Abstract— Evaluating wide-band performance of ground-penetrating radar (GPR) antennas is a challenging task due to the complex electromagnetic coupling effects between the GPR antennas and the platform. Typically, the efficiency of conventional methods utilized to deal with the problem is quite low. However, there are various frequency sweeping techniques which can achieve fast analysis of antennas over a broadband. Accordingly, this paper describes an efficient hybrid scheme, based upon the electric field integral equation (EFIE), for modeling a GPR antenna which is mounted on an electrically large platform.

In this paper, an antenna with two half-elliptical-shape arms, which is an improvement of bowtie antennas, is presented with resistances loaded in the terminal. A shallow rectangular conducting backed cavity is attached to the antenna. On the other hand, the best uniform rational approximation technique is applied to analyze the wide-band property of the antenna since it can avoid repeatedly solving the integral equation at each single frequency point. The main scheme of the frequency sweeping method is as follows: 1) determining the Chebyshev nodes within a given frequency range; 2) computing the equivalent surface currents of antennas at the frequency points corresponding to those Chebyshev nodes; 3) calculating the wide-band response of surface currents according to the Chebyshev series. Finally, the Maehly approximation is utilized to improve the accuracy by matching the Chebyshev series to a rational function.

In the hybrid scheme, the adaptive integral method (AIM) is applied to accelerate matrix-vector products as the IE algorithm and the impedance matrix is stored in a sparse form to facilitate analysis of large antenna-platform system. It is easy to combine the best uniform rational approximation technique with AIM but also other IE methods which are suited for modeling radiation of antennas. This hybrid method greatly extends the range of conventional numerical modeling for GPR antenna system. Furthermore, the efficiency and capability of the presented algorithm can be validated by the designed GPR antenna.

Simulations of Scattering of Electromagnetic Waves by Bicontinuous Media for Applications in Microwave Remote Sensing of Terrestrial Snow

Leung Tsang[1], **Shurun Tan**[1], **Wenmo Chang**[1], **and Xiaolan Xu**[2]

[1]Department of Electrical Engineering, University of Washington, Seattle, WA 98195, USA
[2]Jet Propulsion Laboratory, California Institute of Technology, Pasadena, CA 91109, USA

Abstract— We study the scattering properties of bicontinuous random media with discrete permittivities. The bicontinuous model is based on a continuous representation of interfaces between inhomogeneities within the medium, which are constructed from a large number of stochastic, continuous, sinusoidal waves with random phases and in random directions [1]. The random structure is then defined by setting a level on this Gaussian random process according to the required volume fractions of inhomogeneities. The three dimensional bicontinuous structures generated by such random processes can be characterized by correlation functions [2]. Discrete permittivities are assigned to the structures. Advantages of bicontinuous medium are that the computer generated microstructures resemble real life media such as terrestrial snow and that the microstructures can be characterized by correlation functions and specific surface areas [2]. The correlation functions and specific surface areas of bicontinuous media can be directly compared to those extracted from real-life measurements.

In Monte Carlo simulations, the bicontinuous medium is generated for each realization. Then Maxwell's equations can be solved through volume integral equations. We perform 3D simulations of bicontinuous media and calculate the phase matrix and extinction coefficients [2, 3]. These are then combined with dense media radiative transfer equations to calculate the overall backscattering and emissivities [3]. Full multiple scattering effects under the dense media radiative transfer equation are included. Distinct features of the bicontinuous model compared with Rayleigh scattering and Rayleigh phase functions are: (i) weaker frequency dependence, (ii) weaker size dependence, (iii) moderate forward scattering and strong cross polarization [2, 3]. The weaker frequency dependence is in agreement with broadband measurements.

In radar backscatter calculations, we use the full multiple scattering of radiative transfer equations for active remote sensing. However, the model does not include backscattering enhancement because only the ladder terms are used to derive DMRT equations. We further include the backscattering enhancement effect. When the scattering path of the wave is the opposite of the path of another wave, their backscattering coefficients will add coherently. The multiple scattering effects are accounted for by solving the dense media radiative transfer equation using an iterative approach. Backscattering enhancement is accounted for by the inclusion of cyclical terms. The inclusion of the cyclical terms is performed for each iteration. Backscattering enhancement only contributes in active and does not contribute to passive. The net result is an increase in radar backscattering without the decrease in passive emissivity.

The model is applied to compare with active and passive remote sensing measurements conducted in the NoSREx terrestrial snow campaign in northern Finland. In this campaign, tower based measurements were conducted in Sodankyla, Finland. The instruments include a multi-frequency radiometer called SodRad, and an ESA-owned scatterometer called SnowScat. The tower based measurements include both microwave radiometry measurements and radar backscatter measurements. In addition to the microwave measurements, extensive ground measurements were taken in Sodankyla, including grain size, snow depth, snow density (or fraction volume), and Specific Surface Area (SSA).

REFERENCES

1. Berk, N. F., "Scattering properties of a model bicontinuous structures with a well defined length scale," *Phys. Rev. Lett.*, Vol. 58, 2718–2721, 1987.
2. Ding, K.-H., X. Xu, and L. Tsang, "Electromagnetic scattering by bicontinuous random microstructures with discrete permittivities," *IEEE Transactions on Geoscience and Remote Sensing*, Vol. 48, No. 8, 3139–3151, Aug. 2010.
3. Xu, X., L. Tsang, and S. Yueh, "Electromagnetic models of co/cross-polarization of bicontinuous/DMRT in radar remote sensing of terrestrial snow at X- and Ku-band for CoReH$_2$O and SCLP applications," *IEEE Journal of Selected Topics in Applied Earth Observations and Remote Sensing*, Vol. 5, No. 3, 1024–1032, Jun. 2012.

Electromagnetic Characterization of Tunable Bandpass Filters with a PET-controlled Perturber

G. C. Wan, J. X. Hong, Z. G. Zhou, X. W. Zhang, and M. S. Tong
Department of Electronic Science and Technology
Tongji University, Shanghai, China

Abstract— Tunable bandpass filters (BPFs) are vital microwave components and they have been widely used in communication systems. The design of tunable BPFs is challenging because they require a low loss and compact size. Recently, the tunable BPF with a magnetodielectric perturber controlled by a piezoelectric transducer (PET) was developed [1] and it looks very promising. Such a tunable BPF uses a perturber as a superstrate touching on the microstrip and its position can be controlled by a PET. The perturber is made of a high-permeability ferrite film and a high-permittivity dielectric Rogers material in a sandwich style. The resonant frequency of the BPF can be tuned by applying different bias DC voltages to the PET or by using different layers of magnetodielectric sandwich. The tunable BPF can be easily fabricated with a compact size and low loss and its resonant frequency could be adjusted in a wide range.

Characterizing the tunability of the BPF relies on the electromagnetic modeling and analysis although a costly experimental method can be used. The structure is of multiscale characteristic because some dimensions are very small compared with others in geometry. Although the thickness of microstrip and ground may be ignored to simplify in analysis, the small thickness of high-permeability ferrite film cannot be ignored due to its significant influence and should be accounted for carefully. The structure can be modelled by surface integral equations (SIEs) when all materials are assumed to be homogeneous, but the SIEs may not generate well-conditioned system matrices, especially for multiscale structures. Also, the SIEs need to use appropriate basis functions to represent the electric and magnetic current densities, respectively, in the method of moments (MoM) solution and the choice of the basis functions or testing schemes could strongly affect the accuracy of solutions. In this work, we use volume integral equations (VIEs) to describe the dielectric substrate and magnetodielectric perturber, and form volume-surface integral equations (VSIEs) after combining with the SIE governing the conducting microstrip and ground. The VIEs or VSIEs are usually well-conditioned because they include the second-kind of integral equations. We present a numerical example to demonstrate the analysis of the BPF and its effectiveness has been verified.

A Combined Method for Computing Installed Radiation Patterns of Antennas on Large Conducting Platforms

H. Zhao*, **S. Gao**, **B.-F. Wang**, **and W.-J. Zhao**
Institute of High Performance Computing, 1 Fusionopolis Way, 138632, Singapore

Abstract— The installed radiation patterns of antennas on large platforms are of great interest when installing antennas. The computation of installed radiation patterns is challenging due to the large size of the platform. To reduce the effort of modeling the large platform, this work adopts the hybridization of the method of moments (MoM) and physical optics (PO) method. The multi-level fast multipole method is used to accelerate the solution of matrix equations, so that a large MoM region can be used to improve the accuracy of modeling the antenna and its surrounding structures. Another challenge of modeling antennas on large platforms comes from the complexity of the antennas. Furthermore, when an antenna is outsourced, detailed design information may be unavailable to those who install the antenna, which hinders direct modeling of antennas on large platforms. In this case, equivalent models of antennas are derived based on their uninstalled far field radiation patterns. Using the equivalent models, installed radiation patterns of antennas can be computed without knowing their detailed design information. Furthermore, the equivalent model avoids direct modeling of complex antennas, thus reducing the CPU time and memory requirements. By combining the hybrid method with the equivalent model, the installed radiation patterns are computed efficiently.

*Corresponding author: H. Zhao (huapengzhao@ieee.org).

Multi-scale Electromagnetic Modeling by Integral Equation Domain Decomposition Method with Hybrid Basis Functions

Ran Zhao, **Mi Tian**, **Jun Hu**, **and Zai Ping Nie**
School of Electronic Engineering, University of Electronic Science and Technology of China
Chengdu 611731, China

Abstract— In this paper, a novel electromagnetic (EM) modeling method by integral equation domain decomposition method with hybrid basis functions is developed for the solution of multi-scale problems. Based on the integral equation domain decomposition method, the original multi-scale object were decomposed into several closed sub-domains and transmission condition is enforced on the touching faces to maintain the continuity of current across the interfaces. The higher order hierarchical vector basis functions and low order Rao-Wilton-Glisson (RWG) basis functions are used in different sub-domains to reduce remarkably the number of unknowns. Because the domain decomposition method provides an effective preconditioner, the convergence history will be much better than traditional method of moments (MoM). And because of the non-conformal property of the domain decomposition method, each sub-domain can be meshed independently, which enables the mesh generation be much easier than the traditional method, especially for complex multi-scale objects. Finally, some numerical results are given to validate the ability of the present method.

Dyadic Green's Function, Spectral Function, Local Density of States, and Fluctuation Dissipation Theorem

W. C. Chew[1] and W. E. I. Sha[2]

[1]Department of Electrical and Computer Engineering
University of Illinois, Urbana-Champaign, USA
[2]Department of Electrical and Electronic Engineering
The University of Hong Kong, Hong Kong SAR, China

Abstract— In this talk, we will discuss the relation between dyadic, spectral function, local density of states, and fluctuation dissipation theorem in electromagnetics. Using a retarded and advanced Green's function, one can define a spectral function that is non-causal, but Hermitian. From this spectral function, one can derive the local density of states and density of states quite easily. Since the system is Hermitian, the energy density can be related to quantized electromagnetic field, and hence, the Planck distribution function can be used to derive it.

For lossy dispersive media, this connection is less obvious, but a connection to Planck distribution law can still be made. Moreover, this path of deriving the energy density can be related to the fluctuation dissipation theorem for lossy, dispersive media.

We will derive useful formulas and show the connection by solving Maxwell's equations in vacuum, lossless, lossy, and inhomogeneous dispersive media.

ISAR Scattering/Imaging and Reconstruction for a Space Target Observed in Multi-station and Multi-orbit Modes

Ya-Qiu Jin
Key Laboratory for Information Science of Electromagnetic Waves (MoE)
Fudan University, Shanghai 200433, China

Abstract— With increased number of space targets (satellite, spacecraft, debris, etc.), the space environment becomes more complex and crowded. To ensure the safe utilization of space, the space monitoring and surveillance technologies from observations of multi-station and multi-orbit modes have been of greatly indispensable. High resolution inverse synthetic aperture radar (ISAR) is playing an important role for imaging and signal processing of moving space target in two dimensional (2D) and three dimensional (3D) configurations.

Scattering from a complex target is usually dominated by a limited number of strong scattering centers, which yields strong spatial sparsity. Sparse sensing is a key technology to achieve improved performance, such as super-resolution, feature enhancement and simplicity of data acquirement. Compressed sensing (CS) techniques may offer a framework for detection and allocation of sparse signals with reducing the sample number. Recently, it is known that an unknown sparse signal can be exactly recovered from a very limited number of measurements by exploiting the signal sparsity (SS). CS-SS can be served as a catalyst for future radar imaging.

As a successful integration of scattering issues with physics, mathematics, and computer techniques, computational electromagnetics has been in great advance, e.g., the method of moment (MOM), finite element method, the finite difference time domain method (FDTD), multilevel fast multipole method (MLFMM) and many others have been developed. However, all of these methods may create a huge amount of computations, especially for the issues of imaging and reconstruction of an electrically large complex target under multi-station and multi-orbit observation.

We present numerical approach for ISAR scattering/imaging simulation of a space target under in multi-orbit and multi-station modes, and 2D/3D reconstruction using CS-SS. The bidirectional analytic ray tracing (BART) method is employed to calculate polarized electromagnetic scattering from a satellite-like target. Scattering under multi-station and multi-orbit modes makes 2D and 3D ISAR imaging, and achieve 2D/3D reconstructions under CS-SS. Some examples of ISAR imaging and reconstruction of the models for an Aura satellite and the X-37B vehicle are presented.

A CAV-DDM Method for Scattering by Cavity with Thin Thickness

Jun Hu, Ran Zhao, Ming Jiang, and Zai Ping Nie
School of Electronic Engineering
University of Electronic Science and Technology of China, Chengdu 611731, China

Abstract— In this paper, a novel non-overlapping integral equation domain decomposition method (DDM) named as CAV-DDM is developed for solving electromagnetic (EM) scattering problems of very thin, conducting cavity. By sealing the aperture with a fictitious sheet, and imposing equivalent electric and magnetic currents on the aperture, the original domain is decomposed into two sub-domains, the interior sub-domain and exterior sub-domain. Different from traditional method based on interior-exterior equivalence principle, the coupling of the exterior and interior sub-domains is done only through the transmission condition on the aperture. Based on this CAV-DDM, a well-conditioned combined field integral equation is successfully developed to realize fast solution of the EM scattering of open-ended cavity with extremely thin or zero thickness instead of traditional electric field integral equation. Numerical results are investigated to demonstrate the validity of the present method.

Applying CEM Techniques to Solve Nano-scale Quantum Transport Problems

Jun Z. Huang[1], **Weng Cho Chew**[2], **and Li Jun Jiang**[3]

[1]Purdue University, West Lafayette, IN 47907, USA
[2]University of Illinois, Urbana, Champaign, IL 61801, USA
[3]The University of Hong Kong, Hong Kong SAR, China

Abstract— Continuous technology innovations make it possible to fabricate electronic devices on the order of 10 nm. In this nanoscale regime, quantum physics becomes critically important, like energy quantization effects due to the narrow transistor channels and the leakage currents due to tunnel- ing. It has also been utilized to build novel devices, such as the band-to-band tunneling field-effect transistors (FETs). Therefore, it presages accurate quantum transport simulations [1, 2], which not only allow quantitative understanding of the device performances but also provide physical insight and guidelines for device optimizations. However, quantum transport simulations usually require solving repeatedly the non-equilibrium Greens function (NEGF), or the wave function of the whole device region with open boundary treatment (via self energy matrices) [3], which are computationally cumbersome. Moreover, to overcome the short-channel effects, modern devices usually employ multi-gate structures that are three-dimensional, making the computation very intensive. To enhance the simulation efficiency, fast CEM algorithms are very useful in improving this computational nanotechnology (nanoelectronics) area, since the propagation of electron waves in nanoscale devices bears many similarities with the propagation of electromagnetic waves. Hence, many methods developed to understand and improve wave physics calculations in electromagnetics can be used to improve our understanding of wave physics calculations in nanoscale devices. In this paper, we demonstrate two of these approaches, the asymptotic waveform evaluation (AWE) technique and the model order reduction (MOR) mode matching method, which are widely used algorithms in computational electromagnetic (CEM) society. They are employed to calculate electron wave propagation in novel nanoelectronic devices.

REFERENCES

1. Datta, S., *Electronic Transport in Mesoscopic Systems*, Cambridge University Press, 1995.
2. Datta, S., *Quantum Transport: Atom to Transistor*, Cambridge University Press, 2005.
3. Huang, J. Z., W. C. Chew, Y. Wu, and L. J. Jiang, "Methods for fast evaluation of self-energy matrices in tight-binding modeling of electron transport systems," *J. Appl. Phys.*, Vol. 112, No. 1, 013711, 2012.

Thin Plasmonic Materials to Stop or Filter Waves

Yadong Xu, Qiannan Wu, and Huanyang Chen
School of Physical Science and Technology, Soochow University, Suzhou, Jiangsu 215006, China

Abstract— We will show that thin plasmonic materials can change the properties of a parallel plated waveguide, with a tunable band gap so that the waves could be stopped or filtered in the structure.

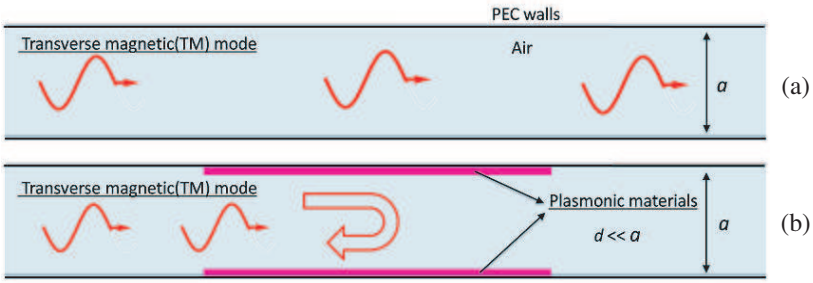

Figure 1: (a) Transverse magnetic modes propagate freely for any frequency in a parallel plated waveguide. (b) When two thin plasmonic materials are attached to the metal walls of the waveguide, the waves can be stopped or filtered.

REFERENCES

1. Xu, Y., Q. Wu, and H. Chen, "Manipulating transverse magnetic modes in waveguide using thin plasmonic materials," *Laser & Photonics Reviews*, 2014.

Giant Circular Dichroism Enhancement and Chiroptical Illusion in Hybrid Molecule-plasmonic Nanostructures

Yineng Liu[1] and Xiangdong Zhang[2]

[1]Beijing Normal University, China
[2]Beijing Institute of Technology, China

Abstract— Recently, there are great interest in studying the interaction between chiral molecules and plasmonic particles, because a weak circular dichroism (CD) signal in the ultraviolet (UV) region from chiral molecules can be both enhanced and transferred to the visible wavelength range by using plasmonic particles. Thus, ultrasensitive probe of tiny amounts of chiral substance by CD are worth waiting for. Here we present another way to strongly enhance CD of chiral molecules by using plasmonic particle cluster, which need not transfer to the visible wavelength. We have presented a multiple scattering method to calculate CD signals of the hybrid system consisting of a molecule and nanosphere cluster. The CD spectra for a chiral molecule inserted into clusters with various metallic nanospheres have been calculated. Our calculated results show that giant enhanced CD of the molecule in the UV region, more than 2 orders of magnitude enhancement in some cases, can be realized by using metallic nanosphere clusters. The enhanced CD resonances are very sensitive to structures and symmetries of the cluster, and they are also very sharp around the wavelength of molecule resonances. Thus, it brings some advantages to perform direct ultrasensitive detection on the chiral molecule in the UV region, which need not transfer to the visible wavelength. Furthermore, we have also found that the mirror symmetry of CD signals can be broken by introducing nanostructures. Therefore, the chiroptical illusion phenomenon of CD signals caused by nanostructures has been disclosed. In addition, quantum size correction on the phenomenon has also been considered. The physical origin for the phenomena has been analyzed. The proposed effects offer an alternative avenue for the ultrasensitive probing of chiral molecules in the UV region.

Analysis of New Phenomena Caused by the Interaction between Electromagnetic Fields and Charged Particles

Jian Wei You and Tie Jun Cui
State Key Laboratory of Millimeter Waves, School of Information Science and Engineering
Southeast University, Nanjing 210096, China

Abstract— Produced from different sources (e.g., cosmic rays, point discharges, and field emissions), charged particles exist inevitably in microwave components. When microwave devices operate under high-power EM fields in the vacuum or close-to-vacuum condition, the interaction between charged particles and EM fields should be considered.Charged particles can be driven by EM fields, while the motion of charged particles can generate a time-varying convection current in return. Based on our previous researches [1, 2], we present some novel and interesting phenomena caused by such complicated interactions.

Multipactor is a special phenomenon caused by such interaction. The initial charged particles driven by EM fields will impact against the metallic surface of components with different incident energies. If the energy is high enough, one or more new electrons can be generated. When some of them synchronize with EM fields, the above electron generation process is repeated until the multipactor avalanche takes place in microwave components. Multipactor breakdown results in a number of undesirable effects including electron noise, signal distortion, additive heating, and even device damage. These harmful effects can noticeably degrade the performance of microwave components. Multipactor occurs in many scenarios, such as space-borne systems, particle accelerators, and high-power microwave (HPM) devices. Today, with the growth of the input power, the risk of the multipactor breakdown has been increased.

Passive intermodulation (PIM) is another interesting phenomenon caused by the interaction between EM fields and charged particles. When charged particles are advanced by EM fields, the motion of charged particles can generate a time-varying convection current in return. In some cases, the resonant convection current radiates EM fields whose frequencies are the function of input frequencies. Thus, PIM can be presented when microwave components are excited by a multicarrier signal. In communication systems, PIM can distort the propagating signal and then degrade their performance. The worse situation is that, PIM cannot be eliminated by filtering, thus is often treated as the dominant source of nonlinear distortion in multichannel communication systems. For such reasons, it is extremely important and worthy to accurately analyze such nonlinear phenomena in microwave systems.

REFERENCES

1. You, J. W., H. G. Wang, J. F. Zhang, W. Z. Cui, and T. J. Cui, "The conformal TDFIT-PIC method using a new extraction of conformal information (ECI) technique," *IEEE Trans. Plasma Sci.*, Vol. 41, No. 11, 3099–3108, Nov. 2013.
2. You, J. W., S. R. Tan, X. Y. Zhou, W. M. Yu, and T. J. Cui, "A new method to analyze broadband antenna-radome interactions in time-domain," *IEEE Trans. Antennas Propag.*, Vol. 62, No. 1, 334–344, Jan. 2014.

Electromagnetic Wave Characterization in the Magnetized Cold Plasma

Ping Li and Li Jun Jiang
Department of EEE, The University of Hong Kong, China

Abstract— The propagation of electromagnetic waves in the cold plasma are being studied because of its importance in many areas. Among various methods, the finite difference time domain (FDTD) models have been well developed to model the wave propagating through the magnetized plasma slabs. The discontinuous Galerkin method (DG) has recently attracted extensive attentions due to many of its advantages, such as its various types and shapes of elements, unstructured and non-conformal meshes, etc. However, to model the electromagnetic waves in a magnetized plasma slab, the convolution relation between the permittivity and electric field in the time domain has to be properly handled since the direct convolution is prohibitive.

In this talk, we will introduce a high order discontinuous Galerkin finite element time domain method (DFTD) to model the electromagnetic wave propagation through magnetized plasma. It uses the auxiliary differential equations (ADE) instead of the recursive convolution method for the constitutive relation. ADE can support the highorder time integration scheme. The effect of the external static biasing magnetic field to the wave propagation is demonstrated through the comparison with the un-magnetized case. To generalize the proposed model, plasma effects contributed from both ion and electron are studied. Numerical results agree very well with analytical solution and plasma theory.

Session 2P2a
SC2: THz Metamaterials and Applications

Performance Enhancement of RMPA Using ESRR Metamaterial at THz

Parul Dawar[1] **and Asok De**[2]

[1]Department of ECE, Guru Tegh Bahadur Institute of Technology
G-8 Area, Rajouri Garden, New Delhi-110064, India
[2]National Institute of Technology, Patna, Bihar-800005, India

Abstract— Left handed materials which have both negative permittivity and permeability, have been the area of potential research over a decade. This paper elucidates antenna parameter optimization using Double Negative Group (DNG) Electric SRR, having 19.13 THz as resonant frequency forming metamaterial array embedded in antenna substrate at high frequency (THz). Ansoft HFSS has been used to design and analyse the RMPA (Rectangular Microstrip Patch Antenna) with design frequency 22.5 THz and operating range of 20 THz to 25 THz having FR4 ($\varepsilon_r = 4.4$) as substrate material. Nicolson Ross Wier (NRW) method has been used to retrieve the material parameters from transmission and reflection coefficient. Upon incorporation, remarkable enhancement in parameters is observed whereby bandwidth increases by factor of 3.75, directivity increases by 5% and front to back lobe ratio improves by 31% with ESRR metamaterial.

Supercontinuum Generation in Elliptical Silicon Nanowire Embedded Spiral Photonic Crystal Fiber

Abdosllam M. Abobaker[1], E. Gunasundari[2], K. Senthilnathan[2], S. Sivabalan[3], K. Nakkeeran[4], and P. Ramesh Babu[2]

[1]Department of Communications Engineering, College of Electronic Technology, Bani Walid, Libya
[2]Photonics, Nuclear and Medical Physics Division
School of Advanced Sciences, VIT University, Vellore 632 014, India
[3]School of Electrical Engineering, VIT University, Vellore 632 014, India
[4]School of Engineering, University of Aberdeen, Aberdeen AB24 3UE, UK

Abstract— In recent times, the generation of supercontinuum in photonic nanowire (PhN) have attracted significant interest with their sub-wavelength diameter due to their unique properties. It finds wide applications in photonic devices for computing, communications and sensing. The dielectric waveguides with a nanocore diameter exhibit a remarkably strong field confinement, enhanced light-matter interactions and strong controls over dispersions. Nanowires are generally fabricated from materials such as silica glass, silicon, etc.. Silicon has excellent transmission properties compared to silica and does not require high power density to bring in nonlinearity owing to its huge nonlinear coefficient. When a nanowire made of silicon is embedded into a photonic crystal fiber, the resulting structure is referred to as a silicon nanowire embedded photonic crystal fiber (SN-PCF) wherein the core diameter is lesser than the operating wavelength. This SN-PCF provides the enhanced linear and nonlinear optical properties and hence, it has attracted considerable interest in the recent past. Thus, with this nanowire, it is possible to generate supercontinuum within a short length of fiber with less input power. In this paper, we design an elliptical core silicon nanowire embedded spiral photonic crystal fiber (SN-SPCF) using fully vectorial finite element method. Further, we analyze the various optical properties, namely, waveguide dispersion, birefringence and effective nonlinearity by varying the ellipticity for a wide range of wavelengths from 0.450 µm to 2.050 µm. The proposed structure exhibits a high birefringence of 0.74143 for a small ellipticity of 0.3 at a longer wavelength of 2.05 µm. Besides, we investigate the evolution of supercontinuum generation both in spectral and temporal domains as a function of ellipticity at 1.550 µm wavelength for an input pulse of width 10 fs and peak power of 50 W in a fiber of 2 mm length. The numerical results corroborate that the proposed SN-SPCF provides a wider bandwidth of supercontinuum (1.2 to 2.4 µm) and the findings of this work may be useful in ultrahigh-resolution optical coherence tomography.

Design of the Proposed SN-PCF: Geometrical structure and mode field distribution of the proposed structure.

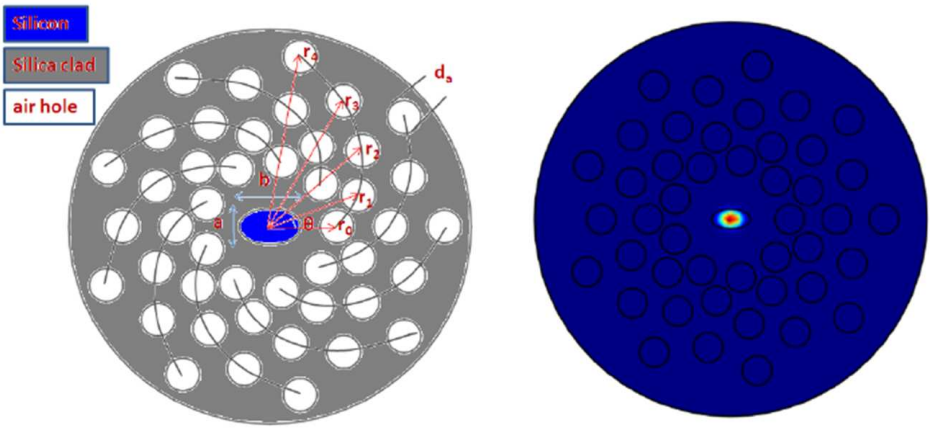

Observation and Phenomenological Interpretation of Shifts in Electrical Resonance of Square Shaped Planar THz Split Ring Resonators

Rahul Kumar[1], **Ankit Arora**[1], **Shaumik Ray**[2], **Bala Pesala**[2], **Enakshi Bhattacharya**[1], **and Ananth Krishnan**[1]

[1]Department of Electrical Engineering
Indian Institute of Technology Madras, Chennai 600036, India
[2]CEERI, CSIR Campus, Chennai 600113, India

Abstract— Electrical resonance in square shaped split ring resonators (SqSRR) has been observed earlier at all polarizations of the incident wave [1, 2], while magnetic resonances occur precisely at certain orientation of the SqSRR to the incident wave. The occurrence of the electrical resonance has been conventionally attributed to dipole oscillations in the arms parallel to the incident E-field, while neglecting the effect of arm perpendicular to external E-field (referred to as horizontal arm) [1–3]. This has been described in the past as the cut-wire approximation of SqSRR as shown in Fig. 1(a) [1–3]. In this work, several modified SqSRR structures with varying lengths of horizontal arm were simulated, fabricated (as shown in Fig. 1(b)) and characterized using a continuous wave THz system from 0.1 THz to 0.3 THz. A significant blue shift in the electrical resonance frequency was observed for decreasing values of the length of the horizontal arms, i.e., moving from closed ring to vertical stripes. The results indicated that, contrary to the cut wire approximation, the arms perpendicular to the incident E-field do play a significant role in determining the effective plasma frequency and resonance frequency in these structures.

In order to explain the role of the horizontal arms, the surface current density of the oscillatory modes was calculated and considerable surface current density was observed in the horizontal arms. The origin of current densities in the horizontal arms was attributed to the diffusion of electrons from the right and left extrema to the center of these arms. An analytical expression for the plasma frequency (f_p) [4] and the resonant frequency (f_0) [5] was modified to include the effect of the horizontal arms. The calculated shifts in f_p and f_0 (based on modified equations) were compared with the measured shifts in the frequency of minimum transmission (f_m; $f_0 < f_m < f_p$) and were found to be in excellent agreement as shown in Fig. 1(c).

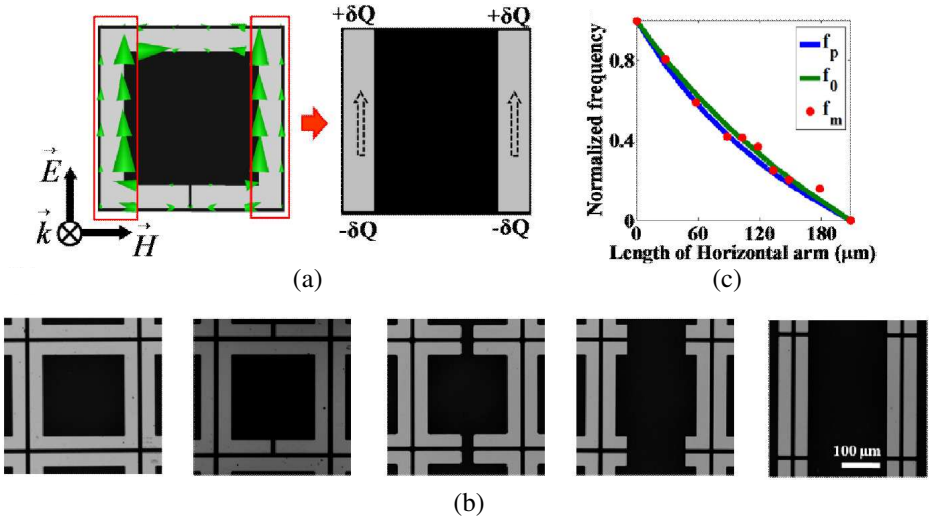

Figure 1: (a) Conventional cut-wire approximation of SqSRR. For shown orientation of electromagnetic wave, arrows and δQ depict direction of instantaneous surface current and instantaneous charge accumulation at the end of vertical arm respectively. (b) Micrograph of fabricated structures. Common scale bar is shown in last figure. (c) Normalized plasma frequency (f_p), electrical resonance frequency (f_0) and the measured frequency of minimum transmission (f_m) versus length of horizontal arm. These frequencies are normalized w.r.t. the corresponding cut-wire response.

REFERENCES

1. Katsarakis, N., et al., "Electric coupling to the magnetic resonance of split ring resonators," *Applied Physics Letters*, Vol. 84, No. 15, 2943–2945, 2004.
2. Koschny, T., et al., "Effective medium theory of left-handed materials," *Physical Review Letters*, Vol. 93, No. 10, 107402, 2004.
3. Linden, S., et al., "Magnetic response of metamaterials at 100 terahertz," *Science*, Vol. 306, No. 5700, 1351–1353, 2004.
4. Pendry, J. B., et al., "Extremely low frequency plasmons in metallic mesostructures," *Physical Review Letters*, Vol. 76, No. 25, 4773, 1996.
5. Koschny, T., et al., "Resonant and antiresonant frequency dependence of the effective parameters of metamaterials," *Physical Review E*, Vol. 68, No. 6, 065602, 2003.

Development of 3D Anisotropic Artificial Dielectric Metamaterial for THz Frequency Range

E. A. Gurvitz, S. A. Andronaki, S. I. Gusev,
V. Y. Soboleva, Y. D. Nazarov, and M. K. Khodzitsky
Saint-Petersburg National Research University of Informational Technologies, Mechanics and Optics
ITMO University, Russia

Abstract— The paper is devoted to development of 3D lossless anisotropic dielectric artificial structure. The proposed structure was simulated by CST Microwave studio and the tensors of refractive index were obtained. Dielectric structure was made by 3D printer. The transmission and reflection spectra were obtained using the time domain spectrometry technique and the tensors of permittivity and refractive index were calculated. The simulation and experimental results are presented and analyzed for 0.1–2 THz frequency range.

Introduction: Nowadays, the metamaterials [1] and their applications challenge the customary view on the physics of optics and photonics. The developments of composite structures based on artificial metallic resonators prove the opportunity to change permittivity and permeability in wide frequency range, indeed, make them negative. Unfortunately the high losses of metallic structures do not allow to effectively use them for the most actual applications such as cloaking, filters, wave polarizators, beam splitters, wave front rotators and etc.. Therefore design of lossless dielectric metamaterials may be the solution of such problem especially for the THz frequency range due to the lack of the natural materials and absence of effective composites for these frequencies. The present work proposes anisotropic artificial dielectric metamaterial manufactured by 3D printing for THz frequency range.

Results and Conclusion: CST Microwave Studio commercial software was used for the numerical simulation of the structure. The sample of the dielectric medium (Fig. 1) was perforated by square holes. Such simple construction was chosen because of limit of spatial resolution of the 3D printer.

The geometry parameters of the unit cell of design were carefully estimated and the more capable parameters were applied. Refractive index spectra for different sides of the structure were calculated from obtained S-parameters matrix and refractive index anisotropy was shown. Using THz time-domain spectrometer the refractive index of the anisotropic structure were also obtained and analyzed for 0.1–2 THz.

The simulated results sufficiently well correlate with the experimental data. The new approach to construct anisotropic artificial dielectric composite structures by 3D printing was proposed.

ACKNOWLEDGMENT

This work was financially supported by Government of Russian Federation, Grant 074-U01.

REFERENCES

1. Capolino, F., *Theory and Phenomena of Metamaterials*, CRC Press, New York, 2009.

Enhancement of Terahertz Surface Plasmon Polaritons Using Tapered Graphene Waveguide

L. Ye[1], **L. Zhang**[1], **Y. Liu**[1], **and Q. H. Liu**[2]

[1]Department of Electronic Science, Xiamen University, China
[2]Department of Electrical and Computer Engineering, Duke University, USA

Abstract— Graphene is one of very few two-dimensional materials with a crystalline structure, which has great potential applications in many fields. Since its extraordinary electrical properties, especially for its tunable complex surface conductivity property leads to efficiently manipulate surface plasmon polaritons (SPPs), which has attracted sparked keen interest in graphene plasmonics. In this paper, firstly, the conductivity of graphene is studied by starting from the Kubo formula and the propagation of SPPs of a single sheet of graphene in terahertz (THz) regime is investigated. Then, a tapered graphene waveduide (TGW) is proposed to achieve terahertz SPPs enhancement. Since graphene's complex conductivity depends on the operating frequency f, charged particle scattering rate Γ, temperature T, and chemical potential μ_c, hence, the terahertz SPPs propagation and enhancement properties would also depend on these parameters. The numerical simulation results show that, by properly choosing the graphene's chemical potential distributions in different segments (however, keep other parameter the same), high enhancement of terahertz SPPs in this TGW can be obtained. Here, we assume operating frequency $f = 9\,\text{THz}$, $\Gamma = 0.43\,\text{meV}$, temperature $T = 3\,\text{K}$, chemical potential $\mu_{c1} = 5\,\text{eV}$ and $\mu_{c2} = 20\,\text{meV}$, respectively. Calculated from Kubo fomula, the conductivity values of the two segment are $\sigma_{g1} = 0.2391 - j10.3604\,\text{mS}$ (corresponding equivalent permittivity $\varepsilon_{g1} = -69068 + j1593.8$) and $\sigma_{g2} = 0.007 - j0.022\,\text{mS}$ (corresponding equivalent permittivity $\varepsilon_{g2} = 149 - j47.1$). As shown in Fig. 1, by comparing to graphene wavguide (GW), the terahertz SPPs enhancement factor of this TGW is greater than 6. This excellent property offers a new perspective on field confinement and should benefit future developments in graphene plasmonics and THz technology.

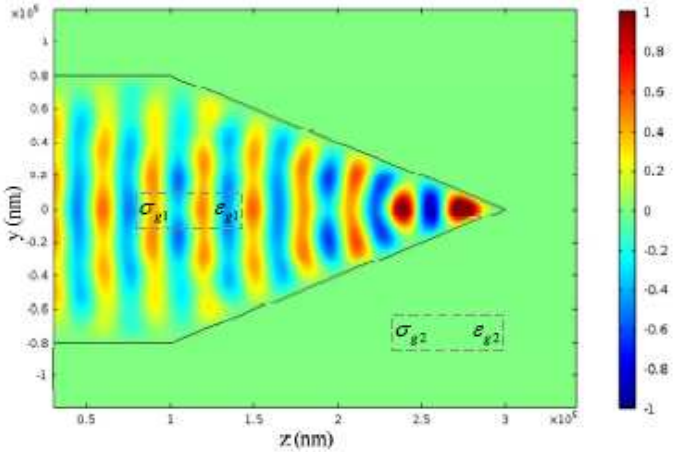

Figure 1: Electric field distribution of TGW.

Fabrication and Characterization of Fused Silica-based Metamaterials for High Temperature Resistant Radome Applications

Xigeng Miao, Qingwen Feng, Xiaowei Fang, Fabrizia Ghezzo, Zhiya Zhao, and Ruopeng Liu
Kuang-Chi Institute of Advanced Technology, Shenzhen, Guangdong 518057, China

Abstract— Polymeric or ceramic laminated composites with at least a layer of frequency selective surface (FSS) or metamaterials, both consisting of conductive periodic cellular architectures, are potential candidates for radome applications due to their unique high efficiencies of transmitting electromagnetic waves in a wide range of frequency. While polymeric laminated composites are relatively easy to be manufactured, they are not suitable for high-temperature resistant radome applications. For achieving the high-temperature resistance, ceramic metamaterials consisting of fused silica ceramic substrates are desirable, as fused silica ceramics have a low dielectric constant, a low dielectric loss, and a microporous structure, which is beneficial for the evaporation of organic species involved in the processing of ceramic metamaterials. However, the processing methods for fabricating ceramic metamaterials are very limited. The currently used low temperature co-fired ceramic (LTCC) technique suffers from the shortcoming of large sintering shrinkage rates, which unfortunately affect the accuracy of the designed geometry and dimensions of the periodic cellular architectures, and thus hinder the processing ability of ceramic-based metamaterials. In this paper, a novel method of a low temperature co-fired ceramic (LTCC) technique combined with a technique of ceramic joining via green tapes was developed to fabricate symmetric fused silica ceramic laminates. The laminates sandwiched a layer of periodic cellular architectures consisting of Ag-Pd conducting wires and patches. The newly developed ceramic laminates exhibited near-zero sintering shrinkage of the periodic cellular architectures in the planar direction, and the property of near-zero sintering shrinkage was significantly advantageous over the large sintering shrinkage of the conventional LTCC process. The near-zero sintering shrinkage was achieved by combining the following mechanisms: (1) constrained sintering of the LTCC laminates due to the presence of the rigid fused silica ceramic substrates; (2) self-constrained sintering of the LTCC laminates themselves due to the use of two different green tapes of different sintering temperatures; (3) pressure-assisted sintering of the LTCC laminates via sintering shrinkage only in the laminate thickness direction. The achieved near-zero sintering shrinkage of the ceramic laminates favored the preservation of the conductive elements in terms of shape and dimensions, and resulted in largely predictable low transmission losses (< 1 dB) of electromagnetic microwaves (7–18 GHz) for incident angles of $+/-30$ degrees and for both the transverse electric (TE) and the transverse magnetic (TM) polarization modes. Thus the fused silica based metamaterials were able to overcome the poor transmission efficiencies (below 11 GHz) of pure fused silica ceramic substrates with an identical thickness.

Multiband and Polarization Insensitive Terahertz Absorption Using a Vertical Nanowire Metamaterial

Yongqiang Pang, **Shaobo Qu**, **Jiafu Wang**, **Hua Ma**, **Jieqiu Zhang**, **Yongfeng Li**, **Mingbao Yan**, **and Hongya Chen**
College of Science, Air Force Engineering University, Xi'an, Shaanxi 710051, China

Abstract— We have investigated a terahertz metamaterial absorber consisting of a periodic quadrangular prism array embedded with vertical metal nanowires. It is found that the parallel nanowires terminated by a metal layer could support a cavity-like resonance when the nanowire height is equal to an odd multiple of quarter wavelengths, and thus a multiband absorption feature can be achieved by dissipating the localized fields in loss metal and dielectric medium. The four-fold rotational symmetry of the quadrangular prim attributes the insensitivity of the response to the polarization state. It is believed that the proposed nanowire array can be employed to design ultra-broadband absorbers.

Session 2P2b
SC3: Optical Microcavities in Biosensing

Optical Sensing and Particle Manipulation Using Silicon-based Optofluidic Chips

Andrew W. Poon, Jiawei Wang, and Zhanshi Yao
Photonic Device Laboratory, Department of Electronic and Computer Engineering
The Hong Kong University of Science and Technology, Clear Water Bay, Hong Kong, China

Abstract— In this talk we will report our latest experimental demonstration in optical sensing and particle manipulation using silicon-based optofluidic chips.

For optical sensing, we demonstrate coupled-resonator optical waveguides (CROWs) on a silicon-based platform as a bulk refractive index (RI) sensorusing what we termed "pixelized spatial detection." The key principle is based on imaging the light elastic scattering patterns from a CROW at a fixed laser wavelength within the CROW transmission band, and integrating the light scattering intensity from each coupled cavity as a pixel. Thus, the pixelized light scattering patterns from a CROW enables a spatial detection of the CROW responses to changes in the bulk refractive index. Unlike the conventional use of optical microcavities in the spectral domain for biosensing, where high quality factors (high Q's) are preferred for the microcavities and sophisticated wavelength-tunable lasers are often needed for spectral alignment with the high-Q resonances, our sensing method given a calibrated chip only requires a fixed-wavelength laser source with the wavelength within the relatively wide CROW transmission band and a camera for recording the light scattering patterns. We will discuss our recent proof-of-concept experiments on the silicon-on-insulator (SOI) platform in 1550 nm and the silicon-nitride (SiN)-on-silica platform in 680 nm.

For optical manipulation,we will highlight our recent work on using SiN microresonators and waveguide components for trapping and sorting sub-micrometer-sized polystyrene particles in a microfluidic channel. We will also briefly discuss our latest studies on using a two-dimensional optical lattice generated on a silicon chip for optical manipulation of particles including biological cells.

Photonic Crystal Slabs for Biosensing

S. Jahns, F. von Oertzen, T. Karrock, Y. Nazirizadeh, and M. Gerken
Institute of Electrical and Information Engineering, Christian-Albrechts-Universität zu Kiel, Germany

Abstract— We investigated the biofunctionalization of photonic crystals slabs for the label-free detection of biomolecules. Photonic crystal slabs are slab waveguides with a periodic nanostructure that supports quasi guided modes coupling to far field radiation. Measurements were performed with light at normal incidence to the photonic crystal slab. Transmission and reflection spectra reveal changes in the guided mode resonances upon binding of biomolecules to the surface. An overview on the design of photonic crystal slabs for biosensing, the fabrication of the photonic crystal slabs, and possible system approaches is given. In the design of photonic crystal slabs for protein binding the sensitivity to small refractive index changes in a thin layer above the surface needs to be optimized. This "surface sensitivity" typically requires a different optimal structure compared to the bulk sensitivity (refractive index change in the complete half space above the photonic crystal slab). The influence of the nanostructure period and duty cycle as well as the high index layer thickness and refractive index were investigated. Nanoimprint lithography with subsequent deposition of a high index layer and biofunctionlization is presented as one approach for fabricating photonic crystal slab biosensors. In comparison photonic crystal slabs fabricated by injection-molding are considered. Oblique angle layer deposition is introduced as a means to achieve structured high index layers. System approaches evaluating the guided mode wavelength and the guided mode intensity are compared. Results obtained with wavelength dependent measurements are compared to simple intensity measurements in a particular wavelength range. Both methods are applicable for label-free detection. In a spectrometer-free setup we measured the binding kinetics of a 2.5 nM solution of the protein streptavidin to a biotinylated photonic crystal surface. Furthermore, we employed aptamers for biofunctionalization. The miniaturization potential of a system based on an intensity measurement is evaluated paving the way towards smartphone biosensing. This approach is particularly promising for mobile biosensors applicable, for example, for home diagnostics.

Polymer-based Two Dimensional Photonic Crystal for Biosensing Application

Tatsuro Endo
Department of Applied Chemistry, Osaka Prefecture University, Osaka, Japan

Abstract— Photonic crystals (PhCs) are an attractive sensing platform because PhC provide strong light confinement which depend on the size and periodicity. In addition, optical response of PhCs are sensitive to surrounding refractive index changes. Hence, using PhCs, we have been developed polymer-based high sensitive biosensors that utilize the detection of surrounding refractive index change by the antigen-antibody reaction. However, to develop the more sensitive PhC-based label-free biosensor, investigation on the PhC design is significant challenge.

In this study, we developed an ultra-sensitive and polymer-based two-dimensional PhC (2D-PhC) cavity for label-free biosensor application. The device was fabricated with polymer on silicon substrate by using electron beam lithography (EBL) and operated near its resonance at 532 nm. Using our 2D-PhC cavity, reflection intensity was 60 times higher than without cavity. In addition, coating the sensor surface using layer-by-layer (LbL) assembly methodology by deposition of cationic (poly (sodium 4-styrenesulfonate)) and anionic (poly (allylamine hydrochloride)) layers for produces a different reflection intensity change. By deposition of LbL layers using 2D-PhC cavity, reflection intensity was decreased systematically and high sensitively (at least 1 layer (thickness: 2 nm)).

PhCs can be designed to localize the electric field in the low refractive index region (e.g., air gap), which makes the sensors extremely sensitive to a small refractive index change. By introducing a point cavity into a PhC, defect states can be pulled down from the air band or up from the substrate band. The corresponding optical spectrum shows narrow reflection peaks inside the photonic band gap (PBG), whose precise position is determined by the refractive index of the gap. Thus, the presence of molecules inside the gaps can be detected by monitoring a large reflection intensity change. In this study, we designed a 2D-PhC cavity optical sensor that is capable of monitoring of surrounding refractive index change on the gap walls.

For the fabrication of the polymer-based 2D-PhC cavity optical sensor, negative tone electron beam resist (NEB22) was coated onto the silicon substrate. The triangular configurated pillar array 2D-PhC cavity patterns (pillar diameter: 168 nm, pitch: 112 nm) were prepared on the electron beam resist-coated silicon substrate using EBL. To investigate the sensing performance using EBL patterned 2D-PhC cavity, a LbL assembly methodology for deposition of cationic and anionic layers by electrostatic interaction for changing of the surrounding refractive index, and the reflection intensity change by the irradiation of green laser (532 nm, 1 mW) was employed.

In addition, 2D-PhC cavity was applied to detect the DNA hybridization. The probe DNA was immobilized onto the 2D-PhC cavity surface. And the reflection intensity change due to the DNA hybridization-based refractive index change was monitored. As a result, the refractive index change with target DNA concentration could also be observed. From these results, this sensor has great potential for high sensitive detection of target molecules in visible region.

Refractive Index Sensing Utilizing Photonic Crystal Nanobeam Cavity

Yaocheng Shi
State Key Laboratory of Modern Optical Instrumentation
Centre for Optical and Electromagnetic Research
Zhejiang Provincial Key Laboratory for Sensing Technologies
Zhejiang University, Zijingang Campus, Hangzhou 310058, China

Abstract— Optical sensors based on one-dimensional Photonic Crystal (PhC) stack nanobeam cavities have been designed, fabricated and characterized. Finite width slots and pillar structures have been introduced to increase the sensitivity of the sensor. The majority of optical field distributes in the sensing area and the light matter interaction with the analytes has been enhanced. The geometry parameters of the cavity are optimized to achieve a high sensitivity while keeping a high Q-factor. The small footprint of the sensing part suggests a strong potential in on-chip biochemical sensing arrays.

Organic Lasers for Biochemical Sensing

Parag B Deotare, **Tom Mahony**, **and Vladimir Bulovic**
Massachusetts Institute of Technology, Cambridge, MA 02139, USA

Abstract— Extensive research is being carried out today to improve sensitivity in chemical and biological sensing to enable detection of single molecules. Recent work using optical microcavities has demonstrated the potential of such cavity based sensors to achieve very high sensitivities. We explore the possibility of improving the detection sensitivity by not only using a microcavity but also by coupling it to a non-linear amplifying medium. Semiconducting organic polymers are well known to have high absorption and emission properties along with good optical transparency. At the same time, the photophysical properties of these polymers gets altered by the slightest addition of impurities. The detection scheme relies on the change in the laser threshold due to introduction of non-radiative decay paths because of adsorption of molecules on the cavity surface. We report a compact, waveguide integratable, low threshold organic laser in a Alq_3 : DCM system. The device uses a photonic crystal nanobeam cavity which provides very high ratio of quality factor to mode volume (Q/V). The inherent waveguide geometry of the structure enables easy on-chip integration and along with the simplistic readout method makes such sensors ideal for biochemical sensing.

Single Nanoparticle Detection Using Microcavity Mode Broadening

Yun-Feng Xiao
State Key Lab for Mesoscopic Physics, Department of Physics, Peking University, Beijing 100871, China

Abstract— Optical microcavity biosensing has emerged as one of the most sensitive detection technologies. We report a new label-free detection method of single nanoparticles by employing nanoparticle-scattering-induced mode broadening in a free-space-coupled deformed microcavity. By monitoring the change of resonance linewidth, our method transcends the detecting ability limited by the intrinsic resonance linewidth and demonstrates the biosensing ability to detect single lentiviruses.

Long intracavity photon lifetimes and strong light confinement of the whispering gallery mode (WGM), described by high quality factors (Q) and small mode volumes (V) respectively, enhance light-matter interactions in optical microcavities, and show therefore a promise for ultrasensitive biosensing applications. Binding of polystyrene (PS) nanoparticles, viruses, DNA oligonucleotides and proteins on microcavities has been successfully detected by essentially monitoring either the resonance wavelength shift [1, 2] or the nanoparticle scattering-induced mode splitting [3, 4]. However, environmental thermal noise and unintended frequency drift of the probe laser hinder detection limit by monitoring the resonance wavelength shift, while the hardness in fabrication of ultra-high-Q modes supported microcavities, typically approaching or even exceeding 10^8, not only restricts the material of microcavities to silica, but also hinders the real sensor application.

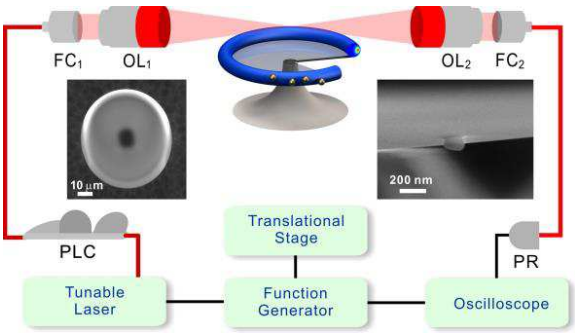

Figure 1: Experimental setup for PS nanoparticles and lentivirus detection using a free-space coupling system. PLC: polarization controller, FC: fiber collimator, OL: objective lens, PR: photoreceiver. Left Inset: SEM image (top view) of a deformed microtoroid. Right Inset: SEM images of a PS nanoparticle with a radius of 70 nm deposited on the microtoroid surface.

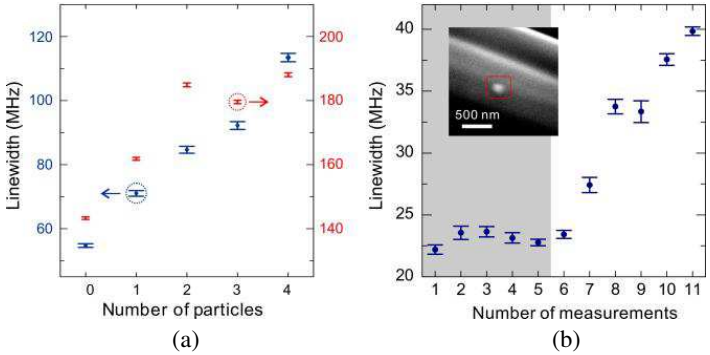

Figure 2: (a) Mode broadenings and fitting errors of two resonant modes versus number of bound 70 nm-radius PS nanoparticles. (b) The linewidth measured after each bath in DMEM solution. The solution used before the first five measurements did not contain lentiviruses; the second solution contained lentiviruses with a concentration of 5 fM. Inset: SEM image of a lentivirus deposited on the microtoroid surface.

Here, we report a new detection, that is monitoring nanoparticle-scattering-induced mode broadening in a free-space-coupled deformed microcavity, which would remove the strict requirement

concerning ultra-high-Q mode cavities, while still remaining reliable and sensitive. With this advantage, large quantity production of microcavities in practical applications is therefore promised, and biocompatible materials, such as polymers, can be used in fabrication.

Controlling Dynamical Tunneling in a Deformed Microcavity

D. Lippolis[1], L. Wang[2], X. F. Jiang[2], and Y. F. Xiao[2]

[1]Institute for Advanced Study, Tsinghua University, China
[2]Department of Physics, Peking University, China

Abstract— Deformed microcavities are characterized by the coexistence of high-Q and chaotic modes, supported on regions of the classical phase space where the dynamics is integrable and chaotic, respectively. Light can be transferred between the two through a classically forbidden process known as dynamical tunneling. As a result, we may observe states that are supported on both the regular and the chaotic regions of the phase space. Experimental evidence for dynamical tunneling can be given for example by the detection of high-Q whispering-gallery modes in the emission spectrum of a cavity where only the chaotic modes can be directly excited by a laser beam via free-space coupling. Originally introduced to enhance the overall output power of a laser, deformed microcavities using free-space coupling may also provide a valuable experimental tool for the investigation of chaotic tunneling. In the present work, we develop theory and experimental realization of a deformed cavity with tunable coupling between chaotic and whispering-gallery modes. The deformed microcavity consists of a quasi-2d silica toroid, on the top of a silicon pillar of significantly higher refractive index, which we use as absorber for the light fields in the silica. The rim of the silica, where most of the whispering-gallery modes live, is slightly thicker than the rest of the toroid. Varying the radius of the pillar also changes the amount of loss inside the microcavity, and, as it turns out, the effective coupling between chaotic and regular modes. For that reason such an absorber may be used to control dynamical tunneling. Theoretically, the electric field localized in the rim of the microcavity couples to the field inside the disk, the strength of the coupling being inversely proportional to the power loss inside the cavity. As a consequence, the probability of excitation of a whispering-gallery mode decreases with the radius of the silicon absorbing pillar. Experimentally, we look at the cavity emission spectra, and count the number of modes whose Q-factor exceeds a fixed threshold, finding it to decrease with the radius of the silicon pillar, the data showing qualitative agreement with the curve predicted. We finally discuss the statistics of the decay rates of the chaotic modes, as a function of the size of the absorber, and how our measurements could be improved in this direction to test the expectations of Random-Matrix-Theory or the fractal Weyl law.

Fabrication and Sensing Capability of Rolled-up Tubular Optical Microcavity

Jiao Wang, Gaoshan Huang, and Yongfeng Mei
Department of Materials Science, Fudan University, Shanghai 200433, China

Abstract— Optical mcirocavities with whispering-gallery-modes (WGMs) have large potential and in particular, those with a tubular geometry have attracted increasing attention due to their special geometry and interesting properties such as trimmed resonant modes, simplicity as fluidic channels, three-dimensionally (3D) mode confinement, unique evanescent wave, and so on. Optical microcaivities with the tubular geometry meet the challenge of assembly of conductive, semi-conductive and insulating materials into a tubular geometry thus spurring multifunctional applications to optofluidic devices, optical micro-devices like micro-lasers, and bio/chemical sensors. In this talk, we will address the rolled-up tubular optical microcavities from the perspectives offabricaiton method, theoretical consideration, optical characterization, and potential sensing applications.

Optical Detection of Ultrasound Using Polymer Microring Resonators and Applications in High Resolution Photoacoustic Imaging

L. Jay Guo
Department of Electrical Engineering and Computer Science
The University of Michigan, Ann Arbor, MI 48109, USA

Abstract— Optical detection of ultrasound is an emerging technique based on the interaction of strain field and optical field, modulating the optical properties of the resonance cavity for sensitive detection. Such a detection scheme can have several unique advantages, such as broadband response and relatively size-independent sensitivity, compared with conventional piezoelectric transducers. This talk will introduce polymer microring detector [1] made by nanoimprint process [2], possessing high sensitivity that is essential for deep penetration depth [3], especially for high-resolution imaging because of the strong attenuation of high-frequency ultrasound. Besides, small element size has the advantage of realizing wide acceptance angle of ultrasound detection [4], and for array [5] and microscopy [6] implementation. Examples of photoacoustic tomography and microscopy will be discussed [7].

Recently we demonstrated a microring detector with unprecedented broad bandwidth and high sensitivity. It has acoustic response up to 350 MHz at −3 dB and noise limited detectable pressure as low as 105 Pa in this frequency range. Application of such detector in photoacoustic imaging leads to improved axial resolving ability than using conventional ultrasound detector and sub-3 μm axial resolution is achieved, which is more than two folds improvement with respect to the reported record. Elastic-optic effect has been identified as the primary interaction mechanism between microring and acoustic field. The device miniaturized cavity height guarantees its superior broadband response, and its high Optical quality factor ensures detection sensitivity. This work suggests that the polymer based miniature microring resonator has the potential for acquiring volumetric photoacoustic images with cellular/sub-cellular resolution in three dimensions.

REFERENCES

1. Chao, C. Y., S. Ashkenazi, S.-W. Huang, M. O'Donnell, and L. J. Guo, "High-frequency ultrasound Sensors using polymer microring resonators," *IEEE Trans. Ultrason., Ferroelect., Freq. Contr.*, Vol. 54, 957–965, 2007.
2. Chao, C. Y. and L. J. Guo, "Polymer micro-ring resonators fabricated by nanoimprint technique," *J. Vac. Sci. & Technol. B.*, Vol. 20, No. 6, 2862–2866, 2002.
3. Ling, T., S.-L. Chen, and L. J. Guo, "Fabrication and characterization of high Q polymer micro-ring resonator and its application as a sensitive ultrasonic detector," *Opt. Exp.*, Vol. 19, 861–869, 2011.
4. Ling, T., S.-L. Chen, and L. J. Guo, "High-sensitivity and wide-directivity ultrasound detection using high Q polymer micro-ring resonators," *Appl. Phys. Lett.*, Vol. 98, 204103, 2011.
5. Maxwell, A., S.-W. Huang, T. Ling, J.-S. Kim, S. Ashkenazi, and L. J. Guo, "Polymer microring resonators for high-frequency ultrasound detection and imaging," *IEEE J. Special Topics in Quantum Electronics (on Biophtonics)*, Vol. 14, 191–197, 2008.
6. Chen, S.-L., Z. Xie, T. Ling, L. J. Guo, X. Wei, and X.-D. Wang, "Miniaturized all-optical photoacoustic microscopy based on microelectromechanical systems mirror scanning," *Opt. Lett.*, Vol. 37, 4263–4265, 2012.
7. Xie, Z., S.-L. Chen, T. Ling, L. J. Guo, P. L. Carson, and X.-D. Wang, "All optical photoacoustic microscopy," *Opt. Exp.*, Vol. 10, 9027–9034, 2011.

Session 2P3a
MS-1.5: Organic and Hybrid Solar Cells 2

Control of Molecular Packing via Evaporation Rate of Small Molecule Organic Solar Cell

Po-Sheng Wang[1], **Jiun-Haw Lee**[1], **Shun-Wei Liu**[2], **Chin-Ti Chen**[3], **Yung-Chih Cheng**[4], **Mau-Kuo Wei**[4], **Chih-Chien Lee**[5], **Wei-Cheng Su**[5], **Tien-Lung Chiu**[6], **and Chi-Feng Lin**[7]

[1]Graduate Institute of Photonics and Optoelectronics and Department of Electrical Engineering
Taiwan University, Taipei, Taiwan
[2]Department of Electronic Engineering, Ming Chi University of Technology
New Taipei City 24301, Taiwan
[3]Institute of Chemistry, Academia Sinica, Taipei 10617, Taiwan
[4]Department of Materials Science and Engineering, Dong Hwa University
Hualien 97401, Taiwan
[5]Department of Electronic Engineering, Taiwan University of Science and Technology
Taipei 10617, Taiwan
[6]Department of Photonics Engineering, Yuan Ze University, Chung-Li, Taiwan
[7]Department of Electro-Optical Engineering, United University, Miaoli 36003, Taiwan

Abstract— In this paper, we demonstrate that the molecular stacking was affected by the deposition rate of organic thin films, bis (naphthylphenylaminophenyl) fumaronitrile (NPAFN) and boron subphthalocyanine chloride (SubPc), which were used as the donor materials of organic solar cells. With lower deposition rate, the inter-molecular interaction increases, which results in higher hole mobility. However, it also increases the reverse saturation current and reduces the open circuit voltage. With suitable tuning the deposition rate, maximum power conversion efficiency can be obtained by compromising the open circuit voltage and serial resistance.

Small-molecule Organic Cathode Interfacial Materials for Organic Photovoltaics

Wan-Yi Tan[1], **Rui Wang**[2, 3], **Min Li**[1], **Gang Liu**[1], **Ping Chen**[5], **Xin-Chen Li**[4], **Shun-Mian Lu**[4], **Hugh Lu Zhu**[4], **Qi-Ming Peng**[5], **Xu-Hui Zhu**[1], **Wei Chen**[2, 3], **Wallace C. H. Choy**[4], **Feng Li**[5], **Junbiao Peng**[1], **and Yong Cao**[1]

[1]State Key Laboratory of Luminescent Materials and Devices (SKLLMD)
Institute of Polymer Optoelectronic Materials and Devices
South China University of Technology (SCUT), Guangzhou 510640, China
[2]Department of Physics, National University of Singapore
3 Science Drive 2, Singapore 117543, Singapore
[3]Department of Chemistry, National University of Singapore
3 Science Drive 3, Singapore 117543, Singapore
[4]Department of Electrical and Electronic Engineering
The University of Hong Kong, Pokfulam Road, Hong Kong, China
[5]State Key Lab of Supramolecular Structure and Materials, Jilin University
2699 Qianjin Avenue, Changchun 130012, China

Abstract— Organic small molecules with different functional moieties have been investigated as cathode interfacial materials (CIMs) for organic photovoltaics. These small-molecule compounds show many favorable features, for instance: (i) Ease of synthesis and purification. Analytically pure sample can be obtained without sublimation. (ii) Non-hygroscopy. (iii) Multi-processability. Thin films can be deposited by facile vacuum deposition or spin-cast from polar solvents. The photovoltaic devices that contained a thermally deposited interlayer **Phen-NaDPO** and Ag or Al cathode produced a considerably improved PCE, due largely to a simultaneous increase in V_{oc} and FF relative to the reference devices without a CIM. Notably, a PCE of 7.51% was obtained for the **Phen-NaDPO**/Ag device utilizing the active layer PTB7:$PC_{71}BM$, which far exceeds that of the reference Ag device and even compares well to that of the Ca/Al device. The increased PCE to 8.56% of the **Phen-NaDPO**/Al device (with $J_{sc} = 16.81\,\mathrm{mA\ cm^{-2}}$, $V_{oc} = 0.75\,\mathrm{V}$, $FF = 0.68$) appears comparable to that of the similar device involving a widely studied conjugated polymer interlayer "PFN". Ultraviolet photoemission spectroscopy (UPS) studies reveal that a thin film of **Phen-NaDPO** can significantly lower the work function of the Ag metal, as well as ITO and HOPG. The impacts of the chemical structures and thickness of the CIMs as well as processability on photovoltaic performances are discussed.

Application of Electrode Interlayers for Highly Efficient Polymer Solar Cells

Youchun Chen[1], **Shuheng Sun**[1], **Weilong Zhou**[1], **Fenghong Li**[1], **and Yuguang Ma**[1, 2]

[1]State Key Laboratory of Supramolecular Structure and Materials
Jilin University, Changchun 130012, China
[2]State Key Laboratory of Luminescent Materials and Devices
Institute of Polymer Optoelectronic Materials and Devices
South China University of Technology, Guangzhou 510640, China

Abstract— Interfacial modification of electrode and active layer has attracted increased attention to improve device efficiency by minimizing charge injection/extraction barriers and forming ohmic contact between electrode and active layer in organic optoelectronic devices [1]. Significant improvements of device efficiency in polymer solar cells (PSCs) have recently appeared due to an introduction of anode interlayer or cathode interlayer [2, 3]. Herein we report our efforts in terms of interfacial modification of electrode and active layer and particularly highlight application of doped conjugated microporous polymer (CMP) films as a anode interlayer in the PSCs. The doped CMP film presents not only inherently uniform micropores and large surface areas but also a high work function and good conductivity. It indicates the doped CMP film is a promising anode interlayer replacing PEDOT : PSS. Our results show that the doped CMP film as an anode interlayer has simultaneously enhanced the open circuit voltage, short circuit current and fill factor of PSCs. It results in an obvious increase of power conversion efficiency of PSCs compared to the PEDOT:PSS-only device. These findings demonstrate the great potential of our CMP film as a universal electrode interlayer in organic optoelectronic devices. In addition, we also compared effects of alkali metal salts or alcohol/water-soluble molecules as a cathode interlayer on the device performance of PSCs. By combined optimization of anode interlayer and cathode interlayer, highly efficient PSCs have been achieved.

REFERENCES

1. Chen, L. M., Z. Xu, Z. R. Hong, and Y. Yang, *J. Mater. Chem.*, Vol. 20, 2575, 2010.
2. He, Z. C., C. M. Zhang, X. Huang, W. Y. Wong, H. B. Wu, L. W. Chen, S. J. Su, and Y. Cao, *Adv. Mater.*, Vol. 23, 4636, 2011.
3. Gu, C., Y. C. Chen, Z. B. Zhang, S. F. Xue, S. H. Sun, K. Zhang, C. M. Zhong, H. H. Zhang, Y. Y. Pan, Y. Lv, Y. Q. Yang, F. H. Li, S. B. Zhang, F. Huang, and Y. G. Ma, *Adv. Mater.*, Vol. 25, 3443, 2013.

Graphene Oxide Derivatives as Hole- and Electron-extraction Layers for Efficient Polymer Solar Cells

Jun Liu
State Key Laboratory of Polymer Physics and Chemistry, Changchun Institute of Applied Chemistry
Chinese Academy of Sciences, 5625 Renmin Street, Changchun 130022, China

Abstract— Polymer solar cells (PSCs) have recently received great attention due to their low cost and flexibility. The electron- and hole-extraction layers play an important role in determining photovoltaic efficiency of PSCs. Recently, graphene oxide (GO) has been demonstrated to be an effective hole-extraction layer for PSCs. However, PSCs based on GO suffer from poor device performance owing to insulating property of GO, which significantly increases series resistance of the PSC devices [1].

We have developed a variety of GO derivatives to be used as hole- and electron- extraction layers for efficient PSCs. For example, sulfated graphene oxide (GO-OSO_3H), in which $-OSO_3H$ groups are introduced to the basal plane of reduced graphene oxide, is an excellent hole-extraction material for PSC due to its improved conductivity and solution processability [2]. Graphene oxide ribbon (GOR), which is developed by unzipping of single-walled carbon nanotubes, was also an excellent hole-extraction layer for PSCs with improved efficiency and lifetime [3]. Cesium-neutralized graphene oxide (GO-Cs), which is synthesized by neutralization of GO aqueous solution with Cs_2CO_3, is an electron-extraction layer for PSCs [4]. The reason for the electron-extraction property of GO-Cs is the work function change of GO-Cs-modified electrode.

REFERENCES

1. Liu, J., M. Durstock, and L. M. Dai, *Energy Environ. Sci.*, 2014, in press.
2. Liu, J., Y. H. Xue, and L. M. Dai, *J. Phys. Chem. Lett.*, Vol. 3, 1928, 2012.
3. Liu, J., G.-H. Kim, Y. H. Xue, J. Y. Kim, J.-B. Baek, M. Durstock, and L. M. Dai, *Adv. Mater.*, Vol. 26, 786, 2014.
4. Liu, J., Y. H. Xue, Y. X. Gao, D. S. Yu, M. Durstock, and L. M. Dai, *Adv. Mater.*, Vol. 24, 2228, 2012.

Ultra-thin Hybrid Photovoltaics with Angle-insensitive Color Appearance, Transparency and High Quantum Efficiency

Jae Yong Lee, **Kyu-Tae Lee**, **Sungyong Seo**, **and L. Jay Guo**
Department of Electrical Engineering and Computer Science
The University of Michigan, Ann Arbor, MI, 48109, USA

Abstract— Most current solar panels are made by complex processes using expensive semiconductor materials, and they are rigid, heavy, and with a dull, black appearance. As a result of their non-aesthetic appearance and weight, they are primarily installed on rooftops so as to minimize the negative appearance. Large surfaces and interiors of the modern buildings are not efficiently utilized for potential electric power generation. Here, we introduce dual-function solar cells based on ultra-thin doping-free amorphous silicon embedded in optical cavity that not only efficiently extract the photogenerated carriers but also display distinctive colors with the desired angle-insensitive appearances. Light-energy harvesting colored signage and colored transparent PVs were demonstrated [1]. Furthermore a cascaded photovoltaics scheme by tunable spectrum splitting can be employed to increase power efficiency by absorbing broader band of light energy. This study points a new direction to architecturally compatible and decorative thin-film photovoltaics.

Conventional thin-film photovoltaic cells have too thick photoactive layer to be utilized for tuning and transmitting various colors. Even typical plasmonic and photonic color filters are not acceptable to be integrated into photovoltaics, hindered by the angle-dependent property, a key challenge for practical use. We address these distinct challenges by investigating ultra-thin ($6 \sim 31$ nm) undoped a-Si/organic hybrid solar cells, producing colors with high angular tolerance. Rather than using the doped p- and n-region in conventional thin film PVs, we borrow the concept of charge transport layers from organic PVs and designed hybrid PV structure to satisfy both the electrical and optical requirement. Since the undoped a-Si is over an order of magnitude thinner than the conventional a-Si PVs, and the thickness smaller than the charge carrier diffusion lengths, very high quantum efficiency have been achieved in these hybrid colored PV cells, clearly demonstrating most of the absorbed photons in the undoped a-Si layer contribute to the photocurrent due to the suppressed electron-hole recombination. We also show the resonance is invariant with respect to the angle of incidence up to $+-70$ degrees regardless of the incident polarization. Our exploration provides a design to realize energy harvesting colored panels, potentially creating innovative applications.

REFERENCES

1. Lee, J. Y., K. T. Lee, S. Y. Seo, and L. J. Guo, "Decorative power generating panels creating angle insensitive transmissive colors," *Sci. Rep.*, Vol. 4, 4192, 2014.

Plasmonic-electrical Effects of Metal Nanoparticles for Highly Efficient Organic Solar Cells

Wallace C. H. Choy, **Fengxian Xie**, **Di Zhang**,
Wei E. I. Sha, **Xinchen Li**, **and Baofu Ding**
Department of Electrical and Electronic Engineering
The University of Hong Kong, Pokfulam Road, Hong Kong

Abstract— Optical effects of the plasmonic structures and materials effects of the metal nanomaterials have recently been individually studied for enhancing performances of organic solar cells (OSCs). In this work, differently, the effects of plasmonically induced carrier generation and enhanced carrier extraction of the carrier transport layer (i.e., plasmonic-electrical effects) in OSCs are investigated. We propose and demonstrate enhanced charge extraction in TiO_2 as a highly efficient electron transport layer by the incorporation of metal nanoparticles (NPs). While OSCs using pristine TiO_2 can only operate by UV activation (< 400 nm, otherwise poor S-shape J-V characteristics are exhibited), efficient device performance is demonstrated by using Au NPs incorporated TiO_2, at a plasmonic wavelength (560–600 nm) far longer than the originally necessary UV light. By optimizing the amount of Au NPs doped into TiO_2, the performances of OSCs with various polymer active layers are enhanced and efficiency of 8.74% is reached [1]. In order to understand the fundamental physics, an integrated optical and electrical model (i.e., a multi-physics model), which takes into account hot carrier tunneling probability and extraction barrier between TiO_2 and active layers, is introduced here. From experimental and theoretical studies, we attribute the enhanced charge extraction under plasmonic wavelength illumination to the strong charge injection of plasmonically excited electrons from NPs into TiO_2. The mechanism favors better energy alignment at the TiO_2 interface which facilitates carrier transport in OSCs. Recently, we also find that the TiO_2-metal NPs composite can enhance the carrier accumulation which can fill the trap states in TiO_2 and thus improve the electrical conduction of TiO_2 and thus improve the device performances of OSCs [2]. The work can contribute to new approaches and knowledge to utilize plasmonically electrical nanostructures in organic optoelectronic devices for enhancing device performances.

REFERENCES

1. Zhang, D., W. C. H. Choy, F. Xie, W. E. I. Sha, X. Li, B. Ding, K. Zhang, F. Huang, and Y. Cao, "Plasmonic-electrically functionalized TiO_2 for high performance organic solar cells," *Adv. Funct. Mat.*, Vol. 23, No. 34, 4255–4261, 2013, Doi: 10.1002/adfm.201203776.
2. Xie, F. X., W. C. H. Choy, W. E. I. Sha, D. Zhang, S. Zhang, X. Li, C. W. Leung, and J. Hou, "Enhanced charge extraction in organic solar cells through electron accumulation effects induced by metal nanoparticles," *Energy Environ. Sci.*, Vol. 6, 3372–3379, 2013.

Light Manipulation for Organic Optoelectronics Using Bio-inspired Moth's Eye Nanostructures

Jian-Xin Tang, Lei Zhou, Qing-Dong Ou, Jing-De Chen, and Yan-Qing Li
Institute of Functional Nano & Soft Materials (FUNSOM)
Collaborative Innovation Center of Suzhou Nano Science and Technology
Soochow University, Suzhou 215123, China

Abstract— Organic optoelectronic devices, including organic light-emitting devices (OLEDs) and organic solar cells (OSCs) have been attracting considerable interest as next-generation lighting source and renewable energy applications. Significant progress on the device performance of OLEDs and OSCs with nearly 100% internal quantum efficiency has been made in recent years via the incorporation of new materials, morphology control, interface engineering, and device fabrication processes. However, further improvement in efficiency remains a daunting challenge due to limited light extraction or absorption in conventional device architectures. Here we report a universal method of optical manipulation of light by integrating a dual-side bio-inspired moth's eye nanostructure with broadband anti-reflective and quasi-omnidirectional properties for use in the performance improvement of organic optoelectronic devices of various material systems. Light out-coupling efficiency of OLEDs with stacked triple emission units is over 2 times that of a conventional device, resulting in drastic increase in external quantum efficiency and current efficiency to 119.7% and 366 cd/A at a luminance of 1,000 cd/m^2 without introducing spectral distortion and directionality. Similarly, the light in-coupling efficiency of OSCs is increased 20%, yielding an enhanced power conversion efficiency of 9.33%. The light-coupling enhancement in OLEDs and OSCs with MEN is the combined result of both the two-dimensional sub-wavelength structures and the continuously tapered morphology on the patterned surface with a superior gradient refractive index profile at the interface. The light is therefore manipulated in all azimuthal directions over the entire emission wavelength range. The optical simulations provide an understanding of optical manipulation of light out-coupling and in-coupling process in OLEDs and OSCs. Note also that the method developed here brings about an invaluable advantage, which enables the processing compatibility with the high-throughput large-area roll-to-flat and roll-to-roll manufacturing techniques in future mass production of low-cost organic optoelectronic devices.

REFERENCES

1. Zhou, L., Q. D. Ou, J. D. Chen, S. Shen, J. X. Tang, Y. Q. Li, and S. T. Lee, *Sci. Rep.*, Vol. 4, 4040, 2014.
2. Chen, J. D., L. Zhou, Q. D. Ou, Y. Q. Li, S. Shen, S. T. Lee, and J. X. Tang, *Adv. Energy Mater.*, 2014, DOI: 10.1002/aenm.201301777.

Engineering Nanostructured Materials for Organic/Inorganic Hybrid Solar Cells

Tao Chen
Department of Physics, The Chinese University of Hong Kong, Shatin, N. T. Hong Kong, China

Abstract— Conversion of solar energy into electricity through photovoltaic (PV) effect is one of the most promising approaches to cope with the energy shortage in the future. To date, various PV devices have been developed, among which dye-sensitized solar cell (DSSC) is a kind of solution processable organic/inorganic hybrid solar cells with low fabrication cost. In addition, the devices can be fabricated with different colors and transparencies, these characteristics are attractive in the building-integrated photovoltaics. In this talk, I will mainly introduce our recent work on the nanostructured materials for both the anode and cathode applications in DSSCs.

In specific, I will firstly present the utilization of plasmon nanostructures for the improvement of light harvesting [1]. In DSSCs, most of the dye molecules only possesses strong light absorption in specific ranges. To improve the weak absorption and finally achieve strong full-color spectral response, we apply the noble metal nanostructure to selectively improve the light response in the low extinction coefficient region of the dye molecules.

Afterwards, I will also talk about our research in the development of the low cost, printable techniques for catalysts on the counter electrodes of DSSCs. To develop FTO- and Pt-free counter electrode, we fabricated carbon supported CZTS nanodots on the Mo based soda lime glass for the counter electrodes of DSSCs [2]. The final results show that the carbon supported CZTS nanodots on the Mo/glass outperform the conventional Pt nanoparticles on FTO coated glass, which is featured as high cost in terms of both the transparent conducting glass as well as the noble metal element.

In addition, we also found that the application of few-layer $MoSe_2$ on Mo/glass can also outperform the conventional counter electrodes [3]. The solar to electrical power conversion efficiencies of the DSSCs based on $MoSe_2$ and Pt catalysts are 9.0% and 8.7% respectively. Notably, the synthesis can be simply conducted by annealing Mo/glass in the selenium vapor. Both the fabrication of the two types of FTO- and Pt-free counter electrode is scalable for the large-area applications.

REFERENCES

1. Chang, S., Q. Li, X. Xiao, K. Y. Wong, and T. Chen, "Enhancement of low energy sunlight harvesting in dye-sensitized solar cells using plasmonic gold nanorods," *Energy Environ. Sci.*, 9444–9448, 2012.
2. He, J., L. T. L. Lee, S. Yang, Q. Li, X. Xiao, and T. Chen, "Printable highly catalytic Pt- and TCO-free counter electrode for dye-sensitized solar cells," *Acs Appl. Mater. & Interfaces*, Vol. 6, 2224–2229, 2014.
3. Lee, L. T. L., J. He, B. Wang, Y. Ma, K. Y. Wong, Q. Li, X. Xiao, and T. Chen, "Few-layer $MoSe_2$ possessing high catalytic activity towards iodide/tri-iodide redox shuttles," *Sci. Rep.*, Vol. 4, 2014.

Photovoltage Loss in Excitonic Solar Cells

Sai-Wing Tsang[1, 2], **Song Chen**[2], **Tzung-Han Lai**[2], **John R. Reynolds**[3], **and Franky So**[2]

[1]Department of Physics and Materials Science, City University of Hong Kong, Hong Kong, China
[2]Materials Science and Engineering Department, University of Florida, USA
[3]School of Chemistry and Biochemistry, School of Materials Science and Engineering
Center for Organic Photonics and Electronics, Georgia Institute of Technology, USA

Abstract— Polymer solar cells with power conversion efficiencies (PCEs) over 8% have been demonstrated in laboratories with advances of novel materials, device processing, and device architectures. However, some critical physical properties of the polymer:fullerene bulk hetero junctions (BHJs) such as the donor-acceptor interface energetics which controls the charge transfer process are not well understood. In a BHJ photovoltaic cell, the open-circuit voltage (V_{OC}) is determined by the energy level difference of the highest-occupied-molecular-orbital (HOMO) of the donor and the lowest-unoccupied-molecular orbital (LUMO) of the acceptor. However, there is lack of experimental approach to directly probe such alignment in a working device.

In this presentation, we will demonstrate a technique — charge modulated electro absorption spectroscopy (CMEAS) to directly determine the effective bandgap and the interface effective force in a polymer:fullerene BHJ system [1]. By measuring the electro absorption (EA) signal due to charge-modulation (CM) in the polymer, we are able to observe a clear sub-bandgap signal through direct excitation of excitons to the charge transfer states. Such a differential spectrum measured by CMEAS has a much higher signal-to-noise ratio than that measured by linear optical absorption techniques. Compared to the conventional electrochemical method, CMEAS can probe the energy level alignment at the electron donor-accept or interface in a working BHJ photo vltaic cell. Using CMEAS, for the first time we are able to directly probe the effective bandgap in polymer:fullerene systems. The results also bring insight into the details of the charge transfer states and the origin of V_{OC} in polymer photovoltaic cells.

REFERENCES

1. Tsang, S.-W., S. Chen, and F. So, *Adv. Mater.*, Vol. 25, 2434, 2013.

High-efficiency All-polymer Solar Cells Enabled by a Low Bandgap Polymer

He Yan
The Hong Kong University of Science and Technology, Hong Kong, China

Abstract— We report high-performance all-PSCs based on a donor polymer with an optical bandgap of 1.55 eV. A high J_{sc} of 11.5 mA/cm^2 and PCE of 5% were achieved largely due to the low optical bandgap and the reasonably large EQE of the cell. AFM and R-SoXS characterizations together support that the NT:N2200 blend film is smooth and exhibits an average domain size of about 100 nm, which is comparable to the corresponding NT:fullerene blend films that have 6.2% with $\sim$ 90 nm thick films. These characterizations combined can largely explain the great performance of NT:N2200-based all-PSCs. Lastly, it is important to note that NT:N2200-based all-PSCs exhibit a near ideal LUMO offset of $\sim$ 0.3 eV, which is the reason why NT:N2200-based cells can obtain low-bandgap and high V_{oc} at the same time. With a reasonably small LUMO offset, NT:N2200-based PSCs offer the potential for further optimization and improvement in device efficiencies.

Design Rule of Plasmonic Materials for High Performance Organic Solar Cells

Jung-Yong Lee
Graduate School of Energy, Environment, Water, and Sustainability (EEWS), Graphene Research Center
Korea Advanced Institute of Science and Technology (KAIST), Daejeon 305-701, Republic of Korea

Abstract— Here, we present a design rule how to utilize the plasmonic materials in organic solar cells (OSCs) as an efficient approach to improve the power conversion efficiency of the OSCs. We successfully manipulated the external quantum efficiency (EQE) and absorption enhancement in OSCs in entire visible wavelength range with controlling the size and shape of metal nanoparticles (MNPs). We found that the *forward scattering efficiency* depending on the size of AgNPs considerably influences the device performance. Then, we propose a metal-metal core-shell nanocube (NC) as an advanced plasmonic material for highly efficient organic solar cells (OSCs). We covered an Au core with a thin Ag shell as *a scattering enhancer* to build Au@Ag NCs, which showed stronger scattering efficiency than Au nanoparticles (AuNPs) throughout the visible range. Highly efficient plasmonic organic solar cells were fabricated by embedding Au@Ag NCs into an anodic buffer layer, poly (3, 4-ethylenedioxythiophene):poly (styrenesulfonate) (PEDOT:PSS). We proved the strongly enhanced plasmonic scattering efficiency of Au@Ag NCs embedded in organic solar cells *via* theoretical calculations and detailed optical measurements.

Session 2P3b
MS-1.2: Graphene Photovoltaics

Graphene-Silicon Heterojunction Photovoltaic Device

Xinming Li
National Center for Nanoscience and Technology
No. 11, Zhongguancun, Beiyitiao, Beijing 100190, China

Abstract— Graphene-silicon heterojunction structures have been attracting increasing interests for both scientific fundamentals and potential applications in various new optoelectronic devices, e.g., solar cells, photodetectors and so on. More and more studies are promoted to realize the full potential of this new type of photovoltaic device.

Graphene-silicon heterojunction photovoltaic devices were first studied in 2010 [1]. This graphene-based heterojunction showed the well-defined diode and photovoltaic effect. When intrinsic p-doped or metallic graphene and n-Si with a prominent work function difference were in contact with each other, electrons on the Si side were depleted, which bent the energy band to form a built-in electric field. This built-in potential splitted the excess electrons and holes generated by incident light, hence converting light energy into electric energy [2.] The solar energy conversion efficiency (η) of this heterojunction solar cells was 6.5%. To further improve the photovoltaic performance, acid doping was employed to optimize the work function of graphene as well as to introduce the nitrate anions into the surface of the film for charge separation and easier transport [3]. Acid doping effectively boosted the energy conversion efficiency of the graphene-based heterojunction solar cells by a factor of $\sim$2 up to 9.6%, which is significantly higher than using the undoped graphene films [4]. Furthermore, a colloidal antireflection coating TiO_2 were involved onto graphene-silicon solar cell and enhanced the efficiency to 14.5% [5]. Recently, this model has been extended to the development of photodetectors, and this device exhibited the excellent performance indicating this also should be a promising field for graphene-silicon heterojunction applications [6]. This simple concept of graphene-silicon heterojunction, with an improved understanding of electronic coupling, surface passivation, doping, and junction formation, will lead to a new trend in the development of graphene-based photovoltaic devices.

REFERENCES

1. Li, X. M., H. W. Zhu, K. L. Wang, et al., "Graphene-on-silicon Schottky junction solar cells," *Advanced Materials*, Vol. 22, 2743–2748, 2010.
2. Lin, Y. X., X. M. Li (co-first author), D. Xie, et al., "Graphene/semiconductor heterojunction solar cells with modulated antireflection and graphene work function," *Energy & Environmental Science*, Vol. 6, 108–115, 2013.
3. Li, X. M., D. Xie, M. Zhu, et al., "Ion doping of graphene for high-efficiency heterojunction solar cells," *Nanoscale*, Vol. 5, 1945–1948, 2013.
4. Li, X. M., D. Xie, H. S. Park, et al., "Anomalous behaviors of graphene transparent conductors in graphene-silicon heterojunction solar cells," *Advanced Energy Materials*, Vol. 3, 1029–1034, 2013.
5. Shi, E. Z., H. B. Li, L. Yang, et al., "Colloidal antireflection coating improves graphene–silicon solar cells," *Nano Letters*, Vol. 13, 1776–1781, 2013.
6. Zhu, M., X. M. Li, Y. B. Guo, et al., "Vertical junction photodetectors based on reduced graphene oxide/silicon schottky diodes," *Nanoscale*, 2014, DOI: 10.1039/C4NR00056K.

Low Temperature Reduction of Free-standing Graphene Oxide Films by Metal Iodide Acidic Aqueous Solutions

Songping Luo, **Chenyang Liu**, **and Hong Lin**
State Key Laboratory of New Ceramics & Fine Processing
School of Materials Science and Engineering, Tsinghua University, Beijing 100084, China

Abstract— Here we report a green and facile route for highly efficient reduction of free-standing graphene oxide (GO) films with metal iodide aqueous solutions at low cost. The metal iodides (MgI_2, AlI_3, ZnI_2, FeI_2) were synthesized directly from metal and iodine powder with water as a catalyzer. An extremely high bulk conductivity of 55088 S/m for reduced graphene oxide (rGO) films were obtained with FeI_2 solution of which pH = 0 at 95°C for 6 hours. The catalytic effect of strong Lewis acid for the promotion of the nucleophilic substitution reaction is responsible for the greatly improved bulk conductivity. Furthermore, it was found that the layer-to-layer distance (d_L) and the crystallinity of the rGOfilms are regarded as two main factors affecting the bulk conductivity rather than C/O ratio and defect concentration.

PEDOT:PSS/planar-Si Hybrid Solar Cells with 12.70% Efficiency

Yuanfan Zhao[1], **Dan Xie**[1], **Jianlong Xu**[1], **Tingting Feng**[1], **Xiaowen Zhang**[1], **Tianling Ren**[1], **Miao Zhu**[2], **and Hongwei Zhu**[2]

[1]Tsinghua National Laboratory for Information Science and Technology (TNList)
Institute of Microelectronics, Tsinghua University, Beijing 100084, China
[2]State Key Laboratory of New Ceramics and Fine Processing
Key Laboratory of Materials Processing Technology of MOE
School of Materials Science and Engineering, Tsinghua University, China

Abstract— The hybrid solar cells with high power conversion efficiency (PCE) and low costs have attracted much research interests. Recently, a transparent and hole transporting polymer of Poly (3, 4-ethylenedioxythiophene):poly (styrene sulfonic acid) (PEDOT:PSS) is used to form a hybrid device with the N-type silicon, which stands out due to its high power conversion efficiency and simple device structure. In the paper, we demonstrate the PEDOT:PSS/planar-Si structure with a hydrogen-terminated Si (H-Si) surface instead of a SiO_x surface layer or any surfactant added into PEDOT:PSS, resulting in high PCE value. H-Si surface is achieved by HF solutions treatment of the device before fabrication of PEDOT:PSS films, which ensures that there was almost no native silicon oxide layer remained. Cells show high power conversion efficiency (PCE) of 8.27 $\sim$ 12.70%, and cell with the PCE of 12.70% presents short circuit current density (J_{SC}), open circuit voltage (V_{OC}) and fill factor (FF) of 20.92 mA/cm^2, 0.63 V and 70.26% under standard illumination (Air mass 1.5, 73 mW/cm^2), respectively. The better contact of PEDOT:PSS film with the Si substrate is contributed to the formation of effective PEDOT:PSS/Si heterojunction, resulting in the enhanced photovoltaic performances.

Reduced Graphene Oxide/n-Si Schottky Junction Photodetector

Miao Zhu and Hongwei Zhu
State Key Laboratory of New Ceramics and Fine Processing
Key Laboratory of Materials Processing Technology of MOE
School of Materials Science and Engineering, Tsinghua University, China

Abstract— Graphene/Si Schottky junction has been widely reported for applications in photovoltaic fields such as solar cell and photodetector due to its high light transmittance and carriers mobility. Recently, such a model has been investigated to be used for photodetecting of ultraviolet and infrared illumination. However, most of these studies were based on graphene prepared by chemical vapor deposition or mechanical exfoliation, which wereof low productivity and complicated in process. Besides, the semi-metal band structure of pristine graphene severely limited its optimization. Reduction of the graphene oxide, which can be easily synthesized based on Hummers method, is another important way to prepare graphene with high productivity and simple proceduress. Moreover, the oxygen functional groups (OFGs) contained in the reduced graphene oxide (r-GO) provides more flexibility to open and control the band gap of graphene. Meanwhile, OFGs can also influence the transportation of carriers across the r-GO/Si interface as well as the separation and recombination of them both in the r-GO film and Si substrate. Here, we present an effective way to fabricate r-GO/n-Si Schottky diodes by a simple drop-casting with following thermal reduction. As-assembled devices show excellent light sensing performance in terms of ON/OFF ratio ($> 10^4$), responsivity, detectivity and response/recovery time. Other characteristics such as the Schottky barrier height, ideal factor, and the photoelectric conversion efficiency dependent on the reduction level are also investigated to analyze influences of OFGs on the performance of the devices.

Photo-detecting Behaviors of MoS_2 Transistors

Xiaowen Zhang[1], **Dan Xie**[1], **Jianlong Xu**[1], **Tingting Feng**[1], **Yuanfan Zhao**[1], **Tianling Ren**[1], **Miao Zhu**[2], **and Hongwei Zhu**[2]

[1]Tsinghua National Laboratory for Information Science and Technology (TNList)
Institute of Microelectronics, Tsinghua University, Beijing 100084, China
[2]State Key Laboratory of New Ceramics and Fine Processing
Key Laboratory of Materials Processing Technology of MOE
School of Materials Science and Engineering, Tsinghua University, Beijing 100084, China

Abstract— Since 2004, graphene has attracted much attention and widely investigated as one of the most promising 2D materials due to its excellent electrical, physical, mechanical and optical properties. But it is also limited in logic circuits and photo detector devices application areas due to the absence of bandgap. Recently, another 2D material MoS_2, one of the transition-metal dichalcogenides, hasemerged as one of the alternatives of graphene due to its large ON/OFF ratio ($\sim 10^8$), existence of band gap, thermal stability and compatibility with CMOS process. It is theoretically computed and experimentally measured that single layer MoS_2 exhibit a direct bandgap of about 1.8 eV, which is suitable for photodetector applications.

In this study, we fabricate the few layers MoS_2 base phototransistor and then investigate its light-induced electric properties. The few layers MoS_2 sheet was exfoliated from bulk MoS_2 and then transferred to Si/SiO_2 substrate. The source and drain electrodes were patterned and fabricated by e-beam lithography and evaporation of Ti/Aumetal. The photocurrent generation solely depends on the illuminating optical power at a constant drain or gate voltage in the same device and the photo responsivity can be tuned by gate voltage. Several phototransistors with different MoS_2 layer numbers were fabricated and showed different photocurrent with the same gate voltage, drain voltage and illuminating optical power because the bandgap value may change with the MoS_2 layer numbers.

Session 2P4
SC2: Wave Manipulations by Metasurfaces

Polarization Multiplexer by Plasmonic Metasurface

Tao Li, Lei Wang, Lin Li, and S. N. Zhu
National Laboratory of Solid State Microstructures
College of Engineering and Applied Sciences
School of Physics, Nanjing University, Nanjing 210093, China

Abstract— Polarization always plays an important role for people in steering the light or photon as an information carries. Over the last decades, great successes have been achieved in manipulating the optical polarizations based on the plasmonic structures or metamaterials, e.g., optical rotation, polarization conversion, etc.. Recently, many researchers turn their eyes to using polarization for multiplexing information, which are proved to be more and more important in this information explosive world nowadays. Here, I would like to report two interesting progresses in advancing the information multiplexing by polarizations within the so-called plasmonic metasurfaces, which are constructed by well designed nano hole arrays in a flat metal surface. Firstly, I will demonstrate an active display device that is implemented by integrating a metasurface with a electrically pumped LED chip. This metasurface is made of a rectangular hole array, in which every unit orientation is particularly designed for a polarization selection. Based on the plasmonic dependent local plasmonic excitations, microscopic active displays of Letter-encoding, gray-scale photos and animations are realized, revealing the function of polarization division multiplexing. Next, I will report a recently achieved plasmonic spin router with reconfigurable polarization. In this process, an incident light with circular polarization will be launched into SPP by two crossed "slit-couplers" into four quadrants in a metal surface. Within the quadrants, the superposed SPPs will interfere and result in versatile reconfigurable polarizations at different local positions. These SPP field can be selectively radiate out in a preferred manner by a well designed nano array. For examples, left and right circular polarized beams are demultiplexed and focused into different focal points. Moreover, a combined 2×2 spatial and polarization multiplexer are demonstrated based on two kinds of spin incidences.

Self-control of Light Polarization by Meta-surface

H. Liu
National Laboratory of Solid State Microstructures & Department of Physics
Nanjing University, Nanjing 210093, China

Abstract— In this work, we reported a meta-cavity composed from meta-surfaces. The resonance cavity modes can be tuned through nonlinear light-controlling effect. As a result, the polarization state of transmission wave through this meta-surface can be manipulated through changing itself power of the incident laser. Both x-polarized and y-polarized state can be obtained in the process. The novel technique will have potential applications in microstructural nonlinear polarizer.

Dynamic Control of Electromagnetic Wave Propagation with Tunable Metasurface

Bo O. Zhu and Yijun Feng
School of Electronic Science and Engineering, Nanjing University, Nanjing, China

Abstract— Dynamic control of electromagnetic (EM) wave propagation (both the amplitude and phase) is essential to many practical applications. For example, the reflection phase control is important in EM wave propagating mode to surface mode conversion, anomalous reflection, EM wave absorber, high impedance surface or artificial magnetic conductor, reflect-array antennas, beam forming and beam scanning antennas, etc.. In order to have full control for the reflection phase, tunable impedance surface with full 360° phase tuning range is desired. Conventional tunable impedance surfaces suffer the deficiency in phase tuning range. In this presentation, we will present a novel approach which employs metasurface having dual resonance poles and one zero in between. In this way, the 360° reflection phase variation is confined within a finite frequency band. Hence, full 360° dynamic control can be achieved within a certain frequency band. This new approach removes the phase tuning deficiency in the conventional methods, and allows the reflection phase to take arbitrary value actively. It can be applied in the case that the reflection phase needs to be fully and finely tuned, such as in beam steering reflect-array antennas. With geometrical scalability, this concept can also be further extended to terahertz or optical regions.

We will also report our recent work on equivalent principle inspired tunable metasurface. It enjoys the advantage of independent tuning for the magnitude and phase in either transmission or reflection. The equivalent principle is employed to analyze the required surface electric and magnetic impedances of a passive metasurface to produce either arbitrary transmission magnitude and phase or arbitrary reflection magnitude and phase. Detailed theoretical analysis, simulation as well as experiment on prototype of tunable metasurface will be demonstrated. This proposal may have many potential applications, such as for dynamic EM beam forming and scanning.

ACKNOWLEDGMENT

This work is partially supported by the National Nature Science Foundation of China (61301017, 61371034, 60990322, 61101011), the Key Grant Project of Ministry of Education of China (313029), the Ph.D. Programs Foundation of Ministry of Education of China (20100091110036, 201200911100-32), and partially supported by Jiangsu Key Laboratory of Advanced Techniques for Manipulating Electromagnetic Waves.

Broadband Unidirectional Propagation Using Gradient Index Metamaterials

Yadong Xu[1], **Chendong Gu**[1], **Bo Hou**[1], **Yun Lai**[1], **Jensen Li**[2], **and Huanyang Chen**[1]

[1]School of Physical Science and Technology, Soochow University, Suzhou, Jiangsu 215006, China
[2]School of Physics and Astronomy, University of Birmingham, Birmingham B15 2TT, UK

Abstract— We employed the recent concept of metasurefaces to design a waveguide with unidirectional propagation of light, independent of polarization. The device blocks both transverse electric and magnetic polarized modes in one direction but transmits them in the other for a broadband spectrum. Experiments in the microwave region verify our findings.

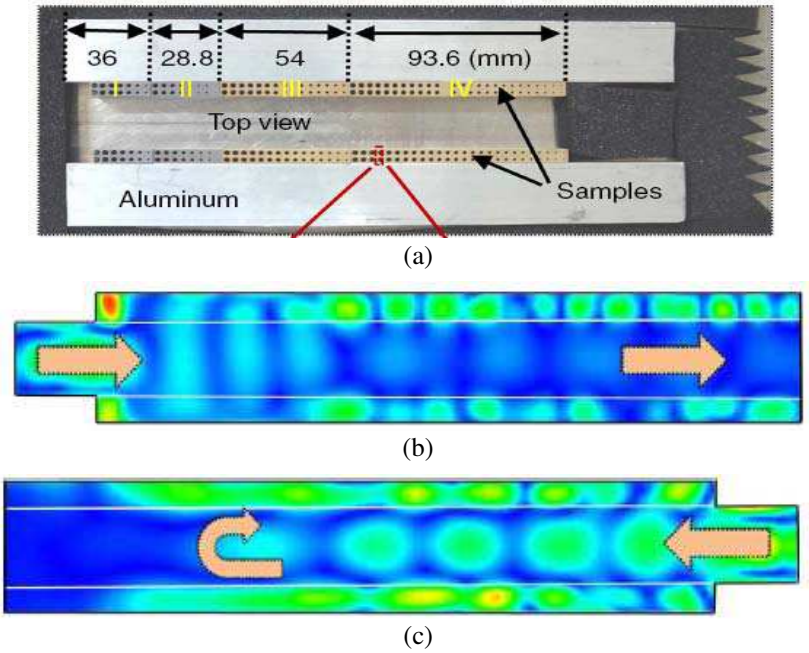

Figure 1: (a) The waveguide sample for broadband unidirectional transmission. (b) The wave coupled from the left port can transmit through the structure. (c) The wave coupled from the right port cannot transmit through the structure.

REFERENCES

1. Xu, Y., C. Gu, B. Hou, Y. Lai, J. Li, and H. Chen, "Broadband asymmetric waveguiding of light without polarization limitations," *Nature Communications*, Vol. 4, 2561, 2013.

Efficient Coupling of Microwave Surface-Plasmon-Like Mode to Propagating Waves

Jun Jun Xu, Hao Chi Zhang, Qian Zhang, and Tie Jun Cui
State Key Laboratory of Millimeter Waves, Southeast University, Nanjing 210096, China

Abstract— Surface plasmon polaritons (SPPs) are highly localized electromagnetic (EM) waves with exponential field decay from the interface of metal and dielectric. Due to the advantages of confining EM waves in a subwavelength scale, SPPs have found a lot of applications. Originally, SPPs were mainly investigated in the optical frequency. In order to realize subwavelength properties of SPPs at lower frequencies, plasmonic metamaterials have been proposed [1–3], in which the corrugated metallic structures are efficient models to support and propagate SPP-like modes in microwave frequency. Such modes are called as spoof SPPs. Controlling the launching efficiency and directionality of spoof SPPs and their coupling to freely propagating wave is a major goal for the application of plasmonic devices and systems. Due to the mismatch of momentum between such two kinds of waves, the excited SPPs are confined to the corrugated metallic structure surface, which are impossible to be converted directly. In this work, we present an efficient approach to convert SPPs into propagating waves by using gradient index metasurface, which is equivalent to a reflective wave vector along the interface to bend wave propagations, especially to emanate perpendicularly to the sample. The precise manipulation of phases using metasurfaces plays a fundamental role in generating synthetic scattering diagrams of macroscopic objects. We demonstrate theoretically and experimentally that a specific gradient index metasurface, which is composed of a periodic arrangement of unit cells, can convert SPPs to radiation waves with high efficiency. Experiments in the microwave region, including both far-field and near-field characterizations, are in excellent agreements with full-wave simulations. The launching scheme is also applicable to other areas, such as the communication system, detector, and high directivity antennas.

Three Dimensional Subwavelength Focusing by a Near-field Plate Lens

Wei Jiang, Lu Lan, and Yungui Ma
Department of Optical Engineering, Centre for Optical and Electromagnetic Research
Zhejiang University, Hangzhou 310058, China

Abstract— Thin artificial plates with unique electromagnetic properties (meta-surface) have gained great attentions in the last few years. In this talk we will report our recent work on a meta-surface focusing lens implemented by the inverse design method. Our thin near-field lens can produce a desired subwavelength focus by manipulating the near fields of a magnetic dipole source. This inverse design method was firstly introduced by Merlin [1] and later experimentally demonstrated in two dimensions by Gribic et al. using an artificial impedance surface lumped with reactive elements (capacitor and inductor) [2]. Our contribution is to extend this technique into three dimensions operating on a spatial incident wave pattern. To realize this, we first define a desired focal field distribution and then expand it into the summation of Fourier components that are spatially inversed to acquire the output field of the lens. With the input and output fields known, the impedance profile of the near-field plate is calculated by a circuit equation derived from the boundary consistent condition. Our near-field lens is implemented by lumped electric elements printed on a thin circuit board (Rogers 6006) by a standard lithography technique. In the experiment, a desired annular focusing spot with a characteristic size nearly three times smaller than that allowed by the diffraction limit is achieved at 3.2 GHz. Besides high-resolution imaging, the proposed near-field plate could be extended for other interesting applications, such as wireless power transfer or complex wavefront/beam shaper [3].

REFERENCES

1. Merlin, R., "Radiationless electromagnetic interference: Evanescent-field lenses and perfect focusing," *Science*, Vol. 317, No. 5840, 927–929, 2007.
2. Grbic, A., L. Jiang, and R. Merlin, "Near-field plates: Subdiffraction focusing with patterned surfaces," *Science*, Vol. 320, No. 5875, 511–513, 2008.
3. Kurs, A., A. Karalis, R. Moffatt, et al., "Wireless power transfer via strongly coupled magnetic resonances," *Science*, Vol. 317, No. 5834, 83–86, 2007.

Helicity-switchable Metasurfaces for Controlling Light Propagation

Benfeng Bai
State Key Laboratory of Precision Measurement Technology and Instruments
Department of Precision Instrument, Tsinghua University, Beijing 100084, China

Abstract— Metasurfaces, a class of monolayered metamaterials, have shown great potential for achieving full control of light without requiring complicated 3D nanofabrication [1, 2]. Various novel functionalities and applications based on metasurfaces have been demonstrated recently, such as ultrathin metalens [3], aberration-free wave plates [4], and spin controlled photonics [5]. In this talk, I will review our recent serial work on a new type of metasurface composed of gold nanorod antenna array. Based on the Berry phase principle, the metasurface can produce dispersionless interfacial phase discontinuities under the illumination of circularly polarized light. Since the phase of light can be controlled in each subwavelength unit cell and can be switched by the helicity of incident light, such metasurfaces show some special advantages such as the dispersionless property, the helicity-switching property, and the separate modulation of light phase and amplitude. Several novel functionalities and applications based on the metasurface have been proposed and experimentally realized, including the anomalous refraction of light, the generation of broadband vortex beam, a dual-polarity metalens, a helicity-switchable unidirectional SPP launcher, and 3D holographic display. All these applications show intriguing and superior properties of the metasurfaces working in the visible and near-IR range. The ultra-thin metasurfaces may pave the way towards novel nano-devices for beam shaping, large capacity data storage, optical information processing, holography-based techniques and so on.

REFERENCES

1. Yu, N., P. Genevet, M. A. Kats, F. Aieta, J.-P. Tetienne, F. Capasso, and Z. Gaburro, *Science*, Vol. 334, 333, 2012.
2. Ni, X., N. K. Emani, A. V. Kildishev, A. Boltasseva, and V. M. Shalaev, *Science*, Vol. 335, 427, 2012.
3. Ni, X., S. Ishii, A. V. Kildishev, and V. M. Shalaev, *Light: Sci. & Appl.*, Vol. 2, e72, 2013.
4. Yu, N., F. Aieta, P. Genevet, M. A. Kats, Z. Gaburro, and F. Capasso, *Nano Lett.*, Vol. 12, 6328, 2012.
5. Litchinitser, N. M., *Science*, Vol. 337, 1054, 2012.

Controlling Electromagnetic Waves with Two-dimensional Gradient Meta-surfaces

Shiwei Tang[1,2], **Meng Qiu**[1,2], **Qiong He**[1,2], **Shulin Sun**[1,2], **and Lei Zhou**[1,2]

[1]State Key Laboratory of Surface Physics, Fudan University, Shanghai 200433, China
[2]Key Laboratory of Micro and Nano Photonic Structures (Ministry of Education)
Fudan University, Shanghai 200433, China

Abstract— Gradient metasurfaces (GMs) can provide additional parallel wave-vectors to an incident wave so that the reflected/refracted waves follow the generalized Snell's law. Such a unique property offers GMs strong abilities to control EM waves. In particular, it was shown in [1, 2] that a GM with a sufficiently large phase gradient can convert an incident propagating wave to a bounded surface wave when the incidence angle is larger than a critical value.

However, previous efforts were mainly devoted to GMs with phase gradient along one dimension. Here, we show that two-dimensional (2D) GMs with tailored gradient properties along two directions can have stronger abilities to control EM waves. For example, we found that a carefully designed 2D GM can work as a polarization beam splitter to separate EM waves with different polarizations into different directions, and another 2D GM can robustly convert incident EM waves to bounded surface waves independent of the incidence angle and polarization. More strikingly, we show that a particular 2D GM can manipulate the polarization of a surface wave and essentially arbitrary polarization state can be realized for a SW on such a system. We have designed realistic GMs and performed microwave experiments to verify these theoretical concepts, and more details will be presented in the conference.

REFERENCES

1. Sun, S., Q. He, S. Xiao, Q. Xu, X. Li, and L. Zhou, *Nature Materials*, Vol. 11, 426–431, 2012.
2. Sun, S., K. Yang, C. Wang, T. Juan, W. T. Chen, C. Y. Liao, Q. He, S. Xiao, W. Kung, G. Guo, L. Zhou, and D. P. Tsai, *Nano Lett.*, Vol. 12, 6223–6229, 2012.

Spoof Plasmonic Analogue of 2D Topological Insulator

Fei Gao[1], **Zhen Gao**[1], **and Baile Zhang**[1, 2]

[1]Division of Physics and Applied Physics, School of Physical and Mathematical Sciences
Nanyang Technological University, Singapore 637371, Singapore
[2]Centre for Disruptive Photonic Technologies
Nanyang Technological University, Singapore 637371, Singapore

Abstract— Strong spin-orbital coupling induces a new phase incondensed matters termed as topological insulators, which shows striking spin-polarized edge states in 2D version. Topologically protected edge states are very robust against various nonmagnetic impurities and defects, which now have been introduced into photonic communities. Much experimental effort has been directed towards realizing 2D photonic topological insulators with dielectric waveguide, bianisotropic metamaterials or resonator arrays. Here we would like to further extend Topological Insulators into plasmonics; and proposed a practical scheme to realize with Spoof SPP resonator arrays. These Spoof SPP resonators are made of Domino structures which consist of metal pillars standing on metal plates. In lattice resonators, flowing directions of Spoof SPP is an analogue of spins of electrons; clockwise flow is for pseudo-spin-up component and anti-clockwise for pseudo-spin-down component. Strong spin-orbital coupling is supported by coupling resonators which play the role of bond and can also conserve spins when wave propagates. Our simulation results unambiguously show the edge state in a bulk array, which is the unique property of topological insulators. When we increase the working frequency to tune down the coupling coefficient, the bulk state has also been observed.In addition, we take away one lattice ring and its three neighbouring coupling rings at the upper edge to generate defect. The reason is that if one 'atom' is taken away, the bond surronding it also vanishes.In this senario, we have observed that edge states bypass the defect and take the newly formed edge to go along.

Recycling Radio Waves with Smart Walls

N. Kaina, M. Dupre, G. Lerosey, and M. Fink
Institut Langevin, ESPCI ParisTech, France

Abstract— We propose to use electronically reconfigurable ultrathin metasurfaces as smart walls to reflect more intelligently the waves in indoor environments. We experimentally prove at 2.47 GHz that it is possible to use these as spatial microwave modulators, using a simple energy feedback. In particular, we show that we can enhance the transmission between two antennas by orders of magnitude or locally conceal a volume from the penetration of waves in a typical office room. We also provide a theoretical model of wavefront shaping in reverberating media. We believe our concept paves the way to greener telecommunication systems as well as it could be an efficient tool to study the wave propagation in highly scattering or reverberating media.

An increasing amount of data is nowadays conveyed wirelessly by radio waves in dense environments such as cities or buildings [1]. While propagating, the electromagnetic waves carrying the information are reflected several times off obstacles such as walls and furnitures, thus causing a spread of the associated electromagnetic energy throughout those complex and reverberating media. This raises health issues and wastes energy. Here we show that part of this seemingly lost energy can be recycled by reflecting more intelligently these multiply scattered waves using smart walls rather than bare ones. To do so we propose to use ultrathin metasurfaces [2] that we design to be electronically reconfigurable in real time as spatial microwave modulators. We show that they can be utilized to cover part of the walls of a typical office room, hence transforming these dumb surfaces into smart ones. We demonstrate that, akin to the spatial light modulators which can focus light through complex media [3, 4], those spatial microwave modulators can passively turn a random electromagnetic field resulting from reverberated and multiply scattered waves into a shaped one using a simple energy feedback and simple optimization algorithms [5]. Specifically, we prove that such smart walls can, in real time, increase by orders of magnitude the energy of a wireless signal received by any antenna or locally conceal a volume from penetration of microwaves. We will present simulation and experimental results as well as a quantitative estimation of the benefits brought by the approach, by introducing and modeling the notion of wavefront shaping in reverberating media.

Our smart walls have applications in green wireless communications and electromagnetic protection, but they are also amazing tools for fundamental physics related to the propagation of waves in complex, highly scattering or reverberating media.

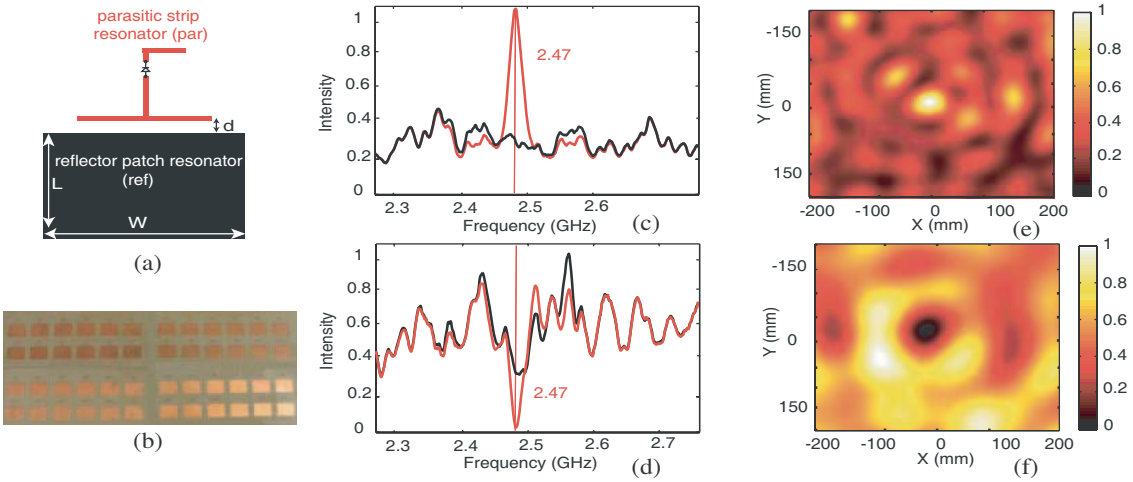

Figure 1: (a) Scheme of the unit cell (up) and picture of the metasurface. Average transmission spectra for a (b) field maximization and (c) field minimization. Average maps of the field after (d) maximization and (e) minimization.

REFERENCES

1. Paulraj, A., R. Nabar, and D. Gore, 277, Cambridge University Press, 2003.
2. Kildishev, A. V., A. Boltasseva, and V. M. Shalaev, *Science*, Vol. 339, 1232009–1232009, 2013.
3. Mosk, A. P., A. Lagendijk, G. Lerosey, and M. Fink, *Nat. Photon.*, Vol. 6, 283–292, 2012.
4. Aulbach, J., B. Gjonaj, P. M. Johnson, A. P. Mosk, and A. Lagendijk, *Phys. Rev. Lett.*, Vol. 106, 103901, 2010.
5. Vellekoop, I. M. and A. P. Mosk, *Opt. Lett.*, Vol. 32, 2309–2311, 2007.

High-efficiency SPP Couplers Based on Gradient Meta-surfaces

Wujiong Sun, Shulin Sun, Qiong He, and Lei Zhou
State Key Laboratory of Surface Physics
Key Laboratory of Micro and Nano Photonic Structures (Ministry of Education)
Fudan University, Shanghai 200433, China

Abstract— Meta-surfaces, ultra-thin metamaterials composed by planar artificial sub-wavelength units with purposely determined electromagnetic (EM) responses, have drawn much attention recently [1–3]. By designing meta-surface in such a way that its reflection/transmission phase distribution exhibits certain profile (e.g., linear, parabolic, etc.), various fascinating wave-manipulation effects have been realized, such as anomalous light reflection/refraction satisfying a generalized Snell's law and light focusing by a planar lens. In particular, it was shown in Ref. [1, 4] that when the phase gradient contributed by a meta-surface is larger than a critical value, a carefully designed reflective meta-surface can perfectly convert an incident propagating wave (PW) to a surface wave (SW) bounded on the meta-surface [1, 4]. Such a PW-SW conversion mechanism is completely different from conventional techniques such as prism or grating couplers, and thus has attracted lots of efforts to design high-efficiency surface plasmon polariton (SPP) couplers.

However, since the gradient meta-surface (GM) itself is inhomogeneous and thus does not support the eigen SPPs, the converted SW can only exist on the meta-surface under the illumination of the incident PW. To guide such driven SW out of the system, a periodic/homogeneous system supporting eigen SPP has to be placed adjacent to the GM. Unfortunately, it was theoretically argued that the scatterings contributed by the super periodicity on the GM are non-negligible, and the efficiency can not be very high for a GM with more super cells.

Here, we propose a new design for high-efficiency SPP coupler based on the GM concept, which can overcome the above issues. To verify our idea, we have designed a realist structure working at 10 GHz, and found by full-wave simulations that the SPP conversion efficiency of the designed device can be as high as 88%. We compared our proposed scheme with available ones, particularly the prism coupler, and found that our new scheme exhibits many advantageous. We are now performing microwave experiments to verify the ideas and more details will be presented in the conference.

REFERENCES

1. Sun, S., Q. He, S. Xiao, Q. Xu, X. Li, and L. Zhou, "Gradient-index meta-surfaces as a bridge linking propagating waves and surface waves," *Nature Materials*, Vol. 11, 426–431, 2012.
2. Yu, N., P. Genevet, M. A. Kats, F. Aieta, J.-P. Tetienne, F. Capasso, and Z. Gaburro, "Light propagation with phase discontinuities: Generalized laws of reflection and refraction," *Science*, Vol. 334, 333, 2011.
3. Ni, X., N. K. Emani, A. V. Kildishev, A. Boltasseva, and V. M. Shalaev, "Broadband light bending with plasmonic nanoantennas," *Science*, Vol. 335, 427, 2012.
4. Qu, C., S. Xiao, S. Sun, Q. He, and L. Zhou, "A theoretical study on the conversion efficiencies of gradient meta-surfaces," *Europhys. Lett.*, Vol. 101, 54002, 2013.

Meta-line

Hong Chen Chu, **Jie Luo**, **and Yun Lai**
School of Physical Science and Technology, Soochow University, Suzhou, China

Abstract— Meta-surface has not only shown extraordinary ability to control the reflection and refraction of waves [1], but also the ability to change propagating waves into surface waves along the surface [2].

Here, we investigate the 1D counterpart of a meta-surface: meta-line, i.e., a line with gradually changing parameters [3]. Our study shows that such a line is also capable of turning incident propagating waves into guided localized waves along the line. The efficiency of such a transition from propagating waves to evanescent waves can be very high. However, the criterion is different for incident waves with different angular momentums.

Our work finds a new way to perfectly couple propagating waves to evanescent waves along a line.

REFERENCES

1. Yu N. F., et al., *Science*, Vol. 334, 333, 2011.
2. Sun S. L., et al., *Nature Materials*, Vol. 11, 426, 2012.
3. Chu, H. C., J. Luo, and Y. Lai, to be Submitted.

Controlling Surface Plasmon Polaritons by Holographic Surfaces

Zhi-Yuan Li[1] and Yue-Gang Chen[2]

[1]Institute of Physics, Chinese Academy of Science, Beijing 100190, China
[2]Department of Physics, Guizhou University, Guiyang 550025, China

Abstract— Surface plasmon polaritons (SPPs) are collective resonances of electron gas in metal surface, which have unique properties of strong confinement of light energy to subwavelength scale and giant enhancement of local field intensity. The manipulation of SPPs on metal surface is of vital importance to construct ultracompact integrated micro/nano optical devices and systems. Many plasmonic structures have been proposed to achieve the exciting, propagating, and focusing of SPPs, and the key issue is to manipulate the SPP wavefront. Recently we invented a novel methodology called surface wave holography (SWH) to design plasmonic nanostructures for complicated wave-front shaping of light. In this talk we will introduce the principles and applications of this method.

First, we discuss the principle of SWH in application to plasmonic wavefront shaping. This method involves writing and reading process of object wave under a given illumination surface wave, and it allows one to directly determine the surface groove morphology in the metallic plate easily without the need of complicated electromagnetic inverse-problem solutions. Analytically, we have derived the morphology equations of an arbitrary single-point focusing and plane-wave collimation by surface-wave holographic structures. Carving grooves on a metallic surface according to these equations, we have obtained numerical and microwave experimental results as predicted by the analytical theory. Second, we present design of plasmonic holographic structures to shape the wave-front of infrared light at 1064 nm wavelength passing through a 400 nm hole into a Latin letter "L" and a letter "O" at a given position [2]. Good agreement between numerical and experimental results confirms the power of this method. In addition, we have been able to shape the wavefront of visible light at 633 nm diffracted from an arbitrary shaped aperture, e.g., a narrow slit of various aspect ratios, into a focusing point by using the methodology [3]. Third, we have expanded the scope of the SWH methodology and developed a direct method to control SPPs propagating on the metal surface by using hologram composed of appropriately determined groove patterns. Several functionalities of SPP wavefront manipulation are demonstrated, in which the pre-designated functionalities have been fully implemented by the designed plasmonic holographic structures [4]. We expect that this novel concept and methodology can find applications not only in holography and plasmonic structures design but also in sensing and information storage.

REFERENCES

1. Chen, Y.-H., J.-X. Fu, and Z.-Y. Li, "Surface electromagnetic wave holography," *Optics Express*, Vol. 19, 23908–23920, 2011.
2. Chen, Y.-H., L. Huang, L. Gan, and Z.-Y. Li, "Wave-front shaping of infrared light through a subwavelength hole," *Light: Science & Applications*, Vol. 1, e26, 2012.
3. Chen, Y.-H., M. Zhang, L. Gan, X. Wu, L. Sun, J. Liu, J. Wang, and Z.-Y. Li, "Holographic plasmonic lenses for surface plasmons with complex wavefront profile," *Optics Express*, Vol. 21, 17558–17566, 2013.
4. Chen, Y.-G., Y.-H. Chen, and Z.-Y. Li, "Direct method to control surface plasmon polaritons on metal surface," *Optics Letters*, Vol. 39, 339–342, 2014.

Manipulating Electromagnetic Waves with GEometric MetaSurfaces (GEMS)

Lingling Huang[1, 2], **Xianzhong Chen**[1], **Holger Mühlenbernd**[3], **Guixin Li**[4], **Benfeng Bai**[2], **Qiaofeng Tan**[2], **Guofan Jin**[2], **Thomas Zentgraf**[3], **and Shuang Zhang**[1]

[1]School of Physics & Astronomy, University of Birmingham, Birmingham, B15 2TT, UK
[2]State Key Laboratory of Precision Measurement Technology and Instruments
Department of Precision Instruments, Tsinghua University, Beijing 100084, China
[3]Department of Physics, University of Paderborn
Warburger Straße 100, Paderborn D-33098, Germany
[4]Department of Physics, Hong Kong Baptist University, Hongkong, China

Abstract— Benefitting from the flexibility in engineering their optical responses, metamaterials have been used to achieve control over the propagation of light to an unprecedented level, leading to highly unconventional and versatile optical functionalities in comparison to their natural counterparts. Recently the emerging field of meta-surfaces consisting of a monolayer of artificial atoms has offered attractive functionalities of shaping the wave front of light by introducing an interfacial abrupt phase discontinuity. Among the various type metasurfaces demonstrated so far, the metasurface consisting of rotating metallic nanorods is capable of the most robust control of the wavefront of light, since the phase of the scattered light is inherently a Berry phase, or geometric phase, controlled solely by the orientation of each individual nanorod, instead of its specific configuration or constituent material. We therefore term this type of metasurface 'geometric metasurface', or GEMS. In this talk I will talk about the mechanism of phase control and device applications of GEMS. In particular, I will focus on two examples of device applications: a dual polarity metalens that can functions either a convex or a concave lens and helicity switchable unidirectional excitation of surface plasmon polaritons.

Lens is the most essential part of any imaging systems. Conventional lens are made from dielectric materials, such as glass, with spatially varying topography. The polarity of conventional lens cannot be altered after fabrication, i.e., either positive (convex) or negative (concave), depending on the surface topography. We have experimentally demonstrated a counter-intuitive bipolar flat lens with switchable polarity at visible frequencies by controlling the phase discontinuities for the circularly polarized light. The positive and negative polarities are interchangeable in one identical flat lens under inversion of the helicity of the input light. Both focusing and imaging are observed for visible light. We further apply GEMS to the design of a novel type of helicity dependent SPP unidirectional excitation at normal incidence. Selective unidirectional excitation of SPPs along opposite directions is experimentally demonstrated at optical frequencies by simply switching the helicity of the incident light. This approach, in conjunction with dynamic polarization modulation techniques, opens gateway towards integrated nanoplasmonic circuits with electrically reconfigurable functionalities.

Design of the Surface Pseudo-Bessel Lens by Using Artificial Impedance Metasurfaces

Yunbo Li, Bengeng Cai, and Tiejun Cui
State Key Laboratory of Millimeter Waves
Department of Radio Engineering, Southeast University, China

Abstract— We propose a method to design the two-dimension surface pseudo-bessel lens by using artificial impedance metasurfaces. The impedance metasurfaces are composed of sub-wavelength metallic patches on a grounded dielectric substrate, which are distributed quasi-periodically so that the basic unit can be simulated under the period boundary condition. We can extract the surface impedance of the texture by using the dispersion character obtained by eigen-mode simulation. Comparing with the most existing bessel lenses based on spatial wave, the two-dimension pseudo-bessel lens of our design can support the surface wave of TM mode.

The surface pseudo-bessel lens is realized by two parts, which are the surface half Maxwell's eye lens and the surface flat lens. The half Maxwell's eye lens is used to shape the surface cylindrical wave excited by a point source (SMA connector) to the surface plane wave and the flat lens can generate the diamond-shaped focus area according to the theory of the pseudo-bessel lens. So the whole surface lens system can transform a point source to the 2-D surface pseudo-bessel beam. By changing the different beam deflection angles of the flat lens, we can obtain different focus lengths of the pseudo-bessel lens.

We have simulated the surface lens system by CST Microwave Studio and the simulate results have good agreements to our theoretical design. The 2-D surface pseudo-bessel lens can be used as the surface wave source characterized as the narrow beam and the high energy focusing in the near-field. The operating frequency of the lens system is 12 GHz, and it also can be extended to the millimeter wave or terahertz wave bands.

Simultaneously Realize Luneburg Lens and Maxwell Fisheye Lens with a Single Anisotropic Metasurface

Xiang Wan and Tie Jun Cui
State Key Laboratory of Millimeter Waves, Department of Radio Engineering
Southeast University, Nanjing 210096, China

Abstract— In the classical physics, Luneburg lens and Maxwell fisheye lens are two typical optical devices with the spherical symmetry. The Luneburg lens can make the image of a point source on the lens surface to an infinite distance in the opposite direction; while the Maxwell fisheye lens makes the image of a point source on the lens surface to the opposite point on the surface. Both Luneburg and fisheye lenses have important applications in the optical and microwave frequencies, such as collimating lights, radar antennas, and wide-angle cameras. Now a raised question is: Can we integrate the Luneburg lens and fisheye lens together? That is to say, can we make a single lens to serve as either Luneburg or fisheye? The answer is: it is possible by using anisotropic materials to control the refractive indexes along the two optical axes. We propose a method to control the inhomogeneous indexes of refraction independently along the two optical axes by designing anisotropic and non-uniform metasurface, which can provide the required distributions of refractive indexes approximately for Luneburg and fisheye lenses watching from the two optical axes. Experiments in the microwave frequency demonstrate very good performance of the planar bi-functional Luneburg-fisheye lens. The proposed method opens a venue to design other kinds of bi-functional devices using metasurfaces in the microwave, terahertz, and even optical frequencies.

Session 2P5a
SC2: Thermal and Acoustic Metamaterials

Acoustic Metasurface with Hybrid Resonances

Ping Sheng
Department of Physics, Hong Kong University of Science and Technology
Clear Water Bay, Kowloon, Hong Kong, China

Abstract— An impedance-matched surface has the property that an incident wave generates no reflection. To diminish reflection from a hard reflecting surface, it is traditionally the practice to add a gradient-index interfacial layer or a quarter-wavelength layer, accompanied by dissipation. For acoustic sound, such additions can be bulky and cumbersome, owing to the large wavelength. Recently, it was shown that for the electromagnetic waves, structuring the interface between two different materials can lead to metasurfaces with diverse functionalities such as phase discontinuity, anomalous refraction/reflection, and polarization manipulations. Here we demonstrate that by using simple construct, an acoustically reflecting surface can acquire hybrid resonances and becomes impedance-matched to airborne sound at tunable frequencies, so that no reflection is generated. The hybrid resonance cell is deep-subwavelength in all its spatial dimensions, breaking the quarter-wavelength constraint by two orders of magnitude. It has two degrees of freedom that can be independently tuned; one is the average membrane displacement, which can be tuned to impedance match with the air-borne sound, and the other is the variance of the membrane displacement, which is decoupled from the radiation mode and hence "deaf". At the particular tunable hybrid resonant frequency of 152 Hz, for example, the membrane's maximum displacement amplitude can reach 45 μm, more than an order of magnitude larger than that of the incident sound with an intensity of 120 dB, even though the surface-averaged displacement is much smaller and matches that of the incident sound. As there can be no transmission, the acoustic wave is hence either completely absorbed at one or multiple frequencies, or converted into other form(s) of energy such as electrical current. A high acoustic-electrical energy conversion efficiency of 23% is achieved.

ACKNOWLEDGMENT

Work done in collaboration with Guancong Ma, Min Yang, Songwen Xiao, and Zhiyu Yang.

Decorated Membrane Resonators as Acoustic Metamaterials

Guancong Ma[1], **Min Yang**[1], **Jun Mei**[2], **Zhiyu Yang**[1], **and Ping Sheng**[1, 3]

[1]Department of Physics, Hong Kong University of Science and Technology
Clear Water Bay, Kowloon, Hong Kong, China
[2]Department of Physics, South China University of Technology, Guangzhou 510641, China
[3]Institute for Advanced Study, Hong Kong University of Science and Technology
Clear Water Bay, Kowloon, Hong Kong, China

Abstract— Centimeter-sized elastic membranes with various decorations can exhibit strong resonant features in sub-kilo Hertz airborne sound field. Some of the resonant characteristics can be explained using effective acoustic constitutive parameters [1]. We show that single negative mass density [2], bulk modulus, as well as double negativity in both mass density and bulk modulus [3], can be realized using decorated membranes. These characteristics can lead to novel functionalities such as total reflection [2, 4], near total transmission [5], and total absorption [6].

REFERENCES

1. Yang, M., G. Ma, Y. Wu, Z. Yang, and P. Sheng, "Homogenization scheme for acoustic metamaterials," *Phys. Rev. B*, Vol. 89, 064309, 2014.
2. Yang, Z., J. Mei, M. Yang, N. H. Chan, and P. Sheng, "Membrane-type acoustic metamaterial with negative dynamic mass," *Phys. Rev. Lett.*, Vol. 101, 204301, 2008.
3. Yang, M., G. Ma, Z. Yang, and P. Sheng, "Coupled membranes with doubly negative mass density and bulk modulus," *Phys. Rev. Lett.*, Vol. 110, 134301, 2013.
4. Ma, G., M. Yang, Z. Yang, and P. Sheng, "Low-frequency narrow-band acoustic filter with large orifice," *Appl. Phys. Lett.*, Vol. 103, 011903, 2013.
5. Park, J. J., K. J. B. Lee, O. B. Wright, M. K. Jung, and S. H. Lee, "Giant acoustic concentration by extraordinary transmission in zero-mass metamaterials," *Phys. Rev. Lett.*, Vol. 110, 244302, 2013.
6. Mei, J., G. Ma, M. Yang, Z. Yang, W. Wen, and P. Sheng, "Dark acoustic metamaterials as super absorbers for low-frequency sound," *Nat. Commun.*, Vol. 3, 756, 2012.

Facile Thermal Metamaterials to Manipulate Heat Signatures

Cheng-Wei Qiu[1], **Tiancheng Han**[1], **Xue Bai**[1, 2], **Dongliang Gao**[1], **Baowen Li**[2], **and John Thong**[1]

[1]Department of Electrical and Computer Engineering, National University of Singapore
4 Engineering Drive 3, Singapore 117583, Republic of Singapore
[2]Department of Physics and Centre for Computational Science and Engineering
National University of Singapore, Singapore 117546, Republic of Singapore

Abstract— Manipulation of various physical fields, including optics, electromagnetics, acoustics, thermotics, etc. through different materials has been a long-standing dream for many researchers over the decades. Analogous to invisible cloak and wave-dynamic illusion, thermal metamaterials can potentially transform an actual perception into a pre-controlled perception, thus empowering unprecedented applications in thermal cloaking and camouflage. Here we report our recently two works about thermal cloak and thermal illusion based on simulation and experimental validation. We demonstrate a bilayer thermal cloak made of bulk isotropic materials [1]. Our simulation work derived directly from thermal conduction equation, has been validated as an exact cloak, and we experimentally verified its ability to maintain the heat front and its heat protection capabilities. Also we propose and realize a functional thermal illusion device [2], which is capable of creating multiple expected images off the original object's position in heat conduction. The thermal scattering signature of the object is thus metamorphosed and perceived as multiple ghost targets with different geometries and compositions. The thermal illusion effect is experimentally confirmed in both time-dependent and temperature-dependent cases, demonstrating excellent thermotics performance.

REFERENCES

1. Han, T., X. Bai, D. Gao, J. T. L. Thong, B. Li, and C.-W. Qiu, "Bilayer thermal cloak: Keeping heat away while maintaining invisibility," *Phys. Rev. Lett.*, 2013, in press.
2. Han, T., X. Bai, J. T. L. Thong, B. Li, and C.-W. Qiu, "Full control and manipulation of heat signatures: Cloaking, camouflage and thermal metamaterials," *Adv. Mater.*, 2013, in press.

A Simple Thermal Cloak with Three Dimensional Realization

Baile Zhang
School of Physical and Mathematical Sciences, Nanyang Technological University, Singapore

Abstract— While the majority of cloaking research in the past few years focused on various wave fields, recently diffuse-field cloaks are attracting more and more attention. A typical example is the thermal cloak that can hide objects from diffusive heat by guiding conductive thermal flux smoothly around a hidden object. Most already reported demonstrations of thermal cloaks were based on transformation thermodynamics that utilized artificial thermal metamaterials implemented mainly in the 2D geometry. A 3D thermal cloak that can hide a 3D object in a thermal environment is still difficult.

Here we move one step forward to extend the 2D geometry in previous reports to three dimensions, and we demonstrate the first successful realization of a 3D thermal cloak working in the 3D space. We choose an air bubble as the object to be cloaked, since it is well known that stationary air is a poor conductor of heat which approximates to a heat insulator in many cases, and small air gaps can seriously block the channel for heat exchange and cause local overheating the main reason of thermal failure in mechanical and electronic devices. It is worth mentioning that what allows us to successfully fabricate a 3D cloak is a specially designed 3D machining process that is introduced for the first time in thermal cloaking research. Another unique aspect of our 3D cloak is its ultrathin thickness, which allows the cloak to perform satisfactorily even in transient and inhomogeneous temperature fields. To the best of our knowledge, our demonstration is the only one so far that provides cloaking evidence for both the transient and the inhomogeneous temperature fields in 3D space.

Total Absorption of Elastic Waves in Ultrathin Layers

Yue Tao Duan, **Jie Luo**, **and Yun Lai**
School of Physical Science and Technology, Soochow University, Suzhou, China

Abstract— Absorption of ultrathin layers has been verified for both acoustic waves [1] and electromagnetic waves [2]. Here, we investigate the case of elastic waves and find that elastic waves can also be perfected absorbed by using ultrathin layers under certain circumstances [3]. The conditions can be derived under three categories: continuous displacement or continuous stress across the ultrathin layer, and both displacement and stress are not continuous across the ultrathin layer. From an effective medium description, we try to fabricate such special absorptive ultrathin layers by using parameters in real materials.

REFERENCES

1. Mei, J., et al., *Nature Communications*, Vol. 3, 756, 2012.
2. Li, S. C., et al., Submitted.
3. Duan, Y. T., J. Luo, and Y. Lai, to be Submitted.

Photonic Flat Band for Broad-angle Acousto-optic Bragg Diffraction

Jensen Li[1], **Charles Croenne**[2], **Fu Liu**[2], **Shiyi Xiao**[1], **Wontaek Seo**[3], **Seunghoon Han**[3], **Hong-Seok Lee**[3], **and U-In Chung**[3]

[1]School of Physics and Astronomy, University of Birmingham, Birmingham, UK
[2]Department of Physics and Materials Science
City University of Hong Kong, Kowloon, Hong Kong, China
[3]Samsung Advanced Institute of Technology, Samsung Electronics
Yongin, Gyeonggi 446-712, South Korea

Abstract— Acousto-optic (AO) effect is induced when there is a change in refractive index from the interaction between acoustic waves and electromagnetic (EM) waves. Very often, such an interaction comes from a travelling acoustic wave, which creates an artificial refractive index grating to modulate an incident optical wave. Here, we investigate how acoustic-optic effect can be enhanced through tailoring band structure of a photonic crystal. In particular, we design a SiO_2/SiN-based photonic crystal, whose dispersion diagram exhibits a flat dispersion at a particular photon wavelength. Such a flat dispersion relaxes the momentum matching rule and can make the acousto-optic Bragg diffraction working for a larger range of incidence angles. We will also discuss experimental realization.

Tailoring Specific Heat and Density in the Design of Thermal Transformation Media

Yu-Lin Tsai and Tungyang Chen
Department of Civil Engineering, Cheng Kung University, Tainan 70101, Taiwan

Abstract— The transformation optics or acoustics in the design of metamaterials has been successfully applied to a number of physical phenomena. This novel method provides simple routes to attain certain significant effects such as invisibility cloaks, concentrators, and others. Given a mapping between two geometric configurations, the material properties of the transformed domain can be accordingly determined. They are in general anisotropic, position varying and sometimes of extreme values at certain points. This in fact restricts the practicality of real fabrication. Here we are concerned with the transient behavior of heat conduction. An inverse algorithm is presented here in the design of transformed medium based on the invariance of governing equation between physical and virtual configurations. We will demonstrate that the thermal capacity (thermal conductivity and heat capacity) can be tailored in specific forms, spatially uniform, linear or quadratic functions of positions, so that the design can be materialized more easily. Numerical illustrations are also presented for 2D and 3D thermal cloak for transient thermal conduction.

Localization of Flexural Waves in Random Locally Resonant Plate

Marc Dubois, Gautier Lefebvre, and Patrick Sebbah
Institut Langevin, CNRS UMR 7587, ESPCI ParisTech, 1 rue Jussieu, 75238 Paris Cedex 05, France

Abstract— Anderson localization has been extensively studied in various fields, from optics [1] to microwave [2], and also in acoustics [3, 4]. Such phenomenon appears in strongly scattering disordered systems. In order to enhance localization, one can take advantage of intrinsic resonances of the scattering elements to increase the scattering cross section and reduce the mean free path [5]. Here, we consider elastic waves propagating in a randomly structured thin plate. A dense random collection of strongly resonant non-through holes is shown to spatially localized modes. This is confirmed numerically. The phase relation between the resonators and the plate in these modes is specific and can be compared to hybridization bandgap observed in locally resonant media.

In the field of flexural waves in thin plates, blind holes represent very convenient resonators, whose frequency and quality factor are both simply tunable by choosing the size of the hole, and the thickness of its bottom. The modes of the resonator are actually similar to those of an equivalent circular clamped membrane. For a constant diameter, the resonance frequency increases with the bottom thickness, while the quality factor is reduced. This means that with a sufficiently thin membrane in the hole, we can obtain a sub-wavelength resonator, and thus we can design a high-density scattering media. We chose to simulate a 560 µm thick, 20 mm by 20 mm clamped square plate. The membrane left at the bottom of the holes is 30 µm thick and the hole diameter is 1 mm.

Using finite element method (FEM) to model this system, we obtain the eigenmodes of the global system including the plate and the blind holes. To estimate the spatial extension of each mode, we use the inverse participation ratio (IPR), defined as: IPR $= \frac{\int a^2(x,y)dS}{(\int a(x,y)dS)^2}$, where a is the amplitude of the envelope, and the integration is done over all the plate. This function represents the inverse of the surface occupied by the mode, which is a standard way to measure localization.

Spatial localization of the energy is seen both within the holes and in-between. Modes on each side of the gap are of different nature. Below the gap, localized modes show in-phase relationship between the holes and the plate whereas above the band-gap, we find antiphase relationship exclusively. Localization length is also variating within these two regimes as the wavevector of the eigenmodes is strongly reduced by the hybridization band gap obtained from the blind holes resonance.

REFERENCES

1. Wiersma, D. S., P. Bartolini, A. Lagendijk, and R. Righini, *Nature*, Vol. 390, 671–673, 1997.
2. Laurent, D., O. Legrand, P. Sebbah, C. Vanneste, and F. Mortessagne, "Localized modes in a finite-size open disordered microwave cavity," *Phys. Rev. Lett.*, Vol. 99, 253902, 2007.
3. Graham, I., L. Piché, and M. Grant, *Phys. Rev. Lett.*, Vol. 64, 3135–3138, 1990.
4. Macon, L., J. P. Desideri, and D. Sornette, *Phys. Rev. B*, Vol. 44, 6755–6772, 1991.
5. Chabanov, A. A. and A. Z. Genack, *Phys. Rev. Lett.*, Vol. 87, 2001.

Session 2P5b
SC2: Optical Metamaterials and Applications

Hyperbolic Metamaterials for Super-resolution Imaging and Deep Sub-wavelength Cavities

Junsuk Rho[1, 2, 3, 4] **and Xiang Zhang**[3, 4]

[1]Department of Mechanical Engineering
Pohang University of Science and Technology (POSTECH), Pohang, Korea
[2]Department of Chemical Engineering
Pohang University of Science and Technology (POSTECH), Pohang, Korea
[3]NSF-Nanoscale Science and Engineering Center, University of California, Berkeley, CA 94720, USA
[4]Lawrence Berkeley National Laboratory, Materials Sciences Division, Berkeley, CA 94720, USA

Abstract— Metamaterials, artificially structured nanomaterials, have enabled unprecedented phenomena such as invisibility cloaking and negative refraction. Especially, hyperbolic metamaterials also known as indefinite metamaterials have unique dispersion relation where the principal components of its permittivity tensors are not all with the same signs and magnitudes. Such extraordinary dispersion relation results in hyperbolic dispersion relations which lead to a number of interesting phenomena, such as super-resolution effect which transfers evanescent waves to propagating waves at its interface with normal materials and, the propagation of electromagnetic waves with very large wavevectors comparing they are evanescent waves and thus decay quickly in natural materials. In this abstract, I will focus discussing our efforts in achieving the unique optical property overcoming diffraction limit to achieve several extraordinary metamaterials and metadevices demonstration. First, I will present super-resolution imaging device called "hyperlens", which is the first experimental demonstration of near- to far-field imaging at visible light with resolution beyond the diffraction limit in two lateral dimensions [1]. Second, I will show another unique application of metamaterials for miniaturizing optical cavity, a key component to make lasers, into the nanoscale for the first time. It shows the cavity array which successfully captured light in 20 nm dimension and show very high figure of merit experimentally [2]. I believe our efforts in sub-wavelength metamaterials having such extraordinary optical properties will lead to further advanced nanophotonics and nanooptics research.

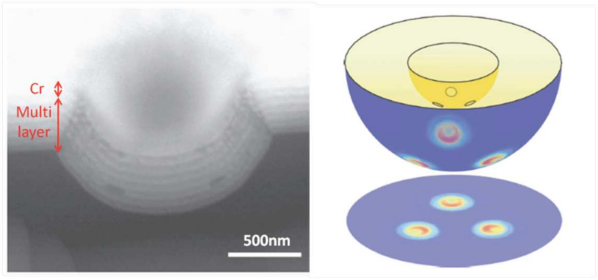

Figure 1: Device and schematic of optical hyperlens.

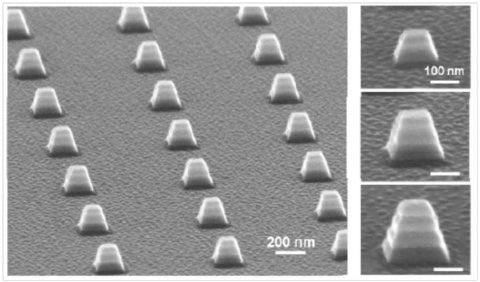

Figure 2: SEM of tunable hyperbolic nanocavities.

ACKNOWLEDGMENT

This work has been supported by the U.S. Department of Energy, Office of Basic Energy Sciences under contract No. DE-AC02-05CH11231 at the University of California Berkeley and Lawrence Berkeley National Laboratory. J. Rho acknowledges fellowships from the U.S. Department of Energy and the Samsung Scholarship Foundation, Republic of Korea.

REFERENCES

1. Rho, J., et al., "Spherical hyperlens for two-dimensional sub-diffractional imaging at visible frequencies," *Nature Communications*, Vol. 1, 143, 2010.
2. Rho, J., et al., "Experimental realization of three-dimensional indefinite cavities at the nanoscale with anomalous scaling laws," *Nature Photonics*, Vol. 6, 450–454, 2012.
3. Rho, J., et al., "Real-time super-resolution bioimaging based on 2D optical hyperlens," in Preparation.

Atomically Thin Transition Radiation of Surface Plasmons

Xiao Lin[1, 2, 3], **Hongsheng Chen**[1, 3], **and Baile Zhang**[2, 4]

[1]State Key Laboratory of Modern Optical Instrumentation, Zhejiang University, Hangzhou 310027, China
[2]Division of Physics and Applied Physics, School of Physical and Mathematical Sciences
Nanyang Technological University, Singapore 637371, Singapore
[3]The Electromagnetics Academy at Zhejiang University, Zhejiang University, Hangzhou 310027, China
[4]Centre for Disruptive Photonic Technologies
Nanyang Technological University, Singapore 637371, Singapore

Abstract— Transition radiation, first predicted by Ginzburg and Frank, occurs with uniform motion of a charged particle in a spatially inhomogeneous medium, and it differs in principle from the Cherenkov radiation, where it occurs for any velocity of the particle, not necessarily exceeding the phase velocity of light in the medium. Transition radiation, understood in a rather broad sense, is of generally physical importance and gets wide practical applications, especially the transition counter in high-energy physics. There is a so-called formation zone that limits the possibility of creating transition radiation. For example, the high-energy cosmic rays do not create transition radiation on the cosmic dust grains, where the usual size of dust grain of the order of 10^{-3}–10^{-4} cm is much smaller than the length of formation zone up to 10^{3} m. It might be due to the above limitation that transition radiation has been rarely studied in the atomically thin system, such as graphene. Graphene is a promising photonic material and can support surface plasmons with the advantages of reduced losses and widely tunable frequency ranges from THz to near-infrared. One arising challenge is creating transition radiation by using a fast-moving charged particle through atomically thin graphene.

We theoretically study the forward and backward transition radiations in graphene monolayer in frequency and time domains, respectively. The far-field and near-field radiation are found strongly dependent on frequency, the charge's moving velocity, and graphene's chemical potential. In particular, transition radiation of grapehene' surface wave ranging from THz to near-infrared frequencies is predicted to exist, indicating the fast moving charge particles may be an alternative excitation source to the graphene plasmonics.

Nanocavity Enhancement for Ultra-thin Film Photo-harvesting

Haomin Song and Qiaoqiang Gan
Department of Electrical Engineering, The State University of New York at Buffalo
Buffalo, NY 14260, USA

Abstract— In most thin-film energy harvesting/conversion applications, there is a long-existing trade-off between optical absorption and thickness of active materials. Particularly, research on two-dimensional (2D) atomic crystals and Van der Waals heterostructures receives intense efforts in recent years, which is promising for the development of new functional ultra-thin electronic and optoelectronic energy efficient devices, such as photodetectors, phototransistors and light sources. However, due to their atomically thin nature, the optical absorption is inherently weak. Consequently, absorption enhancement strategies will introduce revolutionary advances to these ultra-thin-film materials/devices [1]. Here we propose a design by placing an ultra-thin absorptive material on top of a predesigned lossless spacer layer and a metal reflector to realize spectrally tunable resonances absorbed in the top ultra-thin layer, as shown in Figure 1 [2]. As the incident light is coupled into this structure, the reflected components will cancel the incident light at the top surface, resulting in a destructive interference absorber. Since the bottom metal reflector does not absorb much light, most energy will dissipate in the top ultra-thin layer resulting in the significant absorption enhancement. By tuning the thickness of the spacer layer, the destructive interference resonance is spectrally tunable for ultra-thin absorptive materials down to atomic thickness, and therefore overcoming the conflict between the optical absorption and film thickness of energy harvesting/conversion materials. This principle exploits the wave property of light in ultra-thin absorptive nanocavities and will pave the way towards the spectrally tunable absorption enhancement of ultra-thin materials including semiconductor films and monolayers of 2D atomic crystals.

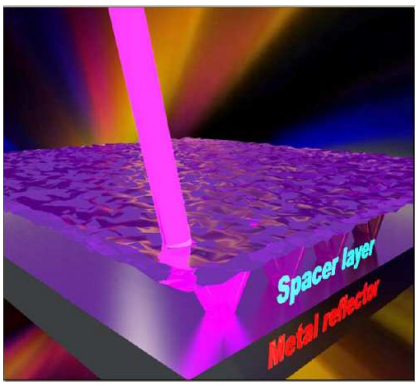

Figure 1: We demonstrated that a 1.5-nm-thick Ge film on nanocavity can absorb over 80% at the resonant wavelength (figure is adopted from the online image for Ref. [2]©Wiley).

REFERENCES

1. Kats, M. A., R. Blanchard, P. Genevet, and F. Capasso, *Nat. Mater.*, Vol. 12, 20, 2013.
2. Song, H., L. Guo, Z. Liu, K. Liu, X. Zeng, D. Ji, N. Zhang, S. Jiang, and Q. Gan, *Adv. Mater.*, published online, DOI: 10.1002/adma.201305793.

Design, Fabrication and Measurement of MRI Enhancement Devices

Chunlai Li, Jie Guo, Zhiya Zhao, and Lin Luan
Shenzhen Key Laboratory of Optical and Terahertz Meta-RF
Kuang-Chi Institute of Advanced Technology
Software Building, No. 9 Gaoxinzhong 1st Road, High-Tech Industrial Estate
Nanshan District, Shenzhen, Guangdong, China

Abstract— Basically there are three types of the MRI (magnetic resonance imaging) enhancement devices based on metamaterials. One is composed of metallic wires, the another one has the Swiss roll structure, and the last one has the microstructure of a capacitively loaded split-ring with a high precision ($\sim 1\%$) capacitor. However, those metamaterial devices yet have long way to go for practical MRI applications. The one with wires has a significant thickness and an inconspicuous image enhancement, the one with the Swiss roll structure also has considerable thickness and in fact its intrinsic resolution is limited by the diameter size of element rolls except for its high loss. The one with split-rings is much less thick than the others but not thin enough for application yet, moreover the addition of high precision capacitors increases cost dramatically and not friendly for fabrication. Examining those structures carefully, one can find that the only reason to use capacitors is to reduce the resonance frequency of the split-rings. Hence it is not necessary to utilize capacitors if the resonance frequency of the microstructure is low enough. One effective way to reducing the resonance frequency of a winding is to fabricate rings on both sides of PCB (printed circuit board) and connect the windings by a via, a standard PCB fabrication technology. We designed a magnetic superlens for 1.5 T MRI system, i.e., the permeability equaling to -1 at working frequency (63.6 MHz) with a windings microstructure, only 1 mm thickness and without capacitors. Also the metamaterials is easy to fabricate and replica. The magnetic field intensity was increased as high as 42.4% at the position about 3 cm after the superlens. The MRI images in animal vitro experiment demonstrated that the quality of images improved distinctly, especially in intensity and SNR (signal to noise ratio), and suggested that the designed metamaterials could offer a very promising practical application for MRI.

Near-field Optical Storage System with a Real Artificial Negative Index Film

Taikei Suyama[1], **Xiaowei Ji**[2], **Akira Matsushima**[2], **and Yaoju Zhang**[3]

[1]Department of Electrical and Computer Engineering
Akashi National College of Technology, Akashi, Japan
[2]Graduate School of Science and Technology, Kumamoto University, Kumamoto, Japan
[3]Department of Physics and Electronic Information, Wenzhou University, Wenzhou, China

Abstract— We report a new method of enhancing the intensity of spot and improving the air-gap width of a near-field optical storage system with a real artificial negative index film (NIF). This method is based on surface plasmas excited by NIF combining a polymer film. In 2004, a near-field SIL optical storage system utilizing a negative index material was proposed [1]. In this paper, we develop the concept of the near-field optical storage using a NIF and propose a new near-field solid immersion lens (SIL) optical recording system. Our method is based on the surface plasmas (SP) excited by a NIF-polymer composite nano-layer which is attached on the plane surface of the SIL. An experimentally-fabricated negative index material comprising silver nanorods [2] is chosen as the NIF and the refractive indices mismatching effect is considered in our simulations. The proposed system may be much more close to an actual near-field optical recording system. Numerical results based on the simple vector diffraction theory show that the present system can reduce energy loss markedly and substantially increase the gap's width of the near-field optical storage system with a SIL.

REFERENCES

1. Liu, L. and S. He, "Near-field optical storage system using a solid immersion lens with a left-handed material slab," *Opt. Express*, Vol. 12, 4835–4840, 2004.
2. Jen, Y. J., A. Lakhtakia, C. W. Yu, and C. T. Lin, "Vapor-deposited thin films with negative real refractive index in the visible regime," *Opt. Express*, Vol. 17, 7784–7789, 2009.
3. Richards, B. and E. Wolf, "Electromagnetic diffraction in optical systems II. Structure of the image field in an aplanatic system," *Proc. Roy. Soc. A*, Vol. 253, 358–379, 1959.
4. Zhang, Y. and J. Bai, "Improving the recording ability of a near-field optical storage system by higher-order radially polarized beams," *Opt. Express*, Vol. 17, 3698–3706, 2009.
5. Yao, J., Z. Liu, Y. Liu, Y. Wang, C. Sun, G. Bartal, A. M. Stacy, and X. Zhang, "Optical negative refraction in bulk metamaterials of nanowires," *Science*, Vol. 321, 930, 2008.

Polarization-independent Metamaterial with Unnaturally High Refractive Index in the Terahertz Region

Zhengxian Liu and Shumin Xiao
Department of Material Science and Engineering Shenzhen Graduate School
Harbin Institute of Technology, Shenzhen 518055, China

Abstract— Refractive index is the most important property of material in optics and most naturally existing transparent materials possess small positive indices of refraction. With the progress of metamaterials, we can manipulate the electromagnetic properties of materials. Metamaterials promise unexpected physical phenomena through creating artificial "atoms" with an array of period metallic structure. However most researches are focusing on the negative refractive index materials at present, on the contrary the opposite side of high refractive index materials attracts far less attention. Previous approaches using metamaterials were not successful in realizing broadband isotropy high refractive indices. Here we design a broadband, isotropy three-dimensional metamaterial with extremely high index of refraction in terahertz region which composed of strongly coupled unit cells. We increase the effective permittivity through strong capacitive coupling and decrease the diamagnetic response with a thin metallic structure in the unit cell. A peak refractive index of 55 at 1.9 THz is observed under TE mode and a peak refractive index of 48 at 2.0 THz under TM mode. Both of polarizations maintain low loss with figure of merit go to as high as 2.3 and 2.7 separately. Moreover, the refractive index does not fall sharply at higher frequencies, and shows an extremely broadband behavior with a full-width at half-maximum (FWHM) of more than 2 THz. Experiments are also launched to match the numerical results.

Photon Hopping and Nanowire Based Hybrid Plasmonic Ring-resonator

Zhiyuan Gu[1], **Shumin Xiao**[2], **Shuai Liu**[1], **Shang Sun**[2], **Kaiyang Wang**[1], **and Qinghai Song**[1, 3]

[1]Department of Electrical and Information Engineering
Harbin Institute of Technology, Shenzhen, Guangdong 518055, China
[2]Department of Materials Science and Engineering
Harbin Institute of Technology, Shenzhen, Guangdong 518055, China
[3]National Key Laboratory on Tunable Laser Technology
Harbin Institute of Technology, Harbin 158001, China

Abstract— Hybrid plasmonic waveguide modes consist of plasmonic and dielectric cylinder waveguide modes open up a new avenue for the design of nano scale optical circuits and light operation at deep sub-wavelength. Several structured are proposed which have two end-to-end nanowires with an air gap. Light jumps the air gap with acceptable energy loss. We numerically demonstrate novel properties of the hybrid plasmonic waveguide that guiding light via photons hopping and systematically investigate the transmission and reflection. Furthermore, full ring resonator and open-ring resonator with high Q factor and smaller mode volume are introduced.

Session 2P6
FocusSession.SC3: Biophotonics — Clinical and Preclinical Applications

Compact Diode Laser-based Systems for Biophotonics Application

P. E. Andersen[1], **O. B. Jensen**[1], **A. Müller**[2], **B. Sumpf**[2], **A. K. Hansen**[1], **P. M. Petersen**[1], **Peter M. Skovgaard**[3], **A. Unterhuber**[4], **and W. Drexler**[4]

[1]Technical University of Denmark, Roskilde, Denmark
[2]Ferdinand-Braun-Institut, Leibniz-Institut für Höchstfrequenztechnik, Berlin, Germany
[3]Norlase ApS, Roskilde, Denmark
[4]Medical University of Vienna, Vienna, Austria

Abstract— Diode lasers are by far the most efficient lasers currently available. With the ever-continuing improvement in diode laser technology, this type of laser has become increasingly attractive for a wide range of biomedical applications. Compared to the characteristics of competing laser systems, diode lasers simultaneously offer tunability, high-power emission and compact size at fairly low cost. Therefore, diode-based lasers are increasingly preferred in important applications, such as photocoagulation, optical coherence tomography, diffuse optical imaging, fluorescence lifetime imaging, and terahertz imaging.

Diode lasers have proven to be versatile light sources for pumping Ti:Sappphire lasers offering advantages over current solid-state lasers in terms of compactness, noise characteristics, and no need for water cooling. Whilst direct green laser diodes at several Watts of output power are not available, nonlinear frequency conversion of high brightness diode lasers has recently resulted in visible light power levels in the watts range enabling an increasing number of applications within biophotonics.

This talk review provides an overview of the developments within nonlinear frequency converted high power laser diodes in the blue-green spectral range. Single-pass nonlinear frequency doubling is presented as a non-sophisticated method to achieve watt-level output powers. Furthermore, potential routes to higher power and increased conversion efficiency are discussed. In particular, so-called cascaded frequency-doubling will be discussed as a means of power scaling, involving one laser and several nonlinear crystals. By beam combining, sum-frequency generation can be achieved, thus combining several lasers in one crystal to obtain higher power. Application examples within pumping of mode-locked Ti:sapphire lasers and implementation of such lasers in optical coherence tomography are presented showing the application potential of these lasers. An example of OCT images and the advantages of using diode laser-based systems in terms of their noise characteristics is shown in Figure 1.

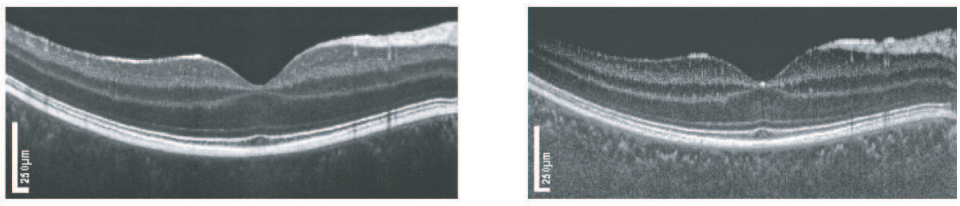

(a) (b)

Figure 1: OCT tomograms using Ti:Sapphire for retinal imaging in spectral domain OCT. (a) Ti:Sapphire pumped by diode-based system (50 frames averaging). Ti:Sapphire pumped by commercially available solid-state laser (50 frames averaging). Tomograms are displayed in a 1 : 3 ratio (horizontal: vertical) for better visualization of the layered structure.

Development of New LED Light Sources for Improved Visualization of Bio-samples

Aikaterini Argyraki, **Jakob Munkgaard Andersen**, **Søren Stentoft Hansen**, **Jørgen Stubager**, **Dennis Dan Corell**, **and Paul Michael Petersen**
Department of Photonics Engineering, Technical University of Denmark, Roskilde DK-4000, Denmark

Abstract— Visual examination is the initial tool used by clinical doctors in all classes of medical diagnostics. Many medical imaging techniques have emerged over the recent years, thereby offering extended "vision" to surgeons and medical doctors. However, immediate visual clarity is still an unresolved issue. Human visual perception can be significantly affected by the spectral power distribution (SPD) of the available light. Though, the diagnostic luminaires are chosen only by taking into account the illumination level, shadow, glare and heating reduction. LED technology allows control over SPD and can, as well, address all above mentioned factors. Simulation programs for predicting the optimal spectral distribution of illuminant, for enhanced color difference between abnormal and normal tissue, has recently been reported successfully [1]. Moreover, exploration of color contrast through computation (NIST color quality simulation program software) according to CIE standards has showed that it is possible to enhance the contrast between color patches typical of tissue color by using special illuminant spectral distribution [2].

In this work, in order to bring into life the simulation work [1, 2], a multi-channel LED lamp was developed. The various channels were allowing modifying the intensities of colored (blue, green, red and cyan) and white LEDs (warm, neutral and cold). The LED light source could provide white light with color temperature ranging from 2700–5400 K, with high color rendering index in the range 90–95. A systematic optimization procedure was followed in order to achieve optimal visual perception of contrast on bio-samples. It was shown that higher color temperatures (above 4500 K) resulted in better visual perception of bio-samples. Furthermore, colored light (mixture of RGBC) resulted in surprisingly better contrast than conventional light sources, but resulted in eye fatigue quicker than white light. Human eye spectral sensitivity combined with reflection measurements of bio-samples, were used as a guide for selecting the optimal spectral power distribution of the colored light. Human acceptance, for the proposed spectral power distributions, and preference over conventional light sources was statistically recorded (population: 35 participants).

A first step towards statistical validation of the human preference for the proposed optimal light source over conventional light sources was done, though confirmation in medical practice is still critical for the implementation of the method. Moreover, the universality of the success of the method for varying bio-samples needs still to be tested, and is of fundamental importance. It is believed that the prospect of improving visual perception of doctors and clinical practitioners by using highly energy efficient and environmentally friendly light sources, as LEDs, could improve the lifecycle of hospitals and benefit medical society.

REFERENCES

1. Murai, K., H. Kawahira, and H. Haneishi, "Improving color appearance of organ in surgery by optimally designed LED illuminant," *Proceedings of IFMBE, World Congress on Medical Physics and Biomedical Engineering*, Vol. 39, 1010–1013, Beijing, China, May 2012.
2. Litorja, M., S. W. Brown, C. Lin, and Y. Ohno, "Illuminants as visualization tool for clinical diagnostics and surgery," *Proceedings of SPIE 7169, Advanced Biomedical and Clinical Diagnostic Systems VII*, Vol. 7169, B1-9, San Jose, CA, January 2009.

Laser-activated Plasmonic Particles for Cancer Theranostics: Novel Targeting Strategies Tested in Vitro and in Vivo

Roberto Pini[1], **Fulvio Ratto**[1], **Francesca Tatini**[1], **Sonia Centi**[2], **Ida Landini**[3], **Stefania Nobili**[3], **Ewa Witort**[2], **Franco Fusi**[2], **Sergio Capaccioli**[2], **and Enrico Mini**[3]

[1]Institute of Applied Physics, National Research Council of Italy, Florence, Italy
[2]Department of Experimental Biomedical and Clinical Science, University of Florence, Italy
[3]Department of Health Science, University of Florence, Italy

Abstract— The combination of pulsed and CW near-infrared laser light with plasmonic particles such as gold nanorods is gaining relevance for the photoacoustic imaging and photothermal ablation of cancer. Selective targeting of malignant cells with these contrast agents may rely on complementary biochemical and biological strategies, including the use of specific probes or the exploitation of cellular vehicles.

Here we move from a platform of PEGylated gold nanorods with plasmonic bands around 800 nm, good biological profiles, stability and efficiency of photoacoustic and photothermal conversion as well as potential to passively accumulate into solid tumors by their enhanced permeability and retention.

In order to enhance this potential, we implemented different approaches for active delivery by functionalization with (i) antibodies against cancer antigen 125 (CA125), which is a common biomarker for ovarian lesions; (ii) inhibitors of carbonic anhydrases 9 and 12 (CAIX and CAXII), which are expressed by hypoxic cells such as those found in solid tumors; and (iii) by introducing macrophages as a versatile model of cellular vehicles that would phagocytose the particles and home to inflammatory lesions

We challenge these alternatives in vitro under relevant conditions and discuss issues and perspectives behind their optimization and synergy.

Microcirculation Imaging with Light and Sound

Martin J. Leahy, Haroon Zafar, Sean O'Gorman,
Aedán Breathnach, and Hrebesh M. Subhash
Tissue Optics & Microcirculation Imaging Group, School of Physics
National University of Ireland, Galway, Ireland

Abstract— Imaging in deep tissue using linear microscopic and mesoscopic techniques requires the use of diffuse light. Improper functioning of the microcirculation is a characteristic of many diseases such as diabetes mellitus, heart disease, peripheral vascular disease and arteriosclerosis. Hence the assessment of both the structural and dynamic properties of the capillaries in the upper dermis and the vessels which supply them are of vital importance.

Methods: We have developed 2D devices based on polarization spectroscopy [1] which output colour-coded maps which are sensitive to the concentration of red blood cells in the skin tissue. The hardware design consists of two orthogonally placed polarisation filters over the light source and sensor of a standard digital camera and utilises the video mode to provide an acquisition frequency of 15/30 Hz at a resolution of ~ 200 m. We have also developed correlation mapping optical coherence tomography (cmOCT) [2, 3] to render the 3D microcirculation. To obtain microvascular maps without motion artefact, we used the full-field technique developed by Boccara [4] and others and applied the cmOCT algorithm to the data [5]. Since the depth is limited to one or two mm with OCT and much less with full-field OCT, we have recently begun to work with photoacoustic tomography. We believe that a reflection type probe, similar to existing clinical ultrasound, is most likely to succeed in real clinical applications. Its advantages include ease of use, speed and familiarity for radiographers and clinicians.

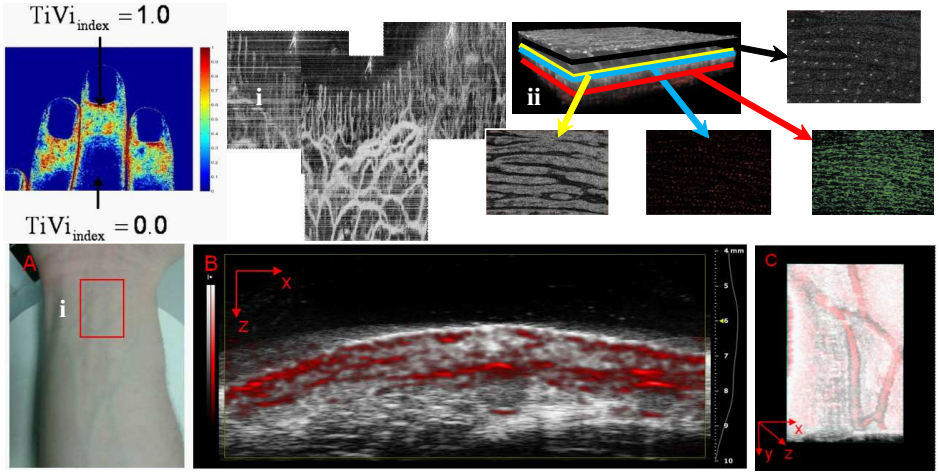

Figure 1: Imaging the microcirculation i) TiVi, ii) cmOCT of the nailfold plexus, iii) 3D cmOCT on the fingertip with structure and iv) 3D photoacoustic and ultrasound imaging of the volar aspect of human wrist.

Conclusion: Light and sound provide complementary techniques for imaging the microcirculation within its native structural context and adds functional information.

ACKNOWLEDGMENT

This study was supported by NBIP Ireland funded under the Higher Education Authority PRTLI Cycle 4, co-funded by the Irish Government and the EU — Investing in your future and IRCSET, the Science Foundation Ireland (SFI). Haroon Zafar is supported by a Hardiman Fellowship from NUI Galway.

REFERENCES

1. McNamara, P., J. O'Doherty, M. L. O'Connell, J. Henricson, B. W. Fitzgerald, C. Anderson, G. E. Nilsson, R. Toll, and M. J. Leahy, "Tissue viability (TiVi) imaging: Temporal effects of local occlusion studies in the volar forearm," *J. Biophotonics*, Vol. 3, Nos. 1–2, 66–74, 2010.

2. Enfield, J., E. Jonathan, and M. J. Leahy, "In vivo imaging of the microcirculation of the volar forearm using correlation mapping optical coherence tomography (OCT)," *Biomedical Optics Express*, Vol. 2, No. 5, 1184–1193, 2011.
3. Zam, A., R. Dsouza, H. M. Subhash, M. O'Connell, J. Enfield, K. Larin, and M. J. Leahy, "Feasibility of correlation mapping optical coherence tomography (cmOCT) for anti-spoof subsurface fingerprinting," *J. Biophoton.*, Vol. 6, No. 9, 663–667, 2013.
4. Grieve, K., et al., "In vivo anterior segment imaging in the rat eye with high speed white light full-field optical coherence tomography," *Opt. Express*, Vol. 13, No. 16, 1094–4087, 6286–6295, 2005.
5. McNamara, P. M., H. M. Subhash, and M. J. Leahy, "In vivo full-field en face correlation mapping optical coherence tomography," *J. Biomed. Opt.*, Vol. 18, No. 12, 126008, 2013.

Transfer of Angular Momentum of Light in Optical Tweezers and Applications

Halina Rubinsztein-Dunlop
Quantum Science Laboratory, School of Mathematics and Physics
The University of Queensland, Brisbane, QLD 4071, Australia

Abstract— The way light can apply forces to a microscopic object is easily understood as an exchange of momentum between the light beam and the object. This applies both to linear momentum and to angular momentum exchange. Methods based on these phenomena promise high flexibility and an opportunity for driving these objects in microfluidic devices or even inside a biological cell. Optical drive of micron scale devices promises the ability to carry out measurements and operations on microscopic systems in a flexible way. The energy that is needed can be transmitted without harm through many materials including a membrane of a cell. Optical tweezers have been already used to measure mechanical properties of cells and their components, and also for studies of molecular motors. The stimulation of cells by forces and torques applied to them has allowed studies of cell response and signal transduction.

The use of the angular momentum of light enables introduction of rotation of microscopic objects. Quantitative measurements of this rotation are possible through a measurement of the change of polarisation state of light after passing through the object. The transfer of the angular momentum can then be used for several applications in biology and medicine. One of such application is microrheology of complex fluids that exhibit both viscous and elastic behaviours.

Viscoelastic fluids are prevalent in many biological systems, from the synovial fluid between bone joints to the cytoplasm inside a cell. Many of these fluids are highly inhomogeneous or preferably available in ultra-small volumes so their precise mechanical properties, rheology, are largely unknown and difficult to test. To enable studies of such systems, we have developed an optical tweezers microrheometer capable of conducting viscoelastic measurements in picoliter volumes with the highest spatial resolution available to particle tracking microrheometers. By observing the rotation of the probe driven by alternating angularly offset traps our method finds rheological information about the local region in which the probe is positioned unhindered by close boundaries.

Cortical Functional Connectivity Revealed by Optical Brain Imaging

Jun Li and Lina Qiu
Centre for Optical and Electromagnetic Research
South China Normal University, Guangzhou 510006, China

Abstract— Optical brain imaging is emerging as a novel technique for non-invasively investigating functioning brain. It uses near-infrared light to probe human cortex through intact scalp and skull, providing cerebral hemodynamic parameters closely associated with neuronal activity. In addition to investigating various task-related brain activities, very recently optical brain imaging has been demonstrated to be able to assess resting state functional connectivity (RSFC) by recording the cortical spontaneous fluctuations. The temporal correlations of these fluctuations reflect the connectivity strength in the functional networks. In this work, we use a continuous-wave optical brain imaging system to record the cerebral spontaneous hemodynamic signals (including oxygenated-, deoxygenated- and total hemoglobin) for 8 minutes, and compute the correlation coefficients for all optical channel pairs. The cortical areas measured include the temporal and the prefrontal cortices. The data from the temporal area show that there are significant differences in the network characteristics (including network connectivity and network range) between children and adults, implying the developmental differences in language skills. For the prefrontal measurements, the data show significant differences between males and females in the RSFC, which may shed light on the underlying physiological basis for sex-related differences in cognitive control and emotional regulation in healthy people, and may also provide insight into sex-related differences in the prevalence of some neurological diseases. Our results suggest using optical brain imaging to assess RSFC may uncover more unrevealed details on functioning brain, which encourages further exploration of this novel technique.

Atypical Activation Pattern of Children with Autism Spectrum Disorder (ASD) in Language Area During Listening Comprehension: A fNIRS Study

Huilin Zhu[1], **Xinge Li**[2], **Guixion Xu**[1], **Rongwei Zhang**[3], **Qianqian Gao**[1, 2], **Ziqiang Hu**[1, 2], **and Sailing He**[1]

[1]Centre for Optical and Electromagnetic Research, ZJU-SCNU Joint Research Center of Photonics South China Normal University (SCNU), Guangzhou 510006, China
[2]School of Psychology, South China Normal University (SCNU), Guangzhou 510631, China
[3]Department of Social Sciences, Fujian Polytechnic of Information Technology, Fuzhou 350003, China

Abstract— Autism spectrum disorder (ASD) is a neuro-developmental disorder, characterized by delays or abnormal functioning started before the age of three years in one or more of the following domains: social interaction, communication and restricted, repetitive and stereotyped patterns of behaviors and interests. Previous studies have found that children with ASD showed language comprehension impairments and atypically functional and anatomical development in language area of the brain, which include bilateral inferior frontal gyrus and bilateral temporal cortex. In the present study, for the first time, fNIRS was used to examine the neural correlation of sentence comprehension in the language areas of brain in the children with ASD and reveal the effect of different kind of comprehensions and promptings.

In this study, a 44-channel functional near infrared spectroscopy (fNIRS) was adopted to measure changes in blood oxygenated hemoglobin (HbO) in the language areas of the brain, and compared the differences of neural activation between children with ASD and typically developing (TD) children between 6–13 years of age during listening sentence comprehension. All the children were informed to listen to a list of sentences and then perform three kinds of comprehension tasks with different level of sociality (to infer emotions of people, to infer identities of peoples, and to infer names of items) and answered the questions with two different types of promptings (pictures and words).

Results were shown that in listening sentence comprehensions, children with ASD showed pervasively reduced activation in language area both in scope and strength. When inferring identities of people under picture promptings, children with ASD showed significant lower response than TD children. However, children ASD did not showed any significant difference (as compared to TD children) in brain response when inferring emotion of people and names of items. Considering the effect promptings, it was indicated that promoting with pictures could activate more regions in language area but with low intensity in the brain with ASD. Meanwhile, promoting of words could activate fewer regions but with higher intensity and showed a compensated activation in the left inferior frontal gyrus and right temporal cortex in the brain with ASD. ASD children with more severe symptom would show less activation in ventral stream (left superior temporal gyrus) of speech processing and more compensated activation in dorsal stream (left inferior gyrus) of speech processing and right temporal cortex when promoted with words.

These results supported the feasibility of using the fNIRS method to assess atypical cortical hemodynamic responses of ASD and to reveal the neural mechanism under language deficits of ASD.

Optical Diagnosis of Middle Ear Infection Using Spectroscopic Techniques — Phantom Experiments

Hao Zhang[1], **Jing Huang**[1], **Tianqi Li**[1], **Sune Svanberg**[1, 2], **and Katarina Svanberg**[1, 2]

[1]Center for Optical and Electromagnetic Research, South China Normal University
University City Campus, Research Building 5, Guangzhou 510006, China
[2]Lund Laser Center, Lund University, SE-221 00 Lund, Sweden

Abstract— Otitis media is an inflammation of the middle ear, and is one of the most common infectious diseases in early childhood. There are three principal types of ear infections — acute otitis media (AOM), otitis media with effusion (OME) and chronic otitis media with effusion (COME), with each type having different symptoms. AOM is the common ear infection, which is related to an upper respiratory infection with blockage of the Eustachian tube and liquid aggregation in the middle ear. In normal conditions, gas exchange through the Eustachian tube plays a very important role to regulate the middle ear pressure [1]. Generally, the diagnosis of otitis media is achieved by using an otoscope for eardrum inspection — A red and bulging eardrum may indicate an ear infection. However, the crying of an upset child can also cause symptoms similar to those of otitis media. We are investigating additional noninvasive optical techniques for improved diagnosis of the ear infection. In recently years, Gas in Scattering Media Absorption Spectroscopy (GASMAS) has been used for diagnosis of sinusitis [2]. In the present study, middle ear phantoms were constructed with a cavity, e.g., a fish swimming bladder, surrounded by strongly scattering material, and were used to investigate the potential of spectroscopic ear infection diagnosis. Two types of gas are detected in backscattering detection geometry, molecular oxygen at 760 nm and water vapor at 935 nm. It is noted, that if the cavity is filled with liquid, the sharp imprints by the free gas are absent. The model was flushed with pure nitrogen and pure oxygen to investigate the gas exchange processes. Experimental results are shown in the Figure 1(a). By studying the oxygen gas response when the nasal cavity is flushed with nitrogen, the ventilation through the Eustachian tube can be assessed. We are now developing an instrument where GASMAS can be combined with reflectance spectroscopy to provide objective assessment of ear infection. A reflectance spectrum from a fish swimming bladder wall, mimicking an eardrum, is also included in the Figure 1(b), showing characteristic absorptive imprints from blood.

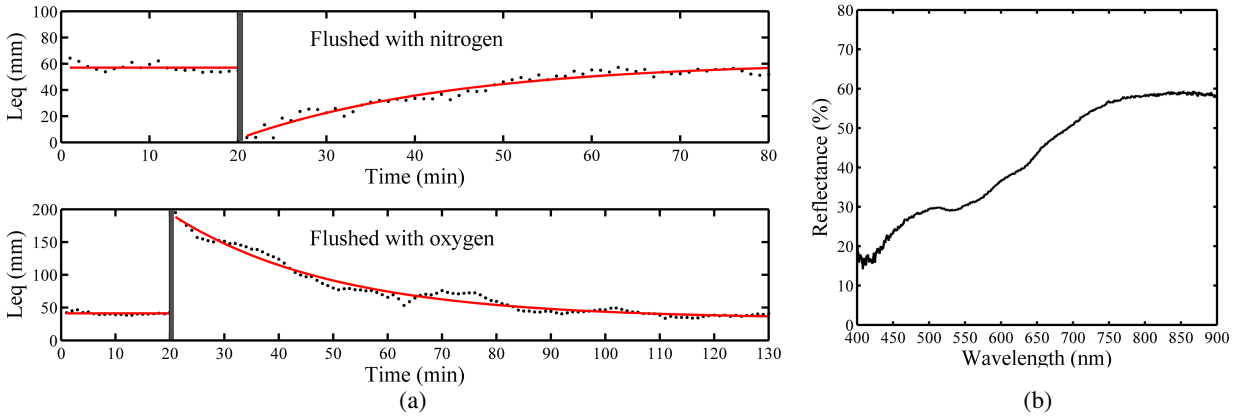

Figure 1.

REFERENCES

1. Ingelstedt, S. and B. Jonson, "Mechanisms of the gas exchange in the normal human middle ear," *Acta Oto-Laryngologica*, Vol. 63, 452, 1967.
2. Persson, L., M. Andersson, M. Cassel-Engquist, K. Svanberg, and S. Svanberg, "Gas monitoring in human sinuses using tunable diode laser spectroscopy," *J. Biomed. Optics*, Vol. 12, 054001, 2007.

Assessment of Human Sinus Cavity Air Volume — Temporal Study

Hao Zhang[1], **Jing Huang**[1], **Tianqi Li**[1], **Katarina Svanberg**[1, 2], **and Sune Svanberg**[1, 2]

[1]Center for Optical and Electromagnetic Research
South China Normal University, University City Campus
Research Building 5, Guangzhou 510006, China
[2]Lund Laser Center, Lund University, Lund SE-221 00, Sweden

Abstract— Sinusitis is a very common disorder, leading to extensive use of antibiotics, warranted if caused by bacterial infection, but not effective if of viral origin, which is the most common case. Growing resistance to antibiotics is a major concern, calling for new diagnostic methods. It has been shown in a clinical study, that sinus cavity data obtained with the technique Gas in Scattering Media Absorption Spectroscopy (GASMAS) [1], show a good agreement with results from computerized tomography [2]. GASMAS can access the size of air-filled cavities (by the size of the water-vapor related signal, and the ventilation status (through the ratio of oxygen and water-vapor related signals). An absolute assessment of oxygen concentration or absolute size of the sinus gas-filled volume is difficult. However, changes over time for a given patient could yield important diagnostic information, especially in patients with recurrent or chronic disease. In order to assess the reproducibility of the technique we have studied the water-vapor GASMAS signal from the frontal sinuses for a number of healthy volunteers, subject to measurements separated by one week. The size of the signal varies between subjects, as does the left-right hand side measured asymmetry as shown in Figure 1(a), showing data for 4 volunteers on one measurement occasion. Data for a single volunteer from 6 occasions over a day are shown in Figure 1(b). The stability of the GASMAS signals from frontal as well as maxillary sinuses are assessed for volunteers free from sinus-related problems, to evaluate the potential to quickly determine anomalies related to disease.

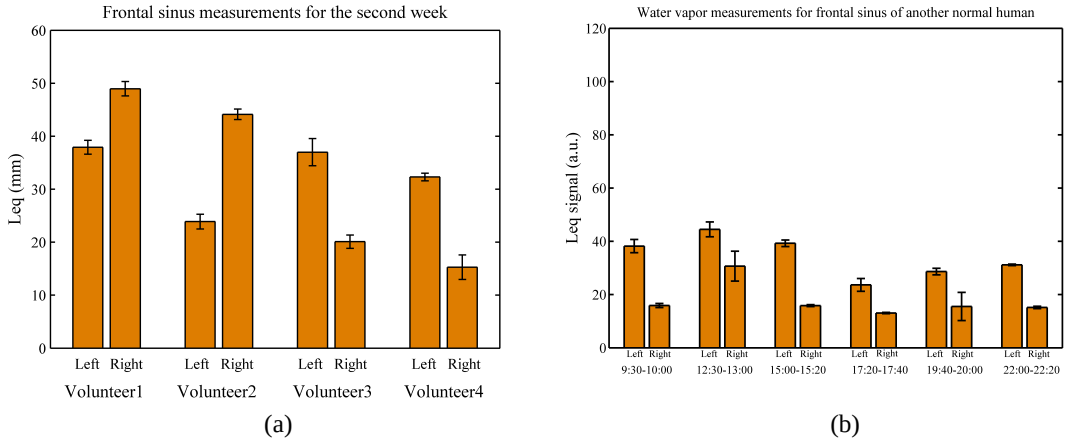

Figure 1.

REFERENCES

1. Svanberg, S., "Gas in scattering media absorption spectroscopy," *Encyclopedia of Analytical Chemistry*, M. Sigrist (Ed)., John Wiley & Sons, 2014.
2. Lewander, M., S. Lindberg, T. Svensson, R. Siemund, K. Svanberg, and S. Svanberg, "Clinical study assessing information on the maxillary and frontal sinuses using diode laser gas spectroscopy," *Rhinology*, Vol. 50, 26, 2011.

Studies of Oxygen and Oxygen Exchange in Fruits Using Gas in Scattering Media Absorption Spectroscopy

Jing Huang[1], **Hao Zhang**[1], **Tianqi Li**[1], **Guangyu Zhao**[1], **Sune Svanberg**[1, 2], **and Katarina Svanberg**[1, 2]

[1]Center for Optics and Electromagnetic Research
South China Normal University, University City Campus, Guangzhou 51006, China
[2]Lund Laser Center, Lund University, Lund SE-221 00, Sweden

Abstract— The concentration of the biologically active molecular oxygen gas is of crucial importance for fruits in the maturation and ripening processes. In metabolic respiration, oxygen is consumed to break down organic compounds of the fruits to release energy necessary to maintain the life activity, and carbon dioxide is produced in the process. By increasing the carbon dioxide and decreasing the oxygen surrounding concentrations, a prolonged fruit shelf-life, because of a decreased respiration rate, will result. However, anaerobic respiration happens when the oxygen is below a limit — the fruit tissue can be damaged by too high carbon dioxide concentrations. Thus, the fruits need an optimal surrounding gas concentration in storage. The skin of the fruits is of critical importance in regulating the gas diffusion in fruits. We have studied oxygen and oxygen exchange in fruits non-invasively by using Gas in Scattering Media Absorption Spectroscopy (GASMAS) [1]. This technique employs a narrow-band tunable diode laser to measure gases in pores and cavities in solid-state matrices. GASMAS relies on the fact that free gases typically have 10,000 times narrower absorption features than the surrounding tissue. The GASMAS imprint is quite small — thus wavelength modulation spectroscopy (WMS) is used for high sensitivity detection. We have studied how the GASMAS oxygen signal changes during the ripening process of different kinds of tropical fruits — nectarine (NE), mango (MG), papaya (PA), and guava (GU) [2]; see Fig. 1(a). L_{eq} is the equivalent path length in normal 21% oxygen air. Combining with measurements of reflectance and fluorescence, we show that optical techniques are very powerful in evaluating the state of ripeness of fruits. To study the role of the skin in regulating gas transport in fruits, oxygen diffusion measurements on peeled and unpeeled apples were performed. The apples were stored over-night in a high concentration oxygen atmosphere prior to the measurements. As illustrated in Fig. 1(b), the skin strongly influences the gas exchange with the environment.

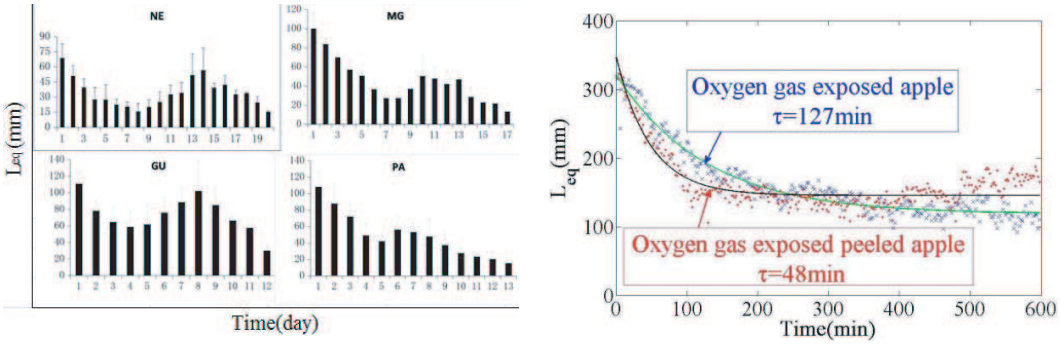

Figure 1.

REFERENCES

1. Svanberg, S., "Gas in scattering media absorption spectroscopy — From basic studies to biomedical applications," *Laser & Photonics Reviews*, Vol. 7, 779–796, 2013.
2. Zhang, H., J. Huang, T. Q. Li, X. X. Wu, S. Svanberg, and K. Svanberg, "Studies for tropical fruit ripening using three different spectroscopic techniques," submitted.

Modulation of Cellular Signaling and Processes by Femtosecond Laser

Hao He[1, 2]

[1]Med-X Research Institute, School of Biomedical Engineering
Shanghai Jiaotong University, Shanghai 200030, China
[2]Ultrafast Laser Laboratory, College of Precision Instrument and Optoelectronics Engineering
Tianjin University, Tianjin 300072, China

Abstract— Regulation of cell signaling is a very attractive challenge to life science which provides good potential for better understanding of cellular processes, cell development, and cell physiology, as well as potential application for gene therapy, economical metabolic engineering and biopharmaceutical production. A lot of approaches have been developed for specific stimulation of cell molecules, signaling pathways, functions. But most of those approaches are based on biochemical techniques, for example, optogenetics and introducing some signaling proteins to cells. Hence usually such techniques are invasive and complicated. In this report, we present series of all-optical methods to modulate cell signaling and processes simply by femtosecond laser. Cellular Ca^{2+} store and reactive oxygen species (ROS) can be released and regulated by a short flash of femtosecond laser irradiation. The open of Ca^{2+} channel in cell membrane and mitochondrial release of ROS can be controlled. Therefore we developed an optical method to regulate gene expression since some transcription factors can be activated by this optical treatment, by which some specific differentiation regulators in mesenchymal stem cells are upregulated for potential induced differentiation. The tightly focused femtosecond laser can further induce precise insult and oxidative flashes in single mitochondria. Mitochondrial contraction, fragmentation and swelling can be induced with no perturbing to surroundings, but the membrane potential and permeability transition pores are inflenced. Localized translocation of Bax and cytochrome C can be precisely controlled by this optical method. Hence we propose that femotosecond laser has a promising application potential in cell research, mitochondrial diseases, gene therapy, and stem-cell medicine.

Effective Bioimaging by Using Two-photon Absorbing Chromophores and Nanoparticles

Kwang-Sup Lee
Department of Advanced Materials, Hannam University, Daejeon 305-811, South Korea

Abstract— In recent years, photoluminescence based bioimaging forms a major thrust of biophotonics. Much focus has been given to the development of efficient, inexpensive, stable, and tunable exogenous optical agents in biological systems, such as quantum dots/rods, silica nanoparticles, metal nanoparticles carbon nanomaterials and up-converting nanophosphores. Although organic fluorophores exhibit remarkably high photoluminescence quantum efficiencies, their applications in the area of biological imaging are still limited due to their intrinsic hydrophobic property and instability in bio-environments. To overcome these problems, our group has been developed unique approaches.

In this lecture we present the preparation and use of aggregated enhanced PL chromophores and nanoparticles with two-photon absorbing activity for effective bioimaging. We firstly present the synthesis of two-photon absorbing chromophores capable of forming effective fluorescent nanoparticle in the J-aggregated state. These chromophores are further combined with materials like hyperbranched polysiloxane and phospholipids to induce celluar uptake and penetration into tumor cells. Polysiloxane polymers exhibited desirable characteristics, including amphiphilicity for nanoparticle formation, and contained various terminal groups for surface-charge control on the nanoparticles or for further bioconjugation for targeted imaging. We also studied *in-vivo* bioimaging using phospholipids [e.g., phospholipids-PEG (polyethylene glycol)] forming fluorescent nanomicelles with brighter fluorescence and make fluorophores more stable in various bio-environments. In addition this, we also developed water-soluble chromophores based on porphyrin and perylenediimide. In vitro test, cellular uptake efficiency has been enhanced by simple modification of molecular structure through changing the number of PEG unit without any support such as polymer-encapsulated inorganic nanoparticles.

REFERENCES

1. Kim, W. J., A. C. Bonoiu, T. Hayakawa, C. Xia, M. Kakimoto, H. E. Pudavar, K.-S. Lee, and P. N. Prasad, *Int. J. Pharmaceutics*, Vol. 376, 141–152, 2009.
2. Kim, W. J., M. S. Kang, H. K. Kim, Y. T. Kim, T. Chang, T. Ohulchanskyy, P. N. Prasad, and K.-S. Lee, *J. Nanosci. Nanotechnol.*, Vol. 9, 7130–7135, 2009.
3. Wang, D., J. Qian, S. He, J. S. Park, K.-S. Lee, S. Han, and Y. Mu, *Biomaterials*, Vol. 32, 5880–5888, 2011.

Optical Remote Monitoring of Flying Insects

M. Brydegaard[1, 2] and S. Svanberg[1, 3]

[1]Applied Molecular Spectroscopy and Remote Sensing Group
Department of Physics, Lund University, Lund SE-221 00, Sweden
[2]Centre for Animal Movement, Department of Biology, Lund University, Lund SE-223 62, Sweden
[3]Center for Optics and Electromagnetic Research, South China Normal University
University City Campus, Guangzhou 51006, China

Abstract— Optical techniques, including spectroscopy, are powerful tools for diagnostics in the biophotonics field. Human tissue can be studied non-intrusively in patients using reflectance, back-scattering, fluorescence and Raman techniques, e.g., for early detection of malignant disease [1]. Similar techniques can be applied in remote sensing implementations, where environmental parameters, such as air or water pollution levels, and vegetation status can be assessed remotely [2]. Ecological studies aiming at flying insect monitoring fall in the intermediate area between these two fields and have extensively been developed in our group following pioneering experiments by Shaw et al. [3]. Insects are interesting to study from a basic science point of view, but also because of the importance in their capacity of being agricultural pests or vectors for spreading disease, e.g., malaria. We have demonstrated fluorescence lidar techniques for insect assessment [4, 5]. Elastic backscattering from a laser beam can provide wing-beat frequencies which are species specific [1]. A particularly simple and powerful variety utilizes backscattering of sunlight from insects, which are observed remotely with a telescope against a background, which is as dark as possible [6]. An overview of our insect monitoring work, including collaborative projects with scientists in developing countries, will be given.

REFERENCES

1. Svanberg, S., "Laser spectroscopy in medical applications," Ch. 10, *Lasers for Medical Applications: Diagnostics, Therapy and Surgery*, H. Jelinkova, Ed., 286–324, Woodhead Publishing, Cambridge, 2013.
2. Svanberg, S., *LIDAR*, Invited Book Chapter for F. Träger, Ed., *Springer Handbook of Lasers and Optics*, 1031–1052, Springer, Heidelberg, 2007.
3. Hoffman, D. S., A. R. Nehrir, K. S. Repasky, J. A. Shaw, and J. L. Carlsten, "Range-resolved optical detection of honeybees by use of wing-beat modulation of scattered light for locating land mines," *Appl. Optics*, Vol. 46, 3007–3012, 2007.
4. Guan, Z. G., M. Brydegaard, P. Lundin, M. Wellenreuther, E. Svensson, and S. Svanberg, "Insect monitoring with fluorescence LIDAR techniques — Field experiments," *Appl. Optics*, Vol. 48, 5668, 2010.
5. Mei, L., Z. G. Guan, H. J. Zhou, J. Lv, Z. R. Zhu, J. A. Cheng, F. J. Chen, C. Löfstedt, S. Svanberg, and G. Somesfalean, "Agricultural pest monitoring using fluorescence lidar techniques," *Applied Physics B*, Vol. 106, 733–740, 2011.
6. Runemark, A., M. Wellereuther, H. Jayaweera, S. Svanberg, and M. Brydegaard, "Rare events in remote dark field spectroscopy," *IEEE JSTQE*, Vol. 18, 1573, 2011.

Session 2P7a
SC3: Advanced Micro-/Nano-fabrication for Optical Sensing and Imaging Applications

Infinitely Long One-nanometer Gaps for Terahertz Funneling

Dai-Sik Kim
Centre for Subwavelength Optics, Department of Physics and Astronomy
Seoul National University, Seoul 151-747, Korea

Abstract— We discuss terahertz nano phenomena whereby millimeter waves funnel through nano antennas enhancing molecular cross sections by 10^3; enhancing nonlinearities and lowering transition temperatures of vanadium dioxide; creating intensity enhancements of 10^9 [1–4]. We push this technology into one-nanometer regime using atomic layer deposition combined with photolithography and exfoliation [5, 6]. One-centimeter long, one-nanometer wide gaps, essentially *infinitely long* for the purpose of terahertz applications, are manufactured. Nano and terahertz technologies have much to offer to each other, providing insights into the smallest possible gaps interacting with largest available wavelengths.

REFERENCES

1. Seo, M. A., H. R. Park, S. M. Koo, D. J. Park, J. H. Kang, O. K. Suwal, S. S. Choi, P. C. M. Planken, G. S. Park, N. K. Park, Q. H. Park, and D. S. Kim, "Terahertz field enhancement by a metallic nano slit operating beyond the skin-depth limit," *Nat. Photonics*, Vol. 3, 152, 2009.
2. Park, H. R., Y. M. Park, H. S. Kim, J. S. Kyoung, M. A. Seo, D. J. Park, Y. H. Ahn, K. J. Ahn, and D. S. Kim, "Terahertz nano-resonators: Giant field enhancement and ultrabroadband performance," *Appl. Phys. Lett.*, Vol. 96, 121106, 2010.
3. Bahk, Y. M., H. R. Park, K. J. Ahn, H. S. Kim, Y. H. Ahn, D.-S. Kim, J. Bravo-Abad, L. Martin-Moreno, and F. J. Garcia-Vidal, "Anomalous band formation in arrays of terahertz nanoresonators," *Phys. Rev. Lett.*, Vol. 106, 013902, 2011.
4. Seo, M., et al., "Active terahertz nanoantennas based on VO_2 phase transition," *Nano Lett.*, Vol. 10, 2064, 2010.
5. Im, H., K. C. Bantz, N. C. Lindquist, C. L. Haynes, and S. H. Oh, "Vertically oriented sub-10-nm plasmonic nanogap arrays," *Nano Lett.*, Vol. 10, 2231–2236, 2010.
6. Chen, X., H. R. Park, et al., "Atomic layer lithography of wafer-scale nanogap arrays for extreme confinement of electromagnetic waves," *Nat. Comm.*, Vol. 4, 2361, 2013.

Nanogap-enhanced Raman Scattering (NERS) Controlled by DNA

Yung Doug Suh[1, 2]

[1]Lab. for Adv. Molecular Probing (LAMP), Research Center for Convergence Nanotechnology (RC2NT)
Korea Research Institute of Chemical Technology (KRICT)
Yuseong, P. O. Box 107, DaeJeon 305-600, Korea
[2]School of Chemical Engineering, Sungkyunkwan University, Suwon 440-746, Korea

Abstract— Since smSERS (single molecule Surface-Enhanced Raman Scattering) was independently reported by S. Nie group and K. Kneipp group in 1997 [1, 2], tremendous amount of interest has been shown to this field because Raman spectroscopy can provide molecular fingerprint together with multiplexing capability in bioassay. Regarding to the origin of this smSERS phenomena, so called "SERS hot spot", Kneipp group reported they could observe smSERS signal only from colloidal aggregation in solution. Later on, Brus group and others showed that SERS hot spots, formed at the junction of two nanoparticles, likely play a major role in smSERS [3, 4]. Theoretical calculations also support that SERS electromagnetic enhancement factors can approach up to $\sim 10^{11}$ when inter-particle spacing reaches down to a few nanometer or less at the junction between two nanoparticle pair. However, formation of these smSERS-active nanostructures with a nano-gap at the SERS hot-spot junction, mostly dimer or colloidal aggregation of Ag or Au nanoparticles adsorbed with Raman active molecules (e.g., Rhodamine 6G), is a random process driven by salt-induced non-specific aggregation. This fact has been a main hurdle for smSERS toward advanced applications.

Based on the idea that controlling this nano-gap between two noble metal nanoparticles is the key to realize reliable smSERS, we have designed a gold-silver nano dumbbell (GSND) and Gold Nanobridged Nanogap Particles (Au-NNP) to exhibit Nanogap-Enhanced Raman Scattering (NERS) controlled by DNA. As for GSND, two gold nano particles with different sizes were linked to each other by double helix DNA (30mer), with a single Raman dye molecule at the center position, to fix the two at a known gap distance ($\sim 10\,\mathrm{nm}$). Then we narrowed the gap down to $< 1\,\mathrm{nm}$ by standard silver staining method to endow the GSND with single molecule sensitivity. We have successfully detected smSERS signals, as well as typical single molecular blinking and polarization behaviors, from each GSNDs by Nano Raman spectroscopy at the single particle level [5]. As for Au-NNP, hollow spherical gap ($\sim 1\,\mathrm{nm}$) between the gold core and gold shell can be precisely loaded with quantifiable amounts of Raman dyes labeled on DNA backbone which is anchored at the gold core and then covered by gold shell [6].

REFERENCES

1. Nie, S. and S. R. Emory, *Science*, Vol. 275, 1102, 1997.
2. Kneipp, K., Y. Wang, H. Kneipp, L. T. Perelman, I. Itzkan, R. R. Dasari, and M. S. Feld, *Phys. Rev. Lett.*, Vol. 78, 1667, 1997.
3. Michaels, A. M., M. Nirmal, and L. E. Brus, *J. Am. Chem. Soc.*, Vol. 121, 9932, 1999.
4. Suh, Y. D., G. K. Schenter, L. Zhu, and H. P. Lu, *Ultramicroscopy*, Vol. 97, 89, 2003.
5. Lim, D., K.-S. Jeon, H.M. Kim, J.-M. Nam, and Y. D. Suh, *Nature Materials*, Vol. 9, 60, 2010.
6. Lim, D., K.-S. Jeon, J. H. Hwang, H. Y. Kim, S. H. Kwon, Y. D. Suh, and J.-M. Nam, *Nature Nanotechnology*, Vol. 6, 452, 2011.

Fabrication, Controlling and Application of Nanoscale Light Sources

Yuanpeng Wu, Pengfei Xu, Xiaowei Liu, Jiabei Li, Haoliang Qian, and Qing Yang
State Key Laboratory of Modern Optical Instrumentation
Department of Optical Engineering
Zhejiang University, Hangzhou 310027, China

Abstract— Nanophotonics has emerged as an exciting new arena concerned with the interaction of light with nanostructured materials. The exploitation of optical phenomena on the nanoscale (nanophotonics) is opening up a diverse field of study that promises to deliver novel technological solutions. Localized intense monochromatic light is highly desired and suitable for coupling light into nanomaterials such as quantum dots, metallic nanoparticles and nanowires (NWs), biological specimens and so on. Precise characteristics and controlling of nanoscale light are highly important for achieving practical applications. We present our work on fabrication, controlling and application of nanoscale light. First of all, we fabricated various NW light sources: semiconductor NW-microfiber hybrid lasers [1, 2] and NW/p-type film hybrid LEDs [3, 4]. Secondly, we focus on achieving tuning/modulating/enhancing the afore-mentioned NW light sources. We demonstrate an efficient way to achieve wide wavelength tunable lasers on single non-doped CdSe NWs [5]. The laser wavelengths are tuned from 746 nm to 706 nm by changing the length of a single NW (402-nm-diameter), spanning a range as large as 40 nm. We investigate the bending effects on NW lasers [6]. We improve the efficiency of LEDs by piezophototronics effect [3, 4]. We also work on the modulation of nanoscale light for example SPP and lasers by electrical tuning [7]. Finally, we investigate the applications of the nanosale light and the behind new physical mechanism. Our work pioneered in nanosale light field may provide a way of fabricating ultra-compact nanophotonic devices and may find its applications in single molecule detection, integrated optical circuits, and optical communications etc..

REFERENCES

1. Yang, Q., X. Jiang, X. Guo, Y. Chen, and L. Tong, "Hybrid structure laser based on semiconductor nanowires and a silica microfiber knot cavity," *Appl. Phys. Lett.*, Vol. 94, 101108, 2009.
2. Ding, Y., Q. Yang, X. Guo, S. Wang, F. Gu, J. Fu, Q. Wan, J. Cheng, and L. Tong, "Nanowires/microfiber hybrid structure multicolor laser," *Opt. Express*, Vol. 17, 21813, 2009.
3. Yang, Q., W. Wang, S. Xu, and Z. L. Wang, "Enhancing light emission of ZnO microwire-based diodes by piezo-phototronic effect," *Nano Lett.*, Vol. 11, 4012–4017, 2011.
4. Yang, Q., Y. Liu, C. Pan, J. Chen, X. Wen, and Z. L. Wang, "Largely enhanced efficiency in ZnO nanowire/p-polymer hybridized inorganic/organic ultraviolet light-emitting diode by piezo-phototronic effect," *Nano Lett.*, Vol. 13, 607–613, 2013.
5. Li, J., C. Meng, Y. Liu, X. Wu, Y. Lu, Y. Ye, L. Dai, L. Tong, X. Liu, and Q. Yang, "Wavelength tunable CdSe nanowire lasers based on the absorption-emission-absorption process," *Adv. Mater.*, Vol. 25, 833–837, 2013.
6. Yang, W., Y. Ma, Y. Wang, C. Meng, X. Wu, Y. Ye, L. Dai, L. Tong, X. Liu, and Q. Yang, "Bending effects on lasing action of semiconductor nanowires," *Opt. Express*, Vol. 21, 2025–2031, 2013.
7. Qian, H., Y. Ma, Q. Yang, B. Chen, Y. Liu, X. Guo, S. Lin, J. Ruan, X. Liu, L. Tong, and Z. L. Wang, "Electrical tuning of surface plasmon polariton propagation in graphenenanowire hybrid structure," *ACS Nano*, 2014, DOI: 10.1021/nn406221s.

Electric and Magnetic Apertured NSOM Probes

Dilip K. Singh[1], **Jae Sung Ahn**[2], **Sukmo Koo**[3], **Taehee Kang**[2], **Joonyeon Kim**[2], **Sukho Lee**[2], **Namkyoo Park**[3], **and Dai-Sik Kim**[2]

[1]Quantum Phenomenon and Photon Physics
CSIR — National Physical Laboratory, New Delhi 110012, India
[2]Centre for Subwavelength Optics, Department of Physics and Astronomy
Seoul National University, Seoul 151-747, Korea
[3]Photonic Systems Laboratory, School of EECS
Seoul National University, Seoul 151-744, Korea

Abstract— We report about physical parameters governing the field vector scattering profiles of near-field scanning optical microscope (NSOM) probes: a method to fabricate electric NSOM probes and Magnetic NSOM probes selectively. Selective field sensitivity was affirmed by mapping spatial variation of field of vertical Hertz standing wave formed upon reflection at oblique incidence. These NSOM probes enable us to uniquely determine randomly oriented electric and magnetic fields.

Search for materials with engineered electromagnetic properties for next generation technologies has triggered strong research interests for sensing [1–3], confinement [4] and enhancement [5, 6] of optical magnetic field of light This work provides a recipe to fabricate NSOM probes selectively sensitive to electric and magnetic field of light.

The sensitivity of NSOM probes to electric or, magnetic field was decided by monitoring the effect of asymmetrically polarized (ϕ) light at oblique incidence angle ($\theta = 72^\circ$), schematically shown in Fig. 1(a). The variation of angle of polarization for the collected signal ψ_{sc} with incident polarization ϕ at oblique incidence angle ($\theta = 72^\circ$) for probe-I is shown in Fig. 1(b) and its FESEM image is shown in Fig. 1(c). At oblique incidence, Probe-I at asymmetric incident polarization states (for $0 < \phi < \pi/2$) shows smaller angle for the scattered polarization angle (ψ_{Sc}) as compared to the incident polarization angle (φ), as governed for Electric type dipoles. It shows stronger collection intensity for TE polarization ($\phi = 0^\circ$) than the TM polarization ($\phi = 90^\circ$), and follows the projected incident electric field ($\vec{E}_t$) and hence such probes are termed as electric NSOM probes.

The variation of ψ_{sc} for Probe-II is shown in Fig. 1(d) and its FESEM image is shown in Fig 1(e). While the scattered radiation collected through Probe-II shows higher polarization angle than the incident polarization angle ($\psi_{Sc} > \phi$), as expected from Bethe's pseudo magnetic dipoles. For probe-II at oblique incidence angle as shown in Fig. 1(d), the scattered polarization direction for asymmetric incident polarization states is larger than the incident polarization (ϕ) and the collected signal has polarization direction perpendicular to the projected incident magnetic field ($\vec{H}_t$) for all arbitrary polarization directions (ϕ) and is independent of the polarization direction of projected incident electric field ($\vec{E}_t$). It shows weaker intensity for TE polarized light and stronger intensity for the TM polarized state and hence probe-II is called as "Magnetic NSOM probe".

We fabricated NSOM probes with different geometrical parameters to investigate the factors governing the selective electromagnetic field sensitivity of these metal coated apertured NSOM probes. The experimental results along with the theoretical understanding will be presented in terms of electromagnetic field coupling coefficients (α) and (β), as shown by fit to the experimental data (solid line) shown in Figs. 1(b) and 1(d). Further, FDTD simulation results confirm the physical understanding of selective sensitivity.

Using these probes we mapped the electric and magnetic field maxima of an optical frequency Hertz standing wave formed upon reflection from the metal surface, schematically as shown in Fig. 1(f). We re-confirm the electric and magnetic nature of our tips by monitoring the collection signal and scattering signal simultaneously and observing relative phase difference between two signals with the electric (Fig. 1(g)) and magnetic probe (Fig. 1(h)). Through this work, we establish the geometrical factors governing the selective EM field sensitivity of NSOM probes and the physics behind it.

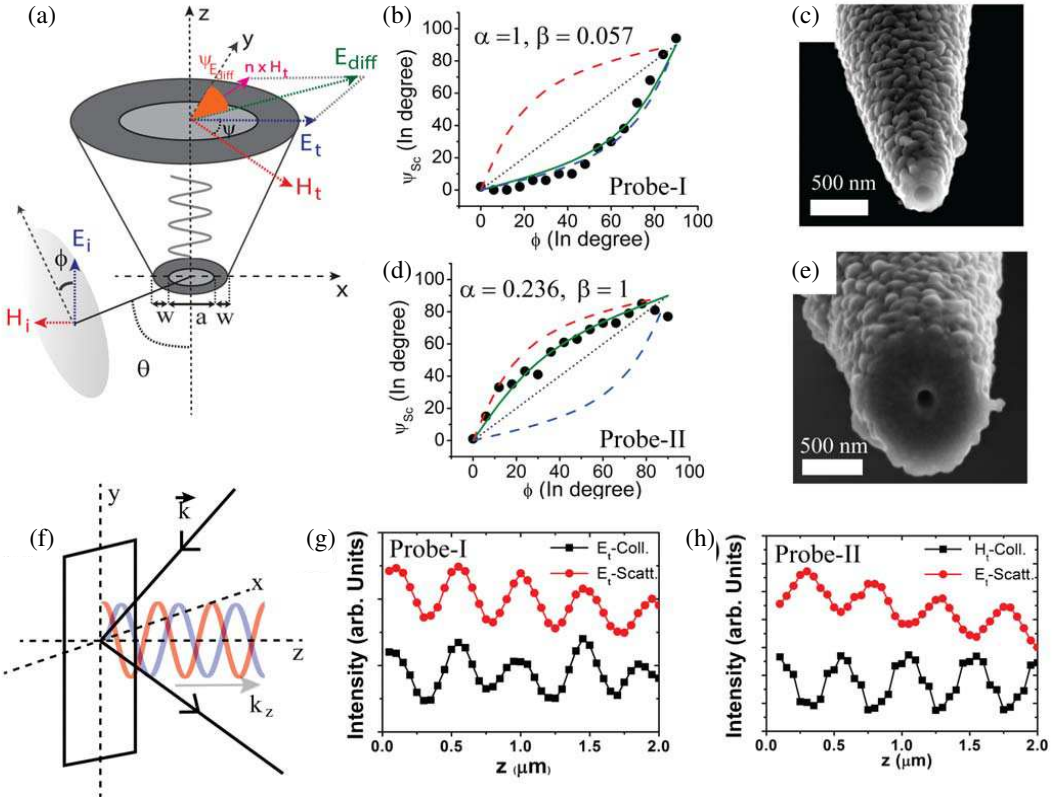

Figure 1: (a) Schematic of the probe and experiment. (b) Variation of scattering polarization ψ_{sc} of Probe-I with ϕ at oblique incidence ($\theta = 72°$). (c) FESEM image of Probe-I. (d) Variation of ψ_{sc} of Probe-II with ϕ. (e) FESEM image of Probe-II. (f) Schematic of formation of vertical Hertz's standing wave upon reflection. Collection and scattering measurement of the vertical standing wave with the electric probe: Probe-I and using the magnetic probe: Probe-II are shown in Fig. 1(g) and Fig. 1(h) respectively.

REFERENCES

1. Kihm, H. W., et al., *Nat. Commun.*, Vol. 2, 451, 2011.
2. Burresi, M., et al., *Science*, Vol. 326, 550, 2009.
3. Taminiau, T. H., et al., *Nat. Commun.*, Vol. 3, 979, 2012.
4. Grosjean, T., et al., *Nano. Lett.*, Vol. 11, 1009, 2011.
5. Koo, S., et al., *Phys. Rev. Lett.*, Vol. 103, 263901, 2009.
6. Karaveli, S., et al., *Phys. Rev. Lett.*, Vol. 106, 193004, 2011.

Recent Progress in Scalable Nanofabrication toward Optical Metamaterials and Metadevices

Junsuk Rho[1, 2, 3, 4]

[1]Department of Mechanical Engineering
Pohang University of Science and Technology (POSTECH), Pohang, Korea
[2]Department of Chemical Engineering
Pohang University of Science and Technology (POSTECH), Pohang, Korea
[3]NSF — Nanoscale Science and Engineering Center
University of California, Berkeley, CA 94720, USA
[4]Materials Sciences Division, Lawrence Berkeley National Laboratory
Berkeley, CA 94720, USA

Abstract— Metamaterials, artificially structured nanomaterials, have enabled unprecedented phenomena such as invisibility cloaking and negative refraction. Especially, hyperbolic metamaterials also known as indefinite metamaterials have unique dispersion relation where the principal components of its permittivity tensors are not all with the same signs and magnitudes. Such extraordinary dispersion relation results in hyperbolic dispersion relations which lead to a number of interesting phenomena, such as super-resolution effect which transfers evanescent waves to propagating waves at its interface with normal materials and, the propagation of electromagnetic waves with very large wavevectors comparing they are evanescent waves and thus decay quickly in natural materials. In this abstract, I will discuss our efforts in achieving the unique optical property overcoming diffraction limit to achieve several extraordinary metamaterials and metadevices demonstration. First, I will present super-resolution imaging device called "hyperlens", which is the first experimental demonstration of near- to far-field imaging at visible light with resolution beyond the diffraction limit in two lateral dimensions [1]. Second, I will show another unique application of metamaterials for miniaturizing optical cavity, a key component to make lasers, into the nanoscale for the first time. It shows the cavity array which successfully captured light in 20 nm dimension and show very high figure of merit experimentally [2]. Then, I will show the recent achievements of photo-induced switching of reconfigurable negative index metamaterial device and large scale negative index metasurface with anomalous spin-Hall effect [3, 4]. Finally, if time allows, I will show how those proof-of-concepts in scientific level can be applied to real engineering applications as a solution in current nanoscience and nanotechnology. It will include the examples of high-resolution and high-throughput flying head nanolithography, super-resolution real-time bioimaging applications and scalable manufacturing methods for future nanosciencne where metamaterials becomes metadevices. I believe our efforts in sub-wavelength metamaterials and scalable manufacturing methods will lead extreme light control and manipulation with development of metamaterials and metadevices, and further advanced nanophotonics, nanomaterials and nanomanufacturing.

ACKNOWLEDGMENT

This work has been supported by the U.S. Department of Energy, Office of Basic Energy Sciences under contract No. DE-AC02-05CH11231 at the University of California Berkeley and Lawrence Berkeley National Laboratory. J. Rho acknowledges fellowships from the U.S. Department of Energy and the Samsung Scholarship Foundation, Republic of Korea.

REFERENCES

1. Rho, J., et al., "Spherical hyperlens for two-dimensional sub-diffractional imaging at visible frequencies," *Nature Communications*, Vol. 1, 143, 2010.
2. Rho, J., et al., "Experimental realization of three-dimensional indefinite cavities at the nanoscale with anomalous scaling laws," *Nature Photonics*, Vol. 6, 450–454, 2012.
3. Zhang, S., J. Rho, et al., "Photoinduced handedness switching in terahertz metamolecules," *Nature Communications*, Vol. 3, 946, 2012.
4. Yin, X., J. Rho, et al., "Photonics spin hall effect at metasurfaces," *Science*, Vol. 339, 1405–1407, 2013.
5. Pan, L., J. Rho, et al., "Maskless plasmonic lithography at 22 nm resolution," Scientific Reports, Vol. 1, 175, 2011.

6. Kante, B., et al., "Symmetry breaking and optical negative index of closed nanorings," *Nature Communications*, Vol. 3, 1180, 2013.
7. O'Brien, K., J. Rho, et al., "Ultrafast acousto plasmonic control and sensing in complex nanostructures," *Nature Communications*, Vol. 5, 4042, 2014.

Ultrahigh-resolution Nano-transfer Printing for Surface-enhanced Raman Spectroscopy (SERS) Analyses

Jae Won Jeong and Yeon Sik Jung
Department of Materials Science and Engineering
Korea Advanced Institute of Science and Technology (KAIST)
291 Daehak-ro, Yuseong-gu, Daejeon 305-701, Republic of Korea

Abstract— Nanotransfer printing (nTP) technology offers outstanding simplicity and throughput in the fabrication of transistors, metamaterials, epidermal sensors, and other emerging devices. Nevertheless, the development of a large-area sub-50 nm nTP process has been hindered by fundamental reliability issues in the replication of high-resolution templates and in the release of generated nanostructures. This talk will present a solvent-assisted nanotransfer printing (S-nTP) technique based on high-fidelity replication of ultrahigh-resolution (8–20 nm scale) patterns using a dual-functional bilayer polymer thin film. The master substrates were prepared by patterning the surface of a silicon wafer through photolithography and/or block copolymer (BCP) lithography followed by plasma etching. In particular, we employed BCP nanolithography for the fabrication of 8–20 nm scale templates. For uniform and fast release of nanostructures on diverse receiver surfaces, interface-specific adhesion control was realized by employing a polydimethylsiloxane (PDMS) gel pad as a solvent-emitting transfer medium, providing unusual printing capability even on biological surfaces such as human skin and fruit peels. Based on this principle, facile printing of plasmonic nanostructures for non-destructive and rapid surface-enhanced Raman spectroscopy (SERS) analyses will be introduced. The utilization of S-nTP can significantly enhance the analysis throughput of SERS by decreasing the analysis preparation time (for the attachment of plasmonic nanostructures on analytes) to 1 sec. As another example of a near-term application, this talk will also demonstrate that Ag nanowires printed on the inner surface of a vial glass can enhance SERS signals, enabling direct and convenient detection of molecules dispersed in a solution at an extremely low concentration.

Laser-based Photothermal Synthesis of Metal Oxides for Optoelectronic Applications

Kyoungsik Yu
Department of Electrical Engineering, KAIST, Daejeon, Korea

Abstract— In this work, we introduce the application of micro-scale photothermal process on a light-absorbing metal layer for in-situ localized deposition/synthesis of metal oxide materials. Focused electromagnetic energy incident on micro-/nano-scale metal structures can be efficiently converted to thermal energy, and thereby stimulates highly localized hydrothermal material synthesis in optofluidic environments by increasing the chemical reaction rates and precursor supply at elevated temperatures. For example, we experimentally demonstrate that a pulsed semiconductor diode laser source can grow a diffraction-limited hemispherical bump of metal oxides, such as zinc oxide and copper oxide, within a few seconds on a metal film in aqueous solution. When applied between two separated metal nanowires, the proposed in-situ fabrication technique can readily form a metal-semiconductor-metal device, which can be used for a number of applications such as ultraviolet photodetectors and memresistors. The laser-based photothermal method allows a simple and facile fabrication process for joining micro-/nano-scale building blocks with electrical and optoelectronic functionalities. Taking advantages of semiconducting properties of metal oxide materials, the proposed technique may open up numerous applications in heterogeneous electric and optoelectronic interconnections with resistive, memristive, and/or gating device components connected with metal nanowire meshes and circuits.

Self-aligned Fabrication of Hybrid Nano-antenna/Nano-particle Systems for Optical Sensing and Spectroscopy

M. Fleischer, J. Fulmes, C. Schäfer, A. Horrer, and D. P. Kern
Institute for Applied Physics, Eberhard Karls University Tuebingen
Auf der Morgenstelle 10, Tuebingen 72076, Germany

Abstract— In optical sensing and spectroscopy the optical signal is often integrated over larger areas for increased signal intensity and high signal-to-noise ratio. At the same time, for many applications the trend goes towards smaller sample volumes and detecting ever smaller concentrations of specific molecules in fluids and gases down to single molecule sensitivity.

Plasmonic nanostructures acting as optical antennas are employed to locally create areas of high electric near-field enhancement, which in their turn are used to enhance the fluorescence or the Raman signal from quantum dots or molecules positioned in these hot-spots.

To use the near-field enhancing structures most efficiently, a large fraction of particles should be positioned in the hot-spots. At the same time, by combining single optical antennas with few or single emitters, hybrid nanostructures with interesting fundamental properties can be prepared. Coupling and energy transfer pathways between the two constituents can be investigated, and the polarization and emission characteristics of the emitter can be modified via the antenna.

To prepare such hybrid systems, single digit control over the positioning of the components relative to each other is desirable. Also the positions of the hotspots are often determined through numerical simulations of idealized structures, while the actual positions may depend on details of the fabrication or local surface roughness.

For these reasons we develop self-aligned strategies for the fabrication of hybrid nanostructures, making use of the unique nanoantenna geometry and near-field properties. The techniques will be demonstrated by the example of plasmonic nanocones [1]. These antennas have widely tunable resonances [2] and can be used as surface-enhanced Raman spectroscopy platforms [3]. The creation and imaging of individual hybrid nanostructures through geometrical self-alignment, self-alignment by near-field ablation, and dielectrophoretic self-alignment will be shown.

ACKNOWLEDGMENT

Financial support by Baden-Wrttemberg Foundation, Carl Zeiss Foundation, German-Israeli Foundation for Scientific Research and Development, and the Office of Science, Office of Basic Energy Sciences, of the U.S. Department of Energy are gratefully acknowledged.

REFERENCES

1. Fleischer, M., D. Zhang, K. Braun, S. Jäger, R. Ehlich, M. Häffner, C. Stanciu, J. K. H. Hörber, A. J. Meixner, and D. P. Kern, *Nanotechnology*, Vol. 21, 065301, 2010.
2. Schäfer, C., D. A. Gollmer, A. Horrer, J. Fulmes, A. Weber-Bargioni, S. Cabrini, P. J. Schuck, D. P. Kern, and M. Fleischer, *Nanoscale*, Vol. 5, 7861, 2013.
3. Horrer, A., C. Schäfer, K. Broch, D. A. Gollmer, J. Rogalski, J. Fulmes, D. Zhang, A. J. Meixner, F. Schreiber, D. P. Kern, and M. Fleischer, *Small*, Vol. 9, 3987, 2013.

Nanoarray-enhanced Implantable Intraocular Pressure Sensor with Remote Optical Readout

Jeong Oen Lee[1], **Trong-Tuong Nguyen**[2], **David Sretavan**[2], **and Hyuck Choo**[1]

[1]Department of Electrical Engineering, California Institute of Technology, CA, USA
[2]Department of Ophthalmology, UC San Francisco, CA, USA

Abstract— An elevated intraocular pressure (IOP) is a major risk factor of glaucoma, which is the second leading cause of blindness [1]. Traditional IOP-detection techniques such as tonometry cannot provide direct, accurate, and continuous IOP measurements [2]. Recently explored LC-resonator IOP-sensing implants are limited by their large sizes and short readout distances [3]. Our compact, robust IOP-sensing implant can greatly improve clinical management of glaucoma and accelerate related drug discoveries.

We demonstrate a compact implantable IOP sensor with remote optical readout for glaucoma research and patient management. Using non-invasive white light, we excite the sensor's pressure-sensitive optomechanical cavity and detect the reflected light, whose optical signature changes as a function of IOP. The sensor has provided robust measurements of hydrostatic pressure between 10–60 mmHg with an accuracy of 0.15 mmHg.

The core of the device, the optomechanical cavity, is formed by a flexible Parylene membrane (diameter: 100 μm; thickness: 3 μm) and rigid silicon substrate whose surfaces are embedded with resonance-enhancing 50×50-μm^2 gold nanodot arrays (pitch: 1000 nm, nanodot diameter: 800 nm). As the pressure is increased from 1 atm, the initial 2-μm gap between the Parylene membrane and the silicon (Si) substrate decreases, which shifts the resonant wavelength of the cavity. To obtain the optimal sensor design parameters that result in highly linear mapping between spectral resonance shifts and pressure changes (1.5 nm/mmHg or about three times the typical spectral resolution of a mini-spectrometer), we ran a series of optomechanical FEM and FDTD simulations using COMSOL and CST, and also made experimental measurements.

We tested the device inside a water-filled pressure chamber connected to a pressure gauge and regulator. Using a broadband source (780–1150 nm for minimum absorption in water and tissue) and a mini-spectrometer (0.22-nm spectral resolution), we remotely acquired reflection spectra from the sensor in the chamber at a 7-mm distance (measurement-setup limited). We linearly varied the chamber pressure and tracked the locations of the major peaks in the spectra, which produced a highly linear mapping (a linear fit of 0.966) of resonance shifts to pressure changes. The average values and standard deviation of the peak locations were determined from over 300 measurements. The sensitivity of the device is 1.53 nm/mmHg over the range of 10–60 mmHg with an accuracy of 0.15 mmHg. The presence of the nanodot array significantly enhances the signal-to-noise ratio of the sensor by a factor of seven and enables robust remote detection. As a next step, we are pursuing measurements in ex vivo rabbit eyes.

REFERENCES

1. Morrison, J. and I. Pollack, *Glaucoma: Science and Practice*, Thieme, 2002.
2. Katuri, K. C., S. Asrani, and M. K. Ramasubramanian, "Intraocular pressure monitoring sensors," *IEEE Sensors Journal*, Vol. 8, No. 1, 12–19, 2008.
3. Chen, P. J., S. Saati, R. Varma, M. S. Humayun, and Y. C. Tai, "Wireless intraocular pressure sensing using microfabricated minimally invasive flexible-coiled LC sensor implant," *J. of Microelectromechanical Systems*, Vol. 19, No. 4, 721–734, 2010.

Session 2P7b
SC3: Nonlinear Optics: Structured Materials, Functional Devices and Applications 2

Third-harmonic Generation in Graphene-clad Microfiber

Yingxin Xu, Shangliang Yu, Bigeng Chen, and Wei Fang
State Key Laboratory of Modern Optical Instrumentation
Department of Optical Engineering, Zhejiang University, China

Abstract— Optical microfibers have attracted much attention in recent years for a range of nonlinear applications due to their strong modal confinement. Though the effective nonlinearity of microfibers can be orders of magnitude higher than that of conventional single mode fibers, the relatively low χ^3 of silica material makes a relatively long interaction length required for efficient third harmonic generation. On the other hand, despite its single atomic layer thickness, graphene shows remarkably strong 3rd order nonlinear optical response due to broadband interband electronic transitions. Utilizing microfiber's unique properties as strong evanescent field and tunable chromatic dispersion via adjusting diameter, in this work, we demonstrated third-harmonic generation from a graphene-clad microfiber (GCM) structure, with a graphene covering length of mere 5 microns

Microfiber sample was fabricated using a flame-heated taper-drawing technique with both ends tapered down from a standard single mode telecom fiber. The diameter of the microfiber was about 1 micron, and the waist length was around 1 mm, with the transmission over 90% from visible to infrared band. Graphene dispersions was prepared by liquid phase exfoliated method, then coated on the microfiber via optical deposition through the combining effects of optical trapping and heat convection with typical coating length of 5 microns. Femtosecond pulsed laser at 1560 nm was launched into the GCM, and transmitted light was measured by a spectrometer after proper filtering the pumping light. Third-harmonic signal at 520 nm was observed, and verified by the signal intensity cubic dependence on the incident laser power. Phase matching condition was investigated both experimentally and theoretically.

All-optical Wavelength Conversion for 16-QAM Signal Using FWM in a Silicon Waveguide

Xiaoyan Wang, Lingchen Huang, Ke Yi, Qiang Yan, Wei Pan, and Shiming Gao
Centre for Optical and Electromagnetic Research
State Key Laboratory of Modern Optical Instrumentation, Zhejiang University, Hangzhou 310058, China

Abstract— Higher-order modulation formats, such as N-QAM (quadrature amplitude modulation), have been considered as promising technologies to increase the spectrally efficient, transmission data rate, and channel capacity for fiber optical communication networks. Also, all-optical wavelength conversion is essential to ensure the function of wavelength routing networks and offer optimized bandwidth utilization. In recent years, four-wave mixing (FWM) in silicon waveguides has been observed and used for integrated wavelength converters with advantages of strict transparent to the signal bit rate and modulation format. So far, wavelength conversion operations have been demonstrated based on FWM either in a semiconductor optical amplifier (SOA) and a highly nonlinear fiber (HNLF), or in a silicon-based waveguide for several kinds of modulation formats, such as amplitude shift-keying (ASK) and quaternary phase shift keying (QPSK), etc. In this talk, we will show all-optical wavelength conversion for 36 Gbit/s 16-QAM signal based on FWM in a silicon waveguide with digital coherent detection technology. The constellation diagrams of the converted idlers are clearly observed. The bit error rate (BER) of the converted signals as a function of the input optical signal-to-noise ratio (OSNR) is measured and a low power penalty (< 1 dB) when the FEC threshold limit is satisfied.

REFERENCES

1. Xie, Y., S. Gao, and S. He, "All-optical wavelength conversion and multicasting for polarization-multiplexed signal using angled pumps in a silicon waveguide," *Opt. Lett.*, Vol. 37, No. 11, 1898–1900, 2012.
2. Ettabib, M. A., K. Hammani, F. Parmigiani, L. Jones, A. Kapsalis, A. Bogris, D. Syvridis, M. Brun, P. Labeye, S. Nicoletti, and P. Petropoulos, "FWM-based wavelength conversion of 40 Gbaud PSK signals in a silicon germanium waveguide," *Opt. Express*, Vol. 21, No. 14, 16683–16689, 2013.
3. Zhou, X. and J. Yu, "Multi-level, multi-dimensional coding for high-speed and high-spectral-efficiency optical transmission," *J. Lightwave Technol.*, Vol. 27, No. 16, 3641–3653, 2009.
4. Ip, E., A. P. T. Lau, D. J. F. Barros, and J. M. Kahn, "Coherent detection in optical fiber systems," *Opt. Express*, Vol. 16, No. 2, 753–791, 2008.

Influence of an Intense Electromagnetic Wave on Magnetoconductivity and Hall Coefficient in Compositional Semiconductor Superlattices: Optical Phonon Interaction

B. D. Hoi[1, 2], **H. V. Ngoc**[1], **and N. Q. Bau**[1]

[1]Department of Physics, College of Natural Science, Vietnam National University, Hanoi, Vietnam
[2]Department of Physics, National University of Civil Engineering, Hanoi, Vietnam

Abstract— We theoretically study the influence of an intense electromagnetic wave (EMW) on the Hall effect in compositional semiconductor superlattices (CSSLs) with a periodical superlattice potential in the z direction, subjected to a crossed dc electric field $\vec{E}_1 = (E_1, 0, 0)$ and magnetic field $\vec{B} = (0, 0, B)$. By considering the electron — optical phonon interaction at high temperatures, we obtain analytical expressions for the magnetoconductivity (MC) and the Hall coefficient (HC) with a dependence on external fields, the temperature of the system, and characteristic parameters of the CSSL. These expressions are fairly different in comparison to those obtained for bulk semiconductors. The influence of the EMW is interpreted by using the dependencies of the MC and the HC on the amplitude and the frequency of the EMW. The analytical results are computationally evaluated for two CSSLs: AlGaAs/GaAs and AlGaN/GaN with the same Al content. The optically detected magnetophonon resonance conditions are obtained. The HC reaches saturation when the magnetic field or the EMW frequency increases.

Calculating the Current Density of the Radio Electrical Effect in Parabolic Quantum Wells

B. D. Hung, N. D. Nam, and D. Q. Vuong
Department of Physics, College of Natural Sciences, Hanoi National University
No. 334, Nguyen Trai Str., Thanh Xuan Dist., Hanoi, Vietnam

Abstract— We study the current density of charge carries of the radioelectrical effect in parabolic quantum wells (PQW) subjected to a dc electric field $\vec{E}_0 = (0, 0, E_{0z})$ and in a linearly polarized electromagnetic wave (EMW) ($\vec{E}(t) = \vec{E}(e^{-i\omega t} + e^{i\omega t})$, $\vec{H}(t) = [\vec{n}, \vec{E}(t)]$), ($\omega \ll \bar{\varepsilon}$; $\bar{\varepsilon}$ is an average carrier energy, in this paper, we select $\hbar = 1$), in the presence of a laser radiation $\vec{F}(t) = \vec{F}\sin\Omega t$; $\Omega\tau \gg 1$ (τ is the characteristic relaxation time). By using the quantum kinetic equation method for electrons interacting with acoustic phonon at low temperatures, we obtain the expressions for the drag of the charge carriers in case the electron gas is completely degenerate. The dependence of the current density on the intensity F and the frequency Ω of the laser radiation, the frequency ω of the linearly polarized EMW, the frequency ω_0 of the parabolic potential are obtained. The analytic expressions are numerically evaluated and plotted for a specific quantum wells, GaAs/AlGaAs, to show clearly the dependence of the current density of charge carriers on the radioelectrical effect on above parameters. The results of current density calculation in this case are compared with bulk semiconductors to show the dissimilarity.

Session 2P8
SC2&3: Light Harvesting for Energy and Optoelectronic Applications

Plasmonic and Nanophotonic Enhanced Organic Photovoltaics: Breaking the Power Conversion Efficiency Barrier

Qiaoqiang Gan, Kai Liu, and Haomin Song
Department of Electrical Engineering
The State University of New York at Buffalo, Buffalo, NY 14260, USA

Abstract— Present photovoltaic technology offers a promising source of clean and sustainable renewable energy, but suffers from relatively high fabrication cost. Solar cell technologies are being actively pursued based on solution-processable organic photovoltaic materials that can be sprayed like inexpensive paint or printed over large areas on rigid or flexible substrates. Recent advances in molecular organic photovoltaics have brought 10% power conversion efficiency for single-junction cells, placing them in direct competition with amorphous silicon solar cells. However, due to the poor electrical conductivity of most organic materials, organic photovoltaics are inherently very thin leading to poor solar light absorption, and relatively low power conversion efficiency. Incorporation of plasmonic nanostructures for light trapping in these thin-film devices offers an attractive means to realize higher-efficiency organic photovoltaics with power conversion efficiency significantly larger than 10%. Particularly, researchers have been working hard to develop new approaches to increase solar light absorption without altering the thicknesses of the organic photovoltaic devices. In this talk, we will provide an overview of recent progress on plasmonic and nanophotonic enhanced organic photovoltaics, one of the most promising solutions for enhancing the power conversion efficiency of an organic photovoltaic device [1]. Focus will be on surface dispersion engineering and ultra-thin-film interference mechanisms which are compatible with thin-film devices [2]. A renewed focus on the science and technology of nanophotonics for light management and trapping in organic photovoltaics will lead to power conversion efficiencies surpassing currently achieved performance levels.

REFERENCES

1. Gan, Q., F. J. Bartoli, and Z. H. Kafafi, *Adv. Mater.*, Vol. 25, 2385, 2013 (front cover article).
2. Liu, K., B. Zeng, H. Song, Q. Gan, F. J. Bartoli, and Z. H. Kafafi, *Optics Communications*, Vol. 314, 48, 2014 (invited paper).

Metallic Core-dielectric Shell Nanoparticles Boosting the Power Conversion Efficiency of Dye-sensitized Solar Cells

Dang Yuan Lei[1, 2]

[1]Department of Applied Physics, The Hong Kong Polytechnic University, Hong Kong, China
[2]Shenzhen Research Institute, The Hong Kong Polytechnic University, Shenzhen, China

Abstract— Plasmonics has been widely demonstrated to be an efficient means to improve the power conversion efficiency of dye-sensitized solar cells (DSSCs). The proposed enhancement mechanisms mainly include nanoparticle scattering-induced increased light absorption path, plasmonic near-field-enhanced absorption of both semiconductors and dyes, and transfer of plasmonic hot electrons from metals to semiconductors at the metal-semiconductor Schottky junction. However, a decreased efficiency has also been observed in other studies with inclusion of metal nanoparticles, and attributed to the reduced surface area of the underlying semiconductor in direct contact with the absorbing dyes, Forster-type energy transfer from the semiconductor or from the dyes to the metallic nanoparticles, and the electron trapping at the metal surface. These controversial results have made plasmon-enhanced DSSCs an open study. To clarify these disagreements, we will present a systematic study on the plasmonic effects in the power conversion efficiency of DSSCs by using metallic core-dielectric shell nanoparticles with adjustable shell thickness. This is because the respective contribution from each of the aforementioned mechanisms strongly depends on the distance between the metal nanoparticle and the semiconductor. For example, since the plasmonic near-field amplitude exponentially decays from the nanoparticle surface, it is expected that the plasmon-enhanced absorption of both semiconductors and dyes will decrease with increasing the dielectric shell thickness. On the other hand, the dielectric shell on the metal nanoparticle can also rule out the possibility of electron trapping at the metal surface, thus clarifying the negative contribution by inclusion of metal nanoparticles in DSSCs. Specifically, we will investigate the power conversion efficiency as a function of the shell thickness varying from 0 to 20 nm, aiming at providing a complete scenario of the contribution channels and their respective dominant ranges.

Advanced Light Trapping Designs for High Efficiency Crystalline Silicon Thin Film Solar Cells

Pingqi Gao and Jichun Ye
Ningbo Institute of Material Technology and Engineering, Chinese Academy of Sciences
Ningbo 315201, China

Abstract— Elaborating reliable and versatile strategies for efficient light trapping is of crucial importance for c-Si thin film solar cells, which are important for reducing cost and endowing flexibility. We report a significant reflection reduction over a broadband light spectrum in crystalline silicon (c-Si) via introduction of low aspect-ratio honeycomb nanobowl front surface textures. A restructuration technique is developed to shape nanopores into nanobowls, enabling excellent impedance matching and efficient mode coupling. As a result, an overall reflection down to 2% in the spectrum range of 400–1100 nm wavelength is achieved. Meanwhile, an inverted-nanopyramid grating based on nanosphere lithography is also developed to achieve high efficient broad-band absorption. Although the two nanostructures both demonstrate overall outstanding light-trapping capabilities in bulk c-Si the conclusion may argue in case of thinner c-Si In this talk, the light trapping effects of the two individual nano-structures, and their combinational configurations (double sided texture design), on c-Si are discussed in details from both theoretically and experimentally scaling with the c-Si thickness from 180 μm down to 10 μm.

Transparent Conductor of Aluminum Thin Film and Integrated Organic Solar Cells

Qing Guo Du[1], **Chan Hin Kam**[2], **Xiao Wei Sun**[2], **and Ching Eng Png**[1]

[1]Institute of High Performance Computing
1 Fusionopolis Way, #16-16 Connexis, Singapore 138632, Singapore
[2]LUMINOUS! Center of Excellence for Semiconductor Lighting & Displays
School of Electrical and Electronic Engineering, Nanyang Technological University
Nanyang Avenue, Singapore 639798, Singapore

Abstract— Transparent conductors (TCs) are essential components of optoelectronic devices such as solar cells and light-emitting diodes (LEDs). Indium tin oxide (ITO) is the commonly used TC in the commercial market due to the high transparency in visible wavelength range and low sheet resistance. However, ITO is high cost because of the limited source of indium on earth. Moreover, ITO is too brittle which prevent it to be used in devices on flexible substrate. Due to these disadvantages of ITO, many materials and structures have been studied in order to replace it including metallic nano meshes [2], ultrathin metallic films, metallic nanowires, carbon nanotube networks and graphenes. Although the electrical and optical properties of one dimensional (1D) patterned metallic nanowires have been studied extensively, the electrical and optical properties of two dimensional (2D) nanohole patterned metallic thin film still need to be studied and optimized because they have quite different optical and electrical properties compared to 1D patterned one. Without loss of generality, here, aluminum (Al), a cheap yet commonly used metal is chosen for the study.

The electrical properties of the Al thin film is optimized firstly. According to the percolation theory, for a 2D nanohole patterned thin film, the large scale effective conductivity is written as $\sigma_c = \sigma_0(\phi_f - \phi_{crit})^t$, where σ_c is the conductivity of the patterned structure, σ_0 is the conductivity of the conductor, ϕ_f is the volume fraction of the patterned conductor, ϕ_{crit} is the percolation threshold where the conductivity of the patterned structure is zero, and t is the critical exponent. Here, $\phi_{crit} = (1 - \frac{\pi}{2\sqrt{3}})$, $t = 1.1$. The sheet resistance of the thin film is obtained by $R_{sh} = \frac{1}{\sigma_c \cdot h}$. The sheet resistances of different hole filling ration f (the area ratio of void region and the whole unit cell) are obtained. The corresponding relationship of average transmittance and sheet resistance is calculated. it is shown that when the sheet resistance of the nanohole patterned Al thin film is larger than 8.4 Ω/sq, the average transmittance is larger than 80%.

The optical properties of the 2D nanohole patterned Al thin film are optimized accordingly. With proper choosing lattice constant, for example $a = 400$ nm, the transmittance at the whole visible wavelength range is exceed 80% while the filling ration f is only 0.8. This is mainly due to the enhanced transmittance originated from both localized and surface plasmonics.

The organic solar cell integrated with nanohole patterned aluminum electrode with hexagonal lattice is analyzed in detail. With properly design, a wave guide mode is excited at 671 which attributes to the large absorption enhancement around 671 nm. The absorption has been enhanced 19.5 times compared to conventional organic solar cell with ITO electrode at the same wavelength. The electric field intensity distribution at two wavelengths of 500 nm and 671 nm are used to identify the support localized surface plasmon mode and wave guide mode. The E-filed intensity distribution shows that the light is highly localized in the active layer due to the waveguide mode with a maximum intensity 20 times larger than that of the incident light. The solar cell with nanohole aluminum electrode also shows excellent angular response.

Extensive Study of Electromagnetic Functionality of Sub-wavelength Metallic Metamaterials

Yifang Chen, Yaqi Ma, Jianpeng Liu, Jinhai Shao, Sichao Zhang, and Bingrui Lu
Nanolithography and Application Research Group, State Key Lab of Asic and System
School of Information Science and Engineering, Fudan University, Shanghai 200433, China

Abstract— Sub-wavelength metallic metamaterials have experimentally demonstrated a wealth of special functionalities such as light harvesting, resonating absorbance, magnetic mirroring, cloaking, extraordinary transmission and super resolution focusing, etc., when they meet electromagnetic waves in free space. All these observations are only available when the cutting-edge nanotechnology is developed. The discoveries of these novel functionalities are the eve of the evolution or even the revolution toward a new era of nanophotonics for their applications in daily life of new generations of opto components. In this talk, I will review both technological developments and research advances in subwavelength metamateials as we have been working on, including chiral fish scales, multiple layer of chiral structures, quasi photonic crystals as super resolution nanolens based on super oscillations, high aspect ratio nano pillars as local surface plasmonic resonators. Part of the above-mentioned work was conducted in the Nanolithography group at Fudan University in China. Future applications of these metamateirals will be proposed and discussed.

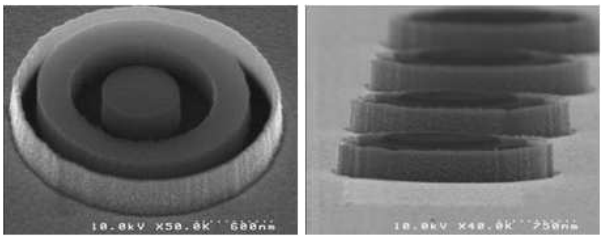

Figure 1: Super resolution nanolens based on super oscillations.

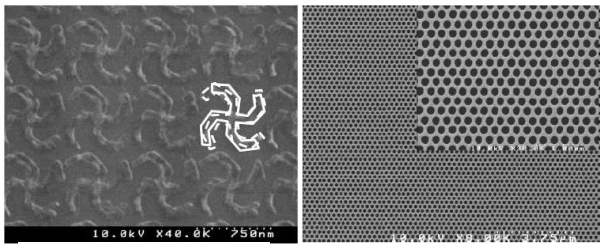

(a) (b)

Figure 2: (a) Double layer of chiral structures by registration in EBL. (b) Nanophotonic structures.

First Experimental Demonstration of Solar Cell Efficiency Enhancement via External Photon Recycling

Jeffrey Gordon
Department of Solar Energy & Environmental Physics, Blaustein Institutes for Desert Research
Ben-Gurion University of the Negev, Sede Boqer Campus, 84990, Israel

Abstract— Although one way to improve the conversion efficiency of ultra-efficient solar cells is through optical concentration (mainly by increasing open-circuit voltage), an equally potent alternative is reducing the cell's recombination current — an aim that can be realized by externally recycling cell photon emission (i.e., by angular confinement of the solar cell's luminescence). The basic physics that describes how the entropy generation associated with photon capture and photon emission affects conversion efficiency places the potential benefits of flux concentration versus angular confinement of cell luminescence on an equal footing. There is a fundamental bound for the degree to which this is attainable, based on the Second Law of Thermodynamics.

While the theory for the potential benefit of photon recycling has recently been elucidated, experimental proof-of-concept had proven elusive — requiring a photovoltaic device possessing a high external luminescent efficiency, combined with efficient light recycling optics. The associated prospect of approaching — and even surpassing — the nominally fundamental (Shockley-Queisser) limit for solar cell conversion efficiency is tantalizing and, in principle, achievable.

Here, we offer experimental evidence of enhancing the performance of today's champion single-junction commercial GaAs cells by external recycling of photon emission from the cell's front surface. We also explain why no improvement of this nature had been demonstrated previously — basically because all solar cells (prior to those fabricated for this study) possessed exceptionally low external luminescent efficiencies (below 0.01).

The magnitude of the measured efficiency enhancement effectis placed in the perspective of the fundamental bounds for voltage enhancement. The potential and the strategies for future improvements via modified solar cell architecture and novel angular confinement micro-optics arealso evaluated.

Light-trapping and Electrical Response of GaAs-based Single-nanowire Solar Cells with Multi-shell Design

Xiaofeng Li, Yaohui Zhan, Chinhua Wang, and Shaolong Wu
Institute of Modern Optical Technologies
& Collaborative Innovation Center of Suzhou Nano Science and Technology
Key Lab of Advanced Optical Manufacturing Technologies of Jiangsu Province
& Key Lab of Modern Optical Technologies of Education Ministry of China
Soochow University, Suzhou 215006, China

Abstract— Single-nanowire solar cells (SNSCs) belong to a new kind of photovoltaic devices by focusing on the compatibility of the device which could be used for applications in optoelectronic devices, optical sensors, biotechnological devices, etc.. We report a device-oriented simulation for coaxial gallium arsenide SNSCs with multiple electrically and optically functional nanoshells, by considering both optical absorption and light-conversion characteristics. The light-absorbing capability based on specific mechanisms, such as the leaky-mode resonances, cavity resonances, etc., will be discussed in a detailed way. A further simulation is performed by modelling the internal carrier transport and collection process in the cylindrical light-conversion devices. Especial attention is paid for the carrier loss due to strong surface recombination as well as the effective control of the carrier recombination loss by introducing a window layer with a large semiconductor bandgap, which allows internal quantum efficiency $\sim 100\%$ in $\sim 75\%$ of the absorption band of gallium arsenide. Results also reveal the role of nanofocusing effect in enhancing the performance of nanowire devices that show both absorption and external quantum efficiencies over 100% under resonances. A dielectric cladding shell is introduced and optimized, which enhances the nanofocusing effect and leads to extraordinary enhancement of both absorption and light-conversion capabilities in a very broad band. This design contributes a short-circuit current density increased by 2.4 times and an open-circuit voltage over 1.1 V.

Incorporation of Cascaded Metallic Gratings into Thin Film Solar Cells for Broadband Plasmonic Light Trapping

Long Wen, **Fuhe Sun**, **and Qin Chen**
Key Laboratory of Nanodevices and Applications-CAS
Collaborative Innovation Center of Suzhou Nano Science and Technology
Suzhou Institute of Nano-Tech and Nano-Bionics, Chinese Academy of Sciences (CAS)
Suzhou 215123, China

Abstract— Plasmonic nanostructures have been regarded as a promising light trapping strategy towards boosting solar cell efficiency recently. However, the absorption enhancement stemming from surface plasmon excitations always suffers from an inherent limitation of narrow bandwidths, which may hamper the complete utilization of the solar radiation in a broadband spectrum for solar cells. In this paper, we present a new concept to achieve broadband absorption in ultrathin amorphous Silicon thin film solar cells (TFSCs). We theoretically show that by cascading metal gratings with different sizes atop the cells, the enhanced light absorption band of the ultrathin active layer is extended due to the excitation of multiple localized surface plasmon resonances (LSPRs). For one-dimensional (1D) cascaded grating structure, the metallic gratings with different widths act as discrete nanoantennas which independently and efficiently collect the incoming photons at the resonance wavelengths, leads to an enhancement of 60% in photocurrent for the TM-polarized incident illumination. Furthermore, we show that the localized nature of the LSPRs beneath each grating leads to a spectral behavior in-dependent of the incidence angle. In order to obtain a polarization-independent enhancement, two-dimensional (2D) metallic gratings assembled TFSCs were applied. By breaking the continuity of 1D grating and shrinking its length in the direction parallel to grating groove, the impact of geometric transformation from 1D to 2D grating structures are thoroughly analyzed with such a straightforward and physically intuitive procedure. It appears that both the coupling of plasmonic/photonic modes and their inter-coupling effects contribute to the light trapping in the 2D grating structures. Finally, we demonstrate a cascaded 2D grating structure with a broadband and polarization-insensitive absorption enhancement which gives rise to a 66.5% increase in the photocurrent over the bare TFSCs. This work paves a promising way for spectral broadening of plasmonic light trapping in TFSCs.

Taper Structures to Harvest Light: Effective-medium Description and Optimum Shape

Baocheng Zhu, Shiyi Xiao, and Lei Zhou
State Key Laboratory of Surface Physics
Key Laboratory of Micro and Nano Photonic Structures (Ministry of Education)
Physics Department, Fudan University, Shanghai 200433, China

Abstract— Recently, metallic taper structures have drawn much attention in photonic research, owing to their application potentials in solar cell [1] and nano-focusing [2]. These structures typically consist of array of metallic objects with gradually varying cross-section size (see Fig. 1(a)), so that they can squeeze electromagnetic (EM) fields into sub-wavelength regions without much reflections within a broad frequency bandwidth. An interesting scientific question is that, within a fixed thickness, what is the optimum taper shape to realize the best functionalities (i.e., wide working bandwidth and high local EM field enhancement)?

Theoretically, both analytical and numerical methods have been employed to study the optical properties of such structures. Analytical understandings usually made some approximations and are valid only in limited cases. Numerical simulations are time-consuming and can give little physical insight. Therefore, a simple criterion derived from an analytical theory, which can help understand the inherent physics and find an optimum taper shape, is highly desired.

Here, we first develop an effective-medium theory (EMT) [3] for such periodic taper structures, based on which we show that waves inside these structures are governed by a Schrödinger-like equation with an "*effective potential*" term solely dictated by the taper shape. Such a mapping not only simplifies our theoretical treatments, but also yields a simple criterion to judge the performance of a given structure and thus helps finding an optimum taper shape to realize the best functionality. Our theoretical results match well with finite-difference-time-domain (FDTD) simulations (see Fig. 1(b)), and show that for the optimum structure a 10^4 field strength enhancement can be easily realized within an ultra-wide frequency bandwidth.

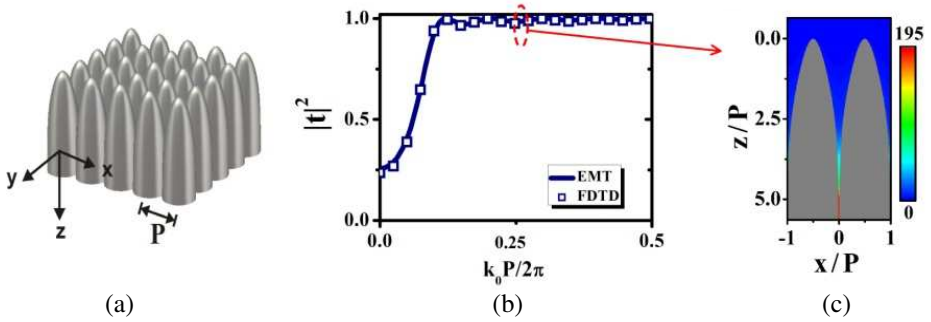

(a) (b) (c)

Figure 1: (a) Schematic picture of the periodic taper array. (b) The transmittance spectra calculated both by our EMT and FDTD simulations. (c) The field strength distribution inside the optimized taper array.

REFERENCES

1. Wang, K. X., Z. Yu, V. Liu, Y. Cui, and S. Fan, *Nano Lett.*, Vol. 12, 1616, 2012.
2. Søndergaard, T., S. M. Novikov, T. Holmgaard, R. L. Eriksen, J. Beermann, Z. Han, K. Pedersen, and S. I. Bozhevolnyi, *Nat. Commun.*, Vol. 3, 969, 2012.
3. Zhu, B. C., S. Xiao, and L. Zhou, Unpublished.

Antireflection Performance of SiN Nanostructure Textured Si Surface for High Efficient Si Solar Cells

Zhen Zhang[1, 2, 3, 4], **Yanyan Wang**[1, 2, 3, 4], **Jian Zhu**[1, 2], **Xuemei Wu**[3, 4], **and Ruiying Zhang**[1, 2]

[1]Division of Nano-devices and Related Materials
Suzhou Institute of Nano-tech and Nano-devices, Chinese Academy of Sciences, Suzhou 215123, China
[2]Key Labs of Nanodevices and Applications
Suzhou Institute of Nano-tech and Nano-bionics, Chinese Academy of Sciences, Suzhou 215123, China
[3]Department of Physics, Soochow University, Suzhou 215006, China
[4]Key Laboratory of Thin Films of Jiangsu, Soochow University, Suzhou 215006, China

Abstract— To achieve high conversion efficiency, it is prerequisite for Si solar cells to reduce both the surface reflection and surface nonradiative combination. In recent years, a variety of Si nanostructures has experimentally and theoretically exhibits broadband and omnidirectional antireflection [1]. However, all these surface nanostructures will induce a great amount of the surface area and surface defects, which undoubtedly increase their surface nonradiative recombination and degrade their conversion efficiency finally. SiN is well known as surface passivation material in conventional semiconductor field However, when SiN film deposited on Si surface, antireflection can be achieved only at specific wavelengths based on interference principle [2].

Here SiN nanostructure and its film coated Si surface as shown in Fig. 1(a) is proposed, which aims at achieving broadband omnidirectional antireflection and passivation simultaneously Such structure was realized by SiN deposition, nanosphere lithography and Reactive Ion Etching (RIE). By controlling the time of etching, we obtained two groups of SiN nanorods one group of samples have different thickness (t) of remaining SiN layer with the same height (h) of SiN nanorods, but the other group of samples have different h with the same t. The reflectivity of all these samples was measured and shown in Figs. 1(b) and (c) respectively. Compared to the planar Si solar cell, the surface reflectivity of these SiN nanorods and its film decorated Si surface is significantly suppressed. For the samples with the same height of SiN nanorods, the thicker the SiN film, the lower the reflectivity can be observed. Meanwhile, thicker SiN film is beneficial to reduce the surface recombination. When they have the same thickness of SiN film, the samples decorated by 600 nm thick SiN nanorods exhibit the lower reflectivity. Based on the above observation, the lower reflection is inferred in the samples decorated by 600 nm high SiN nanorods and thicker SiN film.

In one word, we propose SiN nanorods and SiN film decorated Si surface, by which, broadband antireflection and surface passivation are expected. Here, we demonstrate their broadband antireflection behavior of these SiN composite structure decorated Si surface. Such research should benefit nanostructure being employed in Si solar cells and truly enhancing their conversion efficiency.

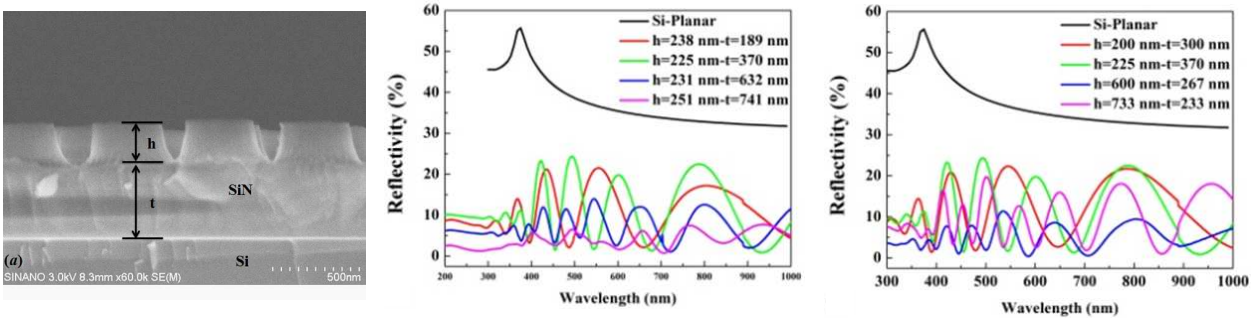

(a) (b) (c)

Figure 1: (a) SEM cross-section pictures of Si solar cell with SiN nanostructure, (b) the surface reflectivity of Si solar cells with same h and different t and (c) same t and different h.

REFERENCES

1. Zhang, R. Y., B. Shao, J. R. Dong, J. C. Zhang, and H. Yang, *J. Appl. Phys.*, Vol. 110, 113105, 2011.
2. Dekkers, H. F. W., L. Carnel, and G. Beaucarne, *Applied Physics Letters*, Vol. 89, 013508, 2006.

Experimental Realization of Broadband Super Absorber Based on Rainbow Trapping in Hyperbolic Metamaterials

Dengxin Ji, **Haomin Song**, **Xie Zeng**, **Haifeng Hu**,
Kai Liu, **Nan Zhang**, **and Qiaoqiang Gan**
Department of Electrical Engineering, University at Buffalo
The State University of New York, Buffalo, NY 14260, USA

Abstract— Thin-film perfect absorbers are important optical/thermal components required by a variety of on-chip applications, including photon/thermal-harvesting, thermal energy recycling, and vacuum heat liberation. Recently, researches on metal-insulator-metal (MIM) metamaterials based perfect absorber and trapped "rainbow" storage of light have attracted considerable interests. However, these researches are limited by either narrow absorption band or relatively low coupling efficiency. In this work, we experimentally realize a patterned hyperbolic meta-film with engineered and freely tunable absorption band from near-IR to mid-IR spectral regions based on multilayered metal/dielectric hyperbolic metamaterial (HMM) waveguide taper [1]. By cascading resonant MIM perfect absorber elements with gradually tuned widths along the vertical direction, the absorption band of the patterned HMM film is extended significantly. As the incident light is coupled into the HMM waveguide taper, the group velocity of the waveguide mode at different wavelength can be reduced significantly at their corresponding critical widths, resulting in the enhanced light-matter interaction [2]. In addition, multi-patterned HMM metafilms is also demonstrated to reduce the required number of metal/dielectric layers, and therefore simplifying the sample preparation and experimental realization of on-chip broadband super absorbers. The ability to efficiently produce broadband, highly confined and localized optical fields on a chip is expected to create new regimes of optical/thermal physics, which holds promise for impacting a broad range of energy technologies ranging from photovoltaics, to thin-film thermal absorbers/emitters, to optical-chemical energy harvesting.

REFERENCES

1. Ji, D., H. Song, X. Zeng, H. Hu, K. Liu, N. Zhang, and Q. Gan, *Sci. Rep.*, 2014, accepted.
2. Hu, H., D. Ji, X. Zeng, K. Liu, and Q. Gan, *Sci. Rep.*, Vol. 3, 1249, 2013.

A MZI Based Integrated Optical Accelerometer

Wei Hu[1, 3], **Guang Qian**[1, 3, 4], **Ruo-Zhou Li**[2, 3, 4], **Feng-Hua Wan**[1, 3], **Jie Tang**[1, 3], **and Tong Zhang**[1, 2, 3, 4]

[1]School of Instrument Science and Engineering, Southeast University, Nanjing 210096, China
[2]School of Electronic Science and Engineering, Southeast University, China
[3]Key Laboratory of Micro-Inertial Instrument and Advanced Navigation Technology Ministry of Education, Nanjing 210096, China
[4]Suzhou Key Laboratory of Metal Nano-Optoelectronic Technology Suzhou Research Institute of Southeast University, Suzhou 215123, China

Abstract— Accelerometers with high sensitivity have been researched as an important field for several decades as accelerometers are widely applied in guidance systems, impact detection, and automation control systems. Various physical principles have been utilized to design different types of accelerometers so far. With the development of integrated optical technique, researches of accelerometers based on Micro-Opto-Electro-Mechanical-Systems (MOEMS) have attracted a lot of attention in past few years, as optical sensors possess several advantages over conventional counterparts. The advantages include low manufacturing cost, light weight, immunity to electromagnetic interference, etc.

We demonstrate an optical accelerometer based on asymmetric Mach-Zehnder interferometer which is proposed to be fabricated on a flexible substrate. The asymmetric MZI based device made by polymer waveguides and substrate to realize the elastic property with a double arms cantilever beam. As the acceleration to be measured exerts a force on the flexible beam, the long arm waveguide of the MZI experiences strain which causes optic transmission phase to change due to strain-optic effect and the physical elongation of the waveguide. The device meters the acceleration through measuring the interference optic intensity of the light beams in the two arms. The special flexible waveguide fabrication technology is utilized to manufacture flexible multilayer substrate based waveguides in order to gain tunable sensitivity and higher stability. The relation between the structure parameters and the sensitivity are analyzed. A prototype is fabricated and a detecting experiment scheme designed for this flexible optical accelerometer is proposed. Due to simplicity of the structure, the sensor is suitable for mass production.

Graphene Photodetector Based on Metamaterial Perfect Absorber

Shichao Song[1], **Long Wen**[1], and **Qin Chen**[1, 2]

[1]Key Lab of Nanodevices and Applications-CAS
Collaborative Innovation Center of Suzhou Nano Science and Technology
Suzhou Institute of Nano-Tech and Nano-Bionics, Chinese Academy of Sciences (CAS)
Suzhou 215123, China
[2]Peking University Shenzhen SOC Key Laboratory, PKU-HKUST Shenzhen-Hong Kong Institute
Hi-Tech Industrial Park South, Shenzhen 518057, China

Abstract— Graphene-based optoelectronic devices in recent years have already attracted a huge amount of interest. Its high carrier mobility, broadband optical absorption and ultra-thin properties have potential applications in high-speed and broadband optical processing and communication with low power consumption. However, monolayer or few layer graphene has very weak light absorption due to the nm-scale thickness, resulting in very low photoresponsivity, especially in graphene photodetectors. In this article, we propose a graphene-metamaterial composite structure for high-efficiency photodetection, where the graphene monolayer is embedded in a metamaterial perfect absorber (MPA) as shown in Figure 1(a). The electromagnetic properties of the sandwich structure are optimized to perfectly meet the impedance match condition. As a result of the high reflection back mirror and the impedance matching, a nearly unit absorption could be achieved on resonance, in which 40% incident light is absorbed in graphene, 17 times enhancement compared to graphene intrinsic absorption. The resonance wavelengths can be readily tuned by changing the dimensions of the metallic nanostructure. Furthermore, spectrum engineering can be achieved in a composite structure consisting of graphene and cascaded MPA. Benefiting from graphene's ultra-wideband optical absorption and high electron mobility, we can obtain a photodetector with high speed, broad band and high photoelectric conversion efficiency. This novel idea using MPAs to enhance the interaction between light and graphene not only presents a new solution to graphene photodetectors, but also could be adopted in other graphene optoelectronic devices.

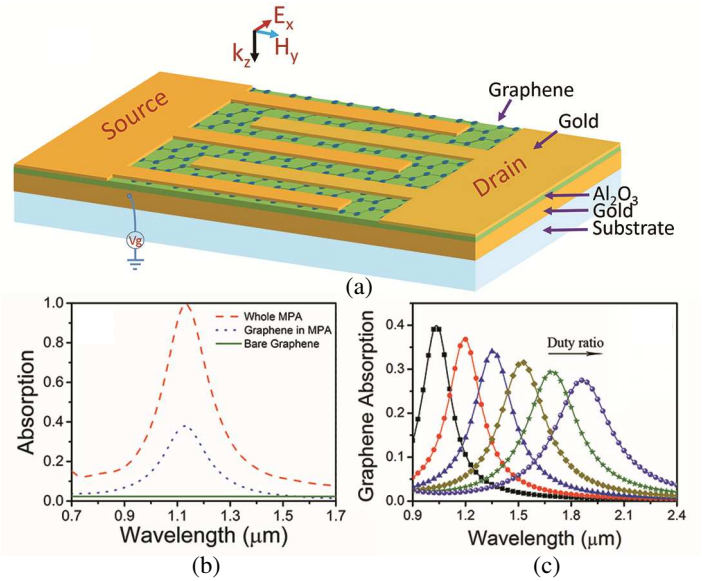

Figure 1: (a) Schematic of a graphene photodetector with graphene embedded in metamaterial perfect absorber. (b) Absorption spectrum of a graphene monolayer in a metamaterial perfect absorber, the absorption spectra of the whole MPA and a bare graphene monolayer are shown for comparison. (c) The resonant wavelengths can be linearly tuned by the duty ratio of the metallic nanostructure.

Photothermal Microbubbles Generation under a Graphene Oxide-microheater

Xiaobo Xing[1], **Debin Zhu**[1], **Liang Lei**[2], **Jiapeng Zheng**[3], **Fengjia Li**[3], **Xiang Cai**[4], **and Ting Wu**[4]

[1]Education Ministry's Key Laboratory of Laser Life Science & Institute of Laser Life Science
College of Biophotonics, South China Normal University, Guangzhou, Guangdong 510631, China
[2]School of Physics and Optoelectronic Engineering
Guangdong University of Technology, Guangzhou 510006, China
[3]School of Physics & Telecommunication Engineering
South China Normal University, Guangzhou, Guangdong 510631, China
[4]Department of Light Chemical Engineering
Guangdong Polytechnic, Foshan 528041, China

Abstract— Microbubbles have enabled highly versatile functions for applications in medical imaging, biomedical analysis, drug delivery, and microfluidic elements. Recent years have witnessed the growing tendency of microbubbles generation based on photothermal effect in the optically controlled systems. Graphene oxide (GO) possesses extraordinary photothermal property in the near-infrared region. Herein, we present a representative and novel device which can serve as a photothermal microheater by combining optical microwire and GO. GO nanosheets (GONs) suspended in DMF were successfully trapped and deposited on the surface of the microwire by injecting near-infrared light into an optical microwire. The GO-deposition exhibited strong photothermal properties, serving as a line-shaped heater with a length of several hundred micrometers.When the GO-micro heat worked, the temperature of the surrounding liquid such as GONs-DMF suspension increased rapidly. Two kinds of microbubbles were introduced in the report. When the GO-microheater was immersed in GONs-DMF suspension, superheat limit of the liquid was possible to reach. A lot of microbubbles with diameters from tens to hundreds of micrometers were generated directly on the microheater based on nucleate boiling. When the GO-microheater was located at the DMF-air interface and its neighboring microwire was immersed in GONs-DMF suspension, microbubbles with novel conformation were indirectly generated on the smooth microwire based on heterogeneous nucleation and continuously grew in the thermal gradient field governed by GO-microheater. Interestingly, each microbubbles exhibited a symmetrical conformation with respect to the microwire axis and took a shape of approximative ellipsoid.

ACKNOWLEDGMENT

The work thanks for Prof. Da Xing from Education Ministry's Key Laboratory of Laser Life Science & Institute of Laser Life Science, College of Biophotonics, South China Normal University, for his support in experiments. This work was supported by National Natural Science Foundation of China (61177077, 61107029, 81071790, 61204102), Guangdong Excelent Doctoral Dissertation Funded Project (SYBZZM201126).

Session 2P9a
SC3: Fiber Optic Sensing Technologies for Structural Health Monitoring and Applications

Fiber Optic Nerve Functions Realized by Optical Correlation Domain Techniques

Kazuo Hotate
Department of Electrical Engineering and Information Systems
The University of Tokyo, 7-3-1 Hongo, Bunkyo-ku, Tokyo 113-8656, Japan

Abstract— Brillouin Scattering in an optical fiber can act as sensing mechanism for strain and/or temperature. By applying schemes to analyze distribution of the Brillouin frequency shift (BFS) along the fiber, "fiber optic nerve systems" are realized to sense damages induced in materials and structures, in which the fiber is embedded. Time domain techniques with pulsed lightwave have been studied for distribution sensing, and much improved recently. However, these have difficulties in realizing ultimate performances, such as quite a high spatial resolution and high speed measurement. In this paper, recent achievements in Brillouin Optical Correlation Domain Analysis/Reflectometry (BOCDA/BOCDR) are presented [1].

Through synthesizing interference nature of a semiconductor laser by modulating lasing frequency with an appropriate waveform, stimulated Brillouin scattering (SBS) can be generated position-selectively at one specific position along an optical fiber. This is called BOCDA [1], in which the SBS is used with launching the pump and the probe continuous lightwave through both the ends of the fiber in opposite directions. The specific position can be changed, for example, by the modulation frequency. Then, distributed measurement of strain or temperature is realized. Superior functions have already been achieved, such as 1.6 mm spatial resolution, 1,000 times/s Brillouin gain spectrum (BGS) measurement speed, and 14,700 ratio between measurement range and spatial resolution. In BOCDA, it is possible to realize random accessibility to arbitrary multiple points along the fiber. With this function, dynamic strain measurement at arbitrary points have been demonstrated with a total sampling rate of 500 times/s, recently.

By synthesizing the interference between the spontaneous Brillouin scattering (SpBS) and a reference lightwave, the position-selective detection of the SpBS can also be realized by modulating the laser frequency. This is called BOCDR [1], in which 10 mm spatial resolution, 50 times/s BGS measurement speed, and 23,500 ratio between the range and the resolution have been demonstrated. Figure 1 shows an BOCDR system, in which back-ground noise spectrum has been reduced with additional intensity modulation (IM) [2]. Then, 10 mm spatial resolution and strain dynamic range beyond 7,000 με have been achieved, as shown in Figure 2 [2].

When the stimulated Brillouin scattering is excited in one polarization axis in a polarization maintaining fiber, acoustic-wave generated refractive-index grating, which is associated with the SBS, can also make the Bragg reflection in the orthogonal polarization axis. This phenomenon is called Brillouin dynamic grating (BDG) [1]. By measuring both the SBS and the BDG characteristics, a BOCDA system has provided with discriminative and distributed measurement of strain and temperature along a fiber with a spatial resolution of about 10 cm.

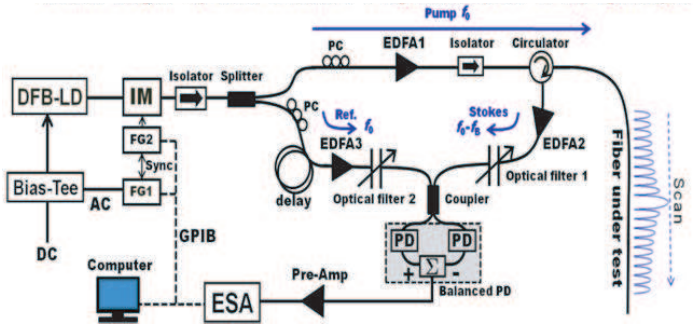

Figure 1: BOCDR system [2]. Intensity modulation scheme is adopted to reduce the back-ground noise spectrum to enhance spatial resolution and strain dynamic range.

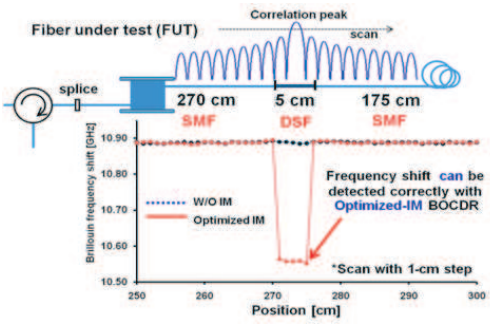

Figure 2: BFS distribution measured by the BOCDR system in Figure 1 [2]. Spatial resolution of 10 mm and strain dynamic range beyond 7,000 were realized.

Applications of the BOCDA systems have been demonstrated, including aircraft structural health monitoring (SHM), pedestrian deck monitoring, dynamic strain monitoring of tall building model, and so on. Distributed strain monitoring, dynamic strain monitoring at arbitrary multiple points, and discriminative distributed measurement of strain and temperature have been demonstrated for aircraft SHM in flight conditions.

REFERENCES

1. Hotate, K., "Fiber distributed Brillouin sensing with optical correlation domain techniques," *Optical Fiber Technology*, Vol. 19, 700–719, 2013, Invited.
2. Manotham, S., M. Kishi, Z. He, and K. Hotate, "1-cm spatial resolution with large dynamic range in strain distributed sensing by Brillouin optical correlation domain reflectometry based on intensity modulation," *Asia Pacific Optical Sensors Conference*, Th-C23, Sydney, Jan. 2012.

Intramodal and Intermodal Stimulated Brillouin Scattering in Few-mode Fibers

Kwang Yong Song
Department of Physics, Chung-Ang University, Seoul 156-756, Korea

Abstract— Introduction to experimental and theoretical studies on the stimulated Brillouin scattering (SBS) in a two- or few-mode fiber (TMF or FMF) is presented. The measurement schemes and the spectral characterization of the Brillouin gain spectra are explained for the intramodal SBS between the same modes and the intermodal SBS between different modes, with the comparison between the theoretical and the experimental results.

Introduction: Space-division multiplexing (SDM) is widely studied as a promising technology for increasing the capacity of optical communications, and mode-division multiplexing (MDM) based on a two- or few-mode fiber (TMF or FMF) is attracting considerable attention as practical implementation of the SDM for realizing multiple and parallel channels [1, 2]. Stimulated Brillouin scattering (SBS) is a nonlinear effect in optical fibers with the lowest threshold, and its characterization has provided useful information for designing and enhancing optical fibers and sensors [3, 4]. Recently, the experimental characterization of the SBS in an elliptical-core TMF and a circular-core FMF has been reported, where a strong intermodal SBS between different optical modes is observed as well as an intramodal SBS between the same modes [5, 6]. In this talk, the measurement results of Brillouin gain spectra (BGS) in a TMF and a FMF are presented. The origin of the intermodal SBS is theoretically explained for the comparison with the experimental results. As one of possible applications of the SBS, the result of a feasibility study on the Brillouin dynamic grating (BDG) in a TMF is briefly introduced.

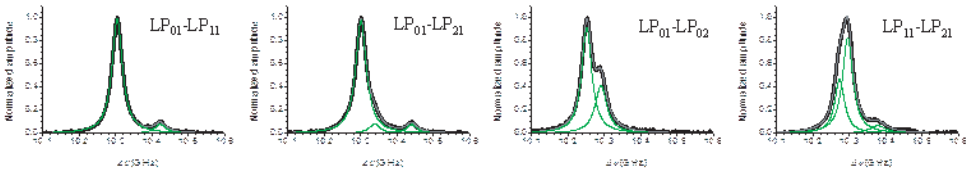

Figure 1: Examples of the BGS of the intermodal SBS in a FMF fitted with multiple Lorentzian curves for each. The table shows the Brillouin frequencies of the BGS peaks.

REFERENCES

1. Randel, S., R. Ryf, A. Sierra, P. J. Winzer, A. H. Gnauck, C. A. Bolle, R. J. Essiambre, D. W. Peckham, A. McCurdy, and R. Lingle, Jr., "6 × 56-Gb/s mode-division multiplexed transmission over 33-km few-mode fiber enabled by 6 × 6 MIMO equalization," *Opt. Express*, Vol. 19, 16697–16707, 2011.
2. Kobyakov, A., S. Kumar, D. Q. Chowdhury, A. B. Ruffin, M. Sauer, S. R. Bickham, and R. Mishra, "Design concept for optical fibers with enhanced SBS threshold," *Opt. Express*, Vol. 13, 5338–5346, 2005.
3. Nikles, M., L. Thevenaz, and P. A. Roberts, "Brillouin gain spectrum characterization in single-mode optical fibers," *J. Lightwave Technol.*, Vol. 15, 1842–1851, 1997.
4. Song, K. Y., Y. H. Kim, and B. Y. Kim, "Intermodal stimulated Brillouin scattering in two-mode fibers," *Opt. Lett.*, Vol. 38, 1805–1807, 2013.
5. Song, K. Y. and Y. H. Kim, "Characterization of stimulated Brillouin scattering in a few-mode fiber," *Opt. Lett.*, Vol. 38, 4841–4844, 2013.

Improved Calibration Method for Raman Distributed Temperature Sensor

K. Oishi, T. Umeno, N. Takeuchi, and S. Adachi
Yokogawa Electric Corporation, Japan

Abstract— In recent years, the Raman Distributed Temperature Sensor (DTS) has been successfully adopted in the oil & gas fields. According to DTS principle, temperature T at the point of scattering can be determined by knowing the temperature T_0 of the temperature reference fiber, the ratio of anti-Stokes and Stokes intensities, and Raman shift wave number of the sensing fiber. Under actual conditions, however, the temperature measurement accuracy may be affected by optical device characteristics such as light source (wavelength), optical filter, photodiode, reference thermometer (uncertainty), optical switch, optical connector, splice, and sensing fiber. We already reported the novel calibration technique to find out the accurate Raman shift wave number of the sensing fiber (fiber having the differential characteristics from built-in fiber) to perform highly accurate temperature measurements over a wide range of temperatures although the conventional linear approximation method is only effective over small temperature range. But the deferential loss (attenuation difference at the Stokes and anti-Stokes wavelengths) should be corrected beforehand.

In this paper, we propose an improved calibration method that automatically calculates the calibration parameters such as the Raman shift wave number and the differential loss of the sensing fiber simultaneously and simply. Demonstrated results are well agreed with proposed method.

Structural Health Monitoring Based on Strain Distributions Measured by Fiber-optic Sensors

Hideaki Murayama[1], **Daichi Wada**[1], **and Hirotaka Igawa**[2]

[1]School of Engineering, The University of Tokyo
7-3-1 Hongo, Bunkyo-ku, Tokyo 113-8656, Japan
[2]Japan Aerospace Exploration Agency
6-13-1 Ohsawa, Mitaka, Tokyo 181-0015, Japan

Abstract— The purpose of structural health monitoring (SHM) is to lead a structure, such as the aerospace, ship,and civil and mechanical engineering infrastructure, to be safer at the lower cost. SHM systems capable of assessing structural integrity during manufacturing or in-service operation would allow actions that can result in the improved quality, optimal operation, timely maintenance, and longer service life.

Strain is a parameter which directly relates deformation and has sensitivity to damage ofstructural members subjected to a load. It is also an elemental measurand for typical fiber-optic distributed sensors. Fiber-optic distributed sensors return a value of the measurand as a function of the linear position along an optical fiber, as they are having useful characteristics of optical fiber sensors for SHM, such as immunity of electromagnetic interference, durability and capability to be embedded into composite materials. Among the fiber-optic distributed sensors, various distributed sensing techniques based on Brillouin scattering have been proposed for strain measurement. Fiber Bragg grating (FBG) sensors with advanced interrogation systems can be also applied to distributed sensing as well as quasi-distributed one.

We have developed sensing techniques that can provide strain distributions along a sensing fiber with high spatial resolution. In our techniques we map the strain profile along FBG sensors based on optical frequency domain reflectometry. Measured strain distributions has been usedfor damage detection and load identification in structures. We have confirmed the applicability of fiber-optic distributed sensors to SHM experimentally and also developed the simulation based design process for distributed strain measurements by optical fibers.

Optic Fiber Sensors Fabricated by Laser-micromachining

Yun-Jiang Rao and Zeng-Ling Ran
Key Laboratory of Optical Fiber Sensing and Communications (Ministry of Education)
University of Electronic Science and Technology of China, Chengdu, Sichuan 610054, China

Abstract— This talk presents an extensively review of recent progress in using excimer lasers to fabricate functional fiber-optic sensing devices in UESTC. Excimer lasers are used to create fiber gratings and in-line fiber interferometers for measurements of strain, acceleration, pressure, temperature and refractive index. In this talk, the following works will be presented.

A novel fiber-optic tip accelerometer based on Fabry-Perot (F-P) interferometer is directed fabricated on a large cladding fiber end by using the 157 nm laser-micromachining technology. With the calibration of a micro electro mechanical systems (MEMS) accelerometer, the sensitivity of such a fiber-optic F-P accelerometer is 1.764 rad/g. The minimum detective acceleration is estimated to be 20 µg. Two laser-machined high-sensitivity fiber-optic Fabry-Perot (F-P) high temperature sensors are demonstrated based on sapphire and silica fibers. The temperature characteristics of the sapphire and silica fiber sensor are investigated over a temperature range from 100°C to 1100°C. Experiment result shows that the sapphire F-P sensor has a temperature sensitivity of ~ 50 pm/°C with a linearity of 0.999, which is 5 times higher than that of the silica F-P sensor.

And two fiber-optic cascaded micro Fabry–Perot (F-P) cavities fabricated by 157-nm laser micromachining are demonstrated for simultaneous measurement of high temperature and refractive index, or high temperature and strain, or high temperature and high pressure, respectively. The sensor head consists of a short air extrinsic F-P cavity and an intrinsic single-mode fiber F-P cavity. These two micro cavities possess different response coefficients to temperature, strain, pressure, and refractive index, which are utilized for dual parameters measurement. Experimental results show that dual parameters measurement could have been achieved from 50°C to 380°C based on such a sensing structure. Moreover, in another work, we presented a highly integrated structure for the simultaneous and co-located measurement of temperature and strain under high temperature (300°C). The FP cavity is fabricated on a GeO_2 doped photon sensitive fiber by using the 157 nm laser micro-machining technique and the FBG is written at the same position of the FP cavity by using the standard 248 nm laser method. As the FP cavity and the FBG have different sensitivity coefficients to temperature and strain, they can be utilized for realization of simultaneous measurement of dual parameters.

For signal processing, subcarrier technology and dual-wavelength demodulation method are combined for tracking the cavity length variation of a micro fiber-optic Fabry-Perot (F-P). Compared with conventional dual-wavelength demodulation method, two operation wavelengths for demodulation are modulated with two different carrier frequencies, respectively, and then injected into optical link connected with the F-P cavity. Light power reflected for the two wavelengths is obtained by interrogating the powers of Fast Fourier Transform (FFT) spectrum at their carrier frequencies. Because the light at the two wavelengths experiences the same optical and electrical routes, measurement deviation resulting from the drift of optical and electrical links can be entirely eliminated.

Compared with conventional optical fiber sensors, these novel micro optical fiber sensors fabricated by laser-micromachining could offer outstanding advantages, such as fast and direct formation, easy mass-production with ultralow-cost, good reproducibility, high temperature stability, low temperature cross-sensitivity, etc..

From Structural Health Monitoring to Earth Crustal Deformation Monitoring

Zuyuan He[1], **Qingwen Liu**[1], **and Tomochika Tokunaga**[2]

[1]State Key Laboratory of Advanced Optical Communication Systems and Networks
Shanghai Jiao Tong University, Shanghai 200240, China
[2]Department of Environment Systems, The University of Tokyo, Chiba 277-8563, Japan

Abstract— For geo-science applications, it is required to monitor the earth's deformation continuously at locations as many as possible with a resolution better than 10 nano-strains ($n\varepsilon$), which corresponds to the crustal deformation induced by oceanic tide. Traditionally, sensors such as extensometers and laser strain-meters installed underground are used for this purpose. These conventional sensors, however, are difficult to be installed widely due to their size of tens to hundred meters in length. Also due to their length, they can only give integrated strain information over that length. Recently, we started a project to investigate the feasibility to employ fiber optic sensors, specifically, fiber Bragg grating (FBG) sensors for geophysics applications. FBG sensors are small in size, and thus low-cost in installation, and can easily be multiplexed, making them attractive for geophysics if they can provide a resolution down to nano-strains ($n\varepsilon$). They have already been widely adopted in strain measurement for applications in smart materials and structures. For most of these applications, a strain resolution about 1 micro-strain ($\mu\varepsilon$) is generally satisfactory.

Although there are several reports of dynamic FBG strain sensing at kHz region realizing even better than $n\varepsilon$ sensitivity, the realization of static strain sensing is much more difficult. A dynamic sensing can be self-referenced, but a static strain sensor has to be compared with an extra standard. In fact the static strain resolution is mainly limited by environmental temperature disturbance, because FBGs are sensitive to both strain and temperature. For strain measurement with high resolution, a common way is to employ a strain-free reference FBG for temperature compensation. The reference FBG is also useful in eliminating other common drift such as the influence from light source wavelength/intensity variation. Strain information can be retrieved by evaluating the different wavelength shift between the sensing FBG and the reference FBG. Many demodulation algorithms have been proposed to determine the Bragg wavelength of FBGs, among which the cross-correlation algorithm can determine the Bragg wavelength difference directly and exhibits good ability of suppressing random uncertainty.

In this paper, we introduce the realization of a nano-strain-resolution FBG static strain sensor. The theoretical analysis and experimental demonstration are reviewed. With this sensor, a resolution of $2.6n\varepsilon$ without strain applied and a resolution of $17.6n\varepsilon$ with strain applied were demonstrated, respectively, and crustal deformations induced by oceanic tide and by earthquake were clearly observed, for the first time to the best of our knowledge.

REFERENCES

1. Liu, Q., T. Tokunaga, and Z. He, "Realization of nano static strain sensing with fiber Bragg gratings interrogated by narrow linewidth tunable lasers," *Opt. Express*, Vol. 19, No. 21, 20214–20223, 2011.
2. Liu, Q., T. Tokunaga, K. Mogi, H. Matsui, H. F. Wang, T. Kato, and Z. He, "Ultra-high resolution multiplexed fiber Bragg grating sensor for crustal strain monitoring," *IEEE Photon. Jour.*, Vol. 4, No. 3, 996–1003, 2012.
3. Liu, Q., T. Tokunaga, and Z. He, "Ultra-high-resolution large-dynamic-range optical fiber static strain sensor using Pound-Drever-Hall technique," *Opt. Lett.*, Vol. 36, No. 20, 4044–4046, 2011.
4. Liu, Q., T. Tokunaga, and Z. He, "Sub-nano resolution static strain fiber sensor using a sideband interrogation technique," *Opt. Lett.*, Vol. 37, No. 3, 434–436, 2012.

Session 2P9b
SC3: Ultrasensitive Optical Sensors

Distributed Measurement of Intense Magnetic Fields by Means of Optical Fibers

L. Palmieri[1] **and A. Galtarossa**[1, 2]

[1]Department of Information Engineering, University of Padova, Padova, Italy
[2]IIUSE, Southeast University, Nanjing, China

Abstract— Optical fiber sensors (OFS) are finding wide and successful applications in the monitoring of several structures as diverse as civil buildings, natural sites, energy plants and mechanical components. OFSs offer two main advantages over electro-mechanical sensors; namely, they enable distributed, or quasi-distributed, monitoring and they are intrinsically immune to electromagnetic interference.

The measurement of magnetic field, based on Faraday rotation of polarization, has been one of the earliest application of OFS. Nonetheless, all magnetic-field OFS developed so far are point sensors, being able to measure the magnetic field only at a specific location. Recently, however, a new distributed optical fiber sensors (DOFS) able to measure the spatial variation of magnetic field along the fiber has been introduced.

This novel sensor is based on the measurement of the state of polarization (SOP) of the field backscattered by the fiber, as a function of the scattering position. This SOP is of course affected by the magnetic field acting on the fiber through Faraday rotation, therefore it can in principle provide information on it. There are however two main difficulties. Actually, the backscattered SOP does not directly provide information on the local Faraday rotation, but rather it is the cumulated effect of forward propagation up to a specific point in the fiber, Rayleigh scattering and subsequent back-propagation to the fiber input. Furthermore, the SOP in an optical fiber is not affected only by magnetic field, but also by other perturbations like bending, twist, anisotropy, geometrical asymmetries, etc., which are well known to impair the effectiveness of standard magnetic field OFS. These difficulties have been however overcome by means of an accurate theoretical model, which has enabled the solution of the inverse scattering problem.

As a result, this novel polarization-sensitive DOFS is able to measure the magnetic field tangent to the fiber at arbitrary positions along the fiber itself, paving the way to new applications. Presently, the system has a sensitivity of about 100 mT and a spatial resolution of few centimeters, over a fiber length of few tens of meters. This paper will review the present state of art, describing the measurement technique and showing some examples of application. Specifically, it will be shown how by means of this technique it is possible to make a 2-dimensional vectorial map of the magnetic field in the area spanned by the fiber (see Fig. 1). The possibility of performing 3-dimensional vectorial measurements will be discussed, too.

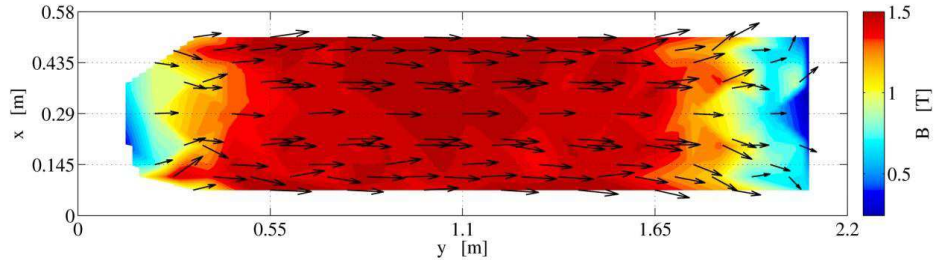

Figure 1: 2D map of amplitude and direction of the magnetic field component that is tangent to the sensor plane.

Surface Roughness and Plasmon Excitation in Metal Films

J. Canning
Interdisciplinary Photonics Laboratories, School of Chemistry
The University of Sydney, 222 Madsen Building F09, Sydney 2006, Australia

Abstract— The complex dielectric of materials is described as a sum of the two parts: $\tilde{\epsilon} = \epsilon' + i\epsilon'' = (n + i\kappa)^2$. For transparent dielectrics such as air and silicate, the dielectric reduces to $? = n^2$. Light of p-polarisation impinging on a thin metal film deposited on silica from the side will generate a time dependent polarization charge at the interface whereas s-polarised light does not. The plasma does not have an instantaneous response in practice, since the electrons have a finite mass and scatter energy as phonons or through defect states producing the resistive scattering measured as Ohmic loss (and often as a detectable temperature change). The two-dimensional nature of the surface also constricts perfect oscillations. This means in practice as a result of the added contribution from the expansion in the full dielectric expression surface wave excitation is separated from the traditional Brewster transmission of p-polarised light where when the film is very thin (nanoscale) can be treated similar to a transparent dielectric for some of the light. In the case of thin films, Equation (1) remains valid when determining the SPR coupling condition since it is only the evanescent field associated with some absorbed light which is coupled into an SPR, despite the fact that on the nanoscale absorption is not 100%.

For such thin films is there a familiar Brewster condition established where p polarised light can in principle transmit through a thin film at the Brewster angle neglecting any absorbed light? Observations indicate there is suggesting the thin film case is not entirely equivalent to the bulk case as is ordinarily assumed. When the film thickness is on the order used to generate plasmons such that light coupled according to (1) can reach and excite the far surface via evanescent waves, there can also be some transmission of p polarized light observed through the film when only the classical Brewster condition is met. In this situation there is no obvious evanescent field as such and no phase matching is satisfied so no SPR generation occurs. Could a non-uniform film lead to omnidirectional scattering of the p-transmitted light such that some quasi-phase matching condition might be generated by the time the light reaches the far-side? Given the high proportion of light potentially achievable at the Brewster condition, this could compensate for a reduced efficiency in coupling that might otherwise be expected at the traditional SPR condition. We have in fact observed that it is indeed possible to launch SPR not at the traditional SPR condition but closer to the Brewster condition, which for gold is $\sim 7^\circ$ from the orthogonal. The implications of this near-orthogonal launch are significant: there is no need for a prims coupling method and we demonstrate that a normal spectrophotometer in reflection mode can excite an SPR and measure the shift with different refractive index liquids (Figure 1).

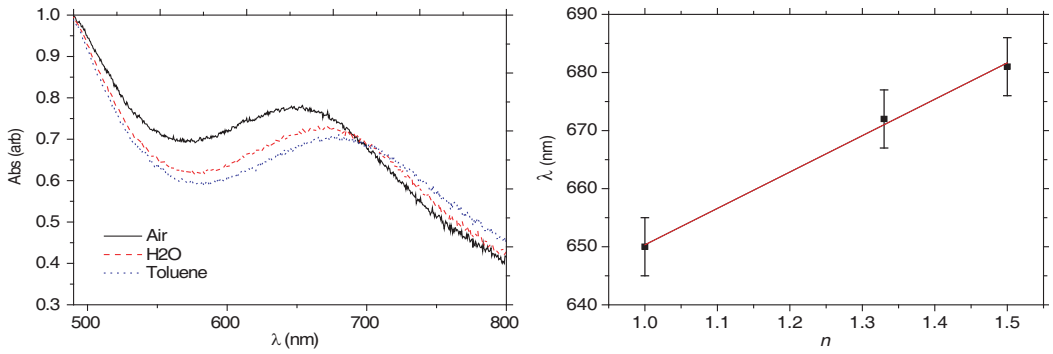

Figure 1: The spectra for near-orthogonal ($\sim 5^\circ$) excited SPR in the presence of air, water and toluene; (a) the peak wavelength shift from (b) as a function of refractive index of each species.

Pd/Ag Coated Photonic Crystal Fiber Hydrogen Sensor

Yuanhong Yang[1], **Fuling Yang**[1], **Huan Wang**[1], **Qirong Liu**[2], **and Xungang Diao**[2]

[1]Department of Opto-electronics Engineering
School of Instrumentation Science and Opto-electronics Engineering
Beihang University, Beijing 100191, China
[2]School of Physics and Nuclear Energy Engineering, Beihang University, Beijing 100191, China

Abstract— Optical fiber hydrogen sensor has attracted intensive research interests due to its potential application at fuel cells, nuclear energy and so on. In this paper, An intrinsic optical fiber hydrogen sensor based on polarization-maintaining photonic crystal fiber (PM-PCF) Sagnac interferometer was proposed. The birefringence of PM-PCF can be modified by the deformation of film after absorbing hydrogen, and the measurement of hydrogen concentration can be realized by detecting the wavelength shift. The facing target sputtering technique with special Pd/Ag plate target structure was developed to deposit Pd/Ag composite film on PM-PCF. The characteristic of Pd/Ag film was measured and analyzed. The deposit rate and atom ratio of Pd:Ag were investigated with different depositing condition and parameters. An experimental setup for hydrogen sensing was built. The sensing characteristic was studied under different film thickness and atom ratio of Pd:Ag. The wavelength shift at different hydrogen concentration and the temperature interference were tested. The results showed the sensitivity was higher at low concentration range and good repeatability was obtained within measuring range of 4%. The PM-PCF used in the hydrogen sensor was designed specially and insensitive to temperature. The experimental result shows that the temperature coefficient was less than 0.08 pm/°C. This is much smaller than the hydrogen concentration sensitivity coefficient and indicates the temperature affect is weak.

Microfiber-based Ultra-sensitive Refractive Index Sensors

Bai-Ou Guan, Li-Peng Sun, Jie Li, and Long Jin
Institute of Photonics Technology, Jinan University, Guangzhou 510632, China

Abstract— Polarimetric interferometer that employs separation of two orthogonal polarizations of light in a highly birefringent (HiBi) fiber has been of great promise in the potential applications of tunable comb filtering, sensing, multi-wavelength lasing, nonlinear resonating, and etc. [1, 2]. Recently, HiBi microfibers, that may be fabricated by heating and tapering a flat glass preform [3], a femtosecond-laser-cut fiber [4], a rectangular fiber [5], or a CO_2-laser-milled fiber [6], have attracted much attention mostly due to their extremely high birefringence [3, 4] and unique group birefringence [5]. Especially, when acting as a refractive index (RI) sensor in a polarization Sagnac interferometer, HiBi microfibers exhibit ultrahigh sensitivity. Simultaneously, the temperature-cross sensitivity is suppressed due to the low silica thermo-optic coefficient and the very similar temperature coefficient between the two polarized lights of interaction.

In this paper, we present a brief review of our recent works on refractive index sensors based on highly birefringent microfibers. Microfibers with birefringence in the order of 10^{-2} are fabricated by heating and tapering the rectangular or elliptic cladding raw fibers. Ultra-sensitive refractive index sensor with sensitivity as high as 195,348 nm/RI at RI = 1.35887 is implemented by inserting the microfiber into a Sagnac loop. Application for relative humidity sensing is also demonstrated.

ACKNOWLEDGMENT

This work is supported by the National Science Fund for Distinguished Young Scholars of China (61225023), the National Natural Science Foundation of China (11374129), the Planned Science and Technology Project of Guangzhou (2012J5100028), the Project of Science and Technology New Star of Zhujiang in Guangzhou city (2012J2200062), and the Guangdong Natural Science Foundation (S2013030013302).

REFERENCES

1. Noda, J., K. Okamoto, and Y. Sasaki, "Polarization-maintaining fibers and their applications," *Journal of Lightwave Technology*, Vol. 4, No. 8, 1071–1089, 1986.
2. Mortimore, D. B., "Fiber loop reflectors," *Journal of Lightwave Technology*, Vol. 6, No. 7, 1217–1224, 1988.
3. Jung, Y. M., G. Brambilla, K. Oh, and D. J. Richardson, "Highly birefringent silica microfiber," *Opt. Lett.*, Vol. 35, 378–380, 2010.
4. Xuan, H. F., J. Ju, and W. Jin, "Highly birefringent optical microfibers," *Opt. Express*, Vol. 18, 3828–3839, 2010.
5. Li, J., L. P. Sun, S. Gao, Z. Quan, Y. L. Chang, Y. Ran, L. Jin, and B. O. Guan, "Ultrasensitive refractive index sensors based on rectangular silica microfibers," *Opt. Lett.*, Vol. 36, 3593–3595, 2011.
6. Sun, L. P., J. Li, L. Jin, S. Gao, Z. Tian, Y. Ran, and B. O. Guan, "High-sensitivity temperature sensor based on highly-birefringent microfiber," *Proc. Asia Pacific Optical Sensors Conference*, 89240C-89240C-4, 2013.
7. Sun, L. P., J. Li, Y. Z. Tan, X. Shen, X. D. Xie, S. Gao, and B. O. Guan, "Miniature highly-birefringent microfiber loop with extremely-high refractive index sensitivity," *Opt. Express*, Vol. 20, 10180–10185, 2012.

High Sensitivity Elastic Wave Sensing Using Fabry-Perot Filters Based on Fiber Bragg Gratings

B. Srinivasan
Department of Electrical Engineering, Indian Institute of Technology Madras, Chennai, India

Abstract— Elastic waves propagating in solid media carry a rich variety of signatures which can be used to monitor the health of mechanical structures [1]. Conventional methods of sensing such waves using piezo-electric transducers (PZTs) are prone to electromagnetic interference (EMI), require heavy cabling, and provide narrowband response owing to their inherent resonances. Fiber Bragg gratings (FBGs), on the other hand exhibit a flat response for a range of frequencies up to 1 MHz, and are amenable to array sensing [2].

One of critical requirements for FBG-based elastic wave sensing is a dynamic interrogator that can support sensing up to 1 MHz frequency with ultra-high sensitivity. In this talk, we will discuss the development of a dynamic interrogator for elastic wave using FBG based Fabry-Perot filters (FP) along with the relevant signal capturing and processing electronics [3]. Based on detailed simulations, specific grating sensor/interrogator elements were fabricated and integrated with appropriate opto-electronics in a compact, portable box. Transient response of the dynamic interrogator was evaluated through standard ball drop tests as well as pulsed elastic wave excitations in an aluminium plate.

In the second part of the talk, directional sensing of elastic waves with FBGs will be discussed. It is observed that FBG is quite sensitive not only to the direction of the elastic wave propagation, but also to the propagating acoustic mode [4]. Depending on the orientation of the FBG with respect to the propagating mode, different modes may be picked up. By comparing the experimental dispersion curves with theory, the different acoustic modes have been identified.

ACKNOWLEDGMENT

The author would like to acknowledge funding from the Indira Gandhi Center for Atomic Research, and technical inputs from A. V. Harish and Bibin Varghese.

REFERENCES

1. Achenbach, J. D., "Wave propagation in elastic solids," *Applied Mathematics and Mechanics*, Vol. 16, 425, doi:10.1002/zamm.19920720607, 1973.
2. Betz, D. C., G. Thursby, B. Culshaw, and W. J. Staszewski, "Identification of structural damage using multifunctional Bragg grating sensors: I. Theory and implementation," *Smart Materials and Structures*, Vol. 15, No. 5, 1305–1312, doi:10.1088/0964-1726/15/5/020, 2006.
3. Srinivasan, B., B. Varghese, and H. V. Achar, "Enhanced detection of vibrations using fiber Fabry Perot filters and spectral estimation techniques," *Advanced Photonics*, JTuB25, OSA, Washington, D.C., doi:10.1364/ANIC.2011.JTuB25, 2011.
4. Achar, H. V., R. Ramakrishnan, K. Balasubramanian, and B. Srinivasan, "Investigation of the directional response of fiber Bragg grating-based acoustic emission sensor," *Imaging and Applied Optics Technical Papers*, SM4F.5, OSA, Washington, D.C., doi:10.1364/SENSORS.2012.SM4F.5., 2012.

High-sensitive Optical Sensors Based on In-fiber Air Bubbles

Yiping Wang, Changrui Liao, and Shen Liu
Key Laboratory of Optoelectronic Devices and Systems of Ministry of Education and Guangdong Province
Shenzhen University, Shenzhen 518060, China

Abstract— We reported a few high-sensitive optical sensors based on different types of in-fiber air bubbles those were fabricated by use of a commercial fusion splicer. A high-sensitivity strain sensor based on an in-fiber Fabry-Perot interferometer (FPI) with an air cavity was demonstrated by means of splicing together two sections of standard single-mode fibers. The sensitivity of this strain sensor was enhanced to 6.0 pm/με by improving the cavity length of the FPI by means of repeating arc discharges for reshaping the air cavity. Moreover, such a strain sensor has a very low temperature sensitivity of 1.1 pm/°C, which reduces the cross sensitivity between tensile strain and temperature.

We also demonstrated a nanoscale silica diaphragm based fiber-tip Fabry-Perot interferometer for pressure sensing applications. The thinnest silica diaphragm with a thickness of ∼ 320 nm has been achieved by use of an improved electrical-arc-discharge technique. Such a nanoscale silica diaphragm breaks the sensitivity limitation imposed by traditional all-silica Fabry-Perot interferometric pressure sensors. As a result, a high pressure sensitivity of ∼ 1036 pm/MPa at 1550 nm and a low temperature cross-sensitivity of ∼ 960 Pa/°C are achieved when a silica diaphragm with a thickness of ∼ 500 nm is employed. Moreover, the all-silica spherical structure enhanced the mechanical strength of the micro-cavity sensor, making it suitable for high sensitive pressure sensing in harsh environment.

Moreover, we presented a type of phase-shifted fiber Bragg gratings based on an in-grating air bubble to develop a promising temperature, strain, and refractive index sensor and/or tunable optical filter. A microchannel vertically crossing the bubble is drilled by use of a femtosecond laser to allow liquid to flow in or out the air bubble. By filling different refractive index (RI) liquid into the bubble, the phase-shift peak is found to experience a linear red shift with the increase of RI, while little contribution to the change of phase shift comes from the temperature and axial strain.

ACKNOWLEDGMENT

This work was supported by the National Natural Science Foundation of China (grants Nos. 11174064, 61308027, and 61377090), the Science & Technology Innovation Commission of Shenzhen (grants Nos. KQCX20120815161 444632, and JCYJ20130329140017262), and the Distinguished Professors Funding from Shenzhen University and Guangdong Province Pearl River Scholars.

A Plasmonic Nano-resonator in Nano-structured Metal-coated Fiber Taper

Ming Ding[1], **Wei Quan**[1], **and Gilberto Brambilla**[2]

[1]School of Instrument Science and Opto-Electronics Engineering
Beihang University, Beijing 100191, China
[2]Optoelectronics Research Centre, University of Southampton
Highfield, Southampton SO171BJ, UK

Abstract— In recent years, research in plasmonics has attracted considerable interest because of their extraordinary potentials in energy confinement and nanoantennas. Nanoscale apertures in thin noble-metal films, with dimensions comparable to the light wavelength, can form plasmonic nano-resonators and show astonishing optical properties leading to enhanced and selective light transmission and confinement. A number of different nano-structures have been considered and studied in detail for their ability to concentrate light. At resonance, such structures can concentrate an incident light field into a small volume with orders-of-magnitude intensity enhancement.

In this paper, we study theoretically a strongly-coupled 3D plasmonic slot nano-resonator (PSNR) by embedding a slot nano-cavity in a plasmonic cylindrical waveguide formed by a thin-metal-film coated fiber taper. Theoretical analysis on a strongly-coupled 3D PSNR by embedding a slot nano-cavity in a metal-coated fibre taper was carried out using a 3D finite element method. Light is launched from one of the fibre pigtails into the 1 μm diameter taper coated with a 30 nm gold layer (see Fig. 1(a)) and the various resonances can be identified simply monitoring the transmitted and reflected spectral features. Fig. 1(b) gives the top-view of the bow-tie PSNR. Fig. 1(c) shows the transmissivity and the reflectivity of the composite structure when the bow-tie PSNR has $L = 400\,\text{nm}$, $D = 200\,\text{nm}$, and $d = 34.4\,\text{nm}$. There are several dips observed in the transmission spectrum and associated peaks in the reflection spectrum, which corresponds to different type of resonances of the embedded PSNR. The resonances at $\lambda = 1524\,\text{nm}$ and 2050 nm correspond to first-order PSNR resonances, with only one intensity maximum along the bow-tie length. A single resonator shows enhancement factor in excess of 9×105, which we believe is the biggest enhancement factor calculated in all types of nano-resonators so far.

Different bow-tie PSNRs with different waist and different edge width, multiple cascaded bow-tie PSNR, and rectangular PSNR were numerically investigated. Wavelength shift rates were found to be strongly dependent on the nature of the associated resonance and the plasmonic waveguide characteristics. Since the PSNR has extremely small size (less than 0.1 μm^2) and it is sensitive to the surrounding environment, the PSNR can be used as a compact refractometer in small areas. Fig. 1(d) shows transmissivity of PSNR when the surrounding refractive index (RI) changes from $n = 1$ to $n = 1.15$. The wavelength changes linearly with the refractive index. The

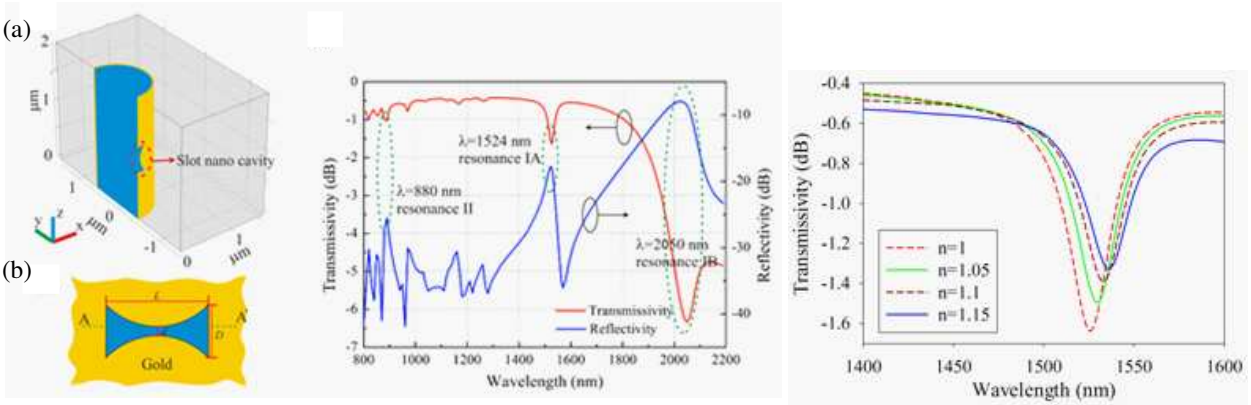

Figure 1: (a) Geometry of the PSNR embedded in the plasmonic microfibre; (b) top-view of the bow-tie; (c) transmissivity (red) and reflectivity (blue) of the bow-tie PSNR embedded in the microfiber; (d) transmissivity of PSNR when the surrounding RI changes from $n = 1$ to $n = 1.15$.

PSNR sensitivity resulted to be 66.7 nm/RIU, with a resolvable index change of 1.5×10^{-4} for a resolvable wavelength change of 0.01 nm.

Also, for the first time, both theoretically and experimentally, the transverse excitation of a strongly-coupled 3D PSNR is investigated by embedding a rectangular slot nano-cavity in a plasmonic structure formed by a thin-metal-film coated optical fiber tip. In the experiment, a rectangular PSNR was inscribed on the surface of a gold-coated fiber tip. The fabrication process involved three main steps: manufacture of optical fiber tip, deposition of a thin gold layer and focused ion beam (FIB) nanopatterning. The strongest enhancement factor 7.24×103 was achieved for the resonance at the wavelength $\lambda \sim 1450$ nm, recorded when light was polarized perpendicularly to the PSNR. The refractive index dependence of PSNR experiment is in progress.

Optical Spectroscopy for Food Applications: A Photonic Tasting

Anna Grazia Mignani, **Leonardo Ciaccheri**, **and Andrea Azelio Mencaglia**
CNR Istituto di Fisica Applicata "Nello Carrara", Sesto Fiorentino (FI), Italy

Abstract— The quality and safety of the food we eat attracts a great deal of publicity, and a demand for fresher, better-tasting, safer, healthier and higher quality food is escalating in every country.

We live in a global marketplace, and we eat a great variety of foods from many different countries. Many fruits, vegetables and dairy products now on the market were not available ten years ago. These are grown using a variety of production practices, from small organic operations to large-scale mechanized farms. On the one hand, produce buyers want to be reassured that farmers are taking reasonable steps to ensure that the produce delivered is safe and free from human pathogenic bacteria and mycotoxins. On the other hand, consumers and food handlers (restaurateurs, retailers, etc.) need to know that the food which they eat and serve is safe and healthy.

In addition to conventional analytical techniques, new instruments and tools are being envisaged that are capable of reducing the costs of quality control and of alerting people of the onset of risks. Also, new instruments for traceability and certification are needed, especially those based on low-cost techniques. The associations of producers and small farmers are increasingly demanding cheap and effective control devices, which are mainly considered as marketing tools for the protection of 'locally-grown' traditional foods. These foods are renowned, and need to be protected from adulteration and imitation, in view of their high qualitative standards, safety, and nutritional excellence.

Sensors based on optic and micro-optic techniques are found to offer effective and low-cost solutions for many industrial and process control applications. Especially in the case of spectroscopy-based devices, the intrinsic optical and mechanical characteristics of optical fibers, together with the wide availability of bright LEDs and portable spectrometers, have made it possible to implement compact instrumentation with a high potential for many applications in the food sector.

This talk presents a selection of spectroscopy-based, fiber-optic and micro-optic devices that have been designed and tested for monitoring the quality and safety of typical foods, such as extra virgin olive oil, wine, whisky and other spirits, beer, milk and other dairy products.

Fiber Optical Distributed Vibration Sensing with High Frequency Response and Spatial Resolution

Tao Zhu and Qian He
Key Laboratory of Optoelectronic Technology & Systems (Ministry of Education)
Chongqing University, Chongqing 400044, China

Abstract— High-frequency vibration incidents always refer to material damages in infrastructures, e.g., leakage of high-pressure gas pipeline and crack of material. Our research mainly focused on distributed vibration detection with high frequency response and spatial resolution. Fortunately, phase-sensitive optical time domain reflectometry (φ-OTDR) applies an ultrasensitive performance in vibration measurement, which is the main technology adopted in our study. Our work are introduced in detail as follows.

Firstly, we applied a new signal processing method, moving averaging and moving differential method, in φ-OTDR. Experimental results show that higher SNR can be achieved with less average number compared with conventional method. In that case, the frequency response was enhanced. Based on the moving averaging and moving differential method, we recently propose a novel system, which is shown in Fig. 1. The frequency information of vibration is acquired by monitoring the backscattering light intensity, which can be treated as a discrete sampling process. According to the Shannon sampling theorem, the maximum frequency response of the sampling system can be enhanced by increasing sampling rate. In experiments, a frequency-difference probe pulse pair with a short time delay is used, and the experimental results agree well with the theory. This method allows the maximum detectable frequency response no longer restricted by the sensing fiber length.

Another configuration is based on the merge of φ-OTDR and interferometers, shown in Fig. 3. A distributed optical fiber sensing system merged Mach-Zehnder interferometer and phase sensitive optical time domain reflectometer (φ-OTDR) system for vibration measurement with high-frequency response and high spatial resolution is demonstrated, where modulated pulses are proposed to be used as sensing source. Frequency response and location information are obtained

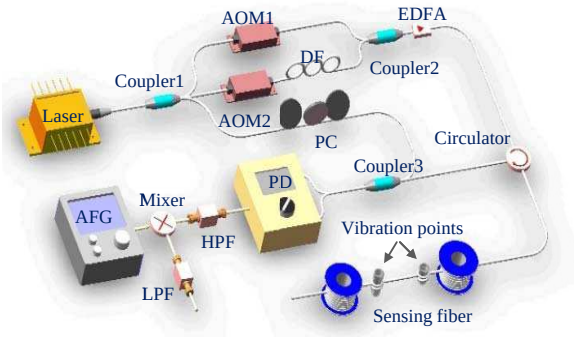

Figure 1: Experimental arrangement.

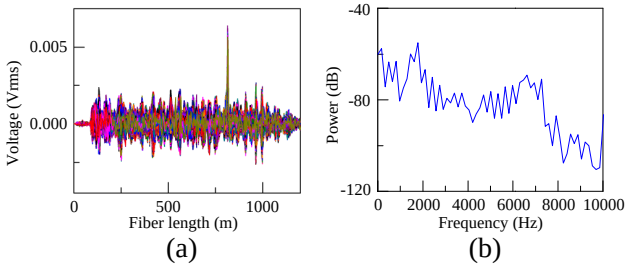

Figure 2: Experimental results of wide-frequency vibration detection.

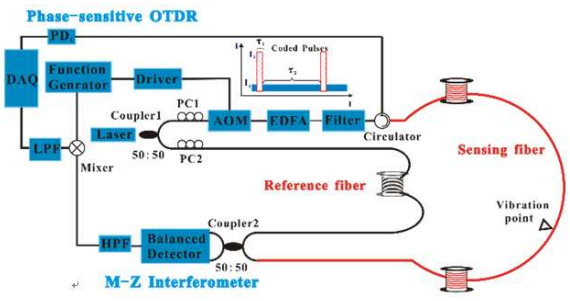

Figure 3: Experimental arrangement.

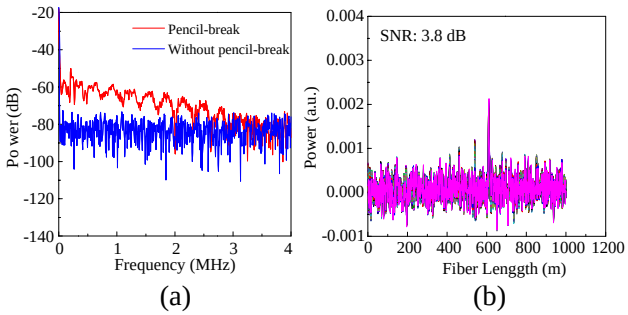

Figure 4: Experimental results of pencil-break.

by Mach-Zehnder interferometer and φ-OTDR technology, respectively. Spatial resolution of 5 m and the maximum frequency response of $\sim$3 MHz are achieved in 1064 m fiber link when the narrow pulse width is 50 ns.

Session 2P10a
SC1&3: Physics and Applications of Photonic Crystals, Materials, and Nanostructures

A New Kind of Leaky Wave Antenna Based on Low Frequency Surface Plasmon Polaritons

Jin Jei Wu[1], **Chien-Jang Wu**[2], **Her-Lih Chiueh**[3], **Tzong-Jer Yang**[1], **and Yao-Huang Kao**[1]

[1]Department of Electrical Engineering, Chung Hua University, Hsinchu 30012, Taiwan
[2]Institute of Electro-Optical Science and Technology, Taiwan Normal University
Taipei 116, Taiwan
[3]Department of Electronic Engineering, Lunghwa University of Science and Technology
Kueishan, Tayouan 333, Taiwan

Abstract— In this paper, based on low frequency surface plasmon polaritons (SPPs), we propose a new kind of leaky wave antenna constructed by periodic metallic bricks with open slot on the top. Numerical analysis shows that by introducing the open slot on the metallic blocks, there will appear extra spoof SPPs mode in the band gap of metallic solid blocks. The dispersion curve of such spoof SPPs mode passes through light line and enters into the radiation region and consequently it can generate a frequency steering pencil-like radiation. Experimental verification agrees with our theoretical results.

Phase Modulation and Refraction of Bloch Surface Waves: A Rigorous Theoretical Analysis

E. A. Bezus[1, 2] and L. L. Doskolovich[1, 2]

[1]Image Processing Systems Institute of the Russian Academy of Sciences, Samara 443001, Russia
[2]Technical Cybernetics Department, Samara State Aerospace University, Samara 443001, Russia

Abstract— Electromagnetic waves supported by the interfaces between photonic crystals and homogeneous media (Bloch surface waves, BSW) have recently attracted considerable research interest due to their potential applications in all-optical integrated systems such as optical sensors or photonic circuits [1, 2]. In some applications, BSW are considered as an alternative to surface plasmon polaritons (SPP) because they can propagate in all-dielectric structures and have negligible absorption losses.

In the present work, we study numerically and theoretically the phase modulation and refraction of a BSW propagating along the interface of a one-dimensional photonic crystal and a homogeneous dielectric medium. The modulation is performed by changing the geometrical parameters of the microrelief in the form of a ridge or a groove located on the surface of the photonic crystal. We show that the phase modulation can be performed by varying the length of the ridge (or the groove) in the upper layer of the photonic crystal at fixed height, or by varying its height at fixed length. The results of the rigorous electromagnetic simulations for BSW are compared both with an analytical model based on the conventional Fresnel equations for plane electromagnetic waves and with similar simulation results for SPP [3]. A reflecting Bragg grating is calculated as an example of an optical element for BSW.

ACKNOWLEDGMENT

This work was financially supported by RSF grant No. 14-19-00796, RFBR grants Nos. 13-07-00464 and 12-07-00495, RF Presidential grant No. NSh-3970.2014.9 and scholarship No. SP-4554.2013.5, and by the Dynasty foundation grant.

REFERENCES

1. Liscidini, M. and J. E. Sipe, "Analysis of Bloch-surface-wave assisted diffraction-based biosensors," *J. Opt. Soc. Am. B*, Vol. 26, 279–289, 2009.
2. Yu, L., E. Barakat, T. Sfez, L. Hvozdara, J. Di Francesco, and H. P. Herzig, "Manipulating Bloch surface waves in 2D: A platform concept-based flat lens," *Light Sci. Appl.*, Vol. 3, e124, 7 pages, 2014.
3. Bezus, E. A., L. L. Doskolovich, N. L. Kazanskiy, V. A. Soifer, and S. I. Kharitonov, "Design of diffractive lenses for focusing surface plasmons," *J. Opt.*, Vol. 12, 015001, 7 pages, 2010.

Analysis of Nanoimprinted TiO_2 Sol-gel Guided-mode Resonance Sensors

Wen-Kai Kuo and Ning-Chi Huang
Department of Electro-Optics Engineering, Formosa University
64 Wenhua Rd., Huwei, Yunlin 63208, Taiwan

Abstract— In this study, characteristics of an optical sensor based on guided-mode resonance structure fabricated by nanoimprinting TiO_2 sol-gel is numerically investigated using finite-difference time-domain (FDTD) simulation. Guided-mode resonant (GMR) grating waveguide structure can reflect the incident p-polarized light maximally when the incident wave is phase matched to a leaky waveguide mode [1]. Since this GMR reflective peak is very sensitivity to the refractive index of the film on the surface of the structure, it has been used for biosensor application [2]. In the traditional GMR sensor, a low refractive index linear grating surface structure is coated with a high-index film. In the paper, we investigate a GMR structure fabricated by newly-developed nanoimprinting TiO_2 sol-gel technique [3]. The sensor structure is shown in Fig. 1. The reflectivities of scanning the incident angle with different refractive index solution (1.33, 1.35, and 1.37) on the sensor surface were calculated by the FDTD method and results are shown in Fig. 2. The refractive indexes of substrate and grating in this structure for simulation are $n_{\text{sub}} = 1.457$ (SiO_2) and $n_{\text{grating}} = 2.25$, respectively. The grating pitch (Λ) modulation depth (h), and thickness (d) are 555 nm, 70 nm, and 200 nm, respectively. The incident light wavelength is 685 nm. The simulation results confirm that the nanoimprinting TiO_2 sol-gel GMR structure can be used as a biosensor.

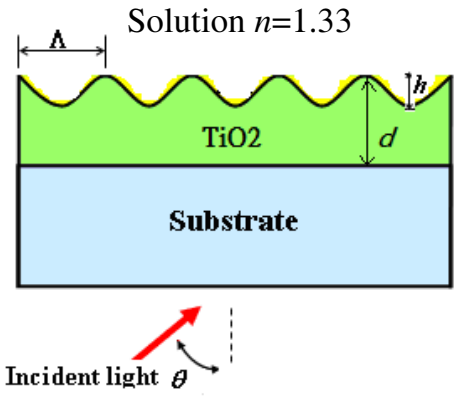

Figure 1.

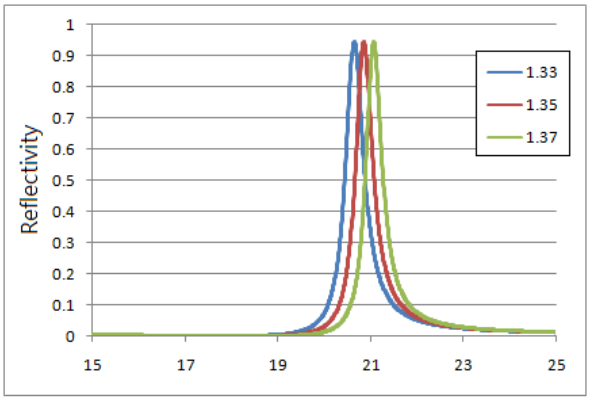

Figure 2.

REFERENCES

1. Wang, S. S. and R. Magnusson, *Appl. Opt.*, Vol. 27, 2606, 1993.
2. Block, I. D., L. L. Chan, and B. T. Cunningham, *Sensor and Actuators B*, Vol. 120, 187, 2006.
3. Hampton, M. J., S. S. Williams, Z. Zhou, J. Nunes, D. Ko, and J. L. Templeton, *Advanced Materials*, Vol. 20, 2667, 2008.

Study of Tunable Negative Refraction in a Doped and Lossy Semiconductor

Yi Min Zeng[1], **Jin Jei Wu**[2], **Tzong-Jer Yang**[2], **and Chien-Jang Wu**[1]

[1]Institute of Electro-Optical Science and Technology
Taiwan Normal University, Taipei 116, Taiwan
[2]Department of Electrical Engineering, Chung Hua University, Hsinchu 300, Taiwan

Abstract— It is known that negative refraction (NR) can be found when a wave is obliquely incident from a normal medium to a negative-index medium (NIM) also called as a double-negative (DNG) medium. However, the phenomenon of NR can also be obtained in an interface of air/lossy normal medium especially when the incident wave is p-polarized. In this work, according to the theory of inhomogeneous wave, we study the tunable NR based on the consideration of doped and lossy semiconductor of InSb. A p-polarized wave is assumed to be incident from air to semi-infinite InSb and the NR is indeed obtainable at suitable conditions. The behavior of NR is shown to be tunable, i.e., it can be tuned by temperature and/or doping concentration at a fixed operating frequency. In addition, the NR is also frequency dependent when the temperature and doping concentration are fixed. All results will be clearly numerically demonstrated.

Simulation Analysis of a Dielectric Hole Plasmonic Nanoantenna

Gung Jing He, Wayne Yang, and Yuan-Fong Chau
Department of Electronic Engineering, Chien Hsin University of Science and Technology
No. 229, Jianxing Rd., Zhongli City, Taoyuan County 32097, Taiwan

Abstract— We have numerically investigated a DH dipole antenna which is composed of two identical DH nanometal with a dielectric medium filled inside the hollow by using a finite element method with three-dimensional calculations. The proposed nanoantenna is composed of two identical hollow nanometal filled dielectric media inside the central part. We examine the influence of the shell thickness, gap width and dielectric media filled inside the hollows on the antenna resonance conditions. Simulation results show that the resonant wavelength of the proposed nanoantenna may be tuned over a broad spectral by considering the dielectric hole (DH) nanoantenna and introducing the design parameters (gap width, media filled inside the DH). The antenna resonance generates a peak in scattering spectra, while the cavity resonances lead to multiple peaks in the scattering spectra. The cavity resonant frequency can be tuned by varying the value of the dielectric constant. The local field enhancement inside the hollows (cavity) is maximized when the gap width, shell thickness and the medium inside the DHs when the cavity and antenna resonant frequencies coincide with each other. Through these simulations, we show that it is possible to tune a plasmonic nanoantenna with a constant length over a broad spectral range. This new nanoantenna promises applications in single molecule surface enhanced Raman spectroscopy (SERS) owing to its high local field enhancements and large scale manufacturability.

ACKNOWLEDGMENT

This work was supported by Ministry of Science and Technology of the Republic of China (Taiwan) under Grant No. NSC 102-2112-M-231-001-.

Numerical Investigation of a High-birefringence Photonic Crystal Fiber by Asymmetric Defect Structures

Wayne Yang and Yuan-Fong Chau
Department of Electronic Engineering, Chien Hsin University of Science and Technology
No. 229, Jianxing Rd., Zhongli City, Taoyuan County 32097, Taiwan

Abstract— We numerically investigated a high birefringence photonic crystal fiber (PCF) by a asymmetric defect structure in fiber core. Several different cases (case A-D) of PCF structures have been investigated for comparison. The birefringence and mode field area of these PCFs have been numerically estimated by employing a finite element method (FEM). An endlessly single mode, high birefringence above 7.0×10^{-3} is found at the excitation wavelength of $\lambda = 1550\,\text{nm}$. The merit of the designed PCFs is that their optimum birefringence can be easily achieved by introducing asymmetric in the fiber core region.

ACKNOWLEDGMENT

This work was supported by Ministry of Science and Technology of the Republic of China (Taiwan) under Grant No. NSC 102-2112-M-231-001-.

Guiding Properties of the Wedge Plasmon Polaritons

T.-J. Yang[1], **J. J. Wu**[1], **D. J. Hou**[2], **L. F. Shen**[3], **H. L. Chiueh**[4], **and C.-J. Wu**[2]

[1]Department of Electrical Engineering, Chung Hua University, Hsinchu 30012, Taiwan
[2]Institute of Electro-Optical Science and Technology
Taiwan Normal University, Taipei 116, Taiwan
[3]Institute of Space Science and Technology, Nanchang University, Nanchang 330031, China
[4]Department of Electronic Engineering, Lunghwa University of Science and Technology
Kueishan, Tayouan 333, Taiwan

Abstract— Subwavelength guiding of wedge plasmon polaritons (WPPs) is realized by a structured metallic wedge at frequencies well below the plasma frequency of metal. The phenomena of the designer WPPs with subwavelength confinement in the transverse plane is experimentally verified at microwave frequencies, whose characteristics resemble those of WPPs at telecom and optical frequencies. Additionally, electromagnetic field focusing and slowing down based on the proposed wedge waveguides are presented.

Supercontinuum Generation at 1.55 μm in a Silicon Nanowire Embedded Photonic Crystal Fiber

E. Gunasundari[1], **Abdosllam M. Abobaker**[2], **K. Senthilnathan**[1], **S. Sivabalan**[3], **K. Nakkeeran**[4], **and P. Ramesh Babu**[1]

[1]Photonics, Nuclear and Medical Physics Division, School of Advanced Sciences
VIT University, Vellore 632 014, India
[2]Department of Communications Engineering, College of Electronic Technology, Bani Walid, Libya
[3]School of Electrical Engineering, VIT University, Vellore 632 014, India
[4]School of Engineering, University of Aberdeen, Aberdeen AB24 3UE, UK

Abstract— Photonic nanowire with a sub-wavelength diameter has recently attracted a significant interest due to its ultrahigh nonlinearity accompanied by tight mode confinement and strong anomalous waveguide dispersion. Nanowires are generally fabricated from materials such as silica glass, silicon, etc.. Silicon has excellent transmission properties compared to silica and does not require high power density to bring in nonlinearity owing to its huge nonlinear coefficient. Silicon nanowires embedded photonic crystal fiber with core diameters smaller than the operating wavelength have attracted considerable interest due to their unique dispersion profiles and nonlinear properties, which, in turn, result in a wide range of applications. With this nanowire, it is possible to generate supercontinuum and ultrashort pulses based on soliton effect pulse compression. Much effort has been dedicated in generating pulses in the few-optical-cycle regime which has permitted important achievements in diverse fields such as the study of ultrafast dynamics in matter, high-order harmonic generation, extreme nonlinear optics, and attosecond physics. In this paper, we design an elliptical silicon nanowire embedded photonic crystal fiber (SN-PCF) using fully vectorial finite element method. Further, we analyze the various optical properties, namely, waveguide dispersion, birefringence, fractional power inside the core and effective nonlinearity by varying the ellipticity for a wide range of wavelengths from 0.8 to 1.8 μm. The proposed structure exhibits a high birefringence of 0.4815 for a small ellipticity of 0.3 at a longer wavelength of 1.8 μm. Besides, we investigate the evolution of supercontinuum at 1.55 μm wavelength for an input pulse width of 25 fs by varying the peak power of the input pulse as well as length of the SN-PCF. The numerical results corroborate that the proposed SN-PCF provides a wider supercontinuum bandwidth of 800 nm for a less input power of 1 W in a 2 mm length of fiber. The findings of this work may be useful in ultrahigh-resolution optical coherence tomography and optical communication systems.

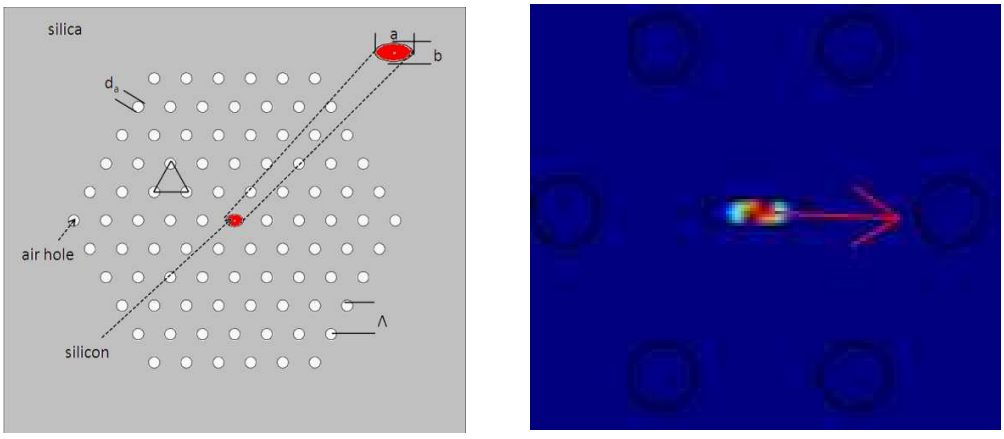

Figure 1: Design of the proposed SN-PCF: geometrical structure and mode field distribution of proposed structure.

Session 2P10b
SC3&2: Photonic Crystals

One-way Slow-light Waveguide by Gyromagnetic Photonic Crystals

Rui-Xin Wu, **Yan Yang**, **and Yin Poo**
School of Electronic Science and Engineering, Nanjing University, Nanjing 210093, China

Abstract— Slow light, the electromagnetic (EM) wave with group velocity reduced to a fraction of its speed in vacuum, has been the subject of extensive research in the last few years. Slow light could facilitate increasing light-matter interaction and enhancing linear and nonlinear effects, which is of both scientific and technological importance. Among many geometries in which the slow light has been observed, photonic crystal waveguides (PCWs) have played a significant part. A broad range of applications in telecommunications exploiting slow light in PCWs have been demonstrated, from delay lines to optical buffers, modulators,switches and so on.

For the slow wave devices or systems, back scattering is particularly worrisome since it may dominate over all other loss mechanisms as group velocity of waves becomes very small. The recently found chiral edge states (CESs) in photonic crystals (PCs), at which light propagates unidirectionally and is not affected by any disorders along the wave channel may provide a way to overcome the backscattering problems in slow light systems.

In this talk, we will show some demonstrations of one-way slow-light waveguide in microwave regime. The waveguide was made of gyromagnetic photonic crystal (GMPC) and a metal cladding. Using phase shift measurement method, we measured dispersion curve of the waveguide at the frequencies about the CES of GMPC, then retrieved the group velocity vg (or equivalently, group index $ng = c/vg$) of the EM wave in the one-way waveguide. The experiments show the group velocity of the one-way wave could be more than one order of magnitude less than the speed of light. By modifying the waveguide configuration, this waveguide can further support slow light with group index in excess of 2000. Meanwhile, the experimental results also show that, in certain frequency range, the variation of group velocity is small, implying the one-way slow light waveguide may have potential applications in information communication system, such as on-chip optical buffers and nonreciprocal slow-light devices.

ACKNOWLEDGMENT

This work was supported by the NSFC (61271080, 61071007), and RFDP (20110091110030). R.X.W. thanks partial support from STP of Jiangsu Province (BK2012722) and Jiangsu Key Laboratory of Advanced Techniques for Manipulating Electromagnetic Waves.

From Microfiber Bragg Gratings to Microfiber Photonic Crystal Devices

Wei Ding, Yang Yu, and Zhi-Yuan Li
Institute of Physics, Chinese Academy of Sciences, Beijing 100190, China

Abstract— Adiabatic fiber tapering technique provides ideal transition from a buried waveguide in a conventional fiber to an open waveguide in a microfiber. Introducing longitudinal structures along these microfibers, a lot of photonic functionalities can be realized. In this talk, we report our manufactures of microfiber Bragg grating and photonic crystal (PhC) devices by utilizing variant technologies.

Using metal deposition or reactive ion etching, thousands of periodic structures consisting of Au strips or corrugations have been fabricated on one side of a 10 μm diameter fiber taper [1, 2]. The periodic patterns are previously produced on a layer of photoresist by using laser interference

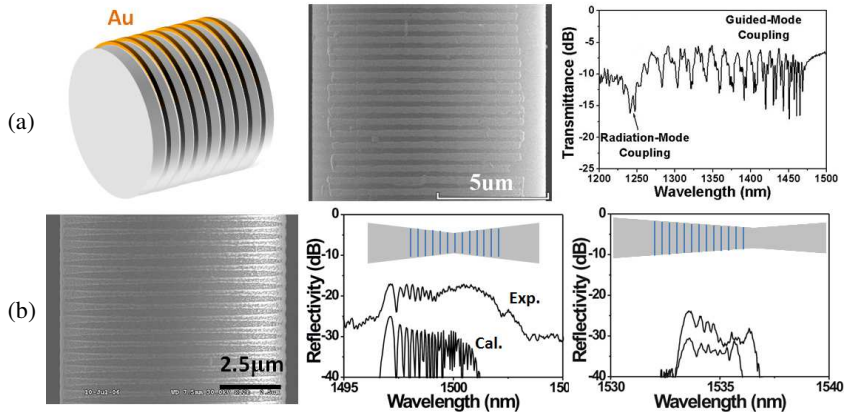

Figure 1: (a) Periodic gold strips on a microfiber lead to many dips in the transmission spectrum. Each dip corresponds to the coupling from the input fundamental mode to one backward mode. (b) Microfiber Bragg gratings consisting of air corrugations give rise to different reflection spectra, if the taper diameter varies in the longitudinal direction.

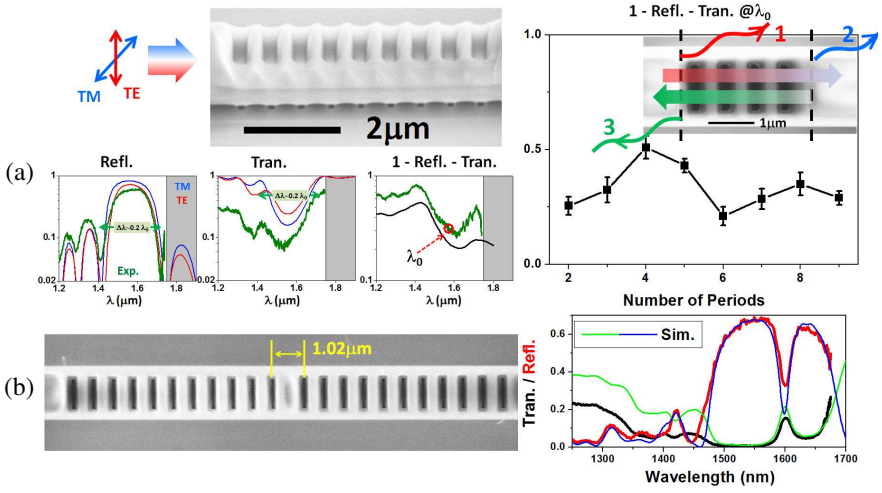

Figure 2: (a) A microfiber with nine rectangular through-holes, i.e., a PhC reflector, exhibits a broad reflection peak and transmission pit. The measured loss at the central wavelength of the stop band shows an undulation with variation of the number of periods. This could be understood by interference between the radiation components 1–3 depicted in the insert. (b) A cavity surrounded by two PhC reflectors shows resonant features in its transmission/reflection spectra. Both the PhC reflector and the microcavity fit well with FDTD simulations.

lithography. We demonstrate functionalities of these microfiber Bragg gratings by exploiting the large index contrast between gold and environment and by varying the diameter profile of the fiber taper respectively. The metal gold has a large negative dielectric constant in near infrared ($\varepsilon_{\mathrm{Au}} \sim -60$), and varying the diameter of the microfiber while maintaining the grating period leads to varied Bragg resonant wavelengths.

Pushing further ahead, a PhC stop band with fractional bandwidth in excess of 10% is demonstrated in a 1.72 µm diameter microfiber by perforating arrays of rectangular through-holes along it [3]. This freely-suspended microfiber PhC device is much compacter than its Bragg grating counterpart and could form the basic building block in many nano-photonic applications. We also show that the radiation loss, which is partly determined by optical interference, can be suppressed by design [4] and a microcavity combining two microfiber PhC reflectors has a Q-factor of ~ 75 and a modal volume of $0.65\lambda_0^3$.

REFERENCES

1. Ding, W., S. R. Andrews, T. A. Birks, and S. A. Maier, *Opt. Lett.*, Vol. 31, 2556, 2006.
2. Ding, W., S. R. Andrews, and S. A. Maier, *Opt. Lett.*, Vol. 32, 2499, 2007.
3. Yu, Y., W. Ding, L. Gan, Z. Y. Li, Q. Luo, and S. R. Andrews, *Opt. Express*, Vol. 22, 2528, 2014.
4. Ding, W., R. J. Liu, and Z. Y. Li, *Opt. Express*, Vol. 20, 28641, 2012.

Metal-ferroelectric Photonic Crystal All-optical Switching

Xiaoyong Hu
State Key Laboratory for Mesoscopic Physics, Department of Physics
Peking University, Beijing 100871, China

Abstract— Nanoscale all-optical switching is one of the core components of optical computing systems and ultrahigh-speed information processing chips. Photonic crystal provides a excellent basis for the realization of nanoscale integrated photonic devices due to its strong ability to control the propagation states of photons based on photonic band gap effect. The basic realization method of photonic crystal all-optical switching is based on the photonic bandgap shift or defect mode shift originating from the pump light induced effective refractive index variation of photonic crystal. However, owing to the relatively small third-order optical nonlinearity of the conventional nonlinear optical materials, it is of a great challenge to realize an ultrafast response time and a low threshold pump power for photonic crystal all-optical switching simultaneously. Moreover, the threshold pump intensity was as high as GW/cm^2 order. This also restricts the practical applications of photonic crystal all-optical switching. We fabricated a one-dimensional metal-ferroelectric photonic crystal, which is composed of four 10-nm-thick gold layers alternating with 150-nm-thick polycrystalline lithium niobate ($LiNbO_3$) layers. Because of the resonant nature of multiple Bragg reflections at the metal-ferroelectric interfaces, pump light can penetrate highly nonlinear metal and ferroelectric layers, which leads to a large nonlinear optical response for the one-dimensional metal-ferroelectric photonic crystal. Moreover, the nanoscale crystal grains of polycrystalline $LiNbO_3$ could provide strong quantum confinement effect, which also contributes to the nonlinearity enhancement of the one-dimensional photonic crystal. The operating threshold pump intensity was reduced by three orders of magnitude, reaching only 9 MW/cm^2. A high switching efficiency of 80% was also obtained. The fast relaxation dynamics of non-equilibrium electrons in gold ensured an ultrafast response time of 24.2 ps. A low-power and ultrafast photonic crystal all-optical switching with a high switching efficiency was realized.

Design and Fabrication of Silicon-polymer Hybrid Photonic Crystal Nanobeam Structures for Achieving Integrated Ultrafast All-optical Switching

Zi-Ming Meng[1] and Zhi-Yuan Li[2]

[1]School of Physics and Optoelectronic Engineering
Guangdong University of Technology, Guangzhou 510006, China
[2]Laboratory of Optical Physics, Institute of Physics, Chinese Academy of Sciences
P. O. Box 603, Beijing 100190, China

Abstract— Integrated ultrafast all-optical switching is highly desirable for on-chip fast and large-data optical interconnect and communication [1]. The design and fabrication of silicon-polymer hybrid photonic crystal nanobeam (HPCN) structures for achieving integrated ultrafast all-optical switching are presented in this talk. Theoretically based on the three-dimensional FDTD method the design of high-Q silicon-polymer HPCN microcavities are explicitly investigated and the total switching time and switching power are also extracted for realizing all-optical switching [2, 3]. Experimentally the fabrication of HPCN structures is divided into two independent parts. One part is to build the PCN structures in silicon-on-insulator (SOI). The other part is to infiltrate the air void region of the PCN with highly nonlinear polymer to form the hybrid structures. Using the electron beam (e-beam) lithography and inductive coupled plasma etching we successfully build high-quality PCN structures in SOI. Specifically we discuss the importance of dosage control in the process of e-beam lithography when using PMMA as the electron beam sensitive mask. Previously high-quality silicon-polymer hybrid PC structures had been fabricated by using the nanoimprint lithography method [4]. We discuss the possible fabrication procedure for constructing high-quality hybrid PCN structures utilizing the nanoimprint lithography method.

REFERENCES

1. Li, Z. Y. and Z. M. Meng, "Polystyrene Kerr nonlinear photonic crystals for building ultrafast optical switching and logic devices," *J. Mater. Chem. C*, Vol. 2, 783, 2014.
2. Meng, Z. M., Y. H. Hu, C. Wang, X. L. Zhong, W. Ding, and Z. Y. Li, "Design of high-Q silicon-polymer hybrid photonic crystal nanobeam microcavities for low-power and ultrafast all-optical switching," *Phot. Nano. Fund. Appl.*, Vol. 12, 83, 2014.
3. Meng, Z. M., X. L. Zhong, C. Wang, and Z. Y. Li "Numerical investigation of high-contrast ultrafast all-optical switching in low-refractive-index polymeric photonic crystal nanobeam microcavities," *EPL*, Vol. 98, 54002, 2012.
4. Qin, F., Z. M. Meng, X. L. Zhong, Y. Liu, and Z. Y. Li, "Fabrication of semiconductor-polymer compound nonlinear photonic crystal slab with highly uniform infiltration based on nano-imprint lithography technique," *Opt. Exp.*, Vol. 20, 13091, 2012.

Tunable Photonic Band Gaps for Strong 1-D Light-matter Interaction

Rong-Juan Liu[1, 2], **Wah Tung Lau**[1], **Sajeev John**[1, 3], **and Zhi-Yuan Li**[2]

[1]Department of Physics, University of Toronto
60 St. George St., Toronto, Ontario M5S1A7, Canada
[2]Institute of Physics, Chinese Academy of Sciences, Beijing 100190, China
[3]Department of Physics, King Abdulaziz University, Jeddah, Saudi Arabia

Abstract— A photonic band gap (PBG) is a frequency window in which light can be localized, spontaneous emission of radiation from atoms is suppressed and novel strong-coupling effects between photons and atoms are predicted [1, 2]. From a fundamental perspective, a 1-D PBG within a larger 3-D PBG provides a testing ground for the physical realization of non-classical multi-photon states [3]. Near a 1-D photonic band edge, the electromagnetic density of states is singular and varies rapidly with frequency. This has a direct bearing on the emission properties of band-edge lasers. Flat bands in photonic crystal waveguides are also excellent candidates for slow light with potential applications in optical information processing, quantum information, spontaneous emission engineering, and sensing. Tunability of the electromagnetic density of states and the slow-light dispersion relations offers novel flexibility to these applications.

In this talk, we design, fabricate and optically characterize a waveguide containing a tunable 1-D PBG, centered at a frequency near 12.5 GHz, within the larger, complete 3-D PBG of a woodpile photonic crystal [4–6]. Waveguide modes are created in the 3-D PBG by cutting dielectric rods, lying in a single plane, to form a line of adjustable air-gaps. When the periodicity of the air-gaps is twice the rod spacing, the single-mode waveguide band splits into two bands separated by a 1-D PBG, with bandwidth and band edge frequencies determined by the air-gap modulation amplitude. The waveguide dispersion is fitted using a simple two-band tight-binding photonic Hamiltonian. Our structure provides highly tunable slow-light modes, localized states of light and adjustable electromagnetic density of states for the experimental study of strong light-matter coupling in one-dimension. Using a suitable split-ring resonator design, we predict a large, discernible vacuum Rabi splitting that is more than one part in a thousand of the original resonance frequency.

REFERENCES

1. John, S., *Phys. Rev. Lett.*, Vol. 58, 2486, 1987.
2. Yablonovitch, E., *Phys. Rev. Lett.*, Vol. 58, 2059, 1987.
3. John, S. and V. Rupasov, *Phys. Rev. Lett.*, Vol. 79, 821, 1997.
4. Li, Z. Y. and K. M. Ho, *J. Opt. Soc. Am. B*, Vol. 20, 801, 2003.
5. Liu, R. J., Z. Y. Li, F. Zhou, and D. Z. Zhang, *Optics Express*, Vol. 15, 15531–15538, 2007.
6. Liu, R. J., Z. Y. Li, F. Zhou, and D. Z. Zhang, *Optics Express*, Vol. 16, 5681–5688, 2008.

Interesting Periodic and Quasiperiodic Photonic Band Gap Networks

Xiangbo Yang, Zhenyu Wang, and Jian Lu
MOE Key Laboratory of Laser Life Science, Institute of Laser Life Science
College of Biophotonics, South China Normal University, Guangzhou 510631, China

Abstract— Periodic dielectric structures on a wavelength scale exhibit photonic band gaps (PBGs), where the transmission of electromagnetic (EM) waves is forbidden. It makes PBG materials be able to control and confine the propagation of EM waves.

Periodic and quasiperiodic networks made of one-dimensional (1D) optical waveguides are also a kind of PBG structures and overcome many shortcomings of PBG materials. Firstly, the structures are flexible, so they can be experimentally easily realizable. Secondly, the phase and amplitude of EM wave function can be measured anywhere inside these systems. Thirdly, the symmetry of a unit cell of the waveguide networks can be changed conveniently and defects or randomness can be easily drawn into the structures. Fourthly, strong scattering can be easily introduced in a unit cell to produce large full gaps in any dimension, unlike usual PBG systems, these networks do not require a material with a large dielectric constant.

In this paper, we construct several kinds of interesting periodic and quasiperiodic optical waveguide networks and investigate the features of PBG and photonic localization of these systems. We find that huge PBGs can be generated by a so-called 1D two-segment-connected periodic tetrahedral waveguide network with the matching ratio of waveguide length of $2:1$, where the gap-midgap ratio of the largest PBG arrives at 146%. On the other hand, we also find that extreme narrow photonic passbands, very strong photonic localization, and tens of hundreds of comb-like photonic bands can be produced by some interesting periodic and quasiperiodic optical waveguide networks. These interesting PBG structures may be useful for the designing of optical switches, optical narrowband filters, high capacity telecommunications, and multichannel filters, etc..

ACKNOWLEDGMENT

This work was supported by the National Natural Science Foundation of China, Grant Nos. 11374107 and 10974061.

Negative Optical Scattering Force in Photonic Crystal Background

Weiqiang Ding, Tongtong Zhu, and Yongyin Cao
Department of Physics, Harbin Institute of Technology, Harbin 150001, China

Abstract— Recently, the optical negative scattering force, which is an unusual optical pulling force opposite to the propagation direction of a light beam, has been attracted much interests due to the interesting physics underground and also potential applications in optical manipulation. Hereto, however, most of the negative pulling forces exerted on scatters are usually considered in uniform backgrounds, such as water or air. More recently, it has been shown that the structure of the background (such as an interfaces of water-air) plays an important role in optical force, which provides rich scattering behaviors, and in turn contributes to the optical forces and optical manipulations significantly. Here, we show that a well-designed periodic background, i.e., a photonic crystal (PC) structure, can be used to generate negative optical pulling force efficiently over extremely long distance by using the self-collimation (SC) mode supported in the PC background. The SC mode can keep a constant and finite transverse size without diffraction along the propagation direction. Then, a carefully designed scatter is used to adiabatically broaden the transverse size of the SC mode from a smaller value to a larger value. Angular spectrum and linear momentum conservation analysis of this process results in a negative scattering force to the scatter. The results presented here provide a new way for the tractor beam long distance optical manipulation.

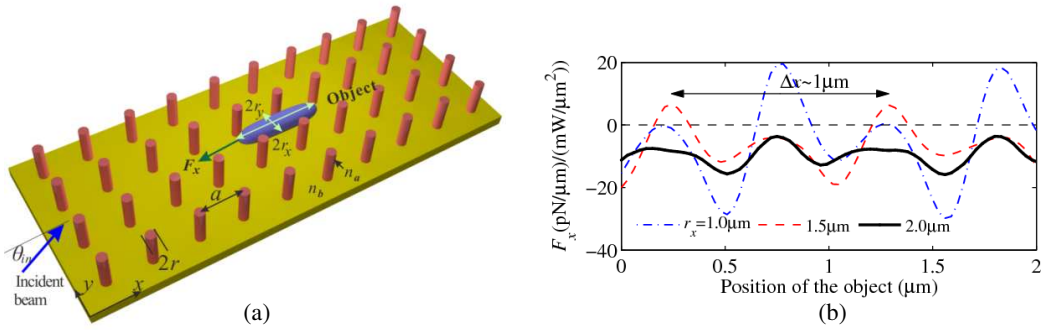

Figure 1: (a) Schematic configuration of the system investigated in this work. The elliptical scatter in the photonic crystal background is illuminated by the self-collimation mode of the PC, and then a negative pulling force on the scatter is obtained. (b) Periodical changes of optical force F_x with the position x at the case of $r_x = 1.0\,\mu\text{m}$, $1.5\,\mu\text{m}$ and $2.0\,\mu\text{m}$.

Session 2P11a
SC1: Computational Techniques in Electromagnetics and Applications

Energy Distribution of Dielectric Waveguides by Various Circular Cylinder Array with Defect Layers

Ryosuke Ozaki and Tsuneki Yamasaki
Department of Electrical Engineering, College of Science and Technology, Nihon University, Japan

Abstract— By progress of optical nanotechnology such as photonic crystals or metamaterial, various optical devices have been widely employed as an optical waveguide filter, optical coupler, and so on. In particular, light propagation property in periodic structure waveguide such as photonic crystal waveguide has been both theoretical and practical interest in many areas of physics and engineering. In periodic structures such as photonic crystals structure, it is known that a frequency stop band occurs. Also, in general, photonic crystals such as optical nanostructures with periodically permittivity distribution are known as technology which can be controlled the light in the periodic structure by interaction of both the wave nature of light and periodicity. Therefore, in the design of photonic crystals structure as much as optical wavelength, it is very important to investigate the stop band region or photonic band gaps. Though it is not analyzed the stop band area in Bragg region in detailed, many numerical results are shown only fields distribution by utilizing the FDTD method, FEM method based on variational method, and another numerical techniques.

In recent papers, we have analyzed the propagation characteristics of dielectric waveguide composed of dielectric circular cylinders array loaded with dielectric circular cylinders, dielectric triangular cylinders, and rhombic dielectric structure in the middle layer by using the combination of improved Fourier series expansion method and multilayer method, and investigated the influence of complex propagation constants at the first stop band region and distribution of energy flow in the defect region for TE and TM mode.

In this paper, we have analyzed the distribution of energy flow for dielectric waveguide by various circular cylinder array with defects layer composed of air-hole and dielectric cylinder array as shown in Fig. 1(a), and investigated the influence of distribution of energy flow in the defect region. Consequently, the aim of this paper is to obtain optimum dielectric waveguide structure to concentrate the energy into the defect area for TE mode. Numerical results are given for the complex propagation constants at the first stop band region and the distribution of energy flow by using the propagation constants at the guided area for TE_0 mode.

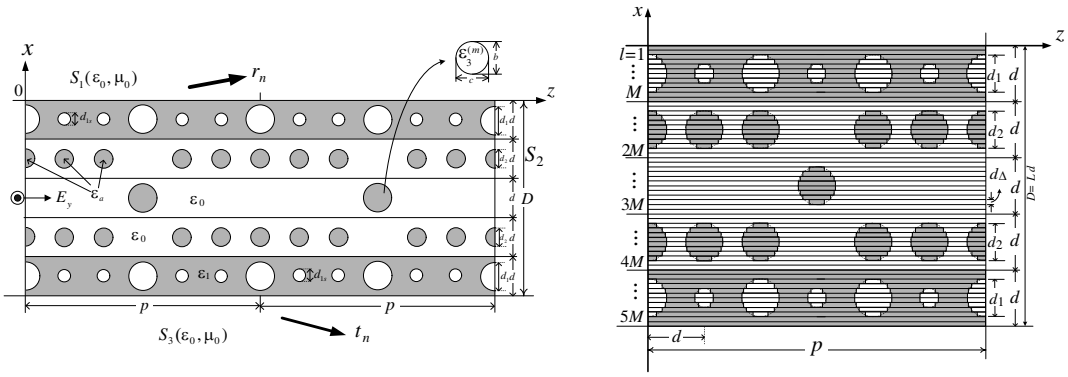

(a) Coordinate system (b) Approximated multilayer method

Figure 1: Structure of dielectric waveguides formed by air-hole and dielectric cylinder array with defects layer.

Fractal Labyrinths: Path Matrices and Borders Topology

V. I. Grachev
Kotel'nikov Institute of Radio Engineering and Electronics, Russian Academy of Sciences, Russia

Abstract— Application of fractal formalism to the analysis of complex weakly formalized processes and systems, to problems of image reconstruction of stochastic nanostructures [1], genetic and self-affine synthesis of antenna arrays [2], to analysis of multidimensional signals etc. intensively is developing at the present time. In this paper, the extension of the class of fractal-scaling approaches is made in considering of a fundamentally new types of self-similar (hierarchical) dendritic structures — fractal labyrinths [3]. Are presented elements of the labyrinthine fractals theory with use of the mathematics of fractional calculus and basic models random walk [4]. Based on the existence and uniqueness theorems of curves of finite length in locked labyrinthine fractals [5] is proposed an algorithm for constructing conductive pathways of the fractal tree with accuracy to isomorphism with respect to rotation and flipping. Matrices of path are calculated with use of Jordan decomposition. It is shown that, in general case, dendritic fractals are more efficient than the classic fractals type Sierpinski carpet for the identification of parameters of nanostructures and signals. Effectiveness of using the fractal labyrinths concept also is demonstrated in the analysis of more general problems, such as the anomalous transport processes in complex systems, which are governed by the non-exponential relaxation model, for example, subdiffusion and superdiffusion in disordered media [3, 6].

REFERENCES

1. Grachev, V. I., A. A. Potapov, and V. A. German, "Fractal labyrinths and planar nanostructures," *PIERS Proceedings*, 122–125, Stockholm, Aug. 12–15, 2013.
2. Potapov, A. A. and V. I. Grachev, "The labyrinth structure in the synthesis of fractal antennas," *PIERS Proceedings*, 1584–1587, Moscow, Russia, Aug. 19–23, 2012.
3. Grachev, V. I., A. A. Potapov, and V. A. Potapov, "Fractal labyrinths," *RENSIT: Radioelectronics, Nanosystems, Information Technologies*, Vol. 3, No. 2, 103–109, 2011 (in Russian).
4. Metzler, R. and J. Klafter, "The random walk's guide to anomalous diffusion: A fractional dynamics approach," *Phys. Rep.*, Vol. 339, 1–77, 2000.
5. Cristea, L. L. and B. Steinsky, "Curves of infinite length in 4×4-labyrinth fractals," *Geom. Dedicata*, Vol. 141, 1–17, 2009.
6. Potapov, A. A. and V. I. Grachev, "Fractal labyrinths: Physics and fractional operators," *PIERS Proceedings*, 1584–1587, Moscow, Russia, Aug. 19–23, 2012.

Radiation Directivity of an Antenna Installed in an Automobile

Zicai Zheng and Hiroshi Shirai
Course of Imformation Security Science, Graduate School of Science and Engineering
Chuo University, 1-13-27 Kasuga, Bunkyo, Tokyo 112-8551, Japan

Abstract— With the development of wireless communication technology in recent years, various wireless communication services such as cell phone, PCS, and wireless LAN are provided. In order to ensure a stable wireless communication environment, it is necessary to understand that how electromagnetic waves emitted from communication equipment propagate in a complicated urban environment. Specially, cell phone are used inside an automobile, while the radiation wave essentially propagates through the window aperture, radiation characteristics will be dramatically affected by the existence of nearby metal frame structure of the automobile. In order to analyze such a complicated environment, numerical technologies such as Finite Difference Time Domain(FDTD) method may be applied to investigate the surrounding radiation field. However, the analysis may be confined for a certain near field region due to the sampling memory limitation.

In this paper, far field radiation pattern of an antenna inside an automobile has been analyzed via near field to far field transformation through equivalence theorem. Firstly, near radiation field of an antenna with automobile is calculated by FDTD method for continuous time harmonic excitation with appropriate absorbing boundary condition. Then, using the principle of equivalent source, far field may be derived from the equivalent source distribution on a postulated closed surface which encloses the antenna and the automobile structure. The validity of this far field derivation is confirmed by comparing the radiation pattern with the theoretically estimated one. It has been found a good agreement between them.

In this presentation, various radiation pattern when an antenna is placed in front or back seat of the automobile will be shown with different tilted angles.

Kd-tree Based Shooting and Bouncing Ray Method for Fast Computation of Near Field Scattering

P. C. Gao, Z. C. Liang, and W. Gao
Science and Technology on Electromagnetic Scattering Laboratory, China

Abstract— In this paper, we propose an efficient kd-tree based shooting and bouncing ray (SBR) method for solving near field modeling problems in radar-target end-game scenarios. The procedure of the SBR involves two steps: ray tube tracing and electromagnetic computing. In near field analysis, the incident field is approximated as a spherical wave, not a plane wave. Bundles of rays radiating from source instead of a grid of parallel rays are shot toward the target. The density of the rays on the virtual aperture should be greater than about ten rays per wavelength in view of the convergence. Thus, the ray tube tracing in the SBR is very time-consuming for electrically large and complex targets. By recursively employing the axis-perpendicular plane to split the target space into uneven axis-aligned boxes according to the greedy Surface Area Heuristic (SAH), the kd-tree is highly effective in handling the irregularly distribution of triangles of the target and can significantly decrease the number of ray-triangle intersection tests. Therefore, we utilize the kd-tree to accelerate the ray tube tracing in the SBR. In the procedure of electromagnetic computing, the geometrical optics (GO) is applied to calculate the reflected field, and the scattered filed of each ray tube can be approximated by the physical optics (PO) integral. However, the far-field assumption results in the decrease of the accuracy of the standard PO in the near field observation. By partitioning the target surface into small pieces, the observation point and the source point are in the far field zone of each small piece. Additionally, each piece has a distinct wave propagation direction towards its local coordinate origin. The proposed modifications to standard PO can extend the region of validity of the SBR to near field scattering. Finally, the results obtained by the proposed method are compared with the results calculated by well-known commercial EM software FEKO. Numerical examples demonstrate that the proposed method can efficiently handle the near field scattering problems of realistic complex targets with high accuracy.

Analysis of the Fluorescence Imaging of Surface Plasmon-coupled Emission Microscopy

X. Ji[1], **T. Suyama**[2], **A. Matsushima**[1], **Y. Zhang**[3], **and Y. Okuno**[4]

[1]Graduate School of Science and Technology, Kumamoto University, Kumamoto, Japan
[2]Akashi National College of Technology, Akashi, Japan
[3]Department of Physics and Electronic Information, Wenzhou University, Wenzhou, China
[4]South China Normal University, Guangzhou, China

Abstract— Surface plasmon-coupled emission microscopy (SPCEM) that makes use of a thin layer of metal deposited on glass slides to efficiently excite fluorophore and to collect the emission light is a widely used imaging technique that has found a number of applications in areas such as biotechnology and biological measurements. SPCEM is a relatively new imaging technique that potentially promises better detection sensitivity and higher signal-to-noise ratio than conventional total internal reflection fluorescence (TIRF) imaging. However, recent theoretical studies suggest that the sensitivity of SPCEM is actually reduced due to the metal layer. We have designed a metal-dielectric multilayer film structure which consists of Ag-Si_3N_4 layers, and we have analyzed the transmission of two counter-propagation lights from the multilayer film by using the characteristic matrix method in the film optics. In this paper, optimization is utilized in the design of the multilayer film structure. And it is coated on the glass slides to improve the quality of microscopic imaging. We mainly use the optimization method to design the thickness of the metal layer and the dielectric layer. We analyze the transmission coefficient of two counter-propagation lights from the multilayer film with different thickness and different number of layer. The refractive indexes with different number of the layer of multilayer film are also discussed.

REFERENCES

1. Török, P., P. Varga, Z. Laczik, and G. R. Booker, "Electromagnetic diffraction of light focused through a planar interface between materials of mismatched refractive indices: An integral representation, *J. Opt. Soc. Am. A*, Vol. 12, 325–332, 1995.
2. Lakowicz, J. R., "Directional surface plasmon-coupled emission: A new method for high sensitivity detection," *Biochem. and Biophys. Res. Comm.*, Vol. 307, No. 3, 435–439, 2003.
3. Van de Nes, A., L. Billy, S. Pereira, and J. Braat, "Calculation of the vectorial field distribution in a stratified focal region of a high numerical aperture imaging system," *Opt. Express*, Vol. 12, 1281–1293, 2004.
4. Tang, W. T., E. Chung, Y. H. Kim, P. T. C. So, and C. J. R. Sheppard, "Investigation of the point spread function of surface plasmon-coupled emission microscopy," *Opt. Express*, Vol. 15, No. 8, 4634–4646, 2007.
5. Suyama, T., X. Ji, and Y. Zhang, "A metal-dielectric composited film applied to enhance the fluorescence imaging," *PIERS Proceedings*, 1409–1414, Stockholm, August 12–15, 2013.
6. Suyama, T., X. Ji, and Y. Zhang, "Enhancement of fluorescent labeling via a composited thin film," *International Journal of Polymer Science*, No. 921489, 2014.

Analysis of Plasmon Resonance in a Multilayer-coated Bigrating

Xun Xu[1], **Yoichi Okuno**[2], **and Taikei Suyama**[3]

[1]Kyushu Sangyo University, Fukuoka, Japan
[2]South China Normal University, Guangzhou, China
[3]Akashi National College of Technology, Akashi, Japan

Abstract— Periodically corrugated thin metal films have an interesting property such as the partial or total absorption of incident light energy. The absorption is associated with the excitation of the surface plasmons and is then termed the resonance absorption [1, 2]. Most of studies on the resonance absorption have mainly dealt with a thin metal film grating whose surfaces are periodic in one direction. We investigate the resonance absorption of a multilayer-coated bigrating which consists of thin-films corrugated periodically in two directions. The absorption in a multilayer-coated bigrating has been of considerable interest since we can expect more complex behaviors in the absorption phenomena by virtue of the presence of double periodicity and multilayer structure. We describe a numerical algorithm based on Mode-matching method [3] for analyzing diffraction of a plane wave by a multilayer-coated bigrating. Using the algorithm we numerically examine characteristics of the resonance absorption in the grating.

REFERENCES

1. Glass, N. E., A. A. Maradudin, and V. Celli, "Surface plasmons on a large-amplitude doubly periodic corrugated surface," *Phys. Rev. B*, Vol. 26, 5357–5365, 1982.
2. Inagaki, T., J. P. Goudonnet, J. W. Little, and E. T. Arakawa, "Photoacoustic study of plasmon-resonance absorption in a doubly periodic grating," *J. Opt Soc. Am. B*, Vol. 2, 432–439, 1985.
3. Okuno, Y., "Mode-matching Method," *Analysis Methods for Electromagnetic Wave Problems,* E. Yamashita, Ed., 107–138, Artech House, Boston, 1990.

Electromagnetic Behaviour of Carbon Fibre Composite Airfoils

Xuesong Meng, **Phillip Sewell**, **Ana Vukovic**, **and Trevor M. Benson**
The University of Nottingham, UK

Abstract— Modern electromagnetic devices are becoming increasing complex and their simulation must take into account geometrical features that are both large and small compared to the wavelength of interest. This often results in large computational problems that may not feasible, even with modern computational resources. A way of reducing computational requirements is to embed electromagnetic models of small features within an otherwise coarse mesh. We have previously reported on embedded models for both carbon fibre composite (CFC) films and optical thin films within the numerical Transmission Line Modelling (TLM) method [1]. In this paper, the embedded thin film model [1] is extended to curved thin panels and used to investigate the electromagnetic behaviour of an CFC airfoil with the profile NACA4415 [2].

The paper outlines the methodology for embedding thin curved panels which can be separated into two steps: a) linearization and b) embedding the structure within a coarse TLM mesh. A section of a curved panel crossing the node (n_x, n_y) is shown in Fig. 1(a), where the crossing red lines denote link lines of the TLM node of length Δ. The curved panel is firstly approximated by linear piece-wise segments, which is achieved by connecting the cross points of the arc and the link lines of the TLM node. The linear segment may split the link line into two parts, as in the case of the point B shown in Fig. 1(a). In this case, the whole section of transmission line, together with the thin layer, is modelled as a three-layer stack and embedded between the neighbouring TLM nodes. The transmission line model of the three layer stack is shown in Fig. 1(b), in which transmission lines of length l_1 and l_2 represent the link lines on either side of the thin film panel.

By way of illustration of the application of this technique, the scattering of a CFC airfoil with the profile NACA4415 with the 1.063 GHz TE wave illumination is shown in Fig. 2. The figure shows that weak fields exist in the airfoil which is consistent with the fact that CFC materials behave as imperfect metals. The full paper will outline the methodology and accuracy of the embedded model and analyse the shielding effectiveness of the airfoil.

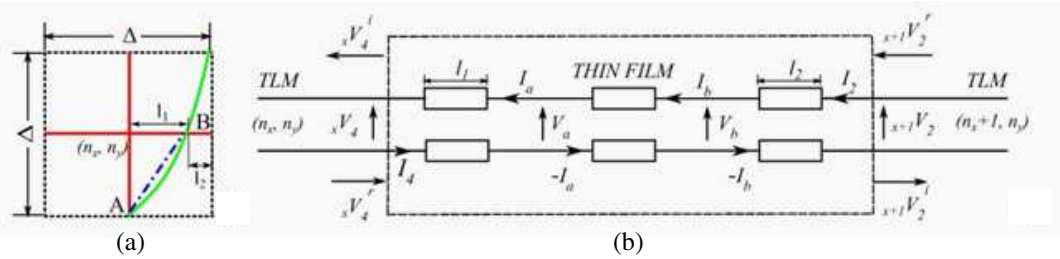

Figure 1: (a) A section of curved panel cross a TLM node, (b) its transmission line model as a three-layer stack embedded between two TLM nodes.

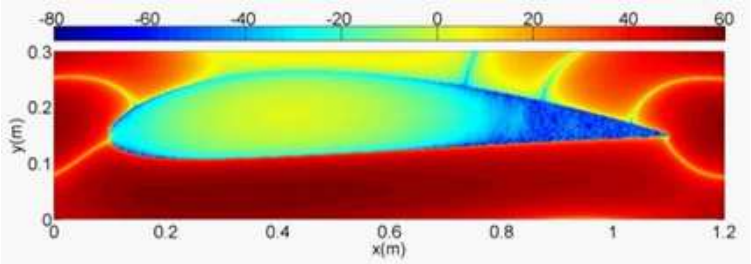

Figure 2: The scattering of the CFC airfoil NACA4415 upon the 1.063 GHz TE wave illumination. The discretisation size is 2 mm.

REFERENCES

1. Meng, X., P. Sewell, A. Vukovic, H. G. Dantanarayana, and T. M. Benson, "Efficient broadband simulations for thin optical structures," *Optical and Quantum Electronics*, Vol. 45, No. 4, 343–348, Oct. 2012.
2. Jacobs, E. N., K. E. Ward, and R. M. Pinkerton, "The characteristics of 78 related airfoil sections from tests in the variable-density wind tunnel," *NACA Report*, No. 460, 1933.

RCS Computation of 3D-wake Vortex Using Method of Moments

Venkat Prasad Padhy[1], **N. Balakrishnan**[1], **and P. Srinivasa Murthy**[2]

[1]SERC, Indian Institute of Science, Bangalore 560012, India
[2]Aeronautical Development Establishment (ADE), Bangalore 60075, India

Abstract— An efficient and accurate 3D full wave numerical solution model for computing the radar cross section (RCS) of wake-vortex is presented, by solving Euler equation to compute the pressure in the aircraft wake region by computational fluid dynamics model and parallel integral equation (IE), based on method of moments (MoM) is used to compute the volume polarization currents, under the plane wave incidence. Then the currents are used to compute far-field from the vortex region.

The scattering of radio waves in the atmosphere has drawn attention of many researchers in recent times, particularly in the areas of radio acoustic sounding system (RASS) and wake-vortex studies. In clear air, the radar reflectivity of wake vortex is mainly caused by Bragg scattering from the refractive index variations. Since wake turbulence is inevitable to all flying aircrafts, remote detection and tracking of wake vortices is important for hazard avoidance especially near airports during landing and take-off phases. Aircrafts that fly through these hazardous vortices experience sudden induced roll. In order to avoid the wake vortex encountering hazard, efforts have been made in the past to monitor and detect wake vortices, and the existing technologies include lidar, sodar and radar. Among them, the radar detection is considered to be the potential candidate for its long working range and under different weather conditions.

In the past studies, aircraft wake is evolved by known vortex model derived from experiment based on aircraft geometry and inertial properties. Also vortex wake is based on wing alone model; body and tail vortex effect are not considered and these models are confined to 2D cross sections in the wake region. And the RCS is computed using Born approximation with highly oscillatory integrand, with the aid of quadrature methods. The validity and applicability of Born approximation is well studied in the low frequency regime, and more recently even at high frequency regime.

However, there is still a need to improve the accuracy and efficiency of wake vortex problem, which demands for a rigorous full wave solution method such as method of moment's. In the present work aircraft wake is computed by solving 3D Euler equations using CFD method. Complete aircraft flow field is computed including vortex generated by all the components such as body, wing and tail units. CFD based wake flow computation is more accurate than the vortex model based computation. Typical aircraft used for the wake computation is the geometry which was used for the AIAA drag prediction workshop. Moreover, IE solution is more accurate for scattering and radiation problems, with Sommerfeld radiation condition implicitly defined. By applying suitable basis and testing functions the IE can be cast as system of linear equations, then solved to obtain the unknown currents, from the currents the back-scattered far-field can be readily obtained,. In essence, this proposed method can be used to model RCS enhancement, in vicinity of the inhomogeneities caused by the flow field.

Session 2P11b
SC2,3&4: Electronics and Optoelectronics Using Two-dimensional Materials and Their Heterostructures

Photonics of Two-dimensional Materials Beyond Graphene

Qiaoliang Bao[1, 2], **Yunzhou Xue**[1], **Shenghuang Lin**[1], **and Shaojuan Li**[1]

[1]Department of Materials Engineering, Melbourne Centre for Nanofabrication
Monash University, Clayton, Victoria 3800, Australia
[2]FUNSOM, Collaborative Innovation Center of Suzhou Nano Science and Technology
Soochow University, Suzhou 215123, China

Abstract— The success in graphene with fascinating and technologically useful properties [1] has stimulated the study of two-dimensional (2D) atomic-layer materials other than graphene, such as single layers of transition metal dichalcogenides (TMDCs, e.g., MoS_2, WS_2, WSe_2, etc.) [2] and a few quintuple layers of topological insulators (TIs, e.g., Bi_2Se_3, Bi_2Te_3, Sb_2Te_3 etc.) [3]. The rapid pace of progress in graphene, TMDCs and TIs and some demonstrated applications have led to the exploration of new type of electric and optoelectronic devices constructed by vertically stacking different layered materials [4, 5].

Here we would like to review our recent progresses on the photonic applications of 2D layered materials other than graphene. A few photonics devices based on these 2D materials or their heterostructures have been successfully fabricated, including pulse laser, photodetector, solar cell, modulator and ring filter. Firstly, we use graphene as template to grow graphene/topological insulator heterostructure and investigate the linear and nonlinear optical properties. Strong saturable absorption was observed and the material was further applied for mode-locked laser to generate ultrafast laser pulse. Secondly, we directly grow large area TMDCs on graphene to form van deer waals heterojuctions for efficient charge transfer and carrier separation at the interface [4], which is the basis for fabrication of new type of flexible thin film photodetectors and solar cell devices. Last, based on the good CMOS-compatibility of 2D materials [5], we fabricate chip-integrated modulator and resonator devices and incorporate graphene/TMDCs heterostructure for the signal modulation and processing. The advances of photonics of these new 2D materials may pave the way for the integration of next generation hybrid silicon photonic circuits.

REFERENCES

1. Bao, Q. L. and K. P. Loh, *ACS Nano*, Vol. 6, 3677–3694, 2012.
2. Chhowalla, M., et al., *Nat. Chem.*, Vol. 5, 263–275, 2013.
3. Zhang, H., et al., *Nature Physics*, Vol. 5, 438–442, 2009.
4. Britnell, L., et al., *Science*, Vol. 340, 1311–1314, 2013.
5. Yu, W. J., et al., *Nat. Nanotech.*, Vol. 8, 952–958, 2013.
6. Pospischil, A., et al., *Nat. Photon.*, Vol. 7, 892–896, 2013.

Two-dimensional Semiconductors for Versatile Photonic Applications

Jun Wang
Key Laboratory of Materials for High-Power Laser
Shanghai Institute of Optics and Fine Mechanics, Chinese Academy of Sciences, Shanghai, China

Abstract— Owing to the specific two-dimensional (2D) confinement of electron motion and the absence of interlayer perturbation, 2D semiconductors possess unique optoelectronic properties and has become a research hot-spot in recent years. Whereas the electronic and luminescent properties of 2D transition metal dichalcogenide (TMDC) nanosheets, say, MoS2, MoSe2, WS2, etc., have been generating much research interest, the ultrafast nonlinear optical (NLO) properties remain largely unexplored. Realized that the sizable and thickness-dependent bandgap offers TMDCs a huge potential in the development of photonic devices with high performance and unique functions, we studied extensively the ultrafast NLO property of a range of TMDC nanosheets. 2D TMDC nanosheets with high-quality layered nanosheets were prepared using liquid-phase exfoliation and CVD techniques. Ultrafast saturable absorption, two-photon absorption, ultrafast nonlinear photoluminescence were observed from the 2D nanostructures. The exciting results open up the door to 2D photonic nano-devices, such as optical switches, pulse shaping devices, mode-lockers, optical limiters, etc., capable of ultrafast response and broadband tunability.

REFERENCES

1. Wang, G., S. Zhang, F. A. Umran, X. Cheng, N. Dong, D. Coghlan, Y. Cheng, L. Zhang, W. J. Blau, and J. Wang, "Tunable effective nonlinear refractive index of graphene dispersions during the distortion of spatial self-phase modulation," *Applied Physics Letters*, Vol. 104, No. 14, 141909, 2014.
2. Wang, K., Y. Ju, J. He, L. Zhang, Y. Chen, W. J. Blau, and J. Wang, "Nonlinear optical propagation in a tandem structure comprising nonlinear absorption and scattering materials," *Applied Physics Letters*, Vol. 104, 021110, 2014.
3. Wang, K., J. Wang, J. Fan, M. Lotya, A. O'Neill, D. Fox, Y. Feng, X. Zhang, B. Jiang, Q. Zhao, H. Zhang, J. N. Coleman, L. Zhang, and W. J. Blau, "Ultrafast saturable absorption of two-dimensional MoS2 nanosheets," *ACS Nano*, Vol. 7 , No. 10, 9260–9267, 2013.
4. Cheng, X., N. Dong, B. Li, X. Zhang, S. Zhang, J. Jiao, W. J. Blau, L. Zhang, and J. Wang, "Controllable broadband nonlinear optical response of graphene dispersions by tuning vacuum pressure," *Optics Express*, Vol. 21, No. 14, 16486–16493, 2013.

Modulating the Optical and Optoelectronic Properties of MoS_2

Haiyan Nan[1], **Zheng Liang**[2], **and Zhenhua Ni**[1]

[1]Southeast University, China
[2]Graphene Research and Characterization Center, Taizhou Sunano New Energy Co., Ltd., China

Abstract— There is a great need for controlling the properties of two dimensional (2D) materials to fulfill the requirements of various applications. Among the mostly investigated 2D layered materials, single and multilayer molybdenum disulphide (MoS_2) are semiconductors with bandgap of $\sim$ 1.2–1.8 eV, which make them promising candidates for optoelectronic applications. Here, we present our results on the modulation of the optical and optoelectronic properties of MoS_2 by plasma thinning and defect engineering.

Firstly, a simple, efficient, and nondestructive way to layer-by-layer control the thickness of MoS_2 by Ar^+ plasma will be discussed. AFM, high resolution TEM, Raman, and photoluminescence (PL) spectra suggest that the top layer MoS_2 is totally removed by plasma while the bottom layer is almost unaffected. We also demonstrate that this method can be used to prepare two dimensional heterostructures with periodical single and bilayer MoS_2, by utilizing standard lithographic techniques. Secondly, structural defects have been observed both in pristine/as-grown MoS_2 and electron beam/plasma irradiated samples. The proper utilization of these defects to improve the optical properties of MoS_2 is highly desirable. We report a strong PL enhancement of monolayer MoS_2 through defect engineering and oxygen bonding. High resolution micro- PL and Raman images clearly reveal that the PL enhancement occurs at defects of MoS_2. The PL enhancement at defect sites can be as high as thousands of times after considering the laser spot size. Finally, we will also present results on the optoelectronic properties of MoS_2 after defect engineering. The above results provide new routes for modulating the optical and optoelectronic properties of 2D semiconductors.

Chip-integrated Graphene Optoelectronic Devices

Xuetao Gan[1], **Ren-Jye Shiue**[2], **and Dirk Englund**[2]

[1]School of Science, Northwestern Polytechnical University, Xi'an 710072, China
[2]Department of Electrical Engineering and Computer Science
Massachusetts Institute of Technology, Cambridge, MA 02139, USA

Abstract— Graphene has attracted great interesting in the development of optoelectronic devices due to its broadband optical response, ultrahigh carrier mobility, and potentially CMOS-compatible. Here, we present our recent work on graphene modulators and photodetectors integrated on silicon photonic crystal cavities and channel waveguides.

By electrically gating a graphene monolayer coupled with a planar photonic crystal cavity, electro-optic modulation of the cavity reflection was possible with a contrast in excess of 10 dB and a switching energy of 300 fJ, as shown in Fig. 1(a) [1]. Moreover, a novel modulator device based on the cavity-coupled graphene-boron nitride-graphene capacitor was fabricated, showing a modulation speed up to 1.2 GHz [2]. A cavity-coupled graphene photodetector was also demonstrated with an enhancement of the photocurrent by a factor of 26 at resonant wavelengths [3].

A waveguide-integrated graphene photodetector that simultaneously exhibits high responsivity, high speed and broad spectral bandwidth has also been reported, as shown in Fig. 1(b) [4]. Using a metal-doped graphene junction coupled evanescently to the waveguide, the detector achieves a photoresponsivity exceeding 0.1 A/W together with a nearly uniform response between 1,450 and 1,590 nm. Under zero-bias operation, a response rate exceeding 20 GHz and an instrumentation-limited 12 Gbit/s optical data link. The demonstrated graphene active devices indicate a new generation of compact, energy-efficient, and ultrafast optoelectronics for on-chip optical communications.

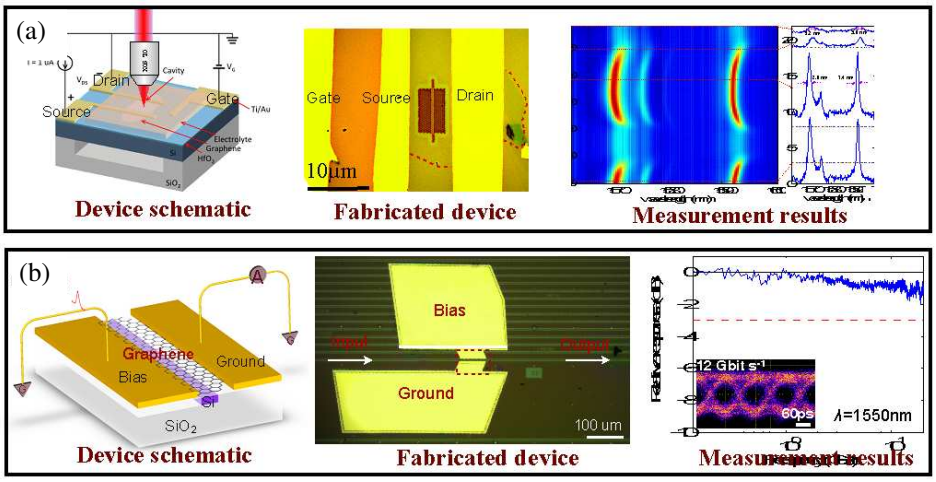

Figure 1: (a) Graphene modulator integrated on photonic crystal cavity; (b) Graphene photodetector integrated on silicon waveguide.

REFERENCES

1. Gan, X., R. Shiue, Y. Gao, K. F. Mak, X. Yao, L. Li, A. Szep, D. Walker, J. Hone, T. F. Heinz, and D. Englund, *Nano Lett.*, Vol. 13, 691, 2013.
2. Gan, X., R. Shiue, Y. Gao, S. Assefa, J. Hone, and D. Englund, *IEEE J. Sele. Top. Quant. Electron.*, Vol. 20, 6000311, 2014.
3. Shiue, R., X. Gan, Y. Gao, L. Li, X. Yao, A. Szep, D. Walker, J. Hone, and D. Englund, *Appl. Phys. Lett.*, Vol. 103, 241109, 2013.
4. Gan, X., R. Shiue, Y. Gao, I. Meric, T. F. Heinz, K. Shepard, J. Hone, S. Assefa, and D. Englund, *Nature Photon.*, Vol. 7, 883, 2013.

Graphene, Topological Insulator and Other 2-dimensional Layered Materials for Ultra-fast Laser Photonics

Han Zhang
Shenzhen University, China

Abstract— We experimentally found that beyond graphene, other two-dimensional layered materials such as topological insulators, MoS2 etc. also possess wideband nonlinear optics response, indicating great potentials in ultrafast laser photonics. By using the saturable absorption property of those 2-D materials, different types of optical saturable absorber devices have been developed for the passive mode locking or passive Q-switching of lasers. In this talk, we will discuss on the nonlinear optics studies of some of typical 2D nanomaterials. Based on the femtosecond z-scan measurement, we then uncovered that, like graphene [1], topological insulators also have both the saturable absorption and nonlinear optical Kerr effects [2]. The saturable absorption of the topological isolators could be used for the passive mode locking of lasers: from an erbium-doped fiber laser at the telecommunication band [3], passive Q-switch an in-band pumped 1645 nm Er:YAG ceramic laser [4], and to an Nd: YAG solid-state laser at 1064 nm with topological insulator [5]. Our recent experiment shows that few-layer MoS2-based mode locker allows for the generation of stable mode-locked laser pulse, centered at 1054.3 nm, with a 3-dB spectral bandwidth of 2.7 nm and a pulse duration of 800 ps. Our finding suggests that few-layered MoS2 nanoplatelets can be useful nonlinear optical material for laser photonics devices, such as passive laser mode locker, Q-switcher, optical limiter, optical switcher and so on [6]. It is expected that the research of two-dimensional nano-materials photonics is rising with more and more ultra-fast photonics and/or optoelectronic devices applications.

REFERENCES

1. Zhang, H., S. Virally, Q. L. Bao, K. P. Loh, S. Massar, N. Godbout, and P. Kockaert, "Z-scan measurement of the nonlinear refractive index of graphene," *Opt. Lett.*, Vol. 37, 1856–1858, 2012.
2. Lu, S. B., C. J. Zhao, Y. H. Zou, S. Q. Chen, Y. Chen, Y. Li, H. Zhang, S. C. Wen, and D. Y. Tang, "Third order nonlinear optical property of Bi2Se3," *Opt. Exp.*, Vol. 21, 2072–2082, 2013.
3. Zhao, C. J., H. Zhang, X. Qi, Y. Chen, Z. T. Wang, S. C. Wen, and D. Y. Tang, "Ultrashort pulse generation by a topological insulator based saturable absorber," *Appl. Phys. Lett.*, Vol. 101, 211106, 2012.
4. Tang, P. H., X. Q. Zhang, C. J. Zhao, Y. Wang, H. Zhang, D. Y. Shen, S. C. Wen, D. Y. Tang, and D. Y. Fan, "Topological insulator: Bi2Te3 saturable absorber for the passive Q-switching operation of an in-band pumped 1645 nm Er:YAG ceramic laser," *IEEE Photon. J.*, 10.1109/JPHOT.2013.2250494, 2013.
5. Yu, H. H., H. Zhang, Y. C. Wang, C. J. Zhao, B. L. Wang, S. C. Wen, H. J. Zhang, and J. Y. Wang, "Topological insulator as an optical modulator for pulsed solid-state lasers," *Laser & Photonics Reviews*, DOI: 10.1002/lpor.201300084, 2013.
6. Zhang, H., S. B. Lu, J. Zheng, J. Du, S. C. Wen, D. Y. Tang, and K. P. Loh, "Molybdenum disulfide (MoS2) as a broadband saturable absorber for ultra-fast photonics," *Opt. Express*, Vol. 22, 7249–7260, 2014.

Coupling Light with Supramolecular Systems

Jialiang Xu, **Sergey Semin**, **Alan E. Rowan**, **and Theo Rasing**

Institute for Molecules and Materials, Radboud University Nijmegen
Heyendaalsweg 135, Nijmegen 6525 AJ, The Netherlands

Abstract— Subwavelength scale architectures are of critical importance as building blocks for light generation, propagation, amplification, and modulation. Since the advent of the laser and the subsequent discovery of nonlinear optics (NLO), there has been an untiring search for novel NLO materials with wide applications ranging from light frequency conversion, optical telecommunication, information processing, to the data storage. Currently most photonic components are based on inorganic nonlinear optical materials, though organic materials intrinsically have higher hyper polarizabilities, come with diverse architectures, and show very fast NLO responses. The challenge for organic NLO materials lies in the use of weak noncovalent interactions between the organic molecules to construct suitable and stable organizations for generating NLO effects, in particular second-order ones for which non-centrosymmetric arrangements are essential. We intend to pursue supramolecular approaches, which can be be summarized by the combination of complementary nonconvalent interactions with a "$1 + 1 > 2$" amplification, to constructing organic based low dimensional photonic materials towards the subwavelength scale architectures.

Two types of supramolecular systems are developed for multifunctional nonlinear optics, namely hydrogen-bonded molecular chains [1] and helical supramolecular scaffolds [2]. Multi-chromophores are arranged into suitable organizations in both systems, with the assistance of subtle supramolecular interactions, for generation of both second- and third-order NLO (Fugure 1). More importantly, the supramolecular systems are fabricated into subwavelength scale low dimensional superstructures by facile solution processed self-assembly or electro-spinning techniques. The resulted microfibers are ideal platforms for combined NLO, waveguiding, and lasing cavity. Detailed polarization dependence analysis also demonstrates that the well-oriented dipole moments in both ground and excited states are vital for the generation and tunability of the combined NLO.

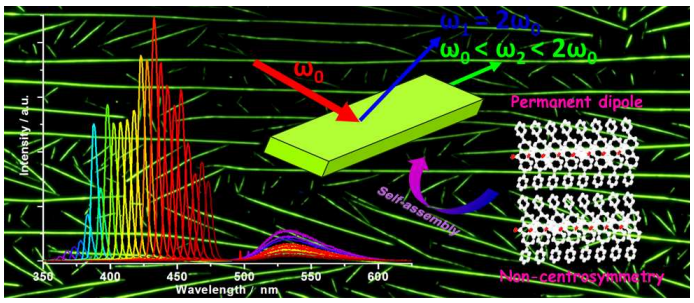

Figure 1: Schematic representation of the hydrogen-bonded molecular chains towards microsized architectures with tunable second- and third-order NLO.

REFERENCES

1. Xu, J., S. Semin, D. Niedzialek, P. H. J. Kouwer, E. Fron, E. Coutino, M. Savoini, Y. Li, J. Hofkens, H. Uji-I, D. Beljonne, T. Rasing, and A. E. Rowan, *Adv. Mater.*, Vol. 25, 2084, 2013.
2. Schwartz, E., M. Koepf, H. J. Kitto, R. J. M. Nolte, and A. E. Rowan, *Polym. Chem.*, Vol. 2, 33, 2011.

Phase Noise Performance in the Mode-locked Fiber Lasers with Carbon Nanotubes and Graphene Oxide Thin Films as Mode Locker

Kan Wu[1], **Xiaohui Li**[2], **and Jianping Chen**[1]

[1]State Key Laboratory of Advanced Optical Communication Systems and Networks
Department of Electronic Engineering, Shanghai Jiao Tong University, Shanghai 200240, China
[2]OPTIMUS, Centre of Excellence for Photonics
School of Electrical and Electronic Engineering, Nanyang Technological University
50 Nanyang Ave., 639798, Singapore

Abstract— Various nano-materials have been demonstrated to be suitable for saturable absorbers (SAs) in the mode-locked lasers. In this paper, we investigate the potential of low-phase-noise operation when two carbon nano-materials, single-wall carbon nanotubes (CNT) and graphene oxide (GO), are incorporated in the mode-locked fiber lasers as mode lockers. These carbon nano-materials are compounded in the polyvinyl alcohol (PVA) films as thin film SAs. With this design, CNT-PVA and GO-PVA thin films can be easily incorporated in an Er-doped fiber laser cavity for mode locking operation and ultrafast pulse generation. The saturable intensity, modulation depth, non-saturable loss and purity of the thin film SAs are all found to be important for low-phase-noise operation of the mode-locked lasers.Thin film design allows to modify the saturable intensity and modulation depth by choosing different number of thin film layers. Since each single thin film is $\sim$ 30–50 µm thick, stacking a few layers will not introduce additional coupling loss between the fiber connectors. By optimizing the number of thin film layers, both CNT-PVA and GO-PVA SAs can allow low-phase-noise mode locking operation without any relexation oscillation peak in the electrical spectrum after photodetection (Fig. 1 and Fig. 2). Especially, the laser mode locked by CNT-PVA obtain a phase noise value 10 dB lower at 10 kHz

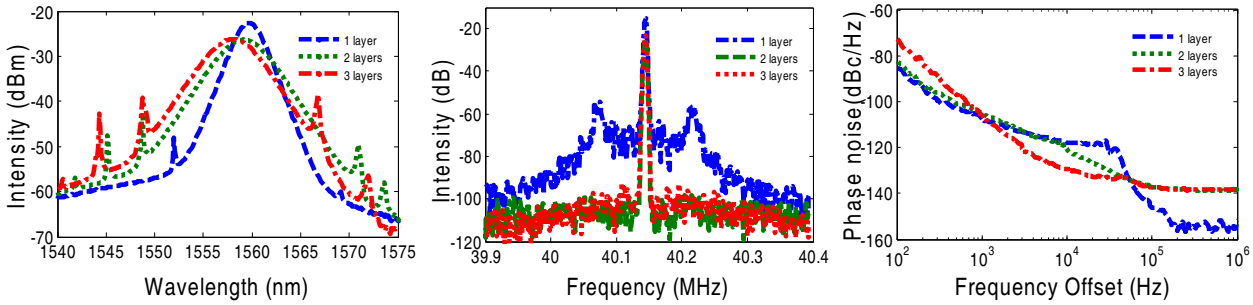

(a) (b) (c)

Figure 1: (a) Optical spectra, (b) electrical spectra and (c) phase noise spectra of different number of layers of CNT-PVA SAs.

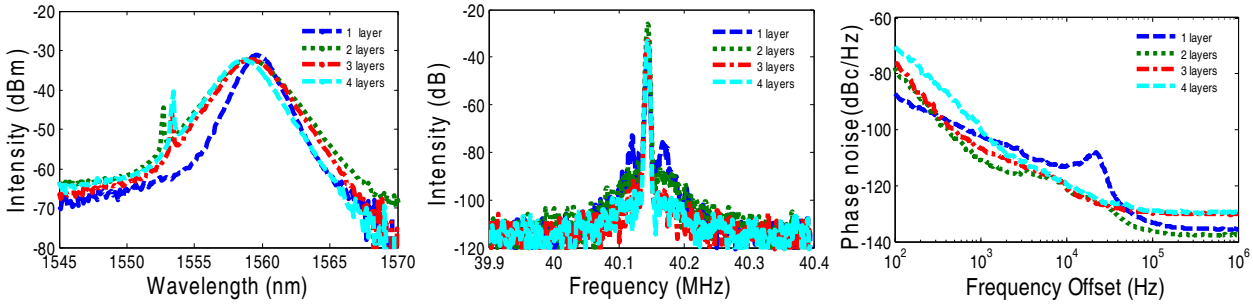

(a) (b) (c)

Figure 2: (a) Optical spectra, (b) electrical spectra and (c) phase noise spectra of different number of layers of GO-PVA SAs.

offset frequency than the laser by GO-PVA. Moreover, the slow saturable absorption effect is also discussed by comparing the noise performance in the lasers mode locked by SESAM, CNT-PVA and GO-PVA, respectively. Our work will pave the way to obtain a high-quality mode-locked fiber lasers with various nano-materials.

Passively Q-switched Linear-cavity Erbium-doped Fiber Laser with MoS_2 Saturable Absorber

Yizhong Huang and Zhengqian Luo
Department of Electronic Engineering, Xiamen University, Xiamen 361005, China

Abstract— Since graphene was discovered and was employed as saturable absorber (SA) to achieve pulsed lasers successfully, 2D materials have attracted growing attention for enormous potential in photonic applications especially for pulsed lasers. Besides graphene and topological insulators (TIs), few-layered transition-metal dichalcogenides (TMDs) was demonstrated exhibiting strong light absorption that was distinct from their bulk states. As a typical TMD, Molybdenum sulfide (MoS_2) nanosheets have hexagonal structure and display outstanding saturable absorption for ultrafast lasers. Moreover, MoS_2 bandgap can be reduced to 0.08 eV (15.4 μm) by the introduction of Mo or S atomic defects, indicating that MoS_2 could be used as Q-switcher or mode-locker in a broad waveband.

We propose and experimentally demonstrate a passively Q-switched linear-cavity erbium-doped fiber laser (EDFL) based on broadband few-layer MoS_2 saturable absorber. The 3–4 layers MoS_2 used in our experiment is firstly prepared by the liquid-phase exfoliation method, and then the filmy polyvinyl alcohol (PVA)-MoS_2 combined with the sandwich structure is adopted to fabricate the fiber compatible SA. The modulation depth and saturable intensity of PVA-MoS_2 are measured to be 1.8% and 7.5 MW/cm^2. Two fiber loop mirrors (FLMs) are used to form the linear resonant cavity. By further inserting the PVA-MoS_2 into the linear cavity, stable Q-switched laser operating at 1556.5 nm is achieved successfully. The obtained Q-switched fiber laser has the minimum pulse duration of 2.74 μs. As increasing the pump power, the repetition rate is tunable in the range of 22.6 $\sim$ 49.5 KHz. In addition, the output power of this Q-switched EDFL is also measured and the single pulse energy is correspondingly calculated. The results of our experiment clearly suggest that few-layer MoS_2 could be a candidate of high-performance SA.

2 μm Passively Q-switched Double-clad Fiber Laser Based on Few-layer MoS_2 Saturable Absorber

Zhengqian Luo, Jianyu Wu, and Yizhong Huang
Department of Electronic Engineering, Xiamen University, Xiamen 361005, China

Abstract— 2 μm passively Q-switched Tm-doped fiber lasers are of particular interest to a wide range of applications in medicine, defence, remote sensing, molecular spectroscopy, and mid-infrared generation, etc.. The key element for 2 μm passive Q-switching is saturable absorber (SA) which can operate at 2 μm wavelength. In past decades, there are always strong motivations to seek for the ideal SAs at 2 μm. In this paper, Molybdenum sulfide (MoS_2), a new type of 2D material, is exfoliated successfully and shows strong saturable absorption, like graphene and topological insulators (TIs). Moreover, the few-layer MoS_2 as a SA is further employed to Q-switched fiber laser at 2 μm wavelength for the first time.

The few-layer MoS_2 used in our experiment is prepared by the liquid-phase exfoliation technique, and the thickness of the MoS_2 nanosheets is characterized to be 3–4 layers. The as-prepared MoS_2 solution is dispersed in the polyvinyl alcohol (PVA) and the mixture is evaporated to form the PVA-MoS_2 film. By inserting the PVA-MoS_2 film between two fiber ferrules, the fiber-compatible MoS_2-SA device is constructed and has a low saturable intensity of 7.5 MW/cm^2 and a modulation depth of 1.8%. By further incorporating the MoS_2-SA device into a Tm^{3+}-doped double-clad fiber laser, passive Q-switching operation at 2010 nm is achieved successfully. As increasing the pump power from 2.74 W to 3.04 W, the repetition rate of the Q-switched pulse can be tuned from 21.1 KHz to 30.3 KHz. The maximum output power is measured to be 3.62 mW, and the corresponding pulse energy is 142 nJ. The higher output power and the larger pulse energy could be obtained by: 1) further improving the modulation depth and decreasing the nonsaturable loss of the MoS_2 SA, 2) optimizing the resonant cavity structure. The results of our experiment clearly show that the PVA-MoS_2 SA is suitable for pulsed laser operation in eye-safe region of 2 μm, potentially exploited as an ultra-broadband and high-performance SA for large pulse-energy laser.

Session 2P12
SC4: Compact Microwave Filters

Synthesis of Dual-wideband Bandpass Filters with Transversal Structure

Runqi Zhang[1] **and Lei Zhu**[2]

[1]School of Electrical and Electronic Engineering, Nanyang Technological University, Singapore
[2]Faculty of Science and Technology, University of Macau, Macau SAR, China

Abstract— A class of dual-band bandpass filters (BPFs) have been exactly synthesized and practically designed by a transversal array structure. The LC equivalent circuits of the proposed filters include two major sub-circuits, the transversal structure and the -shaped inductor/capacitor coupling network. For the former part it introduces a doublet response in the passband, and the latter one exhibits different coupling effect between the source-load ports. When combining these LC sub-circuits, different filter circuits are obtained. The ideal filtering response is closely related to the targeted design specifications and their corresponding LC equivalent circuits. Once the filtering function is theoretically derived, these LC circuits are transferred into their respective microstrip circuits by the Richard's transformation. To analyze the schematics of these microstrip filters, the even-/odd-mode analysis method has been used. In the end,

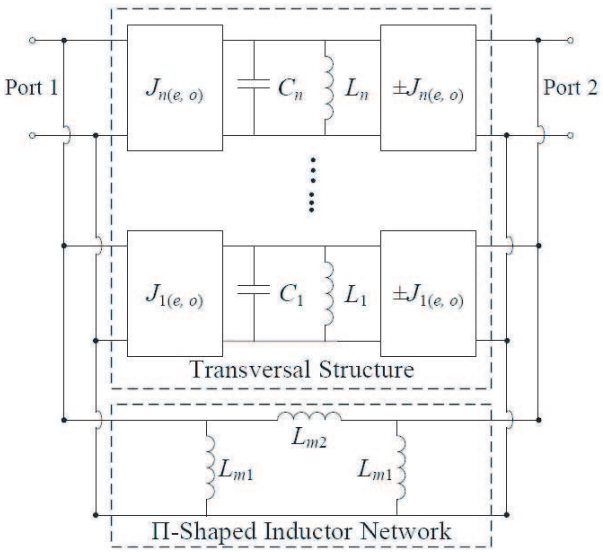

Figure 1: Equivalent circuit of an Nth-order dual-band filter with transversal structure and Π-shaped inductor network ($C_i = 1$ and $L_i = 1/\Omega_{ri}^2$, where Ω_{ri} is the resonant frequency of the ith resonant path).

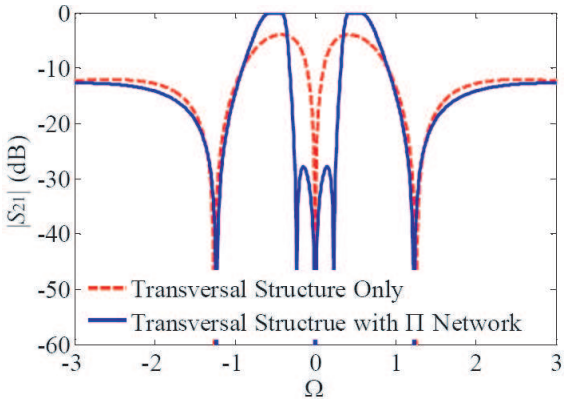

Figure 2: Comparison between frequency responses of the transversal structure with and without the Π-shaped inductor network (source-load coupling network) under other parameters of $C_{oe} = 1.00\,\mathrm{F}$, $L_{oe} = 1.00\,\mathrm{H}$, $C_{oo} = 1.00\,\mathrm{F}$, $L_{oo} = 2.00\,\mathrm{H}$, $J_{oe} = 0.11$, $J_{oo} = 0.15$, $L_{m1} = 80\,\mathrm{H}$ and $L_{m2} = 500\,\mathrm{H}$.

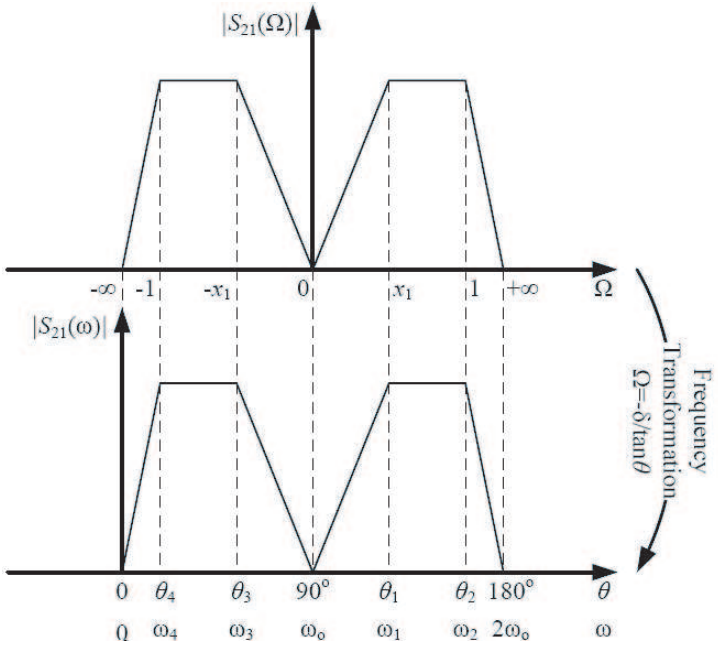

Figure 3: Frequency transformation of the filtering function from the Ω-plane to the θ-plane.

the transfer function of the microstrip filter is forced to be equal to the derived filtering function. Thus, the overall design parameters of the circuit can be directly obtained. That is, the proposed synthesis method is mainly divided into the following three parts. (a) A generalized Chebyshev filtering function is formulated to meet the design specifications. (b) The chosen circuit prototype is analyzed to derive its transfer function. (c) All the circuit parameters are accordingly determined by equating these two aforementioned functions. Some microstrip topologies have been successfully analyzed, designed and implemented with this synthesis method. They include the filter structures of parallel connecting two transmission lines, coupled stepped-impedance resonator to form source-load coupling and the coupled open- or short-circuited stubs with mixed coupling nature. With this technique, the second-, third- and higher-order dual-wideband BPFs with sharp rejection skirt and good band-to-band isolation near both sides of the two passbands have been obtained.

Dual-band Planar Microwave Bandpass Filter with $\lambda/4$ Stepped Impedance Resonators

Songbai Zhang[1] **and Lei Zhu**[2]

[1]School of Electrical and Electronic Engineering, Nanyang Technological University, Singapore
[2]Faculty of Science and Technology, University of Macau, Macau SAR, China

Abstract— A 4th-order microstrip-line dual-band bandpass filter based on quarter-wavelength ($\lambda/4$) stepped impedance resonators (SIR) is presented in this paper. This proposed dual-band filter has a few advanced features as compared to those reported ones, inclusive of compact size, large spacing or ratio and adjustable bandwidths of two operating passbands. To achieve maximum number of finite transmission zeros and enhanced near-band selectivity, this filter is synthesized and designed based on the 4th-order fully-canonical coupling topology. First, the normalized coupling matrix is synthesized with two pairs of finite transmission zeros: $\Omega = \pm j2.28$ and $\pm j10.0$. A compact dual-band bandpass filter with central frequencies of 1.8 and 5.8 GHz and respective fractional bandwidths of 11.0% and 6.0% is then constructed and designed using this efficient synthesis approach. For the constructed filter structure, four dual-band $\lambda/4$ SIRs are serially coupled by alternative J and K inverters in the mainline path. Meanwhile, the magnetic cross coupling $\mathbf{K_{14}}$ between resonators 1 and 4, and capacitive cross coupling $\mathbf{J_{SL}}$ between source and load ports, are introduced and analytically regulated to produce two pairs of finite transmission zeros at both sides of each passband.

In our design, the dual-band inverters $\mathbf{K_{12}}$ and $\mathbf{K_{34}}$ are realized with quasi-lumped metallic via holes, whose dispersive coupling strength increases monotonically with frequency. As a result, the physical dimensions for the $\lambda/4$ SIRs are analytically chosen not only to satisfy the prescribed dual-band central frequencies, but also to compensate different K inverter's values as desired at two central frequencies. Fig. 1 shows a set of design graphs to accomplish this design task. With the determined $\lambda/4$ SIRs, coupling structures for the distributed dual-band mainline $\mathbf{J_{23}}$ coupling and cross $\mathbf{K_{14}}$ coupling are further implemented in the forms of coupled-line structures to meet the prescribed dual-band bandwidths. As such, a $\lambda/4$ SIR dual-band filter is formed up and designed. Lastly, a U-folded coupled-line is proposed to realize the dual-band external and I/O cross couplings as desired by the prescribed dual-band filtering property. To verify its predicted performance, a microstrip dual-band bandpass filter is in final fabricated and measured to experimentally demonstrate the attractive fully canonical dual-passband filtering performance. Fig. 2 plots the three sets of results, which are derived from the coupling matrix approach, fullwave simulation and measurement. The simulated and measured results are in reasonable agreement

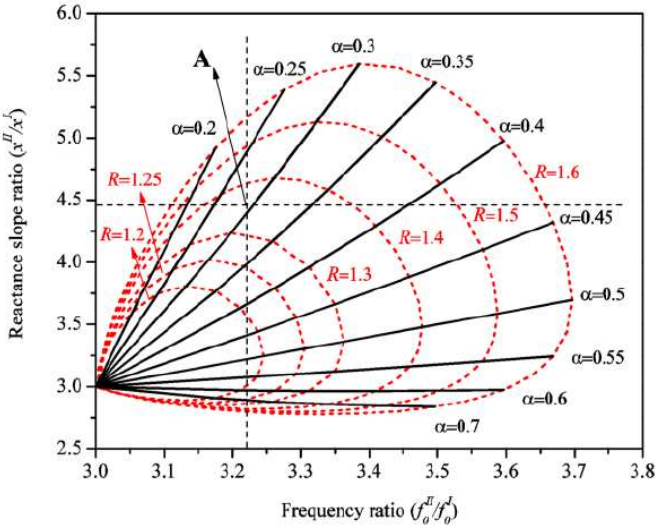

Figure 1: Dual-band reactance slope ratio versus the dual-band resonant frequency ratio of a $\lambda/4$ stepped impedance resonator.

with the synthesized. High insertion loss in the 2nd passband is attributed to the fact that the 2nd passband has a narrow fractional bandwidth against its 1st counterpart. Fig. 3 displays its broadband frequency response, illustrating good out-of-band rejection skirt and level.

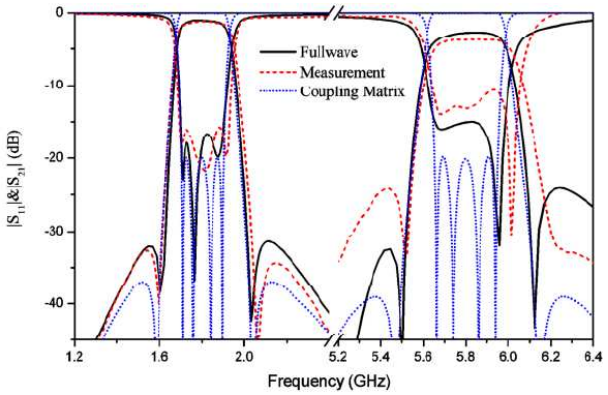

Figure 2: Comparison among in-band theoretical, fullwave simulated, and measured frequency responses.

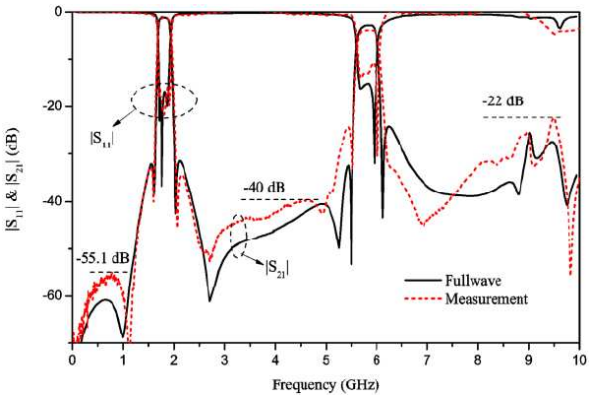

Figure 3: Comparison between broadband fullwave simulated and measured frequency responses.

A Compact Diplexer Composed of Quarter-wavelength Resonators for Ultra-wideband (UWB) System

Kai Wang[1], **Zai-Cheng Guo**[1], **Yu-Fa Zheng**[1], **Jing-Yu Lin**[2], **Sai Wai Wong**[1], **and Qing-Xin Chu**[1]

[1]School of Electronic and Information Engineering, South China University of Technology
Guangzhou, Guangdong 510641, China
[2]School of Information Science and Technology, Southwest Jiaotong University
Chengdu, Sichuan 611756, China

Abstract— A high performance compact diplexer is designed and implemented in this paper. The primary structure is shown in the figure above, this microstrip diplexer is mainly composed of two bandpass filters, which operates at 3.1–5 GHz (L-BPF) and 6.1–10 GHz (H-BPF), respectively. Each filter is composed of three shorted-circuit quarter-wavelength resonators (with respect to the center frequency of each filter at 4 GHz and 8 GHz, respectively). Port 1 is the input port and the microstrip feed line is coupling with two resonators. The coupling coefficient (K) of two resonators and the coupling strength of the input/output ports (Q) are extracted, then according to the theory of coupling mechanism, the bandwidth can easily be adjusted by varying the coupling coefficient (K) and the good passband can be easily achieved by controlling the quality factor (Q), which offers several design freedoms. In full-length paper, the design concept will be proposed in detail and the specific dimensions of the diplexer structure will be given.

The structure of the proposed diplexer is quite simple, but the performances are fairly good. After optimizing the performance using Agilent Technologies' 2013 Advanced Design System (ADS), the highest return loss of each filter in the desired passband is −14 dB and −18 dB, respectively. For both filters, the insertion loss is below 1 dB and the wide stopband rejection is greater than 20 dB. The isolation between two channels is more than 25 dB. The size is compact with overall dimension of $18.5 \times 18 \times 0.8\,\text{mm}^3$.

In the existing communication system, to avoid the frequency use of 5–6 GHz for IEEE 802.11a wireless networks (WLANs), the direct sequence ultra-wideband (DS-UWB) specifications for wireless personal area network (WPANs) need to be divided into a low band of 3.1–4.9 GHz and a high band of 6.2–9.7 GHz. The proposed diplexer satisfies the desired operation passbands.

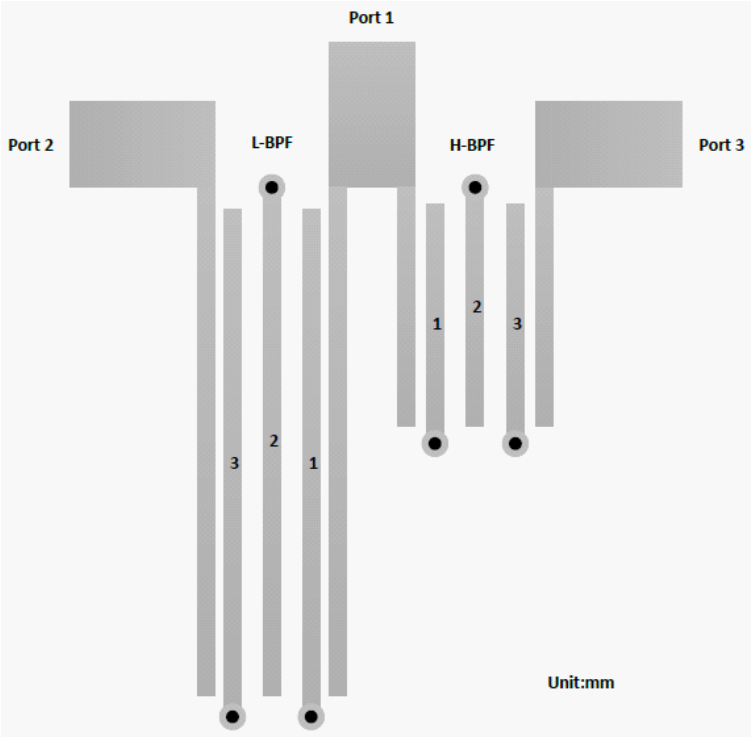

Figure 1: Layout of the designed diplexer.

Synthesis of Phasers for Real-time Signal Processing Using Filter Techniques

Qingfeng Zhang[1] and Christophe Caloz[2]

[1]Department of Electronics & Electrical Engineering
South University of Science and Technology of China, Shenzhen, Guangdong 518055, China
[2]Department of Electrical Engineering, École Polytechnique de Montréal
Montréal, Québec H3T1J4, Canada

Abstract— Radio analog signal processing (R-ASP), inspired by ultra-fast optics [1] and surface acoustics wave signal processing [2], has recently attracted increasing attention due to the exploding demand for more reliable, more ubiquitous and faster communication technology. Conventional digital signal processing (DSP) techniques suffer from high power consumption associated with signal sampling and limited frequency bandwidth due to A/D and D/A limitations. R-ASP technology is immune of these issues and thereby promising for applications in instrumentation, radar, sensors and communications. Some typical applications are reviewed in [3].

The core of a R-ASP system is a phaser, a component exhibiting an arbitrary group delay response versus frequency. A pulse passed through a phaser with linear group delay gets its spectrum mapped onto time, which is a phenomenon exploited in real-time Fourier transformation [4]. Phasers are different from filters in that phasers focus on group delay (or phase) to disperse signals whereas filters are mostly intended to alter the magnitude of signals.

Phasers may be synthesized using two distinct approaches: material (sub-wavelenth and periodic) and filter network (distributed and non-periodic, typically half-wavelength cells). This paper reviews some synthesis techniques for phasers, with a special emphasis on filter-network-based phasers including reflection-type [5], transmission-type allpass [6] and transmission-type bandpass ones [7]. Both closed-form synthesis techniques and optimization techniques [6, 8] are reviewed in this paper.

REFERENCES

1. Saleih, E. A. and M. C. Teich, *Funamentals of Photonics*, 2nd Edition, Wiley, 2007.
2. Lewis, M., "SAW and optical signal processing," *IEEE Proc. Ultrason. Symp.*, Vol. 24, 800–809, Sep. 2005.
3. Caloz, C., S. Gupta, Q. Zhang, and B. Nikfal, "Analog signal processing: A possible alternative or complement to dominantly digital radio schemes," *IEEE Microw. Mag.*, Vol. 14, No. 6, 87–103, Sep. 2013.
4. Laso, M. A. G., T. Lopetegi, M. J. Erro, D. Benito, M. J. Garde, M. A. Muriel, M. Sorolla, and M. Guglielmi, "Real-time spectrum analysis in microstrip technology," *IEEE Trans. Microw. Theory Tech.*, Vol. 51, No. 3, 705–717, Mar. 2003.
5. Zhang, Q., S. Gupta, and C. Caloz, "Synthesis of narrowband reflection-type phasers with arbitrary prescribed group delay," *IEEE Trans. Microw. Theory Tech.*, Vol. 60, No. 8, 2394–2402, 2012.
6. Gupta, S., A. Parsa, E. Perret, R. V. Snyder, R. J. Wenzel, and C. Caloz, "Group delay engineered non-commensurate transmission line all-pass network for analog signal processing," *IEEE Trans. Microw. Theory Tech.*, Vol. 58, No. 8, 2392–2407, Aug. 2010.
7. Zhang, Q., D. Sounas, and C. Caloz, "Synthesis of cross-coupled reduced-order dispersive delay structures (DDSs) with arbitrary group delay and controlled magnitude," *IEEE Trans. Microw. Theory Tech.*, Vol. 61, No. 3, 1043–1052, Mar. 2013.
8. Zhang, Q., J. W. Bandler, and C. Caloz, "Design of dispersive delay structures (DDSs) formed by coupled C-sections using predistortion with space mapping," *IEEE Trans. Microw. Theory Tech.*, Vol. 61, No. 12, 4040–4051, Dec. 2013.

Design of High Isolation Diplexer with Source-load Coupling

Fu-Chang Chen, Hao-Tao Hu, Fu-Xiang Guo, and Qing-Xin Chu
School of Electronic and Information Engineering, South China University of Technology
Guangzhou, Guangdong 510640, China

Abstract— Compact microstrip diplexer with high isolation is presented in this paper. The diplexer consists of two compact cascaded triplet (CT) filters with quarter-wavelength resonators coupled by the metallized via. The utilization of $\lambda/4$ resonators not only makes the filter compact, but also allows the inductive cross coupling to be realized conveniently. This results in a transmission zero of finite frequency on the high side of each passband. The source-load coupling is also proposed to introduce two tunable transmission zeros, which can improve the selectivity of each passband. A trial diplexer is designed and measured, and the measured results show that the isolation greater than 45 dB can be obtained.

A Bandpass Filter Using HMSIW-DGS Cell

Y.-M. Huang, **Z.-S. He**, **P.-K. Li**, **Z.-H. Shao**, **C.-J. You**, **and D. Jiang**
School of Communication and Information Engineering
University of Electronic Science and Technology of China, Chengdu 611731, China

Abstract— In this paper, a half mode substrate integrated waveguide-to-defected ground structure (HMSIW-DGS) cell, and its embedded form are proposed to miniaturize a bandpass filter. Both cells can purchase wideband frequency response and low insertion loss, as well as simple and easy fabrication. By cascading two of them according to design requirement, a X-band bandpass filter is designed and measured to meet compact size, low insertion loss, good return loss as well as second harmonic suppression.

Compact and Sharp-rejection Dual-band Bandstop Filter Based on Transversal Signal-interaction Concept

Lei-Lei Qiu and Qing-Xin Chu
School of Electronic and Information Engineering
South China University of Technology, Guangzhou 510640, China

Abstract— A compact dual-band bandstop filter with sharp-rejection using transversal signal-interaction concept, consisting of a transmission line path and a cascaded coupled line path, is proposed. Folded structure is adopted to build the coupled path and decrease the size, simultaneously. By tuning the coupling coefficient and length of the coupled path, the centre frequency and bandwidth can be controlled, respectively. Meanwhile, the odd-mode impedance can be utilized to allocate the transmission poles without influence on transmission zeros, which sharps the attenuation rate. Furthermore, the impedance of the transmission line path can be used to improve the return loss of the passband thus reduce the insertion loss in passband.

Since four parameters control the performance of the filter independently, the design is simple and flexible. Firstly, circuit models are analyzed to obtain transmission zeros. Then, the influence of the parameters on its performance and design steps are given. Finally, a compact and sharp-rejection dual-band bandstop filter centring at 2.4 GHz and 3.7 GHz with a size of $0.22\lambda_g * 0.15\lambda_g$ (the free space wavelength at the centre frequency of the first stopband) is designed and fabricated to verify the validity. Fig. 1 illustrates the simulated and measured results of the dual-band bandstop filter. When compared with several reported dual-band bandstop filters, the proposed filter shows a few advanced features, such as miniaturization, sharp skirt selectivity and low insertion loss in passband. The simulation and measurement results agree well, which also illustrates the possibility of the application of the proposed filter in WLAN/WiMAX communication systems.

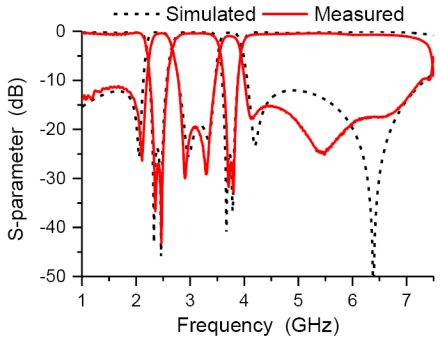

Figure 1: Simulated and measured results of the fabricated dual-band bandstop filter.

Wide-stopband Millimeter-wave Bandpass Filter Based on Discriminating Coupling on GaN MMIC

Jie Kai Lin[1], **Xiu Yin Zhang**[1], **Qing Yi Guo**[1], **and Hsuan-Ling Kao**[2]

[1]School of Electronic and Information Engineering
South China University of Technology, Guangzhou 510640, China
[2]Department of Electronic Engineering, Chang Gung University, Taoyuan, Taiwan

Abstract— This paper presents a third-harmonic suppressed bandpass filter on GaN MMIC (Monolithic Microwave Integrated Circuit). The filter consists of two symmetric quarter-wavelength resonators and they are folded to reduce the size. The feed lines are coupled with the resonators and the ports are tapped at the middle of the feed line. By analyzing the voltage distribution at fundamental frequency and third harmonic of the resonators, suitable coupling region between the feed line and resonator can be selected to make the coupling coefficient at third harmonic to be zero while the coupling coefficient at fundamental frequency can be tuned to the desired value. Therefore, the third harmonic can be suppressed by the discriminating coupling scheme while the fundamental mode responses are unaffected and it can be easily controlled. Meanwhile, to improve the selectivity, source-load coupling is employed to introduce transmission zeros near the passband.

For demonstration, a millimeter-wave filter with good performance is achieved. The filter is designed based on the technology of GaN MMIC with center frequency of 33.5 GHz and insertion loss of 3.2 dB. Two transmission zeros are realized near the passband, the left one is created by source-load coupling and the right one is caused by quarter wavelength of the feed line. Another transmission zero is generated at about 95 GHz, which is introduced by discriminating coupling. This transmission zero help enhance the rejection level within the upper stopband. Due to these transmission zeros, high selectivity and wide-stopband is realized. The circuit area of the filter is only 410 µm × 210 µm, featuring very compact size.

Hybrid Microstrip/Slotline Bandpass Filter with Dual-wideband Characteristics

Xuehui Guan[1], **Tao Xiong**[1], **Lei Zhu**[2], **and Haiwen Liu**[1]

[1]School of Information Engineering, East China Jiaotong University, Nanchang 330013, China
[2]Faculty of Science and Technology, University of Macau, Macau SAR, China

Abstract— A hybrid microstrip/slotline bandpass filter with dual-wideband characteristics is proposed in this paper. Firstly, a multimode stub-loaded slot-line resonator is designed. Two slotline stubs are symmetrically loaded to an open-loop slotline resonator. Secondly, the slotline resonator is fed by two microstrip feed lines and a wideband passband frequency response is realized. Thirdly, a notched band is introduced in the wide passband, thus forming up a dual-wideband bandpass filter. Physically, this notched band is achieved by loading a triangular ring resonator to the slotline resonator. A patch is then added to the top-side corner of the triangular ring resonator, resulting to excite two degenerate modes of the resonator. In this aspect, the bandwidth of this notched band can be controlled by the size of the patch. Finally, the filter is designed, simulated and fabricated. Experimental results demonstrate and verify the existence of two wide passbands with the fractional bandwidth of 54.7% and 34.2%, respectively. The schematic of the proposed filter and its simulated frequency response are depicted in Fig. 1 and Fig. 2.

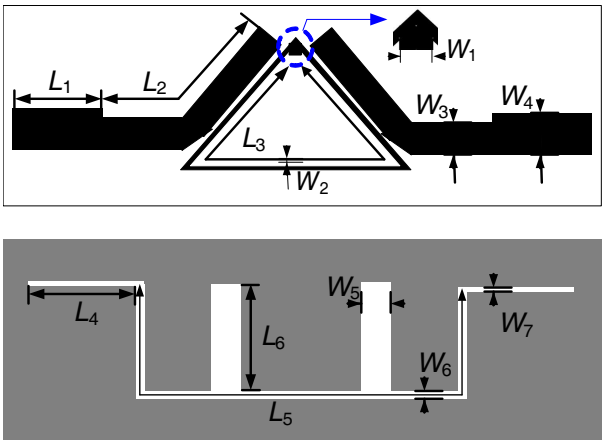

Figure 1: Schematic of the proposed filter.

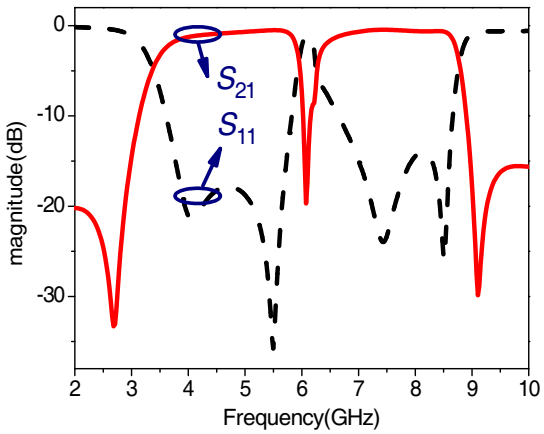

Figure 2: Simulated frequency response.

Reconfigurable WIFI Filter with Isolation Enhancement

Yuan Jiang, Jiawei Yu, Xian Qi Lin, Fei Cheng, and Yong Fan
EHF Key Laboratory of Science, School of Engineering
University of Electronic Science and Technology of China, Chengdu 611731 China

Abstract— Due to the requirements of multifunction and multiband reconfigurable, filters are more and more important in modern communication systems [1]. In his paper a reconfigurable WIFI filter with three modes: 2.4 GHz bandpass filter mode, 5.8 GHz bandpass filter and dual-band bandstop filter mode is proposed. Two half-wavelength resonators and switchable microstrip lines are used to realize the WIFI filter. A half-wavelength resonator coupled with the switchable microstip line is the core structure. When the switchable microsrip is blocking by the reverse biased PIN diode A, the structure is bandpass mode. On the contrary, the structure is bandstop mode. The resistor R and capacitor C of resonator A is used to suppress the second harmonic of 2.4 GHz which is close to 5.8 GHz [2]. This proposed reconfigurable filter technology is also promising in other modern communication system.

In order to test the performance of the reconfigurable WIFI filter, substrate F4B with thickness of 0.8 mm and dielectric constant of 2.65 was used in the EM simulation with Ansys HFSS. Capacitor C0 is a DC blocking capacitor. When PIN A is biased forward direction and PIN B is biased reverse direction, the WIFI filter is working at 5.8 GHz, and isolation of 2.4 GHz is more than 40 dB. On the other hand, when PIN A is biased reverse direction and PIN B is biased forward direction, the WIFI filter is working at 2.4 GHz, and isolation of 5.8 GHz is more than 40 dB. What's more, if both PIN A and B are biased forward direction, the WIFI filter is a dual-band bandstop filter at 2.4 GHz and 5.8 GHz.

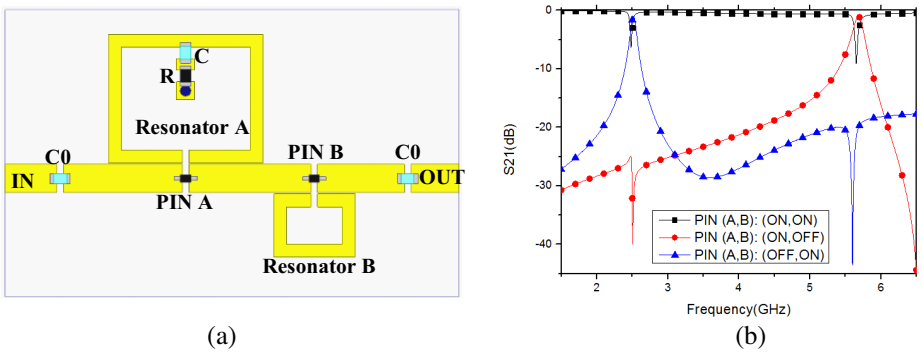

(a) (b)

Figure 1: (a) Layout of the WIFI filter. (b) Reconfigurable status of the WIFI filter.

REFERENCES

1. Chiou, Y.-C. and G. M. Rebeiz, "Tunable 1.55 GHz 4-pole elliptic bandpass filter with bandwidth control and 50 dB rejection for wireless systems," *IEEE Transactions on Microwave Theory and Techniques*, Vol. 61, 117–124, 2013.
2. Zhang, X. Y. and Q. Xue, "Novel centrally loaded resonators and their applications to bandpass filters," *IEEE Transactions on Microwave Theory and Techniques*, Vol. 56, 913–921, 2008.

Reconfigurable Substrate Integrated Waveguide

Yue Feng Hou, Yuan Jiang, Xian Qi Lin, Fei Cheng, and Yong Fan
EHF Key Laboratory of Science, School of Engineering
University of Electronic Science and Technology of China, Chengdu 611731, China

Abstract— Substrate integrated waveguide (SIW), due to its low profile, high Q-factor, low insertion loss and can be easily integrated with other planar circuits, has been widely used in microwave and millimeter wave system and circuit. Electrically tunable technologies, which are required in many wireless communication and radar systems, have been combined with SIW structures in several microwave components, such as phase shifters [1] and filters [2]. In this paper, a new substrate integrated waveguide structure with electrically tunable technology is been proposed, and we call it reconfigurable substrate integrated waveguide (RCSIW). It is realized by replacing the side-wall metal posts of SIW with several grounded varactors. The cutoff frequency of RCSIW can be tuned by changing the capacitance of the varactors, and the varators are placed in the two sides of the RCSIW with very low level electric field, which means the displacement current flowing through series resistance of the varactors is rather small leading a quite safe situation of the varacors. RCSIW with these features is promising in microwave applications.

In order to test the performance of RCSIW, substrate F4B was used in the EM simulation with Ansys HFSS. By changing the capacitance (C) of the varactors, we can conveniently tune the cutoff frequency of RCSIW. Figure 1(a) illustrates structure and electric field of RCSIW. It shows TE_{10} mode is excited in RCSIW, and the electric field is very small near the position of the varactors. Figure 1(b) shows the cutoff frequency varies with the capacitance of varactors.

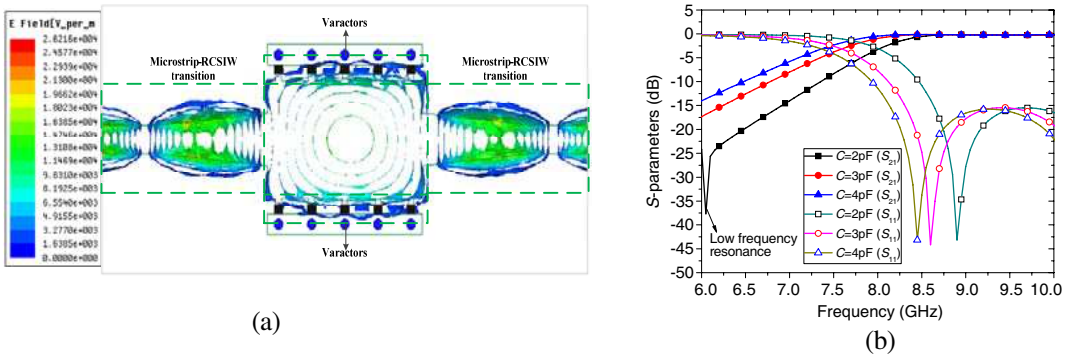

Figure 1: (a) Structure and electric field of RCSIW. (b) Cutoff frequency varies with the capacitance of varactors.

REFERENCES

1. Wu, L.-S., X.-L. Zhou, W.-Y. Yin, C.-T. Liu, L. Zhou, J.-F. Mao, and H.-L. Peng, "A new type of periodically loaded half-mode substrate integrated waveguide and its applications," *IEEE Trans. on Microw. Theory Tech*, Vol. 58, 882–893, 2010.
2. Yan, D. and W. Ke, "Varactor-tuned substrate integrated waveguide phase shifter," *IEEE MTT-S International in Microw. Symp. Digest (MTT)*, 1–4, 2011.

A Compact Substrate Integrated Waveguide Diplexer Using Dual-mode Filters

F. Cheng, X. Q. Lin, Y. Jiang, K. J. Song, and Y. Fan
EHF Key Lab of Fundamental Science, School of Electronic Engineering
University of Electronic Science and Technology of China, Chengdu 611731, China

Abstract— Microwave diplexers are widely used in communication systems to allow two different devices to share a common communications channel. For example, one application of diplexers is to allow two receivers working at different frequencies to share one antenna. Such a diplexer typically consists of two channel filters connected to the common input port through impedance transformers. However, the impedance transformers usually occupy a large area.

In order to solve the problem mentioned before, we have proposed an approach for designing compact integrated substrate waveguide (SIW) diplexer using dual-mode filters. SIW resonators have higher unloaded Q than microstrip resonators and can be easily fabricated using the Printed Circuit Board (PCB) technology. The dual-mode resonator is composed of a square SIW cavity with two perturbation vias in the diagonal line. The resonant frequencies of the two modes can be controlled by the position of the vias. It is very easy to achieve required bandwidth of the filter by moving the perturbation vias. By employing the dual-mode SIW resonator, lower insertion loss can be achieved. It is contributes to the fact that the unloaded Q of the dual-mode is higher than that of the fundamental mode. To reduce the size of the whole circuit, conventional T-junction for impedance matching and isolation at the input port is replaced by the coplanar-waveguide-fed structure. This feeding structure is shared by the both channel filters which are vertically stacked. A diplexer with lower and upper channels centered at 10 and 11 GHz, respectively, is designed to verify the proposed concept. Good agreements are achieved between measurement and simulation.

Ka-band Wideband Filter with a Reconfigurable Mode of Bandpass-bandstop Switching

Yuan Jiang, Jiawei Yu, Xian Qi Lin, Fei Cheng, and Yong Fan
EHF Key Laboratory of Science, School of Engineering
University of Electronic Science and Technology of China, Chengdu 611731, China

Abstract— Recently, reconfigurable filters are taking an increasing attention for their multi-functional and low-profile features in modern wireless and mobile communication systems [1]. In this paper, a bandstop-bandpass switchable Ka-band filter which is always narrow-band is proposed with a wideband performance (showed in Figure 1(a)). As a low-Q resonator [2], a rectangle ring with a straight "tail" is inserted into the central E-plane of a waveguide to realize the wideband performance. With the "ON" or "OFF" state of the PIN diode, the EM field driving by the resonator may be the same direction with or suppress the TE10 of the waveguide, which makes the filter be reconfigurable.

In order to test the performance of the reconfigurable Ka-band filter, Ka-band standard waveguide and substrate F4B with thickness of 0.8 mm and dielectric constant of 2.65 was used in the EM simulation with Ansys HFSS. Figure 1(b) shows reconfigurable modes of the Ka-band filter. When the PIN is bias forward direction, the filter is working with a bandpass feature, the insertion loss is less than 1 dB at frequency range of 33 GHz–37 GHz. And the filter is working as bandstop filter with an insertion loss of more than 15 dB, and at the center frequency of 35 GHz, it reaches a high insertion loss of 65 dB.

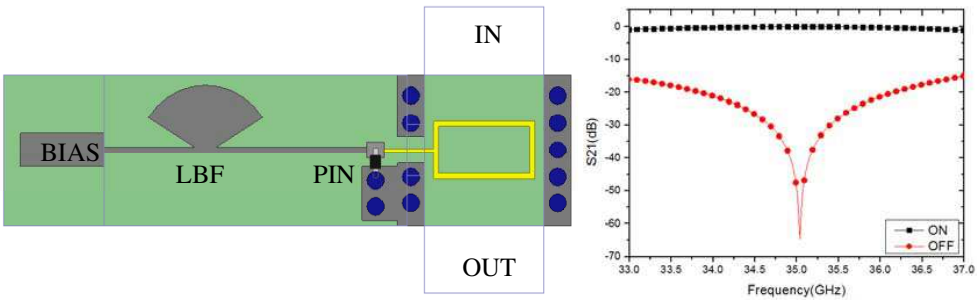

Figure 1: (a) Layout of the proposed Ka-band filter. (b) Reconfigurable modes of the Ka-band filter.

REFERENCES

1. Tsai, H. J., N. W. Chen, and S. K. Jeng, "Center frequency and bandwidth controllable microstrip bandpass filter design using loop-shaped dual-mode resonator," *IEEE Transactions on Microwave Theory and Techniques*, Vol. 61, 3590–3600, 2013.
2. Lin, X. Q., J. W. Yu, Y. Jiang, J. Y. Jin, and Y. Fan, "Electromagnetically induced transparencies in a closed waveguide with high efficiency and wide frequency band," *Applied Physics Letters*, Vol. 101, 093502–093502-3, 2012.

Microstrip Filters with Adjustable Transmission Zeros Using Inductive-coupled Open Stub-loaded Resonators

F. Cheng, X. Q. Lin, Y. Jiang, K. J. Song, and Y. Fan
EHF Key Lab of Fundamental Science, School of Electronic Engineering
University of Electronic Science and Technology of China, Chengdu 611731, China

Abstract— Microwave filters with transmission zeros are highly favorable due to their ability to suppress the unwanted frequencies and improve the selectivity. Many methods have been proposed to create transmission zeros in the previous literatures, such as cross-coupling, extracted pole and so on.

This paper presents two compact microstrip bandpass filters using inductive-coupled open stub-loaded resonator. The character of the open stub-loaded resonator is studied. By properly choosing the impedance ratio and length ratio of the resonator, the spurious frequency and frequency of transmission zero can be designed. One adjustable transmission zero above the pass band of the filters is got by the open stub, which greatly improves the stopband rejection of the filter. The merit of such resonator is that the frequency of the transmission zero is only related to the length of the open stub which is not sensitive to the coupling between resonators. The short-circuited stub is introduced to generate inductive-coupling between the resonators. This coupling strength between adjacent resonators can be easily controlled by length and width of the short stub. To demonstrate the validity of the proposed concept, two filters with center frequency at 2 GHz are designed. The first filter has a fractional bandwidth of 14% and a transmission zero at 2.26 GHz. In order to create more transmission zeros, cross-coupling between the source and load is introduced in the second filter design. Two transmission zeros are located at 1.6 GHz and 2.6 GHz. The simulated and measured results agree very well which has demonstrated the validation of our design.

Design of Wideband Non-equiripple Filtering Response Using Genetic Algorithm Based Neural Network

Shiqing Cui[1], **Sheng Sun**[1], **Shan Shan Gao**[2], **and Lei Zhu**[3]

[1]Department of EEE, The University of Hong Kong, Hong Kong, China
[2]Chengdu University, Chengdu, China
[3]Department of ECE, The University of Macau, Macau, China

Abstract— In this paper, the wideband multiple-mode-based bandpass filter with non-equiripple response is designed using genetic algorithm based neural network. The neural network is first employed to reduce the complexity in the design of wideband in-band equiripple response. Without deriving analytic solutions or solving non-linear equations, the coefficients of polynomials for the filters with non-equiripple responses can also be determined. Finally, the filters with both the five-pole equiripple and non-equiripple bandpass responses are designed and demonstrated. The accuracy of the proposed optimization method is also discussed in details.

Session 2P13a
FocusSession.SC4: Recent Progresses in Monolithic and Multilayer/Planar Integrated Circuits and Components

High Performance RF Front-End Devices/Circuits on VLSI-standard Si Substrate

Albert Chin
Department of Electronic Engineering, Chiao Tung University, Hsinchu 30010, Taiwan

Abstract— Power consumption is one of the most difficult challenges for mobile wireless system, where the power consumes significantly in RF Frond-End (FE) of the overall battery life. Here the RF FE is the interface between transceiver and antenna, which contains RF power amplifier (PA), envelope power tracker, DC supply modulator, transmit/receive (T/R) switch, antenna matching tuner, filters, and passive devices. Besides, the RF FE also needs to operate at multiple bands that complicate the System-on-Chip design. To reduce the size of Printed Circuit Board, it is highly desirable to integrate the RF FE circuitries using Si CMOS technology as much as possible. However, it is well known that the Si MOS Transistor has much poorer power performance than GaAs Hetero-junction Bipolar Transistor. Furthermore, the RF output power degrades monotonically with transistor down-scaling, although the scaled device can deliver a higher operation frequency for RF IC. Nevertheless, the power performance is crucial for both PA and RF T/R switch.

To address this issue, we invented the Asymmetric-LDD MOS Transistor. Using novel Asymmetric-LDD design, the 0.18 µm RF power MOSFET shows twice DC breakdown voltage of 6.9 V, much better 0.54 W/mm power density at 2.4 GHz, higher 115 GHz $f_{\max}$ than conventional MOS Transistor at the same size. The RF PA based on Asymmetric-LDD MOSFET and on-chip inductors has good performances of a power gain of 20.4 dB, an output 1-dB compression point ($P_{1\,\mathrm{dB}}$) of 21.5 dBm and a power-added-efficiency (PAE) of 29.6% at 2.4 GHz.

The T/R switch circuit, using Asymmetric-LDD MOS Transistors, exhibits $2.7 \sim 2.3$ dBm better $P_{1\,\mathrm{dB}}$ than those using conventional MOSFETs and good insertion loss of $0.6 \sim 1.2$ dB for T/R, at 2.4 and 5.8 GHz dual bands.

These novel CMOS power technologies have been successfully adopted by IC foundries.

HBT PA MMIC for WCDMA/LTE Applications

Bumman Kim, **Yunsung Cho**, **Jooseung Kim**, **and Kyunghoon Moon**
Pohang University of Science and Technology, Pohang, Korea

Abstract— Recent development of HBT power amplifier MMICs for WCDMA and LTE applications are introduced. The PA is based on the class AB biased F amplifier, which provides the power density and efficiency comparable to the class F PA, while maintains the linearity. All the linear PAs have a second harmonic short circuit to suppress the second harmonic up-conversion to the third harmonic distortion. The open circuited third harmonic can disturb the fifth harmonic but the distortion level is very low. Therefore, the class F circuit is suited for the linear PA with good power performance. A current PA can amplify a multimode/multiband (MMMB) signal with low-high power mode operation. Envelope tracking (ET) technique is a very popular for the PA since the ET PA can provide a high efficiency for amplification of a highly modulated signal with a high peak-to-average power ratio. Also the ET PA is well suited for the MMMB operation because the mode can be handled easily by the supply modulator and the band can be handled by the PA without any other restrictions. We will introduce the POSTECH approaches for these MMIC PA circuits. Further enhanced circuits including the analog PD optimized for ET operation and multilevel supply modulator optimized for a low power operation are also described. Doherty amplifier is another contender for the applications. However, the load modulation circuit in Doherty amplifier limits the operation band width. In this talk, we will introduce POSTECH approach for a broadband Doherty power amplifier design. The Doherty amplifier is further enhanced for a dual power mode operation and will be discussed.

4-way Power Divider Using Common DGS and Stacked-substrate Structure

Jongsik Lim[1], **Junhyung Jeong**[2], **Phirun Kim**[2], **Yongchae Jeong**[2], **Sang-Min Han**[1], **and Dal Ahn**[1]

[1]Soonchunhyang University, Republic of Korea
[2]Chonbuk National University, Republic of Korea

Abstract— A miniaturized 4-way Wilkinson power divider designed with common defected ground structure (DGS) and stacked-substrate structure is proposed. Fig. 1 shows that the stacked multi-layer structure is composed of 4 dielectriclayers, 3 pattern-layers for transmission lines, and 2 common ground planes in which the common DGS patterns are realized. The signal lines of transmission lines are connected by signal via-holes which penetrate the dielectric layers as depicted in Fig. 1. The beginning of design is to arrange the layout of the normal 4-way divider using stripline and microstrip lines as shown in Fig. 2. This can be simply folded for size-reduction. It is well known that periodic perturbation structures such as DGS and photonic bandgap patterns play a role of size-reduction due to their additional equivalent inductive- and capacitive-elements when they are adopted into transmission lines. In addition, a common DGS located in the common ground plane of double-sided transmission line structures has been proposed previously. So if common DGS patterns are combined to the folded divider, the final size may be quite smaller than that of normal 4-way divider (Fig. 3). It is noted that output port 2 and port 3 are on the upside, while port 4 and port 5 bottom side. So the connecting part between input layer and two output layers should be designed very carefully after taking the identical electrical length and symmetry into consideration (Fig. 4). Fig. 5 shows the S-parameters of the designed size-reduced 4-way divider. It is shown that the power division ($-6.26\,\mathrm{dB}$ and $-6.58\,\mathrm{dB}$), matching ($-12.97 \sim -21.07\,\mathrm{dB}$) and isolation ($-13.76 \sim -29.25\,\mathrm{dB}$) are so good even after the size has become only 1/3 of normal 4-way divider. It is expected the proposed size-reduction using common DGS and stacked-substrate structure are well applicable to multi-layered LTCC and RFIC for microwave and wireless applications.

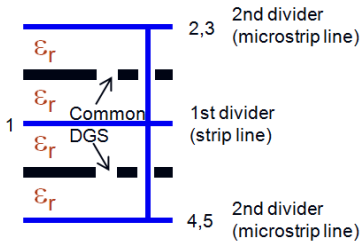

Figure 1.

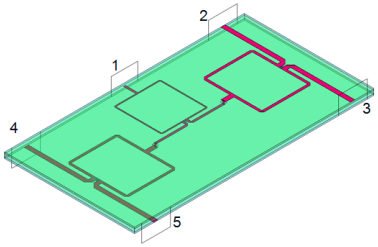

Figure 2.

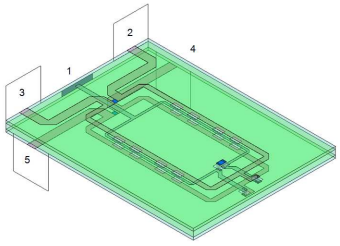

Figure 3.

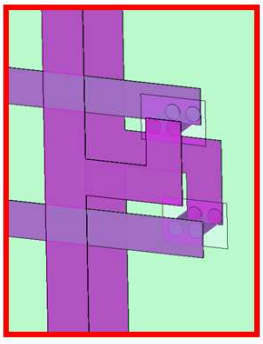

Figure 4.

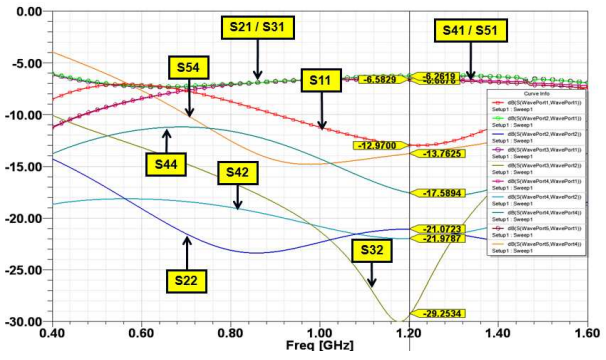

Figure 5.

Multilayer Thick-film and Next Generation Millimetre-wave Embedded Components and System Integration

Kamal K. Samanta[1, 2]

[1]Milmega/AMETEK Ltd., Ryde, Hampshire, PO33 2DD, England
[2]Institute of Microwaves and Photonics, University of Leeds, Leeds, LS2 9JT, UK

Abstract— Until recently, applications of millimetre-wave were mostly confined within some special domain/sectors, like defence and space. But, due to overcrowding towards lower frequency bands and next generation wideband and high resolution requirements, millimetre-wave has been experiencing an ever-increasing demand even for commercial applications, including that for high-speed multimedia and wireless, automotive radar and medical and security imaging. Monolithic circuit (MMIC/RFIC) technologies are quite matured and cost-effective for volume production. However, on semiconductor, it is difficult to realize passive components with required quality. At the same time, interconnecting and packaging of ICs retaining their performances are very critical. As a result, the circuit or system assembling and packaging techniques are more complex and costlier at mmW frequencies. The multilayer Multi-Chip-Module (MCM) and System-in/on-Package are widely regarded as an excellent solution for realising compact and high performance modules or systems.

Using conventional thick-film technology, there are difficulties to achieve a fine conductor geometry with trench-filled visa (to realize compact passives and SIW), or a precise IC mounting pocket, for reliable integration of next generation mmW circuits/systems. In a millimetre-wave MCM, the stray inductance of interconnections can seriously degrade the performance. More often, MMICs/RFICs are mounted onto pedestals inside substrate cavities formed mechanically or by laser cutting. This is a post-processed method which involves additional time and cost, and at the same time, suffers from additional misalignments and fabrication tolerances which cause difficulties to achieve the accuracy requirement or to keep the length of interconnections under control. To address the lack of fabrication precision, as well as circuit/system integration difficulties, advanced multilayer photoimageable thickfilm technology is being shown to be very promising, and meeting the high frequency requirements at a low cost [1]. The technology is highly suitable to produce multilayer SIWs giving operation at mmW and beyond, and also a wide range of precisely passive components and modules are realized with remarkably high performance and miniaturization [1, 2].

This paper will describe a novel and highly efficient mounting and integration technique, and the realization of millimetre-wave embedded components and integrated systems with superior performance, using advance photoimageable thick-film technology. The mounting cavities are formed from large photo-imaged via holes, without any limit on the shape and size. The gap between the MMIC and the edge of the mounting cavity are reduced drastically. The cavities are formed as part of the standard fabrication process and are sufficiently repeatable that the parasitic effects can be incorporated in the design stage, reducing the need for a post-production tuning. Further, will discuss the techniques used to meet the accuracy requirements for assembling MMIC and SMD components, and to maintain the compactness, as well as stable high performance for advanced mmW circuits and systems.

REFERENCES

1. Samanta, K. K., D. Stephens, and I. D. Robertson, "Design and performance of a 60 GHz multi-chip-module receiver employing substrate integrated waveguides," *IEE Proc. of MAP*, Vol. 1, 961–967, Oct. 2007.
2. Samanta, K. K. and I. D. Robertson, "Advanced multilayer thick-film system-on-package technology for miniaturized and high performance CPW microwave passive components," *IEEE Trans. on CPMT*, Vol. 1, No. 11, 1695–1705, Nov. 2011.

Microwave and Millimeter Wave 2D and 3D Integration

Tauno Vähä-Heikkilä[1] and Markku Lahti[2]

[1]Millimeter Wave Laboratory of Finland, MilliLab.
VTT Technical Research Centre of Finland, Finland
[2]Intelligent Sensor Systems, VTT Technical Research Centre of Finland, Finland

Abstract— Most of consumer related radio applications are in the range from few hundreds of MHz to 6 GHz currently. However, trends in last years have been towards higher frequencies. Automotive radars are already used in microwave region at 24 GHz and products are also available around 77 GHz. Also, demand for higher data rate transmission (several G/bits per second) systems has pushed telecommunication systems similarly for millimeter wave frequencies, where wider bandwidths are available. As an example, short range high data rate communication standards have been defined for V-band (50–75 GHz) applications around 60 GHz as well as for E-band (60–90 GHz) point to point applications.

VTT Technical Research Centre of Finland and MilliLab — The millimetre wave laboratory of Finland has been a forerunner in component, circuit and module research and development as well as in characterization of from on-wafer wafer level testing to module and sub-system integration. This presentation is focusing to RF to millimeter wave integration aspects. There will be shown examples from technology and material development to component and circuit realizations. VTT has as in-house technologies low temperature co fired ceramics (LTCC) and integrated passive device (IPD) technologies which are well suitable from below 1 GHz up to 300 GHz and even above (IPD) as component and especially integration technologies. In addition to VTT's in-house technologies, this presentation will cover examples of printed circuit board and other such as liquid crystal polymer (LCP) technologies for possible integration technologies.

Hybrid and Monolithic Planarization and Integration of Non-planar Metallo-dielectric Waveguides for High-density Electromagnetic Circuits and Systems

Ke Wu
Montreal University, Canada

Abstract— Recent research effort in exploring and exploiting substrate integrated circuits (SICs) has fundamentally changed the landscape of high-frequency circuit and system integration and development. In particular, substrate integrated waveguide (SIW) technology, which is part of the SICs family, has created a great enthusiasm in the applied electromagnetic and integrated circuit community worldwide for a wide range of low cost-enabled commercial and high-performance-oriented defense applications from MHz to THz. The critical enablers in this disruptive technology lie in the successful hybrid and monolithic planarization and integration of non-planar metallo-dielectric waveguides through the structure synthesis made of various microfabrication processing techniques. Following the tidal wave of the SIW technology development, which is based on substrate integrated non-planar metallic waveguides, dielectric and metallo-dielectric waveguides becomes an emerging focal point for the next generation millimeter-wave and terahertz integrated circuits and systems. This paper reviews the recent developments and accomplishments of various substrate integrated metallo-dielectric waveguide techniques with emphasis on dielectric image waveguides and non-radiative dielectric waveguides as well as their hybrid forms in connection with the popular SIW structures. Transmission loss and dispersion characteristics of those substrate integrated dielectric waveguides are presented and physical behaviors of their electromagnetic modes are explained with reference to the mono-mode bandwidth and bandgap effects. Integration and interconnect schemes with conventional planar and SIW structures are described for mode conversion and signal transfer applications. Practical examples are shown for their applications in the design and development of innovative integrated passive circuits and antenna arrays for millimeter-wave applications. Future development trends of metallo-dielectric waveguides are discussed and illustrated for various integrated circuits and systems, which include a series of original, non-invasive and/or contact less high-performance measurement and characterization techniques over millimeter-wave and terahertz frequency ranges. This paper is also concerned with grand challenging issues behind the development of metallo-dielectric waveguide techniques such as the lack of accurate knowledge on fundamental metallic-dielectric parameters and the arising of unprecedented problems in passive-active circuits integrations.

Multilayered Integration of Microwave Components by Substrate Integrated Waveguide Technology

Maurizio Bozzi, Riccardo Moro, Stefano Moscato, and Luca Perregrini
Department of Electrical, Computer and Biomedical Engineering, University of Pavia, Pavia 27100, Italy

Abstract— Substrate integrated waveguide (SIW) technology allows for the easy and low-cost integration of microwave and millimeter wave waveguide-like components in planar form. A variety of SIW active and passive components and antennas have been proposed in the last decade [1, 2]. Compared to other planar structures (e.g., microstrip and coplanar waveguide), SIW components provide complete shielding, lower losses, and higher quality factor. On the other hand, compared to classical waveguide components, SIW technology offers low weight and compact size, cost-effective fabrication, and easy integration with active devices.

The development of multilayered structures offers new opportunities for SIW technology, providing additional features and compact size of the circuits. Thanks to the size reduction, for instance, multilayered SIW components can be adopted even at low frequency (a few GHz), where the complete shielding offered by this technology permits to overcome spurious coupling and radiation issues of classical solutions based on microstrip line technology. In the case of filters, multilayered configurations permit to easily implement transmission zeros, and the coupling slots between different layers can be used to introduce additional poles in the frequency response [3].

Different multilayered SIW components will be presented in this work, including a wideband transmission line based on the ridge SIW concept [4], compact filters in folded SIW technology, and folded cavity-backed antennas.

REFERENCES

1. Garg, R., I. Bahl, and M. Bozzi, *Microstrip Lines and Slotlines*, 3rd Edition, Artech House, 2013.
2. Bozzi, M., A. Georgiadis, and K. Wu, "Review of substrate integrated waveguide (SIW) circuits and antennas," *IET Microwaves, Antennas and Propagation*, Vol. 5, No. 8, 909–920, Jun. 2011.
3. Bozzi, M., F. Mira, and A. Georgiadis, "A novel multilayered SIW filter with two mono-modal cavities and three poles," *44th European Microwave Conference (EuMC 2014)*, Rome, Italy, Oct. 5–10, 2014.
4. Bozzi, M., S. A. Winkler, and K. Wu, "Broadband and compact ridge substrate integrated waveguides," *IET Microwaves, Antennas and Propagation*, Vol. 4, No. 11, 1965–1973, Nov. 2010.

Recent Developments in Microwave and Millimeter-wave Integrated Circuits (MMICs) and Systems

Xin Jiang, Wei Hong, Jixin Chen, Debin Hou, and Zhe Chen
State Key Laboratory of Millimeter Waves
School of Information Science and Engineering, Southeast University, Nanjing 210096, China

Abstract— It has been more than 45 years since the first microwave and millimeter-wave monolithic integrated circuit (MMIC) on the three-five compound gallium arsenide (GaAs) substrate was demonstrated in 1968 by Texas Instruments. MMIC technology has evolved with enormous progress and the major driving forces come from changes in manufacture, substrate materials, modeling, design and testing tools. Among them, improvements in manufacture process are the leading factors for the changes in the past and expected to be the major driving force in the future as well. In addition, demands for higher integration with silicon (Si)-based digital circuits and rapid advances of Si-based maximum oscillation frequency ($f_{\max}$) surpassing 400 GHz [1] are currently driving many MMIC designs towards pure Si-based solutions.

This presentation will summarize recent progress in MMIC technologies based on various materials and manufacture processes such as GaAs, InP, GaN, SiGe and Si. Key "front-end" functional blocks and their state-of-the-art performances such as noise factor for LNA, phase noise for VCO, output power for PA and their operation frequencies will be reviewed and compared among volume-production manufacture processes with data collected from the latest publications. Some of the emerging trends in millimeter-wave market demands, especially in China market, and potential solutions use novel system on chip (SOC) solution will also be discussed. Meanwhile, this presentation will briefly introduces some of the recent works in MMIC designs using GaAs and Si processes completed at the State Key Laboratory of Millimeter Waves, Nanjing, China.

CMOS Terahertz Synthesized Left-handed Transmission Lines

Hsien-Shun Wu and Ching-Kuang C. Tzuang
School of Electronic Information Engineering, Tianjin University, Tianjin 300072, China

Abstract— This paper presents the multi-layered synthesized left-handed transmission lines using CMOS technology. The series capacitor and the shunt inductor are constructed in the multi-layered platform, realizing the size of the unit cell in the order of 1.0% of the wavelength in terahertz frequencies. A periodical perforated ground plane, which defines the periodicity of the unit cell, is designed beneath the completed left-handed transmission lines to provide more structural parameters to synthesize the guiding characteristics. Two kinds of the monolithic prototypes are implemented. One is the single left-handed transmission line, and the other is two left-handed transmission lines with the edge-coupling. The rigorous two-port $ABCD$ matrix representations are derived to access accurately the theoretical and the measured complex propagation constants of the transmission lines, enabling the design methodology for the wideband left-handed metamaterial implementations. The extracted results based on the theoretical and experimental multi-port scattering parameters reveal the following unique characteristics of the proposed terahertz left-handed transmission lines. From 100 GHz to 500 GHz, the slow-wave factors of two kinds of the transmission lines, which are defined by the normalize phase constants, has the maximum values exceeding thirty. The bandwidth of the single transmission line in left-handed operation exceeds 250 GHz. The coupling bandwidth of the left-handed edge-coupled line is wider than 200 GHz.

Session 2P13b
SC4: Reconfigurable Antennas

Magnetically Tunable Dual-polarized Dual-band SIW Slot Antenna

Li-Rong Tan[1, 2], **and Rui-Xin Wu**[1]

[1]School of Electronic Science and Engineering, Nanjing University, Nanjing 210093, China
[2]Nanjing College of Information Technology, Nanjing 210046, China

Abstract— With the rapid development of the wireless communication, tunable or reconfigurable antennas with small size become important for the systems in which more than one communication standard is integrated. To meet the demand, electronically tunable SIW antennas [1, 2] or magnetically tunable SIW antennas [3] have been investigated. Here, we propose a novel magnetically tunable dual-polarized dual-band substrate integrated waveguide (SIW) slot antenna. The proposed antenna is composed of a grounded coplanar waveguide (GCPW), two ferrite slabs, and a SIW resonant cavity structure with a crossed radiation slot. The multimode characteristic of SIW resonant cavity helps to realize multiband characteristics of the antenna, and the crossed radiation slot causes the radiating element to radiate desired polarized radiation. By properly choosing the length of two arms of the crossed slots, the radiations from the slots can be adjusted to having equal magnitude and 90 phase difference at one frequency, i.e., a circularly polarized radiation, while linearly polarized radiation at one other frequency.. Further, the operation frequency of the antenna can be tuned by means of the applied magnetic field because of loaded ferrite slabs.

The proposed design is verified by experiments. The antenna is fabricated and whole size of the antenna is 19.8 mm × 23.8 mm. The measurement results shows that the tunable frequency range is more than 8.1% for the circularly polarized radiation (from 8.98 GHz to 9.74 GHz) and 5.5% for the linearly polarized radiation (from 9.98 GHz to 10.54 GHz). The radiation pattern of the proposed antenna is almost not affected by the changes of the applied magnetic field. The antenna gain is more than 5.1 dBi within the frequency tuning range. Furthermore, the proposed antenna also possesses the advantages of low profile, light weight, low fabrication cost, and easy integration with planar circuits.

ACKNOWLEDGMENT

This work is supported by the National Nature Science Funds of China (61301016, 61271080 and 61071007).

REFERENCES

1. Giuppi, F., A. Georgiadis, A. Collado, M. Bozzi, and L. Perrerini, "Tunable SIW cavity backed active antenna oscillator," *Electronics Letters*, Vol. 46, No. 15, 139–141, July 2010.
2. Sam, S. and S. Lim, "Frequency reconfigurable substrate integrated waveguide antenna," *Proc. IEEE ISAP*, 822–825, 2012.
3. Tan, L. R., R. X. Wu, C. Y. Wang, and Y. Poo, "Magnetically tunable ferrite loaded SIW antenna," *IEEE Antennas and Wireless Propagation Letters*, Vol. 12, No. 1, 273–275, 2013.

Dual-polarized Unit-cell of Continuous Reflective Phase-shift for Reconfigurable Reflectarrays

M. T. Zhang[1, 2], S. Gao[1], J. X. Wan[2], B. N. Tian[2], and C. B. Wu[2]

[1]School of Engineering and Digital Arts, University of Kent, Canterbury, CT2 7NT, UK
[2]Xi'an Institute of Space Radio Technology, Xi'an, Shaanxi 710100, China

Abstract— This paper presents a Ku band dual-polarized patch unit-cell of continuous phase shift for reconfigurable reflectarray antennas, and the unit-cell can twist the polarization of incident wave. The radiator in the unit-cell for receiving the waves and radiating into space is a dual-polarized aperture-coupled microstrip patch structure with H-shaped coupling slots in the ground, and arrangement of the H-shaped coupling slots in the element's ground is specially selected, the design to optimize the slots and to save the space for circuit of reflective phase-shifter is completed, as shown in Figure 1. The scheme of reflective phase-shifter based on hybrid coupler can be integrated with this radiator for phase shift in the unit-cell. For continuous phase tuning, the varactor is preferred in the reflective phase-shifter because of its easy integration. A transmission microstrip line with biasing line loaded with a single varactor diode can create a phase variation in the reflected field by varying the bias voltage, thus varactor diodes loaded two microstrip lines can reflect a pair of tunable reflected phase as phase-shifters, after connected to the two ports of the hybrid coupler like the presentation in Figure 2, the reflective phase shifter with power transmission between two ports can be constructed. By controlling the bias voltage, the equivalent reflected phases of β is achieved in the varactor loaded line, and the hybrid coupler transforms the reflected waves to aggregate the waves at one port and to cancel at another port. After assembling the reflective phase-shifter with the dual-polarized radiator of two ports, the reflective phase-shifter can reflect the wave from one linear polarized port after tunable phase-shift to anther port, which is excited for the orthogonal polarization. The varactor loaded microstrip line endow the reflective phase shifter with a continuous reflective phase shift, further the unit-cell can transform the incident wave into the reflected wave of polarization twist with a continuous phase tuning. This varactor tuned reflectarray unit-cell is able to offer a continuous phase tuning over a range of nearly 360°, which is of critical importance to the performance improvement for reconfigurable reflectarray antenna.

The dual-polarized unit-cell of continuous reflective phase-shift can be used in the classic folded reflectarray for beam scanning with a low profile structure. In reconfigurable folded reflectarray based on the polarizing grid, the continuous phase-shift unit-cell of polarization twist is required necessarily for high performance realization. This reconfigurable unit-cell can reflect the incident wave with polarization twist for the application in folded reflectarray configuration, while the continuous phase shift in the reflection ensures the high aperture efficiency in the antenna radiation. Therefore, this unit-cell gives a good optional element for the advanced reconfigurable reflectarray antenna.

$$\vec{\mathbf{E}}_{\mathbf{r}}^{1} = 0, \qquad \vec{\mathbf{E}}_{\mathbf{r}}^{2} = \mathbf{j}e^{-j\beta}\vec{\mathbf{E}}_{\mathbf{i}} \tag{1}$$

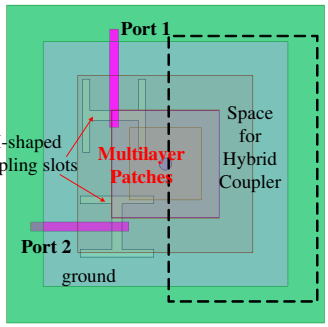

Figure 1: Configuration of dual-polarized H-slot coupled patch unit-cell for reconfigurable reflectarray.

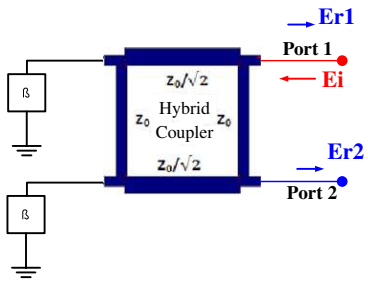

Figure 2: Scheme of reflective phase-shifter based on hybrid coupler for reconfigurable reflectarray unit-cell.

ACKNOWLEDGMENT

This work is funded by China Scholarship Council and Xi'an Institute of Space Radio Technology.

A Reconfigurable Folded Antenna for Mobile Phone Applications

Liu Hu, Ying Liu, Cao Yu, and Shuxi Gong
National Laboratory of Science and Technology on Antennas and Microwaves
Xidian University, Xi'an 710071, China

Abstract— As an important feature of the information age, wireless communication technology has been developing at an unprecedented rate. Since antennas form an initial part of communication systems, their performance plays a significant role in the communication quality of the systems. In the field of a new generation of mobile communication, more requirements are needed to satisfy the demand of the users. Thus how to realize multiband and broadband mobile phone antennas has been a research hotspot in recent years

A folded reconfigurable antenna using three PIN diodes is proposed for personal communication handset applications. In a compact volume of $60 \times 9 \times 8\,\mathrm{mm}^3$, the antenna has a simple metal structure comprising a folded loop strip, a Y-shape folded strip and three PIN diodes. By independently controlling the on/off states of the three PIN diodes located on the radiating element, the proposed structure can operate in the inverted-F antenna (IFA) andloop modes, respectively. While operating in the IFA mode, the 6 dB reflection coefficient bandwidth is sufficient to cover the DCS (1710–1880 MHz), PCS (1850–1990 MHz) bands. Owing to the additional Y-shape folded strip, the bandwidth which is generated by multiple resonant of the loop mode easily covers GSM850 (824–894 MHz), GSM900 (880–960 MHz), GPS (1560–1590 MHz), UMTS (1920–2180 MHz), LTE2300 (2305–2400 MHz), WLAN (2400–2480 MHz) bands. To optimize the antenna structure in both modes, a parametric analysis is performed by sweeping the length and width of the radiators. The proposed antenna is fabricated and all simulated results are confirmed with measured data. Good radiation efficiency and antenna gain at frequencies over the desired operating bands are also obtained. The proposed antenna with the properties of simple structure, wide bandwidth and easy fabrication can be useful for an upcoming generation of personal communication handset.

Pattern Reconfigurable Printed Antennas with High Gain and Broadband

Xue-Xia Yang, **Zhong-Liang Lu**, **Guan-Nan Tan**, **and Yong-Jin Zhou**
School of Communication and Information Engineering, Shanghai University
Shanghai 200072, China

Abstract— Reconfigurable antennas with adjusting beams are demanded in the wireless communication systems such as small base stations. Planar printed antennas are preferred because of the low profile and low cost. Some kinds of beam adjusting planar antennas have been presented while the gains were not illustrated or were very low. This paper reports several latest researches on the beaming adjusting printed antenna with high gain and broadband. The first one is a printed Yagi antenna with six elements and six adjustable beam directions. A tie-shape dipole with the two arms being printed on the opposite side of the dielectric-slab is adopted as the driven element to extend the bandwidth. Six PIN diode switches are simply attached between the ground and the driven dipole on the ground to control the radiation directions. The measured results shows that the bandwidth of the reflection coefficient less than 10 dB is 400 MHz, and the gains are all 7.5 dBi on the main radiation directions of 30°, 90°, 150°, 210°, 270°, 330° with the half power beam width being about 60°. The second one is a Vivaldi-shaped tapered slot antenna with four elements and four adjustable beam directions. The antenna is coupling fed by a microstrip feedline. The four beam directions around 360° range are controlled by four PIN diodes without bias circuits being required. This pattern reconfigurable antenna has wideband from 1.5 GHz to 3.3 GHz and high gain of 6.8 dBi at the center frequency of 2.4 GHz. The further approaches of gain enhancement are discussed.

A Thin Planar Antenna Based on Gradient Metasurface

Bo Chen, Hongyu Shi, Anxue Zhang, and Juan Chen
School of Electronic and Information Engineering, Xi'an Jiaotong University, China

Abstract— Gradient metasurface (GM) can have a pre-defined large wave vector along its surface. It has shining attributes as field enhancement and sub-wavelength transmission. In former works, GMs were excited mostly by plane waves illuminated from high above, and experts concentrated on waveform converting or anomalous reflection. This letter analyses electromagnetic field distribution above GM with some plane waves vertically illuminating. Then it provides a new way to excite GM on one of its edges using parallel plate waveguide, from which we can get an escaping plane wave towards above, and this is the inverse process of plane wave vertical incidence. After a delicate parameter sweep, the simulation shows our design has comparatively high directivity and efficiency within a bandwidth of 0.6 GHz (7.7 GHz to 8.3 GHz). The impact of some important size parameters to the antenna performance is discussed in the letter. On account of the fact that GMs are usually constructed by a mass of unit cells, their shapes are variable and they can cover many facilities, which have great potential in both civil and military use. With the development of metasurfaces, the unit cells will become smaller, and the adjustability of the antennae shapes will rise. To excite GMs with the same unit cells but different shapes, it is possible that we only need to tune their matching structure but not the unit cells. Then a new way to design reconfigurable antennae presents. And with the help of metasurfaces, reconfigurable antennae will be more various and flexible and will have better performance.

Wideband RCS Reduction of Microstrip Antenna by Frequency Reconfigurable Electromagnetic Band Gap

Y. Liu, **Y.-W. Hao**, **Y.-T. Jia**, **and S.-X. Gong**
Xidian University, China

Abstract— In recent years, more and more attention is paid to the radar cross section (RCS) reduction of antennas since the rapid development of the stealth technology. The methods of the RCS reduction of antennas are different from the other devices in a low RCS platform because the radiation characters of the antenna must be considered first. As a result, it becomes a tough problem to consider the radiation characters and RCS of the antenna simultaneously. Electromagnetic band gap (EBG) structure is widely used in RCS reduction of antennas. The principle of its operation is based on the cancellation of the reflection from the EBG structure and the perfect conductor of the antennas. When the reflection phase of the EBG is less than $\pm 90^\circ$, the effect of RCS reduction can be achieved. Because the EBG is a LC resonant structure, the operation frequency band is relatively narrow. However, a wideband RCS reduction is usually required in modern battleground environment. So in this paper, a frequency reconfigurable EBG is designed and used to reduce the RCS of microstrip antenna in a wide frequency band. The frequency reconfigurable EBG structure consists of spiral conductor and two diodes. The diodes are used as switches. By controlling the length of the spiral conductor, the inductance of the EBG structure can be changed and the operation frequency shifts. The length of the spiral conductor can be adjusted by making the diodes on or off. As a result, the EBG can work in a wide frequency band. So, the wideband RCS reduction of microstrip antenna with frequency reconfigurable EBG can be realized.

Frequency Reconfigurable Narrow-frame Antenna for WWAN/LTE Smartphone Applications

Zhong-Xiang Chen and Yong-Ling Ban
Institute of Electromagnetics, University of Electronic Science and Technology of China
2006 Xi-Yuan Avenue, Western High-Tech District, Chengdu, Sichuan 611731, China

Abstract— A compact narrow-frame antenna loaded a PIN diode for hepta-band smartphone applications is presented. The greatest highlight is that the edge of the no-ground planet is quite narrow of only 5 mm, which meets the requirements of the popular narrow-frame smartphone designs with larger touch-screens. Furthermore, the reconfigurable technology is applied to realize a wide coverage with a small volume and a compact structure. The hepta-band operation is successfully achieved by combining the two working states. Detailed considerations of the design are studied in this paper and the proposed antenna is successfully simulated, fabricated, and measured.

Session 2P14a
SC5: Remote Sensing of the Atmosphere, Ocean, Hydrology and Cryosphere

Numerical Simulation of Scattering from Rough Surface/Subsurface and Inversion Application for Extra-planetary Exploration

Ya-Qiu Jin
Key Laboratory for Information Science of Electromagnetic Waves (MoE)
Fudan University, Shanghai 200433, China

Abstract— Scattering from rough surface has been extensively studied in electromagnetic scattering theory ad application. Analytic approaches, such as the KA (Kirchhoff approximation), SPM (small perturbation method), two scales, IEM (integral equation) etc., and numerical approaches, such as MoM, FBM, FEM, FDTD etc. have been developed for many applications, e.g., remote sensing (RS) of earth terrain and sea surfaces.

Great advances of CEM (computational electromagnetics) and deep space RS have been promoting new studies of electromagnetic scattering from complex rough surface/subsurface in several space missions. We present herewith two works on numerical simulation and inversion of rough surface scattering for Moon and Mars explorations.

(1) Multi-angular radar echoes during CE-3 landing on the Moon surface

The main objective of Chinese Chang'E-3 (CE-3) lunar satellite is to achieve soft-landing and roving exploration on lunar surface. Multi-angular radar of the lunar lander measures the echoes from cratered rough surface during descending. The speed of the descending lander is then derived from measurements. Numerical simulation of multi-angular radar echoes and speed inversions from Doppler frequency are presented. An area of the Lunar Sinus Iridum bay, as landing site, is specifically selected. The rough surface is divided into triangular patches for numerical Kirchhoff calculation. Backscattering of multi-angular radar beams of CE-3 is numerically calculated, and the radar echoes during the whole process of soft-landing over rough lunar surface are numerically simulated. The Doppler frequency, the phase changes, and the descending speed are numerically derived to show the landing process.

(2) Radar range echoes imaging and parameters inversion of the Mars surface/subsurface

A two-layer model of Mars cratered rough surface/subsurface is presented for numerical simulation of scattering and range image of radar echoes. Geometric ray tracking for scattering of rough surfaces, which are digitalized by the triangulated network, is applied to calculation of scattering and imaging simulation of radar range echoes. Numerical simulations of a cratered rough surface generated by the Monte Carlo method analyze the functional dependence of radar range echoes at 1–50 MHz center frequencies upon the surface/subsurface feature and parameters of layering media, i.e., layer depth and dielectric properties. The radar range echoes from two areas of real Mars surface, which is described by DEM data with a resolution of 1 m × 1 m and vertical error less than 1 m, are also simulated and analyzed. Based on these simulations, this study presents a design of radar center frequencies for Chinese future Mars exploration. Finally, inversions of the dielectric constants of two-layer media and the regolith layer thickness are developed.

Estimation of Wind-direction Using the Bayesian Approach Retrieved from Marine Radar-image Sequences

Ketao Ma, Xiongbin Wu, Li Wang, Xiaofeng Chen, and Jianfei Liu
Wuhan University, China

Abstract— A new method for wind-direction retrieval with spatially and temporally high-resolution using marine radar-image sequence is presented. The method is based on analyzing the movement of wind gusts, which is visible in radar image sequence because of the change in the radar cross section (RCS). In contrast to previous methods, this new technique requires no calibration by other systems. The wind directions are retrieved from wind induced streaks by using the optical flow based motion estimation technique (OFM) with consideration the errors emerging from estimating wind directions These errors often lead to ill-conditioned directions. Therefore, a function of the wind directional distribution is imported for the correction. This correction for the accurate estimation uses the Bayesian approach through the function of the wind directional distribution, which was used in the field of regression analysis problems where the number of the parameters to be determined was large, when compared with the sample size. Considering the smoothness of the function, the new algorithm takes a continuous an smooth function as the prior distribution for the Bayesian approach. This method is applied to radar image sequences acquired by the computer simulation. The derived wind-directions from these radar image sequences with the Bayesian approach are compared to wind-directions set in the simulation and wind-direction without the Bayesian approachIn contrast to traditional offshore wind sensors, the retrieval of the wind field from the backscatter of the ocean surface makes the system independent and reduces the effects due to platform induced blockage and turbulence effects.

Theoretical Analysis and Experimental Verification of Microwave Radiation Features of Fractured Rock

Shanjun Liu[1], **Zhongyin Xu**[1], **Lixin Wu**[1, 2], **and Bo Tang**[1]

[1]Institute for Geo-informatics & Digital Mine Research, Northeastern University, Shenyang 110819, China
[2]IoT & Perception Mine Research Center, China University of Mining and Technology, Xuzhou, China

Abstract— Rock fracture and failure is a common phenomenon in nature, many geological disasters including earthquake, landslide, collapse, ground subsidence, slope instability, mine water inrush, rock burst, mine earthquake and roof caving etc. are related to rock fracture and failure. Since the beginning of this century, many strong earthquakes have happened in the world, which caused serious disasters to mankind. So, are there microwave radiation abnormal phenomenon before these disasters, can the passive microwave sensors detect these anomalies? To answer these questions, many researchers carried out the microwave detecting experiment of loading rock, and found the microwave radiation changed significantly when the rock fractured, which indicates that the passive microwave is probable to detect the phenomenon of rock fracture and failure, including earthquakes.

But it is unclear by now about the patterns and rules of microwave radiation variation in rock fractures, and the theoretical foundation is also unclear. In this paper we first analyze the microwave radiation characteristics and the influence factors of fractured rock based on the microwave radiation theory of layered medium, and the microwave radiation feature is compared with that of intact rock. Then the theoretical analysis results are verified by a series of passive microwave detecting experiment of fractured rocks.

The main results are (1) the microwave brightness temperature of layered rock is smaller than that of intact rock under same conditions; (2) the environmental radiation have an important influence to brightness temperature of layered rock, and the brightness temperature increase with the increase of environmental temperature in the front of rock; (3) the brightness temperature of layered rock decrease with the increase of the observing angle; (4) the brightness temperature of layered rock increase with the increase of the microwave frequency.

The experiment results indicated that it is possible to use the microwave remote sensing to monitor the fracturing of rock masses, including earthquakes.

Surface Scattering Characteristics and Snow Accumulating-melting Behaviors from GNSS Reflectometry

Shuanggen Jin and Nasser Najibi
Shanghai Astronomical Observatory, Chinese Academy of Sciences, Shanghai 200030, China

Abstract— GNSS-R (Global Navigation Satellite System-Reflectometry) can remotely sense Earth's surface geophysical parameters, e.g., snow depth and soil moisture. However the surface reflectivity interaction and scattering characteristics from GNSS signals are not clear. In this paper, we model the scattering properties and investigate the surface's reflectivity characteristics interacting with GPS L1 and L2 signals in order to retrieve multipath signals and precisely infer surface characteristics. Furthermore, the effects of snow accumulating and melting together with bare soil and fixed snow depth are studied by GNSS-R. Some cases of studies from GPS observations at BAKE and KUUJ sites are also presented as well as discussed.

Study on Microwave Radiation Variation of Typical Ground Features in Yushu

Xiaojing Liu[1], **Shanjun Liu** [1], **and Lixin Wu**[1, 2]

[1]Institute for Geo-informatics & Digital Mine Research, Northeastern University, Shenyang 110819, China
[2]IoT & Perception Mine Research Center, China University of Mining and Technology, Xuzhou, China

Abstract— The study on satellite thermal infrared anomalies before earthquakes has a long history. However, it is difficult to recognize the anomaly in cloudy conditions as the infrared radiation from the Earth's surface cannot pass through clouds and arrive to the satellite. Compared with thermal infrared, microwave has a strong cloud penetrability, which means less weather interference and better data continuity. Therefore, it makes microwave better than other bands in earthquake prediction. Nevertheless, microwave radiation from the Earth's surface is affected by many factors such as geography, coversphere, and weather conditions. The microwave radiation anomaly recognition is a complex process due to seeking the weak signal under the strong interference. Therefore, insight into the microwave radiation characteristics and variation of ground features under non-earthquake condition is undoubtedly helpful to extract abnormal information related to earthquake.

In this study, the region around the Ms 7.1 Yushu earthquake was took as an example. Ground features were classified into 7 main types in the study area: forest, grass, cropland, shrub, snow and ice, barren, and water body. We used microwave brightness temperature data derived from AMSR-E sensor at 3 frequencies (6.9 GHz, 18.7 GHz, and 36.5 GHz) to analyze the microwave radiation characteristics and variation of ground features.

The main results show that the microwave radiation signal of ground features can be divided into two parts, signal with regular variation and signal with random variation: (1) Signal with regular variation mainly refers to the constant and periodical ingredient of microwave brightness temperature (BT), depending on geography, terrain, latitude and seasons. This part of BT in a region keeps constant due to the stability of geography, terrain, and latitude, and it also presents characteristics of period due to the seasonal cycle. It is always negatively related to the latitude and altitude; (2) Signal with random variation is the disorder part of BT, depending on the random variation of weather. The influence of weather on different type of ground features is different. The impact on water is more obvious than other categories, both in the range and the trend.

Application of Computational Electromagnetics to Quantitative Interpretation of Observations with a Polarimetric Weather Radar

Djordje Mirković[1, 3, 4], **Dušan Zrnić**[2], **and Alexander Ryzhkov**[1]

[1]National Severe Storm Laboratory, University of Oklahoma CIMMS, Norman, OK, USA
[2]National Severe Storm Laboratory, NOAA, Norman, OK, USA
[3]School of Electrical and Computer Engineering, University of Oklahoma, Norman, OK, USA
[4]School of Electrical Engineering, University of Belgrade, Serbia

Abstract— Polarimetric weather radar WSR-88D observations brought significant improvement to understanding of weather phenomena allowing for better discrimination of hydrometeor habits. Traditionally hydrometeor scattering has been investigated using simple spheroidal models to represent most of the observed atmospheric particles. These simple models provide satisfying interpretation of polarimetric radar observations for most of precipitation types, but may fail in the case of the scatterers of particularly complex shapes, such as: dry and wet snowflakes, large hailstones with irregular shapes and internal structure, insects, birds, or military chaff. Such models are notorious for being unable to replicate significant reduction of the cross-correlation coefficient commonly observed in the melting layer or hail. Thus, a more sophisticated approach allowing for the quantitative discrimination between different precipitation types on the basis of the measured differential reflectivity Z_{DR}, specific differential phase K_{DP}, backscattered differential phase δ, and correlation coefficient ρ_{HV} is needed.

The proposed approach relies on using a Method of Moments (MoM) EM solver for modeling complex geometries of hydrometeors that can be part of larger ensembles. The complete modeling process is separated into two operations. The first uses the WIPL-D software for calculation of individual hydrometeor scattering coefficients which are then stored in a library. An ensemble of the scattering coefficients with prescribed statistical properties is drawn to then compute second order moments representing radar measurements from which the polarimetric variables are obtained.

The proposed modeling architecture proves to be useful in a variety of cases, as it assumes that ensembles are created off of the statistically independent scatterers. Furthermore it is possible to account for multiple scattering using independent scattering coefficients in the ensemble creation. Because the ensemble creation is "unaware" of the objects' topology, it allows for the ensembles of non-meteorological scatterers such as insects or birds, ipso facto providing a new tool for the research in this area.

To the best of our knowledge, this is the first application of WIPL-D, and one of the first attempts to use MoM for hydrometeor scattering. We suggest specific topologies, orientations, sizes, distribution and EM properties for the sampled scatterers. Specifically we suggest models of giant hail resembling observations to replicate observations made by weather radars.

Session 2P14b
SC5: Synthetic Aperture Radar Imaging and Advanced Radar Techniques

A Novel Keystone Transform Based Algorithm for Moving Target Imaging with Radon Transform and Fractional Fourier Transform Involved

Jiefang Yang[1, 2] **and Yunhua Zhang**[1]

[1]The Key Laboratory of Microwave Remote Sensing, Chinese Academy of Sciences, China
[2]University of Chinese Academy of Sciences, China

Abstract— At present, ground-moving target imaging (GMTI) and motion parameter estimation (MPE) is becoming an important research topic for modern SAR systems. The moving targets are defocused and dislocated in SAR images since their range cell migration (RCM) are different from that of stationary scene due to their unknown relative motions. The Keystone Transform (KT) and the second-order KT (SKT) can be used to correct the RCM of moving targets with no need for any prior knowledge about their motion parameters. However, both KT and SKT suffer from the Doppler ambiguity problem. In a real-world situation, Doppler ambiguity usually occurs for SAR imaging of fast moving target due to the limited PRF. In this paper, we propose an algorithm applying KT and Modified SKT (MSKT) for SAR GMTI and MPE in Doppler ambiguity situation. The algorithm is summarized as follows. First, KT is conducted to correct the range walk induced by baseband Doppler frequency. Second, the number of integer PRF ambiguity is estimated through the searching algorithm, and then the range walk induced by integer PRF ambiguity is compensated. Third, the MSKT is conducted to correct the range curvature. Thus, the target trajectory becomes an oblique line along azimuth direction. Fourth, Radon Transform (RT) is utilized to estimate the slope of the target trajectory, and then the residual range walk can be corrected. At this moment, the target trajectory becomes a straight line along azimuth direction. In the meantime, the target true Doppler frequency can be calculated with the integer PRF ambiguity and the baseband Doppler frequency obtained according to the slope. Fifth, Fractional Fourier Transform (FrFT) is applied to estimating the Doppler rate of target, and then the azimuth matched filtering function and the third-order phase compensation function can be constructed. Finally, the moving target is focused after azimuth matched filtering and the third-order phase compensation, and the target motion parameters can be calculated according to the Doppler frequency and Doppler rate. The effectiveness of the proposed algorithm is demonstrated by the simulated airborne SAR data.

Why Optical Images are Easier to Understand Than Radar Images? — From the Electromagnetic Scattering and Signal Point of View

Yunhua Zhang and Jingshan Jiang
The Key Laboratory of Microwave Remote Sensing
Center for Space Science and Applied Research, Chinese Academy of Sciences
No. 1 Nanertiao, Zhongguancun, Haidian, Beijing 100190, China

Abstract— As the bandwidth of SAR/ISAR system continuously increases as well as the synthetic aperture technique develops, the spatial resolution of radar images is higher and higher. However, the high resolution of radar image does not mean the resolving ability for targets is high. We all have the experience that the optical images are much easier to understand than radar images even if they have less resolution. A simple and frank explanation is due to the wavelengths of optical waves are much shorter than that of microwaves at which radars usually work, e.g., in the order of $10^{-5} \sim 10^{-4}$. Are there any deep reasons for this? Are there any common points between optical camera and SAR/ISAR? We give our answers to these questions in this paper from the aspects of imaging geometry and principle, electromagnetic scattering, signal characteristics, and so on.

We know that the human eye's vision system is similar to a camera, or in another words, the human eye is indeed a camera. The basic imaging principle of optical camera is "smallhole" imaging, it gets the two dimensional resolutions about the target through angular discrimination, but for SAR/ISARs, they get the range resolution through discriminating the arriving times from different targets or different parts of the same target, which is proportional to the signal bandwidth, and thus is inversely proportional to the time duration of the compressed pulse signal, while get the azimuthal resolution through aperture synthesis, which is inversely proportional to the coherent integration time. So radar images have unavoidable and severe geometric distortion compared with optical images, e.g., layover and foreshorten, which makes the radar images more difficult to read

For ordinary optical camera, the signal (light) comes from the sun or other artificial sources, it is random and incoherent. During the imaging process, the light signals interact with the target, where reflections and scattering occur. Due to the short wavelength, which is in the order of several hundreds of nanometers, the scattering exhibits diffusion characteristics and is localized for almost all natural or man-made targets (the surfaces are rough compared with the wavelength of the light), i.e., the scattered signals from every part (structure) of the target go through the lens and sensed by different part of CCD matrix to form a pixel The pixel is formed by incoherently summing the single scattering and multi-scattering signals from the same part of the target so there is only additive noise, at the same time the scattering center (referred to as the pixel) is very stable and independent on the direction of incident light if the looking direction is fixed But for SAR/ISAR, the transmitted signals and the scattered signals are both coherent, and the image is reconstructed by coherent processing the echoes, where the pixel position is not stable but dependent on the direction of incident wave, i.e., one may get different radar images for the same target even if the looking direction is fixed but the incidences are different The role of multi-scattering effect is very positive for camera in some degree for increasing the randomness of incident light, which makes the image looks more uniform and smooth, but for radar, it is very harmful because it leads to the scattering centers deviating from their geometric position or induces ghost scattering centers The noise in SAR/ISAR images is composition of additive and multiplicative noises, so it is very hard to remove. For camera, the signals come from the surface scattering of the target, but for radars, the signals come from both the surface scattering and the volume scattering for general nonmetal target, and the volume scattering makes the scattering centers even more complicated.

As for the signal point of view, for camera, the light waves are continuous, non coherent of one octave. But for SAR/ISAR, the signals are usually pulsed and coherent. So integration time for optical image can be much longer than that of radar image, i.e., the signal to noise ratio (SNR) of optical image could be much higher than that of radar image If look into general lidar images one can obviously find that they are very noisy compared with optical images. The reason is the same as for radar: the signals are pulsed, so the integration time is short and the SNR is lower

As addressed above, the optical camera and SAR/ISAR are both active sensors, i.e., they all have transmitters and receivers as well as antennas. Nevertheless the transmitter for optical

camera is the sun or other man-made light sources, e.g., flasher, which is usually non-cooperative and non-coherent with the receiver (CCD), but the transmitter and receiver of SAR/ISAR are cooperative and coherent.

Optical images and SAR images are presented and compared to illustrate the similarity and the difference between them.

Landslide Displacement Monitoring Using Multi-aperture InSAR and D-InSAR

Liming He[1], **Lixin Wu**[1, 2], **Shanjun Liu**[1], **and Chang Su**[1]

[1]Institute for Geo-informatics & Digital Mine Research
College of Resources and Civil Engineering, Northeastern University, Shenyang 110819, China
[2]IoT & Perception Mine Research Center
China University of Mining and Technology, Xuzhou 221116, China

Abstract— The largest open-pit mine in Asia is Fushun west open-pit mine, which located in Fushun city, Liaoning province, Northeast of China. At present, Fushun west open-pit mine has been the formation of 6,600 meters from east to west, 2,200 meters from north to south, with an average depth of about 420–520 meters, covering an area of about 10,870,000 square meters of open-pit mining. It has a long history of more than one hundred years and made important contributions to China's economic development. However, serious geological disasters, especially large-scale landslides, has become a direct threat to the residents and factories in Fushun city due to excessive and long-term coal mining. The direct economic loss has reached as much as 1.5 billion Yuan. Therefore, it is important to investigate the geological disaster situation, determine the location and size of landslides. Compared to traditional methods, for example leveling measurements and global positioning system (GPS) measurements, interferometric synthetic aperture radar (InSAR) has many advantages such as lager coverage and lower cost, and it can work in all-weather conditions to monitor surface deformation (Massonnet and Feigl, 1998).

A special feature of landslides at Fushun west open-pit mine is that the main deformation occurred along the north-south direction. However, the conventional differential SAR interferometry (D-InSAR) technique can only measure one-dimensional (1-D) deformation along the line-of-sight (LOS) direction. It means that any component of motion orthogonal to the LOS cannot be detected. In the nearly north-south flight pattern of current commercial SAR satellites, the D-InSAR method are only sensitive to the deformation along the up-down and east-west direction (Wright et al., 2004). Therefore, it is almost unable to measure the displacements occurring in the north-south direction at Fushun west open-pit mine with conventional interferometry.

In 2006, a significant improvement in measuring along-track deformation was made by Bechor and Zebker (2006) with a new approach: multiple-aperture InSAR (MAI). In this paper, we aim to extend this method to landslide monitoring at Fushun west open-pit mine due to its main displacements along the north-south direction. By integrating multiple-aperture InSAR and traditional D-InSAR, we explore to reveal the 2-D deformation field of landslides caused by coal mining from the overall perspective via multi-temporal remote sensing data.

A PolSAR Classification Method Based on Scattering Model and Polarization Correlation Coefficient

Jianbo Wang[1, 2], **Chao Wang**[1], **Hong Zhang**[1], **Fan Wu**[1], **and Bo Zhang**[1]

[1]Key Laboratory of Digital Earth Sciences
Institute of Remote Sensing and Digital Earth, CAS, Beijing 100094, China
[2]University of Chinese Academy of Sciences, Beijing 100049, China

Abstract— Recently, many PolSAR image classification methods have been proposed. One commonly used method is based on the scattering model. However, traditional classification based on scattering model usually overestimates the volume scattering contributions, especially in urban areas, resulting in buildings not orthogonal to radar Line-Of-Sight (LOS) misjudged as forests. To solve this problem, an improved PolSAR classification method based on scattering model and polarization correlation coefficient is presented in this paper. By introducing two types of polarization correlation coefficients, circular-pol correlation coefficient (CCC) and normalized circular-pol correlation coefficient (NCCC), the oriented buildings can be effectively extracted from the volume scattering. Since the amplitude values of CCC of forests are very small, while that of buildings orthogonal to radar LOS or with small orientation angles are close to 1. Therefore, the CCC parameter is firstly used to extract some slightly tilted oriented buildings form the initial volume scattering category. Then, the NCCC parameter is introduced to distinguish the buildings with large orientation angles from the remainder volume scattering components. Since these buildings hold strong non-reflection symmetry and larger orientation angles, the values of NCCC of this kind are much larger than that of forests. Finally, the extracted buildings are reclassified into a new oriented buildings category. In order to maintain the dominant scattering mechanism characteristics, the classification method preserving scattering characteristics is utilized to classify the corrected scattering categories. The proposed classification algorithm remedies the defect of traditional scattering-model-based classification method and the experiment result of an E-SAR L-band PolSAR image of Oberpfaffenhofen, Germany demonstrates the effectiveness of the proposed method.

A Case Study of Precursor Aspects of L'Aquila Earthquake Using Spaceborne InSAR Data

Kamel Hasni, **Jie Chen**, **and Nabil Hamdadou**
Signal and Information Processing Department
Electronic and Information Engineering School, Beihang University, Beijing, China

Abstract— The study of pre-seismic deformation field is very important for the understanding of the temporal evolution of active faults, and for the prevention of any possible earthquake. Till now scientists can predict an earthquake within period of 30 years. Interferometric Synthetic Aperture Radar (InSAR) offers a unique tool for mapping ground deformation with subcentimeter precision, when data of other sources cannot be acquired, especially for the period before the earthquake. With the increasing number of radar satellites these last years, a big archive of SAR images was build. New methods were developed for the study of earthquake cycle using radar remote sensing techniques. InSAR was applied to measure the pre-, co- and post-seismic deformation related to earthquakes since the lunch of ERS-1 satellite.

In this work, we are trying to assess the feasibility of the detection of small deformation of the crust, just few weeks before an earthquake using InSAR. The SAR data made available by the European Space Agency (ESA) after the L'Aquila earthquake (06 April 2009) Mw 6.3, was used for this purpose. Three tracks 079 (descending), 129 and 401 (ascending) of Envisat satellite spanning the period from 2002 to 2009 are available. Two of them (079 and 401) was used in this study, because of the availability of images for at least one month before the earthquake (8 days for track 401). An anomaly in the topography was reveled in the interferograms generated for the period of one month before the earthquake. This anomaly quantified as half fringe = 1.4 cm in both ascending and descending couples, in an area where the annual displacement measured by PSInSAR doesn't exceed 1 cm/year. This anomaly was not present in the previous interferograms. We are doing a further study to eliminate the atmospheric contribution correlated with the topography, to get a precise amount of this deformation.

PSInSAR was applied to two tracks of Envisat satellite to measure the displacement near L'Aquila city for over 7 years; the deformation doesn't exceed 1 cm/years. A displacement measured as 1.4 cm was revealed by InSAR just one month before the main shock. A correction of the atmospheric contribution in the interferograms is an important task for the analysis of the real deformation, this investigation can highlight precursors or triggering phenomena for L'Aquila earthquake.

Analysis of Optimal Panel Geometry for Self-illustration Corner Reflector

C. R. Li[1, 2], **Y. S. Zhou**[1, 2], **and L. L. Ma**[1, 2]

[1]Key Lab of Quantitative Remote Sensing Information Technology, Chinese Academy of Sciences, China
[2]Academy of Opto-Electronics, Chinese Academy of Sciences, China

Abstract— Trihedral corner reflectors are usually employed as standard point targets because of their large radar cross section (RCS), extremely wide RCS pattern, light weight, cheap and simple to manufacture. The panel geometry for trihedral corner reflector has been traditionally chosen as triangular shape. However, not all the panel area is the effective area which contributes to the nominal RCS of the reflector. The additional 'tip' reflecting area, if interacting with ground plane, will yield an increase of RCS. This problem will affect SAR radiometric and phase calibration accuracy. The self-illuminating corner reflectors are proposed to solve this problem [1]. All the rays that enter the reflector's cavity experience the triple reflection on the panel and return to the radar. There are many types of self-illuminating corner reflectors, e.g., square, hexagon. Note that the nominal RCS of trihedral corner reflector is calculated by the panel area and radar wavelength, however this is true only when the leg length is very large compared to the radar wavelength. Otherwise, the contribution from edge diffraction becomes an issue. Since edge diffraction is proportional to the panel external edge length, the optimal panel geometry is the one that has the minimal external edge length for the same panel area. In [1], the panel geometry was assumed as polygon and optimum hexagon panel geometry was obtained. According to the isoperimetric theorem, the circle has the shortest perimeter among all planar shapes with the same area, so the external edge length of a circular arc panel should be even smaller than that of hexagon panel, theoretically. In this paper, general expressions for the panel area and panel external edge length of arbitrarily self-illuminating corner reflectors were described by parameter equation. Then the edge of reflector panel is assumed as circular arc, ellipse. Through a numerical approximation approach, the external edge lengths of those self-illuminating trihedral corner reflectors are derived and compared. The method proposed in this paper and the Optimal Panel Geometry will help to improve SAR image quality and radiometric calibration based on corner reflectros.

REFERENCES

1. Sarabandi, K. and T. C. Chiu, "Optimum corner reflectors for calibration of imaging radars," *IEEE Transactions on Antennas and Propagation*, Vol. 44, No. 10, 1348–1361, 1996.

Remote Detection of Human Vital Sign with SFCW Radar

Sixin Liu[1] and Lanbo Liu[2]

[1]Jilin University, Changchun, Jilin, China
[2]University of Connecticut, Storrs, CT, USA

Abstract— The stepped-frequency continuous wave (SFCW) radar technique was used to detect cardio-respiratory signals as the vital sign from a human subject positioned behind obstacles under laboratory conditions. The experiments were organized with a number of detection scenarios by collecting data from a group of human subjects. The experiments also investigated the effect of varying thickness of the obstacles, human subject postures, status of breathing, position of radar antenna relative to human subject's chest, as well as the length of survey times. The experimental results have shown that respiration as the primary vital sign can be detected with very high confidence and should be highlighted in developing radar systems for search and rescue for earthquake disaster survivors. Among the four human subject postures of faceup, facedown, faceleft, and faceright, detection of the cardiologic signals can solely be achieved possibly when the subject was facing up. When the radar antennas to be placed at certain offset, not directly above the human subject's chest, it is still possible for good detection of the breathing signal. The minimum recording time for extracting respiration signal can be as short as 5 s. Even be conservative, a period of 30 s should be long enough for catching the respiratory signal with high signal to noise ratio.

Beam Pattern Reconfiguration Based on Fourier Constrained Rotman Lenses

Yunhua Zhang[1, 2], **Vincent Fusco**[2], **and Guoqiang Zhu**[1]

[1]School of Electronic Information, Wuhan University, 430072, China
[2]The ECIT, Queen's University of Belfast, Belfast BT3 9DT, UK

Abstract— Beam pattern reconfigurable antenna is highly desirable for wireless communication systems and Radar systems, as it provides flexibilities for these systems to accommodate different scenarios and different functionalities. In this paper, a Rotman lens constructed with Fourier constraint is developed to perform beam pattern reconfiguration. A classical Rotman lens can be used for beamwidth reconfiguration without resorting to any digital processing, thus it provides a fast and low-cost solution for beam pattern reconfiguration. However, when it comes to the configuration of arbitrary beam patterns, the results will serverly deteriorate due to the intrinsic interference between the neighbouring beams. To overcome this disadvantage, constraining factors for converting a classical Rotman lens to a Fourier transform Rotman lens are derived, such that the constrained Fourier Rotman lens can produce orthogonal beams through a simple discrete Fourier transform (DFT) from its beam ports to its array ports and vice versa. The Fourier constraint is implemented by adding additional delay lines to the beam ports and locating beam ports with non-uniform spacing.

To validate the proposed Fourier Rotman lens design and its applications in beam pattern reconfiguration, a Fourier constrained Rotman lens operating at X-band has been designed, fabricated and measured. The resulting Fourier lens can perform over approximately 20% bandwidth when constructed with RMS error of 20%. Even when compared to an ideal classical Rotman lens model the above fabricated Fourier Rotman lens yields at least 7 dB improvement in beam orthogonality. Later, the Fourier constrained Rotman lens is employed to reconfigure beam patterns. It is demonstrated that arbitrary beam patterns, including arbitrary beam width and multiple beams with arbitrary phase front, can be readily achieved with the control of a simple switch matrix. Moreover, it has also been demonstrated that the Fourier constrained Rotman lens has a superiority over a classical Rotman lens in beam pattern reconfiguration, which is originated from its beam orthogonality.

As a summary, the paper shows the Fourier constrained Rotman lens provides a means for direct Fourier pattern synthesis and for improved beam forming. The improved beam pattern reconfiguration can be obtained without increased fabrication complexity. The reconfigurable antenna should find use in surveillance and tracking applications. And the Fourier Rotman lens has direct application in real-time microwave signal processing, and low cost beam forming applications, MIMO systems, or for millimeter wave imaging pre-processing.

Session 2P15
SC3: High-speed Optical Communications and Advanced Optical Signal Processing

SNR Comparison of Coherent Optical Receivers

M. Y. Leong[1,2], **S. Popov**[1], **G. Jacobsen**[1,2], **and S. Sergeyev**[3]

[1]KTH Royal Institute of Technology, Sweden
[2]Acreo Swedish ICT, Sweden
[3]Aston University, UK

Abstract— Using a unified approach, we directly compare theoretical SNRs of various receivers.

Coherent optical systems are impaired by additive white Gaussian noise (AWGN). This comes from amplified spontaneous emission (ASE) in fiber inline amplifiers and shot noise in photodetectors. Various architectures have been analyzed to establish theoretical limits of signal-to-noise ratio (SNR) [1–3]. However, previous publications only cover a few receivers each and use different definitions, so it is difficult to compare results. In this paper, we use a unified approach to derive SNRs for many architectures, and compare them directly. We consider the receivers in Fig. 1.

At (i) in Fig. 1, signal power P_s and ASE two-sided power spectral density (PSD) $\xi/2$ are fixed. Optical LO power of $E_{LO}(t)$ is also fixed. For all cases, we calculate SNR at (ii). Heterodyne with image-reject OBPF, heterodyne with optical image-reject receiver, and dual-quadrature homodyne have SNR $P_s/[(\xi+q/R)B]$, where q is electron charge and R is photodetector responsivity. Heterodyne without image rejection has SNR $P_s/[(2\xi+q/R)B]$. Single-quadrature homodyne is like heterodyne without image rejection but with zero IF. The transmitted signal has no quadrature component, e.g., BPSK. Its SNR is $P_s/[(\xi+q/[2R])B]$. Extending to dual-polarization, ASE per polarization is constant. If we assume that signal power per polarization is constant, then dual-polarization receivers have the same SNRs as their single-polarization counterparts.

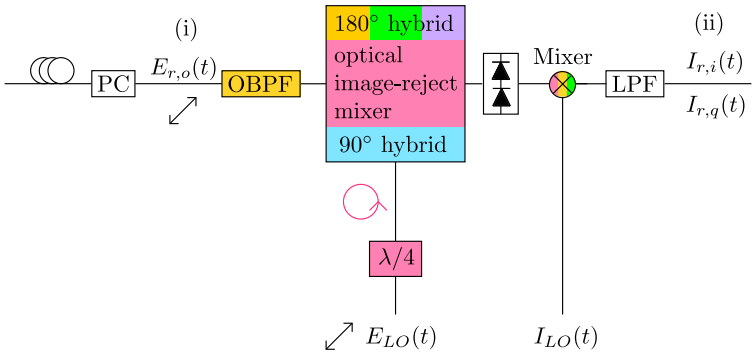

Figure 1: Single-polarization optical receiver. The (white) polarization controller (PC), balanced photodetectors, and low-pass filter (LPF) are always present. We consider five configurations: 1. (green) heterodyne without image rejection, 2. (yellow) heterodyne with image-reject optical bandpass filter (OBPF), 3. (pink) heterodyne with optical image-reject receiver [2], 4. (blue) dual-quadrature homodyne, and 5. (purple) single-quadrature homodyne. The input optical signal + noise is $E_{r,o}(t)$. The optical LO signal is $E_{LO}(t)$ and the electrical LO signal is $I_{LO}(t)$. The output electrical signal + noise in-phase and quadrature components are $I_{r,i}(t)$ and $I_{r,q}(t)$.

ACKNOWLEDGMENT

Work supported by Vetenskapsrådet (No. 0379801) and FP7-PEOPLE-2012-IAPP (No. 324391).

REFERENCES

1. Derr, F., "Comparison of electrical and optical BPSK and QPSK," *J. Opt. Commun.*, Vol. 10, No. 4, 127–131, 1989.
2. Jorgensen, B. F., B. Mikkelsen, and C. J. Mahon, "Analysis of optical amplifier noise in coherent optical communication systems with optical image rejection receivers," *J. Lightw. Technol.*, Vol. 10, No. 5, 660–671, 1992.
3. Ip, E., A. P. T. Lau, D. J. F. Barros, and J. M. Kahn, "Coherent detection in optical fiber systems," *Opt. Express*, Vol. 16, No. 2, 753–791, 2008.

Optical Digital-to-analog Converter Based on Microring Resonators and Optical Splitters

Fanfan Zhang, Ping Zhou, Qiaoshan Chen, Lei Zhang, and Lin Yang
State Key Laboratory on Integrated Optoelectronics
Institute of Semiconductors, Chinese Academy of Sciences, China

Abstract— There are many advantages to process and store data in digital format, which can represent an analog signal in arbitrary resolution and reduce the noise accumulation in signal transmission. The accompanying cost of employing digital signals is that we should always transform analog signals to digital forms and vice versa. So analog to digital converters (ADC) and digital to analog (DAC) converters are the key elements in electronic and photonic data transmission and signal processing. Optical DAC can provide high-speed conversion with the advantages of high-speed clock and sampling.

Silicon-based microring resonators is compatible with complementary metal-oxide-semiconductor (CMOS) process and has the advantages of low power consumption and high compactness, which make it an ideal component to construct integrated optoelectronic circuits.

We propose an N-bit optical digital to analog converter (DAC) based on an integrated optoelectronic circuit consisting of N microring resonators and N 1×2 optical splitters, which can transform an N-bit electrical digital signal to an optical analog signal. As the proof of concept, a 2-bit optical DAC is fabricated in the silicon-on-insulator platform by CMOS-compatible process. The 2-bit electrical digital signal is firstly converted to two electrical analog signals and then employed to modulate the two microring resonators through the electric-field-induced carrier injection in forward biased PIN diodes embedded in the ring waveguides. The analog optical output is detected at the output port of the circuit. A 2-bit optical DAC operating at 100 Mbps is demonstrated.

Multi-band Superchannel Coherent Optical Orthogonal Frequency-division Multiplexing Based on Offset QAM (OFDM/OQAM) System

Qi Yang
State Key Laboratory of Optical Communication Technologies and Networks
Wuhan, Hubei 430074, China

Abstract— We propose a multi-band super-channel coherent optical orthogonal frequency-division multiplexing based on offset QAM (OFDM/OQAM) system. Unlike the conventional orthogonal band-multiplexed OFDM system, no timing or frequency synchronization is required for the OFDM/OQAM system. We also investigate the influence of guard band, and find that very trivial guard band spacing ($< 20\,\mathrm{MHz}$) is required without any performance degradation. It would significantly reduce the implementation constrains for the band-multiplexed super-channel coherent optical OFDM system.

Programmable All-fiber Structured Optical Signal Processing for Flexible Optical Networks

Ming Tang[1], **Ruoxu Wang**[1], **Hailiang Zhang**[1], **Zhiyong Zhao**[1], **Songnian Fu**[1], **and Perry Ping Shum**[2]

[1]Next Generation Internet Access National Engineering Lab (NGIA)
School of Optical and Electronic Information
Huazhong University of Science and Technology, Wuhan, China
[2]Photonics Centre of Excellence, School of Electrical and Electronic Engineering
Nanyang Technological University, 50 Nanyang Avenue, Singapore

Abstract— We proposed and experimentally demonstrated all-fiber structured devices/modules for all-optical signal processing. Our proposed all-fiber devices are fully programmable by using computer software or working alone with MCU controller. The all-optical signal processing technology utilizes optical fiber with periodic structures or functional materials filled The optical property is tailored by applying digital controlled thermal effect.

At first, programmable waveshaper based on linearly chirped fiber Bragg grating (LCFBG) and digital thermal controller will be introduced. We used a standard commercial thermal print head (TPH) to introduced a phase shift of π into the LCFBG, and then aultra-narrow transmission peak will be generated within the stop band of the LCFBG transmission spectrum. The bandwidth of the filter is variable by adjusting the length of the heating area. Since the wavelength of obtained ultra-narrow transmission filter has a linear relationship with the heating position. We can simply obtained one or several filters with controllable shape by choosing the suitable heating area of the LCFBG.

Multi-wavelength filter with Mach-Zehnder interferometer embedded in ethanol filled photonic crystal fiber. We demonstrated a free spectrum range tunable comb filter based on a thermo-controlled Mach-Zehnder interferometer. The device is constructed by sandwiching a length of ethanol-filled photonic crystal fiber between two single mode fibers connected by two ceramic ferrules. In the PCF, the HE11 mode and the HE21 mode are propagating together. Sincethe effective refractive index of the ethanol-filled PCF can be modulated by thermo-optical effect, a thermal print head (TPH) is used to alter the core and the cladding refractive index. By controlling the parameter of the TPH, different variation of the refractive index will be obtained, the phase difference can be adjusted, and thus the interference between HE11 mode and HE21 mode willconstruct a digital-controlled comb filter. The FSR of the comb filter can be digitally tuned conveniently.

We further proposed and experimentally demonstrated an all-fiber structured wavelength-tunable and bandwidth-variable second-order temporal differentiator based on linearly chirped fiber Bragg grating (LCFBG) and thermal print head (TPH). A notch filter can be implemented by heating suitable area of the LCFBG, and the central wavelength and the shape of the notch filter can be controlled by adjusting the heated elements and unheated spacing elements of the TPH. To adjust those parameter, we can obtain a transfer function of second-order differentiator. The central wavelength and the operation bandwidth can be simply accomplished using computer software to shift the right heated and unheated regions along the TPH without moving any components.

The technologies mentioned above are promising for flexible all-optical network, acting as flex-grid tunable optical filter, flexible wavelength selective filter, and all-optical signal generation & processing.

Polarization Demultiplexing in Stokes Space for Coherent Optical Fiber Communications

Xingwen Yi[1], **Zhenming Yu**[1], **Qi Yang**[2], **and Kun Qiu**[1]

[1]Key Laboratory of Optical Fiber Sensing and Communications, Ministry of Education
University of Electronic Science and Technology of China, Chengdu 611731, China
[2]State Key Lab of Optical Communication Technology and Networks, Wuhan, Hubei 430074, China

Abstract— In high-speed and long-distance optical fiber transmissions, polarization multiplexing is widely used to double the spectrum efficiency. However, the polarization states cannot be maintained in the transmission fiber. Therefore, polarization demultiplexing must be applied in receivers for polarization multiplexing systems. As an alternative to conventional constant modulus algorithm (CMA), polarization demultiplexing in Stokes space (SS-PDM) could tolerate chromatic dispersion (CD) and polarization dependent loss (PDL). In this paper, we discuss our recent work to apply SS-PDM both in single-carrier systems and coherent optical OFDM systems:

1. We apply SS-PDM in coherent optical PDM-OFDM system, which could realize polarization multiplexing without inserting train symbols. With a lower overhead, it works well for different modulation formats of OFDM subcarrier. We verify this method in experiment and also show a faster convergence speed.
2. We propose a modified method of constant modulus algorithm (CMA) based on SS-PDM in single-carrier systems. The singularity problem of CMA is avoided effectively in a much wider range of PDL and its convergence speed is also improved. We demonstrate this modified CMA in a simulation of 100-Gbit/s PDM-QPSK with different PDL values. We also experimentally demonstrate this method.

Coherent Detected Temporal Optical Code Division Multiplexing System with High Spectral Efficiency Using Nyquist Pulse Shaping

Lin Chen, Xuezhi Hong, and Changjian Guo*
ZJU-SCNU Joint Research Center of Photonics
South China Normal University (SCNU), Guangzhou 510006, China

Abstract— By using dedicated orthogonal codes for each channel, optical code division multiplexing (OCDM) system offers several attracting features [1], e.g., asynchronous access, soft-capacity and high security, etc.. However, the spectral efficiency of system is decreased in the spectrum spreading process if the number of codes N_c employed is less than the spreading length N_l. In traditional OCDM systems, the spectral efficiency is further limited by the large carrier spacing (> baud rate) in spectral coded systems [2] or non-ideal pulse shaping (not Nyquist) in temporal coded systems [3]. In [4], we have proposed a high SE spectral coded system based on orthogonal frequency multiplexing (OFDM) with carrier spacing equal to baud rate. In this paper, to improve the SE of the temporal coded system, we present a coherent detected OCDM scheme using Nyquist pulse shaping. The schematic description of our proposal is shown in Fig. 1. With Nyquist pulse shaping after temporal encoding, the spread spectrum width of temporal coded signal can be reduced to chip-rate. Therefore, the SE of proposed system is improved compared to conventional temporal OCDM system [3] whose spectrum width could be several times of chip rate.

The transmission of Nyquist-shaped temporal OCD Msignal over 400 km standard single mode fiber with coherent detection is evaluated using Mentor Carlo simulations. The Walsh codes are employed in the encoding/decoding blocks. The OCDM encoding/decoding and Nyquist pulse shaping are conducted in electrical domain, which can share the existing facilities with other DSP functions in the coherent system. The BER performance of the proposed system with different input power under different laser line width is presented (Fig. 2).

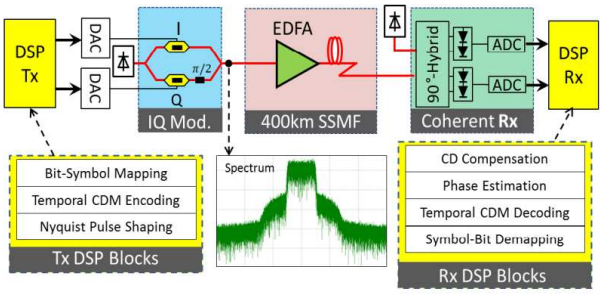

Figure 1: Schematic description (inset: optical spectrum after Nyquist shaping).

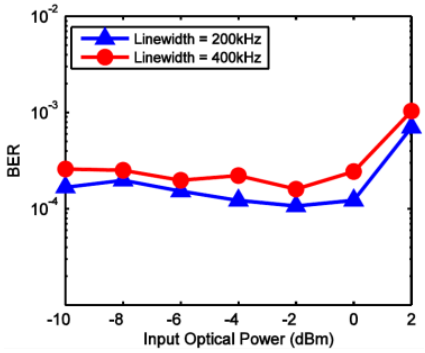

Figure 2: BER vs. input optical power after 400 km transmission.

REFERENCES

1. Ghafouri-Shiraz, H. and M. Massoud Karbassian, *Optical CDMA Networks: Principles, Analysis and Applications*, Wiley, New York, 2012.
2. Toliver, P., et al., "Demonstration of high spectral efficiency coherent OCDM using DQPSK, FEC, and integrated ring resonator-based spectral phase encoder/decoders," *Proceedings of OFC/NFOEC*, PDP 7, 2007.
3. Wang, Z. X., et al., "Secure optical transmission in a point-to-point link with encrypted CDMA codes," *IEEE Photonics Technology Letters*, Vol. 22, No. 19, 1410–1412, 2010.
4. Hong, X., et al., "Coherent detected secure point-to-point optical fiber transmission using ultra-dense optical spectral phase coding (UD-SPC) and multilevel BCJR equalization," *Proc. of Asia Communications and Photonics Conference*, ATh4C.3, 2012.

*Corresponding author: Changjian Guo (changjian.guo@coer-scnu.org).

Chaos Optical Time-domain Reflectometry

Anbang Wang[1,2], **Xiangyu Dong**[1,2], **and Yuncai Wang**[1,2]

[1]Key Laboratory of Advanced Transducers and Intelligent Control System
Ministry of Education and Shanxi Province, China
[2]College of Physics and Optoelectronics
Taiyuan University of Technology, Taiyuan 030024, China

Abstract— Wavelength-division-multiplexing passive optical network (WDM-PON) is considered as a promising optical accessing network [1]. Optical time domain reflectometry (OTDR) has been the main technique for measuring fiber loss distribution and analyzing the causation and location of fault or damage events. But its resolution is not competent for detection of optical accessing network in which faults may happen densely. We proposed a novel OTDR of using broadband chaotic light. This chaos optical time domain reflectometer (COTDR) [2] has the advantage over the conventional OTDR whose spatial resolution are about tens of meters, determined by the pulse duration, in range-independent spatial resolution. Using this broadband chaotic laser, we experimentally demonstrate the proposed COTDR for locating the fiber reflection events, and realize a range-independent resolution of 4 cm and measurable distance of about 70 km. Moreover, according to this experiment setup, we have developed a prototype COTDR.

Furthermore, we propose a method to locate precisely faults in WDM-PON by using a wavelength tunable chaotic laser [3], the experimental setup shown in Fig. 1. The chaotic laser consists of a multiple-longitudinal-mode Fabry-Perot (FP) laser diode whose modes match the channels of WDM-PON, and an optical feedback loop including a filter. By adjusting the filter frequency, we can tune the wavelength of the chaotic light, and diagnose the corresponding branch of WDM-PON. We demonstrate a proof-of-concept experiment for detection of three ITU channels. The results show that spatial resolution of 2 cm and dynamic range of about 20.8 dB can be achieved. Figs. 2(a)–(c) show the logged measure curves (5 log) of the three channels, respectively.

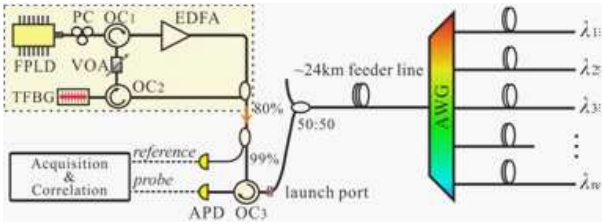

Figure 1: Experimental setup of the tunable COTDR.

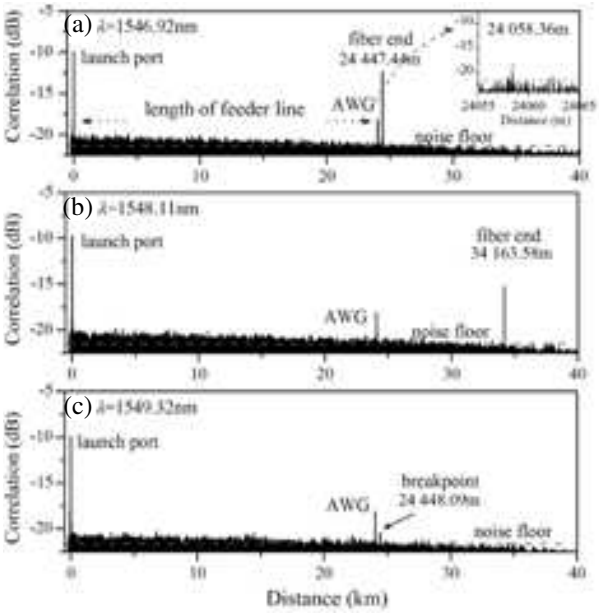

Figure 2: Experimental measure results for channels at wavelength of (a) 1546.92 nm, (b) 1548.11 nm, and (c) 1549.32 nm.

REFERENCES

1. Park, S.-J., C.-H. Lee, K.-T. Jeong, H.-J. Park, J.-G. Ahn, and K.-H. Song, "Fiber-to-the-home services based on wavelength-division-multiplexingpassive optical network," *J. Lightw. Technol.*, Vol. 22, No. 11, 2582–2591, Nov. 2004.

2. Wang, Y. C., et al., "Chaotic correlation optical timedomain reflectometer utilizing laser diode," *IEEE Photon. Technol. Lett.*, Vol. 20, 1636–1638, 2008.
3. Wang, A. B, et al., "Precise fault location in WDMPON by utilizing wavelength tunable chaotic laser," submitted to *J. Lightw. Technol.*, 2012.

Sub-symbol Based Carrier Phase Recovery in CO-OFDM System with Linear Interpolation

Xiaojian Hong, Xuezhi Hong, and Sailing He
ZJU-SCNU Joint Research Center of Photonics
South China Normal University (SCNU), Guangzhou 510006, China

Abstract— Coherent optical orthogonal frequency division multiplexing (CO-OFDM) has been intensively studied for its high tolerance to chromatic dispersion (CD) and polarization mode dispersion (PMD) [1, 2]. However, the performance degradation caused by laser phase noise is more pronounced in CO-OFDM with respect to the single carrier counterpart. When phase noise is large, conventional common phase error compensation (CPEC) is not sufficient to maintain the system performance. In [3], we proposed to use sub-symbol CPEC (S-CPEC) to improve the phase noise tolerance of CO-OFDM system. Better approximation of the phase noise is achieved by linear interpolation (LI) of the CPE estimation of the consecutive CO-OFDM symbols [4]. In this paper, a novel phase noise suppression algorithm combing sub-symbol processing and LI (i.e., LI-S-CPEC) is proposed. Details of LI-S-CPEC algorithm are depicted in Fig. 1(a).

The key idea of the algorithm is to divide a full symbol into several sub-symbols to get an accurate estimation of phase noise inside one symbol. The coarse carrier phase is first estimated using conventional full symbol CPE and then the estimated CPE value is set equal to the middle time domain sample of the corresponding symbol. The phase noise values of the remaining intermediate samples of each symbol in time domain are obtained by linear interpolating the CPE estimation of the adjacent symbols. After tentative decision on coarse compensated signal, the IFFT of tentative decision and received data are partitioned to several sub-symbols to get CPE for the corresponding sub-symbols. A 10 GS/s, 256-IFFT, 16QAM modulated CO-OFDM system is simulated. As shown in Figs. 1 (b), (c), the linewidth tolerance of above system for 4 dB OSNR penalty (BER = 10^{-3}) are 125 kHz (CPEC), 189 kHz (LI), 342 kHz (S-CPEC) and 512 kHz (LI-S-CPEC). Therefore, LI-S-CPEC improves system tolerance of laser phase noise evidently.

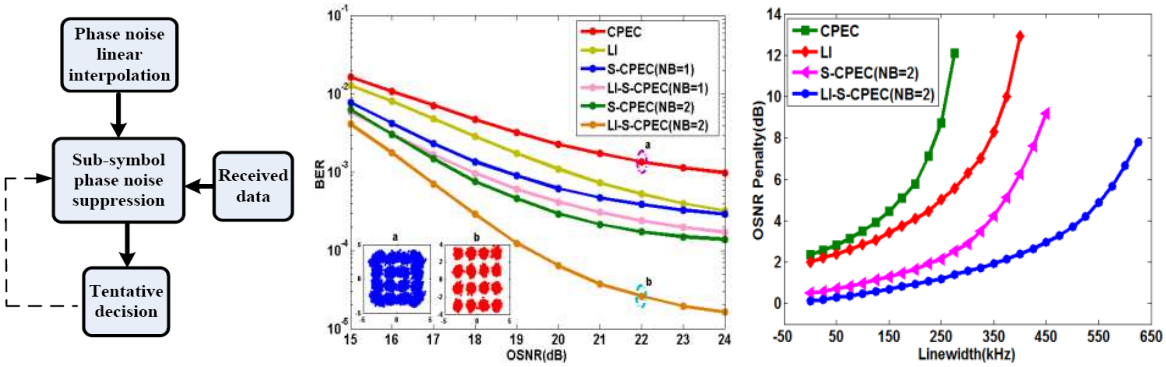

Figure 1: (color online) (a) Block diagram of LI-S-CPEC algorithm. (b) B2B performances for laser linewidth = 250 kHz, insets show the corresponding constellations of point a or b. (c) OSNR penalty curves at BER = 10^{-3} for different laser linewidth.

REFERENCES

1. Shieh, W. and I. Djordjevic, *OFDM for Optical Communications*, Elsevier, 2009.
2. Yi, X., W. Shieh, and Y. Ma, "Phase noise effect on high spectral efficiency coherent optical OFDM transmission," *IEEE Journal of Lightwave Technology*, Vol. 26, No. 10, 1309–1316, 2008.
3. Hong, X. and S. He, "Sub-frame carrier phase estimation for coherent optical orthogonal frequency multiplexing system," *PIERS Proceedings*, Stockholm, Sweden, Aug. 12–15, 2013.
4. Mousa-Pasandi, M. E. and D. V. Plant, "Non-iterative interpolation-based partial phase noise ICI mitigation for CO-OFDM transport systems," *IEEE Photonics Technology Letters*, Vol. 23, No. 21, 1594–1596, 2011.

Phase-conjugated Twin Waves for Optical OFDM Transmissions

Dengke Zeng, Xingwen Yi, Zhenming Yu, Jing Zhang, and Kun Qiu
Key Laboratory of Optical Fiber Sensing and Communications, Ministry of Education
University of Electronic Science and Technology of China, Chengdu 611731, China

Abstract— The emerging coherent optical orthogonal frequency division multiplexing (CO-OFDM) provides major advantages in spectral efficiency and in mitigating the chromatic dispersion and polarization-mode-dispersion impairments. However, a main problem intrinsic to OFDM is its susceptibility to nonlinearity due to high peak-to-average power ratio. In order to mitigate nonlinear impairments in OFDM systems, we propose an OFDM transmission system based on phase-conjugated twin waves (PCTW). PCTW is recently proposed in [1] as a method to cancel nonlinear signal-to-signal interactions. Because it is on per symbol basis, PCTW is a modulation format independent technique which can be applied to OFDM signal symbols. We manipulate the two polarizations to obtain the PCTW in the frequency domain and conduct the digital coherent superposition (DCS) after channel equalizations.

Simulations are performed to compare the conventional PDM-COOFDM system with the proposed PCTW-COOFDM system. In this paper, we also discuss the robustness of PCTW-COOFDM system in the presence of single-channel fiber nonlinearity and the different nonlinear performance between PCTW-QPSK systems and PCTW-OFDM systems. Fig. 1 shows the Q-factor as a function of the signal launch power after 3200-km standard single-mode fiber (SSMF) transmission. At a launch power of 4 dBm, the overall Q-factor improvement by PCTW is ~ 7.1 dB, which corresponds to a reduction of nonlinear signal variance of ~ 8.1 dB when the impact of the linear noise is excluded.

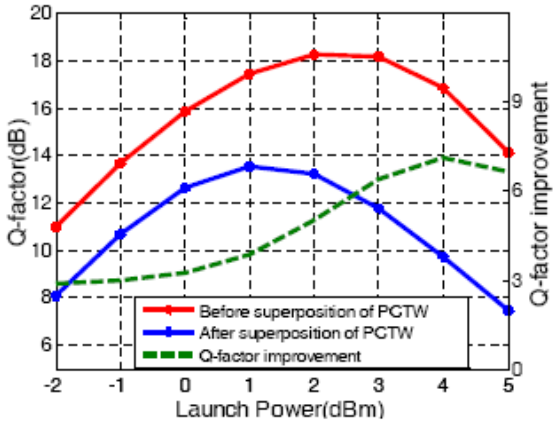

Figure 1: Q-factor as a function of launch power.

REFERENCES

1. Liu, X., A. R. Chraplyvy, P. J. Winzer, R. W. Tkach, and S. Chandrasekhar, "Phase-conjugated twin waves for communication beyond the Kerr nonlinearity limit," *Nature Photon.*, Vol. 7, 560–568, 2013.

SSBI Cancellation Method for IMDD-OFDM System with a Single Photodiode

Xuebing Zhang, Jianping Li, and Zhaohui Li
Institute of Photonics Technology, Jinan University, Guangzhou, Guangdong 510632, China

Abstract— A novel approach is proposed to cancel the SSBI effect for direct-detection double-sideband optical OFDM (DD-DSB-OFDM) signal. Simulation results indicate that the proposed approach can cancel the SSBI effectively and has achieved large power efficiency improvement compared with the conventional scheme.

Quantum Cascade Lasers for Free Space Communications

Xiaohui Li[1] **and Qi Jie Wang**[1, 2]

[1]School of Electrical and Electronic Engineering
Nanyang Technological University, 50 Nanyang Ave., Singapore 639798, Singapore
[2]School of Physics and Mathematics Sciences
Nanyang Technological University, 50 Nanyang Ave., Singapore 639798, Singapore

Abstract— Quantum cascade laser (QCL) is a semiconductor device based on multiple quantum wells/barriers designed to emit light in the mid-infrared and Terahertz ranges, roughly from 3–300 micrometer. Because the emission wavelength of this device is not determined by the bandgap of the material but by suitable engineering the thicknesses of those multiple quantum wells/barriers, it has been widely used to generate arbitrary wavelength emission in the midinfrared and Terahertz for various applications, including free-space communications.

In this talk, I will first introduce the current work in free space communications with mid-infrared and Terahertz QCLs, followed by the introduction of the operation principle of QCLs. Then I will talk about our recent development of high power low beam divergence mid-infrared and Terahertz QCLs, which are suitable for free space communications. After that, I will introduce our recent work on achieving high speed modulation of mid-infrared and THz QCLs based on injection-locked design and nanomaterial modulation, respectively. Our recent work on graphene-based high responsivity mid-infrared photodetector will also be discussed.

Carbon Materials for Ultrafast Photonics

Xiaohui Li[1] **and Qijie Wang**[1, 2]

[1]OPTIMUS, Centre of Excellence for Photonics, School of Electrical and Electronic Engineering
Nanyang Technological University, 50 Nanyang Ave., Singapore 639798, Singapore
[2]Centre for Disruptive Photonic Technology, School of Physical and Mathematical Sciences
Nanyang Technological University, Singapore 637371, Singapore

Abstract— Ultrashort optical pulses have been highly demanded in scientific studies and applications, e.g., high-speed optical laser sources for optical communication, optical frequency comb for optical metrology and time-resolved studies of ultrafast nonlinear phenomena, seeds sources for laser amplifiers and supercontinuum sources, as well as the optical nano-machining for the materials processing etc.. Various nano-materials have been demonstrated to be suitable for the generation of ultrashort pulses. In this paper, we summarized our recent work about the short pulse generation based on the carbon materials, single-wall carbon nanotube (SWNT), graphene oxide (GO). We summarize the carbon materials preparation as saturable absorber (SA) and characterization (Fig. 1). And then we demonstrate the application in high energy pulse generation (Fig. 2), the carbon materials induced inverse operation for the passively mode locked fiber lasers (Fig. 3). We also report the phase noise reduction by controlling the SA in the laser systems (Fig. 4).

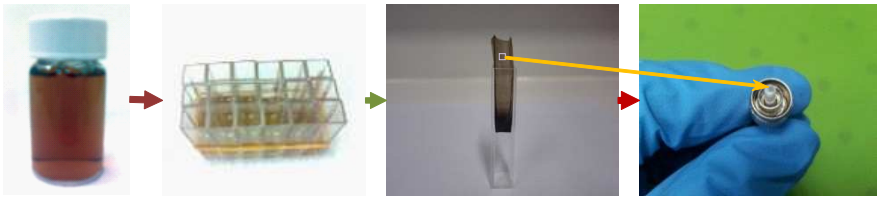

Figure 1: The SA components preparation for SWNT- and Go-PVA SAs

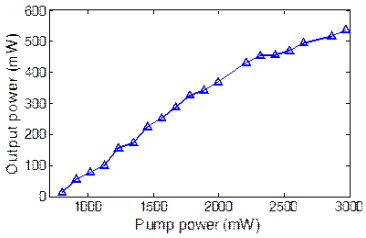

Figure 2: The amplified output power versus the pump power.

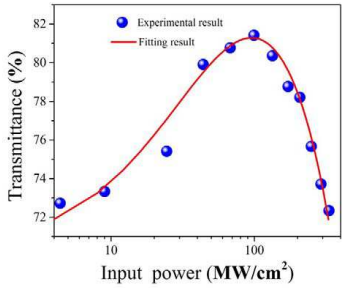

Figure 3: Nonlinear transmittance of the SWNT/PVA film, which shows the inverse saturable absorption.

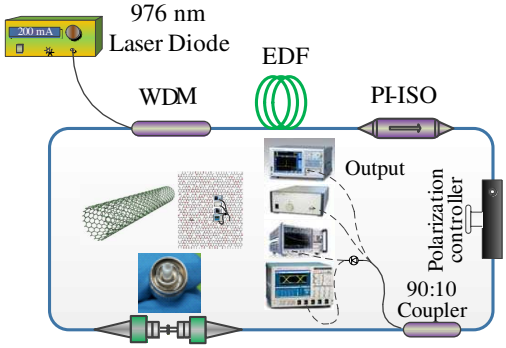

Figure 4: Schematic experimental setup of the passively mode-locked erbium-doped fiber laser based on SWNT- or GO-PVA SAs for the phase noise reduction.

ACKNOWLEDGMENT

We would like to acknowledge financial support from A*STAR SERC grant (Grant No. 112-290-4018) and A*STAR SERC Advanced Optics in Engineering Programme (Grant No. 122 360 0004).

Session 2P0
Poster Session 3

A Wideband Wide-angle Polarization-insensitive Metamaterial Absorber

Peng Cheng Zhang, **Xian Qi Lin**, **Fei Cheng**, **Rui Shen**, **and Yong Fan**
EHF Key Lab of Fundamental Science, School of Electronic Engineering
University of Electronic Science and Technology of China, Chengdu 611731, China

Abstract— Matematerial absorber (MMA) reported by Landy et al. in 2008 [1] has attracted considerable attention in recent years. More recently, several efforts have been made to improve its electromagnetic characteristics, such as polarization-insensitive [2], wide incident angle and wideband absorption. However, the current MMAs still have imperfections in achieving the three above features simultaneously. In this article, an efficient design is present to achieve a wideband, wide-angle, polarization-insensitive MMA. The absorptivity A is simulated by using one cell and infinite period model. In more directive perspective, the absorption is defined as $A = 1 - T - R = 1 - |S_{21}|^2 - |S_{11}|^2$. To maximize the absorption rate, we can minimize the reflection and transmission simultaneously at the same frequency range. Due to the metal background of the structure, the transmission $|S_{21}|$ is equal to zero. Figure 1 shows the geometry of the present absorber cell. The top layer consists of resonators lumped resistors R set in a periodic pattern and bottom layer is a metal plane. Figure 2 illustrates the simulated refraction indexes with wide incident angle ranging from 0 to 60 degree for transverse electric polarization.

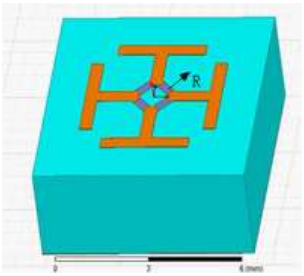

Figure 1: Geometry of MMA cell.

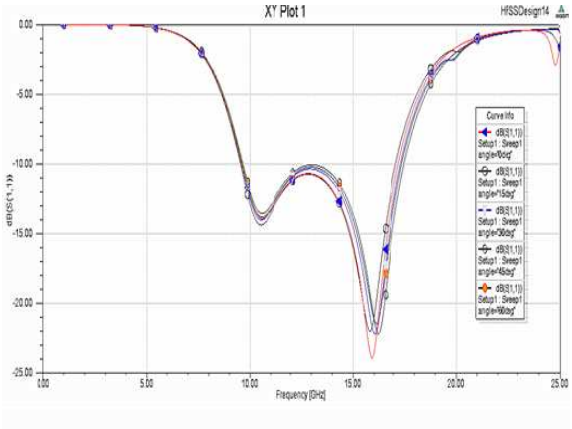

Figure 2: Simulated refraction indexes for different incidence angles for TE polarization.

REFERENCES

1. Landy, N. I., S. Sajuyigbe, J. J. Mock, D. R. Smith, and W. J. Padilla, "Perfect metamaterial absorber," *Phys. Rev. Lett.*, Vol. 100, 207402, 2008.
2. Landy, N. I., C. M. Bingham, T. Tyler, N. Jokerst, D. R. Smith, and W. J. Padilla, "Design, theory, and measurement of a polarization-insensitive absorber for terahertz imaging," *Phys. Rev. B*, Vol. 79 125104, 2009.

Design and Analysis of a Wideband Metamaterial Absorber Applied to Radome

Zhiwen Mao, Shaobin Liu, Xiangkun Kong, Borui Bian, Beiyin Wang, and Lin Chen
Key Laboratory of Radar Imaging and Microwave Photonics, Ministry of Education
College of Electronic and Information Engineering
Nanjing University of Aeronautics and Astronautics, Nanjing 210016, China

Abstract— In this paper, a detailed study of a single-layer wideband metamaterial absorber (MMA) applied toradome, which is transparent at the operating frequency and is absorption at frequencies ranging from 2.5 GHz to 7 GHz. The design is discussed by the unit cell and equivalent circuit model. A unit cell of the periodic structure for the absorber is designed and simulated. The MMA consists of a two-dimensional periodic array of resistor-loaded square loops and crosses. The composite structure is thoroughly analyzed by an efficient equivalent circuit approach and by full-wave numerical simulations. Simulation results show that the proposed MMA has a wideband absorption range that covering most of the C-band and S-band. A pass-band at the frequency 11.2 GHz is obtained, which is operating in X-band. It also shows that the MMA sample is polarization insensitive for TE and TM incident wave and high absorption for wide angle of incidence is up to 60°.

Preliminary Experimental Results along a Horizontal Path for Adaptive Rate-controlled FSO

Changqi Yang[1], **Juan Zhao**[1], **and Anqi Liu**[2]

[1]School of Science, Xi'an Shiyou University, Xi'an 710065, China
[2]Advanced Technology Institute, Hubei University, Hubei 430062, China

Abstract— Free-space optical communication is a focus in recent research. Because of the influence of weather conditions, the transmission channel of free-space optical communication dramatically changes. This paper describes the design of a new adaptive rate-controlled optical communication system. The rate adaptively changes through the estimation of the received signal strength. Usually estimate the channel conditions with a low rate of radio frequency feedback. Previously the author used a new technique to design an adaptive rate-controlled optical communication system. It used beacon calibration instead of radio frequency feedback. In this paper an outdoor experiment is performed along a 186 meters horizontal path. On-off Keying modulation is used. The preliminary results with adaptive rate control are compared with that of without adaptive rate control. It appears to be at least an order of magnitude decrease of the bit-error rate.

A Transmission-typed Broadband Absorber

Hai-Ming Li[1], **Shao-Bin Liu**[1], **Hai-Feng Zhang**[1, 2], **and Xiang-Kun Kong**[1]

[1]Key Laboratory of Radar Imaging and Microwave Photonics, Ministry of Education
College of Electronic and Information Engineering
Nanjing University of Aeronautics and Astronautics, Nanjing 210016, China
[2]Nanjing Artillery Academy, Nanjing 211132, China

Abstract— In this paper, we theoretically found that a wide, near complete absorption in a large range of incident angles for both polarizations can be realized in a heterostructure composed of a dielectric layer and truncated photonic crystals with a lossy dielectric defect. A dielectric layer is put on the top of the truncated photonic crystals to gain a relative flatter broadband absorptions. It is shown that 80% absorption for transverse magnetic (TM) and transverse electric (TE) wave is obtain when the ranges of incident angles is 0 to 60° and 0 to 40°, respectively. Owing to the zero-n gap, the broadband absorption weakly depend on incident angles. The wide absorption band is located within pass band of photonic crystals, which is different of some previous designs.

Realization of XOR and OR Logic Gate with One Configuration in the Two-dimensional Photonic Crystals

Yuchi Jiang[1, 2], **Shao-Bin Liu**[1], **Hai-Feng Zhang**[1], **and Xiang-Kun Kong**[1]

[1]Key Laboratory of Radar Imaging and Microwave Photonics, Ministry of Education
Nanjing University of Aeronautics and Astronautics, Nanjing 210016, China
[2]School of Physics and Electronic Engineering, Changshu Institute of Technology, Changshu 215500, China

Abstract— Based on the theory of light beam interference effect, a new configuration is designed to realize two types of all-optical logic gates including XOR and OR logic gate in two-dimensional photonic crystals, and the distribution of the electrical field is simulated by the Finite-difference in time-domain method. The results show that through this new configuration, not only the two types of all-optical logic gates can be realized, but the higher light contrast ratio of the logic state "1" and "0" can also be obtained. The realization of two types of all-optical logic gates in one configuration is helpful and significant to the optical device integration and potential in the optical communications. It is noticed that the logic state of "1" and "0" at output port are defined as the transmission is larger than 0.5 and less than 0.1, respectively.

Efficient Localization of Terahertz Waves within a Gradient Dielectric-filled Metallic Grating

Wenyu Zhao[1], **Dongquan Ju**[1], **and Yongyuan Jiang**[1, 2]

[1]Department of Physics, Harbin Institute of Technology, Harbin 150001, China
[2]Key Lab of Micro-Optics and Photonic Technology of Heilongjiang Province, Harbin 150001, China

Abstract— Recently reported plasmonic graded metallic grating has opened a new approach for trapping SPPs over a wide spectral band at THz frequency and offers potential applications in optical delay lines, buffers, storage and enhanced nonlinear effects. In this paper, we proposed a gradient dielectric-filled metallic grating to spatially localize a wide-band terahertz wave at different locations for different frequencies, which is called "rainbow trapping". The dispersion relations for terahertz waves propagating along gratings with different filling-depths dielectric were studied under the first-order approximation based on the spoof surface plasmon theory. The dispersion relation curves of THz waves have been dramatically modified by the grating parameters, and the cutoff frequency decreases as filling-depths increases. Spoof SPPs with frequency that is lower than the cutoff frequency are capable of propagating along the metallic grating, while that with frequency higher than the cutoff frequency are prohibited. In particular, as the SPPs frequency approaches the cutoff frequency, the group velocity reduces to zero and indicates that dielectric-filled metallic grating with a certain filling-depths can trap the THz waves near the cutoff frequency. The gradient dielectric-filled metallic grating can localize terahertz waves at the frequency regime from 0.7 to 1.3 THz as the filling-depth gradually increasing from $H = 0$ to 50 μm. Through filling with nematic liquid crystal (4'-n-pentyl-4-cyanobiphenyl, 5CB), the structure can act as an active device. The effective refractive index is able to be tuned by controlling the direction of applied magnetic field, thus, the trapping locations can be varied for different field directions. The structure has a compact size which can be further reduced by filling higher refractive index dielectric, and has potential applications in multi-channel switch, controllable storage and filter.

Nonreciprocal Self-collimation Transmission in Two-dimensional Gyromagnetic Photonic Crystals

Qing-Bo Li[1, 2], **Zhen Li**[1], **and Rui-Xin Wu**[1]

[1]Department of Electronic Sciences and Engineering, Nanjing University, Nanjing 210093, China
[2]School of Physics and Electronic Electrical Engineering, Huaiyin Normal University, Huaian 223300, China

Abstract— We studied self-collimation properties in two-dimensional gyromagnetic photonic crystals (GPCs) composed of semi-circle ferrite YIG rods. Because of the asymmetry in the unit cell of GPC in square lattice, we obtained progressively tilting flat contours in the band structure for transverse magnetic modes. The asymmetry in the unit cell and time reversal symmetry breaking of GPC leads to the equifrequency contours (EFCs), which are nearly flat, asymmetric in certain direction. Therefore, the wave incident on GPC in certain direction will be selfcollimating transmit but may completely reflected from the opposite direction.

This phenomenon was proved by the simulations of wave propagation in GPC. For example, at $a = 10\,\text{mm}$ and frequency $0.594(2\pi c/a)$, the wave incident along $+19^\circ$ to the normal of GPC shows self-collimated propagation with almost no diffractions inside the GPC, and nearly totally reflected at the interface at incident angle -19° to the normal. This nonreciprocal propagating mode avoids beam severe broadening and keeping its profile unchanged due to diffraction. In particular, the designed structure ensures that the collimated mode stays single mode over the operating frequency interval from about $\omega = 0.59(2\pi c/a)$ to $0.64(2\pi c/a)$. The working principle is believed to have enjoyed rapidly growing interest of microwave diode based on the self-collimation characteristics.

ACKNOWLEDGMENT

This work was supported by the NSFC (61271080, 61071007), and RFDP (20110091110030).

The Effect of Structural Parameters on Terahertz Quantum Cascade Lasers

Norihiko Sekine and Iwao Hosako
National Institute of Information and Communications Technology, Japan

Abstract— Terahertz quantum-cascade lasers (THz QCLs) have been attracting much attention as compact coherent light sources and are expected to be applicable to a variety of applications, such as bio-sensing, security, and environmental monitoring [1]. However, the operation of THz QCLs is restricted at low temperatures, and to be of practical use, they must operate even at higher temperatures (room temperature and above). To this date, the highest operating temperature of THz QCLs is still less than 200 K [2]. In this work, we have studied the effects of structural parameters of active regions in THz QCLs on lasing characteristics for improving the performance of the THz QCLs.

In THz QCLs, the active region is composed of a lot of gain units (more than 100 periods) which include upper-/lower-laser states and electron extraction states for realizing efficient creation of population inversion, and small change in thickness of semiconductor layers has considerable influence on gain characteristics etc.. Therefore, we have focused on a gain unit consisting of two quantum wells (QWs) for simplicity, and investigated optimum structures from the view point of the peak gain and the carrier leakage. Assuming the lasing frequency is in the range between 3 to 4 THz, the thicknesses of two GaAs QWs were set to be 9.4 and 10.8 nm, respectively, from the simple calculation. Then, we calculated the oscillator strength (f_{ij}) and the ratio between the scattering time from the upper to the lower laser-states (τ_{ul}) and the LO-phonon scattering time from the lower-laser state (τ_{LO}) by solving self-consistently the Poisson and the Schrödinger equations as good measures. Since these values reflect the peak gain at low temperature, the larger values are preferable for both low threshold current and high dynamic range in the operating temperature. On the other hand, energetic positions of higher states are also important for high-temperature operation because more carriers leak to the next gain unit through these states without THz emission as temperature rises. Therefore the energy difference between the upper laser-state and the lowest-lying leak state (ΔE) was also investigated as another good measure. By changing thickness of two AlGaAs barrier layers, we obtained optimum combination of barrier thicknesses by plotting all three values (f_{ij}, τ_{ul}/τ_{LO}, ΔE).

ACKNOWLEDGMENT

The authors would like to thank H. Yasuda and Y. Sakasegawa for fruitful discussions. This work is partly supported by JSPS KAKENHI Grant Number 24560434.

REFERENCES

1. Tonouchi, M., *Nature Photon.*, Vol. 1, 97, 2007.
2. Fathololoumi, S., et al., *Opt. Express*, Vol. 20, 3866, 2012.

Low Reflectance GaAs Nano-cones Fabricated by Colloidal Lithography for Solar Cells

Nan Liu, **Yu Hu**, **and Jian-Jun He**
State Key Laboratory of Modern Optical Instrumentation, Centre for Integrated Optoelectronics
Department of Optical Engineering, Zhejiang University, Hangzhou 310027, China

Abstract— Semiconductor nanostructures have attracted great attention for photovoltaic applications. Solar cells with surface modified by nanowires are demonstrated to have much lower reflectance, and thus higher absorption of photons. However, nanowires are usually cylindrical, which makes it difficult to fill the gaps between adjacent nanowires with other materials to form electrodes or p-n junctions (e.g., hybrid solar cells). A cone-shaped nanostructure can mitigate this problem. In this paper, we present a method of fabricating large-area well-ordered nano-cones using colloidal lithography and inductively coupled plasma (ICP) dry etching, and discuss the anti-reflectance performance. In the fabrication, we use SiO_2 nano-particles as the mask. Its selectivity in different reacting gases in ICP can result in different shapes of nanostructures. Before the etching, we use methanol-assisted self-assembly at the air/water interface to form the patterns. This method is simple and convenient, without using sophisticated equipment and is far less time consuming. The fabricated patterns are uniformly-distributed and the area can be as large as $2 \times 2\,\mathrm{cm}^2$, or even larger. Different ICP etching recipes are used to form rod-shaped and cone-shaped nanowires with the same height and period. The resultant nano-cone structures are well-shaped with smooth side walls. After the fabrication, the anti-reflection performance is measured and compared, which shows that cone-shaped nanowires can reduce the surface reflection to lower than 4% over the wavelength range of 400–900 nm, while nano-rods can only keep this value at approximately 6%. Theoretical simulations are also carried out using Comsol, which confirm that nano-cones provide better anti-reflectance performance.

Experimental Analysis of Thin Graphite Periodic Structures in the THz Band

M. P. M. Colleoni and B. Vidal
Nanophotonics Technology Center, Universitat Politècnica de València
8F Building, Camino de Vera, sn, Valencia 46022, Spain

Abstract— The THz gap has attracted considerable interest in the last decade in a wide range of applications (from astronomy to biology) due to the low energy of the THz waves and their capability to provide chemical recognition and non-destructive inspection [1]. To implement THz-based solutions, a wide range of components have been developed and efforts are being done to reduce the system cost through the use of inexpensive materials [2].

This work analyzes the development of metal wire grids by using the conductive properties of graphite. The aim is drawing the wire grid using a simple graphite lead pencil on standard paper. This would reduce the cost of several wire grid base components, such as polarizers or filters.

An 8B pencil is used because of its high graphite contents [3]. Parameters such as the pitch of the structure and its fill factor are set to study the behavior of the metal grid in a frequency range from 0.1 to 0.7 THz. The samples are analyzed using a fiber-based pulsed THz Time Domain Spectrometer in transmission mode. An ultrafast laser pulse impinges on a photoconductive antenna generating the THz beam that is detected by a similar switch. Preliminary experimental results with single samples of 800 micrometer average pitch and a fill factor of 0.8 show that the increase of the angle between the horizontally-polarized incoming electric field and the graphite periodic structure corresponds to a decrease of the THz absorption, hinting at a polarizer behavior (with an extinction ratio of 2 dB).

ACKNOWLEDGMENT

Spanish Ministry of Economy and Competitiveness, project TEC2012-35797.

REFERENCES

1. Tonouchi, M., "Cutting-edge Terahertz technology," *Nature Photonics*, Vol. 1, 2007.
2. Scherger, B., M. Scheller, N. Vieweg, S. Cundiff, and M. Koch, "Paper terahertz wave plates," *Opt. Express*, Vol. 19, No. 25, 1064–1076, 2011.
3. Abraham, E., A. Younus, J. C. Delagnes, and P. Mounaix, "Non-invasive investigation of art paintings by Terahertz imaging," *Appl. Phys., A Mater. Sci. Process.*, Vol. 100, No. 3, 585–590, 2010.

Label-free Multiscale Multiview and Multiwavelength Whole Body Photoacoustic Tomography of Small Animals in Vivo

Jeesu Kim[1], **Mansik Jeon**[2], **and Chulhong Kim**[3]

[1]Department of Electrical Engineering, Pohang University of Science and Technology, Republic of Korea
[2]Future IT Innovation Laboratory, Pohang University of Science and Technology, Republic of Korea
[3]Department of Creative IT Engineering, Pohang University of Science and Technology, Republic of Korea.

Abstract— We have developed a multiscale photoacoustic tomography (PAT) system. We performed multiscale PAT imaging of small animals in vivo by switching ultrasound transducers with different center frequencies in a single platform. The PAT images acquired with low ultrasound frequency (i.e., 5 MHz) shows vasculatures of small animals up to $\sim$ 10 mm and the axial spatial resolution is $\sim$ 150 μm. Further, the PAT images obtained with high ultrasound frequency (i.e., 40 MHz) shows microvasculatures of small animals up to $\sim$ 3 mm, and the axial spatial resolution is $\sim$ 50 μm. In addition, we have extended the scanning range of the system to the entire bodies of small animals, and acquired the whole body PAT images of small animals at four different imaging planes such as right sagittal, left sagittal, front coronal, and back coronal planes.Further, we have used four kinds of the excitation optical wavelength: 532, 700, 850, and 1064 nm. At each imaging view and wavelength, internal organs (e.g., spleens, intestines, etc.) as well as major blood vessels (e.g., carotid arteries, jugular vein, etc.) of small animals are clearly visible. The whole body PAT images at each wavelength verify the spectral optical absorption response of the internal structure. After PAT imaging, we have confirmed the position and identification of each organ in the PAT images with invasively acquired photographs.The developed multiscale multiview and multiwavelength PAT imaging system would be potentially an essential imaging modality for small animal researches.

Analysis, Design and Simulation of a Compact Wide Band VHF High Power Tubular Band Pass Filter

Zohre Pourgholamhossein, Gholamreza Askari, Hamid Mirmohammad Sadeghi, and Mehdi Fadaei
Information and Communication Technology Institute (ICTI)
Isfahan University of Technology (IUT), Isfahan 84156, Iran

Abstract— Lumped element filters are used at microwave frequency to about 18 GHz [1]. Dimensions of theses filters are much smaller than distributed filters, which is their major advantages. Actually one of the most important problems of high power transmitter is harmonic radiation and the interfering effects on other communication system. Major efforts are been done to reduce the interferences. To remove the spurious radiation various filters have been presented [2–4]. Also various type of high power filters in [5, 6] have been proposed. These filters constructed by dielectric resonator and sinusoidal quasi periodic waveguide structures. In order to solve the large dimension and power handling difficulties, semi lumped technology was used. Significant development have taken place since 1998 [7], Super conductor technology and microstrip lumped element circuits has been introduced as a tubular BPF with fractional band width about 0.6% (narrow band). But super conducting filter technology is not employed as a high power filter. The later method has been presented in 2006 [8] as a wide band case which is tubular filter terminated with inductor.

This paper present analysis, design and simulation of a wide band VHF coaxial high power tubular band pass filter terminated with capacitor. A semi-lumped structure is used to decrease the size of the filter and improve its power handling. In this analysis all effects of critical distributed and lumped structures are considered. Basic filter design will be introduced and filter geometry and prototype values are discussed. The realization process of the filter and the physical parameters of capacitors and inductors are obtained. Important criteria in choosing reactive elements such as inductors, dielectric gap and air gap with considering average and peak power handling are completely discussed. As it is shown in Fig. 1 considering the topology of 4 orders band pass filter, the filter in coaxial form realized by 5 series coupling capacitors and 4 resonators that

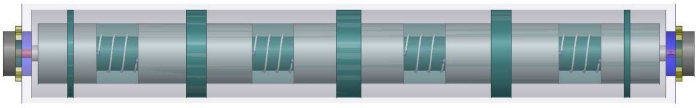

Figure 1: Configuration of a semi coaxial band-pass filter.

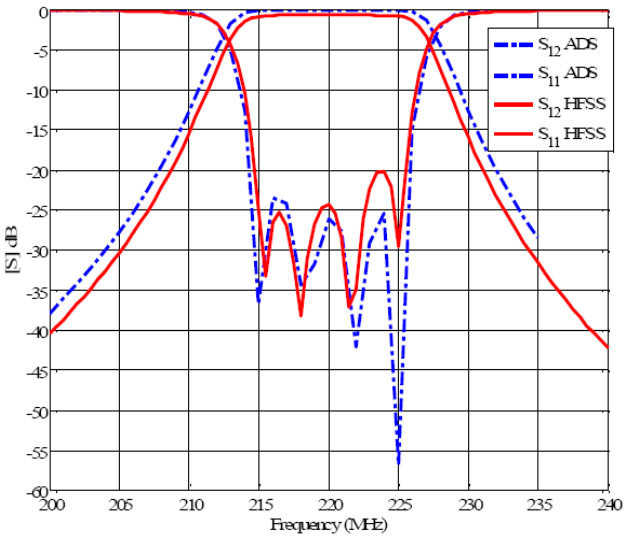

Figure 2: Simulated frequency response of the experimental Band pass filter (solid & dot-dash lines on HFSS and ADS, respectively.

constructed by lumped and distributed elements. To realization of the complete coaxial filter, design and optimization of filter is done stage by stage. Designed n-order filter, will be divided into $2n + 1$ stage that consists pi network capacitors or series inductors. In this procedure, first stage will be optimized separately, and then the new stage will be added and optimized when the values of first stage remain steady and the process of increasing stage continues until $n + 1$ stage. The result of full EM simulator (HFSS) will be compared with design analysis of ADS, to verify the design process. Finally EM simulation is done for the whole filter. As it is shown in Fig. 2, full wave analysis of the filter confirms the designed filter and performance of the full wave simulation of the complete structure. In high power handling, average power and peak power should be considered, which are discussed completely. Another important factor to determine performance of a high power filter is breakdown that is discussed completely. For high power analysis, it is necessary to survey the electrical field and peak voltage on surface and volume of lumped and distributed components in all the circuit. So full wave analyzing must be done to determine critical points in the structure. A vector plot is used arrows to illustrate the magnitudes and direction of electrical field which is shown in Fig. 3. The electric field strength in all over the filter is less than breakdown voltage in air (3e6 V/m) and Teflon with input power of 10 KW (by applying some considerations). The filter has a center frequency of 220 MHz, 0.2 dB bandwidth of 10 MHz (B.W. 5%), insertion loss of about 0.6 dB, better than 30 dBc rejection in 10 MHz offset from the 0.2 dB bandwidth and a return loss better than 20 dB.

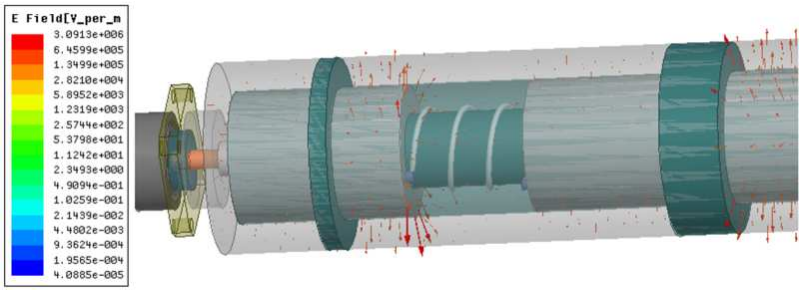

Figure 3: Vector E-field strength (V/m) across the filter in frequency 220 MHz.

REFERENCES

1. Levy, R., R. V. Snyder, and G. Matthaei, "Design of microwave filters," *IEEE Transactions on Microwave Theory and Techniques*, Vol. 50, No. 3, 783, 793, Mar. 2002.
2. Stone, R. H., "High power microwave filter," presented at the *1964 General Electric Co. High Power Tube Symp.*, TWT Business Section, Palo Alto, Calif., MD036, 1960.
3. Price, V. G., "Measurement and control of harmonic and spurious microwave energy, final rept., change B," General Electric Microwave Lab., Contract AF30(602)-1670, May 1960.
4. Yamashita, S. and M. Makimoto, "Miniaturized coaxial resonator partially loaded with high dielectric constant microwave ceramics," *IEEE Transactions on Microwave Theory and Techniques*, Vol. 31, 697–703, 1983.
5. Arregui, I., I. Arnedo, A. Lujambio, M. Chudzik, D. Benito, R. Jost, F. Görtz, T. Lopetegi, and M. A. G. Laso, "A compact design of high-power spurious-free low-pass waveguide filter," *IEEE Microwave and Wireless Components Letters*, Vol. 20, No. 11, 595, 597, Nov. 2010.
6. Bunin, A., V. Gevorkyan, Y. Kazantsev, S. Mikhalin, and S. Vishnyakov, "Resonant section for Ku-band high-power bandpass filter," *2010 IEEE Region 8 International Conference on Computational Technologies in Electrical and Electronics Engineering (SIBIRCON)*, 549, 551, Jul. 11–15, 2010.
7. Huang, Q. and J.-F. Liang, "Direct synthesis of tubular band pass filters with frequency-dependent inductors," *IEEE MTT-S, Digest*, 371–374, 1998.
8. Wu, B., T. Su, B. Li, and C.-H. Liang, "Design of tubular filter based on curve fitting method," *Journal of Electromagnetic Waves and Applications*, Vol. 20, No. 8, 1071–1080, 2006.
9. Hong, J. S. and M. J. Lancaster, *Microstrip Filters for RF/Microwave Applications*, Wiley, 2001.
10. Matthaei, G., et al., *Microwave Filters, Impedance-matching Networks, and Coupling Structures*, Artech House, 1980.

Analysis, Design and Implementation of a Broadband Coaxial-to-microstrip Transition for UWB Radars

Gholamreza Askari[1, 2], **Mahmoud Kamarei**[1], **Mahmoud Shahabadi**[1], **and Hamid Mirmohammad Sadeghi**[2]

[1]School of Electrical and Computer Engineering, College of Engineering
University of Tehran, North Kargar St., Tehran, Iran
[2]Information and Communication Technology Institute
Isfahan University of Technology, Isfahan 84156, Iran

Abstract— Microstrip lines are the most widely used planar transmission lines for microwave circuit applications due to their low cost and ease in circuit layouts [1]. Also in near mm-wave frequency band, some functional modules are realized by plane structure of hybrid integration, and again microstrip is the most common transmission line [2]. On the other hand, for most equipment used for microwave circuit measurements, coaxial structures are normally employed for signal inputs and outputs. Thus, coaxial-to-microstrip transitions are required [1]. There are many coaxial connectors employed to implement coaxial-to-microstrip transitions. Despite the impedance matching between the coaxial connectors and the microstrip lines, a discontinuity exists due to the different electromagnetic (EM) field distributions of these two transmission lines and so signal reflection and radiation are expected. These problems become worse when the operating frequencies are higher [3]. For the past few decades, many techniques have been proposed to improve the high-frequency performance of coaxial — to microstrip transitions by modifying the structures of coaxial connectors or microstrip lines for better matching of the EM field distributions at the transitions [3, 4, 7]. However in some of these transitions, only the impedance is match in a narrow frequency bands and in some others, complicated structure, high cost and large size make it undesirable. Furthermore it is important to have simplex, low-cost and wideband coaxial-to-microstrip transition.

In this paper a useful, simplex and broadband transitions between Air-Coaxial SMA connector and microstrip line is designed and implemented. This transition is designed by the use of a simple and small size ground coplanar waveguide (GCPW) as a pre transition. The CPW and its various configurations such as GCPW have several attractive features in comparison with microstrip line. For example these lines have low wave propagation dispersion up to very high frequency [8]. There have been intensive studies on transition from CPW to other planner transmission lines [9–11]. However, in the conventional method that connects the coaxial inner conductor and CPW center conductor on the same plane, higher-order modes arise at the connection section. This results in the insertion of unnecessary reactance in the line at discontinuous sections in a serial or parallel manner thereby generating a large mismatch [11].

The GCPW, pre-transition section is utilized to provide a smooth transition from coaxial to microstrip. The signal and ground current paths through a transition are also critical and these paths must often be continuous and as close as possible together, to suppress radiation [4]. In this transition the effects of the field and impedance matching on the bandwidth are discussed. To study the effects of GCPW section on the transitions, electromagnetic fields of transition structure in different cut are completely analyzed with CST. Moreover the influence of the possible fabrication and assembly errors such as slightly gap, height of laminate, misalignment between microstrip and center of SMA connector, excitation of higher order modes of SMA in connections and uncertainty of measurement instruments in total performance are completely analyzed and considered. The simulation results using CST and ADS softwares indicate that the bandwidth is increased to maximum operating frequency of SMA connector and the experimental results are in good agreement with simulation results.

The material used in the design and implementation are Rogers RT Duroid 5880 with $\varepsilon_r = 2.2$ and $\tan\delta = 0.0009$, the metal thickness is 0.017 mm and the substrate thickness is 10 mil and 20 mil. The SMA connector is 23_PC35-50-0-53/199_UE from Huber-Suhner Company [12]. The photos of the final implemented transition with the 50 mm Microstrip line is shown in Fig. 1. The experimental results of a 50 mm length of Microstrip line with back-to-back transitions and SMA connectors is presented in Fig. 2. which show that a wideband transition with return loss better than −10 dB and in the worth case, total insertion loss; by removing the insertion loss of the 50 mm Microstrip line and connectors; is less than 1 dB up to 30 GHz. These good performances and its simplicity, easy fabrication and good performances make this transition very useful in

Figure 1: Photos of the proposed transition and the 50 mm microstrip line, (a) gap view, (b) misalignment view, and (c) overall top view.

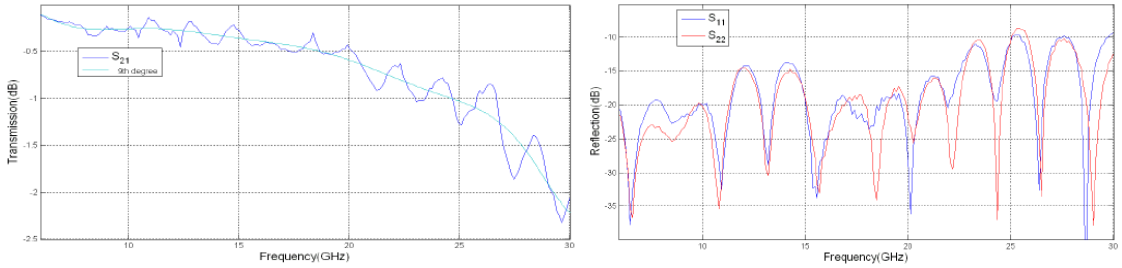

Figure 2: Experimental transmission and reflection results of the proposed transition considering 50 mm Microstrip line.

many applications such as UWB short range Radars up to 30 GHz and make it a very good candidate for higher frequencies [13].

REFERENCES

1. Zhou, Z. and K. L. Melde, "Development of a broadband coplanar waveguide-to-microstrip transition with vias," *IEEE Trans. Adv. Packag.*, Vol. 31, No. 4, 861–872, Nov. 2008.
2. Xu, H.-J., Y.-H. Zhang, and Y. Fan, "Analysis of the connection section between K connector and microstrip with electromagnetic bandgap (EBG) structure," *Progress In Electromagnetics Research*, Vol. 73, 239–247, 2007.
3. Cheng, J.-C., E. S. Li, W.-F. Chou, and K.-L. Huang, "Improving the high-frequency performance of coaxial-to-microstrip transitions," *IEEE Trans. on Microw. Theory and Tech.*, Vol. 59, No. 6, Jun. 2011.
4. Holzman, E., *Essentials of RF and Microwave Grounding,* Artech House, Norwood, MA, 2006.
5. Gupta, K. C., R. Garg, I. Bahl, and P. Bhartia, *Microstrip Lines and Slotlines,* Artech House, Norwell, MA, 1996.
6. Agarwal, K. and R. Harlan, "Coax-to-microstrip transition," US Patent 5552753, Sep. 1996.
7. Quan, C., S. W. Drost, M. Y. Hashimoto, and R. M. Jorgenson, "Microstrip to coax vertical launcher using fuzz button and solderless interconnects," US Patent 5886590, Mar. 1999.
8. Simons, R. N., *Coplanar Waveguide Circuits, Components, and Systems,* Wiley, New York, 2001
9. Chiu, T. and Y. Shen, "A broadband transition between microstrip and coplanar stripline," *IEEE Microw. Wireless Components. Lett.*, Vol. 13, No. 2, 66–68, Feb. 2003.
10. Nedil, M., T. A. Denidni, and A. Djaiz, "Ultra-wideband microstrip to CB-CPW transition applied to broadband filter," *IEEE Electronics Lett.*, Vol. 43, No. 8, Apr. 2007.
11. Kamei, T., Y. Utsumi, N. Q. Dinh, and N. Thanh, "Wide-band coaxial-to-coplanar transition," *IEICE Trans. Electron.*, Vol. E90-C, No. 10, 2030–2036, Oct. 2007.
12. Data Sheet, Online Avalible: http://www.hubersuhner.co.th.
13. Son, H., S. Lee, K. Min, "FPGA implementation of UWB radar signal processing for automotive application," *Proceedings of the 3rd European Wireless Technology Conference*, Paris, France, Sep. 27–28, 2010.

A Broadband UHF RFID Tag Antenna with a Novel T-matching Network

Zhibin He[1], **Te Pan**[1], **Hui Liu**[1], **Yuan Zhang**[1], **and Sailing He**[1, 2]

[1]Centre for Optical and Electromagnetic Research
Academy of Advanced Optoelectronics, South China Normal University, Guangzhou, China
[2]The Royal Institute of Technology, Stockholm, Sweden

Abstract— Radio frequency identification (RFID) technology is a wireless communication technology which use radio frequency signal to identify and read and write the data no touching target. RFID system consists of reader, tags and application software systems. The tag divided into passive tags, semi-active tags and active tags according to whether there is an internal power supply. The tag is the device that carries data on the RFID systems. The tag consists of an electronic chip and an antenna. In RFID system, the read distance of the tags is a most important index.

In the paper an ultra high frequency (UHF) passive broadband radio frequency identification (RFID) Tag Antenna with T-matching network is presented. The T-matching network is applied to help us to achieve a broad impedance bandwidth. The complex impedance matching could be easily attained by slightly tuned the arm lengths of the T-matching network. Thanks to the bent radiating element, the size reduction of the proposed antenna is realized. The bandwidth ($S_{11} < -20$ dB) of the proposed antenna is 133 MHz (835–968 MHz) and the whole global UHF RFID frequency band has been covered. To better embody the broadband character, the power reflection coefficient (PRC) is also introduced here to define the impedance bandwidth. The 3 dB PRC bandwidth of the presented passive UHF tag antenna is 88 MHz (882–970 MHz) which is still wide enough to cover the required frequency band. In late simulation result, a smooth and stable gain curve between 0.19 dBi to 0.85 dBi is found throughout the entire operating frequency band, and a gain of 0.6 dBi is obtained at the desired operating frequency point (915 MHz). In conclusion, the designed antenna owns the advantages of low-profile, compact size (56×56 mm^2), low cost and stable gain. Based on the simple structure, the designed tag antenna can be easily manufacture and widely used in practical applications.

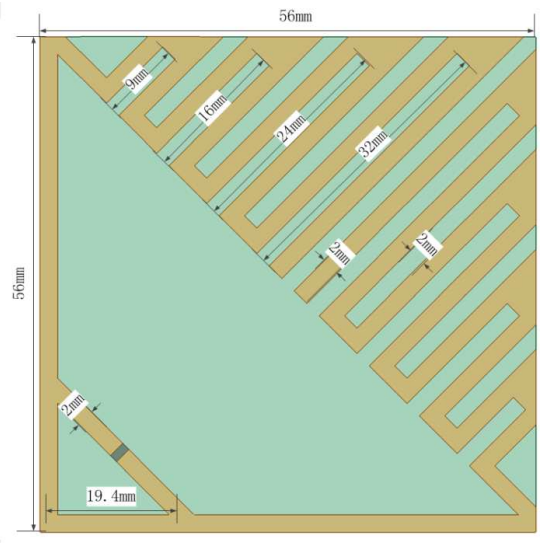

Figure 1: The Geometry of the proposed unground tag antenna (thickness = 1.6 mm).

Capacitively Coupled-fed Electrically Small Loop Antenna with High Efficiency for WiFi Application

Qingchong Liu[1], **Yufeng Yu**[2], **and Qi Liu**[1]

[1]Centre for Optical and Electromagnetic Research, Zhejiang University, Hangzhou 310058, China
[2]China Jiangnan Electronics Communication Institute, Jiaxing 314000, China

Abstract— With the rapid development of mobile communication technology, the demand for antennas with miniaturized size, high radiation efficiency and broad bandwidth keeps increasing. However, as is known to all, due to the small radiation resistance, electrically small antennas (ESAs) without external matching networks are poorly matched to 50-ohm feeding lines, leading to low radiation efficiency and small bandwidth. In this paper, an efficient electrically small planar loop antenna with capacitive feed is proposed for WiFi applications. The loaded capacitor provides needed capacitance to compensate the large inductance of electrically small loop antennas. The capacitive feed offers good impedance matching of the antenna. Thus the proposed antenna provides larger radiation resistance, which leads to higher radiation efficiency, gain and impedance bandwidth. The radiating element of the proposed antenna is comprised of a planar printed loop with an interdigital capacitor inserted on one side and a copper loop wall with height of 6 mm and thickness of 0.3 mm attached to the printed loop. The attached loop wall enables the antenna occupies more volume, which lowers its Q value and contributes to larger bandwidth. The interdigital capacitor loading creates self-resonance of the loop. The feeding element of our antenna is a printed T-shaped monopole, which is capacitively coupled to the radiating capacitively-loaded loop and good impedance matching is achieved through the capacitive coupling mechanism. The antenna exhibits a simulated -10 dB bandwidth of 240 MHz from 2.36 GHz to 2.60 GHz, which is suitable for WiFi application. Other characteristics of such an electrically small loop like the reduced current on the ground plane, the tunable operating frequency, and potential pattern diversity implies its promising use in MIMO applications.

25 G/s Passive Current Board Design of PRBS Generator

Chih-Wei Yu, Jia-Jin Wu, C. L. Chiu, Jau-Ji Jou, and Tien-Tsorng Shih
Department of Electronics Engineering, Kaohsiung University of Applied Sciences
No. 415 Chien Kung Road, Kaohsiung, Taiwan

Abstract— The 25 Gb/s BER test set comprises a signal generator that drives an passive current board including microstrip line (R6C) through Gennum EB-GN2426A IC and SEMTECH GN2426A chip generated with a Pseudo Random Binary Sequence (PRBS) of digital 1's and 0's, representing a random data stream. The simple 25 Gb/s testing of passive current board converts the PRBS data stream from electrical to optical components. The R6C price for 25 Gb/s passive current board of PRBS generator only almost 1/400 by the measurement equipments. R6C is six layers, Jitter of 12.614 ps, Bit rate of 25.5 Gb/s, fall time of 14.5 ps and rise time of 12.5 ps. R6C has a useful role under mass production. It is very cheap and simple high speed testing for 25 Gb/s.

No.	Layer	thickness	Dielectric Constant	Dielectric Loss Tangent
1	0.5 oz + plating	0.03 mm	1	0
2	Rogers 4350B	6.6 mil	3.66	0.004
3	0.5 oz	0.017 mm	1	0
4	PP	10 mil	4.2	0.017
5	0.5 oz	0.017 mm	1	0
6	FR4	6 mil	4.2	0.02
7	0.5 oz	0.017 mm	1	0
8	PP	10 mil	4.2	0.017
9	0.5 oz	0.017 mm	1	0
10	FR4	6 mil	4.2	0.02
11	0.5 oz + plating	0.03 mm	1	0

R6C board structure of six layers

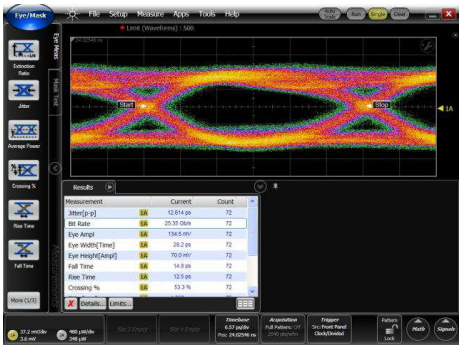

Eyes diagrams

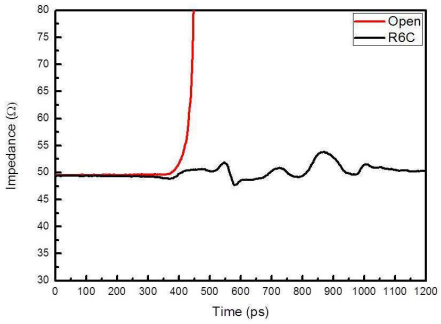

Time-Domain Reflectrometry (TDR)

A Quasi-hexagon Shaped Band-stop FSS in Wideband RCS Reduction

Peng Cheng Zhang, Xian Qi Lin, Fei Cheng, Rui Shen, and Yong Fan
EHF Key Lab of Fundamental Science, School of Electronic Engineering
University of Electronic Science and Technology of China, Chengdu 611731, China

Abstract— Band-stop frequency selective surface (FSS) [1] is from time to time used as antenna reflection ground to improve the antenna gain as well as reduce the out-of-band RCS.

In terms of structural mode scattering, we design a kind of band-stop FSS as a substitute for the common metal reflection board grounded on a hexagon FSS prototype and the typical Koch fractal curve [2]. A wideband RCS reduction can also be obtained by suppressing the spurious stop-bands resonance of FSS units. Patch dipole antenna is used to confirm the validity of this method and result of simulation and experiment agree well. Figure 1 illustrates the unit of the FSS and the refraction indexes with different l_1. Figure 2 shows the measured RCS with two different ground planes, it can be seen that there is a considerable RCS of the patch antenna with band-stop FSS ground plane, about 27 dB reduction in 6.8 GHz.

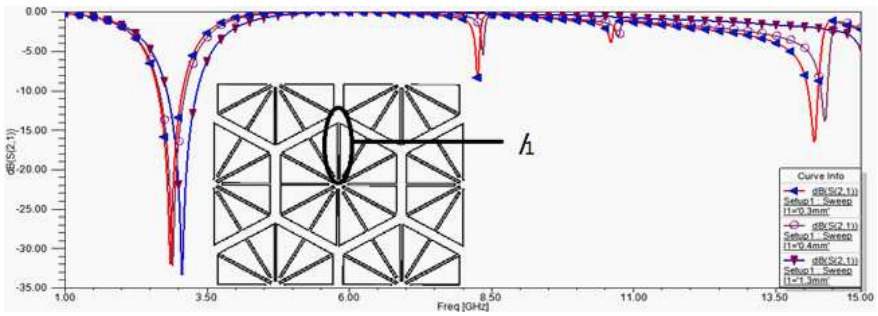

Figure 1: The quasi-hexagon shaped band-stop FSS unit and refraction indexes. ▲l_1 = 5.7 mm, ◯l_1 = 5.6 mm, ▼l_1 = 4.7 mm.

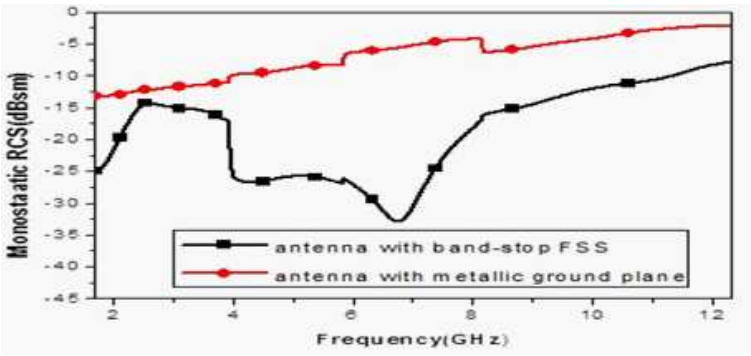

Figure 2: The comparison of the RCS for different ground planes.

REFERENCES

1. Lee, D. H., Y. J. Lee, and J. Yeo, "Design of novel thin frequency selective surface superstrates for dual band directivity enhancement," *Microwaves Antennas & Propagation*, Vol. 1, No. 1, 248–254, 2007.
2. Ismahayati, A., P. J. Soh, R. Hadibah, and G. A. E. Vandenbosch, "Design and analysis of a multibandkoch fractal monopole antenna," *IEEE International RF and Microwave Conference (RFM)*, 58–62, 2011.

A Spiral Antenna with Integrated Planar Feeding Structure

Huifen Huang, Zonglin Lv, and Junfeng Wu
School of Electronic and Information Engineering
South China University of Technology, China

Abstract— Planar spiral antennas have the advantages of great performance on circular polarization, easy impedance matching, and the superior radiation efficiency. However, the conventional feeding structure for planar spiral antennas is situated in the center of the spiral and extends into the third dimension. In practical applications, the low-profile spiral antennas suffer from the lack of proper planar feeding ways. The vertical balun always has a significantly long length, inconsistent with the requirements of the low profile spiral antenna geometry. Feeding the spiral with a transmission line that follows the metal layer beneath the spiral arm to the center point is proposed before. This method is used to feed equiangular spiral antenna and achieves axial ratio below 5 dB over the frequency range of 3–10 GHz, but it is impossible to feed the Archimedean spiral antenna in the same way because of its long and thin arms. However, the Archimedean spiral antenna has a noticeable advantage at axial ratio bandwidth over its equiangular counterparts. On this condition, this paper uses the similar feeding way to feed a newly designed spiral antenna. The antenna designed has largely improved axial ratio compared to the equiangular spiral antenna at comparable size, and the arms are wider and largely shorter than the Archimedean spiral antenna to make it possible to feed the antenna in similar way. The spiral antenna and a Dyson-style balun have been integrated into a multi-layer structure. The resulting structure maintains the typical radiation behavior and broadband operation of spiral antennas, and achieves good axial ratio performance without the vertical balun. The overall size of the spiral antenna is largely reduced.

A Novel Compact UWB Antenna with Triple Band-notched Characteristics

Lin Chen[1], **Shaobin Liu**[1], **Xiangkun Kong**[1, 2], **Borui Bian**[1], **and Zhiwen Mao**[1]

[1]Key Laboratory of Radar Imaging and Microwave Photonics, Ministry of Education
College of Electronic and Information Engineering
Nanjing University of Aeronautics and Astronautics, Nanjing 210016, China
[2]Jiangsu Key Laboratory of Meteorological Observation and Information Processing
Nanjing University of Information Science and Technology, Nanjing 210044, China

Abstract— In this article, a novel compact ultra-wideband (UWB) planar monopole antenna with tri-notched bands is presented. The proposed antenna is fed by a microstrip line and a partial ground plane. The antenna achieves an operating bandwidth ranging from 2.9 to more than 11 GHz and triple band-notched properties of 3.22–3.91, 5.15–5.44, 5.70–5.91 GHz. Throughout this article, the simulated and experimental results of impedance characteristic, gain, and radiation patterns are presented and discussed. A tapered radiating patch is designed to cover UWB working frequency band. The radiation patch and ground plane of the original antenna are all cut by arc which is aimed at impedance matching over the whole UWB. Resonating element etched out above the ground plane generates the rejection at WLAN band. To achieve the lower and higher WLAN band-notched characteristics, two independent curved slots is embeded into the radiation patch. Moreover, the proposed antenna here is significantly smaller and exhibits omni-directional radiation patterns which makes it a suitable candidate for the UWB system. The proposed antenna has an overall dimension of $20 \times 21.1\,\mathrm{mm}^2$.

Quasi-coherent Noise Jamming Based on Interrupted-sampling and Pseudo-random Serials Phase-modulation

Ning Tai, Yu-Jian Pan, Deping Zhang, Chao Wang, and Naichang Yuan
College of Electronic Science and Engineering
National University of Defense Technology, Changsha, China

Abstract— Using the idea of pseudo-random serials phase modulation for reference, an active jamming method of quasi-coherent noise suppression is proposed for countering wideband radar of pulse compression system. The basic idea is that the jammer processes interrupted sampling in range direction and modulates phases on sampled radar signal according the values of pseudo-random serials, and then sends the jamming signal to victim radar. A train of false targets will be achieved after the interrupted-sampling jamming signal passing through the matched filter. The spectrum of radar signal will be spread after pseudo-random serials phase modulation. The combination of these two methods will form large amounts of noise around the pulse compression output of target echo. Given enough jamming power, the radar can't distinguish the true target from the jammed situation.

After detecting radar signal, the jammer first down converts radio frequency radar signal to mediate frequency signal and processes interrupted-sampling in range direction. Meanwhile the pseudo-random serials are created by a shift register. After modulating $+180^\circ$ or -180° phase according the values of pseudo-random serials on sampled radar signal in range direction we produce the jamming signal. At last the jammer up converts mediate frequency jamming signal to radio frequency and transmits the jamming signal to radar.

At last the implementation of jamming signal on a jammer with a receive-transmit time-sharing antenna based on FPGA is introduced. Compared with other non-coherent radio frequency jamming signal, this method obtains some processing gain and the jamming effect is quite good when there is not too much information about victim radar. The proposed method of good real-time is effective and flexible in engineering.

Validation Analysis and Test of Semiconductor Device Simulator GSRES

Yong Li[1], **Gong Ding**[1], **Haiyan Xie**[1], **Chun Xuan**[1], **Hong-Fu Xia**[1], **and Jian-Guo Wang**[1, 2]

[1]Northwest Institute of Nuclear Technology, Xi'an 710024, China
[2]School of Electronic and Information Engineering, Xi'an Jiaotong University, Xi'an 710049, China

Abstract— Basic drift-diffusion model (DDM) of carriers in semiconductor using in a numerical simulator: General Semiconductor Radiation Effect Simulator (GSRES), is studied in order to identify and reduce the numerical errors of this semiconductor simulator. Numerical approximations of the semiconductor device EMP effect simulator is analysed. Numerical errors caused by approximation of the field distribution of lattice temperature, and approximation the of the recombination rate and generation rate are studied. Application range of this simulator is analysed according to the numerical errors caused by these approximations. Terms of the simulator that should be improved and enhanced precision are given.

A Triple-band Planar Inverted-F Antenna for WLAN Application

Huifen Huang and Yuanhua Hu
School of Electronic and Information Engineering
South China University of Technology, Guangzhou, China

Abstract— A novel tri-band PIFA antenna operating at WLAN frequency is proposed. The proposed antenna has a two-layer structure, resembling a capital E. By folding the E-shaped structure down, It can largely reduce the size of the antenna. The antenna is feed by the probe, which extends from the ground plane to connect to the radiating strip. The short-circuit strip connects with the ground plane is realized by the probe or shorting wall. The whole structure is the three-dimension version of the simple inverted-F antenna. Three electric current path consititute three resonant mode, corresponding to 2.4/5.2/5.8 GHz, respectively. At the frequency 2.4 GHz, the current is mainly distributed along the short-circuit to the open end, from the current distribution pattern, the current path is about quarter-wavelength. The majority of the current is concentrated on the strip from the feeding point to the open end, the current path is close to three quarter-wavelength at 5.2 GHz. The third current path is from the feeding point to the short-circuit point, two null in the current distribution pattern shows the current path is approximately one-wavelength. the antenna is not completely controllable independently, however it can adjust the impedance match of some frequency without the shift of other frequency largely. In order to reduce the size of the antenna and reduce the dependence of the ground length, a slit is etched into the ground plane, which can lengthen the current path, further improving the impedence match. The tri-band PIFA occupies $30 \times 25 \times 6\,\mathrm{mm}^3$, operating at the following frequency bands: 2.39–2.51, 5.13–5.37, 5.69–6.03 GHz.

Radiation from Microstrip Patch Antennas Located on Elliptical Surfaces

R. Lech, **A. Kusiek**, **and W. Marynowski**
Gdansk University of Technology, Poland

Abstract— Conformal antennas are interesting due to the possibility of merging them into curved surfaces. They becoming popular due to their advantages and possibilities of applications in airplanes, spacecraft, speedboats and other high-speed vehicles where aerodynamic or hydrodynamic considerations necessitate their use. The other advantage is their wider, relatively to planar antennas, visible angular range. The arrays of radiators located on the surface of a cylinder may be the examples of such antenna that provide omni-directional radiation patterns in azimuth plane or provide, in this plane, the possibility of beam control. These arrangements can find their application in base stations for mobile communications systems.

In the literature there are many solutions of the problem of patch antennas localized on circular cylinder [1–3]. The analysis is commonly carried out by solving the electric field integral equation with the method of moments. In the case of circular cylinder this techniques is very effective and the appropriate Green's functions can be developed in closed-form. In the case of radiation sources located on elliptical surfaces one can find the results based on asymptotic techniques, e.g., [4] or hybrid full wave technique (BI-FEM) [5]. Results concerning layered elliptic cylinder are mainly available for the scattering by TM or TE plane waves or the radiation by 2D structures. The analysis of microstrip patch antenna located on single-layer dielectric coated conducting ellipse employing a modal expansion was presented in [6, 7].

A multi-patch configuration of rectangular microstrip antennas located on an elliptic cylinder, with electrically small radius, is investigated in this paper. The configuration contains an arbitrary number of substrate and superstrate layers (which can also be analyzed as air gaps). A full-wave analysis is employed considering the expansion of the field as a series of Mathieu functions with unknown coefficients. The presence of the electric current is considered in the boundary conditions at interface between the layers and the Galerkin method is applied to obtain the unknown coefficients. The unified procedure for creating proper matrices for the geometry with arbitrary numbers of layers, presented before for antennas located on circular cylinders [8] is employed here for the investigated structure. Numerical results for the radiation patterns are calculated and verified by comparing them with results from the literature and other numerical techniques. The behavior of the radiated field as a function of ratio minor/major axes of elliptic cylinder is investigated. The existence of superstrate layer and the air gaps under substrate and superstrate layers and their influence on radiation pattern of single and multipatch antennas is considered.

ACKNOWLEDGMENT

This work was supported from sources of National Science Center under grant decision No. DEC-2011/01/D/ST7/06639.

REFERENCES

1. Ali, S. M., et al., "Resonance in cylindrical-rectangular and wraparound microstrip structures," *IEEE Trans. Microw. Theory Techn.*, Vol. 37, No. 11, 1773–1783, Nov. 1989.
2. Habashy, T. M., et al., "Input impedance and radiationpattern of cylindrical-rectangular and wraparound microstrip antennas," *IEEE Trans. Antennas Propag.*, Vol. 38, No. 5, 722–731, May 1990.
3. Wong, K.-L., et al., "Resonance in a superstrate-loaded cylindrical-rectangular microstrip structure," *IEEE Trans. Microw. Theory Techn.*, Vol. 41, No. 5, 814–819, May 1993.
4. Jha, R. M. and W. Wiesbeck, "The geodesic constant method: A novel approach to analytical surface-ray tracing on convex conducting bodies," *IEEE Trans. Antennas Propag. Magazine*, Vol. 37, No. 2, Apr. 1995.
5. Wu, C. W., et al., "Hybrid finite element boundary integral method for cavity recessed in an elliptic cylinder," *IEEE Trans. Antennas Propag.*, Vol. 51, No. 8, 1829–1836, Aug. 2003.
6. Angiulli, G., et al., "Radiation from dielectric coated elliptic conducting cylinder by assigned electric current distribution," *Progress In Electromagnetics Research*, Vol. 57, 131–150, 2006.

7. Amendola, G., "Analysis of the rectangular patch antenna printed on elliptic-cylindrical substrates," *IEE Proc Microw., Antennas and Propag.*, Vol. 147, No. 3, 187–194, Jun. 2000.
8. Lech, R., et al., "An analysis of probe-fed rectangular patch antennas with multi-layer and multi-patch configurations on cylindrical surfaces," *IEEE Trans. Antennas Propag.*, in Print, Doi: 10.1109/TAP.2014.2313137.

Nonuniform Cylindrical Ferrite Coupled Line Junction

A. Kusiek, W. Marynowski, and J. Mazur
Gdansk University of Technology, Poland

Abstract— Nonreciprocal devices have been extensively used in modern microwave and millimeter wave system. Recently, the longitudinally magnetized ferrite coupled strip- or slotlines [1, 2] are being developed and employed to realize integrated nonreciprocal devices. Significant interest in these devices results from their advantages, which are weak biasing magnetic field and wide operation bandwidth. So far, studies concerning FCL devices have been focused mainly on structures realized in planar line technology. Such structures allow one to obtain fully integrated FCL devices. However, the main drawback is high level of insertion losses occurring in the ferrite material [3].

The promising results concerning losses reduction were obtained for cylindrical ferrite coupled line (CFCL) junction [4]. In such configuration strong gyromagnetic coupling occurs which is a result of high magnetic field concentration in the ferrite medium. This makes possible to design shorter ferrite junctions ensuring lower insertion losses in comparison to planar ones. Based on the proposed cylindrical junction the isolator and four-port circulator were designed and fabricated [4, 5]. However, for the fabricated prototypes the narrow operation bandwidth was obtained.

The operation bandwidth of ferrite coupled line junction can be improved by applying nonuniformly coupled lines in ferrite section [2]. Hence, in this paper the nonuniform cylindrical ferrite coupled line junction is proposed. In comparison to uniform CFCL, the proposed nonuniform ferrite coupled line is corrugated with different contours on the coupling slots. In the analysis the own software based on hybrid approach combining finite difference, method of moments and mode matching technique is utilized. The nonuniform CFCL junction ensuring $\pi/4$ Faraday rotation is designed and applied to three port circulator. Numerical and experimental results of the circulator are presented and discussed.

ACKNOWLEDGMENT

This work was supported by the Polish Ministry of Science and Higher Education from sources for science in the years 2012-2013 under Contract IP2011 028271 (decision No. 0282/IP3/2011/71).

REFERENCES

1. Cao, M. and R. Pietig, "Ferrite coupled-line circulator with reduced length," *IEEE Transactions on Microwave Theory and Techniques*, Vol. 53, No. 8, 2572–2579, August 2005.
2. Yang, L.-Y. and K. Xie, "Design and measurement of nonuniform ferrite coupled line circulator," *Journal of Electromagnetic Waves and Applications*, Vol. 25, No. 1, 131–145, 2011.
3. Marynowski, W. and P. Kowalczyk, "Analysis of magnetic losses in ferrite coupled lines using SDA and hybrid root finding algorithm," *Progress In Electromagnetics Research Symposium Abstracts*, 635, March 25–28, Taipei, 2013.
4. Kusiek, A., W. Marynowski, and J. Mazur, "Investigations of four-port circulator utilizing cylindrical ferrite coupled line junction," *Progress In Electromagnetics Research*, Vol. 134, 379–395, 2013.
5. Kusiek, A., W. Marynowski, and J. Mazur, "Investigations of nonreciprocal devices employing cylindrical ferrite coupled line junction," *Journal of Electromagnetic Waves and Applications*, Vol. 26, No. 13, 1685–1693, 2012.

Rigorous Analysis of Multilayered Elliptical Striplines

A. Kusiek, R. Lech, and W. Marynowski
Gdansk University of Technology, Poland

Abstract— Elliptical and cylindrical waveguides have been considered for applications such as slotted lines, transition adapters and baluns. Due to the development of conformal antennas such lines can also be utilized as feeding lines of antennas printed on the cylindrical or elliptical surface [1]. Recently, the cylindrical coupled strip/slotlines with ferrite rod have been applied in Faraday nonreciprocal devices, allowing for their length reduction [2, 3].

In order to determine the wave properties of cylindrical/ellitpical guides the conformal mapping technique (CMT) have been commonly utilized in the literature. Based on this approach the formulas for effective permittivity and characteristic impedance were derived and presented for single-layer or multilayered cylindrical or elliptical microstrip lines and striplines [4–6]. Since, the presented formulas are for quasi-static case they are valid at low frequencies. For accurate analysis of conformal guides at higher frequencies the full-wave techniques have to be utilized. Moreover, contrary to CMT, the full-wave techniques provide additional results concerning field distribution or insertion losses, required in designing of many microwave devices.

In the case of cylindrical guide the analytical full-wave technique based on method-of-moments have been presented in [2]. However, in the case of elliptical one the analytical solution has not been encountered in general literature. Hence, in this paper the rigorous analysis of multilayered elliptical stripline is conducted. In the analysis a full-wave technique is utilized based on expansion of the fields as a series of Mathieu functions with unknown coefficients. The presence of electric current is considered in the boundary conditions at interface between the layers and the Galerkin method is applied to obtain the unknown coefficients. The developed technique is applied to the analysis of multilayered elliptical guides with different number and angular location of the strips. Numerical results concerning propagation constants, field distribution and characteristic impedance are calculated and presented for investigated structures.

ACKNOWLEDGMENT

This work was supported in part from sources of National Science Center under grant decision No. DEC-2011/01/D/ST7/06639 and under funding for Statutory Activities for ETI Gdansk University of Technology.

REFERENCES

1. Angiulli, G., G. Amendola, and G. Di Massa, "Radiation from dielectric coated elliptic conducting cylinder by assigned electric current distribution," *Progress In Electromagnetics Research*, Vol. 57, 131–150, 2006.
2. Kusiek, A., W. Marynowski, and J. Mazur, "Investigations of cylindrical ferrite coupled line junction using hybrid technique," *Progress In Electromagnetics Research*, Vol. 120, 143–164, 2011.
3. Kusiek, A., W. Marynowski, and J. Mazur, "Investigations of four-port circulator utilizing cylindrical ferrite coupled line junction," *Progress In Electromagnetics Research*, Vol. 134, 379–395, 2013.
4. Du, Z., K. Gong, J. S. Fu, Z. Feng, and B. Gao, "CAD models for asymmetrical, elliptical, cylindrical, and elliptical cone coplanar strip lines," *IEEE Transactions on Microwave Theory and Techniques*, Vol. 48, No. 2, 312–316, Feb. 2000.
5. Akan, V. and E. Yazgan, "Quasi-static solutions of multilayer elliptical, cylindrical coplanar striplines and multilayer coplanar striplines with finite dielectric dimensions — Asymmetrical case," *IEEE Transactions on Microwave Theory and Techniques*, Vol. 53, No. 12, 3681–3686, Dec. 2005.
6. Majumdar, P. and A. K. Verma, "Analytical model of losses for symmetric elliptical coplanar strip lines," *International Conference on Communications and Signal Processing (ICCSP 2011)* 37–41, Feb. 2011.

Dual Polarization Circular Slot Antenna Using Microstrip and CPW Feeding Structures

W. Marynowski, A. Kusiek, and R. Lech
Gdansk University of Technology, Poland

Abstract— Due to dynamic development of wireless communication systems their diversity of performance is required. One of the method to increase the capacity of the channel is the usage of the multiple-input-multiple-output (MIMO) systems. In the literature there are several structures of dual polarization antenna operating in wide bandwidth with good isolation between ports [1–7] which are proposed for modern wireless communication applications especially for mitigating fading in multipath propagation environments.

In this paper we proposed the dual polarization slot antenna which is based on a single polarization UWB antenna realized in CPW technology [8, 9]. In the antenna the radiating element is a circular slot which is excited by circular patch. This patch is fed from two ports to achieve dual polarization structure. One polarization is excited directly from 50 Ω CPW line placed on one side of the dielectric sheet. The second polarization is excited from 50 Ω microstrip line ended with open radial stub located on the opposite side of the dielectric.

The antenna structure was designed using full wave simulation. The obtained results show that the antenna operates from 4.5 GHz to 6.5 GHz with the refection losses at two ports better than 10 dB and isolation between them better than −18 dB. The simulated gains of the antenna equal 3.24 dB and 2.51 dB for the CPWand microstrip ports feeding, respectively. The designed antenna was manufactured and the simulation results were verified via measurement of the prototype.

ACKNOWLEDGMENT

This work was supported in part by Polish Ministry of Science and Higher Education from sources for science in the years 2012–2013 under Contract No. 0340/IP2/2011/71.

REFERENCES

1. Guo, Y.-X., K.-M. Luk, and K.-F. Lee, "Broadband dual polarization patch element for cellular-phone base stations," *IEEE Transactions on Antennas and Propagation*, Vol. 50, No. 2, 251–253, Feb. 2002.
2. Li, Y., Z. Zhang, W. Chen, Z. Feng, and M. F. Iskander, "A dual-polarization slot antenna using a compact CPW feeding structure," *IEEE Antennas and Wireless Propagation Letters*, Vol. 9, 191–194, 2010.
3. Li, H., J. Xiong, Z. Ying, and S. L. He, "Compact and low profile co-located mimo antenna structure with polarisation diversity and high port isolation," *Electronics Letters*, Vol. 46, No. 2, 108–110, Jan. 2010.
4. Baek, S. and S. Lim, "Compact planar MIMO antenna array with polarisation diversity on single layer," *Electronics Letters*, Vol. 46, No. 13, 880–882, Jun. 2010.
5. Li, Y., Z. Zhang, Z. Feng, and M. F. Iskander, "Dual-mode loop antenna with compact feed for polarization diversity," *IEEE Antennas and Wireless Propagation Letters*, Vol. 10, 95–98, 2011.
6. Gou, Y., S. Yang, Q. Zhu, and Z. Nie, "A compact dual-polarized double E-shaped patch antenna with high isolation," *IEEE Transactions on Antennas and Propagation*, Vol. 61, No. 8, 4349–4353, Aug. 2013.
7. Zheng, W. C., L. Zhang, Q. X. Li, and Y. Leng, "Dual-band dual-polarized compact bowtie antenna array for anti-interference MIMO WLAN," *IEEE Transactions on Antennas and Propagation*, Vol. 62, No. 1, 237–246, Jan. 2014.
8. Lech, R., A. Kusiek, W. Marynowski, and J. Mazur, "Coplanar waveguide-fed broadband microwave devices with (or without) a thin dielectric substrate for use in flexible electronic systems," *International Journal of Antennas and Propagation*, Vol. 2014, Jan. 2014.
9. Marynowski, W. and J. Mazur, "Design of UWB coplanar antenna with reduced ground plane," *Journal of Electromagnetic Waves and Applications*, Vol. 23, No. 13, 1707–1713, 2009.

The Investigation of the Performance of Crossovers Placed on Curved Surfaces

W. Marynowski, **A. Kusiek**, **and R. Lech**
Gdansk University of Technology, Poland

Abstract— The increasing speed of the wireless communication systems increases the complexity of nowadays microwave integrated devices. The system designers deal with many problems, one of which is a crossing of the lines placed on the same layer. In the literature there are several structures of crossovers dedicated for narrow as well as broad band applications [1–6]. The most simple solution of crossing two lines is the utilization of the airbridges or wire bondings. However, these non-planar structures significantly degrade electrical parameters of crossovers and increase their fabrication costs. Another group of the crossovers are the circuits, which are realized as a planar structures on one side of the dielectric layer [1–4]. Such devices operate in a narrow frequency range and usually offer poor level of isolation between lines, which not exceeds −15 dB. In the literature one can find several configurations of planar multilayer crossovers [5–7]. These devices work in narrow or broad band with isolation usually better than −20 dB.

Conformal components (especially antennas and their feeding structures) are becoming popular due to their many advantages and the possibilities of their application [8]. The advantages of using devices with a curved surface arise from the possibility of integrating them with the object on which they are mounted. The conformal devices find application in a variety of fields, such as airborne, space-borne, ship-borne and missile-borne radar, space vehicles, wireless communication and sonar. Besides the conformability of the flexible devices, they can find application in the field of flexible electronics.

In this paper, we investigate a few example of crossovers working in a narrow or wide frequency range. The main goal of this work is to investigate the influence of devices' curvatures on their performance. The obtained simulation results are verified by the measurements of the fabricated prototypes.

ACKNOWLEDGMENT

This work was supported in part from sources of National Science Center under grant decision No. DEC-2011/01/D/ST7/06639 and under funding for Statutory Activities for ETI Gdansk University of Technology.

REFERENCES

1. Lee, Z.-W. and Y.-H. Pang, "Compact planar dual-band crossover using two-section branch-line coupler," *Electronics Letters*, Vol. 48, No. 21, 1348–1349, Oct. 2012.
2. Shao, J., H. Ren, B. Arigong, C. Li, and H. Zhang, "A fully symmetrical crossover and its dual-frequency application," *IEEE Transactions on Microwave Theory and Techniques*, Vol. 60, No. 8, 2410–2416, Aug. 2012.
3. Henin, B. and A. Abbosh, "Design of compact planar crossover using sierpinski carpet microstrip patch," *Microwaves, Antennas Propagation, IET*, Vol. 7, No. 1, 54–60, Jan. 2013.
4. Wang, Y., A. M. Abbosh, and B. Henin, "Broadband microwave crossover using combination of ring resonator and circular microstrip patch," *IEEE Transactions on Components, Packaging and Manufacturing Technology*, Vol. 3, No. 10, 1771–1777, Oct. 2013.
5. Kusiek, A., W. Marynowski, and J Mazur, "A design of a broadband microstrip crossover for ultra-wideband applications," *Microwave and Optical Technology Letters*, Vol. 52, No. 5, 1100–1104, Mar. 2010.
6. Abbosh, A. M., "Wideband planar crossover using two-port and four-port microstrip to slotline transitions," *Microwave and Wireless Components Letters, IEEE*, Vol. 22, No. 9, 465–467, Sept. 2012.
7. Liu, W., Z. Zhang, Z. Feng, and M. F. Iskander, "A compact wideband microstrip crossover," *Microwave and Wireless Components Letters, IEEE*, Vol. 22, No. 5, 254–256, May 2012.
8. Lech, R., A. Kusiek, W. Marynowski, and J Mazur, "Coplanar waveguide-fed broadband microwave devices with (or without) a thin dielectric substrate for use in flexible electronic systems," *International Journal of Antennas and Propagation*, Jan. 2014.

Design and Implementation of a New One Layer Microstrip Antenna Array with CSC2 Pattern for SSR

M. Abdolahi[1], **Gh. Askari**[2], **and H. Mirmohammad Sadeghi**[2]

[1]Department of Electricaland Computer Engineering
Isfahan University of Technology (IUT), Isfahan 84156, Iran
[2]Information and Communication Technology Institute
Isfahan University of Technology (IUT), Isfahan 84156, Iran

Abstract— The most common beam shapes in radar antennas are fan beams. A special case of the fan beam is cosecant squared beam which has significant features. The cosecant squared beam shape in elevation plane is ideal for detection of targets at any range. In some radars, a desired pattern in radar applications is a cosecant squared pattern that in high elevation angles its gain will be more than a typical cosecant squared pattern [1]. Synthesis of cosecant squared pattern was achieved using reflectors [2], non-uniform arrays [3] and serial fed uniform arrays [4, 5]. One of the most uses of cosecant squared pattern is in secondary surveillance radar (SSR) antennas. These antennas work at two frequencies, 1030 ± 10 MHz for sending signals and 1090 ± 10 MHz for receiving responses. For this application several structures were introduced in the past. A prototype integrated microstrip antenna column [8], a two-layer microstrip antenna for monopulse [9] and microstrip patch array that the coupling aperture is centered under the patch [10] are some of designed antennas for SSR applications. In all of above structures multi layers are used to have an acceptable bandwidth (nearly 8% bandwidth), for this, their fabrication are difficult and cost and have complicate structures.

In this paper, an array antenna with a shaped cosecant squared pattern in elevation plane for working as a radiating vertical array of SSR's antenna is designed. A new and simple microstrip structure is adopted to design as the feed network and 11 elements of parallel strip half-wave dipoles with $0.6\lambda_0$ apart used as radiating elements. Desired pattern (modified cosecant square) is synthesized and amplitude and phase of elements are specified. Several methods for synthesizing pattern can be used to obtain amplitude and phase of elements [11–13]. The pattern synthesis was performed using the Orchard-Elliot method [13]. In order to provide specification amplitudes, Wilkinson power dividers are used in a special corporate feed network with constant group delay to provide wide frequency bandwidth (nearly 500 MHz bandwidth). In order to match feed network with elements, a new parallel strip to microstrip balun is designed and used. The proposed structure of the complete antenna array and its feed array is shown in Fig. 1. Fig. 2 shows simulated elevation patterns at center (1060 MHz) and edge frequencies (1030 MHz and 1090 MHz) and compared with desired and synthesized pattern. It can be seen beam shaping has been obtained according to the objectives in the whole band. It has to be noted that the synthesis was done with considering isotropic elements, therefore the differences between the synthesized and simulated pattern at out of 10 dB beam width, are due to the element radiation pattern. Rogers's RT Duroid 5880 with thickness of 31 mil is used as laminate in designing of antenna. For design verification, especially in mutual coupling effect, an element and a two element array fabricated and measured that simulation and measurement have same results.

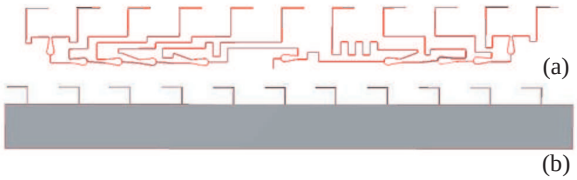

Figure 1: Designed antenna, (a) top view, (b) bottom view.

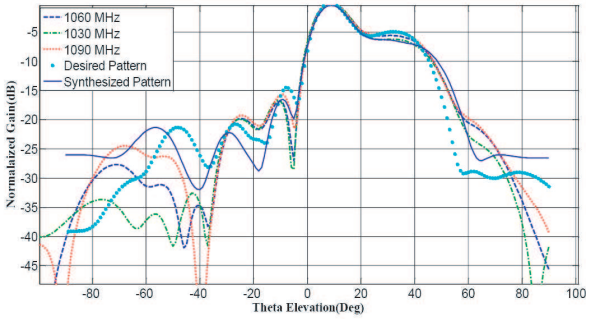

Figure 2: The simulated cosecant squared pattern.

The main beam of designed antenna has about 9 degrees tilt above the ground in the elevation plane, nearly 10 dB gain and 50 degree elevation beam width in −10 dBc. The return Loss in 1030 MHz and 1090 MHz are 13 and 31 dB. The proposed one-layer microstrip array with low complexity and low manufacturing and maintenance cost can be used in all SSR antennas.

REFERENCES

1. Skolnik, M. I., *Radar Handbook*, 3rd Edition, 2-96, 2-97, McGraw-Hill, 2008.
2. Silver, S., *Microwave Antenna Theory and Design*, Sec. 5.7, McGraw-Hill, New York, 1949.
3. Stutzman, W. L., "Synthesis of shaped-beam radiation patterns using the iterative sampling method," *IEEE Tran. Ant. Prop.*, Vol. 19, No. 1, 36–41, January 1971.
4. Jones, B., Y. M. F. Chow, and A. W. Seeto, "The synthesis of shaped patterns with series-fed microstrip patch arrays," *IEEE Tram. Atit. Prop.*, Vol. 30, No. 6, 1206–1202, November 1982.
5. Freytag', L. and B. Jecko, "Cosecant-squared pattern antenna for base station at 40 GHz," *IEEE*, 2004.
6. Madany, M., "The analysis of wideband conformal microstrip array antenna with cosecant-squared beam shaping," *IEEE Trans.*, 2006.
7. Schrank, H. and N. Herscovici, "A simple cosecant squared microstrip array: The shovel microstrip array," *IEEE Antennas and Propagation Magazine*, Vol. 35, No. 4, August 1993.
8. Borowiec, R., A. Jankowski, and Z. Langowski, "Microstrip radiolocation antenna with electronically controlled beam built using composite technology," *IEEE Trans. Microwave*, Vol. 57, No. 4, 815–823, 2009.
9. Biswas, D. and R. Vulapalli, "A two-layer microstrip antenna to generate cosecant squared fan beam for monopulse tracking," *IEEE Proceeding of International Conference on Microwave*, 2008.
10. Kreczkowski, A., T. Rutkowski, and A. Buda, "The microstrip IFF antenna for the airborne radar," *IEEE*, 2005.
11. Zhang, X., K. M. Luk, Q. Wu, and T. Ying, "Cosecant-square pattern synthesis with particle swarm optimization for nonuniformly spaced linear array antennas," *IEEE*, 2008.
12. Stutzman, W. L., *Antenna Theory and Design*, 3rd Edition, John Wiley and Sons, Inc., 2012.
13. Orchard, H. J., "Optimizing the synthesis of shaped beam antenna patterns," *IEEE Proceedings*, Vol. 132, No. I, February 1985.

A Simple Minimized Polarization Reconfigurable Slot Antenna

Maziar Hedayati[1], **Mohsen Abdolahi**[1],
Gholamreza Askari[2], **and Hamid Mirmohammad Sadeghi**[2]

[1]Department of Electrical and Computer Engineering
Isfahan University of Technology (IUT), Isfahan 84156, Iran
[2]Information and Communication Technology Institute
Isfahan University of Technology (IUT), Isfahan 84156, Iran

Abstract— Wireless communication systems have been developed rapidly in recent years Recent developments in the wireless communication industry continue to drive the requirements for small, compatible, and affordable reconfigurable antennas. Concept of a reconfigurable antenna was proposed a few years ago [1] to obtain switchable ability of the antenna Frequency, radiation pattern [2, 3], and polarization [4–6] reconfigurable antennas are alternatives to broadband/multiband antenna, beam forming array, and dual polarized antenna, respectively. But few polarization reconfigurable antennas have been presented in the literature [7, 8]. Polarization-reconfigurable antennas can mitigate multipath fading loss and provide a double-transmission channel for frequency reuse but they are difficult to simultaneously realize a good impedance matching for circular and linear polarizations.

In this paper, a very simple polarization-reconfigurable antenna for satellite communication is proposed. This antenna is designed to have linear and circular polarization. The design process consists of several parts such as designing of the single slot and calculation of its coupling factor second slot length calculation and, the design of reconfigurable antenna. An overall layout of the designed slots is shown in Fig. 1. In the proposed design a new shape of slot antenna based on SIW structures with special tapered microstrip for its excitation at center frequency 31 GHz is presented. To decrease the total area occupied by the antenna, the slot configuration was altered from its standard straight form to an S-shape It was shown that their characteristics are same as standard slot except their polarization. The slot must be placed in a point on SIW surface which the transverse and longitudinal current distribution components of the TE_{10} mode be equal ($x = a/\pi(\tan^{-1}(\lambda_g/2a)$ which $\underline{a}$ and $\underline{\lambda_g}$ are the width and guided wavelength of SIW, respectively. If an s-slot be cut at the x point, the produced transverse and longitudinal components of the electrical field are not exactly the, so it is necessary to optimize the slot to achieve 45 deg polarization which θ in Fig. 1 must be 20° and $(L_1 + L_3)/L_2 < 0.37$. The coupling factor of first slot is obtained 0.59 which to have the uniform amplitude distribution length of second slot is obtained 4.32 mm. There are various elements and techniques implemented in order to achieve the tune ability: micro electromechanical switches (MEMS), varactors, PIN diodes, FET transistors, and special substrate materials like ferroelectric or ferromagnetic materials. In this paper PIN diodes are used because of their reliability, compact size, high switching speed, small resistance and capacitance in the ON and OFF state. The switch bias network must be presented for PIN diode. An inductor is necessary for RF signal isolation but lumped elements do not have appropriate behavior in high frequencies because their self-resonance frequency is less than 31 GHz. The stub is designed by two $\lambda_g/4$ open circuit radial stub line which enhance stub bandwidth. Furthermore two 2.7 pF capacitors are used to improve the DC isolation. Computed return loss shows that the antenna operate in 30–32 GHz in both case (diode on and off). The small ON state resistance also affects the antenna performance and particularly its input impedance. Full wave analysis was

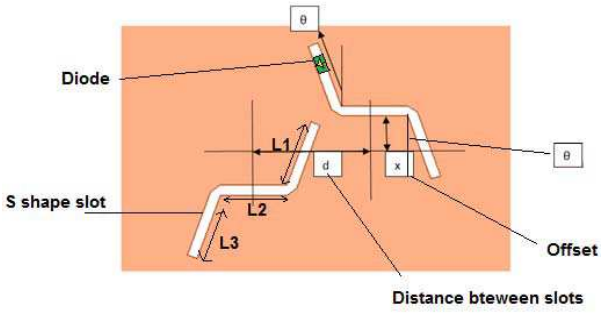

Figure 1: The layout of the designed slots.

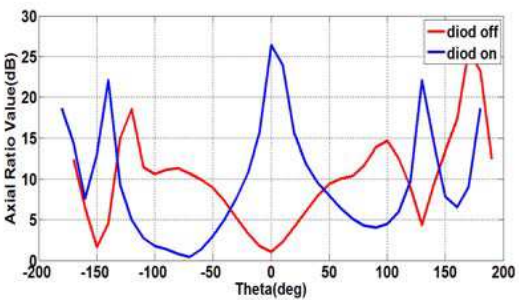

Figure 2: The axial-ratio of the proposed antenna.

used to model these effects. For a first order approximation, the diode resistance was modeled as a thin film resistor on top of the slot and the packaging parasitic elements were neglected in this analysis. As it is shown, the parasite resistance does not affect on antenna performances and the antenna radiation is acceptably the same. Accordingly, the axial-ratio of the proposed antenna is shown in Fig. 2. As it is shown in this figure when the diode is off and on the axial ratio is less than 3 dB and greeter than 15 dB between $-25°$ and $25°$, respectively. Also when the diode is on, the gain of antenna is 0.5 dB less than another one and the side lobe level is more than when diode is off. But In either case, the antenna have the maximum radiation in $\theta = 0$. The results show that the antenna is very useful in satellite communication.

REFERENCES

1. Peroulis, D., K. Sarabandi, and L. P. B. Katehi, "A planar VHF reconfigurable slot antenna," *IEEE Antennas and Propagation Society International Symposium*, Vol. 1, 154, 157, Jul. 8–13, 2001.
2. Chen, S.-H., J.-S. Row, and K.-L. Wong, "Reconfigurable square-ring Patch antenna with pattern diversity," *IEEE Trans. Antennas Propag.*, Vol. 55, No. 2, 472–475, Feb. 2007.
3. Wu, S.-J. and T.-G. Ma, "A wideband slotted bow-tie antenna with Reconfigurable CPW-to-slot line transition for pattern diversity," *IEEE Trans. Antennas Propag.*, Vol. 56, No. 2, 327–334, Feb. 2008.
4. Sung, Y., "Investigation into the polarization of asymmetrical-feed triangular microstrip antennas and its application to reconfigurable antennas," *IEEE Trans. Antennas Propag.*, Vol. 58, No. 4, 1039–1046, Apr. 2010.
5. Simons, R. N., D. Chun, and L. P. B. Katehi, "Polarization-reconfigurable patch antenna using microelectromechanical-system (MEMS) actuators," *IEEE Antennas Propag. Soc. Int.*, Vol. 2, 6–9, 2002.
6. Yang, F. and Y. Rahmat-Samii, "A reconfigurable patch antenna using Switchable slots for circular polarization diversity," *IEEE Microw. Wireless Compon. Lett.*, Vol. 12, No. 3, 96–98, Mar. 2002.
7. Qin, P.-Y., A. R. Weily, Y. J. Guo, and C.-H. Liang, "Polarization reconfigurable U-slot patch antenna," *IEEE Trans. Antennas Propag.*, Vol. 58, 3383–3388, Oct. 2010.
8. Parihar, M. S., A. Basu, and S. K. Koul, "Polarization reconfigurable microstrip antenna," *Proceedings of the Asia-Pacific Microwave Conference APMC'09*, 1918–1921, Singapore, 2009.

Microwave Radiation Interferometry High Resolution Reconstruction Based on Mixed Orthogonal Basis

Chao Song, **Lu Zhu**, **Yuanyuan Liu**, **and Suhua Chen**
School of Information Engineering
East China Jiaotong University, Nanchang 330013, China

Abstract— Microwave radiometry is the primary means of soil moisture remote sensing and capable of observation soil moisture all-time, all-weather. But the imaging method of traditional microwave radiometry has complex structure and low resolution, which limited largely the application in regional soil moisture remote sensing. In this paper, we propose a new inversion method for microwave radiation interferometry imaging based on compressed sensing (CS), by mining the sparse and compressible information of the microwave radiation image. The proposed method can break through the limit of the inherent spatial resolution of the imaging system which based on the Nyquist sampling, achieving the spatial resolution image closely obtained by the expensive large aperture imaging system, and reducing the complexity and the cost of the hardware of the imaging system configuration. Due to the complexity of microwave radiation image scene, it is difficult to sparsely represent the microwave radiation image by single orthogonal basis, so we make use of the sparse representation in mixed orthogonal basis and the constraint conditions of total variation regularization of microwave radiation image, and establish the optimal reconstruction model of microwave radiation image. We solve the optimal solution of reconstruction model by adopting the alternating direction method (ADM), achieve high resolution microwave radiation image reconstruction from low-dimensional measurements to high -dimensional data, and solve the contradiction between the high resolution and the complexity of the system, and establish evaluation methods of spatial resolution. The simulation results show that, compared with the orthogonal matching pursuit (OMP) algorithm, the proposed algorithm can achieve higher spatial resolution.

Development of DC Current Distribution Mapping System for Solar Panels Using an HTS-SQUID Gradiometer

Shohei Kasuya, **Kohei Tanaka**, **Mohd Mawardi Saari**, **Kenji Sakai**, **Toshihiko Kiwa**, **and Keiji Tsukada**
Graduate School of Natural Science and Technology, Okayama University
3-1-1 Tsushima-naka, Kita-ku, Okayama-Shi, Okayama Prefecture, 700-8530, Japan

Abstract— Solar panels provide a sustainable source of energy with a low environmental load. To develop highly efficient and high quality solar panels, it is useful to evaluate solar panels in a non-destructive manner.

In the previous study, we developed an electrical property mapping system for solar panels using a conventional conducting pickup coil and HTS-SQUID (High-T_c Superconductor Superconducting QUantum Interference Device), which is a highly sensitive magnetic sensor. This measurement system can evaluate the magnetic signal that reflects the differential conductance of the solar panels. The measurement unit is easy to operate because an HTS-SQUID with a cooling system can be separated from solar panels using a pickup coil that transfers the magnetic signal of the solar panel to the SQUID. However, this measurement system has to apply a frequency-modulation voltage to the solar panel because the pickup coil cannot detect a DC magnetic field. Using this method, it is difficult to evaluate the magnitude of the current in the solar panels. Therefore, we developed a new type of system that can detect the DC current distribution of the solar panels directly using an HTS-SQUID gradiometer. In this system, it is possible to detect the magnetic field of two independent components generated on its surface ($\partial Bz/\partial x$, $\partial Bz/\partial y$), which is perpendicular to the solar panel. As the measured signals using the developed system are a magnetic field gradient generated by the current through the solar panel, it is possible to calculate the magnitude and the flow of the current through the solar panel using the obtained data. As a result of evaluation of the solar panel using this system, we succeed in mapping the uniformity of the DC current flowing through the solar panel.

ACKNOWLEDGMENT

This work is supported by the "Strategic Promotion of Innovative R&D" of the Japan Science and Technology Agency (JST).

Highly Sensitive Detection Method for Rotating Sample Magnetometer Using HTS-SQUID

Naohiro Okamoto, Yuta Watanabe, Mohd Mawardi Saari, Kenji Sakai, Toshihiko Kiwa, and Keiji Tsukada

Graduate School of Natural Science and Technology, Okayama University
3-1-1 Tsushima-naka, Kita-ku, Okayama-Shi, Okayama Prefecture 700-8530, Japan

Abstract— A superconducting quantum interference device (SQUID) can detect very weak magnetic fields and it is applied to a wide range of fields, such as biomagnetism measurement and non-destructive testing, etc.. For these applications, a highly sensitive magnetometer is important for evaluating magnetic properties precisely. Previously, we developed a rotating sample magnetometer using a high-temperature superconductor (HTS)-SQUID. In this study, we improved the detection method of the developed measurement system to increase the S/N ratio.

The measurement sample is fixed on a turntable and moved by rotating the turntable using the electromagnetic motor. When the sample passes between the permanent magnet, the sample is mag-netized. At this time, a magnetic signal is generated from the sample, and detected by the pick-up coil. Then, the detected signal is transmitted to the HTS-SQUID through an input coil that is con-nected in series with the pick-up coil. First, the shapes of the pickup coils were examined. Elliptical and circular coils are used and the S/N ratios of these two coils were compared. The S/N ratio of the elliptical shape was higher than that of the circular shape. In addition, the noise was also reduced by averaging the data of many rotations and the high frequency component of the signal, which is high-er than that caused by the sample, was removed using a low-pass filter (LPF). Moreover, the accu-racy of the rotation speed of the turntable was investigated because stable rotation is required for the averaging of many rotations. Although an ultrasonic motor has a low electromagnetic noise and does not affect the output signal, the speed of rotation continues to decrease gradually. On the other hand, the rotation speed of an electromagnetic motor is stable and the noise caused by the electromagnetic motor is almost the same as that of an ultrasonic motor. Therefore, an electromagnetic motor was employed in this study.Under optimized conditions, the magnetic signal from 10 ml of water was measured using the developed magnetometer, which has very small magnetic susceptibility. As a result, a very weak magnetic signal could be detected by the developed system with a high S/N ratio.

ACKNOWLEDGMENT

This work is supported by the "Strategic Promotion of Innovative R&D" of the Japan Science and Technology Agency (JST).

Surface Effect of the Two-dimensional Photonic Crystal on Imaging Property

Yuan-Wei Tong, Peng-Fang Liu, and Zao-Jie Zhu
College of Science, University of Shanghai for Science and Technology, Shanghai 200093, China

Abstract— Negative index material become one of wide research object because of its unique characteristic, especially perfect imaging of photonic crystal (PC) slab. In this paper, Si cylindrical rods are designed into hexagonal pattern in air to build a 2D photonic crystal flat. Good-quality images and focusing, with relative refractive index of −1, have been observed in this system for TE mode waves. In order to achieve a high-quality image, an appropriate surface is chosen. In addition, by adjusting the radius of outmost dielectric rods of the PC slab, or shifting the outermost layer rods synchronously, the imaging quality can be further improved. Coupled-mode theory analysis shows that the optimized surface can excite two kinds of surface modes that can couple with the Bloch wave in the PC. With the help of these surface modes, the intensity of image of this triangular lattice PC slab can be improved greatly.

ACKNOWLEDGMENT

This work was supported by the National Key Basic Research Special Foundation of China at No. 2005CB724304, the National Natural Science Foundation of China at No. 60777045, and the support form Tongji University.

REFERENCES

1. Veselago, V. G., "The electrodynamics of substances with simultaneously negative values of ε and μ," *Sov. Phys. Usp.*, Vol. 10, 509, 1968.
2. Pendry, J. B., A. J. Holden, D. J. Robbins, and W. J. Stewart, "Magnetism from conductors and enhanced nonlinear phenomena," *IEEE Trans. Microwave Theory Tech.*, Vol. 47, 2075, 1999.
3. Smith, D. R., W. J. Padilla, D. C. View, S. C. Nemat-Nasser, and S. Schultz, "Composite medium with simultaneously negative permeability and permittivity," *Phys. Rev. Lett.*, Vol. 84, 4184, 2000.
4. Aydin, K., K. Guven, M. Kafesaki, L. Zhang, C. M. Soukoulis, and E. Ozbay, "Experimental observation of true left-handed transmission peak in metamaterials," *Opt. Lett.*, Vol. 29, 2623, 2004.
5. Aydin, K., K. Guven, N. Katsarakis, C. M. Soukoulis, and E. Ozbay, "Effect of disorder on magnetic resonance band gap of split-ring resonator structures," *Opt. Express*, Vol. 12, 5896, 2004.
6. Shelby, R. A., D. R. Smith, and S. Schultz, "Experimental verification of a negative index of refraction," *Science*, Vol. 292, 77, 2001.
7. Parazzoli, C. G., R. B. Greegor, K. Li, B. E. Koltenbah, and M. Tanielian, "Experimental verification and simulation of negative index of refraction using Snell's law," *Phys. Rev. Lett.*, Vol. 90, 107401, 2003.
8. Houck, A. A., J. B. Brock, and I. L. Chuang, "Experimental observations of a left-handed material that obeys Snell's law," *Phys. Rev. Lett.*, Vol. 90, 137401, 2003.
9. Aydin, K., K. Guven, C. M. Soukoulis, and E. Ozbay, "Observation of negative refraction and negative phase velocity in left-handed metamaterials," *Appl. Phys. Lett.*, Vol. 86, 124102, 2005.
10. Cummer, S. A. and B. I. Popa, "Wave fields measured inside a negative refractive index metamaterial," *Appl. Phys. Lett.*, Vol. 85, 4564, 2004.
11. Tong, Y. W., Y. Mao, and S. L. Zhuang, "Numerical study on 2-d photonic crystal with negative refractive index at multiple frequency bands," *Acta Phys. Sin.*, Vol. 59, 5553, 2010.
12. Aydin, K., I. Bulu, K. Guven, M. Kafesaki, C. M. Soukoulis, and E. Ozbay, "Investigation of magnetic resonances for different split-ring resonator parameters and designs," *New J. Phys.*, Vol. 7, 168, 2005.

13. Guibing, X., G. Tao, and W. Yan, "Negative refraction properties of anisotropic magnetic materials at ferromagnetic resonance," *J. University of Shanghai for Science and Technology*, Vol. 35, No. 5, 439, 2013.
14. Pendry, J. B., "Negative refraction makes a perfect lens," *Phys. Rev. Lett.*, Vol. 85, 3966, 2000.
15. Cubukcu, E., K. Aydin, E. Ozbay, S. Foteinopoulou, and C. M. Soukoulis, "Negative refraction by photoniccrystals," *Nature*, Vol. 423, 604, 2003.
16. Cubukcu, E., K. Aydin, S. Foteinopolou, C. M. Soukoulis, and E. Ozbay, "Subwavelength resolution in a two-dimensional photonic-crystal-based superlens," *Phys. Rev. Lett.*, Vol. 91, 207401, 2003.
17. Grbic, A. and G. V. Eleftheriades, "Overcoming the diffraction limit with a planar left-handed transmission-line lens," *Phys. Rev. Lett.*, Vol. 92, 117403, 2004.
18. Smith, D. R., D. Schurig, M. Rosenbluth, S. Schultz, S. A. Ramakrishna, and J. B. Pendry, "limitations on subdiffraction imaging with a negative refractive index slab," *Appl. Phys. Lett.*, Vol. 82, 1506, 2003.
19. Fang, N. and X. Zhang, "Imaging properties of a metamaterial superlens," *Appl. Phys. Lett.*, Vol. 82, 161, 2003.
20. Lagarkov, A. N. and V. N. Kissel, "Near-perfect imaging in a focusing system based on a left-handed-material plate," *Phys. Rev. Lett.*, Vol. 92, 077401, 2004.
21. Rao, X. S. and K. C. Ong, "Subwavelength imaging by a left-handed material superlens," *Phys. Rev. E*, Vol. 68, 067601, 2003.
22. Tong, Y. W., S. Tian, and S.-L. Zhuang, "Imaging properties of triangular lattice photonic crystal at multi-bands," *Optik*, Vol. 123, 590, 2012.
23. Tong, Y. W. and S. L. Zhuang, "Intensity depending on object distance in a two-dimensional photonic crystal," *Optik*, Vol. 124, 361, 2013.
24. Luo, C., S. G. Johnson, J. D. Joannopoulos, and J. B. Pendry, "All-angle negative refraction without negative effective index," *Phys. Rev. B*, Vol. 65, 201104(R), 2002.
25. Foteinopoulou, S. and C. M. Soukoulis, "Negative refraction and left-handed behavior in two-dimensional photonic crystals," *Phys. Rev. B*, Vol. 67, 235107, 2003.

Measurement of Moisture Content Using HTS-SQUID Magnetometer

T. Kusaka, M. M. Saari, Y. Ishihara, Y. Tsukamoto, K. Sakai, T. Kiwa, and K. Tsukada
Graduate School of Natural Science & Technology, Okayama University, Japan

Abstract— It is important to evaluate the moisture content in mortar because mortar is used in the construction of various structures, and its strength is correlated to water content. In this study, we propose a moisture content evaluation method using our developed vibrating sample compact magnetometer using HTS-SQUID. This method enables non-destructive measurement of the moisture content by detecting the magnetic properties of the water. The magnetic signal from the sample was detected as follows. The sample is placed in a DC magnetic field. The sample generates a secondary magnetic field due to its magnetization and the secondary magnetic field is detected by a pickup coil.

The detected signal is then transmitted to a SQUID by a superconducting input coil. The signal detected by the SQUID is measured as the phase and intensity of the magnetic field strength using a lock-in amplifier. To evaluate the moisture content in mortar using the magnetometer, we measured the M-H curve by changing the applied DC magnetic field. The measurement sample of mortar consists of sand, cement and water. To measure changes in moisture content, five samples with different moisture content were prepared. Although the difference in signal intensity is not observed in the low magnetic field region, the signal intensity decreased with increasing the moisture content in the strong magnetic field region because the magnetic signal caused by ferromagnetism is saturated, and the signal change caused by the diamagnetism of water is dominant.

Based on this result, the moisture content can be measured by the M-H curve in a strong magnetic field using the developed highly sensitive magnetometer.

ACKNOWLEDGMENT

This work is supported by the "Strategic Promotion of Innovative R&D" of the Japan Science and Technology Agency (JST).

Stereo-SAR Technique without Using Control Points to Estimate Terrain Height

Hsi-Tseng Chou[1], **Shih-Chung Tuan**[2], **and Kung-Yu Lu**[1]

[1]Department of Communication Engineering, Yuan Ze University, Chung-Li, Taiwan
[2]Department of Communication Engineering, Oriental Institute of Technology, Pan-Chiao, Taiwan

Abstract— Estimation of terrain profiles remains very interested in the applications of remote sensoring. In particular, the high-resolution images obtained by the Airborne or satellite-borne synthetic aperture radars (SARs) were effectively used in conjunction with the applications of stereo techniques to perform the estimation. Many simulation models were thus developed and applied in the stereo techniques to process the optical images to estimate terrain profiles such as the digital elevation model (DEM) and digital terrain model (DTM). Some typical examples of technologies revealed in the literatures are summarized in the following. The works in proposed a new hybrid radar grammetric model as a function of terrain's slope to establish the stereo DEM without the need of using any reference cartographic data. The accuracy was examined by using the topographic 1959 DEM, and Ice, Cloud, and land Elevation Satellite (ICESat) data. It was applied to ice-covered areas with 1-sigma 25- or 18-m accuracy over less than 30° or 5° slopes, respectively. In addition, a systematic elevation lowering of around 10 m computed between 1959 DEM and recent elevation data (R-2 and ICESat) could be due to icefield wastage over the last 50 years.

Detection of Selected Chemical Substances by Means of Nuclear Quadrupole Resonance

M. Steinbauer[1], **B. Kral**[2], **I. Fiala**[2], **M. Stanek**[2], **M. Prochazka**[1], **P. Fiala**[1], **J. Seginak**[1], **and P. Drexler**[1]

[1]Department of Theoretical and Experimental Electrical Engineering
Brno University of Technology, Technická 12, Brno 616 00, Czech Republic
[2]Prototypa, Hudcova 533/78c, Brno 612 00, Czech Republic

Abstract— Nuclear Quadrupole Resonance (NQR) is an advanced diagnostic method for spectroscopy of solid state substances. NQR exploits the presence of electrical quadrupole moment of atomic nuclei of certain isotopes. In case of this isotope, the electrical charge is distributed non-symmetrical within its nucleus. Hence, a gradient electric field is imposed in the nucleus and the nuclear electric multi-pole moment arises. Generally, the nuclear electric field gradient produces electric multi-poles with pole counts 2^n, where n is even number. Therefore the monopole, quadrupole, oktupole moment and so on may occur. However, the manifestations of the moment strongly decrease with raising n. Thus, in solid substances the quadrupole moment is practically the only detectable moment. The principle of NQR method is the detection of resonance of certain nuclear quadrupole moments. A broad set of substances, inorganic and organic also, have their quadrupole resonance in the range of ones to tens of megahertz. An important fact is, that significant quadrupole resonance can be detected in case of substances, which are part of the chemical composition of explosives, drugs and medicaments. Utilization of NQR represents a promising method for non-contact, non-destructive diagnostic method for chemical research, material science and for security applications. A compact experimental NQR spectrometer has been built at DTEEE, Brno University of Technology. The spectrometer allows experimental verification of impact of various functional blocks on the detection abilities. Selected chemical substances containing chlorine and nitrogen isotopes were analyzed with the spectrometer. The spectral patterns of the substances were recorded and there was also investigated the minimal detectable amount of selected substances. The paper will presents the results of spectral patterns measurement and the conclusions on the exploitation of NQR method for chemical substances detection and identification.

Subsurface Imaging 3-D Objects in Multilayered Media by Using Electromagnetic Inverse Scattering Series Method (EISSM)

J. G. Wang[1], **Z. Q. Zhao**[1], **Z. P. Nie**[1], **and Q. H. Liu**[2]

[1]School of Electronic Engineering
University of Electronic Science and Technology of China, China
[2]Department of Electrical and Computer Engineering, Duke University, USA

Abstract— Subsurface imaging 3-D objects buried in multilayered media with electromagnetic waves has recently attracted significant interests and been extensively studied. It has widespread applications such as the detection of land mines, unexploded ordnance, and underground structures. Owing to the uncertainty of dielectric properties of layered background media in practice, most of existing electromagnetic inverse methods reconstruct the buried objects unfaithfully.

In order to accurately reconstruct the objects buried in multilayered media with unknown dielectric parameters, a modified inverse scattering series method based on the inverse scattering series (ISS) theory was developed in hydrocarbon exploration for 1-D and 2-D scenarios. The modified inverse scattering series method reconstructs the electric conductivity of objects with an approximation that the dielectric permittivity is constant and equal to the value of water.

Different to the modified inverse scattering series method, we develop an imaging method named electromagnetic inverse scattering series method (EISSM) for imaging 3-D objects buried in multilayered media. The proposed 3-D EISSM combines the ISS idea with a multi-array tomographic approach. It directly reconstructs the positions of the buried objects (not their dielectric properties) solely with the dielectric parameters of free space according to the discontinuities of dielectric properties. Moreover, the effects of multilayered media to the position error predicted by EISSM are also analyzed and discussed. Aiming to validate the feasibility of the proposed 3-D EISSM, some numerical simulations are given as well as the results reconstructed by commonly used time reversal mirror (TRM) technique. Through the simulations, the proposed EISSM is capable of positioning 3-D targets buried in multilayered media with less error than traditional TRM.

Multi-wavelength Thulium-doped Fiber Laser near 2 μm Based on a Sagnac Loop Filter

Yizhen Wei[1, 2] **and Xiong Yang**[1]

[1]Centre for Optical and Electromagnetic Research, Zhejiang University, China
[2]College of Communication Engineering, Hangzhou Dianzi University, China

Abstract— Multi-wavelength fiber lasers (MWFL) are of great interest over the past several years because of their many applications, such as precise spectroscopy, optical component testing, optical sensing, and especially in high capacity wavelength division multiplexing systems. Stable MWFLs at room temperature near 1.55 μm have been accomplished using various techniques, for instance, injecting a high repetition rate mode-locked pulse train into the nonlinear fiber to generate multi-wavelength source, combining a comb filter and inhomogeneous line broadening gain medium in the laser cavity, employing four-wave-mixing effect to provide channel equalization and expansion, and utilizing successive stimulated Brillouin scattering (SBS) in the Brillouin-erbium fiber laser, which combines the high gain from EDFA and nonlinear gain from SBS process. On the other hand, the ever increasing demand for high bandwidth Internet applications is inspiring the research community to develop systems capable of delivering higher capacities, like exploring new transmission windows. The thulium doped fiber amplifier is an ideal candidate for new wavelength MWFLs due to its remarkable merits. For instance, the possibility of achieving quantum efficiency greater than one thanks to cross relaxation energy transfer processes makes this class of fiber lasers efficient and powerful. The thulium doped fiber amplifier also exhibit a broad gain from 1800 nm to 2100 nm, enabling a wide transmission window.

In this paper, a multi-wavelength thulium-doped fiber laser near 2 μm was realized. A Sagnac loop filter, which is formed by a segment of polarization maintained fiber (PMF), a 3 dB optical coupler, and a polarization controller (PC), is used as the comb filter. By pumping the thulium-doped fiber with two high-power fiber lasers at 1560 nm, an ultra-wide gain centered at 1950 nm can be obtained and multi-wavelength lasing with low ripple of the MWFL is achieved.

Data Acquisition System for Body-to-body Radio Communication Channel

H. A. Rahim[1], **F. Malek**[1], **K. K. Goh**[1], **V. Ganesan**[1], **F. A. A. Fuad**[1], **N. A. A. Talib**[2], **and F. S. Abdullah**[2]

[1]Embedded, Network and Advanced Computing Research Cluster (ENAC)
School of Computer and Communication Engineering, Universiti Malaysia Perlis
P. O. Box 77, d/a Pejabat Pos Besar, Kangar, Perlis 01000, Malaysia
[2]School of Electrical System Engineering, Universiti Malaysia Perlis
P. O. Box 77, d/a Pejabat Pos Besar, Kangar, Perlis 01000, Malaysia

Abstract— This paper presents data acquisition system for dynamic body-to-body radio propagation channel by using Labview software. The aim of this work is to provide an automate system in data collection of S-parameters which involves a large set of data. The data acquisition system is designed using Labview software. The designed software is integrated in the measurement system that utilizes an Agilent vector network analyzer (VNA) (model PNA E8362B), general purpose interface buses (GPIB)-USB cable and a personal computer (PC). The acquisition of the measurement data is performed by a computer, connecting to the VNA via GPIB-USB cable. The measurement data of dynamic body-to-body radio propagation channel, frequency response, S_{21} parameter, is recorded and stored for offline processing. The comparison of data acquisition between with and without the integrated software for dynamic body-to-body radio propagation channel is presented in the paper by setting the sweep time parameter for every 1 second.

Beam Switching Antenna

W. L. Lim[1], **F. H. Wee**[1], **F. Malek**[2], **K. Y. You**[3], **Y. S. Lee**[1], **H. A. Halim**[2], **and F. S. Abdullah**[2]

[1]School of Computer and Communication Engineering, Universiti Malaysia Perlis (UniMAP)
Pauh Putra Campus, Arau, Perlis 02600, Malaysia
[2]School of Electrical Systems Engineering, Universiti Malaysia Perlis (UniMAP)
Pauh Putra Campus, Arau, Perlis 02600, Malaysia
[3]Faculty of Electrical Engineering
Universiti Teknologi Malaysia, Skudai, Johor Bahru, Johor 81310, Malaysia

Abstract— In this paper is showing about Beam Switching Antenna that able to shift the antenna direction by using four microstrip antenna and aluminum. The antenna is using FR-4 and the size is 40 mm × 78 mm. By using aluminum it able increase the gain from 5.269 dB to 8.128 dB while the directivity is from 7.126 dBi to 11.09 dBi. With this antenna it able to control the direction of the radiation pattern up to four location.

A technique that able to switch the beam of the signal of an antenna with durable material that able make the signal stronger. The reason for switching the signal for the place that unwanted for signal is to reduce energy that did not used. It also able use as for security reason that for switch the location that only authorize people in the longing place of the area.

With using aluminum it able support four antenna in different direction and it also able to increase the gain by 64% and increase dielectric by 64.25%. The compounds of greatest importance are aluminum oxide, the sulfate, and the soluble sulfate with potassium (alum). The oxide, alumina, occurs naturally as ruby (AL_2O_3), sapphire, corundum, and emery, and is used in glassmaking and refractories. Synthetic ruby and sapphire are used in lasers for producing coherent light.

The Fig. 1 shows the front view of a microstrip antenna that able to generate 2.45 GHz frequency with the gain of 5.269 dB and the directivity is 11.09 dBi. The saiz of the antenna is 60 × 80 mm. This antenna is using FR-4 material. FR-4 is a grade designation assigned to glass-reinforced epoxy laminate sheets, tubes, rods and printed circuit boards (PCB). FR-4 is a composite material composed of woven fiberglass that flame retardant, chemical resistance and water absorption. The Fig. 2 it show that the antenna is attached with two plate of aluminums that not only to hold the antenna but also to increase the gain of the antenna.

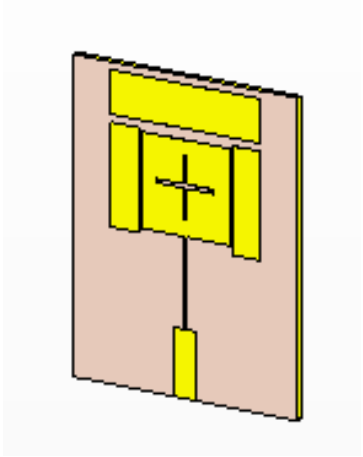

Figure 1: Single microstrip antenna.

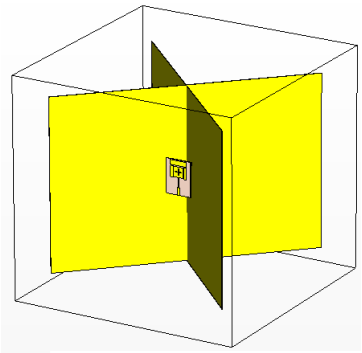

Figure 2: Antenna with aluminum.

A Wideband Metamaterial Absorber Based on Multilayer Rings and Lumped Resistors

Yujie Liu, Wei Tang, and Yuehe Ge
College of Information Science and Engineering, Huaqiao University, Xiamen, Fujian 361021, China

Abstract— Metamaterials attracts much attention of researchers in the past decade. Various novel theories and applications based on metamaterials were proposed and studied. Metamaterial perfect absorber, proposed by David Smith, is able to provide a good absorbance due to the simultaneous electric and magnetic resonances, however, with a narrower bandwidth. Wideband metamaterial absorbers has been studied using interference theory and implemented at higher frequency band. Low-profile planar absorbing materials have also been designed by using the left-handed transmission line theory, achieving a reduction of 10 dB over a bandwidth of 50% at the center frequency of 2 GHz.

In this paper, a novel low-profile metamaterial absorber, composed of square-circular metal rings and lumped resistors, is proposed for wideband absorptive applications. The proposed structural model is original from the typically square and circular loops, which have strongly magnetic resonances. Additionally, the result of the absorber is well explained with the interference theory, which shows that the metamaterial absorber can obtain wide absorptive bandwidth in the low frequency stage. Simulated results show that this composite structure metamaterial absorber has a low-frequency wideband absorption in the range of 1.96 GHz to 7.44 GHz, almost 116.6% absorptive bandwidth. What is more, this design provides a low-profile height of 0.094 free-space wavelength at the lowest operating frequency.

Design of Broadband Dual-polarized Antenna with Inverted L-probe Feed

K. S. Phoo[1], **M. Z. A. Abd Aziz**[1], **B. H. Ahmad**[1], **M. A. Othman**[1], **M. K. Suaidi**[1], **and F. Abd. Malek**[2]

[1]CeTRI, FKEKK, Universiti Teknikal Malaysia Melaka (UTeM), Durian Tunggal, Melaka, Malaysia
[2]School of Computer and Communication Engineering, Universiti Malaysia Perlis, Perlis, Malaysia

Abstract— In practical wireless communication application, broadband application antenna received much attention. In this paper, two broadband dual polarized antennas with different structure of feeding line which connected with the inverted L-probe feed are proposed. One of the antennas is designed with single straight feeding line. Another antenna is designed with bending feeding line. Both antennas are designed with combination of left-handed circular polarization (LHCP) and right-handed circular polarization (RHCP) which operating at 2.4 GHz for WLAN application. The proposed antennas are designed with inverted suspended rectangular microstrip patch antenna (MSA). Both antennas have been designed, simulated and fabricated by using FR4 substrate with dielectric constant, ε_r of 4.4, tangent loss, $\tan\delta$ of 0.019 and thickness, h of 1.6 mm. In order to present in dual-polarization at the same time, two rectangular patches are printed upon the FR4 substrate. Besides, each antenna is excited with single coaxial probe feed to the feeding line which printed on opposite side of the inverted rectangular patch. The inverted rectangular patches are printed with one rectangular notch and double circular slots which will affect the orientation of polarization. The inverted rectangular patch and copper ground plane is separated with 10 mm air gap. This approach is proposed to enhance the bandwidth and gain of the antenna. The simulated and measured S-parameter results presented that the bandwidth of the designed antennas is more than 200 MHz which meet broadband application. Based on the simulation result, antenna with bending feeding line achieved wider bandwidth than the antenna with straight feeding line. The bandwidth for bending feed line and straight feed line are 364 MHz and 222 MHz respectively. The frequency range for antenna with bending feed line is from 2.31 GHz to 2.68 GHz; meanwhile the frequency range for antenna with straight feed line is from 2.22 GHz to 2.44 GHz. The return loss of the proposed antenna is less than −10 dB which achieved at least 90% matching efficiency. Based on the simulation result, the return loss of the antenna with bending feed line is −28.8 dB and this is better than the antenna with single straight feed line which only achieved −12.89 dB. Other than that, the gain for the antenna with bending feeding line also achieved better result than the antenna with straight feeding line. The gain for the antenna with bending feed line and single straight feed line are 8.73 dB and 7.49 dB respectively.

Scrambling Study of Modal Power Distribution in Polygonal Fibers for Exoplanet Detection

Jian Han, **Dong Xiao**, **and Huiqi Ye**
Nanjing Institute of Astronomical Optics & Technology, National Astronomical Observatories, CAS
Bancangstreet 188, Xuanwu District, Nanjing, Jiangsu, China

Abstract— Optical fibers are of a great importance in diverse areas of modern observational astronomy. Particularly, in the field of exoplanet detection, they have become an essentialpart of most current and future instruments because of their filtering and stabilizing capability.In astronomical apparatusInstrumental noise can be broken down into two main components: errors due to couplingof the light to the instrument (varying fiberillumination due to guiding, tracking, seeing andfocusing) andenvironmental instability (mechanical, temperature or pressure), among above, coupling errors are the dominant source of instrumental noise. In order to measure spectral line shifts smaller than one ten-thousandth of apixel and stable for many months, we must reduce errors in our instrumental profile, whichcross-talks with our measurement of the Doppler shift. Optical fibers with octagonal, square and rectangular core shapes have been proposed as alternative to the circular fibers to link the telescopes to spectrographs in order to increase the accuracy of radial velocity measurements. Theoreticallythey offer better scrambling properties than their circular counterparts.

We need to construct the test bench to explore the geometric properties of the new fibers and the corresponding statistical arithmetic. The field is measured through scanning the core of the tested fiber with the different section shape (square,rectangular and octagonal geometry) at the entrance, analyze the role of the fiber section shape in the mode coupling and the light power distribution. Establish a mathematical fiber model of the light transmission. The simulation outcome of the model is agreement with the result of the measurement at the different coupling condition and the fiber section shape, so as to provide a theory insight and experiment direction thathelps to apply the polygonal fiber in observation, scrambling and the stability improvement of the optical power distribution.

Self-reconstruction and Rectification of Non-diffracting Beams after Focusing

Lan Liu[1], **Haitao Zhang**[1], **and Pengtie Wu**[2]

[1]Luohe Medical College, Luohe 462002, China
[2]Huaqiao University, Quanzhou 362021, China

Abstract— Based on Huygens-Fresnel diffraction integral, the expression of intensity distribution of the self-reconstruction beam is obtained and used to study the intensity evolution of self-reconstruction beams. It is shown that the intense central spot size of the self-reconstruction beam is larger than that of the non-diffracting beam before focusing. This property limits the application of the self-reconstruction beams.

An Improved Method of Diagnosis of Failed Elements in Arrays Using Genetic Algorithm

Jing Miao, Bo Chen, and Wuqiong Luo
University of Electronic Science and Technology of China, China

Abstract— The failed elements in antenna arrays made the side lobe level increased and caused unacceptable pattern distortion. The radiation pattern could be restored by re-distributing their feeding method with the failed elements being found in the array. However diagnosis of the failed elements of an array was a problem in practice, especially in the large-scale antenna arrays and fixed arrays which could not be brought to laboratory for inspection.

A cost function was used to compare the calculation pattern (associated to the chromosome encoded by GA) with the degraded pattern at the samples measured from the far field radiation pattern. Genetic algorithm was used to minimize the cost function to locate the failed elements. However, it was found that when using GA to diagnose the failed elements in an array, this method could not accurately distinguish symmetrical positions if the excitation of the array was symmetrical.

In order to solve this ambiguity problem, an asymmetry factor was introduced in the mentioned diagnosis method to the excitation distribution (amplitude or phase) of the arrays artificially. This improved method was exploited to a linear array and a planar array to validate the method. From the comparison between the symmetrical and asymmetrical excitation distributions of the above two arrays, it was showed that the improved method was applicable.

The constitution of this paper was as following. In the first section, the background and development about the method of diagnosis of failed elements in arrays were introduced. In the second section, the improved method was described about diagnosis of failed elements in arrays using GA. This improved method was exploited to a linear array and a planar array to validate the method in the third section. The conclusion and future work were given at last.

Design of a C-band Coaxial Cavity Band Pass Filter

Xingxing Du, Pu Tang, and Bo Chen
University of Electronic Science and Technology of China, China

Abstract— With the development of modern communication technology, the current communication system required a lower noise figure and a higher frequency selectivity, forcing the filter must satisfied low insertion loss, high band rejection, and can withstand high power. At this point, cavity filter is one of the best solution. However, the classical cavity filter had a bulky, heavy disadvantage, therefore, the development of miniaturized portable cavity filter is a hot issue in the industry.

In this paper, a coaxial cavity band pass filter was presented with the volume of 28 mm × 15 mm × 13 mm working at 4.88 GHz with the pass-band of 654.52 MHz. The classical comb lines structure in the coaxial cavity filter was un-applicable for small size. The dressing-line structure was introduced in the coaxial cavity. By adding the capacitance circular plate on the cavity resonant column, the resonant frequency was increased with the volume of the cavity reduced greatly, and requirement of small-size was achieved. The designed filter was fabricated and measurement was conducted. From measurement, the insertion loss at the center frequency is less than 0.7 dB. The band rejection is greater than 49 dB at 1–2 GHz, and greater than 39 dB at 8 GHz–18 GHz. These showed that the designed filter met the requirements.

The constitution of this paper was as following. In the first section, the background about the cavity filter were introduced. In the second section, the design process of the proposed filter was introduced with the parameters discussed. In the third section, results of measurement was showed. In the last section, conclusion and future work were given.

Three-component Decomposition for Polarimetric SAR Images Based on Coherency Matrix

Yongjun Cai[1, 2], **Xiangkun Zhang**[2], **and Jingshan Jiang**[2]

[1]University of Chinese Academy of Sciences, China
[2]CAS Key Laboratory of Microwave Remote Sensing, National Space Science Center, CAS, China

Abstract— Original Freeman three-component decomposition was found useful in information extraction from a mix of area: city blocks, forest, ocean and land surfaces, etc.. However, it always suffers from some inconsistencies with real situation such as negative power and scattering mechanism ambiguity. It is probably because of the overestimate of volume scattering power. In Freeman decomposition, the volume model was always subtracted prior to other scattering mechanisms owing to the assumption that the entire HV component was contributed by volume scattering. The nonnegative eigenvalue constraint was proved effective to limit the volume scattering power significantly. But it should be noted that the nonnegative eigenvalue method was intrinsically a coercive measure to avoid negative power, which takes the biggest one from all the values that ensure the residual matrix is still positive semi-definite, in other words, the rank of the residual coherency matrix is set equal to two. In some sense, it is based on the assumption that the volume scattering is always dominant, with the result that the surface or dihedral scattering component is partly replaced by volume scattering component, which is obviously not reasonable for all pixels. Consequently, the scattering mechanism ambiguity is inevitable. The deorientation method was initially found useful to alleviate this problem to some degree. However, because of the boundedness of deorientation, it is sometimes noneffective, the ambiguity is still not resolved. For example, if in one pixel, there exist buildings orientated in different directions not orthogonal to radar line of sight, even though the deorientation is implemented, one cannot think that the buildings are readjusted to the direction orthogonal to radar line of sight. What's more, the orientation angle sometimes is out of the scope of deorientation angle, so the orientation angle is not compensated sufficiently. Therefore, we will start with the assumed models, and focus on developing a generalized model-based decomposition. Because for model-based scheme, we insist that one should radically start from the models. In this paper, a generalized three-component model-based decomposition is proposed, which consist of the surface, double bounce and volume scattering. Among it the generalized scattering mechanism proposed by Cloude is adopted, which provides a more accurate model for surface and dihedral scattering, and the dominant scattering component will be figured out according to the alpha angle parameter to be solved in the generalized model. Through this solution, the dominant scattering mechanism in one pixel will be preserved better. The performance of this approach is demonstrated and evaluated using the airborne AIRSAR and E-SAR data sets. The results show the advantages and improvements especially for alleviating the scattering mechanism ambiguity of oriented buildings from vegetation.

An Improved Model-based Polarimetric Decomposition Preserving Dominant Scattering Characteristics

Yongjun Cai[1, 2], **Xiangkun Zhang**[2], **and Jingshan Jiang**[2]

[1]University of Chinese Academy of Sciences, China
[2]CAS Key Laboratory of Microwave Remote Sensing, National Space Science Center, CAS, China

Abstract— Owing to the overestimation of volume scattering power in the classical Freeman three-component decomposition, research on model-based polarimetric decomposition has reached a climax in recent several years. To take into account the areas where the reflection symmetry assumption doesn't hold, Yamaguchi added a helix scattering component to the original three component decomposition. Notably, the volume scattering model is also revised to better fit the real situation. By these steps, the power assigned to volume scattering is decreased, and the negative power problem and the scattering mechanism ambiguity are both spontaneously alleviated to some degree. However, these two problems are still serious. Afterwards, the orientation angle compensation is also incorporated into model-based method, but intrinsically, the deorientation is a measure to fit the PolSAR data into the assumed surface and dihedral models by rotating the scattering matrix, in some pixels the oriented buildings are still misinterpreted as vegetation. Probably, it is because of the inconsistency between the assumed models and the actual data. For example, in the most existing model-based approaches, the volume scattering was always subtracted prior to other scattering mechanisms, furthermore, owing to the simplified selection criterion of volume model according to the relative magnitude between HH and VV component, which may often cause mistakes in extracting scattering mechanism. Nonnegative eigenvalue constraint is found wonderful to avoid the negative powers. But it is under the assumption that the rank of residual coherency matrix is two. These all default to that the volume scattering is always dominant, which is distinctly unreasonable for all cases. In this paper, we intend to solve the overestimation of volume scattering power, an improved model-based scheme is proposed, in which the decomposition will be hierarchical. If volume scattering is dominant, a revised nonnegative eigenvalue decomposition is adopted, for which the volume scattering employs the model proposed by Yamaguchi, and if volume scattering is not dominant, a revised four-component decomposition is adopted, for which the volume scattering employs the model proposed by Freeman. Through this revision, the decomposition will be more accurate and the dominant scattering mechanism in each pixel will be preserved better. To verify and demonstrate the performance and advantages of the proposed decomposition, the L-band airborne AIRSAR San Francisco data and E-SAR Oberpfaffenhofen polarimetric data are used. Comparison studies are also carried out to show the improvements by the proposed method.

A Method for Pose Estimation of Ship Target from SAR ROI Based on Ellipse Fitting

Xiaoqiang Zhang, Boli Xiong, Ganggang Dong, and Gangyao Kuang
National University of Defense Technology, China

Abstract— Pose estimation of target ROIs (region of interest) is an essential approach in Synthetic Aperture Radar (SAR) image interpretation. It brings high efficiency and fine accuracy in the process of target recognition and classification with accurate pose estimation. In this paper, firstly, the typical methods of target pose estimation are introduced, and the advantages and disadvantages of them are analyzed. Then, focusing on ship targets in SAR images, a novel method based on ellipse fitting is proposed to estimate the pose of the ship. According to the fact that the contour shape of ship target is generally similar to an ellipse in medium resolution SAR images, the principal axis of the fitted ellipse can be used to estimate the attitude angle of the ship. The ship target ROI is separated from the background and the contour of the target is extracted to fit an ellipse through a least squares ellipse fitting method. Although the contour of the ship target is generally coarse, the ellipse can be stably achieved by the complex real contour and a minority of singular points do not affect the final result significantly. At last, a number of experiments with ship target ROIs from TerraSAR-X SAR data are explored, and the accuracy of pose estimation in the range of 5.0° error is more than 92.0% and the mean error is less than 4.0°, which show the robustness and validity of the proposed method in ship pose estimation with SAR images.

Design of a Doherty Power Amplifier for Performance Enhancement

Yang Liu, **Huaibao Xiao**, **and Guizhen Lu**
Communication University of China, Beijing, China

Abstract— As the new wireless communications access technologies develop rapidly, the constraints imposed are becoming more and more stringent. In fact, linearity and power efficiency are both crucial factors in the design of communication transmitters because of the fact that they permit signal integrity upholding, base-station deployment, operating cost reduction and an increase in battery life for mobile stations.

Since future wireless transmitters need to meet various modulation formats, signal bandwidths and frequency bands, there seems to appear a strong demand for high efficiency power amplifiers (PAs). Among the existing PAs proposed to solve the efficiency problem, the Doherty PA (DPA) is an outstanding design both simple and effective.

This work presents theory, design and simulation of an improved power amplifier based on the Doherty topology. By using multiple iterations of the source-pull and the load-pull with an amplifier topology in the platform of ADS including bias circuits into the load and source traction, we got the optimum load impedance and the optimum source impedance after several steps of multiple iterations. With the design of new matching circuits, an improved main PA is done.

It is theoretically shown that, balancing the effects on the efficiency and linearity of the whole amplifier by the following factors such as the Drain Voltage of the main amplifier and the Gate Voltage of the peak amplifier, we determined the final optimum data of the design.

In this paper, an improved design of Doherty PA has been proposed. The simulation results show that the proposed Doherty PA has a power-added efficiency (PAE) much higher than the traditional one with an even better power gain both at full output power and at back-off power. It tends to approve that this design has a significant improvement in simulation performance compared to traditional one, thus validating practical effects of the design and demonstrating a promising prospect of the design to be used in the future wireless transmitter applications.

Application of the Method of Fresnel Zone Analysis in Base Station Location Survey

Zhiyuan Song, Feng Gao, Kai He, and Wentao Zhu
China Mobile Group Design Institute Co., Ltd., Beijing 100080, China

Abstract— Along with the LTE mobile communication network rapid demand in China, it appears more trouble and difficulties in network plan and needs a faster and relative accurate scientific method to support the BS (base station) location survey with a view to the weakness transmissibility of the radio wave above 2 GHz.

The BS location survey project is one of the important items in mobile communication network plan before construction; however there are less computation model methods and theoretical arithmetic based on measured data to be utilized. The conclusion of BS location survey projection is mainly depended on the experiences and subjective judgments of survey stuffs. In considering of objective factors of surroundings parameter collection, length of work time and etc. in location survey, the common methods including propagation model, ray tracing and etc. have such difficulties and incompetence to apply.

Huygens-Fresnel principle is one of most key point characters of radio wave. In the propagation of radio, every point on the surface of the wave is a secondary radiation wave of spherical wave. And space for a bit of radiation field is surrounded by the wave of each point on the arbitrary closed surface wave from the secondary waves in which the result of superposition of mutual interference. Take advantage of Huygens-Fresnel principle, it has greater possibility to adapt the ability range of BS location survey tools and the requirement of work time with the rapid computation method of Fresnel Zone in BS location survey project. In this paper, it is reported that Fresnel Zone method for the mobile communication will be studied in-depth and the application and the propagation criterion selection of this method will be analyzed concretely.

High-performance Ambipolar Organic Field-effect Transistors Based on Solution-grown TIPS-pentacene Single Crystals

Guobiao Xue, Congcheng Fan, Jiake Wu, Shuang Liu, and Hanying Li
State Key Laboratory of Silicon Materials
MOE Key Laboratory of Macromolecular Synthesis and Functionalization
Department of Polymer Science and Engineering, Zhejiang University, Hangzhou, Zhejiang 310027, China

Abstract— Organic semiconductors have been forming the basis of organic electronics, contributing to the development of electronics devices such as flexible, low-cost, disposable electronics, organic solar cells, light-emitting displays, smart tags, and molecular sensors. Field-effect-transistors (FETs) fabricated from organic semiconductor single crystals exhibit the highest charge carrier mobility among organic semiconductors due to the crystals' high orientation and high purity. Although, ambipoar transport is desired for complementary circuits, most of the organic single crystals show unipolarity, favoring either hole or electron transport, especially when symmetric source and drain electrodes are used.

Here, we have achieved, for the first time, the ambipolar performance of 6, 13-bis(triisopropylsilylethynyl) pentacene (TIPS-Pen) single crystal using Au as both source and drain electrodes. TIPS-Pen crystals were grown using the droplet pinned crystallization (DPC: During drying of a droplet of a semiconductor solution on a substrate, crystals nucleate near the contact line and grow along the receding direction (toward the center) of the droplet) method and FETs were constructed in a top-contact, bottom-gate configuration. The hole mobilities are around $1\,\mathrm{cm^2V^{-1}s^{-1}}$, close to the previously-reported values for TIPS-pen. The highest electron mobility can be as high as $0.069\,\mathrm{cm^2V^{-1}s^{-1}}$.

Large-area Fabrication of Organic Single Crystal Field-effect Transistors via Solution Growth

Shuang Liu, Congcheng Fan, Guobiao Xue, Jiake Wu, and Hanying Li
State Key Laboratory of Silicon Materials
MOE Key Laboratory of Macromolecular Synthesis and Functionalization
Department of Polymer Science and Engineering, Zhejiang University, Hangzhou, Zhejiang 310027, China

Abstract— Organic field-effect transistors (OFETs) have made a tremendous progress since the first demonstration in 1986 by Tsumura and coworkers. Some OFETs now perform as well as amorphous silicon FETs. Compared to their inorganic counterparts, organic materials have several advantages, such as flexibility, inherent compatibility with plastic substrates, and amenability to low-cost and low-temperature processing methods. However, the crystal growth and device fabrication in large-area is still challenging, which is a criterion desired for most organic electronic products. Herein, we propose a facile approach to deposit periodic well-aligned single crystals in large area. A solid needle was used as a pinner to pin a receding droplet of solution. As the solvent slowly evaporated, crystals of the organic semiconductors nucleated near the contact line of the droplet. Subsequently, the nuclei grow along the receding direction (toward the needle) of the droplet. Using this method, the ordered crystalline arrays of TIPS-pentacene were obtained on $1\,\mathrm{cm} \times 2\,\mathrm{cm}$ substrates and up to 70% of the substrates could be covered. FETs were constructed based on the well-aligned TIPS-pentacene single crystals with precise position registration between the crystals and electrodes. A hole mobility above $1\,\mathrm{cm}^2\mathrm{V}^{-1}\mathrm{s}^{-1}$ was obtained. This method is not restricted by the size of substrates and it is easily scalable. This novel one step method may have significant potentials for the large-scale and low-cost production of optoelectronic devices.

Multiband Printed Monopole Antenna Loaded with Slot-type Resonator for WLAN/WiMAX Applications

Kai He, **Feng Gao**, **Zhi-Yuan Song**, **and Wen-Tao Zhu**
China Mobile Group Design Institute Co., Ltd., Beijing 10080, China

Abstract— With the boost in modern wireless communication systems and the integration of WiMAX and WLAN, there is a growing requirement for antennas which are capable of operating in dual- or multi-band. As a result, the coplanar waveguide (CPW)-fed slot antennas have become a promising candidate due to their attractive features of multi-frequency operation capabilities, compact size, low cost, uniplanar structure, and easy integration with RF front-end circuitry. In this paper, a compact CPW-fed tri-band monopole antenna is presented for WLAN and WiMAX applications. The antenna comprises a Y-shaped monopole fed by a 50 Ω CPW transmission line on the top layer of the substrate and a slot-type resonator, which is realized by etching slots on a rotated rectangular patch, on the bottom layer. By properly tuning the coupling between the monopole and the slot-type resonator, good antenna performances are achieved. The antenna is simple in configuration outlining an overall size of $45.74 \times 40 \times 0.8\,\text{mm}^3$. The measured 10 dB bandwidth for return loss is from 2.36–2.54 GHz, 3.37–3.78 GHz and 5.08–6.07 GHz for WLAN and WiMAX applications. Good radiation characteristics and antenna gains for the operating bands can also been observed. Monopole-like radiation patterns are stable in each operating band. The peak antenna gain in the 2.46 GHz band (2.36–2.54 GHz) is about 1.7–2.8 dB, while that in the 3.61 GHz band (3.37–3.78 GHz) is about 2.8–2.9 dB and in the 5.66 GHz (5.08–6.07 GHz) is about 3.5–4.6 dB.

A Novel Mutual Coupling Matrix Monitoring Method in Two Dimensional Rectangle Antenna Array

Junhe Zhou[1], **Jian Zhang**[1], **Hui Wang**[1], **Xuefeng Yin**[1], **Meisong Tong**[1], **and Jian Li**[2]

[1]Department of Electronics Science and Engineering
Tongji University, Shanghai 200092, China
[2]2012 Communication Technology Lab, Huawei Technologies, Shanghai, China

Abstract— Mutual coupling is caused by the electro-magnetic interactions between the antenna elements inside the array. It will greatly impact the performance of the beamforming algorithms and the directional finding algorithms.

It is generally accepted that the mutual coupling effect mainly exists between the closely arranged antenna elements. To monitor the coupling effect, injecting of independent excitation voltage vectors and measuring of the voltages on all of the antenna elements are required. Furthermore, a matrix inversion is necessary during the final calculation of the coupling coefficients.

In this work, a novel method to characterize the mutual coupling matrix of the rectangle antenna array is proposed. The coupling matrix of the array can be decomposed into the product of the discrete sine transform matrix, a diagonal matrix and the transpose of the discrete sine transform matrix provided that only the coupling between the neighboring and the diagonal elements in the array is considered.

Based on this fact, the measuring of the mutual coupling between the neighboring the diagonal elements can be accomplished by monitoring only one element within the array. It is accomplished as follows, the excitation voltage vector of the array is set to be the eigen vector of the coupling matrix, i.e., the row vector of the discrete sine transform matrix. It can be derived that the voltage of the loads of the antenna terminal will also be the row vector of the discrete sine transform matrix, albeit with a constant, which relates to the mutual coupling effect. By varying the voltage with respect to the row vectors of the discrete sine transform matrix and measuring the ratio of the excitation voltage over the load voltage on the monitoring antenna element, one is able to determine the mutual coupling coefficients.

The simulations based on the method of moments are provided to illustrate the concept.

Research on Subwavelength Metal-based Waveguide Structures

Wen Zhou[1], **Qilong Tan**[1], **Jieer Lao**[2], **and Xu Guang Huang**[1]

[1]Laboratory of Nanophotonic Functional Materials and Devices
School for Information and Optoelectronic Science and Engineering
South China Normal University, Guangzhou, China
[2]Laboratory of Photonic Information Technology
South China Normal University, Guangzhou 510006, China

Abstract— The optical waveguide is a basic building block for photonic integrated circuits. For high-density photonic integrations, subwavelength mode confinement along integrated plane of the circuits, chip-scale long propagation length, very compact direct bends with high efficiency and a tiny center-to-center separation between adjacent waveguides with negligible crosstalk are the four indispensable requirements for a valuable candidate. However, few waveguides can be of all of the above essential features simultaneously. In this talk, two different subwavelength metal-based waveguide structures including surface plasmons will be presented.

A long-range metal/periodic hole modulated dielectric waveguide structure is first discussed. The configuration can be considered as a hybrid waveguide combining an MDM waveguide with a photonic crystal-like waveguide. The research shows that the waveguide is of subwavelength mode confinement, long-range propagation distance in broad bandwidth, subwavelength 90 and 120 direct bends with high transmittance, and high waveguide isolation in a tiny center-to-center separation. And a few functional components including WDM filters based on the waveguide platform are also addressed. The reflective filters possess characters of high extinction ratio over 17 dB with narrow bandwidth. The drop efficiencies of a 1×3 wavelength demultiplexer can be enhanced up to 60%. In addition, a new splitter polarization beam splitter based on the localized surface plasmons is introduced. It includes nanoscale metal cylinders as the polarization selection between two silicon waveguides of a directional coupler. The transverse-magnetic polarization light excites localized surface plasmons and is coupled into the cross port of the directional coupler with a low insert loss, while the transverse-electric polarization light is under restriction. The splitter has very compact footprint with an ultra-short coupling length.

Plasmon Lasing Action in Gain-assisted Gold Nanoparticle-array-on-film Geometry

Lina Shi and Changqing Xie
Key Laboratory of Microelectronics Devices & Integrated Technology
Institute of Microelectronics, Chinese Academy of Sciences, Beijing 100029, China

Abstract— Recently, surface plasmon lasers and spaser has attracted tremendous attention due to its ultrafast dynamics and ultrasmall mode volumes since it was first proposed by Bergman and Stockman [1, 2]. Unfortunately, it suffers from large radiative losses and lacks beam directionality. In a further development of the spaser concept, the lasing spaser was suggested to power up a nanoscale source of coherent radiation [3]. Zhou observed experimentally the lasing action from band-edge lattice plasmons in arrays of plasmonic nanocavities in a homogeneous dielectric environment [4]. However, the homogeneous dielectric environment is usually difficult to realization experimentally since the index matching of superstrate and substrate needs some tricks.

Here, we numerically deomonstrate plasmon lasing behaviors in a gold nanoparticle-array-on-film geometry under an unhomogeneous dielectric environment by using a self-consistent Maxwell-Bloch method. More importantly, the coupling of modes here is mediated by SP waves propagating on the gold film. Therefore, this nanoparticle-array-on-film structure can act as out-couplers from the coherent plasmon source to in-plane SPs due to the continuous feature of the gold film. At the same time, the coherent plasmon also can be transformed to directional emitted photons since the array periodicity can compensate the momentum mismatch between photons and SPs. By carefully designing parameters, we demonstrate the dynamic amplification and co-existence of bright and dark modes as well as the mode competition and suppression of both modes. We also show that the field enhancement of dark mode and the vertical emission of bright mode.

Our work is based on a self-consistent Maxwell-Bloch (MB) approach, which deals with time-dependent wave equations by coupling the Maxwell equations with the rate equations of electron populations. The advantages of this self-consistent approach are that one can follow the dynamical evolution process of the amplified electric field inside the system, and the amplification is nonlinear and saturated. The active medium, dye molecules (Rhodamine B), are described by a four-level atomic system in semi-classical theory.

We investigate the lasing characteristic of modes in such system and find that the electric field at some point versus time is firstly amplified, then over-saturated and finally becomes steady after a long relaxation time. And we also find that it lases with two modes when the gain is really big. In addition, the input-output curves shows a well-defined lasing threshold and linear dependence on the pump rate above and below threshold.

We find that the co-existence phenomena of two modes results from the fact that they concentrate their energy at different places. Therefore, at different places, their strong electric fields force the electrons of the upper level to jump down to the lower level by stimulated emission. This leaves enough upper electrons for stimulated emissions of each other and then they can both exist in the same system.

The demonstrated phenomena suggest that large area plamon lasers can be realized in a single platform. Our results imply a broad possibility of applications such as low threshold surface plasmon sources, surface enhanced Raman scattering, solid-state lighting emission, and so on.

REFERENCES

1. Bergman, D. J. and M. I. Stockman, "Surface plasmon amplification by stimulated emission of radiation: Quantum generation of coherent surface plasmons in nanosystems," *Phys. Rev. Lett.*, Vol. 90, 027402, 2003.
2. Noginov, M. A., et al., "Demonstration of a spaser-based nanolaser," *Nature*, Vol. 460, 1110–1168, 2009.
3. Zheludev, N. I., S. L. Prosvirnin, N. Papasimakis, and V. A. Fedotov, "Lasing spaser," *Nat. Photonics*, Vol. 2, No. 6, 351–354, 2008.
4. Zhou, W., M. Dridi, J. Y. Suh, C. H. Kim, D. T. Co, M. R. Wasielewski, G. C. Schatz, and T. W. Odom, "Lasing action in strongly coupled plasmonic nanocavity arrays," *Nat. Nanotechnology*, Vol. 8, 506–511, 2013.

Design and Optimization of Millimeter Wave SPP Devices

Qian Zhang, Xiaopeng Shen, Hao Chi Zhang, and Tie Jun Cui
State Key Laboratory of Millimeter Waves, Southeast University, Nanjing 210096, China

Abstract— Metal behaves as a perfectly electric conductor (PEC) in microwave, millimeter-wave and terahertz frequencies, which originally does not support the surface plasmon polaritons (SPPs). Recently, to realize SPPs in microwave and terahertz frequency bands, researchers have proposed the concept of spoof SPPs, which are formed by drilling periodic holes or grooves on metal surfaces. In this work, we numerically explore while also experimentally implement several spoof SPP devices in millimeter wave frequencies. Firstly, we present the unit-cell structure of plasmonic waveguide together with its dispersion characteristics and transmission performance. Secondly, for efficiently converting guided waves to spoof SPPs at millimeter waves, a highly efficient and broadband transition section is proposed. Based on the above designs, we present millimeter-wave SPP straight waveguide, S-bend, right angle-bend, splitter, and ring-resonator models. The commercial software, CST Microwave Studio, is used for all numerical simulations. The field distributions and dispersion relations show that the proposed plasmonic waveguide is able to confine electromagnetic waves in a very small region. Both simulation and experiment results are in good agreements, demonstrating that the straight waveguide, S bend, and right-angle bend can realize broadband transmissions with high efficiency. The splitter is shown to divide the electromagnetic waves efficiently into two separated SPP waveguides. The ring resonator can realize the effect of periodically selective frequencies. This work may pave the way for development of SPP-based integrated circuits at millimeter-wave frequencies.

Multiband THz Metamaterial Absorber Based on Snowflake-type Resonators

Junchuan Zhuge, **Di Bao**, **Xiaopeng Shen**, **and Tiejun Cui**
State Key Laboratory of Millimeter Waves, Southeast University, Nanjing 210096, China

Abstract— Recently, the devices operating in the terahertz (THz) frequency band have aroused tremendous interests of researchers because of their gigantic potential applications in the areas such as security, public health, and biomedicine [1–4]. In this work, ultrathin multiband THz metamaterial absorbers are proposed, in which the design, simulation, fabrication, measurement, and theoretical analysis of the absorbers are presented. First, a dualband absorber consisting of snowflake-type resonator array is investigated and designed, which is printed on a grounded polyimide dielectric spacer (see the inset of Fig. 1). The commercial software, CST Microwave Studio 2011, is used for numerical simulations, which shows that the proposed structure has two perfect absorption peaks at 0.952 and 1.818 THz with absorption rates reaching 99.7% and 99.9%, respectively, as shown in Fig. 1. By carefully designing the geometrical parameters and layout of the snowflake-type resonators, a quad-band absorber with four perfect absorption peaks is implemented, as illustrated in Fig. 2(a). The numerical simulations show that four different absorption peaks appear at 0.752, 0.950, 1.454, and 1.696 THz with the absorption rates of 98.8%, 97.8%, 92.1%, and 90%, respectively, as given in Fig. 2(b). We present the experimental results

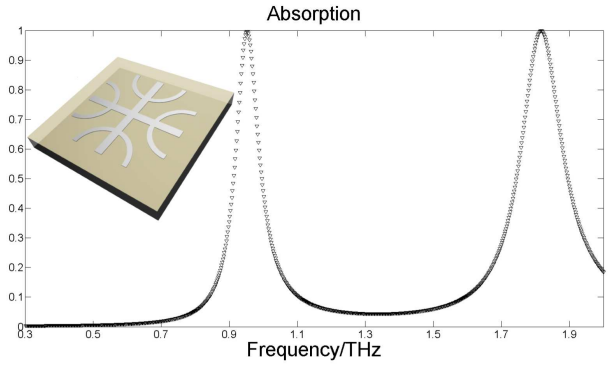

Figure 1: The simulated absorption spectra under the normal incidence of TE polarized waves. The inset shows the unit cell of the dual-band metamaterial absorber. The material properties of the snowflake pattern structure (gray) and the metallic ground plane are set to be aluminum, and the spacer (light yellow) between them is set to be polyimide.

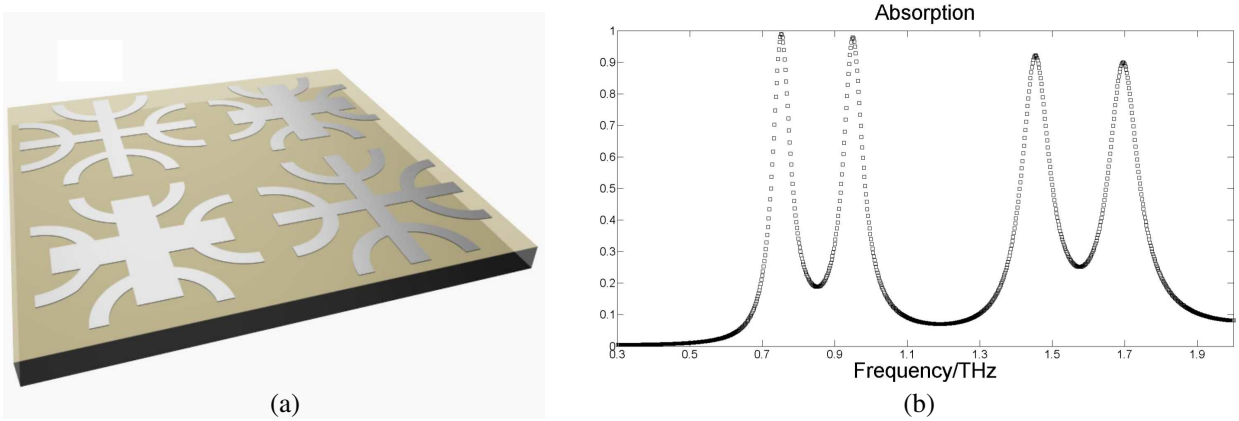

Figure 2: (a) The unit cell of the quad-band metamaterial absorber. The material properties of the top layer pattern (gray) and the metallic ground plane are set to be aluminum and the spacer (light yellow) between them is set to be polyimide. (b) The simulated absorption spectra under the normal incidence of TE polarized waves.

of such metamaterial absorbers, which have good agreements to the simulations, demonstrating excellent absorptive performance at the designed frequency bands over wide angles of incident waves. Finally, the multiple-reflection theory [5, 6] is employed to explain the physics mechanism of the multiband metamaterial absorbers. With this theory, we also explore the influence of the thickness and loss tangent of the dielectric spacer on the absorptive performance.

REFERENCES

1. Federici, J. F., B. Schulkin, F. Huang, et al., "THz imaging and sensing for security applications — Explosives, weapons and drugs," *Semiconductor Science and Technology*, Vol. 20, No. 7, S266, 2005.
2. Kemp, M. C., P. F. Taday, B. E. Cole, et al., "Security applications of terahertz technology," *International Society for Optics and Photonics, AeroSense 2003*, 44–52, 2003.
3. Pickwell, E. and V. P. Wallace, "Biomedical applications of terahertz technology," *Journal of Physics D: Applied Physics*, Vol. 39, No. 17, R301, 2006.
4. Kim, S. M., F. Hatami, J. S. Harris, et al., "Biomedical terahertz imaging with a quantum cascade laser," *Applied Physics Letters*, Vol. 88, No. 15, 153903, 2006.
5. Chen, H. T., "Interference theory of metamaterial perfect absorbers," *Optics Express*, Vol. 20, No. 7, 7165–7172, 2012.
6. Shen, X., Y. Yang, Y. Zang, et al., "Triple-band terahertz metamaterial absorber: Design, experiment, and physical interpretation," *Applied Physics Letters*, Vol. 101, No. 15, 154102, 2012.

Analysis and Design of Multi-band Absorber with Periodic Three-dimensional Square Ring Units

Guorui Zhang, Yang Zhou, Nan Zhang, Peiheng Zhou, Haiyan Chen, and Longjiang Deng
State Key Laboratory of Electronic Thin Film and Integrated Devices
National Engineering Research Center of Electromagnetic Radiation Control Materials
University of Electronic Science and Technology of China, Chengdu 610054, China

Abstract— Broadband electromagnetic (EM) wave absorbers have attracted considerable attention due to their wide practical applications such as antenna, stealth, and electromagnetic (EM) compatibility. Traditionarily, the broadband design is usually a superposition of several sandwiched structures, resembling the Jaumann absorber, with different geometrical dimensions. Herein, we present the simulation, implementation, and measurement of a unconventional multi-band metamaterial absorber, which appears as a cube and is composed of square ring resistive sheets with a metal plane laid at the bottom of the structure. Benefiting from the square ring resistive sheets which are perpendicular to the metal plane, the structure eliminates the total reflection of planer structure whose thickness equals to half of the operating wave length quite well In addition, due to the interreaction between the lateral square ring resistive sheets of the cube and the incident wave, the square ring resistive sheets near the top of the cube offers strong absorption for low frequency EM wave while the ones near the bottom of the cube strongly absorb the high frequency EM waves. As a result, with the help of fullwave commercial solver CST, two absorption peaks have been observed respectively at 3.8 GHz and 16 GHz with absorptivity of nearly 99%. Simultaneously, the absorber shows good absorption larger than 80% at a broadband from 2 GHz to 18 GHz. By means of free-space measurement, a good agreement between simulation and experimental results have been achieved. The result demonstrated that the referred EM absorber could exhibits a promising and flexible method to control the propagation of the EM wave and to extend the absorption bandwidth greatly.

Metamaterial-based Absorption Optimization of Microwave Magnetic Absorbers

Peiheng Zhou, Linbo Zhang, Huibin Zhang, Yangqiu Xu, Haiyan Chen, and Longjiang Deng
State Key Laboratory of Electronic Thin Films and Integrated Devices
National Engineering Research Center of Electromagnetic Radiation Control Materials
University of Electronic Science and Technology of China, China

Abstract— Electromagnetic perfect absorber has to be considered as one of the most important applications in metamaterial. Since the simultaneous electrical and magnetic resonances can be tailored independently, it is of engineering interest to combine the resonance tunability of metamaterial structure with the high energy loss in traditional magnetic absorbing material. In other words, to enforce the incident electromagnetic energy into the high loss medium at the given frequency ranges. Therefore, we can make full use of the advantages of both artificial structure and natural material.

In this work, optimization methods of the traditional microwave magnetic absorbing materials are proposed by incorporating with the metamaterial structures. In our designs, periodic holes and resistive patterns are utilized to fix the operating frequency of magnetic absorber at oblique incidence, thin-films of high magnetic loss are rolled up to absorb in-plane magnetic field, specific metal arrays introduce additional resonance bands to extend the absorption bandwidth, and so on. Based on transmission line and equivalent circuit method, the origin of absorption optimization is discussed associated with the electric field and current distribution in the composite structure. Limitations of the metamaterial incorporated absorption are also found following the impedance matching relation with the equivalent circuit components.

In conclusion, this work emphasized on the approaches for microwave absorbing material design based on the concept of metamaterial. As we found, structural design could effectively improve the performance of traditional magnetic absorbing material as the local electric and magnetic fields within the material was changed. Optimization methods may solve the critical microwave absorption problems of oblique incidence, broad bandwidth, and so on.

High Gain and High Efficient Antenna

Zui Tao, **Shuo Liu**, **Mei Qing Qi**, **and Tie Jun Cui**
State Key Laboratory of Millimeter Waves, Southeast University, Nanjing 210096, Chin

Abstract— Recently, metamaterials have been greatly introduced and widely used as a technique to increase the performance of antennas. Many metamaterial antennas have been proposed to fulfill different functionalities like beam deflection and low side lobes. In this paper, a high-efficient and high-gain antenna is studied and presented. To get high gain and high efficiency, a metamaterial lens is put in front of a transformed horn antenna. It is noted that the metamaterial lens will improve the antenna performance significantly, but not increase the size of antenna aperture, which is critical for antenna applications. The transformed antenna is a standard horn loaded with some metal patches. Such metal patches can make the antenna have higher gain by changing the electromagnetic distribution in the horn antenna. To validate the design, full-wave simulations are conducted by using commercial software, CST Microwave Studio. The maximum gain reaches 26.99 dBi at 14.25 GHz, which increases nearly 6 dB over a standard horn antenna that has the same aperture size. The proposed antenna has a very high efficiency of 0.9677. From the simulated results, we observe that the waves transmitted from the antenna are almost plane waves in the near-field region. The side lobes are both -13 dB in the E-plane and H-plane. Hence the proposed antenna almost has the same far-field performances as an ideal uniform current plane which has the same aperture size.

Electromagnetic Scattering Controlling for a Rectangular Groove with High Impedance Surfaces Loading

Dongjiao Guo, Haiyan Chen, Peiheng Zhou,
Xingxing Huang, Jianliang Xie, and Longjiang Deng
National Engineering Research Center of Electromagnetic Radiation Control Materials
State Key Laboratory of Electronic Thin Film and Integrated Devices
University of Electronic Science and Technology of China, Chengdu 610054, China

Abstract— As a common defect in aircraft, most of grooves exist on the aircraft surface. The groove can become a major potential scattering source of stealth objects in some polarizations and incident angles. Different from the traditional ways of filling materials in the groove, in this paper, a possible solution for controlling electromagnetic scattering from a rectangular groove is presented based on a high impedance surface (HIS) loaded on the two sides of the considering groove. The HIS is realized by H-type frequency selective surface loading on a grounded substrate. The HIS structure is optimized according to the relationship between the size of HIS and surface wave band gaps. As in case of scattering from a rectangular groove in a finite PEC plane, most of the backscattering is induced due to surface waves which flowing through the ground plane. The optimized HIS is loaded on the two sides of the rectangular groove to suppress the surface waves induced by the groove. It is observed that the use of HIS results in a significant scattering suppression of the rectangular groove in a wide angular in the case of vertical polarization, and the maximum reduction of mono-static radar cross section (RCS) can be reached 12 dB compared with that of the original structure and the case with loading other materials on the two sides of the groove. Moreover, the surface wave band gap properties of the HIS and the energy distribution of the proposed structure are also discussed for analyzing the phenomenon of mono-static RCS reduction.

Design and Analysis of 81 to 86 GHz 3-Stages Cascode Low Noise Amplifier with π-type Matching Network Using 65 nm CMOS Process

Hsuan-Der Yen[1], **Yi-Chun Lee**[2], **Guo-Wei Huang**[2, 3], **and Fon-Shan Huang**[1]

[1]Institute of Electronics Engineering, Tsing Hua University
101, Sec. 2, Kuang-Fu Rd., Hsinchu 300, Taiwan
[2]Nano Device Laboratories, 26, Prosperity Rd. 1, Hsinchu 300, Taiwan
[3]Department of Electronics Engineering, Chiao Tung University
1001, University Rd., Hsinchu 300, Taiwan

Abstract— This paper presents an 81 to 86 GHz 3 stages cascode topology low noise amplifier (LNA) with π-type matching network using 65 nm COMS process for millimeter-wave point-to-point high-bandwidth communication links applications. To resolve the low Max-Gain issue of amplifier above V-band applications, 3-stages cascade configuration is chose to improve gain and π-type transmission line matching network is used to provide wide band matching characteristics. The first stage is related to matching and NF design stage, the π-type matching network provides wide matching bandwidth and more fine tuning conditions for noise figure matching for the first stage. The second stage plays as the power gain enhancement and uses π-type matching network for matching between stages 1 and 3. The linearity, gain and output matching are determined by the stage 3. The π-type matching network is used based on CPW transmission line structure with lower losses to improve gain and wide bandwidth matching. Based on simulation results, this cascode configuration amplifier showed high gain, low noise figure (NF), good isolation and low power consumption. Small-signal gain S_{21} is higher than 20 dB while noise figure $7.1 \sim 7.5$ dB between 81 and 86 GHz. The input/output return losses (S_{11}/S_{22}) are better than -10 dB and S_{22} is below -60 dB. As for the linearity characteristic, P1dB is -27 dBm and IIP3 is -8 dBm at 84 GHz. This LNA is implemented by 65 nm 1P6M CMOS technology in chip area of $0.50 \times 0.78\,\mathrm{mm}^2$.

A Novel Tri-band Patch Antenna Based on Complementary Triangle Split Ring Resonator Pair

J.-G. Liang[1], **Z.-J. Song**[1], **L.-J. Yu**[2], **and X.-F. Zhang**[1]

[1]Air and Missile Defense College, Air Force Engineering University, Xi'an 710051, China
[2]Center for Health Management and Policy, Shandong University, Jinan 250012, China

Abstract— A new resonant-type composite right/left-handed transmission line (CRLH TL) is proposed based on the combination of a complementary triangle split ring resonator pair (CTSRRP) etched on the ground plane and a series gap embeded in the conductor strip of a microstrip line. The CTSRRP, which is composed of two identical complementary triangle split ring resonators (CTSRRs) with back-to-back splits, demonstrates negative permittivity. Besides, a center branch is added to the middle of each triangle split ring to divide it into wo parts. In virtue of this, two current paths of different length are formed which primely improve the multi-band characteristic of the transmission line. The equivalent capacitor-inductor circuit model is put forward to analyze the transmission line. The S parameters are derived from electromagnetic full-wave simulation through simulation engine Ansoft HFSS13. Then the dispersion curve of the proposed structure is calculated based on S parameters to attest the left-handed characteristics. Two left-handed and two right-handed bands are observed from the dispersion curve. To demonstrate the applicability of the new type transmission line, a tri-band patch antenna of C band is designed and fabricated. Good agreement between simulated and measured return loss is obtained. Measured results present that three available bands centered at 4.45 GHz, 5.55 GHz, and 7.35 GHz respectively are acquired. Peak gain of more than 7 dB and invariable radiation characteristics can be observed from the simulated radiation patterns. And the cross polarization in working bands is less than -15 dB with the minimal touching bottom of -55 dB.

Plasmon Enhanced F-P Lasing from Flower-like ZnO Microsphere

Jitao Li, **Yi Lin**, **Chunxiang Xu**, **Yueyue Wang**, **and Junfeng Lu**
State Key Laboratory of Bioelectronics, School of Biological Science and Medical Engineering
Southeast University, Nanjing, China

Abstract— Surface plasmon (SP) is a spatially confined electromagnetic field originating from the collective oscillation of free electrons at the metal/semiconductor or dielectric interfaces. SP has attracted much interest due to its applications in enhancement of the weak physical process, such as the absorption of light in molecules and Raman scattering intensities. The metal SP coupling with semiconductors has been demonstrated as an effective approach to improve the quantum efficiency of light emitting materials and devices. In this work, flower-like ZnO microsphere was synthesized by a vapor phase transport (VPT) method, and Au nanoparticles (NPs) was decorated on the microspheres. Fabry-Pérot (F-P) lasing from the microsphere was observed, and SPs mediated emission enhancement has also been observed experimentally. The mechanism of this enhancement was investigated systematically.

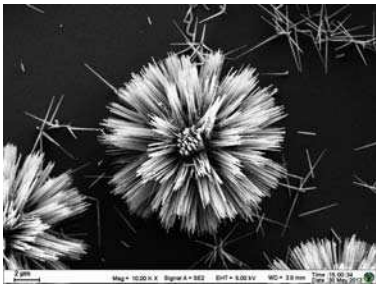

Figure 1: SEM image of an individual flower-like ZnO microsphere.

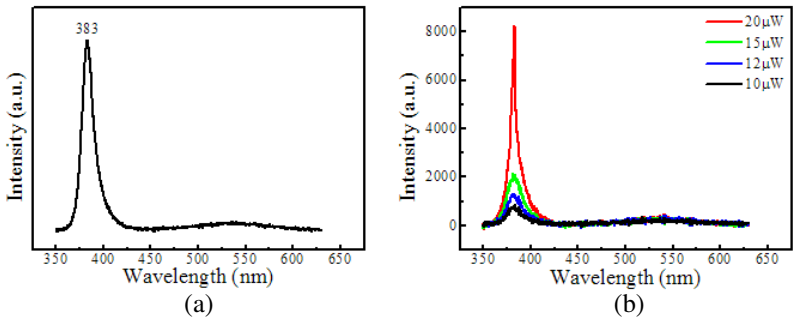

Figure 2: (a) PL spectrum of the microsphere under low excitation power and (b) PL spectra of the microsphere under different excitation powers.

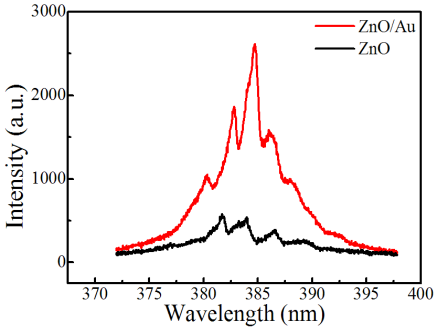

Figure 3: PL spectra of the microsphere with and without Au NPs under the same excitation power.

ACKNOWLEDGMENT

This work was supported by "973" Program (2011CB302004 and 2013CB932903), NSFC (61275054), MOE (20110092130006) and JSIS (BE2012164).

REFERENCES

1. Cheng C. W., E. J. Sie, B. Liu, C. H. A. Huan, T. C. Sum, H. D. Sun, et al., "Surface plasmon enhanced band edge luminescence of ZnO nanorods by capping Au nanoparticles," *Applied Physics Letters*, Vol. 96, 071107, 2010.
2. Niu, B. J., L. L. Wu, W. Tang, X. T. Zhang, and Q. G. Meng, "Enhancement of near-band edge emission of Au/ZnO composite nanobelts by surface plasmon resonance," *Cryst. Eng. Comm.*, Vol. 13, 3678, 2011.
3. Lin, Y., C. Xu, J. Li, G. Zhu, X. Xu, J. Dai, et al. "Localized surface plasmon resonance-enhanced two-photon excited ultraviolet emission of Au-decorated ZnO nanorod arrays," *Advanced Optical Materials*, n/a, 2013.

Electron-Hole Plasma Induced Band Gap Renormalization in ZnO Microlaser Cavities

Jun Dai, **Chunxiang Xu**, **Yueyue Wang**, **Jitao Li**, **and Yi Lin**
State Key Laboratory of Bioelectronics,Southeast University, Nanjing 210096, China

Abstract— Electron-hole plasma (EHP) lasing in hexagonal ZnO microrods and ultrathin nanobelts were investigated. Under the excitation of 325 nm line femtosecond pulsed laser, ultraviolet whispering gallery mode (WGM) lasing was observed from hexagonal ZnO microrods. When EHP was formed at high excitation energy density, the center wavelength of the WGM lasing band presented a redshift from 387.5 nm to 397.5 nm, and the full width of half maximum of the WGM lasing band increased from 2.5 nm to 7 nm. Each lasing mode showed obvious redshift and broadening. Such lasing characteristics were attributed to the band gap renormalization (BGR) due to the high carrier concentration at the EHP condition. In addition, the EHP Fabry-Perot (F-P) mode lasing from an ultrathin ZnO nanobelt was also observed and discussed. Based on values of the renormalized band gap at different carrier density state, the BGR coefficient was fitted as 5.4×10^{-5} meV·cm.

Electromagnetic Force in the Complex Quaternion Space

Zi-Hua Weng
School of Physics and Mechanical & Electrical Engineering
Xiamen University, Xiamen 361005, China

Abstract— In 1873, J. C. Maxwell described the physical feature of electromagnetic field with the vector analysis as well as the quaternion analysis. W. R. Hamilton invented the quaternion in 1843. The octonion, as the ordered couple of quaternions, was invented by J. T. Graves and A. Cayley independently and successively. Later the scientists and engineers separated the quaternion into the scalar part and vector part, to facilitate its application in the engineering. In the works about the electromagnetic theory, J. C. Maxwell mingled naturally the quaternion analysis and vector terminology to depict the electromagnetic feature. Similarly the scholars begin to study the physics feature of gravitational field with the algebra of quaternions.

The ordered couple of quaternions compose the octonion. On the contrary, the octonion is able to be separated into two parts, the quaternion and the S-quaternion (short for the second quaternion), and their coordinates can be chosen as the complex numbers. In the paper, the quaternion space and the S-quaternion space can be introduced into the field theory, in order to describe the physical feature of gravitational and electromagnetic fields. One will be able to conclude that the quaternion space is suitable to describe the gravitational features, while the S-quaternion space is proper to depict the electromagnetic features. This method can deduce the most of conclusions of the electromagnetic and gravitational fields described with the vector.

In the electromagnetic theory described with the complex quaternion, it is able to deduce directly the Maxwell's equations in the classical electromagnetic theory, without the help of the current continuity equation. In this approach, substituting the S-quaternion for the quaternion, one can obtain the same conclusions still. On the basis of this approach, the paper is able to deduce directly the force and the current continuity equation etc in the electromagnetic theory described with the S-quaternion. And the paper can apply the quaternion to research the gravitational theory, deducing directly the force and the mass continuity equation etc..

In the paper, the electromagnetic field and gravitational field can be combined together to become one united field in the theoretical description, to depict simultaneously the physics features of two fields. The different terms of the force can be unified into the single formula in the electromagnetic and gravitational fields, analyzing the related physics features. The force includes the inertial force, gravity, electromagnetic force, and energy gradient etc in the classical field theory. The force and the continuity equations are vital deductions and inevitable components of the field theory described with the quaternion/S-quaternion.

ACKNOWLEDGMENT

The authors are grateful for the financial support from the National Natural Science Foundation of China under grant number 60677039.

Computing Illuminated Area and Scattering for Double-bounce for SAR Manmade Target's Characteristic Modeling

Kai Yang, Kefeng Ji, and Huanxin Zou
College of Electronics Science and Engineering, National University of Defense Technology
Changsha, Hunan 410073, China

Abstract— SAR targets' scattering modeling is of great importance in SAR image interpretation, etc. It can be derived by a variety of approaches, such as Physical Theory of Diffraction (PTD), Geometric Optics (GO), Physical Optics (PO), and Uniform Theory of Diffraction (UTD), and so on. Model using a hybrid GO-PO maintains high computational efficiency and excellent accuracy under certain conditions. However, it is difficult to determine the illuminated area of the double-bounce, as the primary task of this model. What's more, double-bounce scattering effect dominates the scattering of some canonical scatterer, such as dihedral, top-hat, etc. and can be found in a variety of manmade targets in real world scenes, such as vehicle-to-ground, ship-to-sea, building-to-ground, etc. Thus, deriving a general and complete solution, which can easily and accurately determine the integration limits, is deeply desired.

Taking the perfect electrical conductor (PEC) right-angle dihedral with large size for example, under the assumption of high-frequency and farfield, this paper analyzed the double-bounce's illumination cases of the right-angle dihedral and found that there existed six classes of different integral(s) domain along with the transmit angle varying. Then the completeness of the illumination cases was proved by rigorous mathematical reasoning and the range of the transmit aspect angle corresponding to each integral case was also offered. After this, the dihedral's double-bounce scattering effect corresponding to each integral case was computed based on PO integral equation, and the existed singularities of each integral case were also avoid by implementing L'Hopital's rule. At last, combining the results of the double-bounce scattering effect with the single-bounce scattering, we got the total scattering field of the right-angle dihedral.

An experiment displaying the illuminated area along with transmit angle varying was done firstly. The results validate the completeness of the illumination cases in the point of experiment. And then six classes of experiments corresponding to six different integral cases were also set, which were used to compare with FEKO. The results show that the dihedral's double-bounce scattering effect is computed right for each integral case. The proposed method can be extended to many other scatterers whose scattering are dominated by double-bounce scattering effect.

ACKNOWLEDGMENT

This work was supported in part by the National Natural Science Foundation of China under Grant 61372163 and Grant 61331015.

Target Angular Scintillation Measurement of Wide-band Range Comparison Monopulse Radar in Anechoic Chamber

Yang Bai, **Chao Ning**, **Ming Jin**, **Chao Gao**, **and Yanjie Cui**
Science and Technology on Electromagnetic Scattering Laboratory, Beijing 100854, China

Abstract— The range comparison monopulse radar measures angles by comparing the range of the difference-channel signals with the range of the sum-channel signal. Practically, It has been generally accepted that what the radar measures is not the directions of the target, but angular glint errors. In order to realize this characteristic of radar target, a wide-band radar simulate system based on CATR (Compact Antenna Test Range) was designed in this researching, which was constituted with the waveguide slot array antenna, vector network analyzer, and microwave difference-sum network principally. With paying close attention to the complex dimension expend radar target, an algorithm including HRRP (high resolution range profile) method was used to extract and describe the nicety of angular scintillation. By making use of high-frequency phase shift correcting algorithm, the effect of test errors caused by the difference-sum channels' non-equilibrium was weakened. In the anechoic chamber with CATR measurement results of a radar target can be considered as same as the real condition that it is explored by the practical monopulse radar. Therefore, the glint errors were independent of distance between the target and the testing antenna for the experiment was satisfied the electromagnetic far field factor. At last, the scintillation measurement theory was verified by test classical target, such as Standard body, double balls union and airplane model. The high resolution test result was well identical with the simulate result that have been confirmed.

Effective Implementation of the CFS-PML Using DSP Techniques for Truncating Dispersive Medium FDTD Domains

Naixing Feng[1], **Yongqing Yue**[1], **Chunhui Zhu**[1], **and Qing Huo Liu**[2]

[1]Institute of Electromagnetics and Acoustics, Xiamen University, Xiamen, China
[2]Department of Electrical and Computer Engineering, Duke University, Durham, NC 27708, USA

Abstract— Efficient and unsplit-field finite-difference time-domain (FDTD) implementation of the complex frequency-shifted perfectly matched layer (CFS-PML), based on the digital signal processing (DSP) techniques and the material independence relations via applying the electric flux density (D) and the magnetic flux density (B), is proposed for truncating two dimensional FDTD computational domain entirely composed of dispersive material realized with a Drude model. The CFS-PML implementation is introduced based on the stretched coordinate PML (SC-PML) and the uniaxial anisotropic PML (UPML), respectively. The implementation of the proposed CFS-PML formulations is based on the SC-PML due to the fact that has advantage of simple implementation in the corners and the edges of the PML regions. Moreover, these proposed formulations are completely independent of the material properties of the FDTD computational domain and hence can be applied to truncate arbitrary media without any modification because of the D-B constitutive relations used in Maxwell's equations. Besides, the DSP techniques include the Bilinear Z-transform (BZT) method and the Matched Z-transform (MZT) method, respectively. However, from the point of view of the Courant-Friedrichs-Levy (CFL) condition, to the best of our knowledge, time step based on the BZT only needs to meet CFL condition, whereas time step based on the MZT method has to make it smaller for retaining stability and desirable accuracy. Consequently, the former one is introduced into the proposed formulations. A numerical example has been carried out in a two dimensional (3-D) FDTD computational domain to validate the proposed formulations. It is clearly shown that the proposed formulations with CFS scheme are efficient in attenuating evanescent waves and reducing late-time reflections.

Continuously Moving Target Simulator Design

Deping Zhang, Chao Wang, Chang Zhu, and Naichang Yuan
College of Electronic Science and Engineering, National University of Defense Technology, Changsha, China

Abstract— The delay time of echo generated by the moving target simulator is discrete, and the moving trace of simulated target is discontinuous. In order to solve this problem, firstly, the radar digital signal processor must adjust the range gate, and the range error will be limited within one range cell. Then the rest error cannot be removed but can be adjusted by phase pre-compensation in simulator. The idea is that let the phase of simulated target be equal to the one of the real target at sampling time. After the phase pre-compensation, a real continuously moving target will be generated and the problem will be solved. Then MATLAB simulation of the method is done for linear frequency modulation radar system. The simulated results can be used to validate the effectiveness of the method.

Accurate Statistical Modeling Method for Dynamic RCS

Ya-Qiang Zhuang, Chen-Xin Zhang, and Xiao-Kuan Zhang
Air and Missile Defense College, Air Force Engineering University, Xi'an 710051, China

Abstract— Due to dynamic RCS value of radar target fluctuate with no pattern; it is often use the fluctuation distribution to describe it. A method simulate the RCS of moving target is introduced firstly in this paper. Then, the brief introduction of two conventional fluctuation distributions was given, and the Gaussian Mixture distribution as well as its parameter estimation method was investigated. The statistical characterization of dynamic RCS using Chi2 distribution, lognormal distribution and Gaussian Mixture distribution is analyzed. The comparative fitting results show Gaussian Mixture distribution is the best fitting distribution to characterize the dynamic RCS among three distributions.

A Method for Predicting Far Field Radar Cross-section from Near Field Measurements on Cylindrical Scanning Mode

C. Gao[1, 2], J. W. Chen[1, 2], M. Jin[2], and Y. Bai[2]

[1]Information Engineering School, Communication University of China, Beijing 100024, China
[2]Science and Technology on Electromagnetic Scattering Laboratory, Beijing 100854, China

Abstract— RCS measurement is necessary for designing stealth weapon system as well as for the research of the electromagnetic scattering properties of radar-illuminate target. The theory and algorithm of electromagnetic scattering computation can be verified by RCS measurement, moreover, it's difficult to compute electromagnetic scattering of complex and large objects, but the data can be obtained visually by RCS measurement.

For studying the EM signatures of full-size target, it demands outdoor or indoor room large enough for measurement, but the construction of outdoor and indoor room which satisfy the far field conditional both lead to costly installation and require extraordinary elaborate technique, say nothing of carrying out the imaging and RCS diagnostic for stealth weapon in active service. This paper meets the demand of the development with the stealth and anti-stealth weapon, aims at the shortage of outdoor and indoor measuring of the far field electromagnetism feature, presents a research on 3-D near-field to far-field transformation algorithm, in which the far-field condition could not be satisfied on both vertical and horizontal plane for the target under test, and the target is illuminated by a spherical wave. A 3-D multi-scattering center model is built for the target and the near-field data is sampled by 3-D scan, using the extensions of spherical-wave function in cylindrical coordinates, the relationship between far-field and near-field scattering field is deduced under the condition that the antenna works at cylindrical-scan mode. The RCS and image pattern can be achieved by the 3-D IFFT algorithm and interpolation technique. The simulation results show that the algorithm is precise and effective.

Relationships between Surface Wave Attenuation and the Reflection Properties of Thin Surface Wave Absorbing Layer

Hai-Yan Chen, **Li-Juan Lu**, **Dong-Jiao Guo**, **Hai-Peng Lu**,
Pei-Heng Zhou, **Jian-Liang Xie**, **and Long-Jiang Deng**
State Key Laboratory of Electronic Thin Films and Integrated Device
National Engineering Research Center of Electromagnetic Radiation Control Materials
University of Electronic Science and Technology of China, Chengdu 610054, China

Abstract— Compared and analyzed the surface impedance defined by the basic definition of surface wave and by the reflection coefficient of thin radar absorbing material (RAM) layers backed with a perfect electric conductor (PEC) plate, the relationships between its surface wave attenuation property and its reflection characteristics can be founded. Equivalent surface impedance for a perfect electrical conductor (PEC) plate coated by a thin layer of RAM can be easily obtained based on the reflection coefficient for an infinite plate coated with same thin RAM layers, which can be regarded as a function for computing the attenuation of surface wave in this RAM layers. In this paper, two kinds of reality RAM for single layer coating and two layers coating will be considered for verifying this approach respectively. For two layers coating, the mono-static radar cross section (RCS) reduction properties of a slab coated with this RAM are discussed for evaluating the attenuation of surface wave because the equivalent medium theory is not appropriated under this condition. The proposed approach is effective and advantageous especially for thin multi-layers RAM coating.

The RF Immunity Characteristics Analysis of SSD Performance due to Wireless Communications Emission in Proximity

Han-Nien Lin[1], **Po-Yan Wang**[1,], **Hung-Yun Tsai**[1], **and Yung-Chi Tang**[2]

[1]Department of Communications Engineering, Feng-Chia University
No. 100 Wen-Hua Rd., Taichung 40724, Taiwan
[2]Section of EMC, Bureau of Standards, Metrology and Inspection, M.O.E.A
No. 4, Sec. 1, Jinan Rd., Zhongzheng Dist., Taipei City 100, Taiwan

Abstract— To facilitate the high speed data access/storage with vibrating and swaying proof, the Solid State Drive (SSD) is now commonly integrated with mobile or portable device like Ultrabook with its compact size. Besides RFI noise generated from such high speed digital device is observed imposing an inferior impact on RF wireless communications performance, it is also possible that the SSD storage module might be failed for data accessing caused by high level RF transmitted power from various transmitters of wireless communications systems. In addition, when WiFi tethering is used for cloud applications with the 3G/4G WWAN network through smart phone, the transmitted RF power from mobile phone might also affect the data access/storage of SSD memory. Because when we use WWAN network for Internet surfing, we would usually place the mobile phones by side of ultrabook/notebook computer with built-in SSD and thus the high level output signal from nearby mobile phone might cause memory mapping error of SSD. To analyze the EM immunity characteristics of SSD and related memory module, we will categorize the coupling mechanism of RF power between SSD and RF transmitter into antenna coupling, circuitry coupling, and cavity resonance coupling. With the help of dedicated near-field RF signal generator and stripline for closely located digital modules like SSD and flash memory in this study, we can identify the location and root cause of data accessing and storing degradation to benefit the manufacturers for proper SSD integration with mobile or portable device with compact design form limitation. We also evaluated the pass/fail EM immunity characteristics for SSD storage module, and hope to apply the IEC 63132 series IC-EMS measurement techniques on the component level to help solving the problem and further improve the integrating design to meet the EMC/performance requirement in the future study.

Modified 2D-Luneburg Lens Using Metamaterials

Hai Bing Chen, Qiang Cheng, Ai Hua Huang, Jun Yan Dai, and Hui Ying Lu
State Key Laboratory of Millimeter Waves, Southeast University, Nanjing 210096, China

Abstract— Recently, there have been increased interests in the design of Luneburg lens based on metamaterials [1–4]. Different from the previous works we present the design simulation and experimental verification of a modified Luneburg lens constructed by bulk metamaterials with its focus close to the center [5–8]. The lens is composed by a number of concentric layers. By varying the geometric dimensions of the unit cells in each layer, a gradient refraction index distribution required by the modified Luneburg lens can be achieved and therefore leads to the beam forming in pre-set mode [9, 10]. Numerical simulations have been made and as shown in Fig. 1 plane waves generated from a line source located at the focus of the lens could be transformed into cylindrical wave as desired. The exciting source can be rotated around a specific circle with the outgoing waves deflected accordingly. As a modification of the traditional Luneberg lens, the proposed lens is more flexible in real applications since the location of the focus can be adjusted by changing the distributions of the refraction index. By choosing the I-shaped resonator as the basic unit, we have realized broadband modified Luneburg lens within the whole X band. The fabricated lens was measured within a two-dimensional microwave scanning apparatus and the near field distributions validate the properties of the modified Luneburg lens.

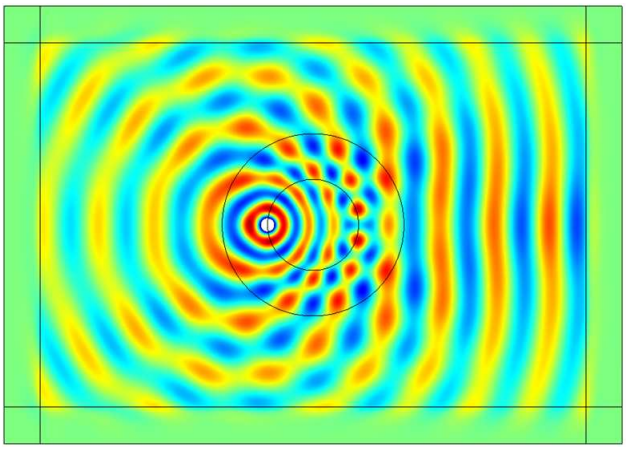

Figure 1: Simulated electric field distributions for the designed lens. The line source is set in the middle of circle center and the outer ring.

REFERENCES

1. Kundtz, N. and D. R. Smith, "Extreme-angle broadband metamaterial lens," *Nature Materials*, Vol. 9, No. 2, 129–132, 2010.
2. Demetriadou, A. and Y. Hao, "Slim Luneburg lens for antenna applications," *Optics Express*, Vol. 19, No. 21, 19925–19934, 2011.
3. Ji, S., et al., "A bio-inspired polymeric gradient refractive index (GRIN) human eye lens," *Optics Express*, Vol. 20, No. 24, 26746–26754, 2012.
4. Hunt, J., et al., "Planar, flattened Luneburg lens at infrared wavelengths," *Optics Express*, Vol. 20, No. 2, 1706–1713, 2012.
5. Gutman, A. S., "Modified Luneberg lens," *Journal of Applied Physics*, Vol. 25, No. 7, 855–859, 1953.
6. Hunt, J., T. Tyler, S. Dhar, et al., "Planar, flattened Luneburg lens at infrared wavelengths," *Optics Express*, Vol. 20, No. 2, 1706–1713, 2012.
7. Headland, D., W. Withayachumnankul, M. Webb, et al., "Beam deflection lens at terahertz frequencies using a hole lattice metamaterial," *38th International Conference on Infrared, Millimeter, and Terahertz Waves (IRMMW-THz)*, 1–2, 2013.

8. Wu, X. and J. Laurin, "Fan-beam millimeter-wave antenna design based on the cylindrical Luneberg lens," *IEEE Transactions on Antennas and Propagation*, Vol. 55, No. 8, 2147–2156, 2007.
9. Gabrielli, L. H. and M. Lipson, "Integrated Luneburg lens via ultra-strong index gradient on silicon," *Optics Express*, Vol. 19, No. 21, 20122–20127, 2011.
10. Huang, H., et al., "Tunable two-dimensional liquid gradient refractive index (L-GRIN) lens for variable light focusing," *Lab on a Chip*, Vol. 10, No. 18, 2387–2393, 2011.

A Simple High-resolution Imaging System Made of Metamaterials

Shuo Ge and Wei Xiang Jiang
State Key Laboratory of Millimeter Waves, Southeast University, Nanjing 210096, China

Abstract— High resolution imaging or super resolution imaging is always a hot topic in the field of artificial metamaterials. Since the conventional optical imaging lenses suffer from the so-called diffraction limit, the resolution is limited to half a wavelength. In order to break this restriction, many metamaterial-based superlenses and hyperlenses have been proposed and investigated. In this work, we present a simple high-resolution imaging system, which is composed of a magnifying lens and a planar focusing lens. The all-dielectric metamaterial magnifying lens is a modified hemispherical solid immersion lens (SIL) with impedance-matching layer, which is made of gradient-index materials. The high permittivity materials in the core of the magnifying lens can magnify evanescent waves that carry subwavelength imaging information. The magnified waves will propagate smoothly to the free space by the matching layer outside the core region. The planar focusing lens will gather the imaging information and produce the image. Therefore, the image formed by the focusing lens contains the magnified subwavelength-imaging information. The planar focusing lens is designed by geometry optics and cylindrically symmetrical. In the simulation, two point sources with a distance of less than half a wavelength are embedded in the core of the magnifying lens. Thus, the two point sources are imaged at the focus of the planar focusing lens with enlarged distance. Both of the magnifying lens and planar focusing lens are made of isotropic dielectric metamaterials, hence, such a simple high-resolution imaging system works efficiently in a broad band.

A Metasurface for RCS Reduction in X Band

Di Sha Dong, **Qiang Cheng**, **Jie Chen**, **Jie Zhao**, **and Li Hua Gao**
State Key Laboratory of Millimeter Waves, Southeast University, Nanjing 210096, China

Abstract— In recent years, more and more stealth technologies based on metamaterial have been proposed for the RCS reduction of targets, including the absorbent material, transformation optics and active cancellation. Here, we will introduce an ultrathin metasurface, which is based on destructive interference between the incident and reflected waves and therefore leads to electromagnetic diffusion in the backward directions. The main lobe and some of the side lobes of the scattering pattern of the targets could be suppressed significantly. The proposed metasurface is composed by metallic patches with different dimensions printed on a grounded substrate. The phase shifts of the metallic patches can be controlled within 0° to 360° uniformly by carefully choosing their geometric dimensions. When the phase shifts of metallic patches are designed to be randomly distributed, the reflected energy from the random metasurface will be scattered in various directions, resulting in the RCS reduction. For broadband RCS reduction applications, the metasurface is usually realized with multilayer structures to achieve the full phase range. In this design, only one single layer is utilized, which is more compact in size and easier to fabricate. By comparing the scattering pattern of the designed metasurface and a pure metallic plate with the same dimensions, the backward RCS can be reduced by more than 10 dB within the whole X band. We believe this metasurface may find potential applications in the stealth technology in the future.

Polarization Conversion and Splitting by Using Thin Reflective Anisotropic Metasurface

Gui Zhen Wang, Hui Feng Ma, and Gu Sheng Kong
State Key Laboratory of Millimeter Waves, School of Information Science and Engineering
Southeast University, Nanjing 210096, China

Abstract— A kind of bi-reflective anisotropic metasurface has been proposed, which can manipulate the polarization states of the electromagnetic waves independently. The bi-reflective anisotropic metastufaces are made up of two mutually perpendicular I-shape structures, which have capacities to control the vertical and horizontal polarizations by using each of I-shape structures, respectively. Two typical devices of such reflective anisotropic metasurfaces have been proposed: polarization converters and polarization beam splitters. Polarization converters are designed by using of homogenous anisotropic metasurfaces with thickness of $\lambda_0/10$, which can transform a linearly polarized incident wave into a circularly or crossly polarized wave in a broad frequency band. Polarization beam splitters are designed by using of graded anisotropic metasurfaces with thickness of $\lambda_0/15$, which can manipulate the vertical and horizontal polarizations to different directions independently. The full-wave simulated results of polarization converters and polarization beam splitters are calculated by using of CST, and good polarization conversion and splitting are clearly observed, which verify the capacities of such reflective anisotropic metasurfaces to manipulate the polarization states of electromagnetic waves.

Variable Gravitational Mass in the Electromagnetic Field Described with the Complex Quaternion

Zi-Hua Weng
School of Physics and Mechanical & Electrical Engineering
Xiamen University, Xiamen 361005, China

Abstract— In the twentieth century the scholars began to apply the complex quaternion/octonion to depict the electromagnetic theory, and even the gravitational theory. In the paper, it is able to deduce directly the Maxwell's equations and the force equilibrium equation, and refine the inference that the gravitational mass varies with the fluctuation of field strength. Moreover the energy gradient associated with the variable gravitational mass will impact the movement of the particle. The deduction can be applied to capture the neutral particle with the low-speed.

Up to now the Eotvos experiment has only been validated in the weak gravitational field, but has never been tested in the strong gravitational field, electromagnetic field, and ever the high-speed situation. So the scholars never stop doubting the validity of Eotvos experiment. In the force equilibrium equation, the force includes the inertial force, gravity, energy gradient, and Lorentz force etc. As long as the energy distribution is no uniform, the energy gradient, as one part of force, will impact the equilibrium relation of the inertial force and the gravity.

The field theory described with the complex quaternion believes that the comparative strong gravitational and electromagnetic strength will evidently result in the fluctuation of gravitational mass. In the gravitational field, the gravitational acceleration will decrease the gravitational mass. For the gravitational mass in the electromagnetic field, the contribution coming from the electric field intensity is different to that from the magnetic flux density. The electric intensity will increase the gravitational mass, while the magnetic flux density will decrease the gravitational mass.

The energy gradient associated with the field strength may be called as the 'gradient force' for the moment. For the magnetic flux density, the gradient force is an attractive force. For the electric field intensity, the gradient force is a repulsive force. When the gradient force is an attractive force, the particle will be in the repeating motion within one local region. When the gradient force is a repulsive force, the particle will be in the repeating motion within one local region, which stays in between two face-and-face gradient forces.

ACKNOWLEDGMENT

The authors are grateful for the financial support from the National Natural Science Foundation of China under grant number 60677039.

Study on Barium Strontium Titanium (BST)-based Metamaterial

J. Yuan, G. Yin, G.-B. Yin, and Y.-G. Ma
Centre for Optical and Electromagnetic Research, Zhejiang University, Hangzhou 310058, China

Abstract— In this paper, the barium strontium titanium (BST) is employed to form the modem layer in the metamaterial. We demonstrate an active metamaterial device capable of efficient real-time control and manipulation of microwave radiation. It is demonstrated that both the resonance frequency and bandwidth of the metamaterial can be tuned by varying the external electric voltage. Because the BST film has a high dielectric constant in the microwave and could be modulated by the external electric voltage. This paper introduces a new method of modulating structure resonance frequency by voltage. The equivalent capacitance of the structure can be tuned, and the resonance frequency shifts subsequently.

Figure 1 shows the $LaAlO_3$-based metamaterial unit, the substrate is made by $LaAlO_3$ which permittivity is 25, the top electrode is made by gold and the BST films is between them. The surface impedance can be characterized as a capacitor.

We get the variation range of dielectric constant is 74.6% from 0 to 1500 V/mm of the biased voltage [1]. Therefore, we will know the reflectivity under different dielectric constant due to applied voltage.

Then we simulated the results in different parameter of the geometry structure. In this work, we introduce a new structure of BST-based metamaterial. It shown that the frequent resonance will shift by the applied voltage.

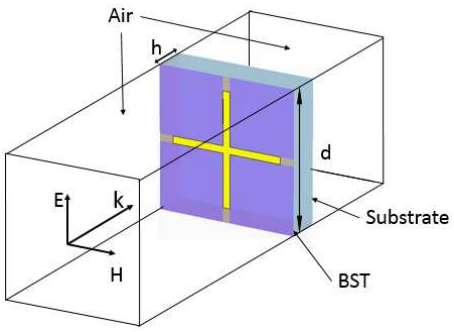

Figure 1: Schematic of the AMC unit, the parameter: d is 3.5 mm, h is 251 μm (includes the thickness of BST film is 1 μm).

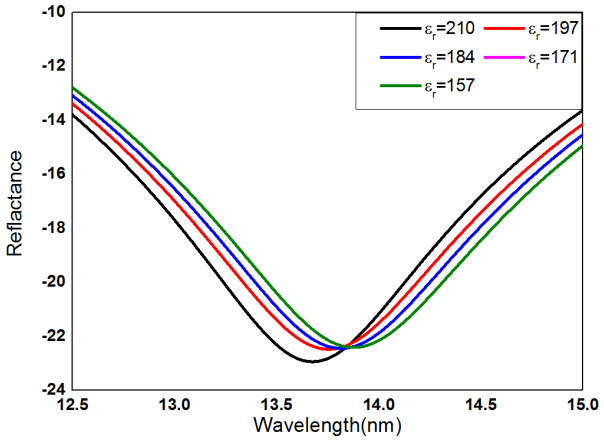

Figure 2: Reflectance of the structure made by Au, relative dielectric constant are 220, 206, 192, 178, 164 [2].

REFERENCES

1. Liang, R. H., X. L. Dong, Y. Chen, F. Cao, and Y. L. Wang, "Mechanism of nonlinear dielectric constant of $BaTiO_3$-based ceramics under high DC electric field," *Acta Physica Sinica*, Vol. 54, No. 10, 2005.
2. Sheng, S., X. Y. Zhang, P. Wang, and C. K. Ong, "Effect of bottom electrodes on dielectric properties of high frequency $Ba_{0.5}Sr_{0.5}TiO_3$ parallel plate varactor," *Thin Solid Films*, Vol. 518, 2864–2866, 2010.

Near-infrared Virtual Intraoperative Surgical Photoacoustic Microscopy for Needle Image Guiding Surgery

Changho Lee[1], **Mansik Jeon**[1], **Jeehyun Kim**[2], **and Chulhong Kim**[3]

[1]Futrue IT Innovation Laboratory, Pohang University of Science and Technology, Republic of Korea
[2]School of IT Engineering, Kyungpook National University, Republic of Korea
[3]Department of Creative IT Engineering, Pohang University of Science and Technology, Republic of Korea

Abstract— We proposed a near infraredvirtual intraoperative surgical photoacoustic microscopy (NIR-VIS-PAM) system by fusing a laser-scanning based optical-resolution photoacoustic microscopy (LS-OR-PAM) with 1064 nm pulsed laser and commercial surgical microscope. By sharing the same optical path of sample part in the LS-OR-PAM and microscope system, a cross-sectional PAM and microscope image was acquired simultaneously. Moreover, using a small-sized commercial beam projector and simple optical device, we have projected cross-sectional PAM images on microscope view plane as augmented reality. It does not require additional display tool for the PAM image monitoring. Therefore, surgeons can monitor both 2D PAM and microscopic images via an ocular lens of the microscope without movement of their sights during surgeries. To demonstrate the feasibility of the NIR-VIS-PAM system, needle intervention in phantom with human hairs was successfully monitored. Finally, we successfully guided needle insertion into tumor of mice by visualizing position of target from the PAM images and the magnified skin surfaces from the conventional microscopic images simultaneously.

Propagation of Surface Plasmons at Semiconductor/Dielectric Interfaces

Dalibor Blažek[1, 2], **Michael Čada**[1, 2], **and Jaromír Pištora**[1]

[1]Nanotechnology Centre, VŠB — Technical University of Ostrava
17, listopadu 15., Ostrava, Poruba 708 33, Czech Republic
[2]Department of Electrical and Computer Engineering, Dalhousie University, Halifax, B3H 4R2, Canada

Abstract— Plasmonic structures are a promising solution for overcoming the diffraction limit of light and for developing novel integrated optics devices. While metals have shown to support plasmon oscillations at optical frequencies, doped semiconductors have been studied for surface plasmons at millimeter waves (terahertz frequencies). It has been shown recently [1] that heavily doped semiconductors support surface plasmons at infrared frequencies. This is possible at much lower free carrier concentrations compared to the ones in metals due to very low effective mass of free electrons in semiconductors such as GaAs or InP. The advantage of using semiconductors is the possibility of tuning the semiconductor properties by changing the composition and doping of a given material. In order to fully understand the resulting surface plasmon propagation characteristics, one needs to investigate properties of the lattice permittivity, the plasma frequency, and the damping.

While the above mentioned material properties may be regarded as the material constants, the relevant surface plasmon properties such as its phase velocity, group velocity, and propagation length are dispersive.Focusing on the surface plasmon of a chosen wavelength, its characteristics may be tuned by a semiconductor's doping level. There exists a minimum dopant concentration that is required to support achosen surface plasmon with its group velocity being low and its propagation length being extremely short. These two parameters rise with increasing doping concentrations. At some level the secondary effects, such as decreasing electron mobility and increasing effective mass, will significantly affect plasmon damping. The imaginary part of the permittivity grows rapidly and it becomes dominant at some doping concentration depending on the type of the studied semiconductor. With the group velocity determined mainly by the permittivity of the interfacing dielectric medium and the increase in damping, a further increase of doping levels appears to be less consequential.

This contribution presents the influence of doping levels on the surface plasmon propagation properties. The calculations are based on the Drude model using the real semiconductor properties. Interestingly, it is shown that the propagation length of the surface plasmon increases monotonically with increasing doping levels despite the extremely large damping (i.e., the dominant imaginary part of the permittivity).

REFERENCES

1. Cada, M. and J. Pistora, "Optical plasmons in semiconductors," *ISMOT-2011 Proceedings*, 23–29, Prague, Czech Republic, June 20–23, 2011.

The Roles of Different NiO Compact Blocking Layers in P-type Sensitized Solar Cells

Huan Wang, Xianwei Zeng, Wenjun Zhang, and Wei Chen
Michael Grätzel Centre for Mesoscopic Solar Cells, Wuhan National Laboratory for Optoelectronics
Huazhong University of Science and Technology, Wuhan 430074, China

Abstract— Compact blocking layers made of wide band gap semiconductors, such as TiO_2, ZnO, are widely used to suppress recombination at the conductive FTO substrate/electrolyte interface in dye or quantum dot sensitized solar cells, especially in the solid-state devices. Though sharing similar mechanism, blocking layers in p-type sensitized solar cells are rarely studied. Our recent works have demonstrated that the compact NiO films dependent upon the preparation ways play important roles in both p-type dye and quantum dots sensitized solar cells. In p-type dye sensitized NiO solar cell, the compact NiO layer, prepared by spin-coating of a sol-gel film, can prevent the recombination at the FTO glass/electrolyte interface and retard the whole cell's recombination kinetics. Therefore, the fill factor and photovoltage can be increased, leading to a 40.77% improved performance of p-type solar cell. In p-type organometal halide perovskite sensitized mesoporous NiO solar cell, it is found that only the spray pyrolysis deposited NiO dense film is effective for selective hole gathering, rather not the sol-gel deposited NiO dense film. The difference may be ascribed to their coverage status on the rough FTO glasses. The existence of such a NiO block layer not only effects on the cell performance but also determines the current flow direction in the p-type perovskite sensitized NiO solar cell.

Performance Analysis of Photonic Phase Shift Network for OAM-beam Antenna Array Receiver

Jian Jian, **Hui Chen**, **Yujie Chen**, **Yanfeng Zhang**, **and Siyuan Yu**
State Key Laboratory of Optoelectronic Materials and Technologies, School of Physics and Engineering
Sun Yat-sen University, Guangzhou 510275, China

Abstract— Transmitting electromagnetic (EM) waves carrying orbital angular momentum (OAM) is potentially capable of increasing the information transmission capacity via utilizing different OAM states (valued by topological charge ℓ) multiplexing. In radio frequency (RF) transmission system, the generated EM waves with different OAM states possess helical wavefronts, hence demultiplexing on the receiver end requires an antenna array, in which each antenna demands a precise phase tune capability enabled by a phase shift network. Using RF photonic technique to realize such phase shift network has the advantage of wide spectral width and high phase shift resolution, over the conventional electrical shifters.

The photonic phase shift network under study comprises multiple directly modulated distributed feedback (DFB) laser diodes with different wavelengths in ITU-C grid. They are modulated by antenna baseband frequency of 10 GHz carrying phase difference induced by the OAM wave phase front received from different antenna elements. These modulated optical signals, each carries the phase shifted carrier coherently superposition by different OAM states, are combined with a wavelength division multiplexer (WDM), and subsequently go through series of phase delay units. The phase delay units have a wavelength-dependent true time delay, and in turn induce a phase compensation to the baseband frequency for the demodulation of a specific OAM channel upon the photodiodes.

The performance of the RF OAM demodulation relies on the photonic phase delay unit. We will compare two structures with wavelength dependent delay: one with the chirped fiber Bragg grating (CFBG), and another with WDM having each wavelength port connected to fibers with high-reflection terminal. The former one provides a relatively low loss solution, whereas the latter one has strength in feasible phase adjustment. Combining the model of the nonlinearity induced by the DFB laser, we numerically study and compare these two solutions on the OAM demodulation performance, including sensitivity, signal distortion, and channel crosstalk.

The phase information received is also dependent to the antenna array shape and relative position to the OAM EM wave. It may deviates from the ideal phase front of each OAM state. Without a calibrated phase delay network, this may deteriorate the demodulation performance. Hence, a study on the phase distortion on the mismatched receiver will be discussed, showing the relative phase tuning range for each phase delay unit is essential for practical implementation.

Session 3A1
FocusSession: Sesquicentennial Commemoration Session for Maxwell's Equations 1

Transformation Optics — Part of Maxwell's Enduring Legacy

John Pendry
The Blackett Lab, Imperial College London, London SW7 2AZ, UK

Abstract— Published 150 years ago Maxwell1s equations were at least as startling as any of the modern advances in physics. They identified electricity and magnetism as the components of light, and laid the foundations for the special theory of relativity by requiring that they were reconciled with Newton1s equations of motion. On their foundations mighty industries have been founded and to this day they still have new facets to be revealed. The equations are known to be invariant under a coordinate transformation and this observation has been exploited in the new tool of transformation optics. Modern studies in electromagnetism go far beyond traditional optics often working in regimes where the length scales are much shorter than the wavelength where such intuitive but approximate rules such as Snell1s law lose their validity. Transformation optics discards the concept of a ray and works instead with the electric and magnetic field lines which obey Maxwell1s equations. Manipulating these fields gives back the intuitive feel of the ray picture but at the same time is exact. Distortion of a field line can be represented as a transformation, which in turn tells what values of permittivity and permeability are needed to shape the fields in this way. Whilst adding nothing to the accuracy of the Maxwell1s equations, this concept provides a picture on which we can unleash our imaginations. I shall describe applications to cloaking devices and to the sub wavelength design of plasmonic devices.

Representing Maxwell's Equations in Vector Diagram Form

Donald R. Wilton[1], **Robert D. Nevels**[2], **and Kuo-Ho Yang**[3]

[1]Department of ECE, University of Houston, Houston, TX 77204, USA
[2]Department of ECE, Texas A&M University, College Station, TX 77843, USA
[3]Department of Engineering and Physical Sciences, St. Ambrose University, Davenport, IA 52803, USA

Abstract—

Maxwell's Equations in the Daily Practice of Near-field Techniques

Jean-Charles Bolomey
University Paris-Sud and Supelec, France

Abstract— Claiming that Maxwell's equations have become a common tool for electromagnetic engineers is nothing but a truism. What a road traveled to get there! Indeed, in their early form involving no less than twenty equations, they just concerned a very limited and closed circle of physicists. They still had to wait, about one century later, the irruption of computers before being increasingly and systematically exploited to solve realistic problems of practical relevance. If computers are unanimously recognized for their efficiency to solve Maxwell's equations, it is usually less clearly realized how these equations have deeply impacted the experimental practice. The purpose of this paper is to review the evolution of experimental techniques and, more particularly, to focus on so-called Near-Field Techniques (NFT's) which make an intensive use of Maxwell's equations. Taken in their broadest sense, NFT's consist in a hybrid approach aiming to obtain, via calculation, a maximum of information from a reduced set of experimental data. As such, they efficiently take profit of the flexibility of computer-aided numerical processing while minimizing the cumbersome collection of experimental data. But this computational aspect would be insufficient to explain the dramatic craze for NFT's in electromagnetic measurement community. After being heavily penalized by the slowness of mechanically scanned single probe measurement, they were stunningly impacted by the probe array technology, whose acceptance was only reached after a long maturation process initiated in the mid 80's. Both NFT's computer and probe array issues related to Maxwell's equations are developed in the following.

Today, several electromagnetic codes are available on the market. Coupled to appropriate optimization algorithms, they are routinely used to design antennas, RF components, etc.. However, codes work on models, and the value of the results they provide depend on the model validity in reproducing the realty. Models validity may be questionable, either for discretization reasons or due to an incomplete and/or uncertain description of the realty. For instance, model validity is more particularly critical in scenarios involving out-of-band behavior of components, or back-door coupling mechanisms in complex systems, or interactions between waves and living structures .... Consequently, the validation by experiment remains, in many applications, an obliged passage, especially, but not only, when the compliance to standards is required.

For a long time, experiments have been conducted on a *cut-and-try* basis, to control and empirically improve first order intentional effects of radiating systems, such as the far-field pattern of antennas. But, rapidly, the development of radio communications or radars, and, recently, the explosion of wireless devices, have resulted in a growing utilization of the electromagnetic spectrum and a need to carefully look at second order non-intentional effects of electromagnetic radiations on electronic systems (ElectroMagnetic Compatibility, EMC) and human beings (Dosimetry). Exposition standards have been progressively defined and the compliance with these standards became mandatory before introducing any new device on the market. For all these reasons, the electromagnetic field needs to be measured on real systems at an increasing number of points and frequencies. For instance, a base-station antenna must not only be tested in its far-field region, but also in its vicinity to ensure compatibility with near-by systems using closely located antennas or safe exposition levels for persons staying outside a prescribed safety perimeter.

To collect such an amount of measured data, two major strategies have been considered. The first one is direct and consists of measuring the field where needed. The advantage of this strategy is that the field value is immediately obtained, but shows the drawback to be renewed at all the points of interest, some of them being possibly difficult to reach. The second one, on the contrary, is indirect and consists to derive by calculation the field at the desired locations from the field measured elsewhere. NFT's belong to this indirect approach, which requires to define an appropriate domain where the measurement can be easily done, and to minimize the required number of measurement points in this domain. Furthermore, a major problem is to accurately extrapolate the field until the domain of interest from the measured data. The analyticity of the electromagnetic field in a source-free region provides a theoretical answer. Practically, usual analytic continuation techniques are severely limited by the achievable measurement accuracy. On the contrary, Maxwell's equations and their derived "products" (mode expansions, source integrals, etc.) appear as a particularly efficient extrapolation scheme, even over long distances.

Several examples will be given to illustrate the practical implementation of NFT's. While initially dedicated to electrically large antennas, they are now currently used for small antennas,

whatever they are fixed or mobile, body-worn, mounted on cars or planes, etc. thanks to rapid in-door or portable measurement setups, optimally combining electronic and mechanical scans for maximum rapidity/accuracy/cost efficiency. Consequently, probe array-based NFT's have had a strong economical impact in reducing the duration, and hence, the cost of experimental programs. Furthermore, they are now recognized to provide the highest possible degree of accuracy, due to the possible control and compensation of various sources of errors they offer. Equivalence theorems and inverse source techniques provide a high degree of flexibility in combining numerical models and experimental data. As an example, the contribution of an antenna measured in a given environment may be de-embedded and used as a source to predict its behavior in another environment. This can be advantageously used in antenna metrology to filter out the parasitic effects of the unavoidable structures supporting the antenna under test. Such equivalent source models are also increasingly used for EMC purposes to model, over broad frequency bands, parasitic and possibly random emissions, for instance, those stemming from components on a printed circuit board or radiated by a power converter. NFT's are also a good candidate for dosimetry applications, where low-invasiveness and high sampling rate of high-reactive fields are required in lossy tissue-simulating phantom materials. NFT-based probe array solutions offer a very attractive alternative to time consuming single probe Specific Absorption Rate measurements, as stipulated by current standards.

All these examples demonstrate that, during the few last decades, NFT's have gained a full acceptance in a large spectrum of applications, thanks to a proper exploitation of the available computer and probe array technologies. They can be considered as the result of a fruitful synthesis between usual numerical modeling and experimental techniques. As such, much more than a simple measurement technique, they constitute a powerful tool and, even to some extent, a new way of approaching electromagnetic problems. Involving a high theoretical background, NFT's perfectly illustrate the omnipresence of Maxwell's equations in the daily practice of electromagnetic engineering.

Casimir-Lifshitz Forces: Designer Quantum Fluctuations, Quantum Levitation and the Future of Nanomachines

Federico Capasso
School of Engineering and Applied Sciences, Harvard University, Cambridge, MA 02138, USA

Abstract— Attractive forces exist between any uncharged surfaces in vacuum due to quantum mechanical fluctuations (zero point energy). Known as Casimir-Lifshitz forces, they can be tailored by suitable choice of the materials and their shape and even turned into repulsive by interleaving a suitable liquid. Measurements of these exotic forces will be presented [1]. These results have implications for future scaled-down MicroElectro Mechanical Systems (MEMS) opening the door to new actuators, nanoscale position sensors and frictionless bearings based on quantum levitation. The talk will conclude with a brief discussion of future exciting possibilities such as the vacuum torque and the "holy grail" of quantum electrodynamics, light generation by "shaking the vacuum".

REFERENCES

1. Rodriguez, A. W., F. Capasso, and S. G. Johnson, *Nature Photonics*, Vol. 5, 211, 2011.

Reflections on Maxwell's Treatise

Arthur D. Yaghjian
Electromagnetics Research Consultant, 115 Wright Road, Concord, MA 01742, USA

Abstract— On many occasions during the past forty years, I have turned to Maxwell's Treatise on Electricity and Magnetism to find out how he approached various topics in electromagnetics ranging from the definition of electric and magnetic fields to the speed of light. I have continually been surprised by the depth and rigor of his derivations as well as the similarity of his notation to that of present-day books on electromagnetism. However, the greatest surprise has been the few important places where Maxwell provided insight into the development of his equations that appears to have been overlooked by many if not all textbooks and historical reviews based on his work. Therefore, in hopes that it is not presumptuous, I will try to explain what has most captured my attention as I reflect upon my periodic excursions into Maxwell's Treatise.

In particular, we will address the questions of what free-space fields Maxwell took to be primary, E and H or E and B, and how he defined these fields; did Maxwell average microscopic fields to get macroscopic fields and, if not, how did he obtain fields in source regions, especially those source regions that contain polarization densities; did Maxwell begin with the integral form or the differential form of the equations of electricity and magnetism; did he use vectors and vector equations or just scalar equations and what was the extent of his use of quaternions; did he depend strongly on the molecular-votices model for electromagnetic fields; did he express his equations in the same way we do today; did he always use the Coulomb gauge ($\mathrm{div}A = 0$); how did Maxwell determine the speed of light.

The 150th Birthday of Maxwell Equations

Giorgio Franceschetti[1, 2]

[1]University Federico II of Naples, Italy
[2]Jet Propulsion Laboratory, United States

Abstract— In this communication this 150th birthday anniversary of Maxwell Equations is celebrated, and their accomplishments over these 150 years commented. Note that, here and in the following, reference is always made to Maxwell Equations, and not to Maxwell's equations, because the children family name is usually that of the father that generated them.

In the late seventeenth and eighteenth century, mysterious electric and magnetic different phenomena were exciting curiosity of people, and interest of scientists. In UK the Health Temple was offering a supposedly electrified bed to help females to become pregnant; in Italy Alessandro Volta assembled the electric battery, thus rendering easy generation of d.c. currents; in Denmark Christian Oerstead was playing with electric currents and magnetic needles in the back of a Pharmacy, as well as Michael Faraday with solenoids and magnetic needles again, in some secluded room of the Royal Institution in UK. These and many other curiosities were analysed by scientists, essentially in France and UK, and formalised by two laws, Biot & Savart and Faraday equations, the first stating that electric currents generate magnetic fields, and vice-versa the second, provided that the magnetic field is time-varying. But no more then that: the electric and magnetic arenas remained separated.

And then James Clerk Maxwell took these two equations, and added a new term: no derivation from other experiments, he just invented it... and, as a sort of miracle, the two fields married for ever, coupled as the electromagnetic field! Accordingly, the electromagnetic waves were created by Maxwell, and later on experimentally verified by Heinrich Rudolf Hertz in Germany, and extensively applied in the communication arena by Guglielmo Marconi in Italy and UK, finally changing our life style.

This communication briefly presents the birth of Maxwell equations, created and not derived from preliminary experiments, and the successive steps of their usage for a number of applications that changed, and are still changing our physical and social life. At the end of the communication, a just one minute additional comment will be added: no detail is given here, to hide a thrilling conclusion!

Session 3A2
MS-2.1: Focus Session on Microwave Photonics Components and Systems

Ultra-high-speed Fiber-wireless Transport Technology

A. Kanno and T. Kawanishi
National Institute of Information and Communications Technology, Japan

Abstract— Fiber-wireless transport technology is essential for configuring future networks that will allow optical and radio networks to be seamlessly connected. Advanced optical fiber communication using high-speed digital signal processing can be diverted into wireless communication channels to increase the capacity to greater than 10 Gb/s. End-to-end modulation and demodulation with transmission impairment compensation over the fiber-wireless link showed not only a reduction in transmission latency, but also a possible reduction in the total power consumption of the network.

To enhance the resilience of the network to disasters and to increase the functionality of the entire network, including optical and wireless networks, fiber-wireless transport technology with seamless connectivity between optical and wireless signals is required. From the viewpoint of capacity, there is a big gap between the 100 Gb/s of optical transport and the less than 1 Gb/s of existing wireless services, which causes a bottleneck in signal transport. Millimeter-wave and terahertz-wave radio are possible candidates for realizing high-speed wireless signal transport. In particular, using a radio-over-fiber (RoF) technique, a seamless connection between the optical and radio signals can help realize high-speed wireless transport with retaining the waveform, including the modulation format.

Coherent RoF techniques, which use digital signal processing (DSP) diverted from advanced optical coherent communication, will result in advantages in terms of low latency and possible low power consumption features over the entire transmission link [1]. This is because the DSP set only at the transmitter and receiver in end-to-end transmission link can mitigate transmission impairments throughout the link; that is, any DSP at an optical-to-wireless conversion or a wireless-to-optical conversion can be excluded.

In the W-band (75–110 GHz) and the terahertz band (> 300 GHz), coherent transmission over optical fiber as an optical signal and over free space as a radio signal is demonstrated with a capacity greater than 10 Gb/s using a multi-level modulation and demodulation technique with the DSP. The waveform of the signal is seamlessly converted between the optical and radio links. This means that the waveform of the signal is maintained over different media; that is, the "waveform-over- fiber" technology can realize signal transport via various transmission media using an end-to-end transmission link [2].

In the talk, we will discuss a demonstration of high-speed wireless communication connected to an optical fiber link using the DSP. Analog signal transmission and its characteristics using advanced optical fiber communication technology will be also discussed.

ACKNOWLEDGMENT

The authors are thankful for financial support from the project entitled "Research and Development of high-precision imaging technology using 90 GHz band linear cells," with funding from "Research and Development to Expand Radio Frequency Resources," supported by the Ministry of Internal Affairs and Communications, Japan.

REFERENCES

1. Kanno, A., T. Kuri, I. Hosako, T. Kawanishi, Y. Yoshida, Y. Yasumura, and K. Kitayama, "Coherent optical and radio seamless transmission based on dsp-aided radio-over-fiber technology," *Proc. Optical Fiber Commun. Conf.*, paper OTu3D.7, Anaheim, USA, Mar. 2013.
2. Kawanishi, T., "Ultra high-speed fiber-wireless transport," *Proc. Optical Fiber Commun. Conf.*, paper M2D.1, San Francisco, USA, Mar. 2014.

Delay-stabilized Optical Fiber Link for Frequency and Signal Transfer

Yitang Dai, Anxu Zhang, Zhongze Jiang, Zhongle Wu, Feifei Yin, Jianqiang Li, and Kun Xu
State Key Laboratory of Information Photonics and Optical Communications
Beijing University of Posts and Telecommunications
P. O. Box 72, Beijing 100876, China

Abstract— The capability of transferring a radio frequency (RF) standard to a remote location ranging from several to hundred kilometers with high stability and accuracy is highly desired in many occasions, such as the test of fundamental physical principles, development of next-generation accelerator-based x-ray sources, long-baseline coherent radio telescope arrays, and the accurate mapping of the Earth's geoid. The delay-stabilized transfer of broadband signal is also desired in connected-element interferometry applications where signal phase alignment among all antennas is required to successfully correlate received signals and achieve higher angular resolution, detective sensitivity, and larger viewing angle. To meet these long-distance stability requirements, optical fiber link has been used to transfer frequency reference or RF signal, which however still suffers from mechanical perturbation and temperature variation along the link and degrades the delay or phasestability at the remote end.

In this presentation, we will review the pastefforts on the stabilized fiber link, from the electronic or optic voltage controllable oscillator to the optical tunable delay line. Then we will show our recent work where the tunable optical carrier wavelength assisted by the fiber dispersion can provide a broadband and large tunable delay range. Such technique supports both point-to-point delivery and multi-point access of frequency reference and time signal, as well as broadband signal downlink. The advantages, performance, and key issues will be discussed.

Fully Monolithic Photonic Integrated Circuits for Microwave and Millimeter Wave Signal Generation

G. Carpintero[1], K. Balakier[2], C. Gordón[1,3], G. Kervella[4], R. Guzmán[1], A. Jiménez[1], M. J. Fice[2], M. Chitoui[4], F. Van Dijk[4], and X. Leijtens[5]

[1]Universidad Carlos III de Madrid, Madrid 28911, Spain
[2]Department of Electronic and Electrical Engineering, University College London
Torrington Place, WC1E 7JE, UK
[3]National Secretary of Science, Technology and Innovation, Senescyt, Quito, Ecuador
[4]III-V Lab, Palaiseau Cedex 91767, France
[5]COBRA Research Institute, Eindhoven University of Technology
Den Dolech 2, Eindhoven 5612AZ, The Netherlands

Abstract— Recent technology roadmaps point to the need of increasing the data rates used in wireless communication systems into the multi-gigabit-per-second to cope with the future needs based in current trends of the demand [1]. A current cost effective solution is to increase the carrier wave frequency into the millimeter wave region, moving to the E-band — 60 to 90 GHz — and beyond [2]. The difficulties to generate, amplify and modulate signals at these frequencies have been overcome by combining electronic with photonic techniques. Currently, most if not all of the reported wireless communication links operating above 100 GHz employ photonic generation of the carrier frequency. There are many different photonic techniques available to generate continuous-wave (CW) frequencies, such as optical heterodyning using two frequency-tunable laser diodes, optical heterodyning using two modes filtered from a multi-wavelength source, combining a CW laser with external modulator and using mode-locked lasers [3].

On several of these approaches, fiber optic components were needed in the photonic system to generate the signal. It has been demonstrated that slight integration efforts lead to significant improvement in the generated millimeter wave signal quality, highlighting the importance of monolithic integration [4]. Currently, InP generic foundry models offer active-passive integration technology to fabricate Photonic Integrated Circuits (PIC) on Multi-Project Wafer (MPW) runs. Complex functionalities can be integrated on a single chip combining a small number of standardized basic building blocks (BB) with high performance [5]. In addition, because generic integration technologies can serve a large market, this allows approaching costs provided by economy of scale. In this work, we demonstrate recent advances in the development of PICs for microwave and millimeter wave signal generation, ranging from the monolithic integration of dual distributed feedback (dual-DFB) lasers to fully monolithic Mode locked laser diodes (MLLD).

On the first approach, we show a fully monolithic millimeter-wave wireless transmitter, including two DFB lasers and optical combiners for the dual wavelength generation, electro-optic modulators (EOM) for data modulation, and, crucially, integrated high-speed photodiodes (PD) to generate the millimeter electrical signal. Semiconductor optical amplifiers (SOA) are also included to compensate the optical losses. This approach, which has the great advantage of continuous tuning of the wavelength spacing, requires a dedicated fabrication process flow to develop all these components in the same chip.

On the monolithic mode-locked approach, we show a novel cavity structure using multimode interference mirrors (MIR) that is fully integrated in the PIC, without need of cleaved facets. This is a step forward since in a MLLD, the length of the resonator defines the repetition rate. With this approach we have a lithographic control of the cavity length. Also, we address the drawback of using cleaved facets that prevents its integration with other optical components into a PIC.

REFERENCES

1. Ericsson Mobility Report, Nov. 2013.
2. Stohr, A., "Photonic millimeter-wave generation and its applications in high data rate wireless access," *IEEE Top. Meeting on Microwave Photonics (MWP)*, Oct. 5–9, 2010.
3. Nagatsuma, T., "Radio spectral evolution with photonics," *International Topical Meeting on Microwave Photonics*, Sept. 9–Oct. 3, 2008.
4. Nagatsuma, T., H. Ito, and K. Iwatsuki, "Generation of low-phase noise and frequency-tunable millimeter-/terahertz-waves using optical heterodyning techniques with uni-traveling carrier photodiodes," *36th European Microwave Conference*, Sept. 10–15, 2006.

5. Smit, M., X. Leijtens, E. Bente, J. van der Tol, H. Ambrosius, D. Robbins, M. Wale, N. Grote, and M. Schell, "Generic foundry model for InP-based photonics," *IET Optoelectronics*, Vol. 5, No. 5, 187, 194, Oct. 2011.

Dual-wavelength Semiconductor Laser with Two Asymmetric Phase-shifts

Xiangfei Chen
National Laboratory of Solid State Microstructures
College of Engineering and Applied Sciences, Nanjing University
Nanjing, China

Abstract— Dual-wavelength lasers have attracted great interests for the ability of photonic generation of microwave. Compared with other lasers, semiconductor laser has the advantages of compact size, stable operation, integration capability and so on. In this work, we propose the dual-wavelength semiconductor lasers with two asymmetric phase shifts. Stable dual wavelength lasing is established by the grating structure consisting of two asymmetric phase shifts $\pm\theta$. In such a grating structure, the power distributions of the two wavelengths along the laser cavity can be spatially separated and the mode competition can be suppressed effectively. The phase shifts are equivalently obtained by specially designed sampling structures with uniform seeding grating based on reconstruction-equivalent-chirp (REC) technique. The uniform seeding grating is obtained by conventional holographic exposure and the sampling structures are formed by another μm-level photolithography. The other processes of the fabrication are the same with the normal ridge semiconductor lasers. Hence, the fabrication of the devices is mature, fast and cost effective. The abrupt phase shifts are replaced by phase-arranging-regions (PARs) for the advantages of separating power distributions in large θ, overcoming the small sampling linewidth on photo mask in small θ and reducing the spatial hole burning (SHB). Stable dual-wavelength lasing with about 0.51 nm wavelength spacing is experimentally demonstrated. A microwave signal at about 64 GHz can be generated by beating the two wavelengths. The -3 dB bandwidth of the beat frequency is 800 kHz. The stability of beating signal is measured every 10 minutes for 1.5 hour and the standard deviation of the microwave frequency is about ± 2.5 MHz. The dual-wavelength semiconductor laser array with varying wavelength spacings by different phase shifts is obtained as well. The wavelength spacing decreases with the value of phase shift increasing.

Microwave Photonic Frequency Mixer for Distributed Antenna System

Shilong Pan and Zhenzhou Tang
Key Laboratory of Radar Imaging and Microwave Photonics, Ministry of Education
Nanjing University of Aeronautics and Astronautics, Nanjing 210016, China

Abstract— Microwave frequency mixing is a basic function of transmitters and receivers in distributed antenna systems (DASs). Compared to a conventional electrical mixer, the microwave photonic frequency mixer has the advantages of large bandwidth, low loss and immune to electromagnetic interference. This paper describes the techniques developed in the last few years in microwave photonic frequency mixers for DAS, with an emphasis on the recent developed ultra-compact microwave photonic frequency mixers without LO and RF signals leakage based on a single dual-drive Mach-Zehnder modulator (DMZM) or a dual-parallel MZM (DPMZM). In addition, with two MZMs placed in parallel, a polarization-insensitive photonic microwave down-converter is realized. Several expected future developments of the microwave photonic frequency mixer are discussed.

Advances in Photonic-assisted Microwave Signals Measurement, Detection, and Analysis

Xihua Zou
Center for Information Photonics and Communications, Southwest Jiaotong University, China

Abstract— A variety of photonic-assisted approaches and methods have been released to enrich and to enhance the measurement, the detection, and the analysis of wideband microwave signals, due to the intrinsic features of photonics technology in wide instantaneous bandwidth and the immunity to electromagnetic interference. In this talk, recent advances with respect to such photonic-assisted approaches and methods are outlined, which have already found applications in the instantaneous frequency measurement, the arrival of angle (AOA) and the time-difference-of-arrival estimation, the Doppler frequency shift estimation.

Then, more attentions are paid the corresponding work and the achievements from Southwest Jiaotong University. For the instantaneous frequency measurement, optical comb filter or filter array are designed and fabricated to perform optical frequency to optical intensity mapping in the proposed approaches, with large wide-open frequency coverage (e.g., 40 GHz or even larger), digital outputs being obtained. For the AOA estimation, the AOA is equivalently converted into a phase shift between two replicas of a microwave signal received at two cascaded modulators. Thus, by measuring the optical power, the phase shift is estimated and this parameter is then used to derive the AOA Also, a high-resolution and frequency-independent solution for the estimation of the Doppler frequency shift and the radial velocity is realized. The Doppler frequency shift between the transmitted microwave signal and the received echo signal is estimated with an improved resolution by a factor of 2 (e.g., measurement errors lower than $\pm 0.5\times 10^9$ Hz) within the range from 0 to 30 GHz. These results indicate a range from 0 to 450 m/s for the radial velocity measurement of a moving object and a velocity resolution of 2.25×10^{-8} m/s at the 30-GHz band.

Linear Optical Filtering Techniques for Optical Signal Processing

Ming Li[1, 2], Reza Ashrafi[2], Ninghua Zhu[2], Tae-Jung Ahn[3], Sophie LaRochelle[4], and José Azaña[1]

[1]Institute of Semiconductors, Chinese Academy of Sciences, No. 35, Tsinghua East Road, Beijing, China
[2]Institut National de la Recherche Scientifique-Énergie, Matériaux et Télécommunications (INRS-EMT) Varennes, Québec J3X 1S2, Canada
[3]Department of Photonic Engineering, Chosun University, Seosuk-dong, Gwangju 375, Korea
[4]Centre d'Optique, Photonique et Laser, Université Laval, Québec, QC G1V0A6, Canada

Abstract— The implementation of all optical circuits for computing, information processing, generation and networking could overcome the severe speed limitations currently imposed by electronic-based systems [1–31]. A promising approach toward the implementation of ultrafast all-optical circuits is to emulate the developments in the electronic domain, i.e., to follow similar component and design strategies, using photonic technologies [1–4]. For this purpose, high-speed optical signal processors, such as optical differentiator [5–11], integrator [12–15], Fourier transformer [16, 17] and Hilbert transformer [18, 19], have recently attracted an increasing interest for optical communications, pulse shaping or sensing applications that use optical signals [20–24].

Sub-picosecond pulse shaping has also attracted an increased interest for its important applications in the areas of ultrahigh speed communications, optical signal processing, and analysis of ultrafast nonlinear processes [20–24]. In the context of optical communications and signal processing, pulse shaping down to the sub-picosecond regime is needed as the bit rates are pushed into the Tb/s range. Sub-picosecond optical pulses with customized temporal shapes can be generated based on linear spectral shaping using a spatial light modulator (SLM) [32]. The major advantage of an SLM-based pulse shaping system is that the system can be programmed to generate different shapes with a large flexibility. The major limitations of an SLM-based pulse shaping system are associated with its implementation involving free-space optics, i.e., large size, relatively poor stability and high insertions losses for incorporation in fiber-optics systems. Alternatively, picosecond or sub-picosecond pulse shaping can be implemented using linear optical filtering with a fiber-optic or integrated-waveguide device. In particular, grating-assisted mode coupling devices have proved particularly successful for this purpose [9, 20–22].

In this paper, recent advances in optical signal processors such as optical differentiator based on a directional coupler, a flat-top pulse shaper using an integrated Mach-Zehnder interferometer (MZI) and high speed bit stream generation with fiber long period gratings (LPGs) are reviewed. The optical pulse shaping capability of the above mentioned devices is also addressed.

REFERENCES

1. Venema, L. M., "Photonics technologies," *Nat. Insight*, Vol. 424, 809, 2003.
2. Azaña, J., C. K. Madsen, K. Takiguchi, and G. Cincontti, "Special issue on 'Optical signal processing'," *J. Lightwave Technol.*, Vol. 24, 2484–2767, 2006.
3. Ngo, N. Q., S. F. Yu, S. C. Tjin, and C. H. Kam, "A new theoretical basis of higher-derivative optical differentiators," *Opt. Commun.*, Vol. 230, 115–129, 2004.
4. Azaña, J., "Ultrafast analog all-optical signal processors based on fiber-grating devices," *IEEE Photon. J.*, Vol. 2, 359–386, 2010.
5. Slavík, R., Y. Park, M. Kulishov, R. Morandotti, and J. Azaña, "Ultrafast all-optical differentiators," *Opt. Express*, Vol. 14, 10699–10707, 2006.
6. Park, Y., J. Azaña, and R. Slavík, "Ultrafast all-optical first- and higher-order differentiators based on interferometers," *Opt. Lett.*, Vol. 32, 710–712, 2007.
7. Ashrafi, R., M. Li, and J. Azaña, "Coupling-strength-independent long-period grating designs for THz-bandwidth optical differentiators," *IEEE Photonics Journal*, Vol. 5, No. 2, 7100311, 2013.
8. Li, M., D. Janner, J. Yao, and V. Pruneri, "Arbitrary-order all-fiber temporal differentiators based on fiber Bragg gratings: design and experimental demonstration," *Optics Express*, Vol. 17, No. 22, 19798–19807, 2009.
9. Li, M., H.-S. Jeong, J. Azaña, and T.-J. Ahn, "25-terahertz-bandwidth all-optical temporal differentiator," *Optics Express*, Vol. 20, No. 27, 28273–28280, Dec. 2012.

10. Li, M. and J. P. Yao, "Multichannel arbitrary-order photonic temporal differentiator for wavelength-division-multiplexed signal processing using a single fiber Bragg grating," *IEEE/OSA J. Lightw. Technol.*, Vol. 29, No. 17, 2506–2511, Sep. 2011.
11. Li, M., L. Y. Shao, J. Albert, and J. P. Yao, "Continuously tunable photonic fractional temporal differentiator based on a tilted fiber Bragg grating," *IEEE Photonics Technology Letters*, Vol. 23, No. 4, 251–253, Feb. 2011.
12. Ferrera, M., Y. Park, L. Razzari, B. E. Little, S. T. Chu, R. Morandotti, D. J. Moss, and J. Azaña, "On-chip CMOS-compatible all-optical integrator," *Nat. Commun.*, Vol. 1, 29–33, 2010.
13. Azaña, J., "Proposal of a uniform fiber Bragg grating as an ultrafast all-optical integrator," *Opt. Lett.*, Vol. 33, 4–6, 2008.
14. Slavík, R., Y. Park, N. Ayotte, S. Doucet, T.-J. Ahn, S. LaRochelle, and J. Azaña, "Photonic temporal integrator for all-optical computing," *Opt. Express*, Vol. 16, 18202–18214, 2008.
15. Malacarne, A., R. Ashrafi, M. Li, S. LaRochelle, J. P. Yao, and J. Azaña, "Single-shot photonic time-intensity integration based on a time-spectrum convolution system," *Opt. Lett.*, Vol. 37, No. 8, 1355–1357, Apr. 2012.
16. Li, M. and J. P. Yao, "Ultrafast all-optical wavelet transform based on temporal pulse shaping incorporating a two-dimensional array of cascaded linearly chirped fiber Bragg gratings," *IEEE Photon. Technol. Lett.*, Vol. 24, No. 15, 1319–1321, Aug. 2012.
17. Li, M. and J. P. Yao, "All-optical short-time Fourier transform based on a temporal pulse shaping system incorporating an array of cascaded linearly chirped fiber Bragg gratings," *IEEE Photon. Technol. Lett.*, Vol. 23, No. 20, 1439–1441, Oct. 2011.
18. Li, M. and J. Yao, "Experimental demonstration of a wideband photonic temporal Hilbert transformer based on a single fiber Bragg grating," *IEEE Photonics Technology Letters*, Vol. 22, No. 21, 1559–1561, Dec. 2010.
19. Li, M. and J. Yao, "All-fiber temporal photonic fractional Hilbert transformer based on a directly designed fiber Bragg grating," *Optics Letters*, Vol. 35, No. 2, 223–225, 2010.
20. Ashrafi, R., M. Li, S. LaRochelle, and J. Azaña, "Superluminal space-to-time mapping in grating-assisted co-directional couplers," *Optics Express*, Vol. 21, 6249–6256, 2013.
21. Ashrafi, R., M. Li, et al., "Experimental demonstration of superluminal space-to-time mapping in long period gratings," *Optics Letters*, Vol. 38, No. 9, 1419–1421, 2013.
22. Ashrafi, R., M. Li, and J. Azaña, "Tsymbol/s optical coding based on long period gratings," *IEEE Photonics Technology Letters*, Vol. 25, No. 10, 910–913, 2013.
23. Fernandez, M. R., M. Li, et al., "Picosecond optical signal processing based on transmissive fiber Bragg gratings," *Optics Letters*, Vol. 38, 1–3, 2013.
24. Li, M., P. Dumais, R. Ashrafi, H. P. Bazargani, J.-B. Quélène, C. Callender, and J. Azaña, "Ultrashort flat-top pulse generation using on-chip CMOS-compatible Mach-Zehnder interferometers," *IEEE Photon. Technol. Lett.*, Vol. 24, No. 16, 1387–1389, Aug. 2012.
25. Li, M., Z. Li, and J. P. Yao, "Photonic generation of a precisely pi phase shifted binary phase-coded microwave signal," *IEEE Photon. Technol. Lett.*, Vol. 24, No. 22, 2001–2004, Nov. 2012.
26. Li, Z., M. Li, H. Chi, X. Zhang, and J. P. Yao, "Photonic generation of phase-coded millimeter-wave signal with large frequency tunability using a polarization-maintaining fiber Bragg grating," *IEEE Microwav. Wireless Compon. Lett.*, Vol. 21, No. 12, 694–696, Dec. 2011.
27. Li, M. and J. P. Yao, "Photonic generation of continuously tunable chirped microwave waveforms based on a temporal interferometer incorporating an optically-pumped linearly-chirped fiber Bragg grating," *IEEE Trans. Microw. Theory Tech.*, Vol. 50, No. 12, 3531–3537, Dec. 2011.
28. Li, M., Y. Han, S. Pan, and J. P. Yao, "Experimental demonstration of symmetrical waveform generation based on amplitude-only modulation in a temporal pulse shaping system," *IEEE Photon. Technol. Lett.*, Vol. 23, No. 11, 715–717, Jun. 2011.
29. Li, M., L. Y. Shao, J. Albert, and J. P. Yao, "Tilted fiber Bragg grating for chirped microwave waveform generation," *IEEE Photonics Technology Letters*, Vol. 23, No. 5, 314–316, Mar. 2011.
30. Li, M., C. Wang, W. Li, and J. Yao, "An unbalanced temporal pulse shaping system for chirped microwave waveform generation," *IEEE Transactions on Microwave Theory and Techniques*, Vol. 58, No. 11, 2968–2975, Nov. 2010.

31. Wang, C., M. Li, and J. Yao, "Continuously tunable photonic microwave frequency multiplication by use of an unbalanced temporal pulse shaping system," *IEEE Photonics Technology Letters*, Vol. 22, No. 17, 1285–1287, Aug. 2010.
32. Weiner, A. M., J. P. Heritage, and E. M. Kirschner, "High-resolution femtosecond pulse shaping," *J. Opt. Soc. Amer. B*, Vol. 5, 1563–1572, Aug. 1988.
33. Lepetit, L., G. Chériaux, and M. Joffre, "Linear techniques of phasemeasurement by femtosecond spectral interferometry for applications in spectroscopy," *J. Opt. Soc. Amer. B*, Vol. 12, No. 12, 2467–2474, Dec. 1995.

Novel High Performance Microwave Photonic Phase Shifters Based on Stimulated Brillouin Scattering

Mattia Pagani, Benjamin J. Eggleton, and David Marpaung
CUDOS, School of Physics, University of Sydney, NSW 2006, Australia

Abstract— Phase shifters are essential components of phased arrays and beamforming systems. These applications require continuously tunable, full 360° phase shift range over wide multi-GHz bandwidths. Microwave photonic phase shifters are capable of operating over much wider frequency bands than their electronic counterparts. Among microwave photonic phase shifters, a scheme that stands above all others exploits optical carrier processing in combination with single sideband modulation, to map a narrow band optical phase shift to an ultra-wide band phase shift in the electrical domain. This results in an operating bandwidth limited only by the bandwidth of the transmitter and receiver employed. Stimulated Brillouin scattering (SBS) is ideal for optical carrier processing due to its narrow bandwidth, and low threshold power. For years SBS phase shifters were restricted to operate in kilometre-spools of fibre which, aside from being bulky, are also susceptible to changes in the environment. Here we present the first phase shifter that makes use of on-chip SBS. Using a 6.5 cm long chalcogenide rib waveguide, we obtained 180° phase shift tuning range over 2–15 GHz frequency band.

All SBS-based phase shifters to date exploits both SBS gain and loss to achieve gain-transparency, which is a major requirement for all phase shifters. However, this technique is fundamentally limited by an unwanted SBS response that restricts the operating bandwidth to only two times the Brillouin frequency shift (~ 11 GHz in silica fibre). In this work, we introduce for the first time a novel SBS-based scheme that not only solves the bandwidth limitation, but also achieves unprecedented gain-transparency. The new phase shifter relies on shaping the SBS pump to independently adjust the magnitude and phase of the optical carrier. We demonstrate gain fluctuations of less than ± 0.2 dB, and full 360° phase shift range over 28 GHz bandwidth, limited only by the modulator used.

Terahertz Communications Based on Coherent Photonics

Tadao Nagatsuma[1], **Yasuyuki Yoshimizu**[1], **Yu Yasuda**[1], **Kazuki Oogimoto**[1], **Shogo Horiguchi**[1], **Yusuke Minamikata**[1], **Shintaro Hisatake**[1], **and Kazutoshi Kato**[2]

[1]Graduate School of Engineering Science, Osaka University
1-3 Machikaneyama, Toyonaka, Osaka 560-8531, Japan
[2]Graduate School of Information Science and Electrical Engineering
Kyushu University, Japan

Abstract— Recently, there has been a growing interest in the application of terahertz (THz) waves, whose frequencies range from 100 GHz to 1 THz, to ultra-broadband wireless communications [1–3]. Photonic techniques have been efficiently employed to generate and modulate THz carrier signals. Real-time and error-free transmission experiments have so far been demonstrated at bit rates of 40 Gbit/s and 48 Gbit/s for a single polarization system and a polarization-multiplexed one, respectively, using a photonics-based transmitter and a direct detection receiver at 300 GHz [3].

In order to further increase the bit rate, introduction of multi-level modulation technique such as QPSK using coherent THz carrier signals together with a coherent detection scheme is effective and practical. Use of the coherent detection scheme also enhances the receiver sensitivity, leading to the increase of transmission distance without an amplifier.

In this paper, we will present our recent studies on THz wireless communications based on photonically-assisted coherent signal generation and detection at carrier frequencies from 100 GHz to 300 GHz.

REFERENCES

1. Kleine-Ostmann, T. and T. Nagatsuma, "A review on terahertz communications research," *J. Infrared Milli. Terhz. Waves*, Vol. 32, No. 2, 143–171, Feb. 2011.
2. Song, H.-J. and T. Nagatsuma, "Present and future of terahertz communications," *IEEE Trans. on Terahertz Science and Technology*, Vol. 1, No. 1, 256–263, Sep. 2011.
3. Nagatsuma, T., S. Horiguchi, Y. Minamikata, Y. Yoshimizu, S. Hisatake, S. Kuwano, N. Yoshimoto, J. Terada, and H. Takahashi, "Terahertz communications based on photonics technologies," *Optics Express*, Vol. 21, No. 20, 23736–23747, Oct. 2013.

Using Single Dual-drive Modulator Generating Arbitrary Waveforms and UWB Signal

Bo Dai[1], **Zhensen Gao**[2], **Satoshi Shimizu**[3], **Naoya Wada**[3], **and Xu Wang**[1]

[1]Institute of Photonics and Quantum Sciences, School of Engineering and Physical Sciences
Heriot-Watt University, Edinburgh EH14 4AS, UK
[2]Bell Laboratories, Alcatel-Lucent Shanghai Bell, Shanghai 201206, China
[3]Photonic Network Research Institute
National Institute of Information and Communications Technology (NICT), Tokyo 184-0015, Japan

Abstract— We demonstrate a novel scheme using a single dual-drive Mach-Zehnder modulator to generate versatile waveforms from a continuous light with a sinusoidal RF signal. A comprehensive mathematic model is derived and the algorithm to decide the variables for generating various waveforms is developed. The theoretical predictions agree with our experimental results. This reveals a new mechanism for arbitrary waveform generation, which has many applications in different fields.

Photonic Time Stretch Channelizer for Broadband Microwave Spectrum Sensing

Chao Wang
School of Engineering and Digital Arts, University of Kent, Canterbury, CT2 7NT, UK

Abstract— Microwave spectrum sensing is of critical importance in wireless communications, radars and electronic warfare. Measuring high-frequency and broadband RF signals in a high-speed and high-resolution while low-cost manner is challenging. Photonically assisted techniques have shown superior performance over their electronic counterpart. Particularly, optical spectral channelizer based technique has attracted great interest as it enables lost-cost spectrum measurement for multi-tone microwave signals. One difficulty of this technique is its relatively poor measurement resolution, limited by the channel spacing.

Based on photonic time-stretch technique, which mirrors the spectrum shape of a largely chirped optical pulse to its temporal waveform, here we propose to use an optical channelizer to equivalently sample the modulated optical pulse. Since no high-speed photodetector is required, system cost is greatly reduced. More importantly, the method features greatly improved measurement resolution, which is more than two orders of magnitude higher than the channel spacing. The technique was verified by experimental demonstrations. Means to further improve the measurement resolution and operational bandwidth will be discussed as well.

ACKNOWLEDGMENT

This work was support in part by the Royal Society of UK (IE131158), and the European Commission Marie-Curie Career Integration Grant (631883).

Time-frequency Manipulation in Real-time Instruments

Mohammad H. Asghari[1], **Jacky Chan**[1], **and Bahram Jalali**[1, 2, 3]

[1]Department of Electrical Engineering, University of California, Los Angeles
420 Westwood Plaza, Los Angeles 90095, USA
[2]Department of Bioengineering, University of California, Los Angeles
420 Westwood Plaza, Los Angeles 90095, USA
[3]Department of Surgery, David Geffen School of Medicine, University of California, Los Angeles
420 Westwood Plaza, Los Angeles 90095, USA

Abstract— We describe compression and expansion of the time bandwidth product of signals. Time bandwidth engineering is enabled by the recently introduced Stretched Modulation Distribution, a mathematical tool that describes the bandwidth and temporal duration of signals after arbitrary transformations. We show application of the Distribution function to design of time bandwidth engineering systems that employ engineered group delay. We derive closed-form mathematical equations governing the operation of such systems. These equations identify an important criterion on the curvature of warped group delay that must be met in order to achieve time bandwidth compression. We also show application of the Distribution to analysis of tolerance to non-idealities. The tools presented here can be used to design data compression and expansion systems that solve the bottlenecks in the real-time capture and generation of wideband data.

Session 3A3a
MS-1.7: Light Emtting Diodes

Fluorescent SiC for White Light-emitting Diodes

Mikael Syväjärvi
Department of Physics, Chemistry and Biology, Linköping University, Linköping SE-58183, Sweden

Abstract— Fluorescent silicon carbide is the host material of a new type of white LED. It converts the light from a UV-LED to white light. Due to the optical conversion process, the light is pure white and does not need any rare earth metals since it is based on a mechanism using n and p-type co-doping.

Such white LED requires thick layers, 250 μm, that are produced by a growth method that should also provide the doping as the layer is growing and maintain a high crystal quality. Defects will strongly influence the optical recombination. Since this is a new research field, not much is known about the details of recombination mechanisms. We have developed a Fast Sublimation Growth Process (FSGP) that is suitable for growth and doping of silicon carbide layers.

In fact, fluorescent SiC can be a foundation for new technologies. Today the 6H and 4H-SiC polytypes are commercially available. In addition, there is 3C-SiC. These polytypes provide a range of different lattice sites, some which are common in all three polytypes and some which are unique for each polytype. Thereby growth and studies of optical properties in fluorescent 6H, 4H and 3C-SiC can be used to understand details of fluorescent properties in SiC, as well as pave the way for a range of novel technologies based on fluorescent SiC.

We will review the research in fluorescent SiC for white LEDs, and discuss potential research routes that can explore novel properties in silicon carbide as optoelectronic material. Important issues are in preparation of the doped source material, to growth of doped layers without deteriorating the crystal quality. Thus there is a strong link between the growth mechanism and optical properties.

Plasmon Enhanced Green GaN Light-emitting Diodes

Haiyan Ou[1], **Ahmed Fadil**[1], **Daisuke Iida**[1, 2], **Yuntian Chen**[1, 3], **Motoaki Iwaya**[2], **Tetsuya Takeuchi**[2], **Satoshi Kamiyama**[2], **and Isamu Akasaki**[2, 4]

[1]DTU Fotonik, Technical University of Denmark, Ørsteds Plads 343, Kgs. Lyngby 2800, Denmark
[2]Faculty of Science and Technology, Meijo University
1-501 Shiogamaguchi Tempaku, Nagoya 468-8502, Japan
[3]School of Optical and Electronic Information
Huazhong University of Science and Technology, Wuhan, China
[4]Akasaki Research Center, Nagoya University, Furo-cho Chikusa, Nagoya 464-8603, Japan

Abstract— High-efficiency garnium nitride (GaN) based blue light-emitting diode (LED) paves the way for solid state lighting to take the place of the conventional incandescent bulbs and fluorescent light tubes. Compared to the traditional light sources, solid state lighting is more efficient, more flexible in spectral design, more compact etc.. The III-nitride (GaN, InN etc.) semiconductors are attracting a lot of research effort because the combination of both could emit light with wavelength range from UV to infrared. Basically one material platform could provide all the solutions to light sources However huge amount of material development is needed before high efficiency devices are achieved. Among them, one effort area is the so called 'green gap', i.e., low efficiency for green color LEDs due to the large piezoelectric field in the quantum wells (QWs) when the In composition is high. From the material growth point of view, the efficiency of green LED is being improved by growing the GaInN material on non-polar or semi-polar surface of sapphire substrate. In parallel with the material growth effort, surface plasmons are implemented by taking use of the interaction between metals and active areas to increase the efficiency.

In this paper, our work on using silver (Ag) nanoparticles (NPs) to enhance the efficiency of the green LEDs is reviewed. Both random and periodic Ag nanoparticles are studied. The random Ag nanoparticles are formed by thermal annealing of thin films. Periodic Ag nanoparticles are formed through nanosphere lithography. For both cases, emission enhancement is demonstrated. For periodic Ag nanoparicles, a photoluminescence enhancement of 2.7 is observed with a nanodisk diameter of 330 nm. It is found that an optimal pitch exists for a given particle size. For the random Ag nanoparticles, low temperature photoluminescence (LTPL) was measured and internal quantum efficiency (IQE) enhancement by the surface plasmons was derived. Excitation power dependence of IQE enhancement is derived as well from the PL measurement under different excitation power densities. It was found that the strong PL enhancement was partly due to LSP-QW coupling, and partly due to excitation source enhancement from the Ag NPs, and separating these effects we noted an IQE improvement due to LSP-QW coupling at 530 nm emission from 19.4% to 44.1% using large sized Ag NPs at 756 W/cm^2. It was also found that the IQE enhancement is strongly dependent on excitation power density, yielding highest enhancement factors at low free carrier densities. Where an IQE enhancement by a factor of 2.3 was observed at 756 W/cm^2, an enhancement factor of 8.1 was observed at 1 W/cm^2.

Future Solid State Lighting Based on Light Emitting Laser Diodes

Paul Michael Petersen and Ole Bjarlin Jensen
DTU Fotonik, Department of Photonics Engineering
Technical University of Denmark, Frederiksborgvej 399, Roskilde 4000, Denmark

Abstract— Solid state lighting (SSL) based on LEDs is today the most efficient light source for generation of high quality white light. Diode lasers, however, have the potential of being more efficient than LEDs for the generation of white light. A major advantage using diode lasers for solid state lighting is that the high efficiency can be obtained at high light lumen levels in a single element emitter and therefore less light sources are required to achieve a desired light level. Furthermore, the high directionality of the generated light from laser diodes increases the energy savings in many applications.

Within the coming years, it is expected that the efficiency of blue laser diodes will approach the efficiency of infrared diode lasers. This will enable high efficiency white light generation with very high lumen per watt values.

SSL today is mainly based on phosphor converted blue light emitting diodes (LEDs). Blue emitting 445–460 nm LED chips with conversion in phosphorescent materials have undergone tremendous development in the last decade with ultra high efficiencies. However, the technology suffers from a decrease in efficiency at high input current densities, known as the "efficiency droop" [1]. This efficiency droop limits operation to relatively low output lumen levels for single element emitters. The cause of the efficiency droop is still not completely clear and thus a solution is not easily found. In the literature it has been suggested that carrier overflow in the quantum wells and non-radiative recombination could be the causes. Recently, Auger recombination was proposed as the dominant mechanism for efficiency droop [2].

In the talk, we discuss the mechanisms of the efficiency droop in LEDs and we show how this problem can be eliminated in laser diodes. With the introduction of diode laser based lighting, high luminous flux levels and high efficiency can be available at the same time. Laser diodes operate in a fundamentally different regime using stimulated emission for light generation as opposed to spontaneous emission in LEDs

The recent progress in solid state lighting based on diode lasers will be reviewed and we will present a new diode laser architecture that emits as high as 2100 lumen green light with an efficiency of 70 lm/W.

REFERENCES

1. Wierer, Jr., J. J., J. Y. Tsao, and D. S. Sizov, "Comparison between blue lasers and light-emitting diodes for future solid-state lighting," *Laser Photonics Rev.*, Vol. 7, No. 6, 963–993, 2013.
2. Iveland, J., L. Martinelli, J. Peretti, J. S. Speck, and C. Weisbuch, "Direct measurement of auger electrons emitted from a semiconductor light-emitting diode under electrical injection: Identification of the dominant mechanism for efficiency droop," *Phys. Rev. Lett.*, Vol. 110, 177406, 2013.

Plasmonic Control of Quantum-well Luminescence for Enhanced Efficiency and Beam Shaping

R. Paiella
Department of Electrical and Computer Engineering, Boston University, USA

Abstract— Metallic nanostructures can be used as optical antennas to control the radiation properties of nearby light emitters, via the near-field excitation and subsequent radiative decay of plasmonic oscillations. Here this basic idea is applied to LED materials based on InGaN/GaN quantum wells. Large enhancements in the radiative efficiency are obtained through the use of plasmonic excitations and lattice surface modes in periodic arrays of Ag nanocylinders. Furthermore, unidirectional beaming at geometrically tunable angles is demonstrated via the excitation and diffractive scattering of surface plasmon polaritons on a Ag film patterned with a periodic array of asymmetric Ag nanoantennas.

Physics of High Efficiency and Efficiency-droop in III-Nitride Light-emitting Diodes

Nelson Tansu, Chee-Keong Tan, Peifen Zhu, and Wei Sun
Center for Photonics and Nanoelectronics, Department of Electrical and Computer Engineering
Lehigh University, Bethlehem, Pennsylvania, USA

Abstract— The materials and device innovations have driven the performance of III-Nitride based light-emitting diodes (LEDs). Various strategies by using new active regions and nanostructure designs resulted in improved internal quantum efficiency in III-Nitride LEDs via charge separation suppression and Purcell factor enhancement. The development of new technique for reducing the dislocation density in III-Nitride LEDs will be presented. New understanding and strategies to suppress the efficiency droop in InGaN-based LEDs will also be presented. The implementation of these strategies to address green gap and droop issue in device level will be compared.

Analysis of Light Extraction Efficiency Enhancement in GaN-based LEDs with Self-assembly Approach

Peifen Zhu, Wei Sun, Chee-Keong Tan, and Nelson Tansu
Center for Photonics and Nanoelectronics
Department of Electrical and Computer Engineering
Lehigh University, Bethlehem, Pennsylvania, USA

Abstract— The thin-film flip-chip (TFFC) light-emitting diodes (LEDs) are the state-of-the-art LED technology, which combined with phosphor materials to generate white light for general illumination and display technologies. However, the efficiency needs to be further improved and the manufacture cost needs to be reduced in order to widely adopt the GaN-based solid-state lighting technology. In this work, the cost-effective methods were employed to improve the efficiency of LED. Specifically, we investigated the light extraction efficiency of LED by using self-assembly method. Comprehensive studies were carried out to investigate the light extraction efficiency of InGaN TFFC LEDs with microsphere arrays, microlens arrays, and microconcave array structures. The use of microlens arrays structure enabled further enhance the light extraction efficiency to 86%, which corresponds to 1.3 times higher than that of the state-of-the-art TFFC LED with surface roughness approach. Light extraction efficiency of 44% was achieved by employing PDMS concave structures on the top of TFFC LED.

Study of Defects in InGaN

Nazir A. Naz[1], **M. Imran**[1], **and Akbar Ali**[1, 2]

[1]Department of Applied Physics
Federal Urdu University of Arts, Science and Technology Islamabad, Pakistan
[2]Department of Basic Sciences, Riphah International University, Islamabad, Pakistan

Abstract— Deep level transient spectroscopy of InGaN-LEDs was carried out to characterize the defects in the material. Nine defects at energy positions 0.54 eV, 0.91 eV, 1.00 eV, 1.24 eV, 1.37 eV, 1.46 eV, 1.68 eV, 2.25 eV, 3.81 eV were observed. Capture cross-sections of the defects measured at infinite temperature are e 1.25×10^{-14}, 2.27×10^{-17}, 4.39×10^{-29}, 1.37×10^{-20}, 9.58×10^{-22}, 4.61×10^{-28}, 2.19×10^{-24}, 8.23×10^{-22}, 4.16×10^{-64} cm^2 respectively. The respective defect concentrations were estimated to be 1.1×10^4, 4.6×10^4, 2.7×10^4, 19.2×10^4, 6.9×10^4, 6.9×10^4, 5.9×10^4, 6.3×10^4 and 11.3×10^4 (cm^3).

Session 3A3b
MS-1.6: Organic Light Emitting Diodes 1

Universal Bipolar Host Materials and Exciplex for White OLEDs

Ken-Tsung Wong
Department of Chemistry, Taiwan University
1, Sec. 4, Roosevelt Rd., Taipei 10617, Taiwan

Abstract— The introduction of heavy metal-based phosphorescent emitters in organic light-emitting diodes (OLEDs) is a major breakthrough for improving the electroluminescence efficiency to achieve 100% internal quantum efficiency (IQE). The high IQE is based on the use of the host-guest strategy with triplet emitter (guest) homogeneously dispersed into a suitable organic matrix (host). This method can suppress the detrimental effects such as aggregation quenching and/or triplet-triplet annihilation of phosphors. As a consequence, the selection of host materials is of great importance for highly efficient OLEDs. Recent research trends have shifted to the development of host materials possessing bipolar property, which can give balance carrier transport, well-defined electron-hole recombination zone within the emitting layer and reduced efficiency roll-off. The physical properties of bipolar host materials can be manipulated by rational molecular design with the judicious selection of hole-transporting (HT) and electron-transporting (ET) subunits and their linking topology. In this conference, our recent efforts on the development of carbazole-based bipolar host materials equipped with various ET-type functional moieties suitable for efficient red, green, blue and white electrophosphorescent devices will be reported. Another emerging strategy to harvest the electrically generated triplet exciton is to take advantage of delay fluorescence through a reverse intersystem crossing (RISC) process. The essential requirement to give efficient RISC is the low singlet-triplet energy difference, which can be feasibly achieved by the subtle intramolecular and/or intermolecular charge transfer state. In this conference, our new progress of using exciplex to generate efficient OLEDs and a new strategy for giving high efficiency ($> 10\%$) pure fluorescence white OLED will also be presented.

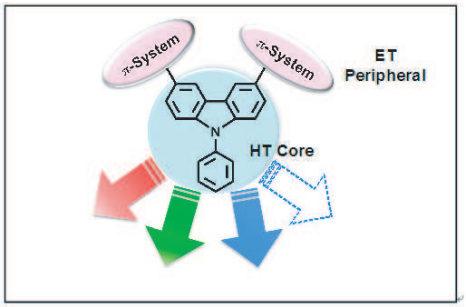

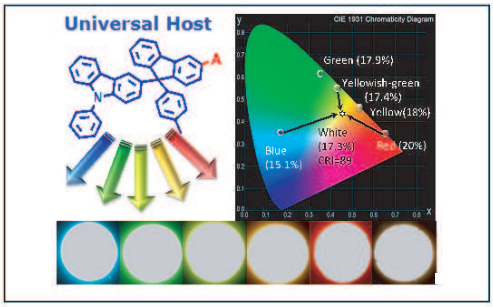

REFERENCES

1. Hung, W.-Y., G.-C. Fang, Y.-C. Chang, T.-Y. Kuo, P.-T. Chou, S.-W. Lin, and K.-T. Wong, "Highly efficient bilayer interface exciplex for yellow organic light-emitting diode," *ACS Applied Materials & Interfaces*, Vol. 5, 6826, 2013.
2. Mondal, E., W.-Y. Hung, Y.-H. Chen, M.-H. Cheng, and K.-T. Wong, "Molecular topology tuning of bipolar host materials composed of fluorene-bridged benzimidazole and carbazole for highly efficient electrophosphorescence," *Chem. Euro. J.*, Vol. 19, 10563, 2013.
3. Mondal, E., W.-Y. Hung, H.-C. Dai, and K.-T. Wong, "Fluorene-based asymmetric bipolar universal hosts for RGBW OLEDs," *Adv. Funct. Mater.*, Vol. 23, 3096, 2013.
4. Lin, M.-S., L.-C. Chi, H.-W. Chang, Y.-H. Huang, K.-C. Tien, C.-C. Chen, C.-H. Chang, C.-C. Wu, A. Chaskar, S.-H. Chou, H.-C. Ting, K.-T. Wong, Y.-H. Liu, and Y. Chi, "A diarylborane-substituted carbazole as a universal bipolar host material for highly efficient electrophosphorescence devices," *J. Mater. Chem.*, Vol. 22, 870, 2012.
5. Hung, W.-Y., L.-C. Chi, W.-J. Chen, E. Mondal, S.-H. Chou, K.-T. Wong, and Y. Chi, "A carbazole-phenylbenzimidazole hybrid bipolar universal host for high efficiency RGB and white PhOLEDs with high chromatic stability," *J. Mater. Chem.*, Vol. 21, 19249, 2011.

High Performance, Single Phosphorescence Dopant, Hybrid White or Multi-color OLEDs Based on Platinum Complexes and a New Host Material

Anurach Poloek[1, 2, 3], **Chieh Wang**[2, 4], **Chao-Tsen Chen**[3], **and Chin-Ti Chen**[2, 4]

[1]Nano Science and Technology Program, TIGP, Academia Sinica, Taipei 11529, Taiwan
[2]Institute of Chemistry, Academia Sinica, Taipei 11529, Taiwan
[3]Department of Chemistry, Taiwan University, Taipei 10617, Taiwan
[4]Department of Applied Chemistry, Chioa Tung University, Hsinchu 30050, Taiwan

Abstract— A series of mixed hetrolepticplatinum (II) complexes, **FPtXND**, where **XND** = 8-substituted 4-hydroxy-1, 5-naphthyridine derivates and **F** = 2-(2, 4-difluorophenyl) pyridine, have been newly synthesized and structurally characterized. Corresponding photophysical properties also have been examined. Each **FPtXND** complex forms variable degree of aggregation in solid state depending on the structural feature of substituent **X** at 8-position of 1, 5-naphthyridine. Therefore, the electroluminescence (EL) from the excimer/aggregate of each **FPtXND** is variable. Using blue light-emitting material, such as conventional NPB (1-naphthylphenylbiphenyl diamine) or newly used (for platinum complex) 4P-NPD (1-naphthylphenylquaterphenyl diamine), and/or host material for **FPtXND** single dopant, high performance hybrid white OLEDs have been achieved with a simple device configuration. Color rendering index of the hybrid white OLEDs fabricated herein can be as high as 90, which is uncommon among single phosphorescent dopant devices. Depending on the phosphorescence dopant concentration, multi-color EL, ranging from blue, green, yellow, orange to red can be obtained.

Device Engineering for High Efficiency Blue Phosphorescence Organic Light-emitting Diode

Tien-Lung Chiu[1], **Hsin-Jen Chen**[1], **Man-Kit Leung**[2], **and Yu-Hsuan Hsieh**[2]

[1]Department of Photonics Engineering, Yuan Ze University
135 Yuan-Tung Road, Chung-Li 32003, Taiwan
[2]Department of Chemistry, Institute of Polymer Science and Engineering
Taiwan University, 1 Roosevelt Road Section 4, Taipei 106, Taiwan

Abstract— A novel ambipolar material CbzTAZ was employed to be the host of the efficient blue phosphorescence organic light-emitting diode (PhOLED) with blue emitter (FIrpic). The original layer structure of blue PhOLED was ITO anode/ NPB (50 nm)/mCP (10 nm)/ CbzTAZ:FIrpic (30 nm)/TAZ(40 nm)/LiF (1 nm)/Al (100 nm). By scanning the doping ratio between host and emitter in emitting layer, and then adjusting the thickness of electron transporting layer and emitting layer, the high efficiency blue PhOLED was obtained. The doping ratio scanning was to find the best condition of energy transfer from host to emitters. The thickness adjustment of electron transporting layer and emitting layer was to achieve the electron-hole balance and the maximum carrier recombination area in emitting layer. Finally, the blue PhOLED perform the current efficiency 48.0 cd/A, power efficiency 42.2 lm/w, and external quantum efficiency 22.9%.

Session 3A4
FocusSession.SC2: Tunable and Reconfigurable Metamaterials and Plasmonics 2

Probing Local Conductivity at Atomic-scale Graphene Defects by Near-field Plasmon Interferometry

J. Chen[1,8], M. L. Nesterov[3], A. Yu. Nikitin[1,2], S. Thongrattanasiri[4], P. Alonso-González[1], T. M. Slipchenko[3], M. Ostler[6], Th. Seyller[6], I. Crassee[7], F. Koppens[5], L. Martin-Moreno[3], J. G. Abajo[4,5], A. B. Kuzmenko[7], and R. Hillenbrand[1,2]

[1]CIC nanoGUNE Consolider, Donostia-San Sebastian 20018, Spain
[2]IKERBASQUE Basque Foundation for Science, Bilbao 48011, Spain
[3]Instituto de Ciencia de Materiales de Aragón and Departamento de Física de la Materia Condensada, CSIC-Universidad de Zaragoza, Zaragoza E-50009, Spain
[4]IQFR-CSIC, Serrano 119, Madrid 28006, Spain
[5]ICFO — Institut de Ciéncies Fotoniques, Mediterranean Technology Park Castelldefels 08860, Barcelona, Spain
[6]Lehrstuhl für Technische Physik, Universität Erlangen-Nürnberg Erwin-Rommel-Str. 1, Erlangen 91058, Germany
[7]Département de Physique de la Matière Condensée, Université de Geneve, Genève 1211, Switzerland
[8]Institute of Physics, Chinese Academy of Science, Beijing 100190, China

Abstract— Understanding the impact of defects in graphene on its optical and electronic properties is essential for future graphene-based applications and devices. Noninvasive and nanoscale resolved mapping of local electronic and optical properties, however, is still a challenging task. Here we employ tip-enhanced infrared near-field microscopy [1] for the contactless and quantitative analysis of local conductivity at substrate steps and wrinkles in epitaxial graphene on SiC. The infrared field concentration at the tip apex launches graphene plasmons, which are back-reflected at these defects, yielding interference patterns in the near-field images [2, 3]. Interestingly, both types of defects induce a strong plasmon reflection, even if their height is only 1 nm [4]. Theoretical analysis of the patterns provides information about the carrier concentration and conductivity variations induced by defects. Near-field plasmon interferometry thus holds great promise for quality control and defect screening in graphene. From a different point of view, the strong plasmon reflection at nanoscale structural and electronic defects could find interesting application potential for the development of active plasmonic graphene devices and circuits.

REFERENCES

1. Ocelic, N., et al., *Appl. Phy. Lett.*, Vol. 89, 101124, 2006.
2. Chen, J., et al., *Nature*, Vol. 487, 77, 2012.
3. Fei, Z., et al., *Nature*, Vol. 487, 82, 2012.
4. Chen, J., et al., *Nano Letters*, Vol. 13, 6210, 2013.

Strong Confinement of Flexible Graphene Plasmons and Its Application

J. Wang, W. B. Lu, X. B. Li, J. Hu, and X. F. Gu
State Key Laboratory of Millimeter Waves, School of Information Science and Engineering
Southeast University, China

Abstract— The intrinsic strong confinement of flexible graphene plasmons (FGPs) is investigated in this paper, such unique property is interpreted by the ultra small thickness and metal like effective dielectric constant from the perspective of classical electromagnetic analysis. Utilizing this advantage, signals and energy can naturally propagate along curved surfaces with little curve-induced radiation loss and acceptable intrinsic propagation loss. Meanwhile, the metal plasmons (MPs) and graphene plasmons (GPs) on curved waveguides are simulated to illustrate the different property. At last, a stereo resonator is proposed as an application for the FGPs based devices.

Enhancing Spontaneous Emission Rates of Molecules Using Nanopatterned Multilayer Hyperbolic Metamaterials

Dylan Lu[1], **Jimmy J. Kan**[2], **Eric E. Fullerton**[1, 2], **and Zhaowei Liu**[1, 2, 3]

[1]Department of Electrical and Computer Engineering, University of California
San Diego, 9500 Gilman Drive, La Jolla, California 92093-0407, USA
[2]Center for Magnetic Recording Research, University of California
San Diego, 9500 Gilman Drive, La Jolla, California 92093-0401, USA
[3]Materials Science and Engineering, University of California
San Diego, 9500 Gilman Drive, La Jolla, California 92093-0418, USA

Abstract— Plasmonic-enabled manipulation of light emission process has been widely investigated for controllable spontaneous emission rates and improved radiative efficiency. This can be achieved by modifying the electromagnetic environment via Purcell effect on metal films. However, such Purcell enhancement, enabled by aligning the surface plasmon mode of a metal film with spontaneous emission spectra, only works for a few narrow bands of frequencies due to the limited plasmonic materials existing in nature. This limitation can be overcome by utilizing hyperbolic meta-materials (HMMs), a type of nanoscale artificial materials with hyperbolic dispersion relations, but with moderate spontaneous emission rate enhancement and weak radiative power demonstrated so far. Here we report nanopatterned Ag-Si multilayer HMMs that not only strongly enhance spontaneous emission rates at desired frequencies but also significantly improve the far-field radiative power. A 76-fold spontaneous emission-rate enhancement is observed by time-resolved photoluminescence on the nanopatterned HMM, which is close to one order of magnitude faster than on pure Ag with the same out-coupling geometry. About 80-fold emission intensity enhancement is simultaneously achieved in our experiment compared to the case without the out-coupling structures. The experimental results are quantitatively explained using a dynamic Lorentzian model describing the spontaneous emission processes in the time domain.

Nonlinear Terahertz Transmission Change with Controllable Graphene Devices

Bumki Min
Department of Mechanical Engineering, KAIST
291 Daehak-ro, Yuseong-gu, Daejeon 305-751, Republic of Korea

Abstract— Graphene, an atom thick two dimensional sheet of carbons, has drawn great attention for its outstanding mechanical, thermal, and electronic properties. As much of its other exotic properties, graphene shows exceptional amount of light-matter interaction that can be controlled efficiently. The control of the light-matter interaction in graphene-based devices was achieved by two major means; optical conductivity control with Fermi level shifting and resonance manipulation with graphene plasmons or meta-atom hybridization. Although nonlinear light-matter interaction of graphene under intense optical fields has even been applied for laser mode-locking in the optical frequencies, its experimental demonstration has only been recently achieved in the terahertz frequencies. In this work, we show the first experimental demonstrations of extrinsic control over the light-matter interaction of graphene under intense terahertz field. The induced transparencies of graphene under intense terahertz field can be controlled by tuning the factors that affect momentum scattering in graphene; changing number of carriers through Fermi level shifting, and altering terahertz field enhancement by resonance manipulation. This scheme of control over light-matter interaction with graphene would open the early steps toward utilization of controllable nonlinear optical behavior.

Graphene Metamaterials and Couplers

Ilya V. Shadrivov[1], **Daria A. Smirnova**[1], **Ivan V. Iorsh**[2, 3], **Andrey V. Gorbach**[4], **Ivan S. Mukhin**[2, 5], **Pavel A. Belov**[2], **and Yuri S. Kivshar**[1]

[1]Nonlinear Physics Centre, Australian National University, Canberra ACT 0200, Australia
[2]National Research University of Information Technologies, Mechanics and Optics (ITMO) St. Petersburg 197101, Russia
[3]Department of Physics, Durham University, DH1 3LE Durham, UK
[4]Centre for Photonics and Photonic Materials, Department of Physics University of Bath, Bath BA2 7AY, UK
[5]St. Petersburg Academic University, Nanotechnology Research and Education Center St. Petersburg 194021, Russia

Abstract— We study propagation of electromagnetic waves in two closely spaced graphene layers and demonstrate that double-layer graphene waveguide can operate as an optical coupler for both continuous plasmons and for spatial plasmon-solitons. We study multilayer graphene structures and show that they are good candidates for realizing hyperbolic metamaterials for THz frequencies. We show theoretically that tuning from elliptic to hyperbolic dispersion in such structure can be achieved with an external gate voltage.

Graphene is a two-dimensional crystal of carbon atoms, which exhibits remarkable characteristics. Recently, its unique optical properties have generated significant interest in the research community [1]. An optical response of graphene is characterized by a surface conductivity which is related to its chemical potential and Fermi energy. At certain frequencies, graphene behaves as a metal, and its coupling to electromagnetic waves may support different types of surface plasmon polaritons, which are described theoretically and have been already observed in experiments [2]. These features make graphene a promising material for plasmonics, paving a way towards the development of optical metadevices. Nonlinear optical properties of graphene structures have attracted attention only recently. Large values of nonlinear optical susceptibilities have been predicted theoretically, and recently they were verified experimentally for the third order nonlinear response. This finding opens a way for the exploration of strong nonlinear photonic effects in graphene structures, including nonlinear self-action of surface plasmons in graphene and the generation of subwavelength spatial solitons [3].

We study analytically and numerically the nonlinear propagation of light in two coupled layers of graphene, and demonstrate that this simple double-layer structure can operate as an efficient optical coupler for both continuous plasmon polaritons and for subwavelength spatial solitons. We demonstrate the nonlinearity-induced symmetry breaking in this graphene coupler and discuss a physical mechanism for optical beam control and manipulation [4].

We also suggest a novel class of hyperbolic metamaterials where individual graphene sheets are separated by host dielectric layers [5]. We demonstrate in this work, a periodic structure of graphene layers creates a special type of metamaterial with strong nonlocal response and hyperbolic properties of its dispersion curves for TM-polarized waves in the THz frequency range and superior characteristics such as a giant Purcell effect and tunability by a gate voltage or magnetic field. Although hyperbolic metamaterial for the THz range can be realized by using conventional metal-dielectric structures, large negative permittivity of metals significantly limits the increase of the radiation efficiency of the emitters placed in such structures.

We present the study of the nonlocal response of such a multi-layer structure, as well as the tunability by external magnetic field. In the presence of a strong magnetic field the longitudinal and Hall part of graphene conductivity are governed by the electron transitions between the discrete Landau levels. We find that, although the imaginary part of the longitudinal conductivity is negative and we would expect the elliptic contours for both the eigenmodes, the coupling via the Hall conductivity term changes the properties dramatically, and the isofrequency contours have a complicated shape, which is neither elliptical nor hyperbolic [5]. We analyse the Purcell factor in the structure, and predict that it can achieve giant values. This suggests that graphene-based hyperbolic metamaterial is an excellent candidate for boosting THz emission by sources placed on a surface of such a medium [5].

REFERENCES

1. Nair, R. R., P. Blake, A. N. Grigorenko, K. S. Novoselov, T. J. Booth, T. Stauber, N. M. R. Peres, and A. K. Geim, *Science*, Vol. 320, 1308, 2008.
2. Fei, Z., A. S. Rodin, G. O. Andreev, W. Bao, A. S. McLeod, M. Wagner, L. M. Zhang, Z. Zhao, M. Thiemens, G. Dominguez, M. M. Fogler, A. H. Castro Neto, C. N. Lau, F. Keilmann, and D. N. Basov, *Nature*, London, Vol. 487, 82, 2012.
3. Nesterov, M. L., J. Bravo-Abad, A. Yu. Nikitin, F. J. Garcia-Vidal, and L. Martin-Moreno, *Laser Photonics Rev.*, Vol. 7, L7, 2013.
4. Smirnova, D. A., A. V. Gorbach, I. V. Iorsh, I. V. Shadrivov, and Yu. S. Kivshar, *Phys. Rev. B*, Vol. 88, 045443, 2013.
5. Iorsh, I. V., I. S. Mukhin, I. V. Shadrivov, P. A. Belov, and Yu. S. Kivshar, *Phys. Rev. B*, Vol. 87, 075416, 2013.

Single Nanoparticle Couplers for Plasmonic Nanocircuits

Shunping Zhang[1] **and Hongxing Xu**[1, 2]

[1]Center for Nanoscience and Nanotechnology, School of Physics and Technology
Wuhan University, Wuhan 430072, China
[2]Beijing National Laboratory for Condensed Matter Physics
Institute of Physics, Chinese Academy of Sciences, Box 603-146, Beijing 100190, China

Abstract— Plasmonic nanowires receive intensive interest due to their potential application as subwavelength waveguides, thanks to the modal confinement of surface plasmon polaritons (SPPs) [1]. Recently, different prototypes of subwavelegnth optical elements have been demonstrated, such as routers [2], quarter waveplates [3] and high performance waveguides [4]. However, the efficiencies of fueling light into a nanowire are quite low due to the impedance mismatch between the waveguides and the free space. In this contribution, we report a strategy of tuning the in-coupling efficiency of light into a nanowire by a single optical antenna [5]. For off-resonant antenna, the coupling between free space radiation and the nanowire SPPs can be suppressed to about 0.05. For resonant ones, the in-coupling efficiency is enhanced by a factor of 8. This finding paves a simple way to control the coupling efficiency between a plasmonic waveguide and the free space which is an important aspect in nanophotonic devices.

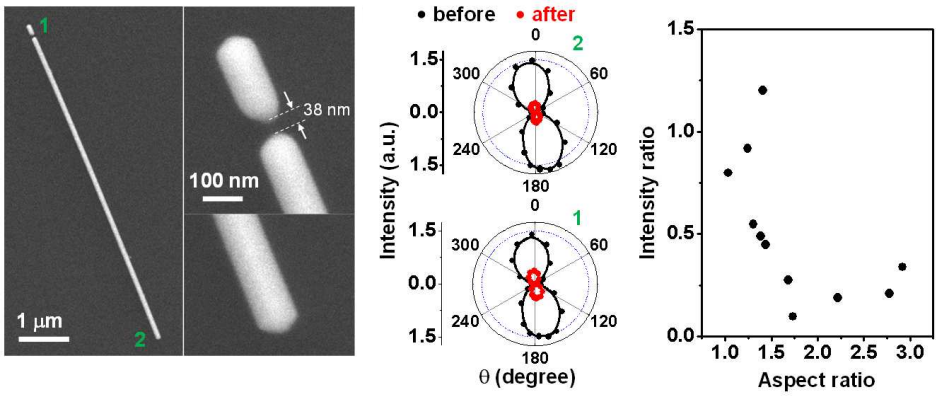

Figure 1: (a) Scanning electron microscopy images of a cut Ag nanowire. (b) Polarization dependence of the transmission light before (black) and after (red) FIB cut. (c) Transmission enhancement as a function of the aspect ratio of the nanorod.

REFERENCES

1. Takahara, J., S. Yamagishi, H. Taki, A. Morimoto, and T. Kobayashi, *Opt. Lett.*, Vol. 22, 475, 1997.
2. Fang, Y. R., Z. P. Li, Y. Z. Huang, et al., *Nano Lett.*, Vol. 10, 1950, 2010.
3. Zhang, S. P., H. Wei, K. Bao, et al., *Phys. Rev. Lett.*, Vol. 107, 096801, 2011.
4. Zhang, S. P. and H. X. Xu, *ACS Nano*, Vol. 6, 8128, 2012.
5. Zhang, S. P., C. Z. Gu, and H. X. Xu, submitted.

Active THz Plasmonic Metamaterials: From Metals to Superconductors

Ranjan Singh
Center for Disruptive Photonic Technologies
Division of Physics and Applied Physics, School of Physical and Mathematical Sciences
Nanyang Technological University, 21 Nanyang Link, 637371, Singapore

Abstract— Recent development in the field of superconductor metamaterials and plasmonics has opened up avenues for reducing losses in these systems and their behaviors could be actively tuned either by changing the temperature, exciting with ultra-short pulses of light, or by applying external magnetic field. There are also very close similarities between the electromagnetic response of metals at optical frequencies and superconductors at terahertz frequencies. In my talk I would discuss about the role of superconductors in designing THz metamaterial and plasmonic devices and compare their responses with traditional plasmonic metals.

Excitation of Surface Plasmon Polaritons at Terahertz Superconducting Hole Array

J. B. Wu[1], X. Zhang[2], B. B. Jin[1], H. Liu[2], Y. H. Chen[3], Z. Y. Li[3], L. Kang[1], W. W. Xu[1], J. Chen[1], and P. H. Wu[1]

[1]School of Electronic Science and Engineering, Research Institute of Superconductor Electronics (RISE)
Nanjing University, Nanjing 210093, China
[2]Key Lab of Opto-electronic Information Science and Technology (MOE)
Institute of Modern Optics, Nankai University, Tianjin 300071, China
[3]Lab of Optical Physics, Institute of Physics, Chinese Academy of Science, Beijing 100190, China

Abstract— The prominent kinetic inductance and low Ohmic loss, combined with wide tunability, make superconductors promising plasmonic medium at terahertz (THz) frequencies [1]. In this talk the plasmonic property of superconducting NbN film at THz frequencies was comprehensively studied by the transmission spectra of a series of superconducting NbN subwavelength hole array both in experiment and microscopic theory. Due to the ultra low loss of superconducting film and periodic subwavelength hole array, the incident THz radiation could be efficiently transformed into surface wave propagate along the surface. We can find experimentally that a long-duration damped transmitted pulse existed after a 1 ps incident THz pulse, which corresponds to about $0.03\,\mathrm{ps}^{-1}$ propagation loss for surface wave. The transmission spectra experienced obvious changes both in amplitude and resonance frequency with temperature, indicating that the plasmonic property could be tuned by changing the density of superconducting carriers. The microscopic hybrid wave (HW) model could well predicate the temperature dependent transmission spectra and intrinsic mechanism of tunability [2, 3]. From the calculated the components of surface plasmon polaritons (SPPs) and quasi-cylindal wave (CW) on the interface of NbN and substrate, the excitation efficiency of SPPs was quite low at resonance frequency. However, the SPPs excitation would be remarkably enhanced when approaching critical temperature and energy gap frequency.

REFERENCES

1. Wu, J., H. Dai, H. Wang, et al., *Opt. Express*, Vol. 19, 1101–1106, 2011.
2. Liu, H. and P. Lalanne, *Nature*, Vol. 452, 728–731, 2008.
3. Liu, H. and P. Lalanne, *J. Opt. Soc. Am. A*, Vol. 27, 2542–2550, 2010.

Modular Assembly of Optical Nanocircuits

Jinwei Shi
Beijing Area Major Laboratory, Department of Physics and Applied Optics
Beijing Normal University, Beijing 100875, China

Abstract— The development level of integration of photonic devices is significantly lagging behind compared with microelectronics, due to diffraction limit and the difficulty of realizing basic functionalities with "lumped" photonic circuit elements at the nanoscale and achieving versatile operations by combining these elements in large circuits.

Here we demonstrate the design, assembly and characterization of various photonic nanocircuits with increasing complexity by accurately positioning a number of metallic and dielectric nanoparticles (NPs) in a reconfigurable way with atomic force microscope (AFM) manipulation, in analogy to what an electrical engineer does when building an electronic circuit. The NP clusters are shown to produce the designed spectral response, qualitatively predicted by simple circuit rules, with fixed optical lumped impedance value of each NP for different nanocircuit configurations. Additionally, such nanophotonic circuits exhibit stereo-functionality, i.e., a response that can be controlled by the polarization of impinging light. Our work represents an important step toward transplanting and extending the powerful design tools of electronic circuits to nanophotonic systems.

Session 3A5
FocusSession.SC2: Microwave Metamaterials 1

Microwave Metamaterials: Promises, Realities and Future Challenges

Raj Mittra
EMC Lab, The Pennsylvania State University, 319 EE East, University Park, PA 16802, USA

Abstract— There are a number of definitions of Metamaterials (MTMs), the most popular among them being "materials that don't exist in nature." This definition, which was introduced when everyone was looking for Doubly-Negative (DNG) materials to realize a perfect lens, has created much confusion, and has also given a bad name to MTMs that are often labeled as being narrowband, dispersive and lossy. While that description indeed does fit materials that are artificially synthesized to realize either DNG characteristics, or those with $\varepsilon < 1$, or $\mu < 1$, it should not be a real concern to us, however, since none of them have ever found their place in any practical device anyway. On the other hand, what has worked for us — when we have attempted to enhance the performance of various antennas — resembles an FSS (Frequency Selective Surface), an EBG (Electronic Band Gap) structure, or a filter comprising of lumped or distributed L's and C's. These structures have been found to be useful for enhancing the performance of an antenna by realizing a higher gain or increased scan capability, or by reducing the mutual coupling between two adjacent antenna elements. The question before us is: "Is it correct to refer to these structures as MTMs, which seems to be the trend and the vogue at present?". This question is particularly relevant for thin surfaces, e.g., FSS screens, or AMCs, for which it is difficult, if not impossible, to come up with a material description. Furthermore, the material description in terms of effective medium parameters would be of little use if it is anisotropic (tensor ε and μ), as is the case more often than not. This is because the simulation of devices, e.g., antennas, loaded with such materials would be difficult, as compared to modeling the original physical structure instead. We should also bear in mind that extracting the anisotropic material parameters from the measurement of Reflection and Transmission coefficients is a very challenging task indeed, not to mention the question of uniqueness which remains open as yet.

Even if we set aside the issue of what to call an artificially synthesized material, we need to ask the question: "Do we have any evidence that using materials with ENG, MNG or DNG characteristics gains us in terms of performance of an antenna?". We would argue that such examples are few, if any; and, hence, we should only narrow our scope to DPS (Doubly-Positive) materials and ignore those that fall in other three quadrants, i.e., ENG, MNG and DNG types, at least when our interest is confined to the microwave regime. That said, we should further probe into the question, whether there is any reason to use DPS materials whose parameters are in the range that is outside that of conventional materials, for instance $\varepsilon < 1$, $\mu < 1$, $\varepsilon \gg 1$, $\mu \gg 1$, all of which are also typically referred to as metamaterials, since they can only be realized via artificial synthesis by using inclusions in a background medium, operating in a frequency region which makes them lossy, narrowband and dispersive. We believe we should stay away from this type of metamaterial as well, except for very narrowband applications, and those for which the loss is acceptable and justifiable. It should be obvious that these applications are expected to be very limited indeed.

Finally, having narrowed down our target for artificially synthesized materials to a relatively narrow regime where the ε and μ values are moderate as well as reasonable — and they are in the *range* that *can be found* in nature — we should turn to the important question: "How do we realize the ε and μ values that we desire, if we face the situation that they are not readily available from the vendors with those precise parameters? We answer this question by saying that we perceive a critical need for a systematic procedure to control the dielectric properties to achieve our goal stated above, and that we will present an approach for achieving this goal by utilizing COTS (commercial-off-the-shelf materials). We add that the technique we will describe is considerably more systematic and easier to use from the fabrication point of view, and it is different from just drilling a hole in a dielectric material to control its effective dielectric constant, a technique that is widely used today.

Lightweight Broadband Microwave Absorber Designed with Multilayer Metamaterial Sheets

Zuojia Wang and Hongsheng Chen
The Electromagnetics Academy at Zhejiang University, Zhejiang University, Hangzhou 310027, China

Abstract— Perfect absorber, a particular branch of metamaterials, has gathered interests due to its unity absorptivity of electromagnetic waves. Since its first experimental demonstration in 2008, the perfect metamaterial absorber has developed rapidly with designs shown across the electromagnetic spectrum, from microwave to optical. However, suffering from narrow bandwidth is the major bottleneck that hampers its extensive applications. Circuit analog absorbers, consist of both resistive and reactive components in front of a single ground plane, can achieve high absorption over broad band. Nevertheless, due to the complexities in design and fabrication, multilayer circuit analog absorbers have been rarely discussed in practice. In this paper, we employ lossy metamaterial sheets as resistive and reactive components to construct a multilayer broadband microwave absorber. By applying transmission line theory, metamaterial sheets are modeled as equivalent loads between dielectric media. Genetic algorithms combined with numerical simulation methods have been used to reduce the thickness and achieve high absorption. Lossy metamaterial surfaces with appropriate effective surface impedances are then designed by a retrieval method. Experimental results show that this absorber has a bandwidth ranging from 5 to 26 GHz for 11 dB reduction of reflectivity with the total thickness 10 mm. Moreover, using polymethacrylimide based rigid foams as the dielectric substrates can effectively reduce the weight of absorber, showing potential applications in microwave engineering.

Arbitrary Control of Electromagnetic Flux in Inhomogeneous Anisotropic Zero-index Media

Jie Luo[1], **Yun Lai**[1], **and C. T. Chan**[2]

[1]School of Physical Science and Technology, Soochow University, Suzhou, China
[2]Department of Physics, The Hong Kong University of Science and Technology, Hong Kong, China

Abstract— In order to control electromagnetic flux in sub-wavelength scales, it is usually assumed that surface plasmons or spoofed surface plasmons that exist on the surface of metal or corrugated metals are necessary, which can guide flux along the surface.

Here, we propose a method to control electromagnetic flux in an almost arbitrary way in wavelength and sub-wavelength scales. The capability of sub-wavelength flux control is enabled not by surface waves, but by the evanescent waves induced by a near zero permittivity component. By designing the spatial profile of the other permittivity component in such inhomogeneous media, the flow and distribution of energy flux can be conveniently manipulated. This method provides another approach to efficiently control electromagnetic flux [1].

The principle of our method is also fundamentally different from transformation optics which relies on coordinate transformation.

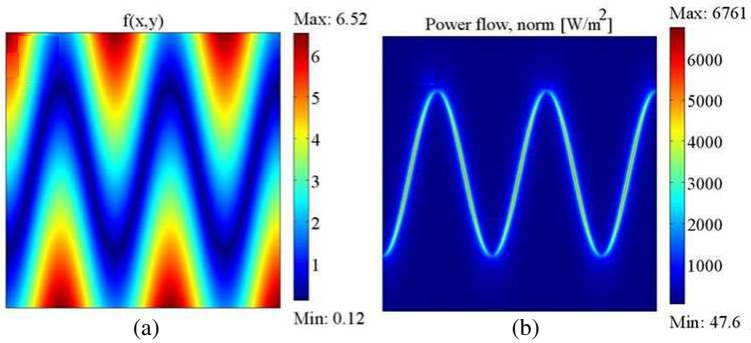

Figure 1: (a) $\varepsilon_y = f(x, y)$ distribution maps and (b) routing of energy flux in a designed sinusoidal path.

REFERENCES

1. Luo, J., W. X. Lu, Z. H. Hang, H. Y. Chen, B. Hou, Y. Lai, and C. T. Chan, *Phys. Rev. Lett.*, Vol. 112, 073903, 2014.

A New Type of Spoof Plasmonic Waveguide

Zhen Gao[1], **Fei Gao**[1], **and Baile Zhang**[1, 2]

[1]Division of Physics and Applied Physics, School of Physical and Mathematical Sciences
Nanyang Technological University, Singapore 637371, Singapore
[2]Centre for Disruptive Photonic Technologies
Nanyang Technological University, Singapore 637371, Singapore

Abstract— We propose a new type of spoof plasmonic waveguide that consists of a single row of coupled planar ring resonator. Unlike other types of spoof plasmonic waveguide, waveguiding in this ultrathin spoof plasmonic coupled-resonator waveguide (SPCRW) is achieved through the weak coupling between otherwise spoof localized surface plasmons (LSPs) cavity.From theoretical simulation, we demonstrate that such a planar plasmonic waveguide can sustain highly confined surface plasmon waves. Additionally, directional couplers,waveguide bends, and super resonators are characterized,demonstrating the flexibility of the proposed concept and the prospects in integrated plasmonic circuits and system.

In recent years, surface plasmon polaritons (SPPs) have attracted a great deal of attentions owning to the possibility of subwavelength confinement and enhancement of electromagnetic (EM) field at metal-dielectric interfaces. In optical frequency, natural SPPs provide us a prominent way to miniaturize compact photonic circuits, whereas localized surface plasmon (LSPs) are widely used in near-field optics, surface-enhanced spectroscopy, and optical nanoantenna. However, at low frequency, metals behave like perfect electric conductors (PECs) and do not support surface plasmons. To exporting the exciting properties of natural SPPs and LSPs to low frequencies (far infrared, terahertz, microwave), the concept of spoof (designer) SPPs was developed by Pendry et al., that is, by cutting holes or grooves in metal surfaces to increase the penetration of EM fields into the metal, thus the EM wave can be highly confined on the engineered metal surface. After that, numbers of waveguiding structures based on this concept have been already suggested. In this work,we present a new mechanism to realize an ultrathin spoof plasmonic surface waveguide based on evanescent-field coupling between individual plasmonic ring resonators. The separation between individual resonators are sufficiently large that the resonators are weakly coupled. Consequently, the eigenmode of electromagnetic field in such a coupled-resonator waveguide will remain essentially the same as the eigenmode in a single plasmonic ring resonator.

Electromagnetic Cloaks Made of Isotropic Materials

Yichao Liu and Yungui Ma
Centre for Optical and Electromagnetic Research, Department of Optical Engineering
Zhejiang University, Hangzhou City 310058, China

Abstract— There are different mathematical Schemes to design electromagnetic cloaks using the coordinate transformation including the general full-wave transformation [1], conformal mapping [2], quasi-conformal mapping [3] and non-Euclidean mapping [4]. Among them the conformal method allows designing a cloak with many unique advantages, such as isotropic material requirement, broadband and low loss, but gets less attentions mainly due to the technical challenges to implement such a device with rapid index variations in a large range. In our talk, we will report our recent work on isotropic electromagnetic cloaks strictly designed conformal transformation and demonstrate both unidirectional and carpet-type cloaking behaviors in a wide band of microwave frequency [5]. Artificial electromagnetic materials with permittivity from 1 to 12 have been implemented to fulfill the stringent spatial dielectric distribution. Microwave measurement shows our samples have very good cloaking performance consistent with numerical simulations. Besides, we also employ the topology optimization to design and fabricate a pure dielectric cloak. Topology optimization is a mathematical approach that optimizes material layout, and it has been used as another strategy for designing cloaks in recent years [6]. The main advantage of this method is its easy and fast fabrication process. We use a precise engraving machine to fabricate a structure on Teflon in order to achieve a unidirectional cloak which works at 15 GHz frequency [7].

REFERENCES

1. Pendry, J. B., D. Schurig, and D. R. Smith, "Controlling electromagnetic fields," *Science*, Vol. 312, No. 5781, 1780–1782, 2006.
2. Leonhardt, U., "Optical conformal mapping," *Science*, Vol. 312, No. 5781, 1777–1780, 2006.
3. Li, J. and J. B. Pendry, "Hiding under the carpet: A new strategy for cloaking," *Physical Review Letters*, Vol. 101, No. 20, 203901, 2008.
4. Leonhardt, U. and T. Tyc, "Broadband invisibility by non-Euclidean cloaking," *Science*, Vol. 323, No. 5910, 110–112, 2009.
5. Ma, Y., Y. Liu, L. Lan, et al., "First experimental demonstration of an isotropic electromagnetic cloak with strict conformal mapping," *Scientific Reports*, Vol. 3, 2013.
6. Andkjær, J. and O. Sigmund, "Topology optimized low-contrast all-dielectric optical cloak," *Applied Physics Letters*, Vol. 98, No. 2, 021112, 2011.
7. Lan, L., F. Sun, Y. Liu, et al., "Experimentally demonstrated a unidirectional electromagnetic cloak designed by topology optimization," *Applied Physics Letters*, Vol. 103, No. 12, 121113, 2013.

Electric and Magnetic Localized Surface Plasmons on Textured Metallic Particles

Xiaopeng Shen[1, 2], **Tie Jun Cui**[2], **Paloma A. Huidobro**[3], **and F. J. Garcia-Vidal**[3]

[1]Department of Physics, China University of Mining and Technology, Xuzhou 221116, China
[2]State Key Laboratory of Millimeter Waves, School of Information Science and Engineering Southeast University, Nanjing 210096, China
[3]Departamento de Fisica Teorica de la Materia Condensada and Condensed Matter Physics Center (IFIMAC), Universidad Autonoma de Madrid, Madrid 28049, Spain

Abstract— Most of the investigations and promising applications of localized surface plasmons (LSPs) have been limited to the optical frequency due to the metal performs like PEC at the low frequency regime. Spoof LSPs have been conducted theoretically and numerically, which showed that a two-dimensional periodically textured metallic cylinder was able to support spoof LSPs in the microwave and terahertz frequencies [1]. We propose and experimentally demonstrate the electric and magnetic spoof LSPs on a planar textured metallic disk at microwave frequencies. We design and realize the plasmonic metamaterial using ultrathin metal film printed on a thin dielectric substrate and observe electric and magnetic dipole resonance, simultaneously [2], as well as multimode plasmon resonance [3], in both numerical simulations and experiments, which have good agreements. We also show that the spoof LSP resonances are sensitive to the disk's geometry and local dielectric environments by simulations and experiments. Hence localized surface plasmon have important practical implications not only in the RF or terahertz ranges of the EM spectrum but also at infrared energies in which spectroscopic tools are essential in many technologies devoted to the analysis of material properties.

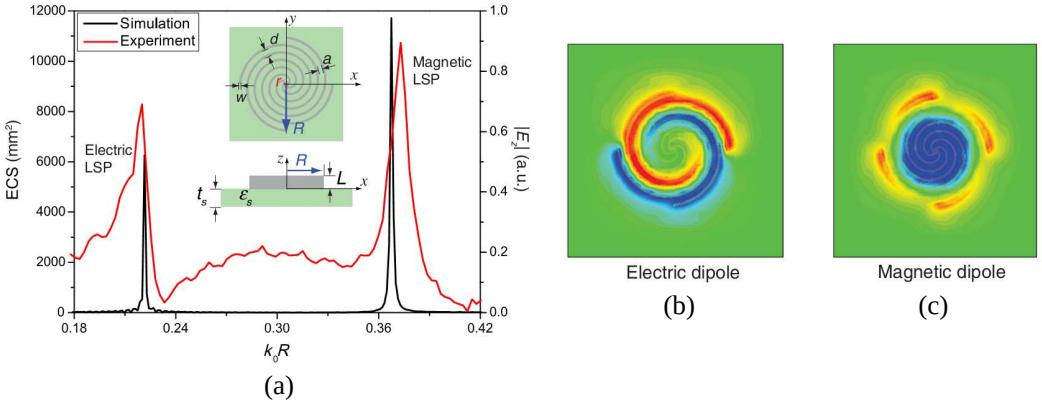

Figure 1: Resonance spectrum for subwavelength ultrathin textured metallic disks.

REFERENCES

1. Pors, E. M., L. Martin-Moreno, J. B. Pendry, and F. J. Garcia-Vidal, "Localized spoof plasmons arise while texturing closed surfaces," *Physical Review Letters*, Vol. 108, 223905, 2012.
2. Huidobro, P. A., X. Shen, J. Cuerda, E. Moreno, L. Martin-Moreno, F. J. Garcia-Vidal, et al., "Magnetic localized surface plasmons," *Physical Review X*, Vol. 4, 021003, 2014.
3. Shen, X. and T. J. Cui, "Ultrathin plasmonic metamaterial for spoof localized surface plasmons," *Laser & Photonics Reviews*, Vol. 8, 137–145, 2014.

Frequency Dependant Microwave Properties of Aramid Paper Based Honeycomb Substrate Impregnated with Carbonaceous Solution

L. Liu, C. Z. Fan, Z. Y. Zhao, G. X. Xu, and R. P. Liu
Kuang-Chi Institute of Advanced Technology
Gaoxin Zhong 1st Road, Nanshan District, Shenzhen 518057, China

Abstract— Composites with sandwich structures have been widely utilized in aircraft and high-speed trains due to their light weight, high specific strength as well as relatively low cost. One of the most useful types of sandwich structures is honeycomb, which contains periodic hexagonal walls normally made of aramid paper and phenolic resin. For electromagnetic composites, honeycomb cores may need to have high dielectric permittivity, as well as high dielectric loss. Applying a lossy polymeric coating on top of honeycomb walls could be a convenient solution. Commonly used fillers include conductive carbon black, magnetic microfiber or magnetic powder with both high dielectric and magnetic properties.

The outstanding properties of carbonaceous nano-particles, like carbon nanotubes (CNT), carbon nanofibers and graphene, were one of the main research focuses in the last decade, which mainly include the remarkable electrical conductivity, mechanical strength and thermal conductivity. Carbonaceous powders are ideal fillers for composites with various applications, for example, electrostatic discharge and electromagnetic interference suppression, as well as electromagnetic wave absorption for indoor anechoic chambers or anti-reflection purposes. In fact, carbonaceous fillers, such as carbon black (CB) and carbon fibers (CF), have been employed for decades to improve the electrical conductivity or to tailor the dielectric dispersion of composite materials. Due to its spherical shape, high concentrated CB is needed to fabricate composites with significantly improved properties, which may compromise their mechanical performance and increase the fabrication cost. Compared with CB or CF, CNTs can be fillers of composites of high permittivity and distinct frequency dispersion at extremely low concentrations. The small diameter and large aspect ratio of CNTs may result in fillers with high permittivity and low percolation ratio, as well as with some distinct properties, like adjustable permittivity under bias electrical field [1–3].

In this paper, a theoretical and experimental study was carried out to measure the effective electromagnetic (EM) permittivity of honeycomb substrates impregnated with carbonaceous particles composites. The effective EM properties were also calculated based on the homogenization and percolation theory. The potential applications of such impregnated honeycomb include microwave devices for waves absorption and noise suppression.

ACKNOWLEDGMENT

I would like to thank the financial support from National High-Tech Projects (863, No. 2012AA030 401), Guangdong Innovative Research Team Program (No. 2009010005), Guangdong Science and Technology Plan (No. 2011A091103003) and Shenzhen Key Laboratory of Transformation Optics and Spatial Modulation (No. CXB201109210100A).

REFERENCES

1. Liu, L., S. Matitsine, Y. Gan, L. Chen, L. B. Kong, and K. Rozanov, *J. Appl. Phys.*, Vol. 101, 094106, 2007.
2. Liu, L., L. B. Kong, and S. Matitsine, *Appl. Phys. Lett.*, Vol. 93, 113106, 2008.
3. Liu, L., Z. H. Yang, L. B. Kong, W. Y. Yin, and S. Wang, *Appl. Phys.*, Vol. 108, 4, 2012.

Slowing Microwaves with Deeply Subwavelength Metamaterial Waveguides

N. Kaina, **M. Fink**, **and G. Lerosey**
Institut Langevin, ESPCI ParisTech, France

Abstract— We study resonant wire media that are scaled at very subwavelength scales. We show that introducing local defects permits to guide the waves with a transverse confinement of the order of one period in any direction, independently of the spatial organization of the medium. We prove that the propagation within these waveguides exhibit a very low group velocities that can be tuned by modifying the geometrical and frequency parameters of the neighboring wires. We present simulation and experimental results.

Slowing down the waves is one stake of time-signal processing, signal energy compressing, wave-matter interaction enhancements and device miniaturization. This can be achieved using strong material dispersion, for example very high index media, or with engineered systems such as photonic crystals waveguides (PCW) or coupled resonator optical waveguides (CROWS). If those are valid solutions for optical signals, photonic crystal based systems become very bulky for microwaves and telecommunication signals. In previous work [1], we demonstrated that is was possible to steer waves at scales independent of the wavelength in a deeply subwavelength wire-medium metamaterial by locally introducing defects whose frequency lie in the hybridization bandgap of the metamaterial. Whithin those waveguides, the wave tunnels from one defect to its neighbour thus providing a very low group velocity propagation as in photonic crystals. Contrarily to PCWs however, our waveguides can have arbitrarily small transverse dimensions, solely limited by the size the wires. The direct consequence is that we can achieve very high δk and hence much lower group velocities $\delta\omega/\delta k$ than in photonic crystals for similar frequency bandwidth.

Here, we investigate the properties of the waveguides in terms of group velocity both in simulations and experiments in media with periodicities up to $\lambda_0/40$. We particularly study the influence of the surrounding medium parameters on the propagation in the waveguide. We show that both the density and the frequency detuning between the wires in the medium and the defects can be adjusted to get the smaller group velocity possible. First simulation results (Fig. 1) show the quasi loss less transmission through $\lambda_0/10$ wide guides, exhibiting a 36 ns delay ($n_g = 135$) which can be further increased. We also show that a similar behaviour occurs in spatially disordered media.

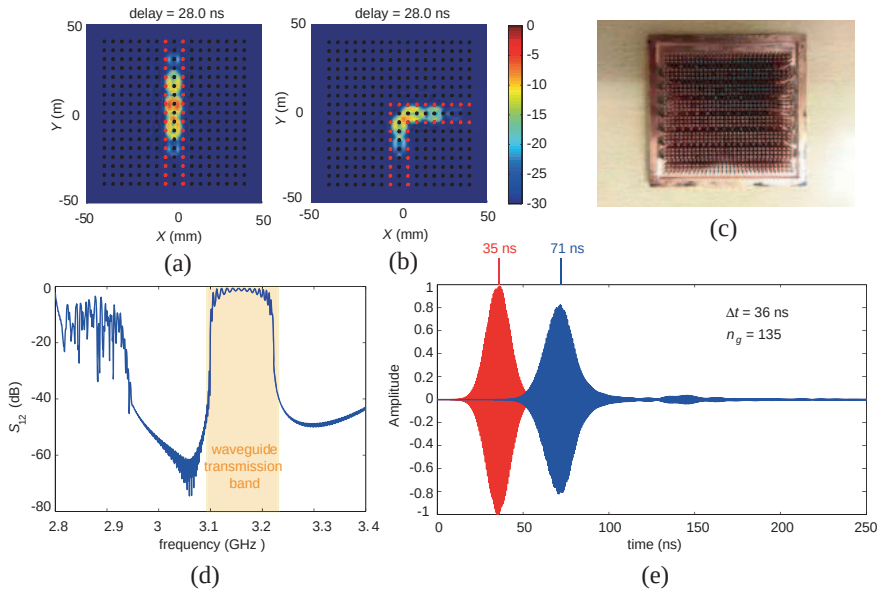

Figure 1: (a), (b) Energy of a pulse propagating in a straight and a 90 deg bended waveguide 28 ns after excitation. (c) 3D printed copper coated sample. (d) Spectral transmission along the straight waveguide (dB). (e) Temporal excitation (red) and guided (blue) signal.

We believe that our deeply subwavelength slow propagation waveguides in the microwave are promising candidates for the miniaturization of delay lines, filters, multiplexers as well as for more fondamental wave-matter enhancement studies.

REFERENCES

1. Lemoult, F., N. Kaina, M. Fink, and G. Lerosey, *Nature Physics*, Vol. 9, 5560, 2013.

Dual-band Hybrid Metacomposites Containing Ferromagnetic Microwire Arrays

Y. Luo[1], **H. X. Peng**[1], **F. X. Qin**[1, 2], **M. Ipatov**[3], **V. Zhukova**[3], **A. Zhukov**[3], **and J. Gonzalez**[3]

[1]Advanced Composite Centre for Innovation and Science, Department of Aerospace Engineering
University of Bristol, University Walk, Bristol, BS8 1TR, UK
[2]1D Nanomaterials Group, National Institute for Material Science
1-2-1 Sengen, Tsukuba, Ibaraki 305-0047, Japan
[3]Departamento de Fisica de Materiales, Facultad de Quimicas
Universidad del Pais Vasco, San Sebastian 20009, Spain

Abstract— Recent years have witnessed the prosperity of the left-hand metamaterials possessing remarkable electromagnetic properties that are unavailable in nature. We have demonstrated that by embedding Fe-based ferromagnetic wire arrays into polymer composites, single-band left-handed features could be achieved [1] accompanied by other merits such as low functional filler concentration [2–4], high mechanical properties [5], and excellent sensing properties [6]. From the application point of view, it is always a challenging task to broaden the double-negative (DNG) operating bandwidth in the metamaterial system. In the present talk, we will introduce a new class of metacomposite containing microwire arrays and pave an effective path to enhance the DNG frequency bandwidth without jeopardizing metamaterial features via the hybridization of Fe-based and Co-based amorphous glass-coated ferromagnetic microwires arrays in the high performance polymer composites. Experimentally, the free space measurement was employed to examine the microwave properties of the metacomposites in the frequency range of 0.9 to 17 GHz with external magnetic bias up to 3000 Oe. We will demonstrate that a transmission window is noted in the frequencies of 1.5 to 5.5 GHz without the assistance of external field associated with the natural ferromagnetic resonance (NFMR) of Fe-based microwires, indicating that DNG characteristics are revealed where no burden magnets is needed to initiate such effect. On the other hand, a high frequency EM wave-induced transparency is realized in the corresponding band of 9 to 17 GHz. Considering the spacing between the Fe-based and Co-based wire array is relatively small (approximately 1 mm), the identified high frequency transmission window can be explained by the long-range dipolar resonance between the microwire arrays [1]. In particular, it indicates that the obtained transmission window is independent of the intrinsic properties of Co-based microwires with/without external field. This is due to the mitigated dynamic coupling between the EM waves and the single Co-based microwire array arisen from the large magnetic loss, rendering that the Co-based wire array purely act as a dielectric component in the composite system. The permittivity spectra showcase that the plasma frequency (f_p) is significantly compensated with the addition of Co-based wire array into the composite. We have proposed a term of effect diameter (a_{eff}) to account for the circumferential domain volume that can interplay with EM waves and basically contribute to the dielectric performance [1, 7]. Hence, this f_p enhancement is arisen from the compensation of the a_{eff} due to the dynamic wire-wire interactions between the Co- and Fe-based wire pairs. Overall, the presented hybrid metacomposites provide essential perspectives in designing and manufacturing the multi-band metamaterial for microwave applications such as sensors and cloaking devices.

REFERENCES

1. Luo, Y., et al., *Appl. Phys. Lett.*, Vol. 103, 251902, 2013.
2. Qin, F. X., et al., *Appl. Phys. Lett.*, Vol. 102, 122903, 2013.
3. Qin, F. X., et al., *Appl. Phys. Lett.*, Vol. 105, 152905, 2012.
4. Qin, F. X., et al., *Appl. Phys. Lett.*, Vol. 99, 252902, 2012.
5. Qin, F. X., et al., *J. Appl. Phys.*, Vol. 107, 09A314, 2010.
6. Qin, F. X. and H. X. Peng, *Prog. Mater. Sci.*, Vol. 58, 183, 2013.
7. Pendry, J. B., et al., *Phys. Rev. Lett.*, Vol. 76, 4773, 1996.

Integrated Circuits Based on Spoof Surface Plasmon Polaritons

Hao Chi Zhang, Xiao Peng Shen, Shuo Liu, and Tie Jun Cui
State Key Laboratory of Millimeter Waves, Southeast University, Nanjing 210096, China

Abstract— In the past decades, spoof surface plasmon polaritons (SPPs), formed on metal surfaces decorated with arrays of subwavelength grooves or holes, have aroused tremendous interests of researchers both in physics and engineering. Various types of plasmonic waveguide supporting spoof SPPs have been reported, including recently proposed conformal surface plasmons (CSPs) consisting of corrugated metal strips printed on a flexible and ultrathin substrate. Owing to the unique features such as good field confinement, deep subwavelength effect, flexibility, and easy fabrication, spoof SPPs may predict promising applications in the low interference transmission and miniaturized microwave circuits. In this work, we present the numerical analyses and experimental realizations of several circuit devices based on the spoof SPPs. Firstly, two different types of plasmonic waveguides, designed by cutting periodic grooves on one side (asymmetric structure) or two sides (symmetric structure) of a metal strip, are introduced and explored. By analyzing their dispersion characteristics and field distributions, we notice that the symmetric structure supports both symmetric and asymmetric eigenmodes and is able to localize the electromagnetic fields in a smaller region than the asymmetric structure. However, since the symmetric structure is more lossy than the asymmetric structure, the latter is mainly adopted in the following designs. Secondly, three different spoof SPP devices are presented: the beam splitter, directional coupler, and ring resonator. The commercial software, CST Microwave Studio, is employed for the full-wave simulations of the realistic three-dimensional model of such devices. All these devices show similar functions to the conventional microwave devices implemented with microstrip lines, whereas exhibit better performance in certain aspects such as highly field localization. Finally, an integrated spoof SPPs circuit combining the above three separated devices is realized by dividing the input electromagnetic wave into two beams and then separately lead to a ring resonator and a directional coupler, respectively. Good agreement is clearly observed from the simulations and experiments. This work has paved the way for the implementation of spoof-SPPs-based integrated circuits.

Measurement of Enhanced Radiation Force on a Parallel Metallic-plate System in the Microwave Regime

Z. H. Hang[1, 2], Z. Marcet[2, 3], S. B. Wang[2], C. T. Chan[2], and H. B. Chan[2]

[1]School of Physical Science and Technology, Soochow University
1 Shizi Street, Suzhou 215006, China
[2]Department of Physics and William Mong Institute of Nano Science and Technology
The Hong Kong University of Science and Technology
Clear Water Bay, Kowloon, Hong Kong, China
[3]Department of Physics, University of Florida, Gainesville, Florida 32611, USA

Abstract— Artificial electromagnetic resonating material, also known as metamaterials have successfully been used to demonstrate various interesting wave guiding properties, including negative refraction, super-imaging, cloaking et al. at a broad frequency range from optics to microwave. In addition, the use of laser paved the path to non-contact particle manipulation by light induced forces, which leads to various applications in physics, chemistry and biology. Here, we show that the measured force exerted by microwave radiation on a centimeter-sized parallel-plate metallic resonant unit can be orders larger than the conventional radiation force [1]. Accompanying the excitation of microwave resonance as well as the microwave induced force, thermal effect due to Ohm loss is evitable and could lead to some photothermal effect. By varying the ambient environment, we distinguish carefully between the direct radiation force and the indirect photothermal component. At the microwave resonance, the former is measured quantitatively to be 100 times larger than the conventional radiation force. Furthermore, the observed radiation force has opposite direction to that of the incident radiation. Both the direction and the magnitude of the measured force agree well with numerical calculations. Our technique of differential capacitance shall be useful for radiation induced force characterization to other frequency range.

REFERENCES

1. Marcet, Z., Z. H. Hang, S. B. Wang, J. Ng, C. T. Chan, and H. B. Chan, "Measurement of enhanced radiation force on a parallel metallic-plate system in the microwave regime," *Phys. Rev. Lett.*, Vol. 112, 045504, 2014.

Session 3A6
FocusSession.SC3: Laser Spectroscopy for Sensing and Environmental Monitoring 1

Laser Remote Sensing for Environmental Monitoring — From Scandinavia to China

Zuguang Guan
Sailhero Environmental Technology Co., Ltd., No. 251 Xiangjiang Road, Shijiazhuang 050035, China

Abstract—

Introduction: Environmental problems have different appearances in different areas of the world but usually induce equally great public concerns. In megacities in developing counties like China, where the industries are blooming, it is highly possible to expose to local hazardous air quality, polluted water and soil. While on Scandinavia peninsula, Nordic people are more nervous to global issues since local pollutions have been fairly well controlled. Carbon budget and global warming, aerosol transport and climate effect, etc., are therefore hot topics in Nordic to both governmental environmental protection agencies (EPAs) and research institutes.

Despite of different measurement focuses, optical methods, for their highly sensitive and noninvasive advantages, are commonly selected by EPAs in different counties as regular instruments. Laser remote sensing techniques, with large-scale coverage, 3D scanning and range resolved capabilities, are especially useful for those environmental applications requiring global-scale considerations. This talk, based on the author's experiences in Nordic and China, reviews different optical detection and remote sensing techniques, and their usage in environmental monitoring.

Environmental Issues: Environmental issues are real modern problems ranging from local industrial pollution to global climate change. For instance excessive anthropogenic emissions have significantly modified the concentrations and distributions of aerosols and trace gases in the earth atmosphere, which is essential to support life. The abnormalities originate at urban area and distribute globally. They are usually harmful to human beings and the natural environment. For example, Sulfur dioxide (SO_2) from coal combustion and nitrogen oxide (NO_x) from traffic are both acid gases and will further pollute water and soil by washout. Another traffic pollutant, carbon monoxide (CO), from exhaust of internal combustion engines, is extremely poisonous to organism. A side product generated from the reaction between Nitric oxide (NO) and Nitrogen dioxide (NO_2) is ground ozone (O_3), which is toxic to agriculture; meanwhile the O_3 layer in the stratosphere is being consumed and holes appear in Antarctic and even Arctic recently. The above four pollutants are regularly measured by EPAs world widely, including in Scandinavia and China, to evaluate the ambient air quality index. Carbon dioxide (CO_2) and methane (CH_4) are non-toxic; however, through green house effect they induce global warming which is attracting more and more public attentions, especially in Nordic countries where the social environmental responsibility is attached higher importance. Another atmospheric pollutant, aerosol, defined as fine particles suspended in gases, is abundantly produced by combustions or industries. Fine particles can exist in the atmosphere long and accumulate in human alveolar through breath. The aerosol pollution makes haze phenomenon in most Chinese cities more and more often. Sufficient public awareness for environmental protection has thus been awaked. Aerosols affect global climate through green house effect meanwhile blocking the energy from the sun radiation. Due to their varied sources and distributions, the net effect is difficult to predict, and thus still attracting much research interests. PM_{10} and $PM_{2.5}$, indicating particulate matters with aerodynamic diameter less than 10 and 2.5 micrometer respectively, are two regular measurands at EPAs.

Optical Detection: Quantitative monitoring is the first step to know the environment and offers possibilities for further control and improvement. Optical methods are natural for environmental monitoring since human being observes the world firstly by vision. Suspended dusts in the air become visible when a ray of sunlight enters a dark room. The same physics, i.e., light scattering, is used in a modern nephelometer or laser particle counter for aerosol detection [1, 2]. In early 19 century, scientists had started the study on sun atmosphere, by finding the existence of dark lines in the solar spectrum. The technology, now called (atomic/molecular) absorption spectroscopy, has been broadly employed for trace gas detection [3, 4]. Regardless for an O_3 meter simply measuring the direct absorbance in UV, or for a CO analyzer applying the more advanced gas filter correlation (GFC) technique, the gas induced absorption in a certain optical path length is used to quantify the gas concentration according to the Beer-Lambert law. A more complex physical phenomenon, fluorescence, is well known for its application in security print on, e.g., identification documents. It can actually reveal the existence of certain trace gases in a very

sensitive way. The low concentration of SO_2 in ambient air can be analyzed in such a method. All the above mentioned optical instruments have been completely commercialized and adopted by most EPAs in the world into their measurement standards [5].

Laser Remote Sensing: Optical methods have instinct noncontact property, and can realize remote sensing applications. In environmental monitoring, remote sensing technology has obvious advantages since in measurement no complicated sampling is required and large space scale can be covered. For instance, a technique called gas-correlation imaging [6] principally applies the GFC technique in front of IR camera(s). Employing the background thermal radiation, the camera can thus see the explosive gas leakage inducing differential absorptions in certain pixels. To watch a full scene in situ and real time is a unique advantage of such a gas camera comparing with normal point sampling instruments. The technique was initialized at Lund University in Sweden and prototypes were commercialized and installed at Statoil Norway who is also an investor of the project. Differential optical absorption spectroscopy (DOAS) [7] is another type of optical remote sensing which usually employs long measurement path length up to kilometers. By properly setting the white light source and the spectrum analyzer, the optical path can cross an entire urban area where multiple pollutants can be measured simultaneously. A Swedish company Opsis AB was generated through spin-off from Lund decades ago and now is a world leader in DOAS techniques.

The invention of laser revolutionized the field of optical remote sensing for its high degree of spatial/temporal coherence and short-pulsed emission. The first ruby laser (invented in 1960) has already been in 1962 applied in a technology called light detection and ranging (lidar), also known as laser radar. By counting the delay between the emitted laser pulses and the backscattered photons, the range information is determined. In the past half century, lidar technology has experienced significant improvement and has been developed into an advanced tool for the environmental monitoring especially for the atmospheric study. Lidar extremely extends the capability of traditional optical environmental instruments into much higher and wider space. Normal aerosol lidars [8] can usually cover the troposphere ($<$ ca. 10 km), the most inner atmosphere layer where contains 80% of air mass and most weather activities. The advanced RMR lidar [9] at ALOMAR observatory in Northern Norway can measure until 80 km and observe noctilucent cloud there besides quantifying atmospheric temperature and wind speed in a spatial resolution of 7.5 m. Differential absorption lidar (dial) maps out the distribution of trace gases in scale of kilometers by 3D scanning or gives the concentration profile (of e.g., O_3 layer in the stratosphere) by vertical sounding [10]. By analyzing the laser induced fluorescence, lidar can also study remote targets, including trace gases, in molecular/atomic level [11]. One extreme example is the state-of-the-art resonance fluorescence lidar [12] at ALOMAR, measuring the sodium layer (ca. 90 km) in mesosphere, where meteors burn up.

Conclusion: Laser remote sensing not only offers possibilities of long term continues measurements in some extreme occasions where in-situ equipment meets difficulties, but also provides full temporal and spatial information in a global-scale measurement. It is still cutting-edge technology in many environmental applications, which however indicate a development trend of modern instruments.

REFERENCES

1. Muller, T., M. Laborde, G. Kassell, and A. Wiedensohler, *Atmospheric Measurement Techniques*, Vol. 4, 1291–1303, 2011.
2. Guan, Z. G., M. Gausa, S. Blinheim, and A. Danielsen, *Proceeding of 26th ILRC*, Vol. S1P-01, 77–80, 2012.
3. Guan, Z. G., M. Lewander, and S. Svanberg, *Optics Express*, Vol. 16, 21714–21720, 2008.
4. Lewander, M., Z. G. Guan, L. Persson, A. Olsson, and S. Svanberg, *Applied Physics B*, Vol. 93, 619–625, 2008.
5. U.S. EPA, *List of Designated Reference and Equivalent Methods*, 2012.
6. Sandsten, J., P. Weibring, H. Edner, and S. Svanberg, *Optics Express*, Vol. 6, 92–103, 2000.
7. Edner, H., P. Ragnarson, S. Spannare, and S. Svanberg, *Applied Optics*, Vol. 32, 327–333, 1993.
8. Lundin, P., Z. G. Guan, L. Mei, G. Somesfalean, E. Swietlicki, and S. Svanberg, *Proceeding of 25th ILRC*, Vol. S4P-50, 663–666, 2010.
9. Von Zahn, U., G. von Cossart, et al., *Annales Geophysicae*, Vol. 18, 815–833, 2000.
10. Guan, Z. G., P. Lundin, L. Mei, G. Somesfalean, and S. Svaberg, *Applied Physics B*, Vol. 101, 465–470, 2010.
11. Guan, Z. G., M. Brydegaard, et al., *Applied Optics*, Vol. 49, 5133–5142, 2010.
12. Chu, X. and G. C. Papen, *Laser Remote Sensing*, Chap. 5, 179–432, CRC, 2005.

LED Mini-lidar and Its Applications

Tatsuo Shiina
Graduate School of Advanced Integration Science, Chiba Unibersity, Japan

Abstract— Lidar technologies have expanded in 50 years thanks to laser developments and adequate optical methods for each atmospheric target. On contrary, lidar is not a popular device because installation fields are restricted. Military use, atmospheric monitoring for study, and crisis detection in airport, where is no other way except for lidar, are lidar installation fields.

Lidar has potential to become an essential sensor in dairy human life. The main problem to block it is fragility of laser and especially its optical arraignment with high precision. Another task is its safety in human activity. There are a lot of efforts to get the lidar techniques to be easy-to-use. They are MPL (Micro Pulse Lidar), LD-lidar, and Eye-safe lidar, etc..

In this study, LED lidar is introduced. LED lamp becomes a light source of lidar. It is not a special lamp. It is for small sign and illumination use. In this study, the LED lamp is pulsed with a pulse width of 10 ns. It can emit light energy of > 100 mW ($= 1$ nJ/10 ns). The average power is less than 1 mW. The key point is pulse repetition frequency. It is increased up to 1 MHz. LED light is weak, but the enough signal-to-noise ratio is kept in the observation range of a few hundred meters by the high repetition frequency. To catch the high repetition signals, the original high-speed photon counter is developed.

The LED mini-lidar becomes compact, lightweight, and low power consumption, that it, the whole system becomes handy. At first, LED mini-lidar was designed for student education purpose. Its applications, however, start to expand in various fields. They are not only to monitor the near range atmosphere, but also to detect dust, gas, and movable target. Now, its applications have been realized with concrete demands.

Lidar Monitoring of Atmospheric Atomic Mercury and Sulfur Dioxide in Guangzhou, China

Guangyu Zhao[1], **Xiuxiang Wu**[1], **Ming Lian**[1], **and Sune Svanberg**[1, 2]

[1]Center for Optics and Electromagnetic Research
South Normal China University City Campus, Guangzhou 51006, China
[2]Department of Physics, Lund University, Lund SE-221 00, Sweden

Abstract— A Differential Absorption Lidar (DIAL) system based on a dye laser pumped by a 20 Hz Nd:YAG laser was constructed and used for range-resolved atomic mercury and sulfur dioxide monitoring. These gases are both severe pollutants in China, and there is a considerable interest to map such gases. DIAL is a powerful technique for such purposes [1]. Measurements were performed from a fixed laboratory, with the eye-safe laser beam pointing upwards at a slant angle, to assess the vertical distribution of the gases. In particular, the influence of weather conditions (temperature and rainfall) was studied during prolonged measurement sequences. A first version of our lidar system, constructed with a 30 cm diameter receiving telescope, is described in [2], where also initial studies of atomic mercury (the only air pollutant present in atomic form) are reported. The mercury absorption line at 253.729 nm (vacuum) is quite narrow, putting stringent requirements on the laser transmitter. We have now studied prominent wash-out effects on mercury due to rainfall. Some results for mercury are given in Fig. 1(a). Mercury concentrations are also sensitive to temperature, especially in industrial areas with deposited mercury, since the metal is very volatile. Generally speaking, the concentration of mercury falls off with increasing altitude, also related to mercury being a heavy atom. For sulfur dioxide with a peak absorption at 300.03 nm, longer measurement ranges, up to 3 km, are possible, related to reduced atmospheric scattering and higher available output pulse energies. Compared to mercury, sulfur dioxide measurements are less demanding due to broader absorptive features. Quite high concentrations measured in Guangzhou, were observed to fall drastically at rainfall due to wash-out; acid rain formation. Some raw DIAL data are shown in Fig. 1(b). Our lidar system is now being integrated into a fully mobile facility, capable to be deployed into the field for remote sensing measurements in the atmospheric, aquatic, agricultural and cultural heritage sectors. Besides DIAL, fluorescence and Raman lidar, as well as remote laser-induced break-down spectroscopy (LIBS) lidar studies will be pursued.

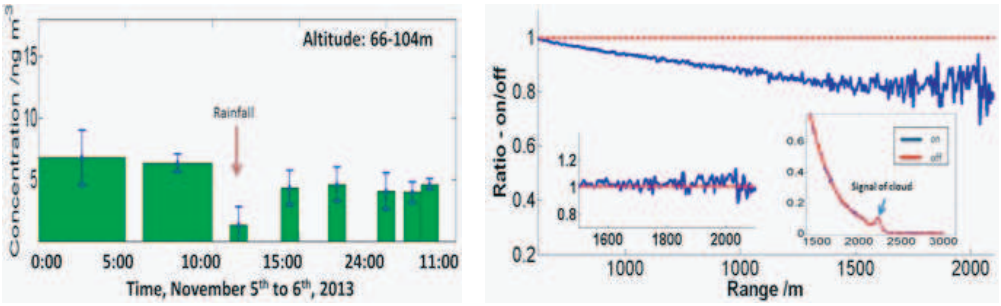

(a) (b)

Figure 1: (a) Mercury wash-out effects. (b) SO_2.

REFERENCES

1. Svanberg, S., "LIDAR," *Springer Handbook of Lasers and Optics*, F. Träger, Ed., 1031–1052, Springer, Heidelberg, 2007.
2. Mei, L., G. Y. Zhao, and S. Svanberg, "Differential absorption lidar system employed for background atomic mercury vertical profiling in South China," *Opt. Lasers Eng.*, Vol. 55, 128, 2014.

Ultraviolet Plasma Grating Triggered Enhancement of Filament-induced Remotely Nonlinear Spectroscopy

Heping Zeng
State Key Laboratory of Precision Spectroscopy, East China Normal University, Shanghai 200062, China

Abstract— Due to the higher multi-photon ionization rate and lower electron temperature inside the ultraviolet filaments, its potential application in remotely nonlinear fluorescence spectroscopy is proposed. The method of ultraviolet plasma grating plus infrared dual-color filamentation in mixed gaseous media was introduced to enhance the plasma fluorescence intensity and signal-to-noise ratio. A semi-classical three-step-excitation model was verified by the fluorescence emission from the impact excitation of high potential atoms such as neon and helium. Firstly, the interference between two nearly-parallel 267-nm ultraviolet filamentary pulses produced periodic wavelength-scale plasma channels surrounding with air molecules. Such a periodic refractive index modulation functioned as effective plasma gratings that supported efficient Bragg diffraction of probe laser pulses. As a result of the nonlinear interaction between ultraviolet filaments, enhanced ionization was produced, which launched waveguide walls for laser beams to suppress their divergence, resulting in a dramatic increase of the ionization rate. Secondly, a subsequent intense infrared pulse was tightly coupled and guided into the preformed plasma channels through nonlinear Bragg diffraction, where the well-confined free electrons were driven by the laser electric field along its polarization direction. A host of free electrons were further peeled through these energetic electrons collision ionization. As a result, the local electron density was enhanced up to $2 \times 10^{19}\,\mathrm{cm}^{-3}$, and electron acceleration therein triggered inelastic collisional ionization. Enhanced impact ionization was observed as electrons were driven to collide with nearby atoms or molecules other than their parent cores. Electron acceleration and impact ionization were well-confined in filamentary plasma gratings. Thirdly, some neutral neon or helium atoms in excited states approaching ionization potential were kicked into ionic states through the collisions of these hot electrons, facilitating the impact ionization of neon atoms. Consequently, more high-lying excited states were populated through ion conversion and dissociative recombination. Such a fluorescence enhancement method may benefit in the laser spectroscopy for remote pollutant monitoring.

REFERENCES

1. Shi, L., et al., *Phys. Rev. Lett.*, Vol. 107, 095004, 2011.
2. Yang, X., et al., *Opt. Lett.*, Vol. 34, 3806, 2009.
3. Yang, X., et al., *Appl. Phys. Lett.*, Vol. 95, 111103, 2009.
4. Yang, X., et al., *Appl. Phys. Lett.*, Vol. 98, 111103, 2011.
5. Yang, X., et al., *CLEO 2008*, CTuE6, 2008.

Femtosecond Laser Filamentation for Remote Sensing

Huailiang Xu
State Key Laboratory on Integrated Optoelectronics
College of Electronic Science and Engineering, Jilin University, Changchun 130012, China

Abstract— The ability to measure atmospheric species and control weather conditions over a long distance is of essential importance in dealing with a variety of environment issues from global warming, rainfall or snowfall and stratospheric ozone depletion to early-warning of biological and nuclear power plant's leak that threatens public and defense security. Recent studies demonstrated that femtosecond laser pulses have high potential in application to atmospheric science. Because of the properties of ultrafast, broadband and high power the propagation of femtosecond laser pulses in the atmosphere leads to a unique nonlinear optical phenomenon of "filamentation", which can result in a constant high field of $\sim 10^{13}$–10^{14} W/cm^2 (intensity clamping) and a broad supercontinuum spectrum from UV to infrared at a distance as far as a few kilometers. This enriches remote spectroscopy techniques and promotes new challenges for atmospheric applications.

The high clamped intensity inside the filament core can induce in all matters in the path of filaments ionization and fragmentation, resulting in characteristic optical emissions from the excited fragments, which could be used for identifying the substances. In this talk, the feasibility of femtosecond laser pulses for remote sensing will be first introduced by demonstrating "clean" spectra from various targets ranging from gases, aerosols to solids [1]. This will be followed by the introduction of several newly developed methods for coherent control of the fingerprint emissions of molecules [2–6]. Finally, the underlying mechanisms responsible for the characteristic emissions of molecules in intense laser fields are discussed based on the understanding of strong-field-molecule interaction in atmospheric as well as in vacuum environments [7–9].

REFERENCES

1. Xu, H. L. and S. L. Chin, *Sensors*, Vol. 11, 32, 2011.
2. Xu, H. L., A. Azarm, S. L. Chin, *Appl. Phys. Lett.*, Vol. 98, 141111, 2011.
3. Yao, J. P., B. Zeng, H. L. Xu, et al., *Phys. Rev. A*, Vol. 84, 051802(R), 2011.
4. Chu, W., B. Zeng, J. P. Yao, et al., *EPL*, Vol. 97, 64004, 2012.
5. Zhang, H., C. Jing, J. Yao, et al., *Phys. Rev. X*, Vol. 3, 041009, 2013.
6. Chu, W., H. L. Li, J. Ni, et al., *Appl. Phys. Lett.*, Vol. 104, 091106, 2014.
7. Jing, C., H. Zhang, W. Chu, et al., *Opt. Express*, Vol. 22, 3151, 2014.
8. Ni, J., W. Chu, H. Zhang, et al., *Opt. Express*, Vol. 20, 20970–20979, 2012.
9. Yao, J. P., G. H. Li, C. R. Jing, et al., *New J. Phys.*, Vol. 15, 023046, 2013.

Mid-IR Laser-spectroscopic Sensing of Gases

Markus W. Sigrist
ETH Zürich, Switzerland

Abstract— Laser-based gas sensing offers high sensitivity and specificity, large dynamic range, multi-component capability, and lack of pretreatment or preconcentration. The availability of broadly tunable sources like difference frequency generation (DFG) and external cavity quantum cascade lasers (EC-QCLs) or the most recent development of diode-pumped lead salt vertical external cavity surface emitting lasers (VECSELs) has certainly eased the implementation of laser-based sensing devices. I shall discuss the setups and performance of two systems developed and implemented in our laboratory in more detail.

The first example concerns the analysis of surgical smoke that is produced during minimal-invasive surgery with an electro-knife in the University hospital in Zurich. There is a controversial discussion going on whether or not this smoke contains compounds that could be hazardous for the medical personnel and/or the patient. We collected gas samples during the course of several operations and recorded infrared spectra with a broadly tunable DFG system in our laboratory. The spectral analysis was then performed with a principal component analysis [1]. Besides water vapor, mainly traces of methane, ethane, ethylene, CO and the anesthetic gas sevoflurane were found in varying concentrations. With the exception of sevoflurane, concentrations were below recommended exposure limits.

A second example concerns first measurements with a novel lead-salt VECSEL [2]. The VECSEL is pumped with a near-IR diode laser and tuning is performed by simply applying a voltage ramp (0 to 100 V) on the VECSEL piezo element. The main features are a broad and fast tuning (e.g., between 2950 cm^{-1} and 3100 cm^{-1} within 2 s). This wavelength range is of special interest in petrochemical industry and other areas for monitoring, e.g., C1 to C4 alkanes (i.e., methane, ethane, propane and butanes) in gas mixtures. With this laser source and a simple multipass absorption cell we achieved sub-ppm detection limits for all these hydrocarbons in mixtures even in the presence of a high water vapor content.

REFERENCES

1. Gianella, M. and M. W. Sigrist, "Chemical analysis of surgical smoke by infrared laser spectroscopy," *Appl. Phys. B*, Vol. 109, 485–496, 2012.
2. Fill, M., P. Debernardi, F. Felder, and H. Zogg, "Lead-chalcogenide mid-infrared vertical external cavity surface emitting lasers with improved threshold: Theory and experiment," *Appl. Phys. Lett.*, Vol. 103, 201120, 2013.

Photonic Monitoring of NO_3, N_2O_5 and NO_2 in VOC Oxidation Process by Long Optical Pathlength Absorption Spectroscopy

Hongming Yi[1, 2], Tao Wu[3], Amélie Lauraguais[1], Vladimir Semenov[4], Cecile Coeur-Tourneur[1], Eric Fertein[1], Xiaoming Gao[2], and Weidong Chen[1]

[1]Université du Littoral Côte d'Opale, France
[2]Anhui Institute of Optics and Fine Mechanics, China
[3]Nanchang Hangkong University, China
[4]General Physics Institute, Russia

Abstract— Nitrate radical (NO_3) and dinitrogen pentoxide (N_2O_5, formed through the reaction of NO_3 with NO_2 and is a large reservoir for NO_3) are two key intermediates components in atmospheric nitrogen chemistry [1]. They affect directly the oxidation capacity of the atmosphere through reaction of NO_3 with volatile organic compounds (VOCs). It's highly desirable to be able to perform in situ, simultaneous and continuous monitoring of NO_3 and N_2O_5 concentrations with high selectivity and fast response time. N_2O_5 is usually indirectly measured via optical measurement of NO_3 after thermal dissociation of N_2O_5 to NO_3 [2]. In this paper, we report on the recent development and application of optical method for in situ direct concentration measurements of NO_3 and N_2O_5 in smog chamber. NO_3 (as well as NO_2) were simultaneously measured by open-path incoherent broadband cavity enhanced absorption spectroscopy (IBBCEAS) [3] based on a light emitted diode operating in the range of 635–675 nm, and N_2O_5 was monitored by means of open-path multi-pass absorption spectroscopy of an external cavity quantum cascade laser tunable from 1223 to 1263 cm^{-1} ($\sim 8\,\mu m$). Reaction of NO_3 with VOCs (such as isoprene, formaldehyde, 2-methoxyphenal) as well as the equilibrium between NO_3 and N_2O_5 during the VOCs oxidation by NO_3 radical have been on-line traced with high temporal resolution: 1 s for NO_3-NO_2 and 25 s for N_2O_5. Experimental detail and preliminary results will be presented. Our present work demonstrated that modern photonic technologies can provide a direct and highly selective analytical tool for chemical kinetic study, for instance, bringing insight into reactive uptake for NO_3 and N_2O_5 on the organic particles [4], which remain still unexplored with few exceptions.

ACKNOWLEDGMENT

This work is mainly supported by the IRENI program of the Région Nord-Pas de Calais. The financial supports from the French national research agency (ANR) under the NexCILAS (ANR-11-NS09-0002) and the CaPPA (ANR-10-LABX-005) contracts are acknowledged.

REFERENCES

1. Monks, P. S., "Gas-phase radical chemistry in the troposphere," *Chem. Soc. Rev.*, Vol. 34, 376–395, 2005.
2. Varma, R. M., S. M. Ball, T. Brauers, H.-P. Dorn, U. Heitmann, R. L. Jones, U. Platt, D. Pöhler, A. A. Ruth, A. J. L. Shillings, J. Thieser, A. Wahner, and D. S. Venables, "Light extinction by Secondary Organic Aerosol: An intercomparison of three broadband cavity spectrometers," *Atmos. Meas. Tech. Discuss.*, Vol. 6, 6685–6727, 2013.
3. Wu, T., C. Coeur-Turneur, G. Dhont, A. Cassez, E. Fertein, X. He, and W. Chen, "Simultaneous monitoring of temporal profiles of NO_3, NO_2 and O_3 by IBBCEAS for atmospheric applications," *J. Quant. Spectrosc. Radiat. Transfer*, Vol. 133, 199–205, 2013.
4. Brown, S., T. Ryerson, A. Wollny, C. Brock, R. Peltier, A. Sullivan, R. Weber, W. Dubé, M. Trainer, J. Meagher, F. Fehsenfeld, and A. Ravishankara, "Variability in nocturnal nitrogen oxide processing and its role in regional air quality," *Science*, Vol. 311, 67–70, 2006.

Spectral Reference Data for Environmental Monitoring

M. Vainio[1, 2], **J. Peltola**[1, 2], **T. Fordell**[1],
T. Hieta[1], **M. Merimaa**[1], **and L. Halonen**[2]

[1]Centre for Metrology and Accreditation, P. O. Box 9, FIN-02151 Espoo, Finland
[2]Laboratory of Physical Chemistry, Department of Chemistry
University of Helsinki, P. O. Box 55, FIN-00014, Finland

Abstract— Trace gas detection by laser absorption spectroscopy is an important tool in, e.g., environmental and atmospheric monitoring. The usefulness of trace gas detection in these applications often relies on the use of spectroscopic databases, such as HITRAN [1]. These databases list absorption line parameters, including line strength, center frequency, width, and line broadening coefficients for several molecular species and isotopologies. Using the listed parameters it is possible to simulate molecular absorption spectra, which helps to find the optimum spectral region for spectroscopic detection of a given molecular species. The simulations are essential for data retrieval, which is based on fitting of the simulated spectra to the measured absorption spectrum. The measurement accuracy in trace gas analysis therefore directly depends on the quality of spectroscopic data in the databases, and severe errors can result from inaccuracy of such data [2].

In our conference contribution, we report on our recent activities that aim to improve the accuracy of spectroscopic databases by developing traceable methods for the measurement of molecular absorption line parameters [3]. We focus on accurate measurements of center frequencies, pressure shifts, and profiles of absorption lines in the mid-infrared region. Our new method for such measurements is based on a continuous-wave optical parameter oscillator (cw OPO), which can be used for high resolution spectroscopy between 3 and 4 µm mid-infrared wavelengths [4]. This is one of the most important spectral regions for trace gas detection applications. The frequency of the mid-infrared (idler) beam of the cw OPO is referenced to the SI second via a fully stabilized optical frequency comb. Absolute-frequency spectroscopy of methane (CH_4) with sub-Doppler resolution is reported as an example. The use of cavity-ring-down spectroscopy also makes it possible to accurately measure the strengths of the molecular absorption lines under study.

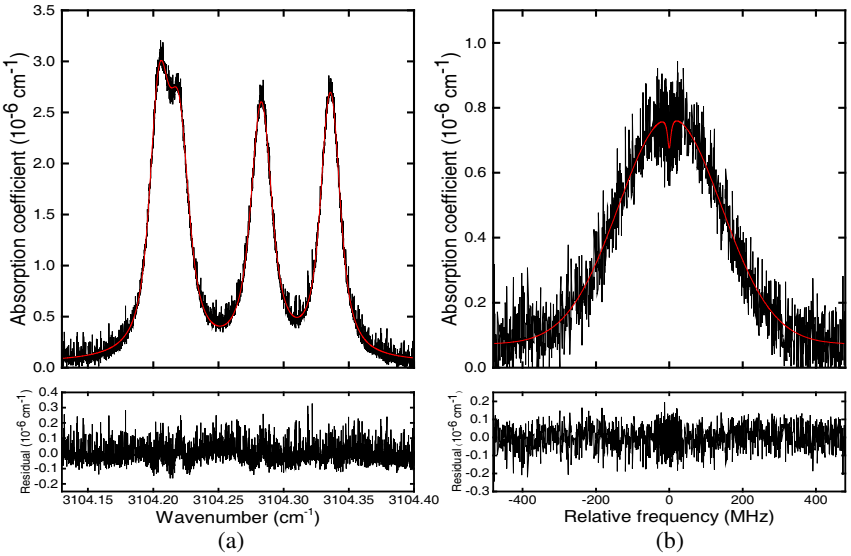

Figure 1: Examples of high-accuracy spectra of CH_4. (a) The $F_2^{(2)}$, $E^{(2)}$, $F_1^{(2)}$ and $F_2^{(1)}$ components of the R(8) transition in 50 mbar pressure. (b) Lamb dip of the $F_1^{(2)}$ component in 1 mbar pressure, demonstrating the sub-Doppler resolution of the frequency-comb referenced cavity-ring-down spectrometer.

REFERENCES

1. Rothman, L. S., et al., "The HITRAN 2012 molecular spectroscopic database," *JQSRT*, Vol. 130, 4–50, 2013.
2. Frankenberg, C., et al., "Tropical methane emissions: A revised view from SCIAMACHY onboard ENVISAT," *Geophys. Res. Lett.*, Vol. 35, L15811, 2008.
3. This work is part of European Metrology Research Programme (EMRP) Joint Research Project (JRP), "Spectral reference data for atmospheric monitoring," *EUMETRISPEC*, http://www.eumetrispec.org. The research was carried out with funding by EURAMET and the European Union. The EMRP is jointly funded by the EMRP participating countries within EURAMET and the European Union.
4. Vainio, M., M. Merimaa, and L. Halonen, "Frequency-comb-referenced molecular spectroscopy in the mid-infrared region," *Opt. Lett.*, Vol. 36, 4122, 2011.

Pathlength Evaluation and Gas Concentration Measurements in Porous Scattering Media

Liang Mei[1], **Gabriel Somesfalean**[1], **and Sune Svanberg**[1, 2]

[1]Atomic Physics Division, Lund University, P. O. Box 118, Lund SE-22100, Sweden
[2]Center for Optical and Electromagnetic Research
South China Normal University, Guangzhou 510006, China

Abstract— Gas monitoring in porous scattering media such as food packages, certain human tissues and ceramics has been developed during the last ten years. The technique to measure enclosed gas concentration in scattering media, is referred to as gas in scattering media absorption spectroscopy (GASMAS), which is a variety of tunable diode laser absorption spectroscopy (TDLAS). By employing wavelength modulation techniques, the very weak absorption imprint superimposed on the transmitted light signal can be detected for gas concentration analysis.

The challenge of measuring the gas concentration in scattering media is that the gas absorption pathlength is unknown due to heavy light scattering, which prevents successful concentration evaluation through the Beer-Lambert law. There are generally a few methods which can, to some extent, retrieve the gas concentration from scattering media. The first approach is to simultaneously measure another gas with known concentration, e.g., H_2O, the saturated concentration of which only depends upon temperature. The absorption pathlength of H_2O is obtained and used for the target gas (e.g., oxygen) to retrieve its concentration. The second approach is to measure the total pathlength, i.e., mean optical pathlength or physical pathlength, with other methods. An average concentration can be obtained by using the total pathlength as the gas absorption pathlength. This method provides the possibility to measure gas concentrations, especially in media with very high porosity or with few large cavities surrounded by a scattering medium, e.g., in food packages. The third method is to analyze the gas absorption line shape of another gas, which depends upon the concentration of buffer gases due to intermolecular collisions. Thus, the concentration of the target gas can be obtained without knowing its absorption pathlength. All these methods open up new, multi-disciplinary applications of the GASMAS technique.

REFERENCES

1. Mei, L., G. Somesfalean, and S. Svanberg, "Pathlength determination for gas in scattering media absorption spectroscopy," *Sensors*, Vol. 14, 3871–3890, 2014.

Development of Advanced Laser-based Concepts for Diagnostic Challenges in Combustion Research

Joakim Bood
Department of Physics, Combustion Physics, Lund University, Lund, Sweden

Abstract— Laser-diagnostic techniques have for more than thirty years added very valuable input for a deepened understanding of combustion processes. Although substantial progress in laser-based combustion diagnostics during this period, a number of difficult challenges remain, especially for diagnostics in practical combustion devices. The present talk will focus on a few major challenges; namely limited optical access, large probe volumes, quantification of species concentrations from laser-induced fluorescence (LIF), and imaging of non-fluorescing species. Our group has developed measurement concepts based on short (picosecond) laser pulses to deal with the first three of these issues. Performing light detection and ranging with picosecond pulses (ps-LIDAR) provides probing of large volumes with high spatial resolution. Thus, being a single-ended technique, ps-LIDAR is an attractive tool for diagnostics in full-scale power plants. The next challenge to be addressed regards quantification of LIF measurements. The difficulty in accounting for radiationless relaxation of the excited species through collisions with other molecules/atoms, i.e., quenching, is the major reason why quantitative data are still rarely extracted from LIF measurements. However, quenching rate constants can be determined by measuring fluorescence lifetimes. Here, a novel method for two-dimensional fluorescence lifetime imaging will be presented. Finally, although many combustion species are detectable using various laser techniques, there are still several important species which have been difficult to measure using these techniques. Our group has developed a technique based on photofragmentation laser-induced fluorescence (PF-LIF) for imaging of molecules having only weakly or non-fluorescing excited states. Using this method, two-dimensional visualization of hydrogen peroxides in a flame has been demonstrated for the first time. Furthermore, quantitative results from PF-LIF measurements of H_2O_2 in an internal combustion engine will be presented. At the end of the presentation possibilities for high-speed visualization, 3-dimensional imaging, and the potential to visualize species requiring multi-photon excitation will be highlighted.

Multimode Diode Laser Correlation Spectroscopy Using Off-axis Cavity Enhancement Techniques

Xiutao Lou and Dongcheng Wu
Department of Physics, Harbin Institute of Technology, Harbin 150001, China

Abstract— Tunable diode laser absorption spectroscopy, TDLAS, has proven to be an effective tool for gas sensing because of its high sensitivity, high specificity, and high speed. In TDLAS, single longitudinal mode operation is an essential requirement for spectroscopic analysis. Recently, light sources with well-behaved multi-wavelength emissions have been used for gas detection such as broadband frequency combs, multi-wavelength laser, multimode laser, displaying a large potential for multi-gas sensing. An alternative TDLAS-based approach for gas detection has been developed by using cheap Fabry-Pérot type multimode diode lasers in combination with correlation spectroscopy. In our previous work, the technique, multimode diode laser correlation spectroscopy (MDL-COSPEC), has been successfully demonstrated for molecular and atomic gas detections, presenting advantages of low cost and simplicity. However, compared with single mode DL based TDLAS, the general sensitivity achieved by MDL-COSPEC is degraded because of the dilution of the absorption magnitude by the non-absorbed laser modes.

In laser absorption spectroscopy, a straight-forward and effective approach to improve sensitivity is to increase the optical pathlength by folding laser beams in particularly designed gas cells. Typical embodiments include multipass cells, optical cavities, integrating spheres, and porous scattering media. By comparison, cavity based methods including cavity ring-down spectroscopy (CRDS) and integrated cavity output spectroscopy (ICOS) [or cavity enhanced absorption spectroscopy (CEAS)] can achieve the longest pathlength. Both CRDS and ICOS exploit the long pathlength using highly reflective mirrors. CRDS requires active cavity stabilization to guarantee efficient coupling of the laser frequency to one of the cavity modes and high-speed electronics to record the ring-down signal with a sufficient time resolution. ICOS monitors the cavity transmission without active frequency locking and averages the cavity mode structure, therefore possessing advantages of robust and low-cost.

In this work, we demonstrate the introduction of OA-ICOS to MDL-COSPEC to enhance its sensitivity. Oxygen in laboratory air was measured by using a free running FP type MDL. The center wavelength of the MDL is around 760 nm overlapping the A-band absorption of oxygen. Although the MDL employed has poor beam quality, nonlinear wavelength tunability and intermittent mode hops, the resultant interferences to measurement were mostly suppressed by the COSPEC scheme. OA-ICOS was performed by using an open cavity consisting of two high-finesse concave mirrors. Piezoelectric transducers on the input mirror were modulated sinusoidally in time to create a more dense-mode spectrum and thus facilitate the average of the resonant modes. Although fall short of resonant-coupling, OA-ICOS presented a merit of less complexity to apply. The wavelength modulation technique with second harmonic detection was finally employed to show its capability of improving the SNR of OA-ICOS. An order of magnitude sensitivity enhancement was obtained by WM-OA-ICOS compared with OA-ICOS alone.

Session 3A7
SC3: Optical Signal Processing

Parametric Phase-sensitive and Phase-insensitive All-optical Signal Processing on Multiple Nonlinear Platforms

C. Peucheret[1], F. Da Ros[2], D. Vukovic[2], Y. Ding[2], K. Dalgaard[2], M. Galili[2], A. Gajda[3, 4], J. Xu[5], Y. Fukuchi[6], H. Hu[2], L. Lei[5], H. Ou[2], L. Zimmermann[4], L. K. Oxenløwe[2], B. Tillack[3, 4], and K. Petermann[3]

[1]FOTON Laboratory, CNRS UMR 6082, University of Rennes 1, ENSSAT, Lannion 22305, France
[2]Department of Photonics Engineering, Technical University of Denmark, Kgs. Lyngby 2800, Denmark
[3]Fachgebiet Hochfrequenztechnik, Technische Universität Berlin, Berlin 10587, Germany
[4]IHP, Frankfurt (Oder) 15236, Germany
[5]Huazhong University of Science and Technology, Wuhan, Hubei 430074, China
[6]Department of Electrical Engineering, Tokyo University of Science, Tokyo 125-8585, Japan

Abstract— Parametric processes in materials presenting a second- or third-order nonlinearity have been widely used to demonstrate a wide range of all-optical signal processing functionalities, including amplification, wavelength conversion, regeneration, sampling, switching, modulation format conversion, optical phase conjugation, etc.. The recent evolution of optical fiber communication systems towards advanced modulation formats making use of the phase dimension, as well as polarization and, more recently, space-multiplexing, has created new requirements, as well as new opportunities, for parametric all-optical signal processing.

In this presentation, we will review our recent results on the demonstration of all-optical parametric signal processing using different nonlinear platforms, including highly nonlinear optical fibers (HNLFs), silicon nanowires, and periodically-poled lithium niobate (PPLN) waveguides. In particular, we will show how phase-sensitive processes can be engineered to demonstrate phase-quadrature separation, which we have recently demonstrated in HNLFs [1] and PPLN waveguides [2]. Silicon nanowires are particularly attractive for signal processing thanks to their compact size, CMOS compatible fabrication process, degrees of freedom in dispersion engineering, and high nonlinear coefficient. However, the detrimental effect of free-carrier absorption induced by two-photon absorption has so far prevented them from being used for the demonstration of phase-sensitive processing. Thanks to the introduction of p-i-n junctions across silicon waveguides, we have recently been able to demonstrate phase-sensitive extinction ratios as high as 20 dB, allowing the phase regeneration of phase-modulated signals under continuous wave pumping operation [3]. One of the well-known limitations of planar waveguide devices for all-optical signal processing is their inherent polarization sensitivity. We will show how the introduction of polarization-diversity circuits relying on efficient and wideband polarization splitters and rotators [4] can overcome this limitation. Finally, we will also discuss the introduction of signal processing functionalities that are compatible with the novel dimension of space multiplexing. More specifically, we will show how mode-selective wavelength conversion based on four-wave mixing can be realized in a multimode silicon waveguide [5].

ACKNOWLEDGMENT

This work was partly funded by the Danish Research Council for Technology and Production Sciences (project 09-066562), the German Research Foundation (DFG) in the framework of Sonderforschungsbereich SFB787, and Villum Fonden via the NATEC Centre.

REFERENCES

1. Da Ros, F., K. Dalgaard, L. Lei, J. Xu, and C. Peucheret, "QPSK-to-2 × BPSK wavelength and modulation format conversion through phase-sensitive four-wave mixing in a highly nonlinear optical fiber," *Opt. Express*, Vol. 21, No. 23, 28743–28750, 2013.
2. Da Ros, F., K. Dalgaard, Y. Fukuchi, J. Xu, M. Galili, and C. Peucheret, "Simultaneous QPSK-to-2 × BPSK wavelength and modulation format conversion in PPLN," to appear in *IEEE Photon. Technol. Lett.*, 2014.
3. Da Ros, F., D. Vukovic, A. Gajda, K. Dalgaard, L. Zimmermann, B. Tillack, M. Galili, K. Petermann, and C. Peucheret, "Phase regeneration of DPSK signals in a silicon waveguide with reverse-biased p-i-n junction," *Opt. Express*, Vol. 22, No. 5, 5029–5036, 2014.

4. Ding, Y., H. Ou, and C. Peucheret, "Wideband polarization splitter and rotator with large fabrication tolerance and simple fabrication process," *Opt. Lett.*, Vol. 38, No. 8, 1227–1229, 2013.
5. Ding, Y., J. Xu, H. Ou, and C. Peucheret, "Mode-selective wavelength conversion based on four-wave mixing in a multimode silicon waveguide," *Opt. Express*, Vol. 22, No. 1, 127–135, 2014.

High-speed Silicon Photonic Devices for Photonic Signal Processing

Xi Xiao[1], **Zhiyong Li**[2], **Yu Yu**[3], **Lei Wang**[1], **Anastasia Nemkova**[2], **Hao Xu**[2], **Xianyao Li**[2], **Miaofeng Li**[1], **Ying Qiu**[1], **Qi Yang**[1], **Shaohua Yu**[1], **Yude Yu**[2], **and Jinzhong Yu**[2]

[1]State Key Laboratory of Optical Communication Technologies and Networks
Wuhan Research Institute of Posts and Telecommunications, Wuhan 430074, China
[2]State Key Laboratory on Integrated Optoelectronics
Institute of Semiconductors, Chinese Academy of Sciences, P. O. Box 912, Beijing 100083, China
[3]Wuhan National Laboratory for Optoelectronics, School of Optical and Electronic Information
Huazhong University of Science and Technology, Wuhan, Hubei 430074, China

Abstract— Silicon photonics, which is enabled by the high index contrast silicon-on-insulator (SOI) platform and the highly advanced CMOS process, has shown alluring performances on the monolithic integration capacity, compactness, power efficiency, layout flexibility, and multifunctionality. The advances of the silicon photonic devices in the past few years unveil the possibility of the photonic signal processing integrated circuit (PSPIC) on a chip.

In this talk, we will review our recent efforts on demonstrating and improving the performances of several essential photonic devices for the silicon-based PSPIC:

a. High-speed silicon modulators

The interleaved and zigzag PN junctions are both firstly proposed and demonstrated by us to overcome the poor modulation efficiency of the plasma-dispersion-effect in silicon waveguides. Modulation bandwidth of around 40 GHz and serial speed over 60 Gb/s are both achieved by the silicon Mach-Zehnder modulators and the microring modulators.

b. Fast-tunable microring devices

Tunable microring resonators are widely utilized in optical modulation and switching, filtering, multiplexing and slow light. Ultra-fast elctro-optical responses of $\sim$ 10 ps were demonstrated by optimizing the resonance-peaking effects of the microring integrated with the PN junctions. Rapid thermal-optical tuning with the 330/450 ns on/off time was also demonstrated by using the reverse breakdown current of the PN junctions.

c. Ge-on-Si waveguided photodetectors

The Ge-on-Si photodetector was monolithically integrated with the silicon modulators. The dark current of 50 pA and 3-dB detection bandwidth of 38 GHz were simultaneously demonstrated by optimizing the absorption length.

d. Efficient grating couplers with nanoimprint process

The adiabatic grating coupler with non-uniform grating periods and filling factors have demonstrated low coupling losses of 0.64 dB/end. The narrow grating grooves down to 40 nm were patterned with the fully-CMOS compatible nanoimprint lithography.

By using the devices introduced above, some investigations on the photonic signal processing including the optical pulse generation, the temporal optical differentiation, all-optical wavelength conversion of the OFDM signals, and the silicon-based optoelectronic oscillator will also be presented.

Transmission Analysis of a Ternary Diversity Reception Based on OFDM FSO System over Correlated Log-normal Fading Channel

Yuwei Su, **Fan Bai**, **and Mitsuji Matsumoto**
Global Information and Telecommunication Studies, Waseda University, Japan

Abstract— With the increasing requirements for larger bandwidth and higher data rate transfer of information, optical wireless communication (OWC) has received growing attention in recent years. Free space optical (FSO) communication belongs to the class of OWC, which has the advantages of not only the high-efficiency using of frequency and bandwidth, but also the lighter, smaller and energy-efficient device with high information security. Although FSO communication has these benefits, atmospheric factors give a serious influence to the performance of the system. Channel fading would be rising from the temporal and spatial fluctuations of the laser beam caused by scintillation. In this paper, orthogonal frequency division multiplexing (OFDM) is chosen for the purpose of against channel dispersion and time varying environment. Spatial diversity is another efficient way to mitigate the effects of scintillation. With increasing of the lens' radius, the cost and the weight of the reception terminal would increase exponentially. It is a kind of trend to replace one big lens to several smaller receivers. We investigate the performance of OFDM FSO system of ternary receivers with EGC reception combining scheme in atmospheric turbulence channel. We analyzed the effects of the distance between different receivers and tried to figure out a proper position to set them. Based on the simulation results, we compared OFDM modulation with single carrier modulations over FSO links, and present a comparison of the transmission performance among ternary receivers, dual receivers and single receiver system over correlated log-normal weak turbulence fading channel. The results would be useful for design and evaluation of optical wireless communication system.

The Principle of the Technology and Design of the Parabolic Strip Telescope

J. Červený, V. Kosejk, and G. Chadzitaskos
Department of Physics, Faculty of Nuclear Sciences and Physical Engineering
Czech Technical University, Břehová 7, CZ-115 19, Prague

Abstract— Contribution of this paper is a proposal of the new special type of telescope with a parabolic strip as a primary element for astronomical observations or for measurements with good angular resolution in one direction. The observed objects are displayed as lines in the image plane of a length equal to the width of the mirror strip. If we observe a sufficiently bright objects, the observation allows us to distinguished fine detail or fine movements on the sky. Each line segment corresponds to the integral intensity of the incident light from the observed object in the direction perpendicular to the mirror strip.

For the reconstruction of the whole image with good resolution we need a parabolic mirror strip to rotate around the optical axis, and a series of sequential snaps with a special camera. Different algorithms for reconstruction of the image are used.

The main advantage of this rotating telescope is mechanical and manufacturing technological simplicity and innovative design. Nothing comparable has yet been made. Currently constructed large telescopes are made up of segments, using adaptive optics, and generally it is technologically challenging. Systems of interfering telescopes are built (the effective diameter of 30 m to the get better resolution. The proposed telescope can be made of tape of length 50 m without any technological problems.

We were created two prototypes of telescopes. One is small with mirror strip length 0.3 m, and second telescope is bigger one with mirror strip of length 1.4 m.

Both telescopes are supported by parallactic mountings, and both are equipped by special cameras with optics, electronics, computer with special controlling software, special servo stepper motors fitted with mechanical transmission, construction of lightweight alloys, plastics and composites.

Electro-optic OR/NOR Logic Gate at 10 Gbps Using Cascaded Micro-ring Resonators

Ping Zhou, Lei Zhang, Jianfeng Ding, and Lin Yang
State Key Laboratory on Integrated Optoelectronics
Institute of Semiconductors, Chinese Academy of Sciences, P. O. Box 912, Beijing 100083, China

Abstract— Directed logic is an innovative optics-inspired architecture proposed to implement high-speed Boolean functions [1–3]. Recently, many directed logic devices based on silicon micro-ring resonators (MRR) have been proposed and demonstrated. We have demonstrated a thermo-optic OR/NOR and AND/NAND logic circuit at 10 Kpbs [4], and an electro-optic AND/NAND logic circuit at 100 Mbps employing electric field-induced carrier injection in PIN junctions [5]. In this paper, we report a 10 Gbps OR/NOR directed logic device using carrier-depletion based silicon micro-ring resonators.

The OR/NOR logic circuit consisting of two cascaded micro-ring resonators are proposed, and the reverse-biased PN junctions embedded in the ring waveguides are designed to implement high-speed modulation. The gap between the straight waveguide and the ring waveguide is designed to be 400 nm so that the Q factor reaches 12000, which is vital for the carrier-depletion modulation since the tuning efficiency is low. After the silicon waveguides are formed, the p-type and n-type doping regions with concentrations of $1 \times 10^{18}\,\mathrm{cm}^{-3}$ and $8 \times 10^{17}\,\mathrm{cm}^{-3}$ respectively are formed around the two ring waveguides. The p+ and n+ doping concentrations are $5.5 \times 10^{20}\,\mathrm{cm}^{-3}$, and the edge to edge distance from heavy doping region to the ring waveguide is 800 nm. Two TiN micro-heaters, with thickness of 150 nm, are fabricated on the top of the MRRs to compensate for the detuning resonances of two MRRs, which are induced by the limited fabricating accuracy.

The working parameters, including working wavelength and voltages reversely applied to the PN junctions of two MRRs, are extracted by analyzing the response spectra of four working states. The extracted working parameters are used in the dynamic experiment. In the dynamic experiment, the OR and NOR results are observed synchronously with the pulse signals (i.e., the operands) applied to MRR1 and MRR2. Experimental results prove that the device can implement OR and NOR operations simultaneously at the speed of 10 Gbps.

REFERENCES

1. Hardy, J. and J. Shamir, *Optics Express*, Vol. 15, 150, 2007.
2. Caulfield, H. J. and S. Dolev, *Nature Photonics*, Vol. 4, 261, 2010.
3. Soref, R., *Advances in Opto Electronics*, Vol. 2011, 627802, 2011.
4. Tian, Y., L. Zhang, R. Ji, L. Yang, P. Zhou, H. Chen, J. Ding, W. Zhu, Y. Lu, and L. Jia, *Optics Letters*, Vol. 36, 1650, 2011.
5. Tian, Y., L. Zhang, and L. Yang, *Optics Express*, Vol. 20, 16794, 2012.

Advances of Ultra-narrow Photonic Filters and Their Applications in Optical/Microwave Signal Processing

Xihua Zou
Center for Information Photonics and Communications, Southwest Jiaotong University, China

Abstract— To date, both a large bandwidth and a high resolution are urgently required for optical/microwave signal processing. Subsequently, powerful photonic filters are emerging as a promising solution to fulfill the two requirements, in particular ultra-narrow photonic filters. In this talk, recent advances in ultra-narrow photonic filters will be presented, including for instance resonator ring/disk/sphere based filters, waveguide grating based filters, fiber Bragg grating (FBG) based filters, and stimulated Brillouin scattering (SBS) based filters. Photonic filter samples and corresponding experimental result are shown, and the point lies in that a 3-dB bandwidth of ∼GHz or lower has been achieved

Especially, the development regarding the FBG based filters and the SBS based filters in my research group will be highlighted. FBG based filters with a large number of phase shifts are designed and fabricated. The obtained spectral response shows a 3-dB bandwidth of 650 MHz and a rectangular shape factor of 1.95 at the 25-dB bandwidth. This might be the narrowest rectangular band-pass response ever reported for an all-fiber filter, to the best of our knowledge. Meanwhile, for the SBS based filters, a 3-dB bandwidth as small as tens MHz and a resulting shape factor less than 2 have been simultaneously obtained owing to the SBS gain. What is more the corresponding bandwidth and the shape can be flexibly controlled by adjusting the spectral shape of the pump source In addition, arising from the SBS based filters, a microwave channelizer can be formed under the wavelength division multiplexing (WDM) mode. Other characteristics including the bandwidth, the channel spacing, and the channel profile can be tuned simply.

These ultra-narrow photonic filters are greatly beneficial for optical/microwave signal processing. Associated application demonstrations including microwave photonic filters, microwave channelizers, spectrum analyzers, opto-electronic oscillators, and phase arrayed antennas, are shown, to reveal the significance and the contributions of these filters

Spectrally Efficient FDM for Optical Communication System

Tao Gui, Yuan Bao, and Zhaohui Li
Institute of Photonics Technology, Jinan University, China

Abstract— Spectrally efficient FDM (SEFDM) systems have been proposed from wireless communications to further improve the spectral efficiency of future communication systems. It offers significant bandwidth gains by relaxing the orthogonal condition at the expense of receiver complexity. In this paper, we investigate the application of this frequency packing technique to optical communication System under coherent and incoherent (direct-detected) detection, respectively. The results show that this technique provide a significant spectral efficiency increase and represent a viable alternative to overcome the theoretical and technological issues related to the use of high-order modulation formats. Meanwhile, due to the inter-carrier interference (ICI) results in the system becoming ill-conditioned, the SEFDM has a strong affecting on accuracy of the conventional equalization method for channel and phase estimation. Therefore, in this work, we introduced the time domain based methods for channel and phase estimation to tackle the ill-conditioning of frequency domain.

Research Progress of On-chip OFDM m-QAM Transmissions for Photonic Interconnections

Jian Wang
Wuhan National Laboratory for Optoelectronics, School of Optical and Electronic Information
Huazhong University of Science and Technology, Wuhan, Hubei 430074, China

Abstract— We report recent research progress of on-chip signal transmissions by employing advanced multi-carrier multi-level modulation formats and integrated photonic devices. Using fabricated silicon microring resonators, silicon vertical slot waveguides and hybrid plasmonic waveguides, we demonstrate on-chip OFDM/OQAM m-QAM signal transmissions in a silicon microring resonator and terabit-scale WDM OFDM 16-QAM signal transmissions in silicon vertical slot waveguides and hybrid plasmonic waveguides. The experimental results of on-chip OFDM m-QAM transmissions imply possible photonic interconnection applications.

Chip-scale optical interconnections based on photonic integrated circuits (PICs) offer relaxed interconnection latency, wide bandwidth, and high resistance to electromagnetic interferences, and low power consumption [1]. Silicon photonics is considered to be a promising technology to address ever increasing challenges of future chip-to-chip and on-chip photonic interconnections owing to the compactness for high-density integration and complementary metaloxide-semiconductor (CMOS) compatible platforms for low-cost mass production [2]. Previously, on-chip binary onoff keying (OOK) signal transmissions in a silicon waveguide and binary differential phase-shift keying (DPSK) signal transmission through a silicon microring switch were demonstrated with impressive performance [3, 4]. Driven by the unabated exponential growth of data traffic, advanced multi-level modulation formats and multiplexing techniques, e.g., m-ary quadrature amplitude modulation (m-QAM), orthogonal frequency-division multiplexing (OFDM) and wavelength-division multiplexing (WDM) have been widely used in fiber optical transmissions to increase the transmission capacity [5, 6]. In this scenario, a laudable goal would be to transmit advanced multi-carrier multi-level modulation signals through integrated photonic devices for possible on-chip photonic interconnection applications.

In this paper, we review our recent works in on-chip signal transmissions with advanced multi-carrier multi-level modulation formats for photonic interconnections. By exploiting our fabricated silicon microring resonators, silicon vertical slot waveguides and hybrid plasmonic waveguides, we achieve: 1) on-chip low-penalty data transmission of OFDM based on offset QAM (OFDM/OQAM) 64-QAM, 128-QAM, 256-QAM and 512-QAM signals in a silicon microring resonator; 2) on-chip ultra-wide bandwidth 1.8-Tbit/s (161 WDM channel 11.2-Gbit/s OFDM 16-QAM) data transmission through silicon vertical slot waveguides [7]; 3) on-chip ultra-wide bandwidth 1.8-Tbit/s (161 WDM channel 11.2-Gbit/s OFDM 16-QAM) data transmission through hybrid plasmonic waveguides [8].

ACKNOWLEDGMENT

This work was supported by the National Natural Science Foundation of China (NSFC) under grants 61222502, 11274131 and 61077051, the Program for New Century Excellent Talents in University (NCET-11-0182), the National Basic Research Program of China (973 Program) under grant 2014CB340004, the Wuhan Science and Technology Plan Project under grant 2014070404010201, the Fundamental Research Funds for the Central Universities (HUST) under grants 2012YQ008 and 2013ZZGH003, and the seed project of Wuhan National Laboratory for Optoelectronics (WNLO).

REFERENCES

1. Miller, D. A. B., *Proc. IEEE*, Vol. 88, 728, 2000.
2. Barwicz, T., et al., *J. Opt. Netw*, Vol. 6, 63, 2007.
3. Lee, B. G., et al., *IEEE Photon. Technol. Lett.*, Vol. 23, 615, 2011.
4. Xu, L., et al., *IEEE Photon. Technol. Lett.*, Vol. 24, 473, 2012.
5. Winzer, P. J., et al., *J. Lightwave Technol.*, Vol. 26, No. 20, 3388, 2008.
6. Li, Z., et al., *Opt. Express*, Vol. 21, 21924, 2013.
7. Gui, C. C., et al., *OECC*, paper 381.00, 2014.
8. Du, J., et al., *CLEO*, paper JTh2A.35, 2014.

Spatial Transformation of Optical Beams Using Phase-shifted Bragg Grating

L. L. Doskolovich[1, 2], **D. A. Bykov**[1, 2], **and N. V. Golovastikov**[1, 2]

[1]Image Processing Systems Institute of the Russian Academy of Sciences, Samara 443001, Russia
[2]Samara State Aerospace University, Samara 443001, Russia

Abstract— Spatiotemporal optical beam transformations are of great interest in a wide variety of applications, including ultrafast all-optical data processing and optical computing. For differentiation and integration of temporal optical signals, various types of Bragg gratings [1, 2] and resonant diffraction gratings [3, 4] have been proposed. In a recently published paper we have demonstrated for the first time that a phase-shifted Bragg grating (PSBG) is able to perform spatial differentiation of 2D optical beams in reflection regime [5]. In this way, the PSBG structure can be considered as an ultra-compact analogue of a classic $4f$ Fourier-transform correlator consisting of a pair of lenses with a spatial filter in the Fourier plane. However, the article [5] does not consider the general class of spatial beam transformations which can be realized with a PSBG.

In the present work, we derive a first-order differential equation describing the general form of the optical 2D beam spatial transformation implemented by a PSBG. In particular, we demonstrate that under certain conditions the above differential equation describes the spatial differentiation of the incident 2D beam in reflection regime and the spatial integration in transmission regime. The proposed approach is generalized to the case of resonant diffraction gratings having more complex form of the reflection or transmission coefficient and thus extending the class of possible spatial transformations. In particular, dielectric resonant diffraction gratings can be used to perform spatial differentiation in transmission regime. Numerical simulations based on the rigorous coupled-wave analysis demonstrate high-quality spatial differentiation and spatial integration in reflection and transmission regimes.

ACKNOWLEDGMENT

The work was financially supported by Russian Science Foundation (RSF) grant 14-19-00796, Russian Foundation for Basic Research (RFBR) grants 12-07-00495, 13-07-00464, 14-07-00339, by the ministry of education and science of the Russian Federation (RF), and by RF Presidential scholarship SP-1665.2012.5.

REFERENCES

1. Rivas, L. M., S. Boudreau, Y. Park, R. Slavík, S. LaRochelle, A. Carballar, and J. Azaña, "Experimental demonstration of ultrafast all-fiber high-order photonic temporal differentiators," *Opt. Lett.*, Vol. 34, No. 12, 1792–1794, 2009.
2. Ngo, N. Q., "Design of an optical temporal integrator based on a phase-shifted fiber bragg grating in transmission," *Opt. Lett.*, Vol. 32, No. 20, 3020–3022, 2007.
3. Bykov, D. A., L. L. Doskolovich, and V. A. Soifer, "Temporal differentiation of optical signals using resonant gratings," *Opt. Lett.*, Vol. 36, No. 17, 3509–3511, 2011.
4. Bykov, D. A., L. L. Doskolovich, and V. A. Soifer, "Single-resonance diffraction gratings for time-domain pulse transformations: Integration of optical signals," *J. Opt. Soc. Am. A*, Vol. 29, No. 8, 1734–1740, 2012.
5. Doskolovich, L. L., D. A. Bykov, E. A. Bezus, and V. A. Soifer, "Spatial differentiation of optical beams using phase-shifted Bragg grating," *Opt. Lett.*, Vol. 39, No. 5, 1278–1281, 2014.

Microwave Optical Signal Fading for Chromatic Dispersion Measurement of Fibers

Shangjian Zhang, Xinghai Zhou, Heng Wang, Yali Zhang, Rongguo Lu, and Yong Liu
State Key Laboratory of Electronic Thin Films and Integrated Devices
School of Optoelectronic Information
University of Electronic Science and Technology of China (UESTC), Chengdu 610054, China

Abstract— Chromatic dispersion of optical fibers should be accounted for when developing optical equipments for use in high-speed optical fiber communications and microwave photonics links. The widely used phase shift method and transfer function method are suitable for characterization of large dispersions with temporal resolution on the order of picoseconds. However, the phase shift method needs the complicated systems to compensate the fiber length variation caused by the thermal fluctuation with a reference light. The traditional transfer function method requires chirp-free operation of intensity modulators, or at least two notches for correcting the chirp error, which leads to a limited measurement range. We proposed two methods for accurately measuring chromatic dispersion of optical fibers based on the fading of phase-modulated signals and chirp intensity-modulated signals, respectively. The phase-modulation-based method holds inherent bias-free feature, while the intensity-modulation-based method not only eliminates the chirp error but also achieves an improved measurement range through adjusting the chirp parameters of intensity modulators. Both methods allow fast and accurate measurement of the magnitude and sign of chromatic dispersion at different operating wavelengths for any kinds of optical fibers simply by a vector network analyzer.

Optical Serial Coherent Analyzer of Radio-frequency (OSCAR)

Cheng Lei, **Hongwei Chen**, **Ruiyue Li**, **Minghua Chen**, **Sigang Yang**, **and Shizhong Xie**
Tsinghua National Laboratory for Information Science and Technology (TNList)
Department of Electronic Engineering, Tsinghua University, Beijing 100084, China

Abstract— Broadband instantaneous radio frequency (RF) measurement has always been a hot research topic for its critical application in radar and electronic warfare. With the frequency of the radar goes higher and higher, photonics assisted implementations have been considered as a promising solution for its inherent large bandwidth, among which, optical serial coherent analyzer of radio-frequency (OSCAR) is a novel scheme that enables fast RF measurements in a large frequency span. The measurements are based on serial channelization, which utilizes recirculating frequency shifting (RFS) and coherent receiving structure.

Considering the wide frequency range of the broadband instantaneous RF signal and the limited processing capacity of the available electrical devices, the basic principle of the proposed OSCAR is to serially channelize the signal by the frequency shifting effect of the RFS loop, and then detect each channel with coherent receiver.

Specifically, there are two kinds of system configurations according to the characteristics of the incoming RF signal. For the RF signal with relatively stable frequency components and high temporal continuity: to make sure all the RF pulses involved, a frequency scanning local oscillator (LO), which is produced by the RFS loop, is applied to mix with the upconverted RF signal, so the RF signal will be temporally partitioned and analyzed. While, for the RF signal with high time-varying property and high temporal sparsity, in case that some instantaneous frequency component might be lost, we use the RFS loop to store the upconverted RF signal, and each time the center frequency of the RF signal is shifted, the coherent receiver will downconvert and analyzed a piece of the RF signal. Moreover, at the receiver, a balanced photodetector (BPD) instead of ordinary photodetector is utilized for coherent detection, which guarantees the accuracy of measurement and gets rid of interferences of RF's self-beating.

With the proposed OSCAR, not only instantaneous multi-frequency measurement, but also the detailed phase information of RF signals can be obtained successfully. In the experimental demonstration, a RF measurement ranging from baseband to 40 GHz with MHz order resolution is successfully realized within several micro-seconds. Furthermore, this system is promised to extensible measurement range and further improvement in various RF vector measurements applications.

ACKNOWLEDGMENT

This work was supported by National Program on Key Basic Research Project (973) under contract 2012CB315703, by the NSFC under contract 61322113, 61335002, 61120106001, 61271134, 61090391, 61132004, and by Program for New Century Excellent Talents in University (NCET-10-0520), and by the young top-notch talent program sponsored by Ministry of Organization, China.

Session 3A8
SC3: Luminescent Materials, Devices and Application

Interface Engineering and Hybrid Structure for Graphene Transistors and Photodetectors in the Vicinity of Substrates

Jian-Bin Xu, Xi Wan, Kun Chen, Xiao-Mu Wang, Zhen Zhou Cheng, and Hon Kin Tsang
Department of Electronic Engineering and Materials Science and Technology Research Centre
The Chinese University of Hong Kong, Shatin, Hong Kong SAR, China

Abstract— In this talk, we will present our efforts on interface engineering of substrate surface for graphene synthesis and device fabrication, as well as their applications in high-quality graphene transistors and photodetectors.

A substrate surface is a ubiquitous supporting platform for graphene sheet formation and the vicinity of carrier generation and transport in the active graphene layer. The surface functionalities play a pronounced role for effectually controlling graphene synthesis and substantially minimizing the interface scattering effect, as well as increasing the carrier mobility. Our recent results have shown that high-quality graphene sheets can be synthesised from different solid polycyclic hydrocarbon precursors on catalytic metal surfaces, and high-performance graphene devices can be achieved on passivated SiO_2 surface on Si substrate with self-assembled monolayers (SAMs). Here we will discuss different interface engineering strategies in producing graphene layers, improving graphene transistor performance, and exploring hybrid graphene optoelectronic devices.

So far we have achieved the highest mobility of graphene on SiO_2/Si substrates at room temperature, and the high performance graphene/siliconheterostructure waveguide photodetector in the mid-infrared range at room temperature. We believe that the ultrasmooth surface platform provided by SAM passivation will be applicable for other 2D materials for achieving high-performance device performance.

ACKNOWLEDGMENT

The work is in part supported by Research Grants Council of Hong Kong, particularly, via Grant Nos. AoE/P-03/08, CUHK4179/10E, CUHK4165/12E, N_CUHK405/12, and CUHK Group Research Scheme 2013. We express our gratitude to Mr. Frank Ng, Mr. Stephen Chan, and Mr. Roger Wong of Information Technology and Service Center of CUHK for HPC technical support. J. B. Xu thanks the National Science Foundation of China for the financial support, particularly, via Grant No. 61229401.

REFERENCES

1. Wan, X., K. Chen, D. Q. Liu, J. Chen, Q. Miao, and J. B. Xu, *Chem. Mater.*, Vol. 24, 3906–3915, 2012.
2. Wan, X., K. Chen, J. Du, D. Liu, J. Chen, X. Lai, W. G. Xie, and J. B. Xu, *J. Phys. Chem. C*, Vol. 117, 4800–4807, 2013.
3. Chen, K., X. Wan, D. Q. Liu, Z. W. Kang, W. G. Xie, J. Chen, Q. Miao, and J. B. Xu, *Nanoscale*, in press.
4. Wang, X. M., J. B. Xu, C. L. Wang, J. Du, and W. G. Xie, *Adv. Mater.*, Vol. 23, 2464–2468, 2011.
5. Wang, X. M., W. G. Xie, J. Du, C. L. Wang, N. Zhao, and J. B. Xu, *Adv. Mater.*, Vol. 24, 2614–2619, 2012.
6. Chen, K., X. M. Wang, J. B. Xu, L. J. Pan, X. R. Wang, and Y. Shi, *J. Phys. Chem. C*, Vol. 116, 6259–6267, 2012.
7. Tian, X. Q., J. B. Xu, and X. M. Wang, *J. Phys. Chem. B*, Vol. 114, 11377–11381, 2010.
8. Wang, X. M., Z. Z. Cheng, K. Xu, H. K. Tsang, and J. B. Xu, *Nature Photonics*, Vol. 7, 888–891, 2013.

Electrically Pumped Homojunction ZnO Nanowire Lasers

Jianlin Liu
Department of Electrical Engineering
University of California Riverside, CA 92521, USA

Abstract— ZnO ultraviolet (UV) semiconductor nanolasers have potential for various applications, such as photonics, information storage, and medical therapeutics thanks to its direct wide bandgap (3.3 eV) and large exciton binding energy (60 meV) at room temperature. Although optically pumped ZnO nanowire lasers have been studied widely, there lacks high-efficiency electrically pumped laser diodes. This is in part due to the lack of reliable p-type ZnO materials. With recent advancement of p-type doping of ZnO, many functional nanowire optoelectronic devices emerged. In this presentation, we report the first homojunction ZnO nanowire laser diodes. These devices consist of p-type Sb-doped or N-doped ZnO nanowires on n-type ZnO films. The p-type characteristics of ZnO nanowires were comprehensively studied. Both electrically pumped random lasing and Fabry Perot (FP) lasing were achieved from these homojunction nanowire diode lasers. Both FP and random ZnO UV nanowire diode lasers exhibited very low threshold currents. Output power and far-field emission characteristics were also studied. Distributed Bragg reflectors were used to further enhance the nanolaser performance.

The Right Way to Dope ZnO p-type, for Lasing

Lei Liu and Dezhen Shen
State Key Laboratory of Luminescence and Applications, Changchun, China

Abstract— As a well-known II-VI semiconductor, ZnO with the direct band gap of 3.37 eV at room temperature has a large exciton binding energy of 60 meV. In comparison, GaN, with almost the same band gap, shows the exciton energy at about 20 meV. Due to its large exciton energy, ZnO has been taken as a promising material to fabricate ultraviolet (UV) light emitters. But, it suffers notoriously the doping asymmetry problem, i.e., it can be easily doped n-type but not p-type. Unlike GaN, whose light-emitting diodes (LEDs) and laser diodes have been successfully fabricated and commercialized, the optoelectronic application of ZnO has been hindered by lack of a practical and efficient p-doping method.

In this talk, by analyzing the surface reaction pathway of N in ZnO with first-principles density functional theory calculations, I will discuss the right way to dope ZnO p-type experimentally for making high efficiency ZnO laser diodes.

REFERENCES

1. Liu, L., J. Xu, D. Wang, M. Jiang, S. Wang, B. Li, Z. Zhang, D. Zhao, C.-X. Shan, B. Yao, and D. Z. Shen, "P-type conductivity in N-doped ZnO: The role of the NZn-VO complex," *Physical Review Letters*, Vol. 108, 215501, 2012.

Plasmon Enhanced Whispering-gallery Mode Lasing from ZnO Microrod

Chunxiang Xu, Junfeng Lu, Yi Lin, Jitao Li, and Yueyue Wang
State Key Laboratory of Bioelectronics, School of Biological Science and Medical Engineering
Southeast University, Nanjing, China

Abstract— Surface plasmons (SPs) are collective electronic oscillations on a metal-dielectric interface with a much smaller wavelength than the excitation or emitted photons, and have emerged as a promising solution to overcome such a barrier. In addition, SPs has attracted intense scientific interest due to its applications in enhancement of the weak physical process, such as the absorption of light in molecules and Raman scattering intensities. In this paper, plasmon enhanced spontaneous emission and whispering-gallery mode (WGM) lasing from hexagonal ZnO microrod has been investigated through monolayer graphene coated ZnO microrod and Al nanoparticles (NPs) decorated ZnO microrod. In both cases, besides the distinct enhancement of spontaneous and stimulated emission, the obviously reduced lasing threshold and the remarkably improved quality factor (Q) were also observed. The underlying mechanism for these two cases were proposed. These research presented here would be potentially important for designing high efficient optical and photo-electronic devices.

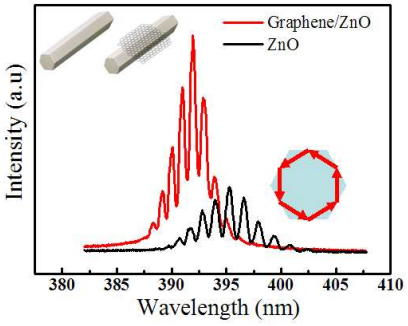

Figure 1: Comparison of the lasing spectra of the same ZnO microrod covered with/without graphene under the same excitation power of 325 nm laser. Upper left insets the schematic of a ZnO microrod covered without and with graphene. Bottom right insets the diagram of a WGM lasing microcavity of the hexagonal ZnO microrod.

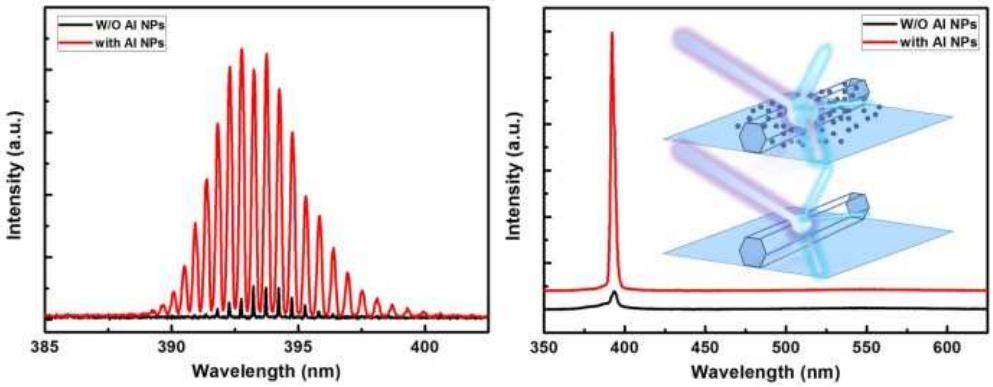

Figure 2: (a) The lasing spectra of the same ZnO microrod with/without Al NPs coating under the same excitation power. (b) Comparison of the μ-PL spectrum between the same ZnO microrod with and without Al NPs coating under the same excitation power. Inset: Schematic diagram of the excitation and emission.

ACKNOWLEDGMENT

This work was supported by "973" Program (2011CB302004 and 2013CB932903), NSFC (61275054), MOE (20110092130006) and JSIS (BE2012164).

REFERENCES

1. Dai, J., C. X. Xu, and X. W. Sun, "ZnO-microrod/p-GaN heterostructured whispering-gallery-mode microlaser diodes," *Advanced Materials*, Vol. 23, 4115–4119, 2011.
2. Huang, M. H., et al., "Room-temperature ultraviolet nanowire nanolasers," *Science*, Vol. 292, 1897–1899, 2001.
3. Oulton, R. F., V. J. Sorger, X. Zhang, et al., "Plasmon lasers at deep subwavelength scale," *Nature*, Vol. 461, 629–632, 2009.
4. Sorger, V. J. and X. Zhang, "Spotlight on plasmon lasers," *Science*, Vol. 333, 709–710, 2011.
5. Oulton, R. F., V. J. Sorger, X. Zhang, et al., "A hybrid plasmonic waveguide for subwavelength confinement and long-range propagation," *Nature Photonics*, Vol. 2, 496–500, 2008.
6. Novoselov, K. S., et al., "Electric field effect in atomically thin carbon films," *Science*, Vol. 306, 666–669, 2004.

Rational Tuning the Optical Properties of Colloidal II-VI Semiconductor Nanowires

Gaoling Yang[1], **Ruibin Liu**[1], **Bingsuo Zou**[2], **and Haizheng Zhong**[1]

[1]Beijing Key Laboratory of Nanophotonics and Ultrafine Optoelectronic Systems
School of Materials Science & Engineering, Beijing Institute of Technology
5 Zhongguancun South Street, Haidian District, Beijing 100081, China
[2]Micro Nano Technology Center, Beijing Institute of Technology
5 Zhongguancun South Street, Haidian District, Beijing 100081, China

Abstract— One-dimensional inorganic semiconductor nanowires form an attractive class of materials for nanoscale optical devices, in particular as optical materials for lasers, waveguide, and polarized light emitting diodes [1, 2]. Numerous synthetic methods have been developed in recent years to realize high-quality semiconductor nanowires with controllable dimensions, shape, and morphology [3, 4]. Solution technology offers great prospects to fabricate untrathin colloidal semicondcutor nanowires with quantum confinement effects for rational design and construction of nanodevices [5]. Since the first report of successful solution solid-liquid-solution (SLS) synthesis [6], various colloidal semicondcutor nanowires have been synthesized [7]. However, much work is still highly needed for tailoring the optical properties and finding effective strategy for practical applications. Recently, we worked on the synthetic chemistry to tailor the optical properties of II-VI semiconductor nanowires [8, 9]. By adapting the tuning strategies (doping, alloying and cation exchange) from colloidal quantum dots, we are able to synthesize high quality nanowires color tunable with tunable light emissive peroperties This may pave the way to fabricate polarized light-emitting devices with using colloidal nanowires.

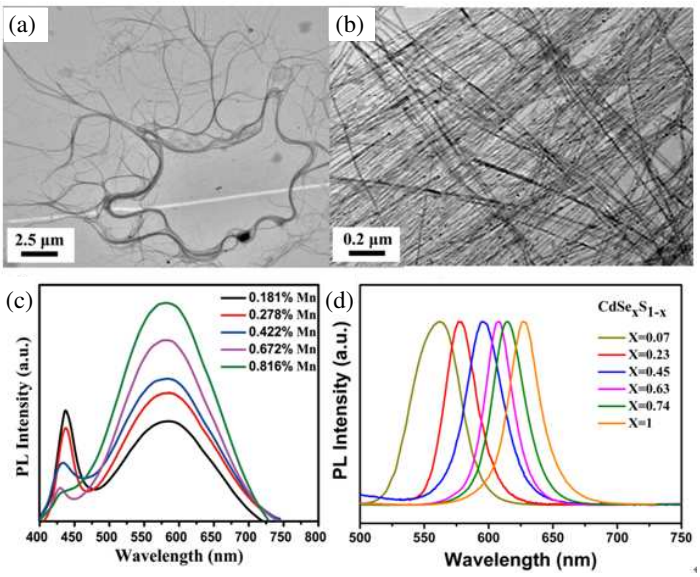

Figure 1: (a), (b) TEM image of $CdSe_xS_{1-x}$ nanowires and the photoluminescence spetra of (c) doped and (d) alloyed nanowires.

REFERENCES

1. Guo, X., Y. B. Ying, and L. M. Tong, "Photonic nanowires: From subwavelength waveguides to optical sensors," *Acc. Chem. Res.*, Vol. 47, No. 2, 656–666, 2014.
2. Yan, R., D. Gargas, and P. D. Yang, "Nanowire photonics," *Nat Photonics*, Vol. 3, No. 10, 569–576, 2009.
3. Calarco, R., M. Marso, T. Richter, A. I. Aykanat, R. Meijers, A. vd Hart, T. Stoica, and H. Lüth, "Size-dependent photoconductivity in MBE-grown GaN nanowires," *Nano Lett.*, Vol. 5, No. 5, 981–984, 2005.

4. Liu, R., Z. A. Li, C. H. Zhang, X. X. Wang, M. A. Kamran, M. Farle, and B. S. Zou, "Single-step synthesis of monolithic comb-like CdS nanostructures with tunable waveguide properties," *Nano Lett.*, Vol. 13, No. 6, 2997–3001, 2013.
5. Wang, F., A. G. Dong, J. W. Sun, R. Tang, H. Yu, and W. E. Buhro, "Solution-liquid-solid growth of semiconductor nanowires," *Inorg Chem.*, Vol. 45, No. 19, 7511–7521, 2006.
6. Trentler, T. J., K. M. Hickman, S. C. Goel, A. M. Viano, P. C. Gibbons, and W. E. Buhro, "Solution-liquid-solid growth of crystalline III-V semiconductors: An anology to vapor-liquid-solid growth," *Science*, Vol. 270, No. 5243, 1791–1794, 1995.
7. Puthussery, J., T. H. Kosel, and M. Kuno, "Facile synthesis and size control of II-VI nanowires using bismuth salts," *Small*, Vol. 5, No. 10, 1112–1116, 2009.
8. Yang G. L, G. Y. Xu, B. K. Chen, S. Y. Zou, R. B. Liu, H. Z. Zhong, and B. S. Zou, "General synthesis and white light emission of diluted magnetic semiconductor nanowires using single-source precursors," *Chem. Mater.*, Vol. 25, No. 15, 3260–3266, 2013.
9. Yang G. L., R. B. Liu, B. S. Zou, and H. Z. Zhong, Unpubilshed Results.

Large Scale Carbon Nanodots Based Remote Phosphor for White-light Light-emitting Diodes

Wenfei Zhang[1] and Siu Fung Yu[2]

[1]The Hong Kong Polytechnic University Shenzhen Research Institute, Shenzhen 518057, China
[2]Department of Applied Physics, The Hong Kong Polytechnic University
Hung Hom, Kowloon, Hong Kong, China

Abstract— Extensive investigations have been carried out to studythe optical characteristics of carbon nanodots (C-dots) since the first observation of photoluminescence (PL). Recently, fluorescent C-dots have been adopted as an alternative technology platform to realize white-light light-emitting devices under ultraviolet (UV) excitation. However, the trend of white-light light-emitting diodes (LEDs) design — remote phosphor LED technology requires the suspension of solid phosphor film to be excited bylow-cost blue (460 nm) LEDs. Hence, the practical applications of C-dots in white-light light-emitting devices are still limited by the use of expensive UV excitation sources.

In this work, we demonstrated for the first time the fabrication of a large scale white-light C-dots based remote phosphor that can be excited by commercial blue (460 nm) LEDs. The C-dots is fabricated by a one-step pyrolysis method which is easy to scale up. The as-prepared C-dots are functionalized with organic groups which is compatible with polymer matrix (i.e., epoxy resin) to form a remote phosphor film. The polymer matrix can provide mechanical support as well as prevent the aggregation of C-dots. The PL quantum efficiency of the C-dots phosphor can achieve as high as 67% when excited at 460 nm. Hence, we verify that the proposed C-dots phosphor films can replace the conventional solid phosphor film using rare-earth materials to generate white-light emission.

ACKNOWLEDGMENT

This work was supported by National Natural Science Foundation of China (grant No. 61378071).

Electrical and Optical Probing of Extremely Large Planar Polymer Light-emitting Electrochemical Cells

Yufeng Hu[1, 2], **Jun Gao**[2], **Yanbing Hou**[1], **Zhidong Lou**[1], **Zhenbo Deng**[1], **and Feng Teng**[1]

[1]Key Laboratory of Luminescence and Optical Information, Ministry of Education
Institute of Optoelectronic Technology, Beijing Jiaotong University, Beijing 100044, China
[2]Physics Department, Queen's University, Kingston, Ontario, Canada

Abstract— Polymer light-emitting electrochemical cells (LECs) are unique solid-state light-emitting devices operating on the principle of *in situ* electrochemical doping and the formation of a *p*-*n* junction. However, the underlying operating mechanism of LECs has been the subject of intense scrutiny and debate. With time-lapse fluorescence imaging, we have demonstrated the existence of the electrochemical doping and the *p*-*n* junction in an operating LEC. The electric potential and conductivity distributions of extremely large planar LECs have been mapped with two-probe measurements. In addition, the optical beam induced current (OBIC) measurement has been explored to map the built-in electric field of extremely large planar LECs. The result clearly shows that a large electric field exists only around the junction region rather than in the electrode region. Moreover, the result confirms that the LEC electronic structure is a graded *p*-*n* junction.

Luminescence and Doping of Lanthanides in Quantum Dots

Rosa Martin Rodriguez, Robin Geitenbeek, Yiming Zhao, Freddy Rabouw, Cees van Walree Celso de Mello Donega, and Andries Meijerink
Debye Institute, Utrecht University, The Netherlands

Abstract— The present popularity of everything that involves 'nano' is not just a hype. In case of semiconductor and metal nanoparticles new physical and chemical properties arise for sizes in the nanometer regime. This results in fascinating size dependent optical and electrical properties: the particles change color when the size is tuned in the nanometer regime. The incorporation of optically active dopants into quantum dots (QDs) can give additional functionality and combine the strong and size tunable QD absorption with efficient size-independent narrow line or band emission from lanthanide ions. Incorporation is however not trivial. In this presentation two methods will be discussed that yield luminescent lanthanide-doped chalcogenide nanocrystals. A single source precursor synthesis method yields ~ 8 nm CaS and SrS nanocrystals which can be doped with Eu^{2+} and Ce^{3+}, yielding yellow-orange emission. CdSe can be doped by Yb^{3+} through surface adsorption followed by incorporation through overgrowth (Fig. 1). Excitation, emission and luminescence life time measurements provide convincing evidence for the introduction of Yb^{3+} and energy transfer from the CdSe QD exciton states to the localized $4f$ states of Yb^{3+}, yielding narrow line 980 nm IR emission [1].

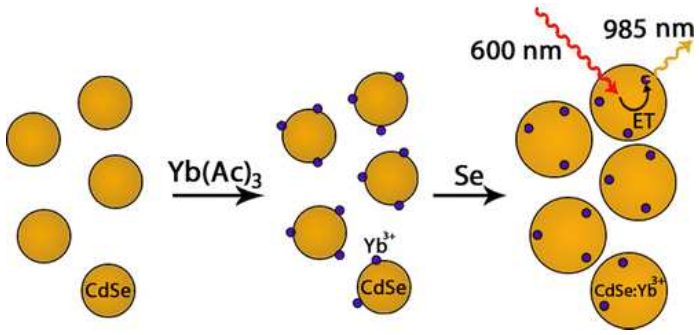

Figure 1: Incorporation mechanism for Yb^{3+} in CdSe quantum dots, yielding narrow band IR emitting quantum dots with efficient broad band visible light absorption.

REFERENCES

1. Rodriguez, R. M., R. Geitenbeekm, and A. Meijerink, *J. Am. Chem. Soc.*, Vol. 135, 13668, 2013.

Polymer Light-emitting Electrochemical Cells: Operating and Degradation Mechanisms

Jun Gao[1], **Yufeng Hu**[1], **Faleh AlTal**[1], **Xiaoyu Li**[2], **and Guojun Liu**[2]

[1]Department of Physics, Engineering Physics and Astronomy
Queen's University, Kingston, Ontario K7L 3N6, Canada
[2]Department of Chemistry, Queen's University, Kingston, Ontario K7L 3N6, Canada

Abstract— Polymer light-emitting electrochemical cells (LECs) are unique among organic semiconductor devices because the operation of LECs involves the *in situ* electrochemical p- and n-doping of the luminescent polymer and the formation of a light-emitting p-n junction. The dynamic doping process can be visualized via time-lapse fluorescence imaging of an extremely large planar LEC under bias.

At the heart of an LEC is the electrochemically-induced pn junction. However, little is known about the electronic structure of the pn junction such as the doping profile and the width of the space charge region. Here we present experimental studies of large, frozen-junction planar LECs using scanning photocurrent and photoluminescence techniques. The photoluminescence profile allows for the precise identification of the junction location. The photocurrent is only expected in the space charge region where there is a built-in electric field. Our results confirm that the p-n junction itself is responsible for the photovoltaic response of the LEC. For a planar LEC with an interelectrode spacing of about 700 microns and probed with a focused laser beam. The width of the space charge region is determined to be less than 10 microns.

A drawback of LECs is their relatively short lifetime when compared to polymer lightemitting diodes made with the same luminescent polymer. In this presentation we show that the apparent luminance decay in sandwich LECs is in fact largely the result of doping-induced fluorescence quenching, and therefore recoverable when the device is allowed to relax without bias. Moreover, LECs display de-coupled luminance decay and voltage drift. Under forwardcurrent operation, the luminance decreases by half while the operating voltage remains nearly unchanged. Under reverse-current operation, the luminance remains constant for over 200 hours while the operating voltage more than doubles. We discuss the likely cause of such highly unusual decay behavior which has not been reported in polymer light-emitting devices.

Effect of Tm_2O_3 Addition on the Spectral Properties of Bismuth Containing Alumino-borosilicate Glasses

Dong Hoon Son[1], **Bok Hyeon Kim**[2], **Seung Ho Lee**[1], **and Won-Taek Han**[1]

[1]Department of Physics and Photon Science, School of Information and Communications
Gwangju Institute of Science and Technology
123 Cheomdan-gwagiro, Buk-Gu, Gwangju 500-712, South Korea
[2]Advanced Photonics Research Institute, Gwangju Institute of Science and Technology
123 Cheomdan-gwagiro, Buk-Gu, Gwangju 500-712, South Korea

Abstract— A broad near-infrared (NIR) emission of bismuth containing glasses has drawn much attention for applications in broadband optical amplifier. Especially, the bismuth containing glasses with various host glass compositions have been intensively studied [1–3].

In this study, we investigated the effect of Tm_2O_3 addition in bismuth containing alumino-borosilicate glasses (SBAB) on spectral properties upon pumping with the 800 nm Ti:sapphire laser. Tm^{3+} emission was found to appear at 1634 nm when 2 mol% of Tm_2O_3 was incorporated but intensity was negligibly small. It was found that the intensity of the broad NIR emission band from bismuth upon pumping considerably decreased by increasing the Tm_2O_3 concentration from 0 to 2 mol%. Because the sensing capability of InGaAs detector considerably decreased with the increase of wavelength over 1600 nm, the full emission band of Tm^{3+} was not observed but instead the fictive emission band near 1643 nm was obtained. The emission spectra of the glasses in visible wavelength were also measured. The strong Tm^{3+} emission band near 693 nm was obtained and intensity was considerably increased with the increase of concentration of Tm_2O_3, indicating that the observed energy from bismuth was transferred to upper state of Tm^{3+} ions and the observed pump energy from Tm^{3+} ions was transferred dominantly to higher energy level then emitted visible light rather than emitting NIR light. To understand the obtained spectral properties, optical absorption in the range of 300–2000 nm and the energy transfer efficiency through lifetime measurement were examined, and possible energy transfer processes were proposed.

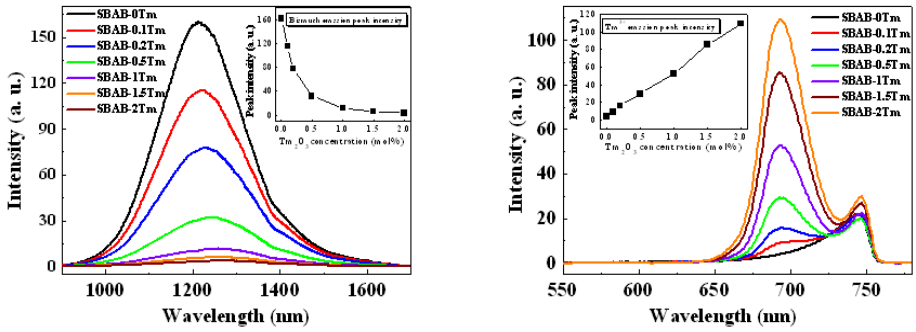

Figure 1: (a) NIR and (b) visible emission spectra of the SBAB glasses with different Tm_2O_3 concentrations under the excitation of 800 nm Ti:sapphire laser.

ACKNOWLEDGMENT

This work was partially supported by the New Growth Engine Industry Project of the Ministry of Trade, Industry and Energy, the Research Programs through the National Research Foundation of Korea (NRF) funded by the Ministry of Education (No. 2013R1A1A2063250, No. 20100020794), the Korea government (MSIP) (No. 2011-0031840), the Asian Laser Center Program and the Brain Korea-21 Plus Information Technology Project through a grant provided by the Gwangju Institute of Science and Technology, South Korea.

REFERENCES

1. Fujimoto, Y. and M. Nakatsuka, "Infrared luminescence from bismuth-doped silica glass," *Jpn. J. Appl. Phys.*, Vol. 40, L279–L281, 2001.

2. Peng, M., J. Qiu, D. Chen, X. Meng, and C. Zhu, "Superbroadband 1310 nm emission from bismuth and tantalum codoped germanium oxide glasses," *Opt. Lett.*, Vol. 30, 2433–2435, 2005.
3. Son, D. H., B. H. Kim, S. H. Lee, S. Y. Yim, and W.-T. Han, "Spectral properties of Bi-Er-Yb triply doped borosilicate glasses with 805 nm excitation," *Ceramic Transactions*, Vol. 231, 209–217, 2011.

Upconverting Fluorescent Nanoparticles with NIR Excitation for Bioimaging and Photoactivation

Yong Zhang[1, 2, 3] **and Kai Huang**[1]

[1]Department of Biomedical Engineering, Faculty of Engineering
National University of Singapore, 117575, Singapore
[2]NanoCore, Faculty of Engineering, National University of Singapore
Block EA-04-27, 117576, Singapore
[3]NUS Graduate School for Integrative Sciences and Engineering
National University of Singapore, 117456, Singapore

Abstract— Traditional fluorophores such as fluorescent dyes/proteins and quantum dots (QDs) are based on 'downconversion fluorescence', emitting low energy fluorescence when excited by high energy light (such as UV or short wavelength visible light). They have somedisadvantages: photobleaching, autofluorescence, shortlight penetration depth and tissue damage. Upconversion nanoparticles (UCNPs) emit detectable photons of higher energy upon irradiation with low energy near-infrared (NIR) light based on a process termed 'upconversion'. UCNPs show absolute photostability, negligible autofluorescence, high penetration depth and minimum photodamage to biological tissues. They can be used for ultrasensitive interference-free bioimaging because most biomolecules do not have upconversion properties. UCNPs are also useful for light based therapy with enhanced efficiency such as photodynamic therapy (PDT). PDT involves two individually non-toxic components that are combined to kill cancer cells. The first component is photosensitizer, a photosensitive molecule that localizes to a target cell and/or tissue. The second component involves the administration of light of a specific wavelength that activates the sensitizer. The photosensitizer transfers energy from light to molecular oxygen, to generate reactive oxygen species which can kill cancer cells. Most of photosensitizers are activated by visible light only. However, visible light has limited penetration depth in biological tissues. For this reason, PDT is usually used to treat tumors on or just under the skin or on the lining of internal organs or cavities, and is less effective in treating large tumors or deep-seated tumors. UCNPs are used for enhanced PDT in deep tissues, because NIR light can go much deeper in tissues than visible light. They are used not only as a light converter but also a carrier for photosensitizers.

Session 3A9
SC3: Quantum Optics

Quantum Plasmonics: Surface-plasmon-induced Quantum Interferences

Ying Gu, Luojia Wang, Dongxing Zhao, Hongyi Chen, Juanjuan Ren, and Qihuang Gong
State Key Laboratory for Mesoscopic Physics, Department of Physics
Peking University, Beijing 100871, China

Abstract— Local field effects of surface plasmons enable strong and nonlinear light-quantum mitter interactions far below the subwavelength scale. Compared with other photonic structures, plasmon nanostructures possess large and anisotropic Purcell factors, which will greatly modify the quantum interferences of coherently prepared quantum system and benefit to quantum information processes. In this talk, I will present our recent progresses in quantum plasmonics, such as polarized resonance fluorescence [1], intrinsic quantum beats [2], modification of spontaneous emission spectra [3], electromagnetically induced transparency (EIT) of the atomic ensemble [4] near metallic nanostructures (Fig. 1), and some dark-plasmon-induced quantum interferences effects in hybrid quantum dots-metallic nanoparticle system [5]. The hybrid system may have applications in ultracompact tunable quantum dot lasers and quantum logic gates.

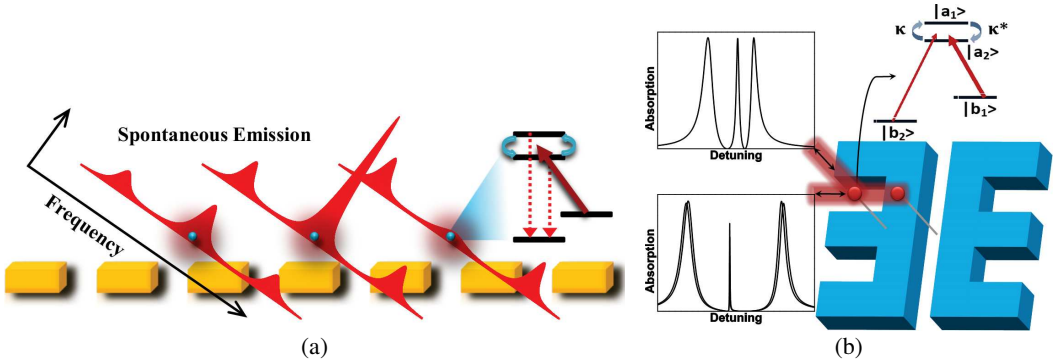

Figure 1: (a) Spontaneous emission spectra of a four-level system in a periodic gold nanostructure. (b) Position-dependent linewidth-controllable polarized EIT spectra of a double-Λ system in a resonant silver nanocavity.

REFERENCES

1. Gu, Y., L. Huang, et al., *Phys. Rev. B*, Vol. 81, No. 19, 193103, 2010.
2. Gu, Y., L. Wang, et al., *Plasmonics*, Vol. 7, 33, 2012.
3. Gu, Y., L. Wang, et al., *Nano Lett.*, Vol. 12, 2488, 2012.
4. Wang, L., Y. Gu, et al., *Sci. Rep.*, Vol. 3, 2879, 2013.
5. Zhao, D., Y. Gu, et al., under review.

Analysis of Hong-Ou-Mandel Interference Behavior of Photons Carrying Orbital Angular Momentum

Xiaoyan Chen, **Guoxuan Zhu**, **Yanfeng Zhang**, **Hui Chen**, **Yujie Chen**, **and Siyuan Yu**
State Key Laboratory of Optoelectronic Materials and Technologies
School of Physics and Engineering, Sun Yat-sen University
Guangzhou 510275, China

Abstract— Quantum interference plays a crucial role in quantum teleportation and optimal quantum state cloning technology. Quantum entanglement in multi-dimensional states requires a higher dimension of freedom. Orbital angular momentum (OAM) is promising for providing such kind of new spatial degree of freedom.

Here, by using quantum matrix mechanics, we investigate the HOM effect of two photons carrying OAM. When it comes to calculation, we use HG_{01} mode (odd mode) and HG_{10} mode (even mode) to form OAM modes. More specifically, OAM modes of $\ell \pm 1$ are generalized by the superposition of HG_{01} mode and HG_{10} mode. We also find out matrix expression about optical components in the Mach Zehnder Interferometer (MZI). Two superposition-mode photons are launched from different input ports of the MZI, in which relationships between the input modes and output ones are revealed.

After a series of matrix calculations, we obtain the common output of photon states from the MZI. Analyzing the results, we can reach the conclusion that if two photons carry OAM with same topological charge ℓ, the HOM coalescence will lead photons to emit from the same output. However, this coalescence can be shifted off by using photons carrying OAM with different ℓ. Furthermore, we find that even interference between two photons carrying OAM of $\ell = +1$ and $\ell = -1$ respectively does not show perfect HOM effect, which means that OAM is an essential quantity in the generation of HOM effect.

This is valuable to interpret the multimode interference about photons carrying diverse OAM states. What's more, these results suggest that OAM has potential to be added to quantum communication protocols as an extra degree of freedom.

Photon Echo Quantum Memories in a Single Mode Resonator

E. S. Moiseev[1] **and S. A. Moiseev**[2, 3]

[1]Institute for Quantum Science and Technology, University of Calgary, Canada
[2]Quantum Center, Kazan National Research Technical University, Russia
[3]Zavoisky Kazan Physical-Technical Institute of KSC RAS, Russia

Abstract— We have analyzed the photon echo quantum memories in the optimal single mode resonators. Following to the time reversibility concept we have discussed the basic properties of such quantum memories specified by the recovering of macroscopic atomic coherence for the input signal field retrieval. Here, special attention has been paid to the well-known photon echo quantum memory schemes (CRIB, AFC, GEM) and we have also discussed the potential advantages of new recently proposed protocol for such quantum memory exploiting natural inhomogeneous broadening and off-resonant Raman atomic transitions.

Finally we have proposed a novel scheme for the quantum random access memory (QRAM) based on the photon echo technique where the single photon field is coupled with the resonator via three-level control atom We have found the following matching conditions for the light-atom interactions [1]:

$$\Omega = 2q^2/\kappa, \tag{1}$$

$$\Delta_{\text{in}} = \frac{2q^2\kappa}{\kappa^2 - 4q^2}, \tag{2}$$

where $\Omega = Nf^2/\Delta_{\text{in}}$, N and f are the number of atoms and photon-atom coupling in the resonator, Δ_{in} — is an inhomogeneous broadening of the resonant atomic transition, κ is a decay constant of the light field in the empty resonator, q is a coupling constant for the resonant interaction between three level atom and resonator field mode.

We have assumed that three-level atom stays close to the resonator and interacts with evanescent part of the resonator field mode. The matching conditions in Eqs. (1), (2) provide a perfect transfer for broadband single photon field in the resonator. Based on the coherent inversion of three-level atom between the ground and blockade level, we have demonstrated the basic scenarios for QRAM operations in storage and recall of the photonic qubits.

REFERENCES

1. Moiseev, E. S. and S. A. Moiseev, "Quantum RAM in QED cavity," Prepared to Press.

Quantum Computing with Multi-photon Entanglement

Chao-Yang Lu
University of Science and Technology of China, China

Abstract— Entangled photons generated from spontaneous parametric down conversion have proven an excellent workhorse for tests of foundation of quantum mechanics, studies of quantum optics and demonstrations of quantum information processing tasks. So far, entanglement up to eight individual single photons have been achieved, and various algorithms including Shor's quantum factoring algorithm, quantum simulation of anyon statistics, loss-tolerant quantum encoding and topological error correction have been demonstrated. In this talk, I will present recent advances in optical quantum computing, with focus on experimental realizations of quantum algorithms for efficiently solving systems of linear equations and for machine learning. The experiment results indicate that quantum computers could offer a useful toolkit for the big data.

REFERENCES

1. Lu, et al., *Nature Physics*, Vol. 3, 91, 2007.
2. Lu, et al., *Phys. Rev. Lett.*, Vol. 99, 250504, 2007.
3. Lu, et al., *PNAS*, Vol. 105, 11050, 2008.
4. Lu, et al., *Phys. Rev. Lett.*, Vol. 102, 030502, 2009.
5. Yao, et al., *Nature Photonics*, Vol. 6, 225, 2012.
6. Cai, et al., *Phys. Rev. Lett.*, Vol. 110, 230501, 2013.
7. Cai, et al., Manuscript submitted Apr. 2014.

Raman Quantum Memory for Light Based on Control Field Frequency Modulation

Alexey Kalachev[1,2], **Xiwen Zhang**[1], **and Olga Kocharovskaya**[1]

[1]Department of Physics, Institute for Quantum Studies
Texas A&M University, College Station, TX 77843-4242, USA
[2]Zavoisky Physical-Technical Institute, 10/7 Sibirsky Trakt Str., Kazan 420029, Russia

Abstract— Optical quantum memories are usually assumed to store and recall optical pulses, such as single-photon wave packets, exploiting inhomogeneous broadened atomic transitions or temporally modulated control fields [1, 2]. Another approach, which requires neither inhomogeneous broadening nor temporal modulation of the control field amplitude but resorts to continuous phase-matching control in an extended resonant medium, has been developed recently [4, 5]. In the present work we propose one more technique that does not require a direct control of the atomic resonant levels. We consider off-resonant Raman interaction of a weak signal field and a strong control field in a Λ-type atomic ensemble assuming that the frequency of the control field is modulated along the direction of propagation of the signal one. In the case of a linear frequency modulation the scheme is equivalent to gradient echo memory (GEM), while in the case of a stepped frequency modulation it becomes a combination of GEM and atomic frequency comb (AFC). However, contrary to GEM, the proposed scheme can be realized without additional electric or magnetic fields. It means that materials demonstrating neither linear Stark nor Zeeman effects can be used and/or materials which are placed in specific external fields remain undisturbed. In addition, compared to AFC, the optical frequency comb is not limited by the inhomogeneous broadening of the atomic levels, and it can be easily created without any background absorption and modified between storage and retrieval. These features make the proposed scheme promising from the viewpoint of experimental realization. The possibilities of implementing the scheme in the solid-state materials such as NVD and rare-earth-ion doped crystals are discussed.

REFERENCES

1. Tittel, W., et al., *Laser & Photonics Reviews*, Vol. 4, 244, 2010.
2. Simon, C., et al., *Eur. Phys. J. D*, Vol. 58, 1, 2010.
3. Zhang, X., A. Kalachev, and O. Kocharovskaya, *PRA*, Vol. 87, 013811, 2013.
4. Kalachev, A. and O. Kocharovskaya, *PRA*, Vol. 88, 033846, 2013.

Generation of Subnatural-linewidth Polarization-entangled Paired Photons

Hui Yan
Laboratory of Quantum Engineering and Quantum Materials
School of Physics and Telecommunication Engineering
South China Normal University, Guangzhou 510006, China

Abstract— Recently, subnatural linewidth biphotons are generated using continuous-wave spontaneous four-wave mixing (SFWM) in laser-cooled atomic ensembles with electromagnetically induced transparency (EIT) [1, 2]. Photons produced from this method not only have narrow bandwidth but also automatically match the atomic transitions. However, while this method provides a natural entanglement mechanism in the time-frequency domain, it is extremely difficult to produce polarization entanglement because of the polarization selectivity of EIT in a non-polarized atomic medium [3, 4].

Here, we report the demonstration of an efficient experimental scheme for producing polarization-entangled photon pairs from spontaneous four-wave mixing (SFWM) in a laser cooled ^{85}Rb atomic ensemble, with a bandwidth (as low as 0.8 MHz) much narrower than the rubidium atomic natural linewidth [5]. By stabilizing the relative phase between the two SFWM paths in a Mach-Zehnder interferometer configuration, we are able to produce all four Bell states. The long coherence time (up to 900 ns) and narrow bandwidth (about 1 MHz) make them ideal flying qubits for connecting remote atomic quantum nodes in a quantum network.

REFERENCES

1. Du, S. W., P. Kolchin, C. Belthangady, G. Y. Yin, and S. E. Harris, *Phys. Rev. Lett.*, Vol. 100, 183603, 2008.
2. Chen, J. F., S. Zhang, H. Yan, M. M. T. Loy, G. K. L. Wong, and S. Du, *Phys. Rev. Lett.*, Vol. 104, 183604, 2010.
3. Chen, Y. C., C. W. Lin, and I. A. Yu, *Phys. Rev. A*, Vol. 61, 053805, 2000.
4. Yan, H., S. C. Zhang, J. F. Chen, M. M. T. Loy, G. K. L. Wong, and S. W. Du, *Phys. Rev. Lett.*, Vol. 106, 033601, 2011.
5. Liao, K., H. Yan, J. He, S. Du, Z.-M. Zhang, and S.-L. Zhu, *Quantum Physics*, arxiv: 1402.2530, Feb. 11, 2014.

Compressive Quantum Sensing

John C. Howell
Department of Physics and Astronomy, University of Rochester, Rochester, NY 14627, USA

Abstract— Compressive sensing utilizes sparsity to realize efficient image reconstruction. It is a valuable processing technique when cost, power, technology or computational overhead are limited or high. In the quantum domain technology usually limits efficient acquisition of weak or fragile signals. I will discuss the basics of information theory, compression, and compressive sensing. I will then discuss our recent work in compressive sensing. The topics of discussion include low-flux laser Radar, photonic phase transitions, high resolution biphoton ghost imaging, Ghost object tracking, 3D object tracking and high dimensional entanglement characterization. I will touch lightly on our current work of rapid wavefunction reconstruction and wavefront sensing. As an example (shown below), we were able efficiently and rapidly reconstruct high dimensional joint probability functions of biphotons in momentum and position. With conventional raster scanning this process would take approximately a year, but using double-pixel compressive sensing, the pictures were acquired in a few hours with modest flux.

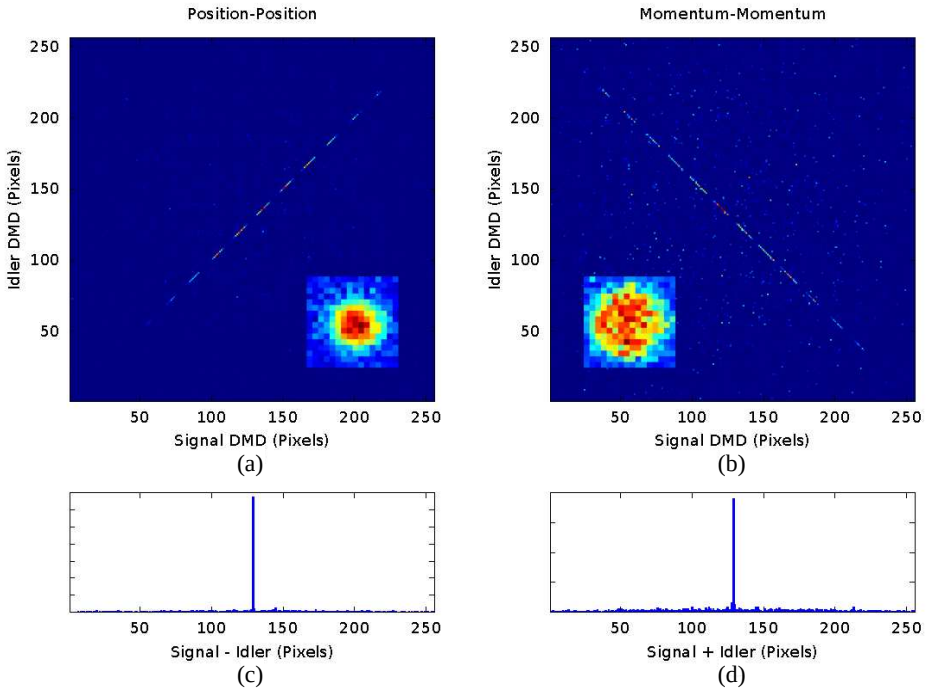

Detection Loophole-free Entanglement Verification

Xiao Yuan[1], **Ping Xu**[2, 3], **Luo-Kan Chen**[2, 3], **He Lu**[2, 3], **Xing-Can Yao**[2, 3], **Xiongfeng Ma**[1], **Yu-Ao Chen**[2, 3], **and Jian-Wei Pan**[2, 3]

[1]Center for Quantum Information, Institute for Interdisciplinary Information Sciences
Tsinghua University, Beijing 100084, China
[2]Hefei National Laboratory for Physical Sciences at Microscale, Department of Modern Physics
University of Science and Technology of China, Hefei, Anhui 230026, China
[3]Shanghai Branch, CAS Center for Excellence and Synergetic Innovation Center in Quantum Information
Quantum Physics University of Science and Technology of China, Shanghai 201315, China

Abstract— Entanglement, the essential resource in quantum information processing, needs to be witnessed in many tasks such as quantum communication and quantum computing. The conventional entanglement witness method, relying on trustful implementations of measurements, could wrongly conclude a separable state to be entangled due to imperfect detection devices. Inspired by the idea of the time-shift attack, we construct an attack on the conventional entanglement witness process and demonstrate that a separable state can be falsely identified to be entangled. To close such detection loopholes, we design and experimentally demonstrate a measurement-device-independent entanglement witness for a variety of two-qubit states. By the new scheme, we show that an entanglement witness can be realized without detection loopholes.

Introduction: Quantum entanglement plays an important role in the nonclassical phenomenons of quantum mechanics. A conventional way to detect entanglement is called entanglement witness (EW), which gives one of two outcomes: Yes or No, corresponding to the conclusive result that the state is entangled or to failure to draw a conclusion, respectively. A faithful conclusion of such witness relies on the correctness of the experimental implementation, imperfections of detection devices could wrongly conclude a separable state to be entangled.

Main Result: On the other hand, there is a strong connection between the EW and the quantum key distribution (QKD) where an entanglement-breaking channel would cause insecurity. For the varieties of attacks in the QKD we construct and experimentally realize a time-shift attack that manipulates the efficiency mismatch between detectors used in an EW process [1]. Under this attack, any state could be witnessed to be entangled, even if the input state is separable. By this example, we demonstrate that there do exist loopholes in the conventional EW procedure.

In quantum key distribution, the technique of measurement-device-independent is immune to all hacking strategies on detection [2]. Due to the similarity between the QKD and the EW, Branciard et al. proposed a measurement-device-independent (MDI) entangelement-witness (MDIEW) method [3], where they proved that there always exists an MDIEW for any entangled state with untrusted measurement apparatuses. Based on this proposal, we design and implement the MDIEW for the bipartite scenario, which is immune to all detection loopholes [1].

ACKNOWLEDGMENT

This work has been supported by the National Basic Research Program of China Grants No. 2011C BA00300, No. 2011CBA00301, No. 2011CB921300, and No. 2013CB336800, the National Natural Science Foundation of China Grants, and the Chinese Academy of Sciences.

REFERENCES

1. Xu, P., X. Yuan, L. K. Chen, et al., "Implementation of a measurement-device-independent entanglement witness," *Phys. Rev. Lett.*, Vol. 112, No. 14, 140506, 2014.
2. Lo, H. K., M. Curty, and B. Qi, "Measurement-device-independent quantum key distribution," *Phys. Rev. Lett.*, Vol. 108, No. 13, 130503, 2012.
3. Branciard, C., D. Rosset, Y. C. Liang, et al., "Measurement-device-independent entanglement witnesses for all entangled quantum states," *Phys. Rev. Lett.*, Vol. 110, No. 6, 060405, 2013.

Efficient Raman Conversion Based on the Atomic Coherence

Liqing Chen[1], **Z. Y. Ou**[1, 2], **and Weiping Zhang**[1]

[1]Quantum Institute of Light and Atoms, State Key Laboratory of Precision Spectroscopy
Department of Physics, East China Normal University, Shanghai 200062, China
[2]Department of Physics, Indiana University-Purdue University Indianapolis
402 N. Blackford Street, Indianapolis, Indiana 46202, USA

Abstract— We will report on our latest experimental results on efficient Raman conversion. Firstly, we studied experimentally the phase relation between the atomic spin wave and Stokes field produced by the spontaneous Raman scattering. Due to the spontaneous nature of the Raman process [1, 2], the phase of the Stokes field and the atomic spin wave change randomly from one realization to another but are anti-correlated to each other [3]. Then based on this phase correlation, we demonstrated a phase sensitive Raman scattering [4] by injecting a Stokes light seed into atomic vapor, whose internal state is set in such a way that it is coherent with the input Stokes seed. The phase sensitive property is a result of interference effect due to the phase correlation between the injected Stokes light field and the internal state of the atomic ensemble in the Raman process. The constructive interference leads to an enhanced Raman efficiency that is larger than other kinds of Raman processes such as stimulated Raman process with Stokes seed injection alone or enhanced Raman scattering with initially prepared atomic coherence. We applied this constructive enhancement effect combined with coherent feedback effect to achieve an efficient Raman conversion at a low Raman pump power of a few 100 μW [5]. The conversion efficiency is about 40–50% for the Stokes field and 20–30% for the anti-Stokes field, respectively. At last, based on such coherent feedback Raman scattering, we improved the retrieval efficiency in reading out the atomic spin wave in a hot ^{87}Rb atomic vapor cell. As high as 90% stored information can be read out from atomic ensemble and is converted into photon using a read laser with low power (~ 50 mW) and a large detuning frequency (~ 3 GHz). These technologies may find applications in precision spectroscopy, quantum optics and precise measurement.

REFERENCES

1. Chen, L., G.-W. Zhang, C.-L. Bian, Z. Y. Ou, and W. Zhang, *Optics Letters*, Vol. 36, 2740, 2011.
2. Chen, L., C.-L. Bian, G.-W. Zhang, Z. Y. Ou, and W. Zhang, *Physical Review A*, Vol. 82, 033832, 2010.
3. Bian, C.-L., L. Chen, G.-W. Zhang, Z. Y. Ou, and W. Zhang, *EPL*, Vol. 97, 34005, 2012.
4. Yuan, C.-H., L. Q. Chen, Z. Y. Ou, and W. Zhang, *Phys. Rev. A*, Vol. 87, 053835, 2013.
5. Chen, B., K. Zhang, C. Bian, C. Qiu, C.-H. Yuan, L. Q. Chen, Z. Y. Ou, and W. Zhang, *Optics Express*, Vol. 21, 010490, 2013.

Exploring a New Scheme for Ramsey-CPT Atomic Frequency Standard

Jing Yang[1], **Yuan Tian**[2], **Bozhong Tan**[2], **and Sihong Gu**[1, 2]

[1]Key Laboratory of Atomic Frequency Standards
Wuhan Institute of Physics and Mathematics, Chinese Academy of Sciences, Wuhan, China
[2]Wuhan National Laboratory for Optoelectronics
Huazhong University of Science and Technology, Wuhan, China

Abstract— The narrow linewidth Ramsey Coherent Population Trapping (CPT) interference fringe obtained from phase interference between separately generated CPT resonances can be used to implement atomic clock, and a short term frequency stability of $10^{-13}\tau^{-1/2}$ has been achieved with a Ramsey-CPT atomic clock [1, 2]. However, in prevalent Ramsey-CPT atomic clock schemes atoms interact with the pulsed laser and an acousto-optic modulator (AOM) is used to generate the pulsed laser [1–3], and the AOM prevents the clock from a compact one. We propose a frequency switching Ramsey-CPT atomic clock scheme. In the scheme a vertical cavity surface emitting laser (VCSEL) drove by periodically microwave modulated current is employed to provide laser for interacting with atoms, and the VCSEL's output switches between monochromatic and multichromatic laser. When the multichromatic laser illuminating atomic vapor cell its two frequency components interact with atoms to generate CPT resonance and when the monochromatic laser illuminating the cell there is no interaction due to off resonance between laser and the atom. Therefore Ramsey-CPT interference can be realized by twice resonances between multichromatic laser and the atoms. We have experimentally studied the scheme and compared with the prevalent one, our experimental results reveal that the frequency stability of the proposed Ramsey-CPT atomic clock could be competitive with that of the prevalent schemes. With eliminating AOM, the physics package is basically the same as that of the conventional CPT atomic clock, while the resource budget of the electronics will also be close although a microwave switch will be added Therefore, it is promising to realize a competitive compact Ramsey-CPT atomic clock through the proposed scheme.

REFERENCES

1. Boudot, R., S. Guerandel, E. de Clercq, N. Dimarcq, and A. Clairon, "Current status of a pulsed CPT Cs cell clock," *IEEE Trans. Instrum. Meas.*, Vol. 58, 1217–1222, 2009.
2. Castagna, N., R. Boudot, S. Guerandel, E. de Clercq, N. Dimarcq, and A. Clairon, "Investigations on continuous and pulsed interrogation for a CPT atomic clock," *IEEE Trans. Ultrason., Ferroelect., Freq. Contr.*, Vol. 56, 246–253, 2009.
3. Peter, Y., Z. Yi, L. Guobin, D. Wei, Y. Li, and G. Sihong, "Multipulse Ramsey-CPT interference fringes for the ^{87}Rb clock transition," *Europhys. Lett.*, Vol. 97, 1–5, 2012.

Sub-MHz Narrow-band Biphoton Generation

Luwei Zhao, Xianxin Guo, Chang Liu, Yuan Sun, M. M. T. Loy, and Shengwang Du
Hong Kong University of Science and Technology, China

Abstract— We report our recent progress in generating biphotons with sub-megahertz bandwidth from cold atomsby spontaneous four-wave mixing. These narrow-band paired photons, having a long coherence time up to about 2 μs, are ideal for single-photon interferometry, quantum storage and teleportation, as well long distance quantum communication. We will describe both theory and experiment.

Holographic Microscopy at Quantum Limits

Saijun Wu
Department of Physics, Fudan University, China

Abstract— We theoretically develop and experimentally demonstrate a holographic method for imaging large objects at diffraction and photon shot noise limits. Aided by a double point source reference field, a simple iterative algorithm robustly removes the twin image of an ^{87}Rb cold atom sample during the image reconstruction. Shot-noise limited phase shift and absorption images are consistently retrieved at various probe detunings, and during the laser cooling process. We consistently resolve less than 2 mrad phase shift (0.4% attenuation) of the probe light, outperforming shot-noise limited phase-contrast (absorption) imaging by a factor of 4 or more if the same camera is used without pixel saturation. In the second part of the presentation I will discuss possible extension of this work for holographic imaging beyond diffraction and shot noise limits using non-classical state of light.

Session 3A10a
SC3: Nanoimprint and Applications

Nanoimprint on a Curved Surface

Xin Hu, Yushang Cui, Changsheng Yuan, and Haixiong Ge
Department of Materials Science and Engineering, College of Engineering and Applied Sciences
Nanjing University, Nanjing 210093, China

Abstract— The ability to pattern curved surfaces with high resolution is desired in many fields, such as MEMS, electronic devices, and optics. We developed a hybrid nanoimprint-soft Lithography (HNSL) technique and demonstrated its capability of patterning highly curved surface with sub-100 nm resolution. The key component of the technology was the mold, which consisted of an ultrathin rigid cross-linked patterning layer on an elastic PDMS support. The complementary mechanical properties of the rigid crosslinked patterning layer and elastic support of the hybrid mold are crucial factors for ideal imprinting results. The high mechanical strength of the rigid patterning layer is the key point to achieve high lithographic resolution. On the other hand, a soft and elastic support with high flexibility allows a conformal contact between mold and substrate without applying large imprint pressure. The flexible nature of the hybrid mold makes it suitable for curved and non-flat substrates.

A thin, uniform resist film is critical to the fabrication of nanostructures via a lithographic technique as required by the subsequent high-fidelity pattern transfer process. There are few existing resist coating methods that would provide resist films with sufficiently thin and uniform thickness on curved substrates. To solve this problem, based on HNSL, we introduce a double transfer UV-curing nanoimprint technique that is capable of forming a thin, uniform patterned resist film on substrates with flat, highly curved or even irregular surface topography. A lift off process is achieved by a degradable UV-cured resist without the assistance of a thermal plastic under-layer, and metal gratings are successfully fabricated on cylindrical optical fiber.

High Contrast Gratings Fabricated Using Nanoimprint Lithography for Full Color Reflective Display

He Liu, **Yuhan Yao**, **Shujin Huang**, **Yifei Wang**, **and Wei Wu**
Department of Electrical Engineering
University of Southern California, Los Angeles, CA 90089, USA

Abstract— Reflective displays are widely used in e-book readers for their unique properties, such as printing-like looking and low power consumption. These properties also bring about a number of potential applications in signage, electronic shelf-labels and display for portable devices [1]. So far, several approaches have been reported and commercialized on reflective displays, i.e., electrophoretic display [2], electrowetting display [3, 4], and cholesteric liquid crystal display [5]. However, most approaches are still suffering from some common drawbacks, like low brightness, low color saturation and small gamut volume [1]. In addition, to fully utilize the ambient light, a three-layer architecture is required, in which red, green and blue tunable band reflectors are stacked. Such architecture prefers each layer to have square function transmission and reflection spectra, which cannot be realized using inks based on dyes or pigments. Subwavelength dielectric grating filter has the potential to fulfill the above requirements [6]. However, to our knowledge, no methods to tune the reflectance of resonant grating filters have been reported. Here we report a full color reflective display based on high contrast gratings in which the reflectance is tuned by driving liquid to/from the grating region.

Three different types of 2-dimentional subwavelength SiNx gratings on glass substrates are designed to reflect blue, green and red light respectively, in order to operate in a RGB trichromatic model. The three resultant reflection spectra cover most parts of the visible spectrum, and a reasonable saturation of each color has also been obtained. The gamut of these filters is comparable with the traditional LCD display. There gratings are fabricated by nanoimprint lithography (NIL) with flexible molds. The mother molds for the NIL are fabricated using interference lithography with a 266 nm laser.

The reflection of a resonance grating is intimately related to the index contrast between the grating material and that of its environment. Hence, when the grating is emerged in some liquid, the reflectance is greatly reduced, and most of the light will be transmitted, achieving a dark state of the filter. More details in design, fabrication and characterization will be presented.

REFERENCES

1. Heikenfeld, J., P. Drzaic, J.-S. Yeo, and T. Koch, "Review paper: A critical review of the present and future prospects for electronic paper," *Journal of the Society for Information Display*, Vol. 19, No. 2, 129, 2011.
2. Ota, I., J. Ohnishi, and M. Yoshiyama, "Electrophoretic image display (EPID) panel," *Proceedings of the IEEE*, Vol. 61, No. 7, 832–836, 1973.
3. Beni, G., "Electro-wetting displays," *Applied Physics Letters*, Vol. 38, No. 4, 207, 1981.
4. Hayes, R. A. and B. J. Feenstra, "Video-speed electronic paper based on electrowetting," *Nature*, Vol. 425, No. 6956, 383–385, Sep. 2003.
5. Yan, J., S.-T. Wu, K.-L. Cheng, and J.-W. Shiu, "A full-color reflective display using polymer-stabilized blue phase liquid crystal," *Applied Physics Letters*, Vol. 102, No. 8, 081102–081102, 2013.
6. Uddin, M. J. and R. Magnusson, "Highly efficient color filter array using resonant Si_3N_4 gratings," *Optics Express*, Vol. 21, No. 10, 12495, May 2013.

Strategy of High Aspect Ratio Structure Fabrication by Nanoimprint for Sub-wavelength Optical Elements

Yoshihiko Hirai
Graduate School of Engineering, Osaka Prefecture University
1-1 Gakuencho, Nakaku, Sakai, Japan

Abstract— Fabrication of high aspect ratio structure by nanoimprint lithography is investigated for polymer deformation and de-molding processes. Variable pressured process for polymer deformation and push back method for de-molding process are discussed for low defective high aspect ratio pattern fabrication.

Introduction: Fabrication of high aspect ratio pattern is demanded for sub-wavelength optical elements such as 1/4 wavelength plate or optical-optical switches. Nanoimprint lithography is one of the promising methods to fabricate high aspect ratio structure in cost effectively. However, defects in polymer deformation process and de-molding process are significant issues for industrial application. In this report, strategy of high aspect ratio structure fabrication by nanoimprint is reviewed in simulation and experimental works.

Polymer Deformation Process: High pressure is required in polymer deformation process, however it causes stress concentration in the polymer body and induces defects. To eliminate the defects, the pressure is reduced in the cooling process in thermal nanoimprint below glass transition temperature of the polymer. Using the variable pressured process, high aspect ratio pattern as high as 10 is demonstrated for 1/4 wavelength plate.

De-molding Process: Even if the polymer is successfully deformed, polymer stretching is induced in the de-molding process, which also causes stress concentration in the polymer and induces polymer breaking defects. The resist separation from the mold is simulated and low defective process is newly proposed by alternation of the mold pulling up and pushing down (push back method). Using the de-molding process, the defect is successfully eliminated because the separation occurs not only pulling up the mold but also pushing down. As a result, the separation is proceeded under lower de-molding load and eliminate the defects.

Conclusion: Strategy of high aspect ratio structure fabrication by nanoimprint is presented by the use of the variable pressured process for polymer deformation and push back method for de-molding process based on simulation works and experiments.

REFERENCES

1. Hirai, Y., et al., *J. Vac. Sci. Technol. B*, Vol. 21, 2765, 2003.
2. Kitagawa, T., et al., *Abstract of Micro and Nano Technology Conference (MNC) 2013*, 6A-3-4, Sapporo, 2013.

Nanoimprint Lithography Using Hydrogen Silsesquioxane Templates Fabricated by Helium Ion Beam Lithography

Wen-Di Li[1], **Jingxuan Cai**[1], **Wei Wu**[2], **Paul Alkemade**[3], **and Emile van Veldhoven**[4]

[1]Department of Mechanical Engineering, The University of Hong Kong, Hong Kong, China
[2]Department of Electrical and Computer Engineering, University of Southern California, Los Angeles, USA
[3]Delft University of Technology, Delft, Netherlands
[4]TNO, Delft, Netherlands

Abstract— Since the recent introduction of helium ion microscopes, the value of this unique tool has been immediately recognized for high-resolution nanolithography [1, 2]. Helium ion beam lithography (HIBL) exhibits important advantages over conventional electron-beam lithography, such as smaller beam spot size, higher sensitivity and very low proximity effect. These advantages combine to offer the capability of single-digit nanopatterning of dense structures over a large area, which is ideal for making unprecedented nanoimprint templates and duplicating high-resolution nanopatterns with a much reduced cost.

In this work, we will demonstrate our sub-4 nm nanoimprint results using a template fabricated by HIBL. Standard nested L patterns with various half pitches were fabricated in hydrogen silsesquioxane (HSQ) using a Carl Zeiss Orion Plus helium ion microscope equipped with a Raith ELPHY pattern generator. The developed nested L patterns in HSQ were used as a NIL template after properly treated with s surface release agent layer. Ultraviolete-curable nanoimprint lithography was carried out in a custom-built nanoimprinter with successful transfer of sub-4 nanometer patterns.

We further studied the three-dimensional energy dissipation of focused helium ions in the HSQ resist. Thick HSQ resist on a thin silicon nitride membrane was used to experimentally visualize the interaction volume of focused helium ions in the resist. Experimental results were compared with numerical modeling results and critical energy density to cross-link HSQ resist in HIBL was obtained. These results are important to fabricate practical nonoimprint templates with relatively high aspect ratios and may also open a new path to three-dimensional fabrication of nanostructures on membranes.

REFERENCES

1. Winston, D., et al., "Scanning-helium-ion-beam lithography with hydrogen silsesquioxane resist," *JVST B*, Vol. 27, No. 6, 2702–2706, 2009.
2. Sidorkin, V., et al., "Sub-10-nm nanolithography with a scanning helium beam," *JVST B*, Vol. 27, No. 4, L18–L20, 2009.

Fabrication and Integration of Memristive Nanodevices with Nanoimprint Lithography

Qiangfei Xia
Nanodevices and Integrated Systems Laboratory, Department of Electrical and Computer Engineering
University of Massachusetts, Amherst, MA 01003, USA

Abstract— Memristive devices (resistance switches) emerge as promising nanoelectronic components for a broad spectrum of applications in the next generation data storage and unconventional computing. As a non-volatile, two-terminal electronic device, the memristor has variable resistance that changes with the polarity and amplitude of the applied voltage. The typical structure of a memristor consists of a layer of switching material that is sandwiched between two electrodes. Using a cross-point structure these devices offer great scalability since the junction area is dependent solely on the width of the two nanowires.

We used nanoimprint lithography as the primary patterning tool and successfully fabricated crossbar arrays with each device as small as $8 \times 8\,\mathrm{nm}^2$. Due to the small size, the switching current of the device was as low as a few hundredpicoamperes. We also developed a self-aligned cross-bar fabrication technique using only onenanoimprint lithography step for all three layers (two electrodes and the switching layer), achieving forming-free memristive devices with low switching current. In this fabrication technique, a mold with cross-bar structures instead of nanowire arrays was used to pattern cross-bar-shaped trenches in the resist stack, followed by angle evaporation for metal electrodes, sputtering deposition of switching layer and liftoff. Finally, we integrated memristor crossbar arrays with CMOS substrates using nanoimprint lithography, leading to the first memristor/CMOS hybrid integrated circuits built on foundry-made CMOS substrates. The memristors served as the configuration bits and switches in a data routing network and were connected to gate-level CMOS components that acted as logic elements, in a manner similar to a field programmable gate array (FPGA). We demonstrated the ability to configure individual devices, use them to wire up various logic gates and a flip-flop, and then reconfigure devices. Our recent progress in integrating planar memristors with CMOS will also be presented.

Continuous Fabrication of Bio-inspired Dry Adhesives via Roll-to-roll Imprint Lithography

Hoon Eui Jeong[1] and Moon Kyu Kwak[2]

[1]Department of Mechanical Engineering
Ulsan National Instititue of Science and Technology, Ulsan 689-798, South Korea
[2]School of Mechanical Engineering, Kyungpook National University
1370 Sankyuk-dong, Buk-gu, Deagu 702-701, South Korea

Abstract— We report a continuous fabrication of bio-inspired dry adhesives by using a roll-to-roll process and modulated, elastic PUA (e-PUA). The e-PUA combined the major benefits of commercial PUA and PDMS, production speed and softness. Production speed can be increasing upto a few seconds as PUA and adhesion of fabricated sample was good like PDMS. A roll-type fabrication system consisted with a rigiflex mold and a UV exposure unit was developed for the continuous process. By integrating the apparatus and materials for roll-to-roll process on production of dry-adhesive, dry adhesives with mushroom shaped tips in the form of a thin flexible film can be produced in a highly continuous and scalable manner. The fabricated mushroom-like microstructures with controlled geometries exhibit good structural integrity, pull-off strength, and structural durability.

Beyond Conventional Nanoimprint — New Methods and Observations

Xing Cheng[1], **Zhong Zhang**[1], **Bingqing Luo**[2], **Yunbum Jung**[2], **Youwei Jiang**[2], **and Yi-Chen Lo**[2]

[1]Department of Materials Science and Engineering
South University of Science and Technology of China, Shenzhen, Guangdong 518055, China
[2]Department of Electrical and Computer Engineering
Texas A&M University, College Station, TX 77843-3128, USA

Abstract— Nanoimprint lithography (NIL) is alithographic technique that can fabricate nanoscale structures with high resolution, low cost and high throughput. However, conventional thermal NIL needs long process cycle time and has the issues of thermal expansion mismatch and mechanical abrasion. UV NIL is usually done at room temperature and has its own limitations, such as liquid resist films that can increase the possibility of sticking to molds. In the first part of this talk, we discuss a new method to perform nanoimprint. In this method, nanoimprint mold with integrated heater is designed for synergistic thermal and UV NIL so that the advantages of both thermal and UV NIL can be utilized. We expect that the synergistic thermal and UV NIL can fabricate nanostructures with much more versatile processes.

In thermal nanoimprint, thermoplastic polymers are shaped into patterns by polymer flow under pressure at a temperature above the glass transition temperature (Tg) of the polymer. It is well known that nanoimprinted thermoplastic polymer micro- and nanostructures are not stable and pattern decay due to internal stress relaxation can occur at a temperature close to or even below the polymer's Tg. Such thermal instability negatively impacts the applications of thermoplastic polymer micro- and nanostructures patterned by nanoimprint. In the second part of this talk, we report that shallow nanostructures of thermoplastic polycarbonate have exceptional thermal stability on chromium layer even at temperatures well above the Tg of polycarbonate. The implications of such observation for thermal nanoimprint will bed is cussed in detail, including fine pattern control through polymer reflow and step-and-repeat thermal nanoimprint.

Session 3A10b
SC3: Heterogeneous Photonic Integration Technologies and Devices on Silicon

Selective Epitaxial Growth of III-Vs on Patterned 300 mm Si Substrate

Zhechao Wang[1], **Clement Merckling**[2], **Bin Tian**[1], **Weiming Guo**[2], **Marianna Pantouvaki**[2], **Joris Van Campenhout**[2], **and Dries Van Thourhout**[1]

[1]INTEC-department, Ghent University-IMEC, Sint-Pietersnieuwstraat 41, Ghent 9000, Belgium
[2]IMEC, Kapeldreef 75, Heverlee 3001, Belgium

Abstract— Emerged more than a decade ago, silicon photonics has been widely recognized as the best integration platform for various applications of optical data transmission, mainly due to its direct compatibility with CMOS infrastructure and its very compact size. While most of the required building blocks have been demonstrated, the key functionality of light generation has become the most challenging task, and the co-integration of other materials becomes essential. III-V material is the dominating material platform for active optoelectronic devices. The introduction of III-Vs on a silicon photonics chip has been widely explored by using bonding technology, and great achievements have been made. Nevertheless, bonding technology has its own limitations, e.g., the relatively high cost, the incompatibility with CMOS, the low yield, etc. Therefore, integration of III-Vs on silicon by epitaxial growth can be the optimal solution, as long as the huge lattice constant and polarity difference between the two materials can be effectively overcome.

In this report, we present the selective growth of InP and InGaAs on patterned 300 mm (001) silicon substrate. CMOS compatible processes were carried out to form nano-scale SiO_2 trenches on silicon, and the defect-trapping effect of the narrow trench dramatically reduces the defect density of the III-Vs selectively grown inside and outside of the trench. To address the polar/non-polar interface obstacle for high quality growth, a unique design of the III-V/Si interface shape and also an optimized nucleation procedure was developed. Micro-PL measurement results show almost defect free III-Vs on silicon has been achieved. It is also interesting to find that the In content of InGaAs material grown on the intermediate InP buffer layer changes and hits the 1550 nm window by optimizing the trench width.

Hybrid InGaAsP-Si Distributed Feedback Laser Based on Selective-area Metal Bonding

Li Tao[1], **Lijun Yuan**[2], **Yanping Li**[1], **Hongyan Yu**[2], **Weixi Chen**[1], **Jiaoqing Pan**[2], **and Guangzhao Ran**[1]

[1]State Key Laboratory for Artificial Microstructure and Mesoscopic Physics
School of Physics, Peking University, Beijing 100871, China
[2]State Key Laboratory of Semiconductor Materials Science
Institute of Semiconductor, Chinese Academy of Science, Beijing 100083, China

Abstract— The integrated silicon photonics can afford complex higher functionality, higher speed interconnect and parallel many-core computation with low cost, and an electrical silicon light source (laser) is a key element for that, it has been shown that silicon evanescent lasers based on silicon-on-insulator (SOI) platform which evanescently couple the optical mode to a silicon waveguide show great potential for industrial scale fabrication. a few of bonding methods have been used to develop silicon evanescent lasers, such as direct wafer bonding, BCB bonding, and selective-area metal bonding (SAMB).

Based on the existing bonding technology, an increasing attention has been paid to the single mode laser, Distributed feedback lasers are attractive for these because of its stable and highly reliable single-mode operation. This paper reports a Hybrid InGaAsP-Si distributed feedback laser based on selective-area metal bonding. The laser has a typical threshold current of 50 mA and emitting at 1546 nm with sidemode suppression ration of 20 dB at room temperature. Compared to the other bonding methods to developing silicon evanescent lasers, the bonding step is performed after all the silicon components and III-V ones are finished in parallel, avoiding the crossover of the silicon and III-V process flow.

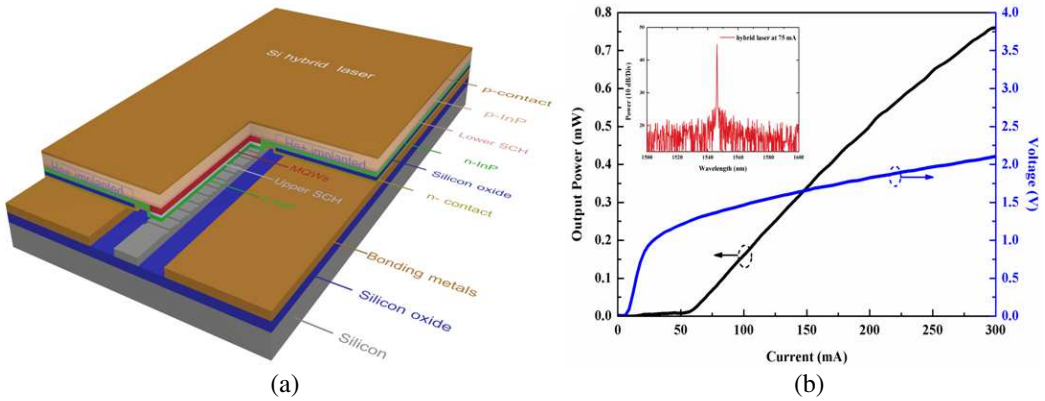

(a) (b)

Figure 1: (a) Schematic drawing of the InGaAsP-Si hybrid laser (not to scale). (b) Typical curves of voltage and light output power versus pulsed injection current of the hybrid laser at room temperature. Inset figure is the lasing spectrum.

Graphene-based Transparent Nano-heater for Thermally-tuning Silicon Nanophotonic Integrated Devices

Longhai Yu, Sailing He, Jiajiu Zheng, and Daoxin Dai
State Key Laboratory for Modern Optical Instrumentation
Centre for Optical and Electromagnetic Research
Zhejiang Provincial Key Laboratory for Sensing Technologies
Zhejiang University, Zijingang Campus, Hangzhou 310058, China

Abstract— For the traditional metal heaters used for silicon-on-insulator (SOI) nanowires, a thick SiO_2 upper-cladding layer is usually required between the metal heater and the silicon core to isolate metal absorption, which however introduces some disadvantages (e.g., low response speed, low heating efficiency, and low maximal temperature). In order to solve these problems, in this paper we propose and demonstrate a graphene-based transparent nano-heater on SOI nanowires. The present transparent graphene nano-heater is designed to contact directly with the silicon core of an SOI nanowire by utilizing the transparency of graphene. The lack of the thick SiO_2 upper-cladding layer between the heater and the core region helps make a fast thermally-tuning nanophotonic integrated device. It is also beneficial to improve the heating efficiency because the heating volume is shrunk significantly. The graphene nano-heater is designed optimally to avoid any significant excess loss for the guided modes in the SOI nanowires. For example, the theoretical propagation losses of TE- and TM-polarization modes of a 600 nm-wide SOI nanowire with a 100 nm-wide graphene nano-heater are as low as $\sim 0.005\,\mathrm{dB/\mu m}$ and $\sim 0.013\,\mathrm{dB/\mu m}$ respectively. With this graphene-based transparent nano-heater, we present a thermally-tuning silicon Mach-Zehnder interferometer (MZI). The power consumption to have π phase-shift is $\sim 7.6\,\mathrm{mW}$ and $\sim 8.1\,\mathrm{mW}$ for TE- and TM-polarization modes, respectively. The theoretical response time is at the order of sub-microsecond, which is about two orders faster than that for the case of using a traditional metal heater. In addition, the temperature of the silicon core is almost the same as that of graphene nano-heaters. In contrast, for the case of traditional metal heaters, the silicon core has much lower temperature than the metal heater while the metal heater has a limited maximal operation-temperature. This indicates that one can achieve higher achievable temperature for the silicon core with the present graphene nano-heater than the traditional metal heater. Graphene can also be used as a heat conductor (other than heater) by utilizing its high thermal conductivity of up to $5300\,\mathrm{W/m{\cdot}K}$. The excellent thermal properties of graphene make it very useful to enable efficient thermally-tuning nanophotonic integrated devices including optical switches, optical filters, etc..

Nanoscale Integrated Photonic Devices Based on Plasmonic Microstructures

Xiaoyong Hu
State Key Laboratory for Mesoscopic Physics, Department of Physics
Peking University, Beijing 100871, China

Abstract— Plasmonic microstructures can confine light into subwavelength scale regions and exhibit strong plasmonic enhancement, which provides an excellent platform to construct nanoscale photonic devices and to realize direct integration with solid-state chips. Photon router is an essential integrated photonic device widely used in fields of optical interconnection networks and ultrahigh-speed information processing chips. Photon router has the function of routing different signal lights to different terminal channels. Various schemes have been proposed to demonstrate photon router by using different phenomena and configurations, such as utilizing photonic crystal slow light waveguides, waveguide side-coupled microcavities, and optical fiber Sagnac interferometers. The feature size was larger than 100 μm for photon router based on conventional dielectric materials, which restricts the practical on-chip applications of these devices. We realized an ultrawide-band photon routing based on rainbow-trapping like effect in a chirped plasmonic grating. The photon routing sample was fabricated by using focused ion beam etching method, which was composed of a gold film coated with a chirped dielectric grating made of organic polymer poly [2-methoxy-5- (2-ethylhexyloxy)-1, 4-phenylenevinylene] (MEH-PPV). The length and the width of the photon routing sampler were 16 μm and 10 μm respectively. The operating bandwidth reached 200 nm through scanning near-field optical microscopy measurement. The photon routing function could be modulated through adjusting the structural parameters of chirped plasmonic grating. A shift of 0.5 μm in the terminal channel was achieved for the 850-nm incident laser when the groove width changes from 150 to 180 nm. Moreover, an ultrafast and low-power nanoscale all-optical switching was also realized by using a plasmonic microstructure composed of polycrystalline lithium niobate and gold.

Session 3A11
SC1: Advanced Mathematical and Computational Methods in Electromagnetic Theory and Their Applications

On an Application of the Hypothesis for the Identity of the $L_2(c, \rho, n)$ and $\hat{L}_2(\hat{c}, \hat{\rho}, \hat{n})$ Numbers

Mariana Nikolova Georgieva-Grosse[1] and Georgi Nikolov Georgiev[2]

[1]Consulting and Researcher in Physics and Computer Sciences, D-70839 Gerlingen, Germany
[2]Faculty of Mathematics and Informatics
University of Veliko Tirnovo "St. St. Cyril and Methodius", BG-5000 Veliko Tirnovo, Bulgaria

Abstract— Recently, it has been suggested [1] that if it holds: $c = \hat{c}$, $\rho = \hat{\rho}$ and $n = \hat{n}$, where c and $\hat{c}$ are limited arbitrary real numbers, ρ and $\hat{\rho}$ are real positive ones, less than unity, and n and $\hat{n}$ are natural and positive integer, resp., then it is fulfilled: $L_2(c, \rho, n) \equiv \hat{L}_2(\hat{c}, \hat{\rho}, \hat{n})$, where $L_2(c, \rho, n)$ and $\hat{L}_2(\hat{c}, \hat{\rho}, \hat{n})$ are finite real positive numbers, connected with the positive purely imaginary, resp. real zeros in x, resp. in $\hat{x}$ of a special function, constructed by two complex $\Phi(a, c; x)$ and $\Phi(a, c; \rho x)$, resp. real $\hat{\Phi}(\hat{a}, \hat{c}; \hat{x})$ and $\hat{\Phi}(\hat{a}, \hat{c}; \hat{\rho}\hat{x})$ Kummer, and two complex $\Psi(a, c; x)$ and $\Psi(a, c; \rho x)$, resp. real $\hat{\Psi}(\hat{a}, \hat{c}; \hat{x})$ and $\hat{\Psi}(\hat{a}, \hat{c}; \hat{\rho}\hat{x})$ Tricomi confluent hypergeometric ones [2] of appropriately picked out complex a and real c, resp. real $\hat{a}$ and $\hat{c}$ parameters and a positive purely imaginary x or ρx, resp. real $\hat{x}$ or $\hat{\rho}\hat{x}$ variable. This assumption has been called Hypothesis for the identity of the $L_2(c, \rho, n)$ and $\hat{L}_2(\hat{c}, \hat{\rho}, \hat{n})$ numbers [1]. It has been substantiated numerically with different degree of accuracy, depending on the values of parameter $c(\hat{c})$ [1].

In this investigation an application of the above statement in the theory of azimuthally magnetized coaxial ferrite waveguides [3–5], is considered. It has been found out earlier that there are $En_{1-} - (\hat{E}n_{1-}-)$ envelope curves in the the $\bar{\beta}(\bar{r}_0) - [\bar{\hat{\beta}}^{(1)}(\bar{\hat{r}}_0^{(1)})-]$ phase diagram of the normal TE_{0n} [3–5] (of the the $T\hat{E}_{0\hat{n}}^{(1)}$ wave which is the one of the two possible slow $T\hat{E}_{0\hat{n}}$ [4]) modes of equation $\bar{\beta}_{en-} = \bar{\beta}_{en-}(\bar{r}_{0en-})$ $[\bar{\hat{\beta}}_{en-}^{(1)} = \bar{\hat{\beta}}_{en-}^{(1)}(\bar{\hat{r}}_{0en-}^{(1)})]$, written in parametric form as: $\bar{r}_{0en-} = L(c, \rho, n)/[|\alpha_{en-}|(1-\alpha_{en-}^2)^{1/2}]$, $\bar{\beta}_{en-} = (1-\alpha_{en-}^2)^{1/2}(\bar{\hat{r}}_{0en-}^{(1)} = \hat{L}_2(\hat{c}, \hat{\rho}, \hat{n})/\{|\hat{\alpha}_{en-}^{(1)}|[1-(\hat{\alpha}_{en-}^{(1)})^2]^{1/2}\}$, $\bar{\hat{\beta}}_{en-}^{(1)} = [1-(\hat{\alpha}_{en-}^{(1)})^2]^{1/2})$ with $c = \hat{c} = 3$ [3–5]. Here $\bar{\beta}$ and $\bar{r}_0$ ($\bar{\hat{\beta}}^{(1)}$ and $\bar{\hat{r}}_0^{(1)}$) are the normalized in a special way phase constant and guide radius, $\rho(\hat{\rho})$ is the relative thickness of the central switching conductor of the structure, $\alpha(\hat{\alpha})$ is the off-diagonal ferrite Polder permeability tensor, $n(\hat{n})$ — order of the mode. All quantities without (with) hats relate to the normal (slow) modes, those with the superscripts (1) — to the slow $T\hat{E}_{0\hat{n}}^{(1)}$ waves and the ones with the subsript "$en-$" — to the envelopes. (Note that both α and $\hat{\alpha}^{(1)}$ are less than unity.) The $En_{1-}-(\hat{E}n_{1-}-)$ line for specific $n(\hat{n})$ restricts from above (below) the phase characteristics for negative (clockwise) ferrite magnetization. It follows from the Hypothesis for identity of numbers that if $\rho = \hat{\rho}$ and $n = \hat{n}$, the envelopes in question for a TE_{0n} and a $T\hat{E}_{0\hat{n}}^{(1)}$ mode of the same order in two waveguides of the same relative thickness of the inner wire (or in given configuration) coincide. Accordingly, it could be regarded as a line at which the normal mode is transformed to a slow one when the normalized radius (i.e., frequency) grows. Graphical results for different parameters $\rho(\hat{\rho})$ are presented and juxtaposed, assuming $n = \hat{n} = 1$.

REFERENCES

1. Georgiev, G. N. and M. N. Georgieva-Grosse, "Hypothesis for the identity of the $L_2(c, \rho, n)$ and $\hat{L}_2(\hat{c}, \hat{\rho}, \hat{n})$ numbers and its application in the theory of waveguides," *Progress In Electromagnetics Research Symposium Abstracts*, 805–806, Stockholm, Sweden, August 12–15, 2013; *PIERS Proceedings*, 940–945, Stockholm, Sweden, August 12–15, 2013.
2. Tricomi, F. G., *Funzioni Ipergeometriche Confluenti*, Edizioni Cremonese, Rome, Italy, 1954.
3. Georgiev, G. N. and M. N. Georgieva-Grosse, "New elements in the theory of the coaxial waveguide with azimuthally magnetized ferrite," *Proc. Int. Sem. Days Diffr. 2005, DD'05*, 81–93, in Abstracts, 29, St. Petersburg, Russia, June 28–July 1, 2005.
4. Georgiev, G. N. and M. N. Georgieva-Grosse, "A property of the $L(c, \rho, n)$ numbers and its application to waveguide propagation," *Proc. XXIX URSI General Assembly*, BK.6(120), CDROM, Chicago, IL, USA, August 7–16, 2008.
5. Georgieva-Grosse, M. N. and G. N. Georgiev, "Transmission properties of the circular waveguide completely or partially filled with azimuthally magnetized ferrite: Review of recent results," *Proc. 1st IEEE-APS Topical Conf. Antennas Propagat. Wireless Commun. IEEE*

APWC'11, 865–868, Turin, Italy, September 12–16, 2011 (Invited Paper in the Special Session "Advances in wireless communications and their applications" organized by M. N. Georgieva-Grosse and G. N. Georgiev).

Solving Nonlinear Helmholtz Equation via Fourier Series

M. S. Sautbekova and S. S. Sautbekov
Eurasian National University, Kazakhstan

Abstract— In recent work we represent a new way of solving non-linear Helmholtz equation. Undefined solution Helmholtz equation is reduced to the system of non-linear algebraic equations by spreading it in a Fourier series, in which we find Fourier coefficients. Later on, by these coefficients we can define our unknown function.

REFERENCES

1. Vladimirov, V. S., *Equations of Mathematical Physics*, Nauka, Moscow, 1981 (in Russian).
2. Schwartz, L., *Mathematics for the Physical Sciences*, MIR, Moscow, 1965 (in Russian).
3. Ferreira, A. C., M. B. C. Costa, A. G. Colho Jr., C. S. Sobrinho, J. L. S. Lima, J. W. M. Menezes, M. L. Lyra, A. S. B. Sombra, C. Xu, J. Weng, H. Li, and W. Xiong, "Analysis of the nonlinear optical switching in a Sagnac interferometer with non-instantaneous Kerr effect," *Optics Communications*, No. 5, 23–38; Vol. 285, No. 6, 1408–1417, 2012.
4. Mukherjee, P. K., "Pretransitional Kerr effect and nonlinear dielectric effect in the isotropic phase of the isotropic to smectic-E phase transition," *Journal of Molecular Liquids*, Vol. 175, 1–3, 2012.

Modeling of Electrical Contact with Dissimilar Materials

Y. Y. Lau, Peng Zhang, and R. M. Gilgenbach
Department of Nuclear Engineering and Radiological Sciences
University of Michigan, Ann Arbor, MI 48109-2104, USA

Abstract— Electrical contact is an important issue to high power microwave sources, pulsed power systems, field emitters, thin film devices and integrated circuits, and interconnects, etc.. Contact problems account for 40 percent of all electrical/electronic failures [1, 2], ranging from small scale consumer electronic devices to large scale military and aerospace systems.

For decades, the fundamental model of electrical contact has been that of Holm's a-spot [3], which consists of two semi-infinite cylinders of radius b placed together. Current can flow through them only via a circular hole of radius a ($\ll b$) at the interface. Thus Holm's a-spot is a poor representation of a realistic contact. By solving Laplace Equation exactly using Fourier series analysis, we vastly generalized Holm's model to include the effects of higher dimensions and of dissimilar materials, for vertical contacts both in bulk [4] and in thin film [5], as well as the horizontal contacts in thin film [6]. The analytic theory was spot-checked against the MAXWELL 2D code and validated in various limits. The current flow patterns from the exact theory are displayed. Scaling laws for, and bounds on, the contact resistance are presented. In the limit of small film thickness, we show that current crowding in the vertical contact is far less serious than the current crowding in the horizontal contact.

Most recently, we have extended our theory to include a resistive layer at the interface between the contact members, to model a typical metal-semiconductor contact. The regimes dominated by the specific contact resistance or by the spreading resistance are identified and compared with experimental data.

ACKNOWLEDGMENT

This work was supported by an AFOSR grant on the Basic Physics of Distributed Plasma Discharges, AFOSR Grant FA9550-09-1-0662, and L-3 Communications Electron Device Division.

REFERENCES

1. "Review of federal programs for wire system safety," National Science and Technology Council Final Report, 2000.
2. Kuzniar, J. S. and G. A. Slenski, "Wire integrity field survey of USAF legacy aircraft," ADP014075, Defense Technical Information Center, 2001.
3. Holm, R., *Electric Contact*, 4th Edition, Springer-Verlag, Berlin, 1967.
4. Zhang, P. and Y. Y. Lau, "Scaling laws for electrical contact resistance with dissimilar materials," *J. Appl. Phys.*, Vol. 108, 044914, 2010.
5. Zhang, P. and Y. Y. Lau, "Constriction resistance and current crowding in vertical thin film contact," *IEEE J. Electron Devices Soc.*, Vol. 1, 83, 2013.
6. Zhang, P., D. Hung, and Y. Y. Lau, "Current flow in a 3-terminal thin film contact with dissimilar materials and general geometric aspect ratios," *J. Phys. D: Appl. Phys.*, Vol. 46, 065502, 2013; Corrigendum, ibid, Vol. 46, 209501, 2013.

Numerical Analysis of the Plane Wave Scattering by the End-face of a Waveguide System

Akira Komiyama
Osaka Electro-Communication University, Hatsu-cho, Neyagawa-shi 572-8530, Japan

Abstract— An image fiber is composed of a large number of cores embedded in a single cladding, which is used to transmit directly an optical image. By illuminating the end-face of an image fiber with a laser beam a diffraction pattern reflecting the arrangement of cores can be simply observed. We can see experimentally that the diffraction pattern does not almost depend on the polarization of the laser beam. We are interested in the problem from a theoretical point of view.

The reflection and transmission of a guided mode by the cut-end of a dielectric slab waveguide and the coupling of a beam wave to a dielectric slab waveguide have been treated by the boundary integral equation [1, 2]. In their papers the approximated form of the Green's function in a waveguide region has been used and the integral equation has been solved numerically. The analytical treatment of the boundary integral equation is very difficult.

The scattering of an electromagnetic wave from a dielectric body has been treated by the volume integral equation for the electric field [3]. The scattered field is the field radiated from the electric polarization induced in a dielectric body by the incident field and the physical image is very clear. The solution of the volume integral equation can be easily expanded into a perturbation series and each term of the series can be derived analytically. The analytical representation gives a deep understanding of the scattering properties of a dielectric body.

The scattering of a plane wave by the end-face of a waveguide system composed of a large number of cores and a single cladding has been treated by the volume integral equation for the electric field [4]. The first order term of the perturbation solution has been derived and it has been shown that the far scattered field does not almost depend on the polarization of an incident wave.

In this paper, the scattering of a plane wave by the end-face of a two-dimensional waveguide system is treated by a numerical method based on the sinc function. The electric field at the end-face is expanded in terms of sinc functions and the expansion coefficients are determined from the boundary conditions. It is shown that the results are in good agreement with the results obtained by the perturbation method.

REFERENCES

1. Nishimura, E., N. Morita, and N. Kumagai, "Theoretical treatment of arbitrary shaped cut-ends of dielectric optical waveguide," *IECE Trans. Electron.*, Vol. J65-C, No. 7, 537–544, 1982 (in Japanese).
2. Nishimura, E., N. Morita, and N. Kumagai, "Theoretical study on the coupling of two-dimensional Gaussian beam to a dielectric slab waveguide," *IECE Trans. Electron.*, Vol. J67-C, No. 5, 474–481, 1984 (in Japanese).
3. Richmond, J. H., "Scattering by a dielectric cylinder of arbitrary cross section shape," *IEEE Trans. Antennas and Propagation*, Vol. 13, No. 3, 334–341, 1965.
4. Taki, A. and A. Komiyama, "Scattering of plane wave from the end-face of a threedimensional waveguide system," *IECE Trans. Electron.*, Vol. E94-C, No. 1, 63-67, 2011.

Numerical Solution of the Helmholtz Equation with Nonlinearity

O. V. Kravchenko and Ya. Yu. Konovalov
Bauman Moscow State Techinal University, Russian Federation

Abstract— The Helmholtz equation with a nonlinear term is considered from the numerical point of view. The corresponding boundary value Dirichlet problem is examined by finite-difference and collocation methods. Numerical techniques are also tested on a benchmark problems with an analytical solutions.

Synthesis of the Sparse Conformal Arrays with Convex Optimal Method

Xiaowen Zhao[1,2], **Qingshan Yang**[1], **and Yunhua Zhang**[1]

[1]Key Laboratory of Microwave Remote Sensing
Center for Space Science and Applied Research, Chinese Academy of Sciences, Beijing 100190, China
[2]University of Chinese Academy of Sciences, Beijing 100049, China

Abstract— Conformal antenna arrays have been widely used in various fields because of its low profile and easy for fitting to the structures. For conformal arrays, on one hand, the well-known Fourier transform relationship between element excitations and far field pattern breaks down and on the other hand, the array factor theory does not hold any more since that each element pattern depends on its own orientation, which make the corresponding synthesis problem significantly difficult. In previous works, the iterative least square techniques and the stochastic optimization approaches, such as the genetic algorithms (GA), the particle swarm (PS) and the ant colony optimization (ACO) algorithms have been widely applied to the synthesis of conformal array. However, fewer works have been done on thinning the conformal arrays in matching the desired pattern.

In this work, the convex optimal technique is applied to the synthesis of sparse conformal arrays for fitting the predefined patterns. The synthesis problem can be formulated by minimizing the number of active elements subjected to the constraints on the pattern requirements. To form the optimization problem, much dense elements are first assigned to equally spaced dense positions, which compose the conformal array aperture. And then, the element patterns attributed to the candidate positions are respectively transformed to expressions in global coordinate system. The conformal array pattern after discretization is written as the product of an excitation vector and a matrix, which is formed by the Kronecker product of element pattern matrix and the steering matrix. The number of active elements at candidate positions is equal to the l_0-norm of the excitation vector. It is worth noting that the l_0-norm should be replaced with its convex approximation, i.e., l_1-norm so as to avoid the NP-hard problem. By this way, the synthesis problem becomes convex, which is easy to form and can be efficiently solved using off-the-shelf numerical routines such as CVX. In numerical experiments, a 22-element sparse ring array (see Fig. 1(a)) is synthesized to achieve the desired pattern of a 30-element uniform ring array. Furthermore, the pattern of a uniformly spaced cylindrical array of 96 elements is used as a reference. The conformal array aperture in azimuth direction is discretized only. A sparse array composed of 79 elements has been synthesized. Fig. 1(b) shows the arrangement and excitation of the corresponding sparse array. In these two cases, the total matching errors of patterns in 3D are as small as 1.862×10^{-4} and 1.047×10^{-2}, respectively. Moreover, the reconstructed array would be sparser if we discrete the cylindrical aperture in axial direction further. These numerical simulations validate that the proposed algorithm is effective and efficient for synthesizing a sparse conformal array.

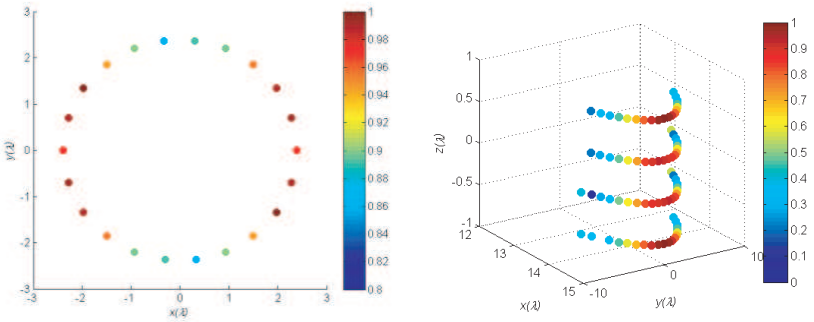

Figure 1: Layouts with excitations of the synthesized arrays: (a) a sparse ring array; (b) a sparse cylindrical array.

Airy Beams and an Analysis of Ray Superposition

Yuanhui Wen, Jiangbo Zhu, Yujie Chen, Yanfeng Zhang, Hui Chen, and Siyuan Yu
State Key Laboratory of Optoelectronic Materials and Technologies
School of Physics and Engineering, Sun Yat-sen University, Guangzhou 510275, China

Abstract— Since Siviloglou et al. observed the Airy beam within the context of optics in 2007 [1], a great deal of research work has been carried out toward Airy beams for its unique properties. Airy beams are non-diffracting, self-bending and self-healing waveforms, which makes them attractive to a variety of applications, such as optical micromanipulation, energy transmission and imaging. Moreover, as the only non-spreading packet for the two-dimensional (2D) paraxial wave equation, Airy wave packets are also promising in the field of plasmonics.

In this work, we start from the angular spectrum theory to study Airy beams in free space under the paraxial approximation and analyze the contribution to an Airy beams propagation by different parts of the spatial spectrum, given that the Airy beam passes through a spatial filter. Imitating the distinct frequency characteristic of Airy beams, we construct several similar beams called Airy-like beams. We find that some of these beams resemble the Airy beams with the characteristic of self-bending within a certain distance. During the investigation of Airy beams propagation, we conceive a different viewpoint to analyze the spread of light beams. Based on the idea of stationary phase approximation, the major contribution to the integral of angular spectrum theory is attributed to the points where its phase function is stationary. Therefore, taking the derivation of the phase function with respect to spatial frequency m, we can obtain the phase stationary point for its corresponding location in the space. Interestingly, all the locations in the space with the same phase stationary point fall into a line, which can be interpreted as each spatial frequency (m) corresponding to a light ray. And the optical field distribution becomes a superposition of all these light rays with the weight factor to be the function value. Using such a ray-superposition theory, we analyze the ideal Airy beams, exponentially modulated Airy beams, Kalnins-and-Miller-Airy beams, partial Airy beams, Airy-like beams we constructed, and do so even beyond the paraxial approximation. The results are consistent with that of the angular spectrum theory, which confirms the reliability of using such a ray-superposition theory to analyze the optical field distribution.

Such an analytical method constructed from a viewpoint of the ray-superposition and not limited to the paraxial approximation provides us a new understanding of the light beams propagation and intuitively explains the self-healing property of Airy beams as well as Airy-like beams. Moreover, such a method is beneficial in greatly simplifying the numerical calculation of optical field distribution at the cost of a little accuracy.

EM Scattering Computation of Electric-large Lossy Dielectric Target Based on Ray Tracing

Hao Zheng and Hongxia Ye
Key Lab of Wave Scattering & Remote Sensing Information, Fudan University, China

Abstract— The high frequency (HF) PO/GO computation based on ray tracing approach is presented to fast compute the EM scattering from arbitrary dielectric target with electric-large size. For lossy medium, the generalized Snell-Descartes and Fresnel laws are introduced to determine the propagation direction of equi-phase and equi-amplitude plane of reflection and refraction wave, which is the main difference from the classical ray tracing approach. The GO reflection and refraction rays are traced according to the propagation direction of equi-phase surface step by step. Accompany with the wave propagation, the phase delay is computed along the normal direction of equi-phase, and the energy attenuation is computed along the normal direction of equi-amplitude. On the exiting surface, the PO integration of surface field is considered for outgoing field computation. For lossy dielectric surface, the PO surface field is inhomogeneous, and this paper derives an analytical integral formula for arbitrary triangular patch to avoid the numerical integral on the dense meshing of 1/8 wavelength. In numerical simulation, the target is constructed with triangular dielectric patches according to its geometry CAD model, not need to mesh according to the electric wavelength. Several models, such as multi-layer dielectric plate, dielectric coating plate, lossy dielectric cubic, et al., are used for validation and comparison with FEKO software, taking the requirements of memory and CPU time into consideration. The numerical simulation indicates that the new HF method is valid and efficient for electric-large target with arbitrary dielectric medium.

ACKNOWLEDGMENT

This work was supported by the National Natural Science Foundation of China No. 61001007.

Effect of a Linear Frequency Modulation on the Nonlinear Dynamics of an Electromagnetic Pulse in a Graded-index Waveguide

I. M. Oreshnikov and M. A. Bisyarin
Faculty of Physics, Saint-Petersburg University, Saint-Petersburg, Russia

Abstract— In the recent years optical vortices has been widely researched and applied to the problems of optical trapping and manipulation, in quantum information processing and astronomy. Applied to communication systems OAM is often viewed as an additional degree of freedom that can be used for channel multiplexing. There are experiments demonstrating OAM light being used to increase channel capacity and spectral efficiency both in free space [1] and optical fibers [2].

The present paper deals with the nonlinear propagation of a vortex mode of a short electromagnetic pulse with a linear modulation of the carrier frequency in a waveguide with a strong dependence of the refractive index on the radial coordinate and a weak dependence on the longitudinal coordinate. Three different types of propagation modes are considered — ordinary radial modes (independent of the azimuth angle in waveguide's cross-section), azimuthal modes (stationary field distribution with respect to the azimuthal angle), and vortex modes (angular momentum modes). Nonlinear envelope dynamics is studied using the approach of [3] and its features conditioned by mutual action of vortex structure and chirp are distinguished.

The propagation process is described with a nonlinear wave equation

$$\Delta f - \left(\beta^2(\rho, s) + \frac{1}{2}\alpha^2(\rho, s)\,|f|^2\right)\frac{\partial^2 f}{\partial t^2} = 0$$

with a Kerr-like dependence of the refractive index on the EM field intensity. The waveguide is produced by a dependence of the linear part of the refractive index on the radial coordinate, with waveguide properties varying along its axis. The asymptotic solution of this equation with respect to a small parameter δ is sought for as

$$f(\rho, \varphi, s, t) = \delta F(\rho, \varphi, s, \theta) e^{i\left(R(s)/\delta^2 - t - \delta^3 \mu(s) t^2\right)} + \text{c. c.}$$

t the dimensionless time (related to high-frequency oscillations), s the stretched ($\propto \delta^2$) longitudinal coordinate, ρ the radius and φ the azimuth within the cross-section, $\mu(s)$ the quadratic phase modulation coefficient, $\theta = Q(s)/\delta - \delta t$ the phase of envelope, $Q(s)$ and $R(s)$ functions to be determined in course of the solution. The principal approximation to the complex amplitude F and the propagation constant $r(s) = R'(s)$ result from equation

$$\frac{\partial^2 F}{\partial \rho^2} + \frac{1}{p}\frac{\partial F}{\partial \rho} + \frac{1}{\rho^2}\frac{\partial^2 F}{\partial \varphi^2} + \left(\beta^2(\rho, s) - r^2(s)\right) F = 0$$

its solution must be bounded for $\rho = 0$, vanish for $\rho \to \infty$, and be 2π-periodic with respect to φ. The propagation modes of the types above mentioned are chosen as eigenvalues and eigenfunctions of this equation, with $\cos(m\varphi)$ dependence for azimuthal and $\exp(im\varphi)$ for vortex modes. General nonlinear evolution equations for envelopes of these modes are derived with coefficients depending on the longitudinal coordinate. For a quadratic dependence of β^2 on ρ explicit expressions can be presented for pulse shape, amplitude, width and velocity, thus illuminating the features imposed by the vortex structure of the chirped pulse on nonlinear dynamics of its envelope.

REFERENCES

1. Wang, J., et al., "Terabit free-space data transmission employing orbital angular momentum multiplexing," *Nature Photonics*, Vol. 6, 488–496, 2012.
2. Bozinovic, N., et al. "Terabit-scale orbital angular momentum mode division multiplexing in fibers," *Science*, Vol. 340, 1545, 2013.
3. Bisyarin, M. A., "Short chirp pulses in graded-index light guides," *Radiophysics and Quantum Electronics*, Vol. 49, No. 1, 58–64, 2006.

Session 3A12
SC4: Novel Frequency Selective Structures

Challenges in Designing Frequency Selective Surfaces to Yield Wide-angle Response over a Wide Frequency Band

Raj Mittra and Chiara Pelletti
EMC Lab, The Pennsylvania State University, 319 EE East, University Park, PA 16802, USA

Abstract— Frequency Selective Surfaces (FSSs) find a number of applications, for example as sub-reflectors in frequency reuse systems and as radomes for high performance aircrafts. One of the challenging problems encountered while designing FSSs is to simultaneously achieve a wide bandwidth, as well as a sharp transition from pass- to stop-band. In the past, several techniques have been applied to control the bandwidths of FSSs, which includes choosing certain element shapes to provide sharp frequency transitions, e.g., screens with thick apertures, and employing multiple layers of printed FSS screens.

Many practical applications of FSSs require that their filtering characteristics be wide-band and elliptical in nature. Conventional single-layer thin-screen versions of FSSs, which typically consist of two-dimensional periodic arrays of patches or slots, seldom ever satisfy this criterion. Approaches to improving the filtering performances of FSSs for broadband applications include dielectric loading and cascading; however, in most cases, the resulting frequency responses are Butterworth or Chebyshev functions with relatively narrow pass-bands.

A number of methods have been proposed to improve the performance of frequency selective surfaces, in a manner such that they exhibit a filtering response with a sharp rejection skirt similar to those of elliptical filters. In this paper we will begin by reviewing a number of different approaches that have been used to widen the *frequency* responses of FSSs Next, we will examine FSS configurations that have wide *angular* responses. Finally, we will discuss strategies for realizing responses of FSSs that are not only wideband, but also simultaneously cover a wide angular range; furthermore, their responses have relatively sharp roll-offs as well.

Our final topic in this presentation will be that of out-of-band-RCS reduction of FSSs, which is a very challenging problem, to say the least. This is because a typical FSS screen which is transparent in the desired frequency band is highly reflecting at out-of-band frequencies, whereas we desire it to be absorbing at these frequencies instead. We will identify the challenges and propose some possible solutions that appear to be promising.

Design and Optimization of a Wideband Circular Polarization Selective Structure

Andreas Ericsson and Daniel Sjöberg
Department of Electrical and Information Technology
Lund University, Box 118, Lund 221 00, Sweden

Abstract— We present a multi layer meander line circular polarization selective structure (CPSS). The design shows a significant increase in bandwidth and stability with respect to the angle of incidence compared to previous CPSS designs. The concept of operation is explained, and a three step iteration scheme is performed to find an optimized design with respect to predefined constraints. A sensitivity analysis has been performed indicating that the design is relatively robust with respect to variations in the design parameters, and that the key parameter is the distance between the meander line sheets.

Introduction: The satellite communication situation of today consist of crowded orbits, where the available reflector space of each satellite is very limited. To fulfill the constant demand of increased data rates, it is crucial to maximize the number of communication channels on each satellite. This can be achieved by utilizing frequency and polarization reuse schemes [1, Ch. 18]. Polarization reuse can be implemented either with a shared aperture reflector antenna or with a polarization diplexing surface, to achieve this in circular polarization is a hot topic in satellite communication as of today [1]. Several resonant CPSS concept designs has been presented through the last 40 years by Pierrot [2], Tilston [3] and Morin [4]. These designs have a limited bandwidth of about 7% and the performance of these structures deteriorates at oblique angles of incidence.

Concept Design: The concept design consists of cascaded periodic metal meander line sheets arranged with a pre-determined spacing, where each layer is rotated with respect to the previous layer in proportion to the distance. By arranging a number of meander line sheets after each other, the reflection of one handedness of circular polarization can be maximized while the reflection of the orthogonal handedness of circular polarization is minimized, thus circular polarization selectivity can be achieved. The fact that this design is non-resonant implies a significant increase in bandwidth with respect to previously presented CPSS designs. A three step iteration scheme is performed to find an optimized design with respect to predefined constraints. A sensitivity analysis has been performed indicating that the design is relatively robust with respect to variations in the design parameters, and that the key parameter is the distance between the meander line sheets.

The CPSS was implemented in a realistic design case as a flat circular polarization diplexer in the Fixed Satellite Service (FSS) K_a downlink band at $18\,\text{GHz} < f < 22\,\text{GHz}$. A simulation model was implemented in CST Studio Suite, where the meander line strips are printed on a kapton substrate, and the substrates are separated by a low permittivity stiffener material.

ACKNOWLEDGMENT

The work reported in this paper was performed under ESA Contract No. 4000108854/13/NL/MH.

REFERENCES

1. Imbriale, W. A., S. Gao, and L. Boccia, *Space Antenna Handbook*, Wiley Online Library, 2012.
2. Pierrot, R., "Reflector for circularly polarized waves," Mar. 30, 1970, US Patent 3,500,420, (French Patent No. 89 609, 1 512 598, Dec. 30, 1966).
3. Tilston, D., M. Tilston, S. Tilston, W. V. Tilston, and T. Tralman, "Polarization selective surface for circular polarization," Oct. 1, 1991, US Patent 5,053,785.
4. Morin, G., "Circular polarization selective surface made of resonant spirals," Jan. 18, 1994, US Patent 5,280,298.

Three-dimensional Loaded Dipoles for Applications in Frequency Selective Structures

A. K. Rashid[1, 2], **S. Ullah**[3], **and S. A. Nauroze**[2]

[1]Namal College Mianwali, Pakistan
[2]National University of Computer and Emerging Sciences, Pakistan
[3]National University of Science and Technology, Pakistan

Abstract— Conventional frequency selective surfaces consist of simple two-dimensional (2-D) unit-cell shapes like dipoles, loops, etc. [1, 2]. A number of variations to earlier simple shapes have been proposed over the last three decades, which lead to an advantage in certain applications [3–5]. This quest for finding the best shape continues till date, and more recently, a few three-dimensional unit-cell shapes have also been considered [6, 7]. Freedom of variation in third dimension actually offers more flexibility in designing innovative unit-cell geometries. It appears prudent to efficiently use the third dimension (thickness) of a frequency selective structure (FSS) in order to obtain improved performance of certain parameters. Based on that, it may be useful to reconsider the conventional FSS shapes, and modify them to utilize the freedom of third dimension. This may lead to better and interesting FSS designs, which may also be easy to analyze and fabricate with the present computational and manufacturing technology.

Dipole constitutes one of the earliest shapes used in FSS designs [1]. It has been a preferred choice for application in linearly polarized FSSs. A number of other FSS shapes have actually been derived from a dipole unit-cell, and they include loaded-dipoles [3], meander-lines [4], crossed-dipoles [8], Jerusalem cross [9], tri-poles [10], etc.. These modified forms basically lead to more compact shapes, which can also be applied in dual-polarized FSS.

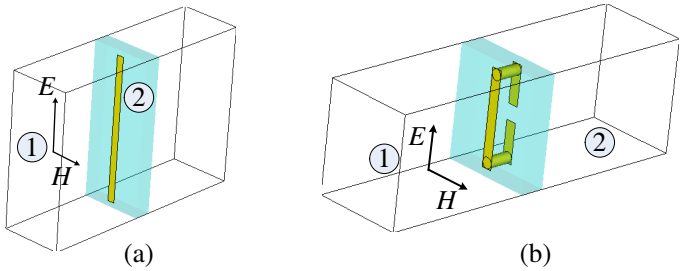

Figure 1: Unit-cell of (a) a conventional FSS consisting of unloaded strip dipoles. (b) The proposed FSS based on three-dimensionally loaded strip dipoles.

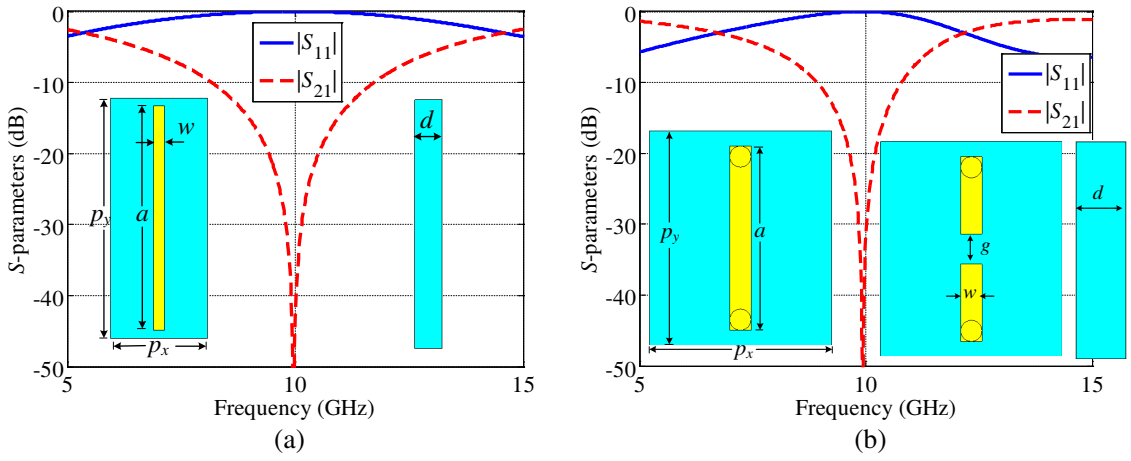

Figure 2: S-parameters of a conventional FSS compared with those of the proposed FSS, when two structures are printed on the same substrate ($\varepsilon_r = 2.2$) and designed for the same resonant frequency. $p_x = 6\,\text{mm}$, $w = 0.7\,\text{mm}$, $d = 1.6\,\text{mm}$. (a) Unloaded case: $p_y = 15\,\text{mm}$, $a = 14\,\text{mm}$, (b) loaded case: $p_y = 7.1\,\text{mm}$, $a = 6.1\,\text{mm}$, $g = 1\,\text{mm}$.

We study an FSS consisting of a 2-D periodic array of strip dipoles, which have been loaded with two cylinders and strips, along the thickness of the FSS. The two cylinders represent the two via-holes, which connect the opposite sides of a printed circuit board (PCB). Fig. 1 compares the unit-cell shape of a conventional FSS with that of our proposed structure. We print strips on the opposite sides of a PCB, and then join them through via-holes. Unlike the 2-D loading of dipoles [3], our proposed loading along the thickness of an FSS, does not affect the horizontal period of the original unloaded dipoles. With the proposed loading, it appears possible to realize a desirably small vertical period. A quick example is shown in Fig. 2, whereby the unit-cell dimensions of a conventional FSS (unloaded dipoles) can be compared with that of our proposed FSS when both are designed for the same resonant frequency. It is seen that the vertical period p_y of the loaded dipole is less than half of the vertical period of an unloaded dipole. Horizontal period p_x, spacing between the elements $p_y - a$, substrate height d, dielectric constant ε_r, and width of the strips w has been kept identical for the two cases. More results and comparisons are part of the full paper.

REFERENCES

1. Munk, B. A., *Frequency Selective Surfaces: Theory and Design*, John Wiley & Sons Inc., 2000.
2. Wu, T. K., *Frequency Selective Surface and Grid Array*, John Wiley & Sons Inc., 1995.
3. Munk, B. A., R. G. Kouyoumjian, and L. Peters, "Reflection properties of periodic surfaces of loaded dipoles," *IEEE Trans. on Antennas and Propag.*, Vol. 19, No. 5, 612–617, Sep. 1971.
4. Parker, E. A. and A. N. A. El-Sheikh, "Convoluted array elements and reduced size unit cells for frequency selective surfaces," *IEE Proc. Microwaves, Antennas and Propag.*, Vol. 138, No. 1, 19–22, Feb. 1991.
5. Zheng, S. F., Y. Z. Yin, H. L. Zheng, Z. Y. Liu, and A. F. Sun, "Convoluted and interdigitated hexagon loop unit cells for frequency selective surfaces," *Electron. Lett.*, Vol. 47, No. 4, 233–235, Feb. 2011.
6. Luo, G. Q., W. Hong, Q. H. Lai, K. Wu, and L. L. Sun, "Design and experimental verification of compact frequency-selective surface with quasi-elliptic bandpass response," *IEEE Trans. on Microwave Theory and Tech.*, Vol. 55, No. 12, 2481–2487, Dec. 2007.
7. Rashid, A. K., Z. Shen, and B. Li, "An elliptical bandpass frequency selective structure based on microstrip lines," *IEEE Trans. on Antennas and Propag.*, Vol. 60, No. 10, 4661–4669, Oct. 2012.
8. Hamdy, S. M. A. and E. A. Parker, "Influence of lattice geometry on transmission of electromagnetic waves through arrays of crossed dipoles," *IEE Proc. Microwaves, Antennas and Propag.*, Vol. 129, No. 1, 7–10, Feb. 1982.
9. Anderson, I., "An the theory of self-resonant grids," *The Bell System Technical Journal,* Vol. 54, No. 10, 1725–1731, 1975.
10. Pelton, E. L. and B. A. Munk, "Periodic antenna surface of triple slot elements," United States Patent 3,975,738, Aug. 17, 1976.

Split Ring Resonator Based Bandstop Frequency Selective Surface for Antenna RCS Reduction

Jiawei Yu, Jin Zhang, Yuan Jiang, Fei Cheng, and Xian Qi Lin
EHF Key Lab of Fundamental Science, University of Electronic Science and Technology of China, China

Abstract— Frequency Selective Surface (FSS) was first proposed in 1960s, a lot studies have focused on it for its potential military applications. Like filters, FSS can be roughly categorized by its frequency response. For antenna RCS reduction, bandstop FSS often works as antenna reflection plane which performance like a metal ground at the working band and reduce reflection on other frequency [1].

In this paper we proposed a bandstop FSS based on SRR for antenna RCS reduction. The main idea of design is to introduce an even mode to the SRR and turn it into a dual-mode resonator. Two metal trips and a via hole forms the basic SRR structure, and then a horizontal metal strip is add at the via hole which work as a virtual ground. This will add an even mode to the SRR but won't affect the odd mode [2].

To testify the design, a model is set up in HFSS and simulated using periodic boundary. The FSS unit cell is shown in Fig. 1. Six slots are cut on the horizontal strip symmetrically to add length to even mode current thus lower the resonant frequency of the even mode and bring two modes' resonant frequencies together. Fig. 2 shows the simulated S_{11} and S_{21}. A stop-band centered at 15 GHz is observed with a bandwidth of 2 GHz. Two transmission poles locate at 14.36 GHz and 21 GHz respectively and outside of the stop-band, reflection is below −10 dB which will lead to a RCS reduction when working as an antenna ground.

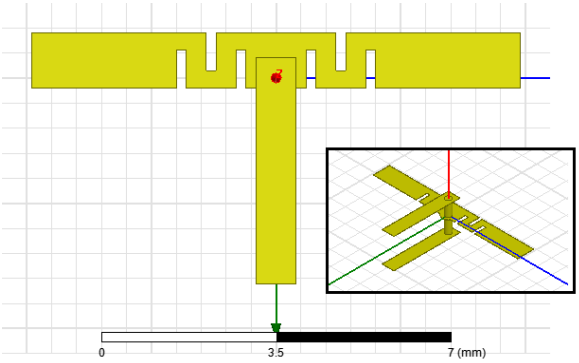

Figure 1: Top and isometric view (enclosed picture) of the FSS unit cell.

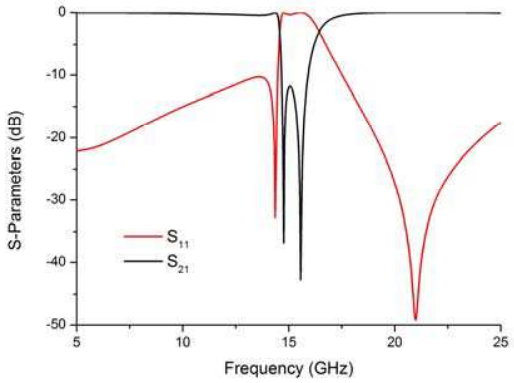

Figure 2: Simulated S_{11} and S_{21} of the proposed FSS.

REFERENCES

1. Bayatpur, F., "Metamaterial-inspired frequency-selective surfacesm" Ph.D. diss., The University of Michigan, 2009.
2. Zhang, X.-Y. and Q. Xue, "Novel centrally loaded resonators and their applications to bandpass filters," *IEEE Transactions on Microwave Theory and Techniques*, Vol. 56, No. 4, 913–921, April 2008.

A Printed Collinear Antenna with a Controllable Main Beam

Radhwan J. Mahmoud and Jonathan M. Rigelsford
Department of Electronic & Electrical Engineering, The University of Sheffield
Mappin Street, Sheffield S1 3JD, United Kingdom

Abstract— This paper presents a reconfigurable antenna with a controllable main beam. The antenna is capable of changing the beamwidth and pointing direction of its main radiating beam. The antenna design comprises a planar printed collinear antenna positioned above a novel active 3-dimensional hybrid electromagnetic band gap (EBG) structure. The design has been chosen to operate at 2.4 GHz and is therefore suitable for intelligent Wi-Fi or smart building applications.

The active ground plane comprises of a solid vertical metallic strip 200 mm long and a quarter of a wavelength wide, and an array of 13 horizontal metallic strips extending to either side. A section of the structure is illustrated in Fig. 1. Each horizontal arm is a quarter of a wavelength long and of width, w. The overall width of the antenna is therefore 91.8 mm ($3\lambda/4$). The arms are vertically separated by a distance g. The horizontal strips are individually isolated from each other and the central portion of the active ground plane by a 1 mm gap, and are electrically connected with capacitors). Normal to, and symmetrically on either side on the central ground plane are similar arms, each split into two sections, each being a sixth of a wavelength long. Again, each strip is electrically connected with capacitors. This results in a ground plane resembling a pair of nested extruded U-shapes.

The EBG can be controlled using variable capacitance diodes (varactor diodes) or PIN diodes connected vertically to the distal end of each horizontal strip. This enables the azimuthal pointing direction of the antenna's main beam to be switched. A voltage potential is supplied to the diodes via a bias-T in the RF feed.

Simulated s-parameter and far-field radiation patterns will be presented and compared to those obtained experimentally.

3D Frequency Selective Absorbers: Concept, Design and Application

Bo Li, Zhongxiang Shen, and Yuping Shang
School of Electrical and Electronic Engineering, Nanyang Technological University
50 Nanyang Avenue, Singapore 639798, Singapore

Abstract— Frequency selective absorber (FSA) is a special kind of frequency selective surface (FSS), which is transparent to incident plane electromagnetic waves in the passband, while absorbs the reflected waves outside the passband. Based on this special characteristic, an FSA has wide applications in target invisibility and interference reduction. So far, most of the reported FSA designs [1–5] were realized by cascading lossy arrays of Salisbury/Jaumann/circuit analog absorbers [6] and conventional 2D frequency selective surfaces with a quarter-wavelength spacer. The transmitting characteristic of these FSAs was provided by the conventional frequency selective surfaces, and the absorption outside the passband was realized by the lossy arrays. Unfortunately, 2D frequency selective surfaces and lossy array consisting of planar periodic arrays of identical resonant cells suffer from large unit-cell size and unstable filtering response over a broad frequency range.

In this work, we first conduct a brief review of 2D FSA designs to understand their operating principles and to identify their advantages and limitations. A 2.5D FSA design with bandpass filtering response and dual-band absorbing characteristic is presented and discussed, as shown in Fig. 1. After that, a 3D FSA with stable bandpass filtering response and wide absorption characteristics is proposed, as shown in Fig. 2. The operating principle of the 3D FSA is explained with the aid of its equivalent circuit model. Experimental verifications are also provided for both design examples. Finally, comparisons are made between the designed 2.5D and 3D FSAs.

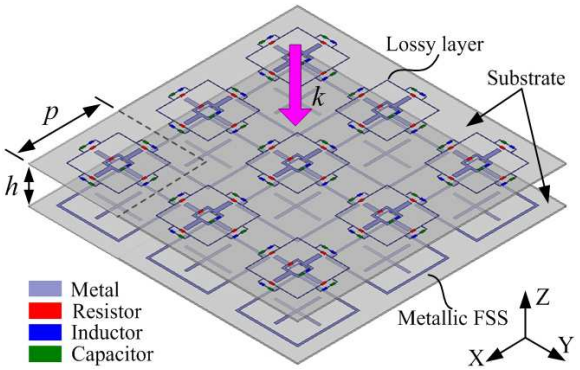

Figure 1: Perspective view of the designed 2D FSA.

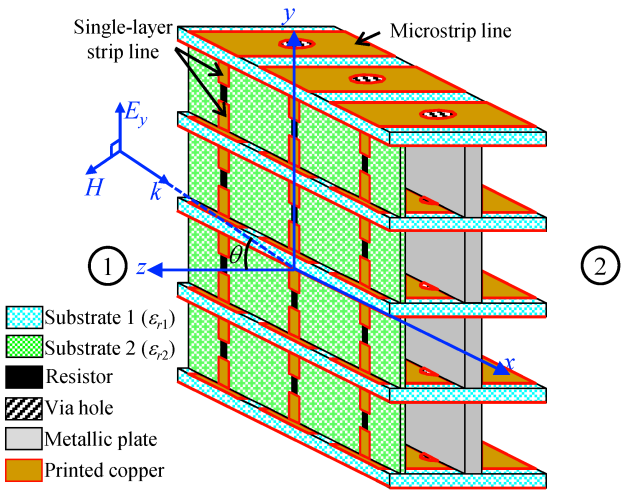

Figure 2: Perspective view of the designed 3D FSA.

REFERENCES

1. Kiani, G. I., A. R. Weily, and K. P. Esselle, "A novel absorb/transmit FSS for secure indoor wireless networks with reduced multipath fading," *IEEE Microw. Wireless Compon. Lett.*, Vol. 16, No. 6, 378–380, 2006.
2. Kiani, G. I., K. L. Ford, K. P. Esselle, A. R. Weily, and C. J. Panagamuwa, "Oblique incidence performance of a novel frequency selective surface absorber," *IEEE Trans. Antennas Propag.*, Vol. 55, No. 10, 2931–2934, 2007.
3. Motevasselian, A. and B. L. G. Jonsson, "Design of a wideband rasorber with a polarization-sensitive transparent window," *IET Microw. Antennas Propag.*, Vol. 6, No. 7, 747–755, 2012.
4. Costa, F. and A. Monorchio, "A frequency selective radome with wideband absorbing properties," *IEEE Trans. Antennas Propag.*, Vol. 60, No. 6, 2740–2747, 2012.

5. Mias, C., "Frequency selective absorption using lumped element frequency selective surfaces," *Electron. Lett.*, Vol. 39, No. 11, 847–849, 2003.
6. Munk, B. A., *Frequency Selective Surfaces: Theory and Design*, John Wiley & Sons Inc., 2000.

Semi Analytical Model for Non-Resonant Layered Frequency Selective Surfaces (FSS)

Poojali Jayaprakash and Kavitha Arunachalam
Department of Engineering Design, Indian Institute of Technology Madras, 600036, India

Abstract— Periodic metallic structures comprising of non-resonant inductive grids and capacitive patches stacked on thin low loss dielectric substrate are widely used in satellite communication and remote sensing systems [1]. In non-resonant FSS, the element size (D) of the unit cell, i.e., building block of the periodic structure is typically smaller compared to the operating wavelength for realization of finite sized FSS [2]. Though 3D full wave EM simulations yield an accurate frequency response, they are time consuming and do not provide insight to understand the behavior of non-resonant FSS for an incident plane wave. Equivalent circuit models provide a quick and easy means to predict and understand the frequency response of layered non resonant unit cells [2–5]. In [2], authors introduced a transmission line model to explain frequency response of non resonant FSS based on the theory in [3]. The proposed model comprised of cascaded LC network in which the dielectric substrate is correctly represented as a delay line. In the generalized equivalent circuit model proposed in [4], the dielectric substrate is represented as a cascaded LC network, this approach needs further optimization in HFSS.

In this work, we present a simplified equivalent circuit model for non-resonant FSS design consisting of inductive grids and capacitive metallic patches. This method gives the modified formulae of [3] based on curve fitting with HFSS results obtained for the individual unit cells. The equivalent capacitance and inductance estimated for the individual unit cells using the modified formulae are then used to build a cascaded transmission line model to predict frequency response of the multilayered FSS. Here, the dielectric substrate is modeled as delay line as in [2]. The agreement between the proposed semi analytical model and HFSS numerical simulations is studied for a second order X band (8–12 GHz) FSS with unit cell dimension, $D = \lambda/15$. Full wave simulations for this structure yielded transmission loss (S_{21}) as low as 0.6 dB in the entire X-band. HFSS model used in this work for FSS analysis was validated with simulations reported in [2, 4]. Frequency response predicted by the proposed equivalent circuit model and the approach of [2] were calculated and compared with full wave simulations. A comparison of the numerical results is summarized in Table 1. It can be observed that the performance of the cascaded transmission line using the modified formulae is in very good agreement with simulations unlike the equivalent circuit model of [2].

Table 1: Comparison of the proposed equivalent circuit model and approach of [2] with full wave simulations.

SI. No.	**Frequency (GHz)**	**Transmission Loss, S_{21} (dB)**		
		HFSS	**Modified formulae**	**Ref. [2]**
1	8.7	−0.6	−0.8	−4.4
2	9.0	−0.5	−0.7	4.8
3	9.5	−0.4	−0.7	−5.3
4	10.0	−0.5	−0.7	−5.8
5	10.5	−0.4	−0.4	−6.3
6	11.0	−0.2	−0.1	−6.7
7	11.5	−0.1	−0.04	−7.5

REFERENCES

1. Munk, B. A., *Frequency Selective Surfaces: Theory and Design*, Wiley-Interscience, New York, 2000.
2. Sarabandi, K. and N. Behdad, "A frequency selective surface with miniaturized elements," *IEEE Trans. Antennas Propag.*, Vol. 55, No. 5, 1239–1245, May 2007.
3. Marcuvitz, N., *Waveguide Handbook*, Boston Technical Publishers, Lexington, MA, 1964.

4. Al-Joumayly, M. A. and N. Behdad, "A generalized method for synthesizing low-profile, band-pass frequency selective surfaces with non-resonant constituting elements," *IEEE Trans. Antennas Propag.*, Vol. 58, No. 5, Dec. 2010.
5. Al-Joumayly, M. and N. Behdad, "A new technique for design of low-profile, second-order, bandpass frequency selective surfaces," *IEEE Trans. Antennas Propag.*, Vol. 57, No. 2, 452–459, Feb. 2009.

Ultra-wide Tuning Frequency Range Active Frequency Selective Surface Based on Enhanced Magnetic Coupling

L. Zhang[1], **L. Ye**[1], **Y. Liu**[1], **and Q. H. Liu**[2]

[1]Department of Electronic Science, Xiamen University, China
[2]Department of Electrical and Computer Engineering, Duke University, USA

Abstract— In this work, a novel compact Active Frequency Selective Surface (AFSS) is presented. The tuning ability is archived by mounting varactors on the unit cells. The varactors are controlled by a DC voltage variable from 0 V to 30 V. This work is realized on a single layer PCB, and no stand-alone biasing grid is needed. To choke high frequency signal, resistors are added. With carefully choosing the value of resistors, DC voltage drop between unit cells is ignorable, while high frequency signal is choked at the same time. Simulation results show that this structure is vertical polarizing sensitive, and the frequency tuning range is from 0.65 GHz to 2.17 GHz that is 1 : 3.34 tuning ratio, which means through the whole frequency range, this AFSS is able to be re ective or transparent. According to the datasheet of this varactor, the tunable range is from 9.3 pF to 0.75 pF, so the theoretical tuning ratio is 1 : 3.52. The simulation results are very close to the physical limits. This wide tuning range is archived by a special design which strongly enhanced the coupling, especially the magnetic field coupling, between the unit cells. Also, similarly to previous work, this AFSS is biased at the end of unit cell columns, which is orthogonal to the direction of unit cell extending; also the presented AFSS is developed for building high performance electronically steerable antenna. According to previous research, if a wide band omnidirectional radiator, which is not difficult to design, is put in the central of the AFSS columns, a wideband steerable antenna would be realized. Also, the power consumption is very low, since the varactors are reverse biased.

Slanted-comb Frequency Selective Surfaces for Passive Reduction in Specular Scatter

Christopher J. Davenport and Jonathan M. Rigelsford
Department of Electronic & Electrical Engineering, The University of Sheffield
Mappin Street, Sheffield S1 3JD, United Kingdom

Abstract— The concept of a wireless friendly building has been of increasing research interest over the past few years. Many novel frequency selective surfaces (FSS) have been developed, offering the ability to filter wireless signals. These can be designed to either pass or block a range of frequencies, depending on user preference. However, these surfaces require expensive printed circuit boards and active components, making large scale adaption expensive or infeasible. Furthermore, traditional FSS can only be used effectively when positioned on a partition wall which is otherwise shielded by metallic insulation. In many applications, a wireless signal can easily propagate down corridors, entering adjacent walls through doors, and causing unwanted interference. It is thus advantageous to prevent the propagation of signals at certain frequencies down corridors.

Underlying principles of passive three-dimensional comb and pin surfaces have been reported by the authors; however, many variations in structure design remain unexplored. This paper presents the use of a slanted-comb frequency selective surface, optimised for use in applications

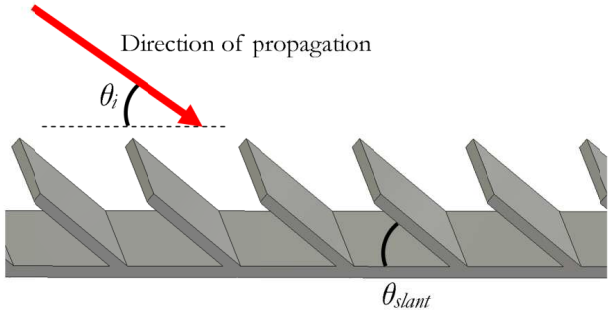

Figure 1: The slanted-comb FSS, with angle of slant, θ_{slant} pointing in the direction of the incident plane wave.

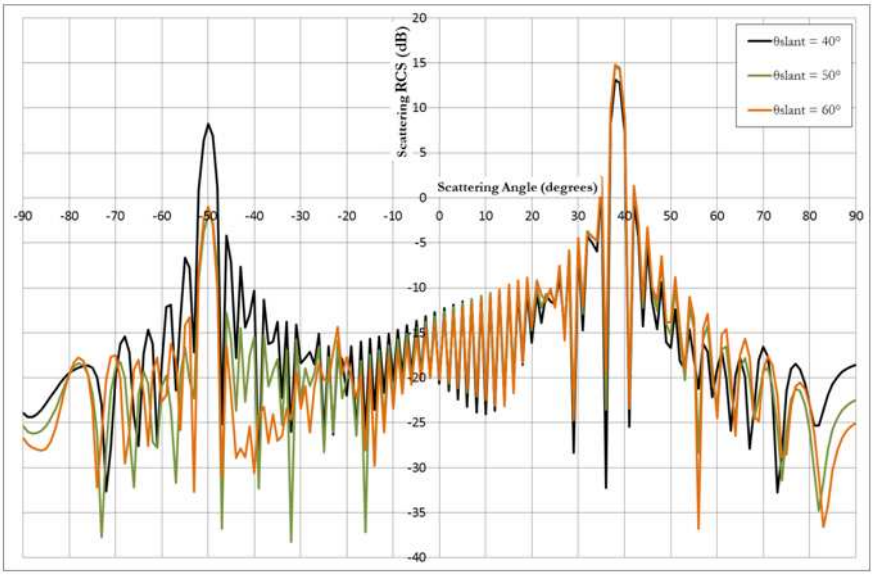

Figure 2: Plot of the specular scatter (negative scattering angles) and the backscatter (positive scattering angles) for a range of slant angles.

where oblique incidence of signals is likely, as shown in Fig. 1. Simulations performed using CST microwave studio illustrate the effect slant angle has on specular and backscatter reflections. Scattering plots clarify the behaviour for a range of slant angles. Additionally, the reduction in specular scatter of the slanted-comb surfaces compared to a flat perfect electrical conductor is represented in frequency graphs, which reveal important features of the surface. Changes in the specular scatter and backscatter are illustrated in Fig. 2 for varying θ_{slant}. Initial analysis shows that both main and side lobe levels can be decreased, depending on both θ_{slant} and θ_i. Finally, three-dimensional mesh plots are used to quantify the choice in slant angle for a range of incidence angles.

A Novel Miniaturized and Multiband Frequency Selective Surface

Mingbao Yan, Shaobo Qu, Jiafu Wang, Hongya Chen, Yongqiang Pang, Yongfeng Li, Lin Zheng, and Wenjie Wang
College of Science, Air Force Engineering University, Xi'an 710051, China

Abstract— Frequency Selective Surface (FSS) have been the subject of extensive studies in recent years, because of their widespread applications as electromagnetic spatial filters for microwave and optical signals, such as: reflector antenna systems, radomes, microwave absorbers, artificial electromagnetic bandgap materials and others. In modern buildings, selective spatial filters are used to provide wireless security for indoor environments and to optimize wireless local area network (WLAN) coverage. For instance, FSSs may be integrated, in the walls and windows of a building, for example, to modify the physical indoor propagation environment, isolating and or avoiding interference among WLAN radios.

However, One problem that FSS encounter when applied to buildings is that the wavelengths in the bands used by most of the mobile, radio and wireless technologies employed in indoor communications are not insignificant when compared with the size of an ordinary office room. So, to obtain of lower resonant frequency, the periodicity may be increased. the directly result is that the grating region may appear fast. To solve the above problem, the size of unit cell must be reduced.

In this paper, a novel miniaturized and multiband frequency selective surface (FSS) is presented. The FSS structure acts like a band reject filter having three broad bands in parts of C, X and Ku band. Due to symmetrical nature of the design, the proposed FSS is insensitive to incident angle and polarization. The performances under different dimensions of the main parameters are further discussed. The simulations are done by CST Microwave studio. To validate the proposed FSS, the measurement is carried out by free space method. Both measurement and simulation results show that the proposed FSS has the excellent performances.

Session 3A13a
SC4&2: Graded Index Structures and Metamaterials for Antenna Applications

Index Profiles with Zero Reflection over a Wide Range of Angles

S. A. R. Horsley
University of Exeter, Stocker Road, Exeter, UK

Abstract— Reflection from material interfaces can be reduced in a number of ways; through impedance matching — as is the case in transformation optics [1]; layering materials as is done for anti-reflection coatings; or through using exotic media with zero index [2] or PT-symmetry [3]. In this talk I will show some theoretical results concerning the problem of finding index profiles that do not reflect radiation over a wide range of angles. The results demonstrate that a planar medium will reflect zero radiation for all angles of incidence onto one side of a slab if the permittivity profile across the slab obeys the Kramers-Kronig relations in space. For a known $\mathrm{Im}[\epsilon(x)]$ we demonstrate that applying the Kramers-Kronig relations gives a $\mathrm{Re}[\epsilon(x)]$ such that there is zero reflection. In principle the slab can be thin (on the order of the wavelength) and highly absorbing, which might be useful in low frequency applications.

The basic theory we have developed can be understood through the following example. Suppose we have a slab of material that is inhomogeneous in the x coordinate, and has translational symmetry in the y-z plane. We write the permittivity of the system as,

$$\epsilon(x) = \epsilon_b + \delta\epsilon(x) \tag{1}$$

where ϵ_b is some background value of the permittivity, and $\delta\epsilon(x)$ is the spatially dependent part describing the slab. For simplicity consider scalar waves within this profile, obeying the Helmholtz equation,

$$\left[\boldsymbol{\nabla}^2 + \frac{\omega^2}{c^2}\epsilon(x)\right]\varphi(x) = 0 \tag{2}$$

If the wave is divided into an incident wave, $\varphi_i = Ae^{i(K_x x + \mathbf{K}_\parallel\cdot\mathbf{x})}$, plus a reflected one φ_s, we find that the reflected wave must obey the equation,

$$\left[\boldsymbol{\nabla}^2 + \frac{\omega^2}{c^2}\epsilon_b\right]\varphi_s = -\frac{\omega^2}{c^2}\delta\epsilon(x)\left[Ae^{i(K_x x + \mathbf{K}_\parallel\cdot\mathbf{x})} + \varphi_s\right] \tag{3}$$

where $\sqrt{K_x^2 + \mathbf{K}_\parallel^2} = \omega\sqrt{\epsilon_b}/c$. The solution to Equation (3) can be written as an infinite series of terms that are integrals involving products of Green functions [4]. The first order term of this series is the well known result,

$$\phi_s^{(1)} = -\frac{\omega^2}{c^2}Ae^{i\mathbf{K}_\parallel\cdot\mathbf{x}}\int_{-\infty}^{\infty}\frac{dk}{2\pi}\frac{e^{ikx}}{\frac{\omega^2}{c^2}\epsilon_b - k_x^2 - \mathbf{K}_\parallel^2}\tilde{\delta\epsilon}\left(k - K_x\right) \tag{4}$$

where a tilde indicates a Fourier transform. Therefore, if we wish the reflection to vanish to first order, then we must have the integrand of (4) vanish for $k < 0$. Examining all orders of $\phi^{(n)}$ we find that for the *total* reflection to vanish then it is also sufficient to have, $\tilde{\delta\epsilon}(k < 0) = 0$. Therefore the profile of a reflectionless slab must take the form,

$$\delta\epsilon(x) = \int_0^\infty \tilde{\delta\epsilon}(k)e^{ikx}\frac{dk}{2\pi} \tag{5}$$

Notice that we have no restriction on $\mathbf{K}_\parallel$, only the sign of K_x. Therefore if the permittivity profile across the slab can be written in the form (5) then it ought not to reflect any radiation, whatever the value of $\mathbf{K}_\parallel$ (which determines the angle of incidence). Notice also that the permittivity (5) is necessarily a complex number, so that the medium must have some combination of either absorption or gain. Indeed, because we are including only positive k in (5), the function $\delta\epsilon(x)$ is analytic in the upper half complex position plane, and therefore obeys the Kramers–Kronig relations in *space*,

$$\mathrm{Re}[\delta\epsilon(x)] = \frac{1}{\pi}P\int_{-\infty}^{\infty}\frac{\mathrm{Im}[\delta\epsilon(y)]}{x - y}dy \tag{6}$$

Figure 1 illustrates an example of an index profile that obeys (6), showing that there is indeed zero reflection, which we have found to be true for the full angular range.

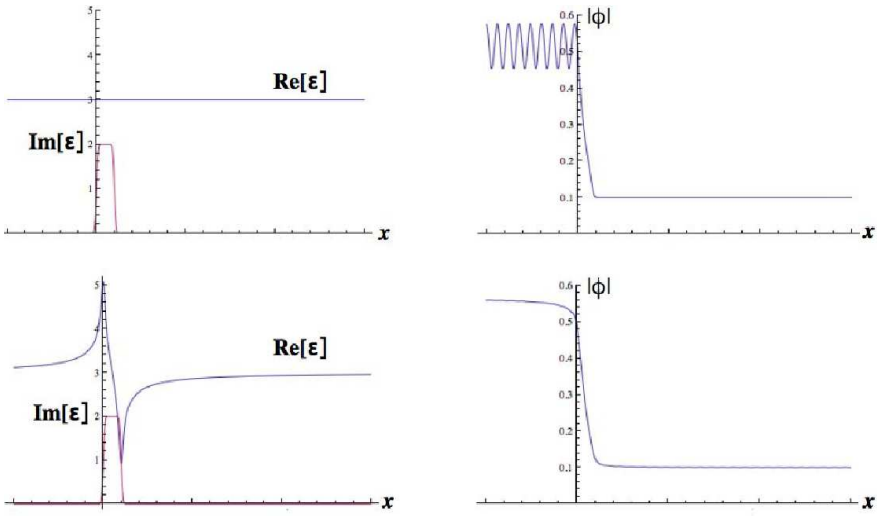

Figure 1: Left hand panels show cross sections of the permittivity of a slab, plotted as a function of x (arbitrary units). The right hand panels show the absolute value of a field that is incident from the left onto this slab (remembering that oscillations in the absolute value indicate reflection). The upper two panels show the case of a highly absorbing material that does not obey the Kramers-Kronig relations (6) in space, where there is clearly a significant reflection from the profile. When the real part of $\delta\epsilon(x)$ is adjusted to satisfy (6) then the reflection vanishes, as the lower panels show.

REFERENCES

1. Cai, W. and V. Shalaev, *Optical Metamaterials*, Springer, 2010.
2. Nguyen, V. C., L. Chen, and K. Halterman, *Phys. Rev. Lett.*, Vol. 105, 233908, 2010.
3. Lin, Z., H. Ramezani, T. Eichelkraut, T. Kottos, H. Cao, and D. N. Chrisodoulides, *Phys. Rev. Lett.*, Vol. 106, 213901, 2011.
4. Roach, G. F., *Green's Functions*, Cambridge University Press, 1970.

Anisotropic Metamaterials for Polarization-controlled Devices

Hui Feng Ma, **Wen Xuan Tang**, **Di Bao**, **and Tie Jun Cui**
State Key Laboratory of Millimeter Waves, School of Information Science and Engineering
Southeast University, Nanjing 210096, China

Abstract— Two polarization-controlled functional devices by using of anisotropic metamaterias have been proposed in this presentation. One device is polarization beam splitter by using of anisotropic gradient-index metamaterials, which can separate the vertical and horizontal polarizations to different directions independently. Two three-dimensional slab lenses have been proposed to design such a polarization beam splitter, which has capacity to make arbitrary beam deflections for the vertical (horizontal) polarization but have no response to the horizontal (vertical) polarization, respectively. Another device is polarization-controlled single metamaterial lens by using of anisotropic homogenous metamaterials, which can act as a spatial filter, a transparent cloak and a polarizer under the illumination of differently polarized waves. A special metamaterial unit cellhas been proposed to realize about two polarization-controlled devices. For one special polarization, the unit cellhas both electric and magnetic responses simultaneously to make equal effective permittivity and permeability for one specially polarized incident waves, hence excellent impedance matching is achieved between the anisotropic lenses and air, but the effective index of refraction can be changed gradually by tuning the dimensions of the unit cells. For another orthogonally polarized incident waves, the unit cell has neither electric nor magnetic responses in whole frequency band with effective index of refraction of unit, which make the waves pass through the lens without any reflection. Both devices are designed, simulated and measured, which show excellent performance of the polarization beam splitter and polarization-controlled multiple functionalities of the single lens.

Conformal Surface Wave Luneburg Lenses

R. C. Mitchell-Thomas[1] and O. Quevedo-Teruel[2]

[1]Department of Physics and Astronomy, University of Exeter, EX4 4QL, England, UK
[2]School of Electrical Engineering, KTH Royal Institute of Technology, Stockholm SE-10044, Sweden

Abstract— Luneburg lenses [1] perform the very desirable function of converting a point source located on its edge to a directive beam, or conversely, are able to focus a plane wave input to a point source on the opposite side of the lens [2–4]. These lenses have been implemented in three dimensions to create steerable, directive beams for communication systems. These lenses are fabricated using a multilayered discretized version of the graded index profile, and are composed of progressively larger spherical structures. These lenses are, however, rather bulky, therefore it is often phased arrays that are chosen to perform the same function due to their planarity.

More recently, Luneburg lenses have been implemented in surface wave devices [5, 6], avoiding the problems of large volume requirements. These flat, two dimensional lenses can achieve the required graded index using metasurfaces [7]. By gradually altering one parameter of the periodic surface structure, a radially-dependent gradient lens can be implemented. All of the current studies have focused upon lenses applied to flat surfaces, however, application of these lenses to more general curved surfaces provides an opportunity to employ them for a wider range of scenarios, such as to the surface of vehicles. In order to retain the electromagnetic behavior, the index profile must be modified, according to the curvature of the surface, and this is achieved using a geometrical optics technique [8, 9]. This will be detailed during the presentation, and will also be verified with numerous numerical simulations.

ACKNOWLEDGMENT

This work was funded by the Engineering and Physical Sciences Research Council (EPSRC), UK under a Programme Grant (EP/I034548/1) "The Quest for Ultimate Electromagnetics using Spatial Transformations (QUEST)".

REFERENCES

1. Luneburg, R. K., *Mathematical Theory of Optics*, Cambridge University Press, 1964.
2. Quevedo-Teruel, O. and Y. Hao, "Directive radiation from a diffuse Luneburg lens," *Optics Letters*, Vol. 38, 392, 2013.
3. Quevedo-Teruel, O., W. Tang, and Y. Hao, "Isotropic and non-dispersive planar fed Luneburg lens from hamiltonian transformation optics," *Optics Letters*, Vol. 37, 4850, 2012.
4. Kundtz, N. and D. R. Smith, "Extreme-angle broadband metamaterials lens," *Nature Materials*, Vol. 9, 129, 2010.
5. Dockrey, J. A., M. J. Lockyear, S. J. Berry, S. A. R. Horsley, R. J. Sambles, and A. P. Hibbins, "Thin metamaterial Luneburg lens for surface waves," *Physical Review B*, Vol. 87, 125137, 2013.
6. Jackson, D. R., C. Caloz, and T. Itoh, "Leaky-wave antennas," *Proceedings of the IEEE*, Vol. 100, 2194, 2012.
7. Maci, S., G. Minatti, M. Casaletti, and M. Bosiljevac, "Metasurfing: Adressing waves on impenetrable metasurfaces," *IEEE Antennas and Wireless Propagation Letters*, Vol. 10, 1499, 2011.
8. Mitchell-Thomas, R. C., T. M. McManus, O. Quevedo-Teruel, S. A. R. Horsley, and Y. Hao, "Perfect surface wave cloaks," *Physical Review Letters*, Vol. 111, 213901, 2013.
9. Leonhardt, U. and T. G. Philbin, *Geometry and Light: The Science of Invisibility*, Dover Publications, New York, 2010.

GRIN Fractal Metamaterial and Its Applications in Novel Broadband Highly-directive Emission System

He-Xiu Xu and Guang-Ming Wang
Air Force Engineering University, Xi'an 710051, China

Abstract— In this section, I will introduce the most recent work of the authors on the research of a new kind of gradient-refractive-index (GRIN) metamaterial, which is constructed by non-uniform fractal geometries. Numerical results show that the GRIN fractal metamaterial element exhibits non-resonant, deep-subwavelength, and broadband features. Then the possible applications of the GRIN fractal metamaterial are explored in two highly-directive emission systems. The former is composed of a three-dimensional (3D) half Maxwell fish-eye (HMFE) lens and an omnidirectional microstrip trapezoid printed monopole while the latter is composed of the same microstrip trapezoid printed monopole and several 3D slab lenses. Numerical and experimental results indicate that both the highly-directive emission systems are with an octave bandwidth in the superextended C band and enable a considerable gain enhancement of the monopole near 10 dB from 3 to 7.5 GHz while without significantly affecting the cross-polarization patterns and impedance matching. Moreover, both the lenses are capable of accurately manipulating the quasi-spherical waves to plane waves due to the deep subwavelength feature of proposed GRIN fractal meta-atom, giving rise to the high directivity and high gain of the emission systems.

Making Geometrical Optics Exact

T. G. Philbin
University of Exeter, UK

Abstract— Geometrical optics (GO) is widely used in studies of electromagnetic materials because of its ease of use compared to full-wave numerical simulations. Exact solutions for waves can, however, differ significantly from the GO approximation. In particular, effects that are "perfect" for waves cannot usually be derived using GO. Here we give a method for designing materials in which GO is exact for some waves. This enables us to find interesting analytical solutions for exact wave propagation in inhomogeneous media. Two examples of the technique are given: a material in which two point sources do not interfere, and a perfect isotropic cloak for waves from a point source. We also give the form of material response required for GO to be exact for all waves.

The method works as follows. We consider monochromatic scalar waves, satisfying the Helmholtz equation

$$\left[\boldsymbol{\nabla}^2 + \frac{\omega^2}{c^2} n^2(\mathbf{r},\omega)\right] \psi(\mathbf{r},\omega) = 0. \tag{1}$$

If the complex wave $\psi(\mathbf{r},\omega)$ is written in terms of its amplitude and phase,

$$\psi(\mathbf{r},\omega) = R(\mathbf{r}) e^{iS(\mathbf{r})}, \tag{2}$$

where $R(\mathbf{r})$ and $S(\mathbf{r})$ are real, then (1) gives the two real equations

$$(\boldsymbol{\nabla} S)^2 - \frac{\boldsymbol{\nabla}^2 R}{R} - \frac{\omega^2}{c^2} n^2(\mathbf{r},\omega) \;=\; 0, \tag{3}$$

$$\boldsymbol{\nabla} \cdot \left(R^2 \boldsymbol{\nabla} S\right) \;=\; 0. \tag{4}$$

The geometrical-optics approximation corresponds to neglecting the second term in (3), which gives the eikonal equation of geometrical optics:

$$(\boldsymbol{\nabla} S)^2 - \frac{\omega^2}{c^2} n^2(\mathbf{r},\omega) = 0. \tag{5}$$

Comparing (3) with (5), we see that geometrical optics (GO) gives an approximate solution for the phase $S(\mathbf{r})$ of the wave.

Note from (3) and (5) that if the amplitude $R(\mathbf{r})$ of the wave satisfies

$$\frac{\boldsymbol{\nabla} R}{R} = 0, \tag{6}$$

then GO is exact and the solution of (5) gives the exact phase $S(\mathbf{r})$ and therefore the exact wave fronts. The amplitude $R(\mathbf{r})$ can then be found by solving (4).

If

$$S(\mathbf{r}) \propto \frac{1}{R(\mathbf{r})} \tag{7}$$

then the exact wave Equation (4) becomes

$$\boldsymbol{\nabla}^2 R = 0 \tag{8}$$

which gives (6) (barring any zeros in amplitude), and this in turn implies (5). We can therefore generate refractive index profiles in which GO is exact as follows. Choose a solution of the Laplace Equation (8) for the amplitude $R(\mathbf{r})$ and choose the phase $S(\mathbf{r})$ to be inversely proportional to $R(\mathbf{r})$. Then one part of the exact wave equation, namely (4), is automatically satisfied and the second part, Equation (3), reduces to the eikonal Equation (5) which can be solved for $n(\mathbf{r},\omega)$ since $S(\mathbf{r})$ is known. We apply this method to find a material in which two point sources do not interfere, and to find a perfect isotropic cloak for waves from a point source.

Removing Singular Refractive Indices with Sculpted Surfaces

S. A. R. Horsley[1], **I. R. Hooper**[1], **R. C. Mitchell-Thomas**[1], **and O. Quevedo-Teruel**[2]

[1]Electromagnetic and Acoustic Materials Group, Department of Physics and Astronomy
University of Exeter, Stocker Road, Exeter, EX4 4QL, UK
[2]School of Electrical Engineering (EES)/Electromagnetic Engineering (ETK)
KTH Royal Institute of Technology, Teknikringen 33, Stockholm SE-100 44, Sweden

Abstract— There exists a family of graded index devices that require infinities in their refractive index profiles, and can therefore only be fabricated in imperfect truncated forms. Recently, a transformation optics [1–4] based technique (named transmutation [5, 6]) was developed to overcome this problem through the use of an appropriate coordinate transformation that removes the singularity. While this is a promising advance, it is often difficult to implement the required anisotropy, severely limiting its utility.

For waves propagating on surfaces there is a geometrical equivalence between the surface shape and the refractive index similar to that used in transformation optics [7]. We will demonstrate that, through an appropriate deformation of the surface, one can manipulate the rays in a way that would require points of infinite refractive index on a flat surface. This means that it is possible to reproduce the propagation characteristics of devices with singular refractive indices by utilising surface curvature and finite refractive index profiles, allowing one to implement in two dimensions devices that are practically impossible to realise in three. We demonstrate the principle with three singular devices: the Eaton lens [8] (see Figure 1), the Invisible sphere [9] and the generalised Maxwell fish eye [5].

The theory is confirmed using full wave simulations of the three devices in a parallel plate waveguide implementation that mimics the propagation of homogeneous plane waves upon a surface. We also report on initial attempts to fabricate and test such devices. These surfaces could potentially be used to modify the radiation pattern of antennas by altering both their directivity and efficiency.

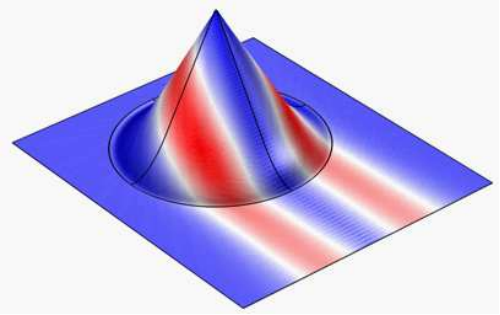

Figure 1: Finite element modelling of a 2D implementation of the Eaton lens using a sculpted parallel plate waveguide. The device is excited using a planar narrow Gaussian beam with a wavelength of 1/10th of the radius of the deformed region offset to one side of the device. The time-averaged electric field is shown.

REFERENCES

1. Leonhardt, U., "Optical conformal mapping," *Science*, Vol. 312, 1777–1780, 2006.
2. Pendry, J. B., et al., "Controlling electromagnetic fields," *Science*, Vol. 312, 1780–1782, 2006.
3. Lai, Y., et al., "Illusion optics: The optical transofmation of an object into another object," *Phys. Rev. Lett.*, Vol. 102, 253902, 2009.
4. Pendry, J., et al., "Transformation optics and subwavelength control of light," *Science*, Vol. 337, 549–552, 2012.
5. Tyc, T., et al., "Transmutation of singularities in optical instruments," *New Journal of Physics*, Vol. 10, 115038, 2008.
6. Hooper, I. R., et al., "Transmutation of singularities and zeros in graded index optical instruments: A methodology for designing practical devices," *Opt. Exp.*, Vol. 21, 32313–32326, 2013.

7. Sarbort, M., et al., "Spherical media and geodesic lenses in geometrical optics," *J. Opt.*, Vol. 14, 075705, 2012.
8. Eaton, J. E., "On spherically symmetric lenses," *IRE Trans. Antennas Propag.*, Vol. 4, 66–71, 1952.
9. Minano, J. C., "Perfect imaging in a homogeneous three-dimensional region," *Opt. Exp.*, Vol. 14, 9627–9635, 2006.

Session 3A13b
Antenna and Array 1

Patch Antenna with Electrically Tunable Ferrite-ferroelectric Bilayer

Kaida Xu[1], **Ronald J. Spiegel**[2], **Yonghong Zhang**[1], **William T. Joines**[2], **and Qing Huo Liu**[2]

[1]EHF Key Lab of Science, University of Electronic Science and Technology of China, Chengdu, China
[2]Department of Electrical and Computer Engineering, Duke University, Durham, NC, USA

Abstract— We designed a coaxial-fed patch antenna comprised of a regular alumina substrate (relative permittivity $\varepsilon_r = 9.9$, thickness $h = 2\,\text{mm}$), a ferrite-ferroelectric bilayer [1], a copper patch and a ground plane (See Fig. 1). The ferrite-ferroelectric bilayer, multiferroic heterostructure, consists of a near-single-crystal ferrite yttrium iron garnet (YIG) film layer and a ferroelectric ceramic barium strontium titanate (BST) film layer with thicknesses of 1 µm and 0.5 µm, respectively. The tunable electric field is applied across the BST layer to change its permittivity [2]. The two thin electrodes deposited on both surfaces of the BST and electromagnet for biasing the YIG can be neglected in the simulation model of the antenna. When the electric field applied across the BST layer changes from 2.5 V/µm to 15 V/µm, the operating frequency of the antenna will be shifted from 2615 MHz up to 2716 MHz (See Fig. 2). We also analyze the influence of the static magnetic field variation to the operating frequency of the antenna.

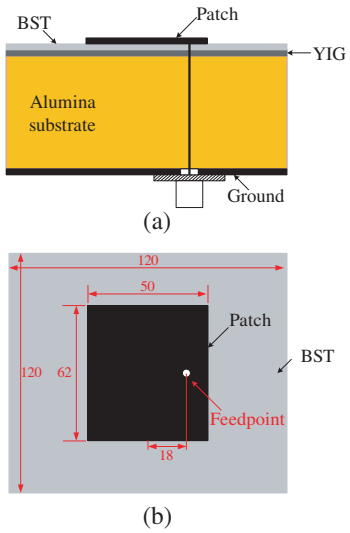

Figure 1: The proposed patch antenna. (a) Side view, and (b) top view (units: mm).

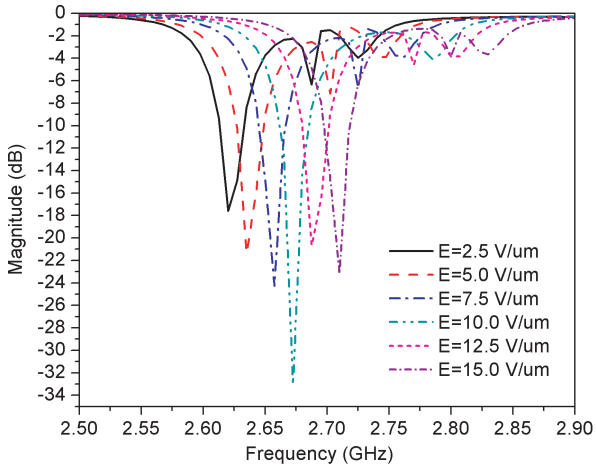

Figure 2: S_{11} of the antenna with tunable E-field across the BST layer.

REFERENCES

1. Ustinov, A. B., G. Srinivasan, and B. A. Kalinikos, "Ferrite-ferroelectric hybrid wave phase shifters," *Applied Physics Letters*, Vol. 90, 031913, 2007.
2. Das, J., Y. Song, N. Mo, P. Krivosik, and C. Patton, "Electric-field-tunable low loss multiferroic Ferrimagnetic-ferroelectric heterostructures," *Advanced Materials*, Vol. 21, 1–5, 2009.

Compact Triple-band Planar Monopole Antenna with Single Metamaterial Unit

Jian Li, **Guangjun Wen**, **Yongjun Huang**, **Kaimin Wu**, **and Weijian Chen**
Centre for RFIC and System Technology, School of Communication and Information Engineering
University of Electronic Science and Technology of China, Chengdu, China

Abstract— In this paper, we present a novel design for compact triple-band planar monopole antenna by integrating with a single metamaterial unit. The single metamaterial unit (single loop ring resonator which can exhibit three resonances) is set as part of radiation patch. The whole antenna structure including the metamaterial inspired patch and optimized ground plane contribute to an eight-like radiation pattern due to the monopole antenna configuration. Such antenna is first numerical analyzed and optimized by finite element method based simulator (Ansoft HFSS V14), and then the fabricated antenna sample are measured within a commercial near field measurement system (Satimo SG 32). Both numerical and experimental results demonstrate that the designed antenna exhibits three distinct operating frequencies and the eight-like radiation patterns at such three frequency bands are all obtained. At the same time, a compared conventional monopole antenna with the same dimensional sizes is also analyzed. Results show that the metamaterial inspired antenna has more compact size. The proposed novel antenna can be exibly used for modern wireless communications including both stationary and portable terminal areas.

High Gain Antenna Using Double Side Paired S-shaped Split Ring Resonator as Metamaterial Superstrate for ku-band Applications

Abdulkareem S. Abdullah and Ali A. Saleh
Department of Electrical Engineering, College of Engineering, University of Basrah, Basra, Iraq

Abstract— A metamaterial unit cell with a very low refractive index over a wide frequency band, from 10.33 GHz to 13 GHz, is proposed and designed. The effective material parameters of the unit cell are retrieved using modified Nicolson-Ross-Weir (NRW) approach. The unit cell forms a planar three-layer metamaterial structure used as a superstrate for gain enhancement of a patch antenna working at 12.15 GHz. The gain of antenna is increased from 6.7 dBi to 13.7 dBi, 7 dBi higher than the original patch. The 3 dB beamwidth becomes narrower from 80° to 34° and from 122° to 30° in E-plane and H-plane respectively. The simulation results are given using Ansoft's HFSS, which is based on the finite element method (FEM).

A metamaterial unit cell of Figure 1 is used as the building block of the antenna superstrate. The substrate type of the unit cell is Rogers 4003 with thickness of 0.508 mm, dielectric loss tangent of 0.0027, and relative permittivity $\varepsilon_r = 3.55$. The dimensions of the unit cell shown in Figure 1 are: $a = 3$ mm, $b = 5.8$ mm, $c = 0.508$ mm, $d = 2$ mm, $e = 2$ mm, $f = 0.4$ mm, and $g = 0.3$ mm. These parameters of the unit cell have been chosen to design a metamaterial in the frequency region (10.33–13) GHz, where the effective electric permittivity, effective magnetic permeability, and refractive index approach zero.

Figure 2(a) presents the calculated effective electric permittivity and effective magnetic permeability of the metamaterial unit cell extracted from the simulated S parameters. At the frequency of 12.15 GHz, the effective refractive index is found to be $0.001127 - j0.003458$, which is very

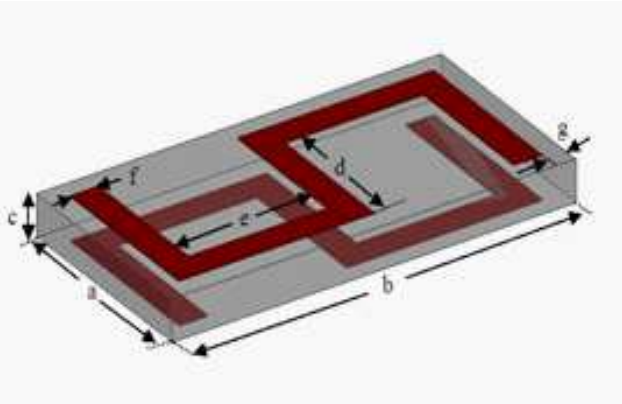

Figure 1: The zero-index metamaterial unit cell.

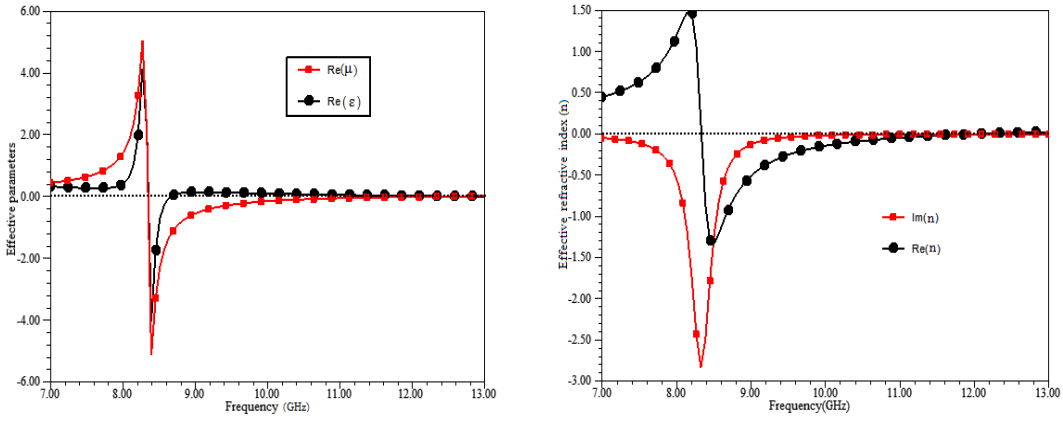

(a) (b)

Figure 2: (a) The extracted relative permittivity and permeability of the metamaterial unit cell; (b) the extracted refractive index of the metamaterial unit cell.

close to zero. Figure 2(b) shows the extracted effective refractive index of the metamaterial unit cell. This extraordinary property of the DNG unit cell can be applied to the antenna in order to congregate the incident radiation field of the antenna and increase the gain. The unit number of the antenna arrays could be reduced for the same gain, which has great significance of minimization design of the antenna array.

Figures 3(a) & (b) show the side view and the top view of the constructed antenna incorporated with the metamaterial superstrate. Three layers are used to form the superstrate, each layer has 5 by 7 unit cells in both x- and y-directions. The distance between any two adjacent cells is $t = 0.6\,\text{mm}$. For supporting purpose, additional rim space on the superstrates with $q = 6.3\,\text{mm}$ width is reserved. The superstrate is fixed above the antenna using four plastic bolts at the corners. The distance from the radiation patch to the bottom layer is kept at $h_1 = 14\,\text{mm}$, and the distance from the bottom layer to the upper layer is kept at $h_3 = 11\,\text{mm}$. The position of the middle layer can be adjusted so that the same characteristics of the original patch (resonant frequency and bandwidth) are got. To validate the beam focusing ability of the metamaterial superstrate within the working frequency range, the patch antenna is designed with working frequency resonant at 12.15 GHz. The patch antenna, used as radiation source, composed of a rectangular patch with dimensions: $W = 7.44\,\text{mm}$, $L = 5.77\,\text{mm}$ etched on a Rogers 4003 substrate of dimensions $W_g = 41\,\text{mm}$, $L_g = 33\,\text{mm}$, thickness of 0.508 mm, relative permittivity $\varepsilon_r = 3.55$, and loss tangent of 0.0027, which is identical to that of the superstrate layers. The center of the patch is aligned with the center of the superstrate. The patch antenna is fed by

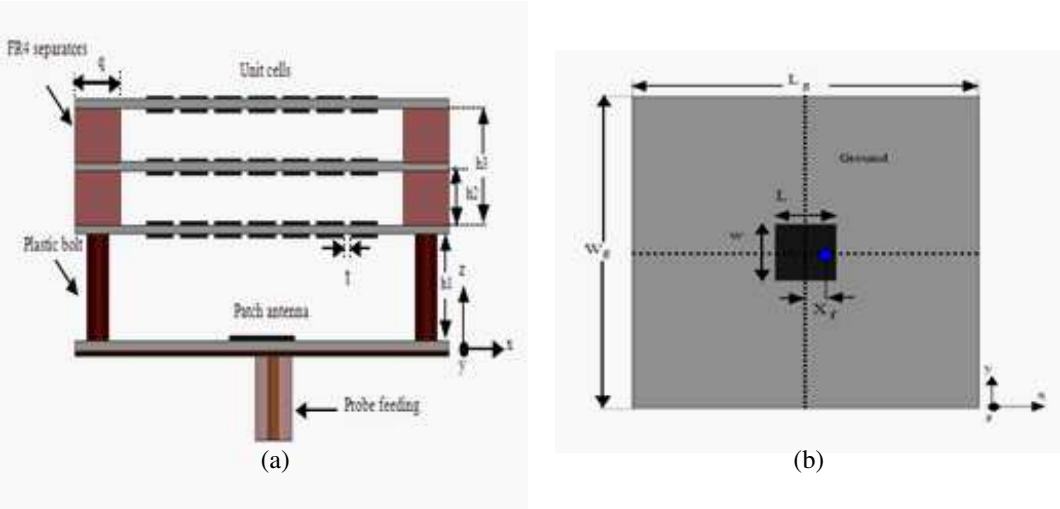

Figure 3: (a) The side view of the patch antenna along with metamaterial superstrate; (b) the top view of the patch antenna.

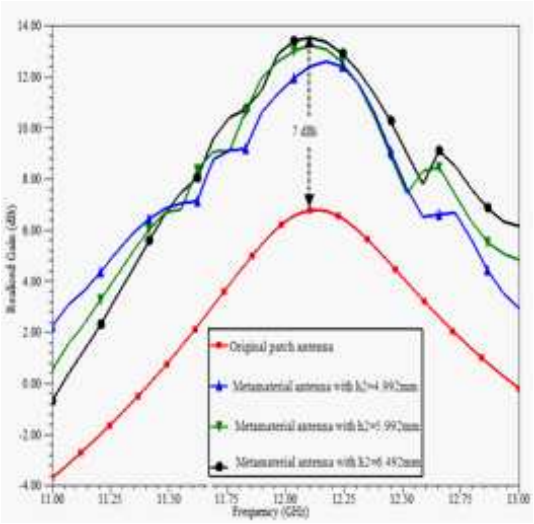

Figure 4: The realized gain of metamaterial antenna.

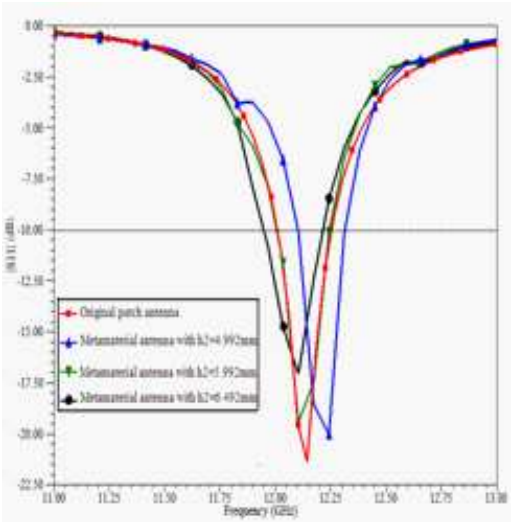

Figure 5: The return loss of the metamaterial antenna for different distances.

coaxial probe with an input impedance of 50 Ω. The position of the probe is $X_f = 1.02$ mm as shown in Figure 3(b).

Figure 4 shows the simulated $|S_{11}|$ for different distances, which presents an optimum distance of $h_2 = 6.492$ mm. At this distance, the simulated -10 dB bandwidth extends from 11.945 GHz to 12.213 GHz with a relative bandwidth of 2.2%. For the original patch antenna, the relative bandwidth is found to be 2%. The operation frequency of the metamaterial antenna is still in the range of zero-index metamaterial superstrate. It is observed that the resonance of the original patch antenna matches the resonance for metamaterial antenna at the optimum distance. In Figure 5, it is shown that the gain of the metamaterial antenna is significantly increased at its resonant frequency for different space distances. For the optimum distance $h_2 = 6.492$ mm, the gain of the metamaterial antenna is enhanced from 6.7 dBi to 13.7 dBi at a working frequency of 12.15 GHz. Since the relative permittivity, relative permeability, and effective refractive index approach zero at around 12.15 GHz, antenna can get a more gain as shown in Figure 5.

Antenna Pattern Reconstruction Using Deconvolution Based Method from Non-anechoic Measurements

Jinhwan Koh
Gyeongsang National University, South Korea

Abstract— This paper focuses on de-convolution method to reconstruct antenna pattern from from non-anechoic measurements. In fact, the de-convolution method uses an impulse response in the angular domains of the reverberant environment and the free space pattern of the device under test is estimated.

The purpose of this paper is, as the pattern reconstruction based on de-convolution methodology, to show that the performance such as the accuracy of the 2D-FFT used on de-convolution based method carried out simultaneously both in azimuth and elevation dimension. The simulation results illustrate validity of this approach.

Discovery and Theory of Small Antenna Near-field Dissipation and Frequency Conversion with Implications for Antenna Efficiency, Beverage Antenna Noise Reduction, Maxwell's Equations and the Chu Criterion

Michael J. Underhill
Underhill Research Ltd., Lingfield, UK

Abstract— The thermal efficiency measured on surface of small antenna conductors is generally found to be much larger than the radiation efficiency measured outside the near-field region. The difference can reach 10 to 20 dB or more at some frequencies. High thermal efficiency means that the surfaces of the antenna conductors do not get excessively hot even with several hundred watts input. Low radiation efficiency with high thermal efficiency means that RF has 'disappeared' in the near-field region. But how?

Measurements made by a Protek thermal camera with a 0.1°C resolution, on a small 80 cm diameter loop-monopole [1] show no sign of a rise in air temperature. It is possible that 'the local ether' itself is being heated. It is proposed that the temperature of this heat is related to the cut-off frequency and power spectral density (per Hz) P of white thermal noise so that $P = kT\,\mathrm{m}^{-2}$ as is found for the thermal noise into a radio antenna of a given capture area. On this basis the temperature of the 'lost radiation', even for a few hundred ($\sim$ 700) watts into a typical HF small antenna, is too low for it to be detectable on the thermal camera.

Another 'null' experiment was based on the hypothesis was that the lost radiation could exert an outward pressure on the 'local ether fabric' surrounding the small loop-monopole antenna. The loop-monopole small antenna [1] has been found to be unidirectional below about 5 MHz. So the loop part was suspended to be a pendulum so that it would be sensitive to any sideways force on it. No force was found down to an estimated limiting sensitivity level of about 100 dynes.

Next it was supposed that the lost radiation in the limit would be completely 'frequency converted' to white noise radiation spectrum with a cut-off at twice the carrier frequency. For a 50% efficient small antenna at 5 MHz we would then expect to find a measured sideband noise to carrier ratio of −70 dBC. Measurements showed that complete spectrum conversion to white noise was not being achieved. The lost radiation was being preferentially converted to increase the power level of some of the discrete spur sidebands of the low cost DDS source (Elecraft XG3) used for the measurements. The excess power has to come from a reduction of the white noise between the spur signals below the −70 dBc level. Figure 1 shows that after propagation from the small loop-monopole to an antenna outside the near-field spur sideband energy is increased relative to the carrier level and the carrier level is decreased more than predicted by the Friis formula. This indicates that some of the power lost from the carrier has been transferred preferentially into the sideband spurs. Note some spurs are unstable in time as seen on the right of Figure 1.

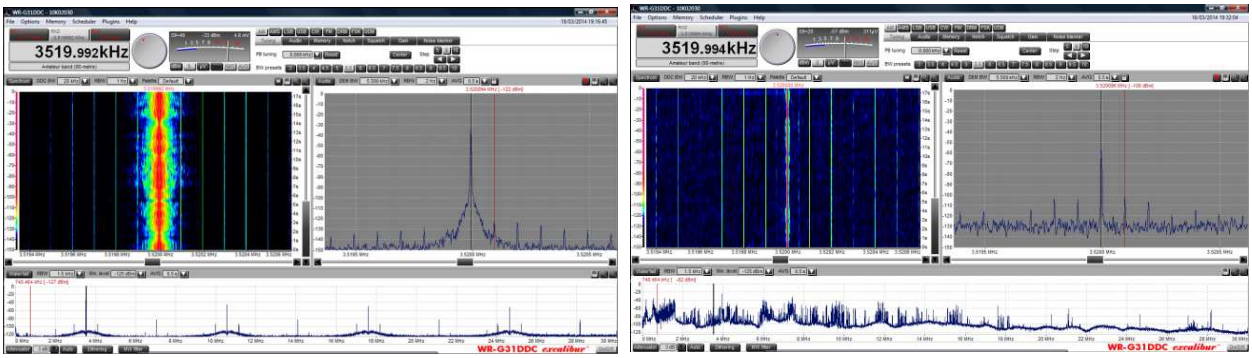

(a) (b)

Figure 1: (a) 17s time waterfall and spectrum of Elecraft XG3 DDS source showing first 100 Hz upper sideband at −89 dBc. (b) Waterfall and spectrum of XG3 after propagation from a loop-monopole to an 83 m perimeter loop at 13 m distance above the loop monopole and showing first upper 100 Hz sideband at only −51 dBc.

The discovery of this small antenna dissipation and frequency conversion process has widespread implications for example for antenna efficiency, Beverage antenna noise reduction, Maxwell's Equations and the Chu Criterion. Theory for this effect has been developed based on [2] and subsequent papers.

REFERENCES

1. Underhill, M. J., "Wideband small loop-monopole hf transmitting antenna with implications for Maxwell's equations and the Chu criterion," *PIERS Proceedings*, 764–768, Taipei, March 25–28, 2013.
2. Underhill, M. J., "A physical model of electro-magnetism for a theory of everything," *PIERS Online*, Vol. 7, No. 2, 196–200, 2011.

Session 3A14
SC5: Inverse Problems, Diagnostics, and Estimation

Image Reconstruction from Total Electric Field Data with No Knowledge of Incident Field

Takashi Takenaka and Toshifumi Moriyama
Graduate School of Engineering, Nagasaki University, 1-14 Bunkyo-machi, Nagasaki 852-8521, Japan

Abstract— In most inversion algorithms, the information of incident fields illuminating the region of interest (ROI) is assumed. To avoid computational complexity, the incident field in the ROI is often modeled as a field radiated by a line source or a set of dipole sources which fits the measured data in the absence of the unknown object. In some measurement situations, the transmitting antenna producing an incident field is placed close to ROI. This implies the incident field in the presence of the object might be different from the measured data in the absence of the object since the antenna characteristics are affected by the object in the near-field zone of the antenna. Using a wave splitting technique, Gustafsson and He showed that inversion can be carried out without the knowledge of incident field [1]. We have proposed an alternative approach based on the field equivalence principle [2]. These methods use both electric and magnetic field data. The measurement of either electric or magnetic field is preferable to avoid measurement complexity.

In this paper, we present an inversion method with only electric field data. Let us consider the scattering by an object placed in an infinitely extending region. The impressed current producing the incident field is assumed to begin to flow at time $t = 0$. We can set up an interior boundary value problem in which the solution is the same as that of the original scattering problem in the finite region Ω bounded by a surface S enclosing the object. The boundary value is given by the tangential components of total electric field of the original scattering problem on the surface S. Suppose we measure the total electric field on S till the time $t = T$ when the electromagnetic fields disappear almost entirely in the interior region Ω. Then, the electromagnetic field $\mathbf{u}(\mathbf{r}, t)$ of the equivalent problem is also null after $t = T$. If the material in the interior region is different from that of the original problem, the equivalent field $\mathbf{u}(\mathbf{r}, t)$ does not become null at $t = T$. Therefore, the value of $\mathbf{u}(\mathbf{r}, t)$ at $t = T$ can be used as an indicator of misfit between an estimated and the original objects. The inverse scattering problem considered here is cast as an optimization problem where the cost functional consisting of the stored energy in the interior region Ω at $t = T$. Numerical simulations were carried out using a genetic algorithm for minimization of the cost functional and the results indicate the effectiveness of the method.

REFERENCES

1. Gustafsson, M. and S. He, "An optimization approach to two-dimensional time domain electromagnetic inverse problems," *Radio Sci.*, Vol. 35, 525–536, Jan. 2000.
2. Takenaka, T. and T. Moriyama, "Inverse scattering approach based on the field equivalence principle: inversion without a priori information on incident fields," *Optics Letters*, Vol. 37, 3432–3434, Aug. 2012.

Reconstruction of Continuous Deformations in a Coaxial Cylindrical Waveguide Using Effects of the Higher Order Modes

Mariana Dalarsson, **Seyed Mohamad Hadi Emadi**, **Martin Norgren**
Electromagnetic Engineering Department, KTH Royal Institute of Technology
Teknikringen 33, SE-100 44 Stockholm, Sweden

Abstract— The power transformer is one of the most critical components in the electric power grid and a failure may result in large consequences for the power supply ability of the grid. The present study is a step towards the development of an online method to detect local mechanical deformations of power transformer windings, and thus avoiding transformer malfunctions. We employ a cylindrical model of an outer power transformer winding surrounded by the transformer tank wall, where the winding is viewed as a continuous metallic structure with deformations described by suitable continuous functions. Thus the perturbation theory for waveguide conductor boundaries can be used and the computation complexity is reduced as compared to the discrete conductor models. Assuming that waves may be launched at both ends of the waveguide, the objective is to reconstruct the continuous deformation functions from measurements of the scattered microwave fields at both ends. Generally speaking, the analysis of the measured signals and their complex relations to the structure parameters that reflect mechanical deformations is an inverse problem. In this study, we present a simple and computationally efficient first order perturbation method to solve the inverse problem of reconstructing continuous axially symmetric deformations in the cylindrical waveguide model described above. We study first the ground mode and then incorporate some effects of the higher order modes. Using a waveguide environment, the cut-off frequencies of the modes imply restrictions on how much information can be obtained from measurements at various frequencies. The dominant TEM-mode yields information at all frequencies, while the higher order modes enter as the frequency increases. Hence, an important question is whether we can utilize multiple modes to improve the reconstructions. The model is tested using synthetic measurement data from simulation of the structure in the commercial FEM program HFSS. The reconstruction results so far indicate an agreement between the reconstructed and true continuous functions that describe the deformations of the waveguide boundary.

Analysis of Probability Distribution of Inverse Problem of Nonlinear Model

Xiaolin Tong[1, 2, 3], **Zhenzhan Wang**[2], **and Qingxia Li**[1]

[1]Department of Electronics and Information Engineering
Huazhong University of Science and Technology, Wuhan 430074, China
[2]Key Laboratory of Microwave Remote Sensing, National Space Science Center
Center for Space Science and Applied Research, Chinese Academy of Sciences, Beijing 100190, China
[3]Department of Basic Experiment Teaching Centers, Henan University, Kaifeng 475001, China

Abstract— In the remote sensing field, the SNR is very low and the model is nonlinearity usually. Thus, it is important to analyze the impact of model nonlinearity. Probability distribution can be used to analyze the parameter distribution directly. Some issues involving priors and posteriors were proposed for models with significant nonlinearity and low signal to noise ratio (SNR). Two important issues are as follows: (1) The unimodal probability density function (PDF) of the observation quantity can give rise to a multi-modal PDF of the parameter (parameter). This property could lead to an incorrect maximum a posteriori estimate or a biased mean central estimate. It means that the biased evaluation results could be derived from statistical methods; (2) The rules for assigning non-informative priors in the measurement approach are different from the principle of maximum entropy. The authors point out the distinctions between PDF and probability distribution of non-linear models in the parameter space based on the resolution relationship between the observation space and the parameter space. For models with significant nonlinearity, if the unit grid interval of the observation space is considered regular, then the unit grid interval of the parameter space is considered irregular. The distribution obtained from regular grid is an approximation to the PDF. The probability should be calculated by integrating the PDF in the corresponding irregular grid. The difference between PDF and probability distribution gives rise to the difficulty in reverse problems. Analyzing the properties of the parameter by using the probability distribution instead of the PDF in the parameter space is necessary. The corresponding relationship between the observation and the parameter is researched based on resolution limit analysis. The non-uniform prior PDF was derived from uniform prior probability distribution in accordance with the principle of maximum entropy. Nonlinear analysis of the nature of the probability density distribution is necessary to eliminate bias caused by statistical methods.

Source Reconstruction from Near- and Far-field Data

Mats Gustafsson
Department of Electrical and Information Technology, Lund University
Box 118, SE-221 00 Lund, Sweden

Abstract— Visualization of currents and electromagnetic field is instrumental for our understanding of the interaction between electromagnetic fields and devices. This is easily integrated in numerical simulation software where the electromagnetic fields are computed and hence directly accessible for display. Visualization is much harder in measurement situations where we often are restricted to far-field data or near-fields on a circumscribing sphere. The near fields and currents must instead be reconstructed from measurements of the fields outside the object or volume of interest. This reconstruction is performed as the solution of an inverse source problem. The inverse problem is ill-posed and the solution requires regularization. Source reconstruction is useful in applications such as non-destructive testing of antennas and radomes [1–8].

In this presentation, we review source reconstruction for near- and far-field data. The theory is illustrated with application in radome diagnostics [5–8].

REFERENCES

1. Alvarez, Y., F. Las-Heras, and M. R. Pino, "Reconstruction of equivalent currents distribution over arbitrary three-dimensional surfaces based on integral equation algorithms," *IEEE Trans. Antennas Propagat.*, Vol. 55, No. 12, 3460–3468, 2007.
2. Cappellin, C., A. Frandsen, and O. Breinbjerg, "Application of the SWE-to-PWE antenna diagnostics technique to an offset reflector antenna," *IEEE Antennas and Propagation Magazine*, Vol. 50, No. 5, 204–213, 2008.
3. Eibert, T. F. and C. H. Schmidt, "Multilevel fast multipole accelerated inverse equivalent current method employing Rao-Wilton-Glisson discretization of electric and magnetic surface currents," *IEEE Trans. Antennas Propagat.*, Vol. 57, No. 4, 1178–1185, 2009.
4. Jörgensen, E., D. W. Hess, P. Meincke, O. Borries, C. Cappellin, and J. Fordham, "Antenna diagnostics on planar arrays using a 3D source reconstruction technique and spherical near-field measurements," *Proceedings of the 6th European Conference on Antennas and Propagation (EUCAP), IEEE*, 2547–2550, 2012.
5. Persson, K. and M. Gustafsson, "Reconstruction of equivalent currents using a near-field data transformation — with radome applications," *Progress In Electromagnetics Research*, Vol. 54, 179–198, 2005.
6. Persson, K., M. Gustafsson, and G. Kristensson, "Reconstruction and visualization of equivalent currents on a radome using an integral representation formulation," *Progress In Electromagnetics Research*, Vol. 20, 65–90, 2010.
7. Persson, K., M. Gustafsson, G. Kristensson, and B. Widenberg, "Source reconstruction by far-field data for imaging of defects in frequency selective radomes," *IEEE Antennas and Wireless Propagation Letters*, Vol. 12, 480–483, 2013.
8. Persson, K., M. Gustafsson, G. Kristensson, and B. Widenberg, "Radome diagnostics-source reconstruction of phase objects with an equivalent currents approach," *IEEE Trans. Antennas Propagat.*, Vol. 62, No. 4, 2014.

Determination of Quantum Initial States in Optical Fibres

Börje Nilsson[1], **Sven Nordebo**[2], **and Andrei Khrennikov**[1]

[1]Department of Mathematics, Linnæs University, Växjö, Sweden
[2]Department of Physics and Electrical Engineering, Linnæs University, Växjö, Sweden

Abstract— There have been intensive efforts during recent years in the area of quantum information. Of particular interest is quantum cryptography to secure the information to be transferred. For long distances, optical fibres are the only realistic alternative for which quantum communications above 100 km have been established.

In particular two of the electrical properties of the fibre obstruct the transfer over long distances. One such property is dispersion that reduces the maximum bit rate. Dispersion is with modern fibres with a high degree of purification the major limiting factor in classical fibre communication. The other electrical property is the material loss that annihilates emitted photons and create new ones due to quantum fluctuations. Losses constitute the major limiting factor in quantum communication provided that the bit rate is not an issue.

Besides the fibre properties, the photon source is of major interest for the quality of communication. To this end methods are required to determine the source properties in terms of the photon initial state, repeatability, independence of sequentially emitted photons etc.. We suggest that the source properties can be determined using statistics of the arrival times of the emitted photons provided that the fibre properties can be modelled with sufficient accuracy. The current paper is limited to the determination of the initial state assuming that the fibre losses can be neglected and that the photons are identically generated and independent. Only one fibre mode is excited and the detection is based on energy making the modelling scalar.

The photon initial state, which determines the probability density for the photon arrival time, maximizes a maximum likelihood function based on arrival time statistics. This optimization problem is in general not convex. However, if the photon detection is made in the so-called asymptotic radiation zone where the probability density can be determined to a sufficient degree with asymptotic methods, the distance to the detector being the large parameter, then the optimization problem is convex. These results are presented and discussed in the current paper.

Complex Permittivity Extraction Using a Leaky-lens Antenna System

Iman Vakili, Lars Ohlsson, Lars-Erik Wernersson, and Mats Gustafsson
Department of Electrical and Information Technology
Lund University, P. O. Box 118, Lund S-221 00, Sweden

Abstract— A time-domain material characterization using a wideband non-dispersive antenna system over the mm-wave frequencies is investigated. A leaky lens antenna [1] consisting of a synthesized hemispherical high resistivity float zone silicone (HRFZ-Si) lens with relative permittivity $\epsilon_r = 11.67$ integrated with a planar feeding structure is connected to an inhouse fabricated wavelet generator [2]. The wavelet generator consists of a fast switching metal-oxide-semiconductor field-effect-transistor (MOSFET) in series with a resonant tunneling diode (RTD) [3]. The wavelet generator modulates 80 ps baseband pulses produced by an Agilent N4906B Serial BERT into 60 GHz and transmit them to the leaky lens antenna. The transmitted pulse is then sent through the material and is received by an identical leaky lens antenna connected to the sampling head of a LeCoryWaveExpert 100 H sampling oscilloscope. The received pulse shape is delayed and distorted by the material under test. For a non-dispersive material, the received signal is just delayed and attenuated due to the losses in the material and the impedance mismatch at the material interface. In this case the permittivity of the material can be estimated directly from the time delay and the amplitude difference between the reference pulse and the received signal in the presence of the material. A dielectric sample of Plexiglas (PMMA) material with the dimensions of $2 \times 30 \times 30\,\mathrm{cm}^3$ is placed at the midpoint between the two antennas. Since PMMA is a low loss material, the delay of the signal determines the relative permittivity to $\epsilon_r = 2.53$. The permittivity over the frequency range of the measurement, i.e., [20, 100] GHz is also estimated using the Fourier transform to $\epsilon_r = 2.54 + j0.01$ which is approximately frequency independent.

REFERENCES

1. Neto, A., "UWB, non dispersive radiation from the planarly fed leaky lens antenna-part I: Theory and design," *IEEE Trans. Antennas Propagat.*, Vol. 58, No. 7, 2238–2247, 2010.
2. Vakili, I., L. Ohlsson, M. Gustafsson, and L.-E. Wernersson, "Wideband and non-dispersive wavelet transmission using leaky lens antenna," *Electronic Letters*, Vol. 49, No. 5, 321–322, 2013.
3. Egard, M., M. Ärlelid, L. Ohlsson, B. M. Borg, E. Lind, and L.-E. Wernersson, "$In_{0.53}Ga_{0.47}As$ RTD-MOSFET millimeter-wave wavelet generator," *IEEE Electron Device Letters*, Vol. 33, No. 7, 970–972, 2012.

A 3D Electromagnetic Data Inversion Algorithm in Wavelet Domain

Maokun Li[1], **Yun Lin**[1], **Aria Abubakar**[2], **and Tarek M. Habashy**[1]

[1]Schlumberger-Doll Research, Cambridge, MA, USA
[2]Schlumberger, Houston, TX, USA

Abstract— Imaging 3D electromagnetic models using nonlinear inversion algorithms is still a challenge because of the large number of parameters required to model the image, leading to extensive computing time and memory usage. In this paper, we extended the model compression scheme to three dimensional (3D) electromagnetic data inversion algorithm to alleviate this challenge. The inversion algorithm is based on a regularized Gauss-Newton algorithm using an efficient finite-difference forward solver in frequency-domain. Using the model compression scheme, we convert the unknown model parameters to reconstruct from 3D voxels in spatial domain to wavelet coefficients of the 3D model. Because images are inherently sparse in wavelet domain, we only need to keep a subset of the wavelet coefficients in the inversion. Hence, the model may then be represented by a set of reduced number of coefficients. This number is usually much less than the number of the discretization using spatial voxels. The reduction can significantly reduce the size of the Hessian or Jacobian matrix in the Gauss-Newton inversion algorithm. It improves the efficiency of the inversion algorithm in both CPU time and memory. In this work, we observe the speed up we can obtain for 3D problems through using the model compression is even larger than the one for 2D problems, when we employ the same level of wavelet truncation. In addition, we can also develop a multiscale inversion scheme by iteratively increasing the resolution in the wavelet domain. Therefore, a compressed representation of the model parameters in wavelet domain can also help to improve the robustness of the inversion. We validated the algorithm using synthetic and field data examples, both results show that the proposed method has potential for reducing the computational complexity of three-dimensional electromagnetic inversions.

RCS Diagnostics Using ISAR

Christer Larsson[1, 2]

[1]Electrical and Information Technology, Lund University, Box 118, SE-221 00 Lund, Sweden
[2]Saab Dynamics, SE-581 11 Linköping, Sweden

Abstract— The definition of the Radar Cross Section (RCS) is based on that the target is illuminated with a planar electromagnetic field, i.e., that the target is at infinite distance from the radar. For practical purposes the definition of "faraway" from the radar is given by the far field criterion,

$$r > \frac{2d^2}{\lambda}, \tag{1}$$

where r is the distance from the radar antenna to the target, d is the dimension of the target and λ is the wavelength. For common radar frequencies the far field criterion means that it is often difficult to meet this condition unless the target is small. In particular, this problem is commonly encountered for indoor measurement ranges.

There are two main methods to solve this problem. The first is to use a compact range where a large reflector is used to obtain a planar wave at the target. The second method is to measure the RCS in the near field but use an algorithm to transform the data to far field RCS for the target. This paper deals with the second method where Inverse Synthetic Aperture Radar (ISAR)is used to obtain geometrically correct images and far field RCS by image gating.

A straight forward way to image the RCS data recorded in the near field is to use the back projection algorithm. The amplitude and location for the scatterers are then determined in a pixel by pixel imaging process. The most complicated part of the processing is the correction to give the correct incidence angles in all parts of the imaged area.

The images obtained show the geometrically correct locations of the target scatterers with exceptions for some target features e.g., when there is multiple or resonance scattering. Separate features in the images can be gated in the image domain and an inverse processing step can be performed to obtain the RCS of selected parts of the image, i.e., collections of scatterers on the target, as a function of angle and frequency. It is also possible to do an approximate near field to far field transformation of the RCS data using image gating.

Examples from RCS diagnostics using imaging in two and three dimensions will be provided.

Inverse Scattering in Inhomogeneously Filled Rectangular Waveguides

Daniel Sjöberg and Christer Larsson
Electrical and Information Technology, Lund University, Box 118, Lund 221 00, Sweden

Abstract— It is common practice to measure material parameters through the reflection and transmission properties of a rectangular sample filling up a standard hollow waveguide, for instance using the Nicolson-Ross-Weir algorithm. This algorithm relies on the exact solution of reflection and transmission of plane waves for a slab, but the corresponding information can of course be obtained for scattering against an object of arbitrary shape. The evaluation of material parameters from measured scattering parameters is then typically done using optimization techniques.

In this paper we present results where the samples are not filling the cross section of the waveguide. Two basic configurations are considered: 1) circular cylindrical rods of various diameters centered in the waveguide, and 2) a single rectangular sample which is rotated in three basic orientations of the waveguide. In the first case, analytical solutions can be used to do a quick optimization, whereas in the second case, only full wave simulations are available, leading to quite long simulation times.

It is found that the cylindrical samples are not reliable for diameters less than $a = 10$, where a is the width of the rectangular waveguide. This is mostly due to limited manufacturing accuracy, and better results are found for larger diameters. Using rectangular samples in different orientations, the well known singularity of the NRW algorithm at half-wavelength thickness is shown to be lifted. These results show that the two configurations provide additional freedom to characterize material properties in rectangular waveguides, in addition to the standard approach.

Reconstruction of Line Currents from Magnetic Field Data: Strategies to Handle the External Disturbance Field

F. Ghasemifard, M. Johansson, and M. Norgren
KTH Royal Institute of Technology, Sweden

Abstract— We consider an inverse source problem of reconstructing the currents in parallel conductor structures. In electric power engineering, such inverse source problems appear in contact-free measurements of currents in e.g., power lines, bus bars and cables. The magnetic field is measured by a set of sensors located in the vicinity of the conductors, and the currents are determined by inversion of the direct map from the currents to the magnetic field, using a suitable model of the problem.

Apart from modeling errors and measurement noise, a deteriorating factor is the disturbance magnetic field from sources in the vicinity of the conductor structure. Theoretically, the influence of two-dimensional disturbance fields can be cancelled by measuring the magnetic field on a closed contour that circumscribes the structure. However, practically, the measurement must be limited both in the angular coverage and in the number of measurement points. The influence of such approximations will be discussed.

Another approach to handle disturbances is to represent the external field, in the measurement region, with a set of multipole coefficients, to be reconstructed together with the currents. This approach can be used to handle three-dimensional disturbance fields, regardless of whether the conductor structure is modelled in 2D or 3D. When truncating to a finite number of multipole coefficients, there is a trade-off between the influences of disturbance fields and measurement noise — a too small truncation number cannot handle the disturbances while a too large number increases the sensitivity to noise.

Typically, in e.g., an out-door measurement situation, the ground will influence the magnetic field. If not incorporated into the model, all currents induced in the ground must be considered as sources to the disturbance fields. However, if the ground properties are known with reasonable accuracy, their incorporation into the model can to some extent offload the above mentioned approaches to handle the disturbance fields. Numerical examples will be shown, demonstrating the performances of the reconstruction algorithms, with and without modeling of the ground.

Inverse Source Problem for Cable Measurements with Finitely Supported Excitation

Sven Nordebo[1], **Mats Gustafsson**[2], **and Börje Nilsson**[3]

[1]Department Physics and Electrical Engineering
Linnæus University, Växjö 351 95, Sweden
[2]Department Electrical and Information Technology
Lund University, Box 118, Lund SE-221 00, Sweden
[3]Department Mathematics, Linnæus University, Växjö 351 95, Sweden

Abstract— There is a growing interest to develop an improved modeling regarding the wave propagation characteristics of power cables and its dependency on various material and structural parameters, see, e.g., [1, 2]. Important application areas are with fault localization and monitoring, transient signal analysis and partial discharge diagnostics to enable cable maintenance and repair without (or with very short) power losses, see, e.g., [3]. The application of a (generalized) matched filter is a generic approach to localize the position of a fault [3]. However, for an accurate fault localization it is naturally very important that the matched filter is based on an accurate cable model.

An electromagnetic model for HVDC power cables is given in [2] which is based on a magnetic frill generator excitation that can be calibrated to the current measured at the input of the cable. A detailed analysis shows that higher-order modes as well as the non-discrete radiating modes (contributions from the branch-cut) can be neglected for the frequency range 0–100 kHz, and it is therefore sufficient to consider the dominant quasi-TEM mode of the cable. Hence, in the frequency domain the transfer function of the cable "channel" can be expressed as $H(\omega, z) = R(\omega)\mathrm{e}^{\mathrm{i}\alpha(\omega)z}$, where ω is the frequency, $\alpha(\omega)$ the propagation constant (the pole), $R(\omega)$ the corresponding residue and z the distance to the source.

Let $s(t)$ denote the unknown excitation signal which is assumed to be supported in the finite time interval $[0, \pi]$. The optimum generalized matched filter is defined here by the optimization problem

$$\min_{s(t),z} \left\| H(\omega, z) \int_0^\tau s(t)\mathrm{e}^{\mathrm{i}\omega t}\mathrm{d}t - Y(\omega) \right\|, \tag{1}$$

where $Y(\omega)$ is the measured signal. It is noted that (1) can be solved by using linear inversion techniques (SVD) to obtain $s(t)$ and by exhaustive search to obtain the unknown distance parameter z.

An alternative, ad hoc blind deconvolution approach is to directly apply the inverse filter on the measurement $Y(\omega) = S(\omega)H(\omega, d)$ where d is the true distance, to get $\hat{S}(\omega, z) = Y(\omega)H^{-1}(\omega, z) = S(\omega)\mathrm{e}^{\mathrm{i}\alpha(\omega)(d-z)}$, and adopt the hypothesis that $\hat{s}(t, z)$ will have minimum support when $z = d$. This ad hoc approach can also be supplemented with different ways of parameterizing the signal $s(t)$.

In this presentation, we will address general issues regarding the inverse source problem for cable measurements with finitely supported excitation and present numerical examples based on pulse measurements on an 82 km long HVDC power cable in the frequency range 0–100 kHz.

REFERENCES

1. Habib, S. and B. Kordi, "Calculation of multiconductor underground cables high-frequency per-unit-length parameters using electromagnetic modal analysis," *IEEE Trans. Power Del.*, Vol. 28, No. 1, 276–284, 2013.
2. Nordebo, S., G. Cinar, S. Gustafsson, and B. Nilsson, "Dispersion modeling and analysis for multilayered open coaxial waveguides," arXiv:1401.4978 [math-ph], 2014.
3. Veen, J. and P. C. J. M. van der Wiellen, "The application of matched filters to PD detection and localization," *IEEE Electrical Insulation Magazine*, Vol. 19, No. 5, 20–26, 2003.

Session 3A15
SCNU Special Session on Biophotonics — Analytical Biophotonics

Single-molecule Detection and Its Biomedical Application

Chun-Yang Zhang
Shenzhen Institutes of Advanced Technology, Chinese Academy of Sciences, Shenzhen 518055, China

Abstract— Due to its remarkable advantages of high signal-to-noise ratio, low sample consumption, and improved sensitivity, single-molecule detection has become a promising approach in the research of chemical analysis, molecular assembly, medical diagnosis, and dynamic study of biological processes. We have made some progress in the development of single-molecule detection technique and further apply it to sensitively detect DNA, microRNA, proteins, and even post-translational modification. We believe that the combination of single-molecule detection with new technologies will expand its application in clinical diagnosis and biomedical research.

Quantitative FRET Measurement Using Emission-spectral Unmixing with Independent Excitation Crosstalk Correction

Tongsheng Chen and Jianwei Zhang
MOE Key Laboratory of Laser Life Science & Institute of Laser Life Science
College of Biophotonics, South China Normal University, Guangzhou 510631, China

Abstract— Current spectral unmixing methods for quantitative measurement of both fluorescence resonance energy transfer (FRET) efficiency (E) and the relative abundances of donors and acceptors need a acceptor-only reference and a linked FRET construct reference in addition to the system calibration to rescale the fluorescence signal for given fluorphores on a particular instrument. Furthermore, all measurements for references and FRET samples must be performed under the same instrument settings. Based on a novel notion to predetermine the extinction coefficient ratio of acceptor-to-donor for the acceptor excitation crosstalk correction, we present here a robust and independent emission-spectral unmixing FRET methodology, Iem-spFRET, which can simultaneously measure the E and the acceptor-to-donor concentration ratio (R_C) of FRET sample without any external references, such that Iem-spFRET circumvents the rigorous restriction of keeping the same imaging condition and can be used for the direct measurement of FRET sample. We validate Iem-spFRET by measuring the absolute E and R_C values of constructs with different acceptor-to-donor stoichiometry expressed in living cells. Our results demonstrate that Iem-spFRET is a simple and powerful tool for real-time monitoring the dynamical intermolecular interaction within single living cells.

Long-lived NIR Emissive Probe for Cell Imaging, Biomolecular Detection and Photodynamic Therapy

Tao Zhang and Da Xing
MOE Key Laboratory of Laser Life Science & Institute of Laser Life Science
College of Biophotonics, South China Normal University, Guangzhou 510631, China

Abstract— Cell imaging and bioactive molecules detection in living cells with long-lived lanthanide-based probes based on time-resolved fluorescence microscope, recently, have emerged as promising tools for the diagnosis of human diseases. In this research, a series of amphiphilic lanthanide (Ln = Yb^{III}, Er^{III}, Gd^{III}) porphyrinate with high NIR emission quantum yield and specific cell location were constructed. The ytterbium complex (Yb-Rh) was found not only impressive NIR emission with linear and nonlinear excitations in water but also mitochondria specific in HeLa cells. Moreover, an ytterbium complex (Yb-N) was found that it can recognize *in-vitro* anionic phospholipids confirmed with the investigation of their performance in five cancer cell lines and three normal cell lines. The primary research goals are directed toward understanding basic photoproperties of the porphyrinate lanthanide complexes for the construction of long-lived NIR emissive probes to detect specific bioactive analytes in living cells. Furthermore, with the replacement of the lanthanide center, the gadolinium complex (Gd-N) was found to be not only cancer cell-specific but also exhibit high singlet oxygen quantum yield, which proved that Gd-N can serve as smart photosensitizer for photodynamic therapy *in vitro* and *in vivo*.

Binomial Distribution-based Quantitative Measurement of Multiple-acceptors Fluorescence Resonance Energy Transfer by Partially Photobleaching Acceptor

Lili Zhang and Tongsheng Chen
MOE Key Laboratory of Laser Life Science & Institute of Laser Life Science
College of Biophotonics, South China Normal University, Guangzhou 510631, China

Abstract— Acceptor photobleaching-based fluorescence resonance energy transfer (FRET) measurement is the most simple and straightforward method to quantify FRET efficiency (E). However, current published PbFRET methods for single-acceptor constructs are unsuitable for multiple-acceptors FRET constructs. We recently proposed an empirical formula (emp-PbFRET) and a linear approximate method (Ma-PbFRET) for multiple acceptors FRET constructs by partially photobleaching acceptors. In this report, we find that binomial distribution depending on acceptor photobleaching degree can be used to characterize the proportions of various kinds of FRET constructs resulted from partial acceptor photobleaching of multiple-acceptors FRET system. On this basis we set up a rigorous quantitation theory for multiple-acceptors FRET construct named as Mb-PbFRET which is not affected by the imaging conditions and fluorophore properties. We experimentally validate Mb-PbFRET with FRET constructs consisted of one donor and two or three acceptors inside living cells on confocal and wide-field microscopes.

A Novel miRNA Assay Based Optical Probe and Enzyme-free Nucleic Acids Circuits

Yuhui Liao, **Xiaoming Zhou**, **and Da Xing**
MOE Key Laboratory of Laser Life Science & Institute of Laser Life Science
College of Biophotonics, South China Normal University, Guangzhou 510631, China

Abstract— MicroRNAs (miRNAs) participate in important processes of life course. Because of their characters of small sizes, vulnerable degradabilities, and sequences similarities, the existing detection technologies mostly contain enzymatic amplification reactions for acquisition of high sensitivities and specificities. However, specific reaction conditions and time-dependent enzyme activities are caused by the accession of enzymes. Herein, we designed a target-triggered enzyme-free amplification platform that is realized by circulatory interactions of two hairpin probes and the integrated electrochemiluminescence (ECL) signal giving-out component. Benefiting from outstanding performances of the enzyme-free amplification system and ECL, this strategy is provided with a simplified reaction process, high sensitivity, and operation under isothermal conditions. Through detection of the miRNA standard substance, the sensitivity of this platform reached 10 fmol, and a splendid specificity was achieved. We also analyzed three tumor cell lines (human lung adenocarcinoma, breast adenocarcinoma, and hepatocellular liver carcinoma cell lines) through this platform. The sensitivities of 103 cells, 104 cells, and 104 cells were, respectively, achieved. Furthermore, clinical tumor samples were tested, and 21 of 30 experimental samples gave out positive signals. Thus, this platform possesses potentials to be an innovation in miRNA detection methodology.

Applications of Laser Spectroscopy to Meet Challenges in Medicine

Katarina Svanberg[1, 2]

[1]Centre for Optical and Electromagnetic Research
South China Normal University, University City Campus, Guangzhou 510006, China
[2]Department of Oncology, Lund University Hospital, Lund University, Lund SE-221 85, Sweden

Abstract— Laser based spectroscopic techniques can be used in the detection and therapy of human diseases. Examples from oncology as well as from the specialities of ear, nose and throat and pediatrics will be given.

Laser spectroscopy has been shown to be a valuable tool both in the detection and the therapy of human malignancies. The most important prognostic factor for cancer patients is early tumour discovery. If malignant tumours are detected during the non-invasive stage, most tumours show a high cure rate of more than 90%. Even though there are many conventional diagnostic modalities, very early tumours may be difficult to discover. Laser-induced fluorescence (LIF) for tissue characterisation is a technique that can be used for monitoring the biomolecular changes in tissue under transformation from normal to dysplastic and cancer tissue before structural tissue changes are seen at a later stage. The technique is based on UV or near-UV illumination for fluorescence excitation. The fluorescence from endogenous chromophores in the tissue alone, or enhanced by exogenously administered tumour seeking substances can be utilised. The technique is non-invasive and gives the results in real-time. LIF can be applied for point monitoring or in an imaging mode for larger areas, such as the vocal cords or the portio of the cervical area [1–4].

Photodynamic therapy is a selective treatment technique for human malignancies. To overcome the limited light penetration in superficial illumination interstitial delivery (IPDT) with the light transmitted to the tumour via optical fibres has been developed. Interactive feed-back dosimetry is of importance for optimising this modality and such a concept has been developed. The technique has special interest for tumours where there are no other options, such as for recurrent prostate cancer after ionising radiation [5, 6]. For correct dosimetry it is important to asses the optical properties of tissue; this can be done by time resolving propagation techniques [7].

Another technique which has been developed for medical application is based on gas in scattering media absorption spectroscopy (GASMAS). The technique is used to detect free gas (oxygen and water vapour) in hollow organs in the human body and has been applied to the detection of of the human sinus cavities [8–11]. The GASMAS technique might also be used for surveillance of prematurly born infants [12]. Approximately 10–15% of all deliveries in Europe and in the US are preterm. As the organs are not fully developed there is a risk of morbidities. In particular the lung function is limited and the babies may develope respiratory distress symptom resulting in decreased oxygen saturation affecting risk organs, such as the brain. GASMAS may also be developed for detection of other diseases, such as middle ear infection in small kids. A certain proportion of these infections are viral induced and in these cases no antibiotics should be prescribed. GASMAS has a potential to discriminate the origin of the disease and thus guide in the desicion of appropriate therapy. Such aspects are presently persued at SCNU, Guangzhou.

Many of these techniques can also be applied to study other organic material, e.g., food. As an example a recent study on fruit maturing combines the techniques of fluoresence, reflectance and GASMAS [13].

REFERENCES

1. Xie, H., H. Liu, P. Svenmarker, J. Axelsson, C. T. Xu, S. Gräfe, J. Holm Lundeman, H. P. H. Cheng, S. Svanberg, N. Bendsoe, P. E. Andersen, K. Svanberg, and S. Andersson-Engels, "Drug quantification in turbid media by fluorescence imaging combined with light-absorption correction using white Monte Carlo simulations," *J. Biomed. Optics*, Vol. 16, 066002, 2011.
2. Thompson, J., S. Coda, M. Brydegaard-Sörensen, G. Kennedy, R. Papalay, U. Waitong-Brämming, P. A. A. Beule, M. A. A. Neil, S. Andesson-Engels, N. Bendöe, P. M. W. French, K. Svanberg, and C. Dunsby, "In vivo measurements of diffuse reflectance and time-resolved autofluorescence emission spectra of basal-cell carcinomas," *J. Biophonics*, DOI: 10.1002/jbio.201100126, 2011.

3. Vogler, N., T. Meyer, D. Akimov, I. Latka, Ch. Krafft, N. Bendsoe, K. Svanberg, B. Dietzek, and J. Popp, "Multimodal imaging to study the morphochemistry of basal cell carcinoma," *J. Biophotonics*, 1–9, DOI 10.1002/jbio.201000071, 2010.
4. Rydell, R., C. Eker, S. Andersson-Engels, P. Wahlberg, and K. Svanberg, "Fluorescence investigations to identify laryngeal lesions in vivo," *Head and Neck*, Vol. 30, 419–426, 2008.
5. Svanberg, K., N. Bendsoe, J. Axelsson, S. Andersson-Engels, and S. Svanberg, "Photodynamic therapy — Superficial and interstitial illumination," *J. Biomed. Optics*, Vol. 15, 041502, 2010.
6. Swartling, J., J. Axelsson, G. Ahlgren, K. M. Kälkner, S. Nilsson, S. Svanberg, K. Svanberg, and S. Andersson-Engels, "System for interstial photodynamic therapy with online dosimetry: First clinical experiences of prostate," *J. Biomed. Optics*, Vol. 15, 058003, 2010.
7. Svensson, T., M. Einarsdóttir, K. Svanberg, and S. Andersson-Engels, "In vivo optical characterization of human prostatic tissue using near-infrared time-resolved spectroscopy," *J. Biomed. Opt.*, Vol. 12, 014022, 2007.
8. Lindberg, S., M. Lewander, T. Svensson, R. Siemund, K. Svanberg, and S. Svanberg, "Noninvasive diagnostics of the maxillary and frontal sinuses based on diode laser gas spectroscopy," *Annals of Otology, Rhinology & Laryngology*, Vol. 121, 217, 2012.
9. Lewander, M., S. Lindberg, T. Svensson, R. Siemund, K. Svanberg, and S. Svanberg, "Clinical study assessing information of the maxillary and frontal sinuses using diode laser gas spectroscopy and correlating it with CT," *Rhinology*, Vol. 50, 26, 2011.
10. Lindberg, S., M. Lewander, T. Svensson, R. Siemund, K. Svanberg, and S. Svanberg, "The gas composition in the mastoid using laser spectroscopy," *Otolaryngology — Head and Neck Surg.*, Vol. 141, 92, 2009.
11. Lewander, M., Z. G. Guan, K. Svanberg, S. Svanberg, and T. Svensson, "Clinical system for non-invasive in situ monitoring of gases in the human paranasal sinuses," *Optics Express*, Vol. 17, 10849–10863, 2009.
12. Lewander, M., A. Bruzelius, S. Svanberg, K. Svanberg, and V. Fellman, "Non-intrusive gas monitoring in neonatal lungs using diode laser spectroscopy — Feasability study," *J. Biomed. Optics*, Vol. 16, No. 12, 127002, 2011.
13. Zhang, H., J. Huang, G. Y. Zhao, S. Svanberg, and K. Svanberg, "Studies on fruit ageing by fluorescence spectroscopy and diode laser absorption spectroscopy," Submitted to *ACP 2013*, Beijing, 2013.

Photoionization-dissociation Mechanisms of Small Organic Molecules and Clusters in the Gas Phase

Yongjun Hu[1], **Weixin Li**[1], **Weizhan Xiao**[1], **Fuyi Liu**[2], **and Liusi Sheng**[2]

[1]College of Biophotonics, South China Normal University, Guangzhou 510631, China
[2]National Synchrotron Radiation Laboratory
University of Science and Technology of China, Hefei, Anhui 230029, China

Abstract— Study of the molecular photoionization and fragmentation in the gas phase is an important way at a molecular level to understand some biological effects such as actinic effect of laser. In the present report, we have studied the photoionization and fragmentation reaction dynamics of the jet cooled biological related molecules and its clusters by the use of VUV synchrotron radiation time of flight mass spectrometry. We found: 1) the cleavage of C-C in the acetic acid dimer is related to the multi-conformers; 2) site-selected ionization occurred in the photoionization of ethanol dimer under different VUV photon energies; 3) hyperconjugative effects could act some roles in the dissociative photoionization processes of the ethanol; 4) migration of methyl has been observed in the photoionization and fragmentation under the higher photon energies radiation. Those results provide a clear picture of the photoionization and dissociation processes of small organic molecules and its clusters under the VUV synchrotron radiations.

Low-level Laser Therapy Promotes Dendrite Growth via Upregulating Brain-derived Neurotrophic Factor Expression

Chengbo Meng, **Zhiyong He**, **and Da Xing**
MOE Key Laboratory of Laser Life Science & Institute of Laser Life Science
College of Biophotonics, South China Normal University, Guangzhou 510631, China

Abstract— Downregulation of brain-derived neurotrophic factor (BDNF) in the hippocampus occurs early in the progression of Alzheimer's disease (AD). Since BDNF plays a critical role in neuronal survival and dendrite growth, BDNF upregulation may contribute to rescue dendrite atrophy and cell loss in AD. Low-level laser therapy (LLLT) has been demonstrated to regulate neuronal function both *in vitro* and *in vivo*. In the present study, we found that LLLT rescued neurons loss and dendritic atrophy via the increase of both BDNF mRNA and protein expression. In addition, dendrite growth was improved after LLLT, characterized by upregulation of PSD95 expression, and the increase in length, branching, and spine density of dendrites in hippocampal neurons. Together, these studies suggest that upregulation of BDNF with LLLT can ameliorate Aβ-induced neurons loss and dendritic atrophy, thus identifying a novel pathway by which LLLT protects against Aβ-induced neurotoxicity. Our research may provide a feasible therapeutic approach to control the progression of Alzheimer's disease.

High-throughput and Rapid Foodborne Pathogen Detection Using Segmented Continuous-flow Multiplex Polymerase Chain Reaction Microfluidics

Bowen Shu and Da Xing
MOE Key Laboratory of Laser Life Science & Institute of Laser Life Science
College of Biophotonics, South China Normal University, Guangzhou 510631, China

Abstract— The development of rapid, reliable and high-throughput molecular tools to detect foodborne pathogens has attracted considerable concern. Here, we present a segmented continuous-flow multiplex polymerase chain reaction (SCF-MPCR) on a spiral-channel microfluidic device, for the high-throughput and rapid identification multiple foodborne pathogens. The proposed microdevice consists of a disposable polytetrafluoroethylene (PTFE) capillary coiled on three isothermal blocks. Within the capillary, n segmented flow regimes are sequentially generated, and m-plex PCR is individually performed in each regime when each mixture is driven to pass three temperature zones, thus providing a rapid analysis throughput of $m \times n$. On the microdevice, continuous-flow multiplex PCR in a single segmented flow is performed in about 19 min, and it enables the detection of down to 10^2 copies$\cdot\mu L^{-1}$ of the genomic DNAs from *Salmonella enterica, Listeria monocytogenes*, E. *coli 0157:H7* and *Staphylococcus aureus*. Furthermore, the multiple air-segmented continuous-flow multiplex PCR is also performed to simultaneously amplify the four bacterial pathogens from banana, milk, and sausage, displaying a throughput of 4×3 with no detectable cross-contamination.

The Interplay of Light Capture, Thermal Dissipation and Plant Disease Responses

Jun Zhou, Lizhang Zeng, and Da Xing
MOE Key Laboratory of Laser Life Science & Institute of Laser Life Science
College of Biophotonics, South China Normal University, Guangzhou 510631, China

Abstract— Chloroplasts are the metabolic factories for photosynthesis, which is recently shown linked with various plant-pathogen interactions via providing energy, reducing equivalents and carbon skeletons. The xanthophyll cycle is well-known involved in dissipating excess light energy to protect the photosynthetic apparatus in a process termed as non-photochemical quenching (NPQ). Here, we found that the xanthophyll cycle was modulated by various pathogens at the early stage of infection. Incubation of pathogens led to localized increase or decrease in NPQ at the normal growth light intensity (PAR = 133 μmol m^{-2} s^{-1}). Further studies showed that this abnormal NPQ was closely correlated with the various ambient pH at the infected area. Moreover, HPLC analysis revealed that the NPQ changes has different impact onxanthophyllsmetabolism including zeaxanthin, viola xanthin and neoxanthin. The following immunoassays showed that the decrease or increase of xanthophyll precursors affected the abscisic acid (ABA) biosynthesis and subsequently altered the tissue defense responses, resulting in the plant susceptibility or resistance to pathogens. Collectively, these findings present novel mechanisms of how photo protective metabolites integrate into plant defense against various pathogens, which will contribute to understanding the plant-pathogens interaction at the early infection stages.

Session 3A0
Poster Session 4

Perovskite Sensitized Mesoporous NiO Based P-type Solar Cells

Xianwei Zeng, Huan Wang, Wenjun Zhang, and Wei Chen
Michael Grätzel Centre for Mesoscopic Solar Cells, Wuhan National Laboratory for Optoelectronics
College of Optoelectronic Science and Engineering, Huazhong University of Science and Technology
Wuhan 430074, China

Abstract— To significantly improve the performance of p-type half cells is prerequisite for the realization of highly efficient pn tandem cells in the future. Since the seminal work of Miyasaka et al. in 2009, organometal halide perovskites have attracted great attention as a new class of light absorbers due to their high molar extinction coefficient and specific ambipolar charge transfer property. Herein, for the first time we report highly efficient p-type solar cells based on organometal halide perovskites ($CH_3NH_3PbBr_3$, $CH_3NH_3PbI_3$ and $CH_3NH_3PbI_2Cl$) sensitized mesoporous NiO photocathodes, which are deposited on top of a about 50 nm thick NiO compact layer. It is particularly necessary to point out that the compact NiO blocking layer deposited by spray pyrolysis holds the key on the "p-type" current flow in the perovskites sensitized NiO solar cells. Among those three different sensitizers, $CH_3NH_3PbI_2Cl$ sensitized device shows remarkably higher efficiency than the other two sensitizers, which is mainly due to its higher hole injection efficiency at the perovskite/NiO interface and the higher hole collection efficiency through the mesoporous NiO network. Time-resolved photoluminescence spectroscopy and transient photocurrent/photovoltage decay measurements have been carried out to characterize the kinetics of the related interfacial processes. A close to 100% internal photon to current conversion efficiency has been approved in $CH_3NH_3PbI_2Cl$ sensitized NiO solar cell, despite the light harvesting loss caused by glass substrate and NiO film. Additionally, the compatibility with the iodine based electrolyte of these perovskites sensitized p-type solar cells makes them very promising to combine with efficient n-type dye-sensitized solar cells, to construct efficient pn tandem cells.

30×100 GHz Digitally Wavelength Switchable V-coupled-cavity Laser with Cleaved Facets

Yuan Zhuang, Xin Zhang, and Jian-Jun He
State Key Laboratory of Modern Optical Instrumentation, Centre for Integrated Optoelectronics
Department of Optical Engineering, Zhejiang University, Hangzhou 310027, China

Abstract— Widely tunable lasers are of vital importance for the modern optical communication systems. With the development of dense wavelength division multiplexing (DWDM) systems, tunable lasers are required to have large wavelength tuning range, large side-mode-suppression-ratio, low cost and low manufacture complexity. Recently, V-coupled-cavity laser (VCCL) has been proposed and excellent wavelength tuning performance has been demonstrated using etched facets. In this paper, we present some latest results on the V-coupled-cavity laser (VCCL) with cleaved facets. A standard ridge waveguide laser structure with InGaAsP/InP multiple quantum wells (MQW) was used to fabricate the laser. The measured photoluminescence peak wavelength of the structure is at about 1.55 μm. The V-coupled-cavity laser comprises a fixed gain cavity, a channel selector cavity with different optical path length and a 2 × 2 half-wave coupler. The lengths of the fixed gain cavity and the channel selector cavity are 466 μm and 512 μm, respectively. The channel selector cavity is a little longer than the fixed gain cavity so that the wavelength tuning range can be magnified by the Vernier effect. Over 30 channels with 100 GHz spacing and side-mode-suppression-ratio above 30 dB are achieved with single electrode tunning. The fabrication process is the same as that of a Fabry-Perot laser and the device size is only 500 μm × 300 μm. Since the device size is comparable to conventional DFB or Fabry-Perot lasers, it can be easily fit into a small-form-factor package. Such a simple, compact and high-performance laser is a promising alternative to the existing tunable lasers and has great potential for wide use in access and data center optical networks.

Experimental Characterization of the Distortion of Signal Propagating with Negative Group Velocity

Dexin Ye[1], **Yannick Salamin**[1], **Qinyi Lv**[1], **Qingyang Meng**[1], **Shan Qiao**[2], **and Lixin Ran**[1]

[1]Laboratory of Applied Research on Electromagnetics (ARE)
Zhejiang University, Hangzhou 310027, China
[2]Zhejiang University City College, Hangzhou 310015, China

Abstract— In Physics, causality is a fundamental postulation arising from the second law of thermodynamics. It constrains a cause temporally preceding its effect. In the context of Electromagnetics, the relativistic causality limits the upper bound of the velocity of information, which is carried by electromagnetic wave packets, to the speed of light in free space c. Although wave packets appear to transmit with superluminal or negative group velocities in anomalously dispersive media, Sommerfeld and Brillouin pointed out that the "front" of such wave packets, known as the initial point of the Sommerfeld precursor, always travels at c, thus these packets can be strongly distorted due to the anomalous dispersion. In this paper, we experimentally observe the wave front and the distortion of modulated wave packets propagating with negative group velocity in a passive artificial medium in the microwave regime. Different from previous literatures that reported superluminal optical Gaussian pulses without notable distortion, a strongly distorted sinusoidal packet with a subluminal wave front is clearly observed. This result validates Brillouin's assertion, i.e., the severe distortion of seemingly superluminal wave packets makes the definition of group velocity physically meaningless.

Influences of Embedded Plasmonic Metallic Nanostrips on Absorption by the Activen Layer in Organic Solar Cells

Yanxia Cui[1, 2], **Shou Zhang**[1], **Yuying Hao**[1], **and Furong Zhu**[2]

[1]College of Physics and Optoelectronics, Taiyuan University of Technology, Taiyuan 030024, China
[2]Department of Physics, Hong Kong Baptist University, Kowloon Tong, Hong Kong, China

Abstract— Organic solar cells (OSCs) have attracted considerable research interests due to their advantages of low cost, solution fabrication process, semi-transparency, large-area production and use of flexible substrate etc.. Plasmonic elements, made of metallic subwavelength structures, have great potentials on light harvesting. There are a series of theoretical and experimental work indicating the incorporation of plasmonic elements into organic solar cells can indeed enhance the absorption of light by the active layer. However, very little work has discussed the relative increase of light absorption by the active layer for the plasmonic organic solar cells, with respect to the corresponding planar cell with best performance. Instead, most of the experimental work has compared the performances of devices by keeping the thickness of the active layer the same before and after incorporating the plasmonic elements. Thus, it would be possible that the performance of the control case may not be the best results of the planar device, resulting in the actual increase of light absorption by the active layer produced by plasmonic elements overrated. Here, we select one typical case that is with plasmonic metallic nanostrips embedded in the active layer for detailed theoretical investigation of this issue. The control devices have inverted architecture and two types of blenders are studied (P3HT:PCBM and PTB7:PC70BM). In this work, we systematically simulate the performances of the plasmonic devices with all the geometrical parameters of the strips (width, height, period, embedded position) tuned. Then we compare their performances with the highest AM1.5 integrated total absorption of light by the active layer for the corresponding planar devices. Based on comparison, we summarize the rules of the influences of the plasmonic nanostrips on light absorption by the active layer in organic solar cells.

Attaining Higher Mobility IGZO-TFT by Annealing Than by Quenching

Peng Xiao, Linfeng Lan, Zhenguo Lin, and Junbiao Peng
State Key Laboratory of Luminescent Materials and Devices, South China University of Technology, China

Abstract— Thin film transistors (TFTs) based on amorphous oxide semiconductors (AOS) are widely applied in display as the key part of the TFT-LCD and AMOLED, due to the advantages of high mobility, good uniformity, visible-light transparency, low-temperature process, low cost, etc. [1–3]. With the development of high-resolution, high-frame rate or 3D displays, the AOSs TFT with high mobility and good stability are required. Usually, AOSs TFT with high performance can be achieved by the following method: 1) changing different semiconductor materials, 2) choosing high-k dielectric layer [4], 3) introducing protection layer, which can protect back-channel from the atmosphere such as H_2O or O_2 [5, 6], 4) optimizing the fabrication process of semiconductor layer, 5) annealing in different surroundings (vacuum, atmosphere, N_2, dry O_2, humid O_2 etc.). But the methods mentioned above are usually complicated and it is difficult to control in practice, especially for the previous two.

In this contribution, we compared the performance of quenched and annealed IGZO-TFTs with the temperature of 400°C at the same conditions. Figure 1 shows the schematic structure of the IGZO-TFT. The results showed that the annealed TFTs exhibited the better electrical properties with a mobility of $10.45\,cm^2 \cdot V^{-1} \cdot s^{-1}$ than the quenched one, as shown in Figure 2. This may ascribed to the formation of the orderly structure and less trap states in the IGZO layer during the annealing process, while the quenched one experienced a shock cooling process which will not have enough time to eliminate the large number of trap states and will bring in negative effect on the device properties. We believe that it is a good way to realize the fabrication of high performance TFT.

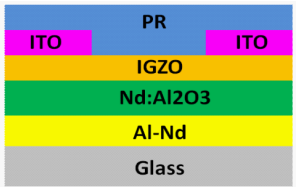

Figure 1: Schematic of the TFT based on IGZO.

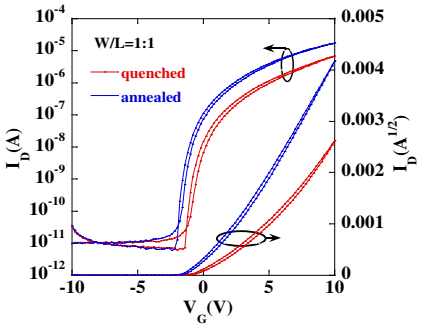

Figure 2: Transfer curves for quenched and annealed IGZO-TFTs.

REFERENCES

1. Nomura, K., H. Ohta, A. Takagi, T. Kamiya, M. Hirano, and H. Hosono, *Nature*, Vol. 432, 488, 2004.
2. Kamiya, T., K. Nomura, and H. Hosono, *Sci. Technol. Adv. Mater.*, Vol. 11, 044305, 2010.
3. Lan, L., N. Xiong, P. Xiao, W. Shi, M. Xu, W. Xu, R. Yao, and J. Peng, *J. Soc. Inf. Disp.*, Vol. 20, 175, 2012.
4. Park, J.-S., J. K. Jeong, Y.-G. Mo, and S. Kim, *Appl. Phys. Lett.*, Vol. 94, 042105, 2009.
5. Park, J.-S., J. K. Jeong, H.-J. Chung, Y.-G. Mo, and H. D. Kim, *Appl. Phys. Lett.*, Vol. 92, 072104, 2008.
6. Kang, D., H. Lim, C. Kim, I. Song, J. Park, and Y. Parka, *Appl. Phys. Lett.*, Vol. 90, 192101, 2007.

Radiation of Inverted Pendulum with Hysteretic Nonlinearity

Mikhail E. Semenov[1, 2, 3], **Peter A. Meleshenko**[1, 2],
Hang T. T. Nguyen[4], **Alexander F. Klinskikh**[2], **and Anton G. Rukavitcyn**[2]

[1]Zhukovsky-Gagarin Air Force Academy, Russia
[2]Voronezh State University, Russia
[3]Voronezh State University of Architecture and Civil Engineering, Russia
[4]Institute of Technology, Vietnam National University — Ho Chi Minh City, Vietnam

Abstract— The inverted pendulum problem (IP) is of more than 100 years history [1, 2], however it remains relevant even in the present days [3–5]. As is well known the model of the IP plays the central role in the control theory [6]. Because of their nonlinear nature pendulums have maintained their usefulness and they are now used to illustrate many of the ideas emerging in the field of nonlinear control [7]. Here we would like to note that, for our knowledge, the problem of charged IP was not considered in the literature. In this way the problem of stabilization of the IP using, e.g., an electrical field, seems novel and promisingly.

Let us recall that the equation of motion of pendulum has the form:

$$\ddot{\phi} - \frac{1}{l}\left[g + \ddot{f}(t)\right]\sin\phi = 0, \tag{1}$$

where ϕ is the angle of vertical deviation of the pendulum, l is the pendulum's length, g is the gravitational acceleration and $f(t)$ is the law of motion of the suspension point (it should be noted that such an equation describes the vertical oscillations of the suspension point and can be used in the problem of stabilization of the pendulum's upper position [5]).

In order to make an adequately description of the dynamics of real physical and mechanical systems it is necessary to take into account various effects with a hysteretic nature such as "backlash", "stops" etc.. Such a nonlinearities, of course, can be included in a corresponding law of motion of the suspension point $f(t)$.

In this work we investigate the radiation of the charged IP with a hysteretic nonlinearity in the form of backlash in the suspension point. Such a radiation can be obtained using the standard methods of classical electrodynamics. Namely, the expression for radiated power has the following form:

$$P = \frac{2q^2l^2}{3c^3}|\ddot{\phi}|^2,$$

where q is a charge of a pendulum, c is the speed of light. Law of motion of a pendulum ϕ can be obtained from numerical solution of the Equation (1) with the law of motion of the suspension point $f(t)$ which contains a hysteretic nonlinearity. Due to the presence of hysteretic nonlinearity there are some interesting results take place. In particular, the numerical simulations show that the radiated power turns in to zero during the hysteretic nonlinearity acts. This fact opens a new way for control of the IP's dynamics (e.g., using the electrical field).

REFERENCES

1. Stephenson, A., "On an induced stability," *Phil. Mag.*, Vol. 15, 233, 1908.
2. Kapitza, P. L., "Pendulum with a vibrating suspension," *Usp. Fiz. Nauk*, Vol. 44, 7–15, 1951 (in Russian).
3. Arinstein, A. and M. Gitterman, "Inverted spring pendulum driven by a periodic force: Linear versus nonlinear analysis," *Eur. J. Phys.*, Vol. 29, 385–392, 2008.
4. Butikov, E. I., "Oscillations of a simple pendulum with extremely large amplitudes," *Eur. J. Phys.*, Vol. 33, 1555–1563, 2012.
5. Semenov, M. E., D. V. Shevlyakova, and P. A. Meleshenko, "Inverted pendulum under hysteretic control: Stability zones and periodic solutions," *Nonlinear Dynam.*, Vol. 75, 247–256, 2014.
6. Huang, J., et al., "Modeling and velocity control for a novel narrow vehicle based on mobile wheeled inverted pendulum," *IEEE Transactions on Control Systems Technology*, Vol. 21, 1607–1617, 2013.
7. Åström, K. J. and K. Furuta, "Swinging up a pendulum by energy control," *Automatica*, Vol. 36, 287–295, 2000.

Aharonov-Bohm Control of Optical Properties in System of Parallel Coupled Quantum Wells

Peter A. Meleshenko[1, 2], **Hang T. T. Nguyen**[3], **and Alexander F. Klinskikh**[2]

[1]Zhukovsky-Gagarin Air Force Academy, Voronezh, Russia
[2]Voronezh State University, Voronezh, Russia
[3]Institute of Technology, Vietnam National University — Ho Chi Minh City, Ho Chi Minh City, Vietnam

Abstract— In recent time various one-dimensional (quantum wires, quantum rings [1] etc.) and two-dimensional systems (such as graphene [2]) have particular interest in connection with the development of low-dimensional technologies. In particular, such systems is widely used (or proposed to be used) in different fields, such as optics [3], spintronics [4], quantum interferometry [5] etc.. It should be noted that the charge transport process in such structures is of purely quantum nature. A special kind of such a low-dimensional systems are quantum interference devices (such as quantum graphs and quantum rings). Using these devices it is possible to observe the "delicate" quantum effects that are connected with the changes in the electron's wave function phase.

In this work we consider (our consideration is based on the scattering theory which allow to investigate not only the continuous spectrum of charge carriers, but also the discrete spectrum) the system of parallel coupled identical one-dimensional quantum wells (such a system can be presented as a multi-arm quantum ring) with a given properties, namely, a width and a depth. State of an electron in such a system has an interesting properties, namely, if one change the number of parallel coupled quantum wells the new bound states in such a system will not appear (as is known, when the quantum wells are arranged in series, i.e., the width of the resulting quantum well increases, there are many bound states in such a system and addition of new wells leads to increasing of the number of bound states) just only shift to the limiting value which determines by the parameters of a single well. In the case of quantum wells with two bound states we have the same result, however the distance between the bound states (it should be noted that the distance between the bound states corresponds to THz frequencies) decreases when the number of wells in a system increases. As a result, the characteristics of such a system, e.g., the optical properties (namely, the frequencies of laser transitions), can be changed by addition of new wells only. Addition of the Aharonov-Bohm flux at origin of such a "ring of quantum wells" allows to change the distance between the bound states as well as their positions just only by changing the magnetic flux. Thereby, the Aharonov-Bohm flux can be considered as a "strong" driven parameter for the optical properties of the system under consideration.

Our simulations are based on the following expression for the transmission amplitude

$$t_n(k) = \frac{4inkq \sin(ql) \cos\left(\frac{\alpha}{2n}\right)}{(2nq)^2 \cos^2\left(\frac{\alpha}{2n}\right) + k^2 \sin^2(ql) \left(1 + 2inq \cot(ql)\right)^2},$$

where k is a wave number of an electron, $q = \sqrt{k^2 - V}$, $V = 2m_e U/\hbar^2$, U is the well's depth and l is the well's width, n is a number of quantum wells in a system, α is a dimensionless Aharonov-Bohm flux. As is known the energies of bound states correspond to simple poles of the transmission amplitude. In order to determine the bound states energies $E_{bound} = -\hbar^2\kappa^2/2m_e$ we construct the analytic continuation of the transmission amplitude $t(i\kappa)$.

REFERENCES

1. Fuhrer, A., S. Lüsher, T. Ihn, et al., "Energy spectra of quantum rings," *Nature*, Vol. 413, 822–825, 2001.
2. Castro Neto, A. H., F. Guinea, N. M. R. Peres, et al., "The electronic properties of graphene," *Rev. Mod. Phys.*, Vol. 81, 109–162, 2009.
3. Suarez, M., T. Grosjean, D. Charraut, et al., "Nanoring as a magnetic or electric field sensitive nano-antenna for near-field optics applications," *Opt. Commun.*, Vol. 270, 447–454, 2007.
4. Cohen, G., O. Hod, and E. Rabani, "Constructing spin interference devices from nanometric rings," *Phys. Rev. B*, Vol. 76, 235120, 2007.
5. Liu, D.-Y., J.-B. Xia, and Y.-C. Chang, "One-dimensional quantum waveguide theory of Rashba electrons," *J. Appl. Phys.*, Vol. 106, 093705, 2009.

Broadband Coaxial Spatial Power Combiner Formed by Tapered Slot Antenna

Mohsen Abdolahi, Gholamreza Askari, Hamid Mirmohammad Sadeghi, and Mehdi Fadaei
Information and Communication Technology Institute (ICTI)
Isfahan University of Technology (IUT), Isfahan, Iran

Abstract— In most of microwave and millimeter wave systems, amplifiers are most important parts. Output power, wide bandwidth, low noise and linearity performances are most important goals in designing a power amplifier. Design and fabrication of an amplifier with these features is too difficult. Nowadays spatial power combiners provide these goals. Quasi optical or spatially combined amplifier arrays attempt to integrate a large number of devices in a planar radiating structure. Tray and Tile configurations [1, 2] are some of these structure. In tile configuration arrays have been reported in a grid configuration on using more conventional planar antennas such as patches and slots [3]. In both cases, the devices are distributed in a single layer transverse to the beam propagation and quietly small resonant antennas must be used that limits bandwidth. In tray configuration because planar radiating structure are in direct of incident wave, wideband antennas can be used and reach high power in wide bandwidth. In tray approach, several structure are introduced, tapered slot antenna [7] in rectangular waveguides [4–6], Yagi-uda antennas between horns [8–10] and radially trays in coaxial waveguides [11] are some of these structures. Rectangular waveguides have cutoff frequency in order of its aperture size, bandwidth of this structure isn't good and thermal management is difficult in these structures. Because dominant mode in this structure is TE_{10}, the rectangular waveguide combiner is facing a big challenge of non-uniform illumination. The sinusoidal field distribution of the dominant waveguide mode TE_{10} will lead to different drive power at the input of MMIC array. When input power increase, MMIC amplifiers at outside trays begin to reach P1 dB output power in which the MMIC amplifiers at inner trays are already overdriven into deep saturation therefore distortion will occurred.

In this paper, a coaxial waveguidebased combining scheme with broadband performance is presented In this approach one or more combined power amplifier circuits are integrated between nonresonant tapered slot antennas and stacked radiating to form a unite power amplifier. These cards can then be stacked together and make a coaxial waveguide which confines the energy and also serves as a heat sink In coaxial waveguides, dominant mode is TEM therefore uniform field distribution will occurred in all trays In this structure cutoff frequency is zero which is useful in wideband operation. This structure is shown in Fig. 1. Designing of this structure include several parts, at first impedance of coaxial waveguide is selected (in this paper impedance considered 40 ohm) in which inner and outer radius of coaxial waveguide is designed in which trays

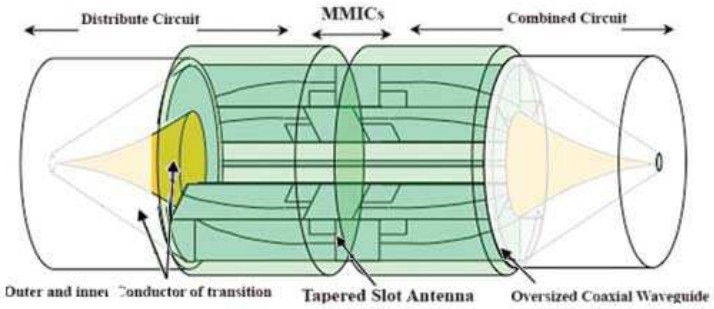

Figure 1: Overall structure of spatial combiner in coaxial waveguide.

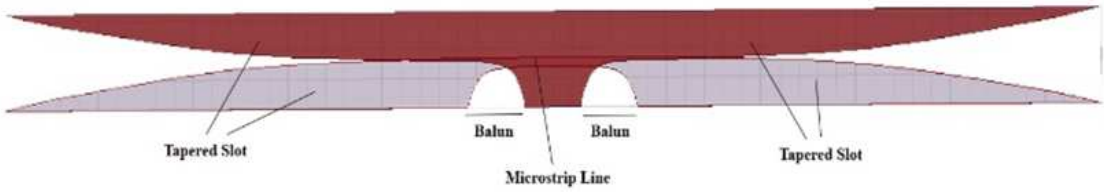

Figure 2: A designed tray in coaxial waveguide.

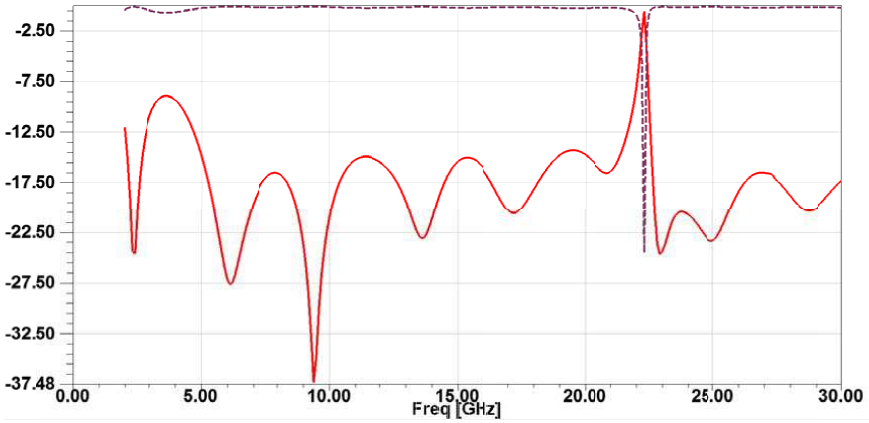

Figure 3: The result of simulated tray.

can be placed between them next the coaxial transition between N type connector and oversized coaxial connector with using Klopfenstein taper is used to obtain inner (a) and outer (b) radius of coaxial taper in which higher modes aren't propagated and return loss is considered better than 20 dB (In this designed taper, return loss was obtained better than 18 dB) After that double sided taper slots with considering 20 trays in coaxial waveguide and taper slot to microstrip balun is presented. Tapered slot and balun which are designed in RT-Duroid 5880 substrate with 31 mil thickness are shown in Fig. 2. The return loss of the designed tray is shown in Fig. 3. As it is shown in this figure, return loss in 2.5–22.5 GHz is better than 10 dB and insertion loss is less than 0.1 dB. By using this tray and other components of the whole power combiner that are discussed in this paper, a full coaxial power combiner in 2.5–22.5 GHz that can be used in many systems, is introduced.

REFERENCES

1. Kim, M., et al., "A grid amplifier," *IEEE Microwave and Guided Wave Letters*, Vol. 1, No. 11, 322-4, 1998.
2. Alexanian, A. and R. A. York, "Broadband waveguide-based spatial combiners," 1999.
3. Tsai, H. S., M. J. W. Rowell, and R. A. York, "Planar amplifier array with improved bandwidth using folded-slots," *IEEE Microwave and Guided Wave Letters*, Vol. 4, No. 4, 112-14, 1999.
4. Chen, L.-Y., N.-S. Cheng, and R. A. York, "Design of waveguide finline arrays for spatial power combining," *IEEE Transactions on Microwave Theory and Techniques*, Vol. 49, No. 4, 609, 614, Apr. 2005.
5. York, R. A., "Broadband spatially combined amplifier array using tapered slot transitions in waveguide," *IEEE Microwave and Guided Wave Letters*, Vol. 7, No. 2, 42, 44, Feb. 2000.
6. Cheng, N.-S., A. Alexanian, M. G. Case, and R. A. York, "20 watt spatial power combiner in waveguide," *IEEE MTT-S International Microwave Symposium Digest*, Vol. 3, 1457, 1460, Jun. 7–12, 2002.
7. Jia, P., "Broadband power combining device using antipodal finline structure," U. S. Patent 7215220, Cap Wireless Inc., May 7, 2007.
8. Tsai, F.-C. E. and M. E. Bialkowski, "An X-band tray-type spatial power combiner using uniplanar quasi-Yagi antennas," *IEEE Antennas and Propagation Society International Symposium*, Vol. 4, 4140, 4143, Jun. 20–25, 2004.
9. Song, H. J. and M. E. Bialkowski, "Broadband power combiner using trays of uniplanar quasi-Yagi microstrip antennas," *2000 Asia-Pacific Microwave Conference*, 241, 244, 2000.
10. Song, H. J. and M. E. Bialkowski, "Spatial power combiner formed by uniplanar quasi-yagi antennas," *30th European Microwave Conference*, 1, 4, Oct. 2000.
11. Jia, P., L.-Y. Chen, A. Alexanian, and R. A. York, "Multioctave spatial power combining in oversized coaxial waveguide," *IEEE Transactions on Microwave Theory and Techniques*, Vol. 50, No. 5, 1355, 1360, May 2002.

S-band Circular Polarization Patch Antenna Design for the Large Curvature Conformal Structure

Yuan Yuan and Zhi Xu
Aviation Key Laboratory of Science and Technology on AISSS
China Leihua Electronic Technology Research Institute, Wuxi, China

Abstract— A circular polarization patch antenna operating at S-band is proposed which is complaint with a large curvature column structure. The coupling effects between the conformed antenna and the based structure are considered accurately in the refined simulation models and impedance performance has been illustrated in the paper. The designed maximal gain in the normal direction of the antenna aperture reaches 7 dBi possessing the polarization axial ratio from 0.3 dB to 3.2 dB within $\pm 45^\circ$ scanning volume.

Application of Artificial Magnetic Conductor in Aperture-coupled Microstrip Antenna

Chao Fang and Guizhen Lu
Communication University of China, China

Abstract— A new technology of the slot waveguide transmission line has been concerned. The application of this technology in aperture of coupled microstrip antenna is studied in this paper. The dispersion characteristics are analyzed in the communication bands. The design and analysis of aperture-coupled microstrip antenna adding artificial magnetic conductor (AMC) has been done.

Aperture-coupled microstrip antenna has been used widely in wireless communication technology. But the drawback of the aperture-coupled antenna is the back radiation effects. This drawback limits the application of the coupling slot antenna in communication. In order to overcome the back radiation effects, the traditional method is to add the reflecting plate or a cavity on the back of antenna. However, the reflective plate tends to produce unwanted radiation.

Development of artificial magnetic materials technology provides the technical foundation for the realization of artificial magnetic conductor technology. The application of artificial magnetic conductor coupled to the coupled microstrip antenna is studied in this paper. The back radiation effect can be reduced by adding artificial magnetic conductor on the back of antenna. The results showed that the feeder matching characteristics of antenna which has artificial magnetic conductor have not changed. Just some of the best match frequency shift position slightly. The size of the artificial magnetic conductor can be adjusted to improve the feeder matching characteristics. There is a small increase in the gain of the antenna with artificial magnetic conductor. The back radiation effect of the antenna has greatly reduced. The result reaches the expected design goals by using artificial magnetic conductor.

Design of Broadband Vector Modulator Based on HMC500LP3 Chip

Qian Xu, Jungang Miao, and Chen Chen
Electromagnetics Laboratory, Beihang University, China

Abstract— Active phased array antenna system has already become the popular field of the antenna technology research. The problem of improving the precision of phase shifting has not been addressed until M. Tuckman proposed the concept module of the vector modulator in 1988. Vector modulator technology in active phased array antenna has been used as a replacement of conventional digital phase shifter and digital attenuator, that reduces the size of the component, and improves the flexibility of amplitude modulation and phase modulation.

In this paper, the vector modulator is realized by a vector modulation HMC500LP3 chip from Hittite by using Agilent ADS software. The HMC500LP3 chip is a high dynamic range Vector Modulator RFIC with the differential input, and thus the Balun BD1631J50100AF is designed to transform the single input into the differential input. The differential characteristic impedance of the output Balun is increased to 100 ohm from 50 ohm. The traditional power supply circuit, namely PI type circuit network, is used. Furthermore, this paper systematically presents the vector modulator measure setup which uses Agilent USB/GPIB control module 82357B to have logic control of vector network analyzer and DC voltage source analyzer by MATLAB software. The R&S ZVA24 vector network analyzer is used to measure the circuit S parameter measurement. Finally, the DEEMBDING calculation for SMA connector is completed by the MATLAB software.

The measurement results show that the chip of the HMC500LP3 vector modulator can realize a continuously controlled 360° phase shifting range and a range of (−9 dB)–(−41 dB) for the amplitude over the 1.8 GHz–2.2 GHz band, Measured S_{11} and S_{22} are below −17 dB and −15 dB. The phase linearity is satisfactory. Moreover, the different power supply voltagehas little influence on the linearity. Compared to a digital phase shifter, the vector modulator can not only realize modulation on phase shift and amplitude simultaneously, but also possesses more accurate phase resolution.

A Novel Substrate Integrated Waveguide Back-cavity Antenna with Bow-tie Shaped Slot

Chuang-Ming Tong[1, 2], **Weijian Pang**[1], **Xiong Zou**[1], **and Tong Wang**[1]

[1]School of Air and Missile Defense, Air Force Engineering University, Xi'an 710051, China
[2]State Key Lab. of Millimeter Waves, Nanjing, Jiangsu 210096, China

Abstract— As substrate integrated waveguide cavity-backed antenna with narrow rectangular slot always be narrow banded, a novel cavity-backed antenna with bow-tie shaped slot is proposed. Bow-tie shaped slot is integrated on the SIW cavity to wide the bandwidth. Design and simulation process are also given in this paper, the key parameters affecting the performance of antenna is studied, and test sample is fabricated and tested. Test results show that 3.96% relative bandwidth and 4.9 dBi gain are obtained at the antenna center frequency 5.3 GHz. The simulation results coincide well with simulated results, verify the validity of the designing.

A Novel UWB Antenna with Dual-band Notched Characteristics

Yongfan Lin, Jiangang Liang, Zimu Yang, Zhiyong Xu, and Rui Wu
Air Force Engineering University, Xi'an, Shanxi 710051, China

Abstract—

Introduction: Since the Federal Communications Commission in 2002, approved rules for the commercial use of the ultra-wideband (UWB) with a frequency range of 3.1–10.6 GHz for commercial purposes. Recently, UWB technology has been widely used in various radars and it pay an important role in the communication system, because it's narrowband system incomparable advantage like low cost, high speed and anti-multipath effect. But, the frequency range for UWB antenna will cause interference with existing narrowband wireless communication systems, for example WIFI (5.470 GHz–5.725 GHz) and WiMAX (3.3 GHz–3.8 GHz). Therefore, in order to reduce and prevent the interference between the spectrum, improve the utilization rate and independence of spectrum, it is particularly important to research UWB antenna with the stopband characteristics. In aspect of implementing spectrum coexistence the antenna will gets better application.

Mainwork: A novel omni-directional ultra-wide band (UWB) antenna with dual-stopband characteristics is designed in this paper. To obtain extended impedance band-width, a small rectangular-shaped defected ground structure is used. The antenna has a good performance on immpedance characteristics with the bandwidth from 2.0 GHz to 13.7 GHz. A U-shaped defected patch structure as well as a L-shaped defected patch structure are designed aims at getting a dual-stopband characteristic, and they are realized at bandwidth of 5.29 GHz–6.608 GHz and 3.30 GHz–3.87 GHz, containing WIFI (5.470 GHz–5.725 GHz) and WIMAX (3.3 GHz–3.8 GHz) working frequency bandwidth. The problem of interference among spectrum can be solved effectively and spectrum coexistence can also be realized.

Spurious Modes Reduction in a Patch Antenna Using a Novel DP-EBG Structure

Zhi-Yong Xu, Hou Zhang, Rui Wu, and Yong-Fan Lin
School of Air and Missile Defense, Air Force Engineering University, Xi'an, Shaanxi 710051, China

Abstract— The active integrated antenna, which integrates active devices directly into the antenna platform, is prospective in communication systems for its simplification of the circuitry and downsizing of the transmission system, but this configuration easily occur the spurious radiation at harmonic frequencies due to the inherent features of the oscillation circuit in this system. To overcome this problem, a novel dual planar electromagnetic bandgap (DP-EBG) microstrip structure is investigated to suppress the spurious radiation of patch antenna. The calculated and experimental results all verify that the application of this DP-EBG structure not only drastically diminishes spurious radiations of 2nd $\sim$ 5th harmonics in a broad frequency band, but also overcome some shortages of other EBG microstrip antennas introduced in previous research such as large back radiation or beam squint.

A Novel DP-EBG Structure for Low-pass Filter of Wide Stopband

Hou Zhang, **Zhi Yong Xu**, **Yong Fan Lin**, **and Rui Wu**
School of Air and Missile Defense, Air Force Engineering University, Xi'an, Shan'xi 710051, China

Abstract— In this letter, a novel dual planar electromagnetic bandgap (DP-EBG) microstrip low-pass filter structure is investigated. The presented structure is realized by superposing two different one-dimensional (1-D) electromagnetic bandgap (EBG) structures which have different center frequency of the stopband into a coupled dual-plane configuration. Both simulation and experimental results have verified that only two cells of the proposed structure are enough for the measured 20 dB stopband from 3.7 GHz to 14 GHz with a excellent low-pass performance in a small circuit area. Since this novel design demonstrates superior low-pass filtering functionality, we expect this novel structure is widely used for wideband monolithic circuit applications.

A Novel Method for Sparse Array Antenna Through-the-wall Imaging Radar Wall Clutter Elimination Using Independent Component Analysis

Chi Zhang, **Yue-Li Li**, **and Zhi-Min Zhou**
College of Electronic Science and Engineering
National University of Defense Technology, Changsha, Hunan 410073, China

Abstract— An independent component analysis (ICA) based wall clutter elimination method for the sparse array antenna through-the-wall imaging radar (TWIR) is proposed in this paper. ICA is a statistical method for transforming an observed multidimensional random vector into independent components. It is recently used to reduce the effect of wall clutter in TWIR since it can decompose data into components containing primarily target information and clutter information respectively.

The synthetic aperture radar (SAR) imaging approach is often adopted by the monostatic radar, in which the ICA algorithm can be applied to the B-scan (two-dimensional data presentation) matrix. While the single-input multiple-output or multiple-input multiple-output (MIMO) processing techniques are suitable for multistatic system using an array antenna. Sometimes, the sparsity of array elements limits the number of range profiles (RP), i.e., observed signals obtained in one single scanning, which will hinder the effectiveness of ICA method. Unlike the conventional manner, a multiple scanning based ICA method is proposed based on the analysis of the weak fluctuation among RP signals in different periods, which implements multiple scanning of the array antenna, then applies ICA to a RP matrix for each transmit/receive antenna pair and remove the wall clutter components.

The paper first discusses the formation of RP as well as ICA model. Then it analyses the fluctuation of RP in the real radar system. It shows that ICA can be applied on a RP matrix for each transmit/receive antenna pair, which is crucial for the proposed method. The experiment with a four-element fixed array antenna is carried out for detection two trihedrals in a room surrounded by concrete wall. The results show that, compared with the single scanning based ICA, the proposed method can separate target and clutter components effectively. The signal-to-clutter ratio (SCR) is promoted in final image after removing the wall clutter components.

A Dual Band U-shaped Slot Antenna for WLAN and WiMAX Applications

Zimu Yang[1], **Hou Zhang**[1], **Ning Zhou**[2], **and Biao Wu**[2]

[1]Air Force Engineering University, China
[2]Electronic Systems Engineering Corporation of China (ESECC), China

Abstract— A compact dual band antenna with two U-shaped slots is presented. The antenna structure consists of rectangular patch and a ground plane at the same side. By using two U-shaped slots, the dual band characteristics are successfully obtained. Utilizing a CPW (Coplanar Waveguide) feeding line, the overall dimension of the antenna is 32 mm × 40 mm × 0.8 mm, which printed on an FR4 substrate with a dielectric constant of 2.95 and a substrate thickness of 0.8 mm. Simulated and measured results show that the antenna impedance bandwidth covers the frequency range of 2.3 to 2.8 GHz and 3.1 to 3.8 GHz. With almost omnidirectional radiation pattern, the proposed antenna configuration can be applied to WLAN and WiMAX devices.

Two Miniaturized Microstrip Patch Antenna for Chinese Compass Navigation Satellite System Based on High-permittivity Substrate

Hangying Yuan, Shaobo Qu, Jieqiu Zhang,
Jiafu Wang, Hua Ma, Lin Zheng, and Mingbao Yan
College of Science, Air Force Engineering University, Xi'an 710051, China

Abstract— With the rapid development of navigation satellite systems, China is accelerating the pace of development of its own Compass Navigation Satellite System (CNSS for short). In CNSS system, miniaturized antennas are more attractive. However, conventional CNSS antennas work at low operation frequency (L band, 1.616 ± 5 MHz and S Band, 2492 ± 5 MHz) which lead to large scale by using low-permittivity ceramic substrate. Consequently, in this paper, we present two miniaturized CNSS microstrip antennas based on high-permittivity ($\varepsilon_r = 16$) ceramic substrate. One is corner-cut-patch structure, and the other is two-pair-slot-patch structure. They work at S Band (2492 ± 5 MHz, right-handed circular polarization, RHCP) to receive position information. An experiment was carried out to verify our design. For corner-cut structure, numerical results show that impedance bandwidth ($S_{11} < -10$ dB), 3 dB axial ratio bandwidth and gain are about 62 MHz, 15 MHz, and 3.48 dB, and measured results shows that impedance bandwidth ($S_{11} < -10$ dB) and 3 dB axial ratio bandwidth are about 66 MHz, 12 MHz, respectively. Meanwhile, for slot structure, numerical results show that impedance bandwidth ($S_{11} < -10$ dB), 3 dB axial ratio bandwidth and gain are about 94 MHz, 23 MHz, and 3.96 dB, and measured results shows that impedance bandwidth ($S_{11} < -10$ dB) is about 132 MHz and 3 dB axial ratio bandwidth is much larger than 22 MHz, respectively. Obviously, the characteristics of slot-patch structure are better than the characteristics of corner-cut structure. Measured results fit well with the simulation results. The two antennas can fully meet the requirement of CNSS. Meanwhile, comparing with the conventional low-permittivity substrate antennas, the two antennas remain their well performances with a reduced size by 75% to 80%. Such advantages make it proper to practical applications.

Investigating the Dual-passbands Frequency Selective Surface with Complementary Structure

Lin Zheng, Shaobo Qu, Jieqiu Zhang, Jiafu Wang, Hang Zhou, Mingbao Yan, Zhiyuan Zhang, Hangying Yuan, Yongfeng Li, and Yongqiang Pang
College of Science, Air Force Engineering University, Xi'an 710051, China

Abstract— The frequency selective surface (FSS) has found widespread applications, such as antennas and radomes for aircraft and communication fields. With the development of radome's performance and the improvement of communication devices, the requirements of multi-frequency communication become more and more significant. For those applications, the multi-band FSS have been used especially when multiple independent transmission bands are required. Therefore the multi-band FSS designs have been investigated extensively. In the past, several techniques have been used to design multi-band FSS, include cascading multi-layer different unit cell to obtain multi-resonance and single-layer FSS with the fractal structures. Recently, in substrate-integrated waveguide technology, dual-band FSS was constructed to obtain a large band separation, band-reject response. In this letter, the dual-passbands performance of frequency selective surface (FSS) with complementary structure is presented. The complementary loop element resonators are used in each FSS unit cell to obtain this ability. We designed three styles FSS composed of circle loop squared loop and hexagonal loop arranged in a 2-D periodic lattice. These FSSs are engineered a hybrid of three layers closely coupled FSS. The outer layers of elements and a middle layer of complementary elements are etched either side of a dielectric substrate. The proposed FSS structure is independent of incident polarization and angle because of centrosymmetric of the unit cell. We investigate the frequency responses of such periodic structures induced field distribution. It is demonstrated that transmission zeros occur in passbands formed by the mode of aperture resonance and aperture coupled patch resonance. By simulating their transmission and reflection coefficients under normal and oblique TE and TM incidences, show that it has a stable frequency response at different oblique incident angles and the advantages of high selectivity. Moreover, there are two passbands separated by a distinct null. These FSSs are also easy to fabricate.

An Ultra Wideband Printed Helical Antenna with Low Profile

Xihui Tang[1], **Ruirui Li**[2], **Jihong Pei**[2], **and Yunliang Long**[3]

[1]Shenzhen Key Lab of Advanced Communications and Information Processing
College of Information Engineering, Shenzhen University, China
[2]College of Information Engineering, Shenzhen University, Shenzhen, China
[3]Department of Electronics and Communication Engineering
Sun Yat-Sen University, Guangzhou, China

Abstract— This paper presents a compact ultra-wideband strip helical antenna with circular polarization. In order to achieve circular polarization and impedance matching with helix of 1.1 turns, the helix is made of uniform metallic strip instead of traditional metallic wire. Considering the convenience in manufacture, the uniform metallic strip is firstly printed on a substrate with $\varepsilon_r = 2.2$, $h = 0.5\,\text{mm}$, then the substrate is rolled into the shape of cylinder such that a helix is formed. A $50\,\Omega$ coaxial cable is directly connected to the helix without an impedance matching section. The ground plane, which is printed on another substrate with $\varepsilon_r = 2.2$, $h = 3\,\text{mm}$, is placed under the helix. To demonstrate this method, a 1.1-turns helical antenna is fabricated, measured and analyzed. Measured results show that the proposed antenna has an impedance bandwidth ($S_{11} \leq -10\,\text{dB}$) of more than 70%, and an axial ratio (AR) bandwidth ($\text{AR} \leq 3\,\text{dB}$) of 55%. These wideband circular polarized (CP) characteristics indicate that the proposed antenna has a potential application in wide-band/multi-band wireless communication systems.

Discussions on the FSS Transmitted Beam Shift in Quasi-optic Instruments

M. Jin, Y. Bai, and C. Gao
Science and Technology on Electromagnetic Scattering Laboratory, Beijing 100854, China

Abstract— The Quasi-Optical (QO) instruments have become popular in feeding the reflector antenna systems, because of the advantages of high transmission efficiency and low dispersion. The frequency selective surface (FSS) is the key component in a multiband QO feed, because of that beams from corrugated horns in different frequency bands can be combined onto a shared feeding aperture. To the transmitted beam, the FSS structure will introduce both degradation and shifting effects, which bring difficulties in developing an multiband QO instrument. Therefore, it is significant to evaluate the FSS transmitted beam aberrations in the design and optimization process.

Hybrid methods based on the plane-wave spectrum (PWS) concept have been constructed and validated, for finding the transmitted fields through periodic structures due to beam incidence. In those methods, the incident and the transmitted beams are expanded in the plane wave spectrum and the influence on each PW component by FSS can be included in analysis. Consequently, results of a 2-D angular sweeping of simulations under periodic boundary conditions (PBC) are required to implement the PWS method.

In a multiband QO instrument, the FSS is deployed among a serial of components in each beam path, where systematic design has to be performed. In this case, an even-more efficient method to investigate the transmitted beam aberrations would help in the early design stage. Recently, we reported a prediction method for the transmitted beam shift caused by FSS. That method is based on the phase analysis of the plane-wave transmission functions of FSS within a range of incident angles, and only the results of a 1-D sweeping of PBC simulations is required. In the reported work, the prediction method for tangential beam shift was validated by results of PWS algorithms. In this work, we are to discuss more FSS unit types and the Longitudinal transmitted beam shift will also be addressed.

Retrieval of Bare-surface Soil Moisture from Simulated Brightness Temperature Using Least Squares Support Vector Machines Technique

Fei Xu, Qinghe Zhang, and Qiyuan Zou
School of Science, Three Gorges University, Yichang, Hubei 443002, China

Abstract— Soil moisture is an important parameter for hydrological and climatic investigations. It also plays a critical role in the prediction of erosion, flood or drought. Passive microwave remote sensing data has great potential for providing estimates of soil moisture. In this paper, we explore the use of the support vector machine technique for modeling soil moisture inversion, like as Least Squares Support Vector Machines (LS-SVM). LS-SVM, put forward by J. A. K. Suykens, is improved by the standard SVM and has more attractive properties, for instance, simpler operation, fast convergence, rate high accuracy, small training sample is needed. Experimental tests are carried by using the different sets of training and test data for each method. The methodologies have been applied to two sets of data to retrieve soil moisture from bare-surface soils and obtained the root mean squared error (RMSE) and the correlation coefficient (R^2). The emissivity model by Wang and Choudhury (Q/H model) is applied to acquire the brightness temperature and generate the datasets, large range of soil moisture and surface roughness are simulated. The frequencies of interest include 1.4 GHz (L-band) of the soil moisture and ocean salinity (SMOS) sensor at two incidence angles and 6.9 GHz (C-band) of the advanced microwave scanning radiometer (AMSR) viewing angle of 55 degree. The effectiveness in this application is assessed by considering various combinations of the input features (i.e., different microwave sensor frequencies, polarizations, and incidence angles). Designed schemes as follows: 1) two L-band 1-D modes — emissivity H and V polarizations at L-band at angles of either 20, or 40 degree; 2) one C-band mode — emissivity dual-polarization at C-band at angle of 55 degree; 3) one L-band 2-D mode — emissivity H and V polarizations at L-band at angles of 20 and 40 degree. A combination of two angles corresponds to one L-band 2-D mode; 4) Three integrate C- and L-band modes — emissivity at C-band combined with those prepared in steps 1 and 3 to become integrated C-band and L-band multiple dimensional emissivity modes. This study demonstrates the great potential of LS-SVM in the inversion of soil moisture from passive microwave remotely sensed data.

A Method of Two-dimensional MIMO Planar Array Design Based on Sub-array Segmentation for Through-wall Imaging

Pengfei Liu, Biying Lu, and Xin Sun
College of Electronic Science and Engineering
National University of Defense Technology, Changsha 410073, China

Abstract— Facing the needs of city against terrorism, street fighting, as well as the personnel rescue buried in the ruins of fires, earthquakes and other disasters, ultra-wideband through-wall imaging (TWI) technology has been widely studied. As two-dimensional (2-D) imaging is just the result of a 2-D projection of the real 3-D space, the imaging obtained by 2-D imaging are mostly suffered from the shadowing effect and space ambiguity phenomena. To get the 3-D information of target scene by 2-D spatial distribution of antennas becomes an urgent need. In order to circumvent the real-time problem of synthetic aperture imaging and the prohibitive cost of real aperture imaging in 3-D TWI, MIMO imaging, which uses the virtual array concept to get a larger imaging aperture while maintaining the actual number of array elements, are mostly preferred. In this paper, the concept of equivalent array is introduced to design the 2-D MIMO array. Derived from a detailed analysis of the split transmit virtual aperture (STVA) that has the shortest physical size when given the virtual aperture, a method named sub-array segmentation is used to resolve the de-convolution process between the equivalent array and MIMO array. As the equivalence condition is valid only at a small range of angle, a concept of comprehensive size, based on the information of sub-array segmentation, is used to select the smallest physical size of the MIMO array among the de-convolution results. Finally, the method is promoted to the 2-D planar case and a 2-D UWB-MIMO array for TWI is designed as an example to validate the proposed method.

Analysis of the Low Intensity Terahertz Radiation Influence on Lymphocyte Early Activation Markers

M. V. Duka (Tsurkan)[1], **M. K. Serebriakova**[2, 4], **I. V. Kudryavtsev**[2, 3], **A. S. Trulioff**[2, 4], **and O. A. Smolyankaya**[1]

[1]ITMO University, Russia
[2]Institute of Experimental Medicine of the NorthWest Branch of the Russian Academy of Medical Sciences, Russia
[3]Far Eastern Federal University, Russia
[4]Saint-Petersburg State University, Russia

Abstract— According to the literary date, terahertz radiation has some effects on different blood cells. Our study focuses on the determining the level of some cell surface antigenes of lymphocytes when exposed to broadband terahertz range 0.05–1.2 THz. These data indicate that terahertz radiation with power density 9.55, 0.63 and 0.03 mW/cm^2 for 1 minute does not alter the functional activity of lymphocytes.

At the moment you can find in the literature a number of papers devoted to study of the influence of terahertz (THz) radiation on the functional activity of human blood cells. In the case of lymphocytes research was focused on the role of various power THz radiation in the regulation of cell cycle [1, 2], violation of the integrity of genetic material of cells and DNA stability [2, 3]. However, to correctly assess the functional state of the cell can be used different approach, based on determining the level of surface antigens that characterize the functional state of the cell, i.e., cellular activation markers. Lymphocyte activation markers spectrum is very wide. During the study, we selected two antigens — CD38 and CD69, up-regulation of these markers is commonly used to estimate the state of functional cells in culture conditions in vitro.

We took as a basis the circuit of a THz radiator developed for the irradiation of nerve cells [4]. It was updated for the irradiation of cells immersed in a liquid medium. The generated THz radiation had a frequency band of 0.05–1.2 THz with a maximum signal at 0.5 THz, and the THz pulse was 2.5 ps wide. The samples were irradiated for 1 min. The power of the THz radiation, allowing for absorption by the plate, was 30, 2, and 0.1 μW. The irradiation area was 3.14 cm^2. The power density was accordingly 9.55, 0.63, and 0.03 μW/cm^2.

For the each power 1 sample from each one donor was irradiated (18 donors). 18 control wells were not subjected to irradiation. Lymphocyte suspension was prepared from the venous blood of healthy donors . After irradiation, staining of antibodies against surface antigens was performed. To assess the level of expression of activation markers isotype controls were used. For each of the samples were analyzed at least 20,000 lymphocytes by flow cytometer Navios ("Beckman Coulter", USA). Analysis of the results was performed using software Kaluza ("Beckman Coulter", USA).

Analysis of the level of expression of cell activation markers (CD38 and CD69) of lymphocytes (T-lymphocytes, B-lymphocytes, natural killer cells and NKT-cells) showed that in response to pulsed terahertz radiation range 0.05–1.2 THz with a power density 9.55; 0.63; 0.03 mW/cm^2 for 1 min is no significant increase in the number of lymphocytes that contain these markers.

ACKNOWLEDGMENT

This work was financially supported by Government of Russian Federation, Grant 074-U01.

REFERENCES

1. Scarfi, M. R., M. Romano, R. Di Pietro, O. Zeni, A. Doria, G. P. Gallerano, E. Giovenale, G. Messina, A. Lai, G. Campurra, D. Coniglio, and M. D'Arienzo, "THz exposure of whole blood for the study of biological effects on human lymphocytes," *Journal of Biological Physics*, Vol. 29, 171–177, 2003.
2. Doria, A., G. P. Gallerano, E. Giovenale, G. Messina, A. Lai, A. Ramundo-Orlando, V. Sposato, M. D'Arienzo, A. Perrotta, M. Romano, M. Sarti, M. R. Scarfi, I. Spassovsky, and O. Zeni, "THz radiation studies on biological systems at the ENEA FEL facility," *Infrared Physics & Technology*, Vol. 45, 339–347, 2004.

3. Korenstein-Ilan, A., A. Barbul, P. Hasin, A. Eliran, A. Gover, and R. Korenstein, "Terahertz radiation increases genomic instability in human lymphocytes," *Radiation Research*, Vol. 170, No. 2, 224–234, 2008.
4. Tsurkan, M. V., O. A. Smolyanskaya, V. G. Bespalov, V. A. Penniyainen, A. V. Kipenko, E. V. Lopatina, and B. V. Krylov, "Changing growth of neuritis of sensory ganglions by terahertz radiation," *Proc. SPIE*, Vol. 8261, 82610S, 2012.

Influence of Terahertz Radiation with a Frequency 0.05 ÷ 1.7 THz on Mitochondrial Membrane Potential of Tumor Cells

M. V. Duka (Tsurkan)[1], **M. K. Serebriakova**[2, 4], **I. V. Kudryavtsev**[2, 3], **A. S. Trulioff**[2, 4], **A. S. Nazarova**[4], **and O. A. Smolyankaya**[1]

[1]ITMO University, Russia
[2]Institute of Experimental Medicine of the North-West Branch of the Russian Academy of Medical Sciences, Russia
[3]Far Eastern Federal University, Russia
[4]Saint-Petersburg State University, Russia

Abstract— In order to ensure safety in the use of terahertz radiation for medical problems, impact assessment of broadband terahertz radiation in the frequency range of 0.05–1.2 THz was made to investigate functional activity of tumor cells in vitro. According to the results of flow cytometry we can speculate that pulsed terahertz radiation with a power density of up to near 10 mW/cm^2 and duration of 1 minute does not change functional activity of tumor cells.

In recent years, application of sources of terahertz (THz) radiation is rapidly growing. It is estimated that it can be used in medical diagnosis of skin diseases and skin cancer. However, the divergent data on the effects of THz radiation are questioning the safety of its use. To assess the effects of THz radiation at the cellular level, the mitochondrial membrane potential and the permeability of the cell membrane of certain cells of transplanted crops were investigated after exposure by flow cytometry.

Cell cultures of the following lines were chosen as objects of study: A-549 (carcinoma cells of human lung), BT-20 (adenocarcinoma cells of the mammary gland), COLO320HSR (carcinoma cells of the sigmoid intestine); U937 (a cell line of leukosis of human histocytes), HL-60 (cells of human promyeloid leukemia).

In the layout of the apparatus, the radiation of femtosecond laser with an Yb : KYW active medium (wavelength 1040 nm, pulse width 120 fs, pulse-repetition rate 75 MHz, mean power 1 W) was modulated by a mechanical modulator and was then fed to an InAs crystal located in a special system with magnetic induction $B = 2.2$ T. THz radiation generated in the InAs crystal was collimated by an off-axis parabolic mirror to a beamsplitter plate. The femtosecond radiation reflected from the crystal was absorbed in a fluoroplastic filter. Next, the part of the radiation transmitted through the beamsplitter plate was focused by a lens onto a GC-1P optoacoustic detector, another part of the radiation was directed by parabolic mirror toward the object. The loss of THz radiation on the plate in which the cells are held was 20%. The generated THz radiation had a frequency band of 0.05–1.2 THz with a maximum signal at 0.5 THz, and the THz pulse was 2.5 ps wide, exposure time was 1 min. The irradiation area was 3.14 cm^2. The power density was 9.55, 0.63, and 0.03 μW/cm^2. Three series of experiments were carried out for each cell culture. The irradiation was done three times in each series at each power. As a control, wells in the plate that were not subjected to the action of the irradiation were used for each of the powers.

It was shown that the terahertz radiation 30, 2 and 0.1 mW and 1 minute exposure have no significant effect on the change in the functional activity of mitochondria, nor gives integrity on their bilayer outer membranes. Including no statistically significant changes in the ratio of live and at different stages of apoptotic cells.

ACKNOWLEDGMENT

This work was financially supported by Government of Russian Federation, Grant 074-U01.

The Baroque Music's Influence on Learning Efficiency Based on the Research of Brain Cognition

Rong Gu, **Jie Zhang**, **Junhe Zhou**, **and M. S. Tong**
Department of Electronic Science and Technology
Tongji University, 4800 Cao'an Road, Shanghai 201804, China

Abstract— Brain is the organ of learning. Human intelligence activities are closely related to the states of human brain. Only by following the brain activity patterns, the learning efficiency could be promoted and the brain function could be furtherly developed. In recent years, by the technologies such as EEG and fMRI, the brain's memory, thinking, learning, emotional and other advanced features are in-depth studied, which confirms that the brain science is bound up with education and has important guiding value to educational practise. The research on brain science is widely used in the field of education, as the important basis of reforming the traditional teaching methods. Therefore, the rational use of the human brain cognitive rules can help improve students' learning efficiency. For the past few years, the research on close integration of brain science and education has been carried out and become a hot spot. The scientists of many countries are researching it.

To let the brain be in the best condition for learning is the task faced to teachers for improving the students' abilities of memory, attention, thinking and so on, which is also a work of great significance for improving the teaching quality. This article discusses the influence of the Baroque music on learning state from the perspective of electroencephalogram analysis. First electroencephalogram (EEG) data of the n-back experiments are collected before and after listening to the Baroque music. Then its frequency, the energy, α wave distribution, scalp, event related potential and other components are compared. Specially, the brain's memory and attention are analyzed and estimated by extracting useful EEG information in time-domain, frequency-domain and spatial distribution. The experimental results show that Baroque music has a positive influence on improving learning efficiency. So that teachers can use Baroque music to assist teaching as reform means, which will provide an effective way to improve the learning efficiency and teaching quality.

Analysis of Spectral Characteristics of the Human Cornea Obtained in the Terahertz Frequency Range

M. I. Sulatsky[1], **E. A. Strepitov**[1], **O. A. Smolyanskaya**[1], **M. K. Khodzitskiy**[1], **I. V. Prozheev**[1], **E. L. Odlyanitskiy**[1], **A. G. Zabolotniy**[2], **and I. A. Geyko**[2]

[1]ITMO University, Saint-Petersburg, Russia
[2]Krasnodar Branch of "S. N. Fyodorov Eye Microsurgery Complex", Krasnodar, Russia

Abstract— The spectral characteristics and optical properties of the human cornea were analyzed for development of non-invasive methods of cornea diagnosis for terahertz frequency range.

Introduction: Currently, the studies of various degenerative processes in the cornea are of considerable interest for ophthalmic diagnosis and therapy. Among the therapeutic measures aimed at enhancing the regeneration and restoration of cornea function, are dominated mainly symptomatic agents. However, medicinal drugs have their drawbacks. Therefore, the development of non-invasive methods of cornea diagnosis and therapy is today very actual task.

Results and Conclusions: In this work, we investigated two different samples of the cornea of the human eye. Experimental spectral characteristics and optical properties of the biological samples were obtained using the universal pulsed broadband THz spectrometer [1] working on transmission and reflection modes. Study of the spectral features of cornea was carried out in 3D numerical simulation environment CST Microwave Studio. The changes of terahertz reflection spectra of the cornea of the human eye in the frequency range of 0.1–2.0 THz was experimentally investigated. It should be referred attributed to the results of the cornea reflection spectra. On the Figure 1 there are the reflection spectra of two different biological samples of human cornea.

The differences in the reflection spectra of the 1st and 2nd cornea are well marked. It can be selected high-intensity expressed peaks at frequencies 0.97, 1.09 and 1.38 THz, as well as spectral peaks of weak intensity at frequencies of 1.00, 1.18, 1.33, 1.19 and 1.41 THz, respectively.

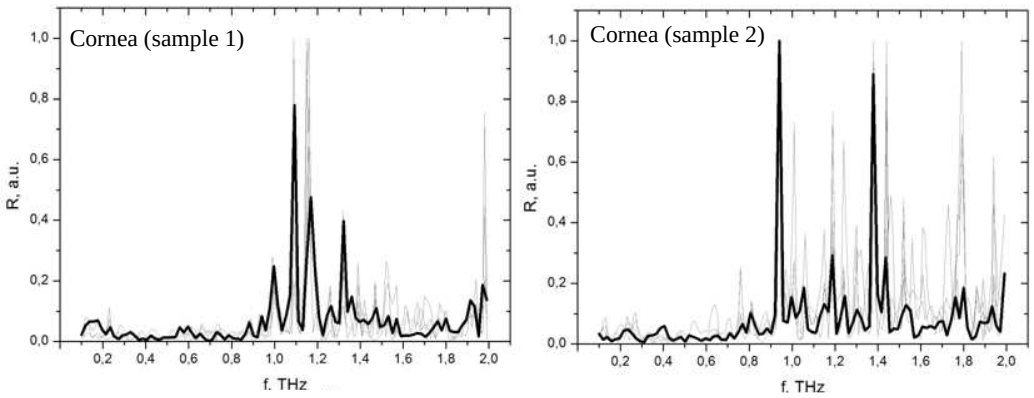

Figure 1: Reflection spectra of the human eye cornea.

ACKNOWLEDGMENT

This work was financially supported by Government of Russian Federation, Grant 074-U01.

REFERENCES

1. Bespalov, V. G., et al., "Methods of generating superbroadband terahertz pulses with femtosecond lasers," *Journal of Optical Technology*, Vol. 75, No. 10, 636–642, 2008.

Study of Penetration Depth Dispersion of THz Radiation in Human Pathological Tissues

I. V. Prozheev, **O. A. Smolyanskaya**, **M. V. Duka**, **A. A. Ezerskaya**, **V. V. Orlov**, **E. A. Strepitov**, **N. S. Balbekin**, **and M. K. Khodzitsky**
ITMO University, Saint Petersburg, Russia

Abstract— The dispersion of penetration depth of terahertz radiation in various human pathological tissues were obtained and analyzed for development of subcutaneous diseases diagnostics in terahertz frequency range.

Introduction: The terahertz (THz) radiation is an electromagnetic radiation in the wavelength range of 3 mm–30 mkm (the frequency range of 0.1–10 THz). One of the most important areas of application for terahertz radiation is the diagnosis of pathological changes in the skin, including cancer, inflammatory and morphological [1, 2]. This paper is devoted to investigation of penetration depth of radiation in human normal and pathological tissues (chemical and thermal burn, etc.) for development of subcutaneous diseases diagnostics in the frequency range of 0.1–2 THz.

Material and Methods: We investigated in vivo several samples of human tissues: normal skin tissue, thermal burn skin tissue, chemical burn skin tissue, skin covered by ointment, phantom skin. The reflection spectra were obtained by THz time domain reflection spectroscopy, utilizing ultrashort electromagnetic pulses generated from a InAs semiconductor in magnetic system driven by femtosecond laser pulses. The THz spectrometer has the following characteristics: the average power of 30 μW; the frequency range of $0.1 \div 2.0$ THz, the pulse duration of 3 ps, the spectral resolution about of 15 GHz) [3]. The signals measured by the spectroscopy system are time domain waveforms that are directly proportional to the terahertz electric field. By mathematical Fourier transformation of the time domain waveforms spectra are obtained in the THz frequency range. Thus, it is possible to recover both phase and amplitude information, which provides a direct measure of the frequency-dependent refractive index of the tissue sample, absorption coefficient and penetration depth.

Results and Conclusions: The characteristic spectral lines for different types of human skin samples in-vivo were observed in the THz reflection spectra, especially in the vibration modes frequency range of 0.2–1.0 THz. The dispersion of THz radiation penetration depth in various skin pathological tissues were obtained using the waveforms of terahertz pulses reflected from air/dielectric window and dielectric window/tissue interfaces. This work contributes to the understanding of the interaction of pulses of THz radiation and tissue and explains the difference between pathological and normal tissue in THz spectra and penetration depth which may lead to improvements in THz technology for medical applications.

ACKNOWLEDGMENT

This work was financially supported by Government of Russian Federation, Grant 074-U01.

REFERENCES

1. Ezerskaya, A. A., et al., "Research of specific peculiarities of THz reflection spectra of abnormal human tissues," *Proceedings of the 15th Int. Conference Laser Optics*, 433–434, 2012.
2. Nazarov, M. M. et al., "Terahertz impulse spectroscopy of biological tissues," *Quantum Electronics*, Vol. 38, No. 7, 647–654, 2008
3. Bespalov, V. G., et al. "Methods of generating superbroadband terahertz pulses with femtosecond lasers," *Journal of Optical Technology*, Vol. 75, No. 10, 636–642, 2008.

A Comparative Study of Analytical and Numerical Analysis for Coaxial Probe Aperture in a Dissipative Media

K. Y. You[1], **C. Y. Lee**[2], **and C. W. Lee**[1]

[1]Department Communication Engineering, Faculty of Electrical Engineering
Universiti Teknologi Malaysia (UTM), Johor 81310, Malaysia
[2]Faculty of Bioscience and Medical Engineering
Universiti Teknologi Malaysia (UTM), Johor 81310, Malaysia

Abstract— This paper presents an analysis of the coaxial probe aperture immersed in a dissipative medium using Levine's integral calculation and Nevels's MoM routines. The analytical integration and MoM are programmed with MATLAB code. The comparison between simplicity and accuracy of both methods has been discussed in detail. This paper intends to enhance the compatibility study of analytical and numerical methods for coaxial probe, since literature on this study for coaxial probe is less compared to linear monopole.

Time-frequency Spectrum and Path Loss by Wind Turbine Forward Scattering

M. B. Raza and T. Fickenscher
Helmut Schmidt University, Hamburg, Germany

Abstract— The growing number of wind farms being deployed around the globe leads to an increase in the possibility of electromagnetic interference with nearby radar and radio communication systems. Reflection, scattering and diffraction from the electrically large wind turbine (WT) structure can seriously deteriorate their performance. A time variant loss and phase shift is observed for the forward scattered signal due to the rotating blades. The subsequent time variant frequency shift presents a figure of interest for the analysis of WT interference to radar and communication systems, in particular to radars dealing with low Doppler frequencies (e.g., weather radar).

Generally, WT interference studies have focused mostly on the back scattered signals [1], while investigations on the forward scatter of WT have concentrated on the shadowing and range effects [2]. Particularly the impact of WT forward scatter on Doppler shift, which is a well-known problem in the context of weather radars, has not yet been quantified. In this paper we use a one dimensional Fresnel approximation for a fast analytical investigation of the WT forward scatter which also includes near-field effects [3]. Short time Fourier transform (STFT) is used to obtain time-dependent frequency information for the WT forward scattered signals. The calculated results are verified by using UTD solver of EM software FEKO. Moreover, the effects of ground plane on the forward scattered signals are presented. Three dimensional radars like Weather radars are less susceptible to the ground plane reflections, owing to their extremely narrow beams. However, the ground plane effects become significant for fixed radio links and hence ground reflections must be taken into account. A thorough investigation is carried out by positioning the WT at different locations along the radio link. Moreover, different transmitter and receiver orientations for varying antenna height and signal path are also considered for outlining the worst case scenario of WT interference.

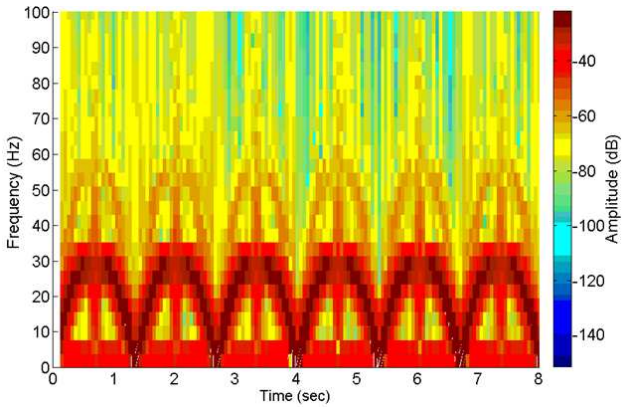

Figure 1: Normalized Spectrogram of the frequency shift due to WT forward scatter (1.3 GHz, 15 RPM).

REFERENCES

1. Brenner, M., "Wind farms and radar," JSR-08-126 prepared by The Mitre Corporation, January 2008.
2. Greving, G., W. Biermann, and R. Mundt, "Wind turbines as distorting scattering objects for radar-clutter aspects and visibility," *11th International Radar Symposium (IRS)*, 1, 4, June 16–18, 2010.
3. Fickenscher, T. and M. B. Raza, "Diffraction loss and phase modulation of terrestrial radio-link by wind turbine," *International Workshop on Antenna Technology iWAT*, Sydney, March 4–6, 2014, in press.

Experimental the Microwave Absorption of Rice Husk/Ash Mixture

Y. S. Lee[1], **F. Malek**[2], **E. M. Cheng**[3], **Wei-Wen Liu**[4], **N. A. C. Ali**[3], **F. H. Wee**[1], **M. N. Iqbal**[1], **L. Zahid**[1], **F. S. Abdullah**[2], **and M. Othman**[2]

[1]School of Computer and Communication Engineering, Pauh Putra Campus
Universiti Malaysia Perlis (UniMAP), Arau, Perlis 02600, Malaysia
[2]School of Electrical Systems Engineering, Pauh Putra Campus
Universiti Malaysia Perlis (UniMAP), Arau, Perlis 02600, Malaysia
[3]School of Mechatronic Engineering, Pauh Putra Campus
Universiti Malaysia Perlis (UniMAP), Arau, Perlis 02600, Malaysia
[4]Institute of Nano Electronic Engineering (INEE)
Universiti Malaysia Perlis (UniMAP), Kangar, Perlis 01000, Malaysia

Abstract— This paper is to study the performance of rice husk and rice husk ash (RH-RHA) mixture material as a microwave absorber. The microwave absorption and materials properties permittivity, ε of RH-RHA mixture with different ratio were investigated in microwave frequency region 8.2 to 12.4 GHz (X-band). A waveguide transmission line method (Nicholson-Ross-Weir) was used to measure the complex permittivity of RH-RHA with different weight ratio mixture. The RH and RHA are lossy material due to their dielectric properties which suitable used as microwave absorber. The dielectric properties are playing one of the main roles in microwave absorption of any material. Before simulate the result, the sample must be defined the dielectric constant and loss factor in CST-MWS over 8.2 GHz–12.4 GHz frequency range. In this simulation, two port method was use to simulate the result. The result of port 1 will be the reflected signal where port 2 will be the transmitted signal. The RH-RHA microwave absorber has been designed and simulated in CST-MWS. The various ratio RH-RHA mixturesshow the different dielectric properties and the microwave absorption. The microwave absorption was calculated by $A = 1 - (S_{11})^2 - (S_{21})^2$. Where A, S_{11}, and S_{21} are the percentage of absorption signal, reflection loss, and transmission loss respectively. The 60%RH-40%RHA microwave absorber has the best microwave absorption. The thickness of the RH-RHA microwave absorberwas influence the absorptionof the Microwave absorber. The thicker of the RH-RHA microwave absorber sample has better absorption compared to the thinner sample absorber. The thickness of the rice husk sample with 10 mm thickness has the highest absorption.

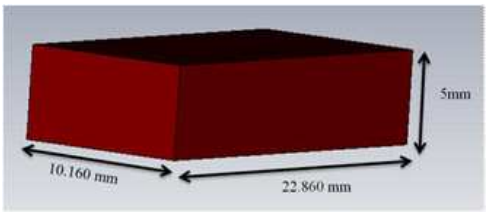

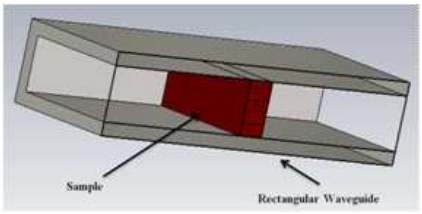

Design of a Dual and Wideband Monopole Antenna with Flattened Ground Plane

T. K. Ong[1], **B. H. Ahmad**[1], **M. Z. A. Abd. Aziz**[1], **M. A. Othman**[1], **M. K. Suaidi**[1], **and F. Abd. Malek**[2]

[1]CeTRI, FKEKK, Universiti Teknikal Malaysia Melaka (UTeM)
Durian Tunggal, Melaka, Malaysia
[2]School of Computer and Communication Engineering
Universiti Malaysia Perlis, Perlis, Malaysia

Abstract— In order to efficiently utilize the wideband technology with minimal radio frequency interference, this paper has proposed a dual and wideband monopole antenna. This antenna is able to operate at 2.4 GHz for WLAN application as well as a wide frequency band from 4.62 GHz to 10.23 GHz with at least 90 percent of matching efficiency. The antenna proposed has a standing rectangular monopole patch and a flattened ground plane fed by a coaxial probe. The ground plane of the antenna is placed perpendicularly to the patch to provide a wide bandwidth. The antenna is designed and fabricated by using FR4 epoxy board with epsilon of 4.4 and thickness of 1.6 mm while the thickness of copper patch and ground plane is designed to be 0.035 mm. In addition, the antenna is simulated by using Computer Simulation Technology (CST) in open space environment. In the design process, parametric study has been done on the antenna design parameter, width and length of the patch to obtain the optimum result of antenna. This antenna operates from 2.23 GHz to 2.83 GHz for the first frequency band of WLAN and the second wide frequency band from 4.62 GHz to 10.23 GHz in return loss less than −10 dB. The minimum antenna gain, directivity, and efficiency for WLAN application are 1.34 dB, 1.86 dBi, and −0.52 dB respectively. Along the second frequency band, the antenna gain increases gradually from 2.90 dB to 6.66 dB whereas the directivity also increases gradually from 3.4 dBi to 7.39 dBi. This antenna has a good total efficiency of more than 79% in the second wide frequency band. The radiation pattern of the antenna at 2.4 GHz is in omnidirectional. In the wideband, the directivity of the main lobe has been shifted from both sides of the antenna to the upper left and upper right of the patch as the frequency increases.

The Performances of Sugarcane Bagasse (SCB) — Rubber Tire Dust Composite as Microwave Absorber in X-Band Frequency

Liyana Zahid[1], **Mohd Fareq Abd Malek**[2], **Ee Meng Cheng**[3], **Wei Wen Liu**[4], **Seng Yeng Lee**[1], **Muhammad Nadeem Iqbal**[1], **and Supri A. Ghani**[5]

[1]School of Computer and Communication Engineering, Pauh Putra Campus
Universiti Malaysia Perlis, Arau, Perlis 02600, Malaysia
[2]School of Electrical Systems Engineering, Pauh Putra Campus
Universiti Malaysia Perlis, Arau, Perlis 02600, Malaysia
[3]School of Mechatronic, Pauh Putra Campus
Universiti Malaysia Perlis, Arau, Perlis 02600, Malaysia
[4]Institute of Nano Electronic Engineering (INEE), Pauh Putra Campus
Universiti Malaysia Perlis, Arau, Perlis 02600, Malaysia
[5]School of Material Engineering, Pauh Putra Campus
Universiti Malaysia Perlis, Arau, Perlis 02600, Malaysia

Abstract— In this work, the performances which are the reflection loss and absorption for composite of sugarcane bagasse (SCB) and rubber tire dustas microwave absorber were investigated in the range frequency of 8.2–12.4 GHz (X-Band). Sugarcane bagasse (SCB) is one of the major agricultural wastes. This residue agricultural waste material has potential to be used as an alternative material for microwave absorber in Radio Frequency (RF) anechoic chamber. Rubber tire dust is one of the residues from tire wear. This paper shows the method about how the sample which is the composite of sugarcane bagasse with rubber tire dust was fabricated and the measurement to get the reflection loss (S_{11}) and transmission coefficient (S_{21}). The thickness of the sample is 5 mm. The methodology included in this work are defining the dielectric properties, measurement of the samples using transmission line technique (waveguide), designing and simulation using CST Microwave Studio Software. The dielectric constant, ε' from the transmission line measurement of the composite of sugarcane bagasse-rubber tire dust is 3.35. The S_{11} results showed that the SCB-rubber tire dust composite absorber was found to be better which means lower than -10 dB. The results proved that SCB-rubber tire dust was a good alternative to be used as microwave absorber. The goal of this investigation is to have the better electromagnetic reflection (S_{11}) which is less that -10 dB with the usage of the new agricultural waste such as sugarcane bagasse (SCB) and rubber tire dust. These can help save the nature and environmental friendly.

Investigation of Combination Circle Loop for Frequency Selective Surface at 5.2 GHz

N. A. Md Fauzi[1], **M. Z. A. Abd. Aziz**[1], **M. A. Meor Said**[1], **M. A. Othman**[1], **and M. F. Abd. Malek**[2]

[1]Center for Telecommunication Research and Innovation
Universiti Teknikal Malaysia Melaka, Melaka, Malaysia
[2]School of Computer and Communication Engineering, Universiti Malaysia Perlis, Perlis, Malaysia

Abstract— This paper presents a new design of combination circle loop frequency selective surface (FSS) for band pass microwave transmission application. The used of energy saving glass where the glass that is coated to absorb free energy and retain internal heat has increased rapidly. Despite this energy saving glass will reduce the heat from outside during daylight, the used of this glass will reduce the performance of the wireless communication system where the signal transmit through it will be reduced. Thus, this FSS can be used on energy saving glass to improve the transmission of wireless communication signals through the glass. The design of combination circle loop frequency selective surface has been simulated and analyzed by using CST software where this simulation and analyzation process are based on characteristics of the transmission (S_{21}) and reflection (S_{11}) of the FSS. In this paper, there are three design were introducing in order to identify the most ideal design. The first design of FSS is a combination of double circle loop in a horizontal plane surface. The second design of FSS is a combination of double circle loop in a vertical plane and the last design is a combination three circle loop on the surface. The results shown the bandwidth of the horizontal circle loop obtained is 421.32 MHz at frequency range from 5 GHz to 5.4213 GHz. Then, the bandwidth obtained for the vertical circle loop is 350.9 MHz which covered the frequency range from 5.0135 GHz to 5.3835 Hz. Meanwhile, the bandwidth is 1.0129 GHz for the combination of three circle loop, where it's covered requency range from 4.7355 GHz to 5.7484 GHz. The optimum reflection (S_{11}) can be obtained for all designs is 17.08 dB, 17 dB and 23.255 dB respectively at frequency 5.2 GHz. This FSS is suitable as a microwave filter for WLAN 5.2 GHz application.

Study on the Relationship between the Size of Resin Sprue on GIS and Intensity of UHF Electromagnetic Waves Radiated from Partial Discharge

Xingwang Li[1], **Siyang Wu**[2], **Qizheng Ye**[2], **and Chu Yang**[2]

[1]Electric Power Research Institute of Guangdong Power Grid Corporation, Guangzhou 510600, China
[2]State Key Laboratory of Advanced Electromagnetic Engineering and Technology
Huazhong University of Science and Technology, Wuhan 430074, China

Abstract— Detection of partial discharge (PD) using the UHF technique is becoming increasingly important in gas insulated substations (GIS) applications However, GIS of different manufacturers have different size of resin sprue, and the size of resin sprue has direct effects on the UHF electromagnetic waves motivated by PD, which brings about many difficulties in accurate estimate of the severity of PD. On the platform of a 252 kV GIS, we used UHF sensors which were mounted on resin sprues of different size that had been set up in advance to detect electromagnetic wave signals emitted by the needle-plane PD model in GIS and found that with an increase of the length of the long side of the sprue, the signal intensity enhances first and weakens later and get its maximum on 75 mm. Another simulation experiment which used pulse signal generator to provide excitation source for the transmitting antenna in GIS to simulate PD and detected signals in the same way to the former also found the same conclusion. The calculation results in XFDTD — An electromagnetic wave simulation software based on finite difference time domain (FDTD) method also proved the same conclusion. This conclusion offers important references for the options of the best size of resin sprue and development of external UHF sensor.

HALT Test of Tower Mounted Amplifier (TAM) Module Used in 4G Communication

Soon-Mi Hwang, Chul-Hee Kim, and Kwan-Hun Lee
Korea Electronics Technology Institute (KETI), Korea

Abstract— Tower Mounted Amplifier (TMA) is normally used to improve cell coverage, capacity and quality of a wireless communication system [1]. TMA is used to expand signal coverage through enhancing the uplink receiving sensitivity in the area where call drops and handoff failure happen frequently Improved receiving sensitivity at base station, TMA also helps to improve signal quality, enhance voice clarity and increase data transmission speed. Usually TMA is installed near to transmit and receive antenna at the top of a cell tower [2]. In general, TMA module is exposed to the outside, it should be guaranteed sufficient immunity for a variety of environmental stresses that can occur in the Outdoor.

HALT is Highly Accelerated Life Test and is a great process used for quickly finding failure mechanisms in a hardware design and product [3]. HALT is special types of accelerated reliability techniques that is very effective and is being used by companies around the world from many different industries. HALT is used at the design stage of a project to quickly expose the weak-points of a design so that the product can be re-designed to remove these weak-points, thereby expanding the margins of the design [4]. By applying various kinds and extreme level of stresses, we can find the operating limits of products; uncover the design flaws and defects of components. Understanding the test results and problems can also help design engineers to find the root causes and develop corrective actions for further improvements [5]. In this paper, we evaluate HALT of TMA module for export to Japan.

HALT test was carried out in five steps such as thermal step (high and low temperature), thermal shock, vibration step and combined stress (thermal and vibration) Real-time measurement system (measuring Insertion Loss, Return Loss, Gain, Current) of was used to determine the failure of product.

Qualmark Typhoon 3.0 is the selected major test equipment for HALT process. It utilizes the resistive wire heater coils and liquid nitrogen (LN2) for heating and cooling system and the temperature ramp rate can reach 60°C/min maximum. In addition, vibration for the test equipment is provided by a six DOF vibration table and the maximum value of acceleration is 50 Grms on random frequency ($10 \sim 10000$ Hz).

As a result, TMA had a low temperature resistance of −60°C. And there was no change in characteristics of 140°C. TMA did not fail at low temperature to −60°C and did not fail at vibration test to 40G. Thermal shock test and combination test were progressed to 5 cycles and there was no change in characteristics.

REFERENCES

1. Amir Razif, A. R. and M. Benyazwar, "Performance analysis of uplink WCDMA tower mounted amplifier," *RF and Microwave Conference*, 80–24, Oct. 5–6, 2004.
2. Lee, H.-K., A. K.-CS, H.-M. Fuad, and T. C.-CK, "A low noise figure high linearity balanced amplifier module for cellular band base station's tower mounted amplifier application using E-mode pHEMT technology," *Asia-Pacific Microwave Conference*, 1–4, Dec. 16–20, 2008.
3. McLean, H., "From HALT results to an accurate field MTBF estimate," *Reliability and Maintainability Symposium*, 1–5, Jan. 25–28, 2010.
4. Silverman, M., "Summary of HALT and HASS results at an accelerated reliability test center," *Reliability and Maintainability Symposium*, 30–36, Jan. 19–22, 1998.
5. Chan, H. A. and P. J. Englert, *Accelerated Stress Testing Handbook*, IEEE Press, New York, 2001.

Failure Mechanisms Analysis of Metal-tag Used in 900 MHz

Soon-Mi Hwang and Kwan-Hun Lee
Korea Electronics Technology Institute (KETI)
#68 Yatap-Dong, Bundang-Gu, Sungnam-Si, KyungGi-Do, Republic of Korea

Abstract— RFID (Radio Frequency IDentification) is a technology which reads the information built in products and objects by using radio frequency in definite distance. Due to the longer read distance, lower cost, faster read rate and many other advantages, the UHF (900 MHz) RFID technology are receiving much attention in the world [1]. RFID Tag is classified into label, metal and plastics types according to the materials. And there is a high demand for metal tags in a ubiquitous RFID system, since they are usually more environmentally resistant than non-metal tags [2].

RFID Tag is a product where modules like IC chip, antenna, and battery are integrated, and 'product reliability' is important as much as the function of each part. If products are developed and used without an enough environment conformance test as RFID Tag is applied in various applied environment and overall society, social chaos and economical damage will be expected from the disorder and malfunction of RFID working system [3, 4].

In this paper, we analyze field failure of metal-type RFID Tag which the most widely used in the domestic market. And then we analyze major failure modes and failure mechanisms of metal-type RFID Tag through environmental stress tests.

Result of failure analysis of field failure product, major failures of metal-type RFID Tag are body bending phenomenon due to mechanical shock or friction by accidental, performance failure due to high temperatures and high humidity and corrosion in saltwater environments.

To reproduce a failure of metal-type RFID tag in the field, high temperature test and mechanical shock/vibration test which are expected to have a major impact on tag's failure were conducted. In the high-temperature test, metaltag was failed. After a period of time, all products recognition rate on the signal was reduced. But in vibration test and mechanical shock test, there has been little change in recognition rate on the signal.

After the environments test, we analyzed fail samples using optical microscope and FIB (Focused Ion Beam). Failures of metal-type RFID tag in high-temperature environments are classified as bending of the pattern (microstrip line), desorption of tag chip and the pattern, failure of tag chip.

REFERENCES

1. He, Y. and Z. Pan, "Design of UHF RFID broadband anti-metal tag antenna applied on surface of metallic objects," *Wireless Communications and Networking Conference*, 4352–4357, April 7–10, 2013.
2. Xi, J. and T. T. Ye, "Ultra low-profile metal tag antenna design with an emphasis on radiation efficiency," *International Conference on RFID*, 42–49, April 30 2013–May 2, 2013.
3. Lu, F., X. S. Chen, and T. T. Ye, "Performance analysis of stacked RFID tags," *IEEE International Conference on RFID*, 330–337, April 27–28, 2009.
4. Karmakar, N., "Introduction to RFID Systems," *Handbook of Smart Antennas for RFID Systems*, 13–56, 2010

Printed Inverted-F MIMO Antenna for TD-LTE Mobile Terminal

Hui Liu[1, 2], **Youhuan Guo**[1], **Te Pan**[2], **Zhibin He**[2], **and Sailing He**[2, 3]

[1]Computer Science and Engineering Department, Guangdong Peizheng College, Guangzhou, China
[2]Centre for Optical and Electromagnetic Research, Academy of Advanced Optoelectronics
South China Normal University, Guangzhou, China
[3]The Royal Institute of Technology, Stockholm, Sweden

Abstract— With the rapid growth and development of the mobile communication technologies in recent years, many mobile communication technologies appeared one after another, of particular concern is 3GPP long term evolution (LTE). TD-SCDMA, has been widely accepted and approved by other countries in the internationalis one of the third generation (3G) international communication standard technologies defined proposed by China. TD-LTE, as the subsequent evolution technology of TD-SCDMA, is growing rapidly in China and is also widely considered in the forth generation (4G) mobile communication now. MIMO technology, which utilizes multiple antenna to improve spectrum efficiency and increase the system channel capacity, is one of the 4G key technologies.

As more and more TD-LTE base-stations are under construction in China, there will be a huge need for TD-LTE mobile terminal antenna. In this paper, a MIMO antenna, operating on TD-LTE frequency band for TD-LTE mobile terminal is designed. The proposed MIMO antenna consists of two printed inverted-F structures has the advantage of small size and multiband for 4G handheld devices. The antenna designed to cover the TD-LTE frequency band of 1880–1900 MHz and 2575–2635 MHz for China Mobile. The printed MIMO antenna is modeled by using Ansoft High Frequency Structure Simulation (HFSS) and electromagnetic simulation software of Computer Simulation Technology (CST). The simulated results show that the proposed system has a good isolation at the central frequency of TD-LTE frequency band and the S_{11} parameters of the proposed MIMO antenna can meet TD-LTE mobile communication requirements. Both results of simulation and test parameters suit the requirement of the TD-LTE communication for mobile terminals.

Compact Circularly Polarized RFID Tag Antenna with an Embedded U-shaped Feedline for Metallic Surfaces

Te Pan[1], **Shuai Zhang**[2], **Zhibin He**[1], **Hui Liu**[1], **and Sailing He**[1, 2]

[1]Centre for Optical and Electromagnetic Research
Academy of Advanced Optoelectronics, South China Normal University, Guangzhou, China
[2]The Royal Institute of Technology, Stockholm, Sweden

Abstract— A passive UHF radio frequency identification (RFID) tag antenna with circular polarization (CP) radiation is proposed to operate at 902–928 MHz band for mounting on metallic surfaces. A terminal short-circuited U-Shaped feedline welded to a tag-chip is embedded in a rectangular slot to achieve a proximity coupled feeding. By slightly tuning the length of the feedline according to the short-circuited transmission line theory and the electromagnetic coupling effect, a good impedance mating could be acquired. Moreover, by employing the rectangular slot, two truncated corners and two L-shaped slots with unequal length on the patch, a compact size and excellent left-hand circular polarization (LHCP) is obtained. Additionally, the operating frequency band of the proposed antenna can be easily tuned by changing the sizes of the rectangular slot and the L-shaped slots. Some rational parameter analysis of our antenna will also be proposed in the following section. Furthermore, the radiation patterns and some measurement results of the read range are presented to intuitively show the good CP radiation performance of our antenna. The power reflection coefficient (PRC) is introduced here to define the impedance bandwidth. And the 3 dB PRC bandwidth of our antenna is 32 MHz (902–934 MHz) which is broad enough to cover the required bandwidth, while the corresponding 3-dB CP bandwidth is 6 MHz (912–918 MHz). The proposed tag antenna possesses reasonable and longer read ranges when mounted on a metal plate in the following experiment.

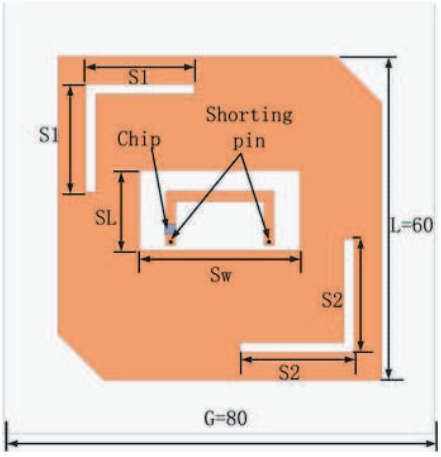

Figure 1: The geometry of the proposed circularly polarized patch tag antenna (unit: mm).

The Research and Application of Array Antenna Element Detecting System

Wentao Zhu, Feng Gao, Zhiyuan Song, and Kai He
China Mobile Group Design Institute Co., Ltd., China

Abstract— Array antenna is commonly used in wireless communication base station, which can form a higher gain and specific shaped electromagnetic beam. Nowadays, base station antenna with more elements has become the mainstream and tendency, especially in the TD-SCDMA system and LTE MIMO system. The arrangement of array is applied not only in one direction (e.g., vertical line array), but also in the orthogonal direction to form planar antenna array.

Array antenna has many elements, while one antenna element does not work properly for some reason (such as rosin joint, short circuit, destroy of mechanical structure), the reflection coefficient of the main port does not deteriorate badly, and thus the antenna will not give out a warning of the VSWR. But the array pattern will be significantly affected at this moment, such as asymmetrical antenna pattern, poor side lobe suppression, decrease of antenna gain, etc..

The existing detection techniques only detect the VSWR of the base station antenna and give out different levels of warning, and thus the abnormal situation of the internal element can't be detected. This paper proposes an antenna element detection system, which was composed of electromagnetic induction sensor and detection circuit. And this paper also supplies weights revision method for smart antenna when some antenna element doesn't work.

Figure 1 is a schematic diagram of the array antenna element detection system. The detection circuit has independent power supply (12 V), which is similar to the RCU (Remote control unit). The signal collected by the detection circuit is transmitted to the base station server by AISG cable; the adapter is mainly used to implement the connection between RS485 and RS232. RS485 has a smaller transmission loss, and it is easy to realize long-distance signal transmission. RS232 interface can be easily connected with PC to facilitate the control of this system.

Based on the comparison of the coupling signal and the reference standard signal, you can achieve the detection of array antenna element station. If the damaged element is detected by the system above, the amplitude and phases on the remaining elements can be adjusted to revise the broadcast beam.

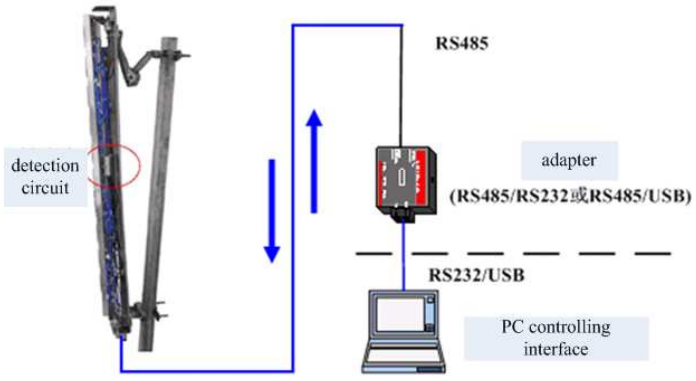

Figure 1: Array antenna element detection system schematic.

Theoretical Analysis and Test of EMF in TDFI Bus

Wentao Zhu, Feng Gao, Zhiyuan Song, and Kai He
China Mobile Group Design Institute Co., Ltd., China

Abstract— The fourth generation of mobile communications is expected to deliver multimedia services anywhere, anytime, with global support and integrated wireless solutions. TDFI is equipment which transform TD-SCDMA/TD-LTE network signal into WIFI signal, Using TDFI solution, people riding in buses can experience rapid and stable LTE TDD data services using WIFI-enabled smart phones.

Meanwhile, the electromagnetic radiation generated by TDFI is drawing the public's increasing attention. Although the radiation power of TDFI is little, it has both TDS/TDL antenna and WIFI antenna; passengers and drivers are likely to locate in the strong electromagnetic radiation field when riding in buses. For the above reason, we performed some tests and theoretical analysis to provide some insight for RF exposure assessment of TDFI equipment.

In this paper, the bus, which has been installed the TDFI equipment, is named TDFI bus. TDFI has both TDS/TDL antenna and WIFI antenna, TDS/TDL module has 2 elements, In the TDFI bus, the received power S is the sum of TDS/TDL antenna and WIFI antenna radiation energy. For propagation distances d much larger than the antenna size, transmit antenna modeled as a point source. As the propagation distance increases, the radiated energy is spread over the surface of a sphere of radius d.

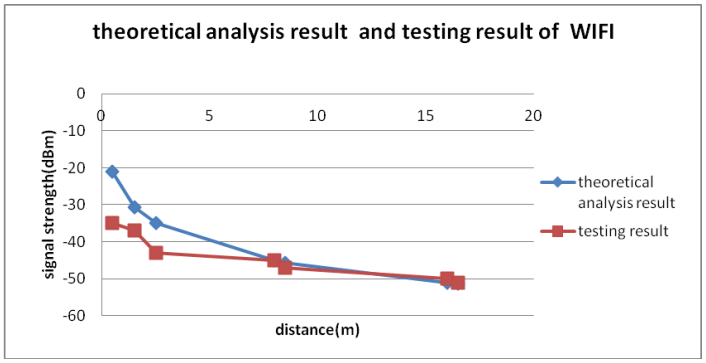

Figure 1: Theoretical analysis result and testing result of WIFI in TDFI bus.

Measured value is identical with the theoretical value. Two tools were used to test the EMF in the 307 TDFI bus, one is broadband field meter NBM 550, and anther is Wi-Fi Analytics app in mobile phone. The Amped Wireless Wi-Fi Analytics Tool analyzes the Wi-Fi networks. It provides advanced signal strength graphs of Wi-Fi network. The result of EMF testing in TDFI bus shows that the EMF level generated by TDFI equipment is less than 0.5 $\mu W/cm^2$, which is much less than international standard (20 $\mu W/cm^2$).

Body Channel Study for Wearable Devices at 2.4 GHz

Kun Zhao[1, 2], **Zhinong Ying**[2], **and Sailing He**[1]

[1]Department of Electromagnetic Engineering, School of Electrical Engineering
KTH-Royal Institute of Technology, Stockholm SE-100 44, Sweden
[2]Research and Technology, Corporate Technology Office
Sony Mobile Communications AB, Lund SE-221 88, Sweden

Abstract— In recent years, the body centric commination has drawn signification attentions from the mobile phone industry due to the rapidly incensement of the wearable device market. Most of wearable devises in the market now need to operate with a mobile terminal in pair through Bluetooth or Wi-Fi when these devices are on users' body, for instance the case shown in Fig. 1(a): A wrist band with a 2.4 GHz Wi-Fi antenna inside and a LTE MIMO terminal mockup with are paired. At 2.4 GHz, the communion mainly relies on the surface wave and the creep wave. However, it is a challenge to control the communication distance within the area approximate to human body at this frequency. In this paper, we investigate the body channel for the communication between a Wi-Fi antenna in a smart wrist band and an antenna in a mobile terminal mockup at 2.4 GHz on a user's body, by measuring the S_{21} between the transmitting and the receiving antennas. The measured S_{21} is compared in three user cases, which are shown in Figs. 1(a)–(c). The three cases represented when the wrist band and the phone are on the same hand, on the different hand and when the phone is in pocket, respectively. Moreover, different positions of the Wi-Fi wrist band antenna and different antennas in the terminal mockup are also compared (Fig. 2), in order to find out the best antenna configuration for body centric communication. In Fig. 3, the S_{21} for the same hand is presented, and it is easy to see that the bottom antenna has the best transmission coefficient due to the closest distance and same polarization with the Wi-Fi wrist band antenna. In the full paper, results for all cases will be presented, and more theory analysis with FDTD simulations will also be given.

(a) (b) (c)

Figure 1: The user cases for body centric communications (a) the same hand, (b) different hand and (c) phone in pocket.

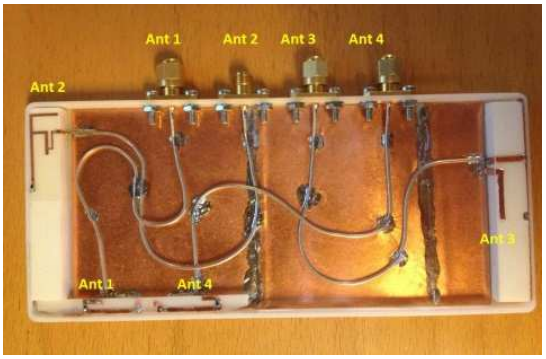

Figure 2: The antenna layout for the mobile terminal mockup.

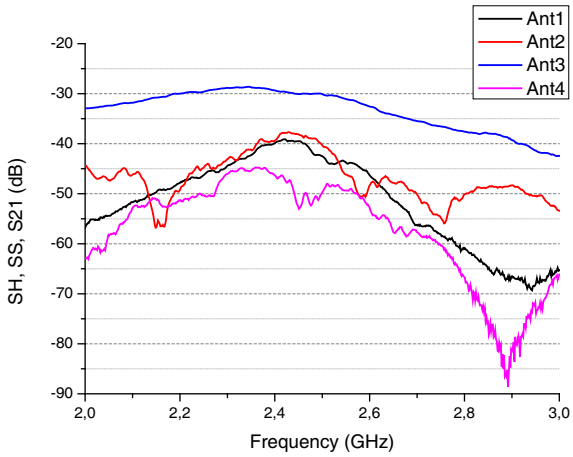

Figure 3: The S_{21} for the same hand case.

Conical Beam Leaky-wave Antenna Using Subwavelength Grooved Metal Structure

Bengeng Cai, Yunbo Li, and Tie Jun Cui
Southeast University, China

Abstract— We present a conical beam leaky-wave antenna using subwavelength grooved metal structure. The shape of antenna is disk made up of metal aluminum. The above of the disk is corrugated with grooved metal structure to support spoof surface plasmon polaritons (SPPs) or transverse magnetic (TM) surface waves. The distribution of surface impedance for grooved metal structures is sinusoidally modulated as hologram, where TM surface wave excited by dipole is taken as reference wave, and leaky-wave or conical beam is taken as object wave. The surface impedance of grooves is varied by adjusting the depth of grooves from 2 mm to 3 mm, the periodicity is 3 mm, and the radius of disk is about 180 mm with a thickness of 10 mm. The TM surface wave is excited by a dipole in the center of the disk structure. As the TM surface wave propagating along the radial direction of the disk, it obeys the Floqeut's theorem due to the periodicity of the hologram, leaky-wave is then radiated to form a conical beam by considering circular symmetry. The polar angle of the conical beam or leaky-wave is determined by the sinusoidally modulated hologram, which is in accord with the periodic leaky-wave mechanism. Both forward leaky-wave and backward leaky-wave in 17 GHz with a polar angle $\theta = 15^\circ$ are simulated to get the conical beam. The full-simulation result agrees well with the design, and confirms that subwavelength grooved metal structure as metasurface could radiate leaky-waves. This method based on holographic metasurface shows both simplicity and accuracy when comparing with previous similar works, where grooved metal structure is not in subwavelength.

Optimal Waveform Design in Through-the-wall Application Based on the Information Theory

Xin Sun, **Bi-Ying Lu**, **Peng-Fei Liu**, **and Zhi-Min Zhou**
College of Electronic Science and Engineering
National University of Defense Technology, Changsha, Hunan 410073, China

Abstract— Ultra-wideband (UWB) through-wall-imaging (TWI) approaches that can detect objects through obstacles, such as walls, doors and other opaque materials, are considered as a powerful tool for a variety of civilian and military applications. With the adaptive radar technology developing, waveform design is becoming one of the most important research directions, and will play a more important role in through-the-wall applications, especially in obtaining the information about the target behind the wall.

In recent years, the waveform design methods have largely developed. The typical contributions are the method based on maximal SINR principle and the method based on the condition mutual information theory. The maximal SINR method gets the optimal waveform by calculating the eigenvector of the autocorrelation matrix corresponding to the largest eigenvalue. The principle of the waveform design method based on the information theory is to maximize the condition mutual information between the target response and the received signal.

Waveform design is one of the hot topics presently. However, it is not pay enough attenuation in through-the-wall applications. Aimed at this problem, we design an waveform for through-the-wall use. As compared with previous work, the main work and contributions of our manuscript are as follows:

1) We construct the signal model of through-the-wall scene based on information theory. The transfer function of the wall is derived.
2) The mutual information based waveform design method is revised. Based on the derived signal model, the optimal waveform used in through-the-wall application is proposed.
3) The optimal waveform can be propitious to get more information of the target, which is very important in further process. And this method concentrates most of the energy into the frequency band, corresponding to the large value of the whole spectrum variance. So it eliminates the narrow-band problem of the maximal SINR method at a certain extent. Furthermore, the comparison between the optimal waveform and the conventional LFM waveform shows that the mutual information by the optimal waveform is obviously better than the LFM signal.

Analysis of EMF and Interference in the Wireless Charging Robot System

Jung-Ick Moon, In-Kui Cho, Seong-Min Kim, Jae-Hun Yun, and Woo-Jin Byun
Radio Technology Research Department
Electronics and Telecommunications Research Institute (ETRI), Korea

Abstract— Many researchers have developed the wireless charging system using the magnetic coupling or magnetic resonance [1]. In this paper, the analysis of EMF and interference in the service robot with the wireless charging system is shown.

As shown in Fig. 1, to transfer the high power energy into the service robot, the wireless power transmission technology using magnetic resonance was used. The resonance frequency and transfer distance is about 1.80 MHz and 20 cm, respectively. The wireless charging system is composed of the spiral type resonators, transceiver with communication module, and Pb-battery. Both resonators are made of litz wires to decrease the loss and have two layers to increase inductance.

For the analysis of EMF and interference, the uniform body model defined in IEC 62369-11 and the harmonic analysis of the resonators was used. Finally, the strength of the electromagnetic field and SAR (Specific Absorption Ratio) nearby the service robot was obtained and the recommended transfer power and service region could be suggested.

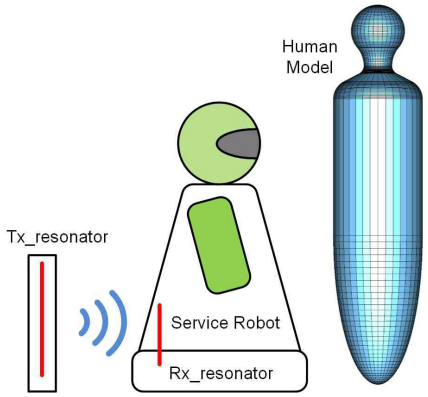

Figure 1: The service robot with the wireless charging system and human model.

ACKNOWLEDGMENT

This research was funded by the MSIP (Ministry of Science, ICT & Future Planning), Korea in the ICT R&D Program 2014.

REFERENCES

1. Cheon, S., et al., "Wireless energy transfer system with multiple coils via coupled magnetic resonances," *ETRI Journal*, Vol. 34, 2012.

Design of Wireless Power Charging Using Coupled Magnetic Resonance to 12 V, 20 Ah LiFePO4 Battery

Seong-Min Kim, Jung-Ick Moon, In-Kui Cho, Jae-Hun Yun, and Woo-Jin Byun
Radio Technology Research Department
Electronics and Telecommunications Research Institute (ETRI), Korea

Abstract— In this paper, a wireless charging system using the coupled magnetic resonance method is presented. The wireless charging system is applied to a walking assistance vehicle with a 12 V, 20 Ah LiFePO4 battery. The charging system is composed of a 130 W power transmitter, a 100 W full-bridge receiver and a constant current battery charging circuit. The power is implemented using DDS (Direct Digital Synthesizer) and a Class-F power amplifier. The operating frequency range of the power transmitter is from 1.6 MHz to 2.0 MHz. The transmit resonator is designed as a two layer spiral structure and its resonance frequency is 1.78 MHz. The diameter of the transmit resonator is 40 cm. The receive resonator is designed as same structure and same resonance frequency with 20 cm diameter. The 100 W power receiver is implemented using a full-bridge diode rectifier, active dummy load circuit and OVP (Over Voltage Protection) circuit. The active dummy load circuit is designed to maintain the receiver input impedance even when the road changes. The constant current charging circuit is designed for battery charging and communication to the power transmitter. The communication between the power transmitter and the charging circuit is implemented for the purpose of transmit power control. The power control algorithm is designed to maintain the system power efficiency. The communication scheme is 400 MHz band 9.6 kbps FSK. By the measurement results, the average charging power is 45 W and the average transmit power is 80 W. The DC/DC system efficiency is about 51%

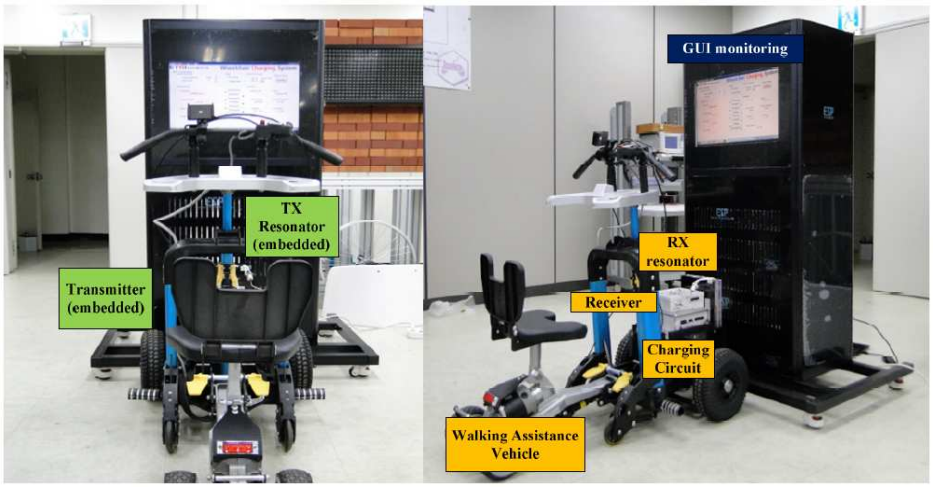

Figure 1: Implemented wireless charging system using walking assistance vehicle.

ACKNOWLEDGMENT

This research was funded by the MSIP (Ministry of Science, ICT & Future Planning), Korea in the ICT R&D Program 2014.

REFERENCES

1. Kurs, A., A. Karalis, R. Moffatt, J. joannpoulos, P. Fisher, and M. Soljacic, "Wireless power transfer via strongly coupled magnetic resonances," *Science Magazine*, Vol. 317, No. 5834, 83–86, 2007.
2. Cheon, S. H., Y. H. Kim, S. Y. Kang, M. L. Lee, and T. Y. Zyung, "Wireless energy transfer system with multiple coils via coupled magnetic resonances," *ETRI Journal*, Vol. 34, No. 4, 527–535, Aug. 2012.

Solar Thermoelectric Co-generators Comprising Parabola trough Collectors and Thermoelectric Modules

Lei Miao[1], **Chao Li**[1, 2], **Yi Pu Kang**[3], **Ming Zhang**[4], **and Jianhua Zhou**[1]

[1]Key Laboratory for Renewable Energy
Guangzhou Institute of Energy Conversion, Chinese Academy of Sciences
No. 2 Nengyuan Road, Tianhe District, Guangzhou 510640, China
[2]Graduate University of Chinese Academy of Sciences, Beijing 100049, China
[3]Department of Frontier Materials, Graduate School of Engineering
Nagoya Institute of Technology, Gokiso-cho, Showa-ku, Nagoya 466-8555, Japan
[4]Department of Physics, Graduate School of Engineering
Yokohama National University, Yokohama 240-8501, Japan

Abstract— Solar thermoelectric co-generators (STECGs) are an attractive means of supplying electric power and heat simultaneously and economically. A parabolic trough concentrator system with the rectangular opening size of $2 * 2\,\mathrm{m}^2$ was constructed in this work. Six Bi_2Te_3 thermoelectric (TE) modules were arranged in series and the hot sides of them were directly bonded to solar absorber metal coated with solar selective absorbing film. The cold sides of them were bonded to the microchannel heat sink system which was essentially cooled down by running water.

The effects of environmental factors on the conversion efficiencies of a new type of STECG was examined Simulations show that the performance of such a system strongly depends on ambient conditions such as solar insolation, temperature and wind velocity. As each of these factors increases, the thermal losses of the STECG system also increase, resulting in decreased solar conversion efficiency, despite the increased radiation absorption. However, the impact of these factors is relatively complicated. Although the electrical efficiency of the system increases with increasing solar insolation, it decreases with increasing ambient temperature and wind velocity. At the best environment and solar conditions, the hot side temperature of the TE module reached up to 152°C. The obtained electronic conversion efficiency and the thermal conversion efficiency was 1.1% and 50% respectively in the best condition. For this evaluation, the thermal network diagram was used to analyze the thermal transfer and thermal losses of the system. Consequently, the electronic power 18 W was generated and the water with 2 L/min at 37°C being deposited in the insulating bucket.

Investigations into Practical Resolution Limits in Microwave Holography Produced with the Bi-polar near-field Measuring Method in X- and K-bands

Pawel Kabacik and Arkadiusz Byndas
Faculty of Electronics, Wroclaw University of Technology, Wroclaw 50-370, Poland

Abstract— There are urgent needs to develop techniques capable to provide high resolution imaging for situation awareness in medical applications, industrial and security areas. In this paper, we summarize some major findings of our studies aiming at possible use of microwave holography to detect objects hidden under dielectrics or submerged in relatively thin water (50 mm). Microwave holography has been originally developed as a follow-up idea to the planar near-field antenna measurements. Presently, there are efforts to extent it on spherical scanning system to the degree required by practical applications. In this paper, metal and dielectric objects reconstruction is presented with use of the bi-polar near-to-far-field transformation by making further computations with respect to far-field data derived with the bi-polar system.

Our main applications are in medical robots — the topic is getting on urgency, as such robots offer major progress to surgical interventions. We also make experiments with spherical near-field system. That applications introduce a particular difficult challenge due to non-homogenous environment for propagation electromagnetic waves (human tissues) and losses related to microwave signals propagation. To optimize radio wave energy propagation from the source to human body, a stratified transformer in a form of several dielectric layers has been considered and numerically analyzed.

The bi-polar scanner does not involve translational moveable parts, as all kinematics required to run scanning probe and element under investigations is ensured exclusively with three revolving axis. That makes the bi-polar system interesting for minimizing phase errors when operating at higher frequencies. The system used in our studies has been developed in-house. As the radiation source we have used antenna arrays (up to 20 GHz) and horn probes featuring up to 15 dBi gain (22–40 GHz).

In our analysis, we scan E-field components on a scanning plane set above the radiation source in a distance from up to 50 cm. Measurements at two orthogonal polarization, usually last a few hours and are run concurrently on 16 to 25 frequencies. Measuring probe is moved along the bi-polar grid within the horizontal scanning plane. After acquiring data on the bi-polar grid, the far-field is calculated and then a backward projection on the specific image plane is computed. Amplitude and phase components are computed. Figure 1 presents results obtained in one of the cases we have investigated.

As shown by experiences gained so far, the most informative is the projection made on the plane where is the radiation source. In the studies we have tried to reconstruct 3D images with a

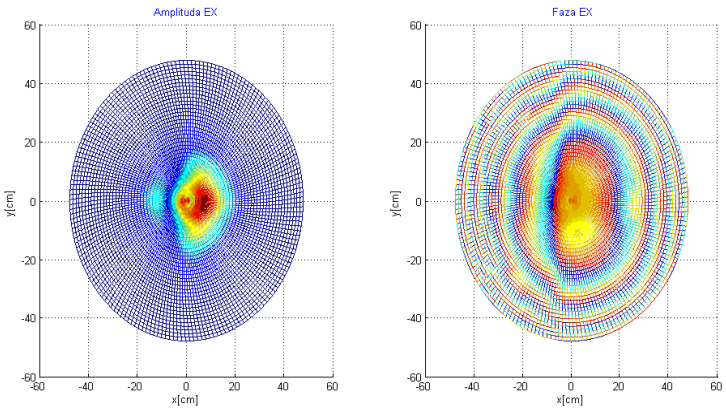

Figure 1: Amplitude and phase microwave holography image for the EX field components, taken for the metal-foil O-ring (53/47 mm) placed 50 mm above the radiation source, $f = 9.05$ GHz. The ring is seen on the image with with phase components.

series of 2D microwave holography images. We have attempted to find a method to get focused images on different planes that brings information capable to precisely reconstruct objects hidden between the radiation source and the scanning plane. The results obtained with that approach reveal existing great challenges to the methodology and computing algorithms.

In the bi-polar grid, we have used the Optimal Sampling Interpolation (OSI) and FFT approach to reconstruct microwave holography image. With the OSI there is more comfort in processing sampling points close to the perimeter of the scanning circle in the bi-polar system. Such a comfort vanishes with several other interpolation algorithms, due to fast sample phase variations far from the grid center. The results presented learnt us, concurrent use of both amplitude and phase computed data is required to investigate practical resolution limits, as particular features are revealed the same way in both field components.

A fundamental factor directly linked with resolution is frequency (wavelength). As wavelength is much shorten in human tissue with respect to air, in these studies we have put considerations to metal elements (such as surgical tools) submerged in some water held by a plastic box. The key point of studies was how the hidden object can be revealed if sounding radiowaves propagates through air and partly through water. In a case of actual implementation, measuring time and data processing/visualization must be made as short as quasi real-time capabilities to provide the image can become feasible.

REFERENCES

1. "Information on medical robot development," The Foundation for Cardiac Surgery Development, Poland, www.frk.pl.
2. Kabacik, P., "The bi-polar near-field antenna measuring system at Wroclaw University of Technology," *IEEE Antennas and Propagation Magazine*, Vol. 45, No. 5, 74–83, Oct. 2003.

Effect of the Air Wave on Marine Controlled Source Electromagnetic Exploration and Its Mitigation Methods

Jinsong Shen[1, 2, 3], **Xuan Wang**[1], **Shuaishuai Wei**[1], **and Man Li**[1]

[1]Geophysical Department, China Petroleum University (Beijing), Beijing 102249, China
[2]State Key Laboratory of Petroleum Resource and Prospecting
China University of Petroleum, Beijing 102249, China
[3]CNPC Key Lab of Geophysical Exploration, Beijing 102249, China

Abstract— In recent years, Marine Controlled Source Electromagnetic Method (MCSEM) has been gradually adopted as a routine geophysical technique in deep sea hydrocarbon exploration. Contract service companies show significant potential of the method in direct identification of hydrocarbon. However, up to now most of the published MCSEM cases are limited to deep water regions where their water depth is larger than about 300 m because of the significant effects on the electromagnetic (EM) signal of the air wave interference. Besides deep water areas, there are larger amounts of license blocks where water depth is shallower than 300 m and EM data acquired by present MCSEM equipments cannot be accurately processed and interpreted because of the contamination of the air wave interactions with the signals. The airwave contribution masks the effective signal reflected and/or refracted from the under seafloor formations. In the study, the air wave interactions with the sea water, seafloor formations and air above the sea surface have been analyzed through the EM wave mode decomposition method. First, the solutions of the electromagnetic fields are expressed in terms of two potential functions that correlate with the transverse electric (TE) and transverse magnetic (TM) modes. Secondly, general potential functions of the horizontal electric dipole (HED) in sea water and layer models are derived from the Maxwell equations and corresponding boundary conditions. Next, the electric and magnetic fields which were deduced from two potential functions have been numerically computed by using the integrals of the Bessel function. Finally, the effects of the air wave interactions with sea surface air, sea water and sub-sea formation have been analyzed through multilayer models with different water depths. It is found that EM field components of TE and TM modes have significant differences in responding to the air wave interaction and we may mitigate or reduce the air wave interference through acquiring multi-components EM fields. Through mode decomposition, we may combine different components and eliminate the airwave.

MCSEM has been proposed since 1980s (Young and Cox, 1981), but its application in direct hydrocarbon identification has not been widely exploited until recently (Eidesmo, et al., 2002). At present, MCSEM has been carried out successfully to determine the presence and extent of hydrocarbon-bearing reservoirs in deep waters. Its primary structure is shown schematically in Figure 1. By studying the received signal as the source is towed through the array, the bulk electrical resistivity of the seafloor formation can be determined at spatial scales of a few tens of meters to several kilometers.

Early applications of the MCSEM in hydrocarbon exploration mainly concentrated on sub-sea targets in water depths of 300 m and greater. This is because, in shallower water domains, signals that have interacted with the air dominate the received EM responses. These signals have been dubbed the airwave using the seismic parallel analysis. However, many exploration targets lie in areas where the water depths are much shallower than 300 m. Several approaches have been proposed to mitigate the effect of the airwave, based on the wavelike procedure of the airwave feature, such as up and down going wave decomposition (Amundsen et al.,2006) and time domain approaches (Constable and Weiss, 2006).

In this study, we adopted the mode decomposition method (David and Lucy, 2008) to understand the mechanism of the air wave interaction with air, sea water and sub-sea formations and revealed that boundary between shallow and deep water domains should not be a fixed depth of 300 m, it depends on resistivity of sub-sea formations and the excitation frequency. First, we use a simple 1D approach to derive the potential functions of the TE and TM field modes and the electric and magnetic fields which were deduced from two potential functions have been numerically computed by using the integrals of the Bessel function. Next, the effects of the air wave interactions with sea surface air, sea water and sub-sea formations have been analyzed through multilayer models with different water depths. And finally, two kind methods of airwave mitigation have been suggested and compared on the basis of the air wave analytic expressions and corresponding simulation results of the layered half-space resistivity model. The first of the bucking method is

based on the electromagnetic responses of different offsets by weighting bucking, and the second of the frequency derivative method is based on the derivation of the electromagnetic response to the radian frequency. Having compared the numerical simulation result of electromagnetic response from background model and reservoir model, we concluded the application conditions and drawbacks of the two methods.

Design of TFOSC Compatible Polarimeter for Polarimetric Observations

S. Helhel[1, 2], **G. Kahya**[1, 2], **I. Khamitov**[1], **and C. Bayar**[1]

[1]TUBITAK National Observatory (TUG), Akdeniz University Campus, Antalya, Turkey
[2]E.E.E. Department, Engineering Faculty, Akdeniz University, Campus, Antalya, Turkey

Abstract— This study proposes a design steps of a TFOSC (TUG Faint Object Spectrograph and Camera) focal plane instrument compatible optical polarimeter in order to investigate the physical parameters of targets (such as albedo, diameter, taxonomy of asteroids, porosity) based on the polarization properties of light. TFOSC has been used in order to determine the reflection spectroscopy and taxonomy of the asteroids, during the last observation campaign of Apophis's close approach with 1.5 m diametertelescope RTT150 at TUG. Since the brightness of object is fainter than 17th magnitude and the class of asteroid detection limit is 16th magnitude with RTT150 telescope, more observation time is required. Asteroids are the rigid rock objects which change the energy distribution of sun beams that impinge on Asteroids and reflect by polarizing them. This emerging variation strictly depends on the physical properties of asteroids such as albedo, diameter, shape, chemical structures, surface geometry and porosity. Meanwhile, images captured with Polarimeter will be free of the atmospheric effect and device errors.

WeDoWo (Wedged Double Wollaston) prism is one of the methods used for determining the celestial body originated light polarization rate throughout the world wide observatories. The light impinging on WeDoWo prism is divided into four different images which is polarized at 0°, 45°, 90°, 135° and used to determine Stokes' parameters of electromagnetic waves. First three elements of Stokes' vector can be determined without needing neither simultaneously obtained light component that have $\lambda/2$ variation nor other moving components.WeDoWo prism has been designed by using commercial optical design software named ZEMAX, it is 35 mm in diameter and has a thickness of 18 mm.

Numerical Investigation of a Novel Two-stage Spectral Compression Structure Employing a Logarithmic DIF Cascading with a HNLF-NOLM

Fan Yang[1], **Ying Chen**[1, 2], **Xiaojun Zhou**[1], **Zhiyao Zhang**[1], **Xiangning Chen**[1], **and Yong Liu**[1]

[1]State Key Laboratory of Electronic Thin Films and Integrated Devices
School of Optoelectronic Information
University of Electronic Science and Technology of China, Chengdu 610054, China
[2]Department of Optoelectronics, Academy of Equipment, Beijing 101416, China

Abstract— A novel all-optical spectral compression structure is proposed, which employs a logarithmic dispersion increasing fiber cascading with a highly nonlinear linear fiber-nonlinear optical loop mirror. Numerical simulation is carried out by solving the generalized nonlinear Schrödinger equation using split-step Fouier method, where the soliton number is in the range of $0.5 \leq N \leq 1.4$. The results show that the spectra are well compressed, and the maximal spectral compression ratio can reach 10.93 with a little of pedestal when $N = 1.4$.

Design and Performance Evaluation of Single Antenna SSD (Simultaneous Single Band Duplex) System Using Turbo Equalizer

Changyoung An[1], **Hongsik Keum**[2], **and Heung-Gyoon Ryu**[1]

[1]Department of Electronic Engineering, Chungbuk National University, South Korea
[2]Electromagnetic Wave Technology Institute, Rapa, South Korea

Abstract— In this paper, we propose a single antenna SSD (simultaneous single band duplex) system using turbo equalizer. The proposed system communicates simultaneously on single band. That is the proposed system is full-duplex system. The proposed system uses balanced feed network circuit to improve isolation in single antenna structure. Also, the proposed system uses RF cancellation and digital cancellation to cancel self-interference. Additionally, the proposed system uses turbo equalizer to equalize ISI by harsh multipath fading and to collect bit errors by residual self-interference signals. By using turbo equalizer, the proposed system guarantees QoS (quality of service). In this paper, we uses Simulink simulation program to analyze system performance of the proposed system. The simulation results confirm that proposed system can communicate simultaneously by using balanced feed network, RF cancellation, digital cancellation and turbo equalizer in harsh multipath channel on single band.

Preparation Technique of AlN Piezoelectric Thin Film

Guanbo Yin[1, 2], **S. Imran**[3], **and Yungui Ma**[2]

[1]Department of Materials Science and Engineering
Nanjing University of Science and Technology, Nanjing, China
[2]State Key Lab of Modern Optical Instrumentation
Department of Optical Engineering, Zhejiang University, Hangzhou, China
[3]South China Academy of Advanced Optoelectronics
South China Normal University, Guangzhou, China

Abstract— AlN piezoelectric thin films were prepared by DC magnetron reactive sputtering. A good c-axis orientation is essential for obtaining high piezoelectric coefficients. Therefore, the experiments were designed about the four parameters of the sputtering power, volume ratio of N_2 and Ar, gas pressure, and substrate temperature, in order to make sure the deposition parameters of the *c*-axis orientation AlN film. The crystal structure and full width at half maximum (FWHM) of the thin films were analyzed by X-ray diffraction (XRD). The results show that the optimal process parameters were the sputtering power of 200 W, volume ratio of N_2 and Ar of 2 : 8, gas pressure of 3.75 mT. The results provide the experiment evidence and process base for the next study.

REFERENCES

1. Dimitrova, V., D. Manova, and E. Valcheva, "Optical and dielectric properties of dc magnetron sputtered AlN thin films correlated with deposition conditions," *Materials Science and Engineering B*, Vol. 68, No. 1, 1–4, 1999.
2. Cheng, H., Y. Sun, J. X. Zhang, Y. B. Zhang, S. Yuan, and P. Hing, "AlN films deposited under various nitrogen concentrations by RF reactive sputtering," *Journal of Crystal Growth*, Vol. 254, Nos. 1–2, 46–54, 2003.
3. Venkataraj, S., D. Severin, R. Drese, F. Koerfer, and M. Wuttig, "Structural, optical and mechanical properties of aluminium nitride films prepared by reactive DC magnetron sputtering," *Thin Solid Films*, Vol. 502, Nos. 1–2, 235–239, 2006.
4. Cho, S., "Effect of nitrogen flow ratio on the structural and optical properties of aluminum nitride thin films," *Journal of Crystal Growth*, Vol. 326, No. 1, 179–182, 2011.
5. García-Méndez, M., S. Morales-Rodríguez, R. Machorro, and W. De La Cruz, "Characterization of ALN thin films deposited by DC reactive magnetron sputtering," *Revista Mexicana de Fisica*, Vol. 54, No. 4, 271–278, 2008.
6. Drüsedau, T. P. and K. Koppenhagen, "Substrate heating by sputter-deposition of AlN: The effects of DC and RF discharges in nitrogen atmosphere," *Surface and Coatings Technology*, Vol. 153, Nos. 2–3, 155–159, 2002.
7. Vispute, R. D., H. Wu, and J. Narayan, "High quality epitaxial aluminum nitride layers on sapphire by pulsed laser deposition," *Applied Physics Letters*, Vol. 67, 1549–1551, 1995.
8. Mahmood, A., N. Rakov, and M. Xiao, "Influence of deposition conditions on optical properties of aluminum nitride (AlN) thin films prepared by DC-reactive magnetron sputtering," *Materials Letters*, Vol. 57, Nos. 13–14, 1925–1933, 2003.

Statistical Modelling of Variations of Medical Characteristics in Time of Near Earth Electromagnetic Indignations

A. V. Sazanov[1, 2], **E. A. Sazanova**[3], **N. P. Sergeenko**[2], **V. G. Ionova**[4], **and Yu. Ya. Varakin**[4]

[1]Moscow State University, Moscow, Russia
[2]Pushkov Institute of Terrestrial Magnetizm, Ionosphere and Radiowave Propagation, Moscow, Russia
[3]Troitsk Hospital of Russian Academy of Sciences, Moscow, Russia
[4]Scientific Center of Neurology, Moscow, Russia

Abstract— In spite of the fact that for last years heliobiological researches have become more active, there is no full understanding of the mechanisms of the interaction in system the Sun-biosphere yet. Therefore the forecast of biotropic effects during the Earth's area electromagnetic disturbances as well as the geophysical forecast in large measure is defined by empirical laws and has probability character. The adequate statistical model should be developed for realisation of the probability forecast. This problem solved in this work.

Medical time series have undergone to trend processing. The received samples have been sorted depending on a heliogeophysical conditions and statistical distributions and invariants to the fourth order were counted. The analysis has shown, that the received distributions differ from the Gauss law in time of disturbances. Therefore attempt of the description of statistical variability of the strokes number on a basis Poisson models has been undertaken. The characteristic function of exponential kind in the assumption, that time series are superposition of some determined and casual process, has been chosen for investigated medical samples. Through Fourier's transformation characteristic function is transformed into function of density of probability.

Statistical distributions calculated for medical samples in disturbances periods have been compared with the received modelling function of distribution. Probabilities of coincidence of the experimental distributions with the theoretical by Kolmogorov criterion is P$\sim$0.7–0.9. The carried out analysis has allowed to draw a conclusion on applicability of the model constructed on base Poisson casual process for the statistical description and probable estimations of change of variations of number of vascular shifts and strokes during electromagnetic disturbances.

Research on the Magnetic Field Space-time Distribution in the Air-core Pulse Transformer

Xiao Yang, **Jianhua Yang**, **Xinbing Cheng**, **Jiajin Lin**, **and Lin Lian**
College of Optoelectronic Science and Engineering
National University of Defence Technology, Changsha 410073, China

Abstract— In the large-scale pulse power device, the transient strong magnetic field, which may make effects on the insulation of the whole pulse power system, usually appears with the transient high current. Therefore, it is necessary to investigate the magnetic field space-time distribution in the pulse power device. By the use of the circuit simulation and transient magnetic field simulation, the space-time distribution of axial magnetic field in the air-core pulse transformer is studied, and the influence generated by the axial magnetic field on the insulation performance in each part of the transformer is discussed in this paper. In the circuit simulations, it can be found that the coupling coefficient makes much influence on the phase difference between the magnetic field and the load voltage. As the coupling coefficient reduces appropriately, the magnetic field in the vicinity of the peak load voltage increases obviously. The magnetic field distribution in the space is much related to the structure of transformers. The magnetic field in the air core of the transformer is uniform along the radial, while a little higher near the rim. The magnetic field decreases fast relatively along the axial when it approaches the edge of the coils. Moreover, an air-core pulse transformer with a coupling coefficient of 0.8 is constructed, and the magnetic field space-time distributions in the air core and the area between primary and secondary coils are measured, which are the same as the results of simulations. The conclusions are favorable to analyze the insulation of this type of transformer, and design a transformer whose transient strong magnetic field can be used reasonably.

A Compact Relativistic Magnetron with a TE_{10} Output Mode

Di-Fu Shi, Bao-Liang Qian, Wei Li, Hong-Gang Wang, and Lin Lian
College of Optoelectronic Science and Engineering
National University of Defense Technology, Changsha, Hunan 410073, China

Abstract— An S-band compact A6 relativistic magnetron which operates in the π-mode is proposed, and its radiation can be extracted as a TE_{10} mode axially through a rectangular waveguide which is designed to match radially with the anode. Compared with the magnetron with diffraction output (MDO), the magnetron of this structure can reduce the dimension of the output port of the magnetron, and therefore reduce the volume of the coil of the applied magnetic field, and also reduce the distance between the electron dump and the anode block so that both the diameter and the axial length of the magnetron can be minimized. In addition, as a result of the limit to the dimension of the output waveguide, such a simple converter of the magnetron can provide a much purer radiated mode. The softwares of high-frequency field analysis and CHIPIC particle-in-cell (PIC) simulation have been used to analyze and optimize the operating performance of the magnetron proposed in this paper. Simulation results show that under the condition of the applied voltage of 360 kV, the input power of 1.87 GW and the applied magnetic field of 0.4 T, the output microwave power is 409.2 MW and the power conversion efficiency can reach 21.9%, while the resonant frequency of π-mode is 2.5 GHz and the radiated mode is TE_{10} in the rectangular waveguide.

Kind of Dual-band Horn Antenna with Coaxial Feed Structure for High Power Microwave Applications

Qiang Zhang, Sheng-Ren Peng, Cheng-Wei Yuan, Yi-Ming Yang, and Jing Liu
College of Optoelectronic Science and Engineering
National University of Defense Technology, Changsha 410073, China

Abstract— With the development of high power microwave (HPM) technologies, great efforts have been made on increasing the output power levels and the frequency spectrum of the HPM systems. As one of the most important sectors in the HPM system, transmission and radiation system mainly determines the whole structure of the HPM system. On the other hand, narrow-band HPM source usually operates at single band and has limited output power at present. An alternative method for enhancing the output capacity of HPM system is taking advantage of waveguide-based power combining technologies, not only for increasing the output power levels, but also for the frequency spectrum of the HPM systems. In this paper, a new kind of dual-band horn antenna for S/X band radiation with high power handling capacity is proposed, which consists of coaxial feed structure and flare angle horn. Low band microwave is fed by TE_{11} coaxial waveguide mode (Coa.TE_{11} mode), and high band microwave is fed by TE_{11} circular waveguide mode (Cir.TE_{11} mode). Based on the specific structure of the horn antenna, mode matching method is utilized to determine scatter matrix of each discontinuity in cross section. To obtain the overall scatter matrix of the antenna, it is necessary to progressively cascade the scatter matrixes, and the overall scatter matrix determines the propagation properties of the horn antenna. Farfield radiation pattern of the dual-band antenna can easily get by using mode expansion technology. Furthermore, a dual-band antenna at 3.6 GHz and 9.5 GHz is designed, and theoretical and numerical simulations agree well with each other. It reveals that the dual-band antenna has high power handling capacity with several GWs level, and good farfield radiation pattern at each band has been achieved. The theoretical and numerical simulation investigations show that it is a promising method for realizing multi-channel multi-band HPM integrative radiation, which is significant for HPM in some special applications.

Highly Luminescent Carbon Dots: Multi-color Composites Andion Sensors

Xiaoming Li[1, 2] **and Haibo Zeng**[1, 2]

[1]Institute of Optoelectronics & Nanomaterials, College of Materials Science and Engineering
Nanjing University of Science and Technology, Nanjing 210094, China
[2]College of Materials Science and Technology, Nanjing University of Aeronautics and Astronautics
Nanjing 210016, China

Abstract— Luminescent carbon dots (L-CDs) with high quantum yield values and controllable emission wavelengths were prepared via a facile hydrothermal method.As a next step, composites containing different L-CDs and polymers were fabricated and exhibited blue, green, and even white luminescence. Finally, the excellent excitation-independent luminescence of L-CDs prepared at low temperature was tested for detecting various metal ions. As an example, the detection limit of toxic Be2+ ions, tested for the first time, was as low as 23 µm.

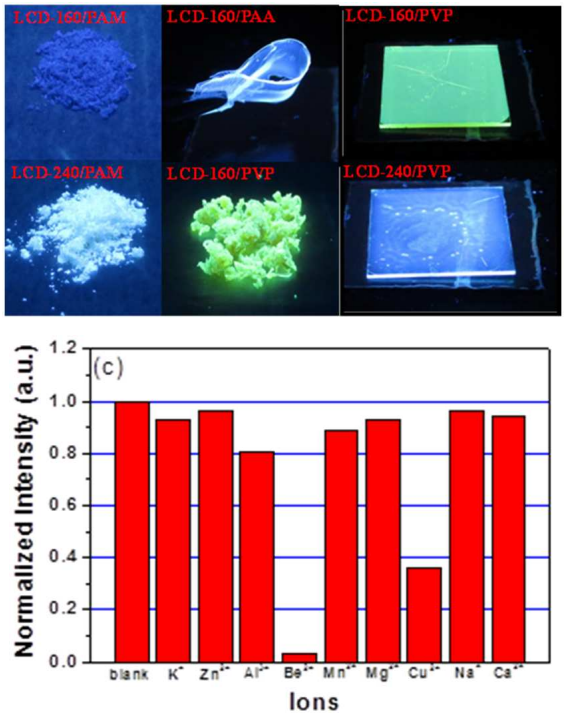

Comparison of B_1^+ Field and Specific Absorption Rate (SAR) between Birdcage, Transverse Electromagnetic and Microstrip Coil for Ultra High Field MRI at 9.4 Tesla

J. Slim, B. Abu Suheil, D. Hoelscher, and D. Heberling
Institute of High Frequency Technology, RWTH Aachen University, Germany

Abstract— The radio frequency (RF) coil is an essential part of magnetic resonance imaging (MRI) systems. In ultra-high field (UHF) MRI, the design of RF coils is a challenging task. The RF coil should resonate at a particular frequency (the Larmor Frequency) and must provide a highly homogeneous B_1^+ field. It must be also safe to use by maintaining a low specific absorption rate (SAR) value.

Homogeneity of the B_1^+ is a supremely important factor in MRI systems. A homogenous B_1^+ allows the spin in different mediums having different electromagnetic properties to "see" the same B_1^+ field. When the field-tissue interaction takes place, the spin interacts differently in a unique manner making it possible for materials to be imaged. Generally speaking, this allows higher resolutions images with high contrast increasing therefore the sensitivity of the MRI system.

The specific absorption rate is a safety indicator. It is an indicator that reflects how much electromagnetic energy is absorbed in the biological tissues. SAR value must be kept as low as possible.

The task of this paper is to provide a quantitative comparison between three common volume RF coils at 9.4 Tesla. The comparison is held in terms of the homogeneity of the B_1^+ both in the loaded and unloaded cases and also as a function of the SAR. Additionally, a comparison with the performance of 7 Tesla RF coils published earlier is considered in order to quantify the gain of increasing the frequency.

Before comparing the coils, the coils must be first built. A novel design for each type of coils is shown. The *s*-parameter as a clue of resonance at the Larmor frequency is presented accompanied with a comparison with measurements performed.

A quantitative approach to assess the interaction between the electromagnetic fields and phantoms is provided and discussed in the context of dielectric resonance. Additional visual clues are provided.

A detailed statistical study of the local homogeneity/inhomogeneity is performed. This makes it possible to conduct local field corrections, increasing therefore the homogeneity and consequently the sensitivity of the MRI system.

A Scaled Simulated Method of Sea Clutter Based on Non-metal Materials

Yajun Wu, Zichang Liang, Li Li, Xiaobing Wang, and Jun Gu
Science and Technology on Electromagnetic Scattering Laboratory, Shanghai, China

Abstract— As we know, it always very difficult to get the composite scattering characteristics between the vehicles on the sea at different sea states. A new kind of method that can easily be used to simulate sea clutter in laboratory was proposed in this paper. By employing the scaled measurement technology, we can obtain the electromagnetic scattering characteristics of different sea states. According to the sea clutter scaled theory and the dielectric properties of non-metallic materials construction technique, we use epoxy mixing metal powder to construct a new kind of composite material which reflectivity and complex permittivity meet the electromagnetic character of scaled simulated sea water. The composite material's permittivity can be controlled over a broad range while the volume ratio of metal powder and epoxy changes. Whereas different sea surface samples of various sea states can be made of the composite materials. According to the geometric similarity conditions of scaled principle the data of scaled sea surface sample is produced, the data of different sea states' surface, which are generated basing on the classic sea spectrum model proposed by the oceanographer, can be converted into the three-dimensional modeling data. Then the surface of the scaled material is processed by CNC machine. In the end, we have measured the reflectivity and RCS at the incident angle of scaled PM (Pierson-Moskowitz) spectrum sea surface sample made of the composite material proposed, and compared the results with theoretical simulation. The compared results verify the feasibility of method proposed basing on scaled simulated sea clutter. So that the scaled sea materials can be used to do the research the composite scattering characteristics of the vehicles on a controlled sea surface.

RCS Measurement of Large Target in Non-cooperative Near Field Environments

Xiuli Xu, Guangde Tong, Li Li, Kun Cai, Xiaobing Wang, and Chao Wang
Science and Technology on Electromagnetic Scattering Laboratory, China

Abstract— Generally speaking, Radar Cross Section (RCS), which is an important indicator to value the electromagnetic scattering characteristic of a target, has been paid more attention as time goes by since WWI. As we know, when RCS measurement is carried out, the accuracy of RCS measurement results always depends on the testing site and the system, and if the target is too large or the frequency is too high, a cooperative and vast measuring area or a costly compact range facility will be needed. As the testing site sometimes is not large enough for some cases, so the radiation pattern of the transmitting-receiving antenna can't be dealt as the far filed pattern. To solve these problems, this paper presents a new method of RCS measurement basing on SAR imaging by a scanner in near field. And also we employ a new SAR imaging method instead of the traditional ISAR imaging method to transform the electromagnetic scattering near field data of target to the far field RCS. That's saying, the near field data is collected by a portable 1-D scanner SAR imaging system, with the new method, we can obtain the far field by the transformation. Furthermore, in order to get the accurate far-field RCS data of the target, we use a new method to correct the effects of transmitting-receiving antenna's pattern and the difference of the distance from scattering center of the antenna to target in near-field imaging measurement, which we usually call corrected-imaging method. The compared results of theoretical simulation and experimental data show that RCS obtained by the proposed method is satisfied the condition and can be used widely.

Scattering Analysis of Reflectarray Antennas Illuminated by a Point Source for Near Field Focus Applications

Shih-Chung Tuan[1] **and Hsi-Tseng Chou**[2]

[1]Department of Communications Engineering, Oriental Institute of Technology, Pan-Chiao, Taiwan
[2]Department of Communications Engineering, Yuan Ze University, Chung-Li, Taiwan

Abstract— The scattering and diffraction mechanisms of reflecting and transmitting arrays illuminated by the radiation of a point source for a general near-field focus problem are summarized. In particular, the phenomena are interpreted by the ray decompositions of Floquet waves and result in the solutions, analogous to the ordinary UTD-type formulations for the phased array antennas with a proper parameter mapping. In this approach, the radiations of periodically located current sources are first decomposed into Floquet modes, in which every mode is equivalent to the radiation of continuous current sources with additional linear phase impressions. Fast convergence in the radiation computation can be achieved because relatively few modes will propagate to the target zone with the rest being evanescent. The ray decomposition is performed by asymptotically evaluating the radiation integral of each Floquet mode and interprets the total fields in terms of rays directly radiated from the aperture and diffracted from aperture truncations.

Nonlocal Theory for Charged Metallic Nanoparticle

H. Y. Chung[1], **P. T. Leung**[1, 2, 3], **and D. P. Tsai**[1, 4]

[1]Research Center for Applied Sciences, Academia Sinica, Taipei 115, Taiwan
[2]Institute of Optoelectronic Sciences, Taiwan Ocean University, Keelung, Taiwan
[3]Department of Physics, Portland State University, P. O. Box 751, Portland, Oregon 97207, USA
[4]Department of Physics, Taiwan University, Taipei 106, Taiwan

Abstract— A theory for light scattering from a charged metallic nanoparticle is formulated with the spatial dispersion effects accounted for in the optical response of the particle. This is achieved via the merging of two theories: the nonlocal Mie theory of Ruppin and the charged sphere theory of Bohren and Hunt. Since these two theories are established via modifying the boundary conditions of the original Mie scattering theory in different ways, the consistency between these theories are also discussed.

REFERENCES

1. Ruppin, R., *Phys. Rev. B*, Vol. 11, 2871, 1975.
2. Bohren, C. F. and A. J. Hunt, *Can. J. Phys.*, Vol. 55, 1930, 1977.
3. Chung, H. Y., P. T. Leung, and D. P. Tsai, *J. Chem. Phys.*, Vol. 138, 224101, 2013.
4. Chung, H. Y., P. T. Leung, and D. P. Tsai, *Opt. Express*, Vol. 21, 26483, 2013.

Non Destructive Method for Detection Wood-destroying Insects

P. Fiala[1], **M. Friedl**[1], **M. Cap**[1], **P. Konas**[1], **P. Smira**[2], **and A. Naswettrova**[2]

[1]Department of Theoretical and Experimental Electrical Engineering
Brno University of Technology, Technicka 3082/12, Brno 616 00, Czech Republic
[2]Thermo Sanace s.r.o., Chamradova 475/23, Ostrava, Kuncicky 718 00, Czech Republic

Abstract— The problem of finding a suitable diagnostic procedure for the examination of structural elements has been closely analyzed in recent years. In this connection, the main material of interest is wood as a sort of heterogeneous matter, and the diagnostic procedure is directed towards enabling industrial application in the future. A new diagnostic method based on X-ray imaging and acoustic electromagnetic wave; the X-ray technique utilizes the reduction of imaging information into 2D planar projection and acoustic recording system allows to find out activity of the wood — destroying pests. After researching activities and localization of wood-destroying pests, there are two methods for its disposal — thermal sanitation and microwave system.

X-ray method is known as nondestructive diagnostic methods in the medical or veterinary practice. This X-ray mobile system was designed for evaluate of the wood quality and presence of wood-boring insects and wood-destroying fungi. Special software are single parts of the X-ray system and enable automatic/semi-automatic diagnostic of the level of damage wood and localization of wood-destroying pests.

Field X-ray monitoring of vital activity of wood-destroying insects is very robust and ineffective in comparison with the acoustic method, which seems like a much better solution. Therefore was designed acoustic system for the initial detection of wood-destroying insects in building construction.

ACKNOWLEDGMENT

The research described in the paper was financially supported by the GACR 13-09086S grant, a project of the BUT Grant Agency, No. FEKT-S-11-5/1012 and project from Education for Competitiveness Operative Programme CZ.1.07.2.3.00.20.0175 and CZ.1.07/2.3.00/30.0005.

REFERENCES

1. Prosser, V., *Experimentální Metody Biofyziky*, Academia Praha, 1989.
2. Koňas, P., M. Rybníček, and T. Kolář, "Statistical processing and usage of incomplete tree-ring series," *Proceedings of Abstracts of TRACE*, s. 44, 2011.
3. Vavrčík, H., V. Gryc, and P. Koňas, "Comparison of wood density in relation to growth rings of English oak and Sessile oak," *TRACE — Tree Rings in Archaeology, Climatology and Ecology, Proceedings of the Dendrosymposium*, 8. vyd. 2010, s. 157–163, ISSN 1610-0956, 2009.
4. Gryc, V., H. Vavrčík, J. Šlezingerová, and P. Koňas, "Asic density of spruce wood, wood with bark, and bark of branches in locations in the Czech Republic," *TRACE — Tree Rings in Archaeology, Climatology and Ecology, Proceedings of the Dendrosymposium*, 8. vyd. 2010, s. 151–156, ISSN 1610-0956, 2009.
5. Trcala, M. and P. Koňas, "Modelling of coupled moisture and heat transfer during wood drying," *Wood Research*, sv. 57, č. 1, ISSN 1336-4561, 2012.
6. "Thermosanace: Likvidace dřevokazného hmyzu horkým vzduchem [online]," [cit. 2012-03-08], Dostupné z: http://www.thermosanace.eu/.

A Novel Miniaturized Frequency Selective Surface with Stable Performances

Rui Wu, Hou Zhang, Zhiyong Xu, Zimu Yang, and Yongfan Lin
School of Air and Missile Defense, Air Force Engineering University, China

Abstract— In this letter, a novel miniaturized periodic element for constructing a band-notch frequency selective surface (FSS) is proposed. The FSS proposed has a good miniaturization. This structure can also improve the stability of the characteristics with respect to incident angles of waves illuminating. Both simulation and measurement will be taken to validate the proposed performance.

Metamaterials-based High-gain Antenna with Wide Viewing Angle

Yang Cao[1, 2] **and Xiaobing Wang**[1, 2]

[1]Shanghai Radio Equipment Institute, Shanghai 200090, China
[2]Shanghai Key Laboratory of Electromagnetic Environmental Effects for Aerospace Vehicle
Shanghai 200090, China

Abstract— Metamaterials (MMs) refer to a class of artificially engineered structures comprised of electric/magnetic resonant building blocks much smaller than the operating wavelength [1]. The extraordinary electromagnetic responses of MMs, not available for naturally occurring materials, have attracted intensive investigations on the underlying physics as well as related applications. In recent years, MMs-based antennas are widely studied and proved to have great potential in improving the radiation performance [2]. In this paper, a MMs-based Febry Perot cavity antenna with wide viewing angle is proposed near 14 GHz. The antenna consists of a high-impedance surface which works as an artificial magnetic conductor (AMC) at resonant frequency and a partially reflective surface (PRS). The AMC loading contributes to the low-profile and high-gain property of the antenna, as the AMC ground plane gives a near-zero phase shift in contrast to conventional metal sheet ground plane [3]. The lateral size of the antenna is only about $3\lambda \times 0.6\lambda$; and the thickness is about $\lambda/5$. Metal walls surrounding the limited aperture are introduced to prevent the leakage of cavity mode and improve the radiation pattern, which also protects the antenna from external electromagnetic environment. The maximum realized gain is 11.5 dB at 13.8 GHz. Meanwhile, the proposed antenna has a wide viewing angle in H-plane for spatial coverage. The 3 dB beam width is found to be 88° in H-plane. This MMs-based antenna may be applied in ETC and RFID system.

REFERENCES

1. Engheta, N. and R. W. Ziolkowski, *Metamaterials: Physics and Engineering Explorations*, Wiley & Sons., 2006.
2. Sievenpiper, D., L. J. Zhang, R. F. J. Broas, N. G. Alexopolous, and E. Yablonovitch, "High-impedance electromagnetic surfaces with a forbidden frequency band," *IEEE T. Microw. Theory*, Vol. 47, 2059, 1999.
3. Zhou, L., H. Q. Li, Y. Q. Qin, Z. Y. Wei, and C. T. Chan, "Directive emissions from subwavelength metamaterial-based cavities," *Appl. Phys. Lett.*, Vol. 86, 101101, 2005.

Surface Electromagnetic Waves Excitation Using a Reflective Phase Gradient Metasurface

Yongfeng Li, Shaobo Qu, Jieqiu Zhang, Jiafu Wang, Hongya Chen, Mingbao Yan, Hang Zhou, Hangying Yuan, Lin Zheng, and Yongqiang Pang
College of Science, Air Force Engineering University, Chna

Abstract— Phase gradient meta-surface are artificial surfaces that can provide pre-defined in-plane wave-vectors to manipulate the shape of the wavefront, propagation direction and polarization of refracted/reflected waves. In this paper, a reflective phase gradient meta-surface is proposed to serve as a surface electromagnetic wave coupler under circular polarized wave incidence. The electric dipole is chosen as the sub-unit resonators to create the phase gradient meta-surface under circular polarized wave incidence. The designed reflective phase gradient meta-surface is composed of three layers: the spatial arranged electric dipoles, a metal ground plate and a dielectric spacer between them. By spatial arrangement of the electric dipole resonators, a dispersionless phase gradient is achieved in X-band, which provides the necessary in-plane moment for surface wave excitation. When the designed phase gradient meta-surface is illuminated by a circular polarized wave, the in-plane wave-vector after compensating is greater than the wave-vector in free space. Thus, the reflection is zero and surface electromagnetic wave is excited by this phase gradient meta-surface and propagating along the phase gradient meta-surface. For a left-handed circular polarized incident wave, the excited surface wave is propagating along $+x$ direction and the excited surface wave is propagating along $-x$ direction for the right-handed circular polarized incident wave. The simulated coupling efficiency for surface wave excitation and distributions of electromagnetic fields indicate that surface electromagnetic wave is high efficiently excited by this phase gradient meta-surface over a wide frequency range from 8 GHz to 12 GHz. It is of significant application values in surface waves coupling.

Dipolar Metastability Progression

K. F. Kaspareck
CTE — Consulenze Tecniche Energia, Italy

Abstract— Metastability progression sustained by thermo-dipolar forces is described and simulated with physical/mathematical modeling of liver tomographic intensity images, before and after chemical therapy cycle.

In the model, energy density changes reciprocal to entropy and temperature, are path independent and functions of chemical potential and density within a system thermodynamically "close-to-open". A central thermo-dipolar nucleus is depleted by metastases growth and strengthened by their regression. Metastable areas are assimilated to a black body, with mass-to-energy conversion and "charge" complementary to the main dipolar nucleus. Re-radiation feeds a main dipolar nucleus within a reversible reaction.

The dipolar reaction ignites over an optical flat, with a central phase transition (phase ghost) at adiabatic inversion. The reaction starts from differential temperature absorption and tends to rebalance electromagnetically by energy exchange. The geometrical progression/decay can be described by Nash equilibrium, where the geometrical opportunity set has an angle like or equal the one of main dipolar axis.

A timeless function, derived as per the 4th law of thermodynamics from integrated image intensity along a cold-warm image scale, is simulated for set chemical and physical parameters. The simulation indicates 0.3 J at 40 degrees Cherenkov angle shifts near red towards lower frequencies close to 5%. The apparent nuclear x section for 5 J power dynamic range is near a factor of 2.

Design of 90°-switched-line Phase Shifter with Constant Phase Shift Using CRLH TL

Jun Zhang[1] and S. W. Cheung[2]

[1]Tongyu Communication Inc., Zhongshan, Guangdong, China
[2]Department of Electrical and Electronic Engineering, The University of Hong Kong, Hong Kong, China

Abstract— The design of a 90°-switched-line phase shifter using composite right/left handed transmission line (CRLH TL) is presented in this paper. To achieve a relatively constant phase shift over a large bandwidth, a CRLH TL implemented using lumped elements and a right-handed transmission line (RH TL) are used as the reference and delay arms, respectively, of the phase shifter. Computer simulation is used to study and design the phase shifter. The phase shifter is also fabricated and measured to verify the simulation results. For comparison, a conventional 90°-switched-line phase shifter is also designed and simulated. Simulation and measurement results show that, the proposed phase shifter has a constant phase shift, a high return loss and a low insertion loss across the operating frequency band.

Design of Oscillator Using Zeroth-order Resonator Based on Composite Right/left-handed Transmission Line

Juanjuan Gao and Guizhen Lu
Communication University of China, China

Abstract— The researches and applications of composite right/left-handed (CRLH) transmission lines have received substantial attention in the scientific and engineering communities. Because of the unique feature of CRLH metamaterials that a β of zero can be achieved, zeroth-order resonators have been proposed and developed. Zeroth-order resonator has the advantage that resonant frequency is not related to the physical length of the TL, therefore it can be realized, theoretically, arbitrarily small. Researches on zeroth-order resonator are popular in recent years; however the applications in RF circuit, such as oscillator, are not very much.

The application of novel zeroth-order resonator in RF circuit is investigated in this paper. The zeroth-order resonator is composed by composite right/left handed transmission lines, full-wave simulations with 1-cell and 4-cell resonators are carried out, respectively. The resonators are constituted by interdigital capacitors, stub inductors and a transmission line, and the transmission line is used to satisfy the phase relation. Zeroth-order resonators can be exited in open- and short-ended case, as well as variable reactance loads at both ends. By changing load impedance at the terminals the resonant condition of the zeroth-order resonator can be controlled. The physical length of designed zeroth-order resonators is smaller than that of traditional transmission line resonators. Microwave oscillators used zeroth-order resonators, which performed as tuning network, are proposed. In order to act in oscillator, resonator should obtain good frequency selectivity in oscillation frequency, phase condition also should be satisfied. The zeroth-order resonators in oscillators determine the frequency. The simulation frequencies of oscillators are 10.7 GHz of 1-cell resonator and 10.51 GHz of 4-cell resonator, respectively. Because of the better frequency selectivity of 4-cell resonator, oscillator using 4-cell resonator has better performance at the magnitude of output signal and phase noise. The research we have carried out indicates that increasing the number of CRLH unit could improve the performances of resonator and oscillator.

Transponder Impact on Power and Spectral Efficiencies in WDM Links Based on 10–40–100 Gbps Mixed-line Rates

Vjaceslavs Bobrovs, Peteris Gavars, Girts Ivanovs, Ilja Trifonovs, and Aleksejs Udalcovs
Institute of Telecommunications, Riga Technical University, Riga, Latvia

Abstract— It has been proved that optical networks which architecture is based on the Mixed-Line Rate (MLR) could in a cost-efficient manner scope with heterogeneity of constantly increasing traffic demands comparing to the Single-Line Rate (SLR) solutions. In the same time, the total power consumption required to ensure the transmission of 1 bps over a Wavelength Division Multiplexing (WDM) transport system depends on the number factors such as (*i*) number of wavelengths operating with the particular bitrate and modulation format; (*ii*) energy efficiency of transponder (*iii*) spectral efficiency which will define the transparent optical reach and, hence, the number of 3R (re-timing, re-shaping, re-amplification) regenerations; (*iv*) distance between two network nodes between whom an end-to-end connection should be provisioned; and (*v*) signal quality need to be guaranteed at the receiving node.

In this paper, we focus on MLR solution which employs three different bitrates — 10, 40 and 100 Gbps. Commonly used optical signal modulation format for the 10 Gbps wavelengths is the non-return-to-zero (NRZ) on-off keying (OOK), for the 100 Gbps — dual polarization quadrature phase-shift keying (DP-QPSK). Although several options are considered for the 40 Gbps such as the NRZ differential phase-shift keying (NRZ-DPSK), the optical duobinary (ODB) format or even the differential QPSK (DQPSK), the NRZ-DPSK is selected due to its very simple realization and lower OSNR (optical signal-to-noise ratio) requirements.

Hence, this papers aims at exploring the power efficient 10 Gbps, 40 Gbps and 100 Gbps wavelength assignment approach as well as the minimum optical bandwidth required to allocate these wavelengths in an end-to-end WDM link where the signal quality ($Q \geq 6$) is mainly limited by a linear crosstalk. In addition, in this paper we (*i*) report about power consumption values for different transponder and 3R types; (*ii*) explores the minimum allowable frequency intervals between collocated wavelengths to fulfill the signal quality requirements; (*iii*) compare the power efficiency of proposed MLR solution with the SLR ones; and (*iv*) analyze the gained transponder load as a function of average aggregated traffic.

While evaluating the power consumption of WDM transport system, we made these assumptions: (*i*) signal quality at the receiving node should be higher than $Q = 6$ (corresponds BER $=10^{-9}$); (*ii*) spectral efficiency is fixed to the maximum value that is mainly defined by the linear crosstalk; (*iii*) frequency intervals used to separate neighboring channels is selected using ITU-T Recommendation G.694.1 while using finer granularity −6.25 GHz; (*iv*) transparent optical reach is fixed to the one sector of transmission line consisted from the booster amplifier, 40 km of standard single mode fiber (SSMF) based on ITU-T Recommendation G.652.D and 8 km of dispersion compensating fiber (DCF). For the further transmission, 3R operations need to be done to secure the defined signal quality. And, finally, (*v*) connection is provisioned over end-to-end link without crossing any optical crossconnect (OXC).

It is revealed that the lowest overall transponder power consumption is secured when not more than there 10 Gbps wavelengths are used to transmit the data and not more than one 40 Gbps wavelength is used regardless to the total capacity need to be transmitted, while the number of 100 Gbps wavelength should be increased as average aggregated traffic grows. This is explained with the highest energy efficiency of 100 Gbps transponders comparing to the 10 Gbps and 40 Gbps. If the number of each wavelength is selected using this proposed algorithm then the total power consumption required to ensure data transmission over one section of transmission line is: (*i*) the same as it would be for the 10 Gbps SLR solution and the capacity less than 30 Gbps; (*ii*) the lowest one for the traffic between 30 and 60 Gbps; (*iii*) not higher as it would be for 100 Gbps SLR solution.

Temperature Dependence of Amplified Spontaneous Emission (ASE) Peak Position Shift of MEH-PPV

Liang Qin, **Yufeng Hu**, **Zhidong Lou**, **Yanbing Hou**, **and Feng Teng**
Key Laboratory of Luminescence and Optical Information
Ministry of Education, Institute of Optoelectronic Technology, Beijing Jiaotong University
Beijing 100044, China

Abstract— We investigated the temperature dependent ASE spectral shifting in poly [2-methoxy, 5-(2'-ethyl-hexyloxy)-1, 4-phenylene vinylene] (MEH-PPV). The films were spun from the MEH-PPV solutions using terahydrofuran, toluene, or cyclohexanone as the solvent onto glass, quartz, and sapphire substrates. We observed a spectral shift in the peak position of the ASE spectra with temperature. Possible explanations for the temperature dependence of ASE peak position are discussed with the role of the morphology and the refractive index of waveguide.

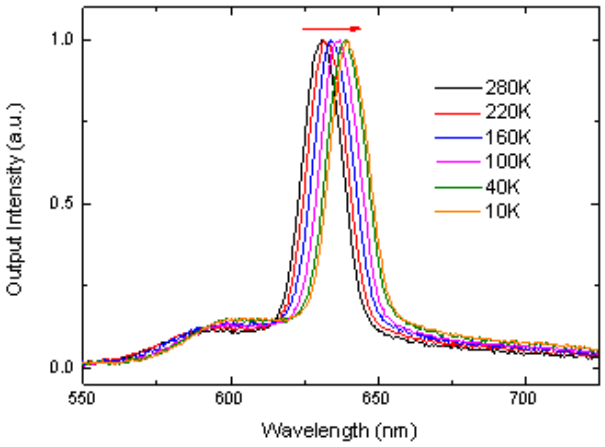

Figure 1: ASE spectral shift of MEH-PPV at the temperature from 280 K to 10 K.

Organic Bistable Devices Based on Poly- (N-vinylcarbazole)/zinc Sulfide Nanocomposites

Yapeng Cao, Jiantao Li, Haihang Ye, Xu Li, Yufeng Hu, Aiwei Tang, and Feng Teng
Key Laboratory of Luminescence and Optical Information, Ministry of Education
Institute of Optoelectronic Technology, Beijing Jiaotong University, Beijing 100044, China

Abstract— Polymer-inorganic nanocomposites have attracted much attention due to their unique advantages, of low cost, high mechanical flexibility, and light weight. The hybrid organic/inorganic devices are excellent candidates for potential applications in the next-generation transistor and memory devices. In this work, electrically bistable devices were fabricated based on blends of n-dodecanethiol capped zinc sulfide (ZnS) nanocrystals and poly (N-vinylcarbazole) (PVK). The reproducible electrical bistability and negative differential resistance effects were observed in current-voltage characteristics. A large ON/OFF current ratio of 104 at negative voltages could be obtained by applying different amplitude of sweeping voltages and varying the mass ratios of ZnS nanocrystals to PVK. The observed conductance switching seems to be resulted from electric-field-induced charge transfer between the nanocrystals and the polymer, and negative differential resistance behavior could be attributed to the charge trapping in the nanocrystals.

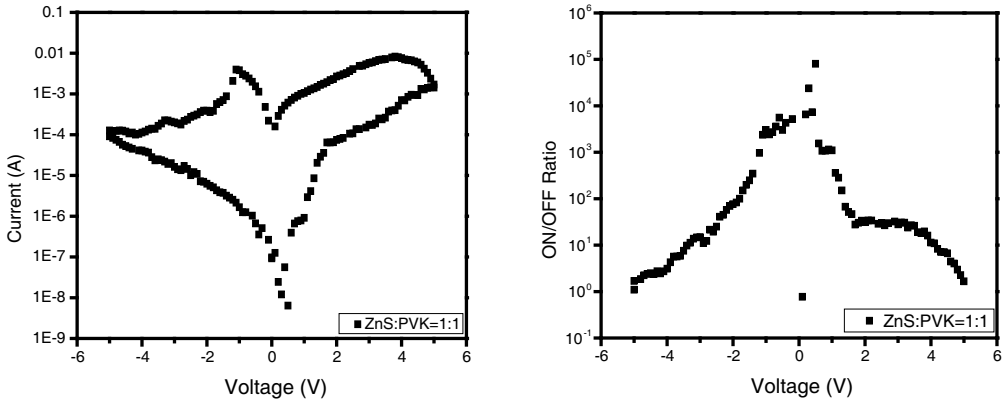

REFERENCES

1. Tang, A., F. Teng, Y. Hou, Y. Wang, F. Tan, et al., *Applied Physics Letters*, Vol. 96, 163112, 2010.
2. Reddy, V. S., S. Karak, and A. Dhar, *Appl. Phys. Lett.*, Vol. 94, 173304, 2009.
3. Yang, Y., J. Ouyang, L. Ma, R. J. H. Tseng, and C. W. Chu, *Advanced Functional Materials*, Vol. 16, 1001–1014, 2006.
4. Heremans, P., G. H. Gelinck, R. Müller, K. J. Baeg, D. Y. Kim, and Y. Y. Noh, *Chem. Mater.*, Vol. 23, 341, 2011.
5. Onlaor, K., B. Tunhoo, T. Thiwawong, and J. Nukeaw, *Current Applied Physics*, Vol. 12, 331–336, 2012.

Light Emission from Pentacene/Tris-(8-hydroxyquinolinato) Bilayer Transistors

Shaobo Cui, Yufeng Hu, Zhidong Lou, Yanbing Hou, and Feng Teng
Key Laboratory of Luminescence and Optical Information
Ministry of Education, Institute of Optoelectronic Technology
Beijing Jiaotong University, Beijing 100044, China

Abstract— The top-contact light-emitting field-effect transistors (OLETs) based on pentacene/tris-(8-hydroxyquinolinato) (Alq_3) bilayer films were fabricated, with poly (methyl methacrylate) (PMMA) as gate dielectrics. Pentacene enables hole transport in the device, while Alq_3 serves both as electron transport and light emitting materials on the top of the pentacene. In order to enhance the device performance, asymmetric electrodes were applied. The drain current versus gate voltage curves of the devices show behavior characteristic of field-effect transistors. The green light emission from Alq_3 is controlled by the gate voltage and is naked-eye visible in the dark.

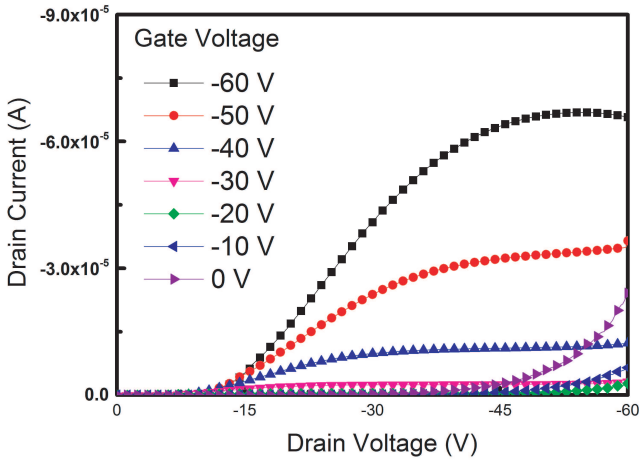

EMI Study of Transformerless Photovoltaic Array System

Wenjie Chen, **Xiaomei Song**, **Hao Huang**, **and Xu Yang**
State Key Laboratory of Electrical Insulation and Power Equipment
Xi'an Jiaotong University, Xi'an, China

Abstract— Nowadays, electromagnetic interference (EMI) seems to be one of the major constraints of photovoltaic inverters, particularly for transformerless grid-tied system. The common mode (CM) leakage current through the parasitic capacitance of the PV array may cause very serious EMI problems. Unfortunately, it is too often regarded as the last phase of the development of the system since it represents the last step of its marketing. The estimation of CM current by mathematic calculation offers a considerable gain from economic point of view. In this paper, a novel high frequency model for PV array is proposed. It shows how relatively simple models can be used to forecast CM leakage current, taking into account various control strategies. Based upon the proposed model, it is found the PV cell to frame capacitance C_{cf} is the most dominant parasitic parameter. The generally accepted PV cell to ground capacitance is smaller than C_{cf} and can be omitted. The corresponding numerical analysis results were successfully verified by the laboratory test measurements. The proposed model can be used as a novel computational

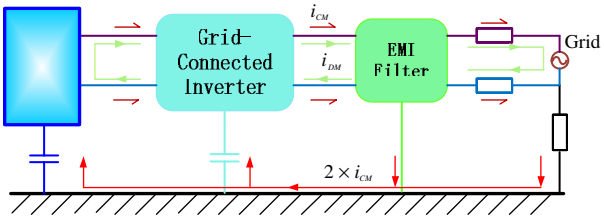

Figure 1: Generally used model for transformerless PV system.

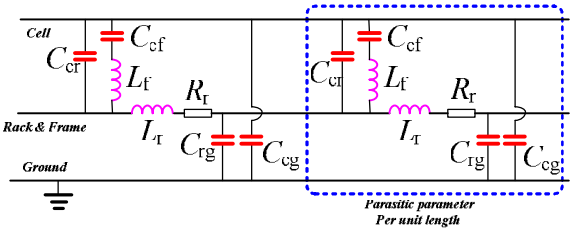

Figure 2: Proposed PV array high frequency model.

Figure 3: Photo of the PV inverter prototype.

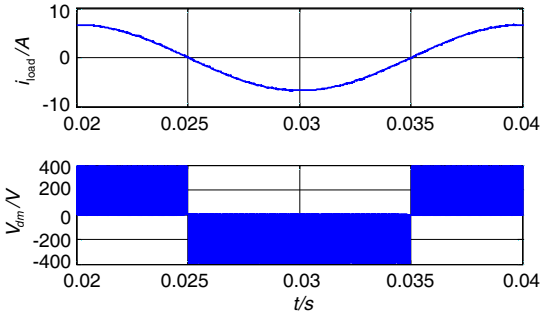

Figure 4: Inverter load current and output voltage waveform.

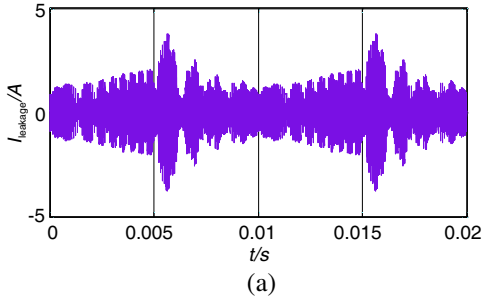

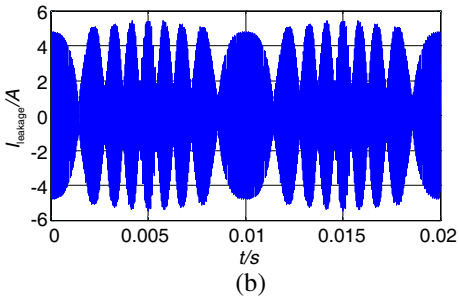

Figure 5: Calculation of the leakage current within DC side of the PV inverter. (a) With improved unipolar SPWM method. (b) With improved unipolar double frequency SPWM method.

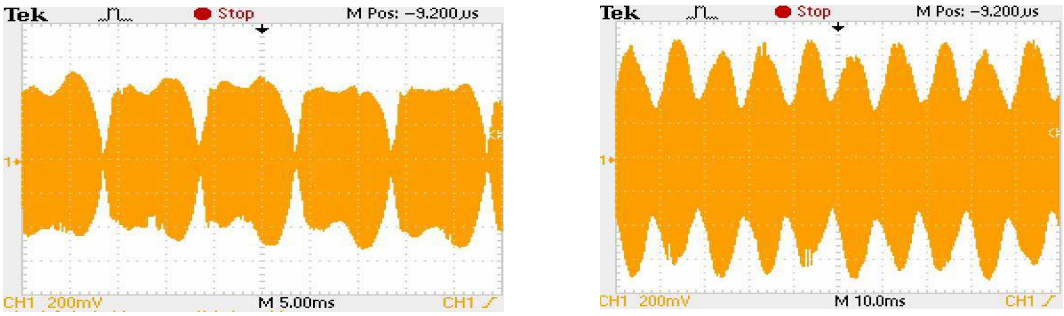

(a) (b)

Figure 6: Experimental results of the leakage current within DC side of the PV inverter. (a) With unipolar SPWM method. (b) With unipolar double frequency SPWM method.

prototyping tool which would allow the development to design and final product stages to be completed without the need for repeated build and test procedures in an industrial environment. The objective is to approach by "fast" calculations the EMI to consider optimization processes.

Demonstration of Polarization Muiltiplexed Signals Division Using a Fiber Optical Parametric Amplifier

S. Olonkins, **I. Lyashuk**, **and J. Porins**
Institute of Telecommunications, Riga Technical University, Azenes st. 16, Riga LV-1048, Latvia

Abstract— The main goal of this paper is to demonstrate the ability of a single pump fiber optical parametric amplifier with linearly polarized pumping radiation to divide orthogonally polarized optical signals, by emphasizing a signal with certain state of polarization from a combination of orthogonally polarized signals. Such additional application of parametric amplifiers can be very promising, as potentially it can lead to significantly increasing spectral efficiency in systems, where fiber optical parametric amplifiers are used for optical signal amplification. In the implemented solution two orthogonally polarized optical signals are intensity modulated on the same wavelength, and, after being highly attenuated, processed by the parametric amplifier in such a way, that only a signal with a certain state of polarization is amplified. Such additional application of parametric amplifiers requires to use linearly polarized pumping radiation, the state of polarization of which would coincide with the state of polarization of the signal to be processed. The parametric amplifier with the chosen configuration was placed as a preamplifier at the input of the receiver, and produced on-off gain up to 20.05 dB. The configuration of the preamplifier was chosen in a way to obtain higher level of amplification using as low pumping power as possible, therefore the peak of amplification had to coincide with the wavelength of the amplified signal.

The obtained results have shown that such level of amplification was high enough to ensure that the bit-error-rate values of the processed signal are below the 10^{-12} mark. Such additional application of parametric amplifiers, to the best of our knowledge, has not been demonstrated so far.

Photoelectrochemical Water Splitting Enhanced by Plasmon Resonance under Visible Light Illumination

Yuqing Zhong, **Yuko Mori**, **Kosei Ueno**, **Tomoya Oshikiri**, **and Hiroaki Misawa**
Research Institute for Electronics Science, Hokkaido University
N21, W-10, Kita-ku, Sapporo, Hokkaido 001-0021, Japan

Abstract— Noble metal nanoparticles showing localized surface plasmon resonance (LSPR) deposited on a semiconductor photoelectrode have the potential to promote photoelectrochemical water splitting due to the light harvesting effect in visible wavelength region. Interestingly, the LSPR significantly separates the photogenerated electrons and holes at the semiconductor/metal interface following the charge transfer from an excited metallic nanoparticle to the conduction band of n-type semiconductor, so that results in promoting a photocurrent enhancement and water oxidation. Herein, we report on the plasmon-induced water splitting device that responds to visible light using gold nanoparticles loaded semiconductor photoelectrode.

Gold nanoparticles were fabricated on the 0.05 wt% Niobium doped strontium titanate ($SrTiO_3$) substrate. The LSPR band was peaking at around 600 nm. The water splitting device contains two solution compartments based on the use of both sides of the same $SrTiO_3$ single-crystal substrate to separate H_2 and O_2, respectively. Gold nanoparticles-loaded surface was on the front side of the $SrTiO_3$, which was irradiated by visible light to induce O_2 evolution, whereas a Pt board was used for H_2 evolution on the backside via Ohmic contact. To promote water splitting, chemical bias was applied by pH regulations of these compartments instead of using external electrochemical apparatus. The xenon light spectrally filtered to the wavelength from 550 nm to 650 nm with an intensity of 0.32 W/cm^2 was irradiated onto the gold nanoparticles to excite LSPR.

Sectionalized yield of the H_2 evolution dependent on the irradiation wavelength was measured with the increment as 100 nm. H_2 yield was almost consistent with the segmented integral area of the plasmon resonance spectrum. Thus, plasmon-induced water splitting was clearly demonstrated. Fig. 1 depicts irradiation time dependence of H_2 and O_2 evolution obtained in back and front side compartment, respectively. The pH value in the back side compartment was set at 1 while that in the front side compartment is 11. As the irradiation time extended, the evolution of both H_2 and O_2 almost linearly increased under the visible irradiated conditions. Importantly, the quantity of H_2 evolved from the surface of Pt used as a co-catalyst of $SrTiO_3$ is twice that of O_2 evolved from gold nanostructured surface. Therefore, stoichiometric evolution of H_2 and O_2 was obviously demonstrated. From the pH dependent experiments, the water splitting was induced at the pH combination of 3 and 6.8, which is corresponding to 0.23 V as a minimum chemical bias. The detailed principle will be exhibited in this presentation.

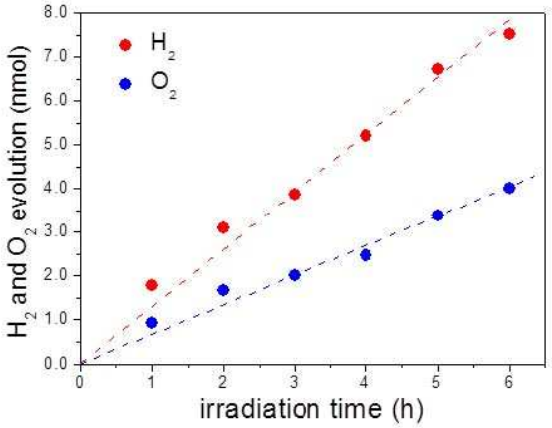

Figure 1: The irradiation time dependence of H_2 and O_2 evolution obtained in back and front side compartment, respectively.

Cooperative Opto-electrical Operation of Parallel Photonic Devices for Broadening Optical Transport Capacity

Naokatsu Yamamoto, Toshimasa Umezawa, Atsushi Kanno, and Tetsuya Kawanishi
National Institute of Information and Communication Technology
4-2-1 Nukui-kita, Koganei, Tokyo 184-8795, Japan

Abstract— The increasing demand for high data transmission capacity necessitates the use of ultra-high-speed photonic devices such as electro-optic modulators, optical switches, and photodetectors. Further, it is generally known that photonic devices capable of ultra-high-speed and ultra-broadband electrical frequency operations are required for the generation of high-baud-rate optical signals in photonic networks. In our study, we have focused on achieving cooperative opto-electrical operation of multi-parallel photonic devices. In this concept, multiple high-speed and narrowband photonic devices are connected and cooperatively operated in serial and/or parallel to achieve high-baud-rate optical data signals. Figures 1(b) and 1(c) show the schematics of our concept in comparison with the conventional system shown in Figure 1(a). A high-baud-rate data signal is directly decomposed in the electrical frequency domain using electrical low-pass and band-pass filters. The multi-parallel electro-optic modulators generate optical signals with decomposed electrical signals, and subsequently, the original high-baud-rate data signal can be reconstructed with the multiplexing of the optical signals. We believe that the technological complexities of operating photonic devices at ultra-broad frequencies can be overcome using this concept. In this study, we first computationally demonstrated 10-Gbps on-off keying (OOK) optical data signal generation using three parallel electro-absorption modulators operated with decomposed electrical signals in a selected frequency range. Figure 1(d) shows the power spectra of 10-Gbps pseudo-random bit sequence (PRBS) electrical signals decomposed using three filters. We successfully demonstrated clear eye-opening (Figure 1(e)) of the reconstructed 10-Gbps optical data signal using three parallel optical modulators operated with the decomposed electrical signals, as shown in Figure 1(d). From the simulated results, we believe that our concept of cooperative opto-electrical operation of parallel photonic devices will lead to further developments in achieving high-baud-rate photonic data transmission.

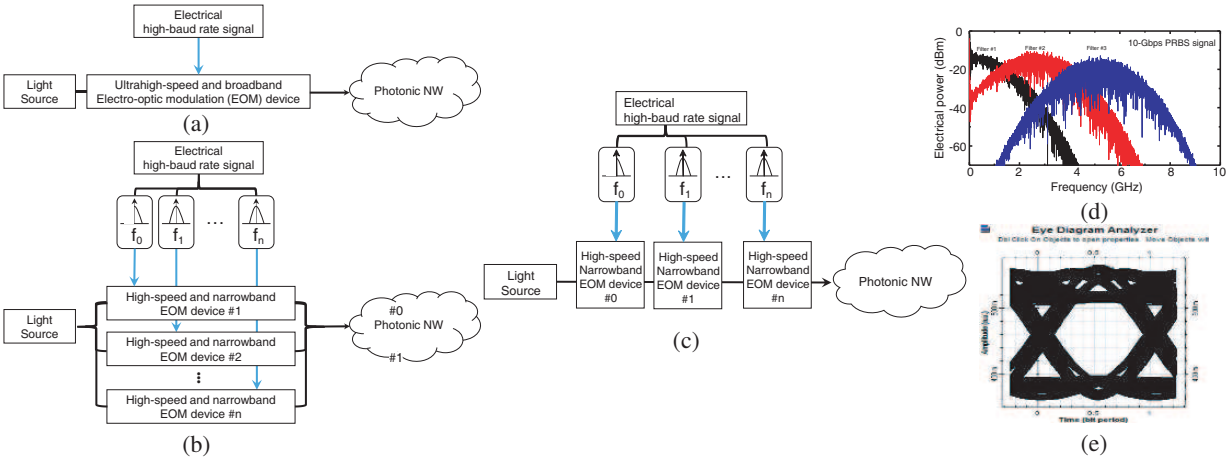

Figure 1: (a) Conventional setup for optical data signal generation. Cooperative opto-electrical operation of multiple photonic devices connected in (b) parallel and (c) serial. (d) Decomposed power spectra of electrical signal. (e) Reconstructed 10-Gbps optical signal.

Efficiency Measurement of Antenna with Lumped Elements Based on Improved Wheeler Cap Method

A. S. Rusakov, **R. V. Salimov**, **D. V. Vasilyev**, **and R. I. Tikhonov**
LG Electronics, Russia R&D Lab, St. Petersburg, Russia

Abstract— Antenna efficiency is one of the most important antenna parameters that shall be considered in design. Often developers don't pay attention to this parameter because it is rather difficult to evaluate it both in theory and in practice. However, this essential parameter shall not be ignored, especially for electrically small antennas, because radiation efficiency of such antennas reduces significantly by decreasing the size of antenna. Efficiency plays a fundamental role in designing real portable devices, such as mobile phones with material losses and with antenna matched by lumped elements (LC).

Among the well-known methods of antenna efficiency measurement such as the directivity/gain method, the radiometric method, and the Wheeler cap method, the last one is the most attractive due to its advantages: low cost, ease of implementation, accuracy and repeatability of the results. In 1959 H. A. Wheeler first presented the possibility of measuring antenna efficiency by completely enclosing an antenna by a metal cap. Later, this method, named Wheeler cap method, has been revisited many times. At the moment, there are several independent technologies of efficiency measurement, and each is still called Wheeler cap method.

The paper presents the possibility of applying the improved Wheeler cap method to measure efficiency of electrically small antennas containing lumped elements. A method for calculating efficiency on the basis of the measured S-parameters of an antenna in free space and the same antenna inside a metal box is followed up. Using one metal box of constant size for a wide frequency range allows to simplify and speed up the measurement process based on the improved Wheeler cap method. However, it does not exclude the box resonances excited by the antenna. In this paper we propose a new algorithm to eliminate parasitic box resonances and their impact on the efficiency calculation of an antenna with lumped elements by recognition of lumped LC resonances. Five antennas have been developed to verify the approach: lossless patch antenna, lossless IFA, low-loss dual-band PIFA, dual-band PIFA loaded with lumped resistor, and dual-band PIFA matched by lumped LC. Only one small box with constant size of about 0.7lamda at 1.2 GHz is used. Measured efficiency of all five antennas has good agreement with calculated values in the frequency range of 0.5–3 GHz. The advantage of the proposed method over existing ones is shown. Disadvantages of the method are also specified.

The Analysis of Receiving Sensitivity Degradation of WLAN Performance due to EMI Noise from SSD Module

Han-Nien Lin[1], **Po-Yu Chiang**[1], **Wang-Chwen Tsai**[1], **and Cheng-Chang Chen**[2]

[1]Department of Communications Engineering, Feng-Chia University
100 Wen-Hua Rd., Taichung 40724, Taiwan
[2]Section of EMC, Bureau of Standards, Metrology and Inspection, M.O.E.A., Taipei, Taiwan

Abstract— The Solid State Drive (SSD) is nowadays commonly installed in mobile devices or Ultrabook owing to its compact size and fast processing speed. However, due to ever shrinking space on edge of lid, the WLAN antennas are now usually located at base of Ultrabook computer and thus suffers EMI noise power generated from high speed SSD. Therefore the broadband EMI noise resulted from SSD operation would usually invade the RF communication channel, and thus degrades the receiving sensitivity of the system. In addition, when WiFi tethering is used for cloud applications with the 3G/4G WWAN network through smart phone, the EMI noise from SSD would also affect the file down-loading of mobile phone. Because when Internet accesses with WWAN network, the users always place the mobile phones by side of notebook computer with built-in EMI aggressive SSD. Since the receiving sensitivity of wireless system is the key issue for cloud applications as required by CTIA and related organization, this study investigates the EMI noise coupling mechanism from SSD to antenna and also analyzes the effect on WLAN performance. The coupling mechanism of EMI noise between SSD and RF modules can be categorized as antenna coupling, circuitry coupling, and cavity coupling. With the help of near-field EMC analysis for closely located RF and digital modules in this study, we can identify the root cause of receiving sensitivity degradation and benefit the manufacturers for proper SSD integration with mobile device or Ultrabook computer from compact form design limitation. We also evaluated the noise limit and frequency range for platform noise of wireless communications, and hope to apply the noise budget concept and IC-EMI measurement techniques on the component level to help SSD-related manufacturers and wireless communications system manufacturers to improve the integrating design to meet the performance and EMC requirement in the future study.

Research in Modeling and Dynamic Simulation of Linear Eddy Current Braking Force of High-speed Train

X. R. Zhang, Q. Y. Guo, J. Zhang, and M. S. Tong
School of Electronic and Information Engineering, Tongji University, Shanghai 200092, China

Abstract— In this paper, we introduce the principle of high speed train eddy current braking, and establish a complete mathematical model for solving eddy current force definite solution problem. The eddy current braking process is a dynamic process. The air gap distance between the magnetic pole and guide rail induction plate is constantly changing, and the change of air gap and the eddy current brake force are mutually coupled. Obviously, the dynamic coupling process of eddy current braking force with air gap cannot be characterized by static analytical expressions. We propose a method to calculate the dynamic simulation of eddy current braking force considering the change of air gap. First, the finite element method is used to establish the 2-dimensional (2D) model, and then the ANSYS software is applied to simulate the calculation. Finally, the results of eddy current brake force (i.e., horizontal braking force) and the normal force change with speed are obtained. We did the analysis on the simulation results, which were further compared with the experimental data. The reasons of the error were analyzed too. This paper provides a reference for the design of high speed train eddy current device.

Enhance the Magnetic Properties of Fe-Si-Al-Cr Flaky Particles by Annealing

Nan Zhang, Xin Wang, Peiheng Zhou, Jiangliang Xie, and Longjiang Deng
National Engineering Research Center of Electromagnetic Radiation Control Materials
State Key Laboratory of Electronic Thin Film and Integrated Devices
University of Electronic Science and Technology of China, Chengdu 610054, China

Abstract— Fe-Si-Al-Cr flaky particles were used as microwave absorbing material. Iron-Silicon-Aluminum-Chromium ingots with nominal compositions $Fe_{73}Si_{15}Al_{10}Cr_2$ were produced by alloying the pure elements in an induction melting furnace under argon atmosphere at 0.03 MPa, and then the ingots were crushed into irregular shaped particles. As-crushed alloy had been milled by planetary miller for 32 h. In order to increase the effective permeability, the material was annealed under different conditions. The morphology of the powders was characterized by scanning electron microscope (SEM). The phases of powders were estimated by X-ray diffractometer (XRD). The microwave permeability dispersion spectra of annealed powders within a frequency range of 0.5–8 GHz was measured. The SEM results showed that particles had been successfully transformed into the flaky shape. The average thickness of flakes is about 43 μm. The average aspect ratio (width/thickness) of flakes is about 28. The XRD results showed that the DO3 ordered phase coexisted with α-Fe(Si,Al,Cr) matrix phase by annealing above 500°C. When the annealing temperature increased from room temperature to 800°C, the grain size grown from 10.4 nm to its maximum 29.8 nm and part of α-Fe(Si,Al,Cr) matrix phasetranslated into DO3. The imaginary part of the effective permeability increased with the annealing temperature, and decreased when the temperature was above 500°C. The resonance frequency decreased with the annealing temperature, and increased when the temperature was above 400°C. The effective permeability of the powders, obtained by 500°C annealing, had a maximum value of 6.0 at 2.5 GHz.

Design of Controlling Edge Scattering Based on Tapered Periodic Surfaces Loading

Li-Juan Lu, **Hai-Yan Chen**, **Pei-Heng Zhou**, **Di-Fei Liang**, **and Long-Jiang Deng**
National Engineering Research Center of Electromagnetic Radiation Control Materials
State Key Laboratory of Electronic Thin Film and Integrated Devices
University of Electronic Science and Technology of China, Chengdu 610054, China

Abstract— In this paper, a novel method for controlling trailing edge scattering is proposed based on tapered periodic surfaces (TPS) loading. The TPS is realized by periodic square metallic patches with tapered dimensions at the direction perpendicular to the considered edge but keeping its period unchanged. The backscattering properties from the trailing edge with the proposed TPS loading are analyzed and compared with that of original trailing edge for various frequencies. Considered that strong trailing edge scattering occurs for VV-polarization, the analysis is limited electromagnetic scattering properties at VV-polarization. The term VV-polarization means the electric field vector is perpendicular to the considered edge. It is observed that wide angular radar cross section (RCS) reduction can be achieved and the average reduction of mono-static RCS up to 20 dB when the pitching angle is between 60° and 80°. Moreover, the maximum reduction of mono-static RCS is 25 dB in the special angle. To further demonstrate that the method of TPS loading is feasible, the mono-static RCS of the trailing-edge serration, a popular design method, is proposed for comparison. Serration is widely applied to the trailing edges of wings, which can avoid reflection in the direction of the incoming wave so as to reduce the backscattering from the edges. It is found that with the azimuth angle deviating from 0°, the serrated edge is increasingly close to and even surpasses to the original edge. However, for the TPS loading case proposed in this paper, the RCS reduction is rather considerable for a wide range of azimuth angles.

Shock Wave Dynamics in the Cleaning of Container Surfaces

M. Janíček, R. Kadlec, and P. Fiala
Department of Theoretical and Experimental Electrical Engineering
Brno University of Technology, Technická 12, Brno 616 00, Czech Republic

Abstract— Lockable containers are commonly applied in both long-term and short-term storage of materials, substances and commodities. In repeatedly used containers, however, cleaning is a crucial problem: traces of previously stored materials have to be removed quickly and effectively, especially in the case of biological compounds or toxic, radioactive, and otherwise hazardous substances. The chemical mechanical methods for the elimination of dirt can be excessively complicated or costly (also due to the use of special equipment), and in some materials the cleaning procedure is difficult to control.

ACKNOWLEDGMENT

The research described in the paper was financially supported by a grant of the BUT science fund, No. FEKT-S-11-5/1012, and the authors also received assistance from projects within the Education for Competitiveness Operative Programme, Nos. CZ.1.07.2.3.00.20.0175 and CZ.1.07/2.3.00/30.0005.

REFERENCES

1. Foerster, C. L., C. Lanni, R. Lee, G. Mitchell, and W. Quade, "Tests of an environmental and personnel safe cleaning process for Brookhaven National Laboratory accelerator and storage ring components," *J. Vac. Sci. Technol. A*, Vol. 15, No. 3, 731–735, May/Jun. 1997.
2. Mathewson, G., J. P. Bacher, K. Booth, R. S. Calder, G. Dominichini, A. Grillot, N. Hilleret, D. Latorre, F. L. Normand, and W. Unterlerchner, "Comparison of chemical cleaning methods of aluminum alloy vacuum chambers for electron storage rings," *J. Vac. Sci. Technol. A,* Vol. 7, No. 1, 77–82, Jan./Feb. 1989.
3. Fleischner, P., *Hydromechanika (Hydromechanics)*, 186 s., ISBN 80-214-0266-1, Skripta VUT FS, VUT Brno, 1990.
4. Černoch, S., *Strojně Technická Příručka*, 386 s. SNTL, Praha, Czech, 12. přepracované vydání, 1968,.
5. Buchar, J. and J. Voldřich, *Terminální Balistika*, Academia, AV ČR Praha, Praha, 2003.
6. *ANSYS Manuals*, V 12.0, Huston, USA 2009.
7. Brdička, M., L. Samek, and S. Brnuno, *Mechanika Kontinua (Continuum Mechanics)*, Academia, No. CV 2000, sv. 481, CS AV Praha, 2000.

Elimination of a Fire through Shock Wave Interference: The Numerical Model and Application Scenarios

M. Janicek, P. Fiala, and R. Kadlec
Department of Theoretical and Experimental Electrical Engineering
Faculty of Electrical Engineering and Communication
Brno University of Technology, Technicka 12, Brno 616 00, Czech Republic

Abstract— The authors present and discuss a non-traditional approach to the elimination of large-scale fire events, for example road and railway tanker accidents. The proposed solution consists in utilising the interference of shock waves generated by highly explosive substances. Within the analysis, the authors introduce the results obtained by the numerical modelling of the dynamical system behaviour and include the basic verification of the solution, which is carried out by means of the related experimental model. The paper also contains a comparison of the results as well as a SWOT analysis table characterising the proposed technology.

ACKNOWLEDGMENT

The research described in the paper was financially supported by a grant of the BUT science fund, No. FEKT-S-11-5/1012, and the authors also received assistance from projects within the Education for Competitiveness Operative Programme, Nos. CZ.1.07.2.3.00.20.0175 and CZ.1.07/2.3.00/30 .0005.

REFERENCES

1. Government Decree No. 172/2001 Coll., "Laying down the rule of procedure for the act on fire prevention,".
2. Janíčk, M., *Dizertační práce: Využití trhací techniky při mimoř'adných událostech,* ev. č'ıslo: 28900220103001, Žilinská univerzita v Žilině, Fakulta špeciálného inžinierstva, Žilina, 2010, (Dissertation: *Application of Blasting Technics in Emergencies*, Reg. No. 28900220103001, Žilinská univerzita v Žiline, Faculty of Special Engineering).
3. Zákon, ČNR č 61/1988 Sb., *O hornické činnosti, výbušninách a o státní báňké správě,* ve znění pozdějších předpisů 240/2006 Sb., *O hornické činnosti, výbušninách a o státní báňdké správě v případě výbušných předmřtů*, (Act No. 61/1988 Coll., *On Mining, Explosive Substances and the State Mining Authority*, as amended by Decree No. 240/2006 Coll., *On Mining, Explosive Substances and the State Mining Authority as Related to Explosive Articles*).
4. Novotný, M., *Vybrané kapitoly z teorie výbušin*, OIST Polivcka, Polivcka, 1981, (*Selected Problems of the Theory of Explosives*).
5. ???
6. Buchar, J. and J. Voldvrch, *Terminální Balistika*, Academia, AV vCR Praha, Praha, 2003, (*Terminal Ballistics*).
7. *ANSYS Manuals*, V 12.0, Houston, USA, 2009.
8. Brdivcka, M., L. Samek, and S. Brnuno, *Mechanika Kontinua*, Academia, No. CV 2000, sv. 481, CS AV Praha, 2000, (*Continuum Mechanics*).
9. *Combustion, Explosion, and Shock Waves*, Journal No. 10573, Editor-in-Chief: Vladimir M. Titov, Springer US.
10. Kaushik, B., G. Franklin, V. N. Doug, and M. Suresh, *Numerical Study of Blast Characteristics from Detonation of Homogeneous Explosives,* © Springer-Verlag, October 13, 2009.

High Gain Electromagnetically Coupled Stacked Circular Disk Patch Antenna for Wideband Application

N. P. Yadav, W. Wu, and D. G. Fang
School of Optoelectronic, Nanjing University of Science and Technology, China

Abstract— Broadband behaviour of an electromagnetically coupled stacked circular patch antenna is investigated theoretically. The effects of feed point locations, radius of parasitic disk, and air gap-spacing are analyzed to achieve optimum conditions for broadband operation. The antenna shows a bandwidth as large as twelve times of that of a single circular patch antenna. The radiation patterns of the antenna are similar to that of single disk antenna. The theoretical results are in reasonable agreement with the IE3D simulated results.

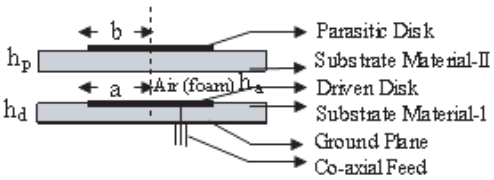

Lower disk Upper disk

(a)

Lower disk Upper disk

(b)

Analysis of Spectral Characteristics of Normal Fibroblasts and Fibroblasts Cultured with Cancer Cells in Terahertz Frequency Range

E. A. Strepitov[1], **I. V. Prozheev**[1], **N. S. Balbekin**[1], **M. I. Sulatsky**[1], **M. K. Khodzitsky**[1], **O. A. Smolyanskaya**[1], **A. S. Trulioff**[2],**and M. K. Serebryakova**[2]

[1]ITMO University, Saint-Petersburg, Russia
[2]Saint-Petersburg State University, Saint-Petersburg, Russia

Abstract— New method of oncology identification based on definition of characteristic cancer spectral lines in the frequency range of 0.1–2 THz was proposed. Using terahertz spectral database of normal and pathological human tissues we could monitor the slightest changes caused by the appearance of oncology at early stages.

Introduction: Nowadays due to enlarged influence of cancer diseases it becomes necessary to conduct accurate diagnosis of cancer tumors at the early stages with high reliability. Among various methods of cancer diagnosis the invasive methods like biopsy are dominant. The invasive methods are gradually being replaced by non-invasive terahertz (THz) imaging and tomography methods, but they don't allow uniquely identifying cancer tumor. In this paper we propose the new method of identification based on definition of characteristic cancer spectral lines.

Results and Conclusions: The reflection and transmission spectra of normal fibroblasts, cancer cells, and fibroblasts cultured with pathological cells (A549, COLO 320 HSR) were obtained using standard THz pulsed spectroscopy technique in the frequency range of 0.1–2 THz. In case the fibroblasts with A549 cells one high intensity reflection peak at the frequency of 1.43 THz appears, the peaks at other frequencies are suppressed. In case the fibroblasts with COLO 320 HSR cells the intensity of reflection peaks at the frequencies of 1.11 and 1.33 THz decreases and one increases at 1.77 THz.

Thus, we could monitor the appearance of oncology at early stages using THz database of characteristic cancer spectral lines.

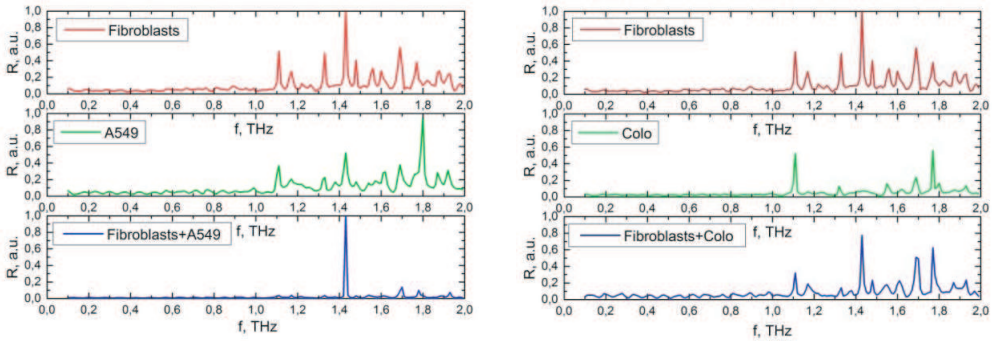

Figure 1: Reflection spectra of normal cells of fibroblasts and fibroblasts cultured together with cancer cells.

ACKNOWLEDGMENT

This work was financially supported by Government of Russian Federation, Grant 074-U01.

REFERENCES

1. Travis, W. D., et al., "Pathologic diagnosis of advanced lung cancer based on small biopsies and cytology: A paradigm shift," *Journal of Thoracic Oncology,* Vol. 5, No. 4, 411–415, 2010.
2. Bespalov, V. G., et al., "Methods of generating superbroadband terahertz pulses with femtosecond lasers," *Journal of Optical Technology*, Vol. 75, No. 10, 636–642, 2008.

Localized Surface Plasmon Enhanced Luminance in Organic Light Emitting Diode

Bei Liu, Bo Liu, Kou-Chen Liu, and Chao Sung Lai
Organic Electronic Device Laboratory, Engineering College, Chang Gung University, Tao-Yuan, Taiwan

Abstract— This paper is about the effect of localized surface plasmon resonance used in Organic Lighting-emission device. We use a bottom emission structure OLED and luminance enhancement is found when incorporate metal nanoparticles in OLED structure. Different size, material and position of metal nanoparticles will be used to discuss the property of LSPR and optimized the best enhancement condition. The LSPR enhancement condition and mechanism in OLED will be discuss in this paper.

Session 3P1a
FocusSession: Sesquicentennial Commemoration Session for Maxwell's Equations 2

Maxwell-like Equations for Gravitational Fields from the Linearized Theory of General Relativity: Are There Experimental Tests of These Equations?

Raymond W. Chiao[1], **Nader Inan**[1], **Gerardo Munoz**[2], **Douglas Singleton**[2], **Xiuhao Deng**[1], **Luis Martinez**[1], **Bong Soo Kang**[1], **Alessandro Castelli**[1], **and Jay Sharping**[1]

[1]University of California, Merced, USA
[2]California State University, Fresno, USA

Abstract— Einstein's theory of general relativity yields four Maxwell-like equations for weak gravitational fields which are formally identical to Maxwell's equations for electrodynamics. Experimental tests for the validity of these Maxwell-like equations would greatly help advance our understanding of gravitational radiation. We propose a specific test involving the use of a moving superconducting membrane as the active element of a parametric amplifier for gravitational radiation. The moving boundary conditions for the superconducting membrane arise naturally from these equations. Calculations show that the threshold for parametric oscillation are practical to achieve in the laboratory. Thus an analog of the maser or the laser for gravitational radiation can be constructed.

Complete Construction of EM Green's Dyadics from Maxwell's Equations and Their Subsequent Asymptotic HF Approximations

Prabhakar Pathak
Ohio State University, USA

Abstract—

Generalized Gauge for Multi-scale Inhomogeneous Media

W. C. Chew[1], **Q. I. Dai**[1], **S. Sun**[2], **A. Y. Liu**[1],
C. J. Ryu[1], **S. Chen**[1], **Y. L. Li**[2], **and W. E. I. Sha**[2]

[1]University of Illinois at Urbana-Champaign, USA
[2]The University of Hong Kong, Hong Kong SAR, China

Abstract— The vector potential $\mathbf{A}$ has no direct physical meaning in classical electromagnetics. However, it manifests itself in quantum physics in terms of the Aharonov-Bohm effect. The vector potential $\mathbf{A}$ is similar to momentum. By itself, it is hard to detect classically, but its time variation generates a force in terms of electric field. Hence, the $\mathbf{E}$ field is of the form

$$\mathbf{E} = -\partial_t \mathbf{A} - \nabla\Phi \tag{1}$$

where the electric field, which exerts a force on a charge, is generated by a time varying $\mathbf{A}$ and the gradient of the scalar potential Φ. The magnetic flux is given by $\mathbf{B} = \nabla \times \mathbf{A}$

By using Lorentz gauge

$$\nabla \cdot \mathbf{A} = -\mu\varepsilon\partial_t\Phi \tag{2}$$

Maxwell's equations in vacuum reduce to

$$\nabla^2\Phi - \mu\varepsilon\partial_t^2\Phi = -\rho/\varepsilon, \tag{3}$$

$$\nabla^2\mathbf{A} - \mu\varepsilon\partial_t^2\mathbf{A} = -\mu\mathbf{J} \tag{4}$$

For inhomogeneous medium, we pick the generalized gauge

$$\varepsilon^{-1}\nabla \cdot \varepsilon\mathbf{A} = -\mu\varepsilon\partial_t\Phi. \tag{5}$$

Then it can be shown that Maxwell's equations reduce to

$$\varepsilon^{-1}\nabla \cdot \varepsilon\nabla\Phi - \mu\varepsilon\partial_t^2\Phi = -\rho/\varepsilon, \tag{6}$$

$$-\mu\nabla \times \mu^{-1}\nabla \times \mathbf{A} - \mu\varepsilon\partial_t^2\mathbf{A} + \mu\varepsilon\nabla\frac{1}{\mu\varepsilon}\varepsilon^{-1}\nabla \cdot \varepsilon\mathbf{A} = -\mu\mathbf{J}. \tag{7}$$

For homogeneous medium, (6) and (7) reduce to (3) and (4).

The above equations have no low-frequency breakdown when solved numerically irrespective of how small the meshes are. Moreover, since $\mathbf{A}$ and Φ are needed in writing the Hamiltonian of an atom-field system, it is particularly suited for solving Maxwell-Schrodinger system of equations.

The discretization of the above equations can be inspired by differential forms from differential geometry. The vector potential $\mathbf{A}$ can be regarded as a one form which is curl-conforming. But the permittivity function can be regarded as a Hodge operator that converts a one form to a two form. Hence, $\varepsilon\mathbf{A}$ becomes a two form which has to be divergence conforming. The Hodge operator can also be implemented numerically.

Session 3P1b
SC2: Plasmonics: Beyond Local-response Dynamics

Electronic Tunneling Effects in Nanoplasmonic Structures

Joseph W. Haus[1, 2], **Domenico de Ceglia**[2], **Maria Antonietta Vincenti**[2], **and Michael Scalora**[3]

[1]Electro-Optics Program, University of Dayton, Dayton, OH 45469-2951, USA
[2]National Research Council — AMRDEC
Charles M. Bowden Research Center, Redstone Arsenal, AL 35898, USA
[3]Charles M. Bowden Research Center
AMRDEC, RDECOM, Redstone Arsenal, AL 35898-5000, USA

Abstract— An electronic quantum tunneling approach, that we call the Quantum Conductivity Theory (QCT), is applied to survey the optical properties of metal-insulator-metal structures with sub-nanometer sized insulator gaps [1, 2]. In our simulations the nonlocal and quantum tunneling effects are treated on the same footing. The close proximity of metallic objects generates a tunneling, ac current density that endows the insulator gap region with additional linear and nonlinear coefficients that in turn trigger linear and nonlinear absorption,and second- and third-harmonic generation of scattered light. Strong field localization inside the insulator gap ensures that harmonic generation arising from the gap region overwhelms intrinsic, metal second- and third-order nonlinearities. Experiments designed to test critical aspects of QCT will be presented.

REFERENCES

1. Haus, J. W., D. de Ceglia, M. A. Vincenti, and M. Scalora, "Quantum conductivity for metal-insulator-metal nanostructures," *J. Opt. Soc. Am. B*, Vol. 31, 259, arXiv 1309.3263, 2014.
2. Haus, J. W., D. de Ceglia, M. A. Vincenti, and M. Scalora, "Nonlinear quantum tunneling effects in nano-plasmonic environments: Two-photon absorption and harmonic generation," *J. Opt. Soc. Am. B*, accepted (2014).

Nonlocal and Quantum Effects in Nanoplasmonics

Yu Luo
The Blackett Laboratory, Department of Physics, Imperial College London, London, UK

Abstract— The miniaturization trend in experimental nano-optics is currently approaching the subnanometer regime. On such small length scales, the nonlocal screening of electrons in metals plays a key role and classical macroscopic electromagnetism breaks down. Previous approaches based on full-quantum or semi-classical descriptions demand high computational resources, preventing their applicability to realistic nanophotonic devices. Using a metamaterial-inspired approach, I will introduce a simple and efficient model able to describe the nonlocal and quantum nature of metallic electrons at the nanoscale. I will show that, remaining in the usual local approximation, an effective composite material can be used to replace a more complex nonlocal system. Our approach incorporates radiative, nonlocal, and quantum tunnelling effects, and thus can be applied to investigate realistically-sized plasmonic systems with Angstrom-sized geometrical features. As an example, I will show how this model can be used to design practical nanophotonic devices for sub-diffraction-limited image and high-harmonic generation.

Surface Effects in the Hydrodynamic Model

G. Toscano[1], **C. Rockstuhl**[1], **M. Wubs**[2, 3], **and N. A. Mortensen**[2, 3]

[1]Institut für Theoretische Festkörperphysik
Karlsruhe Institute of Technology, D-76128 Karlsruhe, Germany
[2]Department of Photonics Engineering
Technical University of Denmark, DK-2800 Kongens Lyngby, Denmark
[3]Center for Nanostructured Graphene (CNG)
Technical University of Denmark, DK-2800 Kongens Lyngby, Denmark

Abstract— The study of the free-electron optical response of metallic nanostructures is usually based on the classical Drude model. The ongoing miniaturization of nanoplasmonic structures down to sizes comparable to the Fermi wavelength of the electrons, calls for a description that captures the emerging quantum effects. To this end, we proposed the use of the hydrodynamic Drude model (HDM), a semiclassical model that describes the free-electron gas in a metal as a Fermi gas subject to the electromagnetic force, as described by the Navier-Stokes like equation [1–5]. New in this description is the presence of longitudinal electromagnetic waves, that are associated with charge density oscillations, and give rise to a spatially nonlocal optical response. The HDM correctly accounts for the blueshift of the resonance peaks for noble metals nanoparticles, and it allows to calculate the fields close to sharp tips, where the classical model gives divergent results. The HDM assumes that the electrons are confined into the metal nanoparticle (hard-wall approximation), therefore it is not suitable for treating electron spill-out and surface effects, that play an important role in plasmonic nanostructures [6, 7].

Here I will survey a more general formulation of the hydrodynamic model (GHDM), that goes far beyond the Thomas-Fermi description of the electron gas, and it allows to treat surface effects self-consistently. I will discuss the implementation of this model as an add-on to standard commercial software (COMSOL 4.2a), and I will show the results obtained for both sodium and silver nanoparticles. The accuracy of the generalized hydrodynamic model is comparable with that of fully quantum mechanical methods, and it allows to treat large systems that are of interest in the plasmonic applications.

REFERENCES

1. Raza, S., G. Toscano, A.-P Jauho, M. Wubs, and N. A. Mortensen, "Unusual resonances in nanoplasmonic structures due to nonlocal response," *Phys. Rev. B*, Vol. 84, 121412(R), 2011.
2. Toscano G., S. Raza, A.-P. Jauho, M. Wubs, and N. A. Mortensen, "Modified field enhancement and extinction by plasmonic nanowire dimers due to nonlocal response," *Optics Express*, Vol. 20, No. 4, 4176–4188, 2012.
3. Toscano G., S. Raza, S. Xiao, M. Wubs, A.-P. Jauho, S. I. Bozhevolnyi, and N. A. Mortensen, "Surface-enhanced Raman spectroscopy (SERS): Nonlocal limitations," *Optics Letters*, Vol. 37, No. 13, 2538–2540, 2012.
4. Mortensen, N. A., G. Toscano, S. Raza, N. Stenger, W. Yan, A.-P. Jauho, S. Xiao, and M. Wubs, "Nanoplasmonics beyond Ohm's law," *AIP Conf. Proc.*, Vol. 1475, 28, 2012.
5. Toscano, G., S. Raza, W. Yan, C. Jeppesen, S. Xiao, M. Wubs, A.-P. Jauho, S. I. Bozhevolnyi, and N. A. Mortensen, "Nonlocal response in plasmonic waveguiding with extreme light confinement," *Nanophotonics*, Vol. 2, 161, 2013.
6. Teperik, T. V., P. Nordlander, J. Aizpurua, and A. G. Borisov, "Quantum effects and nonlocality in strongly coupled plasmonic nanowire dimers," *Optics Express*, Vol. 21, No. 22, 27306–27325, 2013.
7. Stella, L., P. Zhang, F. J. García-Vidal, A. Rubio, and P. García-González, "Performance of nonlocal optics when applied to plasmonic nanostructures," *J. Phys. Chem C*, Vol. 117, 8941–8949, 2013.

Generalized Nonlocal Optical Response

Søren Raza[1], **Thomas Søndergaard**[2], **Martijn Wubs**[3], **Sergey I. Bozhevolnyi**[4], **and N. Asger Mortensen**[3]

[1]Department of Photonics Engineering and Center for Electron Nanoscopy
Technical University of Denmark (DTU), Kongens Lyngby DK-2800, Denmark
[2]Department of Physics and Nanotechnology, Aalborg University, Aalborg DK-9220, Denmark
[3]Department of Photonics Engineering and Center for Nanostructured Graphene
Technical University of Denmark (DTU), Kongens Lyngby DK-2800, Denmark
[4]Institute of Sensors, Signal and Electrotechnics
University of Southern Denmark, Odense DK-5230, Denmark

Abstract— Plasmon hybridization between metallic nanoparticles has attracted a lot of attention in the field of plasmonics due to the tuning of the plasmon resonance energy with gap/particle size and the presence of large electric field enhancements. Such features are exploited in areas such as surface-enhanced Raman spectroscopy, refractive index sensing, biooptics and so on. Recently, using techniques such as electron microscopy or atomic force microscopy, the distance between two metallic nanoparticles has been controlled down to few nanometers ($< 5\,\mathrm{nm}$), allowing for the study of quantum effects due to nonlocal response and the free-electron spill-out effect. Such experiments have so far been interpreted using models based on quantum tunneling.

In this study, we show that features usually attributed to quantum tunneling can be described using a semiclassical nonlocal response model — without the inclusion of quantum tunneling. Using our generalized nonlocal optical response (GNOR) model, which incorporates effects due to both diffusion and hydrodynamic pressure of free electrons, we present results on the plasmon hybridization between two nanowires excited by a plane wave, see Fig. 1. We examine in the detail the touching case ($g = 0$) and present simple equations for the resonance energies of the hybridized plasmon modes.

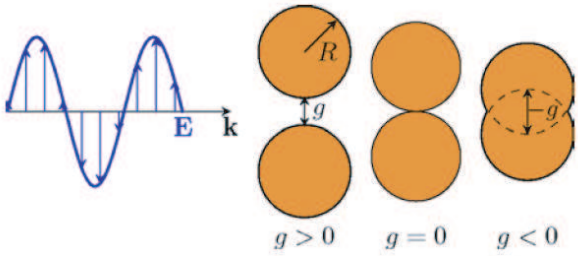

Figure 1: Sketch of the considered system, displaying the incident electric field, which is polarized along the dimer axis, impinging on a dimer consisting of two identical cylinders with radii R and separated by a gap g. The three cases of a separated dimer ($g > 0$), touching dimer ($g = 0$) and overlapping dimer ($g < 0$) are shown.

The Impact of Nonlocality on Gap-plasmon Resonators and Multilayered Structures

A. Moreau[1, 2], C. Ciracì[2, 3], J. Benedicto[1], M. Dchaux[1], E. Centeno[1], and D. R. Smith[2]

[1]Institut Pascal, Clermont University, France
[2]Center for Metamaterials and Integrated Plasmonics, Duke University, USA
[3]Istituto Italiano di Tecnologia, Center for Biomolecular Nanotechnologies, Arnesano, Italy

Abstract— Recent experimental works have attracted a lot of attention on the problem of nonlocality in metals [1] — that is to say the influence of interactions between free electrons on the optical properties of metallic nanostructures. This subject has been studied a lot in the seventies and eighties, but has stopped attracted much interest for almost two decades due to the lack of any reliable experimental data. These new results show moreover that for tiny gaps, the hydrodynamical model is sufficient to describe correctly the physics of the structure.

The gap-plasmon is the fundamental mode of a metallic (metal-insulator-metal) waveguide when the thickness of the waveguide is typically smaller than 50 nm. Due to plasmonic effects, this mode becomes extremely slow for extremely small (below 5 nm) gaps and because of this high effective index, it becomes sensitive to the nonlocality due to interactions between free electrons.

In the case of multilayered structures and in the framework of the hydrodynamical model, it turns out that the reflection coefficients as well as the dispersion relations are analytical [2]. For instance, the dispersion relation of the gap-plasmon in analytical, and shows very clearly that the non-local terms are proportional to the square of the effective index of the mode: the slower the mode, the larger the impact of nonlocality.

All structures that are likely to support gap-plasmons, like patch antennas [3] or nanogratings [4], can thus be expected to be sensitive to nonlocality. Since everything is analytical in a multilayered structure, we have generalized the scattering matrix method to take nonlocality into account. The code, that will soon be made public, allows to see the impact of nonlocality on at lenses made with hyperbolic multilayers, for instance.

Our conclusion is that, while the impact of nonlocality is generally small, it can be important and it should be taken quantatively into account in situations where plasmonics effects are intense — and the theoretical and numerical tools we propose here should help the community to do so.

REFERENCES

1. Cirac, C., R. T. Hill, J. J. Mock, Y. Urzhumov, A. I. Fernndez-Domnguez, S. A. Maier, J. B. Pendry, A. Chilkoti, and D. R. Smith, "Probing the ultimate limits of plasmonic enhancement," *Science*, Vol. 337, 1072–1074, 2012.
2. Moreau, A., C. Cirac, J. J. Mock, R. T. Hill, Q. Wang, B. J. Wiley, A. Chilkoti, and D. R. Smith, "Controlled-reflectance surfaces with film-coupled colloidal nanoantennas," *Nature*, Vol. 492, 86–89, 2012.
3. Moreau, A., C. Cirac, and D. R. Smith, "Impact of nonlocal response on metallodielectric multilayers and optical patch antennas," *Phys. Rev. B*, Vol. 87, 045401, 2013.
4. Le Perchec J., P. Quemerais, A. Barbara, and T. Lopez-Rios, "Why metallic surfaces with grooves a few nanometers deep and wide may strongly absorb visible light," *Phys. Rev. Lett.*, Vol. 100, 066408, 2008.

Session 3P2
FocusSession.SC3: Photonics and Optoelectronics in Industry

Optimization of Nonlinear Coefficient Map in Back-propagation

Yanru Cao and Junhe Zhou
Department of Electronics Science and Engineering, Tongji University, Shanghai 200092, China

Abstract— In optical communication systems, chromatic dispersion and fiber nonlinearities are the main effects that limit the system performance. Compensation of these effects is essential to realize high speed and ultra-long distance fiber transmission.

Back-propagation (BP) algorithm is one of the most extensively used methods which can jointly compensate the chromatic dispersion and the fiber nonlinearities. The algorithm can virtually inverse the fiber transmission by adopting the digital signal processing (DSP) technique. During the application of the algorithm, the dispersion and nonlinearity interplay with each other. The amount of the dispersion should be exactly compensated, while the nonlinearity should be partially compensated [1]. The nonlinear coefficient used in the BP algorithm should between 0 and the actual fiber nonlinear coefficient. It was further proposed in [2] that the nonlinear parameter used in the simulation can be optimized with respect the fiber locations in the span, and this optimal nonlinear compensation map should change with respect to dispersion. However, no systematic approaches have been proposed to optimize the nonlinear compensation map in the BP algorithm.

In this paper, we propose to use two parameters to control the value of the nonlinear coefficient map. The nonlinear coefficient in the BP algorithm changes linearly with respect to the span number and is evaluated as $an + b$, where a and b are two constants to be optimized, n the span number. It is shown in the numerical simulation that by adopting this optimized BP algorithm, the BER performance can be greatly improved.

REFERENCES

1. Ip, E. and J. M. Kahn, "Compensation of dispersion and nonlinear impairments using digital backpropagation," *IEEE Journal of Lightwave Technology*, Vol. 26, 3416–3425, 2008.
2. Ip, E. and J. M. Kahn, "Nonlinear impairment compensation using backpropagation," *Optical Fiber New Developments*, Intech, 2009.

Generic InP-based Integration Technology: RF Crosstalk in High-capacity Optical Transmitter PICs

W. Yao[1], **G. Gilardi**[1], **M. K. Smit**[1], **and M. J. Wale**[1, 2]

[1]COBRA Institute, Photonic Integration Group, University of Technology Eindhoven, The Netherlands
[2]Oclaro Technology Ltd., Caswell, Towcester, Northamptonshire, NN12 8EQ, UK

Abstract— Photonics is a key enabling technology that is used in many areas such as in telecom, datacom or sensing applications. Photonic integrated circuits (PICs), combining several optical components in one chip, are essential for its success but need to be low-cost, mass producible and easily accessible by a broad user range. Generic photonic integration technology can achieve that and is recently gaining increased popularity.

The generic foundry approach for photonics follows the same idea as for microelectronics. A small number of basic building blocks (BBs) with basic functions and well-known performances are available and can be monolithically integrated on InP. The user can use them to build more complex circuits that suit their specific needs. The fabrication is performed by a foundry and R&D costs can be reduced using multi-project wafer runs, where designs from different users are collected and realized on the same wafer, so that the total wafer cost is shared by everyone and the entry-cost per user is reduced. Dedicated design kits with component libraries and behavioral models are available and ease the design process for the user and detach him from the actual fabrication process. With this approach, PICs can be brought to many application fields where their full potential can be exploited.

One such application field lies in optical communications, where low-cost high-capacity optical transmitters and receivers are needed for fiber-to-the-home or datacenter connections. An optical transmitter consisting of a single wavelength laser and a high-speed modulator can be easily realized in the generic integration technology. Using wavelength division multiplexing (WDM) the channel count can be scaled up to achieve very high transmit capacity on a small PIC. One of several challenges for scaling up the channel count and integration density lies in radiofrequency (RF) crosstalk between modulators. With the help of suitable simulation techniques and measurements, RF crosstalk effects on the transmitter performance are analyzed. Proper care needs to be taken in the design of both the transmitter PIC and also the electronic package to minimize crosstalk effects.

The presentation gives an overview of the generic photonic integration technology and its applications in industry and then focuses on RF crosstalk in high-capacity transmitter PICs realized within the generic integration platform.

Design of an Efficient and a Compact Optical Pulse Compressor Using a Tapered Photonic Crystal Fiber

A. Manimegalai[1, 2], D. R. Divya[2], Abdosllam M. Abobaker[3], K. Senthilnathan[1], S. Sivabalan[4], K. Nakkeeran[5], and P. Ramesh Babu[1]

[1]Photonics, Nuclear and Medical Physics Division, School of Advanced Sciences
VIT University, Vellore 632 014, India
[2]Department of Electronics and Communication Engineering
Ganadipathy Tulsi's Jain Engineering College, Vellore 632 102, India
[3]Department of Communications Engineering, College of Electronic Technology, Bani Walid, Libya
[4]School of Electrical Engineering, VIT University, Vellore 632 014, India
[5]School of Engineering, University of Aberdeen, Aberdeen AB24 3UE, UK

Abstract— Ultrashort pulses (USPs) at shorter wavelengths extending down to the ultraviolet region with a high repetition frequency range (GHz-THz) have found wide applications, especially, in bio-photonic sensors, optical coherence tomography, materials processing, etc.. There are some desirable features that USPs need to satisfy such as being pedestal-free and transform-limited for their suitability in communication as well as non-communication based applications. However, it is very difficult to meet out these desirable characteristics even with the carefully configured laser systems. Hence, pulse-compression techniques have been the ultimate solution for generating USPs, in recent times.

Having realized the importance of generating USPs through pulse compression, we aim at designing a novel but practicable pulse compressor using a tapered photonic crystal fiber (PCF) operating down to ultraviolet regime. The pulse propagation in a tapered PCF is governed by the nonlinear Schrödinger (NLS) type equation. We adopt the self-similar scaling analysis for generating USPs. Based on the analytical results, we model a tapered PCF such that the dispersion decreases exponentially while the nonlinearity increases exponentially along the propagation direction. Here, the required tapering is achieved by exponentially decreasing the diameter of the air hole as well as its pitch. We envisage that the proposed pulse compressor would turn out to be an excellent tool for generating high quality USPs down to ultraviolet regime, which, in turn, might be very much useful in bio-photonic related applications.

History, Present and Future of High Speed Transponders and Systems

Anhui Liang
Nanjing University of Posts and Telecommunications, China

Abstract— In this paper, we shall review the history of 10 G, 40 G, especially we shall discuss the history of first commercial 40 G transponder which was designed and developed by the us in 2004. We shall discuss the significances of the invention of 40 G transponders, including the 40 G transponders' important roles in the Iphone's deployment in carriers networks. We shall discuss the major techniques used in 40 G systems. We shall review the history of first commercial deployment of dual carrier and single carrier 100 G transponders in 2009 and 2010 respectively, we shall discuss the progress and issues on 100 G transponders and systems. We shall discuss the important devices and modules used in both line side and client side, including tunable lasers, tunable XFP and CFP etc.. Furthermore, we shall discuss the R&D efforts on 400 G and 1 T transponders and systems. In 2012, we proposed the concept of giant capacity which means the capacity per fiber is larger than 10 P, and we proposed the design concept for 100 P/fiber. We shall discuss the important techniques used in 100 P/fiber systems. We first proposed the dense periodical fibers in 1990s, and we find FWM can be very low over a giant bandwidth (e.g., over 300–1100 nm). Finally, we shall discuss the potential applications of dense periodical fibers in undersea, long haul, metro and access systems.

Applications of High Pulse Energy Femtosecond Fiber Lasers

Xiangdong Cao[1, 2]

[1]WuHan Hongtuo New Technology Co., Ltd., China
[2]Wuhan Natitional Lab for Opto-electronics, Huazhong University of Science and Technology, China

Abstract— High pulse energy femtosecond fiber lasers are becoming important tools for both scientific research and industrial applications due to their high reliability and cost effectiveness. In this presentation, a novel femtosecond fiber laser with 10 W average power, 10 μJ pulse energy at 1 MH repetition will be summarized. Typical applications of this high pulse energy femtosecond laser including photonic waveguides, nano-micro surface modifications, bio-microfluidics will be discussed.

LD and LED Manufacture with Nanoimprint Process v1.0

Wen Liu
Institute of Advance Technology, University of Science and Technology of China
800 Wangjiang West Road, Hefei, AnHui 230088, China

Abstract— As the application of nanophotonics increasing in various fields, the critical dimension becomes smaller and smaller, the pattern complexity becomes higher and higher. Nanoimprint Lithography (NIL), with the advantages of high resolution, low cost, high throughput and high flexibility, has become one of the most promising research interest in micro and nano fabrication.

We presentation a few improvements on NIL itself and demonstrates its application in DFB laser array and light emitting diode (LED) chip manufacturing. Including specific experiment program for each step of NIL: proposing the method of E-beam lithography combining with electroforming to fabricate the metal stamp in order to greatly increase the life of stamp. Soft mold ultraviolet (UV) imprint process is present to improve the yield of large area imprint. A multi-layer mask method is layer mask method developed

Based on these technologies, monolithic integrated 4 channel DFB array with MMI coupled has been fabricated successfully. The average threshold current is less than 10 mA, the sidemode suppression ratio (SMRS) is larger than 50 dB. The monolithic integrated 16 channel DFB array with AWG coupled has also been fabricated Another work is using NIL to fabricate nano patterned sapphire substrate (nPSS) in order to enhance the output efficiency. The photoluminescence (PL) output efficiency of the modified chip is nearly doubled compared with ordinary chip, and after packaging the output power increase by 22.6%.

The Application of Micro-interferometer on Optical Coherent Detection

Jay Hsieh
Optoplex Corporation, USA

Abstract— In optical communication, as the data rate reaches 40G/sec or above, the phase modulation format is a preferred scheme, for its superior SNR capability. Phase modulation includes DPSK (differential phase shift keying), DQPSK (differential quadrature phase shift keying), and coherent detection (DP-QPSK-dual polarization quadrature phase shift keying, or DP-8PSK).

Optical phase demodulators are the key components for the phase modulation scheme. With the demodulator, the phase information carried by a light beam is converted into amplitude modulation, and then sends to the light detection system to decode the signal. In this talk, two types of interferometers are introduced to achieve the function of phase demodulators. Those interferometers are used to mix the input optical signal with phase modulated and the local oscillator to form the amplitude modulated output beams.

Session 3P3
MS-1.6: Organic Light Emitting Diodes 2

Highly Efficient Flexible and Stretchable Polymer Light Emitting Diodes

Lu Li, **Jiajie Liang**, **Shu-Yu Chou**, **Xiaodan Zhu**, **Xiaofan Niu**, **ZhibinYu**, **and Qibing Pei**
Department of Materials Sciences and Engineering, California NanoSystems Institute
Henry Samuli School of Engineering and Applied Science, University of California
Los Angeles, California 90095, USA

Abstract— We report the synthesis of transparent nanocomposite electrodes comprising a percolation network of silver nanowires in the surface layer. The mechanical properties of the electrodes are determined by the polymer matrix employed, and ranges from being rigid to flexible to elastomeric. The composite electrodes have been used to fabricate a variety of thin film electronic devices including flexible polymer light emitting didoes and solar cells. The current efficiencies of polymer OLEDs show significantly improved electroluminescent efficiency than control devices on ITO/glass. Green PLED fabricated on the nanocomposite electrode exhibit a maximum current efficiency of 118 cd/A at 10,000 cd/m^2 with the calculated external quantum efficiency being 39%. The efficiencies of white PLEDs are 47 cd/A and 30%, respectively. These efficiencies are higher than any reported flexible OLEDs without the use of light extraction structures. The viewing angle of the PLEDs is wider than Lambertian distribution, and the emission color from the 90° angle is almost identical to the normal angle. Elastomeric polymer light emitting devices (EPLED) have also been demonstrated employing a pair of elastomeric transparent electrodes to sandwich a layer of light emitting polymer. Balanced charge injections are accomplished by either admixing with a solid electrolyte or employing an electron-injection layer. The EPLED exhibit rubbery elasticity at room temperature, is collapsible, and can emit light when exposed to strains as large as 130%. It can also survive repeated continuous stretching cycles, and small stretching is shown to significantly enhance its light-emitting efficiency. The fabrication process is scalable and was readily adapted for the demonstration of a simple passive matrix monochrome display featuring a 5×5 pixel array.

Room-temperature Solution-processed Transition Metal Oxides as Efficient Carrier Extraction Layer for High Performance Organic Optoelectronics

Wallace C. H. Choy, **Fengxian Xie**, **Xinchen Li**, **and Chuandao Wang**
Department of Electrical and Electronic Engineering
The University of Hong Kong, Pokfulam Road, Hong Kong

Abstract— An essential aspect in designing efficient and stable organic solar cells (OSCs) and organic light emitting diodes (OLEDs) is the engineering of interfacial carrier transporting layers between the organic layer and metal electrodes. Among various materials available for interfacial layers, transition metal oxides (TMOs) have great potential owing to their wide range of energy level aligning capabilities. Bearing the compatibility with large-area, low-cost, high-throughput production and all-solution technology, we propose a one-step method to synthesize low-temperature solution-processed TMOs such as molybdenum oxide and vanadium oxide for hole transport layers through the synthesis of hydrogen molybdenum bronze and hydrogen vanadium bronze. Interestingly, the hydrogen metal oxide bronzes (HMOs) are dispersed uniformly and stably into water-free solvents which are particularly beneficial to the device stability and processing. With low temperature treatment or even at room temperature, the TMO films with small amount oxygen vacancies exhibit high film quality and desirable electrical properties. Through the analysis of UPS and XPS results, we identify the importance of oxygen vacancies for TMOs as HTL. Notably, the synthesized HMOs can be dispersed uniformly and stably into water-free solvents. By using our TMOs to make OSCs with polymer blend of P3HT:PCBM, the power efficiency (PCE) reaches 4% (vs 3.7% for PEDOT:PSS control device) and PCE of 7.75% using polymer blend of PBDTTT-C-T:PCBM (vs 7.24% for the corresponding PEDOT:PSS control device) [1]. Recently, we have achieved solution process of TMOs at room temperature [2] and the PCE performance can reach about 8% in inverted OSCs with polymer blend of PBDTTT-C-T:PCBM as the active layer. Consequently, the results of our newly-synthesized TMOs demonstrate that oxygen vacancy plays an essential role for TMOs as effective HTL for applications on organic electronics.

REFERENCES

1. Xie, F., W. C. H. Choy, C. Wang, X. Li, S. Zhang, and J. Hou, "Low-temperature solution-processed hydrogen molybdenum and vanadium bronzes for efficient hole transport layer in organic electronics," *Adv. Mat.*, Vol. 25, 2051–2055, 2013.
2. Li, X. C., W. C. H. Choy, F. Xie, S. Zhang, and J. Hou, "Room-temperature solution-processed molybdenum oxide as hole transport layer with Ag nanoparticles for highly efficient inverted organic solar cells," *J. Mater. Chem. A*, Vol. 1, 6614–6621, 2013.

High Performance Inverted Organic Light-emitting Diodes with $WO_3/Ag/MoO_2$ Multilayer as Transparent Cathode

Shun-Wei Liu
Department of Electronic Engineering, Ming Chi University of Technology
New Taipei City 24301, Taiwan

Abstract— A transparent conducting oxide (TCO) thin film based on dielectric/metal/dielectric multilayer structure, which can be used to replace a common TCO electrode of indium tin oxide (ITO), has attracted considerable attention because of their low sheet resistance, simplified fabrication process, and high transparency in the visible light range to enhance the device performance of optoelectronic devices. In this work, we present highly efficient and inverted organic light-emitting diodes (OLEDs) with a high conductive transparent $WO_3/Ag/MoO_2$ (WAM) multilayer as transparent cathode electrode on PET substrate. The WAM electrode by thermal deposition process shows a low sheet resistance of $8\,\Omega$/sq and high optical transmittance of of $\sim 82\%$ at range of visible light from 400 to 550 nm. With electrical characterizations (Conductive atomic-force microscopy and current density-voltage measurements), WAM device using a electron only structure has a high electron injection property at WAM/BPhen: CS_2CO_3 interface as compared with the standard ITO electrode. From the device characterization, the device performance of optimal green emission inverted OLED [PET/WO_3(27.5 nm)/Ag(16.5 nm)/MoO_2(3.5 nm)/BPhen: 5%CS_2CO_3(10 nm)/BPhen(20 nm)/CBP: 8%Irppy$_3$(15 nm)/TAPC(55 nm)/MoO_3(7.5 nm)/Al (150 nm)] exhibiting a power efficiency of 65 lm/W, current efficiency of 68 cd/A, and external quantum efficiency of 19.5% at a brightness of 100 cd/m^2 has been achieved. More importantly, the emission property of the WAM device obviously appeared the wide viewing profile for light emission due to the weak microcavity in the device structure, which is much better than that of the device based on ITO electrode or other multilayer system.

Sophisticated Architecture Designs for Blue, Green, and Red Inverted Organic Light-emitting Diodes

Chih-Hao Chang, **Yu-De Su**, **Hao-Xiang Huang**, **Ming-Kuan Hsu**, **and Ying-Chieh Wu**
Department of Photonics Engineering, Yuan Ze University, Chung-Li 32003, Taiwan

Abstract— Inverted OLEDs (IOLEDs) have drawn considerable attention for use in active-matrix OLED displays because of their easy integration with n-channel thin film transistors (TFTs). The electron-injection capability of the bottom cathode used in IOLEDs influences TFT requirements. To meet the stringent requirement of the TFTs, it is highly desirable to decrease the operation voltage of the IOLEDs Previous studies have reported that the turn-on voltages of FIrpic-based IOLEDs fall within a range of 4 to 8 V. Here, we focus on developing bottom-emission IOLEDs with low operating voltages through the use of effective electron injection layers (EILs) consisting of an alkali metal oxide layer and an organic layer doped with alkali metal oxide. This sophisticated EIL is integrated into IOLEDs to simultaneously reduce the operation voltages and to achieve carrier balance. We successfully demonstrated respective turn-on voltages of 3.5 V, 3.2 V, and 3.2 V for the blue, green, and red phosphorescent IOLEDs. Furthermore, the blue, green and red IOLEDs with identical architectures exhibit high efficiency, confirming that the architecture is conducive to easily obtaining the carrier balance. In addition, based on our previous studies, higher performance could be achieved by employing an external light-extraction structure (EES). Thus, the silicon dioxide (SiO_2) nanocomposite film was adopted for light scattering as well as to mitigate the difference between the refractive indices of glass and air. The peak efficiencies of the blue, green, and red IOLEDs with additional EES were further improved by about $1.3 \sim 1.4$ times, and up to 21.0%, 21.3%, and 10.1%, respectively. Moreover, the EQEs of these IOLEDs declined by half of the current density ($J_{1/2}$) to 138.9 (blue), 63.6 (green), and 68.7 (red) mA/cm^2. As a result, the device's efficiency roll-off was less pronounced due to the bipolar host and improved carrier balance. The extended carrier recombination zone could reduce the concentration of excitons in a narrow space. These results indicate the great potential of this architecture design for use in phosphorescent IOLEDs with various emission colors.

Enhancing the Performance of Organic Light Emitting Diodes by Varying Device Structure

Shui-Hsiang Su and Meiso Yokoyama
Department of Electronic Engineering
I-Shou University, Section 1, Hsueh-Cheng Rd., Ta-Hsu Hsiang, Kaohsiung County, Taiwan

Abstract— Organic light emitting diodes (OLEDs) have attracted lots of attention because of their advantages in emission with a wide visible region for application in flat-panel display and lighting. OLEDs are current injection devices and the improvement of electron injection is essential for efficient and stable OLED. An efficient electron injection could be achieved by using low work function metal. In order to further improve the luminous efficiency of OLED, an external electron injection is introduced to impact into device. The field emission organic light emitting diodes (FEOLEDs) [1] utilize organic electroluminescent (EL) layer instead of inorganic phosphor thin film in field emission diode (FED). FEOLEDs mechanism differs from the traditional FED.

The FEOLED is constructed by an OLED and a carbon nanotubes (CNTs) template. OLED comprises with multilayer organic structure of ITO-glass/hole transporting layer/emission layer/electron injection layer/cathode. CNT-base field emitting cathodes act as an electron source. The electrons are excited and accelerated by the electrical field under vacuum so as to become sufficiently energized to supplement the OLED extra electrons to emit light. The collision increase the number of electrons reaching the organic EL light emitting layer, thus enhance the luminous efficiency of the OLED. Therefore, FEOLED balances quantity of electrons and holes in OLED, which let the exciton to be increased and further increased the luminous efficiency of OLED. Under the same current density compare with the OLED and FEOLEDs, the luminous efficiency which work in FEOLEDs was higher than traditional OLED. Various device structure based on the concept of FEOLED is proposed and discussed in this study.

REFERENCES

1. Yokoyama, M., US Patent 7,456,562 B2, November 2008.

Regulating Carriers and Excitons in Simplified Hybrid WOLEDs by Using a Bipolar Interlayer Switch

Baiquan Liu[1], **Jianhua Zou**[1], **Miao Xu**[1], **Lei Wang**[1], **Hong Tao**[1], **Yueju Su**[2], **Dongyu Gao**[2], **Linfeng Lan**[1], **and Junbiao Peng**[1]

[1]Institute of Polymer Optoelectronic Materials and Devices
State Key Laboratory of Luminescent Materials and Devices
South China University of Technology, Guangzhou 510640, China
[2]New Vision Opto-Electronic Technology Co., Ltd, Guangzhou 510530, China

Abstract— As phosphorescent (P) emitters allows for a conversion of up to 100% of injected charges into emitted photons, resulting in a theoretical internal quantum efficiency of unity, P materials are usually imperative to boost the efficiency of white organic light-emitting diodes (WOLEDs). Unfortunately, there is still no proper blue P material in terms of operational lifetime and color-stability until now, limiting the development of all-phosphor devices. To solve the above conflicts, the hybrid WOLEDs, combining blue flourescent (F) emitters with P green-red/orange emitters, are considered to be an effective way due to their merits, such as high efficiency, stable color and long lifetime. A key feature of designing HWOLEDs is utilizing an appropriate interlayer, which locates between the F emitter and the P emitter. Herein, by mixing 4,4-N,N-dicarbazolebiphenyl (CBP) with bis[2-(2-hydroxyphenyl)-pyridine] beryllium ($Bepp_2$) as the interlayer, a simple hybrid with dual-emitting-layer a realized. The device with the bipolar interlayer shows higher performance than the device with CBP, $Bepp_2$ interlayer and the device without interlayer. The reasons can be attributed to the bipolar interlayer which not only regulating the carriers in the device, but also eliminate the both the non-radiative Dexter energy Förster energy transfer between the two layers. The resulting device exhibits a total current efficiency of 23.6 cd/A and power efficiency of 16.2 lm/W at the illumination-relevant luminance of 1000 cd/m^2, respectively. Besides, a Commission Internationale de L'Eclairage (CIEx, y) variation of (0.311, 0.411) and a high color rendering index of 85 at 1000 cd/m^2 can be obtained. Moreover, the lifetime of the device is also discussed.

Efficiency and Color-tunability of Fluorescent-phosphorescent Organic Light-emitting Diodes with Regular, Inverted, and Symmetrical Structures

Su-Hua Yang and Po-Jen Shih
Department of Electronic Engineering
Kaohsiung University of Applied Sciences, Kaohsiung, Taiwan

Abstract— White organic light emitting diodes (OLEDs) were fabricated for color-tunable lighting applications. Four devices with regular-, inverted-, compensated- and symmetrical-EML structures were prepared. Fluorescent and phosphorescent hybrid emission layers (EMLs) were used to enhance the luminance and stability of the devices. The influence of composition and structure of the EMLs on the electroluminescence (EL) properties of the devices were investigated from the viewpoint of their emission spectra. The possible exciton harvesting, diffusion, transport, and annihilation processes occurring in the EMLs were also evaluated.

The emission of device with an inverted-EML was color-stable. However, its EL efficiency degraded significantly at high current density. This was resulted from the luminescence quenching effect and the excitons diffusion from EML to the hole transporting layer. On the contrary, a color-tunable white OLED was obtained when a compensated-EML was prepared. The purity of the white color was improved when an red-EML was inserted between the phosphorescent sensitized EML and the electron-transporting layer. The chromatic coordinates linearly shifted from pure white (0.300, 0.398) to cold white (0.261, 0.367) when the applied voltage was varied from 10 to 14 V. These CIE coordinates correspond to CCTs ranging from 6500 to 8750 K. Furthermore, the device with a quantum-like symmetrical-EML confined carriers efficiently, consequently, high EL efficiency was measured. Stable EL efficiency was obtained from regular-, compensated-, and symmetrical-devices. The highest EL efficiency of 11.4 cd/A was obtained from the inverted-device, and the efficiency of symmetrical-device was slightly lower than that of regular-device but higher than compensated-device by a factor of 2.72.

New AMOLED Pixel Circuits Based on a-IGZO TFTs Compensating for TFT V_{TH} Shift and OLED Degradation

Chih-Lung Lin, Chia-Che Hung, Po-Chun Lai, and Po-Syun Chen
Department of Electrical Engineering, Cheng Kung University, Tainan 701-01, Taiwan

Abstract— Active-matrix organic light-emitting diode (AMOLED) displays have gained much attention in the recent years because of numerous merits such as high brightness, high contrast ratio, wide viewing angle, flexibility, and fast response time. For driving OLEDs, the pixel circuits using hydrogenated amorphous silicon thin-film transistors (a-Si:H TFTs) have been developed. However, the mobility of a-Si:H TFT is too low which results in a low aperture ratio and a large layout area. Consequently, recent AMOLED displays mostly adopt low temperature poly-silicon TFTs (LTPS TFTs) due to high mobility. Nevertheless, LTPS TFTs still have some issues such as high manufacturing process temperature, threshold voltage (V_{TH}) variations, and mobility variations. Therefore, the amorphous indium-gallium-zinc-oxide thin-film transistors (a-IGZO TFTs) have become more considerable owing to numerous benefits such as low cost, visible transparency, low processing temperature, good initial uniformity, and high mobility in the amorphous phase. Although the a-IGZO TFTs have many merits mentioned above, the V_{TH} of a-IGZO TFT still shifts under the gate-source driving voltage stress and there will be negative threshold voltages if depletion mode a-IGZO TFTs are used. Moreover, the OLED luminance drops also need to be considered. Hence, this work proposes two compensating pixel circuits both adopt a-IGZO TFTs. The first pixel circuit can ameliorate OLED material degradations and uses the diode-connection structure to compensate for TFT V_{TH} shifts. However, this structure will fail to compensate for V_{TH} variations when the V_{TH} is a negative value. Thus, the second pixel circuit utilizes the source follower structure to compensate for both negative and positive threshold voltages of a-IGZO TFTs and also ameliorates the OLED degradations.

Optical Modeling in OLED Structures

Y.-P. Chiou[1, 2, 3] **and W.-L. Yeh**[1]

[1]Graduate Institute of Photonics and Optoelectronics, Taiwan University, Taipei 10617, Taiwan
[2]Graduate Institute of Communication Engineering, Taiwan University, Taipei 10617, Taiwan
[3]Department of Electrical Engineering, Taiwan University, Taipei 10617, Taiwan

Abstract— In this talk, we are going to give the optical modeling of OLED structures. The modeling can be divided into wave optics and ray optics. In the wave optics, the modeling is from a simple layered structure and then a grating is added into it. There is a transition from wave optics to ray optics. A substrate layer and optical components such as a polarizer, a color filter, an anti-reflection film, and a microlens film are modeled with transmittance and reflectance. Output post process is calculated for real application and graphic user interface (GUI) is developed.

First, a layered structure is modeled. A dipole source is assumed and then expanded by plane waves in terms of their transverse vectors k_t. According to the wave vectors, the wave behaviors can be classified as surface plasmon modes, waveguide modes, substrate modes, and out-coupled air modes. The transfer matrix method (TMM) is then adopted to treat each plane wave in the layered OLED. Finally, the amplitude of each wave is obtained, and hence the overall wave behavior of the layered OLED is obtained. Second a periodic structure is added into the layered structure. The periodic structure is actually treated as another layer in the layered structure, except that there are coupling between different wave vectors. Rigorous coupled wave analysis (RCWA) is adopted to get the coupling between different wave vectors. Therefore, the whole simulation is similar to that of the simple layered structure, except that the vectors and matrices are expressed in terms of all wave vectors instead for a single wave vector. In the ray optics, the approach is similar to wave optics. The substrate, polarizers, anti-reflection film, and color filter are also treated as layered structure and it is also solved in each wave vector but incoherently. The microlens film also results in coupling between wave vectors. In the post process and GUI, the spectrum of different wave vectors, light extraction efficiency, color analysis, parameter scanning etc. are calculated and plotted. Finally, some simulation and experiment results may be compared in the presentation.

Efficient Light-extraction Microlens Arrays for Organic Light-emitting Devices

Mao-Kuo Wei[1], **Di-Hong Lin**[1], **Yu-Lin Liou**[1], **Jiun-Haw Lee**[2], **and Hoang-Yan Lin**[2]

[1]Department of Materials Science and Engineering, Dong Hwa University, Hualien, Taiwan
[2]Department of Electrical Engineering, Graduate Institute of Photonics and Optoelectronics Taiwan University, Taipei, Taiwan

Abstract— The organic light-emitting devices (OLEDs) have many advantages such as high internal quantum efficiency, energy saving, light weight, and environmental protection. The OLEDs are not only truly planar lighting devices, but also have ability to emit light with a low color temperature that is friendly to the health of mankind at night. Therefore, they seem to be one of the best candidates for next-generation indoor lighting sources. However, only 20%–30% of the generated light from the OLEDs can propagate into air due to total internal reflection in the substrate and anode waveguides, and energy loss in surface plasmonic mode. Many types of micro- and nanostructures were thus proposed to increase efficiency of the OLED in recently years. Among these micro- and nanostructures, the fabrication of microlens arrays is simple, reliable, and economic in processing.

In this study, spherical microlens arrays with different fill factors, heights, and bottom shapes were employed to extract light from the substrate waveguide in the OLEDs. The microlenses were fabricated by the combination of photolithography, thermal reflow, polydimethylsiloxane (PDMS) molding, and UV forming techniques. The height of microlenses was adjusted by changing the spin speed during the coating of photoresist layers. The fill factor and bottom shape of microlenses are normally defined by the Cr patterns on the photomask but the fill factor can be varied to some extent by controlling the heating temperature carefully. The results showed that the luminous current efficiency and power efficiency of the OLEDs can be improved up to 64% and 56%, respectively. It was also found both the luminous current efficiency and power efficiency increased with increasing the fill factor and the height of microlenses. Round-based microlenses enhanced more efficiency of the OLEDs than the square-based ones when having the same parameters. In addition, the emitting spectra and CIE coordinates of the OLEDs with/without microlenses were also measured and analyzed.

Formation of Internal Micro-lens-like Structure for Organic Light-emitting Diodes

C. M. Hsu, Y. X. Zeng, B. T. Lin, W. M. Lin, and W. T. Wu
Department of Electro-Optical Engineering, Southern Taiwan University of Science and Technology
1, Nan-Tai St., Yung-Kang District, Tainan City 710, Taiwan

Abstract— Micro-lens-like structures have been fabricated internally in an organic light-emitting diode (OLED) to promote the light extraction efficiency. Formation of the internal micro-lens-like structure was conducted first by chemically etching surfaces of indium tin oxide (ITO) film to yield 200-nm-deep circular recesses. This surface recessed ITO film was employed to serve as an anode for the OLED. A series of organic layers and an aluminum cathode were then coated on the surface recessed ITO anode to complete the OLED with arrays of recessed light-emitting area or the micro-lens-like structure. The surface recesses were patterned to 4 arrays with various recess coverage ratios of 7.9%, 14.1%, 20.9% and 27.7%. Results showed that the current efficiency of OLEDs could be improved by the internally formed micro-lens-like structure. The current efficiency was enhanced by up to 26.5% for the recessed device with a 14.1% coverage ratio (4.82 cd/A) compared with the planar device (3.81 cd/A). The current efficiency enhancement was attributed to the additional light-emitting area generated on the recess wall as well as the light scattering effects on the recessed surfaces. The enhancement in current efficiency however was found independent with the increasing coverage ratio of micro-lens like structure. The device with the highest recess coverage ratio (27.7%) actually performed the lowest current efficiency among all the recessed devices. This suggested that the light extraction could be effectively raised by the micro-lens-like structure but limited by the arrangement of the recesses.In other words, although more light can be generated on the recess wall for devices with high recess coverage ratios, these light might have high possibility to be redirected to directions that total reflection can happen when the recesses are too much close to each other. Overall, this work has demonstrated that light extraction can be enhanced by introducing an internal micro-lens-like structure in an OLED and this leads to an improved current efficiency.

Balanced Charge Transport Organic Semiconductors for Highly Efficient Organic Light-emitting Diode

Li-Yin Chen, Jin-Kai Chang, Yi-Ru Wu, and Li-Zhong Cai
Department of Photonics, Sun Yat-sen University, Kaohsiung 804, Taiwan

Abstract— Organic light-emitting device (OLED) is one of emerging technology with potential impact in lightings, which is mercury-free and energy-saving illumination light source. Efficiency, cost, and reliability are the challenges in commercializing OLEDs. By incorporating OLEDs into substrates with embedded scattering and wavelength converting architecture, the device structure of OLEDs can be sufficiently simplified, which results in a high efficient and low cost design. We report herein novel substrates with embedded fluorescent and scattering structure for OLEDs. Both of the simulation and experiment of the OLED employing the substrates were demonstrated. The surface roughness of the substrates was qualified to fabricate OLEDs, and wavelength down-conversion could be also achieved by the substrates. The substrates are beneficial to OLEDs in lighting applications due to their potential in simplifying device structure especially in the category of white-OLEDs.

ACKNOWLEDGMENT

This research was supported by the National Science Council under the Grants NSC-102-2221-E-110-064 and NSC-102-2923-E-110-001-MY3.

The Impurity Effect on OLED Via Transient Electroluminescence Analysis

Chi-Feng Lin[1], **Chia-Cheng Jian**[1], **Tien-Lung Chiu**[2], **and Jiun-Haw Lee**[3]

[1]Department of Electro-Optical Engineering, United University, Miaoli 36003, Taiwan
[2]Department of Photonics Engineering, Yuan Ze University, Chung-Li, Taiwan
[3]Graduate Institute of Photonics and Optoelectronics, Department of Electrical Engineering
Taiwan University, Taipei 10617, Taiwan

Abstract— Organic light-emitting devices (OLEDs), with the advantages of light weight, low cost, high efficiency, fast response, self-emission, and flexibility, have received a lot of attentions in recent years. There are many issues that influence OLEDs performance, one of the key issues is the purity of the organic materials. The purity of the organic materials not only lowers the device performance, but also influences the stability and device operation life time seriously. Many researches have discussed the relation between materials purity and device performances with various materials purify methods, such as recrystallization, chromatography, and zone refining. However, owing to the costs and the application to mass production, the sublimation method is still the most popular way on material purification.

In this report, we study the impurity effect on carrier mobility and device efficiency with the conventional electron transporting material, Alq_3. The Alq_3 was purified with thermal sublimation method and the purity was analysis through differential scanning calorimetry (DSC). After the purification, the purity of Alq_3 was improved from 98.94% to 99.85% and the device performance was enhanced from 3.33 cd/A to 4.12 ca/A owing to the decrease of the impurities which act as the trap center in the device. Furthermore, the carrier mobility was calculated by transient electroluminescence analysis, the various delay time of the devices shows that the carrier mobility was increase from $3.30 \times 10^{-6}\,\mathrm{cm}^2$/V-s to $1.32 \times 10^{-6}\,\mathrm{cm}^2$/V-s after Alq_3 purification.

Blue Phosphorescent Organic Light-emitting Diode with Carbozole-triazole Host

Po-Sheng Wang[1], **Bo-Yen Lin**[1], **Jiun-Haw Lee**[1], **Yu-Hsuan Hsieh**[2], **Man-Kit Leung**[2], **Tien-Lung Chiu**[3], **and Chi-Feng Lin**[4]

[1]Graduate Institute of Photonics and Optoelectronics and Department of Electrical Engineering Taiwan University, Taipei, Taiwan
[2]Department of Chemistry, Taiwan University, Taipei 10617, Taiwan
[3]Department of Photonics Engineering, Yuan Ze University, Chung-Li, Taiwan
[4]Department of Electro-Optical Engineering, United University, Miaoli 36003, Taiwan

Abstract— In this paper, we demonstrate a blue phosphorescent organic light-emitting diode based on bis[2-(4, 6-difluorophenyl)pyridinato-C^2, N] (picolinato)iridium(III) (FIrpic) as the emitter in a bipolar carbozole-triazole host. With engineering the organic layer thicknesses and dopant concentration, $> 50\,\mathrm{cd/A}$ in current efficiency can be achieved, corresponding to external quantum efficiency of $> 25\%$.

Voltage Reduction of Blue Phosphorescent Organic Light-emitting Diode with Mixed Host

Chuan-En Lin[1], **Bo-Yen Lin**[1], **Jiun-Haw Lee**[1], **Tien-Lung Chiu**[2], **and Chi-Feng Lin**[3]

[1]Graduate Institute of Photonics and Optoelectronics and Department of Electrical Engineering Taiwan University, Taipei, Taiwan
[2]Department of Photonics Engineering, Yuan Ze University, Chung-Li, Taiwan
[3]Department of Electro-Optical Engineering, United University, Miaoli 36003, Taiwan

Abstract— In this paper, we demonstrate a blue phosphorescent organic light-emitting diode based on bis[2-(4,6-difluorophenyl)pyridinato-C^2, N] (picolinato)iridium(III) (FIrpic) as the emitter in a mixed host consisting of hole-transporting 1, 3-bis(carbazol-9-y1)benzene (mCP) and electron-transporting 1, 3, 5-tris(N-phenylbenzimidazole-2-yl)benzene (TAZ). When varying the mixing ratio of mCP and TAZ, driving voltage decreased and increased because the charge balance condition was achieved.

Session 3P4
SC2: Graphene for Plasmonics and Sensing

Graphene Metamaterials and Plasmonics from Terahertz to Optical Frequencies

Philippe Tassin
Department of Applied Physics, Chalmers University, Sweden

Abstract— There has been quite some interest in graphene metamaterials and plasmonics in the past few years. In this contribution, we will review graphene metamaterials and plasmonics in the terahertz, mid-infrared and optical domains. We will draw conclusions regarding the feasibility and advantages of graphene in each of these frequency domains. In particular, we will highlight the ease of changing the Fermi level in graphene, which may lead to a new generation of tunable metamaterials and plasmonics technology.

REFERENCES

1. Tassin, P., T. Koschny, M. Kafesaki, and C. M. Soukoulis, "A comparison of graphene, superconductors and metals as conductors for metamaterials and plasmonics," *Nature Photonics*, Vol. 6, 259–264, 2012.
2. Zou, Y., P. Tassin, T. Koschny, and C. M. Soukoulis, "Interaction between graphene and metamaterials: Split rings vs. wire pairs," *Opt. Express*, Vol. 20, 12198–12204, 2012.
3. Tassin, P., T. Koschny, and C. M. Soukoulis, "Graphene for terahertz applications," *Science*, Vol. 341, 620–621, 2013.

Design and Analysis of Tunable/Broadband Terahertz Absorbers Based on Graphene Metasurface

Xianjun Huang, Xiao Zhang, Zhirun Hu, Mohammed Aqeeli, and Abdullah Alburaikan
School of Electrical and Electronic Engineering, University of Manchester, Manchester M13 9PL, UK

Abstract— Terahertz technology has attractive application potentials on areas of medical imaging, security and communications, etc.. However, traditional microwave sensors cannot be used to detect and measure THz, which results to increasingly intensive research on THz sensors, including the essential sensing device, THz absorber.

This paper works on the design and analysis of graphene metasurface based absorbers with wide absorption band and tunability. The proposed absorber consists of graphene metasurface and metal-backed dielectric, and the metasurface is the combination of graphene patch array and a continuous graphene layer separated by extremely thin dielectric. Employed with equivalent circuit theory and transmission line theory, the equivalent circuit model is built to analyze the working principles, and the study of absorption structure is converted to simple resonant circuit analysis.

Thanks to the electrical tunability of graphene sheet, more controlling parameters are introduced, which makes the graphene metasurface based absorber flexible in applications. With full wave electromagnetic simulations, this structure is proved to be eligible for broadband and tunable absorbers. When two resonances are introduced, the effective absorption (above 90%) can be as large as 70%, revealing that graphene metasurface based absorber can provide ultra wide broad absorption in low THz spectrum.

Furthermore, tunability of this absorber is also demonstrated to be exceptional compared with previous works. In those reported designs, due to impedance mismatch the absorption peak substantially degraded when the graphene based absorber's resonant frequency was electrically tuned. In contrast, as shown in Fig. 1, the peak absorption frequency of this absorber is tunable within 1.5–2.5 THz, while the value of maximum absorption peak keeps almost constant (nearly 100%), highly desirable in THz sensing applications. Besides, the influences of the key dimensions are discussed to guide the design and the effective absorption bandwidth is also verified to be stable when incident wave angle ranges from 0° to 50°.

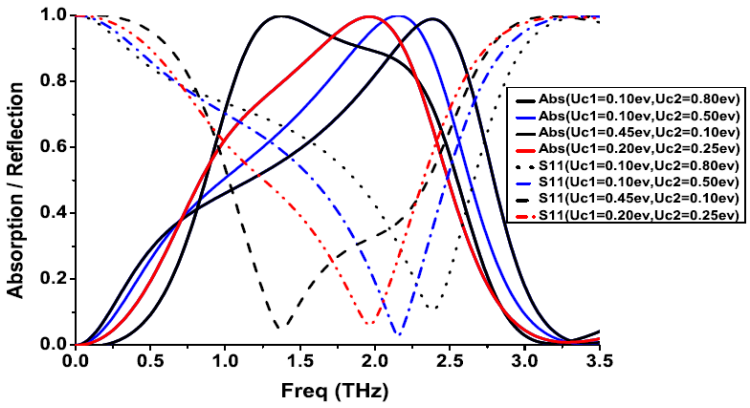

Figure 1: Tunability of the graphene metasurface based absorber.

Strong Light-matter Interaction in Graphene

Sanshui Xiao[1, 2]

[1]Department of Photonics Engineering, Technical University of Denmark
DK-2800 Kongens Lyngby, Denmark
[2]Centre for Nanostructured Graphene (CNG), Technical University of Denmark
DK-2800 Kongens Lyngby, Denmark

Abstract— Graphene has attracted lots of attention due to its remarkable electronic and optical properties, thus providing great promise in photonics and optoelectronics. However, the performance of these devices is generally limited by the weak light-matter interaction in graphene. The combination of graphene with noble-metal nanostructures is currently being explored for strong light-graphene interaction. We introduce a novel hybrid graphene-metal system for studying light-matter interactions with gold-void nanostructures exhibiting resonances in the visible range [1]. The hybrid system is further explored for sensing of Rhodamine 6G molecules with respect to the strong surface-enhanced Raman scattering. The interaction between graphene plasmon (supported by nanodot and antidot arrays) and the substrate phonons [2] is also experimentally demonstrated and structural control is used to map out the hybridization of plasmons and phonons, where the graphene is structured by the nanosphere lithography with structural control down to the sub-100 nanometer regime.

REFERENCES

1. Zhu, X., L. Shi, M. S. Schmidt, A. Boisen, O. Hansen, J. Zi, S. Xiao, and N. A. Mortensen, "Enhanced light-matter interaction in graphene-coved gold nanovoid array," *Nano Lett.*, Vol. 13, No. 10, 4090–4096, 2013.
2. Zhu, X., W. Wang, W. Yan, M. B. Larsen, P. Boeggild, T. G. Pedersen, S. Xiao, J. Zi, and N. A. Mortensen, "Plasmon-phonon coupling in large-area graphene dot and antidot arrays fabricated by nanosphere lithography," *Nano Lett.*, 2014, in press.

Optical Properties of Graphene on Quartz and Polyethylene Substrates in Terahertz Frequency Range

A. K. Denisultanov, **S. E. Azbite**, **N. S. Balbekin**, **S. I. Gusev**, **and M. K. Khodzitsky**
Department of Photonics and Optoinformatics, ITMO University
Kronverkskiy pr. 49, Saint-Petersburg 197101, Russia

Abstract— We report measurements of the optical properties of graphene (refractive index, permittivity, conductivity, penetration depth) in the far-infrared region from 0.1 to 2.0 THz at the temperature of 300 K.

Introduction: Last years graphene increasingly attracts attention of scientists by unusual properties such as high electric and thermal conductivity etc. [1]. Also terahertz (THz) radiation has tremendous potential for applications in imaging, medical diagnosis, health monitoring, environmental control, chemical & biological identification, security infrastructure, military industry. So, using graphene in terahertz optics it would be useful to know dispersion of grapheme optical properties, such as refraction index $n(\omega)$, optical conductivity $\sigma(\omega)$ etc.. The purpose of this paper is to experimentally obtain of optical properties of graphene for THz frequency range.

Results and Conclusion: In our measurements extremely thin graphene monolayers (Graphenea, Inc) were investigated. The quartz (SiO_2) and polyethylene (PET) substrates were chosen, because graphene is successfully transferred on this type substrates and quartz and PET have minimal absorption of terahertz radiation [2]. The data have been obtained with the use of THz time domain reflection spectroscopy, utilizing ultrashort electromagnetic pulses generated from a InAs semiconductor in magnetic system driven by femtosecond laser pulses. The typical waveform of terahertz pulses reflected from air/substrate and substrate/graphene interfaces is shown on Fig. 1. Graphene refraction index $n(\omega)$, optical conductivity $\sigma(\omega)$, dielectric permittivity $\varepsilon(\omega)$, penetration depth $\sigma(\omega)$ and absorption coefficient $\mu_a(\omega)$ were extracted from experimental THz pulse waveforms for the frequency range of 0.1–2 THz. The optical properties of quartz and polyethylene substrates with graphene and substrates without graphene were compared. These data may be used for development of filters based on graphene for THz spectroscopy.

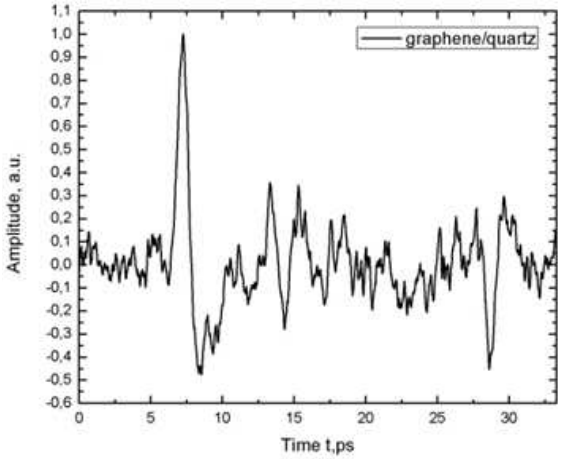

Figure 1: Waveform of THz pulse.

ACKNOWLEDGMENT

This work was financially supported by Government of Russian Federation, Grant 074-U01.

REFERENCES

1. Warner, J. H., *Graphene: Fundamentals and Emergent Applications*, Elsevier, Amsterdam, 2013.
2. Grischkowsky, D., S. Keiding, M. van Exter, and Ch. Fattinger, "Far-infrared time-domain spectroscopy with terahertz beams of dielectrics and semiconductors," *J. Opt. Soc. Am. B*, Vol. 7, No. 10, 2006–2015, 1990.

Recent Developments in Graphene-based Optical Modulators

Ran Hao, J. M. Jin, and E. P. Li
Department of Information Science and Electronics Engineering
Zhejiang University, Hangzhou 310027, China

Abstract— Graphene has shown promising perspectives in optical active components due to the large active-control of its permittivity-function. This paper symmetrically reviews the recent developments of graphene-based optical modulators, including the material property, the different integration schemes, the single-layer graphene-based modulator, the multi-layer and the few-layer graphene-based modulator, the corresponding figure-of-merits, the wavelength/temperature tolerance, and the graphene-based fiber-optic modulator. The different treatments for graphene's isotropic and anisotropic property are also discussed. The results show graphene is an excellent material for enhancing the modulation effect in silicon, and has great potentials for CMOS compatible high efficiency optical modulator, showing significant influence for optical interconnects in future integrated optoelectronic circuits.

Broadband Impedance Matching with Graphene Layers in Terahertz Region

Xinlong Xu
State Key Lab Incubation Base of Photoelectric Technology and Functional Materials
International Cooperation Center for National Photoelectric Technology and Functional Materials, and
Institute of Photonics & Photon-Technology, Northwest University, Xi'an 710069, China

Abstract— There is an urgent demand of terahertz (THz) components for THz wave manipulation. Among them, impedance maching layers are needed to minimize the reflections at the interfaces of the THz components. This is especially useful for the THz time-domain spectroscopy system (THz-TDS), as the reflections limit the spectral resolution. In visible-infrared region, quarter-wavelength dielectric films are the mostly used as antireflection coatings. However, they are not suitable for THz wave due to the broadband characteristics. Graphene as a two-dimensional atomic crystal has excellent mechanical, electrical, optical, magnetic, and thermal properties. In microwave and THz region, metal films and metamaterials are also used as impedance matching layers. However, metal films still need to overcome the complexity of fabrication and high cost, and metamaterials work at narrow bandwidth. Thus new materials with better performances are still in great demand. Here, we present the impedance matching properties of graphene in both theory and experiment in THz region. Graphene samples are synthesized by chemical vapor deposition (CVD), and multi-layer graphene are fabricated by layer-by-layer random stack on both quartz and silicon substrates. We examined the potential of stacked multilayer graphene as broadband terahertz (THz) antireflection coating based on the impedance matching effect. The reflected pulses from the quartz and silicon substrates were observed to change with the layer number and doping concentration of the graphene coating. Remarkable broadband impedance matching was achieved due to optimized THz conductivity. Theoretical analysis based on Drude model and thin film Fresnel coefficients have been used to explain the experimental phenomena, which indicated the shift of Fermi level caused by chemical doping. This work paves the way for graphene-based broadband THz antireflection coating.

Graphene-ferroelectric Nonvolatile Memory and Reconfigurable Logic Metadevices

Bumki Min
Department of Mechanical Engineering, KAIST
291 Daehak-ro, Yuseong-gu, Daejeon 305-751, Republic of Korea

Abstract— Memory metamaterials are artificial media that sustain their transformed electromagnetic properties without persistent external stimuli. Previous memory metamaterials were implemented with phase change materials and graphene. However, they should be operated in a specifically-designed environment for long retention of transformed states. In this work, we demonstrate electrically-driven nonvolatile memory metadevices and extend the concept further to implement reconfigurable logic metadevices, which are all realized by the hybridization of ferroelectric, graphene and meta-atoms. For a memory metadevice having an electrical single-input, amplitude, phase and even the polarization states were clearly distinguishable to multi-states, the values of which are maintained over 10^5 s at room temperature. Furthermore, logic gates and 2-bit digital-to-analog convertor operations were demonstrated for reconfigurable logic metadevices having electrical two-inputs, each of which corresponds to the distinct graphene-ferroelectric layers, respectively. The nonvolatile memory and reconfigurable logic metadevices would provide more functionalities to emerging optoelectronics applications.

Graphene-based THz Broadband Copolanar Waveguide (CPW) Fed Monopole Antenna

Xiao Zhang[1], **Gregory Auton**[2], **Xianjun Huang**[1], **Zhirun Hu**[1], **and Zeyu Long**[1]

[1]School of Electrical and Electronic Engineering, University of Manchester, Manchester M13 9PL, UK
[2]Manchester Centre for Mesoscience and Nanotechnology
University of Manchester, Manchester M13 9PL, UK

Abstract— Graphene is a two-dimensional (2D) planar layer of carbon atoms packed in a honeycomb lattice. It has been drawing a great attention from both research institutes and industry due to its potential applications since it was firstly peeled from graphite in 2004.

In this paper, a broadband graphene terahertz (THz) coplanar waveguide (CPW) fed monopole antenna is proposed and analyzed. Monopole-like plasmonic resonance of the graphene is investigated for efficient THz radiation. Thanks to graphene unique electric band structure, the 2D graphene is modeled by the complex surface conductivity at THz. The proposed antenna has demonstrated very good omnidirectional radiation pattern, return loss and radiation efficiency. It has wide impedance bandwidth from 0.33 THz to 0.44 THz with return loss better than −10 dB

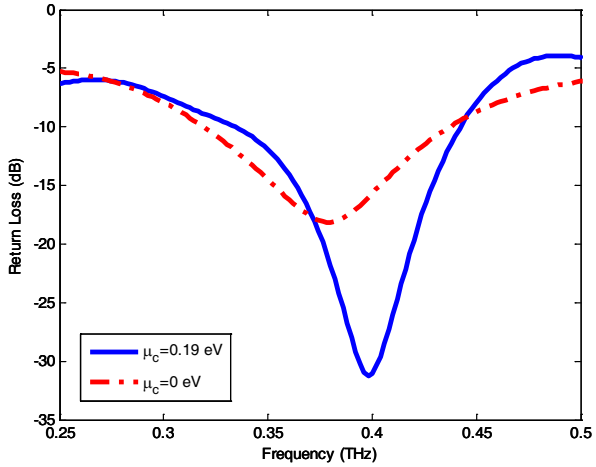

Figure 1: Return loss of the proposed antenna for $\mu_c = 0$ eV and $\mu_c = 0.19$ eV.

Figure 2: Graphene viewed in a microscope (Nikon Eclipse LV100D with a 20x).

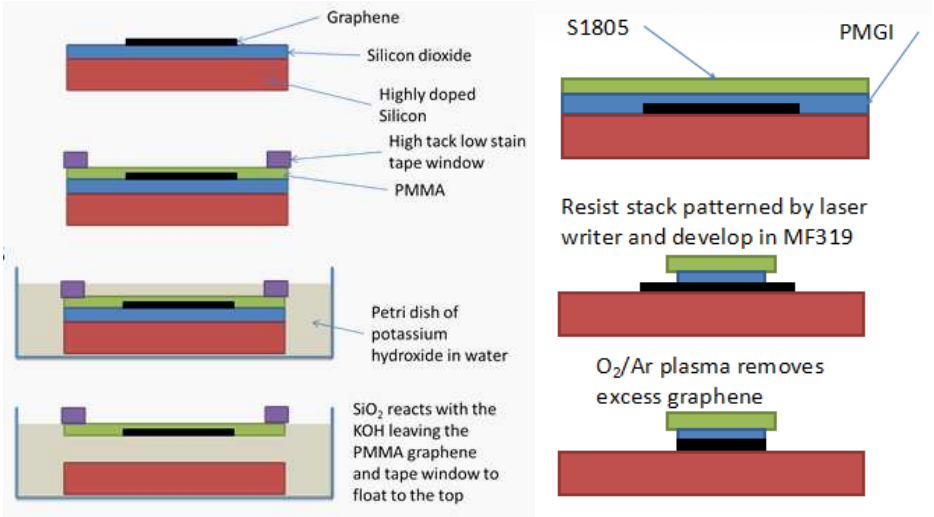

Figure 3: Fabrication illustration of the proposed graphene-based antenna.

and radiation efficiency over 50% around the central frequency of 0.385 THz, as shown in Fig. 1. Parametric study on the antenna performance with the antenna geometrical and material properties have been carried out. The results reveal that the graphene monopole antenna can find its applications for future graphene multi Terabit wireless data transmission and transparent all-graphene THz sensing systems. At last, to get the measurement of the proposed graphene-based monopole antenna, an introduction to the fabrication of graphene antenna on Gallium Arsenide (GaAs) substrate is also included (Fig. 2 and Fig. 3).

Controlling the Propagation of Graphene Plasmons with Nanoantennas

Pablo Alonso-González[1], **Alexey Yu Nikitin**[1,5], **F. Golmar**[1,2], **A. Centeno**[3], **A. Pesquera**[3], **S. Vélez**[1], **J. Chen**[1], **F. Koppens**[4], **A. Zurutuza**[3], **F. Casanova**[1,5], **L. E. Hueso**[1,5], **and R. Hillenbrand**[1,5]

[1]CIC nanoGUNE, Donostia-San Sebastián 20018, Spain
[2]I.N.T.I.-CONICET, Av. Gral. Paz 5445, Ed. 42, B1650JKA, San Martín, Bs As, Argentina
[3]Graphenea SA, Donostia-San Sebastián 20018, Spain
[4]ICFO-Institut de Ciéncies Fotoniques, Mediterranean Technology Park
Casteldefells, Barcelona 08860, Spain
[5]IKERBASQUE, Basque Foundation for Science, Bilbao 48011, Spain

Abstract— Forthcoming information and communication technologies demand the manipulation of not only electrons but also optical fields at the nanoscale. A promising solution for an active control of light in such small regions is the excitation and manipulation of graphene plasmons, which offer ultra-short wavelengths, long lifetimes, strong field confinement, and tuning possibilities by electrical gating. The huge momentum mismatch between graphene plasmons and photons, however, presents a major technological challenge. Here, we will present a versatile platform technology that, based on resonant optical antenna structures (Fig. 1), allows for an efficient coupling of incoming light into propagating graphene plasmons. More importantly, it also allows for controlling the graphene plasmons wavefronts, constituting an essential step for the development of graphene plasmonic circuits.

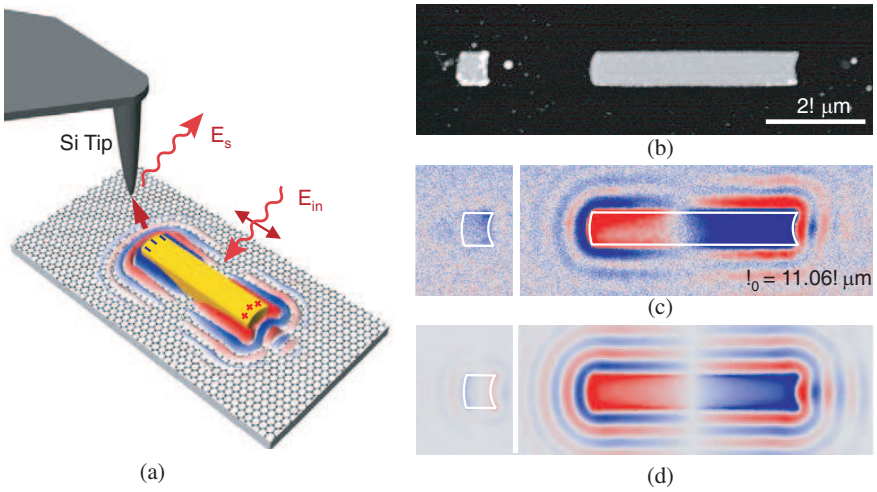

Figure 1: Experimental verification of an antenna-based graphene plasmon device. (a) Illustration of the near-field imaging method. An illuminating plane wave with electric field E_{in} drives an antenna resonance in a metal nanorod. The subsequently generated near fields at the rod extremities launch plasmons in the graphene sheet, which covers the substrate. A dielectric Si tip scans the sample surface and scatters the local near fields at the sample surface. (b) Topography image of an off- and on-resonance dipole antenna (left and right, respectively). (c), (d) Experimental near-field images, showing the real part of the vertical near-field component of the antenna shown in (b).

Novel Tunable Mid-infrared Graphene Plasmonic Waveguide with a Trenched Structure

Jiajiu Zheng, Longhai Yu, and Daoxin Dai
Centre for Optical and Electromagnetic Research
State Key Laboratory for Modern Optical Instrumentation
Zhejiang Provincial Key Laboratory for Sensing Technologies
Zhejiang University, Zijingang Campus, Hangzhou 310058, China

Abstract— Recently, great progress on graphene plasmonics in mid-infrared (MIR) has been made because of some superiorities of graphene to noble metals. One of the most significant features of graphene plasmonics is the tunability by the means of chemical doping or applying a gate voltage. In this paper, we propose a novel nanoscale silicon-based graphene plasmonic waveguide with a pattern-free graphene sheet on the top of a nano-trench. The present graphene plasmonic waveguide is designed with a silicon-on-insulator (SOI) wafer. The top silicon layer is patterned to have a nano-trench and then covered by an Al_2O_3 layer so that the nano-trench is filled by Al_2O_3. The top surface of the Al_2O_3 layer is flattened with a chemical-mechanical-polishing process to achieve a spacer layer with an inverted ridge. Finally a pattern-free graphene sheet is put on the top of the flattened Al_2O_3 spacer layer. Since the Fermi level of graphene is dependent on the thickness of the Al_2O_3 spacer layer, the nano-trench structure introduces stepped Fermi levels for the graphene sheet when applying a gate voltage to the structure of graphene/Al_2O_3/Si. In this way, the graphene sheet is patterned electrostatically to form a graphene plasmonic waveguide enabling nanosclae light confinement. Furthermore, with the present design, single gate voltage is needed only to apply to the structure of graphene/Al_2O_3/Si and a large attenuation ratio can be achieved with a low bias voltage, so that the fabrication and the electrical operation is simple. The mode properties of the present graphene plasmonic waveguide is analyzed with a finite-element method (FEM) mode-solver. It shows that the present graphene plasmonic waveguide enables a significant modulation on the phase shift as well as the attenuation over a broad band by applying a low gate voltage, which is promising for the realization of optical modulators and tunable optical filters in nanoscale.

ACKNOWLEDGMENT

This project was partially supported by a 863 project (No. 2011AA010301), the Nature Science Foundation of China (No. 11374263), Zhejiang provincial grant (Z201121938), the Doctoral Fund of Ministry of Education of China (No. 20120101110094).

Comparisons of Classical, Semiclassical, and Quantum Plasmonics in Graphene Nanodisks

Weihua Wang, Thomas Christensen, Martijn Wubs,
Antti-Pekka Jauho, and N. Asger Mortensen
DTU Fotonik, DTU Nanotech, Center for Nanostructured Graphene
Technical University of Denmark, Denmark

Abstract— We study the transitions from classical, semi-classical, and quantum plasmonic behavior in graphene nanodisks in the quasistatic limit. Specifically, we investigate four hierarchies of approximation: **1**. Local-reponse approximation (LRA), embodying the traditional approach in plasmonic light-matter interaction. **2**. Hydrodynamic response, adapted to the response of graphene, including the first nonlocal correction to its optical response. **3**. Realspace random phase approximation (RPA) formulation with electron states calculated from the Dirac-Weyl equation, with infinite mass and zigzag boundary conditions (BCs). **4**. Real-space RPA with electron states calculated from a nearest-neighbor tight-binding (TB) treatment. In all cases graphene nanodisks are considered. See Figure 1 for a summary of the considered hierarchies. Below we explicate the essence of the four approaches:

1. Local-response Approximation: Taking the localresponse limit of the low-energy dispersion $\epsilon = \pm\hbar v_F k$ response result, the conductivity of graphene is given by summation of intra-(Drude) and inter-band contributions

$$\sigma_D(\omega) = \frac{ie^2\epsilon_F}{\pi\hbar(\omega + i\gamma)}, \qquad \sigma_I(\omega) = \frac{ie^2}{4\pi\hbar}\log\left|\frac{2\epsilon_F - \hbar\omega}{2\epsilon_F + \hbar\omega}\right|. \tag{1}$$

with Fermi level ϵ_F and loss rate γ.

2. Hydrodynamic Reponse in Graphene: A Taylor approximation of the low-energy response result to first non-vanishing component in momentum, k, yields:

$$\sigma(k,\omega) \simeq \sigma_D(\omega)\left(1 + \frac{\beta_D^2}{\omega^2}k^2\right) + \sigma_I(\omega)\left(1 + \frac{\beta_I^2}{\omega^2}k^2\right), \tag{2}$$

where the plasma velocities $\beta_D = \sqrt{3/4}v_F$ and $\beta_I = \sqrt{1/2}v_F$ differ. Neglecting this difference and letting $\beta_I \to \beta_D$, which induces only a small error since the Drude contribution is usually dominant, allows recasting the response as a single hydrodynamic equation for the current $\mathbf{J}$ and electric field $\mathbf{E}$:

$$\mathbf{J}(\mathbf{r},\omega) + \frac{\beta_D^2}{\omega^2}\nabla_\parallel\left[\nabla_\parallel \cdot \mathbf{J}(\mathbf{r},\omega)\right] = \sigma_D(\omega)\mathbf{E}(\mathbf{r},\omega). \tag{3}$$

3. Dirac-Weyl and RPA: The Dirac-Weyl equation for uncoupled Dirac valleys can be cast as a two-spinor equation $\hat{\mathcal{H}}\psi = \epsilon\psi$ with the Hamiltonian $\hat{\mathcal{H}}^\kappa = v_F\sigma\cdot\hat{\mathbf{p}}$ for the $\mathbf{K}$-valley (and $\hat{\mathcal{H}} = v_F\sigma^*\cdot\hat{\mathbf{p}}$ for the $\mathbf{K}'$ valley), and spinor components associated with the A- and B-sublattice. BCs corresponding to zigzag, armchair, and mass confinement can be imposed.

The non-interacting polarizability, χ^0, is computed in a real-space formulation according to:

$$\chi^0(\mathbf{r},\mathbf{r}';\omega) = 2\sum_{\kappa\nu\nu'}\frac{\left[\psi_{\nu'}^{\kappa\dagger}(\mathbf{r})\psi_\nu^\kappa(\mathbf{r})\right]\left[\psi_\nu^{\kappa\dagger}(\mathbf{r}')\,\psi_{\nu'}^{\kappa\dagger}(\mathbf{r}')\right]}{\hbar\omega + i\hbar\eta - (\epsilon_\nu^\kappa - \epsilon_{\nu'}^\kappa)}(f_{\nu'}^\kappa - f_\nu^\kappa) \tag{4}$$

with the summation extending over the state index ν, and also over the valley index κ, with Fermi-Dirac functions f_ν^κ, and with electron relaxation-rate $\eta = \gamma = 2$.

4. Tight-binding and RPA: The TB Hamiltonian, including only nearest-neighbor interaction with energy γ, reads as $\hat{\mathcal{H}} = \gamma\sum_{\langle j,j'\rangle}\hat{a}_j^\dagger b_{j'} + b_{j'}^\dagger\hat{a}_j$, with A- and B-sublattice annihilation (creation) operators $\hat{a}_j^{(\dagger)}$ and $\hat{b}_j^{(\dagger)}$ for $2p$ orbitals at site j and position $\mathbf{r}_j$. Diagonalization of this Hamiltonian yields the electron states. The polarizability is evaluable at the lattice sites, i.e., it takes a discrete representation in real-space $\chi^0(\mathbf{r}_j,\mathbf{r}_{j'};\omega)$. It is determined following the scheme above.

The interaction with external potentials ϕ^{ext}, for both the Dirac-Weyl and TB approaches, is introduced by selfconsistently coupling the total potential ϕ and the induced charge ρ through the equations $\rho(\mathbf{r}) = \int \chi^0(\mathbf{r}, \mathbf{r}')\,\phi(\mathbf{r}')\,d\mathbf{r}'$ and $\phi(\mathbf{r}) = \phi^{\text{ext}}(\mathbf{r}) + \int V(\mathbf{r}, \mathbf{r}')\,\rho(\mathbf{r}')\,d\mathbf{r}'$, with $V(\mathbf{r}, \mathbf{r}')$ denoting the Coulomb interaction, thereby applying the RPA.

In our comparison of the above four approaches for graphene nanodisks we examine and focus on the following aspects: (**a**) The emergence of nonclassical features in the optical response of nanodisks at small radii, being distinct but qualitatively similar in the Dirac-Weyl and TB approaches. These features are due in part to near-zero energy edge states and in part due to energy level quantization. (**b**) Assessing the role of nonlocality in the optical response. We find excellent agreement between the Dirac-Weyl and hydrodynamic approaches at larger radii, both exhibiting quantitatively identical blueshifts compared with the LRA result. These predictions of blueshifts, however, stand in contrast with the predictions of TB which predict minor redshifts of the dipole resonance. (**c**) The sensitivity of TB calculations to atomistic configuration variations, for fixed radii, and sensitivity to polarization-angle.

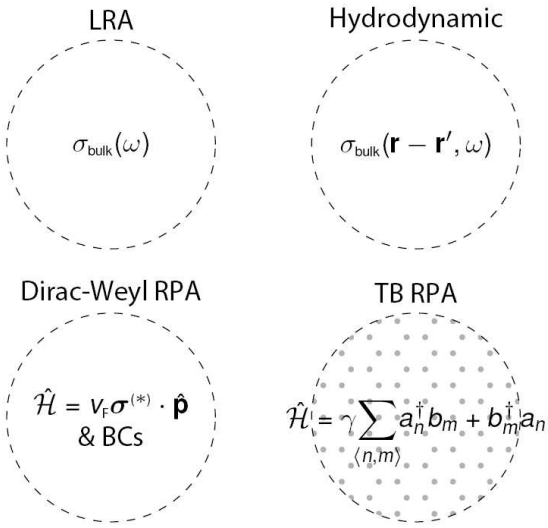

Figure 1: Schematic illustration of the considered levels of approximation in our treatment.

Boosting Tunable Terahertz Absorption in a Monolayer Graphene

Yuancheng Fan[1, 2] and Hongqiang Li[2]

[1]Key Laboratory of Space Applied Physics and Chemistry
Ministry of Education, Department of Applied Physics, School of Science
Northwestern Polytechnical University, Xi'an 710072, China
[2]Key Laboratory of Advanced Micro-structure Materials (MOE)
School of Physics Science and Engineering, Tongji University, Shanghai 200092, China

Abstract— Graphene as a realistic two-dimensional material is emerging in photonics and optoelectronics [1]. As a new optoelectronic material, graphene exhibit a strong binding of surface plasmon polaritons and support its relatively long propagation. Linear dispersion of the 2D Dirac fermions also provides ultrawide band tunability through the electrostatic field, magnetic field or chemical doping. One remarkable feature of the graphene is that as an extremely thin film graphene is almost transparent to optical waves. However, an optical insulator similar to gapped graphene for nanoelectronics is frequently required in a myriad of applications for all-optical systems and components of much miniaturized optical circuits. Artificially constructed micro-structure, i.e., metamaterial, as a platform for enhancing light-matter interactions have been introduced for this purpose. Some pioneering studies [2, 3] reported that optical absorption enhancement can be achieved in periodically doped graphene nanodisks.

We propose to enhance infrared extinction and absorption in a monolayer graphene sheet by patterning split ring resonators (SRRs) [4]. By introducing asymmetric split ring resonators (ASRRs) into the monolayer graphene sheet, we excited both fundamental magnetic mode and electric mode, and the contributions on enhancement of terahertz extinction and absorption of these two modes are comparatively studied. It is found that the electric mode performs better than the magnetic mode and higher order modes in strengthening terahertz absorption (with a 50% maximum absorption)

We will also present some new results on tunable coherent perfect absorption (CPA) within a monolayer graphene at terahertz frequencies [5].

REFERENCES

1. Bonaccorso, F., Z. Sun, T. Hasan, and A. C. Ferrari, *Nat. Photon*, Vol. 4, 611, 2010.
2. Thongrattanasiri, S., F. H. L. Koppens, and F. J. García de Abajo, *Physical Review Letters*, Vol. 108, 047401, 2012.
3. Yan, H., X. Li, B. Chandra, G. Tulevski, Y. Wu, M. Freitag, W. Zhu, P. Avouris, and F. Xia, *Nat. Nano.*, Vol. 7, 330, 2012.
4. Fan, Y., Z. Wei, Z. Zhang, and H. Li, *Opt. Lett.*, Vol. 38, 5410, 2013.
5. Fan, Y., et al., to be submitted.

Plasmon-phonon Hybridization in Graphene Nanostructures on Hexagonal Boron Nitride

Xiaoxia Yang, Mingju Liu, and Qing Dai
National Center for Nanoscience and Technology, Beijing 100190, China

Abstract— Hexagonal boron nitride (h-BN) may be served as a perfect insulating substrate for graphene because both systems share the same lattice structure, with a lattice mismatch of $\sim 1.8\%$. The electronic carriers in graphene on h-BN exhibit very large mobilities because of its atomically smooth surface that is relatively free of dangling bonds and charge traps. In addition, h-BN is an insulator with a $\sim 5.2\,\mathrm{eV}$ gap and the dielectric properties of h-BN is comparable with those of silica. These properties also made h-BN an excellent substrate for graphene plasmonic components. Moreover, the study of surface phonon polaritons in h-BN indicates that h-BN can serve as layered van der Waals crystals such as graphene not only as electrically insulating spacers but also as waveguides for weakly damped polaritons capable of traveling over considerable distances. Here we report the plasmonic properties of graphene nanostructures on h-BN substrate by using a Fourier transform infrared microscopy. The graphene plasmon interacts strongly with h-BN optical phonon in mid-infrared, and the plasmon resonance feature in graphene on silica was totally changed after the intercalation of a single layer of h-BN under graphene. The plasmon-phonon coupling results in a sharp cut-off in the resonance peaks at the optical phonon frequencies of h-BN and a narrow resonance width which means a low plasmon damping rate. The plasmon resonance frequency of graphene on h-BN was hardly electrical tunable. It was also experimentally demonstrated that the plasmon-phonon coupling in monolayer graphene is strong at all densities by showing the hybridization peaks over a large range from ~ 650 to $1400\,\mathrm{cm}^{-1}$.

Session 3P5a
SC2&3: Functional Chiral Metamaterials

Eight-fold Intergrowth of Gyroid Nets: A Chiral Dielectric Material with Optical Activity Comparable to That of Meta-materials

G. E. Schröder-Turk[1], **M. Saba**[1], **M. D. Turner**[2], **K. Meck**[1], **and M. Gu**[2]

[1]Theoretische Physik, Friedrich-Alexander-Universität Erlangen-Nürnberg, Erlangen 91058, Germany
[2]CUDOS & Centre for Micro-Photonics, Swinburne University of Technology, Victoria 3122, Australia

Abstract— The Single Gyroid or srs nanostructure, which occurs as a photonic crystal in butterfly wingscales [1], has attracted interest as a circular-polarisation sensitive photonic material [2–5]. We here develop a group theoretical and scattering matrix method, applicable to any photonic crystal with symmetry $I432$, to demonstrate the remarkable chiral-optical properties of a generalised structure called 8-srs, obtained by intergrowth of eight equal-handed srs nets [6]. We use group or representation theory and scattering matrix calculations to derive analytical results for the band structure topology and the scattering parameters, applicable to any chiral photonic crystal with body-centered-cubic symmetry $I432$ for circularly polarized incident light. We demonstrate in particular that all bands along the cubic [100] direction can be identified with the irreducible representations $E_{\pm}$, A, and B of the $C4$ point group. E_+ and E modes represent the only transmission channels for plane waves with wave vector along the $\triangle$ line, and E and E_+ are identified as noninteracting transmission channels for right- and left-circularly polarized light, respectively. Scattering matrix calculations provide explicit relationships for the transmission and re ectance amplitudes through a finite slab which guarantee equal transmission rates for both polarizations and vanishing ellipticity below a critical frequency, yet allowing for finite rotation of the polarization plane. All results are verified numerically for the so-called 8-srs geometry, consisting of eight interwoven equal-handed dielectric gyroid networks embedded in air. The combination of vanishing losses, vanishing ellipticity, near-perfect transmission, and optical activity comparable to that of metallic metamaterials makes this geometry an attractive design for nanofabricated photonic materials.

REFERENCES

1. Schröder-Turk, G. E., et al., "The chiral structure of porous chitin within the wing-scales of Callophrys rubi," *J. Struct. Biol.*, Vol. 174, 290–295, 2011.
2. Saba, M., et al., "Circular dichroism in biological photonic crystals and cubic chiral nets," *Physical Review Letters*, Vol. 106, 103902, 2011.
3. Turner, M. D., et al., "Fabrication and characterization of three-dimensional biomimetic chiral composites," *Optics Express*, Vol. 19, 10001, 2011.
4. Turner, M. D., et al., "Miniature chiral beamsplitter based on gyroid photonic crystals," *Nature Photonics*, Vol. 7, 801–805, 2013.
5. Cumming, B., et al., "Adaptive optics enhanced direct laser writing of high refractive index gyroid photonic crystals in chalcogenide glass," *Optics Express*, Vol. 2014, 689–698, 2014.
6. Saba, M., et al., "Group theory of circular-polarization effects in chiral photonic crystals with four-fold rotation axes applied to the eight-fold intergrowth of gyroid nets," *Physical Review B*, Vol. 88, 245116, 2013.

Pushing and Pulling Chiral Particles with Light

K. Ding[1], **S. B. Wang**[1], **J. Ng**[2], **L. Zhou**[3], **and C. T. Chan**[1]

[1]Department of Physics and Institute for Advanced Study
The Hong Kong University of Science and Technology, Clear Water Bay, Hong Kong, China
[2]Department of Physics, Institute of Computational and Theoretical Studies
Hong Kong Baptist University, Kowloon Tong, Kowloon, Hong Kong, China
[3]Department of Physics, Fudan University, Shanghai, China

Abstract— Light can exert radiation pressure on any object it encounters and that resulting optical force can be used to manipulate particles. It is commonly assumed that light should pusha particle forward. However, our results indicate that under certain conditions light can push particle in the "wrong" way. We will show that the optical force acting on a chiral particle is qualitatively different from an achiral particle due to chirality dependent terms which couple mechanical linear momentum and optical spin angular momentum. We show that such chirality induced coupling can make light to pull the particle towards the light source instead of pushing the particle [1, 2]. We also show that an anomalous lateral force can be induced in a direction perpendicular to that of the incident phonon momentum if a chiral particle is placed above a substrate that does not break any left-right symmetry [3]. Analytical theory shows that the lateral force emerges from the coupling between the handedness of the chiral particle and the light reflected from the substrate surface. Such coupling induces a sideway force that pushes chiral particles with opposite handedness in opposite directions.

REFERENCES

1. Chen, J., J. Ng, Z. F. Lin, and C. T. Chan, "Optical pulling force," *Nat. Photon.*, Vol. 5, 531, 2011.
2. Ding, K., J. Ng, L. Zhou, and C. T. Chan, "Realizing optical pulling force using chirality," *Physics Optics*, arXiv:1307.3074, 2013.
3. Wang, S. B. and C. T. Chan, "Lateral optical force on chiral particles near a surface," *Nat. Commun.*, accepted, 2014.

Chiral-light Generation with Helical and Multipolar Metamaterials

Manuel Decker, Isabelle Staude, Sergey S. Kruk, Dragomir N. Neshev, and Yuri S. Kivshar
Nonlinear Physics Centre, Research School of Physics & Engineering
Australian National University, Australia

Abstract— Plasmonic nanoparticles have proven to provide a very effective way to control and enhance the photoluminescence properties of localized quantum emitters due to their ability to strongly confine light to ultra-small volumes. Particularly, more complex-shaped nanoparticles that can be incorporated as meta-atoms in metamaterials can be used to specifically tailor the spontaneous emission of semiconductor quantum dots (QDs) beyond the mere enhancement of the photoluminescence signal. However, manipulation of the polarization state of emission to create, e.g., circular-polarization light sources still is a challenging task. Here, we show two routes towards the generation of chiral light.

The first way of achieving this goal are chiral metamaterials that offer remarkable opportunities to manipulate the polarization properties of circularly polarized light, leading to pronounced optical activity and circular dichroism [1–4]. However, the fabrication of 3D-chiral metamaterials optimized for operation in the near-infrared/telecom spectral range, has proven technologically demanding and to date their realization seems to be out of reach.Hence, we employ our novel hybrid fabrication approach [5], combining direct laser writing with electron-beam lithography (EBL) metal nanostructure fabrication to demonstrate 3D-tapered double-helix metamaterials with feature sizes well below 100 nm, enabling operation in the near-infraredspectral range.

We also demonstrate a second route creating chiral emission of light that, remarkably, doesn't require 3D-or even chiral structures at all. By coupling QDs to a single-element multipolar nanoantenna like a split-ring resonator we show that emission of chiral light of opposite handedness is generated by the coupled QD-metamaterial system. This effect is based on the radiation properties of the split-ring-resonator resonance which is characterized by a several resonant multipolar contributions (e.g., electric/magnetic dipole moments, quadrupole moments, etc.) with a fixed phase difference relative to each other. The superposition of the radiation patterns of these multipole components ultimately leads to spin-polarized light emission of opposite handedness for complementary directions of emission that can be easily selected in the back-focal plane, i.e., in the Fourier space.

Our results on spin-controlled light emission with achiral antennas exhibiting two or more multipoles open a new efficient route towards spin-controlled photonics with a range of possible applications in entangled photon sources or display technology.

REFERENCES

1. Plum, E., et al., "Giant optical gyrotropy due to electromagnetic coupling," *Appl. Phys. Lett.*, Vol. 90, 223113, 2002.
2. Decker, M. et al., "Strong optical activity from twisted-cross photonic metamaterials," *Opt. Lett.*, Vol. 34, 2501, 2009.
3. Liu, N., H. Liu, S. Zhu, and H. Giessen, "Stereometamaterials," *Nature Photon.*, Vol. 3, 157, 2009.
4. Gansel J. K., et al., "Gold helix photonic metamaterial as broadband circular polarizer," *Science*, Vol. 325, 1513, 2009.
5. Staude, I., et al., "Hybrid high-resolution three-dimensional nanofabrication for metamaterials and nanoplasmonics," *Adv. Mater.*, Vol. 25, 1259, 2013.

Nonlinear Chiroptical Effects in Plasmonic Meta-surfaces

Ventsislav K. Valev[1], **Jeremy J. Baumberg**[1], **Nuno Braz**[2], **Jan Mertens**[1], **Claire Blejean**[1], **Paul Warburton**[2, 3], **Victor Moshchalkov**[4], **Nicolae-Coriolan Panoiu**[2, 5], **and Thierry Verbiest**[6]

[1]NanoPhotonics Centre, Cavendish Laboratory, University of Cambridge, UK
[2]Department of Electronic and Electrical Engineering, University College London, London, UK
[3]London Centre for Nanotechnology, University College London, London, UK
[4]Nanoscale Superconductivity and Magnetism & Pulsed Fields Group, KU Leuven, Leuven, Belgium
[5]Thomas Young Centre, London Centre for Nanotechnology, University College London, London, UK
[6]Molecular Electronics and Photonics, KU Leuven, Leuven, Belgium

Abstract— We demonstrate a surprising direct relationship between an important linear optical property of light (superchirality) and a nonlinear one (second harmonic generation — SHG) [1]. By varying the dimensions of our meta-molecules, we tune the superchiral light and identify optimal material dimensions for enhanced nonlinear optical response. We then construct such meta-surfaces optimized for enhanced nonlinear interaction and use their strong optical response to reveal a fundamental physical property, i.e., non-reciprocity with respect to space-time reversal, in meta-surfaces.

Recently, chirality in metamaterials has attracted substantial attention [2]. Chiral metamaterials could enable key applications such as negative refractive index and large optical activity, which can lead to nano-levitation and frictionless nano-motors. Additionally, chiral metamaterials can reduce the helical pitch of circularly polarized light thereby achieving superchiral light. Just as plasmonic local field enhancements can be used to increase the interaction of light with molecules (10^{14} in the case of Raman scattering), superchiral light can increase the interaction within chiroptical (chiral optical) effects.

In optical SHG two photons at a fundamental frequency ω are annihilated to generate a single photon at 2ω (half the wavelength). Chiroptical effects in SHG are usually 10^3 larger than their linear optical counterparts. Therefore, nonlinear metamaterials and meta-surfaces are anticipated to achieve record-high chiroptical values compared to those of natural materials and consequently to serve as highly sensitive probes for exploring chiral molecular chemistry. At the moment though, little has been done towards fulfilling these high expectations. Basic understanding of the nonlinear chiroptical properties of meta-surfaces is also lacking; for instance, fundamental physical properties, such as reciprocity, have not yet been investigated. The question of reciprocity in meta-surfaces is crucial as they are the basic building blocks of bulk metamaterials.

Our work brings together ideas from physics, chemistry, material science and engineering. We combine state of the art linear and nonlinear experimental probes with cutting edge theoretical developments to piece together a comprehensive and coherent picture of SHG chiroptical properties. This work also provides a framework for exploiting the benefits of chiral nonlinear meta-surfaces.

REFERENCES

1. Valev, V. K., J. J. Baumberg, B. De Clercq, N. Braz, X. Zheng, E. J. Osley, S. Vandendriessche, M. Hojeij, C. Blejean, J. Mertens, C. G. Biris, V. Volskiy, M. Ameloot, Y. Ekinci, G. A. E. Vandenbosch, P. A. Warburton, V. V. Moshchalkov, N. C. Panoiu, and T. Verbiest, "Nonlinear superchiral meta-surfaces: Tuning chirality and disentangling non-reciprocity at the nanoscale," *Adv. Mater.*, 2014, in Press.
2. Valev, V. K., J. J. Baumberg, C. Sibilia, and T. Verbiest, "Chirality and chiroptical effects in plasmonic nanostructures: Fundamentals, recent progress and outlook," *Adv. Mater.*, Vol. 25, 2508–2628, 2013.

Anisotropy and Non-reciprocity in Boundary Conditions: Generalized PEMC Surface

A. Sihvola, **H. Wallén**, **P. Ylä-Oijala**, **and S. Kiminki**
Department of Radio Science and Engineering
Aalto University School of Electrical Engineering, Espoo, Finland

Abstract— Boundary conditions play an important role in electromagnetics, and not the least in connection with metamaterials and metasurfaces. In this paper, we present a generalization of the PEMC (perfect electromagnetic conductor) boundary. The generalization extends the isotropic and non-reciprocal character of the PEMC boundary into anisotropic and reciprocal dimensions. The effect of the generalized boundary on the polarization of incident waves is analyzed.

Radiation of Chiral Molecules in Chiral Meta-enviroment

Vasily Klimov
Lebedev Physical Institute, Russian Academy of Sciences, Russia

Abstract— Within Classical and Quantum Electrodynamics we have considered spontaneous emission of chiral (optically active) molecule placed in different chiral meta-environments: half-space, chiral layer, sphere and antenna made of 2 chiral nanoparticles. For all these geometries we have found analytical description of the problem for arbitrary parameters of environment, including chiral double negative (DNG, "left-handed") metamaterials. It turns out to be that one can effectively control radiation of "right" and "left" molecules separately by tuning parameters of chiral nano-meta particles indeed. In particular, we have shown that chiral layer with negative refraction can be used to focus right and left polarized waves from point source at different points. Moreover using chirality one can control focus position in wide range what is impossible with nonchiral slab with negative refraction. We have also shown that chiral particles can transform usual plane wave into spiral beam.

An applications of results obtained to separate racemic mixtures of drug enantiomers and to develop nanodetectors sensitive to right or left polarization are discussed.

ACKNOWLEDGMENT

The author thanks the Russian Foundation for Basic Research (grant No. 14-02-00290), the Russian Quantum Center and the Skolkovo Foundation for financial support of this work.

REFERENCES

1. Klimov, V. V., D. V. Guzatov, and M. Ducloy, "Engineering of radiation of optically active molecules with chiral nano-meta-particles," *Europhys. Lett.*, Vol. 97, 47004, 2012.
2. Guzatov, D. V., V. V. Klimov, "The influence of chiral spherical particles on the radiation of optically active molecules," *New J. Phys.*, Vol. 14, 123009, 2012.
3. Guzatov, D. V., V. V. Klimov, and N. S. Poprykailo, "Spontaneous radiation of a chiral molecule located near a half-space of a bi-isotropic material," *J. Exper. Theor. Phys.*, Vol. 116, 531, 2013.
4. Guzatov, D. V. and V. V. Klimov, "Focusing of dipole radiation by chiral slab with negative refraction," *Quant. Electronics*, submitted.
5. Klimov, V. and D. Guzatov, "Engineering of radiation of optically active molecules with chiral nano-meta-particles," *Singular and Chiral Nanoplasmonics*, N. Zheludev and S. Boriskina, Eds., Pan Stanford Publishing, in print.

A Modal Approach to Metamaterials and Nanophotonics

D. A. Powell
Nonlinear Physics Centre, The Australian National University, Canberra, ACT, Australia

Abstract— In characterising modern microwave and nanophotonic structures, the concept of a mode is often invoked. For meta-atoms, nano antennas and similar particles, strong resonant features are observed which clearly correspond to the excitation of some mode. In closed electromagnetic systems, where losses can be treated as a perturbation, these modes are easily found by casting Maxwell's equations into an eigenvalue problem, where the modal field corresponds to the eigenvector. Meta-atoms are in a *completely different regime* from such closed cavities, and their strong radiation losses mean that modes should be considered in terms of the scattering problem. For special cases such as spheres, we can rely on the Mie solution, but few structures of practical interest have such closed-form solutions.

It is shown in this work that the modes of arbitrary small three-dimensional scatterers can be determined robustly and independently of any excitation field. This is based on an integral equation model of the meta-atom, which only needs to consider the polarisation within the object, automatically accounting for the far-field radiation conditions. The system is fully described by an impedance matrix $\mathrm{Z}(s)$, which relates the conduction and polarisation currents to an arbitrary incident field. Such approaches are well-established in microwave modelling, and are increasingly finding application in nano-photonic systems [1]. Utilising concepts from the singularity expansion method [2], a search is made for the complex eigenfrequencies s_n where this integral operator becomes singular, i.e., $\det \mathrm{Z}(s_n) = 0$.

The currents j_n satisfying the homogeneous equation are the modes, and an arbitrary incident field can be projected onto them. Each mode obeys a simple scalar impedance equation $z_n(s)$, which fully describes its dynamics over a broad frequency range, and which can be well approximated by a simple analytical function. This allows the impedance matrix of the system to be decomposed as

$$\mathrm{Z}(s) = \sum_n z_n(s)\mathrm{j}_n(s) \otimes \mathrm{j}_n(s)$$

The advantage of this decomposition is that for many systems of interest, only a small number of modes need to be considered, and their frequency dependence can be neglected, greatly reducing the dimensionality of the problem. This gives a simple yet highly accurate model of the excitation and radiation of meta-atoms, including interaction between near or far neighbours, local stored energy, coupling to a local emitter, scattering and interference. This method reported here is implemented in an open source code [3].

REFERENCES

1. Zheng, X., N. Verellen, V. Volskiy, V. K. Valev, J. J. Baumberg, G. A. E. Vandenbosch, and V. V. Moshchalkov, *Opt. Express*, Vol. 21, 31105, 2013.
2. Baum, C. E., *Proc. IEEE*, Vol. 64, 1598–1616, 1976.
3. "OpenModes: An eigenmode solver for open electromagnetic resonantors," http://pythonhosted.org/OpenModes/.

Planar Chiral Metamaterials: From Twisted to Conjugated Designs

Rongkuo Zhao
The Blackett Laboratory, Department of Physics, Imperial College London, London SW7 2AZ, UK

Abstract— Chiral metamaterials, whose unit cell lacks any plane of mirror symmetry in all directions, possess strong ability to rotate the polarization of electromagnetic waves. For a normally incident light, a single layer of planar chiral structure cannot give us nonzero chirality due to the presence of mirror symmetry in the propagation direction (the mirror symmetry in the propagation direction could be slightly broken by the substrate or different trace widths due to fabrication imperfection). To break the symmetry, twisted double-layer designs had been adopted for the strong chirality purpose (e.g., twisted-rosettes, twisted-cross wires, and twisted-SRRs in Fig. 1). However, because the lattice is fixed, the twisted double-layer structure may look different and result in different reflections from front and back sides. For example the twisted-rosettes design, the reflection from each side is different. This will result in troubles if we want to retrieve its optical parameters. To overcome this problem, we proposed the conjugated principle that the back layer is 180 degree rotated from the top layer so that the structure looks the same from both sides (e.g., the conjugated-gammadions in Fig. 1) and meanwhile the mirror symmetry remains broken. Using this conjugated principle, we can easily design other chiral metamaterials shown in Fig. 2. This flexible and general design principle paves a way to design more complex chiral metamaterials with stronger chirality, smaller unit cell size, and tunable ability.

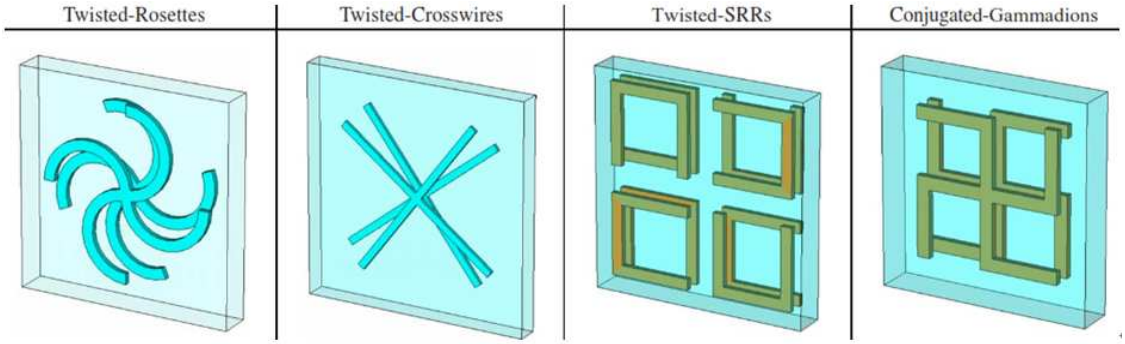

Figure 1: Four kinds of planar chiral metamaterial designs: twisted-rosettes, twisted-crosswires, twisted-SRRs, and conjugated gammadions.

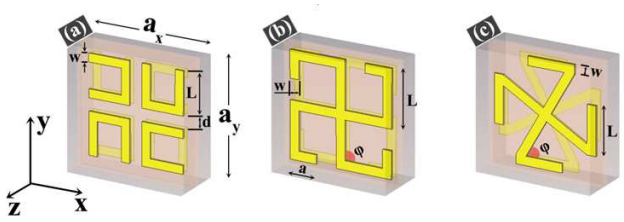

Figure 2: Other chiral metamaterials designs based on the conjugated principle.

Session 3P5b
SC3: Structured Light

Experimental Observation of "Pseudospin" and Edge States in Structured "Photonic Graphene"

Daohong Song[1], **Liqin Tang**[1], **Jingjun Xu**[1], **and Zhigang Chen**[1, 2]

[1]The MOE Key Laboratory of Weak-Light Nonlinear Photonics, TEDA Applied Physics Institute
Nankai University, Tianjin 300457, China
[2]Department of Physics and Astronomy, San Francisco State University
San Francisco, CA 94132, USA

Abstract— Graphene, a single layer of carbon atoms, has attracted tremendous attention in condensed matter physics and other related fields. One of the most important features of graphene is the band gap structure exhibiting Dirac points, where the dispersion relation is linear. The electrons around such Dirac points behave as massless Dirac particles obeying the Dirac-like equation. As such, many exotic quantum physical phenomena including Klein tunneling, zitterbewegung effect and anomalous quantum hall effect have been observed in such materials [1]. Recently, "photonic graphene" — optical equivalent of graphene, structured by periodic waveguide arrays arranged in a honeycomb lattice has been demonstrated as a useful platform to simulate the fundamental graphene physics [2]. Moreover, the reconfigurability and stability of these structured photonic graphene bring about the possibility to demonstrate novel phenomena difficult or impossible to observe in real carbon-based graphene.

In this work, two types of fundamental phenomena — the pseudospin and the edge states in graphene are explored based on a photonic system from structured light. Specifically, we demonstrate experimentally both phenomena in the photonic graphene (a honeycomb photonic lattice optically induced in a nonlinear crystal). For the pseudospin experiment, the pseudospin-mediated vortex generation and topological charge flipping in such an induced photonic graphene were observed in both real space and momentum space. Our results show that the concept of pseudospin in graphene is not just a mathematic formality, but also has real angular momentum, and our experimental results are confirmed by directly solving the Dirac-like equations. For the edge-state experiment, honeycomb photonic lattices with different type of edges were successfully created by employing the optical induction method, and the edge states residing on the zigzag edges were directly observed by selectively excitation of the corresponding modes in momentum space [3]. Our work demonstrated the feasibility of using structured light to develop simple optical and photonic systems to study intriguing fundamental physics.

REFERENCES

1. Castro Neto, A. H., F. Guinea, N. M. R. Peres, K. S. Novoselov, and A. K. Geim, "The electronic properties of graphene," *Reviews of Modern Physics*, Vol. 81, 109–162, 2009.
2. Peleg, O., G. Bartal, B. Freedman, O. Manela, M. Segev, and D. N. Christodoulides, "Conical diffraction and gap solitons in honeycomb photonic lattices," *Physical Review Letters*, Vol. 98, 103901, 2007.
3. Plotnik, Y., M. C. Rechtsman, D. Song, M. Heinrich, J. M. Zeuner, S. Nolte, Y. Lumer, N. Malkova, J. Xu, A. Szameit, Z. Chen, and M. Segev, "Observation of unconventional edge states in 'photonic graphene'," *Nature Materials*, Vol. 13, 57–62, 2014.

Structured Light in the Meta-world

Jingbo Sun, **Mikhail I. Shalaev**, **Jinwei Zeng**, **and Natalia M. Litchinitser**
Electrical Engineering Department
University at Buffalo, The State University of New York, Buffalo, NY 14260, USA

Abstract— We discuss fundamental optical phenomena at the interface of singular optics and metamaterials, including theoretical and experimental studies of linear and nonlinear light-matter interactions of vector and singular optical beams in optical metamaterials. Understanding the physics of the interaction of complex beams with nanostructured "engineered" media is likely to bring new dimensions to the science and applications of complex light, including novel regimes of spin-orbit interaction, extraordinary possibilities for dispersion engineering, and novel possibilities for nonlinear singular optics.

We report theoretical and experimental studies of linear and nonlinear interactions of complex light beams with orbital angular momentum with fiber-based magnetic and negative-index metamaterials. We show that unique optical properties of metamaterials open unlimited prospects to "engineer" light itself. For example, we demonstrate a novel way of complex light manipulation in few-mode optical fibers using metamaterials highlighting how unique properties of metamaterials, namely the ability to manipulate both electric and magnetic field components, open new degrees of freedom in engineering complex polarization states of light. We discuss several approaches to ultra-compact structured light generation, including a nanoscale beam converter based on an ultra-compact array of nano-waveguides with a circular graded distribution of channel diameters that coverts a conventional laser beam into a vortex with configurable orbital angular momentum and a novel, miniaturized astigmatic optical element based on a single biaxial hyperbolic metamaterial that enables the conversion of Hermite-Gaussian beams into vortex beams carrying an orbital angular momentum and vice versa. Such beam converters is likely to enable a new generation of on-chip or all-fiber structured light applications. We also present our initial theoretical studies predicting that vortex-based nonlinear optical processes, such as second harmonic generation or parametric amplification that rely on phase matching, will also be strongly modified in negative index materials. Here we predicted that second harmonic generation with structured light carrying orbital angular momentum and propagating in a negative index material results in a possibility of generating a backward propagating beam with simultaneously doubled frequency, orbital angular momentum, and reversed rotation direction of the wavefront. Finally, we discuss a macroscopic invisibility cloak, based on structured light, operating at optical wavelengths.

These studies may find applications for multidimensional information encoding, secure communications, and quantum cryptography as both spin and orbital angular momentum could be used to encode information; dispersion engineering for spontaneous parametric down-conversion; and on-chip optoelectronic signal processing.

Separating and Transforming Arbitrary Orthogonal Beams Automatically — An Adaptive Universal Linear Optical Component

David A. B. Miller
Stanford University, USA

Abstract— To make the most use of structured light beams, we need to be able transform them flexibly. This is especially challenging if we want to use multiple orthogonal beams at the same time — for example, as separate communications channels. Though we can generate any one structured beam relatively easily, it has not been clear how we could generate or separate multiple arbitrary overlapping orthogonal beams at the same time and without fundamental splitting or combining loss. The problem becomes one of making an arbitrary mode converter [1]. Though solutions are known for specific and highly symmetric cases, it has not even been clear if it was fundamentally possible to solve this arbitrary "mode-converter" problem. This mode-converter problem is provably equivalent to asking if we can perform an arbitrary linear transformation on a light field, and hence to the problem of making an arbitrary linear optical component [1].

Recently, we were able to prove that, at least insofar as we can approximate light beams by finite numbers [2] of "patches" — essentially stepwise approximations to continuous function — it is possible in principle to design any such mode converter, linear transformer or linear optical component [3, 4]. The proof is constructive, showing at least one way of making the device. Such a device can be implemented by an appropriate array of beamsplitters and phase shifters or, equivalently, of Mach-Zehnder interferometers.

Furthermore, we have been able to show how to make this device design itself, based only on local feedback loops between detectors and the controllable beam splitters and/or phase shifters, and a progressive, non-iterative algorithm [3, 4]. Thus the device can be self-configuring, based on training it with the desired input and output beams [3, 4]. This self-configuration and adaptation also makes it easier to make such a device, avoiding precise calibration of components and allowing self-stabilization. This approach is well suited for implementation in silicon photonics, and could be quite practical for beams of low to moderate complexity. Note that this self-configuration means that this device can be designed without any calculations. Extensions of this idea allow devices that can automatically find the best coupled channels through any linear scatterer [5], and reconfigurable spatial add-drop multiplexers [6].

This approach is therefore both a novel fundamental proof in optics and a potentially practical method for novel and highly functional linear optical components.

REFERENCES

1. Miller, D. A. B., "All linear optical devices are mode converters," *Opt. Express*, Vol. 20, 23985–23993, 2012.
2. Miller, D. A. B., "How complicated must an optical component be?," *J. Opt. Soc. Am. A*, Vol. 30, 238–251, 2013.
3. Miller, D. A. B., "Self-aligning universal beam coupler," *Opt. Express*, Vol. 21, 6360–6370, 2013.
4. Miller, D. A. B., "Self-configuring universal linear optical component," *Photon. Res.*, Vol. 1, 1–15, 2013.
5. Miller, D. A. B., "Establishing optimal wave communication channels automatically," *J. Lightwave Technol.*, Vol. 31, 3987–3994, 2013.
6. Miller, D. A. B., "Reconfigurable add-drop multiplexer for spatial modes," *Opt. Express*, Vol. 21, 20220–20229, 2013.

Efficient Detection of Information Encoded in Orbital Angular Momentum of Light

Zhimin Shi[1, 2], **Mohammad Mirhosseini**[2], **Mehul Malik**[2, 3], **and Robert W. Boyd**[2, 4]

[1]Department of Physics, University of South Florida, Tampa, Florida 33620, USA
[2]The Institute of Optics, University of Rochester, Rochester, New York 14627, USA
[3]Institute for Quantum Optics and Quantum Information (IQOQI)
Austrian Academy of Sciences, Boltzmanngasse 3, Vienna A-1090, Austria
[4]Department of Physics, University of Ottawa, Ottawa, Ontario K1N 6N5, Canada

Abstract— Orbital angular momentum (OAM) of light has been found as a useful tool in a variety of classical applications. In addition, it offers an attractive degree of freedom for fundamental studies in quantum mechanics. Circular light beams with different values of the OAM number ℓ form a large orthonormal set of discrete functions that can be used to encode information. It has been suggested that OAM encoding can be used alongside other means to increase the capacity of both classical and quantum communication systems. Additionally, the use of a multi-level encoding basis such as the OAM basis can increase the tolerance of quantum key distribution systems to eavesdropping.

When using OAM of light as an information channel, the ability of unambiguously separating photons carrying different OAM number becomes crucial for the operation of a robust, efficient and secure communication system. However, state-of-the-art methods for separating single photons carrying a large number of different OAM values are limited to a theoretical separation efficiency of approximately 77 percent.

Here we experimentally implement an architecture of a series of unitary optical transformations, including a log-polar coordinate mapping and refractive beam copying, to substantially enhance the separation of the transformed OAM modes. Furthermore, we use a variation of this method for sorting angular(ANG) modes, which form a mutually unbiased basis set with respect to the OAM modes. We achieve a separation efficiency of 92.1 ± 0.7 for a set of 25 OAM modes and 92.7 ± 0.5 for the corresponding 25 ANG modes, which are equivalent to mutual information values of 4.18 and 4.16 bits per detected photons respectively. The high degree of certainty achieved by our method makes our approach particularly attractive for enhancing the information capacity of multi-level quantum cryptography systems.

Propagation and Modulation of 1D Airy Beams

Fei Zhuang[1], **Yuanyuan Pan**[1], **Yuqian Ye**[1], **Xinyue Du**[1], **Xuan Li**[1], **and Zhimin Shi**[2]

[1]Department of Physic, Hangzhou Normal University, Hangzhou 310036, China
[2]Department of Physics, University of South Florida, Tampa, Florida 33620, USA

Abstract— In recent years, the Airy beam has attracted great attention for its abnormal propagation behavior in various media. We here report both numerical and experimental studies on the propagation of one-dimensional Airy beams under three specific scenarios.

We first study the evolution of Airy beams in chiral media. We numerically demonstrate that the circularly polarized Airy beams of opposite handedness can be separated when traveling through the chiral media. The constructive interference of the Airy beams in the near- and far-zone is explicitly analyzed by varying the chirality parameter of the medium. It is interesting to find that the self-acceleration of the beam is sensitive to the interference term.

Secondly, we study the propagation properties of an Airy beam through a four-level EIT atomic vapor. The analytical expression for the Airy beam passing through the ABCD optical system of the EIT vapor is deduced and employed to analyze the propagation characteristics of the beam. It is shown that both the deflection position and the intensity of the Airy beam can be modulated by the Rabi frequency of the control light. Such a tunable optical behavior can find new applications in medicine science.

Lastly, we investigate the healing properties of 1D Airy beams both in simulation and experimental observation. We analyze asymmetry of initial field distribution of 1D Airy beam in detail. We adopt a modified black body radiation function to fit the field distribution of the main lobe of an Airy beam at the initial plane, and consequently derive an analytic expression of the beam propagation through the use of diffraction integral theory. As the initial field distribution is blocked by obstacles with different methods in laboratory, we observe the evolution of the beam, and compare it with the simulations in detail. We find that the deflection and healing properties of 1D Airy beams are mainly determined by the asymmetry of initial optical field distribution.

Structured Light Meets Structured Material: Concepts and Applications

Ebrahim Karimi
Department of Physics, University of Ottawa
150 Louis Pasteur, Ottawa, Ontario K1N 6N5, Canada

Abstract— Optical beams are solution to the Maxwell equations — neglecting a small longitudinal component along propagation direction in the paraxial regime — are fairly transverse. Beside linear momentum (wavevector) and polarisation (spin angular momentum), there are at least two independent indices that define the transverse structure of an optical field, which are associated with the transversality of the optical field [1]. These transverse degrees of freedom are associated with phase structures of the azimuthal and radial modes of a photon in the cylindrical coordinates [1, 2]. A beam with specific transverse modes and polarisation states results in a complex space-variant distribution known as vector beam and in some particular cases reduces into vector-vortex beams [3, 4]. Surprisingly, such a beam in the single photon regime leads to a single photon multi-degrees of freedom entangled state suitable for novel quantum applications such as dense-coding and implementing novel quantum protocols [5, 6]. On the other hand, since the beginning of optics materials — in different geometrical topologies — are widely used to manipulate optical beams. Lenses and prisms are the most simple and common examples in which are used to adjust the beam phase front or wavenumber (in terms of dispersion). However, more recently it has been shown that material possessing specific topology can be used to make different degrees of freedom of light into interact, resulting complex vector beams. In my talk, I will discuss such a concept and application of such a novel designed devices in the classical [7, 8] and quantum information applications [9].

REFERENCES

1. Allen, L., S. M. Barnett, and M. J. Padgett, *Optical Angular Momentum*, Institute of Physics, Bristol, 2003.
2. Karimi, E. and E. Santamato, "Radial coherent and intelligent states of paraxial wave equation," *Optics Letters*, Vol. 37, 2484–2486, 2012.
3. Cardano, F., E. Karimi, et al., "Polarization pattern of vector vortex beams generated by q-plates with different topological charges," *Applied Optics*, Vol. 51, C1–C6, 2012.
4. Cardano, F., E. Karimi, et al., "Generation and dynamics of optical beams with polarization singularities," *Optics Express*, Vol. 21, 8815–8820, 2013.
5. Karimi, E., et al., "Spin-orbit hybrid entanglement of photons and quantum contextuality," *Physical Review A*, Vol. 82, 022115, 2010.
6. Karimi, E., et al., "Hardys paradox tested in the spin-orbit Hilbert space of single photons," *Physical Review A*, Vol. 89, 032122, 2014.
7. Karimi, E., et al., "Efficient generation and sorting of orbital angular momentum eigenmodes of light by thermally tuned q-plates," *Applied Physics Letters*, Vol. 94, 231124, 2009.
8. Karimi, E., et al., "Generating optical orbital angular momentum at visible wavelengths using a plasmonic metasurface," *Light: Science & Applications*, Vol. 3, e167, 2014.
9. Karimi, E., et al., "Exploring the quantum nature of the radial degree of freedom of a photon via Hong-Ou-Mandel interference," *Physical Review A*, Vol. 89, 013829, 2014.

Vectorial Modes in Continuous Variable Quantum Optics

Ch. Marquardt[1, 2, 3], **I. Rigas**[1, 2], **C. Gabriel**[1, 2], **S. Berg-Johansen**[1, 2], **A. Aiello**[1, 2], **P. van Loock**[4], **U. L. Andersen**[1, 2, 3], **and G. Leuchs**[1, 2, 5]

[1]Max Planck Institute for the Science of Light
Guenther-Scharowsky-Str. 1/Bldg. 24, Erlangen 91058, Germany
[2]Institute for Optics, Information and Photonics, University Erlangen-Nuremberg
Staudtstr. 7/B2, Erlangen 91058, Germany
[3]Department of Physics, Technical University of Denmark, Kongens Lyngby 2800, Denmark
[4]Institute of Physics, University of Mainz, Staudingerweg 7, Mainz 55128, Germany
[5]Department of Physics, University of Ottawa, Ottawa, Canada

Abstract— In this talk we will review the application of vectorial modes in quantum optics, particularly in the continuous variable regime. An interesting property of radial and azimuthally polarized modes is the fact, that one cannot factorize the spatial and polarization degrees of freedom. This structural inseparability or "classical entanglement" can lead to quantum correlations between these different degrees of freedom. We will report on the generation of squeezed vectorial modes and their characterization and possible applications in quantum information processing.

Vectorial modes of the light field are interesting both in foundational studies and possible technical applications. A remarkable property of some vectorial modes is the fact, that the polarization and spatial degree of freedom cannot be factorized. This can be illustrated with a radially polarized beam of light which can be written as

$$\mathbf{u}_R(x, y, z) = \frac{1}{\sqrt{2}} \left(\hat{x}\psi_{01} + \hat{y}\psi_{10} \right), \tag{1}$$

where the functions ψ_{nm}, n, $m \in \{0, 1\}$ are the first-order Hermite-Gauss paraxial solutions of the scalar wave equation, and $\hat{x}$ and $\hat{y}$ are unit vectors denoting linear polarization along the x and y axes respectively [1–3]. These modes possess remarkable similarities to entangled states in quantum mechanics [1, 2]. We will discuss the consequences of these properties in continuous variable quantum states. We showed that a squeezed radially polarized light beam can be used to generate two modes that are both squeezed and entangled in two different degrees of freedom [3]. Furthermore these vectorial modes can be transformed to continuous variable cluster states and thereby can act as a resource for measurement based quantum computing [4].

ACKNOWLEDGMENT

We would like to acknowledge financial support from the European Union Integrating Project Q-ESSENCE and the BMBF grant QuOReP.

REFERENCES

1. Spreeuw, R. J. C., "A classical analogy of entanglement," *Foundations of Physics*, Vol. 28, No. 3, 361, 1998.
2. Holleczek, A., A. Aiello, C. Gabriel, C. Marquardt, and G. Leuchs, "Classical and quantum properties of cylindrically polarized states of light," *Opt. Express*, Vol. 19, 9714, 2011.
3. Gabriel, C., A. Aiello, W. Zhong, T. G. Euser, N. Y. Joly, P. Banzer, M. Foertsch, D. Elser, U. L. Andersen, C. Marquardt, P. St. J. Russell, and G. Leuchs, "Entangling different degrees of freedom by quadrature squeezing cylindrically polarized modes," *Phys. Rev. Lett.*, Vol. 106, 060502, 2011.
4. Rigas, I., C. Gabriel, S. Berg-Johansen, A. Aiello, P. van Loock, U. L. Andersen, Ch. Marquardt, and G. Leuchs, "Compact generation of easy-to-access continuous-variable cluster states," arXiv:1210.5188 [quant-ph], 2012.

Measuring a 27-dimensional Orbital Angular Momentum State with Quantum Weak Values

Mehul Malik[1, 2], **Mohammad Mirhosseini**[1], **Martin P. J. Lavery**[3], **Jonathan Leach**[4, 5], **Miles J. Padgett**[3], **and Robert W. Boyd**[1, 5]

[1]The Institute of Optics, University of Rochester, Rochester, New York 14627, USA
[2]Institute for Quantum Optics and Quantum Information (IQOQI), Austrian Academy of Sciences Boltzmanngasse 3, A-1090, Austria
[3]School of Physics and Astronomy, University of Glasgow, Glasgow, UK
[4]School of Engineering and Physical Sciences, Heriot-Watt University, Edinburgh, UK
[5]Department of Physics, University of Ottawa, Ottawa, ON K1N 6N5, Canada

Abstract— First introduced in 1988, quantum weak values [1, 2] have long dwelled in the realm of abstract theoretical physics. Over the last decade, however, there has been an explosion of laboratory experiments that use weak values for a variety of applications, such as the amplification of a small interaction parameter. More recently, weak values have been used to "directly" measure the quantum state itself [3, 4]. The direct measurement method relies on the ability to expand a quantum state in terms of measurable "weak values." A weak value is defined as the average result of a weak measurement of a quantum state, followed by a strong measurement, or post-selection of another observable of the state.

Here, I will describe quantum weak values in terms of real, measurable quantities in the lab. Then, through the use of an experimental example, I will go on to explain how they are measured. We have used this method to measure a quantum state in the discrete, infinite-dimensional space of orbital angular momentum (OAM) [5]. In our direct measurement technique, the OAM weak value $\langle \pi_\ell \rangle_w$ is equal to the average result obtained by making a weak measurement of a projector in the OAM basis ($\hat{\pi}_\ell = |\ell\rangle\langle\ell|$) followed by a strong measurement in the conjugate basis of angular position (θ). By measuring the OAM weak value for each ℓ, we can directly obtain the probability amplitudes that describe a 27-dimensional OAM state vector. Using this technique, we have also measured the effects of rotation on our 27-dimensional state vector in the OAM basis. The rotation manifests as an OAM mode-dependent phase and allows us to observe the action of the angular momentum operator as a generator of rotations.

Direct measurement may offer distinct advantages over conventional methods of quantum state characterization such as tomography. This method does not require a global reconstruction, a step that involves prohibitively long processing times for high-dimensional quantum states such as those of OAM. Consequently, the quantum state is more accessible in that it can be measured locally as a function of OAM quantum number ℓ. Such advantages may allow us to use direct measurement for characterizing very large quantum states of OAM much more efficiently, with significant potential applications in high-dimensional quantum and classical communication systems.

REFERENCES

1. Aharonov, Y., D. Z. Albert, and L. Vaidman, "How the result of a measurement of a component of the spin of a spin-1/2 particle can turn out to be 100," *Phys. Rev. Lett.*, Vol. 60, 1351–1354, 1988.
2. Dressel, J., M. Malik, F. M. Miatto, A. N. Jordan, and R. W. Boyd, "Colloquium: Understanding quantum weak values: Basics and applications," *Rev. Mod. Phys.*, Vol. 86, 307–316, 2014.
3. Lundeen, J. S. and C. Bamber, "Procedure for direct measurement of general quantum states using weak measurement," *Phys. Rev. Lett.*, Vol. 108, 070, 402, 2012.
4. Salvail, J. Z., M. Agnew, A. S. Johnson, E. Bolduc, J. Leach, and R. W. Boyd, "Full characterization of polarization states of light via direct measurement," *Nat. Phot.*, Vol. 7, 316–321, 2013.
5. Malik, M., M. Mirhosseini, M. P. J. Lavery, J. Leach, M. J. Padgett, and R. W. Boyd, "Direct measurement of a 27-dimensional orbital-angular-momentum state vector," *Nature Communications*, Vol. 5, 3115, 2014.

Session 3P6a
FocusSession.SC2: Novel Techniques for Subwavelength-focusing and Super Resolution Imaging 1

Negative Refraction of Sub-wavelength Imaging

John B. Pendry
The Blackett Laboratory, Department of Physics, Imperial College London, London SW7 2AZ, UK

Abstract— Some time ago it has been shown how a negatively refracting medium can produce a sub wavelength image. However these results are confined to the near field and therefore not of immediate use in an everyday microscope where the observer sits many wavelengths away from the object. Here I discuss a scheme in which a sub wavelength lens is employed to give "standoff" between devices used to form sub wavelength structured illumination and the specimen itself, giving the possibility of sub-wavelength resolution observed in the far field.

Electron Induced Near Field Optical Microscopy for Plasmonic Nanostructures

Nicholas X. Fang
Department of Mechanical Engineering, Massachusetts Institute of Technology, USA

Abstract— Recently, low-energy excitation by swift electrons has been applied to explore the optical response of nanostructured materials with unmatched spatial resolution. For example, the measurement of photon emission rate using cathodo-luminescence techniques can provide a direct quantification of local radiative energy transfer from electron to photons at spot size close to 10 nanometers, which compliment other experimental techniques such as photoluminescence. Such tightly localized excitation source and a high-resolution mapping technique is particularly suited to study the spontaneous emission rate of a plasmonic nanostructure with sub-wavelength mode volume

In this talk, we show that dark plasmons in metal nanoantenna and nanocavities can strongly enhance the interaction between moving electron and photon even though dark plasmon itself interacts weakly with photon. Such a counterintuitive experimental result is well-explained by our model based on eigen-response theory as well as numerical simulations. Our finding may offer new opportunity to improve single-photon emission and detection in nanostructures. I will also discuss our recent effort on the development quantum jellium model applied to these metallic nanostructures.

Beating the Diffraction Limit with Resonant Metalenses: Microwaves, Acoustics and Optics Demonstrations

F. Lemoult, M. Fink, and G. Lerosey
Institut Langevin, ESPCI ParisTech & CNRS, Paris, France

Abstract— In order to image objects below the diffraction limit, we propose the concept of resonant metalens which uses a medium made of resonant scatterers (which one can call a metamaterial). By illuminating such a medium with polychromatic light, which gives time (frequency) dependency of waves, one can control wavefields on a subwavelength scale inside the medium. We first show experimental proofs of concept in the low frequency regime of subwavelength focusing and imaging below the diffraction limit from the farfield. Then, we numerically demonstrate that such a device is transposable to the visible frequency range with a realistic medium made of silver nanorods.

To image object with a resolution better than the diffraction limit, one needs to collect information on a scale thinner than this limit which is typically equal to the wavelength. Unfortunately, this information is carried by wavenumbers that correspond to evanescent waves: they do not propagate towards the farfield region but vanish exponentially away from the object. Therefore, one solution that has been proposed to image below the diffraction limit is to probe the field near the object, and it has led to the development of near field scanning optical microscopes. The main drawback of these devices is that one needs to scan the field point by point, whcich avoids their use for real time imaging. In the last decades, there have been many proposals to overcome this limitation such as superlenses, hyperlenses, high numerical aperture lenses, or structured illumination methods. During this presentation, we introduce the concept of resonant metalenses. Based on metamaterials and the use of polychromatic light we will show a way to do super-resolution imaging from the farfield.

We first show two experimental proofs of concept of such a resonant metalens at low frequencies: an example in the microwaves range which uses a wire medium [1], and an example with airborne acoustic waves wich is based on an array of Helmholtz resonators [2]. We then show that this approach is transposable to the visible frequency range [3]. We numerically prove that a resonant metalens made out of plasmonic nanoparticles can potentially focus optical waves onto 30 nm wide foci, that is $\lambda/23$ at the central wavelength of the emitted pulse. We use this lens to demonstrate a real time far field imaging scheme based on light pulse echo interferometry, which can image a low contrast index object with a resolution of 100 nm. This technique is at the frontier of what is achievable with nowadays experimental techniques but given the incredible recent breakthroughs in the spatio-temporal control of light, we believe that it is experimentally realizable.

REFERENCES

1. Lemoult, F., G. Lerosey, J. de Rosny, and M. Fink, "Resonant metalenses for breaking the diffraction barrier," *Phys. Rev. Lett.*, Vol. 104, 203901, 2010.
2. Lemoult, F., M. Fink, and G. Lerosey, "Acoustic resonators for far-field control of sound on a subwavelength scale," *Phys. Rev. Lett.*, Vol. 107, 064301, 2011.
3. Lemoult, F., M. Fink, and G. Lerosey, "A polychromatic approach to far-field superlensing at visible wavelengths," *Nature Communications*, Vol. 3, 889, 2012.

Super Focusing with Electromagnetic Cavities and Subwavelength Gratings

M. Dupré, M. Fink, and G. Lerosey
Institut Langevin, ESPCI ParisTech & CNRS, France

Abstract— Imaging and focusing instruments are known to have a resolution which is limited by the diffraction. Beating this theoretical limit requires to use not only propagative waves, but also evanescent waves. There has been propositions do design lenses that handle evanescent waves to beat the diffraction limit. They mostly rely on a resonant amplification of the evanescent waves supported by a metamaterial such as the superlens [1] or the resonant metalens [2].

Here, we show in the microwave domain that a system composed of a cavity opened with a fractal grating of subwavelength dimensions can effectively focus waves well below the diffraction limit. First and due to their multidimensional scales, space filling curves support modes for wavelengths which are larger than their footprint [3]. Secondly, the long lifetime of the photons in the cavity gives rise to a large number of **k** vectors and that can couple to the modes of the fractal, hence leading to a huge number of degrees of freedom. Figs. 1(a) and (b) show the near field of the grating for a mode of the cavity, and exhibit a complex field at a subwavelength resolution. Thirdly, such degrees of freedom can be coherently controlled with time reversal. Indeed cavities are particularly well suited for that purpose, as they offer an excellent time reversal mirror even with a single antenna. Experimentally, we use a cavity of about 1 m^3 with a single antenna inside. The spectral response of the cavity is measured in the near field of the grating in a bandwidth around 3 GHz for a corresponding wavelength of 10 cm. Finally time reversal is realized to achieve subwavelength focusing at $\lambda/10$ as shown in Fig. 1(c). We investigate and compare different types of fractals, and the influence of the fractal order.

In addition to propose a way to achieve super focusing, this work brings new insights on fractal gratings and fractal metamaterial properties.

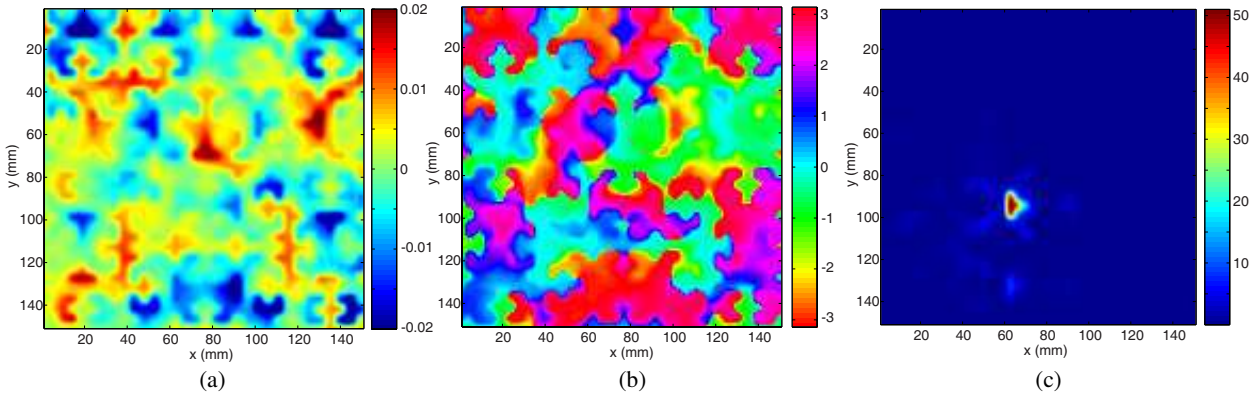

Figure 1: (a) and (b) S_{12} measurements at 2.014 GHz between an antenna inside the cavity and a small probe place in the near field of the grating. The grating is an order 5 Hilbert fractal of 150 × 150 mm. (a) Real part and (b) angle. (c) Time reversal focusing with such a grating (arbitrary unit) with the cavity modes between 2 and 3 GHz. Spot size is about 10 mm ($\lambda/10$).

REFERENCES

1. Pendry, J. B.,"Negative refraction makes a perfect lens," *Phys. Rev. Lett.*, Vol. 85, No. 18, 3966, 2000.
2. Lemoult, F., G. Lerosey, J. de Rosny, and M. Fink, "Resonant metalenses for breaking the diffraction barrier," *Phys. Rev. Lett.*, Vol. 104, No. 20, 203901, 2010.
3. Mc Vay, J., N. Engheta, and A. Hoofar, "High impedance metamaterial surfaces using hilbert-curve inclusions," *IEEE Microw. Wireless Compon. Lett.*, Vol. 14, No. 3, 1–4, 2004.

Subwavelength Light Focusing and Imaging via Wavefront Shaping in Complex Media

Yong Keun Park
Department of Physics, Korea Advanced Technology of Science and Technology (KAIST)
Republic of Korea

Abstract— We present a novel method exploiting multiple scattering to achieve sub-diffraction limited focusing and imaging using visible light. The sub-wavelength information at evanescent near-field are controlled by or transferred into propagating far-field components by elastic scattering from disordered nanoparticles.

We demonstrate that multiple scattering can be controlled via wavefront shaping in order to obtain a sub-diffraction limited focus at an arbitrary position [1] and the full-field dynamic sub-wavelength imaging [2]. Due to the random structure of the highly scattering media there are no restrictions on the physical position of the focus giving the system a high degree of freedom. We first demonstrate that the multiple scattering can be used to steer and focus sub-diffraction limited light spots with arbitrary polarization [3] or wavelength [4] within its inhomogeneous structure.

We also present that the full-field dynamic sub-wavelength imaging can be obtained by transferring the optical near-field into propagating far-field components by multiple light scattering from disordered nanoparticles, which was previously demonstrated in microwave regime [5]. We achieve sub-wavelength light focusing by far-field wavefront control or imaging from a single-shot measurement of a speckle field. This new concept can be regarded as aperture-less scan-free near-field nanoscopy. Two-dimensional imaging can also be readily obtained by scanning the near-field focus or employing the concept of the transmission matrix [6, 7]. This technique can also be utilized for reflection-type optical tomography of biological tissue based on optical coherence tomography [8] or digital phase conjugation technique for suppressing multiple light scattering [9].

REFERENCES

1. Park, J.-H., et al., "Subwavelength light focusing using random nanoparticles," *Nature Photonics*, Vol. 7, No. 6, 454–458, 2013.
2. Park, C., et al., "Scattering super lens for sub-wavelength imaging," under review.
3. Park, J. H., C. Park, H. Yu, Y. H. Cho, and Y. K. Park, "Dynamic active wave plate using random nanoparticles," *Optics Express*, Vol. 20, No. 15, 17010–17016, 2012.
4. Park, J. H., C. H. Park, H. Yu, Y. H. Cho, and Y. K. Park, "Active spectral filtering through turbid media," *Opt. Lett.*, Vol. 37, No. 15, 3261–3263, 2012.
5. Lerosey, G., J. De Rosny, A. Tourin, and M. Fink, "Focusing beyond the diffraction limit with far-field time reversal," *Science*, Vol. 315, No. 5815, 1120–1122, 2007.
6. Yu, H., et al., "Measuring large optical transmission matrices of disordered media," *Physical Review Letters*, Vol. 111, No. 15, 153902, 2013.
7. Popoff, S. M., et al., "Measuring the transmission matrix in optics: An approach to the study and control of light propagation in disordered media," *Physical Review Letters*, Vol. 104, No. 10, 2010.
8. Jang, J., et al., "Complex wavefront shaping for optimal depth-selective focusing in optical coherence tomography," *Optics Express*, Vol. 21, No. 3, 2890–2902, 2013.
9. Hillman, T. R., et al., "Digital optical phase conjugation for delivering two-dimensional images through turbid media," Scientific Reports, Vol. 3, 2013.

Non-invasive Real-time Imaging through Scattering Layers and around Corners via Speckle Correlations

Ori Katz[1,2], **Pierre Heidmann**[1], **Mathias Fink**[1], **and Sylvain Gigan**[1,2]

[1]Institut Langevin, ESPCI ParisTech and CNRS, UMR7587
INSERM ERL U979, 1 Rue Jussieu, Paris 75005, France
[2]Laboratoire Kastler Brossel, Université Pierre et Marie Curie
Ecole Normale Supérieure, CNRS, 4 Place Jussieu, 75252 Paris Cedex 05, France

Abstract— Imaging with optical resolution through and inside complex samples is a difficult challenge with important applications in many fields. The fundamental problem is that inhomogeneous samples, such as biological tissues, randomly scatter and diffuse light, impeding conventional image formation. Despite many advancements, no current method enables to non-invasively image in real-time using diffused light. Here, we present a technique that allows to non-invasively image hidden objects through visually opaque layers and around corners in real-time, using incoherent light and a standard digital camera. We show that a single image of the scattered incoherent light that diffuses through a scattering medium encodes all of the information that is required to image through it, with diffraction limited resolution. Specifically, derived from concepts used in 'stellar speckle interferometry', and the angular 'memory-effect' for speckle correlations exploited in Bertolotti et al. technique [1], we show that the autocorrelation of the scattered light pattern is essentially identical to the autocorrelation of the object's image itself. We then reconstruct the object's image from its autocorrelation using an iterative Fienup-type algorithm. As proofs of concept, we experimentally demonstrate our single-shot noninvasive imaging technique through a variety of highly scattering samples, from optical diffusers to dynamically varying biological tissues. In addition, we demonstrate imaging 'around corners' by recording the diffuse light back-scattered off white-painted 'walls' [2].

In contrast to all present methods for imaging through turbid media or 'around corners' our non-invasive, single-shot technique does not require coherent laser sources, interferometric detection, raster-scanning, wavefront-shaping, nor time-gated detection, and it can be simply realized using just a camera phone, as we demonstrate experimentally.

REFERENCES

1. Bertolotti, J., et al., "Non-invasive imaging through opaque scattering layers," *Nature*, Vol. 491, 232–234, 2012.
2. Katz, O., et al., "Non-invasive real-time imaging through scattering layers and around corners via speckle correlations," arXiv:1403.3316, 2014.

Sparsity-based Sub-wavelength Imaging and Super-resolution in Time-resolved and Spectroscopic Instruments

P. Sidorenko[1], **Y. Shechtman**[1], **Y. C. Eldar**[2], **O. Cohen**[1], **and M. Segev**[1]

[1]Department of Physics, Solid State Institute, Technion, Haifa 32000, Israel
[2]Department of Electrical Engineering, Technion, Haifa 32000, Israel

Abstract— We demonstrate recovery of sub-wavelength optical images based on prior knowledge that the object is sparse, and analogous concept in the time and spectral domains.

A fundamental restriction of optical imaging is set by the diffraction limit, stating that the maximal recoverable resolution cannot exceed one half of the optical wavelength λ. This is a direct result of the evanescent nature of all plane-waves associated with spatial frequencies exceeding $1/\lambda$ [1]. Consequently, spatial frequencies higher than $1/\lambda$ are lost, even after propagation of just a few wavelengths. Hence, using optics to resolve sub-wavelength features from the far-field is virtually impossible. Reaching beyond the diffraction limit barrier is a subject of intense research, culminating in several sophisticated approaches. However, all of these approaches do not capture images in real time: they either require point-by-point scanning in the optical near-field, or necessitate averaging over multiple experiments of distributing florescent particles on the specimen. Likewise, resolution of temporal/spectral measuring device is limited by its time-frequency-bandwidth, and set a fundamental limit on measurements.

In recent papers [2–4], we have shown that sub-wavelength information can be recovered from the far-field of an optical image, based on prior knowledge that the information is sparse in a known basis, and only that. Knowing that the image is sparse seems perhaps a restricting assumption, but in fact sparse optical images are very common in nature, e.g., living cells, where the fraction of non-zero pixels is $\sim$5%. Moreover, some objects may not be sparse in real space but sparse in another basis.

We first proved the concept of sparsity-based sub-wavelength imaging theoretically and provided a proof of concept for coherent light [2] as well as for spatially-incoherent light [3]. Consequently, we demonstrated the ideas experimentally with true sub-wavelength objects, reconstructing 100nm features borne on 532nm laser light [4], Moreover we combined phase retrieval of optical signals with sub-wavelength resolution and performed a proved the concept experiment with extreme UV radiation [5].

However, the concept of sparsity-based super-resolution is not limited to the spatial domain, but can be extended into the temporal and spectral domains. We demonstrated theoretically and experimentally the recovery of the waveforms of short temporal pulses containing features much faster than the response time of the photodetector [6] and reconstruction of ultrafast laser pulses from truncated spectral information [7]. Likewise, in the spectral domain, we demonstrated the recovery of signal at a resolution greatly exceeding the resolution limit of the spectrum analyzing device (FTIR) in general mathematical basis [8].

We believe that our results open the gate to a new age of microscopy and sensing in the domains of space, time, frequency, as well as others measurable variables where the resolution of many physical systems can be improved considerably beyond the physical limitation of the detection apparatus.

REFERENCES

1. Goodman, J. W., *Introduction to Fourier Optics,* 3rd Edition, Roberts & Company Publishers, 2005.
2. Gazit, S., A. Szameit, Y. C. Eldar, and M. Segev, *Opt. Exp.*, Vol. 17, 23920, 2009.
3. Shechtman, Y., S. Gazit, A. Szameit, Y. Eldar, and M. Segev, *Opt. Lett.*, Vol. 35, 1148, 2010.
4. Szameit, A., et al., "Sparsity-based single-shot subwavelength coherent diffractive imaging," *Nature Mat.*, Vol. 11, 455, 2012.
5. Sidorenko, P., et al., "Sparsity-based super-resolution coherent diffractive imaging of (practically) 1D images using extreme UV radiation," Paper QF1C.7, CLEO, 2013.
6. Sidorenko, P., et al., "Exceeding the inherent resolution limit of photo-detectors in pulse-shape measurements by implementing sparseness-based algorithms," *Frontiers in Optics*, Paper FThE2, 2010

7. Sidorenko, P., et al., "Sparsity-based super-resolution in instruments for diagnostics of short pulses," Paper CW1H.2, CLEO, 2013.
8. Sidorenko, P., et al., "Super-resolution spectroscopy by compact representation," *Frontiers in Optics*, Paper FM3F.5, 2012.

Session 3P6b
FocusSession.SC1&2: Nonreciprocal Electromagnetics and Photonics

Optical Nonreciprocal Devices Based on Magneto-optical Phase Shift in Silicon Photonics

T. Mizumoto and Y. Shoji
Department of Electrical and Electronic Engineering, Tokyo Institute of Technology
2-12-1, S9-9 Ookayama, Meguro-ku, Tokyo 152-8552, Japan

Abstract— We have investigated optical nonreciprocal devices based on a magneto-optical garnet. The devices are fabricated on a silicon waveguide [1, 2] as well as a III-V compound semiconductor [3] waveguide. In order to make full use of a strong magneto-optical effect, we adopt a plasma-assisted surface activated direct bonding technique to integrate a single-crystalline magneto-optical garnet on silicon or any other waveguide platforms. Our approach gives an optical nonreciprocal effect most effectively by avoiding an interlayer between a waveguide core and an over cladding garnet.

Optical isolators and circulators are fabricated in Mach-Zehnder interferometer (MZI) configurations. The devices are composed of $\pm\pi/2$ nonreciprocal phase shifters arranged in a push-pull manner together with a reciprocal phase shifter. The phase shifters bring about constructive and destructive interferences in an MZI depending on the light propagation direction and, hence, a unidirectional transmittance between port pairs. The performance of silicon waveguide isolators and circulators has been successfully demonstrated with an isolation > 30 dB in a 1550 nm wavelength range [1, 2].

The insertion losses of the devices are $11 \sim 13$ dB. The losses are due mainly to the absorption of magneto-optical garnet $(CeY)_3Fe_5O_{12}$ (Ce:YIG) and the scattering at the interfaces between air and garnet cladded waveguides. The remaining issues are a narrow isolation bandwidth and a temperature dependence of isolation. The isolation bandwidth can be broadened by introducing a reciprocal phase shift of $\pi/2$, which is realized by adjusting the optical path difference between two interferometer arms [4]. The temperature dependence is brought about by the temperature dependent refractive indices of constituent materials and the magneto-optical effect of Ce:YIG. We measured the temperature dependences of Ce:YIG and proposed an isolator design for reducing the temperature dependence of isolation.

REFERENCES

1. Shoji, Y., et al., "Magneto-optical nonreciprocal devices in silicon photonics," *Sci. Technol. Advanced Mat.*, Vol. 15, 014602, 2014.
2. Mizumoto, T., et al., "Silicon waveguide optical nonreciprocal devices based on magneto-optical phase shift," *Proc. SPIE*, Vol. 8988, 89880C, 2014.
3. Sobu, Y., et al., "GaInAsP/InP MZI waveguide optical isolator integrated with spot size converter," *Opt. Express*, Vol. 21, 15373–15381, 2013.
4. Shoji, Y., et al., "Silicon Mach-Zehnder interferometer optical isolator having 8 nm bandwidth for over 20 dB isolation," *Jpn. J. Appl. Phys.*, Vol. 53, 022202, 2014.

The Growth and Magneto-optical Properties of Large Size Single-crystal Thick TmBiIG Films from Lead-free Flux by LPE Technology

Bing Mei, Huai-Wu Zhang, Qing-Hui Yang,
Shu-Chen Jin, Xiao-Jie Tian, and Ying-Heng Rao
State Key Laboratory of Electronic Films and Integrated Devices
University of Electronic Science and Technology, Chengdu 610054, China

Abstract— In this paper, we prepared the 3-inch magneto-optical (MO) single crystal garnet film with the composition of $(TmBi)_3(FeGa)_5O_{12}$ by Liquid phase epitaxy (LPE) from lead-free flux. The MO garnet films are grown on $Gd_3Ga_5O_{12}$ (GGG (111)) substrate because of the good lattice match between the film and the substrate. In our experiment, we choose the Bi_2O_3 as the fluxing agent not frequently-used PbO because the latter is poisonous and brings negative impact to the growth film. The good films with low defects, mirror surface, high Faraday Rotation angle (FR) and big thickness have been obtained by optimizing the flux ratio and LPE technological parameters. The thickness of the film can reach about 50-60micrometers in 3-inch GGG substrate. The optimal growth rate is 0.85 ... 0.95 μm/min, and mismatch between TmBiIG film and GGG substrate gets its smallest and good magnetic and MO properties have been obtained with this growth rated. The biggest FR is 0.54 degree/μm as the external magnetic field is as small as 25 Oe. The Ms and Hc of TmBiIG film reaches its biggest and smallest value as the growth rate is 0.92 μm/min, respectively, and the value is 50 emu/cm^3 and 5 Oe.

Experimental Observation of Photonic Topological State in a Uniaxial Metacrystal Waveguide

Wen-Jie Chen[1, 2], **Shao-Ji Jiang**[1], **Xiao-Dong Chen**[1], **Jian-Wen Dong**[1, 3], **and C. T. Chan**[2]

[1]State Key Laboratory of Optoelectronic Materials and Technologies
Sun Yat-Sen University, Guangzhou, China
[2]Department of Physics and the Institute for Advanced Study
The Hong Kong University of Science and Technology, Hong Kong, China
[3]School of Physics and Engineering, Sun Yat-Sen University, Guangzhou, China

Abstract— Photonic analogue of topological insulator was recently predicted by arranging ε/μ-matched bianisotropic metamaterials into 2D superlattice [1]. Similar to its electronic counterpart [2–5], the transport of electromagnetic wave at the edge is robust against disorder. However, the experimental observation of such photonic topological insulator (PTI) is challenging as bianisotropic metamaterial is usually highly dispersive due to its resonant characteristic, so that the ε/μ-matching condition can only be satisfied in a narrow frequency range. Here, we experimentally realized a PTI by embedding non-bianisotropic and non-resonant metacrystal into a metallic plate waveguide [6]. Theoretical derivations demonstrate that the cross coupling between transverse electric (TE) and transverse magnetic (TM) that naturally exists between waveguide modes mimics effective bianisotropy. By this means the ε/μ-matching condition is satisfied in a broad frequency range which facilitates experimental observation. The uniaxial metacrystal waveguide can exhibit topological phase transition if one continuously changes its material parameters. The topologically nontrivial bandgap was confirmed by experimentally measured transmission spectra and calculated nonzero Z_2 index. Gapless spin-filtered edge states were demonstrated experimentally by measuring the magnitude and phase of the fields. The transport robustness of the edge states was also observed when an obstacle was introduced near the edge. The concept of crystal waveguide in this work can be a useful platform to experimentally investigate photonic topological state.

REFERENCES

1. Khanikaev, A. B., S. H. Mousavi, W.-K. Tse, M. Kargarian, A. H. MacDonald, and G. Shvets, "Photonic topological insulators," *Nat. Mater.*, Vol. 12, 233–239, 2012.
2. Hasan, M. Z. and C. L. Kane, *Rev. Mod. Phys.*, 2010.
3. Fu, L. and C. L. Kane, *PRB*, Vol. 76, 045302, 2007.
4. Bernevig, B. A., T. L. Hughes, and S. C. Zhang, *Science*, Vol. 314, 1757, 2006.
5. Qi, X. L., et al., *Science*, Vol. 323, 1184, 2009.
6. Chen, W.-J., S.-J. Jiang, X.-D. Chen, J.-W. Dong, and C. T. Chan, "Experimental realization of photonic topological insulator in a uniaxial metacrystal waveguide," 2014, arXiv:1401.0367.

Photonic Networks Realizations of Floquet Topological Insulators

Yidong Chong
College of Science, Singapore

Abstract— Photonic topological insulators consisting of coupled optical elements can be described using Chalker-Coddington network models, which were originally formulated for studying disorder in the quantum Hall effect. Such networks are also mathematically equivalent to the Floquet states of periodically-driven lattices. An interesting feature of all these systems is that the quasi-energy is an angle variable; as a consequence, there can exist unusual bandstructures where all bands have zero Chern number, but every bandgap contains topologically-protected edge states. Such edge states can be counted by a topological invariant based on the winding number associated with the reflection coefficient from one edge of the network.

Faraday Polarisation Rotation in Semiconductor Waveguides Incorporating Periodic Garnet Claddings

D. C. Hutchings[1], C. Zhang[1], B. M. Holmes[1], P. Dulal[2], A. D. Block[2], and B. J. H. Stadler[2]

[1]University of Glasgow, Glasgow, Scotland, UK
[2]University of Minnesota, Minneapolis, MN, USA

Abstract— The nonreciprocal optical effect of Faraday rotation is widely exploited in optical isolators to suppress back-reflections protecting optical sources and other devices from injection noise, or in optical circulators routing counter-propagating signals in a single physical channel to different ports. To date, these devices are assembled manually from bulk components, with consequences due to assembly costs and yields when scaling-up the number of implemented devices. Consequently, the prospect of a monolithically integrated on-chip, waveguide based isolator defined by lithography is attracting considerable attention. Our approach to the development of a waveguide isolator capable of being integrated is to use an evanescent interaction in conventional semiconductor photonic platforms with a magneto-optic iron garnet (with lower refractive index) as an upper cladding. However, the waveguide birefringence introduced with a planar format severely limits the extent of the polarisation mode conversion achievable. This limitation can be overcome by quasi-phase-matching where the upper cladding alternates either between a magneto-optic cladding and a non-magneto-optic cladding or between magneto-optic claddings of opposite sign. Therefore, we have developed a lift-off technique, with a bilayer PMMA resist mask written using electron-beam lithography, that allows definition of iron garnet segments on semiconductors. Precursors of yttrium iron garnet (YIG), terbium iron garnet (TIG) and cerium-substituted yttrium iron garnet (Ce:YIG) have been deposited by multi-target RF sputtering in an oxygen atmosphere and subsequently annealed to form the garnet phase.

The waveguides studied here are fabricated in 500 nm thick silicon-on-insulator. The garnet segments are formed by sputtering YIG to 120 nm thickness for a range of periods 15–20 µm, and subsequent lift-off. The samples are annealed at 800°C for 120 s in oxygen at 130 mbar. Silica waveguide masks aligned to the YIG segments are written by electron-beam lithography of spun HSQ, with widths from 600 to 1100 nm. Silicon-core waveguides are formed with a chlorine-based etch in an ICP etcher. Initially, a longitudinal magnetic field (> 1 kOe) was applied to saturate the magnetisation of the samples. TE polarised radiation was coupled into the guides using the end-fire technique and the output passed through a polarising beam-splitting cube in order to separate the TE- and TM-polarised components. Significant polarisation mode conversion (up to 80% TM-polarised at the output) was observed around the wavelength corresponding to the fulfillment of the phase-matching criteria. However, this polarisation mode-conversion with the periodic YIG cladding is dominated by the reciprocal polarisation mode conversion due to the slight transverse offset of the garnet segments with respect to the etched waveguides.

In order to discern the nonreciprocal magneto-optic component of the quasi-phase-matched polarisation mode conversion, the sample was placed between a pair of Helmholtz coils (providing a $\sim \pm 100$ Oe magnetic field) with the current modulated at a period of a few seconds. The optical output was analysed with a polarimeter. The Stokes S_3 parameter was observed to be modulated by ~ 0.1 at the same frequency as the coil current, providing a first demonstration of quasi-phase-matched Faraday rotation with segmented garnet claddings fabricated using the novel lift-off technique. Further samples, with potentially larger Verdet coefficients, will be characterised with periodic segments of TIG and Ce:YiG on a 5 nm MgO buffer layer. The reciprocal polarisation mode conversion will also be mitigated by overcladding the waveguides with the nonmagneto-optic dielectric Si_3N_4, which has a similar refractive index to the garnet.

Feasibility of Fabrication of Plasmonic Optical Isolator for Photonic Integrated Circuits

V. Zayets[1], **A. Baryshev**[2], **H. Saito**[1], **K. Ando**[1], **and S. Yuasa**[1]

[1]Spintronics Research Center, AIST, Tsukuba, Japan
[2]All-Russia Research Institute of Automatics, Moscow, Russia

Abstract— An optical isolator is an important component of an optical network. At present, there is a significant commercial demand for an optical isolator, which can be integrated into the Photonic Integrated Circuits (PIC). An optical isolator utilizing surface plasmons propagating at a surface of a transition metal is a good option for such integration. Important advantages of the proposed plasmonic isolator are a small size of only a few micrometers and the good technological compatibility with the fabrication technology of a PIC.

We studied theoretically and experimentally optical and magneto-optical properties of a Fe plasmonic waveguide integrated with an AlGaAs rib waveguides and a Co plasmonic waveguide integrated with Si wire waveguides.

It was demonstrated experimentally that by utilizing a double-dielectric plasmonic waveguide it is possible to reduce significantly the optical loss in a plasmonic waveguide. For $Fe/SiO_2/AlGaAs$ double-dielectric plasmonic waveguide the low optical loss of $0.03\,dB/\mu m$ is obtained. As far as we know at present it is a lowest optical loss demonstrated for a plasmon propagating at a surface of a ferromagnetic metal.

Figure 1 illustrates a monolithical integration of Si nanowire waveguide with $Co:SiO_2$ plasmonic waveguide. The designs of an isolator utilizing a ring resonator (Figure 1(c)) or a non-reciprocal coupler were studied. For an efficient coupling between a plasmonic waveguide and a rib waveguide, a side-coupler (Figure 1(e)) was utilized.

The origin and features of the transverse non-reciprocal magneto-optical (nMO) effect will be discussed. The methods to enlarge the transverse nMO for the better isolator performance will be demonstrated.

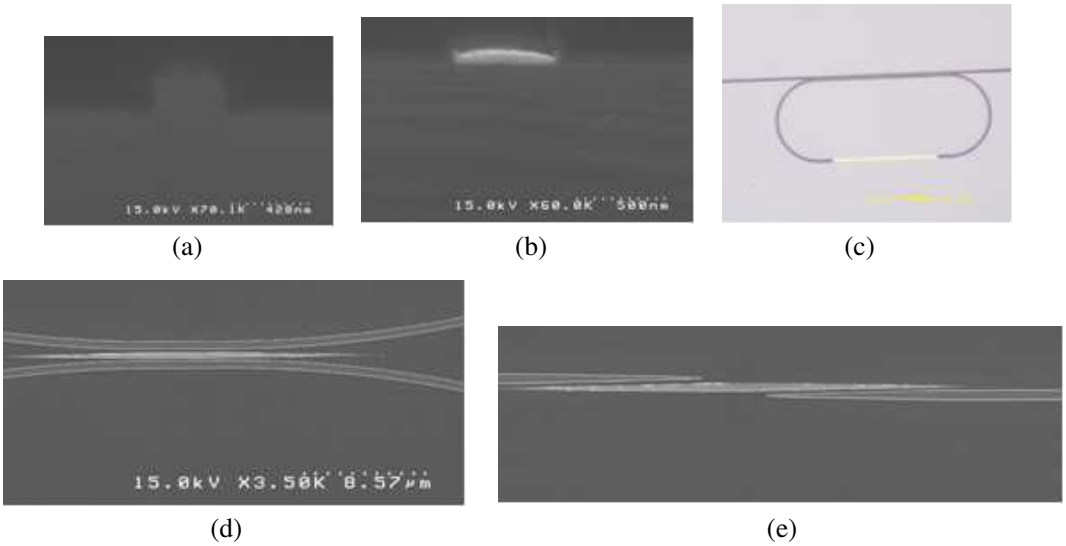

(a) (b) (c) (d) (e)

Figure 1: SEM image of monolithically integrated a Si nanowire waveguide and a Co/SiO_2 plasmonic waveguide. Cross-sectional images of (a) a Si nanowire waveguide and (b) plasmonic waveguide. Top-view images of (c) plasmonic waveguide integrated into a ring resonator; (d) non-reciprocal coupler with a 100-nm-wide plasmonic waveguide; (e) plasmonic-waveguide/Si-wire-waveguide side-coupler. In all pictures the plasmonic waveguides are whiter.

REFERENCES

1. Zayets, V., H. Saito, S. Yuasa, and K. Ando, *J. Appl. Phys.*, Vol. 111, 023103, 2012.
2. Zayets, V., H. Saito, S. Yuasa, and K. Ando, *Materials*, Vol. 5, 857, 2012.

Optical Forces in Photonic One-way Waveguides

Zheng Wang
The University of Texas at Austin, USA

Abstract— Photonic chiral edge states are one-way modes that are strongly protected from backscattering induced by any disorder. The lack of reflection fundamentally changes the optomechanical properties of waveguide containing chiral edge states, allowing one to synthesize arbitrary optical potentials and negative radiation pressures. The response theory of optical forces helps to elucidate the design principles of these unconventional optomechanical devices.

Tunable Nonreciprocity Based on Nonlinear Fano Resonance

Yi Xu[1] and Andrey E Miroshnichenko[2]

[1]Department of Electronics, College of Information Science and Technology
Jinan University, Guangzhou 510632, China
[2]Nonlinear Physics Centre, Research School of Science and Engineering
Australian National University, Canberra, ACT 0200, Australia

Abstract— Manipulation of nonreciprocity in electromagnetic and photonics receive great attentions these years [1–13]. Here, we propose a dynamically tunable nonreciprocal response for wave propagations by employing nonlinear Fano resonances [14]. We demonstrate via a toy model that the transmission contrast between waves propagating in opposite directions can be manipulated by an excitation signal [15]. In particular, the unidirectional transmission can be flipped at different pulse time, resembling a Fano diode with dynamical reconfigurable nonreciprocity. The key mechanism is the interaction between a linear and a nonlinear Fano resonance that allows for the tunable unidirectional wave propagation and ultrahigh transmission contrast ratio. We further provide a realistic photonic example which demonstrates the properties of nonreciprocity can be dynamically manipulated using a pump pulse, based on the general theoretical model.

ACKNOWLEDGMENT

Y. Xu acknowledges the support from NNSF (Grant No. 11304047), Foundation for Distinguished Young Talents in Higher Education of Guangdong Province (Grant No. 2013LYM0067). The work of A. E. Miroshnichenko was supported by the Australian Research Council through Future Fellowship program (FT110100037).

REFERENCES

1. Wang, Z., Y. Chong, J. D. Joannopoulos, and M. Soljačić, *Nature*, Vol. 461, 772, 2009.
2. Yu, Z. and S. Fan, *Nature Photonics*, Vol. 3, 91, 2009.
3. Bi, L., J. J. Hu, P. Jiang, D. H. Kim, G. F. Dionne, L. C. Kimerling, and C. A. Ross, *Nature Photon.*, Vol. 5, 758, 2011.
4. Kang, M. S., A. Butsch, and P. St. J. Russell, *Nature Photonics*, Vol. 5, 549, 2011.
5. Fan, L., J. Wang, L. T. Varghese, H. Shen, B. Niu, Y. Xuan, A. M. Weiner, and M. H. Qi, *Science*, Vol. 335, 447, 2012.
6. Lira, H., Z. Yu, S. Fan, and M. Lipson, *Phys. Rev. Lett.*, Vol. 109, 033901, 2012.
7. Scalora, M., J. P. Dowling, C. M. Bowden, and M. J. Bloemer, *J. Appl. Phys.*, Vol. 76, 2023, 1994.
8. Mingaleev, S. F. and Y. S. Kivshar, *J. Opt. Soc. Am. B*, Vol. 19, 2241, 2002.
9. Lin, X. S., J. H. Yan, L. J. Wu, and S. Lan, *Opt. Express*, Vol. 16, 20949, 2008.
10. Miroshnichenko, A. E., E. Brasselet, and Y. S. Kivshar, *Appl. Phys. Lett.*, Vol. 96, 063302, 2010.
11. Hu, X. Y., C. Xin, Z. Q. Li, Q. H. Gong, *New J. Phys.*, Vol. 12, 1023029, 2010.
12. Hu, X. Y., Z. Q. Li, J. X. Zhang, H. Yang, Q. H. Gong, and X. P. Zhang, *Adv. Funct. Mater.*, Vol. 21, 1803, 2011.
13. Cakmakyapan, S., H. Caglayan, A. E. Serebryannikov, and E. Ozbay, *Appl. Phys. Lett.*, Vol. 98, 051103, 2011.
14. Miroshnichenko, A. E., S. Flach, and Y. S. Kivshar, *Rev. Mod. Phys.*, Vol. 82, 2257, 2010.
15. Xu, Y. and A. E. Miroshnichenko, to be Appeared in *Phys. Rev. B*.

Theoretical Study on the Optical Properties of $Y_3Fe_5O_{12}$ and $Ce_xY_{3-x}Fe_5O_{12}$

Xiao Liang, Longjiang Deng, Jianliang Xie, and Lei Bi
State Key Laboratory of Electronic Thin-Films and Integrated Devices
University of Electronic Science and Technology of China, Chengdu 610054, China

Abstract— We report a first principle study of the electron structure and optic properties of yttrium iron garnet ($Y_3Fe_5O_{12}$) (YIG) and $Ce_{0.41}Y_{2.59}Fe_5O_{12}$ (CeYIG) from the framework of density functional theory (DFT) with Hubbard-U corrections. With a choice of the parameters $U = 4.5\,\text{eV}$ for Fe and $U = 3.0\,\text{eV}$ for Ce respectively, the calculation results are in good agreement with experiments for photon energy ranging from 0 to 6 eV. In particular, we demonstrate that Ce^{3+}-Fe^{3+} (tetrahedral) charge transfer is the dominating mechanism for enhanced near infrared absorption in Ce doped YIG. By changing the value of U to $-2.0\,\text{eV}$ for Ce^{3+} and 2.0 eV for a Fe^{3+} (tetrahedral) which is nearest of Ce^{3+} respectively, the system has converted to a higher-energy charge state of $Ce^{4+}Fe^{2+}$ pairs The energy difference of the two charge states represents the energy barrier of oxidizing Ce^{3+} into Ce^{4+}, which is critical to the magneto-optical properties. On the contrary, when an oxygen vacancy is present near the Ce^{3+}, it is not possible to converge Ce^{3+} into Ce^{4+} state by the +U method, and the Fe^{3+} (both tetrahedral and octahedral) connect to the deprived O would be reduced. Therefore the oxygen vacancy stabilizes the Ce^{3+} which improves the magneto-optical property of this material. This is consistent with recent experimental observations in polycrystalline CeYIG films fabricated under various oxygen partial pressures [1, 2]. However, the oxygen vacancy would produce two additional near infrared absorption peaks in the optic absorption spectrum The trade-off between absorption and magneto-optical property of CeYIG thin films will be analyzed, and the influence on magneto-optical figure of merit will be discussed.

REFERENCES

1. Bi, L., J. Hu, G. F. Dionne, L. C. Kimerling, and C. A. Ross, *Proceeding SPIE*, Vol. 7941, 794105, 2011.
2. Goto, T., Y. Eto, K. Kobayashi, Y. Haga, M. Inoue, and C. A. Ross, *J. Appl. Phys.*, Vol. 113, 17A939, 2013.

Session 3P7a
SC3&4: Liquid Crystals

Liquid-crystal Displays Fabricated from AIE-active Luminogens

Ben Zhong Tang

[1]Department of Chemistry, The Hong Kong University of Science & Technology
Clear Water Bay, Kowloon, Hong Kong, China
[2]Guangdong Innovative Research Team, State Key Laboratory of Luminescent Materials and Devices
South China University of Technology, Guangzhou, China

Abstract— Liquid-crystal displays (LCDs) are widely used in our daily life, ranging from handheld personal devices to flat-panel televisions. Since LCDs are passive display devices, they suffer from narrow viewing angles and low brightness. Light-emitting LCDs (LELCDs) are envisioned as energy-saving display devices. To realize LELCDs, fluorescent materials with strong solid-state emissions are required. Many luminophores, however, suffer from aggregation-caused quenching effect in the solid state. To overcome the shortcoming, we designed and synthesized light-emitting liquid crystals (LELCs) consisting of luminogenic cores and mesogenic peripherals. The LELCs show aggregate-induced emission (AIE) and thermotropic liquid crystallinity. By doping a tiny amount of a LELC into a nematic LC host PA0182, linearly polarized emission is obtained on the unidirectional orientated LC cell. The photoluminescence polarization ratio of the LC cell reached to 4.16 in the directions perpendicular and parallel to the rubbing direction. Through utilizing the emission anisotropy of the LELCs, two kinds of LELCDs are successfully fabricated. This approach simplifies device design, lowers energy consumption, and increases brightness of LCD.

Liquid-crystals as a Versatile Tuning Mechanism for Metamaterials

D. A. Powell
Nonlinear Physics Centre, The Australian National University, Canberra, ACT, Australia

Abstract— One of the most practical approaches for metamaterial tuning is by infiltrating the structure with with liquid crystals (LC). LC infiltration is especially attractive because of the large optical anisotropy of LCs and the ability to control molecular reorientation. Liquid crystals allow several different approaches in tunability to be realised, including changing temperature, applying an external voltage or magnetic field, or even all-optical control of their properties by employing the strong nonlinear response of the LCs.

Many ideas for LC tuning of metamaterials were first explored at optical and microwave frequencies. Examples include LC infiltrated metamaterials tunable by electric or magnetic fields at microwaves. At microwave frequencies, the near-fields of metamaterial modes extends over several millimetres, which requires the use of large amounts of LC, making such devices impractical in terms of cost. In optics, thermal, all-optical [1], and electro-optic tunability [2] of metamaterials infiltrated with LCs have also been demonstrated. However, due to the strong anchoring of the LC to the surfaces of the metamaterials, at optical frequencies the tunability is largely suppressed. Because of this strong anchoring, the LC layer adjacent to the surface ($\sim 100\,\text{nm}$ thick, which largely coincides with the near-field zone of the optical metamaterials) appears 'frozen' and no significant reorientation of the LC molecules occurs within this layer [2].

Here, I review our recent advances on LC tunable metamaterials and discuss the advantages and disadvantages of the different techniques of tuning, as well as compare the tuning mechanisms in the different frequency ranges from visible to terahertz frequencies. In particular I show the all-optical tuning of LC fishnet metamaterials operating in the infra-red spectral region [1, 4]; electro-optic tuning of split-ring resonators (SRR) metamaterials the visible spectral range [2]; as well as thermal tunability of electric-SRR terahertz metamaterials [3], as shown in Fig. 1.

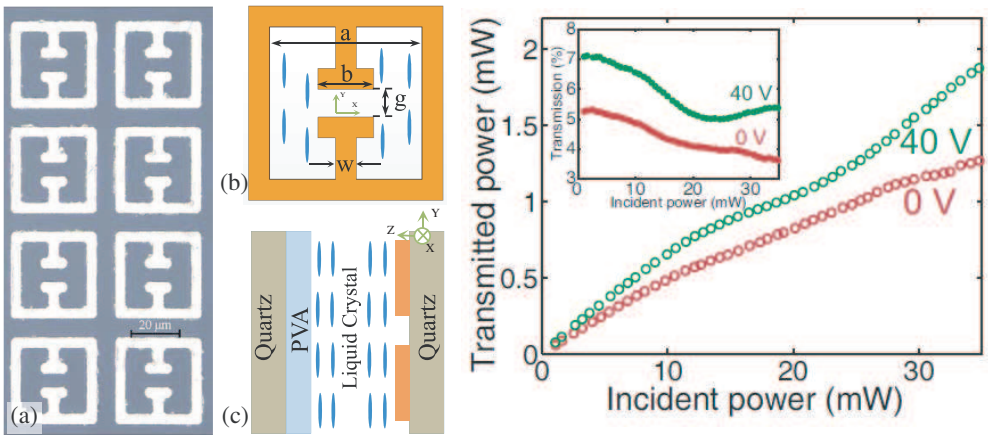

Figure 1: Left: LC-infiltrated terahertz metamaterials which are tuned by temperature. Right: The strong nonlinear response of near-infrared fishnet metamaterials, which can be controlled by the LC bias voltage.

REFERENCES

1. Minovich, A., J. Farnell, D. N. Neshev, I. McKerracher, F. Karouta, J. Tian, D. A. Powell, I. V. Shadrivov, H. H. Tan, C. Jagadish, and Yu. S. Kivshar, "Liquid crystal based nonlinear fishnet metamaterials," *Appl. Phys. Lett.*, Vol. 100, 121113, 2012.
2. Decker, M., C. Kremers, A. Minovich, I. Staude, A. E. Miroshnichenko, H. H. Tan, D. Chigrin, D. N. Neshev, C. Jagadish, and Yu. S. Kivshar, "Electo-optical switching by liquid-crystal controlled metasurfaces," *Opt. Express*, Vol. 21, 8879–8885, 2013.
3. Liu, L., I. V. Shadrivov, D. A. Powell, Md. R. Raihan, H. T. Hattori, M. Decker, E. Mironov, and D. N. Neshev, "Temperature control of terahertz metamaterials with liquid crystals," *IEEE Trans. Terahertz Sci. Technol.*, Vol. 3, 827–831, 2013.
4. Minovich, A., D. N. Neshev, D. A. Powell, I. V. Shadrivov, and Yu. S. Kivshar, "Tunable fishnet metamaterials infiltrated by liquid crystals," *Appl. Phys. Lett.*, Vol. 96, 193103, 2010.

Photonic Band Gap and Nanostructure Tailored Photorefractive and Third Nonlinear Optical Properties Based on Polymer Dispersed Liquid Crystals

Shulei Li and Ming Fu
Key Laboratory of Luminescence and Optical Information, Ministry of Education
Institute of Optoelectronic Technology, Beijing Jiaotong University, Beijing 100044, China

Abstract— Polymer dispersed liquid crystals (PDLC) composed with PMMA, 5CB, C60 are one of the typical photorefractive materials. However, there still are many interesting study points in science when 5CB based PDLC are tailored by photonic band gap structures or nanosheet like structures. The induced redistributions of electromagnetic fields or liquild crystal molecules can strongly improve or modify the photorefractive and third nonlinear optical properties of PDLCs.

As the variation of refractive index is not only the key property of photorefractive materials but also the important factor affecting photonic crystals, photorefractive photonic crystals are one of the most particularly optical materials. The polymer dispersed liquid crystals (PMMA, 5CB, C60), are filled into three-dimensional silica colloidal crystals by solvent-induced phased separation method and fabricate photonic crystals. The stop band shifts to short wavelength when only low voltage is applied. By utilizing the z-scan and two-beam coupling technique, several band gap dependent optical properties of photorefractive photonic crystals have been studied with continuously adjustable wavelength of stop band. The third-order nonlinear-refractive coefficient is enhanced at the edge of photonic stop band. The photorefractive diffraction efficiency gets maximum value when the stop band is overlap with laser beam wavelength.

Because the nanostructure can signifant affect the redistributions of liquid crystals around them, molecular distribution dependent optical properties including photorefractive and third nonlinear properties can be great improved by the doped nanostructures. PDLC doped with different sheet like structures were studied on these nonlinear optical properties. The study will provide us not only the advanced materials for future high performance nonlinear materials but also the understanding of the relationship between graphene and liquid crystals.

Optical Field Processing behind Diffusive Screen Using Spatial Light Modulator

H. X. He[1, 2], **F. J. Wang**[1], **K. S. Wong**[2], **I. C. Khoo**[3], **and J. Y. Zhou**[1]

[1]State Key Laboratories of Optoelectronic Materials and Technology
Sun Yat-sen University, Guangzhou 510275, China
[2]Department of Physics
Hong Kong University of Science and Technology, Clear Water Bay, Hong Kong
[3]Electrical Engineering, The Pennsylvania State University, USA

Abstract— Optical field manipulating and processing, including image recovery, illusion, cloaking, targeted directional heating and induced breakdown behind a diffusive screen using a spatial light modulator is presented, hence demonstrating new possibilities for applications ranging from security, diagnosis to medical therapy.

Self-assembly of Gold Nanorods in Liquid Crystals Confined in a Curved Space and Electric Field for the Application of Optical Cloaking

Nan Wang[1], **Qingkun Liu**[2], **Shaowei Wang**[1], **Iam-Choon Khoo**[1, 3], **and Sailing He**[1, 4]

[1]Centre for Optical and Electromagnetic Research
Zhejiang Provincial Key Laboratory for Sensing Technologies
Zhejiang University, Hangzhou 310058, China
[2]Department of Physics, University of Colorado at Boulder, Boulder, CO 80309, USA
[3]Electrical Engineering Department, Pennsylvania State University, University Park, PA 16802, USA
[4]Department of Electromagnetic Engineering, Royal Institute of Technology, Stockholm S-100 44, Sweden

Abstract— Optical metamaterials comprising artificially nano-structured building-blocks with engineered permittivity and permeability enable the design and fabrication of optical devices with emergent properties such as cloaking, tunable negative-zero-positive indices for manipulate electromagnetic wave in visible spectra [1–5]. However, mass production of such materials based on nano-lithography is a costly and time consuming undertaking. A more viable approach is to utilize self-assembly of the plasmonic nanoparticles with shape anisotropy in a smart host. In this paper, we demonstrate the alignment of gold nanorods (GNRs) in nematic liquid crystal (NLC) in a spherical curved space with surface anchoring imposed by boundary condition. Chemically synthesized GNRs by seed mediated method align along the director of NLC, and result in a strong polarization-dependent surface plasmon resonance (SPR) extinction. The longitudinal SPR at 690 nm is strongest when the polarization of incident light is parallel to the director of LC, while transverse SPR at 530 nm is strongest when the polarization of light is orthogonal to the director. When an alternating electric field is applied on the GNRs-NLC droplet, the orientation of GNRs along with the director of the NLC reorient along the electric field accordingly. Polarized optical microscopy, polarization-dependent spectrometer have been adopted to characterize the spatial orientation and optical properties of GNRs. The unusual optical properties of this hybrid material, and possible application for optical cloaking and other light manipulation operations are discussed [3–5]. The method proposed in this paper is compatible with the state-of-the-art LC display technique and allows for large-scale fabrication of electrically switchable optical metamaterials.

REFERENCES

1. Liu, Q., Y. Cui, D. Gardner, et al., "Self-alignment of plasmonic gold nanorods in reconfigurable anisotropic fluids for tunable bulk metamaterial applications," *Nano Letters*, Vol. 10, No. 4, 1347–1353, 2010.
2. Liu, Q., B. Senyuk, J. Tang, et al., "Plasmonic complex fluids of nematiclike and helicoidal self-assemblies of gold nanorods with a negative order parameter," *Physical Review Letters*, Vol. 109, No. 8, 088301, 2012.
3. Pawlik, G., K. Tarnowski, W. Walasik, et al., "Liquid crystal hyperbolic metamaterial for wide-angle negative-positive refraction and reflection," *Optics Letters*, Vol. 39, 1744–1747, 2014.
4. Khoo, I. C., A. Diaz, J. Liou, et al., "Liquid crystals tunable optical metamaterials," *Selected Topics in Quantum Electronics*, Vol. 16, No. 2, 410–417, 2010.
5. Khoo, I. C., "Nonlinear optics, active plasmonics and metamaterials with liquid crystals," *Progress in Quantum Electronics*, Vol. 38, No. 2, 77–117, 2014.

Blue-phase Liquid-crystal Devices for 3D Applications

Yan Li[1], **Yikai Su**[1], **and Shin-Tson Wu**[2]

[1]National Engineering Lab for TFT-LCD Materials and Technologies
Department of Electronic Engineering, Shanghai Jiao Tong University
Shanghai 200240, China
[2]College of Optics and Photonics, University of Central Florida
Orlando, FL 32816, USA

Abstract— Blue-phase liquid crystal (BPLC) is emerging as a promising candidate for next generation displays due to several attractive features: (1) Submillisecond gray-to-gray response time, which enables field sequential 3D displays while maintaining high spatial resolution, and also enables color sequential display which triples the optical efficiency; (2) Alignment free, which simplifies the fabrication process and reduces the manufacturing cost; (3) Being optically isotropic at voltage-off state, which inherently results in wide and symmetric viewing angle; and (4) insensitivity to cell gap in in-plane-switching (IPS) mode, which is preferable for large-size fabrication. However, there are two major challenges to be confronted before its wide spread application could be realized: (1) high operating voltage and (2) low transmittance. In order to overcome these challenges, great efforts from both material side and device side have been carried out. Large Kerr constant and fast responding blue phase liquid crystal materials have developed by Merck and JNC. Meanwhile, several device designs have been proposed, such as wall-shaped electrode, protrusion electrode, enhanced protrusion electrode, corrugated electrode, vertical field mode, to prove the electro-optical performances of blue phase displays. With these efforts, now, the operating voltage has been reduced from $50\,V_{rms}$ to below $10\,V_{rms}$, and transmittance is increased from 67% to $\sim 100\%$. Moreover, fast responding BPLC lenses could be used for 2D/3D switchable displays, integral 3D imaging and field sequential multi-view 3D displays. Several BPLC lens structures such as hole-patterned structure, curved ITO electrode, multi-electrode, resistive film electrode, and two-BPLC-layer structures are discussed. BPLC lenses could achieve fast response, polarization insensitivity, approximate parabolic phase profile, and thus is very attractive for 3D applications.

Multi-stable Optical Devices Based on Cholesteric Liquid Crystal

Tsung-Hsien Lin
Department of Photonics, Sun Yat-Sen University, Taiwan

Abstract— Cholesteric liquid crystals have received considerable attention for using in various optical devices during recent years. This presentation will demonstrates both optically and electrically switchable tristable optical switches. First is based on the light-matter interactions of dichroic dyes, azo-chiral and liquid crystal. The photo-induced isomerization of the azochiral dopant can alter the thickness/pitch ratio of liquid crystal film and enable the homeotropically aligned device to exhibit three stable fingerprint, focal conic, and homeotropic textures. Second is an electrically activated bistable light shutter that exploits polymer-stabilized cholesteric liquid crystal film. Under double-sided three-terminal electrode driving, the device can be bistable, switched between focal conic and homeotropic textures with a uniform in-plane and vertical electrical field. The dichroic dyes in various textures have different absorptive properties. Multistable attenuation, scattering, and transparent states can be achieved using the dye doped fingerprint, focal conic, and homeotropic textures, respectively. Such a multi-stable optical switch/light shutter exhibits easy switching, a desirable contrast ratio, and low power consumption. It therefore exhibits the potential to be utilized in practical portable information systems and preserve privacy, control illumination and the flow of energy.

REFERENCES

1. Wang, C.-T., Y.-C. Wu, and T.-H. Lin, "Photo-controllable tristable optical switch based on dye doped liquid crystal," *Dyes and Pigments*, Vol. 103, 21, 2014.
2. Wang, C.-T., W.-Y. Wang, and T.-H. Lin, "A stable and switchable uniform lying helix structure in cholesteric liquid crystals," *Appl. Phys. Lett.*, Vol. 99, 041108, 2011.

Some Tunable THz Devices Based on Liquid Crystals

Yan-Qing Lu and Wei Hu
National Laboratory of Solid State Microstructures
College of Engineering and Applied Sciences, Nanjing University, Nanjing 21093, China

Abstract— We developed a serial of large birefringence (> 0.3) nematic liquid crystal (LC) mixtures in the wavelength range from 0.5 to 2 THz. Based on the obtained materials, some THz devices have been developed. Among them, a tunable THz wave plate is demonstrated. We use a metallic grating as front polarizer and electrode. A tree-layer graphene film is used as a transparent and polarization independent back electrode. Photoalignment technique is adopted to obtain a homogeneous LC alignment. If an electric field is applied, the phase retardation of the LC cell changes so that output THz beam is electrically controlled. For a 2.1 THz wave, the polarization state evolution in 0–50 V_{rms} voltage range is recorded, which clearly show the change from a linear polarization, to elliptical polarization, circular polarization then back to an orthogonal linear polarization. The function of a tunable THz half-wave plate (HWP) is well-displayed. Some methods to further cancel the residue phase is also discussed.

In comparison with previous reported LC THz phase shifters, our tunable wave plate shows some interesting advantages, (1) High birefringence LC mixture is used. (2) The polarization rotation and EO tuning are demonstrated with only 50 V_{rms} driving voltage. (3) Unique cell structure containing a built-in metallic grating polarizer/electrode and a lost-cost three layer graphene electrode. (4) A post treatment technique is developed to greatly improve the transmission of porous graphene in THz band. (5) Photo alignment technique is employed so that both the metallic grating and graphene layers could be well protected.

We believe our technologies may pave a road toward many new LC tunable THz apparatuses.

REFERENCES

1. Wang, L., et al., "Large birefringence liquid crystal material in terahertz range," *Opt. Mat. Express*, Vol. 2, 1314–1319, 2012.
2. Lin, X. W., et al., "Self-polarizing terahertz liquid crystal phase shifter," *AIP Advances*, Vol. 1, 032133, 2011.
3. Hu, W., et al., "Polarization independent liquid crystal gratings based on orthogonal photoalignments," *Appl. Phys. Lett.*, Vol. 100, 111116, 2012.
4. Wu, H., et al., "Arbitrary photo-patterning in liquid crystal alignments using DMD based lithography system," *Opt. Express*, Vol. 20, 5384–5391, 2012.
5. Wei, B. Y., et al., "Generating switchable and reconfigurable optical vortices via rewritable photopatterning of liquid crystals," *Adv. Mater.*, Vol. 26, 1590–1595, 2014.

Finite Airy Beam Based on Polymer-stabilized Blue Phase Liquid Crystal

D. Luo and X. W. Sun
Department of Electrical & Electronic Engineering
South University of Science and Technology of China
Xueyuan Road 1088, Shenzhen, Guangdong 518055, China

Abstract— Polymer-stabilized blue phase liquid crystal was used to generate polarization-independent finite energy Airy beam. The intensity of output Airy beam was unchanged while rotating the linear polarization direction of illumination laser. This device also exhibited advantages of simplified fabrication process, and fast opto-electro response time.

Session 3P7b
SC3: Advanced Display Technologies

Electronic Paper Displays: Status and the Trend

Guofu Zhou[1, 2] **and Robert A. Hayes**[1]

[1]Electronic Paper Display Institute
South China Academy of Advanced Optoelectronics, South China Normal University
Building 5, Higher Education Mega Center, Guangzhou 510006, China
[2]Department of Electrical Engineering, Eindhoven University of Technology
P. O. Box 513, 5600 MB Eindhoven, The Netherlands

Abstract— Electronic paper display (EPD) based on electrophoretic principle requires ultra-low power and has superior optical contrast in direct sunlight. Since its successful commercialization in Sony e-reader product in 2004, the worldwide e-reader market has become increasingly attractive and is increased by more than 200% per year in the past several years. Recently, we have made a major step towards the realization of video & color electronic paper displays. The successful industrialization & commercialization of these e-paper displays will further broaden their applications beyond e-readers, particularly interesting for the application in wearable multimedia. In this presentation, we will report the recent progress and share our view on the future development.

Nanofluidics and Optics: Some Experiments

Jan Eijkel
BIOS/the Lab on a Chip Group
MESA+ Institute for Nanotechnology
and MIRA Institute for Biomedical Technology and Technical Medicine
Twente University, The Netherlands

Abstract— Nanofluidic systems offer unprecedented challenges for optical observations due to the short optical path length. We report on the manufacturing of a Fabry-Pérot interferometer with embedded nanochannel, designed for the ultrasensitive observation of filling dynamics of nanofluidic channels. Measurements are demonstrated in channels with height down to 6 nm [1].

Nanofluidic systems also offer unprecedented possibilities for chemical manipulation, due to the extremely high surface to volume ratio. We report on the manufacturing of a gate-controlled nanofluidic proton actuator for the titration of ultrasmall amounts of acid and base in a nanochannel using a fluorescent pH indicator [2].

Finally we report on the production of densely packed emulsion crystals by micro- and nanofluidic technology. Such emulsion crystals could be used as photonic crystals, having a refractive index that can be manipulated by the inner phase composition. We demonstrate production of droplets downto 400 nm diameter [3, 4].

These investigations powerfully demonstrate the usefulness of cleanroom technology for the production of novel nanofluidic systems and functionalities.

REFERENCES

1. Van Delft, K. M., et al., "MicromachinedFabry-Pérot interferometer with embedded nanochannels for nanoscale fluid dynamics," *Nano Lett.*, Vol. 7, 345–350, 2007.
2. Veenhuis, R. B. H., et al., "Field-effect based attomolar titrations in nanoconfinement," *Lab Chip*, Vol. 9, 3472–3480, 2009.
3. Shui, L. L., et al., "Liquid crystallography: 3D microdroplet arrangements using microfluidics," *Soft Matter*, Vol. 5, 2708–2712, 2009.
4. Shui, L. L., et al., "Scalable attolitermonodisperse droplet formation using multiphase nanomicrofluidics," *Microfluid. Nanofluid.*, Vol. 11, 87–92, 2011.

Industrialisation of Electrofluidic Display Technology in China

Robert A. Hayes, Guofu Zhou, Biao Tang, Yuanyuan Guo, Hao Wu, Yingying Dou, Lingling Shui, Mingliang Jin, Xiao Zhang, and Yuan Dong
Institute of Electronic Paper Display
South China Academy of Advanced Optoelectronics, South China Normal University
Building 5, Higher Education Mega Center, Guangzhou 510006, China

Abstract— Electro Fluidic Display (EFD) [1] technology has great potential to produce sunlight readable colour video displays for mobile devices. Commercialisation activities are underway in Europe, the US and Asia. In this presentation, we will report on commercialisation activities being carried out in Southern China. This involves setting up a local supply chain for materials, process development and pilot manufacturing. The current status as well as the remaining challenges will be presented.

REFERENCES

1. Hayes, R. A. and B. J. Feenstra, "Video-speed electronic paper based on electrowetting," *Nature*, Vol. 425, 383, 2003.

Microfluidic Behavior in Micro-pixels of Electrowetting-based Displays

Lingling Shui and Tao He
Institute of Electronic Paper Displays
South China Academy of Advanced Optoelectronics, South China Normal University
Building 5, Higher Education Mega Center, Guangzhou 510006, China

Abstract— Electrowetting-based displays (EWD) have been realized and developed quickly in the previous decade. Typically, the fluid (organic solvent) is confined inside micro-scale confinements (pixels). The fluidic behavior driven by electrowetting is critical for the performance of EWD. Here, we report the effect of geometry and wettablity ofthe display pixels on the microfluidic behavior. Standard lithography process is used for fabricatingthe EWD deviceand self-assembly method is used for fill-in the oil into the micro-sized pixels. The test was carried out using a home-made platform.

Simple Dynamic Model to Describe the Optical Response in an Electrofluidic Based Display Pixel

Jan Groenewold[1, 2], **Biao Tang**[1], **Robert A. Hayes**[1], **and Guofu Zhou**[1]

[1]Institute of Electronic Paper Display
South China Academy of Advanced Optoelectronics, South China Normal University
Building 5, Higher Education Mega Center, Guangzhou 510006, China
[2]Faculty of Science, Utrecht University, The Netherlands

Abstract— The switching time to reach the on state in an electrofluidic based pixel is generally faster compared to the time it takes to reach the off state. In order to optimize the optical response of electrofluidic displays it is desirable to have a model that can predict trends for dependencies on the various system parameters such as: switching voltage, ramps, pixel size, oil film thickness, material properties of the pixel wall, oil volume, surface tension, dielectric layer thickness and general geometric layout of the pixel.

In this contribution, the switching behavior for electrofluidic based pixels is captured in a simple model that is virtually free of adjustable parameters. The asymmetry between on/off switching follows naturally from the model assumptions, which are:

1) Contact line friction described by energy dissipation within the moving contact line.
2) Driving force given by capillary force balance at the contact line.
3) Droplet assumes shape of spherical cap.

In spite of these assumptions being fairly simplistic to describe the optical switching behavior of square or rectangular pixel in an electrofluidic display, they provide nonetheless a remarkable correspondence with the actually observed optical response curve in such devices. It is our aim to calibrate the model with recently manufactured electrofluidic panels and use them to further optimize the switching behavior.

Microfluidics for Electrophoretic Display Technology

Yunfei Zhu, Mingliang Jin, and Lingling Shui
Institute of Electronic Paper Displays, South China Academy of Advanced Optoelectronics
South China Normal University, China

Abstract— This report provides a microfluidic method for the formulation of monodisperse electrophoretic microcapsules by a droplet generator microfluidic device. The image quality and the driven wave forms of Electrophoretic Display (EPD) could be improved by applying monodisperse microcapsules instead of polydisperse microscapsules. The flow-focusing microchannels were used to formulate uniform droplets, and another reservoir was used to polymerize microcapsules surface to precisely controlled thickness. In this device, the whole polymerize process can be observed precisely. The size of microcapsules (60–100 μm) could be controlled by the flow rates of two phases.

When the outer phase values was 10 μl min^{-1} and inner phase is 1 μl min^{-1}, 50 μm diameter-droplets were produced. Figure 4 shows the droplets accumulate in PDMS reservoir after being produced. By controlling the pH value and temperature of the reservoir, the droplets were polymerized. An obviously shrink of the capsules was observed by CCD. Figure 1 shows the sizes and distribution curve of microcapsules produced by agitation emulsification and micro channels. The coefficient of variation (CV) [1] of the microcapsules is 6.35% while the capsules produced in traditional way is 36.18%.

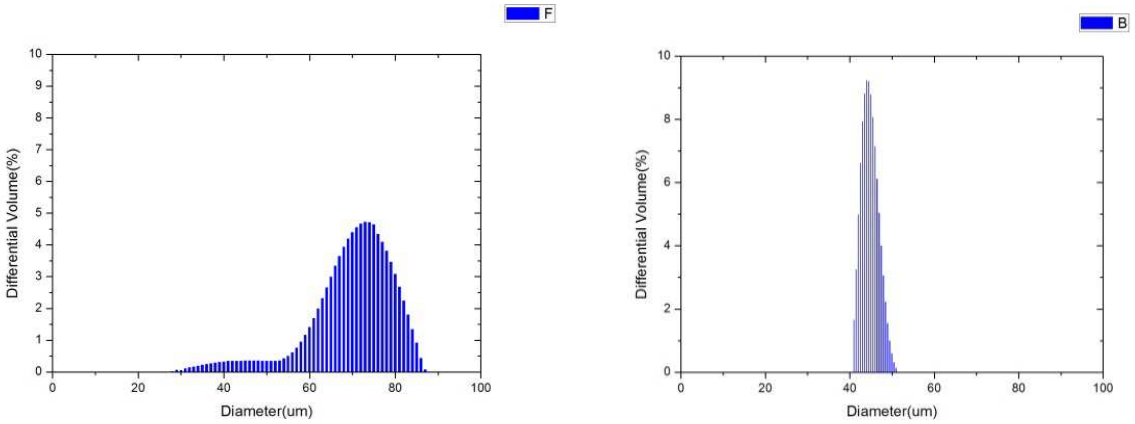

Figure 1: Size and distribution curve of microcapsules produced by agitation emulsification and microfluidics.

REFERENCES

1. Sugiura, S., et al., "Preparation characteristics of water-in-oil-in-water multiple emulsions using microchannel emulsification," *Journal of Colloid and Interface Science*, 2004.

Use of Electro-osmotic Flow in Electrophoretic Displays

Alex Henzen
IRX Innovations B. V., Science Park Eindhoven 5001, Son, The Netherlands

Abstract— Until now, the use of reflective displays has been limited to greyscale displays, like the ones seen in typical e-readers and watch/calculator LCDs, and rare examples of low quality color displays as used in inexpensive children's games. Main reason for this the lack of high quality color displays.

Currently, color displays are made using a black and white switching display (like LCD or EPD), and applying an RGB color filter to this [1]. Predictably, this will lead to dark displays, since color filters remove at least 67% of the incident light, leaving a maximum of 33% brightness. Both LCDs and EPDs show reflectances no better than 45%, which further reduces the brightness to $\sim 15\%$.

The only way around this is to make use of the "classica" way of color reproduction, subtractive color in three layers: cyan, magenta and yellow [2, 3].

We have created the color layers that can switch these primaries with a transmittance of 80%, so that a color display with a reflective brightness of at least 35% is possible. By making use of the fully transparent nature of the display, this brightness can be increased to over 70% without affecting the paper-white appearance of the white state. The new display is called "eCoral", and is based on the electro-osmotic effect.

The underlying principle used is electrophoretic in nature. Colored particles are moved into and out of the field of view. However, to maintain sufficient aperture, the distance between the electrodes needs to be fairly large, i.e., $\sim 30\,\mu$m. Since the speed of the electrophoretic movement of particles is relatively low (up to 100 µm/second), switching speed is limited to approximately 300 ms, and color homogeneity on the pixels is weak.

By applying an electro-osmotic flow inside a pixel, the suspending liquid can be set in motion, in such a way that it flows across the pixel surface (Figures 1, 2). Since the electro-osmotic effect is polarity-independent, the flow will always have the same direction.

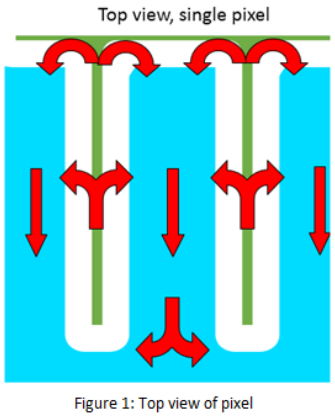

Figure 1: Top view of pixel.

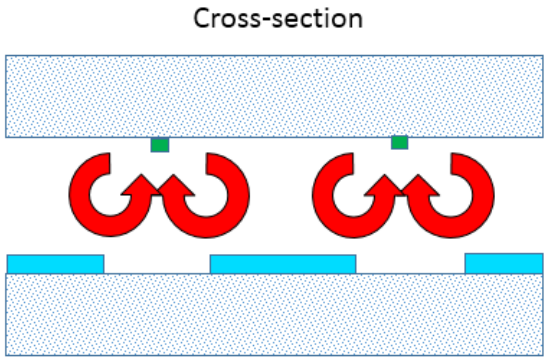

Figure 2: Cross-section of pixel.

Now, the particles in the liquid will see an electric field, attracting them either to the small, opaque pixel electrode, or to the large, transparent field electrode (Figure 3). Once the particles reach the surface they are not carried by the liquid flow anymore, and after a short time the pixel becomes homogenously colored or transparent, dependent on which electrode attracted the particles.

Since the particles only have to travel half the thickness of the cell (in our case 7.5 µm), the particles will swiftly teach the electrode surface. (Theoretically within 100 ms).

We have constructed a high resolution demonstration panel that is capable of displaying 300 PPI resolution images (Figure 4).

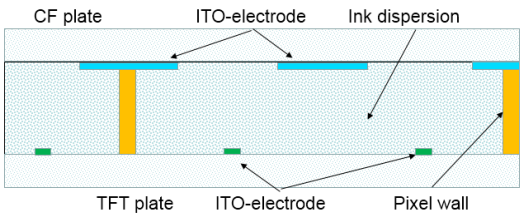

Figure 3: Main pixel elements.

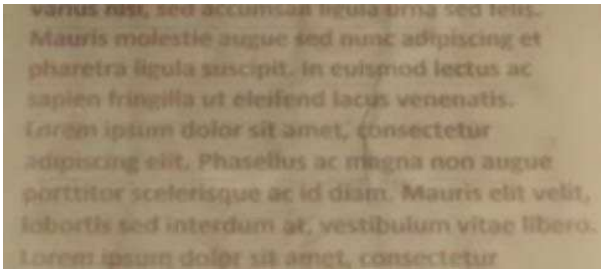

Figure 4: Displayed image.

REFERENCES

1. Bouchard, A., et al., "Advances in active matrix color displays using electrophoretic ink and color filters," *SID Digest of Technical Papers*, 1934–1936, 2006.
2. Lenssen, K.-M., et al., "Novel design for full color electrophoretic paper," *SID Digest of Technical Papers*, 685–688, 2008.
3. Hayes, R. A., et al., "A high brightness Colour 160 PPI reflective display technology based on electrowetting," *SID Digest of Technical Papers*, 1674–1677, 2004.
4. Henzen, A., "Improvements in in-plane electrophoretic displays," *SPIE Photonics West*, 2011.

Session 3P8
SC2: Zero-index Media, Extremely Anisotropic Media, and Nonlocal Photonic Media

Mircowave Devices and Antennas Based on Zero-index Metamaterials

Qiang Cheng, **Hui Feng Ma**, **Wen XuanTang**, **Nan Xiang**, **Bin Zhou**, **Li Hua Yuan**, **and Tie Jun Cui**
State Key Laboratory of Millimeter Waves, Southeast University, Nanjing 210096, China

Abstract— The zero index metamaterials (ZIM)have aroused great interests within the scientific communities due to their special electromagnetic properties like the quasi-infinite phase velocity and infinite wavelength, which are very useful in microwave engineering. In this abstract, we will briefly review some microwave devices based on the ZIM designed by Southeast University, like the spatial power combiner, switchable wave-front converter and electromagnetic tunneling devices. The microwave antennas loaded by the ZIM will also be introduced, which prove that the performance of the antennas can be dramatically improved at the presence of the ZIM. All the examples mentioned above show that the ZIM has provided a new way to design the novel microwave devices and antennas, which is believed to have great potentials in practical applications.

Optic-Null Transformation Optical Media: Realizations and Applications

Qiong He, Shiyi Xiao, Xin Li, and Lei Zhou
State Key Laboratory of Surface Physics and Key Laboratory of Micro and Nano Photonic Structures
Fudan University, Shanghai 200433, China

Abstract— Underpinned by the advent of metamaterials (MMs), transformation optics (TO) offers great versatility to design wave-manipulation devices [1, 2], such as cloaks, beam shifter, superlenses, impedence-matched hyperlenses, and field rotator. Although TO theory developed vigorously, it's is quite obvious that most TO ideas are very difficult to realize in practice, because of the extreme electromagnetic parameters. It's highly desirable to create devices for which real samples can be realized and with which designed functionality can be demonstrated experimentally. In this work, we designed and realized an optically non-existing transformation-media, called "Optic-Null media" (ONM) [3], based on a fractal plasmonic metamaterial. Distinct from epsilon-near-zero media and hyperbolic media, our design is prefect transparent for any incident angle for TE or TM mode at working frequency, without phase accumulation. Based on the coordinate transformation methods, the permittivity tensor and permeability tensor of such media are described as $\vec{\varepsilon} = \vec{\mu} = \begin{pmatrix} 0 & 0 & 0 \\ 0 & 0 & 0 \\ 0 & 0 & \infty \end{pmatrix}$. Employing effective media theory and mode expansion theory [4], we found that under single mode approximation, the tensors of effective permittivity and permeability for Fractal-shaped holey metallic plate are quite similar to those of "optic-null media". We fabricated microwave sample based on the design, demonstrated experimentally several applications of ONM, including the radiation cancellation effect and the hyperlensing effect. The good agreement between full-wave simulation and experimental results verified functionality of our Fractal-shaped holey metallic plate as "Optic-Null media".

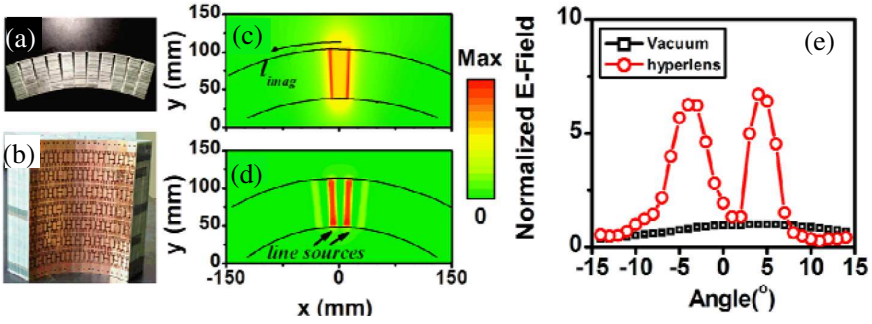

Figure 1: (a) Top-view and (b) side-view pictures of the experiment sample. $|\mathbf{E}/\mathbf{E}_{ref}|$ distributions for the hyperlensing effect realized by (c) a cylindrical ONM and (d) our designed sample obtained by FDTD simulations at frequency 2.63 GHz. (e) Experimental results of normalized amplitude of transmission wave through air and hyperlens.

REFERENCES

1. Pendry, J. B., D. Schurig, and D. R. Smith, *Science*, Vol. 312, 1780, 2006.
2. Leonhardt, U., *Science*, Vol. 312, 1777, 2006.
3. He, Q., S. Xiao, X. Li, and L. Zhou, *Opt. Express*, Vol. 21, 28948, 2013.
4. Xiao, S., Q. He, X. Huang, and L. Zhou, *Metamaterials*, Vol. 5, 112, 2011.

Plasmonic Multilayers Realizing Zero-index Metamaterials

A. A. Orlov[1], **S. V. Zhukovsky**[1, 2], **I. V. Iorsh**[1], **and P. A. Belov**[1]

[1]ITMO University, Kronverksky pr. 49, 197101 St. Petersburg, Russia
[2]DTU Fotonik, Technical University of Denmark, Ørsteds Pl. 343, DK-2800 Kongens Lyngby, Denmark

Abstract— Plasmonic multilayers, or metal-dielectric layered nanostructures, demonstrate a variety of novel electromagnetic phenomena, in particular epsilon-near-zero (zero-index) behaviour in the optical domain. This regime supports subwavelength beam routing, enhanced Purcell effect, and near-perfect cloaking. We study periodic multilayers in the zero-index regime, including the cases of basic and higher-order periodicity. With the introduction of multi-periodicity, we show how to achieve an effective suppression of nonlocality that is the characteristic feature of plasmonic multilayers. We also address the problem of correct extraction of effective index from the scattering parameters in the vicinity of the zero-index point.

Introduction: Plasmonic multilayers are known to support light manipulations at the nanoscale [1, 2], and can be tailored to possess near-zero permittivity [3]. Such zero-index (ZI) behavior of the multilayer implies that one of the components of its effectively permittivity tensor tends to zero. In the corresponding direction, waves in a ZI material can therefore only propagate with infinitely large phase velocities, resulting in a possibility to shape incoming phase distribution and squeeze the radiation throughout almost arbitrary geometries with a small phase variation during propagation.

Zero-Index Plasmonic Multilayers: In this talk we present our recent progress on plasmonic multilayers realizing ZI metamaterials. Basic periodic multilayers, consisting of two kinds of alternating layers, are considered along with more complicated structures containing more than two different kinds of metal or dielectric layers.

Due to the inherent strong optical nonlocality, plasmonic multilayers typically posses a more complicated photonic band structure than the effective-medium theory for an idealized uniaxial ZI material would predict. Nevertheless, we will show how nonlocality can be suppressed, and ZI behaviour can be well reproduced by plasmonic multilayers.

We demonstrate a series of novel phenomena associated with the ZI regime. The most prominent is the dramatic enhancement of the radiative Purcell effect without the need for hyperbolic dispersion. Other intriguing capabilities of the ZI regime include slow-light features and a design of novel optical cloaks with plasmonic multilayers with nearly perfect cloaking behaviour. In addition, we will discuss how to avoid artifacts in characterization of the constitutive parameters of ZI plasmonic multilayers by means of a retrieval procedure from scattering parameters.

ACKNOWLEDGMENT

This work was supported by the Ministry of Education and Science of the Russian Federation (Project 11.G34.31.0020), the President of Russian Federation (Grant SP-2154.2012.1), and the Government of Russian Federation (Grant 074-U01). S.V. Z. wishes to acknowledge financial support from the People Programme (Marie Curie Actions) of the European Union's 7th Framework Programme FP7-PEOPLE-2011-IIF under REA grant agreement No. 302009 (Project HyPHONE).

REFERENCES

1. Orlov, A. A., S. V. Zhukovsky, I. V. Iorsh, and P. A. Belov, "Controlling light with plasmonic multilayers, photonics and nanostructures — Fundamentals and applications," Available online 26 March 2014, http://dx.doi.org/10.1016/j.photonics.2014.03.003.
2. Catrysse, P. B. and S. Fan, "Routing of deep-subwavelength optical beams and images without reflection and diffraction using infinitely anisotropic metamaterials," *Adv. Mater.*, Vol. 25, 194–198, 2013.
3. Subramania, G., A. J. Fischer, and T. S. Luk, "Optical properties of metal-dielectric based epsilon near zero metamaterials," *Appl. Phys. Lett.*, Vol. 101, 241107, 2012.

Semi-Dirac Point in Anisotropic Photonic Crystals

Ying Wu
Division of Computer, Electrical and Mathematical Science and Engineering
King Abdullah University of Science and Technology, Saudi Arabia

Abstract— A semi-Dirac cone refers to a peculiar type of dispersion relation that is linear along the symmetry line but quadratic in the perpendicular direction. Here, I demonstrate that a photonic crystal consisting of a square array of elliptical dielectric cylinders is able to produce such particular dispersion relation in the center of the Brillouin zone. A perturbation method is used to evaluate the linear slope and to affirm that the linear-parabolic behavior of the dispersion relation. Interestingly, it is shown that the linear slope decreases as the k-vector rotates away from the x-direction and eventually becomes zero when the k-vector is along the y-direction. The semi-Dirac point is associated with a topological transition in the geometry of the iso-frequency surface from an open hyperbola to a closed ellipse. Effective medium parameters calculated from a boundary effective medium theory not only unambiguously explain the origin of the topological transition occurring at the semi-Dirac point, but also offer a perspective on the property at that point, where the photonic crystal is a zero-refractive-index material with both effective permittivity and permeability vanish along the x-direction, and an epsilon-near zero material in the perpendicular direction. Drastic change in the wave propagation behavior across the semi-Dirac point is demonstrated.

Acoustic One-way Manipulation with Near-zero Index Metamaterials

Yong Li, Bin Liang, and Jian-Chun Cheng
Key Laboratory of Modern Acoustics, MOE, Department of Physics
Institute of Acoustics, Nanjing University, China

Abstract— As one important and intriguing kind of metamaterials, metamaterials with near zero parameters have been employed to realize a variety of novel types of wave manipulations effects. It is then natural to consider the possibility of applying this kind of metamaterials in realizing one-way manipulations on acoustic waves for yielding unprecedented features. Here we report the design of an acoustic one-way prism comprising acoustic metamaterial with near-zero refractive index. Due to the extremely large phase velocity and the unique acoustic tunneling effect in this kind of metamaterial, the near-zero index metamaterial (ZIM) prism exhibits high angular selectivity for acoustic waves that incident from two opposite sides. As a result, the proposed structure can yield unidirectional acoustic transmission with key capabilities of keeping the output waveform consistent with that of the incident waves and enabling the adjustment of propagation direction of the output waves. Such effects can still hold even in the presence of hard scatters between the input and the output interfaces. Considering the previous designs usually subject to the restrictions of disordered pattern of output wave and unadjustable output angle, these features are of paramount importance for the practical application of acoustic one-way devices in a various situations such as medical ultrasound imaging which generally requires consistence in input and output waveforms. The possibility of experimental realization has also been discussed by demonstrating a potential implementation composed of coiling-up-space metamaterials with properly-designed parameters which are proven to be a good candidate for mimicking the ZIM with desirable parameters. We anticipate our design to have potential for practical applications of acoustic one-way devices in various fields such as ultrasound imaging and treatment where the the above features maybe helpful to prevent unwanted backtracking waves from doing harm to the treatment effect.

Broadband, Strong Diamagnetic Response of Structured Metallic Plates with Fractal Slits at Microwave Frequencies

S. Anwar, S. C. Li, R. R. Chen, S. Li, and B. Hou
School of Physical Science and Technology, Soochow University, Suzhou, China

Abstract— Structured metallic plates have received great attentions in the past decades, enabling the exotic electromagnetic phenomena, such as extraordinary optical transmission (EOT) which refers to greatly enhanced transmission of light through subwavelength hole arrays or apertures in an opaque metallic film [1, 2]. The existence of EOT usually relies on either (spoof) surface plasmon or local resonance on the metal surface which are both critically related to periodicity of the hole array and geometric shape of the apertures [3]. Recently it has been demonstrated both experimentally and theoretically that enhanced transmission can occur in the microwave regime through narrow fractal patterned slits in thick metallic plates even though the aperture is subwavelength all cross section dimension [4].

The deeply subwavelength feature of H fractal slits allows us to employ the effective medium description for the structured plate. In this work, we analyzed the reflection and transmission coefficients to retrieve the effective parameters of the metallic plate with H fractal slits. We found from the retrieved parameters that the effective permittivity has the plasma type behavior and the effective permeability is a near-zero constant over a broad band of microwave frequencies. The broadband strong diamagnetic characteristic is different from the case of metallodielectric composites which is usually predicted by the Maxwell-Garnett formulas. The relevant responsible mechanism lies in the subwavelength local resonance supported by the fractal aperture.

REFERENCES

1. Ebbesen, T. W., H. J. Lezec, H. F. Ghaemi, T. Thio, and P. A. Wolff, *Nature*, Vol. 391, 667, 1998.
2. García de Abajo, F. J., *Rev. Mod. Phys.*, Vol. 79, 1267, 2007.
3. Pendry, J. B., L. Martín-Moreno, F. J. Garcia-Vidal, *Science*, Vol. 305, 847, 2004.
4. Wen, W., L. Zhou, B. Hou, C. T. Chan, and P. Sheng, *Phys. Rev. B*, Vol. 72, 153406, 2005.

The First Field Concentrator Using Fabry-Pérot Resonances

M. M. Sadeghi, Sucheng Li, Lin Xu, Bo Hou, and Huanyang Chen
School of Physical Science and Technology, Soochow University, Suzhou, Jiangsu 215006, China

Abstract— We found that Fabry-Pérot resonances can be used to design various transformation optical devices that are not only easy to realize but also good at working for multiple frequencies. As an example, we fabricated a prototype for a cylindrical field concentrator for microwaves.

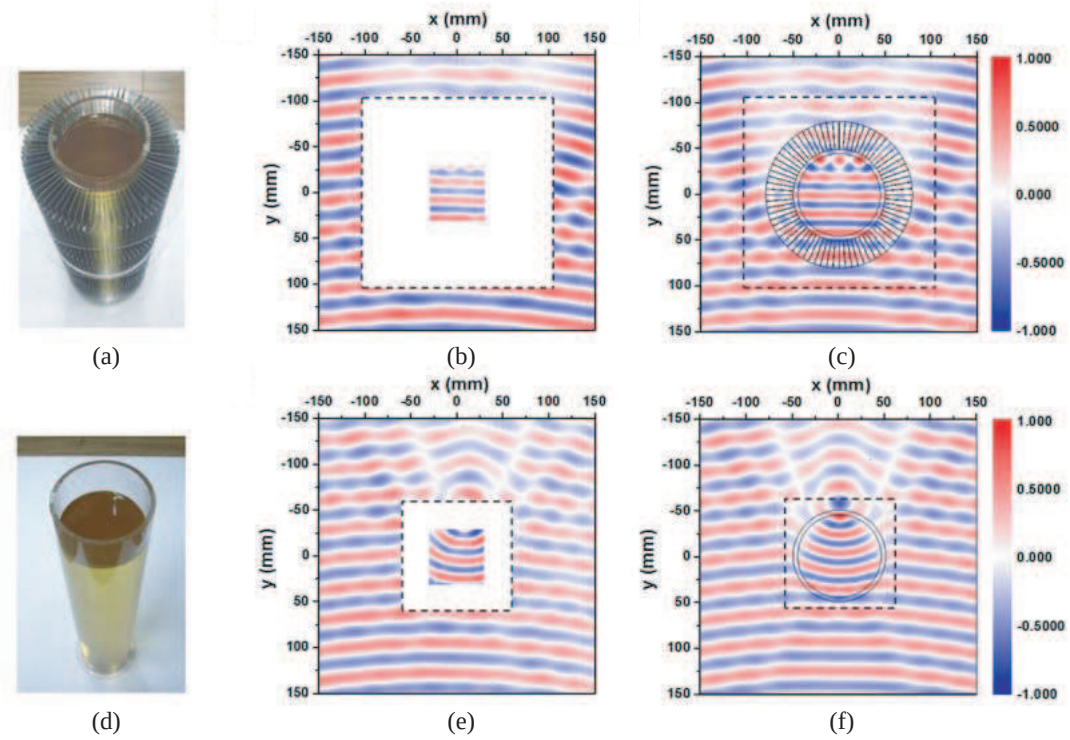

Figure 1: The concentrator with oil cylinder and the effect. (a) The photo of the concentrator with the oil cylinder; (b) The measured Hz field immediately neighboring the concentrator and inside the oil at 9.35 GHz; (c) The simulated result; (d) The photo of the bare oil cylinder; (e) The measured Hz field immediately neighboring the cylinder and inside the oil at 9.35 GHz; (f) The simulated result.

REFERENCES

1. Sadeghi, M. M., S. Li, L. Xu, B. Hou, and H. Chen, "Transformation optics with Fabry-Pérot resonances," *Physical Review Letters*, arXiv:1311.0384, 2014, under review.

Resonant Properties of Subwavelength Voids in Anisotropic Metamaterials

A. V. Vozianova[1], **P. B. Ginzburg**[2], **and A. N. Poddubny**[1, 3]

[1]ITMO University, St. Petersburg, Russia
[2]Department of Physics, Kings College London, Strand, London WC2R 2LS, United Kingdom
[3]Ioffe Physical Technical Institute of the Russian Academy of Sciences, St. Petersburg, Russia

Abstract— Resonant properties of subwavelength voids in strongly anisotropic (hyperbolic) metamaterials were investigated by means of spherical harmonics expansion. These harmonics, being eigen resonances in isotropic environment, are nontrivially coupled by strong anisotropy and corresponding boundary conditions. Eigen resonances of the void are linked to the local field corrections for spontaneous emission rates inside metamaterial environment.

Spontaneous emission processes are efficiently manipulated by nano-structured environment, which could almost on demand control both rates and coherence of quantum emitters. Local density of states, being the key characteristic of electromagnetic space, could be dramatically enhanced by so-called hyperbolic metamaterials — extremely anisotropic artificial composites [1]. However, radiating sources, situated inside a material, strongly interact with their surrounding by inducing additional local polarizations of the matter. One of the well-established approaches, enabling to address this issue, is the Clausius-Mosotti theory, which introduces a virtual cavity around an emitter [2]. This virtual void, being non-resonant for transparent dielectric environment, has nontrivial eigen resonances in the case of hyperbolic metamaterial. Investigation of the nature of these resonances and their impact on the local field correction for emission processes will be studied here.

We consider a spherical void — vacuum cavity of deep subwavelength dimensions, situated inside anisotropic uniaxial medium. The problem of eigen modes of the system was solved in the quasistatic limit by adopting Laplace equation for electric potential and appropriate boundary conditions for normal and tangential field components. In the case of isotropic embedding medium the resonances (material must have negative permittivity in order to support a one) have well-defined sequence — dipole, quadrupole, and higher-poles, defined by spherical harmonic decomposition. However, in the case of anisotropic medium all spherical harmonics are non-trivially coupled via boundary conditions. Uniaxial material, having well-defined crystallographic axis in its natural Cartesian coordinate system, transformed into full 3×3 tensor in the spherical system, appropriated for solution of the spherical cavity. The presents of off-diagonal terms, calculated with the help of scale transformation theory [3], brakes the natural rotation a symmetry of the problem and, as the result, causes the coupling between harmonics Consequently, eigen resonances of the void are described now by infinite series of spherical harmonics. The convergence of these series is strongly dependent on the strength of anisotropy. In the case of extreme anisotropy — hyperbolic metamaterial (ordinary and extraordinary permitivities have different sign) [1] the convergence solely enable by introduction of Joule losses. In order to address the impact of anisotropy on the radiation pattern, the boundary problem with the dipolar extrication was solved. While the

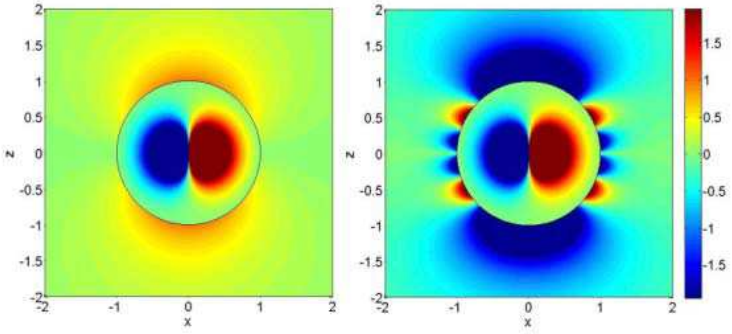

(a) (b)

Figure 1: Radial components of electric field, excited by point vertically polarized dipole, situated in spherical void (a) isotropic medium ($\varepsilon_{in} = 1$, $\varepsilon_{out} = 3$), (b) anisotropic medium ($\varepsilon_{in} = 1$, $\varepsilon_{out} = \mathrm{diag}(2, 2, 3)$).

classical dipole pattern appears at the classic isotropic case (Fig. 1(a)), the strongly anisotropic regime manifest itself in multiple harmonic generations outside the void (Fig. 1(b)). The impact of these harmonics on the radiation will be addressed.

ACKNOWLEDGMENT

This work was supported by Government of Russian Federation (Grant 074-U01) and EPSRC, U.K.

REFERENCES

1. Poddubny, A. N., et al., "Hyperbolic metamaterials," *Nature Photon.*, Vol. 7, 948, 2013.
2. Barnett, S. M., et. al., "Spontaneous emission in absorbing dielectric media," *Phys. Rev. Lett.*, Vol. 68, 3698, 1992.
3. Li, Y.-L. and J.-Y. Huang, "The scale-transformation of electromagnetic theory and its applications," *Chinese Physics*, Vol. 14, 0646, 2005.

Realization of Photonic Functionality in Near-zero Photonic Crystals

Xin-Tao He and Jian-Wen Dong
State Key Laboratory of Optoelectronic Materials and Technologies
Sun Yat-Sen University, Guangzhou 510275, China

Abstract— Zero refraction effects have been demonstrated in photonic crystal with conical dispersions. Here, we employed such interesting phenomenon to realize the functionality: light focus and directional emission. First of all, we designed and fabricated a concave lens comprising Si nanowires that was arranged in square lattice with Dirac dispersion in telecommunication frequency bands. The light focusing in the concave lens has been observed through the out-of-plane radiation. The focusing spot was very close to the center of the concave lens, which indicated zero phase change of near-zero-index medium and was in good agreement with finite-difference time-domain simulations. On the other hand, we found anisotropic Dirac-like cone in the rhombic photonic crystal with C2v symmetry. The photonic bands have linear dispersion along one direction while quadratic dispersions along other directions. Group theory was applied to understand its physics. It is similar to the behavior of semi-Dirac point in electronic systems. Zero phase change and coherent directional emissions were found in the rhombic photonic crystal with Dirac dispersion.

ACKNOWLEDGMENT

This work is supported by the Natural Science Foundation of China, the 973 project, the Program for New Century Excellent Talents in University, the Guangdong Natural Science Funds for Distinguished Young Scholar.

REFERENCES

1. Huang, X., Y. Lai, Z. H. Hang, H. Zheng, and C. T. Chan, *Nat. Mater.*, Vol. 10, 582, 2011.
2. Moitra, P., Y. Yang, Z. Anderson, I. I. Kravchenko, D. P. Briggs, and J. Valentine, *Nat. Photon.*, Vol. 7, 791, 2013.
3. He, X.-T., J.-W. Dong, et al., to be summited.

Surface Mode Formation and Coupling in Honeycomb Lattice Photonic Crystals

Z. H. Hang, J. Wang, and Y. Shao
School of Physical Science and Technology, Soochow University
1, Shizi Street, Suzhou 215006, China

Abstract— Graphene is becoming a promising material for future electronic devices as for its peculiar electron transport behaviors. Moreover, the surface/edge modes in topological insulators attract a lot of research attentions in recent year. As predicted in 2007, the quantum Hall Effect in graphene aroused the interest to study the surface modes of graphene or graphene-like structures. However, due to technical difficulties, the fabrication of graphene sheets with different type of edges is challenging.

At the meantime, the study of topological behavior of photonic crystals brings some new development to this area. Due to the similar band diagram to graphene, especially the existence of Dirac cone dispersions, various interesting electron transport behaviors predicted or observed in graphene have optical analogies in photonic crystals, including pseudo-diffusive transport, Zitterbewegung effect, back-scattering immune surface modes et al.. Due to fabrication easiness, photonic crystal could be a perfect platform for classical simulations of quantum systems.

In this work, we studied an optical analogy to graphene and graphene-like structures: two dimensional photonic crystals with honeycomb lattice. Using finite element method (COMSOL), we can numerically study the eigenmodes of this type of photonic crystals, especially the surface modes with certain lattice truncations. We studied the formation of surface modes as well as the coupling between these surface modes when two photonic crystal sheets are located at proximity. By breaking the inversion symmetry of the lattice, new mechanisms of formation, coupling and annihilation of surface modes are revealed. We hope that our work will help with the development of new optical devices and verify some theoretical predictions from graphene communities.

Nontrivial Flat Bands in Photonic Crystals

Chang Qing Xu, Zhi Hong Hang, and Yun Lai
School of Physical Science and Technology, Soochow University, Suzhou, China

Abstract— Flat bands in photonic crystals have been extensively studied [1, 2]. They are quite useful for slow waves and process optical signals. However, up to now, usual methods to create flat bands in photonic crystals depends on strongly localized modes, such as photonic crystal waveguides and defect modes in band gaps of photonic crystals [3]. Here, we report another method to engineer and achieve nontrivial flat band in photonic crystals, without using strongly localized modes. Comparing to normal flat bands, the eigen-fields of the nontrivial flat bands are more dispersedly distributed and unlocalized. Due to extremely high density of state and character of unlocalized fields, such flat bands may have some interesting applications.

REFERENCES

1. Krauss, T. F., *Journal of Physics D: Applied Physics*, Vol. 40, 2666, 2007.
2. Baba, T., *Nature Photonics*, Vol. 2, 465, 2008.
3. Frandsen, L. H., et al., *Optics Express*, Vol. 14, 9444, 2006.

Some Comments and Applications for Zero-index Metamaterials

Yangyang Fu, Lin Xu, Zhihong Hang, and Huanyang Chen
School of Physical Science and Technology, Soochow University, Suzhou, Jiangsu 215006, China

Abstract— We found that some corrections should be made to the waveguide system of zero index metamaterials with defects when total transmission happens. In addition, we proposed a unidirectional device using array of zero-refractive-index metamaterials (ZIM).

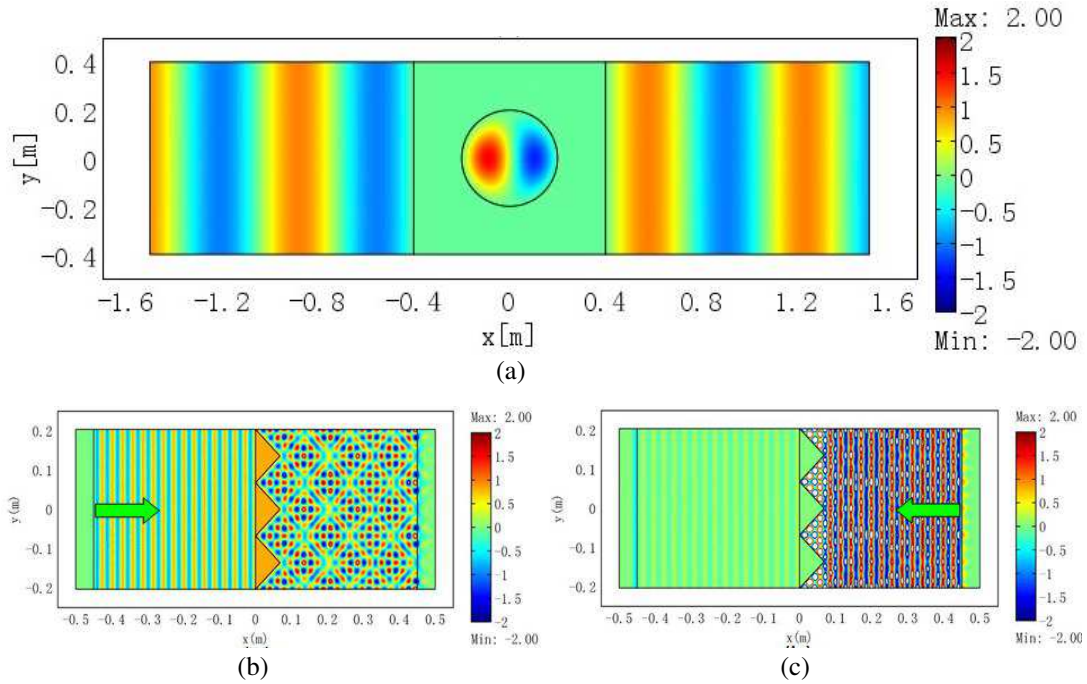

Figure 1: (a) The magnetic field distribution for a new system where is dipole mode excited in the defect. (b) and (c) The field patterns for the left and right incident wave in an array of ZIM prisms.

REFERENCES

1. Fu, Y. and H. Chen, "Comment on 'Total transmission and total reflection by zero index metamaterials with defects'," *Physical Review Letters*, 2014, under Review.
2. Fu, Y., L. Xu, Z. Hang, and H. Chen, "Unidirectional transmission using array of zero-refractive-index metamaterials," *Applied Physics Letters*, 2014, under Review.

Session 3P9a
SC3: Photonic Crystal and Multi-material Fibers

Dynamics of Synchronously Pumped Photonic Crystal Fiber Ring Cavities

N. Y. Joly, M. J. Schmidberger, D. Novoa, F. Biancalanaand, and P. St. J. Russell
Max-Planck Institute for the Science of Light, Guenther-Scharowsky Str. 1, Erlangen 91058, Germany

Abstract— We review ring cavities passively pumped by femtosecond pulses that use photonic crystal fiber as nonlinear element. Precise measurements of timing jitter and the emergence of spontaneous symmetry breaking when pumping synchronously are presented.

Fiber ring cavities are known to exhibit rich and complex dynamics [1]. The use of photonic crystal fiber (PCF), where both dispersion and nonlinearity can be tailored, has recently attracted rising interest as it allows the investigation of various fundamental phenomena such as modulation instability or noise reduction in super continuum generation [2]. Here we present two different aspects of a passive PCF-ring cavity pumped by ultrashort laser pulses. Experimentally, we used an endlessly single mode PCF in a ring cavity pumped by 140 fs-pulses at a repetition rate of 75 MHz. As the temporal walk-off between the round-trip time of the passive cavity and the pump repetition period is tuned, the system exhibits a plethora of different nonlinear dynamics, ranging from a steady state response to highly complex and even chaotic behavior (Fig. 1(a)). We employed the sharp transition between those regimes to precisely determine the combined timing jitter of the pump laser [3]. From a theoretical point of view, we present an extension of the celebrated Lugiato-Lefever model [4] that is usually restricted to continuous-wave pumping. We also show that in the case of a hollow-core fiber filled with a noble gas, the temporal pulse profile can exhibit spontaneous symmetry breaking (Fig. 1(b)). Such unexpected behavior can be explained by the non-trivial phase profile of the circulating pulse, which interferes with the pump pulse at each round-trip [5].

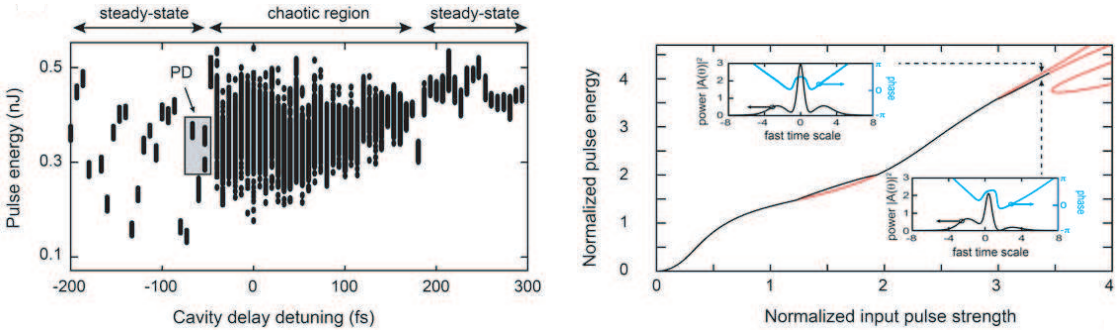

Figure 1: (a) Experimental bifurcation diagram of the total output pulse energy versus cavity detuning. Period-doubling bifurcation occurs in the shaded area (PD). (b) Theoretical bifurcation diagram of the normalized pulse energy for stationary states at zero-detuning, plotted against the normalized input pump energy. Stable states are represented by black lines, and unstable states by red lines.

REFERENCES

1. Ikeda, K., "Multiple-valued stationary state and its instability of the transmitted light by a ring cavity system," *Opt. Commun.*, Vol. 30, 257–261, 1979.
2. Brauckmann, N., M. Kues, P. Gross, and C. Fallnich, "Noise reduction of supercontinua via optical feedback," *Opt. Express*, Vol. 19, 14763–14778, 2011.
3. Schmidberger, M., W. Chang, P. St. J. Russell, and N. Y. Joly, "Influence of timing jitter on nonlinear dynamicsof a photonic crystal fiber ring cavity," *Opt. Lett.*, Vol. 37, 3576–3578, 2012.
4. Lugiato, L. A. and R. Lefever, "Spatial dissipative structures in passive optical systems," *Phys. Rev. Lett.*, Vol. 58, 2209–2211, 1987.
5. Schmidberger, M. J., et al., "Multistability and spontaneous breaking in pulse-shape symmetry in fiber ring cavities," *Opt. Express*, Vol. 22, 3045–3053, 2014.

THz Waveguides, Devices and Hybrid Polymer-chalcogenide Photonic Crystal Fibers

Hualong Bao[1], **Christos Markos**[1], **Kristian Nielsen**[1], **Henrik K. Rasmussen**[2], **Peter Uhd Jepsen**[1], **and Ole Bang**[1]

[1]DTU Fotonik — Department of Photonics Engineering
Technical University of Denmark, Kongens Lyngby Dk-2800, Denmark
[2]DTU Mekanik — Department of Mechnical Engineering
Technical University of Denmark, Kongens Lyngby Dk-2800, Denmark

Abstract— Waveguides and functional devices in Terahertz range have attracted considerable interest in recent years because they can offer the opportunity to develop compact, reliable and flexible THz systems. In this paper, we review our recent activities in the design, fabrication and characterization of polymer THz waveguides.

We will first present a novel polymer (TOPAS) solid-core PCF with ultra-wide bandwidth, which is bendable having low loss and unique dispersion properties. Then we demonstrate both numerically and experimentally a novel band-gap THz fiber design, which consists of a honeycomb cladding structure with a porous core. This structure combines PBG guidance mechanism while keeping the loss at low levels due to its special porous-core. Besides the polymer PCFs, our research activities expand also to THz tubes, which are widely used for guiding THz radiation. We will present a new class of THz tube waveguide, where we deliberately introduce a high-loss, thick cladding which effectively absorbs the cladding field preventing thus the interference with the core modes. Results show that broad transmission bands with low dispersion and low propagation loss can be successfully achieved. Last but not least, we will also demonstrate a novel design of broadband THz directional coupler by using mechanical down-doping of the two cores. Broad bandwidth with relative low device loss is demonstrated for the first time to the best of our knowledge.

At the end, we will briefly show some of our initial results on a novel hybrid polymer photonic crystal fiber with integrated chalcogenide glass layers. The high index glass films introduce antiresonant guiding mechanism in the visible wavelength region, while the ultra-high Kerr nonlinearity of the chalcogenide glass makes the polymer PCF nonlinear. The proposed integration method allows the deposition of nanofilms inside the holes of the polymer PCF using a wide range of different nonlinear glasses and potentially even allows multi-layer deposition of different glasses.

Hybrid Fibers: A Base for Nanophotonic Devices in Fiber Form

Markus A. Schmidt[1, 2]

[1]Max Planck Institute for the Science of Light, Erlangen, Germany
[2]Institute of Photonic Technology, Jena, Germany

Abstract— Hybrid optical fibers are fiber-type waveguides including multimaterial large-aspect ratio nano- and microstructures. Using our pressure-assisted melt-filling approach various hybrid waveguides have been fabricated inside photonic crystal fibers by filling the air holes with materials such as plasmonic metals, semiconductors, fluids or low-melting compound glasses. In this talk I will review our latest results on fiber-based plasmonics, liquid sensing and mid-IR super continuum generation. I will also give an outlook about ongoing experiments in our lab and future developments of in-fiber devices.

Recent Progress in Multimaterial Fibers: From Nanofabrication to Novel Device Architectures

L. Wei, A. M. Stolyarov, A. Gumennik, C. Hou, G. Lestoquoy, X. Jia, B. Grena, A. F. Abouraddy, J. D. Joannopoulos, and Y. Fink
Massachusetts Institute of Technology, USA

Abstract— Multimaterial fiber devices share the basic functional attributes of their traditional wafer-based electronic counterparts, yet are fabricated from materials with disparate optical, electronic, and thermo-mechanical properties using scalable preform-to-fiber processing. A wide range of unique devices have been developed to date in fiber form-factor using this strategy, such as transversely emitting fiber lasers and fibers containing crystalline semiconductor cores. In particular, we describe recent efforts directed at appropriating multimaterial-fiber drawing for chemical synthesis and the fabrication of nanostructures such as structured nanoparticles.

Recent Development and Opportunities of Multi-material Optoelectronic Fibres

Dang Tung Nguyen, Wei Yan, and Fabien Sorin
Photonic Materials and Fibre Devices Laboratory (FIMAP)
Institute of Materials (IMX)
École Polytechnique Fédérale de Lausanne, Switzerland

Abstract— The development of thermally drawn fibers that integrate an assembly of materials with different optical and electronic properties has heralded a novel path towards large area and flexible optoelectronic systems. Complex optoelectronic functionalities can be achieved by combining all of the required materials into a macroscopic preform and using the thermal drawing process to stretch these structures into very long, thin, and flexible functional devices. Micro- and nanostructured materials with widely different optical and electronic properties, in prescribed position and with intimate interfaces, have been demonstrated with this approach. These include sub-hundred nanometers electrically connected semiconducting thin-films that can act as light, heat, or chemical sensors, field effect structures, piezoelectric micro-domains and even extremely long nanowires and complex nanospheres. In that regard, it represents a unique ability to tailor materials, structures and properties spanning the nanometer to kilometer length scales, making these fibres compelling candidates for applications such as remote and distributed sensing, large-area optical-detection arrays, energy harvesting and storage, innovative health care solutions, and functional fabrics.

In this talk, we will focus on the development of multi-material optoelectronic fibres amenable to the distributed detection of optical radiation. After describing the fabrication approach, I will show how successive milestones have enabled improved performance and functionality by engineering new materials and increasingly complex cross-sectional structures. I will in particular highlight some recent results on chemical sensing and give some perspectives as to how, by a judicious choice of architecture, distributed sensing could be achieved. I will conclude by highlighting some directions that the field may take in terms of new materials, structures and functionalities.

Fiber Metamaterials for Subwavelength Imaging at Terahertz Frequencies and Beyond

Alessandro Tuniz[1], **Alexander Argyros**[1], **Simon C. Fleming**[1], **and Boris T. Kuhlmey**[1, 2]

[1]Institute of Photonics and Optical Science (IPOS), School of Physics
The University of Sydney, New South Wales 2006, Australia
[2]Centre for Ultrahigh bandwidth Devices for Optical Systems (CUDOS)
The University of Sydney, New South Wales 2006, Australia

Abstract— Metamaterials are novel artificial composite electromagnetic materials which enable unprecedented control over light. Recent years have been marked by the demonstration of metamaterialdevices with completely novel functionalities, e.g., lenses that resolve objects below the diffraction limit [2]. Most fabrication capabilities provide enormous flexibility over material choice and size [3]. However, since metamaterials are assembled from sub-wavelength optical elements, the geometries that can be achieved for operation at frequencies higher than a few gigahertz (e.g., using lithographic techniques) are typically limited to planar (two-dimensional) geometries, where only small amounts of metamaterial can be produced at a time. In recent years, we have adapted the drawing techniques used to make optical fibers to bulk-produce hundreds of meters of three-dimensional metamaterials in fiber form. Early experiments resulted in metamaterial fibers containing metal micro-wires [4, 5] (possessing a tailored electric permittivity) and metal micro-resonators [6, 7] (possessing a tailored magnetic permeability). Most recently, we produced fibres and tapers containing wire metamaterials that can propagate and focus deeply sub-wavelength images at terahertz frequencies, over optically long distances [8]. Whereas the resolution of conventional lenses is bound by the diffraction limit to about half the wavelength of light, these structures beat this limit by an order of magnitude, due to their large anisotropy [9]. Terahertz imaging (i.e., imaging at frequencies between 0.1–10 THz) is a powerful multidisciplinary tool [10] which has shown applications in detection of bio-molecules [11], cancer diagnosis [12], system inspection [13], and illegal drug detection [14]. Currently, terahertz imaging is under-developed, due in part to the limited availability and functionality of optical components in this region — particularly in terms of resolution. Our fibre geometry improves the fundamental limitation on resolution, and can be made on an industrial scale, promising to be a powerful new tool for medicine, biology, chemistry and physics.

REFERENCES

1. Cai, W. and V. M. Shalaev, *Optical Metamaterials: Fundamentals and Applications*, Springer, 2010.
2. Liu, Z., H. Lee, Y. Xiong, C. Sun, and X. Zhang, "Far-field optical hyperlens magnifying sub-diffraction-limited objects," *Science,* Vol. 315, 1686, 2007.
3. Soukoulis, C. M. and M. Wegener, "Past achievements and future challenges in the development of three-dimensional photonic metamaterials," *Nat. Photonics*, Vol. 5, 523–530, 2011.
4. Tuniz, A., et al., "Drawn metamaterials with plasmonic response at terahertz frequencies," *Appl. Phys. Lett.*, Vol. 96, 191101, 2010.
5. Naman, O. T., et al., "Indefinite media based on wire array metamaterials for the THz and Mid-IR," *Adv. Opt. Mat.*, Vol. 1, 971–977, 2013.
6. Tuniz, A., et al., "Stacked-and-drawn metamaterials with magnetic resonances in the terahertz range," *Opt. Express*, Vol. 19, 16480–16490, 2011.
7. Singh, N., et al., "Fiber-drawn double split ring resonators in the terahertz range," *Opt. Mat. Express*, Vol. 2, 1254–1259, 2012.
8. Tuniz, A., K. J. Kaltenecker, B. M. Fischer, M. Walther, S. C. Fleming, A. Argyros, and B. T. Kuhlmey, "Metamaterial fibres for subdiffraction imaging and focusing at terahertz frequencies over optically long distances," *Nat. Commun.*, Vol. 4, 2706, 2013.
9. Tuniz, A., et al., "Imaging performance of finite uniaxial metamaterials with large anisotropy," *Opt. Lett.*, 2014, in Press.
10. Chan, W. L., J. Deibel, and D. M. Mittleman, "Imaging with terahertz radiation," *Rep. Prog. Phys.*, Vol. 70, 1325–1379, 2007.
11. Korter, T. M. and D. F. Plusquellic, "Continuous-wave terahertz spectroscopy of biotin: Vibrational anharmonicity in the far-infrared," *Chem. Phys. Lett.*, Vol. 385, 45–51, 2004.

12. Yu, C., et al., "The potential of terahertz imaging for cancer diagnosis: A review of investigations to date," *Quant. Imaging Med. Surg.*, Vol. 2, 33–45, 2012.
13. Karpowicz, N., et al., "Compact continuous-wave subterahertz system for inspection applications," *Appl. Phys. Lett.*, Vol. 86, 054105, 2005.
14. Kawase, K., et al., "Non-destructive terahertz imaging of illicit drugs using spectral fingerprints," *Opt. Express*, Vol. 11, 2549–2554, 2003.

Broadband Electrical Interconnects with Multi-electrode Composite Fibers

Zheng Wang
The University of Texas at Austin, USA

Abstract— Electronic interconnects for both digital and analog signals rely on transmission lines with bandwidths fundamentally limited by skin and proximity effects. We present a novel class of electrical transmission line using multi-material fibers to overcomethese fundamental constraints with an order of magnitude improvement on the bandwidth. The design is largely guided by a scaling law that determines the loss and bandwidth from the impedance of fiber. The possibility of realizing extremely low impedance is unique to this system, and are useful for applications requiring large currents.

The Study on Equivalent Models of Finite-size Carbon Fiber Composite Materials

Y. Liao, **Y. Zhang**, **and K. Cai**
Shanghai Key Laboratory of Electromagnetic Environmental Effects for Aerospace Vehicle
846 Minjing RD, Yangpu District, Shanghai 200438, China

Abstract— Carbon fiber reinforced composites (CFRC) are being used more widely in the aerospace and automotive industries as replacement for metals due to their strength and weight properties. However, composite materials are not as electrically conductive and their electromagnetic (EM) properties differ significantly from those of metals such as aluminum and titanium. Composite materials vary considerably in their EM properties and usually have poor performance of shielding effectiveness which may leads to EM Interference problems under EM hazards.

Full numerical approaches are often used to analyze the influence of composite electrical properties on the electromagnetic performance such as reflection coefficient, transmission coefficients, as well as the shielding effectiveness. However, prohibitive computational time and computer memory may be required if thin panels and fibers of composite materials are spatially resolved. Therefore, the equivalent models with effective electromagnetic parameters are usually proposed for the analysis of carbon fiber composite materials. Basically, finite-size CFRCs are often constructed as parts of the large structure system such as aircraft in practical cases, for the analysis of electromagnetic properties.

In this paper, we review different close-form expressions available in the literature based on homogenization technique for approximating the effective permittivity and permeability of fiber composite, and investigate the applicable frequency range for homogenization models. A composite slab example, consists of loose fibers mixed with resins is analyzed to validate the equivalent models. Different thicknesses and sizes of the slab, as well as relative volume of carbon fiber are considered. It is found that the breakdown frequencies of equivalent models vary significantly with the geometries of the composite materials It is important to validate the equivalent models of each finite-size composite block before simplifying them in the whole large structure model.

Session 3P9b
SC3: Fibers and Fiber Devices for Optical Communications

Optical Switching in Nanomechanical Optical Fibers

P. Horak, Z. Lian, M. Segura, N. Podoliak, N. White, X. Feng, and F. Poletti
Optoelectronics Research Centre, University of Southampton, Southampton SO17 1BJ, UK

Abstract— Optical fibers are ubiquitous in optical communication networks as low-loss point-to-point communication channels. On the other hand, signal processing, buffering, and routing are almost exclusively performed in the electronic domain, thus requiring frequent optical-electronic-optical (O-E-O) signal conversion. Finding all-optical and, ideally, all-fiber alternatives to signal processing could remove the O-E-O bottleneck and significantly increase networking speed while reducing power consumption. Here we review our recent progress on developing an all-fiber optical switch based on novel nanomechanically reconfigurable optical fibers.

Our fibers comprise two optically guiding cores suspended individually by thin glass membranes inside a central air hole in the fiber. The separation between the two cores is chosen small enough to ensure overlapping evanescent mode fields and the two cores thus form a directional coupler. Only minute forces are required to mechanically actuate the suspending membranes, modifying the core-to-core separation and therefore the optical coupling strength, which allows for tunable in-fiber switching. We have developed corresponding fiber fabrication techniques and are investigating various different actuation mechanisms theoretically as well as experimentally.

In the first instance, we used pressurization of one of the internal air holes to move one suspended fiber core [1]. This proof of principle experiment demonstrated optical switching between the two fiber cores by applying about 100 m bar of pressure. For practical applications, faster and more robust actuation mechanisms are desirable and we are thus focusing now on electrical actuation. We have developed a multi-material draw technique that allows us to incorporate metal electrodes into the cladding of our dual-core fiber [2]. By running electric currents through the electrodes we can locally heat the fiber structure. Wattlevel powers and corresponding temperature changes of order 10°C were found to modify the optical coupling between cores sufficiently for optical switching by thermal expansion of the fiber structure and the temperature dependence of the refractive index. Another faster and low-power consumption actuation mechanism could be provided by electrostatically induced dipole forces in the fiber cores [3]. We analyzed theoretically various geometries of arranging metal electrodes in the fiber cladding and found that, in an optimized quadrupole configuration, voltages as low as 35 V will lead to optical switching in a 10 cm fiber device.

The fibers used in these experiments [1, 2] were made of lead-silicate glass using an extrusion technique. We are also experimenting with a sheet-stacking technique [4] that allows us to fabricate similar dual- and multi-core fibers with a much larger flexibility of geometries and materials, paving the way to additional functionalities and applications beyond optical switching.

REFERENCES

1. Lian, Z., et al., *Opt. Express*, Vol. 20, 29386, 2012.
2. Lian, Z., et al., *OFC 2014*, paper Tu3K.3, San Francisco, USA, Mar. 9–13, 2014.
3. Podoliak, N., et al., *Opt. Express*, Vol. 22, 1065, 2014.
4. Shi, J., et al., *3rd Workshop on Specialty Optical Fibers and Their Applications*, paper T1.2, Sigtuna, Sweden, Aug. 28–30, 2013.

Wavelength-tunable Dual-concentric-core Photonic Crystal Fibers

Che-Wei Yao[1], **Wei-Hsiang Chuang**[1], **and Jui-Ming Hsu**[1, 2]

[1]Department of Electro-Optical Engineering, United University, Miaoli 360, Taiwan
[2]Optoelectronics Research Center, United University, Miaoli 360, Taiwan

Abstract— We propose a wavelength-tunable dispersion-compensating photonic crystal fiber (WT-DCPCF) based on a dual-concentric-core photonic crystal fiber (DCC-PCF) structure. In general, a single-wavelength dispersion compensating fiber (DCF) has a value of dispersion coefficient considerably larger than a broadband DCF; however it is just suitable for using at a fixed wavelength. In addition to with a high dispersion coefficient close to a single-wavelength DCC-PCF, the proposed WT-DCPCF is even more having a flexible wavelength-variation fabrication.

The Cross-sectional view of the proposed WT-DCPCF structure is shown in Figure 1. To enhance the dispersion compensation effect, we enlarge the size of holes at first layer. The outer ring core with smaller-diameter air holes, which is designed to locate at fourth layer of the WT-DCPCF, separates the cladding region into inner and outer cladding. The mode-couple between inner and outer modes then results in a negative dispersion of the fiber at the phase-matching wavelength. In the inner core, different kinds of liquid with various refractive indices which is colored in orange in the figure, are filled into the central air hole with appropriate diameter. The numeric results show that the operation wavelength is determined by the refractive index of the liquid.

Figure 2 indicates the dependence of the chromatic dispersion coefficients on wavelength for various indices of the liquids filled in the central hole. As shown in the figure, the refractive index of the liquid determines the operation wavelength. The numeric results indicate that the proposed WT-DCPCF with chromatic dispersion coefficients of −32352 ps/km-nm to −41575 ps/km-nm at a wavelength range between 1472 nm to 1617 nm.

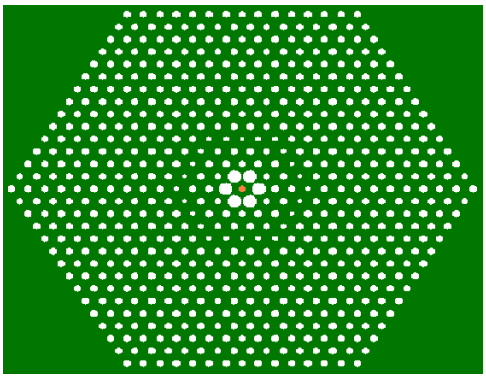

Figure 1: Cross-sectional view of the proposed WT-DCPCF.

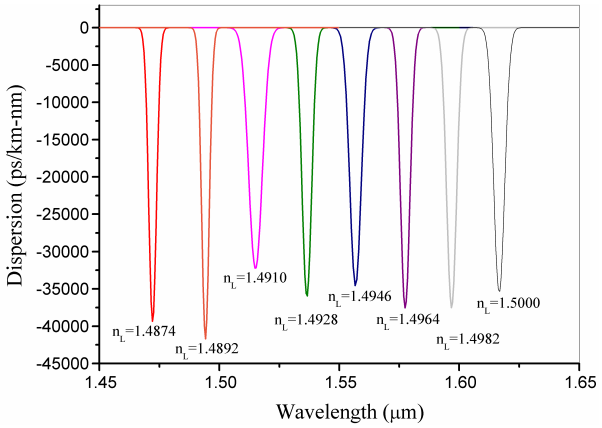

Figure 2: Dependence of the chromatic dispersion on wavelength for various indices of the liquids.

Multi-channel RZ to NRZ Format Conversion Based on a Single Fiber Bragg Grating

Hui Cao[1], **Javid Atai**[2], **Yu Yu**[3], **Qian Dong**[1], **Jun Zuo**[1], **Guo Jie Chen**[1], **and Xuewen Shu**[3]

[1]School of Electronics and Information Engineering, Foshan University, Foshan 528000, China
[2]School of Electrical and Information Engineering, The University of Sydney, NSW, 2006, Australia
[3]Wuhan National Laboratory for Optoelectronics & School of Optoelectronic Science and Engineering
Huazhong University of Science and Technology, Wuhan 430074, China

Abstract— All-optical RZ to NRZ format conversion schemes fall into two categories, namely timedomain waveform processing and frequencydomain signal spectrum tailoring. Generally the spectrum tailoring based converter is all-passive and very attractive compared with active-operation device. This is due to the advantages such as the simplicity of the structure and stable performance. However, their structures are not simple enough, since two filters are used in the reported spectrum tailoring schemes.

In this work, for the first time, we propose a multi-channel RZ-to-NRZ conversion scheme based on a single custom-designed FBG. This customized FBG is a comb filter characterized by the multi-channel reflectivity spectra. Each channel is identical except their central wavelengths. The spectral response of each channel is customized according to the optical spectra algebraic difference between the NRZ signals and the RZ signals. Mathematically, the multi-channel reflectivity spectra are written as follows:

$$r_{FBG,\mathrm{dB}}(\lambda) = \sum_{i=1}^{m} r_{i,\mathrm{dB}}(\lambda-\lambda_{c,i}),$$
$$r_{i,\mathrm{dB}}(\lambda-\lambda_{c,i}) = \begin{cases} \max(n\cdot(FFT_{\mathrm{dB}}(E_{NRZ}(t,\lambda_{c,i}))-FFT_{\mathrm{dB}}(E_{RZ}(t,\lambda_{c,i}))),-25), & |\lambda-\lambda_{c,i}|\le c\cdot T_p, \\ -25, & |\lambda-\lambda_{c,i}|< c\cdot T, \end{cases} \quad (1)$$

where $r_{FBG,\ \mathrm{dB}}(\lambda)$ is the FBG multi-channel reflectivity spectra, $r_{i,\ \mathrm{dB}}(\lambda-\lambda_{c,i})$ is the ith-channel reflectivity spectra, and n is the filter order to be optimized according to the Q-factor of the output NRZ signals.

It should be note that the channel spacing should be chosen according to the signal bit rate. For instance, for the input RZ signals at 40 Gbit/s per channel, the channel spacing should be no less than 80 GHz. Taking into account the crosstalk between adjacent channels as well as

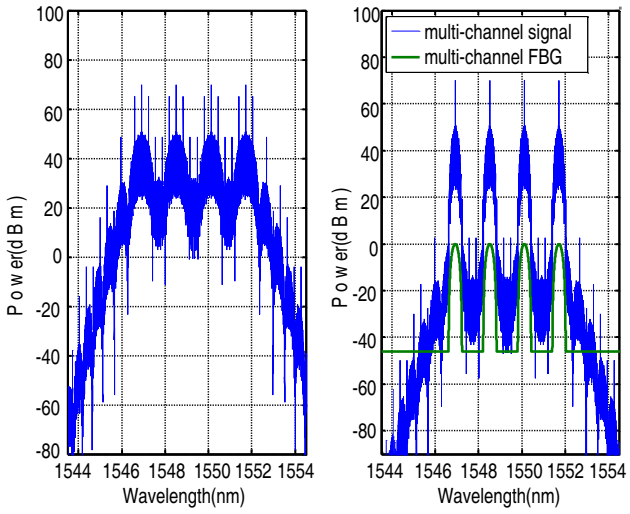

Figure 1: The spectra of (a) the 200 GHz-spaced 4-channel input RZ signal and (b) the corresponding NRZ output.

the ITU WDM grid, we choose 200 GHz spaced 4 channels (1546.92 nm, 1548.51 nm 1550.12 nm and 1551.72 nm) for simulation. By properly matching the FBG multi-channel reflection spectra with the spectra of the input multi-channel RZ signals, the customized FBG is well designed and synthesized using discrete layer-peeling algorithm.

The spectra transformation is shown in Figs. 1(a) and (b). Fig. 1(a) plots the spectra of the input RZ signals before filtering, while Fig. 1(b) presents the spectra of the output NRZ signal after filtering. It is clear that the carriers which are around with strong and periodic spikes in the input RZ spectra can finely pass the FBG, while the sidebands around carriers are suppressed by the FBG. Thus the corresponding NRZ spectra are obtained via the comb filtering introduced by the proposed single FBG.

Recent Advances in Tilted Fibre Gratings and Their Application in Mode-locking Fibre Laser Systems

Lin Zhang, Zhijun Yan, Chengbo Mou, Kaiming Zhou, and Zuxing Zhang
Aston Institute of Photonic Technologies, Aston University, Birmingham, UK

Abstract— Since its first discovery in 1978, side-writing technique establishment in 1989 and booming development in 90's, fibre grating technology has almost matured in terms of fabrication and fibre gratings of variety structures have been widely used in applications in optical communication signal processing, smart sensing and fibre laser systems. This invited talk will report the recent advances in tilted fibre grating structures and functions and their applications in mode-locked fibre laser systems. The talk will briefly review the diffractive fibre grating devices with UV-inscribed index fringe tilted at small, medium and large angles [1] but more focus on 45° tilted fibre gratings (45°-TFGs) implemented as in-fibre high function polarisers [2–4] and Lyot filters [5]. As will be discussed in detail, we will see such 45°-TFG structures can be directly written into standard telecom, polarisation maintaining (PM) and custom-designed fibres, achieving polarisation extinction ratio as high as 35–55 dB. The 45°-TFGs in PM fibre has made it possible to construct true in-fibre single- and multi-stage Lyot polarisation interference filters with arbitrarily tailored transmission response of single polarisation status. For applications, the 45°-TFGs have been utilised as intra-cavity polarisation element enabling all-fibre passively mode-locked lasers to generatefemtosecond pulses of relatively high power (8 mW in average and 1.68 nJ in peak) and repetition rate (48 MHz) [6, 7]. The 45°-TFG based Lyot polarisation interference filter has been employed to achieve picosecond soliton mode locking laser with single polarisation output and capable of tuning over 20 nm range using low cost thermal tuning technique [8].

REFERENCES

1. Zhou, K., L. Zhang, X. Chen, and I. Bennion, "Low thermal sensitivity grating devices based on ex-45° tilting structure capable of forward propagating cladding modes coupling," *J. Lightwave Technol.*, Vol. 24, No. 12, 5087–5094, Dec. 2006.
2. Zhou, K., G. Simpson, X. Chen, L. Zhang, and I. Bennion, "High extinction ratio in-fibre polarizers based on a 45° titled fibre Bragg gratings," *Opt. Lett.*, Vol. 30, No. 11, 1285–1287, Jun. 2005.
3. Yan, Z., C. Mou, K. Zhou, X. Chen, and L. Zhang, "UV-inscription, polarisation dependant loss characteristics and applications of 45° tilted fibre gratings," *IEEE Journal of Lightwave Technology*, Vol. 29, No. 18, 2715–2724, 2011.
4. Yan, Z., K. Zhou, and L. Zhang, "In-fiber linear polarizer based on UV-inscribed 45° tilted grating in polarization maintaining fiber," *Opt. Lett.*, Vol. 37, No. 18, 3819–3821, 2012.
5. Yan, Z., H. Wang, K. Zhou, Y. Wang, W. Zhao, and L. Zhang, "Broadband tunable all-fiber polarization interference filter based on 45° tilted fiber gratings," *J. Lightwave Technol.*, Vol. 31, No. 1, 94–98, 2013.
6. Mou, C., H. Wang, B. Bale, K. Zhou, L. Zhang, and I. Bennion, "All-fiber passively mode-locked femtosecond laser using a 45°-tilted fiber grating polarization element," *Optics Express*, Vol. 18, No. 19, 18906–18911, 2010.
7. Zhang, Z., C. Mou, Z. Yan, K. Zhou, L. Zhang, and S. Turitsyn, "Sub-100 fs mode-locked erbium-doped fiberlaser using a 45°-tilted fiber grating," *Optics Express,* Vol. 21, No. 23, Nov. 2013.
8. Yan, Z., H. Wang, K. Zhou, Y. Wang, W. Zhao, and L. Zhang, "Broadband tunable all-fiber polarization interference filter based on 45," *J. Light. Technol.*, Vol. 31, No. 1, 94–98, Jan. 2013.

All-fiber Tunable Notch Filter Based on Longitudinal Acoustic Wave

Fangcheng Shen and Xuewen Shu
Wuhan National Laboratory for Optoelectronics
Huazhong University of Science and Technology, Wuhan 430074, China

Abstract— All-fiber acousto-optic filters (AOTFs) have attracted much attention as they have advantages such as low insertion loss, fast wavelength tuning, and variable attenuation through simple electronic control. Previous studies of AOTFs mainly focused on wavelength selective acousto-optic (AO) mode coupling introduced by flexural and torsional waves. However, the acoustic birefringence of flexural wave leads to a problem of polarization dependence, while polarization control is needed in AOTFs using torsional wave, resulting in the complexity of the devices and additional insertion loss.

Here we propose an AOTF using longitudinal acoustic wave, which needs no polarization control and has a symmetric strain distribution within the cross section of the fiber, and in consequence, less polarization dependence. Fig. 1 depicts the schematic of the proposed filter structure. Longitudinal acoustic wave is exited by a shear-mode piezo-electric transducer (PZT) vibrating horizontally, as indicated by the double-headed arrow, and an acoustic horn made of aluminum. The fiber section where acousto-optic interaction happens is stripped to enhance the amplitude of the acoustic wave. The frequency and amplitude of the acoustic wave are controlled electrically. Fig. 2 shows a simulated transmission spectrum of the AOTF. Here the refractive index modulation induced by acoustic wave is set to have a typical value of 3×10^{-5}, while the modulation period is 450 µm, and the acousto-optic interaction section has a length of 10 cm. Numerical results indicate the feasibility of the proposal, which will be further confirmed experimentally.

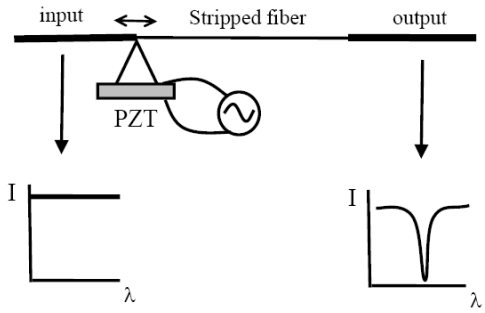

Figure 1: Schematic of the AOTF structure.

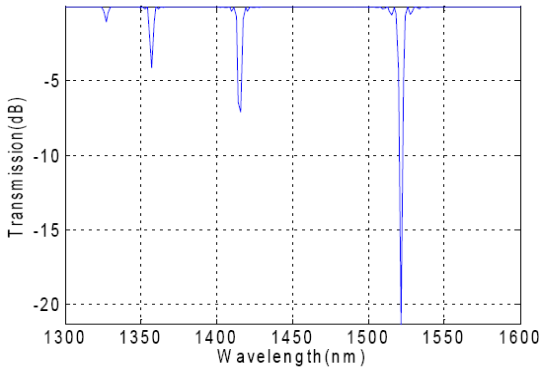

Figure 2: Typical transmission spectrum of the proposed AOTF.

ACKNOWLEDGMENT

This research was partly supported by the Royal Society, UK and the Fundamental Research Funds for the Central Universities, China (HUST: 2013TS047).

Hybrid Fiber-based Distributed Lighting System with Wireless Data Communications

Jau-Jr Lin
Department of Electrical Engineering, Changhua University of Education
No. 2, Shi-Da Road, Changhua City, Taiwan

Abstract— A distributed lighting system, which incorporates with the indoor wireless data communication system, provides both lighting and communication function for households or offices. This hybrid distributed lighting system utilizes both light-emitting diode (LED) light and sunlight to supply the stable lighting and save the electrical power. This fiber-based distributed lighting system spreads out the LEDs, which can reduces the LEDs self-heating effect and indoor cooling system operation fee, for hospital/office-like buildings. Moreover, this fiber-based distributed lighting system provides the communication channels between users in different rooms/floors and the wireless routers. Thus, it is possible to use only one central wireless optical router to cover multi rooms/floors for their wireless data communication needs. This system is energy saving and cost saving. Simulation results demonstrate this system is effective and feasible. Furthermore, the analysis also shows using plastic optical fibers still satisfies the link budget requirement and is a cost-effect solution as well.

Numerical Study on Ring-fiber Lenses Supporting Optical Vortices

Chenxuan Yin, Zhengqian Zhong, Yanfeng Zhang, Yujie Chen, Hui Chen, and Siyuan Yu
State Key Laboratory of Optoelectronic Materials and Technologies
School of Physics and Engineering, Sun Yat-sen University, Guangzhou 510275, China

Abstract— In recent years, optical vortices have become a hot topic in the optics research community. Among many potential applications of vortex beams, using orbital angular momentum (OAM) of such light beams as a means of boosting transmission capacity in optical communication systems has been of great interest. Note that light coupling between the fibre and integrated photonic chips plays an important role in optical fiber communication systems. One convenient way of improving coupling efficiency between optical fibres and waveguide-based photonic devices is using lensed fibres.

In this work, we present numerical simulation results of ring-fiber lenses, using the structure parameters of ring-fibers designed to support various OAM modes. We study the evolution of phase and amplitude in different positions of a ring-fiber lens under different circumstances, including vortex beams with different OAM values and the comparison between coaxial and non-coaxial situations. With different OAM values, our results demonstrate that in the coaxial case, the OAM beams will focus at a distance in a symmetric distribution around the axis outside the fibre lens, which could be utilized to improve the coupling. But with the non-coaxial case, the field around the focal point becomes asymmetric and appears on the away-from-fiber-taper side. We realized the coupling of the focused optical vortices with another identical fiber lens in a head-to-head fashion. Both conical and half-sphere fibre lens are used to demonstrate these coupling and the half-sphere fibre lens has a better performance.

This geometry could be useful for the coupling between devices of optical vortices generation/detection and vortex fibres. These results suggest that optical vortices fibre lenses are feasible and thus can be used in OAM-based fibre communication systems.

Session 3P10a
SC3: Chaotic/Random Lasers and Their Applications

Dynamical Characteristics and Their Applications of Semiconductor Lasers Subject to Both Optical Injection and Optical Feedback

Yi-Huan Liao and Fan-Yi Lin
Institute of Photonics Technologies, Department of Electrical Engineering
Tsing Hua University, Hsinchu 300, Taiwan

Abstract— We experimentally investigate the dynamical characteristics of a semiconductor laser subject to both the optical injection (OI) and the optical feedback (OF). By coupling the OI and the OF lights into the same fiber before injecting into the slave laser (SL), the ratio between the two perturbations can be accurately determined and controlled. The frequency shifts in the cavity resonance frequency of the SL (Δf) induced by the OI and the OF lights are compared quantitatively. Since the main oscillation frequency of the feedback light shifts together with the frequency-pushed cavity resonance frequency of the SL, the frequency-pushing effect induced by the OF light is found to be more significant than that by the OI light. To study the competition between the OI and the OF in the SL, the mapping of the dynamical scenarios and states are plotted in the parameter space. This mapping serves as the guideline for choosing the appropriate operation conditions in various applications employing both the OI and the OF at the same time. In this paper, the suitable feedback strengths to narrow the linewidths of photonic microwave signals generated by the OI are studied. The limitation of using OI in enhancing the bandwidths of the chaos states generated by the OF is discussed. Moreover, we also show that without really plotting the locking regions, the optimal detuning frequency f_{opt} of the OI light to effectively stabilize the unwanted dynamics due to the feedback can be determined by simply measuring the Δf under different feedback strengths.

Classification of Chaotic Codes Using Discriminant Analysis Classifiers and Higher Order Statistical Features

Hend A. Elsayed[1] **and Said E. El-Khamy**[2]

[1]Department of Communication and Computer Engineering, Faculty of Engineering
Delta University for Science and Technology, Mansoura, Egypt
[2]Department of Electrical Engineering, Faculty of Engineering
Alexandria University, Alexandria 21544, Egypt

Abstract— This paper investigates the classification of a new type of Pseudo-Noise codes (PN) which are generated using noise-like chaotic signals. Such signals are very sensitive to initial conditions and hence one can generate a large number of codes using the same chaotic map. Chaotic codes are used in a variety of applications in communications such as code-division multiple-access (CDMA). The classification is made using different discriminant analysis classifiers such as linear, diagonal linear, quadratic, diagonal quadratic, and mahalanobis discriminant analysis classifiers. These classifiers are compared with other classifiers such as neural networks, support vector machines, k-nearest neighbor, and maximum likelihood classifiers. Higher order statistical (HOS) moments and cumulants of the eighth order are used as features. Simulation results illustrates the dependence of the proposed classification method on the type of the used classifier, the type of chaotic map and the initial values used for generating the chaotic code. One dimensional chaotic maps are considered in this work, namely, the logistic map and the Bended up down map. The performance, considered as the probability of correct decision, is shown to differ according to the type of the used classifier and is dependent on the signal to noise ratio. The results show that the quadratic discriminant analysis classifier outperforms the other discriminant analysis classifiers. Also, the performance of two codes generated from one logistic map with two different initial values outperforms the performance of two codes generated from one Bended up down map with two different initial values, two codes generated from logistic map with initial value and Bended up down map with the same initial value, and two codes generated from logistic map with one initial value and Bended up down map with another initial value.

Novel Optical Fast Random Number Generators Based on Integer Domain Chaotic Iterations

Qianxue Wang[1], **Simin Yu**[1], **and Xiaole Fang**[2]

[1]College of Automation, Guangdong University of Technology, China
[2]Land and Resources Technology Center of Guangdong Province, China

Abstract— For cryptography and secure communications, it is very prerequisite that the random number generator (RNG) is based on non-deterministic physical mechanisms, extremely fast generator and robustness to noise are required. In this work, we present novel fast optoelectronic architecture RNGs based on integer domain chaotic iteration (IDCI), with a chaotic semiconductor laser, having time-delayed self-feedback. The solution stems from some well-defined discrete chaotic iterations that satisfy the reputed Devaney's definition of chaos, namely the integer domain chaotic iterations technique, improve the statistical properties of this RNG. Using standard criteria named NIST and DieHARD (famous batteries of tests), the randomness of the output sequences is verified.

Temperature Sensing by Adopting the Optical Wideband Chaos

Di Huang and Li Xia
School of Optical and Electronic Information
Huazhong University of Science & Technology, Wuhan, China

Abstract— The traditional demodulation methods used in the optical sensing are usually based on the optical power/wavelength/phase modulations. However, these modulation methods all can not provide the fiber fault locations. To apply the optical chaos in the optical sensing area was not reported before, as we know. In this letter, we propose a new demodulation method to adopt the optical chaos to achieve the temperature sensing by monitoring the change of correlation peak value. The reflection intensity of optical wideband chaos can be modulated by the temperature induced wavelength spacing between the WDM and the sensing grating.

We use the fiber Bragg gratings (FBGs) to act as the temperature sensors owning to the very mature FBG sensing technology currently. However, the variation of the temperature can normally alter the wavelength shift of the FBGs. As a fact, when the intensity of optical chaotic reflection changes, the peak value located at the correlation spectrum will also change after the cross correlation calculation. Therefore, a plan is designed to convert the wavelength shift of grating into the intensity variation of the chaotic reflection. In the initial, the reflection spectrum of the corresponding sensing grating is chosen to match the transmission spectrum of one specified channel of WDM. When the temperature rises, the wavelength of the grating will shift towards the longer wavelength. Thus, the wavelength spacing between the WDM and the sensing grating will lead to the decrease of the reflection intensity.

Besides the novel demodulation principle, it is also suitable for multi-parameter sensing, long coverage distance, high locating resolution of fiber breakpoint, easy networking and convenient maintenance.

Low Cost Chaos-OTDR Using Laser Diode Modulated by Colpitts Oscillator

Bingjie Wang[1,2], **Hang Xu**[1,2], **Pengcheng Su**[1,2], **Li Liu**[1,2], **Anbang Wang**[1,2], **and Yuncai Wang**[1,2]

[1]Key Laboratory of Advanced Transducers and Intelligent Control System
Ministry of Education and Shanxi Province, Taiyuan 030024, China
[2]College of Physics and Optoelectronics, Taiyuan University of Technology, Taiyuan 030024, China

Abstract— The chaos-OTDR, which uses the chaotic laser as probe signal, has been proposed to detect the faults in single fiber and WDM-PON [1, 2]. The use of chaotic signal not only overcomes the tradeoff in traditional method, but also brings out higher resolution than sequence OTDR. In this paper, we present a low cost chaos-OTDR. The experimental setup is shown in Fig. 1. The chaotic source is a 1550 nm laser diode. The laser driver is direct triggered by an improved Colpitts oscillator programmed to continuously transmit the chaotic waveform. The chaotic signal is divided into the probe and reference signal. The fault location is realized by calculating the echo probe from the fault and the reference signal. In experiment, different types of reflection points are tested, as shown in Fig. 2. A spatial resolution of 6 cm independent of distance and a maximum distance of 98.5 km are achieved. In order to locate the faults in WDM-PON, we also use the wavelength tunable chaotic laser as probe signal which generated by a FP laser direct modulated by the Colpitts Oscillator. A tunable fiber Bragg grating (TFBG) is employed to filter out a single-wavelength light. By adjusting the filter frequency, we can tune the wavelength of the chaotic light, and diagnose the corresponding branch of WDM-PON. The results show that a spatial resolution of 14 cm independent of distance and a dynamic range of 20 dB are achieved.

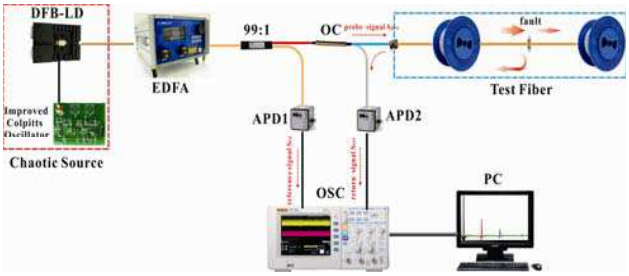

Figure 1: Experimental setup.

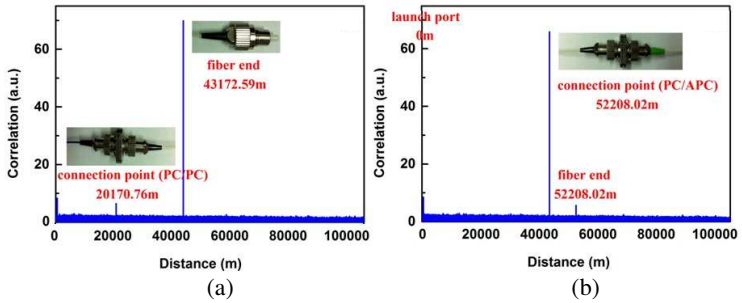

Figure 2: Experimental results with different faults.

REFERENCES

1. Wang, Y. C., B. J. Wang, and A. B. Wang, "Chaotic correlation optical time domain reflectometer utilizing laser diode," *IEEE Photo. Tech. Letters*, Vol. 20, No. 19, 1636–1638, 2008.
2. Wang, A. B., N. Wang, Y. B. Yang, B. J. Wang, M. J. Zhang, and Y. C. Wang, "Precise fault location in WDM-PON by utilizing wavelength tunable chaotic laser," *J. Lightwave Technol.*, Vol. 30, No. 21, 3420–3426, 2012.

From Chaotic to Random Lasers

Wei Li Zhang, **Shi Wei Li**, **Rui Ma**, **and Yun Jiang Rao**
University of Electronic Science & Technology of China, Chengdu 611731, China

Abstract— Chaos is one typical and interesting kind of nonlinear dynamics of lasers. In lasers systems, i.e., semiconductors lasers subjected to delayed coupling, chaos may emerge if the delay time and coupling strength is proper. To form a delayed coupling regime of chaotic light, a distant mirror providing self-feedback injection or a second laser providing external injection is needed. By now, different self-feedback and external injections have been reported, for example, conventional, phase conjugated, polarization controlled, frequency selected, and so on. One hot research topics of chaotic lasers is chaos synchronization, owning to their potential applications to spread spectrum, private, and secure communications. Usually, the transmitter laser is rendered chaotic through optical or optoelectronic feedback. Messages masked in the chaotic outputs of the transmitter can be recovered at the receiver, taking advantage of the chaos pass filtering (CPF) effect. Besides the peer-to-peer optical chaos communications, several efforts have been made to enable chaos communications in more complex optical networks, i.e., chaotic message broadcasting and relaying, multichannel, cascade, and ring synchronization.

Generally speaking, chaotic lasers are ordered optical structures in which light waves exhibit quasi-random fluctuations in time domain, and the fluctuations frequencies are within the RF spectrum. One different type of laser like chaos laser is random laser, which is disordered optical structure of stimulated emission wherein light waves are both multiply scattered and amplified. In random lasers, optical feedback is provided by light scattering in a gain medium rather than a cavity, as in chaotic lasers. Hence, 'random' means that the resonance feedbacks, namely, longitudinal modes, are formed randomly by disorder scatters. Apart from the rich physics involved, random lasers have unique characteristics compared to conventional lasers, like low spatial coherence and high temporal coherence. The coexistence of the high temporal coherence and low spatial coherence makes random lasers an ideal light source in occasions, i.e., imaging, which require high photon radiance while free of coherent artifacts. By now, random laser using different materials in bulk structures as well as low dimensional structures like optical fiber has been reported.

In this presentation, a brief introduction to chaotic lasers and random lasers and their typical applications will be discussed, based on the authors' former studies on chaotic semiconductors lasers and random fiber lasers.

Chaotic Brillouin Optical Coherent Domain Reflectometry

Zhe Ma and Mingjiang Zhang
Key Lab of Advanced Transducers and Intelligent Control System
Ministry of Education and Shanxi Province, Taiyuan University of Technology, Taiyuan 030024, China

Abstract— Distributed optical fiber sensing technology has important applications in construction, mining, petroleum, electric power, aerospace, and so on. Distributed optical fiber sensing technology based on Brillouin scattering has the advantages of simultaneous measurement of strain and temperature with the high precision. However, the drawback of these methods is that they cannot simultaneously achieve high spatial resolution and long distance in sensing measurements. In this letter, we propose a kind of chaotic laser coherent method to realize a long-distance and high resolution method of distributed optical fiber sensing, which called chaotic Brillouin optical coherent domain reflectometry (CBOCDR).

The experimental setup of CBOCDR is depicted in Fig. 1. A distributed-feedback laser diode (DFB-LD), subject to optical feedback via a fiber ring cavity, is used as the chaotic light source. The strength and polarization state of the feedback light are adjusted by a variable attenuator (VA) and polarization controller (PC). A narrow line-width tunable laser was used as a light source, and the light beams inject into an electro-optic modulator (EOM) modulated by the chaotic light source. A mini-MBC was used to control the EOM. The output chaotic light with narrow line-width was divided into two light beams by a coupler. One of the beams was directly used as the reference light of self-heterodyne detection, after passing a 16-km delay fiber and tunable delay line for controlling the correlation peaks. The other beam was injected into the sensing fiber (8 km SMF) as the pump light, after being amplified by an Er-doped fiber amplifier (EDFA) to 15.98 dBm. An optical filter composed of fiber Bragg grating (FBG) with a 3-dB bandwidth of about 10 GHz was inserted in order to suppress the Rayleigh scattering and the Fresnel reflection in the sensing fiber. The optical beat signal of the reference light and the Stokes light was detected by balanced photo-diodes (BPD) and converted to an electrical signal. The relative polarization state of the two light beams was optimized by adjusting polarization controllers manually. By adjusting the tunable optical delay line to control the position of coherence peaks, the optical beat signal of the reference light and the backscattered light was detected by balanced photo-diodes (BPD) and converted to an electrical signal. In experiments, we obtain the result of the distribution of the BGS along the sensing from 8000 m to 8000.16 m.

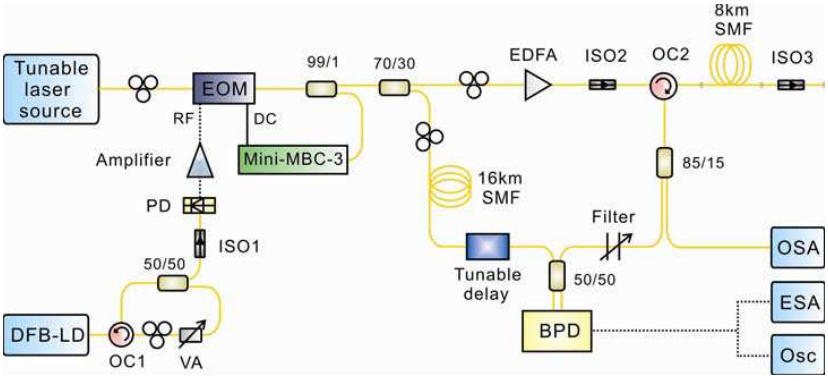

Figure 1: Experimental setup of the CBOCDR.

Random Fiber Laser with the Polarized Pump

Mengqiu Fan, Han Wu, Zinan Wang, and Yunjiang Rao
Key Lab of Optical Fiber Sensing & Communications
University of Electronic Science & Technology of China
Chengdu, Sichuan 611731, China

Abstract— We experimentally investigate the characteristics of Raman gain based random fiber laser with the polarized pump. The results show that the output lasing's spectrum, power and degree of polarization (DOP) can change drastically by changing the state of polarization (SOP) of the pump, suggesting the lasing's emission efficiency is highly dependent on the polarization state of the pump.

Since the distributed feedback random fiber laser (RFL) solely based on SMF was reported in 2010 by Turistsyn, et al. [1], many works about the RFLs have been done and some valuable achievements have been acquired such as a long-distance fiber-optic point-sensing system based on random fiber lasers [2], the low threshold RFL [3] and highly efficient, higher order random fiber laser [4] were reported in succession. But all these devices are using depolarized pump so there is no evidence suggest that the polarization properties of random fiber laser associated with the state of polarization of pump light.

To investigate the polarization properties of random fiber laser, we designed the experimental setup shown in Fig. 1. The 1365 nm pump is a depolarized fiber laser pump source which has a measured degree of polarization (DOP) about 5%. Then we insert a polarizer to make the 1365 nm pump polarized. The polarization controller (PC) is used to adjust the state of polarization (SOP) of 1365 nm pump before injecting into the 50 km long SMF. The 1455 nm random lasing towards the pump side is extracted from the 1365/1455 nm WDM and split by the 1 : 99 and 1 : 1 couplers. The output ports A, B and C are used for monitoring output power, optical spectrum and output polarization simultaneously.

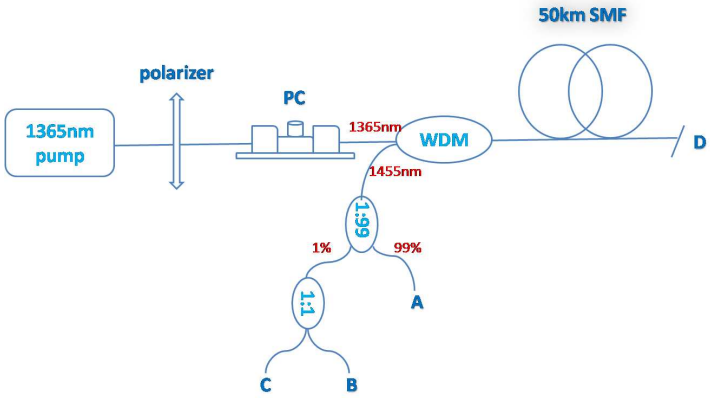

Figure 1: Experimental setup.

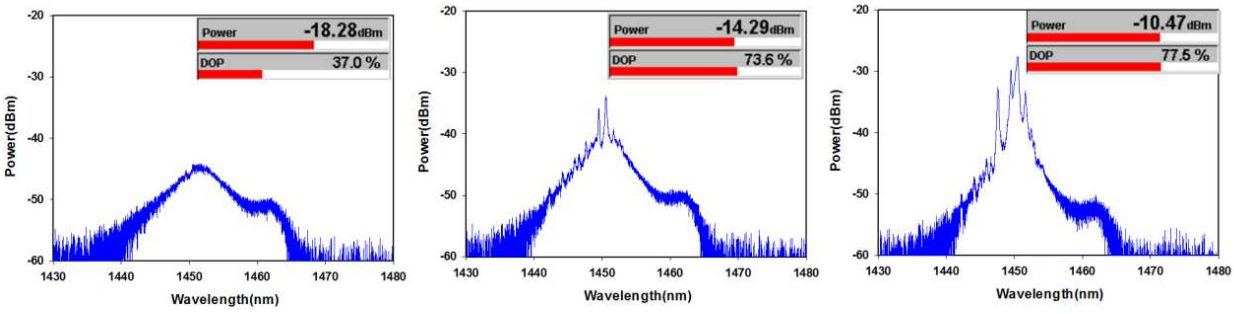

Figure 2: Random lasing's properties under different PC states with pump power 1.3 W.

When we rotate the PC and thus change the SOP of injected pump, the random lasing's spectrum, output power and the degree of polarization (DOP) all drastically change. Fig. 2 shows the spectra (record at port B), output power and DOP (record at port C) under different PC states at pump power 1.3 W. We can clearly see the SOP of pump can alter the threshold and the excited state of random lasing, the output power and DOP also vary substantially with the PC state at the same time. It should be noted that in all cases, the SOP of the output lasing is very stable and keep as a point on surface of the Poincare Sphere.

ACKNOWLEDGMENT

This work is supported by Natural Science Foundation of China (61205048, 61106045, 61290312), Research Fund for the Doctoral Program of Higher Education of China (20120185120003), Fundamental Research Funds for the Central Universities (ZYGX2012J002, ZYGX2011J001), 111 project (B14039) and PCSIRT (IRT1218).

REFERENCES

1. Turitsyn, S. K., S. A. Babin, A. E. El-Taher, et al., "Random distributed feedback fibre laser," *Nature Photonics*, Vol. 4, No. 4, 231–235, 2010.
2. Wang, Z. N., Y. J. Rao, H. Wu, et al., "Long-distance fiber-optic point-sensing systems based on random fiber lasers," *Optics Express*, Vol. 20, No. 16, 17695–17700, 2012.
3. Zhang, W. L., Y. Y. Zhu, Y. J. Rao, et al., "Random fiber laser formed by mixing dispersion compensated fiber and single mode fiber," *Optics Express*, Vol. 21, No. 7, 8544–8549, 2013.
4. Wang, Z., H. Wu, M. Fan, et al., "Third-order random lasing via Raman gain and Rayleigh feedback within a half-open cavity," *Optics Express*, Vol. 21, No. 17, 20090–20095, 2013.

Performance Analysis of a Yb^{3+}-doped Chaotic Fiber Ring Laser

Lingzhen Yang, **Li Zhang**, **Feifei Wang**, **Naijun Xu**, **and Jun Zhang**
College of Physics and Optoelectronics, Taiyuan University of Technology, Taiyuan 030024, China

Abstract— Chaotic dynamics of the Ytterbium-doped chaotic fiber ring laser has been demonstrated. The fiber ring cavity shown in Fig. 1 is composed of a wavelength division multiplex (WDM), an Yb^{3+}-doped fiber with a length of 15-m, a polarization independent isolator, a polarization controller and a 20-m single-mode fiber. A 980-nm laser diode with the maximum pump current of 500 mA is used to pump Yb^{3+}-doped fiber through a 980/1064-nm WDM. Due to the nonlinear interaction, the period-doubling and quasi-periodicity route to chaos is achieved by increasing the pump power and the chaotic autocorrelation exhibits high side-lobes character as shown in Fig. 2. In order to analysis the chaotic noise performance, the Mach-Zehnder interferometer composed of two fiber coupler is launched. The experimental results show a relatively stable chaotic state. These Performances are related to the interaction, iteration and interference of the Mach-Zehnder interferometer.

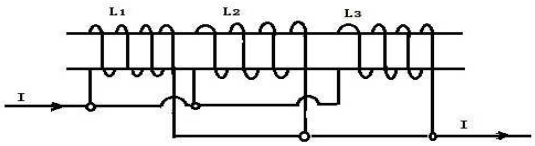

Figure 1: The experimental configuration of the Yb^{3+}-doped fiber ring laser.

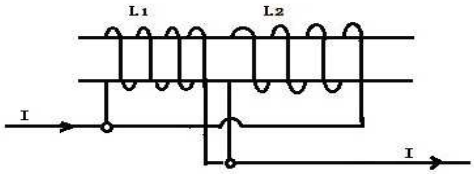

Figure 2: the chaotic dynamics with the pump power of the 124.90-mW from (a), (c), (e) the Yb^{3+}-doped fiber ring laser and (b), (d), (f) the b^{3+}-doped fiber ring laser with a Mach-Zehnder interferometer, respectively. (a), (b) Time series, (c), (d) power spectrum, and (e), (f) autocorrelation trace.

Session 3P10b
SC3: Spectroscopy and Nanoscopy for Sensing and Imaging

Modification of Simplified Modal Method for Subwavelength Triangular Grating with Very High Efficiency

Bin Wang[1,2], **Yihui Wu**[1], **Peng Hao**[1], **and Wenchao Zhou**[1,2]

[1]State Key Laboratory of Applied Optics, Changchun Institute of Optics, Fine Mechanics and Physics Chinese Academy of Sciences, Changchun 130033, China
[2]University of Chinese Academy of Sciences, Beijing 100039, China

Abstract— A modification of simplified modal method (MSMM) is presented to calculate the transmission efficiencies of subwavelength fused-silica grating. In order to consider the reflection of grating, which is neglected in simplified modal method (SMM), the grating region is divided into N thin planer grating slabs and regarded as multilayer films. Then the reflectance is characterized by the effective admittances of air and grating which are complete characteristic of multilayer films. This proposes a manner of reducing the reflection loss of dielectric grating. By analyzing the effective index and admittance of grating, we designed a triangular fused-silica grating with more than 99.9% diffraction efficiency for both TE and TM- polarization. This method offers a clear physical insight of diffraction characteristic: A deep-etched grating would get a high efficiency when the average difference of its mode indices is odd times of e and the admittance of the grating is approximate to that of air. Due to tiny deviation between this method and RCWA, MSMM can be used to design and optimize fused-silica gratings directly. It is better than SMM which only gives starting value of grating parameters. Contrast to RCWA, the starting parameters values of subwavelength dielectric grating can be predicted by the formulas in MSMM when the transmission efficiency is known. However, the starting values are got by cut-and-try procedure in RCWA.

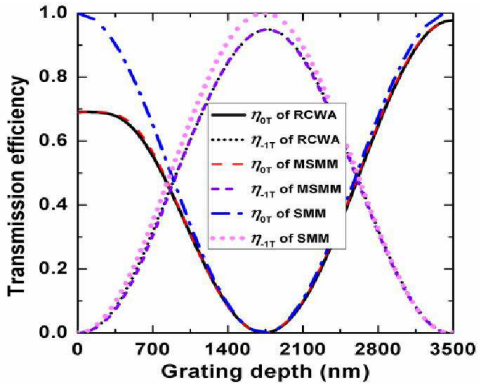

Figure 1: Transmission efficiencies (TE) of atriangular grating calculated by MSMM, SMM and RCWA respectively versus the grating depth.

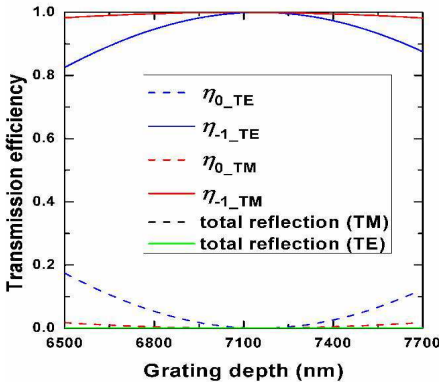

Figure 2: The efficiency versus the grating depth for period $p = 747\,\text{nm}$.

Optical Third-harmonic Generation in Au-CdTe

Liwei Liu, Yue Wang, Yueshu Feng, and Jiaqi Zhang
School of Science, ChangChun University of Science and Technology
ChangChun, Jilin 130022, China

Abstract— In general, third-harmonic generation (THG) is a third-order nonlinear process, the third-order nonlinear optical effects in nanoparticles are remarkably strong, leading to studies that include saturable absorption, optical limiting, two-photon absorption, four-wave mixing (FWM). Herein, we report on nonlinear optical experiments performed on Au-CdTe particle pumped by femtosecond laser pulses. We conduct a theoretical simulation and experiments to determine their third harmonic generation characteristics. The result revealed that there is a more stronger from Au-CdTe than CdTe QDs. Our studies suggest that THG can be used as an optical microscopy probe of these particles, bioimaging, biosensing, and electric detection.

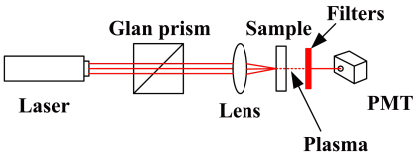

Figure 1: Experimental setup.

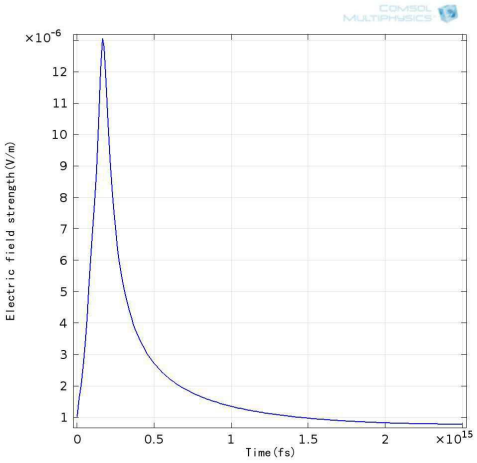

Figure 2: Spectrum of THG from CdTe QDs.

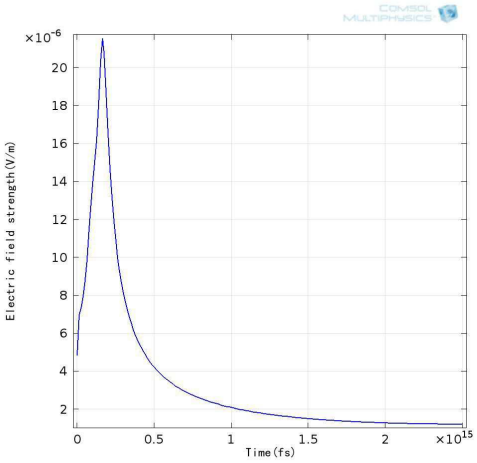

Figure 3: Spectrum of THG from Au- CdTe.

Femtosecond Laser Nanofabrication: An Enabler for Multifunctional Microfluidic Devices

Hong-Bo Sun
State Key Laboratory on Integrated Optoelectronics, College of Electronic Science and Engineering
Jilin University, 2699 Qianjin Street, Changchun 130023, China

Abstract— Recent years have witnessed a rapidly increased research interests in nanofabrication technologies towards tailoring artificial materials with desired nanostructures [1]. Particularly, as two types of classical nanofabrication techniques, "bottom-up" approaches and "top-down" methods have revealed great potential in the fabrication of novel nanostructures and the manufacture of functional nanodevices. Generally, the former method makes use of weak and reversible noncovalent interactions between molecules to have molecular-level components built up into complex assemblies, whereas the later rotes aim at creating nanostuctures from bulky materials. However, despite the fact that the above-mentioned techniques have revealed a cornucopia in the fabrication of micronanostructures, inherent limitations such as poor controllability with respect to "bottom-up" approaches, and 3D processing incapability with respect to "top-down" method, continues to trigger the development of novel techniques that can overcome such limitations.

Femtosecond laser nanofabrication has been established as a nano-enabler to solve problems that are otherwise impossible in versatile scientific and industrial fields [2]. The powerful 3Dl processing capability, arbitrary-shape designability, and high fabricating accuracy up to tens of nanometers, far beyond the optical diffraction limit make it a promising nanofabrication technique for modern functional nanodevices [3]. Herein. we briefly introduce the fundamentals and the underlying mechanisms for achievement of the super high fabrication spatial resolution and surface smoothness; the rule and photochemical strategies that are currently exploited for femtosecond laser nanofabrication has been discussed. Finally, applications of the delicate nanoprototyping approach in the development of multifunctional micro?uidic devices are introduced [4–7].

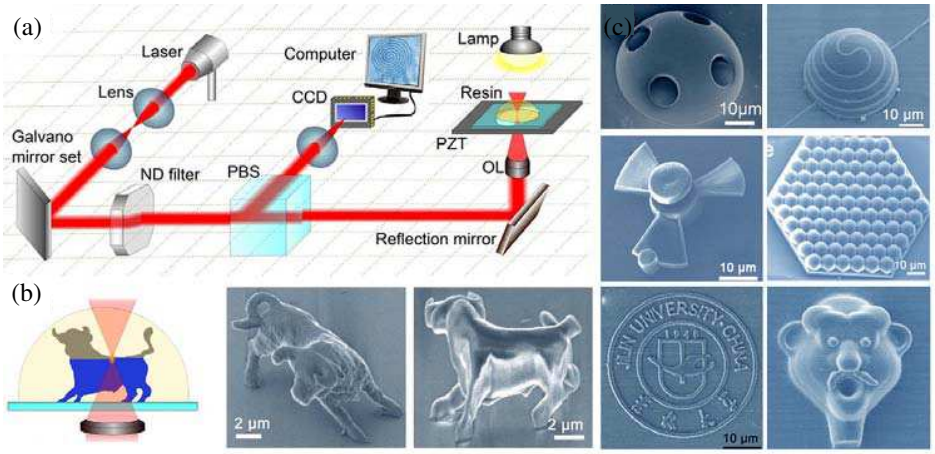

Figure 1: (a) Schematic illustration of the femtosecond laser nanofabrication system; (b) Scheme for the fabrication of 3D microstructures; (c) Various nanostructures fabricated based on diver materials.

REFERENCES

1. Jin, Y., et al., *Adv. Mater.*, Vol. 24, 1187, 2012.
2. Zhang, Y. L., et al., *Nano Today*, Vol. 5, 15, 2010.
3. Xu, B. B., et al., *Small*, Vol. 6, 1762, 2010.
4. Sun, Y. L., et al., *Angew. Chem. Int. Ed.*, Vol. 51, 1558, 2012.
5. Xia, H., et al., *Adv. Mater.*, Vol. 22, 3204, 2010.
6. Zhang, Y. L., et al., *Nano Today*, Vol. 5, 15, 2010.
7. Xu, B. B., et al., *Lab Chip*, Vol. 13, 1677, 2013.

Raman Microscopy beyond the Diffraction Limit

Satoshi Kawata
Osaka University and RIKEN, Japan

Abstract— Without the help of fluorescent molecules or quantum dots to label the molecule of interest, bio-molecules can be detected and analyzed with Raman scattering spectroscopy [1, 2]. The scattering cross-section of spontaneous Raman process is extremely low, so that it would take an enormous time for constructing a distribution of individual molecules as an image. Nonlinear Raman process such as coherent Anti-Stoke Raman and stimulated Raman scattering enhances the signal, while the resolution is limited if confocal microscope configuration is adapted. Resonant Raman scattering would be promising to have a large cross-section, in which deep UV sources/detectors and optics are used [3]. By setting a sample on the metal nano-island substrate, Raman signal is extraordinarily enhanced due to the excitation of localized mode of surface plasmons. Rather than preparing metal islands on substrate, I have proposed to use a metallic tip which scans on the sample surface [4, 5]. The spatial resolution is typically 10–20 nm [6]. This scanning microscopy is now called tip-enhanced Raman scattering (TERS) microscopy, and has been used for analytical imaging of various nano materials.

REFERENCES

1. Palonpon, A., et al., *Nature Protocols*, Vol. 8, 677, 2013.
2. Okada, M., et al., *Proc. Natl. Acad. Sci.*, Vol. 109, 28, 2012.
3. Kumamoto, Y., et al., *J. Biomed. Opt.*, Vol. 7, 076001, 2012.
4. Inouye, Y. and S. Kawata, *Opt. Lett.*, Vol. 19, 159, 1994.
5. Kawata, S., et al., *Nature Photonics*, Vol. 3, 388, 2009.
6. Yano, Y., et al., *Nature Commun.*, Vol. 4, 2592, 2013.

Nanopatterning beyond the Far-field Diffraction Limit Using Photochromism

Rajesh Menon
Department of Electrical and Computer Engineering, The University of Utah
Salt Lake City, Utah 84112, USA

Abstract— Diffraction limits the size of the smallest features that can be fabricated using conventional optical lithography to approximately half the wavelength of the illuminating light. In order to circumvent this limit we have developed an alternative optical lithographic technique that exploits unique combinations of spectrally selective reversible and irreversible photochemical transitions in a family of photochromic molecules to achieve deep sub-wavelength resolution patterning.

In this presentation, I will discuss recent developments in two methods both of which utilize photochromism to achieve deep sub-wavelength resolution patterning. These approaches have the potential for massive parallelism, enabling the creation of nanostructures and devices at a speed surpassing what is currently possible with scanning e-beam lithography.

In the first approach that we refer to as Absorbance-Modulation-Optical Lithography (AMOL), a thin layer of a photochromic material is placed atop a conventional photoresist film. Upon illumination by a ringshaped spot at one wavelength, λ_2 and a focused bright spot at another wavelength, λ_1, a sub-diffractionlimited region of the photochromic layer retains one isomeric form that is transparent to λ_1. Subsequently, those photons at λ_1 penetrate this region and expose the underlying photoresist, resulting in a deepsubwavelength spot [1, 2]. This technique can also be extended to near-field optical microscopy.

In the second approach that we refer to as Patterning via Optical Saturable Transformations (POST), the photochromic film itself is used as the recording medium. Upon irradiation with UV, the open-ring isomer converts to the closed-ring isomer. When exposed to a focused node at a visible wavelength, the molecules are converted back to the open-ring isomer, except in the near-vicinity of the node. By optically saturating this transition, the molecules in the closed-ring isomer remain in a region that is far smaller than the far-field diffraction limit. Then, a "locking" step selectively and irreversibly modifies the closed-ring isomer. This sequence of steps can be repeated with intervening displacements of the sample relative to the optics in a "dot-matrix" fashion to create arbitrary geometries with features spaced much smaller than the far-field diffraction limit [3–5].

REFERENCES

1. Menon, R. and H. I. Smith, "Absorbance modulation optical lithography," *J. Opt. Soc. Am. A*, Vol. 23, 2290, 2006.
2. Andrew, T. L., H. Tsai, and R. Menon, "Confining light to deep subwavelength dimensions to enable optical nanopatterning," *Science*, Vol. 324, 917–920, 2009.
3. Brimhall, N., et al., "Breaking the far-field diffraction limit in optical nanopatterning via repeated photochemical and electrochemical transitions in photochromic molecules," *Phys. Rev. Lett.*, Vol. 107, 205501, 2011.
4. Cantu, P., et al., "Subwavelength nanopattering of photochromic diaryethene films," *Applied Physics Letters*, Vol. 100, 183103, 2012.
5. Cantu, P., et al., "Nanopatterning of diarylethene films via selective dissolution of one photoisomer," *Applied Physics Letters*, Vol. 103, 173112, 2013.

Session 3P11a
SC4: Microwave and Millimeter-wave Measurements and Sensing

Broadband Measurement of Complex Permittivity for Liquids Using the Open-ended Cut-off Circular Waveguide Reflection Method

Kouji Shibata
Department of Electrical and Electric Systems, Hachinohe Institute of Technology
88-1, Aza-oubiraki, Ouaza-myou, Hachinohe, Aomori 031-8501, Japan

Abstract— Recently, the impact of electromagnetic wave exposure on the human body has become a matter of concern. In such a background, health effects using liquid phantoms that imitate human body tissues have been carried out [1]. In order to establish the health effects of electromagnetic wave exposure, a faithful mockup of human body tissue is needed. Thus the Complex Permittivity of these materials is measured. For measuring the complex permittivity of the liquid material, the reflection method that uses a coaxial probe [2] and the cavity resonator method that inserts a Teflon tube are well known. In this study, the complex permittivity of tap water, methanol, ethanol (99.5) and isopropanol with high permittivity and high loss were measured by the reflection method using the coaxial feed open-ended cut-off circular waveguide for the purpose of decrease the effect of the liquid spill when it filled the sample materials [3].

The liquid phantom is measured by the method explained here. First, input impedance is measured at the front of the material by inserting a liquid using a measurement jig assembled from combinations of a cutting worked brass and a SMA connector. Next, the complex permittivity of the sample material is obtained by comparing the calculated result with numerical analysis and the measurement result of the input impedance. Input normalize impedance at the reference plane as seen from the right-hand side is calculated by applying the Mode matching method as a termination as the Perfect Magnetic Condition (PMC) in Fig. 1.

Firstly, the complex permittivity was estimated as an inverse problem by measuring the input impedance when filled with tap water measured here at frequencies of 2.49806 GHz where $2a = 4.1\,\text{mm}$, $2b = 1.3\,\text{mm}$, $d = 5.0\,\text{mm}$, $\varepsilon_{r\cdot A} = 2.05$. The mean value by the present method becomes $73.55 \pm 0.93 - j8.49 \pm 0.41$. Next, the complex permittivity of these liquid materials was measured at frequencies ranging from 50 MHz to 3.0 GHz. Measurement results are shown in Fig. 2. As a result, the real and imaginary parts of the complex permittivity of tap water become 82.0 to 72.0 and 3.0 to 9.0, respectively.

Therefore, the frequency characteristics of the complex permittivity for a wide variety of these high-loss liquid materials were confirmed. Measurement of complex permittivity was operated under the condition that nose section was open. As a result, the effectiveness of the liquid spill is reduced. Thus we consider that this method can respond easily to a small amount of liquid material using a cheap measurement in a broad frequency range.

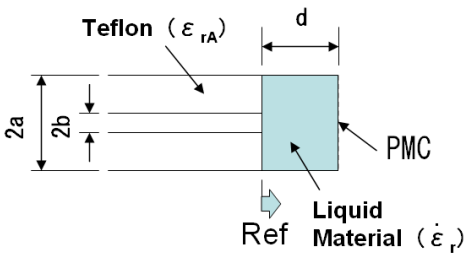

Figure 1: Analytical model.

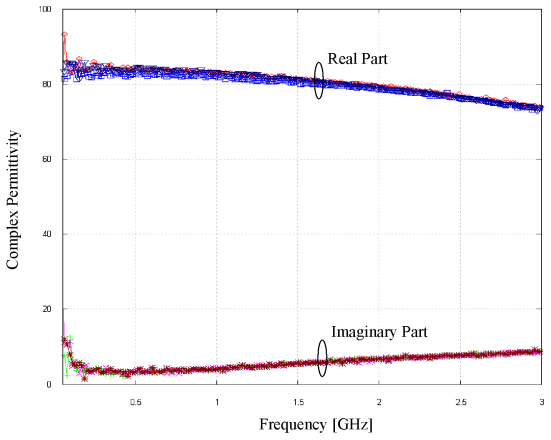

Figure 2: Frequency characteristics of complex permittivity (tap water).

REFERENCES

1. Fukunaga, K., S. Watanabe, K. Wake, and Y. Yamanaka, "Time dependence of tissue-equivalent dielectric liquid materials and its effect on SAR," *Intl. Symp. on Electromagn. Compat.*, 763–767, Sorrento, Sep. 2002.
2. Mosig, J. R. and J. C. Ebesson, "Reflection of an open-ended coaxial line and application to nondestructive measurement of materials," *IEEE Trans. on Instru. and Meas.*, Vol. 30, No. 1, 46–51, Mar. 1981.
3. Shibata, K., "Measurement of complex permittivity for liquid materials using the open-ended cut-off waveguide reflection method," *IEICE Trans. Electron.*, Vol. E93-C, No. 11, 1621–1629, Nov. 2010.

Electromagnetic Surface Wave Scattering with Microwaves

M. Chamtouri[1], **O. Merchiers**[1], **M. Francoeur**[3],
H. Tortel[2], **J.-M. Geffrin**[2], **and R. Vaillon**[1]

[1]Université de Lyon, CNRS, INSA-Lyon, UCBL, CETHIL UMR 5008, F-69621 Villeurbanne, France
[2]Aix Marseille Université, CNRS, Centrale Marseille
Institut Fresnel UMR 7249, 13013 Marseille, France
[3]Department of Mechanical Engineering, University of Utah, Salt Lake City, UT 84112, USA

Abstract— We present a microwave analogy experiment of evanescent surface wave scattering by dielectric objects. The apparatus provides the amplitude and the phase of the scattered fields in both near- and far-field regions. We compare the experimental results against numerical simulations, which take into account particle-substrate interaction. This allows to assess the validity of the numerical methods.

Introduction: Microwave-analog-to-light-scattering is a powerful method to analyze electromagnetic scattering properties of systems, which are difficult to manipulate and hence to study in the optical domain. Furthermore, modern detection techniques give direct experimental access to the field value (amplitude and phase), which is much harder for optical frequencies. The linearity of the Maxwell equations is the physical principle underlying the method; it allows rescaling wavelength together with object size, keeping field distributions invariant. These properties make it suitable as a proof of concept tool (near-field optical microscopy, metamaterials, cloaking, Kerker conditions), but also as an experimental validation tool of numerical methods [1–3].

Experimental Set Up and Results: Here we present a facility in which evanescent waves are generated on top of a dielectric substrate; this allows to study how the electromagnetic fields are scattered by objects, placed on top of the substrate, in both near- and far-field regions. This problem has attracted a lot of attention the past decade due to the development of near-field imaging techniques where knowledge of the precise interactions between tip and substrate are fundamental. On the other hand, only recently, numerical methods started to emerge capable of handling correctly particle-surface interactions [4, 5]. These methods are, however, still in a process of development and require experimental validation. Our setup offers ideal conditions to perform such tests.

In this work we will present experimental results obtained with our facility for the scattering of evanescent waves by dielectric cubes and spheres and demonstrate its capabilities for near- and far-field in terms of detection sensitivity, object size resolution and object separation resolution. We compare the measurements against Finite Element Method and Discrete Dipole Approximation including surface interactions.

ACKNOWLEDGMENT

The authors would like to thank Institut Carnot I@L, Institut Carnot STAR for their financial supports of the project SPLM.

REFERENCES

1. Greenberg, J. M., N. E. Pedersen, and J. C. Pedersen, "Microwave analog to the scattering of light by nonspherical particles," *Journal of Applied Physics*, Vol. 32, No. 2, 233–242, 1961.
2. Gustafson, B. A. S., "Microwave analog to light scattering measurements: A modern implementation of a proven method to achieve precise control," *J. Quant. Spectrosc. Radiat. Transf.*, Vol. 55, 663–672, 1996.
3. Vaillon, R., et al., "A new implementation of a microwave to light scattering measurment device," *J. Quant. Spectrosc. Radiat. Transf.*, Vol. 112, No. 11, 1753–1760, 2011.
4. *At. Transf.*, 2014, in Press.
5. Yurkin, M. A. and A. G. Hoekstra, "The discrete-dipole-approximation code ADDA: Capabilities and known limitations," *J. Quant. Spectrosc. Radiat. Transf.*, Vol. 112, 2234–2247, 2011.

On Capacity Performance of 2×2 Satellite-earth Link at 30 GHz in Rain Environment

Jing Yang, Xiaowei Xue, and Shuhong Gong
School of Physics Optoelectronic Engineering, Xidian University, China

Abstract— The channel model of MilliMeter Wave (MMW) bands single-polarization earth-satellite Multiple-Input Multiple-Output (MIMO) communication systems is presented, which comprehensively considers the propagation and scattering effects induced by rain environment. Based on the channel model, electromagnetic wave propagation theory and information theory, the expression of the channel capacity of MIMO systems is given. The influences of rainy environment on the channel capacity of MIMO systems (2×2 earth-satellite communication system in circular polarization as an example) are investigated. Give the equivalent model of STBC, VBLAST schemes for analyzing their channel capacity. The channel capacity performances of SISO, 2×2 STBC and 2×2 VBLAST schemes in 20 mm/h rain environment are simulated and discussed based on an assumed 2×2 satellite-earth link at 30 GHz in circular polarization as an example.It is obvious that channel capacity can be improved by adopting MIMO technology in satellite communication system. It is natural that VBLAST scheme is the best scheme to improve channel capacity, however it is at the cost of bit error rate. STBC should be the ideal scheme because of its potential merit of both capacity and bit error rate. We will give more comprehensive and deeper investigation in future. The conclusions given in this paper are meaningful for exploiting MIMO communication systems at MMW bands. And the method used in this paper is valid for studying the effects on channel capacity of MIMO systems induced other bad weather (snow, fog, dust, storm etc., for example).

Error in Phase Verification Results for Vector Network Analyzer Measurements in Coaxial Line System

Masahiro Horibe and Ryoko Kishikwa
National Metrology Institute of Japan, Japan

Abstract— An air dielectric coaxial line (air line) is commonly used as the reference impedance and absolute phase standard in a vector network analyzer (VNA) measurement. Phase verification method by using air line as a phase standard has been published by N. Ridler and M. Horibe. In the method, phase measurement accuracy is verified by comparing between dimensional length and electrical length, analyzed by measured value of transmission phase, of air line. However, reflection characteristics of air line at connection parts affects to error of analytical results of electrical length. Above method and its error analysis are presented.

Dielectric Loss at Millimeter Range and Temperatures 300–950 K, and Electrophysical Properties in Diamonds Grown by the Arc Plasma Jet Technology

B. M. Garin[1], **V. I. Polyakov**[1], **A. I. Rukovishnikov**[1], **A. V. Khomich**[1], **V. V. Parshin**[2], **E. A. Serov**[2], **Ch. Ch. Jia**[3], **F. X. Lu**[3], **and W. Z. Tang**[3]

[1]Kotelnikov Institute of Radio Engineering and Electronics of Russian Academy of Sciences
Fryazino Branch, 1, Vvedensky Sq., Fryazino, Moscow Region 141190, Russia
[2]Institute of Applied Physics of Russian Academy of Sciences
46, Ulianov Str., Nizhny Novgorod 603950, Russia
[3]Beijing University of Science and Technology, 30, Cellege Str., Beijing 100083, China

Abstract— The results of study of the dielectric loss at millimeter (MM) wavelengths range and temperatures 300–950 K in different diamonds grown by the arc plasma jet (APJ) technology are presented. Two samples of the APJ diamonds have been investigated: disks with diameter of 18 mm (sample D1) and with diameter of 63 mm (sample D2). The measuring technique at the base of high-Q open resonator is used. The electrophysical properties and parameters of point defects (such as concentrations, activation energies, and capture cross-sections) are investigated also by the charge-based deep level transient spectroscopy (Q-DLTS) technique (for the first time in APJ diamonds). A "strict" Ni and Ti contacts have been used that allowed to obtain quantitative data.

A comparison of results was made for these samples and with the diamonds which have been grown up by the technology of microwave plasma chemical vapor deposition (MPCVD).

It is revealed that the APJ diamonds essentially differ from the MPCVD diamonds. In particular:

1. The dielectric loss tangent $\tan\delta$ in the APJ diamond D1 increases with the frequency ($\tan\delta \sim f$) whereas in the MPCVD diamonds it decreases (at $f < 200$ GHz). It means that the loss mechanism differs from the known for the MPCVD diamonds. It corresponds to the loss mechanism induced by the lattice disorder is offered.
2. The loss tangent temperature dependences are measured in the APJ diamond D2 at the range $T = 300$–950 K on two frequencies: 157 and 313 GHz. The investigated sample essentially differs on the temperature-frequency loss dependences both from the MPCVD diamonds and the APJ diamond D1. In particular, the loss weakly depends on temperature not only at low but also at high temperatures. The theoretical explanation of these dependences on the basis of a combination of contributions of two mechanisms of losses is offered: the lattice loss, induced by the lattice disorder, and the loss related to electroconductivity in intercrystalline areas.

The received results show, that in the APJ diamond D2 the loss tangent and the concentration of lattice disorder is much lower than in the sample D1.

The APJ diamonds are very perspective for application as material for the layers and covering in the high power electronics at the millimeter and terahertz ranges that combines the low loss, insulating property, extreme high thermal conductivity, and relatively low cost.

Chaos Time Domain Reflectometry for Locating Faults on Live Wires

Hang Xu[1,2], **Bingjie Wang**[1,2], **Jianguo Zhang**[1,2], **Li Liu**[1,2], **Jingxia Li**[1,2], **and Yuncai Wang**[1,2]

[1]Key Laboratory of Advanced Transducers and Intelligent Control System
Ministry of Education and Shanxi Province, Taiyuan 030024, China
[2]College of Physics and Optoelectronics, Taiyuan University of Technology, Taiyuan 030024, China

Abstract— Location of faults on live wires has become an area of international concern, and there are several emerging technologies that can help to locate and characterize faults on live wires. The most widely used technique for fault location in automobile wiring is reflectometry [1]. In this paper, we propose a chaos time domain reflectometer (CTDR) [2, 3] for locating wires faults and experimentally demonstrate its ability for testing live wires. As shown in Fig. 1, the chaotic signal generated by a chaotic circuit (such as Boolean chaotic circuit and Colpitts oscillator) is divided into two parts: one serves as a reference signal, and the other serves as a probe signal which is mixed with the existing signal (such as 2-MHz NRZ code) and sent down to the wire under test. The faults are detected by correlating the reference signal and the mixed signal back-reflected from the faults. The experimental results show that the proposed CTDR can be used to locate faults on live wires. Figs. 2(a)–(b) shows the time series of reference signal and mixed signal back-reflected from the faults. Fig. 2(c) gives the detection results of open-circuit point at a distance of 101.4 m on a live wire, which carried a 2-MHz NRZ code. It is reasonably believed that the CTDR is a promising candidate for diagnosing live wires.

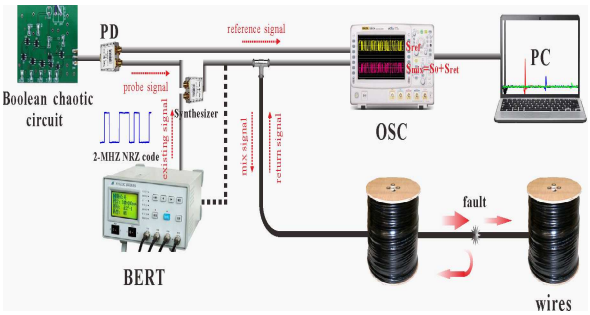

Figure 1: The Experimental setup of the CTDR for locating faults on live wires.

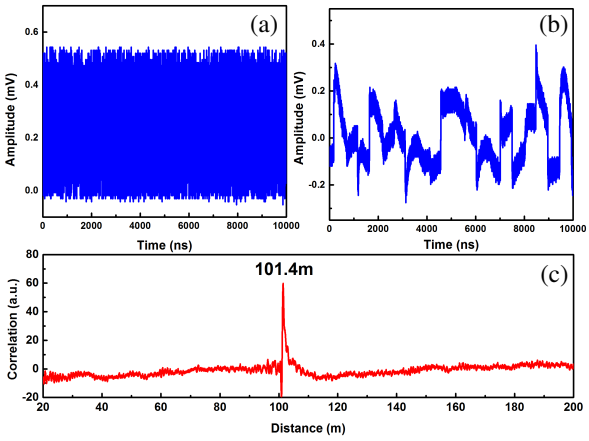

Figure 2: The time series of (a) reference signal, (b) mixed signal back-reflected from the faults. (c) The experimental results of live test for a 2-MHz NRZ code.

REFERENCES

1. Furse, C., Y. C. Chung, C. Lo, and P. Pendayala, "A critical comparison of reflectometry methods for location of wiring faults," *Smart Struct. Syst.*, Vol. 2, No. 1, 25–46, 2006.
2. Wang, A. B., M. J. Zhang, H. Xu, and Y. C. Wang, "Location of wire faults using chaotic signal," *IEEE Electron Dev. Lett.*, Vol. 32, No. 3, 372–374, 2011.
3. Xu, H., B. J. Wang, J. X. Li, A. B. Wang, and Y. C. Wang, "Location of wire faults using chaotic signal generated by an improved Colpitts oscillator," *International Journal of Bifurcation and Chaos*, Vol. 24, No. 4, 14500531–145005310, 2014.

Chaotic Radar Based on Microwave Nonlinear Circuit

Jingxia Li[1,2], **Hang Xu**[1,2], **Jianguo Zhang**[1,2], **Bingjie Wang**[1,2], **and Yuncai Wang**[1,2]

[1]Key Laboratory of Advanced Transducers and Intelligent Control System
Ministry of Education and Shanxi Province, China
[2]College of Physics and Optoelectronics
Taiyuan University of Technology, Taiyuan 030024, China

Abstract— Ultrawideband chaotic signal radars have been studied extensively in recent years since they possess the advantages of high range resolution, low probability of intercept, and high electrical counter-countermeasures performance. In this paper, a chaotic signal radar system based on an improved Colpitts oscillator is experimentally investigated. The chaotic signal is divided into two parts: the probe and reference. By calculating the cross-correlation of the echo probe and the reference signal, we can obtain the target position from the main peak position in the correlation trace. The results show that a maximum range of about 26 m can be achieved. And a ranging resolution of 3 cm for single target and 14 cm for double targets are obtained experimentally. In addition, this system is capable of locating the target behind walls.

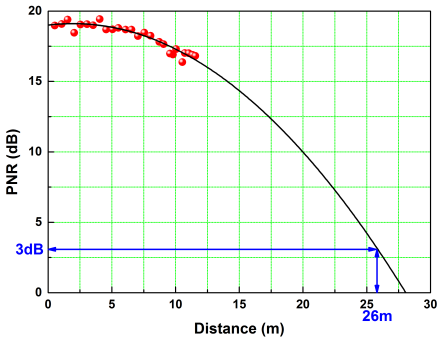

Figure 1: Dynamic range measurements of experiments (the black curve is the fitted linear function and the red spots are obtained by the experimental data).

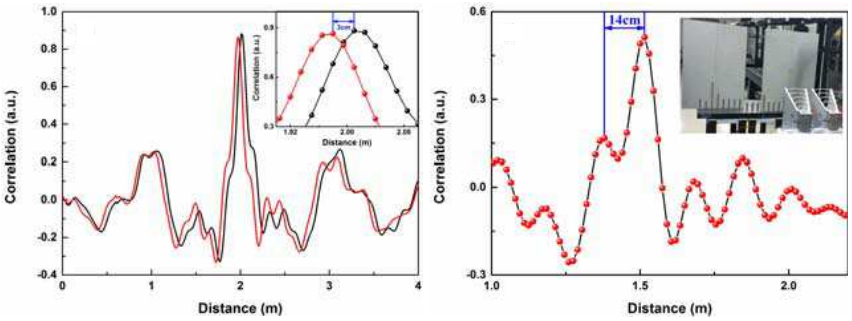

Figure 2: (a) The spatial range resolution of single-target ranging. (b) The spatial range resolution of double-target ranging.

Session 3P11b
SC4: Novel Materials and Technologies for Microwave Components

Coupled Line 180° Hybrids with Modified Trans-directional Couplers

Hongmei Liu, Shaojun Fang, and Zhongbao Wang
Information Science and Technology Institute, Dalian Maritime University, Liaoning 116026, China

Abstract— Rat race couplers are essential component used extensively in various microwave circuits, such as balanced amplifiers, balanced mixers, phase shifters, and feed networks in antenna arrays. It consists of a $3\lambda/2$ perimeter microstrip ring at the operating frequency with four ports connected along the ring.

Recently, an alternative realization of a 180° hybrid is proposed. It is based on a cascade connection of the two identical parallel coupled line couplers. It features the characteristics of simple structure, easy fabrication, and wide range of coupling values. However, the coupling levels of the parallel coupled line couplers are smaller due to fabrication constraints on the spacing of the coupled lines. Thus, it is hard to realize a tight coupling 180° hybrid on a substrate with arbitrary height and permittivity.

Based on the structure, coupled line 180° hybrids with non-TEM directional couplers and Near-TEM Lange couplers are presented. If non-TEM directional couplers are used to construct the coupled line 180° hybrid, single frequency of equal power division or symmetrical over-coupling is not possible, since the even and odd mode velocities of the coupled lines are different. Though the near-TEM Lange couplers tends to compensate for the unequal even and odd mode phase velocities, the closed narrow lines and the necessary bonding wires across the lines are difficult to fabricate using PCB technology.

To realize compact planar coupled line 180° hybrids, a novel 180° hybrid comprises of two modified trans-directional (TRD) couplers and one half-wave transmission line is proposed. The two identical TRD couplers are perpendicular connected to each other at two end points with one directly and the other through a $\lambda/2$ line section. The proposed hybrid can be easily realized on a single-layer substrate by using general printed circuit board (PCB) technology with a low cost. Modified TRD couplers with arbitrary coupling are presented in the paper to construct the hybrid with simple structure, easy fabrication, and wide range of coupling values. Theoretical analysis of the modified TRD coupler and detailed design procedures of the hybrid is given. To validate the structure, test circuit with a 3 dB coupling value was also designed and fabricated. Simulation results are compared with the measurements, and a good agreement is observed. The results show that the proposed 180° hybrid can be a suitable candidate for microwave applications.

Brush-painted Silver Nanoparticle UHF RFID Tags on Fabric Substrates

Johanna Virkki, Toni Björninen, Lauri Sydänheimo, and Leena Ukkonen
Department of Electronics and Communications Engineering
Tampere University of Technology, P. O. Box 692, FI-33101 Tampere, Finland

Abstract— Brush-painting is simple and fast additive manufacturing method for electronics, which also enables mass production in the future. The manufacturing process involves only two process steps: painting and sintering, and it is possible to fabricate antennas with only one brushed layer, which means the fabrication method can offer a great competitiveness in future RFID tag antenna manufacturing. In our study, the tag antennas were brush-painted through a stencil on two different fabric substrates (Fabric 1 was a mix of polyester and viscose used in pants and Fabric 2 was 100% cotton used in coveralls) by using only one layer of ink. The used ink was Harima NPS-JL silver nanoparticle ink.After brushing the ink through the stencil, the tag antennas were sintered with a Xenon photonic sintering system or by heat sintering in an oven. See Fig. 1 for the manufacturing process steps and Fig. 2 for the prototype antennas. The IC manufacturer had mounted the chip in a fixture patterned from copper on a plastic film. We attached the $3 \times 3\,\mathrm{mm}^2$ pads of the fixture to the sintered antennas using conductive epoxy.

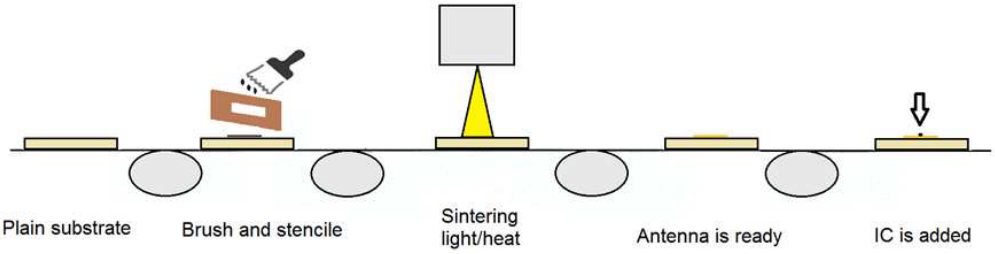

Figure 1: Brush-painting process.

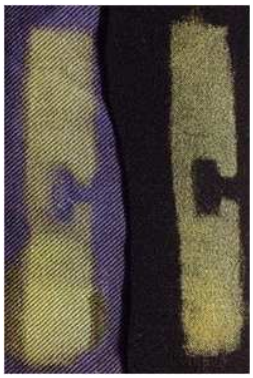

Figure 2: Prototype RFID tags antennas.

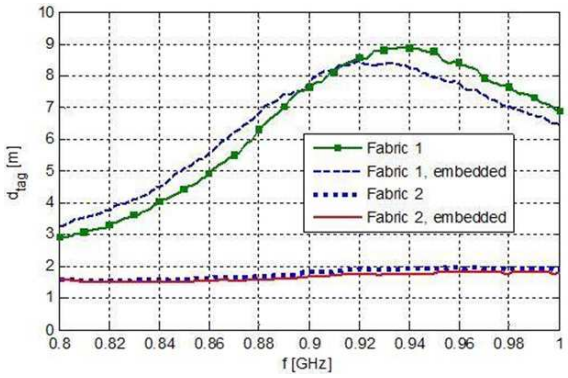

Figure 3: Measurement results.

The RFID tags were measured in an anechoic chamber, using a measurement system containing an RFID reader unit with a capability to power-frequency sweeps. For tag performance evaluation, we recorded the minimum transmitted power from the reader to activate the tag (threshold power) in the frequency range from 800 MHz to 1 GHz. Globally, UHF RFID systems operate within the regionally regulated sub-bands of this range. From the measured result, we computed the maximal read range of the tag in the absence of multipath propagation, which is a widely used tag performance indicator. The results, referred to the emission limit EIRP = 3.28 W are presented in Fig. 3. The RFID tags with heat sintered antennas did not respond. However, the RFID tags with photonic sintered antennas on Fabric 1 showed peak read ranges of over 8 meters both on top of the fabric and while embedded between two layers of fabric. We used normal textile glue join the two fabric layers.The RFID tags on Fabric 2 showed read ranges

of 1.5–2 meters throughout the UHF RFID bandboth on top of the fabric and while embedded between two layers of fabric. Thus, the characteristics of the fabric substrate have a huge effect on the characteristics of the brush-painted RFID tag antennas.The manufacturing process and the results will be further discussed in the full paper.

Combining SIW Techniques and Textile Materials for High Performance Wearable Antennas

Sam Agneessens, Sam Lemey, and Hendrik Rogier
Department of Information Technology (INTEC), Ghent University, Belgium

Abstract— The continuing developments in the area of wearable electronics are opening up new, exciting possibilities for smart fabric/integrated textile (SFIT) systems. Yet, some important impediments, such as robustness, compactness, and user comfort still need to be resolved before these systems are reliable enough for every day use. By combining substrate integrated waveguides techniques and textile materials with a dedicated design methodology, a new generation of wearable antennas can be conceived that yield high performance even in very close proximity of the human body.

A wearable antenna should guarantee robust and reliable body-worn performance, i.e., its characteristics should be independent of the morphology of the wearer or the body area on which it is deployed, both in terms of impedance matching and radiation performance. This behavior is achievable by designing the antenna such that the radiation pattern of the design is directed away from the wearer. The advantage of this is threefold: The body is 'invisible' to the antenna, meaning it will not have an in uence on the antenna's characteristics. It allows for a power efficient design, as no power is lost due to unnecessary RF energy absorption into the human body. Related to this is the final advantage: the design is safe for the user, as he or she will not be exposed to electro-magnetic radiation.

Cavity-backed slot topologies can fulfill these conditions, as the resonant cavity of the antenna is completely isolated from the outside world, with the obvious exception of the radiating slot, and transmission and reception of radiation only occurs in a single hemisphere. Furthermore, they offer possibilities in terms of size reduction by using miniaturization techniques that rely on the symmetry of the field distribution in the cavity. In addition, they can be implemented into textile materials by relying on substrate integrated waveguide (SIW) techniques, which use rows of metalized vias to form effective electrical walls for the resonant cavities. In this contribution, we will present the design and fabrication procedure of two on-body antennas, implemented in SIW technology on textile materials, which can boast excellent on-body performance.

The two realized prototypes show the potential of the SIW-textile combination for wearable antenna design: a wideband SIW topology [1] and a dual-band HMSIW topology [2] miniaturized to be compact and robust when used on-body. The wideband antenna covers two adjacent bands: the 2.4 GHz ISM and the LTE 7 band, both in uplink and downlink. It features a total bandwith of 409 MHz or 15.1% and a maximal measured gain of 6.6 dBi and 83% efficiency. The dual-band design covers two separate ISM bands: the 2.4 GHz and 5.8 GHz ISM bands. In the lower and upper ISM band, the bandwidth is 4.9% and 5.1%, the measured maximal gain equals 4.1 dBi and 5.8 dBi, and the efficiency is 72.8% and 85.6% The performance of both antennas has been measured in case of on-body deployment and when subjected to bending. For each design, very robust performance was demonstrated.

REFERENCES

1. Lemy, S., F. Declerrcq, and H. Rogier, "Dual-band substrate integrated waveguide textile antenna with integrated solar harvester," *IEEE Antennas Wireless Propagat. Lett.*, Vol. 13, 269–272, 2014.
2. Agneessens, S. and H. Rogier, "Compact half diamond dual-band textile HMSIW on body antenna," *IEEE Trans. Antennas Propagat.*, Vol. 62, 2014, in press.

Paper-based Substrate Integrated Waveguide Technology for the Future Generation of Eco-friendly Microwave Components

Stefano Moscato, Riccardo Moro, Maurizio Bozzi, and Luca Perregrini
Department of Electrical, Computer and Biomedical Engineering
University of Pavia, Pavia 27100, Italy

Abstract— The widespread deployment of wireless systems for the future generation of wireless sensor networks and for the Internet of Things requires to establish the right balance of electromagnetic performance, manufacturing costs, and environmental impact. In fact, the implementation of a very large number of wireless devices could determine a significant impact on the environment. For this reason, several research groups in industry and academia are active in the investigation of novel materials and fabrication technologies that, at the same time, guarantee a good performance and are environmentally friendly.

The use of paper as a dielectric substrate represents an ideal solution for the implementation of low cost and environmentally friendly microwave components and antennas [1]. On the other hand, substrate integrated waveguide (SIW) technology represents an emerging approach for the implementation of waveguide-like components at low cost, by using the standards technology of planar circuits [2]. SIW structures are practically shielded, thus avoiding spurious radiation and allowing closely packed interconnects and components. In addition, SIW structures appear particularly suitable for implementation on paper, due to the possibility to easily realize multilayered topologies and conformal geometries.

Different manufacturing technologies have been proposed for the implementation of SIW components on paper. Inkjet printing was adopted in [3], for the fabrication of interconnects, filters and slotted waveguide SIW antennas. In this case, a special printed is used to deposit the conductive layers on the side of the paper substrate: a particular ink with silver particles is adopted, and a following curing step is required. Another approach is based on the classical milling technique: the paper substrate is preliminary prepared, by gluing aluminum sheets at the opposite sides of the paper sheet. Subsequently, the substrate is processed by milling, in the same way as standard laminates. Classical SIW interconnects and half-mode SIW structures have been implemented by using this second technique.

The features and advantages of both fabrication technologies will be presented, along with several examples of SIW components and antennas.

REFERENCES

1. Rida, A., L. Yang, R. Vyas, and M. M. Tentzeris, "Conductive inkjet-printed antennas on flexible low-cost paper-based substrates for RFID and WSN applications," *IEEE Antennas and Propagation Magazine*, Vol. 51, No. 3, 13–23, June 2009.
2. Bozzi, M., A. Georgiadis, and K. Wu, "Review of substrate integrated waveguide (SIW) circuits and antennas," *IET Microwaves, Antennas and Propagation*, Vol. 5, No. 8, 909–920, June 2011.
3. Moro, R., S. Kim, M. Bozzi, and M. Tentzeris, "Inkjet-printed paper-based substrate integrated waveguide (SIW) components and antennas," *International Journal of Microwave and Wireless Technologies*, Vol. 5, No. 3, 197–204, June 2013.

Using Subwavelength Diffraction Gratings to Design Open Electromagnetic Cavities

M. Dupré, M. Fink, and G. Lerosey
Institut Langevin, ESPCI ParisTech & CNRS, France

Abstract— Cavities and gratings are major topics of interest in physics and engineering. Up to date, most works devoted to wave propagation in cavities concentrated on the study of the wave fields inside said cavities, since the latter are usually 2D or 3D shapes enclosed by metallic walls which conceal the electromagnetic fields perfectly. The usual way to couple such cavities to the exterior consists in carving a hole which supports propagating modes in one of its metallic walls, hence realizing so called open microwave cavities in fundamental physics, or cavity backed slot antennas in electrical engineering [2]. In the optical domain, however, open cavities have been studied for a long time. Indeed, at those frequencies metals are no longer good conductors, and a silver film a hundredth nanometers thick constitutes a semi-transparent mirror. High contrast subwavelength gratings have been used recently in so called vertical-cavity surface-emitting laser [3].

Here we propose to use binary subwavelength gratings, which are periodic patterns of metal and dielectric organized at the subwavelength scale, as semi-transparent mirrors for cavities at any frequency. We show that tuning the geometrical parameters of such gratings permits to obtain a mirror with any desired transparency. Replacing one of the walls of a cavity by a subwavelength grating, we achieve a quasi 2 dimensional microwave open cavity. We show that it gives rise to a specific radiation pattern in the far field with only discrete frequencies and angles of emission, as one can see on Fig. 1(a). Then we discuss what is expected if we introduce disorder in the cavity, by considering a disordered cavity or a random grating. We show that the emission pattern tends to become isotropic. Indeed, randomizing the grating broadens the angular pattern at a given frequency, while a chaotic cavity gives rise to distribution of wave vectors that is no longer discrete.

Finally, we show how, using subwavelength grating, we can retrieve Green functions in 2D cavities in a simple and practical way (Figs. 1(b) and (c)). Our method consists in scanning a probe in the near field of the grating that opens a 2d cavity. Hence it is much more simple than techniques used in previous works [4, 5] and could contribute to study disordered and chaotic cavities.

We believe that this type of open microwave cavity will have many applications, for instance to design highly directive antennas, MIMO antennas, radars or detectors, or to study the physics of open cavities.

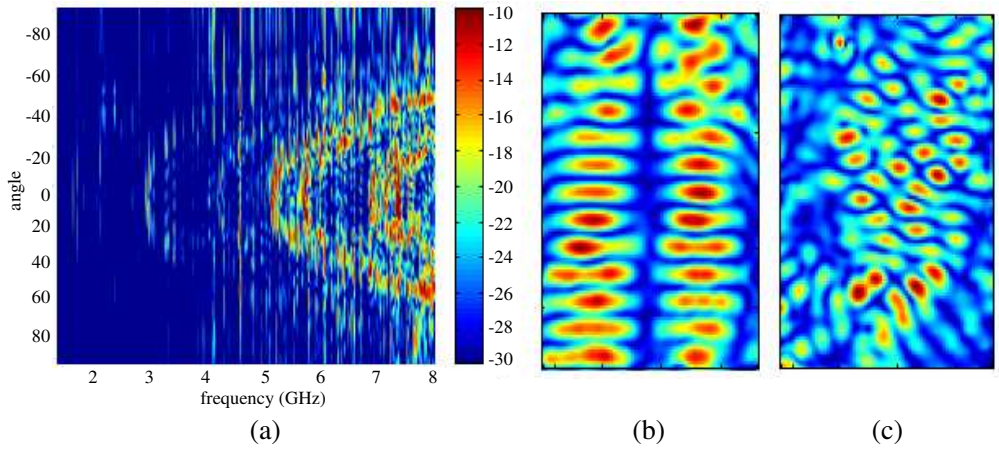

Figure 1: (a) Radiation pattern in dB as a function of the angle of emission and of the frequency. (b), (c) Accessing the Green functions of a 2D (b) ordered and (c) disordered cavity through the exterior.

REFERENCES

1. Dupré, M., M. Fink, and G. Lerosey, "Using subwavelength diffraction gratings to design open electromagnetic cavities," *Phys. Rev. Lett.*, Vol. 112, No. 4, 043902, 2014.
2. Stevenson, A. F., "Theory of slots in rectangular wave-guides," *Journ. of Appl. Phys.*, Vol. 19, No. 1, 24–38, 1948.
3. Huang, M. C. Y., Y. Zhou, and C. J. Chang-Hasnain, "A surface-emitting laser incorporating a high-index-contrast subwavelength grating," *Nat. Photon.*, Vol. 1, No. 2, 119–122, 2007.
4. Stein, J. and H.-J. Stöckmann, "Experimental determination of billiard wave functions," *Phys. Rev. Lett.*, Vol. 68, No. 19, 2867–2870, 1992.
5. Laurent, D., O. Legrand, P. Sebbah, C. Vanneste, and F. Mortessagne, "Localized modes in a finite-size open disordered microwave cavity," *Phys. Rev. Lett.*, Vol. 99, No. 25, 253902, 2007.
6. Bethe, H. A., "Theory of diffraction by small holes," *Phys. Rev.*, Vol. 66, No. 7–8, 163–182, 1944.

Session 3P12a
SC4: MIMO Systems and Applications

On Coordinated Multi-Point Transmission for Cellular Environments

Mário Marques da Silva[1,2], **Américo Correia**[1,3], **Rui Dinis**[1,4], **and Paulo Montezuma**[1,4]

[1]Instituto de Telecomunições, Portugal
[2]Universidade Autónoma de Lisboa, Portugal
[3]ISCTE-IUL, Portugal
[4]DEE-FCT-UNL, Portugal

Abstract— An important requirement of 4G systems is the ability to deliver a homogenous service, regardless the users' positions [1]. Users located at the cell edge may experience a degradation of the Signal-to-Noise Ratio (SNR) due to inter-cell interference, additional path loss or limited Base Station (BS) transmit power. In these scenarios, Coordinated Multi-Point Transmission (CoMP) plays an important role, as it allows the exploitation of additional diversity or the delivery of a high and constant throughput, regardless the users' positions.

The basic concept of Multiple Input Multiple Output (MIMO) relies on the transmission of signals through multiple paths, between multiple transmit and multiple receive antennas [2, 3]. Instead of representing an additional interference level, these multiple paths can be used as an

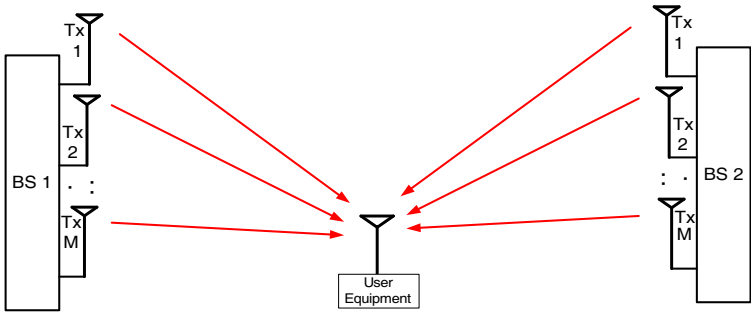

Figure 1: CoMP implemented as a downlink MIMO.

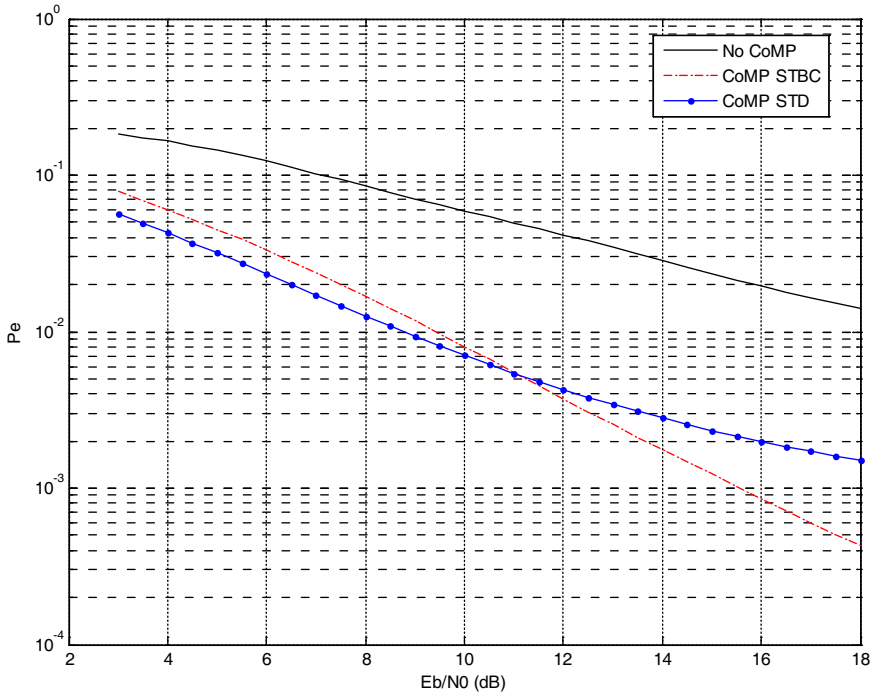

Figure 2: Pedestrian a propagation model (single receive antenna).

advantage. While in MIMO systems the multiple transmit or the multiple receive antennas are co-located, advanced cellular network architectures may also achieve the same level of diversity, but using antennas belonging to different base stations or relay nodes. Nevertheless, a certain level of synchronization or coordination is normally required between those stations [4].

Using CoMP transmission, independent antenna elements of different BSs are grouped together, forming a cluster, and the UEs can experience a throughput increase or performance improvement. In case each BS uses the MIMO scheme, the resulting MIMO can be viewed as a "giant MIMO" (see Figure 1).

Figure 2 shows the performance results concerning the Pedestrian A propagation environment, and assuming a single receive antenna, with and without CoMP (with different techniques). As can be seen, through the exploitation of diversity the CoMP STBC and CoMP STD allows a performance improvement relating to the "No CoMP". Note that the STD performs better than the STBC for E_b/N_0 below 12 dB. Since the Pedestrian A presents a propagation environment close to the single path (flat fading), the selective diversity allows selecting the antenna which presents less instantaneous frequency selectivity, leading to good results even under noisy conditions. Nevertheless, since the STBC always transmits the signals by the two antennas (antenna diversity), and since the corresponding channel presents low level of multipath diversity, it is only able to perform better than the STD for low levels of noise.

REFERENCES

1. Marques da Silva, M., et al., *Transmission Techniques for 4G Systems*, CRC Press Auerbach Publications, ISBN: 9781439815939, FL, USA, November 2012, http://www.crcpress.com/product/isbn/9781466512337.
2. Foschini, G. J., "Layered space-time architecture for wireless communication in a fading environment when using multiple antennas," *Bell Laboratories Technical Journal*, Vol. 1, No. 2, 41–59, Autumn 1996.
3. Alamouti, S. M., "A simple transmitter diversity scheme for wireless communications," *IEEE JSAC*, 1451–1458, October 1998.
4. Marques da Silva, M. and F. Monteiro, *MIMO Processing for 4G and Beyond — Fundamentals and Evolution*, CRC Press, 1st Edition, FL, USA, accepted for publication, May 2014.

Path Loss Model with Multiple-antenna

Hae-Gyu Park[1], **Hongsik Keum**[2], **and Heung-Gyoon Ryu**[1]

[1]Department of Electronic Engineering, Chungbuk National University, South Korea
[2]ElectroMagnetic Wave Technology Institute, RAPA, South Korea

Abstract— In this paper, we propose a path loss model with the multiple antennas using diversity effect. Currently wireless communication systems use the multiple antennas in order to improve the channel capacity or diversity gain. However, until recently, many researches on path loss model only consider geographical environment between the transmitter and the receiver. There is no study about path loss model considering diversity effect. Nowaday wireless communication use the multiple antennas and we in common find examples using diversity scheme that is method in order to enhance a channel capacity. Moreover we anticipate that it work harder in future researches. But in this communication system, path loss model isn't established that predict strength of received signal. So, in order to predict strength of received signal, we take changing SNR by diversity gain. When exceeding the number of antenna of reciever are 7 in proposed model, diversity effect is saturated. Therefore we consider the number of antenna of reciever until 10. We find difference between proposed model and value of calculation is 1 dB. Proposed model can predict loss of received signal in system using multiple antennas.

Coordinated Multi-Point MIMO Processing for 4G

C. Reis[1], **A. Correia**[1,2], **N. Souto**[1,2], **and M. Marques da Silva**[2,3]

[1]ISCTE-Instituto Universitário de Lisboa, Portugal
[2]Instituto de Telecomunicações, Portugal
[3]Universidade Autónoma de Lisboa, Portugal

Abstract— The concept of cooperative MIMO also named as network MIMO or coordinated multipoint transmission (CoMP) was standardized in 3GPP Release 11. The goal of CoMP is to improve the coverage of high data rates and cell-edge throughput, and also to increase system throughput. In this paper we analyze the second scenario using system level simulations in accordance with 3GPP guidelines. It is shown that the use of joint coordinated multipoint transmission achieves additional throughput gains. However, the gains obtained depend on the schedulers employed. This paper also indicates that the criterion of fairness is important when the number of users is increasing.

Features such as coordinated multipoint transmission/reception, machine type communication and energy saving are among the new features introduced in Release 11. This paper presents system level simulations for CoMP transmissions considering the scenarios defined by 3GPP. In Section 2 CoMP is introduced, while Section 3 provides a description of the system level simulations. Numerical results and conclusions are then presented in Sections 4 and 5.

The primary difference between standard MIMO and CoMP is that for the latter, the transmitters are not physically co-located. In the case of downlink CoMP, however, there is the possibility of linking the transmitters at baseband to enable sharing of payload data for the purposes of coordinated precoding. For the standard network topology in which the BSs are physically distributed, the provision of a high capacity and low latency baseband link is challenging and would probably require augmentation of the X2 inter-BSs interface using fiber. However, a cost-effective solution for inter-BSs connectivity is offered by a network architecture in which the baseband and RF transceivers are located at a central site with distribution of the RF to the remote radio heads (RRHs) via fiber.

In PtP scenario, every UE is served individually, and the link established by any given UE. If a user does not receive a packet properly, there is the option to retransmit the lost packet. Therefore, coverage in this type of system is assured. In this scenario, service delay or outage can be experienced (e.g., due to large waiting times when scheduling), being outage one of the aspects that is analyzed here. Another important aspect is the overall system capacity (that is, how many users per cell can the system serve).

The throughput distribution versus the geometry of CoMP with SU-MIMO, $M = 4$ per site, for $Nu = 20$ users per sector is illustrated in Figure 1. LDF presents an almost constant throughput independently of the location of the mobiles. The opposite is MCI with a big linear increase of throughput for users moving towards the base station site. RR provides a small linear increase of throughput for increasing geometry values. PF behavior is explained as a mix of MCI and LDF, as a result it presents a nonlinear throughput increase with increasing throughput value.

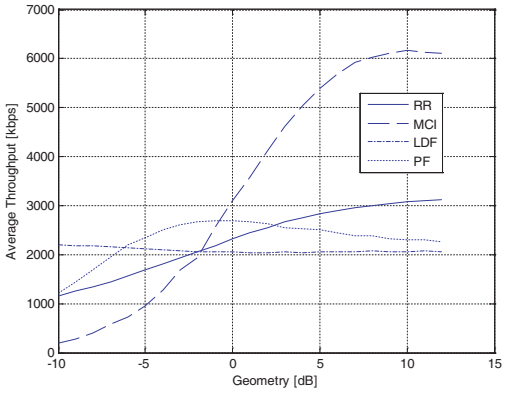

Figure 1: Throughput vs Geometry, $Nu = 20$.

In this paper it is shown that the influence of the type of scheduler employed and the cell loading were analyzed in this paper. There is no difference between the schedulers performance when the average load per user is small compared to the higher capacity of MIMO 4×4 transmission scheme. For such a traffic load it does not matter what the chosen scheduler is. In order to increase the spectral efficiency on average and/or at the cell borders, or when the number of users is increasing, CoMP with fair scheduling should be employed. The use of joint coordinated multipoint transmission achieves additional throughput gains. However, the gains obtained depend on the schedulers employed. The performance results indicate that the criterion of fairness giving priority to users at the cell border is important when the number of users is increasing and CoMP is employed.

REFERENCES

1. 3GPP, "Requirements for further advancements of E-UTRA (LTE-Advanced)," TR 36.913, V11.0.0.
2. 3GPP, "Evolved universal terrestrial radio access (E-UTRA) and evolved universal terrestrial radio access network (E-UTRAN); Overall description; Stage 2," TR 36.300, V11.3.0.
3. 3GPP, "Further advancements for E-UTRA physical layer aspects," TS 36.814, V9.0.0, 2010.
4. 3GPP, "Coordinated multi-point operation for LTE physical layer aspects," TS 36.819, V11.1.0, 2011.
5. ITU-R, "Guidelines for evaluation of radio interface technologies for IMT-advanced," M.2135, 2008.
6. Marques da Silva, M., et al., *Transmission Techniques for 4G Systems,* CRC Press Auerbach Publications, FL, USA, November 2012, ISBN: 9781439815939, http://www.crcpress.com/product/isbn/ 9781466512337.

Multiple Input Multiple Output System with Multi User Support Based on Directive Information Transmission

Paulo Carvalho[1, 2, 3], **Mario Marques da Silva**[2, 4], **and Rui Dinis**[1, 2]

[1]DEE, FCT Universidade Nova de Lisboa, Portugal
[2]IT, Instituto de Telecomunicações, Av. Rovisco Pais, Lisboa, Portugal
[3]Uninova, Instituto de Desenvolvimento de Novas Tecnologias
Quinta da Torre, Caparica, Portugal
[4]Universidade Autonoma de Lisboa, Portugal

Abstract— Low interference and privacy are crucial requirements for system reliability and security. Present and further mobile communication must support multiple users achieving at same time low interference levels. Several solutions can be adopted to reduce interference between users, such as spreading codes or beam forming. For very high bit rates first solution must be discarded. On the other hand, in environments with a very high number of users beam forming can impose demanding hardware requirements in mobile devices, which is undesirable. Moreover, other requirements such as spectral and power efficiency are also important to support the high bit rates and maximize battery life of mobile devices. These requirements can be achieved through multilevel modulations and power efficient amplification techniques. Here we present a new transmitter where the directivity is introduced at information level, since the transmitted constellation is only optimized in the desired direction. In this approach, the constellations are decomposed into several BPSK (Bi Phase Shift Keying) or QPSK components (Quadri Phase Shift Keying), being each one separately amplified and transmitted independently by an antenna. Therefore, power efficiency on amplification can be achieved due to low envelope fluctuations of each sub-constellation and the interference between users can avoided since each user can receive a constellation optimized for a specific direction. Under these conditions each user must know the configuration parameters associated to the constellation configuration, i.e., the direction in which the constellation is optimized, otherwise receives a degenerated constellation with useless data. The simulation results show the effectiveness in user data stream separation of the proposed approach.

Efficiency of MIMO and Receive Diversity in Semi-arched Tunnels

M. Lienard[1], **J. M. Molina-Garcia-Pardo**[2], **C. Sanchis-Borras**[3], **and P. Degauque**[1]

[1]University of Lille, France
[2]University of Politecnica di Cartagena, Spain
[3]University of Catolica San Antonio of Murcia, Spain

Abstract— To improve the performances of data transmission in subway tunnels, either in terms of channel capacity or of bit error rate, MIMO techniques have been proposed, despite the guiding effect of the tunnel leading to a small angular spread of the rays [1]. Indeed, for frequencies of the order or larger than 1 GHz, the transverse dimensions of the tunnel are much larger than the wavelength and the numerous hybrid modes propagating in the tunnel give rise to a modal diversity. However, high order modes suffer high attenuation at large distance from the transmitter (Tx) and the channel transfer matrix becomes ill-conditioned. It thus appears that the increase of correlation between array elements leads to bad performances of spatial multiplexing techniques [2]. Consequently, only space time block codes (STBC) or quasi STBC (QSTBC) will be envisaged for a $(2, 2)$ array or (M, M) array with $M > 2$, respectively. A parametric study has been carried out to show the influence of the element spacing for $(2, 2)$ and $(4, 4)$ MIMO schemes on the bit error rate (BER). The calculation of the BER is based on a simulation of the transmission in presence of white Gaussian noise and using a Monte Carlo method. The transfer matrices introduced in the software are those measured in a straight semi arched tunnel at a frequency of 2.8 GHz. It was assumed that the frequency band is smaller than the coherence bandwidth of the channel, of about 50 MHz, such that the hypothesis of a flat channel is valid. The statistical distribution of the BER is interpreted in terms of correlation between array elements and of the distribution of the eigenvalues of the transfer matrix.

Another way to improve the BER referred to the Single Input Single Output (SISO) case, is to implement a SIMO scheme, thus using diversity only at the receiver (Rx), taking the guiding effect of the tunnel into account. Indeed SIMO is easiest to implement and thus MIMO is justified only if its performances are, by far, much better that those of SIMO. To make a fair comparison between MIMO and receive diversity, the number of array elements, both for Tx and Rx, is the same for these two cases. This means that for SIMO, the M elements of Tx are fed in-phase, corresponding to a broadside antenna. The usual diversity techniques as maximum ratio combining and selection combining are considered. BER for MIMO and SIMO for a number of array elements $M = 2$, 4 are compared for a 16 QAM modulation, spacing between elements varying from 6 to 27 cm (i.e., from 0.56 to 2.5 wavelengths). Conclusions are drawn on the optimization of the transmission scheme depending on the desired value of the BER.

REFERENCES

1. Garcia-Pardo, C., J. M. Molina-Garcia-Pardo, M. Lienard, D. P. Gaillot, and P. Degauque, "Double directional channel measurements in an arched tunnel and interpretation using ray tracing in a rectangular tunnel," *Progress In Electromagnetics Research M*, Vol. 22, 91–107, 2012.
2. Sanchis-Borras, C., J. M. Molina-Garcia-Pardo, M. Lienard, and P. Degauque, "Performance evaluation of MIMO-OFDM in tunnels," *IEEE Antennas Wirel. Propag. Lett.*, Vol. 11, 301–304, 2012.

Channel Capacity Experiment of a Polarization Controlled MIMO Antenna for Wearable Applications

Kun Li, Kazuhiro Honda, and Koichi Ogawa
Graduate School of Engineering, Toyama University
3190 Gofuku, Toyama-shi, Toyama 930-8555, Japan

Abstract— A Small Cell era is coming for realizing ultra-high-capacity mobile communications using multiple-input multiple-output (MIMO) technique as a result of the development of LTE, LTE-Advanced and Beyond 4G cellular systems. Since mobile terminals are close to base stations in the urban area, the cross polarization power ratio (XPR) will increase and vary significantly. Furthermore, a polarization mismatch will also occur easily due to the variation in the inclination angle of an antenna caused by the operator's dynamic motions. In order to solve such difficulties, we had proposed a 3-axis weighted-polarization active antenna that can realize a large-capacity transmission in wearable radio applications in an analytical way [1].

For the purpose of confirming the validity of the proposed antenna, this paper presents a preliminary experiment for evaluating the channel capacity of a polarization-controlled MIMO antenna (see Fig. 1(a)). Firstly, the radiation pattern of the polarization-controlled MIMO antenna was measured in an anechoic chamber, which coincides well with the analytical results calculated by the method of moment, as show in Fig. 1(b). Then, the MIMO channel capacity measurement has been carried out under different use scenarios by an OTA apparatus. From agreement between the measured data and analytical outcomes, the effectiveness of proposed antenna is verified, which is useful for testing the gigabit mobile communication applications in future.

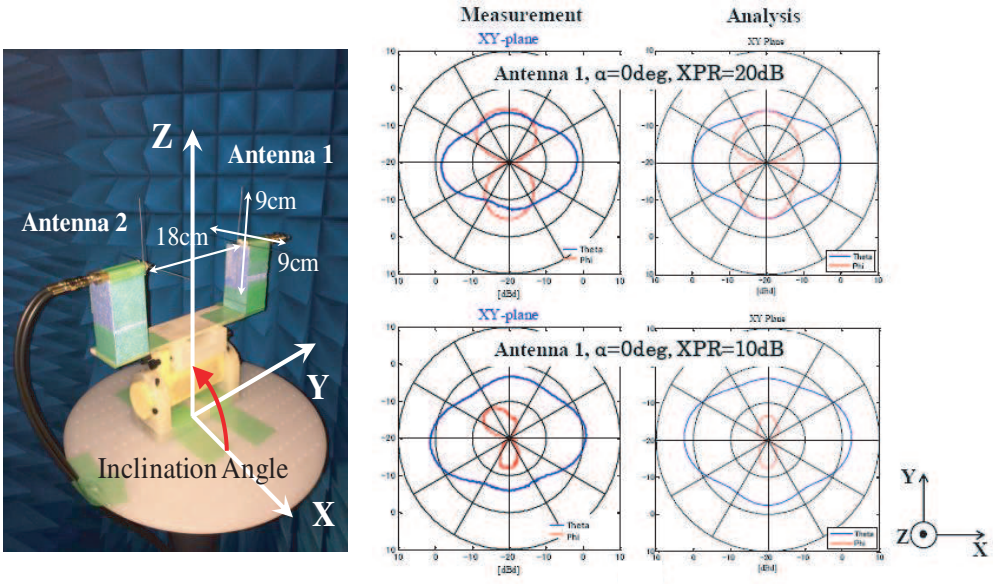

Figure 1: (a) Configuration of the polarization-controlled MIMO antenna, (b) measured and analyzed results of the radiation pattern with different XPRs.

ACKNOWLEDGMENT

This work was partly supported by the SCOPE 2013 grant number 135005102.

REFERENCES

1. Honda, K., K. Li, and K. Ogawa, "An 8 × 8 MIMO 3-axis weighted polarization active antenna for wearable radio applications," *31st URSI General Assembly and Scientific Symposium*, Beijing, China, Aug. 2014, to be presented.

Model Analysis and Isolation Enhancement of Multiple Antennas

Zhi Li, **Qi Wu**, **and Donglin Su**
School of Electronics and Information Engineering, Beihang University, Beijing 100191, China

Abstract— Modern wireless systems usually utilize multiple antennas for transmitting or receiving electromagnetic signals, however, system performance is always limited mutual coupling effects between closely placed antennas. In this paper the mutual coupling effects are studied by using the theory of characteristic modes. Several important coupling modes are separated and their contributions are evaluated in the form of modal admittance. Some higher modes, contribute little to wave radiation but increase the mutual coupling levels, are depressed by using lump element loading and also structural design. This theory provides some useful insights and can be applied to various MIMO systems.

Technical details are explained as follows. First of all, we construct the antenna model and get the triangular mesh. By using the method of moments, the impedance matrix of multiple antenna system is obtained and then the coupling modes are separated by using an eigenvalue solver. Contributions of the separated modes are evaluated through a modal excitation procedure, taking account of specified excitations. From the current distribution diagrams of the separated modes, it is easy to distinguish the high-order modes and find the entry points for antenna optimization. Lump components are introduced into the entry points in order to depress the high-order modes, and then the isolation between multiple antennas can be considerably improved. Parasitic effects of surface mounting components for standard PCB can be also considered in the simulations. Two examples are provided to verify the proposed methods, in the form of simulation and also experiments. This method does not change the dimension or function of each antenna as an important favor.

Session 3P12b
SC4: Antenna-channel Interactions and Multipath Wireless Channels

Non-stationarity Characterization for Vehicle-to-vehicle Channels Using Correlation Matrix Distance and Shadow Fading Correlation

Ruisi He[1, 2], **Olivier Renaudin**[2], **Veli-Matti Kolmonen**[3], **Katsuyuki Haneda**[4], **Zhangdui Zhong**[1], **Bo Ai**[1], **and Claude Oestges**[2]

[1]State Key Laboratory of Rail Traffic Control and Safety, Beijing Jiaotong University, Beijing, China
[2]Institute for Information and Communication Technologies, Electronics and Applied Mathematics Université Catholique de Louvain, Louvain-la-Neuve, Belgium
[3]Philips Medical Systems, MR, Finland
[4]Department of Radio Science and Engineering, Aalto University, Aalto, Finland

Abstract— Vehicle-to-Vehicle (V2V) radio channels have been considered as non-stationary due to the dynamic scatterers in V2V environments. To characterize its stationarity is of great importance as it determines the time-variant V2V channel statistics. In the past, the non-stationarity of V2V radio channels was mostly characterized by using MIMO correlation matrix distance (CMD), however, a more traditional measure of the changes in channel statistics, shadow fading correlation, has so far not been considered for V2V channels. Therefore, in this paper, we analyze the non-stationarity of V2V radio channels using two metrics: the CMD and the shadow fading correlation, and compare the estimated stationarity region.

The analysis is based on the measurements conducted in as uburban area in Finland at 5.3 GHz. We use the Aalto channel sounder and a 30×4 MIMO system, where the Rx array is a dual-polarized semi-spherical antenna array and Tx array is a uniform linear array. We cluster the antenna elements at Rx by defining the "front" and "back" elements, which correspond to the pure line-of-sight (LOS) and the blocked LOS cases, respectively. This grouping enables us to evaluate the impacts of different array configurations on the channel stationarity.

The power delay profile (PDP), CMD, and shadowing are estimated from the measured channel impulse responses. The equivalent stationarity distance is estimated using the two metrics and is found to be around 6 m. It is observed from the PDP and CMD that regions with large delay spreads correspond to smaller stationarity regions. The auto-correlation coefficient of shadow fading is found to follow an exponential decay model and the decorrelation distance is considered as the shadowing-based equivalent stationarity distance. Based on the comparison of the equivalent stationarity distances estimated by the two metrics, it is found that the CMD metric is more sensitive to the changes of direction-of-arrival/departure, whereas the shadowing metric takes only into account the power variations over time. We also note that the estimation of shadowing metric is close to the results from CMD, which shows that the shadow correlation can also be used to characterize the non-stationarity of radio channels. As the measurements of shadowing do not require MIMO system and sometimes are easier to be conducted, for some applications the shadowing correlation metric may have a wider application range in the characterization of channel non-stationarity.

On Effective Gain Variability with Antenna Orientation

Hassan El-Sallabi, Mohamed Abdallah, and Khalid Qaraqe
Electrical and Computer Engineering Department, Texas A&M University at Qatar, Qatar

Abstract— Antenna characteristics, in particular its gain, have major impact on link quality and performance of wireless communication system. Antenna gain is a crucial parameter in design of communication systems where direct line-of-sight (LOS) exists between transmitter and receiver such as in microwave links, where both transmitter and receiver are fixed. Such communication links require maximum gain of antenna in pointing direction to the other communications end. For such applications, the maximum antenna gain is a useful parameter to characterize and improve communications link quality. However, in other applications such as mobile communications, the mobile terminal could be in any direction relative to the main pointing direction of maximum gain of the fixed station (e.g., base station) antenna. The position of mobile terminal could be in LOS or non-line-of-sight (NLOS). In LOS, direct signal may arrive to a fixed antenna from directions other than that of maximum antenna gain and similarly with NLOS propagation conditions. It is well known that in multipath environment, the effective gain of antennas cannot be characterized by directive gain with sufficient accuracy. In multipath channel, the maximum directive gain can be used to increase coverage in particular geographical regions but it does not maximize the gain in a specific direction. Mean effective gain (MEG) has been introduced in literature as a more descriptive parameter for multipath propagation environment that accounts for mutual relationship between antenna radiation pattern and strength of multipath components from different directions. MEG is a statistical average measure over a series of measurements along a "route" that is considered as environment measure. The MEG of antenna is usually given in a single number for fixed antenna orientation. This fixed number could be acceptable in in fixed antenna orientation but not for variable orientation.

Communication systems based on reconfigurable antenna adopt switching between different antenna states in order to enhance its performance. Hence, neither directive gain nor MEG are anymore good metrics that are needed for switching decisions. Switching between antenna states has to be based on instantaneous information. This leads to the concept of instantaneous effective gain (IEG), which is based on instantaneous signal power distribution. The IEG is more suitable than MEG to applications, where antenna pattern switching takes place.

In this work, we present variability of MEG with average cross polarization ratio (XPR) and antenna orientation in order to find the critical angle for half-wavelength dipole antenna, where the MEG is independent of XPR and find parameters that affect the critical angle. We also present variability of IEG with orientation angle for fixed and random parameters of vertical plane angle of arrivals in terms of cumulative distribution function (CDF). The statistics of IEG in terms of its mean are also presented as a function of inclination angle of dipole antenna. Then, we discuss our investigations on the statistics and variability of SEG in order to provide more insight in its variability with instantaneous XPRs and azimuthal and elevation angle of arrivals. We present how the CDF and statistics of the SEG vary with antenna orientation angles.

Broadband Channel Measurements inside Metro Station

Ke Guan[1], **Zhangdui Zhong**[1], **Cesar Briso-Rodríguez**[2], **Carlos Rodríguez-Sanchez**[3], **Juan Moreno**[3], **Sergio Perez**[2], **and Bi Ai**[1]

[1]State Key Laboratory of Rail Traffic Control and Safety
Beijing Jiaotong University, Beijing 100044, China
[2]Radio Communications Research Group (GRC)
Universidad Politécnica de Madrid, Madrid 28031, Spain
[3]Metro de Madrid, Madrid 28013, Spain

Abstract— This paper presents a set of broadband channel measurements conducted in a real metro station in Madrid at 2.45 GHz and 1 GHz, respectively. The power delay profile (PDP) of broadband channels at these two frequencies are obtained. Based on the PDPs, two preliminary tapped delay line models are established. The measured results and corresponding models provide the first-hand information of broadband channel and, therefore, are useful to design and assess the next generation of broadband communication systems in the metro environment.

Impact of Shadowing Correlation on Microdiversity and Marcodiversity of Cellular System in High-speed Railway Environments

Bei Zhang, Zhangdui Zhong, Bo Ai, and Ruisi He
State Key Laboratory of Rail Traffic Control and Safety, Beijing Jiaotong University, China

Abstract— A good understanding of large scale parameters in different radio propagation scenarios is crucial in future wireless network planning. In high-speed railways (HSR), wireless service providers have been striving to improve the coverage of systems to ensure the safety of HSR. One approach is to choose either one or a combination of two different diversity techniques, namely, micro-diversity and macro-diversity. Performance of diversity is significantly affected by the propagation channels, especially by the correlation of shadow fading. However, the shadow fading correlation has been largely ignored when evaluating the link capacity of cellular systems. In HSR environments, correlated shadowing has been widely observed, mainly because the signals from two neighboring base stations (BSs) are likely to be shadowed by the same obstacles. In this paper, the impact of correlated lognormal shadow fading on outage probability of narrow-strip-shaped cells in HSR communication systems with both micro-diversity and macro-diversity techniques are investigated. A cross-correlation model of shadow fading from two BSs based on empirical measurements is employed in our analysis.

First of all, the power density function of signal-to-noise ratio is derived in order to obtain a close form of the outage probability for the narrow-strip-shaped cells in HSRs. It is noted that a Rice distribution is more realistic for modeling small-scale fading in HSRs, what's more, a classical lognormal distribution is adopted to model the shadowing component. Then, the outage probability with the existence of micro-diversity with maximal ratio combining and macro-diversity with selection combining is deduced, considering correlation property of shadow fading among the base stations. It is computed as a function of the shadowing correlation coefficient. Here, the shadowing cross-correlation is defined as correlations of links from the same MS to multiple BSs. Finally, the attenuation of signal amplitude caused by carriage passing loss in outage analysis for HSR is investigated.

The contributions of our work mainly focus on the impact of shadowing correlation on macro-diversity in HSRs. Numerical simulations show that a higher correlation of shadow fading leads to a high value of outage probability. It should be noted when the base stations in a cellular system are very closely spaced, therefore, the effect of correlated shadowing on system performance cannot be ignored. Simulation demonstrates the potential use of adding correlation property in the analysis of wireless systems in HSR channels.

A Novel 3D Ray-tracing Acceleration Technique Based on Kd-tree Algorithm for Radio Propagation Prediction in Complex Indoor Environment

Xiaowei Mei, Yong Zhang, and Hai Lin
State Key Laboratory of CAD&CG, Zhejiang University, Hangzhou, Zhejiang, China

Abstract— With the rapid spread of wireless communication technology, it has become a trend to achieve 5 W (whoever, whenever, wherever, whomever, whatever) of personal communication systems. Therefore, fast and accurate prediction of the indoor radio coverage trends is achieving more and more attention. At present, the ray-tracing technique has been widely used in site-specific models because of its attractive features: high accuracy, low economic cost, ease of procedures, etc.. However, the ray tracing method faces the problem of lacking of computational efficiency when applied to complex indoor environment. This paper presents a new 3D ray tracing acceleration technique based on the kd-tree algorithm for predicting radio coverage in complex indoor environment.

For each ray emitted from the source transmitter, all the ray propagation paths can be searched for by combining Shooting and Bouncing Rays (SBR) and the image source method, with the limitations of the number of reflection, transmission and diffraction. Once all the legal propagation paths are determined, the power strength in the receiving point can be calculated based on Geometry Optics (GO) and Uniform Theory of Diffraction (UTD). The kd-tree algorithm is mainly used to accelerate the core operations of ray tracing: intersection test between a ray and an obstacle. Based on the space-division and traversal features of kd-tree, it greatly reduces the number of intersection test, which as a whole obviously enhance the computational efficiency.

A typical simulation scenario — a family room, which is about 140 square meters of three bedrooms, two bathrooms and two living rooms is analyzed for comparison. The proposed acceleration method and the commercial maturity software winprop are adopted to obtain simulated results respectively. As shown in Fig. 1, the proposed method shows basically the same trend with the measured data and the winprop's results for randomly selected 15 receiving points. To demonstrate the efficiency of the proposed technique, the simulated results of the proposed method are also compared to the conventional ray-tracing technique. Therefore, it can be summarized that the proposed acceleration ray-tracing technique based on the kd-tree algorithm obtains not only high computational accuracy but also satisfactory computational efficiency.

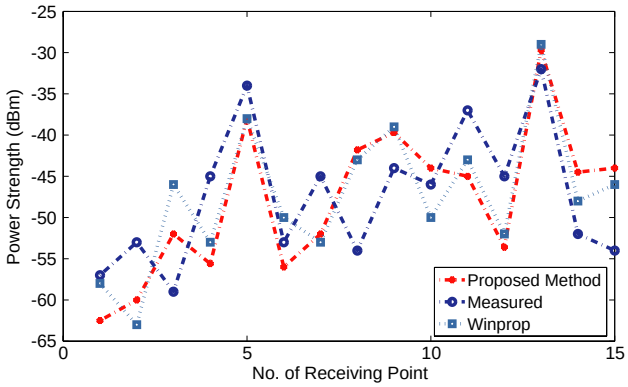

Figure 1: Comparison of measured data,Winprop and the proposed method.

Similarity Measure of Fading Profiles of Different Antenna States of Reconfigurable Antennas

Hassan El-Sallabi, Mohamed Abdallah, and Khalid Qaraqe
Electrical and Computer Engineering Department, Texas A&M University at Qatar, Qatar

Abstract— Smart antenna research has been well explored and investigated based on array signal processing theories. It was considered that at least two antennas are needed to achieve a performance gain from array signal processing theories. However, this research field assumed that the antenna pattern of each antenna element is assumed to be fixed. Reconfigurable antenna is a field that adds one more degree of freedom for wireless communications. It is based on possibility of altering some of antenna characteristics such as antenna pattern, pointing direction, polarization and resonance frequency. This makes wireless system based on either a single antenna or a multiple antennas to be more flexible than conventional antenna technology. Reconfigurable antennas usually have several antenna states, where each state defines some particular antenna characteristics. The interplay between each antenna state with multipath component of propagation environment results in different fading profiles. For similar directional radio channel response, there will be different fading levels with different antenna states.

Design of antenna states in reconfigurable antenna based wireless communication system require careful characterization process based on interplay between pattern of an antenna state and directional impulse response of propagation channel. This work introduces similarity and distance (i.e., dis-similarity) measures that are used in other field of science for characterizing interaction of antenna pattern and propagation channel. The dissimilarity measures indicate the amount of differences between fading profiles by providing information on how much we can gain from diversity of antenna states. The distance/similarity measures are presented in cumulative distribution functions that characterize the interplay of different antenna states with propagation channels and show which antenna states that behave similarly. The presented approach may help in devising a design process to select the antenna state that may enhance the performance of wireless communication systems. The presented results are for dissimilarity (or distance) measures named as Sorenson coefficient and Canberra distance. The Canberra distance is normalized to feature vector length to transform it to Canberra coefficient. The presented results for similarity measure are for Jaccard coefficient.

Algorithms for Indoor Localization on WLAN Networks Applications

S. Helhel and A. Kocakusak
Department of Electrical and Electronics Engineering, Akdeniz University, Turkey

Abstract— This paper proposes algorithms for location applications for indoor scenarios over Wireless Local Area Networks (WLAN). We compare the use of radio frequency (RF) power levels based on ray-tracing as detection methods to estimate the localization of a set of mobile station using the fingerprint technique. Wi-Fi (802.11x) and Wi-Max (802.16x) standards play an important role in applications of high frequencies techniques for locations as a detection method. The proposed algorithm computes the Euclidean distance between the samples of signals received from each known source position and radio-map obtained using EMUMAM's simulation tool. The Euclidean distance has been compared with others similarity distance measures. Experimental results show that more precision can be obtained at same level instead of different floor location of transmitter and receiver. An effect of increasing the number of transmitters has also been investigated and compared. Proposed algorithm allows to obtain very precise indoor localization over WLAN networks.

Three Dimensional (3D) Electromagnetic Field Distributions in the Air and Relative Diversity Gain

Selçuk Helhel[1, 2], Şükrü Özen[2], Yalcın Albayrak[2, 3], and I. Bahadir Basyigit[4]

[1]Tübitak National Observatory, Akdeniz University Campus, Antalya, Turkey
[2]Engineering Faculty, Department of EE, Akdeniz University, Antalya, Turkey
[3]Engineering Faculty, Department of EE, Sakarya University, Adapazarı, Turkey
[4]School of Distance Education, S. Demirel University, Isparta, Turkey

Abstract— Polarization discrimination (XPD) or equivalently polarization diversity is commonly used to improve quality in wireless communication systems such as mobile equipments' applications, LAN and WLAN applications. MIMO antennas have very big applications in wireless communications especially for broadening channel capacity. Diversity reception, especially polarization diversity, for mobile communication systems results in decreasing transmitting power as well as in receiving power which allows to control interfering signals. The measurements were performed at the Antalya Gulf in 1800 MHz network. Two routes were selected as to be driven that they are shore road connecting Antalya City and Kemer City and hill side road patched on hills. An avoiding Rayleigh fading during measurements requires having enough samples over the wavelength, and thus a vehicle speed was kept as 30 km/h and less. Thus, results have a good correspondence on slow-moving equipment. A Type-18 isotropic electric field probe compatible with NARDA SRM3000 is preferred during the measurements.

There exists 3-dimensional (3D) electromagnetic field distribution (EMFD) in the air and its components can be used for polarization discrimination (XPD) or equivalently diversity improvement. Measured values of 3 different components of electromagnetic field let us to calculate cross polarization discrimination values (relative to one another) $XPD_{xy} = 20\log(\frac{E_x}{E_y})$, $XPD_{xz} = 20\log(\frac{E_x}{E_z})$, and $XPD_{yz} = 20\log(\frac{E_y}{E_z})$. Measurements were carried out through shore roads and hillsides. The results show that through the shore side road average XPD value is about 23 dB which extremely high than expected values, and 4.69 dB through hillside road is also important value for solving communication problems. Calculated values point out that 30 dB extra relative gain can be obtained by using suitable 3 dimensional antenna design at shore sides, while 4.6 dB by hill-side roads.

Session 3P13a
Advanced Antenna Theory and Techniques

Analysis and Design of Beam-scanning Reflectarray with Circular Polarization

Zuoxing Dai[1], **Yuanbo Shang**[1], **Fengwei Yao**[2], **and Xiaobo Xuan**[1]

[1]Shanghai Radio Equipment Research Institute, Shanghai, China
[2]Science and Technology on Electromagnetic Scattering Laboratory, Shanghai, China

Abstract— The design of a electronically beam-scanning reflectarray with circular polarization is presented. First, the electrical characteristics of various elements that can be used as spatial phase shifters in circularly polarized reflectarrays are contrasted. For each element type, results are presented for the reflection phase, polarization purity and reflection loss. Then, the reconfigurable reflectarray element be chosen consists of an quadrilateral ring microstrip patch, printed on the TLY-5 substrate, vertical interconnected to a two bits switch phase shifter by coaxial connector. The designed element allows tuning of the reflected signal's phase over a 360 range with a maximum loss of 2.0 dB at 21 GHz, and the spiral antenna is adopt as the feed of the reflectarray. By full-wave commercial simulation software HFSS, the model of the antenna is simulated and optimized. At last, two reflectarray prototypes with different compensate methods for phase delays are designed and proceed, of which one is with different length of stubs, the other is with different rotated angle. The performance of two antennas is also comparison and analysis. The measured results on a 186-element reflectarray prototype with circular aperture show that by changing the different switch state on each element the main beam can be steered to large angles, up to 20 degree from broadside in both H-plane and E-plane. Due to the four states of the switch phase shifter, the first sidelobe of antenna is high, up to -7.6 dB when beam scanning to 20 degree. A loss analysis of the proposed reflectarray is also presented.

A Novel Hybrid Reconfigurable Antenna for Portable Wireless Terminal Applications

Wenxing Li, Lei Bao, Si Li, and Yingsong Li
College of Information and Communications Engineering
Harbin Engineering University, Harbin, Heilongjiang 150001, China

Abstract— In this paper, a dielectric embedded antenna with hybrid reconfigurable characteristics is proposed for portable wireless terminal applications, which is used as frequency or radiation pattern antennas. The proposed hybrid reconfigurable antenna consists of a driven element, two parasitic elements and eight switches. By controlling the ON/OFF states of these switches set on the driven element, the proposed antenna can operate at two different frequencies, namely, 0.85 GHz and 1.9 GHz. The radiation pattern reconfigurable characteristic is achieved by switching six switches installed on the parasitic elements. The proposed antenna has three modes of the radiation patterns at each frequency, has the potential to reduce noisy interference, and hence can improve the performance of the wireless systems. The simulation results demonstrated that the proposed antenna with flexible frequency and radiation pattern reconfigurable is small in size and is promising for portable wireless devices.

Novel Hepta-band Coupled-fed Antenna for WWAN/LTE Metal-ring-frame Smartphone Applications

Li-Wan Zhang and Yong-Ling Ban
Institute of Electromagnetics, University of Electronic Science and Technology of China
2006 Xi-Yuan Avenue, Western High-Tech District, Chengdu, Sichuan 611731, China

Abstract— A novel hepta-band coupled-fed antenna is presented for WWAN/ LTE metal-ring-frame (MRF) smartphone applications in this paper. Unlike the conventional solutions simply removing the redundant resonances generated by the metal ring, A creative couple-fed scheme is utilized in this proposed antenna to take full advantage of the metal ring resonances. With compact size occupation and wide band coverage, the proposed antenna for smartphones enhances the bandwidth coverage, as well as user experience of cosmetic appearance and mechanical strength.

A Hepta-band WWAN/LTE Antenna Design for Metal-rimmed Smartphone Applications

Yun-Fei Qiang and Yong-Ling Ban
Institute of Electromagnetics
University of Electronic Science and Technology of China
2006 Xi-Yuan Avenue, Western High-Tech District, Chengdu, Sichuan 611731, China

Abstract— A simple direct-fed dual-loop antenna capable of providing hepta-band WWAN-/LTE operation under surroundings of an unbroken metal rim in smartphone applications is proposed. The greatest highlight of this proposed antenna is that it provides a simple and effective solution for an unbroken metal-rimmed smartphone. The unbroken metal rim with 5 mm in height embraces the system circuit board of $130 \times 70\,\mathrm{mm}^2$. Two no-ground portions of $10 \times 70\,\mathrm{mm}^2$ and $5 \times 70\,\mathrm{mm}^2$ are set on the top and bottom edge of the system circuit board, respectively. In-between the two separate no-ground portions, there is a system ground of $115 \times 70\,\mathrm{mm}^2$ connected with the unbroken metal rim by a small grounded patch. This proposed dual-loop antenna is capable of covering GSM850/900/DCS /PCS/UMTS2100/LTE2300/2500 operating bands. Detailed design considerations of the proposed antenna are described and both experimental and simulation results are also presented and discussed.

Printed Multi-band Slot Antenna Surrounded by a Metal Ring for WWAN Smartphone Applications

Peng-Peng Li and Yong-Ling Ban
Institute of Electromagnetics
University of Electronic Science and Technology of China
2006 Xi-Yuan Avenue, Western High-Tech District, Chengdu, Sichuan 611731, China

Abstract— A printed monopole slot antenna for WWAN metal-ring frame (MRF) smartphone applications is presented and studied in this paper. The greatest highlight of the proposed antenna is that the band of 824–960 MHz scarcely affected by the modified MRF and achieves great stability. The MRF resonance is also utilized to enhance the bandwidth of the upper band of 1710–2170 MHz. With small size of $8 \times 40\,\text{mm}^2$ occupation and wide band coverage, the proposed antenna is a promising candidate for the MRF smartphone applications.

Tunable Antenna Introductions, Challenges and Opportunities

Guangli Yang[1], **Hao Wang**[1], **and Li Yang**[2]

[1]Shanghai University, China
[2]Northeastern University, China

Abstract— In this paper we systematically summarized tunable technologies in mobile terminal applications with various aspects, including the benefits, popular applications techniques, tunable switch and capacitor selections, closed and open loop tunable system architecture as well as the future opportunities and challenges. The **completed data and graphs** will be included in the presentation at the conference.

Introduction: With the increased demand of the 4G mobile technology, LTE (long term evolution) technology has been adopted in modern mobile terminal for the better broadband and multimedia service than traditional WWAN mobile network, which means that, in addition to GSM850 (824–894 MHz), GSM900 (880–960 MHz), DCS1800 (1710–1880 MHz), PCS1900 (1850–1990 MHz), UMTS (1920–2170 MHz), the LTE antenna also need to support **LTE700 (704–787) and LTE2600 (2500–2690 MHz)** for global applications. This is a big challenge for slim phones with limited space available for antenna. One the other hand, more and more carriers require not only free space but also user's performance. It is well known that the head, hand will detune antenna frequency. Traditional passive antenna is getting very difficult to balance performances at all these conditions.

Tunable antenna is the trend to overcome the passive antenna limitations to support more bandwidth and bands and minimize the head and hand or the user environment impacts. In this paper, we will briefly introduce tunable antenna technologies in application, element selection, antenna design and system integration etc..

Tunable antenna can be used for any antennas such as WAN, WLAN, RFID, mobile TV etc.. In this paper we only focus on the WAN antenna because it is the most challenge we are facing. The other antenna applications will be similar.

Two Common Tuning Techniques: Tunable matching is to put switch (connected with inductor or capacitor, or grounded) or tunable capacitor in series or shunt to the antenna feeding structure. At each stage a different inductance or capacitance will be applied to the antenna impedance matching therefore shifted frequency to what we planned, for example, from GSM850 to LTE700. To reduce the additional loss, usually shunt element positioning is preferred. The antenna matching can improve S_{11} and system efficiency accordingly but do not improve the antenna radiation efficiency because antenna structure is not changed. Tuning antenna structure, on the other hand, is to put tunable component on antenna structure (for example, connect or disconnect an arm when Switch is ON and OFF) or between PCB and antenna grounded leg to change the antenna radiation principle. If used properly, in experiment we saw less loss than tunable matching and could improve antenna radiation efficiency, but sometimes it is challenging to find a smart way to implement. Which method to select is totally depending on user's practical situation, including tunable frequency required range, tunable element increased loss to system, tunable element harmonics, ease of manufacturing, cost etc..

Tunable Switch and Capacitor: After decided the methods to tune antenna, the next important thing is to select proper tuning element, RF switch or tunable capacitor. Thanks to the global R&D from different companies, we have options to use digital tunable capacitor, BST varactor diode, RF switch, MEMS etc. [1]. Which company solution to use varies depending on the application requirements in many factors like tuning range, harmonics, loss, cost, bias voltage, maximum supported power etc.. According our limited experience, most switch and tunable capacitor can support frequency up to 3 GHz, support power more than 35 dBm, 2×2 or 3×3 mm in size. Usually the claimed loss is 0.5 dB or less, but be careful that the loss could be much higher if not used properly. For tunable capacitor, the typical tuning range is from 1 to 5 pF.

Open Loop and Closed Loop: In terminal system level, tunable component can be controlled by so called open loop or closed loop. For the open loop, it has a look-up table with pre-measured data installed in the device to call switch or tunable capacitor to react at defined situation, such as that at free space the switch will ON and antenna works at certain frequency and at head + hand case switch will be OFF so that antenna can make the frequency detune adjustment. It will help many situations. The main limitation is that it only works at the pre-defined situation and

can't be adjusted dynamically. Closed loop will be much better, means that at anytime whenever antenna is detuned, the system will noticed it and tune the antenna resonance to normal, it will be more complicated in terms of return loss S_{11} detection and system level support. A closed loop includes tunable capacitor, coupler, power detector and CPU/microcontroller. Coupler used to detect the incident and reflected RF power and give to power detector to convert to DC respectively, then microcontroller will calculated the return loss S_{11} (used to determine antenna is good or bad) and decide how to change the tunable capacitor value and will stop tuning when S_{11} is reached a preset value like -10 dB.

In early 2013, Qualcomm announced the antenna tuner chip called QFE1510 with size of 3.9×5.8 mm.) [2]. In this chip the tunable capacitors, coupler, AtoD converter, filter etc are integrated together, a big step for closed loop tuning commercialization. Also, they proposed a closed loop system schematic to make both main and diversity antenna tunable and controlled by one MSM controller. In antenna design, mobile terminal designer can play with this chip and find a better way to use it in antenna matching or tuning antenna structure.

Opportunities and Challenges: Tunable components and antenna technologies have been studied for over 10 years. The challenges are mainly from how to minimize the tunable component, nonlinearity issue impacts to the system, loss reduction, size reduction, and stable integration to the antenna for mass production. With the improvements on RF switch or tunable capacitors and more antenna integrations from various vendor and mobile terminal developers, open loop tunable solutions started to be used in mobile terminal such as Samsung Galaxy II and HTC ONE [3]. On the other hand, closed loop antenna is more challenging in terms of system integration with mobile terminal and so far none have been seen in the mobile terminal. The questions need to be answered as follows: How to work with reference design like Qualcomm? When and how often do we need to detect and tune antenna to save battery life? How fast antenna tuning is required to avoid dropping call in moving or cell changing condition? How to combine sensor technology for smarter tuning? With more and more research going forward, it is cautiously optimistic that closed loop tunable antenna solutions will be used in the mobile terminal in the near future. When to use tunable antenna depends on the many factors, try to use passive antenna first if it can do the job because of the simplicity and low cost, otherwise consider tunable antenna with very careful design and plan from system level such as cost impact, additional PCB area, power consumption, circuit tuning/settling speed and potential regulatory risks etc..

Conclusions: Smart tunable antenna is the trend to support more bandwidth and bands, minimize antenna size, and reduce user condition like hand, hand effects. With the maturity of the RF switch and tunable capacitor and proper integration to antenna, it becomes possible and is already started to implement on mobile terminals. Currently antenna tuning is mainly used as open loop to support different bands. Next big thing will be closed loop tunable solution to dynamically optimize antenna performance, it will come soon when more mobile terminal developers are developing new solutions.

ACKNOWLEDGMENT

We like to thank research funding support from Shanghai Eastern-Scholar Professorship Award and xFDTD simulation support from Remcom Inc..

REFERENCES

1. "Tunable switch and capacitor public information from different venders like Peregrine," Skywork, Sony, Wistry, Agile.
2. Qualcomm publich QFE1510 information.
3. Samsung Galaxy II and HTC ONE public information.

Session 3P13b
SC4: RFID Antennas

Cross-dipole Tag Antenna with AMC for UHF RFID On-body Applications

Chien-Wen Chiu, Chen-An Ou, and Xun-Ping Guo
Department of Electronic Engineering, Ilan University
1, Sec. 1, Shen-Lung Road, Yilan City, Yilan County, 260, Taiwan

Abstract— RFID techniques have been applied to logistics, inventory management or bioengineering. The reader antenna of a UHF RFID system is usually circularly polarized since a tag is always oriented at random A linearly polarized antenna may cause 3 dB polarization mismatch loss if its orientation is random. If the tag antenna is circularly polarized, it does not have 3 dB polarization mismatch loss. In other words, the reading range of a circularly polarized antenna is better about 41% than that of a linearly polarized antenna. In this presentation, a circularly polarized cross-dipole tag antenna printed on FR4 is proposed to avoid polarization loss and thus increase reading range. Two asymmetrically orthogonal cross-dipoles are combined to generate degenerate modes for circularly polarization. A symmetric T-matching transformer is employed to conjugate match with a Monza® 4 tag chip. The reading range from the reader to the constructed CP tag is measured in the aisle near our lab and compared with that predicted by Friis formula as the tag is put in free space.

UHF RFID tag does not work well when it is placed close to a human body or held in hand. The input impedance, radiation pattern, and realized gain of the tag antenna are influenced because of the body-proximity and absorption effects. The performance of an RFID tag near a human body is seriously degraded. Therefore, the body-proximity effects must be investigated in advance when a tag is to be designed. Some literatures have studied the effect of a human body on designed tags [1] and some scholars proposed artificial magnetic conductors (AMCs) to insulate the effect of the human body for wearable antenna applications [2]. In this presentation, a Jerusalem cross frequency selective surface (JC-FSS) artificial magnetic conductor (AMC) placed on the back plane of the proposed cross-dipole tag is studied in order to insulate the influence from the human body. To reduce AMC size, a high permittivity substrate RT/Duroid 6010 with $\varepsilon_r = 10.2$ and loss tangent = 0.0023 is designed. The AMC unit cell size is $34.1 \times 34.1\,\text{mm}^2$ and the substrate thickness is 8 mm. The strip width on the substrate is 4 mm and the gap between each unit cell is 1 mm. In order to achieve maximum benefit and minimum size, we uses 5×5 JC-FSS AMC unit cells.

The maximum realized gain of the proposed cross-dipole in free space is about 2.2 dBic, just like that of a half-wavelength dipole antenna. The measured reading range is about 12.6 m as the UHF RFID reader has 4 W EIRP output power. The practical reading range of the measurement is improved about 38.5% as compared to a linearly polarized antenna. Considering body-proximity effects on the tag, we finish a CP tag design with AMC. The designed cross-dipole on the JC-FSS AMC raises realized gain up to 5.19 dBi since the AMC help insulate the effect of the human body. The maximum radiation efficiency is up to 75% but the AR bandwidth is only 5% (891–938 MHz). The reading range still achieves 12.9 meters since the tag antenna gain is raised about 3 dBi as compared to a linearly polarized dipole antenna. The design will be presented in the conference.

REFERENCES

1. Tsai, M. C., C. W. Chiu, H. C. Wang, and T. F. Wu, "Inductively coupled loop antenna design for UHF RFID on-body applications," *Progress In Electromagnetics Research*, Vol. 143, 315–330, 2013.
2. Raad, H. R., A. I. Abbosh, H. M. Al-rizzo, and D. G. Rucker, "Flexible and compact AMC based antenna for telemedicine applications," *IEEE Transactions on Antennas and Propagation*, Vol. 61, 524–531, Feb. 2013.

A Novel Method to Measure the Two States RFID Chip Impedance

Hongbin Ge[1], **Yuan Yao**[1], **Junsheng Yu**[1], **and Xiaodong Chen**[2]

[1]School of Electronic Engineering, Beijing University of Posts and Telecommunications, China
[2]School of Electronic Engineering and Computer Science, Queen Mary, University of London, UK

Abstract— In conventional passive RFID system, the tag chip switches impedance between two states to modulate the backscattered signal from tag to reader. It's crucial to know the two states impedance with respect to frequency and input power to design the proper tag antenna. Several methods have been published, which either needs customized instruments or special algorithm. In this paper, we describe a relatively efficient and accurate solution for measuring the two states input impedance of UHF band RFID transponder chips and present experimental results for an Impinj Monza 4 chip. The presented method is simple and practical since it does not require a specialized Vector Network Analyzer (VNA) that allows external source to activate the chip under test. Besides, no additional matching between chip and VNA is needed. Generally speaking, the main tasks to measure the two states impedance of UHF RFID chip are: 1) Generate a modulated carrier with command sequence which is compliant to the EPCglobal Gen2 UHF RFID Protocol Standard to make the chip to respond; 2) Measure the impedance while the chip is still responding. In the measurement set up as shown in Fig. 1, the tag chip is directly soldered to a SMA connector, and then connected to a VNA and a commercial RFID Reader through a three ports power combiner. An attenuator is included between the power combiner and the RFID Reader in order to protect the chip from damage. The monitoring PC will control the RFID Reader and get the measurement data from VNA via GPIB/USB/LAN interface. This method can also be applied to chips in other packages. Similarly, we can use some other device (e.g., RFID emulator) to replace the commercial RFID Reader as long as it can send RFID-specific modulated commands.

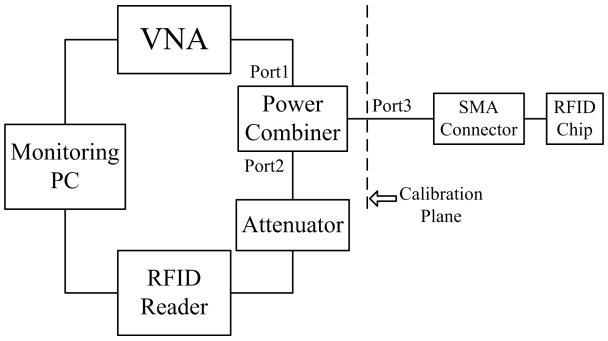

Figure 1: Block diagram of the measurement set up.

A RFID Tag Based on MIT Technology

Y. F. Hou, J. W. Yu, J. Zhang, F. Cheng, and X. Q. Lin
EHF Key Laboratory of Science, School of Engineering
University of Electronic Science and Technology of China, Chengdu 611731, China

Abstract— Today, there is a growing demand for the application of chipless RFID tags with simple structure and high-density identification data. In many resonant-based RFID designs, resonant frequencies can't be brought too close or they will merge into one broadband frequency response. Metamaterial induced transparency (MIT), realized by using fish-net pattern, was firstly reported can generate an EIT-like phenomenon [1] which has a narrow transmission window in a wide absorpting band [2] and provides an extremely large group delay.

In this letter, we propose a new passive RFID tag design using the concept of MIT. The transmission windows in MIT has high Q factor and each transmission pole comes along two transmission zeros on its side, so the resonant frequencies can be brought very close thus achieve high density data coding. By inserting an arc slot on the circular loop and adjusting the length of the slot, a narrow passband will appear in the stopband when the resonance frequency of circular loop is similar to the resonance frequency of arc slots. To make high density coding, we can add more arc slots on the circular loop to generate multiple zero and pole distributions in a relatively narrow frequency band.

In order to verify the structure of high-density identification data, we simulate the case of slotted-ring structures illustrated in Figure 1(a) when 4-bit chipless RFID tags is formed. By locating some stubs along the slot, illustrated in Figure 1(a), we can delete the relevant codes because the resonator is nulled. Figure 1(b) shows two codes of 1111 and 1110.

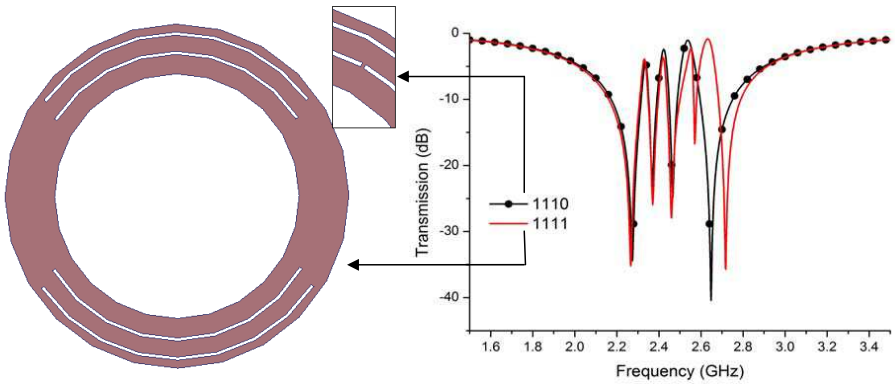

Figure 1: (a) Structure of codes of 1111 and 1110 (enclosed picture). (b) Simulated transmission coefficient.

REFERENCES

1. Papasimakis, N., V. A. Fedotov, and N. I. Zheludev, "Metamaterial analog of electromagnetically induced transparency," *Phys. Rev. Lett.*, Vol. 101, 253903, 2008.
2. Fleischhauer, M., A. Imamoglu, and J. P. Marangos, "Electromagnetically induced transparency: Optics in coherent media," *Rev. Mod. Phys.*, Vol. 77, 633, 2005.

Design of Robust UHF RFID Tag Antenna for Free-space and Metal Surface

Ye Qi[1], **Yuan Yao**[1], **Hongbin Ge**[1], **Junsheng Yu**[1], **and Xiaodong Chen**[2]

[1]School of Electronic Engineering, Beijing University of Posts and Telecommunications, Beijing, China
[2]School of Electronic Engineering and Computer Science, Queen Mary, University of London, London, UK

Abstract— Nowadays, RFID tags have covered a wide range of applications in various areas. As we know, tags are usually designed for a specific environment, and thus are very sensitive when this particular environment changes. The key reason is that the performance of the UHF antennas such as impedance and radiation efficiency will change along with the environment changes. In order to ensure the flexible operation, it will be vital to overcome the performance degradation from underlying or nearby materials. The robust antennas with good performance in different environments would bring convenience to the practical application.

The robust tag antennas including an inserted ground plane have been proposed. However, their rigid, bulky, and complicated geometry, especially the hemisphere radiation characteristic, limits their practical applications. Here, we present a robust tag antenna (see Fig. 1) with an appropriate structure that would operate adequately as a dipole in free space and as a microstrip antenna when placed on a metal surface. We choose a useful T-matching network that is commonly used for the efficient matching of UHF tags and use a folded radiating element to realize the miniaturization characteristic. For low-cost fabrication and simple structure, the antenna will be printed on a single-layer substrate without a ground plane or shorting. The simulated results (see Fig. 2) by optimizing the configuration of the feeding loop and the folded element in HFSS present both a near-optimal impedance match when operating as a dipole (in free space) and an excellent performance when operating as a microstrip with a thin foam backing material (attached to metal). Finally, we will mainly measure the readable ranges in the both environments.

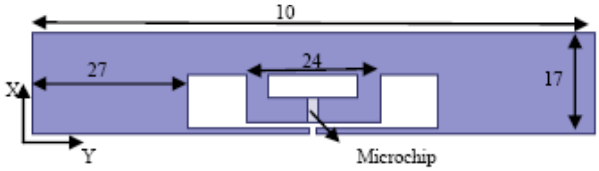

Figure 1: The geometry of the proposed tag antenna.

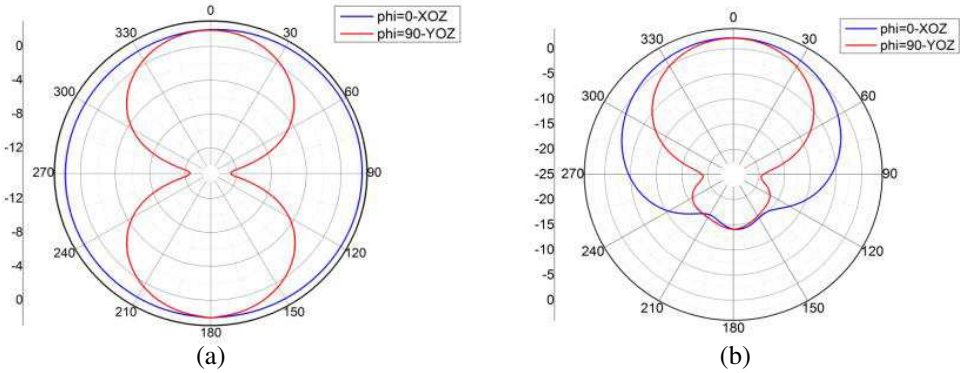

Figure 2: The simulated radiation pattern of the proposed antenna at 915 MHz, (a) in free space, (b) on the metal surface.

Modified Miniature Tri-band CPW-fed Antenna for RFID Applications

Huihui Li[1], **Yongjin Zhou**[2], **and Lei Wang**[1]

[1]Shenzhen Institutes of Advanced Technology, Chinese Academy of Sciences, China
[2]Shenzhen University, China

Abstract— A modified tri-band CPW-fed antenna is designed on a PCBoard with $\epsilon_r = 4.4$ for RFID applications. The design is optimized to operate at 0.915 GHz, 2.44 GHz, 3.55 GHz using the finite element method. In this design, two U-shaped branches are added as additional resonators to achieve multi-band operation based on our previous design. Simulation shows that the $30 \times 30\,\mathrm{mm}^2$ antenna achieves less than -10 dB return loss at the targeted frequencies. Furthermore, the antenna achieves less than -8 dB of S_{11} at 5.8 GHz. Simulated current distribution and radiation patterns are given in the paper.

REFERENCES

1. Li, H. H., X. Q. Mou, Z. Ji, H. Yu, Y. Li, and L. Jiang, "Miniature RFID tri-band CPW-fed antenna optimised using ISPO algorithm," *Electronics Letters*, Vol. 47, No. 3, 161–162, 2011.

Study of CO_2Z Hexaferrite Magnetodielectric Material as Substrate for RFID Reader Antenna

Haiyang Yu[1], **Yuan Yao**[1], **Junsheng Yu**[1], **Xiaodong Chen**[2], **and Xiaoming Liu**[1]

[1]School of Electronic Engineering, Beijing University of Posts and Telecommunications, China
[2]School of Electronic Engineering and Computer Science, Queen Mary, University of London, UK

Abstract— This paper presents investigation on the Co_2Z hexaferrite magneto-dielectric material as substrate for UHF RFID reader antenna. A number of studies on the magneto-dielectric material have shown that the specific permeability and permittivity are useful for designing microwave antennas. Therefore, Co_2Z hexaferrite material with high quality factor, high initial permeability and low dielectric loss is a promising substrate material for microwave antennas design with compactness characteristic.

In this paper, Co_2Z material as the substrate is applied to design a microstrip patch antenna at 920 MHz for UHF RFID reader antenna application with simulation software CST. As the frequency decreases, permeability and permittivity change in different physical structure of Co_2Z hexaferrite materials, is noticed in this paper. The limitations of Co_2Z material in the application of microstrip patch antenna design and improving methods will also be discussed in this article.

The geometry of the proposed antenna is shown in Fig. 1 and the simulated S_{11} is illustrated in Fig. 2. According to the analysis and simulation results, the material of the patch antenna using Co_2Z hexaferrite material have a greater degree of size reduction than the antenna with high K dielectric substrate material. The proposed antenna has good impedance matching and circular polarization characteristics. The simulation and measurement results show that this innovative hexaferrite magnetodielectric material is useful in antenna miniaturization, beneficial to achieve greater bandwidth, and there will have more performance optimizations in the design. With the increasing demand of device miniaturization for RFID reader antenna, it is foreseeable that Co_2Z hexaferrite materials will have a good application prospect in this kind of antenna design.

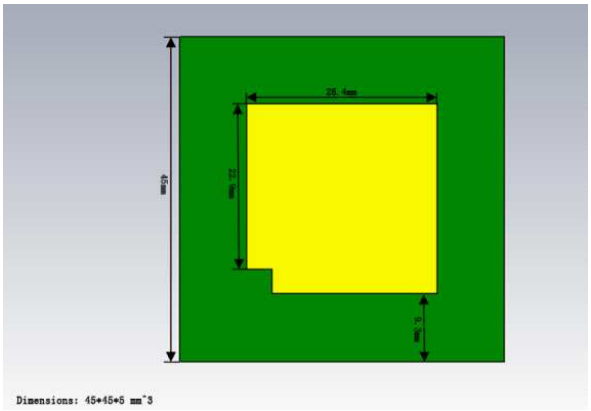

Figure 1: Geometry of the antenna.

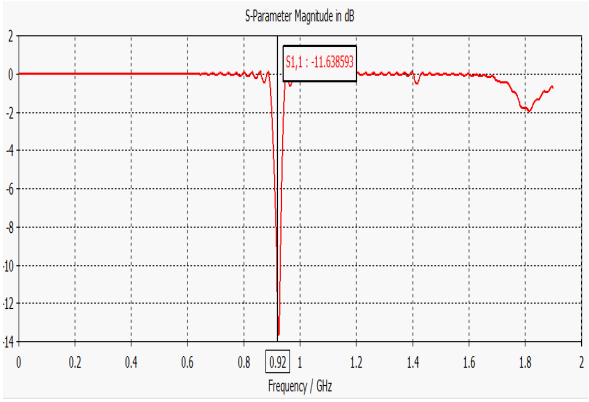

Figure 2: S_{11} parameter.

A Novel Fully Printed 28-bits Capacity Chipless RFID Tag Based on Open Conical Resonators

Raji Nair[1], **Marvin Barahona**[1], **Diego Betancourt**[1], **Georg Schmidt**[2], **Maxi Bellmann**[2], **Daniel Höft**[2], **Dirk Plettermeier**[3], **Arbed Hübler**[2], **and Frank Ellinger**[1]

[1]Circuit Design and Network Theory, TU Dresden, Dresden, Germany
[2]Institute for Print and Media Technology, TU Chemnitz, Chemnitz, Germany
[3]RF Engineering, TU Dresden, Dresden, Germany

Abstract— Printed Chipless RFID provides a feasible approach to obtain a wireless automatic identification solution to the conventional barcode cost. This is achieved by designing the tag using merely conductive printed strips and without placing any surface mounted devices (SMD) on it. The previous simplifies the fabrication process and therefore the production costs are reduced dramatically.

In this work, a novel fully printed chipless tag based on open conical resonators is proposed. The tag is developed on flexible substrate using screen-printing process which enables the fabrication of low cost tags for mass production applications. The proposed 12 resonators tag can encode 28 bits within a compact size ($4.2 \times 3\,\mathrm{cm}^2$). Currently, a "fully printed" passive chipless tag with coding capacity higher than 19 bits can be seldom found [1].

The encoding is performed using frequency shifting, by means of the backscattered Radar Cross Section (RCS) of the tag. As shown in Fig. 1(a), a vertically polarized electromagnetic wave is impinged on the surface of the open conical resonator producing an RCS with sharp peaks at particular frequencies. These frequencies correspond to the physical length of the each resonator. Simulations have been done in order to verify the effect of each design parameter.

One significant design parameter which determines the performance of the conical resonator is the aperture angle "φ". It has been found that decreasing the angle, increases the coupling between the two arms making the frequency peaks to become highly selective with suppression in the even mode, while generating an odd mode. These highly selective peaks with suppression in the even mode allow a more efficient use of frequency bandwidth, since more frequency peaks can be placed, which increases the overall tag encoding capacity.

Taking the previous into consideration, the frequency of operation has been defined between 3.1 GHz and 9.3 GHz; this means that for the used UWB frequency band from 3.1 GHz to 9.3 GHz, one resonator could be placed per almost 500 MHz bandwidth.

Several tags with different code words were printed on flexible PET substrate using the screen printing process, and their respective RCS values were measured experimentally and shown in Fig. 1(b). The obtained results proved the concept and the compact tag is suitable for automatic wireless identification applications.

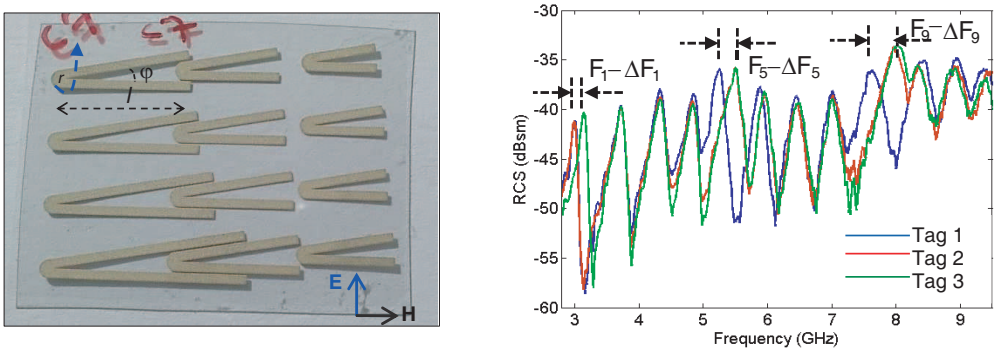

(a) (b)

Figure 1: (a) Open conical resonators tag along with the design parameters. 'l' is the length, 'φ' is the cone angle and 'r' is the radius of the curvature nose edge. In this example $l = 28\,\mathrm{mm}$, $r = 1\,\mathrm{mm}$ and $\varphi = 10°$. (b) Measured RCS response of different tag combinations with 12 resonators.

REFERENCES

1. Vena, A., E. Perret, and S. Tedjini, "High capacity chipless RFID tag insensitive to the polarization," *IEEE Transactions on Antennas and Propagation*, Vol. 60, No. 10, 2012.

Design of a Material-in-container Level Detecting RFID Sensor Antenna

Yilong Huang[1], **Yuan Yao**[1], **Junsheng Yu**[1], **and Xiaodong Chen**[2]

[1]School of Electronic Engineering
Beijing University of Posts and Telecommunications, Beijing, China
[2]School of Electronic Engineering and Computer Science
Queen Mary University of London, London, UK

Abstract— In recent years, increasing efforts have been made on researching how to design a type of RFID antenna which can be used for communication and sensing at the same time without any specific sensor. The rationale of such tag-as-sensor bases on the fact that any physical/chemical change near the tag or antenna's geometrical variation causes changes of the tag's impedance and gain, then we may achieve the information of the environmental variation that we want to know.

This kind of device should be able to properly track the evolution of the environmental variation information under observation while the performance of communication is assured. But the capabilities of sensing and communication have opposite requirements/demands because good performance of communication needs a good impedance matching of chip and tag antenna, and a good capability of sensing needs the variation of antenna impedance to be as great as possible so that the observation of environmental variation information could be clear and obvious.

In this paper, we present an RFID sensor (T-Match antenna) prototype attached on a box container that can detect the sands level in the box through the variations of tag antenna's impedance with respect to the change of sands level. In the meantime, using this example, we discussed the relationship of sensing and communication, and described how to analyze and calculate the theoretical possible maximum capabilities of sensing and communication, and how the change of sands level could be properly tracked. We described the procedure of designing geometrical parameters of the tag antenna to optimize the capabilities of sensing and communication like reading distance, sensing range and precisions, and introduced how to evaluate the performances. The simulation results and measured data will be given in the last parts of the paper.

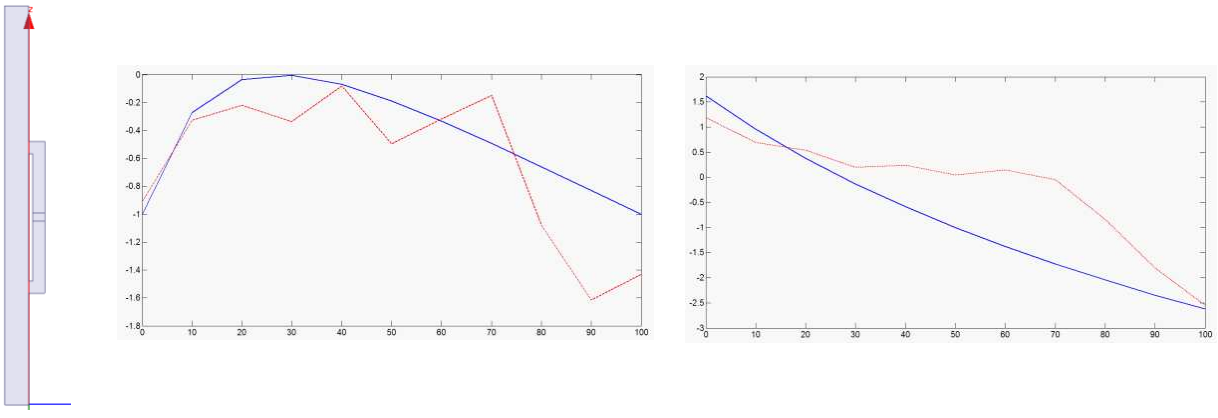

Figure 1: (a) RFID sensor antenna layout. (b) Theoretical and simulated data of communication capability. (c) Theoretical and simulated data of sensing capability.

Session 3P14
Application/Effects of EM Field/Radiation in Medicine/Bio and in Ecological Industrial Technologies

Classification of Acrylonitrile-butadiene-styrene and Polypropylene with Use of Microwave Resonance

Yuya Mori[1], **Ken Tahara**[2], **and Takehiko Kobayashi**[1]

[1]Wireless Systems Laboratory, Tokyo Denki University, Japan
[2]Kanto Electronic Application and Development Corporation, Japan

Abstract— Plastic recycling has been attracting great attention due to its ecological and economic impacts. It is often necessary to perform selecting operation on mixed composition of various plastics; however, it is very challenging to distinguish acrylonitrile-butadiene-styrene (ABS) and polypropylene (PP) resins from the mixture. A conventional selecting method utilizes sink-float separation, based on the difference in specific gravities, but the selection accuracy will be significantly reduced when foreign objects or small amount of air bubbles are adhered to the surface of the material. Another method is electrostatic selecting, which utilizes the difference in charging rate. This method employs an electrostatic field exerts a force on frictionally charged plastics and utilizes a difference in travel distances for selection. However, since the ABS and PP resins are very close in the triboelectric series, difference of surface conditions may reverse their electrification polarity.

In this paper, we propose a method for classifying the ABS and PP by means of microwave cavity resonator perturbation, which is commonly used for evaluating microwave complex permittivity. In this method, a small piece of sample material is inserted into a cavity resonator at a point when the electric and magnetic fields mark the maximum and the minimum values, respectively. The presence of the material yields shifts in resonant frequency and Q factor, in comparison with its absence. This method achieves higher accuracy than others, such as a transmission-line method, for low-loss materials. The shifts in the resonant frequency and the Q factor mainly depend on the difference in respectively real and imaginary parts of the relative permittivity ($\dot{\varepsilon} = \varepsilon' + \varepsilon''$). While ε' of ABS is slightly higher than that of PP, ε'' of ABS is much higher than that of PP (typically ten times), and therefore a large difference in the shift of Q factor is expected between ABS and PP.

Experimental evaluation was carried out with use of a TM_{010}-mode resonator at 1 GHz, whose Q factor was $15,400 \pm 200$ (depending on the temperature) when no sample was inserted. Both ABS and PP were provided by two different companies, denoted by A and B. The samples were parallelepiped whose cross section was either 1.0×1.0 or 1.0×2.0 mm, denoted by 1×1 or 1×2. These samples were inserted into the center hole of the resonator, as shown in Fig. 1. A microwave vector network analyzer was used to measure the resonant characteristics. The measured shifts in the resonant frequency and the Q factor are presented in Fig. 2, where a clear difference was observed between ABS and PP, particularly in the shift of Q factor. This result indicates a potential of microwave resonators applied to classification of ABS and PP resins.

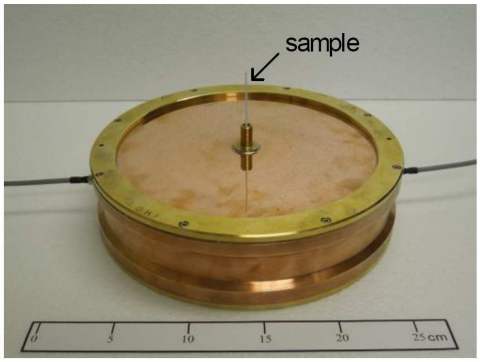

Figure 1: TM_{010}-mode 1-GHz resonator.

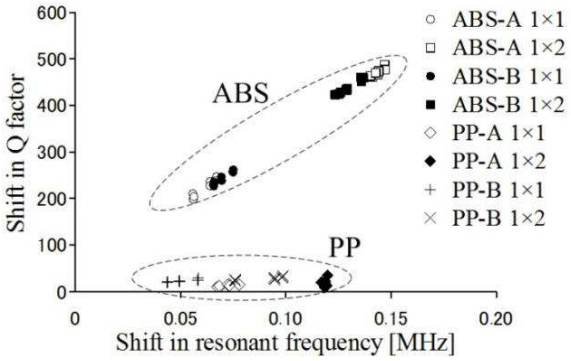

Figure 2: Measured shifts in resonant frequency and Q factor of ABS and PP resins.

Measurement of Temperature Increase of Metal Hip Replacements During Magnetic Resonance Imaging

M. Wiewegh[1] and J. Vrba[2]

[1]Faculty of Biomedical Engineering, Czech Technical University in Prague, Czech Republic
[2]Faculty of Electrical Engineering, Czech Technical University in Prague, Czech Republic

Abstract— With the increasing number of magnetic resonance (MR) systems and the growing number of patients with joint replacements, the question of safety of these patients during magnetic resonance imaging (MRI) arises.

In this paper measurements of temperature increase of three different hip replacements during MRI were carried out. The hip replacements were embedded in an agar phantom which mimics dielectric properties of muscle tissue and were placed into a MRI system with the static magnetic field intensity of $B_0 = 1.5\,\mathrm{T}$. The MRI of the samples took in total 20 minutes. Thermograms of the hip replacements were taken with a thermographic camera.

The considered three hip replacements vary in material and/or in geometry. Two of them were made of stainless steel (AISI 316L) and the third one of cobalt alloy ($Co_{35}Ni_{20}Cr_{10}Mo$). One stainless steel hip replacement was complete, i.e., with an acetabular component. The acetabular component consists of polyethylen liner and metal shell of titan alloy (Ti_6Al_4V). The other stainless steel hip replacement was heated with the MR system without the acetabular component.

Temperature was measured in two different time instances, after ten and twenty minutes of MRI, respectively. After first ten minutes temperature of the stainless steel without the acetabular component rose about 5 to 6°C. After twenty minutes, the temperature of stainless steel with the acetabular component and of the cobalt alloy rose about 7°C and 6°C, respectively. The temperature of the titan alloy rose about 2°C.

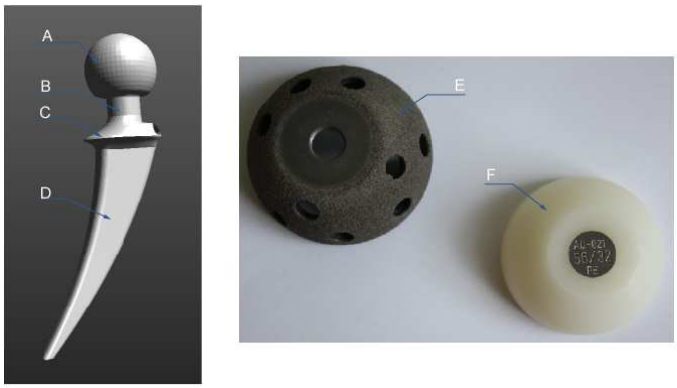

(a) (b)

Figure 1: Figure (a) describes a model of the hip replacement. In the Figure (b) there is metal shell (E) and polyethylene liner (F).

(a) (b) (c)

Figure 2: Figure (a) shows the thermogram of stainless steel hip replacement measured after 10 minutes, maximum temperature rise appears in the region of the head (ball) (A). Figure (b) shows the thermogram of the cobalt alloy after 20 minutes of heating, where the maximum temperature rise appears in the region of head (A), neck (B) and the narrow edges of the stem (D). In the Figure (c) there is the thermogram of metal shell after 20 minutes of MRI.

Electric Fields inside an Ambulance from a Roof Antenna

Hsing-Yi Chen and Chun-Kai Wang
Department of Communications Engineering, Yuan Ze University
135, Yuan-Tung Road, Nei-Li, Chung-Li, Taoyuan Shian 32003, Taiwan

Abstract— All medical devices installed in an ambulance must be correctly designed so that they can be sufficiently immune to electromagnetic interference (EMI). Especially medical devices installed in ambulances used for emergency medical care should be able to function correctly in close proximity to communication instruments. Unfortunately in 1992, a patient attached to a monitor-defibrillator inside an ambulance died because EMI generated from a radio transmitter installed on the ambulance roof prevented the machine from working. Therefore, the interaction between communication instruments and medical devices installed in ambulances should be well studied. The spatial EM field distribution inside a vehicle obtained by simulations and measurements has been reported in the literature. However, only a few studies on the investigation of the spatial EM field distributions inside an ambulance are reported. Investigating the spatial EM field distributions inside an ambulance will be helpful in assessing possible EMI risks on medical devices. In this paper, the FDTD method was used to calculate electric fields inside an ambulance due to the radiation emitted from a transmitter located on the ambulance roof. Simulation results of interior electric fields emitted from the exterior roof transmitter for the ambulance roof made of metallic material are found not to exceed the 3 V/m standard immunity level which is regulated by the IEC Standard 60601-1-2. However, electric field strengths inside the ambulance for the ambulance roof made of non-metallic material are found to exceed the 3 V/m standard immunity level. The obtained results indicate that the interior environment of ambulances can cause considerable challenges to medical devices for the ambulance roofs made of non-metallic materials.

The Effect of Hypomagnetic Field on the Behavior of Adult Male Mice

Weichuan Mo[1], **Jingpeng Fu**[1], **Haimin Ding**[2], **Ying Liu**[1], **Qian Hua**[2], **and Rongqiao He**[1]

[1]State Key Laboratory of Brain and Cognitive Science
Institute of Biophysics, Chinese Academy of Sciences, Beijing 100101, China
[2]School of Preclinical Medicine, Beijing University of Chinese Medicine, Beijing 100029, China

Abstract—

Introduction: Hypomagnetic field (HMF) refers to an extremely weak magnetic field with magnitude lower than 5 μT, which is one of the environmental factors of outer space. It has been reported that HMF exposure decreasesanimal working capacity and learning and memory ability. Therefore, the astronauts would suffer from potential risks due to the HMF exposure during long-term space missions. Investigating the effects of the HMF effect on adult mammals would provide valuable information for the health care in space life science.

Method: Adult male C57BL6 mice (4–6 weeks old) were reared in an HMF simulatedby a 3-axis Helmholtz coils system (< 500 nT). The control animals were maintained in the same room (~ 50 μT). Night vision cameras recorded the daily activities of the HMF-exposed mice and the drinking behaviors of the mice were analyzed. The locomotor ability of the mice was assessed with open field and tread mill tests.

Results and Discussion: After one-month rearing in the HMF, body weight increase of the HMF-exposed mice was slowed down after 2 weeks exposure but the food and water uptakes were not affected. The locomotor activity of the HMF-exposed mice was significantly reduced in open field test and treadmill test. The daily water drinking attempts of the HMF-exposed mice were significantly increased. Our results indicate that HMF exposure weakens the locomotor activity and disturbs the daily activity of adult mice. Further investigations at histological and cellular level would provide useful data for the understanding of the mechanism of the HMF effect and contribute to the development of the counteractive strategy to the HMF exposure.

Fundings: This work was supported by the Queensland-Chinese Academy of Sciences Biotechnology Fund (Grant No. GJHZ1131), the project of Chinese Academy of Sciences for the development of major scientific research equipment (Grant No. YZ201148), the National Nature Science Foundation of China (Grant No. 31200628), and the External Cooperation Program of BIC, Chinese Academy of sciences (Grant No. GJHZ201302).

A Multi-purpose Flexible Antenna for Musculoskeletal MR Imaging at 3T

Rui Zhang[1], **Qunzhi Chen**[2], **Hongyang Yuan**[3], **Fan Jia**[2], **Wenchao Cai**[4], **Kai Zhao**[4], **Jue Zhang**[1, 2], **Xiaoying Wang**[4], **and Jing Fang**[1, 2]

[1]College of Engineering, Peking University, China
[2]Academy for Advanced Interdisciplinary Studies, Peking University, China
[3]Department of Radiology, The University of North Carolina at Chapel Hill, USA
[4]Department of Radiology, Peking University First Hospital, China

Abstract—

Purpose: Flexible coils and antennas for MR imaging have attracted much attention recently because they can highly improve patient comfort and achieve geometrical flexibility to image joint tissues under different flexion angles. Many flexible coils have been proposed for MR imaging different joint tissues, such as knee [1] and wrist [2]. But they can only be used for imaging of one particular joint tissue, there is a strong demand to develop a new flexible coil to cover more regions of the musculoskeletal system. In this study, we proposed a multi-purpose flexible flex cable antenna (MFFCA) for imaging of hand and wrist, shoulder, elbow, ankle and knee, which has the advantages of high flexibility, satisfied comfort, large FOV, high SNR and low cost.

Materials and Methods: Inspired by the loopless monopole antenna [3], we designed the MFFCA which has a flex cable (80 cm in length), a tuning/matching circuit and a signal transmission line (Figure 1). The MFFCA is only employed to receive signal while the body coil is used for exciting. The flex cable has 60 elements. Each element has the diameter of 0.6 mm and the distance between two adjacent elements is 1.0 mm. The tuning and matching circuit consists of 3 tunable capacitors (C_1, C_2, and C_3) and a fixed capacitor (C_4). The antenna is connected to a 3T whole-body MRI system (Signal., GE Medical Systems) through a signal transmission line.

In order to evaluate the feasibility and validity of the proposed MFFCA, the musculoskeletal system of a health volunteer (age 25, male) was examined by using the MFFCA. For imaging of shoulder, ankle and knee, the volunteer was asked to lie down in supine position and the MFFCA was put on the top of the targeted joint tissues by sticking medical plastic tape. For imaging of elbow, the volunteer was required to lie on his stomach with the palm of the hand up and the MFFCA was placed on the top of the arm by sticking medical plastic tape while the arm was in the opposite direction for imaging of hand and wrist. To better demonstrate the high flexibility of our design, we carried out the imaging experiments of elbow, ankle and knee under different flexion angles with the aid of foam blocks and a homemade supporting gadget. The scanning parameters were: sequence: FSE (T1WI: repetition time (TR) = 400.0 ms, echo time (TE) = 12.4 ms; T2WI: TR = 3000.0 ms, TE = 102.0 ms; PDWI: TR = 3000.0 ms, TE = 12.4 ms), slice thickness = 6.0 mm (shoulder, hand and wrist, elbow, ankle) or 7.0 mm (knee), slice spacing = 0 mm, Matrix = 256 × 256, and NEX = 4.0 (shoulder, hand and wrist) or 2.0 (elbow, ankle, knee). The coronal, sagittal and axial images were acquired for shoulder, hand and wrist while the sagittal images under different flexion angles were obtained for elbow, ankle and knee. To evaluate the safety of the MFFCA, we utilized the optical fiber thermometer to measure the temperatures of the surface of flex cable under three different positions during the scan of two continuous sequences (3 min 48 second) and the probes were placed between the tissues around the knee and the flex cable.

Results: As shown in the images of shoulder, hand and wrist, fine anatomic details are rendered and different joints and tissues show clear contrast. The magnetic field distribution of the MFFCA is homogeneous and the SNR of the image is high enough for clinical applications. The images of elbow, ankle and knee under different flexion angles also demonstrate clear contrast between different joints and tissues, high SNR and satisfied homogeneity. Besides, the knee images suggest that the longitudinal coverage of the MFFCA can achieve more than 48 cm, which is much larger than conventional surface coils, birdcage coils and array coils. The largest temperature increment of the three positions during the scan is 1.4°C, which proves the safety of the MFFCA.

Discussion & Conclusion: The results have demonstrated the high flexibility, large FOV, high SNR and safety of the MFFCA. The flex cable is lightweight and can be placed close to the tissues for higher SNR. Actually, the MFFCA is very suitable for joint imaging with different flexion angles under dynamic situations to evaluate joint abnormalities which exhibit

physiological changes only under dynamic conditions, such as neuro-muscular contractures and joint malformations [4]. In the future, we will carry out the real-time MR imaging of joint movement using the MFFCA.

In conclusion, we developed a multi-purpose flexible antenna for musculoskeletal MR imaging with high flexibility, satisfied comfort, large FOV, high SNR and low cost, which can be applied

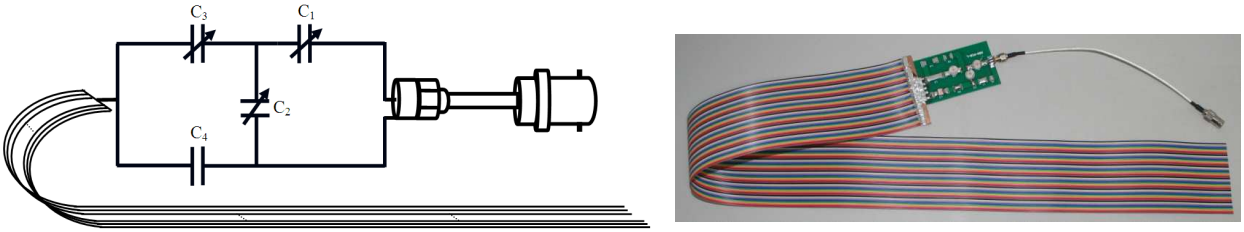

Figure 1: (a) The schematic diagram and (b) photo of the proposed MFFCA.

Figure 2: The MR images of musculoskeletal tissues at different body parts by using the MFFCA ((a) hand and wrist (T1WI, FOV: 28×28 cm), (b) shoulder (T2WI, FOV: 24×24 cm), (c) elbow (PDWI-Sag, FOV: 32×32 cm), (d) ankle (T2WI-Sag, FOV: 30×30 cm), (e) knee (PDWI-Sag, FOV: 48×48 cm)).

in the assessment of musculoskeletal tissues, especially under flexion and dynamic conditions.

REFERENCES

1. Nordmeyer-Massner, J. A., et al., *Magn. Reson. Med.*, Vol. 67, No. 3, 872–879, 2012.
2. Nordmeyer-Massner, J. A., et al., *Magn. Reson. Med.*, Vol. 61, No. 2, 429–438, 2009.
3. Yuan, H. Y., et al., *Magn. Reson. Imaging*, Vol. 31, No. 1, 150–155, 2013.
4. Quick, H. H., et al., *J. Magn. Reson. Imaging*, Vol. 15, No. 6, 710–715, 2002.

System for Animal EM Exposure with Well Defined Dosimetry and First Results of Biological Experiments

Jan Vrba[1], **David Vrba**[2], **Jan Vrba, Jr.**[2], **Frantisek Vožeh**[3], **Jan Barcal**[3], **and Luca Vannucci**[4]

[1]Department of EM Field, Faculty of Electrical Engineering
Czech Technical University in Prague, Prague, Czech Republic
[2]Department of Biomedical Technique, Faculty of Biomedical Engineering
Czech Technical University in Prague, Kladno, Czech Republic
[3]Department of Patophysiology, Medical Faculty in Pilsen
Charles University in Prague, Pilsen, Czech Republic
[4]Institute of Microbiology, Czech Academy of Sciences, Prague, Czech Republic

Abstract— The whole-body exposure system for unrestrained mice was designed in order to analyze the influence of electromagnetic field. The setup operating at 900 MHz was designed with respect to induced uniform field, external radiation elimination, absorbed power determination, sufficient space for mice movement together with even mice exposure and costs. The main aim of this paper is to assure that the dosimetry results reached by computer simulations can be used for determination of absorbed power in the unrestrained mouse. The whole-body exposure chamber with anatomical mouse model was simulated by two different numerical methods: finite-difference-time-domain method (FDTD) and Finite Integration Technique (FIT) and its dosimetry results were compared by computed SAR values. In our contribution we will describe our first results dealing with observed biological effects of EM field, obtained by real exposures of experimental animals.

FEM Analysis of Conical Type Coaxial Open-ended Probe for Dielectric Measurement

H. Arab and C. Akyel
Ecole Polytechnique of Montreal, Canada

Abstract— This paper deals with a numerical modelling technique based on finite elements method (FEM) in microwave frequency for computing the dielectric constant and loss factor of a homogeneous dielectric material by using conical-type coaxial probe. This sort of probe can be easily inserted into a wide range of biological tissue types and semi-rigid materials like rubber, some plastics, and organic materials (ex: dairy, butter, etc. for measuring moisture content). Where his feature is considered to be very important in biological and industrial applications. The measuring principle is based on detecting conductance and capacitance change with respect to the dielectric mass movement in the fringe electrical field. A three-dimensional finite-element formulation is employed in the dielectric material region and a small neighbouring region of the probe structure on which it is mounted. The electrical input admittance as well as the reflection coefficient are found from the finite-element analysis. From this, the conductance and capacitance related to the conical probe and fringing field are calculated and consequently the dielectric constant and loss factor are determined. In contrast to many other modelling techniques used for coaxial probe which are approximate and hence limited, the finite-element model is more

Figure 1: Handmade Probes and network analyzer.

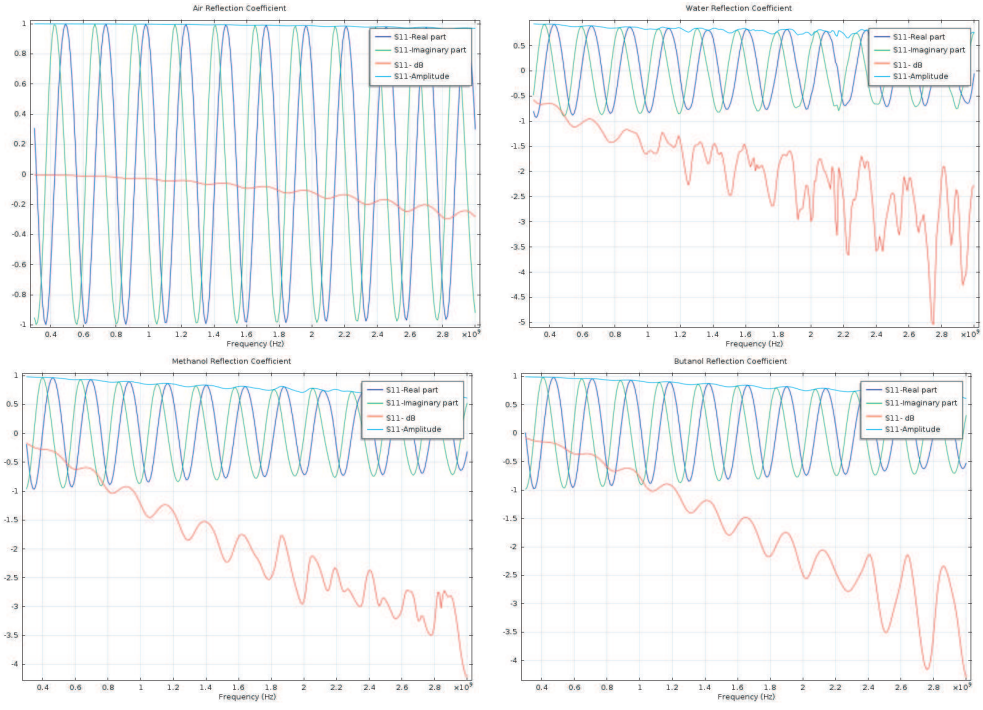

Figure 2: Reflection coefficient for Air, Water, Methanol and Butanol.

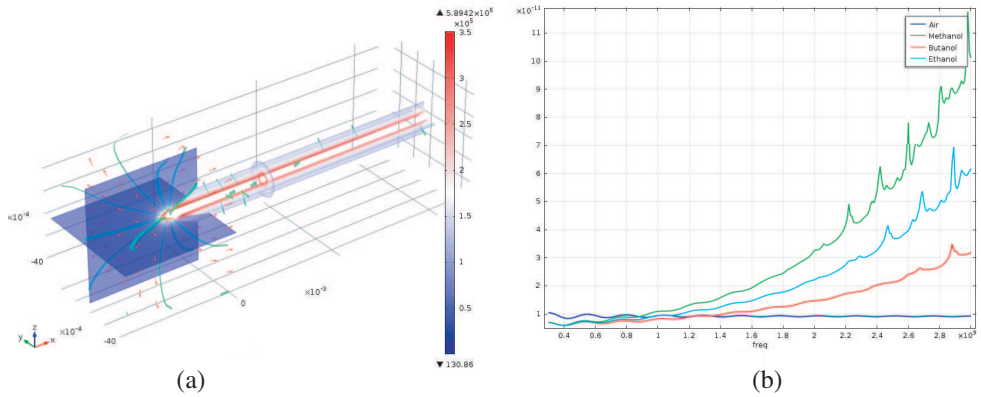

(a) (b)

Figure 3: (a) Electric field. (b) Capacitance for open ended conical coaxial probe (cone angle 30 degree).

exact and is applicable to complicated geometries. To demonstrate the accuracy of the numerical model, a parallel experimental study was carried out in the laboratory for the same geometric dimensions. The two results are compared and show excellent agreement, and also demonstrating that finite-element modelling is a good approach for optimized conical coaxial probe design. The reflection coefficient factor, electromagnetic field at the probe aperture and permittivity of different materials were analyzed in different frequencies (300 MHz to 3 GHz). Figure 2 shows the measured reflection coefficient of Air, Water, Methanol and Butanol at 20 degree with conical type open ended coaxial probe and in Figure 3 calculated electric field and capacitance by FEM method for different material are shown. The results show that open-ended conical coaxial probes can be successfully used especially at low frequencies with the advantage of increased accuracy and sensitivity. Moreover, it is less effected by unavoidable temperature variation when compared to standard at-plan open-circuit coaxial-probe. An additional advantage of the conical-type probe is that it does not have the problem of at coaxial probe with solid surface.

REFERENCES

1. Wagner, N., M. Schwing, and A. Scheuermann, "Numerical 3-D FEM and experimental analysis of the open-ended coaxial line technique for microwave dielectric spectroscopy on soil," Vol. 52, No. 2, 1064–1076, 2014.
2. Panariello, G., L. Verolino, and G. Vitolo, "Efficient and accurate full-wave analysis of the open-ended coaxial cable," *IEEE Transactions on Microwave Theory and Techniques*, Vol. 49, No. 7, 1304–1309, 2001.
3. Lan, F., C. Akyel, et al., "A six-port based on-line measurement system using special probe with conical open end to determine relative complex permittivity at radio and microwave frequencies," *Proceedings of the 16th IEEE Instrumentation and Measurement Technology Conference, 1999, IMTC/99*, 1999.

Zeroth-order Mode Resonator Metamaterial Applicators for Superficial and Deep Local Microwave Hyperthermia

D. Vrba[1], **J. Vrba, Jr.**[1], **M. Wiewegh**[1], **and J. Vrba**[2]

[1]Department of Biomedical Technology, Faculty of Biomedical Engineering
Czech Technical University in Prague, Kladno, Czech Republic
[2]Department of Electromagnetic Field, Faculty of Electrical Engineering
Czech Technical University in Prague, Zikova 4, Prague 166 36, Czech Republic

Abstract—

Aims: It is demonstrated that a theory of zero-order mode resonator (ZOR) metamaterial (MTM) structure can be used for the development of a novel class of applicators for microwave thermotherapy, for example, for hyperthermia in cancer treatment or for physiotherapy. The main idea of creating such an applicator is to generate and radiate a plane electromagnetic (EM) wave into the treated biological tissue, at least in a certain extent. The main aim of this paper is to investigate whether an EM wave generated by ZORMTM structure and emitted into the biological tissue can produce a homogeneous SAR distribution in the planes parallel to the applicator aperture and achieve a penetration depth approaching the theoretical limit represented by SAR distribution and penetration depth of an ideal EM plane wave.

Materials and Methods: EM field distribution inside a virtual phantom of the treated region generated by the applicator that is based on the proposed ZORMTM principle is investigated using a well-proven full-wave commercial simulation tool.

Results: The proposed applicator type shows both a low unwanted leaked electromagnetic field and a fairly homogeneous electric field in its aperture as well as in the virtual phantom of the treated region.

Conclusions: It has been demonstrated, that when penetrating biological tissue EM waves generated by the proposed applicators generate very good SAR homogeneity and achieve penetration depth approaching, to a certain extent, the theoretical limit, that is, close to that of the EM plane wave.

REFERENCES

1. Vrba, D. and J. Vrba, "Novel applicators for local microwave hyperthermia based on zeroth-order mode resonator metamaterial," *International Journal of Antennas and Propagation*, April 2014.

Applicator for Superficial Microwave Hyperthermia Filled with Anisotropic Dielectric Media: Numerical Investigation of Design Degrees of Freedom

J. Vrba, Jr.[1], **D. Vrba**[1], **M. Wiewegh**[1], **and J. Vrba**[2]

[1]Faculty of Biomedical Engineering, Czech Technical University in Prague, Czech Republic
[2]Faculty of Electrical Engineering, Czech Technical University in Prague, Czech Republic

Abstract— From all applicators for superficial microwave hyperthermia proposed in the past and used now in the field of RF/microwave hyperthermia rectangular-waveguide-based applicators excels, in comparison to planar applicators, in:

1. homogeneity of the SAR distribution created in the treated biological tissue,
2. low leaked electromagnetic fields, due to closed metallic walls around the applicator aperture.

On the other hand, the main drawbacks of these applicators are that they are fairly bulky and heavy. Often, in order to decrease the dimensions of these applicators/decrease their working frequency they are completely filled with water that makes them even weightier.

In the past the effective aperture of the rectangular-waveguide applicator with TE_{10} mode was improved using side dielectric slabs of titanium dioxide which shows high relative electric permittivity. The rest of these modified applicators are filled with water.

The numerical investigation performed and presented in this paper is motivated by expectation that by filling a rectangular waveguide with anisotropic media the number of degrees of freedom for the applicator design will increase. The physical parameters like dimensions, weight of the applicator as well as the SAR distribution produced in the treated area are the main investigated properties of the proposed applicator.

The proposed rectangular-waveguide-based applicator is compared with a rectangular waveguide applicator filled completely with water and with the one partially filled with water and partially with titanium dioxide slabs. The numerical simulations will be performed using a full-wave well-proven commercial electromagnetic field simulator COMSOL Multiphysics.

FDTD Analysis of Digitally-modulated Electromagnetic Wave Propagation in Human Head

T. Wuren[1], **Y. Tanaka**[1], **M. Fujii**[2], **K. Kamiyama**[2], **A. Ando**[2], **and F. Costen**[3]

[1]Kurume National College of Technology, Japan
[2]University of Toyama, Japan
[3]The University of Manchester, UK

Abstract— We investigate numerically, for the first time to the best of authors' knowledge, the propagation of digital electromagnetic waves in the human head. It is found that the digital wave exhibits a complicated behavior of scattering and absorption due to the interaction with the high-order resonances of the human head and its complicated dielectric property. The analysis of the digital wave is based on the finite-difference time-domain (FDTD) method, taking into account the frequency dispersion of the human tissues for the frequency range from 1MHz to 20 GHz. The numerical human phantom developed by the National Institute of Information and Communications Technology (NICT), Japan, was used to set the radio environment in the FDTD space; the phantom is anatomically accurate in detail.

Electromagnetic waves, digitally modulated with the binary phase shift keying (BPSK) and the quaternary phase shift keying (QPSK), are launched at the forehead of the human phantom, and the electromagnetic signal has been observed in the human head. We restrict ourselves to the basic modulation schemes of the BPSK and QPSK, not considering any specific wireless communication systems that comprise more sophisticated digital modulation schemes or pulse shaping techniques. We compared the digital signals of 900 MHz and 2400 MHz carrier waves with the digital modulation frequency from 50 MHz to 480 MHz; the unrealistically high modulation frequency of 480 MHz was used to minimize the computational time, while maintaining the generality of the analysis.

Due to the complicated dielectric structure of the human head, including the bone, brain, fluid, eye and so on, together with the frequency dispersion of all the tissues, the digital signals have been found to behave in a manner different from the continuous wave (CW). The electromagnetic wave attenuates inside the human head, but large spike-like signals have been observed at the time of the phase shift of the digital modulation. It is interesting to note that the spike-like signals appear independently of the digital modulation frequencies up to 480 MHz; in contrast, the peak height of the spike-like signals varies unsystematically, depending on the observation positions inside the human head, as well as on the different male and female phantoms.

We are currently investigating other modulation schemes such as the minimum shift keying (MSK), as well as preparing the experimental set-ups. The numerical results will be presented at the conference.

Microwave Technology Based Medical Imaging and Diagnostics

Jan Vrba, Jr. and David Vrba
Department of Biomedical Technique, Faculty of Biomedical Engineering
Czech Technical University in Prague, Kladno, Czech Republic

Abstract— Future trends in medical applications of microwave technique and technology can be seen in development of new diagnostic and imaging methods based on high frequency EM field. A significant importance for the future can be identified for the following methods: Microwave tomography, Microwave radiometry, Measurement of complex permittivity, Imaging in the Terahertz waves band and Microwave diagnostic radars.

Technical Background for Use of Light in Medicine

Jan Vrba
Czech Technical University in Prague, Czech Republic

Abstract—

Session 3P15a
SCNU Special Session on Biophotonics — Biophotonics Imaging

In Vivo Photoacoustic Microscopy and Clinical Applications

Sihua Yang
MOE Key Laboratory of Laser Life Science & Institute of Laser Life Science
South China Normal University, Guangzhou 510631, China

Abstract— Based on the measurement of ultrasonic waves induced by laser pulses, photoacoustic imaging techniques are designed to overcome the poor spatial-resolution of optical imaging and retain the high optical contrasts in heavy scattering tissues. Photoacoustic imaging can reveal optical properties of tissue that are closely related to the physiological and pathological status of tissues, and became the promising clinical imaging modalities. Here we report a clinical-used photoacoustic (PA) microscope with a sound-light coaxial-confocal probe for port wine stain imaging, and a catheter-based intravascular photoacoustic tomography system for in situ meticulous examination of atherosclerotic lesions. Our work will expand the application of photoacoustic microscopy in resolving clinical difficulties.

Multi-dimensional Common Mode Imaging Based on Photoacoustic Microscopy

Zhilie Tang[1, 2]

[1]School of Physics and Telecom Engineering
South China Normal University, Guangzhou 510006, China
[2]Laboratory of Quantum Information Technology, IMOT
South China Normal University, Guangzhou 510006, China

Abstract— Adopted photoacoustic microscopy with high compatibility and high sensitivity, the common mode imaging of the same cell that is used to get the structural and functional information of the cells in the same time and realize the multi-parameter imaging of the cells. In this imaging method, the Raman scattering coefficient, two-photon absorption coefficient, optical absorption coefficient and optical scattering coefficient are used to be the imaging parameters can monitor the dynamic biological behavior that the cells' responses to the medication in real time is realized. Aiming at solving the problem of the poor specific imaging capability, we proposed a common mode imaging method that use photoacoustic raman spectrum and two-photon spectrum which both have molecular recognition ability. This method can greatly improve the specific imaging capability and be used in functional imaging of the cells. The common mode imaging that use the optical absorption coefficient and optical scattering coefficient as the imaging parameters could be used for photoacoustic microscopy of transparent cells without cell staining. It means the interference of the stain can be avoided. We integrate the four kinds of photoacousitic imaging mode into the confocal microscope, then develope the "Photoacoustic-Confocal" microscopy. This common mode imaging with multi-parameter microscopy has not only high resolution which is the characteristic of nonlinear optical microscopy, but also specific imaging ability. It can be used in researching the biological behavior that the cells' responses to the medication at the molecular level. That has important significance in cell morphology, molecular cell biology.

Ultrashort Microwave Pumped Three Dimensional Thermoacoustic Imaging for Depth Tumor Localization: A Phantom Study

Cunguang Lou, Zhong Ji, Yong Fu, and Da Xing
MOE Key Laboratory of Laser Life Science & Institute of Laser Life Science
South China Normal University, Guangzhou 510631, China

Abstract— Ultrashort microwave-induced thermoacoustic imaging (TAI) has attracted considerable interest as a promising imaging modality due to its high resolution and low radiation dose. Previous studies show that TAI has great potential for high contrast breast tumor detection, nevertheless the required microwave energy density and radiation field of view (FOV) can't meet the clinical demand. In this paper, a ultrashort microwave pulse (USMP) pumped TAI system was employed to reduce the demand microwave energy density for imaging, and the FOV was large enough to cover whole breast simultaneously. The experimental results demonstrate that the new USMP-TAI system can be used for high-resolution three-dimensional (3-D) localization of deep breast tumors with low microwave radiation dose over the whole breast.

Label-free and Weakly Absorbing Cellular Differential Photoacoustic Imaging by Combining the Front Scattered Light

Minfang Huang[1] **and Zhilie Tang**[1, 2]

[1]School of Physics and Telecom Engineering
South China Normal University, Guangzhou 510006, China
[2]Laboratory of Quantum Information Technology, IMOT
South China Normal University, Guangzhou 510006, China

Abstract— By combining the front scattered light of the objects, the photoacoustic microscopy (PAM) of label-free and weakly absorbing cell is achieved, which is extremely difficult using existing PAM. Polystyrene microspheres and oral mucosal epithelial cells are used to verify the technique proposed and the contrast of the imaging is improved significantly. Comparing with confocal microscopy using the hematoma carcinoma cells, the method proposed has advantages in delicate imaging. And conjunction of the spatial differential technique, the edges are enhanced, which makes the observation of weakly absorbing objects by PAM much more diversification. The feasible biomedical application of early detection of cancer from the improved differential PAM was demonstrated.

Using Functional Near-infrared Spectroscopy to Investigate Frontal Cortical Response to Joint/non-joint Attention in Children

Jun Li, **Zhifang Zhu**, **and Huilin Zhu**
Centre for Optical and Electromagnetic Research
South China Normal University, Guangzhou 510006, China

Abstract— Functional near-infrared spectroscopy (fNIRS) is an optical technique for non-invasively investigating brain functional activity. It measures cerebral hemodynamic parameters which are closely associated with the neural activity. Recent functional MRI study has demonstrated that individuals with autism show distinct response pattern in prefrontal cortex to joint/non-joint attention stimuli. In this work, we use fNIRS to access cerebral hemodynamic response to the joint/non-joint attention stimuli in children classified as of high and low autistic trait. The stimuli are given by a video which engenders an experience of joint/non-joint attention in observers. 49 channels of fNIRS data are recorded from prefrontal cortex when subjects watch the video. The cortical activation pattern is obtained and the functional connectivity is determined for the joint and the non-joint stimuli. Statistical analysis of data show that the hemodynamic response including changes in oxygenated hemoglobin, deoxygenated hemoglobin and total hemoglobin in prefrontal cortex are significantly different between the high and the low autistic groups for both the joint and the non-joint attention stimuli. These results suggest that fNIRS may have potential to provide objective markers for diagnosing autism.

Two-photon Photoacoustic Microscopy for Label-free Bio-maging Based on Microcavity Transducer

Yongbo Wu[1], **Zhilie Tang**[1, 2], **Yan Chi**[1], **Liru Wu**[1], **and Minfang Huang**[1]

[1]School of Physics and Telecom Engineering
South China Normal University, Guangzhou 510006, China
[2]Laboratory of Quantum Information Technology, IMOT
South China Normal University, Guangzhou 510006, China

Abstract— Label-free nonlinear imaging of biological cells holds the key to uncovering the fundamental mechanism in the cells with high resolution, and the two-photon excitation fluorescence imaging had been proposed in the past two decades. In order to improve the detection efficiency of two-photon signal, here, combining the two-photon absorption and photoacoustic detection, we demonstrate a method for label-free two-photon photoaoustic imaging of biological cells. Our method is based on a microcavity detector with high sensitivity, which is developed based on the bulk modulus of gas five orders of magnitude lower than that of solid. To generate the two-photon photoacoustic signals, we used a high-repetition rate femtosecond laser to induce narrowband excitation. Combining a low-frequency modulation technique and the lock-in detection, the two-photon photoacoustic signal was detected, which is proportional to the square of the incident light energy. By scanning the excitation beam, we performed a two-photon photoacoustic label-free imaging of green bristlegrasss cells, and get the distribution of chlorophyll molecules for label-free with a high contrast.

Study on the Mechanisms of Low-power Laser Irradiation-induced Vascular Endothelial Cell Proliferation

Jie Feng, Yingjie Zhang, and Da Xing
MOE Key Laboratory of Laser Life Science and Institute of Laser Life Science
College of Biophotonics, South China Normal University, Guangzhou 510631, China

Abstract— Angiogenesis, the growth of new blood vessels from pre-existing vessels, represents an excellent therapeutic target for the treatment of wound healing and cardiovascular disease. Herein, we report that LPLI (low-power laser irradiation) activates ERK/Sp1 (extracellular signal-regulated kinase/specificity protein 1) pathway to promote VEGF expression and vascular endothelial cell proliferation. We demonstrate for the first time that LPLI enhances DNA-binding and transactivation activity of Sp1 on VEGF promoter in vascular endothelial cells. Moreover, Sp1-regulated transcription is in an ERK-dependent manner. Activated ERK by LPLI translocates from cytoplasm to nuclear and leads to increasing interaction with Sp1, triggering a progressive phosphorylation of Sp1 on Thr453 and Thr739, resulting in the upregulation of VEGF expression. Furthermore, selective inhibition of Sp1 bymithramycin-A or shRNA suppresses the promotion effect of LPLI on cell cycle progression and proliferation, which is also significantly abolished by inhibition of ERK activity. These findings highlight the important roles of ERK/Sp1 pathway in angiogenesis, supplying potential strategy for angiogenesis-related diseases with LPLI treatment.

Session 3P15b
SC4: Antennas and RF Devices Based on Superconductors and Other Advanced Materials

Pentagonal Shape Antenna with Fractal Slots for Wireless Communication Applications

Sohaib Abbas Zaidi[1], **Mohit Barthwal**[1], **M. R. Tripathy**[1], **and S. S. Pattnaik**[2]

[1]Department of ECE, ASET, Amity University Noida, India
[2]ETV Department, National Institute of Technical Teachers Training & Research, Chandigarh, India

Abstract— This paper presents a pentagonal shape antenna for wireless communication applications. The proposed antenna contains the sierpinski carpet pattern slots. The antenna is resonating at 10.1333 GHz, 11.1333 GHz and 13.1333 GHz for second iteration. The simulated gains of the proposed antenna at respective resonant frequencies are 5.8 dBi, 9.0 dBi and 6.9 dBi. The bandwidth of the proposed antenna is 267 MHz, 529 MHz and 308 MHz in these three frequency bands. The antenna is designed using RT duroid 5880 as substrate which has the permittivity of 2.2. The thickness of substrate is 1.56 mm. The presented antenna can be used for various X band (8 GHz–12 GHz) as well as satellite communication applications in Ku band (12 GHz–18 GHz). The proposed antenna is simulated using HFSS (High Frequency Structure Simulator) software available at NITTTR, Chandigarh, India.

REFERENCES

1. Mandlebrot, B. B., *The Fractal Geometry of Nature*, W.H. Freeman, New York, 1983.
2. Puente, C., J. Romeu, R. Pous, X. Garcia, and F. Benitez, "Fractal multiband antenna based on sierpinski gasket," *Electronics Letters,* Vol. 32, No. 1, 1–2, 1996.
3. Douglas, H. and S. Ganguly, "An overview of fractal antenna engineering research," *IEEE Antennas & Propagation Magazine*, Vol. 45, No. 1, 38–57, 2003.
4. Pahwa, K., P. Mishra, H. P. Sinha, S. S. Pattnaik, and G. J. Joshi, "Design & development of diamond shape fractal antenna for wireless communication," *International Journal of Microwave & Optical Technology*, Vol. 7, No. 2, 2012.
5. Dhaliwal, B. S. and S. S. Pattnaik, "Artificial neural network analysis of sierpinski gasket fractal antenna: A low cost alternative to experimentation," *Advances in Artificial Neural Systems, Hindawi Publishing Corporation*, 1–8, 2013.
6. Chen, W.-L., G.-M. Wang, and C.-X. Zhang, "Small-size microstrip patch antennas combining koch and sierpinski fractal-shapes," *IEEE Antennas and Wireless Propagation Letters*, Vol. 7, 738–741, 2008.
7. Liu, G., L. Xu, and Z. Wu, "Dual-band microstrip RFID antenna with tree-like fractal structure," *IEEE Antennas and Wireless Propagation Letters*, Vol. 12, 976–978, 2013.
8. Fallahi, H. and Z. Atlasbaf, "Study of a class of UWB CPW-fed monopole antenna with fractal elements," *IEEE Antennas and Wireless Propagation Letters*, Vol. 12, 1484–1487, 2013.

Design and Implementation of an UWB Printed Monopole Antenna for Portable Devices

Jamal Nasir[1], **Mohd. Haizal Jamaluddin**[1], **Imdad Khan**[2], **Muhammad Ramlee Kamarudin**[1], **and Muzammil Hussain**[2]

[1]Wireless Communication Center (WCC), Universiti Teknologi Malaysia, Malaysia
[2]COMSATS, Institute of Information Technology, Abbottabad, Pakistan

Abstract— The Federal Communication Commission (FCC) in 2002 allocated the frequency band from 3.1 to 10.6 GHz for Ultra-wide Band wireless communication (UWB). As a result, the academic and industrial communities were motivated to develop novel antennas for UWB communication. During the past few years, the rapid growth in wireless technology has changed our way of life. Small size, high efficiency and large bandwidth are the main requirements of all UWB antennas.

In this paper, a new printed monopole antenna has been proposed for UWB portable device applications. The design has been simulated in HFSS V14 and its results have been tested experimentally. Maximum gain of 2.5 dBi has been achieved at 8.5 GHz and radiation efficiency of 85%–98% is obtained through out UWB range. By using partial ground plane and using slot in radiating plane overall size has been reduced with good radiating efficiency throughout UWB range. Overall size of the proposed antenna is 27.5 mm × 29.5 mm. The presented antenna is printed on FR4 substrate and therefore it is easy to fabricate. Thickness of substrate is 1.6 mm with relative permittivity of 4.8. Fig. 1(a), Fig. 1(b) and Fig. 2, show the top, bottom, and S_{11} plot of the proposed antenna. Fig. 1(c) shows the top and bottom view along with the dimensions of the presented antenna.

A parametric study has been done on various parameters such as ground plane length, slot length and width, to reach an optimum design before fabrication.

The simulated return loss of the presented antenna is shown in Fig. 2. From this figure, it is clearly reveals that the presented antenna will efficiently cover the whole UWB range of 3 to 10 GHz. The antenna is resonating at 6.5 GHz.

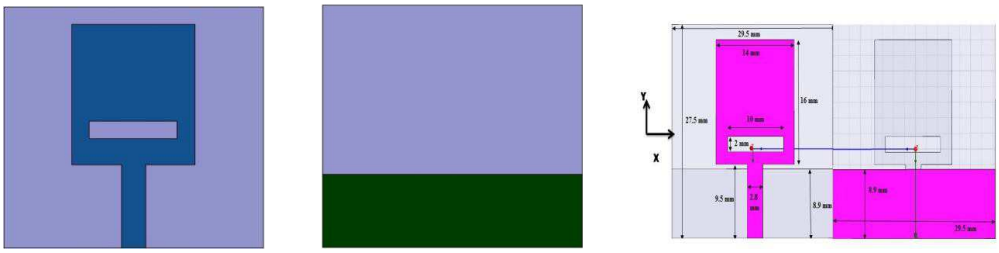

(a) (b) (c)

Figure 1: (a) Front view. (b) Bottom view. (c) Top and bottom view with dimensions.

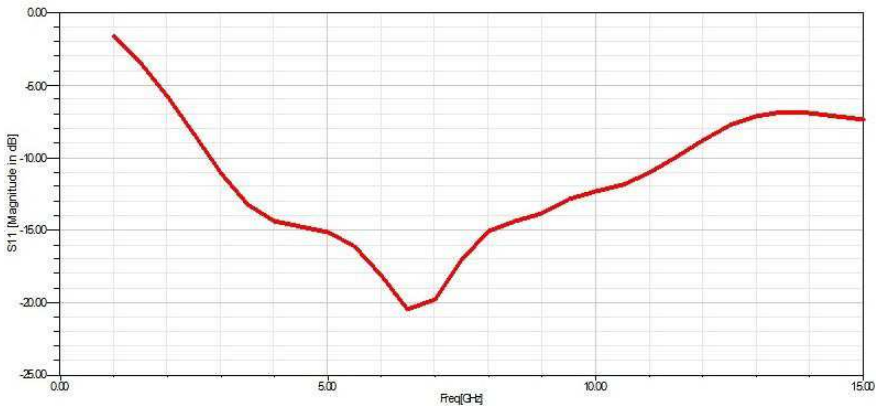

Figure 2: S_{11} magnitude plot.

Tunable S-band RF Front End Receiver for LEO Mission

Geetanjali Sharma, Viral Degarwala, and M. R. Tripathy
Department of Electronics and Communication Engineering
ASET, Amity University, Noida, U.P., India

Abstract— This paper presents the design strategy, simulation results and final schematic of RF-front end (receiver) block level designing with a flexible bandwidth and frequency for S-band (2025–2110 MHz). In this study, with a tunable local oscillators frequency (different channel frequency) the required specification were achieved such as gain < 130 dB, noise figure 2 dB, bandwidth 6 MHz which is targeted for LEO mission. The measured data including gain, noise figure and S-parameter agree well with the simulation results on ADS.

REFERENCES

1. Gonzalez, G., *Microwave Transistor Amplifiers Analysis and Design*, Prentice Hall, 1997.
2. Vendelin, G. D., *Design of Amplifiers and Oscillators by the S-parameter Method*, John Willey & Sons, 1982.
3. Mattaei, G., L. Young, and E. M. T. Jones, *Microwaves Filters, Impedence-matching Networks and Coupling Structure*, Artech House, Norwood, 1980.
4. Hong, J.-S. and M. J. Lancaster, *Microstrip Filters for RF/Microwave Applications*, John Wiley & Son, INC, 2001.
5. Mass, S., *Microwave Mixers*, 2nd Edition, Artech House, Boston, 1993.

Dual Band Rectangular Dielectric Resonator Antenna Design

Raghuraman Selvaraju[1, 2], **Mohsen Khalily**[1], **Muhammad R. Kamarudin**[1], **Mohd H. Jamaluddin**[1], **and Jamal Nasir**[1]

[1]Wireless communication center (WCC), Universiti Teknologi Malaysia, Malaysia
[2]Department of Electronics and Communication Engineering, Periyar Maniammai University, India

Abstract— A frequency reconfigurable rectangular dielectric resonator antenna (RDRA) capable of frequency tunings at two different resonant modes is presented and investigated. In this design two rectangular dielectric resonator's situated on top of substrate is designed with relative permittivity of $\varepsilon_r = 10$ and $\varepsilon_r = 30$ respectively. The antenna is feed by 50 Ω microstrip feedline etched on the top of the fr-4 epoxy printed circuit board (PCB) with a total size of $80 \times 50 \times 1.6\,\text{mm}^3$ and $\varepsilon_r = 4.6$ (loss tangent = 0.02) to ensure good immpedance matching, a $15 \times 15 \times 8\,\text{mm}^3$ rectangualr DRA for bandwidth enhancement is chosen, and a comparative study of the antenna at 2.4 GHz and 4 GHz resonant modes in without DRA the structure does not give any resonance two resonanace frequency have been achived after the DRA's are introduced in the structure. From the parametric study the first DRA is affecting the 4 GHz frequency mode whereas the second DRA is influencing the 2.4 GHz frequency mode. Ansoft HFSS v14 has been used for the simulation of the proposed antenna. The simulation results show that the design can efficiently perform at the lower frequency 2.4 GHz and the upper frequency 4 GHz.

The figures below show the structure of the proposed antenna. Fig. 1(a), Fig. 1(b) and Fig. 1(c) show the 3-D, top, bottom view of the presented antenna.

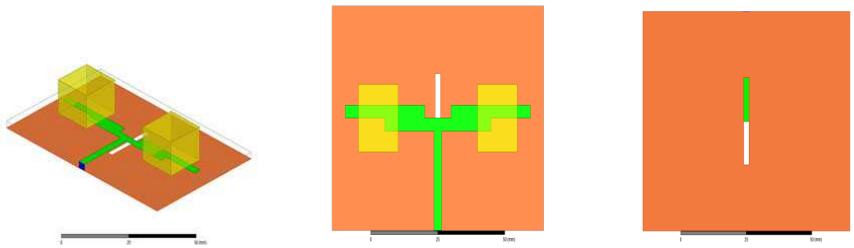

Figure 1: (a) 3-D view, (b) top view, (c) bottom view.

The simulated return loss of the presented antenna is shown in the figure below.

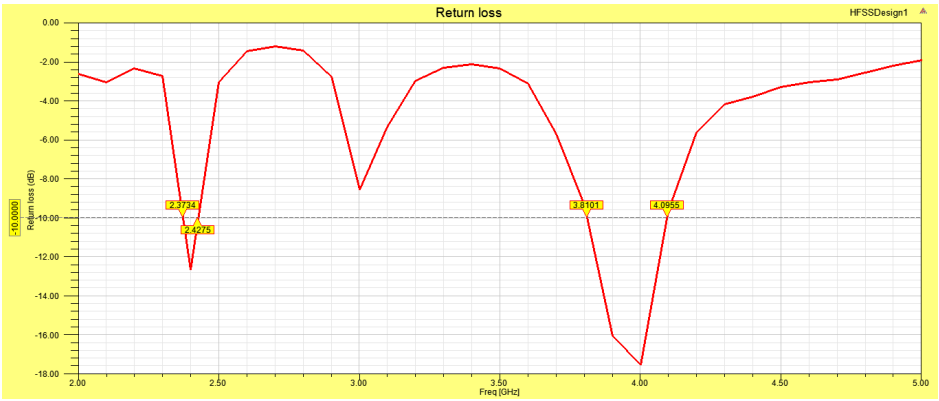

Figure 2: Return loss.

Gain Enhanced UWB Dielectric Resonator Antenna

Mohsen Khalily[1], **Jamal Nasir**[1], **M. R. Kamarudin**[1], **Raghuraman Selvaraju**[1, 2], **and M. H. Jamaluddin**[1]

[1]Wireless communication centre (WCC), Universiti Teknologi Malaysia, Malaysia
[2]Periyar Maniammai University, India

Abstract— A new Dielectric Resonator Antenna (DRA) for UWB applications (2.5 GHz–10.6 GHz) is presented in this work. The antenna has a compact shape with UWB characteristics. The radiator's structure is a split Z shaped DRA with dielectric constant (ε_r) of 10. The antenna is mounted on a copper ground plane of size $75 \times 90\,\text{mm}^2$ and is fed by a rectangular (bevel) shaped strip to improve the impedance matching. Also, an air gap has been introduced to reduce the Q factor and dielectric constant, which in turn improves the impedance bandwidth. The reason for using the split Z shaped DRA is to improve the electric field distribution inside the DRA over the whole UWB frequency range. In order to provide a smooth transition from one mode to another the rectangular (bevel) shaped feeding structure has been employed.

Extensive parametric studies have been carried out on different parameters in order to achieve an optimum structure. Ansoft HFSS v14 has been used for the simulation of the proposed antenna. The simulated S_{11} magnitude (Return Loss) graph in Fig. 2 shows that the antenna can efficiently operate over the frequency range from 2.5 GHz to 10.6 GHz covering the entire UWB range.

The figures below show the structure of the proposed antenna. Fig. 1(a), Fig. 1(b) and Fig. 1(c) show the front, side and 3-D view of the presented antenna.

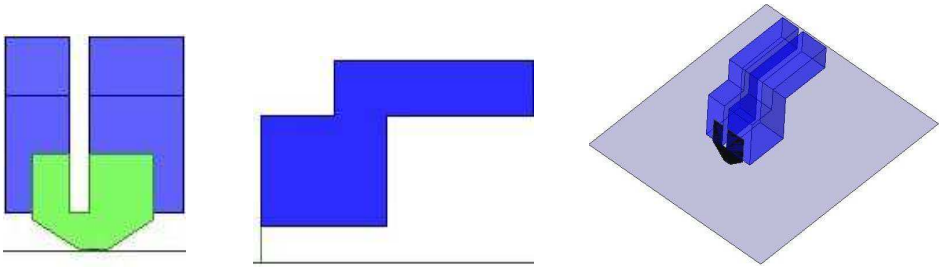

(a) (b) (c)

Figure 1: The proposed structure. (a) Front view, (b) side view and (c) 3-D view.

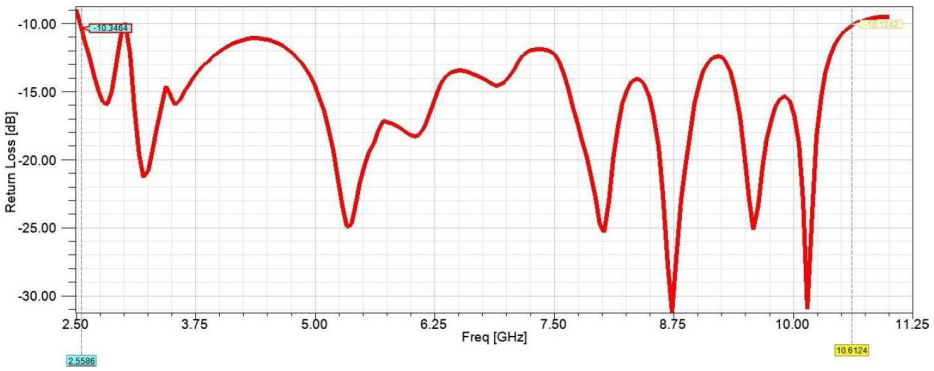

Figure 2: Return loss (S_{11} magnitude).

Session 3P0
Poster Session 5

Calculation of RFID Antenna Characteristic Parameters under the Condition of Near-field Coupling

Guochun Wan, Dongjie Lu, Jie Zhang, and Meisong Tong
Department of Electronic Science and Technology, Tongji University
4800 Cao'an Road, Shanghai 201804, China

Abstract— RFID system is largely used in the area of tracking information. Traditionally, it is only used in some expensive goods or luxuries because of the cost of each RFID tag and the whole system which manufacturers mostly concern about. In this paper, we present an original method to redesign them in order to greatly reduce the cost of each tag and the system so that they can be more widely used in tracking goods. In this work, we analyze some RFID systems to find out the principle of operation and essential designing ideas from them. Then we compare them to find out each system's good aspects and the shortage or some superfluous resources that can be deleted to reduce the cost, so that we can focus on optimizing theoretical principles like some important physical parameters in a mathematical way, such as the optimal radius of the RFID tag's antenna, estimating inductance of the conductor loop, quality factor of the antenna, turning and the magnetic field intensity which will effect the efficiency and the reliability of the whole system. Furthermore, we design the circuit based on what we have optimized, and after that we run the simulation and make some tests in order to meet the expectation of some basic requirements like information storing, transmitting power and system's reliability. Finally, we make the printed circuit board in practical use to make RFID system can be widely adopted in tracking common goods in a cheap way so that more manufacturers can use them to control the tracking information.

An Electrically Small Circular Polarization Radiator with Coupling Feed

Lidong Huang[1], **Jiang Xiong**[2], **and Yufeng Yu**[2]

[1]Computational Electromagnetics Laboratory, UESTC, Chengdu, China
[2]China Jiangnan Electronics Communication Institude, Jiaxing, China

Abstract— In this paper, an electrically small normal-mode helical antenna (NMHA) with capacitive coupling feed has been proposed and studied. An equivalent circuit model of the antenna is proposed and analyzed to understand the working mechanism. Simulated results show the proposed the NMHA has pretty good impedance matching, radiation efficiency and good circular polarization.

Introduction: In this paper, as an extension of our previous work, we have proposed an electrically small NMHA with high radiation efficiency. A monopole feeding structure is used to capacitively feed the NMHA. Full-wave simulation results show that the proposed electrically small NMHA has good impedance matching, radiation efficiency and circular polarization (CP).

Antenna Description: The antenna consists of an electrically small helix of 12 turns as the radiating element and an inner top-loading monopole as a capacitively coupled feeding structure. The feed is connected with the pin (inner conductor) of the 50 ohm coaxial line. Note that the radiating helix is not connected with the ground plane, and in practice it can be fixed with some dielectric posts. Here we choose copper for both the helix and the monopole feed.

The equivalent circuit model of the NMHA (the radiating component of our antenna) is recently described and analyzed in [12]. According to this paper, the NMHA can be modeled with an R-L-C series circuit, whose radiation resistance can be easily obtained. R_{NMHA}, L_{NMHA} and C_{NMHA} represent the resistance, inductance and capacitance of the NMHA, respectively. As a matter of fact, R_{NMHA} includes both the radiation resistance R_r and the loss resistance R_L. L_{NMHA} and C_{NMHA} are the self-inductance and self-capacitance of the NMHA, respectively. The top loading monopole feed can also be considered as an R-L-C series circuit, and R_{fp}, L_{fp} and C_{fp} is its equivalent resistance, inductance and capacitance [15, 16]. Similar to [11], the capacitive coupling between the NMHA and the feeding monopole can be simply represented by a transformer with N_c as its variable ratio. Obviously N_c mainly depends on the inter-space between the radiator and the feed, the height of the feed, the size of the top load, etc..

REFERENCES

1. Kraus, J. D. and R. J. Marhefka, *Antennas: For All Applications*, 228–230, McGraw-Hill, 2001.
2. Balanis, C. A., *Antenna Theory: Analysis and Design*, Wiley, New York, 568–570, 2005.
3. Yamada, Y., W. G. Hong, W. H. Jung, and N. Michishita, "High gain design of a very small normal mode helical antenna for RFID tags," *TENCON 2007 — 2007 IEEE Region 10 Confrence*, 2007.
4. Rowley, J. T., R. B. Waterhouse, and K. H. Joyner, "Modeling of normal — Mode helical antennas at 900 MHz and 1.8 GHz for mobile communications handsets using the FDTD technique," *IEEE Trans. Antennas Propag.*, Vol. 50, No. 6, 812–820, 2002.
5. Erentok, A. and R. W. Ziolkowski, "An efficient metamaterial-inspired electrically-small antenna," *Microw. Opt. Tech. Lett.*, Vol. 49, 1287–1290, Jun. 2007.
6. Erentok, A. and R. W. Ziolkowski, "Two-dimensional efficient metamaterial-inspired electrically-small antenna," *Microw. Opt. Tech. Lett.*," Vol. 49, 1669–1673, Jul. 2007.
7. Erentok, A. and R. W. Ziolkowski, "Metamaterial-inspired efficient electrically-small antenna," *IEEE Trans. Antennas Propag.*, Vol. 56, No. 3, 691–707, Mar. 2008.
8. Jin, P. and R. W. Ziolkowski, "Low Q electrically small, efficient near field resonant parasitic antennas," *IEEE Trans. Antennas Propag.*," Vol. 57, No. 9, 2548–2563, Sep. 2009.
9. Ziolkowski, R. W., "Efficient electrically small antenna facilitated by a near-field resonant parasitic," *IEEE Antennas Wireless Propag. Lett.*, Vol. 7, 580–583, 2008.
10. Ziolkowski, R. W., C.-C. Lin, J. A. Nielsen, M. H. Tanielian, and C. L. Holloway, "Design and experimental verification of a 3D magnetic EZ antenna at 300 MHz," *IEEE Antennas Wireless Propag. Lett.*, Vol. 8, 989–993, 2009.

11. Yu, Y., J. Xiong, H. Li, and S. He, "An electrically small frequency reconfigurable antenna with a wide tuning range," *IEEE Antennas Wireless Propag. Lett.*," Vol. 10, 103–106, 2011.
12. Xiong, J., Y. Yu, Y. Liu, and X. Geng, "An electrically small planar loop antenna with high efficiency for mobile terminal applications," *Journal of Electromagnetic Waves and Applications*, Vol. 26, Nos. 5–6, 744–756, 2012.
13. Liu, Q., Y. Yu, and S. He, "Capacitively-loaded inductively-coupled fed loop antenna with an omnidirectional radiation pattern for UHF RFID tags," *IEEE Antennas Wireless Propag. Lett.*, under review.
14. Shin, D.-R., G. Lee, and W. S. Park, "Simplified vector potential and circuit equivalent model for a normal-mode helical antenna," *IEEE Antennas Wireless Propag. Lett.*, Vol. 12, 1037–1040, 2013.
15. Bulus, U., C. T. Famdie, and K. Solbach, "Equivalent circuit modeling of chassis radiator," *German Microw. Conf. (GeMIC2009)*, Mar. 2009.
16. Bulus, U. and K. Sohlbach, "Modelling of the monopole interaction with a small chassis," *Proc. 3rd EuCAP*, Berlin, Germany, Mar. 23–27, 2009.

A More Practical Patch Used in Microstrip Antenna at Ku-band

Chuanqi Wei, Dawei Liu, Chen Zhu, Jindong Yu, and Jungang Miao
Electromagnetics Laboratory, Beihang University, Beijing 100191, China

Abstract— In the last decade, there is an increasing interest in reflectarray antennas for the following advantage: high gain, light weight, low cost and flexibility and so on.

In this paper, a Ku-band microstrip antenna is analyzed and designed. Due to reflectarray antennas have quasi-periodic structure, infinite periodic unit model is the mainstream approach to analysis the phase shift of patch. In this study, the characteristics of the patch are analyzed and optimized with Ansoft HFSS. It adopts Floquet port and Master-Slave boundary approach. Adifferent patch is evolution of the classic rectangular patch. It has a square loop outside the rectangular patch. We can call it window-patch. Compared with rectangular patch, the window-patch has the following advantages: first, the window-patch has some improvement compared with rectangular patch in range of phase shift; second, the new patch has a smaller slope of the phase shift curve than the rectangular patch. The small slope is an important characteristic for reflectarray patch.

Once the unit element has been fully characterized and a reflectarray designed, an important aspect in the reflectarray analysis is the computation of the radiation patterns. In this literature, a method of Array Element Factor is used to calculate it. For the reflectarray antenna, the ideal range of phase shift should realize $0 \sim 360^\circ$, but sometimes things go contrary. The phase shift of patch would be variable versus electromagnetic wave incident angle. In the last part, we will discuss the effects to the gain carried by the incident angle. Finally, the Ku-band reflectarray antenna will be fabricated and be measured in compact range of Beihang University.

High-Q Weakly Modulated Nanobeam Cavity Based on a Suspended Silicon Dioxide Waveguide

Senlin Zhang and Sailing He
Centre for Optical and Electromagnetic Research
JORCEP [Sino-Sweden Joint Research Center of Photonics]
State Key Laboratory for Modern Optical Instrumentation, East Building No. 5
Zijingang Campus, Zhejiang University, Hangzhou 310058, China

Abstract— Photonic crystal (PhC) cavities have drawn plenty of attentions during the past several decades for the advantages of ultra-high Q factor and small mode volume. Ubiquitous uses can be found in realms such as quantum information processing, low threshold lasers, optomechanics, and nonlinear optics. PhC cavities based on silicon material have been heavily investigated for its compatibility with complementary metal-oxide-semiconductor (CMOS) technology, small feature size and low cost. However, apart from the advantage of high Q factor, silicon based PhC cavities suffer from the drawbacks of high insertion loss because of the mode mismatch with fiber and relatively lower sensitivity. On the other hand, silicon dioxide (silica) waveguide experience relatively smaller loss and owns a similar refractive index to numerous liquid materials to be sensed, which will leads to high sensitivity for a silica based PhC cavity sensor. In this paper, we propose a high Q factor ($Q = 15500$) silica based PhC nanobeam cavity with high sensitivity (the wavelength shift per refractive index unit (RIU) is $S = 338\,\mathrm{nm/RIU}$) at the telecommunication wavelength (1550 nm). Since the refractive index of silica is low for the manufacture of PhC nanobeam cavity, it is essential to utilize a silica waveguide suspended in free space. The PhC nanobeam cavity is then formed by etching a series of elliptical holes, whose dimensions linearly decrease from the center to both ends, directly into the silica waveguide. For the sake of high transmission on-resonance wavelength while maintaining high Q factor, it's important to etch partly into the waveguide, which results in a low-refractive-index perturbation structure. The calculated on-resonance transmission is about 0.28. The novel proposed PhC nanobeam cavity shows sensitivity 3 times larger than silicon based PhC structures and outperforms other low-index-contrast PhC cavities by a higher on-resonance transmission. Such a structure may find applications in sensing, spectrally filtering system, and nonlinear optics.

Design and Analysis of Miniature Fractal Antenna

Ying Suo[1, 2], **Jingyu Han**[1], **Wei Li**[1, 2], **and Weibo Deng**[1]

[1]School of Electronics and Information Technology
Harbin Institute of Technology, Harbin 150001, China
[2]Electronic Science and Technology Postdoctoral Station
Harbin Institute of Technology, Harbin 150001, China

Abstract— There is a rapidly expanding need for highly integrated antenna in both civil and military fields. Fractal antenna designs can meet most of the needs in size reduction. Among those designs, Koch iteration is a widely used and well-evaluated approach in designing wire antenna.

In this paper, Koch iteration technique is applied to a dipole antenna in order to get a miniaturized radar array element. An analysis of the influence caused by fractal dimension on antenna size is first performed using iteration technique. The creation and optimization of a dipole antenna model using proper fractal dimension is then carried out and analyzed according to the miniaturization effects. The results show the characters of this designed antenna, and the simulations and analysis are done in FEKO® software environment.

The dipole antenna with 3rd Koch iteration applied to each of its four segments is designed to operate at a resonant frequency of 500 MHz. The four fractal segments of this antenna spin around the center axis with an angle difference of 90° each, which results to an all-four-direction feature.

The overall size of this dipole fractal antenna at the resonant frequency is reduced by around 33% compared with conventional dipole antenna meanwhile retaining its band characters. It also has great omnidirectional character with satisfactory corresponding gain. The return loss is below −18 dB at 500 MHz. The result of analysis in simulation indicates that the fractal dipole antenna designed above satisfies the application of the miniaturization for antenna array element and can provide a solid foundation for the design of miniaturized antenna array.

An X-band Substrate Integrated Waveguide Vivaldi Array Antenna

Wei Li[1, 2], **Ying Suo**[1, 2], **Jingyu Han**[1], **and Xiaowei Liu**[3]

[1]School of Electronics and Information Engineering
Harbin Institute of Technology, Harbin 150001, China
[2]Electronic Science and Technology Postdoctoral Station
Harbin Institute of Technology, Harbin 150001, China
[3]Department of Microelectronics Science and Technology
Harbin Institute of Technology, Harbin 150001, China

Abstract— In this paper, a kind of compact X-band vivaldi array antenna printed on a substrate is proposed and designed. The antenna is consisted of 4 vivaldi structure radiation elements fed by a 4-way equal power divider with substrate integrated waveguide (SIW) technology.

Based on the SIW theory and technology, the impedance characteristics and transmission characteristics of a 4-way power divider are simulated and analyzed. A SIW is composed with two column metallized via holes in the dielectric substrate and upper and lower metal layers. A SIW-microstrip transition structure is designed to satisfy measurement and connection. The transition section is taper microstrip line. The taper line is able to realize impedance transformation between the 50 Ω microstrip line and the substrate integrated waveguide.

The planar Y-junction multi-way power distribution technology is used in the 4-way SIW equal power divider. The discontinuity of general Y-junction power divider structure results in the higher return loss in pass band. A metal pin inductance in Y-junction power divider is able to decrease the return loss. The electric field distribution of the Y-junction is able to change by surface current distribution of the metal pin inductance.

The vivaldi radiation element is consisted of complementary structure. An element is composed with an index gradient microstrip line are on both sides of the substrate. The reflection coefficient of the X-band SIW vivaldi array antenna is less than −10 dB from 9.1 GHz–10.1 GHz. The gain of the array antenna is 12 dB, and the main lobe width is about 18° with side lobe level less than −12 dB.

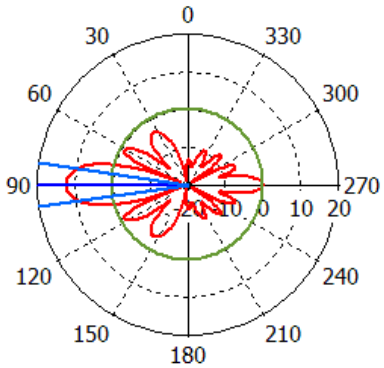

An Omni-directional Circularly Polarized Helical Antenna with an Inductive Feed

Yufeng Yu[1], **Xiaoyi He**[1], **Qi Liu**[2], **and Yufeng Wang**[1]

[1]China Jiangnan Electronics Communication Institute, Jiaxing 314000, China
[2]Center for Optical and Electromagnetic Research, Zhejiang University, Hangzhou 310027, China

Abstract— The paper presents an omni-directional circularly polarized (CP) helical antenna with an inductive feeding structure. The antenna is comprised of a printed helix with six arms on a thin rolled substrate and a feeding loop, which acts as the radiator and the feeding structure, respectively. The helix is fed by the feeding loop without physical connection through inductive coupling, which is convenient to achieve impedance matching. The 90° phase difference between the radiated horizontal and vertical field components is naturally guaranteed by the helix and, therefore, circular polarization is achieved through tuning the height and radius of the helix to ensure equal magnitude of the radiated horizontal and vertical field components. With a size of 67 mm × 67 mm × 41.5 mm, the antenna exhibits a simulated impedance bandwidth ($|S_{11}| \leq -10$ dB) of 5.72% (753.4 MHz to 797.8 MHz) and AR bandwidth (AR$\leq$ 3 dB) of 27.4% (630.5 MHz to 831 MHz). The average right-handed CP gain in the azimuth plane is more than 1.4 dBi over the operating band ($|S_{11}| \leq -10$ dB).

REFERENCES

1. Sakaguchi, K. and N. Hasebe, "A circularly polarized omnidirectional small helical antenna," *International Conference on Antennas and Propagation (ICAP)*, 492–495, 1995.
2. Quan, X., R. L. Li, and M. M. Tentzeris, "A novel broadband omni-directional circularly polarized antenna for mobile communications," *IEEE International Symposium on Antennas and Propagation*, 1777–1779, 2011.
3. Hsiao, F. R. and K. L. Wong, "Low-profile omnidirectional circularly polarized antenna for WLAN access point," *Microw. Opt. Technol. Lett.*, Vol. 46, No. 3, 227–231, August 2005.
4. Park, B. C. and J. H. Lee, "Omnidirectional circularly polarized antenna utilizing zeroth-order resonance of epsilon negative transmission line," *IEEE Trans. Antennas Propag.*, Vol. 59, No. 7, 2717–2720, July 2011.
5. Yu, Y., Z. Shen, and S. He, "Compact omni-directional antenna of circular polarization," *IEEE Antennas Wireless Propag. Lett.*, Vol. 11, 1466–1469, 2012.

A Shared Aperture Millimeter Wave Antenna Using 3D SIW Technology

Zeyang Tian, Jun Ouyang, and Yu Long
School of Electronic Engineering, University of Electronic Science and Technology of China
Chengdu, Sichuan 611731, China

Abstract— This paper presents the design of a shared aperture millimeter wave antenna array based on 3D SIW (Substrate Integrated Waveguide) technology.

The two proposed antenna arrays work at W band and Ka band respectively. We use a SIW slot antenna as the W band antenna array element and will probably use a SIW fed dipole antenna as the Ka band element. The W band array is on the top layer of the substrate and the feed network of the Ka band array is on the bottom layer. Considering that the horizontal space between higher frequency elements is too narrow to place a Ka band antenna since wave length is quite short at W band, the Ka band antenna elements are designed to occupy the vertical space between W band elements. The Ka band antenna is fed by 3D integrated circuits in the gap of W band antennas. There is a slot in the horizontal line which is used for splicing the vertical line. The width of the slot is equal to the vertical line substrate thickness and the length is equal to the vertical line equivalent waveguide width. There is anon-metalized section on the end of the vertical line having the width of the equivalent waveguide and length equal to the substrate thickness of the horizontal line. The vertical line interconnects the horizontal line of the Ka band antennas' feed network to form the 3D architectures of planar circuits. Both the Ka band and W band antenna array generate orthogonal linear polarized waves. RT/Duriod 5880 with thickness of 254 μm and dielectric constant of $\varepsilon_r = 2.2$ is used as the substrate in this work. And all these architectures can be manufactured by using conventional low cost PCB (Printed Circuit Board) fabrication process.

Target Detection Algorithm for SAR Image Based on Visual Saliency

Huijie Xie, **Tao Tang**, **Deliang Xiang**, **and Yi Su**
College of Electronic Science and Engineering, National University of Defense Technology, China

Abstract— Based on visual saliency theory and target detection theory, a target detection algorithm for SAR image is proposed. In a size-fixed sliding window depended on target size, local probability density function statistical feature reflects the difference between target and clutter, which is sensitive to not only the intensity feature but also the shape and size of the target. In the paper, local probability density function statistical feature, hypothesis testing theory and Bayes theorem is used for measuring saliency degree of the SAR image.

Target detection algorithm for SAR image includes four parts: (1) The parameter of the proposed algorithm could be determined according to the sizes of the target. (2) Local saliency and global saliency of each pixel could be calculated respectively according to hypothesis testing theory and Bayes theorem. (3) Saliency map could be acquired by combining local saliency map and global saliency map. (4) Target detection result could be acquired from saliency map by binary segmentation.

The moving and stationary target acquisition and recognition (MSTAR) plan SAR image and airborne X-band SAR image acquired by project term are used for experiment For the SAR images mentioned above, target detections are implemented by the proposed algorithm and CFAR algorithm. The comparison of the detection results shows that the proposed algorithm detects all size-fixed targets with faster computing speed and lower false alarm rate than CFAR algorithm. Moreover, the proposed algorithm is appropriate for target detection in a SAR image with complex background, and solves the problem of CFAR algorithm that mini size strong scatterer must be detected as false alarm.

REFERENCES

1. Rahtu, E., and J. Heikkila, "A simple and efficient saliency detector for background subtraction," *IEEE 12th International Conference on Computer Vision Workshops*, 1137–1144, Kyoto, 2009.
2. Hou, B., W. Yang, W. Shuang, et al., "SAR image ship detection based on visual attention model," *IEEE International Geoscience and Romote Sensing Symposium*, 2003–2006, Melbourne, 2013.
3. Itti, L., C. Koch, and E. Niebur, "A model of saliency-based visual attention for rapid scene analysis," *IEEE Trans. on Pattern Analysis and Machine Intelligence*, Vol. 20, No. 20, 1254–1259, Nov. 1998.
4. Hou, X. D. and L. Q. Zhang, "Saliency detection: A spectral residual approach," *IEEE Conference on Computer Vision and Pattern Recognition*, 1–8, Minneapolis, 2007.

A Wide Tuning-range CMOS VCO with a Tunable Active Inductor

Hsuan-Ling Kao and Ping-Che Lee
Department of Electronic Engineering, Chang Gung University, Tao-Yuan 333, Taiwan

Abstract— Integrated wireless blocks in one chip IC is demanded for high-speed, high-functio nality, small-size and low-cost communication systems. One of the key building blocks is fully-integrated voltage controlled oscillators (VCOs). The challenges of the VCO circuit are die size, cost and power dissipation. This study describes a wide tuning range VCO using tunable active inductor (TAI) topology and cross-coupled pair configuration for radio frequency operation. The major advantage of this structure is the absence of on-chip inductor, thus reducing significantly the chip area. The TAI used two feedback loops form cascode circuit to obtain more degrees of freedom for inductance value and cutoff frequency due to without a load capacitor. The tuning technique was based on the use of a variable-resistance for current-source tuning. The coarse frequency tuning was achieved by the variable-resistance, while the fine tuning was controlled by voltage. The TAI-VCO were fabricated using a 0.18 µm CMOS technology and achieved frequency tuning ranges from 0.6 to 7.1 GHz. The VCO has low phase noise, of −110.38 and −99.04 dBc/Hz, at a 1 MHz offset from a 0.6 and 7.1 GHz carrier (near 168.8% tuning rage), respectively. The output power of the VCO is −4.46 dBm at 2 GHz from a 1.8 V power supply. The power consumption of the VCO with 0.52 mm^2 chip area is 50 mW, from a 1.8 V power supply. The figure of merit was −164 dBc/Hz and the power-frequency tuning-normalized figure-of-merit was −4.6 dB.

A New Local Feature Descriptor for SAR Image Matching

Tao Tang, Deliang Xiang, and Yi Su
College of Electronic Science & Engineering, National University of Defense Technology, Changsha, China

Abstract— A new stable keypoint feature extraction method like SIFT [1] is proposed in this presentation, in which keypoints are detected with Harris detector and Local Gradient Ratio Pattern Histogram (LGRPH) are taken as feature descriptor from the neighbourhood of key points.

In SIFT and SIFT-like algorithm [1–4], main gradient direction histogram is used for feature descriptor of keypoints, which is proper for optical image but improper for SAR image because in SAR image there are much coherent speckle noise that is multiplicative and cannot be overcome by intensity difference. For ROA (Ratio of Average) is robust for multiplicative noise in SAR image, we utilize local gradient ratio pattern histogram (LGRPH descriptor) [5] to represent the feature of local key points.

Gradient information and ratio of intensity is used in LGRPH descriptor. Firstly absolute value of intensity difference of central and neighbour pixels is granted as the gradient of neighbour pixels. The ratio of the gradient and intensity is taken as GRP (Gradient Ratio Pattern) and the average of GRP of all neighbour pixels is granted as GRP of the central pixel. Then the GRP difference between each neighbour pixel and central one is computed and formed a binary code string by criterion function. The value of the binary code string is the LGRP value of central pixel. All LGRP value of neighbourhood of key points will form a histogram named LGRPH.

Local feature extraction for image registration includes three parts: (i) keypoints detection and localization; (ii) keypoint description; (iii) keypoints matching. In our method the first is Harris detector, the second is LGRPH descriptor, the last is similarity measure for matching. Experiments show that this algorithm is robust against coherent speckle noise and local gradient turbulence in SAR images, which is useful for SAR image matching and registration. The novel method shows better performance than other algorithm in experiments.

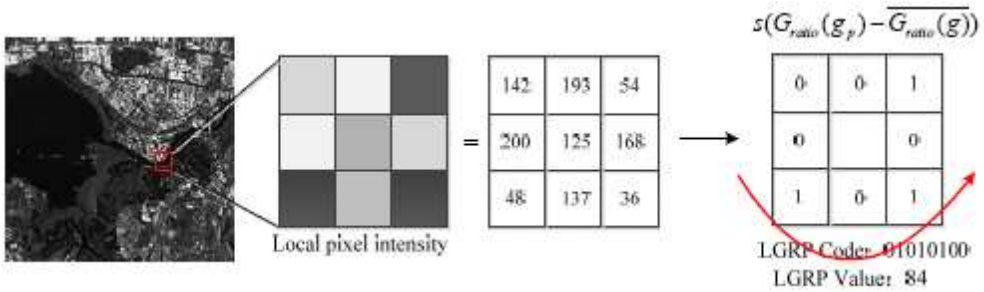

Figure 1: Calculating process of LGRP value. Red: counter-clockwise coding.

REFERENCES

1. Lowe, D., "Distinctive image features from scale-invariant keypoints," *International Journal of Computer Vision*, Vol. 20, 91–110, 2004.
2. Schwind, P., S. Suri, P. Reinartz, and A. Siebert, "Applicability of the SIFT operator to geometric SAR image registration," *Int. J. of Remote Sensing*, Vol. 31, No. 8, 1959–1980, 2010.
3. Dellinger, F., J. Delon, Y. Gousseau, J. Michel, and F. Tupin, "SAR-SIFT: A SIFT-like algorithm for application on SAR images," *Proc. IGRASS 2012*, 3478–3481, Munich, 2012.
4. Ren, S., W. Chang, and X. Liu, "SAR image matching method based on improved SIFT for navigation system," *Progress In Electromagnetics Research M*, Vol. 18, 259–269, 2011.
5. Yuan, X., T. Tang, D. Xiang, et al., "Target recognition in SAR imagery based on local gradient ratio pattern," *Int. J. of Remote Sensing*, Vol. 35, No. 3, 857–870, 2014.

A Dual-band Dual-polarized Antenna and a Switchable Multi-beam Antenna Array

Yu Long, Jun Ouyang, Zeyang Tian, and Yuan Zhang
School of Electronic Engineering, University of Electronic Science and Technology of China
Chengdu, Sichuan 611731, China

Abstract— A dual-band, dual-polarized antenna and a switchable multi-beam antenna array are introduced in this paper. Composed of two orthogonal annular dipoles, the proposed $\pm 45^\circ$ polarization diversity antenna has two simulated impedance bands: 2.39 GHz $\sim$ 2.85 GHz and 3.39 GHz $\sim$ 3.97 GHz, with VSRS < 1.5 and isolation > 28.5 dB. The simulated gain of the antenna is 8.5 dBi at the lower frequency band, and 9.1 dBi at the higher frequency band. In order to compose a $5 * 3$ polarization diversity antenna array, two 3-to-15 feed networks are employed and placed together, one for each polarization. The whole feed network is manufactured using microwave substrate AD255C with thickness of 0.762 mm and dielectric constant of $\varepsilon_r = 2.55$ and its size is limited to 340 mm $*$ 200 mm $*$ 30 mm. The output phase as well as the amplitude of each output port of each network is identical. To realize switchable multi-beam capability in horizontal plane, two microwave switches are used for one array. Connected to 3 out of 6 input ports of the array, one switch has 4 gears and the input phase of the feed network is selected from 4 groups of fixed values. Thus the input phase of the antenna elements can be controlled. In other words, this antenna array can radiate at 4 different angles (within $\pm 30^\circ$ for lower frequency band), yet not simultaneously. Simulated results of the antenna and antenna arrays are presented and discussed. Both the return loss, port isolation and the gain are good enough for civil communication applications.

Design and Analysis of Planar Phased MIMO Antenna for Radar Applications

Nour El-Din Ismail, Sherif Hanafy Mahmoud, Ahmed Hamed, and Alaa Hafez
Faculty of Engineering, Alexandria University, Alexandria, Egypt

Abstract— Phased-multiple-input multiple-output (phased-MIMO) radar using one-dimensional transmit arrays has been thoroughly investigated in the literature. In this paper, we consider two-dimensional phased-MIMO radar array which is called planar-phased-MIMO radar. This new technique aggregates the advantages of the linear-phased-MIMO radar without sacrificing either the main advantage of the planar-phased-array radar, which is the coherent processing gain, or the main advantage of the planar MIMO array radar, which is the diversity processing gain. The essence of the proposed technique is to partition the planar transmit array into a number of planar subarrays that are allowed to overlap. Then, each subarray is used to coherently transmit a waveform which is orthogonal to the waveforms transmitted by other subarrays. Coherent processing gain can be achieved by designing a weight matrix for each subarray to form a beam towards a certain direction in space. Moreover, the subarrays are combined jointly to form a planar-MIMO radar resulting in higher angular resolution capabilities. Substantial improvements is offered by the proposed planar-phased-MIMO radar technique with respect to the linear-phased-MIMO, planar-MIMO and planar-phased-array radar techniques. The achieved improvements are demonstrated analytically and by simulations through analyzing the corresponding beampatterns, the resultant peak side lobe level, mean side lobe level, and directivity. Both analytical and simulation results validate the effectiveness of the proposed planar-phased-MIMO radar.

Non Simultaneous-conjugate-match Technique for S-band Low Noise Amplifier Design

Achmad Munir[1] **and Yana Taryana**[1, 2]

[1]Radio Telecommunication and Microwave Laboratory
School of Electrical Engineering and Informatics, Institut Teknologi Bandung, Indonesia
[2]Research Center for Electronics and Telecommunication, Indonesian Institute of Sciences, Indonesia

Abstract— The design of 2-stage low noise amplifier (LNA) working at S-band frequency is proposed by using non simultaneous-conjugate-match technique. Implementation of the technique is motivated by the circumstance that the gain of LNA designed by the familiar technique, i.e., simultaneous-conjugate-match is almost followed by arise of values in noise figure (NF) and voltage standing wave ratio (VSWR). In the design process, the ADS(R)software is applied to determine the desired trade-off value between LNA parameters such as gain and VSWR. The 2-stage LNA which is deployed on an Arlon DiClad527 applies BJT transistors of BFP420. To achieve the impedance matching condition, microstrip lines are employed at the input and output ports. From the experimental characterization, it shows that the prototype of 2-stage LNA produces the gain of 24.32 dB at 3 GHz which is 4.56 dB lower than the simulated result.

Characterization of Narrowband Hairpin Bandpass Filter Composed of Fractal Koch Geometry

Achmad Munir[1], **Teguh Praludi**[1, 2], **and Mohammad Ridwan Effendi**[1]

[1]Radio Telecommunication and Microwave Laboratory, School of Electrical Engineering and Informatics
Institut Teknologi Bandung, Indonesia
[2]Research Center for Electronics and Telecommunication, Indonesian Institute of Sciences, Indonesia

Abstract— In this paper, a narrowband hairpin bandpass filter (BPF) composed of fractal Koch geometry is characterized numerically and experimentally. The implementation of fractal Koch geometry aims to minimize the dimension of filter which affects to reduce the need of material. The filter which utilizes the 1st iteration of fractal Koch geometry, later referred as fractal hairpin BPF is established using 7 elements deployed on a Rogers RO4350 dielectric substrate with the thickness of 1.52 mm. Prior to hardware realization, the proposed filter is numerically characterized to deal with the required specification. The filter which is intended for radar application is designed to have center frequency of 3 GHz with the 3 dB minimum working bandwidth of 200 MHz. It is shown that the realized fractal hairpin BPF which has the dimension of 16 mm × 47 mm and is approximately 20% smaller than the dimension of conventional one demonstrates the 3 dB working bandwidth of 260 MHz with the center frequency of 3.01 GHz.

The Human Body Can Be Mounted Wearable Antenna

Ho-Jun Lee
Convergence Communication Components Research Center
Korea Electronics Technology Institute, Republic of Korea

Abstract— In this paper, we proposed a novel design of wearable on-body antenna. A wearable antenna is meant to be a part of the clothing used for communication purposes, which includes tracking and notebook and mobile phone. The proposed antenna configuration is shown in Figure 1. Antennas in this paper are simulated by using the CST Microwave Studio (CST MWS). A prototype of this antenna was fabricated on Polyimide substrate with thickness $h = 0.254\,\text{mm}$ and dielectric constant $\varepsilon_r = 3.5$. The measurements of electrical characteristics such as radiation patterns, VSWR, and return loss of the implemented antenna were conducted in an anechoic chamber equipped with a HP 8510C network analyzer and far field measurement system. Figure 2 shows return loss (S_{11}) characteristics. The measured impedance bandwidth of the antenna is from 2.3 to 2.53 GHz for VSWR < 2. Figure 3 shows a photograph of the fabricated antenna. We manufactured the antenna based on the results of optimized simulation results and measured characteristics of the suggested antenna in the anechoic chamber. Details of the proposed antenna designs are described, and typical experimental results are presented and discussed.

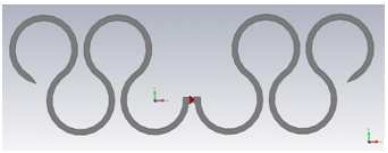

Figure 1: Proposed antenna.

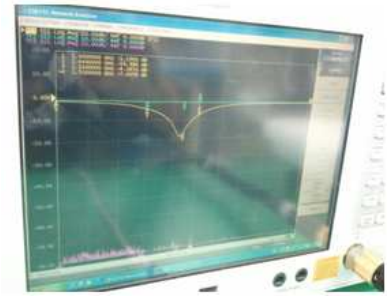

Figure 2: Measured return loss.

Figure 3: Photograph of the fabricated antenna.

REFERENCES

1. Choi, S. H., T. J. Jung, and S. Lim, "Flexible antenna based on composite right/left-handed transmission line," *Electronics Letters*, Vol. 46, No. 17, Aug. 2010.

Memristor-based UWB Antenna with Reconfigurable Notched Band

Kaida Xu[1], **Yonghong Zhang**[1], **Ronald J. Spiegel**[2], **William T. Joines**[2], **and Qing Huo Liu**[2]

[1]EHF Key Lab of Science, University of Electronic Science and Technology of China, Chengdu, China
[2]Department of Electrical and Computer Engineering, Duke University, Durham, NC, USA

Abstract— Memristors have been successfully fabricated by Hewlett-Packard Lab [1] and also applied in microwave devices [2], which offer a nonvolatile resistance as a state variable and retains either a high- or low-resistance state by means of generating or removing oxygen vacancies in the thin film. In this paper, a planar ultra-wideband (UWB) monopole antenna with memristor-based reconfigurable notched band is conceived and presented (See Fig. 1). The reconfigurable rejection frequency band at 3.8–4.1 GHz is achieved by embedding a U-shaped slot in the radiating patch with a memristor across the center of the slot. The nonvolatile memristor is used to activate and deactivate the slotting resonance by retaining either a high- or low-resistance state (See Fig. 2(a)). The transient electric field is observed by a receiver above the proposed antenna using an FDTD model. A sinusoidal wave signal of any frequency point in the notched band as a source could radiate from antenna when the memristor keeps ON state (100–140 ns or 160–200 ns), nevertheless, it would be largely suppressed when the memristor switches from ON to OFF state (140–160 ns).

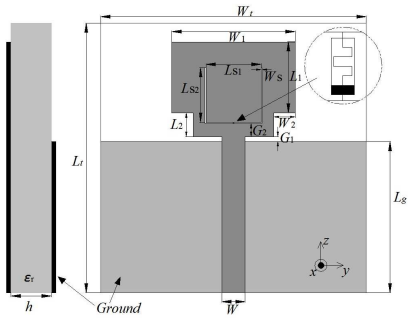

Figure 1: Layout of the proposed antenna. Substrate: $\varepsilon_r = 2.2$, thickness $h = 1.575$ mm.

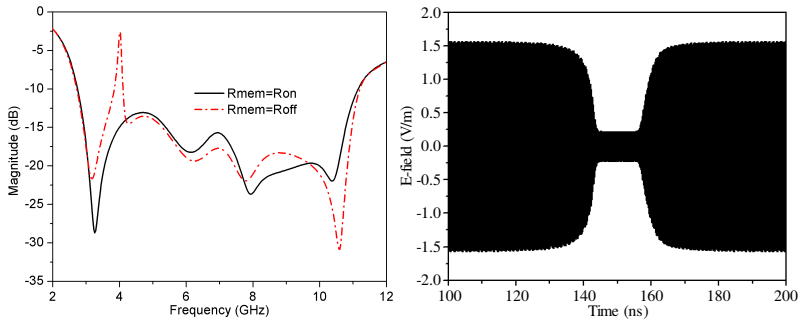

Figure 2: (a) Simulated S_{11} of the antenna when the state of the memristor is ON or OFF. (b) Transient E-field of the antenna when the memristor state is ON → OFF → ON.

REFERENCES

1. Strukov, D. B., G. S. Snider, D. R. Stewart, and S. R. Williams, "The missing memristor found," *Nature*, Vol. 453, No. 7191, 80–83, May 2008.
2. Xu, K., Y. Zhang, L. Wang, M. Yuan, Y. Fan, W. T. Joines, and Q. H. Liu, "Two memristor SPICE models and their applications in microwave devices," *IEEE Trans. Nanotechnol.*, Vol. 13, No. 3, 607–616, May 2014.

Biodegradable Passive RFID Tag for Subcutaneous Implant

Christopher J. Davenport[1], **Baraa F. Al-Azzawi**[1],
Peter Novodvorsky[2], **and Jonathan M. Rigelsford**[1]

[1]Department of Electronic & Electrical Engineering
The University of Sheffield, Mappin Street, Sheffield S1 3JD, United Kingdom
[2]Department of Diabetes and Endocrinology
Royal Hallamshire Hospital, Glossop Road, Sheffield S10 2JF, United Kingdom

Abstract— This paper proposes the use of a biodegradable radio-frequency identification (RFID) tag for the passive monitoring of soft tissue in the human body. Typically, soft tissue trauma can be caused by road accidents, bomb explosions and deep surgery. The RFID tag will be secured in the wound area during initial surgery to monitor for subcutaneous infection. As the tag is biodegradable there is no need for further surgery to remove the device, thus reducing the risk of further infection. This is a distinct advantage over the more common implantable monitoring devices which will need to be removed. The state of degradation of the tag is passively monitored from outside the body, providing information on the level of infection.

To investigate the radiofrequency response of a deteriorating tag, a non-biodegradable prototype has been designed and simulated using CST microwave studio. The design comprises of three overlaying hollow crosses as illustrated in Fig. 1 and has been simulated on thin FR4 substrate. Transmission coefficients are presented for a wideband frequency range spanning from 1 to 18 GHz. Degradation was simulated by methodically removing select parts of the cross, introducing breaks in the metallic elements of the tag. These break points are located in the positions indicated by the green dots in Fig. 1.

Experimental techniques using a vector network analyser (VNA) were used to validate the accuracy of our simulations. A thinner and more flexible non-biodegradable substrate was used to provide similarity with a biodegradable substrate. Finally, results of the tag positioned subcutaneously in a human phantom provide clarification on performance.

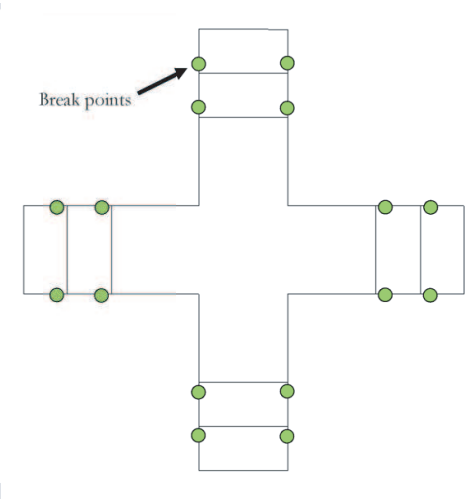

Figure 1: The cross would slowly reduce in size due to degradation, altering the RF measurement.

The Influence of a Magnetic Field on the Behaviour of the Quantum Mechanical Model of Matter

E. Hutova, K. Bartusek, and P. Fiala
Department of Theoretical and Experimental Electrical Engineering
Brno University of Technology, Technická 3082/12, Brno 616 00, Czech Republic

Abstract— The paper presents an experimental measurement of a material inserted in various types of magnetic field. The related model accepts the time component of an electromagnetic field from the perspective of the properties of matter. The relatively moving systems were derived and tested [1], and the influence of the motion on a superposed electromagnetic field was proved to exist already at relative motion speeds. In micro- and nanoscopic objects, such as the basic elements of matter, the effect of an external magnetic field on the growth and behaviour of the matter system needs to be evaluated. We tested the model based on electromagnetic field description via Maxwell's equations, and we also extended the monitored quantities to include various flux densities. Experiments were conducted with growth properties of simple biological samples in pre-set external magnetic fields.

ACKNOWLEDGMENT

The research described in the paper was financially supported from a grant provided by Czech Science Foundation, No. GACR 13-09086S, a project of the internal BUT science fund, No. FEKT-S-11-5/1012, and projects from the Education for Competitiveness Operative Programme, Nos. CZ.1.07.2.3.00.20.0175 and CZ.1.07/2.3.00/30.0005.

REFERENCES

1. Fiala, P., Z. Szabo, and M. Friedl, "EMHD models respecting relativistic processes of trivial geometries," *PIERS Proceedings*, 95–98, Suzhou, China, September 12–16, 2011.
2. Hutova, E. V., K. Bartusek, and P. Fiala, "The effect of a magnetic field on the speed of temperature change," *PIERS Proceedings*, 915–920, Stockholm, August 12–15, 2013.

Optimized Theoretical Analysis of Antimony Selenide (Sb_2Se_3) Chalcogenide Thin Film

Emmanuel Ifeanyi Ugwu
Department of Industrial Physics, Ebonyi State University, P.M.B 53. Abakaliki, Nigeria

Abstract— Theoretical analysis of the optical and Solid State properties of Antimony Selenide (Sb_2Se_3) thin film using beam propagation technique in which a scalar wave is propagated through the material thin film deposited on a substrate with the assumption that the dielectric medium is section into a homogenous reference dielectric constant term, ε_{ref} and a perturbed dielectric term, $\Delta\varepsilon_p(r)$ representing the deposited thin film medium is presented in this work. These two terms, constitute arbitrary complex dielectric function that describes dielectric perturbation imposed by the medium for the system. This is substituted into a defined scalar wave equation in which the appropriate Green's Function was defined on it and solved using series technique. The field value obtained from Green's Function was used in computation the propagated fields for different wavelength within three windows of electromagnetic wave spectrum during which the influence of the dielectric constants of Sb_2Se_3 thin film on the propagating field was considered. The results obtained from the computation were used in turn to obtain the data that were used in turn to compute the band gaps, solid state and optical properties of the thin film such as reflectance, Transmittance, reflectance and band gap of the thin film.

Matlab Extension for 3DSlicer: A Robust MR Image Processing Tool

J. Mikulka
Department of Theoretical and Experimental Electrical Engineering
Brno University of Technology, Technická 12, Brno 616 00, Czech Republic

Abstract— Using magnetic resonance tomography to scan biological tissues is currently a very dynamic approach Based on various image parameters, the method enables us to analyze tissue properties, recognize healthy and pathological tissues, and diagnose the disease or indicate its progression. However, the acquired data must be correctly interpreted and visualized by means of a suitable software tool, such as 3DSlicer (http://www.slicer.org). This well-designed platform provides an interface between the user and the data available in the popular DICOM format, and it facilitates very simple 3D visualization of the MR-based data. One of the main advantages of the open-source software package is undoubtedly its ability to be extended with supplementary modules, for example the Matlab script. The paper describes the open-source environment with a focus on Slicer3D and introduces possible extension of this platform with a module for MR data processing via the three-dimensional, mutiparametric, SVM trainable segmentation method. The module is freely downloadable. The paper also presents a comparison of the processing results with respect to the cycle time and the necessary interactivity. Moreover, the author proposes multiparametric segmentation of a brain tumor edema from T_1 and T_2-weighted images, and the advantages of the SVM technique are compared with corresponding features of both other fast segmentation methods and the one-parameter approach.

Multiparametric Biological Tissue Analysis: A Survey of Image Processing Tools

J. Mikulka
Department of Theoretical and Experimental Electrical Engineering
Brno University of Technology, Technická 12, Brno 616 00, Czech Republic

Abstract— Using magnetic resonance tomography to scan biological tissues is currently a very dynamic approach. Based on various image parameters, the method enables us to analyze tissue properties, recognize healthy and pathological tissues, and diagnose the disease or indicate its progression. These activities are then necessarily accompanied by the processing of the acquired images. The paper introduces a comparison of statistical tools for the trainable segmentation of multiparametric data obtained through magnetic resonance tomography. In this context, the author briefly compares various available tools (Weka, Slicer3D, and RapidMiner) in view of the input data training and testing, applicability of the classification models, and ability of the input/output data to be extended with other systems for further processing. The paper also describes as a multiparametric task the segmentation of a brain tumor performed with real MR data. The source of the data consists in T1 and T2-weighted images. The proposed segmentation method is carried out within the following phases: data resampling; spatial data coregistration; definition of the training points; training of the SVM classification model; testing of the model and interpretation of the classification results.

Automatic Segmentation of Multi-contrast MRI Using Statistical Region Merging

P. Dvorak[1, 2], K. Bartusek[2], and E. Gescheidtova[3]

[1]Department of Telecommunications, Faculty of Electrical Engineering and Communication
Brno University of Technology, Technicka 12, Brno 612 00, Czech Republic
[2]Institute of Scientific Instruments of the ASCR, v.v.i., Kralovopolska 147, Brno 612 64, Czech Republic
[3]Department of Theoretical and Experimental Electrical Engineering
Faculty of Electrical Engineering and Communication, Brno University of Technology
Technicka 12, Brno 612 00, Czech Republic

Abstract— Several methods have been developed for segmentation of MR images. Some of them are fully automated and some of them rely on an expert's assistance, such as determination of a starting point etc.. The fully automated methods are usually based on prior knowledge of a given object and can be used only for particular problem. The purpose of the proposed method is a fully automatic segmentation for general MR images independent on the number of tissues present. The proposed method is based on Statistical Region Merging (SRM) algorithm developed by Richard Nock and Frank Nielsen in 2004. The suitable MR contrasts for this algorithm, as it was confirmed during the test phase, are T1, T2 and FLAIR images. The segmentation process divides to image into regions according the properties in the area, but it does not consider the unconnected areas. For this reason, the algorithm is repeated for created segments without a joint border condition. The algorithm was tested on 5000 axial images with resolution 256×256 pixels. In 2256 slices, the tumor was present. Since the proposed method is fully automatic and independent of image intensities, each image of the database can be considered as unique and independent of others. The Dice coefficient for tissue segmentation varies for particular tissues. The best average result was achieved for grey matter, where the dice coefficient reached value 0.84. The results show the suitability of SRM method for multi-contrast MRI segmentation.

The Optical Angular Momentum in a Vector Vortex Optical Field

Rui-Pin Chen
Department of Physics, Zhejiang Sci-Tech University, Hangzhou 310028, China

Abstract— We study the propagation dynamics of vortex vector field with azimuthally locally uniform and inhomogeneous polarization states by using angular spectrum the electromagnetic beam. The evolution of the polarization states in the field cross section is analyzed numerically in detail during propagation by using the Stokes polarization parameters. The results indicate that the polarization states in the field cross section rotate along the propagation axis due to the existence of vortex field. In particular, the interaction between the central phase singular point (i.e., dislocation) and the polarization singular point (i.e., disclination) leads to the creation or annihilation of optical field in the center of optical field, depending on the number of vortex and polarization topological charges. The transverse energy flux distributions and both spin and orbital optical angular momentum of vector vortex optical field with the different states of polarization in the cross-section of the field are computed and analyzed. Our results indicate that the different states of polarization in the cross-section of the optical vector vortex field can influence and reconstruct the transverse Poyting vector (energy flux) and both spin and orbital optical angular momentum flux distribution in the cross-section of the field. These results, therefore, provide useful information on how to spatially manipulate the angular momentum of laser beams by choosing appropriate states of polarization in the cross-section of the field. This work provides further insight into dynamic behaviors of the vector vortex optical field and sheds light on a new approach in manipulating micro-particles.

Improvement on Optical Microfiber Fabrication Control Technique by Monitoring Mode Cutoff Position

Yang Yu, Xueliang Zhang, Zhangqi Song, Jianfei Wang, and Zhou Meng
College of Optoelectronic Science and Engineering
National University of Defense Technology, Changsha 410073, China

Abstract— By monitoring the intermodal interference pattern, we realize online diameter calibration during optical microfiber (OM) tapering process. By a comparison of LP_{02} mode cut-off position between theoretically prediction and the actual monitoring result, we introduce modifications of tapered parameters, and realize an online and precise feedback control in the OM tapered process. Our online feedback control technology provides an effective tool in acquiring high quality OMs by improving the tapered accuracy while maintaining good repeatability, which is essential for applications in scientific research and engineering areas.

Path Loss of Radio Propagation in an Aircraft Cabin

Wen-Chung Liu, Kuang-Yang Chou, and Chao-Ming Wu
Department of Aeronautical Engineering, Graduate Institute of Aeronautical and Electronic Engineering
Formosa University, Yunlin 632, Taiwan

Abstract— Presently, there is much interest in studying characteristics of wave propagation for a modern aircraft since a large number of navigation, data, and communication systems are usually applied to such aircrafts. Considering use of the personal mobile devices in the modern aircraft is feasible and thus the electromagnetic coupling effect between the personal mobile system and the avionic system has to be avoided. The problem of how to determine the path loss from a personal mobile device radiating in the cabin with a number of passengers becomes important and therefore, the purpose of this research is to establish a numerical model for precisely analyzing the path loss caused from the transmitter inside an aircraft cabin to exterior fuselage antenna. The electromagnetic software CST, base on finite-difference time-domain (FDTD), was applied for the required calculation. An electromagnetic model based on a small civil aircraft T39-A and the passengers was then built for theoretical analysis (Fig. 1). The simulated results of electromagnetic signal loss caused from the location of in-cabin antenna and the passengers when the signal, which operates at around 330 MHz, is transmitted from the antennas situated at the seats in cabin to that situated at the exterior fuselage are presented and discussed. The result shows that exist of the passengers significantly affects wave propagation in the cabin. In addition, to verify the simulation results obtained from the developed simulation model, measurement achieved from the real aircraft platform has also been set up and done. Finally, comparison between simulation and measurement has also been examined.

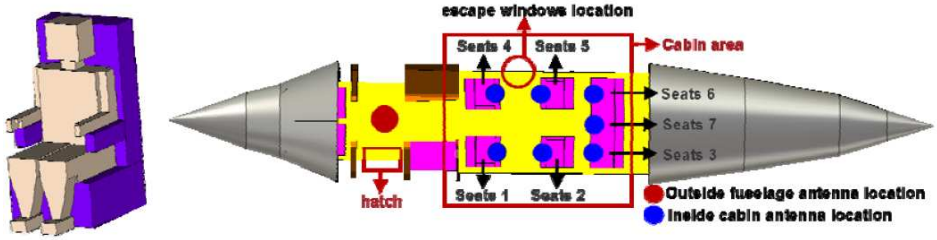

Figure 1: Numerical model of the aircraft and passengers.

ACKNOWLEDGMENT

This work was supported by the Ministry of Science and Technology, Taiwan, under Grant NSC 102-2221-E-150-022.

The Design of Band-pass Frequency Selective Surface with All Dielectric Metamaterial

Fei Yu, Shaobo Qu, Jiafu Wang, Hao Huang, and Jun Wang
Department of Mathematics and Physics, College of Science
Air Force Engineering University, Xi'an, Shaanxi 710051, China

Abstract— The traditional super material and frequency selective surfaces basically is mixed structure of the metal and medium, however, due to the inherent defects of metal materials, the dielectric metamaterial design frequency selective surface is necessary. The constitutive parameters and dielectric resonator theory based on equivalent, can design all dielectric metamaterial frequency selective surface. This paper presents the design of dielectric materials is introduced to the frequency selective surface to, is studied by using high dielectric constant dielectric frequency selective surface design principles and methods, and the design of the band-pass characteristics better dielectric metamaterial frequency selective surface. In this paper, the design principle for all dielectric metamaterial design frequency selective surface has important practical significance and guiding significance.

The Design of Band-pass Frequency Selective Surface with the Grid Dielectric Metamaterial

Fei Yu, **Shaobo Qu**, **Jiafu Wang**, **Hao Huang**, **and Jun Wang**
Department of Mathematics and Physics, College of Science
Air Force Engineering University, Xi'an, Shaanxi 710051, China

Abstract— Metallic parts are indispensable to traditional frequency selective surfaces. However, for millimeter waves, because of surface wave skin effect, the loss of metal-containing FSS is so large that the performance is badly affected. Besides, metal materials are quite unfavorable for high-temperature resistance and corrosion resistant requirements. The article adopt period dielectric structure to achieve band-pass frequency selective properties. The design principles proposed in this paper are of great practical values in designing all-dielectric metamaterials frequency selective surfaces.

Automatic Extraction of Pathological Area in 2D MR Brain Scan

P. Dvorak[1, 2], **K. Bartusek**[2], **and E. Gescheidtova**[3]

[1]Department of Telecommunications, Faculty of Electrical Engineering and Communication
Brno University of Technology, Technicka 12, Brno 612 00, Czech Republic
[2]Institute of Scientific Instruments of the ASCR
v.v.i., Kralovopolska 147, Brno 612 64, Czech Republic
[3]Department of Theoretical and Experimental Electrical Engineering
Faculty of Electrical Engineering and Communication, Brno University of Technology
Technicka 12, Brno 612 00, Czech Republic

Abstract— The aim of this work is to propose the fully automated pathological area extraction from multi-parametric 2D MR images of brain. The proposed method is based on multi-resolution symmetry analysis and automatic thresholding. The extraction is based on thresholding, where the Otsu's algorithm is used for the automatic determination of the threshold. Since the method is based on symmetry, it works for both axial and coronal planes. In both these planes of healthy brain, the approximate left-right symmetry exists and it is used as the prior knowledge for searching the approximate pathology location. It is assumed that this area is not located symmetrically in both hemispheres, which is met in most cases.

Multi-contrast images, concretely T2 and FLAIR, are involved in this task. We are trying to avoid using T1 contrast enhanced images, because they require contrast agent fluid to be injected into the bloodstream. In T2-weighted images, glioma and potential edema produce much stronger signal that the white matter, in which they are mostly located. For this reason, the thresholding is employed here. Since the intensities in image can differ from case to case depending on the data acquisition, it has to be computed from the particular image. Moreover, only pixels in the most asymmetric parts have to be involved in the threshold computation. Otherwise, the threshold would be computed incorrectly in case of small tumors. For this purpose, the asymmetry mask is computed. This mask includes the regions, where the asymmetry reached at least 10% of the maximum asymmetry for particular image. The FLAIR images are employed for taking out CSF from resulting area, because its distinguishing from the glioma or edema is complicated in T2 images.

The algorithm was tested on 357 axial and 443 coronal real images from publicly available BRATS databases containing 3D volumes brain tumor patients. The results were evaluated by Dice Coefficient (axial: 0.85 ± 0.11, coronal 0.82 ± 0.18) and by Accuracy (axial: 0.96 ± 0.05, coronal 0.94 ± 0.09). According to state-of-the-art literatures, $DC > 0.7$ expresses excellent similarity.

Numerical Modeling of Electromagnetic Field in the Biological Cell

E. Vlachova Hutova[1], **T. Kriz**[1], **E. Gescheidtova**[1], **and K. Bartusek**[2]

[1]Department of Theoretical and Experimental Electrical Engineering
Brno University of Technology, Technicka 12, Brno 616 00, Czech Republic
[2]Institute of Scientific Instruments, Academy of Sciences of the Czech Republic
Kralovopolska 147, Brno 612 64, Czech Republic

Abstract— The electric and magnetic field interactions with biological cells are of significant interest in various biophysical and biomedical applications. One reason why it is extremely important to deeply understand the true mode of action of electric or magnetic fields on living organisms (on prokaryotic cells), is the need to protect human health in consideration of the probably future introduction of new technologies such the therapeutic use of magnetic and electric field (e.g., nuclear magnetic resonance). The second reason is also important. It is important to know how cells will responds to external stimullation without disrupting the living cell structure (especially cell membrane). In order to study such important aspect, it is necessary to evaluate the time constant in order to estimate the response time of living cells in the electric or magnetic field. In the present study, the time constant is evaluated by considering the hypothesis of electrical analog of spherical shaped cells and assuming realistic values for capacitance and resistivity properties of cell — nuclear membrane, cytoplasm, and nucleus.

This work demonstrates how a stochastic model can be implemented to obtain a realistic description of the interaction of a biological cell with an external magnetic or electrical fields. In our model formulation, the stochasticity is adopted by introducing various levels of forcing intensities in model parameters. The presence of noise in nuclear membrane capacitance has the most significant effect on the current flow through a biological cell. The increasing amount of data reporting on the biological effects of magnetic and electric fields is leading researchers to understanding of how important it is to fully understand the mode of action of magnetic or electric fields to living organisms. Indeed, even if the perturbations of biological systems by magnetic or electric fields are sublethal at shorter times of exposure, these perturbations could, especially at longer times of exposure, evolve into a progressive accumulation of modifications, whose ultimate effects still need to be clarified.

Study of Electrical Effects of Charged Nanoparticles on a Small Vesicle Using Coarse-grained Molecular Dynamics Simulations

Linying Liu[1], **Jianhua Zhang**[1], **Xiaowei Zhao**[1], **and Qinghuo Liu**[1, 2]

[1]Institution of Electromagnetics and Acoustics, Xiamen University, Xiamen 361005, China
[2]Department of Electrical and Computer Engineering, Duke University, Durham, NC 27708, USA

Abstract— The mechanisms of electrical adsorption and translocation process of nanoparticles onto and across lipid membranes are of great biological and medical importance. They provide insight into the nature of endocytosis and nanoparticle-cell interactions which are critical for guiding the design of drug delivery carriers, biosensors, and biocompatible materials. Biophysical models have been proposed to explain how nanoparticles and their derivatives interact with biological membranes under various conditions of particle shapes, geometry, volume, velocity, and surface chemical properties. However, the mechanism of electrical effects on the adsorption and translocation of nanoparticles have not been determined clearly so far. In this paper, the interactions between charged nanoparticles and a small vesicle (DPPC membrane) are investigated by coarse-grained molecular dynamics simulations. The effects of the charged nanoparticles on a biological vesicle are studied via analyzing the electrical interactions of vesicle and nanoparticles with different surface charge densities. The simulated results demonstrate that the uncharged nanoparticles have no effects on the membrane during the transformation, but the penetration of vesicle has been observed. However, the simulations of positively charged nanoparticles show no preference for their translocation across the DPPC lipid bilayer. On the contrast, they are repulsed by the vesicle membrane. Interestingly, the adsorption of negatively charged nanoparticles on vesicle membrane would occur, which induces vesicle surface reconstruction. With the increase of surface charge density, negatively charged nanoparticles can penetrate through the lipid bilayer to the interior of the vesicle and would create a nanopore on the vesicle membrane. The reconstruction process of vesicle membrane induced by the nanoparticles is also further examined to understand the interaction mechanisms between charged nanoparticles and vesicle. Our analysis provides design criteria for future synthetic nanoparticles with the goal of designing particles that can be used in medical biology.

The Connection of a Micro-hydropower Plant to an Experimental Electrical Network

P. Marcon[1], **Z. Szabo**[1], **Z. Roubla**[1], **and F. Zezulka**[2]

[1]Department of Theoretical and Experimental Electrical Engineering, FEEC
Brno University of Technology, Technicka 12, Brno, Czech Republic
[2]Department of Control and Instrumentation, FEEC
Brno University of Technology, Technicka 12, Brno, Czech Republic

Abstract— The paper describes the connection of the micro hydropower plant to an 24 V experimental smart grid. The principle of the proposed design consists in improving stabilization of the current grid and enabling maximum exploitation of electric energy produced by renewable sources (hydroelectric stations, photovoltaics, wind power plants). In this respect, the authors present a very important block for change the direction of a current flow.

This block denoted as Control Block (in the paper, the block is marked as CB1), which serves both to dispatch energy to the grid and to charge the smart grid batteries. In order to secure correct operation and functioning of the CB1, the authors applied a step-up converter and designed a special step-down converter.

The first mode of CB1 enables to charge the local 12 VDC batteries (whose voltage may range between 11 VDC and 14.5 VDC depending on the battery charge status). The batteries are charged via a DC/DC converter, which behaves like a current source. The 24 VDC smart grid is used as the supporting source. The DC/DC converter is controlled depending on both the current sensed by a HY10 sensor and the voltage determined on a divider; the current and the voltage are measured at the CB1 input. The applied DC/DC converter is a special Linear Technology circuit controlled by a D/A converter via the LabView environment.

The second mode of CB1 allows power the 24 VDC smart grid from local 12 VDC batteries. For this purpose, we used a Vicor DC/DC converter, whose output voltage is controlled via LabView. In general terms, the controlling is performed through a D/A converter in CompactRIO; the output of the converter is connected to the controlling input of the changer. Here, the controlling is also realized depending on the output current and voltage, and sensor types similar to those applied within mode 1 are utilized.

Mutual switching between the two modes is performed using the LabView controlling interface; thus, the activity of only one converter (the step-up or the step-down) at a given moment is secured.

The Statistical Evaluation of Data Obtained via the Manual Segmentation of MRI Images of a Pathological Tissue

P. Marcon[1], **J. Mikulka**[1], **E. Gescheidtova**[1], **K. Bartusek**[2], **and A. Sprlakova**[3]

[1]FEEC, Department of Theoretical and Experimental Electrical Engineering
Brno University of Technology, Technicka 3082/12, Brno 616 00, Czech Republic
[2]Institute of Scientific Instruments of the ASCR
v.v.i, Kralovopolska 147, Brno 612 64, Czech Republic
[3]Radiological Clinic, The University Hospital Brno
Jihlavska 20, Brno 625 00, Czech Republic

Abstract— The authors present a statistical evaluation of the MRI images of bones and soft tissues. MRI imaging of small bones is a problem issue because the measured bone images are loaded with susceptibility artifacts and low signal-to-noise ratio. Therefore, we compare the commonly used MRI contrast (Proton Density — PD; relaxation time T_1; relaxation time T_2; Diffusion Weighted Imaging — DWI). The acquired images are classified in terms of the signal-to-noise ratio, intensity difference and steepness of the edges.

The regions of individual tissues in the measured images were defined. In this context, out interest was directed mainly towards the following tissues: gray matter, white matter, muscle, bone marrow, and bone. The statistical analysis was carried out within selected regions of the tissues. The values of the maximum, minimum, mean, and standard deviations as well as those of the higher statistical orders (skewness and kurtosis) was obtained.

The aim of this research was to statistically evaluate and determine the deviation of MRI images; this step was performed by several experts. These specialists conducted proper segmenting of pathological and healthy tissues, and they also compared the selected areas. In some cases, especially when the boundaries of the area are not clearly visible, the problem is to delimit the bone marrow area. Therefore, it is not possible to use automatic segmentation algorithms, and we focused on the manual evaluation of the statistical data in the area of the patient's bone marrow pathology (e.g., the probability of cyst formation can be determined from abnormal levels of vitamin D and osteocalcin).

In our experiment, an MR tomograph operated by the University Hospital Brno-Bohunice was utilized. The MR tomograph exhibits the static field flux density of $B_0 = 1.5\,\mathrm{T}$.

Uncertainty Determination in Measurements Using a Gerdien Tube

Z. Roubal, **Z. Szabo**, **and M. Steinbauer**
Department of Theoretical and Experimental Electrical Engineering
Brno University of Technology, Technicka 12, Brno 616 00, Czech Republic

Abstract— Light negative air ions demonstrably exhibit positive influence on the human organism. The concentration of these ions can be effectively used as the integral criterion for the evaluation of air purity, and there also exists a multitude of other applications. The presented aspiration method enables us to establish the concentration of air ions in the atmosphere. In a Gerdien tube fitted with a one-piece inner electrode, measurement of the saturation characteristics must be performed to facilitate the determination of the air ion mobility spectrum. This method is very sensitivity to noise and leakage current. In this paper is determination of uncertainty of type B in Gerdien tube and electrometric amplifier. This method is very sensitive to noise and leakage current. In this paper, the determination of uncertainty B in a Gerdien tube and an electrometric amplifier is presented. The uncertainty depends on the input bias current and input noise current of the applied operational amplifier. Another significant source of B uncertainty is the temperature and time instability of the Teflon insulator. This result was used for compared different type of Gerdien tube.

ACKNOWLEDGMENT

The research described in the paper was financially supported by a grant of the BUT science fund, No. FEKT-S-11-5/1012, and the authors also received assistance from projects within the Education for Competitiveness Operative Programme, Nos. CZ.1.07.2.3.00.20.0175 and CZ.1.07/2.3.00/30.0005.

REFERENCES

1. Roubal, Z., M. Steinbauer, and Z. Szabó, "Modeling of saturation characteristic of an aspiration condenser," *PIERS Online,* Vol. 6, No. 1, 26–30, 2010.
2. Kondrashova, M. N., E. V. Grigigorreko, A. N. Tikhonov, T. V. Sirota, A. V. Temnov, I. G. Stavrovskaya, N. I. Kosyakova, N. V. Lange, and V. P. Tikonov, "The primary physicochemical mechanism for the beneficia biological/medical effects of negative air ions," *IEEE Trans. Plasma Scien.*, Vol. 28, No. 1, 230–237, 2000.
3. Roubal, Z. and M. Steinbauer, "Design of electrometric amplifier for aspiration condenser measurement," *PIERS Proceedings*, 1430–1434, Xi'an, China, Mar. 22–26, 2010.
4. Tammet, H. F., *The Aspiration Method for Determination of Atmospheric-ion Spectra*, IPST, Jerusalem, 1970.
5. Bartušek, K., P. Fiala, T. Jirků, and E. Kadlecová, "Accuracy of air ion field measurement," *PIERS Proceedings*, 412–415, Cambridge, USA, Mar. 26–29, 2006.
6. Bartušek, K., "Meření spektrálních charakteristik iontových polí," 2001, Elektrorevue Online: http://www.elektro-revue.cz/clanky/01038/index.html.
7. Steinbauer, M., P. Fiala, K. Bartušek, and Z. Szabó, "Experiments with accuracy of air ion field measurement," *PIERS Online*, Vol. 3, No. 8, 1330–1333, 2007.
8. Roubal, Z. and P. Křepelka, "Estimation of the air ion mobility spectrum by means of a gerdien tube with a segmented inner electrod," *PIERS Proceedings*, 767–771, Stockholm, Sweden, Aug. 12–15, 2013.

SAR Study on MIMO Wi-Fi Antennas in LTE Mobile Terminals

Kun Zhao[1, 2], **Shuai Zhang**[1, 2], **Zhinong Ying**[2], **and Sailing He**[1]

[1]Department of Electromagnetic Engineering, School of Electrical Engineering
KTH-Royal Institute of Technology, Stockholm SE-100 44, Sweden
[2]Research and Technology, Corporate Technology Office
Sony Mobile Communications AB, Lund SE-221 88, Sweden

Abstract— The Specific Absorption Rate (SAR) of mobile terminals is strictly limited by governments, and thus it is important for mobile terminal venders to know the SAR performance of different antenna configurations. SAR performances for cellular antennas have been studied in both SISO and MIMO case. However, the impact of Wi-Fi antennas on the mobile terminals' SAR has not been studied systematically, especially for the MIMO Wi-Fi. With multiple Wi-Fi antennas, the interaction between antennas will be more complicated, and more measurements need to be done in order to get a completed evaluation of the SAR performance. In this abstract, a mobile terminal antenna system with dual elements MIMO LTE antenna and dual elements MIMO Wi-Fi antenna is proposed, we will show the SAR performance with multiple transmitters on both the Specific Anthropomorphic Mannequin (SAM) head phantom and the flat phantom.

The configuration of our proposed MIMO antenna system is shown in Fig. 1(a). Two multi bands monopole antennas are implemented on the top and the bottom of the chassis and compose the LTE MIMO antenna for the mobile terminal. Two PIFA antennas with the same structure are integrated on the corner of the chassis as MIMO Wi-Fi antenna. A plastic case is used to cover the antenna to mock a real mobile terminal. The Simulation Setup on SAM head phantom and flat phantom are shown in Figs. 1(b) and (c).

Figures 2(a) and (b) show the Normalized simultaneous SAR fields when Two Wi-Fi antennas work at 5.4 GHz and the main LTE antenna work at 0.85 GHz and 1.9 GHz on the right side, respectively. We can see that the position of simultaneous peak SAR is mainly decided by the corresponding LTE antenna. This is due to the input power of LTE antenna is much higher than Wi-Fi antenna. In the full paper, the simultaneous SAR of different number of transmitters and different operation schemes will be presented systematically on both phantoms, the impact of MIMO Wi-Fi antenna on the simultaneous SAR will be analyzed deeply.

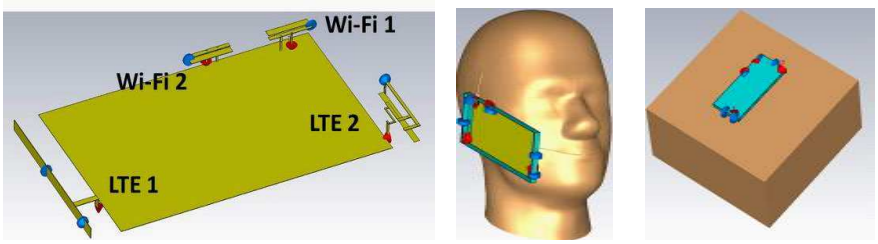

(a) (b) (c)

Figure 1: (a) The structure of proposed MIMO LTE antenna with MIMO WiFi antenna, (b) the SAR simulation setup on SAM head and (c) the SAR simulation setup on flat head.

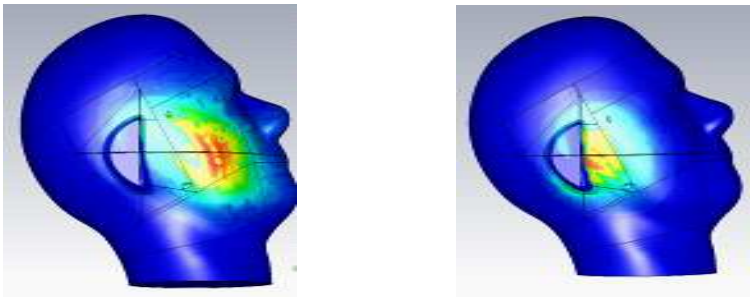

(a) (b)

Figure 2: Normalized combined SAR fields when Two Wi-Fi antennas work at 5.4 GHz and the main LTE antenna work at (a) 0.85 GHz and (b) 1.9 GHz on the right side of SAM head phantom.

Detector for Nuclear Quadrupole Resonance Spectroscopy

J. Chytil and R. Kubasek
Department of Theoretical and Experimental Electrical Engineering
Brno University of Technology, Technicka 12, Brno 616 00, Czech Republic

Abstract— Nuclear quadrupole resonant spectroscopy is method similar to nuclear magnetic resonant spectroscopy also called zero field NMR. The response signal is very low and it is immersed in to the noise. There can be used some methods to harvest signal from noise it can be matched receiver or averaging. This authors describe detector for Nuclear quadrupole resonant spectroscopy based on statistic methods and probability of distribution, that allow to measure repetitive signals below noise level. The paper presents the mathematical model and practical solution of the detector, and problems such as the dynamic range and signal distortion based on the signal-to-noise ratio are also analyzed in the given context. If the time of signal occurrence is known, the repetitive signal below the noise level can be harvested out of noise by averaging because of the wanted signal is correlated therefor highlighted by averaging contrast to the noise which is not correlated so it is supressed by averaging. The same principle we can use in domain of digital signal. So the input signal can be converted to the digital representation. There is an comparator with a triggering level immersed in the noise so the comparator is flipping continuously and the probability of output values is affected by input signal. The output digital signal can be processed by FPGA.

ACKNOWLEDGMENT

The research described in the paper was financially supported by a grant of the BUT science fund, No. FEKT-S-11-5/1012, and the authors also received assistance from projects within the Education for Competitiveness Operative Programme, Nos. CZ.1.07.2.3.00.20.0175.

REFERENCES

1. Somasundaram, S. D., A. Jakobsson, N. R. Butt, M. D. Rowe, J. A. S. Smithand, and K. Althoefer, "Detection of stochastic nuclear quadrupole resonance signals," *Digital Signal Processing*, Vol. 15, 367–370, 2007.
2. Somasundaram, S. D., A. Jakobsson, and E. Gudmundson, "Digital signal processing, 2007," *Journal Title Abbreviation*, Vol. 56, No. 3, 887–894, 2008.
3. Williams, J., "A seven-nanosecond comparator for single supply operation — Linear technology AN72," May 1988.
4. Williams, J., "A high speed comparator techniques — Linear technology AN13," April 1985.
5. Williams, J., "Nanovolt noise measurement for a low noise voltage reference — Linear technology AN124," April 2009.
6. Somasundaram, S. D., A. Jakobsson, N. R. Butt, M. D. Rowe, J. A. S. Smith, and K. Althoefer, "Detecting stochastic nuclear quadrupole resonance signals in the presence of strong radio frequency interference," *Acoustics, Speech and Signal Processing*, Vol. 15, 3645–3648, 2008.

Design of Dual Cross Dipole Antennas with Dual Frequencies and Dual Circularly-polarized

Yu-Feng Wang, Lei Chang, and Yu-Feng Yu
No. 36 Research Institute of CETC, China

Abstract— An integrated antennas are presented with dual frequencies and dual circularly-polarized (CP) in a common aperture. The proposed antennas are consisted of dual dipole antennas (CDAs) with stacked structure, which used 90° self-phase shifting structures for CP wave achieving by adjusting the proportion of the orthogonal arm lengths for 90° phase difference. The upper CDA covers a 4.7% relative bandwith from 1.55 GHz to 1.625 GHz of left-hand CP (LHCP) and the nether CDA covers a 3.4% relative bandwith from 2.44 GHz to 2.525 GHz of right-hand CP (RHCP) with VSWR less than 2 and axial ratio less than 3 dB. Well gains at low elevation angle (larger than 10 deg) are obtained in the proposed antenna with −1 dB at 1.616 GHz and 1 dB at 2.492 GHz.

Design and Study of Multiband Microstrip Antenna

Lei Chang, Jian-Qiang Zhang, Yu-Feng Wang, and Yu-Feng Yu
No. 36 Research Institute of CETC, Jiaxing, China

Abstract— A multiband antenna which is fed by a SMA coaxial probe is investigated in this paper. The proposed antenna is composed of a circular patch and a loop microstrip line. By introducing a loop microstrip line and three probes feeding for the circular patch, the proposed antenna delivers the multiband impedance matching performance. The simulated result shows that the antenna has three frequency bands covering 1.254–1.404 GHz, 1.653–1.746 GHz and 2.142–10.752 GHz for VSWR < 3. Details of the antenna design and results are presented.

REFERENCES

1. Foudazi, A., H. R. Hassani, and S. M. Ali Nezhad, "Small UWB planar monopole antenna with added GPS/GSM/WLAN bands," *IEEE Trans. Antennas Propag.*, Vol. 60, No. 6, 2987–2992, 2012.
2. Mandal, M. K. and Z. N. Chen, "Compact dual-band and ultrawideband loop antennas," *IEEE Trans. Antennas Propag.*, Vol. 59, No. 8, 2774–2779, 2011.
3. Hsieh, C., T. Chiu, and C. Lai, "Compact dual-band slot antenna at the corner of the ground plane," *IEEE Trans. Antennas Propag.*, Vol. 57, No. 10, 3423–3426, 2009.
4. Wu, P., Z. Kuai, and X. Zhu, "Multiband antennas comprising multiple frame-printed dipoles," *IEEE Trans. Antennas Propag.*, Vol. 57, No. 10, 3313–3316, 2009.
5. He, Q. Q., B. Z. Wang, and J. He, "Wideband and dual-band design of a printed dipole antenna," *IEEE Antennas Wireless Propag. Lett.*, Vol. 7, 1–4, 2008.
6. Hsieh, C. and T. Chiu, "Dual-band antenna design using a dual-feed monopole slot," *IET Microw. Antennas Propag.*, Vol. 5, No. 12, 1502–1507, 2011.
7. Quan, X. L., R. L. Li, Y. H. Cui, and M. M Tentzeris, "Analysis and design of a compact dual-band directional antenna," *IEEE Antennas Wireless Propag. Lett.*, Vol. 11, 547–550, 2012.
8. Quevedo-Teruel, Ó., M. N. M. Kehn, and E. Rajo-Iglesias, "Dual-band patch antennas based on short-circuited split ring resonators," *IEEE Trans. Antennas Propag.*, Vol. 59, No. 8, 2758–2765, 2011.

A Polarization Insensitive and High Efficiency Schottky Photodetector Based on Si Ridge Waveguide

Liu Yang and Pengfei Kou
Zhejiang University, China

Abstract— When light radiates on a Schottky contact formed at the metal-silicon interface, internal photoemission (IPE) happens, which is an important way to achieve sub-bandgap detection. Based on this phenomenon, a polarization insensitive and high efficiency plasmonic Schottkyphotodetector is proposed here. The schematic structure is shown in Figure 1(a). Our photodetector consists of a Si ridge waveguide, an Au Schottky electrode (of thickness h_{Au}) covering both the top and sidewalls of the Si ridge, an aluminium (Al) Ohmic electrode on top of the Si slab, and a thin SU8 insulating film (of thickness h_{SU8}) separating the two electrodes. Simulation results show that the new diode is polarization-insensitive and is only 4- μm long, but still absorbs over 85% of light in the wavelength range of 1.2–1.6 μm. All of these excellent properties are attributed to the highly-absorptive plasmonic waveguide with sidewall coverage of Au. What's more, the calculated dark current is also very low, i.e., $I_{dark} = 136$ nA. All of these mean that the new design can be effectively used for applications in high-density silicon photonic integration.

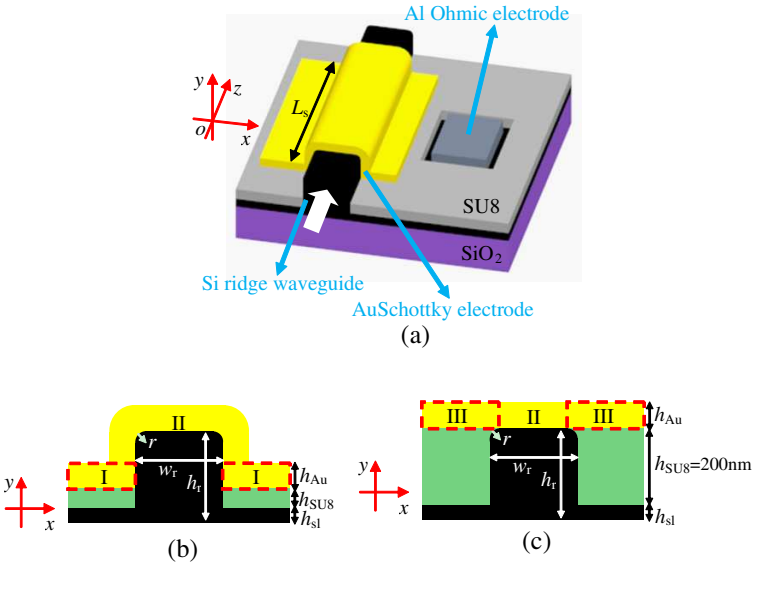

Figure 1: (a) Three-dimensional schematic diagram of our Si PD. Two dimensional schematic diagrams of our Si PD with (b) $h_{SU8} < 200$ nm and (c) $h_{SU8} = 200$ nm.

Narrow-band Tunable Fiber Fabry-Perot Filter Based on Laser Heated Fiber Bragg Gratings

Ying Li[1], **Liang Zhang**[1], **Yebin Zhang**[1], **Shaorui Gao**[1], **Guofeng Yan**[1], **and Bin Zhou**[2]

[1]Centre for Optical and Electromagnetic Research
State Key Laboratory of Modern Optical Instrumentation
Zhejiang University, Hangzhou 310058, China
[2]Centre for Optical and Electromagnetic Research
South China Academy of Advanced Optoelectronic
South China Normal University, Guangzhou 510006, China

Abstract— A tunable fiber Fabry-Perot (FP) filter was developed in a cobalt-doped single mode fiber. The cobalt-doped fiber is an active fiber which can transform optical power into heat effectively due to the nonradiative processes [1, 2]. The core of this special element doped fiber can be heated up to a few hundred degrees Celsius by a heating laser. Two fiber Bragg gratings (FBG) were fabricated inside this fiber, forming a Fabry-Perot resonator. The cavity length is carefully designed to make sure the longitude mode spacing is comparable to the grating bandwidth (typically 0.2–0.5 nm [3]). Thus the cavity supports only one longitude mode within the grating bandwidth. When calculating the FSR, one cannot neglect the effective length of the FBG [4], because of the high-reflectance of the FBG. The distance between the two FBG's adjacent ends is 1 mm, and the efficient length of the FBG is estimated to be 2 mm in our experiment. By adjusting the power of the heating laser, the resonant wavelength of our proposed fiber Fabry-Perot (FP) filter can be easily controlled.

REFERENCES

1. Zhou, B., Z. Chen, Y. Zhang, S. Gao, and S. He, "Active fiber as sensor for methane detecting based on a laser heated fiber Bragg grating," *IEEE Photon. Technol. Lett.*, Vol. 26, No. 11, 1069–1072, Jun. 1, 2014.
2. Davis, M. K. and M. J. F. Digonnet, "Measurements of thermal effects in fibers doped with cobalt and vanadium," *J. Lightw. Technol.*, Vol. 18, No. 2, 161–165, Feb. 2000.
3. Zhang, Y., B.-O. Guan, and H.-Y. Tam, "Ultra-short distributed Bragg reflector fiber laser for sensing applications," *Opt. Express*, Vol. 17, No. 12, 10050–10055, Jun. 8, 2009.
4. Barmenkov, Y. O., "Effective length of short Fabry-Perot cavity formed by uniform fiber Bragg gratings," *Opt. Express*, Vol. 14, No. 14, 6394–9399, Jul. 10, 2006.

5d-4f Luminescence of Rare Earth Ions in New Oxide Hosts

Mattia Trevisani[1], **Konstantin V. Ivanovskikh**[2], **Fabio Piccinelli**[1], **Irene Carrasco**[1], **and Marco Bettinelli**[1]

[1]Luminescent Materials Laboratory, Department of Biotechnology
Strada Le Grazie 15, Verona 37134, Italy
[2]Institute of Physics and Technology, Ural Federal University, Ekaterinburg 62002, Russia

Abstract— The search for new scintillator materials able to convert efficiently high-energy radiation into UV and visible light has been going on for more than fifty years and nowadays is one of the most active research areas in the field of optical materials. In particular, the rapid evolution of nuclear medical imaging techniques such as computed tomography (CT) and positron emission tomography (PET) has generated an increased demand for fast radiation detectors in order to improve the quality of tomographic images.

Most of the scintillators presently used in CT and PET scanners are based on materials activated with the Ce^{3+} ion, which exhibits efficient and relatively fast (20–70 ns) 5d-4f electric-dipole emission in a broad spectral range (350–600 nm). Recently much attention has been focused on the study of the 5d-4f emission of Pr^{3+} ions in wide band-gap compounds. The emitting lowest 5d state of Pr^{3+} ions is located at about 12200 cm^{-1} to higher energy than the one for Ce^{3+} in the same host and its emission lifetime is about 2–3 times shorter allowing the development of scintillators with faster time response. As a result, the choice of the Pr^{3+} ion as an activator ion for wide band-gap hosts may constitute a promising alternative to Ce^{3+} in the development of new scintillators for applications requiring fast response.

Our search for novel materials showing fast 5d-4f emission of lanthanide ions has led us to the synthesis and investigation of the time-resolved spectroscopic properties of Ce^{3+} and Pr^{3+} ions in several classes of mixed oxides, in both nanocrystalline and bulk forms. The synthesis and the structural characterization of these doped materials will be described in detail. Luminescence emission and excitation spectra and decay curves measured using synchrotron radiation will be presented and discussed, together with the prospective applications of these luminescent materials.

ACKNOWLEDGMENT

We would like to thank the European Commission for funding through the Marie Curie Initial Training network LUMINET, grant agreement No. 316906.

A Compact Dual Band Band-pass Filter Using a New Topology of Transmission Line Metamaterial

Akram Boubakri[1], **Fethi Choubani**[1], **Tan Hoa Vuong**[2], **and Jacques David**[2]

[1]Innov'Com Laboratory, Sup'Com, Ariana, Tunisia
[2]Plasma and Energy Conversion Lab, INPT, France

Abstract— Band pass filters are employed in microwave and millimeter wave communication systems to remove signals from an undesired frequency or channel and we often find it before and after the mixer in many kinds of communication systems. With the rapid development of microwave and millimeter wave communication systems, it greatly stimulates the demand on high performance bandpass filters with compact dimensions, low insertion loss, high attenuation in stopband and low cost. However, most of conventional bandpass filters are unsuitable for miniaturized realization demand of modern communication and electronic systems. In this study, we developed a novel compact bandpass filter operating in the X band using a new type of transmission line metamaterial as depicted in Figure l. The aim of using such type of metamaterial is the low cost and the easy achievement using the coupling method to synthesize such a filter.

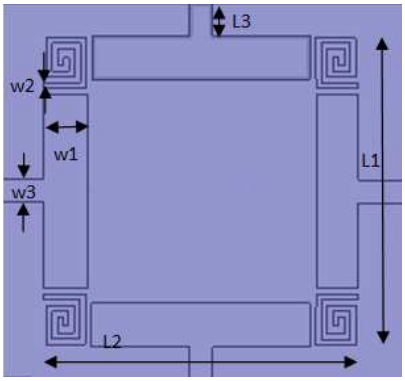

Figure 1: Unit cell of the MTM TL. $L1 = L2 = 5.5\,\text{mm}$, $W1 = 0.788\,\text{mm}$, $W2 = 0.1\,\text{mm}$, $W3 = 0.4\,\text{mm}$, $L3 = 0.5\,\text{mm}$.

A Novel Wideband Wide-angle Frequency Selective Surface Composite Structure

Zhan-Bo Lu, Xue-Quan Yan, and Jian-Jian She
AVIC Leihua Electronic Technology Research Institute, WuXi, China

Abstract— A novel wideband FSS composite structure is proposed, which use modified C-type sandwich cascaded structure and Hexagonal loop element with the characteristics of center symmetry in FSS design resulting in good electrical performance such as high transmission efficiency and stable working frequency band at a wide range of incident angle. The FSS sample is fabricated using low temperature pressing processes and then measured in anechoic chamber, The measured results show relative bandwidth of the FSS composite structure reaches to 45% (Transmission efficiency $> 85\%$) for arbitrary incident angle from 0° to 60° and both polarization. With the increase of the incident angle, the center resonant frequency tends to shift to higher frequency, the maximum offset of which is below 0.5 GHz. Inner envelope relative bandwidth is close to 41% (transmission efficiency $> 85\%$) at a range of $0^\circ \sim 68^\circ$ incident angle of vertical polarization wave and $0^\circ \sim 60^\circ$ incident angle of horizontal polarization wave.

Highly Birefringent Photonic Crystal Fibers with a High-index Doped Rod

Wei-Hsiang Chuang[1], **Che-Wei Yao**[1], **and Jui-Ming Hsu**[1, 2]

[1]Department of Electro-Optical Engineering, United University, Miaoli 360, Taiwan
[2]Optoelectronics Research Center, United University, Miaoli 360, Taiwan

Abstract— A highly birefringent photonic crystal fiber (HB-PCF) are designed and simulated in this article. To achieve a high modal birefringence in the HB-PCF, we designed four types of HB-PCF in sequence by adding some birefringence-enhancing factors. Fig. 1 shows the cross-sectional view of these four types HB-PCF.

To destroy the six-fold symmetry of the fiber and split the degenerated doublet pair for enlarging the modal birefringence, two air holes at the innermost layer of the PCF were replaced with larger holes. This type of structure is named as Type 1 in this article and indicated in Fig. 1(a). In addition to the two larger holes, Type 2 removed two holes in appropriate orientation at the innermost layer of the PCF, which is shown in Fig. 1(b), to enhance the birefringence more. To increase the birefringence of Type 2, one can confine the splitting degeneration modes in a smaller core region. Therefore, as shown in Fig. 1(c), Type 3 was designed by inserting a circular Ge-doped rod with higher refractive index and appropriate diameter in the center of the core. Ultimately, the circular Ge-doped rod was replaced with elliptic one to even more enlarge the modal birefringence. The final structure is named as Type 4 and exhibited in Fig. 1(d).

Figure 2 compares the modal birefringence of these four types of HB-PCF. As shown in Fig. 2, the birefringence values increase in sequence for adding the birefringence-enhancing factors as mentioned previously. For the habitual wavelength $\lambda = 1550\,\text{nm}$ of optical-fiber communications, the numeric values of modal birefringence are 7.919×10^{-3}, 10.562×10^{-3}, 19.33×10^{-3}, and 24.768×10^{-3} with respect to Type 1 to Type 4.

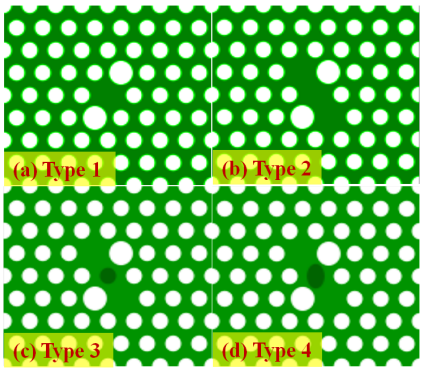

Figure 1: Cross-sectional view of the HB-PCFs. (a) Type 1, (b) Type 2, (c) Type 3, and (d) Type 4.

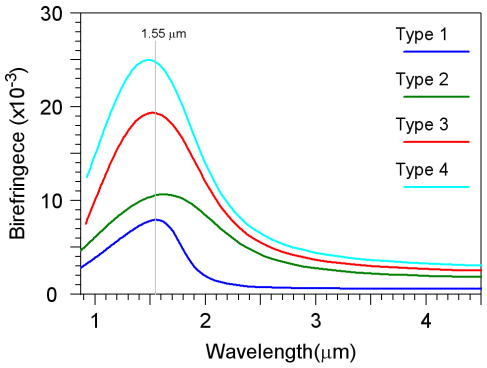

Figure 2: Dependence of birefringence on wavelength for HB-PCFs shown in Fig. 1.

Electromagnetic Field Fluctuations Near a Point-like and an Extended Field Source

R. Passante, L. Rizzuto, and S. Spagnolo
Dipartimento di Fisica e Chimica, Università degli Studi di Palermo
CNISM, Via Archirafi, Palermo 36 90123, Italy

Abstract— We investigate the field fluctuations near a point-like and an extended field source, such as an atom or a polarisable body, and discuss the problem of their singular behavior at the position of the source.

We consider a point-like source interacting with the electromagnetic field, in its dressed ground-state and investigate the local and global properties of the electric and magnetic energy densities in the space around the point-like source, after that the zero-point energy has been subtracted. We show that the assumption of a point-like source leads to a divergence of the renormalized electric and magnetic energy densities at the position of the source. We investigate in detail the mathematical structure of this divergence and show that it is at the origin of a discrepancy between the value of total electromagnetic field energy calculated as expectation value on the dressed ground-state of the field Hamiltonian or as a space integral of the electromagnetic energy density. We discuss that such inconsistency is solved if the singularity at the position of the field source is correctly taken into account. We then consider the case of an extended source, with a finite size and described by an appropriate form factor and investigate in detail the behavior of the electric and magnetic energy densities in the space around the source. We show that the proposed model of extended source eliminates divergences and singularities in local quantities (such as the electric and the magnetic energy density), and also solve the inconsistency between global and space-integrated local self-energies, disappear, for any nonvanishing size of the source.

Solar Cells Efficiency Improvement by Forming a Periodic Structure on the Surface

M. Tomita[1], **Y. Okuno**[2], **T. Suyama**[3], **M. Tanigawa**[4], **and X. Xu**[5]

[1]University of Electro-Communications, Tokyo, Japan
[2]South China Normal University, Guangzhou, China
[3]Akashi National College of Technology, Akashi, Japan
[4]The Kansai Electric Power Company, Inc., Osaka, Japan
[5]Kyushu Sangyo University, Fukuoka, Japan

Abstract— In recent years, many improvements have been attempted on solar cells for the high efficiency. The mode-matching method in the sense of least squares was applied to analyze the transmission coefficient of the solar power with regard to the most upper semiconductor board of solar cell in the case that the board has periodic groove structure on its surface and semiconductors such as GaAs, a-Si and so on are treated in this paper. Problems of this paper are resulted in diffraction problems by two or three-dimensional periodic structures formed on surfaces of those boards with dispersion characteristic. It is concluded from results of analyses that the transmission coefficient of the solar power through the periodic structure is increased considerably over the entire bandwidth of the solar spectra in comparison with the board having flat surface when periodic structures are formed adequately on those surfaces. If the periodic length and the depth of groove are selected as same order as an arbitrary wavelength in the bandwidth of the solar spectra, the transmission coefficient is increased largely on the lower region of the solar spectra than the wavelength mentioned above in comparison with the higher region of that wavelength.

REFERENCES

1. Tomita, M. and Y. Okuno, "Analysis of power transmission coefficient of sunlight into the GaAs board with periodic structure on the surface," *Trans. IEICE Jpn.*, Vol. J97-C, No. 5, 2014, to be published in Japanese.
2. Yasuura, K. and M. Tomita, "Numerical analysis of plane wave scattering from dielectric gratings," *Trans. IECE Jpn.*, Vol. 61-B, No. 7, 662–669, 1978 (in Japanese).
3. Matuda, T and Y. Okuno, "Algorithm of numerical analysis for plane wave diffraction by metallic grating with loss," *Optic*, Vol. 21, No. 8, 541–549, 1992 (in Japanese).

Research on OpenMP Model of the Parallel Programming Technology for Homogeneous Multicore DSP

Minjie Wu, **Weiwei Wu**, **Deping Zhang**, **Hongyu Zhao**, **and Naichang Yuan**
National University of Defense Technology, China

Abstract— As application complexity continues to grow, using multicore processors has been proved to be an effective methodology to meet the ever-increasing processing demand across the industry association. The Master/Slave model the Data Flow model and the OpenMP model are the three dominant models for parallel programming. In this paper, the first two models are briefly discussed while the OpenMP model is focused. Some factors (e.g., the number of threads, the scheduling strategy, the load balance, etc.) that affecting the execution performanceof OpenMP programs were also studied in this paper.

TMS320C6678 DSP is the first delivered industry's homogeneous multicore DSP which supports the OpenMP specification. This paper presents a method of taking advantage of the OpenMP model to realize the image edge detection within the platform of TMS320C6678 DSP. In the process of implementation, atomic operations are introduced instead of lock operations to improve the speedup. Both of them are used for preventing the cores to access the shared memory at the same time. Meanwhile, we also adopt the Master/Slave model to complete the same task in order to compare with the OpenMP model.

At the end of the day, the experimental results show that the OpenMP model has a better advantage on scalability and flexibility compared to the Master/Slave model and the Data Flow model. The best performance can be obtained when the number of threads is equal to the number of cores which are available within the platform. Under the circumstance of using the eight cores of TMS320C6678 DSP simultaneously, an image of 1024×768 pixels just needs 6.192 ms to complete the edge detection. This result is impressive compared to the Master/Slave model's which saves 32.10% in time. Further more, if we use 1 to 8 cores, the respective execution time reduces resulting in the speedup approximately conforms to the Gustafson's law. In the case of 8 cores, the speedup reaches 7.233.

Optical Magnetic Sensor Based on Magnetic Fluid Embedded Fiber Coupler

Guofeng Yan, Liang Zhang, Yebin Zhang, and Sailing He
Centre for Optical and Electromagnetic Research, Zhejiang University, China

Abstract— Magnetic sensors have been widely used in navigation, vehicle detection and current monitoring fields. Due to low cost, small size, immune to electromagnetics, optical fiber magnetic sensors have attracted a great deal of attentions in the past few years. Many fiber-based structures have been proposed for magnetic measurements, such as photonic crystal fibers with microholes in the collapsed region and single-mode-multimode-single-mode interferometers. Most of the sensing schemes are based on wavelength demodulation, which needs broadband light source. Meanwhile, special fibers and complicated fabrication process are needed.

In this paper, we proposed a new kind of magnetic sensor with low cost and ease of fabrication. The sensor is based on a standard single mode fiber coupler. In the coupling section, one arm wasimmersed inmagnetic fluids. When the magnetic field around coupler changes, the refractive index (RI) and absorption coefficient (AC) of the magnetic fluids change as well, thatwill induce the light power fluctuation of both arms. As a result by monitoring the output power of either arm of the coupler, one can easily detect the magnetic field. Simulation was carried out to demonstrate its feasibility, using commercial softwareRsoft. The length of taper waist and the fiber diameter in the waist were set as 1 mm and 10 μm, respectively. Gaussian light beam launched into one arm with magnetic fluids surrounding in the waist section, whose RI and AC parameters were from formal literature. In order to depress the deviation caused by the power fluctuation of the light source, we monitoredthe ratio of both output ports of the coupler. Simulation results showed a linear decreasing ratio from 5.21 to 2.97, when magnetic fields increased from 0 to 160 oe. It's believed that such simple structure with intensity demodulation scheme will have potential applications in magnetic field monitoring.

Atypical Functional Connectivity Development of Children with Autism Spectrum Disorder (ASD) in Prefrontal Cortex of the Brain: A fNIRS Study

Shijing Wu[1, 2], Huilin Zhu[1], Huan Guo[2], Xinge Li[2], Qianqian Gao[1, 2], and Sailing He[1]

[1]Centre for Optical and Electromagnetic Research
ZJU-SCNU Joint Research Center of Photonics
South China Normal University (SCNU), Guangzhou 510006, China
[2]School of Psychology, South China Normal University (SCNU), Guangzhou 510631, China

Abstract— Autism spectrum disorder (ASD) is a neuro-developmental disorder, characterized by delays or abnormal functioning started before the age of three years in one or more of the following domains: social interaction, communication and restricted, repetitive and stereotyped patterns of behaviors and interests. Previous studies have found that children with ASD showed atypically functional and anatomical development in the prefrontal area of the brain, which is considered as region for executive function, including the inferior frontal gyrus, middle frontal gyrus, and superior frontal gyrus. In the present study, for the first time, functional near infrared spectroscopy (fNIRS) was used to examine the resting state functional connectivity in prefrontal cortex of the children with ASD and reveal the different developmental patterns.

In this study, a 42-channel functional near infrared spectroscopy (fNIRS) was adopted to measure the spontaneous hemodynamic activity in prefrontal cortex, and compared the differences of temporal correlation between children with ASD and typically developing (TD) children between 6–13 years of age. The interhemispheric correlation and the inter-region connectivity were analyzed.

Children with ASD showed reduced temporal synchronization and atypical differentiation in the executive function area of the brain, manifesting as significantly reduced interhemispheric correlation and local connectivity in the inferior frontal gyrus, middle frontal gyrus, and superior frontal gyrus, while increased connectivity between the inferior frontal gyrus and superior gyrus

These results supported the feasibility of using the fNIRS method to assess atypical cortical hemodynamic responses of ASD and to reveal the neural mechanism under language deficits of ASD.

Nonlinear Optical Loop Mirror-based Linear Cavity Tunable Multi-wavelength Fiber Laser

B. Huang, H. Y. Meng, R. Xiong, Q. Q. Yao, H. H. Wang, Q. H. Wang, C. H. Tan, and X. G. Huang
Laboratory of Nanophotonic Functional Materials and Devices
South China Normal University, Guangzhou, Guangdong 510006, China

Abstract— We propose and experimentally demonstrate a nonlinear optical loop mirror (NOLM)-based linear cavity tunable multi-wavelength fiber laser. The NOLM, providing intensity-dependent transmissivity, can effectively alleviate the mode competition so that the multi-wavelength lasing can be achieved at room temperature. By adjusting the polarization controllers (PCs), the proposed laser can generate multi-wavelength output. Moreover, the number of the lasing wavelength can be adjusted flexibly from 11 to 13 with a wavelength spacing of 0.4 nm.

REFERENCES

1. Park, N. and P. F. Wysocki, *IEEE Photon. Technol. Lett.*, Vol. 8, 1459-1461, 1996.
2. Wang, W., H. Y. Meng, X. W. Wu, W. Wang, R. Xiong, H. C. Xue, C. H. Tan, and X. G. Huang, *Laser Phys. Lett.*, Vol. 10, 015104, 2013.
3. Wang, W., H. Y. Meng, X. W. Wu, W. Wang, H. C. Xue, C. H. Tan and X. G. Huang, *IEEE Photon. Technol. Lett.*, Vol. 24, 470–472, 2012.
4. Zhang, Z. X., K. Xu, J. Wu, X. B. Hong, and J. T. Lin, *Laser Phys. Lett.*, Vol. 5, 213–216, 2008.

Bending-insensitive Microstructured Polymer Terahertz Fiber with Vortex Cladding Structure

Hongzhi Chen, Guofeng Yan, Xiaochen Ge, and Sailing He
Centre for Optical and Electromagnetic Research, Zhejiang University, China

Abstract— Terahertz spectroscopy systems, as emerging applications in biomedical sensing, noninvasive imaging, non-destructive testing, have weak beam confinement and vulnerability to environmental fluctuations because of the free space propagation of THz wave in the systems. Various types of THz waveguides have been demonstrated in several structures including photonic crystal waveguides, metal wires, dielectric tubes and microstructured polymer fibers. However, most of the THz waveguides suffer high bending loss, which makes them not practical in delivery of THz pulses. Flexible THz waveguides provide a promising approach to overcome these drawbacks, and may lead to compact and low-cost integrated THz systems. In this paper, we proposed a novel microstructured polymer fiber with a vortex cladding structure for terahertz wave guiding. The designed fiber has a solid core with radius of 150 μm, surrounded by 7 spiral air arms with width of 70 μm. Each arm extends along equiangular spiral trajectory. The 7 spiral arms make bridge regions between high refractive index polymer and low refractive index air holes small and narrow, blocking the spread of the field from the solid core to the cladding area. By using the full vector Finite Element method, the guided fundamental mode and cutoff frequency of vortex structure fiber were investigated. In the simulation, the polymer material was set as LDPE with a relatively constant refractive index of 1.514 and frequency dependent absorption coefficient in the form of $\alpha\ [\mathrm{cm}^{-1}] = 0.46\gamma^2 - 0.1\gamma + 0.13$ where γ is working frequency in THz. The modal field of the fundamental mode confined well within the fiber core, as the bending radius decreased from 10 cm to 3 cm, which renders us an ultralow and even constant bending loss of 0.48045 dB/cm. Several structural parameters of the fiber also allow the optimal design of performance over a range of important characteristics. Taking into account of technical limitation of traditional stack- and drill-drawing fiber fabrication method, the fabrication of the vortex structure polymer fiber may be implemented via polymer-jetting rapid prototyping technology.

A New Uniplanar Compact Photonic-bandgap (UC-PBG) Structure in Transmission Line

Wuqiong Luo and Bo Chen
University of Electronic Science and Technology of China, Chengdu, China

Abstract— Recently, the photonic band-gap (PBG) structure has received much interest in microwave and millimeter-wave domain. Applications of PBG in transmission line, microwave components and antennas have been studied and discussed. Especially the compact PBG structure consisting of small metal pads has been demonstrated to improve the performance of microwave circuits and antenna performance.

In this paper, a new uniplanar compact photonic-bandgap (UC-PBG) structure was presented. The proposed PBG structure unit has a two dimensional structure of a rectangle box with two branches intersecting at center. Then this identical unit was connected as a periodical structure. The periodical structure acting as the ground plane of the microstrip transmission line was studied. The transmission line model with the proposed UC-PBG structure ground (TL-UC-PBG) was then studied. An equivalent circuit model of this TL-UC-PBG was suggested to analyze the characteristics of the transmission line with PBG ground. From our study, it was found that this structure has a nice character of low-pass filter. At high-frequency, it showed a broad stop-band. The proposed TL-UC-PBG structure could be used in compact microwave circuit.

In this paper, the structure of the proposed UC-PBG structure would be introduced in the first part with the equivalent circuit model presented to analyze the structure. In the second part, the characteristics of the transmission line with the PBG structure would be shown; the effect of the parameters on the TL-UC-PBG model would be discussed. In the third part, the conclusion and future work would be presented.

Planar Monopole Antenna for WBAN

Ebrahim Sailan Aabidi, **M. R. Kamarudin**, **T. A. Rahman**, **and Mohsen Khalily**
Wireless Communication Centre (WCC), Faculty of Electrical Engineering
Universiti Teknologi Malaysia, UTM Skudai, Johor 81310, Malaysia

Abstract— This paper presents circular-shape monopole antenna for wireless body area network (WBAN) applications at 3.1 to 5.1 GHz and 6.5 to 8 GHz. The design and simulation of proposed antenna for WBAN applications in the free space and close proximity of body surface has been done by using CST Microwave Studio. The proposed antenna was designed on FR4 substrate with dielectric constant (ε_r) of 4.4 and thickness of 1.6 mm. The final optimized design is $50 \times 40\,\text{mm}^2$. Figure 1 shows the geometry of circular-shape monopole antenna. The simulated current distribution on the radiating patch for the proposed circular-shaped monopole antenna frequencies of 3.3 and 7.5 GHz in the free space is presented.

The parametric studies were carried out to investigate different antenna parameters in order to achieve the optimized design. The effect of the slot on the patch has been investigated. The simulated reflection coefficient magnitude is operate at (3.1–5.1 GHz), (5.55–6.28 GHz) and (6.5–8 GHz) without the implementation a slot. While the reflection coefficient magnitude results of the proposed antenna with the slot is (3.1–5.1 GHz) and (6.5–8 GHz) as indicated Figure 2. It can be seen that in section of the slot on the patch of the proposed antenna resulted from 5.55 to 6.28 GHz band rejection. The circular-shaped antenna with the slot is introduced that resulted to avoid interference with WLAN at 5.8 GHz.

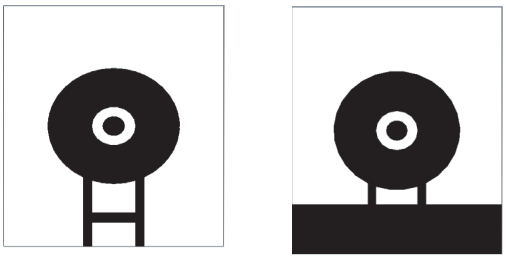

(a) (b)

Figure 1: Geometry of the circular-shape antenna. (a) Front view, (b) back view.

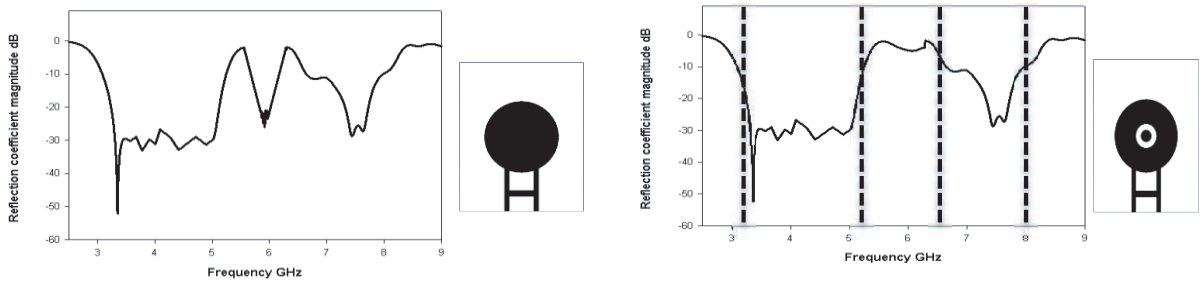

(a) (b)

Figure 2: The reflection coefficient magnitude results of the proposed antenna. (a) Without slot, (b) with slot.

Dynamics of Many-soliton Molecules in Dispersion-managed Optical Fiber

Abdelâali Boudjemâa
Department of Physics, Faculty of Sciences, Hassiba Benbouali University of Chlef
P. O. Box 151, Ouled Fares, Chlef 02000, Algeria

Abstract— We study the stability and the dynamics of many-soliton molecules in dispersion-managed (DM) optical fiber with focus on 4- and 5-soliton molecules by analytical and numerical means. We calculate in particular their binding energy, pulse width and their chirp using a variational approach. A combination of variational and numerical solutions of the nonlinear Schrödinger equation (NLSE) shows that it well describes the intensity profiles of the experimental molecules.

Fibonacci Grating for Far-field Super-resolution Imaging

Kedi Wu and Guo Ping Wang
School of Physics and Technology, Wuhan University, Wuhan 430072, China

Abstract— Optical imaging with high spatial resolution beyond the diffraction limit needs object information carried by evanescent waves, which decay exponentially with distance to the object and are only detectable in the near field. Currently, various superlens configurations such as metal film-based perfect lenses, metal-insulator-metal hyperlenses, and metamaterials-based metalenses are proposed for directly imaging super-resolution information without time-consuming scanning process. However, the image is still bounded in the near field.

By using periodic gratings to transform evanescent waves into propagating waves, or to generate evanescent waves to illuminate sub-wavelength objects, sub-diffraction-limit image of the objects can be recovered through detecting far-field information in free space. However, periodic grating-assisted far-field super-resolution imaging systems suffer from a critical defect, that is, some fine features of objects involved in a certain of spatial frequencies cannot be retrieved. This is due to the fact that a periodic grating can only produce a fixed phase shift in the frequency domain, which leads to a non-continuous frequency shift. As a result, some feature information of the objects will not be obtained.

In this talk, we present a quasi-periodic grating microscope for free-space far-field super-resolution imaging, where a Fibonacci grating is used to transform evanescent waves of objects into propagating waves. By measuring the intensity distributions of light in the far field for one time, we can reconstruct the images of objects with nearly $\lambda/9$ spatial resolution. Comparing to periodical gratings-based microscopy, our quasi-periodic structures can produce a quasi-continuous shift of frequency spectrum, making the case of losing a certain part of sub-wavelength information avoidable. Finally, we also discuss the effect of sampling error on the resolution of retrieved images.

REFERENCES

1. Pendry, J. B., "Negative refraction makes a perfect lens," *Phys. Rev. Lett.*, Vol. 85, 3966–3969, 2000.
2. Durant, S., Z. Liu, J. M. Steele, and X. Zhang, "Theory of the transmission properties of an optical far-field superlens for imaging beyond the diffraction limit," *J. Opt. Soc. Am. B*, Vol. 23, 2383–2392, 2006.
3. Wu, K. and G. P. Wang, "One-dimensional Fibonacci grating for far-field super-resolution imaging," *Opt. Lett.*, Vol. 38, 2032–2034, 2013.

A Single Anisotropic Metasurface to Realize Luneburg Lens and Maxwell Fisheye Lens Simultaneously

Xiang Wan and Tie Jun Cui
State Key Laboratory of Millimeter Waves, Department of Radio Engineering
Southeast University, Nanjing 210096, China

Abstract— The Luneburg lens and Maxwell fisheye lens are well-known microwave and optical devices with distinct focusing properties. Here, we present a planar bi-functional Luneburg-fisheye lens made of anisotropic metasurface, which features as the Luneburg lens along the horizontal optical axis while as fisheye lens along the vertical optical axis.

ACKNOWLEDGMENT

The work was supported in part by the National High Tech (863) Projects (2012AA030402 and 2011AA010202), in part by the National Science Foundation of China (60990320, 60990324 and 61138001), and in part by the 111 Project (111-2-05).

REFERENCES

1. Luneburg, R. K., *Mathematical Theory of Optics*, Brown Univ. Press, Providence, Rhode Island, 1944.
2. Maxwell, J. C., *The Scientific Papers of James Clerk Maxwell*, Dover, New York, 1890.
3. Wan, X., X. Shen, Y. Luo, and T. J. Cui, "Planar bi-functional Luneburg-fisheye lens made of anisotropic metasurface," *Laser & Photonics Reviews*, DOI 10.1002/lpor.201400144, 2014.

Suppression of Scattering Based on an Ultrathin Metasurface

Jie Zhao, Qiang Cheng, Li Hua Gao, Mei Qing Qi, and Tie Jun Cui
State Key Laboratory of Millimeter Waves, Department of Radio Engineering
Southeast University, Nanjing 210096, China

Abstract— The radar system has experienced a rapid development since World War II, which also brings in the requirement to make targets invisible to the electromagnetic waves. Here, we propose a method to suppress the scattering based on an ultrathin metasurface in a broad frequency band. Different from the reflect-array antennas or phase array antennas which can steer the radiation beams based on the constructive interference in the desired directions with pre-adjusted elements, the designed metasurface is composed of two kinds of units with different geometries and opposite reflection phases, which provide destructive interference in most of reflected directions, suppressing the main lobe significantly of the scattering pattern. The random arrangement of the scattering units helps to diminish the side lobes, which makes the present design more useful in monostatic and bistatic radars. Full-wave numerical simulation results show that a large bandwidth of 1.74 GHz is achieved using the proposed metasurface with the thickness 1 mm, which suppresses the scattering by at least 10 dB. The proposed metasurface may find wide applications in a series areas.

Photostimulated Quantum Effects in Quantum Wire with a Parabolic Potential

Hoang Van Ngoc, Nguyen Vu Nhan, and Nguyen Quang Bau
Department of Physics, College of Natural Sciences, Hanoi National University
No. 334, Nguyen Trai Str., Thanh Xuan Dist., Hanoi, Vietnam

Abstract— The quantum theory of the photostimulated effects in quantum wire has been studied based on the quantum kinetic equation for electrons with a parabolic potential $V(z) = \frac{m\omega_0^2 z^2}{2}$. In this case, electrons system in quantum wire is placed in a constant electric field $\vec{E}_0$, an electromagnetic wave $\vec{E}(t) = \vec{E}(e^{-i\omega t} + e^{i\omega t})$ and in the presence of an intense laser field $\vec{F}(t) = \vec{F}\sin\Omega t$. In the presence of laser radiation and polarized electromagnetic wave can influence that current carrier, and do appear an electric field intensity vector $\vec{E}_0$ with open circuit conditions. Hence, the analytic expressions of electric field intensity vector $\vec{E}_0$ ***along the coordinate axes has been calculated***. The dependence of the components $\vec{E}_0$ on the frequency Ω of the laser radiation field, the frequency ω of the electromagnetic wave field, the frequency ω_0 of the parabolic potential are shown. From the analytic results, when $\omega_0 \to 0$, the result will turn back to the photostimulated kinetic effects in semiconductors.

The Influence of the Electromagnetic Wave on the Quantum Acoustomagnetoelectric Field in a Quantum Well with a Parabolic Potential

N. Q. Bau[1] and N. V. Hieu[2]

[1]Faculty of Physics, Hanoi University of Science, Vietnam National University, Hanoi, Vietnam
[2]Faculty of physics, Danang University of Education, Danang, Vietnam

Abstract— The influence of the electromagnetic wave on the quantum acoustomagnetoelectric (QAME) field in a quantum well with a parabolic potential (QWPP) is investigated for an acoustic wave whose wavelength $\lambda = 2\pi/q$ is smaller than the mean free path ℓ of the electrons and in the region $q\ell \gg 1$ (where q is the acoustic wave number). The dependence of the QAME field E^{QAME} on the frequency of acoustic wave ω_q, the temperature T, the magnetic field B, the amplitude E_0 and the photon energy $\hbar\Omega$ of the electromagnetic wave are obtained by using the quantum kinetic equation. Numerical calculation is done, and the result is discussed for a typical AlAs/GaAs/AlAs QWPP. The computational results show that the dependence of the QAME field E^{QAME} on the external acoustic wave frequency ω_q, the temperature T, the magnetic field B and the photon energy $\hbar\Omega$ of the electromagnetic wave is non-monotonic, the cause of appearance peaks attributes the transition between mini-bands $n \to n'$. The quantum theory of the QAME field in a QWPP is newly developed.

Small Design for Wireless Antenna Used by Ultra-wideband Systems

Rashid A. Fayadh[1], **F. Malek**[2], **Hilal A. Fadhil**[1], **Farah Salwani Abdullah**[2], **Sameer A. Dawood**[1], **and Ihsan Jabar Hasan**[3]

[1]School of Computer and Communication Engineering
Universiti Malaysia Perlis (UniMAP), Perlis, Malaysia
[2]School of Electrical System Engineering, Universiti Malaysia Perlis (UniMAP), Perlis, Malaysia
[3]Faculty of Electrical Engineering, Universiti Teknikal Malaysia (UTeM), Melaka, Malaysia

Abstract— The requirements of wireless communication systems continue to increase nowadays steadily. The extending requirements lead to several currently applications in different frequency bands. The propagation capacity in form of latency and data bit rate has been a bottleneck for usage of broadband wireless communications. New wireless communication technologies like ultra wideband (UWB) approach of larger bandwidth than the utilized traditional wireless techniques. This bandwidth is 7.5 GHz according to the Federal Communications Commission (FCC) last report that gave the license for high data rate issues. As the antennas play an important role in UWB systems, the interest of creating the UWB antennas that can be integrated with other system elements on a printed circuit board (PCB). The main objective of this research is to design and implement a small size of UWB antenna with low profile microstrip patch that satisfy the previous technology requirements. Some antenna parameters were studied to extend the antenna bandwidth and several design techniques were used to improve the optimal UWB frequency range performance of the planar antenna design. The performance of the main antenna parameters such as reflection coefficient (S_{11}), Gain, radiation efficiency, and radiation patterns and voltage standing wave ratio (VSWR) of the planar antenna were extensively investigated with software simulations using CST Microwave Studio software. This design supports many UWB modern applications in radar and medical systems for indoor and outdoor propagation. The supporting is based on the size, cost, lightweight, and high performance of the proposed planar antenna. In this UWB antenna, the radiation efficiency is maximized which leads to minimize the dielectric losses to capture most of the radiation energy because of the UWB transmitted power spectral density is low (-41.3 dBM/MHz) compared with other narrow band systems.

Improve the Performance of Multi-users MC-CDMA Based on Critically Sampling Multi-wavelet Transform over Wireless Propagation Channel

Sameer A. Dawood[1], **F. Malek**[2], **M. S. Anuar**[1], **Rashid A. Fayadh**[1], **Farah Salwani Abdullah**[2], **and Mohd Hariz Mohd Fakri**[2]

[1]School of Computer and Communication Engineering
University Malaysia Perlis (UniMAP), Pauh Putra, Arau, Perlis 02000, Malaysia
[2]School of Electrical System Engineering
University Malaysia Perlis (UniMAP), Pauh Putra, Arau, Perlis 02000, Malaysia

Abstract— Third generation of mobile communication systems (3G) will require fast and reliable data transfer to support multimedia services, video conferencing and many more applications. 3G systems will operate at 2 GHz region thus able to provide up to 2 Mbps. Beyond this, future generations of wireless system (4G) will provide even higher data rates, flexibility and able to support a wider range of applications. To achieve high data rate Multi-Carrier Code Division Multiple Access (MC-CDMA) is one suitable choice for next generation wireless communication system. MC-CDMA is the combination of CDMA and Orthogonal Frequency Division Multiplexing (OFDM) schemes, resulting into getting the advantages of both schemes. In this paper, Critically Sampling Inverse Discrete Multi-wavelet Transform (CSIDMWT) are proposed as a modulator technique instead of Inverse Fast Fourier Transform (IFFT) in the realization of the MC-CDMA system to improve the Bit Error Rate (BER) performance. Discrete multi-wavelet transform has two or more low pass and high pass filters, the purpose of this multiplicity is to achieve more BER performance than the conventional MC-CDMA using FFT and Discrete Wavelet Transform (DWT). The proposed approach was applied on the MC-CDMA in Additive White Gaussian Noise (AWGN), flat fading channel and frequency selective fading channel. Walsh-Hadamard code has been chosen for spreading, which reduces the multiple access interference (MAI) in downlink due to its orthogonal property. This system was implemented using MATLAB software (Version 7.8) technical programming language. the performance of the proposed system was compared with the performance of MC-CDMA based on FFT and MC-CDMA based on DWT. It was concluded that the proposed approach gives much better BER performance than the conventional MC-CDMA based on FFT and MC-CDMA based on DWT.

Novel Design of H-plane Bandpass Waveguide Filters Using Complementary Split Ring Resonators

S. Stefanovski[1], **D. Mirković**[1, 2], **M. Potrebić**[1], **and D. Tošić**[1]

[1]School of Electrical Engineering, University of Belgrade
P. O. Box 35-54, Belgrade 11120, Serbia
[2]National Severe Storm Laboratory (NOAA), CIMMS, University of Oklahoma
120 David L. Boren Blvd, Norman, OK 73072, USA

Abstract— For the communication systems where high-power structures with small losses need to be implemented, waveguide filters are of particular interest. These filters are usually implemented by inserting discontinuities of various shapes and positions in the waveguide. It is known that these discontinuities operate as resonators and by setting their parameters and positions, central frequency and bandwidth of the filter can be controlled. For bandpass waveguide filter design, complementary split ring resonators (CSRR) have wide implementation, either as single-mode or multi-mode. In previous publications, various design methods for filters with a single frequency band, using CSRRs, are proposed: implementation in the microstrip technology with defected ground structure as in [1, 2], using substrate integrated waveguide [3] or using rectangular waveguide [4–6]. Multi-band filter design is particularly attractive these days, so this topic calls for closer attention. Therefore, dual-mode resonators can be applied by properly combining single-mode resonators and dual-band filters are developed in this manner. One of the main characteristics of dual-mode resonators used for filter design is that the resonators can be independently tuned [7], hence each frequency band can be independently controlled, as presented in [8].

Herein, we propose novel design of the X-band bandpass waveguide filter using the CSRRs. Resonators are implemented as inserts in a form of metal plates, having properly shaped slots, in the transverse planes of the standard WR90 rectangular waveguide, in order to obtain H-plane bandpass waveguide filters. Design starts from the filter using CSRR attached to the top waveguide wall. It is noticed that the resonator implemented in such a manner provides the same resonant frequency as the one not attached to the waveguide wall, but it is more compact in terms of dimensions. Filter response is investigated for various parameters of the resonator and its position.

Proposed design using CSRRs is recognized as scalable solution applicable for multi-band waveguide filter design. As an example of such design, dual-band filter is presented, along with the filter response (Figure 1). Relatively simple implementation of dual-band filter, obtained by adding the resonator attached to the bottom wall, should be stressed, as another advantage of the proposed design.

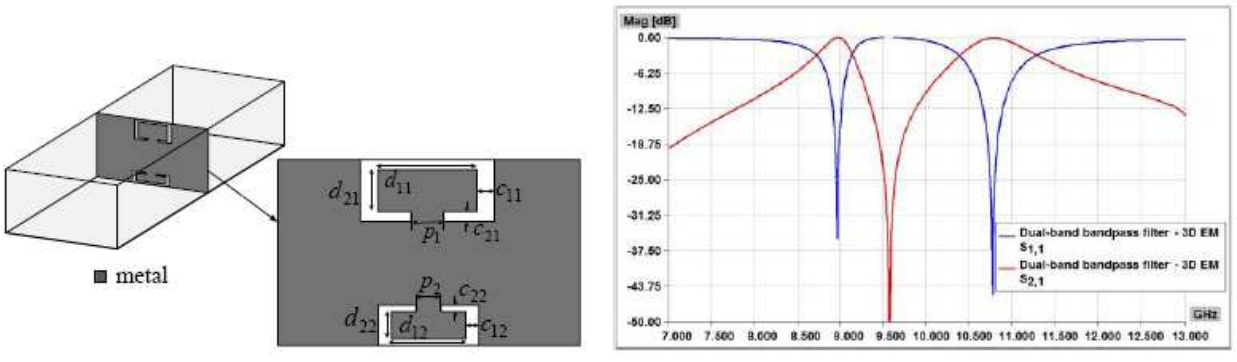

(a) (b)

Figure 1: Dual-band bandpass waveguide filter using CSRRs: (a) 3D EM model, (b) filter response.

REFERENCES

1. Bonache J., F. Martin, F. Falcone, J. D. Baena, T. Lopetegi, J. Garcia-Garcia, M. A. G. Laso, I. Gil, A. Marcotegui, R. Marques, and M. Sorolla, "Application of complementary split-ring resonators to the design of compact narrow band-pass structures in microstrip technology," *Microw. Opt. Techn. Lett.*, Vol. 46, No. 5, 508–512, 2005.
2. Bonache, J., F. Martin, I. Gil, J. Garcia-Garcia, R. Marques, and M. Sorolla, "Microstrip bandpass filters with wide bandwidth and compact dimensions," *Microw. Opt. Techn. Lett.*, Vol. 46, No. 5, 343–346, 2005.
3. Zhang, X.-C., Z.-Y. Yu, and J. Xu, "Novel band-pass substrate integrated waveguide (SIW) filter based on complementary split ring resonators (CSRRs)," *Progress In Electromagnetics Research*, Vol. 72, 39–46, 2007.
4. Ortiz, N., J. D. Baena, M. Beruete, F. Falcone, M. A. G. Laso, T. Lopetegi, R. Marques, F. Martin, J. Garcia-Garcia, and M. Sorolla, "Complementary split-ring resonator for compact waveguide filter design," *Microw. Opt. Techn. Lett.*, Vol. 46, No. 1, 88–92, 2005.
5. Bahrami, H., M. Hakkak, and A. Pirhadi, "Analysis and design of highly compact bandpass waveguide filter using complementary split ring resonators (CSRR)," *Progress In Electromagnetics Research*, Vol. 80, 107–122, 2008.
6. Potrebić, M. M., D. V. Tošić, Z. Ž. Cvetković, and N. Radosavljević, "WIPL-D modeling and results for waveguide filters with printed-circuit inserts," *Proceedings of 28th International Conference on Microelectronics*, 309–312, Niš, Serbia, May 2012.
7. Hong, J. S., *Microstrip Filters for RF/Microwave Applications*, Wiley, New York, 2011.
8. Stefanovski, S. Lj., M. M. Potrebić, and D. V. Tošić, "Design and analysis of bandpass waveguide filters using novel complementary split ring resonators," *Proceedings of 11th International Conference on Telecommunications in Modern Satellite, Cable and Broadcasting Services*, 257–260, Niš, Serbia, October 2013.

Theoretical Investigation on Metallic Nanowire Network as Transparent Conductive Electrodes for Optoelectronic Devices

Bing Han[1, 2], **Ke Pei**[1, 2], **Qiang Peng**[1, 2], **Ruopeng Li**[1, 2], **Krzysztof Kempa**[3], **and Jinwei Gao**[1, 2]

[1]Institute for Advanced Materials (IAM)
South China Normal University, Guangzhou 510006, China
[2]Laboratory of Quantum Engineering and Quantum Materials
South China Normal University, Guangzhou 510006, China
[3]Department of Physics, Boston College, Chestnut Hill, Massachusetts 02467, USA

Abstract— Flexible transparent conductive electrodes (FTCEs) are important components for flexible thin-film solar cells, organic light-emitting diodes, and other optoelectronics. In this paper, we theoretically investigated the optical properties of FTCEs by variation of metallic material, wire shape and wire size, also substrates of silicon and glass. The results show the square structure has a best transmittance of 94.4%, especially using Ni nanowire, and can be potentially applied in thin film solar cell, and display devices.

Optical Remote Sensing of Insects Using Passive Dark-field Techniques

S. M. Zhu[1], **G. Y. Zhao**[1], **T. Q. Li**[1], **M. Lian**[1], **H. Zhang**[1], **K. Svanberg**[1,2], **and S. Svanberg**[1,2]

[1]Center for Optics and Electromagnetic Research, South China Normal University
University City Campus, Guangzhou 51006, China
[2]Lund University Laser Center, Lund University, SE-221 00 Lund, Sweden

Abstract— Ecological studies to investigate the interplay between the fauna and a changing environment are of considerable interest. Insects include agricultural pests having huge economic impact. They are also vectors in spreading diseases, like malaria. Recently, optical remote sensing techniques have been introduced in the study of insects; see, e.g., [1–3]. Fluorescence lidar can provide spectral fingerprints which are related to species [2], and elastic backscattering from a CW laser beam can provide wing-beat frequencies which are species specific [1]. A particularly simple and powerful variety utilizes backscattering of sunlight from insects, which are observed remotely with a telescope against a background, which is as dark as possible [3]. We have recently initiated measurements of this kind on the Chinese scene, and we here report our first results. A 20 cm diameter Cassegrainian reflective telescope was mounted to look into a black box placed in the shadow of the sun, while the path of about 50 m between the telescope and the termination was illuminated by sun or day-light. A photodiode at the output of the telescope was used to observe fast transient oscillations due to, e.g., insect wing beating. Alternatively, the telescope can be fiber-optically coupled to an Ocean Optics compact spectrometer, for recording the reflectance spectra of objects entering the field-of-view. Our set-up is schematically shown in the figure to the left, while a data recording for a butterfly, with a wing-beat frequency of 9 Hz is given in in the figure to the right. Field work related to, e.g., agricultural pests is planned.

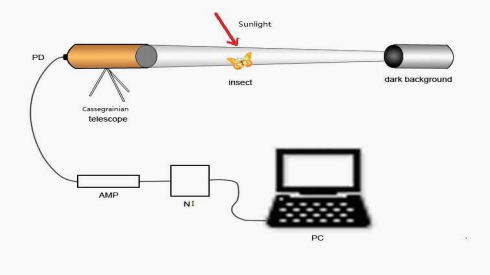

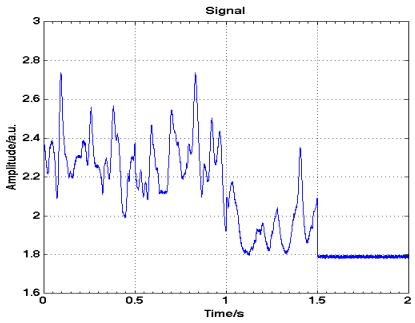

REFERENCES

1. Hoffman, D. S., A. R. Nehrir, K. S. Repasky, J. A. Shaw, and J. L. Carlsten, "Range-resolved optical detection of honeybees by use of wing-beat modulation of scattered light for locating land mines," *Appl. Opt.*, Vol. 46, 3007–3012, 2007.
2. Guan, Z. G., M. Brydegaard, P. Lundin, M. Wellenreuther, E. Svensson, and S. Svanberg, "Insect monitoring with fluorescence LIDAR techniques — Field experiments," *Appl. Optics*, Vol. 48, 5668, 2010.
3. Runemark, A., M. Wellereuther, H. Jayaweera, S. Svanberg, and M. Brydegaard, "Rare events in remote dark field spectroscopy," *IEEE JSTQE*, Vol. 18, 1573, 2011.

Indoor Transparent Antenna for Television Reception

S. N. H. Sa'don, M. R. Kamarudin, and M. Khalily
Wireless Communication Centre (WCC), Universiti Teknologi Malaysia, UTM Skudai 81310, Malaysia

Abstract— The characteristics of indoor transparent antenna are investigated. The purpose of the antenna is applied for television (TV) signal reception which is operating in Ultra High Frequency (UHF) band. The antenna was made from silver coated polyester film (AgHT-4), that is the transparent conductive material and attached with a layer of glass at the backside of the AgHT-4. The antenna size is width and length at 120 mm × 150 mm. It was fed by a co-planar waveguide (CPW) due to the opportunity of low radiation loss and to reduce reflection of the antenna. The frequency range of 500 MHz to 800 MHz has been chosen from the UHF television reception band allocated by Federal Communications Commission (FCC). Due to the television station provide a lot of stations to be watched by Malaysian, each station have different channel with specification frequencies based on the transmitter base station location. This proposed project launches at Universiti Teknologi Malaysia (UTM), Skudai, Johor, Malaysia so all the channel is following the frequency of Gunung Pulai, Johor transmitter base station. The channel utilization are Channel 55 (742–750 MHz): TV1, Channel 10 (209–216 MHz): TV2, Channel 26 (510–518 MHz): TV3, Channel 42 (638–646 MHz): NTV7, Channel 44 (654–662 MHz): TV9 and Channel 46 (670–678 MHz):8TV. The proposed antenna was designed by using Computer Simulation Software (CST) Microwave Studio to obtain the simulation result. The simulated bandwidth of the antenna obtained is 0.524 GHz (0.514 GHz to 1.038 GHz) with simulated impedance bandwidth of 67.53%. It also had potential to be realized because of the omni-directional radiation pattern and gain was more than 2.292 dBi.

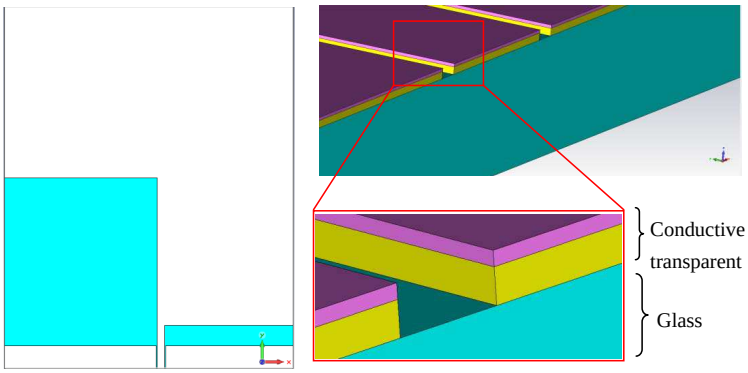

Figure 1: The antenna designed.

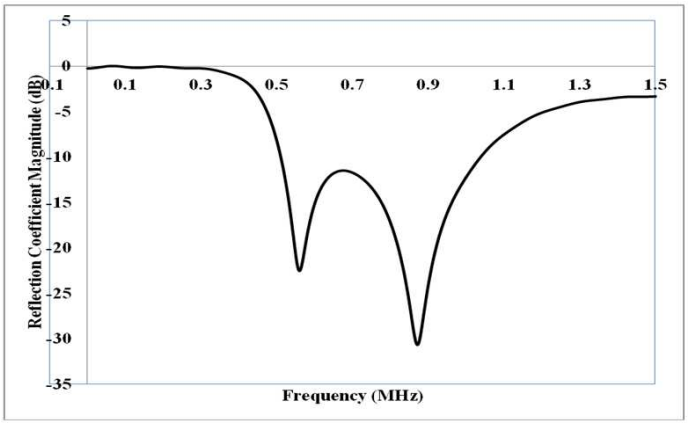

Figure 2: The simulated reflection coefficient magnitude (dB).

Electrical Characterization of GaN

Nazir A. Naz[1], **M. Suleman**[2], **and Akbar Ali**[1, 2]

[1]Department of Applied Physics
Federal Urdu University of Arts, Science and Technology Islamabad, Pakistan
[2]Department of Basic Sciences, Riphah International University, Islamabad, Pakistan

Abstract— GaN based blue light emitting diodes were characterized, using deep level transient spectroscopy technique. Nine defects having ionization energies: 0.06, 0.08, 0.09, 0.14, 0.10, 0.14, 0.14, 0.16 and 0.65 eV and corresponding capture cross-sections (σ_∞) 4.0×10^{-14}, 1.3×10^{-13}, 7.6×10^{-14}, 6.95×10^{-13}, 3.53×10^{-14}, 1.6×10^{-13}, 8.0×10^{-14}, 7.34×10^{-14} and 1.8×10^{-5} cm^2 were identified. Respective concentrations were found to be 8.81×10^{13}, 8.56×10^{13}, 8.90×10^{13}, 8.68×10^{13}, 8.62×10^{13}, 8.56×10^{13}, 8.66×10^{13}, 8.57×10^{13}, 8.54×10^{13}, 8.68×10^{14}, and 8.46×10^{14} (cm^{-3}).

Study of p-type Porous Silicon

Nazir A. Naz, M. Jamil, and Akbar Ali
Federal Urdu University of Arts, Science and Technology, Islamabad G-7/1, Pakistan

Abstract— Porous silicon fabricated by electrochemical etching was studied using Scanning Electron Microscope and Elemental Differential X ray Analyzer. The etched samples found emitting red light when exposed to ultraviolet light of wavelength 254 nm Images of etched surface obtained by Scanning electron microscope showed a formation of sponge like material at the surface. Elemental Differential X ray Analysis provided the evidence of formation of silicon oxide at the surface. Red luminescence emitted from the surface is assumed due to confinement of holes in the pores or oxidized surface of the pores.

Suspended Stripline Bandpass Filter with Very Wide Stop-band

Atallah Balalem, Moayyad M. Abu Khmish, Zekrayat Baidas, and Oday H. Sabi
Faculty of Engineering and Technology, Palestine Technical University, Tulkarm, Palestine

Abstract— In this paper a quasi-lumped fourth order suspended stripline bandpass filter is introduced. The filter consists of quasi-lumped series resonators, each two resonators are connected to each other by capacitive transmission line. The filter has center frequency of 10.4 GHz and bandwidth of 1.5 GHz.

Introduction: Since the field is mainly distributed the air, suspended stripline (SSL) has very low dielectric loss, and due to the existence of the mount, the SSL has no radiation loss, this presents suspended stripline to be a good candidate for filter applications. Moreover, SSL the designer to implement the resonators on both side of the substrate which enhance bandwidth of the filter. Quasi-lumped elements and resonators for (SSL) have been introduced first in [1, 2], different filters including highpass filter have been presented using these elements [1–4]. the presented filters have very small size and very wide band width.

In this paper, a forth order quasi-lumped SSL bandpass filter is introduced. The filter consists of four series resonators, each two resonators are connected to each other be shunt capacitance. The used SSL cross section is shown in Fig. 1.

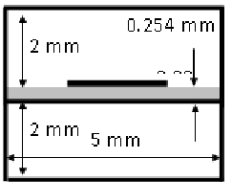

Figure 1: Cross section of the used suspend stripline.

Filter Design: Figure 2 shows the top and backside layout of the filter, the ports and the backside of the shunt capacitance are implemented at the topside of the substrate, while the resonators are implemented at the backside of the substrate. The gap between the 50 ohm line and the wide patch introduce a series capacitance the narrow stripline can be modeled as series inductor. This configuration gives a series resonator. The narrow stripline is connected form the other side by wide patch. This path with this metallization on the other side of the substrate introduced shunt capacitance. The insertion and the return loss of the filter is shown in Fig. 3. The filter has center frequency of 10.4 GHz and bandwidrh of 1.5 GHz. The filter operate up 29 GHz with attenuation higher than 40 dB. The filter in length is 16.9 mm which is considered to be very short.

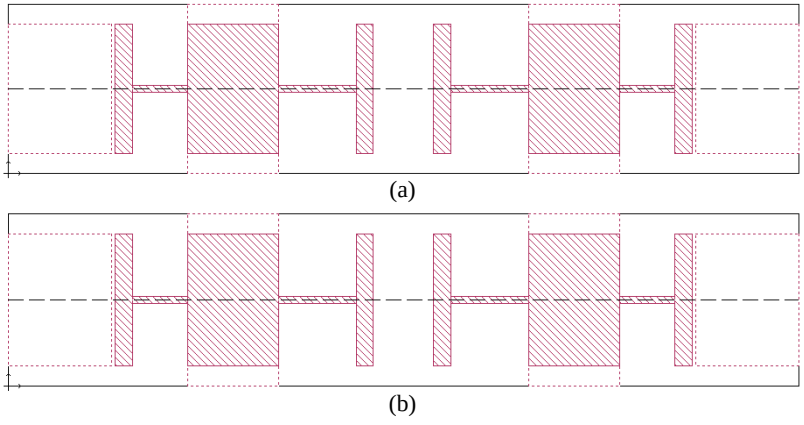

Figure 2: (a) Top and (b) backside layouts of the bandpass filter.

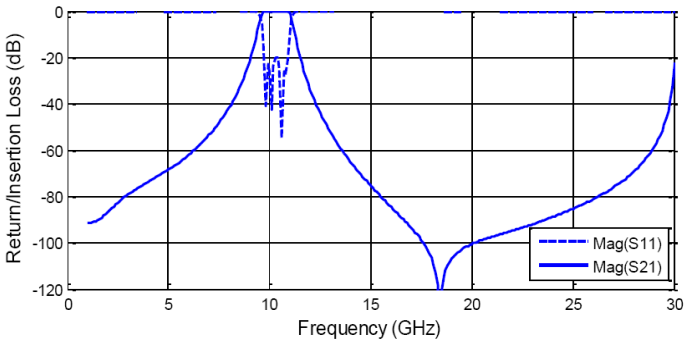

Figure 3: The insertion and return loss of the filter.

Conclusion: a fourth order quasi-lumped SSL bandpass filter has been introduced by using series SSL resonators connected with each other be shunt capacitances. the realized filter has very wide stop-band which reach up to 39 GHz with attenuation higher than 40 dB.

REFERENCES

1. Menzel, W., "A novel miniature suspended stripline filter," *Proc. Euro. Microw. Conf.*, 1047–1050, Munich, Germany, Oct. 2003.
2. Menzel, W. and A. Balalem, "Quasi-lumped suspended stripline filters and diplexers," *IEEE Trans. Microw. Theory Tech.*, Vol. 53, No. 10, 3230–3237, Oct. 2005.
3. Menzel, W. and M. Berry, "Quasi-lumped suspended stripline filters with adjustable zeroes," *IEEE-S Int. Microwve Symp. Dig.*, 1601–1604, Fort Worth, TX, 2004.
4. Menzel, W. and A. Balalem, "Compact suspended stripline quasi-elliptic low-pass filters," *German Microwave Conf.*, 61–64, Ulm, Germany, Apr. 2005.

Wideband Antenna for Microwave Imaging

R. Yahya[1, 2], **M. R. Kamarudin**[2], **and N. Seman**[2]

[1]Faculty of Electrical and Electronic Engineering, Universiti Tun Hussein Onn Malaysia (UTHM)
Parit Raja, Batu Pahat, Johor 86400, Malaysia
[2]Wireless Communication Center (WCC), Universiti Teknologi Malaysia (UTM)
Skudai, Johor Bahru, Johor 81310, Malaysia

Abstract— A robust antenna which designed on fully textile material is presented. A denim jean textile is used as the dielectric substrate while the radiating elements are using conductive shieldit super textile. The thickness of the substrate is 0.7 mm and the conductive textile is 0.17 mm. The conductive textile has surface resistivity less than 0.5 Ohm/sq. The antenna that fed by coplanar waveguide (CPW) technique consists of radiating patch and ground that attached on the substrate with the dimension of 80 mm × 77.5 mm. The grounding element that comprises of slots, slits, and blending edge resulting to wideband frequency antenna. The simulated operating bandwidth of the antenna is 4000 MHz with maximum −10 dB reflection coefficient magnitudes of 1.16–5.16 GHz. The antenna has bi-directional radiation pattern and provides simulated gain values that fluctuate between 2.6 to 6.8 dBi at the entire frequency range. This antenna which operates in the mentioned wideband frequency is highly acceptable for microwave imaging application. In addition, the capability of the textile material to be formed into flexible shape such as bending will be an advantage of its use in flexible microwave imaging purpose.

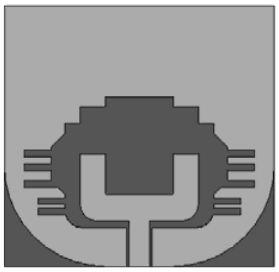

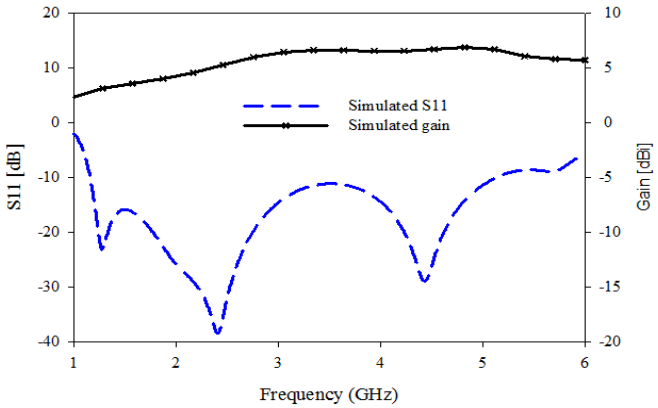

	2 GHz	4 GHz
3D radiation patterns	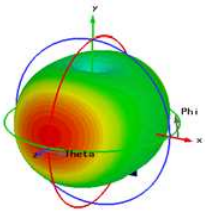	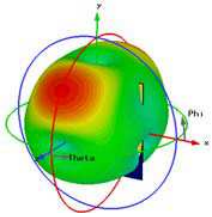

Control of Preferential Orientation (*c*-axis) of Piezoelectric ALN Film for NEMS Applications

S. Imran[1], **Guanbo Yin**[2], **Yungui Ma**[3], **and Sailing He**[1]

[1]South China Academy of Advanced Optoelectronics, Department of Optical Engineering
South China Normal University, Guangzhou, China
[2]Department of Material Science and Engineering
Nanjing University of Technology, Nanjing, China
[3]State Key Lab of Modern Optical Instrumentation, Department of Optical Engineering
Zhejiang University, Hangzhou, China

Abstract— Aluminum nitride (AlN) is is a wide band gap III–V Piezoelectric material with high CMOS compatibility. When ALN thin films are applied to NEMS applications, highly (0002) oriented films are necessary because the electromechanical coupling coefficient of the (0002) oriented films are superior to that of other orientations. Therefore, the influence of different sputtering parameters on the microstructure of AlN thin films with a typical thickness of about 250 nm was investigated.

In this study, AlN films were deposited on Si(100) using DC-reactive magnetron sputtering. Pt was used as a buffer layer. The sputtering pressure was kept constant at 0.4Pa. The influence of the most critical deposition parameters on the AlN thin film crystallography has been investigated by means of X-ray diffraction (XRD) analysis of the rocking curve Full-Width at Half Maximum (FWHM) of the AlN-(0002) peak. Atomic force microscopy (AFM) was used to study the surface morphology of the film.

The relationship between the substrate, the synthesis parameters and the crystallographic orientation of the AlN thin films is discussed. A detail study was done describing how to optimize these conditions to obtain highly c-axis oriented piezoelectric ALN films for NEMS applications.

REFERENCES

1. Kumar, A., H. L. Chan, J. J. Weimer, and L. Sanderson, *Thin Solid Films*, Vol. 406, 308–309, 1997.
2. Muhl, S., J. A. Zapien, J. M. Mendez, and E. Andrade, *J. Phys. D: Appl. Phys.*, Vol. 30, 2147, 1997.
3. Carlotti, G., G. Gbbiotti, F. S. Hickernell, H. M. Liaw, and G. Socino, *Thin Solid Films*, Vol. 310, 34, 1997.
4. Tong, B., X. Yang, Z. Guo, K. Li, J. Ouyang, G. Lin, and S. Chen, *Ceramics International*, Vol. 39, 6853–6859, 2013.
5. Zhang, J. X., H. Cheng, Y. Z. Chen, A. Uddin, S. Yuan, S. J. Geng, and S. Zhang, *Surface & Coatings Technology*, Vol. 198, 68–73, 2005.
6. Karabalin, R. B., M. H. Matheny, X. L. Feng, E. Defaÿ, G. Le Rhun, C. Marcoux, S. Hentz, P. Andreucci, and M. L. Roukes, *Applied Physics Letters*, Vol. 95, 103111, 2009.
7. Venkataraj, S., D. Severin, R. Drese, F. Koerfer, and M. Wuttig, *Thin Solid Films*, Vol. 502, 235–239, 2006.

Polarization-dependent Enhanced Photoluminescence and Polarization-independent Emission Rate of Quantum Dots on Gold Elliptical Nanodisc Arrays

Qiangzhong Zhu, Shupei Zheng, Shijie Lin, Tianran Liu, and Chongjun Jin
State Key Laboratory of Optoelectronic Materials and Technologies
Sun Yat-sen University, Guangzhou, China

Abstract— In the presentation, we report the interaction of the quantum dots with gold elliptical nanodiscs. By tuning the nearest distance between quantum dots and gold elliptical nanodiscs via atomic layer deposition of Al_2O_3, the enhanced photoluminescence (PL) intensity and emission rate of quantum dots near gold elliptical nanodiscs have been studied. The enhancement of the PL becomes larger with the distance decreasing until the thickness of the Al_2O_3 layer is less than 3 nm. It is interesting that the photoluminescence intensity is polarization-dependent with the degree of polarization being equal to that of the light extinction of the gold elliptical nanodiscs; the emission polarization evolves from the quantum dot emission polarization to the dipolar plasmon one as the distance between the quantum dots and gold elliptical nanodiscs decreases, while the emission rate is polarization-independent. This is resulted from the plasmon-coupled emission via the coupling between the quantum dipole and plasmon nano-antenna. Our experiments fully confirm the evidence of plasmophore concept proposed recently in the interaction of the quantum dots with metal nanoparticles.

Projection Method for Solving Scalar Problem of Diffraction of a Plane Wave on a System of Two- and Three-dimensional Obstacles

M. Yu. Medvedik, Yu. G. Smirnov, A. A. Tsupak, and D. V. Valovik
Penza State University, Russia

Abstract— We investigate scalar problems of diffraction of a plane wave on a system of obstacles consisting of piecewise smooth screens Ω_i and volume inhomogeneous bodies Q_j. It is assumed that all obstacles do not intersect each other.

We consider a boundary value problem for the Helmholtz equation in quasi-classical statement and prove the uniqueness of its solution. The original boundary value problem leads to a system of weakly singular integral equations on two- and three-dimensional manifolds $\Omega = \cup\Omega_i,\ Q = \cup Q_j$. The integral operators are treated as pseudo-differential operators in Sobolev spaces on manifolds with boundary.

Using the theory of pseudo-differential operators we obtain several important results: the smoothness of the solution to the system of the integral equations in the interior points of the screens; the equivalence of the integral equations to the original boundary value problem under assumption of infinite differentiability of the incident field. Finally, invertibility of the integral operator results from the unique solvability of the boundary value problem and the Fredholm property of the integral operator.

We propose Galerkin method for numerical solving of the integral equations.

We introduce piecewise constant basis functions in the area of the volume body and on the surface of the "soft" screen. In this work we give a description of the basis functions and prove the approximation property for the basis functions as well as the convergence theorem for Galerkin method.

The software implementation is briefly described and numerical results are given.

Propagation of Electromagnetic Waves along a Nonlinear Inhomogeneous Cylindrical Waveguide

Yu. G. Smirnov and D. V. Valovik
Department of Mathematics and Supercomputing, Penza State University, Russian Federation

Abstract— We investigate guided waves in a nonlinear inhomogeneous cylindrical waveguide filled with Kerr medium. The waveguide is placed in cylindrical coordinate system $O\rho\varphi z$, where axis z coincides with axis of the waveguide. Inhomogeneity is modelled by a function that depends on radius of the waveguide. The permittivity inside the waveguide is $\varepsilon = \varepsilon_2(\rho) + \alpha|\mathbf{E}|^2$, where $\varepsilon_2(\rho)$ is the inhomogeneity, α is a constant in the Kerr law, and $\mathbf{E}$ is the complex amplitude of an electromagnetic field.

Such and similar problems lead to nonlinear transmission eigenvalue problems for ordinary differential equations. Eigenvalues in these problems correspond to propagation constants of the waveguides. In these problems differential equations depend nonlinearly either on sought-for functions and the spectral parameter. The transmission conditions depend nonlinearly on the spectral parameter. The main goal is to prove existence of eigenvalues and determine their localization. Existence and localization can be derived from the dispersion equation (DE). DE is an equation with respect to spectral parameter. There are two ways to obtain the DE. The first one is to integrate the differential equations and obtain, using the transmission conditions, the DE. This way is of very limited applicability, as it is very rarely possible to find explicit solutions of nonlinear differential equations. However, this way works in some cases. The second one is a very general approach based on a reduction of the differential equations to integral equations using the Green function. This approach we call integral equation approach. Here we consider this very method. In spite of the fact that by this method the DE is found in an implicit form, it is possible to prove existence of eigenvalues and find their localization.

In the integral equations approach the original problem is reduced to an integral equation whose kernel depends on the Green function of the linear part of the differential equations of the problem. Two circumstances are important for the following analysis. First, in the case of a homogeneous waveguide ($\varepsilon_2(\rho) \equiv \text{const}$) this Green function can be found explicitly. Second, the dispersion equation of the nonlinear homogeneous case can be written as $\mathrm{DE}_{\mathrm{lin}} + \mathrm{T}_{\mathrm{nonlin}} = 0$, where $\mathrm{DE}_{\mathrm{lin}}$ is a linear problem term and $\mathrm{T}_{\mathrm{nonlin}}$ is an extra nonlinear term. Here the linear problem term is written in an explicit form. Moreover, the equation $\mathrm{DE}_{\mathrm{lin}} = 0$ is well known and examined. Its roots are also known. All this allows proving the existence of the nonlinear problem solutions at least near to the linear problem solutions.

The nonconstant term $\varepsilon_2(\rho)$ dramatically changes the situation. In this case we cannot find explicitly the necessary Green function, so we investigate it in an implicit form. The dispersion equation of the nonlinear inhomogeneous case can be also written as $\mathrm{DE}_{\mathrm{lin}} + \mathrm{T}_{\mathrm{nonlin}} = 0$. However, in this case the term $\mathrm{DE}_{\mathrm{lin}}$ is written in an implicit form as opposed to the case of a homogeneous waveguide, and its roots are unknown. So, at first, we prove that the equation for the linear inhomogeneous problem $\mathrm{DE}_{\mathrm{lin}} = 0$ has roots and define localization of the roots. Then we prove that nonlinear problem has solutions.

Preliminary Study of Embedded Structural Anomalies in Architectural Structures by Microwave Subsurface Tomography

S. Beni[1], **R. Olmi**[1, 2], **F. Micheletti**[2], **and C. Riminesi**[1, 3]

[1]ELab Scientific Srl, Firenze, Italy
[2]Institute for Applied Physics, National Research Council, Firenze, Italy
[3]Institute for the Conservation and Valorization of Cultural Heritage
National Research Council, Firenze, Italy

Abstract— A non-destructive technique (NDT) based on microwave reflectometry has been applied to perform subsurface tomography images. The localization in depth of anomalies in architectural structures such as, for example, inhomogeneity in the masonry texture (cavity of air, metals, and humidity) or on timber structure by means of NDT approach is crucial not only in the diagnostics of the Cultural Heritage, but in general for all civil industry. The target of our research is the development of a robust and user-friendly system to investigate the materials used in architecture until 20 cm in depth, with a resolution less than 1 cm.

This method is implemented with a vector network analyzer and a ridged antenna operating in the range 1.5–6 GHz for the measurement of the reflection coefficient variation (amplitude and phase) due to the dielectric dis-homogeneity into the materials under investigation. The equivalent time-domain response is reconstructed using an inverse Fourier transform of the baseband signal and by a simple model based on TEM approach is determined the constrains on the size of the anomaly (maximum resolution) and on its position into the host medium (maximum non unambiguous range).

The material can be investigated by scanning — step by step — the surface with the ridge antenna. For each step is obtained the reflection coefficient in the frequency range, and subsequently transformed in the time-domain by out-line processing.

Thanks to the penetration of the used microwave radiation, it is possible to sectioning the whole scanned area, in layers 1–2 cm thick (tomogram) parallels to surface scanning, up to 20 cm in depth. Similar sectioning can be obtained for the transversal plain with slices of the same depth. The interdistance between two consecutive slices is related to the distance between the two corresponding scanning lines.

The performance of the proposed technique together with its resolution limits are discussed as regards with other approach proposed in literature. The results on laboratory test materials and on a wooden beam section with structural anomalies induced by biodegradation agents will be presented.

The potentiality of the system as diagnostic tool based on NDT approach for the framework of Cultural Heritage will be discussed together with its limits.

ACKNOWLEDGMENT

The research activity has been partially supported by Tuscany Region, Italy, within the PRIMARTE project (POR CReO FESR 2007-2013 Intervention sector 1.5a 1 1.6).

Session 4A1
FocusSession.SC3: Real-time High-speed Measurements for Communication, Biomedical & Industrial Appl.

Dispersive Fourier Transformation for Fast Real-time Imaging and Spectroscopy

Keisuke Goda[1, 2], **Bahram Jalali**[2], **and Takuro Ideguchi**[1]

[1]Department of Chemistry, University of Tokyo, Japan
[2]Department of Electrical Engineering, University of California, Los Angeles, USA

Abstract— The ability to perform real-time imaging and spectroscopy is crucial for evaluating and characterizing fast non-repetitive or transient processes in a diverse range of industrial and biomedical applications. Such processes include protein folding dynamics, phase transitions in semiconductor materials, shockwave propagation in living cells, enzyme reactions, and turbulent flows in microchannels. Unfortunately, conventional time-resolved measurement techniques based on the pump-probe method fall short in meeting the requirement as they require time-delayed repetitive measurements to construct the time-resolved signal (spectrum or image).

Dispersive Fourier transformation (DFT) [1, 2] is a powerful approach that circumvents the fundamental limitation in the time-resolved measurement techniques. It allows for fast real-time spectral measurements as it eliminates the slow components in conventional spectrometers by replacing the diffraction grating and detector array with a dispersive fiber and photodiode. The operation of DFT is as follows. First, a pulse train is used as an optical source for probing the sample. Second, the reflected, transmitted, or scattered pulse train from the sample via linear or nonlinear processes in the sample is stretched by a sufficient amount of dispersion in the dispersive fiber so that the spectrum of each pulse is mapped into the time domain. Third, the pulse train is measured by a high-speed photodiode for repetitive spectral measurements at the pulse repetition rate. Since the pulse repetition rate of typical mode-locked lasers is 10–90 MHz, spectral measurements can be performed at such a high rate which is at least a few orders of magnitude higher than that of traditional spectrometers.

DFT has been proven effective for fast real-time imaging and spectroscopy [3–7]. Serial time-encoded amplified imaging/microscopy (STEAM) [3, 4] is one of the key techniques based on DFT. STEAM operates at a frame rate which is a few orders of magnitude higher than that of conventional cameras such as CCD and CMOS image sensors. With its superior capability, it has been employed for real-time imaging of laser ablation dynamics, fast surface inspection in manufacturing, and high-throughput image cytometry for cancer detection. DFT holds great promise for these applications in practical settings as well as other potential applications.

REFERENCES

1. Goda, K. and B. Jalali, "Dispersive Fourier transformation for fast continuous single-shot measurements," *Nature Photon.*, Vol. 7, 102–112, 2013.
2. Goda, K., D. R. Solli, K. K. Tsia, and B. Jalali, "Theory of amplified dispersive Fourier transformation," *Phys. Rev. A*, Vol. 80, 043821, 2009.
3. Goda, K., et al., "Serial time-encoded amplified imaging for real-time observation of fast dynamic phenomena," *Nature*, Vol. 458, 1145–1149, 2009.
4. Goda, K., et al., "High-throughput single-microparticle imaging flow analyzer," *Proc. Natl. Acad. Sci. USA*, Vol. 109, 11630–11635, 2012.
5. Solli, D. R., J. Chou, and B. Jalali, "Amplified wavelength-time transformation for real-time spectroscopy," *Nature Photon.*, Vol. 2, 48–51, 2008.
6. Solli, D. R., C. Roper, P. Koonath, and B. Jalali, "Optical rogue waves," *Nature*, Vol. 450, 1054–1057, 2007.
7. Solli, D. R., G. Herink, B. Jalali, and C. Ropers, "Fluctuations and correlations in modulation instability," *Nature Photon.*, Vol. 6, 463–468, 2012.

High-quality Optical Time Stretch: From Real-time Supercontinuum Analysis to Ultrafast Bioimaging

Kevin K. Tsia and Kenneth K. Y. Wong
Department of Electrical & Electronic Engineering, The University of Hong Kong
Pokfulam Road, Hong Kong, China

Abstract— Optical time-stretchis an emerging technique for ultrafast bioimaging and optical spectralanalysis. Its central idea is ultrafast retrieval of any information encoded in the spectrum of a broadband optical pulse by converting it into a serial temporal data format in real time. We here will present a number of *practical and high-quality* optical time-stretch platforms for different applications — ranging from real-time supercontinuum analysis to ultrafast cellular and tissue bioimaging.

On the spectral analysis front, real-time experimental measurements of the spectrally-resolved noise properties of supercontinuum (SC) have been challenging because of the lack of ultrafast optical spectrometer technologies. Understanding the SC noise is increasingly important because it not only can gain new insight of the complex spectral dynamics of SC generation, but also provides clues to search for stable SC source. Driven by the intense interest in the active seeding mechanism for SC generation, we experimentally demonstrate real-time spectrally-resolved, broadband, statistical characterization of minute continuous-wave (CW) seeded SC, enabled by optical time-stretch. It enables us to carry out comprehensive shot-to-shot statistical analysis of the seeded SC at a spectral acquisition rate as high as 20 MHz.

On the bioimaging front, time-stretch microscopy has mostly been operated in bright-field (BF) imaging mode in longer wavelength range, and is thus not capable of revealing high-contrast and detailed morphology of the transparent cells — hindering accurate high-throughput *image-based* cell recognition and screening. To this end, we present a solution by a new imaging approach called *asymmetric-detection time-stretch optical microscopy (ATOM)*, for capturing label-free, high-contrast image of the live cells at ultrahigh speed, in the context of microfluidic flow imaging at a record high *imaging* flow speed of 10 m/s — equivalent to an imaging throughput of $\sim$ 100,000 cells/sec — unreachable by any state-of-the-art image flow cytometersWe also demonstrate interferometric time-stretch (iTS) microscopy for delivering ultrafast quantitative phase cellular and tissue imaging at an imaging line scan rate of more than 20 MHz — orders-of-magnitude faster than conventional quantitative phase imaging (QPI). As many parameters can be further extracted from the phase and served as the intrinsic biomarkers for disease diagnosis, both ATOM and iTS microscopy could find theirniches in high-throughput and high-content cellular assays as well as whole-slide imaging for digital pathology.

We also demonstrate all-optical ultrahigh-speed swept-source optical coherence tomography (OCT) based on amplified optical time-stretch (AOT). We here report an AOT-OCT system which is operated at an A-scan rate of $\sim$ 10 MHz, a superior roll-off performance ($>$ 2 mm/dB), a record-high sensitivity of time-stretch-based OCT ($>$ 80 dB) with a broadband gain bandwidth of 80 nm. Our AOT-OCT system is thus able to, for the first time, perform time-stretch-based OCT of biological tissue in-vivo. It represents a major step forward in utilizing AOT as an alternative for achieving practical MHz OCT, without any long-term mechanical stability concern as in typical swept-source OCT.

ACKNOWLEDGMENT

This work is partially supported by grants from the Research Grants Council of Hong Kong Special Administrative Region, China (HKU 717212E, HKU 717510E, HKU 717911E, and HKU 720112E), and the University Development Fund of HKU.

Fast Surface Imaging by Time-stretch Technique

Hongwei Chen, **Fangjian Xing**, **Cheng Lei**, **Minghua Chen**, **Sigang Yang**, **and Shizhong Xie**
Tsinghua National Laboratory for Information Science and Technology (TNList)
Department of Electronic Engineering, Tsinghua University, Beijing 100084, China

Abstract— Surface imaging (also known as surface inspection or web inspection) is a widely used method for nondestructive evaluation of products during manufacturing. It is widely used for quality control and defect detection on the surface of various materials such as fabrics, paper, plastic bags, strip steel, leather, liquid crystal display panels, thin films, and silicon wafers. The ability to image the surface of such materials or devices at high speed is particularly important for inspecting a large quantity or surface area in a short period of time. Line CCD or CMOS cameras are conventionally used for surface imaging, but has limited frame rate and data throughput. So far the conventional surface inspection systems equipped with line cameras can only operate at a scan rate of 20–40 kHz, meaning that each frame is captured no faster than 25 μs.

By utilizing time-stretch technique in large dispersion fiber, we can get surface imaging with frame rate up to MHz or even GHz, which is almost 100 or 10000 times faster than conventional methods. It employs spatiotemporal dispersion to map the spectrum of a broadband laser pulse into space and time to achieve ultrafast laser scanning at the scan rate equivalent to the laser's pulse repetition rate. So the optical source is a key component in such an imaging system, it determines the scan rate, resolution and field of view. Here, we will introduce three kinds of optical source used for surface imaging, including passively mode-locked laser, actively mode-locked laser and multi-wavelength source. The analysis and demonstration of these three optical sources are given in the talk. Since they have individually imaging performance, therefore can be used for different applications.

ACKNOWLEDGMENT

This work was supported by National Program on Key Basic Research Project (973) under contract 2012CB315703, by the NSFC under contract 61322113, 61335002, 61120106001, 61271134, 61090391, 61132004, and by Program for New Century Excellent Talents in University (NCET-10-0520), and by the young top-notch talent program sponsored by Ministry of Organization, China.

Ultrafast Web-inspecting Laser Scanner

Akio Yazaki[1, 2], **Ata Mahjoubfar**[1, 3], **Chanju Kim**[1, 4], **Jacky Chan**[1], **Keisuke Goda**[1, 5], **Masahiro Watanabe**[2], **and Bahram Jalali**[1, 3, 6, 7]

[1]Department of Electrical Engineering, University of California, Los Angeles, California 90095, USA
[2]Yokohama Research Laboratory, Hitachi, Ltd., Kanagawa 244-0817, Japan
[3]California NanoSystems Institute, University of California, Los Angeles, California 90095, USA
[4]Advanced Photonics Research Institute, Gwangju Institute of Science and Technology Gwangju 500-712, Korea
[5]Department of Chemistry, University of Tokyo, Tokyo 113-0033, Japan
[6]Department of Bioengineering, University of California, Los Angeles, California 90095, USA
[7]Department of Surgery, David Geffen School of Medicine, University of California, Los Angeles California 90095, USA

Abstract— Automated visual inspection (AVI) takes a significant part in the manufacturing process where its functionality encompasses defect detection, component measurement, numbering, orientation recognition and surface examination. Among nondestructive AVI methods, web inspection technology is an important modality when evaluating or characterizing the surface of a sample. Especially for fast and continuous web inspection, a linescan web inspection system with a linear pixel array camera (line scan camera) is most commonly used. Such line scan web inspection systems are deployed in many industrial fields ranging from fabric, paper, semiconductor wafer and flexible film The line rate of the CMOS/CCD detector array imposes limit on the scan speed and the throughput of the system. The line rate of CMOS camera typically goes up to 100 kHz and at the same time it needs to compromise between sensitivity and frame rate

In this work, we propose a solution that achieves continuous line scan rate of 90.9 MHz which represents an increase in speed of three orders of magnitude as compared to modern CMOS/CCD counterparts A Dual Dispersion Dark-field Laser Scanner utilizes temporal dispersion and spatial dispersion as a means for generating a fast inertia-free line scanning beam at a scan rate of 90.9 MHz The pulse train from Ti: Sapphire mode-locked laser is temporally dispersed — the process known as Time-Stretch Microscopy that exploits Dispersive Fourier Transformation (DFT) to map original spectrum into temporal waveform that is slow enough to be digitized in real-time. Then the time-stretched pulse is incident onto a pair of diffraction gratings which spatially disperses the pulse producing a collimated 1D rainbow beam in the line scanning direction with a width of 25 mm (field-of-view) The beam is focused down in the vertical direction and illuminates a target sample. The weak scattered light from the defects on the sample is collected by a Hybrid Photo Detector (HPD) and the electrical signal from the HPD is amplified and recorded by a high-speed digitizer with a sampling rate of 20 GS/s. Serial line scan data is collected by extending the record time duration of oscilloscope and the scattered image for the sample is reconstructed with post processing. To demonstrate the performance of our inspection system, dark-field type imaging tests with our inspection system are performed with 1D rainbow beam normally incident onto the sample After the image reconstruction, we have successfully identified 10 μm × 10 μm sized defects on a film on a rotary roller at a translation speed of 3 m/s and the same sized foreign particles on a hard-disk drive cylinder rotating at the angular speed of 7200 rpm which corresponds to linear translation speed of the defect of 20 m/s. In terms of the system's capability of accommodating broad range of sample types (e.g., non-reflective film, reflective film and semi-transparent film), we expect wide range of applications such as thin film, semiconductor wafer, turbine blade, turbo pumps and train track inspection.

Optical Coding for Ultra-fast Imaging Application

Xu Wang
Institute of Photonics and Quantum Sciences, School of Engineering and Physical Sciences
Heriot-Watt University, Edinburgh EH14 4AS, UK

Abstract— Recently, serial time-encoded amplified microscopy (STEAM) technology emerged as a new approach to real-time imaging. The new imaging method maps a two-dimensional (2D) image into a serial time-domain data stream and simultaneously amplifies the image in the optical domain. An entire 2D image is captured using a single-pixel photodetector and can achieve net image amplification as high as 25 dB. This overcomes the compromise between sensitivity and frame rate without resorting to cooling and high intensity illumination.

STEAM is based on a technique called chirped wavelength encoding and electronic time-domain sampling (CWEETS), which uses chromatic dispersion to transform temporal envelope of a signal into its spectra (wavelength-time mapping) and then the spectrum can be acquired directly in time domain using a single photo-detector and a real-time oscilloscope.

On the other hand, optical code processing technologies have been developed for many years and a number of advanced en/decoding techniques have been proposed and demonstrated for optical communication applications. The image collection stage in STEAM is one kind of the optical code generation process-namely incoherent spectral encoding. In essence, the image collection and recognition process can be regarded as optical code generation/recognition processes. Therefore,the optical code processing technologies that have been developed for optical communication system could be applied for real-time imaging application.

Time-encoded Amplified Microscopy for Ultrafast Imaging Using a Multiwavelength Laser Source

Ming Li[1], **Ye Deng**[1], **Ningbo Huang**[1], **José Azaña**[2], **and Ninghua Zhu**[1]

[1]State Key Laboratory on Integrated Optoelectronics, Institute of Semiconductors
Chinese Academy of Sciences, Beijing 100083, China
[2]Institut National de la Recherche Scientifique-Énergie
Matériaux et Télécommunications (INRS-EMT), Varennes, Québec J3X 1S2, Canada

Abstract— In recent years, ultrafast real-time optical imaging has attracted a lot of interests, because it is an effective and important tool for studying dynamical events, such as shock waves, neural activity, laser surgery and chemical dynamics in living cells [1–6]. For a conventional CCD or CMOS imaging device, although it has many advantages (e.g., high spatial resolution, large number of pixels and low cost), it can not image fast dynamic processes due to limited frame rate [7]. To overcome the limitation, some techniques have been reported. The time-resolved pump-probe technique [8] and framing streak camera can realize high-speed imaging, but they are unable to capture non-repetitive events. Serial time-encoded amplified microscopy (STEAM) technique based on space-frequency mapping combined with frequency-time mapping has been demonstrated as a completely new optical imaging modality [9–14]. By employing a spatial disperser and a dispersive element, the spatial information is converted to a serial sequence in time and can be detected with a single-pixel photodiode and captured by a real-time oscilloscope. However, these methods need a large and high-cost pulsed laser; for this type of lasers, the spectral width is generally limited to about 10 nm which limits the measurement range. In addition, the pulse repetition rate is fixed which in turn means that the imaging frame rate is also fixed.

In this paper, we experimentally demonstrate an incoherent STEAM system by employing a multi-wavelength laser as the light source. This system avoids the need for a broadband coherent laser light source and all the associated limitations, as outlined above. The measurement range can be largely extended by simply increasing the number of laser channels. The frame rate is also reconfigurable by electrically tuning the gating rate. Finally, since an integrated multi-wavelength laser source is commercially available, the incoherent STEAM system has the potential for integration on a photonic chip.

REFERENCES

1. Lee, K. L., M. P. Fok, S. M. Wan, and C. Shu, "Optically controlled Sagnac loop comb filter," *Opt. Express*, Vol. 12, 6335–6340, 2004.
2. Kodama, R., et al., "Fast heating of ultrahigh-density plasma as a step towards laser fusion ignition," *Nature*, Vol. 412, 798–802, 2001.
3. Petty, H. R., "Spatiotemporal chemical dynamics in living cells: From information trafficking to cell physiology," *Biosystems*, Vol. 83, 217–224, 2004.
4. Gridley, T. and R. Woychik, "Laser surgery for mouse geneticists," *Nature Biotechnol.*, Vol. 25, 59–60, 2007.
5. Yanik, M. F., et al., "Functional regeneration after laser axotomy," *Nature*, Vol. 432, 822, 2004.
6. Squires, T. M. and S. R. Quake, "Microfluidics: Fluid physics at the nanoliter scale," *Rev.Mod. Phys.*, Vol. 77, 977–1026, 2005.
7. Holst, G. C. and T. S. Lomheim, "CMOS/CCD sensors and camera systems," *SPIE-International Society for Optical Engine*, 2007.
8. Barty, A., et al., "Ultrafast single-shot diffraction imaging of nanoscale dynamics," *Nature Phys.*, Vol. 2, 415–419, 2008.
9. Goda, K., K. K. Tsia, and B. Jalali, "Serial time-encoded amplified imaging for real-time observation of fast dynamic phenomena," *Nature*, Vol. 458, 1145–1149, 2009.
10. Zhang, C., Y. Qiu, R. Zhu, K. K. Y. Wong, and K. K. Tsia, "Serial time-encoded amplified microscopy (STEAM) based on a stabilized picosecond supercontinuum source," *Opt. Express*, Vol. 19, 15810–15816, 2011.
11. Xing, F., H. Chen, M. Chen, S. Yang, and S. Xie, "Simple approach for fast real-time line scan microscopic imaging," *Appl. Opt.*, Vol. 52, 7049–7053, 2013.

12. Goda, K., K. K. Tsia, and B. Jalali, "Amplified dispersive Fourier-transform imaging for ultrafast displacement sensing and barcode reading," *Appl. Phys. Lett.*, Vol. 93, 131109, 2008.
13. Wong, T. T. W., A. K. S. Lau, K. K. Y. Wong, and K. K. Tsia, "Optical time-stretch confocal microscopy at µm," *Opt. Lett.*, Vol. 37, 3330–3332, 2012.
14. Chen, H., C. Wang, A. Yazaki, C. Kim, K. Goda, and B. Jalali, "Ultrafast web inspection with hybrid dispersion laser scanner," *Appl. Opt.*, Vol. 52, 4072–4076, 2013.

Serial and Parallel Optical Coherence Tomography for Fast Orthogonal Image Slicing

Adrian Gh. Podoleanu
Applied Optics Group, School of Physical Sciences, University of Kent
Canterbury CT2 7NH, United Kingdom

Abstract— Principles of optical coherence tomography (OCT) technologies will be presented comparatively and how their advantages and disadvantages shaped the range of their specific applications. To address disadvantages of spectral domain OCT, research in Kent looked at novel OCT technology of multiplexed channels and parallel processing. So far, OCT progressed as a serial technology, where a Fourier transformation of the signal delivered by a spectrometer (when using a broadband source) or by a photodetector (when using a tunable laser) provided a reflectivity profile in depth (A-scan). In conventional OCT, all scattering centers along the A-scan line in depth are brought into a single step display by a Fourier transformation. This process, however simple and much in use today, presents several important disadvantages, such as the need for data provided to be placed in equal optical frequency slots. Because neither spectrometers nor tunable lasers can provide data linearly in optical frequency, conventional OCT techniques rely on linearization methods. These can be implemented in hardware or in software. Hardware implementations require some sorts of clock generation in the tunable lasers which raise the cost of already expensive systems. Software linearization requires computing resources and so it takes time. In addition, providing all points in an A-scan at once, deprives the current spectral domain OCT technology from the possibility to display *en-face* images in real time. Therefore, modern spectral OCT technology is by excellence an imaging slicing technology that cuts cross section images from the object imaged. Real time *en-face* views (with the more conventional orientation similar to that provided by a microscope or a digital camera) cannot be provided in real time due to the need of signal processing and software cut of the volume of A-scans. There is however a need in medical imaging and in non destructive testing to deliver an *en-face* view alongside the cross section image.

Combinations of time domain with spectral domain principles developed in Kent, address these disadvantages. A novel technology, Master/Slave OCT was proved functional which delivers the points in an A-scan in parallel using spectral domain principles. First reports demonstrated better sensitivity and axial resolution in comparison with the conventional spectral domain technology, along with the possibility to produce an *en-face* image direct, with no linearization and no resampling [1]. This paper will present direct production of *en-face* OCT images and specific parallel processing techniques that can be developed to deliver multiple *en-face* views from different depths, leading to a real time 3D view. The technology of Master/Slave OCT was evolved by more efficient correlation production and utilization of graphic cards. For fast delivery of cross sections, the system still retains the capability of serial signal delivery. A play of serial and parallel signal processing allows a versatile utilization of resources to benefit the user in terms of volume imaging and image inspection for selected parts of the object, with different slicing orientation.

REFERENCES

1. Podoleanu, A. Gh. and A. Bradu, "Master-slave interferometry for parallel spectral domain interferometry sensing and versatile 3D optical coherence tomography," *Opt. Express*, Vol. 21, 19324–19338, 2013.

Coherent Raman Dual Frequency Comb Spectroscopy

Takuro Ideguchi[1, 4], **Simon Holzner**[1], **Birgitta Bernhardt**[1, 2], **Guy Guelachvili**[3], **Nathalie Picqué**[1, 2, 3], **and Theodor W. Hänsch**[1, 2]

[1]Max-Planck-Institut für Quantenoptik, Germany
[2]Ludwig-Maximilians-Universität München, Germany
[3]Institut des Sciences Moléculaires d'Orsay, CNRS, France
[4]The University of Tokyo, Japan

Abstract— Optical frequency comb has harnessed for molecular spectroscopy and showed intriguing potential of broadband and precise measurements. Among direct frequency comb spectroscopy, dual frequency comb spectroscopy with two frequency combs has demonstrated unprecedented measurement speed. Recently, the concept of dual-comb spectroscopy has been applied to nonlinear spectroscopy. A successful demonstration of coherent Raman dual-comb spectroscopy showed a broadband Raman spectrum in the molecular fingerprint region (200–1400 cm^{-1}) within tens of microseconds. A hyper-spectral imaging with this scheme was also demonstrated. This ultrarapid label-free molecular vibrational spectroscopy and imaging could provide new real-time diagnostic methods in a variety of scientific and industrial fields.

A Channelized Wideband Analog to Digital Conversion Based on Coherent Optical Frequency Combs

Yitang Dai, Haijie Yu, Feifei Yin, Jianqiang Li, Kun Xu, and Jintong Lin
State Key Laboratory of Information Photonics and Optical Communications
Beijing University of Posts and Telecommunications
P. O. Box 72, Beijing 100876, China

Abstract— The commercial and military radio frequency (RF) receivers are desired strongly to provide threat information more accurately and more rapidly. The traditional analog-component-based RF receiver is gradually replaced by digital receiver, which is with high flexibility and precision. However, nowadays applications drive the RF receiver towards higher frequencies and larger bandwidths, which poses a significant challenge to digital RF receiver due to the limited sampling ratio of ADC.

Though the photonics-assisted ADC has been studied for many years, in this presentation we will demonstrate a novel photonic ADC scheme. In the new scheme, the broadband RF signal spectrum is channelized into many frequency channels whose bandwidths are compatible with available digital electronics. Compared with the traditional scheme which is essentially a time-division de-multiplexed one, our proposal achieves the demultiplication in frequency domain, and is believed to benefit applications with multiple RF carriers. The division is obtained by two coherent optical frequency combs whose intervals are slightly different. The advantages, performance, and key issues will be discussed.

Characterizing Microwave Modulation Efficiency of an Optical Phase Modulator by Using Dispersion Induced Phase Modulation to Intensity Modulation Conversion

Yong Liu, **Shangjian Zhang**, **Xinghai Zhou**, **Yali Zhang**, **and Rongguo Lu**
State Key Laboratory of Electronic Thin Films and Integrated Devices
School of Optoelectronic Information
University of Electronic Science and Technology of China (UESTC), Chengdu 610054, China

Abstract— Optical phase modulation is very useful for photonic microwave frequency measurement and photonic microwave filtering. In this talk, we investigate phase modulation to intensity modulation conversion in dispersive fibers in the context of characterizing optical phase modulators, and propose a new method for measuring the modulation efficiency through the phase modulation to intensity modulation conversion in fold-back dispersive fiber paths. We theoretically analyze the evolution of phase modulated signals in the dispersive fiber and present the measurement principle with a fold-back configuration to demonstrate our method. The frequency dependent modulation index and half wave voltage are experimentally measured for a commercial phase modulator. During the experiment, our measurements had stable and repeatable results because the optical carrier and its sidebands are affected by the same fiber impairments. Our method works without the restriction of small signal operation, and allows swept frequency measurement with high resolution and accuracy by using a network analyzer, which benefits from the high resolution and swept frequency of developed electrical domain measurement techniques and avoids using an unstable interferometer or additional envelope extraction.

Long-range and Biomedical Measurements Based on Optical Fiber Strain Senor

Changyuan Yu[1, 2, 3], **Zhihao Chen**[1], **and Junhao Hu**[4]

[1]A*STAR Institute for Infocomm Research, Singapore 138632, Singapore
[2]Department of Electrical & Computer Engineering
National University of Singapore, Singapore 117583, Singapore
[3]National University of Singapore (Suzhou) Research Institute, 215123, China
[4]AnSing Technology PTE LTD, Singapore 139951, Singapore

Abstract— Optical fiber strain sensor has wide applications including environment monitoring and biomedical measurement. In this paper, we summarize our research work on two types of optical fiber strain sensors: long distance vibration sensor and biomedical ballistocardiogram (BCG) sensor.

One type of strain sensor is based on Fiber Bragg grating (FBG), which is very attractive in many applications due to its high sensitivity, electro-magnetic immunity, compactness, high resolution and high optical signal-to-noise ratio (SNR) against the noise. For long-range sensing, we need to propagate a broadband light over single-mode fiber (SMF) and then measure the refection of FBG at the far end. However, the measurement distance of this scheme is limited, since the transmission of a broadband light is less than 25 km due to the noise and loss induced by the Rayleigh scattering and attenuation along the fiber, and lasing effects are induced when the pump power is increased to a threshold. To achieve longer distance measurement, complicated setup with a lot of components is generally used to reduce the lasing effect. In practical usage, however, simple long distance sensor systems are desired. We propose a simple structure based on Raman amplification, and demonstrate a 150 km multi-point FBG vibration sensor system.

Another type of strain sensor is based on fiber bending loss. Compared to FBG sensor, the cost is much lower. So it is more suitable for consumer markets. For biomedical application, regular and non-invasive measurement is an important diagnostic method in medical care. Non-invasive methods to monitor vital signs have been of much interest because of their practicality as well as the comfortability for the bedded person. Most developments now have been focused on electrical sensors. Electrical sensors are usually prone to electromagnetic interference (EMI), which is a problem in some clinical examination, e.g., MRI examination. Therefore, the standard electronic monitoring system has significant limits. Optical fiber sensors can inherently immune from electromagnetic interference and chemically inert. Many optical fiber sensing systems have been proposed for monitoring of respiratory rate/body movement in the past. However, most of them are based o fiber gratings which are complex and expensive. We present a new optical fiber strain sensor for non-intrusive vital signs monitoring. Our sensing system is based on measurement of fiber bending loss and consists of a transmitter, optical receiver, a sensor sheet, and a computer. An algorithm was developed to extract breath /body movement/BCG signals. Our system is low cost, which has broken price barrier of optical sensor to industry acceptance. This technology has been commercialized by a Singapore-based company.

Femto-second Arbitral Optical Waveform Synthesis Based on Optical Frequency Comb Synthesizer and Analyzer

Tatsutoshi Shioda
Saitama University, 255 Shimo-Okubo, Sakura-ku, Saitama city, Saitama 338-0835 Japan

Abstract— We have proposed an ultrafast optical arbitrary waveform synthesizer and analyzer in from femtosecond to picosecond time region. Ultrafast waveforms were generated by manipulating the amplitude and phase of a 200 GHz optical frequency comb (OFC) using a customized colorless optical synthesizer. The synthesized waveform was then analyzed on the frequency axis using a custom heterodyne-detection technique based on the dual-heterodyne mixing. The proposed system has been applied to generate 312.5 fs pulses and to synthesize composite amplitude-shift and phase-shift keying signals of 22.4-Tbit/s with 112-bit packets in data processing.

Session 4A2
SC1&3: Design and Simulation of Electromagnetic and Optical Devices 1

Analysis of Post-wall Waveguide Based Bandpass Filters Using a Model of Photonic Crystal Waveguides

Kiyotoshi Yasumoto[1], **Hiroshi Maeda**[1], **and Vakhtang Jandieri**[2]

[1]Faculty of Information Engineering, Fukuoka Institute of Technology, Fukuoka 811-0295, Japan
[2]Department of Computer and Electrical Engineering, Free University of Tbilisi
Tbilisi 0159, Republic of Georgia

Abstract— Post-wall waveguides, also called substrate integrated waveguides, have received a growing attention because of their promising applications to planar circuit components operating in the microwave to millimeter wave frequency range. In this paper, we shall present an approximate analysis of a post-wall waveguide-based bandpass filter using a model of two dimensional photonic crystal waveguides (PCWs).

The post-wall waveguide is formed by two-parallel periodic arrays of conducting circular posts embedded in a dielectric substrate that connect two parallel conducting plates. The periodic arrays play a similar role as the lattice elements in a PCW and confine the guiding fields in the region bounded by two array planes. Using a model of two-dimensional PCWs, we define first a rectangular waveguide with an effective width which is equivalent to the original post-wall waveguide. Since post-wall waveguide based filters are designed by loading metallic or dielectric posts as shown in Fig. 1(a), the original structure is replaced by an equivalent rectangular waveguide structure shown in Fig. 1(b). The vertical post in a rectangular waveguide is regarded as a periodic array of cylinders, being combined with its mirror images with respect to two side walls. When the posts are stacked, a two-dimensional photonic crystal is formed which consists of the original posts and an infinite number of their images. Then we can use again the theory [2] of two-dimensional photonic crystal. The scattering parameters of the circular post are obtained [3] in closed form using the image theory and the lattice sums. The scattering parameters of the post-wall waveguide based bandpass filter shown in Fig. 1(a) have been analyzed by using its equivalent rectangular waveguide model shown in Fig. 1(b). The results are plotted in Fig. 2 and compared with those [4] obtained by a direct numerical analysis using a hybrid method. We can see that our results are in very close agreement with those of the hybrid method.

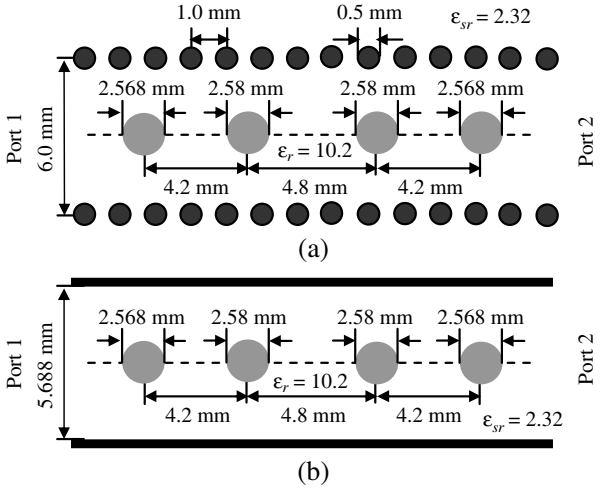

Figure 1: (a) Bandpass filter using a post-wall waveguide and (b) equivalent rectangular waveguide model.

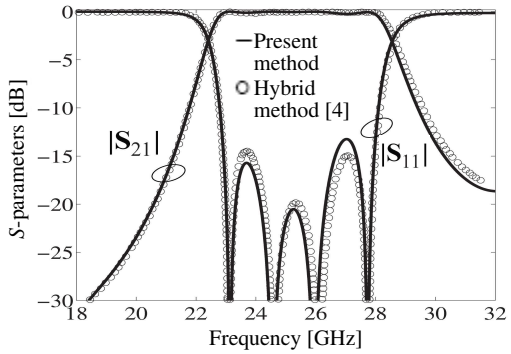

Figure 2: S-parameters of the post-wall waveguide shown in Fig. 1 where four dielectric circular posts are loaded.

ACKNOWLEDGMENT

This work was supported in part by Grant-in-Aid for Scientific Research (C) 24560430.

REFERENCES

1. Yasumoto, K., H. Maeda, and V. Jandieri, *Proceedings of 2013 Kyushu Sec. Joint Conference*, 184, 2012.
2. Yasumoto, K., H. Jia, and K. Sun, *Radio Sci.*, Vol. 40, No. 6, RS6S02, 2005.
3. Yasumoto, K., et al., *IEICE Trans. Electronics*, Vol. E69-C, No. 9, 1324–1329, 2006.
4. Wu, X. H. and A. A. Kishk, *IEEE Trans. Microw. Theory Tech.*, Vol. 56, No. 10, 2270–2276, 2008.

Electromagnetic Modeling and Simulation for Packaging Structures with Lossy Conductors

Y. Q. Zhang, G. Z. Yin, X. W. Zhang, J. Zhang, and M. S. Tong
Department of Electronic Science and Technology
Tongji University, Shanghai, China

Abstract— Accurate electromagnetic (EM) analysis based on numerical modeling and simulation is essential for the optimal design of electronic devices or systems. For interconnect and packaging structures, the conductors are usually lossy and we have to account for the skin effect in numerical solutions. In the integral equation approach for solving the problem, one may use the volume-filament method like the partial equivalent electric circuit (PEEC) solver or surface integral equation (SIE) approach with an approximate surface impedance. However, they are only efficient to model interconnect conductors which are usually long and thin and cannot handle the conductors with irregular shape such as bends and junctions. The SIE approach is preferred whenever available because it only discretizes the boundaries or interfaces of media, resulting less number of unknowns.

To treat arbitrarily-shaped structures with lossy conductors by the SIE approach, the generalized impedance boundary condition (GIBC) approach was proposed by formulating the problem in two regions. The approach treats the lossy conductors as general dielectric media and uses the electric field integral equations (EFIEs) to describe the exterior region of conductors and the magnetic field integral equations (MFIEs) to formulate the interior region of conductors. In this work, we use the EFIEs to describe both the exterior region and interior region of conductors and consider the structural mixture of dielectrics and conductors which were not considered previously. The EFIEs are solved with the method of moments (MoM) in which the the Rao-Wilton- Glisson (RWG) basis function is used to represent the electric current density while the dual basis function is employed to expand the magnetic current density. The two basis functions are also used as testing functions to wisely test the EFIEs so that the conditioning of resulting system matrix can be improved. We present the numerical example for analyzing a typical interconnect structure to illustrate the approach and good results can be observed.

Error Analysis of Superposition Solution Combined with Method of Moments for Electromagnetic Scattering

M. Tanaka
Gifu University, Gifu 501-1193, Japan

Abstract— When the shape of scattering objects is cylindrical in 2-dimensional structure and spherical in 3-dimensional structure, the superposition solution combined with Mie's theory gives an exact solution for electromagnetic scattering from multiple objects.

We employed the method of moments instead of Mie's theory, in order to solve electromagnetic scattering from multiple objects arbitrary in shape. We also performed numerical calculations of the superposition solution combined with the method of moments. However, the method only worked well for the case of small number of objects and low refractive indices of object.

In this paper, we will discuss error analysis of superposition solution combined with the method of moments.

A Numerical Study on 2D Photonic Crystal Devices for Millimeter and Terahertz Wave Applications

T. Kato[1], **K. Kamata**[1], **C. P. Chen**[1], **T. Anada**[1], **Steve Greedy**[2], **and Trevor Benson**[2]

[1]Kanagawa University, 221-8686, Japan
[2]University of Nottingham, NG7 2RD, UK

Abstract— As the demand for greater bandwidth increases alongside the development of the next and future generations of wireless communication systems, the extension of the operating frequency of these systems into the upper-millimeter wave or terahertz region (100 GHz–3 THz) of the electromagnetic spectrum is inevitable. Therefore technologies that enable electronic devices to work in the THz region are required, technologies that perform the operations provided by traditional passive circuits; switches, splitters and filters for example. One technology that has shown promise for the realization of such devices is that of silicon based photonic crystals. Through the introduction of point or line defects in the PhCs, the electromagnetic (EM) wave can be controlled, i.e., confined, guided, or localized.

In this paper, the frequency characteristics of THz functional devices using photonic crystal line defect waveguides/point-defect resonators are then numerically studied by the finite difference time domain (FDTD) method. The validity of our approach is justified through application to examples of; PhC T-junction switching circuits, Pseudo-elliptic function bandpass filter using degenerate modes, and channel drop filter.

A Photonic Crystal Switch Created by Inserting a Small Dielectric Perturbing Rod within T-junction: A novel PhC T-junction switch is proposed here that can control the direction of an EM-wave that propagates along a line defect waveguide. As shown in Fig. 1, the selectivity of the direction is determined by the insertion of a small dielectric perturbing rod. The power transmission efficiency from port 3 to port 4 is seen to be near 95% at frequency $f = 2.10$ THz.

Pseudo-elliptic Function Bandpass Filter Using PhC Degenerate Modes: We propose PhC Pseudo-elliptic function bandpass with an additional large dielectric rod of radius R_d and a small dielectric-perturbing rod of radius r_p as shown in Fig. 2. By laying out the input/output ports orthogonally (90°), both of the degenerate modes are excited and coupled to each other due to the small perturbing rod within the point defect microcavity. By utilizing input-output coupling windows, two transmission zeros can be simultaneously placed below or above the pass-band. Simulation results show that the resulting bandpass filter exhibits a quasi-elliptic response with two transmission zeros at finite frequencies near the passband.

In summary, we can conclude that the photonic crystal planar circuit shows promise as a key technology for constructing high density integrated electromagnetic circuits. In the near future, the PhC devices proposed here will be applied to EM wave propagations in practical photonic crystal circuits.

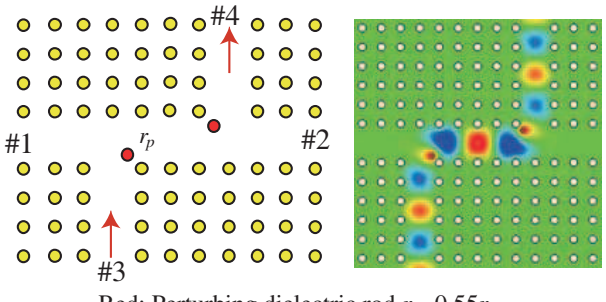

Figure 1: PhC T-junction switch and electric field (Ez).

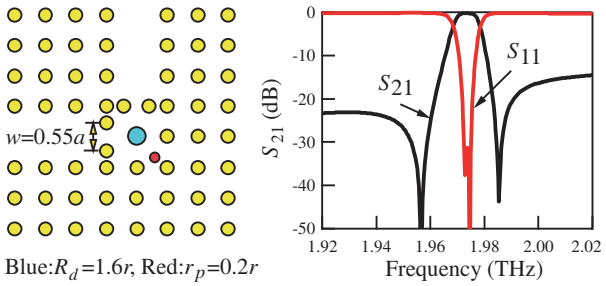

Figure 2: PhC Pseudo-elliptic bandpass filter.

Advance of Research on Coaxial Relativistic Backward Wave Oscillator

Yan Teng, Jun Sun, Zhimin Song, Changhua Chen, and Zhaoyu Du
Northwest Institute of Nuclear Technology, P. O. Box 69-13, Xi'an, Shaanxi 710024, China

Abstract— Coaxial relativistic backward wave oscillator (CRBWO) is a new type of high power microwave (HPM) generator remarked by the conversion efficiency higher than 35%. This paper summarizes the recent progress made on the theoretical and experimental researches on CRBWO. The physical reasons for the high conversion efficiency has been primarily investigated and analyzed. It is found that in CRBWO. It is found that introduction of the inner conductor can promote the beam quality. The distribution of the synchronous wave in coaxial slow wave structure (SWS) benefits the wave-beam interaction. The electron dump on the inner conductor ensures the wave-beam interaction efficiently till the electron vanishes on the inner conductor. According to the special structure and distinguishing physical mechanism of CRBWO, the coaxial reflector has been developed to improve the premodulation of the electron beam, and the structure with coaxial dual annular cathodes has been developed to enhance both the output power and the conversion efficiency up to 3.63 GW and 45%. Making full use of the both rippled conductors of CRBWO by installing an additional set of SWS into the inner conductor results in the generation of the beating wave with the average output power 5.88 GW and conversion efficiency 41.5% consisting of frequency components of 9.0 GHz and 9.7 GHz. It is suggested that the distinct operation mechanism of in CRBWO should be researched further to make full use of its potential of the high efficiency. And the technological problems especially such as coaxiality and power capacity should be delicately considered and optimized to make sure the experimental structure is identical to the physical model.

An Intra-cavity Spatial Light Modulator Laser for Desired Planar Laser Modes

Pengfei Xu, Guoxuan Zhu, Yanfeng Zhang, Hui Chen, Yujie Chen, and Siyuan Yu
State Key Laboratory of Optoelectronic Materials and Technologies
School of Physics and Engineering, Sun Yat-sen University, Guangzhou 510275, China

Abstract— With the invention of the Spatial Light Modulator (SLM), the laser beam shaping becomes efficient and convenient. One can simply acquire a desired optical field distribution by using an accurately generated hologram displayed on the SLM. However, such extra-cavity beam shaping is instable because the modulation requires information on both the intensity and phase profile of the incoming laser beam, which have the significant influence on the outgoing beam.

Recently, the intra-cavity SLM Laser (ICSLM Laser), also called digital laser, which is formed by replacing one of the resonators mirrors with SLM, had an increasing popularity of study. Generally, the output mode of ICSLM laser is determined by the Eigen solution of the Fresnel-Kirchhoff diffraction formula and the boundary conditions of the phase modulating holograms. Once the holograms on SLM is settled, the corresponding output laser beam will stably generating, and that is the advantage of the intra-cavity beam shaping.

We numerically demonstrated that such an ICSLM laser can generate a high resolution custom planar laser pattern, especially for those desired complicated patterns, indicating that the ICSLM lasers can be used as one of the promising candidates of maskless direct-writing photoetching technique. On the other hand, we have analytically derived the creation algorithm of modulating hologram used for the desired laser pattern, and validated its correctness numerically by applying Fox-Li iterative analysis. We have successfully generated several complicated patterns to proved the feasibility of this ICSLM custom-patterned laser.

Finally, we have both analytically and numerically proved that such an ICSLM laser is unable to support the output of high order Hermite-Gaussian (HG) modes and Laguerre-Gaussian (LG) modes, which are the natural solution of paraxial wave function. Due to the symmetric boundary condition of the laser resonator with two identical SLMs, the beam waist in the cavity center can be regarded as the output mode of the ICSLM laser. The ICSLM laser can only support planar laser modes, which complies with the conservation of momentums of the laser system. Therefore, the digital laser for on-demand modes may be limited to planar mode applications only.

A Study on Crosstalk-free Polarization Splitter Based on Single-polarized Photonic Crystal Fibers

Zejun Zhang[1], **Yasuhide Tsuji**[1], **and Masashi Eguchi**[2]

[1]Division of Information and Electronic Engineering
Muroran Institute of Technology, Muroran 050-8585, Japan
[2]Department of Photonics System Technology
Chitose Institute of Science and Technology, Chitose 066-8655, Japan

Abstract— Photonic crystal fibers (PCFs), consisting of single material with periodical array of air holes around the fiber core, also known as holey fibers (HFs), have attracted a lot of attention in the last two decades due to their flexible structure and the special properties that cannot be obtained by the conventional fibers, such as large mode area, endless single mode, high nonlinearity, and so on. One of these properties is absolutely single polarization transmission and a number of single-polarized PCF structures have been proposed. In recent years, elliptical-hole core circularhole holey fiber (EC-CHF), a novel single-polarized holey fiber with a core consisting of elliptical-holes, has been proposed for achieving the single polarization transmission easily [1]. The EC-CHF can be designed to transmit only the x- or y-polarization easily by changing the major axis direction of elliptical-holes in the core region.

Polarization splitter, which can split an arbitrarily polarized light beam into two orthogonal polarization states, is very important component in coherent optical communication systems and optical-fiber sensing systems. Although many new kinds of polarization splitters based on PCF have been proposed, none of them can realize the crosstalk-free polarization. From this point, we have proposed a novel polarization splitter based on EC-CHFs which can split x- and y-polarized waves into different fibers without any crosstalk [2]. The coupling lengths for two orthogonally polarized waves are almost the same, and this makes the splitter easy to be designed. In our research, we use full-vector finite element beam propagation method (FE-BPM) to demonstrate the polarization splitter designed by large hole EC-CHFs (air filling rate in cladding is 38.32%) and small hole EC-CHFs (air filling rate in cladding is 4.39%) can completely divide an arbitrarily polarized light beam into two orthogonal polarization states without any crosstalk. After that, in order to avoid the complex analysis of actual waveguide structure, we employ the fundamental space-filling mode (FSM) of the elliptical holes in the core region to design our proposed splitter effectively. The design accuracy of the FSM method has also been discussed in detail. Finally, we offered the tolerance and wavelength dependence of the proposed polarization splitter with large and small hole EC-CHFs, respectively.

REFERENCES

1. Eguchi, M. and Y. Tsuji, "Design of single-polarization elliptical-hole core circular-hole holey fiber with zero dispersion at 1.55 μm," *J. Opt. Soc. Am. B*, Vol. 25, No. 10, 1690–1701, Oct. 2008.
2. Zhang, Z., Y. Tsuji, and M. Eguchi, "Design of polarization splitter with single-polarized elliptical-hole core circular-hole holey fibers," *IEEE Photon. Technol. Lett.*, Vol. 26, No. 6, 541–543, Mar. 2014.

Reduction of Bend Losses at Sharp Bend in Post Wall Waveguide

Ken'ichiro Yashiro[1] and Ning Guan[2]

[1]Chiba University, Japan
[2]Fujikura Ltd., Japan

Abstract— A post wall waveguide is a promising candidate for the development of low cost circuits in the millimetre-wave region. The post wall waveguide consists of two rows of metallic posts sandwiched between two parallel metallic plates. When one designs a millimeter wave circuit, he wants post wall waveguides to bend sharply. However, some part of incident waves is reflected at sharp bend and the other part is transmitted. Hence there are bend losses.

In this paper, we consider some techniques to reduce the bend losses. We apply the method of moments to analyse the reflection of millimeter waves from the right-angle bend. The global basis functions were used to reduce the number of unknowns per metal post and the necessary computer memory is also reduced. Furthermore, the Galerkin method was used to obtain a system of linear equations. Therefore, the resulting matrix is symmetric. Since the objects were confined to circular metallic posts, the elements of matrix were calculated in closed form and no numerical integration is needed.

It will be shown that only a few additional posts are set at appropriate positions in the post wall waveguide, almost all incident waves go around the corner and the bend losses are minimized. Especially, only one additional metallic post is enough to minimize the bend losses.

The Squarax Amplifier: An Electromagnetic and Thermo-mechanical Innovation

Alberto Leggieri, Davide Passi, and Franco Di Paolo
Dipartimento di Ingegneria Elettronica, Università degli Studi di Roma "Tor Vergata"
Via del Politecnico, 1, Roma 00133, Italy

Abstract— This paper describes a novel broad band Spatial Power Combiner (SPC) Amplifier based on Square Coaxial (Squarax) Transmission Line (TL), able to tolerate the Thermo-Mechanical effects due to the transistor heating.

In the proposed SPC, Fin Line to microstrip transitions (FLuS) are inserted into the Squarax TL, in order to connect many Monolithic Microwave Integrated Circuit (MMIC) Solid State Power Amplifier (SSPA) while maintaining an easy integration.

The proposed structure has some advantages over the traditional SPC's.

The Squarax SPC geometry allows the feeding of a higher number of MMIC than in a Waveguide SPC, and its straight profile allows to connect simple and low-cost square or rectangular heat-sink devices with high thermal dissipation attitude. Conversely, coaxial SPC's need apposite circular heat-sinkers that require expensive custom production.

Squarax structure ensures high power outputs and small sizes, together with theoretical DC frequency cut-off.

In this work, a 16 cards Squarax SPC in the operative bandwidth 4–18 GHz has been designed, able to account for 32 MMIC SSPA's.

Since electromagnetic characteristics depend on various factors, such as the FLuS shape and the number of cards, a computational electromagnetic model has been developed using HFSS version 15.

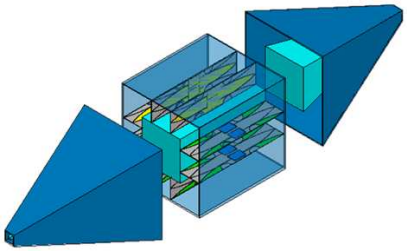

Figure 1: Example of an 8 carriers, each with two FLuS's, inside the central part of the Squarax SPC.

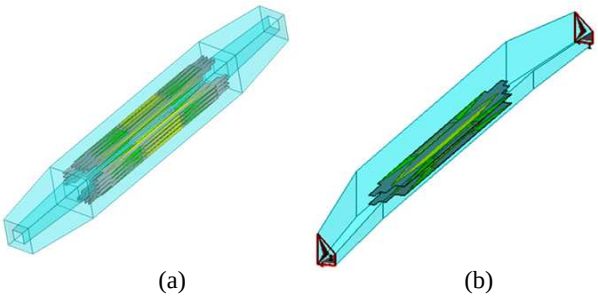

Figure 2: (a) 3D view of the 16 Cards-32 MMIC's designed Squarax and (b) the simulated octave of the device.

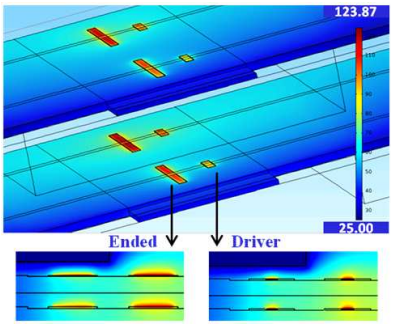

Figure 3: Temperature inside the GaAs FET channels. Maximum temperature reached by the channels is less than 124°C, perfectly respecting the maximum ratings reported by the SSPA vendor.

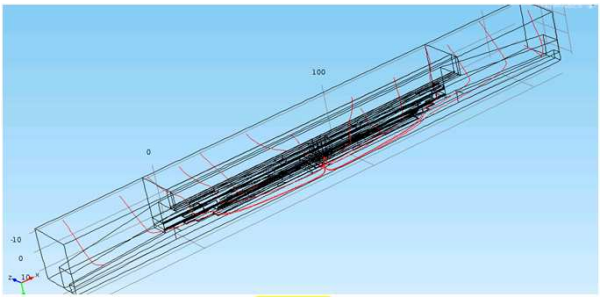

Figure 4: Heat Flux Streamlines described in a quarter of the SPC structure. Heat Flux is directed towards the Squarax TL walls, ensuring the correct heat sinking.

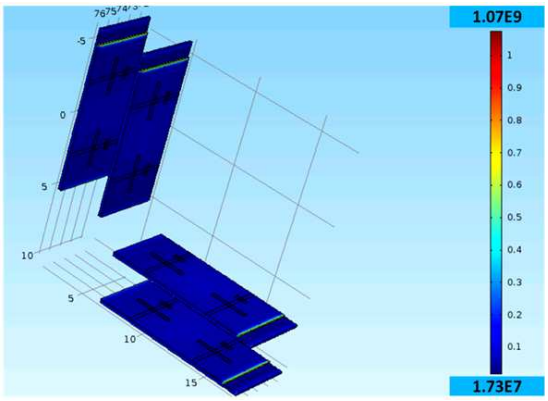

Figure 5: The maximum stress, which is less than $1.1\,\mathrm{GN/m^2}$, is located on the GaAs SSPA near the connection between the copper carrier and the Squarax TL walls.

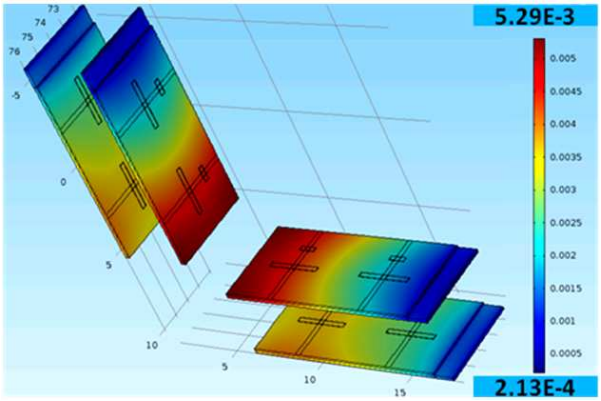

Figure 6: The maximum displacement in the MMIC SSPA's volumes, due to heat generation, is 5.3 µm. For this reason, CuMo layers have been inserted between the back of the GaAs MMIC and the copper carrier.

The power dissipation of the MMIC SSPA's produces a considerable temperature increase and induces a thermal expansion of both the PA's and the connected structure. Transistor damage or an alteration of the desired electromagnetic behavior may occur. In order to inquire about these multiple aspects, a Thermo-mechanical model has been implemented on Comsol Multiphysic Version 4.

Injection Phase-locking of a High-power Transit-time Oscillator

Lin Lian, Juntao He, Junpu Ling, Zumin Qi, and Yi Hu
College of Optoelectronic Science and Engineering, National University of Defence Technology, China

Abstract— To realize phase-locking of high power microwave (HPM) sources for the purposes of spatial power combining, a Ku-band coaxial transit-time oscillator (TTO) with an injection structure is investigated. Between the independent input cavity and the trinal-cavity buncher, a reflector with reflection efficiency of 99.9% is introduced to prevent the leakage power propagating to the input cavity. The RF signal is injected into the input cavity through a coaxial waveguide along the guiding magnet, which avoids separating the magnet coils, and suppresses the asymmetric modes excited in the device. Particle-in-cell (PIC) simulation results indicate that when the injection power ratio ρ ($\rho^2 = P_{in}/P_{out}$, where P_{in} is the injection power, and P_{out} is the output power of the oscillator) is large ($\rho \sim 0.1$), the phase-locking is achieved for a frequency difference of 67 MHz. When the injection power ratio is small ($\rho \sim 0.01$), the phase of the device with the same frequency can be locked ($\Delta f \sim 2$ MHz). It has also been found that the injected signal of high power results in higher output power and earlier saturation than that of a TTO without the injection structure. Moreover, a wider locking bandwidth is expected by the results than that obtained by the Adler's condition.

Numerical Modeling of Novel Optical Vortex Multiplexer

Qingsheng Xiao, **Shimao Li**, **Jiangbo Zhu**, **Hui Chen**,
Yanfeng Zhang, **Yujie Chen**, **and Siyuan Yu**

State Key Laboratory of Optoelectronic Materials and Technologies
School of Physics and Engineering, Sun Yat-sen University
Guangzhou 510275, China

Abstract— We propose an Ω-shaped optical vortex multiplexer which is an variant of the compact silicon-integrated micro-ring-shaped emitters demonstrated by X. Cai et al. [1]. The proposed emitter comprises an Ω-bend waveguide structure with inner-wall angular gratings. In such structure, the circular grating waveguide does not form a full circle, therefore allowing access to the inner circles of multiple devices integrated in a concentric configuration.

The broken ring waveguide differs from the ring resonator-based device in two major aspects. Firstly, it removes the wavelength-selective characteristic of the ring-resonator emitter and provides the device with a continuous linear relationship between its orbital angular momentum (OAM) value and signal wavelength, making it an optically broadband device for OAM order but also liable to emitting fractional OAM mode orders due to wavelength drift. Secondly, the missing grating elements at the notch of the Ω-bend may also deteriorate the output OAM mode quality.

In this work, an azimuthal polarized dipole model is used to analyze OAM beam quality from the emitter. We first fixed the phase difference between the adjacent grating elements given by the resonance condition like that in the ring emitter, and analyze OAM purity as a function of the notch angle, representing reduced grating elements number. The OAM purity, calculated by Fourier analysis of azimuthal (E_ϕ) and radial (E_ρ) electric field, generally deteriorates when the notch angle increases. The deviation from the pure OAM is not significant when the notch angle is below $\pi/6$. However, when the notch angle reaches $7\pi/18$, barely about 50% OAM weights can be retained on the original OAM order, while energy redistributes to the adjacent OAM orders (for both E_ϕ and E_ρ). Note that the OAM spectrum is spreaded by the increasing notch width. This is because the notch of the Ω-shaped emitter give rise to an finite set of samples of light field from the waveguide which makes an essential difference from extracting light infinitely from the micro-ring whispering gallery modes due to the resonance. We then analyze emitting OAM by tuning phase differences between the adjacent grating cells through changing the number of the grating elements, while keeping the notch invariant. The weights of OAM orders are not affected by the phase difference significantly. It is therefore necessary to keep the notch of the Ω-bend small in terms of its opening angle (or as a fraction of the circle) in order to maintain a high OAM mode quality.

REFERENCES

1. Cai, X., et al., *Science*, Vol. 338, 363, 2012.

Session 4A3
MS-1.3-1.4: Organic Transistors/Integrated Circuits and Dye-sensitized Solar Cells

Low Voltage Flexible Organic Thermistor for Temperature Sensing

X. C. Ren and Paddy. K. L. Chan
Department of Mechanical Engineering, The University of Hong Kong, Hong Kong, China

Abstract— Organic devices have been demonstrated to sense variable physical parameters such as light, pressure and temperature. For temperature sensing the sensitivity is related to the conductivity variation of organic thermistor. Due to the low intrinsic activation energy of organic semiconductor, temperature induced activated charges contributed little to conductivity enhancement of organic thermistor made by pentacene or dinaphtho[2,3-b:2′,3′-f]thieno[3,2-b]thiophene (DNTT) therefore leads to poor sensitivity of temperature sensor. At high temperature the environmental issue also brings uncertainty to organic based devices such as oxygen doping effect of pentacene. In this work we co-evaporated air stable organic semiconductor DNTT and Ag nanoparticles (NPs) to form a hybrid organic/metal thermistor. By inserting the Ag NPs into DNTT matrix up to 20% in volume ratio, the activation energy was enhanced to 420 meV and the conductivity variation is thus up to two orders of magnitude during the measured temperature range from 293 K to 373 K. The mechanism of the increasing activation is also discussed and attributed to the extra traps states induced by Ag NPs in band tail of highest occupied molecular orbital (HOMO) of DNTT. When the Ag volume ratio is above 20%, the temperature sensitivity nearly disappeared. Since for increasing number of Ag NPs, a percolation path is started to form and most of current are passing throughout the Ag rather than semiconductor. The hybrid organic/metal thermistor can be fabricated on flexible substrate and operate at low voltage (5 V), making it suitable for portable electronic devices and potentially scale up for electronic skin applications.

Active-matrix Organic Transistor and LED Array on Commercial Printer Paper

Boyu Peng and Paddy K. L. Chan
Department of Mechanical Engineering, The University of Hong Kong, Hong Kong, China

Abstract— Fabricating organic thin film transistors (OTFTs) on unconventional substrates, such as printing paper, banknote and fabric is always a challenging issue due to their dramatically large surface roughness while compared with widely-used silicon wafer. Large roughness makes it difficult to fabricate a highly conductive gate electrode and it is also challenging to deposit a uniform dielectric material to cover the gate electrode with low leakage current, thus resulting in OTFTs have low mobility and low on/off ratio. All the current research about OTFT on paper-based substrate use thick extra planarization layer and are limited to small area, single devices fabrication.

In this work, we demonstrate 8×8 active-matrix organic transistor array on commercial printer paper substrate with excellent uniformity. Parylene-C and DNTT are employed as gate dielectric and semiconductor respectively. All electrodes, including gate, source and drain electrodes together with their connection lines, are all deposited from room temperature screen-printing method. With a carefully designed screen mask and a well-controlled printing process, source-drain electrodes are well patterned with a channel length smaller than $50\,\mu m$. The printed OTFTs show an average mobility of $0.126\,cm^2V^{-1}s^{-1}$, the standard deviation of the mobility is only $0.01\,cm^2V^{-1}s^{-1}$. Specific cut-off frequency test of the transistors is completed by lock-in amplifier, the experimental data fit well with the theoretical calculation. Micro-LEDs are integrated to the each pixel of the active-matrix array to complete a 8×8 active-matrix LED display. With a good mobility number and a large W/L number, the current of the transistors can successfully control the on/off state and the sequence scanning of all the LEDs. A high-frequency lighting up of the whole LED frame and a pre-programmed LED pattern "HKU" are well demonstrated by the active-matrix LED display.

Piezoresistive Wearable Pressure Sensor with Cotton Cloth as Substrate and Spacer

Zongrong Wang and Paddy K. L. Chan
Department of Mechanical Engineering, The University of Hong Kong
Pok Fu Lam, Hong Kong, China

Abstract— Recently, pressure sensors have become critical components in many different applications, including touch panel of electronic devices and blood pressure transducer. Wearable, flexible, stretchable, low operating power and low cost ones will be in great need in the next generation of mobile applications such as rollable touch displays and health monitoring of people's heart and brain. Here, we proposed a wearable piezoresistive pressure with cloth as substrate and spacer. The commercial electrodes are deposited onto cotton cloth by using electric iron (Philips GC4430, MAX power)on two pieces of cloth substrate as the two electrodes. For the spacer, cloth is dipped into Ag nanoparticles (Ag-NPs) solution gets dried by evaporation of low boiling point solvent. The dipping and drying process are repeated for several times. Ag-NPs are reduced with silver acetate as raw material, dodecylamine as phase transfer agent, Tin acetate as reducing agent and toluene as solvent at room temperature. The particles size is ranging from 3 to 20 nm, which is characterized by TEM (TEM, Philips Tecnai G220 S-TWIN), which is tunable with tuning the reducing agent or the reaction temperature. The cross-plane resistor structure is built with Ag-NPs/cloth spacer sandwiched between two cloth electrodes. The resistance change of the Ag-NPs/cloth is measured by the current. The sensitivity (R) under different pressure (P) is calculated by the equation: $R = (I_{load} - I/I)/\Delta P$. The largest resistivity of the piezoresistor proposed here is $0.2\,\mathrm{kPa}^{-1}$, which can be further enhanced by tuning the Ag particle size or other large aspect ratio conductor phase inside, like nanowire or carbon nanotube.

Fiber-shaped Dye-sensitized Solar Cells

Yong Zhou[1, 2, 3]

[1]National Laboratory of Solid State Microstructures
Nanjing University, Nanjing 210093, China
[2]School of Physics, Nanjing University, Nanjing 210093, China
[3]Eco-materials and Renewable Energy Research Center (ERERC)
Nanjing University, Nanjing 210093, China

Abstract— In recently decades, we are forced to find new energy resources to meet our needs because of the increasingly serious environment pollution and energy crisis. The solar energy is the best choice for alternatives energy. As technology improved, electronic device (solar cell) that allows direct conversion solar energy to electrical energy has been a very real idea. Traditional solar cells have typically been fabricated from rigid plates, which restrict the flexibility, shape, weight, and integration of the cells, and also result in some complexities in transport and installation. Fiber-shaped media for solar cell is a natural choice and shows an impressive potential to overcome those disadvantages. Among dye-sensitized solar cells, fiber-shaped dye-sensitized solar cell (FDSSC) is one of major developments.

In this presentation, we will report the utilization of FDSSC to highly efficient conversion of solar energy into electrical energy over certain nanostructured materials. Both high quality photoanode (benefit to electron transportation) and cathode (with high catalytic active) are produced in order to achieve high photoconversion efficiency and low cost of FDDS.

Metal-free Nitrogen Doped Microwave-exfoliated Graphene Nanosheets (N-MEG) as High-electrocatalytic Counter Electrode for Dye Sensitized Solar Cells

Shien-Ping Feng
The University of Hong Kong, China

Abstract— High-efficient metal-free nitrogen-doped microwave-exfoliated graphene (N-MEG) film on rigid FTO glass as counter electrode (CE) for dye-sensitized solar cells (DSSCs) has been fabricated by a facile and low cost process. The N-MEG film exhibits many advantages over graphene and graphene oxide on CE, since it enjoys superior electrocatalytic activity and wettable surface, which is the combined effect of nitrogen doping and mesoporous structure. The film is demonstrated by DSSCs with good electrocatalytic activity in the I-/I3-redox system and high energy conversion efficiency up to 7.18%, which is comparable to that of a DSSC with a Pt CE. This unique N-MEG CE holds great promise in DSSCs.

Highly Conductive Flexible Ni-PET Substrate as Counter Electrode for Efficient Dye-sensitized Solar Cells

Shien-Ping Feng and Chang Liu
The University of Hong Kong, China

Abstract— Highly conductive and flexible nickel-polyethylene terephthalate (Ni-PET) substrate was developed to fabricate a cost-effective and high-performance flexible counter electrode for dye-sensitized solar cells (DSSCs). A facile method including electrodeposition and hot pressing transferring is introduced, which is beneficial for DSSCs towards flexible, rollable, and lightweight. The uniform and continuous Ni film was first fabricated by electroplating metallic Ni on fluorine-doped tin oxide (FTO), and then intactly transferred onto PET via hot-pressing using Surlyn as the joint adhesive. We reported the Ni film electrodeposition mechanism, microstructure, and DSSC performance for the Ni-PET flexible substrate. The transferred Ni-PET substrate film presents high uniformity, low sheet resistance of $0.18\,\Omega/\square$, excellent scalability, and good I^-/I^{3-} electrolyte endurance. A high energy conversion efficiency of 7.89% is achieved based on PtNPs/Ni-PET CE, which presents an improvement of 10.4% as compared with PtNPs/ITO-PEN CE and is also comparable to PtNPs/FTO CE.

High Electrocatalytic and Wettable Nitrogen-doped Microwave-exfoliated Graphene Nanosheets as Counter Electrode for Dye-sensitized Solar Cells

Shien-Ping Feng and Peng Zhai
The University of Hong Kong, China

Abstract— High-efficient metal-free nitrogen-doped microwave-exfoliated graphene (N-MEG) film on rigid FTO glass as counter electrode (CE) for dye-sensitized solar cells (DSSCs) has been fabricated by a facile and low cost process. The pyrrolic and pyridinic N atoms are doped into the carbon conjugated lattice to enhance electrocatalytic activity. N-MEG film having N-doping active sites and large porosity provides a wettable surface to facilitate electrolyte diffusion so that improves fill factor.The film is demonstrated by DSSCs with good electrocatalytic activity in the I-/I3-redox system and high energy conversion efficiency up to 7.18%, which is comparable to that of a DSSC with a Pt CE. This unique N-MEG CE holds great promise in DSSCs.

Session 4A4
SC2&3: Plasmonics for Sensing Applications

Evanescent Wave Microscopy for Cellular and Biomolecular Characterisation

Michael Somekh[1, 2], **Suejit Pechprasarn**[2], **Jing Zhang**[2], **and Melissa Mather**[2]

[1]Department of Electronic and Information Engineering
Hong Kong Polytechnic University, Hung Hom, Hong Kong, China
[2]Institute of Biophysics Imaging and Optical Science, University of Nottingham
Life Sciences Building, Nottingham, UK

Abstract— The use of fluorophores in life science has become an invaluable tool for the investigation of biochemical pathways in living cells. The use of fluorophores is, however, not without its disadvantages in terms of photobleaching and associated phototoxicity. In order to visualize biological material in its 'native' state there is a strong incentive to develop label free methods which can extract crucial information without the need for exogenous fluorescent chemicals.

In this talk we will examine the use of evanescent wave microscopy for these applications. Evanescent waves are excited with a high numerical aperture oil immersion objective through a microscope coverslip. For simple total internal reflection the evanescent wave is excited on an uncoated coverslip whereas for surface plasmon excitation the coverslip is coated with a thin (50 nm) layer of gold. Since evanescent waves are confined to approximately 100 nm they are sensitive to material close to the coverslip and insensitive outside this region, for instance, cell attachment and the ruffling of the cell membrane are well suited to examination by evanescent wave techniques. In our research we have used both total internal reflection imaging as well as surface plasmon microscopy. In some parts of the literature these methods are often presented as being somewhat similar, however, each method has clear advantages which make their domain of application highly distinct.

We explain how total internal reflection microscopy can give far superior images compared to surface plasmon methods on cell structures. Moreover, we discuss a new implementation of our label free total internal reflection microscope which while giving very clear images of cell attachment can gain complementary and quite distinct information in the upper layers of the cell culture by employing a complementary quantitative phase contrast channel. Exemplar studies on neuronal stem cell cultures demonstrate the utility of the technique.

We then turn to surface plasmon methods which while also being capable of imaging cell membranes are more prone to artefacts on account of the fact the surface plasmons propagate across the surface, so are in a sense not localized in the lateral direction to the same extent as an evanescent wave produced at a dielectric interface. The method, however, excels when we want to make a quantitative measurement of local refractive index. We show how a confocal microscope can form a unique and ultrastable interferometer. We also show that the best localization for a surface plasmon measurement is counter-intuitively achieved when the sample is slightly out of focus. We demonstrate how confocal surface plasmon microscopy can be used to measure protein binding as well as local changes in refractive index. We describe the evolution of the confocal system from its earliest implementation through to common path configurations involving pupil function engineering. Using coupled wave diffraction theory we calculate the ultimate detection limit expected of various surface wave microscopy systems.

Finally, we discuss some future developments in evanescent microscopy techniques.

Plasmonic Near-field Localization for Sensing and Imaging of Biomolecular Interactions

Donghyun Kim
School of Electrical and Electronic Engineering, Yonsei University, Republic of Korea

Abstract— In this presentation, we investigate surface plasmon based electromagnetic field localization to break the sensitivity limit of traditional surface plasmon resonance detection. 2D and 3D nanostructures have been used to localize near-field to which target molecular interactions were colocalized. The plasmon-based localization can also be useful to break the diffraction limit of conventional fluorescence microscopy by creating dramatically amplified hot spots at subwavelength metallic nanoaperture surface. We explore locally amplified excitation to induce effective enhancement of detection sensitivity and imaging resolution. In this study, we used random and periodic arrays of optical nanoapertures for plasmonic field localization. Nanoapertures of different sizes and shapes were designed to produce hot spots of different characteristics. The design process was performed numerically based on rigorous coupled wave analysis. The arrays of nanoholes or nanoposts were fabricated on a 50-nm thick gold film surface using electron beam lithography. For surface plasmon resonance detection experiments, colocalization of DNA hybridization was shown to improve the detection limit by more than three orders of magnitude. For optical imaging experiments, the fabricated nanoaperture arrays were mounted in an optical fluorescence microscope and used to image gliding microtubules and intracellular target molecules. By experimental validation, effective resolution less than 100 nm has been confirmed. The results also indicate the feasibility of improving imaging resolution both in the lateral and axial direction to elucidate, for example, axial displacement and positional variations as the molecular movement was reconstructed with a nanoscale resolution. We expect the approach to prove useful for more diverse biological targets.

Vector Beams Assisted Microscopic Phase-sensitive Surface Plasmon Resonance Biosensor

Changjun Min[1], **Chonglei Zhang**[1], **and X.-C. Yuan**[2]

[1]Institute of Modern Optics, Key Laboratory of Optical Information Science and Technology
Ministry of Education of China, Nankai University, Tianjin 300071, China
[2]Institute of Micro and Nano Optics, College of Optoelectronic Engineering
Shenzhen University, Shenzhen 518060, China

Abstract— We proposed a novel phase-sensitivity surface plasmon resonance (SPR) biosensors based on microscopic structure and vector beams, which shows great advantages such as high sensitivity, large dynamic range and high imaging resolution. In the first part, we introduce the use of a tightly focused radially polarized beam to excitation surface plasmon resonance in a microscopic structure, through measuring the dark ring position in reflection image to determine the refractive index of the sample. The measurement principle is similar with the angle-sensitivity surface plasmon resonance based on Kretschmann structure which has a large dynamic range. Furthermore, we introduce the differential interferometry technique between a radially polarized beam and an azimuthally polarized beam to measure the phase at the dark ring, which improves the system sensitivity and achieved a high sensitivity of 7.385×10^{-7} RIU/0.1° with dynamic range of 0.35 RIU in principle. This method solves the problem of a small dynamic range in conventional phase-sensitivity surface plasmon resonance biosensor. Then we introduce the radial/azimuthal polarization alternating mixed vector beams, and the six-step phase shifting technology to achieve common light path measuring, further reducing the noises from environment, light source and PZT, and thus improved the sensitivity of the system. Combined with the scanning imaging technology, we could realize the surface plasmon resonance sensor imaging which has advantages of label free and high imaging resolution. We has measured the phase change to obtain the refractive index profile of fingerprints and live cells with an imaging resolution of 550 nm. This method solves the problem of a small imaging resolution in traditional surface plasmon resonance imaging.

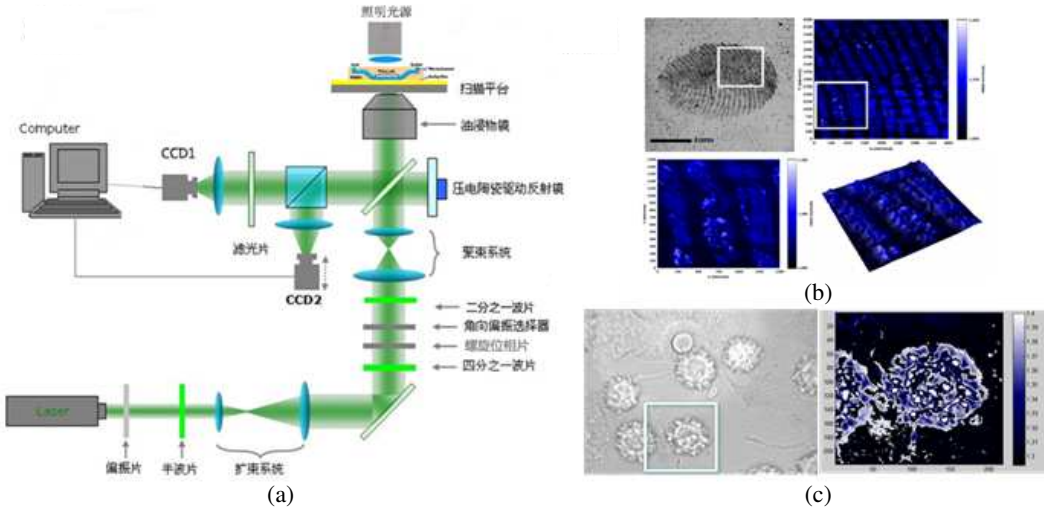

Figure 1: (a) Experimental setup of the SPR biosensor. (b) Measuring the fingerprints refractive index profile. (c) Measuring the live cells refractive index profile.

Evolution of Light-induced Vapor Generation at a Liquid-immersed Metallic Nanoparticle

Jiaming Li and Zheyu Fang
State Key Laboratory for Mesoscopic Physics, School of Physics
Peking University, Beijing 100871, China

Abstract— When an Au nanoparticle in a liquid medium is illuminated with resonant light of sufficient intensity, a nanometer scale envelope of vapor — a "nanobubble" — surrounding the particle, is formed. This is the nanoscale onset of the well-known process of liquid boiling, occurring at a single nanoparticle nucleation site, resulting from the photothermal response of the nanoparticle. Here we examine steam generation at an individual metallic nanoparticle in detail. Incipient nanobubble formation is observed by monitoring the plasmon resonance shift of an individual, illuminated Au nanoparticle, when its local environment changes from liquid to vapor.

The temperature on the nanoparticle surface is monitored during this process, where a dramatic temperature jump is observed as the nanoscale vapor layer thermally decouples the nanoparticle from the surrounding liquid. The subsequent formation of freely diffusing macroscopic bubbles results from the coalescence of the individual, nanoparticle-"bound" vapor envelopes into larger, micron-scale bubbles: the contributions of incident light intensity and nanoparticle density to this process are quantified. These studies provide the first direct and quantitative analysis of the evolution of light-induced steam generation by nanoparticles from the nanoscale to the macroscale, a process that is of fundamental interest for a growing number of applications.

Surface-enhanced Raman Scattering of Nanostuctures

Zhipeng Li[1] and Hongxing Xu[2]

[1]Beijing Key Laboratory of Nano-Photonics and Nano-Structure (NPNS)
Department of Physics, Capital Normal University, Beijing 100048, China
[2]Beijing National Laboratory for Condensed Matter Physics
Institute of Physics, Chinese Academy of Sciences, Box 603-146, Beijing 100190, China

Abstract— Since the discovery of Surface-enhancement Raman scattering (SERS), it has been studied experimentally and theoretically due to its extremely high sensitivity and powerful application on fingerprint spectral sensing [1]. Generally two different SERS mechanisms are recognized — one is the chemical enhancement caused by the molecule-metal charge transfer, the other is the local electromagnetic enhancement originating from the surface plamson resonance in metallic nanostructures. The latter is the main contributor to SERS enhancement, as in most cases it is several orders of magnitude larger than the chemical enhancement. We have investigated the SERS of a single nanoparticle, nanoshell, dimer, trimer and mescoparticles and applications on sensitive sensing. We have experimentally revealed the near-field distribution around the nanoparticle [2], proposed a model for the nano half wave plate [3, 4] and obtained a kind of SERS substrate with relative high enchantment and reproducibility [5, 6].

REFERENCES

1. Xu, H. X., E. J. Bjerneld, M. Käll, and L. Börjesson, "Spectroscopy of single hemoglobin molecules by surface enhanced ranman scattering," *Phys. Rev. Lett.*, Vol. 83, 4357–4360, 1999.
2. Wang, W., Z. P. Li, B. H. Gu, Z. Y. Zhang, and H. X. Xu, "Ag@SiO2 core-shell nanoparticles for probing spatial distribution of electromagnetic field enhancement via surface-enhanced raman scattering," *ACS Nano*, Vol. 3, 3493–3496, 2009.
3. Shegai, T., Z. P. Li, T. Dadosh, Z. Zhang, H. X. Xu, and G. Haran, "Managing light polarization via plasmon-molecule interactions within an asymmetric metal nanoparticle trimer," *Proc. Natl. Acad. Sci. U.S.A.*, Vol. 105, 16448–16453, 2008.
4. Li, Z. P., T. Shegai, G. Haran, and H. X. Xu, "Multiple-particle nanoantennas for enormous enhancement and polarization control of light emission," *ACS Nano*, Vol. 3, 637–642, 2009.
5. Liang, H. Y., Z. P. Li, W. Z. Wang, Y. S. Wu, and H. X. Xu, "Highly surface-roughened 'Flower-like' silver nanoparticles for extremely sensitive substrates of surface-enhanced raman scattering," *Adv. Mater.*, Vol. 21, 4614–4618, 2009.
6. Liang, H., Z. Li, Z. Wang, W. Wang, F. Rosei, D. Ma, and H. Xu, "Enormous surface-enhanced raman scattering from dimers of flower-like silver mesoparticles," *Small*, Vol. 8, 3400–3405, 2012.

Gain-assisted Plasmonic Nanoshells for Biosensing Applications

Shan Yi, Siu-Pang Ng, and Chi-Man Lawrence Wu
Department of Physics and Materials Science, City University of Hong Kong
83 Tat Chee Avenue, Hong Kong SAR, China

Abstract— The subwavelength electromagnetic "hot spots" created by plasmonic nanostructures has drawn enormous attention from the biosensing community. Ultra-sensitive detection schemes of biomolecules, i.e., surface enhance Raman spectroscopy (SERS) and localized surface plasmon resonance (LSPR), are dependent on both field strength and the plurality of these "hot spots" on the plasmonic substrate. Although there are reports on detection of single biomolecule using SERS, it was achieved by coupling plasmonic resonance (CPR) effect between two individual nanoparticles in close vicinity in order to create a "hot spot" of only a few nanometers. While the field strength on the rest of the nanoparticle surface is virtually zero, the SERS signal is only accomplished if the biomolecule is trapped inside the "hot spot", rendering the so-called single molecule detection barely repeatable.

In view of the difficulty, we propose a different direction to tackle the problem by introducing an active dielectric core with optical gain medium into the plasmonic nanoshells. The active core serves two purposes, 1) to compensate the loss of electromagnetic energy due to absorption of the metallic shell, thus enhancing the near-field strength and creating "hot spot", 2) to increase the number of "hot spots" on the nanoshell surface, thus increasing the probability of light-matter interaction for better chance of single biomolecule detection. We have performed computational studies of the gain-assisted nanoshell using both discrete dipole approximation (DDA) and finite difference time domain (FDTD) solver. The absorption (ACS), extinction (ECS) and scattering (SCS) cross sections of the nanoshell at various gain levels were calculated using DDA. At the optimal gain value, the ECS becomes negligible while the ACS turns negative, thus the SCS is amplified from 1×10^{-2} to $1 \times 10^{-4}\,\mu\text{m}^2$, i.e., by 6 orders of magnitude. Besides, the scattering bandwidth (FWHM) is drastically reduced by 3 orders of magnitude, i.e., from 50 nm to 50 ρm which closely resemble a laser emission. These results indicate that the gain-assisted nanoshell amplified the incoming radiation so strong that it re-radiates the energy by lasing. To further investigate the electromagnetic field strength on the surface of the nanoshell, we performed FDTD with the active core-shell structure. With the optimal gain value, the local electric field intensity at the near-field is amplified from 1×10^3 to 1×10^8 V/m, i.e., by 5 orders of magnitude. The near-field pattern resembles the dipolar resonance mode with the field intensity concentrating at the two nanoshell edges parallel to the incident polarization direction of light. Therefore two "hot spots" are created on each nanoshell which is four times those create by CPR on each nanoparticle.

Results of these computational studies clearly indicate that with optimal gain value, the electromagnetic field strength of conventional plasmonic core-shell structure can be amplified enormously. It also creates more "hot spots" on each nanoshell than the existing CPR approach. We believe that these two advantages of the gain-assisted core-shell structure would improve the enhancement factor of SERS and the sensitivity of LSPR for practical single biomolecule detection.

Bifunctional Au@Pt Core-shell Nanostructures for In-situ Monitoring of Catalytic Reactions by Surface-enhanced Raman Scattering Spectroscopy

Zhi Yong Bao[1], **Ruibin Jiang**[3], **Xin Liu**[1], **Jiyan Dai**[1, 2], **Bin Ren**[4], **Jianfang Wang**[3], **Yuen Hong Tsang**[1], **and Dang Yuan Lei**[1, 2]

[1]Department of Applied Physics, The Hong Kong Polytechnic University, Hong Kong, China
[2]Shenzhen Research Institute, The Hong Kong Polytechnic University, Shenzhen, China
[3]Department of Physics, The Chinese University of Hong Kong, Hong Kong, China
[4]State Key Laboratory of Physical Chemistry of Solid Surfaces
College of Chemistry and Chemical Engineering, Xiamen University, Xiamen, China

Abstract— Optical probes of heterogeneous catalytic reactions are of great importance for in-situ determining the catalytic activity and monitoring the reaction process. Surface-enhanced Raman scattering (SERS) spectroscopy could be used as a sensitive optical probe for this purpose provided that plasmonic metal nanoparticles for Raman enhancement are properly integrated

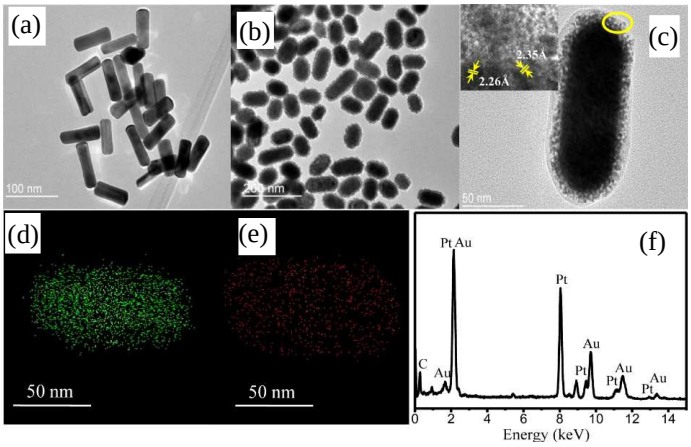

Figure 1: Morphology and composition characterizations of Au@Pt nanostructures. (a) & (b) Low-magnification TEM images of (a) Au NRs and (b) Au@Pt nanostructures. (c) High-magnification TEM image of an Au@Pt nanohybrid with crystal-lattice mapping of the area enclosed by the yellow circle shown in the inset. (d)–(f) Elemental mapping of (d) Au and (e) Pt in the Au@Pt nanostructure and (f) the corresponding EDX spectrum from Au@Pt nanohybrids.

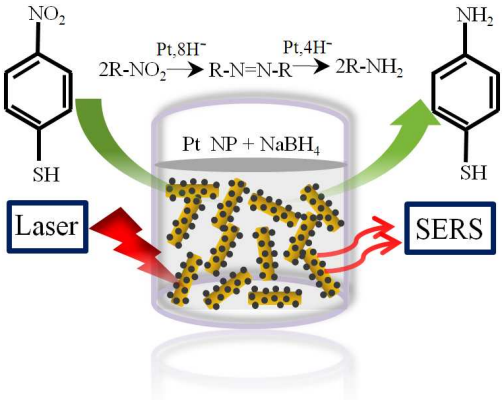

Figure 2: Representation of the reduction of 4-NTP by NaBH4 to 4-ATP, which takes place on Au@Pt superstructure surfaces. The reaction is catalyzed by Pt NPs, while the SERS signal is brought about by local optical fields of the Au NRs.

with catalytic metals as a single entity. Herein we present a facile approach for synthesizing Au@Pt core/shell nanostructures with controllable surface density of sub-5 nm Pt nanoparticles on the surface of Au nanorods (shown in Figure 1). Systematic investigations on both SERS and catalytic activities of the hybrid nanostructures reveal an optimized surface coverage of Pt. More importantly, we demonstrate that, due to their dual functionalities, the hybrid nanostructures are able to track the Pt-catalyzed reaction in real time by measuring the SERS signals of the reactant, intermediate and final products (shown in Figure 2). This SERS-based synergy technique provides a novel approach for quantitatively studying catalytic chemical reaction processes and is suitable for many applications such as reduction and oxidation reactions in fuel cells and catalytic water splitting [1, 2].

REFERENCES

1. Wu, D. Y., L. B. Zhao, X. M. Liu, R. Huang, Y. F. Huang, B. Ren, and Z. Q. Tian, *Chem. Commun.*, Vol. 47, 2520, 2011.
2. Xiao, M. D., R. B. Jiang, F. Wang, C. H. Fang, J. F. Wang, and J. Yu, *J. Mater. Chem. A*, Vol. 1, 5790, 2013.

Micro-analysis of Self-assembly Gold Nanoislands LSPR Biosensor Based on Atomic Force Microscopy

Guangyu Qiu, Siu-Pang Ng, and Chi-Man Lawrence Wu
Department of Physics and Materials Science, City University of Hong Kong
83 Tat Chee Avenue, Hong Kong SAR, China

Abstract— Self-assembly gold nanoislands (SAM-AuNIs) have been explored for label-free biosensing applications. In order to ensure practical its applications, it is very important to study the correlation between the SAM-AuNIs topography and detection sensitivity. The sensing performance can be optimized by changing the fabrication condition, 1) annealing temperature, 2) annealing time and 3) nominal gold film deposition thickness. Using atomic force microscope (AFM) mapping, the topography of SAM-AuNIs shows evident change by varying these conditions. In this presentation, we use stochastic parameters, i.e., height, diameter and interparticle gaps of the nanoislands to evaluate the correlation. These three AFM parameters are regarded as the relevant factors that are directly related to the performance of SAM-AuNIs.

It was found that the fabrication conditions influence the topography in different aspects. The Au nanoislands height decreases with longer annealing time, whereas increasing the nominal gold deposition thickness promotes growth in height and diameter but reduces the interparticle gap, thus it alters the localized surface plasmon resonance (LSPR) extinction wavelength. Guided by a series of topography mapping obtained from AFM data, we changed the fabrication conditions and successfully red shifted the LSPR extinction wavelength from 560 nm to 650 nm. This red shift might imply closing of interparticle gapsamong SAM-AuNIs, leading to coupled plasmonic resonance. Up to now, the most sensitive sample is fabricated with 5.0 nm nominal Au film deposition and achieves 1.98×10^{-7} RIU resolution. According to the AFM data, the average height and interparticle gaps of the SAM-AuNIs are 40 nm and 15 nm respectively.

Dressing Plasmon Resonance with Particle-microcavity Architecture for Efficient Nano-optical Trapping and Sensing

Haixi Zhang[1], **Yanyan Zhou**[3, 4], **Xia Yu**[4], **Feng Luan**[3], **Jianbin Xu**[1], **Hock-Chun Ong**[2], **and Ho-Pui Ho**[1]

[1]Department of Electronic Engineering, The Chinese University of Hong Kong
Shatin, NT, Hong Kong SAR, China
[2]Department of Physics, The Chinese University of Hong Kong
Shatin, NT, Hong Kong SAR, China
[3]School of Electrical and Electronic Engineering
Nanyang Technological University, 50 Nanyang Avenue, Singapore
[4]Precision Measurements Group, Singapore Institute of Manufacturing Technology
71 Nanyang Drive, Singapore

Abstract— We propose a particle-microcavity scheme for efficient optical trapping and sensing. When a resonant plasmonic nanoparticle is placed inside a microcavity with high Q-factor, sensitivity is enhanced in the far-field extinction while near-field around the nanoparticle is barely affected. A schematic of the device is illustrated in Fig. 1. It is assumed that the whole structure is immersed in water. In fact, LPR-based nanosensors may also serve as nano-tweezers if we can make use of the gradient field associated with localization. In this work we show the conditions for having such dual-function particles, which we abbreviate as the ST-NP (sensing-trapping nanoparticle). In this letter, we propose a hybrid ST-NP configuration in which the ST-NP is placed in an external cavity comprising a split micro-ring. We call the split micro-ring a "dressing" device. To modify the LPR of the ST-NP is hence termed as the "dressing plasmon resonance" [1]. Instead of spectral shift, the proposed ST-NP monitors the intensity variation ΔI of the extinction. As compared to the dual beam configuration, our scheme results in higher FOM. More importantly, the structural configuration in our design enables a single monochromatic beam for the ST-NP system.

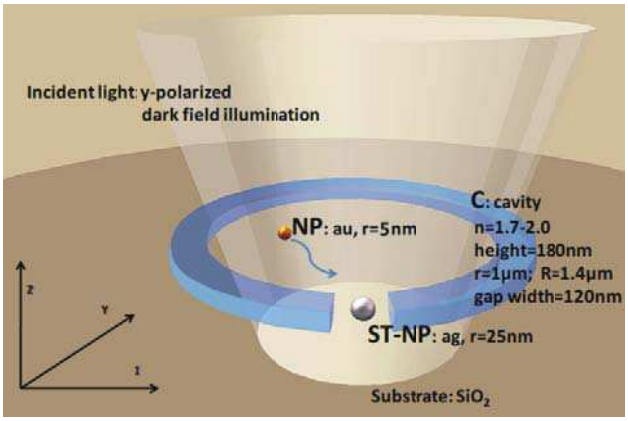

Figure 1: Schematic of the hybrid ST-NP configuration. The micro-ring has a height of 180 nm, a gap width of 120 nm and an outer and inner radius of 0.9 μm and 0.5 μm respectively. The silver ST-NP has a radius of 25 nm. The incident cone of light is used for dark-field spectroscopy.

Figure 2 shows sensing responses from the two configurations: (i) bare ST-NP and (ii) ST-NP with dressing ring cavity. The ring is made of Si_3N_4 which has a refractive index of 2.0. In both cases, the sensing event involves the trapping of a gold NP with a diameter of 10 nm. For simplicity, we abbreviate (i) the bare ST-NP sensor with a trapped NP as the "ST-NP+NP" and (ii) the ST-NP in dressing ring cavity caseas the "C+ST-NP", so that (iii) "C+ST-NP+NP" represents the ultimate case of nanoparticle being trapped and sensed by a C+ST-NP system. As seen from Fig. 2(a) with 2(b) the dressing cavity has introduced a series of peaks in the spectrum of the extinction intensity (I). On the other hand, Fig. 2(b) shows that when a NP is trapped by a simple ST-NP system, the extinction peak changes slightly. However, Fig. 2(a) shows that the C+ST-NP configuration exhibits much larger extinction intensity change (ΔI) caused by the

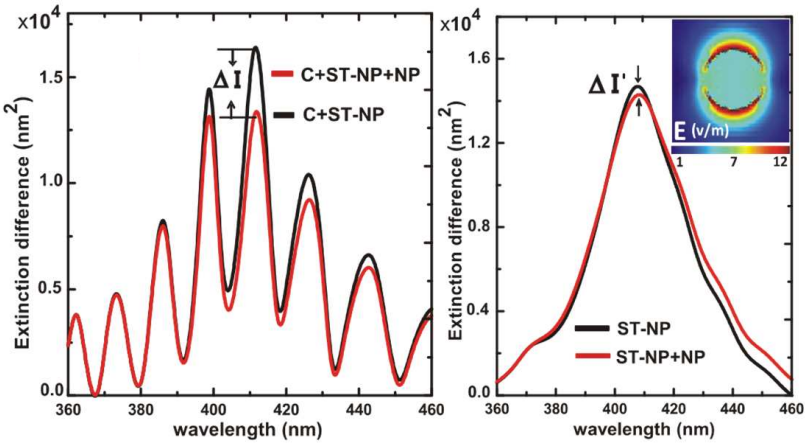

Figure 2: (a) Extinction spectra of the C+ST-NP+NP and C+ST-NP systems with the dressing ring index $n = 2.0$. (b) Extinction spectra of the ST-NP and ST-NP+NP systems; inset shows the ST-NP's near-field distribution in the equatorial plane parallel with the substrate.

trapped NP. We adopt the FOM in terms of $\Delta I/I$ [2]. Calculation reveals a FOM of 7.30 for the C+ST-NP+NP system comparing with the bare ST-NP case at the wavelength of 410 nm [normalized to the value of $\Delta I'/I'$ in Fig. 2(b)]. For single-beam operation in the C+ST-NP system, ΔI is much larger. Compared with the case of bare ST-NP (intensity change denoted as $\Delta I'$), C+ST-NP offers 6.83 times higher sensitivity (i.e., $\Delta I/\Delta I'$). The enhanced ΔI for the proposed C+ST-NP configuration can be straightforwardly explained by the Purcell effect [3].

Stable near-field and high sensitivity for optical trapping and ultrasensitive detection of nano-sized targets are therefore realized simultaneously. Such particle-microcavity system opens up a new hybrid nano-photonic device platform that combines the unique merits of conventional and plasmonic integrated photonics.

REFERENCES

1. Huang, F. M., D. Wilding, J. D. Speed, A. E. Russell, P. N. Bartlett and J. J. Baumberg, *Nano Lett.*, Vol. 11, 1221, 2011.
2. Ameling, R., L. Langguth, M. Hentschel, M. Mesch, P. V. Braun, and H. Giessen, *Appl. Phys. Lett.*, Vol. 97, 253116, 2010.
3. Purcell, E. M., *Phys. Rev.*, Vol. 69, 681, 1946

Tunable Plasmonic Absorption in Random Metallic Nano-islands for Optofluidic Applications

Jiajie Chen, **Zhiwen Kang**, **Guanghui Wang**, **and Ho-Pui Ho**
The Chinese University of Hong Kong, Hong Kong, China

Abstract— Localized surface plasmons (LSPs) are the collective electron oscillations in metal nanoparticles (NPs) excited by incident light. The electron oscillations induced current inside the metal particlesis damped by the metal lattice resistance, therefore, transfer the light energy into thermal energy. Such plasmonic thermal effect has been used in a wide range of applications, such as active microfluidic mixing [1], optofluidic control [2], particle trapping and manipulation via bubbles generated by photo-thermal effects [3], localized heating in microfluidic chips through absorption by gold nanorods [4]. One of the most outstanding properties of LSPs is the sub-wavelength confinement of light energy to create localized heating and temperature gradient in nanometer scale, and thus facilitating energy conversion from optical radiation to hydrodynamic actuation inside microchannels.

Here, we demonstrate a microfluidic flow control technique based on the use of random distributed gold nano-islands substrates (Au-NIS). The random structures are prepared by annealing treatment of a thin layer of continuous gold film deposited on the glass substrate. Simply by changing the annealing temperature, the wettability and absorption peak of Au-NIS can be tuned. Upon receiving radiation from a focused laser beam at sub-mW level, we can guide liquid flow in a microfluidic channel. The flow speed and direction is fully controlled by the laser beam.

As the demand for miniaturization of biomedical testing devices has been increasing constantly over the years, a range of microfluidic sample manipulation techniques have been reported. They are primarily based on complex electronic, ultrasonic or mechanical coupling schemes. The reported plasmonic optofluidic approach offers a high degree of versatility, and the preparation of plasmonic Au-NIS only requires simple thermal annealing steps. We have demonstrated optofluidic devices for performing valving, mixing and dilution of aqueous samples. Further development of this scheme may lead to all optical biomedical microfluidic detection and sensing.

REFERENCES

1. Miao, X., B. K. Wilson, and L. Y. Lin, *Appl. Phys. Lett.*, Vol. 92, 124108, 2008.
2. Liu, G. L., J. Kim, Y. Lu, and L. P. Lee, *Nature Materials*, Vol. 5, 27–32, 2006.
3. Zhao, C., Y. Xie, Z. Mao, Y. Zhao, J. Rufo, S. Yang, F. Guo, J. D. Mai, and T. J. Huang, *Lab on a Chip*, Vol. 14, 384–391, 2014.
4. Li, Z., P. Wang, L. Tong, and L. Zhang, *Optics Express*, Vol. 21, 1281–1286, 2013.

Sensing with Localized Surface Plasmon Resonance of Nanoparticles

Fang Xu, Haifei Lu, Zhiwen Kang, Jiajie Chen, and Hopui Ho
Department of Electronic and Engineering, The Chinese University of Hong Kong
Shatin, Hong Kong SAR, China

Abstract— Recent progress in nano-optics has enabled various highly sensitive and label-free optical biosensors that take advantage of the localized surface plasmon resonance (LSPR) of metal nanostructures. These biosensors can be used in many application fields including clinical diagnosis, biomolecular engineering, drug design, environmental control and food industry. LSPR is an optical phenomenon generated by collective oscillations of the electron gas in metal nanostructure. It takes place when the frequency of the photons matches with the natural frequency of surface electrons oscillating against the restoring force of positive nuclei. The dependence of LSPR extinction peak on the local dielectric environment thus leads to the possibility of performing molecular sensing. Binding between the molecules and the metal nanoparticles will increase the refractive index of the medium around the nanostructures. This will cause a red-shift of the LSPR peak which can be monitored by measuring the extinction spectra.

Compared to other kinds of sensors, the LSPR sensor does not require chemical amplification and additional labeling. It can measure dynamic processes in real time, e.g., binding kinetics of biomolecular interactions. Also, since LSPR based sensor relies only on the optical extinction of the nanoparticles, this approach is not sensitive to temperature and does not require complex equipment.

response to local changes in refractive index, particular when there might only be several molecules involved in the surface binding. The LSPR shifts can be maximized through optimizing the shape, size, composition of the nanoparticles to increase the sensitivity factor. It has been observed that increasing the aspect ratio of the nanoparticles may result in higher sensitivity factor. Nanoparticles with sharp tips offer higher local electric field enhancement and sensitivity factors, which is observed both in experiments and simulations. Uniform dispersity of the nanoparticles improves the LSPR sensitivity by narrowing the spectral line width and increasing extinction. Nanoparticles with smaller size are more sensitive to single molecules. The confined electric field enhancement in the space between nanoparticles is much higher than that of a single nanoparticle, e.g., it is observed that pairs of nanoparticles separated by less than 2.5 particle radii show plasmonic coupling and marked spectral shifts. Thus, designing nanoparticle arrays with optimized nanoparticle size, shape and space distance will prominently improve the LSPR sensing performance.

Double-layer Gold Gratings and Their Applications

Yang Shen, Tianran Liu, and Chongjun Jin
State Key Laboratory of Optoelectronic Materials and Technologies
School of Physics and Engineering, Sun Yat-sen University, Guangzhou 510275, China

Abstract— Modern information acquiring and processing demand ultracompact photonic devices at the chip scale. Surface plasmon polaritons (SPPs) present an intriguing approach to implement ultracompact photonic devices, since with SPPs one may overcome the diffraction limit encountered in conventional optics [1, 2]. Many photonic devices based on SPPs have been investigated in recent years [3, 4], and integrated plasmonic circuits are starting to emerge. Two of the most important application for such a plasmonic nanostructures are biosensor and integrated optical circuits. Here we show that double-layer gold gratings can be served as localized surface plasmon resonance (LSPR) based refractive index sensors with an ultrahigh figure of merit [5] and unidirectional couplers for surface plasmon polariton [6].

We fabricate two-dimensional double-layer gold gratings through interference lithoggraphy and gold deposition, which look like gold-mushroom arrays (GMRAs). We show that the GMRAs can be used as refractive index sensors with an ultimate figure of merit up to 108 resulted from the interference between Wood's anomaly and the LSPRs, which is comparable to the theoretically predicted upper limit (~ 108) for standard propagating surface plasmon resonance (PSPR) based sensors [5]. We further demonstrate these GMRAs as biosensors for detecting Cytochrome c, and alpha-fetoprotein, with their detection limits down to 200 pM and 15 ng/mL, respectively. Our GMRA sensors can be a promising candidate for label-free chemical and biomedical sensing.

We also propose theoretically and demonstrate experimentally a dislocated double-layer metal grating structure, which operates as a unidirectional coupler capable of launching surface plasmon polaritons (SPPs) in a desired direction under normal illumination [6]. The structure consists of a slanted dielectric grating sandwiched between two gold gratings. The upper gold grating has a non-zero lateral relative displacement with respect to the lower one. Numerical simulations show that a grating structure with 7 periods can convert 49% of normally incident light into surface plasmons, with a contrast ratio of 78 between the powers of the surface plasmons launched in two opposite directions. We explain the unidirectional coupling phenomenon by the dislocation-induced interference of the diffracted waves from the upper and lower gold gratings. Furthermore, we developed a simple and cost-effective technique to fabricate the structure via tilted two-beam interference lithography and subsequent shadow deposition of gold. The experimental results demonstrate a coupling efficiency of 36% and a contrast ratio of 43. The relatively simple periodic nature of our structure lends itself to large-scale low-cost fabrication and simple theoretical analysis. Also, unlike the previous unidirectional couplers based on aperiodic structures, the design parameters of our unidirectional coupler can be determined analytically. Therefore, this structure can be an important component for surface-plasmon-based nanophotonic circuits, by providing an efficient interface between free-space and surface plasmon waves.

REFERENCES

1. Barnes, W. L., A. Dereux, and T. W. Ebbesen, *Nature*, Vol. 424, 824–830, 2003.
2. Maier, S. A., P. G. Kik, H. A. Atwater, S. Meltzer, E. Harel, B. E. Koel, and A. A. Requicha, *Nat. Mater.*, Vol. 2, 229–232, 2003.
3. Briggs, R. M., J. Grandidier, S. P. Burgos, E. Feigenbaum, and H. A. Atwater, *Nano Lett.*, Vol. 10, 4851–4857, 2010.
4. Delacour, C., S. Blaize, P. Grosse, J. M. Fedeli, A. Bruyant, R. Salas-Montiel, G. Lerondel, and A. Chelnokov, *Nano Lett.*, Vol. 10, 2922–2926, 2010.
5. Shen, Y., J. Zhou, T. Liu, Y. Tao, R. Jiang, M. Liu, G. Xiao, J. Zhu, Z. Zhou, X. Wang, C. Jin, and J. Wang, *Nature Communications*, Vol. 4, 2381, 2013, DOI: 10.1038/ncomms3381.
6. Liu, T., Y. Shen, W. Shin, Q. Zhu, S. Fan, and C. Jin, "Dislocated double-layer metal gratings: an efficient unidirectional coupler," *Nano Letters*, in print, (dx.doi.org/10.1021/nl501007d).

Session 4A5
FocusSession.SC2: Transfromation Optics 2

Transformation Optics with Nonlocal Photonic Media

Jie Luo, **Yu Ting Yang**, **Zhi Hong Hang**, **and Yun Lai**
School of Physical Science and Technology, Soochow University, Suzhou, China

Abstract— Metamaterials and transformation optics have enormously enriched human's ability to control electromagnetic waves and light, leading to novel applications such as cloaking, exotic lens, illusion optics, etc..

In previous designs of transformation optics devices, local media with special parameters such as negative values and suitable anisotropy have been widely used. The parameters of these local media are often required to have complex spatial distribution, but are usually assumed to be independent of the wave vector. These parameters are difficult to achieve, usually involving both resonances in permittivity and permeability.

However, transformation optics can also be achieved by using nonlocal photonic media with parameters not only dependent on frequency and position, but also on the wave vector.

We theoretically and experimentally demonstrate realization of nonlocal photonic media with suitable k-dependence, so as to achieve interesting applications such as wide-angle Brewster's angle and transformation optics devices [1].

Our work shows the possibility of nonlocal photonic media in controlling electromagnetic waves and light in unprecedented manner.

REFERENCES

1. Luo, J., Y. T. Yang, Z. H. Hang, and Y. Lai, to be Submitted.

Controlling Spontaneous Emission Using Coordinate Transformations

Jingjing Zhang[1] and Anatoly V. Zayats[2]

[1]Department of Photonics Engineering, Technical University of Denmark
DTU Fotonik, Lyngby 2800, Denmark
[2]Department of Physics, King's College London
Strand, London WC2R 2LS, United Kingdom

Abstract— We propose a new approach based on transformation optics methods to designing required density of states and thus controlling the spontaneous emission rate. We show that the SE rate can be either enhanced or suppressed using electromagentic field concentrator devices or invisibility cloaks. Furthermore, the anisotropic material profile of the cloak enables the directional control of the SE rate. Tailoring spontaneous emission properties using transformation optics approach provides a straightforward way for designing emission properties in a complex material environment needed for development of active nanophotonic devices.

One-dimensional Full-parameter Cloak for TM Wave

Yihao Yang and Hongsheng Chen
The Electromagnetics Academy at Zhejiang University
Zhejiang University, Hangzhou 310027, China

Abstract— Invisibility cloaks have aroused considerable interests due to its amazing functions thanks to the advent of metamaterials and transformation optics during the last few years. Here we designed a TM wave one-dimensional full-parameter cloak using a bilayer metamaterial unit cell with negligible spatial dispersive. The size of our cloak is about eight wavelength. Our results show the cloak exhibit a nearly perfect performance at 9.43 GHz with a bandwidth of 0.8 GHz.

Transformation Optics Manipulating the Momentum of Light

V. Ginis[1], **J. Danckaert**[1], **I. Veretennicoff**[1], **C. M. Soukoulis**[2], **and P. Tassin**[3]

[1]Applied Physics Research Group (APHY), Vrije Universiteit Brussel, Pleinlaan 2, Brussel 1050, Belgium
[2]Ames Laboratory — U.S. DOE and Department of Physics and Astronomy
Iowa State University, Ames, IA 50011, USA
[3]Department of Applied Physics, Chalmers University, SE-412 96 Göteborg, Sweden

Abstract— In this presentation, we demonstrate how transformation optics allows for the advanced control of the momentum of light. In the first part of the presentation, we apply the methodology of transformation optics to enhance optical gradient forces. These forces arise when linear momentum is transferred between electromagnetic fields and matter. In the past decade, optical forces have been used in the field of optomechanics, but they still remain too small for dynamic manipulation in photonic actuation systems. We show how transformation optics can enhance optical forces in such systems by altering the perceived separation distance, resulting in a more than tenfold enhancement of the optical force. In the second part, we apply transformation optics to control Cherenkov radiation using anisotropic metamaterials. On the basis of our results, we design a specific anisotropic nanomaterial to enhance the sensitivity of particle detectors in high-energy experiments.

REFERENCES

1. Ginis, V., P. Tassin, C. M. Soukoulis, and I. Veretennicoff, *Phys. Rev. Lett.*, Vol. 110, 057401, 2013.
2. Zhao, R., P. Tassin, T. Koschny, and C. M. Soukoulis, *Opt. Express*, Vol. 18, 25665–25676, 2010.

Transformation Optics: A Universal Design Tool

John Pendry
Imperial College London, London, UK

Abstract— Our intuitive understanding of light has its foundation in the ray approximation and is intimately connected with our vision: As far as our eyes are concerned light behaves like a stream of particles. Here we look inside the wavelength and show how the new concept of transformation optics that manipulates electric and magnetic field lines rather than rays can provide an equally intuitive understanding of sub wavelength phenomena and at the same time be an exact description at the level of Maxwell's equations. Examples will be given of applications to plasmonic structures with dimensions of just a few nanometres: A tenth or even a hundredth of the wavelength of visible light, and an the other extreme to cloaking of static magnetic fields. In both instance the ray picture fails utterly.

Conformal Transformation Optics

Huanyang Chen
School of Physical Science and Technology
Soochow University, Suzhou, Jiangsu 215006, China

Abstract— We reviewed several transformation optical designs using conformal mappings in our group, such as conformal cloaks, conformal lens, directional emitter and so on. Such devices are isotropic materials of non-magnetic response, thus easy to implement.

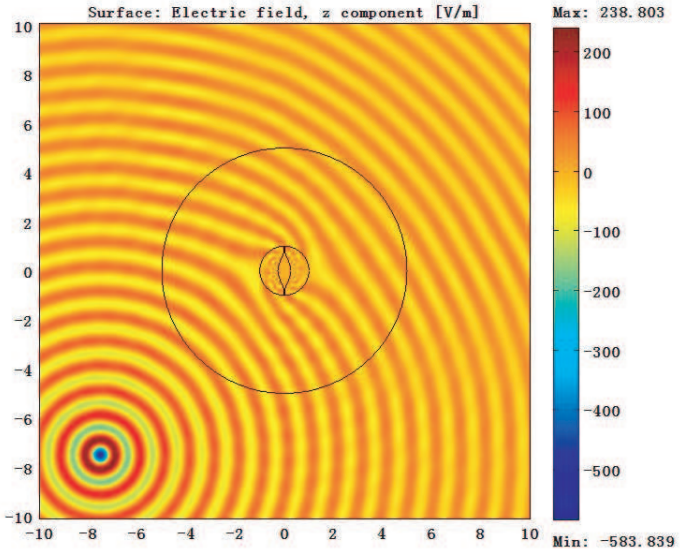

Figure 1: The invisibility effect for a conformal cloak.

REFERENCES

1. Chen, H., U. Leonhardt, and T. Tyc, "Conformal cloak for waves," *Phys. Rev. A*, Vol. 83, 055801, 2011.
2. Jiang, X., K. Yao, Q. Wu, Y. Xu, and H. Chen, "Conformal transformations to achieve unidirectional behaviors of light," *New J. Phys.*, Vol. 14, 053023, 2012.
3. Gu, C., K. Yao, W. Lu, Y. Lai, H. Chen, B. Hou, and X. Jiang, "Experimental realization of a broadband conformal mapping lens for directional emission," *Appl. Phys. Lett.*, Vol. 100, 261907, 2012.
4. Wu, Q., Y. Xu, H. Li, and H. Chen, "Cloaking and imaging at the same time," *EPL*, Vol. 101, 34004, 2013.
5. Li, H., Y. Xu, and H. Chen, "Conformal cloaks at eigenfrequencies," *J. Phys. D: Appl. Phys.*, Vol. 46, 135109, 2013.
6. Chen, H. Y., Y. Xu, H. Li, and T. Tyc, "Playing the tricks of numbers of light sources," *New J. Phys.*, Vol. 15, 093034, 2013.

Three Dimensional Carpet Cloak with Rigorous Transformation Optics

Runren Zhang and Hongsheng Chen
The Electromagnetics Academy at Zhejiang University, Zhejiang University, Hangzhou 310027, China

Abstract— By using rigorous transformation optics, we present a full parameter, three dimensional, broad band carpet cloak working for full polarization waves. We demonstrate a nearly perfect cloaking performance, over a broad bandwidth of 1–4 GHz. The cloak exhibits no lateral scattering shift. The phase of the wave is also preserved when reflecting from the cloak.

Transformation Thermodynamics: Heat Flux Control and Device Applications

Yungui Ma and Yichao Liu

State Key Lab of Modern Optical Instrumentation
Centre for Optical and Electromagnetic Research
Zhejiang University, Hangzhou 310058, China

Abstract— Extended from its electromagnetic counterpart [1, 2], transformation thermodynamics applied to thermal conduction equations can map a virtual geometry into a physical thermal medium, realizing the manipulation of heat flux with almost arbitrarily desired diffusion paths, which provides unprecedented opportunities to create thermal devices unconceivable or deemed impossible before [3, 4]. In this talk, we report our recent work on manipulation of transient heat flux employing this technique and showed two thermal devices: a heat flux cloak and an efficient plate heater. In the cloaking device we will show that heat flux can be guided by a transformed medium to flow around a vacuum obstacle and restore its diffusion direction as if nothing inhomogeneous exists in their trajectories [5]. In the second experiment, we design an efficient plate heater that can transiently achieve a large surface of uniform temperature powered by a small thermal source [6]. As opposed to the traditional approach of relying on the deployment of a resistor network, our approach fully takes advantage of an advanced functional material system to guide the heat flux to achieve the desired temperature heating profile. Our research results are good examples of the powerful application of coordinate transformation on wave/flux manipulation and may help to broaden research in acquiring extraordinary ways to control and utilize heat energy or configure novel heat devices.

REFERENCES

1. Pendry, J., D. Schurig, and D. R. Smith, "Controlling electromagnetic fields," *Science*, Vol. 312, 1780–1781, 2006.
2. Leonhardt, U., "Optical conformal mapping," *Science*, Vol. 312, 1779–1780, 2006.
3. Narayana, S. and Y. Sato, "Heat flux manipulation with engineered thermal materials," *Phys. Rev. Lett.*, Vol. 108, 214303, 2012.
4. Guenneau, S., C. Amra, and D. Veynante, "Transformation therdyamics: Cloaking and concentrating heat flux," *Opt. Express*, Vol. 20, 8207, 2012.
5. Ma, Y. G., L. Lan, W. Jiang, F. Sun, and S. L. He, "A transient thermal cloak experimentally realized through a rescaled diffusion equation with anisotropic thermal diffusivity," *NPG Asia Mater.*, Vol. 5, e75, 2013.
6. Liu, Y. C., W. Jiang, S. L. He, and Y. G. Ma, "An efficient plate heater with uniform surface temperature engineered with effective thermal materials," Unpublished.

Optimization of Nanostructured Lüneburg Lens Based on the Transformation Optics Method

Yinghui Cao[1, 2], **Yongmin Liu**[3, 4], **and Zhenyu Liu**[1]

[1]Changchun Institute of Optics, Fine Mechanics and Physics
3888 East Nanhu Road, Changchun, Jilin 130033, China
[2]College of Computer Science and Technology, Jilin University
2699 Qianjin Street, Changchun, Jilin 130021, China
[3]Department of Mechanical and Industrial Engineering, Northeastern University
360 Huntington Avenue, Boston, MA 02115, USA
[4]Department of Electrical and Computer Engineering, Northeastern University
360 Huntington Avenue, Boston, MA 02115, USA

Abstract— Lüneburg lens is a spherical lens with gradient index (GRIN) structure, which can focus incoming plane wave from any direction into a focal point at the surface of the lens on the opposite direction. However, as a GRIN device, Lüneburg lens is difficult to be fabricated in optical wavelength. In recent years, nanostructured Lüneburg lens which consists of dielectric rods with varying size has been proposed, and designed by the Hamiltonian ray tracing method. In this work, we present the design of nanostructured Lüneburg lens base on the electromagnetic field simulation and optimization method, which is more accurate in the design of compact optical and photonic devices with nanoscale structures. In a previous work, we used the proposed method to design aperiodic photonic crystal devices [1]. In the proposed method, the nanostructured Lüneburg lens is modeled using the Transformed Optics (TO) method, where the dielectric rods with varying size are transformed into an equivalent model that consists of uniform and fixed sized rods, with parameterized permittivity and permeability distributions. By applying the TO technique, small rods of the original device model are now transformed into larger ones, thus mesh refinement around the small rods can be avoided, and efficiency of the simulation is improved. Besides, by using the transformed device model, the nanostructured Lüneburg lens can be simulated and optimized with fixed geometry and mesh grids, eliminating the repetitions of regenerating the geometry and mesh grids during the optimization iterations. The nanostructured Lüneburg lens is optimized with the gradient method. The optimization object is defined as the averaged field intensity in a zone that enclose the focal point, and the gradient is defined as the first-order derivative of the optimization object subject to the rods radii. The gradient are calculated using the Adjoint-Variable Method (AVM), therefore in each optimization iteration only one forward problem and one additional adjoint problem are solved to calculate the gradient for all the design variables. In order to keep symmetry of the optimized Lüneburg lens, gradients of rods at the same distance from the center of the nanostructured Lüneburg lens are averaged. In addition, the nanostructured Lüneburg lens is optimized with the constraints that radii of rods at the inner layers are larger than the rods at outer layers, mimicking the original GRIN Lüneburg lens. Comparing with the GRIN Lüneburg lens, the optimized nanostructured Lüneburg lens has similar field distributions to the GRIN Lüneburg lens. The proposed design method opens up a new avenue to design and optimize a variety of photonic and optical devices with large number of complex structures.

REFERENCES

1. Cao, Y., J. Xie, Y. Liu, and Z. Liu, "Modeling and optimization of photonic crystal devices based on transformation optics method," *Optics Express*, Vol. 22, No. 3, 2725–2734, 2014, http://dx.doi.org/10.1364/OE.22.002725.

Geometry, Topology and Transformation Optics

Yongliang Zhang[1], **Li-Na Shi**[2], **Xian-Zi Dong**[1], **Zhen-Sheng Zhao**[1], **and Xuan-Ming Duan**[3]

[1]Technical Institute of Physics and Chemistry, Chinese Academy of Sciences
No. 29, Zhongguancun East Road, Beijing 100190, China
[2]Institute of Microelectronics, Chinese Academy of Science
No. 3, Beitucheng West Road, Chaoyang District, Beijing 100029, China
[3]Chongqing Institute of Green and Intelligent Technology, Chinese Academy of Sciences
No. 266 Fangzheng Avenue, Shuitu Hi-tech Industrial Park, Beibei, Chongqing 400714, China

Abstract— The behavior of a material medium in response to electromagnetic and gravitational fields is a matter of extensive interest for both fundamental and technological reasons. A recently striking example is the transformation optics [1, 2], which utilizes the formal invariance of Maxwell equations to control the electromagnetic fields by inhomogeneous anisotropic medium computed by a coordinate transformation. Transformation optics enables a variety of unprecedented novel effects ranging from invisibility cloaks, optical illusion, imaging, light harvesting to nonlocal plasmonics.

In principle, the geometry of conventional transformation optics relies on the nontrivial Riemannian structure of transformation media, similar to the general relativistic description of gravity, where light ray follows a null geodesic regardless of its polarization state [3]. However, a complete geometry framework incorporating with the transversal nature of electromagnetic fields, such as chirality, polarization state and singular phase structure, is still lacking. Here [4], we establish the connection between controlling the twisting degree of freedom of light and the torsional affine geometry of transformation optics in the framework of Pendry and Leonhardt. We show that the generic transformation medium is linear bianisotropic material with the magnetoelectric coupling emerging as torsion tensor, reminiscent of the polarization rotating effect due to photon-torsion coupling in the Poincare gauge theory of gravity [5]. We introduce torsion in terms of the spatial gradient of the coordinate transformation, and demonstrate the crucial role of topology in transformation optics by introducing line topological defects. As illustrative examples, we demonstrate the generation of optical angular momentum, both spin and orbital, and analogous gravitational lensing by a toy model of optical cosmic string. Our model not only extends the geometrical and topological aspects of transformation optics but also provides an experimental approach for simulating of classical and quantum physics in curved torsional space in optical laboratory.

REFERENCES

1. Leonhardt, U., *Science*, Vol. 312, 1777, 2006.
2. Pendry, J. B., D. Schurig, and D. R. Smith, *Science*, Vol. 312, 1780, 2006.
3. Leonhardt, U. and T. Philbin, *Geometry and Light: The Science of Invisibility*, Dover, 2010.
4. Zhang, Y. L., L. N. Shi, X. Z. Dong, Z. S. Zhao, and X. M. Duan, arXiv: 1301.6954.
5. Blagojevic, M. and F. W. Hehl, *Gauge Theories of Gravitation: A Reader with Commentaries*, Imperical College Press, 2013.

Session 4A6
FocusSession.SC2: Novel Techniques for Subwavelength-focusing and Super Resolution Imaging 2

Plasmonic Super-resolution Imaging beyond the Plasmonic Limit

Satoshi Kawata[1, 2]

[1]Osaka University, Japan
[2]RIKEN, Japan

Abstract— Surface plasomons have been used for optical super-resolution nano-imaging and nano-spectroscopy, due to their slow and high momentum function [1] and for non-labeling molecular sensing with Raman detection due to the field enhancement effet [2]. In this presentation, I will discuss on the essential limit in plasmonics [3] and the inventions beyond the plasmonic limit. Some latex results including few-nm resolution imaging with tip pressure on the mano-materials [4], rod-array non-scanning imaging with magnification [5], and 3D nano-imaging in a living cell [6] will be shown with related topics such as plasmon holography [7] and molecular imaging during apoptosis [8].

REFERENCES

1. Yano, T., et al., *Nature Commun.*, Vol. 4, 10.1038, 2013.
2. Palonpon, A., et al., *Nature Protcol.*, Vol. 8, 677, 2013.
3. Kawata, S., Y. Inouye, and P. Verma, *Nature Photon.*, Vol. 3, 388, 2009.
4. Yano, T., et al., *Nature Photon.*, Vol. 3, 473, 2009.
5. Kawata, S., A. Ono, and P. Verma, *Nature Photon.*, Vol. 2, 438, 2008.
6. Ando, J., K. Fujita, N. Smith, and S. Kawata, *Nano Lett.*, Vol. 11, 5344, 2011.
7. Ozaki, M., J. Kato, and S. Kawata, *Science*, Vol. 332, 218, 2011.
8. Okada, M., et al., *Proc. Natl. Acad. Sci.*, Vol. 109, 28, 2012.

Plasmonic Structures for Generic Surface Plasmon Generation and Focusing

Shiyi Xiao, **Oscar Byrne**, **and Jensen Li**
School of Physics and Astronomy, University of Birmingham, Birmingham B15 2TT, UK

Abstract— The idea of using surface plasmons (SPs) in holography was suggested by Cowan in 1973 and subsequent proposals of SP holography were reported [1, 2]. In these previous works, SP was used as the reference light to enhance the diffraction efficiency or to realize multiplexing effect, owning to the field enhancement and dispersive band structure of SPs. Conversely, recent works on metasurfaces have focused on exciting SPs using free-space incident wave with designed plasmonic atoms (such as slits or bars) [3, 4], allowing us to apply holographic technique to on-chip applications using SPs. Here we present a specific class of plasmonic atoms (in the later scheme), which can radiate SP with almost isotropic power on a metal surface, based on multiple resonances. By using these atoms with isotropic radiation power, one can construct SP holograms in a more flexible way. As an illustration, we numerically demonstrate how reconfigurable SP focusing can be achieved using these plasmonic atoms.

REFERENCES

1. Cowan, J. J., "The surface plasmon resonance effect in holography," *Opt. Commun.*, Vol. 5, 69, 1972.
2. Ozaki, M., et al., "Surface-plasmon holography with white-light illumination," *Science*, Vol. 332, 218, 2011.
3. Lin, J., et al., "Polarization-controlled tunable directional coupling of surface plasmon polaritons," *Science*, Vol. 340, 331, 2013.
4. Huang, L., et al., "Helicity dependent directional surface plasmon polariton excitation using a metasurface with interfacial phase discontinuity," LSA, Vol. 2, e70, 2013.

Experimental Demonstration of Plasmonic Structured Illumination Microscopy

Feifei Wei, Dylan Lu, Hao Shen, Weiwei Wan, Joseph Ponsetto, Eric Huang, and Zhaowei Liu
Department of Electrical and Computer Engineering, University of California
San Diego, 9500 Gilman Drive, La Jolla, California 92093-0407, USA

Abstract— The optical microscope is an irreplaceable tool for biological research because light can probe bio-specimens non-invasively. Despite its wide application in various research fields, the resolution of an optical microcopy is fundamentally limited by diffraction to the order of 300 nm. To achieve sub-diffraction limited resolution, many novel imaging technologies have been proposed and experimentally demonstrated, such as near-field scanning microscopy (NSOM), far-field superlens (FSL), hyperlens, metalens, stimulated emission depletion microscopy (STED), single molecule localization based microscopy. In this work, we experimentally demonstrate a wide field surface plasmon (SP) assisted super-resolution imaging technique, Plasmonic Structured Illumination Microscopy (PSIM), by combining tunable SP interference (SPI) with structured illumination microscopy (SIM). By replacing the laser interference fringes in conventional SIM with SPI patterns, PSIM exhibits greatly advanced resolving power thanks to the unique properties of SP waves. This new PSIM technique is a wide field super-resolution imaging technique with potential application in the field of high-speed biomedical imaging.

Deep Subwavelength Imaging by Metal-insulator-metal Plasmonic Lens

Xiangang Luo, **Changtao Wang**, **Zeyu Zhao**, **Ping Gao**, **and Na Yao**
State Key Lab of Optical Technologies on Nano-Fabrication and Micro-Engineering
Institute of Optics and Electronics, Chinese Academy of Sciences, P. O. Box 350, Chengdu 610209, China

Abstract— Recently, variant types of plasmonic lens have been proposed and demonstrated both theoretically and experimentally to realize optical imaging beyond the diffraction limit, such as the perfect lens, super lens and hyper lens etc.. However, plasmonic imaging are not only dependent on evanescent waves transfer and amplification ability, but are strongly affected by the polarization states of electric field components in the imaging region. It is found that plasmonic lens in the form of metal-insulator-metal structure give rise to further amplification of evanescent waves in the imaging process, and more importantly, help to tailor the magnitude ratio of electric field components in the normal and tangential directions benefiting from the coupling effect of surface plasmons. As demonstrated in numerical simulations and experiments, this brings significant improvement of plasmonic lens imaging features, like resolution, depth and fidelity of complex pattern images. Nano plasmonic lithography with $4x$-nm, $3x$-nm and $2x$-nm half pitch (critical dimension) resolution and improved resist pattern quality by 365 nm wavelength light is obtained in experiments. Furthermore, this method is employed to enhance the imaging performance of planar hyperlens and plasmonic phase contrast imaging of nano transparent objects, which is believed to find potential applications in high-density optical storage technology.

Application of Wire Metamaterial for Magnetic Resonance Imaging

A. P. Slobozhanyuk and P. A. Belov
ITMO University, St. Petersburg 197101, Russia

Abstract— Wire metamaterial or so-called wire medium is a broad class of electromagnetic metamaterials, which are usually composed of an array of parallel conducting wires embedded in a dielectric matrix [1]. These materials are very promising due to simple fabrication technologies and various breakthrough applications.

In this contribution we will review our recent activities in the area of wire metamaterials. First of all, the experimental study of the magnetic Purcell effect in the wire medium array in the microwave frequency range will be presented. By directly measuring the spatial-frequency map of the Purcell factor we explicitly demonstrate how the Purcell factor is enhanced at the Fabry-Perot resonances of the wire metamaterial block. In addition, we provide comparison between the Purcell factor in the finite and infinite arrays of wire metamaterial. Second of all, the experimental verification of the phenomenon of evanescent waves enhancement inside a wire metamaterial slab with tilted wires will be considered [2]. This phenomenon can be viewed as an improvement of the previously studied wire medium lenses. Without any change in the structure, wire metamaterials are capable of imaging a source with sub-wavelength resolution located at the enhanced distance from the front side of the device, but the image in this case has to be detected inside the slab, this effect was named as internal imaging. Finally, wire metamaterials can be applied for improvement of magnetic resonance imaging in several ways: by using endoscopes in order to obtain possibilities to effectively transport the signal, emitted by an object from the tubes center, for the purpose of its detection in low magnetic field area [3, 4]; by using the wire metasurface, which can increase the signal-to-noise ratio more than twice, the immediate result of this increase is that higher resolution image can be obtained over the same time slot or faster examination can be performed with similar resolution.

REFERENCES

1. Simovski, C. R., P. A. Belov, A. V. Atrashchenko, and Y. S. Kivshar, "Wire metamaterials: Physics and applications," *Adv. Mater.*, Vol. 24, 4229, 2012.
2. Slobozhanyuk, A. P., I. V. Melchakova, C. R. Simovski, and P. A. Belov, "Experimental verification of enhancement of evanescent waves inside a wire medium," *Appl. Phys. Lett.*, Vol. 103, 051118, 2013.
3. Radu, X., D. Garray, and C. Craeye, "Toward a wire medium endoscope for MRI imaging," *Metamaterials*, Vol. 3, No. 2, 90–99, 2009.
4. Slobozhanyuk, A. P., I. V. Melchakova, A. V. Kozachenko, D. S. Filonov, C. R. Simovski, and P. A. Belov, "Endoscope based on highly anisotropic metamaterials for applications in magnetic resonance imaging," *Radiotek. Elektron.*, Vol. 59, No. 4, 1–10, Moscow, 2014.

Super-resolution Focusing with Phononic Crystals

Fabrice Lemoult[1, 2, 3] **and John H. Page**[1]

[1]Department of Physics and Astronomy, University of Manitoba, Winnipeg, MB R3T 2N2, Canada
[2]ESPCI ParisTech, PSL Research University, Institut Langevin, 1 Rue Jussieu, Paris F-75005, France
[3]CNRS, Institut Langevin, 1 Rue Jussieu, Paris F-75005, France

Abstract— Since focusing of acoustic waves by negative refraction in flat phononic crystals was first demonstrated sever-al years ago [1], there has been increasing interest in the possibility that focusing with resolution better than the diffraction limit of $\lambda/2$ may be achievable. In addition to demonstrating negative refraction directly, we show how super-resolution can be realized with two-dimensional phononic crystals in which the equifrequency con-tours are circular and well matched in size to the contours of the medium outside the crystal [2, 3]. The phononic crystals are made of stainless steel rods assembled in a triangular crystal lattice and immersed in a liquid. To achieve matching of the equifrequency contours inside and outside the crystal, the liquid surrounding the rods in the crystal was chosen to have a lower sound velocity than the water outside. At a frequency close to that at which equifrequency contour matching occurs (0.55 MHz for the crystal when the fluid is methanol), an im-age of a subwavelength source was obtained with a resolution of 0.37λ. Our experimental results are compared with theoretical predictions by the Finite Difference Time Domain (FDTD) method, which predicts an optimum resolution of 0.35λ — in good agreement to that observed experimentally (Fig. 1). Super-resolution imaging in these crystals is shown to be related to the coupling between the incident evanescent waves from the source and a bound slab mode of the phononic crystal lens, leading to amplification of evanescent waves by the slab mode. This phenomenon is only observed when the source is located very close to the lens and is very sensitive to the location of the source parallel to the lens surface, as well as to site disorder in the phononic crystal lattice. The dependence of the resolution limit of this steel rod and methanol crystal on various geometric and operational factors such as source frequency, lens geometry and source position will be discussed [4]. The potential for further improvements to the focusing capabilities of such phononic crystal lenses will also be explored.

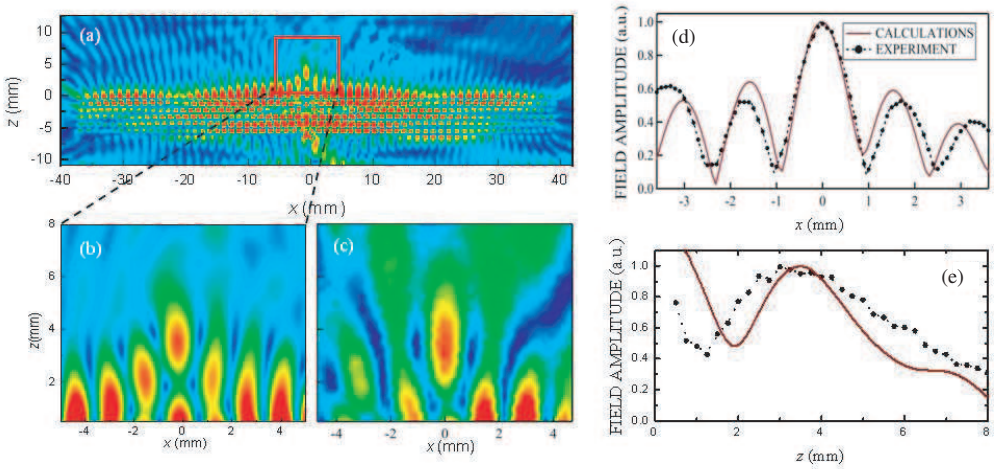

Figure 1: Super-resolution focusing of ultrasound at 530 kHz by a flat 2D phononic crystal consisting 1-mm-diameter steel rods arranged in a triangular lattice and immersed in methanol. The medium outside the crystal is water. (a) FDTD calculations of the average pressure amplitude when a 0.55 mm wide source is placed 0.1 mm below the surface of the crystal, at $x = 0$ mm and $z = -6.35$ mm. The crystal contains 6 layers of rods, with the output side of the crystal at $z = 0$. An image of the source is seen near $x = 0$ and $z = 3.5$ mm, as shown (b) and (c) for FTDT simulations and experiments, respectively. (d) and (e) Comparison of experiment and theory for the field amplitude through the peak of the focal spot along directions parallel and perpendicular to the lens surface. The experimental results and theoretical predictions for the half width of the focal spot parallel to the surface, $\Delta/2$, are found to be 0.37λ and 0.35λ.

ACKNOWLEDGMENT

Work performed with A. Suhkovich, B. Merheb, J.-F. Robillard, J. O. Vasseur, P. A. Deymier, and Cody Friesen.

REFERENCES

1. Yang, S., J. H. Page, Z. Liu, M. L. Cowan, C. T. Chan, and P. Sheng, *Phys. Rev. Lett.*, Vol. 93, 024301, 2004.
2. Sukhovich, A., L. Jing, and J. H. Page, *Phys. Rev. B*, Vol. 77, 014301, 2008.
3. Sukhovich, A., B. Merheb, K. Muralidharan, J. O. Vasseur, Y. Pennec, P. A. Deymier, and J. H. Page, *Phys. Rev. Lett.*, Vol. 102, 154301, 2009.
4. Robillard, J.-F., J. Bucay, P.A. Deymier, A. Shelke, K. Muralidharan, B. Merheb, J. O. Vasseur, A. Sukhovich, and J. H. Page, *Phys. Rev. B*, Vol. 83, 224301, 2011.

Flat Lens for Bending Waves Focusing in Time Domain

M. Dubois[1], **E. Bossy**[1], **S. Enoch**[2], **S. Guenneau**[2], **G. Lerosey**[1], **and P. Sebbah**[1]

[1]Institut Langevin, CNRS UMR 7587, ESPCI ParisTech, 1 rue Jussieu, 75238 Paris Cedex 05, France
[2]Institut Fresnel, CNRS, Aix-Marseille Université, Campus Universitaire de Saint-Jérôme
13013 Marseille, France

Abstract— Flat lens concept proposed in 1968 by V. G. Veselago is extended to elastic waves on a thin plate. A 45°-tilted square lattice of circular holes drilled in a Duraluminium plate has been chosen to experimentally demonstrate focusing of flexural waves. Lamb wave pulse focusing is achieved below the first stop band. If most investigations have been performed in the monochromatic regime, it was recognized that understanding the time development of the superlensing effect is crucial. Finite-difference time-domain simulations confirm the role of lens resonances in pulse reconstruction on opposite side of the platonic crystal. Time-resolved experiments reveal that the focused image shrinks with time below diffraction limit, with a lateral resolution increasing from 1.20λ to 0.37λ.

First proposal of negative index materials by V. G. Veselago [1] has triggered keen interest in materials with simultaneous negative dielectric constant and negative magnetic permeability. In 2000, J. B. Pendry [2] proposed to take advantage of negative refraction and flat lens geometry to achieve subwavelength focusing. Since then, several groups have been working intensively on flat lens designs for optical waves and microwaves [3]. However the design of such double negative constants materials remains extremely challenging. An alternative is based on photonic crystals. Such materials reveal strong anisotropic dispersion relation that may lead to band folding and negative refraction. Flat lens behavior is observable in a spectral range called the All Angle Negative Refraction (AANR), where all incident wave vectors are negatively refracted by the crystal. These concepts have been successfully extended to acoustic waves. Superfocusing has been evidenced in several phononic crystals, for instance through methanol-immersed triangular lattice of steel rods [4]. Design of acoustic metamaterials has promising perspectives. We demonstrate the presence of an AANR around 10 kHz in a 45°-tilted square lattice of circular holes drilled in a Duraluminium. Focusing of flexural wave with this system has been experimentally demonstrated with diffraction limited resolution [5].

The ability of a perfect lens to focus waves at sub-wavelength scales lies in the possibility to amplify evanescent waves through the lens. A mechanism based on resonant coupling of surface modes bounded at each interface of the lens has been proposed by Pendry to explain near-field wave amplification. The dynamics of such a mechanism has been later analyzed in [6–8]. In our case we realized that the lens store energy from the pulse source and release it with longer time decays. We perform a spatial Fourier analysis inside the lens at each time steps in order to confirm the existence of eigenmodes. The presence of a focusing point is supported by the interference between each of these modes in the focal plane. In the case of a monochromatic excitation this interference pattern will be fixed as modes frequency is enforced by the carrier frequency. For pulsed excitation each mode has his own eigenfrequency and interference pattern is no longer constant as time progresses. This time evolution of the interference in the focal plane is experimentally observed and gives rise to better resolution [9]. We observed that evanescent modes do not support this super resolution as the focal spot is away from the interface. We show that a self arrangement of complex interference pattern can create super oscillations [10, 11].

REFERENCES

1. Veselago, V. G., *Sov. Phys. Usp.*, Vol. 10, No. 4, 509–514, 1968.
2. Pendry, J. B., *Phys. Rev. Lett.*, Vol. 85, 3966–3969, 2000.
3. Zhang, X. and Z. Liu, *Nat. Mater.*, Vol. 7, No. 6, 435–441, 2008.
4. Sukhovich, A., B. Merheb, K. Muralidharan, J. O. Vasseur, Y. Pennec, P. A. Deymier, and J. H. Page, *Phys. Rev. Lett.*, Vol. 102, 154301, 2009.
5. Dubois, M., M. Farhat, E. Bossy, S. Enoch, S. Guenneau, and P. Sebbah, *Appl. Phys. Lett.*, Vol. 103, 071915, 2013.
6. Gomez-Santos, G., *Phys. Rev. Lett.*, Vol. 90, 077401, 2003.
7. Wee, W. H. and J. B. Pendry, *Phys. Rev. Lett.*, Vol. 106, 165503, 2011.
8. Archambault, A., M. Besbes, and J. J. Greffet, *Phys. Rev. Lett.*, Vol. 109, 097405, 2012.

9. Dubois, M., M. Farhat, E. Bossy, S. Enoch, S. Guenneau, and P. Sebbah, submitted, arXiv: 1303.3022 [cond-mat.mtrl-sci].
10. Berry, M. V. and S. Popescu, *J. Phys. A*, Vol. 39, 69656977, 2006.
11. Rogers, E. T. F., J. Lindberg, T. Roy, S. Savo, J. E. Chad, M. R. Dennis, and N. I. Zheludev, *Nat. Materials*, Vol. 11, 432, 2012.

Super-focusing by Phase-modulated and Amplitude-modulated Metalens

Cheng-Wei Qiu[1], **Kun Huang**[1], **Hong Liu**[2], **and Jinghua Teng**[2]

[1]Department of Electrical and Computer Engineering
National University of Singapore, 4 Engineering Drive 3, Singapore 117583, Singapore
[2]Agency for Science, Technology and Research,
Institute of Materials Research and Engineering, 3 Research Link, Singapore 117602, Singapore

Abstract— Since the past few decades, intensive efforts have been attributed to achieve optical imaging resolution beyond the diffraction limit. A deep-subwavelength resolution below $\lambda/6$ could be realized via improving the imaging lens, e.g., superlens, hyperlens, micro-lens, metalens or super-oscillatory lens. Our studies focus on the lens design for achieving an ultra-small focusing spot by using amplitude or phase masks with subwavelength features under the illumination with different polarizations (radial polarization, azimuthal polarization, linear polarization and natural polarization, i.e., unpolarized). Based on the focusing properties of metal-lens as well as vectorial and scalar Rayleigh-Sommerfeld diffraction integrals, an optimization-free method is proposed to design a super-focusing lens by numerically solving a nonlinear matrix. Both methods are extended to design lens for achieving a subwavelength spot or needle with purely longitudinal or transverse polarization, or without polarization. With the optimization-free method, we predict theoretically that the spot without significant side lobes by using the far-field diffraction of amplitude or phase masks has a limitation of 0.38λ. Moreover, an analytical model is proposed to describe the far-field diffraction of nano-hole array (nano-seive) with high accuracy. A nano-sieve with high numerical aperture (NA) for achieving a subwavelength spot is well designed and fabricated, which is verified both theoretically and experimentally. Our work paves a roadmap to design various super-focusing lenses for non-invasive imaging, which is benefited for the optical industry related to super-resolution imaging and super focusing.

STED Optical Nanoscopy with Inorganic Fluorescent Labels

Xusan Yang[1], **Zhiping Zeng**[1], **Hao Xie**[1], **Xuanze Chen**[1], **Yujia Liu**[1, 2], **Dayong Jin**[3], **and Peng Xi**[1]

[1]Department of Biomedical Engineering, College of Engineering, Peking University,Beijing, China
[2]School of Biomedical Engineering, Shanghai Jiao Tong University, Shanghai, China
[3]Advanced Cytometry Laboratories, MQ Photonics Research Centre
Macquarie University, Sydney, NSW 2109, Australia

Abstract— Conventional optical microscopy, although been widely applied in biological research, can only yield optical resolution approaching Abbe diffraction limit of $\sim 200\,\text{nm}$. This is still larger than many subcellular organelles whose size is in a few to tens of nanometers. These limitations have driven the development of super-resolution optical imaging methodologies over the past decade.

REversible/Saturable OpticaL Fluorescence Transitions (RESOLFT) is one of the technique that utilizes spatially designed pattern to shrink the effective fluorescence point spread function (PSF) [1]. One of the RESOLFT technique, stimulated emission depletion (STED) microscopy, uses the overlap between the excitation focus and an intense doughnut-shaped spot [2], to instantly de-excite markers from their fluorescent state to the ground state by stimulated emission process [3].

To efficiently dominate the process of emission by stimulated emission, STED induces much faster ON-OFF process and therefore photobleaching is non-negligible for organic dyes. Further, the lifetime of the organic dye is usually very short (in ns scale), so the stimulated emission cross-section is very small. These effects practically hinder STED from obtaining higher resolution.

Here we investigate the possibility of using inorganic dyes for super-resolution microscopy. (1) As the fluorescent nanodiamond lacks the triplet state, it cannot be photobleached. We have compared the imaging result for STED and structured illumination microscopy (SIM), with both FND particles and nitrogen-vacant (NV-) centers grown in bulk diamond [4]. (2) With the long lifetime of upconversion nanoparticles (ms level) [5], and the super brightness of UCNPs [6], we demonstrate the possibility of using UCNPs to achieve super-resolution with very low STED power.

REFERENCES

1. Ding, Y. C., P. Xi, and Q. S. Ren, "Hacking the optical diffraction limit: Review on recent developments of fluorescence nanoscopy," *Chinese Science Bulletin*, Vol. 56, No. 18, 1857–1876, 2011.
2. Xie, H., et al., "Analytical description of high-aperture STED resolution with 0–2 pi vortex phase modulation," *JOSA A*, Vol. 30, No. 8, 1640–1645, 2013.
3. Liu, Y., et al., "Achieving $\lambda/10$ resolution CW STED nanoscopy with a Ti: Sapphire oscillator," *PLoS One*, Vol. 7, No. 6, e40003, 2012.
4. Yang, X., et al., "Sub-diffraction imaging of nitrogen-vacancy centers in diamond by stimulated emission depletion and structured illumination," *RSC Advances*, Vol. 4, 11305–11310, 2014.
5. Lu, Y., et al., "Tunable lifetime multiplexing using luminescent nanocrystals," *Nature Photonics*, Vol. 8, 32–36, 2014.
6. Zhao, J., et al., "Single-nanocrystal sensitivity achieved by enhanced upconversion luminescence," *Nature Nanotechnology*, Vol. 8, No. 10, 729–734, 2013.

Compressing Acoustic Waves with Rainbow Trapping Metamaterial

Jie Zhu[1], **Xuefeng Zhu**[2], **and Xiang Zhang**[1]

[1]NSF Nano-scale Science and Engineering Center (NSEC)
3112 Etcheverry Hall, University of California, Berkeley, California 94720, USA
[2]Huazhong University of Science and Technology, Wuhan, Hubei 430074, China

Abstract— For acoustic imaging, spatial resolution and penetration depth are two of the most crucial judging parameters, yet they are extremely hard to be satisfied at the same time due to the diffraction limited nature of traditional acoustic imaging technology and system. Removing this Achilles' heel will enable our capability to conduct high resolution acoustic imaging with lower frequency sound waves. Previous work has been done in two different directions to provide solutions. One is through promoting harmonic imaging by enhancing the nonlinear effect thus generating harmonic waves. Other methods such as acoustic hyperlens and superlens take advantage of the evanescent waves that contain much larger wave vectors than that of the propagating wave, therefore, contribute to the acoustic imaging with resolution far below the diffraction limit. Here we try to present another road to Rome by experimentally demonstrating a new class of anisotropic acoustic rainbow trapping metamaterials. Such materials are able to efficiently trap broadband acoustic waves and spatially split different frequency components. The effect is due to artificial modulation of acoustic wave velocity through gradient subwavelength unit cell structures that are strongly coupled through the propagation direction. Along the metamaterial, acoustic waves are gradually stopped and successively localized, progressively inducing enhanced acoustic fields that approach the peaks at trapping location. Such spatial evolution of acoustic wave velocity is hardly found in nature materials, revealing the rainbow trapping metamaterial's strong dispersive behavior. Such wave velocity control will leads to the compression of acoustic wave packet with smaller effective wavelength, and eventually, the superfocusing.

Session 4A7
SC3: High Power Fiber Lasers 1

41 W All-fiber kHz-linewidth Single-frequency Linearly-polarized MOPA Laser

Shanhui Xu, **Can Li**, **Changsheng Yang**, **and Zhongmin Yang**
State Key Laboratory of Luminescent Materials and Devices
Institute of Optical Communication Materials
South China University of Technology, Guangzhou 510640, China

Abstract— High-power continuous wave single-frequency fiber lasers at 1.0 µm have demonstrated their potentiality in a wide range of applications, from range finding, coherent and spectrum beam combination, gravitational wave detection, and laser radar [1–3]. Especially, in order to achieve high conversion efficiencies, compact and practical design, laser output with an all-fiber format, kHz-linewidth, linearly-polarized (LP), low noise, and tens of Watts ofpowerisparticularlyrequired.We demonstrated an all-fiber kHz-linewidth single-frequency linearly-polarized laser at 1064 nm by implementing a master-oscillator power-amplifier (MOPA) system, which was seeded by a distributed Bragg reflector (DBR) short cavity Yb-doped phosphate fiber oscillator. A two-stage polarization-maintaining amplification structure was employed, from which the maximal output power is 41.2 W, corresponding to an optical-to-optical conversion efficiency of $> 81\%$. The laser linewidth of < 6 kHz and the signal-to-noise ratio of > 62 dB was achieved. The measured polarization-extinction ratio is greater than 22 dB and the obtained relative intensity noise is less than -140 dB/Hz at frequencies of over 2 MHz. The results indicate that the fiber laser would be a promising candidate as an efficient narrow-linewidth linearly-polarized fundamental laser for nonlinear frequency conversion.

REFERENCES

1. Höfer, S., A. Liem, J. Limpert, H. Zellmer, A. Tünnermann, S. Unger, S. Jetschke, H. Müller, and I. Freitag, "Single-frequency master-oscillator fiber power amplifier system emitting 20 W of power," *Opt. Lett.*, Vol. 26, 1326–1328, 2001.
2. Ma, Y., X. Wang, J. Leng, H. Xiao, X. Dong, J. Zhu, W. Du, P. Zhou, X. Xu, and L. Si, "Coherent beam combination of 1.08 kW fiber amplifier array using single frequency dithering technique," *Opt. Lett.*, Vol. 36, 951–953, 2011.
3. Richardson, D. J., J. Nilsson, and W. A. Clarkson, "High power fiber lasers: Current status and future perspectives [Invited]," *JOSA B*, Vol. 27, B63–B92, 2010.

670 W Single-frequency Retrievable Multi-tone All-fiber MOPA

X. L. Wang, P. Zhou, R. M. Tao, R. T. Su, and X. J. Xu
College of Optoelectronic Science and Engineering
National University of Defense Technology (NUDT), Changsha, China

Abstract— We demonstrated a single-frequency retrievable multi-tone all-fiber laser in master-oscillator power-amplification (MOPA) configuration with the highest recorded power of 670 W. The seed laser runs in multi-tone regime by phase modulating a single-frequency fiber laser using a sine wave signal. Power amplification of the multi-tone master oscillator is then implemented by four cascaded all-fiber power amplifier and a power scaling up to 670 W is achieved. A proof-of-concept experiment for retrieving single-frequency laser from the high power multi-tone laser is carried out by implementing a demodulation signal, which is π phase shift of the modulation signal, on the output laser at a relative low power level. Results indicated that the single-frequency laser can be retrieved with a sideband suppression of more than 20 dB at the power level of 670 W. This method may provide a feasible way for power scaling of single-frequency laser over the SBS limitation in fiber amplifier.

High Power and Widely Tunable Raman Fiber Lasers at ∼1.6 µm Based on Volume Bragg Gratings

Deyuan Shen[1], **Jun Liu**[2], **and Dianyuan Fan**[2]

[1]Department of Optical Science and Engineering, Fudan University, Shanghai 200433, China
[2]Shanghai Institute of Optics and Fine Mechanics, Chinese Academy of Sciences, Shanghai 201800, China

Abstract— Highly efficient and high-power operation of Raman fiber lasers in fixed-wavelength and wavelength-tunable cavity configurations is reported using an in-house constructed high power Er, Yb co-doped fiber laser pump source at 1545 nm and volume Bragg gratings (VBGs) as wavelength control and spectral narrowing element. Fixed-wavelength and wavelength tunable operation are achieved using VBGs with center wavelengths of 1658 nm and 1750 nm, respectively. Based on a graded-index multimode fiber, the fixed-wavelength laser yielded a maximum output power of 10.5 W at 1658.3 nm with a FWHM line width of ∼ 0.1 nm fora launched pump power of 23.4 W, corresponding to a slope efficiency of 82.7% with respect to the launched pump power. The measured beam quality in the form of M^2 factor is ∼ 1.35, corresponding to the fundamental mode of the fiber. For the wavelength-tunable Raman fiber laser, a wavelength tuning range of 37 nm from 1638.5 to 1675.1 nm is obtained with a constant spectral line width of less than ∼ 0.3 nm (FWHM) over the whole tuning range. Besides, lasing characteristics of cladding-pumped Raman fiber lasers are also evaluated. Based on customized double-cladding Raman fibers of 11 µm diameter core (0 : 14 NA) surrounded by a 26.4 µm diameter cladding (0 : 22 NA), a maximum output power of 13.2 W are achieved in a cladding-pumped free-running Raman fiber laser with a beam quality factor M^2 of ∼ 1.22 and a slope efficiency of 120% at the measured power level. The prospects for further improvement in terms of output power, spectral line width and wavelength tuning rang ewill be discussed.

Towards High Power Long-wavelength Ytterbium-doped Fiber Lasers

Pu Zhou, Hanwei Zhang, Hu Xiao, Yu Miao, and Xiaolin Wang
College of Opticelectric Science and Engineering
National University of Defense Technology, Changsha 410073, China

Abstract— Yb-doped fiber (YDF) is one of the most efficient laser gain medium for high level output power with good conversion efficiency. The optical properties of Yb^{3+} ions in silica glass allows one to get lasing over a wide spectral range that covers 1–1.2 μm region. Up to now, most of the reported high power (> 300 W) Yb-doped fiber lasers and amplifiers operates in conventional wavelength (1030 nm ∼ 1100 nm). Actually, long-wavelength ytterbium-doped fiber lasers beyond 1120 nm provide extensive applications. In this paper, we will report our recent progress in high power long-wavelength ytterbium-doped fiber lasers. We have demonstrated. (1) An all-fiber single-mode YDFL operates at 1.173 μm pumped directly by laser diode, a record output power of 15.7 W is obtained when the pump power is 28 W. (2) An all-fiber single-mode YDFL operates at 1.15 μm pumped directly by laser diode, a record output power of 52.6 W is obtained when the pump power is 90.3 W. (3) An all-fiber single-mode YDFL operates at 1.12 μm pumped directly by laser diode, a record output power of 332 W is obtained when the pump power is 450 W. (4) A hundred-watt level random fiber laser operates at 1.15 μm pumped by 1090 nm fiber laser. For the time-being, amplified spontaneous emission (ASE) and parasitic lasing at the conventional wavelength rang limit the power scaling of long-wavelength ytterbium-doped fiber lasers. We have proposed a new system configuration called by Yb-Raman combined nonlinear fiber amplifier, in this configuration the Stokes wave is amplified by ion gain as well as the Raman gain in the YDF, which resulting in more efficient energy transfer. Finally, we achieve a record power of 732 W 1120 nm laser at the pump power of 890 W.

Dual Wavelength Passively Switched Cascade Ho-doped Fluoride Fiber Laser at 3 μm and 2 μm

Jianfeng Li[1, 2], **Hongyu Luo**[1], **Yulian He**[1], **Lin Zhang**[2], **Sergei K. Turistyn**[2], **and Yong Liu**[1]

[1]State Key Laboratory of Electronic Thin Films and Integrated Devices
School of Optoelectronic Information
University of Electronic Science and Technology of China (UESTC), Chengdu 610054, China
[2]Institute of Photonic and Technology (AIPT), Aston University, Birmingham, UK
[3]Department of Electronic Information Engineering, Chongqing University of Technology, China

Abstract— A diode-cladding-pumped dual wavelength passively switched Ho^{3+}-doped fluoride fiber laser based on a saturable mirror (SESAM) was demonstrated. Three main pulsing regimes were exhibited during the launched pump range from 0.48 W to 6.68 W. The laser began to operate at the stable 2.95 μm Q-switching regime after the threshold of ∼ 0.48 W. As improving pump power, increased repetition rate and pulse energy and narrowed pulse duration were observed as that well characterized in typical Q-switched lasers. Once the pump power reached ∼ 3.76 W, stable pulses at 2.074 μm were observed with a μs-level time delay after ∼ 3 μm pulses, and its repetition rate was half of that for ∼ 3 μm pulses. As further increased pump power, the pulse energies and repetition rates of both 2.95 μm and 2.074 μm pulses increased while pulse durations and time delay of them were shortened. After the launched pump power of ∼ 5.84 W, the 2.074 μm pulses tend to operate at same repetition rate with 2.95 μm pulses, but still operated at a competition state between the two different repetition rates. After the pump power of ∼ 6.47 W, the repetition rate of 2.074 μm pulses was same as that of 2.95 μm pulses while with longer pulse time delay. At the highest launched pump power of ∼ 6.68 W, pulse duration of 0.99 μs and 0.85 μs, pulse energy of 7.47 μJ and 2.36 μJ, repetition rate of 108.34 kHz and 108.29 kHz were obtained with respect to 2.95 μm and 2.074 μm pulses, respectively. The pulses at 2.074 μm were also proved to be the cascaded gain-switching pulsed induced by the Q-switching 2.95 μm transition.

Mode-locked Ho-Pr Fiber Laser Operating at 2.86 µm

Darren D. Hudson
Centre for Ultrahigh bandwidth Devices for Optical Systems (CUDOS)
Institute of Photonics and Optical Science, School of Physics
University of Sydney, Camperdown 2006, Australia

Abstract— We present a mode-locked 2.86 µm fiber laser. Using Holmium-Praseodymium codoped ZBLAN fibers we create a 6 ps pulse train with 0.5 kW peak power, and a time bandwidth product of 1.1.

Introduction: The field of long wavelength fiber lasers is growing very rapidly at the moment. Demonstrations of mode-locked, ultrashort pulse systems at 2 µm using Tm and Ho doped fibers has generated significant interest for applications in eye-safe lidar, remote sensing, and spectroscopy. However, moving beyond 2 µm into the mid-IR remains challenging due to the necessary switch from silica fiber to fluoride fiber (ZBLAN). In this paper, we address these challenges and present the first stable, autocorrelation-confirmed mode-locked fiber of the 3 µm class [1].

Experiment and Results: The laser layout consisted of a ring cavity configuration (see Fig. 1(a)) with a transmission based saturable absorber. The Ho-Pr gain fiber was a double-clad fiber with 30,000 : 2500 doping concentration of Ho-Pr. When pumped below 1.25 W, the laser exhibited Q-switched mode-locking; while above 1.25 W, the laser entered the cw mode-locking regime. To characterize the pulse we built a Mach-Zhender 2-photon InGaAs autocorrelator. Using this device we measured 6 ps pulses coming out of the oscillator (see Fig. 1(b)), assuming a sech pulse shape. The average power was nearly 70 mW and the repetition frequency was 24.8 MHz. The calculated peak power was 0.5 kW, and the bandwidth of the laser indicated that the pulse was chirped and could be compressed down to 1.7 ps.

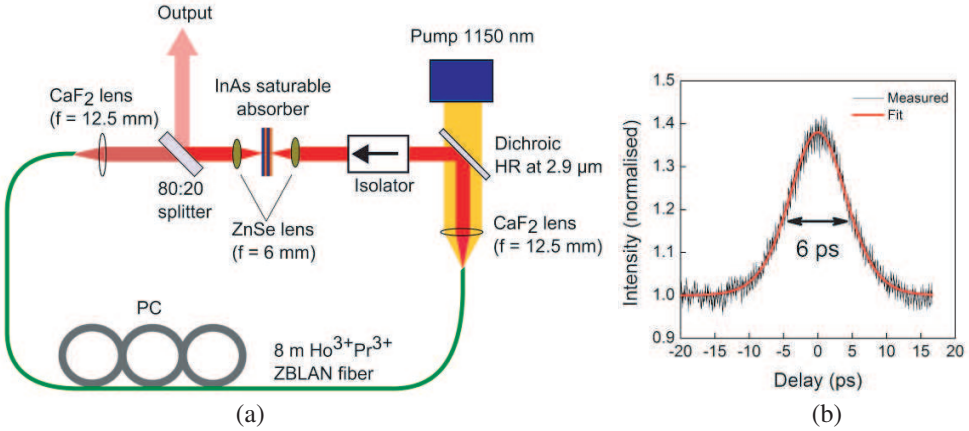

Figure 1: (a) Mode-locked laser cavity layout. (b) Autocorrelation trace showing a stable, 6 ps pulse.

REFERENCES

1. Hu, T., D. Hudson, and S. Jackson, "Stable, self-starting, passively mode-locked fiber ring laser of the 3 µm class," *Opt. Lett.*, Vol. 39, 2133–2136, 2014.

Passively Solitary and Noisy-like Mode-locked Tm-doped Fiber Laser Based on NALM

Hongyu Luo[1], **Yulian He**[1], **Zhuo Li**[1], **Lin Zhang**[2], **Sergei K. Turistyn**[2], **Yong Liu**[1], **and Jianfeng Li**[1, 2]

[1]State Key Laboratory of Electronic Thin Films and Integrated Devices
School of Optoelectronic Information
University of Electronic Science and Technology of China (UESTC), Chengdu 610054, China
[2]Institute of Photonic and Technology (AIPT), Aston University, Birmingham, UK

Abstract— The generation of mode-locked soliton and noise-like pulses is demonstrated in a nonlinear amplifying loop mirror (NALM)-based Tm^{3+}-doped figure-eight fiber laser with net anomalous dispersion. In order to initiate the mode-locking, the launched pump power was increased until the cavity spontaneously mode-locked with multiple pulses and then was reduced to achieve single pulse train. Stable soliton pulses centered at 2030.2 nm with 2.24 nm FWHM were produced at a repetition rate of 10.34 MHz with pulse duration of 1.99 ps and pulse energy of 120.2 pJ. The signal noise ratio (SNR) of $\sim$ 62.5 dB suggested it was stable soliton mode-locking. Once the launched pump power reached 2.8 W, the oscillator can also operate at the noise-like (NL) regime. The NL pulses with SNR of $\sim$ 45 dB, spike width of 573 fs and pulse energy of up to 47.9 nJ were achieved at a center wavelength of 2030.2 nm with a FWHM of 14.87 nm. Decreasing the length of SM 2000 fiber used for generating nonlinear phase shift difference, the initial pump power for both soliton and noise-like mode-locking increased while the pulse duration decreased. Minimum soliton pulse duration of 1.7 ps was achieved by employing 1.0 m SM 2000 fiber. Note that once the length of SM 2000 fiber over than 15.0 m, the mode-locked pulses can not be generated due to the significant large nonlinear phase shift difference which pushed the operating regime to multiple-wavelength regime.

Mid-infrared Supercontinuum Generation in Specialty Optical Fibers

Guanshi Qin
State Key Laboratory on Integrated Optoelectronics, College of Electronic Science and Engineering
Jilin University, 2699 Qianjin Street, Changchun 130012, China

Abstract— Mid-infrared supercontinuum (MIR-SC) light sources have attracted much attention owing to their wide applications in monitoring plasma etching processes, combustion flow monitoring, trace gas sensors for pollution monitoring, and biomedical diagnosis. To generate MIR-SC light source, specialty optical fibers (SOFs, e.g., fluoride, chalcogenide and tellurite fibers) with low loss in the mid-infrared region have been used as the nonlinear medium. In this talk, we will summarize recent progresses on MIR-SC generation in SOFs. Especially, the potential of rare earth ions (e.g., Tm^{3+}, Ho^{3+}) doped SOPs for MIR-SC generation is clarified.

Theoretical Study on Random Laser Based on Active Lasers

Wei Li Zhang, **Shi Wei Li**, **Rui Ma**, **and Yun Jiang Rao**
University of Electronic Science & Technology of China, Chengdu 611731, China

Abstract— Recent years, the studies of fiber lasers have been developed rapidly, many kinds of fiber lasers based on different structures/mechanisms have been reported. In 2010, a novel type of fiber laser, distributed feedback random fiber laser (RFL) based on Raman amplification and distributed Rayleigh scattering (RS) feedback only in a standard single-mode fiber (SMF), was reported by Turistsyn et al. Since then RFLs have been widely studied, due to its simple structure without any 'mirrors' and unique output characteristics. It is believed that RFL is a good candidate of fiber-optic communication and sensing source, due to its stable output with little thermal sensitivity, wide wavelength tenability, excellent noise and modulation characteristics, special incoherence while with a high photonic density of states.

In this paper, we propose a theoretical model to study random lasing in an Er-doped fiber (EDF) and SMF mixed cavity under hybrid pump. In the proposed model, both the Raman gain and stimulated gain mechanisms are considered, which enable us to study random lasing characteristics of different combinations of EDF and SMF. Through a self-consistent iteration method, the model was solved numerically. The results indicate that amplified spontaneous emission (ASE) in the EDF is suppressed and a narrow lasing peak is observed with pump power increasing. Taking use of Rayleigh scattering feedback in SMF and EDF mixed cavity and their hybrid gain, single-wavelength random lasing is obtainable with relative high spectral contrast ratio. All these results are in good accordance with our previous experimental study. This study is useful for fundamental research of random distributed feedback fiber emission, which also provides ways of designing new optical communication and sensing sources.

High Power MOPA Structured Repetition Rates Tunable Tm-doped Fiber Laser

Deqin Ouyang, **Junqing Zhao**, **and Shuangchen Ruan**
Shenzhen Key Laboratory of Laser Engineering
Key Laboratory of Advanced Optical Precision Manufacturing Technology
Guangdong Higher Education Institutes
Shenzhen University, Shenzhen, Guangdong 518060, China

Abstract— We propose a high power MOPA structured 2-μm pulsed all-fiber laser. The pulsed oscillator is self-started by a fiber-coupled acousto-optical modulator (AOM); it can generate pulses with tunable repetition rates due to adjustable working frequencies. The generated pulse durations can also be changed by adjustments of the cavity and the AOM. The tunabilities of the pulsed laser source can offer the most suited choice for power amplification. The seed power was boosted by two-stage double-cladding Tm-doped all-fiber power pre-amplifiers; each stage is pumped by two 12 W, 793 nm LDs. Several watts output power can be obtained after the two-stage power pre-amplification. Six high power 793 nm LDs were used in the main power amplifier stage to boost the output power to tens of watts. The pulses, output power and spectrum properties versus the repetition rates were investigated, respectively. This high power pulsed Tm-doped fiber laser can be used in mid-infrared nonlinear researches, laser processing, laser medicine and radar systems.

The Frequency Gap and SNR Improvement for Self-seeded Multi-wavelength Brillouin-Erbium Fiber Laser

Pinghe Wang and Feng Gao
School of Opto-Electronic Information
University of Electronic Science and Technology of China, Chengdu 610054, China

Abstract— Brillouin-Erbium fiber lasers (BEFL), which integrates the nonlinear gain of single mode fiber and the linear gain of erbium doped fiber, is first demonstrated by G. J. Cowle et al.. The BEFL has drawn a lot of interest in recent years because of its unique properties-narrow linewidth and high output power. Multiwavelength BEFL can be generated by cascaded stimulated brillouin scattering effect. 150 lines are generated by enhanced four wave mixing effect in the cavity. In 2005, Song et al. reported the self-seeded BEFL that generated 120 lines. A little later, a self seeded BEFL with 200 lines was report by the same group.

The frequency gap of the multiwavelength is equal to the Brillouin frequency shift f_B which depends on the fiber material. For single mode fiber (SMF) based on silica, it is about 10 GHz ($\sim$0.08 nm). The narrow frequency gap limits the applications of the multiwavelength BEFL in system implementation. Some researchers are interested in expanding the channel spacing. Recently, Y. G. Shee et al. reported a multiwavelength BEFL with 20 GHz frequency spacing. A four ports circulator is used to combine two cavities. The light output from the unidirectional cavity has the 20 GHz frequency gap.

In this paper, we propose a self-seeded multiwavelength BEFL with 20 GHz frequency gap. The relation between the pump power and the spectra is investigated. 36 output channels with 20 GHz gap are generated when the pump power is 300 mW. The factor that induces the double frequency gap is investigated and proved.

Session 4A8a
SC2: Plasmon Enhanced Light-matter Interactions

Giant Chiroptical Properties of Molecules in Hot Spots

Xiangdong Zhang[1], **Rong-Yao Wang**[1], **Yineng Liu**[1, 2], **Tong Wu**[1], **and Jun Ren**[1]

[1]School of Physics, Beijing Institute of Technology, Beijing 100081, China
[2]Department of Physics, Beijing Normal University, Beijing 100875, China

Abstract— Recently, there are great interest in studying the interaction between chiral molecules and plasmonic particles, because a weak circular dichroism (CD) signal in the ultraviolet (UV) region from chiral molecules can be both enhanced and transferred to the visible wavelength range by using plasmonic particles. Thus, ultrasensitive probe of tiny amounts of chiral substance by CD are worth waiting for. Here we present another way to strongly enhance CD of chiral molecules by using plasmonic particle cluster, which need not transfer to the visible wavelength. The method to calculate CD of chiral molecules in nanosphere clusters has been developed by means of multiple scattering of electromagnetic multipole fields. Our calculated results show that 2 orders of magnitude CD enhancement in the UV region for chiral molecules can be realized. Such a CD enhancement is very sensitive to the cluster structure. The cluster structure can cause chiroptical illusion in which a mirror symmetry in the CD spectra of opposite enantiomeric molecules is broken. The correction of quantum size effect on the phenomenon has also been considered. Our findings open up an alternative avenue for the ultrasensitive detection and illusion of chiral information. Furthermore, we have found that giant superchiral properties of fields in hot spots for the non-chiral structure. We have also found that the enhancement of CD does not necessarily correspond to the enhanced electromagnetic field intensity at hot spots. It is determined by superchiral fields at the hot spots.

Emission of a Point Dipole Mediated by Multiple Fano Resonances in Plasmonic Nanostructures

X. M. Zhang, **Q. Zhang**, **F. F. Qin**, **and J. J. Xiao**
College of Electronic and Information Engineering, Shenzhen Graduate School
Harbin Institute of Technology, Shenzhen, Guangdong 518055, China

Abstract— The optical emission of a dipole-like nano-emitter close to the plasmonic disk-ring structures (DRN) is studied in the frame work of the discrete dipole approximation. By placing the dipole source inside the gap and at the apex of the system in the DRN, we find that multiple Fano resonances are strongly affected by the dipole positions and its polarization and the dipole-multipole hybridization is crucial in engineering the radiative and nonradiative decay rates. Our results may find applications in passive and active plasmonic structure that sustain bight and dark mode coupling.

Absorption and Polarization Manipulation with Stereostructured Metamaterials

X. Xiong, S. C. Jiang, Y. S. Hu, R. W. Peng, and M. Wang
National Laboratory of Solid State Microstructures, Department of Physics
Nanjing University, Nanjing 210093, China

Abstract— The flat metal surface can be used as a reflector (mirror), which has been known for thousands of years. In fact, a metal film just a few tens of nanometer in thickness may have more than 99% reflection and less than 0.1% transmission over a very broad band of frequency. However, once microstructures are introduced to metallic thin film, the situation becomes different. With certain sub-wavelength metallic structures, it is possible to achieve some novel electromagnetic properties, such as negative refractive index, invisibility cloaking and optical magnetics. Among the massive researches in this area, two of the intensively studied subjects are the constructions of metamaterial absorber, and metamaterial wave plate. For metamaterial absorber, it neither reflects nor transmits the incident light, and the energy of the incident light is mostly absorbed. This function makes the absorber promising for applications in photovoltaic solar cell, microbolometers, and high sensitive detectors, etc.. For metamaterial wave plate, traditionally a birefringence crystal plate can realize this function by accumulating the phase difference of light in two orthogonal directions along the optical path. Yet in some circumstances, e.g., in integrated optics, space is extremely limited. It is therefore necessary to find new approaches to construct ultrathin, broadband, and full-function wave plates. Here we report a new type of the absorber and waveplate constructed with 3D stereostructured metamaterials. Electromagnetic absorption and polarization manipulation can be realized with 3D structure design, which offers a new pathway helps to make the ultimate dream of mastering light on the nanoscale come true.

REFERENCES

1. Xiong, X., S. C. Jiang, Y. H. Hu, R. W. Peng, and M. Wang, "Structured metal film as a perfect absorber," *Adv. Mat*, Vol. 25, 3994, 2013.
2. Xiong, X., Z. H. Xue, C. Meng, S. C. Jiang, Y. H. Hu, R. W. Peng, and M. Wang, "Polarization-dependent perfect absorbers/reflectors based on a three-dimensional metamaterial," *Phy. Rev. B*, Vol. 88, 115105, 2013.
3. Jiang, S. C., X. Xiong, P. Sarriugarte, S. W. Jiang, X. B. Yin, Y. Wang, R. W. Peng, D. Wu, R. Hillenbrand, X. Zhang, and M. Wang, "Tuning the polarization state of light via time retardation with a microstructured surface," *Phy. Rev. B*, Vol. 88, 161104(R), 2013.
4. Jiang, S. C., X. Xiong, Y. S. Hu, Y. H. Hu, G. B. Ma, R. W. Peng, C. Sun, and M. Wang, "Controlling the polarization state of light with a dispersion-free metastructure," *Phy. Rev. X*, 2014.

Light-trapping in Single Nanowire Photodetectors by Using Metallic Slits

Yaohui Zhan, Xiaofeng Li, and Shaolong Wu
Key Lab of Advanced Optical Manufacturing Technologies of Jiangsu Province
Key Lab of Modern Optical Technologies of Education Ministry of China
Collaborative Innovation Center of Suzhou Nano Science and Technology
Institute of Modern Optical Technologies, Soochow University, Suzhou 215006, China

Abstract— Single nanowire photodetectors (SNPDs) have recently gained a lot of attention since they are promising candidates of the key components constituting the integrated photonic circuit and integrated electrical circuit. However, due to much reduced photoactive material, the scale down of photodetectors also encounters a fundamental limit of the degraded photoabsorption. To improve the photoresponsivity of SNPDs, we focus on a light-trapping strategy of metallic slits and investigate comprehensively the light-matter interaction in such a slit-coupled system. The results demonstrate that as the germanium SNPD is confined inside a silver slit, properly engineering the slit into superwavelength scale is able to dramatically enhance the SNPD photoresponse to transverse electric incidence. The light absorption of the device with such design can be over 3.7 times higher than its subwavelength counterpart based on plasmonic resonance under transverse magnetic incidence. An extensive investigation on polarization dependence, field profile, photon flux distribution and azimuthal absorption pattern in the SNPD reveals that the underlying mechanisms responsible for the significant performance enhancement is the optimal photodetector-light coupling, benefited from strong light concentration inside the slit cavity. This work provides us new insights into the design of highly sensitive SNPDs.

Silver Plasmonic Supercrystals Synthesized via Bottom-up Strategy for Enhanced Light-matter Interactions

Cuifeng Tian and Jixiang Fang
School of Science, Xi'an Jiaotong University, Shaanxi 710049, China

Abstract— Geometrically precise control of plasmonic periodic structures provides unique optical and photonic phenomena, such as negative refraction, plasmonic waveguide, electromagnetic invisibility cloaks, Fano resonance and surface enhanced Raman scattering (SERS), et al.. Lithographic techniques may successfully fabricate well-ordered patterned arrays. However, these techniques are associated with limitations in throughput and cost. Importantly, it is still difficult to process small nanogaps to sub-5 nm, i.e., 1–2 nm. With the assistance of surface ligands, nanoparticles can be assembled into superlattices, but the introduction of polymer ligands unavoidably sacrifices the coupling effect between light and nanostructures. In this presentation, for the first time, we report the preparation of highly ordered Ag plasmonic supercrystals by a bottom-up strategy using ordered mesoporous silica as a template through chemical reduction approach. The ordered silver plasmonic supercrystals fabricated using large-pore silica as a template, i.e., pore size of ~ 28 nm and wall thickness of ~ 2 nm, exhibit an enhanced light-matter coupling effect. Particularly, we examined the surface enhanced Raman spectroscopy using the obtained silver plasmonic supercrystals, which demonstrate an ultrahigh Raman enhancement with an average enhancement factor of $\sim 10^9$. The current strategy, as a seminal piece of work, could lead to a new class of plasmonic nanostructures and open extraordinary potentials for diverse applications.

REFERENCES

1. Ou, F. S., M. Hu, I. Naumov, A. Kim, W. Wu, A. M. Bratkovsky, X. Li, R. S. Williams, and Z. Li, *Nano Lett.*, Vol. 11, 2538–2542, 2011.
2. Henzie, J., M. Grunwald, A. Widmer-Cooper, P. L. Geissler, and P. D. Yang, *Nature Mater.*, Vol. 11, 131–137, 2011.
3. Tian, C. F., L. Zhang, Y. H. Deng, D. Y. Zhao, and J. X. Fang, submitted.

Threading Plasmonic Nanoparticle Strings with Light

Ventsislav K. Valev[1], **Lars O. Herrmann**[1], **Christos Tserkezis**[2], **Jon S. Barnard**[3], **Oren A. Scherman**[4], **Javier Aizpurua**[2], **and Jeremy J. Baumberg**[1]

[1]NanoPhotonics Centre, Cavendish Laboratory, University of Cambridge, UK
[2]Donostia International Physics Center DIPC and Centro de Física de Materiales CSIC-UPV/EHU
Paseo Manuel de Lardizabal 5, Donostia-San Sebastián, 20018, Spain
[3]Department of Materials Science & Metallurgy, University of Cambridge
27 Charles Babbage Road, Cambridge CB3 0FS, UK
[4]Melville Laboratory for Polymer Synthesis, Department of Chemistry, University of Cambridge, UK

Abstract— Individual plasmonic nanoparticles (NPs) are the constitutive building elements for bottom-up assembled nano- and meta-materials. At the most fundamental level these nanomaterials consist of NP chains, in which single NPs are attached together with molecules. Here we demonstrate the next stage towards achieving continuous bottom-up assembled meta- and nanomaterials. We demonstrate that ultrafast laser pulses can produce a continuous metal thread bridging the chains, thereby allowing charge transfer [1]. The process is characterized by the appearance of a novel plasmon mode, exhibiting both chain- and rod-like features. Upon assembly, real-time monitoring of this plasmon mode enables highly precise control (±3 nm) over the width of the thread.

Novel optical materials are finding increasing applications in transport, communications, healthcare and sensing. Just as light is used to characterize optical materials, light can also be used to build them. Ultrafast lasers have previously been used to shape continuous metal surfaces with diverse micro and nanostructures, such as ripples, needles, nanobumps, cavities and nanojets. Nanojets [2], promising for threading, are columns of liquid material, frozen in the process of surging from the metal surface in the direction opposite to that of the incoming laser pulse. However it is exceedingly difficult to align single nanostructures so that nanojets from opposite nanostructures would face each other. This limitation can be circumvented with surface plasmon resonances — the coherent oscillation of surface electrons. Plasmons enlarge even further the electric field of intense femtosecond pulses and localize it to sub-wavelength regions ('hotspots'). In dimers, or chains of plasmonic NPs, the plasmonic hotspots occur in the regions directly across the gap. It is consequently possible to form a continuous thread in such dimers or chains of nanoparticles, from first stage of nanoscale assembly [3].

In our work, assembly proceeds in water at an unprecedented large scale. Our results indicate that the width of the thread depends on the size of the nanoparticles, on the plasmon resonance wavelength of the chain modes, on the peak-to-peak laser power and on the number of nanoparticles in the chains, which can all be used to tune the optical properties of this novel type of material. Large-scale metamaterial manufacturing is thus in prospect.

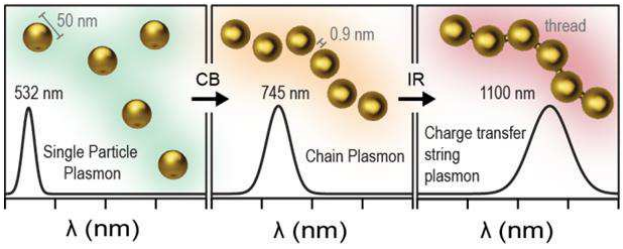

Figure 1: Schematic nano-threading optical assembly.

REFERENCES

1. Herrmann, L. O., et al., "Threading plasmonic nanoparticles with light," *Nat. Commun.*, 2014, submitted.
2. Valev, V. K., et al., "Plasmon-enhanced sub-wavelength laser ablation: plasmonic nanojets," *Adv. Mater.*, Vol. 24, OP29, 2012.
3. Taylor, R., et al., "Precise subnanometer plasmonic junctions for SERS within gold nanoparticle assemblies using cucurbit[n]uril "glue"," *ACS Nano*, Vol. 5, 3878, 2011.

Resonance Enhanced Luminescence of Single Upconversion Nanoparticle Using Plasmonic Gold Nanorods

Xin Zhang, Jing Liu, and Qiuqiang Zhan
Centre for Optical and Electromagnetic Research
South China Normal University, Guangzhou 510006, China

Abstract— Converting near infrared light to visible light via upconversion nanoparticles (UCNPs) has been explored for optical bioimaging [1] and biotherapy [2]. However, the low quantum yield due to small absorption cross-section, slow rate of energy transfer and surface defects have hindered its wide applications [3]. In this work, a novel and facile strategy to enhance the luminescence of UCNPs in single nanoparticle level under microscopy is proposed based on gold nanorods (GNRs) uniformly immobilized chip. Scanning electron microscope (SEM) and atomic force microscopy (AFM) images obtained from different areas of the chips confirmed the uniformity of the monolayer GNRs without any aggregation, and their density are tunable via controlling the concentration of GNRs and the speed of rotator. It was demonstrated that large luminescence enhancement (larger than 50-fold) of single ultrasmall $ZrO_2 : Yb^{3+}$, Er^{3+} UCNP based on single GNR can be achieved. This enhancement could attribute to these two factors: enhancement of excitation and Purcell effect [4]. Significant spectroscopy overlap among longitudinal localized surface plasmon resonances (LSPR) of GNRs, absorption of Yb^{3+}, and the exciting light promote the enhancement of excitation. Purcell effect can change the emission intensity, fluorescence lifetime and quantum yield. Combined with these two effects, the largest enhancement could be acquired at the optimum position of the UCNPs with respect to the GNRs. The green emission bands (523 nm and 542 nm) can be further enhanced by the transverse LSPR of GNRs around 520 nm, contrary to the red emission. This GNRs immobilized chips are easy to manufacture and much cheaper than the other patterned substrates fabricated by physical methods [5]. This promising approach could give a new sight of enhancing luminescence of UCNPs and have important implications for detecting weak upconversion luminescence.

REFERENCES

1. Zhan, Q., J. Qian, H. Liang, et al., "Using 915 nm laser excited $Tm^{3+}/Er^{3+}/Ho^{3+}$-doped $NaYbF_4$ upconversion nanoparticles for in vitro and deeper in vivo bioimaging without overheating irradiation," *ACS Nano*, Vol. 5, No. 5, 3744–3757, 2011.
2. Zhang, P., W. Steelant, M. Kumar, et al., "Versatile photosensitizers for photodynamic therapy at infrared excitation," *Journal of the American Chemical Society*, Vol. 129, No. 15, 4526–4527, 2007.
3. Xu, C. T., Q. Zhan, H. Liu, et al., "Upconverting nanoparticles for pre-clinical diffuse optical imaging, microscopy and sensing: Current trends and future challenges," *Laser & Photonics Reviews*, Vol. 7, No. 5, 663–697, 2013.
4. Purcell, E., "Spontaneous emission probabilities at radio frequencies," *Confined Electrons and Photons*, 839–839, Springer, 1995.
5. Sun, Q.-C., H. Mundoor, J. C. Ribot, et al., "Plasmon-enhanced energy transfer for improved upconversion of infrared radiation in doped-lanthanide nanocrystals," *Nano Letters*, Vol. 14, No. 1, 101–106, 2013.

Session 4A8b
SC1,3&4: Photonics-applied Electromagnetic Measurement: Fundamental Study, Applications, and Standards

Far-field Antenna Factor Measurement for Broadband Antennas Using a Compact Radio on Fiber Modules

Satoru Kurokawa
Electromagnetic Fields Section, Electromagnetic Waves Division
NMIJ/AIST, Japan

Abstract— We propose a simple optical fiber link microwave measurement system that consists of a vector network analyzer, two modules of Electric signal to optical signal converter and a module of optical signal to electric signal converter. The system can measure S-parameters of two-port devices using a vector network analyzer (VNA) in full 2-port calibration. In this paper, we show frequency characteristics, the time stability and the ambient temperature stability of the simple optical fiber link system for the antenna properties measurement. Further, we show the far-field antenna factor measurement results for EMI broadband antennas using our proposed simple optical fiber link modules.

Comparison of Photonic Sensor and OEWG as the Probe for Near-field Antenna Measurements

Masanobu Hirose and Kurokawa Satoru
AIST, NMIJ, Japan

Abstract— We compare and show the advantages on the antenna patterns measured by a photonic sensor and an open-ended waveguide (OEWG) as the probe in the near-field antenna measurements. The photonic sensor can be treated as an infinitesimal dipole antenna below about 10 GHz because the photonic sensor consists of 5 metal strip (3 mm × 0.1 mm) array on a 3 mm × 8 mm × 0.5 $LiNiO_3$ substrate. On the other hand, the OEWG is a metallic rectangular cylinder and it aperture size is about half wavelength. Those characteristics derive all advantages of the photonic sensor and the OEWG used as the probe in the antenna near-field measurements. We demonstrate those by measurements by various antennas.

Product Trends of Optical *E*-field Sensor

Yoshikazu Toba[1], **Jun Ichijoh**[1], **Takehiro Morioka**[2], **Masanobu Hirose**[2], **and Satoru Kurokawa**[2]

[1]SEIKOH GIKEN Co., Ltd. 296-1, Matsuhidai, Matsudo, Chiba 270-2214, Japan
[2]National Institute of Advanced Industrial Science and Technology
1-1-1, Umezono, Tsukuba, Ibaraki 305-8563, Japan

Abstract— We have developed the Optical Electric Field Sensor utilizing the the Pockels effect of lithium niobate ($LiNbO_3$), and proposed it for EMC measurement.

This sensor can measure not only *E*-field strength but also frequency and phase. The feature of this sensor are: mitigating disturbance of the surrounding *E*-field, high-accuracy, elimination of common noise, small sensor head, measurement ability of any kinds of modulations such as AM, FM, CDMA and so on and wide frequency range such as 100 kHz to 10 GHz.

In this paper, I introduce some applications of the optical electric field sensor. And I describe the efforts of some of the future.

Antennas Design for Electric/Optical Sensors of High Sensitivity

Qiang Chen and Hiroto Abe
Tohoku University, Japan

Abstract— The problem of electromagnetic interference between electrical circuits and devices is becoming more and more serious because the clock frequency of the electrical circuits is increasing rapidly, and high-density packaging and multilayer printed circuit board (PCB) technologies are widely applied to PCB design. In order to estimate the radiation source of unnecessary electromagnetic waves inside the electronic devices, it is important to measure the near field distribution on the PCB with a very high resolution. On the other hand, the EM measurement at low frequency band is also very important for some kHz and MHz band applications. In all of these EM measurements, small electromagnetic probe with low interference to distribution of electromagnetic field is desired.

Electric/Optical (E/O) sensor using electro-optical effect is suitable to these measurements because the metal feed cable of the probe is not required and the frequency band of the sensor is very wide especially in low frequency ban. But this technique has a problem of low sensitivity or low gain.

In this research, the design method of the antenna for E/O sensors for measurement of electric field with high sensitivity and high gain is studied. In the antenna design approach, devices including optical modulator, demodulator and active circuit are regarded as a 2-port equivalent circuit. The antenna is developed to match the impedance of the 2-port equivalent circuit based on the measurement results of 2-port scattering parameters of the equivalent circuits. Moreover, the design method of the dipole type antenna is shown as a design example and the performance of the designed antenna is demonstrated by experiment.

ACKNOWLEDGMENT

This work is partly supported by JSPS Grant-in-Aid for Scientific Research (C) of Grant Number 25420353.

Wireless Microwave to Lightwave Signal Converter Using Electro-optic Modulator with Antenna-coupled Electrode

Hiroshi Murata, Takahiro Kohmu, Takashi Ikeda, and Yasuyuki Okamura
Graduate School of Engineering Science, Osaka University, Japan

Abstract— Recently, the photonics-applied electromagnetic field measurement technology is attracting a lot of interest owing to possibility of non-destructive field measurement and remote sensing. A key device of this technology is a converter from wireless microwave to lightwave signal using an electro-optic (EO) modulator. We have proposed several EO modulators utilizing antenna-coupled modulation electrodes for the electromagnetic field measurement. In this presentation, a new device using antenna-coupled electrodes and a thin EO crystal stacked structure is reported. By utilizing a stacked substrate structure composed of a thin ($\sim 50\,\mu$m) $LiNbO_3$ crystal and a low-dielectric-constant base plate, high-efficiency conversion from wireless-microwave to lightwave is obtainable in high-frequency ranges. The proposed device was designed in a 60 GHz band and its basic operations were demonstrated successfully. The design of multi waveguide devices for the directivity control is also reported.

Session 4A9
FocusSession.SC3: Ultrafast Optics

Ultrafast Lasers for Material Processing and Imaging at Miro/Nanoscales

Yong Feng Lu[1], **Yun Shen Zhou**[1], **Wei Xiong**[1], **Li Jia Jiang**[1], **Xi Huang**[1], **Jean-Francois Silvain**[1, 2], **and Lan Jiang**[3]

[1]Department of Electrical Engineering, University of Nebraska-Lincoln
Lincoln, NE 68588-0511, USA
[2]Université Bordeaux 1, Institut de Chimie de la Matière Condensée de Bordeaux (ICMCB)
CNRS, Pessac 33608, France
[3]Department of Mechanical and Automation Engineering
Beijing Institute of Technology, Beijing 100081, China

Abstract— The development of ultrafast lasers has provided tremendous opportunities for material processing and imaging. In this talk, the author will present their recently works in these areas, including additive and subtractive fabrication of three-dimensional (3D) micro/nanostructures, laser direct writing of graphene patterns in ambient air, and 3D imaging of biomedical samples.

Additive nanofabrication by two-photon polymerization (TPP) has recently drawn increased attention due to its sub-100 nm resolution and truly 3D structuring capability. Besides additive processes, subtractive process is also indispensable for various 3D fabrications. In modern 3D micro/nanofabrication, the combination of both additive and subtractive fabrication steps is not only desired but also demanded. However, method possessing both additive and subtractive fabrication capabilities was rarely reported. Recently, we developed a complementary 3D micro/nanofabrication process by integrating both additive two-photon polymerization (TPP) and subtractive multi-photon ablation (MPA) into a single platform of femtosecond-laser direct writing process. Functional device structures were successfully fabricated including: polymer fiber Bragg gratings containing periodic holes of 500-nm diameter and 3D micro-fluidic systems containing arrays of channels of 1-μm diameter. The integration of TPP and MPA processes enhances the micro/nanofabrication efficiency and enables the fabrication of complex 3D micro/nanostructures that are impractical to produce by either TPP or MPA alone. The new 3D micro/nanofabrication method is promising for a wide range of applications including integrated optics, metamaterials, microelectromechanical systems, and micro-fluidics.

Large-scale and high-quality graphene patterns on dielectric substrates have a wide range of promising application such as touch screen display, smart window, flexible solar cells, etc.. Current fabrication methods generally require close-chamber and high-temperature processes for the graphene synthesis plus a multi-step patterning process, which is costly and unsuitable for the industrial manufacturing. We have developed an additive nanofabrication method for fabricating arbitrary graphene patterns at the ambient conditions. Open-air and room-temperature deposition of bi-layer graphene patterns on glass substrates has been achieved via a femtosecond laser direct wring process based on nickel/amorphous carbon (a-C) co-sputtered thin films. Arbitrary patterns of graphene lines can be formed directly on the glass substrates without additional graphene transfer steps. No vacuum and substrate heating are required in the graphene growth process. The formation of graphene in the laser direct writing process follows a solid-state transformation mechanism. Various graphene patterns, including texts, spirals, line arrays, and large-scale integrated circuit patterns, with a feature line width of 800 nm, were successfully fabricated. The laser direct writing technique could provide an innovative, cost-effective way to fabricate large-scale graphene patterns for future practical device applications.

Broadband coherent anti-Stokes Raman spectroscopy (CARS) and microscopy system based on a photonic crystal fiber light source has been used to study biological and medical samples. The pump pulses have a narrow bandwidth and define the spectral resolution. The Stokes pulses are spectrally broad in 700–1100 nm. The pump and Stokes pulses excite multiple Raman transitions within the bandwidth of the Stokes pulses. Vibrationally excited states are probed with a third spectrally narrow probe pulse, usually the same as the pump pulse. In a single shot, the entire CARS spectrum of the excited states is generated. Both the pump and Stokes beams are provided by a single fs laser in conjunction with a supercontinuum generator, which is optimized for performing broadband CARS microscopy. The supercontinuum ensures that broadband anti-Stokes spectra can be obtained without tuning the laser wavelength. The CARS

system has been used to obtain CARS spectra and chemically specific 3D images of biological (such as algal cells) and medical (such as neuro, artery, and liver cells) samples.

Ultrabroadband Infrared Spectroscopy by Chirped Pulse Upconversion

Takao Fuji, Yutaka Nomura, and Hideto Shirai
Institute for Molecular Science, Japan

Abstract— Single-shot detection of an entire MIR spectrum (500–5000 cm^{-1}) has been required for advanced molecular spectroscopy such as pump-probe spectroscopy to trace ultrafast structural dynamics of molecules, real-time molecular imaging of biological tissues, etc.. However, due to low pixel numbers, low sensitivity, and high cost of multichannnel MIR detectors, the bandwidth has been limited to $\sim 500\,\mathrm{cm}^{-1}$ at direct measurement of MIR spectra by using dispersive infrared spectrometers.

Chirped-pulse upconversion is an alternative approach to detect an MIR spectrum with single-shot. By converting the wavelength of coherent MIR pulse to visible range, it becomes possible to detect MIR spectra with a visible spectrometer, which has much higher performance than MIR spectrometers. However, the bandwidth of the chirped-pulse upconversion has still been limited to $\sim 1000\,\mathrm{cm}^{-1}$ because of the limited transmission range of the nonlinear crystals [1].

In this invited talk, we present ultrabroadband detection of MIR spectra on a single-shot basis using chirped-pulse upconversion with four-wave difference frequency generation (FWDFG) in gases [2]. By using a gas as a nonlinear medium, the detection bandwidth becomes dramatically broad due to wide transmission range of gas media.

Experimental demonstration of the scheme was realized with the system described as follows. We generated sub-single-cycle MIR pulses by using four-wave mixing of the fundamental and the second harmonic of Ti:sapphire amplifier (Femtopower compactPro, FEMTOLASERS) output through filamentation in nitrogen, which is basically the same generation scheme as that reported in Refs. [3–5]. A small portion of the fundamental pulse (0.1 mJ) before the compressor of the Ti:sapphire amplifier was used as a chirped pulse, whose pulse duration was 10.3 ps.

The chirped pulse $E_{\mathrm{ref}}(t-\tau)$ and the MIR pulse ($E_{\mathrm{IR}}(t)$, 0.5 μJ) were focused into xenon with a parabolic mirror ($f = 50\,\mathrm{mm}$) and generated a FWDFG signal, $E^2_{\mathrm{ref}}(t-\tau)E^*_{IR}(t)$, which spread from 400 nm to 550 nm. The spectrum of the FWDFG signal was measured with a conventional spectrometer with a camera EMCCD (ProEM+1600, Princeton Instruments). The camera was synchronized with the repetition rate (1 kHz) of the laser and the spectrum was measured with a single shot, namely within 1 ms. Fine structure due to absorption of carbon dioxide ($\sim 2300\,\mathrm{cm}^{-1}$) and water vapor ($\sim 1600\,\mathrm{cm}^{-1}$ and $\sim 3700\,\mathrm{cm}^{-1}$) in air was clearly observed. At the conference, we plan to show the application of the system to attenuated total reflection spectroscopy.

REFERENCES

1. Baiz, C. R. and K. J. Kubarych, "Ultrabroadband detection of a mid-IR continuum by chirped-pulse upconversion," *Opt. Lett.*, Vol. 36, No. 2, 187–189, 2011.
2. Nomura, Y., Y. T. Wang, T. Kozai, H. Shirai, A. Yabushita, C. W. Luo, S. Nakanishi, and T. Fuji., "Single-shot detection of mid-infrared spectra by chirped-pulse upconversion with four-wave difference frequency generation in gases," *Opt. Express*, Vol. 21, No. 15, 18249–18254, 2013.
3. Fuji, T. and T. Suzuki, "Generation of sub-two-cycle mid-infrared pulses by four-wave mixing through filamentation in air," *Opt. Lett.*, Vol. 32, No. 22, 3330–3332, 2007.
4. Nomura, Y., H. Shirai, K. Ishii, N. Tsurumachi, A. A. Voronin, A. M. Zheltikov, and T. Fuji., "Phase-stable sub-cycle mid-infrared conical emission from filamentation in gases," *Opt. Express*, Vol. 20, No. 22, 24741–24747, 2012.
5. Fuji, T. and Y. Nomura, "Generation of phase-stable sub-cycle mid-infrared pulses from filamentation in nitrogen," *Appl. Sci.*, Vol. 3, No. 1, 122–138, 2013.

Multicore Large-mode Area Photonic-crystal-fiber Platform for High-power Ultrashort-pulse Sources

Ming-Lie Hu
Ultrafast Laser Laboratory, College of Precision Instruments and Opto-electronics Engineering
Tianjin University, Tianjin 300072, China

Abstract— Recently, basing on some of these novel properties, photonic crystal fibers have been successfully applied in femtosecond laser technology and pushed the performance of femtosecond fiber laser to match with the solid-state femtosecond laser system. A brief review of recent work on high power femtosecond photonic crystal fiber laser oscillator, amplifier is presented. A compact nonlinear amplification without stretcher is applied in this system and phase locked amplification with multi-core large mode area PCF (which is shown in Fig. 1) greatly enhances the system performance. A 150 MW peak power [1] and 110 W average power femtosecond laser are obtained respectively [2]. Furthermore, a seven-core nonlinear PCF is present and the high power suppercontinuum is generated from this new fiber [3]. We believe that a feasible scenario in future applications of high pulse energy femtosecond PCF laser will come soon.

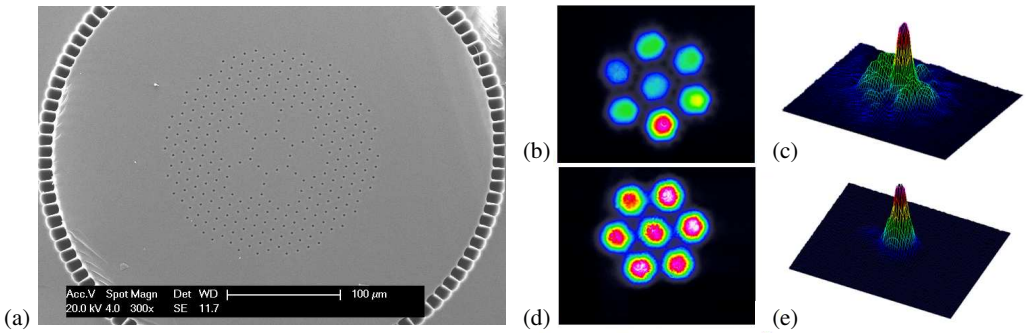

Figure 1: (a) Scanning electron microscope image of the cross section of the seven-core PCF. (b), (c) Beam profiles of the multicore PCF output measured with out of phase and (d), (e) in phase (b), (d) in the near and (c), (e) far fields.

REFERENCES

1. Fang, X.-H., M.-L. Hu, et al., *Opt. Lett.*, Vol. 35, No. 14, 2326–2328, 2010.
2. Huang, L., M.-L. Hu, et al., *Opt. Express*, to be submitted.
3. Fang, X.-H., M. Hu, et al., *Opt. Lett.*, Vol. 37, No. 12, 2292–2294, 2012.

Attosecond-Jitter Fiber Lasers and Their Microwave Photonic Applications

Jungwon Kim
KAIST, Korea

Abstract— In the last few years, we have focused on the characterization and optimization of timing jitter in mode-locked fiber lasers, and different types of fiber lasers with well below 100-attosecond timing jitter [1, 2] have been demonstrated. Using such attosecond-jitter fiber lasers, here we show some new ultrahigh-precision microwave photonic systems.

The first application is ultralow phase noise microwave signal synthesis directly from mode-locked fiber lasers. By using sub-100-attosecond jitter Er-fiber lasers, we could directly generate 10-GHz microwave signals with sub-500-attosecond jitter (integration bandwidth: 10 kHz–10 MHz) and −157 dBc/Hz phase noise at 100 kHz offset frequency [3].

Attosecond-stability synchronization between mode-locked fiber lasers and microwave signals is also demonstrated. By using a differentially-biased fiber-loop Sagnac interferometer idea, we developed an all-fiber phase detector that directly detects the phase error between the optical pulse train and the microwave signals, named the fiberloop optical-microwave phase detector (FLOM-PD). By using this device, we could show 800-attosecond jitter and drift (over 2 hours) synchronization [4] between an Er-fiber laser and a 10-GHz microwave oscillator. This synchronization technique is already used for accelerator-based light sources and ultrafast electron diffraction sources.

Finally, by using the FLOM-PD as a means for fiber link stabilization, we showed that 2.856-GHz microwave signal transfer over a 2.3-km fiber with 6.5×10^{-19} fractional frequency instability [5]. This instability level is so far the lowest for the microwave transfer by frequency combs over km-scale fiber links, and is only limited by the polarization mode dispersion (PMD) of the SMF-28 fiber used.

REFERENCES

1. Kim, T., et al., "Sub-100-as timing jitter optical pulse trains from mode-locked Er-fiber lasers," *Opt. Lett.*, Vol. 36, 4443, 2011.
2. Kim, H., et al., "Sub-20-attosecond timing jitter mode-locked fiber lasers," *IEEE J. Sel. Top. Quantum Electron.*, Vol. 20, 901108, 2014.
3. Jung, K., et al., "Ultralow phase noise microwave generation from mode-locked Er-fiber lasers with subfemtosecond integrated timing jitter," *IEEE Photon. J.*, Vol. 5, 5500906, 2013.
4. Jung, K., et al., "Subfemtosecond synchronization of microwave oscillators with mode-locked Er-fiber lasers," *Opt. Lett.*, Vol. 37, 2958, 2012.
5. Jung, K., et al., "Frequency comb-based microwave transfer over fiber with 7×10^{-19} instability using fiberloop optical-microwave phase detectors," *Opt. Lett.*, Vol. 39, 1577, 2014.

Passively Mode-locked Lasers at Around 2 µm with Optical Superlattice

Xiaopeng Hu, Huan Cheng, Jiong Zou, and Shining Zhu
National Laboratory of Solid State Microstructures and School of Physics
Nanjing University, Nanjing 210093, China

Abstract— Solid-state ultrafast mode-locked lasers in the 2-µm wavelength region have received increasing interests in recent years due to their broad applications in photo-medicine, remote sensing, optical communication, time-resolved molecular spectroscopy, minimally invasive surgery, as well as pumping sources for coherent X-ray generation and synchronously-pumped optical parametric oscillators operating in the mid-infrared region around and above 5 µm. In the past two decades, Tm^{3+}-doped, and Tm^{3+}, Ho^{3+}-co-doped materials have been used as laser gain media to realize ultrafast 2-µm lasers through both active and passive mode-locking approaches. In most passively mode-locked 2-µm lasers, ultrafast pulses are produced by using intra-cavity saturable absorbers (SA). The reported pulses durations range from a few picoseconds to hundreds of femto-seconds with different laser gain crystals. Intra-cavity frequency doubling provides an alternative passively mode-locking scheme other than saturable absorbers. The frequency doubling crystal can be either birefringence-phase-matching (BPM) materials or quasi-phase-matching (QPM) ones. When QPM materials are used as intra-cavity frequency doubling crystals, it is feasible to realize mode-locking at any wavelength in the nonlinear crystal's transparent spectral range, especially for those lasers working at wavelengths where no SESAMs exist. Here we report, for the first time to our knowledge, a diode-pumped Tm : YAP ultrafast laser operating at 1988 nm based on the cascaded second-order nonlinearity mode-locking (CSML) scheme. The nonlinear crystal used in the experiment was a periodically-poled $LiNbO_3$ (PPLN). Near-transform-limit pulses with 6.5-ps and 4.7-ps durations were achieved at the output powers of 1.67 W and 1.05 W respectively, with the repetition rate being 97.09 MHz.

All-optical Ultrafast Control of SOI Waveguide Elements Employing Localized Absorption

Roman Bruck and Otto L. Muskens
Physics and Astronomy, Faculty of Physical Sciences and Engineering
University of Southampton, Southampton SO17 1BJ, UK

Abstract— In telecommunications, the demand for ever increasing data rates drives the development of silicon photonics in this field. The exploitation of ultrafast or instantaneous effects, such as the Kerr effect, e.g., [1], which do not pose limits to achievable date rates, is a promising route for future technologies.

We developed an on-chip technique for all-optical ultrafast control of silicon waveguide based elements, similar to frequency resolved optical gating (FROG) [2]. By introducing localized absorption by free carriers generated with pump or gate pulses (150 fs, $\lambda = 400$ nm), light propagation in silicon photonic elements can be altered. We demonstrated this technique by mapping the light paths in a SOI multimode interference-region. We introduce pump pulses from the top onto the MMI-region and map the response on the transmission of the probe pulse depending on the position of incidence of the pump pulses. Probe pulses (150 fs, $\lambda = 1550$ nm) are coupled into a SOI waveguide, which leads to a symmetrical 1×2 MMI splitter. The transmitted light of one output of the MMI-region is coupled into a fiber and subsequently to a spectrometer.

The pump pulses can be well focused, thus localizing the generation of the free carriers and subsequently absorption. By scanning over the MMI-region, this allows to map the response of probe pulses depending on the position on the MMI-region where the pump pulses are incident, and therefore for a full characterization of the probe pulse propagation in the MMI-region.

For characterizing the MMI-region, the pump-probe time delay (PPTD) was adjusted in a way that the 0.24 nJ pump pulses arrive 4 ps before the probe pulses at the MMI-region. In Fig. 1(b), a map for one wavelength ($\lambda = 1556.45$ nm) is given. Several individual paths contributing to the monitored output can be distinguished.

All-optical ultrafast control of SOI devices can find applications in future telecommunication technology requested by the ever growing demand for higher data rates as well as in analysis of pulse or wave propagation in SOI devices. The exploitation of other ultrafast effects such as a nonlinear change in refractive index is also possible with the developed technique.

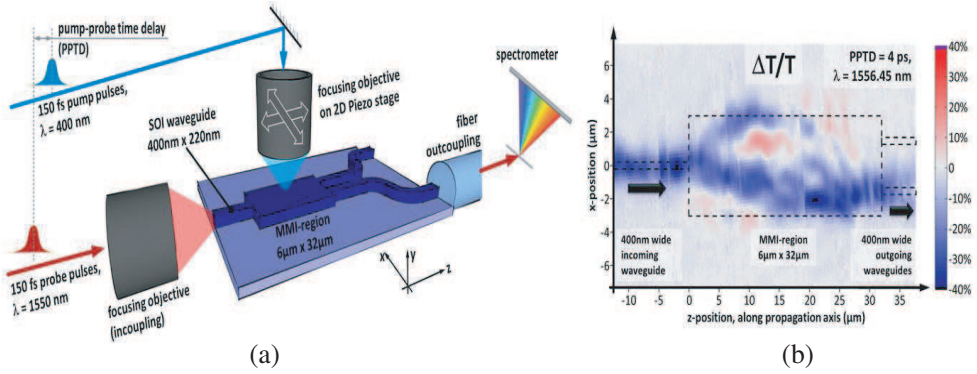

(a) (b)

Figure 1: (a) Schematic of the measurement setup. (b) Map of change in transmission ($\Delta T/T$) of probe pulses when hitting the MMI-region with the pump pulse on the position given by the map.

REFERENCES

1. Dekker, R., A. Driessen, T. Wahlbrink, C. Moormann, J. Niehusmann, and M. Först, "Ultrafast Kerr-induced all-optical wavelength conversion in silicon waveguides using 1.55 μm femtosecond pulses," *Opt. Ex.*, Vol. 14, 8336–8346, 2006.
2. Trebino, R., K. W. DeLong, D. N. Fittinghoff, J. N. Sweetser, M. A. Krumbügel, and D. J. Kane, "Measuring ultrashort laser pulses in the time-frequency domain using frequency-resolved optical gating," *Review of Scientific Instruments*, Vol. 68, 3277–3295, 1997.

Development of 10 PW Ultra-high Power Laser Facility at SIOM

Ruxin Li, Xiaoyan Liang, Yuxin Leng, and Zhizhan Xu
State Key Laboratory of High Field Laser Physics
Shanghai Institute of Optics and Fine Mechanics (SIOM), Chinese Academy of Sciences
390 Qinghe Road, Jiading District, Shanghai 201800, China

Abstract— Generation of ultra-high intensity laser field is one of the most exciting frontiers of laser physics and technology. We report recent progress towards a 10 PW laser system at SIOM. The design target is 300 J energy in 30 fs long pulse at the central wavelength of 800 nm. The laser intensity at focus will be higher than 10^{23} W/cm^2. The laser system is based on the chirped pulse amplification (CPA) and optical parametric chirped pulse amplification (OPCPA) hybrid architecture.

Ti:sapphire (Ti:S) based CPA laser systems have become standard laser sources of high peak power femtosecond pulses. 1 PW class Ti:S laser systems have been developed by several groups worldwide. A number of 10 PW class Ti:S laser systems are under construction, such as the ELI projects in EU. The main technical limitation of larger-aperture Ti:S amplifier is the transverse parasitic lasing (PL). We report on the generation of 26 fs, 2.0 PW high-contrast laser pulses in a typical Ti:sapphire amplifier chain based on chirped-pulse amplification [1]. Combining index-matching cladding and the precise control of the time delay between the input seed pulse and pump pulses, parasitic lasing in the final booster amplifier is effectively suppressed at pump energy of 140 J. The maximum output energy from the final booster amplifier is 72.6 J at pump energy of 140 J at 527 nm, corresponding to a conversion efficiency of 47.2%. The measured spectral width of the amplified output pulse from the final booster amplifier is 60.8 nm for the full width at half-maximum (FWHM) by controlling the spectral evolution in the amplifiers, and the recompressed pulse duration is 26 fs. The technology of cross-polarized wave (XPW) was applied in a broadband front end, and the pulse contrast is improved to $\sim 1.5\times10^{-11}$ (-100 ps before the main pulse).

The PL suppression is still a challenge for 10 PW class CPA amplifiers. OPCPA can support a higher energy amplification without PL issue. LBO is an attractive nonlinear crystal that can support high efficiency and broadband OPCPA near 800 nm. A high peak power laser system can be developed by combining a Ti:sapphire CPA front end and a LBO-OPCPA booster amplifier. We have implemented a hybrid Ti:sapphire-CPA and LBO-OPCPA laser system, which can produce an amplified energy of 28.68 J with spectral bandwidth of 80 nm (FWHM), what the authors believe to be the highest energy amplified in non-collinear LBO-OPCPA centered at 800 nm. Finally, the system demonstrates the compression to 0.61 PW with 33.8 fs pulse duration [2].

REFERENCES

1. Chu, Y., X. Liang, L. Yu, Y. Xu, L. Xu, L. Ma, X. Lu, Y. Liu, Y. Leng, R. Li, and Z. Xu, "High-contrast 2.0 Petawatt Ti:sapphire laser system," *Opt. Express.*, Vol. 21, No. 24, 29231–29239, 2013.
2. Xu, L., L. Yu, X. Liang, Y. Chu, Z. Hu, L. Ma, Y. Xu, C. Wang, X. Lu, H. Lu, Y. Yue, Y. Zhao, F. Fan, H. Tu, Y. Leng, R. Li, and Z. Xu, "High-energy noncollinear optical parametric-chirped pulse amplification in LBO at 800 nm," *Opt. Lett.*, Vol. 38, No. 22, 4837–4840, 2013.

Present Status and Prospects of the High-spatiotemporal-quality Petawatt-class J-KAREN Laser Facility

H. Kiriyama[1], **M. Mori**[1], **A. Kon**[1], **M. Nishiuchi**[1], **H. Sakaki**[1], **K. Ogura**[1], **Y. Fukuda**[1], **A. S. Pirozhkov**[1], **A. Sagisaka**[1], **T. Zh. Esirkepov**[1], **J. Koga**[1], **Y. Hayashi**[1], **H. Kotaki**[1], **M. Kanasaki**[1], **Y. Mashiba**[1, 2], **M. Kando**[1], **S. V. Bulanov**[1], **K. Kondo**[1], **P. R. Bolton**[1], **M. R. Asakawa**[2], **O. Slezak**[3], **D. Vojna**[3], **M. Sawicka-Chyla**[3], **V. Jambunathan**[3], **A. Lucianetti**[3], **and T. Mocek**[3]

[1]Japan Atomic Energy Agency, Kansai Photon Science Institute, Japan
[2]Faculty of Science and Engineering, Kansai University, Japan
[3]HiLASE Centre, Institute of Physics ASCR, Japan

Abstract— The J-KAREN laser system [1] is the flagship system at the Kansai Photon Science Institute (KPSI) of the Japan Atomic Energy Agency (JAEA). The system features a number of innovations, which make it unique. In particular, they include a double CPA architecture, OPCPA preamplifier, two saturable absorbers, and acousto-optic programmable dispersive filter (AOPDF) improving the contrast; cryogenically-cooled power amplifier removing severe thermal effect such as thermal lensing; diffractive optical elements improving the beam profile; extremely high intensity on target with high contrast; possibility of daily operation during long experimental campaigns; and more. The system produces the capability of ~ 600 TW peak power at single-shot with $\sim 10^{12}$ temporal contrast.

We have started the upgrade of the J-KAREN laser toward over PW level at a 0.1 Hz repetition rate. The upgraded system is now called J-KAREN-P laser. The current final amplifier is pumped by a single-shot Nd:glass green laser [2]. This current amplifier stage will be pumped with ~ 50 J of two commercial Nd:glass green lasers at a 0.1 Hz repetition rate. The pulses are further amplified in an additional Ti:sapphire amplifier, which uses a 120 mm diameter Ti:sapphire crystal, that will be pumped at 0.1 Hz with ~ 100 J from four commercial Nd:glass pump lasers. Based on simulation, the achievable broadband energy is calculated to be over 60 J.

Assuming $\sim 70\%$ of the compressor throughput and ~ 30 fs for the recompressed pulse duration, the peak power is expected to be over PW level with the repetition rate of 0.1 Hz. The focal length of the thermal lens of the amplifier is investigated. A 3D finite-element approach (FEM) using Comsol multiphysics software is chosen to model the thermal and stress effects in the amplifier. We have evaluated the impact of the increased repetition rate on thermal lens. The thermal focus length for the amplifier at 0.1 Hz is estimated to be a few km, thus there is no need to consider the thermal lensing effect. Increase in the repetition rate will lead to a more severe thermal issue. This should be helpful and useful as a reference for future higher repetition rate systems.

We suppose that the implementation will be finished at the beginning of 2015. As a first step, J-KAREN-P laser will be used for ~ 100 MeV proton generation and ~ 1 keV ultra-short x-ray generation.

REFERENCES

1. Kiriyama, H., et al., *Appl. Sci.*, Vol. 3, 214–250, 2013.
2. Kiriyama, H., et al., *Opt. Lett.*, Vol. 37, No. 16, 3363–3365, 2012.

Attosecond Control of Electronic Dynamics with Intense Laser Fields

Yong Ju Chen[1, 2], **Chuan Liang Wang**[1, 2], **Song Bo Xu**[1, 2], **Xuan Yang Lai**[1], **Wei Quan**[1], **and Xiao Jun Liu**[1]

[1]State Key Laboratory of Magnetic Resonances and Atomic and Molecular Physics
Wuhan Institute of Physics and Mathematics, Chinese Academy of Sciences, Wuhan 430071, China
[2]University of Chinese Academy of Sciences, Beijing 100049, China

Abstract— Recent advances in ultrafast laser technology have opened the door to deeply insight into intense laser-matter interaction and allowed an unprecedented control of the electronic dynamics on its natural time scale (i.e., attosecond time scale). In this talk, we will report our recent experimental study on the attosecond control of electronic processes in atoms and molecules subject to ultrafast intense laser pulses. With a newly established cold target recoil ion momentum spectrometer (COLTRIMS) and a few-cycle femtosecond laser system, we measure the differential momentum distributions of the ions and electrons emitted from the photoionization of noble gas atoms. By modulating the carrier-envelop phase (CEP) of the few-cycle laser pulse, a distinct change in the ion/electron momentum distribution has been observed. Our analysis shows that the dynamics of ionized electron can be precisely controlled on attosecond time scale.

High-order Harmonic Generation from Carrier-envelope Phase Stabled Few-cycle Intense Laser Pulse

Xinkui He, Hao Teng, Peng Ye, Shiyang Zhong, Minjie Zhan, Lifeng Wang, and Zhiyi Wei
Institute of Physics, Chinese Academy of Sciences (CAS), Beijing 100190, China

Abstract— High-order harmonic generation from the extreme nonlinear interaction between femtosecond laser pulses and atoms or molecules provides an unprecedented attosecond pulse source and simultaneously a coherent XUV source. Carrier-envelope phase (CEP) stabled few-cycle laser gives this extreme nonlinear process further control and finally realized the isolated single attosecond pulse generation. In this talk, I will report our work on few-cycle laser pulse generation, calibration and CEP stabilization. Using this pulse we have obtained the full quantum trajectory resolved high-order harmonic spectrum and generated the first Chinese isolated attosecond pulse. The generated harmonic spectrum in turn gives a new way of calibration the driving few-cycle pulse. Finally I will talk our recent work on noncollinear high harmonic generation, and a new quantum path interference phenomenon will be reported.

Pulse Slice Elongating and Pulse Broadening in a Homogeneous Medium with Only Third Order Susceptibility

Lizhong Wang[1], **Jing Zhang**[1], **Wenxia Bao**[2], **Yong Zhang**[1], **Zhengji Fang**[1], **Peide Zhao**[1], **and Xiaonong Zhu**[2]

[1]School of Science, Hebei University of Technology, Beichen Campus, Tianjin 300401, China
[2]Key Laboratory of Optical Information Science and Technology, Ministry of Education Institute of Modern Optics, Nankai University, Tianjin 300071, China

Abstract— A partial differential equation (PDE) is derived for describing the propagation of ultra-short laser pulses in the isotropic dielectric media of the third order susceptibility. In the case of no molecular two-photon absorption (TPA), the obtained solution of PDE indicates that an incident pulse slice travels with different velocities depending upon the transient intensity, which may lead the slice to noticeable elongating. The elongations in some optical materials are calculated and listed. Solution of the established PDE also shows that the full width at half maximum (FWHM) of a laser pulse can be increased due to pulse shape changes arising from TPA process. Our results suggest that the filamentation with a fixed length perhaps come from the balance of the two effects of pulse slice elongating and pulse broadening when a powerful pulse laser propagates in the third order susceptibility medium. Such a phenomenon may be exploited as an alternative way of determining the third order susceptibility of different optical materials.

Session 4A10
SC2: Nanoantennas

Analysis and Design of the Dielectric Yagi-Uda Nanoantenna with a Double Driven Element

Thanatcha Satitchantrakul and Rardchawadee Silapunt
Department of Electronic and Telecommunication
King Mongkut's University of Technology Thonburi, Bangkok, Thailand

Abstract— Dielectric nanoantennas have recently been explored for their potential as the signal transmitter at optical frequencies. Dielectric materials clearly exhibit low loss at these frequencies and may support both electric and magnetic resonant modes. In this paper, a silicon Yagi-Uda nanoantenna array with a double driven element is proposed. Our goal is to understand and optimize its radiation properties including directivity, gain, and efficiency. In addition, we need to determine the possibility to integrate this nanoantenna to a regular optical waveguide. In our design, the Yagi-Uda nanoantenna consists of the double driven element and four directors,as shown in Figure 1. The dipole source is placed vertically at the left-end of the double driven element. All particles are embedded in SiO_2 to minimize the loss associated with signal refraction. The Finite Intergration Technique (FIT) is used as the simulation tool throughout our study.

The optical characteristics of single nanoparticles with different sizes are initially investigated. The Yagi-Uda structure with the double driven element is then created. In order to optimize the nanoantenna performance, we need to understand the relationship between its geometric parameters and radiation properties. The preliminary numerical model of the nanoantenna directivity derived based on parameter ranges of interest is shown below.

$$D = \left(2.549 + \frac{8.546}{1 + \left(\frac{\frac{rd}{r} - 0.805}{0.173} \right)^2} \right) - a, \tag{1}$$

where D is the nanoantenna directivity, rd is the radius of the driven element, r is the director radius, and a is the gap between particles. At the exciting wavelength of 660 nm, the nanoantenna structure with $r = 74.6$ nm, $rd = 54.47$ nm, and $a = 58.62$ nm provides the maximum directivity of 11.42. The directivity can be further improved to 12.52 by decreasing the distance between the double driven element and the first director. Antenna gain as well as their relationships with the directivity will be further investigated.

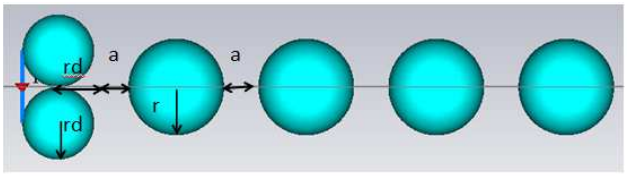

Figure 1: The structure of the silicon Yagi-Uda nanoantenna with the double driven element.

3D Triple-layer Slot Nanoantenna Array

Yu-Bo Wang[1] **and Joshua Le-Wei Li**[1, 2]

[1]Institute of Electromagnetics and School of Electronic Engineering
University of Electronic Science and Technology of China, Chengdu, China
[2]Advanced Engineering Platform and School of Electronic Engineering
Monash University, Selangor/Victoria, Malaysia/Australia

Abstract— Nanoantennas are novel devices flourishing in recent years. Various forms of nanoantennas including aperture and slot nanoantenna [1] has been studied, and intriguing nanoantenna arrays has been made [2, 3]. Here a 3D gold nanoantenna array is demonstrated. We show that a square gold patch (560 nm × 560 nm × 50 nm) with a cross-slot is able to change and enhance the radiation of a single nano emitter. By adding more patch layers with slot, the directivity of the nano emitter can be further increased. Compared with a single square patch without slot which acts as a perfect reflector, the slot nanoantenna, on the contrary, is a guider which can achieve stronger unidirectional radiation.

In addition, beem steering can be realized when introducing phase shift to the array. A 2×2 nanoantenna array is simulated. The normalized directivity reaches 13 and a ± 15 degree beem steering can be realized. Further more, we apply Chebyshev method [4] for excitation amplitude arrangement of a five-element linear slot nanoantenna array, which is proved to be a good way to improve the array performance. The side-lobe level of the Chebyshev array is much lower than linear array with equal amplitude excitation, and because of that, the directivity of the array can still be very high even the scan angle reaches ± 40 degree. It is very promising in applications such as optical information processing and optical linking.

Besides, when optical waves impinge on the array, remarkable absorption is observed over a wide range of frequencies, which does not happen on array without slots. Which means that the array is a potential candidate for photovoltaic.

We apply Drude model for the dielectric constants of gold [5]. And the whole structure is embedded in PMMA (polymethyl methacrylate). The period of the array is 680 nm.

The 3D triple-layer slot nanoantenna array is highly directional and offers much flexibility for optical radiation control. We provide a new way of designing nanoantenna array and optical wave guiding. But many challenges still exist for future applications of nanoantenna arrays including the control of the positioning and the radiation intensity of the quantum emitters (detectors) [6].

REFERENCES

1. Wu, Y.-M., L.-W. Li, and B. Liu, "Gold bow-tie shaped aperture nanoantenna: Wide band near-field resonance and far-field radiation," *IEEE Transactions on Magnetics*, Vol. 46, No. 6, 1918–1921, 2010.
2. Dregely, D., R. Taubert, J. Dorfmüller, R. Vogelgesang, K. Kern, and H. Giessen, "3D optical Yagi-Uda nanoantenna array," *Nature Communications*, Vol. 2, No. 267, 2011.
3. Liu, Z., A. Boltasseva, R. H. Pedersen, R. Bakker, A. V. Kildishev, V. P. Drachev, and V. M. Shalaev, "Plasmonic nanoantenna arrays for the visible," *Metamaterials*, Vol. 2, No. 1, 45–51, 2008.
4. Mailloux, R. J., *Phased Array Antenna Handbook*, Artech House, Boston, 2005.
5. Johnson, P. B and R.-W. Christy, "Optical constants of the noble metals," *Physical Review B*, Vol. 6, No. 12, 4370, 1972.
6. Novotny, L. and N. Van Hulst, "Antennas for light," *Nature Photonics*, Vol. 5, No. 2, 83–90, 2011.

Surface Plasmon Polaritons Focusing by the Plasmonic Chains Illuminated with Linearly Polarized Light

Jiaming Li[1, 2], **Tao Huang**[2], **Feng Lin**[2], **Zheyu Fang**[2], **and Xing Zhu**[2, 3]

[1]Center for Nanoscale Science and Technology, Academy for Advanced Interdisciplinary Studies
Peking University, Beijing 100871, China
[2]State Key Laboratory for Mesoscopic Physics, School of Physics, Peking University, Beijing 100871, China
[3]National Center for Nanoscience and Technology, Beijing 100190, China

Abstract— We theoretically and experimentally demonstrate the focusing of surface plasmon polaritons by half circle and half spiral plasmonic chains illuminated with linearly polarized light. The three-dimensional finite-difference time-domain (FDTD) simulation result demonstrates that there will be a focal spot at the center of the structure when illuminated with linearly polarized light. And the position of the focal spot has nothing to do with the polarization of the incident light. But a structure orientation-dependent transverse shift of the focus is easily observed by comparing the cross sections of the spot. What,s more, the transverse shift of the focus can be adjusted by changing the structural parameters of the chains (such as, from half circle chains to half spiral chains). This focusing properties and shift can be regarded as the optical spin-Hall effect (OSHE), which arises in our structure due to a spin-orbit coupling producing a different spiral geometric phase for opposite chiral photons, because of interference of the SPP waves created by individual columns of our structure, the left and right circularly polarized components of the incident light will propagating to the opposite direction, resulting in the focusing properties and the shift of the focal. The field distribution is characterized by near-field scanning optical microscope (SNOM). A sharp focal spot corresponding to a zero-order Bessel function is observed. In order to proved the conclusion, we also measured with circular polarized light illumination. By using our structure, we can realize surface plasmon polaritons focusing with linearly polarized light easily, and the focal spot is isotropy for any polarization direction of the incident. Our studies are useful to understand the physical mechanism of the plasmonic focusing and have many potential applications for the nano-scale plasmonic devices.

ACKNOWLEDGMENT

Work supported by National Science Foundation of China (Grant Nos. 61176120, 61378059, 11374023).

Paired-strips Gold Nanoantennas for Absorption Enhancement in P3HT Organic Thin-film

Zih-Ying Yang[1] and Kuo-Ping Chen[2]

[1]Institute of Lighting and Energy Photonics, Chiao Tung University
301 Gaofa 3rd Road, Tainan 711, Taiwan
[2]Institute of Imaging and Biomedical Photonics, Chiao Tung University
301 Gaofa 3rd Road, Tainan 711, Taiwan

Abstract— A novel design of nanoantennas, so-called paired-strips nanoantennas, has been proposed for efficient harvesting of light in visible wavelength. The integral localized field of gold paired-strips nanoantennas embedded in absorbing thin-film has been studied. By engineering the thickness of absorbing medium and the dimension of nanoantennas, the optimized effective absorption enhancement could be reached. The localized EM fields in the gaps of paired-strips nanoantennas contribute higher absorption enhancement comparing to single-strip gratings. From the 2D mapping of absorption enhancement, the enhancement factor could reach $\sim$ 20 times larger for gold paired-strips nanoantennas embedded in 100 nm P3HT:PCBM thin film.

REFERENCES

1. Yang, Z. and K. Chen, "Effective absorption enhancement in dielectric thin-films with embedded paired-strips gold nanoantennas," *Opt. Express*, Vol. 22, 12737–12749, 2014.
2. Ferry, V. E., J. N. Munday, and H. A. Atwater, "Design considerations for plasmonic photovoltaics," *Advanced Materials*, Vol. 22, 4794–4808, 2010.
3. Atwater, H. A. and A. Polman. "Plasmonics for improved photovoltaic devices," *Nature Materials*, Vol. 9.3, 205–213, 2010.
4. Bi, G., W. Xiong, L. Wang, K. Ueno, H. Misawa, and J.-R. Qiu, "Fabrication of periodical structure and shape-induced modulating spectroscopy of Au nanoparticles," *Optics Communications*, Vol. 285, 2472–2477, 2012.
5. Pala, R. A., J. White, E. Barnard, J. Liu, and M. L. Brongersma, "Design of plasmonic thinfilm solar cells with broadband absorption enhancements," *Advanced Materials*, Vol. 21, 3504–3509, 2009.

Orthogonal Redirector and Wavelength Selector of SPPs Realized by Using Nano-optical Yagi-Uda Antenna

Xuewei Zhang[1], **Mingcheng Liang**[1], **and Zheyu Fang**[2, 3]

[1]School of Physics, Peking University, Beijing 100871, China
[2]State Key Lab for Mesoscopic Physics, School of Physics, Peking University, Beijing 100871, China
[3]Academy for Advanced Interdisciplinary Studies, Peking University, Beijing 100871, China

Abstract— Direction control of SPPs is a key step to realizing all-optical circuits. And the ability in selecting a specific, wanted wavelength of SPPs is also desirable. To achieve these, an orthogonal redirector and a wavelength selector have been made by utilizing nano-optical Yagi-Uda antennas, which are designed for high directivity as a conventional Yagi-Uda antenna operating in the radiofrequency regime. A structure consisting of two nanorods located in the end of a waveguide has been designed as the redirector. When SPPs propagating along the waveguide emits from the end, the direction can be change to an orthogonal one via the Yagi-Uda antenna-like structure, acting as an orthogonal redirector. Besides, combining this structure with a waveguide consisting of a thick and a thin part, a wavelength selector can be realized. When SPPs along the waveguide reach the junction of two parts, different wavelengths will lead to different reflectivity that to SPP of 600 nm is 75% and to 785 nm is 25% in the simulation. Then SPPs of two different wavelengths can be emitted orthogonally to the waveguide in opposite direction by the redirectors located in the junction and the end of the waveguide, which realizes the separation and selection of SPPs in different wavelengths. Amounts of simulations have been done to obtain parameters for optimal orthogonal redirection and maximum reflectivity distinction due to different wavelengths. Samples of these nano-optical devices have been produced and will be tested to confirm the above properties in experiments soon.

Plamsonic Beaming by Well Designed Nanoscatterers

Tao Li, Lin Li, Xia-Mei Tang, and S. N. Zhu
College of Engineering and Applied Sciences, Nanjing University, Nanjing 210093, China

Abstract— In microwave region, phased array antenna is an important device the development of radar technique. It is reasonable to be extended to the optical region that would possibly arise interesting applications. Different to the macro size in microwave device, the antenna for a light beam are quite small and very difficult to tune its phase individually as in an array. However, if they are carefully arranged with proper excitation, preferred light beam can be formed. Here, I would first briefly introduce an in-plane diffraction method that is adopted to manipulate the surface plasmon polarition (SPP) waves on the metal surface. This process is based on a non-perfectly matched Bragg diffraction, by which the phase modulation in a transverse dimension of SPP beam can be achieved almost at will. As examples, SPP Airy beam, focusing beam, collimated beams are realized [1–4]. Moreover, this method is extended to free space. That means we can convert the near field SPP wave to any desired spatial beams by the diffraction process. In this talk, I will demonstrate the experimental results of the focusing and Airy beams in free space [5]. Interestingly, from another perspective, we found this diffraction (or collective scattering) process can be regarded as a kind of phase selector, which depends on a appropriate selection of the a well distributed wave phase. This finding further deepen our understanding of the beam steering as well as the conversion between SPP and radiation light. More recently, new progresses have been reported in a plasmonic structure covered fiber system to achieve a compact Airy beam generator [6]. It surely implies the potential applications in the wide range of optics.

REFERENCES

1. Li, et al., "Plasmonic Airy beam generated by in-plane diffraction," *Phys. Rev. Lett.*, Vol. 107, 126804, 2011.
2. Li, et al., "Broad band focusing and demultiplexing of in-plane propagating surface plasmons," *Nano Lett.*, Vol. 11, 4357, 2011.
3. Li, et al., "Steering plasmon beam from a point source," *Opt. Lett.*, Vol. 37, 5091, 2012.
4. Li, et al., "Collimated plasmon beam: Nondiffracting versus linearly focused," *Phys. Rev. Lett.*, Vol. 110, 046807, 2013.
5. Tang, et al., "Converting surface plasmon to spatial Airy beam by graded grating on metal surface," *Opt. Lett.*, Vol. 38, 1733, 2013.
6. Guan, et al., "Compact all-fiber plasmonic airy-like beam generator," *Opt. Lett.*, Vol. 39, 1113, 2013.

Plasmonic Photocoupler for Infrared Optoelectronics and Optospintronics

Jie Xu, Fuchun Xi, Lijian Zhang, Qinbai Qian, Peng Gou, Lei Zhou, and Zhenghua An
State Key Laboratory of Surface Physics, Key Laboratory of Micro and Nano Photonic Structures (Ministry of Education), Fudan University, Shanghai 200433, China

Abstract— The intrinsic charge and spin properties of electrons in semiconductors offer us plenty of opportunities in realizing functional nanoelectronic and spintronic devices. Shining electromagnetic waves or photons to these devices enables equally-important (if not more) fields of optoelectronics and optospintronics. To realize optoelectronically or optospintronically functional devices with excellent performance, however, the large mismatch between electron (spin) physical size and the associated wavelength has to be taken account, particularly in the long wavelength (infrared and microwave) regions where photo-active region itself is typically smaller in one or more dimensions than λ. Plasmonic metamaterials (PMM) arise as a promising solution to bridge photon-electron (or spin) coupling, by utilizing the collective motions or plasmons of electrons inside. It is therefore highly desirable to study and optimize the collective motions of electrons in PMM and their coupling with the individual behaviors of electrons in electronic (or spintronic) structures, so that maximal device performance can be expected. We attempt here to use plasmonic cavity coupler to enhance the photo-responsivity of infrared photodetectors and also adopt a modified split-ring antenna to enlarge the spin-rectifying microwave photovoltage of a ferromagnetic device.

High-sensitivity Plasmonic Dipolar Anitbonding Mode of Gold Nanoantennas in Evanescent Waves

Yi-Hsun Chen[1], **Che-Yuan Chang**[2], **Zih-Ying Yang**[1], **and Kuo-Ping Chen**[2]

[1]Institute of Lighting and Energy Photonics, Chiao Tung University
301 Gaofa 3rd Road, Tainan 711, Taiwan
[2]Institute of Imaging and Biomedical Photonics, Chiao Tung University
301 Gaofa 3rd Road, Tainan 711, Taiwan

Abstract— Strong plasmonic dipolar antibonding modes of gold nanoantennas are observed in evanescent waves. For symmetric nanoparticles pairs, the bonding mode, located at a lower energy level, could be strongly excited by normal incidence, but antibonding mode, located at a higher energy level, could hardly excited by normal incident plane wave and which is not easy to be observed. In this work, total internal reflection is used to transfer the energy of incident light to plasmonic antibonding modes resonance in nanoantennas. Comparing to bonding mode in normal incidence, antibonding mode could not only have the higher extinction coefficient, but also achieve higher sensitivity to surrounding environments. Antibonding mode of gold nanoantenna shows 4.84 times higher sensitivity in figure of merit (FOM).

REFERENCES

1. Knight, M. W., H. Sobhani, P. Nordlander, and N. J. Halas, *Science*, Vol. 332, 702, 2011.
2. Liu, Z., A. Boltasseva, R. H. Pedersen, R. Bakker, A. V. Kildishev, V. P. Drachev, and V. M. Shalaev, *Metamaterials*, Vol. 2, 45, 2008.
3. Grosjean, T., M. Mivelle, F. Baida, G. Burr, and U. Fischer, *Nano letters*, Vol. 11, 1009, 2011.
4. Kohoutek, J., D. Dey, A. Bonakdar, R. Gelfand, A. Sklar, O. G. Memis, and H. Mohseni, *Nano Letters*, Vol. 11, 3378, 2011.
5. Yang, S.-C., H. Kobori, C.-L. He, M.-H. Lin, H.-Y. Chen, C. Li, M. Kanehara, T. Teranishi, and S. Gwo, *Nano Letters*, Vol. 10, 632, 2010.
6. Chang, Y.-C., S.-M. Wang, H.-C. Chung, C.-B. Tseng, and S.-H. Chang, *Acs Nano*, Vol. 6, 3390, 2012.
7. Prodan, E., C. Radloff, N. Halas, and P. Nordlander, *Science*, Vol. 302, 419, 2003.
8. Wang, H., D. W. Brandl, P. Nordlander, and N. J. Halas, *Accounts of Chemical Research*, Vol. 40, 53, 2007.
9. Huang, J.-S., J. Kern, P. Geisler, P. Weinmann, M. Kamp, A. Forchel, P. Biagioni, and B. Hecht, *Nano Letters*, Vol. 10, 2105, 2010.

Substrate-mediated Charge Transfer Plasmons in Simple and Complex Nanoparticle Clusters

Ziwei Li[1, 2], **Mingcheng Liang**[1], **and Zheyu Fang**[1, 2]

[1]School of Physics, State Key Lab for Mesoscopic Physics, Peking University, Beijing 100871, China
[2]Academy for Advanced Interdisciplinary Studies, Peking University, Beijing 100871, China

Abstract— A conductive substrate can provide a simple and straightforward way to induce charge-transfer plasmon modes in Au nanoparticle clusters. Charge transfer can connect the isolated nanoparticles together and change the modes distribution. Different thickness of conductive golden films can modulate the Fano resonance in a controlled way. For a simple dimer structure, a remarkably narrow charge transfer plasmon, which differs dramatically from the dipolar plasmon mode of the electrically isolated nanostructure, is clearly observed. A new scattering peak appears and which is considered to be a charge transfer induced monopole mode. For a more complex nonamer cluster that supports a strong Fano resonance on an insulating substrate, a mixed charge transfer-dipole (CTP) mode is observed, where charge transfer is induced on the outer nanoparticles, establishing an opposing dipole on the intervening central particles, resulting in a strongly damped far field response. For both clusters studied, a strong blue shift in the primary plasmon modes is observed, resulting from a decrease in hybridization energy due to screening of the surface charge distributions by the presence of the underlying conductive substrate. Although performed on static structures, one could envision that similar changes in spectral features in active device geometries may be possible, where charge injection by substrate gating would play an analogous role to the underlying conductive film used in these structures.

REFERENCES

1. Wang, Y., Z. Li, K. Zhao, A. Sobhani, X. Zhu, Z. Fang, and N. J. Halas, *Nanoscale*, Vol. 5, 9897, 2013.
2. Huang, S., J. Li, X. Zhang, Y. Kang, Z. Li, F. Lin, and X. Zhu, *Applied Physics A*, DOI: 10.1007/s00339-013-8024-5.
3. Li, J., C. Yang, J. Li, Z. Li, S. Zu, S. Song, H. Zhao, F. Lin, and X. Zhu, *Plasmonics*, DOI: 10.1007/s11468-014-9692-5.

Plasmonic Hot Electron Induced Structural Phase Transition in Monolayer MoS_2

Yimin Kang[1], **Mingcheng Liang**[1], **and Zheyu Fang**[1, 2, 3]

[1]State Key Lab for Mesoscopic Physics, School of Physics, Peking University, Beijing 100871, China
[2]Collaborative Innovation Center of Quantum Matter, Beijing 100871, China
[3]Laboratory for Nanophotonics, Department of Electrical and Computer Engineering
Rice University, 6100 Main Street, Houston, Texas 77005, USA

Abstract— The fascinating properties of molybdenum disulfide (MoS_2) atomic layers have recently been found to support novel physics, such as valleytronics and the quantum Hall effect. The facile and potentially useful semiconducting (2H) to metallic (1T) phase transitions in MoS_2 may be exploited as a means of controlling the electronic and optical properties of devices based on this material [1–10]. The ability to actively control and induce this phase transition by optical means would enable the further development of such applications. In this letter, using Raman scattering and photoluminescence, we demonstrate that hot electrons [11–13] generated by plasmonic Au nanoparticles can induce a 2H-to-1T phase transition in a single MoS_2 layer. Our finding that plasmonic hot electrons can induce phase transitions in nearby low-dimensional materials opens up new possibilities for the development of optoelectronic devices.

REFERENCES

1. Huang, S., J. Li, X. Zhang, Y. Kang, Z. Li, F. Lin, and X. Zhu, *Applied Physics A*, DOI: 10.1007/s00339-013-8024-5.

Session 4A11
SC1: Advanced Numerical Techniques in Computational Electromagnetics

Using Multiple-precision Arithmetic to Prevent Low-frequency Breakdowns in the Diagonalization of the Green's Function

Ö. Ergül and B. Karaosmanoğlu
Department of Electrical and Electronics Engineering
Middle East Technical University, Ankara, Turkey

Abstract— The multilevel fast multipole algorithm (MLFMA) is a powerful method for the solution of electromagnetic problems discretized with large numbers of unknowns [1, 2]. However, conventional implementations of MLFMA are not efficient for low-frequency problems, where dense discretizations with respect to wavelength are used locally or globally on structures. Specifically, box sizes in MLFMA cannot be very small with respect to wavelength [3], and solutions of such problems involving dense discretizations lead to many interactions that must be calculated directly. It is well known that the diagonalization of the Green's function, i.e., expansion of spherical waves in terms of plane waves [4], is responsible for low-frequency breakdowns. Therefore, in the literature, alternative implementations of MLFMA, such as using explicitly multipoles [5, 6] and/or evanescent waves [7, 8] at short distances, are suggested to solve low-frequency problems, as well as multiscale problems involving large objects with dense discretizations.

In this work, we approach low-frequency breakdowns from a different direction and prevent them by using multiple-precision arithmetic (MPA), which has recently become popular in the scientific computation area [9]. Considering breakdowns from a numerical point of view, the standard diagonalization of the Green's function fails to provide accurate subwavelength interactions due to insufficient numbers of digits used in computations. Even when using the double-precision arithmetic, plane waves can be insufficient to represent radiation and receiving patterns of small sources. In addition, translations at short distances may involve addition and subtraction of large numbers due to spherical Hankel functions. Increasing the number of digits by means of MPA, it becomes possible to improve all these computations and perform such critical interactions with a desired level of accuracy using the conventional diagonalization. MPA may easily be used in the existing implementations of MLFMA and convert them to broadband implementations via relatively simple modifications.

REFERENCES

1. Song, J., C.-C. Lu, and W. C. Chew, "Multilevel fast multipole algorithm for electromagnetic scattering by large complex objects," *IEEE Trans. Antennas Propag.*, Vol. 45, No. 10, 1488–1493, Oct. 1997.
2. Ergül, Ö. and L. Gürel, "Accurate solutions of extremely large integral-equation problems in computational electromagnetics," *IEEE Proceedings*, Vol. 101, No. 2, 342–349, Feb. 2013.
3. Chew, W. C., J.-M. Jin, E. Michielssen, and J. Song, *Fast and Efficient Algorithms in Computational Electromagnetics,* Artech House, Boston, MA, 2001.
4. Coifman, R., V. Rokhlin, and S. Wandzura, "The fast multipole method for the wave equation: A pedestrian prescription," *IEEE Antennas Propag. Mag.*, Vol. 35, No. 3, 7–12, Jun. 1993.
5. Zhao, J.-S. and W. C. Chew, "Three dimensional multilevel fast multipole algorithm from static to electrodynamic," *Microw. Opt. Technol. Lett.*, Vol. 26, No. 1, 43–48, Jul. 2000.
6. Jiang, L. J. and W. C. Chew, "A mixed-form fast multipole algorithm," *IEEE Trans. Antennas Propag.*, Vol. 53, No. 12, 4145–4156, Dec. 2005.
7. Jiang, L. J. and W. C. Chew, "Low-frequency fast inhomogeneous plane-wave algorithm (LF-FIPWA)," *Microw. Opt. Technol. Lett.*, Vol. 40, No. 2, 117–122, Jan. 2004.
8. Bogaert, I. and F. Olyslager, "A low frequency stable plane wave addition theorem," *J. Comput. Phys.*, Vol. 228, No. 4, 1000–1016, Mar. 2009.
9. Stefanski, T. P., "Electromagnetic computations requiring high-precision computations," *Antennas Propag. Mag.*, Vol. 55, No. 2, 344–353, Apr. 2013.

Properties of the Gram Matrices Associated with Loop-flower Basis Functions

Yibei Hou and Gaobiao Xiao
Key Laboratory of Ministry of Education of Design and Electromagnetic Compatibility of High-Speed Electronic Systems, Shanghai Jiao Tong University, Shanghai, China

Abstract— In this presentation, loop-flower basis functions are addressed to solve the electric filed integral equation (EFIE) in electromagnetic scattering issues that rise from perfectly conducting objects. A loop basis function and a flower basis function are both defined as the sum of a set of modified RWG basis functions associated with a node in triangular meshes, moreover, they could also be represented by node based Lagrange interpolation polynomials. A flower basis function, which also resembles the star basis function, is named after its shape. In contrast to all previous quasi-Helmholtz decomposition, loop-flower decomposition holds several good characteristics. First, loop-flower decomposition can be used to cure low-frequency breakdown of EFIE spectrum. Second, it can also be directly used to implement Calderón preconditioners for EFIE. Last but not least, the unknown number corresponding with loop-flower basis functions reduces to approximately two thirds of the one associated with RWG. Given that the property of a Calderón preconditioner is largely affected by the Gram matrix that links the range and domain of EFIE operator, this presentation will focus on the properties of Gram matrices associated with loop-flower basis function. Analysis shows the Gram matrices associated with loop-flower basis functions are invertible, and their condition numbers are approximately of the order of (h^{-2}), in which h is the characteristic dimension of a triangular mesh. The theoretical analysis will be demonstrated by several numerical examples.

An Efficient Magnetic Field Integral Equation Based Iterative Solver

Robert Brem and Thomas F. Eibert
Lehrstuhl für Hochfrequenztechnik, Technische Universität München, Munich 80290, Germany

Abstract— Hybrid approaches for electromagnetic scattering computations such as the well-known combination Physical Optics-Method of Moments (PO-MoM) provide a reasonable compromise between asymptotic methods, which are in some cases not accurate enough, and exact methods, which are often too time and memory consuming. Another choice is the Iterative Physical Optics (IPO) technique [1, 2], which tries to solve the magnetic field integral equation (MFIE) in an iterative manner in combination with some simplifications based on neglecting currents in shadow regions. This method was developed for the computation of wave propagation in and scattering from cavity structures, where it typically achieves very good results. The currents and fields show fast convergence and are close enough to the exact solution so that no error correction in the iterative scheme is required in many cases. Problems can arise, however, if IPO is applied on non-cavity-like structures, where the solution is often quickly diverging without control mechanisms. For these cases with mostly convex surfaces the simple PO approximation is typically applied and provides a good prediction of the scattered fields. However, there are cases where the inherent neglect of currents in the shadow region and coupling effects deteriorate the simulation results.

This contribution presents an accurate iterative MFIE based method for perfect electrically conducting (PEC) objects of arbitrary three-dimensional shape which needs fewer approximations than the IPO approach but uses the same efficient and well-proven implementation techniques. The coupling computation between currents on the used triangular surface mesh is based on pulse basis functions and point-matching. The current sampling density can be chosen as approximately one third of the wavelength of the incident field. The total simulation domain is subdivided into blocks among which the coupling matrices are computed. For block pairs whose distance fulfills the far-field condition, the fast far-field approximation (FaFFA) [3] is used for significant acceleration of the computations and reduction of memory requirements. Starting with a good initial current vector obtained by a fast PO or Shooting-and-Bouncing-Rays (SBR) simulation, the MFIE is solved to get the currents after the first iteration. Then, all currents belonging to a certain block are identically weighted with a complex correction factor. Each block has an individual correction factor and the corresponding correction vector is determined by solving a least squares problem so that the currents fulfill the boundary condition as accurate as possible. All subsequent iterations comprise these two steps: computation of a new current vector based on the previous one and improvement of the new currents by multiplication with correction factors. By increasing the number of blocks, a more accurate correction can be achieved.

Similar to the IPO, the goal of this solution scheme is to provide numerical results closer to the exact solution than obtainable by pure asymptotic methods. The quality and robustness of this iterative approach will be demonstrated by numerical examples.

REFERENCES

1. Obelleiro, F., J. Rodriguez, and R. Burkholder, "An iterative physical optics approach for analyzing the electromagnetic scattering by large open-ended cavities," *IEEE Trans. Antennas Propagat.*, Vol. 43, No. 4, 356–361, 1995.
2. Burkholder, R., "A fast and rapidly convergent iterative physical optics algorithm for computing the RCS of open-ended cavities," *Appl. Computational Electromagn. Soc. J.*, Vol. 16, No. 1, 53–60, 2001.
3. Lu, C. and W. Chew, "Fast far-field approximation for calculating the RCS of large objects," *Microwave Opt. Tech. Letters*, Vol. 8, No. 5, 238–241, 1995.

Mixed Spectral Element Method for Maxwell Eigenvalue Problem with Anisotropic and Lossy Media

N. Liu[1], **Z. Mao**[1], **and Q. H. Liu**[2]

[1]Institute of Electromagnetics and Acoustics, Xiamen University, China
[2]Department of Electrical and Computer Engineering, Duke University, USA

Abstract— A higher-order mixed spectral element method (mixed SEM) based on Gauss-Lobatto-Legendre (GLL) polynomials in the mixed finite element framework is applied to solve Maxwell eigenvalue problem with anisotropic and lossy media. The classical spectral element method (SEM) in solving vector Maxwell eigenvalue equations by the finite element method without considering the divergence-free condition yields the presence of spurious zero eigenvalues, and the number of the spurious zero modes is exactly equal to the number of the internal nodes in the whole computation mesh. Therefore, further steps are needed to separate these approximations when the structure does have the physical zero eigenmodes, which is a nontrivial task. In order to avoiding these troubles, in this paper, we extend the Kikuchi's mixed finite element method to the classical SEM to solve the Maxwell eigenvalue problem. It utilizes GLL polynomials to construct the mixed-order curl-conforming vector basis functions in the finite-element framework for the electric field intensity, and scalar node-based basis functions for the auxiliary variable in the weak divergence-free condition as a Lagrange multiplier in the mixed finite-element formulation to calculate the field distributions and eigenvalues of the Maxwell eigenvalue problem. It is shown that the mixed SEM not only can suppress all spurious eigenmodes and well satisfies the divergence-free condition, but also can keep an exponential convergence rate with analytic eigenvalues and superior computational efficiency over the classical SEM. Several numerical examples are given on a rectangular cavity and two PECs cavity in anisotropic and lossy media to verify that the mixed SEM is free of any spurious eigenmodes, has spectral accuracy with analytic eigenvectors and its high efficiency.

Time-domain Analytical Solutions at Each Point of Two-wire Transmission Line Excited by Plane-wave Fields

Mengshi Zhang, Guyan Ni, and Min Zhou
College of Science, National University of Defense Technology, Changsha 410073, China

Abstract— The modeling of transmission line excited by an external electromagnetic (EM) field is a classic topic and plays an important role in performing engineering studies for electrical systems. There are three different approaches for describing the coupling of an external EM field to a line using transmission line theory: including Taylor method, Agrawal method and Rachidi method. Each of these coupling formulations gives the same response for the transmission line. However, it is the most important to realize that transmission line theory does not provide a complete solution for the excitation of a line by an incident EM field. The total induced current in the line has two components: an "antenna mode" current and a "transmission line mode" current. Hence, transmission-line models, which are approximations to a rigorous electromagnetic analysis. In this paper, we discuss the time-domain transmission-line model analytic solutions at each point of the two-wire transmission line excited by a plane-wave field. Applying the superposition principle and the definition of integral, we obtain the frequency-domain Baum-Liu-Tesche (BLT) equation at a point of the two-wire transmission line. Then by the frequency-domain BLT equation, the time-domain analytic solutions are obtained and expressed in an infinite series. But if the current or the voltage is computed in a finite time interval, then the time-domain analytic solution can be expanded in a finite series. Numerical examples are presented.

An Analysis of Energy Conserved Splitting FDTD Method for 3D Maxwell's Equations

Wen Li[1], **Huadong Zhao**[1], **Lei Zhao**[1], **and Wenhua Yu**[2]

[1]Center for Computational Science and Engineering, School of Mathematics and Statistics
Jiangsu Normal University, China
[2]2COMU, State College, PA 16803, USA

Abstract— In this paper, we explore the accuracy limits of an energy conserved splitting finite difference time domain (EC-S-FDTD) method applied to the Maxwell equations which has recently been proposed to solve the Electromagnetic (EM) problem. The EC-S-FDTD methods are based on the combining of the splitting scheme and the implicit scheme. In the proposed methods, a symmetric operator and a uniform splitting are adopted to split the Maxwell's Equations, and then the proposed schemes consist of only two equations at each stage. The rigorous analysis of the schemes is given. The EC-S-FDTD scheme for the 3D Maxwell equations is of second-order accuracy both in time step and spatial steps with unconditional stability. We have verified the accuracy and efficiency of the algorithm by comparing the numerical results with analytical results. The dispersion and dissipation properties of the method are investigated. The results of this analysis are useful for the application of the method, and for the understanding of the behavior of the error of the method. Furthermore, the proposed methods with perfectly matched layer (PML) boundary conditions have been applied to solve EM scattering problems successfully. And the comparison with general FDTD method and alternating direction implicit (ADI) method, in term of computational cost, is also considered. And we develop the high order accuracy of the proposed method by splitting the time step. Subsequently, our result still show that the EC-S-FDTD scheme for the 3D Maxwell equations is with high-order accuracy both in time step and spatial steps with unconditional stability.

Fast Calculation of Response of Scatterers in Uniaxial Laminates

Yu Zhong[1], **Xudong Chen**[2], **Pingping Ding**[3], **Marc Lambert**[3], **and Dominique Lesselier**[3]

[1]A*STAR, Institution of High Performance Computing, 138632, Singapore
[2]Department of Electrical and Computer Engineering
National University of Singapore, 117576, Singapore
[3]Laboratoire des Signaux et Systèmes, Départment de Recherche en Electromagnétisme
UMR8506 (CNRS, Supélec, University Paris-Sud)
3, rue Joliot-Curie, Gif-sur-Yvette cedex 91192, France

Abstract— The volume integral equation method, usually implemented via the method of moments (MoM), is a popular approach to many scattering problems, like when inhomogeneous bodies are embedded within planarly layered media and made to interact with given sources, as henceforth considered.

When the layered media are isotropic, the construction of the impedance matrix of the MoM, the bottleneck of the method, can be fast since one is able to accelerate the calculation of the 1-D Sommerfeld integrals [1]. This is due to the fact that the dispersion relations of the isotropic media enable to calculate the integral along the azimuth direction in closed form.

But, if the uniaxial media are with optical axes parallel with the interfaces, e.g., [2, 3], or if the media are biaxially anisotropic, the above fast methods do not apply anymore. This results in possibly high computational cost to ensure accuracy when dealing with the 2-D inverse Fourier transform (IFT). However, we might still circumvent it, with the rectilinear mesh as done in traditional practice in volume integral equation methods, achieving efficient construction of the impedance matrix.

In a pioneering contribution [4], a method that uses the continuous Fourier transform and a windowing technique is proposed to analyse metal patches within an isotropic multi-layered structure, which can be used to avoid the conventional 2-D IFT. By the generalized Poisson summation formula and the windowing technique, the relation between the discrete Fourier spectrum and the continuous Fourier spectrum of the spatial response is re-derived, which, by using it, enables to efficiently and accurately calculate the response of the multilayer on a rectilinear mesh.

When the continuous Fourier spectrum of the response of the laminates to the current basis function is available, which can be stably and efficiently calculated by the new recurrence relations proposed in our previous contribution [5], we use such a fast method to construct the impedance matrix of the MoM involving uniaxial layered media whose optical axes lie parallel to their planar interfaces. Numerical tests confirm the efficacy of the proposed method.

REFERENCES

1. Alparslan, A., M. I. Aksun, and K. A. Michalski, "Closed-form Green's functions in planar layered media for all ranges and materials," *IEEE Trans. Microwave Theory Tech.*, Vol. 58, 602–613, 2010.
2. Burke, S., "Eddy-current induction in a uniaxially anisotropic plate," *J. Appl. Phys.*, Vol. 68, 3080–3090, 1990.
3. Wasselynck, G., D. Trichet, B. Ramdane, and J. Fouladagar, "Microscopic and macroscopic electromagnetic and thermal modeling of carbon fiber reinforced polymer composites," *IEEE Trans. Magn.*, Vol. 47, 1114–1117, 2011.
4. Catedra, M. and E. Gago, "Spectral domain analysis of conducting patches of arbitrary geometry in multilayer media using the CG-FFT method," *IEEE Trans. Antennas Propagat.*, Vol. 38, 1530–1536, 1990.
5. Zhong, Y., M. Lambert, D. Lesselier, and X. Chen, "Electromagnetic response of anisotropic laminates to distributed sources," *IEEE Trans. Antennas Propagat.*, Vol. 62, 247–256, 2014.

A Derivative-free Broadband Source Reconstruction Method

Ping Li and Li Jun Jiang
Dept. of EEE, the University of Hong Kong, Hong Kong, China

Abstract— Source reconstruction methods (SRM) are being frequently used in the antenna measurement theory, electromagnetic emission diagnosis, and imaging process, etc. Fundamentally it uses the equivalence principle to build up the relationship between the near field and far field. Then the near field represented by equivalence sources is further computed through numerical approaches. Dominantly done in the frequency domain, the recovered equivalence sources are usually constructed at every frequency point being investigated. Thereby when a broadband near field information is needed, the computational load will be tremendous. The asymptotic waveform evaluation (AWE) could be employed to reduce the needed computation. However, it demands the derivatives of the target function, which dramatically makes the process complicated.

In this paper, the Neville-type Stoer-Bulirsch (SB) rational interpolation algorithm is employed to solve the broadband SRM problem. Because the SB algorithm is recursive tabular based, it implements the interpolation over a broadband using a single rational function without any derivative involved. Working together with the bisection method based on the adaptive frequency sampling (AFS) approach, the total number of required sampling data could be significantly reduced. Numerical benchmarks for the antenna array and the broadband spiral antenna both show the efficiency and accuracy of the proposed method.

Numerical Verification of Nanoscale Antenna Performance for Ultra-fast Magnetic Recording

S. Ohnuki, **T. Okuda**, **Y. Ashizawa**, **K. Nakagawa**, **and A. Tsukamoto**
College of Science and Technology, Nihon University
1-8-14 Surugadai, Kanda, Chiyoda-ku, Tokyo 101-8308, Japan

Abstract— All-optical magnetic recording with circularly polarized light has been attracted attention to realize ultra-fast magnetic recording. The experimental results show that the magnetization reversal occurs by ultra-short optical stimulus less than 100 fs [1], therefore the recording speed can be accelerated about 100,000 times faster than those for conventional methods. To achieve higher density for all-optical magnetic recording, nanoscale antennas play an important role to localize circularly polarized light whose spot size determines the storage capacity [2]. However, nanoscale fabrication is still difficult and performance of a fabricated antenna differs from numerically designed one.

In this presentation, we discuss electromagnetic simulation of a fabricated nanoscale antenna which is modeled after an electron micrograph picture [3]. Our computational method is based on a boundary integral equation method [4, 5] and characteristics of the antenna are evaluated in terms of the Stokes parameters.

REFERENCES

1. Stanciu, C. D., F. Hansteen, A. V. Kimel, A. Kirilyuk, A. Tsukamoto, A. Itoh, and T. Rasing, *Phys. Rev. Lett.*, Vol. 99, 047601-1–047601-4 , Jul. 2007.
2. Nakagawa, K., Y. Ashizawa, S. Ohnuki, A. Itoh, and A. Tsukamoto, *J. Appl. Phys.*, Vol. 109, No. 7, 07B735-1–07B735-3, Apr. 2011.
3. Koene, B., M. Savoini, A. V. Kimel, A. Kirilyuk, and T. Rasing, *Proc. of NFO-12, ThP-064*, 285, Sep. 2012.
4. Kishimoto, S., S. Ohnuki,Y. Ashizawa, K. Nakagawa, and W. C. Chew, *Journal of Electromagnetic Waves and Applications*, Vol. 26, No. 8–9, 997–1006, Jul. 2012.
5. Mayergoyz, I. D., D. R. Fredkin, and Z. Zhang, *Phys. Rev. B*, Vol. 72, No. 15, 155412-1–155412-15, Oct., 2005.

Session 4A12
SC1: Extended/Unconventional Electromagnetic Theory, Electro-hydrodynamics/Electro-magneto-hydrodynamics, and Electro-biology

Intelligent Channel Assignment for WI-FI System Based on Reinforcement Learning

R. Urban and P. Drexler
Department of Theoretical and Experimental Electrical Engineering
Brno University of Technology, Technicka 12, Brno 612 00, Czech Republic

Abstract— WI-FI has recently become a dominant wireless technology for local area networks (LAN) and personal area networks (PAN) worldwide. All the modification of IEEE 802.11 [1] came extremely popular during last decades. The WI-FI modules are now installed into various types of devices such as laptops, mobile phones, smart TVs, digital cameras etc.. Even the intelligent buildings require to be connected to the network common house devices, e.g., laundry machines and fridges, etc.. The ISM bands (2.4 GHz and 5 GHz) used for WI-FI systems are quite narrow. There is a lack of the capacity for so many connected devices. Another issue which has to be solved is the demand for high transmission speed. In order to provide higher than 100 Mbit connectivity between receiver and transmitter, new modulation schemes and connection of several consecutive channels (channel aggregation) have to be used. These solutions require high Signal-to-Noise-Ratio (SNR) and precise spectrum planning. The cognitive radio [2] ideas should solve all these following frequency spectrum problems: low SNR, overfilled frequency spectrum and channel assignment. Cognitive radio is an intelligent autonomous system with ability to change its parameters according to the environment (radiation power, modulation, and channel). In this paper we will introduce intelligent channel allocation for single channel WI-FI system or aggregated channels WI-FI system respectively (802.11n) [3]. Based on the real measured data [4] from spectrum survey, the whole WI-FI band will be investigated in detail and channels will be prioritized according to its occupancy. Each channel will receive the score (higher score means less suitable channel) given by weigh function from reinforcement learning algorithms. Afterwards, this score will be updated over the time and the temporary used channel should also decrease its score as a consequence in the next time steps. The learning will be continuous action. Moreover, we are able to distinguish between short-time usage of the channel and long-term unstoppable channel usage. The key parameters of the proposed system are following: total performance of the client to access point transmission and interference count for selected channels. These parameters will be after finally compared with the situation without proposed improvements.

ACKNOWLEDGMENT

This work was supported by the project CZ.1.07/2.3.00/30.0005 of Brno University of Technology.

REFERENCES

1. IEEE, "Part 11: Wireless LAN medium access control (MAC) and physical layer (PHY) specifications," *Amendment 4: Further Higher Data Rate Extension in the 2.4 GHz Band*, The Institute of Electrical and Electronics Engineers, Inc., 2003.
2. Fette, B., *Cognitive Radio Technology*, Newnes, Burlington, 2006.
3. Ortiz, S., "IEEE 802.11n: The road ahead," *Computer*, Vol. 42, 13–15, 2009.
4. Urban, R., T. Korinek, and P. Pechac, "Broadband spectrum survey measurements for cognitive radio applications," *Radioengineering*, Vol. 21, 2012.

Analysis of Conditions on the Boundary between Layers

R. Kadlec and P. Fiala
Department of Theoretical and Experimental Electrical Engineering
Brno University of Technology, Technická 3082/12, Brno 616 00, Czech Republic

Abstract— The authors report on an analysis of conditions on the boundary between layers having varied electromagnetic properties. The research is performed using consistent theoretical derivation of analytical formulas, and the underlying problem is considered also in view of multiple boundaries including the effect of the propagation of electromagnetic waves having different instantaneous speed.

The paper includes a theoretical analysis and references to the generated algorithms. The algorithm was assembled to enable simple evaluation of all components of the electromagnetic field in relation to the speed of the wave propagation in a heterogeneous environment. The proposed algorithms are compared by means of different numerical methods for the modelling of electromagnetic waves on the boundary between materials; moreover, electromagnetic field components in common points of the model were also subject to comparison.

When in conjunction with tools facilitating the analysis of material response to the source of a continuous signal, the algorithms constitute a supplementary instrument for the design of a layered material. Such design enables the realization of, for example, recoilless plane, recoilless transition between different types of environment, and filters for both optical and radio frequencies. This phenomenon occurs in metamaterials.

ACKNOWLEDGMENT

The research described in the paper was financially supported by Czech Science Foundation (13-09086S), a project of the BUT Grant Agency, No. FEKT-S-11-5/1012, and a project from the Education for Competitiveness Operative Programme, No. CZ.1.07.2.3.00.20.0175 (Electro-researcher).

REFERENCES

1. Roubal, Z., M. Steinbauer, and Z. Szabó, "Modeling of saturation characteristic of an aspiration condenser," *PIERS Online*, Vol. 6, No. 1, 26–30, 2010.
2. Steinbauer, M., R. Kubásek, and K. Bartušek, "Numerical method of simulation of material influences in MR tomography," *Progress In Electromagnetics Research Letters*, Vol. 1, 205–210, 2008.
3. Dedek, L. and J. Dedková, *Elektromagnetismus*, Vol. 2, 232, VITIUM, Brno, 2000, ISBN 80-214-1548-7.
4. Drexler, P. and R. Kubásek, "Pulsed magnetic field fiber optic sensor based on orthoconjugate retroreflector," *Proceedings of SCS 2009 International Conference on Signals, Circuits and Systems*, 52–57, Tunisia, 2009, ISBN: 978-1-4244-4398-7.

Fast Calculation of T_2 Relaxation Time in Magnetic Resonance Imaging

J. Mikulka[1] and P. Dvořák[2]

[1]Department of Theoretical and Experimental Electrical Engineering
Brno University of Technology, Technická 12, Brno 616 00, Czech Republic
[2]Academy of Science of the Czech Republic, Institute of Scientific Instruments
Královopolská 147, Brno 612 64, Czech Republic

Abstract— The main parameters displayed by means of magnetic resonance include, for example, relaxation times T_1 and T_2 or diffusion parameters. This paper presents the computation of relaxation time T_2 measured indirectly with the Spin Echo method. The sensing coil of the tomograph provides a signal in which the important factor is the location of the peaks from individual measurements. These points must be interleaved with an exponential function. The relaxation time T_2 can be directly determined from the exponential shape. The described process has to be repeated for each pixel of the sensed tissue, and this requirement makes the processing of larger images very demanding in terms of both the actual computation and the time needed for the entire operation. More concretely, if we assume the common resolution of 256×256, 20 slices, and five measurements with different times T_E, it is necessary to reconstruct $1.3 \cdot 10^6$ exponential functions in total, which requires the processing of more than 6 MB of data. At present, such computation lasts approximately 3 minutes if performed by means of a regular PC. The author discusses various approaches to the parallelization of the given problem. In the described context, the time required for the processing of the applied three-dimensional image was shortened to 300 ms thanks to simple interpolation approach. The final section of the paper comprises a detailed comparison of the computation times characterizing both the sequential and the parallel solutions.

Measuring and Application of NIR Light Absorption Coefficient of Bacteria

Pavel Krepelka[1], **Fernando Camara Martos**[2],
Guiomar Denisse Posada-Izquierdo[2], **and Fernando Pérez-Rodríguez**[2]

[1]Department of Theoretical and Experimental Electrical Engineering
Brno University of Technology, Technická 12, Brno 616 00, Czech Republic
[2]Departamento de Bromatología y Tecnología de los Alimentos, Ed. Darwin-Anexo
Campus Rabanales s/n, Universidad de Córdoba, Córdoba 14014, Spain

Abstract— NIR spectroscopy is a widespread technique in analytical chemistry. However, recently, there is a growing interest in usage of the NIR spectroscopy in microbiological analysis. Due to improvement of the experiment set-up and increase of efficiency of evaluation methods, knowledge about absorption coefficient of sample can be very beneficial. Purpose of this study is to introduce issues that concern measuring and handling with absorption coefficient.

Molecular bonds presented in the examined sample cause absorption of incident light. When the energy quantum from a source of light equals the energy necessary for the transition of a bond to a higher vibration level, the light is absorbed. Considering this effect, it is possible to identify chemical composition of sample. Recent studies proved chemical composition of different bacteria species are sufficiently diverse, thus bacteria can be identified by NIR spectrum. Absorption coefficient is mostly used in Lambert-Beer-Bouguer law. This equation expresses how the optical intensity of the light wave is exponentially reduced while traveling through the sample. In case of NIR spectroscopy, output light intensity is measured. Multiplicative scatter and other unwanted influences of the incoming radiation make direct measurement difficult. For correct computing of absorption coefficient, it is necessary to separate physical light-scattering effect from chemical light absorbance constituted by vibrations of molecule's bonds. Absorption coefficient is function of the energy of photons (wavelength) and its value depends on the position and amplitude of fundamental, overtones or combination types of molecular bonds absorption.

Knowing of absorption coefficient is important due to optimizing measure technique and statistics methods. Because straightforward measuring of bacteria cells requires a special approach, prior knowledge of absorption coefficient can leads to reduce costs in money and time.

Using Diffusion-weighted Images to Identify Brain Tumors

P. Marcon[1], **K. Bartusek**[2], **and A. Sprlakova**[3]

[1]Department of Theoretical and Experimental Electrical Engineering
Brno University of Technology, Technicka, Brno 3082/12, Czech Republic
[2]Institute of Scientific Instruments of the ASCR, v.v.i
Kralovopolska 147, Brno 612 64, Czech Republic
[3]Radiological Clinic, The University Hospital Brno, Jihlavska 20, Brno 625 00, Czech Republic

Abstract— The paper presents an evaluation of the magnetic resonance images of a pathology in the human brain. The experiment involved patients with high-grade glioma tumors in the brain, and an MR tomograph operated by the University Hospital Brno-Bohunice was utilized in the related examinations. The MR tomograph exhibits the static field flux density of $B_0 = 1.5\,\mathrm{T}$. The measurement and processing methods were tested on healthy objects.

In our investigation, we measured images weighted by T_1, T_2, and diffusion. A very interesting technique is diffusion-weighted imaging (DWI), where the measurement sequence comprises a table with 32 vectors of the b-factor orientation. The goal is to perform signal processing in the measured diffusion-weighted images. We proposed a special algorithm for the processing of the DWI image signal. The next step in the procedure was the statistical evaluation of T_1-weighted, T_2-weighted, and DWI images of healthy and diseased human tissues. We also calculated the brain white matter images, such as those of the fraction anisotropy, RA (relative anisotropy), and VR (volume ratio). These indicators are all scaled from zero to one, although the VR contrast is inverted. The diffusion tensor images weighted by eigenvalues and eigenvectors are also of interest for the process of defining the pathology.

All the obtained images are compared and evaluated; the paper contains a figure showing the most visible tumor in the brain area.

Partial Discharge Detection and Localization System

M. Cap, P. Drexler, and P. Fiala
Department of Theoretical and Experimental Electrical Engineering
Brno University of Technology, Technicka 3082/12, Brno 616 00, Czech Republic

Abstract— This article describes the partial discharges (PD) detection and localization system. Localization can be performed on the basis of measured UHF waveforms analysis during activity of the partial discharges. The time-shifts of the waveforms related to transient process occurrence in the signals are the main input parameters for localization methods. In order to estimate the position of the signal source in the 3D space a minimum of four antennas has to be used, since the time of the PD is unknown. Analysis of the PD starts with visual investigation of the signals present inside of the power oil transformer. PD signal level is in comparison to other signals inside the transformer very low. Therefore, signal line contains except amplifiers also controlled attenuators to reach required trigger conditions. Detailed investigation of all signals inside transformer is provided in memory mode in which system store defined number of signals for offline diagnosis a localization. Continual and memory mode of the system also contain differential method for non PD signals removing. Differential method is based on simultaneous detection of the signal inside and outside of the transformer with aim to acquire only signal which comes from inside of the transformer. Localization of the PD origin is based on TDOA algorithm. Resulting position are visualized as point in transformer 2D and 3D scheme.

Numerical Model of a Large Periodic Structure

R. Urban, P. Drexler, P. Fiala, and D. Nešpor
FEEC, BUT, UTEE, Technická 12, Brno 616 00, Czech Republic

Abstract— The aim of this paper is to present a special numerical model of structures used for nano applications. The practical impact of the research consists in enhanced evaluation of electromagnetic parameters: the numerical model will facilitate more efficient designing of nanoelements, and it will also promote dynamic solution of nanotechnology-related problems. The first numerical model of a large periodic structure is conceived to test electromagnetic wave propagation in graphene-based composite materials. According to the current interpretation of the results, the basic design of an applicable structure will be prepared for experimental fabrication.

REFERENCES

1. Castro Neto, A. H., F. Guinea, K. S. Novoselov, and A. K. Geim, "The electronic properties of graphene, reviews of modern physics," Vol. 81, The American Physical Society, January–March 2009.
2. Yan, C., K.-S. Kim, S.-K. Lee, S.-H. Bae, B. H. Hong, J.-H. Kim, H.-J. Lee, and J.-H. Ahn, "Mechanical and environmental stability of polymer thin-film-coated graphene," Vol. 6, No. 3, 2096–2103, ACS, NANO, 2012.
3. Singh, K., A. Ohlan, and S. K. Dhawan, "Polymer-graphene nanocomposites: Preparation, characterization, properties, and applications," INTECH, © 2012, http://dx.doi.org/10.5772/50408.
4. Lincoln Vogel, F., "The electrical conductivity of graphite intercalated with superacid fluorides: Experiments with antimony pentafluoride," *Journal of Materials Science*, Vol. 12, No. 5, 982–986, 1997.
5. Van Vlaenderen, K. J. and A. Waser, "Electrodynamics with the scalar field," *Physics*, Vol. 2, 1–13, 2001.
6. Kikuchir, H., *Electrohydrodynamics in Dusty and Dirty Plasmas, Gravito-electrodynamics and EHD,* Kluwer Academic Publishers, Dordrecht/Boston/London, 2001.
7. Van Vlaenderen, K. J., "A charge space as the orogin of sources, fields and potentials," *Physics*, Vol. 1, 1–13, Oct. 16, 1999, arXiv:physics/9910022.
8. Stratton, J. A., "Teorie elektromagnetického pole," 51–60, SNTL, Praha, Czech Republic, 1985.
9. Fiala, P., "Modeling and design of pulsed power generator," Habilitation Thesis, No. 13, VUT FEKT Brno, Czech Republic, Aug. 2005, ISBN 80-214-1346-8.

Optimization of the Particle Swarm Algorithm

J. Chytil
Department of Theoretical and Experimental Electrical Engineering
Brno University of Technology, Technicka 12, Brno 616 00, Czech Republic

Abstract— Particle Swarm Optimization is a swarm intelligence based and stochastic algorithm to solve the optimization problem. This paper presents the Multidimensional Particle Swarm algorithm with non-equidistant discrete input data such as E-Series or Renard numbers for circuit design. The authors describe the optimization of this method for different circuit designs, agent recycling, and omission of already computed points. The problem of omission of already computed points is to determinate when it is faster to omit the points than compute them. The personal omission history can be used for agent recycling or trajectory corrections. There is also described effect of recycled agents with corrected parameters on the convergence of optimalization. Parameters corrections are based on the principles of genetic algorithms in the other words inheritance from the best rated agents. System of agents rating is described briefly.

REFERENCES

1. Zhang, H. and H. Qing, "Hybrid multiagent swarm optimization: Algorithms, evaluation, and application," *Decision and Control*, 5699–5704, 2012.
2. Ibrahim, I., Z. M. Yusof, S. W. Nawawi, M. A. A. Rahim, K. Khalil, H. Ahmad, and Z. Ibrahim, "A novel multi-state particle swarm optimization for discrete combinatorial optimization problems," *Computational Intelligence, Modelling and Simulation*, 18–23, 2012.
3. Pratiwi, L., Y.-H. Choo, N. A. Muda, and A. K. Muda, "Improving ant swarm optimization with embedded vaccination for optimum reducts generation," *Hybrid Intelligent Systems*, 448–454 2011.
4. Wu, X., "A density adjustment based particle swarm optimization learning algorithm for neural network design," *Electrical and Control Engineering*, 2829–2832, 2011.
5. Anantathanavit, M. and M. A. Munlin "Radius particle swarm optimization," *Computer Science and Engineering Conference*, 126–130, 2013.

Sensitivity Improvement in NQR Based Detection Methods

M. Steinbauer, J. Segiňák, and P. Dohnal
Department of Theoretical and Experimental Electrical Engineering
Brno University of Technology, Technická 12, Brno 616 00, Czech Republic

Abstract— The proposed article will present some approach to sensitivity improvement in nuclear quadrupolar resonance (NQR) based detection method, used for example for explosives detection. We have experimental pulsed NQR apparatus equipped with 250 W pulse power rf amplifier with working frequency range from 0.5 to 50 MHz. This range is suitable for detection of isotopes ^{14}N and ^{35}Cl. Article will describe some improvements in circuitry of NQR system proposed by authors and experimentally verified on above mentioned system. These modifications lead to increased signal to noise ratio (SNR) and thus increase the sensitivity of system during the detection of substances. Main improvements are in rf blocking circuit, which prevents the power rf pulse from reaching the preamplifier of receiver. In this position some impedance transformers with switched coil has been tested. The appropriate quenching circuit further reduces the penetration of excitation pulse to this sensitive preamplifier and thus shortens the recovery time. Next improvement of sensitivity is based on the suppression of false signals interchangeable with FID response, caused by external rf source. This could be either done by differential method with reference external antenna, or alternately by switched magnetic field in the sample, which brings the loss of NQR signals in the sample, so calculating differential measurement with and without static magnetic field affecting the sample can dramatically highlight the NQR peaks in spectrum of detected signal.

Finally, the appropriate pulse sequence parameters as well as level of excitation of sample is important to good SNR of measured signal. For example too high level of excitation pulse cause less or even zero NQR response.

Experimentally verified impact of all the proposed enhancements applied to our pulsed NQR system will be given also.

A Dark Matter Model to Unify Gravity and Electromagnetism

Michael J. Underhill
Underhill Research Ltd, Lingfield, UK

Abstract— In previous papers feasible electromagnetic structures for all particles have been proposed [1–4]. These support the proposition that 'Everything is Electromagnetic' and therefore there is 'An Electromagnetic Theory of Everything'. The prime basis for the 'Physical Electromagnetic Model' is the discovery of Electromagnetic (EM) Coupling [1–8]. Paper [9] suggested how this model could explain the ratio of measured stable masses of all the sub-atomic particles in the Standard Model [10].

Paper [8] also proposed that *any* form of energy has a *gravitational* mass in accordance with $E = mc^2$. It is important to note that this included *the energy in fields* and low density particles such as photons and neutrinos [1, 8]. All forms of energy can be expressed as $E = \Phi \times \Psi$, where Φ is potential and Ψ is *substance* (charges, currents and matter-substance). This definition is common to both Gravity and Electromagnetism and therefore is itself a unifying concept.

In paper [8] an EM coupling mechanism was given for the *inertial* mass of particles having a dense central core. In this case inertial mass is defined to be equal to gravitational mass. The 'core-atmosphere' particle model in [8] is assumed as the basis for finding particle stability conditions [9]. The core consists of concentrated 'substance' which creates the surrounding 'atmosphere'.

Low density forms of energy such as heat, light and electromagnetic and gravitational fields are considered to be *dark matter* having a low inertia but with gravitational mass defined by $E = mc^2$. Thus even the fields created by and emanating from any form of 'substance', such as any type of charge, current, matter, or mass, do themselves have energy and mass and therefore are defined also as *dark matter* having full gravitational mass but low inertial mass. Note that particles are predicted to have line spectra with each spectral component having energy E_n and frequency f_n, given by $E_n = hf_n$. By contrast heat and in general dark matter have continuous broadband spectra. (Frequency is regarded as 'the fifth dimension').

Electromagnetic Coupling is now defined both as a trans-impedance $Z_{12}e^{-j\omega\tau}$ with delay τ and as a trans-conductance $Y_{21}e^{-j\omega\tau}$ with the same delay. The delay value is a (new) fundamental physical constant and can be shown to be the origin of the 'inertial mass of any particle [8]. These definitions also apply to mass and gravity as a result of the common definitions: Energy, $E = mc^2 =$ Potential, $\Phi \times$ Substance, Ψ.

The proposed 'dark matter model of gravitation' is based on the observation of 'process capture' where the fields from two sources overlap. When applied to either EM or gravitational fields, the process capture RSS (Root-Sum-of-the-Squares) rule in general causes a net diminution in total field energy, and hence in total mass when two particles (having mass) are brought together. It is this diminution of energy that is the root cause of gravitational attraction. This concept can be extended to further cases, such as small particles in a large (gravitational) field, self-attraction of dark matter, and black holes.

REFERENCES

1. Underhill, M. J., "The phase noise spectrum and structure of photons?" *Proc. 16th EFTF-2010*, 8 pages, Noordwijk, Netherlands, April 13–16, 2010.
2. Underhill, M. J., "A physical model of electro-magnetism for a theory of everything," *PIERS Online*, Vol. 7, No. 2, 196–200, 2011.
3. Underhill, M. J., "Maxwell's transfer functions," *PIERS Proceedings*, 1766–1770, Kuala Lumpur, Malaysia, March 27–30, 2012.
4. Underhill, M. J., "A local ether lens path integral model of electromagnetic wave reception by wires," *PIERS Proceedings*, 1005–1008, Moscow, Russia, August 19–23, 2012.
5. Underhill, M. J., "Antenna pattern formation in the near field local ether," *PIERS Proceedings*, 1009–1012, Moscow, Russia, August 19–23, 2012.
6. Underhill, M. J., "Wideband small loop-monopole HF transmitting antenna with implications for Maxwell's equations and the Chu criterion," *PIERS Proceedings*, 764–768, Taipei, March 25–28, 2013.

7. Underhill, M. J., "Coupled electromagnetic wave propagation in space and around surfaces and interfaces," *PIERS Proceedings*, 394–398, Stockholm, August 12–15, 2013.
8. Underhill, M. J., "Electromagnetic structures and inertias of particles including the Higgs Boson," *PIERS Proceedings*, 401–405, Taipei, March 25–28, 2013.
9. Underhill, M. J., "The stability of EM particles and predicted mass ratios," *Proc. PIERS*, 399–404, Stockholm, August 12–15, 2013.
10. http://en.wikipedia.org/wiki/Standard_Model.

Interactive Segmentation of Hip Joint Cartilage

Pavel Dvorak[1,2], **Vladimir Juras**[3], **Wolf-Dieter Vogl**[4], **and Jiri Chytil**[2]

[1]Institute of Scientific Instruments of the ASCR
v.v.i., Královopolská 147, Brno 612 64, Czech Republic
[2]Faculty of Electrical Engineering, Brno University of Technology
Technická 12, Brno 612 00, Czech Republic
[3]High Field MR Center, Department of Biomedical Imaging and Image-guided Therapy
Medical University of Vienna, Waehringer Guertel 18-20, Vienna A-1090, Austria
[4]Computational Image Analysis and Radiology Lab, Department of Radiology
Medical University of Vienna, Lazarettgasse 14, Vienna A-1090, Austria

Abstract— This work deals with hip joint cartilage segmentation, which is an important task in joint diseases diagnosis. Since the manual segmentation commonly used nowadays, is a tedious and lengthy task, this work brings a new idea into its automation and simplification of the medical expert work. The proposed method is an interactive algorithm for hip joint cartilage segmentation, and hence it requires some user interaction, which is common and usually desired in medical image processing. The first step of the method is a selection of several points in several slices lying inside the cartilage. The purpose is a rough delimitation of the cartilage area. This delimitation is based on the assumption that the femur head has approximately circular shape. The cartilage is then segmented using the combination of Graph Cut segmentation and K-means clustering techniques. The algorithm was tested on 3D isotropic True-FISP volumes of patients with femoroacetabular impingement and the results were evaluated by commonly used Dice Similarity Coefficient (0.62). The results of the segmentation will be prospectively used for the segmentation of quantitative MR maps (T_1 and T_2) in femoro-acetabular impingement (FAI) investigation.

PIERS: Progress In Electromagnetism — Relativity Superseded

Piers Hutchinson
MA Oxon, 485 Hilson Ave, Ottawa K1Z 6C6, Canada

Abstract— This paper proposes an end to the idea that Time can start in a Big Bang, dilate at speed and stop in a Black Hole. Time and Space are manmade abstracts and do not combine to form an object called space-time that can warp to produce gravity. Maxwell was right: Radiation is not made of particles but is a wave in ether. Ether is made of particles of Plank length and mass here called evrons. Gravity, magnetism and the strong force are not negative quanta but positive surrounding evronic pressure which increases with increasing opposed density. The red-shift and the Microwave Background Radiation are the lengthening of light wave patterns as they spread through evrons in a boundless universe. Nucleons are made of solitons of evrons; instead of orbiting electrons, the nucleons produce waves in the ether described by the Schrodinger wave equation; the photoelectric effect is the creation of electrons from evrons. Matter does not change into energy; $E = mc^2$ is the release of evronic energy; the mass is conserved. The effects of Special Relativity including the perihelion of Mercury are the result of ether drag according to Lorentz's drag formula, $\sqrt{1 - (v/c)^2}$. The proofs of evrons are: (1) The Michelson-Morley experiment conducted on a train which produces an interference wave pattern [Sagnac]; (2) The Two-Slit experiment with the equivalent of one photon at a time which produces an interference wave pattern; (3) WMAP measurements over the last ten years which show the universe is 3-D flat; (4) Hadron collision experiments which produce extra particles from the so-called vacuum; (5) DNA copying which depends on the wave pattern of the original nucleotide locating another nucleotide with a complementary wave pattern among thousands of non-matching molecules; (6) The superposition of waves which allows an animal to see and remember as a dynamic whole, in a single fixation, a scene moving at light speed; (7) The ability of humans to conceptualize at the speed of light and to act freely.

Session 4A13a
Remote Sensing of the Earth, Ocean, and Atmosphere

PO-GO/ECM for Bistatic RCS Modeling of Complex Objects over Rough Sea Surface

Y. Bennani[1] **and R. Talhi**[1, 2]

[1]Department of EECS, University of Tours, Avenue Monge, Tours 37200, France
[2]CNRS/LPC2E, 3A Avenue de la Recherche Scientifique, Orleans Cedex 2 45071, France

Abstract— The work summarized in this paper fits well in the field of remote sensing of the marine environment. It shall include, on one hand the study of interaction of an electromagnetic wave with a sea surface in the presence of a complex target observed in bi-static configuration. Furthermore the work is completed by the study and analysis of the influence on this EM interaction of various parameters related to both the target and also to the environment. In this study context, this paper focuses on two important components. The first is the study and simulation of Radar Cross Section (RCS) of a complex target placed in free space [1]. To address this point, the electromagnetic model held is based on a combination of asymptotic methods (Physical Optics (PO), Optical Geometric (OG), Equivalent Current Method (ECM)) including shadowing effect and multipath. The proposed methodology was evaluated via simulations as well as experiments in anechoic chamber with a generic model of a ship. And a second part deals with the scattering by target over sea surface [2]. In order to introduce the influence of the sea surface on the electromagnetic response of the target in its environment, we opted for a representation of the scene (target + sea surface) by a set of triangular facets. Within this framework, the target discretized by a triangular mesh is generated using a CAD — Computer Aided Design — tool (CATIA, V5); as regards the sea surface, it is generated using the Elfouhaily sea spectrum [3] (and the Debye model to take into account the dielectric parameters of seawater).

The model has been validated by comparing theoretical results to experimental results obtained in the anechoic chamber [4], then it was applied to a marine scene by considering the sea surface and the target as a single complex object. More results will be given in the final version of this paper. Moreover, other applications of our method could be the radar imagery in bistatic representation and 3-D imagery representation.

REFERENCES

1. Xu, F. and Y. Q. Jin, "Bidirectional analytic ray tracing for fast computation of composite scattering from electric-large target over a randomly rough surface," *IEEE Transactions on Antennas and Propagation*, Vol. 57, 1495–1505, 2009.
2. Burkholder, R. J., P. Janpugdee, and D. Colak, "Development of computational tools for pre-decting the radar scattering from target on a rough sea surface," Tech. Rep., Ohio State University, 2001.
3. Elfouhaily, T., B. Chapron, and K. Katsaros, "A unified directional spectrum for long and short wind-driven waves," *Journal of Geophysical Research*, Vol. 102, 15–781, 1997.
4. Bennani, Y., F. Comblet, and A. Khenchaf, "RCS of complex targets: Original representation validated by measurements — application to ISAR imagery," *IEEE Transactions on Geoscience and Remote Sensing*, Vol. 50, 3882–3891, October 2012.

Space-borne Observations and Analysis of Human-generated Electromagnetic Radiations

R. Talhi[1,2], P. Sebire[1], and Y. Bennani[2]

[1]CNRS/LPC2E, 3A Avenue de la Recherche Scientifique, Orleans Cedex 2 45071, France
[2]Department of EECS, University of Tours, Avenue Monge, Tours 37200, France

Abstract— In the last decades human-generated electromagnetic (EM) radiations have increased dramatically, and they are more and more influencing the near-Earth environment (atmosphere-thermosphere-ionosphere system). For example, powerful transmitters (communications and broadcasting systems), electric energy transport systems (or power lines), automotive ignition, industrial areas, heat generated by daily activities in major northern hemisphere metropolitan areas, among others, are the well-known causes produced by human activities [1] and radiated from the Earth's surface, which contribute to polluting our atmosphere. This kind of pollution, actively discussed in scientific community and health care professionals, has led some scientists to consider possible negative effects of EM radiations on human life and living systems in general. Therefore accurate measurements of human-generated EM radiations are necessary to understand the relative power levels in the different frequency bands and their influence on life [2]. EM radiations observed in the near-Earth environment are the superposition of natural (solar activity) and human-generated emissions. In this paper, we only concentrate on the latter case.

Human activities generate EM emissions which cause perturbations in the ionosphere and induce some phenomena in ionospheric plasmas; as we know, most of these phenomena are still poorly understood. Also the continuous monitoring of EM environment on board of LEO (Low Earth Orbit) satellites, can detect and record human-generated EM (HG-EM) radiations, taking into account geophysical conditions, as well as properties of the surrounding satellite environment and noise generated by the payload system.

In this context, the purpose of this paper is to describe in detail some observed and statistically analyzed EM data corresponding to ionospheric plasma characteristics recorded by DEMETER space mission (http://smsc.cnes.fr/Demeter/index.htm) [3] over powerful EM emissions from human-generated activities, mainly VLF-powerful transmitters (VLF-PT), power lines harmonic radiations (PLHR), and industrial areas, during months to years. Our objective is to examine the spatial and frequency distributions of observed perturbations. Upon close examination of data, it appears that a variety of observed phenomena seem connected with VLF-PT, like generation of electrostatic (ES) waves from HF to ELF frequency bands, appearance of strong turbulence, increasing of electrons and ions temperatures (heating of the ionosphere) as well as fluctuations of electrons and ions densities. Moreover, it is shown that above the location of these VLF-PT, an important wave activity exists at MF frequencies, which means that whistler waves generated by lightning strokes are able to reach the ionosphere at MF frequencies. Other types of signatures were observed in the ionosphere. These include sudden noise emissions which are detected at ELF/VLF frequency bands when the space-borne is above industrial areas. Also observed are radiations at high order harmonics of 50 or 60 Hz which are found to be associated with the electric energy transport systems, that is the power lines harmonics radiations (PLHR).

All these experimental observations clearly show that an amount of HG-EM energy is injected in the atmosphere at various frequency bands. In other words, these experimental observations imply the existence of energy flow mechanism from the Earth surface to the ionosphere. A goal is to build up an accurate physical model to account for this mechanism.

REFERENCES

1. Zhang, G. J., et al., "Energy consumption and the unexplained winter warming over northern Asia and North America," *Nature Climate Change*, January 27, 2013.
2. Bianchi, C., et al., "Natural and man-made Terrestrial EM noise: An outlook," *Annals of Geophysics*, June 2007.
3. Parrot, M., Guest Editor, "First results of the demeter micro-satellite," Special Issue of *Planetary and Space Science*, Vol. 54, No. 5, April 2006.

Study on the Variation Characteristics of Land Desertification in Ebinur Lake Basin

L. S. Sun[1], **Y. T. Ma**[1, 2], **and H. Ding**[1]

[1]School of Civil Engineering, Shenyang Jianzhu University, Shenyang, China
[2]School of Resource & Civil Engineering, Northeastern University, Shenyang, China

Abstract— The increasingly serious desertification not only led to huge direct economic losses but also caused the continuously decrease of the quantity and quality of land source which human beings depend on, the frequent occurrence of sand storm and other natural disasters, and the constantly deterioration of ecological environment, which are directly posing a threat to the very existence and development of mankind. Due to aforementioned facts, obviously, the prevention and control of desertification are significant and urgent. Based on the 2006, 2009 and August 2012 MODIS-NDVI data and dimidiate pixel model, the vegetation coverage were estimated in this paper. Furthermore, the remote sensing monitoring of the land sandy desertification in Ebinur Lake Basin was also processed to reflect the dynamic changes of desertification in last 6 years, which offered decision support for regional ecological environment assessment and sustainable development.

The results were found: the sandy desertification in most parts of Ebinur Lake Basin was mild and moderate desertification which were always over the 60 percent of total area; Over 50 percent of area changed from mild desertification to non-desertification during 2006 to 2009 and 2009 to 2012 respectively; Compared to 2006, in 2012, the areas of the severe, moderate and mild desertification were increased and the areas of the micro and non-desertification were decreased. The most significant variation among these was the difference of area of severe desertification which increased by 517.065 square kilometers in 6 years, and its annual variable rate reached 16.332 percent. Meanwhile, the area of the micro desertification decreased by 1786.512 square kilometers, and reached a −6.083-percent annual variable rate, and the area of non-desertification also decreased slightly. It means that the area of micro and non-desertification had been transforming to the area of the severe, moderate and mild desertification. The research method in this paper which examined the variation and degree of soil desertification is low-cost, accurate and feasible.

Analysis of EVI and NDVI Characteristics in Different Land Cover Types in Liaoning Province

J. L. Wang[1], **Y. T. Ma**[1, 2, *], **and L. S. Sun**[1]

[1]School of Civil Engineering, Shenyang Jianzhu University, Shenyang, China
[2]School of Resource & Civil Engineering, Northeastern University, Shenyang, China

Abstract— There are two vegetation index products, Normalized Difference Vegetation Index (NDVI) and Enhanced Vegetation Index (EVI). The monitoring vegetation capacity and the relationship of NDVI and EVI have been studied at home and aboard. It has been found there were some advantages and disadvantages of monitoring vegetation by NDVI and EVI. The characteristics and relationships of the two vegetation index still need to be unceasingly researched, especially on the typical features In Liaoning Province.

Based on vegetation types of data and TERRA/MODIS data in 2011, both EVI and NDVI variations of four types of land cover in Liaoning province were studied in time series. The 16 regions from four types of land cover, including woodland, plowland, water and urban were selected as interest. Their characteristics and relationships of EVI and NDVI were analyzed by the data statistics method. The results were the following.

In the woodland coverage area, the shape of their NDVI and EVI in time series looked like a bell-shaped curve in the period of forests turning green and growing, NDVI was prone to become saturated, and could not show the growth process of trees while EVI could better do that. In the plowland coverage area, the shape of their NDVI and EVI in time series looked like an inverted V-shaped curve in the period of crops growing season. In the water coverage area and urban, the values of their NDVI and EVI were slightly higher in the summer than other seasons, and the annual variation range of their NDVI and EVI was small. In the plowland coverage area, both NDVI and EVI could well show the process of vegetation growth. In the water coverage areas and urban, NDVI sensitively influenced by noise, while EVI could overcome this shortcoming. The curves shapes of NDVI and EVI under different land cover types are of great significance for vegetation classification and extraction in Liaoning province. The figures characteristics of NDVI and EVI indicate that EVI can well monitor the growth of forest in the woodland coverage areas, both NDVI and EVI can monitor the growth of crops in the plowland coverage area, and EVI can well monitor the growth of vegetation in the water coverage areas and urban.

*Corresponding author: Yuntao Ma (mayuntao7@163.com).

On a New Ship Detection Parameter Using Multi-polarization SAR Data

Chan-Su Yang[1, 2, 3] **and Kazuo Ouchi**[2]

[1]Department of Ocean Environmental System Science
University of Science and Technology, Daejeon, Korea
[2]Korea Ocean Satellite Center, Korea Ocean Institute of Science & Technology, Ansan, Korea
[3]Department of Convergence Study on the Ocean Science and Technology
School of Ocean Science and Technology, Busan, Korea

Abstract— In the present article, a new parameter is proposed to improve the accuracy of ship detection based on polarimetric analyses of synthetic aperture radar (SAR) data. The parameter is similar to the normalized difference vegetation index (NDVI) for multispectral optical data, and it is defined as the difference of values in polarimetric entropy from coherence divided by the sum of these two values. It has been known that the polarimetric entropy is high for targets that give rise to random scattering consists of different scattering processes such as ships; while it is low for targets yielding single scattering, for example, surface scattering from sea surface. It is also known that the coherence, i.e., correlation between HH- and VV-polarization images of targets with volume or multiple scattering is low in comparison with targets to give rise to surface scattering. The proposed index by taking the ratio of entropy-coherence difference to their sum, therefore, enhances the images of targets of multiple scattering against the targets of surface scattering in comparison with the entropy or coherence alone; and improves the detection accuracy of man-made targets on the sea such as ships. The validity of this new parameter for ship detection is examined using ALOS-PALSAR data over the Tokyo Bay, Japan.

Experimental Ship Monitoring Using SAR, FMCW Radar and AIS on the Ieodo Ocean Research Station, South Korea

Chan-Su Yang[1, 2, 3] **and Kazuo Ouchi**[2]

[1]Department of Ocean Environmental System Science
University of Science and Technology, DAEJEON, Republic of Korea
[2]Korea Ocean Satellite Center
Korea Ocean Institute of Science & Technology, ANSAN, Republic of Korea
[3]Department of Convergence Study on the Ocean Science and Technology
School of Ocean Science and Technology, BUSAN, Republic of Korea

Abstract— We have developed the ship monitoring system based on Automatic Identification System (AIS) and FMCW RADAR, and a prototype system including Synthetic Aperture Radar (SAR) was introduced in the conference (IGARSS 2013) and the Journal of Navigation (2012). This paper describes the experimental results for an integration system of ships obtained from RADAR, SAR and AIS through the field campaigns on the Ieodo Ocean Research Station (IORS) in the northern part of the East China Sea, South Korea. SAR has been widely used to detect targets of interest with the advantage of the operating capability in all weather and luminance free condition (Margarit and Tabasco, 2011). In general, FMCW radar can play an important role in maritime surveillance, because it has many advantages such as low warm-up time, low power consumption, and its all-weather performance. AIS provides ships information including position, ID number (MMSI and IMO), type, nation, speed, direction, and so on.

Simultaneous observation of RADAR, SAR (Rasarsat-2 Wide Mode: HV, VV) and AIS was conducted on the same date as of the SAR acquisition for the purpose to perform an integration and identification test. The data were acquired from 21th November to 1st December 2013. All data were analysed statistically for assessment of marine traffic environments, and development of database for service of ship information. More details will be provided on the conference.

Session 4A13b
SC4&3: Metamaterials for Antenna Applications: Practical Solutions

Minkowski Fractal Antenna Design with DMS-SRR and DGS-SRR Structure for WLAN Application

H. Nornikman[1, 2], F. Malek[1], M. H. F. Mohd Fakri[1], M. Z. A. Abd Aziz[2], and B. H. Ahmad[2]

[1]School of Computer and Communication, Universiti Malaysia Perlis, Perlis, Malaysia
[2]Center for Telecommunication Research and Innovation (CeTRI)
Faculty of Electronics and Computer Engineering
Universiti Teknikal Malaysia Melaka, Durian Tunggal, Melaka, Malaysia

Abstract— Nowadays, the high gain and compact antennas are the most common issue that commonly considered by many researchers in the telecommunication area, especially in antenna design. There are many types of microstrip patch antenna had been researching to cater this problem. This paper is focused on the combination of defected microstrip structure of split ring resonators (DMS-SRR) and defected ground structure of split ring resonators (DGS-SRR) on the ground plane. The proposed DMS-SRR structure effect to wider the bandwidth and also increase the gain of the Minkowski fractal patch antenna. The other technique used in this design is a double layer substrate of FR-4 to improve the gain of the antenna. This double layer effect to increase the Minkowski fractal antenna gain to 3.827 dB, but it shifted the resonant frequency to 2.634 GHz. The DGS-SRR structure used to shift back the resonant frequency to 2.4 GHz region. Other parameters that had been considered in this work are return loss, radiation pattern and surface current. The first work is started by designing a normal Minkowski patch antenna. Then, three units of DMS-SRR had been added to the front side of the Minkowski fractal antenna. After that, a pair of DGS-SRR had been added to the ground plane of the antenna. The resonant frequency of this antenna is 2.4 GHz used for wireless LAN (WLAN) application. The proposed antenna capability to improve the antenna gain from 2.445 GHz to 3.650 GHz while the bandwidth is improving from from 69.00 MHz (2.368 GHz to 2.437 GHz) to 129.90 MHz (2.407 GHz to 2.537 GHz).

Equivalent Circuit Model of Different Configurations of Loop Elements Using Vector-fitting

Payal Majumdar, Zhiya Zhao, Yutao Yue, Chunlin Ji, and Ruopeng Liu
State Key Laboratory of Meta-RF Electromagnetic Modulation Technology
Kuang-Chi Institute of Advanced Technology, Shenzhen, Guangdong 518000, China

Abstract— A frequency-selective surface (FSS) is a periodic, planar assembly of generally metallic elements on a dielectric layer. It is built in conjunction with the EM waves in order to "tailor" an electromagnetic link in the free-space environment. Acting as a barrier for the waves propagating along the link, the FSS controls the flow of the EM energy. The transfer function of the FSS manipulates the spectral content of the wave. As a result, some of the frequency constituents of the wave are blocked, and some pass through the FSS fence.

For more than four decades, FSS has been an important topic because of their comprehensive applications, such as polarizers, filters, sub-reflectors, hybrid radomes, etc.. Unlike traditional microwave filters, the frequency response of FSS are not only functions of frequency, but also functions of incident angle and polarizations of EM waves. Consequently, it is necessary that an excellent FSS should provide stable performances for both various incidence angles and different polarizations within its operating frequencies. There is a growing demand for developing an accurate equivalent circuit model for FSS so that one can synthesize a desired frequency response (center frequency, bandwidth, insertion loss and tuning range) by an optimization method in a reasonably short time using a circuit simulator.

In this paper, we present the analysis and modeling of different configurations of loop elements in FSS, with resonant unit cells adopting an efficient vector-fitting. The elements studied are 1) Square loop, 2) Double Square loop and 3) Gridded Square loop. The vector-fitting is a new approach for rational macro modeling that ensures high accuracy with arbitrary terminal conditions. The simulations of microstructure are performed with full wave simulation tool CST Microwave Studio on single-substrate for different physical parameters, oblique incidence and effect of TE/TM polarization as well. Then circuit models are extracted and developed using the vector fitting tool and implemented in a circuit simulator enabling both time and frequency analyses along with effect of polarization and angle of incidence. Then ADS SPICE generator is used for verifying circuit models developed using simulated results. The developed model is within 1% of average deviation against reference data.

Antenna Reconfiguration Using Metasurfaces

Hailiang Zhu, S. W. Cheung, and T. I. Yuk
Department of Electrical and Electronic Engineering
The University of Hong Kong, Hong Kong

Abstract— The paper describes the designs of a frequency-reconfigurable, polarization reconfigurable and pattern reconfigurable antennas using metasurfaces (MS). The frequency-reconfigurable and polarization reconfigurable antennas are composed of a simple circular patch antenna or slot antenna as the source antenna and a circular MS with the same diameter, with both source antenna and MS implemented using planar technology. The pattern reconfigurable antenna is composed of a circular patch antenna as the source antenna and a semicircular MS. In all these reconfigurable antennas, the MS is placed directly atop of the source antenna, making the antenna very compact and low profile with a thickness of only $0.05\lambda_0$. By rotating the MS around the center with respect to the source antenna, the frequency, polarization or pattern can be reconfigured.

The geometry of the frequency-reconfigurable antenna is shown in Fig. 1, which has a diameter of $0.67\lambda_0$, with λ_0 being the free space wavelength. The source antenna is a rectangular patch antenna and the circular MS consists of rectangular-loop unit cells placed periodically in the vertical and horizontal directions on a single-sided substrate. Studies show that the MS underneath the patch antenna behaves like a dielectric substrate, and rotating the MS around the center with respect to the patch antenna will change the equivalent relative permittivity of the substrate and hence the operating frequency of the antenna. Results show that rotating the MS can change the operating frequency from 4.76 to 5.51 GHz, a fractional tuning range of 14.6%. The radiation efficiency and a realized peak gain of more than 80% and 5 dBi, respectively, across the tuning range.

In the polarization reconfigurable antenna, the source antenna is a slot antenna as shown in Fig. 2. The diameter of the MS antenna is $0.9\lambda_0$ and is composed of corner-truncated square unit cells on a single-sided substrate. The antenna is designed to operate at around 3.5 GHz. Studies show that, by rotating the MS around the center with respect to the slot antenna, the antenna can be reconfigured to linear polarization (LP), left-hand (LH) and right-hand circular polarizations

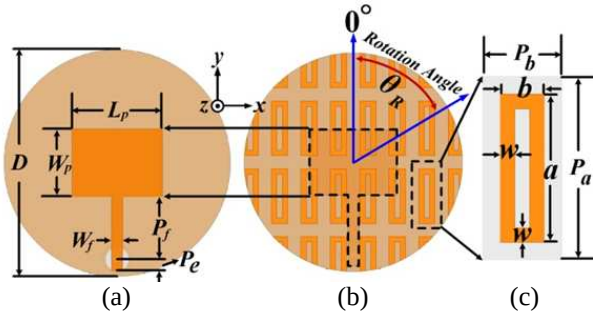

Figure 1: Geometries of frequency-reconfigurable antenna. (a) Patch antenna (source antenna), (b) matesurface, and (c) unit cell.

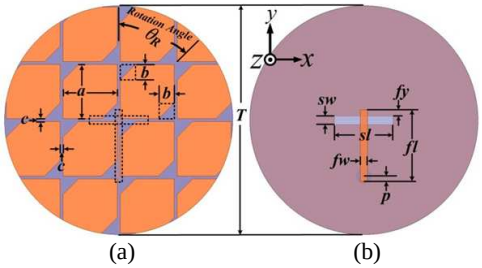

Figure 2: Geometries of polarization reconfigurable antenna. (a) MS and (b) slot antenna (source antenna).

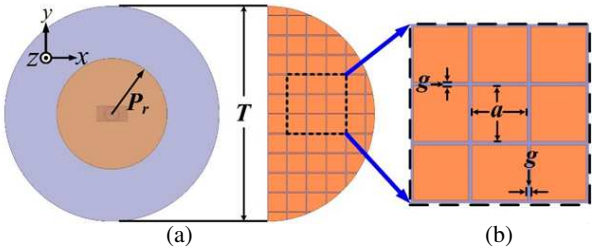

Figure 3: Geometries of polarization reconfigurable antenna. (a) MS and (b) slot antenna (source antenna).

(RHPL). In the paper, an equivalent circuit is used to explain the reconfigurability of the antenna. Results show that the antenna in circular polarization has an operating bandwidth of 3.3–3.7 GHz (i.e., fractional bandwidth 11.4%), a boresight gain of above 5 dBi and high-polarization isolation of larger than 15 dB. While the antenna in linear polarization achieves a gain of above 7.5 dBi with cross-polarization isolation larger than 50 dB.

Figure 3 shows the geometries of the pattern reconfigurable antenna. The source antenna is a circular patch antenna and the MS has a semicircular shape, both having the same diameter $1.2\lambda_0$. The MS uses small square patches as the unit cells. The semicircular structure of the MS underneath the patch antenna makes the antenna to have the beam tilted by 30° from the boresight direction. By rotating the MS around the center of the antenna, the tilted beam can be steered to different directions. The operating bandwidth, radiation efficiency and a peak gain will be presented in the paper.

A Systematic Approach to Synthesizing Artificial Dielctrics (Metamaterials) and Its Application to Antenna Design

Raj Mittra and J. C. Vardaxoglou
Electromagnetic Communication Lab, Pennsylvania State University, USA

Abstract— Historically, Metamaterials (MTMs), were defined as "materials that don't exist in nature." This definition was introduced when everyone was looking for doubly-negative (DNG) materials to realize a perfect lens. Later, the scope as well as the definition of Metamaterials were generalized, and now it is not uncommon to find that almost any artificially synthesized material being referred to as MTMs. Although MTMs were promised to be the magic material for realizing superlenses and invisibility cloaks, difficulties in realizing DNG, MNG (m negative) and e or m materials with values less than unity severely hampered the practical realizations of superlenses and cloaks. This is due primarily to the fact that MTMS with the attributes mentioned above, and realized by embedding resonant inclusion — as they almost always were — turned out to be narrowband, dispersive and lossy, which severely limited their practical usage.

Fortunately, however, other electromagnetic devices were successfully designed later, and were found to be useful for enhancing the performance of antennas and rendering them low-profile — among others — for a number of applications, albeit in some niche areas. This has helped to kindled renewed interest in MTM synthesis in a way that circumvents the problems of narrow bandwidth, dispersion and losses.

The objective of this paper is to examine the problem of synthesizing MTMS, in the context of several practical applications, e.g., flat GRIN lenses, and to propose a strategy of realizing the specified dielectric parameters that avoids the pitfalls in the previous design strategies based on the use of MTMs, which led to narrowband designs that were also lossy. We show a step-by-step procedure for designing a flat GRIN lens by systematically modifying COTS (commercially off-the-shelf) materials, by using inclusions in a background material that are either metallic or dielectric types. We then compare the performance of the lens, designed by using MTMS as described above, and show that the MTM-based lens typically exhibits a superior performance, not only over the conventional MTM/GRIN lenses, but also over those designed by using the recently introduced technique called TO (Transformation Optics).

Next, we present an example of a Metasurface, designed for a Reflectarray (RA) application. It is well known that the conventional reflectarrays are inherently narrowband, because they use resonant-type printed patches to realize the desired phase shit from the flat RA surface to achieve lens-like beam shaping properties. We show that the paradigm for synthesizing desired artificial dielectrics, described in this paper, enables us to achieve a relatively broadband performance, without compromising the gain.

Metamaterial Surfaces for Integrated Multiband Horn Applications

J. (Yiannis) C. Vardaxoglou
School of Electronic, Electrical and Systems Engineering
Loughborough University, Loughborough, LE11 3TU, UK

Abstract— Novel (Integrated Multiband Horn) IMH antenna designs using artificial metamaterial surfaces (FSS, EBG) are presented. A 'horn within a horn' concept is introduced whereby miniaturised metamaterial surfaces (of double ring elements) are embedded in the IMH.

Session 4P1
SC3: Nanoparticle-assisted Bioimaging and Sensing

A Double-amplification Strategy for Quantitative DNA Fluorescent Detection

Xia Liu, **Guofu Zhou**, **and Mingliang Jin**
Electronic Paper Display Institute, South China Academy of Advanced Optoelectronics
South China Normal University, China

Abstract— Sensitive and selective DNA detection has become increasingly important to the investigation of the genetic basis of diseases, clinical diagnosis, and gene therapy. A great number of ingenious methods for DNA detection based on duplicating target DNA (t-DNA) or amplifying detected probes have been developed [1–3]. Most of these technologies are one level signal amplification. In order to improve the detection sensitivity, we try to develop an ultrasensitive DNA assay based on double amplification strategy, as showed in Fig. 1. The method is a combination of magnetic submicrobeads (MSBs) amplification and enzyme amplification [4]. In this method, target DNA (t-DNA) is captured by streptavidin-coated substrate via biotinylated capture DNA (DNAc). The MSBs, modified with streptavidin, are fabricated with probe DNA (DNAp), which is modified with biotin through the absorption between streptavidin and biotin. Then the functionalized MSBs are labeled with alkaline phosphatase (AP) using biotinylated detection DNAs (DNAd) and streptavidin-AP conjugates. Since there are more than 10,000 conjugating position on MSB, the number of AP molecules on one MSB is much larger than the general enzymatic amplification method. Subsequently, the MSBs labeled with AP are conjugated to t-DNA sequences with a ratio of 1 : 1 by the hybridization between t-DNA and DNAp. The 1 : 1 ration means that one t-DNA corresponds to one MSB, which realized the quantification of t-DNA. After the hybridization between the t-DNA and MSBs, the substrate of AP, 4-methylumbelliferyl phosphate (4-MUP) is applied. The 4-MUP is hydrolized to 4-MU and the reaction is catalyzed by AP [5]. Since the 4-MU is a kind of good fluorescent dye, the concentration of 4-MU can be determined by the intensity of fluorescence. Furthermore, the 4-MU concentration is proportional to the number of AP, which is determined by the number of t-DNA. Using this strategy, we detected series concentration of t-DNA, and the limit of detection is 10^{-15} M.

REFERENCES

1. Tosar, J. P., G. Branas, and J. Laiz, "Electrochemical DNA hybridization sensors applied to real and complex biological samples," *Biosens. Bioelectron.*, Vol. 26, No. 4, 1205–1217, 2010.
2. Chen, X. J., et al., "Noble metal nanoparticles in DNA detection and delivery," *Wiley Interdiscip. Rev. Nanomed. Nanobiotechnol.*, Vol. 4, No. 3, 273–290, 2012.
3. De-los-Santos-Alvarez, P., et al., "Current strategies for electrochemical detection of DNA with solid electrodes," *Anal. Bioanal. Chem.*, Vol. 378, No. 1, 104–118, 2004.
4. Zhang, X., et al., "Ultrasensitive electrochemical DNA assay based on counting of single magnetic nanobeads by a combination of DNA amplification and enzyme amplification," *Anal. Chem.*, Vol. 81, No. 5, 1826–1832, 2009.
5. Xiao, K. Y., et al., "Use of fluorescent substrate 4-MUP in the detection of biotin-labeled DNA probes," *J. Tongji Med. Univ.*, Vol. 13, No. 4, 206–208, 1993.

A Quantum-dots-assisted Positioning System for Location Sensing of Nanobots

Lujiang Qian, Yu Zhou, Changyu Wang, Yifan Chen, Rui Wang, and Qingfeng Zhang
Department of Electrical and Electronics Engineering
South University of Science and Technology of China, China

Abstract— This paper presents a novel quantum-dots-assisted positioning system (QPS) for *in vivo* location sensing of medical nanobots. A multi-scale architecture of the QPS is proposed to noninvasively locate the nanobots. The sensing performance of the proposed technique is analyzed using VariPose that provides a realistic computational human phantom.

Applications of nanobots for medical use have attracted much attention recently [1], which require accurate *in vivo* location sensing of nanobots. To this end, we propose a quantum-dots-assisted position system (QPS). Quantum dot (QDot) is an atom-like, zero-dimension semiconductor particle, which emits light with a size-dependent frequency. In the proposed scheme, two different types of QDots are wrapped by a biocompatible container (e.g., liposome, micelle) into one cluster [2], which is attached to a nanobot and functions as a receiver or a transmitter. One type of QDots emits longer-wavelength light (LWL), so as to penetrate human tissues to assist in *macro-scale* exterior sensing while the other type emits shorter-wavelength light (SWL), which can transmit only in blood environment for *micro-scale* interior sensing. These two mechanisms of fluorescence are combined to achieve a *multi-scale* QPS. As illustrated in Fig. 1(a), a laser beam shines upon Nanobot 1 with a known position acting as the anchor, whose QDots emit SWL to stimulate nearby nanobots with unknown positions (i.e., Nanobot 2, 3, and 4). The QDots appended to these nanobots then emit LWL, which is observed by an external detector moving in different locations along the surface of the human body. Thus, the lateral positions of these nanobots can be pinpointed by investigating the LWL intensity peaks. Subsequently, as shown in Fig. 1(b), the laser beam shines upon Nanobot 2, 3, 4 respectively and the detector measures the intensity of light from the position of Nanobot 1 at each shining. Given the dielectric properties of human tissue and blood, the vertical positions of all nanobots can then be calculated by combining these sets of measurement data and by applying the wave diffraction-attenuation model. A comprehensive simulation study using VariPose is currently underway to validate the positioning algorithm.

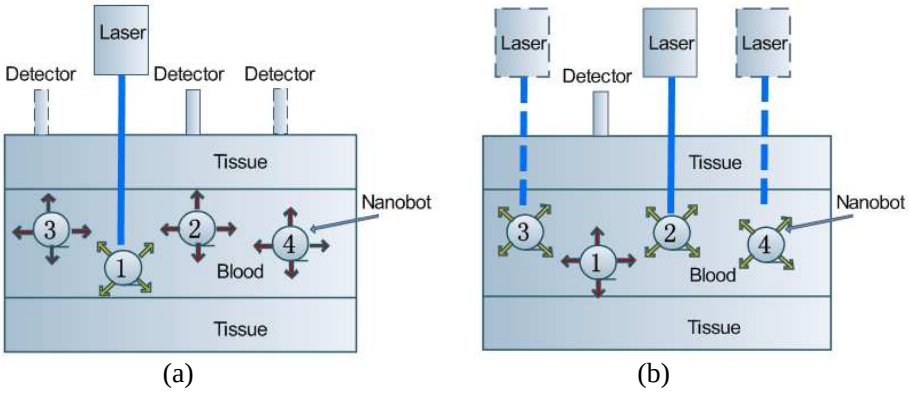

Figure 1: Illustration of the QPS for nano-sensing.

ACKNOWLEDGMENT

This work is supported by 2013 Guangdong Natural Science Funds for Distinguished Young Scholar (S2013050014223).

REFERENCES

1. Cavalcanti, A., B. Shirinzadeh, M. Zhang, and L. C. Kretly, "Nanorobot hardware architecture for medical defense," *Sensor*, Vol. 8, No. 5, 2932–2958, 2008.

2. Dubertret, B., P. Skourides, D. J. Norris, V. Noireaux, A. H. Brivanlou, and A. Libchaber, "*In vivo* imaging of quantum dots encapsulated in phospholipid micelles," *Science*, Vol. 298, No. 5599, 1759–1762, Nov. 2002.

AIE-active Biomaterials Based on 9, 10-bis (4-hydroxystyryl) Anthracene Derivatives

Wenjing Tian, Bin Xu, Xing Li, Hongguang Lv, Zilong Wang, Yan Zang, and Ke Ma
State Key Laboratory of Supramolecular Structure and Materials
College of Chemistry, Jilin University, Changchun, China

Abstract— Recently, due to the excellent luminescent properties, more and more aggregation-induced emission (AIE)-active materials have been used as bioprobes for detecting metal ions or biomolecules (DNA, protein etc.) and visualization tools for bioimaging with high sensitivity. Opposite to the aggregation caused quench (ACQ) effect, AIE-active fluorophores are nonemissive in the molecularly dissolved states, while give highly fluorescent emission when they are in the aggregate states. Taking advantage of AIE characteristic, the AIE bioprobes and bioimaging tools have high fluorescent emission and high sensitive generally which make AIE-active materials remarkable candidates for biological applications.

Here, we exhibit a series of fluorescent probes based on typical AIE molecules 9, 10-bis (4-hydroxystyryl) anthracene (DSA) derivatives. Different kinds of bioprobes based on DSA derivatives were synthesized to detect Pb^{2+}, Hg^{2+}, BSA and ssDNA with low detection limit and high sensitive. And we prepared a novel fluorescent aptasensor with high selectivity and sensitivity by introducing grapheme oxide as a quencher. Meanwhile, different amphiphilic copolymer nanoparticles and mesoporous silica nanoparticles containing DSA core, with low cytotoxicity and high fluorescence quantum yield (Up to 40%) were prepared for target cell imaging. Under the stimulus of these works, we will develop more materials with marvelous bio-medical potential.

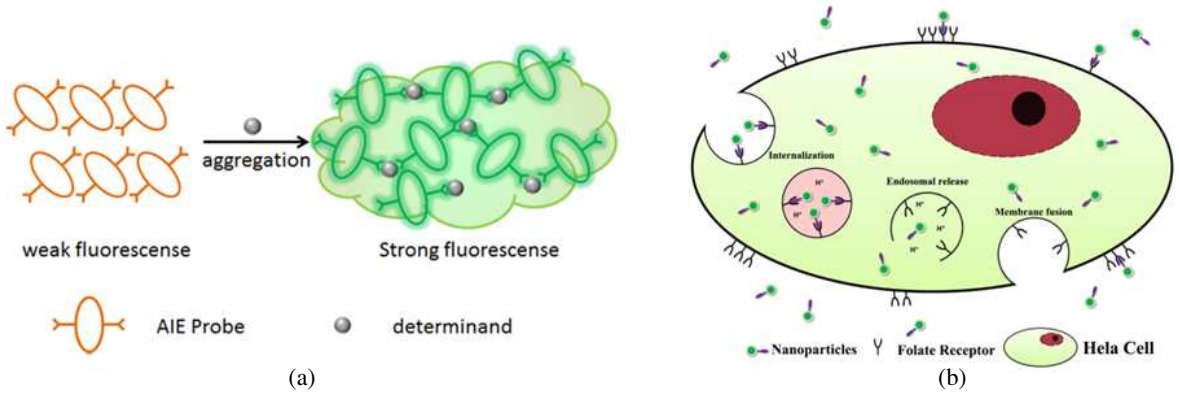

Figure 1: (a) Detectionrationale of AIE probes. (b) Bioimaging scheme of AIE nanoparticles.

REFERENCES

1. Lu, H. G., W. J. Tian, et al., "Novel fluorescent pH sensors and a biological probe based on anthracene derivatives with aggregation-induced emission characteristics," *Langmuir*, Vol. 26, No. 9, 6838–6844, 2010.
2. Lu, H. G., D. R. Meldrum, et al., "A series of Poly[N-(2-Hydroxypropyl)methacrylamide] copolymers with anthracene-derived fluorophores showing aggregation-induced emission properties for bioimaging," *J. Polym. Sci., Part A: Polym. Chem.*, Vol. 50, 890–899, 2012.
3. Lu, H. G., Y. Q. Tian, et al., "Using fluorine-containing amphiphilic random copolymers to manipulate the quantum yields of aggregation-induced emission fluorophores in aqueous solutions and the use of these polymers for fluorescent bioimaging," *J. Mater. Chem.*, Vol. 22, 9890–9900, 2012.
4. Li, X., W. J. Tian, et al., "Label-free fluorescence turn-on detection of Pb^{2+} based on AIE-active quaternary ammonium salt of 9, 10-distyrylanthracene," *Anal. Methods*, Vol. 5, 438–441, 2013.

5. Wang, Z. L., W. J. Tian, et al., "Folic acid-functionalized mesoporous silica nanosphereshybridized with AIE luminogens for targeted cancer cellimaging," *Nanoscale*, Vol. 5, 2065–2072, 2013.
6. Li, X., W. J. Tian, et al., "Fluorescent aptasensor based on aggregation-induced emission probe and graphene oxide," *Anal. Chem.*, Vol. 86, No. 1, 298–303, 2014.
7. Li, X., W. J. Tian, et al., "Highly sensitive determination of ssDNA and real-time sensingof nuclease activity and inhibition based on the controlledself-assembly of a 9, 10-distyrylanthracene probe," *Anal. Bioanal. Chem.*, Vol. 406, No. 3, 851–858, 2014.
8. Ma, K., W. J. Tian, et al., "A sensitive and selective "turn-on" fluorescent probe for Hg^{2+} based on thymine-Hg^{2+}-thymine complex with an aggregation-induced emission feature," *Anal. Methods*, Vol. 6, 2338–2342, 2014.
9. Zhang, Y., W. J. Tian, et al., "Folic acid-functionalized AIE pdots based onamphiphilic PCL-b-PEG for targeted cell imaging," *Polym. Chem.*, DOI: 10.1039/c4py00075g.

Luminogenic Polymers with Aggregation-induced Emission Characteristics for High-performance Sensing Applications

Anjun Qin[1, 2] **and Ben Zhong Tang**[1, 2, 3]

[1] Guangdong Innovative Research Team, State Key Laboratory of Luminescent Materials and Devices
South China University of Technology, Guangzhou 510640, China
[2]Department of Polymer Science and Engineering, Zhejiang University, Hangzhou 310027, China
[3]Department of Chemistry, The Hong Kong University of Science & Technology
Clear Water Bay, Kowloon, Hong Kong, China

Abstract— Luminescent materials have been widely used as chemosensors and bioprobes. These materials, however, suffer from the aggregation-caused quenching (ACQ) effect, which makes their performance greatly decreased in condensed phase. Exactly opposite to the ACQ effect, we observed a unique photo-physical phenomenon of aggregation-induced emission (AIE) in 2001: a series of propeller-shaped molecules such as siloles, are nonemissive when molecularly dissolved but induced to emit efficiently by aggregation [1, 2]. Nowadays, the AIE effect has drawn much attention from the researchers worldwide and hundreds of AIE-active luminogens have been prepared and their applications were explored. Although the research on the AIE-active polymers is in its infancy stage, it has attracted much interesting due to their advantages of good film-forming ability and simply device fabrication procedures [3].

The prevalent strategy for the preparation of AIE-active polymers is to incorporate the AIE-active molecules in the main- or side-chains [4]. In this talk, we will present our recent efforts on preparing AIE-active polytriazoles with linear and hyperbranched structures by $Cu(PPh_3)_3Br$-catalyzed and metal-free click polymerizations [5–7]. Moreover, the quaterization reaction was also used to prepare AIE-active amphiphilic polymer, in which the AIE-active moieties were attached in the side-chain [8]. Thanks to their AIE features, the nanoparticles of polytriazoles could be employed to detect explosives with superamplification effect and that of the amphiphilic polymer could be used for cellular imaging to specifically stain cytosol of cells.

ACKNOWLEDGMENT

We thank the National Science Foundation of China (21222402 and 21174120), National basic Research Program of the Ministry of Science & Technology of China (2013CB834702), and Guangdong Innovative Research Team Program (201101C0105067115) for financial support.

REFERENCES

1. Luo, J., Z. Xie, J. W. Y. Lam, L. Cheng, H. Chen, C. Qiu, H. S. Kwok, X. Zhan, Y. Liu, D. Zhu, and B. Z. Tang, *Chem. Commun.*, Vol. 37, 1740, 2001.
2. Hong, Y., J. W. Y. Lam, and B. Z. Tang, *Chem. Soc. Rev.*, Vol. 40, 5361, 2011.
3. Liu, J., J. W. Y. Lam, and B. Z. Tang, *Chem. Rev.*, Vol. 109, 5799, 2009.
4. Qin, A., J. W. Y. Lam, and B. Z. Tang, *Prog. Polym. Sci.*, Vol. 37, 182, 2012.
5. Qin, A., J. W. Y. Lam, and B. Z. Tang, *Chem. Soc. Rev.*, Vol. 39, 2522, 2010.
6. Qin, A., J. W. Y. Lam, and B. Z. Tang, *Macromolecules*, Vol. 43, 8693, 2010.
7. Li, H. K., J. Z. Sun, A. J. Qin, and B. Z. Tang, *Chinese J. Polym. Sci.*, Vol. 30, 1, 2012.
8. Qin, A., Y. Zhang, N. Han, J. Mei, J. Z. Sun, W. Fan, and B. Z. Tang, *Sci. China Chem.*, Vol. 55, 772, 2012.

Joint SERS-fluorescence Spectrum and Its Applications in Biosensing & Imaging

Zhuyuan Wang, Yiping Cui, and Shenfei Zong
Advanced Photonics Center, Southeast University, Nanjing 210096, China

Abstract— Optical spectra are playing significant roles in biosensing and bioimaging. Up to now, fluorescence technology has been employed as the most widely way for biological sensing or imaging [1]. Although this method is fast-read and straightforward, it might encounter some problems caused by several factors, including photo bleaching, cellular autofluorescence and so on, which means a more effective and accurate monitor method is still required. In addition to fluorescence, SERS is another powerful analytical tool since it can provide rich spectroscopic information of the analyte, which is advantageous for biological detection or imaging [2]. But the relatively long acquisition time of SERS makes it unsuitable for high-speed or dynamic analysis. Considering these factors, integrating both SERS and fluorescence signals into a single nanocomposite can be a good solution toward multiplex analysis with fast readout and easy operation. A fine example of such a SERS-fluorescence dual mode nanocomposite is the SERS-fluorescence joint spectral encoded (SFJSE) nanoparticle we have recently developed [3]. Besides, this joint SERS-fluorescence spectrum also has great potential in the research field of intracellular drug release. Previously, we have presented several SERS traceable nanocarrier through a simple strategy for cancer cell targeted drug delivery [4–7]. In the presented systems, the locations of nanocarriers can be tracked by SERS signals while those of drugs can be monitored through their fluorescence, allowing the simultaneous investigation of the intracellular distribution of both the nanocarriers and the drugs. Thus, this joint SERS-fluorescence spectrum would be more powerful than that based on sole fluorescence or SERS signals in the studies of high-throughput biosensing or intracellular drug release dynamic processes.

REFERENCES

1. Vahrmeijer, A. L., M. Hutteman, J. R. van der Vorst, C. J. H. van de Velde, and J. V. Frangioni, *Nature Reviews Clinical Oncology*, Vol. 10, 507–518, 2013.
2. Wang, Y. Q., B. Yan, and L. X. Chen, *Chemical Reviews*, Vol. 113, 1391–1428, 2013.
3. Wang, Z. Y., S. F. Zong, W. Li, C. L. Wang, S. H. Xu, H. Chen, and Y. P. Cui, *Journal of the American Chemical Society*, Vol. 134, 2993–3000, 2012.
4. Zong, S., Z. Wang, H. Chen, J. Yang, and Y. Cui, *Anal. Chem.*, Vol. 85, 2223–2230, 2013.
5. Yang, J., Z. Y. Wang, S. F. Zong, R. H. Zhang, and Y. P. Cui, *Biosensors and Bioelectronics*, Vol. 51, 82–89, 2014.
6. Wu, X., Z. Wang, D. Zhu, S. Zong, L. Yang, and Y. Cui, *ACS Applied Materials & Interfaces*, Vol. 5, 10895–10903, 2013.
7. Yang, J., Y. P. Cui, S. F. Zong, R. H. Zhang, C. Y. Song, and Z. Y. Wang, *Molecular Pharmaceutics*, Vol. 9, 842–849, 2012.

Nonlinear Optical Properties of Gold Nanorods (GNRs) under FS Laser Excitation near the Third Optical Tissue Window and Application for Multichannel Cellular Imaging

Yalun Wang, Kanghui Li, Zhenfeng Zhu, and Jun Qian
Centre for Optical and Electromagnetic Research
Zhejiang University, Zijingang Campus, Hangzhou 310058, China

Abstract— Gold nanorod (GNR) was a promising bioimaging probe in the third optical tissue window (1600–1800 nm). In this paper, hydrophilic GNRs with proper dimensions were synthesized according to the classical seed mediated method. Their nanostructures were taken with a transmission electron microscope and their extinction spectra were recorded on a UV-vis scanning spectrophotometer. Their nonlinear optical features were recorded by a home built measurement system, under the femtosecond (fs) laser excitation of 1580 nm, which was selected as the demonstration of the third optical tissue window. A sharp third harmonic generation (THG) signal and a mild three photon luminescence (3PL) signal could be clearly distinguished. These signals could be utilized for multichannel nonlinear bioimaging in the third optical tissue window.

Negatively charged polystyrene sulfonate (PSS) and positively charged polyallylamine hydrochloride (PAH) were separately coated onto the positively charged GNRs through electrostatic adherence. The PAH-PSS coated GNRs were added in the culture medium of HeLa cells. Multichannel nonlinear optical imaging of cancer cells stained with GNRs was performed with a 1580 nm fs laser coupled scanning microscope. The signals were filtered by a 665 nm dichroic mirror, and then splitted by another 560 nm dichroic mirror into the green and red imaging channels. HeLa cells can be clearly visualized in both green and red channels with good contrast. For HeLa cells without GNRs treatment, there were no such signals detected in these channels.

This was a pioneer work of the multichannel nonlinear bioimaging in the third optical tissue window with GNRs and would be helpful for our further studies on *in vivo* bioimaging in this window with deeper penetration.

Three-photon Luminescence of High Aspect Ratio Gold Nanorods and Its Applications for High Contrast Tissue and *in Vivo* Imaging

Shaowei Wang and Jun Qian
Centre for Optical and Electromagnetic Research, Zhejiang University, Hangzhou 310027, China

Abstract— Gold nanoparticles display many unique optical properties including localized surface plasmon resonance (LSPR), which makes them ideal enhancement agents for surface-enhanced Ranma scattering and plasmon enhanced fluorescence. Gold Nanorods (GNRs) with well-defined shapes and sizes are very attractive for their plasmon resonant absorption and scattering in the NIR region, making them promising probes for in vitro and in vivo imaging. GNRs have been demonstrated to exhibit strong plasmon enhanced multi-photon luminescence (MPL) with brightness many times stronger than the conventional organic chromophores.

In this study, we synthesized GNRs with high aspect ratio of 6 and correlated longitudinal surface plasmon resonance (LSPR) band of 1000 nm. GNRs with high aspect ratio exhibit large cross sections for multi-photon light absorption processes in the near infrared region due to surface plasmon resonances. To make the gold nanorods a better photoluminescence probe for in vitro and in vivo imaging under multi-photon excitation, PEGylated GNRs with great biocompatibility were intravenously injected through the tail vein into mice and we demonstrated the use of gold nanorods as bright contrast agents for three-photon luminescence (3PL) imaging of mouse ear blood vessels in vivo. And we also investigated the ability to assess the biodistribution of gold nanorods in major organs. Due to the bright 3PL of PEGylated GNRs excited by 1000 nm laser, GNRs targeted in tissues could be clearly visualized without any autofluorescence background. The results indicated that 3PL imaging can be used to assess the distribution of GNRs in tissues with high contrast. In addition, excited by 1000 nm laser, which penetrates deeply into tissues, 3PL imaging of GNRs holds great potential in the applications of deep in vivo imaging and nanoparticle assisted tumor diagnostic and therapeutic.

Near-infrared Fluorophore-doped Nanoparticles for *in vitro* and *in vivo* Bioimaging

Liliang Chu[1], **Shaowei Wang**[1], **Kanghui Li**[1], **Wang Xi**[2], **and Jun Qian**[1]

[1]Centre for Optical and Electromagnetic Research, Zhejiang University, China
[2]Department of Neurobiology, School of Medicine
Zhejiang University, Hangzhou, Zhejiang 310058, China

Abstract— Near-infrared (NIR) imaging technology has been widely used for bioimaging, since it can achieve deep penetration in biological tissues due to less absorption and scattering of NIR light. IR-820 is a typical type of NIR fluorophore which has an absorption peak at 835 nm and an emission peak at 850 nm. In our research, an upright laser scanning confocal microscope (Olympus FV1000) is adopted for NIR bioimaging, and a 635 nm laser is used as the excitation light source. IR-820 doped organically modified silica (ORMOSIL) nanoparticles, as well as IR-820 doped polymer nanoparticles are synthesized, and used for *in vitro* and *in vivo* bioimaging separately. They have many advantages in the application of bioimaging, such as relatively high fluorescence quantum yield, high stability in biological environment, facile surface functionalization and bio-compatibility. Observed from high contrast cell images, HeLa cells are stained with IR-820 ORMOSIL nanoparticles very uniformly and effectively with the help of bright fluorescent signals from IR-820 molecules under the 635 nm-excitation. As for *in vivo* bioimaging, IR-820 doped polymer nanoparticles, which are synthesized by encapsulating IR-820 dyes with PEG amphiphilic molecules and possess excellent photostability in phosphate buffer solution (PBS), are utilized as an optical contrast agent. They are injected into a nude mouse via the tail vein. The images of blood vessels at different depths in the ear of the mouse are obtained with high signal to noise ratio. Furthermore, we perform *in vivo* microscopic imaging of mouse brain vasculature, and three-dimensional reconstructive images of brain vasculature of a mouse are achieved. The results of our experiments show that NIR fluorophore-doped nanoparticles can be utilized as a good candidate for high-contrast and deep-tissue functional bioimaging.

Conjugated Polymer Nanoparticles for Cellular Imaging and Sensing Applications

Changfeng Wu[1], **Gaixia Xu**[2], **and Danni Chen**[2]

[1]State Key Laboratory on Integrated Optoelectronics, College of Electronic Science and Engineering
Jilin University, Changchun, Jilin 130012, China
[2]Key Laboratory of Optoelectronic Devices and Systems of Ministry of Education and Guangdong Province
Shenzhen University, 518060, China

Abstract— While fluorescence based techniques provide unprecedented detail about cellular processes, many advanced applications are limited by the lack of appropriate fluorescence probes. In many cases, currently available fluorescent labels are not sufficiently bright and photostable to overcome the background associated with various fluorescence and scattering processes. Semiconducting polymer nanoparticles have attracted considerable interest due to their outstanding properties as fluorescent probes. These nanoparticles are called polymer dots (Pdots) when they exhibit small particle size and high brightness. Quantitative comparisons of the optical properties of the Pdots indicate their fluorescence brightness is a factor of $10^2 \sim 10^4$ higher than conventional fluorescent dyes, and a factor of $10 \sim 10^3$ than inorganic quantum dots. Single particle fluorescence imaging and kinetic studies indicate much higher emission rates of the Pdots as compared to quantum dots, and but no "blinking" as often encountered for fluorescent dye and quantum dots. In addition, efficient intra-particle energy transfer has been demonstrated in fluorescent dye-doped Pdots, which provides a new strategy to improve the fluorescence brightness and photostability of the Pdots, and design novel sensitive biosensors. In this work, we present recent findings of the photophysical properties of Pdots and their applications in cellular labeling, in vivo fluorescence imaging, photoacoustic imaging, and versatile biosensors.

ACKNOWLEDGMENT

Changfeng Wu acknowledges financial support from "Thousand Young Talents Program" and the National Science Foundation of China (Grant Nos. 61222508 and 61335001). This work is also supported by the Key Laboratory of Optoelectronic Devices and Systems of Ministry of Education and Guangdong Province.

A Photostable AIE Luminogen for Multifunctional Three-photon Bioimaging

Zhenfeng Zhu[1], **Chris Wai Tung Leung**[2], **and Xinyuan Zhao**[3]

[1]Centre for Optical and Electromagnetic Research
Zhejiang Provincial Key Laboratory for Sensing Technologies
Zhejiang University, Hangzhou 310058, China
[2]Department of Chemistry, The Hong Kong University of Science and Technology
Clear Water Bay, Kowloon, Hong Kong, China
[3]Bioelectromagnetics Laboratory, School of Medicine
Zhejiang University, Zijingang Campus, Hangzhou 310058, China

Abstract— Fluorescent probes with the advantages of sensitivity, selectivity, and biocompatibility, have been a powerful tool for bioimaging and biosensing. Multiphoton imaging which takes the advantages of high spatial resolution as well as enabling in vivo deep-tissue imaging, has also played an important role in both preclinical research and clinical diagnostic applications. Three-photon excitation is a process that occurs when three photons are simultaneously absorbed within a luminophore for photo-excitation through virtual states. It requires the fluorescent dye with a high intrinsic quantum efficiency or high concentration. However, due to the accompanying aggregation-induced quenching (ACQ) effect, most luminophore cannot be adopted for bioimaging at high concentration.

We study a fluorescent agent with aggregation induced emission (AIE) feature, which is called tetraphenylethene-triphenylphosphonium (TPE-TPP). It is almost nonfluorescent when molecularly dissolved but becomes highly emissive in the aggregate state with fluorescence increasing along with the increase of fluorophore concentration. Besides, they are highly specific and photostable as an excellent mitochondria tracker. Its maximal absorption is around 320 nm, which is in ultraviolet spectral range with high energy, and excitation in this wavelength may produce harm to cells. We realize multiphoton fluorescence imaging of TPP-TPP and study its two-photon and three-photon photostability, which shows that with the increasing of the order of nonlinear optical effect, the photostability increased accordingly. Besides, compared with one-photon and two-photon imaging, three-photon imaging of TPE-TPP (using a 1020 nm femtosecond laser as excitation) has the advantage of a high resolution over MitoTracker red FM (MT), which is a commercially available mitochondria imaging agent. We here demonstrate that TPE-TPP can light up mitochondria with 1020 nm-excitation in live cells with superior photostability as well as high resolution, enabling the observation of mitochondrial morphological changes, as well as dynamic cellular processes.

Session 4P2a
SC1&3: Design and Simulation of Electromagnetic and Optical Devices 2

New Application Field for Surface Plasmon in Magnetic Recording and Sensing

K. Nakagawa, **Y. Ashizawa**, **A. Tsukamoto**, **and S. Ohnuki**
College of Science and Technology, Nihon University
7-24-1 Narashinodai, Funabashi city, Chiba, 274-8501, Japan

Abstract— Surface plasmon, which appears at the surface between metal and dielectric material, contributes toward confining optical energy into a smaller scale than the optical diffraction limit [1]. Besides, the surface plasmon is very sensitive to the optical characteristics at the surface. First, we found conditions for future high-density magnetic recording, so called thermally assisted magnetic recording (TAMR) [2], to enhance light spot energy as well as to confine the energy into 10 nm in diameter. TAMR is one of the promising future technologies to increase memory density, and it needs to use small optical spot to heat a local small area when a magnetic domain is written by magnetic field. The surface plasmon technique is only the one to generate a spot smaller than the diffraction limit. Second, we also revealed that sensing technique applying surface plasmon on the surface of magnetic layer can contribute to high-sensitive and super-tiny magnetic sensor. The design and simulation for the materials and its metal shape of surface plasmon is very important.

For magnetic recording applying TAMR, localized surface plasmon in a gold antenna was studied by the Finite-Difference Time-Domain (FDTD) method. It was found that the antenna effectively enabled light spot to be confined into less than 10 nm in diameter. We also studied that the waveguide applying the surface plasmon polaritons (SPPs) can effectively increase the optical efficiency to deliver the energy to the antenna [3]. The antenna effect was also confirmed by an experimental study applying femto-second laser [4].

For magnetic sensor, the double-layer film made of noble metal and magnetic metal shows SPPs reflectivity response to magnetic field. We studied non-solid solution single film made of gold and cobalt, and the film shows an effect to increase sensitivity.

The research using surface plasmon give us beneficial electromagnetic and optical devices.

REFERENCES

1. Nakagawa, K., J. Kim, and A. Itoh, *J. Appl. Phys.*, Vol. 101, 09H504, 2007.
2. Kryder, M. H., E. C. Gage, T. W. McDaniel, W. A. Challener, R. E. Rottmayer, G. Ju, Y.-T. Hsia, and M. F. Erden, *Proc. of the IEEE*, Vol. 96, 1810, 2008.
3. Ashizawa, Y., T. Ota, K. Tamura, and K. Nakagawa, *J. Magn. Soc. Jpn.*, Vol. 37, 111–114, 2013.
4. Nakagawa, K., A. Tajiri, K. Tamura, S. Toriumi, Y. Ashizawa, A. Tsukamoto, A. Itoh, Y. Sasaki, S. Saito, M. Takahashi, and S. Ohnuki, *J. Magn. Soc. Jpn.*, Vol. 37, 119–122, 2013.

An Ambient Sensitive Grating Reflector Based on Generalized Guided-mode Resonance

F. C. Huang[1], **L. K. Liao**[1], **and Y. P. Chiou**[1, 2]

[1]Graduate Institute of Photonics and Optoelectronics
Taiwan University, Taipei 106-17, Taiwan
[2]Department of Electrical Engineering
Graduate Institute of Communication Engineering, Taipei 106-17, Taiwan

Abstract— An ambient sensitive grating reflector based on generalized guided-mode resonance has been proposed in this paper. Guided-mode resonance (GMR) properties in resonant grating waveguide structures have attracted considerable attention in researches. GMR related literatures indicate that high zero-order reflected diffraction efficiencies were achieved in a rapid spectral response when GMR occurs [1]. Possible applications based on GMR related properties are optical filters, reflective mirrors in laser systems, electro-optical switches and even security features [2]. And rapid spectral variations of the zero-order reflected diffraction efficiency of GMRs may be suitable for applications in sensor fields [3]. In conventional guided-mode resonance models, gratings are usually viewed as guiding region with higher average refractive index or a perturbative boundary with an infinitely thin thickness of the grating-reflector systems. However, gratings of the grating-reflector system proposed here are especially designed of a comparable thickness and lower average index compared to the sublayer which is the guiding region. Gratings are neither the guiding layer nor perturbation of the boundary of the grating-reflector system.

In this paper, the generalized GMR models are proposed. A three-layer grating-reflector system has been discussed first with thicknesses of gratings especially designed under the subwavelength condition. Designs and analysis of an ambient sensitive grating-reflector system are demonstrated, including estimations of the sublayer thickness and waveguide modes related to the generalized guided-mode resonance. The spectral response and the field distribution of the designed grating reflector are also shown. A significant feature in this generalized GMR design is that the strong evanescent fields distribute outside the grating medium at the transmitted side, namely the region suitable for the analyte, which results in an ambient sensitive grating reflectors with respect to the surroundings. As a result, the designed grating reflector with the ambient sensitive property and rapid spectral variations of the zero-order reflected diffraction efficiency may be suitable for applications in sensor fields. The proposed grating-reflector structure is simple and compact in constitution, making mass production possible, and it may be a good choice as a sensing device. The analyte to be detected can be gaseous or fluid. A sensor must perform sensitive to the analyte while other disturbances like variations of pressure and temperature of the environment are insusceptible [3]. Meanwhile, sensing of refractive index is an useful technique in sensor fields which presents noninvasive and label-free in sensor designs, and it is also feasible in optical systems. Hence, the performance of the proposed ambient sensitive grating reflector with respect to variations of refractive index of the analyte is demonstrated in the end.

REFERENCES

1. Wang, S. S., R. Magnusson, J. S. Bagby, and M. G. Moharam, "Guided-mode resonances in planar dielectric-layer diffraction gratings," *J. Opt. Soc. Am. A*, Vol. 7, No. 8, 1470–1474, 1990.
2. Magnusson R., Y. Ding, K. J. Lee, D. Shin, P. S. Priambodo, P. P. Young, and T. A. Maldonado, "Photonic devices enabled by waveguide-mode resonance effects in periodically modulated films," *Nano- and Micro-optics for Information Systems*, 20–34, San Diego, CA, October 2003.
3. Passaro, V. M. N., F. D. Olio, B. Casamassima, and F. D. Leonardis, "Guided-wave optical biosensors," *Sensors*, Vol. 7, 508–536, 2007.

Application of the Explicit and Implicit FDTD Methods to the Analysis of a Terahertz Plasmonic Grating

J. Shibayama, Y. Wada, J. Yamauchi, and H. Nakano
Faculty of Science and Engineering, Hosei University, Tokyo 184-8584, Japan

Abstract— A surface plasmon polariton (SPP) propagates along a metal-insulator interface at the optical frequencies. Note, however, that the SPP cannot be supported along the interface at the terahertz (THz) frequencies. Recently, the use of a semiconductor material such as InSb has been investigated for guiding the SPP at the THz frequencies [1]. The permittivity of InSb becomes negative, so that the SPP can be guided along the InSb-insulator interface. Another interesting feature of InSb is its permittivity exhibits temperature dependence. This enables us to obtain tunable devices using InSb based on the temperature dependence.

In this presentation, we analyze a THz plasmonic grating made of InSb using the explicit and implicit finite-difference time-domain (FDTD) methods with the frequency-dependent formulation [2]. The permittivity of InSb versus frequency is presented using the Drude model into which the temperature dependence is introduced. With attention to temperature variation, the modification of the eigenmode field is shown for a gap (InSb-air-InSb) waveguide. The eigenmode field is then utilized to launch an input pulse in the following FDTD analysis. We discuss the reflection spectrum of the grating consisting of the gap waveguide with periodic variation of the gap width. The efficiency improvement in numerical calculations is also demonstrated using the implicit FDTD method based on the locally one-dimensional scheme [2, 3].

REFERENCES

1. Isaac, T. H., W. L. Barnes, and E. Hendry, "Determining the terahertz optical properties of subwavelength films using semiconductor surface plasmons," *Appl. Phys. Lett.*, Vol. 93, No. 24, 241115-1–3, Dec. 2008.
2. Shibayama, J., A. Nomura, R. Ando, J. Yamauchi, and H. Nakano, "A frequency-dependent LOD-FDTD method and its application to the analyses of plasmonic waveguide devices," *IEEE J. Quantum Electron.*, Vol. 46, No. 1, 40–49, Jan. 2010.
3. Shibayama, J., M. Muraki, J. Yamauchi, and H. Nakano, "Efficient implicit FDTD algorithm based on locally one-dimensional scheme," *Electron. Lett.*, Vol. 41, No. 19, 1046–1047, Sep. 2005.

Electronic State Control Based on Hybrid Simulation Consisted of Maxwell and Schrödinger Equations — A Singled Electron Constrained in Thin Tube

T. Takeuchi[1], **S. Ohnuki**[1], **T. Sako**[1], **Y. Ashizawa**[1], **K. Nakagawa**[1], **and M. Tanaka**[2]

[1]College of Science and Technology, Nihon University, Japan
[2]Faculty of Engineering, Gifu University, Japan

Abstract— Quantum state control plays an important rule to realize various attractive technologies such as quantum computer and high efficiency photochemical reaction. Light control pulse is one of possible ways to adjust quantum states and has been tried to design both numerically and experimentally [1, 2]. To the best of author's knowledge, all proposed numerical schemes for designing the light control pulse are based on the approximation which ignores the radiated electromagnetic fields from controlled particles having only a few charges.

In this paper, we will demonstrate to control an electronic state for a single electron constrained in a thin tube interacted with the light pulse and validate the approximation neglecting the radiated field. Hybrid simulation consisted of Maxwell and Schrödinger equations will be utilized to accurately simulate the radiated field, i.e., light-electron interaction [3, 4]. The numerical results will indicate that the approximation significantly affects the control accuracy for the electronic state.

REFERENCES

1. Ohtsuki, Y., H. Kono, and Y. Fujimura, "Quantum control of nuclear wave packets by locally designed optimal pulses," *The Journal of Chemical Physics*, Vol. 109, No. 21, 9318–9331, 1998.
2. Daniel, C., J. Full, L. González, C. Lupulescu, J. Manz, A. Merli, Š. Vajda, and L. Wöste, "Deciphering the reaction dynamics underlying optimal control laser fields," *Science*, Vol. 299, 536–539, 2003
3. Pierantoni, L., D. Mencarelli, and T. Rozzi, "A new 3-D transmission line matrix scheme for the combined Schrödinger-Maxwell problem in the electronic/electromagnetic characterization of nanodevices," *IEEE Trans. MTT*, Vol. 56, No. 3, 654–662, 2008.
4. Takeuchi, T., S. Ohnuki, and T. Sako, "Comparison between Maxwell-Schrödinger and Maxwell-Newton hybrid simulations for multi-well electrostatic potential," *IEEE J. Quantum Electronics*, in press.

Scattering Characteristics of Electrically Large IR-reflective/MW-transmissive Beam Combiner

Hui Yan, **Yi Tian**, **Zhiwei Bai**, **Xin Wang**, **and Zhuo Li**
Beijing Key Lab for Precision Optoelectronic Measurement Instrument and Technology
School of Opto-electronics, Beijing Institute of Technology, Beijing 100081, China

Abstract— A beam combiner is a device that combines different beam signals, like IR, MW, laser, and etc., into a common aperture. IR/MW beam combiner is the key element in the hardware-in-the-loop (HWIL) simulation of IR/MW dual-mode compound guidance seeker. Among various beam combiner designs, the multilayered dielectric plate design is the most widely used. The multilayered dielectric plate, coated with IR reflective film, transmits MW signal and reflect IR signal.

Electric field deviations (in both amplitude and phase) in the quiet zone of MW chamber will lead to boresight error, which is the major concern of HWIL systems. The major cause of field deviation is the scattering effect of the finite-sized beam combiner. Current EM simulation algorithms are not suitable for the analysis of scattering field of electrically large MW-transmissive beam combiner. The MoM method is accurate but too inefficient. Applicable high-frequency methods (like PO method) do not offer enough accuracy. Consequently, the scattering characteristics of the beam combiner is yet unclear, and the design of aperture size and edge shape, which dominate the scattering effect, lack theoretical supports.

This paper therefore employed an aperture field integration method (AFIM) for rapid computation of beam combiner's near field. Scattering characteristics were investigated through simulation of a set of example beam combiners with different aperture sizes and edge shapes. Thus the design criteria of aperture size and edge shape were induced.

The AFIM considers the MW-transmissive beam combiner an analogy to the MW-reflective CATR aperture antenna. Aperture field of transmitting wave on the immediate surface of beam combiner is computed using transmission line theory. Then according to the equivalence principle, the scattering field can be obtained by integration of the field of the aperture equivalent source. Simulation of a 550 mm diameter beam combiner at 13 GHz showed that the relative error between AFIM and MoM was within 10% but AFIM could be done in 3 seconds with less than 5 MB of memory.

The rapid AFIM was employed to investigate the scattering characteristics and a set of example beam combiners were simulated. Since the electric field deviation caused by scattering effect is of most concern, the peak-peak value and rms value of electric field were used to evaluate the scattering effect. Varying parameters include: working frequency ($0.8 \sim 40$ GHz), incident angle ($0 \sim 30°$), edge shape (round, square and serrated), aperture size ($1x \sim 4x$ quiet zone size), and distance from quiet zone ($1x \sim 4x$ quiet zone size). Simulation results showed that serrated edge is generally the best and round edge is the worst among the three. The field deviation is smaller with larger aperture size and longer distance from quiet zone, and is also sensitive to incident angle and working frequency. Generally, a neglectable boresight error desires a field deviation of 1 dB in amplitude and 10° in phase. Design criteria of aperture size and edge shape can thus be induced through simulation results. According to the design criteria, the previously simulated 550 mm diameter beam combiner should be enlarged to at least 1100 mm.

Tuned Window for Standing Wave Linear Accelerators

Alberto Leggieri[1, 2], **Alessia Ciccotelli**[2], **Giuseppe Felici**[2], **Leonardo Zappelli**[3], **Davide Passi**[1], **and Franco Di Paolo**[1]

[1]Dipartimento di Ingegneria Elettronica, Università degli Studi di Roma "Tor Vergata"
Via del Politecnico, 1, Roma 00133, Italy
[2]S.I.T. — Sordina IORT Technologies, S.p.A., Via dell'Industria, 1A, Aprilia, LT 04011, Italy
[3]Dipartimento di Ingegneria dell'Informazione, Università Politecnica delle Marche
Via Brecce Bianche, Ancona 60131, Italy

Abstract— This paper describes a Dielectric Window (DW) for Standing Wave Linear Accelerators (LINAC's) which can be tuned after brazing or welding process. Due manufacturing processes, every LINAC has a proper working frequency and characteristic parameters. We propose a DW that includes a Matching Network which is insertable in the low pressure atmosphere side of the window, without brazing or welding on any material, avoiding deformations and consequent electromagnetic behavior alteration.

This study investigates the in-frequency return loss behavior of the LINAC, in order to improve matching and transmitting conditions while maintaining the optimum coupling between LINAC and High Power Microwave source. Design formulas are provided and Computer Aided Design techniques are proposed.

Proposed Window consists of a pill-box-type vacuum DW with alumina ceramics connected to an Input Matching Network (IMN). During the LINAC fabrication, cavities and DW are brazed

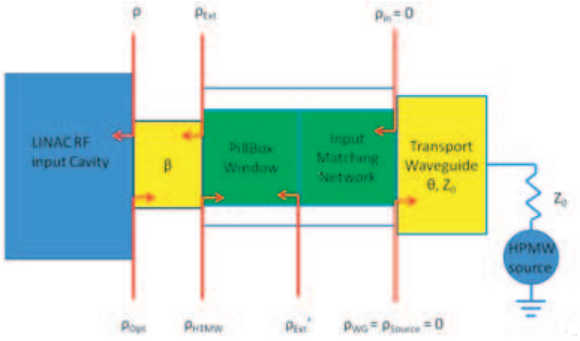

Figure 1: Devices disposition and reflections coefficients at the interfaces.

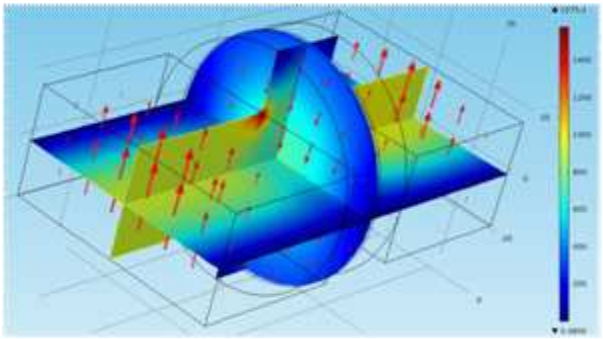

Figure 2: Geometry and normalized electric field distribution in the RWg and DW on bisecting planes @ 2998 MHz (TE_{11}) for $L = 27$ mm with $t = 2.4$ mm.

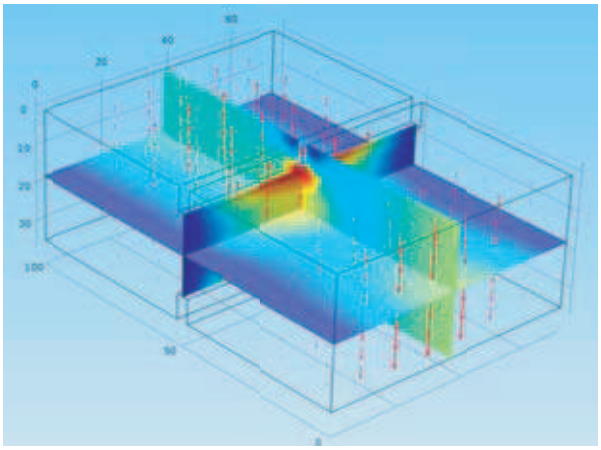

Figure 3: Capacitive iris structure on the RWg sector and fundamental mode (TE_{10}) electric field distribution on bisecting planes at 2998 MHz.

Figure 4: Measured $|S_{11}|$ dB of the LINAC with traditional DW: $RL = 16.5$ dB.

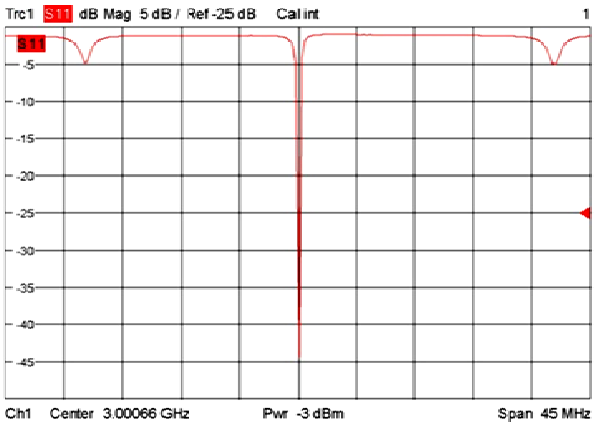

Figure 5: Measured $|S_{11}|$ dB of the LINAC with tuned window: $RL = 44\,\text{dB}$.

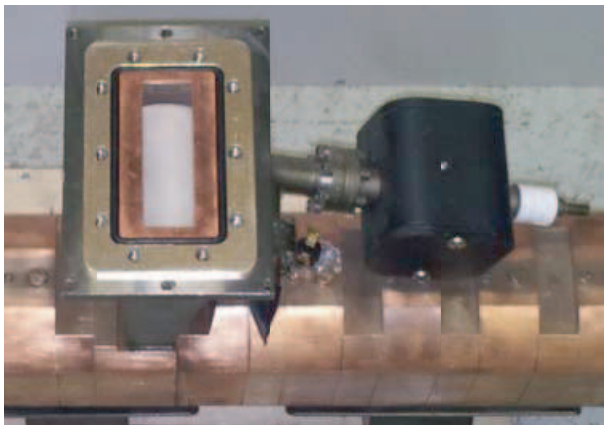

Figure 6: Top view of the HTMW mounted on the NOVAC 11 LINAC.

or welded, so that the input characteristics of the system may be modified. In this paper, we propose to compensate this alteration by introducing a reactive IMN at the low pressure interface of the DW. As the IMN is placed in this section, it can be inserted and locked by screws, without vacuum loss and it can be sized basing on the effective measured input parameters of the post-brazed LINAC.

Pill-box DW consists principally of a Rectangular Waveguide (RWg) to Circular Waveguide (CWg) transitions. Each discontinuity mathematically inserts infinite modes, but only the modes over cut off can propagate. Other modes (evanescent modes) may store and release reactive energy, reducing performances. Such behavior can be avoided if, at the desired frequency, the wave does not view the discontinuity, so that the fundamental mode of the RWg leads only the fundamental mode of the CWg. This is possible if the fundamental mode wavelength propagating into the RWg will remain the same in the CWg. In order to have the maximum power transfer between RWg and CWg, the DW is designed so that at the junction, impedance of the RWg and CWg are matched both in the input and output side.

IMN consists of a RWg section with a capacitive iris. This distributed network moves the reflection coefficient shown by the cascade of the LINAC and the DW to the centre of the Smith Chart at the LINAC operating frequency.

A prototype has been made and tested by performing cold S-parameter. The proposed device offers more energy transport attitude over the traditional DW, as shown by a return loss increase of 167% with a substantial improvement of the LINAC coupling characteristics. This solution can offer a decrease of power line size, weight and cost.

Application of Optical Frequency Comb Synthesizer/Analyzer to 22.4 Tbit/s Composite Amplitude and Phase Shift Keying

Takayuki Miyamoto[1], **Mitsutaka Ito**[1], **Toshiaki Yamazaki**[1], **and Tatsutoshi Shioda**[1]

[1]Department of Electrical and Electronic Systems, Saitama University
255 Shimo-Okubo, Saitama 338-8570, Japan
[2]Department of Electrical Engineering, Nagaoka University of Technology
1603-1 Kamitomioka, Nagaoka, Niigata 940-2188, Japan

Abstract—

Introduction: Recent explosion of data transmission speed over terabit per second in telecommunications requires ultra-high speed optical signal processing technology.

An optical frequency comb (OFC) provides a lot of teeth whose amplitudes and phase spectra is precisely controlled. It has already been proved to create arbitrary optical waveforms using an optical synthesizer [1]. However, the limited channel number of the optical synthesizer has made it difficult to expand the frequency band, because the size of the synthesizer, which integrates an arrayed waveguide grating (AWG) and phase and intensity modulators on a silica waveguide, is limited. Then, we have developed a colorless optical synthesizer consisting of a colorless AWG [2]. On the other hand, multi-heterodyne mixing, which can measure amplitude and phase spectra, and optical waveform can be reconstructed [2–5].

In this study, the results to apply our proposed system to the composite ASK and PSK to control the 22.4-Tbit/s with 112-bit packet are reported.

Experimental Results & Discussions: Figure 1 shows the experimental setup.

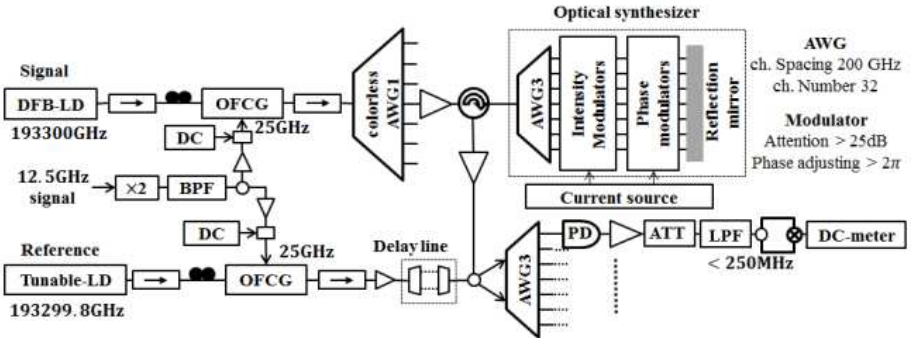

Figure 1: Experimental setup.

As a demonstration, composite signals of 4 values ASK and 32 values of PSK were tried to be operated. The theoretical amplitude and phase spectra were numerically calculated by Fourier transformation of target signals. The PSK signal pattern was set to be a variation of "31 → 29 → 18 → 23 → 9 → 17 → 2 → 19 → 3 → 0 → 1 → 0 → 15 → 16 → 20 → 29" as assignment to angle of 5-bit signal. In addition, ASK signal was set to be with a variation of "3 → 3 → 2 → 2 → 1 → 1 → 0 → 0 → 2 → 2 → 1 → 1 → 0 → 0 → 3 → 3" as a relative values.

Electric-field waveforms were numerically obtained by inverse Fourier transformation of the observed spectra, as shown in Fig. 2. To obtain the phase variations, the observed electric-field waveform was divided into 16 sections and was fitted by a sinusoidal function. Then, amplitude and phase variations were obtained as shown in Fig. 3. The experimental and simulated results of the electric-field waveforms shown in Figs. 2(a) and (b), and also spectra of Fig. 3(a) and Fig. 3(b) are consistent to each other.

As a results, it has been confirmed that the optical frequency comb synthesizer / analyzer can be applied to process composite ASK and PSK signals with 22.4-Tbit/s with 112-bit packets.

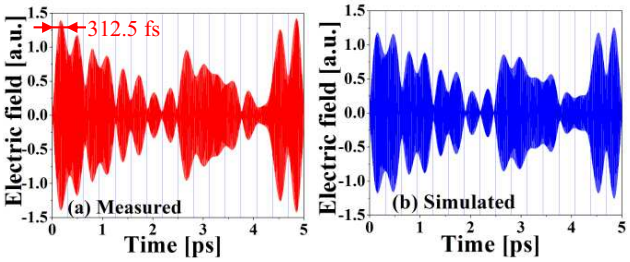

Figure 2: (a) Experimental and (b) simulated waveforms.

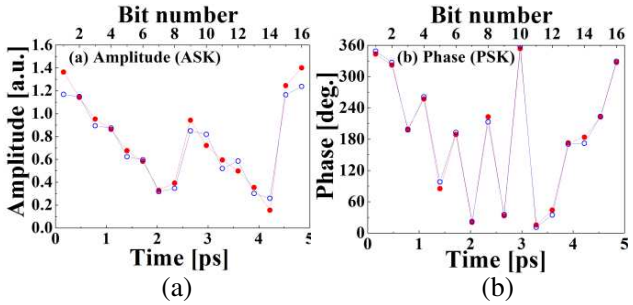

Figure 3: Experimental (closed circles) and simulated (open circles) results of (a) amplitude and (b) phase shift keying modulated signals.

REFERENCES

1. Mandai, K., et al., *IEEE Photon. Tech. Lett.*, Vol. 18, 721–723, 2006.
2. Shioda, T., et al., *Opt. Lett.*, Vol. 37, 3642–3644, 2012.
3. Yamazaki, T., et al., *J. Opt. Soc. Am. B*, Vol. 29, No. 7, 1707–1711, 2012.
4. Shioda, T., et al., *Opt Commun.*, Vol. 23, 4733–4740, 2010.
5. Yamazaki, T., et al., *CLEO Pacific Rim*, TuF2-5, 2013.

Session 4P2b
Optoelectronic and Photonics Devices

Simulation and Design of Monolithically Integrated Tunable Wavelength Converter Based on V-cavity Laser and Delayed Mach-Zehnder Interferometer

Yingchen Wu and Jian-Jun He
State Key Laboratory of Modern Optical Instrumentation, Centre for Integrated Optoelectronics
Department of Optical Engineering, Zhejiang University, Hangzhou 310027, China

Abstract— Tunable wavelength converters are very useful for realizing large scalable wavelength routers. They usually involve complex structures such as non-uniform gratings and multiple epitaxial regrowth. In this paper, we present the design and simulation results of a much simpler structure based on a V-cavity laser and delayed Mach-Zehnder interferometer (MZI) with semiconductor optical amplifiers (SOAs). InP based offset quantum well platform is used for the active and passive integration. The widely-tunable V-cavity laser, which consists of two Fabry-Perot cavities coupled through a half-wave coupler, offers simple and efficient wavelength switching with 100 GHz ITU channel spacing in C band. The probe light emitting out of both branches of V-cavity laser is coupled to MZI-SOAs through deep trenches. The deep-etched passive waveguides are used for the delay line. With a carefully designed taper, the coupling loss between deep-etched passive waveguide and shallow-etched active waveguide is less than 0.1 dB with a center misalignment tolerance of as large as 0.5 μm. The SOAs are carefully designed to realize different functions, such as linear amplification and cross-phase modulation (XPM). The dynamic characteristics of the wavelength converter including optical pulse patterns, frequency chirp and extinction ratio are investigated using the large-signal dynamic model of semiconductor optical amplifier (SOA) with time-dependent transfer matrix method (TD-TMM). The model considers material gain spectrum, facet reflectivity, carrier-induced refractive index change, internal reflection and amplified spontaneous emission (ASE) noise. A 10 Gb/s return-to-zero (RZ) tunable all-optical wavelength converter is achieved with a large extinction ratio, for both wavelength up and down conversions.

Simulated Optimization of the Colorless Laser Transmitter under 10-Gbit/s Direct Encoding and Optical Injection-locking

Yu-Chieh Chi and Gong-Ru Lin
Department of Electrical Engineering, Graduate Institute of Photonics and Optoelectronics
Taiwan University, No. 1, Sec. 4, Roosevelt Road, Taipei 10617, Taiwan

Abstract— The characteristics of free-running and injection-locked colorless laser diode with weak-resonance and long-cavity under 10-Gbit/s direct encoding are simulated, and the analytical modeling based on the modified rate equations for the buildup dynamics improved by the optical injection-locking are also explored. By reducing the front-facet reflectance to 1% and lengthening the cavity length to 600 μm, the key parameters of such a specific laser diode including threshold current of 27.5 mA and the mode spacing of 0.572 nm are utilized for multi-channel application. As compared with the typical FPLD, the colorless laser diode requires overcoming the slightly higher threshold current to show broaden spectral linewidth and extended locking range; however, its limited relaxation resonance frequency is the obstruction for the high-data-rate transmission. Nonetheless, it can be easily overcome by the optical injection-locking.

At free-running condition, the colorless laser diode difficultly carries the 10-Gbit/s non-return-to-zero (NRZ) data because of its limited modulation bandwidth by the insufficient stimulated emitting photons. After optical injection-locking, the relaxation resonance frequency up-shifts to higher frequency at a cost of sacrificing the throughput intensity because of the enhanced accumulation of stimulated emitting photons. With a proper injection ratio of −8 dB, the simulated output characteristics of the colorless laser transmitter under 10-Gbit/s NRZ encoding are improved to exhibit a reduced threshold current of 26.4 mA, an enlarged detuning wavelength of 0.32 nm, a highest Q-factor of 13.2 dB, a lowest timing jitter of 1.8 ps, and a suppressed peak-to-peak chirp of 4.78 GHz. If the injection ratio is overly increased beyond −8 dBm, not only overstretch relaxation resonance frequency but also decreased throughput intensity at the modulated frequency regime are observed, which inevitably degrades the injection-locked and directly-modulated colorless laser output with a delayed rising/falling time. This work explores a selecting role on the injection ratio for the 10-Gbit/s NRZ encoding and injection-locked colorless laser diode for the multi-user services in next-generation passive-optical-network (NG-PON).

Power Conservation in Dual Periodic Dielectric Waveguides

Nai-Hsiang Sun, **Tsum-Yen He**, **Shih-Cing Lei**, **Yu-Wei Liu**, **and Jung-Sheng Chiang**
Department of Electrical Engineering, I-Shou University, Kaohsiung, Taiwan

Abstract— In the paper, the power conservation in dual periodical dielectric waveguide is analyzed. The Floquet-Bloch theory is used to analyze the dispersion relationship. The effect index and the field distribution of a grating structure can be calculated. The discontinuity interfaces between the grating and the non-grating region are evaluated by Mahmoud-Beal's method. By overlapping integrals of the fields, we obtain the transmission efficiency and reflection efficiency of a periodic dielectric waveguide. Moreover, we calculate the energy distribution in the dual grating region. We successfully simulate the power distribution of the dual dielectric waveguides.

Bandgap Engineering of InGaAsP/InP Multiple Quantum Well Structure by Dielectric Sputtering

Hongli Zhu, Yuan Zhuang, Xin Zhang, and Jian-Jun He
Centre for Integrated Optoelectronics, State Key Laboratory of Modern Optical Instrumentation
Department of Optical Engineering, Zhejiang University, Hangzhou 310027, China

Abstract— The InGaAsP/InP multiple quantum well (MQW) heterostructure is a widely used material system for 1.55 μm optical communication lasers. Recently, photonic integrated circuit (PIC) has attracted more and more attention for its high-functionality, low-cost, and low-power-consumption. A key issue in the fabrication of PICs is the bandgap engineering of the MQW wafer in order to monolithically integrate active and passive devices. Quantum well intermixing (QWI) is a promising method that can selectively shift the bandgap post-growth with simple process. In this paper, we present our recent work on QWI by dielectric sputtering method. Different dielectric materials are investigated for the effectiveness of QWI, including Al_2O_3, SiO_2, and Si_3N_4. The InGaAsP/InP MQW laser structure was grown by MOCVD with a 0.5 μm thick InP sacrificial layer. The sample was first pre-processed by argon plasma for 10 seconds. Then, a thin layer of dielectric film was deposited by sputtering in 20 mT argon atmosphere with 200 W RF power for 1.5 hour. After a 750°C rapid thermal annealing (RTA) in nitrogen atmosphere for 120 seconds, the film was removed by lift-off of sacrificial layer in hydrochloric acerbic (HCl) solution. The photoluminescence (PL) spectrum of the sample shows bandgap blue shifts as large as 100 nm or more. Although the PL peak is a little broadened with slightly reduced intensity, Fabry-Perot (FP) lasers with blueshifted wavelength are fabricated without significant increase in lasing threshold current. The waveguide losses are also measured before and after QWI. The results indicate the good quality of the MQW material after bandgap engineering by dielectric sputtering and annealing.

High Stable Exciton Emission from SnO_2 Quantum Dots Grown via a Facile "Top-down" Strategy

Shu Sheng Pan[1], **Wei Lu**[2, 3], **Zhao Qin Chu**[1], **Si Chao Xu**[1], **Yun Xia Zhang**[1], **Yuan Yuan Luo**[1], **and Guang Hai Li**[1]

[1]Key Laboratory of Materials Physics, Anhui Key Laboratory of Nanomaterials and Nanostructures
Institute of Solid State Physics, Chinese Academy of Sciences, Hefei, Anhui 230031, China
[2]Department of Applied Physics, The Hong Kong Polytechnic University
Hung Hom, Kowloon, Hong Kong, China
[3]Materials Research Centre, The Hong Kong Polytechnic University
Hung Hom, Kowloon, Hong Kong, China

Abstract— Abstract-SnO_2 is a promising wide band gap semiconductor for next generation ultraviolet (UV) non-polar optoelectronic devices applications. The development of SnO_2-based optoelectronic devices is obsessed by its low exciton emission efficiency. In this study, quantum confined SnO_2 nanocrystals have been fabricated via pulsed laser ablation in water and ethanol. The SnO_2 quantum dots (QDs) possess high performance exciton emission at 300 nm and 313 nm in water and ethanol, respectively. The exciton emission intensity and wavelength can be slightly tuned by laser pulse energy and irradiation time. Optical gain has also observed in SnO_2 QDs. Therefore, we have shown that SnO_2 QDs can be a potential luminescent material suitable for the realization of ultraviolet B non-polar light emitting devices and lasing devices.

Design and Simulation of 450 nm GaN-based Multiple-quantum-well Tunable V-cavity Laser

Zhipeng Hu, **Jianjun Meng**, **Lin Wu**, **and Jian-Jun He**
State Key Laboratory of Modern Optical Instrumentation, Centre for Integrated Optoelectronics
Department of Optical Engineering, Zhejiang University, Hangzhou 310027, China

Abstract— Tunable blue laser diodes based on gallium nitride are of great interest for wide range of applications, such as chemical or biological hazard detection, laser-induced fluorescence spectroscopy, combustion diagnostics and medical diagnostics. At present, blue light sources based on GaN are mostly based on LED or multimode Fabry-Perot lasers. A tunable blue laser based on external cavity grating structure has recently been reported, which require precise mechanics and alignment, complex structure, bulky and expensive systems. Recently, a compact tunable V-cavity laser (VCL) was proposed and full-band wavelength tuning of up to 50 channels with 100 GHz spacing around 1550 nm was demonstrated experimentally with excellent side-mode suppression ratio (SMSR) in InP based material system. In this paper, we present the design and simulation of the GaN-based tunable laser, where V-cavity laser structure is adopted. The V-cavity laser consists of a fixed gain cavity and a channel selector cavity with different optical path length, which are coupled through a 2×2 half-wave coupler. By using the half-wave coupled cavity design, we show that single-mode lasing with a high SMSR and a large tuning range can be achieved with compact size and simple fabrication process. Vertical optical mode profile are calculated by TMM method. With considering the material properties and processing conditions, we obtain large confinement factor (= 0.1813) with relative high indium doped InGaN guiding layers and aluminum doped AlGaN superlattice structure layers. Since backside contacts are not available with the sapphire substrate, the device geometry is designed to use coplanar electrodes with shallow etched waveguide and deep etched mesa. The waveguide and half-wave coupler are optimized to realize low loss, high SMSR and wide tuning range. The simulation result shows that more than 10 channels with 300 GHz spacing within the tunable range of 4.1 nm and high SMSR over 30 dB is achieved.

Session 4P3a
SC3: Fano Resonance in Nanoscale Structures

Self-Fano Resonance in a Symmetry Broken Ag Nanodisk

Jiaming Li and Zheyu Fang
State Key Laboratory for Mesoscopic Physics, School of Physics
Peking University, Beijing 100871, China

Abstract— We experimentally investigated the Fano resonance of a single symmetry broken Ag nanodisk at a normal incidence. We showed the asymmetric Fano line shape can be controlled by modifying the open angle of the nanodisk, and demonstrated this Fano splitting is the result of the overlap between a plasmonic broad hybridized dipolar mode and a narrow quadrupolar mode. We further introduced a semi-analytical method to calculate the plasmon hybridization and to analyze this quadru Fano resonance. With a good agreement between finite-difference time-domain simulations and detected scattering cross sections, the suggested configuration provides a way to investigate and control the Fano resonance within a single planar nanostructure, and can be applied as a high-performance Fano resonance sensor in the future.

Fano Resonances in Magneto-dielectric Core-shell Nanoparticles

Wei Liu[1, 2, 3]

[1]College of Optoelectronic Science and Engineering, National University of Defense Technology, China
[2]Nonlinear Physics Centre, Australian National University, Australia
[3]The Blackett Laboratory, Imperial College London, United Kingdom

Abstract— We propose a geometric model for localized surface plasmons, which is employed to explain the overlapping of electric and magnetic dipoles in magneto-dielectric core-shell nanoparticles. Then we investigate Fano resonances (FRs) in such nanoparticles, including polarization independent FRs in arrays of nanospheres and FR-based efficient scattering shaping for nanowires.

Introduction: As a ubiquitous wave inference phenomenon, Fano resonance (FR) is attracting surging interest in the currently vibrant fields of plasmonics and metamaterials, due to many related observations and applications in various configurations [1, 2]. However the FRs studied up to now in plasmonic nanostructures usually involve only electric responses and very few investigations have been conducted into FRs induced by optically-induced magnetic responses [3, 4].

Geometrization of Localized Surface Plasmons [4]: In this section, we propose a geometric model based on the Bohr condition for localized surface plasmons, which can provide intuitive explanations for conventional scattering features of plasmonic nanoparticles. Based on this geometric model we further demonstrate anomalous scattering features for plasmonic nanoparticles, e.g., higher order modes supported at lower frequencies, blueshift of the resonance with increasing particle sizes, and multiple resonances of the same order supported at different frequencies. This geometric model can also be employed to explain the overlapping of electric and magnetic responses in magneto-dielectric core-shell nanoparticles. The geometric picture offers new insights into the understanding of the localized resonances, and may shed new light to many related new phenomena and applications (including FRs) based on particle scattering.

Fano Resonances in Core-shell Nanoparticles [5–7]: In this section, we study the scattering properties of arrays of core-shell nanospheres and reveal the existence of polarization-independent FRs. Such FRs occur through the interaction of a pair of degenerate orthogonal electric and magnetic dipoles of the same strength with the spectrally-narrow geometric resonance due to the diffractive coupling in the array. Furthermore, we show that for different polarizations of the incident plane waves, the electric and magnetic dipoles supported by each nanosphere can be selectively enhanced, providing extra freedom for near-field manipulations. We also extend our study to the scattering features of core-shell nanowires, and demonstrate efficient scattering shaping based on FRs, which originate from the interferences of electric quadrupole modes with the broad magnetic dipole modes. FRs involving both electric and magnetic responses can be possibly employed for various applications, including sensing, lasing, nonlinear switching and scattering shaping in the fields of plasmonics and metamaterials.

ACKNOWLEDGMENT

We highly appreciate the significant contributions from Andrey E. Miroshnichenko, Dragomir N. Neshev, Yuri S. Kivshar, Ortwin Hess and Rupert F. Oulton.

REFERENCES

1. Lukyanchuk, B. S., et al., *Nat. Mater.*, Vol. 9, 707, 2010.
2. Miroshnichenko, A. E., et al., *Rev. Mod. Phys.*, Vol. 82, 2257, 2010.
3. Liu, W., et al., *Chin. Phys. B*, Vol. 23, 047806, 2014, invited topical review.
4. Liu, W., "Light manipulation by plasmonic nanostructures," ANU PhD Thesis, 2013.
5. Liu, W., et al., *ACS Nano*, Vol. 6, 5469, 2012.
6. Liu, W., et al., *Phys. Rev. B*, Vol. 86(R), 081407, 2012.
7. Liu, W., et al., *Opt. Lett.*, Vol. 38, 2621, 2013.

Negative Optical Binding Force Induced by Fano Resonances in Plasmonic Heterodimers

Jun Jun Xiao, Qiang Zhang, Xiao Ming Zhang, and F. F. Qin
College of Electronic and Information Engineering, Shenzhen Graduate School
Harbin Institute of Technology, Shenzhen, Guangdong 518055, China

Abstract— Plasmonic nanosystems featuring multiple Fano spectra are shown to have flexible spectral positioning and line shaping functionalities. In view that optical resonances in plasmonic structure dramatically affect their optical force properties, we study the optical binding forces (OBF) induce by Fano resonance in a nanorod heterodimer and a ring-disk resonator. It is shown that there is an OBF reversal between the two nanorods which is due to the out of phase oscillation of the current across the dimer gap. We find that the force reversal may be ubiquitous in the plasmonic structures that sustain Fano resonances and further study the optical force properties in a ring-disk resonator supporting multiple Fano resonance. It is found that the OBF between the disk and the ring shows multiple sign reversals, spectrally from the dipole-quadrupole regime up to the dipole-decapole regime. The zero-force points can be categorized into two types: the positive-to-negative ones resulting from the Fano dip and the negative-to-positive ones associated with the transitions between dipole-multipole modes. Such characters make it possible to organize unusual "optical matters" from individual plasmonic nanoparticles.

Subgroup Decomposition of Plasmonic Resonances in Hybrid Oligomers for Ultrasensitive Biochemical Sensing

Dang Yuan Lei[1, 2]

[1]Department of Applied Physics, The Hong Kong Polytechnic University, Hong Kong, China
[2]Shenzhen Research Institute, The Hong Kong Polytechnic University, Shenzhen, China

Abstract— In this talk, we show how one can easily but significantly tailor the overall spectral profile in plasmonic nanocluster systems, for example, nanoparticle quadrumers and pentamers, by selectively altering the particle shape without a need to change the particle size, inter-particle distance or the number of elements of the oligomers. We also investigate experimentally the sensitivities of these pentamers to the adsorption of self-assembled alkanethiols monolayers, which are found to depend on the nanocluster arrangement, constitute nanoparticle shape and the plasmon resonance wavelength. In the first part of this talk, we will show that the whole spectrum profile of a hybrid nanocluster can be decomposed into two separate contributions from two different subgroups, which are efficiently excited at their spectral peaks, respectively. We further show that in some cases, each subgroup is separately active in distinct frequency windows with only small overlap, leading to a simple convolution of the sub-spectra. Variation in particle shape of either subgroup results in the tuning of the overall spectral lineshape, which opens a novel pathway for shaping the plasmonic response in small nanoclusters. In the second part of this talk, we will study the monolayer sensing sensitivities of the aforementioned nanoparticle quadrumers. Together with full-wave numerical simulation results, we unveil a direct correlation between the sensitivity and the field strength of plasmonic "hot" spots generated in each nanocluster. Our observation is beyond conventional considerations for improving the sensing performance of metal nanoclusters-based biosensors and opens the possibilities of using plasmonic nanoclusters for single-molecule detection and identification.

REFERENCES

1. Rahmani, M., D. Y. Lei, V. Giannini, B. Lukiyanchuk, M. Ranjbar, T. Y. F. Liew, M. Hong, and S. A. Maier, "Subgroup decomposition of plasmonic resonances in hybrid oligomers: Modeling the resonance lineshape," *Nano Lett.*, Vol. 12, 2101–2106, 2012.
2. Rahmani, M., A. E. Miroshnichenko, D. Y. Lei, B. Luk'yanchuk, M. I. Tribelsky, A. I. Kuznetsov, Y. S. Kivshar, Y. Francescato, V. Giannini, M. Hong, and S. A. Maier, "Beyond the hybridization effects in plasmonic nanoclusters: Diffraction-induced enhanced absorptionand scattering," *Small*, Vol. 10, 576–583, 2014.
3. Koenig, M., M. Rahmani, D. Y. Lei, V. Giannini, T. R. Roschuk, M. Hong, S. Schlücker, and S. A. Maier, "Unveiling the correlation between monolayer sensing sensitivities and plasmonic near-field "hot" spots in coupled metal nanoclusters," 2014, under preparation.

Reworking the Understanding of Fano Resonances in Nanoparticle Oligomers

B. Hopkins[1], **A. N. Poddubny**[2, 3], **A. E. Miroshnichenko**[1], **and Y. S. Kivshar**[1, 3]

[1]Nonlinear Physics Centre, Australian National University, Australia
[2]Ioffe Physical-Technical Institute of the Russian Academy of Sciences, Russia
[3]National Research University for Information Technology, Mechanics and Optics, Russia

Abstract— We present a general approach for describing the physics of Fano resonances in nanoparticle oligomers made from metallic or dielectric nanoparticles. It is shown that the interference of nonorthogonal collective eigenmodes is a sufficient condition to produce Fano resonances, where such eigenmodes can be defined explicitly using the coupled-dipole approximation. We then prove analytically that the number of collective eigenmodes that can be excited in symmetric nanoparticle oligomers always permits the existence of Fano resonances, and further demonstrate that the excitation of dark eigenmodes is not necessary. In doing this we are able to unify the understanding of Fano resonances for both plasmonic and all-dielectric oligomers.

Introduction, Results and Conclusions: The sharp interference phenomena in the scattering of nanoscale systems, known as Fano resonances, have generated immense interest due to their extreme dispersion and sensitivity to environment; characteristics which make them very promising candidates for a multitude of high-accuracy sensing applications. The symmetric nanoparticle 'oligomer' geometries are of particular interest due to their polarization-independent response and, therefore, Fano resonances. Until now only metals have been used to induce Fano resonances in these oligomers because only metals support plasmon mode-hybridization, which has been considered as integral for the Fano resonances to exist. However Fano resonances have since been observed in purely all-dielectric oligomers that do not support such plasmon hybridization. Subsequently there must exist a different mechanism which leads to Fano resonances.

Results and Conclusions: Here we revisit the underlying behavior of general oligomers and acknowledge the full consequences of non-Hermitian interactions to rigorously show that Fano resonances can occur purely due to the interference between the nonorthogonal eigenmodes of oligomer systems [1]. As a consequence we show that there exists a simpler mechanism to produce Fano resonances in both plasmonic and dielectric oligomers without the excitation of dark modes. Further, we generalize this approach by proving that the number of eigenmodes that can be excited in an arbitrary oligomer is predominately set by symmetry and not the number of particles. This number of eigenmodes is then doubled when each particle has both electric and magnetic responses, as is the case with high-permittivity dielectric nanoparticles. As such there is seemingly no reason why an all-dielectric oligomer cannot support Fano resonances. On the contrary, we show that the electric and magnetic eigenmodes in all-dielectric oligomers are each independently capable of producing Fano resonances. Such electric and magnetic Fano resonances in all-dielectric oligomers have since been observed experimentally by Filonov et al. [2] at microwave frequencies and Chong et al. [3] at optical frequencies. This now opens the door to new, low-loss, all-dielectric oligomers being utilized in what has been an exclusively-plasmonic field.

REFERENCES

1. Hopkins, B., A. N. Poddubny, A. E. Miroshnichenko, and Y. S. Kivshar, "Revisiting the physics of Fano resonances for nanoparticle oligomers," *Phys. Rev. A*, Vol. 88, No. 5, 053819, 2013.
2. Filonov, D. S., A. P. Slobozhanyuk, A. E. Krasnok, P. A. Belov, E. A. Nenasheva, B. Hopkins, A. E. Miroshnichenko, and Y. S. Kivshar, "Near-field mapping of Fano resonances in all-dielectric oligomers," *Appl. Phys. Lett.*, Vol. 104, 021104, 2014.
3. Chong, K. E., B. Hopkins, I. Staude, A. E. Miroshnichenko, J. Dominguez, M. L. Decker, D. N. Neshev, I. Brener, and Y. S. Kivshar, "Observation of fano resonances in all-dielectric nanoparticle oligomers," *Small*, 2014, DOI: 10.1002/smll.201303612.

Equivalent Permittivity and Permeability and Multiple Fano Resonances for Nonlocal Metallic Nanowires

Yang Huang and Lei Gao
School of Physical Science and Technology, Soochow University, Suzhou 215006, China

Abstract— For metallic nanostructures whose dimensions are of a few nanometers, the conventional local solutions of Maxwell's equations are no longer able to describe electromagnetic properties, when one takes into account the electron-electron interactions in the dielectric response of metals. Actually, when the electric field is applied to metallic particles, due to the Pauli exclusion principle and the classical Coulomb force, the electrons migrating to the surface are not infinitely compressible, and the screening electrons are generally distributed in a layer with thickness of about the Thomas screening length. These intrinsic quantum properties of the metal's conduction electrons may be described by including the nonlocal effects on the interaction between the incident wave and the metallic nanostructures. In the semi-classical electrodynamic descriptions, it is also called spatial dispersion of the dielectric response. In this talk, we establish the nonlocal effective medium theory for a composite in which the parallel nonlocal nanocylinders are embedded in the host medium beyond the long-wavelength approximation, and then derive the equivalent permittivity and permeability (EP) for the nanocylinder with spatial dispersion. In addition, motivated by the anomalous light scattering and Fano resonance from small particles with weak dissipation, we take one step forward to investigate the electro-magnetic scattering from nonlocal nanocylinders with weak dissipation, and find that Multiple Fano resonances exist because of the interference of different longitudinal modes with the dipole moments, and the nonlocal nanocylinder can be designed to yield an abrupt transition between full transparency and strong scattering.

Nonlinear Fano Resonance in Photonic Crystal Waveguide and Cavity System: Physical Properties and Applications

Yi Xu[1] **and Andrey E. Miroshnichenko**[2]

[1]Department of Electronics, College of Information Science and Technology
Jinan University, Guangzhou 510632, China
[2]Nonlinear Physics Centre, Research School of Science and Engineering
Australian National University, Canberra ACT 0200, Australia

Abstract— During last decade, the Fano resonances in nanoscale structures have gained numerous attentions due to their capability of building sensors, switches, filters at a very compact scale [1]. The Fano resonances manifest themselves as asymmetric profiles in transmission or scattering line shape, which originates from the resonant constructive and destructive interference phenomena in waves scattering [2]. Photonic crystal waveguide and side-coupled cavity system provides a superior platform for observing and manipulating Fano resonance [3–5]. Utilizing the Kerr nonlinearity in the photonic crystal cavity, we can obtain tunable response of such system which in principle manifests as the nonlinear Fano resonance. We will discuss the physical properties of nonlinear Fano resonance found in different photonic crystal waveguide and side-coupled cavity system [6–11]. Applications including enhancement of nonlinear response, manipulating optical flow, tunable optical diode and optical biosensor based on these properties are proposed and demonstrated via numerical experiments.

ACKNOWLEDGMENT

Y. Xu acknowledges the support from NNSF (Grant No. 11304047), Foundation for Distinguished Young Talents in Higher Education of Guangdong Province (Grant No. 2013LYM0067). The work of A. E. Miroshnichenko was supported by the Australian Research Council through Future Fellowship program (FT110100037).

REFERENCES

1. Miroshnichenko, A. E., S. Flach, and Yu. S. Kivshar, *Rev. Mod. Phys.*, Vol. 82, 2257, 2010.
2. Fano, U., *Phys. Rev.*, Vol. 124, 1866, 1961.
3. Fan, S., *Appl. Phys. Lett.*, Vol. 80, 908–910, 2002.
4. Miroshnichenko, A. E., S. F. Mingaleev, S. Flach, and Yu. S. Kivshar, *Phys. Rev. E*, Vol. 71, 036626, 2005.
5. Miroshnichenko, A. E., Yu. Kivshar, C. Etrich, T. Pertsch, R. Iliew, and F. Lederer, *Phys. Rev. A*, Vol. 79, 013809, 2009.
6. Xu, Y. and A. E. Miroshnichenko, *Phys. Rev. A*, Vol. 84, 033828, 2011.
7. Xu, Y. and A. E. Miroshnichenko, *Europhysics Lett.*, Vol. 97, 44007, 2012.
8. Xu, Y., A. E. Miroshnichenko, and Anton S. Desyatnikov, *Opt. Lett.*, Vol. 37, 4985–4987, 2012.
9. Weimann, S., Y. Xu, R. Keil, A. E. Miroshnichenko, S. Nolte, A. A. Sukhorukov, A. Szameit, and Y. S. Kivshar, *Phys. Rev. Lett.*, Vol. 111, 240403, 2013.
10. Li, X. Q. and Yi Xu, *Opt. Commun.*, Vol. 301, 7–11, 2013.
11. Xu, Y. and A. E. Miroshnichenko, to be appeared in *Phys. Rev. B*.

Session 4P3b
SC2&3: Active Nanophotonics: Design of Nano-devices/Structures and Their Interaction with Molecules

1.7-nanometer Resolution Structural Analysis of Carbon Nanotube by Tip Enhanced Raman Imaging

Chi Chen[1, 2], **Norihiko Hayazawa**[1], **and Satoshi Kawata**[1, 3]

[1]The Institute of Physical and Chemical Research (RIKEN), Wako, Saitama 351-0198, Japan
[2]Research Center for Applied Sciences, Academia Sinica, Taipei 115, Taiwan
[2]Department of Applied Physics, Osaka University, Suita, Osaka 565-0871, Japan

Abstract— TERS (tip enhanced Raman spectroscopy) opens a new horizon for nanoscale characterization. Atomic force microscopy (AFM) combined with near field Raman spectroscopy is generally used for hybrid imaging and chemical analysis. However, for higher spatial resolution, we constructed a scanning tunneling microscope (STM) based TERS targeting at location-dependent Raman spectroscopy of carbon nanotubes (CNT).

In this talk, TERS imaging of the individual Raman modes of CNT is demonstrated with 1.7 nm lateral resolution based on the enhancement and positioning of a STM tip. CNT is selected as our sample for TERS because it has strong Raman signal and clear morphology. We obtained spectrally resolved TERS images simultaneously with STM scanning. Different Raman modes show characteristic distributions in the length scale of a few nanometers. Local defect is visualized in real space through D-band imaging while G-band and 2D-band provide various structural information. With superior resolution, we observe beautiful underlying physical chemistry of CNTs, including diameter effect, local defect, and bundling effect in real space and further distinguish one of the CNTs as a multiwall CNT. We do not require ultrahigh vacuum and cryogenic environment to reach nanometers scale chemical analysis. This makes STM-TERS a unique analytical tool for "as-made" materials, soft materials, and biological sample with ultrahigh spatial resolution.

Large Kerr Nonlinearity Induced by Anisotropic Purcell Factors

Juanjuan Ren, Ying Gu, Hongyi Chen, Dongxing Zhao, and Qihuang Gong
State Key Laboratory for Mesoscopic Physics, Department of Physics
Peking University, Beijing 100871, China

Abstract— Kerr nonlinearity is the cornerstone of many nonlinear optics phenomena and optical device. Recently, the enhanced Kerr nonlinearity via spontaneously generated coherence (SGC), which originates from the interference of nearly degenerate spontaneous channels, has been researched in three level systems [1]. However, the requirement of nearly parallel dipole moments, which does not exist in natural atoms, constitutes the major barrier in the application of SGC and hence, large Kerr nonlinearity.

Here, via the anisotropic Purcell factor, we find that the Kerr nonlinearity of three-level Λ-type atomic systems can be greatly enhanced with two perpendicular dipole moments, as shown in Fig. 1. Large Kerr nonlinearity with two non-vertical dipole moments has also been investigated. The plasmonic structures possessing large anisotropic Purcell factors [2] will be used to realize the large Kerr nonlinearity at the nanoscale. Without the need of parallel dipole moments, our studies provide an experimentally feasible platform for SGC enhanced Kerr nonlinearity. Such controllable Kerr nonlinearity can apply to optoelectronic devices, such as all-optical switches and logic gates.

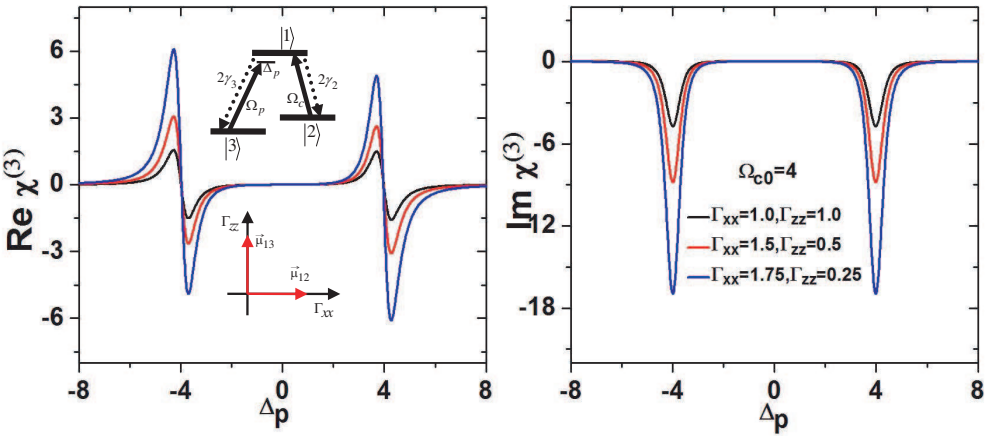

Figure 1: Dispersion and absorption of the Kerr nonlinearity of the Λ-type system with anisotropic Purcell factors. $\vec{\mu}_{12}$ ($\vec{\mu}_{13}$) refers to the dipole moments between transition $|1\rangle \leftrightarrow |2\rangle(|3\rangle)$. Γ_{xx} and Γ_{zz} denote the decay rates along the x and z directions. That $\Gamma_{xx} = \Gamma_{zz} = 1.0$ stands for a vacuum.

REFERENCES

1. Niu, Y. and S. Gong, *Phys. Rev. A*, Vol. 73, 053811, 2006.
2. Gu, Y., L. Wang, et al., *Nano Lett.*, Vol. 12, 2488, 2012.

Hiding the Interior Region of Core-shell Nano-particles Based on Scattering Cancellation

Jeng Yi Lee[1] **and Ray-Kuang Lee**[1, 2]

[1]Institute of Photonics Technologies, Tsing-Hua University, Hsinchu 300, Taiwan
[2]Physics Division, Center of Theoretical Science, Hsinchu 300, Taiwan

Abstract— Based on the scattering cancellation, we provide a method not only making a nano-particle nearly invisible, but also hiding its interior region from the outside probing matter wave. By applying the interplay among the nodal points of partial waves along with the concept of streamline in fluid dynamics for probability flux, a quantum invisible cloak to the electron transport in a host semiconductor is demonstrate by simultaneously guiding the probability flux outside a hidden region and keeping the total scattering cross section negligible. As the probability flux vanishes in the interior region, one can embed any materials inside a multiple core-shell nano-particle without affecting physical observables from the outside. Our results reveal the possibility to design a protection shield layer for fragile interior parts from the impact of transport electrons.

Vortex Energy Flows Generated by the Periodic Nanostructures

Shih-Wen Chen and Jia-Han Li
Department of Engineering Science and Ocean Engineering, Taiwan University
No. 1, Roosevelt Road, Sec. 4, Taipei 10617, Taiwan

Abstract— An optical vortex means that light travels spirally around a zero of an electromagnetic field point and it is also called an optical singularity because of the character of the phase singularity at the zero point. Optical vortices attract a lot of attentions due to its fascinating ability of manipulating the positions of nanostructures [1, 2]. Considering the possibility of a realization of plasmonic on-chip systems, many researches provide ways to create optical vortices in plasmonic regime such as plasmonic vortex lens [3], nanogears [4] and core-shell nanocylinders [5]. Since the extraordinary optical transmission was found in 1998 [6], the periodic hole arrays have been popular plasmonic structures until today. In this study, vortex energy flows are found and generated by periodic nanostructures based on the finite difference time domain method. The rim of a hole in the periodic array behaves like a light source and its strong electric enhancement can be applied to induce optical vortices for specific wavelengths. The electric fields are enhanced when optical vortices occur and the Poynting vector reveals that different shapes give different numbers of vortex energy flows. With different shapes or depths, the optimization of the structures will facilitate the design for the applications of light trapping, biosensing and quantum information.

REFERENCES

1. Paterson, L., M. P. MacDonald, J. Arlt, W. Sibbett, P. E. Bryant, and K. Dholakia, "Controlled rotation of optically trapped microscopic particles," *Science*, Vol. 291, 912–914, 2001.
2. Yan, Z. and N. F. Scherer, "Optical vortex induced rotation of silver nanowires," *J. Phys. Chem. Lett.*, Vol. 4, 2937–2942, 2013.
3. Kim, H., J. Park, S.-W. Cho, S.-Y. Lee, M. Kang, and B. Lee, "Synthesis and dynamic switching of surface plasmon vortices with plasmonic vortex lens," *J. Phys. Chem. Lett.*, Vol. 10, 529–536, 2010.
4. Boriskina, S. V. and B. M. Reinhard, "Molding the flow of light on the nanoscale: From votex naogears to phase-operated plasmonic machinery," *Nanoscale*, Vol. 4, 76–90, 2012.
5. Lu, J. Y. and Y. H. Chang, "Optical singularities associated with the energy flow of two closely spaced core-shell nanocylinders," *Opt. Express*, Vol. 17, 19451–19458, 2009.
6. Ebbesen, T. W., H. J. Lezec, H. F. Ghaemi, T. Thio, and P. A. Wolff, "Extraordinary optical transmission through sub-wavelength hole arrays," *Nature*, Vol. 391, 667–669, 1998.

Shaping the CPML Absorbing Boundary Condition to Eliminate Impinging Light at a Specific Position inside Electromagnetic Simulations

Sergio Cantero, Shuai-Hsun Lee, and Snow H. Tseng
Graduate Institute of Photonics and Optoelectronics
Taiwan University, Taipei 10617, Taiwan

Abstract— The Finite-difference time-domain (FDTD) algorithm is widely used for electromagnetic wave propagation and light scattering problems. Based upon numerical solutions of Maxwell's equations, the electromagnetic wave characteristics can be accurately analyzed. To model light propagation through a macroscopic scattering medium to a target position, an absorber is required to eliminate impinging light. In modeling a physical problem in open space, absorbing boundary conditions (ABC) are applied to terminate the computational grid. ABCs are designed to absorb outgoing electromagnetic energy, allowing modeling an optical system isolated in free space with limited computation memory. The introduction in 1994 by Berenger of perfectly matched layers (PML) ABC effectively reduces the artificial numerical error caused by the simulation boundary. In this research we explore the possibility to implement an optical target that eliminates incoming wave by a modified morphology of an absorbing boundary condition. In particular, our model is based on convolutional perfectly matched layers (CPML) ABC; the CPML algorithm was first introduced by Roden and Gedney using a recursive convolution PML. To validate this method, a cylindrical CPML region is constructed as artificial absorbing material and simulated using a two-dimensional FDTD algorithm. Its performance is analyzed for both omnidirectional incident light and focused beam wave source conditions. Varying the spatial size of the circular CPML, we compute the absorption efficiency for a wide range of applications and demonstrate its performance as a numerical optical target in FDTD simulations. We demonstrate that the reported simulation construct can effectively eliminate impinging light wave for a macroscopic light scattering simulation.

Session 4P4a
SC3&1: Science and Applications of Electromagnetic Vortices and Orbital Angular Momentum (OAM)

Helically Corrugated Metallic Nanowires as Nanovortices Sources

Changming Huang[1], **Fangwei Ye**[1], **Abiola O. Oladipo**[2, 3], **Nicolae C. Panoiu**[2], **and Xianfeng Chen**[1]

[1]Department of Physics and Astronomy, Shanghai Jiao Tong University, Shanghai 200240, China
[2]Department of Electronic and Electrical Engineering, University College London Torrington Place, London WC1E 7JE, United Kingdom
[3]Bio-Nano Consulting, 338 Euston Road, London NW1 3BT, United Kingdom

Abstract— Optical vortices are light beams with a phase change equal to an integer multiple of 2π along a closed trajectory around the center of beams, where the phase of the beam is undermined and thus representing a phase singularity, while the field amplitude is vanishes. Such optical beams can be generated by using different schemes, such as computer-synthesized holograms, spiral phase plates, and nonlinear optical process. Optical vortices may find a series of appealing applications such as in optical tweezers, imaging and quantum information, and thus have drawn substantially research interests.

Optical vortices generated and studied thus far have been diffraction-limited. For their applications at nanoscales, however, it is desirable to generate deep sub-wavelengthed vortices. In this presentation, we put forward a type of nanoscale vortices sources: they are metallic cylinders of deep-subwavelengthed radius a, with their surfaces being periodically and helically corrugated with a period P and a height h ($h \ll a$). The fundamental mode of such nanowires can be excited by a TM Gaussian beam, and then the fundamental mode is found to be transferred into vortex mode, provided that the phase mismatch between the fundamental and the desired vortical mode is compensated. This is true when the period of pitch is carefully selected such that $P = \frac{2\pi}{(\beta_0 - \beta_l)k_0}$, where β_0 and β_l are the effective mode index of the fundamental and vortex mode of topological charge "l", respectively. We demonstrate that such metallic helix structures behave as nanovortices sources, by simulating the beam propagation through the nanowires. The methods we used are not only the direct simulation on Maxwell equations with the help of COMSOL MultiPhysics, but also the coupled mode theory that allows to analytically determine the coupling length, L, over which the fundamental mode is fully converted into vortex mode.

Generation of a Partially Coherent Laguerre-Gaussian Beam and Determination of Its Topological Charge

Yuan Dong, Chengliang Zhao, and Yangjian Cai
School of Physical Science and Technology, Soochow University, Suzhou 215006, China

Abstract— We report experimental generation of a partially coherent Laguerre-Gaussian beam with mode orders 0 and l (i.e., LG_{0l} beam) using a rotating ground-glass plate and a spatial light modulator. Focusing properties of the generated beam are studied both theoretically and experimentally. It is found that the focused intensity of the LG_{0l} beam is shaped through varying the initial spatial coherence, and our experimental results agree well with the theoretical predictions. It is known that one can determine the topological charge of a vortex beam based on the Fourier transform of its intensity. We demonstrate both theoretically and experimentally that this method will be invalid for determining the topological charge of a vortex beam with low coherence. Furthermore, we propose a method to determine the topological charge of a vortex beam with low coherence based on its complex degree of coherence.

Interference of Laser Beams with Different OAMs

Maxime Favier[1] **and Sergei Popov**[2]

[1]Institut d'Optique, Palaiseau Cedex 91127, France
[2]Royal Institute of Technology, Stockholm, SE-16440, Sweden

Abstract— Spatial modulation of laser beam phase with a helix profile allows creating the intensity pattern with a dark spot in the center of beam cross-section. Such waves known as vortex beams, or beams carrying orbital angular momentum (OAM), have a sharp intensity gradient in the central part and find different applications, e.g., manipulating small particles (optical tweezers), free-space communication, and others [1]. The spatial phase pitch along the beam axis defines the order of OAM. OAM beams are generated by the use of phase retardation plates implementing continuous azimuthal phase modulation where the number of integer 2pi rotations corresponds to the order of OAM [2]. Making two beams carrying different OAMs to interfere with each other, it is possible to shift a zero-intensity area away from the beam center (Fig. 1).

In our project we used liquid-crystal spatial light modulator (LQ SLM) to realize reconfigurable phase retardation required to generate a beam carrying different OAMs. Unlike conventional phase plates generating beams with fixed OAMs, the SLM has pixel structure with "dead zones" and does not allow to produce gradually changing azimuthal phase retardation. In addition, each SLM pixel introduces varying birefringence which depends on particular phase retardation in that pixel (due to different control voltage applied to the pixel). Such functionality requires knowledge and implementation of specific polarization eigenstate of the incident beam matching the overall birefringence of the SLM for each particular order of OAM. Measuring the phase retardation response of the SLM and using matrix technique, we can define necessary states of light polarization to compensate local birefringence effect from pixels. Combining two beams with different OAMs, e.g., plane Gaussian beam (zero-order OAM) and beams of OAM orders 1–3, we have experimentally demonstrated possibility to modify intensity distribution via shift of the dark zones (Fig. 2).

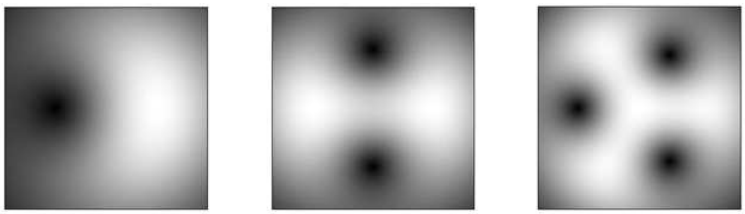

Figure 1: Simulated interference pattern for OAM beams of first 3 orders.

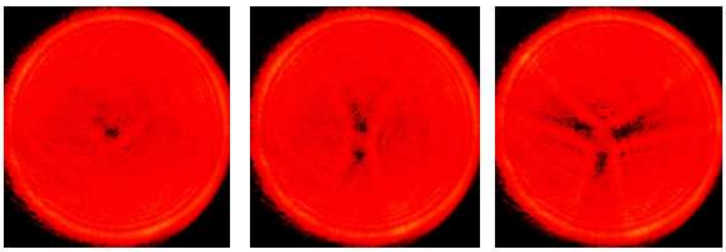

Figure 2: Interference of OAM beams of first 3 orders. Beam polarization eigenstates are properly matched to the SLM phase retardation (experiment).

REFERENCES

1. Allen, L., M. W. Beijersbergen, R. J. C. Spreeuw, and J. P. Woerdman, "Orbital angular momentum of light and the transformation of Laguerre-Gaussian laser modes," *Phys. Rev. A*, Vol. 45, 1992.
2. Heckenberg, N. R., R. McDuff, C. P. Smith, and A. G. White, "Generation of optical phase singularities by computer-generated holograms," *Optics Letters*, Vol. 17, No. 3, 1991.

Breakdown of Optical Vortices at a Dielectric Plane Surface

Yi Wang, Huazhou Chen, Guoxuan Zhu, Shimao Li, Yanfeng Zhang, Hui Chen, Yujie Chen, and Siyuan Yu
State Key Laboratory of Optoelectronic Materials and Technologies
School of Physics and Engineering, Sun Yat-sen University, Guangzhou 510275, China

Abstract— Non-plane wave Laguerre-Gaussian (LG) beams carrying orbital angular momentum (OAM) and known as optical vortices have applications in various areas including optical communications, quantum information processing, imaging and micromanipulation. The ability of generation, detection and manipulation of such beams is crucial for any application. In recent years, research on optical vortices breakdown has been a hot issue for its ubiquity in optical systems. It is found that high order optical vortices are vulnerable to perturbations such as random phase noise, asymmetric aperture and astigmatic focusing. In this paper, we report a simple way of tearing apart high order optical vortices — via refraction at a dielectric plane surface. This phenomenon is observed experimentally and discussed theoretically.

In the experiment, an $|\ell|$-order optical vortex is broken into $|\ell|$ secondary vortices aligned nicely in a row after refraction; meanwhile, the transverse beam pattern undergoes significant deformation to resemble an $|\ell|$-order diagonal Hermite Gaussian (HG) mode. The direction of the diagonal row is determined by the sign of the original optical vortex. As the reflected and refracted beams leave the plane surface, the intrinsic circulation of the optical vortices will reveal themselves in the form of the rotation of overall intensity patterns around the beam axes. At long distances, the transverse intensity pattern of the transmitted beam will return to an elliptical donut while the secondary vortices remain separate. It is also worth noting that the secondary optical vortices are able to propagate independently and thus be studied and processed respectively.

Theoretically, we applied the Wigner function approach to describe the transverse beam patterns. In this process, energy exchanges between the astigmatic part and the vortex part while the total orbital energy is conserved. This discussion is substantiated by the HG expansion method. LG modes are decomposed into several HG modes in the beam cross-section at the dielectric plane surface. Then the HG modes are contracted in one direction due to refraction. Finally, the astigmatic HG modes are added up to form the transmitted beam. The theoretical analysis is consistent with the experimental observation.

Due to the ubiquity of reflection and refraction in optical systems, studies on these vortex breakdown phenomena are vital to optical alignment and subtle experiments. In addition, the unique cross-section pattern of the refracted beam could be readily utilized to determine the order and the sign of an optical vortex. This study could also pave the way for OAM mode filtering crucial to OAM information coding and processing.

Self-imaging of Orbital Angular Momentum (OAM) Modes in Square Multimode Interference Waveguide

Zelin Ma, Hui Chen, Yanfeng Zhang, Yujie Chen, and Siyuan Yu
State Key Laboratory of Optoelectronic Materials and Technologies, School of Physics and Engineering
Sun Yat-sen University, Guangzhou 510275, China

Abstract— Light beams carrying orbital angular momentum (OAM) have found increasing applications in various areas such as optical tweezers, microscopy and optical communication systems. However, much of the research is based on traditional bulk optical components. There is a lack of attention on research of OAM modes propagating in planar photonic integrated components. Multimode interference (MMI) effect in planar waveguides, which results in duplicating of input field in periodic longitudinal locations (i.e., self-imaging), is widely used in integrated optics for fabrication of various couplers, a class of key elements in photonic integrated circuits (PICs). Conventionally the input to MMI couplers are single mode waveguides. When the input is an OAM mode, special phenomenon arise due to the helicity of its phase structure.

As an OAM state can be represented as a combination of even and odd modes with a $\pm\pi/2$ phase shift between them, we consider even and odd modes respectively. Due to the symmetry or anti-symmetry in the transverse (x or y) direction, there occurs the degeneracy of the images. If the input field locates at the center of the MMI cross section, the OAM mode is split at the position of four-fold degeneracy in the z direction. Interestingly, the image at this position is different with different values of the azimuthal index ℓ. And the OAM mode is maintained at the position of double degeneracy while the phase is modified, resulting in $1 \times N^2$ OAM beam splitting. If the OAM input is shifted along the x or y direction, the images are shifted, resulting in the separation of degenerate images. As the phase of the odd/even mode is modified differently, the OAM mode is distorted at such positions. Inversely, we can generate OAM modes in this way. If the OAM input is shifted for identical distance along the x and y directions, the phase of the odd/even mode is modified identically so that the OAM mode is maintained at the image position. We present a 4×4 OAM coupler in square MMI waveguide. A beam propagation (BPM) method is used to numerically verify such analytical expressions.

Such MMI devices can be used as OAM beam splitters and couplers. And because of the unique images at the position of four-fold degeneracy, it can be utilized to determine the order of an optical vortex. In addition, it is also a promising way of generating photons carrying OAM in the fashion of integrated optics. This study could pave the way for OAM integrated components and OAM communication systems.

Session 4P4b
Novel Optical Imaging Methods for Biomedical Applications, Spectroscopic and THz Bioelectromagnetics

Schlieren Confocal Microscopy Enables Confocal Phase-relief Imaging

Hao Xie[1], **Dayong Jin**[2], **and Peng Xi**[1]

[1]Department of Biomedical Engineering, College of Engineering
Peking University, Beijing 100871, China
[2]Advanced Cytometry Labs, MQphotonics Research Centre
Macquarie University, Sydney, NSW 2109, Australia

Abstract— Conventionally, fluorescence confocal microscopy (FCM) can only image the fluorescent signal from the specimen, whereas the phase structural information has been lost. Here an optical phase-relief imaging technique, termed Schlieren confocal microscopy (SCM) had been put forward to enable confocal microscopy with the phase-sensitive imaging modality. Compared to the laser oblique scanning optical microscopy (LOSOM) [1], shift of the detection optical path is no longer required in SCM. Instead, it employs only a piece of fluorescence medium on the top of the specimen, and a partial block in the propagation path of the fluorescence signal. Therefore, it can be more conveniently integrated into confocal laser scanning system.

Two types of Schlieren confocal microscopy are investigated: Type 1 uses a uniform fluorescence medium and partial beam obstruction, and Type 2 uses a half fluorescence plate only. A good linearity between intensity and phase gradient is found, suggesting the potential of quantitative phase imaging with SCM. Also, SCM maintains the same resolution as the confocal microscopy. Mouse kidney and HeLa cell samples are imaged with SCM to obtain multi-modality images of both fluorescence and phase imaging [2].

REFERENCES

1. Ding, Y., H. Xie, T. Peng, Y. Lu, D. Jin, J. Teng, Q. Ren, and P. Xi, "Laser oblique scanning optical microscopy (LOSOM) for phase relief imaging," *Optics Express*, Vol. 20, No. 13, 14100–14108, 2012.
2. Xie, H., D. Jin, J. Yu, T. Peng, Y. Ding, C. Zhou, and P. Xi, "Schlieren confocal microscopy for phase-relief imaging," *Optics Letters*, Vol. 39, No. 5, 1238–1241, 2014.

Dark-field Optical Coherence Tomography for Sidelobe Suppression

Xiaojun Yu, Xinyu Liu, Dongyao Cui, and Linbo Liu
School of Electrical & Electronic Engineering, Nanyang Technological University, Singapore

Abstract— Optical Coherence Tomography (OCT) has been established as a routine clinical diagnostic tool for detection of eye and skin diseases. Recently, intracoronary OCT and endoscopic OCT for diagnosis of coronary artery disease and gastrointestinal cancers have been developed and commercial products have been launched. The current OCT technology is advantageous over ultrasound imaging in spatial resolution, but still not enough for resolving cellular and subcellular structures of human tissue. Therefore, high resolution OCT is highly desired for better device performance and imaging quality. A number of methods have been proposed to improve spatial resolution but all of them have issue of pronounced side lobes.

In this study, a dark-field OCT device is developed using center obscuration techniques. The device is based on a modified spectral-domain OCT (SD-OCT system). The resolution of the system is characterized using a various size of polystyrene beads including 200 nm, 300 nm and 2 µm, and transverse profile of point spread function was acquired. We have demonstrated numerically and experimentally that one of merits of the proposed setup is reduced side lobed compared with other resolution-enhancing techniques.

A High Speed FPGA-based Pseudo-random Bit Sequence Generator

Qiang Zhang[1], **Wei Wang**[1], **Ling Chen**[1], **Tian Dong**[1], **and Nanguang Chen**[1, 2]

[1]Institute of Engineering (Hangzhou), College of Engineering, Peking University, 311121, China
[2]Department of Biomedical Engineering, National University of Singapore, 117576, Singapore

Abstract— We report a novel FPGA based approach to generate ahigh speed pseudo-random bit sequence (PRBS). This sequence is to be used as the modulation signal for the light source in our diffuse optical tomography system. In this system, a pattern 10, 2.5 Gpbs PRBS is required.

An evaluation board (SP605, from Xilinx) has been exploited to develop this generator. In this approach, a 10-stage linear-feedback shift register (LFSR) is set to its initial state (the first 10 bits for PRBS). Abiding by a certain polynomial (e.g., $X^7 + X^{10} + 1$), the subsequent 20 bits are calculated with a combinational logic, within one internal clock cycle. The serializer/deserializer (SerDes) on board then serialize these 20 parallel bits and output to I/O. Thus, to generate a PRBS with data rate of 2.5 Gbps, a 125 MHz (2.5 GHz/20) internal clock frequency will be sufficient. The 10–90% rise time has been measured to be 200 ps, which meets our bandwidth requirement.

Compared to the commercial PRBS generator (TG2P1A, from Centellax) used in our previous system, this approach provides slightly compromised performance, but is much less expensive (less than 500$ vs more than 10000$) and programmable in terms of pattern, polynomial and temporal shift. Compared to the conventional LFSR approach utilizing the sequential logic to output 1 bit per clock cycle, our approach can achieve much higher bit rate given a low clock frequency ($20X$ of clock).

The Influence of Tissue-mimic Outer Layer on Diffuse Optical Imaging of Hemisphere

Ling Chen[1], **Tian Dong**[1], **Qiang Zhang**[1], **Wei Wang**[1], **and Nanguang Chen**[1, 2]

[1]Biomedical Instruments Lab, Institute of Engineering (Hangzhou)
College of Engineering, Peking University, China
[2]Department of Bioengineering, National University of Singapore, Singapore

Abstract— In the early application of diffuse optical breast imaging, hand held planar imaging probe that enabled partial imaging was used. The problem with such probe design was that it introduced many instabilities during scan, such as the vibration of the operator's hand, the deformation of the breast, the mismatch between the imaging geometry and the actual breast shape. In recent developments, the concept of whole breast imaging was receiving constant attentions. Some groups have proposed non-contact imager with the aid of 3D breast surface reconstruction. Such methods require heavy computation in which accurate reconstruction of the breast surface is critical to the imaging accuracy and is intractable. Philips Research have proposed imaging cup associated with liquid infusion. This design reduced the complexity of geometry modelling by replacing the modelling of the irregular breast geometry with the modelling of the imaging cup. However, their focuses were in fluorescence imaging with the contrast agent to enhance the signal contrast, and the influence of the liquid infusion on imaging results was negligible. The influence of the liquid infusion on the imaging accuracy in diffuse optical imaging using an imaging cup, where the setting is sensitive, has yet to be investigated. In addition, issues towards clinical application of whole breast imaging like dimensions of imaging cup also need to be addressed. We proposed a hemisphere imaging cup to image the breast in a hemisphere geometry with the aid of a lipofundin tissue-mimic outer layer. The influence of the tissue-mimic outer layer on the reconstruction accuracy was studied through simulation, including the influence of the mean thickness of the layer and the influence of the mismatch of optical properties between the layer and the breast. Appropriate range of layer thickness in regard to different breast size was proposed for better reconstruction accuracy, along with the recommendation of a set of imaging cup dimensions for clinical application.

Optical Investigation of Nd^{3+}-sensitized Upconversion Nanoparticles for Damage-free *in vivo* Deep Imaging and *in vitro* Microscopy

Yuxiang Zhao and Qiuqiang Zhan*
Centre for Optical and Electromagnetic Research, South China Academy of Advanced Optoelectronics
South China Normal University (SCNU), Guangzhou 510006, China

Abstract— Upconversion nanoparticles (UCNPs) have been presented as the powerful nanoprobes in the field of biophotonics because of its unique optical properties, such as no photobleaching, no blinking, sharp emission band, large anti-Stokes shift, low cytotoxicity, deep detection ability and high spatial resolution [1]. However, traditional 975 nm excitation of Yb^{3+}-sensitized UCNPs have been proved to bring in the overheating effect in biological samples [2] which is a huge barrier to the development of high efficient UCNPs-based biomedical application. In the past year, Nd^{3+}-sensitized UCNPs have been demonstrated as a potential candidate to replace traditional Yb^{3+}-sensitized ones due to the minimized heating effect of 795 nm excitation [3] which has much lower absorption compared with 975 nm excitation However, since it's not easy to evaluate the damage inside tissue in the *in vivo* experiments, there is no quantitative damage study of these two exciting wavelengths with exactly optical parameter setting In recent months, some peer groups have experimentally demonstrated the synthesis and potential applications of this novel Nd^{3+}-sensitized UCNPs [4–6]. However, there is no theoretical investigation of the 795 nm excitation process For example, the deep imaging mechanism of 795 nm excited Nd^{3+}-sensitized UCNPs is not yet clear; The visible emission of 795 nm excited UCNPs has large scattering and absorption in the tissue and will decrease the imaging depth to some extent; The energy transfer efficiency from Nd^{3+} to Yb^{3+} has strong correlation with the deep imaging ability In this work, we for the first time optically modelled for Nd^{3+}-sensitized UCNPs-based bio-applications. The simulation results show the damage-free imaging of 795 nm excitation compared with 975 nm excitation Meanwhile the energy transfer efficiency from Nd^{3+} to Yb^{3+} is discussed to study its impact on the deep imaging ability of 795 nm excitation This work will give a new sight of developing UCNPs-based biomedical applications.

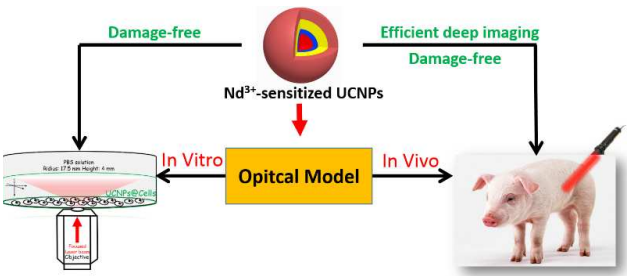

REFERENCES

1. Xu, C. T., Q. Zhan, H. Liu, G. Somesfalean, J. Qian, S. He, et al., "Upconverting nanoparticles for pre-clinical diffuse optical imaging, microscopy and sensing: Current trends and future challenges," *Laser & Photonics Reviews*, Vol. 7, 663–697, 2013.
2. Zhan, Q., J. Qian, H. Liang, G. Somesfalean, D. Wang, S. He, et al., "Using 915 nm laser excited $Tm^{3+}/Er^{3+}/Ho^{3+}$-doped NaYbF4 upconversion nanoparticles for in vitro and deeper in vivo bioimaging without overheating irradiation," *ACS Nano*, Vol. 5, 3744–3757, 2011.
3. Wang, Y.-F., G.-Y. Liu, L.-D. Sun, J.-W. Xiao, J.-C. Zhou, and C.-H. Yan, "Nd^{3+}-sensitized upconversion nanophosphors: Efficient in vivo bioimaging probes with minimized heating effect," *ACS Nano*, Vol. 7, 7200–7206, August 27, 2013.
4. Li, X., R. Wang, F. Zhang, L. Zhou, D. Shen, C. Yao, et al., "Nd^{3+} sensitized up/down converting dual-mode nanomaterials for efficient in-vitro and in-vivo bioimaging excited at 800 nm," Scientific Reports, Vol. 3, 2013.

*Corresponding author: Qiuqiang Zhan (qiuqiang.zhan@coer-scnu.org).

5. Shen, J., G. Chen, A. M. Vu, W. Fan, O. S. Bilsel, C. C. Chang, et al., "Engineering the upconversion nanoparticle excitation wavelength: Cascade sensitization of tridoped upconversion colloidal nanoparticles at 800 nm," *Advanced Optical Materials*, Vol. 1, 644–650, 2013.
6. Xie, X., N. Gao, R. Deng, Q. Sun, Q.-H. Xu, and X. Liu, "Mechanistic investigation of photon upconversion in Nd^{3+}-sensitized core-shell nanoparticles," *Journal of the American Chemical Society*, Vol. 135, 12608–12611, 2013.

Tradeoff Study of Microwave Imaging Based on Frequency Considerations

Dau-Chyrh Chang[1], **Yau-Jyun Tsai**[1], **Chih-Hung Lee**[2, 3], **and Chang-Hsuan Kao**[1]

[1]Oriental Institute of Technology, CRC, OIT, Taiwan
[2]Yuan Ze University, Taiwan
[3]Electronics Testing Center, Taiwan

Abstract— The microwave image can be generated by the radar arrays are appeared in many literatures. The quality of image includes the resolution of pixel and contrast of the pixel. The better the quality of image is with higher the resolution of pixel and larger the contrast. The contrast depends on the signal to noise ratio of the radar receiver. The resolution of pixel depends on the radar frequency. The higher the frequency the better the resolution of pixel will be.

Figure 1 is interesting image area with the geometry of the image area 10 cm by 10 cm and the desired resolution of pixel is 2 mm by 2 mm. The uniform rectangular target pixels with size 2 cm by 2 cm inside the interesting image area will be analyzed. There are 128 circular monostatic radar arrays. The radius of radar arrays is 10 cm. The radar images will be generated by the discrete radar frequencies. Figure 2 is the radar image generated by frequency at 50 GHz. The uniform rectangular target is distorted as in discrete points. Figure 3 is the radar image generated by frequency at 70 GHz. The uniform rectangular shape of target is also distorted. The final image as shown in Figure 4 is the scalar summation of contrast at each pixel for nine frequencies uniform distributed in 40 GHz∼80 GHz.

In this paper, the formulation of radar image, quality of radar image with various frequencies and number of circular radars will be discussed. In order to verify the simulation results, the results of measurement will also be compared at the final paper.

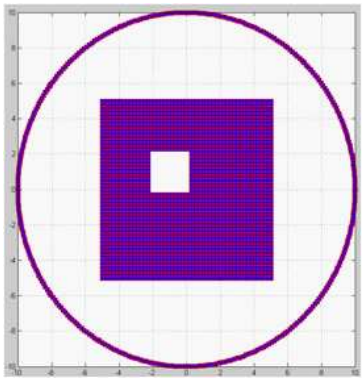

Figure 1: Geometry of image model.

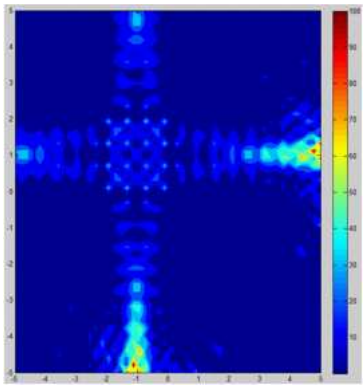

Figure 2: Radar image by 50 GHz.

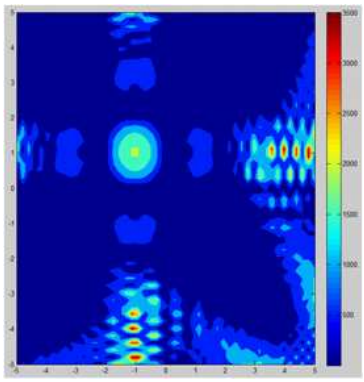

Figure 3: Radar image by 70 GHz.

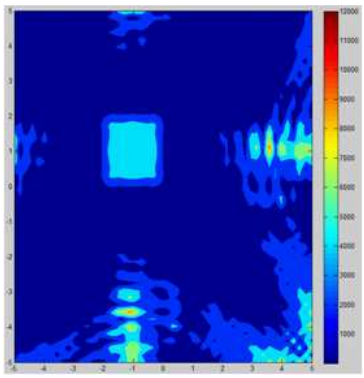

Figure 4: Image by 9 discrete frequencies.

Plasmonics Based Localization Microscopy: Axially Super-resolved Intracellular Imaging Based on Extraordinary Light Transmission

Wonju Lee[1], **Taehwang Son**[1], **Jong-Ryul Choi**[2], **Kyujung Kim**[3], **Youngjin Oh**[1], **and Donghyun Kim**[1]

[1]School of Electrical and Electronic Engineering, Yonsei University, Republic of Korea
[2]Medical Device Development Center
Daegu-Gyeongbuk Medical Innovation Foundation, Republic of Korea
[3]Department of Nanofusion Engineering, Pusan National University, Republic of Korea

Abstract— In recent years, super-resolution imaging techniques have been developed for bimolecular observations in live cells. Many approaches have been investigated to obtain sub-diffraction-limited resolution, ranging from total internal reflection fluorescence (TIRF) to stimulated emission depletion, structured light illumination, and single molecule localization. Plasmonic localization based on subwavelength metallic nanostructures was also utilized to acquire super-resolved images of cells and biomolecules. Most of these imaging techniques have been effective to enhancing resolution in the lateral domain rather than in the axial direction. Relatively few approaches have been attempted to improve axial imaging resolution and to implement axial sectioning. While fluorescence excitation can be localized within evanescent waves under total internal reflection, super-resolved depth imaging is still limited.

In this presentation, we explore super-resolution imaging for axial sectioning of intracellular protein distribution in live cells using plasmonic nanoaperture arrays. The amplitude of transmitted light through subwavelength nanoholes can be dramatically amplified due to plasmon coupling effects, which is known as extraordinary optical transmission (EOT). For EOT-based axial imaging (EOT-AIM), we used linear nanoaperture arrays consisting of nanoapertures of different size. Each nanoaperture induces light transmission by a different penetration depth. Super-resolved depth information was obtained by taking differences in fluorescence excited between neighboring nanoapertures in the arrays. The axial resolution of EOT-AIM was as small as 20 nm in a 500-nm depth range. The axial distribution of ganglioside in mouse macrophage cells were successfully measured using FITC-labeled cholera toxin subunit B. The results confirmed the feasibility of EOM-AIM for axial super-resolution microscopy.

Terahertz Spectroscopic Investigation of Substrate Materials for Biological Application in the Frequency Range of 1–15 THz

Rui Zhang[1], **Ruixue Wang**[2], **Liangliang Zhang**[3], **Jue Zhang**[1, 2], **Cunlin Zhang**[3], **and Jing Fang**[1, 2]

[1]College of Engineering, Peking University, China
[2]Academy for Advanced Interdisciplinary Studies, Peking University, China
[3]Department of Physics, Capital Normal University, China

Abstract— As emerging modalities, terahertz time-domain spectroscopy and imaging have been widely applied to investigate the optical properties of different biological tissues. The substrate materials are always needed for the biological spectroscopic measurements. They should have small absorption coefficients and almost constant refractive indices at terahertz frequency range. For example, in the terahertz reflection geometry, the biological sample is usually placed on a window made of quartz [1]. In the terahertz transmission geometry, the sample holder usually consists of two parallel windows made of quartz or high-density polyethylene (HDPE) [2]. Teflon has the similar absorption coefficient and refractive index to the HDPE in the region of 0.1–3 THz [3]. Paraffin-embedded tissue is a traditional sample modality for biomedical research and has been adopted in the terahertz spectroscopic study of biological tissues [4].

However, the former researches concentrated on the terahertz frequency between 0.1 THz to 3 THz on account of being constrained by the generation and detection technique. The spectroscopy contrast of different biological tissues is low. It is extremely essential to investigate the biological characterizations on the ultra-broadband terahertz frequency range for more spectroscopic information. The terahertz optical properties of the substrate materials in the range of 3–10 THz are still missing. It is fairly necessary to determine whether they can be used as sample substrates in the broadband terahertz system for biological spectroscopy measurement.

In this study, we report on the optical parameters, represented by the refractive index and absorption coefficient, for the typical substrate materials (quartz, HDPE, teflon and paraffin) of biological terahertz spectroscopic measurement. The optical parameters are determined for frequencies spanning from 1 to 15 THz. The terahertz air-biased-coherent-detection (ABCD) system is utilized to cover the broad spectrum.

The results show that HDPE and paraffin have small absorption coefficients under 15 cm^{-1} in the terahertz frequency range of 1–15 THz. In addition, the absorption coefficient of HDPE is lower than that of paraffin, especially in the higher terahertz frequency. The teflon and quartz are almost transparent below 3 THz while exhibit strong absorption with the frequency increase. The results also demonstrate that HDPE and paraffin possess almost constant refractive indices in the terahertz frequency extending from 1 THz to 15 THz.

The nearly constant refractive indices and very small absorption coefficients of HDPE and paraffin mean they can be used as high-quality substrate materials in the ultra-broadband terahertz system. They are good candidates of sample windows for biomedical spectroscopic measurements using broadband terahertz experimental setup. The results also demonstrate that paraffin-embedded tissues can be adopted as one sample modality in the broadband biological terahertz spectroscopy. However, teflon and quartz have strong absorption in the terahertz frequency range over about 5 THz implies that they can not be considered as substrate materials in broadband terahertz spectrometer. The results obtained in this study lay a good foundation for the potential terahertz broadband spectroscopic study of biological tissues.

REFERENCES

1. Huang, S. Y., et al., *Phys. Med. Biol.*, Vol. 54, No. 1, 149–160, 2009.
2. Png, G. M., et al., *Phys. Med. Biol.*, Vol. 53, No. 13, 3501–3517, 2008.
3. Jin, Y.-S., et al., *J. Korean Phy. Soc.*, Vol. 49, No. 2, 513–517, 2006.
4. Nakajima, S., et al., *Appl. Phys. Lett.*, Vol. 90, 041102, 2007.

Development of Ion Measurement Method by a Terahertz Chemical Microscopy

Y. Okawa, K. Akimune, K. Sakai, T. Kiwa, and K. Tsukada
Okayama University, Japan

Abstract— Measurements of the distribution of the ion concentration are important in various fields such as studies of high-performance batteries and biological diagnosis. Our group has been developed a terahertz chemical microscopy (TCM) in order to visualize the chemical potential changes in the water solution.

TCM can detect the distribution of the change in the amplitude of radiated THz wave from a THz sensing plate by irradiating the sensing plate by a femtosecond laser. The amplitude of radiated THz wave is proportional to the electric or chemical potential shifts caused by chemical reactions in the solutions on the THz sensing plate. In this work, the ion selective membranes were immobilized on the sensing plate. When the concentration of the ions in the solutions is changed, the electric potential at the surface of the ion selective membrane is changed. As a result, the amplitude of THz which can be related to the concentration of the ions also changes.

As the demonstration of ion detections, the solutions of sodium ions with the concentration of between 10^{-4} M and 10^{-1} M was dropped on the sensing plate. The THz amplitude changes proportional to the concentration of sodium ions were successfully observed. We also visualize the distribution of the electric potential on the ion selective membranes by scanning the femtosecond laser.

Session 4P5
SC2: Microwave Metamaterials 2

Dual-band Slot-FSS for Improving the Transmission of Wireless Communication Signals through Energy-saving Glass

Hsing-Yi Chen and Tsung-Han Lin
Department of Communications Engineering, Yuan Ze University
135, Yuan-Tung Road, Nei-Li, Chung-Li, Taoyuan Shian 32003, Taiwan

Abstract— Energy-saving glass has been widely used in modern building due to its low-emissivity. This energy-saving glass is manufactured by coating a metallic oxide layer on one side of ordinary float glass. The metallic oxide layer can provide good thermal isolation for blocking energy flowing in or out the building for longer period of time and therefore saving the cost of heat in winter and the cost of cooling in summer. However, the coating layer on glass also attenuates many useful wireless communication signals through it. In order to improve signal transmission, aperture types of frequency selective surfaces may be used to provide a better signal transmission through energy-saving glass while without degrading thermal isolation capability. In this paper, A dual-band slot frequency selective (FSS) consisting of regular Jerusalem-cross elements was proposed to provide a better signal transmission through energy-saving glass at 2.45 and 5.8 GHz for Bluetooth and WLAN applications, respectively. Return losses of the energy-saving glass with the dual-band slot FSS are improved by a factor of 10 dB and 3 dB at 2.45 and 5.8 GHz, respectively. While transmission of the energy-saving glass with the dual-band slot FSS are improved by a factor of 50 dB and 40 dB at 2.45 and 5.8 GHz, respectively. The ratio of area occupied by the dual-band slot FSS to area of the energy-saving glass is 35.6%, which may slightly degrade thermal isolation capability but can greatly improve the communication quality for wireless communications. The structure of the dual-band slot FSS consisting of Jerusalem cross elements is easily fabricated and has a beautiful pattern on building windows.

Minifying and Magnifying Scattering Coefficients by a Metasurface

Fan Yang[1], **Zhong Lei Mei**[1], **and Tie Jun Cui**[2]

[1]School of Information Science and Engineering, Lanzhou University, Lanzhou 730000, China
[2]State Key Laboratory of Millimetre Waves, School of Information Science and Engineering
Southeast University, Nanjing 210096, China

Abstract— We propose that the metasurface can be used for minifying and magnifying scattering coefficients by adjusting the surface impedance. Some previous works have focused on cloaking a medium or metal by an impedance surface, which is realized by scattering cancellation. In view of this, we replace the medium or metal to a source, i.e., to cloak a source. We have analyzed the cloaking of monopole and dipole theoretically, and then the method has been promoted to multipolar situation. Since a source can be expanded to multipolar form, so this method is not only limited to multipolar system, but suitable to a random source. Our simulation results confirm the argument. The weakness of the proposal is that one needs the prior information from the probing source.

The above mentioned metasurface takes advantage of minifying scattering coefficients. And we have also studied the magnification of scattering coefficients by changing a specific order to infinite, while other scattering coefficients are finite. By setting the surface impendence to a value that will lead the zero order scattering coefficient to infinite, the total field will behave as a monopole radiation for the fact that other order fields become incomparable to the magnified field. Similarly, when another order of scattering coefficient is magnified, the total field will behave as that order of scattering field. This property has great potential application in the controlling of antenna radiation. Also, the radiation of an antenna can be realized by easily changing the surface impedance rather than the geometrical shape.

Study on the Scattering Properties of an Artificial Electromagnetic Hard Surface

Xingxing Huang, Peiheng Zhou, Haiyan Chen, Mangui Han, and Longjiang Deng
National Engineering Research Center of Electromagnetic Radiation Control Materials
State Key Laboratory of Electronic Thin Film and Integrated Devices
University of Electronic Science and Technology of China, Chengdu 610054, China

Abstract— An artificial electromagnetic hard surface realized by the longitudinally oriented metal strips loaded on a grounded dielectric substrate is proposed. Electromagnetic scattering properties of the proposed structure are analyzed for both transverse magnetic (TM) polarization and transverse electric (TE) polarization, where *TM* polarization is defined by the polarized direction of the incidence electric field E parallel with the metal strips. The scattering properties of a high impedance surface (HIS) with similar structure are also proposed for comparison. In the case of the HIS, radar cross section (RCS) reduction at broad angles can be obtained for *TE* polarization, but get worse for *TM* polarization. While in the case of the hard surface, RCS reduction at the whole considered angles can be obtained for *TE* polarization, and almost invariable for *TM* polarization, which has the potential advantages in antenna design and stealth technique. To explain this phenomenon, the phase properties and energy distribution of the considered structure are also analyzed.

A Realization Compact Pseudo Chebyshev Low Pass Filters for UHF Band Using RF MEMS Technology

H. F. Liew[1], **S. I. S. Hassan**[2], **M. F. Malek**[2], **Y. Wahab**[1], **M. M. Nurhakimah**[2], **H. Nornikman**[3], **M. Mazlee**[1], **M. Ghauth Sazali**[1], **and S. S. Nadia**[1]

[1]School of Microelectronic, University Malaysia Perlis, Perlis, Malaysia
[2]School of Electrical System, University Malaysia Perlis, Perlis, Malaysia
[3]Faculty of Electronics and Computer Engineering, University Teknikal Malaysia, Melaka, Malaysia

Abstract— This paper describes the development compact Chebyshev microstrip filter is fabricated by using RF MEMS technology, which laser micromachining techniques are selected. The 5th order Chebyshev low pass filter operating within UHF range have been designed, simulated, fabricated, tested, investigated and implemented on silicon substrate with a band pass ripple of 0.01 dB. The design of lumped element and microstrip circuit filters are simulated and implemented by using Advanced Design System. The simulation and measurement results of microstrip low pass filter have been compared and excellent agreement is observed. Laser micromachining can lead to finer finishes, improved accuracy and less process overhead. The purpose for this work has been focus on laser micromachining into develop compact microstrip circuit. To satisfy these challenging in terms of geometry, machining accuracy, surface finish or processing speed, laser micromachining with diffraction limited beam quality offer many benefits such as small spot size, high power density, enhanced processing speeds, reduced heat affected zone for a range of micromachining applications. Laser micromachining has become a great prospective as a MEMS (micro-electro-mechanical systems) fabrication technique in ever-continuing trend of miniaturization in microelectronics, micro-optics and micromechanics for wireless communication system.

A Novel Plasmonic Waveguide Compatible with Conventional Transmision Line

Shuo Liu, Hao Chi Zhang, and Tie Jun Cui
State Key Laboratory of Millimeter Waves, Southeast University, Nanjing 210096, China

Abstract— In the past a few years, geometry-controlled surface plasmon polaritons (SPPs) at microwave or terahertz regime, namely spoof SPPs, have been experimentally realized by drilling holes or cutting grooves on metal surfaces. The recently proposed conformal surface plasmons (CSPs), made of single comb-shaped metal strip printed on a flexible substrate, represents one of the most potential candidates for the application of spoof-SPPs-based circuits operating from microwave to terahertz spectra. However, it is inherently incompatible with the conventional planar waveguide since it only contains one conductor. To solve the problem, we present a novel plasmonic waveguide comprising two comb-shaped metal strips on each side of a substrate with mirror symmetry. This particular design exhibits significant advantages over the previous CSPs, such as the enhanced subwavelength effect and improved field confinement. Most importantly, this two-conductor plasmonic waveguide allows the direct application of most available circuit devices and techniques to the design of spoof-SPPs-based circuits. Both numerical simulations and experiments demonstrate that spoof SPPs are able to efficiently propagate on the plasmonic waveguide from DC to its cutoff frequency with low loss. To feed the plasmonic waveguide with a microstrip line of 50 ohm impedance efficiently, we also propose a novel transition section. This efficient and compact converting device is implemented by momentum and impedance matching between plasmonic and conventional waveguides. Note that the transmission characteristic of the transition section can be optimized according to different applications by simply adjusting its critical geometrical parameters. The features such as highly field localization, high efficiency, broadband operation and easy fabrication of the proposed plasmonic waveguide may advance a significant step toward the combination of spoof-SPP-based circuits with conventional microwave circuits.

Macroscopic Model for Metamaterials

Kirti Inamdar[1], **Y. P. Kosta**[2], **and S. Patnaik**[3]

[1]ECED, SVNIT, Surat, Gujarat, India
[2]MEFGI, Rajkot, Gujarat, India
[3]St. Xavier's Institute of Engineering, Mumbai, India

Abstract— Analysis of any material or medium can be performed either at microscopic level or at macroscopic level. At microscopic level, the interaction of the EM waves with the medium are analyzed explicitly. But at macroscopic levels, only the average bulk effects are considered. The basic properties of any material are permittivity (ε), permeability (μ) and chirality. They all are macroscopic concepts emanating from microscopic electrical response of the matter. This paper presents the macroscopic modeling of metamaterials with the help of which the characteristic material parameter ε and μ are derived. When a matter is electrically excited, the response of it gets polarized. This polarization is the addition of all types of polarizations such as electric, magnetic, atomic, ionic, directional and interfacial polarizations. All these add together to give the macroscopic material properties. MM are analyzed by considering the polarizability of the artificial (introduced/embedded) molecules in isolation. So it is required to apply electromagnetic mixing theory rules that will help to develop and estimate the bulk properties of such artificially created materials. One such theoretical development has been done by A. Shivola and has been followed by the author for the formulation of MM theory. In the history of metamaterials, many famous researchers have given their contribution by proposing several shapes for metamaterials such as Square Split Ring resonator (SRR) with metallic rods, Circular SRR with metallic rods, cross shaped unit cells etc. This paper presents a new shape inspired by Jerusalem cross shape namely 'Criss-Cross' shape. Its effective medium parameters have been derived and their negative behavior has been analyzed by using the theoretical formulation presented in the paper.

Miniaturized Microscript Bandpass Filter Based on the Twist Split Ring Resonators

Jian Li, **Guangjun Wen**, **Yongjun Huang**, **Kaimin Wu**, **and Weijian Chen**
Centre for RFIC and System Technology, School of Communication and Information Engineering
University of Electronic Science and Technology of China, Chengdu, China

Abstract— In this paper, a novel design for miniaturized microscript bandpass filter based on the twist split ring resonators (TSRRs) is analyzed systematically. The proposed TSRRs printed on the conventional dielectric substrate with full size ground plane exhibit two resonance states separated each others. And the two resonance frequencies can be tuned by changing the distance between the two single split ring resonators. We first discuss the resonance characteristics and optimize the designed filter with finite element method based simulator (Ansoft HFSS V14). Then the designed microscript bandpass filters with different distances between the two single split ring resonators are fabricated by standard printed circuit board techniques. Finally, the proposed filters are numerically and experimentally discussed in details, including the passband, out-of-band suppression, and higher order properties. Both results show that the proposed filter exhibits a compact size and well passband characteristics, which can be used in radio frequency/microwave integrated circuits.

Improvement of Oblique Incidence Performance for a Microwave Absorber Based on Magnetic Polymer Composites

Linbo Zhang, Nan Zhang, Peiheng Zhou, Yangqiu Xu, Haiyan Chen, Jianliang Xie, and Longjiang Deng
National Engineering Research Center of Electromagnetic Radiation Control Materials
State Key Laboratory of Electronic Thin Film and Integrated Devices
University of Electronic Science and Technology of China, Chengdu 610054, China

Abstract— In recent years, there has been an increasing interest in the application of metamaterial absorbers. Most investigations of absorbers like Jaumann and circuit analog absorbers consider normal angle of incidence only. There are a few of published information on oblique incidence performance of absorbers. The demand of good oblique incidence performance for various kinds of absorbers with emphasis on the applications in solving electromagnetic pollution problems such as electromagnetic interference (EMI) and electromagnetic compatibility (EMC) has been an increasing concern. Absorbers with good performance at oblique incidence for both transverse electric (TE) and transverse magnetic (TM) polarizations are badly needed.

This paper presents a microwave absorber combing together the frequency selective surfaces (FSSs) and magnetic absorbing sheet for stable absorption under both TE and TM polarizations.The proposed absorber is constructed of magnetic absorbing substrate embedded with a periodic array of cross pattern composing a series of circular-metal-disks, and a bottom metal plane. The absorption characteristics of the magnetic absorbing substrate under both TE and TM polarizations are tuned and improved by introducing the circular-metal-disks. After optimizing the dimensions of the circular-metal-disks, the absorber with a thickness of 2.4 mm achieves a reflection coefficient less than -10 dB from 4.8 GHz to 11.0 GHz with a stable frequency response up to 30° for both polarizations. Meanwhile, the absorber has a wide bandwidth of 10.8 GHz with the incidence angle from 45° to 60° under TM polarization. The study of the impedance characteristic and the current indicates that the improvement of the absorption characteristics is due to both the electric resonance and magnetic resonance.

A Novel Absorptive Frequency Selective Surface with Miniaturized Element

Qiang Chen, Liang Chen, and Yunqi Fu
College of Electronic Science and Engineering, National University of Defense Technology, China

Abstract— In recent years, a concept of an absorptive frequency selective surface (AFSS) has been put forward, which permits the transmission of signals at a given frequency band, while absorbs the electromagnetic waves above the transmission band. An AFSS design presented in [1] has a transmissive property at 1 GHz and a wideband absorptive property over 3–9 GHz. The AFSS is composed of a layer of resistive surface placed above a metallic band-pass FSS. Because the periodicity of the resistive surface (36 mm) is over one wavelength at the highest frequency of the absorbing band (9 GHz), high-order resonance and backward grating globes will appear in the absorbing band when illuminated by oblique incident wave. Therefore an attempt has been made to reduce the size of the AFSS element in this paper. An incurved square loop inserted with lumped resistors is exploited as the element of the resistive surface, with the unit size of 10 mm, just $1/3\lambda$ at 9 GHz; and the element of the band-pass FSS is composed of two layer of metallic patch, whose unit size is miniaturized to be 20 mm, $1/15\lambda$ of the transmissive frequency (1 GHz), by increasing the distributed capacitance by enlarging the coupling area. The similar transmissive/ absorptive property during the band $3 \sim 9$ GHz and at least 10 dB bi-static radar cross-section (RCS) reduction have been observed from simulated results. Besides, the backward grating globes over absorbing band are totally eliminated. Finally, the principle to select the dimension of the resistive elements of AFSS structures for avoiding backward grating globes in absorbing band has been discussed.

REFERENCES

1. Liu, L. G., P. F. Guo, J. J. Huang, W. W. Wu, J. J. Mo, Y. Q. Fu, and N. C. Yuan, "Design of an invisible radome by metamaterial absorbers loaded with lumped resistors," *Chin. Phys. Lett.*, Vol. 29, 2012.

Metamaterial Based Patch Antenna with Broad Bandwidth and Simple Structures

X. S. Li[1], **F. M. Lin**[2], **and D. L. Wu**[2]

[1]School of Automation, Guangdong University of Technology, China
[2]School of Physics and Optoelectronic Engineering
Guangdong University of Technology, China

Abstract— A patch antenna based on metamaterials of composite split-ring-resonators (CSRRs) and strip gaps is presented. The antenna is constructed by using CSRR structures in forms of circular rings on the patch and employing strip gaps on the ground plane. The signal is fed by a common microstrip line that connects the patch and the input port. The antenna is based on a simple structure of an only one-layer substrate. Rogers RO4350 ($\varepsilon_r = 3.66$) is preferred as the dielectric material of the substrate. The antenna has a compact footprint that is only $0.408\lambda_0 \times 0.357\lambda_0$ at the lowest operating frequency of 1.7 GHz. The antenna could operate over two bands that are from 1.70 GHz to 2.98 GHz and from 3.99 GHz to 5.34 GHz. The CSRR and strip gaps are combined with the patch and ground to broaden its operating frequencies as well as to enhance its radiation performance via their coupling with the substrate in a different way. The measured impedance of the antenna shows a smooth variation in the vicinity of 50 Ω over the operating bands. This smooth variation enables the antenna to have broad bandwidth. Additionally, its radiation performance is kept favorable with a peak gain of 6.04 dB. The performances of the antenna were characterized computationally and verified experimentally. Good agreements between the simulations and measurements were observed convincing that the antenna could operate over wide bandwidths and radiate effectively with its simple structure and compact size. The presented design is favorable for its broadband as well as good radiation performance with a simple structure that is comprised of only one layer substrate. The antenna is promising for broadband applications that require the operating bands of WCDMA (1920–2170 MHz), WiMAX (2500–2690 MHz), Bluetooth (2400–2480 MHz) or Wibro (2300–2390 MHz).

Session 4P6a
FocusSession.SC3: Laser Spectroscopy for Sensing and Environmental Monitoring 2

Dual Frequency Comb Spectroscopy for Accurate and Precise Carbon Monitoring over Multi-kilometer Paths

Ian Coddington
Quantum Electronics and Photonics, NIST, USA

Abstract— Accurate sensing of atmospheric trace gases is a challenging problem. Dual frequency-comb spectroscopy is ideally suited to this challenge; it combines broadband spectral coverage for multi-species detection with a diffraction-limited laser output for high sensitivity over long air paths. Equally important, its negligible instrument line shape provides high accuracy spectra that can be reliably cross-compared over different systems, times, and locations. We demonstrate open-air-path dual-comb spectroscopy across a 2-km turbulent path covering $267\,\mathrm{cm}^{-1}$ (8 THz) of bandwidth near $6100\,\mathrm{cm}^{-1}$ ($1.64\,\mu\mathrm{m}$) with a point spacing of $0.0033\,\mathrm{cm}^{-1}$ (100 MHz) and resolution of $\sim 4\times10^{-8}\,\mathrm{cm}^{-1}$ (kHz). Fits retrieved the air temperature, CO_2, CH_4, H_2O, HDO, and $^{13}CO_2$ concentrations, as well as time-resolved dry-mole fraction of CO_2 and CH_4 at $\sim 0.2\%$ stability in five minutes. Future system should also be able to operate in the 2 micron and 0.76 micron spectral regions.

Generation of Impulsive Raman Scattering with an Intense Free-space Air Laser

J. Ni[1], **W. Chu**[1], **B. Zeng**[1], **J. Yao**[1], **H. Xu**[2], **and Y. Cheng**[1]

[1]State Key Laboratory of High Field Laser Physics
Shanghai Institute of Optics and Fine Mechanics, Chinese Academy of Sciences
P. O. Box 800-211, Shanghai 201800, China
[2]State Key Laboratory on Integrated Optoelectronics
College of Electronic Science and Engineering, Jilin University, Changchun 130012, China

Abstract— Recently, we have shown that during femtosecond laser filamentation, stimulated seed amplification at characteristic transition wavelengths of ionized molecules would occur, leading to generation of free-space laser in remote air. Generally, the intensity of such air laser can be several orders of magnitude higher than that of spontaneous fluorescence emission, depending on the conditions of pump laser sources and focal systems [1]. The intense air laser opens many possibilities for atmospheric remote sensing application. In this talk, we show that the air laser can serve as a coherent, narrow-bandwidth pumping source for in situ generation of an impulsive Raman signal, making it possible to perform remote sensing based on Raman fingerprinting [2]. In our scheme, intense air lasing at a wavelength of ∼428 nm is generated in nitrogen ion during femtosecond laser filamentation with the self-broadened supercontinuum light as a seed. S-branch ($J \rightarrow J+2$) rotational Raman lines $S(6)$, $S(8)$, $S(10)$, $S(12)$ and $S(14)$ of neutral nitrogen molecules can be clearly identified from the spectrum.

Compared to the previously reported impulsive Raman scattering scheme, our scheme provides two unique advantages. First, the femtosecond laser and the air laser pulses naturally overlap in time and space, since the latter is generated in the filament induced by the femtosecond laser. Second, the femtosecond laser-filamentation-process offers the potential to realize the Raman fingerprinting in a remote distance. Both these advantages are highly desirable for atmospheric remote sensing.

REFERENCES

1. Yao, J., B. Zeng, H. Xu, et al., "High-brightness switchable multiwavelength remote laser in air," *Phys. Rev. A*, Vol. 84, 051802(R), 2011.
2. Ni, J., W. Chu, H. Zhang, et al., "Impulsive rotational Raman scattering of N_2 by a remote 'air laser' in femtosecond laser filament," *Opt. Lett.*, Vol. 39, 2250, 2014.

High-resolution Spectroscopy with Single-sideband Optical Modulator and Optical Frequency Comb

Tatsutoshi Shioda[1] **and Takashi Kurokawa**[2]

[1]Saitama Univerisity, 255 Shimo-Okubo, Sakura-ku, Saitama city, Saitama 338-0835, Japan
[2]Tokyo University of Agriculture and Technology, 2-24-16 Naka-cho, Koganei-shi, Tokyo 184-8588, Japan

Abstract— We have proposed a 1 MHz resolution with terahertz measurement range spectroscopy using a single-sideband (SSB) optical modulator and an optical frequency comb (OFC). The OFC was generated by a waveguide-type lithium niobate modulator coated with high reflection films on the facets [1, 2]. The SSB modulator acts as an optical frequency shifter with an accuracy less than 1 MHz. The scanning range of the SSB modulator is over 10 GHz that covers a repetition rate of the OFC. Also, the SSB modulator can sweep all comb teeth frequencies lies on 4 THz frequency range at the same time by injecting the comb into the modulator, with which the 1 MHz resolution higher than the 10 GHz comb repetition rate can be realized. The comb peak intensities are detected by an optical heterodyne detection technique with a reference tunable laser light. Absolute optical frequency of the spectroscopy is guaranteed in kilohertz order by locking the frequency of the OFC. Several systems providing the same principle have been proposed and experimentally demonstrated as an absorption spectroscopy using isotope HCN gas appeared in 1.5 micron wavelength region.

REFERENCES

1. Saitoh, T., S. Mattori, S. Kinugawa, K. Miyagi, A. Taniguchi, M. Kourogi, and M. Ohtsu, *IEEE J, Lightwave Technol.*, Vol. 16, 824–832, 1998.
2. Kourogi, M., T. Enami, and M. Ohtsu, *IEEE Photon. Technol. Lett.*, Vol. 6, 214–217, 1994.

Amplitude-to-phase Noise Suppression in 100-W Infrared Optical Frequency Combs

Kangwen Yang, Wenxue Li, Xuling Shen, Jian Zhao, Dongbi Bai, and Heping Zeng
State Key Laboratory of Precision Spectroscopy, East China Normal University, Shanghai 200062, China

Abstract— 100-W infrared frequency comb was accomplished via feedback control of a Ti:Sapphire seed laser and double-clad Yb-fiber amplifier. We compared the linewidth, frequency fluctuation and Allan deviation in different output powers to characterize the performance of amplitude-to-phase noise. Recently, a feed-forward scheme employing an acousto-optic frequency shifter was demonstrated in a nonlinear polarization rotation mode-locked ytterbium-doped fiber laser to dynamically control the carrier envelope phase (CEP) drift with a small linewidth of 1.4 MHz. However, the achievable maximum average power of ultrashort laser pulses with stable CEP was inevitably limited by the damage threshold of acousto-optic crystals. As a widely used approach for CEP stabilization, the electronic feedback method has been proved to be an effective way to achieve high-power frequency comb with average power up to hundreds of watts. In this report, we demonstrated the behavior of amplitude-to-phase noise in $10 \sim 100$ W frequency comb system; the locked offset frequency reveals a linewidth of 2.25 MHz and an Allan deviation of 2.4×10^{-10} for 1 s integration times. The experimental setup consists of a Ti:sapphire femtosecond oscillator, a cascade four-stage Yb-doped fiber amplifier and electronic locking loops for repetition rate and CEP stabilization. The infrared spectral fraction with an average power of 0.2 mW from the 10-fs 79.5 MHz Ti:sapphire oscillator was amplified to 100 W. The pulse width was compressed to 490 fs with a total compressor efficiency of 60%. As for the CEP stabilization, the detected beat signal from cross-referenced f–$2f$ interferometer was sent to the locking electronics (Menlosystems GmbH, XPS 800) in which the error signal $\varepsilon = f_0 - f_{rep}/4$ was calculated and converted to a voltage signal for modulating the pump power of the oscillator. As shown in Fig.1(a), the counts of beat frequency increased from 1.86 MHz in 10 W to 3.88 MHz in 30 W and maintained around 4.30 MHz when the output power rising from 40 W to 100 W. The locked beat signal has a linewidth of 2.25 MHz, as shown in Fig. 2(b). Fig. 2(c) shows the Allan deviation derived from the RMS fluctuation data. The Allan deviation of 10-W locked offset frequency starts at 9.2×10^{-11} for 1 s integration time and drops in accordance with 1/T as expected for the phase-locked signals.

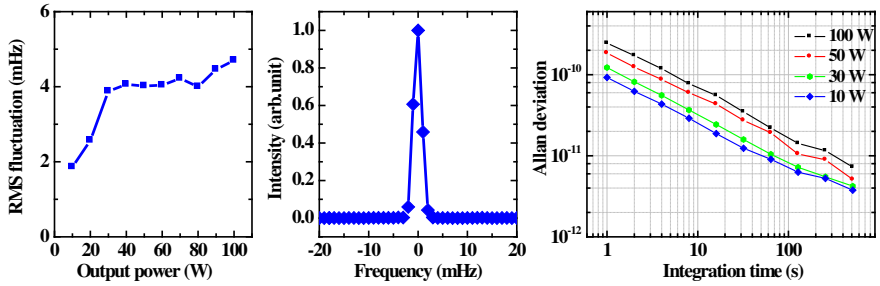

Figure 1: (a) RMS fluctuation of the instantaneous frequency, (b) linewidth, and (c) Allan deviation of the locked CEP versus output power.

Sub-harmonic Generation of Broadband Mid-infrared Frequency Combs for Molecular Spectroscopy

Alireza Marandi, **Nick C. Leindecker**, **Magnus W. Haakestad**, **Tobias P. Lamour**, **Kirk A. Ingold**, **Konstantin L. Vodopyanov**, **and Robert L. Byer**
E. L. Ginzton Laboratory, Stanford University, Stanford CA, USA

Abstract— Broad mid-IR frequency combs in the difficult-to-achieve 2–20 μm range are greatly desirable for molecular spectroscopy, where they promise to dramatically improve precision and sensitivity. Sub-harmonic generation using degenerate optical parametric oscillators has been shown to be an effective way to coherently translate the well-established near-IR frequency combs to the mid-IR spectral region.This technique benefits from simplicity of setup, low-threshold operation, high conversion efficiency, intrinsic phase locking to the pump, and broad instantaneous bandwidth.We discuss the concept of sub-harmonic generation and overview the results of several experiments on generation of frequency combs between 1.8 and 6 μm, and ultrasensitive intracavity molecular spectroscopy.

Surface Plasmon Amplification for High-performance Sensing

Jiafang Li and Zhi-Yuan Li
Institute of Physics, Chinese Academy of Sciences, Beijing 100190, China

Abstract— Plasmonic structures can impose strong enhancement and confinement on electromagnetic field, which find wide applications ranging from sensing, sub-wavelength resolution imaging, plasmonic circuitry, etc.. However, the intrinsic absorption of metal fundamentally limits the performances of these plasmonic systems [1]. Integrating metallic structures with an optical gain medium has been proposed as a feasible solution to this problem in versatile schemes. In this talk we will discuss how surface plasmon (SP) amplification can be used for high-sensitivity biochemical sensing, molecular fluorescence and Raman signal detection.

First we show that metal nanoparticles incorporated with gain medium can efficiently compensate for the absorption loss due to metal dissipation, greatly reduce the linewidth of surface plasmon resonance (SPR) peak, accumulate optical energy and amplify the amplitude of plasmonic mode, finally enhance the local field intensity to an extremely high level of single-molecule Raman detection [1]. Second, we show that GNRs with strong longitudinal SPR modes are more efficient for amplifying SPR and have unique wavelength tunability and polarization sensitivity [2], compared with other nanosystems like gold nanospheres, gold nanocubes and concentric spherical nanoparticles. Third, we show experimentally that amplification of SP can be achieved by pumping dye molecules with their fluorescence emission band matched with the SP in a simple prism setup [3, 4], or the SPR mode in GNRs [5]. Finally, we show that amplification of SPR in plasmonic nanoparticles and nanocavities can be described by an all-analytical semiclassical theory [6], which incorporates the four-level atomic rate equations in association with the classical oscillator model for active materials and Maxwell's equations for fields. As these active plasmonic systems have better plasmonic features in linewidth, dissipation, local field intensity, and light-matter interaction strength, they can find potential application in biochemical sensing, signal detection, and laser spectroscopy.

REFERENCES

1. Li, Z. Y. and Y. N. Xia, *Nano Letters*, Vol. 10, 243–249, 2010.
2. Liu, S. Y., J. F. Li, F. Zhou, L. Gan, and Z. Y. Li, *Opt. Lett.*, Vol. 36, 1296–1298, 2011.
3. Chen, Y. H., J. F. Li, M. L. Ren, B. L. Wang, J. X. Fu, S. Y. Liu, and Z. Y. Li, *Appl. Phys. Lett.*, Vol. 98, 261912, 2011.
4. Chen, Y. H., J. F. Li, M. L. Ren, and Z. Y. Li, *Small*, Vol. 8, 1355–1359, 2012.
5. Liu, S. Y., L. Huang, J. F. Li, C. Wang, Q. Li, H. X. Xu, H. L. Guo, Z. M. Meng, Z. Shi, and Z. Y. Li, *J. Phys. Chem. C*, Vol. 117, 10636–10642, 2013.
6. Zhong, X. L. and Z. Y. Li, *Phys. Rev. B*, Vol. 88, 2013.

Efficient Octave-spanning Supercontinuum Generation Driven by a Compact Yb-fiber Oscillator and All-fiber Amplifier

Qiang Hao[1], **Zhengru Guo**[1], **Qingshan Zhang**[1], **and Heping Zeng**[1, 2]

[1]Shanghai Key Laboratory of Modern Optical System
Engineering Research Center of Optical Instrument and System
Ministry of Education, School of Optical Electrical and Computer Engineering
University of Shanghai for Science and Technology, Shanghai 200093, China
[2]State Key Laboratory of Precision Spectroscopy
East China Normal University, Shanghai 200062, China

Abstract— High power femtosecond fiber lasers and their supercontinuum generation provide effective laser sources for the research of optical coherence tomography, coherent anti-Stokes Raman spectroscopy, and frequency metrology. Specifically, the production of more than one octave-spanning supercontinuum is the necessary way to obtain the f-to-2f self-referencing signal for carrier-envelope offset stabilization. We report here on octave-spanning super-continua pumped by an Yb-fiber laser system which consisted of a femtosecond master oscillator, single-mode fiber pre-amplifier, and nearly-single-mode main-amplifier. The laser oscillator relied on nonlinear polarization rotation to initiate mode-locking. Some integrated optical components, such as a wavelength division multiplexer and an optical isolator integrated with collimators, were used to make a compact size. By adjusting the intracavity grating pairs, as short as 100-fs dechirped pulses were achieved. The average power of laser pulses could be amplified to 150 mW by the pre-amplifier and further boosted to more than 5-W average power by the main-amplifier. The output pulses were compressed to less than 200-fs pulse duration by a transmission-grating pair with a resolution of 1250 line/mm and an efficiency of 60%. A 15-cm-long photonic crystal fiber (PCF) with a diameter of 3.2 μm, a numerical aperture (NA) of 0.36, and a zero-dispersion wavelength of 890 nm was used to generate supercontinuum. By coupling an average power of 150 mW into the PCF, the resulting spectrum covered more than one octave from 540 to 1470 nm. A strong Raman-soliton at 1300 nm as well as a dispersive wave at 650 nm was observed in the supercontinuum and offered two spectral peaks for f-to-2f self-referencing.

InGaAs/GaAs Quantum Well Laser with 40 nm Broad Spectrum of Emission

Huolei Wang[1], **Junping Mi**[1], **Jiaqi Wang**[1], **Weixi Chen**[3], **Jiaoqing Pan**[1], **and Ying Ding**[2]

[1]Key Laboratory of Semiconductor Materials Science
Institute of Semiconductors, Chinese Academy of Science, Beijing 100083, China
[2]School of Engineering, University of Glasgow, Glasgow G12 8LT, UK
[3]State Key Lab for Mesoscopic Physics, School of Physics, Peking University, Beijing 100871, China

Abstract— Semiconductor light sources with broadband and continuous spectrum, high-power and highly efficient are greatly attractive for many applications in sensing, spectroscopy, ultra-short pulse generation, and biomedical imaging [1]. The semiconductor broadband sources are usually included in two classes, based on the operation mode: the superluminescent diodes (SLD), working in the amplified spontaneous emission mode, and the broad inter-subband and inter-band laser diodes, working in the stimulated emission mode. However, it is difficult for SLD to achieve high power, which may limit their applications. The structure of broadband laser diodes usually includes hybrid quantum dot (QD)-quantum well (QW), chirped QD and quantum dash (Qdash). A broad stimulated emission of ~ 50 nm full width at half maximum (FWHM) from an InAs/InP Qdash layer embedded in a strained QW structure [2] and a ~ 40 nm FWHM from an InAs/GaAs QD layer sandwiched by superlattices and thick cladding layers structure [3] have been reported.

In this letter, we report the first demonstration of a 40 nm ultrabroad emission and 35 mW per-facet output power laser using an InGaAs/GaAs QWs PiNiN structure grown by Metal Organic Chemical Vapor Deposition (MOCVD). Contrary to the conventional light emitting and laser diodes, we added a GaAs junction between the two QW active regions. Our results may lead to the realization of more applications, such as mode locking with ultra-short pulse generation, biomedical imaging, broad wavelength tunability, multi-wavelengths generation etc., by using GaAs-based QW structures. In addition, our work is an advancement in achieving ultra-wide lasing bandwidth based on simplex QW active structures.

Tunable and Multi-color Optical Frequency Combs Spanning from Deep UV to Mid-IR for Spectroscopy

Jinghua Sun[1, 2], **Teresa I. Ferreiro**[2], **Richard A. McCracken**[2], **Zhaowei Zhang**[2], **and Derryck T. Reid**[2]

[1]Key Laboratory of Fundamental Physical Quantities Measurement of Ministry of Education
School of Physics, Huazhong University of Science and Technology, Wuhan, China
[2]Scottish Universities Physics Alliance (SUPA), Institute of Photonics and Quantum Sciences
School of Engineering and Physical Sciences, Heriot-Watt University, Riccarton, Edinburgh EH14 4AS, UK

Abstract— Optical frequency combs have shown their revolutionary influences not only on understanding and generating of coherent light sources, but also applications on precision metrology, spectroscopy, atto-science, and fundamental physics [1]. Femtosecond optical parametric oscillators, benefiting from the intrinsic synchronization, phase entanglement, and continuous tunability of the χ^2 nonlinear interactions, have unique advantages for generation of tunable, multi-color, broadly spanning optical frequency combs [2]. Dual optical frequency combs with different repetition rates are also demonstrated in a single OPO system [3]. These combs have important applications in researches spanning from comb FTIR for detecting molecule finger prints [4] to precision deep UV spectroscopy of atoms for testing variation of fundamental physical constants [5].

REFERENCES

1. Udem, T., R. Holzwarth, and T. W. Hänsch, "Optical frequency metrology," *Nature*, Vol. 416, 233, 2002.
2. Sun, J. H., B. J. S. Gale, and D. T. Reid, "Composite frequency comb spanning 0.4–2.4μm from a phase-controlled femtosecond Ti:sapphire laser and synchronously pumped optical parametric oscillator," *Opt. Lett.*, Vol. 32, 1414, 2007.
3. Zhang, Z., C. Gu, J. Sun, C. Wang, T. Gardiner, and D. T. Reid, "Asynchronous midinfrared optical parametric oscillator for dual-comb spectroscopy," *Opt. Lett.*, Vol. 37, 187, 2012.
4. Mandon, J., G. Guelachvili, and N. Picqué, "Fourier transform spectroscopy with a laser frequency comb," *Nature Photonics*, Vol. 3, 99, 2009.
5. Srianand, R., H. Chand, P. Petitjean, and B. Aracil, "Limits on the time variation of the electromagnetic fine-structure constant in the low energy limit from absorption lines in the spectra of distant quasars," *Phys. Rev. Lett.*, Vol. 92, 121302, 2004.

Session 4P6b
SC3: Optical Polarization and Coherence in the Near-field Range

Control of Radiative and Non-radiative Channels of Molecule Fluorescence near Hyperbolic Metamaterials

Vasily Klimov
Lebedev Physical Institute, Russian Academy of Sciences, Russia

Abstract— Now hyperbolic metamaterials (HMM) are considered as promising media to enhance decay rate of simple quantum systems [1, 2]. Due to huge local density of photon states the decay rate of molecule near surface of HMM tends to infinity as

$$\gamma^{rad} \propto \frac{2\sqrt{|\varepsilon_x|\,\varepsilon_z}}{d^3\,(1+|\varepsilon_x|\,\varepsilon_z)} \tag{1}$$

where $d \to 0$ is distance between molecule and HMM surface and $\varepsilon_x = \varepsilon_y,\ \varepsilon_z$ are real components of permittivity tensor.

However if we take into account losses in HMM it is easy to show that non-radiative (Joule) losses also tend to infinity when molecule gets closer to surface of HMM

$$\gamma^{nonrad} \sim \frac{\mathrm{Im}\varepsilon}{d^3} \tag{2}$$

In this work, we will present results of investigation of relations between (1) and (2) for different 1D materials, molecule positions and orientations of its dipole momentum, and find conditions where nonradiative rate is small in comparison with radiative one.

We have shown that neither dielectric lamellar structures nor hyperbolic metamaterials are able to provide any significant enhancement of the radiation performance in comparison with a thin single metal film or metal-dielectric pair. In particular, we have shown that upper limit of the radiative decay rate into half space where molecule is situated is limited by

$$\left(\frac{\gamma}{\gamma_0}\right)_{rad,up} \leq 2 \tag{3}$$

This fundamental restriction puts the theoretical limit to the enhancement of the radiative decay rate near any 1D material half-space, including the quantum emitters near HMMs. Analogous limitations exist also for molecule radiation in opposite half space.

We have also investigated possibility to use nanoantennas to overcome limitations (3). In particular, we have shown that bull eye type nanoantenna can enhance radiative decay rate by factor 10 without substantial increasing of losses inside hyperbolic metamaterials. From physical point of view, this nanoantenna converts Dyaconov surface waves into directed radiation in upper half space. Other possibilities of light extraction from HMM are also considered.

ACKNOWLEDGMENT

The author thanks the Russian Foundation for Basic Research (grant No. 14-02-00290), the Russian Quantum Center and the Skolkovo Foundation for financial support of this work.

REFERENCES

1. Jacob, Z., J. Y. Kim, G. V. Naik, A. Boltasseva, E. Narimanov, and V. M. Shalaev, "Engineering photonic density of states using metamaterials," Paper 696, Birck and NCN Publications, 2010, http://docs.lib.purdue.edu/nanopub/696.
2. Jacob, Z., I. I. Smolyaninov, and E. E. Narimanov, "Broadband purcell effect: Radiative decay engineering with metamaterials," *Applied Physics Letters*, Vol. 100, 181105, 2012.

Purity of Random Electromagnetic Fields

Timo Hassinen[1], **Jani Tervo**[2], **and Ari T. Friberg**[2]

[1]Royal Institute of Technology (KTH), Kista, Sweden
[2]University of Eastern Finland, Joensuu, Finland

Abstract— In optical coherence theory the concept of purity is related to the invariance of some field property under superposition. For example, the spectrum of a cross-spectrally pure field remains unaltered at certain area on the observation plane of Young's two-pinhole experiment, whereas a polarizationally pure field retains its state of polarization in Young's experiment or other diffractive device.

Cross-spectral purity was originally studied by Mandel [1] in the context of scalar coherence theory. His research was fueled by the observation that at some occasions the complex degree of coherence reduces to simpler functions. This kind of reduction property was shown to characterize cross-spectrally pure fields. Cross-spectral purity was later studied also in frequency domain by Mandel and Wolf [2]. In this presentation, we show that cross-spectral purity is a valid field property also in the context of electromagnetic coherence theory [3]. Cross-spectrally pure random electromagnetic fields are also described by a certain reduction formula, and they possess interesting physical properties. The fact that the spectrum of an electromagnetic field is described by the zeroth Stokes parameter raises the question of whether it would be possible to investigate the purity of other Stokes parameters. We show that the concept of cross-spectral purity can indeed be extended to other Stokes parameters as well [4].

Purity of polarization has been addressed before by Santarsiero [5] who studied polarization invariance in Young's experiment. He noted that, in order for a field to retain its state of polarization in the experiment, its cross-spectral density matrix has to separate into parts representing correlation and polarization. In addition, Gori et al. [6] investigated different types of completely unpolarized beams. In this presentation, we review Santarsiero's result and discuss the differences in polarization purity between time and frequency domains [7]. We show that the purity condition in frequency domain is a more general one and that the concept of polarization purity is closely related to the so-called non-quantum entanglement.

REFERENCES

1. Mandel, L., "Concept of cross-spectral purity in coherence theory," *J. Opt. Soc. Am.*, Vol. 51, 1342–1350, 1961.
2. Mandel, L. and E. Wolf, "Spectral coherene and the concept of cross-spectral purity," *J. Opt. Soc. Am.*, Vol. 66, 529–535, 1976.
3. Hassinen, T., J. Tervo, and A. T. Friberg, "Cross-spectral purity of electromagnetic fields," *Opt. Lett.*, Vol. 34, 3866–3868, 2009.
4. Hassinen, T., J. Tervo, and A. T. Friberg, "Cross-spectral purity of the stokes parameters," *Appl. Phys. B*, Vol. 105, 305–308, 2011.
5. Santarsiero, M., "Polarization invariance in a Young interferometer," *J. Opt. Soc. Am. A*, Vol. 24, 3493–3499, 2007.
6. Gori, F., J. Tervo, and J. Turunen, "Correlation matrices of completely unpolarized beams," *Opt. Lett.*, Vol. 34, 1447–1449, 2009.
7. Hassinen, T., J. Tervo, and A. T. Friberg, "Purity of partial polarization in the frequency and time domains," *Opt. Lett.*, Vol. 38, 1221–1223, 2013.

Nanograting with Greatly Enhanced Near Field: A Highly-active Plasmonic Sers Substrate

Benfeng Bai
State Key Laboratory of Precision Measurement Technology and Instruments
Department of Precision Instrument, Tsinghua University, Beijing 100084, China

Abstract— Plasmonic nanostructures with tiny nanogaps [1, 2], such as V-grooves [3], nanoslots [4], and self-similar chain of metal nanoparticles [5], enable strong electromagnetic field confinement at nanoscale due to the excitation of localized surface plasmons (LSPs), which can greatly enhance light-matter interaction and are highly demanded in many applications such as surface-enhanced Raman scattering (SERS). The LSPs can be further steered via the inter-coupling of various LSP resonance modes in complex metallic nanostructures, where the energy splitting of LSP modes may be achieved by an inappreciable change of, e.g., the nanogap size in the nanostructures, leading to pronounced shift of resonance frequencies. Therefore, the fine control of nanogaps or nanotips in such structures is crucial for generating, sustaining, and steering strong field hot spots.

In this talk, a simple M-shaped nanograting with narrow V-shaped grooves of tens of nanometer width is presented to achieve cascaded field confinement and enhancement. The electromagnetic field on the surface of the M-grating can be pronouncedly enhanced due to the LSP mode excitation and inter-coupling in the nanogaps formed by the narrow V-grooves. A technique based on room-temperature nanoimprinting lithography and anisotropic reactive ion etching is developed for fabricating this device, which is cost effective, reliable, and suitable for fabricating large-area nanostructures. The near-field localization and enhancement in the M-grating are numerically analyzed and are experimentally characterized by scanning near-field optical microscopy. As a demonstration of the potential application of this device, the M-grating is used as a SERS substrate for probing Rhodamine 6G molecules. In experiment, an average SERS enhancement factor as high as 5×10^8 has been achieved, verifying the existence of strong localized field hot spots and the greatly enhanced light-matter interaction in the structure.

REFERENCES

1. Barnes, W. L., A. Dereux, and T. W. Ebbesen, *Nature*, Vol. 424, 824, 2003.
2. Schuller, J. A., E. S. Barnard, W. Cai, Y. C. Jun, and J. S. White, *Nat. Mater.*, Vol. 9, 193, 2010.
3. Stockman, M. I., S. V. Faleev, and D. J. Bergman, *Phys. Rev. Lett.*, Vol. 88, 067402, 2002.
4. Dionne, J. A., L. A. Sweatlock, H. A. Atwater, and A. Polman, *Phys. Rew. B*, Vol. 73, 035407, 2006.
5. Li, K., M. I. Stockman, and D. J. Bergman, *Phys. Rev. Lett.*, Vol. 91, 227402, 2003.

Fluorescence Resonance Energy Transfer Scanning Near-field Optical Microscopy: From Spatial Superresolution to Quantum Computing

S. K. Sekatskii and G. Dietler
Laboratoire de Physique de la Matière Vivante, IPSB
Ecole Polytechnique Fédérale de Lausanne, Lausanne CH1015, Switzerland

Abstract— In recent years, a few groups presented first Fluorescence Resonant Energy Transfer Scanning Near-field Optical Microscopy (FRET SNOM) images. However, to realize all advantages of the method [1], truly single-molecule FRET SNOM images should be obtained: the task which proved to be difficult due to the limiting photostability of the fluorescent centers and rapid damage of the "FRET-active" SNOM probes. Here we first discuss what we believe are the first FRET SNOM single molecule images obtained using CdSe nanocrystals as donors (these are spin-coated onto glass slide surface) and AlexaFluor 594 or Texas Red dye molecules as acceptors (these are incorporated into the "self sharpening pencil-type" probes based on thin polystyrene layers stained with dye molecules deposited onto SNOM tip apex) [2]. Very rapid scanning available with our SNOM exploring "double-resonant montage" of a fiber probe onto the tuning fork was used (SNOM image of an area with the sizes of 200–300 nm is recorded during 10–30 seconds), which enables to overcome the photostability problem. Additional advantage consists in the following. Such a fast scanning rate for standard 256×256 or 128×128 pixel images corresponds to expositions of the order of 0.1–2 ms/pixel, hence for typical noise level less than 1000 counts/s we obtain essentially "completely dark background area" (the most pixels contain zero counts) which enables to distinguish isolated single molecules as "extended non-dark spots". Spatial resolution of the order of 10–20 nm is achieved [2]. Our current researches with ultraphotostable NV color centers in nanodiamond crystals will be also discussed.

We also present first results obtained in the field related with coherent FRET SNOM quantum computing [3]. Low temperature (4–8 K) pump-probe laser spectroscopy of resonantly interacting trivalent neodymium ions in calcium fluoride crystal (so called M-centers; these are nothing else than donor-acceptor pairs subject to coherent FRET interaction with the decoherence time of ca. 6 ns which is longer than laser pulse duration) reveals the preparation of Bell's fully entangled vacuum-single exciton and vacuum-double exciton states [4]. We show that at low temperatures principally new type of FRET process, viz. that of coherent cooperative resonance energy transfer between different neighboring rare-earth ions, is possible [5].

REFERENCES

1. Sekatskii, S. K. and V. S. Letokhov, *Appl. Phys. B*, Vol. 63, 525, 1996.
2. Sekatskii, S. K., G. Dietler, and V. S. Letokhov, *Chem. Phys. Lett.*, Vol. 452, 220, 2008.
3. Sekatskii, S. K., M. Chergui, and G. Dietler, *Europhys. Lett.*, Vol. 63, 21, 2003.
4. Basiev, T. T., I. T. Basieva, A. A. Kornienko, V. V. Osiko, K. K. Pukhov, and S. K. Sekatskii, *J. Mod. Opt.*, Vol. 59, 166, 2012.
5. Sekatskii, S. K. and K. K. Pukhov, *Opt. Spectrosc*, Vol. 116, 65, 2014.

Bloch Surface Waves; a Novel Method for 2D Optical Integration

E. Barakat and H. P. Herzig
Optics & Photonics Technology Laboratory
Swiss Federal Institute of Technology in Lausanne (EPFL), Neuchâtel, Switzerland

Abstract— Carefully designed periodic dielectric structures sustain surface electromagnetic states, called Bloch surface waves (BSW), within their photonic bandgaps. There are several advantages provided by BSW propagation. First of all, due to the use of dielectric material, absorption losses are very low when transparent materials are considered at the desired wavelength. This allows the propagation of BSW over long distances and thus, the spectral range is not limited anymore by the material properties. Another advantage of using BSW is the possibility of its excitation at any wavelength by optimizing either the multilayer thicknesses or the incident beam angle. Furthermore, because the maximum intensity associated with the BSW can be tuned on the surface, a strong field intensity, increased by several orders of magnitudes, can be achieved and thereby enhance the light-matter interaction close to the surface.

We propose and demonstrate that a BSW-sustaining multilayer is a suitable general platform for manipulating and control the BSW propagation on its surface in the spectral range of telecom wavelengths. Several 2D optical photonic devices can be implemented starting from an ultrathin ($\sim \lambda/15$) additional layer deposited on the multilayer that can be subsequently shaped as desired. One of the main advantages is that these 2D photonic devices can have arbitrary shapes, which is difficult to obtain in 3D. Since BSW can be considered as a 2D wave which is bound at the surface of the multilayer, near-field imaging is one of the preferred tools to directly monitor and characterize the near-field produced on the structured multilayered surface. Multi-heterodyne scanning near-field optical microscope is used in the near-field characterization. The modification of the top surface to customize a 2D micro-system can be produced, by e-beam writing, optical lithography, stamping and other replication techniques.

Our recent results demonstrated the possibility of developing a robust multilayer platform that would pave the way for integration of photonic components in photonic chips using standard wafer-scale production. Various 2D polymer photonic-components have been fabricated and analysed on top of the platform. We experimentally and theoretically demonstrate that the BSW can be diffracted, focused, coupled and made resonating by locally shaping the geometries of 2D photonic devices on the multilayer, such as lenses, prisms, gratings, bended waveguides and waveguide couplers, etc..

REFERENCES

1. Yeh, P., A. Yariv, and A. Y. Cho, "Optical surface waves in periodic layered media," *Appl. Phys. Lett.*, Vol. 32, 104–105, 1978.
2. Descrovi, E., T. Sfez, L. Dominici, W. Nakagawa, F. Michelotti, F. Giorgis, and H. P. Herzig, "Near-field imaging of Bloch surface waves on silicon nitride one-dimensional photonic crystals," *Opt. Express*, Vol. 16, 5453–5464, 2008.
3. Descrovi, E., T. Sfez, M. Quaglio, D. Brunazzo, L. Dominici, F. Michelotti, H. P. Herzig, O. J. F. Martin, and F. Giorgis "Guided bloch surface waves on ultrathin polymeric ridges," *Nano Lett.*, Vol. 10, 2087–2091, 2010.
4. Yu, L., T. Sfez, V. Paeder, P. Stenberg, W. Nakagawa, M. Kuittinen, and H. P. Herzig, "Concurrent polarization retrieval in multi-heterodyne scanning near-field optical microscopy: Validation on silicon form-birefringent grating," *Opt. Express*, Vol. 20, 23088–23099, 2012.
5. Yu, L., E. Barakat, T. Sfez, L. Hvozdara, J. Di Francesco, and H. P. Herzig, "Manipulating Bloch surface waves in 2D: A platform concept-based at lens," *Light: Science & Applications*, Vol. 3, e124, 2014.

Photon Crystal Surface EM and Their Use for Ultrasensitive Label-free Biosensing and Generation of Ultralong Propagating Blue and Violet Plasmons

S. K. Sekatskii and G. Dietler
Laboratoire de Physique de la Matière Vivante, IPSB, BSP
Ecole Polytechnique Fédérale de Lausanne, Lausanne CH1015, Switzerland

Abstract— This is known that a properly designed Photonic Crystal (PC) supports the propagation of bounded electromagnetic Surface Waves (SW) along the PC-medium to be studied interface, and such an approach can be used with or without the presence of thin metal layer [1]. In a sense, one may say that such a PC, for certain wavelength and incidence angle, can "mimic" the refraction index of an external media thus creating an analogue of symmetrical sandwich configuration known as capable to support ultralong plasmon propagation [2].

This approach was used by us with thin (8 nm) Pd or Au layer deposited onto the surface of a PC. For the case of Pd, this enabled to realize ultrasensitive detection of hydrogen [3, 4] and establish the size-dependent character of the hydrogen uptake for Pd-nanoparticles as well as the donation of hydrogen electrons to the collective electronic band of the metal [4]. Ultralong surface plasmon propagation for the **blue** laser line at 405 nm and sensitive detection of nitrogen dioxide was realized for the case of gold layers [5]; experiments with UV surface plasmons are currently underway. Further perspectives of these researches will be discussed.

For biosensing, we use bare (no metal coating) PC-external medium interface, specially treated to chemisorb protein layers, for the study of kinetics of the interprotein interactions. Besides quite large sensitivity, $0.2\,\mathrm{pg/mm^2}$, this approach has additional advantages due to the possibility to excite simultaneously *s*- and *p*-polarized surface electromagnetic waves having very different penetration depths into an external medium. This enables to segregate surface and volume effects, thus drastically increasing both the sensitivity and reliability of the data obtained, and also to study interactions involving rather thick (of the order of one micron) objects such as bacteria, viruses, and certain cell organells-option, unattainable for usual surface plasmon resonance-based detectors due to the short penetration depth of such plasmons. After first successful tests of the detector for kinetic measurements of a few standard receptor-ligand interactions [6], we apply it for the study of yet uncharacterized interactions between different fragments of faviviral (tick born encephalitis and West Nile viruses) surface glycoprotein *E* with its putative cell receptor laminin binding protein (LBP). Together with the Single Molecule Force Spectroscopy data, the results obtained unambiguously demonstrate force induced globule-coil transition of LBP and its complexes at acid conditions characteristic for viral penetration into cell endosome thus establishing a crucial role of LBP for viral-cell membrane fusion (submitted).

REFERENCES

1. Konopsky, V. N. and E. V. Alieva, *Phys. Rev. Lett.*, Vol. 97, 253904, 2006.
2. Sarid, D., *Phys. Rev. Lett.*, Vol. 47, 1927, 1986.
3. Konopsky, V. N., D. N. Basmanov, E. V. Alieva, et al., *New J. Phys.*, Vol. 12, 063049, 2009.
4. Konopsky, V. N., D. N. Basmanov, E. V. Alieva, et al., *Appl. Phys. Lett.*, Vol. 100, 083108, 2012.
5. Alieva, E. V., V. N. Konopsky, D. V. Basmanov, et al., *Opt. Comm.*, Vol. 309, 148, 2013.
6. Konopsky, V. N., T. Karakouz, E. V. Alieva, et al., *Sensors*, Vol. 13, 2566, 2013.

Session 4P7a
SC3: High Power Fiber Lasers 2

Ultrafast Laser Generation from a Topological Insulator Mode-locked Fiber Laser

Chujun Zhao and Han Zhang
Key Laboratory of Optoelectronic Devices and Systems of Ministry of Education and Guangdong Province
College of Optoelectronic Engineering, Shenzhen University, Shenzhen 518060, China

Abstract— Passively mode-locked ultrafast fiber laser possesses widespread applications, such as optical communications, material processing, military and so on. To achieve passively mode locking in a fiber laser, the key component is the saturable absorber (SA). Some artificial SAs, such as nonlinear polarization rotation, nonlinear amplifying loop mirror, and real SAs have been investigated intensively. Among them, real SA is expected to be a more efficient way to generate ultrafast pulse. After the emergence of the first generation dye SA for passively mode locking Nd:glass laser, the saturable absorber mirror (SESAM) has already largely fostered the development of ultra-fast laser towards the goals of high-power, low-cost, compactness and high-efficiency. With the development of novel materials, the SA is fabricated with the materials evolving from semiconductor towards nanomaterials, including carbon nanotube and graphene. In particular, the graphene, a type of Dirac materials, possesses some advantages, such as wavelength-independent saturable absorption, low saturable absorption threshold, and large modulation depth. The significant advancement in graphene SA renders us to propose one fundamental but interesting question, whether the other type of Dirac materials, except graphene, could exhibit saturable absorption as well?

Recently, a newly rising Dirac material: topological insulators (TI) have attracted much attention in condensed-matter physics. Similar to graphene, TIs are also Dirac materials, exhibiting the Dirac-like linear band dispersion. In 2012, Bernard et al. found that TIs show the saturable absorption behavior around 1550 nm wavelength. Using the saturable absorption behavior of TI-based SA, we further demonstrated the generation of ultrafast fiber laser mode-locked by TI SAs, which was prepared by top-down and bottom-up approaches, respectively. In addition to the saturable absorbing effect, we also found that the TIs possess large nonlinear refractive index with the Z-scan technique. The experimental results clearly evidences that TIs possesses the desired optical properties for laser mode locking and can be considered as another Dirac material type of SA, paving the way for TI based ultrafast photonics.

Numerical Study on High Power and Highly Efficient Random Fiber Laser Operating at 1455 nm

Mengqiu Fan, Han Wu, Zinan Wang, and Yunjiang Rao
Key Lab of Optical Fiber Sensing & Communications
University of Electronic Science & Technology of China, Chengdu, Sichuan 611731, China

Abstract— We proposed a high power and highly efficient random fiber laser with half-open cavity formed by single-mode fiber (SMF) and a fiber loop mirror (FLM) operating at 1455 nm wavelength and we did the numerical study with this scheme. The numerical calculation shows that the threshold is reduced to 1.2 W and the slope efficiency of the laser reach to 85% with the pump power increase above the threshold. Also we obtained the output power of 3.25 W with the pump power of 5 W.

Since the distributed feedback random fiber laser (RFL) solely based on SMF was reported in 2010 by Turistsyn et al. [1], it has attracted a lot of interests for its many unique features such as long-distance signal delivery ability, ultra-low intensity noise, stable output with little thermal sensitivity, and cavity simplicity. Therefore, a long-distance fiber-optic point-sensing system based on random fiber lasers was reported [2]. Recently, studies have focused on the issues of reduction of the threshold [3], slope efficiency, higher order random laser [4] and increase of output power. Indeed, one of the advantages of distributed feedback RFL against the conventional RFL is the possibility of high power first Stokes wave generation that is difficult to achieve in conventional RFL because of generation of higher order Stokes waves.

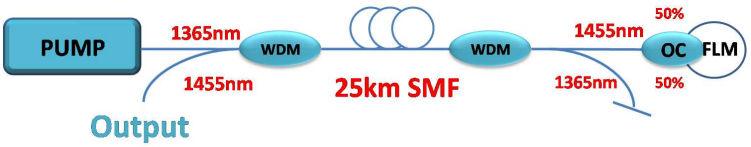

Figure 1: Setup.

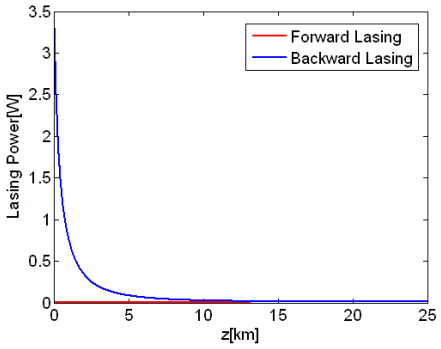

Figure 2: Power distribution along the fiber.

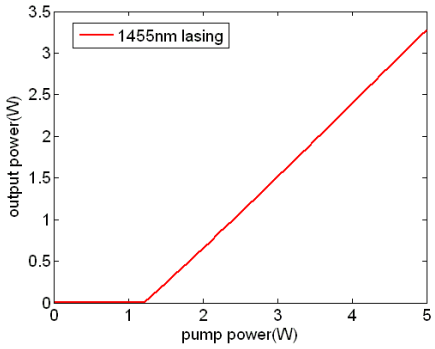

Figure 3: Output power as a function of pump power.

Our lasing cavity is formed by G.652 fiber and a FLM, as shown in Fig. 1, while the former acts as the distributed reflector and the latter acts as the point reflector. To improve the output power of the laser, we place the reflector at the far end of the fiber via connected by a wavelength-division-multiplexer (WDM). Utilizing a optimized SMF (25 km) and a far end point feedback, the threshold is reduced to 1.2 W. The most importantly, because of the far end point feedback, the power distribution along the fiber changes significantly so that we can obtain a high power and highly efficient output from the 1455 nm port of the WDM which at the pump end.

We use the stationary model to calculate the output power and power distribution along the fiber. Fig. 2 shows the calculated output power as a function of the pump. Fig. 3 shows the calculated power distribution along the fiber. It suggests that the majority of the power flow is towards to

the near end of the fiber, thus increasing the output power and slope efficiency compared with the open cavity.

ACKNOWLEDGMENT

This work is supported by Natural Science Foundation of China (61205048, 61106045, 61290312), Research Fund for the Doctoral Program of Higher Education of China (20120185120003), Fundamental Research Funds for the Central Universities (ZYGX2012J002, ZYGX2011J001), 111 project (B14039) and PCSIRT (IRT1218).

REFERENCES

1. Turitsyn, S. K., S. A. Babin, A. E. El-Taher, et al., "Random distributed feedback fibre laser," *Nature Photonics*, Vol. 4, No. 4, 231–235, 2010.
2. Wang, Z. N., Y. J. Rao, H. Wu, et al., "Long-distance fiber-optic point-sensing systems based on random fiber lasers," *Optics Express*, Vol. 20, No. 16, 17695–17700, 2012.
3. Zhang, W. L., Y. Y. Zhu, Y. J. Rao, et al., "Random fiber laser formed by mixing dispersion compensated fiber and single mode fiber," *Optics Express*, Vol. 21, No. 7, 8544–8549, 2013.
4. Wang, Z., H. Wu, M. Fan, et al., "Third-order random lasing via Raman gain and Rayleigh feedback within a half-open cavity," *Optics Express*, Vol. 21, No. 17, 20090–20095, 2013.

Coherent Beam Combining of Two Tm-doped Fiber MOPAs with Output Power of 50 W

Xiaoxi Jin, **Xiong Wang**, **Xiaolin Wang**, **Yanxing Ma**, **and Pu Zhou**
College of Optoelectronic Science and Engineering
National University of Defense Technology, Changsha 410073, China

Abstract— Thulium-doped fiber lasers operating at $\sim 2\,\mu m$ band have significant application prospects in fields such as eye-safe lidar, remote sensing, medical care and nonlinear frequency conversion. However, due to thermal damage, mode instability and nonlinear effects, the output power level of single Tm-doped fiber laser was limited, which confined the development of Tm-doped fiber laser. Coherent beam combining (CBC) is an effective method to improve power level of fiber lasers. In this paper, we demonstrated CBC of two Tm-doped fiber master oscillator power amplifiers (MOPAs) with total output power reaching 50 W. The output powers of the both MOPAs can reach ~ 25 W when the pump power of each MOPA was ~ 55 W. Single frequency dithering technique was used to implement active phase locking in feedback loop of the CBC system. When the feedback loop was implemented, phase noises below 700 Hz in the system were compensated effectively, and the far field intensity patterns were highly stable compared with the fluctuating patterns obtained when the feedback loop did not work. The fringe contrast was increased from ~ 0.34 in open loop to ~ 0.90 in closed-loop. These results indicate that the system we presented is a promising way to increase the output power of Tm-doped fiber lasers. Since the output power of the system is pump-limited, it's reasonable to believe that higher output power at $\sim 2\,\mu m$ could be obtained via CBC, if more channels are combined together and/or the power of each channel is further scaled up.

Numerical Investigation of a Novel Two-stage Structure to Compress Spectrum and Suppress Pedestal Employing a DIF Interconnected with a HNLF-NOLM

Ying Chen[1, 2], **Yu Guo**[3], **Bing Liu**[1], **Fan Yang**[2], **Xiaojun Zhou**[2], **Yong Liu**[2], **and Xiangning Chen**[1]

[1]Department of Optoelectronics, Academy of Equipment, Beijing 101416, China
[2]State Key Laboratory of Electronic Thin Films and Integrated Devices
School of Optoelectronic Information
University of Electronic Science and Technology of China, Chengdu 610054, China
[3]Air Force 95806 Unit, 100076, China

Abstract— A novel all-fiber spectral compression scheme is proposed and demonstrated, which is based on a two-stage structure employing a dispersion increasing fiber interconnected with a nonlinear optical loop mirror. Five sorts of DIF with different distribution of dispersion coefficient is analyzed one by one in the two-stage scheme. Numerical simulation result shows Logarithmic DIF is suitable for the two-stage scheme, obtain a SCR as high as 10.93 without a Raman self-frequency soliton shift under the condition of soliton number is equal to 1.4.

Cr^{2+}: ZnSe Crystal Based High Power Passively Q-switched Tm-doped Fiber Laser

Yulian He, **Zhuo Li**, **Hongyu Luo**, **Lele Wang**, **Lian Han**, **and Jianfeng Li**
State Key Laboratory of Electronic Thin Films and Integrated Devices
School of Optoelectronic Information
University of Electronic Science and Technology of China (UESTC)
Chengdu 610054, China

Abstract— In this paper, Q-switched Tm^{3+}-doped fiber lasers with Cr^{2+}: ZnSe crystal of different initial transmissions as saturable absorbers were demonstrated. Stable Q-switching regime was achieved if inserting the crystal of 70% initial transmission into the cavity with a confocal arrangement after the threshold launched pump power of 1.50 W at which pulse energy of 7.58 μJ, pulse duration of 190 ns and repetition rate of 21.4 kHz were obtained, the Q-switching can maintained stable consistently until the maximum launched pump power of 7.13 W at which the pulse energy of 8.74 μJ, repetition rate of 150.7 kHz and pulse duration of 160 ns were achieved at a SNR of up to ∼ 56 dB and a center wavelength of 1985 nm with FWHM of 15.3 nm. The obtained maximum output power of 1.32 W at a slope efficiency of 20.1% only limited by the available pump power was also, to the best of our knowledge, highest level generating from crystal-based passively Q-switched Tm^{3+}-doped fiber laser. In order to increase the repetition rate of the Q-switched pulses, a Cr^{2+}: ZnSe crystal of 80% initial transmission was introduced into the cavity with other arrangements unchanged. Due to its lower modulation depth and higher initial transmission, pulse energy of 4.72 μJ, pulse duration of 584 ns, repetition rate of 39.97 kHz were achieved at the Q-switching threshold of 1.31 W. The stable Q-switching can be well operating until the launched pump power of 4.19 W at which the pulse energy of 6.92 μJ, repetition rate of 138.1 kHz and pulse duration of 352 ns were achieved at a SNR of up to ∼ 55.7 dB and a center wavelength of 1981 nm with FWHM of 13.4 nm, and maximum pulse power of 0.96 W was delivered at an improved slope efficiency of 25.8%. Once beyond this pump power, however, the stable Q-switched state was broken by another chaotic state with a sharp decline SNR. The stable Q-switched pulses re-appeared if re-adjusting the pump power down to 4.19 W indicating the crystal free from damage.

Session 4P7b
SC3: High Speed Interconnects for High Performance Computing

Through-Silicon-Via Pairs Modelling via Compressed Sensing

Tao Wang, Jun Fan, Yiyu Shi, and Boping Wu
Missouri University of Science and Technology, USA

Abstract— Through-Silicon-Vias (TSVs) are the critical enabling technique for three-dimensional integrated circuits (3D ICs). While there are a few existing works in literature to model the electrical performance of TSVs, they are either for fixed geometry or in lack of accuracy. In this paper, we use compressed sensing technique to model the electrical performance of TSV pairs. Experimental results indicate that with an exceptionally small number of samples, our model has a maximum relative error of 3.70% compared with full-wave simulations over a wide range of geometry parameters and frequencies.

Comprehensive Study of Through Silicon Via (TSV) Modeling and Analysis in High Speed Three Dimensional Integrated Circuits (3D IC)

M. Amimul Ehsan[1], **Zhen Zhou**[2], **Xin Fu**[3], **and Yang Yi**[1]

[1]Department of Computer Science and Electrical Engineering
University of Missouri-Kansas City, Kansas City, MO 64110, USA
[2]Research Lab on Photonic Technology, Intel Crop.
3600 Juliette Ln, Santa Clara, CA 95054, USA
[3]Department of Electrical Engineeringand Computer Science
University of Kansas, Lawrence, KS 66044, USA

Abstract— Through silicon via (TSV) is a chip stacking technology which is very important for three dimensional (3D) system design and analysis. Along with the need for low-cost and high-yield process technology, the successful application of TSV technology requires further optimization of the TSV electrical design, which needs careful consideration of the complex TSV electrical modeling and analysis. Recently, much progress has been made on TSV modeling and analysis to address the impact of TSVs on high speed signals, to analyze the TSV crosstalk, to study the TSV resistance, inductance and capacitance characterization, as well as to apply the full-chip extraction and optimization. These methodologies can be categorized into three classes based on the types of electromagnetic techniques used: full-wave modeling, quasi-static modeling, and analytical modeling. There are three modes being considered: 1) slow wave mode at low frequencies where the electrical field is screened by the silicon substrate and the magnetic field penetrates much further into the substrate; 2) quasi-transverse electromagnetic mode when both electrical and magnetic fields penetrate deep into silicon substrate; and 3) skin effect mode at very high frequency when the skin depth in silicon is smaller than TSV spacing. The full wave analysis methods are accurate, but will be computationally intensive due to the large number and multi-scale dimensions (oxide thickness and aspect ratio) of TSVs in the 3D mmW integrated circuits. Another bottleneck of the full wave methods is that it is difficult to be compatible with SPICE simulators. The full wave methods need computationally expensive field solvers for the electrical modeling of various TSVs arrangements, which will significantly increase the simulation time. The equivalent circuit methods with lumped RLGC elements could be a good alternative. The equivalent methods can provide good compatibility with SPICE simulators. Most of the TSV modeling approaches in equivalent methods focus on the RF applications with operation frequency of several GHz or even lower,whereas the TSV technology specifically for millimeter wave (mmW)/THz applications is seldom reported. The challenges in modeling TSV in 3D mmW integrated circuits comes from the need of accurate broadband model capturing high frequency effect, frequency-dependent losses, coupling, and mismatch.

In this paper, the electrical design and modeling challenges associated with 3D integration using TSVs is discussed at first. In light of the challenges in modeling the TSV operating in mmW/THz frequency range, we investigated the TSV metal oxide semiconductor (MOS) effect and high frequency effect, and then proposed a compact and accurate circuit model for TSV analysis and characterization. A closed-form expression for TSV capacitance in both depletion and accumulation regions is proposed. Since frequent switching of high speed signals can dynamically bias TSV metal insulator semiconductor (MIS) interface and allocate TSV MIS into accumulation or depletion regions, the TSV capacitance is nonlinear and dependent on the biasing of the TSVs. Furthermore, we introduced a rough sidewall TSV model to account the impact on propagation characteristic in the ultra-broad band frequency range.The proposed circuit model accurately captures all the parasitic elements of various TSVs arrangements and accounts for wide frequency range, high frequency skin effect, eddy currents in substrate, metal MOS effect, and surface roughness effect.

Ultra-wideband THz Interconnect Using Micromachined Silicon Dielectric Waveguide

Bo Yu, Yuhao Liu, Jane Gu, and Xiaoguang Liu
University of California, Davis, USA

Abstract— Although the absolute speed of current general purpose microprocessors has slowed down in progression due to their increasing power consumption and thermal dissipation requirements, today's computing systems, be it a personal computer, a supercomputer, or a large datacenter, has roughly maintained performance scaling by taking advantage of parallelism. While alleviating the requirement on each individual processing unit, parallelism shifts the burden to the interconnects between processors and cores. The ever-increasing inter- and intra-chip communication bandwidth imposes a big challenge over decades: interconnect bottleneck. Both electrical interconnects, in the form of metal traces and bondwires, and optical interconnects, in the form of integrated photonic transceivers, have been extensively studied over the last few decades. Electrical interconnects can be easily integrated within current semiconductor design and fabrication processes but face increasing challenges in terms of the usable bandwidth and signal integrity issues. Optical interconnects offer extremely large data bandwidth and very low distortion but suffer significant difficulties in integration with existing semiconductor technologies.

THz interconnect (TI) aims to bridge the gap to enable energy efficient centimeter range communications, and complement EI and OI by integrating both electronic and optic advantages. In this work, we demonstrate the feasibility of using the terahertz frequency band for ultra-high speed chip-to-chip interconnects. In particular, we will demonstrate the use of micromachining technologies for the fabrication of low-loss large-bandwidth single- and multi-mode THz interconnects that can be realistically integrated with existing semiconductor fabrication and packaging processes. We will demonstrate a silicon-based dielectric waveguide interconnect that exhibit loss much lower than 0.1 dB/mm.

Method to Reduce Coupon Lengths for Transmission Line *S*-parameter Measurements through Elimination of Guided-wave Multiple Reflections

Shaowu Huang, Jeff Loyer, Richard Kunze, and Boping Wu
Intel Corporation, 2800 Center Dr, DuPont, WA 98327, USA

Abstract— A new approach is proposed to reduce the length requirements and increase the accuracy for the measurement of transmission line S-parameters in printed circuit boards (PCBs). In addition, the approach improves the accuracy of measurements.

In existing methods, widely adopted by the industry, a trace length of 8 inches is typically chosen to achieve accurate measurements of S-parameters, particularly of insertion loss. For manufacturing, shorter coupons are desired, but two major effects require longer coupons: 1) Limits of receiver sensitivity require insertion loss to be high enough to exceed the noise floor of the instrument, and 2) for non-50 ohm DUTs (or 100 ohms differential), return loss effects can cause errors in insertion loss measurements. A longer trace is chosen so that the effects of multiple reflections on the insertion loss measurements are negligible, compared to the insertion loss measured, and signal amplitude is sufficient for the instrument used.

In this work, we demonstrate that guided-wave multiple reflections of the transmission lines in the signal propagation direction limits use of short transmission lines samples. The reflections can be also interpreted as standing waves, waveguide modes, waveguide resonances, or layered medium multiple reflections. The elimination of the guided-wave multiple reflections is introduced to overcome the coupon length limit for accurate measurements of transmission lines S-parameters. We introduce implementations of the proposed approach in the time and frequency domains. For time-domain measurements, we do corrections to remove the reflection noise signals from received signals: the first is the waveform manipulation for removing the internal reflections, and the second is the novel manipulation of S-parameters to compensate for reflected and transmitted losses. For native frequency-domain measurements, that manipulation of the S-parameters is used as a de-embedding correction method to remove the reflected and transmitted signals' contributions from the S-parameters. Simulation results are presented to demonstrate the efficiency and accuracy of the new approach. Results show that the new approach can reduce the minimum length of high-speed transmission lines from 8 inches in traditional industry standards to only 0.5 inch for both 4-port TDR/VNA measurements and 2-port SET2DIL. This can significantly reduce coupon area, allowing more compact PCB designs, and enabling the ability to include coupons in the actual design, rather than as "outriggers" (dedicated portions of a PCB panel for manufacturing testing).

High-speed Silicon Mach-Zehnder Optical Modulator with Large Optical Bandwidth

Jianfeng Ding and Lin Yang
State Key Laboratory on Integrated Optoelectronics
Institute of Semiconductors, Chinese Academy of Sciences, China

Abstract— As the core of the central processing unit becomes more and more, the bandwidth of the electrical interconnect gradually becomes the bottleneck for improving the computing performance due to its higher power consumption, limited bandwidth and longer latency. Optical interconnect is taken as a promising solution to this problem. Silicon optical modulator, as a device transforming the data from the electrical domain to the optical domain, has been widely studied for many years. Silicon Mach-Zehnder optical modulator is believed to have a large optical bandwidth. However, Most of the reported high-speed silicon Mach-Zehnder optical modulators have optical bandwidths of only several nanometers.

In this letter, we report a carrier-depletion silicon Mach-Zehnder optical modulator with large optical bandwidth by adopting two symmetric arms. The fiber-to-fiber loss of the device is about $7.2 \sim 8$ dB in the wavelength range from 1525 nm to 1565 nm. We have used the truncation method to accurately measure the loss of the optical splitter and combiner, and the on-chip loss is about 3.8 dB. The dynamic extinction ratios at the speed of 40 Gb/s are $4.9 \sim 6.4$ dB in the wavelength range from 1529 nm to 1565 nm. By analyzing the dependence of the optical bandwidth on the optical path difference between the two arms, we find that there is an unexpected optical path difference of around 3.3 μm between the two arms, which is considered to originate from the nonuniform morphologies of the waveguide and the nonuniform doping profiles along the two arms and is responsible for the slight wavelength dependence of the static and dynamic response of the silicon Mach-Zehnder optical modulator.

A Simple Equivalent Circuit Model of Finite Ground Coplanar Waveguide (FGCPW) on MIS for Ultra-fast Monolithic Photodiode Application

M. Amimul Ehsan[1], **Zhen Zhou**[2], **and Yang Yi**[1]

[1]Department of Computer Science and Electrical Engineering
University of Missouri-Kansas City, Kansas City, MO 64110, USA
[2]Research Lab on Photonic Technology, Intel Crop., 3600 Juliette Ln, Santa Clara, CA 95054, USA

Abstract— When the data rate of a digital communication system exceeds 25 Gbps, an optical interconnects using fiber or optical waveguide emerges as an alternative to the copper wired interconnect for an interconnection longer than a few ten inches to conserve the power consumption.

Photodetector (PD), as an optical to electrical signal convertor,is an essential component in an optical interconnects. Its bandwidth directly impacts the achievable data rate of the optical interconnects. The overall bandwidth of a PD is limited by its transit time, junction RC, and the bandwidth of interconnect. PD often uses Finite ground plane coplanar waveguide (FGCPW) on metal-insulator-semiconductor (MIS) as its interconnects to realize the DC bias and connection to the transimpedance amplifier (TIA). To accurately predict the performance of the photodiode, its interconnect needs to be accurately modeled within the device operational frequency band.

Historically, full wave solver such as HFSS can be employed to simulate the FGCPW at frequency domain, and the resulted S-parameters can be used for circuit simulation in time domain. However, the HFSS simulation can be time consuming and inaccurate at low frequency. This is because the transverse dimensions of the interconnects are smaller than $10^5\times$ guided wavelength (λ_g) at frequencies lower than 1 GHz, and HFSS experiences difficulties in obtaining accurate passive solutions. In order to accurately predict the photodiode performance, correctly characterizing the interconnect behavior at DC is important, because it directly affects the bias applied to the photodiode. If the S-parameter or equivalent circuit model created by HFSS is explicitly used in time domain simulation, it is likely that the DC bias condition for the photodiode will be inaccurately predicted. The limitation of the HFSS S-parameter simulation at lower frequency necessitates the development of a lumped equivalent circuit model which can give a more accurate prediction of the interconnect behavior at both DC and high frequency band of interest.

For time domain simulation, a RLC circuit for interconnect is often preferred. The lumped elements in the equivalent circuitare regarded as frequency independent components and are usually obtained by LRC measurements taken at low frequency. The interconnect bandwidth is simply calculated using one pole RC model formed by Rand C. This simplification is valid only when the operation frequency is low and the interconnect length and transverse dimension is much smaller than the guided wavelength. When the operational frequency increases, the one-pole lumped element model is no longer sufficient. In this paper, a new equivalent circuit model for the FGCPW interconnect is proposed. It accounts for the electrical length and physical loss mechanism of the FGCPW interconnects, and the accuracy of the new model is verified. The method for extracting the parameters for the equivalent circuit by using the measured S-parameter from an open structure is illustrated.

Performance Evaluation of an OFDM-based BPSK PLC System in an Impulsive Noise Environment

A. M. Nyete, T. J. O. Afullo, and I. Davidson
Discipline of Electrical, Electronic and Computer Engineering
University of KwaZulu-Natal, Durban, South Africa

Abstract— Power line carrier (PLC) communication provides a ready medium for broadband internet connectivity and as well as monitoring, control and automation functions for both industries and homes. In fact, the power line network is the most expansive network in the world reaching every room in every facility connected to the power grid. Thus, PLC technology is the most economical way to provide internet connectivity and home networking in rural/remote areas. However, the original design of power lines was not for communication purposes but electrical power transmission. Thus, PLC technology provides a readily available channel that is hostile when used for communication purposes. This hostility is due to the many problematic characteristics of the power line network from a communications perspective. They include reflections due to impedance mismatch, frequency varying attenuation, multipath due to the cable joints, as well as the different types of noise inherent in the channel. In this paper, we investigate the impact of impulse noise on the performance of an OFDM based BPSK PLC channel. This is motivated by the fact that the very characteristics of the impulse noise, namely; pulse width, amplitude and interarrival time, have not been studied at an elementary level in terms of their influence on the performance of the PLC channel. The mathematics behind the impulse function is utilized in an attempt to fully characterize the impulse noise for the PLC channel. The performance of the PLC system is compared in terms of the bit error rate (BER) characteristics for given signal to noise ratio (SNR) values for different impulsive noise parameters.

Glass Weave and Rough Surface Effect for High Speed Channel Signal Integrity

Ruihua Ding[1] and Boping Wu[2]

[1]Intel Corporation, Platform Engineering Supergroup, Santa Clara, CA 95054, USA
[2]Intel Corporation, DCG Supergroup, King of Prussia, PA 19406, USA

Abstract— Glass weave and rough surface effect on printed circuit board (PCB) is a manufacturing process effect which is often neglected by the signal integrity engineers in their channel characterization and performance evaluation. As the data link speed increases, these two factors have to be included in the circuit simulation for high speed channel evaluation and optimization. Understanding these effects and their potential signal integrity issues are critical in designing robust high speed data links.

In this paper, we will present an overview of the glass weave effect in a simulation based approach to understand its maximum effect on signal integrity of high speed IO. Several typical glass styles in PCB will be simulated by 3D full wave simulator. We will focus on the structures of microstrips because glass weave has large impact on microstrip compared to the stripline. Single ended microstrip line will be evaluated in a DDR4 channel with 2667 MT/s data speed. Differential microstrip lines will be evaluated in PCIe Gen3 channel with 8 Gb/s. For high speed interface environment, microstrip line performance in frequency domain and time domain will be compared between the PCB with and without glass clothes. By using recessed probe launch technique, effective loss tangent will be adopted to simulate the attenuation of copper roughness for various trace-width and trace-spacing configurations. The design trend of low attenuation Meg6 HVLP PCB will be presented in a clear chart. Eye margin will be used to evaluate the whole channel impact. The paper will conclude on some design guidelines for PCB with glass weave and rough surface effect considered.

Comprehensive Ultra-broadband Design and Mode Suppression Techniques for Bends in a Differential Pair

Chenyuan Zhao[1], **Zhen Zhou**[2], **Yi-Che Lee**[3], **and Yang Yi**[1]

[1]Department of Computer Science and Electrical Engineering
University of Missouri-Kansas City, Kansas City, MO 64110, USA
[2]Research Lab on Photonic Technology, Intel Crop., 3600 Juliette Ln, Santa Clara, CA 95054, USA
[3]School of Electrical and Computer Engineering, Georgia Institute of Technology, Atlanta, GA 30332, USA

Abstract— Differential signaling is widely used in ultra-wideband digital links due to its superior noise immunity, its robustness to crosstalk, and less EMI comparing to single-ended signaling. However, any asymmetry in the signal path can cause mode conversion. Differential to common mode conversion can reduce differential signal bandwidth and introduce EMI. On the other hand, common mode to differential conversion will be received as a noise by the receiver and can cause the link to fail.

Skew induced by length mismatch in a differential pair is one of the main causes of mode conversion. The skew alone can make the pair behave as a low pass filter. The 3-dB bandwidth due to the skew depends on the amount of skew. A bend in a pair is also inevitable and is the most common location where the mode conversions occur. A bend in the pair can introduce more than the length mismatch. If the bend is not designed appropriately, it can cause the impedance mismatch and the propagation speed mismatch in the pair as well.

To eliminate the skew caused bandwidth limitation, de-skew structures are commonly presented in the layout. The rule of thumb for the skew management used to be the 10% of the UI for the overall link including the driver, the interconnects, and the receiver. For an ultra-broadband digital link, the data rate is expected to be 25 Gbps or beyond, thus the absolute allowable skew becomes 4 ps or even less.

However, designing a de-skew structure such as a wiglet can be arduous. Some of the parasitics brought by the de-skew wiglets can severely shadow the benefits that the wiglets may offer and make their presences less preferable. Thus, the PCB layout designer would like to know how much the skew budget the interconnects should have.

In this paper, we firstly provide a criterion to determine the interconnect skew budget. Alternative de-skew structures, such as de-skew meander lines and de-skew bend other than wiglets are simulated and discussed to provide methodology to determine when each de-skew structure shall be considered.

Session 4P8
SC1: Characterization, Propagation and Application of Beams with Controlled Polarization, Coherence and Phase

Effects of Focusing on Scintillations of Higher Order Laser Modes in Non-Kolmogorov Turbulence

Yahya Baykal
Department of Electronic and Communication Engineering, Çankaya University
Yukarıyurtçu Mah., Mimar Sinan Cad., No. 4, 06790 Etimesgut Ankara, Turkey

Abstract— The scintillation index of focused higher order laser beam propagating in non-Kolmogorov atmospheric turbulence is formulated by employing the Rytov method and the equivalence of the structure constant. Our evaluations are performed for even modes. The equivalence formula for the structure constant is extracted from our earlier work in which the equivalence is obtained by equating the scintillation indices found in the Kolmogorov and the non-Kolmogorov turbulence. If not specified otherwise, the focused beam is defined when the focal length is equal to the link length. For the focused higher order laser beams, as the power law exponent of the non-Kolmogorov spectrum decreases, the scintillations decrease. At any power law exponent, the scintillations tend to become larger when the mode order of the focused beam becomes larger, i.e., the focused Gaussian beam is advantageous over the focused higher order laser beams for any realization of the non-Kolmogorov turbulence. Again being valid for any power law exponent, increase in the source size is found to decrease the intensity fluctuations of all the focused higher order mode scintillations. Especially for the larger order beams, focusing the higher order beam at a distance smaller than the link length results in a change in the behaviour of the scintillation index versus the power law exponent. In such cases, the scintillations are observed to increase. Comparison of the focused higher order beam scintillations with the previously obtained collimated higher order beam scintillations yields that the focused higher order beam scintillations are lower. Collimated higher order beams exhibit lower scintillations than the collimated Gaussian beams whereas this is reversed in the focused case. Another observation in such comparison shows that the difference of the intensity fluctuations between the Gaussian and the higher order beams are much larger in the focused case, especially at larger power law exponent values.

Dependence of the Beam Wander of an Airy Beam on Its Kurtosis Parameter in Turbulent Atmosphere

Wen Wei[1, 2], **Xiuxiang Chu**[3], **and Yangjian Cai**[1]

[1]School of Physical Science and Technology, Soochow University, Suzhou 215006, China
[2]Department of Physics and Information Engineering, Huaihua University, Huaihua 418008, China
[3]School of Sciences, Zhejiang Agriculture and Forestry University, Lin'an 311300, China

Abstract— Beam wander which will be affected by many factors is an important characteristic of laser beams in turbulent atmosphere. In present letter the influence of an Airy beam's kurtosis parameter on its beam wander has been studied. The interesting results is that the beam wander of Airy beam has a simple and fixed rule versus its kurtosis parameter regardless of the variation of propagation distance, characteristic scales of Airy beam, inner scales of turbulence and wave length. It can be used in the control of beam wander for Airy beam in practice, such as in the free-space-optical communication and laser defence.

Nonparaxial Propagation of Complex Variable Function Cosh-Gaussian Beams

Dongmei Deng[1, 2], **Chidao Chen**[1], **Yushan Zheng**[3], **Xi Peng**[1], **Bo Chen**[1], **Yulian Peng**[1], **and Meiling Zhou**[1]

[1]Laboratory of Nanophotonic Functional Materials and Devices
South China Normal University, Guangzhou 510631, China
[2]CAS Key Laboratory of Geospace Environment
University of Science and Technology of China, Chinese Academy of Sciences, Hefei 230026, China
[3]Shenzhen Entry-exit Inspection and Quarantine Bureau, Shenzhen 518045, China

Abstract— By applying the superposition of beams, we obtain a group of virtual sources for a complex variable function Cosh-Gaussian wave. We also derive a closed-form expression for the complex variable function Cosh-Gaussian wave that in the appropriate limit yielding the paraxial complex variable function Cosh-Gaussian beam. From the spectral representation of the complex variable function Cosh-Gaussian waves, we derive the nth-order nonpar axial corrections for the corresponding paraxial complex variable function Cosh-Gaussian beam analytically. The angular velocity of then on paraxial complex variable function Cosh-Gaussian beams decreases with the propagation distance increasing.

Experimental Study of the Scintillation Properties of Partially Coherent Beams in Turbulent Atmosphere

Xianlong Liu, **Fei Wang**, **and Yangjian Cai**
College of Physics, Optoelectronics and Energy, Soochow University, Suzhou 215006, China

Abstract— It is well known that one of the fundamental limitations for a laser weapon system in turbulence is the scintillation induced by atmospheric turbulence. Scintillation is caused from the distortion of the phase structure of the field by the turbulence, thus it is extremely important to develop a method to reduce turbulence induced scintillation. It has been revealed that one can reduce turbulence-induced scintillation by use of a partially coherent beam or a coherent beam with special beam properties (i.e., special beam profile, phase, and polarization). By modulating the beam profile, polarization, correlation function, and phase of a partially coherent beam, one can expect to further reduce the turbulence-induced scintillation. Here, we experimentally investigate the scintillation index of a radially polarized beam with controllable spatial coherence and studied the vortex phase-induced reduction in scintillation of a partially coherent beam. Our experimental results have been shown that a partially coherent radially polarized beam can reducing turbulence-induced scintillation compared to linearly polarized partially coherent beam. And with a partially coherent beam-carrying vortex phase (i.e., Gaussian-Schell model vortex beam) has appreciably smaller scintillation than a Gaussian-Schell model beam, the results will be helpful in free-space optical communication and laser weapon system in turbulent atmosphere.

Coherent forward Scattering through a Cold Sr^{88} Atomic Cloud

C. C. Kwong[1], **T. Yang**[2], **P. Symore**[2], **K. Panday**[2], **D. Delande**[3], **R. Pierrat**[4], **and D. Wilkowski**[1, 2, 5]

[1]PAP, School of Physical and Mathematical Sciences
Nanyang Technological University, 637371, Singapore
[2]Centre for Quantum Technologies, National University of Singapore, 117543, Singapore
[3]Laboratoire Kastler Brossel, UPMC-Paris 6, ENS, CNRS; 4 Place Jussieu, Paris 75005, France
[4]Institut Langevin, ESPCI ParisTech, CNRS UMR 7587, 10 rue Vauquelin, Paris 75005, France
[5]CNRS, Institut Non, Linéaire de Nice, Université de Nice Sophia-Antipolis, Valbonne 06560, France

Abstract— The coherent forward scattering in ultra-cold atomic gas is investigated experimentally to verify the theoretical prediction. The light matter interaction in the optical thick medium has be studied theoretically and numerically. A high flux source for ultra cold Strontium atoms is constructed. When an abrupt extinction of the resonant laser incidents through a cold atomic cloud, a coherent flash is emitted in forward direction. A "superflash" with an initial transmission larger than 1 is observed via modifying the phase of the incident beam.

Radiation Force Produced by Tightly Focused Cylindrical Vector Pulse Beam by High Numerical Aperture Lens on Rayleigh Particles

Yiming Dong[1], **Fei Wang**[2], **and Yangjian Cai**[2]

[1]Department of Physics, Shaoxing University, Shaoxing 312000, China
[2]School of Physical Science and Technology, Soochow University, Suzhou 215006, China

Abstract— In the past several years, cylindrical vector beam has been widely investigated due to its unique tightly focusing properties and has important applications in many fields, such as optical trapping, laser making, dark field imaging and data storage, etc.. Compared to continuous-wave laser beams in optical trapping, pulse beams can produce much larger radiation force on micro-particles and can trap particles more stably. In this paper, dynamic evolution of radiation force produced by tightly focused cylindrical vector pulse beam by high numerical aperture lens on Rayleigh particles is investigated by Richards-Wolf vectorial diffraction method. Our numerical results show that the radiation force, for both the transverse and longitudinal components, can be greatly enhanced as the pulse duration decreases. It is further found that for the cylindrical vector pulse with short pulse duration, Rayleigh particles can be trapped much more stably than long pulse duration whereas for the linear polarized pulse beam with short pulse duration, the stably optical trapping is destroyed. Finally we discuss the stability conditions of the effective manipulating the particle by the pulse beam. Our results provide the important information about the trapping mechanism of pulsed tweezers.

Cosine-Gaussian-correlated Schell-model Beams with Rectangular Symmetry

Chunhao Liang, **Fei Wang**, **Xianlong Liu**, **and Yangjian Cai**
College of Physics, Optoelectronics and Energy, Soochow University, Suzhou 215006, China

Abstract— A class of partially coherent beams whose degrees of coherence have position-independent Gaussian profiles have been studied in depth due to its tractability and universality. Since the sufficient condition for devising a genuine correlation function of a scalar or electromagnetic partially coherent beam was established by Gori and collaborators, a wide variety of partially coherent sources and beams became known, such as beams with locally varying spatial coherence, a nonuniformly correlated (NUC) beam, multi-Gaussian Schell model (MGSM) beam, cosine-Gaussian Schell model (CGSM) beam, Bessel-Gaussian (BGSM) and Laguerre-Gaussian Schell-model (LGSM) beam, and a special correlated partially coherent vector beam. All these beams exhibit interesting features. The NUC beam displays a self-focusing effect and a lateral shift of the intensity maximum on propagation. The MGSM beam displays a far-field flat-topped beam profile. The CGSM, BGSM, and LGSM beams display far-field ring-shaped beam profiles. In 2013, Zhangrong Mei et al. proposed the CGSM sources, whose degree of coherence (DOC) is of circular symmetry. Now we have introduced a model for a CGSM beam, whose DOC is the superposition of two 1D cosine-Gaussian-correlated Schell-model sources, i.e., possesses rectangular symmetry as a natural extension of it. The novel model sources and beams we generate are termed rectangular cosine-Gaussian Schell-model (RCGSM). Their features are quite different on propagation, e.g., the RCGSM's intensity in the far field (or in the focal plane) displays a four-beamlet array profile, and the CSGM's intensity in the far field displays ring-shaped beam profiles. Furthermore, we have carried out experimental generation of the proposed beam, and the degree of coherences in the output plane is the Fourier transform of the source intensity distribution on the face of the rotating glass ground-disk (RGGD), thus we can realize modulating the DOC of a partially coherent beam just choosing intensity distribution on the face of the RGGD. The RCGSM is of importance in applications, such as particle trapping and material thermal processing.

Cosine-Gaussian Correlated Schell-model Pulses in Dispersive Media

Chaoliang Ding and Liuzhan Pan
Department of Physics, Luoyang Normal University, Luoyang 471022, China

Abstract— Taking into account the extraordinary properties of stationary cosine-Gaussian correlated Schell-model beams on propagation, an interesting question comes up: Are there some new characteristics of cosine-Gaussian correlated Schell-model (CGSM) pulses in dispersive-media propagation?

In this paper, a new class of partially coherent pulse of Schell type with cosine-Gaussian temporal degree of coherence, i.e., CGSM pulses, is introduced. The analytical expression of the mutual coherence function of CGSM pulses in dispersive media is derived, and used to study the evolution of the intensity and the temporal degree of coherence of CGSM pulses. Numerical calculations are performed to show the dependence of the intensity and the temporal degree of coherence of CGSM pulse on the incident pulse duration, temporal coherence length, parameter n and medium dispersion. It is shown that at some critical propagation distances, one CGSM pulse begins to split into two in dispersive-media propagation. And the critical propagation distance of the two splitting pulses and their evolution depend on the incident pulse parameters and propagation medium coefficient. The main results are interpreted physically.

An Optimal Match between the Ground-based Laser and a Relay Mirror System

Lipeng Luo, Yongte Jiang, Haiqiang Tong,
Chunmei Chai, Chunnan Zhang, and Xiuxiang Chu
School of Sciences, Zhejiang Forestry University, Lin'an 311300, China

Abstract— Based on the application of a relay mirror system, we study the intensity distribution and receiving efficiency of laser beams through a relay mirror system. When Fresnel number is big, this studies shows that the coupling efficiency of power between ground-based telescope and relay mirror is high for collimated beams. Due to small spot and high intensity concentrated on central obscuration, beams focusing to relay mirror is not suitable. For the reason that the distance between the laser source and relay mirror is fixed, and the distance from the relay mirror to a target is various, the intensity distribution is changed with different target. It is impossible to keep in high coupling efficiency when beams focus to target directly through a relay mirror system.

Partially Coherent Vector Beam with Special Correlation Functions

Yahong Chen, **Fei Wang**, **Chengliang Zhao**, **and Yangjian Cai**
College of Physics, Optoelectronics and Energy of Soochow University, Suzhou 215006, China

Abstract— Partially coherent beam with conventional correlation functions (i.e., Gaussian correlated Schell-model functions) have been studied extensively and have found wide applications, such as free-space optical communications, optical imaging, laser scanning, inertial confinement fusion, reduction of noise in photography, remote detection, second-harmonic generation, particle trapping and optical scattering. Since Gori discussed the sufficient condition for devising the genuine correlation function of a scalar or electromagnetic partially coherent beam, more and more attention is being paid to partially coherent beams with nonconventional correlation functions. A variety of partially coherent beams with nonconventional correlation functions, such as non-uniformly correlated Gaussian Schell-model beam, multi-Gaussian Schell-model beam, cosine-Gaussian Schell-model beam, and Laguerre-Gaussian correlated Schell-model, have been introduced. Those partially coherent beams with special correlation functions have been found to exhibit some extraordinary propagation characteristics, such as far-field flat-topped and ring intensity profile formation, self-focusing effect, and a lateral shift of the intensity maximum. However, the previous studies about partially coherent beams with special correlation functions were confined to scalar treatment. In this paper, we introduce a general optical system for synthesis of partially coherent vector beams with a variety of correlation functions. In particular we employ it for generation of the family of beams, termed the specially correlated radially polarized (SCRP) beams and examine their free-space propagation both theoretically and experimentally. Our results clearly show that a SCRP beam exhibits unique features on propagation in comparison with those of beams with conventional correlation function. The technique for modulation of the correlation functions and, hence, the coherence state of a SCRP beam in the source plane leads to efficient control of its intensity distribution and its degree of polarization on propagation, which is of importance in particle trapping and material thermal processing applications.

Spatial Correlation Properties of Partially and Fully Coherent Fields

Yuanjie Yang[1] and Yi-Dong Liu[2]

[1]School of Astronautics & Aeronautics
University of Electronic Science and Technology of China, Chengdu 610054, China
[2]School of Physical Electronics
University of Electronic Science and Technology of China, Chengdu 610054, China

Abstract— Recently, the coherence vortices and the phase singularities of a partially coherent have been studied extensively, and the cross correlation function of a partially coherent beam has been studied theoretically and experimentally. It has been shown that spatial correlation functions have interesting topological properties associated with their phase singularities, and there exist correlation singularities in the regions where the phase is ill-defined. In this paper, the analytical expression for the far-field the mutual coherence function (MCF) of a partially coherent vortex beam is derived. Based on this analytical expression, the far-field correlation properties of partially coherent vortex fields are studied. We show there are many kinds of correlation singularities in partially coherent optical field besides cross-correlation singularity, and the correlation singularities can even exist in the partially coherent field without orbital angular momentum. Furthermore, we show that MCF (x, y; $-x$, $-y$) and MCF (x, y; 0, 0) have the same correlation singularities, and which depends on both radial mode and topological charge. However, the number of correlation singularities of MCF (x, y; $2x$, $2y$) is more different from that of MCF (x, y; $-x$, $-y$) or MCF (x, y; 0, 0). Lastly, we show the link between the far-field cross-correlation function of partially coherent beam and the far-field auto-correlation function of fully coherent beam. Interestingly, it is shown that for given radial mode and topological charge, the far-field cross-correlation function of partially coherent beam, in low coherence cases, is consistent with the far-field auto-correlation function of fully coherent beam.

Analysis of a Vortex Beam in a Non-coaxial Optical Focusing System

Guoxuan Zhu, **Yanfeng Zhang**, **Hui Chen**, **Yujie Chen**, **and Siyuan Yu**
State Key Laboratory of Optoelectronic Materials and Technologies
School of Physics and Engineering, Sun Yat-sen University, Guangzhou 510275, China

Abstract— In recent years, light beams carrying orbital angular momentum (OAM) have attracted lots of interest in the scientific community, especially in the field of optical communication. The OAM of a given symmetric beam is not related to the reference axis selected. However, the distribution of ℓ is dependent on the chosen reference axis. There have been reports on the distribution of ℓ in a misaligned optical beam. Here, we consider the situation where a vortex phase plate (VPP) and a lens are used to generate and focus a vortex beam. The study is key to the coupling of a vortex beam from free space to a ring fiber that can be used to support and transmitted photons carrying OAM for communication systems.

Note that a symmetric beam can be expanded into Fourier series in the azimuth frequency (ℓ) space. These discrete Fourier bases are orthogonal to each other and form the distribution of ℓ. We use this as a tool to analyze the non-coaxial system. An off-axis optical lens will not change the distribution of azimuth frequency if we set the parallel line through the lens center as the reference axis. The off-axis VPP causes a shift in the azimuth frequency space, which brings the separation of the intensity and the geometry center. The situation mentioned above does not change the detected value of OAM. Furthermore, when the spherical lens is tilted, a more complex phenomenon called astigmatism appears. We calculate the situation when the slant angle is small. When a VPP tilts, it changes the purity of ℓ state and the phase distortion depends on the deflection angle. We analyze these situations and use criterion of $\partial\psi/\partial\phi$ to estimate the value of ℓ at each points, in which ψ is the light field distribution function.

The research reveals that an off-axis focusing system will not change the OAM states but will change the distribution of ℓ. It also shows that a deflection focusing system will seriously change the phase and causes the error of detection.

M^2-factor for the Partially Coherent Elegant Laguerre-Gaussian Beam Propagating through the Turbulent Ocean

B. Wang, Y. S. Yuan, Z. F. Cui, and J. Qu
Department of Physics, Anhui Normal University, Wuhu 241000, China

Abstract— On account of the extended Huygens-Fresnel principle and the second order moments of the Wigner distribution function, associated with the spatial power spectrum considering temperature and salinity fluctuations, the analytical expression of the beam propagation factor (M^2-factor) for partially coherent elegant Laguerre-Gaussian (PCELG) beam has been theoretically derived. On the basis of the theoretical formulae, specific numerical calculations are illustrated, to indicate how the beam and the oceanic turbulence parameters influence on M^2-factor of the PCELG beam in oceanic turbulence. Furthermore, the corresponding analysis and discussions reveal that the M^2-factor of the PCELG beam in oceanic turbulence vary with changes in parameters of the beam and the oceanic turbulence. The acquired results may have some certain reference value for laser tracking, remote sensing and optical communication under the water.

Propagation Properties of an Anomalous Hollow Beam with Orbital Angular Momentum through a Paraxial ABCD Optical System

Chenchen Zhao, Chengliang Zhao, and Yangjian Cai
School of Physical Science and Technology, Soochow University, Suzhou 215006, China

Abstract— Based on the Collins integral, an analytical expression of a general anomalous hollow vortex beam passing through a paraxial ABCD optical system is derived by means of the mathematical technique. As a numerical example, the normalized intensity distribution, the phase distribution, and the orbital angular momentum density distribution of anomalous hollow vortex beams propagating in free space are graphically demonstrated. The influences of axial propagation distance and the topological charge on the normalized intensity distribution, the phase distribution, and the orbital angular momentum density distribution of anomalous hollow vortex beams propagating in free space are discussed in detail.

Propagation Properties of Partially Coherent Anomalous Hollow Beams in Uniaxial Crystals

Xingyuan Lu, Chengliang Zhao, and Yangjian Cai
School of Physical Science and Technology, Soochow University, Suzhou 215006, China

Abstract— Analytical propagation formulae for partially coherent anomalous hollow beams in uniaxial crystals are derived. Paraxial propagation of partially coherent anomalous hollow beams in uniaxial crystals orthogonal to the optical axis is investigated based on the beam propagation equations. The propagation properties of partially coherent anomalous hollow beams in uniaxial crystals and in free space are studied numerically and comparatively. It is found that the propagation properties of partially coherent anomalous hollow beams in uniaxial crystals behave very differently from those in free space, and are closely determined by the parameters of the uniaxial crystals and the initial coherence width. The uniaxial crystals provide an effective way for generating astigmatic beams.

Session 4P9
Microwave and Millimeter Wave Circuits and Devices, CAD

Microstrip Diplexer Design Using Three EBG

Ursula Martinez-Iranzo[1], **Bahareh Moradi**[1], **Eva Arasa**[2], **Julian Alonso**[2], **and Joan Garcia-Garcia**[1]

[1]Grupo de Aplicaciones Electromagnéticas Industriales — GAEMI
Electronic Engineering Department, Universidad Autónoma de Barcelona, Campus de Bellaterra
08208 Cerdanyola del Vallès, Barcelona, Spain
[2]Grupo de Sensores y Biosensores, Analytical Chemistry Department
Universidad Autónoma de Barcelona, Campus de Bellaterra, 08208 Cerdanyola del Vallès, Barcelona, Spain

Abstract— A novel diplexer design by combining of three electromagnetic band gap (EBG) structures is presented in this paper. The diplexer is constructed by combining an EBG at the input port with two different EBG at the ouput ports. The proposed diplexer is configured with filter in each arm to reject unwanted signals. The first or the second harmonic falls into the stopband and can be suppressed by EBG structures as well as band pass is controled directly by EBG structure. One of the most important properties of EBG structure is to prohibit the propagation of surface wave. Further the EBG structure demonstrates a better performance to improve the mutual coupling. Practical applications of EBG structure usually have difficulty in accommodating its physical size, because the period of EBG lattices has to be a half-wavelength at the band-gap frequency. The proposed design has been implemented in a Rogers RO3010 substrate with thickness 25 mil. It provide a new idea for designing more efficient electromagnetic structures for microwave circuit applications, such as filters, diplexer, and other passive circuits. This research is only the first step for the feasibility study of the diplexer design by using EBG technology, which can be modified to the other desired frequency bands. The proposed diplexer is simple to fabricate, as it is designed using micro-strip technology, and presents compact dimensions, making use of a low number of elements. The excellent agreement between the electromagnetic simulation and the measurement are an excellent starting point to develop a robust design methodology.

Wide-stopband Millimeter-wave BPF on GaN MMIC Using Asymmetric Feeding Structure

Jin Xu Xu, Xiu Yin Zhang, and Xiao Feng Liu
School of Electronic and Information Engineering
South China University of Technology, Guangzhou 510640, China

Abstract— This paper presents a novel compact bandpass filter for 30 GHz millimeter-wave applications on GaN Monolithic Microwave Integrated Circuit (MMIC). The proposed circuit consists of two symmetrical coupled quarter-wavelength transmission-line resonators and two coupled transmission-line feeding structures. The two coupled quarter-wavelength transmission-line resonators are folded to miniaturize the circuit size and connected by the via to result in both electrical and magnetic coupling. Two feeding lines are designed as asymmetrical structures, which are utilized not only to cause mismatch at the third harmonic frequency between the resonator and feeding lines so that the third harmonic can be suppressed but also to provide source-loaded to generate two transmission zeros near the passband, resulting in high selectivity. To verify the proposed idea, an experiment filter has been implemented. High skirt selectivity and wide stopband are observed in the results. Due to the millimeter-wave MMIC technology and its compact structure, the filter is only 400 µm × 310 µm ($0.092\lambda_g \times 0.069\lambda_g$), where λ_g is the guided wavelength at the operating frequency of 30 GHz.

The filter has a 3-dB bandwidth of about 6.8 GHz at the center frequency of 30 GHz. The insertion loss of the passband is about 3 dB and return loss is better than 15 dB at the center frequency. Also, four transmission zeros appear at the frequency of 10 GHz, 46 GHz, 75 GHz and 85 GHz, which help achieve the wide stopband and high skirt selectivity. The rejection level is more than 25 dB within the frequency range from 41 GHz to 110 GHz.

Substrate Integrated Waveguide Frequency Reconfigurable Filter Controlled by Magnetic Field

Qiu Dong Huang, Xiao Liang Liu, and Yu Jian Cheng
University of Electronic Science and Technology of China, China

Abstract— Frequency tunable/reconfigurable filters have special significance in future smart and miniaturized wireless systems. The currently popular substrate integrated waveguide (SIW) technique combines the best and complementary features of both planar transmission lines and non-planar waveguides. Thus it is found very appropriate in microwave and millimeter-wave tunable filter applications. Researchers try to realize some SIW reconfigurable filters by use of PIN diodes and varactors. Unlike those conventional planar transmission lines, such as the microstrip line, the SIW is a uniconductor guided-wave structure and has the same electric potential for each metallic surface. Therefore, some difficulties exist in electronically tunable SIW designs. Besides, complex DC bias circuits may lead to unwanted leakage and interference. Tuning operation characteristics of SIW components by magnetic field is another possible wayof avoiding these problems.

A novel frequency reconfigurable SIW bandpass filter is presented in this paper. This ferrite-loaded SIW filter can be considered as two sub-components. The first one consists of rectangular ferrite slabs loaded on the sidewall slots of SIW where the magnetic fields are strongest. With the application of an external magnetic bias (dH_1) on the ferrite slabs, the cutoff frequency of the SIW is changed, thereby making the lower sideband of the SIW filter switchable. The second component, which is associated with a wide ferrite slab in a SIW with the magnetic field perpendicular to the direction of propagation, employs the edge-mode effect to achieve the bandstop phenomenon and then form the upper sideband of the SIW filter. This sideband can also be controlled by another external magnetic bias (dH_2) on the ferrite slab. Thus both of this filter's bandwidth and operating band can be adjusted.

After full-wave simulation and optimization implemented by Ansoft HFSS, a ferrite-loaded SIW frequency-agile filter is designed. YIG ferrite is employed in this design. Its saturation magnetization value is 1850 Gs, relative dielectric constant is 14.5, and 3 dB line width is 20 Oe. The used substrate is 0.508 mm thick Rogers6010 substrate. Its permittivity and loss tangent are 10.2 and 0.0023, respectively. The actual SIW width is 6.1 mm, the distance between adjacent metallic vias are 1.2 mm, and the diameter of vias are 0.6 mm. As shown in Fig. 1, the lower sideband of the filter can be adjusted from 8.8 GHz to 10.7 GHz. As shown in Fig. 2, the upper sideband can be tuned from 9.3 GHz to 12.0 GHz. Furthermore, a filter whose operating band can be adjusted from 8.8 GHz to 12 GHz is achieved with approximately 2.5 dB insertion loss as shown in Fig. 3.

Compared to previously reported frequency tunable SIW filters, the proposed filter offers a relatively wide tuning range and flexibly reconfigurable abilities while dramatically reducing the complexity of external control circuit.

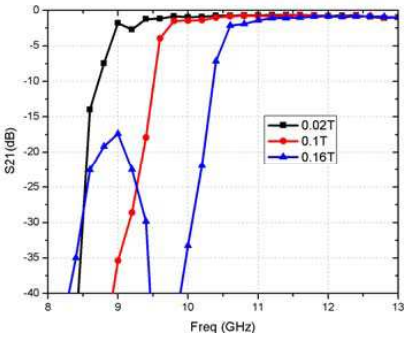

Figure 1.

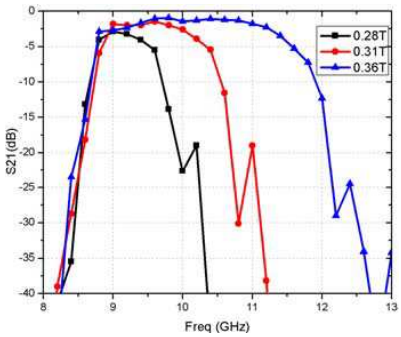

Figure 2.

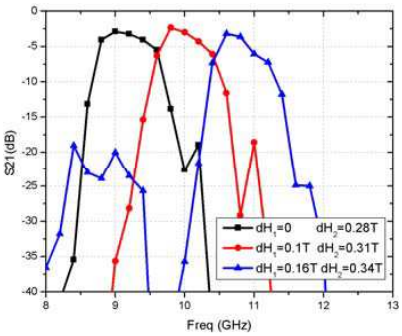

Figure 3.

A Dual-mode Circle Ring Resonator Bandpass Filter

Rong Sheng Li and Ying Hua Lu
School of Electronic Engineering
Beijing University of Posts and Telecommunications, Beijing 100876, China

Abstract— In this article, a novel dual-mode band-pass filter with two transmission zeros in the pass-band using a single ring resonator is proposed. The novel band-pass filter is based on the circle ring resonator with two inner open-circuited stubs which are loaded symmetrically along the ring. Because the proposed structure is symmetrical and the circuit structure for the novel band-pass filter is symmetrical, odd-even mode theory are used to analyze the structure. Based on the theoretical analysis results, we give electrical parameters' values for three band-pass filters. The calculated scattering parameters of three band-pass filter examples are also given. Bandwidth and rejection level of the filter can be designed by choosing different even-mode and odd-mode characteristic impedances values of the transmission lines. By using circle ring resonator with two inner open-circuited stubs, the proposed band-pass filter has two transmission zeros. Without coupling gaps between feed lines and rings, there are no mismatches and radiation losses between them and the novel filter shows low insertion loss. To validate this topology, the proposed band-pass filter is simulated, fabricated and measured. The measured results prove to be largely consistent with the calculated results and the simulated results. There is frequency offset and different insertion loss between the simulated results and the measured results. The filter has many remarkable advantages, such as low insertion loss, simple structure, compact size and high selectivity. Because of its advantages, they have great applications in RF circuits and system.

Additional Cross Coupling Coefficient Used as Matching Ladder Network in Coupled Based Band Pass Filters

B. Moradi, **U. Martinez**, **and J. J. García-García**
Electrical Engineering Department GAEMI
Universitat Autonoma de Barcelona, Cerdanyola Del Valles, Spain

Abstract— A novel design based on three coupling coefficient filter is presented in this paper. The design based on three square open loop resonators in gap between them and a cross coupling between input/output (I/O) port. The novelty of the proposed design is the introduction of a cross coupling interactions that allows to match the impedance achieving excellent performance in the transmission and reflection response. The proposed filter has been implemented in a Rogers RO3010 substrate. The minimal distance of gap between the resonators is 0.2 mm and the distance between the I/O port line and the resonators has been fixed to 0.15 mm which is the more critical distance of the design. The designs based on the coupling coefficient exhibit an inherent limitation fixed by the minimal distance that is fixed by protolaser miling technology. The square shape of the resonators maximize the capacitance of the LC resonant tank, resulting in a final thickness of 3.1 mm. Extensions of the ports with a 90° angle feed the resonators through a capacitive coupling (1.5 mm gap) which intensity depends of the proximity to the extreme resonators. The interaction between resonators and, specially, the interaction between the input-output ports introduces loads in the resonators that affects to the fundamental resonant frequencies as well as to the matching impedance. Measures of the fabricated prototype depicted a well matched wide band pass filter between 1.1 GHz and 1.79 GHz, which correspond to a FBW = 50% and also insertion losses oscillates between −0.66 dB and −1.3 dB. The excellent agreement between the electromagnetic simulation and the measurement are an excellent starting point to develop a robust design methodology. In this paper we propose a small modification of the layout that introduce a cross coupled that can be interpreted as an additional matching ladder network.

Negative Group Delay Network Using CMOS Cascade Amplifier and Bonding-wire

Jaeyeon Kim[1], **Junsik Park**[1], **Girdhari Chaudhary**[1], **Yongchae Jeong**[1], **Namsik Ryu**[2], **and Jongsik Lim**[3]

[1]Chonbuk National University, Republic of Korea
[2]Electronics and Telecommunications Research Institute (ETRI), Republic of Korea
[3]Soonchunhyang University, Republic of Korea

Abstract— Recently, some interesting studies of the negative group delay (NGD) concept have led to its experimental validation through the realization in electronic circuit. Well-synchronization signals are required to maintain the system consistency. In order to enhance the signal synchronization in the RF/microwave and millimeter-wave equipment, various techniques using NGD concept at baseband and microwave bands were presented in previous works. However, there are lacks of researches of NGD network in RFIC using CMOS process as compared with other areas. Therefore, this work seems the first attempt to design NGD network in the field of RFIC.

In this paper, a design of active NGD network is presented based on cascade amplifier in CMOS process which can provide NGD time as well as gain at operating center frequency of 1.95 GHz. The proposed circuit uses two NMOS MOSFET amplifiers in cascade structure and parallel RLC resonator at the source of each NMOS amplifier in order to generate the NGD time as shown in Fig. 1. In order to avoid the use of spiral inductor for miniaturization of circuit, the values of R and L are implemented with bonding wire, which is connected between ground and pad of chip as shown in Fig. 1. The feedback RC circuit between the gate and drain of MOSFET has been used to increase stability. The input/output matching circuits are used to enhance the reflection characteristics. Fig. 2 shows the simulation results of proposed circuit. From simulation, the NGD time of -1.73 ns with gain of 11.35 dB were obtained as shown in Fig. 2. The input and output return loss characteristics are better than -20 dB as shown in Fig. 3.

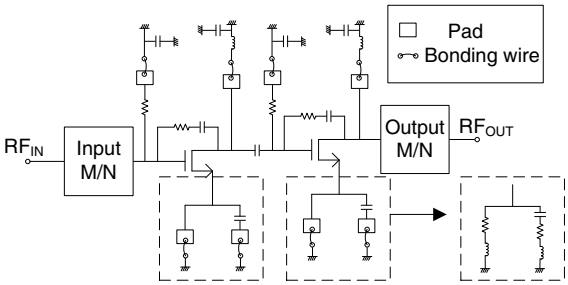

Figure 1.

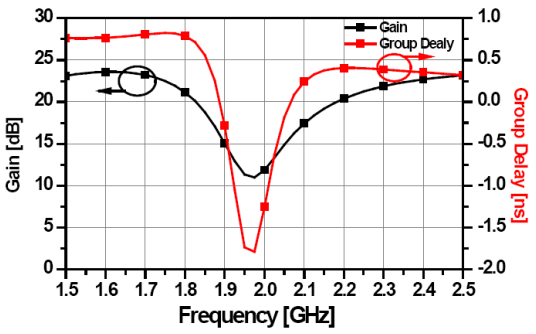

Figure 2.

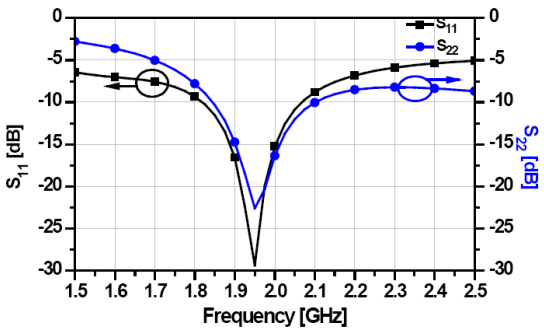

Figure 3.

High Efficiency TM_{01}-mode Cylindrical Waveguide Microwave Reactor for Microwave Material Continuing Processing

Yi-Chen Zhong, Wei-Na Huang, and Yu-Jian Cheng
University of Electronic Science and Technology of China, Chengdu, China

Abstract— In this paper, a cylindrical waveguide microwave reactor is proposed for microwave material continuing processing. This traveling-wave type chemical reactor will be used in food processing, microwave chemistry, coal desulfurization, etc.. Compared with the existing microwave reactor, such as rectangular waveguide types, ridge waveguide types, and folded waveguide types, our structure has obvious advantages in the distribution of the field strength, reaction effect, and energy consumption.

As shown in Fig. 1, a cylindrical waveguide microwave reactor with two axial slits is demonstrated in this paper. It operates with TM_{01} mode, i.e., the first high-order mode. Two axial slits are cut out from the conductor wall of the cylindrical waveguide in order to fix the conveyor belt. In this configuration, the electric field is concentrated on the axis of the cylindrical waveguide as shown in Fig. 2. Thus the sample is located in this region and carried by the low-loss conveyor belt. In this case, the electric field sufficiently reacts with the sample; thereby enhancing the absorption of the microwave power of the sample to accelerate the reaction (the absorbed power $P = 56.62 \times 10^{-12} f E^2 \varepsilon''$ is proportional to electric field strength). The conveyor belt, which goes through the two slits, is connected to the wheels outside to support the sample. However, the TM_{01} mode may be converted into the TE_{11} mode, i.e., the dominant mode of cylindrical waveguide, due to the discontinuity of the waveguide. It should be noted that the slits could inhibit the appearance of the TE_{11} mode by cutting radially current on the inner surface. The coaxial ring coupling feeding method is employed to excite the TM_{01} mode.

As an example, the pulverized coals are placed in this reactor for desulfurization reaction. At 915 MHz, the simulated result implemented by Ansoft HFSS show that the pulverized coal's SAR (Specific Absorption Rate) in this reactor is much higher, i.e., $1.5 \sim 3$ times, than the SAR in a conventional rectangular waveguide reactor or a ridge waveguide reactor with the same condition.

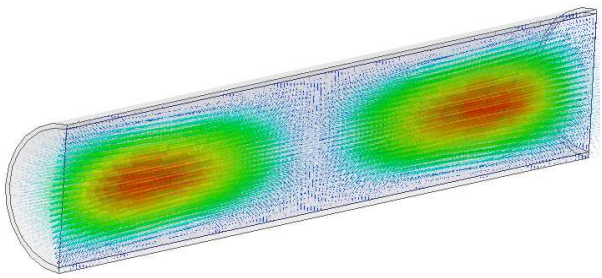

Figure 1: Electric field distribution of TM_{01} mode.

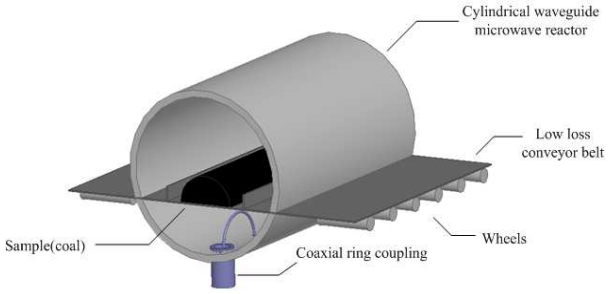

Figure 2: Pulverized coal desulfurization reaction.

A High-efficiency Darlington Power Amplifier Design Using 0.5 μm GaN-on-Silicon HEMT Technology

Min-Li Chou, Hong-Kun Wang, Hsien-Chin Chiu, and Fan-Hsiu Huang
Department of Electronic Engineering, Chang Gung University, Taoyuan 333, Taiwan

Abstract— This paper presents a broadband Darlington power amplifier with high efficiency performance for band and band applications. The proposed power amplifier was fabricated in 0.5 μm GaN-on-Silicon HEMT technology. The schematic of power amplifier is shown in Fig. 1. The broadband performance has been provided by Darlington circuit topology, which is composed of gain stage (M_1 and M_2) and power stage (M_3 and M_4). To further improve the output power characteristic and enhance high-frequency small-signal gain in this circuit, cascode transistor structure was employed by using M_3 and M_4, where transistor M_3 with the bias VG3 plays a common-gate amplifier to achieve a proper output impedance for efficiency improvement. In addition, transistor M_2 with a feedback resistor R_3 can be used to be a self-adjustment resistor while it operates at large signal state. Based on the operation, the node A presents the modification to waveform shape and equivalent dc bias. Thus the rf-to-dc efficiency of first stage can be improved. A signal with AM-PM linearity adjustment also is generated by the function. The linearity of the output signal therefore can be compensated and improved after connecting the power stage circuit.

The chip photograph is shown in Fig. 2, where the passive components were arranged on the chip with dc and rf pads. The complete device small/large-signal modeling for HEMTs and passive components had been built for circuit simulation. The size of the chip is $2000 \times 1300\,\mu m^2$, and the gate width for $M_1 \sim M_4$ are $4 \times 100\,\mu m$, $2 \times 25\,\mu m$, $16 \times 100\,\mu m$ and $16 \times 100\,\mu m$. In the measurement setup, a off-chip inductor to be rf choke was used through bonding wire at the

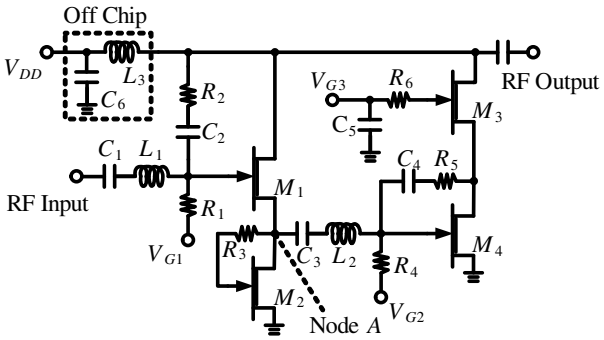

Figure 1: Schematic of the Darlington power amplifier.

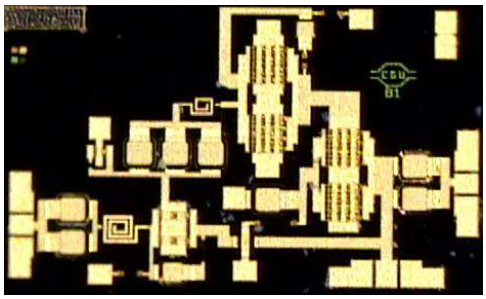

Figure 2: Chip photograph of the proposed PA.

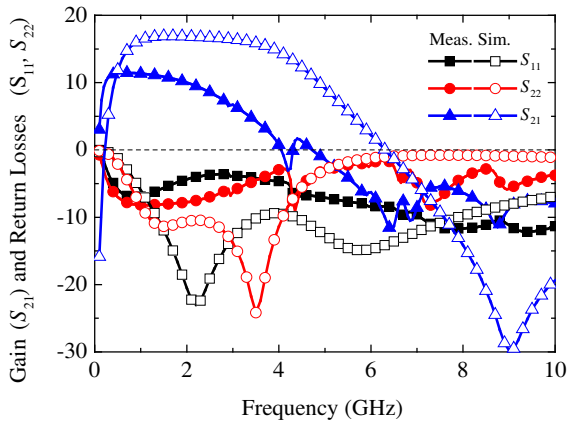

Figure 3: Gain and return loss of proposed PA.

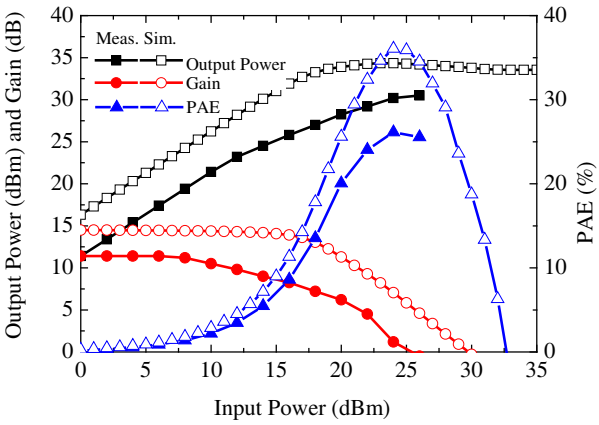

Figure 4: Large-signal performances of the proposed PA.

output port as show in Fig. 1. Fig. 3 shows the measured and simulated small-signal gain and return loss curves. The maximum gain in the measurement is 11.5 dB with a 3-dB bandwidth from 0.2 GHz to 2.5 GHz, where the supply voltage was set to be 25 V with a dc current of 120 mA. Because the process mismatch results in a large characteristic variation in HEMTs, a narrow bandwidth performance therefore was exhibited in this circuit. Fig. 4 shows the output power, gain and PAE along with the rf input power at 1 GHz. The maximum output power of 30.5 dBm can be achieved, and the maximum PAE is about 26% at an input power of 25 dBm.

ACKNOWLEDGMENT

This work was partially supported by the National Science Council, Taiwan, R.O.C., (NSC 102-2221-E-182-070), the High Speed Intelligent Communication (HSIC) Research Center, and the Healthy Aging Research Center (HARC), Chang Gung University.

Design of an All-pass Phaser Using Microstrip C-sections

Weiwei Liao, Qingfeng Zhang, and Yifan Chen
Department of Electrical and Electronics Engineering
South University of Science and Technology of China, China

Abstract— This paper presents a C-section all-pass phaser based on microstrip technology. It consists of eight cascaded coupled C-sections. By controlling the length and coupling coefficient of the C-sections, a linear group delay response with 0.25 ns swing is obtained within the operation frequency range 1–2 GHz. The full-wave simulation result agrees well with the specified response, which validates the proposed design method.

Real-time analog signal processing (R-ASP) is getting popular nowadays with the exploding demand for faster communication technology [1]. The core component of a R-ASP system is a phaser, which exhibits an arbitrary group delay response versus frequency. C-section all-pass phaser, as one of the design technologies, is widely used due to its wide operation bandwidth and simple design principle. However, only stripline implementations were reported so far [2], in which the fabrication requirement is very high due to the multi-layer structure and complicated transitions. This paper presents a microstrip design featuring low fabrication complexity. Fig. 1 shows the layout and full-wave simulation results. Note that a linear group delay with 0.25 ns swing is observed within the frequency 1–2 GHz, which agrees well with the specified response. The reflection magnitude is also suppressed below −20 dB.

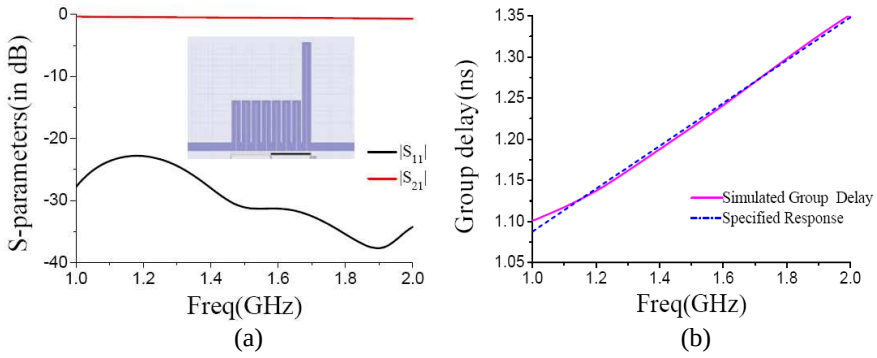

Figure 1: (a) Layout and magnitude response, (b) group delay response.

REFERENCES

1. Caloz, C., S. Gupta, Q. Zhang, and B. Nikfal, "Analog signal processing: A possible alternative or complement to dominantly digital radio schemes," *IEEE Microw. Mag.*, Vol. 14, No. 6, 87–103, Sep. 2013.
2. Gupta, S., A. Parsa, E. Perret, R. V. Snyder, R. J. Wenzel, and C. Caloz, "Group delay engineered non-commensurate transmission line all-pass network for analog signal processing," *IEEE Trans. Microw. Theory Tech.*, Vol. 58, No. 8, 2392–2407, Aug. 2010.

A Double Ended Active Electrode Using SiP with DC and 50 Hz Rejection

Linping Gao, Nikolas Gaio, Jinyong Zhang, and Lei Wang
Shenzhen Institutes of Advanced Technology, Chinese Academy of Sciences, China

Abstract— Active electrode is considered an extremely effective structure for capturing human bio-potential signals when compared with the traditional Ag/AgCl electrodes. This work presents a new configuration for a double ended active electrode included in a System-in-Package (SiP) solution. The chip overcomes the traditional problems of relatively large area and slow time response, and it demonstrates the characteristics of low power consumption, DC and 50 Hz rejection. It has a 2.1 kHz bandwidth with a 40 dB gain, and it reaches the extremely low cut-off frequency of 7.9 MHz. The working voltage is 1.8 V, and the power consumption of per channel is 6.7 µW. This chip has been fabricated with 0.18 µm 1P6M CMOS Process and then inserted in a SiP.

Simulation of a High-convergence Electron Optics System for an X-band High-impedance Relativistic Klystron

Danni Zhu, **Jun Zhang**, **Zumin Qi**, **and Wei Li**
College of Optoelectric Science and Engineering
National University of Defense Technology, Changsha 410073, China

Abstract— As a high-quality, small radius electron beam plays a crucial role in an effective beam-wave interaction, a high-convergence electron optics system is required for an 11.424 GHz high-impedance relativistic klystron, with an output power of 105 MW. With the synthesis of Pierce's electron gun and the cylindrical focusing electrode, a particle in cell model of the electron gun is constructed to generate the electron beam. Based on the electrostatic beam trajectories, a beam-focusing system is designed, with which electron beam can be well focused by adjusting the magnetic field profile especially in the transient region. The PIC simulation results indicate that the balance radius of the reasonably fluctuated beam is about 3 mm, with a fine laminarity, and the transmission, the perveance and the area convergence are 100%, 0.9 μP and 97 : 1 respectively, which satisfy the requirement of the 11.424 GHz high-impedance relativistic klystron.

The Metamaterial Technology Applied to Planar Antennas

E. F. Guelber[1], **A. V. Cardoso**[1], **C. E. Capovilla**[2], **and H. X. Araujo**[1]

[1]Universidade Federal de São João Del Rei — UFSJ, Brazil
[2]Universidade Federal do ABC — UFABC, Brazil

Abstract— In this work, metamaterials structures are applied to electromagnetic devices in order to improve its performance, in terms of gain, bandwidth and resonance. Basically, three topologies are used (Jerusalem cross pair, tripole array and CSRR — complementary split ring resonator), in three different devices: antennas, waveguides and a GTEM chamber. Experimental results are compared to the simulated ones.

Actually, metamaterial is a macroscopic composite of periodic or non-periodic structure, whose function is due to both the cellular architecture and the chemical composition [1]. Therefore, the behavior of a material, in the presence of an electric field, is determined by the macroscopic parameters, permittivity ε and permeability μ. Several metamaterial structures have been investigated along the last years. In particular, ones those are capable to provide artificial magnetic responses and electric walls.

The artificial magnetic conductors can be obtained when a plane wave focus on the capacitive gap, while the artificial electric conductor is obtained through the opposite way.

In fact, the metamaterial pattern is applied to physical devices aiming to obtain specific responses. In [2] a CSRR structure is employed to a UWB antenna in order to provide a rejection characteristic in a desired frequency. On the other hand, in [3] metamaterial structures are applied to an UHF antenna and a better gain is obtained, while in [4] the periodic is structures are applied to the septum of a GTEM — Gigahertz Transverse Electromagnetic chamber, expecting a shift on the resonance frequencies.

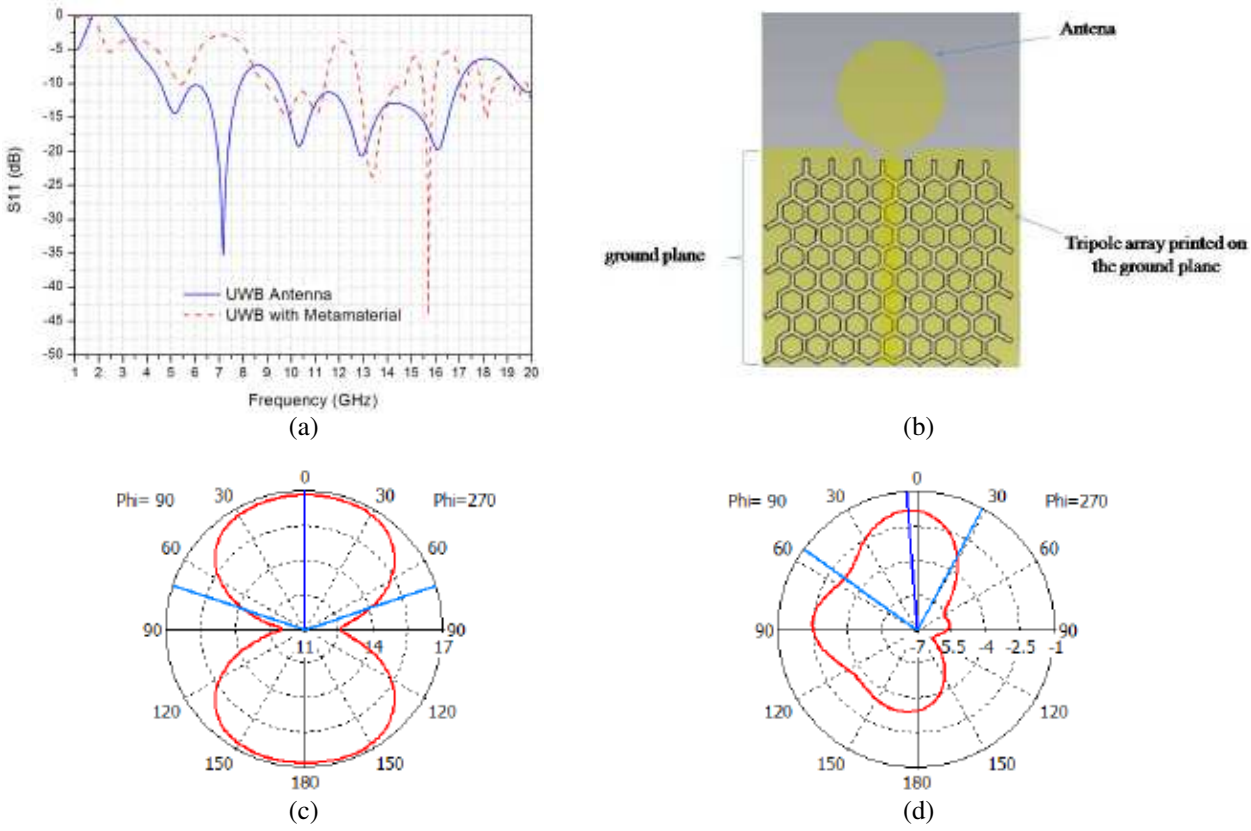

Figure 1: Metamaterial structures applied to a patch antenna. (a) Return loss; (b) prototype; (c) radiation pattern E-plane without metamaterial; (d) radiation pattern E-plane with metamaterial.

In this context, to improve the performance in terms of gain, bandwidth and resonance, of telecommunications devices, three different topologies are employed.

REFERENCES

1. Cui, T. J., "Electromagnetic metamaterials: Recent advances on the theory, experiments, and applications," *IEEE Antennas Propag. Mag.*, 2008.
2. Jo, N.-I, D.-O. Kim, and C.-Y. Kim, "A compact band notched UWB antenna for mobile applications," *PIERS Online*, Vol. 6, No. 2, 177–180, 2010.
3. Araujo, H. X., S. E. Barbin, and L. C. Kretly, "Metamaterial cell patterns applied to quasi-Yagi antenna for RFID applications," *Radio and Wireless Symposium — RWS*, Santa Clara, USA, 2012.
4. De Araujo, H. X. and L. C. Kretly, "The effect of metamaterial patterning to improve the septum GTEM chamber performance," *PIERS Proceedings*, 1224–1228, Marrakesh, Morocco, March 20–23, 2011.

Session 4P10
Antenna and Array 2

Analysis and Design of the Switched-beam Antenna Array for Automotive Radar Applications

Jau-Jr Lin
Department of Electrical Engineering, Changhua University of Education
No. 2, Shi-Da Road, Changhua City, Taiwan

Abstract— More and more vehicles equip the radar system to improve the driving safety. However, the multiple antenna arrays are used to cover different field of view (FOV) for most models. To reduce the multiple modules for different applications, a switched-beam antenna array is designed to cover both long-range and short-range automotive radar applications plus the blind side detection. The FOV is -8° to $+8^\circ$ and -45° to $+45^\circ$ for the long-range and short-range automotive radars, respectively. For the blind side detection, the FOV is -80° to -45° and $+45^\circ$ to $+80^\circ$ to cover the angles, which are often blocked by the vehicle front pillars. This is extremely helpful for the driving situations like leaving the parking spots, exiting the small streets and driving in the curved mountain roads, etc.. Based on the FOV requirements, a switch-beam antenna array is proposed. The simulation demonstrates this antenna array can operate not only over the wide FOV, but also wide bandwidth (76 to 81 GHz).

Compact Printed Ultra-wide Band Antenna with Band-notched Characteristics

Chongzhi Han, Jiaran Qi, and Jinghui Qiu
Department of Microwave Engineering, School of Electronics and Information Engineering
Harbin Institute of Technology, Harbin, Heilongjiang, China

Abstract— In 2002, the Federal Communications Commission (FCC) set the bandwidth of 3.1–10.6 GHz as the bandwidth of working and measuring system. From then on, ultra-wide band (UWB) wire antenna has aroused more and more attention. In this paper, a novel UWB microstrip antenna was proposed in order to suit the UWB communication system. The bandwidth of the antenna is wide enough to cover 3.1–10.6 GHz. Moreover, as it is known to us all that the UWB bandwidth is occupied by some other smaller ones. Such as wireless local area network (WLAN) and worldwide interoperability for microwave access (WiMax). As a result, the proposed antenna was promoted via simulation. Utilizing the parasitic strip and the structure of the gap, the characteristic of dual band suppression has been achieved rejecting the frequency band of 5.15–5.825 GHz and that of 3.3–3.8 GHz. The proposed antenna was modeled and simulated in CST software. The antenna prototype has been made also. The measured and simulated results suit well. The proposed antenna has low profile as well as a small geometric dimensioning. The relative bandwidth can reach as wide as 120%, easily fits the UWB communication system.

A Triangular Antenna with Spiral Slot Arrays for Beidou Navigation

Jianhua Zhou, Kaishuang Zhang, and Baiqiang You
Department of Electronic Engineering, Xiamen University, Xiamen, Fujian, China

Abstract— A dual-band triangular microstrip antenna is presented for Beidou navigation, applying spiral-slot arrays coupling technique. Different with the conventional stacked dual-band antenna, the radiation patch is designed on a single layer of medium loaded with 6-elements feed coupling slot arrays. Thus, the actual current path could be controlled and the size of the proposed antenna is reduced effectively. Dual-band radiation is realized by introducing two triangular vortex rings coupled with 6 meandering slots, covering 1.616 GHz and 2.492 GHz. The three meandering slots are introduced on the ground plane to improve the antenna performance to further. The simulation results show that the 10 dB impedance working bandwidths are 17 MHz and 35 MHz respectively for lower and higher frequencies of Beidou navigation, with quite good radiation stability and high gain performances.

As shown in Fig. 1, the proposed antenna is designed to be printed on a CER-10 (Taconic) substrate with thickness of 3 mm, relative permittivity of 10, and loss tangent of 0.0035. Three large meandering slots and three small meandering slots are introduced on the microstrip patch. Applying fractal and slot technology as the model foundation, these meandering slots are intersected each other and couple with two self-similar triangular ring, in which the small triangular ring could excite the higher resonant frequency while the large one support the lower resonant frequency.

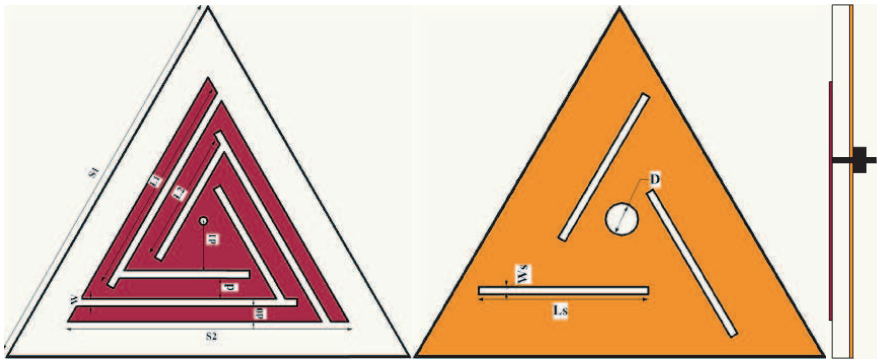

(a) (b) (c)

Figure 1: Configuration of the proposed antenna. (a) Top view. (b) Bottom view. (c) Side view.

A New Spiral Antenna with Improved Axial Ratio and Shorted Arm Length

Huifen Huang and Zonglin Lv
School of Electronic and Information Engineering, South China University of Technology, China

Abstract— Among all frequency-independent antennas, spiral antennas can be a good choice in ultra-wideband systems because of its great performance on circular polarization and maintaining consistent gain and input impedance. A new spiral antenna is proposed in this paper. The developed antenna has improved axial ratio (AR) and shorted arm length. Power spiral antenna, which is designed to improve fidelity factor and pulse compression, aroused our attention. This spiral antenna also achieves noticeable improvement in axial ratio at low frequencies, but the axial ratio degrades at high frequencies. In former work, Archimedean spiral antenna and power spiral antenna are combined to achieve good AR at both low and high frequencies. But the antenna is not a self-complementary structure, and the arm length inevitably becomes longer. The developed spiral antenna in this paper combines the low frequency property of power spiral antenna and high frequency property of Archimedean spiral antenna. The growth rate of radial distance at large winding angle is close to power spiral for improved AR in low frequencies, and the growth rate at small winding angle is close to Archimedean spiral for good AR in high frequencies. The new spiral structure achieves improved axial ratio at the same size with typical Archimedean spiral, and the problem of axial ratio degradation of power spiral antenna is also solved. The arm length is largely shorted by 46.4% than Archimedean spiral antenna, and 63.5% than power spiral antenna. The improved axial ratio also means size reduction of spiral structures. Conventional Archimedean spiral antenna, power spiral antenna, and the new spiral antenna will be discussed in radiation characteristics and arm length in this paper.

Compact Frequency-reconfigurable Antenna for Multi-band Wireless Applications

Abdulkareem S. Abdullah[1], **Yasir I. Abdulraheem**[1], **and Ayman N. Salman**[2]

[1]Department of Electrical Engineering, College of Engineering, University of Basrah, Basra, Iraq
[2]Department of Electrical and Electronics, College of Engineering, University of Thi-Qar, Thi-Qar, Iraq

Abstract— A frequency-reconfigurable multi-band microstrip antenna with two PIN-diode switches is presented here. This antenna engages a compact area of $50 \times 45\,\text{mm}^2$ as a substrate with slotted ground. The antenna is printed on the top of a 1.6-mm thick, FR4 substrate with relative permittivity 4.3, and loss tangent 0.025. In this paper, multiband is achieved by making a slot in the patch with two PIN diode switches located in the proper places along the slots. Loading the slotted patch with switches provides the reconfigurablity property by shifting the frequency from one band to another. By switching the diodes in the ON or OFF states, up to ten different bands from 2.41 to 6.21 GHz are achieved, with impedance bandwidths around 2.5% and 8%. The proposed antenna is designed using Computer Simulation Technology (CST) software based on FDTD method. The advantages of this design is that the different bands of operation for WiMax and Wi-Fi applications with frequency reconfigurabality can be achieved using the same antenna. The schematic diagram of our proposed reconfigurable antenna is presented in Figure 1. It consists of multi slot patch with a single microstrip line feed network, two PIN diode switches on one side of the substrate and a ground plane with two slot on the other side of the substrate. Detailed dimensions of our designed antenna are shown in Table 1.

The dimensions of this antenna are optimized to operate in the 5.2 GHz WLAN band. Since cutting a slot or modifying the dimensions of the patch can create new distributions of current paths. In the other hand, matching circuits of the antenna have been designed and optimized for best possible performance of impedance match. Two PIN diodes are used as a switches. In computer simulation technology, CST microwave studio, these diodes are modeled with a lumped element network which gives $0.9\,\Omega$ as the resistance value of the PIN diode in the ON state (forward biasing) and 0.3 pF as the capacitance value in the OFF state(reverse biasing).

The two PIN diodes provide four possible switching states. Figure 2 shows simulated return loss of the proposed antenna for different states, where a return loss of better than $-14\,\text{dB}$ is observed

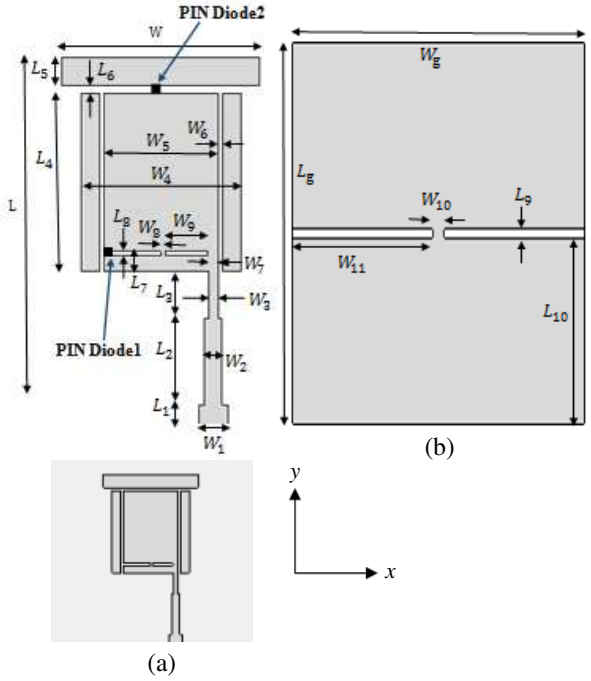

Figure 1: Geometry of the proposed antenna. (a) Front view. (b) Back view.

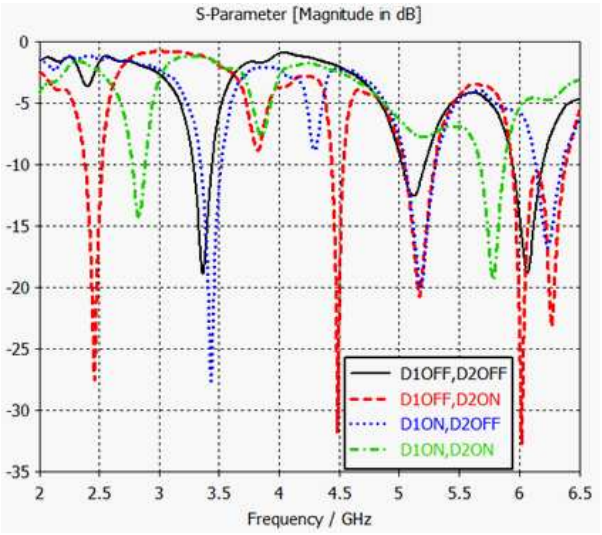

Figure 2: Simulated return loss for the four states.

Table 1: Detailed dimensions of designed antenna (units in mm).

W	W_1	W_2	W_3	W_4	W_5	W_6
21.4	3.11	1.87	1	17.4	12.4	0.5
W_7	W_8	W_9	W_{10}	W_{11}	W_g	h
1.1	0.5	4.6	2	24	50	1.6
L	L_1	L_2	L_3	L_4	L_5	L_6
38.2	2	9	4.85	18.58	3	0.77
	L_7	L_8	L_9	L_10	L_g	
	2.15	0.5	1	22	45	

Table 2: Theoretically calculated resonant frequencies and impedance bandwidths.

Switches configuration		f_r **[GHz]**	**Impedance bandwidth %**
Diode 1	**Diode 2**		
OFF	**ON**	2.41	4.5
		4.41	2.5
		5.19	4.8
		6.2	8
ON	**OFF**	3.4	5.8
		5.2	5.7
		6.21	3.3
OFF	**OFF**	3.35	6
		5.1	4
		6.1	4
ON	**ON**	2.8	3.5
		5.69	4.4

at all resonances. Table 2 shows the four states, the resonance frequencies and the corresponding impedance bandwidth (for reflection coefficient $S_{11} < -10\,\text{dB}$) achieved in each state.

The achieved bandwidths of (D1 OFF, D2 ON) state cover the unlicensed ISM (2.4–2.48 GHz) band used in (IEEE 802.11b/g) and U-NII (5.15–5.35 GHz) band used in (IEEE 802.11a) for WiMax and Wi-Fi applications. (D1 ON, D2 OFF) and (D1 OFF, D2 OFF) states can operate in another bands of WiMax applications. (D1 ON, D2 ON) state can cover the licensed MMDS (2.7–2.9 GHz) band and unlicensed WRC (5.45–5.725 GHz) band required by WiMax applications. The antenna has a peak gain of 4.48 dBi at 5.15 GHz in both (D1 OFF, D2 ON) and (D1 ON, D2 OFF) states, whereas it has a peak gain of 3.9 dBi at 5.19 GHz in the other states. Simulation results for return loss and peak gains for different diodes states show acceptable performance for different WLANs applications.

Tri-band Dual-polarized Multilayer SAR Microstrip Antenna

Hossam Hamza[1] **and Khaled Hussien**[2]

[1]Xidian University, Xi'an, China
[2]Military Technical College, Cairo, Egypt

Abstract— A tri-frequency (at C, X and Ku) bands with dual-linear polarized each, multilayer microstrip antenna single element is proposed and presented. The triple band operation is obtained by using two antenna elements, one for a dual-band resonance at C and X bands with dual linear polarization and above is for the Ku band (also with dual linear polarized behaviour). The feeding mechanism for the dual antenna element is an aperture coupling through cross shaped slot with different shaped feeding ports (to enhance isolation). The Ku band antenna element has an electromagnetically coupled microstrip T-junction feed for one polarization and a direct feeding for the orthogonal polarization. The multilayer microstrip element exhibits a selective frequency band of operation, good isolation among the different feeding ports, good directivity pattern and high gain for both polarizations at all frequency bands. The performance of the proposed antenna was simulated using a commercial software based on the Finite Element Method (FEM) algorithm. The proposed antenna is designed to meet the requirements of Synthetic Aperture Radar (SAR), where multiple frequency with dual linear polarization is needed.

Antenna Design and Simulation: A novel TBDP shared aperture SAR antenna is proposed. The antenna consists of a dual band square patch with two orthogonal feeding ports (for dual polarization) through a cross slot aperture in the ground plane. The two ports are different, one is a line feed and the other is a dual offset feed line. The feed ports are designed over thin Rogers RT/Duroid 6006 (with dielectric constant 6.15) where the antenna is placed over thick foam substrate (with dielectric constant 1.06) to satisfy light weight constraint of SAR systems. The Ku band antenna with two orthogonal feed ports is designed over Rogers RT/Duroid 5880 (with dielectric constant 2.2) and separated from the dual band antenna underneath by a foam substrate. The antenna exhibits return loss less than (-15 dB) at all frequencies. The simulated data is obtained using $\text{HFSS}_{11.1}$ readymade software.

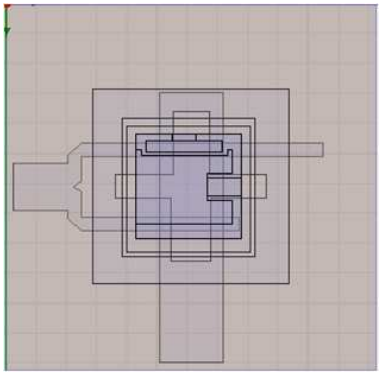

Figure 1: Simulated structure of TBDP antenna (top view).

A Multiple-notch UWB Printed Slot Antenna with CNSS Enhanced

Baiqiang You, Tao Zhou, and Jianhua Zhou
Department of Electronic Engineering, Xiamen University, Xiamen, Fujian, China

Abstract— This paper is focused on the design of a printed slot antenna with multiple-notch function for ultra-wideband (UWB) applications and also enhanced gain for the Compass Navigation Satellite System (CNSS). The proposed antenna consists of a curved radiation patch with an arc gradient microstrip line configuration and a class octagonal-shaped wide slot (with beveled bottom edges and stepped top edges) on a rectangular ground plane, supporting a much wider impedance bandwidth. With a class C-shaped slot on the patch and a class L-shaped strip attached on the ground, the multiple-notch function could be achieved to cover all the 5.2/5.8 GHz WLAN, 3.5 GHz WiMAX and 4 GHz C-bands. By introducing a third-order stepping strip at the upper part of the wide slot on the ground, an additional operating frequency in 2.492 GHz CNSS band can be realize. The simulation results show that the designed antenna is with a small size and relative bandwidth larger than 122% in the band of 3.10 $\sim$ 12.99 GHz. The radiation pattern and current distributions are also analyzed respectively.

As shown in Fig. 1, the proposed multiple-notch antenna is fed by a gradient microstrip line. The antenna is designed to be printed on a FR4 substrate with an area size of $29 \times 23\,\text{mm}^2$ and thickness of 1 mm, relative permittivity of 4.4, and loss tangent of 0.02. The class C-shaped slot on the radiation patch and the class L-shaped stub on the ground act as a quarter-wave resonant structure at the required notch center frequency respectively, perturbing the resonant response.

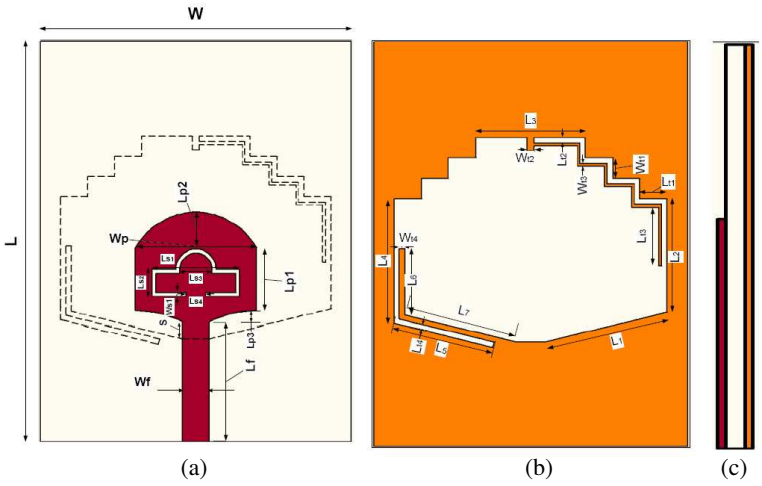

Figure 1: Configuration of the proposed antenna. (a) Top view. (b) Bottom view. (c) Side view.

Active Phased Array Radars as an Effective ECCM systems

Faran Awais Butt, Ahmed Malik, and Madiha Jalil
School of Engineering, University of Management and Technology (UMT), Lahore, Pakistan

Abstract— Phased Array Radars have started to regain some serious attention over the past few decades owing to its high accuracy, efficiency and less susceptible characteristics. The most basic requirement that one could wish for in a good modern radar is its beam agility, low distribution loss, maximum bandwidth, lower cost, maximum efficiency and effective resource management. Modern phased array radars can be best utilized to achieve characteristics of an effective radar system with minimum tradeoffs. The most basic thing that it can achieve is, that the antennas can be arranged to get the desired radiation pattern. Graceful degradation, higher date rate, ease of maintenance and flexibility, effective power management and anti jamming capabilities makes active phased radars far more capable and agile than other types of radars.

Figure 1 shows the normalized pattern of a 2d array with 10 elements on x axis and 100 elements on y axis, where as Fig. 2 shows the normalized pattern with 100 elements on x axis and 100 elements on y axis. Clearly we can see that the side lobes amplitudes have decreased considerably. So by this, jamming can also be countered and more power can be concentrated in particular direction of interest.

Figure 3 is highlighting the pattern for phi squints of 20 and 30 degrees and Fig. 4 is showing the power corresponding to various values of squint angles. The corresponding phi squints give the maximum peak at these values. Taking into consideration different T/R modules, we can

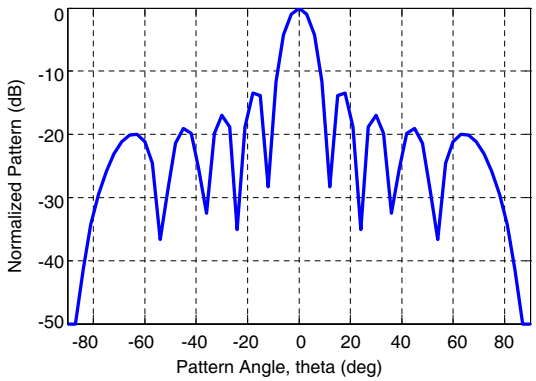

Figure 1: Normalized pattern vs. pattern angle for 10 elements on x axis.

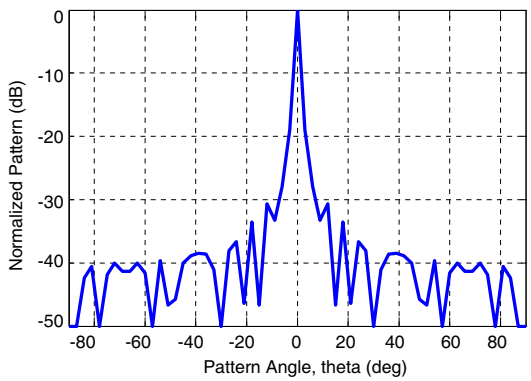

Figure 2: Normalized pattern vs. pattern angle for 100 elements on x axis.

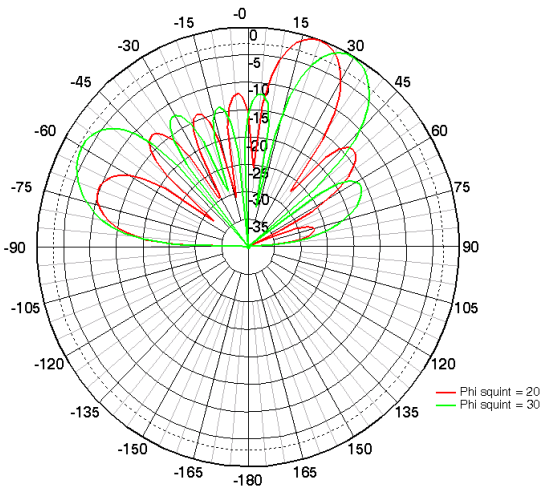

Figure 3: Electric field pattern for azimuth squint of 20° and 30°.

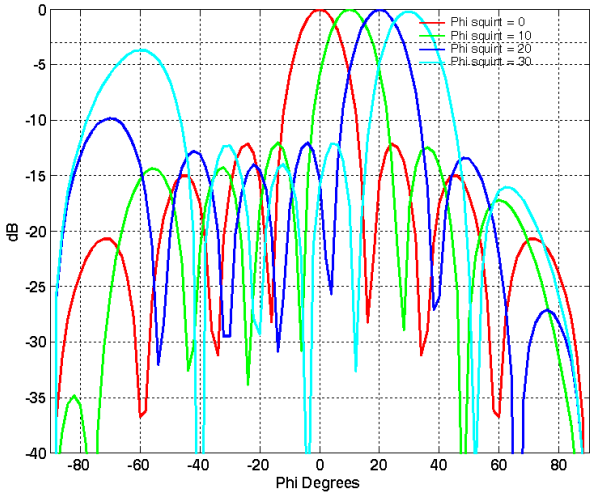

Figure 4: Pattern cuts for azimuth squint of 0°, 10°, 20° and 30°.

also have an effect of a MIMO system and overall system can be able to transmit while having frequency diversity, different polarization and sidelobe blanking. The results shows that offsetting the transmission angle of different radiating elements of active phased array radar can give us a desired radiation pattern and hence can be very useful as it can overcome the effects of various forms of jamming.

Modern active phased arrays radars can be exploited to have all properties that one could wish for in good military based radar. They provide an overall improvement in radar functionality and performance. They also provide improved anti-jamming ability, fast beam scanning and ability to track multiple targets at a time. The benefit we can extract from the active nature of the arrays is the modifications of TR modules which are independent of other TR modules. Hence active phased array radar can be casted by the user according to the demands of the situation. In future, modern phased array systems with MIMO functionality can make an ideal ECCM system. The benefit of active phased array would be the vigilance to approaching threats all across azimuth and elevation angles.

Design and Implementation of a New Missile-borne Conical Conformal Antenna

Ming Li, **Liang Xu**, **Wen Bin Zeng**, **and Guo Liu**
The Institute of Radio Wave Propagation, Xidian University, Xi'an, Shaanxi 710071, China

Abstract— In this paper, a conical missile-borne conformal antenna is proposed to meet a specific application. To achieve good omnidirectional circularly polarized (CP) radiation, the proposed antenna array is consisted of four identical CP microstrip antennas, which are distributed around the projectile. The antenna array is fed by a four power splitter, shifter network and optimized patch is used to get CP performance for each antenna. The measured results are in good agreement with the simulation one. The experimental results show that the axial ratio (AR) of element antenna is less than 3 dB, omni-axis ratio is less than 6 dB, and the 3 dB axial ratio bandwidth is 19 MHz. The antenna array can obtain the impedance bandwidth of 1.18 GHz $\sim$ 1.36 GHz with the relative bandwidth 28.3%. The radiation pattern of antenna in the horizontal direction is circular, with un-roundness less than 2 dB and the vertical pattern is "8", zero depth is about -20 dB. The designed antenna array is compact, low profile, and low cost with good performance. This antenna array is very useful in practice.

A Study of Parameterization on Rectangular Patched Microstrip Antenna Using High Frequency Structure Simulator (HFSS)

Anas Abdu and Hong-Xing Zheng
Tianjin University of Technology and Education, China

Abstract— With low profile nature, light weight, eases of fabrication and conformability with many integrated circuits [1], microstrip antenna makes it very attractive in the world of wireless communication. However, many researchers across the globe are now investing their time to research on the microstrip antennas [2] because of the inherent narrow bandwidth of the patch. In order to design an antenna operating from 1 GHz to 9 GHz to be suitable for the mobiles or vehicles, the size of patch must be considered carefully. It is very essential to study the parameterization of this antenna as it would be a conceptual tool for beginners in the field of antenna design. Effect of the length (L) and width (W) of the patch and the height (h) of the substrate of patched microstrip antenna has been investigated in details in this approach. Using the ansoft software of High Frequency Structure Simulator (HFSS), how the bandwidth and other characteristic affected by L, W and h have been observed [3]. Many operating frequency bands have been observed when these parameters are changed. It was discovered that, these parameters are critical in determining the resonating frequency, improving the bandwidth, impedance and other features of the antenna. Finally a multiple band antenna has been realized.

ACKNOWLEDGMENT

This work was supported by the Tianjin Research Program of Application Foundation and Advanced Technology under Grant 12JCYBJC10500.

REFERENCES

1. Ali, M., G. J. Hayes, H.-S. Hwang, and R. A. Sadler, "Design of a multiband internal antenna for third generation mobile phone handsets," *IEEE Transactions on Antennas and Propagation*, Vol. 51, 1452–1461, 2003.
2. Sami, G., M. Mohanna, and M. L. Rabeh, "Tri-band microstrip antenna design for wireless communication applications," *Journal of Astronomy and Geophysics*, Vol. 2, 39–44, 2013.
3. Ma, X.-B. and H. Zheng, "A wide-band antenna design by using electromagnetic simulation software," *Applied Mechanics and Materials*, Vols. 198–199, 1594–1598, 2012.

Absorption of 30 and 20 GHz Microwave Communication Signal as a Function of Rain Rate

Inderjit Singh Hudiara
Chitkara University, Chandigarh-Patiala National Highway, Rajpura, Punjab 140401, India

Abstract— The attenuation of Microwave communication signals operating at 30 GHz and 20 GHz has been measured as a function of rain rate. The line of sight distance between the transmitters and receivers was 2.3 km. It is experimentally observed that as the rain starts falling the signal received by the receivers at both the frequencies starts decreasing and as the rain rate starts increasing, the signals received by both the receivers starts decreasing and reaches to a minimum value when the rain rate is highest and as the rain rate starts decreasing the signal received at both the frequencies starts increasing and reaches the previous maximum value when the rain stops. This shows that microwave signal is absorbed by water contents of rain and we must transmit more power during rain to get the same power at the receiver. However, the increase in power at the transmitter end will depend on the rain rate. It is observed that the attenuation of microwave signal operating at 30 GHz and 20 GHz follow the same pattern. Line of sight path attenuation as a function of rain rate has also been experimentally measured at these frequencies. It is observed that the rain induced attenuation increases at both the frequencies as the rainfall rate increases. It is observed that the rain induced attenuation at 30 GHz is higher than at 20 GHz for the same rainfall rate. Specific rain induced attenuation has also been calculated using Medhurst technique and compared with Marshal and Palmer and International Telecommunication Union Models.

Rain attenuation parameters as a function of rainfall rate obtained in this experimental study can be used for designing efficient and reliable terrestrial and satellite communication systems.

Session 4P11a
SC1: Novel Mathematical Methods in Electromagnetics

On the Influence of the Electronic Structure of Atoms on the Behavior of Radiation Transition Probabilities in Alternating Electric Fields

E. V. Koryukina
National Research Tomsk State University, 36, Lenin Ave., Tomsk 634050, Russia

Abstract— In this work, it is shown that the behavior of transition probabilities in emission spectra of rare gases, induced by alternating circular electric field, is specified by the electronic structure of atomic states. A simulation of the behavior of transition probabilities in electric fields of different strengths and frequencies has allowed us to classify the behavior of considered probabilities according to the electronic structure of the Stark states participating in the transition.

The method of the energy matrix diagonalization for an atom in the electric field [1] was used for our theoretical calculations. This method free from limitations of perturbation theory was implemented in the computer software package *StarkD*. In the framework of the suggested approach, it has been shown that the degree of the Stark state interactions depends on the electronic structure of atoms, that is, on the quantum numbers n and l of electron from the external electron shell and the quantum number J of the energy level under consideration.

An analysis of the wave functions has shown that, at $J \leq 2$, the absence of the energy state interactions is typical of the low-lying atomic states with small n. The mixture of the states increases with quantum numbers J, n, and l of the energy state from which the transition occurs and with the electric field strength. Based on the electronic structure of atomic states and the degree of the Stark state interactions, the following classification of the types of behavior for transition probabilities $A(JM \rightarrow J'M')$ with changes of the electric field F and electric field frequency ω has been established:

- For weak mixture of the Stark states, all $M \rightarrow M'$ transitions are equiprobable (at $J,\ J' \leq 1$) and pairwise equiprobable (at $J,\ J' \geq 2$), and the transition probabilities decrease with increasing electric field strength. For strong interactions of states, all $M \rightarrow M'$ transitions are unequiprobable, and transition probabilities can either decrease or increase with increasing F;
- For weak mixture of the Stark states, the transition probabilities are practically indifferent to an increase in the electric field frequency. For strong state interactions, an increase in ω causes a tendency of unequiprobable $M \rightarrow M'$ transitions to pairwise equiprobability;
- Both for weak and strong mixtures of states, the behavior of the $A(JM \rightarrow J'M')$ probabilities for $J \leq J'$ and $J > J'$ is noticeably distinguished. If $J \leq J'$, then the probabilities of all transitions drastically diminish with switching on the electric field, and then they become practically insensitive to changes in the electric field strength. On the contrary, if $J > J'$, then at least one of all probabilities is practically independent of the electric field strength, whereas the remaining ones demonstrate the same behavior as that of the transition probabilities for $J \leq J'$;
- Both for weak and strong mixture of states, switching on the electric field leads to the M-ordered distribution of transition probabilities.

These regularities obtained for the first time are interesting from the theoretical viewpoint and can be used for solving practical problems of plasma spectroscopy, gas discharge physics, and astrophysics.

REFERENCES

1. Koryukina, E. V., *J. Phys. D: Appl. Phys.*, Vol. 38, 3296-33, 2005.

Higher-order Surface Modes in the Goubau Line

Ekaterina Kuzmina[1] and Yury Shestopalov[2]

[1]Moscow State Institute of Radio Engineering, Electronics, and Automation (Technical University)
pr. Vernadskogo 78, Moscow, Russia
[2]Department of Electronics, Mathematics and Natural Sciences
Faculty of Engineering and Sustainable Development, University of Gävle, Gävle SE-801 76, Sweden

Abstract— A significant amount of fundamental results of the mathematical theory of wave propagation in open and shielded metal-dielectric waveguides obtained recently [1, 2] open new possibilities for solving forward and inverse problems of electromagnetics. In particular, the description of the spectrum of normal waves is completed for a wide family of waveguides with dielectric inclusions (which actually envelopes all known types of basic guiding structures including slot and strip lines). It is shown that the spectrum is nonempty, forms a countable set of isolated points on the complex plane (there is no continuous spectrum), is located symmetrically in a certain band, and the spectral points enter the spectrum in 'fours'. Consequently, the mathematical background and potential relatedto comprehensive mathematical modeling and analysis of more complicated structures increase. In this work, we apply some of these results to investigate higher-order surface modes propagating in an open metal-dielectric waveguide — the Goubau line (a perfectly conducting cylinder of circular cross section covered by a concentric dielectric layer). We show that analysis of the spectrum of higher-order surface modes reduces to the solution of specific families of Sturm-Liouville boundary eigenvalue problems with the boundary operator depending on the spectral parameter. We prove the existence and analyze the spectrum of the principal and higher-order surface modes revealing some of their important properties that were not reported earlier by solving these spectral problems. The developed techniques enable one to study conducting cylinders, complex waves, and multi-layer lossy dielectric covers.

REFERENCES

1. Shestopalov, Y. and Y. Smirnov, "Eigenwaves in waveguides with dielectric inclusions: Spectrum," *Applicable Analysis*, 22, 2013, DOI: 10.1080/00036811.2013.778980.
2. Shestopalov, Y. and Y. Smirnov, "Eigenwaves in waveguides with dielectric inclusions: Completeness," *Applicable Analysis*, 20, 2013, DOI: 10.1080/00036811.2013.850494.

Inverse Problem Method for Permittivity Reconstruction of Two-layered Media: Numerical and Experimental Results

Yu. V. Shestopalov[1], **Yu. G. Smirnov**[2], **and E. D. Derevyanchuk**[2]

[1]University of Gävle, Sweden
[2]Penza State University, Russia

Abstract— In this paper we consider the inverse problem of finding permittivity of the media filling multi-sectional dielectric diaphragms in a rectangular waveguide. Electromagnetic parameters of composite dielectrics bodies as a rule cannot be directly measured in practice. Therefore mathematical modeling is applied.

In our early studies [1–3] we developed a numerical-analytical method for solving the inverse problem of permittivity determination of layered materials: in [1, 2] permittivity and permeability were scalars and in [3] they were tensors. In all these works we solve the corresponding diffraction problem to get the input data for solving the inverse problem.

This work is a continuation of the investigations performed in papers [1, 2]. The study is devoted to the comparison of numerical and experimental results in the case of a two-sectional diaphragm. For this purpose we use the experimentally obtained input data. By the developed numerical-analytical method [1, 2], we solve the forward diffraction problems and reconstruct electromagnetic parameters of both diaphragm sections with the prescribed accuracy. Then we compare our numerical results with the measured and experimentally obtained data. Analysis of the comparison shows the efficiency of the method. The developed technique can be applied in nanotechnology and optics for the determination of electromagnetic parameters of layered media. A special significance of the results and the developed approach is connected with the possibility of finding permittivities of artificial composite materials with unknown electrodynamic properties on the basis of standard equipment employing network analyzers.

REFERENCES

1. Smirnov, Yu. G., Yu. V. Shestopalov, and E. D. Derevyanchuk, "Permittivity reconstruction of layered dielectrics in a rectangular waveguide from the transmission coefficient at different frequencies," *Inverse Problems and Large-Scale Computations, Series: Springer Proceedings in Mathematics & Statistics*, Vol. 52, 169–181, 2013.
2. Smirnov, Yu. G., Yu. V. Shestopalov, and E. D. Derevyanchuk, "Permittivity determination of multi-sectional diaphragm with metamaterial layers in rectangular waveguide," *PIERS Proceedings*, 135–139, Taipei, March 25–28, 2013.
3. Smirnov, Yu. G., Yu. V. Shestopalov, and E. D. Derevyanchuk, "Reconstruction of permittivity and permeability tensors of anisotropic materials in a rectangular waveguide from the reflection and transmission coefficients at different frequencies," *PIERS Proceedings*, 290–295, Stockholm, August 12–15, 2013.

Propagation of TM Waves in a Double-layer Nonlinear Inhomogeneous Cylindrical Waveguide

E. Yu. Smolkin and D. V. Valovik
Penza State University, Russia

Abstract— The paper focuses on the problem of electromagnetic TM (transverse-magnetic) wave propagation in a two-layered circle cylindrical dielectric waveguide (this is an example of Bragg waveguide) with nonlinear permittivity $\varepsilon = \varepsilon_2(\rho) + f(|\mathbf{E}|^2)$ inside one of its layers (here $\varepsilon_2(\rho)$ is a function of inhomogeneity, which depend on radius of the waveguide; f is a function that models nonlinearity; $\mathbf{E}$ is the complex amplitude of an electric field); the other layer has constant permittivity. We speak only about intensity-dependent permittivity.

The physical problem is reduced to a nonlinear transmission eigenvalue problem for Maxwell's equations, which then reduced to a system of nonlinear ordinary differential equations. Existence of eigenvalues of the considered problem is proved. Eigenvalues of the problem correspond to propagation constants of the waveguide.

Numerical experiments are carried out for three types of nonlinearities:

- $\varepsilon = \varepsilon_2(\rho) + \alpha u^2$ (Kerr law);
- $\varepsilon = \varepsilon_2(\rho) + \frac{\alpha u^2}{1+\beta u^2}$ (nonlinearity with saturation);
- $\varepsilon = \varepsilon_2(\rho) + \alpha(1 - e^{-\beta u^2})$ (nonlinearity with saturation),

where $\varepsilon_2(\rho)$ is one of ρ^{-1}, const, and ρ. Comparisons with linear homogeneous (inhomogeneous) and nonlinear homogeneous (inhomogeneous) cases are given. One of the interesting results is that there are new eigenvalues that correspond to a new nonlinear propagation regime. These eigenvalues can not be obtained from the corresponding linearised problem.

Numerical Analyze of Waveguide Transmission Coefficient with Non-uniform Dielectric Slab

A. P. Smirnov[1], **A. N. Semenov**[1], **and Y. V. Shestoplalov**[2]

[1]Lomonosov Moscow State University, Moscow, Russia
[2]University of Gavle, Gavle, Sweden

Abstract— Propagation in the time domain of electromagnetic waves in a rectangular waveguide with a non-uniform dielectric slab is considered. Electromagnetic field components are computed and investigation of energy transport in the guide is performed by using Finite Difference Time Domain (FDTD) method in different frequency ranges. Parallel high performance FDTD solver, based on Maxwell equations approximation in integral form on Yee lattice and developed by the paper authors is used. A method for calculating the transmission coefficient with respect to all the problem parameters is proposed. The method is based on the analysis of the amplitude of the scattered wave derived from FDTD numerical solution. The pure scattered field method is proposed to specify the waveguide mode with respect to numerical dispersion. Computations for nonstationary Maxwell equations system are performed for the H_{10}-mode scattering from a dielectric slab placed in the waveguide. Multiple numerical computations for the corresponding large-scale problems have been performed on Lomonosov Moscow State University IBM BlueGene/P supercomputer. Using the methods described above, we compute the values of the waveguide transmission, attenuation and propagation factors in a wide range of permittivity and different positions of the dielectric slab inclusions. Continuous curves on the complex plane describing the dependence of the transmission coefficient on the dielectric constant are obtained. The comparison of the transmission coefficient calculated by the present approach and the volume integral equation method is performed.

Near Field Optimization in EM Simulation of Smart Shelf RFID Antenna Radiation

Andrey S. Andrenko
SYSU-CMU Shunde International Joint Research Institute
No. 1, Eastern Nanguo Road, Shunde, Foshan, Guangdong 528300, China

Abstract— This paper presents the accurate analysis and EM simulation of the so-called smart shelf antenna designed for the UHF RFID retail and item-tagging applications. The smart shelf antenna operation utilizes the near field communication in a range close to a wavelength between the planar reader/writer antenna and several tagged items being placed on the shelf. To provide reliable detection of the multiple tags which can generally be distributed within a wide interrogation volume over the shelf surface, uniform and strong near field radiated be the smart shelf antenna is required.

This paper presents the accurate analysis and EM simulation of the so-called smart shelf antenna designed for the UHF RFID retail and item-tagging applications. The smart shelf antenna operation utilizes the near field communication in a range close to a wavelength between the planar reader/writer antenna and several tagged items being placed on the shelf. To provide reliable detection of the multiple tags which can generally be distributed within a wide interrogation volume over the shelf surface, uniform and strong near field radiated be the smart shelf antenna is required.

The design of the proposed smart shelf antenna is based on the EM coupling between the open ended, or shorted-to-the ground microstrip line and periodic metal strips printed on the top surface of a dielectric substrate. Because of the standing wave current-voltage distribution along the microstrip line the parasitic metal strips are placed at the points of maximum voltage so that the uniform phase distribution along antenna aperture is realized. The required uniform near E-field has been provided by optimizing the layout of the periodic strips forming the smart shelf antenna layout. Series of full-wave EM simulations have been carried out to analyze the E-field distribution calculated at the different distances from the antenna surface, in a range from 5 cm to 40 cm. It has been confirmed that the proposed antenna creates strong near field within the entire volume where multiple RFID tags are placed. Two types of the smart shelf antenna have been designed and optimized. The first is the antenna where the periodic EM coupled elements are straight strips of approximately one wavelength so that the smart shelf antenna radiates predominantly linearly polarized E-field. Such an antenna is to be used for library and automated file processing when RFID tags are oriented in a specific direction. The second one has been designed for the apparel tagging applications where tagged items are arbitrary oriented in the plane parallel to the antenna surface. Therefore, EM near field of this antenna has to be quasi-circularly polarized (CP) with quasi here meaning the E-field having also z-component (normal to antenna surface). What is the most important in such an application is that the E-field has to have a well balanced x- and y-components at the different distances from antenna and within an entire interrogation volume. The required quasi-CP near field has been optimized by utilizing the three-section layout of the periodic metal strips and changing the angles of between strip sections that results in both Ex- and Ey-components being produced.

Several prototypes of the proposed smart shelf antenna have been produced and their performance in the UHF RFID system has been verified. 100% detection rate and measured read range for the large number of tagged items have confirmed the simulated near field distribution and excellent performance of the proposed antenna.

Energetic Wave Process of Time-domain Signal Propagation in Hollow Waveguides

Özlem Akgün[1] and Oleg A. Tretyakov[2]

[1]Department of Electrical and Electronics Engineering, Aksaray University, Aksaray, Turkey
[2]Department of Electronics Engineering, Gebze Institute of Technology, Gebze, Kocaeli, Turkey

Abstract— The aim of this study is to focus on the energetic wave process of the time-domain signal propagation utilizing the modal amplitudes proposed recently in [1] where non-sinusoidal modal amplitudes of TE and TM waveguide modes are aimed in a hollow waveguide and expressed explicitly via products of the Bessel and the modified Bessel functions.

It is a well-known fact that power and energy are associated with time-varying electromagnetic fields. For time-harmonic electromagnetic fields, the quadratic characteristics of the fields are derived using the complex spatial forms of the field vectors resulting in time-averaged energy density and complex power. Hence, the opportunity to study the dynamic processes of the aforementioned quadratic characteristics is lost in the classical time-harmonic electromagnetic field concept. To overcome this drawback, the problem of signal propagation in a waveguide should be solved in the time domain directly. In [2], Evolutionary Approach to Electromagnetics (EAE) operating with the real-valued field is proposed to solve the time-domain waveguide modes explicitly. In [3], the EAE is used to explain the energy and surplus of the energy for the time-domain waveguide modes via the modal amplitudes generated by the solutions to the Klein-Gordon Equation (KGE) that are invariant under the relativistic Lorentz transformations and subjected to the causality principle. In [4, 5], the dynamics of the energetic modal characteristics for a lossy waveguide are discussed for TE and TM modes, respectively. However, there still exists various ways to solve the KGE, see Appendix A of [2], which is necessary to extend the analytical solutions yet to be known including the dynamic velocity of wave energy transferred along the waveguide that can be obtained via the modal amplitudes proposed in [1].

In this study, by calculating the exchange with the energy stored in the longitudinal and transverse field components of the time-domain waveguide modes, it is disclosed that the energetic process in the waveguide is also a wave process. The dynamic velocity is calculated to demonstrate how the velocity of wave energy transferred along the waveguide evolves in time.

REFERENCES

1. Akgün, Ö., "A complete set of relativistic time-domain waveguide modes in hollow waveguides," *Progress In Electromagnetics Research Symposium Abstracts*, 119, Stockholm, Sweden, Aug. 12–15, 2013.
2. Tretyakov, O. A. and O. Akgun, "Derivation of Klein-Gordon equation from Maxwell's equations and study of relativistic time-domain waveguide modes," *Progress In Electromagnetics Research*, Vol. 105, 171–191, 2010.
3. Eroglu, E., et al., "Energy education science and technology Part A: Energy science and research," Vol. 29, No. 1, 495–506, 2012.
4. Tretyakov, O. A. and M. Kaya, "The real-valued time-domain TE-modes in lossy waveguides," *Progress In Electromagnetics Research*, Vol. 127, 405–426, 2012.
5. Tretyakov O. A. and M. Kaya, "Time-domain real-valued TM-modal waves in lossy waveguides," *Progress In Electromagnetics Research*, Vol. 138, 675–696, 2013.

Session 4P11b
Computational Electromagnetics

Efficient Method for Field Coupling to Nonuniform Transmission Line Using Cascaded SPICE Model

Haiyan Xie[1], **Jianguo Wang**[2], **Yong Li**[1], **Hongfu Xia**[1], **and Chun Xuan**[1]

[1]Northwest Institute of Nuclear Technology, P. O. Box 69-12, Xi'an, Shaanxi 710024, China
[2]Northwest Institute of Nuclear Technology, P. O. Box 69-1, Xi'an, Shaanxi 710024, China

Abstract— This paper presents a method of equivalent cascaded SPICE model for external field coupling with nonuniform transmission line. In the method, the nonuniform transmission line is approximated by a series of cascaded segments of uniform transmission line first, then the SPICE model for each segment is developed, and at last these SPICE models are cascaded to compose the SPICE circuit of the nonuniform transmission line. Two nonuniform transmission lines excited by an external EMP with different incidences have been studied to validate its accuracy and efficiency. The results show that the induced voltages obtained by the proposed method agree well with those via the software CST even when the segment number is up to three and the proposed method has higher efficiency, where the CST takes several hours while the proposed method takes several seconds. Due to the application of SPICE model and directly computation in the time domain, this method allows for the analysis of nonuniform transmission line terminated with nonlinear loads and integrated circuits.

Self-consistent Simulation of the Nuclear (E1) HEMP

Meiyan Fu and Maoyu Zhang
Northwest Institute of Nuclear Technology, Xi'an 710024, China

Abstract— The early time (E1) nuclear high altitude electromagnetic pulse mostly is simulated in a non-consistent way, that is, just considering the geomagnetic field not the self-consistent magnetic field. But, how does the self-consistent magnetic field influence the waveform of the HEMP Electric field? Especially, when the pulse propagates toward the upward direction? This is a problem. In this paper, a one dimensional Particle-in-cell Parallel code has been developed for self-consistent simulation of the early time (E1) nuclear high altitude electromagnetic pulse. The electromagnetic field is calculated by the outgoing wave approximation, and the physical process of the Compton electrons scattered by the interaction of gamma rays with air molecules turning in the geomagnetic field and self-consistent magnetic field is computed by Particle-in-Cell method. The waveform characteristics of the electromagnetic pulse E1 of the self-consistent simulation are compared with the results from non-consistent simulation. The differences between self-consistent simulation and non-consistent simulation are given and analyzed.

Reduced Vlasov-Maxwell Modeling

P. Helluy[1], **M. Massaro**[2], **L. Navoret**[1], **N. Pham**[2], **and L. T. Strub**[3]

[1]University of Strasbourg & Inria Tonus, France
[2]University of Strasbourg, France
[3]AxesSim, France

Abstract— The Discontinuous Galerkin (DG) approximation is an efficient method for solving the time-dependent Maxwell equations around complex geometries. It is also very well adapted to parallel and GPU computing. In plasma physics or beam physics applications, it is important to couple the Maxwell model with the Vlasov model, which describes the motions of charged particles. The unknown of the Vlasov equation is the distribution function of the charged particles, which depends on time and on a six-dimensional space-velocity variable. It is thus very expensive to solve, even on recent supercomputers. The Particle-In-Cell (PIC) method is a popular Lagrangian method for solving the Vlasov equation. However, the PIC method often produces noisy and inaccurate numerical results. In addition, the PIC method is not well suited to recent multicore and parallel computers architectures. In this work we propose a fully Eulerian DG solver for computing both the electromagnetic field and the charged particles distribution function. The method is theoretically introduced in [1, 2, 4].

We first reduce the Vlasov equation to a space-only first order hyperbolic system compatible with the Maxwell model. We compute the coupled system with a generic DG solver adapted to recent multicore computers [3].

The solver is written in OpenCL and can run on a cluster of GPU, for instance. In the solver, the structure of the underlying hyperbolic system is described in an abstract manner. In this way, it is possible to solve any linear or non-linear hyperbolic system. In the conference, we will present two-dimensional and three-dimensional numerical simulations for the Maxwell or the Vlasov-Maxwell equations. We will compare the accuracy of a DG-PIC solver with the reduced Vlasov-Maxwell DG solver.

REFERENCES

1. Helluy, P., N. Pham, and A. Crestetto, "Space-only hyperbolic approximation of the Vlasov equation," *ESAIM: Proceedings*, Vol. 43, 17–36, 2013, http://hal.archives-ouvertes.fr/hal-00797974.
2. Helluy, P., N. Pham, and L. Navoret, "Hyperbolic approximation of the Fourier transformed Vlasov equation," 2013, http://hal.archives-ouvertes.fr/hal-00872972,
3. Helluy, P. and T. Strub, "Multi-GPU numerical simulation of electromagnetic waves," 2013, http://hal.archives-ouvertes.fr/hal-00919702.
4. Helluy, P., L. Navoret, N. Pham, and A. Crestetto, "Reduced Vlasov-Maxwell simulations," 2014, http://hal.archives-ouvertes.fr/hal-00957045,

Discontinuous Galerkin Time Domain Method for Scattering Problems Simulation with GPU Acceleration

Gen Chen[1], **Lei Zhao**[1], **and Wenhua Yu**[2]

[1]Center for Computational Science and Engineering
School of Mathematics and Statistics, Jiangsu Normal University, China
[2]2COMU, State College, PA 16803, USA

Abstract— An efficient numerical method for large and complex bodies is very important for many practical applications. In this paper, the Discontinuous Galerkin time-domain (DGTD) with GPU acceleration is proposed for simulating the large-scale electromagnetic (EM) scattering problems. DGTD contains the adaptability of the unstructured meshes and spatial superconvergence, which allows us to effectively handle many practical EM problems where the required precision is different over the entire domain, or when the solution lacks smoothness. And furthermore, the DGTD method has an embarrassing performance for parallel processing because the coupling of the elements only exits at interfaces. In the proposed method, we combined GPU calculation with MPI technology for large EM problem, which makes more than one GPU card can be used in the simulation. And the uniaxial perfectly matched layer (UPML) is used to truncate the computational domain, in which the spatial derivative does not need to be calculated. With this implementation, we have done some simulations on a workstation which includes two Intel Xeon E5-2690 CPU, NVIDIA Quadro 6000 Graphics card and 32Gb memory. We have verified the accuracy and efficiency of the algorithm by comparing the numerical results with analytical results. Numerical results show that the proposed method has good parallel performance.

A Fast Algorithm for Calculating Complex Targets Near-field EM Scattering Characteristics

Yanjie Cui, Wenqiang Chen, Xiangyang Zhang, Jianping Zheng, and Bai Yang
Science and Technology on Electromagnetic Scattering Laboratory, Beijing 100854, China

Abstract— In order to meet the requirement of fuse's digital simulation and hard-ware-in-the-loop simulation, a fast algorithm based on the electromagnetic scattering modeling techniques of complex targets in the near field is proposed to calculate the echo power of fuse. The main research work in this paper involves the followings: 1) Considering the influence of antenna pattern and distance as well as spherical wave irradiation, a mathematical model based on the PO and PTD and GO methods is given to calculate the RCS of complex targets in the near field. In addition, the proposed theoretical model is calibrated by actually-measured data and the emulation results are with a good agreement with measured results. 2) We consider the radar target as a set of cubes and its local points. Each cube is an area of target's surface. Each local point is the middle point of all triangles which are located inside of the local cube. For instance, geometrical model of F-117 consists of 20 local points. Then calculate the diagram of RCS of the cube and for distance from antenna to local point of cube in spherical coordinate (angel of vision and angel of azimuth). 3) Establishing the missile-target encounter model though the conversion from different coordinate systems, then calculate the echo power of fuse by integrating those of the local points which are illuminated by radar beam during missile target encounter. Based on the theoretical analysis method proposed in former mentioned, we have developed a program to compute the echo power. Taking F-117 for exampleWe have calculated the echo power by the mentioned method and by the PO and PTD and GO methods, and the emulation results are with a good agreement. It is necessary to note also, the general time of calculation of echo power from F-117 on all trajectory is less than 1 second, but the PO and PTD and GO methods need almost half an hour. Above all, numerical results prove the proposed method high efficiency and preciseness. It would be especially valuable in engineering application.

Fast Iterative Computation of Internal Field Intensity for Cabin on HIRF Based on Energy Conservation Modification

Zichang Liang, Yi Liao, Pengcheng Gao, and Liangshuai Guo
Shanghai Key Laboratory of Electromagnetic Environmental Effects for Aerospace
Shanghai 200438, China

Abstract— With the development of electronic technology, the strength and operating frequency of communications navigation, military radar and other man-made radiation sources increase, which can't be ignored in the aerospace vehicle flight safety. Interior electromagnetic characteristics in the Fuselage under HIRF illumination is the foundation for the aerospace vehicle safety design. For electromagnetic radiation sources with operating frequency up to GHz, the size of aerospace vehicle fuselage can reach thousands of wavelengths and the electromagnetic wave reflects many times in the aerospace vehicle, which are electrically large interior cavity scattering problems which are difficult to converge.

This paper aims to meet the requirement of field strength calculation for the analysis of HIRF effect. We apply the iterative algorithm to calculate the reflection of the fuselage wall, and utilize the domain decomposition and the main beam tracking to accelerate the iterative procedure. Additionally, according to the principle of conservation of energy and the random extent of the field distribution after multiple reflections, we statistically predict the field distribution after the subsequent multiple reflections. The field distribution in the fuselage can be obtained with the method mentioned above. We compare the results obtained by the proposed method with the results of the numerical algorithm, and it demonstrates the effectiveness of the proposed method. The proposed method can be applied to efficiently model HIRF effect on a fuselage with length of 20 m at 40 GHz.

Session 4P12
SC1&4: Antennas, Shielding, HPEM and EMC Measurement

Dual Band Microstrip Antenna

Rafal Przesmycki and Paweł Skokowski
Faculty of Electronics, Military University of Technology
Gen. S. Kaliskiego 2 str., Warsaw 00-908, Poland

Abstract— Portable electronic devices more boldly enter into the daily life of modern man. Society depends not only from simple mobile phones, but also with multimedia equipment, which allows, among others continuous access of the Internet and determining the user's position through the GPS system. It can be assumed that this is a transitional phase to integrate multiple electronic devices with clothing and build a system, which includes many elements will be part of enabling human contact with the world and unlimited access to all the information, but also monitoring his vitals and his alarming and appropriate professionals about the potential dangers and hazards.

The article presents a multi-layered structure of a microstrip antenna operating at frequencies 2.4 GHz and 5.8 GHz. The design of the antenna consists of three dielectric layers and two of the radiating elements, is fed by electromagnetic coupling. The article also addresses the problems occurring in multilayer structures dual frequency.

When designing multilayer dual band microstrip antennas must take into account several important considerations. The main condition for the construction of multi-band antennas is resonant frequency spacing between them. Constructing a dual band microstrip antenna when to two frequencies, one of which is more greater than twice than the second encounter several problems of structural design.

Wideband Microstrip Antenna

Rafal Przesmycki, Marek Bugaj, and Marian Wnuk
Faculty of Electronics, Military University of Technology
Gen. S. Kaliskiego 2 str., Warsaw 00-908, Poland

Abstract— The article concerns the issue of a narrow band of microstrip antennas. The article presents ways to increase bandwidth operation of microstrip antennas, shows examples of the construction of microstrip antenna with a high operating band. The results obtained in the simulation and design of antennas confirmed through measurement. The rapid development of wireless technologies of access to the Internet and the requirements to meet the standards imposed on the WLAN, WiMAX and other wireless technologies necessitate the need for the device, which in addition to reliability and functionality are characterized by small size. As the essential element of any wireless system is an antenna, it also forces on the elements of miniaturization, and also the opportunity to work in more than one frequency band. Antennas, which, due to its characteristics to best meet the above requirements are microstrip antennas.

Narrow bandwidth is a major disadvantage of microstrip antennas. A typical width of the band of the antenna is almost always too low. At the present day wireless communication systems require antennas to the wide frequency band. Let's give an example, cellular systems (GSM 900: Range: 890–960 MHz) require bandwidth of 7.5%, for GSM 1800 (range: 1710–1880 MHz) bands need at 9.5%, and for UMTS systems 12, 2%. Order to meet these requirements is not an easy. Special methods have been developed to extend the frequency band of a microstrip antenna such as: increasing the thickness of the dielectric substrate, the use of structures using electromagnetic coupling with an additional patch radiating elements, multilayer configurations, powered by the coupling of aperture, etc..

Ultra-wideband Antenna with Metamaterial and Periodic Structure

Roman Kubacki, Salim Lamari, and Mirosław Czyżewski
Faculty of Electronics, Military University of Technology
Gen. S. Kaliski 2 Str., Warsaw 00-908, Poland

Abstract— Nowadays the Ultra-WideBand (UWB) technology occupies an important place in the communications systems, thanks to their compelling aspects, and high data rates, low cost and resistance to interferences. During the last decades the microstrip patch antenna has been the most experienced and analyzed antenna because of its simplicity of fabrication by means of lithographic techniques in monolithic circuits, and its low cost, simple structure, conformity and small size.

The advent of the metamaterials which are new materials, predicted by Veselago forty years ago, and having properties not generally found in nature, have offered some new possible solutions. Indeed, many new antenna designs have been proposed to approach this new technique. But one should notice that realization of metamaterials (called also as left handed materials) are classified in two categories; the resonant type and the non-resonant type. The non-resonant type of metamaterials is fundamentally the dual of the conventional transmission line circuit model. The non-resonant model has intrinsically low loss and wide bandwidth characteristics compared with the resonant type of metamaterials, therefore the non-resonant type is preferable from an application point of view. A non-resonant type in two-dimensional configuration can have a planar structure with an array of unit cells periodically arranged on both sides of a substrate.

In this paper, we propose an ultra-wideband microstrip antenna having higher bandwidth and gain. The concept of this metamaterial based antenna consists of a microstrip antenna with planar repetitive patterns etched on the metallic parts (patch and ground plane) of the laminate composing the antenna.

Identification of Interface in the Complex Systems Based on Radiated Emission of Mobile Computer

Rafal Przesmycki, Marian Wnuk, Pawel Skokowski, and Marek Bugaj
Faculty of Electronics, Military University of Technology
Gen. S. Kaliskiego 2 Str., Warsaw 00-908, Poland

Abstract— The electromagnetic energy emitted by any source in general, may depend on the frequency (f), the time (t) and the direction (Φ). The amount sent at the time (t) in the direction of (Φ), the frequency (f), per unit time and unit solid angle per unit frequency range (expressed in the case of three-dimensional space in $[\mathrm{W} \cdot \mathrm{sr}^{-1} \cdot \mathrm{Hz}^{-1}]$), can be called the ability sources emission:

$$\varepsilon = f(\Phi, f, t). \tag{1}$$

Electromagnetic energy emitted by IT devices to the surrounding environment is divided into two groups. The first group are desirable emissions associated with the transmission and processing of signals carrying useful information. Wanted emissions are eliminated through a proper and meticulous allocation of frequency bands or single frequencies. This phenomenon is called the electromagnetic spectrum management, or building resistance of objects to electromagnetic fields. In this paper, particular attention is paid to the second group of electromagnetic emissions, namely undesirable emissions. These emissions are by-products produced inadvertently during the implementation of the basic functions of IT equipment. They arise in electrical circuits containing inductance and capacitance, in which sudden changes of current or voltage, or fluctuating changes in the density of charge carriers occur, or in which a positive feedback or negative resistance take place.

The article describes the construction of complex systems, defined and estimated levels of radiated undesirable emissions coming from modern IT equipment on the market is the European Union. In addition, the article presents an analysis of radiated emissions for different hardware interfaces of PC laptop and the results of the identification of hardware interfaces for the mobile computer characterized by increased radiated emission.

Measurement and Analysis of Compromising Emanation for Laser Printer

Rafal Przesmycki
Faculty of Electronics, Military University of Technology
Gen. S. Kaliskiego 2 Str., Warsaw 00-908, Poland

Abstract— The protection of information against the penetration of electromagnetic devices and electronic systems (information technology) is very important. This problem increases with ever greater use of IT equipment for the processing and transmission of information, which should not fall into the wrong hands. This is due to the fact that every electronic device is a source of undesirable (secondary) emission of electromagnetic energy induced in the surrounding area, any electrical wiring and metal structures.

When the emission undesirable signals are correlated with the non-confidential information, they can be used to reproduce the information by intelligence services. The phenomenon of the emission undesirable is called disclosing emission. The use of disclosing emission by intelligence services we call penetration or electromagnetic infiltration. Projects designed to blocking identifying systems based on disclosing emissions we call information protection against the penetration of electromagnetic emissions or safety emissions.

The article concerns problems of electromagnetic compatibility and disclosing emission that is the information security. The article describes the electromagnetic channels of penetration information. There are three channels of information penetration: conducted, radiated and mixed. The article focuses on the radiated channel of penetration information, and then focuses on laser printers for which shows signals of extortion used during of disclosing emission measurements. The article presents the results of disclosing emissions measurements derived from laser printer. In addition, the article discusses the laboratory stand for measuring disclosing emissions. The laboratory stand to determine the measurements a sources of disclosing emissions should be able to receive the generated test signal propagates as disclosing radiated emissions. The laboratory stand is based on wideband measurement receiver and active, low-noise antennas.

Compromising Emanations from USB 2 Interface

Leszek Nowosielski and Marian Wnuk
Faculty of Electronics, Military University of Technology
Gen. S. Kaliskiego 2 Str., Warsaw 00-908, Poland

Abstract— The article concerns problems connected with eavesdropping risks of PC computers. Compromising emissions are defined as unintentional intelligence-bearing signals which, if intercepted and analyzed, may disclose the information transmitted, received, handled, or otherwise processed by any information-processing equipment. The PC computers interfaces (e.g., USB, ETHERNET, RS-232) can emit unintentional signals from which eavesdroppers may reconstruct processed data at some distance. The article focuses on USB 2.0 interface which is one of the most popular PC interfaces. This interface was designed to standardize the connection of computer peripherals to personal computers, both to communicate and to supply electric power. The article documents eavesdropping experiments on USB 2.0 interface. It discusses the nature and properties of compromising emanations for USB 2.0 interface. The detection equipment used matches the capabilities to be expected from professional eavesdroppers. The article demonstrates the use of cross-correlation to find even weak traces of a data sent by USB 2.0 interface as radiated emissions. The article illustrates how cross-correlation can detect a known signal within noise and in this way provides a sensitive measure for the signal detection. All described experiments were carried out in a shielded anechoic chamber.

Attenuation Measurements of Materials Used in Construction of Buildings

Marek Bugaj
Faculty of Electronics, Military University of Technology
Gen. S. Kaliskiego 2 Str., Warsaw 00-908, Poland

Abstract— Attenuation of walls, ceilings, or other building partitions depends inter alia on the electrical permittivity of the material from which the wall is built, the frequency of the incident radiation and the thickness of the wall. In order to determine the attenuation of electromagnetic waves through the wall should measure each wall individually to determine what level of intensity of the electromagnetic field is attenuated by such a barrier. In order to determine the attenuation of the materials used for building construction perform the analytical calculation of the electric field attenuation or made direct measurement of the sample of the natural material. In order to calculate the analytical attenuation of the electromagnetic field by the shielding material is necessary to determine the electric and magnetic properties of the material from which is made of a construction material. The parameters that define above properties shall suitably permittivity and the magnetic permeability of the material under test. Due to the fact that the construction materials, especially those based on natural raw materials (concrete, brick, gypsum) are characterized by a repeating composition of the rare, the only way to estimate its electrical and magnetic properties is carried out using a laboratory measurement of the natural samples.

In practice has not been possible tested all materials because they used in a wide variety of their assortment and their composition rarely repeated. For this reason, it is impossible to accurately determine the attenuation values of the wall (elevation) or a simple, fast and direct method of measuring its performance. The article focuses therefore on the number of selected types of materials used in the construction of buildings. The article describes the test methodology and laboratory stand to determine the attenuation of the materials used in the construction of buildings. The described test methodology is based on microwave test set based on a coaxial line which guarantees a wide range of performed measurements. The article describes the selected samples of the materials used in the construction of buildings and presents the results of attenuation of these materials.

New Attempt to Building Materials Permittivity Measurements

Roman Kubacki
Faculty of Electronics, Military University of Technology
Gen. S. Kaliskiego 2 Str., Warsaw 00-908, Poland

Abstract— Many recently published investigations and numerical calculations that predict wireless local area network performance claim regarding the propagation losses through the walls at higher frequency range. In the work, measured results for complex permittivity of some commonly used building materials have been presented. The relative permittivity was measured in the coaxial line with TEM fundamental mode. Such a measurement condition corresponds to the free-space test, with a planar incident wave. In the literature different techniques were presented for coaxial lines permittivity determination, basing on measurements of complex values of scattering parameters. In proposed attempt the only magnitude of transmission coefficient (S_{21}) has been used for relative permittivity determination. The relationships for calculating the relative permittivity and analysis concerning the algorithm convergence have been discussed. Proposed calculation method allows applying this method for measuring the electric field, neglecting the phase assessing. Examples of material tested in a laboratory setting are concrete, two kinds of bricks and gypsum board.

Measurements of Wall Attenuation in Closed Spaces inside a Building

Marek Bugaj
Faculty of Electronics, Military University of Technology
Gen. S. Kaliskiego 2 str., Warsaw 00-908, Poland

Abstract— In the present article deals with the issue of attenuation measurements of the walls in the confined spaces inside the building. The methodology of measurement and the measurement results obtained in determining the attenuation walls or other structural elements in a small, enclosed inside the building.

In order to measure the attenuation of walls in confined spaces is required in the test set, which includes a transmitter and a signal strength meter measuring electromagnetic fields. The individual parts of the kit may include a measurement software, which runs on a computer control to automate the measurement process. In the present article illustrates the principle of the measurement set without the use of control software.

The proposed measurement method is the primary method of comparison. On the basis of the results of measurement it is possible to determine the damping elements inside the building, such as walls, ceilings and other structural components for buildings.

Attenuation measurement indoor walls are reduced to perform two measurements of the signal level at the receiver input for a specific frequency. The first measurement is made, as so reference measurement. During the measurement standardization transmitting antenna transmitter and receiving antenna measuring the field strength meter are placed close to each other in direct visibility.

Analytical Model of EMP Pulse

Leszek Nowosielski
Faculty of Electronics, Military University of Technology
Gen. S. Kaliskiego 2 str., Warsaw 00-908, Poland

Abstract— The article concerns problems connected with analytical modelling of high-voltage electromagnetic pulse (EMP) propagated in the anechoic chamber as the electromagnetic dumped sinusoid wave.

The article presents the analytical model of EMP pulse propagated in the anechoic chamber. The analytical model is based on the measurement results of the EMP pulses obtained from the Marx generator DS110 (Diehl BGT Defence, Germany). The maximum electrical field strength generated by the generator is 240 kV/m and the frequency spectrum of the pulse covers the frequency bandwidth 450 MHz from 150 MHz to 600 MHz. The measurements took place in the anechoic chamber with dimensions 10 m × 10 m × 10 m. The chamber is lined inside with the ferrite plates and pyramidal absorbers. The article presents also the description of the laboratory stand, where the measurements were made. The anechoic chamber is located in the Electronics Department at the Military University of Technology in Poland.

In order to validate the elaborated analytical model of EMP pulse the calculated pulse shape in time axis and the frequency spectrum is compared with the pulse shape and the frequency spectrum recorded during measurements in the anechoic chamber.

Measurement of Shielding Effectiveness with the Method Using High Power Electromagnetic Pulse Generator

Leszek Nowosielski and Jerzy Lopatka
Faculty of Electronics, Military University of Technology
Gen. S. Kaliskiego 2 Str., Warsaw 00-908, Poland

Abstract— The article concerns problems connected with electromagnetic compatibility. The method of measuring shielding effectiveness of small shielding chambers was described here which was based on using, as probing signal, high power pulses generated by Marx generator with the value of electric field strength over 90 kV/m with maximum duration of single pulse not exceeding 5 ns. The proposed method is characterized by a large range of shielding effectiveness (SE) measurement dynamics and it can be used for measurement of shielding effectiveness of chambers with small overall dimensions. In the article completion of measuring position was presented which consists of high power pulse generator and meter of the high power pulse level built on the basis of broad-band oscilloscope and sensor with matching block.

The new shielding effectiveness (SE) measurement methodology basing on HPEM RF DS110 pulse generator is described. In order to conduct validation of research methodology the shielding effectiveness measurement results for selected enclosure are presented. During the measurement the worked out methodology was used. The obtained measurement results are compared to shielding efficiency measurement results which are obtained using standard measurement methodology basing on the selective measurement receiver and RF signal generator which is used as source of testing signal.

Honeycomb Ventilation Grill Shielding Effectiveness Measuring Methodology

Leszek Nowosielski and Cezary Piotrowski
Faculty of Electronics, Military University of Technology
Gen. S. Kaliskiego 2 str., Warsaw 00-908, Poland

Abstract— The article concerns problems connected with shielding effectiveness calculation of the honeycomb ventilation grill using computer simulation in CST Microwave Studio environment.

At the beginning the honeycomb ventilation grill shielding effectiveness measurement methodology and laboratory stand diagram basing on the method which uses a selective measuring receiver and tuned RF signal generator has been presented. The described measurement methodology and selected honeycomb ventilation grill was modelled in CST Microwave Studio environment in order to conduct calculation of shielding effectiveness using computer simulation. In the article are presented the shielding effectiveness of selected honeycomb ventilation grill model obtained from computer simulation. The results of shielding effectiveness measurement of selected honeycomb ventilation grill obtained from real measurements using selective measuring receiver and tuned RF signal generator are presented too. The computer simulation and measurements using real laboratory stand were conducted in the frequency range from 300 MHz to 3000 MHz.

In order to validate the elaborated simulation model in CST Microwave Studio the shielding effectiveness simulation results are compared with the shielding effectiveness measured using the method based on a selective measuring receiver and retuned RF signal generator.

Technique of High Power Microwave Pulses Dosimetry of Living Systems

Roman Kubacki and Salim Lamari
Faculty of Electronics, Military University of Technology
Gen. S. Kaliskiego 2 Str., Warsaw 00-908, Poland

Abstract— The novel technique was proposed to improve the dosimetry of living tissues exposed to high power microwaves (HPM) radiation. HPM pulses are characterized by extremely high power in peak (mega or giga watts) and pulse duration less than 100 ns and are called as e-bomb. Many reports demonstrated the destructive effects of e-bombs to electronics exposed to HPM's. Despite the fact that potential health hazard from HPM pulses is not broadly investigated, the generators emitting such HPM pulses have been called non-lethal weapons. Electromagnetic radiation emitted from HPM generators can also be treated as ultra wide-band (UWB) signals because their frequency band is 500 MHz or broader.

In order to investigate the biological effects evoked in the high power electromagnetic fields, the numerical calculation for *in vitro* study has been carried out. The widely used 90 mm Petri dishes filled with human blood was exposed to high power microwave pulses in an anechoic chamber. Electric and magnetic vectors of the incident field were parallel to the surface of Petri dishes. According to the actual safety standards the specific absorption rate (SAR) is a basic restriction parameter for protecting against thermal effects in the risk assessment study. The numerical calculation has been performed to maintain uniformity of the specific absorption rate (SAR) distribution in the specimen. The novel attempt of the dosimetry takes into account the calculation of SAR of all frequency harmonics of the spectrum taking into consideration the function of permittivity of the medium (human blood) in the analyzed frequency range.

Modelling of Electromagnetic Wave Propagation with the Use of the Ray-tracing Method

Leszek Nowosielski, Jerzy Łopatka, and Michał Siłaczuk
Faculty of Electronics, Military University of Technology
Gen. S. Kaliskiego 2 Str., Warsaw 00-908, Poland

Abstract— In widely available literature concerning methods of radio-wave propagation modelling one can find a series of solutions different from each other in:

- modelled propagation environment (open space, urbanized area, building interior),
- dimensionality (two-dimensional, three-dimensional),
- possible to obtain calculation accuracy.

Only a few of them can be used for modelling of radio-wave propagation in semi-anechoic chambers. Despite the development of numerical methods used for solving electromagnetic problems (method of moments, FDTD) writing a program application implementing specific radio-wave propagation models is still very difficult and sometimes even impossible. We can distinguish a group of methods of radio-wave propagation modelling due to which, after some simplifications, it is possible to obtain simulation results with permissible accuracy in its acceptable duration.

The article concerns problems of electromagnetic wave propagation in semi anechoic chambers. Electromagnetic wave propagation modelling using ray tracing methodology is described. The analytical equations which are used in ray tracing methodology are presented. The elaborated program algorithm basing on presented analytical equations is described. The worked out software application basing on the described algorithm is presented. The validation results of elaborated software are presented too.

Electromagnetically Shielded Real-time MANET Testbed

Anna Kaszuba, Radoslaw Checinski, Michal Kryk, Jerzy Lopatka, and Leszek Nowosielski
Faculty of Electronics, Military University of Technology,
Gen. S. Kaliskiego 2 Str., Warsaw 00-908, Poland

Abstract— Mobile ad-hoc networks (MANETs) are fast growing method of efficient wireless communications in highly mobile environment. Such networks can be designed using software simulators. They allow users to design, test and analyze new solutions at low cost. In case of networks, these tools enable analysis of network configuration and protocol used for optimizing radio resources and performing the best Quality of Service (throughput, delays, etc.). However the simulators cause approximations of results due to simplification of EM compatibility issues and propagation phenomena in the electromagnetic environment. Furthermore the most common simulators do not allow the simulation in real time that causes long simulation time.

This problem can be resolved using real time test beds, containing SDR (Software Defined Radio) architecture. The most popular device based on the SDR technology is USRP (Universal Software Radio Peripheral). This device is widely used by researchers to study various transmission protocols or create real-time applications like OpenBTS or MIMO links.

This article describes a real-time testbed for MANET, where each radio node is represented by one USRP. Electromagnetic environment emulation is performed by RF switch matrix, providing attenuation of RF signals. The article presents also the software architecture of radio nodes including implemented physical layer based on OFDM (Orthogonal Frequency-Division Multiplexing) modulation and MAC (Media Access Control) layer based on TDMA (Time Division Multiple Access) radio access. Next, control process whole test bed and RF switch matrix is described. The obtained results show performance of the testbed.

Author Index